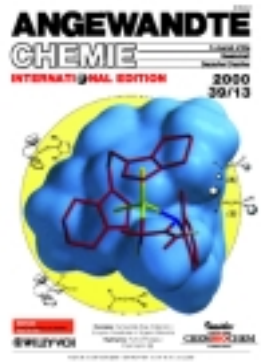
Cover Picture



Zachary K. Sweeney, Jennifer L. Salsman, Richard A. Andersen, and Robert G. Bergman

The cover picture shows a further example of the power of transition metal complexes in organic synthesis: the enantiopure imidozirconium complex, top left, reacts with 1,3-disubstituted racemic allenes (right) in a highly enantioselective, stepwise cycloaddition. Both the enantiomers of an allene react to give the same diastereopure azazirconacyclobutane complex, the structure of which is shown in the center of the picture as a space filling model with the molecular framework superimposed. The reaction with 1,2-propadiene (bottom center) releases the enantiopure allene from the metallacycle. The overall process couples kinetic resolution with the complete inversion of the absolute configuration of a 1,3-disubstituted allene. More about this unusual new method for enantiomer separation and enrichment is reported by R. G. Bergman et al. on page 2339 pp.

New syntheses with oils and fats as renewable raw materials for the chemical industry



ANGEWANDTE CHEMIE
© WILEY-VCH

New Syntheses with Oils and Fats as Renewable Raw Materials for the Chemical Industry

Ursula Biermann, Wolfgang Friedt, Siegmund Lang, Wilfried Lühs, Guido Machmüller, Jürgen O. Metzger,* Mark Rüsch gen. Klaas, Hans J. Schäfer, and Manfred P. Schneider

Oils and fats are the most important renewable raw materials for the chemical industry. Hitherto, industrial oleochemistry has concentrated predominantly on the carboxy functionality of fatty acids but, more recently, modern synthetic methods have been applied extensively to fatty compounds for the selective functionalization of the alkyl chain. Radical, electrophilic, nucleophilic, and pericyclic as well as transition metal catalyzed additions to the C–C double bond of, for example, oleic acid as the prototype of a readily accessible, unsaturated fatty acid have led to a large number of novel fatty compounds from which interesting properties are expected. Functionalization of C–H bonds in the alkyl chain is also feasible with remarkable selectivity. Effective and highly versatile catalysts for the metathesis of esters of unsaturated fatty acids have been developed, which lead to new and interesting ω-unsaturated fatty acids. The epoxidation of unsaturated fatty acids has been developed extensively. Enzymatic reactions allow syntheses with high selectivity and yield of mono- and diglycerides and esters of carbohydrates with a variety of surfactant properties. Regio- and enantioselective microbial hydrations and hydroxylations widen the spectrum of selective reactions. Of considerable significance is that, with the use of gene technology, natural oils and fats have been improved significantly and will be improved still further, insofar as they show a more uniform and often unusual fatty acid spectrum. Numerous fatty acids are now available in a purity which makes them attractive for synthesis and as raw materials for the chemical industry.

Keywords: additions · enzyme catalysis · fatty acids · gene technology · renewable resources

1. Introduction

Sustainable development had become the key ideal of the 20th century.[1] In the search for sustainable chemistry, considerable importance is being attached to renewable raw materials which exploit the synthetic capabilities of nature.[2, 3] Oils and fats of vegetable and animal origin make up the greatest proportion of the current consumption of renewable raw materials in the chemical industry, since they offer to chemistry a large number of possibilities for applications which can be rarely met by petrochemistry. The extent of the use of natural oils and fats in chemistry was summarized in 1988.[4] It stated that "more than 90% of oleochemical reactions have been those occurring at the fatty acid carboxy group, while less than 10% have involved transformations of the alkyl chain. However, future progress will be along the lines of these latter types of reactions with their potential for considerably extending the range of compounds obtainable from oils and fats. Such progress is essential for a growth in the use of oils and fats as renewable raw materials". For the future, this means that "oils and fats of vegetable and animal origin offer possibilities for providing chemistry with a wealth of reaction products which will be of great value in the future. The chemical possibilities of renewable oils and fats are still very far from being fully exploited. Interdisciplinary collaboration involving chemistry, biochemistry, plant breeding, and

[*] Prof. Dr. J. O. Metzger, Dr. U. Biermann
Fachbereich Chemie der Carl von Ossietzky Universität Oldenburg
Postfach 2603, 26111 Oldenburg (Germany)
Fax: (+49) 441-798-3329
E-mail: juergen.metzger@uni-oldenburg.de

Prof. Dr. W. Friedt, Dr. W. Lühs
Institut für Pflanzenbau und Pflanzenzüchtung I
Justus-Liebig-Universität Giessen (Germany)

Priv.-Doz. Dr. S. Lang
Institut für Biochemie und Biotechnologie
Technische Universität Braunschweig (Germany)

Dipl.-Chem. G. Machmüller, Prof. Dr. M. P. Schneider
FB 9 – Organische Chemie
Bergische Universität, GH Wuppertal (Germany)

Prof. Dr. M. Rüsch gen. Klaas
Fachbereich Technologie
Fachhochschule Neubrandenburg (Germany)

Prof. Dr. H. J. Schäfer
Organisch-Chemisches Institut der Universität Münster
(Germany)

 © WILEY-VCH Verlag GmbH, D-69451 Weinheim, 2000 1433-7851/00/3913-2207 $ 17.50+.50/0



Ursula Biermann, born in 1953, studied food chemistry in Hanover and Munich. She received her doctorate at the Deutsche Forschungsanstalt für Lebensmittelchemie, Garching, in 1979 under W. Grosch. Since 1987, she has been a research fellow at the Fachbereich Chemie of the Universität Oldenburg under J. O. Metzger, where she works on the synthesis of novel fatty compounds: natural oils and fats as chemical raw materials.



Wolfgang Friedt, born in 1946, studied agricultural science in Bonn and obtained his doctorate (plant breeding) at the Technische Universität München-Freising. He was a scientific fellow at the Institut für Resistenzgenetik, Grünbach, of the Biologische Bundesanstalt für Land- und Forstwirtschaft, followed by his habilitation (genetics) at the Universität Bayreuth. Since 1985, he has held a professorship for plant breeding in the Fachbereich Agrarwissenschaft und Umweltsicherung at the Universität Giessen. His research includes the genetic basis of plant breeding, cellular and molecular genetics, biotechnology, and cereal and oil plant breeding.



Siegmund Lang, born in 1945, is an Akademischer Oberrat at the Institut für Biochemie und Biotechnologie of the Technische Universität Braunschweig. He received his doctorate in 1975 on the microbiological hydroxylation of steroids under F. Wagner and H. H. Inhoffen at the Technische Universität Braunschweig, and completed his habilitation in 1999 at the same institute. His current research topics are the microbial production of biosurfactants and lipases and microbial marine biotechnology.



Wilfried Lühs, born in 1962, studied agricultural science in Giessen and gained his doctorate (plant breeding) in 1996. His research, at the Lehrstuhl für Pflanzenzüchtung of the Institut für Pflanzenbau und Planzenzüchtung in Giessen, is on the conception, planning, and organization of breeding programs, in particular rapeseed, by bio- and genetic technological methods.



Guido Machmüller, born in 1971, studied chemistry in Wuppertal. For his dissertation under M. P. Schneider, he worked on the bioconversion of renewable raw materials, specializing in enzymatic synthesis of isomerically pure carbohydrate esters and glycosides.



Mark Rüsch gen. Klaas, born in 1965, studied chemistry in Aachen and received his doctorate in 1993 under S. Warwel. During 1993–99, he was at the Institut für Biochemie und Technologie der Fette of the Bundesanstalt für Getreide-, Kartoffel- und Fettforschung. In September 1999, he was appointed Professor for Cosmetic Products and Commodities at the Fachhochschule Neubrandenburg. His particular interests are the use of vegetable oils in the nonfood areas and the development of catalytic oxidations with "clean" oxidizing agents.



Jürgen O. Metzger, born in 1940, studied chemistry in Tübingen, Erlangen, Berlin, and Hamburg. He gained his doctorate in Hamburg in 1970 on Ziegler–Natta catalysts. In 1983, he gained his habilitation at the Universität Oldenburg on the topic "Thermally initiated intermolecular organic reactions at elevated temperatures and pressures, and reactions under supercritical conditions". In 1991, he was appointed Professor of Organic Chemistry. His work areas include sustainability in chemistry, environmentally benign organic synthesis, renewable raw materials, radical chemistry, and mass spectrometry.



Hans Jürgen Schäfer, born in 1937, gained his doctorate on anionic rearrangements at the Universität Heidelberg in 1963. During 1964–66, he worked on the mechanism of chromic acid oxidations at Yale University and he gained his habilitation at the Universität Göttingen in 1970 on the topic "Anodic dimerizations and additions". In 1973, he was appointed professor at the Universität Münster. His main research interests lie in the areas of organic electrosynthesis, the conversion of fatty acids into new oleoproducts and their surface properties, and natural product synthesis.



Manfred P. Schneider, born in 1940, studied chemistry in Stuttgart and Vienna and he received his doctorate in Stuttgart in 1969. After a post-doctoral period at the University of Pittsburgh with P. Dowd, he returned to Stuttgart in 1971 and gained his habilitation there in 1977. Since 1980, he has been Professor of Organic Chemistry at the Bergische Universität in Wuppertal. His central research area is the use of enzymes in organic synthesis for the preparation of enantiomerically pure synthesis building blocks and biologically active compounds such as pharmaceuticals, aromatics, pheromones, "second messengers", and cationic lipids as vectors for gene therapy. A further research topic of current work is the bioconversion of renewable raw materials.

agriculture is necessary to extend the successful applications of this technology." A good example of this is the alkyl polyglycosides, the use and properties of which have been recently reviewed.[5]

We report here the advances made in the chemistry and biotechnology of fatty materials over the last ten years and include the improvements in natural oils and fats by plant breeding.

2. Reactions of Unsaturated Fatty Compounds

By means of simple industrial reactions, fatty materials are available from vegetable oils in such purity that they may be used for further chemical conversions and for the synthesis of chemically pure compounds. Predominantly, oleic acid **1a** and elaidic acid (*E*)-**1a**, petroselinic acid **2a**, erucic acid **3a**, linoleic acid **4a**, and linolenic acid **5a** have been used in the syntheses described below (Figure 1). Ricinoleic acid **6a** carries an additional hydroxyl group which is useful in stereo- and regioselective syntheses. By pyrolysis of **6b** and subsequent hydrolysis, 10-undecenoic acid **7a**, a ω-unsaturated carboxylic acid, is obtained,[4] which is very useful for selective reactions. Both 9-decenoic acid **8a** and 13-tetradecenoic acid **9a** are accessible by the metathesis reaction of ethylene with oleic acid **1a** and erucic acid **3a**, respectively, thus extending the range of ω-unsaturated fatty compounds available (Section 2.3). Conjuenic acid **10a**, with conjugated double bonds, is obtained as a regio- and stereoisomeric mixture by the isomerization of linoleic acid **4a**.[4] The alkyne fatty compounds **11**–**13**, with internal or terminal triple bonds, are readily available on a laboratory scale.[6]

The epoxides **14**–**16**, the synthesis of which has been greatly improved recently, are also available as reactive fatty compounds (see Section 2.1). Methyl ricinoleate **6b** may be oxidized to methyl 12-oxooleate **17** which, in turn, may be readily isomerized to the enone **18**.[7] Similarly, the allyl alcohol **19**, obtained by selenium oxidation of methyl 10-undecenoate **7b** (see Section 3.2.2), can be dehydrogenated to the ω-unsaturated enone **20**.[7b] The fatty compounds **17**–**20** are suitable substrates for interesting follow-up reactions.

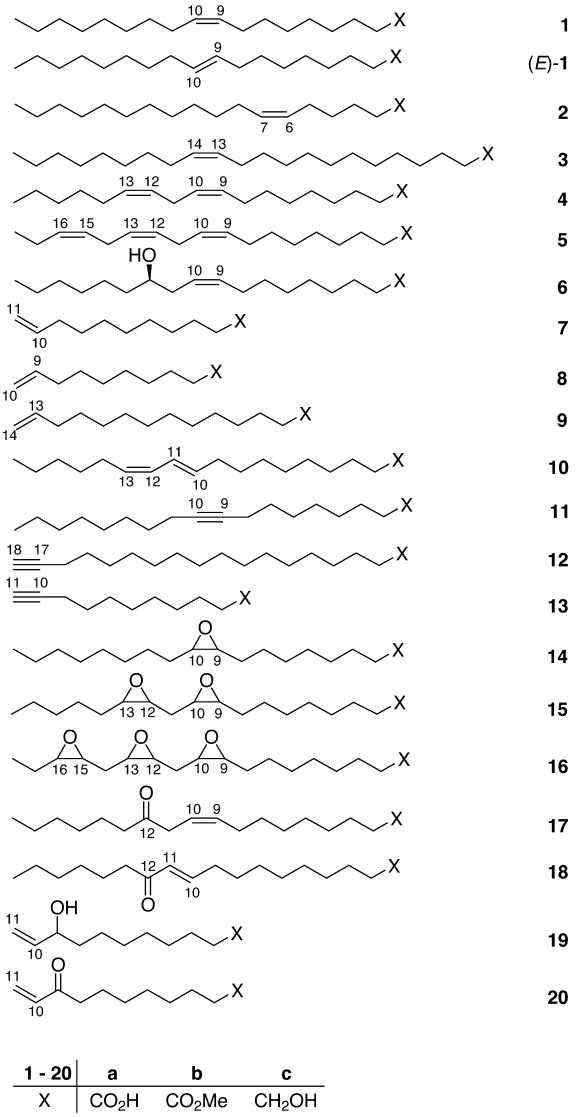


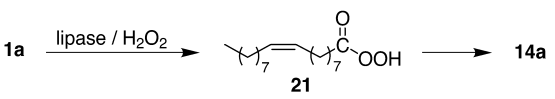
Figure 1. Starting materials for the synthesis of novel fatty acids: Oleic acid **1a**, elaidic acid (*E*)-**1a**, petroselinic acid **2a**, erucic acid **3a**, linoleic acid **4a**, linolenic acid **5a**, ricinoleic acid **6a**, 10-undecenoic acid **7a**, 9-decenoic acid **8a**, 13-tetradecenoic acid **9a**, conjuenoic acid **10a** (regio and stereoisomeric mixture), stearoleic acid **11a**, 17-octadecynoic acid **12a**, 10-undecynoic acid **13a**, *cis*-9,10-epoxyoctadecanoic acid **14a**, *cis*-9,10;*cis*-12,13-bisepoxyoctadecanoic acid **15a**, *cis*-9,10;*cis*-12,13;*cis*-15,16-trisepoxyoctadecanoic acid **16a**, 12-oxooleic acid **17a**, 12-oxooctadec-10-enoic acid **18a**, 9-hydroxy-10-undecenoic acid **19a**, 9-oxo-10-undecenoic acid **20a**, and the respective methyl esters **1b**–**20b** and alcohols **1c**–**20c**.

2.1. Oxidations

2.1.1. New Methods for the Epoxidation of Unsaturated Fatty Acids

Unsaturated fatty compounds are preferably epoxidized on an industrial scale by the in situ performic acid procedure.[4] Numerous new methods have been used, particularly with oleic acid, such as epoxidation with aldehydes and molecular oxygen,[8] dioxiranes,[9–11] H_2O_2/tungsten heteropolyacids,[12, 13] and H_2O_2/methyl trioxorhenium.[14–17] Epoxidation by the Halcon process[18] with alkyl hydroperoxides also succeeds with unsaturated fatty compounds.[19, 20] As yet, however, none of these methods has achieved industrial significance.

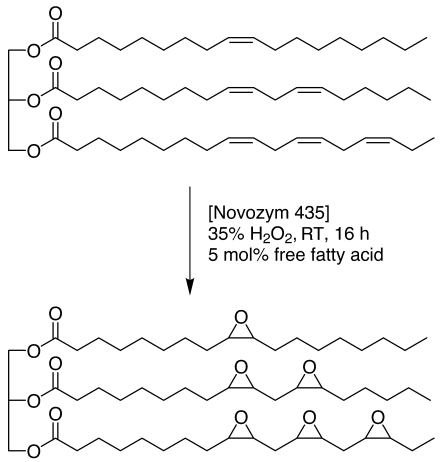
Chemo-enzymatic epoxidation is of considerable interest because this method totally suppresses undesirable ring opening of the epoxide. Initially, the unsaturated fatty acid[21] or ester[22] is converted into an unsaturated percarboxylic acid, such as **21**, by a lipase-catalyzed reaction with H_2O_2 and is then self-epoxidized in an essentially intermolecular reaction (Scheme 1).[23] The second reaction step occurs without involvement of the enzyme, following the rules of the Prileshajev epoxidation.



Scheme 1. Reaction principle of the chemo-enzymatic "self" epoxidation of unsaturated fatty acids: intermediate enzymatic formation of peroxyoleic acid **21** from oleic acid **1a**.[23]

Excellent stability and activity is shown by Novozym 435, a *Candida antarctica* lipase B immobilized on polyacryl. This remarkable, readily separable, heterogeneous biocatalyst can be used several times without loss of activity; a turnover of more than 200000 moles of product per mole of catalyst has been achieved.

If vegetable oils are subjected to perhydrolysis, they are likewise epoxidized by the peroxy fatty acid formed (Scheme 2).[24] The formation of mono- and diglycerides can be fully suppressed by the addition of 5 mol % free fatty acid. Soybean and other vegetable oils have been oxidized by these methods with conversions and selectivities of 90 % and above. Even with the highly unsaturated linseed oil, the selectivity of this reaction is maintained.

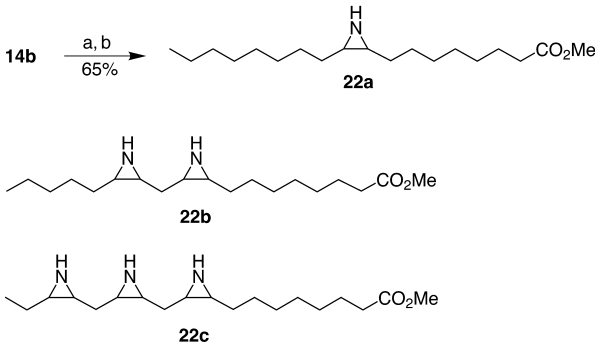


Scheme 2. Chemo-enzymatic epoxidation of vegetable oils.[24]

Industrially, vegetable oil epoxides are currently used mainly as PVC stabilizers. New applications have been opened by the possibility of photochemically initiated cationic curing.[25]

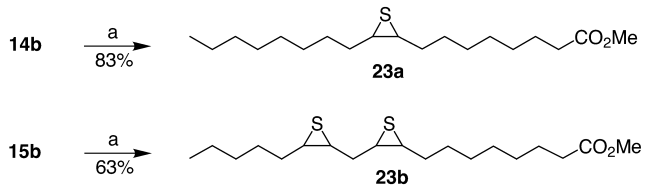
2.1.1.1. Follow-Up Reactions of Epoxides to Aziridines and Episulfides

Epoxidized fats, such as **14**–**16**, are reactive reactants for a number of interesting follow-up processes.[4] The corresponding methyl epiminooctadecanoates **22a**–**c** have been synthesized as potentially bioactive compounds (Scheme 3).[26, 27]



Scheme 3. Synthesis of methyl epiminooctadecanoate **22a** from methyl epoxyoctadecanoate **14b**: a) NaN_3, NH_4Cl, EtOH, H_2O; b) Ph_3P, THF.[26] Methyl di- and triepiminooctadecanoates **22b** and **22c** can be synthesized in a similar manner from the methyl di- and triepoxyoctadecanoates **15b** and **16b**.[27]

The aziridines **22** and the episulfides **23**,[28] the latter being accessible from the epoxides **14b** and **15b** (Scheme 4), are interesting intermediates in the synthesis of heterocyclic and highly functionalized fatty compounds.



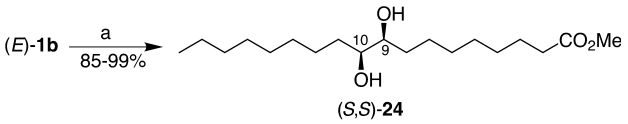
Scheme 4. Synthesis of methyl epithiooctadecanoate **23a** from methyl epoxyoctadecanoate **14b**: a) $HC(=S)N(CH_3)_2$, CF_3COOH, $ClCH_2CH_2Cl$. Methyl diepithiooctadecanoate **23b** can be synthesized in a similar manner from methyl diepoxyoctadecanoate **15b**.[28]

2.1.2. Oxidation to vic*-Dihydroxy Fatty Acids*

Vicinal diols of unsaturated fatty compounds—polyols for polyurethanes based on renewable raw materials—may be prepared by epoxidation and subsequent nucleophilic ring opening of the epoxide. Since harsh reaction conditions are technically necessary for ring opening of fatty epoxides,[29] the direct synthesis of vicinal dihydroxy fatty acids is an interesting alternative.

The hydroxylation of oleic acid **1a** by H_2O_2 and a molybdenum,[30] tungsten, [31] or rhenium-based catalysts[32, 33] affords *syn* diols via the epoxide intermediate.

The enantioselective oxidation of methyl elaidate (*E*)-**1b** to the chiral *syn*-dihydroxyoctadecanoate (*S*,*S*)-**24** and its enantiomer with AD-mix-α and AD-mix-β,[34] respectively, in a yield of 97 % and an enantiomeric excess of 95 % *ee* is especially noteworthy (Scheme 5).[35a] With methyl oleate **1b**, the enantiomeric excess was very low using this method. The enantiomerically enriched carboxylates derived from **24** associate to gels in carbon tetrachloride. Like the corresponding gels from enantiomerically pure ricinoleic acid salts,[36] they form helical fibers which can be visualized with atomic force microscopy.[35b]

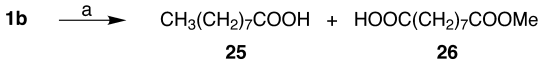


Scheme 5. Enantioselective oxidation of methyl elaidate (*E*)-**1b** with AD-mix-α to methyl (−)-(9*S*,10*S*)- and with AD-mix-β to methyl (+)-(9*R*,10*R*)-dihydroxyoctadecanoate **24**.[35a] a) AD-mix, $MeSO_2NH_2$, H_2O, *t*BuOH, 0 °C.

2.1.3. Oxidative Cleavage

The cleavage of oleic acid **1a** to pelargonic **25** and azelaic acids **26a** with ozone as oxidant is the most important industrial application of ozonolysis.[4, 37] A catalytic alternative, which uses a more suitable and safe oxidant is of considerable interest.[4]

The direct oxidative cleavage of internal C–C double bonds with peracetic acid and ruthenium catalysts or with H_2O_2 and Mo, W, or Re-based catalysts leads to yields of only 50–60 % (Scheme 6).[38] In contrast, terminal C–C double bonds can be

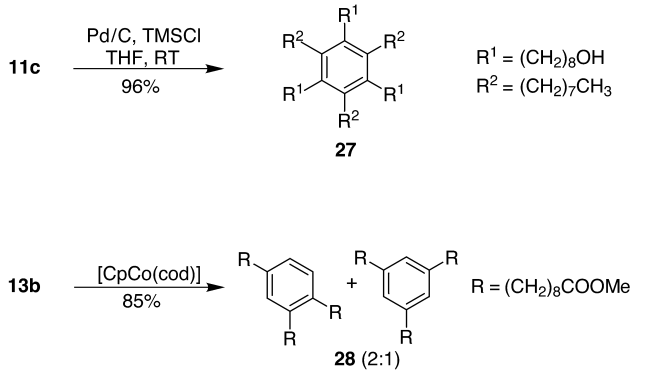


Scheme 6. Transition metal catalyzed oxidative cleavage of methyl oleate **1b** to pelargonic acid **25** and azelaic acid half ester **26** with peracetic acid[39] or hydrogen peroxide.[40] a) $[Ru(acac)_3]/CH_3CO_3H$ or Re_2O_7/H_2O_2.

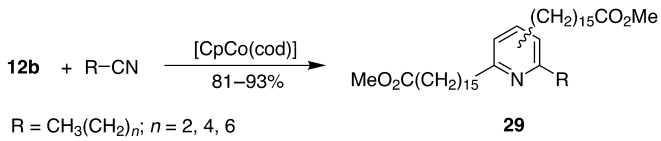
cleaved in yields of 80% with $Ru(acac)_3/CH_3CO_3H$[39] or Re_2O_7/H_2O_2[40] (acac = acetylacetonato). This gives rise to the possibility of initially converting natural, internally unsaturated fatty acids into ω-unsaturated fatty acid methyl esters such as **8b** and **9b** by means of metathesis, followed by oxidative cleavage. The advantage here is that the production of azelaic acid **26** and pelargonic acid **25** can be uncoupled, independent of the oxidation method.

2.2. Transition Metal Catalyzed Syntheses of Aromatic Compounds

The route to aromatic compounds from renewable raw materials is of importance.[4] The transition metal catalyzed trimerization of the alkyne fatty compounds **11** and **13** gives the highly functionalized aromatic species **27** and **28**, respectively (Scheme 7), and co-trimerization with nitrile moieties affords the highly varied and functionalized pyridine derivatives **29** (Scheme 8).[42]



Scheme 7. Cyclotrimerization of the internal alkyne **11c** and the terminal alkyne **13b** to the regioisomeric benzene derivatives **27** and **28**.[42] TMS = trimethylsilyl, Cp = cyclopentadienyl, cod = cycloocta-1,5-diene.

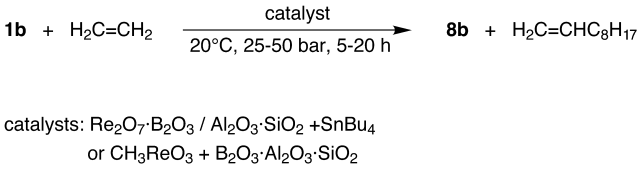


Scheme 8. Cyclization of methyl 17-octadecynoate **12b** with nitrile species to the pyridine derivatives **29**.[42]

2.3. Olefin Metathesis

Transition metal metathesis of olefins, which is used in the industrial petrochemistry and polymer chemistry for the production of special olefins and unsaturated polymers, is also applicable to unsaturated fatty acid esters. However, the low loading of the expensive catalysts has, until now, stood in the way of the technical utilization of this interesting reaction in oleochemistry.[4]

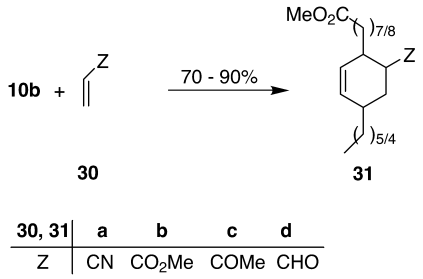
Over the past few years, Warwel et al. have developed significantly more active catalysts in the form of $Re_2O_7 \cdot B_2O_3/Al_2O_3 \cdot SiO_2 + SnBu_4$ and $CH_3ReO_3 + B_2O_3 \cdot Al_2O_3 \cdot SiO_2$ and successfully tested them in a series of metathesis transformations.[43] The industrial application of olefin metathesis to unsaturated fatty compounds thus moves realistically nearer. Scheme 9 illustrates the co-metathesis of methyl oleate **1b** and ethylene to form methyl 9-decenoate **8b** and 1-decene. Similarly, methyl 13-tetradecenoate **9b** and 1-decene are obtained from methyl erucate **3b** and ethylene.[43] Methyltrioxorhenium is also a suitable catalyst for the metathesis of unsaturated fatty compounds.[44]



Scheme 9. Co-metathesis of methyl oleate **1b** and ethylene to methyl 9-decenoate **8b** and 1-decene. The ester **1b** used (new sunflower) was 87% pure, the conversions and selectivities each >90%, and the yields of **8b** were >80%.[43]

2.4. Pericyclic Reactions

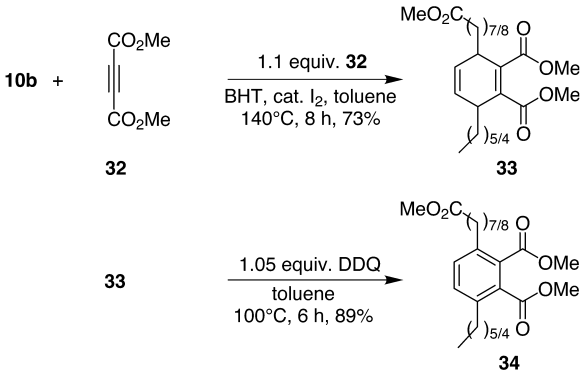
The thermal Diels–Alder reaction of methyl conjuenate **10b** with electron-deficient dienophiles has been thoroughly investigated[4] and is carried out industrially with maleic anhydride. With a Lewis acid, such as boron trichloride or tin tetrachloride, and catalytic amounts of iodine it was possible to obtain the cycloadducts **31** with the dienophiles **30**, even at room temperature (Scheme 10).[45] Building on the cyclo-



Scheme 10. Diels–Alder reactions of methyl conjuenates **10b** with the dienophiles **30a–d** to the regioisomeric addition products **31**.[45].

addition of dimethyl acetylenedicarboxylate **32** to **10b**, a further aromatic synthesis has been developed. Adduct **33** was dehydrogenated with 2,3-dichloro-5,6-dicyano-1,4-benzoquinone (DDQ) to the dimethyl phthalate **34** into which the fatty acid side chain is incorporated (Scheme 11).

In addition, Diels–Alder reactions with the enones **18** and **20** as dienophiles,[45, 46] ene reactions,[47, 48] [2+2] cycloadditions of ketenes,[49] and isocyanates[50] to unsaturated fatty compounds, as well as sigmatropic [3,3] rearrangements of

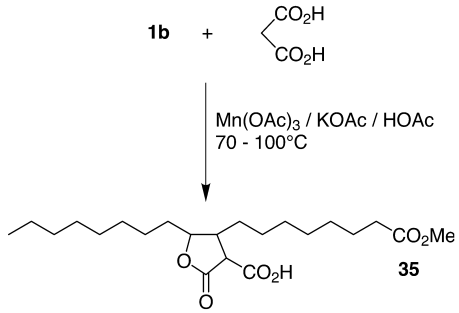


Scheme 11. Diels–Alder addition reactions of methyl conjuenates **10b** and dimethyl acetylenedicarboxylate **32** to the cycloaddition product **33** which was dehydrogenated to the dimethyl phthalates **34** with DDQ.[45] BHT = 4-methyl-2,6-bis[(1,1-dimethyl)ethyl]phenol.

allylvinyl ethers derived from fats,[49] have been investigated, which lead to a number of interesting and novel fatty compounds.

2.5. Radical Additions

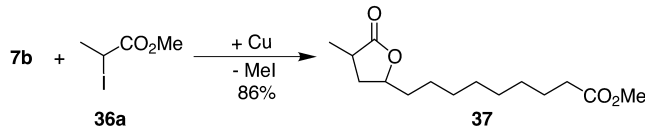
With the development of modern preparative radical chemistry, radical additions to unsaturated fatty compounds with the formation of new C–C bonds have been investigated systematically. Normal tin hydride radical chemistry[51] cannot be applied to the sterically constrained, internal, and electron-rich double bonds, as in **1b**. In contrast, enolizable compounds such as acetic acid, malonic acid, monomethyl malonate, and cyanoacetic acid were added to the fatty acid esters **1b** and **7b** by initiation with manganese(III) acetate[52] to give the respective γ-lactones such as **35** (Scheme 12).[53–55] Unfortunately, higher carboxylic acids cannot be oxidized to radicals with manganese(III) acetate and added to alkenes.[54, 55] For this purpose, a new method was developed.



Scheme 12. Manganese(III) acetate induced radical addition of malonic acid to methyl oleate **1b** with formation of the regioisomeric γ-lactones **35**.[53–55]

2.5.1. Solvent-Free, Copper-Initiated Additions of 2-Halocarboxylates

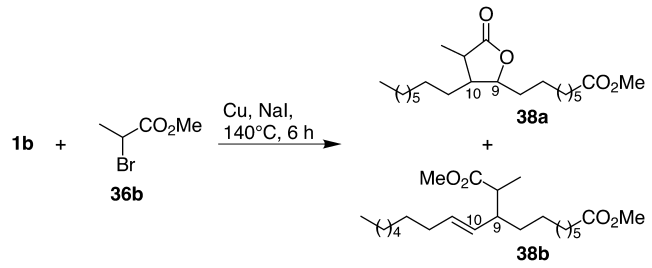
Higher carboxylic acids can be added to alkenes, such as unsaturated fatty compounds, as their α-haloesters, a process initiated by electron transfer from copper.[56–58] The addition of 2-iodocarboxylates, for example, methyl 2-iodopropanoate **36a**, to **7b** gave the γ-lactone **37** in high yields (Scheme 13).



Scheme 13. Copper-initiated addition of methyl 2-iodopropanoate **36a** to methyl 10-undecenoate **7b**.[56–58]

The reaction procedure is very simple: The unsaturated fatty compound, the 2-halocarboxylate, and commercial copper powder are mixed without further pretreatment and heated at 100–130 °C under an inert atmosphere. After a simple work-up, analytically pure products are obtained in good yields. Esters of 2-iodocarboxylic acids can be obtained in situ from the readily available bromo compounds by the addition of a stoichiometric amount of sodium iodide.

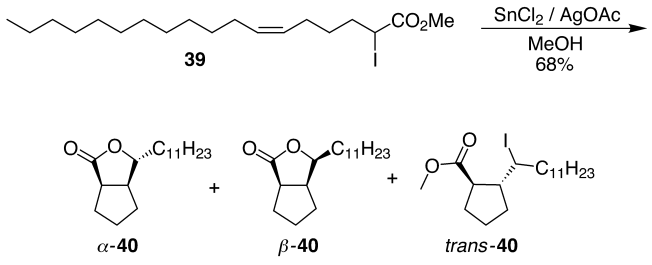
Methyl 2-bromopropanoate **36b** was also added to methyl oleate **1b** with copper by the addition of stoichiometric amounts of sodium iodide. The regioisomeric addition products **38a** were isolated in 58% yield. The addition–elimination product **38b** was isolated as a byproduct (Scheme 14). Comparable results were achieved with methyl



Scheme 14. Copper-initiated addition of methyl 2-bromopropanoate **36b** to methyl oleate **1b** in the presence of sodium iodide yields the regioisomeric γ-lactones **38a** and the addition–elimination product **38b**.[56–58]

petroselinate **2b** and methyl erucate **3b**.[57, 58] This generally applicable addition reaction was also carried out with bromomalonates, 2-bromo-3-alkylsuccinates, and α,α'-diiododicarboxylates, among others, in good to very good yields.[57, 58] In an analogous manner, 2-haloalkane nitriles have also undergone addition.[56–58]

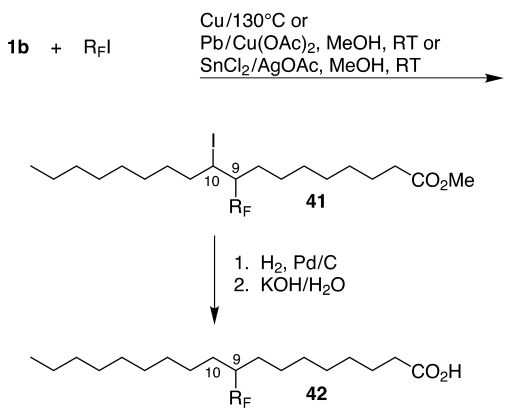
The reaction can also be used for intramolecular cyclization. The cyclization of methyl 2-iodopetroselinate **39** to the cyclopentane derivatives **40** was best carried out with the initiator system AgOAc/$SnCl_2$ (Scheme 15).[59]



Scheme 15. Radical cyclization of methyl 2-iodopetroselinate **39** induced by AgOAc/$SnCl_2$ (α-**40**:β-**40**:*trans*-**40** = 35:31:34).[59]

2.5.2. Addition of Perfluoroalkyl Iodides

Radical additions of perfluoroalkyl iodides to terminally unsaturated carboxylic acids such as 10-undecenoic acid **7a** with 2,2′-azobisisobutylnitrile (AIBN) as initiator give perfluoroalkylated products in good yields.[60] In contrast, for radical additions to alkenes with internal double bonds, such as methyl oleate **1b**, the addition products are only obtained in very low yields by this method.[61] Perfluoroalkyl iodides **41** can be added to both methyl 10-undecenoate **7b** and methyl oleate **1b** with good to very good yields if the reaction is initiated by electron transfer from metals such as finely divided silver,[61] copper powder,[62] or lead with a catalytic amount of copper(II) acetate[62] (Scheme 16). The best yields of addition product **41** are obtained with copper powder or with lead/$Cu(OAc)_2$.[62]



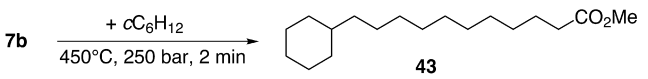
41, 42	a	b	c
R_F	C_4F_9	C_6F_{13}	C_8F_{17}

Scheme 16. Synthesis of 9- and 10-perfluoroalkyloctadecanoic acids **42** as a regioisomeric mixture: Addition of perfluoroalkyl iodides to **1b** give the regioisomeric perfluoroalkylated iodoesters **41**, which were then reduced to iodine-free esters and hydrolyzed to free perfluoroalkylated fatty acids **42**.[61, 62]

Perfluoroalkylated fatty compounds such as **42** are of interest because of their surfactant properties.[63]

2.5.3. Thermal Addition of Alkanes

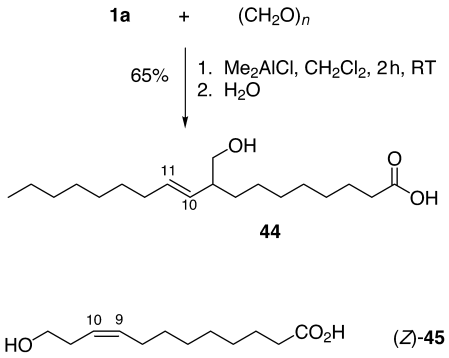
Alkylated fatty acids have interesting properties[64] and an effective synthesis of these products is important.[4] The ane reaction is the thermally initiated radical addition of alkanes to alkenes at elevated temperatures (200–450 °C) and pressures (200–250 bar).[65] The addition of cyclohexane to methyl 10-undecenoate **7b** gave methyl 11-cyclohexylundecanoate **43** (Scheme 17);[66] 11-cyclohexylundecanoic acid is the main lipid of thermophilic archaebacteria.[67]



Scheme 17. Thermally initiated addition of cyclohexane to methyl 10-undecenoate **7b**. The reaction was carried out in a high pressure–high temperature flow reactor.[66]

2.6. Lewis Acid Induced Cationic Addition

ω-Hydroxycarboxylic acids, including alkyl-branched acids such as **44**, which are of interest as polyester components, are obtained with high selectivity by the ene addition of formaldehyde to unsaturated fatty acids (Scheme 18).[68] However, stoichiometric amounts of dimethylaluminum chloride or ethylaluminum dichloride are used as reagents.[69, 70] A catalytic variant would be highly significant. The acid (*Z*)-**45** (Scheme 18), obtained by the addition of formaldehyde to 10-undecenoic acid **7a**, induces wound healing of tissue damage in soybeans by stimulation of callus formation at the damaged site.[71]

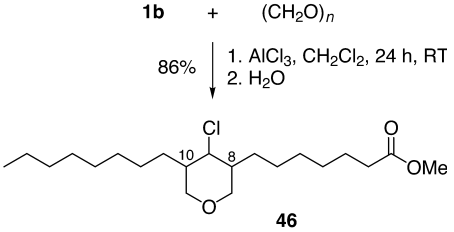


Scheme 18. Me_2AlCl-induced addition of paraformaldehyde to oleic acid **1a** to give the regioisomeric homoallyl alcohols **44**. The corresponding addition to 10-undecenoic acid **7a** gives the homoallyl alcohol **45** [(*E*):(*Z*) = 4:1].[68]

Ene additions of formaldehyde to natural oils proceed with formation of the respective di- and trifunctionalized triglycerides,[72] and jojoba oil gives mixtures of 1:1 and 1:2 adducts.[73] Homoallyl ethers are obtained in an analogous reaction with acetals.[74]

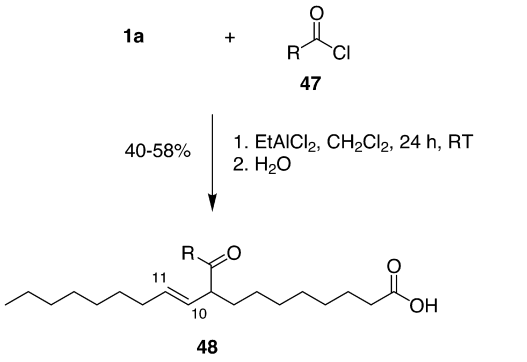
Formaldehyde and higher aldehydes react with unsaturated fatty compounds in the presence of aluminum chloride to form the corresponding alkyl-substituted 4-chlorotetrahydropyrans in good yields and with high selectivity.[75] The reaction of two equivalents of formaldehyde with, for example, methyl oleate **1b**, gave the 3,5-dialkyl substituted 4-chlorotetrahydropyran **46** (Scheme 19). Variation of the alkene, on the one hand, and the carbonyl component, on the other, leads to a broad range of alkyl-substituted chlorotetrahydropyrans.

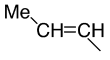
The Friedel–Crafts acylation is an interesting and versatile method for the functionalization of unsaturated fatty com-



Scheme 19. $AlCl_3$-induced addition of two equivalents of paraformaldehyde to methyl oleate **1b** to give the 4-chlorotetrahydropyrans **46** (mixture of two regioisomers).[75]

pounds.[76] The $EtAlCl_2$-induced acylation of oleic acid **1a**, among others, with acyl chlorides **47** gave the (*E*)-configured β,γ-unsaturated oxocarboxylic acids **48** with high selectivity (Scheme 20). Cyclic anhydrides, such as succinic anhydride, gave oxo diacids in a similar manner.[76] The acylation products **48** are substrates for a number of interesting follow-up reactions, for example, **48g** for Nazarov cyclizations.[77]



47, 48	a	b	c	d	e	f	g
R	Me	nC_6H_{13}	$nC_{15}H_{31}$	cC_3H_5	Ph		

Scheme 20. $EtAlCl_2$-induced Friedel–Crafts acylations of oleic acid **1a** with the acyl chlorides **47a–g** give the unsaturated regioisomeric oxocarboxylic acids **48a–g**.[76]

2.7. Nucleophilic Addition to Reversed-Polarity Unsaturated Fatty Acids

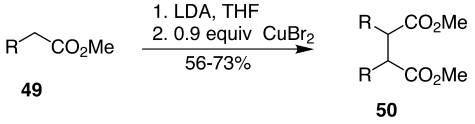
Addition to the double bond of unsaturated fatty acids mainly occurs with electrophiles (Section 2.6), radicals (Section 2.5), or in pericyclic reactions (Section 2.4). Totally new coupling possibilities arise when the polarity of the electron-rich double bond is reversed, as in the enone fatty acids **18** and **20**. In this way, a number of nucleophiles may be coupled to the double bond by Michael additions.[78] Interesting and novel fatty compounds have also been obtained from the enones **18** and **20** in Stetter[7, 78] and Mukaiyama additions.[79] Similarly, methyl conjuenate **10b** has been treated anodically with numerous alcohols to afford methyl dialkoxyoctadecanoates, some of which had interesting surfactant properties.[80] Numerous carbon, oxygen, and nitrogen-based nucleophiles may be inserted into fatty allyl carbonates by palladium catalysis (from the corresponding allyl alcohols; Section 3.2.2) in very good yields.[79b,d]

3. Reactions of Saturated Fatty Compounds

3.1. Radical C–C Coupling

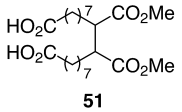
3.1.1. Oxidative Coupling of C2 Anions of Fatty Acids

The C–C coupling, with the concurrent formation of symmetrical products, may be achieved by the dimerization of two radicals. Radicals may be formed selectively under mild conditions in high concentrations by the oxidation of anionic precursors. Unsaturated fatty acids possess several sites with comparably high C–H acidities, which are suitable for anionization and subsequent reactions, particularly the α-positioned C–H bond of the ester group. The fatty acid methyl esters **49** were anionized and treated oxidatively with 0.9 equivalents $CuBr_2$. In this way, the dimers **50** were formed with a (*d,l*):*meso* ratio of about 1.2:1 (Scheme 21).[81a] The dimethyl ester of the tetracarboxylic acid **51** was obtained from **50c** by ozonolysis in 90% yield.



	R	Yield of **50** (%)[a]	
a	C_6H_{13}	67	(84)
b	C_8H_{17}	73	(82)
c	$CH_2{=}CH(CH_2)_7$[b]	69	(81)
d	$C_{10}H_{21}$	64	(82)
e	$C_{12}H_{25}$	66	(81)
f	(*Z*)-7-hexadecenyl[c]	56	(66)
g	(*Z,Z*)-7,10-hexadecadienyl[d]	67	(80)

[a] Yields given in brackets are calculated with respect to conversion; [b] **49c=7b**; [c] **49f=1b**; [d] **49g=4b**



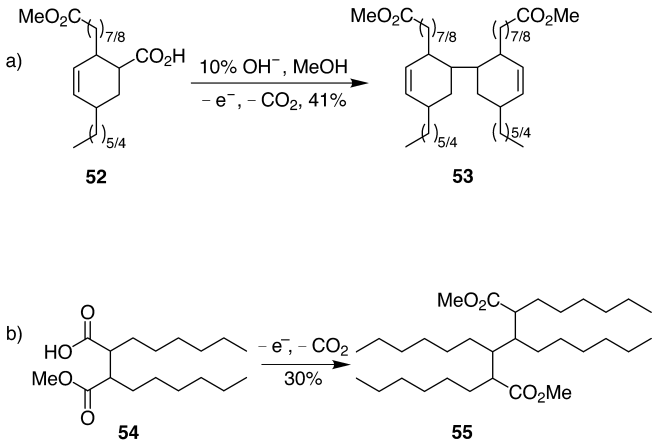
Scheme 21. Radical α,α' dimerization of the fatty acid methyl esters **49**. Ozonolysis of the dimer **50c** gives the dimethyl tetracarboxylate **51**.[81] LDA = lithium diisopropylamide.

3.1.2. Anodic Homo- and Heterocoupling of Fatty Acids (Kolbe Electrolysis)

The anodic decarboxylation of aliphatic carboxylic acids gives a rapid, and also technically useful, path to radicals for dimerization and coupling (Kolbe electrolysis).[82] This efficient synthetic method was used extensively in homocouplings with natural and modified fatty acids, such as in the preparation of specifically functionalized alkanes[83] or in the preparation of long chain diesters. Isostearic acid may be dimerized in 63% yield to a methyl-branched C_{34} hydrocarbon whose cosmetic property profile resembles that of squalane. As the half ester with the currently greatest number of carbon atoms, the methyl ester of the C_{36} dimeric fatty acid was coupled in 38% yield to a C_{70} dimethyl dicarboxylate.[83, 84]

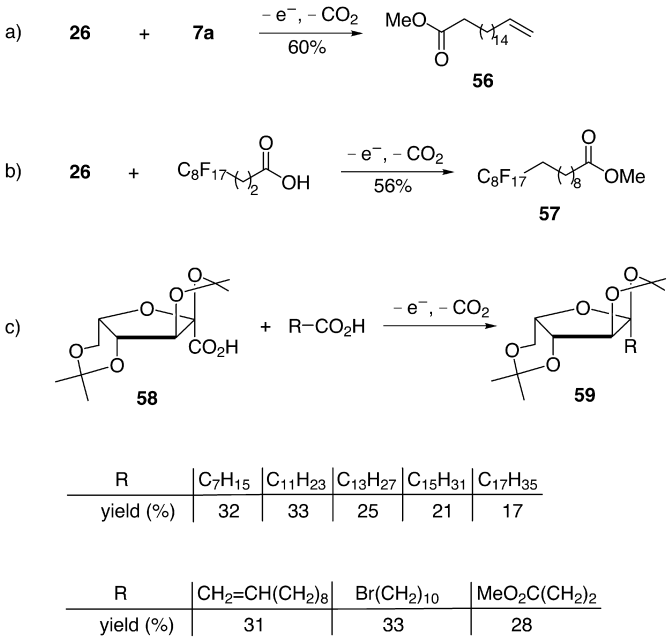
In addition, the dimeric fatty acids **53** may be obtained from Diels–Alder adducts of fatty acids such as **52** (Section 2.4) by homocoupling (Scheme 22a),[47] or dicarboxylic acids with four alkyl chains, such as **55**, are obtained from 2,2′-coupled diacids like **54** (Section 3.1.1; Scheme 22b).[78b]

Through heterocoupling, that is, the electrolysis of two different carboxylic acids, new unsaturated fatty acids are



Scheme 22. Homocoupling of the half esters **52** and **54** by Kolbe electrolysis to give the dimers **53**[45] and **55**,[78b] respectively.

formed,[82a, 84, 85a] such as methyl 17-octadecenoate **56** (Scheme 23a),[84] partially perfluoronated fatty acids like **57** (Scheme 23b),[84] pheromones,[85b] C-glycosides **59** formed by co-electrolysis with carbohydrate carboxylic acids **58** (Scheme 23c)),[86] or long chain diesters.[85b]



R	C_7H_{15}	$C_{11}H_{23}$	$C_{13}H_{27}$	$C_{15}H_{31}$	$C_{17}H_{35}$
yield (%)	32	33	25	21	17

R	$CH_2{=}CH(CH_2)_8$	$Br(CH_2)_{10}$	$MeO_2C(CH_2)_2$
yield (%)	31	33	28

Scheme 23. Kolbe electrolysis of two different fatty acids: Synthesis a) of new ω-unsaturated fatty acids such as **56**,[84] b) of perfluoroalkylated fatty acids such as **57**,[84] and c) of C-glycosides such as **59**.[86a]

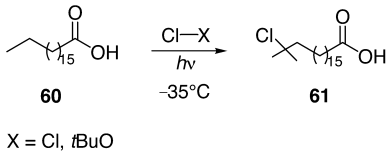
3.2. Functionalization of C–H Bonds

Selective reactions at the alkyl chain of fatty acids are still rare but are of great interest.[4]

3.2.1. Oxidation of Nonactivated C–H Bonds

Nonactivated C–H bonds may be functionalized chemically[87] or enzymatically[88] (Section 4.2.5). Particularly important, but yet to be solved satisfactorily, is the regioselectivity of C–H functionalization.

Notable advances have been achieved by photochemical gas phase chlorination of fatty acids that are adsorbed onto aluminum oxide with chlorine or *t*BuOCl. For this reaction, selectivities increase with increasing chain length of the fatty acid. Stearic acid **60** reacts with chlorine or *t*BuOCl at $-35\,^{\circ}C$ in the ω-(ω-2) position to form the chlorostearic acids **61** in yields of 96% and 93%, respectively (Scheme 24).[89] The selectivity is significantly better than with the more established radical chlorination with dialkylchloramines in an acidic medium.[90, 91] The methyl esters of shorter chain fatty acids and fatty alcohols may be hydroxylated with amine oxides with good conversions and (ω-1)-(ω-2) selectivities.[7a]

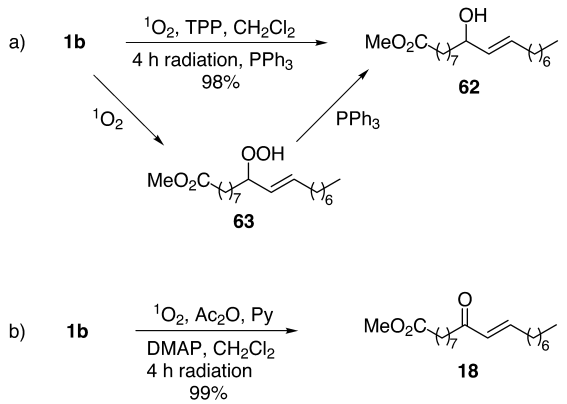


Scheme 24. Photochemical gas-phase chlorination of stearic acid **60** adsorbed on aluminum oxide to chlorostearic acids **61** with chlorine (relative product distribution (rpd): ω-2 14.2%; ω-1 38.4%; ω 43.7%) and *t*BuOCl (rpd: ω-2 11.6%;ω-1 51.5%;ω 30.1%).[89]

3.2.2. Oxidation of Allylic C–H Bonds

The allylic C–H bonds of unsaturated fatty acids are activated C–H bonds, which, in principle, may be functionalized with a number of oxidizing agents. For the allylic oxidation of methyl 10-undecenoate **7b** and methyl oleate **1b**, SeO_2/*t*BuOOH has been shown to be suitable.[7]

The reaction with singlet oxygen has proved to be considerably more suitable for the preparation of the allyl alcohol **62**. For this purpose, **1b** was photoxygenated with oxygen by means of a high pressure sodium-vapor lamp and tetraphenylporphin as sensitizer, and the resulting hydroperoxide **63** was reduced with triphenylphosphine (Scheme 25).[79b,c] In the presence of acetic anhydride, pyridine, and catalytic amounts of 4-dimethylaminopyridine (DMAP), the hydroperoxide may converted directly into the regioisomeric mixture of the enone fatty acids **18**.[79b,c] Since the photoxidation occurs even



Scheme 25. Photooxygenation of methyl oleate **1b** with singlet oxygen and tetraphenylporphin as sensitizer to give a) allyl alcohols **62** and b) α,β-unsaturated ketones **18** (both regioisomeric mixtures form).[79b,c]

in sunlight, unsaturated fatty acids oxidized in the allylic position are available by a route which is particularly favorable from both an economical and an ecological viewpoint.

4. Enzymatic Reactions

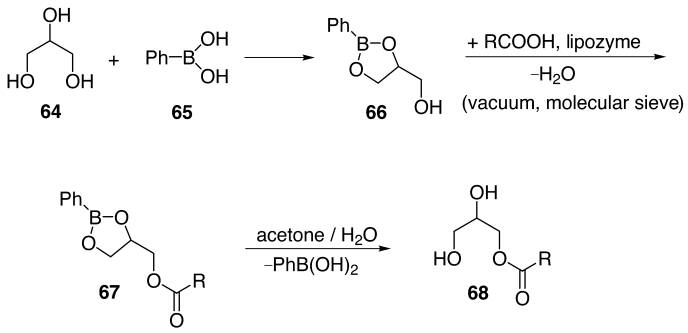
4.1. Lipase Catalyzed Transformations

Lipases and their applications have been reviewed in this journal in 1998.[92] We will limit ourselves therefore to a few examples of selective syntheses of fatty compounds.

4.1.1. Lipase-Catalyzed Syntheses of Monoglycerides and Diglycerides

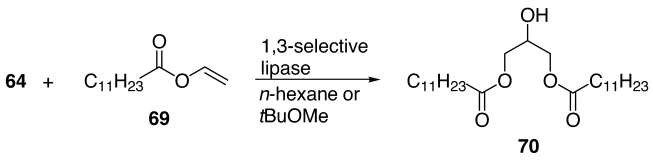
Mono- and diglycerides (partial glycerides) are among the most important nonionic surfactants emerging from oleochemistry. They are used widely as emulsifiers in the preparation of foodstuff. "Monoglycerides" are prepared on a large scale by the glycerolysis of natural fats and oils in the presence of inorganic catalysts and must be subsequently purified by molecular distillation.[92] Biocatalytic transformations offer a more gentle alternative to this process.[4] Considerable advances have been made here in the last few years but no breakthrough could yet be considered economic.

Glycerol, protected as the isopropylidene[93] or phenylboroester[94, 95] derivatives, can be converted into pure monoglycerides **68** with interesting surfactant properties in the presence of a lipase from *Rhizomucor miehei* (lipozyme) and free fatty acids as acyl donors (Scheme 26).



Scheme 26. Lipase-catalyzed synthesis of 1(3)-*sn*-monoglycerides **68** by acylation of glyceryl phenylborates **66** with fatty acids to give **67** once the protecting group is cleaved.[94, 95]

If glycerol is immobilized on silica gel, the esterification runs surprisingly smoothly in aprotic solvents such as *n*-hexane or *tert*-butylmethyl ether in the presence of different lipases and acyl donors (free fatty acids, fatty acid methyl esters, vinyl esters, triglycerides, and so forth).[96–98] Thus, for example, isomerically pure (>98%) 1,3-*sn*-dilaurin **70** is readily obtained with vinyl laurate **69** in the presence of a "1,3-selective" lipase (Scheme 27).[96, 99] Because of their ready accessibility, up to the kilogram scale, and their high purity and stability, these 1,3-*sn*-diglycerides represent interesting building blocks for further surfactant compounds (for example, by coupling with amino acids) and for the preparation of reagents for lipid modification of natural products.[100]



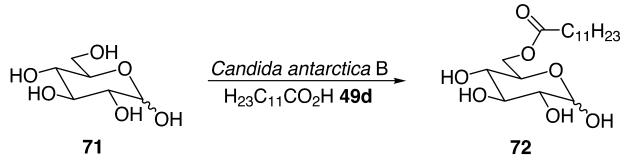
Scheme 27. Lipase-catalyzed synthesis of 1,3-*sn*-diglycerides, such as 1,3-*sn*-dilaurin **70**, by the vinyl lauroate (**69**) acylation of glycerol immobilized on silica gel.[96, 99]

If the 1(3)-*sn*-monoglycerides **68** are prepared by this method, they must be selectively separated from the reaction mixture, since they are very readily esterified by the lipases to 1,3-*sn*-diglycerides. This separation is achieved by exploiting the poor solubility of the monoglycerides **68** at low temperatures in appropriate solvent mixtures.[97, 98] The method has proved to be exceptionally suitable for the conversion of natural fats and oils from palm kernels, coconuts, soybeans, sunflowers, and rapeseeds into the respective monoglyceride mixtures. Such highest-quality products are particularly well suited for uses in the cosmetic and pharmaceutical industries.

4.1.2. Lipase-Catalyzed Syntheses of Carbohydrate Esters

Alkylpolyglucosides (APGs) and (polyethoxylated) sorbitan esters (Span, Tween)—both directly or indirectly derivatives of glucose—are already used extensively as nonionic surfactants or emulsifiers.[5] The lipase-catalyzed synthesis of carbohydrate esters has been recently reviewed.[92]

It is particularly noteworthy, that in aprotic solvents such as tetrahydrofuran, dioxan, monoglyme, or diglyme, monosaccharides such as D-glucose, D-galactose, D-mannose, and D-fructose can be transformed regioselectively and in high yields into the respective 6-*O*-acyl derivatives in the presence of the lipase from *Candida antarctica* B (Novozym SP 435). Thus, for example 6-*O*-lauroyl-D-glucose **72** was obtained directly from glucose **71** and lauric acid **49d** (Scheme 28). The method may also be applied to the esterification of L-ascorbic acid and even, if only to a limited extent, to saccharose. The fatty acids caprylic, capric, lauric, myristic, palmitic, stearic, oleic, 12-hydroxystearic, and erucic acids have been used as acyl donors.[101]



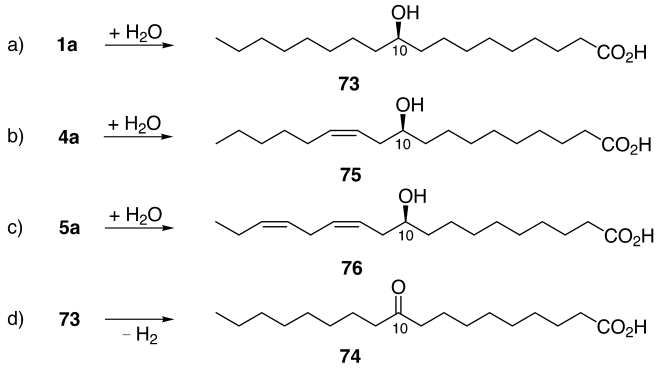
Scheme 28. Lipase-catalyzed selective esterification of glucose **71** with lauric acid **49d** in aprotic solvents to give 6-*O*-lauroyl-D-glucose **72**.[101]

4.2. Microbial Transformations

4.2.1. Microbial Hydration of Unsaturated Fatty Acids

The chemical addition of water to unsaturated fatty compounds such as **1a** is neither regioselective nor stereoselective.[102] In contrast, microbial hydration is frequently both regio- and stereoselective.

Microbial water attachment to an unsaturated fatty acid was first reported by Wallen et al. in 1962.[103] The authors observed that a *Pseudomonas* species, isolated from fat-containing materials, hydrated oleic acid **1a** to (*R*)-10-hydroxystearic acid **73** in 14% yield (Scheme 29a). This water attachment was also observed with the bacterial genera *Nocardia*, *Rhodococcus*, *Corynebacterium*, and *Micrococcus*.[104–106] Compound **73** was obtained in 45% yield with the yeast *Saccharomyces cerevisiae*.[107] The hydration product **73** can be oxidized to 10-oxooctadecanoic acid **74** in a subsequent enzymatic dehydrogenation reaction (Scheme 29d).[107]



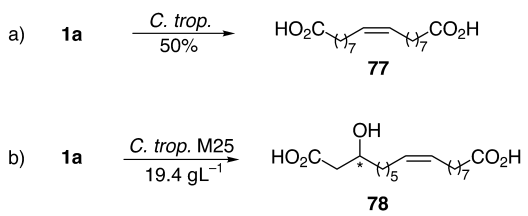
Scheme 29. Microbial enantioselective and regioselective addition of water to a) oleic acid **1a**,[103–106] b) linoleic acid **4a**,[108] and c) linolenic acid **5a**[108] to give the 10-hydroxy fatty acids **73**, **75**, and **76**; further, d) **73** can be enzymatically dehydrogenated to 10-oxooctadecanoic acid **74**.[107]

Microbes *Lactobacillus plantarum* and *Nocardia cholesteriolicum* assited the formation of (*Z*)-10-hydroxyoctadec-12-enoic acid **75** in 71% yield from linoleic acid **4a** (Scheme 29b).[108] α-Linolenic acid **5a** was converted into (12*Z*,15*Z*)-10-hydroxyoctadeca-12,15-dienoic acid **76** in 77% yield (Scheme 29c). [108] The hydratase was not active towards *trans*-unsaturated fatty acids, such as elaidic acid (*E*)-**1a**, and unsaturated fatty acids without a double bond in the 9 position, such as erucic acid **3a**. Enzymatic hydration activity occurred less readily with a greater number of double bonds in the substrate. Since hydratases from a number of bacteria and yeasts convert (9*Z*)-fatty acids into 10-hydroxy fatty acids, it can be assumed that the C10 specificity is universal in nature.[109]

In the future, it is expected that protein structure elucidation in algae, higher plants, and marine lifeforms will advance and these enzymes will cloned in microorganisms so that biocatalysts will be available for synthetic use in ever larger amounts.[110]

4.2.2. Microbial ω- and β-Oxidation of Fatty Acids

Microbial ω-oxidation of fatty acids, which leads to dicarboxylic acids, is of great interest.[4] Advances have been made here in recent years: Yi and Rehm[111] were able to convert oleic acid **1a** into the corresponding unsaturated dicarboxylic acids **77** with yeast of the genus *Candida tropicalis* (Scheme 30a). With alkaline fermentation procedures, it was possible to increase the yields of **77** from 23% to 50% and also to oxidize solid fatty acids, such as palmitic acid,



Scheme 30. Microbial ω-oxidation of oleic acid **1a** to a) (*Z*)-9-octadecendioic acid **77** with *Candida tropicalis*[111, 112a] and b) (*Z*)-3-hydroxy-9-octadecendioic acid **78** with the yeast mutant *Candida tropicalis* M25.[114]

stearic acid, and erucic acid, to the respective dicarboxylic acids.[112a] In a batch fermentation with 70 g L^{-1} palmitic acid, hexadecanedioic acid was obtained in a yield of 36% and a concentration of 28.1 g L^{-1}. In comparison with reported yields,[113] this value is among the highest values that have been obtained with genetically unaltered microorganisms. This reaction is therefore not subject to the gene technology regulations and is therefore of additional industrial interest. The yields are significantly lower with linoleic acid **4a** and ricinoleic acid **6a**.[112b]

Oleic acid **1a** can be transformed into the unsaturated hydroxy diacid **78** with 76% *ee* with the yeast mutant *Candida tropicalis* DSM 3152. The productivity of the strain is improved by *N*-methyl-*N*′-nitro-*N*-nitrosoguanidine (NMG) mutagenesis, and in a Fed batch fermentation with the mutant *Candida tropicalis* M25 19.4 g L^{-1} **78** were obtained from oleic acid (Scheme 30b).[114] Under similar conditions, 6.1 g L^{-1} hydroxydiene diacid were obtained with 30 mL L^{-1} linoleic acid.[115]

4.3. Microbial Conversion of Oils/Fats and Glucose into Glycolipids

The broad structural palette of biosurfactants, along with their numerous applications and biosynthetic pathways, were comprehensively reviewed by Kosaric,[116] Ratledge,[117] Desai and Banat,[118] Banat,[119] and Lang and Wagner.[120] Of particular interest, because of the remarkably high yield, 300–400 g L^{-1}, is the sophorose lipid formation with *Candida bombolica* from glucose and rapeseed oil as substrates.[121, 122] Moreover, natural oils, fatty acid methyl esters, and free fatty acids have been converted into glycolipids in the presence of *Ustilago maydis* DSM 4500. In comparison with natural oils, the use of free fatty acids has brought about an increase in yield to 30 g L^{-1} glycolipid containing 90 wt% of mannosyl erythritolipids.[123]

5. Improvement in Natural Oils and Fats by Plant Breeding

In recent years, knowledge of the biochemical relationships of plant metabolism—in particular, of the biosynthesis of the storage fats in commercial use—has increased considerably.[124] Breeding has always been aimed mainly at an improvement in the yield performance of useful plants. Efforts are also now being made to meet the demands of industry for tailor-made oils and fats. The potential for future

growth in this area is mainly expected where suitability for chemical processing already exists due to the natural structure or purity of the vegetable raw material. Possibilities for the genetic modification of oil plants exist primarily in respect of the composition of the storage lipids, since, where chain length, number, and position of double bonds and functional groups are concerned, nature has already generated an enormous variety of fatty acids. Even drastic variations in the fatty acid pattern of seeds are tolerated by the plants and the seedlings.

5.1. Gene Technology as an Extension of the Methodological Repertoire of Plant Breeding

Concurrent with the increasing demand for renewable raw materials, modern biotechniques, including gene technology, have made enormous steps in extending the methodological repertoire of plant breeding, so that today's breeding procedures are even more efficient and selective. Although classical plant breeding, when combined with experimental mutagenesis ("mutation breeding") and modern in vitro cell- and tissue-culture methods, has frequently proved to be successful in oil plants such as, for example, soybean, rapeseed, sunflower, or linseed,[125, 126] gene technology offers an additional, universal approach for changing the amount and composition of the stored oil.[127, 128]

This development was recently made possible by a series of methodological improvements. This is illustrated by continued progress both in natural vector-transformation systems based upon natural infection by the soil-borne bacterium *Agrobacterium tumefaciens* (or *A. rhizogenes*) and in a series of vector-free transformation systems where, for example, the foreign recombinant gene is integrated into cells lacking a cell wall (protoplasts) or by bombardment of regenerable meristems with DNA-loaded particles.[129, 130] In molecular-biological experiment, the necessary regulatory "gene switches" (promoters) as expression signals are normally combined (cloned) with structural parts of previously isolated genes (structural genes) to form a new functional unit, a chimeric gene.[131] Moreover, selection markers, namely, genes which confer antibiotic or herbicide resistance and thus permit a selection of successfully transformed plant cells, are also frequently inserted.[129]

A widely used method for the genetic modification of useful plants, which are used particularly for the prevention of the undesired expression of species-specific genes, is the "antisense RNA" approach. Although the mode of action in transgenic plants is not yet fully understood, the simplest explanation is that the species-specific sense RNA binds to the transferred, complementary antisense RNA and, thus, the translation and biosynthesis of the relevant protein is inhibited. The resulting double-stranded RNA hybrid appears to be degraded very rapidly by nucleic-acid digesting enzymes (the nucleases, in this case RNAse H).[132] The extent of the gene expression achieved is dependent to a significant extent upon of the transcriptionally active promoter used. Thus, in the preparation of the gene constructs that are to be transferred, bacterial or viral promoters are frequently used. Meanwhile, however, a series of seed-specific promoter sequences such as those of napin, phaseolin, or oleosin genes have also been successfully used.[131, 133] Since at present, almost exclusive reliance is placed upon cell cultures or embryonic tissue in vitro for genetic transformation, further improvements are also indispensable for the regeneration to intact, transgenic plants; this has also been achieved.[129]

5.2. New Oil Qualities by Oil Designed with Available Agricultural Varieties

New genetic variation is fundamental to every commercial breeding activity, that is, selection is only successful if the characteristic to be changed varies in the starting material. Because of the intensive breeding to which they have been subject, the variability for new, desirable quality properties in agriculturally cultivated plants is, in practise, highly restricted. In contrast, a very rich reservoir of genetic resources for industrially interesting raw material for fatty compound in high purity is present in wild plants. These are, for example, medium to very long chain fatty acids as well as fatty acids with unusual functionality resulting from the number and position of double bonds or the presence of hydroxyl, oxo, or epoxy groups.[134, 135] Plant breeding efforts to domesticate wild plants such as species of the genera *Cuphea*, *Calendula*, *Euphorbia*, *Vernonia*, *Lesquerella*, *Crambe*, or *Limnanthes*, in order to develop useful plants that may be more productive, are not lacking.[136]

Where the genetic distance between the wild and the cultivated species is not too large, it is possible, in principle, to transfer the desired, quality improving property into the cultivated form by conventional methods of interspecific and intergeneric hybridization or with the support of biotechniques (for example, "embryo rescue"). Such breeding programs are, among others, very laborious, since many adverse properties of the "gene donor", such as the low yield capability, late ripening, or low shattering resistance of a wild species, is also transferred. These unfavorable properties must once more be eliminated with difficulty through repeated backcrossing and subsequent selection (often even without success). This clarifies why transferring a novel oil quality into a high yielding, agronomically adapted plant species by conventional methods is indeed possible, but is fraught with difficulty.

In this scenario, gene technology is well suited to accelerate breeding progress or, in many cases, to make it even possible. In practice, this grants the ability to implant a specific and desired quality property from distantly related plant species, from microorganisms (such as bacterial or yeasts), or even from mammals without detrimental effects to the genetic background or yield capabilities of the productive species. Numerous genes (*c*DNA clones) exist for the biosynthesis of unusual fatty acids such as, ricinoleic, petroselinic, linoleic, vernolic, or crepenynic acids, which may be cloned and transformed in cultivated plants. With the help of this material, it should become more possible to optimize genotypes (such as species) for the production of oleochemical raw materials.[127, 137–139]

5.3. Overview of Renewable Raw Materials Optimized by Breeding

A series of oil plants of world-wide significance is suitable for the production of renewable raw materials, namely, for the extraction of oils and fats with a specific fatty acid composition. Thus, commercially exploited oil seeds such as soybean (*Glycine max*), rapeseed (*Brassica napus*), sunflower (*Helianthus annuus*), peanut (*Arachis hypogaea*), or linseed (*Linum usitatissimum*) now exhibit a considerable variation in their fatty acid pattern, both in nature and as modified by breeding (Table 1).[126, 140–143] Where "nonfood" uses are concerned, genetic engineering approaches can make a special contribution to the expansion in the wealth of raw materials available to oleochemistry, such as increasing the content of individual fatty acids or drastically changing the oil quality by the introduction of a new fatty acid. Within this context, variants of important oil seeds, which have become available by plant breeding with different methods, will be discussed in the following on the basis of selected examples (Table 2).

5.3.1. Soybean

As a result of intensive quality breeding, the fatty acid pattern of the soya bean is remarkably variable. In addition to the low linolenic acid varieties, which should contribute considerably to the improvement in oxidative stability (mainly in the food oil area), there are further varieties with modified proportions of individual saturated fatty acids (Table 2).[144–146] "High oleic" (HO) soybeans have been produced by routes based on genetic engineering. It has been estimated that 40000 ha of this variety was planted in the USA in 1998.[138, 147]

5.3.2. Rapeseed

For a number of reasons, the intensive, ongoing work inducing alterations in the oil quality of cultivated plants is currently concentrated on rapeseed (*B. napus*). Since both summer and winter forms of this species are available, they can be planted as oil plant in climatically different regions of the world. A further advantage of rapeseed over other cultivated species is in its accessibility to biotechnological methods and, in particular, in its capability for transformation and regeneration.[141, 148]

Rapeseed oil is very rich in erucic acid (**3a**), a widely sought raw material for many nonfood uses.[149, 150] In the context of improvement in nutritional oil quality, the low erucic acid varieties—named zero and double zero or canola types, which exhibit about 60% oleic acid (**1a**)—were developed by

Table 1. Commercially available fatty acid variants of important oil seeds.

Type	Variant	Origin	12:0[a]	14:0	16:0	18:0	18:1	18:2	18:3	20:1	22:1	Others	Source
soybean	conventional		–	–	11	4	23	54	8	–	–	–	[126]
rapeseed	high erucic acid	conventional	–	–	3	1	11	12	9	8	52	4	[126]
	0 or 00 (canola)	natural mutation	–	–	4	2	60	21	10	1	1	1	[126]
	low linolenic acid	mutagenesis	–	–	4	2	61	28	3	1	–	1	[140]
	high lauric acid	gene technology	37	4	3	1	33	12	7	–	–	3	[141]
sunflower	conventional		–	–	7	5	19	68	–	–	–	1	[126]
	high oleic acid (HO)	mutagenesis	–	–	3	4	83	10	–	–	–	–	[126]
peanut	conventional		–	–	12	4	47	31	–	–	–	6	[142]
	high oleic acid (HO)	natural mutation	–	–	6	2	81	3	–	–	–	8	[142]
linseed	conventional		–	–	6	4	18	14	58	–	–	–	[126]
	low linolenic acid (linola)	mutagenesis	–	–	6	3	15	73	3	–	–	–	[143]

[a] 12:0 = lauric acid, 14:0 = myristic acid, 16:0 = palmitic acid, 18:0 = stearic acid **60**, 18:1 = oleic acid **1a**, 18:2 = linoleic acid **4a**, 18:3 = linolenic acid **5a**, 20:1 = eicosenoic acid, 22:1 = erucic acid **3a**.

Table 2. Extreme fatty acid variants in breeding material from important oil seeds.

Type	Variant	Method	14:0[a]	16:0	18:0	18:1	18:2	18:3	20:1	22:1	Others	Source
soybean	low linolenic acid	mutagenesis	–	10.5	4.6	23.2	59.6	2.0	–	–	–	[144]
	low palmitic acid	mutagenesis	–	3.7	3.7	24.1	58.9	8.9	–	–	0.7	[145]
	high palmitic acid	mutagenesis	–	17.3	2.9	16.8	54.5	8.3	–	–	0.2	[146]
	high stearic acid	mutagenesis	–	8.4	28.1	19.8	35.5	6.6	–	–	1.6	[146]
	high oleic acid (HO)	gene technology	–	6.6	3.6	84.9	0.6	1.9	–	–	2.4	[147]
rapeseed	high myristic acid	gene technology	17.7	23.1	2.4	33.7	14.8	3.8	–	–	4.5	[155]
	high stearin	gene technology	–	4	29	15	19	22	1	–	10[b]	[153]
	high oleic acid (HO)	mutagenesis	–	4.2	2.2	80.2	4.5	5.2	1.8	–	1.9	[151]
	high oleic acid (HO)	gene technology	–	4.3	1.4	84.1	5.2	2.9	0.9	–	1.2	[133]
	low linolen	gene technology	–	3.8	1.5	68.5	22.1	1.2	1.1	–	1.8	[133]
sunflower	high palmitin	mutagenesis	–	25.2	3.5	11.4	55.1	–	–	–	4.8[c]	[158]
	high stearin	mutagenesis	–	5.1	26.0	13.8	55.1	–	–	–	–	[158]
	high oleic acid combined with low saturated fatty acids	mutagenesis	–	3.2	2.4	92.1	2.3	–	–	–	–	[144]
linseed	high palmitin	mutagenesis	–	27.8	1.8	17.5	6.0	42.0	–	–	4.8[d]	[164]

[a] 14:0 = myristic acid, 16:0 = palmitic acid, 18:0 = stearic acid **60**, 18:1 = oleic acid **1a**, 18:2 = linoleic acid **4a**, 18:3 = linolenic acid **5a**, 20:1 = eicosenoic acid, 22:1 = erucic acid **3a**; [b] includes 6% arachidic acid (20:0), 2% behenic acid (22:0), 1% lignoceric acid (24:0); [c] includes 3.7% palmitoleic acid (16:1); [d] palmitoleic acid (16:1).

classical breeding methods. The breeding of linolenic acid deficient (< 3 % **5a**) or high oleic acid (> 80 % **1a**) rapeseed forms has been achieved both by induced mutation[151, 152] and genetically by inhibition of the inherent 12- or 15-desaturase genes[133] (Table 2). Anti-sense inhibition of the desaturation step in *Brassica rapa* (a close relative of *B. napus*) yields up to 40 % stearic acid **60** in the seed oil and has been already tested under field conditions.[153] In approaches which promise success, special fatty acid variants, which previously could not be realized in rapeseed, have been developed by gene technology. In this way, success was obtained in establishing the synthesis of short- and medium-chain saturated fatty acids (chain lengths of 8 – 14 carbon atoms), which are of special interest for oleochemistry and which could only be obtained previously from imported tropical fats (coconut, palm kernels).[154, 155] Most advanced is the development of "high lauric acid rapeseed" with about 40 – 50 % lauric acid by Calgene (CA, USA), which depends on the transfer of a thioesterase gene from the Californian bay (*Umbellularia californica*) and which has been already commercially planted.[141, 154]

There is a constant demand for high erucic acid rapeseed oil for industrial use. Here, breeding is devoted to increasing the fraction of this very long chain fatty acid well above the current maximum of 55 – 60 % **3a**. It has been known for a long time that, because of the nonoccupation of the middle of the three triacylglycerol positions by erucic acid **3a**, a (theoretical) maximum of 67 % cannot be exceeded.[149] However, partial success was achieved recently when transgenic rape forms were developed with varying contents of trierucin (trierucoylglycerol) in the seed oil by transfer of the gene for *sn*-2-acyltransferase (lysophosphatidic acid acyltransferase, LPAAT) from different *Limnanthes* species (meadowfoam) and by inhibition of the inherent LPAAT of rapeseed.[141, 156]

5.3.3. Sunflower

In addition to the conventional sunflower oils, which exhibit a high content of linoleic acid (**4a**), HO types were developed experimentally some time ago by mutagenesis.[126, 157] Furthermore, forms with increased proportions of saturated fatty acids, which could provide advantages for margarine production (Table 2), have been produced by mutagenic treatment.[158] However, the industrial use of HO sunflower oil requires that the content of saturated fatty acids should be as low as possible. Breeding has already reduced the content of stearic acid **60** to 1.5 %, which adversely affects the solidification temperature and the cloud point. Under favorable climatic and cultivation conditions, a stable proportion of 90 % **1a** with a concurrently reduced content of stearic acid **60** could be achieved from current HO sunflower lines or hybrids developed in this way.[144] In contrast for nonfood purposes in Germany, economic reasons demand at least 83 % oleic acid **1a** in the product in order to avoid additional purification steps and thus increase the advantage to this production, against **1a** derived from the competing raw material, beef tallow.[159]

5.3.4. Peanut

In the case of the peanut, an HO mutant (breeding line F435 from the University of Florida) was found in the available varieties which was then used to breed varieties which provide an oil with high oxidative stability.[142, 160]

5.3.5. Linseed

If the possibilities for the use of linseed oil in the nonfood areas are considered, its main uses are in the production of dyes, coatings, and linoleum.[135] On the other hand, in the oleochemical area, the high reactivity of the polyene structure of linseed fatty acids results in a pronounced sensitivity towards autoxidation of products based on linseed oil as well as complex reaction pathways which lead to poorly defined products.[161] From this point of view, breeding efforts are being made to improve the variability of linseed oil in respect of its fatty acid and triglyceride composition in order to provide new, specific oil qualities.[162] Here too, the classical approach of mutagenesis has also been used to breed new linseed varieties with a linolenic acid **5a** content of less than 5 % (linola quality)[143, 163] or with an increased palmitic acid content in the oil.[164]

5.4. Concluding Remarks on the Use of Gene Technology

The preceding presentation clearly illustrates that gene technology is a very suitable breeding instrument in order to induce new genetic variation. In the ideal situation, it allows the breeder to introduce totally new qualities into cultivated plant varieties with greater precision without impairing the performance capabilities of the respective genotype. There are certain barriers to the realization and use of gene technology because of the poor acceptance by some end users; this applies especially to the nutritional and feed area (novel food, novel feed). However, since the novel products do not enter the human food chain directly, it is not surprising that the initial applications of modern bio- and gene technology methods are found in the technical and chemical area, where they provide vegetable raw materials of improved quality and yield. In this way, important but limited raw material resources can be saved for future generations. To what extent these "new" plant types achieve practical relevance depends on economic factors. Thus, from the viewpoint of industry, demand will only be generated if new raw materials of vegetable origin are available in sufficient quantities at competitive prices, economically viable isolation of the relevant components is possible, and they are held in a higher esteem and preference to alternatives which come, for example, from the petrochemical industry.

6. Future Prospects

After years of relative stagnation, the synthesis of novel fatty compounds based on oils and fats has made important

advances. With the breeding of new oil plants—including the use of gene technology—numerous fatty compounds of adequate purity are now available which makes them attractive for synthesis. The use of modern synthetic methods together with enzymatic and microbiological methods has lead to an extraordinary expansion in the potential for the synthesis of novel fatty compounds, which are selectively modified in the alkyl chain. These are now being investigated for their action, properties, and possibilities for new applications.

However, numerous synthetic problems remain unsolved and solutions must be found in the coming years. Chemists, biotechnologists, and plant breeders are all challenged to continue development of the advances made in recent years in an integrated, interdisciplinary approach and thus prepare the way for oils and fats to be increasingly used as renewable raw materials in the chemical industry.

We thank the Departments of Bildung und Forschung, and Ernährung, Landwirtschaft, und Forsten of the German government, as well as the companies Bayer AG, Henkel KGaA, Harburger Fettchemie, Brinckmann & Mergel GmbH, Hoechst, BASF AG, Condea Chemie GmbH, Süd-Chemie AG, and Wella AG for inspirational and material support of our work.

Received: 26 March, 1999
Revised: 1 October, 1999 [A336]

[1] *Konzept Nachhaltigkeit, vom Leitbild zur Umsetzung*, Concluding report of the Symposium "Schutz des Menschen und der Umwelt—Ziele und Rahmenbedingungen einer nachhaltig zukunftsverträglichen Entwicklung" of the 13th German Parliament (Ed.: Deutscher Bundestag, Referat Öffentlichkeitsarbeit), Bonn, **1998**.
[2] *Nachwachsende Rohstoffe, Perspektiven für die Chemie* (Eds.: M. Eggersdorfer, S. Warwel, G. Wulff), VCH, Weinheim, **1993**.
[3] *Perspektiven nachwachsender Rohstoffe in der Chemie* (Ed.: H. Eierdanz), VCH, Weinheim, **1996**.
[4] H. Baumann, M. Bühler, H. Fochem, F. Hirsinger, H. Zoebelein, J. Falbe, *Angew. Chem.* **1988**, *100*, 42 – 62; *Angew. Chem. Int. Ed. Engl.* **1988**, *27*, 41 – 62.
[5] W. von Rybinski, K. Hill, *Angew. Chem.* **1998**, *110*, 1394 – 1412; *Angew. Chem. Int. Ed.* **1998**, *37*, 1328 – 1345.
[6] K. E. Augustin, H. J. Schäfer, *Liebigs Ann. Chem.* **1991**, 1037 – 1040.
[7] a) L. Hinkamp, PhD thesis, Universität Münster (Germany), **1993**; b) H. J. Schäfer, M. aus dem Kahmen, L. Hinkamp, R. Maletz in *3. Symposium Nachwachsende Rohstoffe, Perspektiven für die Chemie* (Ed.: Bundesministerium für Ernährung, Landwirtschaft und Forsten) Landwirtschaftsverlag, Münster, **1994**, pp. 217 – 234.
[8] M. C. Kuo, C. T. Chou, *Ind. Eng. Chem. Res.* **1987**, *26*, 277 – 284.
[9] W. Adam, J. Bialas, L. Hadjiarapoglou, *Chem. Ber.* **1991**, *124*, 2377.
[10] P. E. Sonnet, M. E. Lankin, G. P. Lankin, *J. Am. Oil Chem. Soc.* **1995**, *72*, 199 – 204.
[11] M. S. F. Lie Ken Jie, M. K. Pasha, *Lipids* **1998**, *33*, 633 – 637.
[12] Y. Ishii, K. Yamawaki, T. Ura, H. Yamada, T. Yoshida, M. Ogawa, *J. Org. Chem.* **1988**, *53*, 3587 – 3593.
[13] P. Bavaj, PhD thesis, RWTH Aachen (Germany), **1995**.
[14] W. A. Herrmann, R. W. Fischer, M. U. Rauch, W. Scherer, *J. Mol. Catal.* **1994**, *86*, 245 – 266.
[15] W. A. Herrmann, R. W. Fischer, D. W. Matz, *Angew. Chem.* **1991**, *103*, 1706 – 1709; *Angew. Chem. Int. Ed. Engl.* **1991**, *30*, 1638 – 1641.
[16] M. Gerle, PhD thesis, RWTH Aachen (Germany), **1997**.
[17] W. A. Herrmann, J. D. G. Correia, F. E. Kühn, G. R. J. Artus, C. C. Romao, *Chem. Eur. J.* **1996**, *2*, 168 – 173.
[18] R. Landau, G. A. Sullivan, D. Brown, *CHEMTECH* **1979**, 602 – 607.
[19] P. J. Martinez de la Cuesta, E. Martinez, L. M. Cotoluero Minguez, *Grasas Aceites (Seville)* **1985**, *36*, 181 – 185, and references therein.
[20] A. Debal, G. Rafaralahitsimba, E. Ucciani, *Fat Sci. Technol.* **1993**, *95*, 236 – 239.
[21] a) F. Björkling, S. E. Godtfredsen, O. Kirk, *J. Chem. Soc. Chem. Commun.* **1990**, 1302 – 1303; b) F. Björkling, H. Frykman, S. E. Godtfredsen, O. Kirk, *Tetrahedron* **1992**, *48*, 4587 – 4592; c) O. Kirk, F. Björkling,T. Damhus, S. E. Godtfredsen, *Biocatalysis* **1994**, *11*, 65 – 77.
[22] M. Rüsch gen. Klaas, S. Warwel, *J. Mol. Catal. A* **1997**, *117*, 311 – 319.
[23] S. Warwel, M. Rüsch gen. Klaas, *J. Mol. Catal. B* **1995**, *1*, 29 – 35.
[24] a) M. Rüsch gen. Klaas, S. Warwel, *J. Am. Oil Chem. Soc.* **1996**, *73*, 1453 – 1457; b) M. Rüsch gen. Klaas, S. Warwel, *Ind. Crops Prod.* **1999**, *9*, 125 – 132.
[25] J. V. Crivello, R. Narayan, *Chem. Mater.* **1992**, *4*, 692 – 699.
[26] M. S. F. Lie Ken Jie, M. S. K. Syed-Rahmatullah, *J. Am. Oil Chem. Soc.* **1992**, *69*, 359 – 362.
[27] J. O. Metzger, S. Fürmeier, *Eur. J. Org. Chem.* **1999**, 661 – 664.
[28] M. S. F. Lie Ken Jie, Y. F. Zheng, *Chem. Phys. Lipids* **1988**, *49*, 167 – 178.
[29] B. Dahlke, S. Hellbardt, M. Paetow, W. H. Zech, *J. Am. Oil Chem. Soc.* **1995**, *72*, 349 – 353.
[30] "Stets geforscht…Chemieforschung im Degussa-Forschungszentrum Wolfgang": M. Dankowski, G. Goor, G. Prescher, *Degussa AG company publication*, *Vol. 2*, Frankfurt, **1988**, p. 63.
[31] T. M. Luong, H. Schriftmann, D. Swern, *J. Am. Oil Chem. Soc.* **1967**, *44*, 316 – 320.
[32] W. A. Herrmann, D. Marz, J. G. Kuchler, G. Weichselbaumer, R. W. Fischer, DE-A 3902357 A1, **1989**; *Chem. Abstr.* **1991**, *114*, 143714
[33] S. Warwel, M. Rüsch gen. Klaas, M. Sojka, *Chem. Commun.* **1991**, 1578 – 1579.
[34] K. B. Sharpless, H. Kolb, M. S. van Nieuwenhze, *Chem. Rev.* **1994**, *94*, 2483 – 2547.
[35] a) M. Plate, M. Overs, H. J. Schäfer, *Synthesis* **1998**, 1255 – 1258; b) S. Jacobi, L. Chi, M. Plate, M. Overs, H. J. Schäfer, H. Fuchs, *Thin Solid Films* **1998**, *327 – 329*, 180 – 184.
[36] T. Tachibana, T. Mori, K. Hori, *Bull. Chem. Soc. Jpn.* **1980**, *53*, 1714 – 1719.
[37] G. Fayter in *Perspektiven nachwachsender Rohstoffe in der Chemie* (Ed.: H. Eierdanz), VCH, Weinheim, **1996**, pp. 107 – 118.
[38] a) M. Rüsch gen. Klaas, P. Bavaj, S. Warwel, *Fat Sci. Technol.* **1995**, *97*, 359 – 367; b) S. Warwel, M. Rüsch gen. Klaas, *Lipid Technol.* **1997**, 10 – 14.
[39] S. Warwel, M. Sojka, M. Rüsch gen. Klaas, *Top. Curr. Chem.* **1993**, *164*, 79 – 89.
[40] S. Warwel, M. Rüsch gen. Klaas, US-A 5321158, **1994**; *Chem. Abstr.* **1996**, *125*, 136578.
[41] K. M. Draths, J. W. Frost in *Green Chemistry, Frontiers in Benign Chemical Syntheses and Processes* (Eds.: P. T. Anastas, T. C. Williamson), Oxford University Press, Oxford, **1998**, pp. 150 – 165.
[42] K. Augustin, PhD thesis, Universität Münster (Germany), **1991**.
[43] a) B. Wolff, PhD thesis, RWTH Aachen (Germany), **1994**; b) S. Warwel, P. Bavaj, M. Rüsch gen. Klaas, B. Wolff in *Perspektiven nachwachsender Rohstoffe in der Chemie* (Ed.: H. Eierdanz), VCH, Weinheim, **1996**, pp. 119 – 135.
[44] W. A. Herrmann, W. Wagner, U. N. Flessner, U. Volkhardt, H. Komter, *Angew. Chem.* **1991**, *102*, 1704 – 1706; *Angew. Chem. Int. Ed. Engl.* **1991**, *30*, 1641 – 1643.
[45] M. aus dem Kahmen, H. J. Schäfer, *Fett/Lipid* **1998**, *100*, 227 – 235.
[46] M. aus dem Kahmen, PhD thesis, Universität Münster (Germany), **1993**.
[47] J. O. Metzger, K. F. Leisinger, *Fat Sci. Technol.* **1988**, *90*, 1 – 5.
[48] J. O. Metzger, U. Biermann, *Fat Sci. Technol.* **1994**, *96*, 321 – 323.
[49] E. M. Zobel, PhD thesis, Universität Münster (Germany), **1997**.
[50] C. Kalk, Diploma thesis, Universität Münster (Germany), **1998**.
[51] "Carbon radicals": *Methoden Org. Chem. (Houben-Weyl), 4th. ed. 1952 –*, Vol. E19a, **1989**.
[52] G. G. Melikyan, *Synthesis* **1993**, 833 – 850.
[53] J. O. Metzger, U. Riedner, *Fat Sci. Technol.* **1989**, *91*, 18 – 23.
[54] J. O. Metzger, U. Linker, *Fat Sci. Technol.* **1991**, *93*, 244 – 249.
[55] U. Linker, PhD thesis, Universität Oldenburg (Germany), **1991**.
[56] J. O. Metzger, R. Mahler, *Angew. Chem.* **1995**, *107*, 1012 – 1016; *Angew. Chem. Int. Ed. Engl.* **1995**, *34*, 902 – 906.

[57] J. O. Metzger, R. Mahler, G. Francke, *Liebigs Ann.* **1997**, 2303 – 2313.
[58] R. Mahler, PhD thesis, Universität Oldenburg (Germany), **1994**.
[59] J. O. Metzger, R. Mahler, *Liebigs Ann.* **1993**, 203 – 205.
[60] N. O. Brace, *J. Org. Chem.* **1962**, *27*, 4491 – 4498.
[61] J. O. Metzger, U. Linker, *Liebigs Ann*. **1992**, 209 – 216.
[62] J. O. Metzger, R. Mahler, A. Schmidt, *Liebigs Ann*. **1996**, 693 – 696.
[63] J. Greiner, A. Manfredi, J. G. Riess, *New J. Chem.* **1989**, *13*, 247 – 254.
[64] D. V. Kinsman in *Fatty Acids in Industry* (Eds.: R. W. Johnson, E. Fritz), Marcel Dekker, New York, NY, **1989**, pp. 233 – 276.
[65] J. Hartmanns, K. Klenke, J. O. Metzger, *Chem. Ber*. **1986**, *119*, 488 – 499.
[66] J. O. Metzger, F. Bangert, *Fat Sci. Technol.* **1995**, *97*, 7 – 9.
[67] a) H. G. Floss, *Nat. Prod. Rep*. **1997**, *14*, 433 – 452; b) S. Handa, H. G. Floss, *Chem. Commun.* **1997**, 153 – 154.
[68] a) U. Biermann, J. O. Metzger, *Fat Sci. Technol* **1991**, *93*, 282 – 284; b) J. O. Metzger, U. Biermann, *Synthesis* **1992**, 463 – 465.
[69] B. B. Snider, D. J. Rodini, T. C. Kirk, R. Cordova, *J. Am. Chem. Soc.* **1982**, *104*, 555 – 563.
[70] B. B. Snider, G. B. Phillips, *J. Org. Chem.* **1983**, *48*, 464 – 469.
[71] E. Blée, *INFORM* **1995**, *6*, 852 – 861.
[72] J. O. Metzger, U. Biermann in *Chemische Nutzung heimischer Pflanzenöle* (Ed.: Fachagentur Nachwachsende Rohstoffe), Landwirtschaftsverlag, Münster, **1998**, pp. 144 – 176, see p. 145.
[73] J. F. Mc Lellan, R. M. Mortier, S. T. Orszulik, R. M. Paton, *J. Am. Oil Chem. Soc.* **1994**, *71*, 231 – 232.
[74] J. O. Metzger, U. Biermann, *Liebigs Ann.* **1996**, 1851 – 1854.
[75] J. O. Metzger, U. Biermann, *Bull. Soc. Chim. Belg.* **1994**, *103*, 393 – 397.
[76] a) U. Biermann, J. O. Metzger, *Fat Sci. Technol.* **1992**, *94*, 329 – 332; b) J. O. Metzger, U. Biermann, *Liebigs Ann.* **1993**, 645 – 650.
[77] J. O. Metzger, U. Biermann, *Fett/Lipid* **1998**, *100*, 2 – 6.
[78] a) R. Maletz, H. J. Schäfer, R. Quermann, *Fett/Lipid* **1996**, *98*, 370 – 379; b) R. Maletz, PhD thesis, Universität Münster (Germany), **1994**.
[79] a) M. Zobel, Diploma thesis, Universität Münster (Germany), **1994**; b) M. Zobel, PhD thesis, Universität Münster (Germany), **1997**; c) M. Zobel, H. J. Schäfer in *5. Symposium Nachwachsende Rohstoffe* (Ed.: Fachagentur Nachwachsende Rohstoffe), Landwirtschaftsverlag, Münster, **1997**, pp. 186 – 190; d) H. J. Schäfer, M. Zobel in *Recent Developments in the Synthesis of Fatty Acid Derivatives* (Eds.: G. Knothe, J. T. P. Derksen), AOCS Press, Champaign, IL, **1999**, pp. 59 – 79.
[80] a) M. Plate, PhD thesis, Universität Münster (Germany), **1997**; b) M. Plate, H. J. Schäfer in *5. Symposium Nachwachsende Rohstoffe* (Ed.: Fachagentur Nachwachsende Rohstoffe), Landwirtschaftsverlag Münster, **1997**, pp. 195 – 198; c) M. Plate, H. J. Schäfer, M. aus dem Kahmen in *Nachwachsende Rohstoffe*, *Band 12*, Chemische Nutzung heimischer Pflanzenöle, Landwirtschaftsverlag, Münster, **1998**, p. 50.
[81] a) R. Quermann, R. Maletz, H. J. Schäfer, *Liebigs Ann. Chem.* **1993**, 1219 – 1223; b) R. Quermann, PhD thesis, Universität Münster (Germany), **1991**.
[82] a) H. J. Schäfer, *Top. Curr. Chem*. **1990**, *152*, 91 – 151; b) D. Degner, *Top. Curr. Chem.* **1988**, *148*, 1 – 95, see p. 24.
[83] A. Weiper-Idelmann, M. aus dem Kahmen, H. J. Schäfer, M. Gockeln, *Acta Chem. Scand*. **1998**, *52*, 672 – 682.
[84] H. J. Schäfer, A. Weiper, M. aus dem Kahmen, A. Matzeit in *Nachwachsende Rohstoffe* (Eds.: M. Eggersdorfer, S. Warwel, G. Wulff), VCH, Weinheim, **1993**, p. 97.
[85] a) B. C. L. Weedon, *Adv. Org. Chem*. **1960**, *1*, 1 – 60; b) H. J. Schäfer, *Chem. Phys. Lipids* **1979**, *24*, 321 – 333.
[86] a) A. Weiper, H. J. Schäfer, *Angew. Chem.* **1990**, *102*, 228; *Angew. Chem. Int. Ed. Engl*. **1990**, *29*, 195 – 197; b) A. Matzeit, M. Harenbrock, H. J. Schäfer, *Liebigs Ann*. **1996**, 55 – 62.
[87] a) J. A. Davies, P. L. Watson, J. F. Liebman, A. Greenberg, *Selective Hydrocarbon Activation*, *Principles and Progress*, VCH, Weinheim, **1990**; b) D. Mansuy, *Pure Appl. Chem.* **1990**, *62*, 741 – 766; c) O. Reiser, *Angew. Chem*. **1994**, *106*, 73 – 76; *Angew. Chem. Int. Ed. Engl.* **1994**, *33*, 69 – 72; d) H. J. Schäfer in *Chemistry of Alkanes and Cycloalkanes* (Eds.: S. Patai, Z. Rapoport), Wiley, New York, NY, **1992**, pp. 781 – 808.
[88] a) M. Bühler, J. Schindler, in *Biotechnology*, *Vol. 6a* (Eds.: J. Rehm, G. Reed), VCH, Weinheim, **1984**, pp. 329 – 385; b) K. Kieslich, *Microbial Transformations of Non-Steroid Cyclic Compounds*, Thieme, Stuttgart, **1976**.
[89] L. Hinkamp, H. J. Schäfer, B. Wippich, H. Luftmann, *Liebigs Ann. Chem*. **1992**, 559 – 563.
[90] N. C. Deno, W. E. Billups, R. Fishbein, C. Person, R. Whalen, J. Wyckoff, *J. Am. Chem. Soc.* **1971**, *93*, 438 – 440.
[91] a) E. Cramer, H. J. Schäfer, *Fat Sci. Technol*. **1988**, *90*, 351 – 357; b) J. R. L. Smith, R. O. C. Norman, A. G. Rowley, *J. Chem. Soc. Perkin Trans. 1* **1973**, 566 – 571; c) N. C. Deno, D. G. Pohl, *J. Am. Chem. Soc*. **1974**, *96*, 6680 – 6682.
[92] R. D. Schmid, R. Verger, *Angew. Chem.* **1998**, *110*, 1694 – 1720; *Angew. Chem. Int. Ed.* **1998**, *37*, 1608 – 1633.
[93] a) C. C. Akoh, *Biotechnol. Lett.* **1993**, 15, 949 – 954; b) S. Pecnik, Z. Knez, *J. Am. Oil Chem. Soc.* **1992**, *62*, 261 – 265; c) Y. F. Wang, J. J. Lalonde, M. Momongan, D. E. Bergbreiter, C. H. Wong, *J. Am. Chem. Soc.* **1988**, *110*, 7200 – 7205; d) W. A. Szarek, A. Zamojeski, K. N. Tiwari, E. R. Ison, *Tetrahedron Lett.* **1986**, *27*, 3827 – 3830; e) V. Partali, A. G. Melbye, T. Alvik, T. Anthonsen, *Tetrahedron: Asymmetry* **1992**, *3*, 65 – 72.
[94] a) O. Papendorf, B. Steffen, S. Lang, F. Wagner, *Chim. Oggi*, **1995**, *10*, 17 – 20; b) B. Steffen, A. Ziemann, S. Lang, F. Wagner, *Biotechnol. Lett.* **1992**, *14*, 773 – 778.
[95] B. Steffen, S. Lang, D. Hamann, P. Schneider, H. K. Cammenga, F. Wagner, *Fat Sci. Technol.* **1995**, *97*, 132 – 136.
[96] M. Berger, M. P. Schneider, *J. Am. Oil Chem. Soc.* **1992**, *69*, 961 – 965.
[97] M. Berger, K. Laumen, M. P. Schneider, *J. Am. Oil Chem. Soc*. **1992**, *69*, 955 – 960.
[98] C. Waldinger, M. P. Schneider, *J. Am. Oil Chem. Soc*. **1996**, *73*, 1513 – 1519.
[99] a) H. Berger, M. P. Schneider, *Biotechnol. Lett.* **1991**, *13*, 333 – 338; b) P. Villeneuve, T. A. Foglia, *INFORM* **1997**, *8*, 640 – 650.
[100] M. Berger, M. P. Schneider, *Fat Sci.Technol.* **1993**, *95*, 169 – 175.
[101] a) B. Haase, G. Machmüller, M. P. Schneider in *Biokonversion nachwachsender Rohstoffe* (Ed.: Fachagentur Nachwachsende Rohstoffe), Landwirtschaftsverlag, Münster, **1998**, pp. 218 – 224; b) B. Haase, G. Machmüller, M. P. Schneider, DE-B 19 62 6943.1, **1996**; *Chem. Abstr.* **1998**, *128*, 127145t.
[102] T. Lucas, PhD thesis, Universität Münster (Germany), **1991**.
[103] L. L. Wallen, R. G. Benedict, R. W. Jackson, *Arch. Biochem. Biophys.* **1962**, *99*, 249 – 253.
[104] S. Koritala, L. Hosie, C. T. Hou, C. W. Hesseltine, M. O. Bagby, *Appl. Microbiol. Biotechnol.* **1989**, *32*, 299 – 304.
[105] C. W. Seo, Y. Yamada, N. Takada, H. Okada, *Agric. Biol. Chem.* **1981**, *45*, 2025 – 2030.
[106] W. Blank, H. Takayanagi, T. Kido, F. Meussdoerfer, N. Esaki, K. Soda, *Agric. Biol. Chem.* **1991**, *55*, 2651 – 2652.
[107] S. H. El-Sharkawy, W. Yang, L. Dostal, J. P. N. Rosazza, *Appl. Environ. Microbiol.* **1992**, *58*, 2116 – 2122.
[108] a) Y. Yamada, H. Uemura, H. Nakaya, K. Sakata, T. Takatori, M. Nagao, H. Iwase, K. Iwadate, *Biochem. Biophys. Res. Commun.* **1996**, *226*, 391 – 395; b) S. Koritala, M. O. Bagby, *J. Am. Oil Chem. Soc.* **1992**, *69*, 575 – 578.
[109] C. T. Hou in *Advances in Applied Microbiology*, *Vol. 41* (Eds.: S. L. Neidleman, A. I. Laskin), Academic Press, San Diego, **1995**, pp. 1 – 23.
[110] a) I. Gill, R. Valivety, *Trends Biotechnol.* **1997**, *15*, 470 – 478; b) A. Nuñez, G. St. Armand, T. A. Foglia, G. J. Piazza, *Biotechnol. Appl. Biochem.* **1997**, *25*, 75 – 80.
[111] Z.-H. Yi, H.-J. Rehm, *Appl. Microbiol. Biotechnol*. **1988**, *30*, 327 – 331.
[112] a) D. Fabritius, Diploma thesis, Universität Münster (Germany), **1993**; b) D. Fabritius, PhD thesis, Universität Münster (Germany), **1996**.
[113] a) J. Schindler, F. Meussdorfer, H. G. Bühler, *Forum-Biotechnol.* **1990**, 274 – 281; b) N. Uemura, A. Taoka, M. Takagi, *J. Am. Oil Chem. Soc.* **1988**, *65*, 148 – 152.
[114] D. Fabritius, H. J. Schäfer, A. Steinbüchel, *Appl. Microbiol. Biotechnol*. **1996**, *45*, 432 – 438.
[115] D. Fabritius, H. J. Schäfer, A. Steinbüchel, *Appl. Microbiol. Biotechnol*. **1998**, *50*, 573 – 578.
[116] N. Kosaric in *Biotechnology*, *Vol. 6* (Eds.: H. J. Rehm, G. Reed, A. Pühler, P. Stadler), VCH, Weinheim, **1996**, pp. 659 – 717.

[117] C. Ratledge in *Biotechnology*, *Vol. 7* (Eds.: H. J. Rehm, G. Reed, A. Pühler, P. Stadler), VCH, Weinheim, **1997**, pp. 133 – 197.

[118] J. D. Desai, I. M. Banat, *Microbiol. Mol. Biol. Rev.* **1997**, *61*, 47 – 64.

[119] I. M. Banat, *Acta Biotechnol.* **1995**, *15*, 251 – 267.

[120] S. Lang, F. Wagner, *Fat Sci. Technol.* **1995**, *97*, 69 – 77.

[121] A. Albrecht, U. Rau, F. Wagner, *Appl. Microbiol. Biotechnol.* **1996**, *46*, 67 – 73.

[122] a) A.-M. Davila, R. Marchal, J.-P. Vandecasteele, *Appl. Microbiol. Biotechnol.* **1992**, *38*, 6 – 11; b) Q. H Zhou, N. Kosaric, *J. Am. Oil Chem. Soc.* **1995**, *72*, 67 – 71; c) L. Fischer, A. Boger, S. Lang, C. Manzke, S.-H. Park, U. Rau, A. Schlotterbeck, F. Wagner in *Perspektiven nachwachsender Rohstoffe der Chemie* (Ed.: H. Eierdanz), VCH, Weinheim, **1996**, pp. 250 – 254; d) H.-J. Daniel, M. Reuss, C. Syldatk, *Biotechnol. Lett.* **1998**, *20*, 1153 – 1156; e) U. Rau, S. Hammen, R. Heckmann, V. Wray, S. Lang, *Ind. Crops Products* **1999**, in press.

[123] S. Lang, U. Rau, D. Rasch, S. Spöckner, E. Vollbrecht in *Biokonversion nachwachsender Rohstoffe* (Ed.: Fachagentur Nachwachsende Rohstoffe) Landwirtschaftsverlag, Münster, **1998**, pp. 154 – 164.

[124] a) J. B. Ohlrogge, J. Browse, *Plant Cell* **1995**, *7*, 957 – 970; b) J. L. Harwood, *Biochim. Biophys. Acta* **1996**, *1301*, 7 – 56; c) J. B. Ohlrogge, J. G. Jaworski, *Annu. Rev. Plant Physiol. Plant Mol. Biol.* **1997**, *48*, 109 – 136.

[125] A. Thierfelder, W. Lühs, W. Friedt, *Ind. Crops Prod.* **1993**, *1*, 261 – 271.

[126] W. Lühs, W. Friedt in *Designer Oil Crops* (Ed.: D. J. Murphy), VCH, Weinheim, **1994**, pp. 5 – 71.

[127] D. J. Murphy, *Lipid Technol.* **1994**, *6*(4), 84 – 91.

[128] a) R. Töpfer, M. Martini, J. Schell, *Science* **1995**, *268*, 681 – 686; b) W. Friedt, W. Lühs in *Perspektiven nachwachsender Rohstoffe in der Chemie* (Ed.: H. Eierdanz), VCH, Weinheim, **1996**, pp. 11 – 20; c) G. J. Budziszewski, K. P. C. Croft, D. F. Hildebrand, *Lipids* **1996**, *31*, 557 – 569; d) A. J. Kinney in *Genetic Engineering*, *Vol. 19* (Ed.: J. K. Setlow), Plenum, New York, NY, **1997**, pp. 149 – 166; e) M. Lassner, *Lipid Technol.* **1997**, *9*(1), 5 – 9; f) W. Friedt, W. Lühs, *Biol. Unserer Zeit* **1999**, *29*, 142 – 150.

[129] a) M. De Block, *Euphytica* **1993**, *71*, 1 – 14; b) H. J. Fisk, A. M. Dandekar, *Sci. Horti. (Amsterdam)* **1993**, *55*, 5 – 36.

[130] R. Luthra, Varsha, R. K. Dubey, A. K. Srivastava, S. Kumar, *Euphytica* **1997**, *95*, 269 – 294.

[131] a) J. C. Kridl, V. C. Knauf, G. A. Thompson in *Control of Plant Gene Expression* (Ed.: D. P. S. Verma), CRC, Boca Raton, FL, **1993**, pp. 481 – 498; b) T. J. Guilfoyle in *Genetic Engineering*, *Vol. 19* (Ed.: J. K. Setlow), Plenum, New York, NY, **1997**, pp. 15 – 47.

[132] a) J. Green, O. Pines, M. Inouye, *Annu. Rev. Biochem.* **1986**, *55*, 569 – 597; b) G. M. Fader, A. J. Kinney, W. D. Hitz, *INFORM* **1995**, *6*, 167 – 169; c) B. Lewin, *Genes*, 6th ed., Oxford University Press, Oxford, **1997**.

[133] a) W. D. Hitz, C. J. Mauvis, K. G. Ripp, R. J. Reiter, *Rapeseed Today and Tomorrow*, *Vol. 2*, Dorset, Dorchester, **1995**, pp. 470 – 472 (Proc. 9th Int. Rapeseed Congr. (GCIRC)); b) W. D. Hitz, N. S. Yadav, R. J. Reiter, C. J. Mauvis, A. J. Kinney in *Plant Lipid Metabolism* (Eds.: J.-C. Kader, P. Mazliak), Kluwer, Dordrecht, **1995**, pp. 506 – 508.

[134] a) T. P. Hilditch, P. N. Williams, *The Chemical Constitution of Natural Fats*, 3rd ed., Chapman & Hall, London, **1964**; b) C. R. Smith, Jr. in *Progress in the Chemistry of Fats and other Lipids*, *Vol. 11* (Ed.: R. T. Holman), Pergamon, Oxford, **1970**, pp. 137 – 177; c) R. C. Badami, K. B. Patil, *Progr. Lipid Res.* **1981**, *19*, 119 – 153; d) B. G. Muuse, F. P. Cuperus, J. T. P. Derksen, *Ind. Crops Prod.* **1992**, *1*, 57 – 65; e) H. K. Mangold, *Fat Sci. Technol.* **1994**, *96*, 23 – 27; f) K. Aitzetmüller in *Perspektiven nachwachsender Rohstoffe in der Chemie* (Ed.: H. Eierdanz), VCH, Weinheim, **1996**, pp. 209 – 217; g) V. Spitzer, *Fett/Lipid* **1999**, *101*, 2 – 19.

[135] W. Lühs, W. Friedt in *Designer Oil Crops* (Ed.: D. J. Murphy), VCH, Weinheim, **1994**, pp. 73 – 130.

[136] a) F. Hirsinger in *Oil Crops of the World* (Eds.: G. Röbbelen, R. K. Downey, A. Ashri), McGraw-Hill, New York, NY, **1989**, pp 518 – 532; b) *Progress in New Crops*, Proc. 3rd Nat. Symp. New Crops (Ed.: J. Janick), ASHS Press, Alexandria, VA, **1996**; c) *Domestication*, *Production and Utilization of New Crops* (Ed.: J. Smartt, N. Haq), International Centre for Underutilized Crops, Southampton University (UK), **1997**.

[137] a) E. B. Cahoon, J. B. Ohlrogge, *Plant Physiol.* **1994**, *104*, 827 – 837; b) A. S. Reddy, T. L. Thomas, *Nat. Biotechnol.* **1996**, *14*, 639 – 642; c) P. Broun, P. C. Somerville, *Plant Physiol.* **1997**, *113*, 933 – 942.

[138] A. J. Kinney, *Fett/Lipid* **1998**, *100*, 173 – 176.

[139] M. Lee, M. Lenman, A. Banas, M. Bafor, S. Singh, M. Schweizer, R. Nilsson, C. Liljenberg, A. Dahlqvist, P. O. Gummeson, S. Sjoedahl, A. Green, S. Stymne, *Science* **1998**, *280*, 915 – 918.

[140] R. Scarth, P. B. E. McVetty, S. R. Rimmer, *Can. J. Plant Sci.* **1997**, *77*, 125 – 126.

[141] W. Friedt, W. Lühs, *Fett/Lipid* **1998**, *100*, 219 – 226.

[142] J. B. Mugendi, C. A. Sims, D. W. Gorbet, S. F. O'Keefe, *J. Am. Oil Chem. Soc.* **1998**, *75*, 21 – 25.

[143] J. C. P. Dribnenki, A. G. Green, G. N. Atlin, *Can. J. Plant Sci.* **1996**, *76*, 329 – 331.

[144] G. Cole, G. S. Coughlan, N. Frey, J. Hazebroek, C. Jennings, *Fett/Lipid* **1998**, *100*, 177 – 181.

[145] X. Ndzana, W. R. Fehr, G. A. Welke, E. G. Hammond, D. N. Duvick, S. R. Cianzio, *Crop Sci.* **1994**, *34*, 646 – 649.

[146] R. F. Wilson, *INFORM* **1993**, *4*, 193 – 200.

[147] a) E. P. Heppard, A. J. Kinney, K. L. Stecca, G. H. Miao, *Plant Physiol.* **1996**, *110*, 311 – 319; b) A. J. Kinney, S. Knowlton in *Genetic Modification in the Food Industry* (Eds.: S. Roller, S. Harlander), Blackie, London, **1998**, pp. 193 – 213.

[148] a) D. J. Murphy, *Trends Biotechnol.* **1996**, *14*, 206 – 213; b) G. B. Poulsen, *Plant Breed.* **1996**, *115*, 209 – 225; c) B. Fitch Haumann, *INFORM* **1997**, *8*, 804 – 811.

[149] W. Lühs, W. Friedt, *Fat Sci. Technol.* **1994**, *96*, 137 – 146.

[150] a) N. O. V. Sonntag, *INFORM* **1991**, *2*, 449 – 463; b) N. O. V. Sonntag in *Brassica Oilseeds – --Production and Utilization* (Eds.: D. S. Kimber, D. I. McGregor), CAB International, Wallingford, **1995**, pp. 339 – 352; c) K. Coupland, K. B. T. Hatton in *Synthesis in Lipid Chemistry* (Ed.: J. H. P. Tyman), The Royal Society of Chemistry, Cambridge, **1996**, pp. 57 – 66.

[151] D. L. Auld, M. K. Heikkinen, D. A. Erickson, J. L. Sernyk, J. E. Romero, *Crop Sci.* **1992**, *32*, 657 – 662.

[152] B. Rücker, G. Röbbelen in *Rapeseed Today and Tomorrow*, *Vol. 2*, Dorset Press, Dorchester, **1995**, pp. 389 – 391 (Proc. 9th Int. Rapeseed Congr. (GCIRC)).

[153] D. S. Knutzon, G. A. Thompson, S. E. Radke, W. B. Johnson, V. C. Knauf, J. C. Kridl, *Proc. Natl. Acad. Sci. USA* **1992**, *89*, 2624 – 2628.

[154] a) T. A. Voelker, A. C. Worrell, L. Anderson, J. Bleibaum, C. Fan, D. J. Hawkins, S. E. Radke, H. M. Davies, *Science* **1992**, *257*, 72 – 74; b) A. J. Del Vecchio, *INFORM* **1996**, *7*, 230 – 243; c) D. S. Knutzon, T. R. Hayes, A. Wyrick, H. Xiong, H. M. Davies, T. A. Voelker, *Plant Physiol.* **1999**, *120*, 739 – 746.

[155] a) N. Martini, J. Schell, R. Töpfer in *Rapeseed Today and Tomorrow*, *Vol. 2*, Dorset Press, Dorchester, **1995**, pp. 461 – 463 (Proc. 9th Int. Rapeseed Congr. (GCIRC)); b) E. Rudloff, P. Wehling, *Acta Horti.* **1998**, *459*, 379 – 385.

[156] a) D. Weier, C. Hanke, A. Eickelkamp, W. Lühs, J. Dettendorfer, E. Schaffert, C. Möllers, W. Friedt, F. P. Wolter, M. Frentzen, *Fett/Lipid* **1997**, *99*, 160 – 165; b) M. Frentzen, *Fett/Lipid* **1998**, *100*, 161 – 166; c) A. Gräfin zu Münster, W. Lühs, D. S. Borchardt, F. P. Wolter, M. Frentzen in *Advances in Plant Lipid Research* (Eds.: J. Sánchez, E. Cerdá-Olmedo, E. Martinez-Force), Secretariado de Publicaciones de la Universidad de Sevilla, (Spain), **1998**, pp. 671 – 674; d) W. Lühs, A. Voss, J. Han, A. Gräfin zu Münster, D. Weier, F. P. Wolter, M. Frentzen, W. Friedt in *Genetics and Breeding for Crop Quality and Resistance* (Eds.: G. T. S. Mugnozza, E. Porceddu, M. A. Pagnotta), Kluwer, Dordrecht, **1999**, pp. 323 – 330.

[157] a) K. I. Soldatov in *Proc. 7th Int. Sunflower Conf.*, Krasnodar, USSR, Intern. Sunflower Assoc., **1976**, pp. 352 – 357; b) W. Lühs, K. J. Dehmer, R. Bergmann, W. Friedt in *Perspektiven nachwachsender Rohstoffe in der Chemie* (Ed.: H. Eierdanz), VCH, Weinheim, **1996**, pp. 232 – 238.

[158] J. Osorio, J. Fernández-Martínez, M. Mancha, R. Garés, *Crop Sci.* **1995**, *35*, 739 – 742.

[159] a) W. Lühs, W. Friedt, *Anbauempfehlungen für hochölsäurehaltige Sonnenblumen (HO-Sonnenblumen) in Deutschland*, 3rd ed., Universität Giessen (Germany), **1998**; b) W. Lühs, W. Friedt in *Proc. 6th*

Symp. Renewable Resources and 4th. Eur. Symp. on Ind. Crops Prod. (Ed.: Fachagentur Nachwachsende Rohstoffe), Landwirtschaftsverlag Münster, **1999**, pp. 401 – 406.

[160] a) A. J. Norden, D. W. Gorbet, D. A. Knauft, C. T. Young, *Peanut Sci.* **1987**, *14*, 7 – 11; b) T. G. Isleib, C. T. Young, D. A. Knauft, *Crop Sci.* **1996**, *36*, 556 – 558.

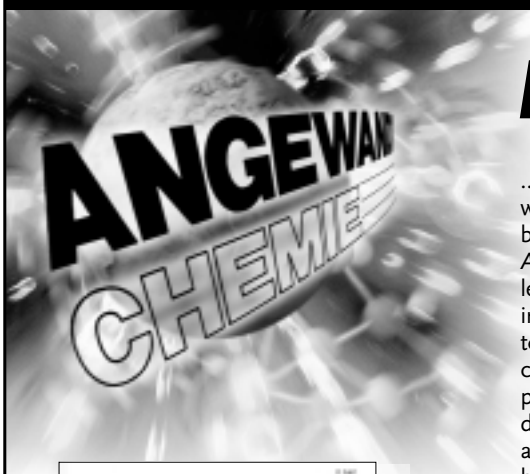
[161] R. Höfer, W. Knörr, A. Westfechtel in *3. Symposium Nachwachsende Rohstoffe*, *Perspektiven für die Chemie* (Ed.: Bundesminsterium für Ernährung, Landwirtschaft und Forsten), Landwirtschaftsverlag, Münster, **1994**, pp. 235 – 256.

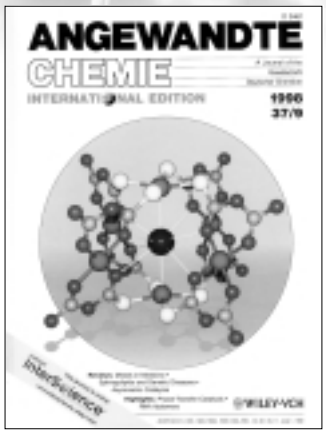
[162] a) C. Bickert, W. Lühs, W. Friedt, *Ind. Crops Prod.* **1994**, *2*, 229 – 237; C. Bickert, W. Lühs, W. Friedt, *Ind. Crops Prod.* **1994**, *2*, 317; b) R. Steiss, A. Schuster, W. Friedt, *Ind. Crops Prod.* **1998**, *7*, 303 – 309.

[163] a) A. G. Green, *Can. J. Plant Sci.* **1986**, *66*, 499 – 503; b) A. G. Green, *Theor. Appl. Genet.* **1986**, *72*, 654 – 661; c) G. G. Rowland, *Can. J. Plant Sci.* **1991**, *71*, 393 – 396.

[164] C. Ntiamoah, G. G. Rowland, D. C. Taylor, *Crop Sci.* **1995**, *35*, 148 – 152.

+++ THE LINK TO INTERNATIONAL CHEMISTRY +++





SCHULZ1299<ACHLINK1>

Reviews? Reviews!

...are indispensable for chemists wanting to keep up-to-date with all branches of chemistry. Reviews in *Angewandte Chemie* are written by leading experts. They summarize the important results of recent research on topical subjects in all branches of chemistry, point to unresolved problems, and discuss possible developments. Their informative approach is ideal for students and fast browsing.

Here are the most cited Review articles from 1998:

- *A. Kraft. A.C. Grimsdale, A.B.Holmes:* Electroluminescent Conjugated Polymers – Seeing Polymers in a New Light
- *Y. Xia, G. Whitesides:* Soft Lithography
- *M. Dobson, A. Sali, M. Karplus:* Protein Folding: A Perspective from Theory and Experiment
- *J.F. Hartwig:* Transition Metal Catalyzed Synthesis of Arylamines and Aryl Ethers from Aryl Halides and Triflates: Scope and Mechanism
- *K.C. Nicolaou, et al.:* Chemical Biology of Epothilones
- *S.R. Batten, R. Robson:* Interpenetrating Nets: Ordered, Periodic Entanglement
- *E.J. Corey, A. Guzman-Perez:* The Catalytic Enantioselective Construction of Molecules with Quaternary Carbon Stereocenters
- *H. Waldmann et al.:* Organic Synthesis and Biological Signal Transduction
- *G.A. Ozin et al.:* A New Model for Aluminophosphate Formation: Transformation of a Linear Chain Aluminophosphate to Chain, Layer, and Framework Structures
- *L. Echegoyen et al:* Electrochemistry of Supramolecular Systems

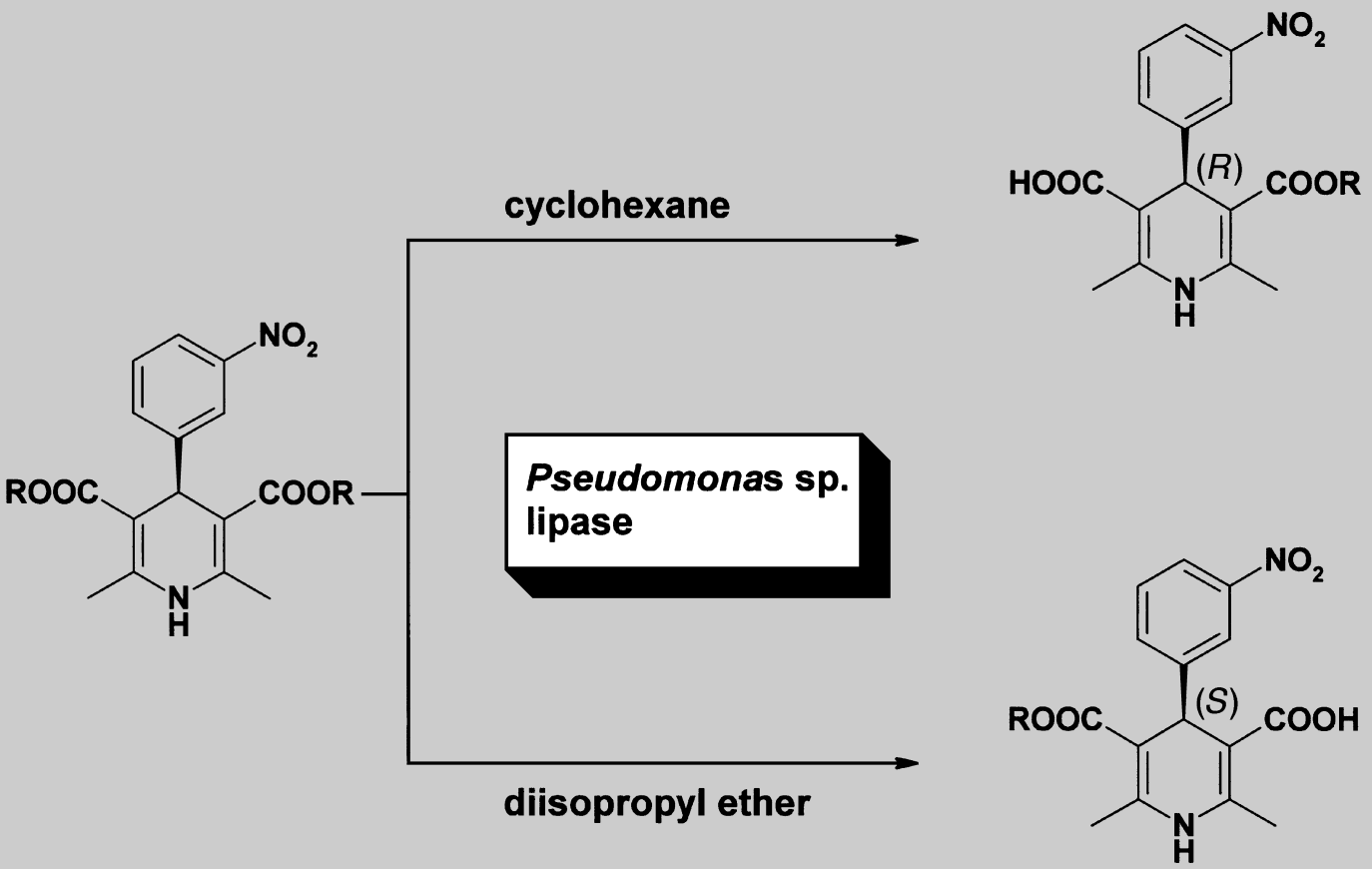
Don't miss out on this important information. Order your personal copy of *Angewandte Chemie* (see the Order Form on the last page of this issue).

WILEY-VCH, P.O. Box 10 11 61, 69451 Weinheim, Germany
Phone +49 (6201) 606-328, Fax +49 (6201) 606-348
e-mail: sales-journals@wiley-vch.de, http://www.wiley-vch.de

WILEY-VCH

ANGEWANDTE CHEMIE © WILEY-VCH

“Medium Engineering” of Enzymatic Reactions:



Enzyme selectivity in organic solvents can differ from that in water and can change, or even reverse, from one solvent to another.

Properties and Synthetic Applications of Enzymes in Organic Solvents

Giacomo Carrea* and Sergio Riva*

Biotransformations already represent an effective and sometimes preferable alternative to chemical synthesis for the production of fine chemicals and optically active compounds. To further widen the versatility of the biological approach, the so-called "nonaqueous enzymology", which now represents an important area of research and biotechnological development, has emerged in the last ten years or so. This new methodology is especially suitable for the modification of precursors of pharmaceutical compounds and fine chemicals, which, in most cases, are insoluble or poorly soluble in water. Even though the idea of carrying out an enzymatic process in organic solvent was initially considered with scepticism, biocatalysis in such media is now investigated and exploited in numerous academic and industrial laboratories. One of the reasons that makes enzymatic catalysis in nonaqueous media so appealing, is the important new properties that enzymes exhibit in organic solvents. For example, they are often more stable and can catalyze reactions that are impossible or difficult in water. Furthermore, enzyme selectivity can also differ from that in water and can change, or even reverse, from one solvent to another. This phenomenon, which can be called "medium engineering", can be exploited as a valid alternative to protein engineering. The first part of this review examines the thermodynamic, kinetic, spectroscopic, and physical approaches that have been adopted to investigate the factors that affect activity, stability, structure, and selectivity of enzymes in organic solvents. These combined studies have brought the understanding of enzyme catalysis in organic solvents to a level almost comparable to that reached for biocatalysis in aqueous media. The second part surveys a number of the synthetic applications of enzymes in organic media, which span from the preparation of milligrams of specifically labeled compounds to the modification of fats on multiton scale and from the preparation of complex key intermediates for the pharmaceutical industry to the synthesis of polymers.

Keywords: enantiomeric resolution · enzyme catalysis · solvent effects · synthetic methods

1. Introduction

In recent years, the employment of biocatalysts for organic synthesis has become an increasingly attractive alternative to conventional chemical methods.[1] In fact, enzymes quite often display high chemo-, regio-, and enantioselectivity, which makes these catalysts especially attractive for the pharmaceutical and agrochemical areas, where the interest for enantiomerically pure and specifically functionalized compounds is continuously growing. Furthermore, enzyme-catalyzed reactions are normally carried out under mild conditions, such as room temperature and neutral or almost neutral pH, which minimizes problems of product isomerization, racemization, or epimerization. In addition, enzymes can be very efficient catalysts, capable of increasing reaction rates by up to 10^{12} times. Finally, biocatalytic processes are less hazardous, polluting, and energy consuming than conventional chemistry-based methodologies, especially those making use of heavy-metal catalysts.

All these reasons have made biocatalysis a popular topic for research in academia and industry and a tremendous number of enzymes have been described in the literature with a claimed potential for practical exploitation. For instance, the database BioCatalysis, based on 8000 articles and patents, describes 18 500 biotransformations carried out with enzymes, microorganisms, and catalytic antibodies.[2] Clearly, most of the described conversions are bound to remain mere laboratory curiosities, but an important part of them already has, or will have, an industrial application.

Unfortunately, there are also some drawbacks, such as the sometimes unsatisfactory stability of the enzymes and/or their laborious isolation and poor productivity. However, the improvement of purification procedures and the use of immobilized or engineered enzymes are progressively reduc-

[*] Dr. G. Carrea, Dr. S. Riva
Istituto di Biocatalisi e Riconoscimento Molecolare, CNR
Via Mario Bianco 9, 20131 Milan (Italy)
Fax: (+390) 02-285-000-36
E-mail: g.carrea@ico.mi.cnr.it, rivas@ico.mi.cnr.it

 © WILEY-VCH Verlag GmbH, D-69451 Weinheim, 2000 1433-7851/00/3913-2227 $ 17.50+.50/0

ing the incidence of these limitations. Another disadvantage, caused by the limited water solubility of many organic substrates, is that reagent concentrations are generally lower in biocatalytic than in chemical processes; this, of course, leads to larger reaction volumes and complicates product recovery.

2. Organic Solvent Systems

Among the various methods adopted to increase the solubility of hydrophobic substrates in biocatalyzed reactions, the most obvious and widely employed is that based on organic solvents. This includes the use of mixtures of water and water-miscible organic solvents,[3] biphasic systems consisting of water and water-immiscible organic solvents (see the pioneering work by Sym[4] and some more recent reviews[5]), reverse micellar systems,[5f, 6] and, finally, organic solvent systems.[5f, 7]

Some features of the various systems that could help in understanding their peculiarities are represented in Figure 1.

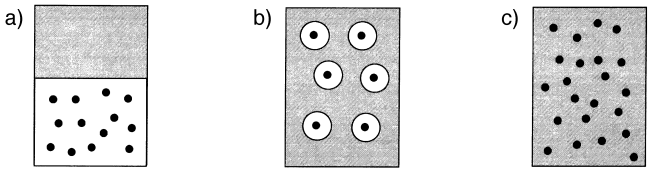


Figure 1. Representations of some organic solvent systems. a) Two-phase system, b) inverse micellular system, c) organic solvent system. Shaded areas: organic phase, white areas: water phase, black dots: biocatalyst.

In biphasic systems (a), the enzymes and hydrophilic compounds are contained in the aqueous phase, where the reaction occurs, while hydrophobic compounds are mostly partitioned in the organic phase. In reverse micellar systems (b), enzyme molecules are solubilized in discrete, hydrated, reverse micelles, formed by surfactants, within a continuous phase of a hydrophobic organic solvent. Under appropriate conditions, the reverse micellar solution is homogeneous, thermodynamically stable, and optically transparent. In organic solvent systems (c), solid enzyme preparations (for example, enzymes lyophilized or adsorbed on an inert support) are suspended in an organic solvent in the presence of enough aqueous buffer (as a rule of thumb $< 5\,\%$ v/v) to ensure enzymatic activity. Although the amount of water added to the solvent may exceed its solubility in that solvent, a visible discrete aqueous phase is not apparent because part of the solvent in the system is adsorbed by the biocatalyst. Visually, the two phases involved in an organic solvent system are liquid (bulk organic solvent and reagents dissolved in it) and solid (hydrated enzyme particles).

Even though each of the systems described above has pros and cons,[8] the organic solvent system is the one which has been most deeply investigated and widely applied and, in this review, we shall exclusively focus on this system. Several advantages account for the interest in this kind of enzyme-catalyzed reaction and for its success, such as:

1) the catalysis of reactions that are unfavorable in water is possible (for example, the reversal of hydrolysis reactions in favor of synthesis),
2) water-induced side reactions, such as hydrolysis of acid anhydrides and halogenate esters, can be suppressed,
3) hydrophobic substrates can be solubilized,

Giacomo Carrea, born in Tortona (Italy) in 1943, graduated in chemistry at the University of Pavia in 1968. In 1969 he joined the Centro Nazionale delle Ricerche (CNR) where he is presently Director of the Istituto di Biocatalisi e Riconoscimento Molecolare (IBRM). He has been working in such fields as enzyme catalysis in organic solvents, synthesis of fine chemicals catalyzed by hydrolases, dehydrogenases, peroxidases, and monooxygenases, the study of the conformation of proteins and polypeptides, and analytical applications of bioluminescent enzymes. He is a member of the Editorial Boards of Trends in Biotechnology *and* Biocatalysis and Biotransformation *and the author of approximately 170 publications.*



G. Carrea



S. Riva

Sergio Riva, born in Milan (Italy) in 1958, is a Senior Research Scientist at the IBRM (Istituto di Biocatalisi e Riconoscimento Molecolare), where he has been working since 1984. He took his Laurea in chemistry at the University of Milan in 1983 and his Diploma di Specialitá in organic synthesis at the Politecnico of Milan in 1989. In 1987, he spent one year at the Massachusetts Institute of Technology (Cambridge, USA) working with Prof. A. Klibanov. In 1993 he was awarded the Ciamician medal by the Organic Chemical Division of the Italian Chemical Society. His research activity is documented by more than 100 publications reporting on the isolation and characterization of enzymes belonging to different classes (hydrolases, dehydrogenases, oxynitrilases, glycosyltransferases) and on the use of these biocatalysts for the mild and selective modification of different natural compounds (steroids, alkaloids, terpenes, sugars, and natural glycosides).

4) some products can be easily recovered,
5) the insoluble biocatalysts can be easily recovered,
6) biocatalyst thermostability is increased, at least at low water levels.

Furthermore, enzyme selectivity can be markedly influenced, and even reversed, by the solvent; this sort of solvent engineering thus provides an alternative to protein engineering. Organic solvent systems are also useful for fundamental studies of the effects of water on enzyme dynamics and catalysis.

In the following sections the properties and synthetic applications of enzymes in organic solvents will be examined.

3. Enzyme Properties in Organic Solvents

Thermodynamic, kinetic, spectroscopic, and physical approaches have all contributed to improve the understanding of the factors affecting activity, stability, structure, and selectivity of enzymes in organic solvents; this understanding is now being developed to a level almost comparable to that of biocatalysis in aqueous media.

3.1. Enzyme Activity

Enzyme activity in organic solvents depends dramatically on such parameters as water activity, substrate–product solvation, pH control, enzyme form, and the nature of the solvent.

3.1.1. Water Activity

It became apparent quite soon that enzyme activity was higher in hydrophobic solvents than in hydrophilic ones and, indeed, Laane et al.[9] found that there was a direct correlation between activity and solvent hydrophobicity, expressed as $\log P$ (where P is the partition coefficient of a given solvent between *n*-octanol and water). The authors ascribed this result to differences in the ability of organic solvents to distort the essential water layer around the biocatalysts.[9]

Shortly afterwards, Zaks and Klibanov[10] demonstrated, with the three unrelated enzymes yeast alcohol oxidase, mushroom polyphenol oxidase, and horse liver alcohol dehydrogenase, that enzyme activity was more or less coincident in the various solvents, provided that the amount of water bound to the enzyme was the same. Figure 2a shows that the more hydrophilic the solvent is, the higher the water content of the solvent has to be to reach high activity. This happens because the water content of the enzyme (W_e, Figure 2b) and not that of the solvent (W_S, Figure 2a) is what actually matters for activity. Thus, depending on the hydrophobicity of the solvent, the same water content results in entirely different amounts of water on the enzyme. These data suggest that the effects of organic solvents on an enzyme are primarily due to interactions with the essential enzyme-bound layer of water rather than with the enzyme itself. The maximal enzymatic activity for the three examined enzymes was attained at about 1000 molecules of water per enzyme

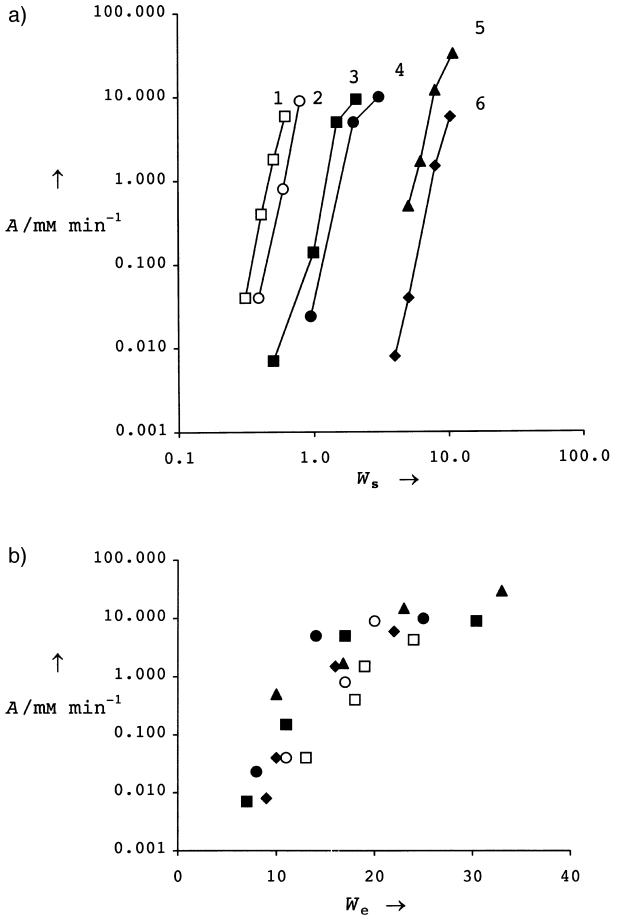


Figure 2. Dependence of yeast alcohol oxidase activity (A) on: a) the concentration of water in various organic solvents (W_s in % (v/v)), b) on the water content of the enzyme (W_e in % (w/w)). Solvents tested: 1 = Diethyl ether (□), 2 = butyl acetate (○), 3 = ethyl acetate (■), 4 = *n*-octanol (●), 5 = *tert*-amyl alcohol (▲), 6 = 2-butanol (◆).

molecule, that is, roughly a monolayer of water on the surface, as had already been found for activity recovery, in air, of dry lysozyme[11] and chymotrypsin.[12] It should be mentioned that at optimal water contents, enzymatic activities in organic solvents of alcohol oxidase, polyphenol oxidase, and alcohol dehydrogenase were in the range from 20 to 40% of those in aqueous solutions.[10] Different degrees of water stripping as a function of solvent polarity were found and quantified by direct measurement of tritiated water desorption from enzymes; water stripping occurred nearly immediately when the enzyme was suspended in organic solvents.[13]

A more rigorous way to correlate enzyme activity with the water present in the reaction medium was proposed by Halling[14] and Goderis et al.,[15] who expressed the water in the medium not in terms of content but of thermodynamic water activity. Water activity (a_w) is correlated to the mole fraction of water (χ_w) and the water activity coefficient (γ_w) by the equation $a_w = \gamma_w \chi_w$. Since, in the first approximation, the water activity coefficient (γ_w) increases as a function of solvent hydrophobicity, it is obvious that a given value of a_w will be obtained at a lower water concentration in a hydrophobic medium than in a hydrophilic medium. Therefore, to attain the same level of enzyme hydration, or of a_w, in the

enzyme, less water is necessary in hydrophobic than hydrophilic solvents. To clarify the water activity concept, Bell et al.[7i] suggested that a_w is like temperature, while water content is like heat content. Two systems can have the same a_w or temperature, but at the same time differ in the water content or heat content. It should be mentioned that, at equilibrium, a_w will be the same for all the components of the reaction system, such as, catalyst, matrix (in the case of immobilized enzymes[16]), reagents, and solvents.

The existence of a direct correlation between enzyme activity and the a_w of the system, was clearly demonstrated in the case of *Mucor miehei* lipase.[17] The lipase showed a similar optimum of activity at $a_w = 0.55$ when used in solvents varying in polarity from hexane to pentanone (Figure 3a). The absolute reaction rates were somewhat solvent dependent, but the shape of the profile was essentially unchanged. Of course, the optimum varied widely when activity was plotted against water concentration in the organic solvents (Figure 3b). In a study carried out with lipases from five different sources, it was also found that the dependence of catalytic activity on a_w varied significantly from enzyme to enzyme, possibly as a consequence of molecular structure differences.[18] A recent study has shown that, contrary to what was observed with nonpolar solvents, with polar solvents such as dioxane, acetonitrile, tetrahydrofuran, and acetone, a_w fails to precisely predict the critical hydration level for enzyme activity; this probably reflects direct solvent effects on the enzyme.[19]

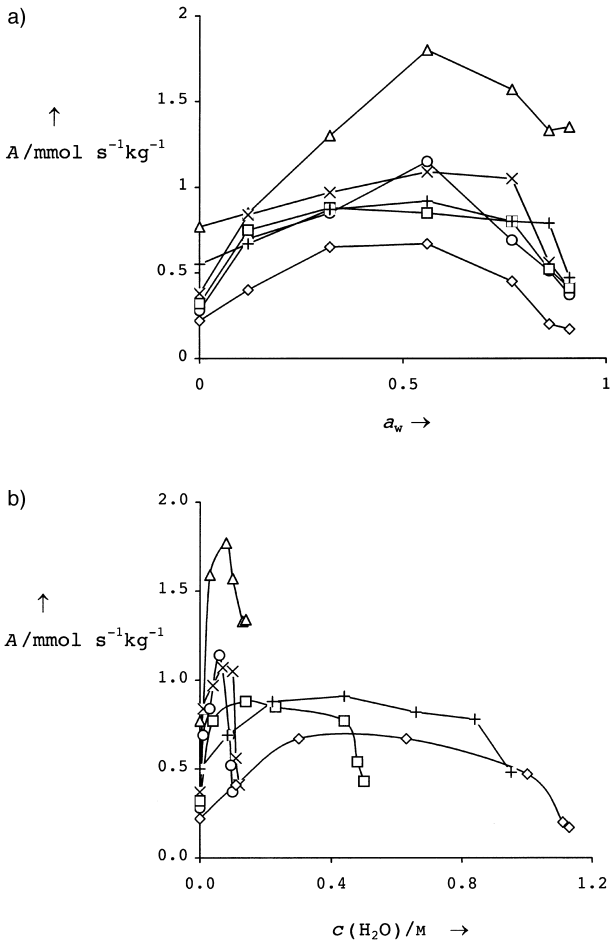


Figure 3. Activity (A) of Lipozyme catalyst: a) as a function of water activity (a_w), b) as a function of water concentration (c) in the organic phase. Solvents tested: Hexane (△), toluene (×), trichloroethylene (○), diisopropyl ether (□), 3-pentanone (◇), dodecanoic acid:dodecanol 1:1 (+).

The increase of a_w or water content can induce an increase of K_m values.[20] This is especially true for the K_m of nucleophiles in hydrolase-catalyzed esterification and transesterification reactions, where water acts as an inhibitor by competing with the substrate for the acyl–enzyme intermediate.[20b–d] This phenomenon is exemplified in Table 1, where the effect of water concentration on the $K_{m,app}$ of subtilisin for the nucleophile 1-hexanol is shown. As expected, the $K_{m,app}$ for the acylating agent vinyl butyrate was not affected. Similarly, a_w influences the equilibrium of hydrolase-catalyzed esterifications or transesterifications because water favors the reverse reaction (hydrolysis of the product) in the case of esterifications or the hydrolysis of the acylating agent (activated esters or enol esters and acid anhydrides) and, again, of the product in the case of transesterifications.[14c, 21]

Table 1. Effect of water concentration on the kinetic parameters of PEG–subtilisin-catalyzed transesterification of vinyl butyrate with 1-hexanol in dioxane.

water [M]	1-hexanol		vinyl butyrate	
	$K_{m,app}$[a]	$v_{max,app}$[b]	$K_{m,app}$[a]	$v_{max,app}$[b]
0	0.72	156	0.17	76
1.1	1.99	142	0.16	67
2.2	3.19	128	0.16	55

[a] Units: molar. [b] Units: μmol per h and per mg protein.

Due to the fundamental role played by water, it is clear that the control of a_w in the enzymatic reactions carried out in organic solvents is of paramount importance and, as a consequence, different methods have been developed to this end.[15, 22] Goderis et al.[15] used the knowledge that some salts have a fixed hydration state which gives a well-defined a_w,[23] and employed saturated salt solutions to equilibrate, through the gas phase, organic solvent reactions. The method can be used to adjust a_w not only initially, but also during a reaction in which water is produced or consumed.[22a,b] The disadvantage of the method is that water transfer is influenced by the design of the equilibration chambers. Another method for a_w control is based on the use of salt hydrates which can act as a_w buffers in organic media; however, they have limited capacity and require additional separation steps if they (and/or the enzymes) are to be reused.[22c,d] More promising, especially for preparative-scale applications, seems to be a recently described method in which a_w control is exerted by circulating salt solutions in silicone tubing submerged in the organic solvent.[22e] The silicone membranes are permeable to water vapors and impermeable to ions; therefore, only water is transferred through them.

3.1.2. Kinetics

Kinetic studies carried out mostly with hydrolases, have shown that enzymes in organic solvents follow conventional models.[24] Thus, various transesterification reactions catalyzed by porcine pancreatic lipase (PPL) in hexane obey

Michaelis–Menten kinetics[24a] and those catalyzed by lipases from *Mucor miehei*[24b] and *Candida antarctica*[24c] follow a bi-bi ping-pong mechanism, with competitive inhibition by substrates and products. The identity of the mechanism of subtilisin-catalyzed ester hydrolysis in water and transesterification in organic solvents has been demonstrated by Chatterjee and Russel,[24d,e] who have also determined individual rate constants and equilibrium constants of the reaction in organic solvents.

Considering kinetic parameters in organic solvents, the values may be very different from solvent to solvent and from those for the same enzyme and substrate in aqueous media; similarly, substrate specificity may change dramatically from solvent to solvent and from water. Table 2, for example, shows that *N*-acetyl-L-serine ethyl ester (*N*-Ac-L-Ser-OEt) is the preferred substrate of subtilisin in dichloromethane, while in *tert*-butylamine the preferred substrate is *N*-acetyl-L-phenylalanine ethyl ester (*N*-Ac-L-Phe-OEt).[25]

Table 2. Substrate specificity (S, $(k_{cat}/K_M)_{Ser}/(k_{cat}/K_M)_{Phe}$) in the transesterification of *N*-Ac-L-Ser-OEt (Ser) and *N*-Ac-L-Phe-OEt (Phe) with 1-propanol, catalyzed by subtilisin Carlsberg in various anhydrous organic solvents.

solvent	S	solvent	S
dichloromethane	8.2	*tert*-butyl methyl ether	2.5
chloroform	5.5	octane	2.5
toluene	4.8	isopropyl acetate	2.2
benzene	4.4	acetonitrile	1.7
N,*N*-dimethylformamide	4.3	dioxane	1.2
tert-butyl acetate	3.7	acetone	1.1
N-methylacetamide	3.4	pyridine	0.53
diethyl ether	3.2	*tert*-amyl alcohol	0.27
carbontetrachloride	3.2	*tert*-butyl alcohol	0.19
ethyl acetate	2.6	*tert*-butylamine	0.12

However, all these effects can be at least partly explained by different solvation of the substrates as the reaction medium changes.[26] Different methods are available to correct for solvation of substrates (and products). As discussed by Janssen et al.,[26f] one of them is based on a transfer of free energy method, where the activation (or binding) energy is calculated from experimental data for v_{max}/K_m (or K_m).[26a,b] This experimental activation (or binding) energy and the transfer of free energy of the substrate, are used to calculate the corrected activation (or binding) energy. Another method of correction is to express the kinetic constants in terms of thermodynamic activities instead of concentrations.[26c,d] A third method is to correct the Michaelis constant by using partition coefficients. In this case, the experimental K_m, which is based on substrates concentration in the organic phase, is corrected to a K_m value which is based on the concentrations in the aqueous phase.[26e] These three methods of correction are essentially equivalent and, once applied, give similar kinetic parameters in the various media[7h] and explain the differences of substrate specificity.[24]

3.1.3. pH Value and pH Control

The protonation state of the various groups of an enzyme is undoubtedly important for enzyme activity, both in aqueous and organic media. However, while protonation in water is simply controlled by adjustments of pH values, this is not the case in organic solvents, where even the concept of pH value itself is challenged.[14c] A way to control the initial state of enzyme protonation and, hence, activity was developed by Zaks and Klibanov,[24a] who showed that enzyme activity in organic solvents was markedly dependent on the pH value of the solution from which the enzyme was recovered (by lyophilization or precipitation). This methodology, which is now widely applied in the field of biocatalysis in organic solvents, is perfectly suitable when there is no alteration of acid/base concentration in the course of the reaction. If this is not the case, as in the synthesis, hydrolysis, or aminolysis of esters, for instance, the enzyme protonation and activity may change during reaction.

To overcome this drawback, the use of buffering systems involving highly hydrophobic acids and their sodium salts, and highly hydrophobic bases and their hydrochlorides, has been proposed.[27] Indeed, these systems can efficiently buffer organic solvent media, as illustrated in Figure 4 where the dependence of subtilisin activity on the composition of some acids pairs and their conjugated bases is shown. The main disadvantage of these buffer systems is that they are appreciably soluble only in solvents with a relatively high polarity (such as, 3-pentanone, dioxane, dimethylformamide, tetrahydrofuran).

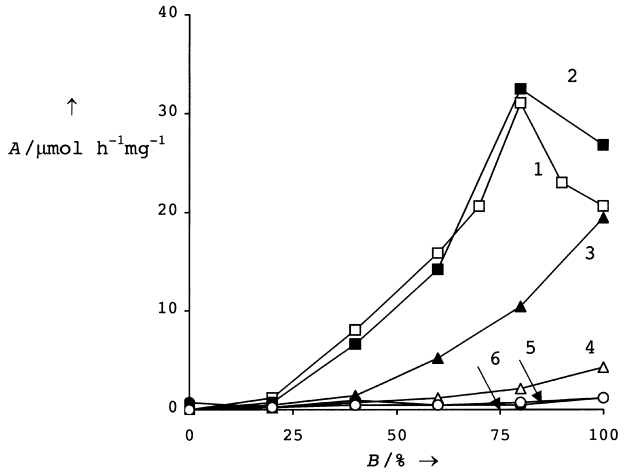


Figure 4. Dependence of the enzymatic activity (A) of subtilisin in 3-pentanone on the base mole fraction (B) of various pairs of acids and their conjugate bases (as sodium salts) added to the enzyme suspension. 1 = Phenylboronic acid (□), 2 = *para*-nitrophenol (■), 3 = triphenylacetic acid (▲), 4 = acetic acid (△), 5 = *para*-toluensulfonic acid (○), 6 = diphenylphosphinic acid (●).

3.1.4. Enzyme Form

Proteins are practically insoluble in most organic solvents[28] and when they do dissolve, as in dimethylsulfoxide and formamide, they lose their native conformation.[29] Therefore, in the absence of any special treatment, enzymes are usually present in organic solvents as a solid–liquid biphasic suspension. This simplifies catalyst–product separation and enzyme reutilization.

The simplest way to prepare biocatalysts for use in organic solvents and, at the same time, to adjust key parameters such

as pH value and associated ions, is enzyme lyophilization or precipitation (by, for instance, addition of acetone) from aqueous solutions. These preparations, however, can undergo diffusional limitations or prevent enzyme–substrate interaction because of protein–protein stacking. The use of small enzyme particles obtained by prior sonication and vigorous shaking or stirring during reaction are recommended to alleviate these disadvantages. In some cases, ultrasonic treatment has also been done during the reaction and this has notably increased reaction rates.[30] Rate enhancements were attributed to the increase of catalyst surface area (better dispersion) or to locally high pressures.[30b] That aggregation can limit enzyme efficiency was also suggested by the finding that chymotrypsin and subtilisin activities in ethanol were inversely correlated to enzyme concentration in the medium.[31] Russell and co-workers have calculated the role of internal and external mass transfer and found that enzyme particles suspended in organic solvents will be subjected to increasing diffusion limitations as the enzyme activity and particle size increase.[32]

Enzyme lyophilization in the presence of ligands, lyoprotectants (various sugars, polyethylene glycol), salts, and micellar amphiphiles has often yielded preparations that are markedly more active than those obtained in the absence of additives.[20d, 33] Various explanations such as "trapping" of the enzyme in a more active conformation (ligands and micellar amphiphiles),[33a,f] prevention of lyophilization-induced partial denaturation of the enzyme that becomes irreversible in organic solvents (lyoprotectants),[33c] protection against deactivation by direct contact with the solvent (salts),[33d] retention of the water shell around the enzyme (sorbitol),[33e] or increased catalyst dispersion in the medium (various additives) have been invoked to rationalize the results.[20d]

Adsorption on solid matrices, which improves, at least at optimal protein/support ratios, enzyme dispersion, reduces diffusional limitations and favors substrate access to individual enzyme molecules. Matrices with different particle size, porosity, and composition (Celite, controlled pore glass, polyamide, polypropylene, alumina, silica, zirconia) were employed and the pros and cons evaluated.[34] A common feature is that for each enzyme and matrix there is an optimal enzyme/support ratio for expression of activity. Figure 5 illustrates the behavior of lipase from *Pseudomonas* sp. adsorbed onto Celite.[34b] When the rate per unit weight of lipase–support material was considered, maximum activity was attained at an enzyme loading of 150 mg per g Celite and then it remained constant (Figure 5a). When the rate per unit weight of lipase was considered (Figure 5b), the highest value was still obtained at an enzyme loading of 150 mg per g Celite and then it decreased. These data suggest that at low loadings the enzyme undergoes conformational modifications and inactivation caused by strong interactions with the matrix,[35] whereas, at high loading, diffusional limitations or substrate inaccessibility to the active site reduce enzyme effectiveness. Inactivation at low enzyme loading can be prevented by carrying out the immobilization in the presence of extraneous proteins (albumin, gelatin, casein) or polyethylene glycol.[34c]

Immobilized lipases with excellent activity and stability were obtained by entrapping the enzymes in hydrophobic sol-

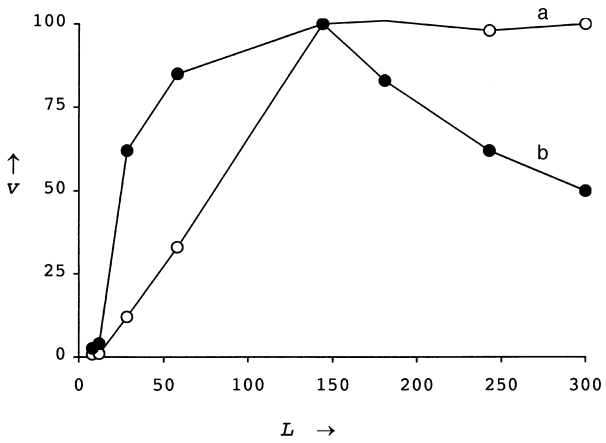


Figure 5. Transesterification rate (v) of lipase from *Pseudomonas cepacia*, adsorbed onto Celite, as a function of enzyme loading (L; in mg enzyme per g Celite). The relative rate is given once as mg of whole material (lipase plus Celite, a) and once as mg of lipase only (b). Transesterification between (±)-sulcatol and vinyl acetate was investigated.

gel materials.[36] With this methodology it would be possible to generate tailor-made gels for each lipase by varying a range of parameters such as the nature of silane monomers and the water/silane stoichiometry. Cross-linked enzyme crystals (CLECs) have proved to be very robust, though rather expensive, catalysts for organic solvent reactions when cross-linked with glutaraldehyde.[37] Several CLEC catalysts (for example, thermolysin, subtilisin, penicillin acylase, and lipases from *Candida rugosa* and *Pseudomonas cepacia*) have already been produced on a multikilogram scale.[37]

In order to minimize substrate-diffusion limitations and maximize enzyme dispersion, various approaches have been used to solubilize the biocatalysts in organic solvents. The most widespread method is based on the covalent linking of the amphiphilic polymer polyethylene glycol (PEG) to enzyme molecules. In this way, a large number of PEG–enzyme complexes have been prepared and they have been shown to give transparent solutions in several organic solvents.[20d, 38] Transparent enzyme solutions can also be obtained with non-covalent PEG–enzyme complexes simply prepared by lyophilization of the enzyme in the presence of an excess of PEG.[39] In both cases, excellent activity in organic solvents was often obtained.[38, 39]

Enzyme complexes with anionic or non-ionic surfactants that dissolve in organic solvents have been described by several groups.[40] For example, chymotrypsin and subtilisin complexed with Aerosol OT (10% w/v solution of bis(2-ethylhexyl)sodium sulfosuccinate in water) and dissolved in isooctane in the absence of reversed micelles, showed k_{cat} values nearly one-third and two-thirds as high as in aqueous buffer, respectively.[40a] Similarly, the lipid-coated lipase from *Pseudomonas fragi* (Lipase B) was found to be twice as active as PEG-grafted enzyme and one hundred times more active than the enzyme powder in the esterification of 1-phenylethanol in isooctane (Figure 6).[40d]

The activities of different forms of lipase from *Pseudomonas cepacia* have been compared in carbon tetrachloride and

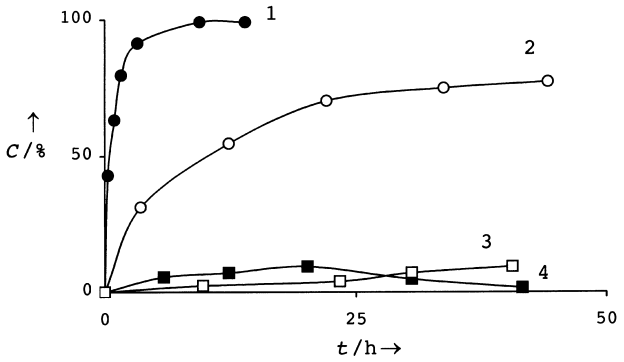


Figure 6. Ester synthesis from (*R*)-1-phenylethanol and lauric acid in anhydrous isooctane at 40 °C, catalyzed by: lipid-coated lipase B (1, ●), PEG-grafted lipase B (2, ○), lipase B in water-in-oil emulsion (3, □), direct dispersion of lipase B powder (4, ■). On the ordinate axis the conversion of (*R*)-1-phenyl ethanol is indicated.

the data are shown in Table 3.[39b] The most active form was the lipase entrapped in the sol-gel matrices, while the crystallized and cross-linked enzyme was less active. It should be mentioned that the activity displayed by the sol-gel lipase in carbon tetrachloride, using *n*-octanol and vinyl acetate as the substrates, was even higher than that displayed by the same amount of lipase protein in the hydrolysis of tributyrin in water.[39b]

Table 3. Relative activity of different forms of lipase from *Pseudomonas cepacia* in carbon tetrachloride.

enzyme form [a]	activity[b]	enzyme form [a]	activity[b]
sol-gel-AK-PC	100	CLEC-PC	2
PEG + PC	30	crude PC	9
PEG-PC	37		

[a] Lipase was entrapped in sol-gel matrices (sol-gel-AK-PC), lyophilized in the presence of PEG (PEG + PC), covalently linked to PEG (PEG-PC), crystallized and cross linked (CLEC-PC), or used as a crude powder (crude PC). [b] The activities of the various enzyme forms refer to the same amount of lipase protein.

3.1.5. Bioreactors

Laboratory-scale transformations catalyzed by enzymes in organic solvents are most commonly carried out in batch reactors with use of enzyme powders or adsorbed enzymes, under continuous stirring or shaking. Water activity and pH value are initially adjusted, respectively, by equilibration with saturated salt solutions and by lyophilization or precipitation of the catalyst from a suitable aqueous solution. However, no continuous control of a_w and pH value are usually done during reaction.

Methods for the scale-up and optimization of bioreactions in organic solvents have been sought for many years, as demonstrated by the development in the eighties of fixed-bed and microporous-membrane reactors for the lipase-catalyzed continuous transesterification[41a,b] or synthesis[41c] of glycerides. More recently, fixed-bed reactors with immobilized lipases and proteases were extended to the production of fine chemicals and optically active compounds such as 2-(4-chlorophenoxy)propanoic acid,[42a] metallorganic intermediates,[42b] and various synthons. The enzyme powder of lipase from *Pseudomonas cepacia* was also employed in a microfiltration membrane reactor for the continuous resolution of the mucolytic drug (±)-*trans*-sobrerol.[42c]

A twin-core packed-bed reactor, which permits a_w control by means of salt hydrate pairs, has been developed for the *Candida rugosa* catalyzed esterification of decanoic acid and dodecanol.[43a] Salt hydrates were confined in the inner core and the enzyme, immobilized on a macroporous polypropylene support, was in in the outer core of the reactor which was continuously fed with the substrate mixture. Complete conversion, albeit at different rates, was obtained with a_w buffering at 0.48 and 0.80 by using salt hydrates of $Na_4P_2O_7$ and Na_2HPO_4, respectively. Continuous a_w control, in this case based on saturated salt solutions, was described for a packed-bed hollow-fiber reactor employed for enzymatic esterification in hexane.[43b] In another approach, the *Candida antarctica* lipase catalyzed synthesis of (*Z*)-3-hexen-1-yl acetate, carried out on kilogram scale, was facilitated by water removal through azeotropic distillation.[43c]

3.2. Enzyme Stability and Structure

Several studies have indicated that enzymes as diverse as porcine pancreatic lipase (PPL),[44a] chymotrypsin,[44b,f] terpene cyclase,[44c] ATPase and cytochrome oxidase,[44d,e] and ribonuclease and lysozyme[44f] are more thermostable in organic solvents than in water. For example, PPL remained active for many hours (halflife longer than 12 hours) when incubated at 100 °C in an almost anhydrous mixture of heptanol and tributyrin (Figure 7).[44a] Lower stability was

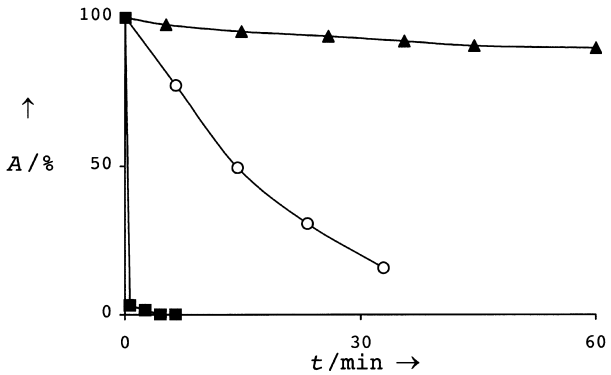


Figure 7. Activity (*A*) decay of the dried powder of porcine pancreatic lipase at 100 °C in water or 0.1 M phosphate buffer (■) and in a 2 M solution of heptanol in tributyrin containing 0.8 % water (○) or 0.015 % water (▲).

observed in the presence of 0.8 % w/v water, while the inactivation was almost instantaneous in aqueous buffer or water (Figure 7). The high thermal stability of enzymes in organic solvents, especially in hydrophobic ones and at low water content, was attributed to increased conformational rigidity and to the absence of nearly all covalent reactions which cause irreversible thermoinactivation in water.[44f] It should be mentioned that, as demonstrated by FTIR spectro-

scopic studies on lysozyme and subtilisin, enzyme structure is much more similar to the native form in pure organic solvents such as acetonitrile, tetrahydrofuran, and 1-propanol than in water–solvent mixtures.[45] This behavior was found to be kinetically controlled, that is, to be due to the inherent restriction on protein conformational mobility in anhydrous media in contrast to aqueous–organic solvent mixtures.[45a] Improvements of enzyme stability (and activity) in aqueous–organic media have been obtained by "rational" design methods[45b] and directed evolution.[45c]

A direct picture of enzyme conformation in organic solvents came from X-ray crystal structures of cross-linked crystals of subtilisin in acetonitrile[46a] and γ-chymotrypsin in hexane.[46b] The subtilisin structure in acetonitrile was essentially identical to the three-dimensional structure of the enzyme in water; the differences observed were smaller than those between two independently determined structures in aqueous solution.[46a] Crystalline γ-chymotrypsin retained its native conformation in hexane and could catalyze both hydrolysis and synthesis reactions in the organic solvent. However, the mobility was decreased and side-chain conformation significantly changed.[46b] A study on hydrogen isotope exchange with high resolution NMR spectroscopy has also shown that the structure of bovine pancreatic trypsin inhibitor is poorly affected by such solvents as acetonitrile, tetrahydrofuran, ethyl acetate, and butanol.[47] In addition, Hammett analysis, a method that provides information on the transition intermediates of reactions, has revealed that the transition state of a subtilisin-catalyzed reaction is the same in water and in organic solvents.[48]

Besides enzyme powders and crystals, other enzyme forms have also been investigated for their stability and structure in organic solvents. Subtilisin covalently linked to PEG was less stable and more prone to autolysis in acetonitrile and dioxane, where it was soluble, than the corresponding enzyme powder.[20d, 49] PEG–subtilisin possessed the same conformation in water and dioxane as evidenced by circular dichroism and intrinsic protein fluorescence measurements.[20d, 49] Subtilisin solubilized in organic solvents by ion pairing with low concentrations of an anionic surfactant (Aerosol OT) was three orders of magnitude more stable in octane than in water, while in tetrahydrofuran 99% of the activity was lost in 10 min.[50]

The relationship between hydration, catalytic activity, and protein dynamics was investigated by several groups with several methods.[51] A study on α-lytic protease suspended in organic solvents showed, by means of deuterium solid-state NMR spectroscopy, that hydration increased enzyme flexibility.[51a] However, no direct link between conformational flexibility and either solvent dielectric properties or catalytic activity was demonstrated. Later works, carried out with electron spin resonance[51b] and time-resolved fluorescence anisotropy[51c] techniques, clearly indicated the existence of a direct correlation between protein hydration and conformational flexibility and activity. A recent paper also established, by proton solid-state NMR, that enzyme flexibility and activity are mostly a function of thermodynamic water activity and not of solvent dielectric properties.[51d]

3.3. Enzyme Selectivity

The ability of enzymes to act as selective catalysts for a broad spectrum of organic reactions has been known and exploited for several years.[1] However, in many cases the selectivity (enantiomeric, prochiral, and regiomeric) of the enzymes is unsatisfactory, and so a number of techniques have been developed to overcome this limitation. Improvements in selectivity have been obtained by modification of enzymes (by, for example, in vitro evolution[52a]), substrates, and reaction conditions (temperature, solvent, and even pressure).[52b] In this review, only the effects of solvents, which are peculiar to the system examined here, will be taken into consideration.

3.3.1. Medium Engineering

The term "medium engineering", which refers to the possibility of influencing enzyme properties by changing the nature of the solvent in which the reaction is carried out, was first coined by Klibanov and co-workers, who indicated it was an alternative to or an integration with protein engineering.[53a] Indeed, a great number of papers have reported that the enantio-, prochiral, and regioselectivity of enzymes can be affected, sometimes very remarkably, by the nature of the organic solvent used as the reaction medium (For recent reviews, see Ref. [53]). In the following paragraphs, a few examples of solvent effects on enzyme selectivity will be considered and the possible rationales discussed.

It should be mentioned that the enantioselective performance of enzymes is generally expressed as the enantiomeric ratio E, which is the ratio of the specificity constants k_{cat}/K_m for the two enantiomers. Equations relating the enantiomeric ratio to the value of the enantiomeric excess of the reagent or of the product, have been developed for kinetic resolutions.[7c] Of course, the higher the enantiomeric ratio, the higher the enantiomeric excess of the product and of the residual substrate.

Table 4 indicates how subtilisin enantioselectivity changes as a function of solvent nature, in the resolution of (±)-1-phenylethanol. The enantiomeric ratio E decreases from 61 in dioxane to 3 in methyl acetamide and shows an inverse correlation with the solvent dielectric constant.[54a] Solvent effects on *Pseudomonas* sp. lipase prochiral selectivity are illustrated in the monohydrolysis of 2-(1-naphtoylamino)trimethylene dibutyrate (Table 5). In this case, it seems that enzyme selectivity is, roughly, inversely correlated with solvent hydrophobicity, expressed as log P.[54b] The resolution of the mucolytic drug (±)-*trans*-sobrerol by lipase from

Table 4. Enantioselectivity (E) of subtilisin in the transesterification of (±)-1-phenylethanol in various organic solvents, and the dielectric constants (ε_r) of the solvents.

solvent	ε_r	E	solvent	ε_r	E
dioxane	2.2	61	dimethylformamide	36.7	9
benzene	2.3	54	nitromethane	35.9	5
triethylamine	2.4	48	acetonitrile	35.9	3
tetrahydrofuran	7.6	40	methylacetamide	191.3	3
pyridine	12.9	31			

Table 5. Effects of the hydrophobicity (log*P*) of solvents on the prochiral selectivity (*S*) of *Pseudomonas* sp. lipase in the monohydrolysis of 2-(1-naphthoylamino)trimethylene dibutyrate.

solvent	log*P*	*S*[a]
acetonitrile	−0.33	>30
nitrobenzene	1.8	>30
acetone	−0.23	18
cyclohexanone	0.96	18
butanone	0.29	16
2-pentanone	0.80	16
chloroform	2.0	9.9
tetrahydrofuran	0.49	9.1
2-hexanone	1.3	8.8
dioxane	−1.1	5.4
t-butyl acetate	1.7	5.3
t-butyl alcohol	0.80	4.9
t-amyl alcohol	1.4	4.8
triethylamine	1.6	4.7
toluene	2.5	3.5
benzene	2.0	3.2
carbon tetrachloride	3.0	2.6

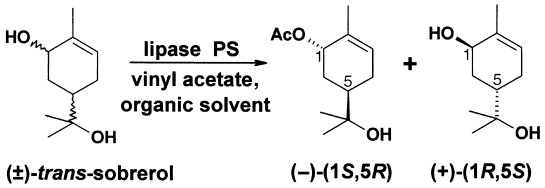
[a] Defined as the ratio of the rate of accumulation of one enantiomer over the other.

Pseudomonas cepacia in various solvents is depicted in Table 6; no correlation between enzyme enantioselectivity and the physico-chemical properties of the solvent related to its hydrophobicity or polarity was found.[54c]

A very striking example of solvent influence on enzyme selectivity and stereochemical preference is that reported by Hirose et al.[54d] In the *Pseudomonas* sp. lipase catalyzed desymmetrization of prochiral dihydropyridine dicarboxylates [Eq. (2)], the (*S*)-monoesters were obtained with *ee* values as high as 99% in water-saturated diisopropyl ether, whereas the (*R*)-isomers were formed preferentially (*ee* = 88–91%) in water-saturated cyclohexane (Table 7).

An interesting study concerning regioselectivity involved the *Pseudomonas cepacia* lipase catalyzed butanolysis of 1,4-dibutyryloxy-2-octylbenzene in several organic solvents.[55a] In cyclohexane, for example, this lipase preferentially deacylated the 4-*O*-butanoate whereas, in acetonitrile, the 1-*O*-butanoate was preferred. The same enzyme was also sensitive to the nature of the solvent regarding the ability to discriminate among the hydroxyls of phenyl 6-*O*-trityl-β-D-glycopyranosides.[55b]

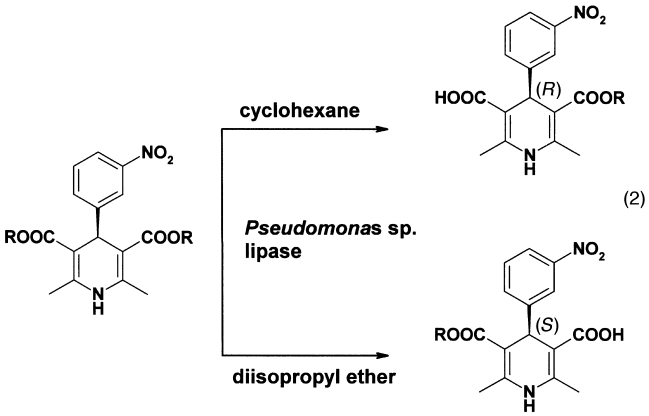
Table 6. Resolution of (±)-*trans*-sobrerol [Eq. (1)]: Optimization of enantioselectivity (*E*) by variation of the solvent.



(1)

solvent	log *P*	ε_r	*E*
tert-amyl alcohol	1.4	5.8	518
3-pentanone	0.80	17	212
dioxane	−1.1	2.2	178
acetone	−0.23	20.6	142
vinyl acetate	0.31	–	89
tetrahydrofuran	0.49	7.6	69

Table 7. Asymmetric hydrolysis of dihydropyridine carboxylates [Eq. (2)]: Influence of solvent on stereochemical preference.



(2)

R	solvent	configuration	*ee* [%] of hemiester
*t*BuC(O)OCH$_2$	cyclohexane	*R*	88.8
*t*BuC(O)OCH$_2$	diisopropyl ether	*S*	>99
EtC(O)OCH$_2$	cyclohexane	*R*	91.4
EtC(O)OCH$_2$	*iso*-propyl ether	*S*	68.1

3.3.2. Rationale

The data reported to date (see above and the reviews in Ref. [53]) show that, in order to modify or improve enzyme selectivity, medium engineering represents a good and convenient alternative to protein engineering and to the time-consuming search for new catalysts. Various hypotheses have been formulated to rationalize this phenomenon. For instance, the solvent, depending on its polarity, could modify the enzyme conformation and, thus, influence the selectivity by altering the molecular recognition process between substrate and enzyme.[54a] According to another theory, selectivity depends on the energetics of substrate solvation,[54b] whereas a third model envisages that solvent molecules could bind within the active site and, depending on their structure, interfere with the association or transformation of one enantiomer more than with that of the other.[54d, 56]

However, both the hypotheses based on the physicochemical properties of the solvents and that based on solvent structure are, at present, unsatisfactory from the point of view of predictive value. In fact, the models either appear to be valid only for the specific enzyme and substrate investigated each time[53a] or, when formation of solvent–enzyme complexes is proposed,[56] no generalization is possible because of the large number of possible solvent–enzyme complexes and because each complex might behave differently depending on the nature of the substrate.[53b]

A theoretical model based on the thermodynamics of substrate solvation was also developed.[57a,b] However, the model, which implies the determination of the desolvated portion of the substrate transition state by molecular modeling and the calculation of the activity coefficient by UNIFAC, gave contradictory results. In fact, it was successful in predicting solvent effects on the prochiral and enantioselectivity of γ-chymotrypsin with 2-substituted 1,3-propanediols[57a] and racemic 3-hydroxy-2-phenylpropionate,[57b]

whereas it failed in the case of subtilisin with racemic *sec*-phenetyl alcohol and *trans*-sobrerol.[57c]

At present, no link among the various hypotheses appears to exist, even though it is likely that the solvent influences enzymatic selectivity through more than a single mechanism.

4. Synthetic Applications

The beginning of detailed investigations into the performances of enzymes in organic solvents can be temporally located approximately fifteen years ago. Since this time, the enthusiastic statements of the pioneers of biocatalysis in nonnatural media have been experimentally verified in several research groups. Specifically, it has been proved true that many enzymes can work in organic solvents, even though it has also been observed that enzymes belonging to different classes need different hydration levels to maintain their catalytic activity, or at least a percentage of it. Additionally, although some enzymes can give really astonishing results, only few classes of these biocatalysts (such as lipases, proteases, oxynitrilases, and a few other enzymes) have proved to be synthetically useful from a practical point of view. These enzymes will be presented in the following paragraphs.

Other enzymes, such as dehydrogenases and glycosidases, despite their synthetic importance, have found limited or no practical applications so far. This is mainly because they either act on polar substrates or coenzymes that are poorly soluble in organic solvents, or because they are inhibited or inactivated by organic solvents. Another more general limitation arises from the fact that numerous biocatalysts are still too expensive or not commercially available at all.

4.1. Hydrolases

Reactions catalyzed by hydrolases are predominant among the reported biotransformations in organic solvents. Several groups of hydrolases exist in nature, but only two of these have been widely used in nonnatural media: lipases—recently redefined as "fat-splitting" esterases[58]—and proteases. These enzymes have been used in the labs all over the world and are now considered normal chemical bench reagents. The reasons for this success arise from the availability of these proteins from different commercial suppliers at reasonably cheap prices, their ease of handling (they do not need sensitive and/or expensive cofactors), and from their stability and versatility of action. From a chemical point of view, lipases and proteases in organic solvents can be seen as mild and selective reagents that are able to activate a generic carboxylate and transfer it to a huge number of nucleophiles. Several reviews and book chapters have already been published on specific synthetic applications of these enzymes. The most recent of them will be indicated in the headlines of the following sections.

4.1.1. Enantioselectivity of Hydrolases

The increasing demand for enantiomerically pure compounds by pharmaceutical and agrochemical companies has surely been one of the driving forces of the exploitation of hydrolases in synthesis, the most recurrent application being the kinetic resolution of racemates.

As has pointed out in Section 3.3.1, enzymatic enantioselectivity can be evaluated by the so-called "enantiomeric ratio", E. Besides being equal to the ratio of the specificity constants for the two competing enantiomers, some seminal papers have shown that E can be more conveniently calculated from the degree of conversion (c) and from the enantiomeric excesses of the products (ee_P) and the residual substrate (ee_S), both for irreversible[59] and reversible[60] reactions.

4.1.1.1. Kinetic Resolution of Alcohols[1c–e, 7c, 61]

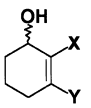
Kinetic resolution of alcohols can be obtained by enzyme catalyzed esterification [Eq. (3)] or, more commonly, by transesterification [Eq. (4)].

$$\mathrm{R^*OH + R'COOH \longrightarrow R'COOR^* + H_2O + R^*OH_{residual}} \quad (3)$$

$$\mathrm{R^*OH + R'COOR'' \longrightarrow R'COOR^* + R''OH + R^*OH_{residual}} \quad (4)$$

As the achiral alcohol component (R″OH) of the acyl transfer reagent (R′COOR″) can be used by the enzyme to catalyze the reverse reaction, which would decrease the optical purity of the products, acyl transfer reagents have to be chosen to make the transformations irreversible.[62] This goal can be achieved when the leaving R″OH is a poor nucleophile, and, accordingly, halogenated alcohols such as trichloro- and trifluoroethanol were used initially.[63] Later on, the use of oximes[64] and anhydrides[65] was suggested, but the reagents of choice for the kinetic resolution of alcohols in organic solvents are now enol esters, such as vinyl and isopropenyl acetate.[66]

The rich literature data can support the neophyte who is approaching an enzyme-catalyzed kinetic resolution for the first time. However, in the absence of generally valid predictive models, the initial experimental approach still requires a screening of several commercially available hydrolases. As exemplified in Table 8, the lipase from *Mucor miehei* was the best catalyst for the kinetic resolution of the cyclic allylic alcohol **1**.[67] Enzymatic behavior can be different with structurally related substrates and, accordingly, the lipase



1: X = Br; Y = H
2: X = H; Y = Br

Table 8. Enantioselectivity (E) of different lipases in the acetylation of **1** and **2** in vinyl acetate.

lipase	E values for **1**	E values for **2**
Pseudomonas cepacia	6	44
porcine pancreatic	34	24
Chromobacterium viscosum	6	26
Mucor miehei	78	15
Humicola lanuginosa	40	18
Penicillium camemberti	7	2
Candida rugosa	16	6

from *Pseudomonas cepacia* became the best catalyst among the lipases reported in Table 8 in the kinetic resolution of the allylic alcohol **2**. Both optically enriched alcohols **1** and **2**, as well as other related cyclic allylic alcohols, were then used as chiral synthons for the preparation of alkaloids by a 1,3-Claisen rearrangement with retention of chirality.[67] Hundreds of published papers are similarly concerned with the chemoenzymatic synthesis of complex compounds from chiral synthons obtained by the kinetic resolutions of racemates.

Once the best enzyme available has been identified, there is usually room for improving the enantioselectivity by exploiting some of the different techniques described in Section 3.3. Usually the most sensitive and most easily manipulatable parameter is the organic solvent. For instance, as already reported in Table 6, when the lipase from *Pseudomonas cepacia* is used, the *E* value for the resolution of *trans*-sobrerol changed from 69 in THF to more than 500 in *tert*-amyl alcohol.[54c] In such a solvent the "ideal" kinetic resolution of the racemic substrate was obtained, as the enzymatic reaction stopped spontaneously at 50% conversion when the (−)-(1*S*,5*R*) enantiomer was completely acylated.

As it is almost impossible to enumerate all the reported examples of kinetic resolutions of racemic primary and secondary alcohols, only some specific applications will be discussed in the following sections (Section 4.1.4.). However, by increasing the number of substrates investigated, active site models for different lipases have been suggested to rationalize the data collected so far and to predict the selectivity with new substrates.

Concerning secondary alcohols, a model based on the extension of Prelog's rule has been suggested for the lipases from *Pseudomonas cepacia* (now reclassified as the lipase from *Burkholderia cepacia*, BCL) and from *Candida rugosa* (CRL, Figure 8a).[68] This empirical rule predicts which

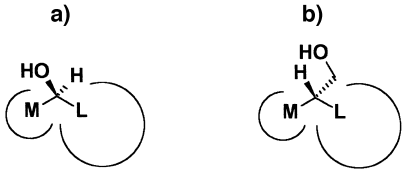
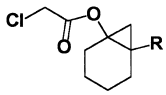


Figure 8. Empirical rules that summarize the enantiopreference of BCL and CRL toward secondary alcohols (a) and the enantiopreference of BCL toward primary alcohols (b, no oxygen linked at the stereocenter).

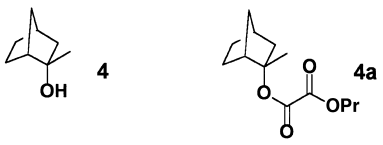
enantiomer reacts faster based on the relative sizes of the substituents at the stereocenter and has been proposed for other commercially available lipases (from *Mucor miehei*,[69], *Arthrobacter*,[70] and *Aspergillus niger* [71]) and for proteases.[72] The so-called "Kazlauskas rule" for BCL has also been extended to primary alcohols,[73] though it proved to be not always reliable for primary alcohols that have an oxygen atom attached to the stereocenter (Figure 8b). A more sophisticated three-dimensional active site model has recently been suggested for the same lipase,[74] while a definite conclusion about the chiral preference of CRL has been drawn from the X-ray crystal structures of covalent complexes of this enzyme with transition-state analogues for the hydrolysis of menthyl esters.[75] As all the lipases and esterases tested so far catalyze the hydrolysis of the same enantiomer of menthol (the 1*R* enantiomer), it is likely that features common to all these enzymes must be responsible for the observed enantiopreference. A combination of empirical rules derived from substrate data bases and high resolution enzymatic X-ray data is likely to support synthetic applications of this methodology very effectively.

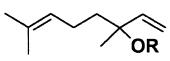
Finally, it has to be mentioned that, for steric reasons, hydrolases do not usually catalyse the transformation of tertiary alcohols, either in organic solvents or in aqueous solutions. An exception is given by the chloroacetate **3**, whose propanolysis was effective when catalyzed by *Mucor miehei* lipase in isopropyl ether (*E* values ranging from 13 to 38) and



3: R = H, Me, Et, Bu, C_6H_{13}

gave the optically active alcohol with the (1*S*,6*S*) absolute configuration.[76] The other (few) reports are related to the hydrolysis of esters in aqueous solutions containing different amounts of organic cosolvents and therefore are beyond the object of this review. However, the approach suggested by Brackenridge et al. for the resolution of the alcohol **4** deserves to be mentioned, that is, the introduction of a spatial separation between the chiral quaternary carbon and the ester which has to be split during the reaction. In this specific example, the formation of an oxalate ester, **4a**, reduced the steric hindrance of the molecule and made it acceptable for different lipases.[77a] In a similar approach, the stereoselective alcoholysis of the butanoyloxymetyl derivative **5a** of linalool (**5**) has been achieved by action of *Candida rugosa* lipase.[77b]

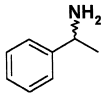




5: R = H
5a: R = $CH_2OCOCH_2CH_2CH_3$

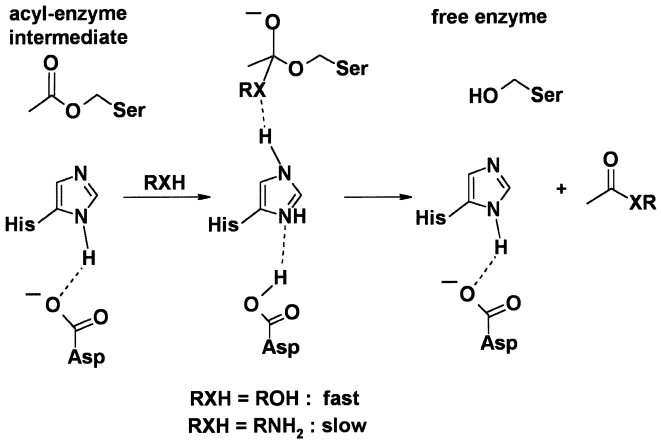
4.1.1.2. Kinetic Resolution of Amines and Thiols[1c–e, 61]

Compared to the hydrolase-catalyzed resolutions of alcohols, the corresponding acylations of racemic amines and thiols are rare. In the first report on this subject,[78] the kinetic resolution of various amines (for example, α-methylbenzylamine, **6**) catalyzed by the protease subtilisin was achieved by modulating the organic medium. Later on, the specificity of three lipases were exploited; lipase B from *Candida antarctica* (CALB) is the most popular for this transformation,[79] although the lipases from *Pseudomonas*



6

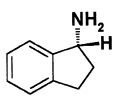
cepacia[80] and *Pseudomonas aeruginosa*[81] have also been used. By comparing the literature experimental data, it is evident that the lipase-catalyzed aminolysis of esters needs a greater amount of enzyme and longer reaction times than the corresponding alcoholysis of esters, even though higher *ee* values are generally obtained. A likely explanation for this phenomenon has been suggested, as shown in Scheme 1.[82] The rate of proton transfer from the acyl acceptor (RNH_2 or



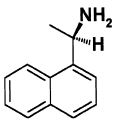
Scheme 1. Decomposition of the acyl–enzyme intermediate by action of alcohols or amines.

ROH) to the His residue of the catalytic triad during the nucleophilic attack on the acyl–enzyme complex is likely to be lower for a neutral amine, which has a significantly higher acid dissociation constant than the corresponding alcohol. On the other hand, the higher enantioselectivity can be explained by taking into account the low reactivity of the formed amides as substrates for lipases (these enzymes do not hydrolyse the peptidic bond in water). Despite the fact that more severe experimental conditions are necessary, the lipase-catalyzed resolution of racemic amines is presently the most successful application of enzymatic catalysis in organic solvents (see Section 4.1.4.).

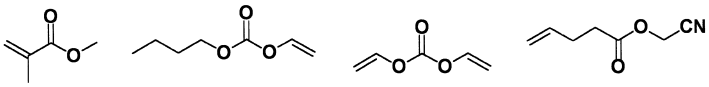
It has been pointed out[72] that proteases and lipases have opposite enantioselectivity. Accordingly, the protease subtilisin has been used for the production of the pharmaceutically important intermediate (*R*)-1-aminoindan (**7**) and the chiral resolving agent (*R*)-1-(1-naphthyl)ethylamine (**8**).[83] By using a continuous-flow reactor containing the enzyme adsorbed on porous glass beads for the kinetic resolution of these compounds, up to 330 g of racemic **7** and 1.6 kg of racemic **8** have been resolved to give 132 g of **7** (40% yield from the racemate, 98% *ee*) and 560 g of **8** (after crystallization of the corresponding hydrochloride, 35% yield, >99% *ee*; 95% *ee* prior to crystallization), respectively. Finally, some papers deserve to be mentioned which describe the enzymatic resolution of amines using as acyl donors acrylic esters (such as **9**),[84a] vinyl carbonates (such as **10**),[84b] homocarbonates (such as **11**),[84c] and cyanomethyl pent-4-enoate (**12**).[84d] These examples begin to show the versatility of hydrolases towards different acyl donors, a property that will be further detailed in the Section 4.1.2.



7

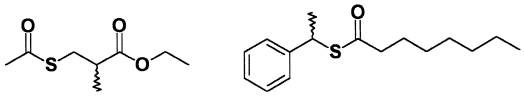


8



9 **10** **11** **12**

Little attention has been paid up to now to the enzymatic resolutions of thiols. The lipases from the porcine pancreas and *Pseudomonas cepacia* catalyzed the regio- and chemoselective alcoholysis of the thioesters **13** to the corresponding thiol with the (*R*) absolute configuration.[85] Similarly, the



13 **14**

thiooctanoate **14** was used as an acyl donor in a reaction catalyzed by CALB to give the corresponding (*R*)-thiol with >95% *ee*.[86] The direct enzymatic acylation of the racemic thiols was unsuccessful, for reasons that are still obviously related to the enzymatic mechanism. In fact, regarding the decomposition of the tetrahedral intermediate (see Scheme 1), the best leaving group is, in this case, the thiol, which is less basic than the active site serine hydroxyl group.

4.1.1.3. Kinetic Resolution of Carboxylic Acids[1c–e, 61]

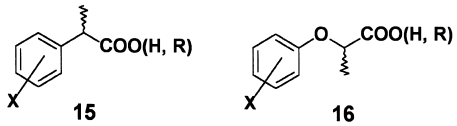
In principle, carboxylic acids in organic media can be enzymatically resolved in two ways, that is, either by hydrolase-catalysed esterification between an acid and an alcohol [Eq. (5)] or by transesterification between an ester and an alcohol [Eq. (6)]. More recently, aminolysis reactions with suitable amines have also been suggested [Eq. (7)].

$$R^*COOH + R'OH \longrightarrow R^*COOR' + H_2O + R^*COOH_{residual} \quad (5)$$

$$R^*COOR' + R''OH \longrightarrow R^*COOR'' + R'OH + R^*COOR'_{residual} \quad (6)$$

$$R^*COOR' + R''NH_2 \longrightarrow R^*CONHR'' + R'OH + R^*COOR'_{residual} \quad (7)$$

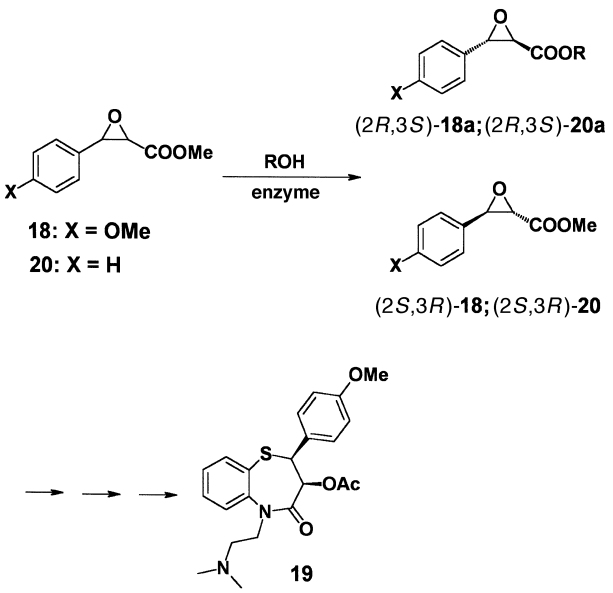
Most of the work has been devoted to the resolution of α-aryl-propionates (**15**) and α-aryloxy-propionates (**16**); the former are nonsteroidal anti-inflammatory drugs (such as naproxen and ibuprofen) and the latter are an important class of herbicides. The (*S*)-enantiomers of **15** are those which show therapeutic activity, while the (*R*)-enantiomers of **16** (which,



15 **16**

by the way, are structurally similar to (*S*)-**15**) are active as herbicides.

One of the very first reports deals with the enantioselective esterification of α-halogen-substituted carboxylic acids **17** (R = alkyl, aryl; X = Cl, Br, *p*-ClC_6H_4O) catalyzed by *Candida rugosa* lipase in hexane.[87] This transformation has been scaled up to a pilot plant.[88] In a previous paper by Cambou and Klibanov,[89] different strategies were compared for the kinetic resolution of 2-(4-chlorophenoxy)propionic acid (**16a**, X = *p*-Cl). The best approach proved to be the transesterification reaction ([Eq. (6)], R′ = Me, R″ = Bu). Another example of this methodology is the kinetic resolution of the *trans*-glycidic methyl ester **18**, whose (2*R*,3*S*)-enantiomer **18a** is a precursor of the calcium channel blocker drug diltiazem (**19**, Scheme 2). The enzymatic resolution has been achieved by α-chymotrypsin suspended in hexane/BuOH 9/1,[90] or by action of *Candida rugosa* lipase suspended in *tert*-amyl alcohol containing *n*-octanol (37% yield, 88% *ee* for the residual **18a**).[91] Similarly, the racemic *trans*-glycidic methyl ester **20** was resolved by action of *Mucor miehei* lipase in hexane in the presence of *i*BuOH ($E = 33$, 42% yield, 95% *ee* for (−)-**20**; 43% yield, 95 *ee* for the (+)-**20**).[92] Both enantiomers were then elaborated to obtain the taxol C-13 side chain.



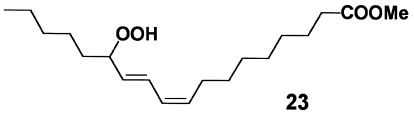
Scheme 2. Enzymatic kinetic resolution of *trans*-phenylglycidic methyl esters.

A disadvantage of the transesterification approach is the similar nature of the substrates and products, which leads to reaction mixtures containing compounds with similar physicochemical properties. As a consequence, serious problems can be encountered in scaling the reactions up if a chromatographic purification has to be avoided. An elegant technique for the separation of the resolved enantiomers was achieved by using poly(ethyleneglycol) as a nucleophile for the alcoholysis of the epoxybutanoate **21**, a precursor of (*R*)-carnitine.[93] Another approach is described in a patent, dealing again with the resolution of racemic **18**; 4-hydroxybutanoic acid was used as a nucleophile using a lipase from *Alcaligenes* species.[94] The corresponding ester **18a** (R = $CH_2CH_2CH_2COOH$) could be separated from the unreacted **18** by washing the reaction mixture with a mild alkaline solution.

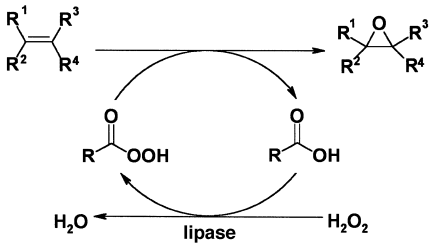
Candida antarctica lipase B catalyzed amminolysis of the 2-chloroethyl ester of ibuprofen (**22**) is a good example of the process described in Equation (7).[95] The use of NH_3 as a nucleophile greatly increased the enantioselectivity of the reaction ($E = 28$, solvent *tert*-butylalcohol) compared to the enzymatic alcoholysis ($E = 3$, same solvent). Lipases from *Candida antarctica* (SP435) and *Humicola* species (SP398) seem to be particularly effective for this reaction, as they are able to tolerate high concentration of NH_3 (up to 2.5 M). Additionally, many amides are sparingly soluble in organic solvents and precipitate during the ammoniolysis reaction, thus facilitating their isolation.

4.1.1.4. Kinetic Resolution of Hydroperoxides and Lipase-Mediated Formation of Peroxycarboxylic Acids

Hydroperoxides can be accepted as nucleophiles by hydrolases suspended in organic solvents. The kinetic resolution of racemic hydroperoxides (such as **23**) catalyzed by *Pseudomonas fluorescens* lipase has been reported,[96] a procedure which also exploits the spontaneous degradation of acylated hydroperoxides to carboxylic acid and ketone. For example, using cyclohexane as a solvent, (*S*)-1-phenylethyl hydroperoxide was prepared enantiopure at 60% conversion.



In an interesting approach, immobilized lipases have been used for generating peroxycarboxylic acids in a suitable organic solvent directly from the parent carboxylic acid and hydrogen peroxide. Furthermore, the peroxy acids formed under these very mild reaction conditions can be applied concomitantly for the nonstereoselective epoxidation of alkenes (Scheme 3).[97]

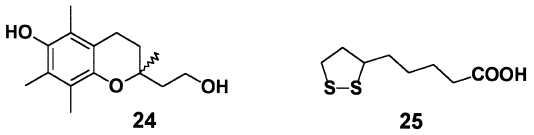


Scheme 3. Chemoenzymatic epoxidation of alkenes by enzymatically generated peroxycarboxylic acids.

4.1.1.5. Kinetic Resolution of Compounds Carrying a "Distant" Stereocenter

In all the examples described so far, enzyme selectivity was acting on stereocenters located adjacent to the site of catalysis. However an enzyme has the potential to discriminate any substrate stereocenter, no matter how remotely it is located from the catalytic site, since the whole active site of the enzyme is chiral. This property is synthetically very appealing, because the control of configurations of stereocenters remote from the chiral auxiliaries or catalysts applied in nonenzymatic methodology remains an unsolved problem. Despite that, the effects of distal chiral centers on the stereoselectivity of hydrolases has not been broadly studied and, consequently, not many examples have appeared in the literature.[1j]

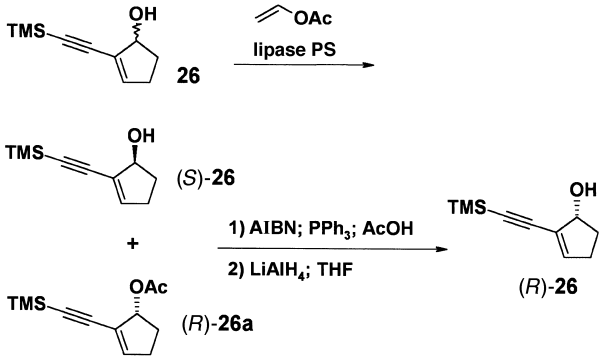
Concerning transformations in organic solvents, the kinetic resolution of compound **24**, a precursor of the α-tocopherol analogue MDL-73404, has been reported. Enzymatic acylation of **24** catalyzed by a lipase from *Pseudomonas* sp. (lipase B, Sapporo) allowed the isolation of the pure (*S*)-enantiomer of **24** in 36% yields.[98] In another example, enzymatic stereoselective esterification of racemic α-lipoic acid (**25**), a compound in which the carboxylic acid and the stereogenic center are four carbon atoms away, was achieved by exploiting the properties of *Candida rugosa* lipase.[99] Different alcohols were tested and the best results were obtained with *n*-hexanol.



24 **25**

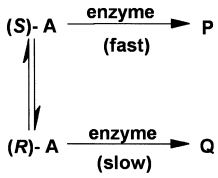
4.1.1.6. Dynamic Kinetic Resolution[100]

The main drawback of the kinetic resolutions described so far is that the maximum yield of one stereoisomer which can be obtained under ideal conditions is limited to 50%. A possible approach to overcome this limitation is chemical elaboration of the crude mixture by enzymatic acylation. For instance, the stereochemical inversion of the residual alcohol with the Mitsunobu protocol[101] has proved to be quite successful, as exemplified in Scheme 4. Following reduction of acetate (+)-(*R*)-**26a** with $LiAlH_4$, the corresponding alcohol (+)-(*R*)-**26** was obtained with an optical purity of 87.5% *ee*, which was increased to $\geq$99% *ee* by a single crystallization (73% overall yield from the starting racemic alcohol **26**).[101]



Scheme 4. Chemoenzymatic kinetic resolution of racemic **26**. AIBN = azobisisobutyronitrile.

A complementary approach is the so-called "dynamic kinetic resolution" (DKR).[100] This process is a type of second order asymmetric transformation,[102] and indicates any procedure which allows in situ racemization of the substrate prior to the enantioselective reaction, so that, in principle, a quantitative conversion of the starting material into a single stereoisomer of the product can be obtained. For DKR to be effective, the reactant isomers must be in rapid equilibrium, to make removal of one isomer the rate determining step (Scheme 5). As the enzyme always faces a racemic substrate during the reaction, the optical purity of the product becomes independent from the extent of conversion and depends only on the enantiomeric ratio *E* [Eq. (8)].

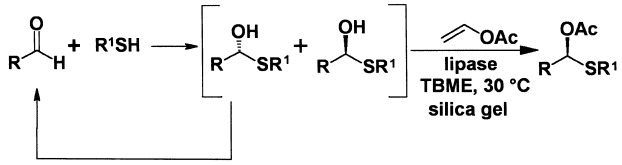


Scheme 5. Dynamic kinetic resolution of a generic racemate. The enzyme generates the products from starting enantiomers which are in fast equilibrium.

$$ee = \frac{E-1}{E+1} \quad (8)$$

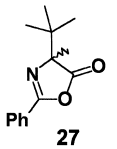
The kinetics of DKR have recently been described,[103] and some examples dealing with the subject of this review have been reported. Of course, in situ racemization occurs by breaking and forming bonds, and this has been achieved either by exploiting the acidity of a proton linked to a specific stereocenter or by formation of a stereocenter from achiral precursors. The latter was the case in the DKR of cyanohydrins[104] (described in detail in Section 4.1.2) and hemithioacetals.[105]

As shown in Scheme 6, different thiols and aldehydes were mixed together to form racemic hemithioacetals, of which essentially a single enantiomer was acylated by *Pseudomonas fluorescens* lipase under the reaction conditions. Racemization of the unrecognized hemithioacetals was obtained by a dissociation–recombination process catalyzed by silica gel. The best substituents ($R = AcOCH_2$, $R_1 = n$-octyl) allowed the isolation of the corresponding acetylated (*S*)-hemithioacetal with >95% *ee* in 85% yield.

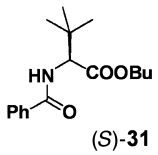


Scheme 6. Enzyme-mediated dynamic kinetic resolution of an epimerising hemithioacetal.

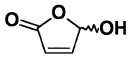
Compounds **27**–**30** are some of the molecules containing a labile stereogenic center that have been successfully subjected to DKR. Alcoholysis of the oxazolin-5(4H)-one (**27**) catalyzed by lipozyme has been scaled up to 200 g L^{-1} and the



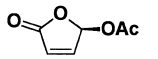
27



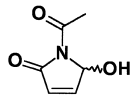
(*S*)-**31**



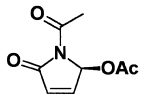
28



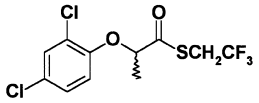
(*R*)-**32**



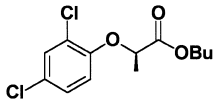
29



(*S*)-**33**



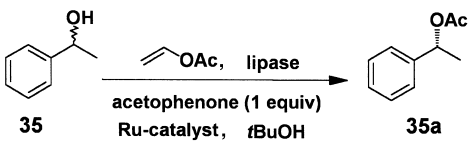
30



(*R*)-**34**

product (*S*)-**31** has been obtained with 97% *ee* at 96% conversion after 24 h.[106] By choosing the appropriate lipase, acetate (*R*)-**32** could be obtained enantiomerically pure (*ee* > 99%) at 90% conversion,[107] and so could acetate (*S*)-**33** (>99% *ee* at 99% conversion after 18 h).[107a] Alcoholysis of the thioester **30** catalyzed by lipase PS gave the corresponding butyl ester (*R*)-**34** with 75% *ee* at 99% conversion.[108]

More recently, DKRs have been obtained by a suitable combination of enzymes and transition metals.[109, 107b] Of course, to utilize these reactions an additional condition must be met, that is, the organometallic catalyst should not influence the enzyme in terms of selectivity or reactivity. In a first report,[110] the model secondary alcohol **35** was acetylated in the presence of *Pseudomonas* sp. lipase and a suitable ruthenium catalyst to give the (*R*)-acetate **35a** with 98% *ee* at 60% conversion after 72 h. Mechanistically, racemization of the unreacted alcohol is achieved by its temporary oxidation, catalyzed by the transition metal in the presence of a base at the expense of a corresponding ketone (such as acetophenone, Scheme 7). Optimization of the



Scheme 7. Dynamic kinetic resolution using a combination of enzyme and transition metals.

reaction conditions (a different ruthenium catalyst and the use of *p*-chlorophenylacetate as acyl donor) allowed the isolation of **35a** with 92% yield and >99.5 *ee*.[111]

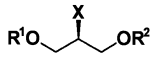
The lipase-catalyzed DKR of amines using palladium catalysts has also been reported.[112] For instance, *N*-acylated phenylmethylamine was obtained with 99% *ee* at 75–77% conversion.

4.1.1.7. Enzymatic Desymmetrization of Prochiral and Meso Substrates[113]

Enzymatic DKR is clearly a very attractive process, but racemization and resolution usually require reaction conditions which are mutually incompatible. Only by finding the required fine balance between the two, could such a process be achieved as described in the previous section.

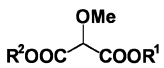
A more versatile approach to the synthetic goal of enantiomerically pure products in quantitative yields is given by the exploitation of another property of hydrolases, that is, their ability to differentiate enantiotopic groups of prochiral and meso compounds. Additionally, the ability to enter into either enantiomeric series in a straightforward fashion, regardless of the enantiomeric outcome of the enzymatic desymmmetrization, is a substantial advantage of working with these molecules. These desymmetrization processes have been discussed in detailed reviews very recently[113] and, therefore, only few cases will be presented as examples in the following paragraphs.

Considering prochiral substrates first, the synthetic versatility of 2-methyl-1,3-propanediol (**36**) and of its equivalents (X = alkyl, benzyl, aryl, alkenyl) has been recognized, and a review entirely dedicated to their preparation, enzymatic desymmetrization, and synthetic applications is also available.[114] For instance, the desymmetrization of diol **37** catalyzed by porcine pancreas lipase has been performed on a 40 g scale.[115] The monobutanoate **38**, obtained with 97.6 *ee* in 74.4% yield, was a key intermediate for the synthesis of both monocarbamate enantiomers of **39**, metabolites of the antiepileptic drug felbamate (**40**).



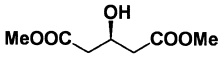
36: X = Me; $R^1 = R^2 = H$
37: X = Ph; $R^1 = R^2 = H$
38: X = Ph; $R^1 = H$; $R^2 = COPr$
39a: X = Ph; $R^1 = H$; $R^2 = CONH_2$
39b: X = Ph; $R^1 = CONH_2$; $R^2 = H$
40: X = Ph; $R^1 = R^2 = CONH_2$

Malonates monosubstituted at the C-2 atom are compounds related to **36**. Attempted enzymatic desymmetrization of **41** under aqueous conditions failed, because the activated C–H in the half ester product undergoes fast exchange accompanied by racemization. On the other hand, the use of enzymes in organic solvents allowed the efficient preparation of both optically labile enantiomers **42a** and **42b**, and their conversion into configurationally stable compounds.[116]

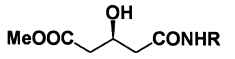


41: $R^1 = R^2 = Me$
42a: $R^1 = Me$; $R^2 = Bn$
42b: $R^1 = Bn$; $R^2 = Me$

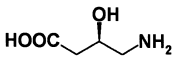
The aminolysis or ammonolysis of the homologous dimethyl 3-hydroxyglutarate (**43**) catalyzed by *Candida antarctica* lipase in dioxane was also highly enantioselective and the corresponding enantiopure amides (*R*)-**44** were obtained in almost quantitative yields.[117] To show the synthetic utility of the optically active compounds (*R*)-**44**, one of them ((*R*)-**44d**) was elaborated into the biologically active (*R*)-4-amino-3-hydroxybutanoic acid ((*R*)-GABOB, **45**).



43

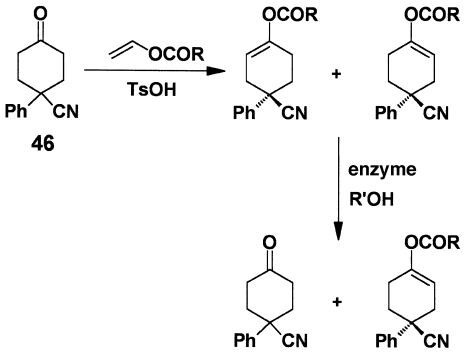


44a: R = Bn; **44b**: R = Bu
44c: R = Allyl; **44d**: R = H



45

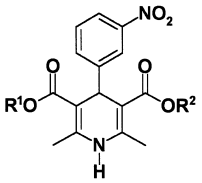
Moving to cyclic compounds, the desymmetrization of the prochiral ketone **46** by enzymatic enantioselective hydrolysis of its enol esters in water-saturated organic solvent has been reported (Scheme 8).[118]



46

Scheme 8. Desymmetrization of the prochiral ketone **46**.

Finally, concerning the desymmetrization of prochiral compounds, the brilliant elaboration of prochiral 1,4-dihydropyridines (**47**) deserves to be mentioned.[119] As previously discussed,[54d] the two enantiomers (*S*)-**48** and (*R*)-**48** could be obtained either by using the same lipase (lipase AH) and modulating the reaction media (iPr_2O to get (*S*)-**48** and cyclohexane to get (*R*)-**48**) or by using the same solvent (iPr_2O) and two different lipases (lipase AH to get (*S*)-**48** and lipase PS to get (*R*)-**48**). Interestingly, by changing just three aminoacids of lipase PS by side-directed mutagenesis, the performance of the mutant enzyme became similar to that of the wild type lipase AH.[119]

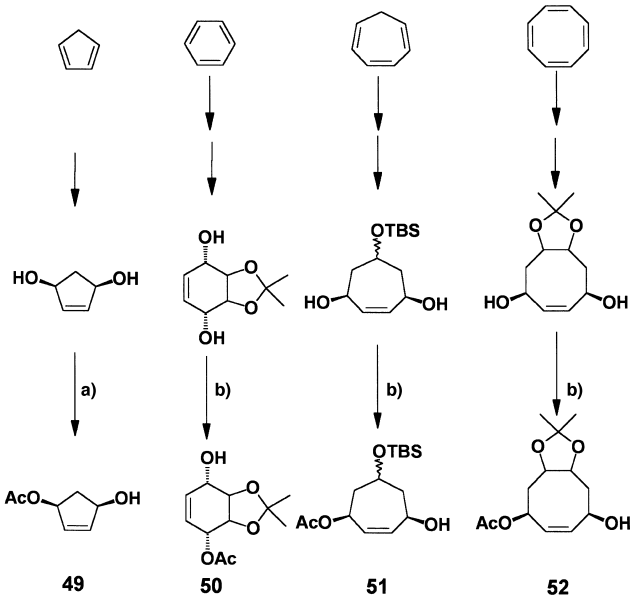


47: $R^1 = R^2 = CH_2OCOtBu$
(*R*)-**48**: $R^1 = H$; $R^2 = CH_2OCOtBu$
(*S*)-**48**: $R^1 = CH_2OCOtBu$; $R^2 = H$

Scheme 9 exemplifies the desymmetrization of some cyclic meso diols (products **49**–**52**),[113a, 113b] while Scheme 10 shows some of the compounds that have been obtained from the synthon **50**. The literature concerning the enzymatic desymmetrization of acyclic meso polyols is also very rich.[113b] Two arbitrarily chosen examples[120, 121] are shown in Scheme 11.

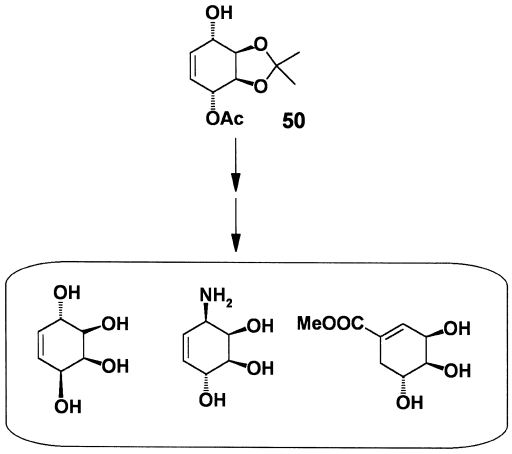
4.1.1.8. Kinetic Resolution of Organometallic Compounds

Organometallic compounds are widely used in modern organic chemistry and hydrolase selectivity can be exploited with these unnatural substrates too. In a very few reports the non-carbon atom was also the stereogenic center. This was the

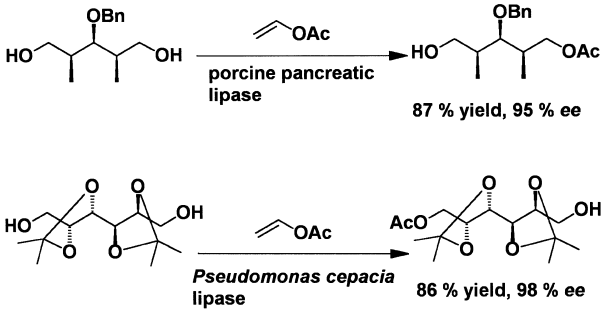


49 **50** **51** **52**

Scheme 9. Desymmetrization of cyclic meso diols with isopropenylacetate as the acylating agent. Enzymes utilized: a) Novozym 435; b) *Pseudomonas cepacia* lipase.

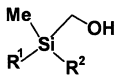


Scheme 10. Chemical elaboration of the enzymatically-produced monoacetate **50**.



Scheme 11. Lipase-catalyzed desymmetrization of acyclic *meso*-polyols.

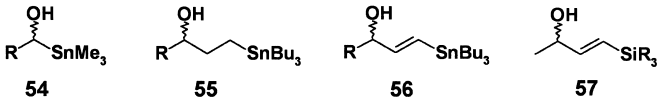
case, for instance, with the silyl methanol derivatives **53**, which were resolved by the protease papain catalyzed acylation with



53

R^1 = Ph, *p*-Me-C_6H_4, *p*-F-C_6H_4
R^2 = Et, Pr

5-phenylpentanoic acid in water-saturated 2,2,4-trimethylpentane.[122] More frequently, like in the case of the organotin and organosilyl compounds **54**–**57**, the metallic atom was just an additional functional group which makes it possible to design a wide variety of synthetic elaboration. Lipase-catalyzed kinetic resolutions of these compounds[123–126] are just a further exemplification of the procedures described in the Section 4.1.1.1.



54 **55** **56** **57**

The compatibility of metallic atoms with enzymatic activity and selectivity is even more important when using planar chiral organometallic compounds (belonging, for instance, to the (arene)$Cr(CO)_3$ series) as a substrate. Thus, the esterification of the chromium complexes **58** with vinyl esters in the presence of *Pseudomonas* sp. lipases gave the corresponding (*S*)-esters and the residual (*R*)-alcohols; the optical purities of the products depended on the nature of the acyl donor.[127] Similarly, the lipase PS catalyzed deacylation of the oxime acetates **59** with *n*BuOH allowed the resolution of the racemic mixture.[128] The *E* value was not very high, but modulation of the reaction medium allowed the inversion of the enzymatic enantioselectivity.



58 **59**

X = Me, OMe, $SiMe_3$ X = Me, OMe, Cl, F

Efficient enzymatic preparations of optically active ferrocenyl alcohols starting from racemic or meso precursors, such as **60** and **61**, have also been described by different authors.[129, 66b]

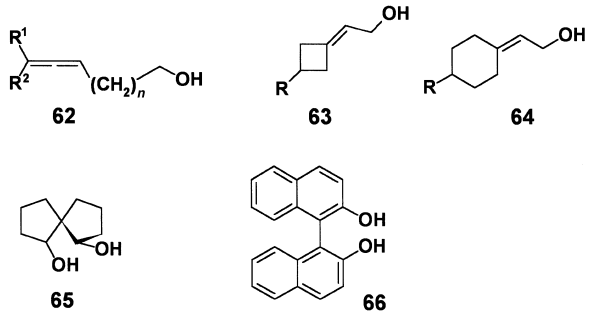


60 **61**

4.1.1.9. Kinetic Resolution of Racemates Without a Chiral Carbon Center

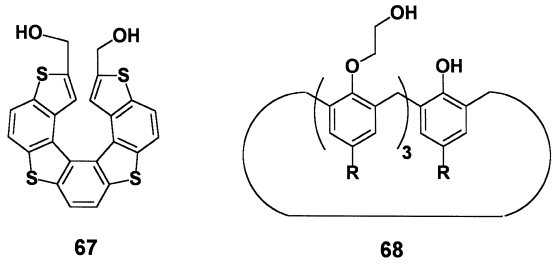
The last examples of the previous paragraph show that, besides being able to selectively recognize molecules containing one or more stereogenic center, hydrolases are also able to catalyze the kinetic resolution of other chiral compounds. Similarly, the resolution of axially chiral primary allenic alcohols of type **62**, as well as of the alkenes **63** and **64**, have also been reported, although with moderate selectivity.[130, 131] On the other hand, resolution of the spiro diol **65** and of the axially chiral [1,1′-binaphthyl]-2,2′-diol **66** were more efficient.[132, 133]

Very interesting results have also been reported on the resolution of racemic bis(hydroxymethyl)[7]thiaheterohelicenes **67**[134] and on the desymmetrization of the calix[4]arene derivative **68**.[135]



62 **63** **64**

65 **66**



67 **68**

4.1.2. Regioselectivity of Hydrolases

According to IUPAC definition "a regioselective reaction is one in which one direction of bond making or breaking occurs preferentially over all the other possible directions".[136] In 1985, the regioselective acylation of the primary hydroxyl groups of simple aliphatic glycols by the action of porcine pancreatic lipase was reported.[137] Since then , the ability of hydrolases to perform this kind of transformation in organic solvents has been extensively exploited in the modification of other diols and of polyfunctionalized compounds, such as carbohydrates, steroids, alkaloids.

Considering carbohydrates first, we have to initially acknowledge Klibanov's pioneering studies on the use of lipases for the regioselective esterification of primary[138] or secondary[139] hydroxyl groups of monosaccharides, and on the use of the protease subtilisin for the modification of primary hydroxyl groups of di- and oligosaccharides, as well as of natural glycosides.[140] The substrates described in these papers (some of which are depicted in Figure 9) offer a good exemplification of the versatility of the methodology and, in a way, they can be considered the "natural ancestors" of the numerous applications that have been reported in the literature since then. As this subject has already been covered in recent reviews and book chapters,[141] only few representative examples will be described and commented on here. Specifically, lipases and proteases have been exploited:

a) To catalyze a protective step in a chemoenzymatic synthesis of sugar derivatives. For instance, subtilisin-catalyzed esterification of lactosides has been used for a chemoenzymatic approach to 6′-deoxy-6′-fluoro- and 6-deoxy-6-fluoro-lactosides.[142] In another example, the acylation of sugar benzylidene derivatives, useful intermediates in the synthesis of oligosaccharides, has been described.

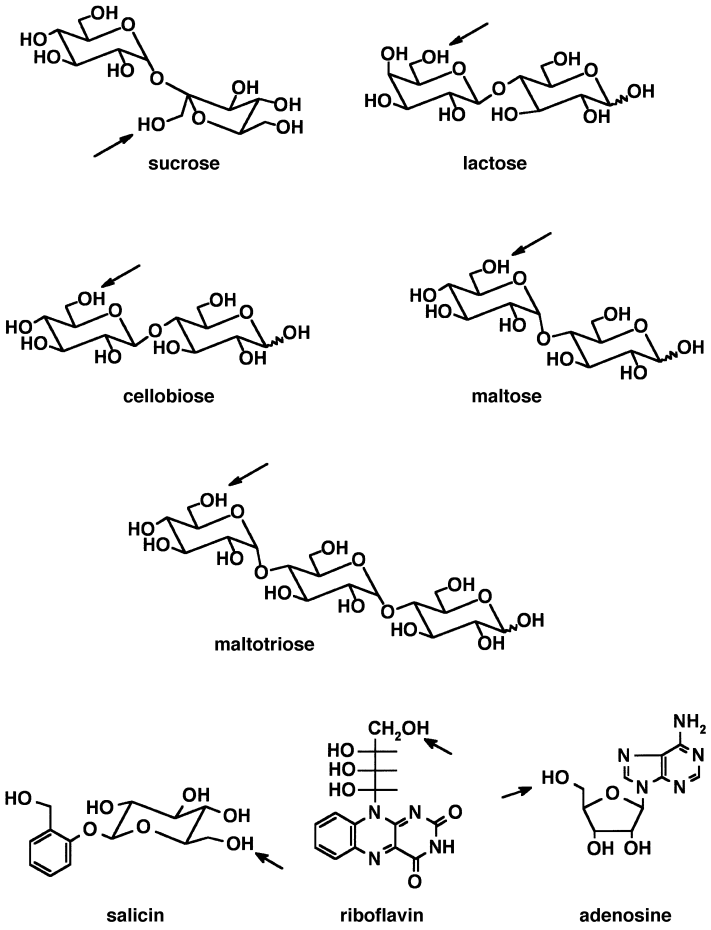
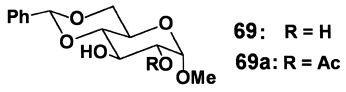


Figure 9. Acylation of sugars and natural glycosides, catalyzed by subtilisin in DMF, occurs at the indicated sites.

For instance, esterification of the 4,6-*O*-benzylidene-α-D-glucopyranoside (**69**) with vinyl acetate by action of *Pseudomonas cepacia* lipase gave the 2-*O*-acetate **69a** quantitatively. Results obtained with similar sugar derivatives were obtained independently by two research groups;[143, 144]



b) To synthesize specific esters of natural glycosides. For instance, a chemoenzymatic approach to malonyl esters of the flavonoid glycosides isoquercitrin, rutin, and naringin,[145] as well as of the ginsenoside Rg_1 has been described;[146]
c) To increase the basic knowledge of hydrolase selectivity. For instance, the rational control of enzyme-catalyzed regioselectivity has been studied using sucrose acylation with vinyl esters in organic media as a model;[147]
d) For the large-scale production of sugar acrylates, suitable monomers for the preparation of new polymeric hydrogels;[148]
e) For the large-scale production of new biosurfactants.[149]

The first paper published on the selective acylation of polyhydroxylated steroids described the complementary regioselectivity of two hydrolases, namely the lipase from *Chromobacterium viscosum* (CvL) and the protease subtilisin, towards different substitution of the tetracyclic skeleton.[150] As shown in Figure 10, the model dihydroxylated steroid 5α-androstane-3β,17β-diol (**70**) was selectively monoacylated at

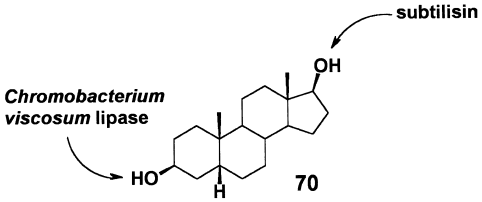
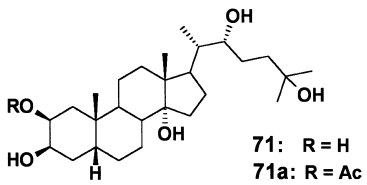
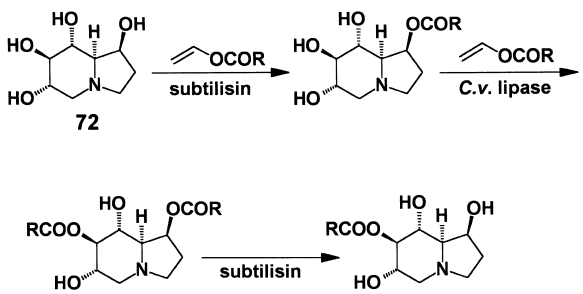


Figure 10. Sites of attack in the acylation of 5α-androstran-3β,17β-diol catalyzed by different hydrolases.

one of its two hydroxyl groups by changing the enzyme used. (This phenomenon is quite common and it has been reported with other polyhydroxy compounds.[139, 151]) The reactivities of numerous hydroxysteroids with these two enzymes were examined and the results showed that CvL lipase was very sensitive to the immediate environment of the C-3 hydroxyl group, accepting only the steroids with an A/B ring fusion in the *trans* configuration and the hydroxyl group in the equatorial (β)-position, but was quite insensitive to variations of the side chain. Conversely, changes in the A or B ring did not dramatically affect the acylation of steroids by subtilisin, confirming the preference of this protease for C-17 or side-chain hydroxyl groups. The performances of two other lipases, from *Candida rugosa*[152] and from *Candida antarctica*,[153] were subsequently investigated with different steroids, these enzymes proving to have less strict stereochemical requirements. The latter enzyme was also used for the regioselective esterification of the C-2 hydroxyl group of several ecdysteroids (such as **71**, to give **71a**).[154]



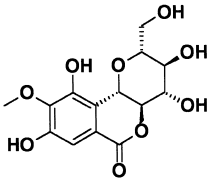
An interesting exploitation of enzymatic regioselectivity was reported by Margolin and co-workers.[155] As exemplified in Scheme 12, the sequential use of different hydrolases



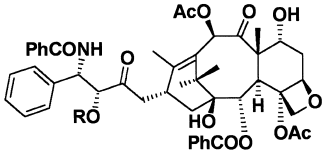
Scheme 12. Synthesis of various acyl derivatives of the alkaloid castanospermine **72** by sequential use of different hydrolases.

allowed the isolation of several *O*-acyl derivatives of the alkaloid castanospermine (**72**), that proved to be as much as 20 times more active that castanospermine itself in inhibiting HIV replication.

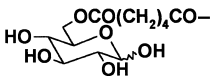
In a way, this paper can be considered a precursor of the so-called "combinatorial biocatalysis", a recent approach to drug discovery.[156] For instance, the same enzymatic strategy was applied to produce a solution-phase combinatorial library of 167 distinct, selectively acylated derivatives of the polyhydroxylated flavonoid bergenin (**73**) on a robotic workstation in a 96-well plate format. Additionally, by exploiting enzymes



73



74: R = H



74a: R =

74b: R = $CO(CH_2)_4COOH$

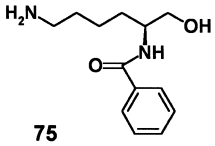
belonging to different classes, up to 600 bergenin derivatives were automatically produced.[157] Other lead compounds that have been similarly derivatized are, for instance, the antibiotic erythromycin and the antitumoral paclitaxel (**74**). The latter compound has a very low water solubility, a problem that could be overcome by selective enzymatic modification of its side-chain C-2′ hydroxyl group, followed by further enzymatic modifications. For example, the glucosylated derivatives **74a** is 60 times more soluble than **74**, while the acid derivative **74b** is more than three orders of magnitude more soluble.[158]

Of course this approach is not limited to complex molecules, but can be used to derivatize any kind of organic compounds carrying a functional group, for instance, polybenzyl esters that were used to produce amide libraries.[159]

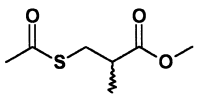
The combinatorial biocatalytic approach shows the versatility of hydrolases towards acylating agents, which are not limited to simple aliphatic acids like acetate and butanoate. However, generally speaking, it is not true that it is possible to acylate any substrate with any kind of ester. As pointed out in some reports,[141, 145] it is likely that a reciprocal steric hindrance occurs between large acyl groups and large nucleophiles, the latter being excluded by the catalytic site and, thus, prevented from attacking the acyl–enzyme intermediate.

4.1.3. Chemoselectivity of Hydrolases

Chemoselectivity is "the preferential reaction of a chemical reagent with one of two or more different functional groups".[136] Exploitation of this property has been reported for the selective monoacylation of aminoalcohols and sulfanylalcohols. In 1989, Klibanov and co-workers described unexpected selectivity of *Aspergillus niger* lipase towards the acylation of 6-amino-1-hexanol, opposite to that of the chemical reaction.[160] The overwhelming preference for the esterification of the hydroxyl group allowed the authors to prepare several *O*-acylated amino alcohols in good yield without requiring protecting groups. This study was then extended and it was reported that the ratio of *O*- to *N*-acylation was markedly dependent on the solvent.[161] For example, this ratio varied from 1.1 in *tert*-butyl alcohol to 21 in 1,2-dichloroethane for the acylation of *N*-α-benzoyl-L-lynisol (**75**) with trifluoroethyl butyrate catalyzed by *Pseudomonas cepacia* lipase. Other authors have reported that porcine pancreatic lipase is able to direct its action to the selective *O*-acylation of 2- mercaptoethanol with ethylcarboxylates.[162] On the other hand, the same lipase, as well as *Pseudomonas cepacia* lipase, exclusively catalyzed the thiotransesterification of the thioester **76** with propanol in hexane.[85]

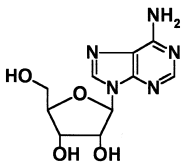


75

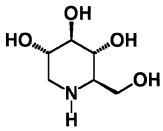


76

The acylation of the sugar moiety of the nucleotide adenosine (**77**)[140] described above (Figure 9), as well as of the hydroxyl group(s) of the alkaloid castanospermine (**72**, Scheme 12),[155] are other examples of chemoselective transformations. Preferential *O*-acylation was also obtained with another bioactive alkaloid, 1-deoxynojirimicin (**78**), which, similarly to castanospermine, was selectively acylated at the C-6 and/or C-2 hydroxyl group by the protease subtilisin, despite the presence of a potentially more reactive amino functional group.[163]



77



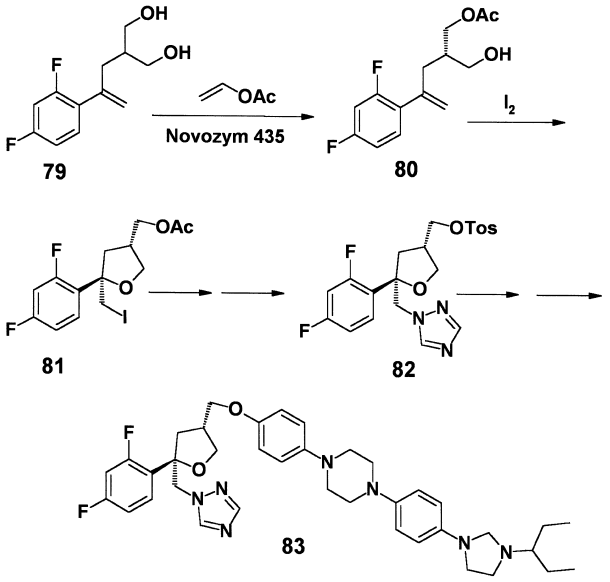
78

Surprisingly, the OH versus NH_2 chemoselectivity of this enzyme is reversed in peptide synthesis. Thus the derivatives of amino acids that contain a hydroxyl group at the side chain (such as serine, threonine, or tyrosine) could be used without protection of the OH group, as was exemplified in the synthesis of dipeptide fragments of the "so-called" octapeptide T.[160]

4.1.4. Large-Scale Applications[164]

Several companies are currently using enzyme-catalyzed reactions in organic solvents for the large-scale production of useful intermediates. However, due to confidentially reasons, it is often quite difficult to get information about the processes or even the substrates and enzymes used. In the following paragraphs we will discuss some examples that can be extrapolated from the patent and scientific literature.

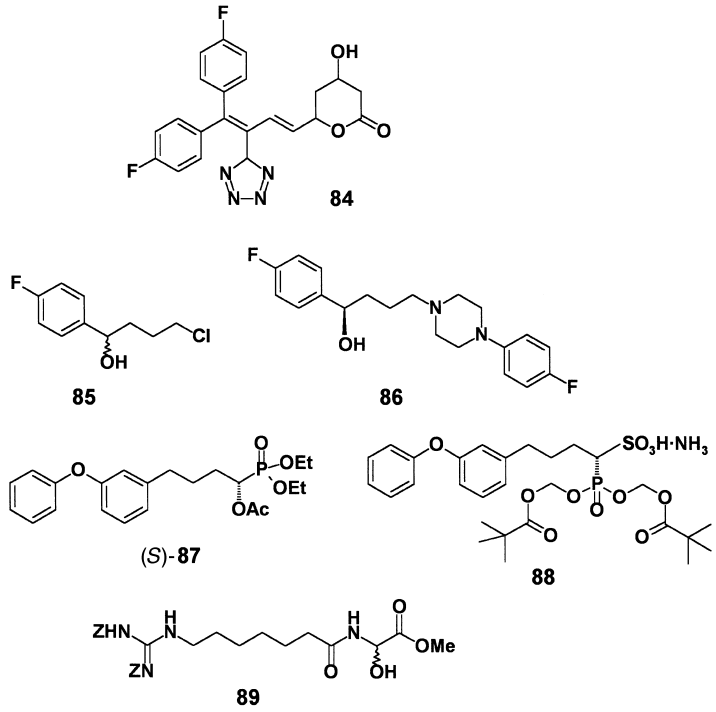
Compound SCH51048 (**83**) from Schering–Plough is an antifungal azole derivative that is now in Phase II clinical trials. The synthetic route to the final drug proceeds through a key intermediate, the (2*R*,4*S*)-phenylsulfonate **82** (Scheme 13). The required stereochemistry at the C-2 and C-4 positions in the tetrahydrofuran ring of **82** is achieved by an



Scheme 13. Synthesis of SCH51048 (**83**).

iodocyclization reaction performed on the chiral monoester **80**, followed by displacement of the iodide in **81** with sodium triazolide. In turn, **80** is synthesized by enzymatic acylation of the symmetric diol **79** under nonaqueous conditions. Using *Candida antarctica* lipase B (Novozym 435) and vinyl acetate in acetonitrile, highly enantioselective acetylation of diol **79** occurs to give the monoacetate **80**. Acetonitrile was selected as the reaction solvent since the subsequent iodocyclization step was carried out in the same solvent at 0 °C, simply by removing the enzyme beads by filtration and carrying out the cyclization on the crude enzymatic reaction mixture. This enzymatic process is continuously running in a pilot plant to supply material for the clinical trial.[165]

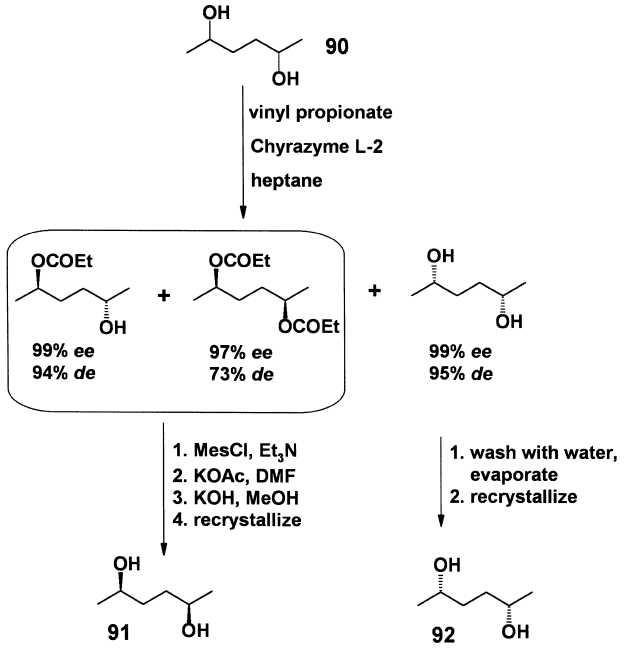
In another example from the Bristol–Myers Squibb Pharmaceutical Research Group, the resolution of racemic **84** by an acetylation reaction catalyzed by lipase PS-30 was scaled up to 640-L batches. The reaction contained 4 g L^{-1} of racemic **84**, 2% (v/v) isopropenyl acetate, 0.05% distilled water (v/v), and 1% (w/v) crude lipase PS-30 powder in toluene. The batch reactor was shaken at 37 °C and 150 rpm for 20 h and gave the unreacted (*R*)-(+)-**84** with an *ee* value of 99.5% in 48% yield.[166] Other pharmaceutical intermediates have been prepared by the same research group on a multigram scale. For instance, racemic α-(3-chloropropyl)-4-fluorobenzenemethanol (**85**), a possible intermediate for the synthesis of the potential antipsychotic agent BMS 181100 (**86**), was resolved using isopropenyl acetate and lipase PS-30 in heptane. The *S* alcohol was obtained in 42% with >99% optical purity, while *R* acetate was obtained with 92.6% optical purity by stopping the reaction at 46% conversion.[167]



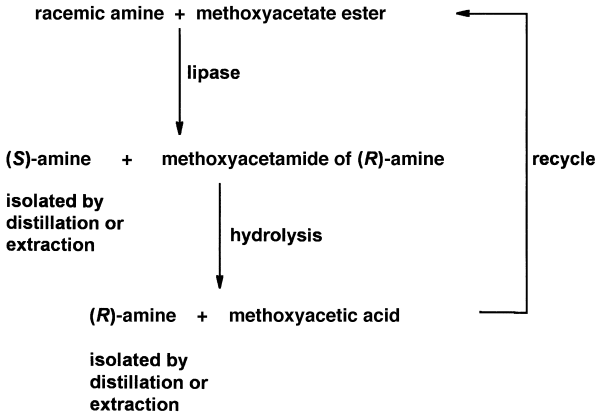
The chiral intermediate (*S*)-**87** was prepared for the total synthesis of a squalene synthase inhibitor effective as an anticholesterol drug, BMS-188494 (**88**). The kinetic resolution of racemic [1-(hydroxy)-4-(3-phenyl)butyl] phosphonic acid, diethyl ester was carried out in toluene using the lipase from *Geotrichum candidum* with isopropenyl acetate as the acylating agent. A reaction yield of 38% and an optical purity of 95% were obtained for the acetate (*S*)-**87**.[168] At variance, the stereoselective acetylation of racemic **89** (Z = benzyloxycarbonyl), a precursor of the antitumor antibiotic and immunosuppressive agent (−)-15-deoxyspergualin, was carried out in methyl ethyl ketone using a lipase from *Pseudomonas* sp. (lipase AK) and vinyl acetate. A reaction yield of 48% and an optical purity of 98% were obtained for the corresponding (*S*)-acetate, while the unreacted alcohol was obtained in 41% yield and 98.5% *ee*.[169]

The research group of Chiroscience Ltd. has developed an efficient lipase-catalyzed transesterification of racemic/*meso*-hexane-2,5-diol (**90**) combined with a mesylation/displacement reaction sequence to give both hexane-(2*R*,5*R*)-diol (**91**) and hexane-(2*S*,5*S*)-diol (**92**) in 99% *ee* and 99% *de*, without the need for chromatography (Scheme 14).[170] These compounds are important intermediates in the synthesis of 2,5-disubstituted pyrrolidines and phospine ligands of interest for asymmetric hydrogenation. This volume-efficient process has been performed on a multikilogram scale and can be extended to alternative diols.

Probably the process that is actually performed on the largest scale is the enzymatic resolution of racemic amines developed by the BASF research group,[171] in which a racemic amine or aminoalcohol is enantioselectively acylated in the presence of an hydrolase with an ester whose acid component bears a fluorine, nitrogen, oxygen, or sulfur atom in the proximity of the carbonyl atom. As shown in Scheme 15, the acylating agent can be ethyl methoxyacetate while, following



Scheme 14. Preparation of enantiomerically pure C_2-symmetric diols.



Scheme 15. BASF process for the kinetic resolution of amines.

the separation of the unreacted (*S*)-amine by extraction or distillation, the methoxyacetamide of the (*R*)-amine can be chemically hydrolyzed and the resulting amine can be either isolated or racemized for recycling.

4.1.5. Miscellaneous Applications of Hydrolases

Enzyme-catalyzed transesterification using 1,3-regiospecific lipases can be used to produce valuable confectionery fats. At present, Unichema in Europe and Fuji Oil in Japan produce several hundred tons of cocoa butter equivalents (cocoa butter is the fat that confers chocolate with its required crystallization and melting characteristics) by transesterification of cheap sunflower oil, particularly rich in oleic acid, with stearic acid.[1i] This process is catalyzed on a solvent-free packed-bed reactor by the lipases from *Rhizomucor miehei* (Unichema)[172] or *Rhizopus* (Fuji Oil).[173]

The use of lipases has proven to be particularly advantageous for the synthesis of partial glycerides containing labile substituents such as 8′-apo-β-carotinoic acid, which would not withstand chemical procedures.[174]

Fatty acid esters of carbohydrates have potentially important applications in detergents, food and feed, cosmetics and pharmaceuticals because of their surface-active properties. A promising enzymatic approach to this class of compounds has been developed at Novo Nordisk. Monoesters of alkyl glycopyranosides have been prepared on a large scale in a more than 90% yield by direct enzyme-catalyzed esterification of glucopyranosides with long chain fatty acids in a solvent free process.[149] Specifically, the procedure was tested in a pilot-plant on a 20 kg scale using a mixture of α- and β-ethyl D-glucopyranoside, prepared by direct glucosylation of glucose in ethanol in the presence of an ion-exchange resin, and 5% of immobilised lipase (w/w) from *Candida antarctica* as the catalyst. The corresponding 6-*O*-monoesters were obtained in 85–90% yield within 24 hours, and the enzyme could be recycled several times with no noticeable loss of activity. In other reports, the low solubility of the sugars in the melted fatty acids has been overcome by the use of butyl glycosides [175] or sugar acetals,[176] as well as by the addition of small amounts of organic solvents serving as adjuvant to maintain a small liquid phase.[177]

Lipases and proteases have also been used for the large scale production of sugar acrylates, which are suitable monomers for the preparation of new polymeric hydrogels.[178] A two step chemoenzymatic synthetic strategy has been developed to prepare polysugar acrylates.[148] In the first step, an enzyme is used to catalyze the regioselective acryloylation of a sugar, then the derivatized sugar is chemically polymerized (typically by a free radical mechanism) to give a long-chain, linear polysugar acrylate.

Following a first report by Klibanov and co-workers,[179] hydrolase-catalyzed processes have been used to prepare various oligomers and polymers through A–B type polycondensation,[180] AA–BB type polycondensation,[181] and ring-opening polymerization.[182]

Another interesting application of hydrolases in organic media is the synthesis of peptides.[183] In one of the first paper published on this subject it was found that the enantioselectivity of serine protease is dramatically relaxed in organic solvents.[184] This finding opened the possibility for the formation of D–L or D–D type peptide bonds by using a protease,[185] a transformation that is not possible in water due to the enzyme's strict selectivity for L-aminoacids. Additionally, this system was found to exhibit unique regio- and chemoselectivity. For instance, when lysine was used as an amino donor without protection of its side chain, subtilisin catalyzed peptide bond formation selectively on the ε-amino group in *tert*-amyl alcohol.[186] Hydrolases that do not have a proteolytic activity in water, like lipases, are instead able to catalyze the acyl transfer to an amino nucleophile. Accordingly, different lipases have been used to catalyze peptidic bond formation.[187]

Finally, the use of lipases in the flavor and fragrances field deserves to be mentioned.[188] In these cases the enzymatic transformation is usually quite trivial, such as the esterification of citronellol with acetic acid in the presence of molecular sieves to remove the water formed,[189] but the products can

have the added value associated with the "natural" label. In fact, legislation of most countries requires that, in order to qualify a product such as a food additive as "natural", its preparation should not involve any 'chemical' steps. Enzymatic transformations are considered by the same legislation to be 'natural'.

4.2. Exploiting Other Enzymes in Organic Solvents

All the examples discussed in the previous sections involved the use of hydrolases. However there are other classes of enzymes that have found useful application in nonaqueous media, as will be discussed in the following paragraphs.

4.2.1. Hydroxynitrile Lyases

Hydroxynitrile lyases (HNLs, also called oxynitrilases) are proteins that catalyze the cleavage of cyanohydrins to aldehydes and hydrogen cyanide, thus supporting the catabolic degradation of cyanogenic glycosides in nature. Under appropriate conditions, these enzymes can catalyze the stereoselective addition of HCN to carbonyl compounds, producing either (*R*)- or (*S*)-cyanohydrins.[190] Eleven different HNLs from six different plant families have been isolated to date,[191] but only four of these enzymes have found interesting synthetic applications.[192] Specifically, these proteins are the (*R*)-HNL from almonds (*Prunus amygdalus*), and the (*S*)-HNLs from *Sorgum bicolor*, *Hevea brasiliensis*, and *Manihot esculenta* (Figure 11). The latter two enzymes have recently been cloned and overexpressed,[193] while the (*R*)-HNL from almond can be easily isolated in sufficient quantities from its natural source and, due to its stability and natural abundance, it has been the first investigated enzyme of this class.

The suppression of the spontaneous chemical addition of HCN to the carbonyl compounds is a prerequisite to obtaining the chiral cyanohydrins in good enantiomeric purity. The extent of this nonenzymatic reaction strongly depends on the reaction conditions; for instance, it was found that an aqueous reaction medium is only suitable if pH values below 4.0 and low temperatures are employed. A decisive breakthrough came when it was discovered that the undesirable chemical addition is more or less suppressed in organic solvents which are not miscible with water, like ethyl acetate or diisopropyl ether.[194] Since then, several papers have been published on this subject by different groups, but most of these reports are beyond the purpose of this review as the reactions were run in "pure" biphasic systems. However, in some of these protocols the water phase was limited to the amount of liquid adsorbed on the solid material upon which the enzyme was supported. Using this methodology, cyanohydrins used as precursors of (*R*)-pantolactone (**93**),[195] thienyl and furyl analogus of ephedrin (**94**),[196] and the adrenergic bronchodilatators (*R*)-terbutaline (**95**)[197]—just to give a few examples—have been prepared on a multigram scale (Scheme 16).

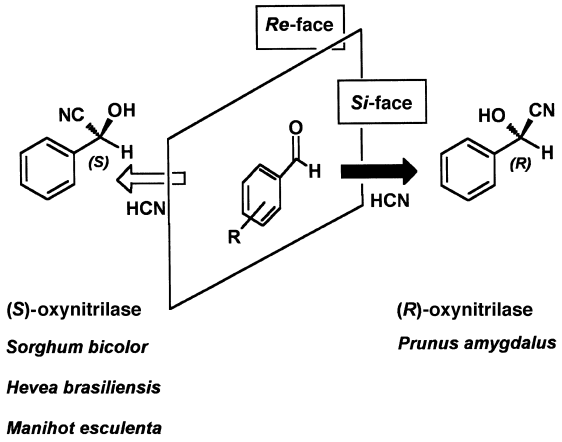
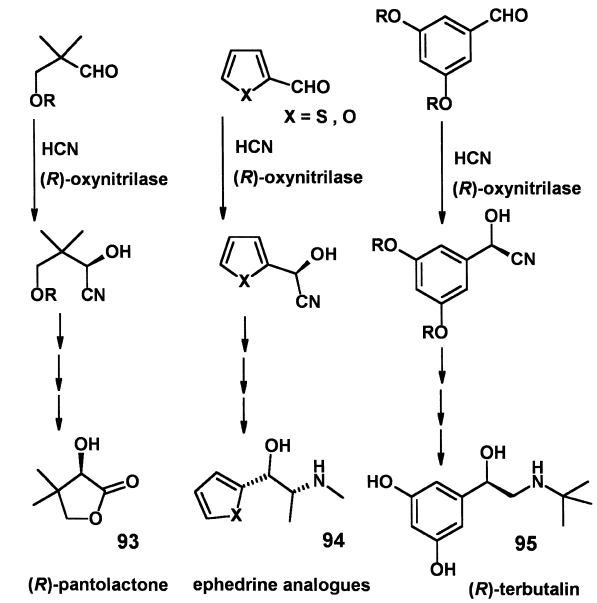


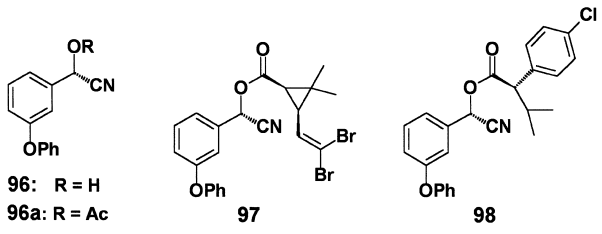
Figure 11. Oxynitrilase-catalyzed enantioselective synthesis of cyanohydrins.



Scheme 16. Chemoenzymatic synthesis of compounds **93**–**95**.

4.2.2. A Case Study: The Chemoenzymatic Synthesis of (S)-α-Cyano-3-Phenoxybenzyl Alcohol (96)

Pyretrine I, a compound extracted from *Chrisanthemum cinerariefolium*, has a strong insecticidal activity. The rapid knock-down of insects, high level of activity, and considerable degree of safety to mammals, accompanied by its relatively low stability, has led to intense interest in the synthesis of chemical analogues of this compound. Many of the present commercially important pyretrine analogues are esters of (*S*)-α-cyano-3-phenoxybenzyl alcohol (**96**) and include Deltametrhin (**97**, Hoechst) and Esfenvalerate (**98**, Sumitomo Chemicals).



Several enzymatic approaches to **96** have been published and most of them are related to the use of enzymes in organic solvents. A *Sorghum bicolor* (*S*)-oxynitrilase catalyzed reaction allowed the isolation of **96** in 93% yield and 96% *ee*.[198] The main drawback of this approach is the difficulty in isolating this enzyme. The recent availability of two other (*S*)-HNLs (from *Hevea brasiliensis* and *Manihot esculenta*), cloned and overexpressed, might allow this biocatalytic transformation to become competitive soon.[199]

An alternative approach is the kinetic resolution of the chemically-produced racemic **96** by lipase-catalyzed transesterification. The enantioselective acetylation of racemic **96** has been achieved by action of a lipoprotein lipase from *Pseudomonas* sp. suspended in *tert*-butyl methyl ether containing vinyl acetate. The (*S*)-acetate **96a** was obtained in 90% *ee* at 41% conversion.[200] The same enzyme was used to hydrolyze (*S*)-**96a** back to **96** (96% *ee* at 82% conversion), which was then coupled with the suitable acyl chloride to give the insecticide **98**.

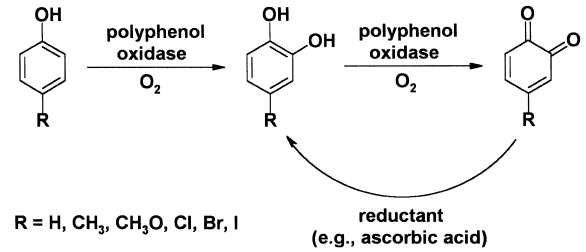
A significative improvement to this approach was obtained by coupling the lipase-catalyzed kinetic resolution with the in situ formation and racemization of cyanohydrins (a further example of dynamic kinetic resolution). Racemic **96**, generated from *m*-phenoxybenzaldehyde and acetone cyanohydrin in diisopropyl ether under the catalysis of a basic anion-exchange resin, was acetylated by *Pseudomonas cepacia* lipase using isopropenyl acetate as the acylating agent.[104] The racemization of the optically active residual cyanohydrin by Amberlite IRA-904 (OH^- form) was found to be much faster than the enzymatic acetylation, confirming the effective second order asymmetric transformation. In this way, the acetate (*S*)-**96a** was obtained in 84% yield and 89% *ee*. Ethanolysis of (*S*)-**96a**, catalyzed by the same lipase in iPr_2O, and coupling of the resulting cyanohydrin with the appropriate acyl chloride afforded the pyretroid **97** in 90% yield and 94% *de*.

Finally, another approach was recently suggested involving the lipase-catalyzed alcoholysis of the racemic cyanohydrin acetate **96a**. The resulting **96** was separated from the unreacted (*R*,*S*)-**96a** by chromatographic techniques, as well as by extraction with hexane, and the residual ester (partially enantiomerically enriched) was then racemized using triethylamine in diisopropyl ether or toluene.[201] Alternatively, the crude enzymatic reaction mixture was directly treated with the appropriate chloride, and the pyretroid product separated from the unreacted (*R*,*S*)-**96a** by bulb-to-bulb distillation. The residual unreacted **96a** was racemized with triethylamine and returned to the process.[202]

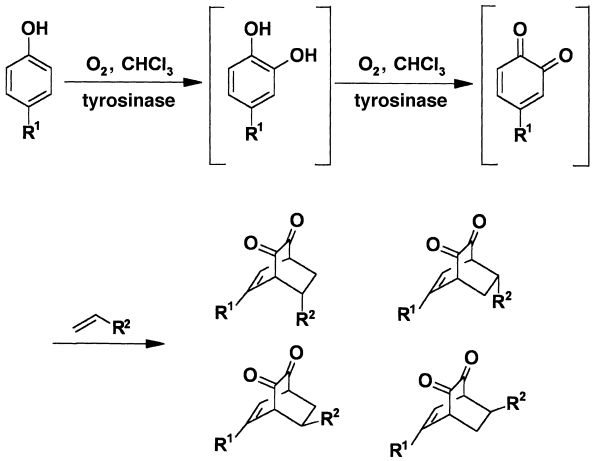
4.3. Miscellanea

Other classes of enzymes have been used in organic solvents, but, despite the high synthetic potential of some of these transformations, the reports are limited to few examples up to now.

Kazandjian and Klibanov showed that it is possible to use a mushroom polyphenol oxidase (also called tyrosinase) adsorbed on porous glass to catalyze the oxidation of a number of phenols to *o*-quinones in chloroform.[203] The authors reported that, while in water the enzymatic oxidation resulted in negligible yields due to rapid inactivation of the enzyme and spontaneous polymerization of the quinones, a quantitative conversion was achieved in chloroform. The quinones produced were then nonenzymatically reduced to cathecols, affording a net regioselective hydroxylation of phenols (Scheme 17). Very recently, Waldmann and co-workers exploited this biotransformation by coupling it with nonenzymatic transformations in a domino reaction sequence.[204] As shown in Scheme 18, the *ortho*-quinones, obtained by action of a mushroom tyrosinase, subsequently underwent a Diels–Alder reaction in the presence of different dienophiles. This three-step reaction cascade allowed the preparation of functionalized bicyclo[2,2,2]octene-diones in a rapid and efficient manner.



Scheme 17. Chemoenzymatic synthesis of cathecols.



Scheme 18. Enzyme-initiated hydroxylation, oxidation, and carbo-Diels–Alder domino reaction.

The enzyme horseradish peroxidase catalyses the free radical polymerization of phenols in the presence of H_2O_2. The poor solubility of the growing polymer chains in water leads to the incorporation of organic solvents into the reaction medium; for example, polymers of *para*-phenylphenol were produced in aqueous dioxane and the molecular weight of the macromolecules increased with decreasing water content.[205]. This methodology might offer a valid alternative for the preparation of phenolic resins avoiding the use of the toxic formaldehyde; the technology is under development, as shown by patent applications.

Horse liver alcohol dehydrogenase (HLADH) was also used in organic solvents (such as isopropyl ether). Both the

enzyme and the nicotinamide cofactor were deposited onto the surface of glass beads, which were then suspended in a water-immiscible organic solvent containing the substrate.[206] Due to the insolubility of the NAD(H) molecule in the organic media, the cofactor could only be regenerated in situ by using the "one enzyme – two substrates" approach. Using HLADH, the cofactor NADH could be regenerated by the oxidation of EtOH to acetaldehyde, while the oxidized NAD could be produced by the reduction of isobutyraldehyde.

A partially purified preparation of (+)-α-pinene cyclase from sage (*Salvia officinalis*) was shown to convert geranyl pyrophosphate to the monoterpene olefins α-pinene, camphene, limonene, and myrcene in hexane. The cyclase was shown to be stabilized with respect to temperature and time by the use of a hydrocarbon solvent, and, in all other characteristics, to exhibit properties closely resembling those observed in aqueous media.[44c]

5. Summary and Outlook

The enzymatic catalysis in organic solvents, described as an unusual phenomenon in some pioneering papers published at the beginning of this century, has turned into an important instrument for organic synthesis in the last decade. As has been pointed out in the previous sections, hydrolases – and particularly lipases – are already a well-exploited tool for transformations performed up to a production-plant scale. Oxynitrilases, a class of enzymes which catalyses one of the most important reactions of organic chemistry, the formation of the carbon – carbon bond, are also on the way to becoming an industrial success. Applications of these biocatalysts ranges from the preparation of milligrams of specifically labeled compounds to the modification of fats on a multiton scale and from the preparation of complex key intermediates for the pharmaceutical industry to the synthesis of polymers. Other enzymes, especially oxidoreductases, have found more limited applications. Additional research is needed to overcome such drawbacks as limited substrate and/or coenzyme solubility and enzyme instability or inhibition in organic solvents.

Besides the overwhelming reports on synthetic applications, enzymatic catalysis in organic solvents has stimulated basic research to address questions related to the performance of enzymes in nonnatural environments, as well as to their catalytic mechanism in such media. In the last few years particular attention has been paid to understanding why the catalytic activity of enzymes in anhydrous organic solvents is, in most cases, drastically diminished relative to that in water. As a result of this effort, different causes of this phenomenon have been elucidated, and the research is now focused on the design of strategies that might restore full enzymatic activity.

Finally, it has been pointed out that optimization of enzymatic performances can be obtained by manipulating the protein structure through genetic engineering, either by site-specific or by random mutagenesis. Enzyme engineering and "medium" engineering are supporting the exploitation of this methodology in a decisive way and expanding the synthetic potentiality even further.

We gratefully acknowledge financial support for our work from the Biotechnology Programme of the European Commisssion (BIO4-CT95-0231) and the CNR Target Project on Biotechnology.

Received: March 25, 1999 [A 335]

[1] a) G. M. Whitesides, C. H. Wong, *Angew. Chem.* **1985**, *97*, 617 – 638; *Angew. Chem. Int. Ed. Engl.* **1985**, *24*, 17 – 638; b) J. B. Jones, *Tetrahedron* **1986**, *42*, 3351 – 3403; c) K. Faber, *Biotransformations in Organic Chemistry*, Springer, Berlin, **1992**; d) E. Santaniello, P. Ferraboschi, P. Grisenti, A. Manzocchi, *Chem. Rev.* **1992**, *92*, 1071 – 1140; e) C. H. Wong, G. M. Whitesides, *Enzymes in Synthetic Organic Chemistry*, Pergamon, Trowbridge, **1994**; f) F. Theil, *Chem. Rev.* **1995**, *95*, 2203 – 2227; g) *Enzyme Catalysis in Organic Synthesis* (Eds.: K. Drauz, H. Waldmann), VCH, Weinheim, **1995**; h) *Chirality in Industry* (Eds.: A. N. Collins, G. N. Sheldrake, J. Crosby), Wiley, Chichester, **1997**; i) R. D. Schmidt, R. Verger, *Angew. Chem.* **1998**, *110*, 1694 – 1720; *Angew. Chem. Int. Ed.* **1998**, *37*, 1608 – 1633; j) R. J. Kaslauskas, U. T. Bornscheuer in *Biotechnology Series*, *Vol. 8a* (Eds.: H. J. Rehm, G. Reed, V. Puhlet, P. J. W. Stadler, D. R. Kelly), Wiley-VCH, Weinheim, **1998**, pp. 37 – 191; k) U. T. Bornscheuer, R. J. Kazlauskas, *Hydrolases in Organic Synthesis—Regio- and Stereoselective Biotransformations*, Wiley-VCH, Weinheim, **1999**.

[2] J. B. Jones, H. Holland, *Biocatalysis*, Synopsis Scientific System, Leeds, **1997**.

[3] L. G. Butler, *Enzyme Microb. Technol.* **1979**, *1*, 253 – 259.

[4] E. A. Sym, *Biochem. J.* **1936**, *30*, 609 – 617.

[5] a) M. D. Lilly, *J. Chem. Technol. Biotechnol.* **1982**, *32*, 162 – 169; b) G. Carrea, *Trends Biotechnol.* **1984**, *2*, 102 – 106; c) A. N. Semenov, Y. L. Khmelnitsky, I. V. Berezin, K. Martinek, *Biocatalysis* **1987**, *1*, 2 – 7; d) L. E. S. Brink, J. Tramper, K. C. A. M. Luyben, K. Van't Riet, *Enzyme Microb. Technol.* **1988**, *10*, 736 – 743; e) R. A. Ramelmeier, H. V. Blanch, *Biocatalysis* **1989**, *2*, 97 – 120; f) *Biocatalysis in Non-Conventional Media* (Eds.: J. Tramper, M. H. Vermue, H. H. Beeftink, U. von Stockar), Elsevier, Amsterdam, **1992**; g) M. G. Wubbolts, O. Favre-Bulle, B. Withold, *Biotechnol. Bioeng.* **1996**, *52*, 301 – 308; h) M. Garguri, M. D. Legoy, *Biochim. Biophys. Acta* **1997**, *1337*, 227 – 232.

[6] a) F. M. Menger, K. Yamada, *J. Am. Chem. Soc.* **1981**, *101*, 6731 – 6734; b) K. Martinek, A. V. Levashov, Y. L. Khmelnitsky, U. L. Klyachko, I. V. Berezin, *Science* **1982**, *218*, 889 – 891; c) P. D. I. Fletcher, G. D. Rees, B. H. Robinson, R. B. Freedman, *Biochim. Biophys. Acta* **1985**, *832*, 204 – 214; d) P. L. Luisi, L. J. Magid, *CRC Crit. Rev. Biochem.* **1986**, *20*, 409 – 474; e) M. Waks, *Protein Struct. Funct. Genet.* **1986**, *1*, 4 – 15; f) R. M. D. Verhaert, R. Hilhorst, M. Vermue, T. J. Schaafsma, C. Veeger, *Eur. J. Biochem.* **1990**, *187*, 59 – 72.

[7] a) A. M. Klibanov, *CHEMTECH* **1986**, *16*, 354 – 359; b) J. S. Dordick, *Enzyme Microb. Technol.* **1989**, *11*, 194 – 211; c) C. S. Chen, C. J. Sih, *Angew. Chem.* **1989**, *101*, 711 – 723; *Angew. Chem. Int. Ed. Engl.* **1989**, *28*, 695 – 707; d) A. M. Klibanov, *Trends Biochem. Sci.* **1989**, *14*, 141 – 144; e) M. N. Gupta, *Eur. J. Biochem.* **1992**, *203*, 25 – 32; f) E. Santaniello, P. Ferraboschi, P. Grisenti, *Enzyme Microb. Technol.* **1993**, *15*, 367 – 382; g) L. Kvittingen, *Tetrahedron* **1994**, *50*, 8253 – 8274; h) J. A. Jongejan, *Chim. Oggi* **1994**, *July/August*, 15 – 24; i) G. Bell, P. J. Halling, B. D. Moore, J. Partridge, D. G. Rees, *Trends Biotechnol.* **1995**, *13*, 468 – 473; j) *Enzymatic Reactions in Organic Media* (Eds.: A. M. P. Koskinen, A. M. Klibanov), Blackie Academic & Professional, London, **1996**; k) S. V. Kamat, E. J. Beckman, A. J. Russell, *Crit. Rev. Biotechnol.* **1995**, *15*, 41 – 71; l) A. M. Klibanov, *Trends Biotechnol.* **1997**, *15*, 97 – 101.

[8] a) F. Borzeix, F. Monot, J. P. Vandecasteele, *Enzyme Microb. Technol.* **1992**, *14*, 791 – 797; b) F. Yang, A. J. Russell, *Biotechnol Bioeng.* **1995**, *47*, 60 – 70; c) R. J. Tweddel, S. Kermasha, D. Combes, A. Marty, *Enzyme Microb. Technol.* **1998**, *22*, 439 – 445; d) E. Catoni, E. Cernia, C. Palocci, *J. Mol. Catal. A* **1996**, *105*, 79 – 86.

[9] C. Laane, S. Boeren, K. Vos, C. Veeger, *Biotechnol. Bioeng.* **1987**, *30*, 81 – 87.

[10] A. Zaks, A. M. Klibanov, *J. Biol. Chem.* **1988**, *263*, 8017 – 8021.

[11] J. A. Rupley, E. Gratton, G. Careri, *Trends Biochem. Sci*. **1983**, *8*, 18 – 22.
[12] S. Bone, *Biochim. Biophys. Acta* **1987**, *916*, 128 – 134.
[13] L. A. S. Gorman, J. S. Dordick, *Biotechnol. Bioeng*. **1992**, *39*, 392 – 397.
[14] a) P. J. Halling, *Enzyme Microb. Technol*. **1984**, *6*, 513 – 514; b) P. J. Halling, *Trends Biotechnol*. **1989**, *7*, 50 – 52; c) P. J. Halling, *Enzyme Microb. Technol*. **1994**, *16*, 178 – 206.
[15] H. L. Goderis, G. Ampe, M. P. Feyten, B. L. Fouwè, W. M. Guffens, S. M. Van Cauwenbergh, P. P. Tobback, *Biotechnol. Bioeng*. **1987**, *30*, 258 – 266.
[16] a) M. Reslow, P. Adlercreutz, B. Mattiasson, *Eur. J. Biochem*. **1988**, *172*, 573 – 578; b) R. H. Valivety, P. J. Halling, A. D. Peilow, A. R. Macrae, *Eur. J. Biochem*. **1994**, *222*, 461 – 464.
[17] R. H. Valivety, P. J. Halling, A. R. Macrae, *Biochim. Biophys. Acta* **1992**, *1118*, 218 – 222.
[18] R. H. Valivety, P. J. Halling, A. D. Peilow, A. R. Macrae, *Biochim. Biophys. Acta* **1992**, *1122*, 143 – 146.
[19] G. Bell, A. E. M. Janssen, P. J. Halling, *Enzyme Microb. Technol*. **1997**, *20*, 471 – 477.
[20] a) S. H. M. van Herp, E. O. Kamenskaya, Y. L. Khmelnitsky, *Eur. J. Biochem*. **1991**, *202*, 379 – 384; b) R. H. Valivety, P. J. Halling, A. R. Macrae, *Biotechnol. Lett*. **1993**, *15*, 1133 – 1138; c) R. Bovara, G. Carrea, G. Ottolina, S. Riva, *Biotechnol. Lett*. **1993**, *15*, 937 – 942; d) R. Bovara, G. Carrea, A. M. Gioacchini, S. Riva, F. Secundo, *Biotechnol. Bioeng*. **1997**, *54*, 50 – 57.
[21] K. Faber, S. Riva, *Synthesis* **1992**, 895 – 910.
[22] a) G. Ljunger, P. Adlercreutz, B. Mattiasson, *Enzyme Microb. Technol*. **1994**, *16*, 751 – 755; b) Y. Dudal, R. Lortie, *Biotechnol. Bioeng*. **1995**, *45*, 129 – 134; c) P. J. Halling, *Biotechnol. Tech*. **1992**, *6*, 271 – 276; d) Z. Yang, D. Robb, *Biotechnol. Tech*. **1993**, *7*, 37 – 42; e) E. Wehtje, K. Jasmedh, P. Adlercreutz, S. Chand, B. Mattiasson, *Enzyme Microb. Technol*. **1997**, *21*, 502 – 510.
[23] L. Greenspan, *J. Res. Nat. Bur. Stand. Sect. A* **1977**, *81*, 89 – 96.
[24] A. Zaks, A. M. Klibanov, *Proc. Natl. Acad. Sci. USA* **1985**, *82*, 3192 – 3196; b) M. Rizzi, P. Stylos, A. Riek, M. Reuss, *Enzyme Microb. Technol*. **1992**, *14*, 709 – 714; c) M. Martinelle, K. Hult, *Biochim. Biophys. Acta* **1995**, *1251*, 191 – 197; d) S. Chatterjee, A. J. Russell, *Biotechnol. Bioeng*. **1992**, *40*, 1069 – 1077; e) S. Chatterjee, A. J. Russell, *Enzyme Microb. Technol*. **1993**, *15*, 1022 – 1029.
[25] C. R. Wescott, A. M. Klibanov, *J. Am. Chem. Soc*. **1993**, *115*, 1629 – 1631.
[26] a) K. Ryu, J. S. Dordick, *Biochemistry* **1992**, *31*, 2588 – 2598; b) C. R. Wescott, A. M. Klibanov, *J. Am. Chem. Soc*. **1993**, *115*, 10362 – 10363; c) A. J. J. Straathof, J. L. L. Rakels, J. J. Heejnen in *Biocatalysis in Non-Conventional Media* (Eds.: J. Tramper, M. H. Vermue, H. H. Beeftink, U. von Stockar), Elsevier, Amsterdam, **1992**, pp. 137 – 144; d) J. B. A. Van Tol, J. B. Odenthal, J. A. Jongejan, J. A. Duine in *Biocatalysis in Non-Conventional Media* (Eds.: J. Tramper, M. H. Vermue, H. H. Beeftink, U. von Stockar), Elsevier, Amsterdam, **1992**, pp. 229 – 235; e) A. Reimann, D. A. Robb, P. J. Halling, *Biotechnol. Bioeng*. **1994**, *43*, 1081 – 1086; f) A. E. M. Janssen, A. M. Vaidya, P. J. Halling, *Enzyme Microb. Technol*. **1996**, *18*, 340 – 346.
[27] a) A. D. Blackwood, L. J. Curran, B. D. Moore, P. J. Halling, *Biochim. Biophys. Acta* **1994**, *1206*, 161 – 165; b) K. Xu, A. M. Klibanov, *J. Am. Chem. Soc*. **1996**, *118*, 9815 – 9819.
[28] S. J. Singer, *Adv. Protein Chem*. **1962**, *17*, 1 – 68.
[29] a) A. A. Klyosov, N. Van Viet, I. V. Berezin, *Eur. J. Biochem*. **1975**, *59*, 3 – 7; b) M. Jackson, H. M. Mantsch, *Biochim. Biophys. Acta* **1991**, *1078*, 2231 – 2235.
[30] a) E. N. Vulfson, D. B. Sarney, B. A. Law, *Enzyme Microb. Technol*. **1991**, *13*, 123 – 126; b) G. Lin, H.-C. Liu, *Tetrahedron Lett*. **1995**, *36*, 6067 – 6068.
[31] Y. Yamamoto, H. Kise, *Biotechnol. Lett*. **1993**, *15*, 647 – 652.
[32] S. Kamat, E. J. Beckman, A. J. Russell, *Enzyme Microb. Technol*. **1992**, *14*, 265 – 271.
[33] a) A. J. Russell, A. M. Klibanov, *J. Biol. Chem*. **1988**, *263*, 11624 – 11626; b) T. Yamane, T. Ichiryu, M. Nagata, A. Ueno, S. Shimizu, *Biotechnol. Bioeng*. **1990**, *36*, 1063 – 1069; c) K. Dabulis, A. M. Klibanov, *Biotechnol. Bioeng*. **1993**, *41*, 566 – 571; d) Y. L. Khmelnitsky, S. H. Welch, D. S. Clark, J. S. Dordick, *J. Am. Chem. Soc*. **1994**, *116*, 2647 – 2648; e) A. O. Triantafyllou, E. Wehtje, P. Adlercreutz, B. Mattiasson, *Biotechnol. Bioeng*. **1995**, *45*, 406 – 414; f) I. Mingarro, H. Gonzales-Navarro, L. Braco, *Biochemistry* **1996**, *35*, 9935 – 9944.
[34] a) P. Adlercreutz, *Eur. J. Biochem*. **1991**, *199*, 609 – 614; b) R. Bovara, G. Carrea, G. Ottolina, S. Riva, *Biotechnol. Lett*. **1993**, *15*, 169 – 174; c) E. Wehtje, P. Adlercreutz, B. Mattiasson, *Biotechnol. Bioeng*. **1993**, *41*, 171 – 178; d) D. K. Oladepo, P. J. Halling, V. F. Larsen, *Biocatal. Biotransform.* **1995**, *12*, 47 – 54; e) G. Pencreac'h, J. C. Baratti, *Appl. Microbiol. Biotechnol*. **1997**, *47*, 630 – 635; f) R. J. Barros, E. Wehtje, P. Adlercreutz, *Biotechnol. Bioeng.* **1998**, *59*, 364 – 373.
[35] M. Wahlgren, T. Arnebrant, *Trends Biotechnol*. **1991**, *9*, 201 – 208.
[36] M. T. Reetz, A. Zonta, J. Simpelkamp, *Angew. Chem*. **1995**, *107*, 373 – 375; *Angew. Chem. Int. Ed. Engl*. **1995**, *34*, 301 – 303.
[37] A. L. Margolin, *Trends Biotechnol*. **1996**, *14*, 223 – 230.
[38] A. Matsushima, Y. Kodera, M. Hiroto, H. Nishimura, Y. Inada, *J. Mol. Catal. B* **1996**, *2*, 1 – 17, and references therein.
[39] a) G. Ottolina, G. Carrea, S. Riva, L. Sartore, F. M. Veronese, *Biotechnol. Lett.* **1992**, *14*, 947 – 952; b) F. Secundo, S. Spadaro, G. Carrea, *Biotechnol. Bioeng*. **1999**, *62*, 554 – 561.
[40] a) V. M. Paradkar, J. S. Dordick, *J. Am. Chem. Soc*. **1994**, *116*, 5009 – 5010; b) M. Goto, N. Kamiya, F. Nakashio, *Biotechnol. Bioeng*. **1995**, *45*, 27 – 32; c) S. Basheer, K. I. Mogi, M. Nakajima, *Biotechnol. Bioeng*. **1995**, *45*, 187 – 195; d) Y. Okahata, T. Mori, *Trends Biotechnol*. **1997**, *15*, 50 – 54.
[41] a) A. R. Macrae, *J. Am. Oil Chem. Soc*. **1983**, *60*, 291 – 294; b) R. A. Wisdom, P. Dunnil, M. D. Lilly, *Biotechnol. Bioeng*. **1987**, *29*, 1081 – 1085; c) M. M. Hog, T. Yamane, S. Shimizu, S. Ishida, *J. Am. Oil Chem. Soc*. **1984**, *61*, 776 – 781.
[42] a) T. Fukui, T. Kawamoto, K. Sonomoto, A. Tanaka, *Appl. Microbiol. Biotechnol*. **1990**, *34*, 330 – 334; b) A. Wickli, E. Schmidt, J. R. Bourne in *Biocatalysis in Non-Conventional Media* (Eds.: J. Tramper, M. H. Vermue, H. H. Beeftink, U. von Stockar), Elsevier, Amsterdam, **1992**, pp. 577 – 584; c) M. Indlekofer, M. Funke, W. Claassen, M. Reuss, *Biotechnol. Prog*. **1995**, *11*, 436 – 442.
[43] a) C. M. Rosell, A. M. Vaidya, *Appl. Microbiol. Biotechnol*. **1995**, *44*, 283 – 286; b) C. M. Rosell, A. M. Vaidya, P. J. Halling, *Biotechnol. Bioeng*. **1996**, *49*, 284 – 289; c) S. Bourg-Garros, N. Razafindramboa, A. A. Pavia, *Biotechnol. Bioeng*. **1998**, *59*, 495 – 500.
[44] a) A. Zaks, A. M. Klibanov, *Science* **1984**, *224*, 1249 – 1251; b) M. Reslow, P. Adlercreutz, B. Mattiasson, *Appl. Microbiol. Biotechnol*. **1987**, *26*, 1 – 8; c) C. J. Wheeler, R. Croteau, *Arch. Biochem. Biophys.* **1986**, *248*, 429 – 434; d) G. Ayala, M. Tuena de Gomez-Puyou, A. Gomez-Puyou, A. Darszon, *FEBS Lett*. **1986**, *203*, 41 – 43; e) G. Garza-Ramos, A. Darszon, M. Tuena de Gomez-Puyou, A. Gomez-Puyou, *Biochemistry* **1989**, *28*, 3177 – 3182; f) D. B. Volkin, A. Staubli, R. Langer, A. M. Klibanov, *Biotechnol. Bioeng*. **1991**, *37*, 843 – 853.
[45] a) K. Griebenow, A. M. Klibanov, *J. Am. Chem. Soc*. **1996**, *118*, 11695 – 11700; b) F. H. Arnold, *Trends Biotechnol.* **1990**, *8*, 244 – 249; c) L. You, F. H. Arnold, *Protein Eng.* **1994**, *9*, 77 – 83.
[46] a) P. L. Fitzpatrick, A. C. U. Steinmetz, D. Ringe, A. M. Klibanov, *Proc. Natl. Acad. Sci. USA* **1993**, *90*, 8653 – 8657; b) N. H. Yennawar, H. P. Yennawar, G. K. Farber, *Biochemistry* **1994**, *33*, 7326 – 7336.
[47] U. R. Desai, A. M. Klibanov, *J. Am. Chem. Soc*. **1995**, *117*, 3940 – 3945.
[48] L. T. Kanerva, A. M. Klibanov, *J. Am. Chem. Soc*. **1989**, *111*, 6864 – 6865.
[49] P. Pasta, S. Riva, G. Carrea, *FEBS Lett*. **1988**, *236*, 329 – 332.
[50] P. P. Wangikar, P. Michels, D. S. Clark, J. S. Dordick, *J. Am. Chem. Soc*. **1997**, *119*, 70 – 76.
[51] a) P. A. Burke, R. G. Griffin, A. M. Klibanov, *Biotechnol. Bioeng*. **1993**, *42*, 87 – 94; b) R. Affleck, Z. I. Xu, V. Suzawa, K. Focht, D. S. Clark, J. S. Dordick, *Proc. Natl. Acad. Sci. USA* **1992**, *89*, 1100 – 1104; c) J. Broos, A. J. W. G. Visser, J. F. J. Engbersen, W. Verboom, A. van Hoek, D. N. Reinhoudt, *J. Am. Chem. Soc*. **1995**, *117*, 12657 – 12663; d) J. Partridge, P. R. Dennison, B. D. Moore, P. J. Halling, *Biochim. Biophys. Acta* **1998**, *1386*, 79 – 89.
[52] a) M. T. Reetz, A. Zonta, K. Schimossek, K. Liebeton, K. E. Jaeger, *Angew. Chem*. **1997**, *109*, 2961 – 2963; *Angew. Chem. Int. Ed. Engl.* **1997**, *36*, 2830 – 2832; b) K. Faber, G. Ottolina, S. Riva, *Biocatalysis* **1993**, *8*, 91 – 132.

[53] a) C. R. Wescott, A. M. Klibanov, *Biochim. Biophys. Acta* **1994**, *1206*, 1 – 9; b) G. Carrea, G. Ottolina, S. Riva, *Trends Biotechnol*. **1995**, *13*, 63 – 70.

[54] a) P. A. Fitzpatrick, A. M. Klibanov, *J. Am. Chem. Soc*. **1991**, *113*, 3166 – 3171; b) F. Terradas, M. Teston-Henry, P. A. Fitzpatrick, A. M. Klibanov, *J. Am. Chem. Soc*. **1993**, *115*, 390 – 396; c) R. Bovara, G. Carrea, L. Ferrara, S. Riva, *Tetrahedron: Asymmetry* **1991**, *2*, 931 – 938; d) Y. Hirose, K. Kariya, J. Sasaki, Y. Kurono, H. Ebike, K. Achiwa, *Tetrahedron Lett*. **1992**, *33*, 7157 – 7160.

[55] a) E. Rubio, A. Fernandez-Mayorales, A. M. Klibanov, *J. Am. Chem. Soc*. **1991**, *113*, 695 – 696; b) D. A. MacManus, E. N. Vulfson, *Enzyme Microbiol. Technol*. **1997**, *20*, 225 – 228.

[56] a) K. Nakamura, J. Takebe, T. Kitayama, A. Ohno, *Tetrahedron Lett*. **1991**, *32*, 4941 – 4944; b) F. Secundo, S. Riva, G. Carrea, *Tetrahedron: Asymmetry* **1992**, *3*, 267 – 280.

[57] a) T. Ke, C. R. Wescott, A. M. Klibanov, *J. Am. Chem. Soc*. **1996**, *118*, 3366 – 3374; b) C. R. Wescott, H. Noritomi, A. M. Klibanov, *J. Am. Chem. Soc*. **1996**, *118*, 10365 – 10370; c) G. Colombo, G. Ottolina, G. Carrea, A. Bernardi, C. Scolastico, *Tetrahedron: Asymmetry* **1998**, *9*, 1205 – 1214.

[58] R. Verger, *Trends Biotechnol.* **1997**, *15*, 32 – 38.

[59] C. S. Chen, Y. Fujimoto, G. Girdaukas, C. J. Sih, *J. Am. Chem. Soc.* **1982**, *104*, 7294 – 7298.

[60] C. S. Chen, S. H. Wu, G. Girdaukas, C. J. Sih, *J. Am. Chem. Soc.* **1987**, *109*, 2812 – 2817.

[61] a) C. J. Sih, G. Girdaukas, C. S. Chen, C. J. Sih in Ref. [7j], pp. 94 – 139; b) L. T. Kanerva in Ref. [7j], pp. 170 – 223.

[62] K. Faber, S. Riva, *Synthesis* **1992**, 895 – 910.

[63] G. Kirchner, M. P. Scollar, A. M. Klibanov, *J. Am. Chem. Soc.* **1985**, *107*, 7072 – 7076.

[64] A. Ghogare, G. S. Kumar, *J. Chem. Soc. Chem. Commun.* **1989**, 1533 – 1535.

[65] D. Bianchi, P. Cesti, E. Battistel, *J. Org. Chem.* **1988**, *53*, 5531 – 5534.

[66] a) M. Degueil-Castaing, B. De Jeso, S. Drouillard, B. Maillard, *Tetrahedron Lett.* **1987**, *28*, 953 – 954; b) Y F. Wang, J. J. Lalonde, M. Momongan, D. E. Bergbreiter, C. H. Wong, *J. Am. Chem. Soc.* **1988**, *110*, 7200 – 7205.

[67] G. Carrea, B. Danieli, G. Palmisano, S. Riva, M. Santagostino, *Tetrahedron: Asymmetry* **1992**, *3*, 775 – 784.

[68] R. J. Kazlauskas, A. N. E. Weissfloch, A. T. Rappaport, L. A. Cuccia, *J. Org. Chem.* **1991**, *56*, 2656 – 2665.

[69] S. M. Roberts, *Philos. Trans. R. Soc. London* **1989**, *324*, 557 – 587.

[70] "Biocatalysis in Agricultural Biotechnology": T. Umemora, H. Hirohara, *ACS Symp. Ser.* **1989**, *389*, 371 – 384.

[71] L. E. Janes, R. J. Kazlauskas, *Tetrahedron: Asymmetry* **1997**, *8*, 3719 – 3733.

[72] R. J. Kazlauskas, A. N. E. Weissfloch, *J. Mol. Catal. B* **1997**, *3*, 65 – 72.

[73] A. N. E. Weissfloch, R. J. Kazlauskas, *J. Org. Chem.* **1995**, *60*, 6959 – 6969.

[74] K. Lemke, M. Lemke, F. Theil, *J. Org. Chem.* **1997**, *62*, 6268 – 6273.

[75] M. Cygler, P. Grochulski, R. J. Kazlauskas, J. D. Schrag, F. Bouthillier, B. Rubin, A. N. Serreqi, A. K. Gupta, *J. Am. Chem. Soc.* **1994**, *116*, 3180 – 3186.

[76] J. P. Branier, L. Blanco, G. Rousseau, E. Guibe′-Jampel, I. Fresse, *J. Org. Chem.* **1993**, *58*, 1570 – 1574.

[77] a) I. Brackenridge, R. McCague, S. M. Roberts, N. J. Turner, *J. Chem. Soc. Perkin Trans. 1* **1993**, 1093 – 1094; b) M. C. R. Franssen, E. L. V. Goetheer, H. Jongejan, A. de Groot, *Tetrahedron Lett.* **1998**, *39*, 8345 – 8348.

[78] H. Kitaguchi, P. A. Fitzpatrick, J. E. Huber, A. M. Klibanov, *J. Am. Chem. Soc.* **1989**, *111*, 3094 – 3095.

[79] a) V. Gotor, E. Menendez, Z. Mouloungui, A. Gaset, *J. Chem. Soc. Perkin Trans. 1* **1993**, 2453 – 2456; b) M. T. Reetz, C. Dreisbach, *Chimia* **1994**, *48*, 570; c) L. E. Iglesias, V. M. Sanchez, F. Rebolledo, V. Gotor, *Tetrahedron*: *Asymmetry* **1997**, *8*, 2675 – 2677.

[80] L. T. Kanerva, P. Csomos, O. Sundholm, G. Bernath, F. Fulop, *Tetrahedron*: *Asymmetry* **1996**, *7*, 1705 – 1716.

[81] K. E. Jaeger, K. Liebeton, A. Zonta, K. Schimossek, M. T. Reetz, *Appl. Microbiol. Biotechnol.* **1996**, *46*, 99 – 105.

[82] M. Soledad de Castro, J. V. Sinisterra Cago, *Tetrahedron* **1998**, *54*, 2877 – 2892.

[83] a) A. L. Gutman, E. Meyer, E. Kalerin, F. Polyak, J. Sterling, *Biotechnol. Bioeng.* **1992**, *40*, 760 – 767; b) A. L. Gutman, E. Shkolnik, E. Meyer, F. Polyak, D. Brenner, A. Boltanski, *Ann. NY Acad. Sci.* **1996**, *799*, 620 – 632.

[84] a) S. Puertas, R. Brieva, F. Rebolledo, V. Gotor, *Tetrahedron* **1993**, *49*, 4007 – 4014; b) M. Pozo, V. Gotor, *Tetrahedron* **1993**, *49*, 4321 – 4326; c) B. Orsat, P. B. Alper, W. Moree, C. P. Mak, C. H. Wong, *J. Am. Chem. Soc.* **1996**, *118*, 712 – 713; d) S. Takayama, W. J. Moree, C. H. Wong, *Tetrahedron Lett.* **1996**, *37*, 6287 – 6290.

[85] D. Bianchi, P. Cesti, *J. Org. Chem.* **1990**, *55*, 5657 – 5659.

[86] N. Ohrner, C. Orrenius, A. Mattson, T. Norin, K. Hult, *Enzyme Microbiol. Technol.* **1996**, *19*, 328 – 331.

[87] G. Kirchner, M. P. Scollar, A. M. Klibanov, *J. Am. Chem. Soc.* **1985**, *107*, 7072 – 7076.

[88] A. M. Klibanov, G. Kirchner, US-A 4601987, **1986**.

[89] B. Cambou, A. M. Klibanov, *Biotechnol. Bioeng.* **1994**, *26*, 1149 – 1154.

[90] A. Gentile, C. Giordano, C. Fuganti, L. Ghirotto, S. Servi, *J. Org. Chem.* **1992**, *57*, 6637 – 6640.

[91] L. T. Kanerva, O. Sundholm, *J. Chem. Soc. Perkin Trans. 1* **1993**, 1385 – 1389.

[92] D. M. Gou, Y. C. Liu, C. S. Chen, *J. Org. Chem.* **1993**, *58*, 1287 – 1289.

[93] J. S. Wallace, K. B. Rede, M. E. Williams, C. J. Morrow, *J. Org. Chem.* **1990**, *55*, 3544 – 3546.

[94] G. Rossey, I. Chekroun, A. Ugolini, A. Wick, B. Gerin, A. Bourbon, J. B. Graux, FR-B 89-246890111, **1989** [*Chem. Abstr.* **1991**, *114*, 81901s].

[95] M. C. de Zoete, A. C. Kock Van Dalen, F. Van Rantwijk, R. A. Sheldon, *J. Chem. Soc. Chem. Commun.* **1993**, 1831 – 1832.

[96] a) N. Baba, M. Mimura, J. Hiratake, K. Uchida, J. Oda, *Agric. Biol. Chem.* **1988**, *52*, 2685 – 2687; b) N. Baba, K. Takeno, J. Iwasa, J. Oda, *Agric. Biol. Chem.* **1990**, *54*, 3349 – 3350.

[97] a) F. Bjorkling, S. E. Godtfredsen, O. Kirk, *J. Chem. Soc. Chem. Commun.* **1990**, 1301 – 1303; b) F. Bjorkling, H. Frykman, S. E. Godtfredsen, O. Kirk, *Tetrahedron* **1992**, *48*, 4587 – 4592.

[98] E. Mizuguchi, T. Suzuki, K. Achiwa, *Synlett* **1994**, 929 – 930.

[99] N. W. Fadnavis, K. Koteshwar, *Tetrahedron: Asymmetry* **1997**, *8*, 337 – 339.

[100] a) H. Stecher, K. Faber, *Synthesis* **1997**, 1 – 16; b) E. J. Ebbers, G. J. A. Ariaans, J. P. M. Houbiers, A. Bruggink, B. Zwanenburg, *Tetrahedron* **1997**, *53*, 9417 – 9476; c) R. S. Ward, *Tetrahedron: Asymmetry* **1995**, *6*, 1475 – 1490.

[101] S. Takano, M. Suzuki, K. Ogasawara, *Tetrahedron: Asymmetry* **1993**, *4*, 1043 – 1046.

[102] E. L. Eliel in *Stereochemistry of Organic Compounds* (Eds.: E. L. Eliel, S. H. Wilen, L. N. Mander), Wiley, New York, **1994**, pp. 315.

[103] M. Kitamura, M. Tokunaga, R. Noyori, *J. Am. Chem. Soc.* **1993**, *115*, 144 – 152.

[104] M. Inagaki, J. Hiratake, T. Nishioka, J. Oda, *J. Org. Chem.* **1992**, *57*, 5643 – 5649.

[105] S. Brand, M. F. Jones, C. M. Rayner, *Tetrahedron Lett.* **1995**, *36*, 8493 – 8496.

[106] N. J. Turner, J. R. Winterman, R. McCague, J. S. Parratt, S. J. C. Taylor, *Tetrahedron Lett.* **1995**, *36*, 1113 – 1116.

[107] a) H. van der Deen, A. D. Cuiper, R. P. Hof, A. van Oeveren, B. L. Feringa, R. M. Kellogg, *J. Am. Chem. Soc.* **1996**, *118*, 3801 – 3803; b) J. Willem, J. F. Thuring, A. J. H. Klunder, G. H. L. Nefkens, M. A. Wegman, B. Zwanenburg, *Tetrahedron Lett.* **1996**, *37*, 4759 – 4760.

[108] P. J. Um, D. G. Drueckhammer, *J. Am. Chem. Soc.* **1998**, *120*, 5605 – 5610.

[109] R. Stürmer, *Angew. Chem.* **1997**, *109*, 1221 – 1222; *Angew. Chem. Int. Ed. Engl.* **1997**, *36*, 1173 – 1174.

[110] P. M. Dinh, J. A. Howarth, A. R. Hudnott, J. M. J. Williams, W. Harris, *Tetrahedron Lett.* **1996**, *37*, 7623 – 7626.

[111] A. L. E. Larsson, B. Anders Persson, J. E. Backvall, *Angew. Chem.* **1997**, *109*, 1256 – 1258; *Angew. Chem. Int. Ed. Engl.* **1997**, *36*, 1211 – 1212.

[112] M. T. Reetz, K. Schimossek, *Chimia* **1996**, *50*, 668 – 669.

[113] a) C. R. Johnson, *Acc. Chem. Res.* **1998**, *31*, 333 – 341; b) E. Schoffers, A. Golebiowski, C. R. Johnson, *Tetrahedron* **1996**, *52*, 3769 – 3826; c) B. Danieli, G. Lesma, D. Passarella, S. Riva in *Advances in the Use*

of Synthons in Organic Chemistry (Eds.: A. Dondoni, A. Padwa), JAI, London, **1993**, pp. 143 – 219.
[114] L. Banfi, G. Guanti, *Synthesis* **1993**, 1029 – 1056.
[115] B. Morgan, G. Bydlinsky, D. R. Dodds, *Tetrahedron: Asymmetry* **1995**, *6*, 1765 – 1772.
[116] a) A. L. Gutman, M. Shapira, A. Boltanski, *J. Org. Chem.* **1992**, *57*, 1063 – 1065; b) M. Shapira, A. L. Gutman, *Tetrahedron: Asymmetry* **1994**, *5*, 1689 – 1700.
[117] S. Puertas, R. Rebolledo, V. Gotor, *J. Org. Chem.* **1996**, *61*, 6024 – 6027.
[118] A. J. Carnell, J. Barkley, A. Singh, *Tetrahedron Lett.* **1997**, *38*, 7781 – 7784.
[119] J. Hirose, K. Kariya, Y. Nakanishi, K. Achiva, *Tetrahedron Lett.* **1995**, *36*, 1063 – 1066.
[120] S. Nagumo, T. Arai, H. Akita, *Tetrahedron Lett.* **1997**, *38*, 5165 – 5168.
[121] C. Bonini, R. Racioppi, L. Viggiani, *Tetrahedron: Asymmetry* **1997**, *8*, 353 – 354.
[122] T. Fukui, T. Kawamoto, A. Tanaka, *Tetrahedron: Asymmetry* **1994**, *5*, 73 – 82.
[123] a) J. M. Chong, E. K. Mar, *Tetrahedron Lett.* **1991**, *32*, 5683 – 5686; b) T. Itoh, T. Ohta, *Tetrahedron Lett.* **1990**, *31*, 6407 – 6408.
[124] T. Itoh, T. Ohta, M. Sano, *Tetrahedron Lett.* **1990**, *31*, 6387 – 6390.
[125] T. Itoh, T. Ohta, *Chem. Lett.* **1991**, 217 – 218.
[126] M. A. Sparks, J. S. Panek, *Tetrahedron Lett.* **1991**, *32*, 4085 – 4088.
[127] a) K. Nakamura, K. Ishihara, A. Ohno, M. Vemura, H. Nishimura, Y. Hayashi, *Tetrahedron Lett.* **1990**, *31*, 3603 – 3604; b) Y. Yamasaki, K. Hosono, *Tetrahedron Lett.* **1990**, *31*, 3895 – 3896.
[128] C. Baldoli, S. Maiorana, G. Carrea, S. Riva, *Tetrahedron: Asymmetry* **1993**, *4*, 767 – 772.
[129] a) G. Nicolosi, A. Patti, M. Piattelli, *J. Org. Chem.* **1994**, *59*, 251 – 254; b) D. Lambusta, G. Nicolosi, A. Patti, M. Piattelli, *Tetrahedron: Asymmetry* **1993**, *4*, 919 – 924; c) T. Izumi, F. Tamura, K. Sazaki, *Bull. Chem. Soc. Jpn*. **1992**, *65*, 2784 – 2788; d) M. J. Kim, H. Cho, K. Chol, *J. Chem. Soc. Perkin Trans. 1* **1991**, 2270 – 2272; e) N. W. Boaz, *Tetrahedron Lett.* **1989**, *30*, 2061 – 2064.
[130] G. Gill, E. Ferre, J. LePetit, C. Triantaphylides, *Tetrahedron Lett.* **1987**, *28*, 1647 – 1648.
[131] J. C. Fiaud, R. Gil, J. Y. Legros, W. A. Konig, *Tetrahedron Lett.* **1992**, *33*, 6967 – 6970.
[132] K. Naemura, A. Furutani, *J. Chem. Soc. Perkin Trans. 1* **1991**, 1879 – 1884.
[133] M. Inagaki, J. Hiratake, T. Nishida, J. Oda, *Agric. Biol. Chem.* **1989**, *53*, 1879 – 1884.
[134] a) K. Tanaka, Y. Shogase, H. Osuga, H. Suzuki, K. Nakamura, *Tetrahedron Lett.* **1995**, *36*, 1675 – 1678; b) K. Tanaka, H. Osuga, H. Suzuki, Y. Shogase, Y. Kitahara, *J. Chem. Soc. Perkin Trans. 1* **1998**, 935 – 940.
[135] J. K. Browne, M. A. McKervey, M. Pitarch, J. A. Russell, J. S. Millership, *Tetrahedron Lett.* **1998**, *39*, 1787 – 1790.
[136] P. Muller, *Pure Appl. Chem.* **1994**, *66*, 1077 – 1184.
[137] P. Cesti, A. Zaks, A. M. Klibanov, *Appl. Biochem. Biotechnol.* **1985**, *11*, 401 – 407.
[138] M. Therisod, A. M. Klibanov, *J. Am. Chem. Soc.* **1986**, *108*, 5638 – 5640.
[139] M. Therisod, A. M. Klibanov, *J. Am. Chem. Soc.* **1986**, *109*, 3977 – 3981.
[140] S. Riva, J. Chopineau, A. P. G. Kieboom, A. M. Klibanov, *J. Am. Chem. Soc.* **1988**, *110*, 584 – 589.
[141] S. Riva in Ref. [7j], pp. 140 – 169.
[142] S. Cai, S. Hakomori, T. Toyokuni, *J. Org. Chem.* **1992**, *57*, 3431 – 3437.
[143] L. Panza, M. Luisetti, E. Crociati, S. Riva, *J. Carbohydr. Chem.* **1993**, *12*, 125 – 130.
[144] M. J. Chin, G. Iacazio, D. G. Spackman, N. J. Turner, S. M. Roberts, *J. Chem. Soc. Perkin Trans. 1* **1992**, 661 – 662.
[145] S. Riva, B. Danieli, M. Luisetti, *J. Nat. Prod.* **1996**, *59*, 618 – 621.
[146] B. Danieli, M. Luisetti, S. Riva, A. Bertinotti, E. Ragg, L. Scaglioni, E. Bombardelli, *J. Org. Chem.* **1995**, *60*, 3637 – 3642.
[147] J. O. Rich, B. A. Bedell, J. S. Dordick, *Biotechnol. Bioeng*. **1995**, *45*, 426 – 434.
[148] X. Chen, A. Johnson, J. S. Dordick, D. G. Rethwisch, *Macromol. Chem. Phys.* **1994**, *195*, 3567 – 3578.
[149] K. Adelhorst, F. Bjorkling, S. E. Godtfredsen, O. Kirk, *Synthesis* **1990**, 112 – 115.
[150] S. Riva, A. M. Klibanov, *J. Am. Chem. Soc.* **1988**, *110*, 3291 – 3295.
[151] F. Nicotra, S. Riva, F. Secundo, L. Zucchelli, *Tetrahedron Lett.* **1989**, *30*, 1703 – 1704.
[152] S. Riva, R. Bovara, G. Ottolina, G. Carrea, *J. Org. Chem.* **1989**, *54*, 3161 – 3164.
[153] A. Bertinotti, G. Carrea, G. Ottolina, S. Riva, *Tetrahedron* **1994**, *50*, 13165 – 13172.
[154] B. Danieli, G. Lesma, M. Luisetti, S. Riva, *Tetrahedron* **1997**, *53*, 5855 – 5862.
[155] A. L. Margolin, D. L. Delinck, M. R. Whalon, *J. Am. Chem. Soc.* **1990**, *112*, 2849 – 2854.
[156] P. C. Michels, Y. L. Khmelnitsky, J. S. Dordick, D. S. Clark, *Trends Biotechnol.* **1998**, *16*, 210 – 215.
[157] V. M. Mozhaev, C. L. Budde, J. O. Rich, A. Y. Usyatinsky, P. C. Michels, Y. L. Khmelnitsky, J. S. Dordick, D. S. Clark, *Tetrahedron* **1998**, *54*, 3971 – 3982.
[158] Y. L. Khmelnitsky, C. L. Budde, J. M. Arnold, A. Y. Usyatinsky, J. S. Dordick, D. S. Clark, *J. Am. Chem. Soc.* **1997**, *119*, 11554 – 11555.
[159] M. Adamezyk, J. C. Gebler, J. Grote, *Bioorg. Med. Chem. Lett.* **1997**, *7*, 1027 – 1030.
[160] N. Chinsky, A. L. Margolin, A. M. Klibanov, *J. Am. Chem. Soc.* **1989**, *111*, 386 – 388.
[161] S. Tawaki, A. M. Klibanov, *Biocatalysis* **1993**, *8*, 3 – 19.
[162] A. Baldessari, L. E. Iglesias, E. G. Gros, *J. Chem. Res. Synop.* **1992**, 204 – 205.
[163] D. L. Delink, A. L. Margolin, *Tetrahedron* **1990**, *31*, 3093 – 3096.
[164] A. Zaks, D. R. Dodds, *Drug Discovery Today* **1997**, *2*, 513 – 531.
[165] B. M. Morgan, D. R. Dodds, A. Zaks, D. R. Andrews, R. Klesse, *J. Org. Chem.* **1997**, *62*, 7736 – 7743.
[166] R. N. Patel, C. M. McNamee, L. J. Szarka, *Appl. Microbiol. Biotechnol.* **1992**, *38*, 56 – 60.
[167] R. L. Hanson, A. Banerjee, F. T. Comezoglu, K. D. Mirfakhrae, R. N. Patel, L. J. Szarka, *Tetrahedron: Asymmetry* **1994**, *5*, 1925 – 1934.
[168] R. N. Patel, A. Banerjee, L. J. Szarka, *Tetrahedron: Asymmetry* **1997**, *8*, 1055 – 1059.
[169] R. N. Patel, A. Banerjee, L. J. Szarka, *Tetrahedron: Asymmetry* **1997**, *8*, 1767 – 1771.
[170] K. E. Holt, U. Berens, R. McCague, S. J. C. Taylor, *Abstr. Pap. Biotrans'97 Conference* (La Grande Motte, **1997**), p. 65.
[171] a) F. Balkenhohl, K. Ditrich, B. Hauer, W. Ladner, *J. Prakt. Chem.* **1997**, *339*, 381 – 384; b) F. Balkenhohl, B. Hauer, W. Ladner, U. Pressler, C. Nubling, US-A 5728876, **1998**.
[172] M. H. Coleman, A. R. MacRae (Unilever NV), DE-B 2705608, **1977** [*Chem. Abstr.* **1977**, *87*, 166366].
[173] T. Matsuo, N. Sawamura, Y. Hashimoto, W. Hashida (Fuji Oil Co.), EP-B 0035883A2, **1982** [*Chem. Abstr.* **1982**, *96*, 4958y].
[174] V. Partali, L. Kvittingen, H. R. Sliwka, T. Anthonson, *Angew. Chem.* **1996**, *108*, 342 – 344; *Angew. Chem. Int. Ed. Engl.* **1996**, *35*, 329 – 330.
[175] J. Fabre, D. Betbeder, F. Paul, P. Monsan, J. Perie, *Carbohydr. Res.* **1993**, *243*, 407 – 411.
[176] G. Fregapane, D. B. Sarney, E. N. Vulfson, *Enzyme Microbiol. Technol.* **1991**, *13*, 796 – 800.
[177] L. Cao, A. Fischer, U. T. Bornscheuer, R. D. Schmid, *Biocatal. Biotrans.* **1997**, *14*, 269 – 283.
[178] J. S. Dordick, R. J. Linhardt, D. G. Rethwisch, *CHEMTECH* **1994**, *24* (1), 33 – 39.
[179] A. L. Margolin, J. Y. Crenne, A. M. Klibanov, *Tetrahedron Lett.* **1987**, *28*, 1607 – 1610.
[180] D. Knani, A. L. Gutmann, D. H. J. Kohn, *Polym. Sci. Part A* **1993**, *31*, 1221 – 1232.
[181] a) C. Berkane, G. Mezoul, T. Lalot, M. Bigodiot, E. Marechal, *Macromolecules* **1997**, *30*, 7729 – 7734; b) A. K. Chaudhary, E. J. Beckman, A. J. Russell, *J. Am. Chem. Soc.* **1995**, *117*, 3728 – 3733; c) D. R. Patil, J. S. Dordick, D. G. Rethwich, *Macromolecules* **1991**, *24*, 3462 – 3463; d) J. S. Wallace, C. J. Morrow, *J. Polym. Sci. Part A* **1989**, *27*, 3271 – 3284; e) J. S. Wallace, C. J. Morrow, *J. Polym. Sci. Part A* **1989**, *27*, 2553 – 2567.
[182] a) K. S. Bisht, F. Deng, R. A. Gross, D. L. Kaplan, G. J. Swift, *J. Am. Chem. Soc.* **1998**, *120*, 1363 – 1367; b) A. Cordova, T. Iversen, K. Hult, *Macromolecules* **1998**, *31*, 1040 – 1045; c) K. S. Bisht, Y. T.

Svirkin, L. A. Henderson, R. A. Gross, D. L. Kaplan, G. Swift, *Macromolecules* **1997**, *30*, 7735 – 7742; d) S. Kobayashi, H. Kikuchi, H. Uyama, *Macromol. Rapid Commun.* **1997**, *18*, 575 – 579; e) K. S. Matsumura, K. Mabushi, K. Toshima, *Macromol. Rapid Commun.* **1997**, *18*, 477 – 482; f) A. R. Nobes, R. J. Kazlauskas, R. H. Marchessault, *Macromolecules* **1996**, *29*, 4829 – 4833.
[183] H. Kitaguchi in Ref. [7j], pp. 224 – 243.
[184] T. Sakurai, A. L. Margolin, A. J. Russell, A. M. Klibanov, *J. Am. Chem. Soc.* **1988**, *110*, 7236 – 7237.
[185] A. L. Margolin, D. F. Tai, A. M. Klibanov, *J. Am. Chem. Soc.* **1987**, *109*, 7885 – 7887.
[186] H. Kitaguchi, D. F. Tai, A. M. Klibanov, *Tetrahedron Lett.* **1988**, *29*, 5487 – 5488.
[187] a) A. L. Margolin, A. M. Klibanov, *J. Am. Chem. Soc.* **1987**, *109*, 3802 – 3804; b) L. Gardossi, D. Bianchi, A. M. Klibanov, *J. Am. Chem. Soc.* **1991**, *113*, 6328 – 6329.
[188] R. A. Sheldon in Ref. [7j], pp. 280 – 284.
[189] F. M. Fonteyn, C. Blecker, G. Lognoy, M. Marlier, M. Severin, *Biotechnol. Lett.* **1994**, *16*, 693 – 696.
[190] F. Effenberger, *Angew. Chem.* **1994**, *104*, 1609 – 1619; *Angew. Chem. Int. Ed. Engl.* **1994**, *33*, 1555 – 1564.
[191] A. Hickel, M. Hasslacher, H. Griengl, *Physiol. Plant.* **1996**, *98*, 891 – 898.
[192] H. Griengl, A. Hickel, D. V. Johnson, C. Kratky, M. Schmidt, H. Schwab, *Chem. Commun.* **1997**, 1933 – 1940.
[193] a) M. Hasslacher, M. Schall, M. Hayn, H. Griengl, S. D. Kohlwein, H. Schwab, *J. Biol. Chem.* **1996**, *271*, 5884 – 5891; b) S. Forster, J. Roos, F. Effenberger, H. Wajant, A. Sprauer, *Angew. Chem.* **1996**, *108*, 493 – 494; *Angew. Chem. Int. Ed. Engl.* **1996**, *35*, 437 – 439.
[194] F. Effenberger, T. Ziegler, S. Forster, *Angew. Chem*. **1987**, *99*, 491 – 492; *Angew. Chem. Int. Ed. Engl.* **1987**, *26*, 458 – 460.
[195] F. Effenberger, J. Eichhorn, J. Roos, *Tetrahedron: Asymmetry* **1995**, *6*, 271 – 282.
[196] F. Effenberger, J. Eichhorn, *Tetrahedron: Asymmetry* **1997**, *8*, 469 – 476.
[197] F. Effenberger, J. Jäger, *J. Org. Chem.* **1997**, *62*, 3867 – 3873.
[198] F. Effenberger, B. Hörsch, S. Förster, T. Ziegler, *Tetrahedron Lett.* **1990**, *31*, 1249 – 1252.
[199] M. Schmidt, S. Hervé, N. Klempier, H. Griengl, *Tetrahedron* **1996**, *52*, 7883 – 7840.
[200] S. H. Hsu, S. S. Wu, Y. F. Wang, C. H. Wong, *Tetrahedron Lett.* **1990**, *31*, 6403 – 6406.
[201] A. Fishman, M. Zviely, *Tetrahedron: Asymmetry* **1998**, *9*, 107 – 118.
[202] J. Roos, U. Stelzer, F. Effenberger, *Tetrahedron: Asymmetry* **1998**, *9*, 1043 – 1049.
[203] R. Z. Kazandjian, A. M. Klibanov, *J. Am. Chem. Soc.* **1985**, *107*, 5448 – 5450.
[204] G. H. Müller, A. Lang, D. R. Seithel, H. Waldmann, *Chem. Eur. J.* **1998**, *4*, 2513 – 2522.
[205] J. S. Dordick, M. A. Marletta, A. M. Klibanov, *Biotechnol. Bioeng.* **1987**, *30*, 31 – 36.
[206] J. Grunwald, B. Wirz, M. Scollar, A. M. Klibanov, *J. Am. Chem. Soc.* **1986**, *108*, 6732 – 6734.

Paradigms Lost and Paradigms Found: Examples of Science Extraordinary and Science Pathological—And How To Tell the Difference**

Nicholas J. Turro*

Scientific Knowledge: Paradigms and Pathologies

One of the most interesting challenges a practicing scientist faces is explaining to a nonscientist how science works and why scientists appear to have a way of knowing that, while not perfect, their discoveries seem to be the best that the human mind has been able to come up with. Scientists, in general, understand the tentative nature of the scientific process and that all conclusions are provisional, at least in principle. Nevertheless, in their everyday activities, scientists often behave as if they are dealing with a set of "truths". This behavior is supported by the manner in which science confidently produces a seemingly unending series of stunning predictions and verifications, which often move rapidly into important technological applications, making the explanatory challenge more difficult. How can one be so sure about what one "knows" and, at the same time, avoid the arrogance of a know-it-all and the pitfalls of intellectual hubris?

In this context, another challenge is to explain how science handles extraordinary claims. How can a scientist tell whether a remarkable idea or experimental observation would lead to the Nobel Prize, which is awarded for science that changes the way that scientists think and know—or would lead to the IgNobel Prize, awarded to pathological science that epitomizes the way the scientific process should *not* work?

Throughout the history of science, the distinction between *revolutionary* science and *pathological* science has not always been so clear. What is the objective scientific process by which one distinguishes genius from nonsense? Both extremes of the scientific spectrum are characterized by a common trait: The ability of the scientist (or a community of scientists) to "think outside the box". But what is this box of which they must be outside? I would identify it as the paradigm, the concept popularized by Thomas Kuhn in *The Nature of Scientific Revolutions*.[1] Science makes quantum jumps when a paradigm shifts but an intricate and complex process with both scientific and sociological components is required to confirm that an extraordinary claim is revolutionary—the content of true paradigm shifts–and separate it from those that are eventually shown to be pathological, destined for the dustbin of scientific history.

For example, during the past century Max Planck published some mathematical computations intended to describe an apparent anomaly in the classical theory of light, which, at the time, was believed to be an unshakable paradigm. The anomaly was termed the "ultraviolet catastrophe", which gives some idea of how severely the anomaly disturbed the scientific community! Planck made the extraordinary suggestion that if light were "quantized" and consisted of bits of energy rather than a continuum of energy, which was the paradigm of the classical theory of light, the anomaly would disappear. At the time (and to some still) this appeared to be a preposterous suggestion, contrary to all known experience and a threat to the reigning paradigm of the classical theory of light. Yet a few years after the paper was published, Einstein connected Planck's suggestion to another anomaly involving the way that light causes electrons to be ejected from a metal (the basis of the photoelectric effect, which operates the "electric eye" of security doors everywhere). The interpretation of the photoelectric effect in quantum terms led to Einstein's Nobel Prize in 1921. For the next several decades the physics community endured a battle royal, with the ideas of quantum mechanics emerging triumphant, if still resistant to explanation in terms of ordinary experience. The emergence of the paradigm of quantum chemistry warns and teaches us that, no matter how bizarre a scientific claim may be or how remote from ordinary experience, it can still be accepted and used by the scientific community and even rapidly applied to technological uses!

But what of the many remarkable claims that have been proposed, debated, and then dismissed by the scientific community as pathological? How was each decision made and how do we know the decision was correct? Are there any rules scientists can follow to minimize the probability of falling into the trap of promoting pathological science?

Mechanisms of Delusion

Troubled science takes many forms, from pseudoscience (irrational or mystical systems of thought dressed up in

[*] N. J. Turro
Department of Chemistry
and Department of Chemical Engineering
Columbia University
3000 Broadway, Mail Code 3119
New York, NY 10027 (USA)
Fax: (+1) 212-932-1289
E-mail: turro@chem.columbia.edu

[**] The author thanks Bill Millard, editor of Columbia University's 21C magazine, for his excellent assistance and collaboration. The support of the NSF (Grant CHE98-12676) is gratefully acknowledged.

 © WILEY-VCH Verlag GmbH, D-69451 Weinheim, 2000 0570-0833/00/3913-2255 $ 17.50+.50/0

ostensibly scientific jargon; often complex but never rigorous) to junk science (methodologically sloppy research usually conducted to advance some extrascientific agenda or to prevail in litigation) to outright fraud. This paper is not concerned with science that results from dishonest practices (which are rarely intellectually interesting) but, instead, with serious investigations leading down pathways that ultimately prove to be erroneous and which may be classified as *pathological science*.[2] As Nobel prize winning chemist Irving Langmuir said in his famous General Electric lecture on the topic, "These are cases where there is no dishonesty involved, but where people are tricked into false results by the lack of understanding about what human beings can do to themselves in the way of being led astray by subjective effects, wishful thinking, or threshold interactions."[3]

The road to greater scientific truth is not just littered with history's errors; it is constructed through a process of constant error correction. If we accept Kuhn's description of scientific progress as a succession of revolutions, or paradigm shifts, resulting from the constant effort to reconcile new results with dominant paradigms, then a scientific field's moments of crisis—when different factions contend over whether an idea or experimental result will turn out to be revolutionary or absurd—tells us a great deal about how knowledge is constructed, tested, defended, and accepted. For this reason, an understanding of pathological science can help a researcher better understand, and perform, reliable science.

Kuhn[1] posits that in the conduct of normal everyday science, researchers sometimes obtain anomalous results; the scrupulous scientist investigates these oddities through experiments intended to disprove the anomalies and reinforce the current reigning paradigm. (We can call this pattern of paradigm-guided scrutiny the First Law of "Parodynamics".) However, if important anomalies persist and resist the best efforts of the community to remove them, a period of intense debate and experimental work results, typically with one community impeaching the correctness of the paradigm and another defending it. A key result may suddenly emerge, supporting the paradigm and revealing the challenging anomaly as pathological; on rare and treasured occasions, a key result convincingly supports a significant revision or "shift" of the paradigm. (Nobel Prizes occasionally follow).

Whatever paradigm may govern a scientific disciple at any given time, it helps to frame and organize a researcher's thinking, acting as a kind of "road map" for inquiries within the specialty and as a safeguard against pathological work. When a science is in a potentially revolutionary phase, a dominant paradigm can be a prison, preventing researchers from following promising new leads, but more often it is a form of conceptual authority, something not to be abandoned without peril. Science often turns pathological when investigators venture outside their familiar paradigm without becoming sufficiently versed in the paradigms of the new field. An informative example[4] is the "cold fusion" controversy of 1989, in which a claim of an extraordinary nuclear process was made, based on some "anomalous" heat measurements made during electrochemical reactions. The investigators, trained as electrochemists, claimed that the nuclear-reaction interpretation was supported by measurements of neutron and gamma-ray emission. However, the latter claims were shown by experts in nuclear physics to be artifacts. The electrochemists could probably have saved themselves quite a bit of opprobrium if they had been better versed in the paradigms of high-energy physicists dealing with the detecting a flux of neutrons or gamma rays in their apparatus.

Since only a few anomalies ever lead to revolutionary change—while most working scientists dream of making exactly that type of discovery of which prestige is made—there is an understandable temptation to interpret unexpected results that can be interpreted as extraordinary as meaningful anomalies. For each community, there is an intuitive evaluation and quantification of an idea's newness, its intellectual potential (in a sense, akin to potential energy in measuring the idea's distance from what an existing paradigm would predict) which might be termed the *surprisal* of the idea or result. A high surprisal implies that the idea or result is well outside of the paradigm. Because high surprisal investigations are both high gain and high risk, the need for the counterpoise of skepticism among investigators studying such topics is acute.

The history of scientific misfires indicates certain patterns, as shown in Figure 1, which I have adapted from a previous publication in this Journal.[5] When a field is in the critical prerevolutionary/prepathological phase, a principle that I will call the Second Law of "Parodynamics" comes into effect: The more drastic the departure from an established paradigm, the greater the chance of either a revolutionary or a pathological outcome—and the more urgent the need for awareness of the mechanisms whereby cognitive errors tend to arise. Figure 1 shows the Second Law of "Parodynamics" for a mature scientific paradigm in action. Everyday, "normal science" follows the uneventful loops in which puzzles endorsed by the paradigm are solved and the paradigm is constantly reinforced.

Figure 1 shows the area of "normal science", consisting of generating puzzles based on the conventional paradigms, solving the puzzles, and thereby reinforcing the paradigms.

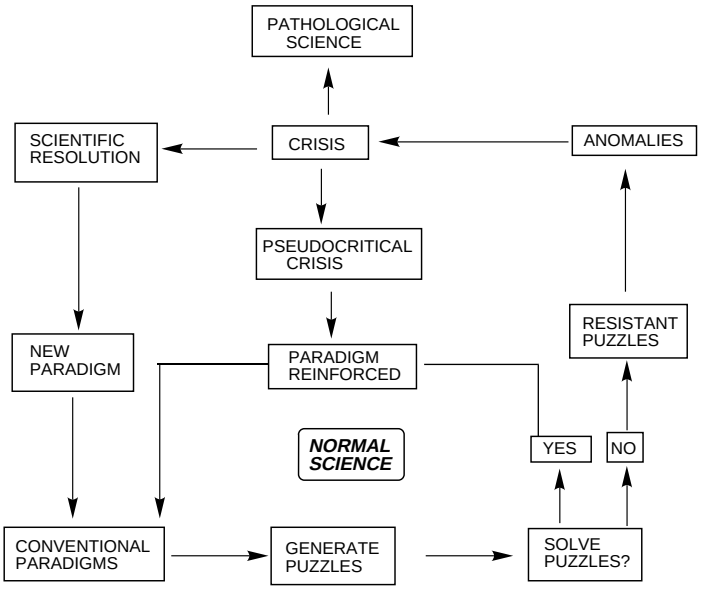


Figure 1. The procedural loops through which science flows.

 © WILEY-VCH Verlag GmbH, D-69451 Weinheim, 2000 0570-0833/00/3913-2256 $ 17.50+.50/0

From time to time, some puzzles become resistant and, if they remain stubbornly resistant even to the best practitioners in the field, may be considered as anomalies by the community. Anomalous results, unexplainable within a field's governing paradigm and important enough to cause true intellectual alarm within the community, can throw the field into crisis—an unpredictable state analogous to a "catastrophe point" in topological mathematics—which might eventuate in reinforcement of the current paradigm, whether the example is of revolutionary science or of pathological science.

Typically, resolution from the crisis point can take one of three forms: 1) The anomaly's revolutionary potential may be revealed as more apparent than real and this "pseudocritical" state resolves to reinforce the original paradigm in the same way as normal science although with more force because of the excursion; 2) The anomaly may foster a true Kuhnian revolution, resulting in a new paradigm; 3) The anomaly may prove pathological, in which case only zealots continue to pursue it, and the conventional paradigm structure is not only untouched but reconfirmed.

From the Possible to the Plausible to the Probable to the Proven

One way confusion can enter a scientist's thinking involves disruption of the natural conceptual progression through four categories of scientific "cognition". For convenience, we can refer to these as the four Ps:

- The *possible* comprises all ideas that do not violate the most basic and global principles of science (for example, the second law of thermodynamics; the conservation of momentum and energy).
- The *plausible* describes ideas that do not violate the possible and which might be tenable if we could envision circumstances under which they could be realized and tested. (In the celebrated case[6] of "polywater" or polymerized H_2O molecules, there was no a priori reason why a chemical reaction yielding such a substance could not occur and move downhill in potential energy as any reaction must; the idea may be considered as implausible but not impossible, since it only requires that a state of polymerized water exists and is more stable than ordinary water under some conditions.)
- The *probable* describes ideas in "normal or everyday science" as Kuhn used the term: The ideas and explorations that apply an established paradigm and which may extend the scope of the paradigm but do not threaten to overturn or shift it. These ideas are so embedded in the community that they are usually not debated but taken as dogma.
- The *proven* applies to unsurprising exercises in puzzle solving, the routine application of testing or "proving" ideas experimentally, working firmly within a stable paradigm.

The borders separating these cognition levels—particularly between the first two—are not as clear in practice as in theory, especially when a result is of interest to two or more distinct specialties possessing different paradigms. A high surprisal hypothesis may appear impossible from one vantage point, while a different field's paradigm makes it clear that the hypothesis is well within the realm of the possible and merely stretches the limits of plausibility or probability. For example, the low temperature "cold fusing" of two deuterium nuclei or the polymerization of water are currently outside of the paradigm of conventional chemistry and might therefore be termed "impossible" if one is constrained to "ordinary" chemical conditions. In fact, it would be more accurate to term them as "implausible" under extraordinary chemical conditions, such as those of high energy physics. Indeed, the cold fusion experiment did not represent an impossibility, since it is known that nuclei can be fused with the release of enormous energy. The cold fusion experiment represented a "catalyzed" fusion that did not require the high energy physics approach. As implausible as it may seem, the history of science has indicated that clever scientists can figure out how to make "implausible" science occur as long as it is "possible".

Only after an idea has run the scientific community's gauntlet—surviving rigorous experimental and interpretive efforts to falsify it—can it be said to move from a question of possibility to a probable or proven status. Pathological science occurs when an investigator cuts this process short, prematurely trading scrutiny for advocacy.

Sometimes There's No "There" There

Langmuir's classic symptoms of pathological science (Table 1) attribute many errors to various forms of subjective judgment. Uncertainty is part of all science and subjective judgments are inescapable in most fields but statistically marginal phenomena on the threshold of human perception, with a low signal-to-noise ratio, are easy to misinterpret. (Langmuir himself detected this phenomenon in the Columbia laboratory of Professors Bergen Davis and Arthur Barnes in 1930; these physicists believed they were detecting a phenomenon called "electron capture" by alpha particles in a magnetic field but Langmuir found that in their six-hour marathon sessions counting scintillations on a screen in a darkened room they also counted visual hallucinations, which are common in such circumstances, and dismissed observations that conflicted with their paradigm.)

Table 1. Langmuir's[3] six recurring patterns in cases of pathological science

- The maximum effect that is observed is produced by a causative agent of barely detectable intensity and the magnitude of the effect is substantially independent of the intensity of the cause
- The effect is of a magnitude that remains close to the limit of detectability or many measurements are necessary because of the very low statistical significance of the results
- There are claims of great accuracy
- Fantastic theories contrary to experience are suggested
- Criticisms are met by ad hoc excuses thought up on the spur of the moment
- The ratio of supporters to critics rises up to somewhere near 50 percent and then falls gradually to oblivion

To these we may add the following:

- The remarkable result is specific for a "special" system
- Some special technique or equipment is involved
- The result requires a stunning departure from the paradigms that fully determine results in all other comparable systems, including those studied by the authors

 © WILEY-VCH Verlag GmbH, D-69451 Weinheim, 2000 0570-0833/00/3913-2257 $ 17.50+.50/0

Scientists commonly select and discard some of their scattered data points because of suspected confounding conditions or experimental error; in some contexts this may border on cheating but more often it is simply a reasonable and acceptable selection process. In all fields, the requirement of reproducibility within statistical limits guards against this kind of observer error.

The red flag of pathology should thus appear any time a researcher offers resistance to the challenge of reproducibility, claiming that only a certain special system (or even certain investigators) can generate the anomalous result. Such an example may be found in the notorious case[7] of "infinite dilution" studies, which held that antibody solutions remained biologically effective even when diluted so thoroughly that no molecules of the solute were detectable in the fluid, implying that water somehow retains a memory of molecules that have been dissolved in it. If confirmed, this hypothesis—highly implausible but not impossible according to chemical paradigms—would have overthrown some of chemistry's fundamental beliefs about the properties of water; independent investigators found that the investigators reporting infinite dilution did not apply proper controls for observer bias or sample contamination, excluded conflicting measurements, "massaged" the statistics, and neglected to investigate reasons for failures of reproducibility. Rather than acknowledge that his group had been pursuing a pathological inquiry, the leader of the laboratory has clung to his theory, and acquired not just one, but two, IgNobel prizes for improbable research. The course of the infinite dilution story matches Langmuir's symptoms smoothly.[2, 3]

Interpreting Something into Existence

Not all scientific pathologies, however, are covered by Langmuir's list. Another instance of pathological science, the debate over polywater[6] in the 1960s, illustrates a common type of shortcut: a failure to consider standard alternate hypotheses with a paradigm to explain an apparently extraordinary result. Deryagin and other researchers were able to produce a dense liquid, through condensation of water in tiny capillaries, that was claimed to be a new, polymerized form of water, polywater. It should be noted the observations made by Deryagin could be made reproducibly and with exhaustive attention to controlling physicochemical variables and answering colleagues' critiques. Nevertheless, the dense liquid ultimately turned out to be an artifact caused by impurities in ordinary water. Deryagin and a worldwide network of adherents to his theory pursued the polywater concept to extraordinary lengths, in part because of plausible theories about the behavior of water molecules in ultrafine capillaries (and probably in part because of heavy funding from the U.S. Navy,[8] which took an interest in possible military applications of polywater!). However, when purification tests using more sophisticated equipment convinced Deryagin to reconsider an obvious hypothesis he had previously rejected—that the dense liquid was not polywater but simply water that was contaminated somehow—he readily and honestly conceded that his original experiments were flawed, invalidating any interpretations based on these results.

The scientific process healed itself in this case, though not as quickly as it would have if Deryagin and others had kept Occam's razor in mind and given more weight to the simplest available explanation, contamination. A favored hypothesis can develop its own momentum, especially when a researcher invests his or her prestige or professional self-identification in one idea to the exclusion of competing (and often more parsimonious) explanations for the results. Having formed a pet conclusion, the scientist often defends it using its own terms, models, and assumptions. Assuming one's conclusion, rather than challenging the hypothesis before accepting a conclusion, the scientist introduces logical circularity into the interpretation of results. Such pathologies, although not in Langmuir's list, certainly are of the same ilk, as they refer to "what human beings can do to themselves in the way of being led astray by…wishful thinking."[3]

A sensational result can also be inextricably confused with a sensational interpretation. Pathological science often involves a relatively sensational interpretation of an unexceptional observation; the cold fusion episode offers an instructive example. The actual experiment involved an anomalous temperature rise during electrolysis. The translation of this observation led to the conclusion that the "only" source was a nuclear process. The observation of an atomic explosion dwarfs any interpretation of the causal relations and scientific principles leading to it and, on some level, the cold fusion investigators may have been comparing the energy-generating potential of cold fusion to that of the H-bomb. Lacking a spectacular observation, they generated all the media "bang" they needed through their interpretation.

It is interesting that the pathological stories of cold fusion, polywater, and infinite dilution, all involve properties of water and provide shining (or perhaps glaring) examples of how implausible ideas can run amok. Perhaps it is because water is essential to life, has numerous properties that are indeed anomalous (or at least ill understood), and is rich in metaphoric connotations, that it seems to bring out the nonskeptical enthusiast in some researchers.

Surrounding all the common shortcuts around established scientific methods are the human flaws that imperil any kind of enterprise. Extrascientific considerations such as media attention, professional standing, promises of monetary gain, ideological predilections, hubris Nobelicus, and pressures from interested parties outside the scientific community can all contribute to and encourage self delusion. The exigencies of funding may tempt even the most scrupulous basic researcher to hype or overstate practical benefits when describing new work to potential supporters. Today's academic environment—which can appear more like a media fishbowl than an ivory tower—also presents the scientist with ample channels to speak to the general public with a considerable risk of misrepresenting the content, purpose, and potential of a scientific discovery, either in an effort to simplify professional jargon (the ever present problem of "dumbing it down") or in the highly contagious enthusiasm over an untested idea or potentially extraordinary but preliminary observation. These are not paradigm questions, of course, just questions of objectivity and professionalism.

 © WILEY-VCH Verlag GmbH, D-69451 Weinheim, 2000 0570-0833/00/3913-2258 $ 17.50+.50/0

Advice for the Working Scientific Revolutionist

Clearly, scientific progress would be impossible if researchers always played it safe within a dominant paradigm, discarding disturbing results, or shying away from daring hypotheses. Some of today's most robust discoveries and most promising research subjects—manned space flight, wave–particle duality, C_{60} (buckminsterfullerene, buckyball) molecules, high temperature superconductivity, and so forth—once struck mainstream scientific opinion as sheer fantasy. Perhaps there are some practical steps that a working researcher can take to lower the chances that today's "eureka!" will be tomorrow's IgNobel:

- Always generate and test several plausible hypotheses to explain experimental results.[9]
- Let the best available paradigm be your guide until you are certain that your results require revision of the paradigm.
- Be conservative about the concepts of statistical significance and margin of error, especially when analyzing phenomena on the threshold between signal and noise and particularly when the results appear to be extraordinary.
- Reproduce, reproduce, reproduce.
- Capture the phenomena by two or more truly independent methods. If the results are consistent by two or more independent methods, you have paid due diligence and earned the right to claim that your observation is real.
- Discuss surprising findings openly with peers (through both formal and informal channels, inside and outside one's own specialty) and make constructive use of the critiques that arise.
- When discussing research with nonscientists—especially those holding microphones, cameras, notebooks, or checkbooks—avoid the temptations to overinterpret results, oversimplify your explanations, or promise direct practical applications.
- If further studies convincingly falsify your hypothesis, and you are convinced also, acknowledge it. Blind leads are nothing to be ashamed of; they are inseparable from the progress of science. After any number of pathological investigations, there is eventually one like quantum mechanics, which necessitated a few adjustments to the law of conservation of mass but ultimately withstood criticism, explained results that Newtonian theory couldn't explain, and revolutionized physics. The same communal corrective processes that falsified one theory verified the other; that is how science operates and why it almost always works.
- Do the unthinkable! Try your very best to find faults in your experiment and to falsify your interpretation in a serious fashion. We should recognize[9] that once a scientist devises an original and satisfactory explanation for an apparently extraordinary phenomenon, from "that moment, affection for one's intellectual child springs into existence, and as the explanation grows into a definite theory one's parental affections cluster about the offspring and it grows more and more dear to the individual…[t]here springs up also unwittingly a pressing of the theory to make it fit the facts and a pressing of the facts to make them fit the theory." The more extraordinary the result, the more the principle investigator should try to destroy their claim by running critical experiments. One must be willing to kill one's own intellectual offspring! After all, if one's "apparently" extraordinary science is correct, one will not be able to destroy it. The best way to separate revolutionary science from pathological science is to be brutal and let the battlefield of ideas and experiment decide the victor. Even if you do turn out to be wrong, you will have been true to your science and will be admired by the community for your intellectual courage and dedication to the scientific ethos.

Conclusions

Kuhn's paradigms[1] and Langmuir's symptoms of pathological science[2, 3], provide the scientist with valuable intellectual tools to avoid pitfalls in the scientific process. The paradigm is conservative and *discourages* revolutionary science. Effectively, the paradigm of a discipline is the sociological, scientific, and intellectual structure that serves as a barrier to caution the community about accepting revolutionary claims. Pathological science, on the other hand, is quick to accept the extraordinary interpretation and rationalize the conservative interpretation that falls within the reigning paradigms. Every scientist has probably felt the tension between paradigmatic and pathological science, between the ordinary, normal result and the extraordinary, amazing result. The author hopes that this essay may be useful as a guide for chemists to recognize and differentiate science extraordinary from science pathological.

[1] T. S. Kuhn, *The Structure of Scientific Revolutions*, 2nd ed., University of Chicago, Chicago, **1970**.

[2] Case studies in pathological science: D. L. Rousseau, *Am. Sci.* **1992**, *80*, 54–63.

[3] Pathological science: I. Langmuir, *Phys. Today* **1989**, *42*, 36–48.

[4] a) F. E. Close, *Too Hot to Handle. The Story of the Race for Cold Fusion*, W. H. Allen, London, **1990**; b) E. F. Mallove, *Fire from Ice: Searching for the Truth Behind the Cold Fusion Furor*, Wiley, New York, **1989**.

[5] "Geometric and topological thinking in organic chemistry": N. J. Turro, *Angew. Chem.* **1986**, *98*, 872–892; *Angew. Chem. Int. Ed. Engl.* **1986**, *25*, 882–901.

[6] Polywater: F. Franks, *MIT Press Energy Lab. Ser.* **1981**.

[7] "High-dilution experiments a delusion": J. Maddox, J. Randi, W. W. Stewart, *Nature* **1988**, *334*, 287–290; Dr. Jacques Benveniste replies: J. Benveniste, *Nature* **1988**, *334*, 291.

[8] Dr. Brian Pethica, currently adjunct senior research scientist at the Henry Krumb School of Mines (Columbia University, NY), was one of the principal Western investigators of polywater while heading the Unilever Research Laboratory near Liverpool (UK) and predicted at the time that chemists "would see polywater papers until the Navy's $4 million runs out."

[9] J. R. Platt, *Science* **1964**, *146*, 347–352.

 © WILEY-VCH Verlag GmbH, D-69451 Weinheim, 2000 0570-0833/00/3913-2259 $ 17.50+.50/0

β-Catenin, Cyclins, and More: New Insights into the Pathogenesis, Treatment, and Prevention of Colon Cancer

Athanassios Giannis*

For quite a long time it has been believed that the protein β-catenin plays a critical role during pathogenesis of colon cancer.[1] This suspicion was strengthened by the discovery that the intracellular concentration of β-catenin is greatly increased in the intestinal epithelial cells of patients with the hereditary disease adenomatous polyposis coli.[2] This disease is caused by a mutation of the *APC* gene and represents a predisposition for colon cancer. Furthermore, the *APC* gene is mutated in the majority of colon cancer patients and the gene seems to be decisively involved in this type of cancer.[3]

In normal cells, the APC protein conjoins with β-catenin and axin.[4] In this complex, the β-catenin is phosphorylated by glycogen synthase kinase 3β (GSK-3β) and subsequently, after ubiquitination, degraded in the proteasomes.[5] However, in colon cells with a mutated *APC* gene, this degradation is interrupted and, thereby, the level of intracellular β-catenin is raised.

Up to now, β-catenin has been known to be an important intracellular component, which enables the connection of the cadherin class adhesion molecules (E-, N-, and P-cadherins) with the actin cytoskeleton and, therewith, enables cell–cell adhesion. Also known, but less well studied, was the fact that β-catenin induces the expression of certain genes after nuclear translocation. These genes are, along with others, responsible for cell division and proliferation. However, the mechanism of this remained a mystery.

The situation changed in 1996 when it was found that β-catenin acts as an transcriptional activator after its complexation with DNA-binding proteins of the T-cell factor (TCF)/lymphoid enhancer-binding factor (LEF) families.[6] The understanding of this background and the fact that the APC protein keeps the level of intracellular β-catenin low was evidence of the importance of the *APC* gene as a decisive negative regulator of the Wnt signaling pathway,[7] whose excessive activation leads to cancer in humans.

Despite this progress, the nature of the genes which are activated by the β-catenin/TCF complex remained undiscovered. At the beginning of 1999, two research groups independently reported a new breakthrough discovery.[8] Due to the fact that the protein cyclin D1 is an important regulator of the progression of the cell cycle, many research efforts were focused on it as a possible target of β-catenin/TCF. It was also known that cyclin D1 is overexpressed in a significant number of colon carcinomas.[9, 10] Interestingly, the inhibition of cyclin D1 expression by antisense oligodeoxynucleotides abolished the growth of certain colon cancer cells.[11] Investigations in the group of Ben-Ze'ev in Israel showed that the β-catenin/TCF complex stimulates the expression of cyclin D1 in SW-480 colon cancer cells by binding at the cyclin D1 promotor.[8a] Transfection of this cancer cell line with the wild-type *APC* gene leads, by the stimulation of the degradation of β-catenin, to a decrease of free β-catenin and, thereby, to the reduction of cyclin D1 expression. The same result was obtained by overexpression of the cytoplasmatic tail of N-cadherin. The reason is most probably the interception of free β-catenin by the cadherin, which finally leads to reduction of β-catenin/TCF complex concentration. Similar results were found by the group of McCormick in the USA.[8b] Additionally, the authors showed that the oncoprotein Valin-12-p21^{ras} enhances the β-catenin-mediated cyclin D1 expression with the support of the Ets-family transcription factors.[12]

All of these findings clearly show that β-catenin is an oncoprotein. The APC protein is an important physiological antagonist of β-catenin and, thereby, an antagonist of the Wnt signal transduction pathway. When lacking extracellular stimuli, the APC protein promotes the degradation of β-catenin and supports the migration of colorectal epithelial cells throughout the column of the Lieberkühn crypts. The stabilization of β-catenin in the presence of the Wnt signal is probably caused by the inhibition of GSK-3β. This finally results in the suppression of apoptosis and stimulation of proliferation (Figure 1).[1]

What are the implications of these new insights for the development of new colon cancer therapies? One possibility could be the overexpression of the cytoplasmatic cadherin tail which would intercept the free β-catenin. The consequences of this interception concept have to be proven with a suitable in vivo model. The *Min* mouse[13] is an appropriate test system for human adenomatous polyposis coli, because it has a mutated *APC* gene and bears a similar syndrome.

Furthermore, the effect of cyclin D1 could be restrained with suitable inhibitors, such as the synthetic flavonoid

[*] Prof. Dr. A. Giannis
Institut für Organische Chemie der Universität
Richard-Willstätter-Allee 2, 76128 Karlsruhe (Germany)
Fax: (+49) 721-608-7652
E-mail: giannis@ochhades.chemie.uni-karlsruhe.de

 © WILEY-VCH Verlag GmbH, D-69451 Weinheim, 2000 1433-7851/00/3913-2261 $ 17.50+.50/0

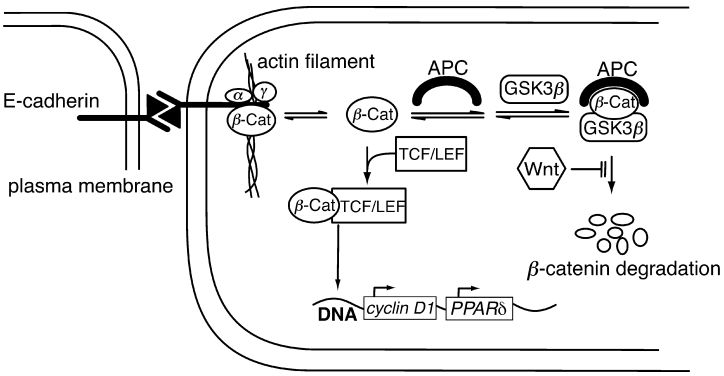
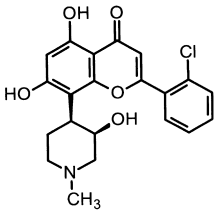


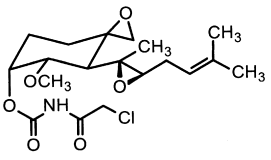
Figure 1. β-Catenin has a dual function: On one hand, it connects the adhesion molecules of the cadherin class with the actin filament of the cytoskeleton. On the other hand, it activates, in the form of a complex with the transcription factor TCF/LEF, the expression of certain genes, such as cyclin D1 and PPARδ. Thereby, proliferation is stimulated and/or apoptosis is inhibited. The effect of the β-catenin is terminated by its proteasomal degradation. For this purpose the proteins APC, GSK-3β, and axin (not shown) are necessary. In the hereditary disease adenomatous polyposis coli, as well as in many cases of colon cancer, the degradation of β-catenin is disturbed, due to a mutation of the *APC* gene. This results in a rise of the intracellular level of β-catenin. Activation of the Wnt signaling transduction pathway enhances the stability of the APC/β-Cat/GSK-3β complex and leads to the same result.

derivative flavopyridol (**1**). Flavopyridol is already in clinical trials and seems to be a promising candidate.[14] It is not only a potent inhibitor for cyclin D1-dependent kinase 4 (cdk4), but also for other kinases which are required for the progression of the cell cycle, like cdk1, cdk2, and cdk7. Interestingly, flavopyridol strongly reduces the expression of cyclin D1. [15]



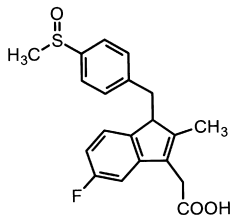
1

Regarding the involvement of Ras proteins and Ets transcription factors in cyclin D1 expression, the use of Ras farnesylation inhibitors[16], in combination with inhibitors of the Ets biosynthesis, seems to be promising for the treatment of colon cancer. Fumagillin and its synthetic analogue TNP-470 (**2**) seem to be suitable, because both are not only potent antiangiogenic agents but also inhibitors of Ets-1 expression.[17]



2

Further possibilities arise from the reports of Kinzler et al. in the USA. This group recently identified the peroxisome proliferator activated receptor δ (PPARδ) as a new target of the β-catenin/TCF complex.[18] PPARδ is a member of the ligand-dependent nuclear receptor superfamily.[19] This family regulates the expression of their target genes by binding the so-called PPAR response element (PPRE) and, thereby, the family controls different aspects of growth, development, and homeostasis. Different polyunsaturated fatty acids and eicosanoid metabolites (such as prostaglandins) were identified as ligands of the PPARs. Kinzler et al. showed that nonsteroidal antiinflammatory drugs (NSAIDs), as sulindac (**3**), inhibit tumor genesis and tumor growth in two distinct ways. On one hand, they inhibit cyclooxygenases (COX-1 as well as the inducible COX-2), which results in the reduction of the formation of prostaglandins. The latter are known to promote the development of colon cancer through paracrine and/or autocrine mechanisms.[20] On the other hand, sulindac can bind to PPARδ and disrupt its DNA binding ability. The sulindac sulfone, which is not an inhibitor of COX, is able to suppress the β-catenin-mediated PPARδ activity.[18] Also, in this case, the "good" APC protein acts as an antagonist of the PPARδ expression, by stimulating the degradation of β-catenin.



3

Selective inhibitors of COX-2 were successfully used for chemopreventation of colon cancer in different studies.[21] The results of Kinzler et al. present a plausible explanation for the molecular mechanisms. They indicate that COX inhibitors, which are also potent inhibitors of PPARδ, may be more useful.[22] In this context, it seems important to point out that cyclooxygenase inhibitors show an additional favorable property for tumor therapy—they block the formation of new blood vessels (angiogenesis).[23]

In summary, one can say that, in the last few years, decisive progress has been made in the understanding of the molecular basis for the pathogenesis of colon cancer. The optimism concerning the development of new efficient agents for prevention, as well as treatment, of this disease is justified. It is an exciting question whether these drugs will simply be aspirin derivatives in the end.[24]

[1] M. Peifer, *Science* **1996**, *272*, 974 – 975.
[2] P. J. Morin, A. B. Sparks, V. Korinek, N. Barker, B. Vogelstein, K. W. Kinzler, *Science* **1997**, *275*, 1787 – 1790.
[3] K. W. Kinzler, B. Vogelstein, *Cell* **1996**, *87*, 159 – 170.
[4] a) L. Zeng, F. Fagotto, T. Zhang, W. Hsu, T. J. Vasicek, W. L. Perry, J. J. Lee, S. M. Tilghman, B. M. Gumbiner, F. Costantini, *Cell* **1997**, *90*, 181 – 192; b) J. Behrens, B. A. Jerchow, M. Würtele, J. Grimm, C. Asbrand, R. Wirtz, M. Kühl, D. Wedlich, W. Birchmeier, *Science* **1998**, *280*, 596 – 599.
[5] H. Aberle, A. Bauer, J. Stappert, A. Kispert, R. Kemler, *EMBO J* **1997**, *16*, 3797 – 3804.
[6] a) J. Behrens, J. P. von Kries, M. Kuhl, L. Bruhn, D. Wedlich, R. Grosschedl, W. Birchmeier, *Nature* **1996**, *382*, 638 – 642; b) M. Molenaar, M. van de Wetering, M. Oosterwegel, J. Peterson-Maduro, S. Godsave, V. Korinek, J. Roose, O. Destree, H. Clevers, *Cell* **1996**, *86*, 391 – 399.
[7] M. Peifer, *Nature* **1999**, *400*, 213 – 215.
[8] a) M. Shtutman, J. Zhurinsky, I. Simcha, C. Albanese, M. D'Amico, R. Pestel, A. Ben-Ze'ev, *Proc. Natl. Acad. Sci. USA* **1999**, *96*, 5522 – 5527; b) O. Tetsu, F. McCormick, *Nature* **1999**, *398*, 422 – 426.
[9] J. Bartkova, J. Lukas, M. Strauss, J. Bartek, *Int. J. Cancer* **1994**, *58*, 568 – 573.
[10] N. Arber, H. Hibshoosh, S. F. Moss, T. Sutter, Y. Zhang, M. Begg, S. Wang, I. B. Weinstein, P. R. Holt, *Gastroenterology* **1996**, *110*, 669 – 674.
[11] N. Arber, Y. Doki, E. K.-H. Han, A. Scambato, P. Zhou, N. H. Kim, T. Delohery, M. Klein, P. R. Holt, I. B. Weinstein, *Cancer Res.* **1997**, *57*, 1569 – 1574.
[12] K. Inoue, C. J. Sherr, L. H. Shapiro, *J. Biol. Chem.* **1998**, *273*, 29188 – 29194.

 © WILEY-VCH Verlag GmbH, D-69451 Weinheim, 2000 1433-7851/00/3913-2262 $ 17.50+.50/0

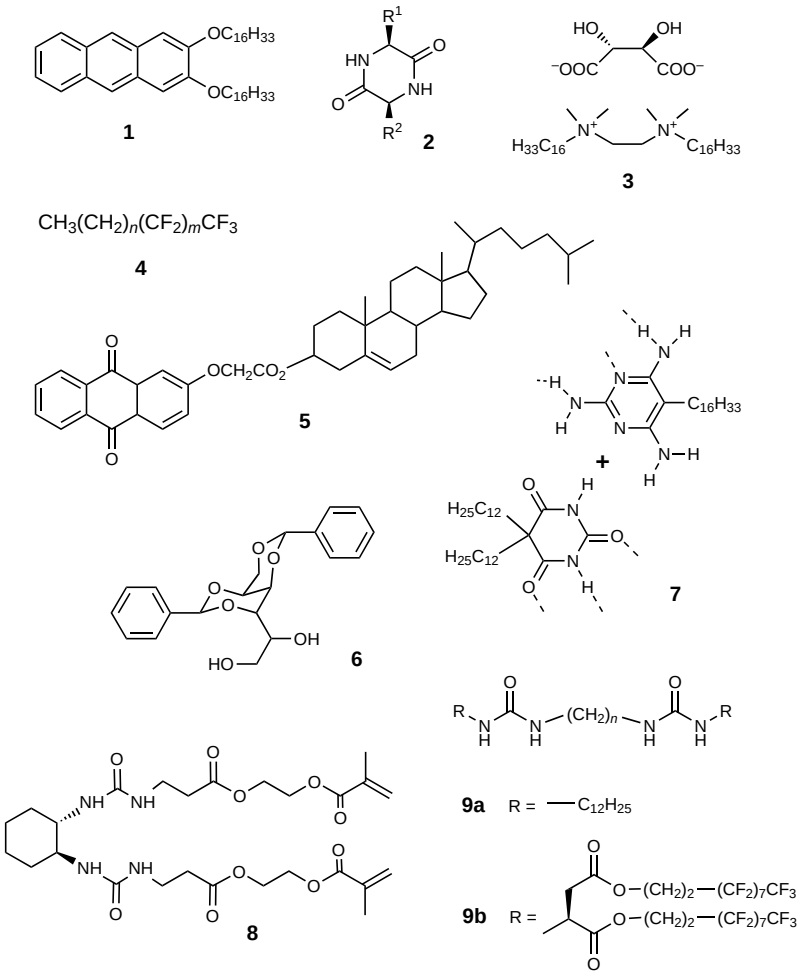
[13] W. F. Dove, K. A. Gould, C. Luongo, A. R. Moser, A. R. Shoemaker, *Cancer Surv.* **1995**, *25*, 335 – 355.
[14] a) H. H. Sedlacek, J. Czech, R. Naik, G. Kaur, P. Worland, M. Losiewicz, B. Parker, B. Carlson, A. Smith, A. Senderowicz, E. Sausville, *Int. J. Oncol*. **1996**, *9*, 1143 – 1168; b) A. J. Kraker, R. N. Booher, *Annu. Rep. Med. Chem*. **1999**, *34*, 247 – 256.
[15] B. Carlson, T. Lahusen, S. Singh, A. Loaiza-Perez, P. J. Worland, R. Pestell, C. Albanese, E. A. Sausville, A. M. Senderowicz, *Cancer Res.* **1999**, *59*, 4634 – 4641.
[16] D. M. Leonhard, *J. Med. Chem*. **1997**, *40*, 2971 – 2990.
[17] N. Wernert, A. Stanjek, S. Kiriakidis, A. Hügel, H. C. Jha, R. Mazitschek, A. Giannis, *Angew. Chem*. **1999**, *111*, 3432 – 3435; *Angew. Chem. Int. Ed.* **1999**, *38*, 3228 – 3231.
[18] T.-C. He, T. A. Chan, B. Vogelstein, K. W. Kinzler, *Cell* **1999**, *99*, 335 – 345.
[19] D. J. Mangelsdorf, C. Thummel, M. Beato, P. Herrlich, G. Schutz, K. Umesono, B. Blumberg, P. Kastner, M. Mark, P. Chambon, *Cell* **1995**, *83*, 835 – 839.
[20] S. M. Prescott, R. M. White, *Cell* **1996**, *87*, 783 – 786.
[21] D. J. E. Elder, C. Paraskeva, *Nat. Med*. **1998**, *4*, 392 – 393.
[22] G. A. Piazza, D. S. Alberts, L. J. Hixson, N. S. Paranka, H. Li, T. Finn, C. Bogert, J. M. Guillen, K. Brendel, P. H. Gross, *Cancer Res.* **1997**, *57*, 2909 – 2915.
[23] M. K. Jones, H. Wang, B. M. Peskar, E. Levin, R. M. Itani, I. J. Sarfeh, A. S. Tarnawski, *Nat. Med*. **1999**, *5*, 1418 – 1423.
[24] S. J. Shiff, B. Rigas, *Nat. Med*. **1999**, 5, 1348 – 1349.

New Functional Materials Based on Self-Assembling Organogels: From Serendipity towards Design**

Jan H. van Esch* and Ben L. Feringa

Everyone knows what a gel is, but from a scientific point of view the term gel encompasses chemically very diverse systems. Gel systems formed by, for instance, dilute solutions of polymers, proteins, and inorganic substances like silica or clays in water and organic solvents have been well studied and are widely used in, for example, photographic, cosmetics, food, and petroleum industries.[1] In recent years there has been a rapidly growing interest in low molecular weight gelling agents, which is motivated not only by the many potential applications of gels, but also by the fact that these systems exhibit striking properties with respect to self-assembly phenomena (Scheme 1).[2, 3]

These "organogels" have in common with other gel systems that the gelling agent forms a continuous three-dimensional entangled network in the solvent, thereby preventing the liquid from flowing.[4] In contrast to their macromolecular and inorganic counterparts, the network structure formed by low molecular weight organogelators is held together solely by noncovalent forces, including hydrogen bonding, π stacking, and solvophobic effects (Figure 1). The self-



Scheme 1. Examples of low molecular weight gelling agents, illustrating the enormous structural diversity among organogelators.

[*] Dr. J. H. van Esch, Prof. Dr. B. L. Feringa
Laboratory for Organic Chemistry
Stratingh Institute, University of Groningen
Nijenborgh 4, 9747 AG Groningen (The Netherlands)
Fax: (+31) 50-3634296
E-mail: esch@chem.rug.nl

[**] The Royal Netherlands Academy of Science is gratefully acknowledged for a fellowship for J.H.v.E.

 © WILEY-VCH Verlag GmbH, D-69451 Weinheim, 2000 1433-7851/00/3913-2263 $ 17.50+.50/0

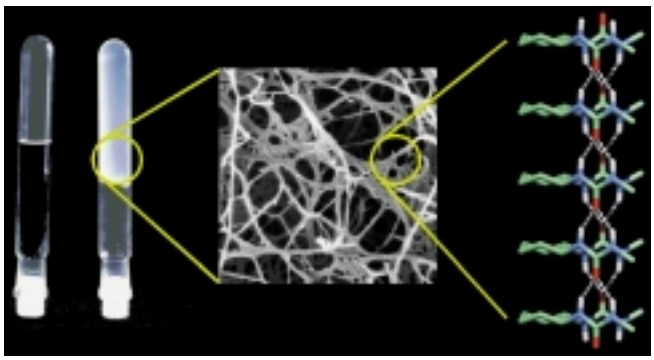


Figure 1. Organic gelling agents self-assemble into one-dimensional fibers (left) and finally an entangled network (middle), which causes gelation of the liquid (right).

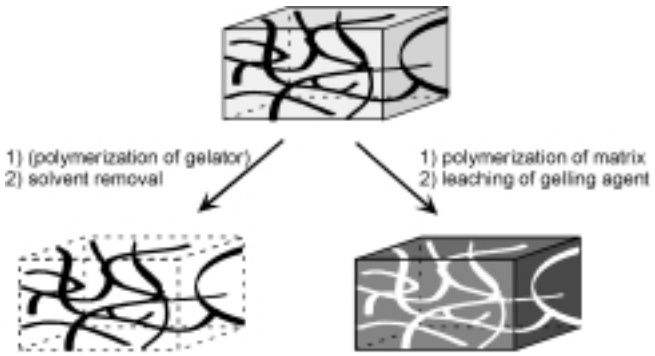


Figure 2. Preparation of organic aerogels (left) and porous membranes (right) from organogels.

assembly process starting from a single molecule to fibers and ultimately an entangled network structure is thus completely reversible, and at the same time also highly efficient as most organogelators already form gels at concentrations well below 1 wt%.

The second distinct feature of organogels is that the network filaments consist of well-ordered arrays of molecules up to micrometer lengths, and different filament architectures like tapes, rods, fibers, sheets, and cylinders have been reported. Although the formation of organogels from small organic molecules is an excellent example of a supramolecular self-assembly process, most organogelators have been found by serendipity rather than design, and many aspects of organogels are still poorly understood. The control of gelation phenomena induced by small molecules and the design of new gelling agents are therefore challenging goals leading to a new area of fascinating organic materials, and it has only been recently that a number of successes have been reported.

In a recent paper in *Science*, Beckman, Hamilton, and coworkers reported on new microcellular organic materials which have been prepared by supercritical drying of organogels in CO_2.[5] The most remarkable feature of this system is that except for the organogelator and CO_2, no other compounds or cosolvents are involved, resulting in a single-step, very clean, and environmentally friendly method to create these materials. The essence of this work is that the authors succeeded in the design of organic gelling agents for CO_2, that is, compounds that strongly associate and form an entangled network structure at lower temperature or pressure, but would dissolve upon increasing the temperature or pressure. For this purpose gelling agents were developed in which urea groups, to achieve association through multiple hydrogen bonding, are combined with groups showing affinity for CO_2 to increase the solubility, in this particular case perfluoroalkanes (e.g. **9b**, Scheme 1).

The results of this very basic design are remarkable. The compounds dissolve very well in supercritical CO_2 at higher temperatures and pressures, but upon cooling the solution turns into an opaque gel. Moreover, upon removal of the solvent by simply lowering the pressure, the network structure is preserved and a highly porous and self-supporting monolithic foam is obtained (Figure 2). The foams combine an extraordinary low density (<5% of the bulk density of the organogelators) with a submicrometer cellular size, properties which could not be obtained with traditional polymers in combination with CO_2 as foaming agent. These organic analogues of silicate aerogels are therefore highly interesting materials for application in separation processes as well as for use as novel low dielectric or insulating materials and as support for catalysts.

The design of novel gelling agents as reported by Beckman, Hamilton et al.[5] is, however, not without precedent. Other research groups including those of Terech, Hanabusa, Weiss, Shinkai, and Boden as well as our group all made significant contributions towards the design of novel gelling agents and the understanding of the gelation phenomena.[2, 6] Important guidelines for the design of novel gelling agents that emerged from these studies are: 1) the presence of strong self-complementary and unidirectional intermolecular interactions to enforce one-dimensional self-assembly; 2) control of fiber–solvent interfacial energy to control solubility and to prevent crystallization; and 3) some factor to induce fiber cross-linking for network formation.

Most new gelling agents that resulted from these studies are based on peptides or carbohydrates because of the strength and high directionality of hydrogen-bond interactions. Especially cyclic dipeptides and bis-urea-based gelling agents appeared to be very efficient gelling agents and combine easy accessibility with a wide solvent scope, and in the case of the bis-urea gelling agents it was shown that the supramolecular architecture can be controlled by the spacer between the urea groups.[6e, 7, 8] The hydrogen bonding core of these cyclic dipeptides and bis-ureas provide a "gelating scaffold" which can easily be functionalized without loss of gelation ability. For example, we reported some years ago that the polymerizable bis-urea **8** (Scheme 1) is a potent gelling agent for apolar solvents.[8b] After photopolymerization of benzene gels and removal of the solvent by freeze-drying, an organic aerogel was obtained with very similar characteristics with respect to density and cellular size as that reported by Beckman, Hamilton et al.[5]

Another exciting development is the use of organogelators as template for the preparation of nanostructured materials. First Möller[9] and later also Weiss[10] and Nolte[11] prepared membranes with nanosized pores by the gel–template–leaching process, taking advantage of the distinct feature of

 © WILEY-VCH Verlag GmbH, D-69451 Weinheim, 2000 1433-7851/00/3913-2264 $ 17.50+.50/0

organogelators to *reversibly* form elongated fibers with well-defined dimensions and geometry. In the gel–template–leaching process, gels of various gelling agents are prepared in polymerizable solvents like methacrylates or styrene in the presence of a cross-linking agent. After polymerization of the matrix, the organic gelling agent is removed again by extraction with a proper solvent (Figure 2). In this way the organogel fiber network is "imprinted" in the cross-linked polymer matrix, resulting in porous membranes with channels of submicrometer and in some cases even nanometer dimensions.

Although this method holds great promises, the preservation of the original fiber morphology in the polymer network is often rather poor, which is most likely due to the flexible nature of the cross-linked polymers used. This drawback was recently overcome by Shinkai and co-workers, who used gels formed by chiral organogelators as a template to control the morphology of silica formed by a concurrent inorganic sol–gel process.[12] After removal of the organic template by calcination, hollow fibers and, under carefully controlled conditions, even helical silica fibers with a single screw sense were obtained. It should be noted that the organic gel network only acts as a template when it bears a significant fraction of cationic groups, indicating the necessity of strong interactions between the organic template network and the growing inorganic silica gel.

The regular arrangement of organic gelling agents in the network filaments has also been exploited as a framework for the spatial organization of covalently attached functional groups, for example fullerene derivatives or other conjugated moieties. It has been shown that this strategy can be very successful for improving collective properties like electron conductivity.[13]

A completely different but very appealing issue in gel research is the development of "smart" or "responsive" gel systems.[14] Pioneering work on smart polymer gels which could reversibly swell or shrink upon exposure to some chemical or physical triggering event has been carried out by Tanaka.[4b] Recently, the Tanaka-group developed a novel gel system which can bind guest molecules by multiple-point noncovalent interactions.[15] Most interestingly, swelling of the gel induced by a temperature change increases the distance between the individual interaction points. As a result the binding changes from a multiple-point to a single-point interaction, and the affinity decreases by more than one order of magnitude. It is foreseen that this principle can be applied for controlled drug-release systems, and gels can be designed to respond to other triggers like solvent polarity or pH value as well.

It should be emphasized that organogels are very attractive systems for the design of novel responsive gels, because their formation is completely reversible. Here the challenge is to couple the self-assembly process to a chemical or physical trigger (Figure 3). Having the feature of reversibility in mind, Aggeli et al. designed various peptide-based gelling agents which self-assemble into extended β-sheet tapes and which, depending on the polarity of the solvents, entangle to form gels.[6d] To make gel systems that are responsive to pH value some basic amino acids have been incorporated in the peptide, and indeed it was found that a change in pH triggers the reversible transition from the gel state to a solution. Gels of other peptides respond to shear by a change of their viscoelastic properties. Shinkai and co-workers have demonstrated already some years ago by using an azobenzene-steroid-based gel system that it is possible to switch by irradiation with UV and visible light from solution to the gel state and back,[16a] and two other recent publications indicate that also host–guest interactions can be employed to control the structure or stability of organogels.[16]

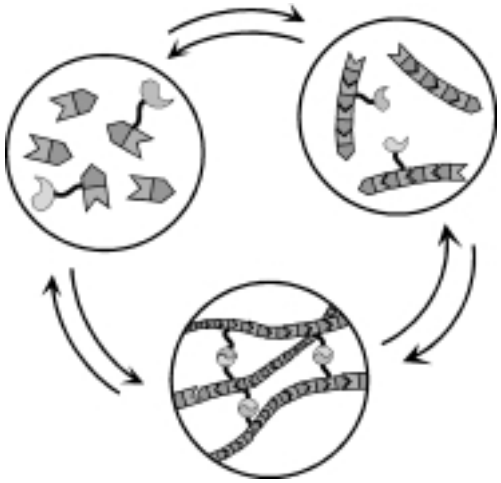


Figure 3. Cartoon of switchable organogels, showing the different levels at which switching might affect the viscoelastic properties.

In conclusion, within a very short period organogels have developed from a chemical and physical curiosity to a highly promising new area of research. Their well-defined structure, the coexistence of these highly ordered fibers with a liquid phase, the large interfacial area, and the possibility to entrap solutes within the network pores make organogels very attractive materials for membrane and separation technology, catalysis, or drug delivery.

[1] a) *Polymer Gels: Fundamentals and Biomedical Applications* (Eds.: D. Derossi, K. Kajiwara, Y. Osada, A. Yamauchi), Plenum Press, New York, **1991**; b) J.-M. Guenet, *Thermoreversible Gelation of Polymers and Biopolymers*, Academic Press, London, **1992**; c) "Gels": Eds.: Kremer, G. Lagaly, *Prog. Colloid. Polym. Sci.* **1996**, *102*; d) R. J. P. Corriu, D. Leclercq, *Angew. Chem.* **1996**, *108*, 1524–1540; *Angew. Chem. Int. Ed. Engl.* **1996**, *35*, 1420–1436; e) M. T. Reetz, *Adv. Mater.* **1997**, *9*, 943–954.

[2] a) P. Terech, R. G. Weiss, *Chem. Rev.* **1997**, *97*, 3133–3159; b) J. van Esch, F. Schoonbeek, M. de Loos, E. M. Veen, R. M. Kellogg, B. L. Feringa, *Nato ASI Ser. C* **1999**, *527*, 233–259.

[3] The first symposium on low molecular weight organogelators was held in Groningen, The Netherlands, in November 1999.

[4] a) P. J. Flory, *Farady Discuss. R. Soc. Chem.* **1974**, *57*, 8; b) T. Tanaka, *Am. Sci.* **1981**, *244*, 110–123.

[5] C. Shi, Z. Huang, S. Kilic, J. Xu, R. M. Enick, E. J. Beckman, A. J. Carr, R. E. Melendez, A. D. Hamilton, *Science* **1999**, *286*, 1540–1543.

[6] a) K. Hanabusa, M. Yamada, M. Kimura, H. Shirai, *Angew. Chem.* **1996**, *108*, 2086–2088; *Angew. Chem. Int. Ed. Engl.* **1996**, *35*, 1949–1951; b) Y. Lin, B. Kachar, R. G. Weiss, *J. Am. Chem. Soc.* **1989**, *111*, 5542–5551; c) K. Yoza, N. Amanokura, Y. Ono, T. Aoka, H. Shinmori, M. Takeuchi, S. Shinkai, D. N. Reinhoudt, *Chem. Eur. J.* **1999**, *5*, 2722–2729; d) A. Aggeli, M. Bell, N. Boden, J. N. Keen, P. F. Knowles, T. C. B. McLeish, M. Pitkeathly, S. E. Radford, *Nature* **1997**,

 © WILEY-VCH Verlag GmbH, D-69451 Weinheim, 2000 1433-7851/00/3913-2265 $ 17.50+.50/0

386, 259 – 262; e) J. van Esch, F. Schoonbeek, M. de Loos, H. Kooiman, A. L. Spek, R. M. Kellogg, B. L. Feringa, *Chem. Eur. J.* **1999**, *5*, 937 – 950; f) R. Oda, I. Huc, S. J. Candau, *Angew. Chem.* **1998**, *110*, 2835 – 2838; *Angew. Chem. Int. Ed.* **1998**, *37*, 2689 – 2691; g) R. J. H. Hafkamp, M. C. Feiters, R. J. M. Nolte, *J. Org. Chem.* **1999**, *64*, 412 – 426.

[7] a) K. Hanabusa, Y. Matsumoto, T. Miki, T. Koyama, H. Shirai, *J. Chem. Soc. Chem. Commun.* **1994**, 1401 – 1402; b) K. Hanabusa, K. Shimura, K. Hirose, M. Kimura, H. Shirai, *Chem. Lett.* **1996**, 885.

[8] a) J. van Esch, S. De Feyter, R. M. Kellogg, F. De Schryver, B. L. Feringa, *Chem. Eur. J.* **1997**, *3*, 1238 – 1243; b) M. de Loos, J. van Esch, I. Stokroos, R. M. Kellogg, B. L. Feringa, *J. Am. Chem. Soc.* **1997**, *112*, 12675 – 12676.

[9] a) H. Gankema, Ph.D. Thesis, University of Twente, The Netherlands, **1995**; b) U. Beginn, S. Keinath, M. Möller, *Macromol. Chem. Phys.* **1998**, *199*, 2379 – 2384.

[10] W. Gu, L. Lu, G. B. Chapman, R. G. Weiss, *Chem. Commun.* **1997**, 543 – 544.

[11] R. J. Hafkamp, B. P. A. Kokke, I. M. Danke, H. P. M. Geurts, A. E. Rowan, M. C. Feiters, R. J. M. Nolte, *Chem. Commun.* **1997**, 545 – 546.

[12] a) Y. Ono, K. Nakashima, M. Sano, Y. Kanekiyo, K. Inoue, J. Hojo, S. Shinkai, *Chem. Commun.* **1998**, 1477 – 1475; b) Y. Ono, K. Nakashima, M. Sano, J. Hojo, S. Shinkai, *Chem. Lett.* **1999**, 1119 – 1120.

[13] a) F. Schoonbeek, J. van Esch, B. Wegewijs, D. B. A. Rep, M. P. De Haas, T. M. Klapwijk, R. M. Kellogg, B. L. Feringa, *Angew. Chem.* **1999**, *111*, 1486 – 1490; *Angew. Chem. Int. Ed.* **1999**, *38*, 1393 – 1397; b) K. Oishi, T. Ishi-i, M. sano, S. Shinkai, *Chem. Lett.* **1999**, 1089 – 1090; c) A. M. Cassell, C. L. Asplund, J. M. Tour, *Angew. Chem.* **1999**, *111*, 2565 – 2568; *Angew. Chem. Int. Ed.* **1999**, *38*, 2403 – 2405.

[14] Y. Osada, J.-P. Gong, *Adv. Mater.* **1998**, *10*, 827 – 837.

[15] T. Oya, T. Enoki, A. U. Grosberg, S. Masamune, T. Sakiyama, Y. Takeoka, K. Tanaka, G. Wang, Y. Yilmaz, M. S. Feld, R. Dasari, T. Tanaka, *Science* **1999**, *286*, 1543 – 1545.

[16] a) K. Murata, M. Aoki, T. Nishi, A. Ikeda, S. Shinkai, *J. Chem. Soc. Chem. Commun.* **1991**, 1715 – 1718; b) J. H. Jung, Y. Ono, S. Shinkai, *Tetrahedron Lett.* **1999**, *40*, 8395 – 8399; c) H. Engelkamp, S. Middelbeek, R. J. M. Nolte, *Science* **1999**, *284*, 785 – 788.

+++ THE LINK TO INTERNATIONAL CHEMISTRY +++

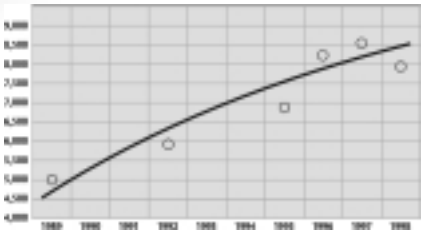


More of the Best, Every Year

More Content:



More Quality as Evidenced by the Impact Factor:



More Service:

1996: - Notification of forthcoming "Hot Papers" on the Internet
1997: - Supporting Information available on the Internet
1998: - Press releases on important communications
1999: - *Angewandte Chemie* goes Online with Wiley InterScience (www.interscience.wiley.com)
- Notification of VIPs (Very Important Papers)
- Simultaneous Publication of German and English versions
2000: - New section
- Essays has its debut
- *Angewandte* is now covered by Medline in addition to a phlethora of other databases

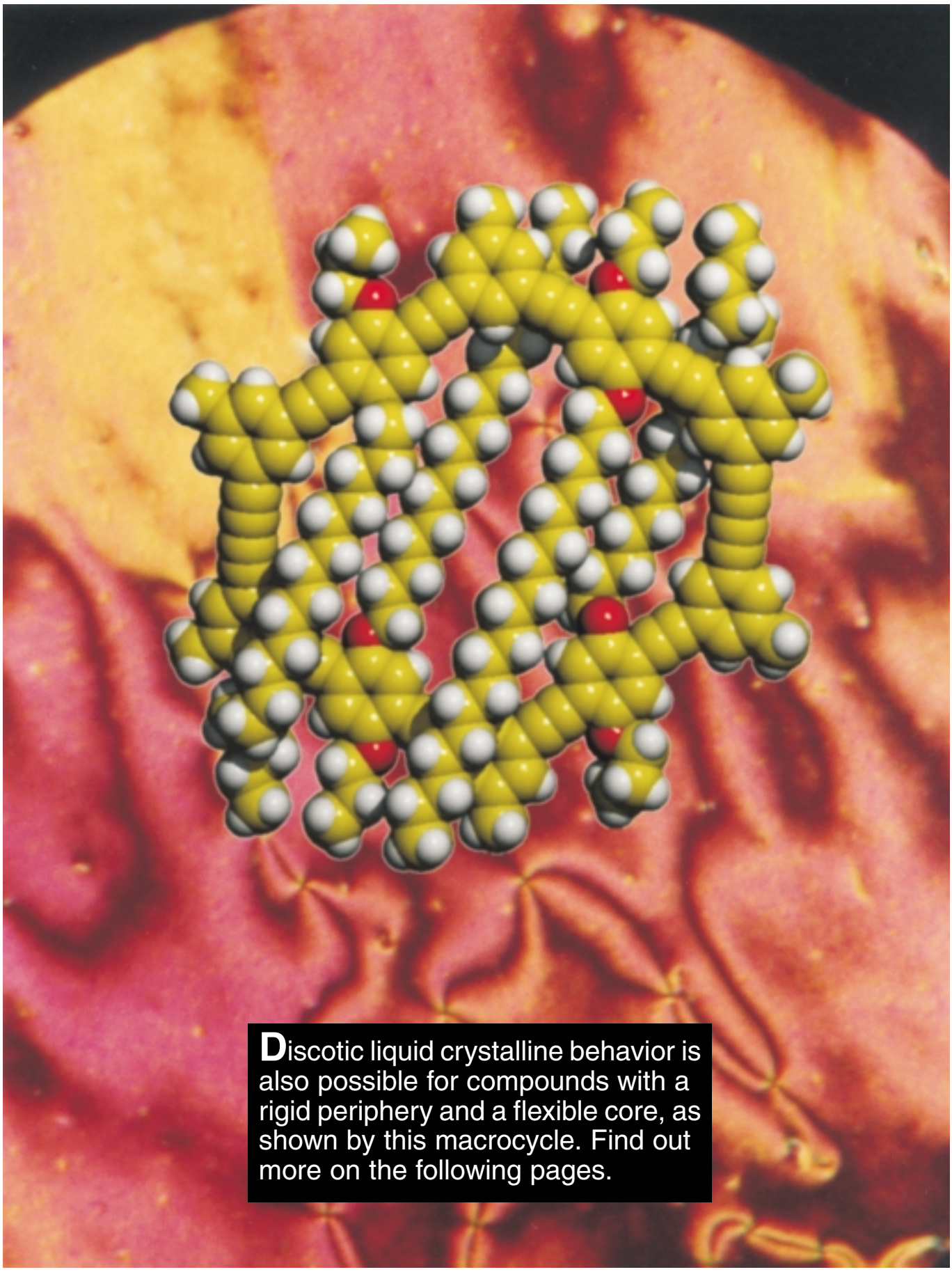
What else would you like to see in *Angewandte*?
E-mail your suggestions to:
angewandte@wiley-vch.de



WILEY-VCH, P.O. Box 10 11 61, 69451 Weinheim, Germany
Phone +49 (6201) 606-328, Fax +49 (6201) 606-348
e-mail: sales-journals@wiley-vch.de, http://www.wiley-vch.de

WILEY-VCH

 © WILEY-VCH Verlag GmbH, D-69451 Weinheim, 2000 1433-7851/00/3913-2266 $ 17.50+.50/0



Discotic liquid crystalline behavior is also possible for compounds with a rigid periphery and a flexible core, as shown by this macrocycle. Find out more on the following pages.

 © WILEY-VCH Verlag GmbH, D-69451 Weinheim, 2000 1433-7851/00/3913-2267 $ 17.50+.50/0

Alkyl-Substituted Shape-Persistent Macrocycles: The First Discotic Liquid Crystal Composed of a Rigid Periphery and a Flexible Core**

Sigurd Höger,* Volker Enkelmann, Klaus Bonrad, and Carsten Tschierske

Dedicated to Professor Gerhard Wegner on occasion of his 60th birthday

More than twenty years ago, Chandrasekhar et al. found that disklike molecules composed of a rigid core and flexible side chains pointing outward (discotics) could form columnar thermotropic mesophases (Figure 1a).[1] Later columnar mesomorphism was also found for molecular architectures, which differ from those of classical discotics.[2] Macrocyclic compounds are of special interest in this context because the formation of channel structures should be possible if the backbone of the rings remains intact and is not collapsed.[3] This can be accomplished in flexible rings by the formation of host–guest complexes,[4, 5] whereas, shape-persistent rings are, per se, noncollapsed (Figure 1b).

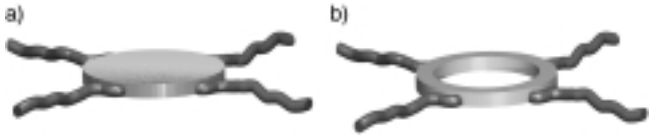
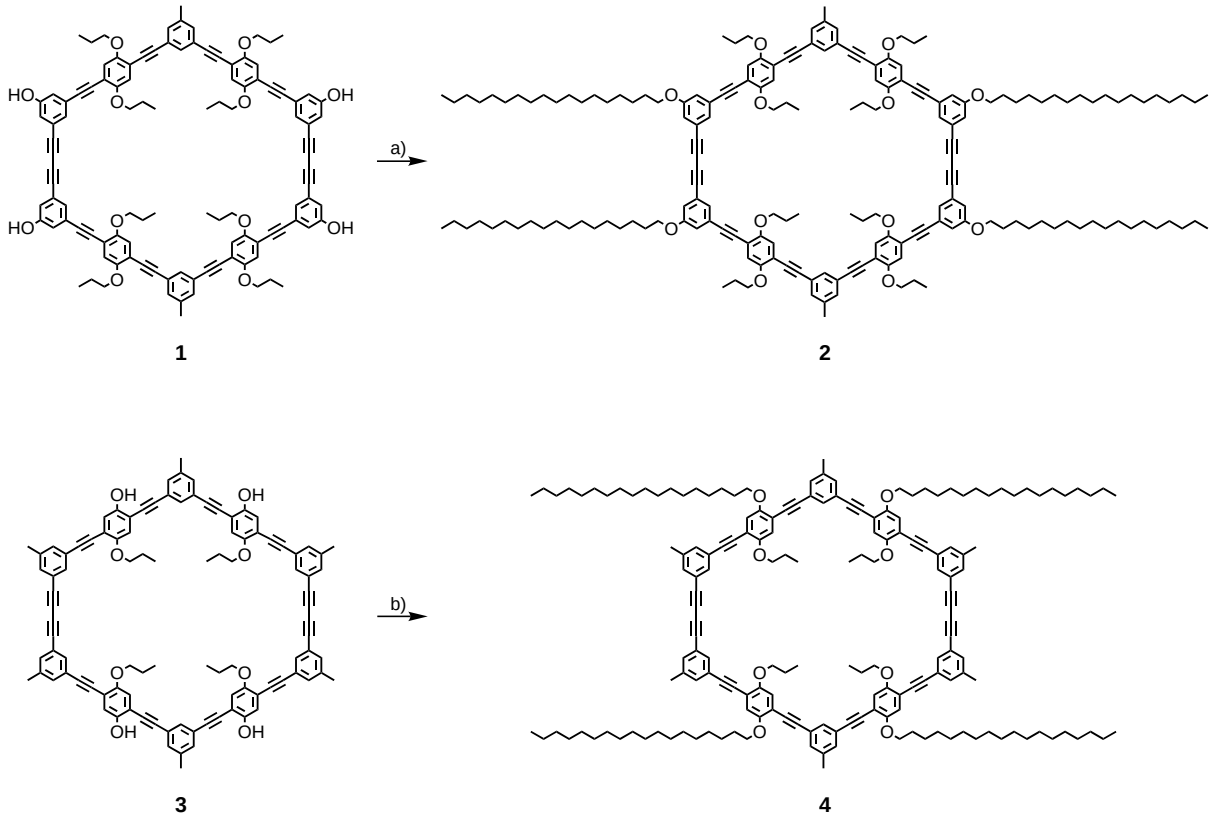


Figure 1. Design principle of disklike (a) and cyclic molecules (b) capable of forming thermotropic mesophases.

During our work on the synthesis and properties of shape-persistent macrocyclic amphiphiles, we also investigated their nonpolar derivatives **2** and **4** (Scheme 1).[6] Compound **2** was prepared by base-catalyzed alkylation of the phenol **1** with 1-bromooctadecane. Efforts to prepare **4** under the same conditions starting from **3** were unsuccessful, we only obtained an intractable mixture of different products. However, alkylation of **3** with 1-octadecanol under Mitsunobu conditions gave **4** in good yields (Scheme 1).



Scheme 1. Synthesis of nonpolar amphiphile derivatives **2** and **4**. a) 1-bromooctadecane, K_2CO_3, DMF, 70 °C, 4 d (14%); b) 1-octadecanol, diethylazodicarboxylate (DEAD), PPh_3, THF, room temperature, 4 h (63%).

At first glance, both compounds contain the same macrocyclic backbone and differ only in the positions where the octadecyl chains are attached to the ring. Both **2** as well as **4** correlate with the principle design of thermotropic liquid crystals described above.[7] Contrary to our expectations, crossed-polarized microscopic investigations revealed that **2**

[*] Dr. S. Höger, Dr. V. Enkelmann, Dr. K. Bonrad
Max-Planck-Institut für Polymerforschung
Ackermannweg 10, 55128 Mainz (Germany)
Fax: (+49) 6131-379-100
E-mail: hoeger@mpip-mainz.mpg.de
Prof. Dr. C. Tschierske
Fachbereich Chemie der Martin-Luther-Universität Halle-Wittenberg
Kurt-Mothes-Strasse 2, 06099 Halle (Saale) (Germany)

[**] A part of this work was supported by the Volkswagen-Stiftung. S.H. thanks the Fonds der Chemischen Industrie and the GDCh (Dr. Hermann Schnell-Stiftung) for support.

 © WILEY-VCH Verlag GmbH, D-69451 Weinheim, 2000 1433-7851/00/3913-2268 $ 17.50+.50/0

melts isotropically at about 220 °C, and even with quenching we were not able to observe the appearance of a texture typical for a mesophase.[8] In sharp contrast, compound **4** exhibits liquid crystalline properties. The compound melts at 185 °C to form a mesophase ($\Delta H = 152.7\ \mathrm{kJ\,mol^{-1}}$) that becomes isotropic at 207 °C ($\Delta H = 0.73\ \mathrm{kJ\,mol^{-1}}$). The observed Schlieren texture suggests the formation of a nematic phase (Figure 2). This is consistent with observed reflections of the crystalline **4** that disappear above the transition temperature. Also we observe only a broad reflection at approximately 4.5 Å, typical for the scattering behavior of liquid or liquid crystalline paraffin chains.[9]

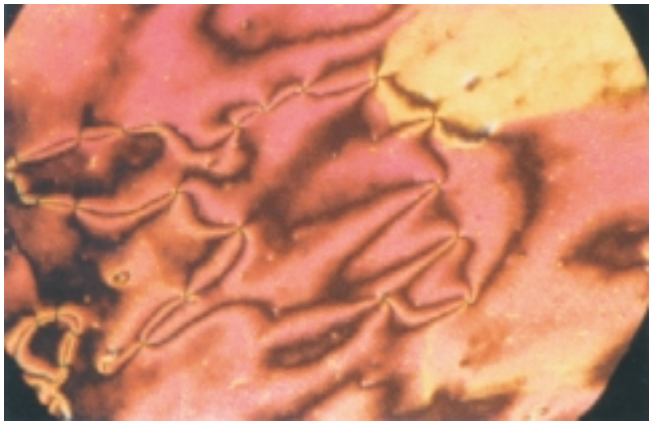


Figure 2. Texture of **4** at 200 °C viewed between crossed polarizers.

The significant difference in the thermic behavior of **2** and **4** can be explained by their different molecular architectures. It can be expected that in the solid state the interiors of the (nonsolvated) macrocycles are filled with alkyl chains. Since these point outward in **2** and backfolding is improbable for enthalpic and entropic reasons, it is expected that the interior of one ring is filled by the alkyl chains of neighboring rings. The interiors of the rings induce an interlocking of the molecules ("physical crosslinks"). According to the structural formulas in Scheme 1, one should expect a similar behavior for **4**. However, single-crystal X-ray analysis shows that in **4** there is an intramolecular interaction between the rings and the alkyl chains, by which each molecule fills its cavity with its *own* side chains (Figure 3a).[10] In this case the molecules become mobile when the alkyl chains melt and can form the liquid crystalline phase by parallel arrangement. Owing to network formation, the mechanical coupling of the rings of **2** does not breakdown before it is completely molten.[11]

It should be pointed out that **4** is not completely planar in the solid state. Therefore the alkyl chains are not arranged in one plane but are located alternately above and below the plane of view. Together with the chains of neighboring rings, they form a dense packing (Figure 3b). The lattice parameters of the alkyl chain subcell are $a = 4.22$, $b = 4.66$, $c = 2.56$ Å, $\alpha = 87.5$, $\beta = 108.4$, $\gamma = 105.2°$.[12] These correlate well with those of the triclinic structure of polyethylene ($a = 4.26$, $b = 4.46$, $c = 2.55$ Å, $\alpha = 90$, $\beta = 107$, $\gamma = 101°$) and show that the side chains can adopt a low-energy packing independent of the cyclic backbone.[13] This side chain packing also separates adjacent rings and prevents intermolecular interactions of the atoms in the aromatic framework.

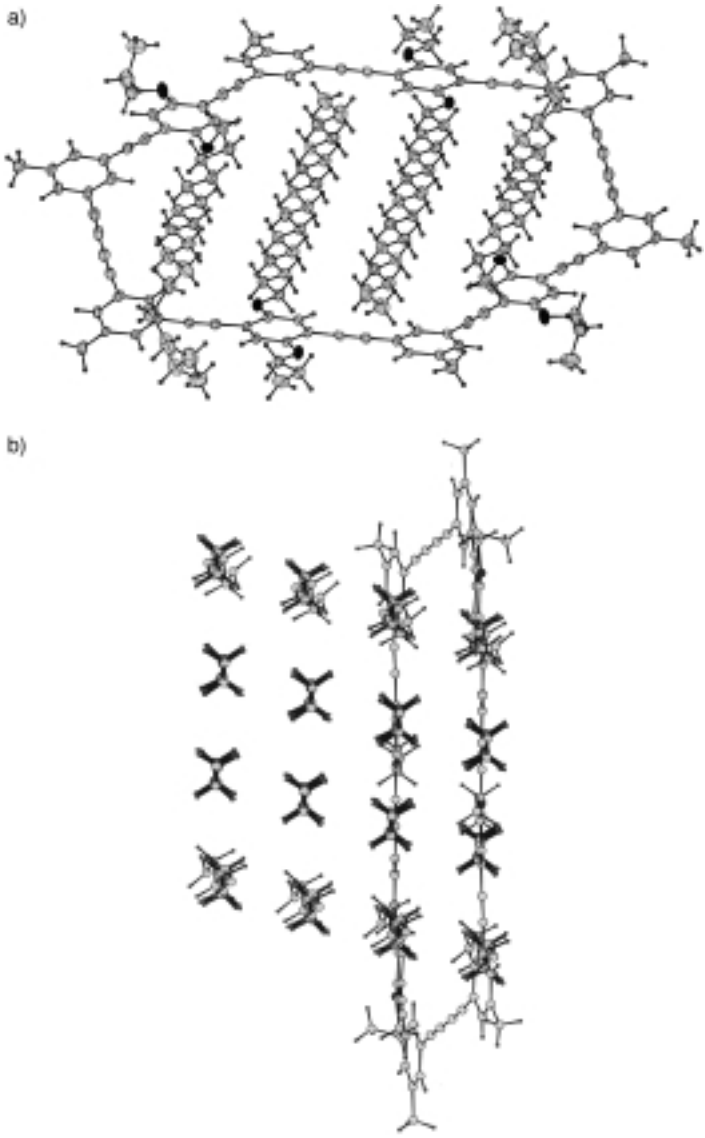


Figure 3. Top: Structure of **4** in the crystal. Projection along *a*. Bottom: View of the alkyl chain packing. For clarity, only one macrocycle is shown.

Unlike **2**, the interior of **4** is filled intramolecularly with its own alkyl chains, and does not act as a crosslinker. It should be pointed out that this has its origin in the ability of the central arene units of the rings to rotate freely, as we have shown earlier.[14] Notable is the fact that the liquid crystalline macrocycle **4** has a topology that is opposite to all discotics described so far: a rigid ring acts as a framework for flexible side groups pointing to the *inside* (Figure 4).[15]



Figure 4. Schematic representation of the arrangement of the alkyl chains in **4**.

Received: January 27, 2000 [Z 14605]

 © WILEY-VCH Verlag GmbH, D-69451 Weinheim, 2000 1433-7851/00/3913-2269 $ 17.50+.50/0

[1] a) S. Chandrasekhar, B. K. Sadashiva, K. A. Suresh, *Pramana* **1977**, *7*, 471; b) S. Chandrasekhar in *Handbook of Liquid Crystals*, *Vol. 2B* (Eds.: D. Demus, J. Goodby, G. W. Gray, H.-W. Spiess, V. Vill), Wiley-VCH, Weinheim, **1998**, p. 749.
[2] C. Tschierske, *J. Mater. Chem.* **1998**, *8*, 1485.
[3] O. Y. Mindyuk, M. R. Stetzer, P. A. Heiney, J. C. Nelson, J. S. Moore, *Adv. Mater.* **1998**, *10*, 1363.
[4] a) J. M. Lehn, J. Malthête, A. M. Levelut, *J. Chem. Soc. Chem. Commun.* **1985**, 1794; b) G. Lattermann, *Mol. Cryst. Liq. Cryst.* **1990**, *182B*, 299.
[5] A. Liebmann, C. Mertesdorf, T. Plesnivy, H. Ringsdorf, J. H. Wendorff, *Angew. Chem.* **1991**, *103*, 1358; *Angew. Chem. Int. Ed. Engl.* **1991**, 30, 1375.
[6] a) S. Höger, A.-D. Meckenstock, S. Müller, *Chem. Eur. J.* **1998**, *4*, 2421; b) S. Höger, *J. Polym. Sci. Part A* **1999**, *37*, 2685.
[7] One of the basic conditions for the formation of columnar liquid crystalline phases is an optimal coverage of the periphery of the central core by lateral chains (B. Kohnke, K. Praefke, *Chem. Z.* **1985**, *109*, 121). Owing to the size of our rigid structure and the attachment of only four octadecyloxy groups, the appearance of such a mesophase is improbable.
[8] When **2** is heated for a longer period above 220 °C, a temperature well above the clearing point of **4**, we cannot eliminate the possibility of partial decomposition.
[9] The exact type of the nematic phase (e.g., nematic discotic, nematic-columnar, etc.) could not be determined yet.
[10] Crystals of **4** were grown from a CH_2Cl_2 solution by slow evaporation. Crystal structure data for **4**: $C_{174}H_{220}O_8$, triclinic, space group $P\bar{1}$, $a = 9.729(4)$ $b = 16.124(4)$ $c = 24.746(7)$ Å, $\alpha = 106.248(21)$, $\beta = 98.083(29)$, $\gamma = 89.741(20)$ °, $V = 3687.6$ Å^3, $\rho_{calcd} = 1.069$ g cm^{-3}, $\mu = 4.633$ cm^{-1}, $T = 165$ K. Nonius CAD4 diffractometer, graphite-monochromated $Cu_{K\alpha}$ radiation, $\lambda = 1.5418$ Å, $\theta/2\theta$ scans, 5958 independent reflections, of which 3028 were observed ($I > 3\sigma(I)$), empirical absorption correction. The structure was solved by direct methods (Shelxs) and refined by full-matrix least-squares analyses on F with anisotropic temperature factors for C an O. The hydrogen atoms were refined with fixed isotropic temperature factors in the riding mode. The refinement converged at $R = 0.0569$ and $R_w = 0.0571$. Crystallographic data (excluding structure factors) for the structure reported in this paper have been deposited with the Cambridge Crystallographic Data Centre as supplementary publication no. CCDC-139443. Copies of the data can be obtained free of charge on application to CCDC, 12 Union Road, Cambridge CB21EZ, UK (fax: (+44) 1223-336-033; e-mail: deposit@ccdc.cam.ac.uk).
[11] Nematic and smectic phases can be also observed for some other alkylated shape-persistent macrocycles, for example, a) C. C. Ling, R. Darcy, W. Risse, *J. Chem. Soc. Chem. Commun.* **1993**, 438; b) N. Usol'tseva, K. Praefcke, D. Singer, B. Gündogan, *Liq. Cryst.* **1994**, *16*, 601. However, in all those cases, the interior of the rings is much smaller, such that a complete intraannular arrangement of the side chains can be excluded.
[12] V. Enkelmann in *Electronic Materials: The Oligomeric Approach* (Eds.: K. Müllen, G. Wegner), Wiley-VCH, Weinheim, **1998**, p. 295.
[13] B. Wunderlich, *Macromolecular Physics*, *Vol. 1*, Academic Press, New York, **1973**, p. 91.
[14] a) S. Höger, V. Enkelmann, *Angew. Chem.* **1995**, *107*, 2917; *Angew. Chem. Int. Ed. Engl.* **1995**, *34*, 2713; b) D. L. Morrison, S. Höger, *Chem. Commun.* **1996**, 2313.
[15] The investigation of the conformation of **4** in the melt as well as the extension of this concept to macrocycles with a fixed intraannular arrangement of the flexible side groups is part of our current studies.

De Novo Prediction of Inorganic Structures Developed through Automated Assembly of Secondary Building Units (AASBU Method)**

Caroline Mellot Draznieks,* John M. Newsam, Alan M. Gorman, Clive M. Freeman, and Gérard Férey*

Simulations of the crystal structures and of the properties of solids are topical and were recognized early in materials science as a challenging task. Several computational approaches to predicting crystal structures have been described, such as:

1) Local optimization of approximate, preconstructed models by potential or first principles methods.[1, 2]
2) Monte Carlo or genetic algorithm based sampling of packing arrangements of molecular crystals.[3]
3) Assembly of atoms or ions assuming unit cell and symmetry by, for example, simulated annealing[4–9] or a genetic algorithm.[10]
4) Operations for combining two-dimensional periodic sheets.[11]
5) Enumeration of framework structures[12–14] given defined symmetry and connectivity constraints.[15]

The motivation for these efforts is to aid the often difficult process of crystal structure determination, to help rationalize different but related structure types, or to help limit the domain of structures that are possible to a given system.[5] In certain cases, combination with other desired structural attributes, for example microporosity, can allow these structure prediction methods to be applied in a genuine design sense.

In general, we lack an ability to develop viable synthesis routes based solely on a knowledge of the crystal structure. Inspired by molecular chemistry, for which rational synthesis routes are almost invariably developed, it is interesting to consider how rational approaches might be developed for the synthesis of inorganic structures, for example, zeolites[16, 17] or larger pore materials.[18–21] The desire to develop virtual libraries that might be accessible by rational synthesis is made more pressing by the recent emergence of combinatorial and high-throughput experimentation approaches to inorganic chemistry (see [22, 23] and references therein).

The prediction of periodic inorganic structures is a difficult task involving many degrees of freedom, which are related to the chemical and structural diversity of inorganic structures.

[*] Dr. C. Mellot Draznieks, Prof. G. Férey
Institut Lavoisier - UMR CNRS 8637
Université de Versailles St. Quentin
45 Avenue des Etats-Unis, 78035 Versailles Cedex (France)
Fax: (+33) 1-3925-4358
E-mail: mellot@chimie.uvsq.fr, ferey@chimie.uvsq.fr
Prof. J. M. Newsam, Dr. A. M. Gorman, Dr. C. M. Freeman
Molecular Simulations, Inc.
9685 Scranton Road, San Diego, CA 92121-3752 (USA)

[**] This work was supported by Centre National de la Recherche Scientifique. We thank F. J. J. Leusen, G. Engel, and A. K. Cheetham for useful assistance and discussions.

 © WILEY-VCH Verlag GmbH, D-69451 Weinheim, 2000 1433-7851/00/3913-2270 $ 17.50+.50/0

Any means to reduce the number of degrees of freedom is potentially valuable. Assuming, where appropriate, the occurrence of specific secondary building units (SBUs) is one such means. Many periodic inorganic structures can be regarded as elementary units, and, more generally, as SBUs assembled in one, two, or three dimensions. Related structures may be differentiated by the mode of interconnection between the SBUs. However, while SBUs have been used widely for descriptive and characterization purposes,[12, 16, 24] the exploitation of SBUs in a computational means of constructing models has not been developed until now.

Here, we describe a general computational methodology (automated assembly of secondary building blocks, AASBU) for producing virtual libraries of viable inorganic structures based on secondary building units (SBUs), implemented according to the following design criteria: 1) no explicit constraints on the nature or size of the SBUs involved, 2) no explicit constraints on unit cell dimensions but, optionally, on space group symmetry, 3) an ability to accommodate one or more types of SBUs, with the possible inclusion also of occludates, such as template molecules, 4) accommodation of differing modes of inter-SBU connection, allowing, for example, corner-, edge-, and face-sharing modes, and 5) broad flexibility in the definition of the linkage points. This use of SBUs reduces dramatically the number of possible structure types, relative to a 'free atom'[6–10] or even 'free tetrahedron' approach;[5] the huge number of generated structures has been a major hindrance to the broader application of previous structure prediction methods.[5] Perhaps more importantly, however, we consider that the virtual libraries of inorganic structures developed by this method will, at least for certain structural families, prove more amenable to rational synthesis. The building unit comprising two octahedra and two tetrahedra in a corner-shared configuration (see Figure 1), for example, is known to form under synthesis conditions[25] that can be adjusted to yield two different periodic assemblages, the three-dimensional structure AlPO-CJ2[26] and its layered form isotype with the minyulite structure.[27]

Apart from the SBU itself, the two assumptions in a given simulation are the number of SBUs per unit cell and the space group symmetry. For the most general case a search can be performed in the space group *P*1. A final determination of the symmetry of the generated structures is systematically performed with a "Find_Symmetry" analysis. The simulations provide a list of candidate structures, sorted by cost, with their final space group, cell parameters, and atomic positions that can then be compared with existing structures by using any of a portfolio of crystallographic tools.

The preliminary step in the AASBU method consists of elaborating a suitable library of SBUs, for example in the subsequent discussion, M_xL_y (M: central metal atom; L: coordinating or 'ligand' atoms). Figure 1 shows illustrative examples of SBUs extracted from known families of inorganic structures. The next step consists of defining the rules that control the possible assembly of the SBUs during the subsequent simulation stages. These rules are encapsulated in a forcefield that includes 'sticky-atom' pairs. The SBUs are treated as rigid bodies, with the inter-SBU interactions parameterized on an atom–atom basis by a simple Lennard-Jones expression for the energy of interaction between pairs of atoms *i* and *j*, as defined in Equation (1). The 'sticky

$$E_{ij} = \varepsilon_{ij}[(r_{ij}^{*}\, r_{ij}^{-1})^{12} - 2(r_{ij}^{*}\, r_{ij}^{-1})^{6}] \quad (1)$$

atom' pairs are those that, when combined, form the inter-SBU linkages; these are parameterized as a highly attractive potential well with a minimum at a very short $L_i \cdots L_j$ separation. This potential function has no direct physical meaning. It serves simply to 'glue' together the SBUs at the linkage points during subsequent simulation steps.

A repulsive potential between $M_i \cdots M_j$ pairs prevents SBUs from overlapping with each other, and this repulsive potential is also tuned in order to favor either corner-, edge-, or face-sharing during the assembly process. This tuning provides a bias in favor of the target mode of linkage, but does not exclude other connection modes, which can then occur also as local minima in the sampled configurational space. A repulsive potential between $M_i \cdots M_j$ pairs discourages undesirable local minima corresponding to proximate, but unconnected SBUs. For example, typical values of the various atom–atom potential parameters in the Lennard-Jones expression for a corner-shared target configuration in the case of octahedra-based and tetrahedra-based building units is given in Table 1. The total cost or "energy" of a given

Table 1. Typical Lennard-Jones potential parameters used in developing the cumulative cost function[a] favoring corner-shared configurations.

	Octahedra-based building units		Tetrahedra-based building units	
	ε_{ij} [kcal mol^{-1}]	r_{ij}^{*} [Å]	ε_{ij} [kcal mol^{-1}]	r_{ij}^{*} [Å]
$L_i \cdots L_j$	400	0.20	400	0.2
$M_i \cdots M_j$	1.00	4.40[b]	1.00	3.9
$M_i \cdots L_j$	1.00	2.24	1.00	1.9

[a] Charge terms are not included in this implementation of the AASBU methodology. [b] A reduction of the r_{ij}^{*} parameter for the $M_i \cdots M_j$ pairs (3.5 Å, for example) favors edge-sharing configurations of octahedra-based building units.

configuration of SBUs in a unit cell, E_{total}, is then computed as the sum over the set of unique SBUs of the Lennard-Jones terms involving dissimilar $L \cdots L$, $M \cdots L$, and $M \cdots M$ pairs, as defined in Equation (2). The magnitude of this cost function

$$E_{\text{total}} = \sum_{\text{SBUs}} (E_{L\cdots L} + E_{M\cdots L} + E_{M\cdots M}) \quad (2)$$

provides an estimate of the degree of connectivity of a given arrangement of SBUs. Since a given SBU is defined by its geometry and its set of potential connection points, specific connection modes are easily favored or discouraged by assigning each ligand atom L with attractive or repulsive parameters. The simulations will then typically yield structures with different degrees of connectivity, their final ranking by cost being dependent on the initial parameter choices. Differing modes of interconnection, such as corner-, edge-, face-sharing, can be promoted, not only through the tuning of the $M_i \cdots M_j$ repulsive potential, but also by direct inclusion of corner-, edge-, face-sharing polyhedra within the SBUs themselves (Figure 1).

 © WILEY-VCH Verlag GmbH, D-69451 Weinheim, 2000 1433-7851/00/3913-2271 $ 17.50+.50/0

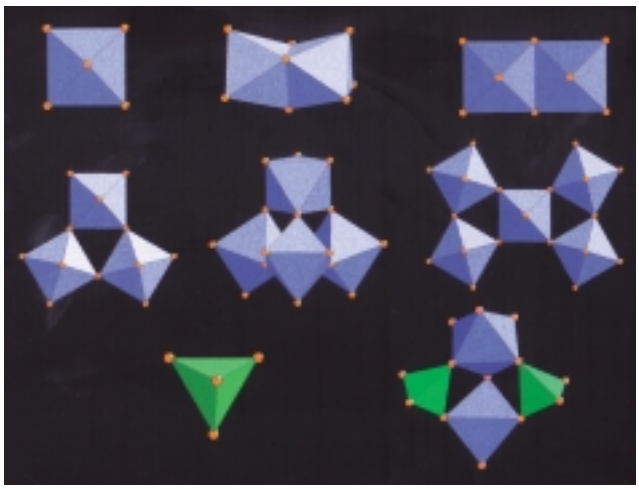


Figure 1. Examples of building units used in the AASBU method (green: tetrahedra, blue: octahedra). Simple polyhedra, including specimens with corner-, edge-, and face-sharing polyhedra, are shown together with a more complex SBU made of both octahedra and tetrahedra.

With the set of SBUs and potentials defined, the candidate periodic structures are generated by using a cascade of simulations[28] that entails five major steps:

1) Periodic SBUs trial arrangements are randomly generated by a simulated annealing procedure.[3] The angular degrees of freedom of each unique SBU are sampled by a Metropolis Monte Carlo algorithm.[29] At each such step, both the cell size and the distances between SBUs are adjusted to relieve close interatomic contacts, leading to successive phases of cell contractions and expansions. As the simulated annealing proceeds configurations of lower cost are stored;[3, 5] a typical simulation run within a 10000–300 K 'temperature' range, yields a final set of some 10^4 trial periodic configurations of SBUs.
2) The trial arrangements are reduced to a set of unique arrangements, corresponding to unique local minima; redundancies are removed through the comparison of radial distribution functions and simulated diffraction patterns.[3]
3) The resulting set, which contains typically some 10^3 unique arrangements, is minimized with respect to the cost (energy).
4) After the structure optimization, the redundant arrangements are removed. At this stage, the simulation yields typically a few hundred possible SBUs configurations, which are ranked by cost or degree of connectivity.
5) For each such configuration, the sets of 'sticky atoms' at short separations (typically pairs) are reduced to single atoms, and the space group symmetry of the arrangement determined automatically by the Find_Symmetry algorithm.[30, 31]

The result is a list of predicted structures sorted according to space group and cost, with cell parameters and atomic positions suitable for direct comparison with other libraries of inorganic crystal structures, or based on corresponding crystallographic data. The computing time depends on the number of atoms in the SBU, the stipulated number of SBUs per unit cell, and the details of the simulated annealing schedule. A typical run for an SBU composed of a trimer of octahedra (Figure 1) requires some three hours CPU time on an Octane SGI R12000 workstation operating at 300 MHz.

To demonstrate the viability of the AASBU method in structure prediction, we use simple building units extracted from known families of inorganic structures. First, to explore structure types based on corner-sharing octahedra, such as the perovskite, bronze, and pyrochlore families, SBUs composed of a discrete octahedron, ML_6, and of the trimer M_3L_{15}, the tetramer M_4L_{18}, and the pentamer M_5L_{24} were built according to the known geometry of TiO_6 in rutile (M–L = 2 Å) (Figure 1). Using a corner-sharing oriented forcefield (Table 1), we generated candidate structures with one SBU per asymmetric unit, either in *P*1 or using various space group symmetry constraints.

The known three-dimensional structure types based on corner-sharing octahedra were sucessfully generated (Table 2). For example, a simulation with ML_6 as the SBU in the space group *C*2/*c*, yields the cubic perovskite-type structure (space group $Pm3-m$). The other well-known tilted perovskite arrangements were also obtained in other space groups.[32] The pyrochlore structure type ($Fd\bar{3}m$) was generated in *P*1 using the tetrameric SBU, M_4L_{18}, appearing ranked as the lowest cost structure among a list of 50 candidates. The AASBU simulations generated all known three-dimensional structure types based on corner-sharing arrangements of the pentameric SBU, M_5L_{24}, namely the $Ba_4CoTa_{10}O_{30}$ type structure, the intergrowth tungsten bronze and the tetragonal tungsten bronze (Figure 2A), demonstrating the ability of the AASBU method to highlight topological affiliations within related materials.

Table 2. Examples of existing structures based on octahedra as predicted by the AASBU method, using various SBUs and space groups.

SBU	Space group used	Predicted structure	Symmetry analysis of the predicted structure
three-dimensional structures based on corner-sharing octahedra			
ML_6	*C*2/*c* (15)	cubic perovskite	$Pm\bar{3}m$ (221)
ML_6	$P2_12_12_1$ (19)	tilted perovskite	$P2_12_12_1$ (19)
M_3L_{15}	*P*1 (1)	hexagonal tungsten bronze	*P*6/*mmm* (191)
M_4L_{18}	*P*1 (1)	pyrochlore	$Fd\bar{3}m$ (230)
M_5L_{24}	*P*1 (1)	$Ba_4CoTa_{10}O_{30}$	*Cmmm* (65)
M_5L_{24}	*C*2 (5)	intergrowth tungsten bronze	*Fmm*2 (42)
M_5L_{24}	*P*4/*m* (83)	tetragonal tungsten bronze	*P*4/*m* (83)
other structures			
ML_6	*C*2/*c* (15)	NaCl	*Cmca* (64)
ML_6	*C*2/*c* (15)	V_2O_5	*C*2/*c* (15)
ML_6	$P2_12_12_1$ (19)	rutile (TiO_2)	$P\bar{4}2_1m$ (113)
ML_6	$P2_12_12_1$ (19)	ramsdellite (γ-MnO_2)	*Pnma* (62)

Using an elementary octahedron as SBU with a corner-sharing oriented forcefield (Table 1), generates a series of known structure types containing both edge- and corner-sharing octahedra in addition to rutile (TiO_2), such as ramsdelite (γ MnO_2), V_2O_5, and NaCl (see Table 2). Combining the use of an edge-shared dimer, M_2O_{10}, as SBU with a corner-sharing oriented forcefield (Table 1) leads to a series of structure types, including both known types such as $CaTa_2O_6$

 © WILEY-VCH Verlag GmbH, D-69451 Weinheim, 2000 1433-7851/00/3913-2272 $ 17.50+.50/0

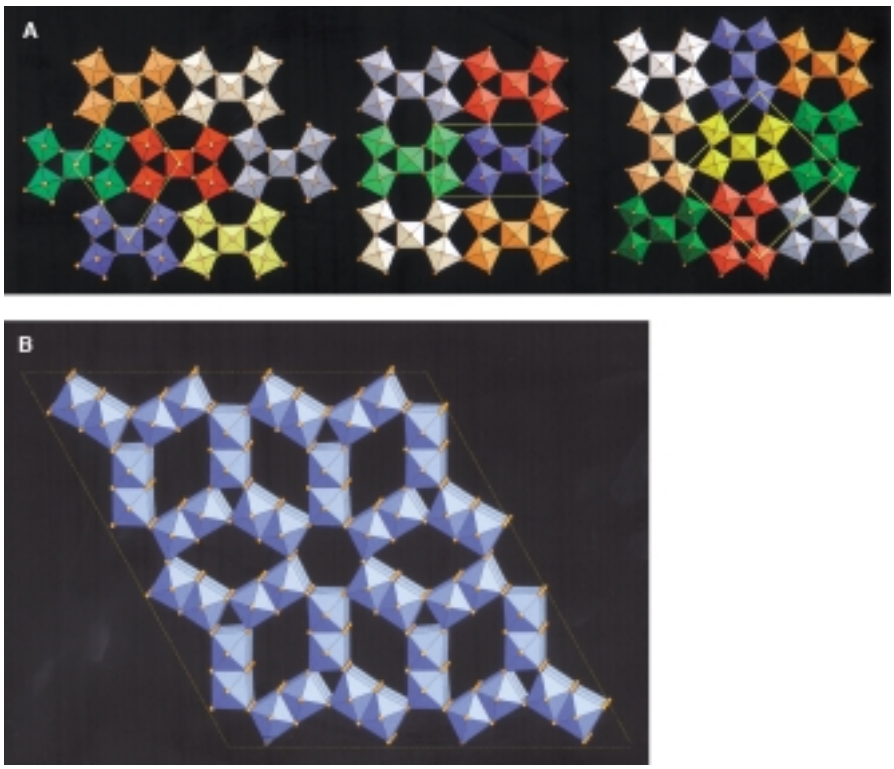


Figure 2. A) Topologic filiation between existing inorganic structures based on the pentameric SBU, M_5L_{24}, as predicted by the AASBU method. Left: $Ba_4CoTa_{10}O_{30}$, center: intergrowth tungsten bronze ($TlCa_2Ta_5O_{15}$), right: tetragonal tungsten bronze. B) New framework topology of a porous oxide (MO_3) as predicted by the AASBU method, using an edge-shared dimer, M_2O_{10}.

and $PbSb_2O_6$, as well as apparently novel microporous frameworks (Figure 2B). New metal oxides with structures based on interlinked octahedral units are topical; for example, several manganese oxide structures show interesting ion-exchange, adsorptive, magnetic, and electrochemical properties.[33] The present simulation results demonstrate the feasibility of the AASBU approach, and suggest possibilities for the a posteriori synthesis of multifunctional microporous oxides.

Continued progress in the synthesis and characterization of zeolites and related crystalline microporous solids has led to an expanding family of more than 100 observed framework structure types;[16] libraries containing many thousands of hypothetical framework structures have already been developed by several authors. Given this history of differing approaches to framework structure prediction, we have applied the AASBU method using a corner-sharing oriented forcefield to the case of an elementary tetrahedron, ML_4 (M–L = 1.65 Å), as SBU (Table 1). The number of structural possibilities is known to be large,[5, 15] so we restricted the simulations to the illustrative cases of one or two SBUs per asymmetric unit, and a selected set of space groups. In each case the anticipated, known structure types were predicted, for example the GME-, FAU-, RHO-, and LTL-frameworks.[16] New frameworks were also produced (Figure 3). Of the two structures ((a) and (b) in Figure 3) that were identified for space group P6/*mmm*, and related to the LTL-framework, the first structure (Figure 3A) is composed of a 3D arrangement of gmelinite cages[12] interconnected through their 6-rings, in contrast to the cancrinite cages[12] in the LTL-framework, but has a similar 12-ring channel system. The second structure (Figure 3B, Table 3) also contains gmelinite cages and has channels that run in the (001) direction circumscribed by 24 tetrahedra, with free aperture dimensions of 17.2×19.4 Å. Each 24-ring channel connects with its six neighbors through gmelinite cages and through six double 8-rings. The pore volume of this hypothetical structure is large; grand canonical Monte Carlo simulations of N_2 adsorption at 1 bar and 298 K, indicate an adsorption capacity of 0.25 mmol g^{-1}. Lattice energy calculations of the LTL-framework and of these two hypothetical frameworks, both with pure silicate compositions, were performed by using the GULP software and default potentials.[34] Relatively small internal energy differences (with -77.10 eV per formula unit, SiO_2, for the LTL-framework, -77.09 eV for structure (a) and -77.05 eV for structure (b)) suggest similar framework stabilities. These results underscore the vast known scope of structural possibilities for microporous framework structures composed of corner-shared tetrahedra, and highlight one advantage of the AASBU method, compared to other approaches, in its being able to accommodate SBUs substantially larger than individual tetrahedra.

In a simple, yet illustrative application of the AASBU method to structures with more than one type of SBU, a series of simulations was performed by using a 1:1 combination of an octahedron and a tetrahedron per asymmetric unit. Figure 4 illustrates a selection of the corresponding structures thus generated.

To conclude, the AASBU method offers a useful means of developing virtual libraries of viable, periodic structures for inorganic solids than can be constructed from predefined secondary building units. The use of a simple cost function developed from atom–atom Lennard-Jones potentials supports both conventional nonbonded interactions and 'sticky atom' pairs parameterized to form the SBU interlinkages during the simulated annealing and minimization procedures. Tailoring of the atom–atom potential parameters allows differing modes of interconnection to be promoted or disfavored. The AASBU method accommodates SBUs of varying complexity and size and its general applicability is demonstrated through generation of both known and apparently novel structures in various families of materials, including bronzes and zeolites. The AASBU approach provides a new de novo methodology for developing virtual libraries of viable structures, a means of rationalizing existing structures in terms of topologic affiliations, and a potential aid

 © WILEY-VCH Verlag GmbH, D-69451 Weinheim, 2000 1433-7851/00/3913-2273 $ 17.50+.50/0

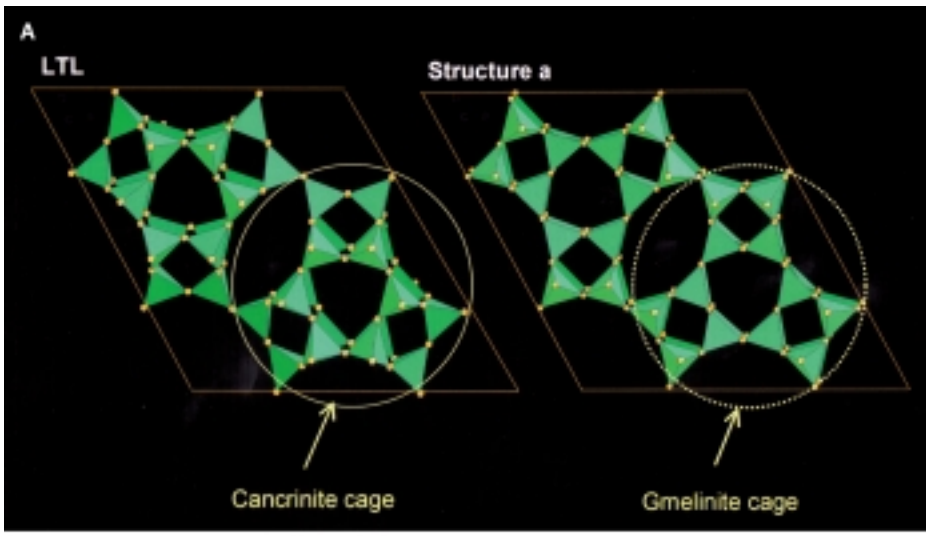


Figure 3. A) Comparison between the LTL-framework and a hypothetical 12-ring channel zeotype-structure (a) as predicted by the AASBU method. B) A second zeotype structure (b) was predicted. The simulated X-ray pattern is shown for its $Si_{48}O_{96}$ form. The associated atomic coordinates as obtained from the simulations are listed in Table 3 (cell volume: 5604.15 Å^3; channels: $24 \times 8 \times 8$; simulated N_2 adsorption capacity at 1 bar and 298 K: 0.25 mmol g^{-1}; framework density: 8.56 tetrahedra (T) per 1000 Å^3).

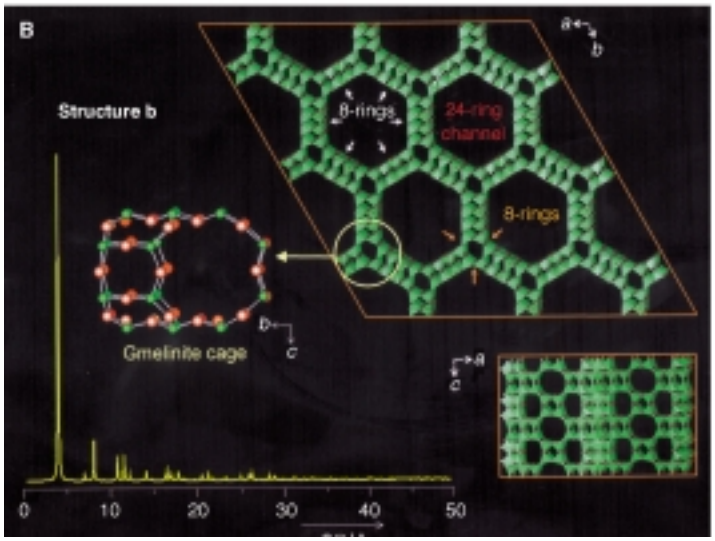


Table 3. Atomic coordinates of the hypothetical zeotype structure given in Figure 3B for the pure silicate form, which was generated by the AASBU method (P6/*mmm* symmetry, $a = b = 24.73$, $c = 10.58$ Å); two elementary tetrahedra served as building units.

Atom	*x*	*y*	*z*
Si(1)	0.530	0.333	0.336
Si(2)	0.466	0.393	0.153
O(1)	0.604	0.396	0.297
O(2)	0.476	0.341	0.264
O(3)	0.526	0.263	0.293
O(4)	0.521	0.333	0.500
O(5)	0.403	0.403	0.192
O(6)	0.455	0.363	0.000
O(7)	0.535	0.465	0.157

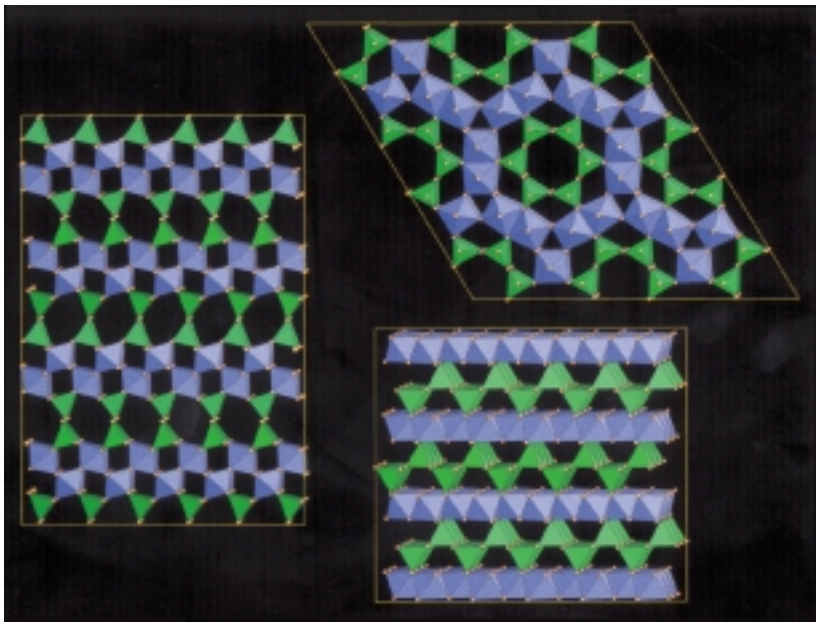


Figure 4. Examples of structures made of two independent SBUs (tetrahedra and octahedra) as predicted by the AASBU method.

in the solution of crystal structures that cannot be solved with conventional methods and for which some insight into the nature of SBUs is available. While not yet proved in practice, it is also considered likely that this SBU-based approach will yield virtual libraries whose members prove more amenable to directed synthesis: this approach opens the field to the a posteriori synthesis of inorganic structures, that is the search for a chemical match between a new predicted topology and adequate framework elements. In addition to more exhaustive studies of tetrahedral, octahedral, and mixed tetrahedral-octahedral frameworks, it will be interesting now to apply the AASBU method to other areas such as the prediction of combined framework plus template structures,[17] the 'design' step in the design-make-test-model high-throughput experimentation cycle, and to the aggregation of larger motifs as SBUs, such as polyhedra, cages, or local structures described in noncrystalline solids.

Received: July 26, 1999 [Z13781]
Revised: March 17, 2000

 © WILEY-VCH Verlag GmbH, D-69451 Weinheim, 2000 1433-7851/00/3913-2274 $ 17.50+.50/0

[1] J. Maddox, *Nature* **1988**, *335*, 201; M. L. Cohen, *Nature* **1989**, *338*, 291; F. C. Hawthorne, *Nature* **1990**, *345*, 297; C. R. A. Catlow, G. D. Price, *Nature* **1990**, *347*, 243.
[2] *New Methods for Modelling Processes within Solids and at Their Surfaces* (Ed.: C. R. A. Catlow), Oxford University Press, London, **1993**; *Journal of Computer-Aided Materials Design*, *Vol. 3* (Eds.: A. K. Cheetham, U. W. Suter, E. Wimmer, S. Yip), ESCOM, Leiden, Netherlands, **1996**.
[3] P. Verwer, F. J. J. Leusen in *Reviews in Computational Chemistry*, *Vol. 12* (Eds.: K. B. Lipkowitz, D. B. Boyd), Wiley, New York, **1998**, p. 327.
[4] S. Kirkpatrick, C. D. Gelatt, M. P. Vecchi, *Science* **1983**, *220*, 671.
[5] M. W. Deem, J. Newsam, *Nature* **1989**, *342*, 260; M. W. Deem, J. Newsam, *J. Am. Chem. Soc.* **1992**, *114*, 7189; M. Falcioni, M. W. Deem, *J. Chem. Phys.* **1999**, *110*, 1754.
[6] J. Pannetier, J. Bassas-Alsina, J. Rodriguez-Carvajal, V. Caignaert, *Nature* **1990**, *346*, 343.
[7] C. M. Freeman, J. M. Newsam, S. M. Levine, C. R. A. Catlow, *J. Mater. Chem.* **1993**, *3*, 531.
[8] J. C. Schön, M. Jansen, *Angew. Chem.* **1996**, *108*, 1358; *Angew. Chem. Int. Ed. Engl.* **1996**, *35*, 1286; H. Putz, J. C. Schön, M. Jansen, *Comput. Mater. Science* **1998**, *11*, 309.
[9] M. B. Boisen, G. V. Gibbs, M. S. T. Bukowinski, *Phys. Chem. Miner.* **1994**, *21*, 269; D. M. Teter, G. V. Gibbs, M. B. Boisen, D. C. Allan, M. P. Teter, *Phys. Rev. B* **1995**, *52*, 11; M. B. Boisen, G. V. Gibbs, M. O'Keeffe, K. L. Bartelmehs, *Micropor. Mesopor. Mater.* **1999**, *29*, 219.
[10] S. M. Woodley, P. D. Battle, J. D. Gale, C. R. A. Catlow, *Phys. Chem. Chem. Phys.* **1999**, *1*, 2535.
[11] D. E. Akporiaye, G. D. Price, *Zeolites* **1989**, *9*, 23.
[12] J. V. Smith, *Chem. Rev.* **1988**, *88*, 149, and references therein.
[13] M. O'Keeffe, B. G. Hyde, *Philos. Trans. R. Soc. London A* **1980**, *295*, 38; M. O'Keeffe, N. E. Brese, *Acta Crystallogr. Sect. A* **1992**, *48*, 663.
[14] J. Klinowski, *Curr. Opin. Solid State Mater. Sci.* **1998**, *3*, 79, and references therein; O. D. Friedrichs, A. W. M. Dress, D. H. Huson, J. Klinowski, *Nature* **1999**, *400*, 644.
[15] M. M. J. Treacy, K. H. Randall, S. Rao, J. A. Perry, D. J. Chadi, *Z. Kristallogr.* **1997**, *212*, 768.
[16] *Atlas of Zeolite Structure Types* (Eds.: W. M. Meier, D. H. Olson, C. Bärlocher), Elsevier, London, **1996**; update on: http://www.iza-sc.ethz.ch/IZA-SC.
[17] D. W. Lewis, D. J. Willock, C. R. A. Catlow, J. M. Thomas, G. J. Hutchings, *Nature* **1996**, *382*, 604; F. Cora, D. W. Lewis, C. R. A. Catlow, *Chem. Commun.* **1998**, 1934.
[18] J. V. Smith, W. J. Dytrych, *Nature* **1984**, *309*, 607.
[19] M. E. Davis, C. Saldarriga, C. Montes, J. Garces, C. Crowder, *Nature* **1988**, *331*, 698.
[20] D. E. Akporiaye, *Angew. Chem.* **1998**, *110*, 2594; *Angew. Chem. Int. Ed.* **1998**, *37*, 2456.
[21] G. Férey, A. K. Cheetham, *Science* **1999**, *283*, 1125.
[22] J. M. Newsam, F. Schüth, *Biotechnol. Bioeng.* **1999**, *61*, 203.
[23] B. Jandeleit, D. J. Schaefer, T. S. Powers, H. W. Turner, W. H. Weinberg, *Angew. Chem.* **1999**, *111*, 2648; *Angew. Chem. Int. Ed.* **1999**, *38*, 2494.
[24] G. Férey, *C. R. Acad. Sci. Ser. II c* **1999**, *1*, 1.
[25] F. Taulelle, M. Pruski, J. P. Amoureux, D. Lang, A. Bailly, C. Huguenard, M. Haouas, C. Gérardin, T. Loiseau, G. Férey, *J. Am. Chem. Soc.* **1999**, *121*, 12148.
[26] F. Taulelle, M. Haouas, C. Gérardin, C. Estournes, T. Loiseau, G. Férey, *Colloids Surf. A* **1999**, *158*, 299; S. Dick, G. Grossmann, G. Ohms, M. Müller, *Z. Naturforsch. B* **1997**, *52*, 1447.
[27] S. Dick, G. Grossmann, G. Ohms, T. Zeiske, *Z. Naturforsch. B* **1997**, *52*, 1439.
[28] Cerius2 Software Suite, Version 3.9, Molecular Simulations Inc., USA.
[29] N. Metropolis, A. Rosenbluth, M. Rosenbluth, A. Teller, E. Teller, *J. Chem. Phys.* **1953**, *21*, 1087.
[30] *Biosym Catalysis 2.0 Software Manuals 1993*, Molecular Simulations Inc., USA. The MSI Catalysis and Sorption Project is supported by a consortium of member companies.
[31] *Accuracy in Powder Diffraction II (NIST Special Publication No. 846)* (Eds.: J. M. Newsam, M. W. Deem, C. M. Freeman, E. Prince, J. K. Stalick), National Institute of Standards and Technology, Bethesda, MD, USA, **1992**, p. 80.
[32] A. M. Glazer, *Acta Crystallogr. Sect. B* **1972**, *28*, 3384.
[33] F. Cora, D. W. Lewis, C. R. A. Catlow, *Chem. Commun.* **1998**, 1943; Q. Feng, H. Kanoh, K. Ooi, *J. Mater. Chem.* **1999**, *9*, 319.
[34] J. Gale, *J. Chem. Soc. Faraday Trans.* **1997**, *93*, 629.

Template-Induced, Stereoselective Cyclizations in the Cyclopolymerization of TADDOL-Dimethacrylate**

Günter Wulff,* Anja Matussek, Christian Hanf, Stefan Gladow, Christian Lehmann, and Richard Goddard

In the context of the synthesis of main-chain chiral copolymers, Kakuchi et al.[1] cyclo-copolymerized[2] 2,3-*O*-isopropylidine-D-threitol-1,4-(dimethacrylate), derived from D-tartaric acid, with styrene. After removal of the 2,3-*O*-isopropylidine-D-threitol template, the resulting copolymers containing methylmethacrylate and styrene units showed relatively small optical rotations, in contrast to copolymers prepared from D-mannitol derivatives previously obtained by us.[2] In order to obtain increased asymmetric induction, we used (*R*,*R*)-TADDOL, introduced by Seebach et al.,[3] instead of the threitol derivative, and prepared for the first time the dimethacrylate **M** (see Scheme 1).[4, 5] Surprisingly, copolymerization with styrene followed by removal of the template resulted in a copolymer with a significantly smaller optical activity. This can only be explained if the methacrylate units are arranged as *meso* diads to one another. Homopolymerization should lead to an isotactic arrangement in the chain, and this was indeed the case. After anionic polymerization, removal of the template, and esterification, the polymethacrylate obtained was completely isotactic, but it exhibited a small but distinct optical rotation, which decreased with increasing molecular weight.

Independent of our work, Sogah, Okamoto, and co-workers[6, 7] also prepared the monomer **M** and homopolymerized it by radical, anionic, and group-transfer polymerization. They obtained a homopolymer with a large optical rotation, from which they assumed that it exists as an atropisomeric single-handed helix, as found for tritylmethacrylate. After removal

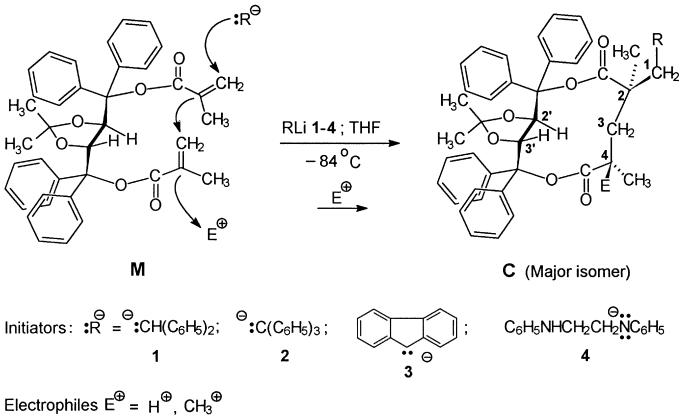
[*] Prof. Dr. G. Wulff, Dr. A. Matussek, Dr. C. Hanf, Dr. S. Gladow
Institut für Organische Chemie und Makromolekulare Chemie
Heinrich-Heine-Universität Düsseldorf
Universitätsstrasse 1, 40225 Düsseldorf (Germany)
Fax: (+49) 211-8114788
E-mail: wulffg@uni-duesseldorf.de
Dr. C. Lehmann, Dr. R. Goddard
Max-Planck-Institut für Kohlenforschung
Kaiser-Wilhelm-Platz 1, 45470 Mülheim/Ruhr (Germany)

[**] This work was supported by the Fonds der Chemischen Industrie.

 © WILEY-VCH Verlag GmbH, D-69451 Weinheim, 2000 1433-7851/00/3913-2275 $ 17.50+.50/0

of the template and conversion to the methyl ester, they similarly obtained a highly isotactic polymethacrylate (PMMA).

We now wanted to investigate more precisely the mechanism of this cyclopolymerization—in particular the first steps—to obtain further details about the polymerization and the structure of the helical polymers, as well as the PMMAs. We therefore attempted to bring about just the first step of the polymerization—the cyclization—using the monomer **M** and various anionic initiators (Scheme 1). By using a



Scheme 1. Anionic cyclization of TADDOL-dimethacrylate **M** with various initiators.

sufficiently large excess of the initiator, a monocyclization was indeed successfully achieved.[8] Subsequently, this anionic intermediate was then allowed to react with MeOH or with CH_3I, whereby the H- or CH_3-terminated cyclic compound was obtained in yields of 60–70%. The termination with CH_3^+ has the advantage that only one new stereogenic center is created, and thus only two diastereomers can be formed. Termination with H^+ results in two stereogenic centers, so that in total four diastereomers are possible. The disadvantage here is that the second step proceeds less stereoselectively, and thus under these conditions one always obtains a mixture. If, however,—as intended in our case—the products so obtained are deprotonated again in order to serve as optically active initiators for anionic polymerization or as chiral building blocks,[9] this is not a considerable disadvantage, since this stereogenic center is removed again in the anion.

Here only the CH_3-terminated monocycles will be described in detail. Diphenylmethyllithium (**1**), triphenylmethyllithium (**2**), fluorenyllithium (**3**), and *N*,*N*′-diphenylethylenediamine-*N*-lithium (DPEDA-Li) (**4**) were used as initiators. The composition of the reaction products were analyzed by ^{1}H NMR spectroscopy; the protons on C-2′ and C-3′ of the TADDOL group, in particular, differ significantly in the diastereomers. As expected, two diastereomers were obtained, which depending on the initiator (diphenylmethyl < trityl < fluorenyl < DPEDA) were formed with diastereoselectivities *de* of between 16.6 and 96.4% (Table 1).

Table 1. Percentage composition of the stereoisomers obtained from the monocyclization of **M** with various initiators.

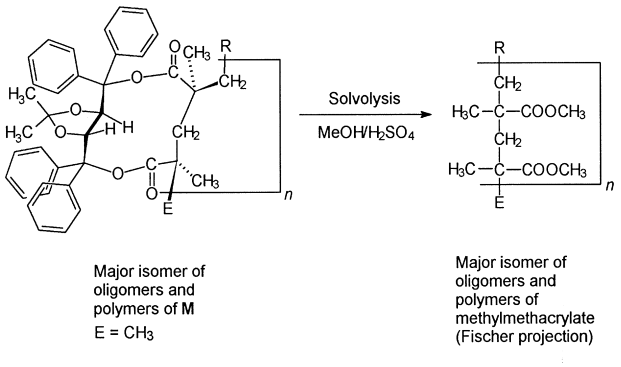
Initiator	Ring system	Product ratio on termination with CH_3I [%][a]		*de* [%]
1	**C1**	58.3	41.7	16.6
2	**C2**	74.9	25.1	49.8
3	**C3**	91.7	8.3	83.4
4	**C4**[b]	98.2	1.8	96.4

[a] The diastereomers produced were identified by NMR analysis. If not otherwise stated, on the left is the amount of the (2*S*) isomer and on the right the (2*R*) isomer. [b] In this case according to the CIP rules, on the left is the (2*R*) isomer and on the right is the (2*S*) isomer; the absolute configurations are, however, the same as those for the other substances given in same columns.

In order to show that in each case C-2 epimers are indeed involved, the isomeric compounds **C2** (major isomer) and **C2′** (minor isomer) cyclized with the trityl derivative **2** were obtained analytically pure by chromatographic separation, and the template was removed by methanolysis.[10] The resulting methacrylate dimers $\mathbf{C_h2}$ (major isomer, Scheme 2) and $\mathbf{C_h2'}$ (minor isomer) prove unequivocally to be enantiomers, by virtue of their equal but complementary optical rotations and their CD spectra. The absolute configuration was then determined by an X-ray structure analysis of **C2**,[11] which shows it to be the (2*S*) compound. Accordingly, **C2′** is the (2*R*) compound.

The first step of the cyclopolymerization to form the 11-membered ring thus proceeds highly stereoselectively for the fluorenyl and DPEDA initiators. Correspondingly, one obtains in these cases one diastereomer in high yields which can be isolated completely pure by crystallization. Subsequent hydrolysis readily affords the pure enantiomer $\mathbf{C_h3}$ and $\mathbf{C_h4}$, respectively (see Scheme 2).

The stereochemical direction of the subsequent polymerization steps can be best investigated by using trityl as initiator, since both epimers are formed in the first step. Whereas it is comparably simple to obtain the monocycles from **M** by using an excess of initiator, the second polymerization step to the dimer with two cycles must be extremely carefully controlled, since the anion of the dimer, and even more so that of the trimer, have higher reaction rates than that of the monocycle. By optimization of the conditions, a mixture



C : *n*=1 ; **B** : *n*=2 ; **T** : *n*=3 ; $\mathbf{P}_n$: *n*=12–90 $\quad$ $\mathbf{C_h}$: *n*=1 ; $\mathbf{B_h}$: *n*=2 ; $\mathbf{T_h}$: *n*=3 ; $\mathbf{P_{nh}}$: *n*=12–90

Scheme 2. Removal of TADDOL from the cyclized compound with formation of oligomers and polymers of methylmethacrylate.

 © WILEY-VCH Verlag GmbH, D-69451 Weinheim, 2000 1433-7851/00/3913-2276 $ 17.50+.50/0 *Angew. Chem. Int. Ed.* **2000**, *39*, No. 13

can be obtained after termination with CH_3I that comprises 16% from monocycles **C2**, 15% from dimers with two cycles **B2**, 1% from trimers with three cycles **T2**, and 60% from oligomers $\mathbf{P_n}$**2** with $n > 10$. The dimers **B2** possess three new stereogenic centers and can therefore form eight diastereoisomers. In fact, one observes only four, in the ratio of 77:15:7:<1 in the NMR spectrum, whereas for the trimer **T2** only one single isomer is detectable.

The major component of the dimers **B2** can be obtained analytically pure by using chromatography. Crystals suitable for X-ray structure analysis can be obtained from $CHCl_3$/pentane.[12, 13] Figure 1 shows the structure, which allows important conclusions to be drawn about the structure of

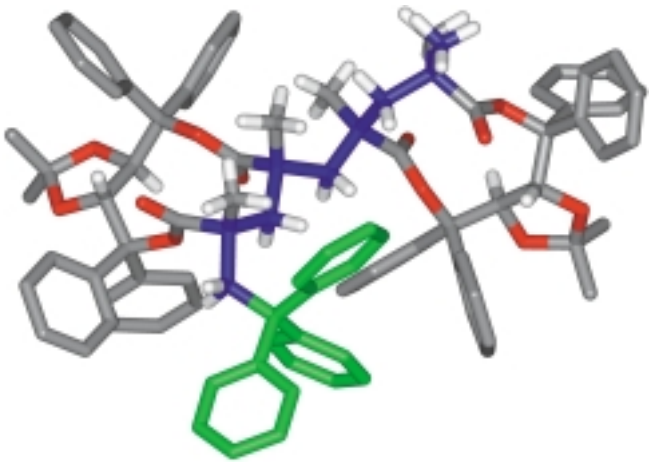


Figure 1. The X-ray crystal structure of **B2**. Initiator group (trityl): green, methylmethacrylate chain: blue.

the polymer. The stereochemistry of C-4, the second stereogenic center of the first monomer unit, has an *S* configuration. The corresponding PMMA diad, formed after removal of the template, corresponds therefore to a *meso* diad, as is present in isotactic polymers. The attack of the anion of the monocycle on a new monomer **M** thus proceeds with high stereoselectivity, as for the first monomer and also for the new stereogenic center of the second monomer (C-6). The anionic monocycle acts thus like a strongly bulky initiator and induces a new center with the same absolute configuration as in **C2**, which, however, because of the CIP rules is designated (6*R*). In the case of the fluorenyl and DPEDA initiators it should be possible to obtain the dimers **B3** and **B4**, respectively, directly in an almost diastereomerically pure form. On hydrolysis of the main isomer of **B2**, the MMA tetramer $\mathbf{B_h}$**2** was also obtained enantiomerically pure.

The trimer **T2**, which is only obtained as a single diastereomer, possesses a similarly configurated structure throughout, which on hydrolysis leads to an enantiomerically pure (2*S*, 4*S*, 6*S*, 8*R*, 10*R*) hexamer $\mathbf{T_h}$**2** of MMA, which is completely isotactic. Evidently, after the formation of the (non-methylated) anionic dimer with two cycles, a change in the steric control occurs by the helix-control mechanism, known also for the polymerization of tritylmethylacrylate,[14] which leads to an increase in the speed of the reaction and an appreciably higher stereoselectivity. For this reason also almost no oligomers $\mathbf{P_n}$ with *n* between 3 and 10 are found. Evidently, here is also a similarity to the helix-sense-selective anionic polymerization of tritylmethacrylate, in which oligomers with the incorrect configuration grow no further.[14]

By increasing the ratio of monomer to initiator, polymers $\mathbf{P_n}$ can be prepared, whose degree of polymerization *n* is extensively controlled by the monomer/initiator ratio. The specific optical rotation increases considerably with *n*. This has been attributed to a single-handed helix,[6, 7] which in this case could be either left- or right-handed. For steric reasons two neighboring monomer units can only occur in a specific relative arrangement to one another. The X-ray structure analysis of **B2** reveals that the two monomer units make an angle of 120.9° to one another, and that both units are arranged in a right-handed helical sense, thus forming a *M* helix. On increasing the length of this chain still further, all the monomer units should maintain this relation to one another, leading to a *M* helix with three monomer units per turn. Accordingly, we are looking at a 3/1 helix with a repeat distance of 13.4 Å. Thus, for the first time an atopisomeric helix of vinyl polymers has been unequivocally and completely described.

Thus, during the anionic cyclopolymerization of **M** the first step involves cyclization to give the 11-membered ring, whereby the *de* value on the first stereogenic center (C-2) lies between 17 and 96%, depending on the bulkiness of the initiator. In the second step the anion of the monocycle attacks a new monomer, during which two new stereogenic centers (C-4 and C-6) are formed. The isolated dimers show that this step proceeds with high stereoselectivity, especially when one considers that a large percentage of the dimers with the "correct" configuration reacts further. The formation of trimers, tetramers, etc., proceeds more rapidly and with higher stereoselectivity, since on the formation of a helix, the new monomer can only attack with a specific stereochemistry (helix-control mechanism). The polymer chain with **M** members can only exist in a helical, atropisomeric form, so that the polymerization is a "helix-sense-selective" polymerization, while at the same time all stereogenic centers in the chain are built up with the same absolute configuration. Correspondingly, after removal of the template one obtains uniform enantiomers of isotactic oligomers or polymers $\mathbf{P_h}$ of methylmethacrylate, which otherwise are very difficult to synthesize.[15] It should also be possible to obtain similar stereochemical control during cyclopolymerization using other monomer units bonded to TADDOL.

Received: February 8, 2000 [Z 14673]

[1] For an overview see: K. Yokota, O. Haba, T. Satoh, T. Kakuchi, *Macromol. Chem. Phys.* **1995**, *196*, 2383–2416.

[2] Review articles: a) G. Wulff, *Angew. Chem.* **1989**, *101*, 22; *Angew. Chem. Int. Ed. Engl.* **1989**, *28*, 21; b) "Synthesis of Polymers": G. Wulff in *Materials Science and Technology Series* (Ed.: A. D. Schlüter), Wiley-VCH, Weinheim, **1999**, p. 375.

[3] D. Seebach, A. K. Beck, R. Imwinkelried, S. Roggo, A. Wonnacott, *Helv. Chim. Acta* **1987**, *70*, 954.

 © WILEY-VCH Verlag GmbH, D-69451 Weinheim, 2000 1433-7851/00/3913-2277 $ 17.50+.50/0

[4] a) G. Wulff, S. Gladow, B. Kühneweg, S. Krieger, presented at the 5th SPSI-Int. Conference in Osaka, Japan **1994**. See: G. Wulff, S. Gladow, B. Kühneweg, S. Krieger, *Macromol. Symp.* **1996**, *101*, 355; b) S. Gladow, Dissertation, Universität Düsseldorf, **1994**.
[5] G. Wulff, U. Zweering, S. Gladow, *Polym. Prepr. Am. Chem. Soc. Div. Polym. Chem.* **1996**, *37*, 448.
[6] T. Nakano, Y. Okamoto, D. Y. Sogah, S. Zheng, *Macromolecules* **1995**, *28*, 8705 – 8706.
[7] a) D. Sogah, S. Zheng, T. Nakano, *Polym. Prep. Am. Chem. Soc. Div. Polym. Chem.* **1996**, *37*, 442 – 443; b) S. Zheng, D. Y. Sogah, *Polym. Prep. Am. Chem. Soc. Div. Polym. Chem.* **1997**, *38*, 60 – 61; c) S. Zheng, D. Y. Sogah, *Tetrahedron* **1997**, *53*, 15469 – 15485; D. Y. Sogah, S. Zheng, *Polym. Prepr. Am. Chem. Soc. Div. Poly. Chem.* **1999**, *40*, 540 – 541.
[8] Synthesis of the monocycle **C2** with $R = C(C_6H_5)_3$, $E = CH_3$: Under inert conditions THF (700 mL) (dried over BuLi) was condensed onto triphenylmethane (10.5 g, 42 mmol). At $-84\,^{\circ}C$ the mixture was stirred with BuLi (25 mL, 40 mmol) for 12 h. Subsequently, **M** (5.5 g, 8.5 mmol) in THF (16 mL) was slowly added in measured quantities over 100 min using a perfusor. After the addition, the mixture was stirred for 8 h. It was then stirred with CH_3I (10 mL) for a further 4 h. After concentration at $40\,^{\circ}C$ the mixture was examined by ^1H NMR spectroscopy, and the major component **C2** purified by chromatography.
[9] A. Matussek, Dissertation, Universität Düsseldorf, **1999**.
[10] Hydrolysis of the monocycles: Compound **C** (1 g) in MeOH (1.4 L) was heated with concentrated H_2SO_4 (420 mL) under reflux for 120 h. After addition of H_2O (700 mL), the mixture was extracted four times with diethyl ether. The organic phase was washed with saturated $NaHCO_3$ solution until it was neutral, then washed with H_2O, and concentrated after drying with Na_2SO_4. The compound was purified by chromatography. Yield $\mathbf{C_h} \sim 30 - 60\,\%$, $\mathbf{B_h} \sim 30\,\%$, $\mathbf{T_h} \sim 43\,\%$, $\mathbf{P_h} \sim 75\,\%$.
[11] Crystal structure data for **C2** · hexane[13].
[12] Crystal structure data for **B2**:[13] Crystals from $CHCl_3$/pentane; $C_{98}H_{94}O_{12}$, $M_r = 1463.73$, orthorhombic, space group $P2_12_12_1$ (no. 19), $a = 15.106(3)$, $b = 17.289(4)$, $c = 38.611(8)$ Å, $V = 10084(3)$ Å^3, 100 K, $Z = 4$, $\rho_{calcd} = 0.96\ g\,cm^{-3}$, $\mu = 0.063\ mm^{-1}$, crystal size $0.35 \times 0.25 \times 0.18$ mm, Nonius KappaCCD diffractometer, $Mo_{K\alpha}$ radiation, $1.05 < \theta < 27.50^{\circ}$, 53982 measured reflections, 21803 independent, and 12130 with $I > 2\sigma(I)$, programs SHELXS-97 and SHELXL-97; both programs are from G. M. Sheldrick, Universität Göttingen, **1997**; 993 parameters, $R1 = 0.083$, w$R2$ (all data = 0.259, $(\Delta/\sigma)_{max} = 0.001$, H atoms riding, max/min residual electron density $0.796/-0.366\ e\,Å^{-3}$.
[13] Crystallographic data (excluding structure factors) for the structures reported in this paper have been deposited with the Cambridge Crystallographic Data Centre as supplementary publication no. CCDC-139662 (**C2**) and CCDC-139663 (**B2**). Copies of the data can be obtained free of charge on application to CCDC, 12 Union Road, Cambridge CB2 1EZ, UK (fax: (+44) 1223-336-033; e-mail: deposit@ccdc.cam.ac.uk).
[14] Y. Okamoto, H. Mohri, T. Nakano, K. Hatada, *J. Am. Chem. Soc.* **1989**, *111*, 5952.
[15] G. Wulff, U. Zweering, *Chem. Eur. J.* **1999**, *5*, 1898 – 1904.

Bicyclo[3.2.1]DNA: On the Structural and Energetic Role of the Furanose Subunit in Complementary Strand Recognition of DNA**

Bernhard M. Keller and Christian J. Leumann*

Dedicated to Professor Richard Neidlein on the occasion of his 70th birthday

The nucleic acids (DNA, RNA) are the molecular "master-tapes" of all genetic information in living systems. In a cell, protein-controlled DNA replication proceeds with high efficiency, high speed, and high fidelity. Only a limited number of mutations, responsible for sequence evolution of DNA and thus the evolution of species, are admitted. The functional properties of DNA and RNA, which have outperformed alternative complementary base-pairing systems during molecular evolution,[1] therefore demand structure – function correlation studies.[2]

Experimental investigations showed that removal of the central ring in the nucleoside units, as in the acyclic DNA analogues glycerol-DNA,[3] 1,2-*seco*-DNA[4] (Figure 1), and

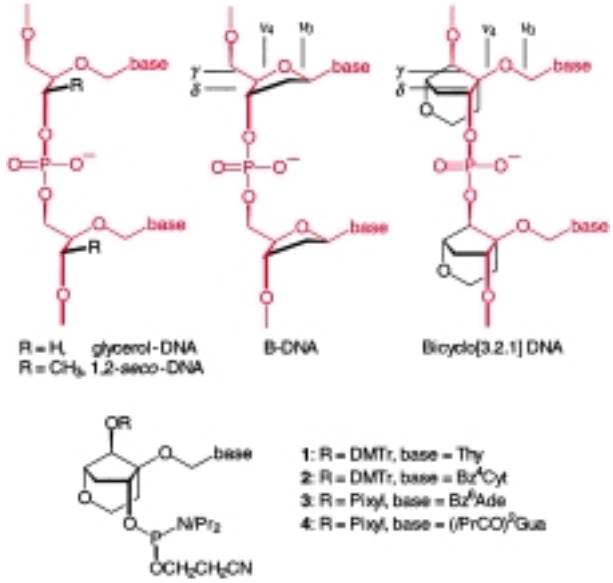


Figure 1. Above: Section of the chemical structures of glycerol-DNA, 1,2-*seco*-DNA, natural B-DNA, and bicyclo[3.2.1]DNA. The commonly shared structural features in the sugar-phosphate backbones of the four systems are drawn in red. The sugar- and backbone torsion angles ν_0, ν_4, γ, and δ differ in their conformational freedom in the three pairing systems. Essentially, no rotational restriction around the four torsion angles ν_0, ν_4, γ, and δ occurs in glycerol- and 1,2-*seco*-DNA. In B-DNA, the torsion angles δ, ν_0, and ν_4, are restricted by the furanose ring. In bicyclo[3.2.1]DNA, the backbone torsion angles γ and δ are frozen in a geometry similar to that observed in B-DNA duplexes, while the endocyclic torsion angles ν_0, ν_4 are conformationally flexible. Below: The bulding blocks for the synthesis of bicyclo[3.2.1]oligonucleotides. DMTr = (4′,4′-dimethoxy)triphenylmethyl, Pixyl = 9′-phenyl xanthenyl, Bz = benzoyl.

[*] Prof. C. J. Leumann, Dipl.-Chem. B. M. Keller
Department of Chemistry and Biochemistry
University of Bern
Freiestrasse 3, 3012 Bern (Switzerland)
Fax: + (41) 31-631-3422
E-mail: leumann@ioc.unibe.ch

[**] Financial support by the Swiss National Science Foundation is gratefully acknowledged. B.M.K. thanks the Roche Science Foundation for a PhD stipendium.

 © WILEY-VCH Verlag GmbH, D-69451 Weinheim, 2000 1433-7851/00/3913-2278 $ 17.50+.50/0

related systems,[5] leads to incompetent complementary base-pairing systems, most likely because of the high entropic costs for conformational reorganization of the single strands upon duplex formation. On the other hand, investigations in the areas of antisense research[6–12] and prebiotic chemistry[13–16] give an increasing number of DNA-like base-pairing systems, based on cyclic nucleoside analogues, that show characteristic structural and functional properties.

From the supramolecular point of view, it remains an open question whether the connection between the bases and the phosphodiester backbone needs to be a ring system in order to obtain a base-pairing system which is sensitive to base mismatches and selective to strand orientation. We decided to address this question with the DNA analog bicyclo[3.2.1]-DNA. In this analogue, the phosphodiester backbone is preorganized in a B-DNA conformation, while the base is attached to the backbone via an acyclic linking unit.[17] While we have already demonstrated that the pyrimidine-containing bicyclo[3.2.1]oligonucleotide forms duplexes with complementary DNA,[18] we show here that bicyclo[3.2.1]DNA is, by itself, a selective base-pairing system.

The synthesis of the bicyclo[3.2.1]oligonucleotides started from the corresponding phosphoramidite building blocks **1**–**4** according to adapted protocols for solid-phase DNA synthesis and will be reported in detail elsewhere. In order to explore the base-pairing properties, a series of 10–20 nucleotide unit sequences were prepared and their integrity verified by ESI^+ mass spectrometry (Table 1). For reasons of their synthethesis, all bicyclo[3.2.1]oligonucleotides bear a natural deoxynucleotide unit at their 3′ end (represented in bold type in Table 1).

To determine the relative differences in stability between duplexes in the bicyclo[3.2.1]DNA and the natural DNA series, UV-melting curve experiments were performed. With the exception of the adenine- and thymine-containing homodecamers, the bicyclo[3.2.1]oligonucleotides formed stable, antiparallel duplexes (Table 2). Their melting temperatures (T_m) were generally lower by 1.5–2.5 K per base pair compared to the natural oligonucleotides. Neglecting the energetic contribution of the terminal base pairs in the duplexes, this represents an average increase in the value of ΔG^0 of 0.7–0.8 kcal mol^{-1} per base pair (25 °C). The decrease in melting temperature for the bicyclo[3.2.1]DNA 15-mer duplex relative to the bicyclo[3.2.1]DNA 13-mer duplex (Entry 2 versus 3 in Table 2) is likely to arise due to the higher content of A-T base pairs in the former duplex and indicates a stronger energetic contribution of G-C base pairs to the duplex stability of bicyclo[3.2.1]DNA.

Table 1. Sequence and mass spectrometric data of the bicyclo[3.2.1]oligonucleotides used in this investigation.

bicyclo[3.2.1]oligonucleotides	ESI^+-MS	
	calcd.	found
5′-AAAAAAAAAA**A**-3′	3574.5	3574.0
5′-AAGAGAGGGAAG**A**-3′	4778.3	4777.8
5′-AGAGAGAGAGAAAAA**A**-3′	5500.8	5500.1
5′-AAAGAAAAAGAGAGGGAAG**A**-3′	7379.1	7379.3
5′-TTTTTTTTTT**T**-3′	3484.5	3482.1[a]
5′-TCTTCCCTCTCT**T**-3′	4473.3	4474.6
5′-TTCTCTCCCTTC**T**-3′	4473.3	4474.6
5′-TCTTCCCCCTCT**T**-3′	4458.8	4459.5
5′-TTTTTCTCTCTCTC**T**-3′	5210.8	5212.6[a]
5′-TCTTCCCTCTCTTTTTCTT**T**-3′	6982.1	6980.2[a]

[a] Determined by MALDI-TOF mass spectometry.

Strand association in bicyclo[3.2.1]DNA is selective to orientation: Duplexes were formed only between antiparallel complementary strands. A test for the formation of a parallel duplex between two parallel complementary bicyclo[3.2.1]-oligonucleotide 13-mers was negative (Entry 5, Table 2). Thus, the mode of strand association is controlled remotely by the geometry of the backbone unit. Furthermore, as in DNA, base mismatch is strongly discriminated in bicyclo[3.2.1]DNA. This is inferred from the observation that within a 13-mer duplex of bicyclo[3.2.1]DNA, an A-C mismatch in the center of the sequence completely forbids duplex formation (Entry 6, Table 2; compare with Entry 2 for the fully matched duplex).

Preliminary information on the structure of bicyclo-[3.2.1]DNA duplexes was obtained from CD spectroscopy and molecular modeling. The CD spectrum of the antiparallel, complementary bicyclo[3.2.1]DNA 20-mer duplex (Entry 4, Table 2) is reminiscent of a Watson–Crick base-paired A-type double helix and different from that of the corresponding DNA duplex, which adopts a B-DNA conformation (Figure 2). This was unexpected, since the backbone torsion angle δ—which is mostly responsible for the conformational

Table 2. Melting points (T_m) from the UV melting curves (260 nm) of a series of DNA and the bicyclo[3.2.1]DNA duplexes of 10–20 base pairs.[a]

Entry	Duplex		T_m [°C]	ΔT_m [K][b]	$\Delta G^{25\,°C}$ [kcal mol^{-1}][c]
1	5′-AAAAAAAAAA	DNA	33		−7.3
	TTTTTTTTTT-5′	[3.2.1]DNA	<0	–	–
2	5′-AAGAGAGGGAAGA	DNA	52.6		−16.0
	TTCTCTCCCTTCT-5′	[3.2.1]DNA	20.8	−2.4	−7.7
3	5′-AGAGAGAGAGAAAAA	DNA	54.9		−17.1
	TCTCTCTCTCTTTTT-5′	[3.2.1]DNA	18.4	−2.4	−6.6
4	5′-AGAAGGGAGAGAAAAAGAAA	DNA	61.9		−25.2
	TCTTCCCTCTCTTTTTCTTT-5′	[3.2.1]DNA	30.6	−1.6	−11.2
5	5′-AAGAGAGGGAAGA	DNA	[d]	–	–
	5′-TTCTCTCCCTTCT	[3.2.1]DNA	<0	–	
6	5′-AAGAG**A**GGGAAGA	DNA	[d]	–	–
	TTCTC**C**CCCTTCT-5′	[3.2.1]DNA	<0	–	

[a] Experimental conditions: c(duplex) = 2 μM, in 10 mM Na cacodylate, 1 M NaCl, pH 7.0. [b] T_m difference between the DNA- and bicyclo[3.2.1]DNA-duplexes per base pair. [c] The values were obtained from curve fitting to the experimentally determined melting curve according to described procedures.[18] [d] Not determined.

 © WILEY-VCH Verlag GmbH, D-69451 Weinheim, 2000 1433-7851/00/3913-2279 $ 17.50+.50/0

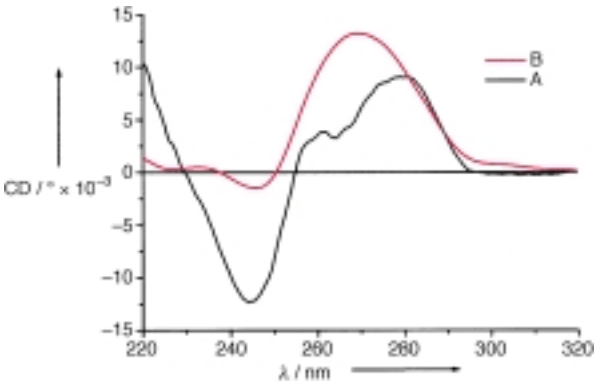


Figure 2. CD spectra of the DNA (A) and the bicyclo[3.2.1]DNA (B) duplexes which correspond to Entry 4 in Table 2 at 4 °C. Buffer conditions as indicated in Footnote [a], Table 2.

difference between the A- and B-DNA families—is restricted in bicyclo[3.2.1]DNA to values that are typical for B-DNA.

A molecular dynamics simulation of the bicyclo[3.2.1]DNA duplex corresponding to Entry 2 (Table 2) on a 200 ps trajectory with the initial structure in a B-DNA geometry revealed a double helical structure which roughly resembles that of a B-DNA double helix (Figure 3). No major differences, relative to DNA, are observed for the backbone torsion

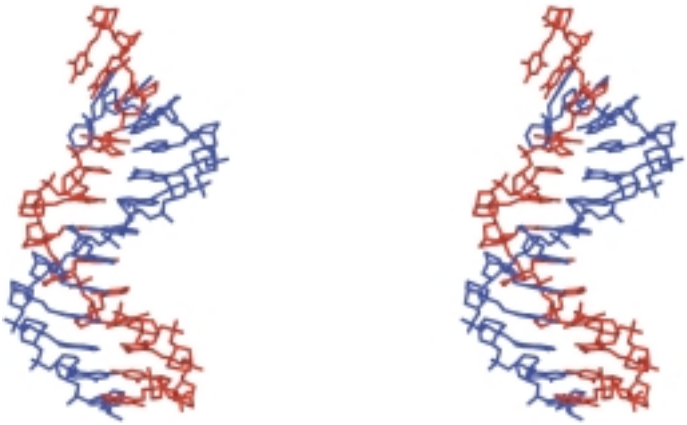


Figure 3. Stereoscopic view of the averaged structure of the last 50 ps of the 200 ps molecular dynamics simulation (Insight II/Discover) of the bicyclo[3.2.1]DNA duplex corresponding to Entry 2 in Table 2. For the simulation,the AMBER force field was used and a distance-dependent dielectric constant of $\varepsilon = 4r$ was used to simulate an aqueous environment.

angles $\alpha - \zeta$. As expected, the linker region between the base and the backbone unit in bicyclo[3.2.1]DNA adopts a nearly perfect, extended conformation and thus differs from the corresponding structural unit in B-DNA. As a result, the base-stacking pattern in bicyclo[3.2.1]DNA becomes similar to A-DNA (Figure 4), which is in accord with the CD spectrum.

From the experimental results, the following conclusions with respect to the structural and energetic role of the furanose ring system in DNA can be drawn. 1) The entropic costs for duplex formation in a phosphodiester-based analogue of DNA, in which the bases are flexibly attached to the backbone, can be overcome if the backbone itself is restricted conformationally. 2) Even without a ring system, which brings the nucleobases into a well defined orientation with respect to the backbone, strand orientation selectivity can be maintained. This is of interest with respect to the acyclic, peptide-based DNA analogue PNA, which only shows a very modest strand-orientation selectivity,[19] and with respect to mixed, α/β-DNA duplexes, in which the preferred strand alignment is opposite (parallel) to that observed for β/β-DNA duplexes (antiparallel).[20] 3) An increase in the translational and rotational degrees of freedom of a base pair in the center of the double helix does not lead to a loss in base-pairing selectivity.

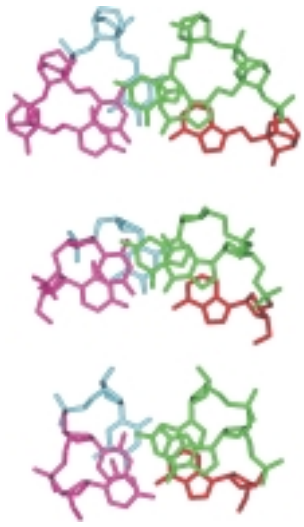


Figure 4. View along the helix axis of the central AGG-CCT unit in the modeled structure of the bicyclo[3.2.1]DNA 13-mer duplex (above), of canonical A-DNA (middle), and of canonical B-DNA (below). The similarity in the base-stacking pattern between A-DNA and the bicyclo[3.2.1]DNA is evident.

Whatever the chemical determinants by which RNA and DNA became selected as a genetic material, phosphodiester-based systems devoid of a ring unit as a connector between the bases and backbone cannot collectively be excluded from the list of potential candidates in the selection process.

Received: February 16, 2000 [Z 14713]

[1] *The RNA World*, (Eds.: R. F. Gesteland, T. R. Cech, J. F. Atkins), 2nd ed., Cold Spring Harbor Laboratory Press, New York, **1999**.
[2] A. Eschenmoser, M. Dobler, *Helv. Chim. Acta* **1992**, *75*, 218 – 259.
[3] K. C. Schneider, S. A. Benner, *J. Am. Chem. Soc.* **1990**, *112*, 453 – 455.
[4] L. Peng, H.-J. Roth, *Helv. Chim. Acta* **1997**, *80*, 1494 – 1512.
[5] P. Nielsen, L. H. Dreioe, J. Wengel, *Bioorg. Med. Chem.* **1995**, *3*, 19 – 28.
[6] A. A. Koshkin, S. K. Singh, P. Nielsen, V. K. Rajwanshi, R. Kumar, M. Meldgaard, C. E. Olsen, J. Wengel, *Tetrahedron* **1998**, *54*, 3607 – 3630.
[7] V. K. Rajwanshi, A. E. Hakansson, B. Dahl, J. Wengel, *Chem. Commun.* **1999**, 1395 – 1396.
[8] C. Hendrix, H. Rosemeyer, I. Verheggen, F. Seela, A. Van Aerschot, P. Herdewijn, *Chem. Eur. J.* **1997**, *3*, 110 – 120.
[9] Y. Maurinsh, H. Rosemeyer, R. Esnouf, A. Medvedovici, J. Wang, G. Ceulemans, E. Lescrinier, C. Hendrix, R. Busson, P. Sandra, F. Seela, A. Van Aerschot, P. Herdewijn, *Chem. Eur. J.* **1999**, *5*, 2139 – 2150.
[10] M. Bolli, C. Litten, R. Schütz, C. Leumann, *Chem. Biol.* **1996**, *3*, 197 – 206.
[11] M. Bolli, H. U. Trafelet, C. Leumann, *Nucleic Acids Res.* **1996**, *24*, 4660 – 4667.
[12] R. Steffens, C. J. Leumann, *J. Am. Chem. Soc.* **1999**, *121*, 3249 – 3255.
[13] M. Beier, F. Reck, T. Wagner, R. Krishnamurthy, A. Eschenmoser, *Science* **1999**, *283*, 699 – 703.
[14] J. Hunziker, H.-J. Roth, M. Böhringer, A. Giger, U. Diederichsen, M. Göbel, R. Krishnan, B. Jaun, C. Leumann, A. Eschenmoser, *Helv. Chim. Acta* **1993**, *76*, 259 – 352.
[15] O. Jungmann, H. Wippo, M. Stanek, H. K. Huynh, R. Krishnamurthy, A. Eschenmoser, *Org. Lett.* **1999**, *1*, 1527 – 1530.
[16] S. Pitsch, R. Krishnamurthy, M. Bolli, S. Wendeborn, A. Holzner, M. Minton, C. Lesueur, I. Schönvogt, B. Jaun, A. Eschenmoser, *Helv. Chim. Acta* **1995**, *78*, 1621 – 1635.

 © WILEY-VCH Verlag GmbH, D-69451 Weinheim, 2000 1433-7851/00/3913-2280 $ 17.50+.50/0

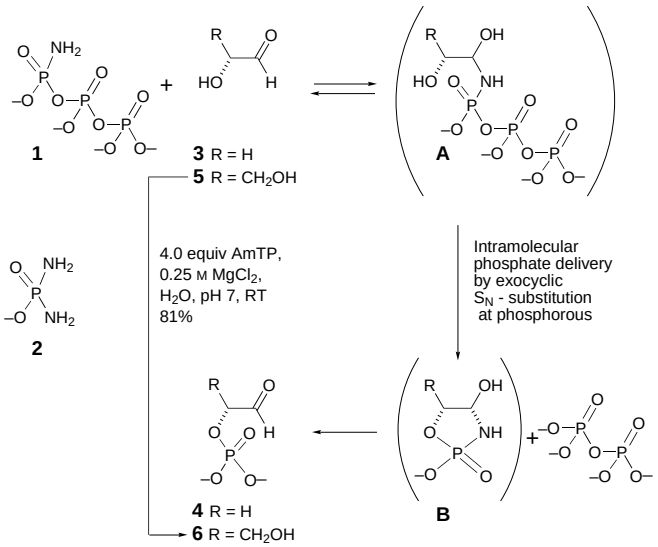
[17] A different nucleoside analogue, based on similar design criteria, was presented in the literature (M. Marangoni, A. Van Aerschot, P. Augustyns, J. Rozenski, P. Herdewijn, *Nucleic Acids Res.* **1997**, *25*, 3034 – 3041). However, only the binding properties of oligonucleotides containing one such modification were described. Hence, no extrapolation to the properties of fully modified oligonucleotides is possible.
[18] C. Epple, C. Leumann, *Chem. Biol.* **1998**, *5*, 209 – 216.
[19] M. Egholm, O. Buchardt, L. Christensen, C. Behrens, S. M. Freier, D. A. Driver, R. H. Berg, S. K. Kim, B. Norden, P. E. Nielsen, *Nature* **1993**, *365*, 566 – 568.
[20] F. Morvan, B. Rayner, J.-L. Imbach, M. Lee, J. A. Hartley, D.-K. Chang, J. W. Lown, *Nucleic Acids Res.* **1987**, *15*, 7027 – 7044.

Regioselective α-Phosphorylation of Aldoses in Aqueous Solution**

Ramanarayanan Krishnamurthy, Sreenivasulu Guntha, and Albert Eschenmoser*

In the context of studies on a potentially prebiotic chemistry of glycolaldehyde,[3] we recently described an efficient conversion of this hydroxyaldehyde into its 2-phosphate in aqueous solution under very mild conditions (Scheme 1).[1] The specific phosphorylation reagent in this process is amidotriphosphate (**1**, AmTP), a compound known to be formed by ammonolysis of cyclotriphosphate ("metatriphosphate") in aqueous solution.[4] Significantly, cyclotriphosphate itself is not effective as a phosphorylation agent under the conditions where its ammonolysis product phosphorylates glycolaldehyde in essentially quantitative yields.[1] The reason for this remarkable difference in reactivity is the specific capability of the amidotriphosphate to reversibly form a carbonyl addition product **A** with glycolaldehyde and to phosphorylate the α-hydroxyl group by intramolecular phosphate group delivery from **A** to the intermediate **B** which then undergoes hydrolysis to **4** (Scheme 1).

This mechanistic concept predicts that AmTP should have the potential to regioselectively phosphorylate the α-hydroxyl groups of aldosugars. Here we report that AmTP indeed reacts with glyceraldehyde, the tetrofuranoses, and the four aldopentoses under mild conditions to form reaction products that are derived from intramolecular phosphate delivery to the hydroxyl group at the C-2 position of the sugar. We also found that a comparably efficient regioselective phosphorylation can be brought about with diamidophosphate (**2**, DAP)[5] instead of AmTP as the phosphorylating reagent; in the case of aldofuranoses, there is even a preparative advantage with regard to product isolation.



Scheme 1. Regioselective intramolecular phosphorylation of glycolaldehyde (R = H) and D-glyceraldehyde (R = CH_2OH) by amidotriphosphate (**1**, AmTP).

D-glyceraldehyde (**5**), under the reaction conditions optimized for glycolaldehyde (0.025 M aqueous solution, 0.25 M $MgCl_2$, room temperature (RT), 5 days),[1] reacts with the sodium salt of AmTP (4 equivalents, pH ≈ 7) slowly but cleanly and with high regioselectivity, to give D-glyceraldehyde-2-phosphate (**6**; Scheme 1; 81 % yield after isolation by ion-exchange chromatography). No discernable glyceraldehyde-3-phosphate formation takes place according to ^1H and ^{31}P NMR spectra of the reaction mixture.[6]

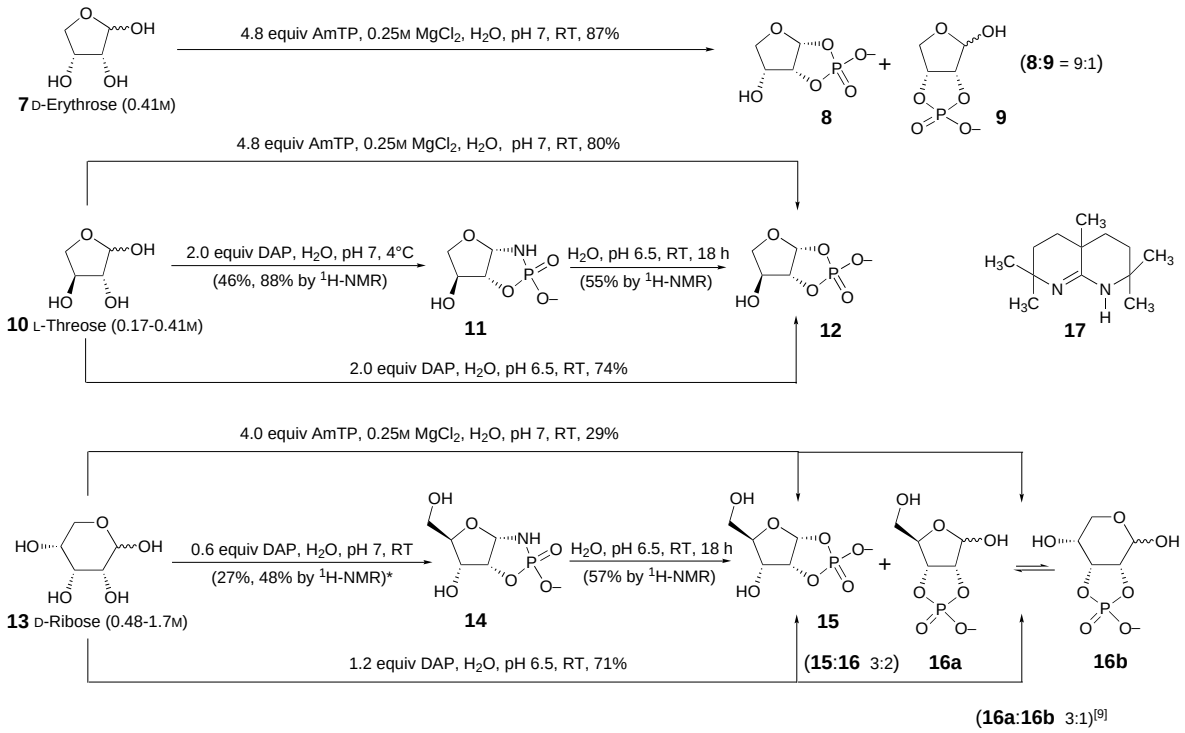
In subjecting the two aldotetroses **7** and **10** to the same treatment, a similarly regioselective phosphorylation of the α-hydroxyl groups occurs, yet this time with a twist: the products are the 1,2-cyclophosphates **8** and **12**, isolated in yields of 87 % and 80 %, respectively. In the erythrose series (2,3-diol in *cis* configuration), about a tenth of the product material is the isomeric 2,3-cyclophosphate **9**, whereas in the threose series (2,3-diol in *trans* configuration) the 1,2-cyclophosphate is free of its 2,3-isomer (Scheme 2). D-ribose (**13**) with 4 equivalents of AmTP under similar conditions reacts more sluggishly and gives the furanosyl 1,2-cyclophosphate (**15**) besides the 2,3-cyclophosphates (**16a** and **16b**), with the latter in somewhat greater proportion than in the erythrose series (Scheme 2). Overall yields are lower (29 %), presumably due to trapping of intermediates in the pyranose form.[7] According to exploratory experiments monitored by ^1H and ^{31}P NMR spectroscopy, the other three pentoses behave similarly to ribose. The reaction of AmTP with hexoses was explored with

[*] Prof. Dr. A. Eschenmoser, Prof. Dr. R. Krishnamurthy, Dr. S. Guntha
Department of Chemistry and
The Skaggs Institute for Chemical Biology
The Scripps Research Institute
10550 North Torrey Pines Road, La Jolla, CA 92037 (USA)
Fax: (+1) 858-784-9573
E-mail: rkrishna@scripps.edu
and
Laboratorium für Organische Chemie
Eidgenössische Technische Hochschule
Unversitätstrasse 16, 8092 Zürich (Switzerland)
Fax: (+41) 1-632-1043

[**] Chemistry of α-aminonitriles, Part 29. Part 28: Ref. [1], Part 27: Ref. [2]. This work was supported by the Skaggs Foundation. S.G. thanks the NASA NSCORT Exobiology program (La Jolla) for a postdoctoral fellowship.

Supporting information for this article is available on the WWW under http://www.wiley-vch.de/home/angewandte/ or from R.K. (rkrishna@scripps.edu).

 © WILEY-VCH Verlag GmbH, D-69451 Weinheim, 2000 1433-7851/00/3913-2281 $ 17.50+.50/0



Scheme 2. Characterized products and intermediates isolated (in yields indicated) from the reaction of aldoses with either the sodium salt of amidotriphosphate (AmTP) or diamidophosphate (DAP). The experiment with AmTP in the threose series was carried out with D-threose. Yields are based on the starting aldose with the exception of the * marked value.[10]

glucose and mannose, in both cases very little phosphorylation (approximately 5%) was observed by ^{1}H NMR spectroscopy, after 14 days.

The relative reactivity of the aldoses towards AmTP is in the order of glycolaldehyde > glyceraldehyde > erythrose > threose ≫ ribose ≫≫ glucose and mannose. While the phosphorylation of the C_2-, C_3-, and C_4-sugars proceeds to completion within two to five days, the reaction with ribose progresses to about one third in two weeks (by ^{1}H NMR spectroscopy). These differences seem related to the relative stabilities of the open aldehyde form of the aldoses in aqueous solution as well as to the position of their furanose/pyranose equilibrium.[7] On the other hand, the "cyclic" aldoses (**7**, **10**, and **13**) are also phosphorylated by AmTP in the absence of $MgCl_2$, although much more slowly, whereas the "acyclic" ones (glycolaldehyde and **5**) are not.

Structural assignments in the ribose series are based on spectral comparisons to authentic samples of ribofuranosyl-1,2-cyclophosphate (**15**)[8] and the corresponding 2,3-cyclophosphate **16**,[9] while assignments for **8** and **12** in the tetrose series are supported by ^{1}H and ^{31}P NMR spectra, as well as ^{1}H–^{1}H and ^{1}H–^{13}C NMR correlation spectra. When the reaction in both the D-threose and D-ribose series is monitored by ^{1}H and ^{31}P NMR spectroscopy in D_2O in the presence of $MgCl_2$, transient signals attributed to 1,2-amidocyclophosphates **11** ($\delta(^1H) = 5.57$, CH anomeric center; $\delta(^{31}P) = 25.7$) and **14** ($\delta(^1H) = 5.35$; $\delta(^{31}P) = 25.9$) can be observed. As the reaction progresses, the intensity of these signals diminishes with concomitant rise of those for the 1,2-cyclophosphates **12** ($\delta(^1H) = 5.95$, CH anomeric center; $\delta(^{31}P) = 18.4$) and **15** ($\delta(^1H) = 5.87$; $\delta(^{31}P) = 18.8$). The constitution of the transiently formed 1,2-amidocyclophosphate **11** was assigned by ^{1}H, ^{31}P, and ^{13}C NMR spectroscopy (Figure 1). Attempts to isolate the intermediate by ion-exchange chromatography led to a mixture that contained the cyclophosphate **12** besides **11**.

According to Feldmann and Thilo,[4b] when cyclotriphosphate is ammonolyzed to AmTP, the reaction can be pushed further to form diamidophosphate (**2**). Preparatively, this compound is conveniently produced by a method starting from $POCl_3$ and stored as a crystalline pentahydrate sodium salt.[5] We have reasoned that DAP (**2**) could also serve as selective phosphorylating reagent of α-hydroxyaldehydes similar to AmTP, since one of its amino groups could act as nucleophile towards the carbonyl group and the second (after protonation) as a leaving group in the intramolecular phosphate delivery process. These expectations were realized in experiments involving L-threose and D-ribose as representative aldoses. Thereby, reaction conditions were found that not only allowed the isolation of the elusive 1,2-amidocyclophosphates **11** and **14**, but also gave better yields of final phosphorylation products in the ribose series.

When L-threose (**10**) is treated with two equivalents of DAP in aqueous solution (0.16 M **10**, RT, pH 9.6) only adduct formation, accompanied by very little phosphorylation, takes place within 24 h (^{1}H and ^{31}P NMR spectroscopy). When such an experiment is run at 4 °C and the pH value of the reaction mixture is lowered to about 7 by addition of ion-exchange resin Amberlite IR-120 (H^+), formation of the 1,2-amidocyclophosphate **11**, as well as minor amounts of **12**, is observed (^{1}H and ^{31}P NMR spectroscopy). Since the phosphorylation slowly raises the pH value of the medium (to approximately

 © WILEY-VCH Verlag GmbH, D-69451 Weinheim, 2000 1433-7851/00/3913-2282 $ 17.50+.50/0 *Angew. Chem. Int. Ed.* **2000**, *39*, No. 13

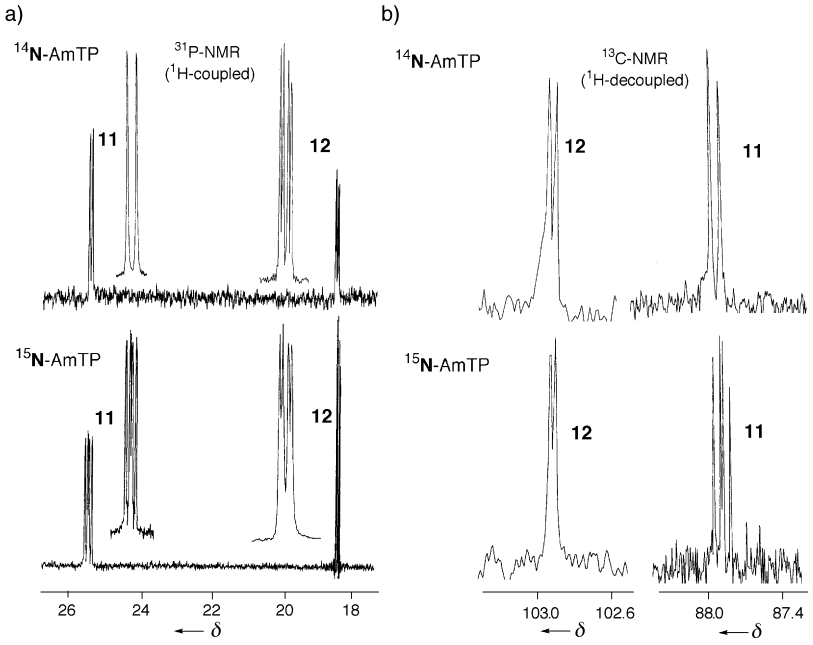


Figure 1. ^{31}P NMR and ^{13}C NMR spectral comparison of reaction mixtures observed in the reaction of threose with ^{14}N-AmTP (top) and ^{15}N-AmTP (bottom) (0.17 mmol **10** in 1 mL D_2O, 4 equivalents 98% ^{15}N-AmTP,[1] 0.25 M $MgCl_2$). ^{1}H-decoupled ^{31}P NMR spectrum (a) and ^{1}H-coupled ^{13}C NMR spectrum (b) recorded after 3 days at RT. a) Effect of ^{15}N-AmTP relative to ^{14}N-AmTP, in the coupling patterns of the ^{31}P{^{1}H} NMR spectrum of **11** where the phosphorous signal at $\delta = 25.9$ appears as a doublet of doublets ($J_{N,P} = 25.8$, $J_{1,P} = 16.2$ Hz), instead of the doublet ($J_{1,P} = 16.2$ Hz) that is in the spectrum when ^{14}N-AmTP is used. The signal of **12** at 18.5 ppm remains, as expected, unchanged in its splitting pattern. Over the course of time, the signal of **11** gradually disappears while that of **12** becomes larger until the end of the reaction when it remains unchanged. b) ^{13}C NMR spectra of the above reaction mixture. In the reaction with ^{14}N-AmTP, the signal at $\delta = 87$ (assigned to the anomeric carbon center of **11** by ^{13}C-^{1}H COSY experiments) appears as a doublet ($J_{C1,P} = 12.6$ Hz); with ^{15}N-AmTP it appears as a doublet of doublets ($J_{C1,P} = 12.5$ Hz, $J_{N,P} = 9.5$ Hz). The signal of **12** at 102.8 ppm (assigned to C-1) is unchanged in its splitting pattern as anticipated (d, $J_{C1,P} = 4.3$ Hz). These observations demonstrate that the nitrogen atom in **11** is attached to both the anomeric carbon atom and the phosphorous atom.

8.5) and therefore ceases to proceed, addition of Amberlite IR-120 (H^+) at 12 h intervals over 4 days is required to maintain a pH value of about 7 and allow complete consumption of L-threose. By such a procedure, **11** is formed in high yield (up to approximately 90% by ^{1}H NMR spectroscopy, as well as about 10% of **12**). About half of it (46%) could be isolated in essentially pure form by ion-exchange chromatography, the loss reflecting the lability of the primary phosphorylation product towards transformation into cyclophosphate **12**.

Isolation of the 1,2-amidocyclophosphate intermediate **14** in the D-ribose series proved more difficult due to its fast conversion into the mixture of the 1,2- and 2,3-cyclophosphates under the conditions of its (slower) formation. In an experiment starting with an excess of D-ribose[10] (1.6 M aqueous solution of **13** and 1 M DAP, RT, pH value kept at about 7 in 4 h intervals over 48 h), amidocyclophosphate **14** was isolated in 27% yield (48% by ^{1}H NMR spectroscopy, with respect to DAP). Its constitution could be fully characterized by ^{1}H NMR spectroscopy (Figure 2) in the form of its DMSO- and $CHCl_3$-soluble salt which is formed with the bicyclic amidine base **17**.[11]

When DAP phosphorylation mixtures in both series are maintained throughout at a pH value of 6.5, the phosphorylation products accumulate as cyclophosphates: in the L-threose series selectively as 1,2-cyclophosphate **12** (74% isolated), in the D-ribose series as a mixture of the 1,2- and 2,3-cyclophosphates **15** and **16** (71%, **15**:**16** ratio 3:2 according to ^{1}H NMR spectroscopy). The fact that under such reaction conditions the 1,2-amidocyclophosphates **11** and **14** convert themselves into the corresponding cyclophosphates was documented in separate experiments monitored by ^{1}H NMR spectroscopy and starting from pure **11** and **14** (Scheme 2).

Preparative phosphorylation of L-threose and D-ribose all the way to the corresponding 2-phosphates **18** and **19** is achieved by gradually lowering the pH value of the DAP reaction from pH 6.5 to about 2, under which conditions the 1,2-cyclophosphates are hydrolyzed within days to the 2-phosphates (Scheme 3). In the ribose series, a minor portion of the hydrolysis product is the 3-phosphate **20**, expected to be derived from the ribofuranosyl-2,3-cyclophosphate component **16** present in the phosphorylation mixture. Structural assignments in the ribose series are again by spectral comparison with known compounds[8, 9] and for **18** in the threose series by ^{1}H, ^{31}P, ^{1}H–^{1}H, and ^{1}H–^{13}C correlation NMR spectra.

The reactions between the ("cyclic") aldoses and AmTP or DAP appear mechanistically transparent with the exception of open questions referring to the structurally detailed role of the magnesium ion as well as the step in which the conversion of the 1,2-amidocyclophosphate to the 1,2-cyclophosphate intermediate is taking place. What seems remarkable is that the hydrolysis of the activated

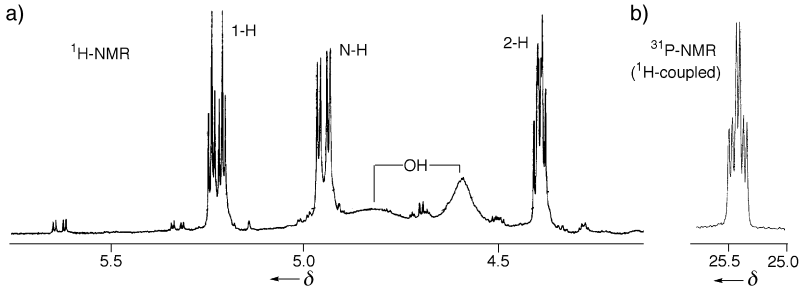
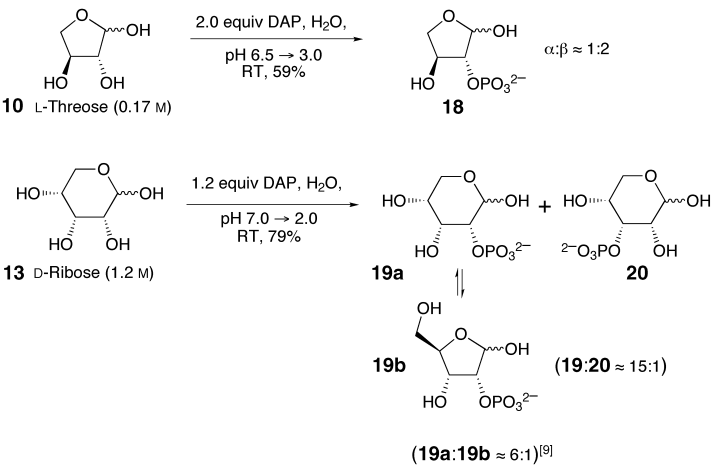


Figure 2. ^{1}H and ^{31}P NMR spectra ((a) and (b), respectively) of ribofuranosyl-1,2-amidocyclophosphate salt **14**·**17** in DMSO. The phosphoramide NH proton at $\delta = 4.96$ appears as a doublet of doublets ($J_{NH,P} = 15.4$, $J_{1,NH} = 5.0$ Hz). The signal at $\delta = 5.25$ which is the 1-H (anomeric center) signal appears as a multiplet ($J_{1,P} = 16.5$ Hz, $J_{1,NH} = 5.0$, $J_{1,2} = 4.9$ Hz). In the ^{31}P NMR spectrum the signal appears at $\delta = 25.5$ as doublet of doublet of doublets ($J_{1,P} = 16.5$ Hz, $J_{NH,P} = 15.4$, $J_{2,P} = 7.4$ Hz). On addition of D_2O, the signal at $\delta = 4.96$ disappears, along with signals assigned to the OH groups, with a concomitant change in the splitting pattern of the signal at $\delta = 5.25$, reverting back to a doublet of doublets. At the same time the ^{31}P NMR signal at $\delta = 25.5$, reduces to a doublet of doublets.

 © WILEY-VCH Verlag GmbH, D-69451 Weinheim, 2000 1433-7851/00/3913-2283 $ 17.50+.50/0



Scheme 3. One-pot transformation of selected aldoses into 2-phosphate derivatives with diamidophosphate (DAP). In separate experiments it was demonstrated by ^{1}H NMR spectroscopy that **11** and **12** (see Scheme 2) react to give **18** and **14**, and the mixture of **15**/**16** (Scheme 2) reacts to give **19**/**20**, under the same reaction conditions but in the absence of DAP.

amidocyclophosphate group takes the path through a primary product in which the phosphate group is still activated (the 1,2-cyclophosphates), before the final hydrolysis products, the stable 2-phosphates, are formed. Such a stepwise deactivation path clearly reflects a transient kinetic control of the hydrolysis process by anchimeric assistance in the cycle forming steps.[12]

The phosphorylation processes reported here exemplify a general strategy for attaining regioselectivity in synthesis, namely, to reversibly attach an activated reagent to a reactant in the structural neighborhood of the site to be functionalized, and to achieve the desired structural transformation by an irreversible intramolecular delivery of the functionalizing group.[13] Apart from the interest the reported reactions can have for the chemistry of carbohydrates[14], the demonstration of the existence of such robust and regioselective phosphorylation processes in aqueous solution is also intended to be a contribution to prebiotic chemistry.[1, 15]

Experimental Section[19]

10 →**12** (Example of a phosphorylation with AmTP): An aqueous solution of sodium salt of AmTP[1] (5 mL, 10.0 mmol) was added to D-threose, **10** (250 mg, 2.1 mmol; Sigma-Aldrich) followed by anhydrous $MgCl_2$ (119 mg, 1.25 mmol). The reaction mixture (pH 8.5) was shaken at RT until a clear solution resulted. After five days (pH 7.1) the turbid solution was diluted with 500 mL of water and subjected to ion-exchange chromatography (DEAE-A25-Sephadex, 40–120 mesh, HCO_3^- form, 5 × 20 cm, washed with 300 mL water, final elution with 0 →0.5 M $Et_3NH.HCO_3$ in 0.01M increments of 50 mL). Fractions containing the product (after concentration to approximately 10 mL, detected by thin layer chromatography: *n*BuOH:AcOH:H_2O 5:3:2, anisaldehyde stain) were combined and concentrated in vacuo (10 mm Hg), coevaporated with water 4 times to remove excess buffer, and dried to constant weight (high vacuum, RT, approximately 24 h) to afford 512 mg of pale yellow powder which contained the triethylammonium salt of **12** (477 mg, 80% yield based on pentaerythritol as the ^{1}H NMR internal reference; purity > 95% according to ^{1}H NMR spectroscopy). **12** · Et_3NH^+: R_f = 0.60; ^{1}H NMR (600 MHz, D_2O): δ = 1.16 (t, J = 7.4 Hz, 9H, CH_3), 3.07 (q, J = 7.4 Hz, 6H, CH_2), 3.86 (dd, J_{gem} = 10.6, $J_{3,4}$ = 1.1 Hz, 1H, 4-H), 4.06 (dd, J_{gem} = 10.6, $J_{3,4}$ = 2.6 Hz, 1H, 4-H), 4.28 (br.m, 1H, 3-H), 4.70 (m, partially masked by HDO signal, 1H, 2-H), 5.95 (ddd, $J_{1,P}$ = 15.7, $J_{1,2}$ = 4.0, $J_{1,3}$ = 1.7 Hz, 1H, 1-H); ^{13}C NMR (151 MHz, D_2O): δ = 8.58 (CH_3), 46.98 (CH_2), 73.19 (C4), 74.54 ($J_{C3,P}$ = 6.9 Hz, C3), 84.27 (C2), 102.78 ($J_{C1,P}$ = 4.3 Hz, C1); ^{31}P NMR (243 MHz, D_2O): 18.7 (dd, $J_{H1,P}$ = 15.7, $J_{H2,P}$ = 5.5 Hz); MS (pos., FAB): *m*/*z* (%): 306 (10, $[M+Na]^+$), 102 (100, $[Et_3NH]^+$); high resolution MS: found: 306.1084 $[M+Na]^+$; calcd: 306.1082.

13 →**15** + **16** (Example of a phosphorylation with DAP): D-Ribose (**13**, 600 mg, 4.0 mmol) was dissolved in water (3.4 mL) and $NaPO_2(NH_2)_2 \cdot 5H_2O$ (500 mg, 2.4 mmol) was added at RT. The pH value of the solution (9.4) was lowered to and maintained at 7, over a 24 h period, by addition of ion-exchange resin Amberlite IR-120 (H^+) at 4 h intervals. Another batch of $NaPO_2(NH_2)_2 \cdot 5H_2O$ (500 mg, 2.4 mmol) was added and pH 7 maintained as before, over a 24 h period. Subsequently the pH of the reaction mixture was lowered to 6.5 and maintained, over 24 h, by addition of Amberlite IR-120 (H^+) as before. The reaction mixture was diluted to 10 mL with 0.05 M aqueous $Et_3NH \cdot HCO_3$, filtered, and the resin washed 3 times with 0.05 M aqueous $Et_3NH \cdot HCO_3$ (10 mL). The washings were combined with the filtrate and subjected to ion-exchange chromatography (Dowex 1X8, HCO_3^- form; 7.5 × 10 cm, elution with 0.05 →0.2 M $Et_3NH \cdot HCO_3$ in 0.01-M increments of 50 mL volume each). The fractions containing the product (after each was concentrated in vacuo, analyzed by ^{31}P NMR spectroscopy (D_2O)) were combined and worked up as described for **12** to yield 960 mg of a white powder containing the triethylammonium salt of **15** + **16** (883 mg, 71% yield based on sodium benzoate as a ^{1}H NMR internal reference; **15**:**16** = 3:2, ^{1}H NMR spectroscopy). **15**(Na^+): R_f = 0.31; ^{1}H NMR (600 MHz, D_2O): δ = 3.64 (dd, J_{gem} = 12.5 Hz, $J_{4,5}$ = 4.5 Hz, 1H, 5-H), 3.88 (d, J_{gem} = 12.5 Hz, 1H, 5-H), 4.04 (br.m, 2H, 3-H, 4-H), 4.82 (m, 1H, 2-H), 5.86 (dd, $J_{1,P}$ = 17.0 Hz, $J_{1,2}$ = 4.1 Hz, 1H, 1-H); ^{13}C NMR (151 MHz, D_2O): δ = 59.68 (C5), 69.74 ($J_{3,P}$ = 6.1 Hz, C3), 78.76 (C2), 80.37 (C4), 101.34 ($J_{1,P}$ = 4.1 Hz, C1); ^{31}P NMR (243 MHz, D_2O): δ = 19.89 (dd, $J_{H1,P}$ = 16.9 Hz, $J_{H2,P}$ = 4.9 Hz); MS (pos., FAB): *m*/*z* (%): 257 (100, $[M+Na]^+$); MS (neg., ESI): *m*/*z* (%): 211 (100, $[M]^-$). Diagnostic signals for **16** (as a mixture of α/β-pyranose and -furanose anomers): ^{1}H NMR (600 MHz, D_2O): δ = 4.88 (d, $J_{1,2}$ = 6.9 Hz, 0.25H, 1-H, β-pyranose), 5.43 (br.s, 0.55H, 1-H, β-furanose), 5.49 (dd, $J_{1,2}$ = 5.1, $J_{2,P}$ = 0.9 Hz, 0.20H, 1-H, α-furanose); ^{31}P NMR (243 MHz, D_2O): δ = 17.73 (d, J = 18.1 Hz, β-pyranose), 21.49 (dd, J = 8.9 Hz, J = 8.7 Hz, β-furanose), 22.89 (t, J = 7.6 Hz, α-furanose).

Received: January 24, 2000 [Z14583]

[1] R. Krishnamurthy, G. Arrhenius, A. Eschenmoser, *Orig. Life Evol. Biosphere* **1999**, *29*, 333–354.

[2] F. Reck, H. Wippo, R. Kudick, M. Bolli, G. Ceulemans, R. Krishnamurthy, A. Eschenmoser, *Org. Lett.* **1999**, *1*, 1531–1534.

[3] D. Müller, S. Pitsch, A. Kittaka, E. Wagner, C. Wintner, A. Eschenmoser, *Helv. Chim. Acta.* **1990**, *73*, 1410–1468; S. Pitsch, A. Eschenmoser, B. Gedulin, S. Hui, G. Arrhenius, *Orig. Life Evol. Biosphere* **1995**, *25*, 294–334; R. Krishnamurthy, S. Pitsch, G. Arrhenius, *Orig. Life Evol. Biosphere* **1999**, *29*, 139–152.

[4] a) O. T. Quimby, T. J. Flautt, *Z. Anorg. Allg. Chem.* **1958**, *296*, 220–228; b) V. W. Feldmann, E. Z. Thilo, *Z. Anorg. Allg. Chem.* **1964**, *328*, 113–126.

[5] a) R. Klement, G. Biberachter, V. Hille, *Z. Anorg. Allg. Chem.* **1957**, *289*, 80–89; b) M. Watanabe, S. Sato, *J. Mater. Sci.* **1986**, *21*, 2623–2627.

[6] Signals of glyceraldehyde-3-phosphate would be expected at δ = 3.95–4.05 (for 2-H and 3-H) in the ^{1}H NMR spectrum and at 3.5 ppm in the ^{31}P NMR spectrum (Data taken from an authentic sample, Sigma-Aldrich). On a related note, D-2-deoxyribose was observed not to be phosphorylated by AmTP under conditions where D-ribose is.

[7] The β-pyranosyl form of the primary AmTP addition product is not expected to undergo intramolecular phosphate delivery and may only slowly equilibrate with the furanosyl form under the reaction conditions. Primary adduct formation of **13** with AmTP (in contrast to the experiments with DAP) is inferred, but could not be reliably monitored by ^{31}P NMR, due to signal overlap. The much higher yield of **15**/**16** obtained by the DAP procedure (see below) is presumably related to acid catalysis in the equilibration of primary adducts. Hexopyranoses with DAP under such conditions again give only a little phosphorylation.

[8] R. Fathi, F. Jordan, *J. Org. Chem.* **1986**, *51*, 4143–4146.

 © WILEY-VCH Verlag GmbH, D-69451 Weinheim, 2000 1433-7851/00/3913-2284 $ 17.50+.50/0

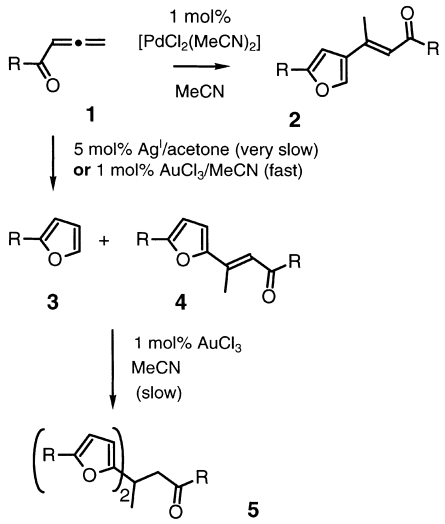
[9] S. Pitsch, C. Spinner, K. Atsumi, P. Ermert, *Chimia* **1999**, *53*, 291 – 294.
[10] In this experiment, excess ribose was used in order to facilitate separation of the product from the reagent in the ion-exchange chromatography.
[11] F. Heinzer, M. Soukup, A. Eschenmoser, *Helv. Chim. Acta.* **1978**, *61*, 2851 – 2874.
[12] This can either be a nucleophilic assistance by an adjacent hydroxyl group in a proton-catalyzed substitution of the NH_2 group in a non-cyclic 2-amidophosphate (formation of 2,3- and 1,2-cyclophosphates in the ribose and erythrose series), and/or a (N →O) exchange at the anomeric center through proton-catalyzed C,N dissociation →C,O recombination and subsequent hydrolytic loss of ammonia.
[13] Examples in synthetic chemistry where this strategy has used are legion. For early examples, see Ref. [16] (regioselectivity in the formation of the porphyrin skeleton in Woodward's chlorophyll synthesis) and Ref. [17] (regioselectivity of a Michael addition step in a colchicine synthesis).
[14] Note that, as the procedures described here involve separation and isolation by ion-exchange chromatography requiring large volumes, scaling up these reactions may therefore have its limits.
[15] High concentrations of substrates and reagents (up to 20% and 30%, respectively) are necessary in order for the reactions to be completed within days (instead of weeks, using lower concentrations). For the special case of ribose, the transformation to the cyclophosphates **15** and **16a** belongs to those functionalizations of the ribose molecule which select the furanose form from the sugar's pyranose/furanose equilibrium (see also Footnote 61 in Ref. [18]).
[16] a) R. B. Woodward, *Angew. Chem.* **1960**, *72*, 651 – 662; b) R. B. Woodward, *Pure Appl. Chem.* **1961**, *2*, 383 – 404.
[17] a) J. Schreiber, W. Leimgruber, M. Pesaro, P. Schudel, A. Eschenmoser, *Angew. Chem.* **1959**, *71*, 637 – 640; b) J. Schreiber, W. Leimgruber, M. Pesaro, P. Schudel, T. Threlfall A. Eschenmoser, *Helv. Chim. Acta* **1961**, *44*, 540 – 597.
[18] A. Eschenmoser, *Science* **1999**, *284*, 2118 – 2124.
[19] Further experimental details of the preparation of and spectral data for **6**, **8** + **9**, **11**, **14**, **18**, and **19** + **20** are given in the Supporting Information.

A New Gold-Catalyzed C–C Bond Formation**

A. Stephen K. Hashmi,* Lothar Schwarz, Ji-Hyun Choi, and Tanja M. Frost

While a manifold on the stoichiometric organometallic chemistry of gold is known, only a few catalytical applications have been reported.[1] As far as the *homogeneous* catalysis of organic reactions is concerned, there exist only two reactions that have reached any importance. The first forms C–X bonds (X = heteroatom) by the addition of O- or N-nucleophiles to alkenes or alkynes, as developed by Utimoto et al.[2] and Teles et al.[3] The second application forms C–C bonds by the asymmetric aldol reaction, as developed by Ito and Hayashi et al. and Togni et al.[4] We now report a new gold-catalyzed reaction that combines both C–O and C–C bond formation and allows the selective cross cycloisomerization/dimerization of terminal allenyl ketones and α,β-unsaturated ketones.

In the course of our investigation of transition metal catalyzed reactions of the readily available allenyl ketones **1**,[5] we observed that certain substrates such as **1a**, in which electron-rich substituents in the Ag^I-catalyzed Marshall reaction[6] lead to **3** as the major product, also form cycloisomers/dimers **4** as minor side products. Compound **4** is a constitutional isomer of the cycloisomer/dimer **2** obtained from the Pd^{II}-catalyzed conversion of **1** (Scheme 1).[7]



1-5	yield [%] of 2	3	4	5
a: R = 4-(TBDMSO)C_6H_4				
Pd^{II}	59	-	-	
Ag^I	-	22	14	
gold catalysis		**3**[a]	**4**[a]	**5**[b]
b: R = CH_2-4-(MeO)C_6H_4		60	31	-
c: R = CH_2-4-(TBDMSO)C_6H_4		35	5	42
d: R = CH_2CH_2-4-(TBDMSO)C_6H_4		38	6	31
e: R = 3-(MeO)C_6H_4		34	38	-
f: R = 4-(O_2N)C_6H_4		88	4	-
g: R = 2-(O_2N)C_6H_4		72	8	-
h: R = 3,4-(OCH_2O)C_6H_3		29	24	-
i: R = 4-(MeS)C_6H_4		48	51	-
k: R = CH_3		47[c]	47	-
m: R = 2,5-$(MeO)_2C_6H_3$		45	36	-

Scheme 1. Cycloisomerization, dimerization, and trimerization of **1**. a) Immediate workup after consumption of the starting material. b) Workup after several hours. c) Determined in the crude product by ^{1}H NMR.

In order to make **4** the major product, we tested Au^{III} catalysts, which combine a Pd^{II}-like d^8 system, with a silver-like metal of the copper triad. These gold catalysts prove to be extremely active and allow the reactions to be conducted under very mild conditions at room temperature or below. Because of the absence of paramagnetic species, the reactions could be easily monitored by NMR. For 1 mol% of catalyst, the required reaction times at 20 °C were, depending on the substrate, over one week for $AgNO_3$, about one hour for $[PdCl_2(MeCN)_2]$, and about one minute for $AuCl_3$! The

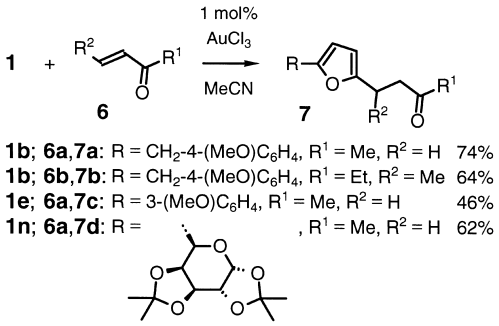
[*] Priv.-Doz. A. S. K. Hashmi, Dipl.-Chem. L. Schwarz, J.-H. Choi, T. M. Frost
Institut für Organische Chemie
Johann Wolfgang Goethe-Universität
Marie-Curie-Strasse 11, 60439 Frankfurt a. M. (Germany)
Fax: (+49) 69-79829464
E-mail: hashmi@chemie.uni-frankfurt.de

[**] This work was supported by the Deutsche Forschungsgemeinschaft (Ha 1932/5-1, Ha 1932/6-1) and the Fonds der Chemischen Industrie. Gold salts were donated by Degussa-Hüls AG. A.S.K.H. is indebted to Prof. M. Göbel for laboratory space.

 © WILEY-VCH Verlag GmbH, D-69451 Weinheim, 2000 1433-7851/00/3913-2285 $ 17.50+.50/0

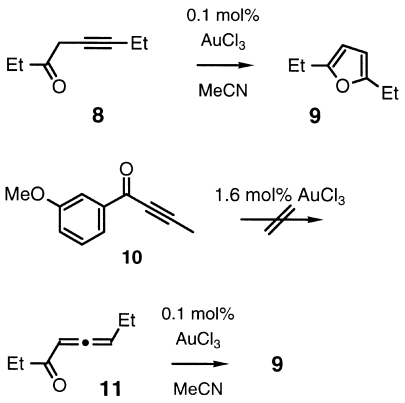
amount of Au^{III} could be reduced to 0.1 mol% with a complete consumption of **1**.

Interestingly, the initial products formed in the gold-catalyzed reactions are still **3** and **4** but the share of **4** increased. Furthermore, on a time scale of several hours, **3** and **4** reacted with each other to form **5** (a trimer of **1**) until either **3** or **4** were fully consumed. The latter observation suggested that, unlike the palladium-catalyzed conversions of **1**, in which a cross dimerization of **1** with other acceptor-substituted olefins failed, gold catalysts might allow such a cross coupling. Indeed, the addition of **1** to a solution of the catalyst and α,β-unsaturated ketones **6** did provide **7** (Scheme 2).



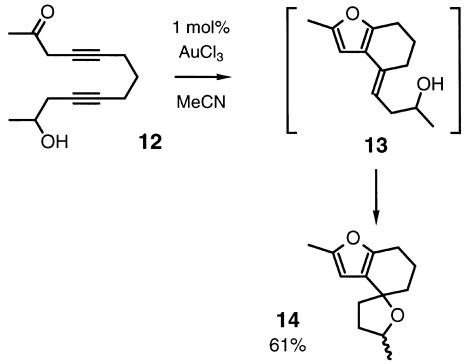
Scheme 2. Cross dimerization of **1** with Michael acceptors **6**.

These gold catalysts were also quite successful in other areas: While the reactions of propargyl ketones such as **8** failed with Ag^{I} as a catalyst and with palladium catalysts only at 100 °C,[8] the Au^{III} catalyst readily transferred **8** to **9** within minutes at room temperature in an essentially quantitative yield (Scheme 3). This saves the extra step of propargyl ketone isomerization to the corresponding allenyl ketone. On the other hand, under similar conditions the (to **1** and **8** isomeric) 1-propynyl ketones **10** did not react with the Au^{III} catalyst.



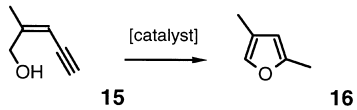
Scheme 3. Other gold-catalyzed cycloisomerizations.

Whereas for substrates like **8** or **11**, that lead to 2,5-disubstituted furans **9**, no intermolecular C–C bond formation was possible but, as shown for **12**, intramolecular C–C bonds could still form. Probably, the intermediate **13** formed and then suffered additional, nondiastereoselective C–O bond formation (no facile selection at the olefin) to provide **14** (Scheme 4).



Scheme 4. Combination of a C–C and two C–O bond forming reactions.

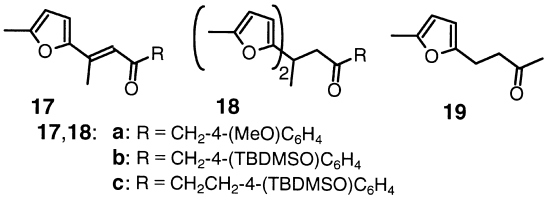
The high activity of the gold catalysts for C–O bond formation, shown already for intermolecular cases by Teles, also applies for intramolecular cases such as the transformation of **15** to **16**. While Dixneuf et al. reported that the transformation requires either 1 mol% of a Ru catalyst for 2 h treatment at 60 °C or 1 mol% of a Pd catalyst for 2 h at 100 °C,[9] and Marshall used 10 mol% of Ag catalysts for 2 h at 20 °C,[10] only 0.1 mol% of the Au catalyst for 1 h at 20 °C are sufficient (Scheme 5).



Scheme 5. Cycloisomerization of (*Z*)-enynol **15**.

Due to the high activity of the gold catalysts, we also tested whether reactions known to be catalyzed by relatively large amounts of silver catalysts are, in fact, a result of gold impurities in the silver. We found that highly pure $AgNO_3$ also showed a normal activity.[11]

For the mechanism of the reactions, the formation of **5** from **3** and **4** suggested already that two separate reactions occur, the first being the cycloisomerization of **1** to **3**, the second being the subsequent reaction of **3** with either a second molecule of **1**, **4**, or **6**. This hypothesis was further supported by the ability of $AuCl_3$ to catalyze the reaction of 2-methylfuran **3k** with **1b–d** or **6a** to form **17** and **18** or **19**, respectively (Scheme 6).

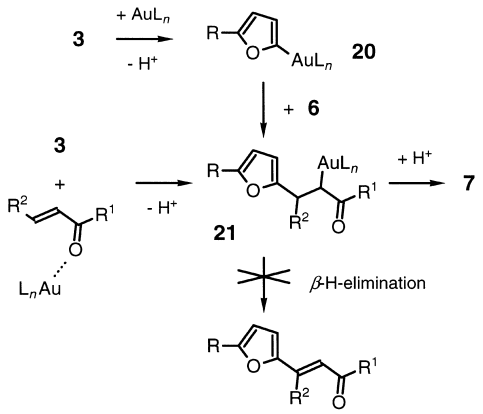


Scheme 6. Products from the cross dimerization of 2-methylfuran with allenyl ketones or methyl vinyl ketone (MVK).

Thus, for the reaction of **3** with the Michael acceptors, there remain two possibilities that both lead to the same intermediate **21**. Either the gold activates the enones, which then form the new C–C bonds by an electrophilic aromatic substitution at the 5-position of the furan to provide **21**, or a direct electrophilic attack of the gold catalyst at the furan

 © WILEY-VCH Verlag GmbH, D-69451 Weinheim, 2000 1433-7851/00/3913-2286 $ 17.50+.50/0 *Angew. Chem. Int. Ed.* **2000**, *39*, No. 13

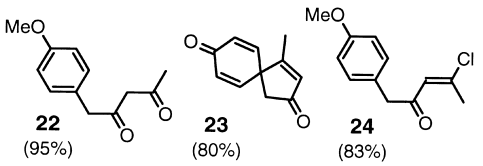
(auration)[12] forms a furyl–gold species **20**, which subsequently undergoes a 1,4-addition to the Michael system (similar to the corresponding organocuprates but generated in a protic environment; Scheme 7).



Scheme 7. Possible mechanisms for the C–C bond formation.

The gold enolate common to both routes does not undergo a β-H elimination but instead protonation by the proton set free during the electrophilic aromatic substitution step. Compound **21** strongly resembles the analogous intermediate of a palladium-catalyzed Heck reaction but, in the latter case, only in rare cases has protonation instead of β-H elimination been observed.[13] There exists one precedent in the literature that reports β-H eliminations are relatively slow with a gold catalyst.[14] As a control experiment, we mixed stoichiometric amounts of a) $AuCl_3$ and methyl vinyl ketone (MVK) or b) $AuCl_3$ and 2-methylfuran and monitored the behavior by NMR spectroscopy. For case (a) no significant change in the spectra was observed, whereas for case (b) an immediate darkening of the solution and a strong change in the spectra was observed. This change was time dependent and only broad signals were visible in the NMR spectra. While an immediate addition of MVK still provided the coupling product, a later addition did not lead to coupling (perhaps because of aggregation of the gold species, multiple aurations, or by a slow reduction of the gold).[12] We consider $AuCl_3$ only to be a precatalyst and we do not know whether the catalytically active species is Au^{III} or Au^{I} (but it should be an electrophilic gold species).[15] We occasionally observed the precipitation of gold in the form of a gold mirror but this always ocurred after the reaction was complete.

In order to prove that the Brønsted acid (H^+) set free in the electrophilic aromatic substitution was not responsible for the C–C bond formation, we treated **1b** as well as 2-methylfuran with MVK in the presence of 5% $HClO_4$. In the first case, the dione **22** was produced; in the second case, an unidentified polymeric material was formed. Compound **1b** is also a substrate that nicely proves the unique behavior of the gold catalyst: With Ag^{I} **3b** is formed; with Pd^{II}, **2b**; with H^+, **22** (Scheme 8); with Hg^{II}, **23**; with a stoichiometric amount of $FeCl_3$, **24**; with Au^{III}, **3b** and **4b**; and with Au^{III} in the presence of **6a**, the cross coupling product **7a**. So, unlike the addition of



Scheme 8. Products from the reactions of **1b** with different catalysts.

O-based nucleophiles to C–C multiple bonds, in which mercury and gold behave similarly, entirely different reactions were observed here.

Experimental Section

A solution of $AuCl_3$ in MeCN ($AuCl_3$ 30.3 mg, MeCN 970 mg) was prepared. An aliquot of this solution (267 mg; $AuCl_3$ 8.1 mg, 1 mol%) was added to **1b** (500 mg, 2.66 mmol) in MeCN (3 mL), at 20 °C. When the reaction was complete (as monitored by thin-layer chromatography (TLC)), the MeCN was removed in vacuo and the residue was purified by column chromatography (silica gel, hexane/ethyl acetate (10/1)). Compounds **3b** (298 mg, 60%) and **4b** (153 mg, 31%) were obtained. **4b**: IR (film): $\tilde{\nu}$ = 2999, 2954, 2933, 2835, 1672 cm^{-1} (C=O); ^1H NMR ($CDCl_3$, 400 MHz): δ = 2.39 (d, J = 1.1 Hz, 3H), 3.74 (s, 2H), 3.80 (s, 3H), 3.81 (s, 3H), 3.93 (s, 2H), 6.03 (d, J = 3.4 Hz, 1H), 6.60 (d, J = 3.4 Hz, 1H), 6.71 (d, J = 1.0 Hz, 1H), 6.87–6.90 (m, 4H), 7.15–7.19 (m, 4H); ^{13}C NMR ($CDCl_3$, 62.9 MHz): δ = 14.98 (q), 33.75 (t), 50.79 (t), 55.08 (q), 55.11 (q), 108.91 (d), 113.86 (d), 113.89 (d, 2C), 113.94 (d, 2C), 117.08 (d), 127.09 (s), 129.05 (s), 129.64 (d, 2C), 130.35 (d, 2C), 141.33 (s), 153.25 (s), 157.47 (s), 158.33 (s), 158.35 (s), 198.31 (s); MS (70 eV): m/z (%): 376 (14)[M^+], 255 (100); elemental analysis for $C_{24}H_{24}O_4$: calcd: C 76.57, H 6.43; found: C 76.31, H 6.50.

A 172 mg sample of a second $AlCl_3$/MeCN solution ($AuCl_3$ 30.3 mg, MeCN 967 mg; $AuCl_3$ 5.2 mg, 1 mol%) was diluted into 500 µL of MeCN containing 180 mg **6a** (2.57 mmol, 1.5 equiv). A solution of **1b** (322 mg, 1.71 mmol) in MeCN (2 mL) was then added slowly. When the reaction was complete (TLC), the MeCN was removed in vacuo and the residue was purified by column chromatography (silica gel, hexane/ethyl acetate (5/1)). Compounds **3b** (22.1 mg, 7%) and **7a** (326 mg, 74%) were obtained. **7a**: m.p.: 30–33 °C; IR (film): $\tilde{\nu}$ = 3000, 2908, 2836, 1716 cm^{-1} (C=O); ^1H NMR ($CDCl_3$, 250 MHz): δ = 2.13 (s, 3H), 2.70–2.77 (m, 2H), 2.83–2.90 (m, 2H), 3.79 (s, 3H), 3.85 (s, 2H), 5.83 (d, J = 3.0 Hz, 1H), 5.87 (d, J = 3.0 Hz, 1H), 6.82–6.87 (m, 2H), 7.11–7.15 (m, 2H); ^{13}C NMR ($CDCl_3$, 62.9 MHz): δ = 22.19 (t), 29.73 (q), 33.48 (t), 41.64 (t), 55.09 (q), 105.60 (d), 106.40 (d), 113.70 (d, 2C), 129.47 (d, 2C), 130.20 (s), 153.12 (s), 153.39 (s), 158.06 (s), 207.25 (s); MS (70 eV): m/z (%): 258 (100)[M^+]; elemental analysis for $C_{16}H_{18}O_3$: calcd: C 74.40, H 7.02; found: C 74.12, H 6.94.

Received: February 2, 2000 [Z 14636]

[1] H. Schmidbaur, A. Grohmann in *Comprehensive Organometallic Chemistry II*, *Vol. 3* (Eds.: E. W. Abel, F. G. A. Stone, G. Wilkinson, J. L. Wardell), Pergamon, New York, **1995**, pp. 1–56; H. Schmidbaur, *Gold: Chemistry, Biochemistry and Technology*, Wiley, New York, **1999**.

[2] Y. Fukuda, K. Utimoto, *J. Org. Chem.* **1991**, *56*, 3729–3731; Y. Fukuda, K. Utimoto, *Bull. Chem. Soc. Jpn.* **1991**, *64*, 2013–2015; Y. Fukuda, K. Utimoto, *Synthesis* **1991**, 975–978.

[3] J. H. Teles, S. Brode, M. Chabanas, *Angew. Chem.* **1998**, *110*, 1475–1478; *Angew. Chem. Int. Ed.* **1998**, *37*, 1415–1418.

[4] Y. Ito, M. Sawamura, T. Hayashi, *J. Am. Chem. Soc.* **1986**, *108*, 6405–6406; A. Togni, S. D. Pastor, *J. Org. Chem.* **1990**, *55*, 1649–1664; T. Hayashi, M. Sawamura, Y. Ito, *Tetrahedron* **1992**, *48*, 1999–2012. For the most recent report on a gold-catalyzed reaction, see: H. Ito, T. Yajima, J. Tateiwa, A. Hosomi, *Tetrahedron Lett.* **1999**, *40*, 7807–7810.

[5] A. S. K. Hashmi, L. Schwarz, *J. Prakt. Chem.* **2000**, *342*, 40–51.

[6] J. A. Marshall, E. D. Robinson, *J. Org. Chem.* **1990**, *55*, 3450–3451; J. A. Marshall, G. S. Bartley, *J. Org. Chem.* **1994**, *59*, 7169–7171.

 © WILEY-VCH Verlag GmbH, D-69451 Weinheim, 2000 1433-7851/00/3913-2287 $ 17.50+.50/0

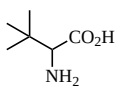
[7] A. S. K. Hashmi, *Angew. Chem.* **1995**, *107*, 1749 – 1751; *Angew. Chem. Int. Ed. Engl.* **1995**, *34*, 1581 – 1582; A. S. K. Hashmi, T. L. Ruppert, T. Knöfel, J. W. Bats, *J. Org. Chem.* **1997**, *62*, 7295 – 7304.
[8] H. Sheng, S. Lin, Y. Huang, *Synthesis* **1987**, 1022 – 1023.
[9] B. Seiller, C. Bruneau, P. H. Dixneuf, *Tetrahedron* **1995**, *51*, 13089 – 13102. For a recent example, see also: B. Gabriele, G. Salerno, E. Lauria, *J. Org. Chem.* **1999**, *64*, 7687 – 7692.
[10] J. A. Marshall, C. A. Sehon, *J. Org. Chem.* **1995**, *60*, 5966 – 5968.
[11] Silver nitrate 99.9999 %.
[12] Comparable aurations have been observed in the stoichiometric coupling of nucleobases by $[AuCl_4]^-$: F. Zamora, P. Amo-Ochoa, B. Fischer, A. Schimanski, B. Lippert, *Angew. Chem.* **1999**, *111*, 2415 – 2417; *Angew. Chem. Int. Ed.* **1999**, *38*, 2274 – 2275; F. Zamora, E. Zangrando, M. Furlan, L. Randaccio, B. Lippert, *J. Organomet. Chem.* **1998**, *552*, 127 – 134. The darkening and polymerization have been discussed already: P. W. J. de Graaf, J. Boersma, G. J. M. van der Kerk, *J. Organomet. Chem.* **1976**, *105*, 399 – 406.
[13] S. Cacchi, A. Arcadi, *J. Org. Chem.* **1983**, *48*, 4236 – 4240; R. Benhaddou, S. Czernecki, G. Ville, *J. Org. Chem.* **1992**, *57*, 4612 – 4616; H. Hagiwara, Y. Eda, K. Morohashi, T. Suzuki, M. Ando, N. Ito, *Tetrahedron Lett.* **1998**, *39*, 4055 – 4058.
[14] R. T. Baker, P. Nguyen, T. B. Marder, S. A. Westcott, *Angew. Chem.* **1995**, *107*, 1451 – 1452; *Angew. Chem. Int. Ed. Engl.* **1995**, *34*, 1336 – 1338.
[15] Au^I, in the form of [AuCl(tetrahydrothiophene)], converted **1b** to **3b** only and no dimer **4b** was observed.

α-Trialkylsilyl-Substituted α-Amino Acids**

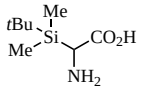
Carsten Bolm,* Andrey Kasyan, Karlheinz Drauz, Kurt Günther, and Gerhard Raabe

Dedicated to Professor Franz Effenberger on the occasion of his 70th birthday

As building blocks of peptides and proteins, α-amino acids are widespread throughout nature.[1] Various methods have been developed to gain access to them,[2] and among these catalytic processes appear particularly attractive.[2d] Among the nonproteinogenic amino acids *tert*-leucine (**1**) has emerged as an outstanding representative.[3] Bearing a hydrophobic and sterically demanding *tert*-butyl substituent, it has proved to be a valuable building block for pharmacologically effective peptide analogues[4] and has been frequently employed in syntheses of chiral auxiliaries.[5, 6] Here, we report the first synthesis of *tert*-leucine-analogous α-trialkylsilyl-substituted α-amino acids **2** and their corresponding, amino- and carboxyl-protected derivatives **4**.[7]

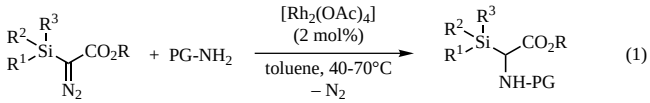


1



2

For the synthesis of **2**, fully protected α-trialkylsilyl-α-aminoacetates **4** play a pivotal role. These are prepared starting from α-trialkylsilyl-α-diazoacetates **3**,[8] which in turn are accessible through reaction of the corresponding α-diazoacetates with trialkylsilyltriflates in the presence of tertiary amine bases.[9, 10] Rhodium-catalyzed cleavage of nitrogen[11, 12] and intermolecular carbenoid-type N,H-insertion[12, 13] leads to the protected α-trialkylsilyl-α-aminoacetates **4** [Eq. (1); PG = protecting group]. The yields in these



(1)

3 **4**

insertion reactions are good (up to 86 %; Table 1). An X-ray crystal structure analysis of ester *rac*-**4a** confirmed its constitution.[14]

Table 1. Synthesis of protected α-trialkylsilyl-α-aminoacetates **4**.

R	R^1/R^2	R^3	PG[a]	Product	Yield [%]
Et	Me	*t*Bu	Tos	**4a**[b]	58
Et	Me	*t*Bu	Boc	**4b**	72
Et	Me	*t*Bu	Z	**4c**	83
Et	Me	Me	Boc	**4d**	65
Et	Me	Me	Z	**4e**	69
Et	Et	Et	Boc	**4f**	77
Et	Et	Et	Z	**4g**	86
Bn	Me	*t*Bu	Boc	**4h**	47
Bn	Me	*t*Bu	Z	**4i**	53

[a] Tos = tosyl = *p*-toluenesulfonyl, Boc = *tert*-butoxycarbonyl, Z = benzyloxycarbonyl. [b] From a reaction sequence as described in the Experimental Section.

The enantiomers of **4a** were separated by means of preparative HPLC using a chiral stationary phase.[15] Enantiopure **4a** is configurationally stable even upon prolonged storing. The absolute configuration of the later-eluted (+)-enantiomer of **4a** was determined to be (*S*) by a second X-ray crystal structure analysis. Figure 1 shows the molecular structure of (*S*)-**4a** in the crystal.[14]

The Si–C11 bond (1.919(5) Å) in (*S*)-**4a** is significantly longer than those between the silicon atom and C13 (1.904(6) Å), C12 (1.862(5) Å), and C17 (1.865(4) Å); the last two bond lengths fall within the range that is considered average for a bond between a four-coordinate Si atom and an

[*] Prof. Dr. C. Bolm, Dr. A. Kasyan, Priv.-Doz. Dr. G. Raabe
Institut für Organische Chemie der RWTH Aachen
Professor-Pirlet Strasse 1, 52074 Aachen (Germany)
Fax: (+49) 241-8888-391
E-mail: Carsten.Bolm@oc.RWTH-Aachen.de
Prof. Dr. K. Drauz[+]
Forschung, Entwicklung und Anwendungstechnik des Geschäftsbereichs Feinchemikalien
Degussa-Hüls AG, Postfach 1345, 63403 Hanau (Germany)
Dr. K. Günther
Analytisch Technische Services
Infracor GmbH, Postfach 1345, 63403 Hanau (Germany)

[**] This work was financially supported by the Fonds der Chemischen Industrie and Degussa-Hüls. We are grateful to Dr. P. Phansavath for preliminary studies in this field.

[+] Transformation of Amino Acids, Part 15. Part 14: A. S. Bommarius, K. Drauz, K. Günther, G. Knaup, M. Schwarm, *Tetrahedron: Asymmetry* **1997**, *8*, 3197.

 © WILEY-VCH Verlag GmbH, D-69451 Weinheim, 2000 1433-7851/00/3913-2288 $ 17.50+.50/0

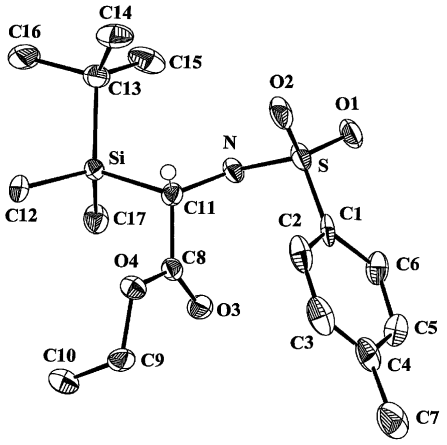
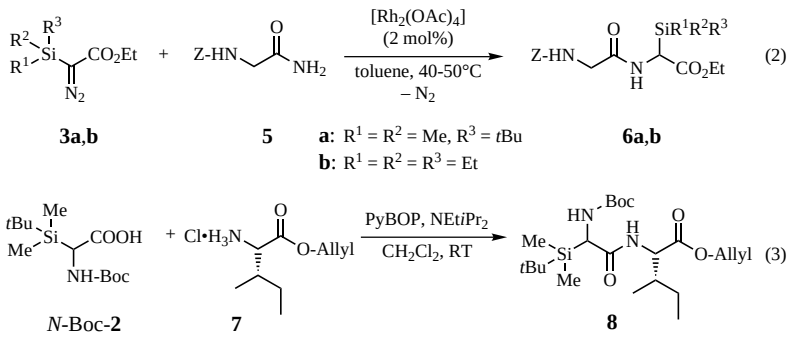


Figure 1. Molecular structure of (*S*)-**4a** in the solid state. Selected distances [Å] and angles [°]: Si-C11 1.919(5), N-C11 1.469(6), C8-C11 1.512(7), C8-O3 1.198(5), C8-O4 1.327(5); C8-C11-Si 108.7(3), N-C11-Si 110.2(3), N-S-C1 109.3(2), C13-Si-C11 110.3(2), C12-Si-C17 112.2(2), C12-Si-C13 109.8(2).



sp^3-hybridized carbon atom (1.863(24) Å).[16] A quantum-chemical calculation at the B3LYP/6-31G* level confirms this tendency. Starting from the experimentally found structure of crystalline *rac*-**4a**, a complete geometry optimization resulted in a bond length of 1.959 Å for Si–C11, while the Si–C13, Si–C12, and Si–C17 bonds of 1.922, 1.895, and 1.892 Å, respectively, are significantly shorter.

In order to allow the incorporation of α-trialkylsilyl-substituted α-amino acids into peptides, processes needed to be devised that selectively released the amino and carboxy termini of protected esters **4** and, in addition, stability of the derivatives formed had to be ensured. Therefore, *N*-Boc derivative **4b** was treated with concentrated trifluoroacetic acid (in CH_2Cl_2 2 h, ambient temperature) and subsequently with tosyl chloride and a base. The formation of tosylated product **4a** (58% yield) may be taken as evidence for the stability of the intermediate α-trialkylsilyl-substituted α-amino ester, which bears a free amino group. Hydrogenolysis of benzyl *N*-Boc-ester **4h** selectively furnished the corresponding, still *N*-protected α-trialkylsilyl-substituted α-amino acid (*N*-Boc-**2**) in 93% yield. In the same manner an entirely unprotected α-trialkylsilyl-substituted α-amino acid was synthesized for the first time. Thus, twofold debenzylation of **4i** afforded **2** in 92% yield. Consequently, starting from either enantiomer of **4i**, amino acids (*S*)-**2** and (*R*)-**2** were obtained in optically pure form.

Two methods exemplifying the synthesis of peptide-type structures were investigated. On the one hand, rhodium-catalyzed reaction of **3a** and **3b** with Z-protected glycine amide **5** gave rise to dipeptides **6a** and **6b** in 20–25% yield; that is α-trialkylsilyl α-diazoacetates **3** could react directly with amides to yield dipeptidic entities [Eq. (2)].[17] A more efficient approach, on the other hand, was the peptide coupling of *N*-Boc-**2** and the HCl salt of L-isoleucineallylester (**7**) under standard conditions involving benzotriazol-1-yloxytripyrrolidinophosphonium hexafluorophosphate (PyBOP), which gave dipeptide **8** in about 88% yield [Eq. (3)].[18]

Experimental Section

Synthesis of **4a**: $[Rh_2(OAc)_4]$ (18 mg, 0.04 mmol, 2 mol%) was added at room temperature to a stirred solution of **3a** (457 mg, 2 mmol) and *tert*-butylcarbamate (586 mg, 5 mmol) in dry toluene (5 mL). The reaction mixture was heated to 50 °C and stirred at this temperature for 24 h. After the mixture had been allowed to cool to ambient temperature, the solvents were removed under reduced pressure and the product was purified by column chromatography (silica gel, petroleum ether/ethyl acetate 5:1). Thus, *N*-Boc-protected ester **4b** (457 mg, 72%) was obtained as a colorless oil. For the synthesis of **4a**, trifluoroacetic acid (0.2 mL) was added dropwise to a solution of **4b** (317 mg, 1 mmol) in dry dichloromethane (3 mL) under argon. The reaction mixture was stirred for 2 h at ambient temperature before the solvent was removed under reduced pressure. The resulting residue was dissolved in dichloromethane (5 mL) and treated sequentially with triethylamine (0.28 mL) and tosyl chloride (190 mg, 1 mmol). After 1 h of stirring the reaction was quenched with water (10 mL) and the mixture was extracted with dichloromethane (2 × 20 mL). The combined organic extracts were dried over $MgSO_4$, and the solvent was removed under reduced pressure. The product was purified by column chromatography (silica gel, petroleum ether/ethyl acetate 3:1) to afford **4a** (216 mg; 58%) as a white solid (m.p. 127–128 °C (ethanol)). The separation of the enantiomers was performed by means of HPLC using a chiral stationary phase.[15]

Received: October 14, 1999 [Z14148]
Revised version: April 7, 2000

[1] a) H.-D. Jakubke, H. Jeschkeit, *Aminosäuren, Peptide, Proteine*, VCH, Weinheim, **1982**; b) H.-D. Jakubke, *Peptide: Chemie und Biologie*, Spektrum, Heidelberg, **1996**; c) *Peptides* (Ed.: B. Gutte), Academic Press, San Diego, **1995**; d) S. M. Hecht, *Bioorganic Chemistry: Peptides and Proteins*, Oxford University Press, New York, **1998**.

[2] a) R. M. Williams, *Synthesis of Optically Active α-Amino Acids*, Pergamon, Oxford, **1989**; b) R. M. Williams, J. A. Hendrix, *Chem. Rev.* **1992**, *92*, 889; c) R. O. Duthaler, *Tetrahedron* **1994**, *50*, 1539; d) M. J. Burk, F. Bienewald in *Transition Metals for Organic Synthesis*, *Vol. 2* (Eds.: M. Beller, C. Bolm), Wiley-VCH, Weinheim, **1998**, p. 13; e) M. Calmes, J. Daunis, *Amino Acids* **1999**, *16*, 215.

[3] a) A. S. Bommarius, M. Schwarm, K. Stingl, M. Kottenhahn, K. Huthmacher, K. Drauz, *Tetrahedron: Asymmetry* **1995**, *6*, 2851; b) K. Drauz, *Chimia* **1997**, *50*, 310.

[4] For examples, see: a) R. J. Andersen, J. E. Coleman, E. Piers, D. J. Wallace, *Tetrahedron Lett.* **1997**, *38*, 317; b) P. Ettmayer, M. Hübner, A. Billich, B. Rosenwirth, H. Gstach, *Bioorg. Med. Chem. Lett.* **1994**, *4*, 2851; c) K. Paulvannan, T. Chen, *Synlett* **1999**, 1371; d) G. Bold, A. Fässler, H.-G. Capraro, R. Cozens, T. Klimkait, J. Lazdins, J. Mestan, B. Poncioni, J. Rösel, D. Strover, M. Titelnot-Blomley, F. Acemoglu, W. Beck, E. Boss, M. Eschbach, T. Hürlimann, E. Masso, S. Roussel, K. Ucci-Stoll, D. Wyss, M. Lang, *J. Med. Chem.* **1998**, *41*, 3387; e) K. Paulvannan, T. Chen, *Synlett* **1999**, 1371.

[5] Reviews: a) A. Studer, *Synthesis* **1996**, 793; b) H. Waldmann, *Synlett* **1995**, 133; c) D. J. Ager, I. Prakash, D. R. Schaad, *Chem. Rev.* **1996**, *96*, 835.

 © WILEY-VCH Verlag GmbH, D-69451 Weinheim, 2000 1433-7851/00/3913-2289 $ 17.50+.50/0

[6] Further recent examples of successful asymmetric metal catalyses involving ligands based on *tert*-leucine: a) C. Bolm, K. Muñiz, J. P. Hildebrand, *Org. Lett.* **1999**, *1*, 491; b) C. Bolm, K. Muñiz-Fernandez, A. Seger, G. Raabe, K. Günther, *J. Org. Chem.* **1998**, *63*, 7860; c) C. Bolm, F. Bienewald, *Synlett* **1998**, 1327; d) C. Bolm, T. K. K. Luong, G. Schlingloff, *Synlett* **1997**, 1151; e) A. Lightfoot, P. Schnider, A. Pfaltz, *Angew. Chem*. **1998**, *110*, 3047; *Angew. Chem. Int. Ed.* **1998**, *37*, 2897; f) M. Peer, J. C. de Jong, M. Kiefer, T. Langer, H. Rieck, H. Schell, P. Sennhenn, J. Sprinz, H. Steinhagen, B. Wiese, G. Helmchen, *Tetrahedron* **1996**, *52*, 7547; g) S. Kudis, G. Helmchen, *Angew. Chem*. **1998**, *110*, 3047; *Angew. Chem. Int. Ed.* **1998**, *37*, 3047; h) D. A. Evans, T. Rovis, M. C. Kozlowski, J. S. Tedrow, *J. Am. Chem. Soc*. **1999**, *121*, 1994.

[7] A fully protected ethyl α-trimethylsilyl-α-amino ester was identified as minor isomer in a product mixture that was obtained by reaction of a lithiated aminosilane with ethyl chloroformate. S. McSieburth, J. J. Somers, H. K. O'Hare *Tetrahedron* **1996**, *52*, 5669.

[8] For the synthesis of benzyl α-diazoacetate, which—like the corresponding, commercially available ethyl ester—can be silylated, see: S. R. Angle, D. S. Bernier, N. A. El-Said, D. E. Jones, S. Z. Shaw, *Tetrahedron Lett.* **1998**, *39*, 3919.

[9] a) M. Martin, *Synth. Commun.* **1983**, *13*, 809; b) A. Fronda, F. Krebs, B. Daucher, T. Erle, G. Maas, *J. Organomet. Chem.* **1992**, *424*, 253; c) G. Maas, S. Bender, *Synthesis* **1999**, 1175; d) general overview of diazocarbonyl chemistry: T. Ye, M. A. McKervey, *Chem. Rev.* **1994**, *94*, 1091.

[10] Reviews on silyl-substituted diazocarbonyl compounds, α-silylcarbenes and -carbenoids: a) G. Maas in *The Chemistry of Organic Silicon Compounds, Vol. 2*, *Part 1* (Eds.: Z. Rappoport, Y. Apeloig), Wiley, Chichester, **1998**, chap. 13, p. 703; b) H. Tomioka, *Methoden Org. Chem. (Houben Weyl)*, *4th ed.*, *1952–*, *Vol. E 19b*, **1989**, p. 1410.

[11] Examples of other Rh-catalyzed reactions of α-silyl-α-diazoacetates: a) G. Maas, M. Gimmy, M. Alt, *Organometallics* **1992**, *11*, 3813; b) V. Gettwert, F. Krebs, G. Maas, *Eur. J. Org. Chem*. **1999**, 1213; c) S. N. Kablean, S. P. Marsden, A. M. Craig, *Tetrahedron Lett*. **1998**, *39*, 5109; d) S. P. Marsden, W.-K. Pang, *Tetrahedron Lett*. **1998**, *39*, 6077; e) S. P. Marsden, E.-K. Pang, *Chem. Commun.* **1999**, 1199.

[12] Simple trialkylsilylcarbenes do not react under *N,H*-insertion: a) R. L. Kreeger, H. Shechter, *Tetrahedron Lett.* **1975**, 2061; b) in ref. [10b], p. 1417.

[13] Examples of N,H-insertions in Rh-catalyzed transformations with other diazocarbonyl compounds: a) S. N. Osipov, N. Sewald, A. F. Kolomiets, A. V. Fokin, K. Burger, *Tetrahedron Lett*. **1996**, *37*, 615; b) L. Ferris, D. Haigh, C. J. Moody, *J. Chem. Soc. Perkin Trans. 1* **1996**, 2885; c) C. J. Moody, L. Ferris, D. Haigh, E. Swann, *Chem. Commun*. **1997**, 2391; d) M. C. Bagley, R. T. Buck, S. L. Hind, C. J. Moody, A. M. Z. Slawin, *Synlett* **1996**, 825; e) G. Mloston, M. Celeda, A. Swiatek, M. Kägi, H. Heimgartner, *Pol. J. Chem.* **1998**, *72*, 1907; f) diastereoselectively (de_{max}: 13%): E. Aller, R. T. Buck, M. J. Drysdale, L. Ferris, D. Haigh, C. J. Moody, N. D. Pearson, J. B. Sanghera, *J. Chem. Soc. Perkin Trans. 1* **1996**, 2879; g) enantioselectively (ee_{max}: 45%): C. F. García, M. A. McKervey, T. Ye, *Chem. Commun*. **1996**, 1465.

[14] Crystallographic data (excluding structure factors) for the structures reported in this paper have been deposited with the Cambridge Crystallographic Data Centre as supplementary publication no. CCDC-135676 (*rac*-**4a**) and -135677 (*(S)*-**4a**). Copies of the data can be obtained free of charge on application to CCDC, 12 Union Road, Cambridge CB21EZ, UK (fax: (+44) 1223-336-033; e-mail: deposit@ccdc.cam.ac.uk).

[15] HPLC separation (analytic): Chiralpak AD (Daicel); 4.6 mm × 250 mm; isohexane/2-propanol 97:3 (v:v); 215 nm; 1 mL min^{-1}; 25 °C; t_R (−)-(*R*)-**4a**: 15 min, t_R (+)-(*S*)-**4a**: 21.4 min. Preparative: as analytical separation but 40 mm × 250 mm and 60 mL min^{-1}.

[16] F. H. Allen, O. Kennard, D. G. Watson, L. Brammer, A. G. Orpen, R. Taylor, *J. Chem. Soc. Perkin Trans. 2* **1987**, S1.

[17] Reactions of the like have already been utilized to synthesize simple dipeptides; cf. ref. [13].

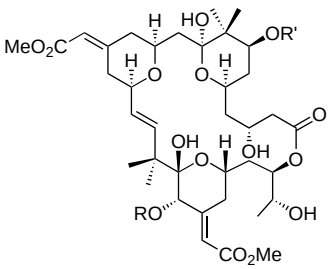
[18] This transformation was performed with racemic *N*-Boc-**2**. It is still to be investigated how enantiopure α-trialkylsilyl-α-amino acids will react.

Total Synthesis of Bryostatin 3**

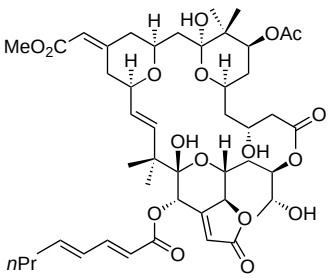
Ken Ohmori, Yasuyuki Ogawa, Tetsuo Obitsu, Yuichi Ishikawa, Shigeru Nishiyama,* and Shosuke Yamamura*

Bryostatins, 18 related macrolides isolated from the marine bryozoa *Bugula neritina Linnaeus* and *Amathia convuluta*, have been known to possess remarkably powerful antineoplastic activities against the murine P388 lymphocytic leukemia and other tumors, and have the potential to activate protein kinase C without tumor promotion, in contrast to the activities of phorbol and aplysiatoxin.[1] In particular, bryostatin 1, which is the most abundant congener in the family, is in phase II of clinical trials.

From the viewpoints of their interesting biological activity and novel macrolide structure, the bryostatins have been attracting the attention of many synthetic chemists.[2] However, only a few bryostatins have been synthesized: bryostatin 7 by Masamune et al.[3] and bryostatin 2 by Evans et al.[4] We have also carried out extensive synthetic studies on the bryostatins.[5] Bryostatin 3 (**1**), which includes the exceptional γ-lactone structure, was taken as a challenging target molecule, because it was isolated as a very minor component from natural sources (a few milligrams from each 100 kilograms of source),[6] yet it is expected to be a promising antitumor agent. We describe herein the total synthesis of bryostatin 3 (**1**).



bryostatin 1: R = COC_7H_{11}, R' = Ac
bryostatin 2: R = COC_7H_{11}, R' = H
bryostatin 7: R = Ac, R' = Ac



1: bryostatin 3

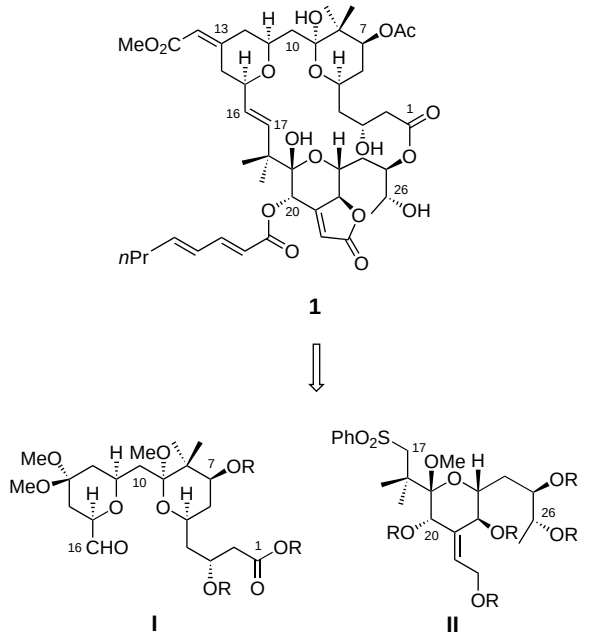
Based on the retrosynthetic analysis depicted in Scheme 1, the molecule of **1** is divided into two fragments (**I** and **II**). The C1−C16 fragment **I**, which is shared by all bryostatins, has been synthesized by a convergent synthetic methodology.[5d]

To accomplish the desired coupling reaction, the functionality of fragment **I** was required in an appropriate form, which was obtained from the intermediate **2**.[5d] As can be seen in

[*] Prof. Dr. S. Nishiyama, Prof. Dr. S. Yamamura, Dr. K. Ohmori, Y. Ogawa, T. Obitsu, Y. Ishikawa
Department of Chemistry
Faculty of Science and Technology
Keio University, Hiyoshi, Yokohama 223-8522 (Japan)
Fax: (+81) 45-566-1697
E-mail: nisiyama@chem.keio.ac.jp, yamamura@chem.keio.ac.jp

[**] This work was supported by the Ministry of Education, Science, Sports, and Culture (Japan). K.O. is grateful to JSPS for a predoctoral fellowship. The authors thank Dr. G. N. Chmurny (NIH) for providing them with ^{1}H and ^{13}C NMR spectra of bryostatin 3 and for helpful discussions.

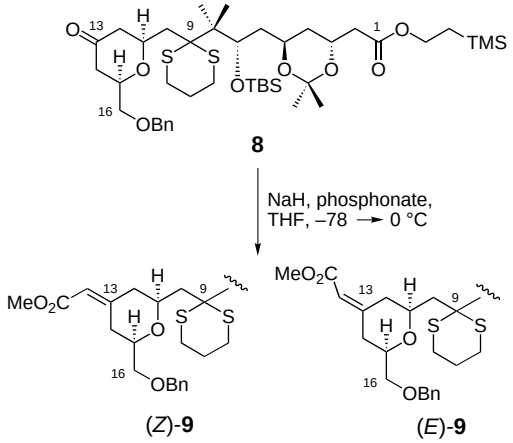
 © WILEY-VCH Verlag GmbH, D-69451 Weinheim, 2000 1433-7851/00/3913-2290 $ 17.50+.50/0



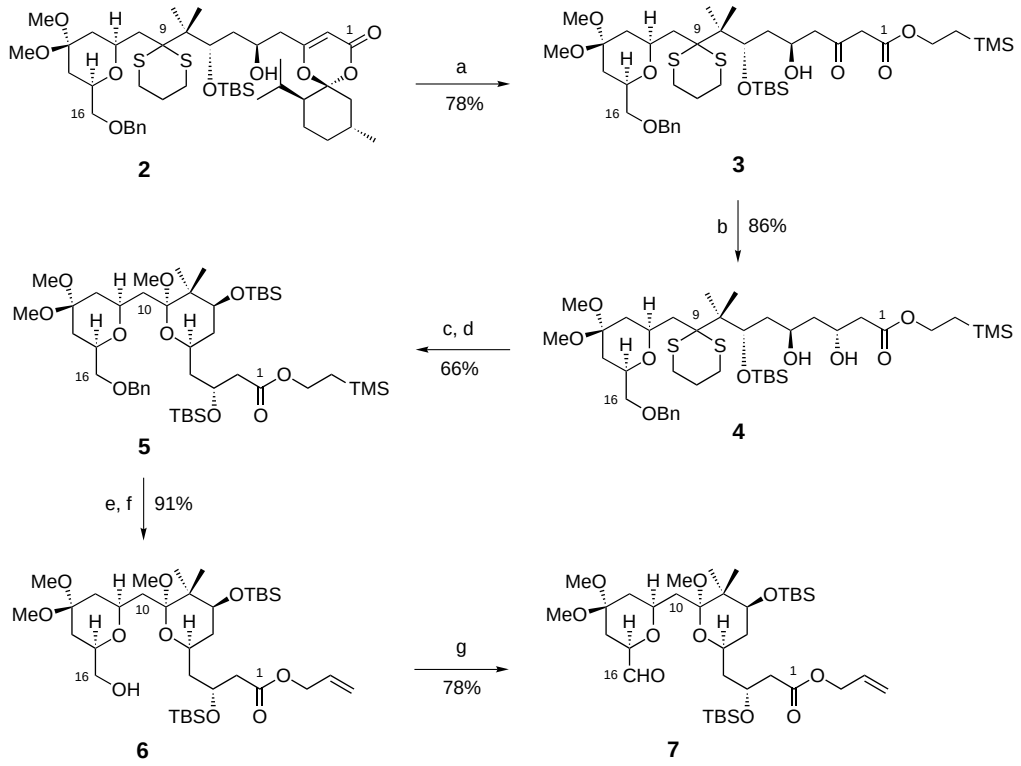
Scheme 1. Retrosynthesis of bryostatin 3 (**1**).

Scheme 2, treatment of **2** with 2-(trimethylsilyl)ethanol gave ester **3**. The resulting ketone group of **3** was selectively reduced with $Me_4NBH(OAc)_3$[7] to afford diol **4**. Subsequently, **4** was subjected to deprotection with $HgCl_2$/HgO in CH_3CN/H_2O (90/10) followed by methyl acetal formation with PPTS in MeOH, and then silylation to give the desired compound **5**, which was smoothly converted into allyl ester **6** in 3 steps. Finally, the desired C1–C16 fragment **7** was synthesized by TPAP oxidation of **6**.

Stereocontrolled introduction of a methoxycarbonylmethylene unit to the C13 position is one of the crucial steps in the bryostatin synthesis. In contrast to the syntheses by Masamune et al.[3] and Evans and co-workers,[4c] we carried out a simple Horner-Wadsworth-Emmons reaction with the known ketone **8**,[5d] as a model experiment (Scheme 3). As previously



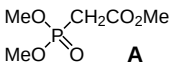
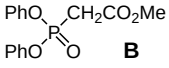
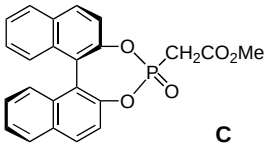
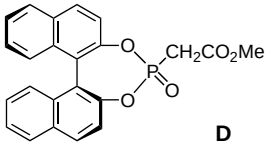
Scheme 3. Indroduction of a methoxycarbonylmethylene unit (**8** → **9**).



Scheme 2. Synthesis of the C1–C16 fragment **7**. a) $TMS(CH_2)_2OH$, toluene, reflux; b) $Me_4NBH(OAc)_3$, AcOH/CH_3CN (1/2), −20 °C; c) 1. $HgCl_2$, HgO, CH_3CN/H_2O (9/1); 2. PPTS, MeOH; d) TBSOTf, 2,6-lutidine, CH_2Cl_2; e) H_2, $Pd(OH)_2$/C, MeOH; f) 1. $LiOH \cdot H_2O$, THF/MeOH/H_2O (1/2/1); 2. CH_2=$CHCH_2Br$, $NaHCO_3$, DMF; g) TPAP, NMO, 4Å molecular sieves, CH_2Cl_2. Bn = benzyl, NMO = *N*-methylmorpholine *N*-oxide, PPTS = pyridinium *p*-toluenesulfonate, TBS = *tert*-butyldimethylsilyl, Tf = trifluoromethanesulfonyl, TMS = trimethylsilyl, TPAP = tetrapropylammonium perruthenate.

reported,[5d] treatment of **8** with an anion generated from $(MeO)_2P(O)CH_2CO_2Me$/NaH gave a mixture of the corresponding α,β-unsaturated esters **9** in 94% yield, with the desired ester (*Z*)-**9** obtained as a major product (*Z*:*E* = 1.6:1), which suggested a possibility for the selective construction of the methylene unit. In order to improve the selectivity, several Horner-Wadsworth-Emmons reagents were examined. The representative entries are shown in Table 1.[8] Clearly, the reagent **C**[9] is the most suitable for the formation of the desired (*Z*)-**9** (*Z*:*E* = 4:1). This result is almost the same as that of the recent Evans investigation.[4a]

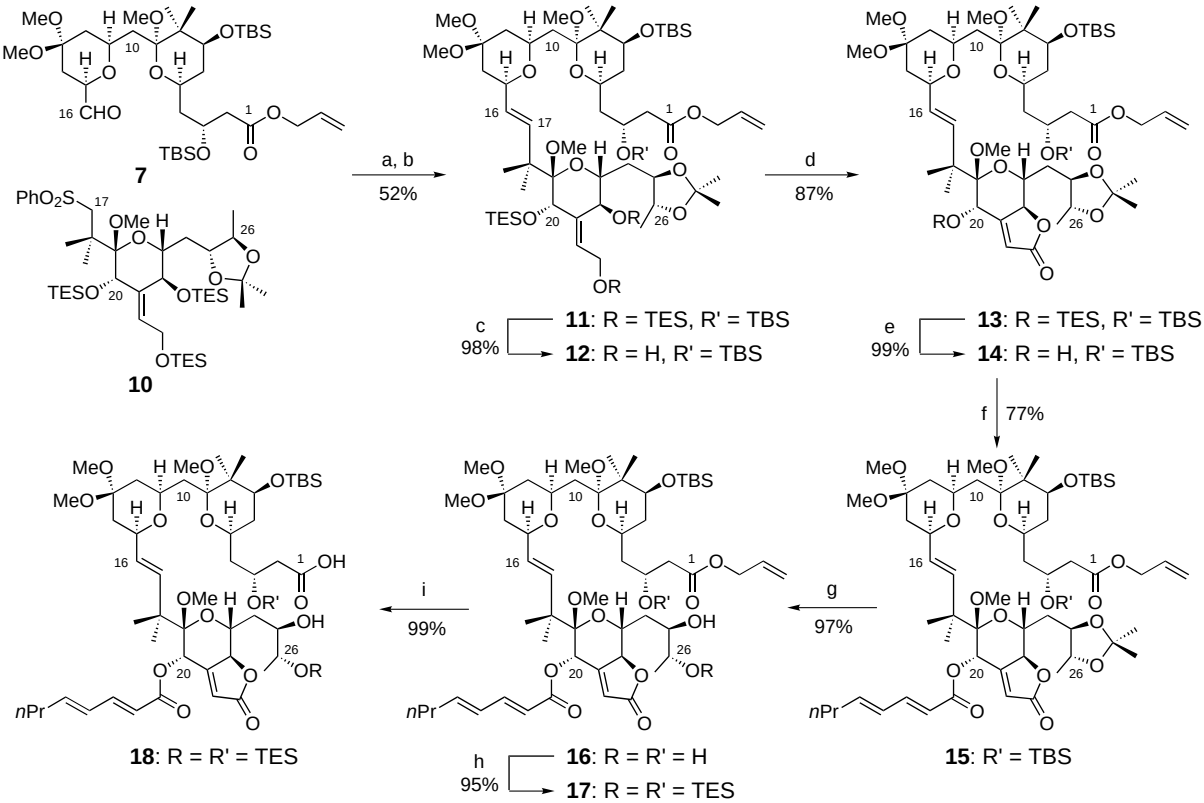
Table 1. Horner-Wadsworth-Emmons reaction of **8** with various reagents.

Phosphonate	Yield [%]	*Z*:*E* ratio of **9**
 **A**	94	1.6:1
 **B**	90	2.0:1
 **C**	92	4.0:1
 **D**	85	2.3:1

The Julia–Lythgoe olefination[10] of the previously synthesized sulfone C17-C27 fragment **10**[5a] with the aldehyde **7** was successively effected under PhLi conditions, and the following treatment with BzCl/DMAP and then 5% Na-Hg (in Na_2HPO_4) gave olefin **11** (Scheme 4), which possesses a *trans* double bond ($^3J_{H16,H17}$ = 16.1 Hz). The olefin **11** was treated with TBAF/AcOH (1/1) in THF (0 °C, 1 h) to selectively afford diol **12** in nearly quantitative yield.

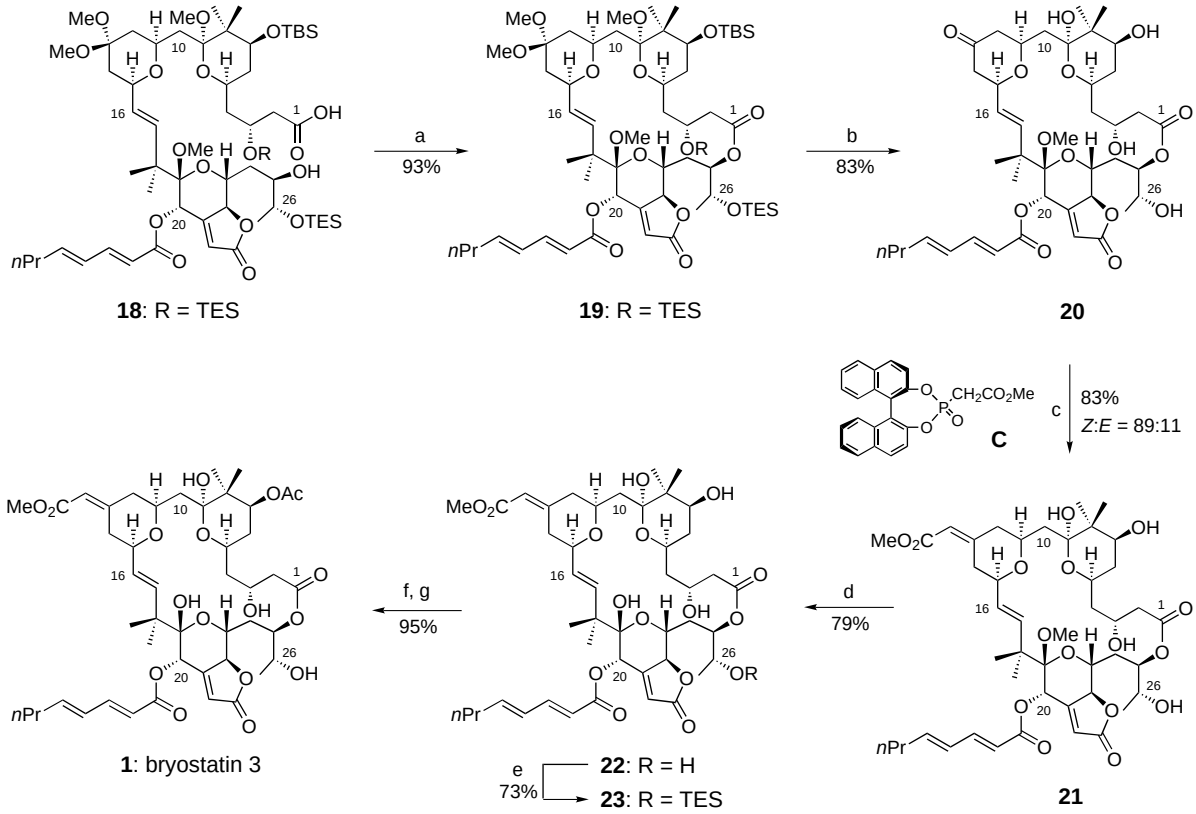
Oxidation of **12** with TPAP/NMO afforded the desired α,β-unsaturated γ-lactone **13**, which on selective deprotection with TBAF/AcOH (2/1) in THF (0 °C, 5 min) gave **14**. According to the Yamaguchi protocol,[11] **14** was treated with (*E*,*E*)-2,4-octadienoic acid to afford ester **15**, which was selectively deprotected with CSA in MeOH to give triol **16**, with the protecting group of the most hindered C7 position being kept intact. Reprotection of **16** with $TESCl/Et_3N$ in DMF (−30 °C, 30 min) was carefully carried out to give the desired disiloxy ether **17** in 95% yield, which was subsequently treated with $[Pd(PPh_3)_4]$/morpholine to give seco acid **18**.

Macrolactonization of **18** was successfully accomplished by using the Yamaguchi protocol[11] to give **19** (see Scheme 5) in 93% yield, which was submitted to deprotection with 46% HF (aq.) in CH_3CN at room temperature overnight to give



Scheme 4. Synthesis of the seco acid **18**. a) **10**, PhLi, THF, −78 °C, then **7**, −78 °C, then BzCl, DMAP, −78 → 0 °C; b) 5% $Na/Hg(Na_2HPO_4)$, MeOH/EtOAc (2/1), −35 °C; c) TBAF, AcOH, THF, 0 °C; d) TPAP, NMO, 4Å molecular sieves, CH_2Cl_2; e) TBAF, AcOH, THF, 0 °C; f) (*E*,*E*)-2,4-octadienoic acid, 2,4,6-trichlorobenzoyl chloride, Et_3N, toluene, then **14**, DMAP, toluene; g) CSA, MeOH; h) TESCl, Et_3N, DMF, −30 °C; i) $[Pd(PPh_3)_4]$, morpholine, THF. Bz = benzoyl, CSA = camphorsulfonic acid, DMAP = 4-dimethylaminopyridine, DMF = *N*,*N*-dimethylformamide, TBAF = tetrabutylammonium fluoride, TES = triethylsilyl.

 © WILEY-VCH Verlag GmbH, D-69451 Weinheim, 2000 1433-7851/00/3913-2292 $ 17.50+.50/0 *Angew. Chem. Int. Ed.* **2000**, *39*, No. 13



Scheme 5. Total synthesis of bryostatin 3 (**1**). a) 2,4,6-trichlorobenzoyl chloride, Et_3N, toluene, then DMAP, toluene; b) 46% HF (aq.), CH_3CN; c) NaH, **C**, THF, 0 °C, then **20**, 50 → −10 °C; d) TFA, H_2O, CH_2Cl_2; e) TESCl, DMAP, CH_2Cl_2, −10 °C; f) Ac_2O, pyridine; g) 46% HF (aq.), CH_3CN/H_2O. TFA = trifluoroacetic acid.

ketone **20** in high yield. At this stage, we carried out the Horner-Wadsworth-Emmons reaction of **20** with an anion generated from reagent **C**/NaH in THF to give a mixture of α,β-unsaturated esters **21** ($Z:E = 89:11$)[12] in 83% yield. In the next step, any efforts made to cleave the methyl acetal at the C19 position were unsuccessful because this acetal is less reactive than that at the C9 position. However, extremely drastic conditions for hydrolysis gave rise to decomposition of the tetrahydropyrane part including the unsaturated γ-lactone. Such a property was quite different from those of other bryostatins.[3a, 4a] Ultimately, **21** was successfully hydrolyzed with TFA/H_2O (10/1) in CH_2Cl_2 (room temperature, 1 h) conditions to afford the desired compound **22** in 79% yield. Based on the ^1H and ^{13}C NMR spectra including ROESY experiments, **22** appears to adopt the same conformation as that of natural bryostatin 1,[13] which is different from that of the methyl acetal **21**, owing to the hydrogen bonding effect of the C19 hydroxyl group.[14]

Furthermore, **22** was treated with TESCl/DMAP to selectively protect the C26 hydroxyl group and form siloxy ether **23**, which on acetylation with Ac_2O/pyridine and desilylation with 46% HF (aq.) in CH_3CN provided bryostatin 3 (**1**) in almost quantitative yield. The synthetic compound is completely identical with natural bryostatin 3 in all respects of the spectral data (IR, ^1H and ^{13}C NMR (in $CDCl_3$), and UV spectroscopy and mass spectrometry). Up to now, we have been able to acquire 25 mg of synthetic bryostatin 3 (**1**), which will be used for a variety of biological tests, as well as for studying interactions with protein kinase C and other substances.

Received: January 18, 2000 [Z 14555]

[1] G. R. Pettit, *Prog. Chem. Org. Nat. Prod.* **1991**, *57*, 153–195; b) G. R. Pettit, *J. Nat. Prod.* **1996**, *59*, 812–821.

[2] a) R. D. Norcross, I. Paterson, *Chem. Rev.* **1995**, *95*, 2041–2114; b) J. Gracia, E. J. Thomas, *J. Chem. Soc. Perkin Trans. 1* **1998**, *17*, 2865–2871; c) R. J. Maguire, S. P. Munt, E. J. Thomas, *J. Chem. Soc. Perkin Trans. 1* **1998**, *17*, 2853–2863; d) J. Baxter, E. G. Mate, E. J. Thomas, *Tetrahedron* **1998**, *54*, 14359–14376; e) S. Kiyooka, H. Maeda, *Tetrahedron: Asymmetry* **1997**, *8*, 3371–3374; f) J. M. Weiss, H. M. R. Hoffmann, *Tetrahedron: Asymmetry* **1997**, *8*, 3913–3920; g) J. DeBrabander, B. A. Kulkatni, R. Garcia-Lopez, M. Vandewalle, *Tetrahedron: Asymmetry* **1997**, *8*, 1721–1724; h) T. F. J. Lampe, H. M. R. Hoffmann, *Tetrahedron Lett.* **1996**, *37*, 7695–7698; i) T. F. J. Lampe, H. M. R. Hoffmann, *Chem. Commun.* **1996**, 1931–1932; j) J. DeBrabander, M. Vandewalle, *Pure Appl. Chem.* **1996**, *68*, 715–718; k) M, Kalesse, M. Eh, *Tetrahedron Lett.* **1996**, *37*, 1767–1770; l) R. W. Hoffmann, H. C. Stiasny, *Tetrahedron Lett.* **1995**, *36*, 4595–4598; m) K. J. Hale, J. A. Lennon, S. Manaviazar, M. H. Javaid, *Tetrahedron Lett.* **1995**, *36*, 1359–1362.

[3] a) M. Kageyama, T. Tamura, M. H. Nantz, J. C. Roberts, P. Somfai, D. C. Whritenour, S. Masamune, *J. Am. Chem. Soc.* **1990**, *112*, 7407–7408; b) S. Masamune, *Pure Appl. Chem.* **1988**, *60*, 1587–1596; c) M. A. Blanchette, M. S. Malamas, M. H. Nantz, J. C. Roberts, P. Somfai, D. C. Whritenour, S. Masamune, M. Kageyama, T. Tamura, *J. Org. Chem.* **1989**, *54*, 2817–2825; d) A. J. Duplantier, M. H. Nantz, J. C. Roberts, R. P. Short, P. Somfai, S. Masamune, *Tetrahedron Lett.* **1989**, *30*, 7357–7360.

 © WILEY-VCH Verlag GmbH, D-69451 Weinheim, 2000 1433-7851/00/3913-2293 $ 17.50+.50/0

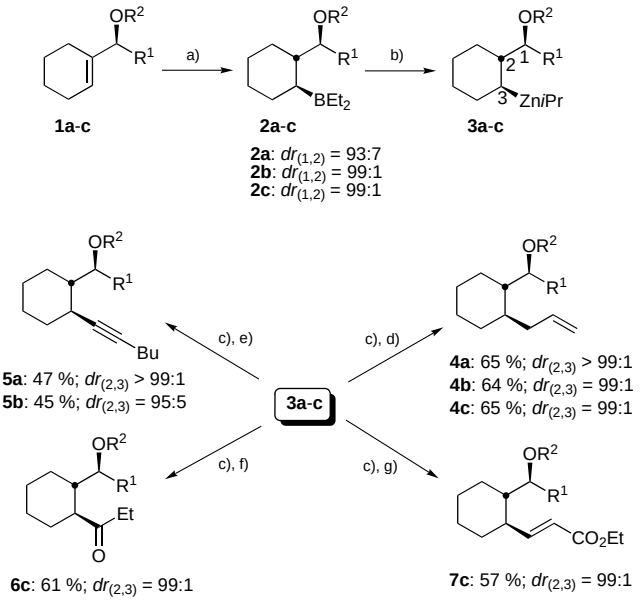
[4] a) D. A. Evans, P. H. Carter, E. M. Carreira, A. B. Charette, J. A. Prunet, M. Lautens, *J. Am. Chem. Soc.* **1999**, *121*, 7540 – 7552; b) D. A. Evans, P. H. Carter, E. M. Carreira, J. A. Prunet, A. B. Charette, M. Lautens, *Angew. Chem.* **1998**, *110*, 2526 – 2530; *Angew. Chem. Int. Ed.* **1998**, *37*, 2354 – 2359; c) D. A. Evans, E. M. Carreira, *Tetrahedron Lett.* **1990**, *31*, 4703 – 4706.
[5] a) T. Obitsu, K. Ohmori, Y. Ogawa, H. Hosomi, S. Ohba, S. Nishiyama, S. Yamamura, *Tetrahedron Lett.* **1998**, *39*, 7349 – 7352; b) K. Ohmori, T. Suzuki, S. Nishiyama, S. Yamamura, *Tetrahedron Lett.* **1995**, *36*, 6515 – 6518; c) K. Ohmori, S. Nishiyama, S. Yamamura, *Tetrahedron Lett.* **1995**, *36*, 6519 – 6522; d) K. Ohmori, T. Suzuki, K. Miyazawa, S. Nishiyama, S. Yamamura, *Tetrahedron Lett.* **1993**, *34*, 4981 – 4984.
[6] a) D. E. Schaufelberger, G. N. Chmurny, J. A. Beutler, M. P. Koleck, A. B. Alvarado, B. W. Schaufelberger, G. M. Muschik, *J. Org. Chem.* **1991**, *56*, 2895 – 2900; b) G. N. Chmurny, M. P. Koleck, B. D. Hilton, *J. Org. Chem.* **1992**, *57*, 5260 – 5264.
[7] D. A. Evans, K. T. Chapman, E. M. Carreira, *J. Am. Chem. Soc.* **1988**, *110*, 3560 – 3578.
[8] K. Ohmori, PhD thesis, Keio University, **1996**.
[9] K. Tanaka, Y. Ohta, K. Fuji, *Tetrahedron Lett.* **1993**, *34*, 4071 – 4074.
[10] a) M. Julia, J. M. Paris, *Tetrahedron Lett.* **1973**, 4833 – 4836; b) P. J. Kocienski, B. Lythgoe, S. Ruston, *J. Chem. Soc. Perkin Trans. 1* **1978**, 829 – 834.
[11] J. Inanaga, K. Hirata, H. Saeki, T. Katsuki, M. Yamaguchi, *Bull. Chem. Soc. Jpn.* **1979**, *52*, 1989 – 1993.
[12] The relative ratio was determined by ^{1}H NMR spectroscopy and the configuration of the resulting olefin was confirmed by ROESY experiments.
[13] a) G. R. Pettit, C. L. Herald, D. L. Doubek, D. L. Herald, *J. Am. Chem. Soc.* **1982**, *104*, 6846 – 6848; b) Y. Kamano, H. Zhang, H. Morita, H. Itokawa, O. Shirota, G. R. Pettit, D. L. Herald, C. L. Herard, *Tetrahedron* **1996**, *52*, 2369 – 2376.
[14] The conformational difference between **21** and **22** had an influence on the stereoselectivity of methoxycarbonylmethylene introduction; the desired stereochemistry (Z:E = 8:1) was obtained by reagent **C** in the case of **21**, whereas **22** gave rise to no reaction under the same conditions. Additionally, reaction of **22** with **A** proceeded in favor of the undesired selectivity (Z:E = 1:4).

Highly Diastereoselective Synthesis of Monocyclic and Bicyclic Secondary Diorganozinc Reagents with Defined Configuration**

Andreas Boudier, Eike Hupe, and Paul Knochel*

Dedicated to Professor Bernd Giese on the occasion of his 60th birthday

The stereoselective formation of new C–C bonds is an important goal in organic synthesis. A requirement for stereoselective coupling is the availability of C(sp^3)-hybridized organometallic compounds having a defined configuration. Organolithium compounds with high configurational stability are obtained only in strained cyclic systems or for organolithium reagents bearing a chelating heteroatom in the α-position.[1, 2] Although remarkable progress has recently been made in this field,[3, 4] a more general approach would be desirable. Recently, we have shown that secondary cyclic and acyclic chiral diorganozinc reagents can be prepared in the absence of any chelating heteroatom with high diastereoselectivity, allowing the stereochemical control of two adjacent stereocenters.[5, 6, 7] Herein, we report the diastereoselective hydroboration of various monocyclic and bicyclic ring systems allowing, after subsequent boron–zinc exchange,[8] the preparation of configurationally stable secondary dialkylzinc compounds with three adjacent chiral centers. Initially, we investigated the diastereoselective hydroboration of allylic ethers[9] of type **1**, since the corresponding alcohols can be readily obtained in optically pure form.[10] Thus, the hydroboration of **1a** (R^1 = Ph; R^2 = CH_2Ph) with Et_2BH in Me_2S[11] produces the corresponding organoborane **2a** with a diastereoselectivity of 93:7 (Scheme 1). An improved stereoselectivity of 99:1 is obtained by using an ethoxymethyl (EOM) protecting group (**2b**, R^2 = EOM). The presence of this acetal function also considerably facilitates the boron–zinc exchange, yielding secondary diorganozinc compounds of type **3**. After transmetalation with CuCN · 2 LiCl,[12] a smooth C–C bond-forming reaction occurs with various electrophiles such as allyl bromide, 1-bromo-1-hexyne,[13] propionyl chloride, or ethyl propiolate furnishing various polyfunctional products of type **4**–**7** (Table 1, entries 1–7).[14] This one-pot sequence proceeds with good overall yields (45–73%) and excellent

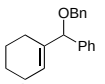
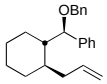
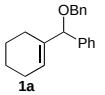
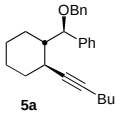
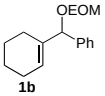
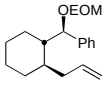
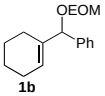
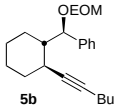
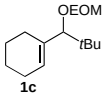
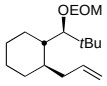
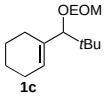
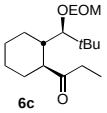
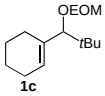
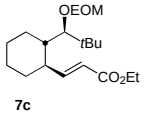
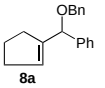
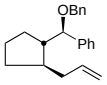
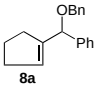
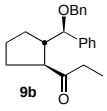
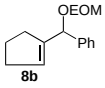
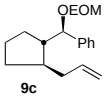
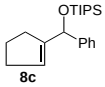
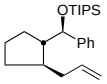
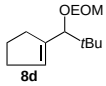
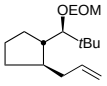
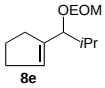
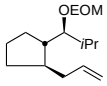
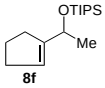
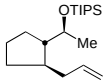
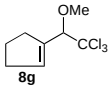
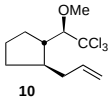


Scheme 1. Diastereoselective hydroboration of **1a**–**c**, boron–zinc exchange and reaction with electrophiles. For compounds of type **1**–**7**: **a**: R^1 = Ph; R^2 = Bn; **b**: R^1 = Ph; R^2 = CH_2OEt; **c**: R^1 = *t*Bu; R^2 = CH_2OEt. Reaction conditions: a) Et_2BH (3 equiv) in Me_2S, 50 °C, 16 h; b) *i*Pr_2Zn (3 equiv), 25 °C, 5 h; c) CuCN · 2 LiCl (1 equiv), −78 °C, 30 min; d) allyl bromide (3 equiv), −78 °C to 25 °C, 12 h; e) 1-bromo-1-hexyne (5 equiv), −55 °C, 2 d; f) EtC(O)Cl (3 equiv, −78 °C to 25 °C, 12 h; g) ethyl propiolate (3 equiv), −78 °C to 25 °C, 12 h.

[*] Prof. Dr. P. Knochel, Dipl.-Chem A. Boudier, Dipl.-Chem. E. Hupe
Department Chemie, Ludwig-Maximilians-Universität
Butenandtstrasse 5–13 (Haus F), 81377 München (Germany)
Fax: (+49) 89-2180-7680
E-mail: Paul.Knochel@cup.uni-muenchen.de

[**] We thank the DFG (SFB 260, Leibniz-Program) and the Fonds der Chemischen Industrie for generous support (Kekulé-scholarship for E. H.). We thank BASF, Degussa-Hüls AG, and Chemetall GmbH AG for the generous gift of chemicals.

Table 1. Cu^{I}-mediated reactions of monocyclic secondary diorganozinc reagents with electrophiles.

Entry	Alkene[a]	EX[b]	Product	dr[c](1,2)	dr[c](2,3)	Yield[d] [%]
1	 **1a**	A	 **4a**	93:7	>99:1	65
2	 **1a**	B	 **5a**	93:7	>99:1	47
3	 **1b**	A	 **4b**	99:1	99:1	64
4	 **1b**	B	 **5b**	99:1	95:5	45
5	 **1c**	A	 **4c**	99:1	99:1	65
6	 **1c**	C	 **6c**	99:1	99:1	61
7	 **1c**	D	 **7c**	99:1	99:1	57
8	 **8a**	A	 **9a**	92:8	99:1	73
9	 **8a**	C	 **9b**	94:6	95:5	54
10	 **8b**	A	 **9c**	88:12	99:1	71
11	 **8c**	A	 **9d**	60:30	99:1	67
12	 **8d**	A	 **9e**	87:13	99:1	73
13	 **8e**	A	 **9f**	73:27	90:10	61
14	 **8f**	A	 **9g**	50:50	78:22	59
15	 **8g**	A	 **10**	99:1	99:1	62

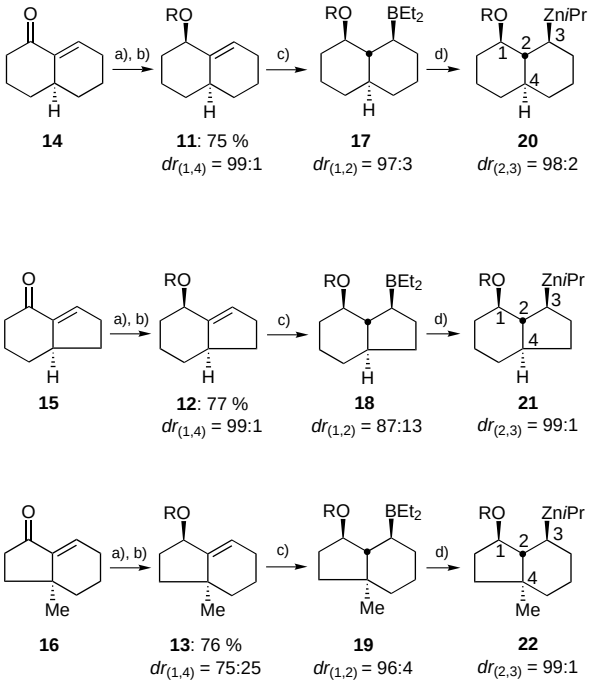
[a] Bn = benzyl, EOM = ethoxymethyl, TIPS = triisopropyl. [b] A = allyl bromide; B = 1-bromo-hex-1-yne; C = propionyl chloride; D = ethyl propiolate. [c] The diastereomeric ratio (*dr*) was determined by GC and NMR analysis of the crude product. [d] Yield of analytically pure product based on the starting alkene.

diastereoselectivities ($dr_{(2,3)}$ = 95:5 to 99:1 and $dr_{(1,2)}$ = 99:1, with R^2 = EOM) allowing a relative control of three adjacent centers and the formation of a new C–C bond (Scheme 1 and Table 1).

The diastereoselectivity of the hydroboration is similarly dependent on the nature of the protecting group for the corresponding cyclopentene derivatives of type **8** (entries 8–15).[15] Excellent diastereoselectivities were obtained for R^2 = Bn or Me ($dr_{(1,2)}$ up to 99:1), whereas protecting groups such as EOM or TIPS reduce dramatically the diastereoselectivity of the hydroboration (for R^2 = TIPS and R^1 = Ph, $dr_{(1,2)}$ = 60:40; for R^2 = EOM and R^1 = Ph, $dr_{(1,2)}$ = 88:12). Thus, by using the same reaction sequence as described in Scheme 1, the products **9a–g** were obtained with satisfactory overall yield. The trichloromethyl derivative **8g** (R^2 = Me and R^1 = CCl_3) leads stereoselectively to the allylated product **10** (Table 1, entry 15).

After these encouraging results, we examined the hydroboration of the bicyclic EOM-protected allylic alcohols **11**, **12**, and **13** (Scheme 2). These compounds were obtained by the reduction of the corresponding enones **14**, **15**,[16] and **16**[17] using $NaBH_4/CeCl_3$ (1 equiv, MeOH, 25 °C, 30 min)[18] followed by a protection reaction with $EtOCH_2Cl$ (Hünig's base, CH_2Cl_2, 25 °C, 16 h).[19]

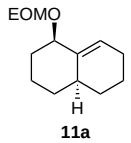
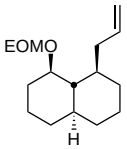
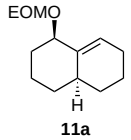
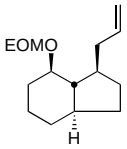
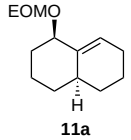
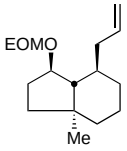
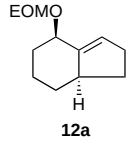
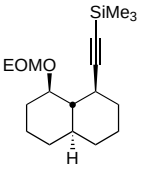
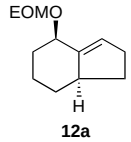
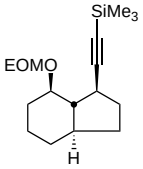
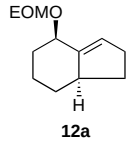
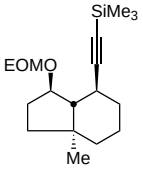
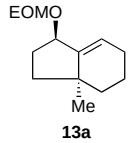
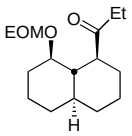
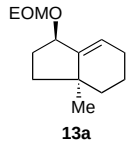
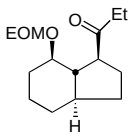
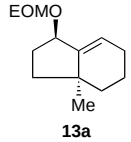
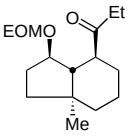
Whereas for the enones **14** and **15** the reduction was highly diastereoselective furnishing the corresponding allyl alcohols as only one diastereomer, for the reduction of **16**, a 3:1 mixture of two separable diastereomers was



Scheme 2. Stereoselective synthesis of bicyclic secondary organozinc reagents and their reaction with electrophiles. R = CH_2OEt; reaction conditions: a) $NaBH_4$ (1 equiv), $CeCl_3 \cdot 7H_2O$ (0.4 M in MeOH, 1 equiv) 25 °C, 30 min); b) $EtOCH_2Cl$ (1.5 equiv), Hünig's base (2 equiv), CH_2Cl_2, 25 °C, 16 h; c) Et_2BH (3 equiv), CH_2Cl_2:Me_2S (4:1), 25 °C, 48 h; d) iPr_2Zn (3 equiv), 25 °C, 5 h.

 © WILEY-VCH Verlag GmbH, D-69451 Weinheim, 2000 1433-7851/00/3913-2295 $ 17.50+.50/0

Table 2. Cu^{I}-mediated reactions of bicyclic secondary diorganozinc reagents with electrophiles.

Entry	Alkene	EX[a]	Product	*dr*[b](1,2)	*dr*[b](2,3)	Yield[c] [%]
1	 **11a**	A	 **23a**	97:3	> 98:2	65
2	 **11a**	B	 **23b**	97:3	> 99: < 1	42
3	 **11a**	C	 **23c**	97:3	94:6	59
4	 **12a**	A	 **24a**	87:13	99:1	65
5	 **12a**	B	 **24b**	87:13	> 99: < 1	43
6	 **12a**	C	 **24c**	87:13	96:4	62
7	 **13a**	A	 **25a**	96:4	98:2	59
8	 **13a**	B	 **25b**	96:4	> 99: < 1	41
9	 **13a**	C	 **25c**	96:4	94:6	61

[a] A = allyl bromide; B = 1-bromo-hex-1-yne; C = propionyl chloride. [b] The diastereomeric ratio (*dr*) was determined by GC and NMR analysis of the crude product. [c] Yield of analytically pure product based on the starting alkene.

obtained. The hydroboration of **11** under the standard reaction conditions (Et_2BH in Me_2S, 50 °C, 16 h) provided a 3:1 mixture of two diastereomeric alcohols (after oxidative work-up). However, the use of CH_2Cl_2 as cosolvent (Me_2S:CH_2Cl_2, 1:4) greatly improved the diastereoselectivity of the hydroboration (Et_2BH, 25 °C, 48 h), furnishing the organoborane **17** ($dr_{(1,2)} = 97{:}3$). Similarly, by using these improved hydroboration conditions, the bicyclic olefins **12** and **13** were converted to the corresponding organoboranes **18** ($dr_{(1,2)} = 87{:}13$) and **19** ($dr_{(1,2).} = 94{:}6$). The boron–zinc exchange of **17**–**19** proceeded smoothly with iPr_2Zn (3 equiv, 25 °C, 5 h), affording the corresponding secondary organozinc reagents **20**–**22** (Scheme 2) which after transmetalation with CuCN · 2 LiCl react under almost complete retention of configuration ($dr_{(2,3)} \geq 96{:}4$) with electrophiles such as allyl bromide, 1-bromoalkynes, or propionyl chloride. Bicyclic products of the type **23**–**25** have been obtained with excellent diastereoselectivities and satisfactory overall yields (Table 2).

Experimental Section

7c: A flame-dried 25-mL flask equipped with a magnetic stirring bar, an argon inlet, and a septum was charged with alkene **1c** (226 mg, 1 mmol). Et_2BH (0.4 mL, 7.3 M in Me_2S, 3 equiv) was added and the resulting mixture was stirred for 16 h at 50 °C. After the volatiles had been removed under vacuum (0.1 mm Hg, 25 °C, 2 h), iPr_2Zn (0.6 mL, 5 M in Et_2O, 3 equiv) was added and the mixture was stirred 5 h at 25 °C. The boron–zinc conversion was about 85 % as monitored by GC analysis of oxidized aliquots (aqueous 3 M NaOH/aqueous 30 % H_2O_2). The volatiles were removed under vacuum (0.1 mm Hg, 25 °C, 0.5 h) and the gray-black residue was diluted with THF (4 mL) and cooled to −78 °C. A freshly prepared solution of CuCN · 2 LiCl (1.5 mL, 1 M in THF, 1.5 equiv) was added over 20 min. The mixture was stirred for 30 min at −78 °C. Then ethyl propiolate (294 mg, 3 mmol, 3 equiv) in anhydrous THF (2 mL) was slowly added (30 min). After stirring for 1 h at −78 °C, the mixture was allowed to warm to room temperature. Usual work-up and purification by flash chromatography (SiO_2, hexanes/Et_2O 19:1 → 9:1) afforded **7c** (186 mg; 57 %) as a colorless oil.

23a: A flame-dried 25-mL flask equipped with a magnetic stirring bar, an argon inlet, and a septum was charged with alkene **11** (210 mg, 1 mmol) in CH_2Cl_2 (2 mL). Et_2BH (0.4 mL, 7.3 M in Me_2S, 3 equiv) was added and the resulting mixture was stirred for 48 h at 25 °C. After the volatiles had been removed under vacuum (0.1 mm Hg, 25 °C, 2 h), iPr_2Zn (0.6 mL, 5 M in Et_2O, 3 equiv) was added and the mixture was stirred 5 h at 25 °C. The boron–zinc conversion was about 80 % as monitored by GC analysis of oxidized aliquots (aqueous 3 M NaOH/aqueous 30 % H_2O_2). The volatiles were removed under vacuum (0.1 mm Hg, 25 °C, 0.5 h) and the gray-black residue was diluted with THF (2.5 mL) and cooled to −78 °C. At −78 °C, a freshly prepared solution of CuCN · 2 LiCl (0.7 mL, 1 M in THF, 0.7 equiv) was added over 1 h. The mixture was stirred for 20 min at −78 °C. Then allyl bromide (363 mg, 3 mmol, 3 equiv) in anhydrous THF (1.5 mL) was slowly added (40 min). After stirring for 1 h at −78 °C, the mixture was allowed to warm to room temperature. Usual work-up and purification by flash chromatography (SiO_2, hexanes/Et_2O = 49:1) afforded **23a** (164 mg; 65 %) as a colorless oil.

Received: January 26, 2000 [Z 14599]

[1] J. Corey, B. De, *J. Am. Chem. Soc.* **1984**, *106*, 2735–2736.
[2] a) W. C. Still, C. Sreekumar, *J. Am. Chem. Soc.* **1980**, *102*, 1201–1202; b) J. M. Chong, E. K. Mar, *Tetrahedron* **1989**, *45*, 7709–7716; c) W. H. Pearson, A. C. Lindbeck, *J. Am. Chem. Soc.* **1991**, *113*, 8546–8548; d) H. J. Reich, M. A. Medina, M. D. Bowe, *J. Am. Chem. Soc.* **1992**, *114*, 11003–11004; e) O. Zschage, D. Hoppe, *Tetrahedron* **1992**, *48*, 5657–5666.

 © WILEY-VCH Verlag GmbH, D-69451 Weinheim, 2000 1433-7851/00/3913-2296 $ 17.50+.50/0

[3] D. Hoppe, T. Hense, *Angew. Chem.* **1997**, *109*, 2376 – 2410; *Angew. Chem. Int. Ed. Engl.* **1997**, *36*, 2282 – 2316.
[4] a) S. T. Kerrick, P. Beak, *J. Am. Chem. Soc.* **1991**, *113*, 9708 – 9710; b) A. Basu, P. Beak, *J. Am. Chem. Soc.* **1996**, *118*, 1575 – 1576; c) D. J. Pippel, G. A. Weisenburger, S. R. Wilson, P. Beak, *Angew. Chem.* **1998**, *110*, 2600 – 2602; *Angew. Chem. Int. Ed.* **1998**, *37*, 2522 – 2524.
[5] L. Micouin, M. Oestreich, P. Knochel, *Angew. Chem.* **1997**, *109*, 274 – 276; *Angew. Chem. Int. Ed. Engl.* **1997**, *36*, 245 – 246.
[6] C. Darcel, F. Flachsmann, P. Knochel, *Chem. Commun*. **1998**, 205 – 206.
[7] a) A. Boudier, F. Flachsmann, P. Knochel, *Synlett* **1998**, 1438 – 1440; b) A. Boudier, P. Knochel, *Tetrahedron Lett.* **1999**, *40*, 687 – 690.
[8] a) F. Langer, L. Schwink, A. Devasagayaraj, P.-Y. Chavant, P. Knochel, *J. Org. Chem.* **1996**, *61*, 8229 – 8243; b) L. Micouin, P. Knochel, *Synlett* **1997**, 327 – 328.
[9] a) D. A. Evans, J. Bartoli, T. Godel, *Tetrahedron Lett.* **1982**, *23*, 4577 – 4580; b) D. H. Birtwistle, J. M. Brown, M. W. Foxton, *Tetrahedron Lett.* **1986**, *27*, 4367 – 4370; c) G. Schmid, T. Fukuyama, K. Akasaka, Y. Kishi, *J. Am. Chem. Soc.* **1979**, *101*, 259 – 260; d) W. C. Still, J. C. Barrish, *J. Am. Chem. Soc.* **1983**, *105*, 2487 – 2489; e) S. S. Bhagwat, P. R. Hamann, W. C. Still, *Tetrahedron Lett.* **1985**, *26*, 1955 – 1958.
[10] I. Klement, P. Knochel, *Synlett* **1996**, 1004 – 1006.
[11] Et_2BH is generated by the reaction of $BH_3 \cdot Me_2S$ (1 equiv) with Et_3B (2 equiv, RT, 4 d); compare with ref. [8].
[12] P. Knochel, M. C. P. Yeh, S. C. Berk, J. Talbert, *J. Org. Chem.* **1988**, *53*, 2390 – 2392.
[13] M. C. P. Yeh, P. Knochel, *Tetrahedron Lett.* **1989**, *30*, 4799 – 4802.
[14] For radical C–C bonding reactions via organoboranes, see: C. Ollivier, P. Renaud, *Chem. Eur. J.* **1999**, *5*, 1468 – 1473.
[15] 2D-COSY and NOESY NMR analysis was used to establish the relative stereochemistry of the hydroboration step for systems **1**, **8**, and **11** – **13**. The monocyclic protected allylic alcohols **1** and **8** had to be converted initially into the corresponding bicyclic acetals (hydroboration, oxidation, *p*-toluenesulfonic acid catalyzed acetalization).
[16] S. A. Bal, A. Marfat, P. Helquist, *J. Org. Chem.* **1982**, *47*, 5045 – 5050.
[17] T. Hiyama, M. Shinoda, H. Saimoto, H. Nozaki, *Bull. Chem. Soc. Jpn.* **1981**, *54*, 2747 – 2758.
[18] J.-L. Luche, *J. Am. Chem. Soc.* **1978**, *100*, 2226 – 2227.
[19] D. Askin, R. P. Volante, R. A. Reamer, K. M. Ryan, I. Shinkai, *Tetrahedron Lett.* **1988**, *29*, 277 – 280.

Distance-Dependent Electron Transfer in Au/Spacer/Q-CdSe Assemblies

Erik P. A. M. Bakkers, Albert W. Marsman, Leonardus W. Jenneskens, and Daniël Vanmaekelbergh*

Long-range electron transfer, that is, over distances of several molecular units, is an important phenomenon in biological systems; its role in protein and DNA function is currently a central issue in biological and chemical research.[1] Long-range electron tunneling also plays a key role in (opto)electronic devices. For instance, further miniaturization of the silicon-based metal/oxide/semiconductor transistor is seriously hindered due to electron tunneling through the oxide layer of molecular thickness.[2] The dependence of electron transfer rate on the tunneling distance is an important topic in chemistry, biology, and physics. The electron transfer rate constant k between a filled (donor) and empty (acceptor) level is given by Equation (1), where H_{DA} describes the electronic coupling between the donor and acceptor, and $F(\Delta G,\lambda)$ is the Franck – Condon factor.[3]

$$k = (2\pi/\hbar)\, H_{DA}^2\, F(\Delta G,\lambda) \quad (1)$$

To enable elastic tunneling, a nuclear reorganization in the donor – acceptor system is often required: The expression $F(\Delta G,\lambda)$ accounts for the thermal activation that depends on the Gibbs free energy change ΔG and the reorganization energy parameter λ of the system. Due to the separation r between the electron donor and acceptor, the electronic coupling is much weaker than the maximum value $H_{DA,max}$ and decays exponentially with r [(Eq. (2)].

$$H_{DA}^2 = H_{DA,\,max}^2\, e^{-\beta r} \quad (2)$$

Much research has been devoted to the experimental determination of the decay parameter β in crystalline and amorphous solids and in biologically relevant (protein, DNA) systems. Interestingly, the values for β, $0.1 - 1.5\ \text{Å}^{-1}$, are considerably smaller than the values for tunneling through a vacuum and depend markedly on the nature of the bridging molecule(s) between the donor and acceptor.[1] An inherent problem in a reliable determination of β is the possible dependence of the Franck – Condon factor $F(\Delta G,\lambda)$ on the separation r because of Coulombic interactions in the reactant, product, and transition state.[1, 3] The electron transfer rate is often investigated by time-resolved optical methods, for instance, fluorescence quenching of the photoexcited electron donor or acceptor. For a reliable interpretation of the data, the mechanism of excited-state decay, which involves light emission, electron transfer, and/or electron – phonon coupling, must be known. In addition, this mechanism must not change when the distance between donor and acceptor is increased by using larger bridging molecules.

Herein, we describe a class of assemblies, in which a photoexcitable entity (here a quantum dot, Q, in the form of a nanocrystalline particle) is covalently linked to a metal by spacer molecules of variable length. Relaxation of the excited state in Q may occur by two electronic transfers between the metal and Q; energy relaxation then occurs in the metal phase. Figure 1 shows an excited state in Q. Decay by two consecutive electron transfers may compete with relaxation of the excited state in Q. For this to occur, the Fermi level of the metal must be below the energy level of the excited electron in Q (the LUMO in Figure 1) but above the empty energy level (the unoccupied trap in Figure 1). Electron transfer between the energy levels in Q and the continuum of electron levels in the metal does not involve thermal activation; this means that the rate is solely determined by the electronic coupling between donor and acceptor [see Eq. (1) and (2)].

[*] Dr. D. Vanmaekelbergh, Dr. E. P. A. M. Bakkers
Chemistry and Physics of Condensed Matter
Debye Institute, Utrecht University
P.O. Box 80000, 3508 TA Utrecht (The Netherlands)
Fax: (+31) 30-253-2403
E-mail: Daniel@phys.uu.nl
Dr. A. W. Marsman, Prof. Dr. L. W. Jenneskens
Department of Physical Organic Chemistry
Debye Institute, Utrecht University,
P.O. Box 80000, 3508 TA Utrecht (The Netherlands)

 © WILEY-VCH Verlag GmbH, D-69451 Weinheim, 2000 1433-7851/00/3913-2297 $ 17.50+.50/0

for 3 h. The solution of the hydroxide form of the template **1** obtained after filtration was used directly in the aluminophosphate synthesis.

Synthesis of FeAlPO-31: To a solution of phosphoric acid (85%, Aldrich) in water, aluminium hydroxide hydrate (Aldrich) and an aqueous solution of iron(II) acetate (Aldrich) was added, and the mixture was stirred until homogeneous. To this, an aqueous solution of **1** was added slowly with vigorous stirring to obtain a gel with the empirical composition $0.04\,FeO : 0.48\,Al_2O_3 : 0.5\,P_2O_5 : 0.8/n\,[C_{12}H_{26}N_2O_2]_n : 40\,H_2O$ (pH 7–8). The gel was sealed in a Teflon-lined stainless steel autoclave and heated at 195 °C under autogeneous pressure for 48 h. The solid product was isolated by filtration, washed with deionized water, and dried in air (90 °C). The as-prepared product was calcined first in nitrogen and then in dry oxygen at 550 °C for 1 h and 10 h, respectively.

In situ XRD/XAS measurements:[20] The combined XRD/XAS measurements were performed at station 9.3 of the Daresbury synchrotron radiation source, which operates at 2 GeV with a typical current 130–250 mA. The station is equipped with a Si(220) double-crystal monochromator and ion chambers for measuring incident (I_0) and transmitted (I_t) beam intensities. For the in situ experiment, 25 mg of FeAlPO-31 was calcined in an situ cell at 550 °C in an O_2 flow. The XRD/XAS measurements were performed during the course of increasing the temperature (5 K min^{-1}) and at the final temperature. The XRD patterns were collected at the wavelength of 1.8088 Å, below the Fe–K edge. Each XRD pattern was measured for 180 s and each XAS spectrum for 380 s associated with a dead time of 40 s, to give a total cycle time of 10 min. The data were analysed using the suite of programs EXCALIB, EXBROOK, and EXCURV98, available at Daresbury laboratory.

Received: December 21, 1999 [Z14431]

[1] D. D. Davis in *Ullmanns Encyclopaedia of Industrial Chemistry, Vol. A1*, VCH, Weinheim, **1985**, pp. 269–276.
[2] D. D. Davis, D. R. Kemp in *Kirk Othmer Encyclopaedia of Chemical Technology, Vol.1* (Eds.: J. I. Kroschwitz, M. Howe-Grant), 4th ed., Wiley, New York, **1991**, pp. 466–493.
[3] K. I. Zamaraev, *J. Mol. Catal.* **1993**, *82*, 275.
[4] M. T. Musser in *Ullmanns Encyclopaedia of Industrial Chemistry, Vol. A8*, VCH, Weinheim, **1985**, pp. 217–226.
[5] E. P. Talsi, V. D. Chinakov, V. P. Babenko, V. N. Sidelnikov, K. I. Zamaraev, *J. Mol. Catal.* **1993**, *81*, 215–233.
[6] T. Maschmeyer, R. Oldroyd, G. Sankar, J. M. Thomas, I. J. Shannon, J. A. Klepetko, A. F. Masters, J. K. Beattie, C. R. A. Catlow, *Angew. Chem.* **1997**, *109*, 1713–1716; *Angew. Chem. Int. Ed. Engl.* **1997**, *36*, 1639–1642.
[7] K. Tanaka, *Chem. Technol. 4*. **1974**, *9*, 555–559.
[8] H. S. Bruner Jr. (DuPont), US pat. 5166421, **1992**.
[9] N. von Kutepow (BASF), US pat. 3876695, **1975**.
[10] R. Platz, R. Kummer, H. Schneider (BASF), US pat. 4258203, **1981**.
[11] J. M. Thomas, R. Raja, G. Sankar, R. Bell, *Nature* **1999**, *398*, 227.
[12] G. Sankar, R. Raja, J. M. Thomas, *Catal. Lett.* **1998**, *55*, 15–23.
[13] R. Raja, G. Sankar, J. M. Thomas, *J. Am. Chem. Soc.* **1999**, *121*, 11926–11927.
[14] P. B. Weisz, *Pure Appl. Chem*. **1980**, *52*, 2091.
[15] P. B. Weisz, W. O. Haag, R. M. Lago, *Nature* **1984**, *309*, 589–591.
[16] R. Raja, J. M. Thomas, *Chem. Commun.* **1998**, 1841-1842; J. M. Thomas, *Angew. Chem*. **1999**, *111*, 3800–3843; *Angew. Chem. Int. Ed.* **1999**, *38*, 3588–3628.
[17] J. M. Bennett, R. M. Kirchner, *Zeolites* **1992**, *12*, 338; A. J. Mora, A. N. Fitch, M. Cole, R. Goyal, R. H. Jones, H. Jobic, S. W. Carr, *J. Mater. Chem*. **1996**, *6*, 1831–1835.
[18] P. A. Wright, R. H. Jones, S. Natarajan, R. G. Bell, J. Chen, M. B. Hursthouse, J. M. Thomas, *J. Chem. Soc. Chem. Commun*. **1993**, 633-635.
[19] P. A. Wright, P. A. Cox, G. W. Noble, V. Patinec in *Proceedings of the 12th International Zeolite Conference III* (Eds.: M. M. J. Treacy, B. K. Marcus, M. E. Fisher, J. B. Higgins), Materials Research Society, Warrendale, PA, **1999**, pp. 1603–1610.
[20] Di-*n*-pentylamine has also been suggested[21] for the preferential synthesis of the AlPO-31 structure. We have not used this template.
[21] O. V. Kikhtyanin, R. F. Vogel, C. L. Kibby, T. V. Harris, K. G. Ione, D. J. O'Rear in *Proceedings of the 12th International Zeolite Conference III* (Eds.: M. M. J. Treacy, B. K. Marcus, M. E. Fisher, J. B. Higgins), Materials Research Society, Warrendale, PA, **1999**, 1743–1749.
[22] R. H. Daniels, G. T. Kerr, L. D. Rollmann, *J. Am. Chem. Soc*. **1978**, *100*, 3097–3100.
[23] J. M. Thomas *Chem. Eur. J.* **1997**, *3*, 1557–1562; G. Sankar, J. M. Thomas, *Top. Catal.* **1999**, *8*, 1–2.

Designing a Molecular Sieve Catalyst for the Aerial Oxidation of *n*-Hexane to Adipic Acid**

Robert Raja, Gopinathan Sankar, and John Meurig Thomas*

Dedicated to Professor H. W. Roesky on the occasion of his 65th birthday

Linear alkanes are so notoriously difficult to oxidize that their very name—paraffins, from the Latin *parum affinis* (slight affinity)—emphasizes their inertness. *n*-Hexane, for example, is not attacked by boiling nitric acid, concentrated sulphuric acid, potassium permanganate, or chromic acid. It is widely acknowledged that the controlled oxyfunctionalization of alkanes is one of the major challenges of modern catalysis;[1–4] particularly desirable products are those that are oxidized at the terminal position (hexanoic acid, for example), since these serve as feedstocks for the chemical and pharmaceutical industries.

A decade ago, following the discovery[5, 6] of molecular sieve titanosilicates such as TS-1, it was reported[7, 8] that *n*-hexane yielded a mixture of four products when hydrogen peroxide was used as the oxidant for the selective oxidation catalyzed by TS-1: 2-hexanol (17%), 3-hexanol (39%), 2-hexanone (34%), and 3-hexanone (10%). In a series of recent papers[9–13] we have reported how aluminophosphate (AlPO) molecular sieves, which contain an appropriate, framework-substituted transition-metal ion, M, in a high oxidation state, serve as effective catalysts for the selective oxidation of alkanes (especially at the terminal position). Molecular sieve catalysts are potentially more powerful for regioselective oxidation and are demonstrably capable of going beyond what may be achieved by Gif reagents developed by Barton et al.[14] for the rather high oxidative selectivity for secondary over tertiary positions in saturated hydrocarbons.[15–17] Here, we report how adipic acid, an

[*] Prof. Dr. Sir J. M. Thomas, Dr. R. Raja, Dr. G. Sankar
The Royal Institution of Great Britain
Davy Faraday Research Laboratory
21 Albemarle Street, London W1X 4BS (UK)
Fax: (+44) 0207-670-2988
E-mail: jmt@ri.ac.uk

[**] We gratefully acknowledge helpful discussions with Dr. R. G. Bell and Prof. C. R. A. Catlow, the support (via a rolling grant to J.M.T.) of the EPSRC, and the award of a research fellowship (for G.S.) from the Leverhulme Foundation.

 © WILEY-VCH Verlag GmbH, D-69451 Weinheim, 2000 1433-7851/00/3913-2313 $ 17.50+.50/0

important chemical feedstock, may be obtained from *n*-hexane in substantial amount using air as oxidant at low temperature and a Co^{III} framework-substituted AlPO as a catalyst.

The key features of this new class of versatile[18] MAlPO (M = Co^{III}, Mn^{III}, Fe^{III}) microporous catalysts that we have designed and developed are the following four points. First, the size and shape of the pores of the solid molecular sieve must be carefully selected so as to ensure that alkane oxidation, which proceeds[11] by a free-radical mechanism, takes place in an essentially shape-selective manner in the spatially restricted environment of the catalytically active sites. Second, these active sites are known[19] (by X-ray absorption spectroscopy) to be isolated M^{III} ions exposed at the inner walls of the molecular sieve used for the particular selective oxyfunctionalization that is being targeted. Third, the M^{III} active sites (in this case, Co^{III} ions, that have replaced a small, controlled fraction of the framework Al^{III} ions) are introduced during the synthesis and calcination of the molecular sieve catalyst (see below). Fourth, we have established[11, 12] that the tetrahedrally coordinated Co^{III} ions in the AlPO framework function as centers for the generation of free radicals and are responsible, in concert with the constraints imposed by the shape and size of the sieve, for the preferential attack by oxygen on the terminal groups of the alkane.

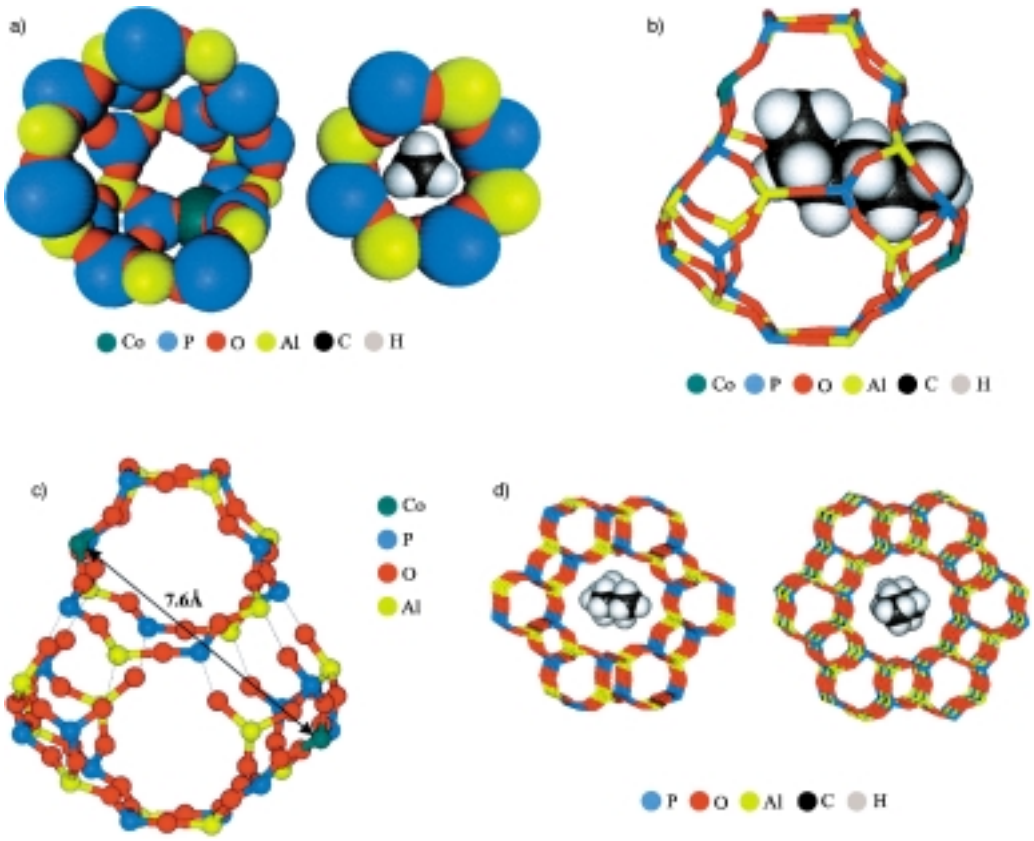


Figure 1. a) Views of (left) interior of the cage in the Co^{III}AlPO-18 catalyst and (right) of the aperture of the cage, which shows a terminal methyl group of an *n*-hexane molecule. b) The energy-minimized configuration (see ref. [11]) of an *n*-hexane molecule at 0 K inside an AlPO-18 framework. Two Co^{III} ions have been placed at the opposite vertices of the cage, at positions compatible (see text) with the composition $Co_{0.1}Al_{0.9}PO_4$. We estimate the separation distance between the van der Waals limits of these two framework ions to be about 7.6 Å. c) Expanded view of a cage in the CoAlPO-18 catalyst. For clarity, the top half has been separated from the bottom, the dotted lines indicating which atoms in the separated halves connnect. d) The structures of the AlPO-36 (left) and AlPO-5 (right) catalysts.

To achieve oxyfunctionalization at both (methyl) ends of *n*-hexane, we argued that a sufficiently large number of framework Co^{III} ions needed to be accommodated on the inner walls of catalysts such as CoAlPO-18—which, with about 4 atom % of Al^{III} replaced by Co^{III} ions, smoothly yields the (single) terminally oxidized products hexanol, hexanal, and hexanoic acid from *n*-hexane in air or oxygen—in such a manner that two framework Co^{III} ions should be separated by about 7–8 Å from one another. In other words, it is highly plausible that there are about two (separated) Co^{III} ions in each cage of the AlPO-18 structure, preferably situated opposite one another (Figure 1).

It is not just AlPO-18 but also AlPO-34 and AlPO-44 frameworks (all of which are closely akin to the aluminosilicate mineral chabazite, of idealized formula $Ca_6[Al_{12}Si_{24}O_{72}]$) that are candidates—in view of their pore dimensions and shape—for the designed catalyst. Experiments showed that AlPO-44 structures are not thermally stable;[20] they were not, therefore, considered further by us in this context. AlPO-34, although difficult to prepare in a phase-pure form with Co:P ratios less than 0.1, are, however, viable candidate catalysts along with AlPO-18 and are prepared through the agency of structure-directing (template) quaternized organic bases according to procedures described elsewhere.[21, 22] (A new template, trimethyl azabicyclooctane, was found to be effective for the preparation of CoAlPO-34 with Co:P ratios of about unity.[23])

It is not, unfortunately, readily possible by direct electron microscopic[24] or other techniques to determine the precise distribution of the Co^{III} ions in the AlPO framework, as the transition metal cation is not ordered within the structure. Simple computational estimates,[25] which assume spatially random substitution of Al^{III} by Co^{III} ions, indicate that with Co:P ratios of 0.08 and higher there is a strong tendency for two Co^{III} ions to be accommodated in each (chabazitic) cage.

Table 1 and Figure 2 summarize the results of our selective oxidation experiments and specifically highlight the contrast in catalytic performance—particularly in regard to production of adipic acid—of low and high Co:P ratios for CoAlPO-18 (namely, 0.04 and 0.10, respectively). It is gratifying to note,

 © WILEY-VCH Verlag GmbH, D-69451 Weinheim, 2000 1433-7851/00/3913-2314 $ 17.50+.50/0 *Angew. Chem. Int. Ed.* **2000**, *39*, No. 13

Table 1. Aerial oxidation of *n*-hexane: comparison of catalysts[a]

Catalyst (Co:P ratio)	Time [h]	Conversion [%]	Product selectivity (mole %)[b]								
			A	B	C	D	E	F	G	H	others
CoAlPO-18 (0.10)	8	5.9	15.8	19.0	32.8	7.3	14.7	6.2	2.5	–	2.3
	24	9.3	4.0	2.4	33.0	31.6	1.9	6.3	18.2	–	2.8
	24[c]	*9.5*	*3.1*	*2.3*	*35.2*	*33.6*	–	*4.5*	*19.7*	–	*2.5*
CoAlPO-18 (0.04)	8	3.5	13.1	24.3	57.1	–	–	3.5	2.1	–	–
	24	7.2	4.5	3.3	53.5	–	–	13.9	22.2	–	4.4
CoAlPO-34 (0.10)	8	6.3	20.5	16.0	26.7	4.0	17.3	8.2	6.2	–	1.5
	24	7.9	7.3	6.2	29.4	19.7	3.9	7.5	23.4	–	2.6
CoAlPO-36 (0.04)	8	3.1	9.9	2.0	2.5	–	–	18.3	12.5	49.6	4.7
	24	5.2	8.7	3.8	10.2	–	–	9.2	19.8	45.1	3.2

[a] Reaction conditions: *n*-hexane ≈50 g; catalyst = 0.51 g; oxidant (air) = 1.5 MPa; $T = 373$ K. [b] Products: A = 1-hexanol; B = 1-hexanal; C = hexanoic acid; D = adipic acid; E = 1,6-hexanediol and 1,6-hexanedial; F = 2-hexanol; G = 2-hexanone; H = 3-hexanol and 3-hexanone; others = traces of fragmentation products such as succinic and glutaric acids. [c] The italicized numbers denote results obtained from a duplicate experiment, in which the same catalyst was washed thoroughly with methanol and recalcined at 550 °C before use.

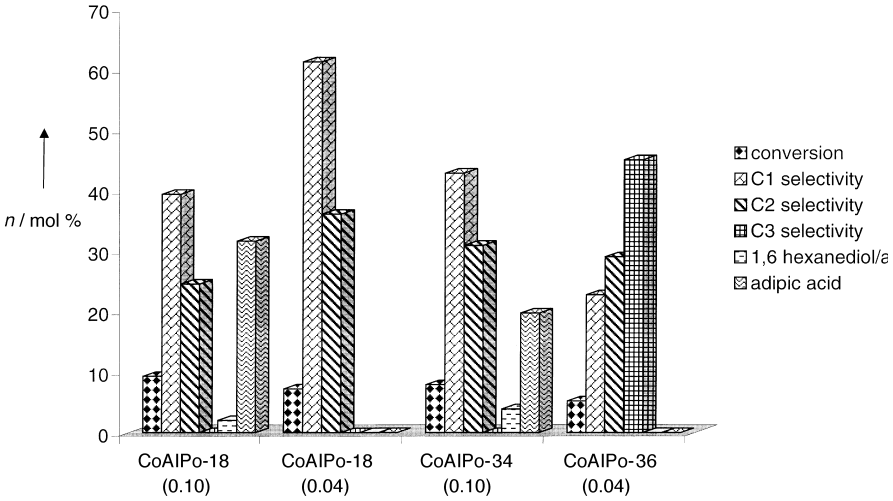


Figure 2. Bar chart to illustrate the efficacy of the cobalt-enriched CoAPO-18 (Co:P = 0.10) as a catalyst for the conversion of *n*-hexane to adipic acid. The values in parentheses refer to the Co:P ratio.

given the essential synonymity of their framework structures, that CoAlPO-18 and CoAlPO-34 (each with Co:P ratios of 0.10) exhibit broadly similar performances. On the other hand, CoAlPO-36 is markedly different, and this is to be expected, because of its larger pore structure and shape (Figure 1 d).

Detailed kinetic studies (Figure 3) are also informative, especially when compared with those reported earlier[11] for CoAlPO-18 with a Co:P ratio of 0.04. With a Co:P ratio of 0.1 for both the CoAlPO-18 and CoAlPO-34 catalysts, hexanol is the major product during the initial stages of the reaction but this is subsequently converted to hexanal and hexanoic acid. After 5 h, 1,6-hexanediol, 1,6-hexanedial, and traces of adipic acid appear in the reaction mixture as well as the three principal products (hexanol, hexanal, and hexanoic acid) observed earlier.[11]

It is noteworthy, that there is no decrease in hexanoic acid selectivity (Figure 3) but, that at prolonged contact times (10–24 h), there is a steady decrease in the concentrations of both 1,6-hexanediol and 1,6-hexanedial and a concomitant increase in the production of adipic acid. Evidently, the production of adipic acid arises as a result of the further oxidation of 1,6-hexanediol and 1,6-hexanedial. Further, when hexanoic acid was taken as the substrate (instead of *n*-hexane), using CoAlPO-18 (Co:P = 0.10) as the catalyst we did not observe any conversion. With a Co:P ratio of 0.04, the CoAlPO-18 catalyst, under identical conditions, produces neither 1,6-hexanediol, 1,6-hexanedial, nor any detectable adipic acid.[26]

The active, adipic acid-producing CoAlPO-18 catalyst, with its Co:P ratio of 0.10, is remarkably stable and we did not observe any leaching of the cobalt ions during the catalysis.[27] Even upon removal of the template molecule by gentle calcination in oxygen, in order to produce empty cages, the X-ray absorption and diffraction data, collected by in situ measurements as previously described,[10, 20] leave no doubt about the retention of structural integrity whilst the oxidation state of Co^{II} ions in the as-prepared solid increases to Co^{III} (Figure 4). This behavior mirrors exactly that of CoAlPO-18, which has a Co:P ratio of 0.04.[28]

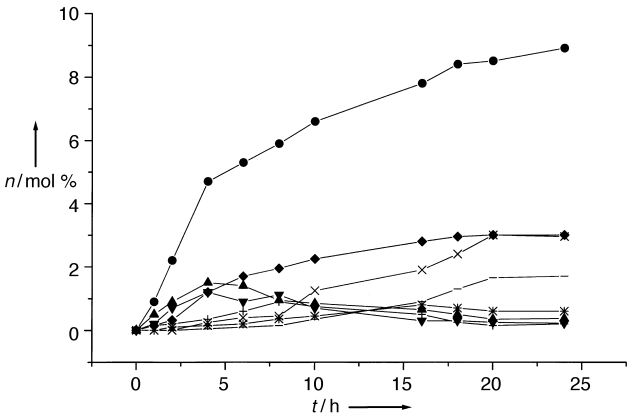


Figure 3. Kinetic plots showing the overall conversion of *n*-hexane and the appearance of various products with the CoAlPO-18 catalyst (Co:P = 0.10): ● = conversion; ▲ = 1-hexanol; ▼ = 1-hexanal; ◆ = hexanoic acid; + = 1,6-hexanediol and 1,6-hexanedial; × = adipic acid; ✱ = 2-hexanol; – = 2-hexanone.

 © WILEY-VCH Verlag GmbH, D-69451 Weinheim, 2000 1433-7851/00/3913-2315 $ 17.50+.50/0

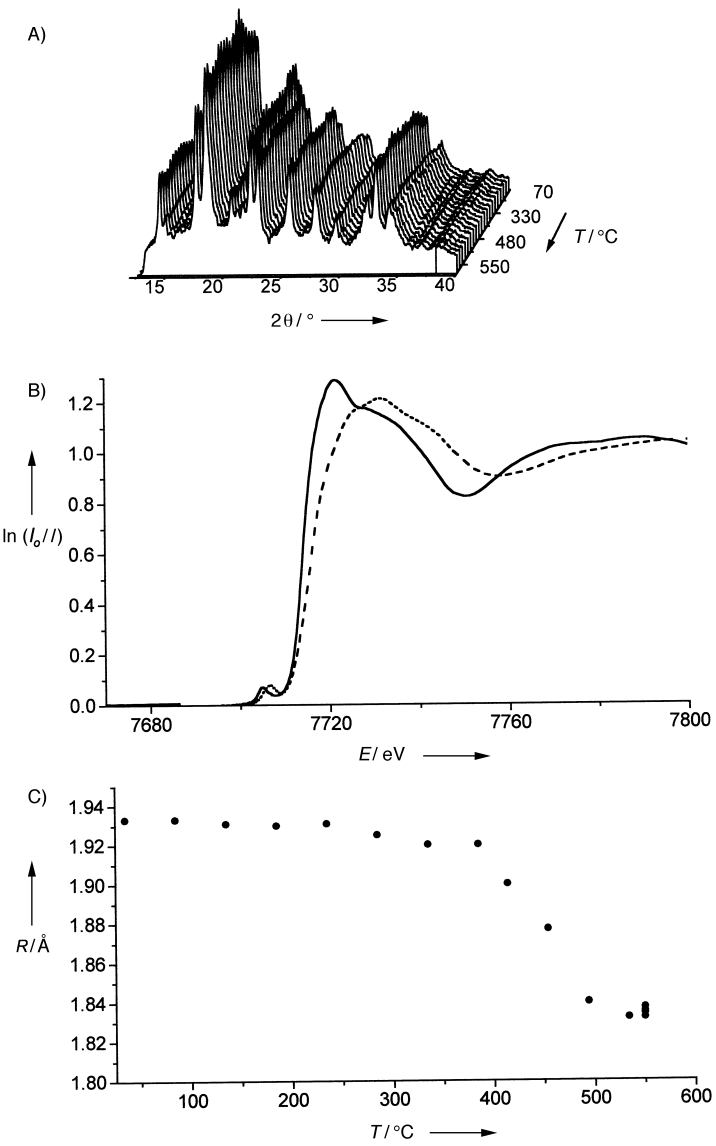


Figure 4. Combined time-resolved X-ray diffraction (XRD) patterns and X-ray near-edge absorption (XANES) spectra[20,28] of the progressively calcined CoAlPO-18 show, when the organic template (*N*,*N*-diisopropylethylamine) is driven off, the framework structure of the microporous catalyst does not collapse and the Co^{II} ions, present in the as-prepared material, are oxidized to Co^{III} at around 550 °C. A) Stacked XRD diffractograms; B) XANES spectra (compare with ref. [28]); C) the progressive decrease of the mean Co–O bond distance (*R*; derived from extended X-ray absorption fine structure (EXAFS) analysis) as the template molecule is removed by calcination.

To our knowledge, this is the first report that describes the formation of substantial amounts of adipic acid directly from *n*-hexane, a process hitherto considered so demanding as to become the quintessence of J. D. Roberts', the famous American chemist, Barton challenge.[15]

Received: February 15, 2000 [Z14705]

[1] P. A. MacFaul, D. D. M. Wayner, K. U. Ingold, *Acc. Chem. Res.* **1998**, *31*, 159–162.
[2] J. A. Cusumano in *Perspectives in Catalysis* (Eds.: J. M. Thomas, K. I. Zamaraev), Blackwells and IUPAC, Oxford, **1992**, pp. 1–33.
[3] *Activation and Functionalization of Alkanes* (Ed.: C. L. Hill), Wiley, Chichester, **1989**, Chap. 6–8.
[4] J. M. Thomas, *Nature* **1985**, *314*, 669–670.
[5] M. Taramasso, G. Perego, B. Notari in *Proc. 5th Int. Conf. Zeolites* (Ed.: L. V. C. Rees), Heydon & Sons, London, **1980**, p. 40.
[6] B. Notari, *Adv. Catal.* **1996**, *41*, 253–334.
[7] T. Tatsumi, M. Nakamura, S. Negishi, H. Tominaga, *J. Chem. Soc. Chem. Commun.* **1990**, 476–477.
[8] J. M. Thomas, *Philos. Trans. R. Soc. A* **1990**, *333*, 173.
[9] R. Raja, J. M. Thomas, *Chem. Commun.* **1998**, 1841–1842.
[10] G. Sankar, R. Raja, J. M. Thomas, *Catal. Lett.* **1998**, *55*, 15–23.
[11] J. M. Thomas, R. Raja, G. Sankar, R. G. Bell, *Nature* **1999**, *398*, 227–230.
[12] R. Raja, G. Sankar, J. M. Thomas, *J. Am. Chem. Soc.* **1999**, *121*, 11926–11927.
[13] M. Dugal, G. Sankar, R. Raja, J. M. Thomas, *Angew. Chem.* **2000**, *112*, 2399–2401; *Angew. Chem. Int. Ed.* **2000**, *39*, 2310–2313.
[14] a) D. H. R. Barton, M. J. Gastinger, W. B. Motherwell, *J. Chem. Soc. Chem. Commun.* **1983**, 731–733; b) D. H. R. Barton, *Chem. Soc. Rev.* **1996**, *25*, 237–240.
[15] J. D. Roberts, *The Chemical Intelligencer* **1999**, *5*, 32.
[16] J. A. Labinger, *CatTech* **1999**, *3*, 18–23.
[17] M. Hartman, S. Ernst, *Angew. Chem.* **2000**, *112*, 916–918; *Angew. Chem. Int. Ed.* **2000**, *39*, 888–890.
[18] Such catalysts are effective for a variety of other reactions, such as epoxidation, the Baeyer–Villiger conversion of ketones to lactones, and the selective oxidation of cyclohexane.
[19] P. A. Barrett, G. Sankar, C. R. A. Catlow, J. M. Thomas, *J. Phys. Chem.* **1996**, *100*, 8977–8985.
[20] G. Sankar, J. M. Thomas, *Top. Catal.* **1999**, *8*, 1–21.
[21] J. M. Thomas, *Angew. Chem.* **1999**, *111*, 3800–3843; *Angew. Chem. Int. Ed.* **1999**, *38*, 3588–3628.
[22] J. S. Chen, J. M. Thomas, *J. Chem. Soc. Chem. Commun.* **1994**, 603–604.
[23] J. K. Wyles, G. Sankar, D. W. Lewis, C. R. A. Catlow, J. M. Thomas, *Proc. 12th Int. Zeolite. Conf.* **1999**, 1723–1730.
[24] D. Ozkaya, W. Zhou, J. M. Thomas, P. A. Midgley, V. J. Keast, S. Hermans, *Catal. Lett.* **1999**, *60*, 113–120.
[25] CERIUS, Biosym Inc., San Diego, USA, **1994**.
[26] In order to verify that the above reaction is not affected by the *n*-hexane:cobalt molar ratio, we carried out two experiments: The first used 0.20 g of CoAlPO-34 (ratio 0.10), so that the number of moles of cobalt corresponds to that used in the CoAlPO-18 (ratio 0.04) experiment; the second used 0.87 g of CoAlPO-18 (ratio 0.04), so that the cobalt concentration corresponds to that used in the present study with CoAlPO-34 (ratio 0.10). Interestingly, in the case of the former, we still observed 1,6-hexanediol, 1,6-hexanedial, and adipic acid in the reaction mixture (although the conversion was only 5.2% after 24 h), whereas for the latter, we did not observe any of the above-mentioned products.
[27] The following experiments have been carried out to rule out the possibility of leaching. 1) In a typical experiment (see Table 1), the solid catalyst (CoAlPO-18; Co:P = 0.10) was filtered from the hot reaction mixture after 8 h and the reaction continued with the resulting filtrate for a further 16 h. No significant change in *n*-hexane conversion or the product selectivity was observed, which indicated that the leached metal ions (if any) are not responsible for the observed activity and selectivity. 2) The resulting filtrate (at the end of the reaction, 24 h) was analyzed independently by ICP and AAS for free or dissolved cobalt ions; only trace amounts (< 3 ppb) were detected. 3) When an equimolar mixture of *n*-hexane and cyclohexane was subjected to a catalytic test over CoAlPO-18 (Co:P = 0.10), there was, unsurprisingly, absolutely no conversion of the cyclohexane molecule, as it is too large to access the active Co^{III} framework sites in the AlPO-18 structure, while the conversion of *n*-hexane remained unaffected. If hexanoic acid or adipic acid leached cobalt from the framework, the cyclohexane molecule would have also been oxidized to cyclohexanol and cyclohexanone. See ref. [12] for further details.
[28] J. M. Thomas, G. N. Greaves, G. Sankar, P. A. Wright, J. S. Chen, A. J. Dent, L. Marchese, *Angew. Chem.* **1994**, *106*, 1922–1925; *Angew. Chem. Int. Ed. Engl.* **1994**, *33*, 1871–1873.

 © WILEY-VCH Verlag GmbH, D-69451 Weinheim, 2000 1433-7851/00/3913-2316 $ 17.50+.50/0

[3] D. Hoppe, T. Hense, *Angew. Chem.* **1997**, *109*, 2376 – 2410; *Angew. Chem. Int. Ed. Engl.* **1997**, *36*, 2282 – 2316.
[4] a) S. T. Kerrick, P. Beak, *J. Am. Chem. Soc.* **1991**, *113*, 9708 – 9710; b) A. Basu, P. Beak, *J. Am. Chem. Soc.* **1996**, *118*, 1575 – 1576; c) D. J. Pippel, G. A. Weisenburger, S. R. Wilson, P. Beak, *Angew. Chem.* **1998**, *110*, 2600 – 2602; *Angew. Chem. Int. Ed.* **1998**, *37*, 2522 – 2524.
[5] L. Micouin, M. Oestreich, P. Knochel, *Angew. Chem.* **1997**, *109*, 274 – 276; *Angew. Chem. Int. Ed. Engl.* **1997**, *36*, 245 – 246.
[6] C. Darcel, F. Flachsmann, P. Knochel, *Chem. Commun*. **1998**, 205 – 206.
[7] a) A. Boudier, F. Flachsmann, P. Knochel, *Synlett* **1998**, 1438 – 1440; b) A. Boudier, P. Knochel, *Tetrahedron Lett.* **1999**, *40*, 687 – 690.
[8] a) F. Langer, L. Schwink, A. Devasagayaraj, P.-Y. Chavant, P. Knochel, *J. Org. Chem.* **1996**, *61*, 8229 – 8243; b) L. Micouin, P. Knochel, *Synlett* **1997**, 327 – 328.
[9] a) D. A. Evans, J. Bartoli, T. Godel, *Tetrahedron Lett.* **1982**, *23*, 4577 – 4580; b) D. H. Birtwistle, J. M. Brown, M. W. Foxton, *Tetrahedron Lett.* **1986**, *27*, 4367 – 4370; c) G. Schmid, T. Fukuyama, K. Akasaka, Y. Kishi, *J. Am. Chem. Soc.* **1979**, *101*, 259 – 260; d) W. C. Still, J. C. Barrish, *J. Am. Chem. Soc.* **1983**, *105*, 2487 – 2489; e) S. S. Bhagwat, P. R. Hamann, W. C. Still, *Tetrahedron Lett.* **1985**, *26*, 1955 – 1958.
[10] I. Klement, P. Knochel, *Synlett* **1996**, 1004 – 1006.
[11] Et_2BH is generated by the reaction of $BH_3 \cdot Me_2S$ (1 equiv) with Et_3B (2 equiv, RT, 4 d); compare with ref. [8].
[12] P. Knochel, M. C. P. Yeh, S. C. Berk, J. Talbert, *J. Org. Chem.* **1988**, *53*, 2390 – 2392.
[13] M. C. P. Yeh, P. Knochel, *Tetrahedron Lett.* **1989**, *30*, 4799 – 4802.
[14] For radical C–C bonding reactions via organoboranes, see: C. Ollivier, P. Renaud, *Chem. Eur. J.* **1999**, *5*, 1468 – 1473.
[15] 2D-COSY and NOESY NMR analysis was used to establish the relative stereochemistry of the hydroboration step for systems **1**, **8**, and **11** – **13**. The monocyclic protected allylic alcohols **1** and **8** had to be converted initially into the corresponding bicyclic acetals (hydroboration, oxidation, *p*-toluenesulfonic acid catalyzed acetalization).
[16] S. A. Bal, A. Marfat, P. Helquist, *J. Org. Chem.* **1982**, *47*, 5045 – 5050.
[17] T. Hiyama, M. Shinoda, H. Saimoto, H. Nozaki, *Bull. Chem. Soc. Jpn.* **1981**, *54*, 2747 – 2758.
[18] J.-L. Luche, *J. Am. Chem. Soc.* **1978**, *100*, 2226 – 2227.
[19] D. Askin, R. P. Volante, R. A. Reamer, K. M. Ryan, I. Shinkai, *Tetrahedron Lett.* **1988**, *29*, 277 – 280.

Distance-Dependent Electron Transfer in Au/Spacer/Q-CdSe Assemblies

Erik P. A. M. Bakkers, Albert W. Marsman, Leonardus W. Jenneskens, and Daniël Vanmaekelbergh*

Long-range electron transfer, that is, over distances of several molecular units, is an important phenomenon in biological systems; its role in protein and DNA function is currently a central issue in biological and chemical research.[1] Long-range electron tunneling also plays a key role in (opto)electronic devices. For instance, further miniaturization of the silicon-based metal/oxide/semiconductor transistor is seriously hindered due to electron tunneling through the oxide layer of molecular thickness.[2] The dependence of electron transfer rate on the tunneling distance is an important topic in chemistry, biology, and physics. The electron transfer rate constant k between a filled (donor) and empty (acceptor) level is given by Equation (1), where H_{DA} describes the electronic coupling between the donor and acceptor, and $F(\Delta G,\lambda)$ is the Franck – Condon factor.[3]

$$k = (2\pi/\hbar)\, H_{DA}^2\, F(\Delta G,\lambda) \quad (1)$$

To enable elastic tunneling, a nuclear reorganization in the donor – acceptor system is often required: The expression $F(\Delta G,\lambda)$ accounts for the thermal activation that depends on the Gibbs free energy change ΔG and the reorganization energy parameter λ of the system. Due to the separation r between the electron donor and acceptor, the electronic coupling is much weaker than the maximum value $H_{DA,max}$ and decays exponentially with r [(Eq. (2)].

$$H_{DA}^2 = H_{DA,\,max}^2\, e^{-\beta r} \quad (2)$$

Much research has been devoted to the experimental determination of the decay parameter β in crystalline and amorphous solids and in biologically relevant (protein, DNA) systems. Interestingly, the values for β, $0.1 - 1.5\ \text{Å}^{-1}$, are considerably smaller than the values for tunneling through a vacuum and depend markedly on the nature of the bridging molecule(s) between the donor and acceptor.[1] An inherent problem in a reliable determination of β is the possible dependence of the Franck – Condon factor $F(\Delta G,\lambda)$ on the separation r because of Coulombic interactions in the reactant, product, and transition state.[1, 3] The electron transfer rate is often investigated by time-resolved optical methods, for instance, fluorescence quenching of the photoexcited electron donor or acceptor. For a reliable interpretation of the data, the mechanism of excited-state decay, which involves light emission, electron transfer, and/or electron – phonon coupling, must be known. In addition, this mechanism must not change when the distance between donor and acceptor is increased by using larger bridging molecules.

Herein, we describe a class of assemblies, in which a photoexcitable entity (here a quantum dot, Q, in the form of a nanocrystalline particle) is covalently linked to a metal by spacer molecules of variable length. Relaxation of the excited state in Q may occur by two electronic transfers between the metal and Q; energy relaxation then occurs in the metal phase. Figure 1 shows an excited state in Q. Decay by two consecutive electron transfers may compete with relaxation of the excited state in Q. For this to occur, the Fermi level of the metal must be below the energy level of the excited electron in Q (the LUMO in Figure 1) but above the empty energy level (the unoccupied trap in Figure 1). Electron transfer between the energy levels in Q and the continuum of electron levels in the metal does not involve thermal activation; this means that the rate is solely determined by the electronic coupling between donor and acceptor [see Eq. (1) and (2)].

[*] Dr. D. Vanmaekelbergh, Dr. E. P. A. M. Bakkers
Chemistry and Physics of Condensed Matter
Debye Institute, Utrecht University
P.O. Box 80000, 3508 TA Utrecht (The Netherlands)
Fax: (+31) 30-253-2403
E-mail: Daniel@phys.uu.nl
Dr. A. W. Marsman, Prof. Dr. L. W. Jenneskens
Department of Physical Organic Chemistry
Debye Institute, Utrecht University,
P.O. Box 80000, 3508 TA Utrecht (The Netherlands)

 © WILEY-VCH Verlag GmbH, D-69451 Weinheim, 2000 1433-7851/00/3913-2297 $ 17.50+.50/0

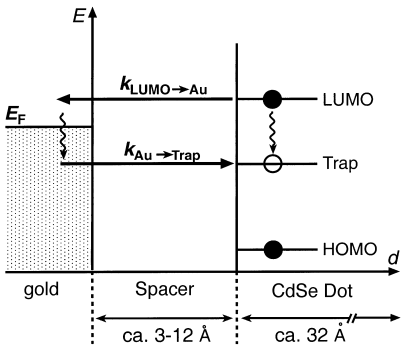
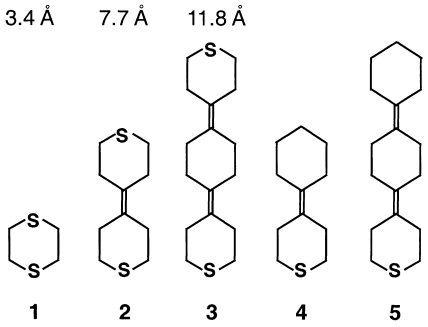


Figure 1. Energy diagram of a photoexcited semiconductive Q particle linked to a metal by a spacer molecule. The relaxation of the photoexcited state by electron transfer between the metal and the Q particle may effectively compete with direct decay (vertical arrow on the right-hand side), if the Fermi level of the metal is located between the energy level occupied by the photoexcited electron (the LUMO) and the unoccupied level (a trapped hole).

This simplification allows a direct interpretation of experimental data. In addition, if the metal/spacer/Q assembly is used as an electrode, the rates of electron transfer can be measured electrically, namely, by time-resolved measurement of the photoinduced current in the external circuit. Clearly, metal/spacer/Q assemblies are ideal systems for the study of the distance dependence of electron transfer.

We present results obtained with an Au/spacer/Q-CdSe system (Q-CdSe is a size-quantized CdSe paticle) used as a working electrode in a photoelectrochemical cell, which contains also a counter and reference electrode. Three bissulfide spacer molecules (**1**–**3**) have been used; they are rigid insulating species with lengths of 3.4, 7.7, and 11.8 Å, respectively. These molecules form compact self-assembled



monolayers (SAM) on gold with a tilt angle of 23° with respect to the normal axis.[4] AOT-stabilized Q-CdSe colloid crystals in heptane (AOT = bis(2-ethylhexyl)sulfosuccinate) were prepared according to a procedure reported in the literature.[5] Figure 2a shows the absorption spectrum of the suspension. The size of the crystals was 32 ± 4 Å, as determined by transmission electron microscopy (TEM) and optical absorbance spectroscopy. The nanocrystals are anchored as a monolayer on the Au/spacer system by immersing this system in the colloidal suspension for several hours. A scanning tuneling microcopy (STM) image of the system is presented in Figure 2b. Evidence for a covalent linking of the nanocrystals to the spacer molecule by S–Cd bonds is

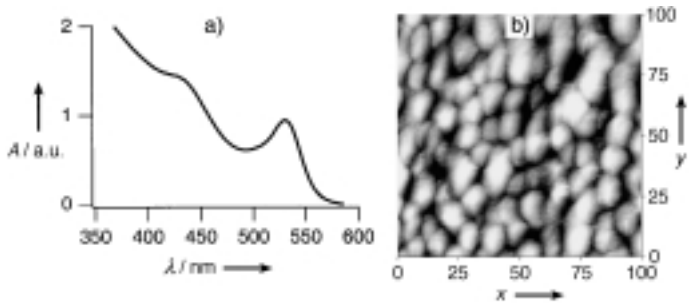


Figure 2. a) Absorption spectrum of a suspension of the size-quantized CdSe colloids (diameter 32 ± 4 Å). b) STM image of the CdSe particles chemisorbed on a gold surface covered with a SAM of **2**.

provided by the robust mechanical properties of the Au/spacer/Q-CdSe system during repeated atomic force microscopy (AFM) and STM scans and also by the fact that the CdSe dots did not attach to the Au/SAM when the monosulfide spacer molecules **4** and **5**, instead of **1**–**3**, were used. Other evidence for covalent S–Cd bonds is provided in ref. [6].

The Au/spacer/Q-CdSe electrode was illuminated with an argon ion laser ($\lambda = 457$ nm). A harmonic contribution to the intensity, $\tilde{\Phi}(\omega)$, was obtained with an acoustooptic modulator (frequency range $1 < \omega < 10^5\ s^{-1}$). The harmonically varying current density $\tilde{j}(\omega)$ was measured in the external circuit between the working and counter electrodes. A typical spectrum of the optoelectrical transfer function $\tilde{j}(\omega)/e\tilde{\Phi}(\omega)$ for Au/**2**/Q-CdSe is shown in Figure 3a; similar spectra are obtained with the spacer molecules **1** and **3**. The spectrum can be explained by assuming a long-lived excited state is formed in Q-CdSe upon excitation with light of energy $h\nu > E_{gap}$. This is confirmed by results from transient luminescence spectroscopy.[7] At sufficiently high frequencies, $\tilde{j}(\omega)/e\tilde{\Phi}(\omega)$ is zero. An "anodic" vector develops with decreasing frequencies, which is indicative of electron transfer from the photoexcited Q-CdSe particles to the gold. The anodic vector reaches a maximum and subsequently diminishes to zero with decreasing frequency; electron transfer from the nanocrystal to gold is gradually compensated by the slower transfer in opposite direction, from the gold to an empty state in Q-CdSe particles. Thus, decay of the excited state by transfer of an electron from Q-CdSe to gold and back to Q-CdSe competes effectively with intraparticle decay (Figure 1). By scanning the Fermi level of the gold electrode, we found that the long-lived state of the Q-CdSe particles consists of an electron in the LUMO, located at around 0.9 eV (versus SCE), and an empty level (trapped hole), 0.5 eV below the LUMO. Thus, photoinduced electron transfer is due to a long-lived state (lifetime ≥ 1 ms, see later) of low energy (0.5 eV). We should remark that this state results from the decay of a primary exciton (electron in the LUMO, hole in the HOMO) in the Q-CdSe particle. From the previous argumentation and from an analytical treatment, it follows that the characteristic frequencies ω_a and ω_b correspond to the rate constants $k_{LUMO \rightarrow Au}$ and $k_{Au \rightarrow Trap}$, respectively.[8] These rate constants are independent of temperature over the range 293–333 K, which shows that electron transfer is not thermally activated. In addition, the rate constants were (nearly) independent of the Fermi level in

 © WILEY-VCH Verlag GmbH, D-69451 Weinheim, 2000 1433-7851/00/3913-2298 $ 17.50+.50/0

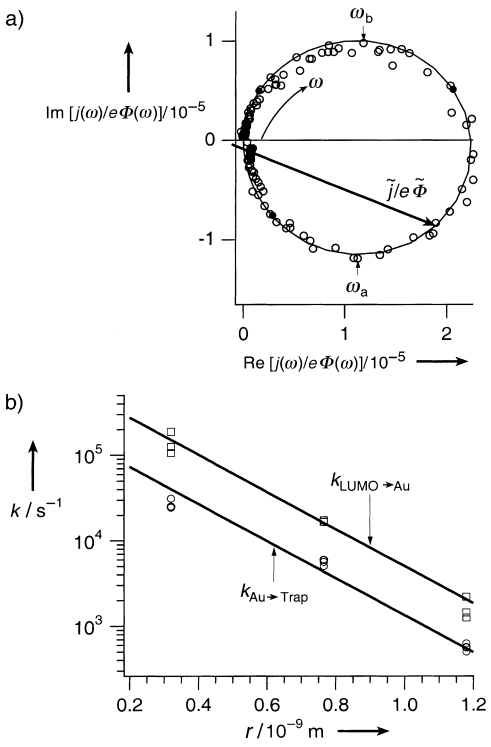


Figure 3. a) Plot of the transfer function $\tilde{j}(\omega)/e\tilde{\Phi}(\omega)$ in the complex plane obtained with a Au/**2**/Q-CdSe electrode in a photoelectrochemical cell (Pt counter electrode, SCE reference electrode, aqueous 1M KCl solution). The spectrum is quantitatively explained by two photoinduced electron transfer steps between Q-CdSe and gold; the characteristic frequencies ω_a and ω_b correspond to the rate constants $k_{LUMO \rightarrow Au}$ and $k_{Au \rightarrow Trap}$, respectively.[8] b) Semilogarithmic plot of the rate constants $k_{LUMO \rightarrow Au}$ and $k_{Au \rightarrow Trap}$ versus the length r of the spacer molecules **1**–**3**; the results shown were obtained for three samples for each spacer.

the gold electrode between 0.5 and 0.9 eV (versus SCE). Both observations show that the Franck–Condon factor $F(\Delta G,\lambda)$ is a constant and, hence, that changes in the rates of electron transfer are directly related to the electronic coupling. It was also found that the optoelectrical transfer function is independent of the background light intensity, to indicate that effects due to two-photon absorption in the Q-CdSe particles are unimportant.

The dependence of $k_{LUMO \rightarrow Au}$ and $k_{Au \rightarrow Trap}$ on the length of the rigid spacer molecule was investigated by measurement of the $\tilde{j}(\omega)/e\tilde{\Phi}(\omega)$ spectrum for each Au/spacer/Q-CdSe system for spacer molecules **1**–**3**. The results are presented in Figure 3b. Both $k_{LUMO \rightarrow Au}$ and $k_{Au \rightarrow Trap}$ decrease exponentially with increasing distance ($k = k_{max} e^{-\beta r}$), the parameter β is 0.50 ± 0.05 Å^{-1}. This β value is about one half of that found for most proteins and comparable to values for DNA strands.[1, 3] Using the Gamow formula for tunneling through vacuum, $\beta = 2\sqrt{2 m_e V/\hbar^2}$, we estimate a β value of 2.2 Å^{-1} assuming an energy barrier V of 4 eV. The much weaker attenuation of the electron transfer rates with distance in the Au/spacer/Q-CdSe system is indicative of strong coupling between Au and CdSe over the disulfide spacer molecules. It shows that there is a strong orbital overlap between Au and S on one side and between Cd and S on the other side of the spacer molecule. In addition, there must be a strong through-bond interaction in the spacer molecules. Photoelectron spectroscopy (He I) of the spacer molecules proves that there is a strong interaction between the two $3p_\pi$ lone pair (Lp) orbitals of the terminating sulfur atoms ($Lp_\pi(S)$) through the olefinic π bond orbitals and the H_{ax}-C-C-H_{ax} σ orbital system of the cyclohexyl rings; the orbital-energy differences $\Delta Lp_\pi(S)$ are for **1**–**3** 0.45, 0.4, and 0.3 eV, respectively.[4] This is in agreement with the weak distance dependence of the rate of electron transfer in the Au/spacer/Q-CdSe assemblies reported here.

In summary, for covalently bound metal/spacer/Q assemblies, in which Q is a light-absorbing nanocrystal, photoinduced electron transfer can occur without thermal activation. This allows an unambiguous determination of the distance dependence of the electron transfer rate using spacer molecules of variable length. This is illustrated with CdSe quantum dots bound to the metal with rigid bisulfide spacer molecules.

Received: January 13, 2000 [Z14532]

[1] a) C. C. Moser, J. M. Keske, K. Warncke, R. S. Farid, P. L. Dutton, *Nature* **1992**, *355*, 796–802; b) G. L. Closs, J. R. Miller, *Science* **1988**, *240*, 440–446; P. F. Barbara, T. J. Meyer, M. A. Ratner, *J. Phys. Chem.* **1996**, *100*, 13148–13168; d) S. O. Kelley, J. K. Barton, *Science* **1999**, *283*, 375–381.

[2] P. A. Packan, *Science* **1999**, *285*, 2079–2080, and references therein.

[3] R. A. Marcus, N. Sutin, *Biochim. Biophys. Acta* **1985**, *811*, 265–322.

[4] a) A. W. Marsman, PhD thesis, University of Utrecht (The Netherlands) **1999**, Chap. 6; b) The He I photoelectron spectra of the spacer molecules **1**–**3** were measured at the University of Heidelberg by Prof. Dr. R. Gleiter and co-workers, A. W. Marsmann, R. W. A. Havenith, S. Bethke, L. W. Jenneskens, R. Gleiter, J. H. van Lenthe, M. Lutz, A. L. Spek, *J. Org. Chem.* **2000**, in press. c) For photoinduced intramolecular electron transfer in donor–acceptor-substituted analogues of **1**–**3**, see: F. J. Hoogesteger, C. A. van Walree, L. W. Jenneskens, M. R. Roest, J. W. Verhoeven, W. Schuddeboom, J. J. Piet, J. M. Warman, *Chem. Eur. J.* **2000**, in press.

[5] M. L. Steigerwald, A. P. Alivisatos, J. M. Gibson, T. D. Harris, R. Kortan, A. J. Muller, A. M. Thayer, T. M. Duncan, D. C. Douglas, L. E. Brus, *J. Am. Chem. Soc.* **1988**, *110*, 3046–3050.

[6] V. L. Colvin, A. N. Goldstein, A. P. Alivisatos, *J. Am. Chem. Soc.* **1992**, *114*, 5221. The capping of the Q particles is the same as used in our work; the SAM layer consisted of hexanedithiol.

[7] M. G. Bawendi, P. J. Carroll, W. L. Wilson, L. E. Brus, *J. Chem. Phys.* **1992**, *96*, 946–954.

[8] E. P. A. M. Bakkers, E. Reitsma, J. J. Kelly, D. Vanmaekelbergh, *J. Phys. Chem. B.* **1999**, *103*, 2871–2788.

 © WILEY-VCH Verlag GmbH, D-69451 Weinheim, 2000 1433-7851/00/3913-2299 $ 17.50+.50/0

Purification and Partial Characterization of Tryptophan 7-Halogenase (PrnA) from *Pseudomonas fluorescens***

Sascha Keller, Tobias Wage, Kathrin Hohaus, Manuela Hölzer, Eric Eichhorn, and Karl-Heinz van Pée*

Dedicated to Professor Franz Lingens on the occasion of his 75th birthday.

The formation of natural organic halocompounds is not unusual.[1] Contrary to what is known about the metabolites, there is a huge lack of knowledge concerning the mechanisms for the formation of these compounds. For many years, haloperoxidases were thought to be responsible for the incorporation of halogen atoms into organic molecules.[2, 3] Haloperoxidases catalyze the incorporation of halogen atoms through the oxidation of the halide ions iodide, bromide, and chloride with the help of hydrogen peroxide. The enzyme-bound intermediates formed during this reaction are very unstable and hypohalous acid ultimately forms, which leads to unspecific halogenation reactions which are not in agreement with expectations from enzyme-catalyzed reactions.[4, 5] Nonetheless, there are situations in which unspecific halogenation reactions play important roles in nature, such as the defence mechanism of mammals against infections. Here, for example, myeloperoxidase has an important function.[6] For the specific formation of complex halogenated natural compounds, however, such a mechanism is not very useful.[3] Hints towards a different mechanism for the formation of halogenated compounds in nature were obtained during the investigation of the biosynthesis of barbamide, which is synthesized by the cyanobacterium *Lyngbya majuscula*. These results point to a radical mechanism for the formation of the trichloromethyl group of barbamide.[7, 8]

Molecular genetic investigations on the biosyntheses of the antibiotics 7-chlorotetracycline and pyrrolnitrin have shown that haloperoxidases are not involved in the formation of these halometabolites.[9–11] During the elucidation of the pyrrolnitrin biosynthesis, the existence of halogenating enzymes, which require NADH for the catalysis of halogenation reactions, was detected.[12] One of the two enzymes involved in pyrrolnitrin biosynthesis catalyzes the regioselective chlorination of tryptophan **1** to 7-chlorotryptophan **2** (see Scheme 1). This tryptophan 7-halogenase (Trp-7-Hal), PrnA, was now purified and partially characterized.

Purification to homogeneity (Figure 1) was achieved by ion exchange, hydrophobic-phase column chromatography, and molecular sieve chromatography (Table 1).

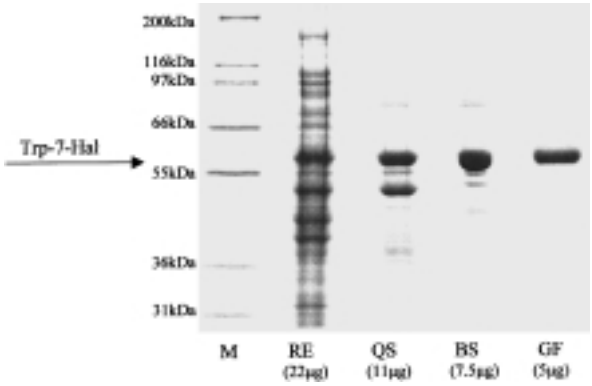


Figure 1. Sodium dodecylsulfate/polyacrylamide gel electrophoresis of the different purification steps for PrnA. M: marker proteins; RE: crude extract; QS: Q-sepharose pool; BS: butyl sepharose pool; GF: gel filtration pool; the amount of protein loaded on each lane is given in brackets.

Table 1. Purification scheme for PrnA (see Figure 1); activities (in units U [mmol min^{-1}]) were determined after addition of reductase. Without reductase, fractions after elution from the molecular sieve column did not show any activity.

Purification	Total protein [mg]	Activity [mU]	Specific activity [μU mg^{-1}]	Recovery [%]	Enhancement
Crude extract	2789.9	96.3	34.5	100.0	1.0
QS pool	221.3	92.6	418.4	96.2	12.1
BS pool	90.2	47.53	527.0	49.4	15.3
GF pool	12.5	9.12	730.0	9.5	21.2

In the first step of the purification, a protein component was partially removed which is absolutely necessary for activity (Figure 2). This protein component is a flavin reductase that reduces FAD to $FADH_2$ with the help of NADH. The FAD required for this reaction is still present after the first chromatographic step; it was, however, also removed during the later purification.

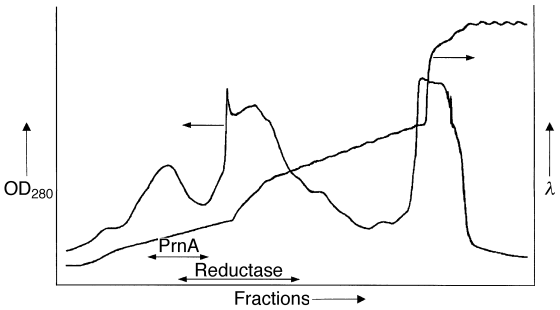


Figure 2. Elution profile from ion-exchange chromatography. QS pool: PrnA-containing fractions which were used for further purification; activator-component-pool: reductase-containing fractions. OD_{280} = optical density at 280 nm.

[*] Prof. Dr. K.-H. van Pée, Dipl.-Chem. S. Keller, Dipl.-Chem. T. Wage, Dr. K. Hohaus, Dr. M. Hölzer
Institut für Biochemie der Technischen Universität Dresden
Mommsenstrasse 13, 01062 Dresden (Germany)
Fax: (+49) 351-463-5506
E-mail: Karl-Heinz.vanPee@chemie.tu-dresden.de
Dipl.-Biotech. E. Eichhorn
Institut für Mikrobiologie, ETH
ETH-Zentrum, 8092 Zurich (Switzerland)

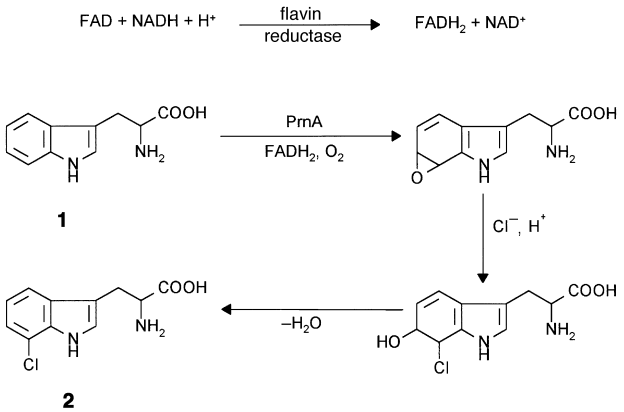
[**] This work was supported by the Deutsche Forschungsgemeinschaft (DFG) through the Graduiertenkolleg "Struktur-Eigenschafts-Beziehungen bei Heterocyclen", the Environment and Climate Research and Technology Development Programme of the European Union, the Sächsische Staatsministerium für Umwelt und Landesentwicklung, the Max-Buchner-Stiftung, and the Fonds der Chemischen Industrie. Samples of *P. fluorescens* BL915ΔORF1-4 with pPEH14-(*prnA*) and pPEH14(*prnC*) were obtained from Dr. J. M. Ligon, Novartis Agribusiness Biotechnology Research, Inc., Research Triangle, NC (USA) and NADH oxidase (from *Thermus thermiphilus*) from Prof. Helmut Erdmann, Fachhochschule Flensburg (Germany).

 © WILEY-VCH Verlag GmbH, D-69451 Weinheim, 2000 1433-7851/00/3913-2300 $ 17.50+.50/0

The necessity of a second component was a surprise since, according to molecular genetic data, it had to be assumed that no second protein component is necessary.[11] Obviously, the gene for this second component is not part of the biosynthetic cluster, which consists of four genes (*prnA – D*). The flavin reductase is an unspecific enzyme because the reductase from the *Pseudomonas* strain can be substituted by flavin reductases from other bacteria, such as SsuE, the flavin reductase component of the alkanesulfonate monooxygenase from *E. coli*[13] or by NADH oxidase from *Thermus thermophilus*.[14] Although flavin mononucleotide (FMN) is the better substrate for these flavin reductases, only FAD is accepted for the halogenation reaction. Obviously, tryptophan 7-halogenase is specific for $FADH_2$.

The possibility of substitution of the flavin reductase from *P. fluorescens* with a flavin reductase from *E. coli* also explains why *E. coli*, which only contains the four genes of the pyrrolnitrin biosynthetic gene cluster on a plasmid without the reductase gene, can synthesize pyrrolnitrin.[11] The other NADH/FAD-dependent halogenase thus far known, monodechloroaminopyrrolnitrin 3-halogenase (PrnC), is also a two-component system and requires a flavin reductase as the second component.

According to the hypothetical mechanism of these halogenases, the incorporation of the chloride ion requires the activation of the organic substrate by oxygen.[12] The oxygen dependence could be demonstrated by incubation under anaerobic conditions. In the absence of oxygen, no halogenating activity could be detected. The absolute requirement for oxygen, FAD, and NADH for the reaction very strongly points towards a monooxygenase-type reaction, as has been postulated earlier.[12] In the case of these monooxygenases,[15–17] a flavin reductase forms $FADH_2$ when treated with FAD and NADH, which together with oxygen then forms a flavin hydroperoxide. This flavin hydroperoxide can then attack double bonds and lead to the formation of an epoxide. By the regioselective incorporation of chloride, a halohydrin is thereby formed. The specific removal of water results in formation of the chlorinated product (Scheme 1). Recently, the genes of such halogenases have also been detected in other halometabolite-producing bacteria.[18–21] This mechanism is clearly one of the main mechanisms for the specific formation of halometabolites.



Scheme 1. Hypothetical reaction mechanism of the $FADH_2$-dependent tryptophan 7-halogenase reaction.

Experimental Section

Purification of tryptophan 7-halogenase: *P. fluorescens* BL915ΔORF1-4 harboring the tryptophan 7-halogenase gene on a plasmid [pPEH14-(*prnA*)] was used.[11] After 3 d incubation in a corn-molasses medium at 30 °C, the cells were collected by centrifugation, washed, resuspended in 100 mM potassium phosphate buffer (pH 7.2), and disrupted by ultrasonication. After the removal of insoluble cell components by centrifugation, the crude extract was dialyzed against 10 mM potassium phosphate buffer (pH 7.2) and passed through an ion-exchange column (Q-sepharose FF, Pharmacia). Elution was achieved with a linear NaCl gradient (0 – 0.5 M). Fractions that contained PrnA, which was detected by sodium dodecylsulfate/polyacrylamide gel electrophoresis (SDS-PAGE), were pooled (QS pool in Table 1). The flavin reductase eluted slightly later in the gradient and partially overlapped with PrnA (see Figure 2). Flavin reductase now free of PrnA was pooled separately and dialyzed against a 10 mM potassium phosphate buffer. For further purification, 1 M ammonium sulfate was added to the PrnA pool, which was then passed through a butyl sepharose 4 FF packed column. Elution was achieved with a linear descending gradient of ammonium sulfate (1 – 0.5 M). Fractions that contained PrnA, detected by SDS-PAGE analysis, were pooled (BS pool), concentrated by ultrafiltration, and loaded onto a HiLoad 16/60 Superdex 200 column. Elution was achieved with a 10 mm potassium phosphate buffer containing 1 M ammonium sulfate. Fractions were analyzed by electrophoresis and those containing PrnA were pooled (GF pool), dialyzed against 10 mm potassium phosphate buffer with 25 % glycerol, and concentrated by ultrafiltration.

Determination of halogenating activity: 55 μL of protein solution containing PrnA was incubated together with 110 μL of protein solution which contained either reductase (3.5×10^{-4} units SsuE from *E. coli*) or NADH oxidase (7×10^{-4} units from *Thermus thermophilus*), 10 μM FAD, 100 mM NaCl, 0.6 mM **1**, and 2.4 mM NADH in a total volume of 200 μL in 10 mM potassium phosphate buffer (pH 7.2). After incubation at 30 °C for 6 h, the reaction was stopped as described previously and analyzed by HPLC.[12]

Enrichment of PrnC: *P. fluorescens* BL915ΔORF1-4 harboring the monodechloroaminopyrrolnitrin 3-halogenase gene on a plasmid [pPEH14(*prnC*)] was used.[11] Cell incubation and preparation of the crude extract was performed as described for PrnA. Enrichment of PrnC was performed by ammonium sulfate precipitation at 25 – 45 % saturation.

Received: January 14, 2000 [Z 14537]

[1] G. W. Gribble, *Prog. Chem. Org. Nat. Prod.* **1966**, *68*, 1 – 5.
[2] S. L. Neidleman, J. Geigert, *Biohalogenation: Principles, Basic Roles and Applications*, Ellis Horwood, Chichester, **1986**.
[3] K.-H. van Pée, *Annu. Rev. Microbiol.* **1996**, *50*, 375 – 399.
[4] M. C. R. Franssen, *Biocatalysis* **1994**, *10*, 87 – 111.
[5] M. Sundaramoorthy, J. Terner, T. L. Poulos, *Chem. Biol.* **1998**, *5*, 461 – 473.
[6] H. B. Dunford, *Heme Peroxidases*, Wiley-VCH, Weinheim, **1999**.
[7] N. Sitachitta, J. Rossi, M. A. Roberts, W. H. Gerwick, M. D. Fletscher, C. L. Willis, *J. Am. Chem. Soc.* **1998**, *120*, 7131 – 7132.
[8] J. Hartung, *Angew. Chem.* **1999**, *111*, 1287 – 1288; *Angew. Chem. Int. Ed.* **1999**, *38*, 1209 – 1211.
[9] T. Dairi, T. Nakano, K. Aisaka, R. Katsumata, M. Hasegawa, *Biosci. Biotechnol. Biochem.* **1995**, *59*, 1099 – 1106.
[10] S. Kirner, S. Krauss, G. Sury, S. T. Lam, J. M. Ligon, K.-H. van Pée, *Microbiology* **1996**, *142*, 2129 – 2135.
[11] P. E. Hammer, D. S. Hill, S. T. Lam, K.-H. van Pée, J. M. Ligon, *Appl. Environ. Microbiol.* **1997**, *63*, 2147 – 2154.
[12] K. Hohaus, A. Altmann, W. Burd, I. Fischer, P. E. Hammer, D. S. Hill, J. M. Ligon, K.-H. van Pée, *Angew. Chem.* **1997**, *109*, 2102 – 2104; *Angew. Chem. Int. Ed. Engl.* **1997**, *36*, 2012 – 2013.
[13] E. Eichhorn, J. R. van der Ploeg, T. Leisinger, *J. Biol. Chem.* **1999**, *274*, 26639 – 26646.
[14] H. J. Hecht, H. Erdmann, H.-J. Park, M. Sprinzl, R. D. Schmid, *Nat. Struct. Biol.* **1995**, *2*, 1109 – 1114.
[15] M. Witschel, S. Nagel, T. Egli, *J. Bacteriol.* **1997**, *179*, 6937 – 6943.
[16] R. J. Parry, W. Li, *J. Biol. Chem.* **1997**, *272*, 23303 – 23311.

 © WILEY-VCH Verlag GmbH, D-69451 Weinheim, 2000 1433-7851/00/3913-2301 $ 17.50+.50/0

[17] M. A. Kertesz, K. Schmidt-Larbig, T. Wüest, *J. Bacteriol.* **1999**, *181*, 1464 – 1473.
[18] A. van Wageningen, P. N. Kirkpatrick, D. H. Williams, B. R. Harris, J. K. Kershaw, N. J. Lennard, M. Jones, S. J. M. Jones, P. J. Solenberg, *Chem. Biol.* **1998**, *5*, 155 – 162.
[19] S. Pelzer, R. Süßmuth, D. Heckmann, J. Recktenwald, P. Huber, G. Jung, W. Wohlleben, *Antimicrob. Agents Chemother.* **1999**, *43*, 1565 – 1573.
[20] B. Nowak-Thompson, N Chaney, J. S. Wing, S. J. Gold, J. E. Loper, *J. Bacteriol.* **1999**, *181*, 2166 – 2174.
[21] K.-H. van Pée, S. Keller, T. Wage, I. Wynands, H. Schnerr, S. Zehner, *Biol. Chem.* **2000**, *381*, 1 – 5.

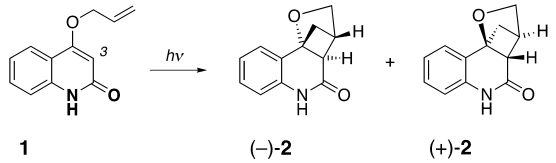
Enantioselective Intramolecular [2+2]-Photocycloaddition Reactions in Solution**

Thorsten Bach,* Hermann Bergmann, and Klaus Harms

Dedicated to Professor Horst Kessler on the occasion of his 60th birthday

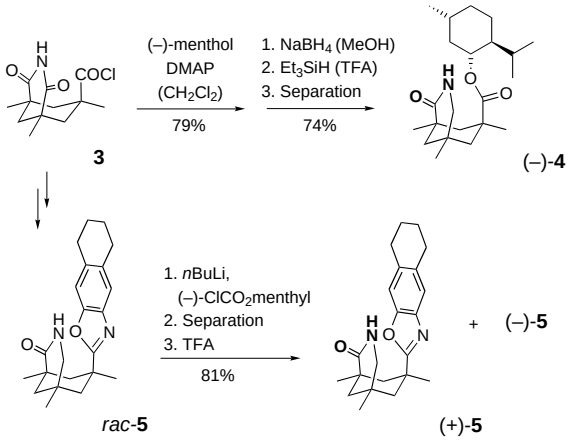
There are various approaches to obtain enantiomerically pure or enriched products from prochiral substrates by photochemical reactions in solution.[1] Whereas chiral auxiliaries which are covalently bound to one of the substrates have been successfully employed in many cases,[2, 3] chiral complexing agents which bind one substrate and thereby induce face discrimination have only been used to a limited extent.[4–8] Enantiomeric excess (*ee*) values achieved in C–C bond forming reactions based on the latter method have been moderate at best. In the solid phase however, complexes of an achiral substrate and a chiral complexing agent have been used more frequently and some excellent enantioselectivities have been recorded.[9, 10] We now report on [2+2]-photocycloaddition reactions in the presence of a chiral host, which proceeded in toluene with high enantioselectivity. Hydrogen bonds facilitate the binding of the prochiral substrate to the host and the transmission of the chiral information.

Our concept is based on the fact that prochiral lactams can coordinate to a chiral amide through their oxygen atom which acts as hydrogen acceptor and their nitrogen-bonded hydrogen atom which acts as hydrogen donor. We have recently shown that certain chiral amides derived from Kemp's triacid (1,3,5-trimethylcyclohexan-1,3,5-tricarboxylic acid) show low self-association and are therefore able to bind prochiral lactams efficiently.[11] A prochiral lactam bound to such a host is expected to undergo a stereoselective reaction. For our studies we have selected the 2-quinolone **1**, which upon irradiation with UV light cleanly yields the chiral cyclobutane (−)-**2** and its enantiomer (+)-**2** by an intramolecular [2+2]-photocycloaddition.[12] The simple diastereoselectivity of the reaction is high; only a single diastereoisomer is formed, as shown in Scheme 1.



Scheme 1. The intramolecular [2+2]-photocycloaddition reaction of the prochiral substrate **1**.

As host compounds, the bicyclic lactams (−)-**4** and (+)-**5** were prepared (Scheme 2). Association of compound **1** to the lactam unit through the atoms shown in bold would lead to an



Scheme 2. The synthesis of the enantiomerically pure host compounds (−)-**4**, (+)-**5**, and (−)-**5**. The transformation of acid chloride **3** into the racemic host *rac*-**5** is discussed in the text. (See also ref. [13]). DMAP = 4-dimethylaminopyridine, TFA = trifluoroacetic acid.

enantioface differentation in the course of the photocycloaddition, favoring enantiomer (−)-**2** (*Re* attack at carbon atom C-3). For the synthesis of host (−)-**4**, acid chloride **3**[13] was treated with enantiomerically pure (−)-menthol. Diastereoselective reduction of one carbonyl group and subsequent separation of diastereoisomers yielded compound (−)-**4** in enantiomerically pure form. The racemic benzoxazole *rac*-**5** was prepared from chloride **3** in 71 % yield by employing the corresponding *ortho*-aminophenol 3-amino-5,6,7,8-tetrahydro-2-naphthol[14] as the nucleophile according to a known procedure.[13] The resolution of enantiomers was performed by chromatographic separation of the corresponding *N*-menthyloxycarbonyllactam and its diastereoisomer. Removal of the chiral alkoxycarbonyl group yielded the enantiomerically pure host (+)-**5**[15] and its enantiomer (−)-**5**.

[*] Prof. Dr. T. Bach,[+] Dipl.-Chem. H. Bergmann, Dr. K. Harms[++]
Fachbereich Chemie der Philipps-Universität
Hans-Meerwein-Strasse, 35032 Marburg (Germany)
[+] New address:
Lehrstuhl für Organische Chemie I
Technische Universität München
Lichtenbergstrasse 4, 85747 Garching (Germany)
Fax: (+49) 89-2891-3315
E-mail: thorsten.bach@ch.tum.de
[++] Crystal structure determination
[**] This project was supported by the Deutsche Forschungsgemeinschaft (Ba 1372-4/1 and -4/2) and by the Fonds der Chemischen Industrie. We would like to thank Stefan Sieber (undergraduate research participant) for skillful technical assistance.

 © WILEY-VCH Verlag GmbH, D-69451 Weinheim, 2000 1433-7851/00/3913-2302 $ 17.50+.50/0

Irradiation experiments with the substrate **1** in the presence of the host molecules depicted in Scheme 2 gave product **2** whose *ee* value was determined by HPLC (Table 1).[16] Host (−)-**4** was suitable for induction of enantioselectivity but the

Table 1. Intramolecular [2+2]-Photocycloaddition Reactions of **1** (Scheme 1) in the Presence of Chiral Host Compounds.[16]

Entry	Host	Equiv[a]	T [°C][b]	Yield [%]	*ee* [%][c]
1	(−)-**4**	2.1	30	74	11
2	(−)-**4**	2.3	−15	89	37
3	(+)-**5**	1	30	76	28
4	(−)-**5**	1	−15	77	−78
5	(−)-**5**	2.1	30	73	−39
6	(+)-**5**	2.6	−15	79	84
7	(−)-**5**	2.6	−60	77	−93

[a] Equivalents of chiral host. The host compounds were recovered almost quantitatively (>90%). [b] Irradiation temperature. Irradiation source at 30°C: Rayonet RPR 3000 Å. Irradiation source at −15°C and at −60°C: Original Hanau TQ 150. [c] The *ee* values were determined by chiral HPLC.

ee values remained low (entries 1, 2). As anticipated, product (−)-**2** was the predominant enantiomer formed. We suspected that the nonplanarity of the menthol ring was responsible for a comparably weak association and insufficient face differentiation. Indeed, the crystal structure of compound (−)-**4** revealed that the methyl group at the menthyl ring might interact unfavorably with an associated substrate (Figure 1).[17] The almost planar tetrahydronaphthalenoxazole

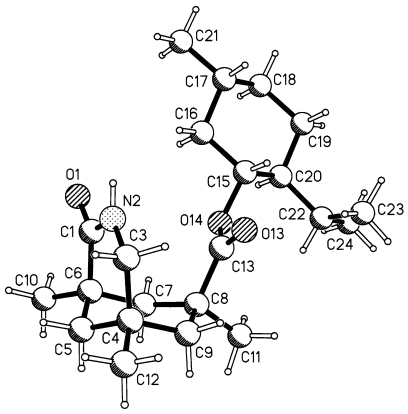
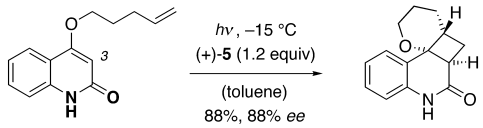


Figure 1. Structure of host (−)-**4** as a crystal.

moiety of compounds (+)-**5** and (−)-**5** should not encounter this problem. Indeed, host **5** proved superior to (−)-**4**. If employed stoichiometrically the *ee* value achieved in the photocycloaddition at −15°C was remarkably high (entry 4). Increased association can be forced by the use of more than one equivalent of the host. This led to an improvement of the *ee* values, both at 30°C (entries 3 and 5) and at −15°C (entries 4 and 6). The best value recorded so far was obtained at −60°C (entry 7). The absolute configuration of (+)-**2** (obtained by irradiation in the presence of (−)-**5**) was proven by single-crystal X-ray crystallography of its *N*-menthyloxycarbonyl derivative.[18]

The application of the enantioselective photocycloaddition is not restricted to the formation of the crossed photocycloaddition product **2**. A high enantiomeric excess was also recorded in the photocycloaddition of substrate **6**[12] which was converted enantioselectively into cyclobutane (−)-**7** (Scheme 3). The product (88% *ee*) was isolated in 88% yield. Its absolute configuration was assigned based on the assumption of *Re* attack at C-3.



6 (−)-**7**

Scheme 3. The intramolecular [2+2]-photocycloaddition reaction of the prochiral substrate **6**.

In summary, the first highly enantioselective [2+2]-photocycloaddition reactions in solution have been described. 2-Quinolones **1** and **6** yield the corresponding photocycloaddition products (−)-**2** and (−)-**7** in the presence of the chiral host compound (+)-**5**. The use of this host in related photochemical reactions of lactams is likely to yield similarly high enantioselectivities. Experiments along these lines are currently under way in our laboratory.

Received: February 21, 2000 [Z14737]

[1] Reviews: a) S. R. L. Everitt, Y. Inoue in *Molecular and Supramolecular Photochemistry: Organic Molecular Photochemistry*, *Vol. 3* (Eds.: V. Ramamurthy, K. S. Schanze), Marcel Dekker, New York, **1999**, pp. 71–130; b) Y. Inoue, *Chem. Rev.* **1992**, *92*, 741–770; c) H. Rau, *Chem. Rev.* **1983**, *83*, 535–547.

[2] Reviews on auxiliary-controlled stereoselective photochemical reactions: a) T. Bach, *Synthesis* **1998**, 683–703; b) S. A. Fleming, C. L. Bradford, J. J. Gao in *Molecular and Supramolecular Photochemistry: Organic Photochemistry*, *Vol. 1* (Eds.: V. Ramamurthy, K. S. Schanze), Marcel Dekker, New York, **1997**, pp. 187–243; c) J.-P. Pete, *Adv. Photochem.* **1996**, *21*, 135–216; d) J. Mattay, R. Conrads, R. Hoffmann, *Methoden Org. Chem. (Houben-Weyl) 4th ed. 1952–*, *Vol. E 21c*, **1995**, pp. 3085–3178; e) M. Demuth, G. Mikhail, *Synthesis* **1989**, 145–162.

[3] Some selected examples from the field of [2+2]-photocycloaddition chemistry: a) L. M. Tolbert, M. B. Ali, *J. Am. Chem. Soc.* **1982**, *104*, 1742–1744; b) H. Koch, J. Runsink, H.-D. Scharf, *Tetrahedron Lett.* **1983**, *24*, 3217–3220; c) A. I. Meyers, S. A. Fleming, *J. Am. Chem. Soc.* **1986**, *108*, 306–307; d) M. Demuth, A. Palomer, H.-D. Sluma, A. K. Dey, C. Krüger, Y.-H. Tsay, *Angew. Chem.* **1986**, *98*, 1093–1095; *Angew. Chem. Int. Ed. Engl.* **1986**, *25*, 1117–1119.

[4] Photopinacolization: a) D. Seebach, H.-A. Oei, H. Daum, *Chem. Ber.* **1977**, *110*, 2316–2333; b) L. Horner, J. Klaus, *Liebigs Ann. Chem.* **1979**, 1232–1257.

[5] Photocyclization: T. Naito, Y. Tada, I. Ninomiya, *Heterocycles* **1984**, *22*, 237–240.

[6] Photochemical rearrangement: D. R. Boyd, R. M. Campbell, J. Grimshaw, D. C. Neill, W. B. Jennings, *J. Chem. Soc. Perkin Trans. 1* **1985**, 849–855.

[7] Photodestruction: N. Levi-Minzi, M. Zandomenegni, *J. Am. Chem. Soc.* **1992**, *114*, 9300–9304.

[8] Photooxygenation: a) L. Weber, I. Imiolczyk, G. Haufe, D. Rehorek, H. Hennig, *J. Chem. Soc. Chem. Commun.* **1992**, 301–303; b) A. Sakai, H. Tani, T. Aoyama, T. Shioiri, *Synlett* **1998**, 257–258, and references therein.

[9] Reviews: a) F. Toda, *Acc. Chem. Res.* **1995**, *28*, 480–486; b) Y. Ito, *Synthesis* **1998**, 1–32.

[10] A. Joy, S. Uppili, M. R. Netherton, J. R. Scheffer, V. Ramamurthy, *J. Am. Chem. Soc.* **2000**, *122*, 728–729, and references therein.

 © WILEY-VCH Verlag GmbH, D-69451 Weinheim, 2000 1433-7851/00/3913-2303 $ 17.50+.50/0

[11] T. Bach, H. Bergmann, K. Harms, *J. Am. Chem. Soc.* **1999**, *121*, 10650 – 10651.
[12] C. Kaneko, T. Suzuki, M. Sato, T. Naito, *Chem. Pharm. Bull.* **1987**, *35*, 112 – 123.
[13] J. G. Stack, D. P. Curran, S. V. Geib, J. Rebek, Jr., P. Ballester, *J. Am. Chem. Soc.* **1992**, *114*, 7007 – 7018.
[14] M. Kajino, Y. Shibouta, K. Nishikawa, K. Meguro, *Chem. Pharm. Bull.* **1991**, *39*, 2896 – 2905.
[15] The absolute configuration of the tetrahydronaphthalenoxazole derivative (+)-**5** was concluded from comparison of its optical rotation ($[\alpha]_D^{20} = +7.4$; $c = 1$ in $CHCl_3$) with the analogous benzoxazole derivative[13] ($[\alpha]_D^{20} = +7.4$; $c = 2$ in $CHCl_3$) and by the absolute configuration of the irradiation product **2**.
[16] The reactions were conducted at the indicated temperature with toluene as the solvent (0.15 M solution of **1**). Further details regarding the irradiation procedure can be found in: T. Bach, J. Schröder, *J. Org. Chem.* **1999**, *64*, 1265 – 1273. The *ee* values ($ee = [(-)\text{-}\mathbf{2} - (+)\text{-}\mathbf{2}]/[(-)\text{-}\mathbf{2} + (+)\text{-}\mathbf{2}]$) were determined by HPLC analysis (column: Chiracel OD; eluent: hexane/2-propanol, 92/8) of the crude product mixture. The separation of host and product is possible by flash chromatography (pentane/*tert*-butylmethylether, 1/2). Both enantiomers of the host **5** were employed. Naturally, the direction of the face discrimination changes if (+)-**5** is replaced by (−)-**5**.
[17] Crystal data of host (−)-**4** ($C_{22}H_{37}NO_3 \cdot CH_2Cl_2$, $M_r = 448.45$): crystal size $0.3 \times 0.3 \times 0.15$ mm^3, orthorhombic, space group $P2_12_12_1$, $a = 852.0(1)$, $b = 1212.3(1)$, $c = 2410.5(1)$ pm, $V = 2489.9(4)$ Å^3, $\rho_{calcd} = 1.196$ g cm^{-3}, $Z = 4$, $F(000) = 968$, $\mu = 2.516$ mm^{-1}, Enraf-Nonius-CAD4 diffractometer, $\lambda = 1.54178$ Å, ω-scans, 4875 measured reflections ($-h, +k, \pm l$), $\Theta_{max} = 65°$, 4245 independent and 3575 observed reflections [$F \geq 4\sigma(F)$], 272 refined parameters, $R = 0.0608$, $wR^2 = 0.2080$, max. residual electron density 0.22 e Å^{-3}, direct methods, carbon-bound hydrogen atoms calculated, N–H atom refined. Crystallographic data (excluding structure factors) for the structure reported in this paper have been deposited with the Cambridge Crystallographic Data Centre as supplementary publication no. CCDC-142268. Copies of the data can be obtained free of charge on application to CCDC, 12 Union Road, Cambridge CB2 1EZ, UK (fax: (+44) 1223-336-033; e-mail: deposit@ccdc.cam.ac.uk).
[18] T. Bach, H. Bergmann, K. Harms, unpublished results.

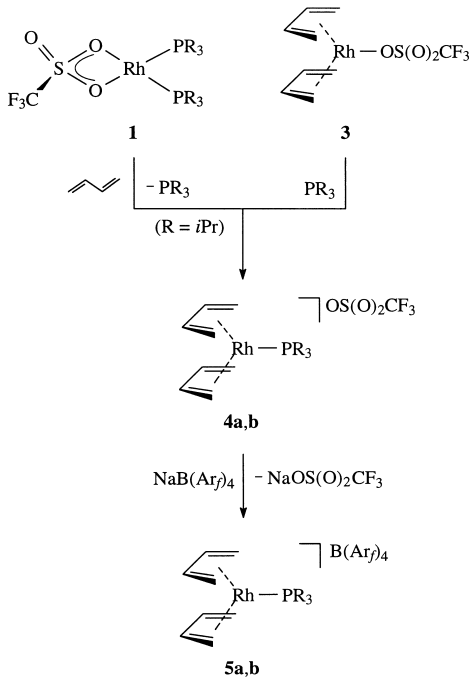
The Rhodium-Catalyzed Cyclotetramerization of Butadiene: Isolation and Structural Characterization of an Intermediate**

Marco Bosch, Maurice S. Brookhart, Kerstin Ilg, and Helmut Werner*

We have recently shown that the square-planar sulfonatorhodium(I) complex *cis*-[Rh{η^2-$O_2S(O)CF_3$}($PiPr_3$)$_2$][1] (**1**) is an active catalyst for the polymerization of butadiene.[2] A remarkable side product of this process was found to be 1,5,9,13-cyclohexadecatetraene. Although in the initial studies the overall yield of this cyclotetramer was rather low (< 5 %), we became interested to find out whether there could be a relationship between this reaction and the well known, "naked-nickel"-catalyzed, cyclo*tri*merization of butadiene discovered by Wilke et al.[3, 4] Since a key step in the reaction leading to *all-trans*-1,5,9-cyclododecatriene is the oxidative coupling of two butadiene ligands in the coordination sphere of nickel(0) to give the labile octadienediylnickel(II) derivative [Ni(η^3:η^3-C_8H_{12})],[4] we focused our efforts on detecting or, if possible, even isolating a related rhodium complex containing a C_8H_{12} ligand.

In a first attempt to elucidate the mechanism of the rhodium-catalyzed cyclo*tetra*merization of butadiene, we treated the triflate [Rh{μ-$O_2S(O)CF_3$}(C_8H_{14})$_2$]$_2$ (**2**) with C_4H_6 and isolated the neutral bis(butadiene)rhodium(I) complex [Rh{η^1-$OS(O)_2CF_3$}(*s-cis*-η^4-C_4H_6)$_2$] (**3**) in almost quantitative yield.[5] Since it was known that the addition of one equivalent of tricyclohexylphosphane to the nickel(0) compound [Ni(*s-cis*-η^4-C_6H_{10})$_2$] induces the coupling of the two coordinated 2,3-dimethylbutadiene ligands to generate the substituted octadienediylnickel(II) complex [Ni(η^1:η^3-$C_{12}H_{20}$)(PCy_3)],[6] we also treated compound **3** with PCy_3. However, under the conditions used (acetone, 5 min, 25 °C), instead of a C–C coupling a substitution of the coordinated triflate occurred and the ionic product [Rh(*s-cis*-η^4-C_4H_6)$_2$(PCy_3)]OTf (**4b**) was formed (Scheme 1, $OS(O)_2CF_3$ = OTF). The triisopropylphosphane analogue **4a**, which like **4b** is a white, moderately air-stable solid, is accessible in a similar way.[5] Salt metathesis of **4a** and **4b** with $NaB(Ar_f)_4$ (Ar_f = 3,5-bis(trifluoromethyl)phenyl) affords the corresponding compounds **5a** and **5b** in 83 and 86 % yield, respectively.

Although both **4a** and **4b** are stable in solution at room temperature and thus can be characterized by ^{1}H, ^{13}C{^{1}H},



Scheme 1. **a**: R = *i*Pr; **b**: R = Cy.

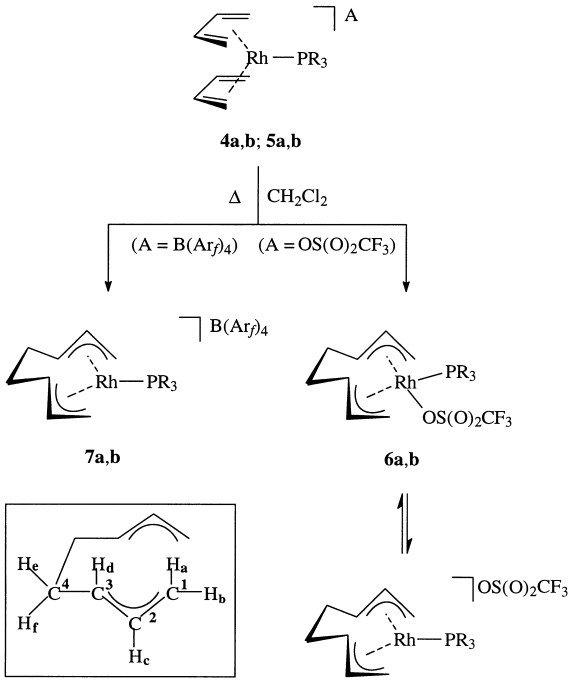
[*] Prof. Dr. H. Werner, Dipl.-Chem. M. Bosch, Dipl.-Chem. K. Ilg
Institut für Anorganische Chemie der Universität
Am Hubland, 97074 Würzburg (Germany)
Fax: (+49) 931-8884605
E-mail: helmut.werner@mail.uni-wuerzburg.de
Prof. Dr. M. S. Brookhart
Department of Chemistry, Venable and Kenan Laboratories
University of North Carolina
Chapel Hill, North Carolina 27599-3290 (USA)

[**] This work was supported by the Deutsche Forschungsgemeinschaft (SFB 347). K.I. thanks the Fonds der Chemischen Industrie for a Ph.D. scholarship.

Supporting information for this article is available on the WWW under http://www.wiley-vch.de/home/angewandte/ or from the author.

 © WILEY-VCH Verlag GmbH, D-69451 Weinheim, 2000 1433-7851/00/3913-2304 $ 17.50+.50/0

and $^{31}P\{^1H\}$ NMR spectroscopy, they react in CH_2Cl_2 under reflux (12 h for **4a** and 6 h for **4b**) to give, after recrystallization from CH_2Cl_2/pentane, the isomeric octadienediyl complexes **6a** and **6b** (Scheme 2). The red crystalline solids are soluble in polar organic solvents and can be stored without decomposition under argon at room temperature for days.



Scheme 2. **a**: R = *i*Pr, **b**: R = Cy.

The result of the X-ray crystal structure analysis of **6a** is shown in Figure 1.[7] The coordination geometry around the rhodium(III) center is distorted octahedral with atoms P1, C1, C6, and C8 occupying the equatorial and C3 and O1 the axial positions. The bond lengths Rh1–C1, Rh1–C3, C1–C2, and C2–C3 together with the bond angle C1-C2-C3 are in good agreement with those in related η^3-allylrhodium[5, 8] and octadienediylruthenium complexes.[9] In contrast to the C1-C2-C3 unit, the C6-C7-C8 fragment is slightly distorted which results in a lengthening of the two C–C bonds by approximately 0.05 Å and of the Rh–C bonds by approximately 0.1 Å. An even more characteristic feature is that the Rh1–O1 bond length (2.473(3) Å) is significantly longer than in the precursor molecule **3** (2.289(1) Å),[5] which explains why, as indicated by the IR spectrum of **6a** in CH_2Cl_2, a dissociation of the neutral compound into the triflate anion and the cation $[Rh(\eta^3{:}\eta^3\text{-}C_8H_{12})(P\mathit{i}Pr_3)]^+$ occurs (see Scheme 2). To the best of our knowledge, compounds **6a** and **6b** are the first octadienediyl complexes of the Group 9 elements (Co, Rh, Ir) described in the literature.[10]

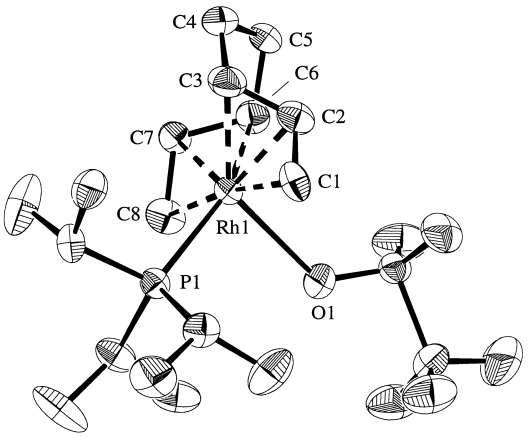


Figure 1. Molecular structure of **6a** in the crystal. Selected bond lengths [Å] and angles [°]: C1-C2 1.398(10), C2-C3 1.412(10), C3-C4 1.501(12), C4-C5 1.528(12), C5-C6 1.508(10), C6-C7 1.461(17), C7-C8 1.453(17), Rh1-C1 2.158(17), Rh1-C3 2.179(6), Rh1-C6 2.262(5), Rh1-C8 2.286(14), Rh1-P1 2.478(1), Rh1-O1 2.473(3); C1-C2-C3 116(1), C6-C7-C8 112(2).

Similarly to **4a** and **4b**, also the $B(Ar_f)_4$ complexes **5a** and **5b**, upon heating in dichloromethane, undergo a C–C coupling process to give the corresponding ionic octadienediylrhodium(III) derivatives **7a**, **b** in approximately 70 % yield (Scheme 2). From a high-level density functional theory (DFT) study using $[Rh(s\text{-}cis\text{-}\eta^4\text{-}C_4H_6)_2(PH_3)]^+$ and $[Rh(\eta^3{:}\eta^3\text{-}C_8H_{12})(PH_3)]^+$ as model compounds, a difference in energy of $\Delta G = -4.1$ kcal mol^{-1} between the two isomers was calculated.[11] This indicates that the C–C coupling reaction is thermodynamically favored. The conversion of the bis(diene) compounds **4a**, **b** and **5a**, **b** to their octadienediyl derivatives **6a**, **b** and **7a**, **b**, respectively, follows a first-order rate law. In nitromethane, the reactions of **4b** and **5b** are somewhat faster than those of the P*i*Pr$_3$ analogues **4a** and **5a**. The free energy of activation $\Delta G^{\neq}$ has been determined as 23.7(1) kcal mol^{-1} (for **4a** and **5a**) and 23.3(1) kcal mol^{-1} (for **4b** and **5b**).

The observation that **1** reacts under mild conditions with C_4H_6 to give **4a** in nearly quantitative yield (Scheme 1) supports the assumption that the bis(diene) complex **4a** plays an important role as an intermediate in the poly- and oligomerization of butadiene catalyzed by triflate **1**. In order to prove this, we treated **4a** as well as **4b** at elevated temperatures with an excess of C_4H_6 and found that a mixture of (cyclo)oligomers and polymers of butadiene in a ratio of 43:57 (**4a**) and 34:66 (**4b**) is formed (see Table 1, entry 1 and 2). GC/MS analysis of the mixture of products revealed that the oligomeric fraction predominantly (ca. 90 %) consists of a mixture of C_{12} and C_{16} hydrocarbons. Among the tetrameric fraction, a high selectivity, 83 % with **4a** and 79 % with **4b** as catalyst, for the *cis,cis,trans,trans* isomer of 1,5,9,13-cyclohexadecatetraene (**8**) is observed (Scheme 3). This results in an overall selectivity for **8** in the oligomeric fraction of 34 and 41 %, respectively. When the catalyst is prepared in situ from **2** and two equivalents of P*i*Pr$_3$ (Table 1, entry 3), both the activity and selectivity compare well with that for **4a**. Raising the temperature to 95 °C (Table 1, entry 4) leads to a higher selectivity for the tetrameric products in the oligomeric fraction (60 %) but also to a significant increase of the relative amount of polymeric material.

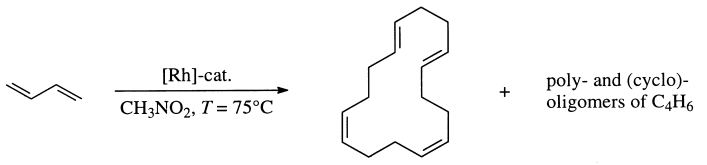
The ^{13}C NMR spectrum of **8**, which can be isolated as a colorless oil, shows four signals of equal intensity at around $\delta = 129$ for the CH carbon atoms, from which the configuration was derived as *c,c,t,t* (and not *c,t,c,t*).

 © WILEY-VCH Verlag GmbH, D-69451 Weinheim, 2000 1433-7851/00/3913-2305 $ 17.50+.50/0

Table 1. Metal-catalyzed poly- and oligomerization reactions of butadiene. Standard conditions for entries 1–4: CH_3NO_2 (10 mL), C_4H_6 (3 mL), 5 h, 75 °C.

Entry	Catalyst	Cat.-loading[a] [mol %]	Yield [%]	TON[b]	Polymer: Oligomer[c]	Product distribution of oligomeric fraction [%]				
						C_8	C_{12}	C_{16}[d]	C_{20}	C_{24}
1	**4a**	0.33	23	69	57:43	–	49	41 (34)	6	4
2	**4b**	0.30	27	88	66:34	–	37	52 (41)	7	4
3	**2** + 2 P*i*Pr$_3$	0.56	39	70	55:45	–	46	44 (31)	6	4
4[e]	**2** + 2 P*i*Pr$_3$	0.45	47	104	72:28	–	28	60 (39)	6	6
5	[Ni(C_3H_5)$_2$]/ [NiCl(C_3H_5)]$_2$[f]	0.26	58	224	56:44	9	41	8 (–)	22	20

[a] Based on the amount of butadiene employed. [b] TON = turnover number = {amount of C_4H_6 [mmol]}/[amount of catalyst [mmol]}. [c] The polymeric product consists of oligobutadienes $(C_4H_6)_n$ with $n \geq 8$. [d] Percentage of *cis,cis,trans,trans*-1,5,9,13-cyclohexadecatetraene (**8**) in parenthesis. [e] C_4H_6 (5 mL), 95 °C. [f] In toluene, 85 h, room temperature.



8

Scheme 3. [Rh]-cat. = **4a**, **4b** or **2** + 2 P*i*Pr$_3$.

In summary, it is rather surprising that, despite the numerous studies about the poly- and oligomerization reactions of butadiene, the transition metal catalyzed cyclo*tetra*merization of C_4H_6 has received little attention in the literature.[4a] There are two reports by Dzhemilev et al.[12] and Miyake et al.[13] who generated a catalytic system in situ, either from $TiCl_4/Et_2AlCl$ and 2-vinylfuran or from π-allylnickel(II) compounds. With the titanium system, a mixture of cyclic *all-trans* tri- and tetramers in a ratio of 7:3 was formed, whereas with the nickel(II) compound a variety of poly- and (cyclo)oligomers of butadiene was obtained (Table 1, entry 5). In contrast, the phosphanerhodium(I) complexes **4a**, **4b**, and **2**, if used as catalysts, have the advantage of a narrow product distribution and a high selectivity for **8** in the oligomeric fraction. With regard to the role that the isolated octadienediyl complex **6a** plays in the rhodium-catalyzed cyclooligomerization of C_4H_6, the results of preliminary NMR experiments indicate that in the initial stage of the reaction the formation of **6a** is the rate-determining step and the bis(diene) compound **4a** is the catalyst resting state.

Experimental Section

6a: A solution of of **4a** (175 mg, 0.34 mmol) in dichloromethane (20 mL) was heated under reflux for 12 h. A gradual change of color from light red to dark red occurred. After the reaction mixture was cooled to room temperature, the solvent was removed in vacuo. The oily residue was washed with pentane (3 × 5 mL) and the resulting red solid recrystallized from dichloromethane/pentane (1:5); yield 131 mg (74%); m.p. 104 °C (decomp); IR (CH_2Cl_2): $\tilde{\nu}$ = 1270–1260 ($OSO_{asymm.}$), 1239 ($CF_{symm.}$), 1162 ($CF_{asymm.}$), 1031 cm^{-1} ($OSO_{symm.}$); ^{1}H NMR (400 MHz, CD_2Cl_2):[14] δ = 5.23 (ddd, 2H, ^3J(H,H) = 11.6 Hz, ^3J(H,H) = 10.6 Hz, ^3J(H,H) = 7.0 Hz; H_c), 4.88 (dd, 2H, ^3J(H,H) = 7.0 Hz, ^4J(H,H) = 1.8 Hz; H_a), 4.21 (br ddd, 2H, ^3J(H,H) = 10.6 Hz, ^3J(H,H) = 3.5 Hz, ^4J(H,H) = 1.8 Hz; H_d), 3.07 (dd, 2H, ^3J(H,H) = 11.6 Hz, ^3J(P,H) = 6.3 Hz; H_b), 2.63 (m, 3H; PC*H*CH$_3$), 2.28 (m, 2H; H_e), 1.53 (m, 2H; H_f), 1.28 (dd, 9H, ^3J(P,H) = 14.3 Hz, ^3J(H,H) = 7.0 Hz; PCHC*H*$_3$), 1.15 (dd, 9H, ^3J(P,H) = 13.8 Hz, ^3J(H,H) = 7.3 Hz; PCHC*H*$_3$); ^{13}C{^{1}H} NMR (100.6 MHz, CD_2Cl_2): δ = 97.0 (d, ^1J(Rh,C) = 5.3 Hz; C^2), 91.1 (dd, ^1J(Rh,C) = 8.4 Hz, ^2J(P,C) = 6.4 Hz; C^3), 69.9 (dd, ^1J(Rh,C) = 6.1 Hz, ^2J(P,C) = 3.8 Hz; C^1), 29.2 (s; C^4), 27.1 (d, ^1J(P,C) = 18.3 Hz; P*C*HCH$_3$), 19.8, 19.7 (both s; PCH*C*H$_3$); ^{19}F{^{1}H} NMR (376.4 MHz, CD_2Cl_2): δ = –78.8 (s); ^{31}P{^{1}H} NMR (162.0 MHz, CD_2Cl_2): δ = 40.2 (d, ^1J(Rh,P) = 170.4 Hz). For assignment of protons and carbon atoms of the C_8H_{12} ligand see Scheme 2.

8: The cyclotetramer was obtained after fractional distillation of the combined oligomeric fractions obtained with **4a**, **4b** and **2**/P*i*Pr$_3$ as catalysts (Table 1, entries 1–4) in a Kugelrohr apparatus; colorless oil; b.p. 100–110 °C (1 mbar); MS (70 eV): *m*/*z*: 216 [M^+]; ^{1}H NMR (200 MHz, $CDCl_3$): δ = 5.41 (br s, 8H, CH), 2.08 (br s, 16H, CH_2); ^{13}C{^{1}H} NMR (50.3 MHz, $CDCl_3$): δ = 129.9, 129.7, 129.6, 129.4 (all s, CH), 32.6, 28.0, 27.7 (all s, CH_2).

The catalytic reactions were carried out as follows: In a typical experiment, a 50-mL glass autoclave was loaded with a solution of **4a** (58 mg, 0.11 mmol), **4b** (65 mg, 0.10 mmol), or a mixture of **2** (89 mg, 0.09 mmol) and P*i*Pr$_3$ (37 mL, 0.18 mmol), in freshly distilled nitromethane (10 mL) and butadiene (3 mL, 33.8 mmol). The mixture was heated for 5 h at 75 °C and then cooled to room temperature. The solvent and excess butadiene were removed, the oily residue was extracted with pentane (2 × 35 mL), and the extract was flash-chromatographed on Al_2O_3 (neutral, activity grade V). Evaporation of the solvent afforded in each case a waxy colorless product which was analyzed by GC/MS; yield 413 mg (**4a**), 488 mg (**4b**), 708 mg (**2**, entry 3) and 1488 mg (**2**, entry 4, Table 1). The relative amount of polymer in the isolated product was calculated from the difference between the yield of product and the yield of oligomers determined by the sum of the integrated signals in the GC spectrum for the C_8–C_{24} hydrocarbons.

Received: February 18, 2000 [Z14732]

[1] H. Werner, M. Bosch, C. Hahn, F. Kukla, M. Laubender, M. Manger, M. E. Schneider, B. Weberndörfer, B. Windmüller, *J. Chem. Soc. Dalton Trans.* **1998**, 3549–3558.

[2] a) M. E. Schneider, H. Werner, *10th International Symposium on Homogeneous Catalysis*, Princeton, **1996**; b) M. E. Schneider, PhD thesis, Universität Würzburg, **1997**.

[3] a) G. Wilke, *Angew. Chem.* **1988**, *100*, 189–211; *Angew. Chem. Int. Ed. Engl.* **1988**, *27*, 185–206; b) G. Wilke, B. Bogdanovic, P. Hardt, P. Heimbach, W. Keim, M. Kröner, W. Oberkirch, K. Tanaka, E. Steinrücke, D. Walter, H. Zimmermann, *Angew. Chem.* **1966**, *78*, 157–172; *Angew. Chem. Int. Ed. Engl.* **1966**, *5*, 151–164; c) G. Wilke, *Angew. Chem.* **1963**, *75*, 10–20; *Angew. Chem. Int. Ed. Engl.* **1963**, *2*, 105–115.

[4] a) G. Wilke, A. Eckerle in *Applied Homogeneous Catalysis with Organometallic Compounds*, *Vol. 1* (Eds.: B. Cornils, W. A. Herrmann), VCH, Weinheim, **1996**, Chap. 2.3.6; b) P. W. Jolly, G. Wilke, *The Organic Chemistry of Nickel*, *Vol. 2*, Academic Press, New York, **1975**, Chap. 3.

[5] M. Bosch, M. Laubender, B. Weberndörfer, H. Werner, *Chem. Eur. J.* **1999**, *5*, 2203–2211.

[6] R. Benn, B. Büssemeier, S. Holle, P. W. Jolly, R. Mynott, I. Tkatchenko, G. Wilke, *J. Organomet. Chem.* **1985**, *279*, 63–86.

 © WILEY-VCH Verlag GmbH, D-69451 Weinheim, 2000 1433-7851/00/3913-2306 $ 17.50+.50/0

[7] Data for the X-ray structure analysis of **6a**: Crystals from dichloromethane/pentane, $C_{18}H_{33}F_3O_3PRhS$ ($M_r = 520.46$); crystal size $0.19 \times 0.18 \times 0.16$ mm; monoclinic, space group $P2_1/c$, $Z = 4$, $a = 8.498(1)$, $b = 15.383(1)$, $c = 16.899(2)$ Å, $\beta = 94.18(2)^\circ$, $V = 2201.9(5)$ Å^3, $\rho_{calcd} = 1.570$ g cm^{-3}; $T = 173(2)$ K; $2\theta = 50.04^\circ$; 17827 reflections measured, 3884 were unique, ($R_{int} = 0.0569$), and 2922 observed ($I > 2\sigma(I)$); IPDS (Stoe), $Mo_{K\alpha}$ radiation ($\lambda = 0.71073$ Å), graphite-monochromated; Lp correction. The structure was solved by direct methods and refined with the full-matrix, least-square method; $R_1 = 0.0360$, $wR_2 = 0.0877$ (for 2922 reflections with $I > 2\sigma(I)$), $R_1 = 0.0509$, $wR_2 = 0.0936$ (for all 3884 data); data-to-parameter ratio 11.99; residual electron density $+0.797/-0.636$. All non-hydrogen atoms were refined anisotropically, and a riding model was employed in the refinement of the hydrogen atom positions. The octadienediyl ligand in **6a** is disordered and found with an occupancy of 0.69:0.31, it was refined anisotropically with restrains.Crystallographic data (excluding structure factors) for the structure reported in this paper has been deposited with the Cambridge Crystallographic Data Centre as supplementary publication no. CCDC-139992. Copies of the data can be obtained free of charge on application to CCDC, 12 Union Road, Cambridge CB2 1EZ, UK (fax: (+44) 1223-336-033; e-mail: deposit@ccdc.cam.ac.uk).

[8] a) R. Wiedemann, R. Fleischer, D. Stalke, H. Werner, *Organometallics* **1997**, *16*, 866–870; b) H. Werner, M. Schäfer, O. Nürnberg, J. Wolf, *Chem. Ber.* **1994**, *127*, 27–38.

[9] a) S. Wache, W. A. Herrmann, G. Artus, O. Nuyken, D. Wolf, *J. Organomet. Chem.* **1995**, *491*, 181–188; b) J. W. Steed, D. A. Tocher, *Polyhedron* **1994**, *13*, 167–173; c) B. Kavanagh, J. W. Steed, D. A. Tocher, *J. Chem. Soc. Dalton Trans.* **1993**, 327–335; d) D. N. Cox, R. Roulet, *J. Organomet. Chem.* **1988**, *342*, 87–95; e) D. N. Cox, R. Roulet, *Organometallics* **1985**, *4*, 2001–2005; f) A. Colombo, G. Allegra, *Acta Crystallogr. Sect. B* **1971**, *27*, 1653.

[10] In the rhodium-catalyzed coupling reaction of butadiene and CO_2 to give 2-ethyl-2,4,9-undecatrien-4-olide, the formation of an octadienediylrhodium complex has been postulated: A. Behr, R. He, K.-D. Juszak, C. Krüger, Y.-H. Tsay, *Chem. Ber.* **1986**, *119*, 991–1015.

[11] The calculated structures of $[Rh(s\text{-}cis\text{-}\eta^4\text{-}C_4H_6)_2(PH_3)]^+$ and $[Rh(\eta^3\text{:}\eta^3\text{-}C_8H_{12})(PH_3)]^+$ are very close to that found in the solid state for the P*i*Pr$_3$ analogues **4a** and **6a** despite the lack of the coordinated triflate anion in the latter (the PH_3 ligand is positioned symmetrically with respect to the octadienediyl moiety); L. Perrin, E. Clot, O. Eisenstein, private communication.

[12] a) U. M. Dzhemilev, L. Y. Gubaidullin, *Zh. Org. Khim* **1976**, *12*, 44–46 [*Chem. Abstr.* **1976**, *84*, 121244]; b) G. A. Tolstikov, U. M. Dzhemilev, L. Y. Gubaidullin, *Ivz. Akad. Nauk SSSR Ser. Khim* **1975**, *2*, 487 [*Chem. Abstr.* **1975**, *82*, 139467].

[13] A. Miyake, H. Kondo, M. Nishino, *Angew. Chem.* **1971**, *83*, 851–852; *Angew. Chem. Int. Ed. Engl.* **1971**, *10*, 802–803.

[14] The ^{1}H and ^{13}C{^{1}H} NMR data of the anionic ligand are omitted for clarity.

Novel 1,2,4-Triphosphole and 1,2,3-Triphosphetene Derivatives from *N,N′*-Bis(2,2-dimethylpropyl)benzimidazolin-2-ylidene and Phosphaalkynes**

F. Ekkehardt Hahn,* Lars Wittenbecher, Duc Le Van, Roland Fröhlich, and Birgit Wibbeling

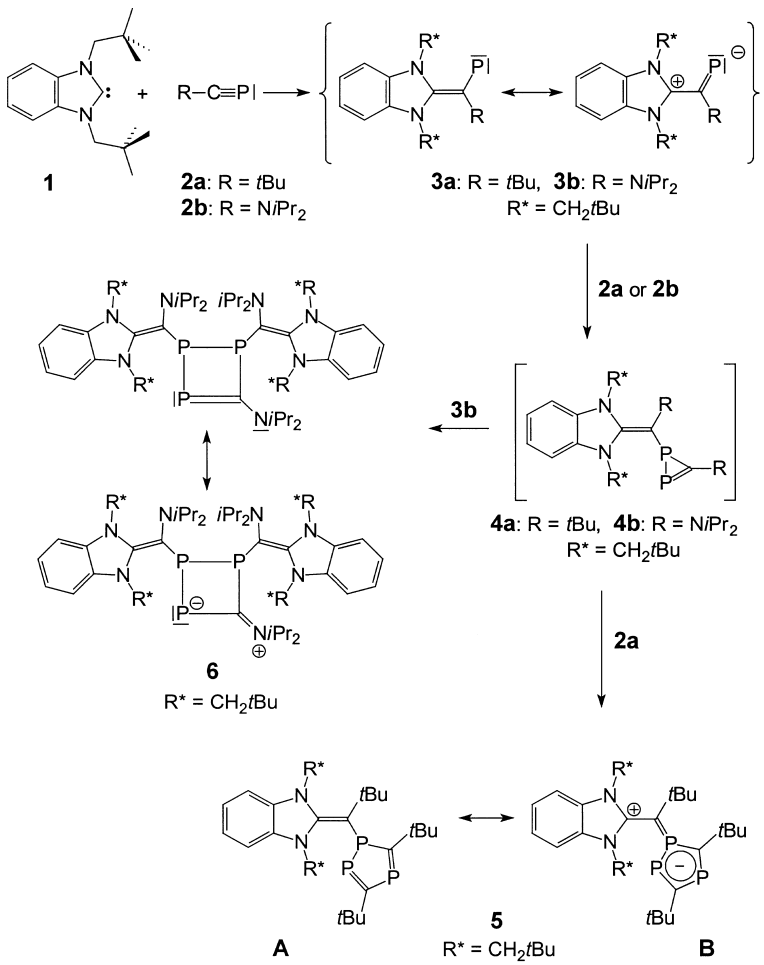
Halocarbenes react with phosphaalkynes primarily to form unstable 2*H*-phosphirenes, which undergo rearrangements through [1,3] halogen shift to yield the isomeric 1*H*-phosphirenes.[1] Addition of the phosphanylsilylcarbene (Bertrand carbene) to *tert*-butylphosphaacetylene affords the stable $1\lambda^5,2\lambda^3$-diphosphetene (probably due to the ring expansion of 2-phosphino-2*H*-phosphirene, which is an intermediate produced through a [1+2] cycloaddition).[2] The analogous reactions of silylenes, germylenes, and stannylenes with P≡CR produce three- or four-membered-ring systems containing a phosphaalkene structural element.[3] However, to date nothing has been reported about the reactivity of the intensively studied N-heterocyclic carbenes[4] toward phosphaalkynes.

We now report the unexpected formation of functionalized 1,2,4-triphosphole[5] and 1,2,3-triphosphetene[6] derivatives by reaction of the recently discovered stable N-heterocyclic annelated carbene *N,N′*-bis(2,2-dimethylpropyl)benzimidazolin-2-ylidene (**1**),[7] with the phosphaalkyne P≡C*t*Bu (**2a**) or P≡C-N*i*Pr$_2$ (**2b**).

Treatment of carbene **1** with the phosphaacetylene **2a** at room temperature in a molar ratio of 1:1 affords the crystalline adduct **5** after 48 h in a near quantitative yield (calculated from **2a**) (Scheme 1). The ^{31}P{^{1}H} NMR spectrum shows an AMX spin system. The positions of the signals and corresponding couplings of the resonances, and in particular the characteristic size of the ^1J(P1,P2) coupling of 528.1 Hz, are similar to those reported for the 1,2,4-triphosphole $P_3C_2tBu_2R$ ($R = CH(SiMe_3)_2$)[5a]. The ^{1}H and ^{13}C NMR parameters also fit well with the literature data.[5a] Information on the structure and bonding in the new 1,2,4-triphosphole derivative **5** is provided by the X-ray crystal structure analysis (Figure 1). The phosphorus heterocycle is almost planar (maximum deviation from the best plane through the ring is 0.016 Å for P2. The sum of the angles at the tricoordinate phosphorus atom is 359.8°). The σ^3-P–C_{Ring} bond (1.721(2) Å) is noticeably shorter than the other σ^2-P–C_{Ring} bonds (1.734(2)–1.738(2) Å). These structural parameters indicate a completely delocalized 1,2,4-triphosphacyclopentadiene system, which is in agreement with the results recently published by Niecke and Nixon et al.[5b] on aromatic 1-[bis-(trimethylsilyl)methyl]-3,5-bis(trimethylsilyl)-1,2,4-triphos-

[*] Prof. Dr. F. E. Hahn, Dr. L. Wittenbecher, Dr. D. Le Van
Anorganisch-chemisches Institut der Universität
Wilhelm-Klemm-Strasse 8, 48149 Münster (Germany)
Fax: (+49) 251-833-3108
E-mail: fehahn@uni-muenster.de
Dr. R. Fröhlich, B. Wibbeling
Organisch-chemisches Institut der Universität
Corrensstrasse 40, 48149 Münster (Germany)

[**] This work was supported by the Deutsche Forschungsgemeinschaft and the Fonds der Chemischen Industrie.



Scheme 1. Proposed mechanism for the formation of **5** and **6**.

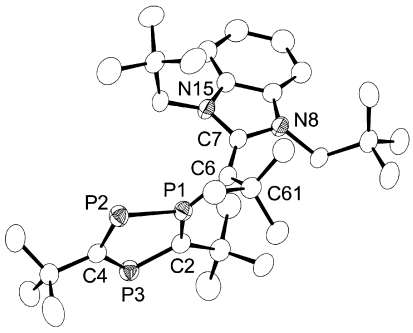


Figure 1. Molecular structure of **5** in the crystal. Selected bond lengths [Å] and angles [°]: P1-P2 2.0853(8), P1-C2 1.721(2), P1-C6 1.757(2), P3-C2 1.736(2), P3-C4 1.739(2), P2-C4 1.734(2), C6-C7 1.406(3), C7-N8 1.394(3), C7-N15 1.380(3); C2-P1-P2 106.33(8), C6-P1-P2 125.31(8), C2-P1-C6 128.15(11), P1-C2-P3 113.83(12), C2-P3-C4 102.97(11), P1-P2-C4 94.90(8), P2-C4-P3 121.92(13), P1-C6-C7 116.1(2), P1-C6-C61 118.0(2), C7-C6-C61 125.9(2), N8-C7-N15 105.5(2), N8-C7-C6 129.2(2), N15-C7-C6 125.1(2).

phole. In contrast to the triphospholes previously described,[5] **5** has mesomerically stabilizing substituents on the tricoordinate phosphorus atom. Both the steric bulk of these ligands,[5b] and the participation of the polar resonance structures **B** in the ground state of the system (Scheme 1), can be considered as possible causes for the leveling out of the ring. The molecular structure of **5** shows a strong twisting (ca. 60°) of the benzimidazol-2-ylidene plane towards the C7-C6-C61-P1 plane, which in turn, is twisted with respect to the plane of the triphosphole ring. An effective conjugation between these sections of the molecule seems to be thus out of the question. Evidently the sterically hindered groups on the C6 atom are also responsible for the lengthening of the C6–C7 double bond to 1.406(3) Å.

Under comparable reaction conditions, the aminophosphaalkyne **2b** behaves differently than **2a** toward **1**. In the reaction of **2b**, the time taken for its complete consumption was only about 15 min (monitored by ^{31}P NMR spectroscopy), during which time the air-sensitive 1,2,3-triphosphetene **6** crystallized out as the only product. The ^{31}P{^{1}H} NMR spectra of **6** show the presence of three stereoisomers (molar ratio 1:1:0.5) in solution. The signal patterns and coupling constants of the isomers are in agreement with the literature data for four-membered rings of this type.[6b, 6c] The strong high-field shift of the signal of the $\lambda^3\sigma^2$-P atom is typical of *C*-aminophosphaalkenes, and demonstrates an effective π-donation from the amino-nitrogen atom. The molecular structure of **6** was unequivocally established by crystal structure analysis[8] (Figure 2). As expected, the four-membered heterocycle is not planar (torsion angle C28-P1-P2-P3 14.2°). The two different bond lengths (P1–P2 2.195(2) Å and P2–P3 2.249(2) Å) are based on the decreased covalent radius of the dicoordinate P atom. The stretching of the P1–C28 bond (1.739(2) Å), the planar environment of the N29 atom (sum of the angles 357.6°), and the shortening of the C28–N29 bond (1.362(2) Å), all suggest a π-delocalization in the N29-C28-P1 fragment. The C–C double bonds on the periphery of the four-membered ring are unusually long in comparison to those in dimerized *N*,*N*′-stabilized carbenes (C1–C2 1.389(3), C41–C42

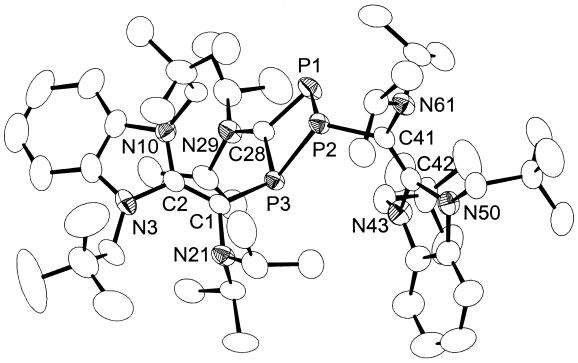


Figure 2. Molecular structure of **6** in the crystal. Selected bond lengths [Å] and angles [°]: P1-P2 2.1952(9), P3-C1 1.832(2), P1-C28 1.739(2), P2-P3 2.2497(9), P2-C41 1.841(2), P3-C28 1.827(2), C28-N29 1.362(2), C1-N21 1.451(2), C1-C2 1.389(3), C2-N3 1.415(2), C2-N10 1.400(3), C41-N61 1.452(2), C41-C42 1.374(3), C42-N43 1.417(2), C42-N50 1.422(2); P1-P2-P3 79.35(3), P1-C28-P3 105.43(10), P2-P1-C28 87.06(7), P2-P3-C28 83.37(6), P1-C28-N29 128.28(14), P3-C28-N29 125.86(14), P3-C1-C2 125.90(14), P3-C1-N21 114.38(14), C2-C1-N21 118.8(2), N3-C2-N10 105.4(2), P2-C41-C42 128.73(14), P2-C41-N61 110.97(14), C42-C41-N61 118.7(2), N43-C42-N50 103.9(2).

 © WILEY-VCH Verlag GmbH, D-69451 Weinheim, 2000 1433-7851/00/3913-2308 $ 17.50+.50/0

1.374(3) Å) and display large torsional angles (N10-C2-C1-P3 −18.7°, N3-C2-C1-N21 −18.2°, N43-C42-C41-P2 22.8°, N50-C42-C41-N61 19.2°). In order to minimize the steric interactions, the two neopentyl groups on the ring nitrogen atom in **6**, as in **5**, and the complex [W(CO)$_5$ (**1**)],[7] are positioned on the same side of the N-heterocycle.

Whilst no intermediates were detected by ^{31}P NMR monitoring of the reaction of the carbene **1** with **2a**, the analogous reaction with **2b** yielded two mutually coupled doublets of the same intensity, which disappeared over the period of a few hours in favor of the phosphorus signal of **6**. The high-field position of these temporary ^{31}P NMR signals (−183.3 and −66.3) and their ^1J(P,P) coupling constants (97.7 Hz) are comparable to the data for the amino-substituted 1*H*-diphosphirenes,[9] and give rise to the suggestion that the nonisolable 1*H*-diphosphirene **4b** is present. On the basis of this assumption, we postulate a multistep process for the selective production of **5** and **6** (Scheme 1). The reaction commences with the addition of the nucleophilic carbene **1** to **2a** or **2b** to form the highly reactive species **3a** or **3b**, respectively. However, the possibility that the 2*H*-phosphirenes are formed first, as with the addition of the halocarbenes to phosphaalkynes,[1] cannot be ruled out. The ensuing [2+1] cycloaddition of **3a** or **3b** to a further molecule of the phosphaalkyne delivers the 1*H*-diphosphirene **4a** or **4b**, respectively. Compound **4a** is capable, after ring opening, of undergoing a [3+2] cycloaddition with the *tert*-butylphosphaacetylene **2a** to form **5**. In the case of **4b**, the insertion previously described in the literature of phosphinidenes into the P–P diphosphirene bond[6a] (here **3b** into **4b**) leads to the four-membered heterocycle **6**. The reaction sequence (**4a** →**5**) has already been discussed in the literature.[10] The cause of the difference in the end products obtained from the reaction of **1** with **2a** or **2b** lies clearly in the difference in the polarity between the two related phosphaalkynes. Compound **2b** is known to have a higher reactivity toward polar reagents than **2a**, due to the donor substituents.[6b, 11]

Compounds **5** and **6** presented herein are not only the first 1,2,4-triphosphole and 1,2,3-triphosphetene derivatives to carry reactive olefinic bonds on their substituents, but they contain a long unknown structural element, namely the combination of two heteroatom-substituted carbenes N(N)C: and P(C)C: or P(N)C:, respectively. In view of the recently demonstrated cleavage of entetramines,[12] compounds of type **6** could in particular find use in the preparation of new N,N,N,P-substituted olefins and of stable N,P-substituted carbenes.

Experimental Section

All reactions were carried out under argon using standard Schlenk techniques. Solvents were dried and then distilled and stored under argon. Reactions were monitored by using ^{31}P NMR spectroscopy.

5: A solution of **2a**[13a] (0.10 g, 1.0 mmol) in C_6D_6 (0.5 mL) was added at room temperature to a solution of **1**[7] (0.26 g, 1.0 mmol) in C_6D_6 (1 mL). The dark red solution was stirred for 48 h at 25 °C, during which time red crystals of **5** were formed in the solution. After filtration and drying at 0.5 Torr, **5** was obtained in 92% yield (0.17 g). Unconverted carbene **1** remained in solution during this procedure. ^{31}P{^{1}H} NMR (81.0 MHz, C_6D_6, 25 °C, numbering: see Figure 1): δ = 224.8 (P3), 178.5 (P2), 111.3 (P1), ^1J(P1,P2) = 528.1, ^2J(P1,P3) = 17.2, ^2J(P2,P3) = 40.5 Hz; ^{1}H NMR (200.1 MHz, C_6D_6, 25 °C): δ = 0.86 (s, 9H; $CH_2CC\mathit{H_3}$), 0.96 (s, 9H; $CH_2CC\mathit{H_3}$), 1.44 (d, ^3J(P,H) = 1.4 Hz, 9H; PCCC$\mathit{H_3}$), 1.60(s, 9H; PCCC$\mathit{H_3}$), 1.85 (d, ^3J(P,H) = 0.8 Hz, 9H; PCCC$\mathit{H_3}$), 4.55 (s, 4H; NCH_2), 6.50 (m, 4H, Ar-H); ^{13}C{^{1}H} NMR (50.3 MHz, C_6D_6, 25 °C): δ = 201.7 (ddd, ^1J(P,C) = 73.4, ^1J(P,C) = 64.8, ^2J(P,C) = 20.5 Hz; PC(4)P), 180.5 (ddd, ^1J(P,C) = 70.4, ^1J(P,C) = 17.6, ^2J(P,C) = 9.7 Hz; PC(2)P), 159.8 (d, ^2J(P,C) = 4.5 Hz; NCN), 67.2 (ddd, ^1J(P,C) = 36.2, ^2J(P,C) = 5.2, ^3J(P,C) = 2.3 Hz, C*C*tBu), 143.6, 135.6, 121.7, 118.9, 110.9, 105.4 (Ar-C), 64.2 (s; CH_2), 57.0 (s; CH_2), 41.7 (ddd, ^2J(P,C) = 40.9, ^2J(P,C) = 18.3, ^3J(P,C) = 8.6 Hz; *C*Me$_3$), 40.0 (dd, ^2J(P,C) = 20.8, ^2J(P,C) = 3.0 Hz; *C*Me$_3$), 36.3 (dd, ^2J(P,C) = 11.4, ^3J(P,C) = 2.5 Hz; *C*Me$_3$), 36.0 (s; CH_2CMe$_3$), 35.8 (s; CH_2CMe$_3$), 34.0 (d, ^3J(P,C) = 4.2 Hz; CH_3), 33.9 (d, ^3J(P,C) = 2.7 Hz; CH_3), 33.8 (d, ^3J(P,C) = 3.2 Hz; CH_3), 30.0 (s; $CH_2CC\mathit{H_3}$), 27.9 (s; $CH_2CC\mathit{H_3}$); MS (70 eV): *m*/*z* (%): 558 (100) [M^+], 543 (54) [$M^+ - CH_3$], 501 (8) [$M^+ - t$Bu], 327 (11) [$M^+ - P_3C_2t$Bu$_2$].

6: As described for **5**, 0.08 g (90%) yellow crystals, suitable for X-ray analysis, were obtained from **1** (0.07 g, 0.28 mmol) and **2b** (0.04 g, 0.28 mmol).[13b] ^{31}P{^{1}H} NMR (81.0 MHz, C_6D_6, 25 °C; mixture of isomers, molar ratio: a:b:c = 1:1:0.5; numbering: see Figure 2), isomer a: δ = 86.5 (P1), −58.5 (P2), 9.5 (P3), ^1J(P1,P2) = 255.8, ^2J(P1,P3) = 55.8, ^2J(P2,P3) = 249.8 Hz; isomer b: δ = 96.3 (P1), −45.0 (P2), 19.8 (P3), ^1J(P1,P2) = 246.8, ^2J(P1,P3) = 62.7, ^2J(P2,P3) = 238.0 Hz; isomer c: δ = 121.1 (P1), −62.1 (P2), 18.0 (P3), ^1J(P1,P2) = 242.0, ^2J(P1,P3) = 64.1, ^2J(P2,P3) = 230.0 Hz; ^{1}H NMR (mixture of isomers, 200.1 MHz, C_6D_6, 25 °C): δ = 0.59–1.29 (72H, CH_3), 2.8–4.2 (br., 14H, CH_2, CH), 6.5–6.8 (m, 8H, Ar-H).

Received: January 25, 2000 [Z14594]

[1] a) O. Wagner, M. Ehle, M. Birkel, J. Hoffmann, M. Regitz, *Chem. Ber.* **1991**, *124*, 1207–1213; b) H. Memmersheimer, M. Regitz in *Advances in Carbene Chemistry*, *Vol. 1* (Ed.: U. H. Brinker), JAI, Greenwich, CT, **1994**, pp. 185–213.

[2] R. Armbrust, M. Sanchez, R. Réau, U. Bergsträsser, M. Regitz, G. Bertrand, *J. Am. Chem. Soc.* **1995**, *117*, 10785–10786.

[3] Silylenes:a) A. Schäfer, M. Weidenbruch, W. Saak, S. Pohl, *Angew. Chem.* **1987**, *99*, 806–807; *Angew. Chem. Int. Ed. Engl.* **1987**, *26*, 776–777; b) M. Weidenbruch, S. Osthoff, K. Peters, H. G. von Schnering, *Chem. Commun.* **1997**, 1433–1434; germylenes: c) A. H. Cowley, S. W. Hall, C. M. Nunn, J. M. Power, *J. Chem. Soc. Chem. Commun.* **1988**, 753–754; stannylenes: d) A. H. Cowley, S. W. Hall, C. M. Nunn, J. M. Power, *Angew. Chem.* **1988**, *100*, 874–875; *Angew. Chem. Int. Ed. Engl.* **1988**, *27*, 838–839.

[4] a) M. Regitz, *Angew. Chem.* **1996**, *108*, 791–794; *Angew. Chem. Int. Ed. Engl.* **1996**, *35*, 725–728; b) W. A. Herrmann, C. Köcher, *Angew. Chem.* **1997**, *109*, 2256–2282; *Angew. Chem. Int. Ed. Engl.* **1997**, *36*, 2162–2187; c) A. J. Arduengo III, *Acc. Chem. Res.* **1999**, *32*, 913–921; d) D. Bourissou, O. Guerret, F. P. Gabbaï, G. Bertrand, *Chem. Rev.* **2000**, *100*, 39–91.

[5] a) V. Caliman, P. B. Hitchcock, J. F. Nixon, *J. Chem. Soc. Chem. Commun.* **1995**, 1661–1662; b) F. G. N. Cloke, P. B. Hitchcock, P. Hunnable, J. F. Nixon, L. Nyulászi, E. Niecke, V. Thelen, *Angew. Chem.* **1998**, *110*, 1139–1142; *Angew. Chem. Int. Ed.* **1998**, *37*, 1083–1086; c) A. Elvers, F. W. Heinemann, B. Wrackmeyer, U. Zenneck, *Chem. Eur. J.* **1999**, *5*, 3143–3153.

[6] a) R. Streubel, L. Ernst, J. Jeske, P. G. Jones, *J. Chem. Soc. Chem. Commun.* **1995**, 2113–2114; b) H. Pucknat, J. Grobe, D. Le Van, B. Broschk, M. Hegemann, B. Krebs, M. Läge, *Chem. Eur. J.* **1996**, *2*, 208–213; c) J. Grobe, D. Le Van, T. Pohlmeyer, B. Krebs, M. Läge, E. Dobbert, L. Weber, *Organometallics* **1998**, *17*, 3383–3386.

[7] F. E. Hahn, L. Wittenbecher, R. Boese, D. Bläser, *Chem. Eur. J.* **1999**, *5*, 1931–1935.

[8] a) X-ray structure analysis of **5** ($C_{32}H_{53}N_2P_3$): M_r = 558.67, red crystals 0.30 × 0.30 × 0.10 mm, a = 9.450(1), b = 24.111(1), c = 14.570(1) Å, β = 97.97(1)°, V = 3287.7(4) Å^3, ρ_{calcd} = 1.129 g cm^{-3}, μ = 2.03 cm^{-1}, empirical absorption correction with SORTAV (0.942 ≤ T ≤ 0.980), Z = 4, monoclinic, space group $P2_1/c$ (no. 14), λ = 0.71073 Å, T = 198 K, ω and φ scans, 13894 measured reflections ($\pm h$, $\pm k$, $\pm l$), [(sinθ)/λ] = 0.65 Å^{-1}, 7512 independent (R_{int} = 0.060) and 5241 observed reflec-

tions [$I \geq 2\sigma(I)$], 349 refined parameters, $R = 0.055$, $wR^2 = 0.133$, max/min residual electron density 0.35/ − 0.34 e Å^{-3}, hydrogen atoms calculated and refined as riding atoms.[14] b) X-ray structure analysis of **6** ($C_{55}H_{94}N_7P_3$): $M_r = 946.28$, yellow crystals 0.25 × 0.20 × 0.10 mm, $a = 10.995(2)$, $b = 15.658(3)$, $c = 17.031(3)$ Å, $\alpha = 80.33(3)$, $\beta = 88.60(3)$, $\gamma = 82.72(3)^\circ$, $V = 2867.1(9)$ Å^3, $\rho_{calcd} = 1.096$ g cm^{-3}, $\mu = 12.46$ cm^{-1}, empirical absorption correction by using ψ scan data ($0.746 \geq T \geq 0.886$), $Z = 2$, triclinic, space group $P\bar{1}$ (no. 2), $\lambda = 1.54178$ Å, $T = 223$ K, $\omega/2\theta$ scans, 12328 measured reflections ($+h$, $\pm k$, $\pm l$), [$(\sin\theta)/\lambda$] = 0.62 Å^{-1}, 11688 independent ($R_{int} = 0.016$) and 9440 observed reflections [$I \geq 2\sigma(I)$], 660 refined parameters, $R = 0.053$, $wR^2 = 0.167$, max/min residual electron density 0.43/ − 0.167 e Å^{-3}, disorder of the *tert*-butyl groups at C12 and C17 are described with split positions and geometric constraints, hydrogen atoms calculated and refined as riding atoms.[14]

[9] a) D. Bourissou, Y. Canac, M. I. Collado, A. Baceiredo, G. Bertrand, *Chem. Commun*. **1997**, 2399 – 2400; b) E. Niecke, R. Streubel, M. Nieger, D. Stalke, *Angew. Chem*. **1989**, *101*, 1708 – 1710; *Angew. Chem. Int. Ed. Engl*. **1989**, *28*, 1673 – 1674.

[10] M. Julino, M. Slany, U. Bergsträßer, F. Merçier, F. Mathey, M. Regitz, *Chem. Ber.* **1995**, *128*, 991 – 997.

[11] a) J. Grobe, D. Le Van, B. Broschk, M. Hegemann, B. Lüth, G. Becker, M. Böhringer, E.-U. Würthwein, *J. Organomet. Chem.* **1997**, *529*, 177 – 187; b) P. Binger, S. Stutzmann, J. Bruckmann, C. Krüger, J. Grobe, D. Le Van, T. Pohlmeyer, *Eur. J. Inorg. Chem.* **1998**, 2071 – 2074.

[12] F. E. Hahn, L. Wittenbecher, D. Le Van, R. Fröhlich, *Angew. Chem*. **2000**, *112*, 551 – 554; *Angew. Chem. Int. Ed.* ***2000****, 39*, 541 – 544.

[13] a) G. Becker, H. Schmidt, G. Uhl, W. Uhl, *Inorg. Synth.* **1990**, *27*, 249 – 253; b) J. Grobe, D. Le Van, B. Lüth, M. Hegemann, *Chem. Ber.* **1990**, *123*, 2317 – 2320.

[14] All data sets were collected on a Enraf Nonius CAD4 or a Nonius Kappa-CCD diffractometer with a rotating anode FR591 (Nonius) used as a radiation source. The following programs were used: EXPRESS (Nonius B. V., 1994) and COLLECT (Nonius B. V., 1998) for data collection; MolEN (K. Fair, Enraf-Nonius B. V., 1990) and Denzo-SMN (Z. Otwinowski, W. Minor, *Methods Enzymol.* **1997**, *276*, 307 – 326) for data reduction; SORTAV for absorption correction of CCD-Data (R. H. Blessing, *Acta Crystallogr. Sect. A* **1995**, *51*, 33 – 37; R. H. Blessing, *J. Appl. Crystallogr.* **1997**, *30*, 421 – 426); SHELXS-97 (G. M. Sheldrick, *Acta Crystallogr. Sect. A* **1990**, *46*, 467 – 473) for structure solution; SHELXL-97 (G. M. Sheldrick, Universität Göttingen, **1997**) for structure refinement. Crystallographic data (excluding structure factors) for the structures reported in this paper have been deposited with the Cambridge Crystallographic Data Centre as supplementary publication no. CCDC-139113 (**5**) and CCDC-139114 (**6**). Copies of the data can be obtained free of charge on application to CCDC, 12 Union Road, Cambridge CB21EZ, UK (fax: (+44) 1223-336-033; e-mail: deposit@ccdc.cam.ac.uk).

Designing a Heterogeneous Catalyst for the Production of Adipic Acid by Aerial Oxidation of Cyclohexane**

Markus Dugal, Gopinathan Sankar, Robert Raja, and John Meurig Thomas*

Dedicated to Professor Helmut Knözinger on the occasion of his 65th birthday

Adipic acid (AA) is an important building block for a variety of commercially useful products such as polyamides (nylon 6.6) and urethanes.[1] Currently, it is manufactured mainly by a two-step process involving nitric acid oxidation of cylohexanone and cyclohexanol. The latter compound is generated from cyclohexane using homogeneous (cobalt-based) catalysts, often in combination with promoters and peroxides.[2–4] Alternative synthetic routes have been developed, such as the one-step oxidation of cyclohexane with either alkyl hydroperoxide as oxidant and a catalyst consisting of cobalt salts[5, 6] or dioxygen as oxidant and a cobalt acetate catalyst in acetic acid.[7] More recent industrial syntheses include the homogeneously catalysed hydrocarboxylation[8, 9] or carboalkoxylation[10] of butadiene. For the research chemist, the intellectual challenge is to devise a strategy for a one-step production of AA from hydrocarbons using an appropriately designed, heterogeneous catalyst that functions with air or dioxygen as the oxidant. Such a catalyst would allow facile separation and recycling while simultaneously avoiding the use of hazardous or corrosive reagents. Herein, we report progress towards this goal. The iron-based, framework-substituted, molecular-sieve catalyst that we describe exhibits good performance in the direct low-temperature conversion of cyclohexane to AA in air.

Based on our recent work on the selective aerial oxidation of alkanes at the terminal position[11] and, in particular, the selective aerial conversion of cyclohexane to cyclohexanol and cyclohexanone using transition metal ion substituted, microporous aluminium phosphates (MAPOs),[12, 13] we argued that it was necessary to assemble an Fe^{III}-substituted MAPO structure in which the pore aperture is significantly smaller than that of FeAlPO-5 (7.3 Å diameter). This structure creates a constrained environment for the cyclohexane oxidation (see Figure 1) and thus modifies the selectivity of the reaction. What we capitalize upon is shape-selective catalysis[14, 15] using a carefully designed microporous solid. In our previous work, we showed[16] for hydrocarbons small enough to enter into a microporous catalyst, the free radical oxidation of these materials proceeds in a highly localized manner in the restricted environment of the catalytically active sites at which the M^{III} ions are exposed on the

[*] Prof. Dr. Sir J. M. Thomas, Dr. M. Dugal, Dr. G. Sankar, Dr. R. Raja
The Royal Institution of Great Britain
Davy Faraday Research Laboratories
21 Albemarle Street, London W1X 4BS (UK)
Fax: (+44) 0207-607-2988
E-mail: jmt@ri.ac.uk

[**] This work was supported by an EPSRC rolling grant to J.M.T. We thank the CLRC for the synchrotron beam time and other facilities at Daresbury Laboratory.

 © WILEY-VCH Verlag GmbH, D-69451 Weinheim, 2000 1433-7851/00/3913-2310 $ 17.50+.50/0

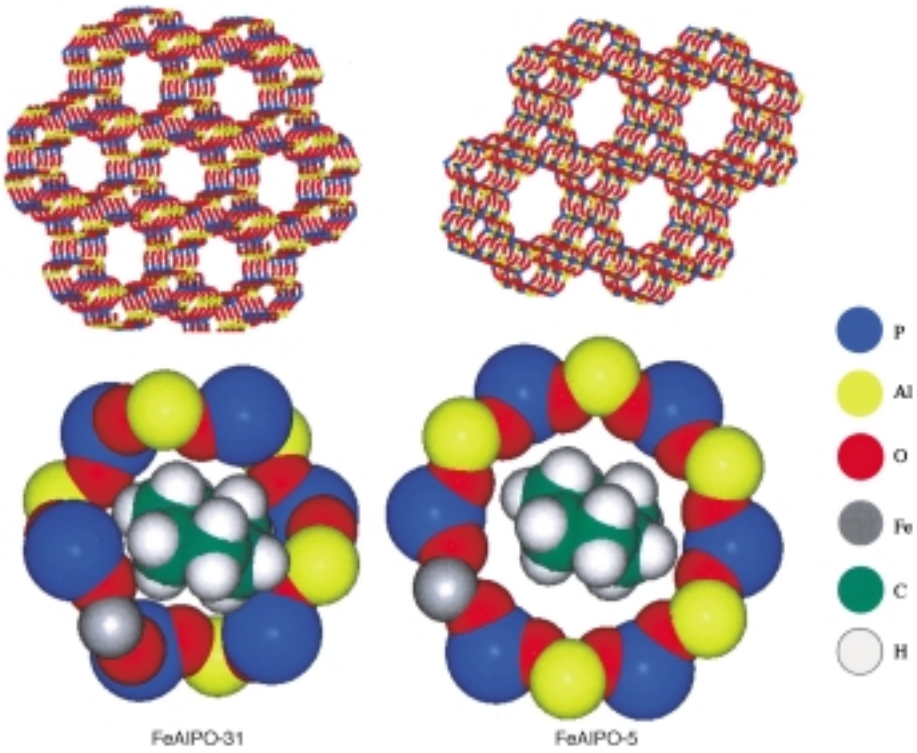


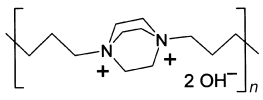
Figure 1. Above: A side view of the microporous AlPO-31 and AlPO-5 structures, which show the one-dimensional channels. Below: Representation of the cyclohexane molecule in the differently sized pore openings of FeAlPO-31 (5.4 Å) and FeAlPO-5 (7.3 Å).

inner walls of the micropores (M = Co, Mn, Fe). In effect, we have here "product shape selectivity"—only those products with appropriate molecular dimensions may diffuse easily out of the pores, whereas larger ones formed in the course of the reaction are trapped inside (on account of their significantly retarded diffusion). Qualitatively, we may envisage the free radical and molecular intermediates (cyclohexanol, cyclohexanone formed from cyclohexyl hydroperoxide[13] or 2-hydroxycylohexanone and 1,2-cyclohexanedione) to be held in the vicinity of the active site until oxidation proceeds further to yield the more mobile (and desired) linear products.

For the present purposes, the framework structure of the microporous catalyst that we have targeted is the one-dimensional channel system, AlPO-31[17] (Figure 1). Because of the more puckered inner walls, compared with AlPO-5,[13, 17] there is a smaller pore of diameter 5.4 Å, which introduces the very kind of constrained environment that is required here.

As with the oxidation of *n*-alkanes at the terminal position over Co^{III}- or Mn^{III}-substituted AlPO-18 catalysts[11] and the conversion of cyclohexane to cyclohexanol over an Fe^{III}AlPO-5 catalyst,[13] framework-isolated, transition metal ions in their M^{III} oxidation states are vital for the catalysis. We therefore devised a facile means of preparing Fe^{III}AlPO-31 microporous samples, in which up to about four atom per cent of the Al^{III} framework ions are replaced by Fe^{III}, and where all these active sites are accessible to cyclohexane at the inner surfaces of the micropores.

Building on our prior experience with quaternized template cations (such as for the synthesis of DAF-1[18]) and the work of Wright et al.,[19] who used several types of polymeric-template ammonium salts to produce various solid acid Mg-substituted aluminophosphates (which include AlPO-5, AlPO-31, and STA-1), we selected the polymeric-template ammonium salt **1**, which strongly favors the production of MAPO-31.[20] This template



1

salt was prepared through a Menshutkin-type reaction from 1,4-diazabicyclo[2.2.2]octane (DABCO) and 1,6-dibromohexane, then followed by ion exchange of the bromide counterion against hydroxide. Employing an optimized modification of the reported literature procedures[18, 22] (see the Experimental Section), the required template was obtained in high yield and purity.

FeAlPO-31 was obtained from a hydrothermal synthesis (see the Experimental Section) in a phase-pure form (Figure 2). The diffraction pattern of the calcined sample, recorded in situ,[23] is essentially identical to that of the as-prepared material, which demonstrates structural stability upon removal of the template. A helpful feature of the in situ combined XRD/XAS study[23] is that, although the diffraction pattern (hence the framework structure) remains the same, there is a significant increase of the pre-edge feature and a decrease in Fe–O distance from 1.94 to 1.85 Å upon calcination. The similarity of the intense pre-edge feature and the Fe–O distance with the corresponding values in either $FePO_4$ or Fe-substituted ZSM-5 shows that the substituted iron ions are present in the Fe^{III} state and with a tetrahedral geometry.

Comparisons of the catalytic performance of FeAlPO-31 and of FeAlPO-5 are summarized in Figure 3 and in Table 1. In addition to a higher turnover number (TON) for FeAlPO-31 compared to FeAlPO-5, there are significant differences in the product selectivities: With FeAlPO-5 as the catalyst, cyclohexanol and cyclohexanone were the major products,[13] whereas FeAlPO-31 predominantly produces adipic acid and comparatively small amounts of other oxidation and fragmentation products. At higher temperatures with FeAlPO-31 there is no significant change in the overall conversion but the formation of tar and other fragmentation products (succinic and glutaric acids) increases. The structure of the catalysts, as we conclude from identical XRD patterns recorded before and after the catalytic reaction, remains unchanged under the chosen reaction conditions. (Further ICP analysis of the reaction mixture gave no indication of any leaching of iron out of the framework.)

 © WILEY-VCH Verlag GmbH, D-69451 Weinheim, 2000 1433-7851/00/3913-2311 $ 17.50+.50/0

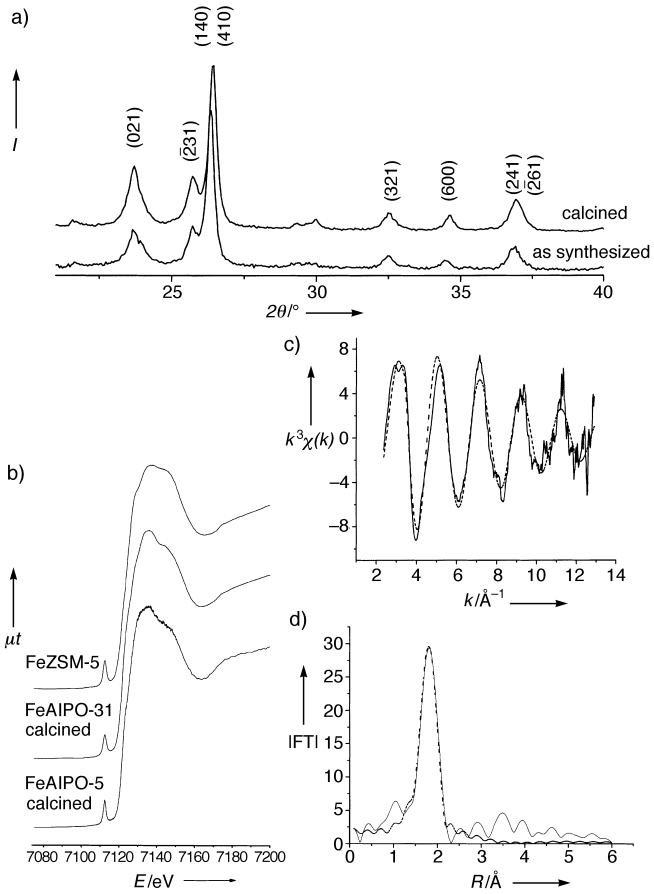


Figure 2. a) XRD patterns of FeAlPO-31 before and after calcination in O_2 at 550 °C recorded by employing the in situ, combined XRD/XAS technique. b) XANES spectra of as-synthesized FeZSM-5[13] and of calcined FeAlPO-31 and FeAlPO-5.[13] Note the similarities in the pre-edge intensities. c) EXAFS and d) the associated Fourier transform of calcined FeAlPO-31. The solid and the dashed curves represent the experimental and calculated data, respectively. The EXAFS derived Fe–O coordination number, bond distance, and Debye–Waller factor are 3.85 ± 0.4, 1.85 ± 0.02 Å, and 0.0045 Å^2, respectively. In (a), only a small range of $2\theta = 22 - 40°$ is displayed for clarity. Note that it is not possible to record XRD data below about 11°, since there is a dead space associated with the INEL detector and hence this detector should be positioned in such a way that transmitted intensity (I_t) for EXAFS measurement is not affected.

The remarkable fact that the selectivity pattern of FeAlPO-31 is so completely different from that of FeAlPO-5, even though the structure of their active sites is identical, is explicable only in terms of the difference in pore dimensions of the two AlPO hosts for the isolated sites. The cyclohexane molecule is much more confined in case of the FeAlPO-31 than in FeAlPO-5. Owing to this constraint, the diffusion of cyclohexane and the cyclic intermediates in the oxidation reaction within the FeAlPO-31 channel system is severely limited and therefore further oxidation of the cyclic intermediates to linear products as adipic acid is facilitated.

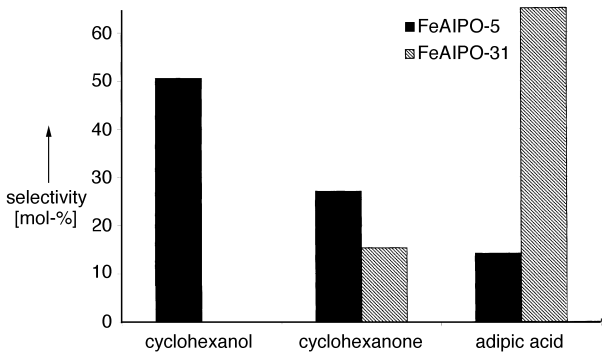


Figure 3. Bar chart comparing the product selectivities (given in mol-%) after 24 h in the aerial oxidation of cyclohexane ($T = 373$ K) with FeAlPO-31 and FeAlPO-5 as catalysts. Only major products are shown.

Although many features of this new catalyst (FeAlPO-31) rival those of commercial catalysts used in the production of AA, our principal aim in this work was not to develop a new industrial procedure but rather to adopt a design approach for the development of many other new catalysts for converting organic molecules to useful products under mild and environmentally benign conditions. We believe that there is scope to extend the free radical, shape selective catalysis described herein to other systems.

Experimental Section

Synthesis of **1**: DABCO (98%, Aldrich, 22.9 g, 0.2 mol) was dissolved in toluene (500 mL) and 1,6-dibromohexane (96%, Aldrich, 50.7 g, 0.2 mol) was added slowly under vigorous stirring. The mixture was heated to 105 °C (oil bath temperature) for 3 h upon which a voluminous white precipitate formed. After cooling, the bromide salt of the template[19, 21] was collected by filtration, washed with toluene (3×150 mL) and pentane (3×150 mL) and dried in vacuo (60.3 g white, hygroscopic powder, 82% yield). Ion exchange was accomplished by stirring a solution of the bromide salt in deionized water (0.45 g mL^{-1}) with an excess amount of a strongly basic ion-exchange resin (Dowex SBR, Aldrich, 150 g resin per 100 g solution)

Table 1. Comparison of the catalytic behavior of FeAlPO-31 and FeAlPO-5 in the aerial oxidation of cyclohexane.[a]

Catalyst	t [h]	T [K]	Conversion [mol-%][c]	TON[b]	Product selectivities [mol-%][c, d]							
					A	B	C	D	E	F	G	H
FeAlPO-31	8	373	2.5	78	6.3	31.0	55.3	1.9	3.2	–	–	2.5
FeAlPO-31	24	373	6.6	211	–	15.3	65.0	5.9	7.7	–	–	6.0(I)
FeAlPO-31	8	403	3.9	121	–	12.5	53.7	14.2	10.0	–	–	9.8(I)
FeAlPO-31	24	403	7.7	239	–	6.8	31.3	24.7	11.3	–	–	26.0(I)
FeAlPO-5	8	373	1.7	20	83.0	6.5	9.2	–	–	–	–	1.5
FeAlPO-5	24	373	5.3	62	50.5	27.0	14.1	–	–	6.3	–	1.8
FeAlPO-5	8	403	2.5	45	41.1	17.9	26.2	–	–	13.	–	1.9
FeAlPO-5	24	403	6.6	113	36.2	15.5	31.0	–	–	9.2	5.4	2.7

[a] Conditions: cyclohexane ≅ 50 g, catalyst 0.75 g, pressure (air) 1.5 MPa. [b] TON = moles of substrate converted per mol of metal (Fe) in the used amount of catalyst, as determined by elemental analysis (FeAlPO-31: Fe = 1.43 wt-% Fe; FeAlPO-5: 3.77 wt-% Fe). [c] Determined by GC against mesitylene (≅2.5 g) as internal standard. [d] Overall yield; product abbreviations: A: cyclohexanol; B: cyclohexanone; C: adipic acid; D: succinic acid; E: glutaric acid; F: valeraldehyde; G: valeric acid; H: probably CO_2, CO, water, and traces of lower olefins in the gas phase; I: tar.

 © WILEY-VCH Verlag GmbH, D-69451 Weinheim, 2000 1433-7851/00/3913-2312 $ 17.50+.50/0

for 3 h. The solution of the hydroxide form of the template **1** obtained after filtration was used directly in the aluminophosphate synthesis.

Synthesis of FeAlPO-31: To a solution of phosphoric acid (85%, Aldrich) in water, aluminium hydroxide hydrate (Aldrich) and an aqueous solution of iron(II) acetate (Aldrich) was added, and the mixture was stirred until homogeneous. To this, an aqueous solution of **1** was added slowly with vigorous stirring to obtain a gel with the empirical composition $0.04\,FeO : 0.48\,Al_2O_3 : 0.5\,P_2O_5 : 0.8/n\,[C_{12}H_{26}N_2O_2]_n : 40\,H_2O$ (pH 7–8). The gel was sealed in a Teflon-lined stainless steel autoclave and heated at 195 °C under autogeneous pressure for 48 h. The solid product was isolated by filtration, washed with deionized water, and dried in air (90 °C). The as-prepared product was calcined first in nitrogen and then in dry oxygen at 550 °C for 1 h and 10 h, respectively.

In situ XRD/XAS measurements:[20] The combined XRD/XAS measurements were performed at station 9.3 of the Daresbury synchrotron radiation source, which operates at 2 GeV with a typical current 130–250 mA. The station is equipped with a Si(220) double-crystal monochromator and ion chambers for measuring incident (I_0) and transmitted (I_t) beam intensities. For the in situ experiment, 25 mg of FeAlPO-31 was calcined in an situ cell at 550 °C in an O_2 flow. The XRD/XAS measurements were performed during the course of increasing the temperature (5 K min^{-1}) and at the final temperature. The XRD patterns were collected at the wavelength of 1.8088 Å, below the Fe–K edge. Each XRD pattern was measured for 180 s and each XAS spectrum for 380 s associated with a dead time of 40 s, to give a total cycle time of 10 min. The data were analysed using the suite of programs EXCALIB, EXBROOK, and EXCURV98, available at Daresbury laboratory.

Received: December 21, 1999 [Z14431]

[1] D. D. Davis in *Ullmanns Encyclopaedia of Industrial Chemistry, Vol. A1*, VCH, Weinheim, **1985**, pp. 269–276.
[2] D. D. Davis, D. R. Kemp in *Kirk Othmer Encyclopaedia of Chemical Technology, Vol.1* (Eds.: J. I. Kroschwitz, M. Howe-Grant), 4th ed., Wiley, New York, **1991**, pp. 466–493.
[3] K. I. Zamaraev, *J. Mol. Catal.* **1993**, *82*, 275.
[4] M. T. Musser in *Ullmanns Encyclopaedia of Industrial Chemistry, Vol. A8*, VCH, Weinheim, **1985**, pp. 217–226.
[5] E. P. Talsi, V. D. Chinakov, V. P. Babenko, V. N. Sidelnikov, K. I. Zamaraev, *J. Mol. Catal.* **1993**, *81*, 215–233.
[6] T. Maschmeyer, R. Oldroyd, G. Sankar, J. M. Thomas, I. J. Shannon, J. A. Klepetko, A. F. Masters, J. K. Beattie, C. R. A. Catlow, *Angew. Chem.* **1997**, *109*, 1713–1716; *Angew. Chem. Int. Ed. Engl.* **1997**, *36*, 1639–1642.
[7] K. Tanaka, *Chem. Technol. 4*. **1974**, *9*, 555–559.
[8] H. S. Bruner Jr. (DuPont), US pat. 5166421, **1992**.
[9] N. von Kutepow (BASF), US pat. 3876695, **1975**.
[10] R. Platz, R. Kummer, H. Schneider (BASF), US pat. 4258203, **1981**.
[11] J. M. Thomas, R. Raja, G. Sankar, R. Bell, *Nature* **1999**, *398*, 227.
[12] G. Sankar, R. Raja, J. M. Thomas, *Catal. Lett.* **1998**, *55*, 15–23.
[13] R. Raja, G. Sankar, J. M. Thomas, *J. Am. Chem. Soc.* **1999**, *121*, 11926–11927.
[14] P. B. Weisz, *Pure Appl. Chem*. **1980**, *52*, 2091.
[15] P. B. Weisz, W. O. Haag, R. M. Lago, *Nature* **1984**, *309*, 589–591.
[16] R. Raja, J. M. Thomas, *Chem. Commun.* **1998**, 1841-1842; J. M. Thomas, *Angew. Chem*. **1999**, *111*, 3800–3843; *Angew. Chem. Int. Ed.* **1999**, *38*, 3588–3628.
[17] J. M. Bennett, R. M. Kirchner, *Zeolites* **1992**, *12*, 338; A. J. Mora, A. N. Fitch, M. Cole, R. Goyal, R. H. Jones, H. Jobic, S. W. Carr, *J. Mater. Chem*. **1996**, *6*, 1831–1835.
[18] P. A. Wright, R. H. Jones, S. Natarajan, R. G. Bell, J. Chen, M. B. Hursthouse, J. M. Thomas, *J. Chem. Soc. Chem. Commun*. **1993**, 633-635.
[19] P. A. Wright, P. A. Cox, G. W. Noble, V. Patinec in *Proceedings of the 12th International Zeolite Conference III* (Eds.: M. M. J. Treacy, B. K. Marcus, M. E. Fisher, J. B. Higgins), Materials Research Society, Warrendale, PA, **1999**, pp. 1603–1610.
[20] Di-*n*-pentylamine has also been suggested[21] for the preferential synthesis of the AlPO-31 structure. We have not used this template.
[21] O. V. Kikhtyanin, R. F. Vogel, C. L. Kibby, T. V. Harris, K. G. Ione, D. J. O'Rear in *Proceedings of the 12th International Zeolite Conference III* (Eds.: M. M. J. Treacy, B. K. Marcus, M. E. Fisher, J. B. Higgins), Materials Research Society, Warrendale, PA, **1999**, 1743–1749.
[22] R. H. Daniels, G. T. Kerr, L. D. Rollmann, *J. Am. Chem. Soc*. **1978**, *100*, 3097–3100.
[23] J. M. Thomas *Chem. Eur. J.* **1997**, *3*, 1557–1562; G. Sankar, J. M. Thomas, *Top. Catal.* **1999**, *8*, 1–2.

Designing a Molecular Sieve Catalyst for the Aerial Oxidation of *n*-Hexane to Adipic Acid**

Robert Raja, Gopinathan Sankar, and John Meurig Thomas*

Dedicated to Professor H. W. Roesky on the occasion of his 65th birthday

Linear alkanes are so notoriously difficult to oxidize that their very name—paraffins, from the Latin *parum affinis* (slight affinity)—emphasizes their inertness. *n*-Hexane, for example, is not attacked by boiling nitric acid, concentrated sulphuric acid, potassium permanganate, or chromic acid. It is widely acknowledged that the controlled oxyfunctionalization of alkanes is one of the major challenges of modern catalysis;[1–4] particularly desirable products are those that are oxidized at the terminal position (hexanoic acid, for example), since these serve as feedstocks for the chemical and pharmaceutical industries.

A decade ago, following the discovery[5, 6] of molecular sieve titanosilicates such as TS-1, it was reported[7, 8] that *n*-hexane yielded a mixture of four products when hydrogen peroxide was used as the oxidant for the selective oxidation catalyzed by TS-1: 2-hexanol (17%), 3-hexanol (39%), 2-hexanone (34%), and 3-hexanone (10%). In a series of recent papers[9–13] we have reported how aluminophosphate (AlPO) molecular sieves, which contain an appropriate, framework-substituted transition-metal ion, M, in a high oxidation state, serve as effective catalysts for the selective oxidation of alkanes (especially at the terminal position). Molecular sieve catalysts are potentially more powerful for regioselective oxidation and are demonstrably capable of going beyond what may be achieved by Gif reagents developed by Barton et al.[14] for the rather high oxidative selectivity for secondary over tertiary positions in saturated hydrocarbons.[15–17] Here, we report how adipic acid, an

[*] Prof. Dr. Sir J. M. Thomas, Dr. R. Raja, Dr. G. Sankar
The Royal Institution of Great Britain
Davy Faraday Research Laboratory
21 Albemarle Street, London W1X 4BS (UK)
Fax: (+44) 0207-670-2988
E-mail: jmt@ri.ac.uk

[**] We gratefully acknowledge helpful discussions with Dr. R. G. Bell and Prof. C. R. A. Catlow, the support (via a rolling grant to J.M.T.) of the EPSRC, and the award of a research fellowship (for G.S.) from the Leverhulme Foundation.

 © WILEY-VCH Verlag GmbH, D-69451 Weinheim, 2000 1433-7851/00/3913-2313 $ 17.50+.50/0

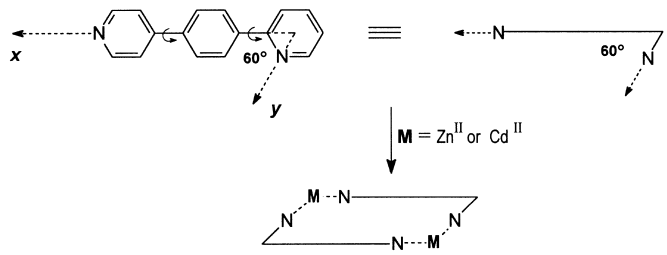
Controlled Assembly of Dinuclear Metallacycles into a Three-Dimensional Helical Array**

Alexander J. Blake, Neil R. Champness,*
Andrei N. Khlobystov, Simon Parsons, and
Martin Schröder*

The family of cyclic nanostructures assembled from transition metal junctions and bridging ligands is now a well-established group of coordination compounds.[1] The variety of different metal cation/donor atom interactions that can be used by the coordination chemist provides significant structural flexibility for such "supermolecules".[1b, 2] The diversity of such coordination nanostructures makes them remarkable examples in the growing library of self-assembled entities,[3] which now can be considered for use as construction blocks for larger supramolecular arrays.[4]

It has been demonstrated recently that if discrete metallosupramolecular species contain additional peripheral binding sites they can assemble into one-dimensional (1D) polymeric structures.[5a] Similarly, the aggregation of metallacycles into 1D polymers can be supported by additional bridging ligands[5b,c] or coordinated counterions.[5d] Understanding the principles of nanostructure formation by polymerization is important not only from the viewpoint of coordination chemistry, but also for the future development of increasingly intricate and functional coordination networks.

We report herein the toposelective self-assembly of a cyclic dinuclear complex using a simple angular ligand, 2,4′-(1,4-phenylene)bispyridine L,[6] and its controlled aggregation into a three-dimensional (3D) infinite framework. The main geometric features of the ligand can be summarized as follows: 1) two heterocycles are linked through a phenylene group, each ring having free rotation around the x axis (Scheme 1); 2) the donor atom separation is 9.5 Å; 3) the angle between the N-donor lone pairs is 60°, which cannot be distorted significantly when the ligand coordinates to metal centers because of the rigid nature of the $C(sp^2)$–$C(sp^2)$ bonds. The rigid bis-monodentate nature of ligand L makes it suitable for the synthesis of cyclic nanostructures, and it can potentially be used to construct a dinuclear metallacycle when combined with a suitable metal center (Scheme 1).



Scheme 1. Geometry of ligand L and its coordination with transition metals.

Treatment of a solution of $Zn(NO_3)_2$ with a solution of ligand L gives the dinuclear complex $[Zn_2(L)_2(NO_3)_4]$ (**1**) in nearly quantitative yield (Figure 1a). The single-crystal X-ray structure analysis[7] of **1** shows a parallelogram-shaped

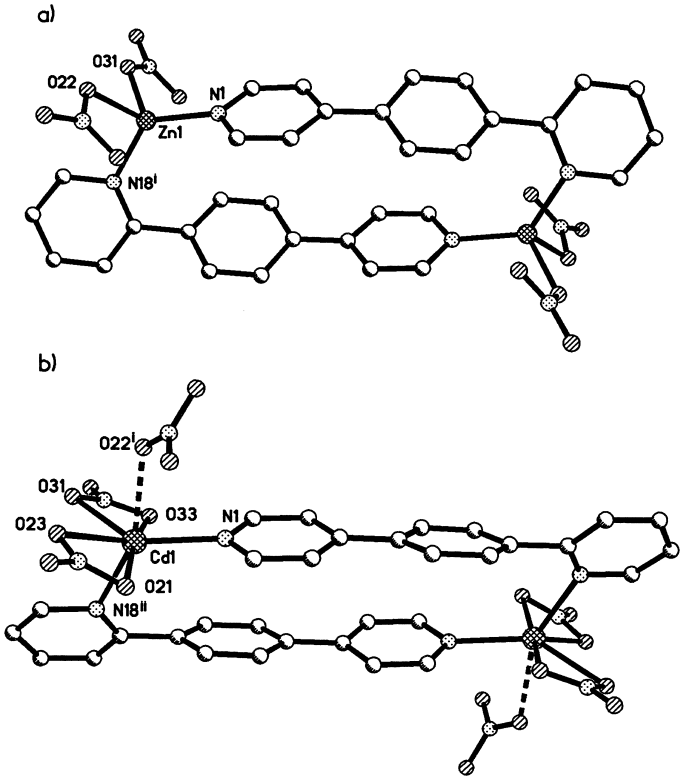


Figure 1. a) Molecular structure of complex **1**. b) Molecular structure of the monomeric unit of **2**; bridging coordination to a NO_3^- ion of a neighboring molecule is shown by a dashed line. Symmetry codes i: $2/3 - x + y, 1/3 - x, 1/3 + z$; ii: $1 - x, -y, 1 - z$.

structural motif with the Zn^{II} cations having a distorted tetrahedral geometry (N1-Zn1-N18^i 127.92(12)°). Two NO_3^- ions are bound to each metal center each by one oxygen donor and function as terminators, preventing further aggregation. The coordinated 2-pyridyl ring is strongly twisted relative to the rest of the ligand molecule (dihedral angle 47.5(2)°) allowing the two other essentially coplanar aromatic rings to be involved in intramolecular π–π stacking with an interplanar separation of 3.394(5) Å. This gives an optimal charge separation which presumably has a beneficial influence on the formation of the metallacyclic entity.[10] The Zn^{II} centers in **1** are coordinatively saturated in their pseudo-tetrahedral

[*] Dr. N. R. Champness, Prof. Dr. M. Schröder, Dr. A. J. Blake, A. N. Khlobystov
School of Chemistry
University of Nottingham
University Park, Nottingham NG7 2RD (UK)
Fax: (+44) 115-951-3563
E-mail: Neil.Champness@nottingham.ac.uk, m.schroder@nottingham.ac.uk.
Dr. S. Parsons
Department of Chemistry
University of Edinburgh
West Mains Road, Edinburgh EH9 3JJ (UK)

[**] This work was supported by the CVCP (Overseas Research Student Scheme) (to A.N.K.), the EPSRC, and the University of Nottingham.

Supporting information for this article is available on the WWW under http://www.wiley-vch.de/home/angewandte/ or from the author.

 © WILEY-VCH Verlag GmbH, D-69451 Weinheim, 2000 1433-7851/00/3913-2317 $ 17.50+.50/0

environment so that the metallacycle is not involved in interactions with neighboring molecules in the solid state, and thus exists as a discrete unit. Complex **1** is very sparingly soluble in common organic solvents but dissolves sufficiently in $MeNO_2$ and MeOH to allow ^1H NMR spectroscopic measurements and electrospray mass spectrometry experiments. The results of these indicate that the metallacyclic structure is maintained in solution. However, in DMSO solution the ^1H NMR spectrum is consistent with disassembly of the complex into its components as would be expected for this more coordinating solvent.

The single-crystal X-ray structure analysis[7b, 11] of the Cd^{II} analogue shows that it forms a similar parallelogram-shaped unit (Figure 1b) which has a more "ideal" structure (N1-Cd1-N18^{ii} 121.5(2)°, when the ligand nondistorted geometry requires an angle of 120° (Scheme 1)) than complex **1**. Cd^{II} is known to have a more flexible coordination sphere than Zn^{II} and it can adopt coordination numbers between four and eight, particularly in the presence of the NO_3^- ion.[12] Despite both NO_3^- ions in complex **2** binding to the Cd^{II} center in a bidentate fashion, not all of the coordination sites of the cation are occupied. As a result, each Cd^{II} cation interacts with a NO_3^- ion of a neighboring molecule.[13] The resulting interaction through the bridging NO_3^- ion allows aggregation to give an infinite $[Cd(NO_3)]_\infty$ helix arranged around a crystallographic $\bar{3}$ axis (Figure 2). The supramolecular arrangement of the metallacycles has the effect of bridging two different helices, of opposite hands, to give a structure with no overall chirality. However, the ligands positioned between adjacent helices form fascinating hydrophobic hexagonal channels with a diameter of about 10 Å which comprise 17% of the volume of the structure[14] (Figure 3). As the network is uncharged, these channels are anion-free and available for the inclusion of guest species, potentially as large as adamantane-sized molecules. Significantly, the crystallographic analysis showed residual electron density inside the channels, but the nature of the included species could not be established because of extreme disorder around a threefold inversion axis. However, elemental analysis and NMR spectroscopic studies of complex **2** dissolved, and disassembled, in DMSO revealed no other organic molecule in its structure except ligand L. The elemental analysis gave a metal:ligand ratio of 1:1.25 indicating that the 1:1 Cd:L complex was supplemented by 0.25 equivalents of uncoordinated L within the channels. The metal:ligand ratio observed by elemental analysis of 1:1.25 corresponds with 4.5 extra molecules of L per unit cell which is consistent with the channel volume.[14] Powder X-ray diffraction studies of bulk samples, with elemental analysis consistent with the formula $\{[Cd_2(L)_2(NO_3)_4]0.5\,L\}_n$, confirmed that the structure observed in the single-crystal X-ray studies was maintained (see Supporting Information). What appears to be preferred inclusion of free ligand guest molecules over other small guests was further supported by the inclusion of *p*-terphenyl (PhC_6H_4Ph) into **2**, when **2** is prepared in the presence of this guest molecule. The inclusion of *p*-terphenyl was confirmed by ^1H NMR spectroscopy of the compound subsequently disassembled in DMSO solution. The elongated π-electronic system (10 Å in length) may even be acting as a template for the formation of the 3D structure observed for **2** through edge–face π interactions.[15] Attempts to include other guest molecules (e.g. C_6H_6, PhOMe, PhCN, MeOH, MeCN, CH_2Cl_2) by using these species as solvents gave crystals of **2** that contained only $Cd(NO_3)_2$ and the ligand in the same 1:1.25 M:L ratio, as confirmed by elemental analysis and by ^1H NMR spectroscopy of crystals dissolved in $[D_6]$DMSO.

We were interested to see whether the guest ligand molecules could be removed from the channels of compound **2** and to this end single crystals of **2** were refluxed in toluene (a

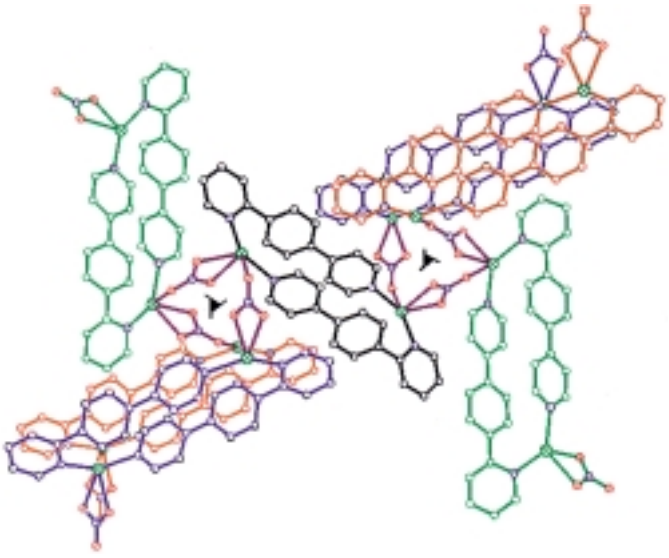


Figure 2. The metallacycle within the structure of **2** (central unit) that forms two helices of opposing hands through NO_3^- bridges; terminating NO_3^- groups are omitted for clarity. Crystallographic symmetry operations are shown to indicate the 3_1 and 3_2 screw axes around which the helices are formed.

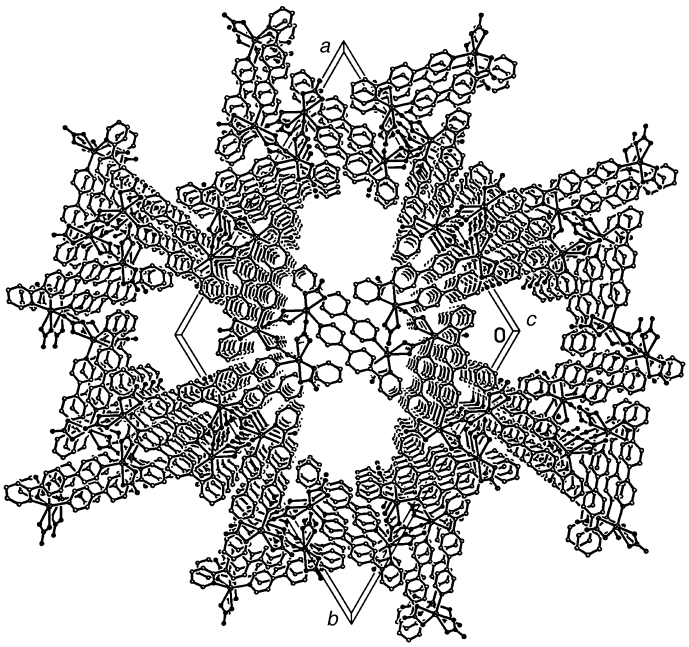


Figure 3. A view of the extended structure of **2**, including the crystallographic unit cell, showing metallacycles aggregated into helices and forming infinite channels with a diameter of about 10 Å.

 © WILEY-VCH Verlag GmbH, D-69451 Weinheim, 2000 1433-7851/00/3913-2318 $ 17.50+.50/0

solvent in which the free ligand is soluble) for 12 h and then dried in vacuo for 5 h at 70 °C. Under these conditions sufficient crystallinity was maintained in the resulting samples **3**, which showed only a slight colorization due to surface decomposition, to allow a redetermination of the single-crystal X-ray structure.[7b],[16] The 3D framework structure was maintained and interestingly *no* residual electron density was observed in the hexagonal channels.[14] The total residual electron density in the channels was assessed by using the SQUEEZE routine[14] giving a value for the residual net electron density of 0.0(17) e^- per unit cell and a total solvent accessible volume of 1597.6 Å^3. Elemental analysis of **3** was also consistent with removal of guest molecules from the channels.[17] This represents a rare example of a coordination framework acting as an analogue of porous zeolite-like frameworks.[18]

In summary, rigid bis-monodentate angular ligand L forms a dinuclear cyclic complex with exclusive "head-to-tail" ligand placement using its self-complementarity. The parallelogram can exist either as a discrete unit when the metal centers are completely coordinatively saturated (Zn^{II}) or assembles into a highly unusual 3D polymeric array when the metal centers have a high coordination number (Cd^{II}). The polymeric complex **2** is an unprecedented supramolecular aggregate of dinuclear cyclic molecules which has a multi-helical structure in which the organic molecules form large hydrophobic channels with a cross-section of about 10 Å. We have also demonstrated removal of the guests from the channels in **2** generating an open "host" framework.

Experimental Section

General: All reagents (Aldrich) were used as received. Ligand L was prepared by the literature method.[6] Elemental analyses (C,H,N) were carried out at the University of Nottingham. Infrared spectra were obtained as KBr pressed pellets using a Perkin-Elmer 1600 series FTIR spectrometer. NMR spectra were recorded at 300 MHz on a Bruker DPX300 spectrometer.

1: A solution of $Zn(NO_3)_2\cdot 6H_2O$ (0.064 g, 2.2×10^{-4} mol) in CH_3CN (12 mL) was layered over a solution of L (0.051 g, 2.2×10^{-4} mol) in CH_2Cl_2 (12 mL). After two weeks yellow crystals suitable for X-ray diffraction were formed (yield 0.182 g, 98 %). Elemental analysis for $C_{32}H_{24}N_8O_{12}Zn_2$ (M_r = 843.33): calcd: C 45.54, H 2.85, N 13.28; found: C 45.25, H 2.79, N 13.32; ^{1}H NMR ([D$_6$]DMSO, 300 MHz, 25 °C): δ = 7.40 (dd, ^1J = 9 Hz, ^2J = 5 Hz, 1H), 7.77 (d, ^1J = 6 Hz, 2H), 7.88–7.91 (m, 1H), 7.94 (d, J = 8 Hz, 2H), 8.04 (d, J = 9 Hz, 1H), 8.23 (d, J = 8 Hz, 2H), 8.70 (d, J = 6 Hz, 2H), 8.75 (d, J = 5 Hz, 1H); ^{1}H NMR (CD_3NO_2, 300 MHz, 25 °C): δ = 7.48–7.54 (m, 1H), 8.00–8.06 (m br., 4H), 8.07–8.13 (m br., 2H), 8.25–8.34 (m br., 2H), 8.73–8.81 (m br., 3H); MS (electrospray in MeOH): m/z: 817 [$M-NO_3^-+2H_2O$].

2: A solution of $Cd(NO_3)_2\cdot 4H_2O$ (0.011 g, 3.6×10^{-5} mol) in CH_3CN (2 mL) was layered over a solution of L (0.008 g, 3.6×10^{-5} mol) in CH_2Cl_2 (2 mL). After one week a solid precipitate was filtered off. Diffusion of Et_2O vapor into the filtrate yielded crystals suitable for X-ray diffraction (yield: 0.006 g, 40 %). Elemental analysis for $C_{20}H_{15}N_{4.5}O_6Cd$ (M_r = 526.9): calcd: C 45.59, H 2.85, N 11.97; found: C 46.01, H 3.15, N 11.59.

Received: December 20, 1999 [Z14421]

[1] a) B. Olenyuk, A. Fechtenkötter, P. J. Stang, *J. Chem. Soc. Dalton Trans.* **1998**, 1707; b) C. Piguet, G. Bernardinelli, G. Hopfgartner, *Chem. Rev.* **1997**, *97*, 2005.

[2] M. Scherer, D. L. Caulder, D. W. Johnson, K. N. Raymond, *Angew. Chem.* **1999**, *111*, 1690; *Angew. Chem. Int. Ed. Engl.* **1999**, *38*, 1588.

[3] J.-M. Lehn, *Chem. Eur. J.* **1999**, *5*, 2455.

[4] M. C. T. Fyfe, J. F. Stoddart, *Acc. Chem. Res.* **1997**, *30*, 393.

[5] a) M. Loi, M. W. Hosseini, A. Jouaiti, A. De Cian, J. Fischer, *Eur. J. Inorg. Chem.* **1999**, 1981; b) C. V. K. Sharma, R. D. Rogers, *Cryst. Eng.* **1999**, *1*, 19; c) M. A. Withersby, A. J. Blake, N. R. Champness, P. A. Cooke, P. Hubberstey, M. Schröder, *Cryst. Eng.* **1999**, *2*, 123; d) M. Albrecht, R. Fröhlich, *J. Am. Chem. Soc.* **1997**, *119*, 1656.

[6] S. I. Didenko, L. V. Akimenko, *Zh. Org. Khim.* **1987**, *23*, 1573.

[7] a) Single-crystal X-ray experiments were performed on a Stoe Stadi-4 four-circle diffractometer equipped with an Oxford Cryosystems open-flow cryostat (graphite-monochromated $Mo_{K\alpha}$ radiation, λ = 0.71073 Å). All structures were solved by direct methods[8] and all non-hydrogen atoms were located by using difference Fourier methods.[9] Crystal structure data for **1** $C_{32}H_{24}N_8O_{12}Zn_2$, M_r = 843.33, triclinic, space group $P\bar{1}$, a = 7.300(2), b = 9.911(3), c = 12.203(5) Å, α = 74.669(17), β = 82.37(2), γ = 72.943(19)°, V = 812.6(5) Å^3, T = 220(2) K, Z = 1, ρ_{calcd} = 1.723 Mg m^{-3}, $F(000)$ = 428, $\mu(Mo_{K\alpha})$ = 1.557 mm^{-1}. Crystal morphology: colorless blocks. Crystal dimensions: 0.23 × 0.16 × 0.12 mm. A total of 3674 reflections was collected, 2873 unique (R_{int} = 0.0501), θ_{max} = 25.03°. Absorption correction by ψ scans. Weighting scheme $w = 1/[\sigma^2(F_o^2) + (0.0397P)]$, where $P = [\max(F_o^2,0) + 2F_c^2]/3$. Goodness-of-fit on F^2 was 0.992, $R1$ (for 2219 reflections with $I > 2\sigma(I)$) = 0.0392, $wR2$ = 0.0755. Data/parameters 2873/244. Largest difference Fourier peak and hole 0.32 and −0.36 e Å^{-3}, respectively. b) Crystallographic data (excluding structure factors) for the structures reported in this paper have been deposited with the Cambridge Crystallographic Data Centre as supplementary publication nos. CCDC-137731 (**1**), CCDC-137732 (**2**), and CCDC-137733 (**3**). Copies of the data can be obtained free of charge on application to CCDC, 12 Union Road, Cambridge CB2 1EZ, UK (fax: (+44) 1223-336-033; e-mail: deposit@ccdc.cam.ac.uk).

[8] G. M. Sheldrick, SHELXS-97, *Acta Crystallogr. Sect. A* **1990**, *46*, 467.

[9] G. M. Sheldrick, SHELXL-97, Universität Göttingen, Germany, **1997**.

[10] a) C. A. Hunter, *Chem. Soc. Rev.* **1994**, 101; b) C. A. Hunter, *Angew. Chem.* **1993**, *105*, 1653; *Angew. Chem. Int. Ed. Engl.* **1993**, *32*, 1584.

[11] Crystal structure data for **2** $C_{20}H_{15}N_{4.5}O_6Cd$, M_r = 526.9, trigonal, space group $R\bar{3}$, a = 36.475(9), c = 7.570(3) Å, V = 8722(5) Å^3, T = 150(2) K, Z = 18, ρ_{calcd} = 1.606 Mg m^{-3}, $F(000)$ = 4176, $\mu(Mo_{K\alpha})$ = 1.165 mm^{-1}. Crystal morphology: colorless columns. Crystal dimensions: 0.47 × 0.15 × 0.13 mm. A total of 12854 reflections was collected, 3808 unique (R_{int} = 0.0727), θ_{max} = 26.00°. Absorption correction by ψ scans. Weighting scheme $w = 1/[\sigma^2(F_o^2) + (0.1089P)^2 + 142.9P]$, where $P = [\max(F_o^2,0) + 2F_c^2]/3$. Goodness-of-fit on F^2 was 1.133, $R1$ (for 2974 reflections with $I > 2\sigma(I)$) = 0.0601, $wR2$ = 0.1740. Data/parameters 3808/244. Largest difference Fourier peak and hole 2.4 and −0.94 e Å^{-3}, respectively.[7b].

[12] a) *Comprehensive Coordination Chemistry*, *vol. 5* (Ed.: G. Wilkinson), Pergamon, Oxford, **1987**; b) A. F. Wells, *Structural Inorganic Chemistry*, 5th ed., Oxford University Press, Oxford, **1984**.

[13] The overall geometry around the Cd^{II} center is a distorted pentagonal bipyramid. Two chelating NO_3^- groups are in the equatorial plane. The axially coordinated 2-pyridyl nitrogen atom and the bridging NO_3^- group form a N18^{ii}-Cd1-O22^{i} angle of 152.2(2)°.

[14] A. L. Spek, PLATON97, University of Utrecht, The Netherlands, **1997**.

[15] a) G. R. Desiraju, *Angew. Chem.* **1995**, *107*, 2541; *Angew. Chem. Int. Ed. Engl.* **1995**, *34*, 2311; b) H. Adams, F. J. Carrer, C. A. Hunter, J. C. Morales, E. M. Seward, *Angew. Chem.* **1996**, *108*, 1628; *Angew. Chem. Int. Ed. Engl.* **1996**, *35*, 1542.

[16] Crystal structure data for **3** $C_{16}H_{12}N_4O_6Cd$, M_r = 468.7, trigonal, space group $R\bar{3}$, a = 36.42(8), c = 7.799(15) Å, V = 8959(33) Å^3, T = 298(2) K, Z = 18, ρ_{calcd} = 1.564 Mg m^{-3}, $F(000)$ = 4176, $\mu(Mo_{K\alpha})$ = 1.134 mm^{-1}. Crystal morphology: pale brown needle. Crystal dimensions: 0.50 × 0.06 × 0.04 mm. A total of 3563 reflections was collected, 2602 unique (R_{int} = 0.1089), θ_{max} = 22.49°. Numerical absorption correction. Weighting scheme $w = 1/[\sigma^2(F_o^2) + (0.0002P)^2 + 813P]$, where $P = [\max(F_o^2,0) + 2F_c^2]/3$. Goodness-of-fit on F^2 was 1.198, $R1$ (for 1381 reflections with $I > 2\sigma(I)$) = 0.111, $wR2$ = 0.2681. Data/

parameters 2602/244. Largest difference Fourier peak and hole 0.74 and −0.99 e Å^{-3}, respectively.[7b].

[17] Elemental analysis for $C_{16}H_{12}N_4O_6Cd$ (M_r = 468.7): calcd: C 40.99, H 2.59, N 11.96; found: C 41.17, H 2.73, N 11.87.

[18] For example, see: a) B. F. Abrahams, P. A. Jackson, R. Robson, *Angew. Chem.* **1998**, *110*, 2801; *Angew. Chem. Int. Ed.* **1998**, *37*, 2656; b) D. M. L. Goodgame, D. A. Grachvogel, D. J. Williams, *Angew. Chem.* **1999**, *111*, 217; *Angew. Chem. Int. Ed.* **1999**, *38*, 153; c) C. J. Kepert, M. J. Rosseinsky, *Chem. Commun*. **1999**, 375; d) O. M. Yaghi, H. Li, C. Davis, D. Richardson, T. L. Groy, *Acc. Chem. Res.* **1998**, *31*, 474.

A Dodecanuclear Copper(II) Cage Containing Phosphonate and Pyrazole Ligands**

Vadapalli Chandrasekhar* and Savariraj Kingsley

Dedicated to Professor P. Natarajan on the occasion of his 60th birthday

Metal phosphates and phosphonates have received a lot of attention in recent years for several reasons.[1] For instance, many members of this family function as cation exchangers which could be very useful in the processing of radioactive waste streams.[2] Other potential applications of these materials include sorption,[3] catalysis,[4] catalyst supports,[4] sensors,[5] and nonlinear optics.[6] Many of these potential applications can be attributed to the extensive structural and compositional diversity of these systems. Although many transition metal phosphonates possess layered structures,[1, 7] other types of formulations such as mononuclear coordination complexes[1] and one-dimensional linear complexes[1, 8] are also known in addition to three-dimensional microporous frameworks.[9] Among the layered compounds further modulation of the structure is possible by varying the transition metal ion and the nature of the alkyl or aryl group attached to the phosphorus, and by post-synthetic changes through addition of appropriate pillaring agents.[1]

In contrast to the layered phosphonates, molecular systems of multimetal aggregates containing the phosphonate moiety as ligand(s) are relatively rare. Recently molecular phosphonate cages containing Group 13 elements[10] have been synthesized by the reaction of an alkyl phosphonic acid with alkyl metal compounds. This reaction is driven by the elimination of an alkane and the formation of a M−O bond. A similar methodology has also been applied to the corresponding arsonates.[11] Other molecular phosphonates containing zinc[12] or vanadium[13] have also been synthesized. In view of the diverse structural types that can result in these systems and also because it is known that the transition metal ions in layered phosphonates can act as Lewis acid sites, we set about preparing molecular phosphonates containing additional chelating ligands such as 3,5-dimethylpyrazolyl in order to gain a better understanding the type of clusters that would result. Apart from the novel structures, polynuclear copper(II) complexes are also of interest because of the growing awareness of the involvement of cluster compounds at the active sites of biological molecules.[14] Herein we report the synthesis and X-ray crystal structure analysis of a novel dodecanuclear copper phosphonate cluster containing 3,5-dimethylpyrazolyl ligands.

The reaction of $Cu^{II}Cl_2$ with 3,5-dimethylpyrazole (3,5-Me_2PzH) and *tert*-butylphosphonic acid in the presence of triethylamine (used as scavenger for the HCl formed in the reaction) afforded a green solid from which the crystals of the title compound **1** were grown [Eq. (1)].

$$12\,CuCl_2 + 10\,3,5\text{-}Me_2PzH + 8\,t\text{BuP(O)(OH)}_2 + 18\,Et_3N \rightarrow [Cu_{12}(\mu_4\text{-Cl})_4(\mu_3\text{-Cl})_2(\eta^1\text{-}3,5\text{-}Me_2PzH)_6(\mu_2\text{-}3,5\text{-}Me_2Pz)_4(\mu_3\text{-}t\text{BuPO}_3)_4\text{-}(\mu_2\text{-}t\text{BuPO}_3)_2(\mu_2\text{-}t\text{BuPO}_2\text{OH})_2]\ (\mathbf{1}) + 18\,Et_3N\cdot HCl \quad (1)$$

The X-ray structure analysis of compound **1** shows that it is a dodecanuclear cluster in which the entire copper assembly is encased in a lipophilic sheath composed of alkyl groups emanating from either phosphorus or from the pyrazolyl units[15] (Figure 1). This structural feature is mainly responsible for the favorable solubility properties of the cluster in many common organic solvents such as benzene. In addition **1** is stable in air and does not undergo any change upon exposure to ambient atmosphere. Compound **1** consists of two symmetry-related hexameric units that are linked with each other (Figure 2). To the best of our knowledge this kind of structural assembly is unprecedented for copper(II) clusters.

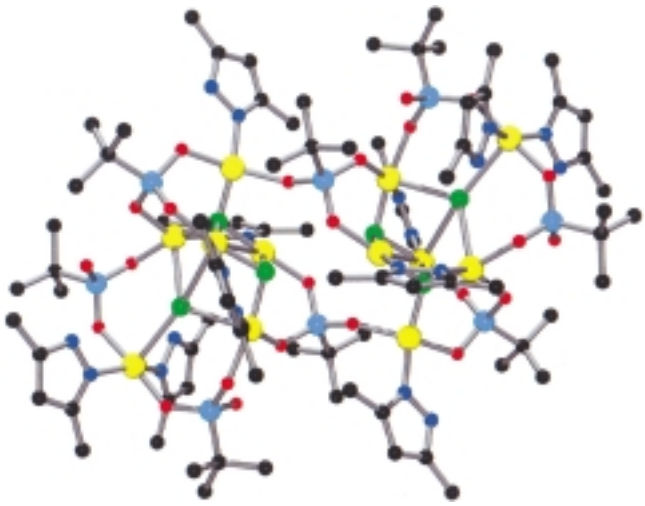


Figure 1. POVRAY diagram of **1** showing the organic lipophilic envelope surrounding the dodecanuclear Cu^{II} metal framework. Hydrogen atoms omitted for clarity. Color code: carbon: black; chlorine: green; copper: yellow; oxygen: red; phosphorus: cyan; dark blue: nitrogen.

[*] Prof. Dr. V. Chandrasekhar, S. Kingsley
Department of Chemistry, Indian Institute of Technology
Kanpur - 208 016 (India)
Fax: (+91) 512-597-436/590-007
E-mail: vc@iitk.ac.in

[**] This work was supported by a grant from the Department of Science and Technology (DST), New Delhi (V.C.). V.C. is also grateful to the Homi Bhabha Fellowship Council for a fellowship. We thank the DST for funding the National Facility for X-ray Crystallography at the Indian Institute of Technology, Kanpur. We thank Prof. Dr. P. K. Bharadwaj for his help in the data collection and X-ray analysis, and Prof. Dr. A. R. Chakravorthy, Department of Inorganic and Physical Chemistry, Indian Institute of Science, Bangalore, India for the magnetic measurements on **1**.

 © WILEY-VCH Verlag GmbH, D-69451 Weinheim, 2000 1433-7851/00/3913-2320 $ 17.50+.50/0

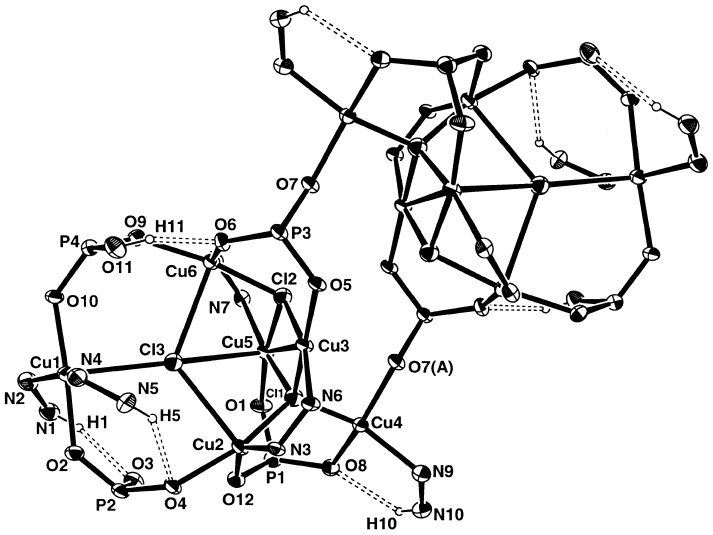


Figure 2. ORTEP diagram of **1** showing the framework of the dodecanuclear copper(II) cluster. All carbon and hydrogen atoms have been omitted. Selected bond lengths [Å]: Cl1-Cu2 1.913(3), Cl1-Cu3 1.935(6), Cl1-Cu4 1.876(12), Cl1-Cu5 1.970(7), Cl2-Cu3 1.988(8), Cl2-Cu5 1.996(4), Cl2-Cu6 1.986(5), Cl3-Cu1 2.670(7), Cl3-Cu2 2.727(1), Cl3-Cu5 2.816(1), Cl3-Cu6 2.721(7), Cu-N (free pyrazoles) range from 1.927–1.966, Cu-N (bridged pyrazoles) range from 1.971–2.012, Cu-O range from 1.919–2.009. This figure also shows the intramolecular hydrogen bonding within **1**: H11···O6 1.800(1), H1···O3 2.098(2), H5···O4 2.349(3), H10···O8 2.122(5).

Furthermore *every* copper center present in the hexameric assembly is unique by way of coordination environment and/or geometry. Specifically the copper centers present all have distorted geometry and are four- or five-coordinate, and the coordination environment around each copper center contains at least three types of ligating atoms (oxygen, chlorine, and nitrogen). In contrast in layered phosphonates such as $Cu(O_3PC_6H_5)\cdot H_2O$ and $Cu(O_3PCH_3)\cdot H_2O$, which are prepared by hydrothermal synthesis, the copper centers are all equivalent and display a distorted tetragonal-pyramidal geometry, in which each copper center is coordinated to five oxygen atoms.[16] Additionally in **1** none of the phosphonate ligands are found in a chelating coordination mode; a feature which is present in several layered phosphonates.[1]

Each of the symmetry-related hexameric copper assemblies in **1** contains a "basket handle" shaped pentameric subunit; the base of the basket is formed by a Cu_2Cl_2 core (Figure 2). Although the two copper atoms involved in this dimeric core (Cu3 and Cu5) are within a distance of 2.967(5) Å, it is unlikely that they are bonded to each other; similar nonbonding distances between copper atoms are found for some tetranuclear copper complexes containing a Cu_4O_4 framework.[14, 17] The structural integrity of the basket arises from two features. One, a μ_4-Cl atom (Cl3) holds four of the copper atoms together in a distorted tetrahedral geometry. Other chlorine atoms (μ_4-Cl1 and μ_3-Cl2) in the Cu_2Cl_2 core are involved in the propagation of the basket. The sides of the basket are stitched together by μ_2-phosphonato ligands (O1, O12, O5, and O6) and μ_2-pyrazolyl ligands (N6, N3, N7, and N8). Additionally μ_3-phosphonato ligands that are present assist not only in holding two copper centers (Cu2 and Cu6) in the pentameric subunits but also provide linkage (O8 and O7) to the copper atom(s) (Cu4) that serve as the bridge between the two pentameric subunits. The structure of **1** also shows the varied coordination modes of the ligands, chloride, 3,5-dimethylpyrazole, and phosphonate. Thus the 3,5-dimethylpyrazole groups that are present are either anionic and function as bidentate (μ_2) ligands or remain neutral and function as monodentate ligands (η^1). Similarly of the four phosphonate units present for each half of the cluster three are completely deprotonated. Of these, two units coordinate through all the three oxygen atoms (μ_3), while the other only provides two oxygen atoms (μ_2) for coordination. The fourth ligating moiety of this family is actually a phosphinate $RP(O)_2(OH)$ and provides coordination through two oxygen atoms (O10 and O9), while the third oxygen atom (O11) remains protonated. Similarly of the three chlorine atoms that are present for each half of the cluster, two function as μ_4 bridges, while one is μ_3 bridging. The presence of hydrogen atoms on the pyrazolyl nitrogen atoms (N1, N5, N10) and on the oxygen atom of $RP(O)_2(OH)$ (O11) causes intramolecular hydrogen bonding within the cluster. This leads to the preferential orientation of the pyrazolyl rings on Cu1 so as to maximize the hydrogen bonding interaction with the phosphonate oxygen atoms O3 and O4. The hydrogen bonding interaction present in **1** is shown in Figure 2. The extensive and elaborate structural diversity in this molecule appears to be truly remarkable and is brought about by the versatile coordination adaptability of the Cu^{II} ion in the presence of the ligand $[RPO_3]^{2-}$ and the ancillary 3,5-dimethylpyrazolyl and chloride ligands. In view of these results it would be of interest to study the structural effects brought out by the replacement of the water molecules found in copper phosphonates $Cu(O_3PC_6H_5)\cdot H_2O$ and $Cu(O_3PCH_3)\cdot H_2O$ by pyrazolyl ligands.

Magnetic susceptibility measurements on the copper cluster **1** were carried out between room temperature and 18 K. The μ_{eff} value decreases with a decrease in temperature. Figure 3 shows the plot of χ_M versus T as well as that of μ_{eff} per copper atom versus T. These plots show that **1** displays weakly antiferromagnetically coupled behavior. This is reflected in the interception of the straight line at $-30\,^{\circ}C$ in the plot of $1/\chi_M$ versus T (Figure 3).

We have described the synthesis of a novel dodecanuclear copper(II) cluster mediated by *tert*-butylphosphonic acid and 3,5-dimethylpyrazole. The combination of these two ligands leads to the assembly of **1** whose structure is completely different from any structural type known in such copper systems so far. Currently we are adapting this synthetic methodology to other transition and lanthanide metal systems.

Experimental Section

1: Anhydrous copper(II) chloride(0.20 g, 1.50 mmol) was taken up in anhydrous dichloromethane (30 mL). To this was added a solution of 3,5-dimethylpyrazole (0.12 g, 1.25 mmol) in dichloromethane (10 mL) at room temperature. This resulted in a green solution to which a solution of *tert*-butylphosphonic acid (0.14 g, 1.0 mmol) and triethylamine (0.23 g, 2.25 mmol) in dichloromethane (20 mL) was added in one portion. The resulting green solution was stirred at room temperature for 20 h. The solvent was removed in vacuo to afford a green solid, which was treated

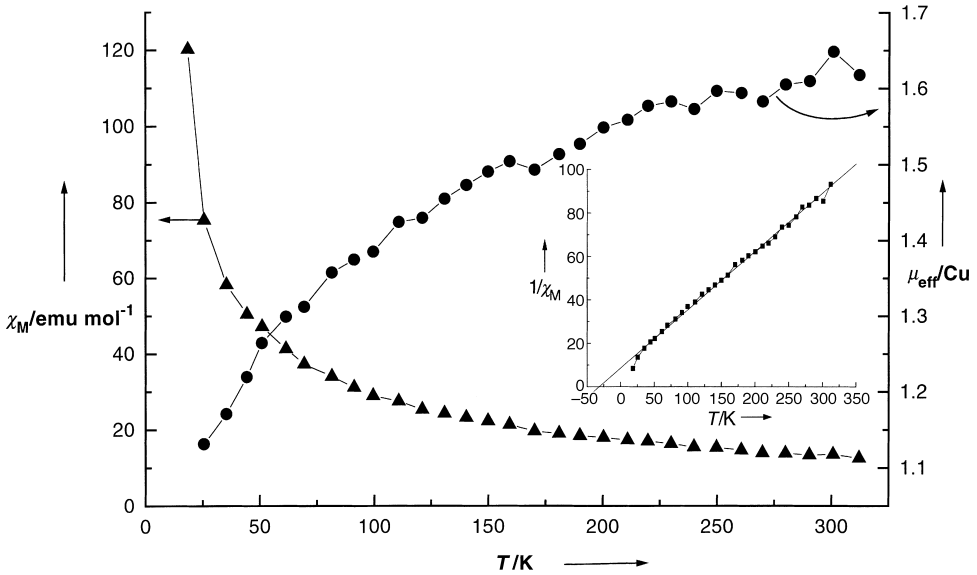


Figure 3. Plots of χ_M versus T/K (▲) and of μ_{eff}/Cu versus T/K (●) for **1**. Inset: Plot of $1/\chi_M$ versus T for **1**.

with benzene (50 mL), filtered, and the solvent was removed from the filtrate affording a crystalline solid (0.31 g) which upon recrystallization from *n*-hexane and dichloromethane (1:1) at room temperature afforded dark green crystals. M.p.: 188 °C. C,H,N analysis: calcd for $C_{82}H_{150}Cl_6Cu_{12}N_{20}O_{24}P_8$ (3023.29): C 32.57, H 5.00, N9.26; found: C 32.45, H 5.10, N 9.12; IR (KBr): $\tilde{\nu}$ = 3340(s), 2947(s), 2866(m), 2493(m), 2172(m), 1571(m), 1477(s), 1422(m), 1268(m), 1120(m), 1046(s), 971(m), 917(m), 831(m), 667(s), 524(s), 431(m) cm^{-1}; UV/Vis (CH_2Cl_2): λ_{max} (ε) = 730 (860), 246 nm (23140).

Received: January 3, 2000
Revised: March 30, 2000 [Z14493]

[1] A. Clearfield, *Prog. Inorg. Chem.* **1998**, *47*, 371; M. G. Walawalkar, *Synthesis and Structural Studies of Model Compounds for Zeolites and Phosphate Materials*, Cuvillier, Göttingen, **1997**; G. Alberti in *Comprehensive Supramolecular Chemistry*, *Vol 7* (Eds.: J. L. Atwood, J. E. D. Davies, D. D. MacNicol, F. Vögtle, J. M. Lehn), Elsevier, New York, **1996**, pp 151–187; M. E. Thompson, *Chem. Mater.* **1994**, *6*, 1168; G. Cao, H.-G. Hong, T. E. Mallouk, *Acc. Chem. Res.* **1992**, *25*, 420.

[2] A. Clearfield, *Inorganic Ion Exchange Materials*, CRC Press, Boca Raton, Florida, **1982**; G. Alberti, *Acc. Chem. Res.* **1978**, *11*, 163; J. D. Wang, A. Clearfield, G.-Z. Peng, *Mater. Chem. Phys.* **1993**, *35*, 208.

[3] F. Fredoueil, D. Massiot, P. Janvier, F. Gingl, M. Bujoli-Doeuff, M. Evain, A. Clearfield, B. Bujoli, *Inorg. Chem*. **1999**, *38*, 1831; G. Cao, V. M. Lynch, L. N. Yacullo, *Chem. Mater*. **1993**, *5*, 583.

[4] B.-Z. Wan, R. G. Anthony, G.-Z. Peng, A. Clearfield, *J. Catal*. **1994**, *19*, 101; D. Deniaud, B. Schollorn, D. Mansuy, J. Rouxel, P. Battion, B. Bujoli, *Chem. Mater*. **1995**, *7*, 995.

[5] G. Alberti, R. Polombari, *Solid State Ionics*, **1989**, *35*, 153; G. Alberti, M. Casciola, R. Polombari, *Solid State Ionics*, **1992**, *52*, 291.

[6] S. B. Ungashe, W. L. Wilson, H. E. Katz, G. R. Scheller, T. M. Putvinski, *J. Am. Chem. Soc*. **1992**, *114*, 8717.

[7] A. Cabeza, M. A. G. Aranda, S. Bruque, D. M. Poojary, A. Clearfield, J. Sanz, *Inorg. Chem*. **1998**, *37*, 4168; B. Zhang, D. M. Poojary, A. Clearfield, *Inorg. Chem.* **1998**, *37*, 249.

[8] D. Grohol, A. Clearfield, *J. Am. Chem. Soc*. **1997**, *119*, 9301.

[9] J. Le Bideau, C. Payen, P. Palvadeau, B. Bujoli, *Inorg. Chem*. **1994**, *33*, 4885; K. Maeda, J. Akimoto, Y. Kiyozumi, F. Mizukami, *J. Chem. Soc. Chem. Commun*. **1995**, 1033; K. Maeda, J. Akimoto, Y. Kiyozumi, F. Mizukami, *Angew. Chem.* **1995**, *107*, 1313; *Angew. Chem. Int. Ed. Engl*. **1995**, *34*, 1199.

[10] M. G. Walawalkar, H. W. Roesky, R. Murugavel, *Acc. Chem. Res.* **1999**, *32*, 117; M. G. Walawalkar, R. Murugavel, H. W. Roesky, H.-G. Schmidt, *Organometallics* **1997**, *16*, 516; M. G. Walawalkar, R. Murugavel, H. W. Roesky, H.-G. Schmidt, *Inorg. Chem*. **1997**, *36*, 4202; M. G. Walawalkar, R. Murugavel, A. Voigt, H. W. Roesky, H.-G. Schmidt, *J. Am. Chem. Soc*. **1997**, *119*, 4656; M. G. Walawalkar, R. Murugavel, H. W. Roesky, I. Uson, R. Kraetzner, *Inorg. Chem*. **1998**, *37*, 473; Y. Yang, J. Pinkas, M. Schafer, H. W. Roesky, *Angew. Chem.* **1998**, *110*, 2795; *Angew. Chem. Int. Ed.* **1998**, *37*, 2650; Y. Yang, M. G. Walawalkar, J. Pinkas, H. W. Roesky, H.-G. Schmidt, *Angew. Chem.* **1998**, *110*, 101; *Angew. Chem. Int. Ed.* **1998**, *37*, 96; M. R. Mason, A. M. Perkins, R. M. Matthews, J. D. Fisher, M. S. Mashuta, A. Vij, *Inorg. Chem.* **1998**, *37*, 3734; A. Keys, S. Bott, A. R. Bott, *Chem. Commun.* **1996**, 2339; C. C. Landry, W. M. Cleaver, I. A. Guzei, A. L. Rheingold, *Organometallics* **1998**, *17*, 5209.

[11] Y. Yang, J. Pinkas, M. Noltemeyer, H.-G. Schmidt, H. W. Roesky, *Angew. Chem.* **1999**, *111*, 706; *Angew. Chem. Int. Ed.* **1999**, *38*, 664.

[12] M. R. Mason, *J. Cluster. Sci.* **1998**, *9*, 1; M. R. Mason, M. S. Mashuta, J. F. Richardson, *Angew. Chem.* **1997**, *109*, 249; *Angew. Chem. Int. Ed. Engl*. **1997**, *36*, 239; M. R. Mason, R. M. Matthews, M. S. Mashuta, J. F. Richardson, *Inorg. Chem.* **1997**, *36*, 6476.

[13] J. Salta, Q. Chen, Y. Chang, J. Zubieta, *Angew. Chem.* **1994**, *106*, 781; *Angew. Chem. Int. Ed. Engl.* **1994**, *33*, 757; Y. Chang, J. Salta, J. Zubieta, *Angew. Chem.* **1994**, *106*, 347; *Angew. Chem. Int. Ed. Engl.* **1994**, *33*, 325; Q. Chen, J. Zubieta, *J. Chem. Soc. Chem. Commun.* **1994**, 1635; Q. Chen, J. Zubieta, *J. Chem. Soc. Chem. Commun.* **1994**, 2663; D. L. Thorn, R. L. Harlow, N. Herron, *Inorg. Chem.* **1995**, *34*, 2629; A. Müller, K. Hovemeier, E. Krickemeyer, H. Bögge, *Angew. Chem.* **1995**, *107*, 857; *Angew. Chem. Int. Ed. Engl.* **1995**, *34*, 779; A. Müller, K. Hovemeier, R. Rohlfing, *Angew. Chem.* **1992**, *104*, 1214; *Angew. Chem. Int. Ed. Engl.* **1992**, *31*, 1192.

[14] X. S. Tan, Y. Fujii, R. Nukada, M. Mikuriya, Y. Nakano, *J. Chem. Soc. Dalton Trans.* **1999**, 2415.

[15] Crystal data for **1**: Crystal dimensions: 0.40 × 0.30 × 0.03 mm. Molecular formula: $C_{82}H_{150}Cl_6Cu_{12}N_{20}O_{24}P_8$, M_r = 3023.29, monoclinic, space group *C*2/c, a = 20.721(2), b = 30.323(5), c = 25.07(3) Å, β = 106.90(4)°, V = 15073(16) Å^3, Z = 4, T = 293(2) K, ρ_{calcd} = 1.331 g cm^{-3}, Enraf Nonius FR590 CAD-4 diffractometer, $Mo_{k\alpha}$ radiation, 9543 reflections collected, 9235 independent reflections (R_{int} = 0.0778), $R1$ = 0.0697, $wR2$ = 0.2042 [$I > 2\sigma(I)$], $R1$ = 0.1658, $wR2$ = 0.2384 (all data), GOF = 1.335. The maximum and minimum residual electron density are 1.058 and −1.526 e Å^{-3}, respectively. The structure was solved by using the WINGX1.61 crystallographic collective package (L. J. Farrugia, WINGX ver 1.61, An Integrated Systems of Windows programs for the Solution, Refinement and Analysis of single-crystal X-ray diffraction data, Department of Chemistry, University of Glasgow). The structure was solved initially with SIR92 and refined with the SHELX-97 package incorporated in WINGX. The structure was refined against F^2 with a full-matrix least-squares algorithm. All hydrogen atoms were included in idealized positions and a riding model was used. Crystallographic data (excluding structure factors) for the structures reported in this paper have been deposited with the Cambridge Crystallographic Data Centre as supplementary publication no. CCDC-138262. Copies of the data can be obtained free of charge on application to CCDC, 12 Union Road, Cambridge CB21EZ, UK (fax: (+44) 1223-336-033; e-mail: deposit@ccdc.cam.ac.uk).

[16] Y. Zhang, A. Clearfield, *Inorg. Chem*. **1992**, *31*, 2821.

[17] L. P. Wu, T. Kuroda-Sowa, M. Maekawa, Y. Suenaga, M. Munakata, *J. Chem. Soc. Dalton Trans.* **1996**, 2179.

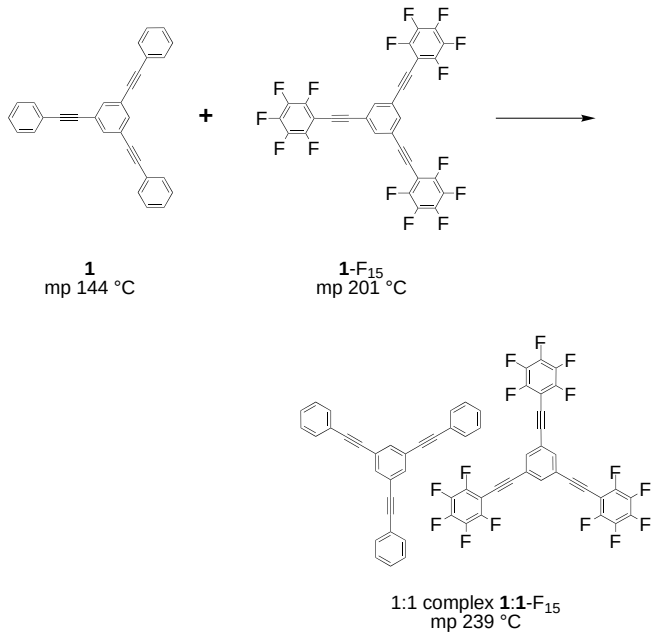
 © WILEY-VCH Verlag GmbH, D-69451 Weinheim, 2000 1433-7851/00/3913-2322 $ 17.50+.50/0

Phenyl/Pentafluorophenyl Interactions and the Generation of Ordered Mixed Crystals: *sym*-Triphenethynylbenzene and *sym*-Tris(perfluorophenethynyl)benzene**

Francesco Ponzini, Ralph Zagha, Kenneth Hardcastle, and Jay S. Siegel*

Although benzene and perfluorobenzene adopt crystal structures with "herringbone" (T-shaped) pairwise orientations,[1, 2] combination of the two liquids produces an intimate 1:1 solid complex in which the basic short range order is a face-to-face stack.[3, 4] The driving force for this specific mixing stems from the quadrupole moment and van der Waals surface of benzene and perfluorobenzene.[5–8] Recent dynamic studies have provided quantitative evidence for a general, polar-π phenyl/perfluorophenyl attraction.[9, 10] These studies of ours and related work have developed a design principle for ordered mixed-crystals of aromatic/perfluoroaromatic compounds.[9–14] Studies on tolan/perfluorotolan and related compounds support these ideas.[15–17] A powerful extension of the principle is to use the attractive phenyl/perfluorophenyl interactions to anchor other groups in a specific order within a crystal, that is, to accomplish crystal engineering.[18] We provide a striking demonstration of such control through the crystal structures and mixing behavior of *sym*-triphenethynylbenzene (**1**) and *sym*-tris(perfluorophenethynyl)benzene (**1**–F_{15}); the pure compounds pack in slipped stacks and the 1:1 complex displays face-to-face stacks alternating **1** and **1**–F_{15}.

Reaction of 1,3,5-tribromobenzene with phenylacetylene under Sonagoshira conditions (Pd^{IV} 5%, dimethylformamide, base) resulted in the formation of **1** in 58% yield. Under similar conditions 1,3,5-triethynylbenzene and pentafluoroiodobenzene were coupled to form **1**–F_{15} in 30% yield. Pure **1** was crystallized from hexanes/dichloromethane to produce needles that melted at 142–146 °C (visual inspection), 144 °C (differential scanning calorimetry (DSC)). Pure **1**–F_{15} was recrystallized from hexanes/dichloromethane to produce needles that melted at 199–201 °C (visual inspection), 201 °C (DSC). Equimolar amounts of **1** and **1**–F_{15} were ground in an agate mortar to produce a fine powder (Figure 1, top). Unlike most solid mixtures, the melting point of the 1:1 mixture was higher than either of the two pure compounds (235–239 °C, visual inspection; 239 °C, DSC). Recrystallization of this powder from hexanes/dichloromethane by evaporation of a clear solution produced crystals (**1**:**1**–F_{15}) with identical melting behavior to the original powder. The sharp and higher melting point of the mixture indicated that a solid compound had formed and it was inferred that the special phenyl/perfluorophenyl interaction was involved.



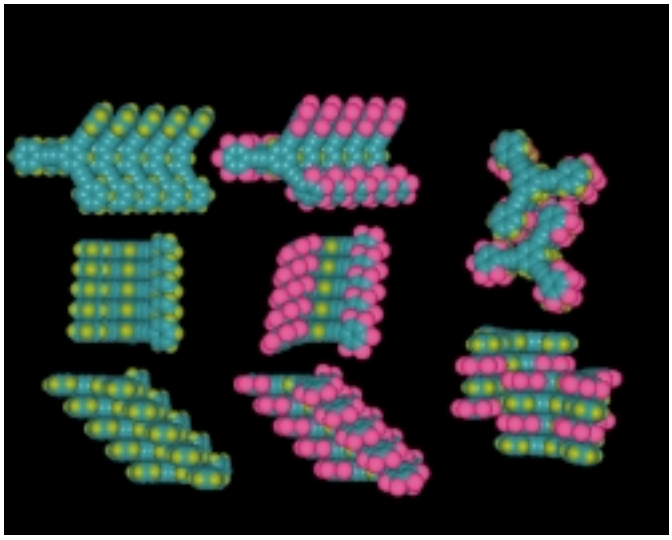


Figure 1. Three views of the stacked structures in (left to right) **1**, **1**–F_{15}, and **1**:**1**–F_{15} (1:1 complex), with reaction scheme and melting points above. From upper to lower: a) top view, b) back view, c) side view.

Crystallographic analysis of single crystals of **1**, **1**–F_{15}, and **1**:**1**–F_{15} (1:1 complex) revealed two structural classes: slipped stacks and columnar stacks (Figure 1, bottom).[19–24] The monoclinic centered (*C*2/*c*) structure of **1** displays a twisted rotor form. The interplanar angles between the radial and central benzene rings are 0, 9, and 80°. The acetylenic bonds are bent slightly (175–180° with an average of 178°). The rings are not face-stacked with respect to one another in the crystal, but rather slipped such that one radial benzene ring sits atop the acetylene of its neighbor within the stack. The acute angle of the vector passing through the middle of the central benzene rings in each stack with the normal to the best

[*] Prof. J. S. Siegel, F. Ponzini, R. Zagha
Department of Chemistry
University of California–San Diego
La Jolla, CA 92093-0358 (USA)
Fax: (+1) 858-822-0386
E-mail: jss@chem.ucsd.edu
Prof. K. Hardcastle
Department of Chemistry
California State University Northridge
Northridge, CA 91330-8262 (USA)

[**] This work was supported by the US National Science Foundation (CHE-9904275).

plane of those rings can be defined as a slip angle. That angle would be 0° for a perfect columnar stacking and 90° for a single lamellar sheet. Assuming a 3.6 Å distance between layers and "normal" benzenoid bond lengths, an angle of 35° (sin of 0.81) would place the hydrogen of one ring over the center of its neighbors, the face-to-face/center-to-edge conformation (Figure 2). In the case of **1** the slip angle is approximately 48°, well beyond the face-to-face/center-to-edge conformation. Packing between the stacks seems to be dominated by shape selection, with each stack nestling into the other.

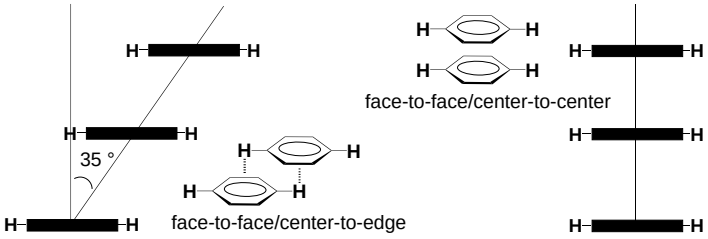


Figure 2. Relation of face-to-face/center-to-edge (left) and face-to-face/center-to-center (right) geometries to the packing slip angle.

A remarkably similar structure is observed for the monoclinic ($P2_1/c$) crystal structure of **1**–F_{15}. Again a twisted structure is adopted, however, with more severe interplanar torsion angles of 4, 28, and 90°. The acetylenic bonds are bent slightly more (171–177° with an average of 174°). The slip-angle of the stack is 46°, only 2° off from the 48° seen in **1**. Thus, again the radial ring in one molecule tends to pack over the acetylenic unit of its neighbors.

Things change markedly for the mixed crystal **1**:**1**–F_{15}. The triclinic ($P\bar{1}$) form displays an alternating motif of **1** and **1**–F_{15} in each stack. The stacks are nestled together by shape complementarity, but are shifted out of register with each other to juxtapose molecules of **1** as lateral neighbors to molecules of **1**–F_{15}. The proximity of hydrogen and fluorine atoms (2.4–2.7 Å) could be viewed as evidence for favorable C–H to F interactions, but it could also be due to the benefit of having commensurate layers (maximum packing density) or to lateral quadrupolar interactions.[25] More importantly, the molecules of **1** and **1**–F_{15} do not adopt twisted rotor conformations but are essentially planar and the slip-angle is only about 20°, significantly less than that predicted for the center-to-edge slipped stacking and approaching columnar stacking. Thus, it would seem that the anchoring principle of benzene-to-perfluorobenzene interactions applies in this case.

In conclusion, design principles and predictability in crystal engineering remain a frontier question in supramolecular chemistry.[26] Simple ideas like hydrogen-bond complementarity have made it possible to reduce the gamut of structures and to increase the chances that short-range supramolecular order will appear in the solid state.[27] The elucidation of other locally favored motifs, such as those induced by polar-π interactions, expands our control in the engineering of solids.[9, 15–17] Indeed, the use of phenyl/perfluorophenyl attractions is a useful and reliable way to control local order in crystal packing.[10] The underlying physics of this interaction is not limited to crystal packing; therefore, one could apply this principle to a number of constructions and exploit it in related short-range packing problems such as receptor–substrate interactions.

Received: January 31, 2000 [Z 14619]

[1] B. E. G. Cox, D. W. J. Cruickshank, J. A. S. Smith, *Proc. R. Soc. London A* **1958**, *247*, 1.
[2] N. Boden, P. P. Davis, C. H. Stam, G. A. Wesselink, *Mol. Phys.* **1968**, *25*, 81.
[3] J. H. Williams, J. K. Cockcroft, A. N. Fitch, *Angew. Chem.* **1992**, *104*, 1666; *Angew. Chem. Int. Ed. Engl.* **1992**, *31*, 1655.
[4] For full eutectic analysis of this mixture, as well as DSC-based thermodynamic analysis of the melting behavior, see: J. S. Brennan, N. M. D. Brown, F. L. Swinton, *J. Chem. Soc. Faraday Trans. I* **1974**, *70*, 1965.
[5] J. M. Steed, T. A. Dixon, W. Klemperer, *J. Chem. Phys.* **1979**, *70*, 4940.
[6] M. Claessens, L. Palombini, M.-L. Stein, J. Reisse, *New J. Chem.* **1982**, *6*, 595.
[7] J. Almlöf, K. Faegri, Jr., *J. Chem. Phys.* **1983**, *79*, 2284.
[8] K. E. Laidig, *Chem. Phys. Lett.* **1991**, *185*, 483.
[9] F. Cozzi, J. S. Siegel, *Pure Appl. Chem.* **1995**, *67*, 683.
[10] F. Cozzi, F. Ponzini, R. Annunziata, M. Cinquini, J. S. Siegel, *Angew. Chem.* **1995**, *107*, 1092; *Angew. Chem. Int. Ed. Engl.* **1995**, *34*, 1019.
[11] These design principles were presented at the ACS Cope Scholar Award address at the ACS National Meeting in Boston, **1998**.
[12] For examples of other related crystal structures, see: T. Dahl, *Acta. Chem. Scand.* **1994**, *48*, 95.
[13] T. Dahl, *Acta Crystallogr.* **1990**, *B46*, 283.
[14] T. Dahl, *Acta Chem. Scand. A* **1988**, *42*, 1.
[15] G. W. Coates, A. R. Dunn, L. M. Henling, D. A. Dougherty, R. H. Grubbs, *Angew. Chem.* **1997**, *109*, 290; *Angew. Chem. Int. Ed. Engl.* **1997**, *36*, 248.
[16] G. W. Coates, A. R. Dunn, L. M. Henling, J. W. Ziller, E. B. Lobkovsky, R. H. Grubbs, *J. Am. Chem. Soc.* **1998**, *120*, 3641.
[17] M. Weck, A. Dunn, K. Matsumoto, G. Coates, E. Lobkovsky, R. Grubbs, *Angew. Chem.* **1999**, *111*, 2909; *Angew. Chem. Int. Ed.* **1999**, *38*, 2741.
[18] G. R. Desiraju, *Angew. Chem.* **1995**, *107*, 2541; *Angew. Chem. Int. Ed. Engl.* **1995**, *34*, 2311.
[19] All data was collected using molybdenum radiation ($\lambda = 0.71073$ Å). Data for **1** and **1**–F_{15} were collected on an Enraf-Nonius CAD-4 diffractometer; data for **1**:**1**–F_{15} (1:1 complex) was collected on a Bruker SMART CCD diffractometer (Center for Molecular Structure, Cal State University Fullerton, Fullerton, CA). Data reduction and LP corrections for **1** and **1**–F_{15} were performed by XCAD4, and for **1**:**1**–F_{15} (1:1 complex) by SAINT V4; structures were solved and refined using SHELXTL/PC v5.0; hydrogen atoms were included in calculated positions (HFIX). All programs: Bruker AXS, Madison, WI, (USA).
[20] Crystallographic data (excluding structure factors) for the structures reported in this paper have been deposited with the Cambridge Crystallographic Data Centre as supplementary publication nos. CCDC-132202, -132203, and -132204. Copies of the data can be obtained free of charge on application to CCDC, 12 Union Road, Cambridge CB2 1EZ, UK (fax: (+44) 1223-336-033; e-mail: deposit@ccdc.cam.ac.uk).
[21] In general, the quality of these room temperature analyses can be viewed as reasonable, R and R^2 factors are 5–8%, the data to parameter ratio exceeds 10, and residuals are small. The density of **1**:**1**–F_{15} falls within 2% of the average for **1** and **1**–F_{15}. The average bond lengths for any given bond type are normal; however, the ranges leave something to be desired. In addition, the average aromatic carbon–carbon bond length is unusually small in the radial benzene rings, but normal for the central benzene rings in all three structures. Some of these range and average anomalies can be explained if thermal motion is focused into librational motion of the outer rings. For our purposes, detailed analyses of the specific bond lengths is not necessary, and this caveat is in place for others who might want to

 © WILEY-VCH Verlag GmbH, D-69451 Weinheim, 2000 1433-7851/00/3913-2324 $ 17.50+.50/0

overinterpret the data. Despite the above mentioned concerns, we believe the supramolecular aspects of the crystal structures to be valid.
[22] Crystal data for **1**: crystal dimensions $0.50 \times 0.25 \times 0.10$ mm^3, monoclinic space group $C2/c$ (No. 15), $a = 35.645(11)$, $b = 4.851(3)$, $c = 24.804(9)$ Å, $\beta = 98.55(3)^\circ$, $V = 4241(3)$ Å^3, $Z = 8$, $\rho_{calcd} = 1.185$ g cm^{-3}, $\mu = 0.067$ mm^{-1}, $F(000) = 1584$; 6107 reflections with $1.16 < \theta < 21.98^\circ$. Structure solution and refinement for 2591 independent reflections ($R_{int} = 0.192$) with $I > 2\sigma(I)$ and 272 parameters, $R = 0.0541$, $R_w = 0.0600$, max./min. residual electron density 0.139/ − 0.140 e Å^{-3}.
[23] Crystal data for **1**−F_{15}: crystal dimensions $0.80 \times 0.08 \times 0.08$ mm^3, monoclinic space group $P2_1/c$ (No. 14), $a = 18.308(7)$, $b = 4.887(4)$, $c = 27.145(14)$ Å, $\beta = 96.38(4)^\circ$, $V = 2414(3)$ Å^3, $Z = 4$, $\rho_{calcd} = 1.784$ g cm^{-3}, $\mu = 0.186$ mm^{-1}, $F(000) = 1272$; 6965 reflections with $1.12 < \theta < 21.97^\circ$. Structure solution and refinement for 2943 independent reflections ($R_{int} = 0.088$) with $I > 2\sigma(I)$ and 406 parameters, $R = 0.0869$, $R_w = 0.0742$, max./min. residual electron density 0.250/ − 0.229 e Å^{-3}.
[24] Crystal data for **1**:**1**−F_{15} (1:1 complex): crystal dimensions $0.30 \times 0.05 \times 0.05$ mm^3, triclinic space group $P\bar{1}$ (No. 2), $a = 7.4913(5)$, $b = 14.0798(9)$, $c = 22.2722(14)$ Å, $\alpha = 94.779(1)^\circ$, $\beta = 92.692(1)^\circ$, $\gamma = 91.580(1)^\circ$, $V = 2337.3(3)$ Å^3, $Z = 2$, $\rho_{calcd} = 1.459$ g cm^{-3}, $\mu = 0.126$ mm^{-1}, $F(000) = 1032$; 23084 reflections with $0.92 < \theta < 28.66^\circ$. Structure solution and refinement for 10394 independent reflections ($R_{int} = 0.162$) with $I > 2\sigma(I)$ and 676 parameters, $R = 0.0628$, $R_w = 0.0582$, max./min. residual electron density 0.144/ − 0.172 e Å^{-3}.
[25] It has been noted that organofluorine almost never accepts hydrogen bonds; see: J. D. Dunitz, R. Taylor, *Eur. J. Chem.* **1997**, *3*, 89.
[26] J.-M. Lehn, *Supramolecular Chemistry*, VCH, Weinheim, **1994**.
[27] a) M. C. Etter, *Acc. Chem. Res.* **1990**, *23*, 120; b) J. Berstein, M. C. Etter, L. Leiserowitz, *Structure Correlation* (Eds.: J. D. Dunitzm, H.-B. Bürgi), VCH, Weinheim, **1994**, Chap. 11.

Inorganic – Organic Hybrid Materials Constructed from $[(VO_2)(HPO_4)]_\infty$ Helical Chains and $[M(4,4'\text{-bpy})_2]^{2+}$ (M = Co, Ni) Fragments**

Zhan Shi, Shouhua Feng,* Shan Gao, Lirong Zhang, Guoyu Yang, and Jia Hua

The design and synthesis of inorganic – organic hybrid materials have generated significant interest for their potential application in the fields of catalysis, biology, and optical and electromagnetic functional materials.[1] Huge structures have been reported for these materials over the past few years, in which various architectures with one- (1D), two- (2D), and three-dimensional (3D) connections between inorganic and organic species are displayed. Polyoxoanions associated with organic templates[2] or with metal coordination compounds[3, 4] have become a well-established class of inorganic – organic materials, among these the major interest has been shown in the few helical or chiral structures reported. For instance, a double helical chain has been described in $[(CH_3)_2NH_2]K_4[V_{10}O_{10}(H_2O)_2(OH)_4(PO_4)_7] \cdot 4H_2O$,[5] spirals of InO_6 octahedra in $RbIn(OH)PO_4$,[6] and a spiral-shaped chain in $[\{Cu(en)(OH_2)\}Mo_5P_2O_{23}]^{4-}$.[7] The rational synthesis of inorganic – organic compounds containing a helical array is a challenging goal.[8] Our aim was to synthesize such helical structures for the inorganic – organic compounds generated from a combination of vanadium phosphates[9] and metal coordination compounds. The diversity of polyhedra and valence states of vanadium together with the coupling characteristics of the components in the synthetic system provide the basis for constructing unusual structures.

Unlike the above examples, herein we report the synthesis and X-ray crystal structure analyses of the inorganic – organic hybrid materials **1** and **2**, which have not only an infinite helical chain $[(VO_2)(HPO_4)]_\infty$, but also both left-handed and right-handed helical chains in one compound.

$[M(4,4'\text{-bpy})_2(VO_2)_2(HPO_4)_4]$
(**1**: M = Co; **2**: M = Ni; bpy = bipyridine)

Compounds **1** and **2** were synthesized by the hydrothermal reaction of $NaVO_3$, NaH_2PO_4, $Co(NO_3)_2$ (for **1**) or $Ni(NO_3)_2$ (for **2**), 4,4′-bpy, and H_2O in a molar ratio 1:1:1:1:556 at 160 °C for five days. The crystalline product in each case was characterized by elemental analysis, IR spectroscopy, thermogravimetric analysis/differential thermal analysis (TGA – DTA), and single-crystal X-ray diffraction analysis.[10]

Single-crystal X-ray diffraction analysis revealed that **1** and **2**, which are analogues, have a novel 3D structure constructed from two subunits, namely $[(VO_2)(HPO_4)]_\infty$ helical chains and $[M(4,4'\text{-bpy})_2]^{2+}$ fragments. These helical chains are composed of alternately corner-sharing HPO_4 tetrahedra and VO_4N trigonal bipyramids (Figure 1). The central axis of each helical chain is a twofold screw axis. Two oxygen atoms from adjacent VO_4N and HPO_4 units in the helical chain chelate an M atom of $[M(4,4'\text{-bpy})_2]$, generating a 3-ring $\{MVPO_3\}$. These 3-rings link the left-handed helical and right-handed helical $[(VO_2)(HPO_4)]_\infty$ chains to produce a layer motif $\{MV_2P_2O_{20}\}$ in the (101) plane (Figure 1a). Adjacent M/V/P/O layers are connected by 4,4′-bpy ligands, which generates a 3D structure (Figure 2).

Each vanadium atom resides in a distorted trigonal-bipyramidal environment, coordinated to four oxygen atoms and to a nitrogen atom from 4,4′-bpy. Three of the four oxygen atoms lie in an equatorial plane; one of these oxygen atoms is terminal, and two are bridging, one with P and one with M. The remaining oxygen atom, which bridges P and the N atom from 4,4′-bpy, is oriented axially, perpendicular to the equatorial plane. PO_4 tetrahedra link two V atoms, an M atom, and a proton. The M atoms reside in octahedral environments, coordinated to four oxygen atoms from VO_4N and HPO_4 in the equatorial plane and to two nitrogen atoms from 4,4′-bpy ligands occupying the axial positions.

When 4,4′-bpy functions as a rodlike ligand it usually coordinates with only central metals. In the case reported herein, it acts as a bifunctional organic ligand, directly linked to M (Co or Ni) and to V atoms in the P-V-O chains. To our knowledge, this coordination mode has not been observed in

[*] Prof. S. Feng, Dr. Z. Shi, Dr. S. Gao, Dr. L. Zhang, Dr. G. Yang, Dr. J. Hua
Key Laboratory of Inorganic Synthesis and Preparative Chemistry
Department of Chemistry
Jilin University
Changchun 130023 (P. R. China)
Fax: (+86) 431-567-1974
E-mail: shfeng@mail.jlu.edu.cn

[**] This work was supported by the National Natural Science Foundation of China and the STMC.

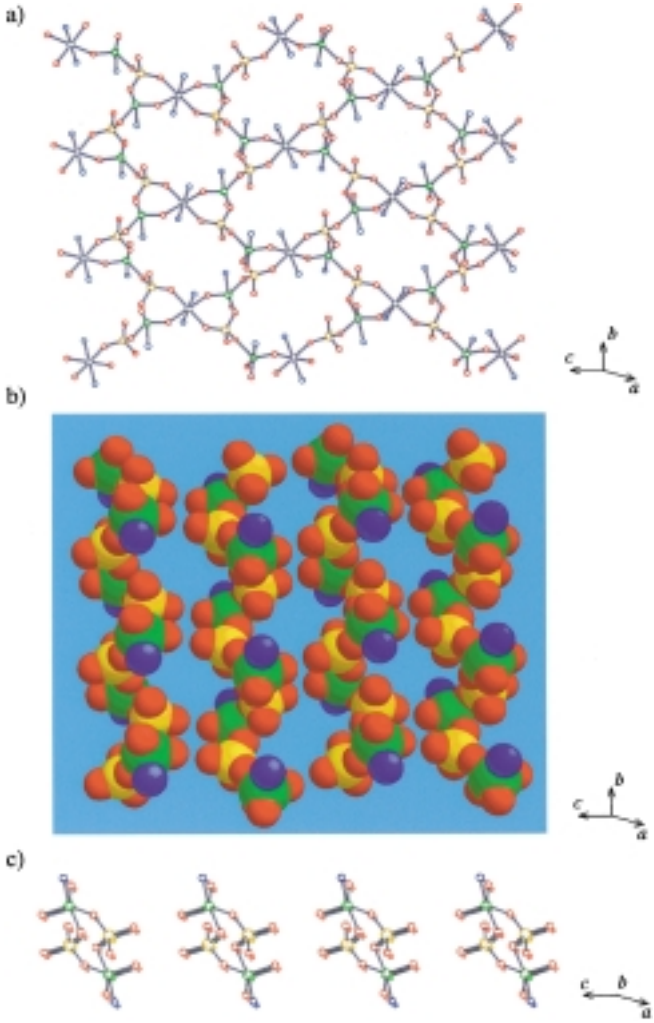


Figure 1. a) View of the structure of the M/V/P/O layer. b) View of the space-filling plot of the left-helical and right-helical V-P-O chains. c) View of the V-P-O helix along the *b* axis. Color code: M (Co or Ni): gray; V: green; P: yellow; O: red; N: blue.

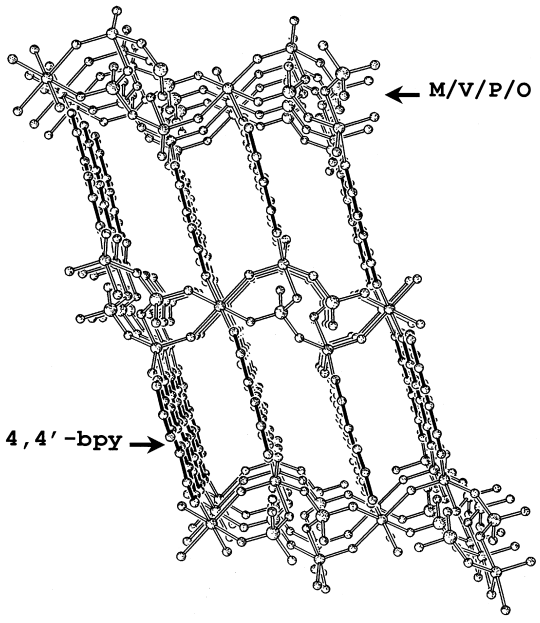


Figure 2. View of the structure of **1** and **2** along the (101) plane, showing the channels.

other compounds. The formation of the helix in the structure may be partly due to the introduction of an extra-force from the $[M(4,4'\text{-bpy})_2]$ fragment. The interaction of the $[M(4,4'\text{-bpy})_2]$ fragment with each vanadium atom on the helical chains may be very important for stabilizing the helix. Moreover, in the (101) plane the M-O-V and M-O-P units form an angle of about 48.5° with the M-N ≈ N-V connection line; this is necessary for building up the helix.

The structures of the two novel inorganic–organic hybrid compounds reported herein not only contain helical chains, but also possess left-handed and right-handed helical chains in one compound. These compounds could be important in terms of the rational synthesis and properties of helical inorganic–organic compounds.

Experimental Section

The syntheses were performed in 20-mL Teflon-lined stainless steel vessels filled to 50% at room temperature.

1: A mixture of $NaVO_3 \cdot H_2O$ (0.158 g), $NaH_2PO_4 \cdot H_2O$ (0.156 g), $Co(NO_3)_2 \cdot H_2O$ (0.291 g), 4,4′-bpy · H_2O (0.192 g), and H_2O in a molar ratio 1:1:1:1:556 was heated at 160 °C for five days. This gave dark red columnar crystals of **1**. Elemental analysis (%) calcd for $C_{20}H_{18}N_4CoV_2P_2O_{12}$: C 32.95, H 2.49, N 7.68, Co 8.08, P 8.50, V 13.97; found: C 32.79, H 2.60, N 7.51, Co 8.11, P 8.62, V 13.82; IR (KBr pellet): $\tilde{\nu} = 1610$ (s), 1537 (m), 1489 (m), 1410 (s), 1304 (m), 1215 (m), 1142 (s), 1078 (m), 1026 (s), 1010 (s), 966 (s), 941 (s), 909 (s), 817 (s), 724 (m), 640 (s), 588 (m), 568 (m), 528 (s), 491 (m), 476 (m), 433 (m) cm^{-1}. Thermogravimetric analysis showed a weight loss of about 44% in the range from 380–520 °C in air corresponding to the removal of 4,4′-bipyridine and the removal of H_2O from HPO_4.

2: A mixture of $NaVO_3 \cdot H_2O$ (0.158 g), $NaH_2PO_4 \cdot H_2O$ (0.156 g), $Ni(NO_3)_2 \cdot H_2O$ (0.291 g), 4,4′-bipy · H_2O (0.192 g), and H_2O in a molar ratio 1:1:1:1:556 was heated at 160 °C for five days. This gave dark red blocks of **2**. Elemental analysis (%) calcd for $C_{20}H_{18}N_4NiV_2P_2O_{12}$: C 32.96, H 2.49, N, 7.69, Ni 8.05, P 8.50, V 13.98; found: C 32.83, H 2.58, N 7.75, Ni 8.00, P 8.61, V 13.84; IR data and results of thermogravimetric analysis were similar to those of **1**.

Received: February 28, 2000 [Z14777]

[1] a) C. L. Bowes, G. A. Ozin, *Adv. Mater.* **1996**, *8*, 13–28; b) S. Kitagawa, M. Kondo, *Bull. Chem. Soc. Jpn.* **1998**, *71*, 1739–1753; c) S. S.-Y. Chui, S. M.-F. Lo, J. P. H. Charmant, A. G. Orpen, I. D. Williams, *Science* **1999**, *283*, 1148–1150; d) C. R. Kagan, D. B. Mitzi, C. D. Dimitrakopoulos, *Science* **1999**, *286*, 945–947; e) P. S. Halasyamani, M. J. Drewitt, D. O'Hare, *Chem. Commun.* **1997**, 867–868; f) P. J. Hagrman, D. Hagrman, J. Zubieta, *Angew. Chem.* **1999**, *111*, 2798–2848; *Angew. Chem. Int. Ed.* **1999**, *38*, 2638–2684, and references therein.

[2] K. H. Lii, Y. F. Huang, *Inorg. Chem.* **1999**, *38*, 1348–1350.

[3] a) Y. Zhang, J. R. D. DeBord, C. J. O'Connor, R. C. Haushalter, A. Clearfield, J. Zubieta, *Angew. Chem.* **1996**, *108*, 1067–1069; *Angew. Chem. Int. Ed. Engl.* **1996**, *35*, 989–991; b) J. R. D. DeBord, Y. Zhang, R. C. Haushalter, J. Zubieta, C. J. O'Connor, *J. Solid State Chem.* **1996**, *122*, 251–258; c) P. J. Zapf, C. J. Warren, R. C. Haushalter, J. Zubieta, *Chem. Commun.* **1997**, 1543–1544; d) J. R. D. DeBord, R. C. Haushalter, L. M. Meyer, D. J. Rose, P. J. Zapf, J. Zubieta, *Inorg. Chim. Acta* **1997**, *256*, 165–168; e) P. J. Zapf, R. P. Hammond, R. C. Haushalter, J. Zubieta, *Chem. Mater.* **1998**, *10*, 1366–1373; f) D. Hagrman, P. J. Zapf, J. Zubieta, *Chem. Commun.* **1998**, 1283–1284; g) L. M. Zheng, J. S. Zhao, K. H. Lii, L. Y. Zhang, Y. Liu, X. Q. Xin, *J. Chem. Soc. Dalton Trans.* **1999**, 939–943; h) Z. Shi, L. Zhang, G. Zhu, J. Hua, H. Ding, S. Feng, *Chem. Mater.* **1999**, *11*, 3565–3570.

[4] a) D. Hagrman, C. Zubieta, D. J. Rose, J. Zubieta, R. C. Haushalter, *Angew. Chem.* **1997**, *109*, 904–907; *Angew. Chem. Int. Ed. Engl.* **1997**,

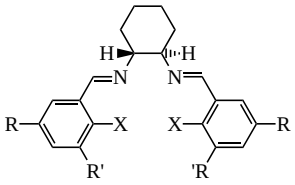
 © WILEY-VCH Verlag GmbH, D-69451 Weinheim, 2000 1433-7851/00/3913-2326 $ 17.50+.50/0

36, 873–876; b) D. Hagrman, R. C. Haushalter, J. Zubieta, *Chem. Mater.* **1998**, *10*, 361–365; c) D. Hagrman, C. Sangregorio, C. J. O'Connor, J. Zubieta, *J. Chem. Soc. Dalton Trans.* **1998**, 3707–3709.
[5] V. Soghomonian, Q, Chen, R. C. Haushalter, J. Zubieta, C. J. O'Connor, *Science* **1993**, *259*, 1596–1599.
[6] K. H. Lii, *J. Chem. Soc. Dalton. Trans.* **1996**, 815–818.
[7] J. Lu, Y. Xu, N. K. Goh, L. S. Chia, *Chem. Commun.* **1998**, 2733–2734.
[8] a) K. Nozaki, T. Terakawa, H. Takaya, T. Hiyama, *Angew. Chem.* **1998**, *110*, 138–140; *Angew. Chem. Int. Ed.* **1998**, *37*, 131–133; b) T. E. Gier, X. Bu, P. Feng, G. D. Stucky, *Nature* **1998**, *395*, 154–157; c) K. Biradha, C. Seward, M. J. Zaworotko, *Angew. Chem.* **1999**, *111*, 584–587; *Angew. Chem. Int. Ed.* **1999**, *38*, 492–495.
[9] a) Z. Bircsak, A. K. Hall, W. T. A. Harrison, *J. Solid State Chem.* **1999**, *142*, 168–173; b) Y. Lu, R. C. Haushalter, J. Zubieta, *Inorg. Chim. Acta* **1998**, *268*, 257–261, and references therein; c) Z. Bircsak, W. T. A. Harrison, *J. Solid State Chem.* **1998**, *140*, 272–277; d) M. Schindler, W. H. Baur, *Angew. Chem.* **1997**, *109*, 88–90; *Angew. Chem. Int. Ed. Engl.* **1997**, *36*, 91–93; e) V. Soghomonian, Q. Chen, R. C. Haushalter, J. Zubieta, *Angew. Chem.* **1993**, *105*, 601–603; *Angew. Chem. Int. Ed. Engl.* **1993**, *32*, 610–612.
[10] Crystal structure analysis: The data were collected at 293(2) K on a Bruker SMART-CCD diffractometer (graphite-monochromated $Mo_{K\alpha}$-radiation: $\lambda = 0.71073$ Å). The structures were solved by direct methods (SHELXTL Version 5.10) and refined by full-matrix least-squares on F^2. All non-hydrogen atoms were refined anisotropically. Crystal data for $C_{20}H_{18}N_4CoP_2V_2O_{12}$ (**1**): Crystal dimensions $0.170 \times 0.070 \times 0.070$ mm, monoclinic, space group *C*2/c (no. 15), $a = 25.1399(15)$, $b = 8.1532(5)$, $c = 15.6510(10)$ Å, $\beta = 127.0030(10)^\circ$, $V = 2561.9(3)$ Å^3. $Z = 4$, $\rho_{calcd} = 1.890$ g cm^{-3}, $\mu(Mo_{K\alpha}) = 1.552$ mm^{-1}. Of the 6086 reflections measured ($2.60 \le \theta \le 23.24^\circ$), 1832 symmetry-independent reflections were used to solve the structure. Based on all these data and 223 refined parameters, $R1 = 0.0349$ (all data), $wR2 = 0.0824$, and goodness-of-fit on F^2 is 1.039. Crystal data for $C_{20}H_{18}N_4NiP_2V_2O_{12}$ (**2**): Crystal dimensions $0.160 \times 0.080 \times 0.050$ mm, monoclinic, space group *C*2/c (no. 15), $a = 25.025(3)$, $b = 8.1660(12)$, $c = 15.610(2)$ Å, $\beta = 127.477(3)^\circ$, $V = 2531.5(6)$ Å^3. $Z = 4$, $\rho_{calcd} = 1.913$ g cm^{-3}, $\mu(Mo_{K\alpha}) = 1.659$ mm^{-1}. Of the 6008 reflections measured ($2.05 \le \theta \le 23.27^\circ$), 1822 symmetry-independent reflections were used to solve the structure. Based on all these data and 223 refined parameters, $R1 = 0.0385$ (all data), $wR2 = 0.0876$, and goodness-of-fit on F^2 is 1.089. Crystallographic data (excluding structure factors) for the structures reported in this paper have been deposited with the Cambridge Crystallographic Data Centre as supplementary publication nos. CCDC-137922 (**1**) and CCDC-137923 (**2**). Copies of the data can be obtained free of charge on application to CCDC, 12 Union Road, Cambridge CB21EZ, UK (fax: (+44) 1223-336-033; e-mail: deposit@ccdc.cam.ac.uk).

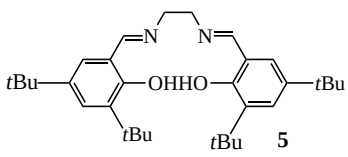
Salen as a Chiral Activator: *anti* versus *syn* Switchable Diastereoselection in the Enantioselective Addition of Crotyl Bromide to Aromatic Aldehydes**

Marco Bandini, Pier Giorgio Cozzi,* and Achille Umani-Ronchi*

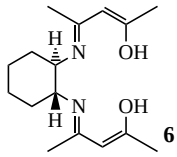
Diastereoselective addition of organometallic reagents is widely used in preparative organic synthesis.[1] The stereochemical outcome of the reaction derives from the ability of the metal to behave as a Lewis acid and therefore to control the addition "via" a cyclic or acyclic transition state. Stereogenic allyl chromium reagents normally add to carbonyl compounds to furnish the corresponding homoallylic alcohols with a high level of *anti* diastereoselection "via" a cyclic Zimmermann–Traxler-type transition state.[2] Moreover, when the above-mentioned nucleophilic addition is performed with a catalytic redox cycle ([Cr] 7 mol%, Mn, Me_3SiCl), the same level of diastereoselection is observed.[3] Herein we report that by changing the amount of the salen ligand (**1**)[4] employed (salen = (*R*,*R*)-*N*,*N*′-bis(3,5-di-*tert*-butylsalicylidene)-1,2-cyclohexanediamine) it is possible to switch the



1: X = OH, R = *t*Bu, R' = *t*Bu;
2: X = OMe, R = *t*Bu, R' = *t*Bu;
3: X = OH, R = *t*Bu, R' = H;
4: X = OH, R = *t*Bu, R' = Br;



5



6

simple diastereoselection from *anti* to *syn* in the catalytic addition of chiral organochromium reagents to aromatic aldehydes. Recently, we described the first enantioselective version of the Nozaki–Hiyama reaction performed in the presence of a catalytic amount of a [Cr(salen)] complex.[5]

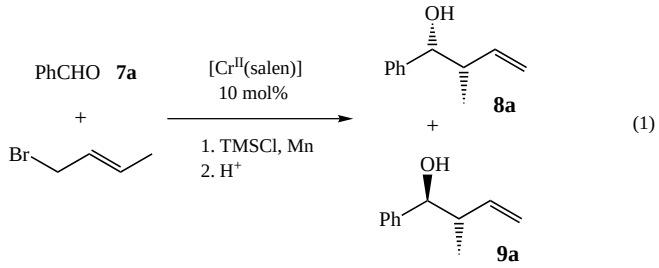
[*] Dr. P. G. Cozzi, Prof. Dr. A. Umani-Ronchi, Dr. M. Bandini
Dipartimento di Chimica "G. Ciamician"
Università di Bologna
Via Selmi, 2, 40126 Bologna (Italy)
Fax: (+390) 51-2099-456
E-mail: pgcozzi@ciam.unibo.it, umani@ciam.unibo.it

[**] We thank the CNR (Rome), M.U.R.S.T. (Rome) "Progetto Stereoselezione in Chimica Organica, Metodologie ed Applicazioni", and the University of Bologna (funds for selected research topics) for financial support of this research.

Supporting information for this article is available on the WWW under http://www.wiley-vch.de/home/angewandte/ or from the author.

 © WILEY-VCH Verlag GmbH, D-69451 Weinheim, 2000 1433-7851/00/3913-2327 $ 17.50+.50/0

Optimal reaction conditions require the preparation of the [Cr^{II}(salen)] catalyst in CH_3CN and the successive oxidative addition of an organohalide. The "in situ" generated organometallic complex was employed in 10 mol% in the presence of Mn and TMSCl to catalyze the addition of allyl chloride to the aldehydes. No reaction was observed when the same protocol was performed with benzaldehyde and (*E*)-crotyl chloride. However, with the more reactive crotyl bromide,[6] we isolated the desired homoallylic alcohol in a satisfactory yield (50%), but with a low degree of distereoselectivity [Eq. 1; *anti*:*syn* = 67:33, **9a** = 5% *ee*, **8a** = 78% *ee*]. After a



(1)

considerable number of trials, we discovered that the amount of salen used was crucial. In fact, good levels of diastereoselectivity and enantioselectivity were obtained with the addition of crotyl bromide to the benzaldehyde by using an excess of the chiral ligand. The simple diastereoselection strictly depends on the amount of salen ligand (Figure 1). The

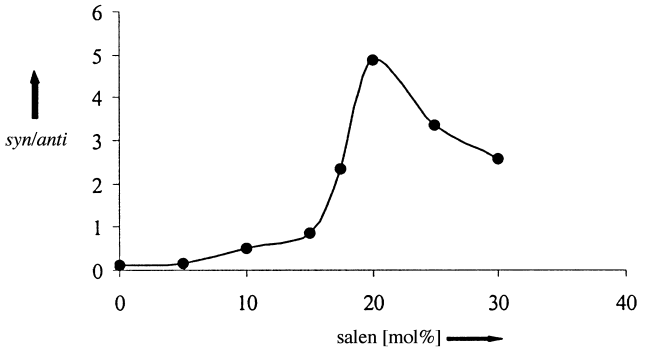


Figure 1. Influence of the amount of salen on the diastereoselectivity of the chromium-catalyzed addition of crotyl bromide to PhCHO.

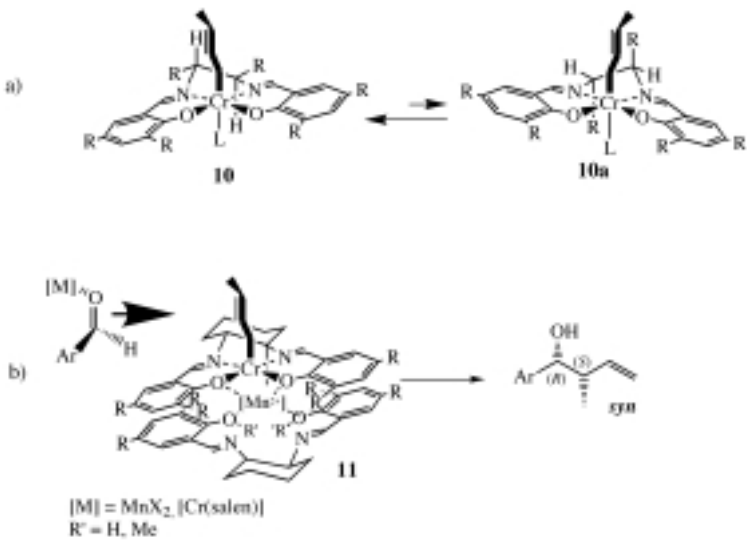
highest diastereoselection (*syn*:*anti* = 83:17) was recorded when a 2:1 salen:chromium salt ratio was utilized (see Supporting Information). Moreover, under these conditions we isolated the *syn* product with excellent enantiomeric excess (ee_{syn} = 89%, ee_{anti} = 36%, Table 1, entry 1). We suggest that the *syn* diastereoselectivity observed can be explained by the formation of an acyclic transition state in which the aldehyde is coordinated by the manganese salts or by a [Cr(salen)] complex. The latter possibility is in accordance with studies by Jacobsen et al., in which it was proven that both [Cr(salen)] and [Co(salen)] catalysts promote asymmetric processes by cooperative mechanisms.[7] Catalytic amounts of coordinating agents,[8] such as DMF, 1,3-dimethylhexahydro-2-pyrimidone (DMPU), 4-(3-phenylpropyl)pyridine *N*-oxide (4-PPNO), phosphorous ligands (Ph_3PO, Ph_3P), and the Schiff bases **4**–**6** structurally correlated to salen, did not afford the same results either in terms of yield or stereoselection (Table 1, entries 4–11).[9] It is important to note that while the simple diastereoselection appears to be strongly correlated to the nature of the additive used, the facial diastereoselection is less affected. This observation is clear evidence of the presence of two competitive mechanisms for the allylation reaction. The singleness of the salen points to the chiral ligand playing a sort of chiral supramolecular recognition.[10] This effect does not appear to be determined by hydrogen-bonding interactions, because the (*R*,*R*)-*N*,*N*′-bis(3,5-di-*tert*-butyl-methoxy-salicylidene)-1,2-cyclohexanediamine (**2**) gives a result similar to **1** (Table 1, entry 2). Probably, a specific noncovalent binding of the chiral organochromium species with another molecule of salen affords this peculiar behavior. At the present time we can only speculate about the probable structure of such an adduct. However, we propose that a previously reported "head to tail" alignment[7a] between the [Cr(III)crotyl(salen)] species and a different molecule of the ligand coordinated with Mn salts could be involved (Scheme 1b). Such a stacking interaction could shift the conformational equilibrium[11] between the speculated nonplanar diastereomeric conformers **10** and **10a** (Scheme 1a). We further suggest that salen preferentially binds to conformer **10** and that the aggregate **11** is responsible for the increase in the stereoselectivity of the process.[12] Moreover, it is noteworthy that this protocol represents the first *syn*-diastereoselective catalytic addition of stereogenic organohalides to aldehydes with chiral organochromium reagents [Eq. (2)]. In fact, the optimized reaction conditions were successfully used with a range of variously substituted

Table 1. Different additives used for modifying the simple diastreoselection in the addition of crotyl bromide to the PhCHO.[a]

Entry	Additive (10 mol%)	Yield [%][b]	**8a**:**9a**[c]	*ee* of **8a** [%][d]	*ee* of **9a** [%][d]
1	**1**	56	83:17	89(1*R*,2*S*)	36(1*S*,2*S*)
2	**2**	40	76:24	88(1*R*,2*S*)	30(1*S*,2*S*)
3	**3**	41	81:19	77(1*R*,2*S*)	22(1*S*,2*S*)
4	**4**	29	56:44	73(1*R*,2*S*)	12(1*S*,2*S*)
5	**5**	20	31:69	48(1*R*,2*S*)	3(1*S*,2*S*)
6	**6**	46	49:51	80(1*R*,2*S*)	11(1*S*,2*S*)
7	DMF	30	59:41	82(1*R*,2*S*)	10(1*S*,2*S*)
8	DMPU	39	53:47	82(1*R*,2*S*)	10(1*S*,2*S*)
9	Ph_3PO	35	62:38	68(1*R*,2*S*)	20(1*S*,2*S*)
10	Ph_3P[e]	39	52:48	90(1*R*,2*S*)	10(1*S*,2*S*)
11	4-PPNO	17	38:62	80(1*R*,2*S*)	0

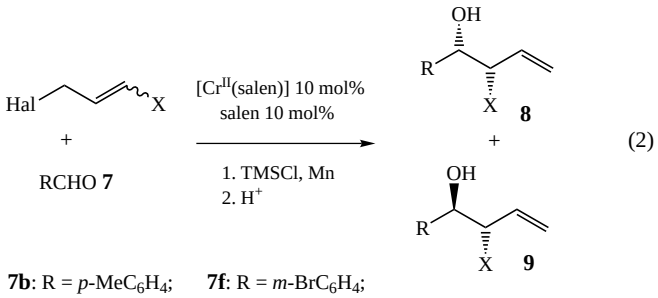
[a] All the reactions were carried out in anhydrous CH_3CN at room temperature. [b] Yield of isolated product after desilylation (HCl/THF) and flash chromatography. The by-product derived from the pinacol coupling was observed. [c] The ratio between **8a** and **9a** was determined by GC analysis of the crude reaction mixture and ^1H NMR analysis after chromatographic purification. [d] Determined by chiral GC analysis of the corresponding *O*-methyl ether. See the Supporting Information for details. The absolute configurations of **8a** and **9a** were assigned by ^1H NMR analysis of the (*R*)-Mosher's esters derivatives (300 MHz, C_6D_6, δ OMe: (1*R*,2*S*) = 3.32, (1*S*,2*R*) = 3.39, (1*R*,2*R*) = 3.22, (1*S*,2*S*) = 3.43); see reference [9]. [e] The reaction was performed employing anhydrous $CrCl_2$ as the chromium source.

 © WILEY-VCH Verlag GmbH, D-69451 Weinheim, 2000 1433-7851/00/3913-2328 $ 17.50+.50/0



Scheme 1. a) Equilibrium mixture of the stepped conformational crotyl(salen)-Cr(III) isomers. b) Plausible approach of an aldehyde to the chiral organochromium complex giving the observed diastereoisomer.

aromatic aldehydes.[13] All the results obtained using the [Cr^{II}(salen)] complex (10 mol%) as the catalyst are summarized in Table 2. Excellent enantiomeric excess values for the *syn* isomers (62–90%) and a good level of diastereoselection (*syn*:*anti* 75:25) were recorded.

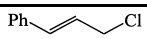
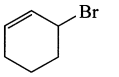
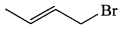


7b: R = *p*-MeC$_6$H$_4$; **7f**: R = *m*-BrC$_6$H$_4$;
7c: R = *p*-FC$_6$H$_4$; **7g**: R = *p*-MeOC$_6$H$_4$;
7d: R = *p*-ClC$_6$H$_4$; **7h**: R = *p*-PhC$_6$H$_4$;
7e: R = *p*-BrC$_6$H$_4$;

In summary, we have shown that high enantio- and diastereoselectivities can be obtained with the [Cr(salen)]-catalyzed addition of stereogenic organohalides to aromatic aldehydes. What is amazing, is the key role played by the amount of chiral ligand in the stereochemical control of the process. In fact, by employing a 10 mol% excess of the Schiff base, complete inversion of the simple diastereoselection *anti* →*syn* was observed. Further studies will be directed at the exploitation of such supramolecolar devices in other [M(salen)]-promoted reactions.

Received: January 12, 2000 [Z14527]

Table 2. Results of the diastereo- and enantioselective addition of organohalides to aromatic aldehydes using chiral [Cr(salen)] catalyst [Eq. (2)].[a]

RCHO	R′X	Yield [%][b]	Product (*syn*:*anti*)[c]	*ee* of *syn* [%][d]	*ee* of *anti* [%][d]
7a		72[e]	75:25[g]	86[g]	26[g]
7a		25[e,f]	75:25[g]	62[g]	25[g]
7b		48	74:26	85(1*R*,2*S*)	26(1*S*,2*S*)
7c	“”	53	74:26	90(1*R*,2*S*)	27(1*S*,2*S*)
7d	“”	46	61:39	82(1*R*,2*S*)	24(1*S*,2*S*)
7e	“”	43	72:28	82(1*R*,2*S*)	28(1*S*,2*S*)
7f	“”	49	66:34	70[h]	43[h]
7g	“”	52	60:40	58(1*R*,2*S*)	15(1*S*,2*S*)
7h	“”	47	71:29[e]	84(1*R*,2*S*)	16(1*S*,2*S*)

[a] Performing the reaction in the presence of $CrCl_3$ as the catalyst (10 mol%), we obtained the *anti* homoallylic alcohols as the major isomer; see Supporting Information. [b] Isolated yield after desilylation (HCl/THF) and flash chromatography. By-products derived from the pinacol coupling reaction were detected by GC analysis. [c] Determined by GC analysis of the crude reaction mixture and ^{1}H NMR analysis after chromatographic purification. [d] Determined by chiral GC analysis of the corresponding *O*-methyl ether. See the Supporting Information for details. The absolute configurations of **8** and **9** were assigned by analogy to the chiral GC analysis of the **8a**/**9a** mixture. [e] Isolated yield after desilylation (Bu_4NF/THF) and flash chromatography. [f] The low yield obtained was derived from the high instability of the chiral organochromium intermediate. In fact, a large amount of bicyclohexyl-2,2′-diene (coupling product) was detected from the MS-GC analysis. [g] Determined by chiral HPLC analysis (Chiralcel OD column). [h] Determined by ^{1}H NMR analysis of the (*S*)-(+)-*O*-acetyl-mandelic ester. See the Supporting Information for details.

[1] J. Mulzer in *Comprehensive Asymmetric Chemistry*, *Vol.1* (Eds.: E. N. Jacobsen, A. Pfaltz, H. Yamamoto), Springer, **1999**, pp. 35–97.
[2] A. Fürstner, *Chem. Rev.* **1999**, *99*, 991–1046, and references therein.
[3] A. Fürstner, N. Shi, *J. Am. Chem. Soc.* **1996**, *118*, 12349–12357.
[4] For the use of chiral [M(salen)] complexes in asymmetric catalysis, see: L. Canali, D. C. Sherrington, *Chem. Soc. Rev.* **1998**, *28*, 85–94, and references therein.
[5] M. Bandini, P. G. Cozzi, P. Melchiorre, A. Umani-Ronchi, *Angew. Chem.* **1999**, *111*, 3558–3561; *Angew. Chem. Int. Ed.* **1999**, *38*, 3357–3359.
[6] Commercially available crotyl bromide (85% tech.) was used.
[7] a) R. G. Konsler, J. K. Karl, E. N. Jacobsen, *J. Am. Chem. Soc.* **1998**, *120*, 10780–10781; b) M. H. Wu, K. B. Hansen, E. N. Jacobsen, *Angew. Chem.* **1999**, *111*, 2167–2170; *Angew. Chem. Int. Ed.* **1999**, *38*, 2012–2014.
[8] For the role of nonchiral additives and cocatalysts in catalytic asymmetric processes, see: E. M. Vogl, H. Gröger, M. Shibasaki, *Angew. Chem.* **1999**, *111*, 1671–1680; *Angew. Chem. Int. Ed.* **1999**, *38*, 1570–1577; for other interesting applications concerning the use of chiral activators in asymmetric catalysis, see: K. Mikami, S. Matsukawa, *Tetrahedron: Asymmetry* **1995**, *6*, 2571–2574; K. Mikami, S. Matsukawa, *Enantiomer* **1996**, *1*, 69–73; K. Mikami, S. Matsukawa, *Nature* **1997**, *385*, 613–615.
[9] D. R. Kelly, *Tetrahedron: Asymmetry* **1999**, *10*, 2927–2934.
[10] J.-M. Lehn, *Angew. Chem.* **1990**, *102*, 1347–1362; *Angew. Chem. Int. Ed. Engl.* **1990**, *29*, 1304–1319.
[11] It is well accepted that oxo(salen)manganese(v) and azide(salen)-chromium(III) complexes exist in an equilibrium mixture of two enantio- or diastereomeric conformers: Y. N. Ito, T. Katsuki, *Bull. Chem. Soc. Jpn.* **1999**, *72*, 603–619, and references therein. On the basis of the similar stepped structures of the oxo(salen)chromium complexes reported, we assumed that an analogous conformational equilibrium could involve the crotyl(salen)chromium(III) adduct **10**, see: E. G. Samsel, K. Srinivasan, J. K. Kochi, *J. Am. Chem. Soc.* **1985**, *107*, 7606–7617; K. B. Hansen, J. L. Leighton, E. N. Jacobsen, *J. Am. Chem. Soc.* **1996**, *118*, 10924–10925.

 © WILEY-VCH Verlag GmbH, D-69451 Weinheim, 2000 1433-7851/00/3913-2329 $ 17.50+.50/0

[12] For studies concerning the influence of additives on the geometry and reactivity of [Mn(salen)] and [Cr(salen)] complexes, see: a) T. Hashihayata, T. Punniyamurthy, R. Irie, T. Katsuki, M. Akita, Y. Moro-oka, *Tetrahedron* **1999**, *55*, 14599–14610; b) K. M. Ryan, C. Bousquet, D. G. Gilheany, *Tetrahedron Lett.* **1999**, *40*, 3613–3616; c) A. M. Daly, C. T. Dalton, M. F. Renehan, D. G. Gilheany, *Tetrahedron Lett.* **1999**, *40*, 3617–3620.

[13] The amount of salen employed with enolizable aliphatic aldehydes does not significantly influence the diastereoselectivity of the reaction (salen 20 mol%, crotyl bromide): *n*-octylaldehyde *anti*:*syn* 71:29 (ee_{anti} = N.D., ee_{syn} = 85%), cyclohexylcarbaldehyde *anti*:*syn* 85:15 (ee_{anti} = 0%, ee_{syn} = 70%), hydrocinnamaldehyde *anti*:*syn* 79:21 (ee_{anti} = 63%, ee_{syn} = 87%).

A Designed β-Hairpin Containing a Natural Hydrophobic Cluster**

Juan F. Espinosa and Samuel H. Gellman*

β-Sheets are a very common substructure in folded proteins,[1] and intermolecular sheet-type interactions play a crucial role in protein–protein recognition[2] and in pathological protein aggregation.[3] Therefore, understanding the balance of noncovalent forces that controls β-sheet formation is a goal of fundamental importance. Recently it has become possible to probe the origins of antiparallel β-sheet stability with short, designed peptides that fold autonomously in aqueous solution.[4] These model systems complement the more traditional approach of examining β-sheets that are embedded within a particular tertiary fold;[5] short peptides allow one to explore small increments of β-sheet in the absence of a specific structural context. Here, we describe a peptide in which a cluster of hydrophobic sidechains from the protein GB1 has been grafted onto a designed sequence. Thermodynamic analysis of folding provides insight on the origins of β-sheet stability.

The "β-hairpin" architectural motif, comprised of two antiparallel strands and a short connecting loop, is essential for creation of short peptides that display antiparallel β-sheet folding in water.[4] β-Hairpins are common in proteins,[6] but natural β-hairpin sequences seldom fold in water when extracted from their native protein context.[4] An exception is a 16-residue segment of the protein GB1, **1**, which displays partial population of a native-like β-hairpin conformation.[7] Peptide **1** differs from other autonomously folding β-hairpins

Gly-Ile-Trp-Thr-Tyr-Asp-Asp-Ala-Thr-Lys-Thr-Phe-Thr-Val-Thr-Glu

1

in the unusually large six-residue loop (Asp-Asp-Ala-Thr-Lys-Thr) that connects the two strand segments; other autonomously folding β-hairpins contain loops of two to four residues.[4, 8] Interstrand interactions within the folded conformation of **1** are limited to residues near the termini.[7] Clustering among the hydrophobic sidechains of Trp 3, Tyr 5, Phe 12, and Val 14 presumably provides a drive for β-hairpin folding, which overcomes the entropic cost of ordering the loop segment.

In order to elucidate the contribution of interstrand sidechain interactions to β-sheet stability, we incorporated the residues of the GB1 cluster into a 12-residue sequence, **2**,[9] that was expected to adopt a more highly defined β-hairpin conformation than does **1**. The arrangement of the Trp, Tyr,

Arg-Trp-Gln-Tyr-Val-Xxx-Gly-Lys-Phe-Thr-Val-Gln-NH_2

2, Xxx = D-Pro
3, Xxx = L-Pro

Phe, and Val residues in **2** allows native-like sidechain juxtapositions if the peptide folds to a β-hairpin conformation with a tight two-residue loop; the D-Pro–Gly segment strongly promotes this type of β-hairpin.[8e, 8g, 10] Our design hypothesis was that the mutually reinforcing effects of the D-Pro–Gly loop and the GB1 cluster in **2** would produce a β-hairpin conformation well-defined over most residues and, therefore, suitable for thermodynamic analysis. Diastereomer **3**, with D-Pro replaced by L-Pro, was expected to serve as a negative control, since L-Pro-Gly discourages formation of tight β-hairpin conformations.[8, 10]

Peptide **2** displays numerous NOE interactions between residues that are not adjacent in sequence, and all of these nonadjacent effects are consistent with the β-hairpin conformation shown in Figure 1. The subset of interstrand NOE interactions involving backbone protons (NH and H_α; Figure 1a, b) verifies antiparallel β-sheet formation at the backbone level. Sidechain–sidechain NOE data (Figure 1c) reveal the anticipated clustering among the GB1 sidechains. No interactions between nonadjacent residues were observed for L-Pro diastereomer **3**, which demonstrates that changing the proline configuration constitutes an "on/off" switch for β-hairpin formation in aqueous solution. The solution structure of **2** was calculated with the program DYANA,[11] using 37 NOE measurements (including all effects between nonadjacent residues) as distance restraints. Among the 20 best structures, the root mean square deviation (RMSD) was 0.58 ± 0.16 Å for the backbone atoms and 1.25 ± 0.22 Å for all heavy atoms, over residues 2–11 (terminal residues 1 and 12 were highly disordered). These results demonstrate that the

[*] Prof. S. H. Gellman, Dr. J. F. Espinosa
Department of Chemistry
University of Wisconsin
1101 University Avenue, Madison, WI 53706 (USA)
Fax: (+1) 608-265-4534
E-mail: gellman@chem.wisc.edu

[**] This research was supported by the National Science Foundation (CHE-9820952). J.F.E. was supported by a fellowship from the Ministerio de Educacion y Cultura (Spain) and the Fulbright Commission. The mass spectrometer was purchased in part with a National Science Foundation grant (CHE-9520868), and the NMR spectrometers were purchased in part with a National Institute Of Health grant (1 S10 RR04981). The CD spectrometer and analytical ultracentrifuge are part of the UW Biophysics Instrumentation Facility (NSF BIR-9512577).

 © WILEY-VCH Verlag GmbH, D-69451 Weinheim, 2000 1433-7851/00/3913-2330 $ 17.50+.50/0

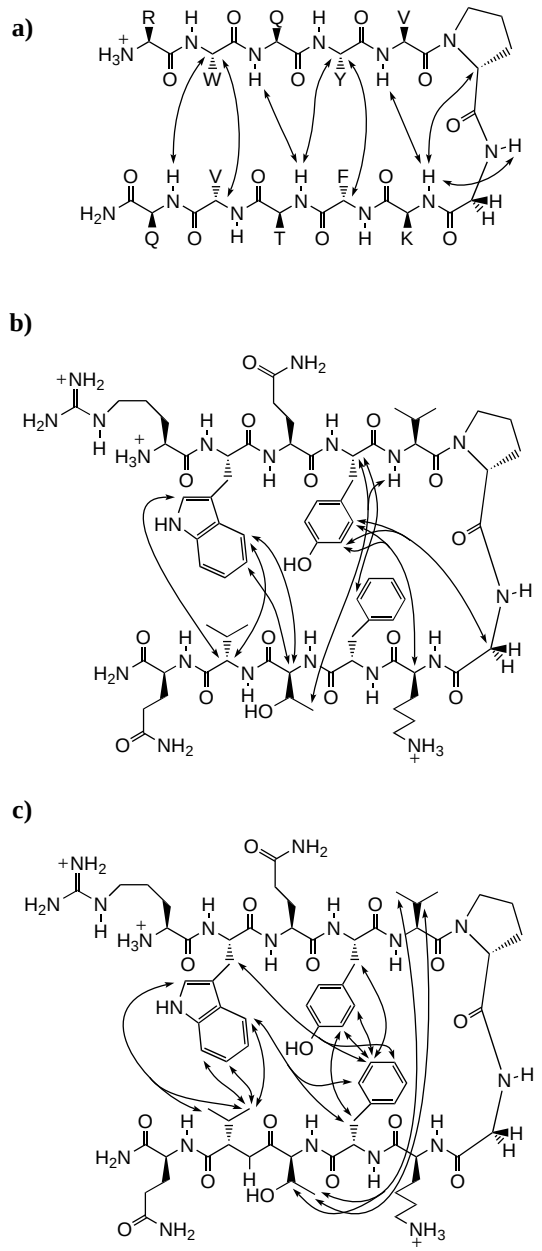


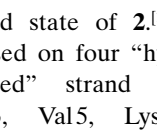
Figure 1. Summary of long-range NOE interactions observed in ROESY analysis for **2** (1.6 mM) in aqueous sodium deuteroacetate buffer (100 mM; H_2O:D_2O 9:1 or D_2O), at pH 3.8 (uncorrected) and 276 K. a) Backbone–backbone NOE interactions (NH–NH, NH–H_α, and H_α–H_α). b) Backbone–sidechain NOE interactions. c) Sidechain–sidechain NOE interactions. Resonance assignments were obtained from a combination of COSY, TOCSY, NOESY, and ROESY data at 500 MHz. Additional ROESY data were obtained at 750 MHz. Analytical ultracentrifugation showed that **2** does not self-associate under the conditions used for NMR structural analysis.

unnatural D-proline residue in the loop promotes native-like pairing of antiparallel β-strands.

NMR data indicate that the extent of β-hairpin folding is comparable at several different sites within **2**, and that the β-hairpin population changes in a coordinated way as a function of temperature throughout the peptide. Thus, β-hairpin formation appears to be cooperative, and we can use a two-state model (unfolded versus β-hairpin) to analyze thermal effects on folding.

NOE data provide two independent estimates for the β-hairpin population of **2**. The intensities of interstrand H_α–H_α NOE interactions between laterally aligned residues[12] can be used to estimate β-hairpin population if one assumes that there is a fixed H_α–H_α separation in the folded state (2.3 Å) and no contribution to NOE intensity from the unfolded state.[13] We calculate that, at 3 °C, **2** has 54% β-hairpin population based on the $H_\alpha4$–$H_\alpha9$ NOE measurement and 76% based on the $H_\alpha2$–$H_\alpha11$ NOE data. These two populations are in reasonably good agreement, given the intrinsic limitations of the NOE-based approach. (Small differences between assumed and actual H–H separations in the folded state lead to large errors because the NOE intensity varies as the inverse sixth power of H–H separation.[12]) The fact that the NOE near the termini is slightly more intense than the NOE near the turn indicates that the hairpin is well-defined over most of its length.

Hα chemical shifts ($\delta_{H\alpha}$) offer an independent basis for population quantification[4, 14] because $\delta_{H\alpha}$ values are highly sensitive to the local secondary structure.[15] This approach requires $\delta_{H\alpha}$ data for each of the two limiting states of **2**, unfolded and β-hairpin, since equilibration is rapid on the NMR time scale. The L-Pro diastereomer **3** provides $\delta_{H\alpha}$ data for the fully unfolded state of **2**, and cyclic peptide **4** serves as a model for the completely folded state of **2**.[14, 16] We focused on four "hydrogen-bonded" strand residues, Gln3, Val5, Lys8, and Thr10. Populations deduced at these four sites[17] vary in a coordinated way as a function of temperature (Figure 2). The α-protons of these residues point away from the opposite



4

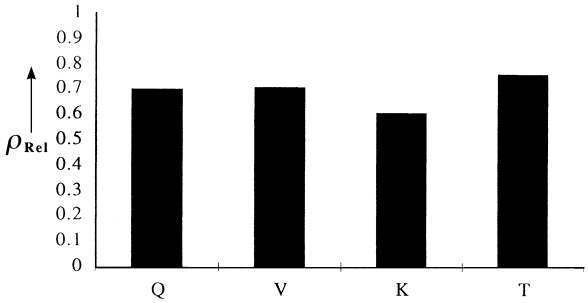


Figure 2. Relative population of the β-hairpin conformation (ρ_{Rel})of **2** at 321 K versus 276 K, as determined from $\delta_{H\alpha}$ data at four hydrogen bonded strand residues, Gln3 (Q), Val5 (V), Lys8 (K), and Thr10 (T).

strand in the β-sheet conformation, and these $\delta_{H\alpha}$ values should therefore be less susceptible than $\delta_{H\alpha}$ values of the "non-hydrogen-bonded" strand residues to secondary effects from the aromatic sidechains on the adjacent strand. Indeed, the $\delta_{H\alpha}$ values of Phe9 and Val11 display an upfield shift relative to unfolded reference **3**, rather than the expected downfield shift,[15] as a result of anisotropic effects of the Trp2 and Tyr4 sidechains that are brought into proximity by β-hairpin formation.[18, 19]

ΔH°, ΔS°, and ΔC_p° for β-hairpin formation by **2** were estimated from $\delta_{H\alpha}$ data obtained between 275 K and 315 K (Figure 3). An average β-hairpin population was determined

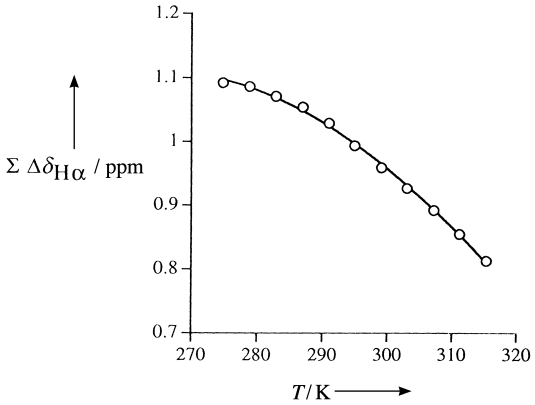


Figure 3. Use of variable-temperature NMR chemical shift data ($\delta_{\alpha H}$) to estimate folding thermodynamics for β-hairpin **2**. $\Sigma\Delta\delta_{H\alpha}$ is the sum of the α-proton chemical shifts for four strand residues in hydrogen-bonded positions, Gln3, Val5, Lys8, and Thr10, for **2**, minus the analogous sum for unfolded reference **3**, at the indicated temperature. These data were fitted to the equation $\Sigma\Delta\delta_{H\alpha} = \Sigma\Delta\delta_{H\alpha limit}[\exp(x/RT)]/[1+\exp(x/RT)$, where $x = [T(\Delta S^\circ_{298} + \Delta C^\circ_p \ln(T/298)) - (\Delta H^\circ_{298} + \Delta C^\circ_p(T-298)]$ and $\Sigma\Delta\delta_{H\alpha limit} = \Sigma\Delta\delta_{H\alpha}(\mathbf{4}) - \Sigma\Delta\delta_{H\alpha}(\mathbf{3})$. This analysis is based on Ref. [20]. The resulting ΔH°, ΔS°, and ΔC°_p values are given in the text.

at each temperature by using the sum of $\delta_{H\alpha}$ values for Gln3, Val5, Lys8, and Thr10 in **2** and in reference peptides **3** and **4**.[17–19] The β-hairpin population was calculated to be 61% at 275K (consistent with NOE-based populations discussed above) and 45% at 315K. A previously reported nonlinear fitting method[20] was used to estimate thermodynamic parameters for the two-state equilibrium (unfolded versus β-hairpin) from the temperature-dependent $\delta_{H\alpha}$ data. This analysis gave $\Delta H^\circ = -3.2 \pm 0.1$ kcal mol^{-1}, $\Delta S^\circ = -10.2 \pm 0.2$ cal K^{-1} mol^{-1}, and $\Delta C^\circ_p = -98 \pm 8$ cal K^{-1} mol^{-1} (the uncertainties arise from the fitting).[21]

The thermodynamic profile deduced for the folding of **2** differs qualitatively from that reported for **5**, a designed peptide that adopts a β-hairpin conformation with a two-residue loop at Asn–Gly.[20] At 298K, the folding of **5** in

Lys-Lys-Tyr-Thr-Val-Ser-Ile-Asn-Gly-Lys-Lys-Ile-Thr-Val-Ser-Ile

5

aqueous solution is enthalpically unfavorable ($\Delta H^\circ = +1.7$ kcal mol^{-1}) and entropically favorable ($\Delta S^\circ = +5.5$ cal K^{-1} mol^{-1}), and formation of this β-hairpin involves a large negative change in heat capacity ($\Delta C^\circ_p = -330$ cal K^{-1} mol^{-1}). This thermodynamic profile is consistent with a classical hydrophobic driving force for β-hairpin formation.[20, 22] In contrast, the thermodynamic profile of β-hairpin folding for **2** does not conform to expectations for a purely hydrophobic driving force, since the process is enthalpically favorable and entropically unfavorable at 298K. The negative ΔC°_p for **2**, however, suggests a classical hydrophobic component to β-hairpin stabilization.[22]

Many lines of evidence indicate that dehydration of hydrophobic surfaces in the folded state provides a major source of protein conformational stability.[22, 23] The data for **2** are interesting because the thermodynamic profile suggests that classical hydrophobic interactions alone are not the major driving force for folding, despite the clustering of the four GB1 nonpolar sidechains. Interstrand hydrogen bonds formed in the β-hairpin state of **2** might explain the ΔH° and ΔS° data for the folding of this peptide,[24] but these contributions, if dominant, should have been evident in the folding of β-hairpin **5** as well.[20, 25] The thermodynamic differences between β-hairpin formation by **2** and **5** can be reconciled through a hypothesis of Diederich et al.,[26] who proposed that tight and loose interactions between nonpolar entities in aqueous solution lead to qualitatively different thermodynamic profiles. The classical hydrophobic signature, involving an entropic driving force at 298K, was proposed to correspond to a loose interaction, while an enthalpic driving force at 298K was proposed to result from a tight interaction.[26] Thus, it is possible that the folded state of **2** allows tighter association among nonpolar sidechains than does the folded state of **5**. In this regard, the higher proportion of aromatic sidechains in **2** relative to **5** may be significant, since it has been argued that aromatic groups have a greater intrinsic affinity for other nonpolar groups than do aliphatic groups.[27]

We have shown that transplantation of a nonpolar sidechain cluster from a β-sheet in a folded protein to a short designed peptide (**2**) generates a well-defined β-hairpin conformation as judged by both backbone and sidechain NMR indicators. These results demonstrate that the tight β-hairpin backbone conformation induced by the D-Pro-Gly segment is compatible with the well-defined cluster of hydrophobic sidechains observed in the protein GB1. Further analysis of the differences between **2** and previously reported β-hairpin **5**[20] should shed additional light on the origins of β-sheet stability; the differences themselves underscore the importance of studying multiple model β-sheet systems.

Received: January 10, 2000 [Z14514]

[1] C. L. Nesloney, J. W. Kelly, *Bioorg. Med. Chem.* **1996**, *4*, 739.
[2] See, for example: W. S. Somers, S. E. V. Philips, *Nature* **1992**, *359*, 387.
[3] J. W. Kelly, *Curr. Opin. Struct. Biol.* **1998**, *8*, 101; P. T. Lansbury, *Acc. Chem. Res.* **1996**, *29*, 317.
[4] For leading references, see: a) F. Blanco, M. Ramírez-Alvarado, L. Serrano, *Curr. Opin. Struct. Biol.* **1998**, *8*, 107; b) S. H. Gellman, *Curr. Opin. Chem. Biol.* **1998**, *7*, 717; c) E. Lacroix, T. Kortemme, M. L. de la Paz, L. Serrano, *Curr. Opin. Struct. Biol.* **1999**, *9*, 487; d) E. de Alba, J. Santoro, M. Rico, M. A. Jiménez, *Protein Sci.* **1999**, *8*, 854; f) S. R. Griffiths-Jones, A. J. Maynard, M. S. Searle, *J. Mol. Biol.* **1999**, *292*, 1051.
[5] a) C. K. Smith, L. Regan, *Acc. Chem. Res.* **1997**, *30*, 153; b) E. Ilyina, V. Roongta, K. H. Mayo, *Biochemistry* **1997**, *36*, 5245.
[6] a) B. L. Sibanda, J. M. Thornton, *Nature* **1985**, *316*, 170; b) B. L. Sibanda, T. L. Blundell, J. M. Thornton, *J. Mol. Biol.* **1989**, *206*, 759; c) B. L. Sibanda, J. M. Thornton, *J. Mol. Biol.* **1993**, *229*, 428; d) K. Gunasekaran, F. Ramakrishnan, P. Balaram, *Protein Eng.* **1997**, *10*, 1131.
[7] F. J. Blanco, G. Rivas, L. Serrano, *Nat. Struct. Biol.* **1994**, *1*, 584.
[8] Representative linear peptides that fold to β-hairpin conformations in aqueous solution: a) F. J. Blanco, M. A. Jiménez, J. Herranz, M. Rico, J. Santoro, J. L. Nieto, *J. Am. Chem. Soc.* **1993**, *115*, 5887; b) M. S. Searle, D. H. Williams, L. C. Rackman, *Nat. Struct. Biol.* **1995**, *2*, 999; c) M. Ramírez-Alvarado, F. J. Blanco, L. Serrano, *Nat. Struct. Biol.* **1996**, *3*, 604; d) E. de Alba, M. A. Jimenez, M. Rico, *J. Am. Chem. Soc.* **1997**, *119*, 175; e) T. S. Haque, S. H. Gellman, *J. Am. Chem. Soc.* **1997**, *119*, 2303; f) A. J. Maynard, M. S. Searle, *Chem. Commun.* **1997**, 1297; g) H. E. Stanger, S. H. Gellman, *J. Am. Chem. Soc.* **1998**, *120*, 4236;

 © WILEY-VCH Verlag GmbH, D-69451 Weinheim, 2000 1433-7851/00/3913-2332 $ 17.50+.50/0

h) Cyclic peptides: J. M. McDonnell, D. Fushman, S. M. Cahill, B. J. Sutton, D. Cowburn, *J. Am. Chem. Soc.* **1997**, *119*, 5321; M. Favre, K. Moehle, L. Jiang, B. Pfeiffer, J. A. Robinson, *J. Am. Chem. Soc.* **1999**, *121*, 2679.

[9] Peptides **2**–**4** were synthesized by solid-phase methods and purified by reverse-phase HPLC. The structures were confirmed by matrix-assisted laser desorption/time of flight mass spectrometry (MALDI-TOF MS) and by high-resolution ^{1}H NMR spectroscopy.

[10] a) T. S. Haque, J. C. Little, S. H. Gellman, *J. Am. Chem. Soc.* **1994**, *116*, 4105; b) S. Awasthi, S. Raghothama, P. Balaram, *Biochem. Biophys. Res. Commun.* **1995**, *216*, 375; c) T. S. Haque, J. C. Little, S. H. Gellman, *J. Am. Chem. Soc.* **1996**, *118*, 6975; d) I. L. Karle, S. K. Awasthi, P. Balaram, *Proc. Natl. Acad. Sci. USA* **1996**, *93*, 8189; e) H. L. Schenck, S. H. Gellman, *J. Am. Chem. Soc.* **1998**, *120*, 4869; f) C. Das, S. Raghothama, P. Balaram, *J. Am. Chem. Soc.* **1998**, *120*, 5812; g) S. R. Raghothama, S. K. Awasthi, P. Balaram, *J. Chem. Soc. Perkin Trans. 2* **1998**, 137; h) C. Das, S. Raghothama, P. Balaram, *Chem. Commun.* **1999**, 967.

[11] P. Guntert, C. Mumenthaler, K. Wüthrich, *J. Mol. Biol.* **1997**, *273*, 283.

[12] K. Wüthrich, *NMR of Proteins and Nucleic Acids*, Wiley, New York, **1986**.

[13] Use of $H_\alpha - H_\alpha$ NOE interactions to determine β-hairpin population: a) Ref. [8b]; b) Ref. [8c]; c) E. de Alba, J. Rico, M. A. Jiménez, *Protein Sci.* **1997**, *6*, 2548; d) M. Ramírez-Alvarado, F. J. Blanco, H. Niemann, L. Serrano, *J. Mol. Biol.* **1997**, *273*, 898.

[14] F. A. Syud, J. F. Espinosa, S. H. Gellman, *J. Am. Chem. Soc.* **1999**, *121*, 11577.

[15] a) D. S. Wishart, B. D. Sykes, F. M. Richards, *J. Mol. Biol.* **1991**, *222*, 311; b) D. S. Wishart, B. D. Sykes, F. M. Richards, *Biochemistry* **1992**, *31*, 1647.

[16] We have recently shown that a cyclic 14-residue peptide containing two D-Pro–Gly loop segments, similar to **4**, displays very high population of the β-sheet conformation in aqueous solution (Ref. [14]); analogous behavior was observed for **4** (manuscript in preparation).

[17] The β-hairpin population of **2** was estimated at each indicator residue and temperature by interpolating the $\delta_{H\alpha}$ value for **2** between the $\delta_{H\alpha}$ value for the corresponding residue in unfolded reference **3** at that temperature and the $\delta_{H\alpha}$ value for folded reference **4** at 276 K. (We assume that **4** is maximally folded at low temperature.)

[18] Attempted population analysis based on $\delta_{H\alpha}$ data for the non-hydrogen-bonded strand residues of **2** (Trp 2, Tyr 4, Phe 9, and Val 11) and reference peptides **3** and **4** provides nonsensical results. For example, at 275 K, $\delta_{H\alpha}$ data for Trp 2 imply 180 % β-hairpin population for **2**, while $\delta_{H\alpha}$ data for Phe 9 imply < 0 % β-hairpin population for **2**. We suspect that subtle differences in aromatic sidechain packing between cyclic peptide **4** and the fully folded state of **3** are responsible for these observations. (This hypothesis requires differences of < 0.3 ppm in non-hydrogen-bonded residue $\delta_{H\alpha}$ values between these two systems.) Although **4** appears not to be a fully accurate model for interstrand sidechain packing in the β-hairpin conformation of **3**, we believe that **4** is a good model for the backbone in the β-hairpin conformation of **3** because of the good agreement among data for the four hydrogen-bonded strand residues (Gln 3, Val 5, Lys 8, and Thr 10) and for the Gly residue in the turn (see Ref. [19]).

[19] The folding equilibrium of a designed β-hairpin has been monitored by the chemical shift separation ($\Delta\delta_{H\alpha}$) between the geminal α-protons of a glycine residue in the loop (loop sequence = Asn–Gly): M. S. Searle, S. R. Griffiths-Jones, H. Skinner-Smith, *J. Am. Chem. Soc.* **1999**, *121*, 11615. We estimated the β-hairpin population of **2** by interpolating between $\Delta\delta_{H\alpha}$ values for reference peptides **3** and **4**. This analysis indicated 66 % β-hairpin population for **2** at 275 K, and 56 % at 315 K; these estimates agree well with those obtained from strand residue $\delta_{H\alpha}$ data.

[20] A. J. Maynard, G. J. Sharman, M. S. Searle, *J. Am. Chem. Soc.* **1998**, *120*, 1996.

[21] After this report was submitted for publication, a thermodynamic analysis of β-hairpin formation by GB1-derived peptide **1** appeared: S. Honda, N. Kobayashi, E. Munekata, *J. Mol. Biol.* **2000**, *295*, 269. These authors concluded that β-hairpin formation is enthalpically favorable ($\Delta H = -13$ kcal mol^{-1}) and entropically unfavorable ($\Delta S = -43$ e.u.) near room temperature. The signs of these thermodynamic parameters match the signs of the parameters we deduce for **2**, but the parameters for **1** are approximately fourfold larger. This quantitative difference may arise because of sequence differences between **1** and **2** and/or because Honda et al. assumed $\Delta C_p = 0$ for β-hairpin formation by **2**, which may not be correct.

[22] a) R. L. Baldwin, *Proc. Natl. Acad. Sci. USA* **1986**, *83*, 8069; b) R. S. Spolar, J. H. Ha, M. T. Record, *Proc. Natl. Acad. Sci. USA* **1989**, *86*, 8382; c) J. R. Livingstone, R. S. Spolar, M. T. Record, *Biochemistry* **1991**, *30*, 4237.

[23] a) K. A. Dill, *Biochemistry* **1990**, *29*, 7133; b) W. Blokzijl, J. B. F. N. Engberts, *Angew. Chem.* **1993**, *105*, 1610; *Angew. Chem. Int. Ed. Engl.* **1993**, *32*, 1545.

[24] Leading references on the contributions of hydrogen bonds to the stability of folded peptides and proteins: a) B. A. Shirley, P. Stanssens, U. Hahn, C. N. Pace, *Biochemistry* **1992**, *31*, 725; b) B. P. P. Huyghues-Despointes, T. M. Klinger, R. L. Baldwin, *Biochemistry* **1995**, *34*, 13267; c) M. P. Byrne, R. L. Manuel, L. G. Lowe, W. E. Stites, *Biochemistry* **1995**, *34*, 13949.

[25] β-Hairpin formation by **5** in 50 % aqueous methanol is enthalpically favorable and entropically unfavorable at 298 K, which has been interpreted to indicate that interstrand hydrogen bond formation provides an enthalpic driving force for folding in this mixed solvent (Ref. [20]).

[26] a) D. B. Smithrud, T. B. Wyman, F. Diederich, *J. Am. Chem. Soc.* **1991**, *113*, 5420; b) D. B. Smithrud, F. Diederich, *J. Am. Chem. Soc.* **1990**, *112*, 339.

[27] G. I. Makhatadze, P. L. Privalov, *Biophys. Chem.* **1994**, *50*, 285, and references therein.

Complimentary Polytopic Interactions**

Ekaterina O. Arikainen, Neville Boden, Richard J. Bushby,* Owen R. Lozman, Jeremy G. Vinter, and Andrew Wood

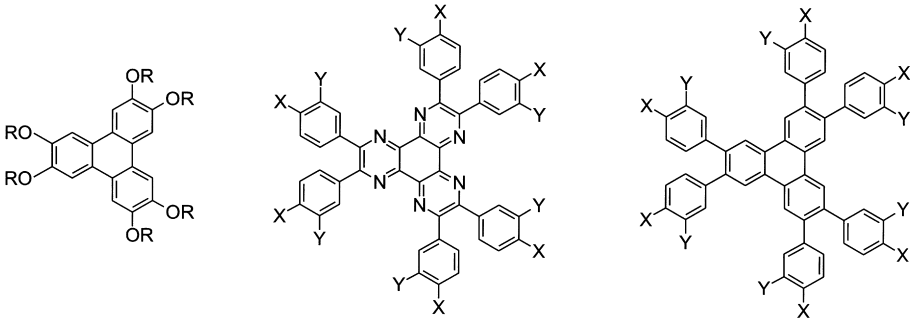
Substantially enhanced mesophase ranges can be obtained by mixing the discotic liquid crystal **1a** with one equivalent of the "larger core" polynuclear aromatic compounds **2a** or **3a** (Scheme 1). The special stability of these novel π-stacked systems is not the result of either charge-transfer or (net) quadrupolar interactions but instead arises from a complimentary polytopic interaction (CPI).

Chemical doping of discotic liquid crystals is well known and, in some cases, it produces enhanced mesophase ranges.[1] Hence, mixtures of the discotic liquid crystal **1a** with 2,4,7-trinitrofluoren-9-one (TNF) have been extensively studied.[2] Although charge-transfer bands are observed in the UV/Vis spectrum of this mixture, they are weak. It is now believed

[*] Prof. R. J. Bushby, E. O. Arikainen, Prof. N. Boden, O. R. Lozman, A. Wood
Centre for Self-Organising Molecular Systems (SOMS)
University of Leeds, Woodhouse Lane, Leeds LS2 9JT (UK)
Fax: (+44) 113-233-6452
E-mail: R.J.Bushby@chem.leeds.ac.uk
J. G. Vinter
The University Chemical Laboratory
Lensfield Road, Cambridge CB2 1EW (UK)

[**] Complimentary Polytopic Interactions, Part 1. This work was supported by BDH (Merck Ltd.) and the EPSRC. The photoconductivity experiment and synthesis of large-core molecules **2** and **3** are reported elsewhere.[4, 12]

 © WILEY-VCH Verlag GmbH, D-69451 Weinheim, 2000 1433-7851/00/3913-2333 $ 17.50+.50/0



1a : R = C_6H_{13}
1b : R = CH_3
1n : R = C_nH_{2n+1}

2a : X = C_9H_{19}, Y = H
2b : X = OCH_3, Y = OCH_3
2c : X = CH_3, Y = H
2d : X = OCH_3, Y = OCH_3

3a : X = C_9H_{19}, Y = H
3b : X = OC_6H_{13}, Y = OC_6H_{13}
3c : X = CH_3, Y= H
3d : X = OCH_3, Y = OCH_3

Scheme 1. Molecules used in this investigation are the small-core discogens **1** and the large-core polynuclear aromatic species **2** and **3**, which differ only by atomic (N, C) substitution.

that quadrupolar interactions between the two components produce the dominant stabilizing effect and that charge transfer is coincidental.[3] Nevertheless, almost all known examples of "chemical doping" of discotic materials have involved electron donor–electron acceptor pairs.

2,3,6,7,10,11-Hexakis(hexyloxy)triphenylene **1a** displays a hexagonal-columnar mesophase between 70 and 100 °C. When mixed with the azatriphenylene **2a** (which has itself two crystalline forms that melt at 71 °C and 81 °C) in a 1:1 ratio, a new liquid crystal **A** is formed, with a hexagonal-columnar phase between 130 °C and 240 °C. The transition at 240 °C is isothermal. The phase behavior of the components **2** and **3** and their mixtures with **1a** are shown in Table 1.[4]

Table 1. Phase transitions of the pure components and mixtures studied in this investigation.

Molecule/mixture	Phase transition T [°C] (ΔH [kJ mol^{-1}])[a]
1a	Cr 70 (48.3), Col_h 100 (7.1), I
2a	Cr 71 (34.3), Cr 81 (variable), I
2b	Cr_1 98 (32.0), Cr_2 147 (6.7), Col_1 150 (10.2), Col_r 194 (31.8), I
3a	Cr 59 (27.0), I
3b	Cr 65 (1.3), Col_h 135 (12.5), I
1a+**2a** (**A**)	Solid ≈130 (0.0), Col_h 240 (37.6), I
1a+**3a** (**B**)	Cr 66 (3.4), Col_h 155 (18.3), I

[a] The transition temperatures and enthalpies were measured by DSC (Perkin-Elmer DSC7, sample 2–3 mg in closed Al pans, heating rate +10 K min^{-1}). Phases were assigned from polarizing optical microscopy and X-ray diffraction data.

Thin-layer chromatography of **A** shows two distinct spots, corresponding to **1a** and **2a**. The UV/Vis (as a solid or a $CHCl_3$ solution), the ^{1}H NMR (as a solution in $CDCl_3$ or C_6D_6), and the IR (as a solid or nujol mull) spectra of the mixture prove to be simply a sum of those of the two components. Apparently, there is no covalent bonding between the two components and their electronic structures are not perturbed in any significant way.

The optical texture of **A** is similar to that obtained for many columnar mesophases (Figure 1). When a thin film between glass slides is annealed at 230 °C overnight, a homeotropic alignment is obtained.

The diffraction maxima in the small-angle region of the X-ray diffraction (XRD) pattern are sharper and more numerous in **A** than those of **1a**. The diffuse wide-angle maximum is typical of a columnar liquid crystal, however, the suggestion is that this phase is much more highly ordered. This is also consistent with the rather high enthalpy associated with the Col→I transition (+37.6 kJ mol^{-1} for **A**, a ½ : ½ molar mixture of **1a**:**2a**, compared to +7.1 kJ mol^{-1} for **1a**). The unit cell parameters

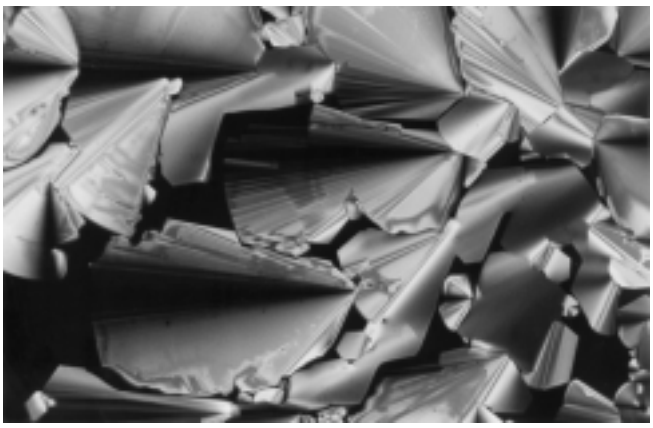


Figure 1. Optical texture of **A** as it appears when viewed through cross-polarizing filters at 240 °C (×100).

for this and the related mixture, **B** (**1a**+**3a**), are given in Table 2.

The fact that there is a single column/column repeat distance C and a hexagonal lattice shows that there cannot be segregated stacks of **1a** and **2a**. There is probably an alternating structure of the type shown in Figure 2.

Over most of the composition range, **A** is immiscible with both **1a** and **2a** (Figure 3). Along with the enhanced phase behavior and changes in ordering, this confirms that there is a very strong interaction between **1a** and **2a**.

Table 2. Calculated cell parameters from XRD measurements[a] on some of the pure components and their mixtures.

Molecule/mixture	a_{hex} [Å]	C [Å]	Number of reflections
1a	24.2	3.55	3
2a	30.5	3.55	7
3a	29.6	3.55	7
1a+**2a** (**A**)	28.3	6.92[b]	11
1a+**3a** (**B**)	27.0	7.07[c]	15

[a] Diffraction patterns were collected on film using a pinhole camera consisting of a Philips generator and tubes, Ni-filtered $Cu_{K\alpha}$ radiation (λ = 0.154 nm), and a Lindemann sample tube (1.5 mm inner diameter) to a plate 135.5 mm distant. [b] Average ring separation 3.46 Å. [c] Average ring separation 3.54 Å.

 © WILEY-VCH Verlag GmbH, D-69451 Weinheim, 2000 1433-7851/00/3913-2334 $ 17.50+.50/0 *Angew. Chem. Int. Ed.* **2000**, *39*, No. 13



Figure 2. Representation of the probable stacking of **1a** and **2a** in **A**.

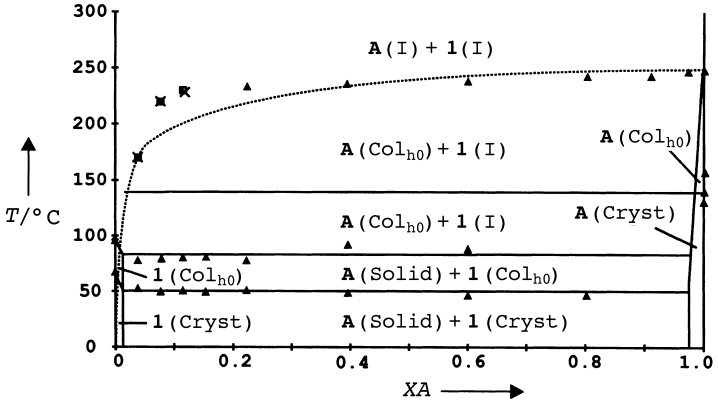


Figure 3. Phase versus composition diagram for binary mixtures of **1a** and **A** (data points are those measured by differential scanning calorimetry (DSC) and optical polarizing microscopy (OPM)). The liquidus of the phase diagram for an ideal mixture of solid **1a**:**2a** (=**A**, which dissociates completely upon melting to **1a** and **2a**) against component **1a** is given by Equation (1), where x_1 is the mole fraction of **1a**, ΔH_A is the enthalpy change at the clearing point of **A** (for a ½:½ molar ratio **1a**:**2a**), T_m is the melting point of pure **A**, and T is the melting point of the mixture (**1a** + **A**).[5].

A stable mixture, **B**, is also formed between **3a** (the carbon-atom analogue of **2a**) and **1a**. The phase diagram for mixtures of **1a** and **B** fits the same thermodynamic model as mixtures of **1a** and **A**. Once again, X-ray diffraction shows the mixture to be more highly ordered than **1a**. In contrast, no stabilized mixture is obtained when **1** is mixed with the more highly substituted molecules **2b** or **3b**.

Stable mixtures formed by the discogen **1a** with TNF have previously been modeled by treating the components as Gay–Berne disks with associated (net) quadrupole moments.[6] On this basis, we expect the molecular components of the stable 1:1 mixtures formed between the discogen **1a** and compounds **2a** and **3a** should carry opposite quadrupoles. Table 3 shows calculated values for the net quadrupoles of the aromatic cores of these molecules and it is evident from these calculations that this is not the case.

In order to understand the nature of the interactions in these π-stacked systems properly, a dispersed, polytopic description of the molecular charge distribution is required. We have modeled these mixtures using an extended electron distribution (XED) based upon that exploited by Hunter.[8, 9] This method involves displacing nonbonded electrons (such as π electrons and lone pairs) from the atomic centers to leave a positive charge at the nucleus.[10] This effectively generates a set of quadrupole moments dispersed on each atom of the system. This provides a more realistic charge distribution than is available using traditional atom-centered charge methods or by assuming that it is the net molecular dipole or quadrupole that dominates.[10] The geometries of the molecules under investigation (**1b**, **2c**, **2d**, **3c**, **3d**) were optimized using the AM1 semiempirical routine in the MOPAC package.[11] After the extended electrons were added, a conformational search was performed. The docking routine then brought one moveable (but conformationally fixed) molecule towards an immobile (and conformationally fixed) molecule from every direction using a free SIMPLEX minimizer. In each case, where stable pairs are formed, the same minima were obtained from many of these starting configurations. The output from the docking experiment gives the overall interaction energy and its van der Waals and coulombic contributions. From this output, the minimum energy intermolecular conformations can also be visualized. By comparing the interactions between the molecules and themselves (such as **1b** + **1b** and **2c** + **2c**) and the mixed system (such as **1a** + **2c**) it is possible to predict whether or not a stable mixture will form. These figures (Table 4) agree with the experimentally observed trends in mixture formation and stability. Representations of the minimum energy "stacks" for **1b** + **1b** and **3c** + **3c** and their mixture (**1b** + **3c**) are shown in Figure 4.

Compounds **2a** and **3a** have different electronic characteristics but similar shapes. Mixtures of both **2a** and **3a** with 2,3,6,7,10,11-hexakis(alkoxy)triphenylenes of varying chain lengths **1*n*** (n = 4–16) behave in a similar manner (Figure 5). In both cases there is an optimum side-chain length for the **1*n***

Table 3. Calculated dipole (μ) and quadrupole (Θ) moments for the pure components.

Molecule[a]	μ [D]	Θ [e A^2]	Observed[b]	Expected[c]
C_6H_6	0.00	−16.8	–	–
C_6F_6	0.00	17.9	–	–
1b	0.02	−47.1	–	–
2c	0.01	−83.4	Yes	No
2d	0.06	106.6	No	Yes
3c	0.03	−71.3	Yes	No
3d	0.08	178.2	No	Yes

[a] Benzene and hexafluorobenzene are shown as an example of a binary mixture that forms an induced phase.[7] [b] Stable mixture with **1** observed experimentally. [c] Stable mixture with **1** expected on the basis of the (net) quadrupolar model.[6]

Table 4. Results from the XED calculations.

Mixture[a]	Mean energy [kJ mol^{-1}]	Observed[b]	Expected[c]
$C_6H_6 + C_6H_6$	−4.7	–	–
$C_6F_6 + C_6F_6$	−5.2	–	–
$C_6H_6 + C_6F_6$	−10.6	–	–
1b + **1b**	−39.8	–	–
2c + **2c**	−37.3	–	–
2c + **1b**	−41.2	Yes	Yes
2d + **2d**	−51.6	–	–
2d + **1b**	−40.9	No	No
3c + **3c**	−36.5	–	–
3c + **1b**	−49.9	Yes	Yes
3d + **3d**	−41.0	–	–
3d + **1b**	−32.6	No	No

[a] Benzene and hexafluorobenzene are shown as an example of a binary mixture that forms an induced phase (see Table 3). [b] Stable mixture with **1** observed experimentally. [c] Stable mixture with **1** expected on the basis of the XED/CPI model.

 © WILEY-VCH Verlag GmbH, D-69451 Weinheim, 2000 1433-7851/00/3913-2335 $ 17.50+.50/0

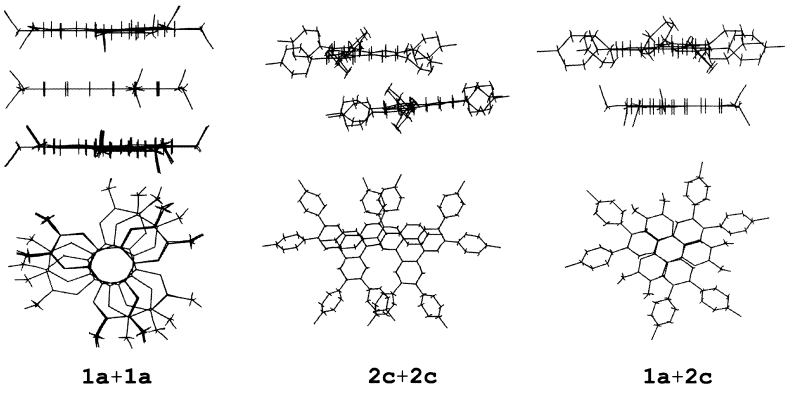


Figure 4. The elevation and plan views of the XED minimum energy dock of two molecules for a system which forms a stable mixture with **1b**. Left: **1b** + **1b**; middle: **3c** + **3c**; right: the mixture **1b** + **3c**.

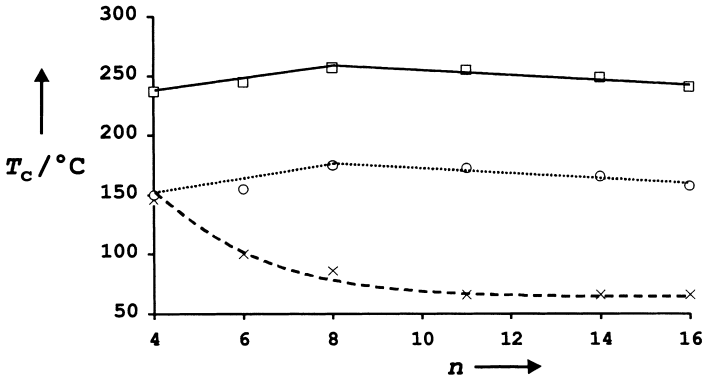


Figure 5. The trends in clearing temperature T_c for binary mixtures of the large core molecules (**2a** and **3a**) with discogen **1*n*** as a function of chain length *n*, measured by DSC and OPM. Upper line (——) = **1*n*** + **2a**; middle line (••••) = **1*n*** + **3a**; lower line (- - - -) = **1*n*** alone.

component, presumably corresponding to the same optimum packing. This stabilizing effect vanishes in those systems where the side chains are too long and no stable mixtures are obtained, or even predicted, for the systems **1a** + **2b** or **1a** + **3b** (**1b** + **2d**, **1b** + **3d**) in which the number of side-chain (x + y) is doubled to twelve. Hence, although the XED – CPI approach seems to be the only way to rationalize the stability of these mixtures, the packing of side chains is also important.

These mixtures not only provide a novel way of designing π-stacked systems but, from the standpoint of some applications, these particular systems are attractive. For example, mixtures obtained in this way are better photoconductors, with higher charge mobilities (for example, the mobility is $\sim 0.02\ cm^2 V^{-1} s^{-1}$ for **3a** + **1*n*** ($n = 11$)) than the discotic liquid crystal **1*n*** alone (**1*n*** ($n = 11$) is $3 \times 10^{-4}\ cm^2 V^{-1} s^{-1}$).[12] This enhanced mobility begins to approach the highest known values for discotic liquid crystals ($0.1\ cm^2 V^{-1} s^{-1}$).[13]

Received: December 14, 1999
Revised: April 13, 2000 [Z14395/Z14397]

[1] K. Praefcke, J. D. Holbery, *J. Inclusion Phenom. Mol. Recognit. Chem.* **1996**, *24*, 19.
[2] W. Kranig, C. Boeffel, H. W. Spiess, O. Karthaus, H. Ringsdorf, R. Wustefeld, *Liq. Cryst.* **1990**, *8*, 375.
[3] M. A. Bates, G. R. Luckhurst, *Liq. Cryst.* **1998**, *24*, 229.
[4] New synthesis of large core discogens: N. Boden, R. J. Bushby, G. Headdock, O. R. Lozman, A. Wood, *Liq. Cryst.*, submitted.
[5] H. A. J. Oonk, *Phase Theory, The Thermodynamics of Heterogeneous Equilibria, Vol. 3*, Elsevier Scientific, Amsterdam, **1981**, pp. 175 – 178.
[6] M. A. Bates, G. R. Luckhurst, *Liq. Cryst.* **1998**, *24*, 229.
[7] T. Dahl, *Acta. Chem. Scand.* **1973**, *27*, 995.
[8] C. A. Hunter, J. K. M. Saunders, *J. Am. Chem. Soc.* **1990**, *112*, 5525.
[9] C. A. Hunter, *Angew. Chem.* **1993**, *105*, 1653; *Angew. Chem. Int. Ed. Engl.* **1993**, *32*, 1584.
[10] J. G. Vinter, *J. Comput. Aided Mol. Des.* **1996**, *10*, 417.
[11] MOPAC and SIMPLEX as implemented in the COSMIC modelling system, J. G. Vinter, Cambridge, **1996**.
[12] Enhanced electronic transport properties: N. Boden, R. J. Bushby, K. J. Donovan, T. Kreouzis, O. R. Lozman, *J. Chem. Phys.*, submitted.
[13] D. Adam, P. Schuhmacher, J. Simmerer, L. Haussling, K. Siemensmeyer, K. H. Etzbach, H. Ringsdorf, D. Haarer, *Nature* **1994**, *371*, 141 – 143.

Rhodium – Rhodium Bonds in Edge-Sharing Coplanar Dinuclear Complexes**

Cristina Tejel, Milena Sommovigo, Miguel A. Ciriano,* José A. López, Fernando J. Lahoz, and Luis A. Oro*

Dinuclear rhodium(II) complexes typically have face-to-face structures with both rhodium atoms in pseudooctahedral or pseudo-square-pyramidal environments. The rhodium – rhodium bond is systematically perpendicular to the two faces, which are disposed in eclipsed or staggered conformations.[1] These characteristics are found in complexes ranging from the large family of lantern complexes with four bridging ligands $[Rh_2(\mu\text{-bridge})_4(L)_n]$ up to the cationic complex $[Rh_2(NCMe)_{10}]^{4+}$ with no bridging ligands.[1c] Analogous rhodium – rhodium bonds are even formed in complexes in which the bridging ligands prevent face-to-face structures.[1d] Here we describe unprecedented dinuclear rhodium(II) complexes with a bond between two metal atoms in coplanar square-planar environments and an unusually low electron count of 30 valence electrons.

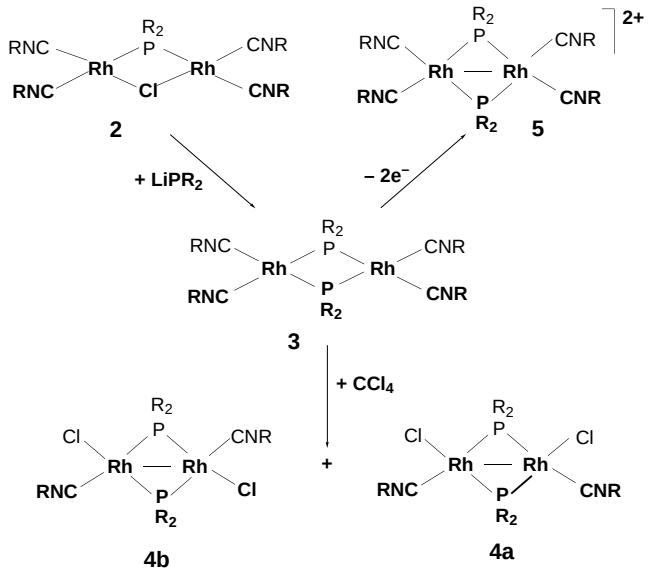
New starting materials with bulky $PtBu_2^-$ ligands can be obtained by circumventing the inertness of known phosphido rhodium(I) complexes. In contrast to the partial replacement of 1,5-cyclooctadiene (COD) in $[\{Rh(\mu\text{-}PPh_2)_2(cod)\}_2]$ by

[*] Dr. M. A. Ciriano, Prof. L. A. Oro, Dr. C. Tejel, Dr. M. Sommovigo, Dr. J. A. López, Dr. F. J. Lahoz
Departamento de Química Inorgánica
Instituto de Ciencia de Materiales de Aragón
Universidad de Zaragoza – C.S.I.C.
50009-Zaragoza (Spain)
Fax: (+34) 976761143
E-mail: mciriano@posta.unizar.es, oro@posta.unizar.es

[**] Generous financial support from DGES (Projects PB98-641, PB95-318, and PB94-1186) and a fellowship (to M.S.) are gratefully acknowledged.

 © WILEY-VCH Verlag GmbH, D-69451 Weinheim, 2000 1433-7851/00/3913-2336 $ 17.50+.50/0

monodentate phosphanes,[2] the complete replacement of the diolefin in [{Rh(cod)}$_2$(μ-P*t*Bu$_2$)(μ-Cl)] (**1**)[3] by CN*t*Bu takes place smoothly to give the dinuclear complex [{Rh(CN*t*Bu)$_2$}$_2$(μ-P*t*Bu$_2$)(μ-Cl)] (**2**) in good yield. Complex **2** lacks a metal–metal bond, as revealed by the high-field chemical shift of the triplet ($\delta = 16.2$, $J_{P,Rh} = 100$ Hz) in the $^{31}P\{^1H\}$ NMR spectrum,[4] and the metal environments are square-planar, since the two signals observed for the CN*t*Bu groups in the ^1H NMR spectrum correspond to ligands *trans* to the P donor and Cl ligands (Scheme 1). Moreover,



Scheme 1. Structural formulas of the new compounds and their transformations. R = *t*Bu.

complexes **1** and **2** show distinct behavior with respect to the replacement of the chloride ligand. Whilst the cyclooctadiene complex **1** does not react with LiP*t*Bu$_2$ under prolonged reflux in THF, the isocyanide complex **2** reacts smoothly with equimolar amounts of LiP*t*Bu$_2$ in diethyl ether to give the new dinuclear bis-phosphido rhodium complex **3** (Scheme 1). Orange solutions of **3** in dichloromethane contain a single species with a planar Rh_2P_2 framework and no rhodium–rhodium bond. No changes in the $^{31}P\{^1H\}$ NMR spectrum were observed on varying the temperature in the range of -80 to 25°C, and therefore the geometric isomerization process involving exchange of the coordination sphere of one metal center from square-planar to tetrahedral that was reported for the related isoelectronic rhodium(I) complex [{Rh(μ-P*t*Bu$_2$)(CO)$_2$}$_2$][5] can be ruled out for **3**.

Complex **3** reacts slowly with chloroform to give a red solution containing several complexes, which evolve into two major species over one day. Both compounds, **4a** and **4b** (Scheme 1), contain a rhodium–rhodium bond, as evidenced by the low-field chemical shift of the $^{31}P\{^1H\}$ NMR signals. Complex **4a** exhibits two triplets of doublets at $\delta = 431.6$ ($J_{P,Rh} = 89$, $J_{P,P} = 14$ Hz) and $\delta = 417.1$ ($J_{P,Rh} = 85$, $J_{P,P} = 14$ Hz), while **4b** shows a multiplet at $\delta = 399.7$, which corresponds to the AA′ part of an AA′XX′ spin system. Further evolution of this mixture at room temperature leads exclusively to **4b** after six days. At this point, the IR spectrum shows a single $\tilde{\nu}$(CN) band at 2160 cm^{-1}. Complex **4b** was obtained in one day by carrying out the reaction in carbon tetrachloride under argon at room temperature. Evaporation of the red solutions in chloroform or carbon tetrachloride and crystallization of the crude product from benzene/*n*-hexane gave red crystals (70% yield of isolated product) of the diamagnetic dirhodium(II) complex **4b**. Most probably, the intermediate **4a** is the *cis* isomer according to the above-described $^{31}P\{^1H\}$ NMR spectrum, since the phosphorus nuclei are inequivalent.

Complex **4b** was studied by single-crystal X-ray diffraction, and its novel structure is shown in Figure 1.[6] Excluding the intermetallic interaction, each metal atom is in a square-planar coordination environment and is bonded to two P*t*Bu$_2$ bridging ligands, a chloride ion, and a *t*BuNC group. The

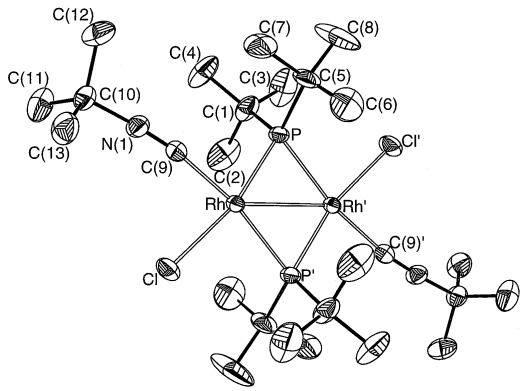


Figure 1. Molecular structure of **4b** (hydrogen atoms omitted; primed atoms are related to the unprimed ones by an inversion center). Selected bond lengths [Å] and angles [°]: Rh-Rh′ 2.7583(6), Rh-P 2.2168(10), Rh-P′ 2.2705(10), Rh-Cl 2.3962(10), Rh-C(9) 1.992(4); P-Rh-P′ 104.15(3), P-Rh-Cl 167.22(4), P-Rh-C(9) 88.67(11), P′-Rh-Cl 88.00(4), P′-Rh-C(9) 166.92(11), Cl-Rh-C(9) 79.41(11), Rh′-Rh-P 52.96(3), Rh′-Rh-P′ 51.20(3), Rh′-Rh-Cl 139.02(3), Rh′-Rh-C(9) 141.55(11), Rh-P-Rh′ 75.85(3).

presence of a crystallographic inversion center makes the Rh_2P_2 core strictly planar; the angle between this plane and that defined by the remaining ligands (calculated through Rh, Cl, and C(9)) is 5.3(2)°. Apart from the coplanarity of the metal coordination planes, the most interesting feature of this complex is the short intermetallic distance of 2.7583(6) Å. This short distance suggests the existence of a Rh–Rh bond, as do the $^{31}P\{^1H\}$ NMR data, and is similar to the bond lengths in the two polymorphs of the square-planar/tetrahedral rhodium(I) complex [{Rh(μ-P*t*Bu$_2$)(CO)$_2$}$_2$] of 2.7609(9) and 2.748 Å, for which a rhodium–rhodium bond was postulated.[5a, 7] For comparison, the square-planar/square-planar isomer of this tetracarbonyl dimer, which does not have an intermetallic bond, has a metal–metal distance of 3.717(1) Å.[5a] In the former isomer the formation of the metal–metal bond was associated with the above-mentioned change of the coordination sphere of one metal center from square-planar to tetrahedral, whereas the intermetallic bond in **4** results from chemical oxidation of the metal centers. The only related example is the recently reported platinum(III) complex [{Pt(μ-PPh$_2$)(C$_6$F$_5$)$_2$}$_2$], which has a Pt–Pt bond length of 2.7245(7) Å.[8]

 © WILEY-VCH Verlag GmbH, D-69451 Weinheim, 2000 1433-7851/00/3913-2337 $ 17.50+.50/0

In the search for additional complexes with this unusual structure, we realized that the reaction of **3** with chloroform or carbon tetrachloride to give **4** implies a formal oxidation of the metal centers and the removal of two CN*t*Bu ligands. Therefore, we investigated the potential generalization of this process by chemical oxidation of dirhodium(I) complexes. Thus, complex **3** was treated with $[FeCp_2]OTf$ (OTf = trifluoromethanesulfonate) in 1:2 molar ratio in acetone. Upon mixing, the dark blue color of $[FeCp_2]OTf$ faded almost immediately to give an orange solution. After evaporating the acetone and washing the crude product with diethyl ether, the residue was recrystallized from dichloromethane/diethyl ether to give orange crystals of $[\{Rh(\mu\text{-}PtBu_2)(CNtBu)_2\}_2](OTf)_2$ (**5**) in 90% yield. Spectroscopic data for **5**, especially the triplet at $\delta = 450.4$ ($J_{P,Rh} = 86$ Hz) in the $^{31}P\{^1H\}$ NMR spectrum, suggest a structure similar to that of **4b**, and thus the validity of this synthetic approach is confirmed.

The molecular structure of the dinuclear complex cation of **5** (Figure 2)[9] is very similar to that of the neutral complex **4b**. The cation also has a crystallographic inversion center at the midpoint of the Rh_2P_2 rhombus and a short intermetallic

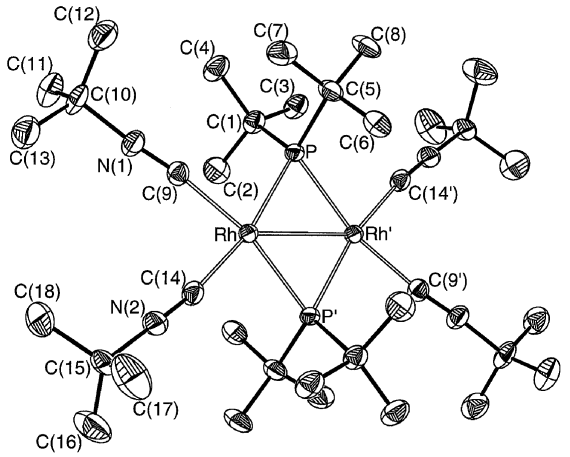


Figure 2. Molecular structure of the complex cation of **5** (hydrogen atoms omitted; primed atoms are related to the unprimed ones by an inversion center). Selected bond lengths [Å] and angles [°]: Rh-Rh′ 2.7403(9), Rh-P 2.2764(10), Rh-P′ 2.2744(10), Rh-C(9) 1.987(4), Rh-C(14) 1.996(4), P-Rh-P′ 105.95(3); P-Rh-C(9) 85.64(11), P-Rh-C(14) 166.82(10), P′-Rh-C(9) 167.22(11), P′-Rh-C(14) 86.89(10), C(9)-Rh-C(14) 81.88(15), Rh′-Rh-P 52.94(3), Rh′-Rh-P′ 53.01(3), Rh′-Rh-C(9) 138.27(10), Rh′-Rh-C(14) 139.80(10), Rh-P-Rh′ 74.05(3).

distance (2.7403(9) Å). Both metal centers have slightly distorted square-planar environments; the deviations from ideal square-planar coordination could be related to the dihedral angle between the Rh_2P_2 planar core and the plane through the terminal ligands [6.7(2)°, calculated through Rh, C(9), and C(14)].

The short metal–metal distances in **4b** and **5**, together with the diamagnetism of the complexes, clearly indicate some kind of Rh–Rh bonding. However, the way in which this spin pairing takes place is not completely clear, since two possibilities are conceivable. One is through a "direct" metal–metal σ bond, as suggested by density functional theory (DFT) calculations on the related diplatinum(III) complex.[8] However, the alternative "through-ring" bonding proposed by Alvarez et al.[10] should not be excluded, since both **4b** and **5** have a framework electron count (FEC) of six.

In conclusion, the combination of the bulky anionic $PtBu_2^-$ ligands and the good σ donor CN*t*Bu promotes the formation of unprecedented coplanar square-planar dirhodium(II) complexes with a metal–metal bond.

Received: February 3, 2000 [Z14644]

[1] a) A wide range of compounds with bridging carboxylate, amidate, pyrazolate, 2-pyridonate, and related ligands form lantern dinuclear rhodium(II) complexes. For a recent paper containing about 130 references to these complexes, see G. Aullón, S. Alvarez, *Inorg. Chem.* **1993**, *32*, 3712; b) C. A. Crawford, J. H. Matonic, J. C. Huffman, K. Folting, K. R. Dunbar, G. Christou, *Inorg. Chem.* **1997**, *36*, 2361, and references therein; F. P. Pruchnik, *Pure Appl. Chem.* **1989**, *61*, 795; c) K. R. Dunbar, L. E. Pence, *Inorg. Synth.* **1992**, *29*, 182; d) For complexes with two bridging ligands and without face-to-face structures see: C. Tejel, M. A: Ciriano, J. A: López, F. J. Lahoz, L. A. Oro, *Organometallics* **1997**, *16*, 4718, and references therein; C. Tejel, M. Bordonaba, M. A. Ciriano, A. J. Edwards, W. Clegg, F. J. Lahoz, L. A. Oro, *Inorg. Chem.* **1999**, *38*, 1108.

[2] P. E. Kreter, D. W. Meek, *Inorg. Chem.* **1983**, *22*, 319.

[3] A. M. Arif, R. A. Jones, M. H. Seeberger, B. R. Whittlesey, T. C. Wright, *Inorg. Chem.* **1986**, *25*, 3943.

[4] Selected analytical and spectroscopic data for the new complexes: **2**: Analysis calcd for $C_{28}H_{54}ClN_4PRh_2$: C 46.77, H 7.57, N 7.79; found: C 46.95, H 7.29, N 7.20; IR (Et_2O): $\tilde{\nu}$(CN) = 2177 (w), 2127 (vs), 2052 (m), 1963 cm^{-1} (w); $^1H\{^{31}P\}$ NMR (300 MHz, C_6D_6, 293 K): $\delta = 2.024$ (s, 18H, P*t*Bu$_2$), 1.121 (s, 18H, CN*t*Bu), 0.855 (s, 18H, CN*t*Bu); $^{31}P\{^1H\}$ NMR (121 MHz, C_6D_6, 293 K): $\delta = 16.2$ (t, $J_{P,Rh} = 100$ Hz). **3**: Analysis calcd for $C_{36}H_{72}N_4P_2Rh_2$: C 52.17, H 8.75, N 6.76; found: C 51.43, H 8.32, N 6.24; IR (CH_2Cl_2): $\tilde{\nu}$(CN) = 2112 (vs), 2050 cm^{-1} (s); $^1H\{^{31}P\}$ NMR (C_6D_6, 293 K): $\delta = 1.440$ (s, 36H, P*t*Bu$_2$), 1.374 (s, 36H, CN*t*Bu); $^{31}P\{^1H\}$ NMR (C_6D_6, 293 K): $\delta = -98.8$ (t, $J_{P,Rh} = 91$ Hz). **4b**: Analysis calcd for $C_{26}H_{54}Cl_2N_2P_2Rh_2$: C 42.58, H 7.42, N 3.82; found: C 42.12, H 7.52, N 3.65; IR ($CHCl_3$): $\tilde{\nu}$(CN) = 2160 cm^{-1} (vs); $^1H\{^{31}P\}$ NMR (C_6D_6, 293 K): $\delta = 1.664$ (s, 36H, P*t*Bu$_2$), 0.988 (s, 18H, CN*t*Bu).; $^{31}P\{^1H\}$ NMR (C_6D_6, 293 K): $\delta = 399.7$ (m). **5**: Analysis calcd for $C_{38}H_{72}F_6N_4O_6P_2S_2Rh_2$: C 40.50, H 6.44, N 4.97, S 5.69; found: C 39.73, H 6.69, N 5.32, S 6.08; IR (CH_2Cl_2): $\tilde{\nu}$(CN) = 2185 cm^{-1} (s); $^1H\{^{31}P\}$ NMR ([D$_6$]acetone, 293 K): $\delta = 1.775$ (s, 36H, CN*t*Bu), 1.567 (s, 36H, P*t*Bu$_2$); $^{31}P\{^1H\}$ ([D$_6$]acetone, 293 K) $\delta = 450.4$ (t, $J_{P,Rh} = 86$ Hz).

[5] a) R. A. Jones, T. C. Wright, J. L. Atwood, W. E. Hunter, *Organometallics* **1983**, *2*, 470; b) S.-K. Kang, T. A. Albright, T. C. Wright, R. A. Jones, *Organometallics* **1985**, *4*, 666.

[6] Crystal data for **4b**·2C$_6$H$_6$: $C_{26}H_{54}Cl_2N_2P_2Rh_2 \cdot 2C_6H_6$, $M_r = 889.59$, monoclinic, space group $P2_1/n$ (no. 14), $a = 11.4245(10)$, $b = 15.2523(14)$, $c = 12.5443(10)$ Å, $\beta = 99.369(10)°$, $V = 2156.7(3)$ Å^3, $Z = 2$, $\rho_{calcd} = 1.370$ g cm^{-3}, $F(000) = 924$, $\lambda = 0.71073$ Å, $T = 173(2)$ K, $\mu(Mo_{K\alpha}) = 0.990$ mm^{-1}. Data were collected on a Siemens–Stoe AED2 diffractometer on a dark red crystal ($0.44 \times 0.30 \times 0.22$ mm). Of the 3865 reflections collected by $\omega/2\theta$ scans ($4 \le 2\theta \le 50°$), 3682 were unique ($R_{int} = 0.0235$) and 2844 observed with $I \ge 2\sigma(I)$. A Ψ scan absorption correction gave min./max. transmission factors of 0.6699/0.8117. The structure was solved by direct methods (A. Altomare, G. Cascarano, C. Giacovazzo, A. Guagliardi, *J. Appl. Crystallogr.* **1994**, *27*, 435) and refined by full-matrix least-squares methods on F^2 for all reflections (G. M. Sheldrick, *SHELXL-97*, University of Göttingen, Germany, **1997**). Final agreement factors were $R_1 = 0.0334$ (observed reflections) and $wR_2 = 0.0687$ (all data) for 230 parameters; GOF: 1.014. Largest peak and hole in the final difference map: 0.701 and -0.447 e Å^{-3}.[9b]

[7] R. A. Jones, T. C. Wright, J. L. Atwood, W. E. Hunter, *Acta Crystallogr. Sect. C* **1986**, *42*, 294.

[8] E. Alonso, J. M. Casas, F. A. Cotton, X. Feng, J. Forniés, C. Fortuño, M. Tomás, *Inorg. Chem.* **1999**, *38*, 5034.

[9] a) Crystal data for **5**: $C_{38}H_{72}F_6N_4O_6P_2Rh_2S_2$, $M_r = 1126.88$, triclinic, $P\bar{1}$ (no. 2), $a = 10.752(2)$, $b = 11.3754(19)$, $c = 12.061(3)$ Å, $\alpha =$

 © WILEY-VCH Verlag GmbH, D-69451 Weinheim, 2000 1433-7851/00/3913-2338 $ 17.50+.50/0

63.021(10), $\beta = 82.579(14)$, $\gamma = 89.386(14)^\circ$, $V = 1301.7(5)$ Å^3, $Z = 1$, $\rho_{calcd} = 1.438$ g cm^{-3}, $F(000) = 582$, $\lambda = 0.71073$ Å, $T = 293(2)$ K, $\mu(Mo_{K\alpha}) = 0.840$ mm^{-1}. Data were collected on a Siemens–Stoe AED2 diffractometer on an orange crystal ($0.26 \times 0.25 \times 0.04$ mm). Of the 7336 reflections collected by $\omega/2\theta$ scans ($4 \le 2\theta \le 50^\circ$), 4586 were unique ($R_{int} = 0.0320$) and 4270 observed with $I \ge 2\sigma(I)$. Data were corrected for absorption (Gaussian face-indexed method) with min./max. transmission factors of 0.8113/0.9672. Structure solution and refinement were as described for **4b**. Final agreement factors were $R_1 = 0.0362$ (observed reflections) and $wR_2 = 0.0760$ (all data) for 296 parameters; GOF 1.024; largest peak and hole in the final difference map 0.737 and -0.440 e Å^{-3}, respectively; b) Crystallographic data (excluding structure factors) for the structures reported in this paper have been deposited with the Cambridge Crystallographic Data Centre as supplementary publication nos. CCDC-139639 (**4a**) and CCDC-139640 (**4b**). Copies of the data can be obtained free of charge on application to CCDC, 12 Union Road, Cambridge CB2 1EZ, UK (fax: (+44) 1223-336-033; e-mail: deposit@ccdc.cam.ac.uk).

[10] a) G. Aullón, P. Alemany, S. Alvarez, *J. Organomet. Chem.* **1994**, *478*, 75; b) S. Alvarez, A. A. Palacios, G. Aullón, *Coord. Chem. Rev.* **1999**, *185–186*, 431.

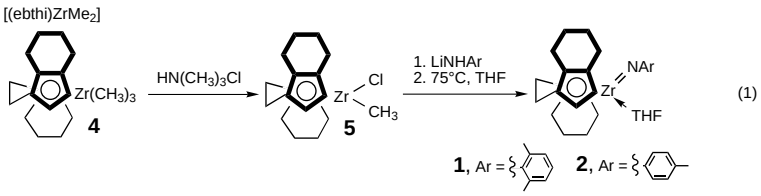
Synthesis of Chiral, Enantiopure Zirconocene Imido Complexes: Highly Selective Kinetic Resolution and Stereoinversion of Allenes, and Evidence for a Stepwise Cycloaddition/Retrocycloaddition Reaction Mechanism**

Zachary K. Sweeney, Jennifer L. Salsman, Richard A. Andersen,* and Robert G. Bergman*

Certain metal–carbon multiple bonds exhibit substantial reactivity toward organic compounds and are important intermediates in many catalytic processes.[1] The analogous reactivity of metal–heteroatom multiple bonds, such as those in metal–imido complexes, has been known for a much shorter time and has only relatively recently been utilized in synthetic applications.[2]

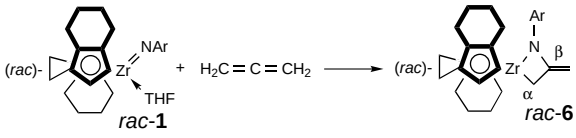
We wish to report a series of highly enantioselective reactions using isolable imido complexes with reactive metal–nitrogen double bonds.[3–9] These involve the reactions of enantiopure (ebthi)(L)Zr=NR complexes with 1,3-disubstituted allenes (L = tetrahydrofuran; ebthi = bis(tetrahydroindenyl)ethane). Our observations a) demonstrate the operation of a general and highly selective kinetic resolution, b) provide the first example of a reaction that can be used to selectively invert the absolute configuration of one (symmetrically or unsymmetrically 1,3-disubstituted) allene enantiomer within a racemic mixture, and c) provide strong mechanistic evidence for the stepwise nature of an organometallic cycloaddition reaction.

Previous work in our laboratories has shown that zirconocene–imido complexes undergo cycloaddition reactions with a wide range of unsaturated organic molecules including alkynes,[10] imines,[11] and certain alkenes.[12] Several of these reactions are important steps in catalytic transformations (for example, hydroamination or imine metathesis) mediated by the imido compounds. To extend this chemistry to systems capable of enantioselective reactions, we decided to examine the reactions of chiral disubstituted allenes with zirconium imido complexes bearing the C_2-symmetric ebthi ligand developed by Brintzinger.[13] The chiral imido complexes were synthesized in two steps from the known dimethyl complex **4**, as shown in [Eq. (1)].[14]



(1)

In order to investigate the products and diastereoselectivity of the chiral zirconocene–allene reactions, we first examined the stoichiometric reactions of racemic ebthi complexes **1** and **2** with achiral allenes and racemic chiral 1,3-disubstituted allenes. The purple metallacycle *rac*-**6** was formed rapidly upon condensation of allene onto a benzene solution of *rac*-**1** [Eq. (2)]. Production of an azametallacycle with the exocyclic methylene group in the β (as opposed to the α) position was indicated by its ^{1}H, ^{1}H NOESY spectrum, which featured a strong NOE between one of the exocyclic methylene protons and the methyl groups on the phenyl ring.

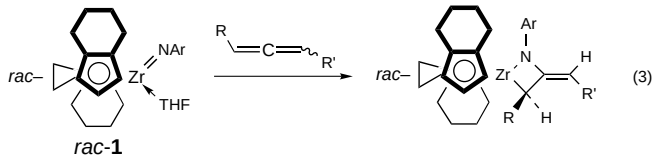


(2)

The reaction of *rac*-**1** with 1 equiv of racemic 1,3-diphenylallene, 3,4-heptadiene, 4,5-nonadiene, or 1,2-cyclononadiene at 23 °C provided a single diastereomeric product in each case, as determined by ^{1}H and ^{13}C NMR spectra ([Eq. (3)]). A bulky imido substituent is required for the selectivity in these transformations, as an 85:15 mixture of diastereomers was formed from the reaction of the *p*-tolylimido complex *rac*-**2** with diphenylallene. These results were encouraging because they suggested that the reactions are stereospecific: (*S*,*S*)-**1**

[*] Prof. R. A. Andersen, Prof R. G. Bergman, Z. K. Sweeney, J. L. Salsman
Department of Chemistry
University of California
Berkeley, CA 94720-1460 (USA)
Fax: (+1) 510-642-7714
E-mail: andersen@actinide.lbl.gov, bergman@cchem.berkeley.edu

[**] This work was supported by the US National Institutes of Health (grant no. GM-25459 to R.G.B.). Z.K.S. acknowledges a fellowship from the Chevron Co. We are grateful to Dr. Jeffrey S. Johnson and Mr. Stephen R. Jenkins for experimental assistance and helpful discussions, Prof. David MacMillan and his co-workers for extensive assistance with chiral gas chromatography, and Boulder Scientific Co. for a gift of *rac*-(ebthi)$ZrCl_2$.



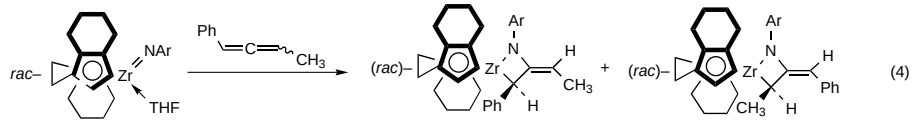
rac-**1** (3)

	R	R'
rac-**7**	Ph	Ph
rac-**8**	C_2H_5	C_2H_5
rac-**9**	C_3H_7	C_3H_7
rac-**10**	$-(CH_2)_6-$	

reacts preferentially with the (*S*) allene, and (*R*,*R*)-**1** with the (*R*) allene, in order to give the diastereoselectivity observed. As the data summarized below shows, the actual situation is more complicated.

Reactions of **1** with the unsymmetrically substituted allenes 1-phenyl-1,2-butadiene and 1-phenyl-1,2-pentadiene can potentially produce a mixture of diastereo- and regioisomers. However, addition of 1 equiv of 1-phenyl-1,2-butadiene to a solution of *rac*-**1** produced only the regioisomers *rac*-**11** and *rac*-**12** (1:1 ratio determined by ^{1}H NMR [Eq. (4)]). Therefore, even though the reaction is not regioselective, it is still highly diastereoselective. Similar results were obtained in the reaction of *rac*-**1** with 1-phenyl-1,2-pentadiene.

Deeper insight into the actual course of these reactions was provided by examining the stereochemistry of the allene cycloaddition reactions with enantiopure **1**. First, the reaction of enantiopure (*S*,*S*)-**1** with the racemic allenes used in excess provided an effective kinetic resolution even at room temperature. Addition of 1.8 equiv of racemic 1,3-diphenylallene to a benzene solution of (*S*,*S*)-**1** at 23 °C resulted in consumption of approximately 50% of the allene.[15, 16] The unreacted 1,3-diphenylallene was highly enriched in the (*R*) enantiomer (>98% *ee*). The results of enantioselective capture experi-



rac-**1** *rac*-**11** *rac*-**12** (4)

ments, in which (*S*,*S*)-**1** was treated with other chiral allenes, are shown in Table 1. Notably, the cycloaddition reaction is selective for both symmetrically and unsymmetrically 1,3-disubstituted allenes with high *ee* values in most cases.[17, 18]

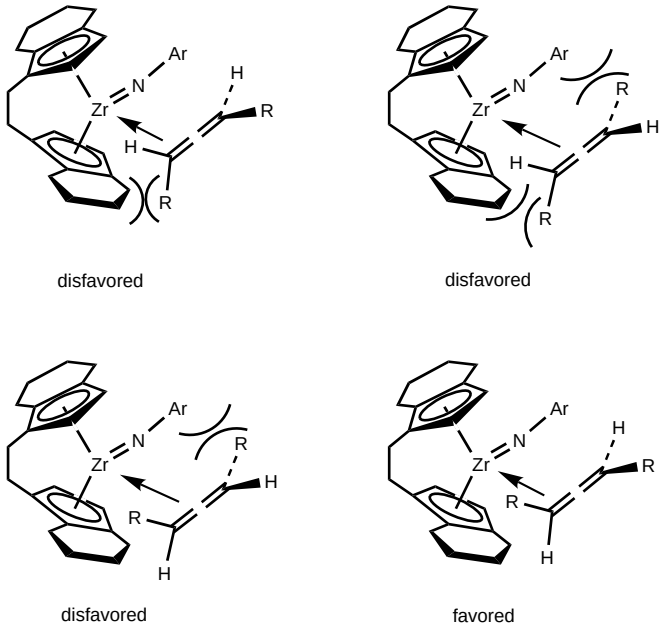
We propose that the selectivity observed in these cycloadditions is the result of mutually reinforcing stereocontrol

Table 1. Enantioselective capture reactions of $(R_1)HC{=}C{=}CH(R_2)$ with (*S*,*S*)-**1**.

Entry	R_1	R_2	Allene consumed [%]	*ee*[a] [%]	Configuration of unreacted allene
1	*cyclo*-$(CH_2)_6$		54	78	(*R*)
2	C_3H_5	C_3H_5	59	>98	(*R*)
3	Ph	Me	61	94	(*R*)
4	Ph	Et	53	>98	(*R*)
5	Ph	Ph	50	>98	(*R*)

[a] Enantiomeric excess of the unreacted allene. See ref. [16] for the method of *ee* determination.

imposed by the combination of the ebthi ligand and the bulky imido substitutent. The ebthi ligand allows the imido complex to add preferentially onto one face of the reacting π bond,[19] while the N–Ar group favors reaction of the allene enantiomer in which one olefin substituent is oriented away from the imido ligand in the cycloaddition transition state (Scheme 1).

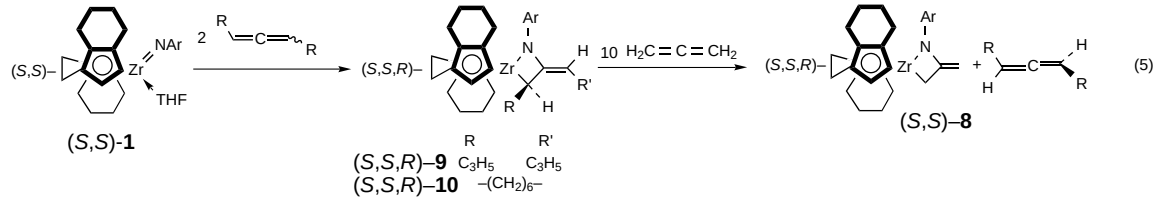


Scheme 1. Alternative structures of the π complexes formed by interaction of (*S*,*S*)-(ebthi)Zr=NAr with the two enantiomers of a 1,3-disubstituted allene.

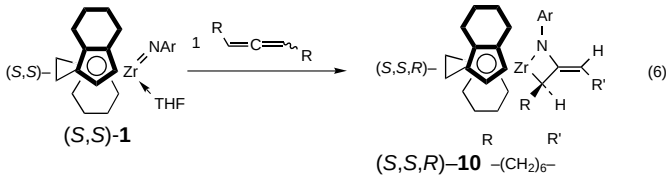
This model is supported by the observation that the reactions of **2**, which contains a smaller imido substituent, appear to be substantially less selective than the reactions of **1**. The proposal is also consistent with the absolute configuration observed in the enantioselective cycloaddition reactions.

A single metallacycle diastereomer is, by NMR spectroscopy, observed to be the major organometallic product in the enantioselective capture reactions. In separate experiments, (*S*,*S*,*R*)-**9** and (*S*,*S*,*R*)-**10** could be isolated by treatment of (*S*,*S*)-**1** with slightly more than 2 equiv of either 4,5-nonadiene or 1,2-cyclononadiene followed by removal of the excess allene in vacuo [Eq. (5)]. The faster reacting allene enantiomer was then regenerated from the metallacycle by treating it with the parent allene, 1,2-propadiene (C_3H_4). Thus, when (*S*,*S*,*R*)-**9** was treated with 1,2-propadiene, retrocycloaddition occurred slowly at 23 °C to produce (*S*,*S*)-**8** and (*S*)-4,5-nonadiene that was highly enantioenriched (93% *ee*, >95% recovery). Similarly, (*S*)-1,2-cyclononadiene (85% *ee*, >95% recovery) was produced from the reaction of 1,2-propadiene with (*S*,*S*,*R*)-**10**. By this method, it is possible to obtain good separation of allene racemates: The slower reacting allene enantiomer is recovered from the initial cycloaddition and the faster reacting allene enantiomer is recovered by displacement from the product metallacycle.

 © WILEY-VCH Verlag GmbH, D-69451 Weinheim, 2000 1433-7851/00/3913-2340 $ 17.50+.50/0



As the allene cycloaddition reactions appeared to be stereospecific, we expected that the reaction of the enantiopure imido complex with only 1 equiv of a racemic disubstituted allene (for example, 1,2-cyclononadiene) would allow reaction of the imido complex with the slower reacting allene enantiomer, once the faster reacting enantiomer had been consumed. This might then lead to a mixture of metallacycle diastereomers. We were therefore surprised to find that (*S*,*S*,*R*)-**10** was the only detectable product of the reaction between 1 equiv of racemic 1,2-cyclononadiene and (*S*,*S*)-**1** [Eq. (6)]. No intermediates were observed when this reaction was followed by ^{1}H NMR spectroscopy. Following treatment of the product mixture with 1,2-propadiene, (*S*)-1,2-cyclononadiene (84 % *ee*, 93 % yield) evolved.



The only way we are able to rationalize this result is to assume that when the slower reacting (*R*) allene reacts with (*S*,*S*)-**1**, its absolute configuration is inverted. To further test this conclusion, we treated (*S*,*S*)-**1** with 1,2-cyclononadiene enriched in the (*R*) enantiomer (67 % *ee*). This again led to (*S*,*S*,*R*)-**10**, and condensation of 1,2-propadiene into the solution regenerated (*S*)-1,2-cyclononadiene (85 % *ee*). Therefore, we suggest that: a) the faster reacting (*S*) enantiomer of 1,2-cyclononadiene forms a metallacycle, which is then regenerated in the retrocycloaddition with *retention* of its absolute configuration, but b) the slower reacting (*R*) enantiomer reacts to produce the same metallacycle as that formed for the (*S*) enantiomer, which is regenerated with overall *inversion* of its absolute configuration. The allene cycloaddition is therefore highly stereoselective but not stereospecific.[20] This system allows quantitative (rather than just 50 %, as would be possible in a conventional kinetic resolution) conversion of racemic allene into material that is highly enriched in the (*R*) enantiomer. Similarly, the (*R*,*R*) imido complex can be used to convert racemic allene quantitatively into material that is highly enriched in the (*S*) enantiomer. Interconversion of (*R*) and (*S*) allenes is very slow under these conditions.

Other reactions of (*S*,*S*)-**1** with racemic chiral allenes behave analogously. The reaction of (*S*,*S*)-**1** with 1 equiv of racemic 1-phenyl-1,2-butadiene at 23 °C produced (*S*,*S*,*R*)-**11**, (*S*,*S*,*R*)-**12**, and a third, unidentified metallacycle diastereomer in a 1.0:1.0:0.5 ratio, respectively (^{1}H NMR). After 1 h, all of the disubstituted allene was consumed in the reaction. Treatment of this product mixture with 1,2-propadiene at 75 °C quantitatively converted it to (*S*,*S*)-**8** and free 1-phenyl-1,2-butadiene. Chiral GC analysis indicated that the released disubstituted allene was enantioenriched ((*S*) 43 % *ee*, 90 % recovery). Enantioenriched 1-phenyl-1,2-pentadiene ((*S*) 33 % *ee*, > 95 % recovery) was also obtained by consecutive treatment of racemic 1-phenyl-1,2-pentadiene with (*S*,*S*)-**1** and 1,2-propadiene.

Previous experimental work has suggested that such organometallic cycloaddition reactions are concerted and stereospecific,[21] and several theoretical studies support this postulate.[22] However, we see no *economical* way to explain our unusual observations by assuming that the imido – allene cycloadditions are concerted processes. We therefore offer the stepwise mechanism illustrated in Figure 1 for (*S*,*S*)-**1** and 1,2-cyclononadiene, which proceeds through the diradical intermediate **C**,[23] as a working explanation for our results. The left-hand side of the diagram accounts for the kinetic resolution. It assumes that when the (*S*,*S*)-imido complex approaches the allene, perhaps to form the initial π complexes **A** and **B**, coordination of the (*S*) enantiomer of the allene gives the lower energy complex **A** because the two allene substituents can lie away from the N–Ar group and in the open quadrant of the metal coordination sphere. In complex **B**, however, the requirement that the external allene substituent lies away from the N–Ar moiety forces the internal allene substituent into the more sterically congested quadrant of the metal coordination sphere, to result in a higher energy complex. Subsequent formation of the C–N bond with rotation about one of the C–C bonds of the developing allyl radical results in the formation of intermediate **C**. However, the transition states $\mathbf{A}^{\ddagger}$ and $\mathbf{B}^{\ddagger}$, which lead to **C** and are not planar about the three carbon atom fragment, must still retain some of the energetics associated with the initial π complexes.[24] This accounts for the observation that one allene enantiomer reacts more quickly than the other. Once **C** has been reached, the chirality of the allene has been destroyed. Therefore a second enantioselective step is required to explain the observed stereochemistry of the metallacycle and the recovered less reactive. To account for this, we assume that ring closure in intermediate **C** can take place by rotation of the internal R group "up" into the open quadrant of the coordination sphere—which is favored—but not "down" into the more hindered quadrant.[25] Thus the same metallacycle (*S*,*S*,*R*)-**10** is formed from both allene enantiomers and the (*R*) allene enantiomer is always regenerated from this metallacycle.[26]

According to this mechanism, the selectivities of both the enantioselective capture and the retrocycloaddition reactions

 © WILEY-VCH Verlag GmbH, D-69451 Weinheim, 2000 1433-7851/00/3913-2341 $ 17.50+.50/0

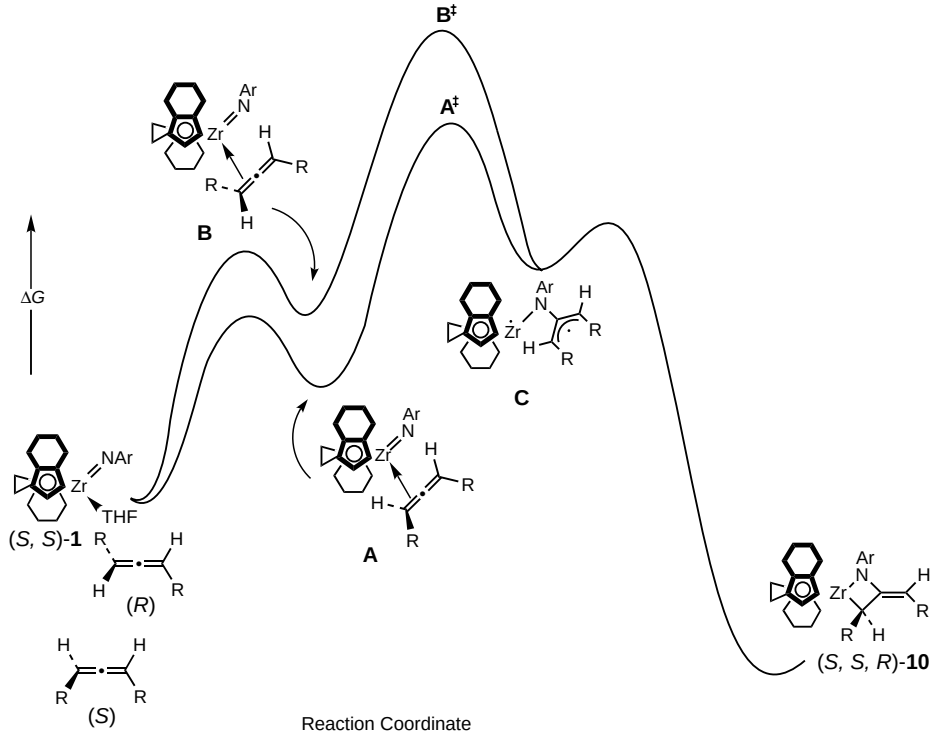


Figure 1. Reaction coordinate diagram illustrating the proposed mechanism of the reaction of imido complex (*S*,*S*)-**1** with both enantiomers of 1,2-cyclononadiene.

are a function of the free energy difference ($\Delta G^{\ddagger}_{A^{\ddagger}} - \Delta G^{\ddagger}_{B^{\ddagger}}$) for transition states $A^{\ddagger}$ and $B^{\ddagger}$. Therefore, if this model is correct, the selectivities of the enantioselective capture and retrocycloaddition reactions should be identical. Analysis of the cyclononadiene cycloaddition and retrocycloaddition reactions confirms that this is indeed the case. The selectivity of the enantioselective capture reaction in which (*S*,*S*)-**1** is treated with excess 1,2-cyclononadiene can be estimated using [Eq. (7)], where *s* is the selectivity of the reaction, *C* is the

$$s = \frac{\ln[(1 - C)(1 - ee)]}{\ln[(1 - C)(1 + ee)]} \qquad (7)$$

percentage of allene consumed in the reaction, and *ee* is the enantiomeric excess of the remaining allene.[27] Using the values in Table 1, a selectivity of 12.0 is calculated. This corresponds to a difference in the activation energies ($\Delta\Delta G^{\ddagger}$) of the reaction of the slower and faster reacting enantiomers of 1.5 kcal mol^{-1} at 298 K. A selectivity of 11.5 ($\Delta\Delta G^{\ddagger} =$ 1.4 kcal mol^{-1}, 298 K) for release of the chiral allene can be calculated directly from the enantiomeric ratio (92:8) of the cyclononadiene enantiomers following the retrocycloaddition reaction. The similarity of these values strongly supports the postulate that the formation and fragmentation of these metallacycles occur via the same pathway.

In summary, **1** undergoes highly enantioselective cycloaddition reactions and, in certain cases, this system allows conversion of an allene racemate into a mixture enriched in one enantiomer. The absolute sense of stereochemistry of these reactions appears to be so predictable that we believe they can be used to assign the absolute configurations of new, optically active allenes.

Experimental Section

(*rac*-**1**): A solution of *n*BuLi (0.50 mL of 1.6 M solution in Et_2O) was added dropwise to a stirred solution of 2,6-dimethylaniline (98 mg, 0.80 mmol) in Et_2O (5 mL) at RT to form a yellow solution. After 10 min, the yellow solution was added dropwise to a stirred suspension of *rac*-**5** (327 mg, 0.80 mmol) in THF (8 mL). This mixture was stirred overnight and the volatile materials were removed in vacuo to give a yellow residue. The yellow residue was dissolved in Et_2O and filtered. The volatile materials were removed in vacuo and the yellow solid was dissolved in THF (5 mL) and heated to 75 °C overnight in a sealed ampoule. The resulting orange solution was cooled to −30 °C overnight to precipitate 265 mg of *rac*-**1** (65 %) as orange crystals.

(*S*,*S*)-**1**: Solid LiNH(2,6-CH_3-C_6H_3) was added to a solution of (*S*,*S*)-**5** (299 mg, 0.73 mmol) in benzene. The resulting yellow solution was stirred for 1 h, the volatile materials were removed in vacuo, and the remaining solid was dissolved in pentane and filtered. The volatile materials were removed in vacuo and the yellow solid was dissolved in THF (7 mL) and heated to 75 °C overnight in a sealed ampoule. The volume of the resulting orange solution was reduced in vacuo and crystallization from THF/Et_2O at −30 °C provided (*S*,*S*)-**1** (210 mg, 53 %). ^{1}H NMR (C_6D_6): $\delta = 7.23$ (d, $J = 7.3$ Hz, 2H), 6.75 (t, $J = 7.3$ Hz, 1H), 6.37 (d, $J =$ 2.7 Hz, 1H), 5.78 (d, $J = 2.7$ Hz, 1H), 5.35 (d, $J = 2.4$ Hz, 1H), 5.30 (d, $J =$ 2.4 Hz, 1H), 3.63 (m, 2H), 3.38 (m, 2H), 3.05 (m, 1H), 2.83 (m, 1H), 2.67 (m, 3H), 2.51 (m, 11H), 2.21 (m, 2H), 1.72 (m, 1H), 1.46 (m, 6H), 1.15 (m, 5H). ^{13}C{^{1}H} NMR ([D_8]THF; assignments made by DEPT spectrum): quaternary: $\delta = 157.2$, 133.1, 130.1, 128.3, 127.5, 117.9, 115.7; methine: $\delta =$ 127.7, 115.0, 109.6, 108.2, 103.7, 100.5; α-methylene in coordinated THF: $\delta = 68.4$; methyl: $\delta = 26.55$; aliphatic CH_2: $\delta = 28.9$, 28.2, 26.4, 25.8, 25.4, 25.3, 24.9, 24.8, 24.7, 24.0. IR (Nujol): $\tilde{\nu} = 3061$, 2881, 1582, 1315, 1005, 844, 761 cm^{-1}. Elemental analysis: calcd for $C_{32}H_{41}NOZr$: C 70.28, H 7.56, N 2.56; found: C 70.07, H 7.83, N 2.50. M.p. (*rac*)-**1**: 145–158 °C; (*S*,*S*)-**1**: 170–185 °C. $[\alpha]_D^{25} = -665.5°$ ($c = 5.27$ mg mL^{-1}, C_6D_6).

Received: January 21, 2000 [Z 14578]

[1] a) B. Cornils, W. A. Herrmann, *Applied Homogeneous Catalysis with Organometallic Compounds*, *Vols. 1 & 2*, VCH, Weinheim **1996**, pp. 318 ff, 557 ff, 1150 ff.; b) M. P. Doyle, D. C. Forbes, *Chem. Rev.* **1998**, *98*, 911; c) K. H. Dötz, P. Tomuschat, *Chem. Soc. Rev.* **1999**, *28*, 187; d) R. H. Grubbs, S. Chang, *Tetrahedron* **1998**, *54*, 4413; e) M. Schuster, S. Blechert, *Angew. Chem.* **1997**, *109*, 2124; *Angew. Chem. Int. Ed. Engl.* **1997**, *36*, 2037; f) J. Feldman, R. R. Schrock in *Prog. Inorg. Chem.*, *Vol. 39* (Ed.: S. J. Lippard), Wiley, New York, **1991**, 1.
[2] a) W. A. Nugent, J. M. Meyer, *Metal–Ligand Multiple Bonds*, Wiley, New York, **1988**; b) D. E. Wigley in *Prog. Inorg. Chem.*, *Vol. 42* (Ed.: K. D. Karlin), Wiley, New York, **1994**; c) R. Taube in *Homogeneous Catalysis with Organometallic Compounds* (Eds.: B. Cornils, W. A. Herrmann), VCH, Weinheim, **1996**, Chap. 2.7.
[3] S. Minakata, T. Ando, M. Nishimura, I. Ryu, M. Komatsu, *Angew. Chem.* **1998**, *110*, 3596; *Angew. Chem. Int. Ed.* **1998**, *37*, 3392.
[4] Z. Li, R. W. Quan, E. N. Jacobsen, *J. Am. Chem. Soc.* **1995**, *117*, 5889.
[5] D. A. Evans, M. M. Faul, M. T. Bilodeau, *J. Am. Chem. Soc.* **1994**, *116*, 2742.
[6] E. A. Kretzschmar, J. Kipke, J. Sundermeyer, *Chem. Commun.* **1999**, 2381.
[7] X.-G. Zhou, X.-Q. Yu, J.-S. Huang, C.-M. Che, *Chem. Commun.* **1999**, 2377.

 © WILEY-VCH Verlag GmbH, D-69451 Weinheim, 2000 1433-7851/00/3913-2342 $ 17.50+.50/0

[8] P. O'Brien, *Angew. Chem.* **1999**, *111*, 339; *Angew. Chem. Int. Ed.* **1999**, *38*, 326.
[9] A. E. Rubin, K. B. Sharpless, *Angew. Chem.* **1997**, *109*, 2751; *Angew. Chem. Int. Ed. Engl.* **1997**, *36*, 2637.
[10] A. M. Baranger, P. J. Walsh, R. G. Bergman, *J. Am. Chem. Soc.* **1993**, *115*, 2753.
[11] S. W. Krska, R. L. Zuckerman, R. G. Bergman, *J. Am. Chem. Soc.* **1998**, *120*, 11828, and references therein.
[12] P. J. Walsh, F. J. Hollander, R. G. Bergman, *Organometallics* **1993**, *12*, 3705.
[13] F. R. W. P. Wild, M. Wasiucionek, G. Huttner, H. H. Brintzinger, *J. Organomet. Chem.* **1985**, *288*, 63.
[14] Enantioresolved complexes **1** and **5** were confirmed to be enantiopure by NMR analysis of the products formed by treating the zirconium complexes with enantiopure (*R*)-mandelic acid, as described by earlier workers: a) A. Schafer, L. Zsolnai, G. Huttner, H. H. Brintzinger, *J. Organomet. Chem.* **1987**, *328*, 87; b) R. B. Grossman, W. M. Davis, S. L. Buchwald, *J. Am. Chem. Soc.* **1991**, *113*, 2321; c) B. Chin, S. L. Buchwald, *J. Org. Chem.* **1997**, *62*, 2267.
[15] The reaction was stopped 10 min after addition of the allene.
[16] Enantioenrichments of the allenes were determined by chiral vapor-phase chromatography, in which the resolution is calibrated using racemic mixtures.
[17] Y. Noguchi, H. Takiyama, T. Katsuki, *Synlett* **1998**, 543.
[18] The configuration of cyclononadiene was assigned by comparison with material prepared in partially enantioenriched form by resolution with $[(-)\text{-(isopinylcampheyl)}_2\text{BH}]_2$. Resolution using this reagent is known to provide cyclononadiene enriched in the *S* enantiomer. See: a) R. D. Bach, J. W. Holubka, C. L. Willis, *J. Am. Chem. Soc.* **1982**, *104*, 3980; b) W. R. Moore, H. W. Anderson, S. D. Clark, *J. Am. Chem. Soc.* **1973**, *95*, 835.
[19] A. H. Hoveyda, J. P. Morken, *Angew. Chem.* **1996**, *108*, 1378; *Angew. Chem. Int. Ed. Engl.* **1996**, *35*, 1263.
[20] E. L. Eliel, S. H. Wilen, L. N. Mander, *Stereochemistry of Organic Compounds*, John Wiley and Sons, Inc., New York, **1994**, p. 837.
[21] B. R. Bender, D. L. Ramage, J. R. Norton, D. C. Wiser, A. K. Rappe, *J. Am. Chem. Soc.* **1997**, *119*, 5628.
[22] a) T. H. Upton, A. K. Rappe, *J. Am. Chem. Soc.* **1985**, *107*, 1206; b) E. Folga, T. Ziegler, *Organometallics* **1993**, *12*, 325.
[23] We postulate a diradical structure for the intermediate because the thermal dimerization of allenes is known to proceed via this type of species. For leading references, see: a) D. J. Pasto, *Tetrahedron*, **1984**, *40*, 2805; b) *The Chemistry of the Allenes* (Ed.: S. R. Landor), Academic Press, London, **1982**. However, with our presently available data, we cannot distinguish between a diradical and the corresponding zwitterion (presumably with a positive charge on Zr and a negative charge on the allyl moiety) or a π-allyl complex in which the C3 fragment in intermediate **C** is coordinated to the Zr center. Evidence has been proposed for diradical intermediates in several organometallic reactions; for examples, see: c) S. L. Buchwald, E. V. Anslyn, R. H. Grubbs, *J. Am. Chem. Soc.* **1985**, *107*, 1766; d) L. Cavallo; H. Jacobsen, *Angew. Chem.* **2000**, *112*, 602; *Angew. Chem. Int. Ed.* **2000**, *39*, 589, and references therein.
[24] The assumption of initial π-complex formation is convenient but not required to explain the enantioselective behavior of this system; the initial interaction between imido complex **1** and the allenes could lead directly to the transition states A^+ and B^+.
[25] There is, of course, a higher energy path leading from intermediate **C** to the more sterically congested isomer of the metallacycle. Because we do not observe detectable amounts of this product, we have omitted this pathway and product from the diagram for the sake of clarity.
[26] One can always postulate more complicated mechanisms that will also account for a particular set of experimental results. Therefore, as noted by two referees, we cannot rule out alternative scenarios in which the faster reacting allene enantiomer reacts by a concerted mechanism and the slower reacting allene reacts by a stepwise process proceeding through intermediate **C** or through a less stable diastereoisomer of (*S*,*S*,*R*)-**10**. Experiments are under way aimed at distinguishing these possibilities.
[27] H. B. Kagan, J. C. Fiaud, *Top. Stereochem.* **1988**, *18*, 249.

Oxygenation of Hydrocarbons Mediated by Mixed-Valent Basic Iron Trifluoroacetate and Valence-Separated Component Species under Gif-Type Conditions Involves Carbon- and Oxygen-Centered Radicals**

Amy E. Tapper, Jeffrey R. Long, Richard J. Staples, and Pericles Stavropoulos*

A remarkable series of iron-based systems for oxidizing hydrocarbons—such as the century-old Fenton reagent,[1] the biologically relevant Udenfriend system,[2] and the more recently developed Gif systems[3]—have received detailed attention, but the nature of the active oxidants involved (free HO•/RO• radicals or metal-bound $Fe^{IV/V}$=O/$Fe^{II/III}$–OO(H) units) and their mode of action (radical or concerted) are topics of current debate.[4, 5] Recent advances towards elucidating the functional behavior of high-valent Fe=O units, presumed to operate in biological monooxygenases (P-450,[6] sMMO[7]), have cast suspicion as to whether similar metal-centered oxidants participate in oxygenated Fenton,[4, 8] Gif,[9] and other allegedly biomimetic systems.[10] There is now consensus[11] that at least *t*BuOOH-dependent versions of these systems involve *t*BuO•/*t*BuOO• and substrate-centered radicals (RO•/ROO•). The recognition that *t*BuOOH-supported shunt pathways of P-450-type mimics[12] frequently generate *t*BuO•/*t*BuOO• radicals limits the usefulness of these systems in probing mechanistic distinctions. Evidence to support a radical mechanism[13] for mainstream H_2O_2- or O_2/Zn-dependent Gif-type systems is currently resting on insufficient experimental basis.[14] Reported in the present study is a persuasive case of a typical Gif reagent which performs oxidation of substrates with H_2O_2 in pyridine/trifluoroacetic acid (py/TFA) by radical pathways.

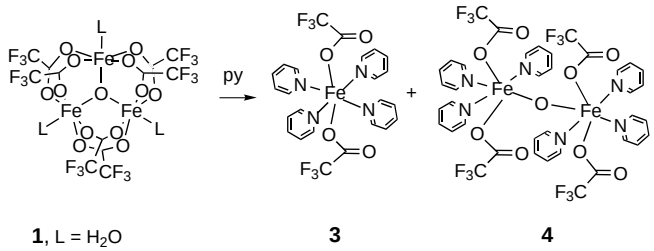
The reaction of $[Fe_3O(O_2CCH_3)_6(H_2O)_3]$ with excess TFA is known[15] to yield $[Fe_3O(O_2CCF_3)_6(H_2O)_3]\cdot 3.5\,H_2O$. In our hands, samples prepared in TFA/H_2O (4/1 v/v) afford red crystals of $[Fe_3O(O_2CCF_3)_6(H_2O)_3]\cdot 2.5\,H_2O\cdot CF_3COOH$ (**1**, see Scheme 1). The structure of **1** at 133 K (see the Supporting Information) indicates a valence-trapped state within the triangular Fe_3O core (av Fe^{III}–O 1.864(8), Fe^{II}–O 2.034(3) Å). In dimethyl sulfoxide (DMSO), **1** affords red $[Fe_3O(O_2CCF_3)_6(DMSO)_3]$ (**2**), whose structure at 213 K (see the Supporting Information) reveals partial valence trapping, as there is only a 0.065 Å difference between the longer and shorter Fe–O distances.

[*] Prof. P. Stavropoulos, A. E. Tapper
Department of Chemistry, Boston University
590 Commonwealth Avenue, Boston, MA 02215 (USA)
Fax: (+1) 617-353-6466
E-mail: stavro@chem.bu.edu.
Prof. J. R. Long
University of California, Berkeley, CA (USA)
Dr. R. J. Staples
Harvard University, Cambridge, MA (USA)

[**] This work was supported by the U.S. Environmental Protection Agency and the NIH/NIEHS (superfund).

Supporting information for this article is available on the WWW under http://www.wiley-vch.de/home/angewandte/ or from the author.

Surprisingly, solutions of **1** or **2** in pyridine afford green $[Fe^{II}(O_2CCF_3)_2(py)_4]$ (**3**) and red $[Fe^{III}_2O(O_2CCF_3)_4(py)_6]\cdot 2\,py$ (**4**, Scheme 1). Apparently, the stronger N-donor moiety



Scheme 1. Dissociation of $[Fe_3O(O_2CCF_3)_6(L)_3]$ (L = H_2O, DMSO) in pyridine.

weakens the *trans*-oriented Fe^{II}–O ligation to cause complete dissociation of the parent Fe_3O core structure. Compound **3** is also obtained from a solution of $[Fe(O_2CCF_3)_2]_n$ in pyridine. The structure of **3** (Figure 1)[16] reveals a distorted octahedral

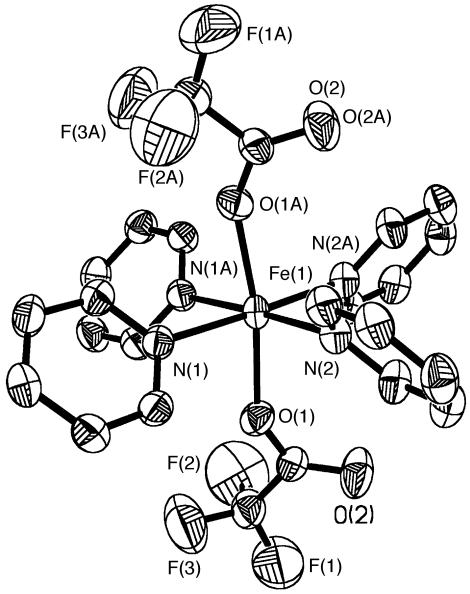


Figure 1. The structure of **3**. Selected bond lengths [Å] and angles [°]: Fe(1)–O(1) 2.069(2), Fe(1)–N(1) 2.220(3), Fe(1)–N(2) 2.205(3); O(1)-Fe(1)-O(1A) 169.90(13), N(1)-Fe(1)-N(1A) 88.95(14).

Fe environment with an imposed C_2 axis bisecting the symmetry-related N(1)-Fe(1)-N(1A) and N(2)-Fe(1)-N(2A) angles. Compound **4**, prepared independently from $[Et_4N]_2[Fe_2OCl_6]$ and CF_3CO_2Na, features a nearly linear μ-oxo bridge, linking two ferric sites that differ slightly in their metrical parameters (Figure 2).[16]

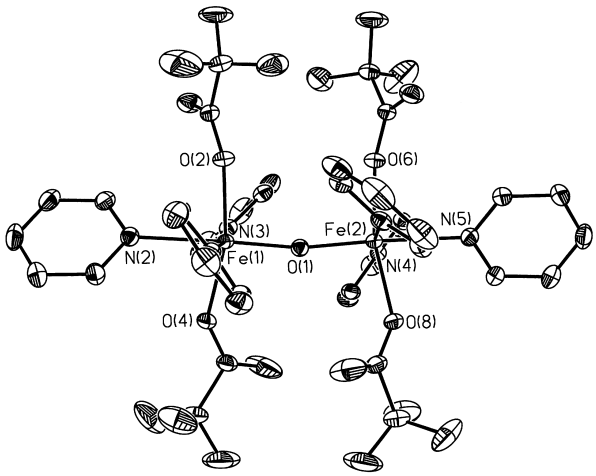
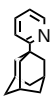
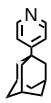


Figure 2. The structure of **4**. Selected bond lengths [Å] and angles [°]: Fe(1)–O(1) 1.7878(13), Fe(2)–O(1) 1.7854(14), Fe(1)–N(2) 2.304(2), Fe(1)–N(3) 2.160(2), Fe(1)–O(2) 2.0341(15), Fe(2)–N(5) 2.310(2), Fe(2)–N(4) 2.195(2), Fe(2)–O(6) 2.0415(15); Fe(1)-O(1)-Fe(2) 169.48(10).

Table 1 shows profiles of products derived from oxidations of the benchmark substrate adamantane (5 mmol) by the system **3** (or **4**)/H_2O_2 (0.2/2.0 mmol) in py/TFA (30.0/3.0 mL) under a stream of Ar, O_2 (4%) in N_2, or pure O_2. Similar results (not shown) are obtained with **1**, apparently because **1** dissociates to **3** and **4** in py/TFA. In addition to the expected oxo products, 2- and 4-adamantylpyridines are obtained not only for the *tert*-adamantyl positions (as previously recognized),[3] but also for the *sec*-adamantyl sites, especially under Ar. The presence of these coupled products provides direct evidence for the generation of *tert*- and *sec*-adamantyl radicals.[17] The reported absence of *sec*-alkylpyridines in the product profile of Gif oxygenations had led Barton and Doller[3] to propose that at least the activation of *sec* C–H bonds is brought about by nonradical pathways. Under O_2, the ratio of products derived due to competition between O_2

Table 1. Product profiles for the oxidation[a] of adamantane by H_2O_2 mediated by **3** or **4** and via authentic adamantyl radicals.[a,b]

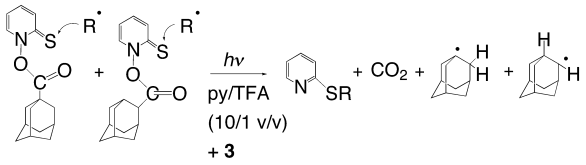
System	Substrate	Products [mmol]							Ratio[c]
									
3/Ar		0.001	nd[d]	0.004	0.124	0.085	0.132	0.124	2.4
3/O_2 (4%)		0.003	0.016	0.117	0.120	0.077	0.018	0.018	3.5
3/O_2		0.034	0.027	0.143	0.128	0.078	0.001	0.001	4.2
4/Ar		0.001	0.002	0.036	0.100	0.065	0.057	0.057	3.3
4/O_2 (4%)		0.003	0.011	0.095	0.088	0.059	0.010	0.011	3.5
4/O_2		0.025	0.015	0.098	0.091	0.056	0.001	nd[d]	4.5
3/O_2 (4%)[b]		0.002	trace	0.027	0.029	0.032	0.002	0.003	

[a] See text for conditions. [b] By photolysis of the PTOC esters of Barton et al.[19] [c] Ratio of products (tertiary/secondary) obtained via tertiary and secondary adamantyl radicals. [d] nd = not detected.

 © WILEY-VCH Verlag GmbH, D-69451 Weinheim, 2000 1433-7851/00/3913-2344 $ 17.50+.50/0 *Angew. Chem. Int. Ed.* **2000**, *39*, No. 13

and $[pyNH]^+$ in trapping adamantyl radicals shifts profoundly in favor of oxo species at the secondary position and to a much lesser extent at the tertiary site. Minisci et al.[18] have traced this behavior to the superior rate constant (by two orders of magnitude) and inferior reversibility for the addition reaction of *tert*-adamantyl versus *sec*-adamantyl radicals to protonated pyridine.

Generation of *tert*- and *sec*-adamantyl radicals in the presence of **3** by photolysis of the appropriate PTOC esters of Barton et al.[19] (Scheme 2) in py/TFA under O_2 (4%) provides ratios of oxo- versus pyridine-trapped adamantyl



Scheme 2. Generation of authentic *tert*- and *sec*-adamantyl radicals.

products (Table 1) which for both the tertiary (0.03) and secondary positions (5.4) are comparable to those obtained by the analogous Gif experiment (*tert* 0.02, *sec* 3.7). Therefore the product profiles of adamantane oxidation are entirely dictated by the generation of *tert*- and *sec*-adamantyl radicals.

The normalized tertiary/secondary selectivities suggest that a fairly indiscriminate oxidant is involved under Ar, coupled to a more selective oxidant in the presence of O_2. The addition reaction of HO$^\bullet$ to DMSO [Eq. (1)] and the competitive hydrogen abstraction from EtOH [Eq. (2)] have been used[20]

$$Me_2S{=}O + HO^\bullet \longrightarrow \underset{(92\,\%)}{MeS(=O)OH} + Me^\bullet \quad (1)$$

$$CH_3CH_2OH + HO^\bullet \longrightarrow \underset{(13.2\,\%)}{^\bullet CH_2CH_2OH} + \underset{(84.3\,\%)}{CH_3{}^\bullet CHOH} \quad (2)$$

to investigate the possible involvement of HO$^\bullet$, by monitoring the formation of pyridine-trapped alkyl radicals produced in these reactions under a constant stream of Ar. Table 2 reveals that the reagent **3**/H_2O_2 oxidizes DMSO/EtOH (5 mmol/3–10 mmol) in py/TFA (30.0/3.0 mL) as predicted by Equations (1) and (2).

Furthermore, the average k_{EtOH}/k_{DMSO} value of 0.32(4), roughly evaluated from the ratio of methylpyridines over hydroxyethylpyridines and the initial concentrations of DMSO and EtOH, is consistent with the ratio of rate constants ($k_{EtOH}/k_{DMSO} = 0.29$) reported[20] by virtue of HO$^\bullet$ attack on DMSO/EtOH in aqueous pulse radiolysis experiments. The reaction in Equation (3), which is known[21] to proceed at near diffusion controlled rates, may limit the preciseness of the assessment, further assisted by the reversibility of the addition reaction of α-hydroxyethyl radicals to $[pyNH]^+$.[17]

$$Fe^{III} + CH_3{}^\bullet CHOH \longrightarrow Fe^{II} + H^+ + CH_3CHO \quad (3)$$

However, the total amount of iron is kept at low levels with respect to py/TFA. Most importantly, it is found that Fe^{III} sites are destabilized by the electron-withdrawing TFA (or picolinate[22]), and are rapidly reduced to Fe^{II} in the presence of stoichiometric amounts of H_2O_2, probably in conjunction with H_2O_2 dismutation. This further argues in support of a central role for the Fe^{II}/H_2O_2 combination in generating the active oxidant. In a reinterpretation of the Gif mechanism, Barton et al.[23] had accepted that the Fe^{II}/H_2O_2 "manifold" (as opposed to Fe^{III}/H_2O_2) produces substrate-based alkyl radicals, but maintained that the active oxidant is $Fe^{IV}{=}O$.

The present results provide compelling evidence that HO$^\bullet$ is the key hydrogen-abstracting oxidant under Ar, coupled to a more selective oxidant (most likely substrate-centered alkoxyl radicals: R$^\bullet \rightarrow$ROO$^\bullet \rightarrow$RO$^\bullet$) under increasing partial pressures of dioxygen. In conclusion, the findings of this report lend further support to the proposition[5] of a preponderant, carbon- and oxygen-centered radical pathway for mainstream Gif systems.

Experimental Section

A typical oxidation of adamantane was conducted as follows: The iron reagent (0.20 mmol) was dissolved under anaerobic conditions in pyridine (30.0 mL) and TFA (3.0 mL) followed by addition of adamantane (681 mg, 5.0 mmol). Degassed H_2O_2 (aq. 30%, 0.28 mL, 2.0 mmol) was added slowly (6 h) using a syringe pump under a flow of specified gas. At the end of the reaction, oxalic acid (5 equiv per Fe) and PPh_3 (2 equiv per H_2O_2) were added followed by the internal standard (1,3,5-triisopropylbenzene). An aliquot (2 mL) was withdrawn for ether extraction and GC (SPB-1 column) or GC/MS analysis.

Received: February 16, 2000 [Z14721]

[1] C. Walling, *Acc. Chem. Res.* **1975**, *8*, 125–131.
[2] S. Udenfriend, C. T. Clark, J. Axelrod, B. B. Brodie, *J. Biol. Chem.* **1954**, *208*, 731–739.
[3] D. H. R. Barton, D. Doller, *Acc. Chem. Res.* **1992**, *25*, 504–512.
[4] a) P. A. MacFaul, D. D. M. Wayner, K. U. Ingold, *Acc. Chem. Res.* **1998**, *31*, 159–162; b) C. Walling, *Acc. Chem. Res.* **1998**, *31*, 155–157; c) S. Goldstein, D. Meyerstein, *Acc. Chem. Res.* **1999**, *32*, 547–550.
[5] M. J. Perkins, *Chem. Soc. Rev.* **1996**, 229–236.

Table 2. Product profiles of the oxidation of DMSO/EtOH by H_2O_2 mediated by **3** in py (30.0 mL)/TFA (3.0 mL) under Ar.

	Products [mmol]							k_{EtOH}/k_{DMSO}
								
1[a]	0.198	0.026	0.099					
2[b]	0.154	0.016	0.078	0.026	0.011	0.003	0.002	0.29
3[c]	0.179	0.020	0.090	0.092	0.038	0.013	0.005	0.36
4[d]	0.118	0.016	0.059	0.080	0.029	0.009	0.004	0.32

[a] DMSO (5 mmol). [b] DMSO (5 mmol)/EtOH (3 mmol). [c] DMSO (5 mmol)/EtOH (7 mmol). [d] DMSO (5 mmol)/EtOH (10 mmol).

 © WILEY-VCH Verlag GmbH, D-69451 Weinheim, 2000 1433-7851/00/3913-2345 $ 17.50+.50/0

[6] M. Sono, M. P. Roach, E. D. Coulter, J. H. Dawson, *Chem. Rev.* **1996**, *96*, 2841 – 2887.
[7] B. J. Wallar, J. D. Lipscomb, *Chem. Rev.* **1996**, *96*, 2625 – 2657.
[8] D. T. Sawyer, A. Sobkowiak, T. Matsushita, *Acc. Chem. Res.* **1996**, *29*, 409 – 416.
[9] M. Newcomb, P. A. Simakov, S.-U. Park, *Tetrahedron Lett.* **1996**, *37*, 819 – 822.
[10] P. A. MacFaul, K. U. Ingold, D. D. M. Wayner, L. Que Jr., *J. Am. Chem. Soc.* **1997**, *119*, 10594 – 10598.
[11] a) F. Minisci, F. Fontana, S. Araneo, F. Recupero, L. Zhao, *Synlett* **1996**, 119 – 125; b) D. H. R. Barton, *Synlett* **1997**, 229 – 230.
[12] B. Meunier, *Chem. Rev.* **1992**, *92*, 1411 – 1456.
[13] M. J. Perkins, *Chem. Soc. Rev.* **1996**, 229 – 236.
[14] M. Newcomb, P. A. Simakov, S.-U. Park, *Tetrahedron Lett.* **1996**, *37*, 819 – 822.
[15] V. I. Ponomarev, O. S. Filipenko, L. O. Atovmyan, S. A. Bobkova, K. I. Turtè, *Sov. Phys. Dokl.* **1982**, *27*, 6 – 9.
[16] Crystal data for **3** (213 K) with $Mo_{K\alpha}$ radiation ($\lambda = 0.71073$ Å): orthorhombic, space group *Pccn*, $a = 16.698(5)$, $b = 9.074(2)$, $c = 16.587(4)$ Å, $V = 2513(1)$ Å^3, $Z = 4$, $R_1 = 0.0478$ for 2156 data with $I > 2\sigma(I)$, GOF (on F^2) = 1.108. For **4** (213 K): orthorhombic, space group $P2_12_12_1$, $a = 13.3830(1)$, $b = 16.4843(2)$, $c = 24.1315(2)$ Å, $V = 5323.60(8)$ Å^3, $Z = 4$, $R_1 = 0.0327$ for 9486 data with $I > 2\sigma(I)$, GOF (on F^2) = 1.055. Further details on the crystal structure investigations may be obtained from the Fachinformationszentrum Karlsruhe, 76344 Eggenstein-Leopoldshafen, Germany (fax: (+49) 7247-808-666; e-mail: crysdata@fiz-karlsruhe.de), on quoting the depository numbers CSD-411108 (**3**) and -411109 (**4**).
[17] F. Minisci, E. Vismara, F. Fontana, *Heterocycles* **1989**, *28*, 489 – 519.
[18] F. Recupero, A. Bravo, H.-R. Bjørsvik, F. Fontana, F. Minisci, M. Piredda, *J. Chem. Soc. Perkin Trans. 2* **1997**, 2399 – 2405.
[19] D. H. R. Barton, F. Halley, N. Ozbalik, M. Schmitt, E. Young, G. Balavoine, *J. Am. Chem. Soc.* **1989**, *111*, 7144 – 7149.
[20] G. V. Buxton, C. L. Greenstock, W. P. Helman, A. B. Ross, *J. Phys. Chem. Ref. Data* **1988**, *17*, 513 – 886.
[21] F. Minisci, A. Citterio, E. Vismara, *Tetrahedron* **1985**, *41*, 4157 – 4170.
[22] S. Kiani, A. Tapper, R. J. Staples, P. Stavropoulos, *J. Am. Chem. Soc.*, submitted.
[23] D. H. R. Barton, B. Hu, D. K. Taylor, R. U. Rojas Wahl, *J. Chem. Soc. Perkin Trans. 2* **1996**, 1031 – 1041.

Synthesis, Characterization, and Catalytic Activity of a Large-Pore Tridirectional Zeolite, H-ITQ-7**

Avelino Corma,* María José Díaz-Cabañas, and Vicente Fornés

Zeolites are probably the most widely used solid catalysts in refining, petrochemistry, and fine chemical production. This is especially true for the acid zeolites, (H-zeolites). Their success is derived from properties such as high surface area, high adsorption capacity, molecular sieve characteristics, and the possibility of preparation with a well defined number of uniformly active sites;[1] these sites are introduced by direct synthesis or by postchemical treatment.[2] Considering the channel size, zeolites are classified as ultralarge (>12 membered rings (MR)), large (12-MR), medium (10-MR) or small (8-MR) pore materials depending on the number of T atoms that limits the pore aperture of their largest channels (T represents atoms from the aluminum and silicon families). While zeolites with small pores have found some specific applications in, for instance, the conversion of methanol to olefins[3], the most successful zeolitic catalysts are those based on zeolites with medium and large pores. More specifically, large-pore zeolites have unique properties for dealing with many of the oil fractions involved in refinery processes (cracking, hydrocracking, hydroisomerization, among others), in petrochemistry (including benzene alkylation with olefins, isomerization and disproportionation of alkylaromatic species), and in fine chemical production (such as alkylation, acylation, isomerization, and esterification).

It must be noted, for many of the processes named above, a rapid diffusion of the reactants and products is desired and this is better achieved with large-pore tridirectional zeolites. Until recently, however, only two large-pore tridirectional zeolites were synthesized, faujasite and Beta, and of these only the Beta zeolite can be directly synthesized with a high Si:Al ratio and therefore does not need, unlike the faujasites, a postsynthesis dealumination. Therefore, owing to the large catalytic interest and very limited number of large-pore tridirectional zeolites, a considerable effort has been devoted in the last decade to produce such structures[4]. Very recently,[5] the pure silica form of a new large-pore tridirectional zeolite has been presented, named ITQ-7 (Instituto de Tecnología Química-7). Unfortunately, the authors were unable to introduce acidity into ITQ-7 by direct synthesis with the trivalent (Al and Ga family) atoms in an isomorphically substituted zeolite[6]. Therefore, this large-pore tridirectional zeolite have had no possibilities in catalysis since only the purely siliceous form was available. Herein, we present the possibility to synthesize ITQ-7 with different T^{III} and T^{IV} elements isomorphically incorporated into the framework and, in this way, acidic, catalytically active ITQ-7 materials have been prepared.

The synthesis of isomorphically substituted zeolites was attempted following two strategies. The first strategy consists of synthesizing a boron-containing ITQ-7 (B-ITQ-7) sample which already should present some weak acidity and then, in a further step, to exchange B with Al to yield materials, named B/Al-ITQ-7, with a much greater acidity than the B-ITQ-7 precursor. The second strategy involves the direct synthesis of Al-ITQ-7. The two synthesis routes will be described below.

B-ITQ-7: Boron-containing ITQ-7 was formed from a gel with the composition SiO_2:B_2O_3:$C_{14}H_{26}NOH$:HF:H_2O in a molar ratio 1.0:0.01:0.50:0.50:3.0, where $C_{14}H_{26}NOH$ is 1,3,3-trimethyl-6-azonium-tricyclo[3.2.1.4^{6,6}]dodecane hydroxide. The gel was prepared by dissolving H_3BO_3 (0.08 g) in a solution of $C_{14}H_{26}NOH$ (0.99 M, 31.98 g). Tetraethylorthosilicate (TEOS, 13.46 g) was then hydrolyzed in the solution and the mixture was stirred gently to completely evaporated the ethanol formed. Finally, HF (1.34 g as 48.1 % in water) and purely siliceous ITQ-7 crystals (0.20 g) were added and the mixture was homogeneized. After 7 days crystallization at

[*] Prof. A. Corma, M. J. Díaz-Cabañas, V. Fornés
Instituto de Tecnología Química
UPV-CVSIC Universidad Politécnica de Valencia
Avda. de los Naranjos s/n, 46022 Valencia (Spain)
Fax: (+34) 96-387-78-09
E-mail: acorma@itq.upv.es

[**] We thank the Spanish CICYT for financial support (Project MAT97-1016-C02-01).

 © WILEY-VCH Verlag GmbH, D-69451 Weinheim, 2000 1433-7851/00/3913-2346 $ 17.50+.50/0

423 K in a PTFE-lined stainless steel autoclave rotating at 60 rpm, the powder obtained was washed, dryed at 373 K, and calcined at 853 K for 3 hours to yield a material whose X-ray diffraction (XRD) pattern closely corresponds to that obtained for the purely siliceous ITQ-7 (Figure 1 a). The ^{11}B MAS NMR spectra of the uncalcined sample showed the

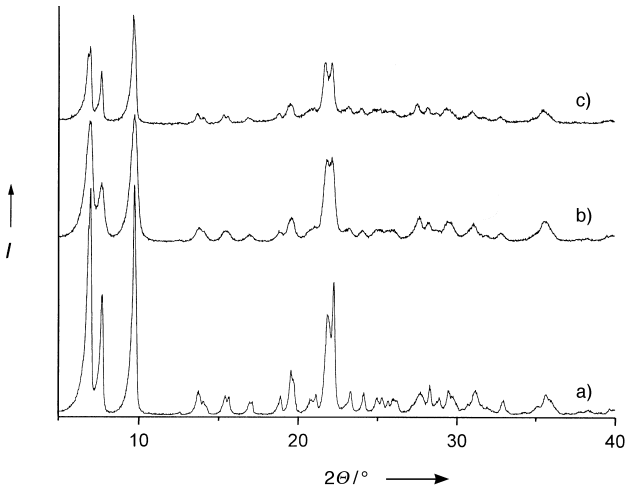


Figure 1. XRD patterns of calcined ITQ-7 samples: a) B-ITQ-7; b) Ge-ITQ-7; c) Al/Ge-ITQ-7.

presence of tetrahedrally coordinated boron (−3 ppm, spectrum not shown).[7] During the activation of the sample by calcination, the thermal decomposition of the structure directing agent (SDA; in this case $C_{14}H_{26}NOH$) was followed by IR spectroscopy. A 10 mg cm^{-2} self-supported wafer of the as-synthesized sample was introduced in an IR cell and the sample was heated to effect the complete disappearance of the IR bands of the SDA. Figure 2 shows the IR spectra of the ITQ-7 sample, in which of IR bands at 2955 cm^{-1} (ν_{asym}), 2873 cm^{-1} (ν_{sym}) and 1460 cm^{-1} (δ_{sciss}) are assigned to CH_2 groups and a shoulder at 2972 cm^{-1} (ν_{asym}) and a band at 1398 cm^{-1} (ν_{asym}) correspond to terminal CH_3 groups. Upon heating in vacuum (10^{-3} Pa), a slow and homogeneous decrease of the IR intensities occur. At 573 K, a new band appears at 1685 cm^{-1} while the intensity of the bands assigned to CH_3 groups decreases. The intensity of this new band increases with temperature up to 673 K and, at the same time, the bands of the methyl groups vanish and the total intensity of the IR spectrum strongly decreases. This change must be related to the partial decomposition of the SDA. The presence of the 1685 cm^{-1} band, tentatively assigned to an imine $\nu_{-C=N-}$ stretching vibration[8], suggests the formation of these compounds during the process. It seems reasonable to assume that the elimination mechanism occurs by breaking the SDA, at the C–N bond, into the five member ring imine and the remainder of the molecule, which includes all of the CH_3 groups. The imine moiety remains in the zeolite structure and the rest of the SDA decomposes. The imine moiety is fully lost at 773 K.

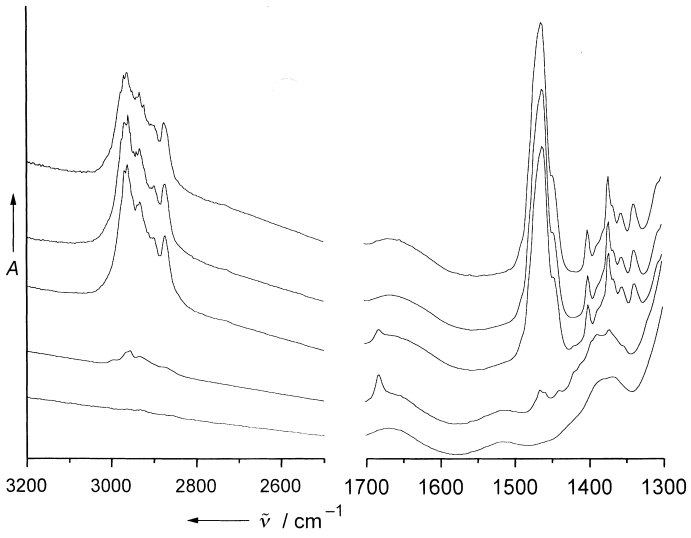


Figure 2. Infrared spectra of as-synthesized B-ITQ-7 sample. From top to bottom, the spectra are at room temperature and heated under vacuum at temperatures of 473, 573, 673, and 773 K.

The B-ITQ-7 sample was calcined and boron was exchanged with aluminum to form B/Al-ITQ-7 by following the procedure of Lobo and Davis[9]. The exchanged sample has a bulk Si:Al ratio of 90:1, as determined by elemental analysis, and the ^{27}Al MAS NMR spectrum (Figure 3 a) shows that most of the Al atoms occupy framework positions (54 ppm).

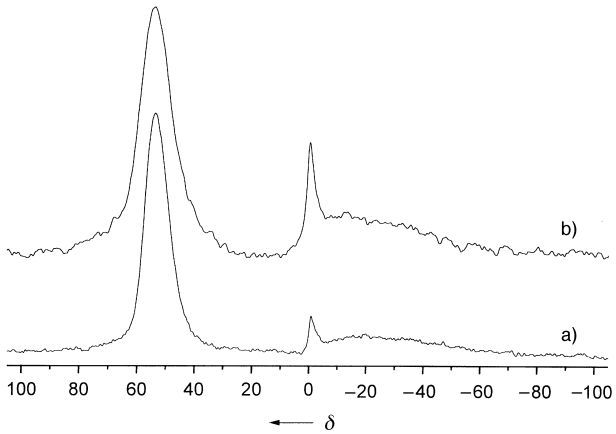


Figure 3. ^{27}Al MAS NMR spectra of calcined ITQ-7 samples: a) B/Al-ITQ-7, b) Al/Ge-ITQ-7.

To determine the Brønsted and Lewis acidities of the aluminum-exchanged sample, pyridine adsorption/desorption experiments were performed. The IR spectrum of the B/Al-ITQ-7 sample in the ν_{OH} region shows (Figure 4 a 1) the presence of three bands at $\tilde{\nu} = 3745$, 3628, and 3595 cm^{-1}. The first band is assigned to silanol groups, while the other two bands should be attributed to exposed hydroxyl groups of the acidic sites, as they vanish upon pyridine adsorption (Figure 4 a 2). The IR spectra of the adsorped pyridine in the 1350–1750 cm^{-1} region (Figure 4 b) show the relative intensities of the 1545 cm^{-1} (Brønsted) and 1455 cm^{-1} (Lewis) acid sites after desorption at different temperatures. This temperature-dependant desorption indicates that the majority of the Brønsted acid sites are of medium strength (423 K) while

 © WILEY-VCH Verlag GmbH, D-69451 Weinheim, 2000 1433-7851/00/3913-2347 $ 17.50+.50/0

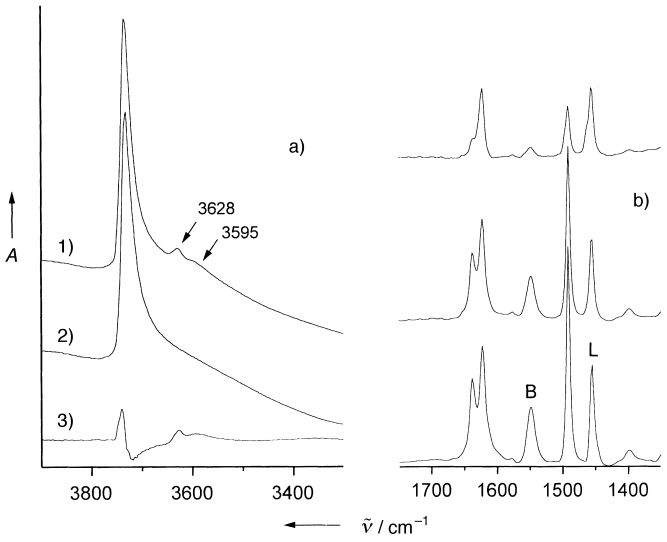


Figure 4. a) IR spectra in the OH stretching region of Al-ITQ-7: 1) after treatment at 673 K in vacuum, 2) after adsorbing pyridine at 523 K and 3) the differential spectrum. b) IR spectra of the adsorbed pyridine, which is then desorbed at (bottom to top) 423, 523, and 623 K. The IR spectra are offset for clarity. Labels B and L represent Brønsted and Lewis acid sites, respectively.

some remaining sites are of high strength (pyridine signal at >623 K). Lewis acid sites are strongly acidic, since pyridine remains adsorbed at temperatures as high as 623 K.

The presence of sites with medium and strong acidities in the B/Al-ITQ-7 sample opened the possibility of using this material as acid catalyst. In order to estimate its catalytic behaviour, the sample was tested by the catalytic cracking of *n*-decane and the conversion was compared with that obtained with a Beta zeolite with the same Si:Al ratio. The results, given in Figure 5, clearly show that the B/Al-ITQ-7 is active and its activity is close to that of Beta zeolite.

Al-ITQ-7: When we have attempted to introduce Al under the synthesis conditions reported previously,[6] an amorphous material was obtained even when using Si:Al ratios of 100:1 in the synthesis gel. When seeded with purely siliceous ITQ-7, an amorphous material with some XRD peaks of ITQ-7 was obtained after 30 days crystallization, while under other synthesis conditions, Beta zeolite was produced when Al was added to the gel. It seems that the distortion created in the framework by introducing Al may complicate the nucleation and growth of the ITQ-7 structure.

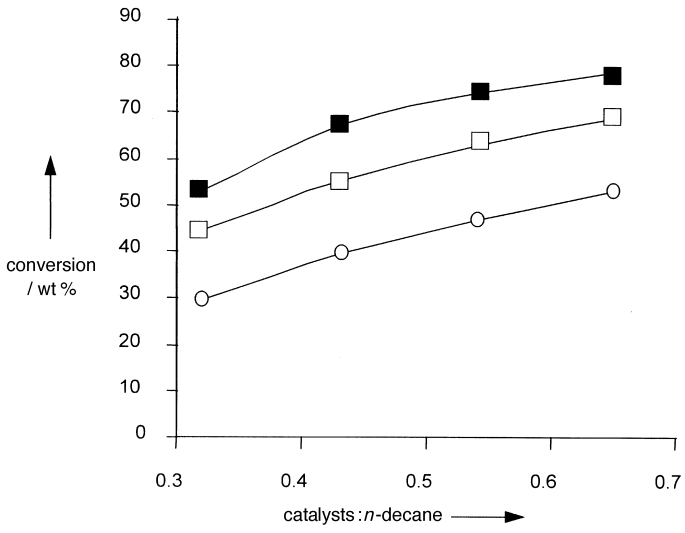


Figure 5. Cracking of *n*-decane on (□) B/Al-ITQ-7, (○) Al/Ge-ITQ-7, and (■) Beta zeolites at atmospheric pressure, 773 K, and 60 s on stream.

Recently, it has been proposed[10] that the addition of T atoms to the synthesis gel that are not Si but which can also coordinate tetrahedrally can produce different zeolitic structures, even when using the same organic SDA. It appears then that the effect of added heteroatoms on the structure of the zeolite should be due to the T-O-T′ bond lengths and angles which can direct the formation of particular secondary building units. In a recent theoretical study,[11] we found, by using periodic models and ab initio methods, that the introduction of germanium in the zeolite framework produces an increase in the framework flexibility because of the less rigid GeO_4 units and, as a consequence, we concluded that structures containing Ge could stabilize other, non-silicon framework cations, such as Ti and Al. Following this concept, we thought that a Si/Ge-ITQ-7 sample, if it could be synthesized, may be better able to cope with the framework distortions created by introducing Al.

The following synthesis gel of composition SiO_2:GeO_2:$C_{14}H_{26}NOH$:HF:H_2O in a molar ratio 1.0:0.10:0.55:0.55:3.30 was thus prepared. A quantity of GeO_2 (0.71 g) was dissolved in a solution of $C_{14}H_{26}NOH$ (1.06 M, 38.60 g). Then, TEOS (14.18 g) was added, allowed to hydrolyse, and the ethanol formed was left to evaporate. Finally, HF (1.56 g as 48.1 % in water) was added. After 7 days crystallization at 423 K, Ge-ITQ-7 was obtained (Figure 1 b) as the unique phase. The ^{29}Si MAS NMR spectra of the calcined sample (Figure 6) shows, in addition to a small concentration of defects (denoted by a resonance around -100 ppm due to Q_3 species), a marked decrease in the resolution of the bands corresponding to Q_4 species as

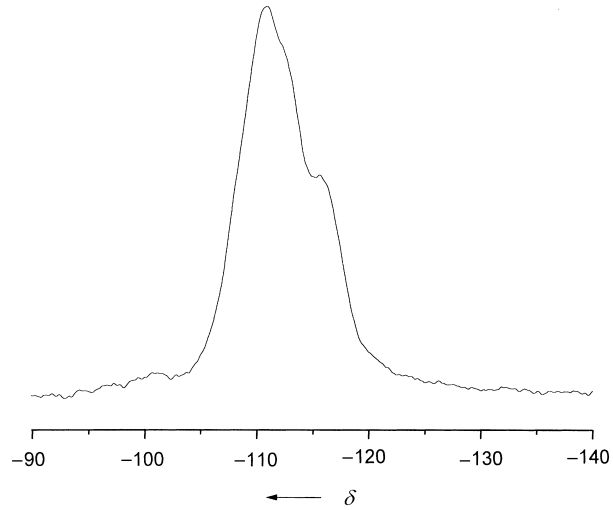


Figure 6. ^{29}Si MAS NMR spectrum of calcined Ge-ITQ-7.

 © WILEY-VCH Verlag GmbH, D-69451 Weinheim, 2000 1433-7851/00/3913-2348 $ 17.50+.50/0

compared with those reported for the purely siliceous ITQ-7[5]. This can probably be attributed to the presence of Ge in the framework. An interesting observation is that while the purely siliceous sample presents crystallite sizes of ~ 2.0 μm, Ge-ITQ-7 forms very small crystallites with dimensions (> 0.1 μm) close to those of nanocrystalline zeolites (Figure 7). This result is extremely interesting, from the catalytic point of view, when treating molecules with smaller diffusion coefficients.

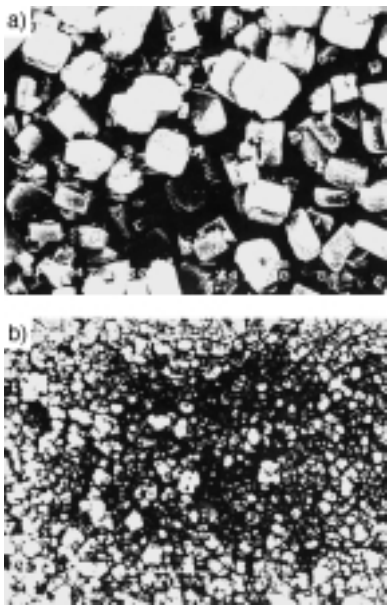


Figure 7. Scanning electron micrographs of a) purely siliceous ITQ-7 and b) Ge-ITQ-7.

After succeeding in the synthesis of Ge-ITQ-7, the incorporation of Al was attempted by preparing a gel with of composition SiO_2:GeO_2:Al_2O_3:$C_{14}H_{26}NOH$:HF:H_2O in a molar ratio 1.0:0.10:0.02:0.55:0.55:3.30. After 7 days crystallization at 423 K, Al/Ge-ITQ-7 was obtained (Figure 1c). The Al content was 1.2 wt % in the form of Al_2O_3. The ^{27}Al MAS NMR spectrum (Figure 3b) indicates that the majority of Al is tetrahedrally coordinated ($\delta = 54$) but some octahedral Al ($\delta = 0$) is present. In the IR spectrum of Al/Ge-ITQ-7 after pyridine adsorption (spectrum not shown), a $\tilde{\nu} = 1545$ cm^{-1} band attributed to pyridinium ions is observed, which indicates that this sample possesses a strong acidity.

The catalytic behaviour of the Al/Ge-ITQ-7 was tested by means of the catalytic cracking of *n*-decane and the results (Figure 5) indicate that the activity of this sample is lower than the B/Al-ITQ-7. This is in agreement with the greater amount of extra-framework Al present in Al/Ge-ITQ-7.

In conclusion, the T^{III}- and T^{IV}-substituted ITQ-7 zeolites have been synthesized and acid catalysts could be derived. For B-ITQ-7, boron occupies framework positions and generates mildly acid sites. The B can be exchanged with Al and, in the resultant B/Al-ITQ-7, the Al is in mostly in tetrahedral framework positions, to generate strongly acid sites that are very active for the cracking of *n*-decane. Germanium can also be introduced in the framework by direct synthesis, with a concomitant modification in the morphology of ITQ-7. When Ge is present in the synthesis gel, Al can be directly introduced in the framework of ITQ-7. The resultant Al/Ge-ITQ-7 zeolite is also acidic and catalyticaly active.

Received: February 21, 2000 [Z 14749]

[1] A. Corma, *Chem. Rev.* **1995**, *95*, 559.
[2] H. Hamdan, B. Sulikowski, J. Klinowski, *J. Phys. Chem.* **1989**, *93*, 350.
[3] S. W. Kaiser, US Patent 4499327, **1985**; [*Chem. Abstr.* **1984**, *101*, 24133v]; C. D. Chang, *Catal. Rev. Sci. Eng.* **1984**, *26*, 323.
[4] Y. Kubota, M. M. Helmkamp, S. I. Zones, M. E. Davis, *Microporous Mater.* **1996**, *6*, 213.
[5] L. A. Villaescusa, P. A. Barret, M. A. Camblor, *Angew. Chem.* **1999**, *111*, 2164; *Angew. Chem. Int. Ed.* **1999**, *38*, 1997.
[6] L. A. Villaescusa, PhD thesis, Universidad Politécnica de Valencia (Spain), **1999**.
[7] R. Bandyopadhyay, Y. Kubota, N. Sugimoto, Y. Fukushima, Y. Sugi, *Microporous Mesop. Mater.* **1999**, *32*, 81.
[8] L. J. Bellamy, *The Infrared Spectra of Complex Molecules*, Chapman and Hall, London, **1975**.
[9] R. F. Lobo, M. E. Davis, *Microporous Mater.* **1994**, *3*, 61.
[10] T. Takewaki, L. W. Beck, M. E. Davis, *Microporous Mesop. Mater.* **1999**, *33*, 197.
[11] C. M. Zicovich-Wilson, A. Corma, *J. Phys. Chem. B* **2000**, *104*, 4134.

Infinite, Linear, Unbranched Borynide Chains in LiB_x—Isoelectronic to Polyyne and Polycumulene**

Michael Wörle* and Reinhard Nesper*

Dedicated to Professor Peter Paetzold on the occasion of his 65th birthday

One of the great challenges in carbon chemistry is the synthesis of unbranched, linear chain modifications of carbon, the carbynes. Such carbynes are expected to have interesting physical properties like exceptional mechanical strength as well as one-dimensional conductivity and display an unusual variety of soliton and polaron states under appropriate doping conditions.[1] An infinite, linear, unbranched carbon chain can adopt the acetylenic $-[C{\equiv}C-]_nC{\equiv}$ (α carbyne) or the cumulenic form $=[C{=})]_nC=$ (β carbyne).[1–3] A main problem in synthesizing these carbon chains is their tendency to undergo interchain polymerization reactions of the Diels–Alder type.[2, 4, 5]

[*] Dr. M. Wörle, Prof. Dr. R. Nesper
Laboratory of Inorganic Chemistry
ETH Zürich
Universitätstrasse 6, 8092 Zürich (Switzerland)
Fax: (+41) 1-632-1149
E-mail: nesper@inorg.chem.ethz.ch

[**] The financial support by the Swiss National Science Foundation (projects 21-36586.92 and 4030-032775) is gratefully acknowledged. We thank Dr. V. Shklover for SEM pictures, Dr. M. Spahr for magnetic measurements, Dr. T. Chatterij and Dr. E. Souard for the neutron diffraction experiments, and Prof. Dr. S. Roth, Prof. Dr. H. Kuzmany, Prof. H. D. Lutz, and Dr. E. Suchanek for spectroscopic investigations.

 © WILEY-VCH Verlag GmbH, D-69451 Weinheim, 2000 1433-7851/00/3913-2349 $ 17.50+.50/0

One way to keep short chains separated from each other is to introduce specific end groups. For chains with up to 16 C_2 units, a stabilization seems to be possible in that way.[6–8] Not long ago, Bauer et al. reported the formation of small boron carbon chains containing up to 13 atoms in a rare earth metal matrix.[9, 10]

We have now extended this idea to a polar, charged, pseudoelement system, namely, a lithium boride in which each boron atom yields one negative charge and thus becomes isoelectronic to carbon. The compound forms from a low-temperature melt of lithium and boron showing increasing viscosity with temperature and time,[11–13] which is traced back to the presence of different oligo and polymeric boron species in the melt before solidification either to an apparently metallic glass or the crystalline LiB_x depending on the actual composition and tempering time. If about 10 % magnesium is added to the lithium melt, the metallic glass behavior is more pronounced.[14] Over more than twenty years, different groups [15, 16] have tried to unravel the nature of the polymerization products and of the compound LiB_x. Lithium-rich boron alloys possibly doped by a few percent of magnesium have been proposed as lithium electrode materials.[17, 18] We now succeeded in preparing pure-phase LiB_x samples with the approximate range $0.82 < x < 1.0$. The upper limit is somewhat unclear, since detection of an excess of poorly crystalline boron in the powder diagrams is very difficult. Furthermore, we were able to solve the crystal structure, which revealed a novel linear borynide chain that can be described as the first linear boron wire of molecular dimension. The borynide chain $[B^-]_n$ is indeed an exciting example of how some longstanding problems in materials science, in this case the synthesis of carbyne C_n, may be circumvented by a pseudoatom approach (B^- instead of C).[19]

We report here on the preparation and structural characterization of LiB_x, which contains linear, unbranched borynide chains in a lithium matrix. A compound with the same powder patterns was described earlier as either Li_5B_4 ($x = 0.80$) or Li_7B_6 ($x = 0.85$).[15, 21] In these investigations a structure containing three rings of boron atoms with unreasonably short distances was proposed based on an erroneous pseudo-cubic, rhombohedral symmetry. Study of the powder patterns showed that there are additional strong Bragg reflections which were misinterpreted in these older investigations. Proper indexing of the pattern led us to a hexagonal metric which depends on the stoichiometry parameter x.[16]

Our investigation is based on pure-phase LiB_x obtained as a brittle, grey, metallic solid upon heating elemental lithium and β-rhombohedral boron in sealed steel or niobium ampoules under an argon atmosphere for 48 h at 723 K. Scanning electron microscopy pictures show that this solid is composed of thin fiberlike crystals (Figure 1).[22] The compound is very sensitive to oxygen, nitrogen, and water and can be handled only under an inert argon atmosphere without decomposition. Finely ground powders are pyrophoric upon contact with air. As expected for such polymers, attempts to grow larger single crystals suitable for crystal structure determination failed up to now. Therefore, we used X-ray and neutron powder diffraction data for solving the structure. A close inspection of the X-ray powder diffraction patterns reveals that the

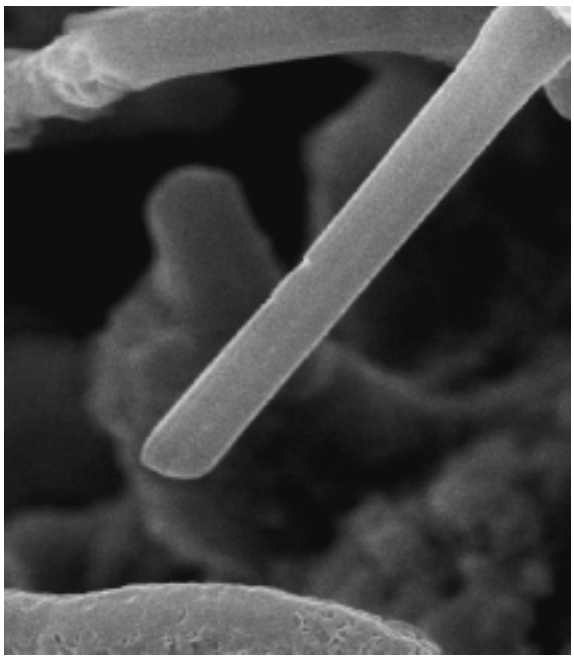


Figure 1. SEM picture of LiB_x crystals (length 36 μm, diameter 4 μm). In the upper left corner one can see partly decomposed fibers, due to exposure to air.

positions of some lines vary with the lithium content of the sample, whereas other lines remain unaffected. Instead of assuming two different phases in the samples (as proposed by Wang et al.),[11, 12] we were able to index all the observed lines consistently on the basis of a single hexagonal unit cell. Depending on the lithium content, the lattice constants vary significantly. For nominal compositions $x = 1.0$ and $x = 0.82$ we find $a = 4.025(1)$ Å, $c = 2.857(2)$ Å, $V = 40.08$ Å^3 and $a = 4.019(1)$ Å, $c = 2.792(1)$ Å, $V = 39.06$ Å^3, respectively. This is a volume reduction of nearly 3 %, which is mainly due to the reduction of the c axis while the variations in the hexagonal base are unspecific. A structure model (Figure 2a) was worked out in space group $P6_3/mmc$ and refined by simultaneous Rietveld refinement of multiple data sets (Figure 3) with X-ray and neutron powder diffraction data from samples of the nominal composition $LiB_{0.82}$.[23]

The structure may be derived from a hexagonal closed packing of Li atoms, but the c/a ratio (0.7098, 0.6947) is so

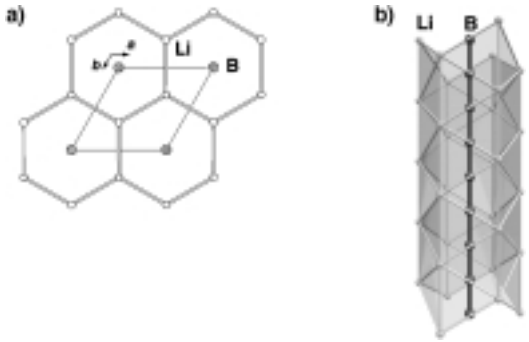


Figure 2. a) The unit cell of LiB_x in the [001] projection; b) a chain of boron atoms surrounded by a lithium shell. One possible location of the B atoms in the disordered borynide chain is shown.

 © WILEY-VCH Verlag GmbH, D-69451 Weinheim, 2000 1433-7851/00/3913-2350 $ 17.50+.50/0

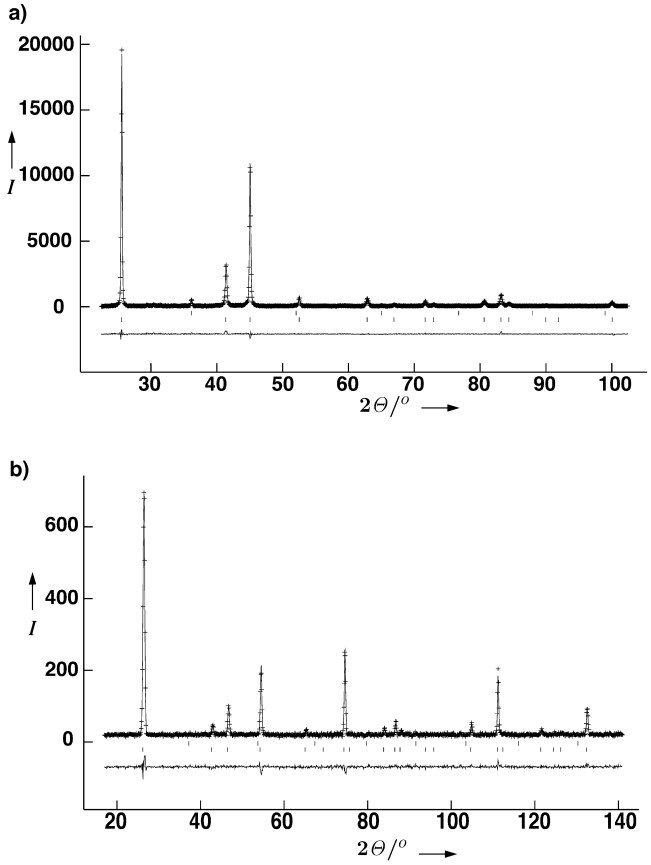


Figure 3. Multiple data set Rietveld refinement (after background correction) with a) X-ray and b) neutron powder diffraction data on samples with the nominal composition $LiB_{0.82}$.

different from the ideal one (1.633) that this correlation would be too far fetched. The original stacks of face-sharing Li_6 octahedra along the *c* direction fuse to a sixfold column which fully encapsulates the boron strand (Figure 2b). The boron positions cannot be defined with atomic resolution in the direction of the chain, as shown by the characteristic electron density section displayed in Figure 4. This is due to the particular bonding requirements of lithium and boron in this compound (see below).

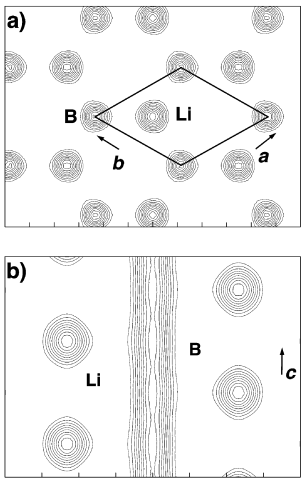


Figure 4. Observed electron density distribution in LiB_x: a) layer perpendicular to [001] at $z = 0.25$; b) layer perpendicular to [110] through the origin of the unit cell to show the disordered boron atom sites (line distance of 0.3 $e^- Å^{-3}$).

Similar electron density distributions are observed in composite structures where two partial structures form incommensurate arrangements. This may either give rise to satellite reflections or regions of expanded diffuse scattering depending on the degree of disorder. In the latter case, layers of diffuse intensity are expected perpendicular to the boron chain direction, and the lower edge of the diffuse intensity is a measure of the average boron – boron distance. Such behavior is observed, for example, in apatites with incommensurate distribution of the anions in the channels.[25] Indeed, very weak diffuse intensity is detected in the X-ray patterns, and strong diffuse scattering appears in the neutron diffraction pattern. In both cases this onset occurs at $d = 1.59$ Å, which we interpret as the average B–B distance in the chains (Figure 5).

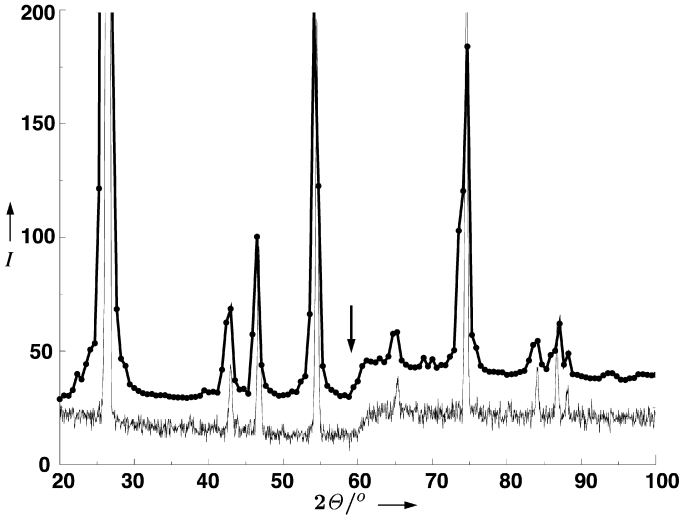


Figure 5. Selected area of the neutron diffraction pattern (lower curve) with the step-like diffuse scattering and simulated pattern (upper curve).

This is significantly longer than the simplest commensurate model with $d(B-B) = c/2 = 1.396$ Å and thus two bonds per unit cell, the latter being too short with respect to the bonding situation of (approximately) four bonds for each boron atom as dictated by the valence electron count. Accordingly, the simulated[26] diffuse intensity step (Figure 5) is based on a model containing 400 boron chains ($20 \times 20 \times 20$ superstructure, 32000 atoms) with alternating single and triple bonds of 1.40 Å and 1.77 Å (av 1.59 Å), respectively, which are randomly shifted against each other along the *c* axis. However, a related conjugated chain model with average spacing between the boron atoms leads to the same result. Thus the diffraction data do not allow discrimination between the two limiting cases. This smeared out appearance of the boron chains based on the diffraction data shows that there is practically no correlation between different chains, but instead disorder. The kink at $d = 1.59$ Å is very well reproduced by this model, as shown in Figure 5.

Comparing the mean boron – boron distances derived from the kinks in the scattering data and the *c* lattice translation, the lithium-to-boron ratio is obtained. The former defines the

 © WILEY-VCH Verlag GmbH, D-69451 Weinheim, 2000 1433-7851/00/3913-2351 $ 17.50+.50/0

(fractional) number of borons and the latter the (integer) number of lithium atoms per unit cell. Compositions of $LiB_{0.90}$ and $LiB_{0.88}$ are calculated, whereas the above-mentioned hyphothetical commensurate chain length would lead to stoichiometric LiB. The composition calculated by means of free occupancy and temperature factor refinement is $LiB_{0.95(1)}$. A composition of $LiB_{0.88}$ can be refined to practically the the same *R* value as in the free refinement, that is, the variation of *R* due to these model changes is insignificant (Table 1). The residual electron density is very weak and featureless (see Figure 4). No substantial number of defects in the boron chains are to be expected, because that would reduce the boron content even further below $\times = 0.88$, resulting in a significant increase of the figure of merit.

Table 1. Atomic coordinates, isotropic thermal displacement parameters ($U_{iso/equi}$), and site occupation factors (Occ.) obtained from free refinement of thermal parameters and site occupation factors.

Atom	Site	*x*	*y*	*z*	Model A[a]		Model B[b]	
					$U_{iso/equi}$ [Å]	Occ.	$U_{iso/equi}$ [Å]	Occ.
Li	2c	1/3	2/3	1/4	0.0305(6)	1	0.0398(5)	1
B1	2a	0	0	0	0.0295(6)	0.48(1)	0.0283(5)	0.44
B2	2b	0	0	1/4	0.0295(6)	0.47(1)	0.0283(5)	0.44

[a] Model A: free refinement leading to the composition $LiB_{0.95(2)}$ ($wRp = 0.159$). The estimated standard deviations of the occupation factors for model A have been multiplied by a factor of 3 with respect to the calculated results, accounting for the well-known oversampling effects in the Rietveld refinement. [b] Model B: for a constrained composition of $LiB_{0.88}$ ($wRp = 0.160$).

A small excess of lithium in the sample with the nominal composition $LiB_{0.82}$ is detected in the X-ray powder diffraction pattern. This excess cannot easily be removed due to the sensitivity of LiB_x to loss of lithium under vacuum conditions.

An interesting question is how much charge the corresponding—still hypothetical—carbyne chain would take up from a surrounding Li matrix. By comparison with n-doped polyacetylene chains it is expected to do so.[27] The chains in LiB_x may also be slightly reduced by population of π^* states depending on the actual composition. Because of the phase width the bond order in the chains can show slight changes. On the other hand, a population of bonding lithium states is more likely and, as such, is reflected by the significant reduction of the *c* axis with increasing lithium content. These two effects induce a metal conductivity ($\sigma = 7 \times 10^6\ S\,cm^{-1}$),[11] which is different from all other lithium borides known so far.[28, 29] The variable lithium content plays the same role here as oxidizing or reducing dopants, which are in general a necessary ingredient for achieving conducting, carbon-based polymers. Considering an ideal valence electron concentration (VEC) of four for the boron atoms, the same bonding situation as for a carbyne chain is present. This is matched by assigning formal charges of -1 to all boron atoms. The bonding situation is expected to be very similar to that calculated for the hypothetical carbon chain, namely, $=[B^{-}=]_nB^{-}=$ or $-[B^{-}\equiv B^{-}-]_nB^{-}\equiv$.

The description of an ionic compound is also in agreement with ^{7}Li NMR measurements which reveal a series of lines around $\delta = 0$ with respect to an aqueous solution of lithium chloride[22] as well as with ab initio and extended Hückel calculations for small boron–carbon chains.[9] The chains of pseudocarbon atoms B^- in LiB_x are the first examples of carbinoid systems (borynide) of a really large size.

According to MP2 calculations, the distances for a B=B bond should lie in the range of 1.629 Å for the hyphothetical molecule $Li_2B_2H_4$, where the $B_2H_4^{2-}$ anion is coordinated by two Li^+ cations, and 1.673 Å for the isolated ion.[30] These bond distances are only marginally shorter than the observed single bond distances in organic derivatives of B_2H_4 (1.698(4), 1.711(6) Å), B_2F_4 (1.67(5), 1.72 Å), B_2Cl_4 (1.75(5), 1.70(7) Å), and B_2Br_4 (1.69(2) Å). A comparison of the boron–boron bond distances for different neutral, singly and doubly reduced organodiborane(4) compounds[31] reveals a shortening upon going from the neutral species (1.706(12) and 1.724(9) Å, bond order of one) to the doubly reduced species (1.627(9) and 1.636(11) Å, bond order two). Apparently, the shortening due to higher bond order is reduced by the increasing coulombic repulsion. In any case, the average boron–boron distance of 1.59 Å in LiB_x is at the short end of the expected values for B=B bonds. A significant shortening of single bond distances is also observed in conjugated carbon chain systems.[32] Furthermore, the coulombic attraction of the lithium matrix, the length of a B≡B bond, and the coulombic repulsion within the boron chains are competing effects and difficult to weigh against each other. The Li–B distances are comparable with those in other lithium borides (2.321(1)–2.424(1) Å).[29, 33] The lithium atoms form a continuous one-dimensional cage which encapsulates and stabilizes the boron chain like an insulation shell around a wire.

Solid-state NMR experiments[22] support a description such as $(Li^+)_x(B^-)$ where the lithium atoms have mainly cationic character. However, a small amount of electron density centered at Li is quite likely, especially because the Li matrix contracts with increasing electron number. This will lead to metallic conductivity as well. The unique structure of this compound leads to very interesting physical and spectroscopic properties.[1] The binary phase system lithium–boron was investigated by several authors. A lithium boride in the mentioned composition range was used as an electrode material due to its unique properties: The material releases and takes up elemental lithium due to its high microporosity, and it exhibits a high mechanical stability even at temperatures above the melting point of lithium.[21, 22] Sanchez and Belin showed that samples of nominal composition Li_7B_3 consist of a refractory matrix of the composition $LiB_{0.943}$ and elemental lithium.[22] This observation can be explained by our results as well as the shape of the crystals formed and the difficulties encountered in growing single crystals.

The high microporosity and the possibility of the inclusion of metal explains the very different values for the experimentally determined densities reported in the literature.[12, 22, 34, 35] Conductivity measurements[11, 16] on the system described here show metallic behavior, in contrast to all other known binary lithium borides. This can be explained by the special charge transfer situation between the boron chains and the lithium matrix. At present, corresponding theoretical investigations are being performed. Magnetic measurements

 © WILEY-VCH Verlag GmbH, D-69451 Weinheim, 2000 1433-7851/00/3913-2352 $ 17.50+.50/0

show a hysteresis of the magnetization curve at 5 K, the nature of which is not understood but which may be due to a Peierls distortion in the borynide chains. This correlates nicely with the observation of additional Bragg reflections in the neutron diffraction pattern at low temperature. To our knowledge, the borynide chain $[B^-]_n$ in LiB_x is the first structurally well characterized linear system which is isoelectronic and isolobal to carbyne.

Received: September 17, 1999
Revised: March 21, 2000 [Z14027]

[1] M. J. Rice, A. R. Bishop, D. K. Campbell, *Phys. Rev. Lett.* **1983**, *51*, 2136.
[2] R. Hoffmann, C. Janiak, C. Kollmar, *Macromolecules* **1991**, *24*, 3725.
[3] F. Cataldo, *Polym. Int.* **1997**, *44*, 191.
[4] F. Diederich, *Nature* **1994**, *369*, 199.
[5] F. Diederich, Y. Rubin, *Angew. Chem.* **1992**, *104*, 1123; *Angew. Chem. Int. Ed. Engl.* **1992**, *31*, 1101.
[6] T. Bartik, B. Bartik, M. Brady, R. Dembinsky, J. A. Gladysz, *Angew. Chem.* **1996**, *108*, 467; *Angew. Chem. Int. Ed. Engl.* **1996**, *35*, 414.
[7] R. E. Martin, F. Diederich, *Angew. Chem.* **1999**, *111*, 1440; *Angew. Chem. Int. Ed.* **1999**, *38*, 1350.
[8] J. Bauer, J.-F. Halet, J.-Y. Saillard, *Coord. Chem. Rev.* **1998**, *178–180*, 723.
[9] J. Bauer, G. Boucekkine, G. Frapper, J.-F. Halet, J.-Y. Saillard, B. Zouchoune, *J. Solid State Chem.* **1997**, *133*, 190.
[10] D. Ansel, J. Bauer, F. Bonhomme, G. Boucekkine, G. Frapper, P. Gougeon, J.-F. Halet, J.-Y. Saillard, B. Zouchoune, *Angew. Chem.* **1996**, *108*, 2245; *Angew. Chem. Int. Ed. Engl.***1996**, *35*, 2098.
[11] F. E. Wang, R. A. Sutula, M. A. Mitchell, J. R. Holden, *Naval Surface Weapons Center*, *TR 77–84*, **1977**.
[12] F. E. Wang, M. A. Mitchell, R. A. Sutula, J. R. Holden, *J. Less-Common Met.* **1978**, *61*, 237.
[13] M. Wörle, Diplom thesis, Universtät Stuttgart, Max-Planck-Institut für Festkörperforschung, Stuttgart, **1990**.
[14] W. B. Pearson, personal communication, **1984**.
[15] F. E. Wang, *Metall. Trans. A* **1979**, *10*, 343.
[16] M. Wörle, PhD thesis, ETH Zürich, no. 11162, **1995**.
[17] R. A. Sutula, F. E. Wang (US Navy), US-A 4162352, **1979** [*Chem. Abstr.* **1979**, *91*, 126104j].
[18] F. Riffault, C. Pathé, S. Ferrier, D. Debattista (Aerospatiale), EP-B 160604, **1985** [*Chem. Abstr.* **1986**, *104*, 53681v].
[19] Recently, Daedalus envisaged a stabilization of carbyne chains by metal coordination.[20]
[20] D. Jones, *Nature* **1995**, *327*, 636.
[21] S. Dallek, D. W. Ernst, B. F. Larrick, *J. Electrochem. Soc.* **1979**, *126*, 866.
[22] P. Sanchez, C. Belin, *C. R. Seances Acad. Sci. Ser. II* **1988**, *307*, 2021.
[23] The simultaneous Rietveld refinement was performed with the Program package GSAS.[24] The X-ray data were obtained on a Stoe STADIP powder diffractometer, and the neutron powder diffraction data were recorded at the D2B beamline at the ILL in Grenoble. The following R values were obtained: neutron: $wRp = 0.107$, $Rp = 0.082$, $R(F^2) = 0.084$ (28 observed reflections); X-ray: $wRp = 0.164$, $Rp = 0.103$, $R(F^2) = 0.096$ (22 observed reflections); total: $wRp = 0.160$, $Rp = 0.102$ (see Table 1). Further details on the crystal structure investigation may be obtained from the Fachinformationszentrum Karlsruhe, 76344 Eggenstein-Leopoldshafen, Germany (fax: (+49) 7247-808-666; e-mail: crysdata@fiz-karlsruhe.de), on quoting the depository number CSD-410955.
[24] A. C. Larson, R. B. Von Dreele, Program GSAS, Los Alamos, **1994**.
[25] P. Alberius-Henning, PhD thesis, Stockholm University, **1999**.
[26] T. Proffen, R. B. Neder, Program DISCUS, *J. Appl. Cryst.* **1997**, *30*, 171. A program to extract powder data from the calculated diffraction patterns was written by us.
[27] S. Roth, *One-dimensional Metals*, VCH, Weinheim, **1995**.
[28] G. Mair, PhD thesis, Universität Stuttgart, **1984**.
[29] G. Mair, H. G. von Schnering, M. Wörle, R. Nesper, *Z. Anorg. Allg. Chem.* **1999**, *625*, 1207.
[30] E. Kaufmann, P. von R. Schleyer, *Inorg. Chem.* **1988**, *27*, 3987.
[31] W. J. Grigsby, P. Power, *Chem. Eur. J.* **1997**, *3*, 368.
[32] G. Gilli in *Fundamentals of Crystallography* (Ed.: C. Giacovazzo), Oxford University Press, Oxford, **1988**, p. 504.
[33] G. Mair, R. Nesper, H. G. von Schnering, *J. Solid State Chem.* **1988**, *75*, 30.
[34] M. A. Mitchell, R. A. Sutula, *J. Less-Common Met.* **1978**, *57*, 161.
[35] V. P. Sorokin, P. I. Gavrilov, E. V. Levakov, *Russ. J. Inorg. Chem.* **1977**, *22*, 329.

A New, Simple Route to Novel Gold Clusters: Structure of an Au_6Ag Wheel with a Gold Rim**

Elena Cerrada, María Contel, A. Delia Valencia, Mariano Laguna,* Thomas Gelbrich, and Michael B. Hursthouse

Gold–silver clusters in which the gold and silver atoms can be formally considered in an oxidation state between 0 and 1,[1–7] have attracted considerable attention during the last decade. Apart from such clusters, few complexes containing nonsupported gold–silver bonds, namely $[\{AuAg(C_6F_5)_2L_2\}_n]$,[8, 9] $[Au_2Ag_2(CH_2PPh_3)_4(ClO_4)_4]$,[10] $[\{Au_3(\mu\text{-bzim-}N^3,C^2)_3\}_2Ag]$,[11] and $[Au_4Ag(CH_2SiMe_3)_4(\mu\text{-dppm})_2]CF_3SO_3$[12] have been reported so far (L = tetrahydrothiophene, benzene; bzim = 1-benzylimidazole). For the latter two, the silver center is coordinated solely by gold atoms in a distorted trigonal prismatic and a distorted tetrahedral fashion, respectively.

In this communication, we report on the synthesis of novel heteronuclear compounds containing Au_5Ag and Au_6Ag cores. The X-ray crystal structure of the complex $[Au_6Ag\{\mu\text{-}C_6H_2(CHMe_2)_3\}_6]CF_3SO_3$ confirms the presence of an almost planar $AgAu_6$ core, in which the silver(I) atom is at the center of a regular hexagon of gold atoms. Thus, a "cart wheel"-like arrangement is achieved, in which the six gold–gold interactions form the rim and the six silver–gold bonds the spokes. To the best of our knowledge, this coordination mode for a silver center does not have a precedent in the literature.

Heteronuclear gold–silver compounds (with nonsupported metal–metal bonds) can be obtained by the addition of silver ions to dinuclear[12] or cyclic trinuclear gold(I) complexes.[11]

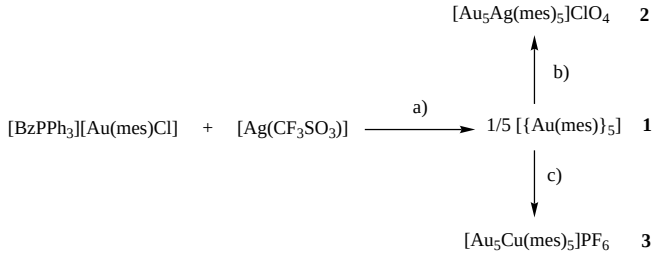
[*] Prof. M. Laguna, Dr. E. Cerrada, Dr. M. Contel, A. D. Valencia
Departamento de Química Inorgánica
Instituto de Ciencia de Materiales de Aragón
Universidad de Zaragoza-C.S.I.C, 50009 Zaragoza (Spain)
Fax: (+34) 976-761187
E-mail: mlaguna@posta.unizar.es
Dr. T. Gelbrich, Prof. M. B. Hursthouse
Department of Chemistry
University of Southampton
Highfield, Southampton, SO171BJ (UK)

[**] This research was supported by the Dirección General de Enseñanza Superior (PB 98-0542) and the Engineering and Physical Sciences Research Council.

 © WILEY-VCH Verlag GmbH, D-69451 Weinheim, 2000 1433-7851/00/3913-2353 $ 17.50+.50/0

We considered that the addition of metal ions to the pentanuclear gold(I) complex $[\{Au(mes)\}_5]$ (**1**, reported by Floriani et al. in the early 1980s; mes = mesityl = 2,4,6-trimethylphenyl)[13, 14] would be of interest, since such a disposition of gold atoms could potentially donate electron density to another metallic center.

The pentameric starting material was synthesized by us in a simpler way than previously reported—the reaction of $[AuCl(CO)]$[15] with $[\{Ag(mes)\}_4]$[14, 16, 17] requires several steps and special care. The preparation sequence is outlined in Scheme 1 and consists of the reaction of the anionic derivative

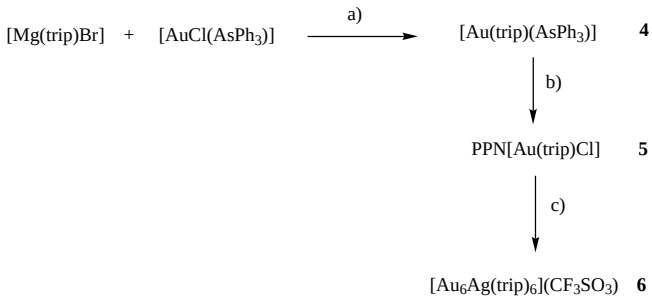


Scheme 1. Synthesis of $[\{Au(mes)\}_5]$ (**1**) and subsquent gold–silver- and gold–copper complexes **2** and **3**. a) $-$AgCl, $-(BzPPh_3)(CF_3SO_3)$ (molar ratio 1:1); b) $AgClO_4$ (molar ratio 1:1); c) $[Cu(NCCH_3)_4]PF_6$ (molar ratio 1:1).

$(PPh_3Bz)[Au(mes)Cl]$[18] with stoichiometric quantities of $[Ag(CF_3SO_3)]$ in dichloromethane (Bz = benzyl). Precipitation of $(BzPPh_3)(CF_3SO_3)$ and AgCl and subsequent workup of the yellow filtrate gave **1** as a solid in a moderate yield. Subsequent reaction of **1** with $AgClO_4$ (Scheme 1b) gave a solution from which $[Au_5Ag(mes)_5]ClO_4$ (**2**) precipitated as a green solid. The reaction of **1** with $[Cu(CH_3CN)_4]PF_6$ afforded $[Au_5Cu(mes)_5]PF_6$ (**3**) as a red solid.

Mass spectrometry (LSIMS$^+$, nitrobenzylalcohol matrix) of complexes **2** and **3** showed the parent ion $[Au_5M(mes)_5]^+$ (M = Ag, Cu) as the base peaks of m/z values of 1687 (100%) and 1643 (100%), respectively, with loss of the anions. The remaining peaks are associated with the pentanuclear species $[Au_4M(mes)_4]^+$ at m/z (%) 1371 (89) and 1327 (54), tetranuclear $[Au_3M(mes)_3]^+$ at 1055 (24) and 1011 (21), trinuclear $[Au_2M(mes)_2]^+$ at 739 (39) and 695 (40), and dinuclear $[AuM(mes)]^+$ at 423 (44) and 379 (37) for **2** and **3**, respectively. The ^{1}H NMR spectrum of **2** showed three resonances of equivalent mesityl groups, from *m*-H, *o*-CH_3, and *p*-CH_3, that are shifted downfield compared to the spectrum of **1**. It is worth noting that, because the two *m*-H and the *o*-CH_3 protons are inequivalent, the ^{1}H NMR spectrum of **3** has five resonances. The spectrum of **2** at $-60\,^\circ$C showed a broadening of the resonances of the *m*-H and *o*-Me protons rather than a split into two signals, as found for **3**.

Unfortunately, it was not possible to obtain crystals suitable for an X-ray diffraction study from **2** and **3**. Hence, we have carried out the analogous reactions (Scheme 2) with an alternative gold(I) precursor in which the mesityl group is replaced by the bulkier tris(isopropyl)phenyl ligand (trip, 2,4,6-$[(CH_3)_2CH]_3C_6H_2$). Starting from Br(trip), we reacted BrMg(trip) with $[AuCl(AsPh_3)]$ to provide $[Au(trip)(AsPh_3)]$



Scheme 2. Synthesis of complexes **4**–**6**. a) 0 °C (molar ratio 1.5:1); b) PPN^+Cl^- (molar ratio 1:1); c) $[Ag(CF_3SO_3)]$ (molar ratio 1:1 or 1.25:1).

(**4**) which, when treated with PPN^+Cl^-, afforded PPN-[Au(trip)Cl] (**5**; PPN = bis(triphenylphosphine)iminium). The reaction of **5** with equimolecular quantities of $[Ag(CF_3SO_3)]$ did not afford the homoleptic trip derivative similar to **1** but the heterometallic green complex $[Au_6Ag(trip)_6]CF_3SO_3$ (**6**) instead. Complex **6** could be obtained in better yield if the reaction was carried out in the presence of a small excess (1–1.25:1) of $[Ag(CF_3SO_3)]$. In contrast to the previously described complex $[\{Au_3(\mu\text{-bzim-}N^3,C^2)_3\}_2Ag]$[11], **6** was not found to be luminescent.

The mass spectrum (LSIMS$^+$) of **6** showed the parent ion $[Au_6Ag(trip)_6]^+$ at m/z (%) 2507 (10) and loss of the $CF_3SO_3^-$ ion. The ^{1}H NMR spectrum of **6** showed eight signals of the equivalent tris(isopropyl)phenyl groups assigned to two *m*-H singlets, three *o*- and *p*-CH septets, and three doublets from the CH_3 moieties. Clearly, the tris(isopropyl)phenyl units do not rotate within the NMR time scale. This behavior is similar to what was observed (for the mesityl groups) in the ^{1}H NMR spectrum of **3** and in the low temperature spectrum of **2** (see above).

The molecular structure of the cation of compound **6**·$\frac{1}{2}CH_2Cl_2$ is shown in Figure 1. It is based upon a ring of six gold atoms with the silver atom at its center. Each Au position deviates slightly (by 0.028 Å) but systematically (alternating above/below) from the least-square plane calculated for the entire Au_6Ag unit. As imposed by crystallographic symmetry, Ag is located exactly on this plane. The gold–silver atomic distances within this novel Au_6Ag core are 2.797(1), 2.802(1), and 2.809(1) Å, which can be considered as formal gold–silver bonds.[11, 12] The gold–gold distances range over 2.795(1)–2.817(1) Å and are slightly longer than those observed for the pentamer **1** (2.697(1)–2.708(1) Å).[13, 14] Furthermore, the C_{ipso} atoms of the tris(isopropylphenyl) groups serve as bridges between two consecutive gold atoms within the hexagon. With values between 2.111(7) and 2.200(7) Å, the Au–C distances are similar to those in other aryl-bridged complexes[13, 18, 19] or in seminal aromatic derivatives.[20] As observed for the previously mentioned mesityl complexes, the planar tris(isopropylphenyl) groups are nearly perpendicular to the mean plane through the gold and silver atoms, so that the angle between the average planes of Au_6Ag and the C11–C16 ring is 85.7°. However, the planes of the phenyl rings are slightly bent towards one of the adjacent gold atoms, for example, the angle Au1-C11-C14 is 125.5° but Au2-C11-C14 is 153.6°. Moreover, the six C_{ipso} atoms around the Au_6 hexagon

 © WILEY-VCH Verlag GmbH, D-69451 Weinheim, 2000 1433-7851/00/3913-2354 $ 17.50+.50/0 *Angew. Chem. Int. Ed.* **2000**, *39*, No. 13

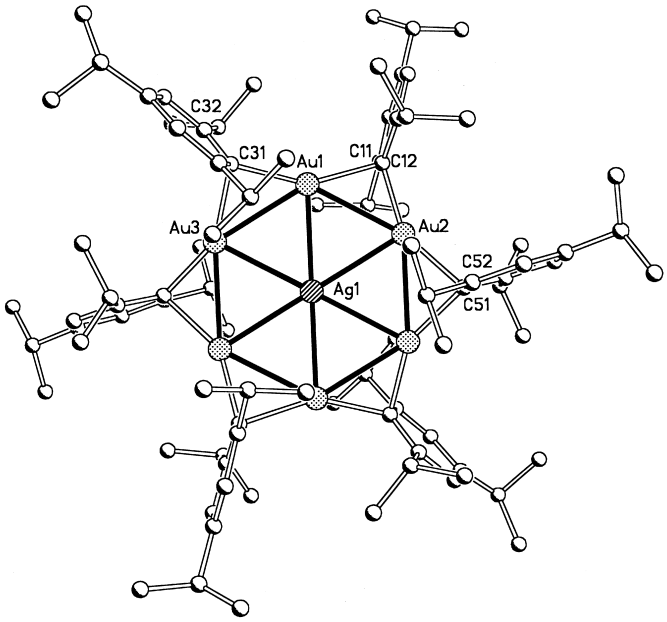


Figure 1. The structure of the cation of complex **6** in the crystal. Atomic radii are arbitrary and H atoms are omitted for clarity. Selected bond lengths [Å] and angles [°]: Ag1-Au1 2.8022(9), Ag1-Au2 2.797(1), Ag1-Au3 2.809(1), Au1-Au2 2.795(1), Au1-Au3 2.798(1); Au1-Ag1-Au2 59.97(3), Au3-Ag1-Au1 60.21(3), Au2-Ag1-Au3 60.05(3).

deviate from the Au_6Ag plane by 0.75 Å, three lie above and three below the plane.

The ^{1}H NMR spectrum of complex **6**, as discussed above, is in accordance with its structure being maintained in solution. Thus, complexes **2** and **3** should present similar structures with five gold–mesityl fragments (indicated by their mass spectra).

In conclusion, the reaction sequence to generate **1** (Scheme 1a) shows a general method to synthesize $[(AuR)_n]$ complexes, which could be extended to other radical and/or metallic centers. In addition, the preparation of **6** is a rare example of template synthesis for a hexaatomic gold rim. We are currently researching reactions with different organic ligands and the effects of addition of different metallic ions to these $[AuR]_n$ species.

Experimental Section

1: To a solution of $(PPh_3Bz)[Au(mes)Cl]$[18] (0.5 mmol) in dichloromethane (40 mL), a solution of $[Ag(CF_3SO_3)]$ (0.5 mmol) in diethyl ether (10 mL) is added. Precipitated AgCl was removed through celite filtration. The solution was concentrated to about 2 mL and addition of diethyl ether (30 mL) precipitated $(BzPPh_3)(CF_3SO_3)$, which was also removed by filtration. Concentration of the solution to about 5 mL and addition of *n*-hexane (30 mL) afforded **1** as a pure solid (yield: 49%).

2 and **3**: To a diethyl ether solutions of **1** (0.25 mmol) 0.05 mmol of $AgClO_4$ [or $[Cu(CH_3CN)_4]PF_6$] were added at 0 °C. Concentration of the deep green [deep red] solution to about 5 mL and addition of *n*-hexane (20 mL) precipitated **2** (yield: 40%) [**3** (yield: 50%)] as a green [red] solid.

Compounds **4** and **5** were obtained in 80 and 90%, respectively. The reactions are similar to those previously reported for their mesityl analogues.[18]

6: To a solution of **5** (0.25 mmol) in dichloromethane (30 mL), $[Ag(CF_3SO_3)]$ (0.042 mmol) was added. Preciptated AgCl was filtered. Addition of of diethyl ether (30 mL) precipitated $PPN(CF_3SO_3)$ which was also separated by filtration. Concentration of the solution to about 5 mL and addition of *n*-hexane (20 mL) afforded **6** as a deep green solid (40%).

Microcrystalline samples of complexes **1**–**6** gave satisfactory elemental analyses. Selected NMR data at room temperature (^{1}H NMR: 300 MHz, $CDCl_3$, $SiMe_4$; $^{31}P\{^1H\}$ NMR: 121 MHz, $CDCl_3$, external 85% H_3PO_4). **1**: ^{1}H: $\delta = 6.75$ (s, 2H; *m*-H), 2.62 (s, 6H; *o*-CH_3), 2.14 (s, 3H; *p*-CH_3). **2**: ^{1}H: $\delta = 6.84$ (s, 2H; *m*-H), 2.76 (s, 6H; *o*-CH_3), 2.14 (s, 3H; *p*-CH_3). **3**: ^{1}H: $\delta =$ 6.88 (s, 1H; *m*-H), 6.86 (s, 1H; *m*-H), 2.67 (s, 3H; *o*-CH_3), 2.63 (s, 3H; *o*-CH_3), 2.14 (s, 3H; *p*-CH_3). **4**: ^{1}H: $\delta = 7.59-7.4$ (m, 15H), 6.97 (s, 2H), 3.6 (sept, 2H, $^2J_{H,H} = 6.9$ Hz; *o*-$CH(CH_3)_2$), 3.6 (sept, 1H, $^2J_{H,H} = 6.9$ Hz; *p*-$CH(CH_3)_2$), 1.35 (d, 12H; CH_3), 1.23 (d, 6H; CH_3). **5**: ^{1}H: $\delta = 7.64-7.21$ (m, 60H; PPN), 6.76 (s, 2H), 3.81 (sept, 2H, $^2J_{H,H} = 6.9$ Hz; *o*-$CH(CH_3)_2$), 2.74 (sept, 1H, $^2J_{H,H} = 6.9$ Hz; *p*-$CH(CH_3)_2$), 1.16 (d, 18H; CH_3); $^{31}P\{^1H\}$: $\delta =$ 21.7 (s; PPN). **6**: ^{1}H: $\delta = 7.08$ (s, 1H), 6.78 (s, 1H), 3.91 (sept, 1H, $^2J_{H,H} =$ 6.8 Hz; $CH(CH_3)_2$), 3.08 (sept, 1H, $^2J_{H,H} = 6.8$ Hz; $CH(CH_3)_2$), 2.74 (sept, 1H, $^2J_{H,H} = 6.8$ Hz; $CH(CH_3)_2$), 1.64 (d, 6H; CH_3), 1.09 (d, 6H; CH_3), 0.56 (d, 6H; CH_3).

Crystal data for $\mathbf{6}\cdot\frac{1}{2}CH_2Cl_2$: $C_{92}H_{140}AgAu_6Cl_2F_3O_3S$, $M_r = 2743.67$, triclinic, space group $P\bar{1}$, $a = 13.532(3)$, $b = 13.973(3)$, $c = 14.240(3)$ Å, $\alpha =$ 90.93(3), $\beta = 105.4(3)$, $\gamma = 95.89(3)^\circ$, $V = 2579.5(3)$ Å^3, $Z = 1$, $\mu =$ 8.802 mm^{-1}, $F(000) = 1314$, $T = 150$ K. 32159 reflections were collected in an Enraf–Nonius Kappa CCD diffractometer, of which 9109 were independent ($R_{int} = 0.060$). Correction were made with the SORTAV program.[21] 33 distance restraints were applied to refine the positions of two disordered isopropyl groups. Hydrogen atoms were placed in calculated positions. The final $wR(F^2)$ was 0.106 for 9109 data, 488 parameters, with a conventional $R(F)[F^2 > 2\sigma(F^2)] = 0.041$. Max./min. electron density = 1.806/−3.400 e Å^3. Crystallographic data (excluding structure factors) for the structure reported in this paper has been deposited with the Cambridge Crystallographic Data Centre as supplementary publication no. CCDC-141781 (**6**). Copies of the data can be obtained free of charge on application to CCDC, 12 Union Road, Cambridge CB21EZ, UK (fax: (+44) 1223-336-033; e-mail: deposit@ccdc.cam.ac.uk).

Received: March 15, 2000 [Z14855]

[1] B. K. Teo, H. Zhang, X. Shi, *Inorg. Chem.* **1994**, *33*, 4086, and references therein.
[2] B. K. Teo, H. Zhang, X. Shi, *J. Am. Chem. Soc.* **1993**, *115*, 8489, and references therein.
[3] T. G. M. M. Kappen, P. P. J. Schlebos, J. J. Bour, W. P. Bosman, G. Beurskens, J. M. M. Smits, P. T. Beurskens, J. J. Steggerda, *Inorg. Chem.* **1995**, *34*, 2121.
[4] T. G. M. M. Kappen, P. P. J. Schlebos, J. J. Bour, W. P. Bosman, J. M. M. Smits, P. T. Beurskens, J. J. Steggerda, *Inorg. Chem.* **1994**, *33*, 754.
[5] R. C. B. Copley, D. M. P. Mingos, *J. Chem. Soc. Dalton Trans.* **1992**, 1755.
[6] R. P. F. Kanters, P. P. J. Schlebos, J. J. Bour, W. P. Bosman, J. M. M. Smits, P. T. Beurskens, J. J. Steggerda, *Inorg. Chem.* **1990**, *29*, 324.
[7] V. G. Albano, M. C. Iapalucci, G. Longoni, M. Monari, A. Paselli, S. Zacchini, *Organometallics* **1998**, *17*, 4438.
[8] R. Usón, A. Laguna, M. Laguna, B. R. Manzano, P. G. Jones, G. M. Sheldrick, *J. Chem. Soc. Dalton Trans.* **1984**, 285.
[9] R. Usón, A. Laguna, M. Laguna, P. G. Jones, G. M. Sheldrick, *J. Chem. Soc. Chem. Commun.* **1981**, 1097.
[10] R. Usón, A. Laguna, M. Laguna, P. G. Jones, C. F. Erdbrügger, *Organometallics* **1987**, *6*, 1778.
[11] A. Burini, J. P. Fackler Jr., R. Galassi, B. R. Pietroni, R. J. Stapler, *Chem. Commun.* **1998**, 95.
[12] M. Contel, J. Garrido, M. C. Gimeno, M. Laguna, *J. Chem. Soc. Dalton Trans.* **1998**, 1083.
[13] S. Gambarotta, C. Floriani, A. Chiesi-Villa, C. Guastini, *J. Chem. Soc. Chem. Commun.* **1983**, 1304.
[14] E. M. Meyer, C. Floriani, A. Chiesi-Villa, C. Guastini, *Organometallics* **1989**, *8*, 1067.
[15] D. Belli-Dell'Amico, F. Calderazzo, *Gazz. Chim. Ital.* **1973**, *103*, 1099.
[16] S. Gambarotta, C. Floriani, A. Chiesi-Villa, C. Guastini, *J. Chem. Soc. Chem. Commun.* **1984**, 870.
[17] R. Usón, A. Laguna, E. J. Fernández, M. E. Ruiz Romero, P. G. Jones, J. Lautner, *J. Chem. Soc. Dalton Trans.* **1989**, 2127.

[18] M. Contel, J. Jiménez, P. G. Jones, A. Laguna, M. Laguna, *J. Chem. Soc. Dalton Trans.* **1994**, 2515.
[19] M. Contel, J. Garrido, M. C. Gimeno, P. G. Jones, A. Laguna, M. Laguna, *Organometallics* **1996**, *15*, 4939.
[20] A. N. Nesmenayov, E. G. Peralova, K. I. Grandberg, D. A. Lemenovskii, T. V. Baukova, U. B. Afanassova, *J. Organomet. Chem.* **1974**, *65*, 131.
[21] R. H. Blessing, *Acta Crystallogr. Sect. A* **1995**, *51*, 33; R. H. Blessing, *J. Appl Crystallogr.* **1997**, *30*, 467.

Photoregulation of the DNA Polymerase Reaction by Oligonucleotides Bearing an Azobenzene**

Akira Yamazawa, Xingguo Liang, Hiroyuki Asanuma, and Makoto Komiyama*

Regulation of bioreactions by external stimuli has been one of the most attractive and urgent themes of recent research.[1] The activities of enzymes have been photomodulated by attaching azobenzene and spiropyran near to their active centers.[2, 3] Furthermore, growth and differentiation of cells have been controlled by applying electric voltage.[4] However, little has been known about artificial control of biosynthesis of DNA. Here we report the first photoregulation of a template-dependent DNA polymerase reaction. By using photoresponsive oligonucleotides as modulators and irradiating with appropriate light, DNA of predetermined length is selectively produced from one template DNA.

The oligonucleotides used here are presented in Figure 1. The modulator **1b** bears an azobenzene for photoinduced *cis–trans* isomerization.[5] Its 3′ terminus is protected by a 3-hydroxypropyl residue to avoid DNA elongation from that point. The primer DNA **3** (18-mer) is labeled with fluorescein isothiocyanate (FITC) at the 5′ end. The template DNA **4** is a 54-mer. When DNA polymerization with T7 DNA polymerase was achieved at pH 7.5 and 34 °C in the dark in the presence of **1b**, only 34-mer DNA was produced (lane 3 in Figure 2). Apparently, the DNA elongation was blocked by **1b**, and stopped at its 5′ terminus. Under irradiation with UV light ($300 < \lambda < 400$ nm), however, the 34-mer DNA was not formed and instead 54-mer DNA was predominantly produced (lane 4, Figure 2). Depending on whether the light is used or not, either of these two DNAs is selectively obtained from one template.[6] The irradiation causes no significant effects on the enzymatic activity, as confirmed by careful control experiments. When unmodified oligonucleotide (**1a**) was used as the modulator, only the 34-mer DNA was produced either in the dark or under UV irradiation (lanes 1 and 2, Figure 2).

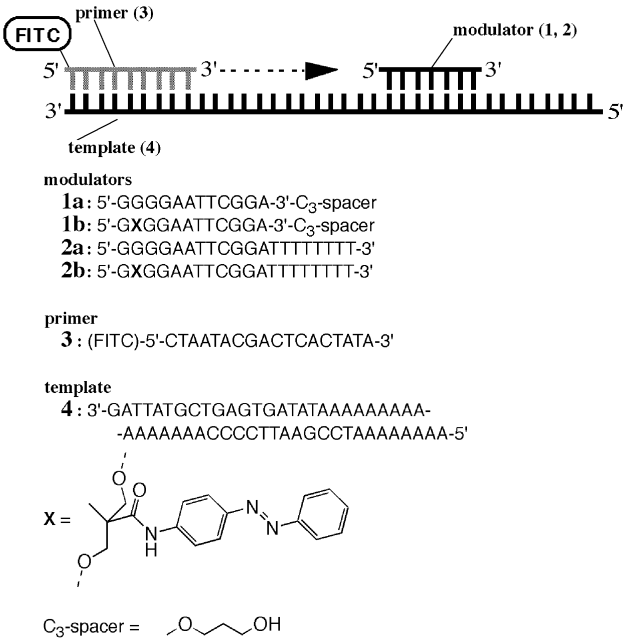


Figure 1. Strategy for the photoregulation of a T7 DNA polymerase reaction. In the modulators, **X** denotes the residue carrying an azobenzene.

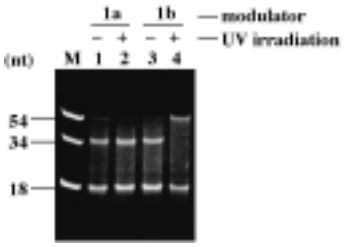


Figure 2. Polyacrylamide gel electrophoresis patterns for the T7 DNA polymerase reactions at pH 7.5 and 34 °C for 20 min. Lane 1: with the unmodified oligonucleotide **1a** in the dark; lane 2: with **1a** under UV irradiation; lane 3: with the modified oligonucleotide **1b** in the dark; lane 4: with **1b** under UV irradiation; lane M: markers (18-mer, 34-mer, and 54-mer).

Before the UV irradiation, the azobenzene in **1b** mostly takes the *trans* form.[5] Here, the melting temperature (T_m) of the duplex between **1b** and **4** is 57 °C (measured at 260 nm under the reaction conditions), and this duplex is almost completely formed at the reaction temperature (34 °C). The *trans*-azobenzene has a planar structure, and is favorably accommodated in the duplex. When the T7 DNA polymerase moves along the template **4** in the 3′→5′ direction during the polymerization, it cannot go through this double-stranded region (This enzyme requires single-stranded DNA as template) and the DNA elongation terminates at the 5′ end of **1b**. Under UV irradiation, the azobenzene in **1b** is isomerized to the *cis* form. This isomer is nonplanar so that its steric repulsion against **4** weakens the binding of **1b** to **4**. This effect

[*] Prof. Dr. M. Komiyama, Dr. A. Yamazawa, X. Liang, Dr. H. Asanuma
Research Center for Advanced Science and Technology
The University of Tokyo
4-6-1 Komaba, Meguro-ku, Tokyo, 153-8904 (Japan)
Fax: (+81) 3-5452-5209
E-mail: komiyama@mkomi.rcast.u-tokyo.ac.jp

[**] We should like to thank Professor Kazunari Taira for valuable comments. This work was partially supported by the Grant-in-Aid for Scientific Research from the Ministry of Education, Science, and Culture, Japan (Molecular Synchronization for Design of New Materials System). The support of the grant from the "Research for the Future" Program of the Japan Society for the Promotion of Science (JSPS-RFTF97I00301) is also acknowledged.

Supporting information for this article is available on the WWW under http://www.wiley-vch.de/home/angewandte/ or from the author.

 © WILEY-VCH Verlag GmbH, D-69451 Weinheim, 2000 1433-7851/00/3913-2356 $ 17.50+.50/0

is especially notable near the 5′ end of **1b**, where the *cis*-azobenzene is covalently bound. Thus, this section is competitively excluded from **4** by the T7 DNA polymerase, when this enzyme comes to the 5′ end of **1b** in the polymerization. Accordingly, the polymerase reaction proceeds further, and provides the full-length DNA (the proposed mechanism is schematically presented in the Supporting Information).[7] Note that T7 DNA polymerase has no 5′→3′ exonuclease activity,[8] and does not cleave **1b** for the complete elongation.

These arguments are supported by the results shown in Figure 3. Here, a modified 20-mer oligonucleotide (**2b**), which covers the template **4** down to its 5′ end, was used as the modulator. This longer modulator forms a more stable duplex

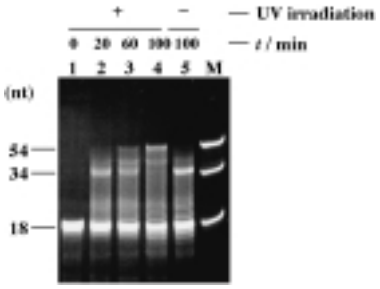


Figure 3. Time-course of the T7 DNA polymerase reaction under UV irradiation in the presence of modulator **2b**. Lane 1: $t = 0$; lane 2: $t = 20$; lane 3: $t = 60$; lane 4: $t = 100$ min. Lane 5 shows the result of the reaction in the dark after 100 min.

with **4** than **1b** does. Thus, the amount of **4** which is free from complex formation with **2b** is virtually nil, even when its azobenzene takes the *cis* form. Yet, the 54-mer DNA is efficiently formed under UV irradiation (lane 4, Figure 3). Evidently, the modulator involving the *cis*-azobenzene is excluded from the template by the enzyme during the polymerization. The breakdown of the stable **2b**–**4** duplex requires considerable energy, so that the elongation is notably retarded at the 5′ end of **2b**. As a result, the 34-mer DNA is somewhat accumulated in the early stages of the reaction (lanes 2 and 3, Figure 3). In dark conditions, however, the 34-mer DNA is the dominant product, even with long reaction times (lane 5, Figure 3).[9]

The present photoregulation is never based on the change of the amount of free **4** which is available as the template. Although the T_m of the duplex between *cis* isomer **1b** and **4** is lower than that of the *trans* isomer,[5] it is still much higher than the reaction temperature, and the duplex is dominantly formed under these conditions.[10] In conclusion, a T7 DNA polymerase reaction has been successfully photoregulated with photoresponsive oligonucleotides as modulators. The application of this finding to various purposes is currently under way.

Experimental Section

The modulators **1b** and **2b** were prepared on an automated synthesizer, with the phosphoramidite monomer carrying an azobenzene.[11] For the synthesis of **1a** and **1b**, 3′ spacer C3 CPG columns from the Glen Research Co. (Virginia) were employed. The diastereomers, with respect to the chirality of the X residue, were completely separated by reverse phase HPLC, and the fraction with the shorter retention time was used for the experiments described in the present paper. The other diastereomer gave almost the same results (see Figure 4 in the Supporting Information).

Reaction conditions for the T7 DNA polymerase reactions: The template (**4**; 3.2 μM), the primer (**3**; 3.2 μM), the modulator (**1a**, **1b**, **2a**, or **2b**; 4.0 μM), each dNTP (200 μM) and NaCl (150 mM) were incubated in Tris-HCl buffer (40 mM, pH 7.5) containing dithiothreitol and $MgCl_2$ (1 and 10 mM, respectively) at 34 °C for 30 min. The mixture was cooled in ice, and then the T7 DNA polymerase (Pharmacia; 1 unit in 25 μL), was added. At the same time, irradiation was started. The reaction was continued at 34 °C for a predetermined period of time, and stopped by addition of 80/20 formamide/water mixture (in the same volume as the reaction mixture). The mixture was denatured at 95 °C for 5 min, and subjected to electrophoresis on 20 % polyacrylamide gel containing 7 M urea. The pattern was visualized by fluorescence from the FITC on a UV illuminator.

For the *trans*→*cis* photoisomerization, UV light from 6 W UV-A fluorescence lamp (FL6BL-A, Toshiba) was shone through a UV-D36C filter (Asahi Technoglass). The intensity of UV light was 0.9 – 1.0 mW cm^{-2}. In order to avoid the thermal reverse isomerization, the irradiation was continued throughout the polymerase reactions. According to the results of reverse phase HPLC,[11] > 90 % of the azobenzene was the *trans* isomer before the UV irradiation, and > 80 % was the *cis* isomer during irradiation.

Received: January 3, 2000 [Z 14499]

[1] I. Willner, *Acc. Chem. Res.* **1997**, *30*, 347.
[2] M. Aizawa, K. Namba, S. Suzuki, *Arch. Biochem. Biophys.* **1977**, *182*, 305.
[3] a) I. Willner, S. Rubin, A. Riklin, *J. Am. Chem. Soc.* **1991**, *113*, 3321; b) T. Hohsaka, K. Kawashima, M. Sisido, *J. Am. Chem. Soc.* **1994**, *116*, 413; c) I. Hamachi, T. Hiraoka, Y. Yamada, S. Shinkai, *Chem. Lett.* **1998**, 537; d) D. G. Weston, J. Kirkham, D. C. Cullen, *Biochim. Biophys. Acta* **1999**, *1428*, 463.
[4] M. Aizawa, S. Koyama, K. Kimura, Y. Yanagida, E. Kobatake, *Denki Kagaku (Electrochemistry)* **1999**, *67*, 118, and references therein.
[5] It was recently reported that the melting temperatures (T_m) of the duplexes between these oligonucleotides and the complementary ones are notably changed on photoirradiation: H. Asanuma, T. Ito, T. Yoshida, X. Liang, M. Komiyama, *Angew. Chem.* **1999**, *111*, 2547; *Angew. Chem. Int. Ed.* **1999**, *38*, 2393. However, the present photoregulation of the polymerase reaction is based on a different chemistry (see text for details).
[6] When another 54-mer DNA was used as the template, the full-length product was produced for 20 min in almost 100 % yield (with respect to the template: see Figure 1 in the Supporting Information). The efficiency of the present photoregulated polymerization considerably depends on the sequences of components. The photoregulation was also successful, when an 89-mer DNA was used as the template.
[7] The proposed "peeling-off mechanism" has been further substantiated by the fact that the azobenzene must be placed near the 5′ end of the modulator in order to accomplish a clear-cut photoregulation. When an azobenzene was introduced near the 3′ terminus of the modulator (5′-GGGGAATTCG**X**A-3′-C_3-spacer), the dominant product was the 34-mer DNA, even with UV irradiation (see Figure 3 in the Supporting Information).
[8] K. Hori, D. F. Mark, C. C. Richardson, *J. Biol. Chem.* **1979**, *254*, 11598.
[9] Consistently, the 34-mer DNA was the dominant product, even under UV irradiation, when the unmodified 20-mer modulator **2a** was used in place of **2b**.
[10] At the reaction temperature, the amount of free **4** should be smaller than 3 %, when the azobenzene in **1b** takes the *cis* form. This value was estimated from the hypochromicity at 260 nm, measured immediately after UV irradiation. Precise determination of the T_m was unsuccessful, since thermal *cis*→*trans* isomerization was too fast at approximate T_m values (> 50 °C).
[11] H. Asanuma, T. Ito, M. Komiyama, *Tetrahedron Lett.* **1998**, *39*, 9015.

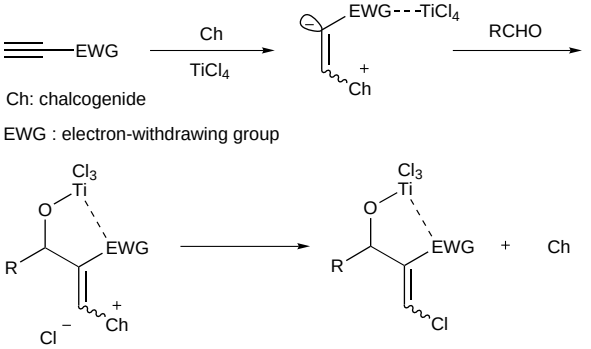
 © WILEY-VCH Verlag GmbH, D-69451 Weinheim, 2000 1433-7851/00/3913-2357 $ 17.50+.50/0

A Convenient Synthesis of α-Halomethylene Aldols or β-Halo-α-(hydroxyalkyl)acrylates Using the Chalcogeno-Baylis–Hillman Reaction**

Tadashi Kataoka,* Hironori Kinoshita, Sayaka Kinoshita, Tatsunori Iwamura, and Shin-ichi Watanabe

The Baylis–Hillman reaction is an efficient carbon–carbon bond-forming reaction that has become of major interest recently.[1] In the course of our studies into the reactions of alkynyl or alkenyl selenonium salts with sodium benzenesulfinate in an alcohol,[2] the chalcogenide-catalyzed Baylis–Hillman reaction was identified as the reverse reaction. After various attempts to find a good catalyst, we developed a reaction catalyzed by chalcogenides and $TiCl_4$, known as the chalcogeno-Baylis–Hillman reaction.[3] This reaction has some merits, namely, that it is complete within an hour[4] and can be applicable to thioesters[5] and ketoesters,[6] for which the Baylis–Hillman reaction gives unsatisfactory results. Dimethyl sulfide, cyclic chalcogenides, and bifunctional chalcogenides are used as the catalysts of the reactions.[4, 7, 8] Asymmetric synthesis using this procedure was attempted, although the enantiomeric excess of the products was not satisfactory.[8]

Most recently, we obtained α-chloromethyl aldols, the hydrogen chloride adducts of the Baylis–Hillman products, after purification of the raw products by column chromatography.[9] An examination of the mechanism of this reaction showed us that the chloride ion generated in the reaction process acts as an important nucleophile. Also, vinyl selenonium salts react with halide ions to give vinyl halides[10] through similar reaction pathways to the reactions of selenonium salts with alkoxides.[2] The outcome of these studies gave rise to the idea that acetylenic compounds should undergo the chalcogeno-Baylis–Hillman reaction [Eq. (1)]. The Baylis–Hillman reaction of active alkynes with aldehydes cannot proceed from the mechanistic viewpoint of the reaction. Therefore, β-branched acrylates, for example, are usually prepared from the reactions of α-metallated acrylates with aldehydes.[11, 12]

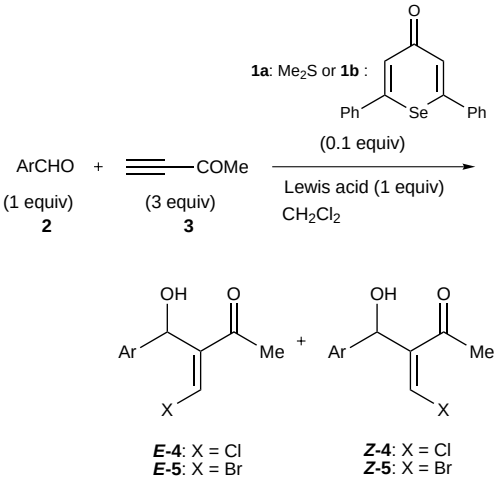


(1)

In this communication, we describe the chalcogeno-Baylis–Hillman reaction of active alkynes with aldehydes giving α-halomethylene aldols or β-halo-α-(hydroxyalkyl)acrylates. The products are highly functionalized by the four groups, that is, the carbon–halogen bond, the conjugated carbon–carbon double bond, the hydroxy group, and the carbonyl group, and can subsequently be transformed into a variety of useful compounds.[13]

Reactions of 3-butyn-2-one (**3**) with some benzaldehydes **2** were conducted [Eq. (2)], and the results are shown in Table 1. The reaction of **3** with *p*-nitrobenzaldehyde (**2a**) proceeded in the presence of dimethyl sulfide (**1a**, 0.1 equiv) and $TiCl_4$ (1 equiv) at 0 °C for 2 h to give the α-chloromethylene aldol **4a** in 86% yield (Entry 1). The product contained the *E* isomer only, and its geometry was determined by NOE enhancement of the ^{1}H NMR spectrum. Reactions with other aldehydes, **2b**–**d**, gave adducts **4b**–**d**, respectively, in high yields (Entries 3–5). The reaction using 2,6-diphenylselenopyran-4-one (**1b**) was slower than that using dimethyl sulfide (**1a**)—achieving a satisfactory result took 5 h at room temperature. Interestingly, the reaction proceeded without chalcogenide to give the product **4a** in 84% yield in an isomer ratio $E:Z = 1:1$ (Entry 7). This finding showed that

Table 1. Reactions of 3-Butyn-2-one (**3**) with Aldehydes (**2**).[a]



(2)

Entry	Ar (ArCHO)	Catalyst	Product	Yield [%]	*E*:*Z* Ratio
1	*p*-$NO_2C_6H_4$ (**2a**)	**1a**/$TiCl_4$	**4a**	86%	*E* only
2	*p*-$NO_2C_6H_4$ (**2a**)	**1b**/$TiCl_4$	**4a**	89%	*E* only
3	*p*-$CF_3C_6H_4$ (**2b**)	**1a**/$TiCl_4$	**4b**	73%	*E* only
4	*p*-ClC_6H_4 (**2c**)	**1a**/$TiCl_4$	**4c**	73%	*E* only
5	*p*-FC_6H_4 (**2d**)	**1a**/$TiCl_4$	**4d**	89%	*E* only
6	*p*-$NO_2C_6H_4$ (**2a**)	**1a**/$TiBr_4$	**5a**	63%	*E* only
7	*p*-$NO_2C_6H_4$ (**2a**)	$TiCl_4$	**4a**	84%	1:1
8	*p*-$NO_2C_6H_4$ (**2a**)	$TiBr_4$	**5a**	49%	*E* only

[a] All reactions were performed at 0 °C for two hours with the exception of the reaction in entry 2, which took place at room temperature for five hours.

[*] Prof. Dr. T. Kataoka, H. Kinoshita, S. Kinoshita, Dr. T. Iwamura, S.-i. Watanabe
Gifu Pharmaceutical University
6-1 Mitahora-higashi 5-chome, Gifu 502-8585 (Japan)
Fax: (+81) 58-237-5979
E-mail: kataoka@gifu-pu.ac.jp

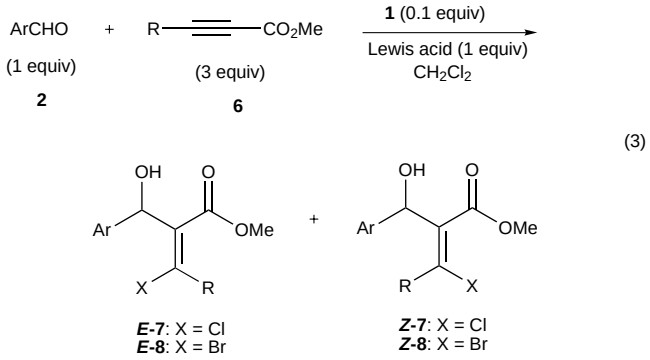
[**] This work was supported in part by a Grant-in-Aid for Scientific Research (Priority Areas Nos. 10133244 and 11120247) from the Ministry of Education, Science, Sports, and Culture, Japan.

 © WILEY-VCH Verlag GmbH, D-69451 Weinheim, 2000 1433-7851/00/3913-2358 $ 17.50+.50/0

the chloride ion generated from $TiCl_4$ acted as a nucleophile, but the isomer ratios between the products of entries 1 and 7 were quite different. Very recently, Li and co-workers reported a $TiCl_4$-mediated Baylis–Hillman reaction.[14] The reaction with $TiBr_4$ afforded the α-bromomethylene aldol **5a** in 49% yield (Entry 8).

Next, reactions of alkyne carboxylic acid esters with aromatic aldehydes were examined [Eq. (3)]. The results are summarized in Table 2. The reaction of methyl propiolate (**6a**) with *p*-nitrobenzaldehyde (**2a**) at room temperature for

Table 2. Reactions of Alkyne Carboxylic Acid Esters (**6**) with Aldehydes (**2**).[a]



(3)

Entry	Ar (ArCHO)	R (Ester)	Catalyst	t [h]	Product	Yield [%]	E:Z Ratio
1	*p*-$NO_2C_6H_4$ (**2a**)	H (**6a**)	**1a**/$TiCl_4$	24	**7a**	53	1:4
2	*p*-$NO_2C_6H_4$ (**2a**)	H (**6a**)	**1a**/$TiCl_4$	41	**7a**	70	1:6
3	*p*-$NO_2C_6H_4$ (**2a**)	H (**6a**)	**1a**/$TiCl_4$	64	**7a**	75	1:7
4	*p*-$NO_2C_6H_4$ (**2a**)	H (**6a**)	**1a**/$TiCl_4$[b]	50	**7a**	34	1:3
5	*p*-$NO_2C_6H_4$ (**2a**)	H (**6a**)	**1b**/$TiCl_4$	24	**7a**	5	ND[c]
6	*p*-$CF_3C_6H_4$ (**2b**)	H (**6a**)	**1a**/$TiCl_4$	50	**7b**	36	1:1.6
7	*p*-ClC_6H_4 (**2c**)	H (**6a**)	**1a**/$TiCl_4$	50	**7c**	47	1:7
8	*p*-$NO_2C_6H_4$ (**2a**)	H (**6a**)	**1a**/$TiCl_4$	50	**8**	37	1:2
9	*p*-$NO_2C_6H_4$ (**2a**)	Me (**6b**)	**1a**/$TiCl_4$	50	**7d**	25	1:1
10	*p*-$NO_2C_6H_4$ (**2a**)	CO_2Me (**6c**)	**1a**/$TiCl_4$	50	**7e**	31	Z only
11	*p*-$NO_2C_6H_4$ (**2a**)	H (**6a**)	$TiCl_4$	50	–[d]	–[d]	–[d]

[a] All reactions were performed at room temperature. [b] One equivalent of **1a** was used, rather than a catalytic quantity. [c] ND = not determined. [d] No reaction took place.

24 h produced adduct **7a** in 53% yield with a ratio of E:Z = 1:4 (Entry 1). Prolonged reaction time increased the yield (Entry 3), but use of one equivalent of **1a**, rather than a catalytic quantity, decreased it (Entry 4). The reaction using 2,6-diphenylselenopyran-4-one (**1b**) as a Lewis base afforded the product **7a** in only 5% yield (Entry 5). Use of $TiBr_4$ as a Lewis acid gave β-bromoacrylate **8** in low yield. Similarly, *p*-trifluoromethyl- and *p*-chlorobenzaldehydes **2b** and **2c** gave the products **7b** and **7c**, respectively, in low yields (Entries 6 and 7). The reaction catalyzed by only $TiCl_4$ did not afford the product **7a** (Entry 11). These results indicate that **6a** was less reactive than 3-butyn-2-one (**3**) and also that dimethyl sulfide (**1a**) worked as an important catalyst for the reactions. The isomer distribution was Z isomer predominant and opposite to that obtained with ketone **3**. β-Substituted alkyne carboxylate **6b** and dimethyl acetylenedicarboxylate **6c** provided the adducts **7d** and **7e** in 25% and 31% yields, respectively (Entries 9 and 10).

In summary, we have described the chalcogeno-Baylis-Hillman reaction of active alkynes as an efficient synthetic method for α-halomethylene aldols or β-halo-α-(hydroxybenzyl)acrylates. The asymmetric synthesis and application of this chemistry in the synthesis of bioactive compounds are currently under investigation.

Experimental Section

4a: *p*-Nitrobenzaldehyde (**2a**; 76 mg, 0.5 mmol) and methyl sulfide (**1a**; 3 mg, 0.05 mmol) were added to a solution of 3-butyn-2-one (**3**; 102 mg, 1.5 mmol) in anhydrous dichloromethane (1.5 mL). $TiCl_4$ (55 μL, 0.5 mmol) was added dropwise at 0 °C. The mixture was stirred for 2 h and then quenched by addition of saturated aqueous $NaHCO_3$ solution (1.5 mL). The inorganic precipitate was removed by filtration through celite, and the filtrate was dried over $MgSO_4$ and concentrated under reduced pressure. The residue was purified by preparative thin layer chromatography on silica gel with hexane/ethyl acetate (1/1) to give (*E*)-4-chloro-3-[1-hydroxy-1-(4-nitrophenyl)methyl]-3-buten-2-one ((***E***)-**4a**) in 86% yield. (***E***)-**4a**: m.p. 117 °C (from hexane/ethyl acetate); ^{1}H NMR (400 MHz, $CDCl_3$): δ = 2.43 (s, 3H, CH_3), 4.41 (d, J = 11 Hz, 1H, OH), 6.01 (d, J = 11 Hz, 1H, benzylic H), 7.56 (s, 1H, vinyl H), 7.55 and 8.19 (each d, J = 8.5 Hz, 2H, ArH); ^{13}C NMR (100 MHz, $CDCl_3$; * denotes two overlapping signals): δ = 26.9, 70.1, 123.7*, 126.0*, 136.9, 142.5, 147.3, 148.9, 197.9; elemental analysis calcd (%) for $C_{11}H_{10}ClNO_4$: C 51.68, H 3.94, N 5.48; found: C 51.66, H 3.99, 5.47.

The (***Z***)-**4a** isomer was also obtained from the reaction of **2a** with **3** in the presence of $TiCl_4$. (***Z***)-**4a**: m.p. 113–114 °C (from hexane/ethyl acetate); ^{1}H NMR (400 MHz, $CDCl_3$): δ = 2.47 (s, 3H, CH_3), 3.42 (d, J = 6 Hz, 1H, OH), 5.62 (d, J = 6 Hz, 1H, benzylic H), 6.81 (s, 1H, vinylic H), 7.55 and 8.23 (each d, J = 8.5 Hz, 2H, ArH); ^{13}C NMR (100 MHz, $CDCl_3$; * denotes two overlapping signals): δ = 32.2, 73.7, 123.7*, 127.1*, 132.1, 142.7, 147.5, 147.9, 200.6; elemental analysis calcd (%) for $C_{11}H_{10}ClNO_4$: C 51.68, H 3.94, N 5.48; found: C 51.86, H 4.03, N 5.38.

Received: January 11, 2000 [Z 14524]

[1] K. Morita, Z. Suzuki, H. Hirose, *Bull. Chem. Soc. Jpn.* **1968**, *41*, 2815; A. B. Baylis, M. E. D. Hillman (Celanese Corp.), German Patent, **1972**, 2155113 [*Chem. Abstr.* **1972**, *77*, 34174q]; H. M. R. Hoffmann, J. Rabe, *Angew. Chem.* **1983**, *95*, 795–796; *Angew. Chem. Int. Ed. Engl.* **1983**, *22*, 795–796; J. Rabe, H. M. R. Hoffmann, *Angew. Chem.* **1983**, *95*, 796–797; *Angew. Chem. Int. Ed. Engl.* **1983**, *22*, 796–797; for reviews, see: S. E. Drewes, G. H. P. Roos, *Tetrahedron* **1988**, *44*, 4653–4670; D. Basavaiah, P. D. Rao, R. S. Hyma, *Tetrahedron* **1996**, *52*, 8001–8062; E. Ciganek in *Organic Reactions, Vol. 51* (Ed.: L. A. Paquette), John Wiley & Sons, Inc., New York, **1997**, pp. 201–350.

[2] T. Kataoka, Y. Banno, S. Watanabe, T. Iwamura, H. Shimizu, *Tetrahedron Lett.* **1997**, *38*, 1809–1812; S. Watanabe, K. Yamamoto, Y. Itagaki, T. Kataoka, *J. Chem. Soc. Perkin Trans. 1* **1999**, 2053–2055.

[3] T. Kataoka, T. Iwama, S. Tsujiyama, *Chem. Commun*. **1998**, 197–198.

[4] T. Kataoka, T. Iwama, S. Tsujiyama, T. Iwamura, S. Watanabe, *Tetrahedron* **1998**, *54*, 11813–11824.

[5] T. Kataoka, T. Iwama, H. Kinoshita, S. Tsujiyama, Y. Tsurukami, T. Iwamura, S. Watanabe, *Synlett* **1999**, 197–198.

[6] D. Basavaiah, K. Muthukumaran, B. Sreenivasulu, *Synlett* **1999**, 1249–1250.

[7] T. Iwama, H. Kinoshita, T. Kataoka, *Tetrahedron Lett*. **1999**, *40*, 3741–3744.

[8] T. Kataoka, T. Iwama, S. Tsujiyama, K. Kanematsu, T. Iwamura, S. Watanabe, *Chem. Lett*. **1999**, 257–258; T. Iwama, S. Tsujiyama, H. Kinoshita, K. Kanematsu, Y. Tsurukami, T. Iwamura, S. Watanabe, T. Kataoka, *Chem. Pharm. Bull.* **1999**, *47*, 956–961.

[9] T. Kataoka, H. Kinoshita, T. Iwama, S. Tsujiyama, T. Iwamura, S. Watanabe, O. Muraoka, G. Tanabe, *Tetrahedron*, submitted.

[10] T. Kataoka, S. Watanabe, unpublished results.

[11] Copper: J. P. Marino, R. J. Linderman, *J. Org. Chem.* **1981**, *46*, 3696–3702; J. P. Marino, R. J. Linderman, *J. Org. Chem.* **1983**, *48*, 4621–

 © WILEY-VCH Verlag GmbH, D-69451 Weinheim, 2000 1433-7851/00/3913-2359 $ 17.50+.50/0

4628; H.-X. Wei, S. Willis, G. Li, *Tetrahedron Lett.* **1998**, *39*, 8203–8206.
[12] Aluminum: Y. Genisson, C. Massardier, I. Gautier-Luneau, A. E. Greene, *J. Chem. Soc. Perkin. Trans. 1* **1996**, 2869–2872; P. V. Ramachandran, M. V. R. Reddy, M. T. Rudd, J. R. de Alaniz, *Tetrahedron Lett*. **1998**, *39*, 8791–8794; G. Li, H.-X. Wei, B. R. Whittlesey, N. N. Batrice, *J. Org. Chem.* **1999**, *64*, 1061–1064; P. V. Ramachandran, M. V. R. Reddy, M. T. Rudd, J. R. de Alaniz, *Tetrahedron Lett*. **1999**, *40*, 627–630.
[13] V. J. Lee in *Comprehensive Organic Synthesis, Vol. 4* (Eds.: B. M. Trost, I. Fleming), Pergamon, Oxford, **1991**, p. 125; A. B. Smith, S. N. Kilenyi, *Tetrahedron Lett*. **1985**, *26*, 4419–4422; R. C. Larock, K. Narayanan, S. S. Hershberger, *J. Org. Chem*. **1983**, *48*, 4377–4380.
[14] G. Li, H.-X Wei, J. J. Gao, T. D. Caputo, *Tetrahedron Lett.* **2000**, *41*, 1–5.

Base-Specific Minor Groove Site Binding in Metallo-Nucleobase Polymers**

Michelle A. Shipman, Clayton Price, Mark R. J. Elsegood, William Clegg, and Andrew Houlton*

The use of metal–ligand bond formation to generate extended molecular assemblies is now a well established aspect of supramolecular chemistry.[1] Recently this approach has been combined with the use of organic ligands which possess hydrogen-bonding functionalities in an effort to further introduce directional interactions for structure building.[1, 2] Nucleobases are a useful set of building blocks for forming such structures through a combination of these interactions, and this has been demonstrated in particular in the work of Lippert.[3] Here we report crystal and molecular structures of two nucleobase coordination polymers containing adenine and guanine. These were formed from reactions of Cu^{II} ions with the respective purine bases derivatized with an alkyldiamine tether.[4] Analysis of the resulting polymers reveals a base-specific metal ion binding to the minor groove site N3, with coordination observed only with adenine, and formation of a polynucleotide analogue in the case of guanine.

Aqueous solutions containing equimolar equivalents of $Cu(NO_3)_2$ and the appropriate nucleobase–alkyldiamine (ethylenediamine-N9-ethylguanine, G-Et-en, and ethylenediamine-N9-ethyladenine, A-Et-en) as the hydrochloride salt showed evidence for the formation of Cu:L complexes in the UV/Vis spectra (characteristic band at $\lambda = 650$ nm).[5] This was also supported by electrospray mass spectrometry data with both solutions indicating the presence of the appropriate $[CuL(NO_3)]^+$ cation (m/z: 362, L = Et-G-en; 346, L = Et-A-en). Slow evaporation of these solutions yielded crystals suitable for single crystal X-ray analyses.[6]

Compound **1**, $[Cu(Et\text{-}N7\text{-}G\text{-}en)(H_2O)_2][NO_3]Cl \cdot (H_2O)_x$, is a coordination polymer in which the metal ion adopts a square pyramidal configuration with a {3N:2O} coordination sphere (Figure 1). The three nitrogen donor atoms are provided by the diamine function of one ligand and the N7 of the guanine from a second ligand. The extended structure contains stacked guanine bases which are rotated by 90° and inclined at 9.6° with respect to the nearest neighbor (related by a crystallographic fourfold screw axis). The 6-membered rings of the purine heterocycles in the stack lie above one another at a separation of approximately 3.157 Å. Figure 2a shows the bond density representation of the polymer chain to highlight the polymer shape. The helical arrangement has a pitch of 12.627 Å (the unit cell c-axis) and the copper ions spiral around the outside of the helical structure with a distance of 6.984 Å between adjacent metal ions in the backbone. Interestingly, this is close to the intrastrand P···P distance observed in duplex B-DNA (approximately 6.7 Å).[7]

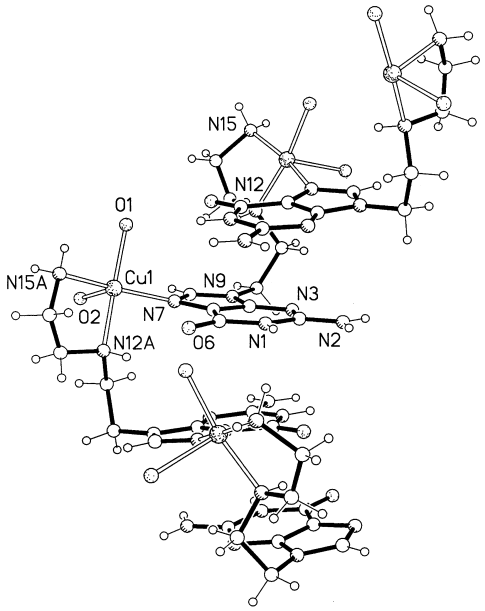


Figure 1. Polymeric chain in **1** formed by coordination through N7 and the diamine function. Metal–ligand bond lengths: Cu-O1 2.012(5), Cu-O2 2.315(7), Cu-N7 1.992(7), Cu-N12A 2.027(6), Cu-N15A 1.977(8) Å. The nucleobase lies at an angle of 70.9° to the plane formed by basal donor atoms (N7/O1/N12A/N15A), with the copper ion lying 0.208 Å above this plane. Each of the guanine residues is hydrogen bonded to uncoordinated nitrate anions ($O4NO_3^- \cdots$ N2 2.873 and $O3NO_3^- \cdots$ N1 2.874 Å).

In fact, **1** may be considered as a cationic polyguaninyl analogue and bears relevance to several aspects of DNA chemistry. For instance, antisense technology requires a means to enhance the binding between target and probe strands.[8] Cationic oligonucleotides based on metal ion linkages, as in **1**, may be an effective approach to this problem.

The analogous adenine complex, $[CuCl(Et\text{-}A\text{-}en)][NO_3] \cdot H_2O$ (**2**), is also polymeric with square pyramidal Cu^{II} ions and a {4N:Cl} donor set of ligands. However, the individual polymer chains exhibit a markedly different topology relative

[*] Dr. A. Houlton, M. A. Shipman, Dr. C. Price, Dr. M. R. J. Elsegood, Prof. W. Clegg
Department of Chemistry
University of Newcastle upon Tyne
Newcastle upon Tyne, NE1 7RU (UK)
Fax: (+44) 191-222-6929
E-mail: andrew.houlton@ncl.ac.uk

[**] This work was financially supported by the EPSRC and the BBSRC. The EPSRC mass spectrometry service at the University of Wales, Swansea, is acknowledged.

 © WILEY-VCH Verlag GmbH, D-69451 Weinheim, 2000 1433-7851/00/3913-2360 $ 17.50+.50/0

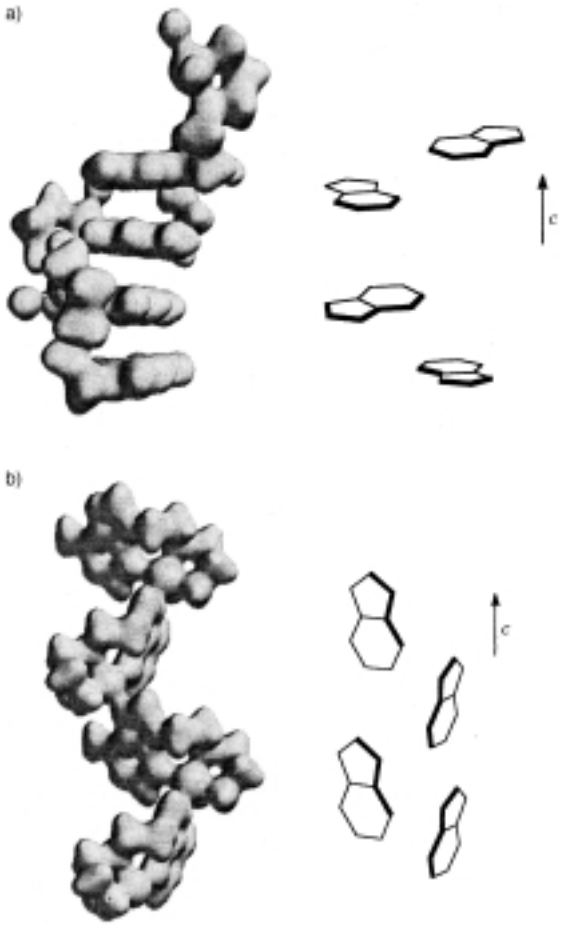


Figure 2. Bond density representation of the polymer topology in **1** and **2** (above and below, respectively).

to **1** (Figure 2b). For example, the nucleobases, no longer essentially parallel, make an angle of 74.4° with neighbors and the Cu ··· Cu distance is increased to 7.296 Å.

The observed topologies of **1** and **2** (Figure 2) can be related to the details of the binding mode of the organic ligands. A significant difference is seen with regard to the minor groove based donor sites. While in **1** the metal–nucleobase interactions are restricted to N7, in **2** both the major groove site N7 and the minor groove site N3 coordinate to copper ions. Hence, Et-A-en acts as a tridentate ligand to one copper ion through the diamine function and N3 of the nucleobase (Figure 3). This binding mode generates two chelate rings (5- and 7-membered) and is analogous to that observed in [CuCl(NO_3)(Prop-A-en)].[9] The Cu–N distances are 2.019 and 2.064 Å to N3A and N7, respectively, indicating that the bond to N3 is not a weak interaction. These structural data indicate that for the minor groove donor site N3, with Cu^{II} ions at least, binding at adenine is preferred over guanine.

To the best of our knowledge, there is only one structurally characterized example of a guanine N3-bound metal complex, the triplatinum derivative [*N1*,*N7*,*N3*-{Pt(NH_3)$_3$}$_3$-9-ethylguanine].[10] For adenine derivatives, however, there is an increasing number of reports of metal ions binding at this site.[11] Examples of crystallographically characterized metal complexes featuring N3 binding can be seen in the work of

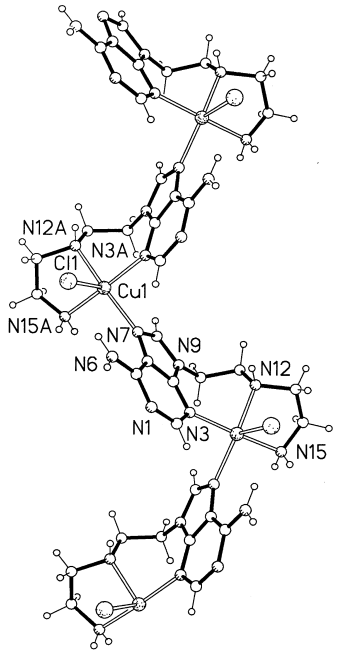


Figure 3. The polymeric chain in **2** involving coordination through N3 and N7 of adenine and through the diamine tether. Metal–ligand bond lengths: Cu-Cl 2.6737(12), Cu-N7 2.064(3), Cu-N3A 2.019(3), Cu-N12A 2.040(4), Cu-N15A 1.980(4) Å. Adenine lies at an angle of 87.9° to the plane of the basel donor atoms (N7/N3A/N12A/N15A) with the copper ion lying 0.198 Å above this plane. The polymer chains propagate along the unit cell *c*-axis.

Lippert, Sigel et al.,[12] Loeb and co-workers,[13] and an example reported by ourselves.[9]

These findings, along with the data here, highlight the issue of base-specific metal ion binding in the minor groove of DNA.[7, 14] This has been attributed in part to the markedly electronegative electrostatic potential found in the vicinity of adenine ··· thymine (AT) regions. This phenomenon has been proposed to account for the intrusion of monovalent cations into the minor groove spine of hydration of B-DNA.[15] Furthermore, Mn^{II} ions have been shown to localize at AT regions in the minor groove of dodecamers.[16] The observed preference for binding at adenine-N3 compared to guanidine-N3 seen here provides a possible contributing factor for these observations.

In conclusion, we have demonstrated that chelate-tethered nucleobases can form extended molecular assemblies by bridging metal ions. Moreover, the resulting structures, as polynucleotide analogues or in highlighting base-specific binding, are relevant to wider aspects of DNA chemistry.

Experimental Section

G-Et-enH · Cl and A-Et-enH · Cl: The appropriate chloroalkyl purine[17] was stirred in excess neat anhydrous ethylenediamine at room temperature for 18 hours under an atmosphere of nitrogen. The ethylenediamine was removed in vacuo and the resulting oil dissolved in ethanol with heating. The solution was concentrated in vacuo to precipitate a white powder. This was collected by filtration, washed with ethanol, and vacuum dried. G-Et-enH · Cl: ^{1}H NMR (500 MHz, $(CD_3)_2SO$): $\delta = 2.66$ (t, NH_2-CH_2-CH_2-NH), 2.73 (t, NH_2-CH_2-CH_2-NH), 2.85 (t, NH-CH_2-CH_2-GuaN^9) 3.98 (t, NH-CH_2-CH_2-GuaN^9), 6.62 (s, NH_2), 7.70 (s, H8); MS: *m*/*z* (%): 238 (100), [M^+ – Cl]; elemental analysis calcd for $C_9H_{16}ClN_7O$: C 39.49, H 5.89, N

 © WILEY-VCH Verlag GmbH, D-69451 Weinheim, 2000 1433-7851/00/3913-2361 $ 17.50+.50/0

35.82; found: C 38.84, H 5.59, N 34.46. A-Et-enH · Cl: ^{1}H NMR (500 MHz, $(CD_3)_2SO$): $\delta = 2.85$ (t, NH_2-CH_2-CH_2-NH), 2.90 (t, NH_2-CH_2-CH_2-NH), 3.13 (t, NH-CH_2-CH_2-AdeN^9), 4.30 (t, NH-CH_2-CH_2-AdeN^9), 7.28 (s, NH_2), 8.24 (s, H2), 8.30 (s, H8); MS: *m/z* (%): 222 (100), $[M^+ - Cl]$; elemental analysis calcd for $C_9H_{16}ClN_7$: C 41.94, H 6.26, N 38.04; found: C 41.24, H 6.11, N 38.20.

1 and **2:** An equimolar aqueous solution of either G-Et-enH · Cl or A-Et-enH · Cl was added to a solution of copper nitrate in distilled water at room temperature. In each case blue crystals were isolated which were suitable for single crystal X-ray analysis. **1**: MS: *m/z* (%):362 (100), $[M^+]$; elemental analysis calcd for $[CuClC_9N_8O_4H_{15}]$: C 27.14, H 3.80, N 28.14; found: C 26.92, H 4.01, N 27.82. (Analyses were for pump-dried samples and correspond to an anhydrous form of **1**.) **2**: MS: *m/z* (%):346 (100), $[M^+]$; elemental analysis calcd for $[(CuClC_9N_7H_{15})(NO_3) \cdot H_2O]$: C 27.00, H 4.28, N 28.00; found: C 27.23, H 3.92, N 27.84.

Received: January 21, 2000 [Z14580]

[1] *Comprehensive Supramolecular Chemistry* (Eds.: J. L. Atwood, J-M. Lehn), Pergamon, New York, **1996**.

[2] See, for example: a) A. D. Burrows, C-W. Chan, M. M. Chowdhry, J. E. McGrady, D. M. P. Mingos, *Chem. Soc. Rev.* **1995**, *24*, 329 – 339; b) D. Braga, F. Grepioni, G. R. Desiraju, *J. Organomet. Chem.* **1997**, *548*, 33 – 43; c) M. D. Ward, *Chem. Soc. Revs.* **1997**, *26*, 365 – 375; d) M. Munakata, L. P. Wu, M. Yamamoto, T. KurodaSowa, M. Maekawa, *J. Am. Chem. Soc.* **1996**, *118*, 3117 – 3124.

[3] See, for example: a) J. A. R. Navarro, B. Lippert, *Coord. Chem. Rev.* **1999**, *186*, 653 – 667; b) H. Rauter, I. Mutikainen, M. Blomberg, C. J. L. Lock, P. Amoochoa, E. Freisinger, L. Randaccio, E. Zangrando, E. Chiarparin, B. Lippert, *Angew. Chem.* **1997**, 109, 1353 – 1357; *Angew. Chem. Int. Ed. Engl.* **1997**, *36*, 1296 – 1301; c) R. K. O. Sigel, S. M. Thompson, E. Freisinger, B. Lippert, *Chem. Commun.* **1999**, 19 – 20; d) J. A. R. Navarro, M. B. L. Janik, E. Freisinger, B. Lippert, *Inorg. Chem.* **1999**, *38*, 426 – 432.

[4] a) C. Price, M. R. J. Elsegood, W. Clegg, N. H. Rees, A. Houlton, *Angew. Chem.* **1997**, *109*, 1823 – 1825; *Angew. Chem. Int. Ed. Engl.* **1997**, *36*, 1762 – 1764; b) C. Price, N. H. Rees, M. R. J. Elsegood, W. Clegg, A. Houlton, *J. Chem. Soc. Dalton Trans.* **1998**, 2001 – 2006.

[5] J. Bjerrum, E. J. Nielsen, *Acta Chem. Scand.* **1948**, 297 – 318; b) H. B. Jonassen, T. H. Dexter, *J. Am. Chem. Soc.* **1949**, *71*, 1553 – 1556.

[6] a) Crystal data for **1**: $[C_9H_{19}CuN_7O_3][NO_3]Cl$, $M_r = 434.3$, tetragonal, space group $I4_1/a$, $a = 25.184(3)$, $c = 12.6272(15)$ Å, $V = 8008.8(16)$ Å^3, $Z = 16$, ρ_{calcd} 1.441 g cm^{-3}; $Mo_{K\alpha}$ radiation, $\lambda = 0.71073$ Å, $\mu = 1.16$ mm^{-1}, $T = 160$ K. 17849 measured reflections were corrected for absorption, 3516 were unique ($R_{int} = 0.152$, $\theta = 25.0°$); $R = 0.0946$ (F values, $F^2 > 2\sigma$), $R_w = 0.2497$ (F^2 values, all data), GOF = 1.075 for 217 parameters, residual electron density between 0.64/ – 0.53 e Å^3. The structure contains substantial regions of diffuse electron density modelled by the SQUEEZE procedure (A. L. Spek, PLATON, University of Utrecht, The Netherlands, **1999**) and corresponding to disordered chloride anion and approximately 6 water molecules per asymmetric unit according to total electron density and volumes. The chloride anion, required for overall charge balance and by chemical analysis results, is included in the chemical formula and derived crystal data above; addition of 6 H_2O gives $M_r = 542.3$, $\rho_{calcd} = 1.799$ g cm^{-3}. This substantial disorder is responsible for the generally weak diffraction data. Other program used: SHELXTL (G. Sheldrick, Bruker AXS Inc., Madison, WI, USA, 1998, Version 5.1). b) Crystal data for **2**: $[C_9H_{15}ClCuN_7][NO_3] \cdot H_2O$, $M_r = 400.3$, monoclinic, space group $P2_1/c$, $a = 10.767(2)$, $b = 11.754(2)$, $c = 11.875(2)$ Å, $\beta = 100.287(4)°$, $V = 1478.7(5)$ Å^3, $Z = 4$, ρ_{calcd} 1.798 g cm^{-3}; $T = 160$ K. The very small crystal size ($0.11 \times 0.03 \times 0.02$ mm) and the relatively poor quality necessitated data collection with synchrotron radiation (SRS at Daresbury Laboratory, station 9.8, $\lambda = 0.6920$, $\mu = 1.69$ mm^{-1}). 8557 reflections were measured, 3135 were unique ($R_{int} = 0.053$, $\theta = 26.0°$); $R = 0.0529$, $R_w = 0.1425$, GOF = 0.976 for 229 parameters, residual electron density between 2.03/ – 0.99 e Å^3 with the largest features close to Cu. c) Crystallographic data (excluding structure factors) for the structures reported in this paper have been deposited with the Cambridge Crystallographic Data Centre as supplementary publication nos. CCDC-139134 (**1**) and -139135 (**2**). Copies of the data can be obtained free of charge on application to CCDC, 12 Union Road, Cambridge CB2 1EZ, UK (fax: (+44) 1223-336-033; e-mail: deposit@ccdc.cam.ac.uk).

[7] *Nucleic Acids in Chemistry and Biology* (Eds. G. M. Blackburn, M. J. Gait), IRL Press, Oxford, **1990**; b) *Bioinorganic Chemistry* (Eds. I. Bertini, H. B. Gray, S. J. Lippard, J. S. Valentine), University Science Books, California, **1994**; c) G. Pratviel, J. Bernadou, B. Meunier, *Adv. Inorg. Chem.* **1998**, *45*, 251 – 312, and references therein.

[8] E. Uhlmann, A. Peymann, *Chem. Rev.* **1990**, *90*, 543 – 584.

[9] C. Price, M. R. J. Elsegood, W. Clegg, A. Houlton, *J. Chem. Soc. Chem. Commun.* **1995**, 2285 – 2286.

[10] G. Rauduschlsieber, H. Schollhorn, U. Thewalt, B. Lippert, *J. Am. Chem. Soc.* **1985**, *107*, 3591 – 3595.

[11] a) C. A. Blindauer, A. Holy, H. Dvorakova, H. Sigel, *J. Biol. Inorg. Chem.* **1998**, *3*, 423 – 433; b) B. Song, S. A. Sajadi, F. Gregan, N. Pronayova, H. Sigel, *Inorg. Chim. Acta* **1998**, *273*, 101 – 105; c) C. A. Blindauer, A. H. Emwas, A. Holy, H. Dvorakova, E. Sletten, H. Sigel, *Chem. Eur. J.* 1997, 3, 1526 – 1536; d) S. S. Massoud, H. Sigel, *Eur. J. Biochem.* **1989**, *179*, 451 – 458; e) H. Sigel, *Coord. Chem. Rev.* **1995**, *144*, 287 – 319, and references therein.

[12] C. Meiser, B. Song, E. Freisinger, M. Peilert, H. Sigel, B. Lippert, *Chem. Eur. J.* **1997**, *3*, 388 – 398.

[13] J. E. Kickham, S. J. Loeb, S. L. Murphy, *Chem. Eur. J.* **1997**, *3*, 1203 – 1213.

[14] a) R. Lavery, B. Pullman, *J. Biomol. Struct. Dyn.* **1985**, *5*, 1021 – 1032; b) L. D. Higgins, M. S. Searle, *Chem. Commun.* **1999**, 1861 – 1862, and references therein.

[15] M. A. Young, B. Jayaram, D. L. Beveridge, *J. Am. Chem. Soc.* **1997**, *119*, 59 – 69.

[16] N. V. Hud, J. Feigon, *J. Am. Chem. Soc.* **1997**, *119*, 5756 – 5757.

[17] a) D. T. Browne, J. Eisinger, N. J. Leonard, *J. Am. Chem. Soc.* **1968**, *90*, 7302 – 7323; b) O. F. Schall, G. W. Gokel, *J. Am. Chem. Soc.* **1994**, *116*, 6089 – 6100; c) M. R. Harnden, R. L. Jarvest, T. H. Bacon, M. R. Boyd, *J. Med. Chem.* **1987**, *30*, 1636 – 1642; d) M. Ashwell, C. Bleasdale, B. T. Golding, I. K. O'Neill, *J. Chem. Soc. Chem. Commun.* **1990**, 955 – 956.

Coordinated and Clathrated Molecular Diiodine in $[Rh_2(O_2CCF_3)_4I_2] \cdot I_2$**

F. Albert Cotton,* Evgeny V. Dikarev, and Marina A. Petrukhina

The tetrakis(trifluoroacetate) dirhodium(II) molecule, $[Rh_2(O_2CCF_3)_4]$, has been shown to be a versatile, bifunctional Lewis acid, able to coordinate in solution an extraordinary variety of donor molecules to the axial positions.[1] Recent work in our laboratory employing a "solventless" synthetic technique has further extended the chemical and structural range of products to include those with aromatic and alkyne ligands, polymeric and oligomeric structures, and reaction products with dirhodium(I) units.[2] As a result of finding $[Rh_2(O_2CCF_3)_4]$ to be such an exceptionally avid

[*] Prof. F. A. Cotton, Dr. E. V. Dikarev, Dr. M. A. Petrukhina
Laboratory for Molecular Structure and Bonding
Department of Chemistry
Texas A&M University
P.O. Box 30012, College Station, TX 77842-3012 (USA)
Fax: (+1) 979-845-9351
E-mail: cotton@tamu.edu

[**] Studies of Dirhodium(II) Tetrakis(trifluoroacetate), part 7. This work was supported by the Robert A. Welch Foundation. Part 6: ref. [2c].

 © WILEY-VCH Verlag GmbH, D-69451 Weinheim, 2000 1433-7851/00/3913-2362 $ 17.50+.50/0

Lewis acid we decided to see if adducts could be obtained with the elemental halogens.

We report here the interactions of I_2 with $[Rh_2(O_2CCF_3)_4]$ using a solid/vapor deposition ("solventless") technique. The resulting product is a zigzag chain polymer $\{[Rh_2(O_2CCF_3)_4\text{-}I_2]\cdot I_2\}_\infty$ formed by alternating $[Rh_2(O_2CCF_3)_4]$ and I_2 molecules and having an unprecedented bidentate bridging coordination mode of molecular diiodine. Another I_2 molecule is clathrated within the channels in the structure. This unusual product further confirms the exceptional acceptor ability of the $[Rh_2(O_2CCF_3)_4]$ molecule and extends the class of halo-transition metal complexes.

We again demonstrate the utility of the solventless synthesis technique for studying weak interactions as the title compound, $[Rh_2(O_2CCF_3)_4I_2]\cdot I_2$ (**1**), was prepared by heating a mixture of unligated $[Rh_2(O_2CCF_3)_4]$ with molecular diiodine. Although we had a slight excess of $[Rh_2(O_2CCF_3)_4]$ in the initial mixture, heating that mixture to 160 °C resulted in an excess of I_2 over the dirhodium units in the gas phase, from which a product with a Rh_2:I_2 composition of 1:2 has been deposited. Interestingly, there was a tendency to form only the given composition in the solid state, as attempts to work with lower diiodine contents resulted in no crystalline product. The solid injection technique of EI mass spectroscopy applied to crystals of **1** showed only $[Rh_2(O_2CCF_3)_n]^+$ fragments, implying immediate thermal cleavage of I_2 from the product. There were indications of gradual iodine loss in the solid state even at room temperature, which prevented obtaining accurate elemental analysis data for **1**. Nevertheless, crystals appeared to be stable at low temperatures and were characterized by X-ray diffraction study.[3]

In the crystal structure of **1** the dirhodium trifluoroacetate units are linked together in a zigzag chain by interacting with neutral I_2 molecules in such a way that each Rh^{II} center has contact with one iodine atom of an I_2 molecule (Figure 1). There are two crystallographically independent dirhodium

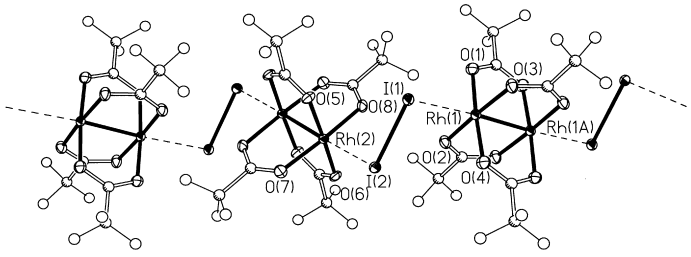


Figure 1. Fragment showing the alternating arrangement of $[Rh_2(O_2CCF_3)_4]$ and coordinated diiodine molecules in the crystal structure of **1**. Atoms are represented by thermal ellipsoids at the 40% probability level. Carbon and fluorine atoms are shown as spheres of arbitrary radii and are not labeled for clarity. Axial contacts to Rh atoms are drawn as dashed lines. Only one orientation of disordered CF_3 groups is depicted.

units in the cell with Rh–Rh distances of 2.417(1) and 2.415(1) Å; other characteristics of the two units are also very similar. The dirhodium fragments are linked by a diiodine bridge with the axial Rh–I contacts being only slightly different at 2.8359(9) and 2.8239(9) Å, while the Rh-Rh-I angles are close to linear (the mean value is 177.04(3)°). Such an orientation of the coordinated iodine minimizes the possible contacts with oxygen atoms of the carboxylate groups. The shortest of those, 3.44 Å, is equal to the sum of the van der Waals radii of I and O atoms. The two Rh-I-I angles have an average value of 95.31(2)°, reflecting a stereochemical activity of the lone electron pairs of the iodine atoms, and the average torsion angle for Rh-I-I-Rh is 106.6°. Another diiodine molecule is clathrated, just filling holes in the structure (Figure 2) without any close contacts to the

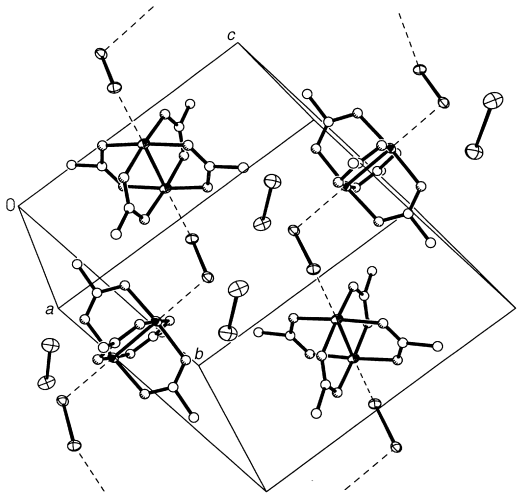


Figure 2. Packing diagram of **1** showing the displacement of both coordinated and clathrated diiodine molecules. Fluorine atoms of CF_3 groups are omitted for clarity. Axial interactions to dirhodium units are drawn as dashed lines. Only the major orientation of clathrated I_2 molecules is depicted.

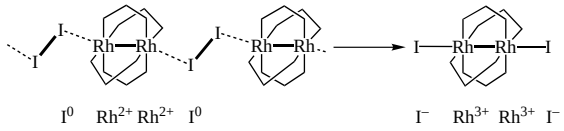
neighboring atoms (all longer than 3.3 Å). It is disordered over two positions with site occupancies of 94.4 and 5.6%. The I–I distance in the "coordinated" I_2 molecule (2.7202(6) Å) is longer than in the "clathrated" one (2.666(2) Å). The latter is the same as the value of free diiodine in the gaseous state (2.667(2) Å).[4]

The bridging coordination mode of I_2 found here is without precedent. There are numerous examples of iodine adducts of transition metal complexes, but most of them have the I_2 forming a part of a polyiodide anion—for instance I_3^-, I_5^-, I_4^{2-}—in both terminal and bridging modes.[5, 6] An example of a complex in which the reactive neutral halogen, I_2, is coordinated directly to a transition metal is the iodine–platinum(II) complex $[PtI\{o,o'\text{-}(Me_2NCH_2)_2C_6H_3\}(\eta^1\text{-}I_2)]$[7a] where there is a linear Pt-I-I arrangement with a long Pt–I distance of 2.895(1) Å. This platinum–iodine bonding resulted in an elongation of the I–I bond distance from 2.667(2) Å in "free" diiodine[4] to 2.822(1) Å. A number of similar Pt–I_2 compounds with the same type of ligand $C_6H_3\{CH_2NR^1R^2\}_2$ bearing various substituents R^1 and R^2 on the N atom have been reported having the same η^1-coordination mode.[7b] In all these Pt-I-I complexes, there is a linear arrangement, which is in sharp contrast to the bent (95°) structure in the present case. It has been suggested[7a] that in the Pt compounds the metal is donating to the σ* orbital of the I_2 molecule, whereas in **1** we believe that the I_2 molecule is functioning as an electron-pair donor to the rhodium atoms. There appears to be no close analogue to the bridging bidentate coordination

 © WILEY-VCH Verlag GmbH, D-69451 Weinheim, 2000 1433-7851/00/3913-2363 $ 17.50+.50/0

mode of molecular diiodine to a transition metal atom found in **1**.

Another interesting synthetic aspect of this result is the resistance of the dirhodium trifluoroacetate unit toward oxidation by I_2 at temperatures above 150 °C. Analogous reactions with different concentrations of Br_2 and $PhI \cdot Cl_2$ (as a dichlorine source) have been attempted over a wide range of temperatures (100 – 180 °C), but no crystalline products were formed under the conditions used. These reactions most probably resulted in the oxidation of $[Rh_2(O_2CCF_3)_4]$ and formation of nonvolatile materials. The oxidation of dirhodium carboxylates by Br_2 is known to take place in solutions at ambient temperatures.[8] The unique halo-metal complex **1** represents a model for probable intermediates during the early stages of oxidative addition reactions by halides (Scheme 1).



Scheme 1. Schematic representation of oxidative addition reactions of halides with $[Rh_2(O_2CCF_3)_4]$, with **1** as a model for probable intermediates.

Experimental Section

All experimental manipulations involving the synthesis of the starting materials were carried out under dry, oxygen-free argon by employing Schlenk techniques. The unligated form of $[Rh_2(O_2CCF_3)_4]$ was obtained using literature procedures.[9] The EI/DP mass spectra were acquired using a VG Analytical 70S high-resolution, double focusing, sectored (EB) mass spectrometer.

The title compound **1** was prepared by heating a mixture of $[Rh_2(O_2CCF_3)_4]$ (65 mg, 0.10 mmol) and freshly sublimed I_2 (20 mg, 0.08 mmol) at 150 – 160 °C for 5 – 6 days in a sealed evacuated Pyrex ampoule. Dark (red-violet on grinding) crystals of **1** were collected in the "cold" zone of the tube where the temperature was set about 5 °C lower; yield: 34 mg (29.2 %). MS (300 °C): *m/z* (%): 657 (38, $[Rh_2(O_2CCF_3)_4]^+$), 544 (47, $[Rh_2(O_2CCF_3)_3]^+$), 431 (65, $[Rh_2(O_2CCF_3)_2]^+$), 318 (9, $[Rh_2(O_2CCF_3)]^+$), 127 (100, $[I]^+$)

The use of FeI_2 as a slow release source of I_2, and lower concentrations of molecular I_2 produced no crystalline iodine-containing products.

Received: January 17, 2000 [Z14543]

[1] a) F. A. Cotton, R. A. Walton, *Multiple Bonds Between Metal Atoms*, 2nd Ed., Oxford University Press, Oxford, **1993**, pp. 432 – 443; b) T. R. Felthouse, *Prog. Inorg. Chem*. **1982**, *29*, 73 – 166.

[2] a) F. A. Cotton, E. V. Dikarev, S.-E. Stiriba, *Organometallics* **1999**, *18*, 2724 – 2726; b) F. A. Cotton, E. V. Dikarev, M. A. Petrukhina, *J. Organomet. Chem*. **2000**, *596*, 130 – 135; c) F. A. Cotton, E. V. Dikarev, M. A. Petrukhina, S.-E. Stiriba, *Organometallics* **2000**, *19*, 1402 – 1405.

[3] Crystallographic data for **1** ($C_8F_{12}I_4O_8Rh_2$): $M_r = 1165.50$, red-violet block, $0.45 \times 0.25 \times 0.18$ mm, triclinic, space group $P\bar{1}$, $a = 10.4259(3)$, $b = 10.671(1)$, $c = 11.924(3)$ Å, $\alpha = 80.35(3)$, $\beta = 89.82(1)$, $\gamma = 68.80(1)°$, $V = 1216.9(3)$ Å^3, $Z = 2$, $\rho_{calcd} = 3.181$ g cm^{-3}, $\mu = 6.553$ mm^{-1}, $2\theta_{max} = 50.14°$, Nonius FAST area detector system, $Mo_{K\alpha}$ radiation ($\lambda = 0.71073$ Å), $T = -60$ °C, 8002 reflections measured, data corrected for Lorentz and polarization effects, absorption correction (transmission coefficients 0.109 – 0.286), direct method solution (SHELXTL V.5), full-matrix refinement on F^2 (SHELXL-93), $R1$ (on F_o) = 0.040, $wR2$ (on F_o^2) = 0.1121 for 316 parameters and 37 restraints, 4061 independent reflections, $R1$ (on F_o) = 0.0381, $wR2$ (on F_o^2) = 0.1094 for 3874 reflections with $I > 2\sigma(I)$, highest residual peak 1.51 e$^-$ Å^{-3}. Crystallographic data (excluding structure factors) for the structure reported in this paper have been deposited with the Cambridge Crystallographic Data Centre as supplementary publication no.CCDC-138682 (entries carrying the suffix *x* represent disordered atoms). Copies of the data can be obtained free of charge on application to CCDC, 12 Union Road, Cambridge CB21EZ, UK (fax: (+44) 1223-336-033; e-mail: deposit@ccdc.cam.ac.uk).

[4] I. L. Karle, *Chem. Phys.* **1955**, *23*, 1739.

[5] a) F. Calderazzo, R. Poli, P. F. Zanazzi, *Gazz. Chim. Ital*. **1988**, *118*, 595 – 601; b) R. Ambrosetti, W. Baratta, D. B. Dell'Amico, F. Calderazzo, F. Marchetti, *Gazz. Chim. Ital*. **1990**, *120*, 511 – 525; c) K.-F. Tebbe, A. Gräfe-Kavoosian, B. Freckmann, *Z. Naturforsch. B* **1996**, *51*, 999 – 1006.

[6] a) M. F. Belicchi, G. G. Fava, C. Pelizzi, *Acta Crystallogr. Sect. B* **1981**, *37*, 924 – 926; b) L. R. Gray, D. J. Gulliver, W. Levason, M. Webster, *Inorg. Chem.* **1983**, *22*, 2362 – 2366; c) R. D. Bailey, L. L Hook, W. T. Pennington, *Chem. Commun*. **1998**, 1181 – 1182; d) P. H. Svensson, L. Kloo, *Inorg. Chem.* **1999**, *38*, 3390 – 3393.

[7] a) J. A. M. van Beek, G. van Koten, W. J. J. Smeets, A. L. Spek, *J. Am. Chem. Soc.* **1986**, *108*, 5010 – 5011; b) J. A. M. van Beek, G. van Koten, G. P. C. M. Dekker, E. Wissing, M. C. Zouberg, C. H. Stam, *J. Organomet. Chem.* **1990**, *394*, 659 – 678.

[8] M. A. Golubnichaya, E. M. Trishkina, G. N. Kuznetsova, A. V. Rotov, I. B. Baranovskii, *Russ. J. Inorg. Chem.* **1989**, *34*, 1493 – 1494.

[9] F. A. Cotton, E. V. Dikarev, X. Feng, *Inorg. Chim. Acta* **1995**, *237*, 19 – 26.

Thermosensitive, Reversibly Cross-Linking Gels with a Shape "Memory"

Babinder K. Samra, Igor Yu. Galaev, and Bo Mattiasson*

Smart polymers/gels are materials that undergo a sharp and reversible change in their microstructure when subjected to an external stimulus such as temperature, pH, ionic strength, solvent composition. When triggered, this change can be seen on a macroscopic level either as phase separation, or else in the case of gels, an order-of-magnitude volume change.[1] The ability of smart materials to change their physical properties according to their environment makes them desirable for a multitude of applications, including drug delivery devices,[2] supports for biocatalysts,[3, 4] bioseparations,[5] and biosensors. The external trigger for a thermosensitive polymer is temperature. The polymer is soluble in water at temperatures below the lower critical solution temperature (LCST) as a result of a thermodynamic balance of the four fundamental forces between the polymeric material and the water.[6]

The polymer-enriched phase formed above the LCST could be either in the form of a compact polymer precipitate or as a physically cross-linked gel. The latter occurs with linear polymer chains where there is an increased physical interaction between neighboring chains.[7, 8] This type of self-

[*] Prof. B. Mattiasson, Dr. B. K. Samra, Dr. I. Yu. Galaev
Department of Biotechnology
Center for Chemistry and Chemical Engineering
Lund University, P.O. Box 124
221 00 Lund (Sweden)
Fax: (+46) 46-222-4713
E-mail: bo.mattiasson@biotek.lu.se

 © WILEY-VCH Verlag GmbH, D-69451 Weinheim, 2000 1433-7851/00/3913-2364 $ 17.50+.50/0

assembling behavior occurs as a consequence of multi-point contacts, mainly by hydrophobic interaction and hydrogen bonding.[9]

Herein we discuss the properties of a thermosensitive, three-component copolymer that undergoes phase separation to form either a compact polymer precipitate or a physically cross-linked gel, depending on the relative composition of the components used. Moreover, an additional feature is that the physically cross-linked gel formed collapses with a further increase in temperature to result in shrunken, shape-remembered gel formation (see Scheme 1).

The polymers were synthesised and their composition determined as follows. The monomer *N*-isopropylacrylamide (NIPAAM; Aldrich, Germany) was recrystallized twice from cyclohexane prior to use, while styrene (Aldrich, Germany) and 2-hydroxyethylmethacrylate (HEMA; Aldrich, Germany) were passed twice through an alumina (ICN; high resolution aluminium oxide, W200 neutral, particle size 18–32 μm) column using a volume ratio of approximately 3:1 alumina:monomer to remove *tert*-butylcatechol and hydroquinone monomethyl ether, respectively. NIPAAM styrene and *N*-acryloxysuccinimide (NASI; Acros, Belgium: used as supplied) or HEMA were dissolved in argon-degassed THF (analysis grade) and 0.2 mol% 2,2′-azobisisobutyronitrile (AIBN; Fluka, Germany: recrystallized from methanol, twice) relative to NIPAAM, was added to a reaction tube, which was sealed and subsequently heated at about 80 °C overnight. The reaction mixture was cooled and poured onto diethyl ether to precipitate the polymer. The polymer was filtered off, redissolved in THF, and precipitated again in diethyl ether to remove any oligomers. The polymer was air dried at room temperature and analyzed by NMR spectroscopy to determine the relative monomer composition. The relative compositions of the copolymers were calculated on the basis of the integrations for the protons from the pendant groups of the different monomer moieties (see Table 1).

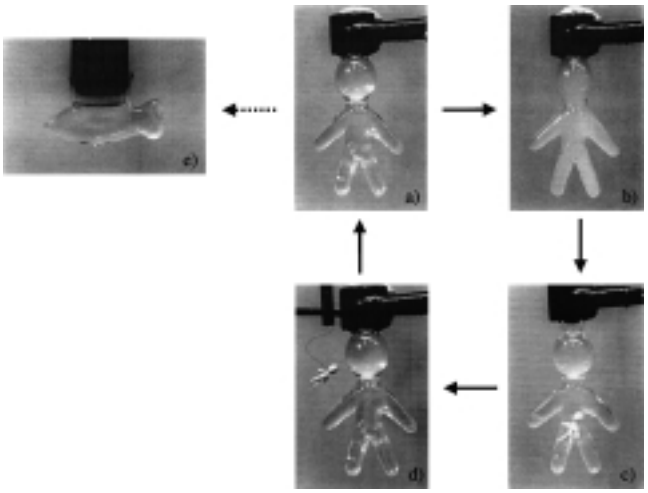
Copolymers of styrene and NIPAAM (Table 1, polymers a–f) have higher LCST values relative to a NIPAAM homopolymer, which has a LCST of 32 °C.[10] The LCST was reduced to a minimum of 11.5 °C by the incorporation of 14 mol% styrene. A higher styrene content rendered the polymer insoluble in aqueous media. Conversely, NASI-NIPAAM copolymers had increased LCST values relative to poly(NIPAAM) (data not shown). However, the resulting gel formed from a three-component polymer demonstrated properties quite distinct from the usual behavior exhibited by thermosensitive gels. A narrow composition range of the three components resulted in the formation of shape-remembered gels (Scheme 1). The difference with this type of physical cross-linked hydrogel compared to a chemically cross-linked gel is that the former gel is formed thermoreversibly. At low temperatures the polymer remained in solution. As the temperature was increased, the polymer thermoprecipitated and the resulting gel had the appearance of a turbid, homogenous, viscous phase, which filled the volume of the vessel. The turbid gel collapsed and shrank with a further increase in temperature. A distinct phase separation was observed as the gel formed a dense white miniaturized version of the original polymer in the vessel, and the water was expelled as a separate phase. The collapsed gel cast was mechanically strong enough to be removed from the aqueous phase and transported into another vessel.

The polymer was resolubilized simply by cooling. The solubilized polymer could then be recast in another form,

Table 1. Relative molar ratio of monomers in the copolymers.

Polymer	Poly(styrene$_x$-NASI$_y$-NIPAAM$_z$)[a]			Comments[b]
	x	*y*	*z*	
a	10	–	90	17.0 °C
b	11	–	89	16.5 °C
c	12	–	88	15.5 °C
d	13	–	87	11.5 °C
e	14	–	86	11.5 °C
f	15	–	85	0
1	19	40	41	0
2	20	35	45	0
3	35	25	40	0
4	13	44	43	–
5	14	37	49	–
6	15	25	60	–
7	16	39	45	–
8	20	22	58	+
9	22	23	55	+
10	23	21	56	+
11	19	29	52	+++
12	19	30	51	+++
13	19	31	50	+++
14	19	32	49	+++
15	19	33	48	+++
16	22	29	49	+++

[a] The relative compositions of the copolymers were calculated from the integrations for the protons from the pendant groups of the different monomer moieties: ^{1}H NMR (500 MHz, [D$_8$]THF, 25 °C, TMS): $\delta = 1.2$ (NIPAAM 6H; $(CH_3)_2$), 2.9 (NASI 4H; $NC(O)(CH_2)_2C(O)$), 7.2 (styrene 5H; $C(CH_2)_5$). The combined signal of the above mentioned protons was taken as 100 mol% of the polymer with the accuracy of determination of the single component to be within 2–3 mol%. [b] 0: aqueous insoluble copolymer, –: forms a flocculated precipitate, +: forms a weak gel which decomposes into a flocculated precipitate on further heating, +++: forms a gel which shrinks on further heating preserving the shape of the vessel.



Scheme 1. Formation (a and b) and form-remembered shrinkage (c) of the poly(styrene$_{19}$-NASI$_{31}$-NIPAAM$_{50}$) physically cross-linked gel on increasing the temperature of an aqueous solution of the polymer. The shrunken gel is mechanically strong enough to be transported to another vessel (d). e) Resolubilization of the shrunken gel in cold water and recasting in another shape.

 © WILEY-VCH Verlag GmbH, D-69451 Weinheim, 2000 1433-7851/00/3913-2365 $ 17.50+.50/0

using a different shaped vessel (Scheme 1). This behavior was exhibited by polymers 8–16 (Table 1) in which the styrene content was around 20 mol % and the NASI around 30 mol %. The polymers outside this relatively narrow composition range (Figure 1) behaved in a more conventional manner,

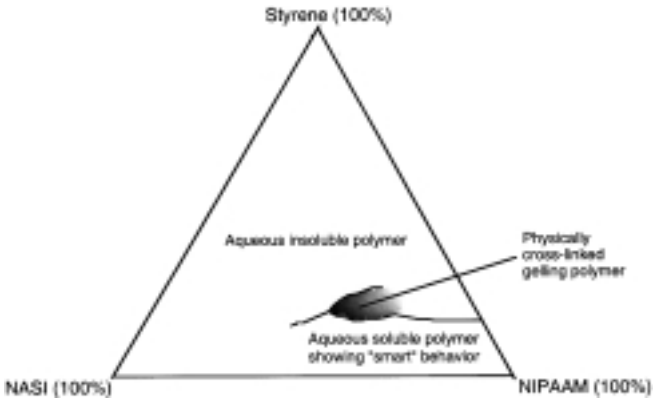


Figure 1. Effect of poly(styrene$_x$-NASI$_y$-NIPAAM$_z$) composition on the behavior of the polymer in aqueous solutions in response to increasing temperature.

forming either a compact polymer precipitate, such as polymers 4–7 (Table 1), or being insoluble, such as polymers 1–3. The insolubility of poly(styrene$_{35}$-NASI$_{25}$-NIPAAM$_{40}$) was the result of a high styrene content. This result was expected owing to the high hydrophobicity of the styrene component. However, for the other two polymers in this group, poly(styrene$_{19}$-NASI$_{40}$-NIPAAM$_{41}$) and poly(styrene$_{20}$-NASI$_{35}$-NIPAAM$_{45}$), it appears the same insolubility effect was also observed with a high NASI content.

The requirements for the formation of thermosensitive, physically cross-linked gels are for the polymeric chain to be composed of "blocks" of copolymers of differing hydrophobicity.[10] The hydrophobic segments form self-aggregating temporary cross-links, whilst the hydrophilic components allow the copolymer to remain in solution. As the degree of blocking in the synthesized polymers is unknown, the explanation for the behavior of the gel could be that the mixture of copolymers of various composition has been created with ongoing conversion. The more hydrophobic copolymers in the mixture may be responsible for the cross-linking effects, whilst the more hydrophilic ones give rise to swelling.

The degree of maximal shrinkage attained within the concentration range (0.1–1.0 % (w/w)) and volume (3 mL) tested, was the same for all the different polymer concentrations. Below 0.1 % (w/w), the shrunken gel did not properly conserve the shape. At 2.0 % (w/w), the shrunken gel was not floating, as with the lower concentrations, but was splattered on the bottom of the vessel, presumably because of the increased density of the collapsed gel. The lowest concentration where the polymers of type poly(styrene$_x$-NASI$_y$-NIPAAM$_z$) could form thermoreversible gels was found to be 0.1 % (w/w), which is much lower than is usually observed for other types of synthetic, thermoreversibly gelating polymers. For example, poly(ethylene glycol-*b*-(DL-lactic acid-*co*-glycolic acid)-*b*-ethylene oxide)[8] or poly(ethylene oxide-*b*-propylene oxide-*b*-ethylene)[10] form gels at polymer concentrations above 15 % (w/w) with increasing temperatures. Natural polymers, such as methylcellulose, form thermoreversibly gels at lower concentrations of 0.5 % (w/w),[7] which is comparable to that of poly(styrene$_x$-NASI$_y$-NIPAAM$_z$)-type polymers.

The degree of shrinkage (the ratio of the volumes of swollen and shrunken state of the gel) of the gels formed by polymers of the type poly(styrene$_x$-NASI$_y$-NIPAAM$_z$) increased with the duration of heating to a maximum of about 150 after 16 h (Figure 2). As the degree of shrinkage

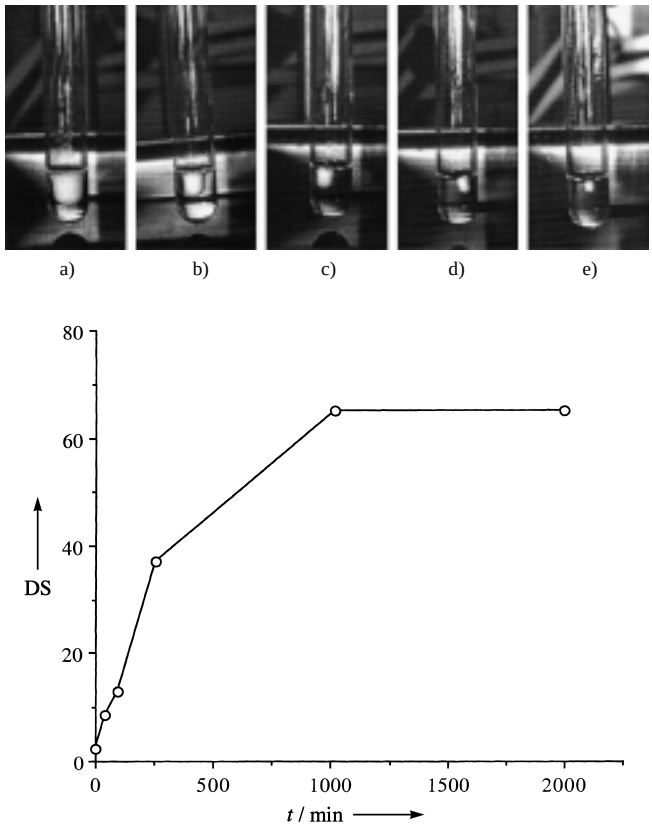


Figure 2. Time dependence of the shrinking of a physically cross-linked gel formed by poly(styrene$_{19}$-NASI$_{31}$-NIPAAM$_{50}$) at 43 °C at a) 0, b) 40, c) 90, d) 260, and e) 1000 min. The graph presents the dependence of the degree of shrinkage (DS) versus time.

increased, more water was expelled from the cross-linked polymer network, and the gel became increasingly impermeable to water. At this stage the gel proved extremely difficult to resolubilize by simple cooling, and required mechanical grinding before resolubilization occurred. Otherwise, the precipitated cross-linked gel was extremely stable and could be stored in water at ambient temperature indefinitely.

The narrowest diameter vessel where the shape of the shrunken polymer gel was conserved was found to be 2 mm. The precipitated gel shape was not observed below this thickness. It is believed that as the thickness decreases the convection flows and surface forces in the water become too strong for the formation of very thin polymer threads.

The preliminary, investigative work described here shows the synthesis of a novel, multifunctional copolymer with an unusual combination of properties, the full potential of which

 © WILEY-VCH Verlag GmbH, D-69451 Weinheim, 2000 1433-7851/00/3913-2366 $ 17.50+.50/0

are beyond the scope of this article. However, this polymer demonstrates a range of different features, and is envisaged to have potential use for the development of new drug-delivery systems, biocatalysts, and biosensors.

Received: January 17, 2000
Revised: March 22, 2000 [Z14542]

[1] I. Yu. Galaev, B. Mattiasson, *Enzyme Microb. Technol.* **1993**, *15*, 354 – 366.
[2] S. Miyazaki, F. Suisha, N. Kawasaki, M. Shirakawa, K. Yamatoya, D. Attwood, *J. Controlled Release* **1998**, *56*, 75 – 83.
[3] Y. Ito, N. Sugimura, H. K. Oh, Y. Imanishi, *Nat. Biotechnol.* **1999**, *17*, 73 – 75.
[4] H. Lee, T. G. Park, *Biotechnol. Prog.* **1998**, *14*, 508 – 516.
[5] Using Stimuli-Responsive Polymers in Bioseparation (Ed.: I. Yu. Galaev), *Bioseparation Special Issue* **1999**, *7*, 175 – 280.
[6] E. Kokufuta, *Responsive gels: Volume transitions II* (Ed.: K. Dusek) Springer, Berlin, **1993**, pp. 158 – 176.
[7] K. Kobayashi, C. Huang, T. P. Lodge, *Macromolecules* **1999**, *32*, 7070 – 7077.
[8] B. Jeong, Y. H. Bae, S. W. Kim, *Macromolecules* **1999**, *32*, 7064 – 7069.
[9] H. Hachisako, R Murakami, *Recent Res. Develop. Pure Appl. Chem.* **1998**, *2*, 547 – 561.
[10] L. E. Bromberg, *J. Phys. Chem.* **1998**, *102*, 1956 – 1963.

+++ THE LINK TO INTERNATIONAL CHEMISTRY +++

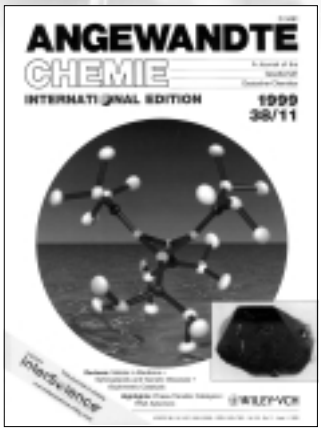


"It is a long time since I have read one issue of a journal [...] which has so much of interest...

...to process R&D chemists and engineers as issue No. 23 in Vol. 36 of *Angewandte Chemie.*

Trevor Laird, Editor of Organic Process Research & Development
[Org. Process Res. Dev. 1998, 2, 64]

The Highlights in *Angewandte* provide concise evaluations of the most important current trends in chemical research.



Have your own Highlights every two weeks. Subscribe to *Angewandte* with the Order Form on the last page of this issue.

The most cited Highlights in 1998 are:

- *A.E. Rowan, R.J.M Nolte:* Helical Molecular Programming
- *N. Krause:* Copper-Catalyzed Enantioselective Michael Additions: Recent Progress with New Phosphorus Ligands
- *O. Geis, H.-G. Schmalz:* New Developments in the Pauson - Khand Reaction
- *J.E. Cosgriff, G.B. Deacon:* Another Surprise from Pyrazolate Ligands
- *C. Schneider:* New Polyol Syntheses
- *A.P. Davis:* Tilting at Windmills? The Second Law Survives
- *J.O. Metzger:* Solvent-Free Organic Syntheses
- *H. Frey:* From Random Coil to Extended Nanocylinder: Dendrimer Fragments Shape Polymer Chains
- *J.D. Smith:* Phosphanides of the Heavier Alkali Metals
- *D. Wolf :* High Yields of Methanol from Methane by C-H Bond Activation at Low Temperatures
- *P. Luger:* Large Molecules from the Virtual Bakery - Filling a Gap in Structure Research
- *V. Fehring, R. Selke:* Highly Enantioselective Complex-Catalyzed Reduction of Ketones - Now with Purely Aliphatic Derivations Too

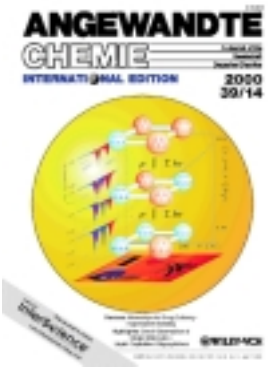
WILEY-VCH, P.O. Box 10 11 61, 69451 Weinheim, Germany
Phone +49 (6201) 606-328, Fax +49 (6201) 606-348
e-mail: sales-journals@wiley-vch.de, http://www.wiley-vch.de

WILEY-VCH

SCHULZ1299<ACHUNK1>

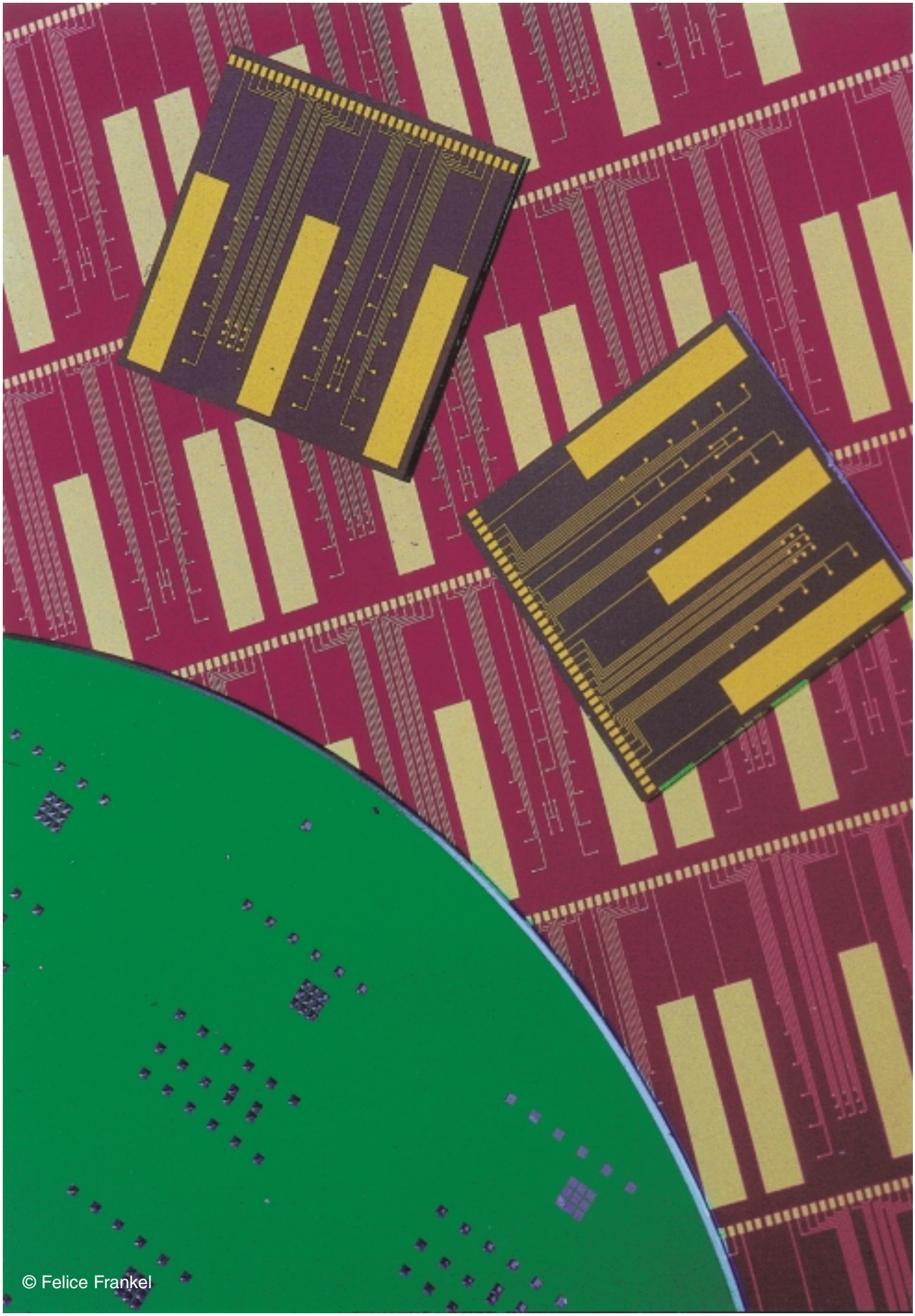
 © WILEY-VCH Verlag GmbH, D-69451 Weinheim, 2000 1433-7851/00/3913-2367 $ 17.50+.50/0

Cover Picture



Esther Breuning, Mario Ruben, Jean-Marie Lehn, Franz Renz, Yann Garcia, Vadim Ksenofontov, Philipp Gütlich, Elina Wegelius, and Kari Rissanen

The cover picture shows how both, fine arts and science, avail themselves of a system of intertwined symbolic and iconic languages. They make use of a common set of abstracted signs to report on their results. Thus, already in 1925, Wassily Kandinsky painted a masterpiece (bottom), which now, 75 years later, might be regarded as a blueprint for a scientific project. In his painting, Kandinsky pictured a grid-shaped sign that resembles in effect an actual molecular switch. Apparently following an enigmatic protocol, the groups of Lehn and Gütlich (see p. 2504 ff. for more details) constructed a grid-type inorganic architecture that operates as a three-level magnetic switch (center) triggered by three external perturbations (p, T, $h\nu$). The switching principle is based on the spin-crossover phenomenon of Fe^{II} ions and can be monitored by Mössbauer spectroscopy (left) and magnetic measurements (rear). Maybe not by chance, the English translation of the title of the painting "signs" is a homonym of "science", since both presented works are a product of the insatiable curiosity of man and his untiring desire to recognize his existence.



Microchips with reservoirs for chemicals that can be filled from the back (lower left part) and electrodes at the front for opening the reservoirs.

ANGEWANDTE
CHEMIE
© WILEY-VCH

Microchips as Controlled Drug-Delivery Devices

John T. Santini, Jr.,* Amy C. Richards, Rebecca Scheidt, Michael J. Cima,* and Robert Langer*

Controlled-release systems are common in a number of product areas, including foods, cosmetics, pesticides, and paper. Microencapsulated systems, for example, are used for the release of flavors and vitamins in foods, fragrances in perfumes, and inks in carbonless copy paper. Controlled-release systems for drug delivery first appeared in the 1960s and 1970s. In the past three decades, the number and variety of controlled release systems for drug-delivery applications has increased dramatically. Many of these use polymers having particular physical or chemical characteristics such as biodegradability, biocompatibility, or responsiveness to pH or temperature changes. However, recent advances in the field of microfabrication have created the possibility of a new class of controlled-release systems for drug delivery, namely, that of small, programmable devices. Their small size, potential for integration with microelectronics, and ability to store and release chemicals on demand could make controlled-release microchips useful in a number of areas, including medical diagnostics, analytical chemistry, chemical detection, industrial process monitoring and control, combinatorial chemistry, microbiology, and fragrance delivery. More importantly, drug-delivery microchips resulting from this convergence of controlled release and microfabrication technologies may provide new treatment options to clinicians in their fight against disease.

Keywords: controlled release · drug delivery · drug research · microchips · microreactors

1. Introduction

Microelectronic devices have become an integral part of our lives. They are present in our automobiles, cellular phones, and personal computers. This review examines an emerging new field: the application of microfabrication technologies to the development of devices for the controlled release of chemicals, including drugs. To provide the proper background for understanding this new field, we begin with an overview of the field of controlled release and then briefly discuss relevant work from the field of microfabrication. The remainder of the article reviews our recent work on the development of controlled-release microchips for chemical- and drug-delivery applications.

[*] Dr. J. T. Santini, Jr.,[+] Prof. R. Langer
Department of Chemical Engineering, Room E25-342
Massachusetts Institute of Technology
Cambridge, MA 02139 (USA)
Fax: (+1) 617-258-8827
E-mail: jsantini@mchips.com, rlanger@mit.edu

Prof. M. J. Cima, A. C. Richards, R. Scheidt
Department of Materials Science and Engineering, Room 12-011
Massachusetts Institute of Technology
Cambridge, MA 02139 (USA)
Fax: (+1) 617-258-6936
E-mail: mjcima@mit.edu

[+] Present Address:
MicroCHIPS, Inc.
45 Spinelli Place
Cambridge, MA 02138 (USA)
Fax: (+1) 617-492-2435

2. Overview of Controlled Release

Controlled release, as used in this review, refers to materials or devices for controlling the release time of a chemical, the release rate, or both. Controlled release has proved useful in areas such as foods, cosmetics, and pesticides,[1] but it has had its largest impact in the field of drug delivery.[2]

The method by which a drug is delivered can have a significant effect on its therapeutic efficacy.[3] Some drugs have an optimum range of concentrations within which the maximum therapeutic benefit is derived. Drug concentrations above or below this range can be toxic or produce no therapeutic benefit. Conventional drug-delivery systems such as tablets or injections typically result in a drug-delivery profile that is initially marked by a sharp increase in concentration to a peak above the therapeutic range. Then, there is a relatively rapid decrease in concentration until the drug falls below the therapeutic range. Therefore, the time spent in the optimum concentration range may be short

 © WILEY-VCH Verlag GmbH, D-69451 Weinheim, 2000 1433-7851/00/3914-2397 $ 17.50+.50/0

(Figure 1 a). Sleeping pills are a good example for illustrating the importance of drug concentration. If the drug concentration is below the therapeutic range, enhancement of sleep is not observed. If the drug concentration is above the therapeutic range, potentially fatal toxicity may be encountered. Therefore, the ideal concentration profile, in some cases, would reside in the therapeutic range and be nearly independent of time (Figure 1 a).

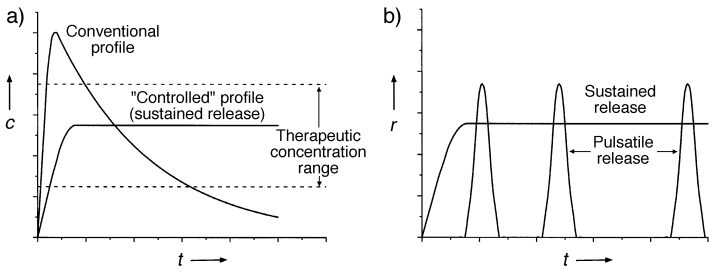


Figure 1. a) Exemplary concentration c vs. time t profiles for conventional and controlled-release drug-delivery devices. The controlled release profile here is characteristic of sustained (or continuous) release. b) Exemplary release rate r vs. time profiles demonstrating the difference between sustained (or continuous) release and pulsatile release.

2.1. Sustained Release

The field of controlled release initially focused on achieving a sustained (or continuous) release of drug over an extended


R. Langer


M. J. Cima


J. T. Santini, Jr.


A. C. Richards


R. Scheidt

Robert Langer is the Kenneth J. Germeshausen Professor of Chemical and Biomedical Engineering at MIT. He received a BSc from Cornell University in 1970 and a ScD from MIT in 1974, both in chemical engineering. He has received honorary degrees from ETH (Switzerland) and Technion (Israel) and over 80 major awards, including the Gairdner Foundation International Award. He has authored 620 scientific publications, 400 abstracts, 365 patents, has edited 12 books and is the only active member of all three United States National Academies (Science, Medicine, Engineering). His research interests include drug delivery, tissue engineering, and polymers.

Michael J. Cima is the Sumitomo Electric Industries Professor in the Materials Science and Engineering Department at MIT. He earned a BSc in chemistry in 1982 and a PhD in chemical engineering in 1986, both from the University of California at Berkeley. He has written 130 scientific publications and nine patents and has received numerous honors, including the International Award of Materials Engineering for Resources, R&D 100 Award, ALCOA Foundation Science Award, and election as a Fellow of the American Ceramics Society. His research interests include ceramics processing, ink-jet and other printing technologies, and drug delivery.

John T. Santini, Jr. received a BSc from the University of Michigan in 1994 and a PhD from MIT in 1999, both in chemical engineering. His graduate study was supported by a National Science Foundation Fellowship and focused on the design, fabrication, and characterization of microchips for chemical and drug-delivery applications. At present he is continuing his drug-delivery research at MicroCHIPS, Inc. and at MIT as a research affiliate in the Harvard-MIT Division of Health Sciences and Technology.

Amy C. Richards received a BSc in materials science and engineering from MIT in 1997. She is currently a National Science Foundation Fellow and is working toward her PhD in materials science and engineering under the guidance of Professor Langer and Professor Cima. Her doctoral research involves the integration of polymer science, polymer processing, and drug delivery to develop and characterize novel controlled-release devices.

Rebecca Scheidt graduated summa cum laude from the University of Missouri-Rolla in 1998 with a BSc in ceramic engineering. She is currently a graduate student and National Science Foundation Fellow in materials science and engineering at MIT working on the electrochemical and microprocessing aspects of drug-delivery microchips.

period of time (Figure 1b) with minimal influence by outside factors such as pH.[4] Much of this work involved polymers that released the drug at a nearly constant rate due to diffusion out of the polymer or by degradation of the polymer over time. These controlled-release systems may be of a macro- or microscopic size and exist in a number of different forms, such as oral tablets, polymer implants (rods, wafers, or pellets), and polymer microspheres. Two examples of commercially available polymeric devices for constant drug release include Gliadel[5] (implantable polyanhydride wafers that release carmustine for the treatment of malignant brain tumors at a nearly constant rate as the polymer degrades) and Lupron Depot[6] (injectable polymer microspheres, for treatment of endometriosis, precocious puberty, or for the nearly constant release of LHRH analogues for prostate cancer therapy).

Transdermal delivery is another method that achieves sustained release of drugs. It has proved successful for small lipophilic drug molecules such as scopolamine (motion sickness), fentanyl (pain), clonidine (hypertension), estradiol (hormone replacement), testosterone (impotence), nicotine (smoking cessation), and nitroglycerin (angina).[2, 7] A major advantage of transdermal delivery is that first-pass metabolism of the administered drug by the liver is reduced.[7b] However, there is typically a lag time between the application to the skin and the establishment of a stable concentration of the drug in the bloodstream, and only a limited number of drugs can penetrate the skin at rates fast enough to reach a therapeutic steady-state concentration in the bloodstream without chemical enhancers or external stimuli such as ultrasound.[8]

2.2. Pulsatile Release

The examples presented in Section 2.1 are designed to release drugs at a nearly constant rate. In numerous cases, however, sustained release is not the optimal method of drug delivery. Instead, delivery of pulses of drug at variable time intervals is the preferred method (Figure 1b) and is commonly referred to as pulsatile release. This delivery method works better in certain cases because it closely mimics the way in which the human body naturally produces some compounds. Insulin is a well-known example of a compound secreted by the body in a pulsatile manner.[9] Another example of compounds produced by the body in a pulsatile or periodic manner are the hormones of the anterior pituitary gland (adenohypophysis), for example gonadotropin and growth hormone, which are important in regulating reproduction and growth, respectively. Many compounds and environmental factors can stimulate or inhibit the production of these hormones. However, compounds secreted by the hypothalamus, called releasing factors or hormones, play a primary role in the regulation of adenohypophysial hormones. For example, women suffering from gonadotropin releasing hormone (GnRH) deficiency may not ovulate normally, making it difficult to conceive a child. Growth hormone releasing hormone (GHRH) deficiency in children may lead to dwarfism. Pulsatile administration of GnRH and GHRH can help reduce the severity of these deficiencies.[10] In fact, continuous adminstration of GnRH results in desensitization of GnRH receptors on the pituitary gland and may actually suppress the release of gonadotropins.[11]

Much previous work on methods of achieving pulsatile release focused on developing polymers that respond to specific stimuli:[12] changes in electric[13] or magnetic[14] fields, exposure to ultrasound,[14b, 15] light,[16] enzymes,[17] changes in pH[18] or temperature,[19] or molecules present in the human body, including antigens.[20] Transdermal delivery, typically a route for sustained delivery, can be modified to produce a more pulsatile release pattern in the presence of ultrasound[8] or voltage pulses (high voltage: electroporation, low voltage: iontophoresis).[21] Pulsatile release systems can be externally regulated (open-loop) or self-regulated (closed-loop).[22] A polymer implant that releases a drug when an oscillating magnetic field is applied is an example of an externally regulated system,[23] while a system that releases drug in response to antigens in the body is an example of self-regulation.[20] An example of oral and implantable polymer devices capable of delivering pulses of drug without the use of an external stimulus are those fabricated by Three Dimensional Printing. They are based on the controlled microstructure of the polymer matrix and release drugs at specified times as determined by the permeability of the polymer and the position of the drug in the device.[24]

An alternative method of pulsatile release involves the use of pumps and catheters. Pumps work well for both sustained and pulsatile release and can be programmed to deliver pulses of drug solutions to a patient through a catheter at different times. In fact, one of the current methods for treating GnRH deficiency in women involves wearing a pump (about the size of an adult fist) on a belt with a subcutaneous or intravenous catheter.[25] The pump delivers a pulse of a solution containing 5 μg of GnRH every 90 min for several weeks to months. However, some external pump and catheter systems can be inconvenient and uncomfortable, can limit the patient's mobility, can be expensive, and may result in irritation or infections at the catheter site. Completely implantable pumps, developed for diabetes, oncology, or analgesia,[26] for example, may improve patient mobility and reduce infections by eliminating transcutaneous catheters, but they may still be hampered by their size, cost, ability to deliver only drugs in solution, and the limited stability of some drugs in solution at 37 °C.

3. Overview of Microfabrication Technology

Microfabrication can be generally defined as the production of microscale features in or on a material by techniques such as deposition, etching, micromolding,[27] along with patterning techniques such as photolithography[27a–c] or microcontact printing.[28] Microfabrication has traditionally been used to produce integrated circuits for microelectronic devices such as computer microprocessors. However, microfabrication has been used increasingly to produce microscale devices whose primary function is mechanical, chemical, or optical in nature. Such devices include microreactors, micro-

pumps, accelerometers, and micromirrors, and are commonly referred to as microelectromechanical systems (MEMS). MEMS are commonly made with silicon and microelectronic processing techniques. However, MEMS can also be made from plastics, glass, metals, or ceramics by processes such as stamping, casting, molding, and laser ablation.

MEMS have found use in a number of fields. Two notable examples are the fabrication of nozzles for ink-jet printers[29] and accelerometers for automotive applications.[30] More recent advances in MEMS include the development of microreactors for the production of chemicals[31] and microturbine engines for aerospace applications.[32] For the purposes of this review, microfabricated devices for biological applications can generally be classified as microfluidic devices and nonmicrofluidic devices.

3.1. Microfluidic Devices

Microfluidics is an area of microfabrication that focuses on the miniaturization of fluid-handling systems such as pumps, valves, and flow channels. The concept of fabricating entire chemical labs-on-a-chip or miniaturized total analysis systems (μTAS) that include pumps, valves, mixers, reactors, and separators has recently generated much interest.[33] The demand for such systems has resulted in the development of numerous microfluidic components such as micropumps and microvalves.[34] Micropumps can be based on moving parts such as diaphragms or piezoelectric components that mechanically pump liquids[35] or they can move ionic fluids by using electric fields (i.e. electroosmotic pumping).[36] Microfabricated valves with pneumatic[37] or thermoelectric[38] actuators can operate reversibly. Irreversible valves based on electrochemical actuation have also been suggested.[39]

Recent interest in microfluidics for biological applications has focused largely on developing microsystems for chemical[33c, 40] or DNA[33b,d, 41] analysis. Other areas where microfluidic devices have been utilized include combinatorial chemistry,[33b] bioassays,[42] and capillary electrophoresis systems. For example, various methods of capillary electrophoresis on polydimethylsiloxane and fused silica microdevices have been used to separate DNA fragments,[43] oligonucleotides,[44] polymerase chain reaction (PCR) products,[45, 46] single DNA molecules,[43a, 47] and single-[41e] and double-stranded[48] DNA. Capillary electrophoresis on microdevices has also been used for DNA genotyping[49] and the separation of neurotransmitters,[45] amino acids,[50] peptides,[43a] insulin, and lysozyme.[43b]

3.2. Nonmicrofluidic Devices

Nonmicrofluidic devices for biological applications do not involve the pumping or controlled movement of fluids and include many biosensors and some "DNA chips". Biosensors can be manufactured from silicon by using semiconductor processes, but their fabrication often involves at least one unconventional step to produce surface features or coat the sensor with a biologically or chemically active compound.[51] Similarly, DNA chips use immobilized materials on the device surface to identify genetic material or other chemicals.[52] Over the last several years, DNA chips have become popular with pharmaceutical companies for high-throughput drug screening and combinatorial chemistry.

The use of microfabrication technology in biological applications has grown tremendously in recent years. However, microfabrication has found limited use in the fields of controlled release and drug delivery. One could envision using microfluidic devices to achieve drug release, but the potential limitations of delivering only liquid drug formulations, the instability of certain drugs in solution, the complexity of some fabrication schemes, and the presence of moving parts that are subject to breakdown may present obstacles to their clinical and commercial use. As a result, the field of controlled release has yet to take full advantage of microfabrication technology.

4. Controlled Release Microchips

The ultimate goal of our work was to develop a microfabricated device with the ability to store and release multiple chemical substances on demand by a mechanism devoid of moving parts.

4.1. Theory of Operation

Figure 2 shows a model embodiment of a controlled-release microchip consisting of an array of reservoirs that extend through an electrolyte-impermeable substrate. Each reservoir is sealed at one end by a thin membrane of material that

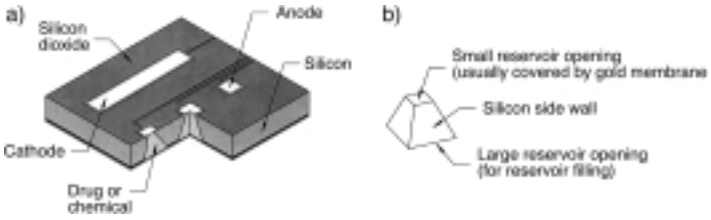


Figure 2. A schematic of a typical controlled-release microchip. a) Cut away section showing anodes, cathodes, and reservoirs, b) shape of an individual reservoir (see Section 4.2 for typical dimensions).

serves as an anode in an electrochemical reaction and dissolves when an electric potential is applied to it in an electrolyte. There must be at least one other electrode on the device surface to serve as a cathode in the electrochemical reaction. The cathode can be made of any conductive material but is usually made of the same material as the anodes to simplify fabrication procedures. In addition, any number of cathodes can be included on a microchip, and they can be of any shape or size to suit the electrode design desired for a particular application. The reservoirs are filled through the open end with the chemical to be released. The open ends of the reservoirs are then sealed with a waterproof material.

The device is submerged in an electrolyte containing ions that form a soluble complex with the anode material in its ionic form. An electric potential is applied to an anode membrane when release from its corresponding reservoir is desired. This causes oxidation of the anode material and formation of the soluble complex with the electrolyte ions. The complex then dissolves in the electrolyte, and the membrane disappears. Figure 3 shows the principle of operation schematically. The chemical in the newly opened reservoir is now exposed to the surrounding electrolyte and is free to dissolve in the electrolyte and diffuse out of the reservoir.

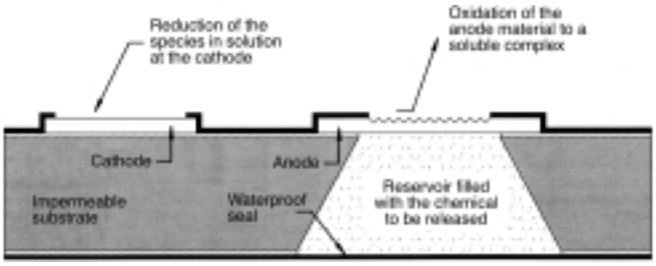


Figure 3. A cross section of a typical controlled-release microchip illustrating the principle of the electrochemical reservoir opening mechanism. The materials used in prototype microchips are described in Section 4.2.

4.2. Experimental Prototype Specifications

Four-inch-diameter silicon wafers were used as the initial model substrate material for the prototype controlled-release microchips. The prototype was a 17×17 mm square silicon device containing thirty-four reservoirs that extended completely through the silicon. The reservoirs were square pyramidal in shape (see Figure 2b) due to the potassium hydroxide etching method used to fabricate them. The small reservoir opening was approximately 50×50 μm, and the large opening approximately 480×480 μm. The thickness of the silicon substrate varied between 295 and 315 μm, so that each reservoir had a volume of approximately 25 nL. Each reservoir was sealed at the small end by a 0.2–0.3-μm gold membrane that served as an anode in an electrochemical reaction. Three thin-film gold cathodes were placed at different intervals across the surface of the device. Some portions of the gold anodes and cathodes were covered by a 0.4–0.6-μm silicon dioxide film to prevent corrosion in those areas during the application of an electric potential. The prototype microchip shown in Figure 4 had only three cathodes for thirty-four anodes. Twenty-one such prototype microchips can be fabricated on one four-inch silicon wafer.

The size of the prototype device was selected strictly for ease of handling during release experiments and compatibility with commercially available device packaging. However, devices are not restricted to that size and could be made much larger or smaller (< 2 mm), depending on the particular application. A device of the size used in these studies (17×17 mm) can accommodate over 1000 reservoirs.

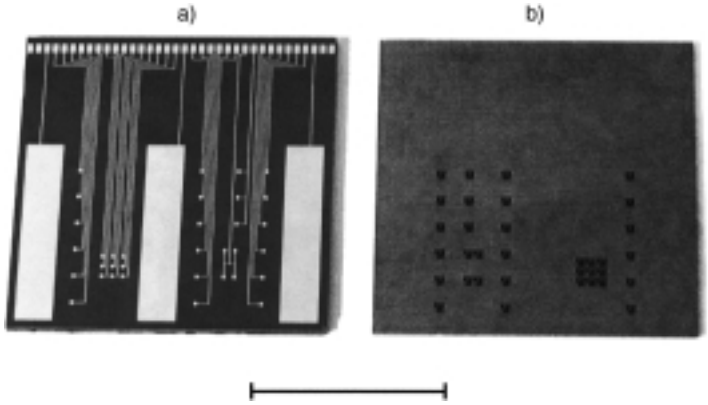


Figure 4. Photographs of a prototype microchip. a) The electrode-containing front side, b) the back side with the openings for filling the reservoirs. (Scale bar: 10 mm; photographs by Paul Horwitz.)

4.3. Selection of the Membrane Material

Selection of the proper membrane material is critical for the reliable operation of controlled-release microchips. A key requirement for the membrane material is that it should remain stable in the solution in the absence of an applied electric potential to prevent premature release of the chemical from the microchip. The membrane material must also be able to dissolve quickly and selectively when a specific electric potential is applied to it. However, selecting a material possessing both of these qualities is difficult because biological fluids contain a small amount of dissolved oxygen and chloride ions, which cause many metals to corrode spontaneously.

Gold was selected as the initial model membrane and electrode material primarily due to its unique electrochemical properties. Gold has long been considered a noble metal. It is easily deposited and patterned, has a low reactivity with other substances, and resists spontaneous corrosion in most aqueous solutions over the entire pH range. The fact that the gold surface remains clean (i.e., the native oxide layer on a gold surface, if present, is very thin) and does not corrode in most environments led to its widespread use in jewelry, currency, medical implants, and microelectronic devices. Pourbaix diagrams indicate the thermodynamically stable species in a solution at any combination of applied potential and solution pH. A computer-generated[53] Pourbaix diagram for gold in aqueous solutions free from complexing substances is shown in Figure 5. The diagram indicates that gold, when no electric potential is applied, is immune to corrosion over the entire domain of water stability (the area between the dotted lines). The species in areas delineated by solid lines are the thermodynamically stable, solid species at each combination of applied potential and solution pH.

The presence of a small amount of chloride ions in solution creates an electric potential/pH region that thermodynamically favors the formation of water-soluble chlorogold complexes.[54] The presence of a complexing substance such as chloride can change the Pourbaix diagram for gold in aqueous solutions (Figure 6a). However, thermodynamics does not tell the whole story. It is also important to look at the kinetics of

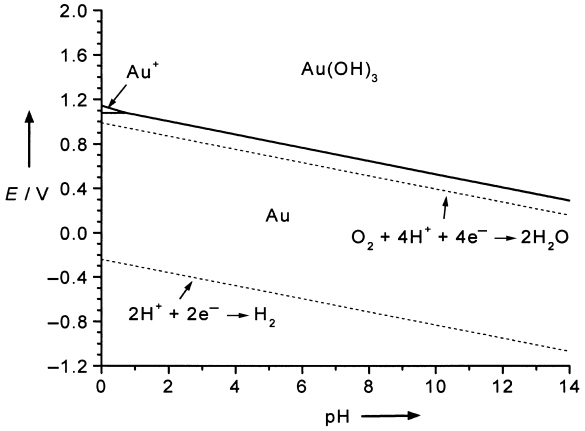


Figure 5. A Pourbaix diagram for the gold–water system in the absence of complexing substances such as chloride ions (applied potential E relative to SCE).

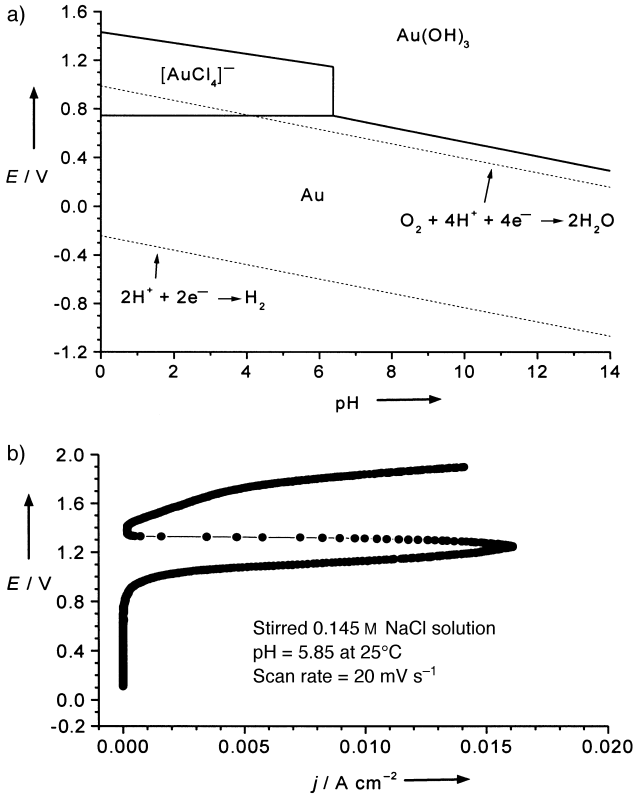


Figure 6. a) A Pourbaix diagram for the gold–chloride–water system containing 0.145 M chloride ion. b) An Evans diagram for the same gold–chloride–water system obtained potentiodynamically. This diagram represents the kinetics of the gold corrosion reaction in chloride-containing solutions.

the formation of chlorogold complexes. Evans diagrams represent the kinetics of corrosion and indicate how the corrosion rate (shown as current density) changes with applied potential. A potentiodynamic Evans diagram for gold in 0.145 M sodium chloride solution (Figure 6b) begins to show a rise in current density corresponding to the formation of tetrachloroaurate(III) at an applied potential slightly above its thermodynamic barrier potential of approximately +0.75 V relative to a saturated calomel electrode (SCE). Gold corrosion by the formation of water-soluble chlorogold(III) complexes is thermodynamically and kinetically favored and occurs at appreciable rates at potentials slightly above +1.0 V versus SCE. Corrosion of gold membranes occurs rapidly (typically 10–30 s for a 0.1–0.3 μm thick membrane at +1.04 V vs. SCE) and is clearly evident in the scanning electron micrographs of Figure 7.

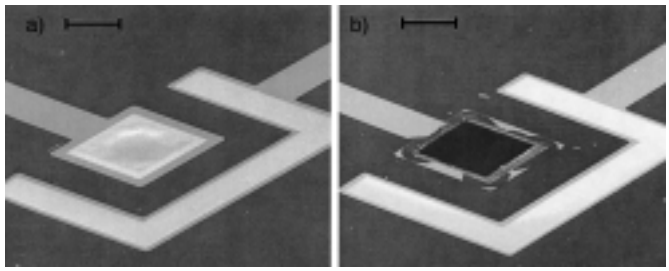


Figure 7. Scanning electron micrographs of a gold anode membrane covering a reservoir a) before and b) after the application of +1.04 V vs. SCE for several seconds in phosphate-buffered saline (PBS). (Scale bar: 50 μm.)

In addition to its favorable electrochemical properties, gold was selected as the initial model membrane material for proof-of-concept experiments due to its biocompatibility. Gold and its ionic compounds have been studied for many years due to their extensive use in dental materials, transdermal gene delivery, and drugs for treating rheumatoid arthritis.[55] Typical cumulative doses of Au^{I} salts used for treatment of rheumatoid arthritis can range from milligrams to grams, and the most common adverse side effects (various forms of dermatitis) are rarely seen in patients with a cumulative dosage of less than 250 mg.[55] The local effects of Au^{III} compounds have been less extensively studied. Some data have been reported for Au^{III} compounds in vitro,[56] but few studies have examined the local effect of Au^{III} in vivo. The quantity of Au^{III} that is locally released due to the opening of one reservoir is small (ca. 2–6 ng), and the diffusion and clearance kinetics of Au^{III}, which affect its local concentration, are dependent on the implantation site.

4.4. Fabrication

Controlled-release microchips are fabricated by standard microelectronic processing techniques such as chemical vapor deposition, photolithography, and plasma etching. The details of the stepwise process of making the prototype controlled release microchips can be found in the literature.[57]

4.5. Proof-of-Principle Release Studies

Proof-of-principle release studies were designed to determine whether chemicals could be stored in a microchip and released on demand. The model chemicals used were selected primarily according to two criteria. The first criterion was the minimum concentration that could be reliably detected (i.e. detection limit). We wanted to be able to detect concentrations as low as 1.0 nM. The second criterion was the ease of

using a particular detection method. We preferred to use a method that would allow us to analyze our release samples with minimal sample preparation. This makes the release studies easier to conduct and reduces the opportunities for introduction of errors by complicated sample preparation. The two chemicals selected were the fluorescent dye sodium fluorescein and radioactive calcium chloride $^{45}CaCl_2$.

Ink-jet printing or microinjection was used to fill the reservoirs from the backside of the microchip with a liquid or gel containing the chemicals to be released. Each reservoir of a given microchip is typically filled with the same volume of liquid or gel. For in vitro experiments, the open ends of the filled reservoirs were covered with a thin film of plastic and then sealed with materials such as water- and solvent-resistant epoxy resins. A more detailed description of the fabrication and preparation of the prototype microchips can be found in the literature.[57]

Microchips filled with one or both of the model chemicals were sealed, packaged, and inserted into 100 mL of saline solution, with or without phosphate buffer. A saturated calomel reference electrode was placed in the solution near the microchip to allow the anode to be held at a particular potential. An electric potential of +1.04 V versus SCE was applied for up to 30 s to an anode when release was desired from the corresponding reservoir. Release of the chemical from the microchip was detected within a few minutes of applying the electric potential to the anode, and typically 70% of the chemical was released within 30 min. However, complete release could take a few hours under these experimental conditions. The rate of release of the chemical may be affected by factors such as the dissolution rate of the chemicals inside the reservoir and the diffusion rate of the chemical out of the reservoir. Figure 8 proves that a single chemical can be stored in and released from a microchip on demand.

It was desired to release several chemicals from a single device in a similar fashion. Figure 9 shows the result for a prototype microchip filled with both model chemicals. This is the first demonstration that several chemicals can be stored in and released independently from a microchip on demand. These results provide proof-of-principle for microchips as chemical delivery devices.

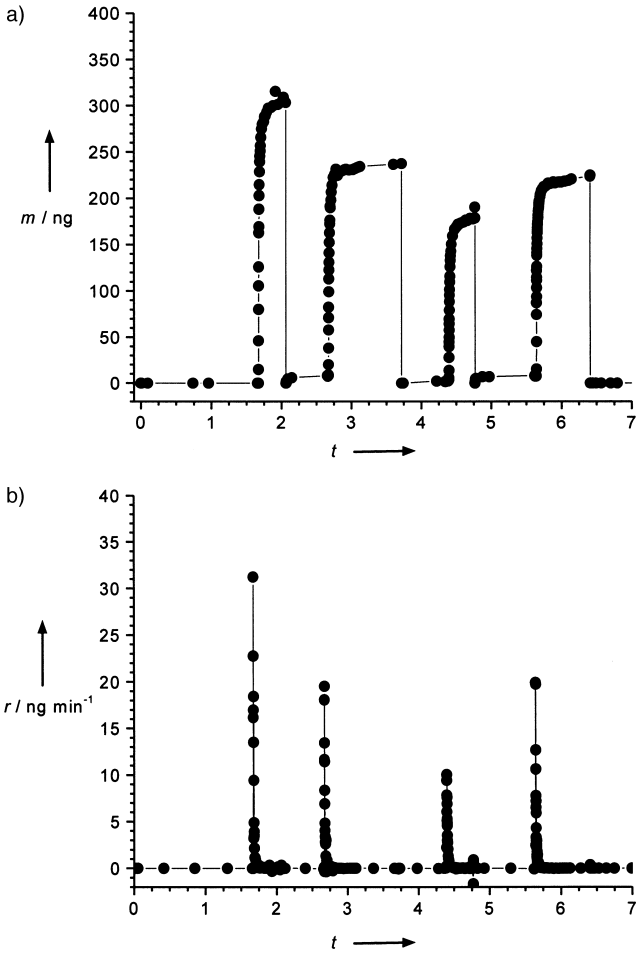


Figure 8. Pulsatile release of a single substance (sodium fluorescein) into PBS from four identically loaded reservoirs of a prototype controlled release microchip. a) Mass m released vs. time t (in days) and b) release rate r vs. time t (in days). In plot (a), m is returned to zero by replacing the release medium with fresh solution between release events.

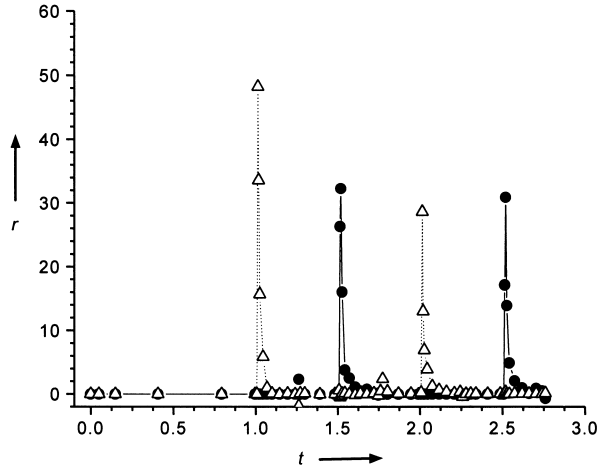


Figure 9. Pulsatile release of multiple substances (sodium fluorescein and $^{45}Ca^{2+}$) from a prototype controlled-release microchip into 0.145 M sodium chloride solution. The release rate r of sodium fluorescein (●) is given in units of ng min^{-1}, and that of $^{45}Ca^{2+}$ (△) in units of 5 nCi min^{-1}. t in days.

4.6. Potential Advantages

The controlled-release microchip has a number of potential advantages, some unique to its design and some stemming from characteristics common to most microdevices (i.e., small size). These are described in the following sections.

4.6.1. Chemicals to be Released

Multiple chemicals can be stored inside and released from the microchip. Each reservoir can be filled with a different chemical or combination of chemicals. Chemicals in any form (solid, liquid, or gel) can be delivered by the microchip. Microfluidic devices such as pumps are limited to delivering liquids. The controlled-release microchip consists of a reservoir covered by a thin membrane of material that can be dissolved on demand. The form of the chemical or drug in the reservoir and the presence or absence of other materials such

as polymer matrices or excipients have little or no effect on the electrochemical behavior of the membrane. Therefore, controlled-release microchips have the potential for a high degree of flexibility in the types of chemicals they can store and release.

4.6.2. Simplicity of Release Mechanism

The microchip has no moving parts. A thin barrier membrane covers each reservoir filled with one or more chemicals. The release of chemicals from the microchip is initiated by the disintegration of the membrane. The membrane is removed by the application of an electric potential, which causes the membrane to dissolve by a simple electrochemical reaction. The absence of moving parts potentially increases device reliability by decreasing the possibility of mechanical breakdown.

4.6.3. Accuracy

A variety of highly potent drugs can potentially be delivered from the microchip in a safe manner. It is important that the amount of drug delivered to a patient matches the amount prescribed, especially for highly potent compounds. It is difficult to accurately measure small quantities of drug for incorporation into conventional drug-delivery vehicles such as pressed tablets. This may lead to large uncertainties in the total amount of drug in the tablet. However, each reservoir of a microchip can be accurately filled with a small amount of the drug by using microinjection or ink-jet-printing techniques. In fact, this dosing approach has been demonstrated in the manufacture of delivery devices by Three Dimensional Printing.[58] The amount of drug administered from a microchip filled by these printing methods can be tightly controlled, and accidental overdose is unlikely because release from active devices can only occur when an electric potential is applied to an anode. Larger doses can be administered by simply opening several reservoirs simultaneously.

4.6.4. Complex Release Patterns

Complex release patterns (such as simultaneous constant and pulsatile release) can be achieved from the microchip. Any complex chemical or drug release pattern can be broken down into a combination of two parameters: release time and release rate. A unique feature of the controlled-release microchip is the potential to control both of these parameters.

The time at which release begins from any reservoir is determined by the time at which the anode membrane covering that reservoir is removed. Spontaneous release from a reservoir will not occur if the anode membrane material is stable in the electrolyte solution. Therefore, an anode membrane material is selected that will not dissolve and open until the correct electric potential is applied. Demultiplexing enables each anode membrane covering a reservoir to have its own conducting path to the power source. This makes each reservoir (or group of reservoirs) "independently addressable," so that electric potential can be applied to any combination of reservoirs at any given time. Incorporation of preprogrammed microprocessors, remote control units, or biosensors may potentially allow tight control over the time at which the membranes are removed and release of chemicals begins.

The rate of release from a reservoir is a function of the dissolution rate of the materials in the reservoir, the diffusion rate of these materials out of the reservoir, or both. Therefore, the release rate from an individual reservoir can be tailored to a particular application by the proper selection of the materials placed inside the reservoir (e.g., pure drug(s), drug(s) with polymers, etc.). For example, pulsatile release can be achieved by using materials that quickly dissolve when the reservoir is opened. Sustained release can be achieved by using materials that dissolve slowly after the reservoir opening, or that do not dissolve but allow the drug to diffuse out at a known rate.

4.6.5. Potential for Local Delivery

The microchip can be made small enough to make local chemical delivery possible. An advantage of local drug delivery is that high concentrations of drug can be achieved at the site where it is needed, while keeping the systemic concentration of the drug at a low level. This technique is particularly useful if the drug has adverse side effects if administered systemically in high doses. For example, BCNU (carmustine) is used extensively in the treatment of malignant brain tumors.[59] Large amounts of BCNU must be administered to a patient systemically to achieve its minimum acceptable concentration at the tumor site in the brain. This is largely due to the impermeability of the blood–brain barrier to most drugs. The resulting large systemic concentration of BCNU causes many extreme side effects in the liver, kidneys, and spleen. Implantation of polymer wafers containing BCNU at the site of the tumor after its removal allows the local concentration of BCNU at the tumor site to be 1000 times higher than that possible with systemic delivery. However, the systemic concentration of BCNU is kept quite low, and this greatly reduces the side effects normally associated with BCNU therapy. This therapy significantly extends life and greatly improves the quality of life of the patient during treatment and is a good illustration of the benefits of local drug delivery.

4.6.6. Stability Enhancement

Some new protein-based drugs have limited stability (i.e., shelf life). Water penetration into these protein drug formulations is one of the most frequent causes of their instability.[60] The membrane covering the filled reservoirs of a microchip will prevent penetration of water into these reservoirs. Thus, the stability of protein drugs is theoretically enhanced first, because the drugs can be isolated from the outside environment (hermetically sealed) and second, because they can be stored in the microchip in their most stable form (solid, liquid, or gel).

5. Summary and Outlook

There is a direct analogy between computer and chemical microchips. Computer microchips break down any complex operation into a series of simple binary symbols, either 0s or 1s. Chemical microchips are analogous in that any complex chemical release pattern can be broken down into a series of small, simple subunits. The small subunit here is a single reservoir that is closed (0) or open (1). Any complex release profile (continuous, pulsatile, or both) can be approximated by the precisely timed emptying of a series of single reservoirs. Figure 10a shows the release profile that can be obtained with

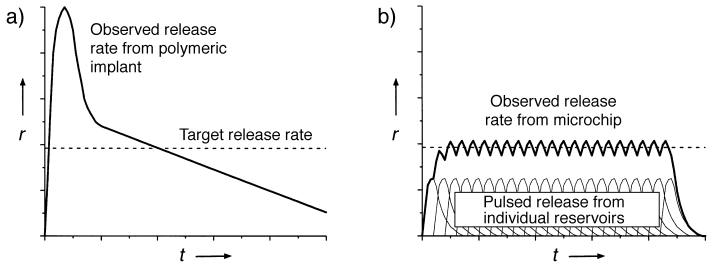


Figure 10. a) A sustained-release profile from a typical controlled-release polymer. b) An example of how a sustained-release profile may be approximated by the precisely timed release of pulses of chemical from a microchip.

a conventional polymer drug-delivery implant from which a sustained, nearly constant release rate is desired. A typical profile is characterized by an initial "burst" release of drug from the device with a slow decrease in the release rate over time as the device is depleted of drug. Microchips cannot only be used for pulsatile release, such as that demonstrated in Figures 8 and 9; Figure 10b shows an example of how a sustained-release rate profile might be approximated by a series of precisely timed pulses of chemical from a microchip. We have termed this the "digitization" of chemical release.

The first demonstration of the storage and release of multiple chemical substances from a microchip,[57] reviewed here, provides the proof-of-principle for the digitization of chemical delivery. Application of this new concept to controlled drug delivery could represent, with further study, a substantial step forward in the development of a "pharmacy-on-a-chip" or other "smart" drug delivery systems. Areas outside of drug delivery where this technology may also find use include medical diagnostics, analytical chemistry, chemical detection, industrial process monitoring and control, combinatorial chemistry, microbiology, and fragrance delivery.

The next step in the development of controlled-release microchips is the integration of active components into the microchip. A battery, a clock, and possibly a reference electrode need to be combined with the microchip into a single package for implantation. Many of the necessary technologies already exist in other areas. For example, cardiac pacemaking is a highly developed field with power and control capabilities that could be applied to microchip drug-delivery devices. Other active components could include a signal receiver for remote control of drug delivery or a biosensor for autonomous, closed-loop operation.

A logical extension of the controlled-release microchip work is the development of a passive, polymer microchip. The term "passive microchip" refers to devices that contain no electronics, power sources, or microprocessors. The passive microchip is similar to the controlled-release microchip discussed in this review in that the substrate contains numerous reservoirs that are filled with the drug(s) to be released or with a matrix material that typically consists of a polymer and the drug. Each reservoir is covered by a layer or "cap" of a degradable material, a cap of a nondegradable material with a known permeability for the drug, or is left uncapped. The time and rate of release from a reservoir is dictated by the degradation rate of the caps or matrix material or the diffusion of the drug through the caps or out of the matrix material. Both parameters can be controlled by varying the composition or thickness of the caps or the formulation of the drug or matrix material within the reservoirs. This type of microchip device could have the additional advantage of being completely biodegradable, so passive microchip implants for drug delivery applications would not have to be removed.

We thank Achim Göpferich, Mateos Llabres, and Lenny Rigione for their contributions in the early stages of the project; Nishla Keiser and Allie Lin for their help with corrosion and release experiments; William Rowe, Wendy Katstra, and Patrick Teung for their assistance with portions of the literature search; and Jörg Lahann for translating the review into German. We would also like to thank the U.S. National Institutes of Health for funding support through Grant No. 1 R24 AI47739-01, and the U.S. National Science Foundation for their graduate fellowship support of John, Amy, and Rebecca. All microfabrication work was carried out at the Microsystems Technology Laboratory at MIT. Figures 2, 7, 8, and 9 were reprinted by permission from Nature **1999**, *397*, 335 – 338.

Received: December 3, 1999 [A 372]

[1] a) L. Brannon-Peppas, *ACS Symp. Ser.* **1993**, *520*, 42 – 52; b) R. Levy, M. A. Nichols, T. W. Miller, Jr., *ACS Symp. Ser.* **1993**, *520*, 202 – 212.
[2] R. Langer, *Nature* **1998**, *392* (*suppl.*), 5 – 10.
[3] E. E. Bakken, K. Heruth, *Ann. NY Acad. Sci.* **1991**, *618*, 422 – 427.
[4] R. Langer, *Science* **1990**, *249*, 1527 – 1533; K. E. Uhrich, S. M. Cannizzaro, R. S. Langer, K. M. Shakesheff, *Chem. Rev.* **1999**, *99*, 3181 – 3198.
[5] *Physicians' Desk Reference* (Ed.: R. Arky), Medical Economics Company, Montvale, NJ, USA, **1998**, pp. 2587 – 2589.
[6] *Physicians' Desk Reference* (Ed.: R. Arky), Medical Economics Company, Montvale, NJ, USA, **1998**, pp. 3139 – 3150.
[7] a) L. R. Brown, R. Langer, *Annu. Rev. Med.* **1988**, *39*, 221 – 229; b) P. Sinko, J. Kohn, *ACS Symp. Ser.* **1993**, *520*, 18 – 41.
[8] a) D. Levy, J. Kost, Y. Meshulam, R. Langer, *J. Clin. Invest.* **1989**, *83*, 2074 – 2078; b) S. Mitragotri, D. Blankschtein, R. Langer, *Science* **1995**, *269*, 850 – 853.
[9] D. R. Matthews, D. A. Lang, M. A. Burnett, R. C. Turner, *Diabetologia* **1983**, *24*, 231 – 237.
[10] a) R. L. Reid, R. Fretts, D. A. Van Vugt, *Am. J. Obstet. Gynecol.* **1988**, *158*, 176 – 185; b) M. C. Gelato, G. R. Merriam, *Annu. Rev. Physiol.* **1986**, *48*, 569 – 591.

[11] J. A. Kuret, F. Murad in *Goodman and Gilman's*, *The Pharmacological Basis of Therapeutics* (Eds.: A. G. Gilman, T. W. Rall, A. S. Nies, P. Taylor), 8th ed., Pergamon, New York, **1990**, pp. 1334 – 1360.

[12] J. Kost, R. Langer, *Adv. Drug Delivery Rev.* **1991**, *6*, 19 – 50.

[13] a) I. C. Kwon, Y. H. Bae, S. W. Kim, *Nature* **1991**, *354*, 291 – 293; b) Y. H. Bae, I. C. Kwon, S. W. Kim in *Polymeric Drugs and Drug Administration* (Ed.: R. M. Ottenbrite), American Chemical Society, Washington, DC, USA, **1994**, pp. 98 – 110; c) L. L. Miller, *Mol. Cryst. Liq. Cryst.* **1998**, *160*, 297 – 301; d) M. Hepel, Z. Fijalek in *Polymeric Drugs and Drug Administration* (Ed.: R. M. Ottenbrite), American Chemical Society, Washington, DC, USA, **1994**, pp. 79 – 97; e) S. F. Schwendeman, G. L. Amidon, R. J. Levy, *Macromolecules* **1993**, *26*, 2264 – 2272.

[14] a) E. R. Edelman, J. Kost, H. Bobeck, R. Langer, *J. Biomed. Mater. Res.* **1985**, *19*, 67 – 83; b) J. Kost, R. Langer in *Pulsed and Self-Regulated Drug Delivery* (Ed.: J. Kost), CRC Press, Boca Raton, FL, USA, **1990**, pp. 3 – 16.

[15] J. Kost, K. Leong, R. Langer, *Proc. Natl. Acad. Sci. USA* **1989**, *86*, 7663 – 7666.

[16] E. Mathiowitz, M. D. Cohen, *J. Membr. Sci.* **1989**, *40*, 67 – 86.

[17] F. Fischel-Ghodsian, L. Brown, E. Mathiowitz, D. Brandenburg, R. Langer, *Proc. Natl. Acad. Sci. USA* **1988**, *85*, 2403 – 2406.

[18] a) R. A. Siegel, M. Falamarzian, B. A. Firestone, B. C. Moxley, *J. Controlled Release* **1988**, *8*, 179 – 182; b) J. H. Kim, J. Y. Kim, Y. M. Lee, K. Y. Kim, *J. Appl. Polym. Sci.* **1992**, *44*, 1823 – 1828; c) A. Gutowska, J. S. Bark, I. C. Kwon, Y. H. Bae, Y. Cha, S. W. Kim, *J. Controlled Release* **1997**, *48*, 141 – 148.

[19] a) Y. H. Bae, T. Okano, R. Hsu, S. W. Kim, *Makromol. Chem. Rapid Commun.* **1987**, *8*, 481 – 485; b) A. S. Hoffman, A. Afrassiabi, L. C. Dong, *J. Controlled Release* **1986**, *4*, 213 – 222; c) T. Okano, Y. H. Bae, S. W. Kim in *Pulsed and Self-Regulated Drug Delivery* (Ed.: J. Kost), CRC Press, Boca Raton, FL, USA, **1990**, pp. 17 – 45.

[20] Y. Suzuki, M. Tanihara, Y. Nishimura, K. Suzuki, Y. Kakimaru, Y. Shimizu, *J. Appl. Biomat.* **1998**, *42*(1), 112 – 116.

[21] a) T. Chen, R. Langer, J. C. Weaver, *J. Invest. Dermatol. Symp. Proc.* **1998**, *3*, 159 – 165; b) M. R. Prausnitz, V. G. Bose, R. Langer, J. C. Weaver, *Proc. Natl. Acad. Sci. USA* **1993**, *90*, 10504 – 10508; c) V. Merino, Y. N. Kalia, R. H. Guy, *Trends Biotechnol.* **1997**, *15*, 288 – 290; d) J. M. Hill, L. P. Gangarossa, N. H. Park, *Ann. NY Acad. Sci.* **1977**, *284*, 604 – 612.

[22] J. Kost, R. Langer, *Trends Biotechnol.* **1992**, *10*, 127 – 131.

[23] J. Kost, J. Wolfrum, R. Langer, *J. Biomed. Mater. Res.* **1987**, *21*, 1367 – 1373.

[24] a) W. E. Katstra, R. D. Palazzolo, C. W. Rowe, B. Giritlioglu, P. Teung, M. J. Cima, *J. Control. Rel.*, in press; b) C. W. Rowe, W. E. Katstra, R. D. Palazzolo, B. Giritlioglu, P. Teung, M. J. Cima, *J. Control. Rel.*, in press.

[25] a) N. Santoro, *Am. J. Obstet. Gynecol.* **1990**, *163*, 1759 – 1764; b) G. W. Creasy, M. E. Jaffe, *Ann. NY Acad. Sci.* **1991**, *618*, 548 – 557; c) G. W. Creasy, M. E. Jaffe, *Adv. Drug Delivery Rev.* **1991**, *6*, 51 – 56.

[26] a) G. Koning, F. Feith in *Neurological Applications of Implanted Drug Pumps*, *Vol. 531* (Ed.: R. D. Penn), New York Academy of Science, New York, **1988**, pp. 49 – 56; b) J. Johnston, S. Reich, A. Bailey, J. Sluetz in *Neurological Applications of Implanted Drug Pumps*, *Vol. 531* (Ed.: R. D. Penn), New York Academy of Science, New York, **1988**, pp. 57 – 65; c) P. Lord, H. Allami, M. Davis, R. Diaz, P. Heck, R. Fischell in *Neurological Applications of Implanted Drug Pumps*, *Vol. 531* (Ed.: R. D. Penn), New York Academy of Science, New York, **1988**, pp. 66 – 71; d) K. T. Heruth in *Neurological Applications of Implanted Drug Pumps*, *Vol. 531* (Ed.: R. D. Penn), New York Academy of Science, New York, **1988**, pp. 72 – 75.

[27] a) M. Madou, *Fundamentals of Microfabrication*, CRC Press, Boca Raton, FL, USA, **1997**, pp. 1 – 323; b) "Process Technology": S. Wolf, R. N. Tauber, *Silicon Processing for the VLSI Era*, *Vol. 1*, Lattice Press, Sunset Beach, **1986**, pp. 124 – 585; c) R. C. Jaeger in *Introduction to Microelectronic Fabrication* (*Modular Series on Solid State Devices*, *Vol. 5* (Eds.: G. W. Neudeck, R. F. Pierret)), Addison-Wesley, Reading, **1993**, pp. 1 – 131; d) R. J. Jackman, S. T. Brittain, A. Adams, M. G. Prentiss, G. M. Whitesides, *Science* **1998**, *280*, 2089 – 2091; e) Y. Xia, E. Kim, X.-M. Zhao, J. A. Rogers, M. Prentiss, G. M. Whitesides, *Science* **1996**, *273*, 347 – 349; f) Y. Xia, J. J. McClelland, R. Gupta, D. Qin, X.-M. Zhao, L. L. Sohn, R. J. Celotta, G. M. Whitesides, *Adv. Mater.* **1997**, *9*, 147 – 149.

[28] a) L. Yan, X.-M. Zhao, G. M. Whitesides, *J. Am. Chem. Soc.* **1998**, *120*, 6179 – 6180; b) Y. Xia, D. Qin, G. M. Whitesides, *Adv. Mater.* **1996**, *8*, 1015 – 1017; c) C. Marzolin, A. Terfort, J. Tien, G. M. Whitesides, *Thin Solid Films* **1998**, *315*, 9 – 12; d) Y. Xia, G. M. Whitesides, *Angew. Chem.* **1998**, *110*, 568 – 594; *Angew. Chem. Int. Ed. Engl.* **1998**, *37*, 550 – 575.

[29] E. Bassous, H. H. Taub, L. Kuhn, *Appl. Phys. Lett.* **1977**, *31*, 135 – 137.

[30] a) M. Madou, *Fundamentals of Microfabrication*, CRC Press, Boca Raton, FL, USA, **1997**, pp. 459 – 468; b) L. M. Roylance, J. B. Angell, *IEEE Trans. Electron Devices* **1979**, *26*, 1911 – 1917.

[31] a) K. F. Jensen, *AIChE J.* **1999**, *45*, 2051 – 2054; b) S. H. DeWitt, *Curr. Opin. Chem. Biol.* **1999**, *3*, 350 – 356; c) W. Ehrfeld, V. Hessel, H. Lehr in *Microsystem Technology in Chemistry and Life Science* (Eds.: A. Manz, H. Becker), Springer, Berlin, **1998**, pp. 233 – 252.

[32] a) A. H. Epstein, S. D. Senturia, *Science* **1997**, *276*, 1211; b) A. H. Epstein, S. D. Senturia, O. Al-Midani, G. Anathasuresh, A. Ayon, K. Breuer, K. S. Chen, F. F. Ehrich, E. Esteve, L. Frechette, G. Gauba, R. Ghodssi, C. Groshenry, S. A. Jacobson, J. L. Kerrebrock, J. H. Lang, C. C. Lin, A. London, J. Lopata, A. Mehra, J. O. Mur Miranda, S. Nagle, D. J. Orr, E. Piekos, M. A. Schmidt, G. Shirley, S. M. Spearing, C. S. Tan, Y. S. Tzeng, I. A. Waitz in *28th AIAA Fluid Dynamics Conference*, *4th AIAA Shear Flow Control Conference*, American Institute of Aeronautics and Astronautics, Snowmass Village, **1997**.

[33] a) M. Freemantle, *Chem. Eng. News* **1999**, *77*(8), 27 – 36; b) R. F. Service, *Science* **1998**, *282*, 399 – 401; c) G. Blankenstein, U. D. Larsen, *Biosens. Bioelectron.* **1998**, *13*, 427 – 438; d) S. Borman, *Chem. Eng. News* **1996**, *74*(50), 42 – 43; e) S. Latta, *The Scientist* **1997**, *11*(18), 1; f) *Micro Total Analysis Systems '98* (Eds.: D. J. Harrison, A. van den Berg), Kluwer, Dordrecht, **1998**.

[34] a) P. Gravesen, J. Branebjerg, O. S. Jensen, *J. Micromech. Microeng.* **1993**, *3*, 168 – 182; b) S. Shoji, M. Esashi, *J. Micromech. Microeng.* **1994**, *4*, 157 – 171.

[35] a) J. G. Smits, *Sens. Actuators A* **1990**, *21 – 23*, 203 – 206; b) W. K. Schomburg, J. Fahrenberg, D. Maas, R. Rapp, *J. Micromech. Microeng.* **1993**, *3*, 216 – 218; c) T. Bourouina, A. Bossebœuf, J. P. Grandchamp, *J. Micromech. Microeng.* **1997**, *7*, 186 – 188.

[36] a) G. Fuhr, R. Hagedorn, T. Müller, W. Benecke, B. Wagner, *J. Microelectromech. Syst.* **1992**, *1*, 141 – 146; b) D. J. Harrison, K. Fluri, K. Seiler, Z. Fan, C. S. Effenhauser, A. Manz, *Science* **1993**, *261*, 895 – 897; c) A. Manz, C. S. Effenhauser, N. Burggraf, D. J. Harrison, K. Seiler, K. Fluri, *J. Micromech. Microeng.* **1994**, *4*, 257 – 265.

[37] C. Vieider, O. Ohman, H. Elderstig, *Abstr. Pap. Dig. Int. Conf. Sensors and Actuators "Transducers '95*, *Eurosensors IX"* (Stockholm) **1995**, pp. 284 – 286.

[38] J. Franz, H. Baumann, H. P. Trah, *Abstr. Pap. Dig. Int. Conf. Sensors and Actuators "Transducers '95*, *Eurosensors IX"* (Stockholm) **1995**, pp. 313 – 316.

[39] M. Madou, *Fundamentals of Microfabrication*, CRC Press, Boca Raton, FL, USA, **1997**, pp. 485 – 486.

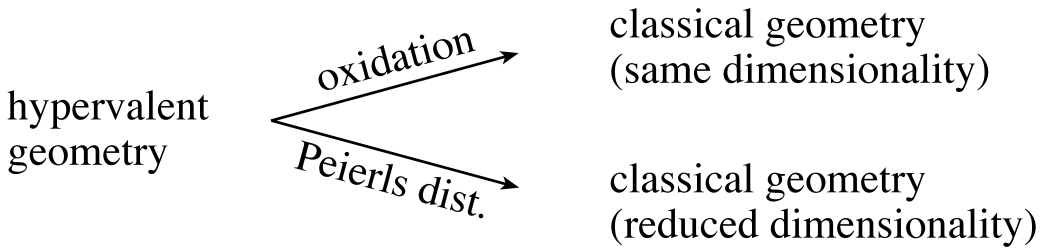
[40] a) S. Nakagawa, S. Shoji, M. Esashi, *Proc. IEEE Microelectromechanical Systems "MEMS '90"*, IEEE (Napa Valley) **1990**, pp. 89 – 94; b) B. H. van der Schoot, S. Jeanneret, A. van den Berg, N. F. de Rooij, *Sens. Actuators B* **1993**, *13 – 14*, 333 – 335.

[41] a) M. A. Burns, C. H. Mastrangelo, T. S. Sammarco, F. P. Man, J. R. Webster, B. N. Johnson, B. Foerster, D. Jones, Y. Fields, A. R. Kaiser, D. T. Burke, *Proc. Natl. Acad. Sci. USA* **1996**, *93*, 5556 – 5561; b) M. A. Burns, B. N. Johnson, S. N. Brahmasandra, K. Handique, J. R. Webster, M. Krishnan, T. S. Sammarco, P. M. Man, D. Jones, D. Heldsinger, C. H. Mastrangelo, D. T. Burke, *Science* **1998**, *282*, 484 – 487; c) C. H. Mastrangelo, M. A. Burns, D. T. Burke, *Proc. IEEE* **1998**, *86*, 1769 – 1787; d) A. D. Mirzabov, *Trends Biotechnol.* **1994**, *12*, 27 – 32; e) D. Schmalzing, A. Adourian, L. Koutny, L. Ziaugra, P. Matsudaira, D. Ehrlich, *Anal. Chem.* **1998**, *70*, 2303 – 2310.

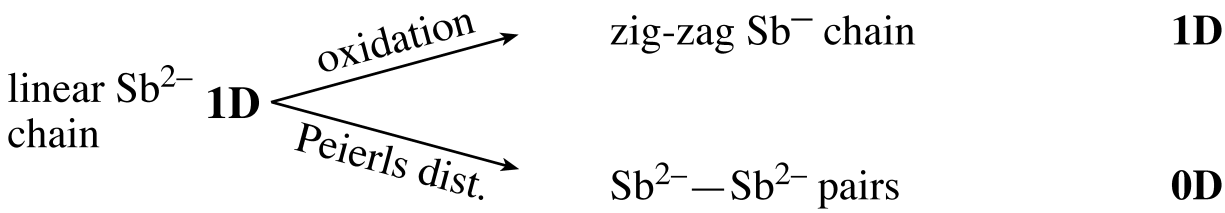
[42] a) E. Delamarche, A. Bernard, H. Schmid, B. Michel, H. Biebuyck, *Science* **1997**, *276*, 779 – 781; b) E. Delamarche, A. Bernard, H. Schmid, A. Bietsch, B. Michel, H. Biebucyk, *J. Am. Chem. Soc.* **1998**, *120*, 500 – 508.

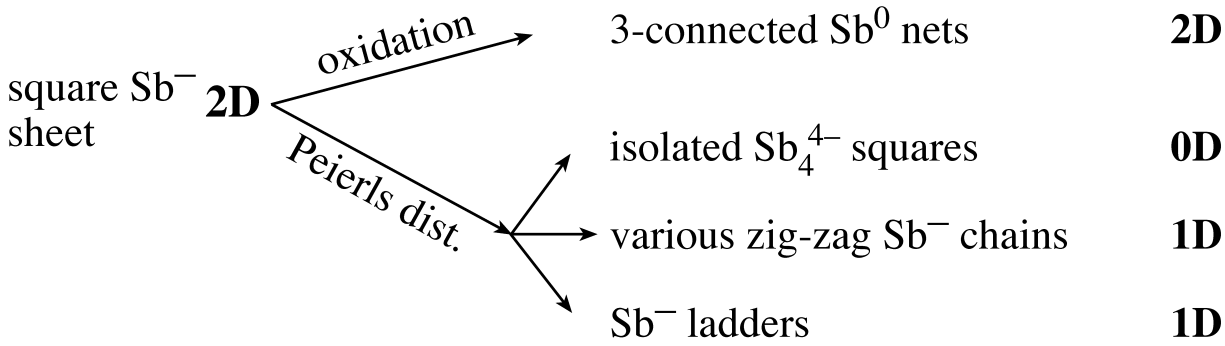
[43] a) C. S. Effenhauser, G. J. M. Bruin, A. Paulus, M. Ehrat, *Anal. Chem.* **1997**, *69*, 3451 – 3457; b) D. C. Duffy, J. C. McDonald, O. J. A. Scheuller, G. M. Whitesides, *Anal. Chem.* **1998**, *70*, 4974 – 4984.

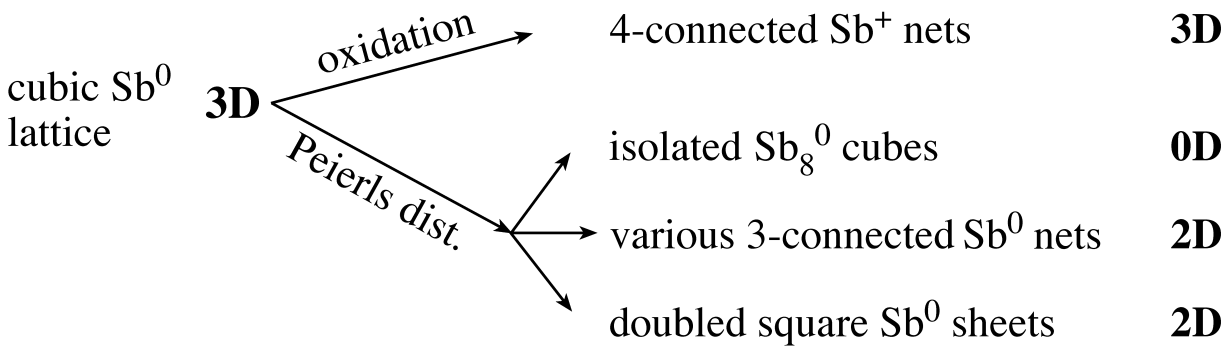
[44] C. S. Effenhauser, A. Paulus, A. Manz, H. M. Widmer, *Anal. Chem.* **1994**, *66*, 2949 – 2953.
[45] A. T. Woolley, K. Lao, A. N. Glazer, R. A. Mathies, *Anal. Chem.* **1998**, *70*, 684 – 688.
[46] A. T. Woolley, D. Hadley, P. Landre, A. J. deMello, R. A. Mathies, M. A. Northrup, *Anal. Chem.* **1996**, *68*, 4081 – 4086.
[47] D. J. Ehrlich, P. Matsudaira, *Trends Biotechnol.* **1999**, *17*, 315 – 319.
[48] R. M. McCormick, R. J. Nelson, M. G. Alonso-Amigo, D. J. Benvegnu, H. H. Hooper, *Anal. Chem.* **1997**, *69*, 2626 – 2630.
[49] A. T. Woolley, G. F. Sensabaugh, R. A. Mathies, *Anal. Chem.* **1997**, *69*, 2181 – 2186.
[50] a) D. J. Harrison, K. Fluri, K. Seiler, Z. Fan, C. S. Effenhauser, A. Manz, *Science* **1993**, *261*, 895 – 897; b) C. S. Effenhauser, Z. Manz, H. M. Widmer, *Anal. Chem.* **1993**, *65*, 2637 – 2642; c) S. C. Jacobson, R. Hergenroeder, A. W. Moore, Jr., J. M. Ramsey, *Anal. Chem.* **1994**, *66*, 4127 – 4132.
[51] a) C. Gonzalez, S. D. Collins, R. L. Smith, *Proc. SPIE* **1997**, *3224*, 207 – 215; b) C. Gonzalez, R. L. Smith, D. G. Howitt, S. D. Collins, *Sens. Actuators A* **1998**, *66*, 315 – 332; c) M. Cohn, K. Böhringer, J. M. Noworolski, A. Singh, C. Keller, K. Goldberg, R. Howe, *Proc. SPIE* **1998**, *3514*, 2 – 16; d) A. Götz, C. Cané, *Proc. SPIE* **1998**, *3514*, 112 – 123.
[52] a) R. F. Service, *Science* **1998**, *282*, 396 – 399; b) M. Eggers, M. Hogan, R. K. Reich, J. Lamture, D. Ehrlich, M. Hollis, B. Kosicki, T. Powdrill, K. Beattie, S. Smith, R. Varma, R. Gangadharan, A. Mallik, B. Burke, D. Wallace, *Biotechniques* **1994**, *17*, 516 – 524; c) G. Yershov, V. Barsky, A. Belgovskiy, E. Kirillov, E. Kreindlin, I. Ivanov, S. Parinov, D. Guschin, A. Drobishev, S. Dubiley, A. Mirzabekov, *Proc. Natl. Acad. Sci. USA* **1996**, *93*, 4913 – 4918; d) R. C. Anderson, G. McGall, R. J. Lipshutz in *Microsystem Technology in Chemistry and Life Science* (Eds.: A. Manz, H. Becker), Springer, Berlin, **1998**, pp. 117 – 130.
[53] HSC Chemistry Computer Program, Version 3.0, Outokumpu Research.
[54] R. P. Frankenthal, D. J. Siconolfi, *J. Electrochem. Soc.* **1982**, *129*, 1192 – 1196.
[55] a) B. Merchant, *Biologicals* **1998**, *26*, 49 – 59; b) S. L. Best, P. J. Sadler, *Gold Bull.* **1996**, *29*, 87 – 93.
[56] a) C. F. Shaw, *Inorg. Perspect. Biol. Med.* **1979**, *2*, 287 – 355; b) A. A. Isab, P. J. Sadler, *Biochim. Biophys. Acta* **1977**, *492*, 322 – 330.
[57] J. T. Santini, Jr., M. J. Cima, R. Langer, *Nature* **1999**, *397*, 335 – 338.
[58] J. Yoo, E. Bornancini, D. Yang, G. Shanahan, D. Monkhouse, *Pharm. Res. Suppl.* **1997**, *14*, S-90.
[59] P. Sampath, H. Brem, *Cancer Control JMMC* **1998**, *5*, 130 – 137.
[60] a) J. L. Cleland, R. Langer, *ACS Symp. Ser.* **1994**, *567*, 1 – 21; b) S. D. Putney, P. A. Burke, *Nat. Biotechnol.* **1998**, *16*, 153 – 157.



Examples







© WILEY-VCH

Hypervalent Bonding in One, Two, and Three Dimensions: Extending the Zintl–Klemm Concept to Nonclassical Electron-Rich Networks

Garegin A. Papoian* and Roald Hoffmann*

We construct a theory for electron-rich polyanionic networks in the intermetallic compounds of heavy late main group elements, building a bonding framework that makes a connection to well-understood hypervalent bonding in small molecules such as XeF_4, XeF_2, and I_3^-. What we do is similar in spirit to the analogy between the Zintl–Klemm treatment of classical polyanionic networks and the octet rule for molecules. We show that the optimal electron count for a linear chain of a heavy main group element is seven electrons per atom, six electrons per atom for a square lattice, and five electrons per atom for a simple cubic lattice. Suggestions that these electron counts are appropriate already exist in the literature. We also derive electron counts for more complicated topologies, including one-dimensional ladders and one dimensional strips cut from a square lattice. We also study pairing (Peierls) distortions from these ideal geometries as well as other deformations. The presence of s-p mixing (or its absence) plays a critical role in the propensity for pairing and, in general, in determining the geometrical and electronic structure of these phases. Hypervalent bonding goes along with the relative absence of significant s-p interaction; there is a continuum of such mixing, but also a significant difference between the second-row and heavier elements. We attribute the existence of undistorted metallic networks of the latter elements to diminished s-p mixing, which in turn is due to the contraction of less-screened s orbitals relative to p orbitals down the groups in the Periodic Table. The number of electrons in the polyanionic network may be varied experimentally. An important general principle emerges from our theoretical analysis: upon oxidation a hypervalent structure transforms into a classical one with the same lattice dimensionality, while upon Peierls distortion the hypervalent structures transform into classical ones with the lattice dimensionality reduced. Dozens of crystal structure types, seemingly unrelated to each other, may be understood using the unifying concept of electron-rich multicenter bonding. Antimonides, which are explored in great detail in the current work, conform particularly well to the set of electron counting rules for electron-rich nonclassical networks. Some deviation up and down from the ideal electron count is exhibited by known stannides and tellurides. We can also make sense of the bonding in substantially more complicated alloys, including $La_{12}Mn_2Sb_{30}$ and Tl_4SnTe_3. The hypervalent electron counting scheme developed in this paper, along with the classical Zintl–Klemm electron counting rules, gives an easy qualitative understanding of bonding in a wide variety of intermetallic compounds of heavy main group elements.

Keywords: bond theory · hypervalent compounds · solid-state structures

1. Introduction

A significant number of pieces of the diverse and important intermetallic mosaic is made up by phases containing heavy late main group elements. The majority of these networks obey classical Zintl–Klemm electron counting rules, among the most important and useful paradigms in solid-state chemistry.[1–3] However, many networks built from main group elements show an unusual, nonclassical local coordination, for instance, a triangular one (in polyhedra) or a linear one, as in one-dimensional linear chains or two-dimensional square sheets. Along with the unusual geometries often come interesting physical properties such as metallic conductivity.

Some intermetallic systems are electron deficient. Indeed, first, second, and Group 13 elements form networks[4] with an abundance of triangular faces. This tendency has been rationalized within the context of a moments theory by a large and energy-controling third moment for the low electron count.[5, 6] Certain groups of extended electron-deficient compounds may be understood by the application of

[*] Dr. G. A. Papoian, Prof. Dr. R. Hoffmann
Department of Chemistry and Chemical Biology
and Materials Science Center
Cornell University, Ithaca NY 14853-1301 (USA)
Fax: (+1) 607-255-5707
E-mail: rh34@cornell.edu

 © WILEY-VCH Verlag GmbH, D-69451 Weinheim, 2000 1433-7851/00/3912-2409 $ 17.50+.50/0

Wade – Mingos rules, which give a guide to magic electron counts for some common polyhedra.[7–10] An important review of bonding in electron-deficient intermetallic compounds has been written by Nesper.[11]

On the right side of the Periodic Table (the late main group elements) bonding in intermetallic phases is very different. These electron-rich compounds often feature locally "linear" nonclassical geometries, two-dimensional square sheets, and a number of fascinating geometries derived from these.

Electron counting schemes for these unusual electron-rich geometries are the main subject of this review and antimony is our entry point. We choose antimony as our workhorse example, prompted by its rich structural chemistry. However, our ideas are applicable to a variety of structures of other late main group elements as well, and we discuss a selection of these.

Suggestions of appropriate electron counts in the nonclassical geometries encountered in the remarkably rich chemistry of antimony have arisen from experimental studies. For instance, Jeitschko and co-workers[12, 13] proposed that one should count long bonds as one electron in the one dimensional (1D) linear Sb chain in U_3TiSb_5 and in the 2D square Sb sheet in $CeAgSb_2$. Nesper[14] suggested one electron per bond in the 1D linear chain in Li_2Sb,[15] also on the basis of the long bond length determined experimentally. He also argued[14] that the square Bi sheet in LiBi is stable because of the relativistic contraction of s orbitals, that is, only p orbitals are involved in bonding. A similar, more general argument concerning the contraction (relativistic and nonrelativistic) of s orbitals down the groups, is one of the cornerstones of our analysis.

Are the electron counts proposed above a general phenomenon characteristic of all late main group elements and, if yes, what are the reasons behind that? We will provide a theoretical rationale for these electron counts in two ways: by using conventional molecular orbital theory[16] and band structure analysis.[17] In addition, we will suggest new optimal electron counts for a 3D simple cubic lattice, 1D strips cut from a square lattice, and a number of other nonclassical frameworks. Most importantly, we will provide and exemplify an aufbau principle for analyzing any hypervalent network.

In the theoretical section we explain a phenomenon that at first seems quite disjoint from the above unusual geometries—the important tendency of heavier late main group elements to remain metallic while lighter elements in the group undergo Peierls distortion[18] to become semiconductors or insulators. We also consider Peierls distortion pathways for various nonclassical bonding geometries, in particular for a square net. This subject has been studied earlier by our group[19] as well as by Lee and co-workers.[20–24] Finally, the electron counting scheme developed for simple networks with electron-rich multicenter bonding will show its utility in an analysis of the bonding in quite complicated anionic sublattices, such as those that occur in the intermetallic phases $La_{12}Mn_2Sb_{30}$ and Tl_4SnTe_3.

2. A Roadmap

In order to facilitate reading of this paper a brief description of the remaining sections is given below:

- Section 3: The many classical and hypervalent Sb networks are reviewed. A general electron counting scheme emerges

Garegin A. Papoian was born in Yerevan, Armenia in 1973. He completed four years of undergraduate studies in the Higher College of the Russian Accadamy of Sciences, carrying out research under the guidance of Pofessor Alexander Pasynskii. After completing an M.S. degree from the University of Kansas in 1995, he was a Ph.D student in the Department of Chemistry at Cornell University working with Roald Hoffmann and completed his studies on a wide variaty of problems in solid-state chemistry and heterogeneous catalysis in 1999. He then joined the research group of Professor Michael Klein at the University of Pennsylvania as a postdoctoral associate. His current research interests lie in the application of quantum mechanical and statistical mechanical methods to important chemical and physical properties of solid-state, surface-catalytic, and biocatalytic systems.



G. A. Papoian



R. Hoffmann

Roald Hoffmann was born in 1937 in Zloczow, Poland. He moved to the U.S. in 1949 and studied chemistry at Columbia University and Harvard University (Ph.D 1962). Since 1965 he has been at Cornell University, now as the Frank H. T. Rhodes Professor of Humane Letters. He has received many of the honors of his profession, including the 1981 Nobel Prize in Chemistry (shared with Kenichi Fukui). "Applied theoretical chemistry" is the way Roald Hoffmann likes to characterize the particular blend of computations which are stimulated by experiment and the construction of generalized models, of frameworks for understanding, that is his contribution to chemistry. Dr. Hoffmann also has a career as a writer, that profession sometimes overlapping his chemistry, sometimes not. He writes poems, essays, nonfiction, and plays.

for hypervalent networks, which applies to all Sb phases known to us.

- Sections 4–8: The major assumptions of our theoretical model are given. A theory is developed which rationalizes electron counting in hypervalent networks. The tendency of heavier elements to form metallic frameworks as well as the distortion pathways of hypervalent networks is explored. The interrelationship of electron counting, dimensionality, and Peierls distortion is highlighted.
- Section 9: The theory developed in Sections 4–8 is applied to a seemingly complicated $La_{12}Mn_2Sb_{30}$ alloy. Retrotheoretical analysis is introduced as a powerful strategy to understand solid-state compounds which contain several sublattices.
- Section 10: We look at linear chains and derivative networks made up of main group elements other than Sb.
- Section 11: Electron counting and the stability of a wide range of binary, ternary, and quaternary phases of Group 14 elements containing square sheets are discussed in detail.
- Section 12: The upper stability range of electron counting in square sheets is examined in chalcogen compounds. The charge density wave (CDW) distortions of the latter sheets are reviewed.
- Section 13: Conclusions.

Now we are ready to take a close look at Sb networks in a wide variety of Sb phases. The observed structures are at the same time striking and complex, begging to be shown and explained.

3. Electron Counting in Individual Structures

The basic idea behind the Zintl–Klemm concept is the transfer of electrons from more electropositive elements to more electronegative elements, with the potential for the formation of strong bonds between the latter. This protocol usually works well with alkali, alkaline earth, and rare earth elements as electron donors. Things are not so simple for the transition metals, where multiple oxidation states are common and the electronegativities approach and even surpass those of some main group elements. Among the hundreds of Sb phases reported we have selected those where the extent of the electron donation to the Sb network is unambiguous. This approach does exclude many transition metal antimonides from Table 1, which is a selective listing of a variety of Sb phases characterized by classical and nonclassical structural elements.

We included some transition metals in our study for the following reasons: Firstly, magnetic measurements have been carried out on some Mn compounds, and this has allowed the assignment of a nonambigious formal charge to Mn. Secondly, FeS_2-m (marcasite) type transition metal diantimonides show a very interesting pattern of stacking of Sb–Sb pairs into a 1D ladder, which is dependent on the metal. Such strips are related to one of the geometrical patterns we analyze. Similarly, zirconium phases of antimony contain 1D strips that are electronically intriguing. We will talk about them in Section 6.2.

In this section we first apply the Zintl–Klemm electron counting concept to Sb phases with classical geometries. We

Table 1. Geometries of Sb subnetworks in various compounds.

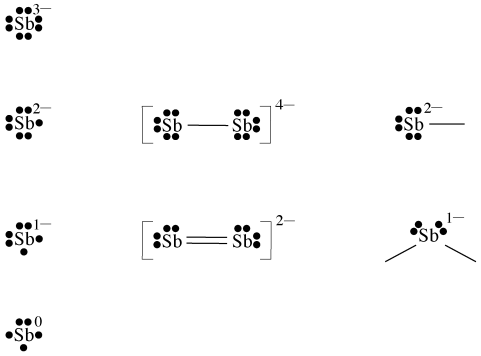
Compound	Structure type	Geometrical patterns	
		classical	hypervalent
Ba_5Sb_4[245]	Sm_5Ge_4	0D pairs, atoms	
$Li_4Sr_3Sb_4$[246]	$Li_4Sr_3Sb_4$	0D pairs, atoms	
Zn_4Sb_3[247, 248]	Zn_4Sb_3	0D pairs, atoms	
ZnSb[249]	CdSb	0D pairs	
$EuNi_{1.51}Sb_2$[250]	$ThCr_2Si_2$	0D pairs	
$CoSb_2$[74]	$CoSb_2$	0D pairs	see the text
$Ca_{11}Sb_{10}$[251]	$Ho_{11}Ge_{10}$	0D squares, pairs, atoms	
$CoSb_3$[33]	$CoAs_3$	0D squares	
REM_4Sb_{12}[a][30, 31]	$CoAs_3$	0D squares	
(Ba_2Sb_3,[36] Eu_2Sb_3,[37] Sr_2Sb_3[38])	Sr_2Sb_3	0D Sb_6 zig-zag units	
KSb[39]	LiAs	1D helical chains	
RbSb[252]	NaP	1D helical chains	
$CaSb_2$,[253] $EuSb_2$[40]	$CaSb_2$	1D zig-zag chains	
KSb_2[254]	KSb_2	1D ribbon; edge-sharing Sb_6 octahedra	
$BaSb_3$[43]	BaP_3	2D 2,3-connected nets	
Sb[44]	As	2D 3-connected nets	
$Eu_{14}MnSb_{11}$[49]	$Ca_{14}AlSb_{11}$	0D atoms	linear 0D Sb_3 units
($CrSb_2$,[255] $FeSb_2$,[72] $CoSb_2$,[256] $NiSb_2$[257])	FeS_2	0D pairs	see the text
Li_2Sb[15]	Li_2Sb	0D pairs	linear 1D chains
U_3MSb_5 (M = Ti, V, Cr, Mn)[12]	"Anti"-Hf_5Sn_3Cu	0D atoms	linear 1D chains
La_3MSb_5(M = Zr, Hf)[58]	"Anti"-Hf_5Sn_3Cu	0D atoms	linear 1D chains
$LaSb_2$, $CeSb_2$, $SmSb_2$[258–260, 62]	$SmSb_2$	0D pairs	2D square sheets
($LaCrSb_3$,[58] $CeCrSb_3$[261])	$CeCrSb_3$	0D pairs, atoms	2D square sheets
$BaCu_2Sb_2$[262]	$BaCu_2Sb_2$	0D pairs, atoms	square 2D sheets
$EuCu_2Sb_2$,[262] $LaNi_{1.51}Sb_2$[250]	$CaBe_2Ge_2$	0D atoms	2D square sheets
REM_xSb_2[b][13, 64–70]	$ZrCuSi_2$	0D atoms	2D square sheets
$YbSb_2$[61]	$ZrSi_2$	1D zig-zag chains	2D square sheets
$M_6M'Sb_{15}$ (M = La, Ce; M′ = Mn, Cu, Zn)[71]	La_6MnSb_{15}	0D atoms, 1D Sb_3 strips, 3D Sb_{10} network	
$ZrSb_2$[105]	Co_2Si	1D Sb_4 strips	
$ZrSb_2$[106]	$ZrSb_2$	1D Sb_6 strips	

[a] RE = La, Ce, Pr, Nd, Sm, Eu; M = Fe, Ru. [b] RE = rare earth element, M = Mn, Fe, Co, Ni, Cu, Zn, Pt, Pd, Cd, Ag, Au.

show that Sb can act as a "well-behaved" Zintl–Klemm element. Then, we examine Sb phases containing unusual 1D linear chains and 2D square sheets, invoking the previously conjectured electron counting generalizations. We finish this section by analyzing the sidewise fusion of two 1D linear chains to produce 1D ladders.

3.1. Classical Geometries: 0D Sb_2 Pairs and Sb_4 Squares

The most commonly occurring Sb substructure with an Sb–Sb bond is an Sb_2 pair. In theory, the pair can have seven, six, or five electrons per Sb, which would formally correspond to single, double, or triple bonds (Scheme 1). However, π



Scheme 1.

bonding is weak and rare for heavier elements, and usually only σ-bonded species are found. The typical range of observed bond lengths for the Sb_2 fragment in these phases is 2.80–2.90 Å. An unambiguous Sb–Sb single bond in a molecular hydrazine analogue, $(CH_3)_2Sb–Sb(CH_3)_2$, is 2.87 Å is used for calibration. Recently, the first Sb–Sb double bond (2.64 Å) in a molecular compound has been reported.[25]

The overwhelming majority of Sb phases containing just pairs and atoms conforms to the Zintl–Klemm concept. Thus, upon completing the octet, an isolated Sb atom should be formally −3 and Sb in a single-bonded pair −2. We considered Ba_5Sb_4 as an example (Entry 1 in Table 1). We do not show the structure, but two of the four Sb atoms per formula unit are isolated and two form a pair. The charges in Ba_5Sb_4 can be assigned as $(Ba_5)^{10+}(Sb_2^{atom})^{6-}(Sb_2^{pair})^{4-}$. The Sb–Sb separation in the pairs is 2.89 Å, which is within the normal range for a single bond. From here on we will use the label "atom" for an isolated or single atom in a structure. Similarly, the formal charges on $Li_4Sr_3Sb_4$ (Entry 2 in Table 1) can be assigned as $(Li_4)^{4+}(Sr_3)^{6+}(Sb_2^{atom})^{6-}(Sb_2^{pair})^{4-}$ on the basis of the multiplicities of Sb positions in the crystal structure. Note that these simple assignments do necessitate a knowledge of the structure of the phase, a typical (and productive) piece of nearly circular chemical reasoning.[26]

Isolated Sb_4 squares are also quite common within antimony phases. If one completes an octet around each Sb in the Sb_4 square, then one is led to a −1 charge to each Sb.[27] For example, $Ca_{11}Sb_{10}$ contains one isolated Sb_4 square, four Sb_2 pairs, and eight Sb atoms per two formula units (Figure 1).

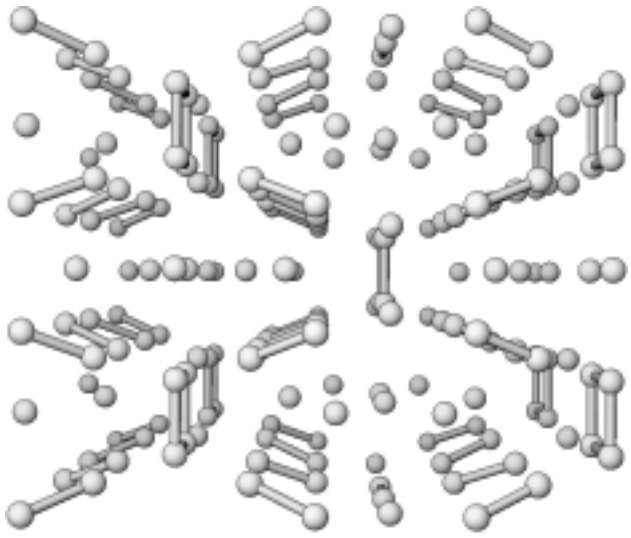


Figure 1. A perspective view of the Sb sublattice of the $Ca_{11}Sb_{10}$ crystal structure.

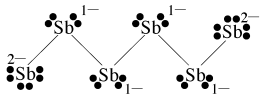
Following the Zintl–Klemm viewpoint, these molecular entities should carry a −1, −2, and −3 charge, respectively. Indeed, taking into account the multiplicities of the different kinds of atoms in the crystal structure, a simple charge assignment is established: $(Ca_{22})^{44+}(Sb_4^{square})^{4-}(Sb_8^{pair})^{16-}(Sb_8^{atom})^{24-}$.

The presence of transition metals complicates the bonding picture for the antimony phases with the relatively popular and fascinating skutterudite[28–31] ($CoAs_3$-type) structure. For a detailed description of bonding in these fascinating solids we refer readers to the original papers of Jung, Whangbo, and Alvarez[32] and Jeitschko and their co-workers.[31]

The picture of bonding is slightly more simple in the binary representatives of the skutterudite family, such as $CoSb_3$.[33] If one assigns a −1 charge to the Sb in squares (classical isolated Sb_4^{4-} squares), then Co becomes 3+ in $CoSb_3$.[31, 32] This d^6 electron configuration on octahedrally coordinated Co satisfies the 18 electron rule. Therefore, one expects semiconducting behavior for $CoSb_3$, and this has been observed for isoelectronic CoP_3, $RhAs_3$, $IrAs_3$, $IrSb_3$, and some other ternary skutterudites.[34, 35]

3.2. Classical Geometries: Zig-Zag Chains

The crystal structure of Ba_2Sb_3,[36] Eu_2Sb_3,[37] and Sr_2Sb_3[38]) contains isolated zig-zag chains of Sb_6 (Scheme 2). The Sb–Sb bond lengths range from 2.86 to 3.00 Å. If one completes an octet around each Sb atom in the chain, then the charges can be assigned as $(Ba_2)^{4+}Sb^{2-}Sb^{-}Sb^{-}$. This compound thus obeys the Zintl–Klemm electron counting rules.



Scheme 2.

In contrast to these isolated Sb_6 units, the zig-zag chains that we discuss next are extended one-dimensional arrays. A perspective view of the Sb sublattice of the KSb crystal structure[39] is shown in Figure 2.

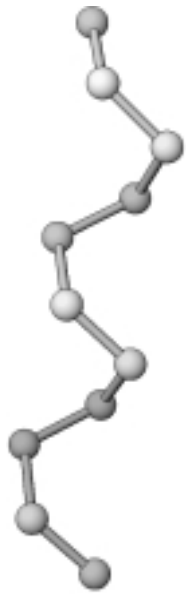


Figure 2. A perspective view of the Sb sublattice of the KSb crystal structure.

The Sb atoms form a helix, with Sb–Sb bonds of 2.83 and 2.88 Å. It is natural to assign a $1+$ charge to the potassium atom, which makes the antimony center -1. The Sb^- ion is isoelectronic to the Te atom, which indeed forms helical chains in its elemental structure. The Sb^- ions in RbSb (Table 1) also forms helical chains, but with a somewhat different conformation.

In contrast to KSb and RbSb the zig-zag chains of Sb ions in $CaSb_2$ and $EuSb_2$ (Table 1) are planar. A perspective view of the $EuSb_2$ crystal structure is given in Figure 3. The Sb–Sb distance in the chains is 2.93 Å. These compounds are also classical, since the cations are divalent (established by magnetic measurements for Eu compounds[40]). This assignment leads one to a -1 charge on the Sb center, which would be consistent with a twofold coordination. In Figure 3 one observes that the Sb chains are planar.

Why are such Sb^- chains sometimes helical and sometimes planar? A hint is provided by the shortest interchain distance in the horizontal planes being 3.54 Å (Figure 3), which can be thought of as a secondary

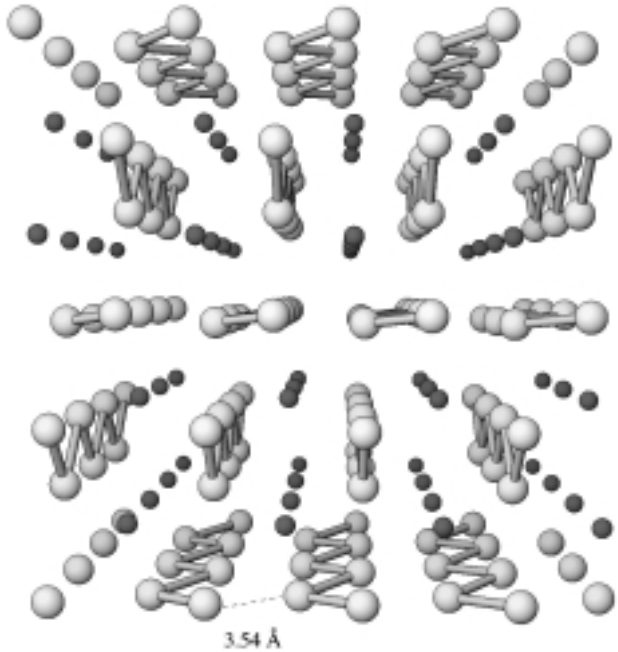


Figure 3. A perspective view of the $EuSb_2$ crystal structure. Eu = small dark spheres; Sb = large light spheres.

interaction[41, 42] (this assumption is supported by the near-linear Sb–Sb···Sb angle). When we examine the $YbSb_2$ and $SmSb_2$ crystal structures, we will consider the possibility of fusing the 1D zig-zag chains to give a square lattice.

3.3. Classical Geometries: Two-Dimensional Structures

We want to discuss two structures in this subsection: that of $BaSb_3$[43] and that of elemental Sb.[44] The former forms a two-dimensional 2,3-connected Sb net (Figure 4). As in the case of

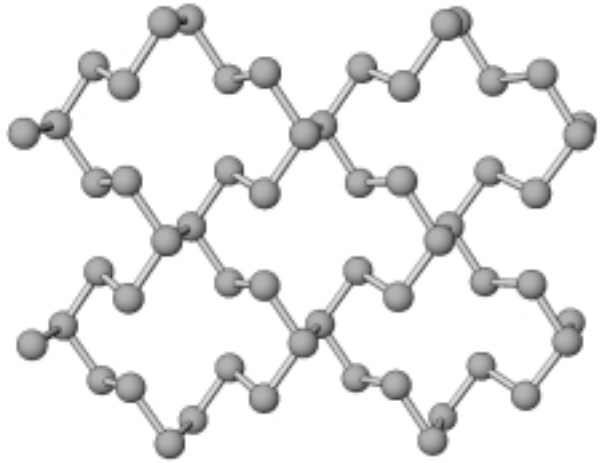


Figure 4. A perspective view of the Sb substructure of the $BaSb_3$ crystal structure.

the ribbons discussed above, we count three-connected Sb centers as neutral and two-connected Sb centers as Sb^-. Taking into account the site multiplicities in the crystal, the charges may be assigned as $Ba^{2+}Sb^0(Sb_2)^{2-}$. The Sb–Sb bonds in the crystal structure are around 2.85 Å, within the normal range. By any criterion, Sb acts as a good Zintl–Klemm element in this compound.

The crystal structure of elemental As-type Sb (Figure 5) is easy to understand, yet has some interesting features in it. If one chooses to ignore the 3.34 Å Sb–Sb inter-sheet contacts,

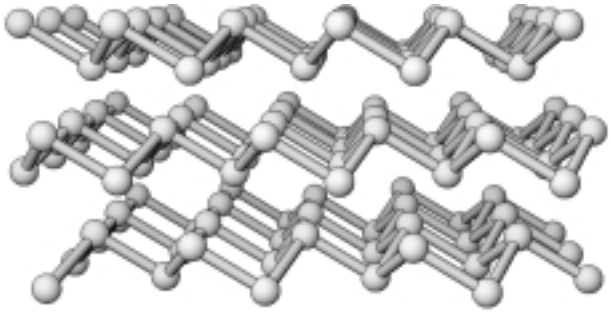


Figure 5. A perspective view of the crystal structure of elemental Sb.

then bonding in elemental Sb can be described as three-connected neutral Sb atoms that form a two-dimensional sheet, with each Sb center being appropriately pyramidal. However, two details of the structure are unsettling. The 3.34 Å inter-sheet contact is significantly shorter than an Sb···Sb van der Waals contact. Another interesting fact is the slight elongation of the Sb–Sb bond within the sheets to 2.90 Å, compared with 2.85 Å found in the sheets of $BaSb_3$. All these facts point to the existence of secondary inter-sheet interactions that also weaken the bonding within the sheets. We

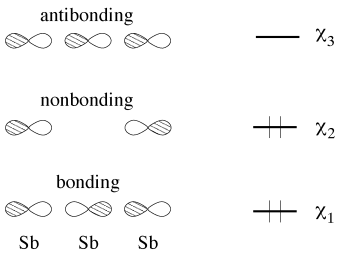
hinted earlier that similar interactions exist between zig-zag chains in $CaSb_2$ and $EuSb_2$. Indeed, under high pressure (between 6 GPa and 7.5 GPa) elemental Sb undergoes a phase transformation[45] to give a simple cubic structure (Po-type), which results in equal inter- and intra-sheet Sb–Sb bonds (2.99 Å). Cubic Sb has also been prepared as a metastable phase by quenching from liquid and vapor.[46] The Sb–Sb bond length in that phase is 3.16 Å, which is longer than that in Sb after high-pressure treatment. One can think of elemental As-type Sb as having undergone a Peierls distortion[18] from cubic Sb.[47] We will return to this viewpoint in the theoretical part (Section 6).

The above sections explore the remarkable range of "normal" Zintl–Klemm type bonding in antimony compounds. But this element does not confine itself to classical structures. Next we examine the numerous Sb phases with nonclassical Sb sublattices.

3.4. Hypervalent Geometries: Linear Chains

The simplest nonclassical Sb structure may be that found in $Ca_{14}AlSb_{11}$[48] (see also $Eu_{14}MnSb_{11}$[49]) in the form of Sb_3 linear units. If the charge on Al is $3+$, the cationic charge is $31+$ per formula unit. In $Eu_{14}MnSb_{11}$ the Eu center is thought to have a charge of $2+$ and Mn correspondingly $3+$. In both structures there are eight isolated Sb atoms, which contribute -24 to the charge balance. Therefore, the remaining Sb_3 group should carry a -7 charge. The Sb_3^{7-} unit is isoelectronic with I_3^- and XeF_2, which are both classical hypervalent or electron-rich four-electron three-center species. The Sb_3 linear geometry and long Sb–Sb bonds (3.20 Å in $Ca_{14}AlSb_{11}$, 3.26 Å in $Eu_{14}MnSb_{11}$) are consistent with this suggestion. Kauzlarich, Fong, and Gallup carried out pseudopotential planewave density functional theory (DFT) calculations[50] on the analogous $Ca_{14}GaAs_{11}$ structure.[51] Their calculations were fully consistent with the existence of hypervalent As_3^{7-} units.

A word is in order here about the general framework of hypervalent or four-electron three-center bonding. Multicenter bonding is a natural extension of covalent electron-pair bonding to electron-deficient or electron-rich systems. In the context of the latter, it was initially described by Rundle for I_3^- (or XeF_2).[52, 53, 54] The reader is also referred to the important paper by Musher.[55] If the terminal atoms contribute only p orbitals (as shown here) or some hybrids of like symmetry, and the central atom only a single p orbital, one obtains the set of MOs shown in Scheme 3. In the four



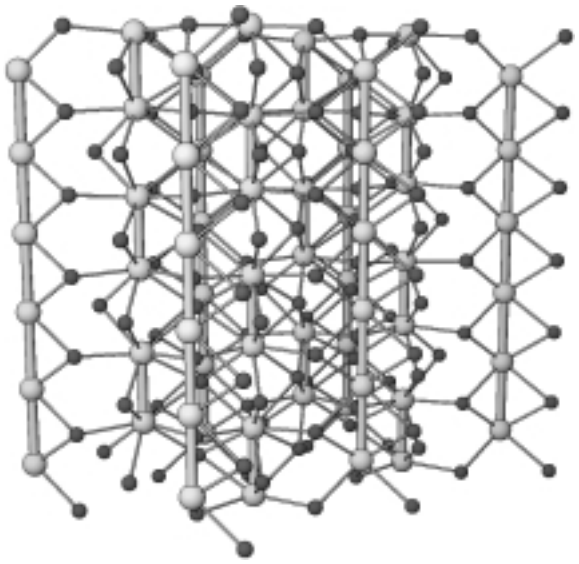
Scheme 3.

-electron system (only p orbitals of σ type are considered) χ_1 and χ_2 are occupied. The bonding scheme is modified slightly by the inclusion of an s orbital on the central atom. In that case χ_2 becomes somewhat antibonding through out-of-phase mixture of the central s orbital.

This bonding pattern may be used in a simple description of the axial bonding in PF_5, SF_4, and BrF_3 as well, though hypervalency in PF_5 has been questioned by Häser.[56] For square-planar systems (XeF_4, $TeBr_4^{2-}$) one has two perpendicular bonds of this type. The octahedral or deformed octahedral XeF_6 (and SbX_6^{3-}) have three such bonds.[57] SF_6 and SbX_6^- have two electrons less; however, a similar octahedral environment is also found in these compounds.[57]

Some people do not like the term hypervalent. We view it as a historically and heuristically useful categorization of bonding in electron-rich systems, and will use the term interchangeably with electron-rich multi-center bonding. Such bonding occurs in Sb_3^{7-}, and we will see it in linear, square net, and cubic sublattices of antimonides.

We return to our perusal of antimony bonding types. Extended linear chains of antimony atoms are found in Li_2Sb,[15] U_3MSb_5 (M = Ti,V,Cr,Mn),[12] La_3MSb_5 (Zr,Hf),[58] and other Sb phases. A perspective view of the Li_2Sb crystal structure is shown in Figure 6. There are two types of Sb in the


Figure 6. A perspective view of the Li_2Sb crystal structure. Li = small dark spheres; Sb = large light spheres.

crystal structure—Sb–Sb pairs and 1D linear chains, and both types occur in equal numbers. The Sb–Sb pairs are also stacked into a chain, but the inter-pair Sb–Sb contact is 3.56 Å, compared to 2.97 Å within the Sb_2 pair. In the linear chains all Sb–Sb bonds lengths are equal to 3.26 Å. This distance is long by comparison with an Sb–Sb single bond, but is definitely in the bonding regime. If one assigns a $1+$ charge to Li ions and a -2 charge to the Sb centers in the pairs, then one can assign a -2 charge also to the Sb atoms in the extended chains.

Before we take up this assignment in the theoretical section, we should mention again that Jeitschko and co-

workers,[13, 12] Nesper,[14] and Mar and co-workers[58] have suggested from empirical calculations that one consider long Sb–Sb bonds as half bonds (that is, one electron per bond). By making an implicit assumption of three additional lone pairs on each Sb atom, these authors have proposed a -2 charge for each Sb center in a linear chain, that is, three lone pairs and one bonding electron per Sb center. We will provide below a more formal theoretical analysis of this proposition.

In the theoretical section we will also consider the formation of Sb_2^{4-} pairs as the result of a Peierls (pairing) distortion in a one-dimensional linear Sb^{2-} chain with a half-filled band. What is surprising is that both Peierls distorted and undistorted chains coexist in the same crystal structure. The geometrical details alone of this fascinating structure indicate, we think, that the potential energy surface for Peierls distortion of Sb networks should be rather soft.

One-dimensional Sb chains are also found in U_3MSb_5 (M = Ti,V,Cr,Mn)[12] and La_3MSb_5 (M = Zr,Hf).[58] The Sb–Sb bonds in the linear chains again are somewhat long for both series of compounds, being around 3.17 Å for the former series and 3.06 Å in the latter. A perspective view of the La_3ZrSb_5 crystal structure is given in Figure 7. For two formula

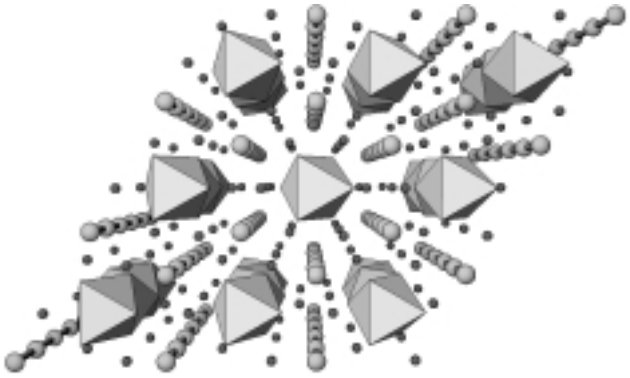


Figure 7. A perspective view of the La_3ZrSb_5 crystal structure. La = small dark spheres; Sb = large light spheres; $ZrSb_6$ octahedra are shown in a polyhedral representation.

units per unit cell, one could assume that cations donate $6 \times (+3) + 2 \times (+4) = (+26)$ electrons to the anionic framework. There are two kind of Sb atoms present in the crystal structure. Isolated Sb atoms, which comprise the Sb part of the face-sharing $ZrSb_3$ octahedral chains, occupy a six-fold Wyckoff position. Thus, they contribute a $6 \times (-3) = -18$ charge to the overall charge balance. The remaining Sb atoms in the linear Sb chains are found in a fourfold position, therefore each should carry a -2 charge in order to preserve the neutrality of the unit cell.[58]

A -2 charge per Sb atom in these linear chains was also suggested for La_3MSb_5(M = Ti,Hf)[58] and U_3TiSb_5.[12] A clear assignment of charges for the Mn analogue of the latter compound was not possible.[12] Sb–Sb bond lengths between Sb atoms in 1D linear chains vary greatly from compound to compound (for example, 3.26 Å in Li_2Sb and 3.06 Å in Sb_5MLa_3 (M = Zr, Hf)).

In summary, there are a number of Sb phases with linear Sb arrays. An electron count of seven electrons per Sb atom for 1D linear Sb chains makes sense of the electron counting in these structures. In these chains the Sb–Sb bonds are significantly elongated relative to a single Sb–Sb bond.

One final point should be made, which is relevant to the longer Sb–Sb bonds found in the linear arrays discussed here and also found in the square nets still to be mentioned. On one hand this is a reflection of the hypervalent bonding being weaker than normal electron pair bonding (compare, for instance, the I–I separation of 2.90 Å in I_3^- with 2.76 Å in diatomic I_2). There is also a connection to be made to donor–acceptor viewpoints of bonding and "secondary bonding" in numerous crystal structures. What we see are manifestations of a continuum between covalent bonding and closed-shell interactions, a subject that we[59] and others[60] have considered in detail elsewhere.

3.5. Hypervalent Geometries: Square Sheets

It is convenient to begin the discussion of square Sb sheets by first revisiting the structures of $CaSb_2$ and $EuSb_2$ (Table 1). We contemplated already the possibility of the horizontal zig-zag chains in Figure 3 collapsing into a square sheet. Indeed, this essentially happens in the $YbSb_2$ case (Figure 8).[61] Actually, the "square" sheets in $YbSb_2$ are slightly puckered,

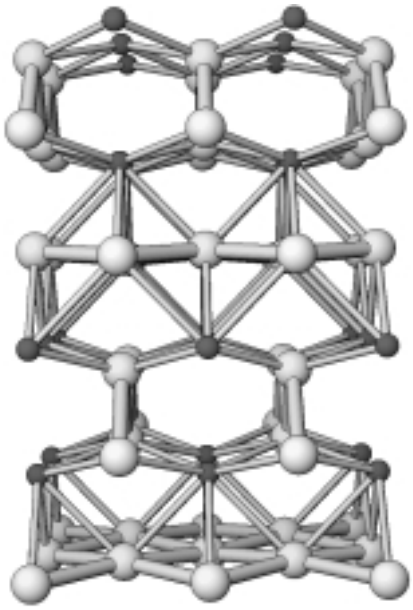


Figure 8. A perspective view of the crystal structure of $YbSb_2$. Yb = small dark spheres; Sb = large light spheres.

with Sb-Sb-Sb angles within the sheet of 93° and 86°. The Sb–Sb bond lengths are significantly longer (3.12 Å) than those found in the zig-zag chains of the $EuSb_2$ crystal structure (2.93 Å).

The magnetic susceptibility data for the Yb ion in $YbSb_2$ are consistent with Yb^{2+}, with a small (2%) admixture of the Yb^{3+} cation. If one assigns a -1 charge to Sb in the zig-zag chains (Figure 8), then Sb must also carry the same -1 charge in the approximately square sheets (there are as many chain Sb

atoms as those in the square sheet). Similar to a Peierls distortion of linear Sb^{2-} chains into the relatively isolated classical Sb_2^{4-} pairs (see the discussion on Li_2Sb in Section 3.4), square sheets of Sb^- ions may distort into classical zig-zag Sb^- chains (which could still have secondary interactions with each other). This, however, does not happen in $YbSb_2$. Tremel and Hoffmann argued that the existence of a small amount of Yb^{3+} ions in $YbSb_2$ suppresses the possible distortion to a zig-zag chain.[19] The electrostatic interactions within the lattice have to be taken into account as well to provide a detailed explanation of this behavior.

The crystal structures of $EuSb_2$ and $YbSb_2$ prompt us to think about what might happen to an Sb network of this type when a divalent rare earth element is replaced by a trivalent one. If we start with the $EuSb_2$ crystal structure (Figure 3), two resolutions come to mind. Upon reduction by one electron per two Sb atoms one of the two types of zig-zag chains might break into isolated pairs ($RE^{3+}(Sb^{zig\text{-}zag})^-(Sb^{pair})^{2-}$). If the newly formed $Sb_2^{pair\,4-}$ pairs are appropriately aligned, they might further fuse into a linear Sb chain. Alternatively, one could begin with the $YbSb_2$ structure with its approximately square sheets and zig-zag chains. One might guess that upon reduction the presumably weaker hypervalent bonds within the square sheets will disrupt before the break-up of classically bonded zig-zag chains. There is an implicit assumption here that the hypervalent bands, being only partially filled, would be occupied more easily by extra electrons than presumably high-lying empty antibonding orbitals of classical zig-zag chains.

Neither of those alternatives takes place in the $SmSb_2$ crystal structure (Figure 9)! Magnetic measurements for the isostructural Ce compound, $CeSb_2$, indicate a trivalency of rare earth cations.[62] Other rare earth atoms are also thought to be trivalent in rare earth diantimonides (La also forms an isostructural phase). The $SmSb_2$ structure is best viewed as derived from the $YbSb_2$ crystal structure by breaking the zig-zag chains into isolated pairs. The approximately square lattice of $YbSb_2$ becomes nearly ideal in $SmSb_2$ (Sb–Sb distances in the sheets are 3.03 Å and 3.09 Å). The Sb–Sb distance of 2.79 Å in Sb_2 pairs is within a normal Sb–Sb single bond range. Again the electron count is consistent with a -1 charge on the Sb atoms in the "square" sheets ($Sm^{3+}(Sb^{sheet})^-$-$(Sb^{pair})^{2-}$).

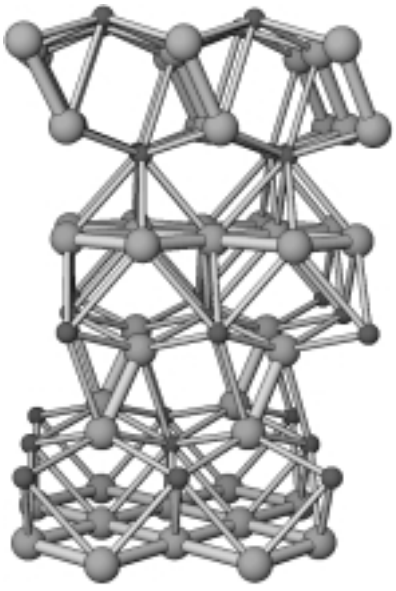


Figure 9. A perspective view of the crystal structure of $SmSb_2$. Sm = small dark spheres; Sb = large light spheres.

Perfect square Sb sheets are found[63] in the $BaZnSb_2$ crystal structure (Figure 10). Zn atoms are surrounded by isolated Sb atoms in a tetrahedral environment. The closest Sb···Sb contact between isolated Sb atoms is 4.49 Å, which is clearly nonbonding. The Sb–Sb bonds in the square sheets are rather long (3.24 Å), which is consistent with the observed trend for other square sheets. It is reasonable to assume that both Ba and Zn are dipositive, which requires again a -1 charge on Sb atoms in the square sheets. The charges on the elements in this compound then can be written as $Ba^{2+}Zn^{2+}(Sb^{sheet})^-(Sb^{atom})^{3-}$.

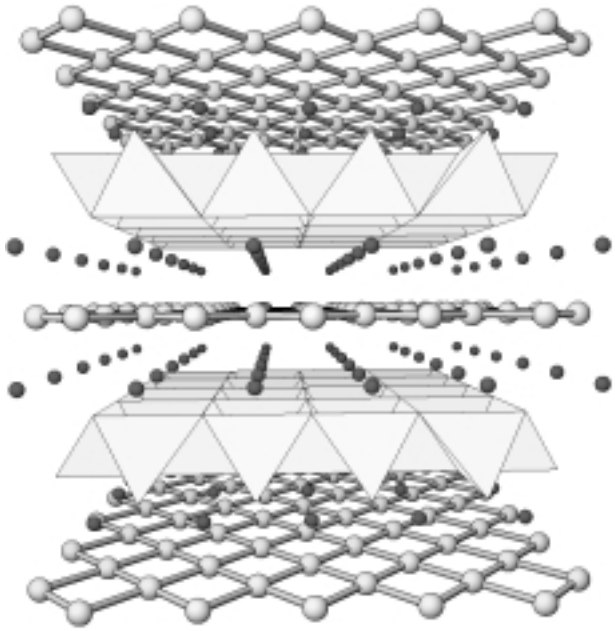


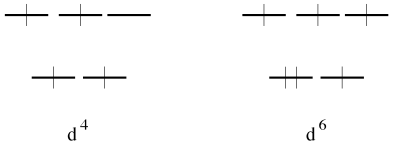
Figure 10. A perspective view of the crystal structure of $BaZnSb_2$. Ba = small dark spheres; Sb = large light spheres; $ZnSb_4$ tetrahedra are shown in a polyhedral representation.

Perfect square sheets exist in a wide variety of other antimonides. Among the most common of these[13, 64, 65, 66, 67, 68, 69, 70] are compounds with a stoichiometry REM_xSb_2, where RE stands for a rare earth, M is a transition metal (M = Mn, Fe, Co, Ni, Cu, Zn, Pt, Pd, Cd, Ag, Au), and x is usually less or equal to one. This structure is a variation of the $BaZnSb_2$ crystal structure given above. The rare earth ions in these compound have been shown[70, 71, 67, 68] to be tripositive. Since that $3+$ charge is exactly canceled out by a -3 charge on isolated Sb atoms (one of the Sb atoms is in the square sheet, one is isolated), the formal charge on Sb in the square sheets is determined solely by the charge on M_x part. If we assume a -1 charge on the square sheet Sb atoms, a count we have seen is consistent in other cases, we are led to a singly charged M ion if x is near one. The structures where this is plausible are $LaCu_{0.82-0.87}Sb_2$,[64] $REAgSb_2$,[67] $LaAuSb_2$,[69] and others. On

the other hand, if x is close to 0.5 then we expect the metal to be dipositive. This assumption seems quite reasonable for $LaZn_{0.52}Sb_2$.[64]

For other transition metals in this group of compounds, the assignment of charges becomes ambiguous. Here we will discuss only the Mn case, where good magnetic susceptibility data are available.[70, 68] The x value for these Mn compounds varies from 0.65 to 0.90. A magnetic moment of 4.3 μ_B, which corresponds roughly to four unpaired electrons, has been calculated for Mn atoms in $CeMn_{0.9}Sb_2$ (in addition to the Ce^{3+} magnetic moment). This result led the authors to assign a $3+$ charge to the Mn ion (d^4 configuration). This electron count then results in a large -2.7 charge per Sb atom in the sheets, but this fails to explain the relatively short Sb–Sb bonds in the sheets (3.10 Å)—there is very little that would hold the $Sb^{2.7-}$ centers together.

The Mn ions are located in a tetrahedral environment, where a high-spin d^6 configuration will also lead to four unpaired electrons (Scheme 4). We think that both the



Scheme 4.

magnetic data and internal consistency of the structural information in $CeMn_{0.9}Sb_2$ allow an interpretation of the Mn oxidation state in these compounds as $+1$. Admittedly, this is not a usual oxidation state for the Mn ion.

In summary, many structures of antimonides which contain square or near-square Sb sheets give a consistent charge partitioning (in the Zintl–Klemm sense) if a -1 charge is assigned to each Sb atom in the square sheet. This is not an absolute requirement, for instance if we think about the $CeMn_xSb_2$ phase just discussed, the relatively large range of x values (0.65–0.9) indicates a fractional band filling in the square sheets. Eventually, by considering other main group elements, we will see a similar range of possible counts. The electron count of six electrons per Sb atom indicates only a preferred electron count, actual fluctuations around that number are to be expected, hopefully within a reasonably narrow range.

3.6. Other Geometries: The Marcasite- and Arsenopyrite-Type Compounds

Hybrid classical-hypervalent Sb subnetworks are present in transition metal dipnictides with the marcasite (FeS_2) crystal structure. A perspective view of the $FeSb_2$ crystal structure[72] is shown in Figure 11. One can view the Sb subnetwork as composed of regular Sb–Sb pairs (2.88 Å) that are stacked to form a one-dimensional ladder structure with an inter-pair Sb–Sb distance of 3.18 Å. An alternative (and perhaps more conventional) view would be to treat the Sb–Sb pairs as noninteracting units. A -2 charge is required to complete an

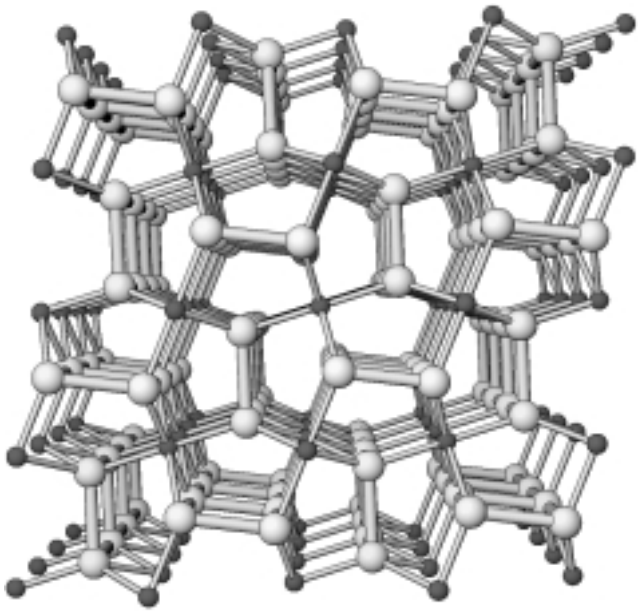


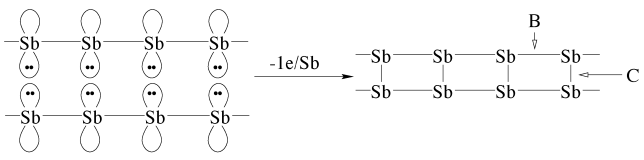
Figure 11. A perspective view of the crystal structure of $FeSb_2$. Fe = small dark spheres; Sb = large light spheres.

octet around each Sb in the latter case, which leads to a $4+$ charge on the metal center. Since the Sb electronegativity is not very high it is hard to justify such a high oxidation state on the transition metal atom, at least for some of the metals listed in Table 2. Relatively short inter-pair Sb–Sb distances also cast doubt on this line of reasoning.

Table 2. Geometrical data for the marcasite-type transition metal dianti-monides.

Compound	$CrSb_2$[255]	$FeSb_2$[72]	$CoSb_2$$[256]	$NiSb_2$[257]
intra-pair Sb–Sb distance [Å]	2.85	2.88 A	2.82 A	2.88 A
inter-pair Sb–Sb distance [Å]	3.27	3.19	3.37	3.84

Another approach would be to construct the Sb subnetwork in $FeSb_2$ beginning with a linear Sb chain (Sb–Sb distance of 3.19 Å). The electron count for such a chain should be seven electrons per Sb, as suggested in Section 3.4 and as we will prove in the theoretical section (Section 4). The next step is to pair up two linear chains to form the ladder structure. This would result in strong lone pair—lone pair repulsion (Scheme 5). To form Sb–Sb bonds between the chains, an



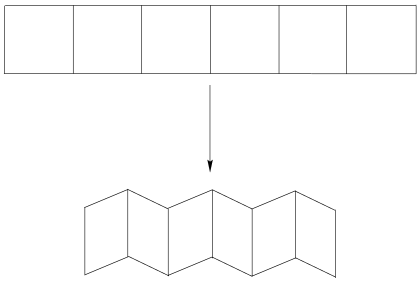
Scheme 5.

electron should be taken away from each Sb atom. This line of reasoning results in a -1 charge on each Sb center, which in turn corresponds to a formal $2+$ charge on Fe ions. The

resulting d^6 configuration for the octahedrally coordinated Fe ion is consistent with the 18e rule.

The analysis for the other metals in Table 2 is less clear. The intra-pair Sb–Sb distance (bond C in Scheme 5) becomes larger for Cr, Co, and Ni. In the Ni case the isolated pair view could be more justified, although again 4+ is an unusual oxidation state for the Ni ion. On the other hand, if the Ni ion had a charge of 2+, then Sb_2^{2-} would have a Sb–Sb double bond, something not supported by the Sb–Sb bond length (2.88 Å). Some experimental indication of the metal oxidation states would be very helpful in clarifying the issue of bonding within the Sb subnetworks of the marcasite type diantimonides. Holseth and Kjekshus[73] carried out magnetic susceptibility measurements on the marcasite-type dipnictides but, unfortunately, could not assign oxidation states to the transition metals. The arsenopyrite–marcasite phase transformation of $CoAs_2$ and $CoSb_2$ has been studied by Siegrist and Hulliger.[74] They have detected a phase transition, but the semiconductor–metal nature of this transition has not been confirmed. One might expect metallic properties for the marcasite structure because of the partial filling of the p_z band (z being the chain axis) in evenly spaced one-dimensional ladders (see the later discussion for more details).

An interesting connection can be made between the marcasite-type structures and the zig-zag ladders of main group elements as well as main group–transition metal elements. If a linear ladder were kinked at every Sb atom, then a zig-zag ladder would be produced (Scheme 6). An



Scheme 6.

isolated zig-zag ladder contains three-connected classical atoms (pyramidal); appropriate to these would be an electron count of five electrons per atom. Zig-zag ladders could be fused together to produce the characteristic four-connected networks found in the $BaIn_2$-type[75] binary compounds and the TiNiSi-type[76] ternary compounds.

In the next section we present theoretical arguments for the conjectured electron counting schemes for nonclassical hypervalent networks.

4. Theory: Basic Principles

4.1. Assumptions of the Model

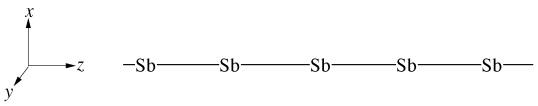
Our calculations, used throughout this work to support qualitative bonding considerations, are based on the extended Hückel (EH) method, an approximate molecular orbital (MO) theory.[77, 78, 79] Parameters for extended Hückel calculations are given in Appendix I (Section 14).

Key to our analysis will be an assumption of weak π interactions and weak (although, still significant) s-p mixing. Heavier main group elements are known to have weak π bonding, presumably because at the E–E distance set by the σ-bonding framework the p–p π overlap is quite small. Hence, the first assumption seems plausible. The weak s-p mixing can be traced to the contraction of the outer s orbital relative to the p orbitals down the groups in the Periodic Table. We will elaborate on this (and so understand the effect of including such mixing) when we discuss the *instability* of a hypothetical linear N^{2-} chain toward a pairing distortion, relative to an Sb^{2-} chain (such as the one that exists in Li_2Sb, for example). For the heaviest elements this contraction is further enhanced by relativistic effects, as was pointed out for these particular systems by Lohr[80] and by Nesper.[14] We will further explore this subject in this Section 4.6.

4.2. The Linear 1D Chain: A Simple MO Approach

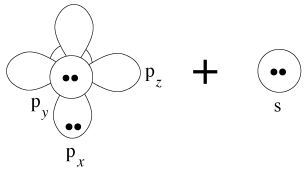
There are several ways to derive an optimal electron count for a linear 1D Sb chain. We begin with a simple molecular orbital picture that does not require a band structure analysis.

The chain coordinate system is given in Scheme 7. By



Scheme 7.

assuming weak π bonding and an excess of electrons, the p_x and p_y orbitals in the chain are essentially lone pairs. Furthermore, if we assume little s-p mixing occurs we can consider the s orbital simply as an occupied lone pair. Three filled lone pairs (Scheme 8) correspond already to six



Scheme 8.

electrons per atom. Therefore, the final electron count will be determined by the occupancy of the remaining p_z orbital, which emerges as responsible for the presence or absence of bonding in the chain.

We consider first the oligomers which develop into this polymer. For a three-atom chain, the molecular orbitals are well known from the analysis of hypervalent bonding in, say, I_3^- or XeF_2.[54, 52, 53, 59] The two lowest orbitals are bonding and nonbonding, and the highest molecular orbital is antibonding (see Scheme 3). General bonding notions[16, 59] suggest the filling of all orbitals that are not strongly antibonding. In the

present instance this leads to four electrons in the p_z σ system and 18 electrons in lone pairs (s, p_x, and p_y), that is, an electron count of 22/3 electrons per atom for hypervalent I_3^- (or the related XeF_2).

Next we consider a linear chain with five atoms. While the orbitals are σ in character, they are "pentadienyl π-system-like" in terms of their phase relationships. The chain has three bonding and nonbonding p_z molecular orbitals (Scheme 9), filling which (along with the s, p_x, and p_y lone pairs) results in a electron count of $(6+5\times 6)/5 = 36/5$ electrons per atom. The extrapolation is clear[81]: an odd numbered *n*-member linear chain has $(n+1)/2$ bonding and nonbonding p_z levels (see Scheme 9) in addition to $3n$ s, p_x, and p_y lone pairs. To fill with two electrons per level all levels except the antibonding ones, one needs $2(3n+(n+1)/2) = 7n+1$ electrons. This amounts to $7+1/n$ electrons per atom. If *n* goes to infinity, as it does for

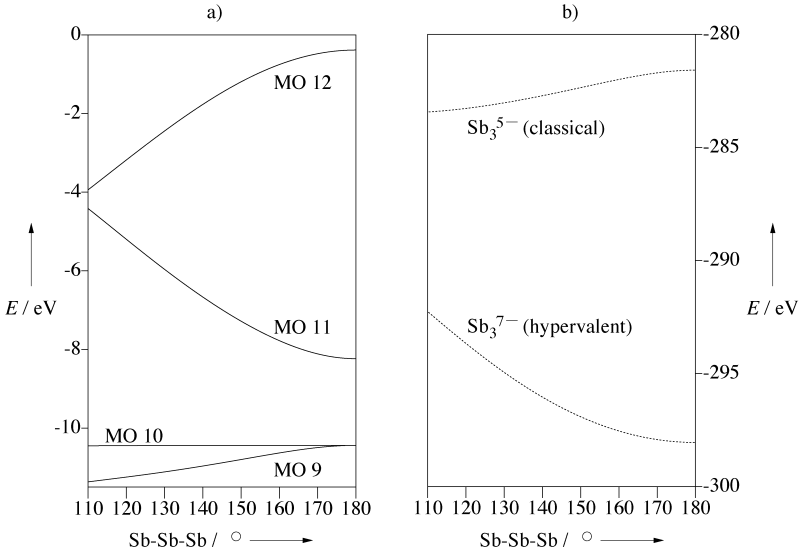
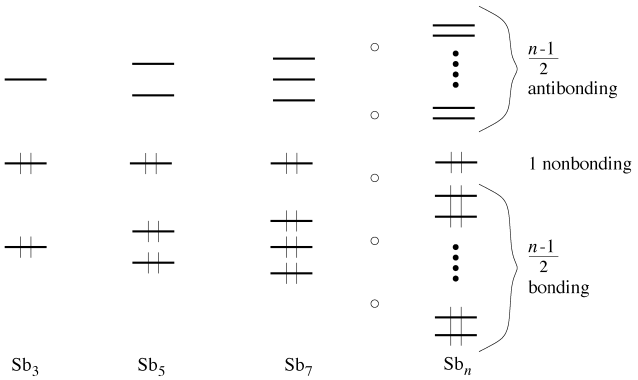


Figure 12. Walsh diagrams for the bending of Sb_3 molecules. a) Individual molecular orbital energies as a function of the bending angle; b) the total energy change for hypervalent Sb_3^{7-} and classical Sb_3^{5-} as a function of the bending angle. For Sb_3^{7-} MO 11 is filled.

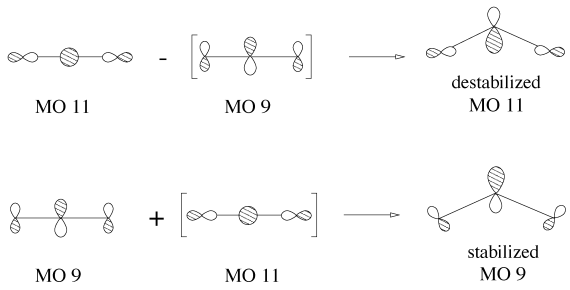


Scheme 9.

a one-dimensional linear chain, the proposed electron count of seven electrons per atom is obtained.

Before we derive the same result from a band structure analysis, we should compare the stability of a linear chain with this electron count with a kinked (zig-zag) chain. This comparison is familiar for the three-atom case, that is, for molecules such as XeF_2 and SF_2. XeF_2 has the hypervalent electron count of $7+⅓$ electrons per atom and it is linear, while SF_2 has a classical electron count, and it is bent. The isoelectronic Sb species, both found in the solid state, are Sb_3^{7-} and Sb_3^{5-}.[49, 71] The former ion is linear, while the latter one is bent, which is consistent with the molecular analogues.

A Walsh diagram for bending the Sb_3 unit is shown in Figure 12. Indeed, the 22 valence electron hypervalent structure prefers to be linear (Figure 12a) while the 20 electron classical one prefers to be bent (Figure 12b). The slope upon bending of the corresponding highest occupied molecular orbital (HOMO; MO 11) is responsible for the observed behavior. This MO is significantly destabilized upon bending, by mixing in an antibonding way with MO 9—one of the degenerate π orbitals (see Scheme 10, top). The HOMOs for the classical electron count are the doubly degenerate π

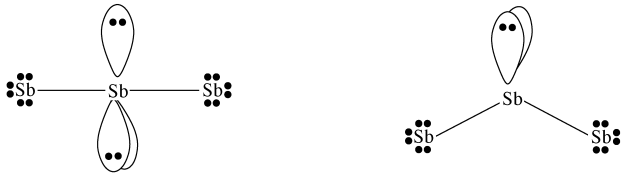


Scheme 10.

orbitals (MO 9 and 10). One of those orbitals becomes stabilized by mixing (now in a bonding way) with the higher lying MO 11 (see Scheme 10, bottom).

The energetic consequences for bending are enormous. For example, bending hypervalent Sb_3^{7-} from 180° to 110° costs 5.8 eV (Figure 12b). For classical Sb_3^{5-} the same bending leads to a stabilization by 1.85 eV. Clearly, the removal of two electrons from Sb_3^{7-} has a profound effect on its geometry. We emphasize this point because the same relationship between the locally linear and locally bent geometries is seen for infinite linear and kinked (zig-zag and helical) chains. And the energetic consequences (studied by us but not detailed here) are similar.

An even simpler explanation for the preferred geometries could be given within the VSEPR model.[82] Three lone pairs on the central atom in hypervalent Sb_3^{7-} occupy the equatorial positions in a trigonal bipyramid (Scheme 11, left), while



Scheme 11.

the side atoms occupy the axial positions of a trigonal bipyramid, in a linear arrangement with the central atom. The corresponding polyhedron for classical Sb_3^{5-} is a tetrahedron, with two lone pairs occupying two vertices, and two side atoms occupying the remaining two vertices (Scheme 11, right), creating an Sb-Sb-Sb bent geometry. The VSEPR picture is useful because it places bonds and lone pairs on a comparable basis.

On going to the extended geometries, the situation does not change much. For the classical electron count of six electrons per atom, zig-zag or helical chains are commonly found (elemental Te is a good example[83]; another example is the Sb sublattice in KSb[39]). On the contrary, the hypervalent electron count of seven electrons per atom is associated with linear chains, as exemplified by the Sb chains[15, 12, 58] which we discussed above. The molecular orbital picture behind this behavior is similar to the Walsh diagram (Figure 12) and VSEPR (Scheme 11) arguments given above.

We should mention that our analysis focuses on the bending coordinate in the structures. The question of the potential surface for an asymmetric stretch distortion, especially of the of the hypervalent Sb_3^{7-} (toward Sb_2^{4-} and Sb^{3-}) is not addressed. This distortion is easy in some analogous hypervalent species (for example, I_3^-) and not in others (PF_5). It is also related to the choice we will see Sb^{2-} chains make between hypervalent lines and paired distorted structures.

4.3. Linear 1D Chains: Band Structure Approach

In the previous subsection we demonstrated in one way that the electron count of seven electrons per atom is comfortable for a linear chain. Another way to come to this result is to use the band structure formalism.[17]

The computed band structure of an Sb chain at a 3.2 Å Sb–Sb distance is shown in Figure 13. If we ignore the s-p mixing (slight but not absent, as we will see), the shape of the resulting crystal orbitals is dictated purely by the symmetry and the topology of orbital interactions. Consider the s band (Figure 13): At Γ the crystal orbital is bonding and at Z it is antibonding. Since the s band is completely filled, its net effect on bonding is vanishing (all Sb–Sb bonding and antibonding combinations are filled), or even slightly antibonding (because of the bigger coefficients on the antibonding orbitals).

The π-interacting p_x and p_y orbitals "run up" along the Γ – Z line in the same manner as the s band (Figure 13). The flatness of the π band is consistent with our assumption of little π bonding. These two bands are also completely filled, therefore they do not contribute to bonding. The remaining band is σ type, based on the p_z orbital. This band "runs down" from Γ to Z. Midway between Γ and Z (at $k = \pm \pi/2a$), the p_z crystal orbital is nonbonding. The upper part of the p_z band is strongly antibonding. Destabilization within the chain would be expected if this part of the p_z band were to be filled. Therefore, a comfortable electron count (no σ-antibonding orbitals filled) is anticipated for a half-filled p_z band. With the completely filled s, p_x, p_y, and half-filled p_z band we arrive at the electron count of seven electrons per atom.

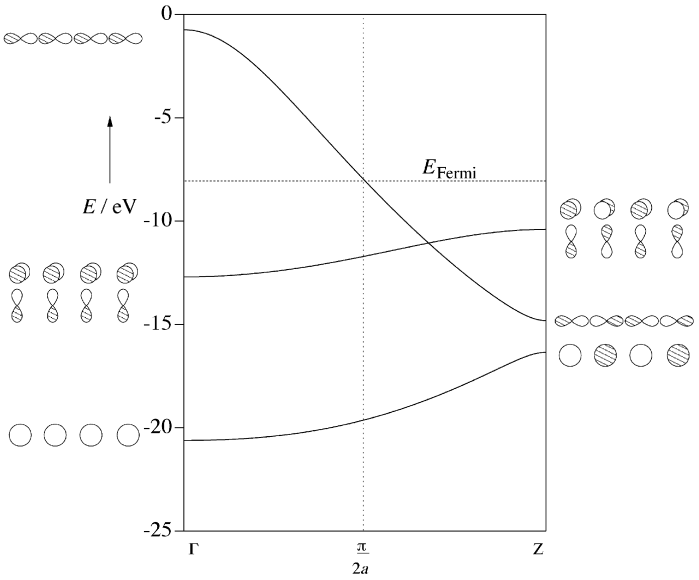


Figure 13. The band structure of a 1D Sb^{2-} chain with the Sb–Sb distance of 3.2 Å.

Note that the differential between σ and π bonding is very important in setting the favored electron count for hypervalent networks in this part of the Periodic Table. The entire width of the π band is below the center of gravity of the p_z σ band, and disparity in the $\sigma(p_z)$ versus $\pi(p_x, p_y)$ bonding exists. If this were otherwise, as in linear carbon chains, classical linear chains would be preferred at much lower electron counts. Instead of constructing the σ chain orbitals from the s lone pair and the p_z "hypervalent" band, as in Sb^{2-} linear chain, two carbon sp hybrids that develop into a band become a better starting point.[84] Taking also into account strong π bonding, linear carbon chains presumably have two double bonds per carbon atom and an electron count of four electrons per atom. It is reasonable to think that relatively strong π bonding ensures the linearity of these chains.

For the electron count of seven electrons per Sb atom, the linear chain is highly resistant to a kinking distortion. Molecular orbital considerations behind this were given in Section 4.2 for the three-atom oligomer Sb_3^{7-} (Scheme 10). In contrast, an electron count of six per atom strongly favors a kinking of the linear chain into a zig-zag chain, much in the same way as for molecular Sb_3^{5-}.

However, the Sb^{2-} linear chain, while possessing a reasonable electron count, is potentially susceptible to a pairing or Peierls distortion—a subject that we take up next. More detailed treatment of bonding patterns in infinite chains is given elsewhere.[85–87]

4.4. Peierls Distortion of a Linear 1D Sb^{2-} Chain

As we saw previously, Li_2Sb is a remarkable compound where both distorted (paired) and undistorted linear Sb

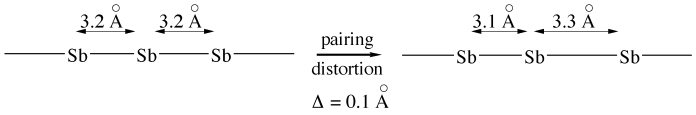
chains coexist in the same crystal structure (see Figure 6). The Sb–Sb distance in the undistorted chains is 3.26 Å and in the distorted (paired) chains the distance alternates between 2.97 and 3.56 Å.

When one sees a pairing one is naturally led to thinking of a Peierls distortion. A Peierls distortion is the extended system analogue of a Jahn–Teller distortion. For a given electron count there is a specific optimal coupling with a lattice vibration—a phonon mode—which reduces the symmetry of the lattice. In particular, a pairing distortion is indicated for a half-filled band.[17, 47, 88–91]

We already discussed the band structure of a linear Sb chain in the previous subsection. The band structure shown in Figure 13 is calculated for a unit cell containing only one Sb atom. It is not a convenient starting point for the Peierls distortion, because in the distorted chain the unit cell is doubled. Therefore, we start our analysis by doubling the unit cell of an ideal linear 1D Sb chain. In the absence of a deformation the physics and chemistry of bonding should not be changed by this hypothetical doubling process and we should obtain the same results as with the single unit cell.

What happens to the band structure in Figure 13 when the unit cell is doubled? There is an inverse relationship between the length of the direct and the reciprocal lattice vectors. By doubling the size of the direct lattice vectors, we halve the reciprocal unit cell. Since the total number of crystal orbitals must be conserved, there should be twice as many bands in the new Brillouin zone to compensate for the reduction of its size. The resulting band structure for the doubled unit cell is shown in Figure 14a. It can be thought of as a band structure for a normal cell (Figure 13) folded around vertical lines drawn at $+\pi/2a$ and $-\pi/2a$. A more detailed account of band structure folding can be found in ref. [17] and references therein by Burdett and Whangbo.

Next we examine a specific pairing distortion of an ideal chain ($\Delta = 0.1$ Å; for the definition of Δ see Scheme 12).



Scheme 12.

Because of the folding, all bands at Z are doubly degenerate. The pairing distortion removes that degeneracy, that is, the lower band of a pair becomes more stabilized and the upper band becomes destabilized. This may be seen for three pairs of bands in Figure 14b.

The susceptibility to the pairing distortion depends on the electron count in the chain. If the original unfolded band was fully occupied, then the stabilization of the lower branch of the folded band would not fully compensate the destabilization of the upper branch. If the original unfolded band was only half-occupied (as it is for Sb^{2-}) then the total energy is clearly lowered. Indeed, a pairing distortion of $\Delta = 0.1$ Å in magnitude occurring in an ideal Sb^{2-} chain (Sb–Sb distance of 3.2 Å) lowers the total energy by 0.16 eV per doubled unit cell in an extended Hückel (EH) calculation. The potential energy curve as a function of distortion parameter Δ is given in Figure 15 (what happens for a N^{2-} chain is discussed in the Section 4.5).

So far in our analysis we have neglected electrostatic and other forces present in real crystals. The simultaneous existence of Peierls-distorted and -undistorted linear chains in Li_2Sb indicates that other factors can overcome the driving force for the Peierls distortion. For this to happen, the potential energy surface for the pairing distortion should be shallow. Indeed, as Figure 15 shows, the energy lowering calculated for the pairing distortion in the Sb^{2-} chain is not large. A Δ value of 0.1 Å lowers the energy of the structure by only 0.16 eV.

The implications of the reasoning in the last paragraph are really important in the general context of the Periodic Table. Compounds that are susceptible to a Peierls distortion have partially filled bands, and that often makes them metallic. If the distortion occurs, then typically a band gap opens up at the Fermi level, and a metal to insulator transition occurs as well. If the potential energy surface for the Peierls distortion is shallow, the "chemical pressure" in solids[23] (this is one way one might think of Madelung and packing energies) may operate to keep the distortion from occurring. Then there will be a reasonable chance of finding late main group compounds with metallic properties. Indeed, the great majority of Sb phases containing linear chains and square sheets are metallic.

One often draws an a "diagonal" line in this region of the Periodic Table, separating nonmetallic and metallic main group elements. Could we explain the existence of the metal–nonmetal "diagonal" line by the shallowness/steepness of the potential energy surface for the Peierls distortion? In order to answer this

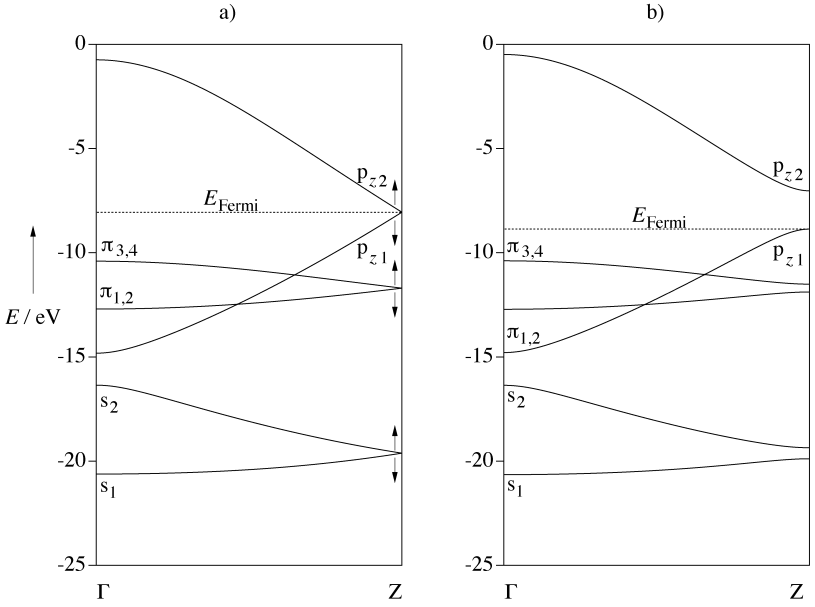


Figure 14. The band structure of a 1D Sb_2 chain with a) uniform Sb–Sb separations of 3.2 Å, b) alternating Sb–Sb distances of 3.1 and 3.3 Å.

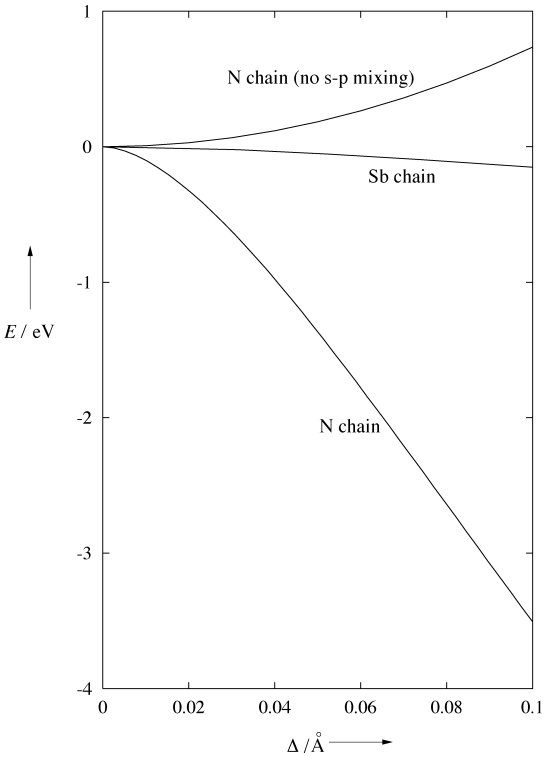


Figure 15. Total energy for Sb^{2-} and N^{2-} chains as a function of the distortion parameter Δ (for a definition of Δ see Scheme 12).

question, we consider next the Peierls distortion of a hypothetical (and nonexistent) linear N^{2-} chain.

4.5. Why a Linear 1D N^{2-} Chain Does Not Exist

The band structure of a linear 1D N^{2-} chain is shown in Figure 16a. We chose an N–N separation of 1.50 Å, a little greater than a single bond; there is no known structure to guide us here. Two assumptions that underlay our qualitative description of the band structure of an Sb chain are no longer valid. First, there are strong π interactions, reflected in the width (ca. 5 eV) of the π band in Figure 16a. Second, one notices immediately the unusually high position of the two "p_z" bands.

We remind ourselves of the bonding features of the p_z band, as we analyzed them for the Sb linear chain. In the picture appropriate for a single unit cell we found that the lower part of the p_z band is bonding (at Z), the middle is nearly nonbonding (at $k = \pi/2a$) and the upper part is antibonding (at Γ). Upon folding, these points come at Γ, Z, and Γ of the doubled unit cell (halved Brillouin zone), respectively (see Figures 14a and 16a). Examination of the N–N crystal orbital overlap population (COOP) curve (Figure 17a) indicates that at the aforementioned three points (indeed throughout the p_z band) the N–N interaction is *antibonding*. Something has changed from the simple picture that worked so well for Sb.

In deriving the band structure for a linear Sb chain we assumed that no s-p mixing occurs. Our calculations actually show that some mixing occurs even for Sb. But since its extent was not large we could safely ignore it. This is not so for the N case; the s-p mixing is in fact so large that an avoided crossing occurs between s and p_z bands. The "p_z" band has purely p_z character at Γ and purely s character at Z.[88] The s band contribution to the p_z band of nitrogen is 30% (averaged over the Brillouin zone), compared to 18% for the Sb case.

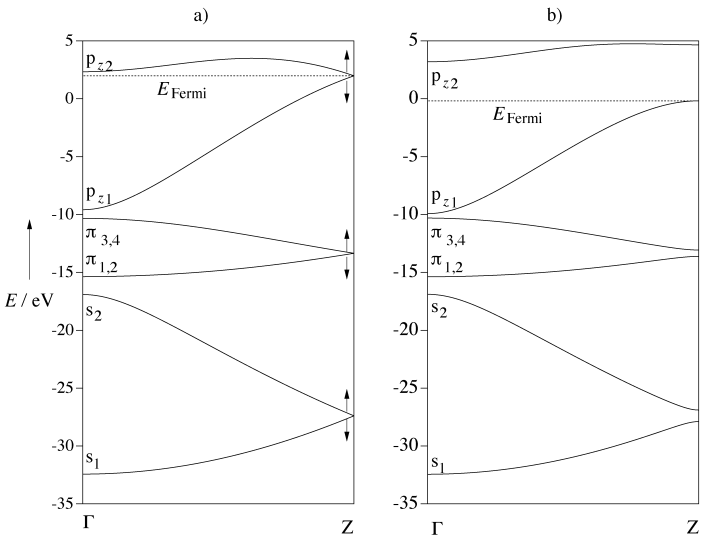


Figure 16. The band structure of a 1D N_2 chain with a) uniform N–N separations of 1.50 Å, b) alternating N–N distances of 1.45 and 1.55 Å.

As a result of the strong s-p mixing, the "p_z" band is greatly destabilized throughout the whole Brillouin zone and is strongly N–N antibonding. One would expect intuitively that a higher energy band would be more stabilized by a Peierls distortion than a lower energy band, given equal changes in the overlaps during the distortion. We provide elsewhere[92]

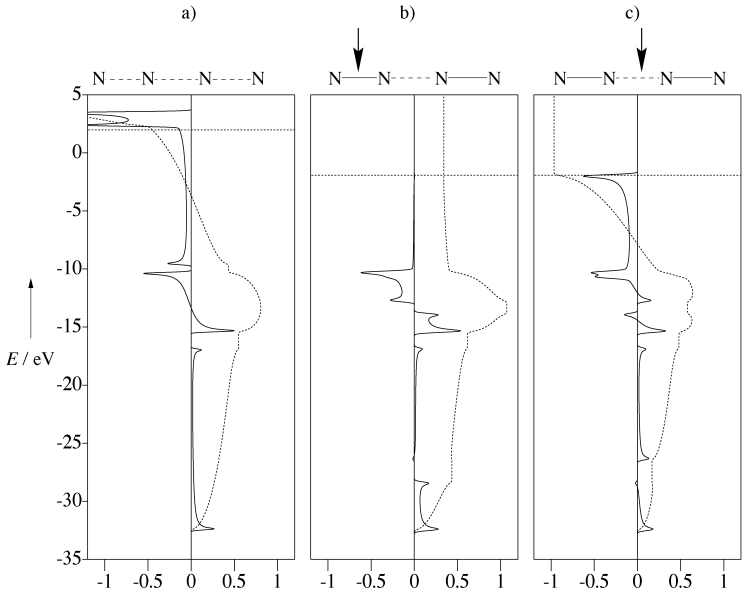
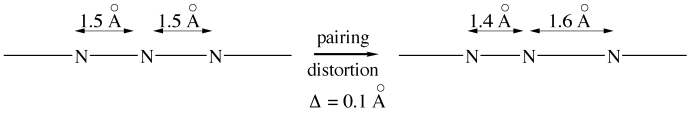


Figure 17. COOP curves (solid lines) and their integrations (dashed lines) between the nearest neighbor nitrogen atoms in an ideal chain (a) in a distorted chain with short (b) and long N–N distances (c); the magnitude Δ of the distortion is 0.1 Å.

the formal basis for this argument with the help of molecular perturbation theory.[93, 94] A word of caution is in order here. Although s-p mixing destabilizes the "p_z" band, and, therefore, creates favorable conditions for the Peierls distortion, the Peierls distortion itself is not driven by s-p mixing. Our calculations indicate that, on the contrary, the magnitude of the s-p mixing diminishes during the Peierls distortion process.

We calculated the effect of a pairing distortion of a relatively small magnitude ($\Delta = 0.10$ Å) of an ideal N chain (Scheme 13). The band structure for an undistorted chain is



Scheme 13.

shown in Figure 16a. The stabilization (3.47 eV per N_2 unit cell) is an order of magnitude higher than for the corresponding distortion in the Sb chain (0.18 eV per Sb_2 unit cell). This relatively small distortion is sufficient to make the lower (filled) "p_z" band (p_{z1} in Figures 16a and b) lose its strongly antibonding character. The p_{z1} band rehybridizes (namely, the extent of s-p mixing in it is changed) in such a way that the sp hybrid lobes grow pointing outward from the new N_2 pairs. This significantly reduces the intra-pair N–N negative overlap population (Figure 17b) more than compensating for the incr;ease in the inter-pair N–N overlap population (Figure 17c). The effects are very clear in the integrated COOP curves.

To clarify further the important role of s-p mixing for the N-chain distortion we carried out a numerical experiment, in which the overlaps between the s and p orbitals of N were simply set to zero (that is, there is no s-p mixing). As may be inferred from Figure 15, this has an overwhelming effect on the stability of an ideal N chain—the pairing distortion becomes strongly disfavored! We trace this unexpected result to the significant stabilization of the p_z band in the ideal N chain. The midpoint of the p_z band (or point Z in Figure 16a) drops below the corresponding point of the π bands, thus making the latter the highest occupied band at Z. Since both bonding and anti-
bonding branches of the π bands near Z are filled (see Figure 16a), the pairing distortion raises the total energy. Clearly, s-p mixing plays an exceptionally important role in the tendency of a linear N chain to undergo a Peierls distortion.

4.6. The Rationale for Variable s-p Mixing

It is apparent that pairing is much more favorable for an N^{2-} chain than for a Sb^{2-} chain (see Figure 15). Actually, neither N^{2-} chains nor N_2^{4-} pairs have yet been found in extended structures, only isolated nitride (N^{3-}) and molecular azide (N_3^-) units. Nevertheless, the theoretically derived trend makes sense; the tendency to pair or, more generally, undergo a Peierls distortion is much more pronounced at the top of any group in the Periodic Table. This observation is important, and is essentially tied to the periodic tendency to undergo a metal–insulator transition. We trace the effect to a substantially greater s-p mixing in the lighter elements in the group.

The last question to be answered in this subsection is more fundamental: *Why* is s-p mixing greater for the lighter elements? From the point of view of first-order molecular perturbation theory two factors influence the strength of an interaction, which is generally proportional to $S_{ij}^2/\Delta E_{ij}$ (S_{ij} is the overlap and ΔE_{ij} is the energy difference between two orbitals i and j).[93, 94] The energy difference between the s and p orbitals of the heavier elements is smaller then for the lighter elements.[95] Therefore, the energy argument would actually suggest greater s-p mixing for the heavier elements. However, the overlap term completely reverses this tendency. As a result of the electron–electron interactions, the poorly screened s orbitals become more contracted[95] down a group in the Periodic Table (Table 3). This contraction of s orbitals is further enhanced by relativistic effects for the heavier elements, which have been discussed by several authors.[96, 14, 80]

Table 3. Average radii and one-electron orbital energies for elements of Group 5 from Hartree–Fock calculations.[95]

	N	P	As	Sb	Bi
$\langle r_s \rangle$ [Å]	0.70	0.91	1.07	1.26	1.34
$\langle r_p \rangle$ [Å]	0.75	1.09	1.33	1.53	1.64
E_s [eV]	– 25.72	– 18.96	– 18.64	– 15.84	– 15.00
E_p [eV]	– 15.44	– 10.66	– 10.06	– 9.10	– 8.71

Consequently, as one goes down a group the s-s and s-p overlaps are much reduced and the s orbitals in general play a lesser role in chemical bonding. As a reviewer pointed out, there are other ways to analyze this problem, such as in terms of polarizability or effective charge. The reader is referred to the important paper of Kutzelnigg for a deeper discussion.[97]

In summary, strong s-p mixing for a N^{2-} chain destabilizes greatly the filled "p_z" band, making a Peierls distortion inevitable. On the other hand, the tendency of an Sb^{2-} chain to undergo a pairing distortion is much less pronounced, which allows the existence of metallic phases that do not do not undergo a Peierls distortion. Gradual dimunition of s-p mixing from N to Bi leads to the enhancement of their potential metallic properties. We think this is a useful, if not complete, way to think about the "diagonal line" separating metals from nonmetals in the right part of the Periodic Table. To deal reliably and quantitavely with the question of the metal/nonmetal transition the effect of electron–electron interactions on the Peierls distortion has to be examined.

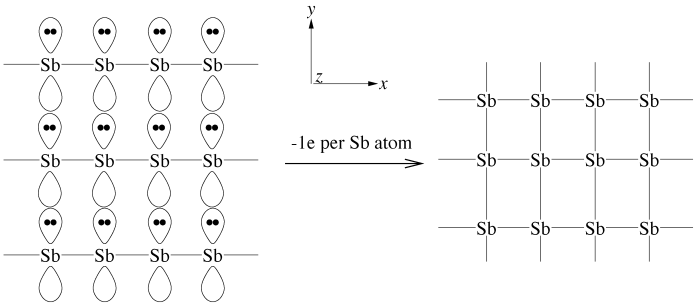
In the last two sections we have described only Peierls distortion of one-dimensional N and Sb chains. For higher dimensional sublattices incomplete Fermi nesting might occur, as has been recently shown by D.-K. Seo and R. Hoffmann for Group 5 elemental structures.[98]

Having described bonding in a linear 1D Sb chain, we are now ready to generalize our ideas to higher dimensions.

5. Theory: Hypervalent Bonding in Two Dimensions

5.1. Electron Counting in a Square Lattice

There are several ways that we might assemble a square lattice. One can think of a square lattice as a 2D collection of individual atoms and simply derive its crystal orbitals. An alternative view is to think of a square lattice as an array of 1D chains (Scheme 14). Since we discussed the band structure of an 1D chain in detail above, let's first use the latter approach.



Scheme 14.

We assemble a square Sb sheet in the *xy* plane, positioning component 1D linear chains along the x direction (Figure 18a). There are three lone pairs per Sb atom in a linear Sb chain, localized now in the s, p_y, and p_z orbitals. If isolated Sb^{2-} chains are brought up to each other in the *xy* plane (see Scheme 14), repulsion would clearly develop between the p_y lone pairs of the chains.

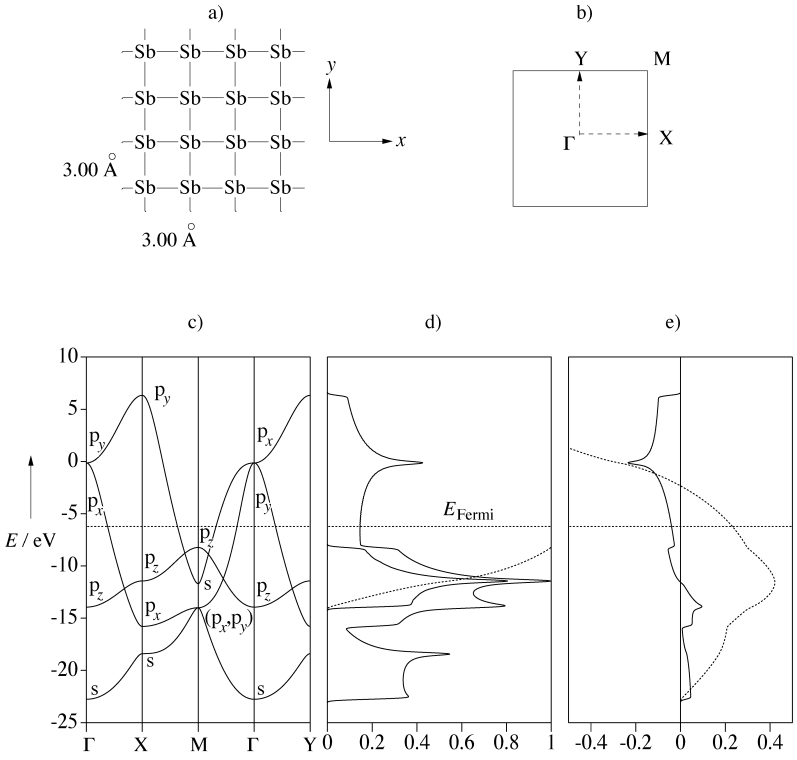


Figure 18. a) Square sheet of Sb, b) Brillouin zone, c) band structure of the square Sb^- sheet, d) p_z contribution to the total DOS, e) nearest neighbor Sb–Sb COOP (solid line) and its integration curve (dashed line).

How can we make the interactions of 1D chains in Scheme 14 attractive? Faced with the same question about two approaching CH_3^- fragments an organic chemist would propose a clear solution: to remove one electron from each CH_3^- lone pair, which in turn would lead to the formation of the stable C–C bond in ethane. We may do the same with the linear Sb chains: remove one electron from each p_y lone pair. Bonding interactions then develop in the *y* direction, much as they exist in the *x* direction (in a perfect square lattice the *x* and *y* directions are equivalent). Since we started with seven electrons per atom in the linear chain, the optimal electron count for the square lattice should be six electrons per atom.

Now we discuss the same idea from the point of view of band structure theory. A square Sb lattice has a square reciprocal unit cell as depicted in Figure 18b. The special points in the first Brillouin zone are Γ, X, Y, and M. The band structure and crystal orbitals for a generic square lattice have been discussed many times in the literature.[17, 19] We have recently described in detail the crystal orbitals for an Sb square lattice.[99] Here we discuss very briefly the band structure of a square Sb^- sheet.

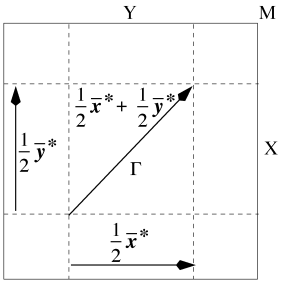
In our discussion of a 1D Sb^{2-} chain in Section 4.2 we found it possible to neglect the influence of π bonding in the system. For a square lattice this assumption is still valid—the p_z band (perpendicular to the sheet) in Figure 18c is relatively narrow and completely filled (Figure 18d). In-plane π interactions of p_x and p_y bands are also small compared to σ interactions. For example, the dispersion of the σ-interacting p_x band along the Γ – X symmetry line is much wider than that of the π-interacting p_y band along the same symmetry line. Our other assumption was the relative unimportance of s-p mixing for heavy elements. For a square lattice, s-p mixing is strongest at M (Figure 18c), where an avoided crossing occurs between the s band and doubly degenerate p_x and p_y bands. Still, s-p mixing for a square Sb lattice is much less than what is found for a square N lattice. Our two major qualitative assumptions continue to hold for a square Sb lattice.

The nearest-neighbor Sb–Sb COOP curves (Figure 18e) shed further light on the bonding in the square sheet. The overlap population generated by the antibonding part of the π band cancels out its bonding part. The COOP near the Fermi level is weakly antibonding, although our qualitative picture implies that it should be nonbonding. The reason for this discrepancy was already discussed for an 1D chain—some s-p mixing does occur. The same part of the band structure for an N^{2-} chain was *strongly* antibonding (see Figure 17a).

As for the 1D chain, we need to make a connection between a square lattice and various classical geometries for the same electron count (six electrons per Sb atom). One way to do this is to examine possible pathways for a Peierls distortion of a square sheet, a subject that we take up in the next section.

5.2. Peierls Distortion of a Square Sb^- Lattice—Classical and Semiclassical Geometries

For a 1D Sb^{2-} chain, the Peierls distortion viewpoint led unambiguously (if weakly) to the formation of classical Sb_2^{4-} pairs. The possibilities for Peierls distortion of a square net are much richer. One systematic way to study them is to use the Fermi surface nesting approach.[20–22, 89–91] In this method the reciprocal lattice vector that maximally nests the Fermi surface is likely to lead to charge density waves (CDW) with the same wavevector. These most often manifest themselves in static distortions of the lattice. Since the Fermi surface topology depends clearly on the number of electrons, the nesting vector is dependent on the electron count. An elegant experimental and theoretical study of this dependency for mixed Sb and Te square lattice has been carried out by Lee and co-workers,[20] and the groups of Whangbo and Canadell have shown the utility of the Fermi surface nesting formalism.[89–91] Our group has used a different approach to study possible distortions of a square lattice.[19] Here we outline qualitatively the main results of these studies and introduce a new hypothetical distortion to ladder chains.



Scheme 15.

For a qualitative discussion we are again going to ignore π interactions and s-p mixing. The Fermi surface of an Sb^- square array is then particularly simple (Scheme 15). We can think of this Fermi surface as a superposition of two one dimensional Fermi surfaces for the p_x and p_y bands. As one may see from Scheme 15, there are several reciprocal vectors that nest the Fermi surface. First consider the nesting by the $\frac{1}{2}\bar{x}^*$ vector. This leads to a pairing distortion in the x direction in real space and has no effect on the y direction. The structural consequence is that 1D ladder chains emerge (Figure 19a). Since a Peierls distortion does not alter the electron count, an electron count for these ladders is also six electrons per atom (the same as for a square lattice). Following a different line of reasoning, we proposed an electron count of six electrons per atom for a ladder structure when discussing the $FeSb_2$ crystal structure. It is encouraging that our model of bonding in extended linear networks is internally consistent.

The 1D ladders that we have obtained are classically bonded in the x direction but are still hypervalent in the y direction. If the ladders become isolated from each other, then a new Peierls distortion may occur in the direction of the chain propagation (nesting vector $\frac{1}{2}\bar{y}^*$ in Scheme 15) leading to isolated Sb_4^{4-} squares (Figure 19b). The electron count for noninteracting squares corresponds to completion of an octet around each Sb, namely, a classical structure. One can also obtain isolated squares from a square sheet by a single Peierls distortion with the nested vector $\frac{1}{2}\bar{x}^* + \frac{1}{2}\bar{y}^*$ (see Scheme 15). It turns out that this unique vector in the reciprocal space does not uniquely determine the arrangement of atoms in the real space; it only tells us that there occurs unit cell doubling in both the x and y directions. However, the movement of individual atoms within the quadrupled unit cell remains uncertain.

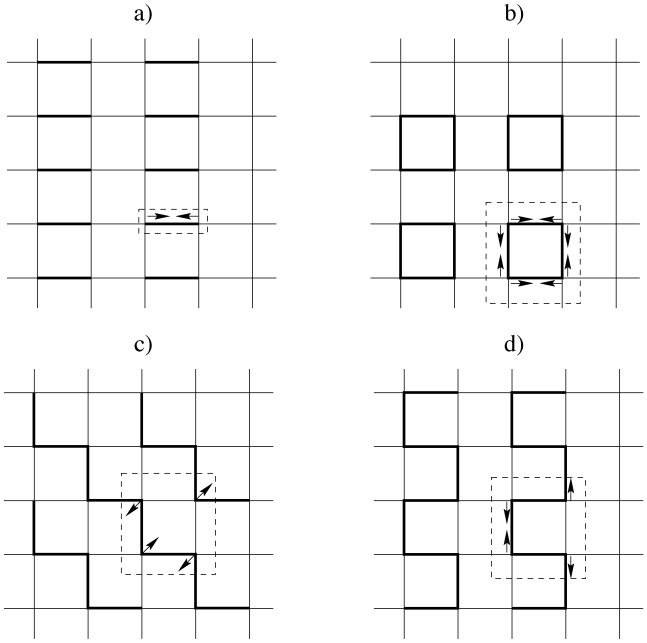


Figure 19. a) Pairing distortion in the x direction ($\frac{1}{2}\bar{x}^*$) leading to laddertype substructures; b) pairing distortions in both the x and y directions ($\frac{1}{2}\bar{x}^* + \frac{1}{2}\bar{y}^*$) resulting in squares; c) zig-zag chain formation ($\frac{1}{2}\bar{x}^* + \frac{1}{2}\bar{y}^*$); d) another distortion corresponding to $\frac{1}{2}\bar{x}^* + \frac{1}{2}\bar{y}^*$; unit cells are given in dashed lines.

In addition to isolated squares, 1D kinked chains may be formed as a result of a Peierls distortion. Two such possibilities are shown in Figures 19c and d. In the case of a zig-zag chain formation (Figure 19c) it is possible to choose an alternative unit cell with only two atoms per unit cell. In order to describe the Peierls distortion in the latter case, a non-orthogonal primitive unit cell in direct space must be used, which in turn complicates the picture in reciprocal space. A detailed treatment of orbital interactions that leads to chains of different topology is given by Tremel and Hoffmann.[19]

It is worthwhile here to introduce a general cautionary note. Sometimes words like hypervalent bonding might be taken to imply a greater stability. This may be so, but it also may well not be so. Consider for instance the salutary and classical example of I_3^-. In the gas phase the molecule is symmetrical. But in the solid state, depending on the countercation, a multitude of geometries is known, which spans pretty much the range between noninteracting $I^- + I_2$ and symmetrical I_3^-. When we get more structures, with linear chains and square nets, we expect to see a range of structures and distances "around" these symmetrical archetypes.

6. Theory: Other Topologies

6.1. Electron Counting in a Simple Cubic Lattice

In Section 5.1 we demonstrated in detail the transition from a one-dimensional chain to a square lattice. The development

of the simple cubic Sb band structure proceeds in an analogous way. The only remaining lone-pair p_z orbitals for the square Sb^- lattice (see coordinate system in scheme 14) interact repulsively when square sheets are brought together to form a cubic lattice. Therefore, as we argued before, one electron should be removed from each p_z lone pair, so bonding interactions can develop in the z direction. If a square sheet had initially six electrons per Sb, this line of reasoning leads to five electrons per Sb in a stable cubic network.

There are not that many compounds which contain formally neutral Sb atoms (five electrons per Sb atom). One of the best known examples, elemental Sb, can be made cubic under high pressure[45] (a similar high-pressure phase is known for Bi[100]). A metastable cubic phase can also be synthesized by quenching from liquid and vapor.[46] Under ambient conditions elemental Sb takes on an As-type structure—three-connected sheets stacked on top of each other in such a way (see Figure 5) that a compression along the stacked direction would result in the formation of a cubic lattice. Turning the reasoning around, one can think of an elemental Sb sheetlike structure as derived from a simple cubic lattice through a Peierls distortion (Figure 20) corresponding to reciprocal nesting vector $\frac{1}{2}\,\bar{x}^* + \frac{1}{2}\,\bar{y}^* + \frac{1}{2}\,\bar{z}^*$.[47] Notice the similarity between Figures 19c and 20.

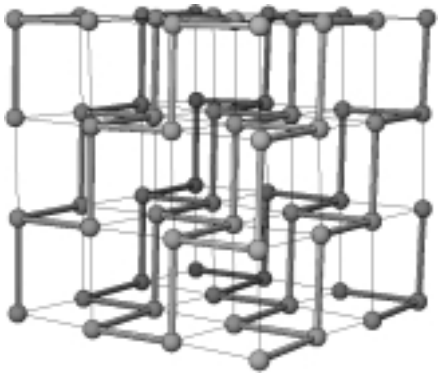


Figure 20. Peierls distortion pathway from a cubic lattice to an As-type three-connected sheet structure (thick lines).

This is hardly the only deformation available to the system.[47] One can come up with many other Peierls distortions of a simple cubic lattice, ones which would lead to classical (for example, kinked sheets) and semiclassical (for example, doubled square sheets) networks.

An interesting problem is posed for us by Po, which has six electrons per atom. This is the archetype, indeed the only element to assume a simple cubic structure under ambient conditions. What might be the source of the seeming contradiction with our argument for an electron count of five electrons per atom in a cubic lattice? The sixth electron of Po adds one third of an electron to each p_x, p_y, and p_z bands, and this might not be enough to destroy Po–Po bonding. Another reason might be the existence of strong relativistic effects that we did not explicitly consider in our derivations. Strong spin–orbit coupling makes $p_{1/2}$ atomic orbitals significantly contracted compared to $p_{3/2}$ orbitals, which in turn changes the bonding patterns in the crystal.[80] The electron counting scheme that we have discussed so far may need to be modified for elements which have pronounced relativistic spin–orbit coupling.

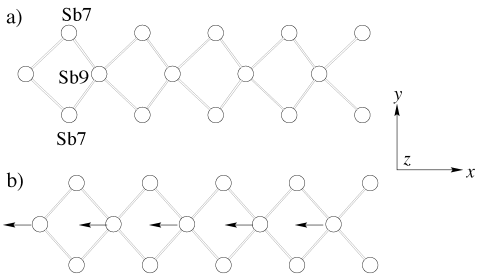
von Schnering has brought to our attention the fact that many binary compounds with an average valence electron count of five undergo high-temperature or pressure transitions to "more symmetrical" structures with cubic coordination. The evolution of structural types is GeS → TlI → NaCl → CsCl.[101–104]

We have considered so far a linear 1D chain, a square lattice, and a simple cubic lattice. The last topology that we examine is a 1D Sb_3 strip, which we can imagine as being cut out from a square lattice.

6.2. Extended Networks Built from Finite Hypervalent Linear Chains

There are a number of structures where an aufbau based on finite hypervalent linear chains can lead to greater insight into their electronic structure. For instance, when two linear three-membered linear chains, which were discussed earlier, share a central atom, then a square-planar coordination of the central atom results. Square-planar units can be further condensed into a 1D ribbon of vertex-sharing squares. The importance of this construction is based on the persistent nature of the three-center four-electrons bonds underlying the extended network, even though these localized three-center orbitals broaden into bands by interaction with each other and other orbitals. Consequently, electron counting rules for such extended structures may be derived in a few easy steps starting with known electron counts for finite linear chains. This point is illustrated by the following examples.

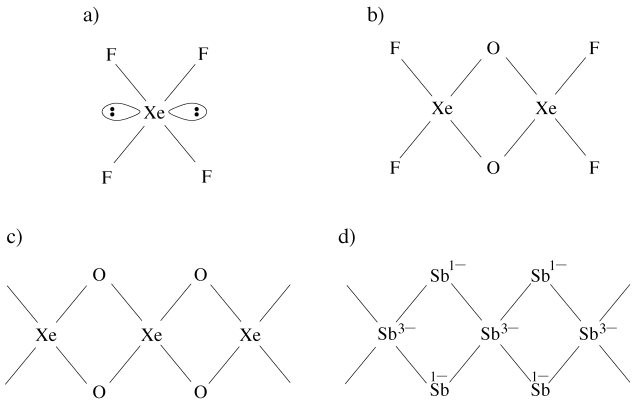
One dimensional Sb strips of various width are found in several binary and ternary Sb phases.[71, 105, 106] For example, 1D Sb strips of slightly distorted vertex-sharing rhombi comprise an isolated part of the Sb subnetwork in $La_{12}Mn_2Sb_{30}$.[71] One can imagine these strips (Scheme 16a)



Scheme 16.

as derived from more-symmetrical undistorted strips (Scheme 16b) through a simple sliding distortion of central atoms.

What is the optimal electron count for a strip of vertex-sharing squares? The central Sb atoms in the strips (Scheme 16b) are located in a square-planar environment, which is unusual for classical compounds of main-group elements. Therefore, as a starting molecular model we choose square-planar hypervalent XeF_4 (Scheme 17a, the lines here



Scheme 17.

are not classical electron pair bonds, just connectivities). In this molecule the Xe atom is hypervalent while F atoms are classical (an octet can be completed around each F atom). If one wants to build a dimer out of XeF_4, one has to replace bridging F atoms by O atoms in order to preserve their classical electron count (Scheme 17b). In a similar manner, if one continues to build a trimer, a tetramer, oligomer, polymer, all the bridging F atoms have to be replaced by oxygen atoms. Therefore, a hypothetical XeO_2 polymer (Scheme 17c) has classical O atoms and hypervalent Xe atoms (12 electrons per Xe atom). The electron count in extended XeO_2 is $8+2\times6=20$ electrons per unit cell. A neutral Sb_3 strip contains only 15 electrons per unit cell, which necessitates an addition of a -5 charge to the unit cell.

An important point must be made about "real" and formal charges, and the way the latter are used in this work. To define theoretically a charge on an atom or a fragment one must choose a wavefunction (namely, the degree of approximation in computing one), and a way of analyzing that wavefunction (Mulliken population analysis, Bader partitioning, etc.).

In our work we use formal charges. As in organometallic chemistry, these are not unambiguous (should C_5H_5 carry a -1 or 0 charge? Should a halide be counted as anionic or neutral?). What is unambiguous is the total electron count, no matter whether one starts from an initial ionic or neutral (covalent) assignment. Thus Xe has ten electrons around it in XeF_2, whether one begins with Xe^{2+} and $2F^-$, or with Xe^0 and $2F^0$.

There is still another way of assigning charges, which has a history in the three-center bonding field, and this is partway between a starting point based on an ionic (or covalent) formal charge and one based on a "real" electron distribution. A Hückel analysis of the distribution of the four electrons in the three-center system puts 1.5 electrons on the terminal and 1.0 on the central atom. Such an assignment would lead to Xe^+ and two $F^{1/2-}$ centers in XeF_2.

In the spirit of Zintl–Klemm formalism, throughout this paper we will use only formal charges and a "covalent" formalism. We do this with full awareness of, and respect for, the other variants prevalent in the literature. To be specific, we will look at XeF_2 as formally being derived from a Xe atom and two F atoms. We will also look at the "isoelectronic" Sb_3^{7-} linear molecule as being made up from formal Sb^{2-} end ions and a central Sb^{3-} ion.

Returning to the Sb_3^{5-} strip (Scheme 17d), its electronic structure is directly related to molecular XeF_4. These considerations are supported by detailed band calculations. As we mentioned above, a sliding distortion is observed in these structures. This deformation can be analyzed as a solid-state analogue of a second-order Jahn–Teller distortion. The details are given in our ref. [99].

The Sb_3 strip is the most narrow one that can be cut out from a square lattice. Wider Sb strips are found in the binary Zr–Sb phases.[105–107] The square two-dimensional Te defect lattice in the binary Cs_3Te_{22} phase can also be thought of as being comprised from finite (five-membered) linear chains.[108, 109] Electron counting rules for these ribbons and sheets will be published elsewhere.[110]

7. Navigating between Classical and Hypervalent Structures: Oxidation versus Peierls Distortion

It is time to face a fundamental question: that of the interrelationship of dimensionality and deformation. The electron counting regularities we derived *did not* emerge from a principle of maximized bonding. Instead they assumed a certain electron count, and traced the bonding and geometrical consequences. For instance, a linear geometry is much favored over the kinked classical geometry for a linear Sb chain with seven electrons per atom (Sb^{2-}). For this electron count, the only classical alternative to the linear hypervalent chain consists of isolated Sb_2^{4-} pairs—the result of the Peierls distortion of the linear chain (Figure 21).

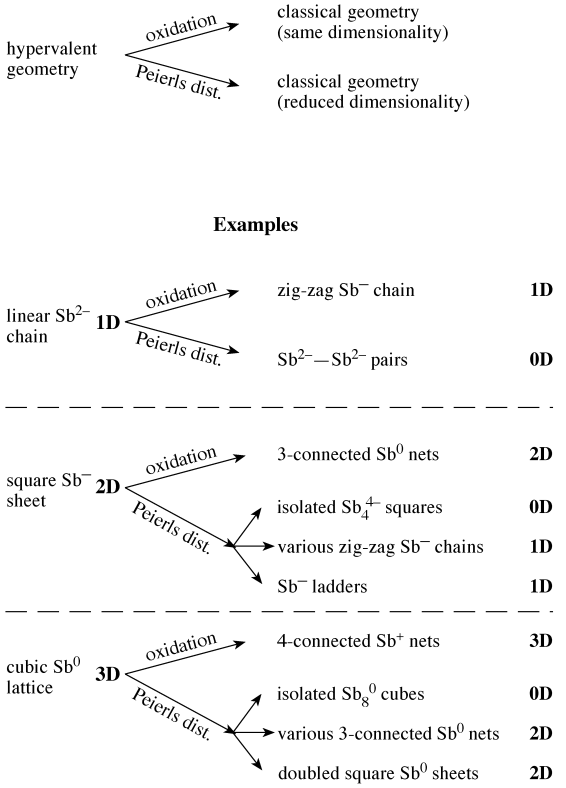


Figure 21. A schematic diagram showing relationships between electron counting, the Peierls distortion, and the dimensionality.

However, if we imagine the anion chain in an ionic atmosphere of cations whose number can vary, the possibility of a change in electron count of the main group sublattice opens up. When Sb^{2-} is oxidized to Sb^{-}, the classical kinked (zig-zag or helical) chain is much preferred over the linear chain.

In general, we have an important principle: if one wants to transform a hypervalent structure into a classical one with the same lattice dimensionality, one has to oxidize the hypervalent structure. The Peierls distortion, which conserves the electron count, transforms the hypervalent structures into classical or semiclassical ones with the lattice dimensionality reduced. Figure 21 summarizes and exemplifies this principle.

We examined briefly in Section 5.2 the Peierls-distortion pathways of a square Sb^{-} lattice (see Figure 19). The resulting classical isolated squares, zig-zag chains, and semiclassical ladders retain the original electron count of six electrons per atom (Figure 21), while their dimensionality is reduced from two to one or zero. Oxidation of the square Sb^{-} sheet can lead to a three-connected classical "As-type" Sb^{0} net with the same dimensionality (2D). A possible mechanism for this transformation might include an intermediate hexagonal net, which then puckers (Figure 22). The transformation of a square lattice into a hexagonal net has been described by Burdett and Lee.[47] We believe that for the electron count of five electrons per atom the As-type net is much more stable than the square net. Nevertheless, kinetic barriers might prevent this transformation, hence creating a metastable square net.

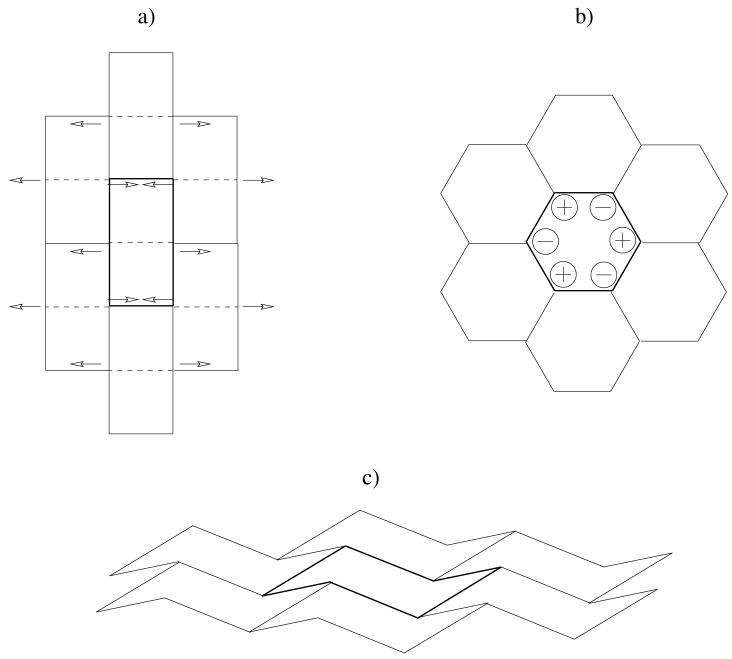


Figure 22. A hypothetical pathway connecting a square lattice into an As-type net. a) Arrows indicate schematically the atom motions and show how a square lattice might transform into a hexagonal network; b) plus and minus indicate the out-of-plane motion of atoms of the As-type net (c).

Oxidation of the cubic Sb^{0} lattice might result in a four-connected Sb^{+} net, with the preservation of the original dimensionality. A hypothetical two-step pathway for the transformation of a simple cubic lattice to a diamond structure is given in Figure 23. It begins by orienting the cubic lattice along (111) and looking at it as a repetition of three double layers (A, A′), (B, B′), and (C, C′; see Figure 23a). In the first step of the transformation, the double layers flatten, creating tetrahedral angles within the sheets and separate from each other (Figure 23b). Next, the double layers are envisioned as sliding on top of each other, adjusting their vertical coordinates so as to create the diamond lattice (Figure 23c). Since extensive bond breaking and bond formation occur during this transformation (six-connected network changes into four-connected one), kinetic barriers may preclude the formation of the diamond lattice.

The Peierls distortion of a cubic lattice reduces its dimensionality from three to two, one, or zero. One may use the schematic (and incomplete) diagram of Figure 21 as an approximate guide for navigating between the hypervalent and classical networks.

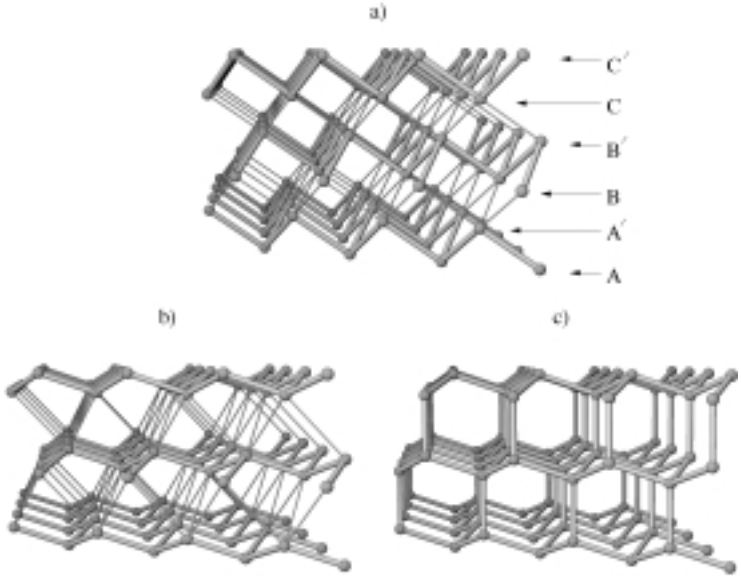


Figure 23. A hypothetical pathway transforming a simple cubic lattice into a diamond lattice. a) The simple cubic lattice represented as a repeated pattern of six layers: A, A′, B, B′, C, C′; b) As-type 3-connected sheets are created with tetrahedral angles; c) diamond lattice.

8. Theory: Summary of the Preceding Sections

In the discussion above we derived optimal electron counting for different hypervalent geometries. We demonstrated that a linear Sb chain is relatively stable with seven electrons per atom, a square Sb sheet with six electrons per atom, and a simple cubic Sb network with five electrons per atom. The Peierls distortion of a square sheet may lead to semiclassical ladders with the same electron count of six electrons per atom. The analogous distortion of a cubic lattice might lead to doubled square sheets, with an electron count of five electrons per atom. By carefully examining the Peierls distortion pathways of a cubic lattice or a square sheet, one

may derive electron counting schemes for many of the resulting classical and semiclassical lattices.

Another topology we considered is that of Sb_3 strips cut from a square lattice. By making a connection to molecular hypervalent XeF_4 we were able to derive an electron count of 20 electrons per unit cell (Sb_3^{5-}). This sublattice (and other strips) are subject to a potential second-order Jahn–Teller distortion, which leads to more stable, classical isolated Sb_3^{5-} units.[99]

At the end we showed the connection between electron counting, the Peierls distortion, and the dimensionality. The electron counting scheme that we have suggested for electron-rich networks is only an approximation, a rough guide to the beautifully complicated reality of antimonide framework bonding. One reason for the complexity is the often metallic character of these networks—fractional filling of the bands is common. The number of electrons that we derived for each network indicates only the most likely number of electrons that can be expected for that particular network. Our derivations apply to the heavier late main group elements, where π bonding and s-p mixing are not important. For the lighter elements where s-p mixing is important, the Peierls distorted classical structures are much more favorable, which is why linear metallic 1D N^{2-} chains do not exist.

The electron counting considerations that we propose can be used as a kind of aufbau, the foundation, for more elaborate analysis. In the following section we demonstrate how Sb–Sb bonding in the fairly complicated alloy $La_{12}Mn_2Sb_{30}$[71] can be understood with the help of these simple electron counting schemes. The applicability of the proposed electron counting principles to other main group elements will be examined next.

9. Building Complex Networks from Low-Dimensional Sb Sheets and Strips

In many cases a given complex structure can be theoretically broken down into simpler pieces, studied as such, and reassembled back. In this "retrotheoretical analysis"[99] the Zintl–Klemm electron counting scheme is indispensable. The electron counting schemes developed in this review make the nonclassical and semiclassical electron-rich multicenter networks new building blocks for such a "retrotheoretical analysis". We exemplify this process in this section, where we analyze qualitatively the Sb–Sb bonding in the $La_{12}Mn_2Sb_{30}$ alloy. For a more complete discussion of the bonding in this structure we refer readers to the original paper.[99]

$La_{12}Mn_2Sb_{30}$ (Figure 24) is a member of a series of new ternary compounds ($RE_{12}M_2Sb_{30}$) reported recently by Rogl, Cordier, and co-workers.[71] Magnetic measurements indicate[71] that rare earth metals are tripositive in all compounds, and the Mn ions are dipositive in $Ce_{12}Mn_2Sb_{30}$. If one assumes that Mn is dipositive also in $La_{12}Mn_2Sb_{30}$, then the number of electrons formally transferred to the Sb network is unambiguously calculated as $12 \times 3 + 2 \times 2 = 40$.

The Sb sublattice of $La_{12}Mn_2Sb_{30}$ crystal structure consists of no less than three noninteracting sublattices—a 3D Sb_{20} network (Figure 25b), 1D Sb_3 strips (see Scheme 16a), and

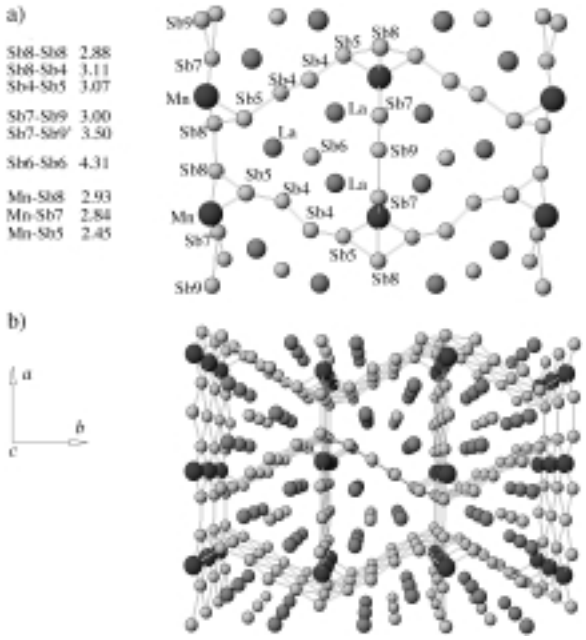


Figure 24. a) Unit cell of $La_{12}Mn_2Sb_{30}$; b) perspective view of the crystal structure of $La_{12}Mn_2Sb_{30}$; Sb = small spheres; La = medium size spheres; Mn = large dark spheres (half-occupied).

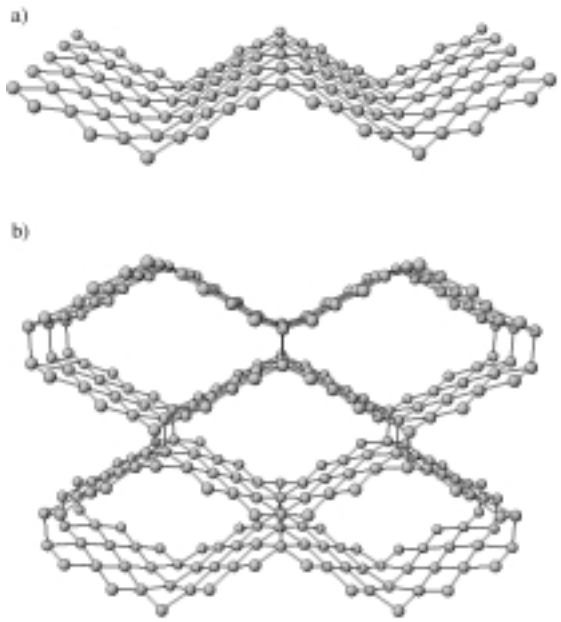


Figure 25. a) A 2D kinked sheet of Sb atoms; b) 3D Sb_{20} substructure.

isolated Sb atoms. By taking into account the crystal site multiplicities, the Sb_{30} substructure can be written as $Sb_{20}^{3D\,net}Sb_6^{1D\,strip}Sb_4^{atom}$. By taking the retrotheoretical approach one step further, we break down the three-dimensional Sb_{20} network into 2D kinked sheets (Figure 25a). The latter sheets can be hypothetically flattened into a square lattice. The stages of this retrotheoretical analysis are indicated in Figure 26.

The simple building blocks that we have to analyze are 1) isolated Sb atoms, 2) 1D Sb_3 strips, and 3) square Sb sheets. According to the Zintl–Klemm concept we assign a -3 charge to isolated Sb atoms, which then contribute a -12

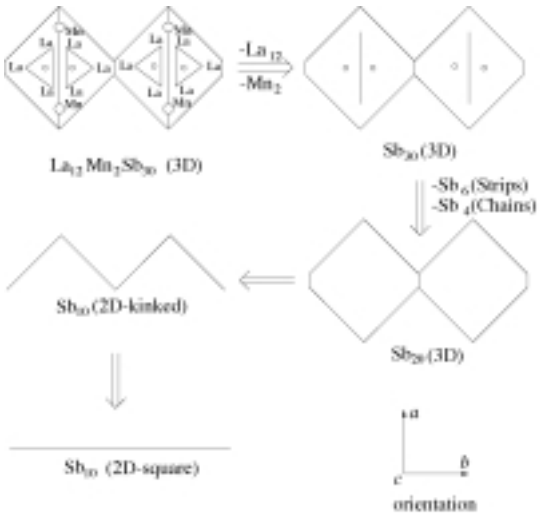
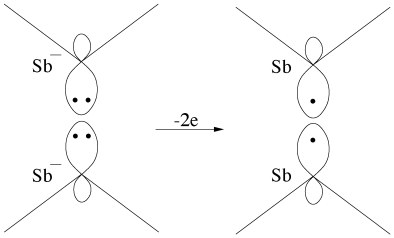


Figure 26. Schematic representation of "retrotheoretical" disassembly of $La_{12}Mn_2Sb_{30}$. A side view parallel to the *c* axis is shown.

charge to the full Sb_{30} network. The 1D Sb_3 strip (Scheme 16) should carry a -5 charge, following our earlier analysis. Since there are two such units in the unit cell of $La_{12}Mn_2Sb_{30}$, they contribute a -10 charge.

We begin by assigning a -1 charge to each Sb atom in a square lattice. The sheet depicted in Figure 25a can be derived from a square Sb sheet by kinking at every fifth diagonal line. A detailed analysis shows that this kinking leads to s-p hybridization and localization of the π orbitals at the kinks, but otherwise does not significantly influence the electronic structure of the square sheet.[99] The electron count remains at six electrons per Sb atom for the kinked sheet. The stacking of the kinked sheets into a three-dimensional network (Figure 25b) would lead to repulsion between neighboring sheets as a consequence of the interaction of lone pairs (Scheme 18). To make the interaction between two neighboring sheets bonding, one electron has to be removed from each Sb atom participating in intersheet linkage (a fifth of the total number of Sb atoms). This translates into the removal of $⅕ \times 20 = 4$ electrons from the Sb_{20}^{20-} unit cell, making it Sb_{20}^{16-}.

The contributions of the isolated Sb atoms, 1D Sb strips, and 3D Sb subnetwork to the total Sb charge are then -12, -10, and -16, respectively. The overall -38 charge on the Sb_{30} substructure falls two electrons short of the -40 charge donated by the La and Mn ions. The disposition of the last two electrons (from a total of 200 electrons in the unit cell) is a matter of some interest, and is no doubt related to the conducting properties of the material. The bonding around the Mn center and the fate of the two electrons are discussed in our original paper.[99]



Scheme 18.

10. Hypervalent Linear Chains and their Derivatives Made of Other Heavy Main Group Elements

The hypervalent bonding patterns in Sb compounds conform surprisingly well to our electron counting scheme. In this section we look at hypervalent linear chains of some other heavy main group elements, mainly Te, Se, and Sn. A selective compilation of binary and ternary phases containing linear chains or their derivatives is given in Table 4.

First, we discuss the linear chains in the compounds where the assignment of the formal oxidation states to cations is more or less straightforward, then we take up more complicated cases. We demonstrate in this section that the electron count of seven electrons per atom in the linear chain serves as a good starting point for the most of these compounds, and that the deviations from this electron count are observed in a rather narrow range. In the process we make sense, we believe, of some pretty incredible structures.

10.1. Simpler Binary Phases

Simple linear Te chains are found in the CuTe crystal structure.[111, 112] The Te–Te bond length between uniformly

Table 4. Heavy main group compounds containing linear chains.

Compound	Related Structures	Geometrical patterns
K_5Se_3, Cs_5Te_3[114]		dumbbells aligned into a linear chain
CuTe[111, 112]		linear chains
TlTe[263]		linear chains with handles
Tl_5Te_3[264]		linear chains condensed into a 3D structure
Tl_4MTe_3 (M = Sn, Pb)[115]	Tl_5Te_3	linear chains condensed into a 3D structure
Tl_9ME_6 (M = Sb, Bi; E = Se, Te)[115]	Tl_5Te_3	linear chains condensed into a 3D structure
UTe_2[118, 120]	β-$ErSe_2$	linear chains
$ErSe_2$[122]	UTe_2	linear chains
$Dy_{0.5}U_{0.5}Te_2$[121]	UTe_2, β-$ErSe_2$	linear chains
ME_3 (M = Ti, Zr, Hf; E = S, Se, Te)[123]	UTe_2	dumbbells aligned into a linear chain
α-UTe_3[265]	$ZrTe_3$	dumbbells aligned into a linear chain
MTh_2Se_6 (M = K, Rb)[125]	$ZrSe_3$	CDW-distorted linear chain
$Tl_{0.56}UTe_3$[129]	$ZrTe_3$	linear chain
$CsTh_2Te_6$[126]	$ZrTe_3$	linear chains
$M_2Th_2E_6$ (M = K, Cs; E = Se, Te)[127]	$ZrTe_3$	linear chains
$CuTh_2Te_6$[128]	$ZrTe_3$	linear chains
$CsTiUTe_5$[266]		linear chains
$Cu_{0.28}LaTe_2$[130]		linear chains
$Dy_3Cu_2Te_7$[131]		linear chains
MM'_3Te_8(M = Cs, Rb; M′ = Ce, Nd) [243]		linear chains kinked at every second atom
UTe_5[267]		linear chains kinked at every second atom

spaced Te atoms within the Te chain is 3.16 Å, a typical distance for a hypervalent Te–Te bond (3.05 Å in hypervalent Te_5^{2-} in Cs_2Te_5[113]). One associates two common oxidation states with the Cu ion, +1 and +2. We believe that the latter is improbable in this compound, since in that case Te^{2-} ions would be expected to be more than 4 Å apart from each other. An assumption of Cu^+ leads to Te^-, which is consistent with our electron counting scheme of seven electrons per atom in the linear chain.

The linear chains in K_5Se_3 and Cs_5Te_3[114] have undergone a pairing distortion, more emphasized for the former compound. The Te–Te intra-pair distance in Cs_5Te_3 is 2.81 Å, while the Te–Te inter-pair distance is 3.85 Å. In addition to Te_2 dumbbells aligned into a linear chain there exist also isolated Te atoms in this compound. Taking into account the crystal site multiplicities, the charges in Cs_5Te_3 may be assigned as $(Cs_{10})^{+10}(Te_2^{pair})^{2-}(Te_4^{atom})^{8-}$. An electron count of seven electrons per atom is reasonable for isolated Te_2 pairs as well as for Te atoms aligned into a linear chain; we have discussed this choice in some detail in Section 3.4.

Simple linear chains and their derivatives are found in the TlTe binary phase (Figure 27). In this compound some of the linear Te chains have "handles" attached to them, with each

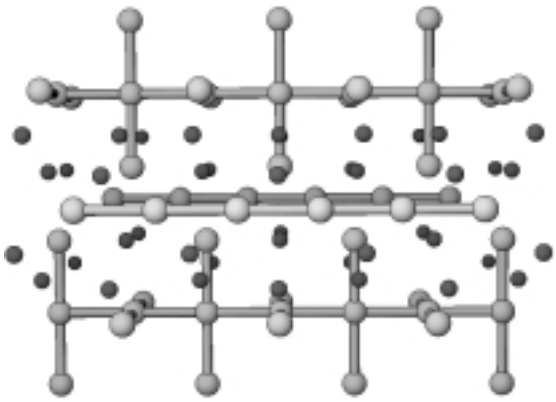
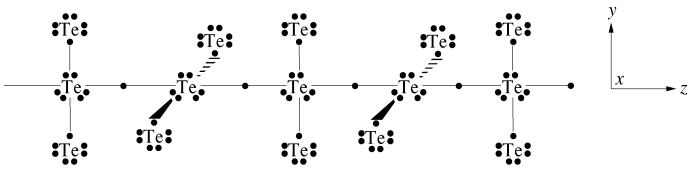


Figure 27. A perspective view of the crystal structure of TlTe. Tl = small dark spheres; Te = large light spheres.

handle oriented perpendicular to the next one. The Te–Te bond length within the chains in both simple linear chains and composite linear chains is 3.09 Å. The distance between the Te atoms in the chain and on the sidearms in the composite linear chains is 3.03 Å. This distance, although shorter than the one within the chains, is still on the hypervalent side of the range of Te–Te bond lengths.

We may use our electron counting scheme for hypervalent bonding in the solid state as a starting point for the rationalization of the stoichiometry of this compound. We begin by assigning a −1 charge to Te atoms in the simple linear chains. For the linear chains with handles we follow a two-step procedure, where we imagine the composite chain being assembled hypothetically from a simple linear chain and isolated side atoms (handles). A −1 charge should be assigned to Te atoms in an isolated linear chain. We prepare "side" Te atoms for subsequent bonding by making them also have a charge of −1, so they can contribute only one electron to bonding. Two such side Te^- ions interact with the lone pair (p_x, p_y) on the central Te atom, forming a three-center four-electron hypervalent bond (Scheme 19). We have seen this picture earlier (see Scheme 3), when discussing the bonding in



Scheme 19.

XeF_2 and I_3^- molecules. All three types of Te atoms (simple chain atoms, central atoms in the composite chain, and sidearm atoms in the composite chain) carry a −1 charge. Since Tl is commonly found monopositive, the Tl^+Te^- formulation seems to be reasonable.

10.2. The Tl_5Te_3 Binary Phase and its Ternary Derivatives

A perspective view of the Tl_4SnTe_3 crystal structure is given in Figure 28. One could perform a retrotheoretical disassembly of the beautiful and intricate $SnTe_3$ subnetwork in this

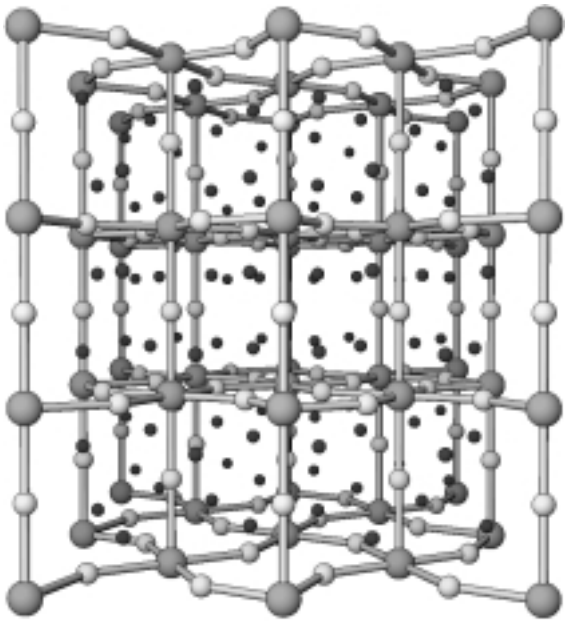


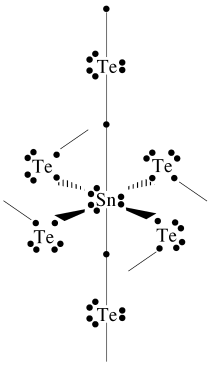
Figure 28. A perspective view of the crystal structure of Tl_4SnTe_3. Tl = small dark spheres; Te = small light spheres; Sn = large light spheres.

compound in various alternative ways. Since we are obsessed with linear chains, we view this network as linear SnTe chains connected together by bridging Te atoms (Figure 28). One could also imagine this network as being composed of vertex-sharing $SnTe_6$ octahedra, similar to the ReO_3 network. Notice that these $SnTe_6$ octahedra are then tilted with respect to each other within horizontal planes. The Sn–Te bond length within the linear chain is 3.26 Å, and between Sn atoms and sidearm

Te atoms is 3.30 Å. These bond lengths indicate hypervalent bonding between Sn and Te atoms.

We carry out the hypothetical assembly of the $SnTe_3$ network in Tl_4SnTe_3 in two distinct steps. First, we form linear SnTe chains and then we connect them with bridging Te atoms. The isolated SnTe linear chain should carry a -4 charge per SnTe unit, since the neutral SnTe unit is short by four of the fourteen electrons per two atoms needed for an ideal linear chain. Given this charge on the SnTe unit, each Sn and Te atom carries three lone pairs (s, p_x, and p_y) and a p_z chain orbital filled with only one electron (the z direction is chosen as the SnTe chain propagation axis).

We prepare the bridging Te atoms for subsequent bonding by making them neutral, which in turn provides two unpaired electrons per Te atom for bonding with the linear chains. As we have discussed for the Te chains with handles in the TlTe phase, three-center four-electron hypervalent bonds form between two side Te atoms and the p_x, p_y orbitals of the Sn atoms in the chains (Scheme 20). This reasoning leads to a -4 charge on the $SnTe_3$ unit, namely, $(SnTe)^{4-}Te_2^{bridging})^0$. To counterbalance the negative charge, the Tl atoms should be monopositive, which is a typical oxidation state for the Tl ion.



Scheme 20.

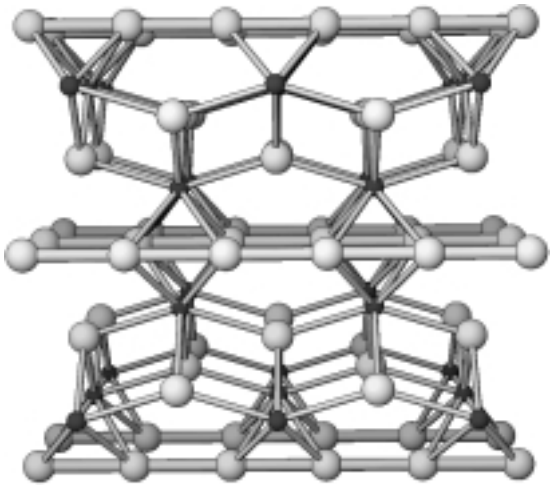
Each Sn atom in this structure plays the role of the hypervalent central atom (compare with Xe in XeF_4 or XeF_6) and participates in two linear three-center bonds. On the other hand, the sidearm Te atoms are classically bonded, since the Sn-Te-Sn angle is not linear (143°). It turns out that if all sidearm Te atoms were made linear then the structure would still keep the same electron count! Therefore, one could expect a soft potential energy surface for bending of the Sn-Te-Sn angle, which in turn might explain the large value observed for the Sn-Te-Sn angle.

A wide variety of compounds isostructural to Tl_4SnTe_3 have also been reported.[115] In the isoelectronic compound Tl_4PbTe_3 Sn is replaced by Pb, with the same geometrical features around the Te and Pb atoms as in Tl_4SnTe_3. The Tl_9BX_6 series of compounds (B = Sb or Bi, X = Se or Te) may be obtained from Tl_4SnTe_3 by first doubling its empirical formula to $Tl_8(SnSn)Te_6$, then by replacing the SnSn unit by TlSb or TlBi units, and finally by replacing all Te atoms by Se atoms if appropriate. The Sn positions in Tl_4SnTe_3 are randomly occupied by Tl and Bi or Sb in Tl_9BX_6. Notice that the substitution of SnSn by TlSb or TlBi keeps the same number of electrons in the system.

Finally, the crystal structure of parent Tl_5Te_3 may be derived from Tl_4SnTe_3 in the same way as Tl_9BX_6 was derived. Only in this case two Sn atoms are replaced by two Tl atoms, leaving the system two electrons less per $Tl_{10}Te_6$ formula unit. If one assumes that these two electrons are removed from p orbitals which are engaged in chain bonding, and given that there are two chain TlTe units in $Tl_{10}Te_6$, the electron count becomes 6.5 electrons per Tl or Te atom in the isolated chain. To learn more about the structural and physical properties of the Tl_5Te_3 family of compounds readers are referred to a recent paper by Böttcher and co-workers.[116] An alternative ionic treatment of Tl_5Te_3 and derivative phases is given by Nordell and Miller.[117]

10.3. UTe_2 and its Derivative Phases

The linear Te chains, found in the UTe_2 crystal structure, are almost uniformly spaced, with Te–Te bond lengths of 3.05 and 3.07 Å.[118, 119] The U atoms are surrounded by Te atoms in a bicapped trigonal-prismatic manner, and they are condensed in the vertical direction through Te_4 rectangular faces (Figure 29). Isolated Te atoms are also found in the UTe_2 structure, with a 1:1 ratio of chain to isolated Te atoms.


Figure 29. A perspective view of the crystal structure of UTe_2. U = small dark spheres; Te = large light spheres.

If one were to assign a $+4$ charge to U, a typical uranium oxidation state, one would force a -2 charge on both the isolated and chain Te atoms. Given the clearly bonding interactions between chain Te atoms, Beck and Dausch propose a $+(3+\delta)$ charge on the U atoms and a $-(1+\delta)$ charge on the chain Te atoms.[120] This assignment of charges is further supported by the substitution of U by trivalent Dy in UTe_2 to form $Dy_{0.5}U_{0.5}Te_2$.[121] The isostructural β-$ErTe_2$ phase was also reported.[122] By taking all these facts into account, we also concur that the oxidation state of U is much closer to $+3$ in UTe_2, and the Te atoms in the linear chains carry approximately seven electrons per atom, which is consistent with our electron counting scheme.

10.4. $ZrTe_3$ and Related Binary Phases

The $ZrTe_3$ crystal structure[123, 124] is closely related to that of UTe_2 (Figure 30). One may arrive at $ZrTe_3$ by inserting an additional plane of linear Te chains into the UTe_2 structure (Figure 29). The nearly equidistant linear Te chains in UTe_2 are more distorted in $ZrTe_3$, the Te–Te bond lengths being 2.79 Å and 3.10 Å, respectively.[123, 124] The U atoms in UTe_2 share rectangular faces in the vertical direction, which is no

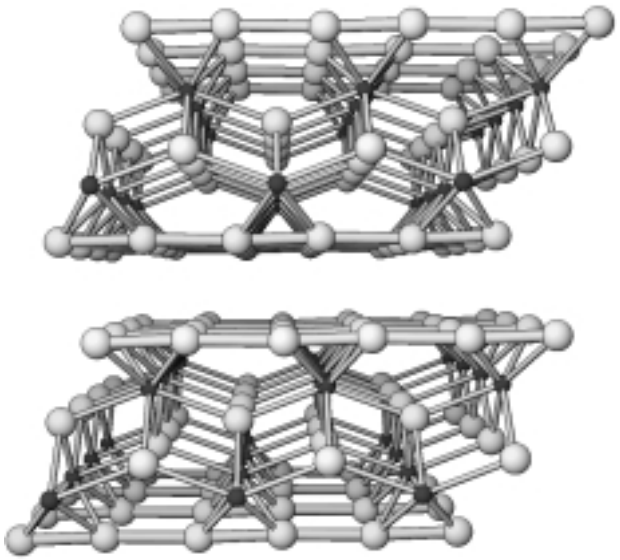


Figure 30. A perspective view of the crystal structure of $ZrTe_3$. Zr = small dark spheres; Te = large light spheres.

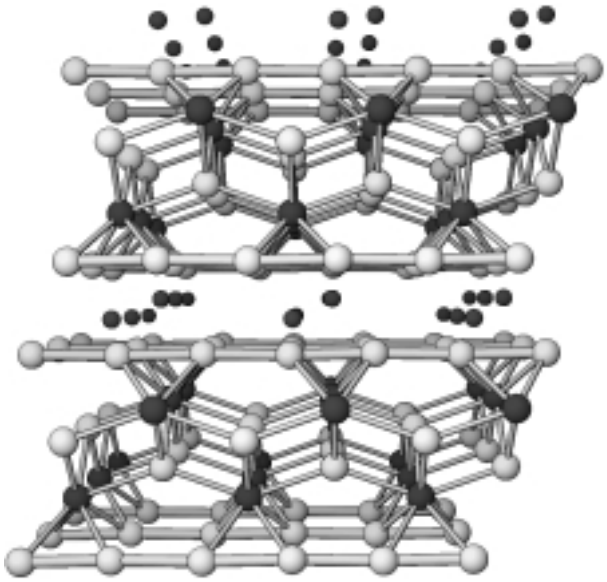


Figure 31. A perspective view of the crystal structure of $CuTh_2Te_6$. Th = large dark spheres; Cu = small dark spheres; Te = large light spheres.

longer the case for the $ZrTe_3$ crystal structure. Zr_2Te_6 slabs touch each other at van der Waals separation through the planes of linear Te chains.

If one assumes a -1 charge on the chain Te atoms and a -2 charge on the isolated Te atoms, then the Te_3 subnetwork should carry a -4 charge $(Te_2^{chain})^{2-}(Te^{atom})^{2-}$. Consequently, this forces a $+4$ oxidation state on Zr, which seems reasonable. Since the linear chains are pairwise distorted in $ZrTe_3$, one would expect a semiconducting behavior from this compound. This is not so, however. Linear muffin tin orbital (LMTO) DFT calculations by Stöwe and Wagner indicated that some Te and Zr bands crossed the Fermi level, and thus rationalized the metallic conductivity.[124] The formal oxidation state of Zr atoms was found to be near $+4$, as expected.[124]

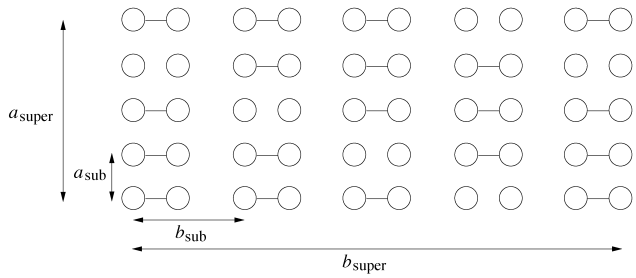
Isostructural TX_3 binary phases were reported for other tetravalent metals (T = Zr, Hf, U) as well as for X = Se.[123] In all of these compounds, Te or Se atoms in the linear chains appear to have a -1 oxidation state, that is, seven electrons per atom.

10.5. AT_2X_6 Compounds: Ternary Phases with the $ZrTe_3$ Structure

A large number of ternary AT_2X_6 (A = K, Rb, Cs, Cu; T = U, Th; X = Se, Te) compounds have been reported which are closely related to the $ZrTe_3$ binary phase.[125–128] In all of these compounds the T_2X_6 slabs are similar to those found in $ZrTe_3$, but with monopositive ions intercalated into the van der Waals gap between the slabs (compare Figures 30 and 31). Two outcomes are possible upon the introduction of an extra electron into the T_2X_6 subnetwork—either the T^{4+} atoms become partially reduced to $T^{3.5+}$ or the X^- atoms in the linear chains are reduced to $X^{1.25-}$.

From the limited data available we suggest that both scenarios actually take place. Magnetic susceptibility measurements carried out for the $CuTh_2Te_6$ ternary phase indicate an effective magnetic moment of $2.06\,\mu_B$ per unit cell.[128] Assuming a $+4$ oxidation state for the Th atoms, and taking into account the presumably nonmagnetic nature of both Cu^+ ions and of the partially filled broad Te chain bands, one would expect diamagnetic behavior from this compound. Therefore, we attribute the paramagnetic behavior of $CuTh_2Te_6$ to the partial reduction of Th^{4+} ions, which could make them magnetic. It would follow that the Te atoms in the chain carry a charge closer to -1 than to -1.25.

The second scenario—the reduction of linear Se chains, happens in $MThSe_6$ (M = K, Rb).[125] These compounds show diamagnetic behavior, which suggests a $+4$ oxidation state of the Th atoms. Extensive physical measurements, including Raman spectroscopy, electron diffraction studies, and pair distribution function analysis, led Kanatzidis and co-workers to the conclusion that the plane of Se chains undergoes a static 4×4 CDW distortion (Scheme 21)[125] with linear Se chains distorting into Se_2^{2-} dumbbells and with the Se^{2-} isolated atoms completing an octet around each Se atom.



Scheme 21.

The limited set of physical property measurements on the compounds with an AT_2X_6 stoichiometry suggests that either tetrapositive T ions are reduced as in $CuTh_2Te_6$ (paramagnetic), or the linear X^- chains are reduced as in $MThSe_6$ (M =

K, Rb; diamagnetic), which results in a distortion of the linear chain into X_2^{4-} dumbbells and isolated X^{2-} atoms. In the former case, the X atoms in the linear chain carry approximately seven electrons per atom.

10.6. Linear Te Chains Which are not Mononegative

The $Tl_{0.56}UTe_3$ crystal is also isostructural to the $ZrTe_3$ binary phase and AT_2X_6 ternary phases discussed in Sections 10.4 and 10.5, respectively.[129] The Te chains, found in this compound, are almost uniformly spaced at 3.04 and 3.05 Å. The magnetic susceptibility measurements indicate an effective paramagnetic moment of 3.27 μ_B, which the authors suggest is close to the typical values for that observed for the U^{4+} ion.[129] If the U ions are indeed tetravalent in this compound, and assuming no CDW distortions, one is led to a -1.28 charge on the Te atoms in the linear chains.

A similar situation is observed for the $Cu_{0.28}LaTe_2$ ternary phase,[130] where uniformly spaced linear Te chains carry a -1.28 charge per Te atom. It is remarkable that in the related $LaTe_2$ binary phase the Te atoms form a square sheet instead of linear chains ($La^{3+}(Te^{atom})^{2-}Te^-$). Thus, when an additional 0.28 electrons are introduced into a square Te^- sheet, the latter disintegrates into linear chains.

Nearly perfect linear Te chains in the crystal structure of $Dy_3Cu_2Te_7$ have been reported recently by Lee and co-workers.[131] Assuming a +3 oxidation state for Dy and a +1 oxidation state for Cu, the authors arrive at a -1.25 oxidation state for the Te atoms in the linear chains.

10.7. Summary

We have examined in this section the bonding patterns and possible electron counting of a selection of binary and ternary phases of heavy main group elements which contain linear chains or their derivatives. It appears that the electron count of seven electrons per atom is dominant in these compounds, with a few exceptions of 7.25–7.28 electrons per chain atom found in Te ternary phases. We argued earlier that an electron count of six electrons per atom would force the linear chain to kink, while no bonding at all is expected at an electron count of eight electrons per atom. We estimate that the effective range for the electron count for a hypervalent linear chain might be between 6.5 and 7.5 electrons. The compounds made and structurally characterized to date point to a still narrower range of electron counts.

Having looked into the range of electron counts for linear chains, we next examine the range of possible electron counts for square sheets of elements of Groups 4 and 6.

11. Square Sheets in the Compounds of Group 4 Elements

Square sheets of Group 4 elements are realized in a wide variety of compositions and structure types and they offer a stringent test of our electron counting scheme. We first look at binary compounds having the $ZrSi_2$ structure type, followed by ternary and quaternary derivatives of $ZrSi_2$. The filled version of the $ZrSi_2$ type, the $CeNiSi_2$ structure type, is also considered. Finally, we examine some ternary compounds having the $CaBe_2Ge_2$ structure type, a ternary derivative of the $BaAl_4$ structure.

11.1 Binary $M^{IV}X_2$ and $M^{II}X_2$ Compounds

We have already encountered the $ZrSi_2$ structure type when discussing the $YbSb_2$ binary phase (see Figure 8). In that compound, which consists of zig-zag chains and square sheets of Sb atoms, we assigned a -1 charge to the Sb atoms in both networks. If one were to replace the divalent Yb cations by tetravalent ones, and the Sb atoms by Group 4 elements, then the total number of electrons remains the same.

However, many $M^{IV}X_2$ phases crystallize in quite different structure types, in particular in the $TiSi_2$, $CrSi_2$, $ThSi_2$, and AlB_2 structures. The crystal structures and electrical properties of $ZrSi_2$ and polymorphs of $TiSi_2$ have been extensively scrutinized recently for their potential application as contact materials in ultra-large-scale integrated circuits (ULSI).[132–135] Indeed, some $M^{IV}X_2$ structures listed in Figure 32 crystallize

	Ti^{4+} 0.74 Å	Hf^{4+} 0.83 Å	Zr^{4+} 0.84 Å	U^{4+} 1.00 Å	Th^{4+} 1.05 Å
Si 1.90 Å	**0.39** $ZrSi_2$ $TiSi_2$	**0.44** $ZrSi_2$	**0.44** $ZrSi_2$	**0.53** $ThSi_2$ AlB_2	**0.55** $ThSi_2$ AlB_2
Ge 2.00 Å	**0.37** $TiSi_2$	**0.42** $ZrSi_2$	**0.42** $ZrSi_2$	**0.50** $ZrSi_2$	**0.53** $ZrSi_2$ $ThSi_2$ $ThGe_2$
Sn 2.16 Å	**0.34**	**0.38** $CrSi_2$	**0.39** $TiSi_2$	**0.46**	**0.49** $ZrSi_2$

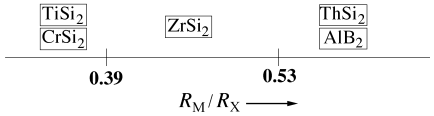


Figure 32. Crystal structure types of $M^{IV}X_2$ compounds, where X = Si, Ge, Sn.[132, 134–147] The ionic radii of M^{IV} ions for coordination number eight (found in the $ZrSi_2$ structure) were taken from the CRC Handbook of Chemistry and Physics,[155] while the corresponding radii of X were estimated from averaged metal–element bond lengths in $HfSi_2$ ($ZrSi_2$-type), $HfGe_2$ ($ZrSi_2$-type), and $ZrSn_2$ ($ZrSi_2$-type) crystal structures. The ionic radii ratio R_M/R_X is given for each pair. Some of the stoichiometries exhibit polymorphism, as indicated by the simultaneous inclusion of several structure types in corresponding fields.

with the same $ZrSi_2$ structure type (shown in Figure 33 a), that is, with zig-zag chains and square sheets of X^{2-} (six electrons per X atom).

Given the same electron count for all the compounds in Figure 32, it is apparent that other factors play a key role in determining the stability of various structure types. Inspired by the structural maps of Villars and co-workers[148, 149] and by earlier work of many other authors, we have been able to separate various structure types into distinct domains using the metal–element ionic size ratio R_M/R_X as a key parameter

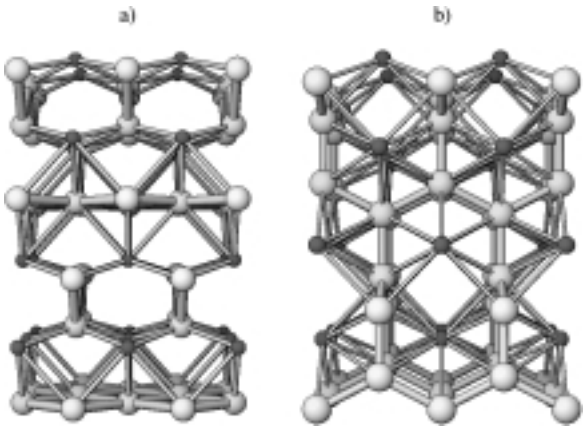


Figure 33. a) A perspective view of the $ThSn_2$ ($ZrSi_2$ type) crystal structure. Th = small dark spheres; Sn = large light spheres. b) A perspective view of the $EuSi_2$ ($ThSi_2$ type) crystal structure. Eu = small dark spheres; Si = large light spheres.

(Figure 32). The $ZrSi_2$ structure is stable between R_M/R_X ratios of 0.39 and 0.53. We will pick up this point in Section 11.2 when discussing the crystal chemistry of rare earth disilicides, digermanides, and distannides.

When Yb^{2+} atoms in the $YbSb_2$ crystal structure are substituted by Sm^{3+} atoms (see the earlier discussion in Section 3.5 on Sb compounds), the zig-zag chains accommodate the extra electron by breaking up into isolated Sb_2 pairs, preserving the electron count of six electrons per atom in the square sheets. One would like to know if this robust electron count for the square sheet is characteristic for sheets comprised of the Group 4 elements as well. For example, what are the consequences of replacing tetravalent cations by trivalent and divalent ones?

The structures provide a straightforward answer for the divalent Ca, Sr, and Eu cations. In these $M^{II}X_2$ compounds the X atoms carry an average -1 charge, that is, five electrons per atom. Such an electron count implies a classical three-connected network. This is indeed what happens: Si atoms in $EuSi_2$ form three-connected networks in both the $ThSi_2$[150] (Figure 33b) and AlB_2[151] structure types (Figure 34a for

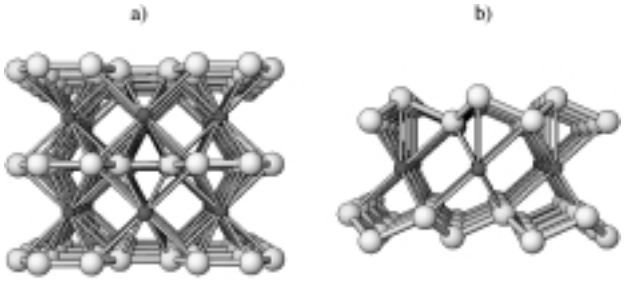


Figure 34. a) A perspective view of the $YbSi_2$ (AlB_2 type) crystal structure. Yb = small dark spheres; Si = large light spheres. b) A perspective view of the $CaSi_2$ ($CaSi_2$ type) crystal structure. Ca = small dark spheres; Si = large light spheres.

$YbSi_2$ in the AlB_2 structure type). In the latter the Si atoms form a graphite-like sheet sandwiching the metal ions. Corrugated three-connected As-like sheets are found[152] in the $CaSi_2$ crystal structure (Figure 34b), which may be transformed under pressure into a three-connected $ThSi_2$ network[153] (Figure 33b). $SrSi_2$ forms yet another three-connected Si network,[154] which also may be transformed into a $ThSi_2$ network under pressure.[153]

If the ratio of the ionic radii is indeed a critical parameter in determining the stability of the $ZrSi_2$ structure type (Figure 32), then the larger size of divalent Ca, Sr, and Eu[155] may be the reason for the absence of this structure type, that is, the R^{II}_M/R_X ratio is well over 0.53 (Figure 32). Therefore, we consider next the substitution of tetravalent cations in MX_2 compounds by trivalent rare earth ones, which have ionic radii comparable to those of Th^{4+} and U^{4+} ions.

11.2. Binary REX_2 Phases

Figure 35 shows in graphic form the major structure types which are assumed by REX_2 compounds. Let it not be said that chemistry is about simplicity—no less than eight structure types are displayed by this isoelectronic group of compounds.

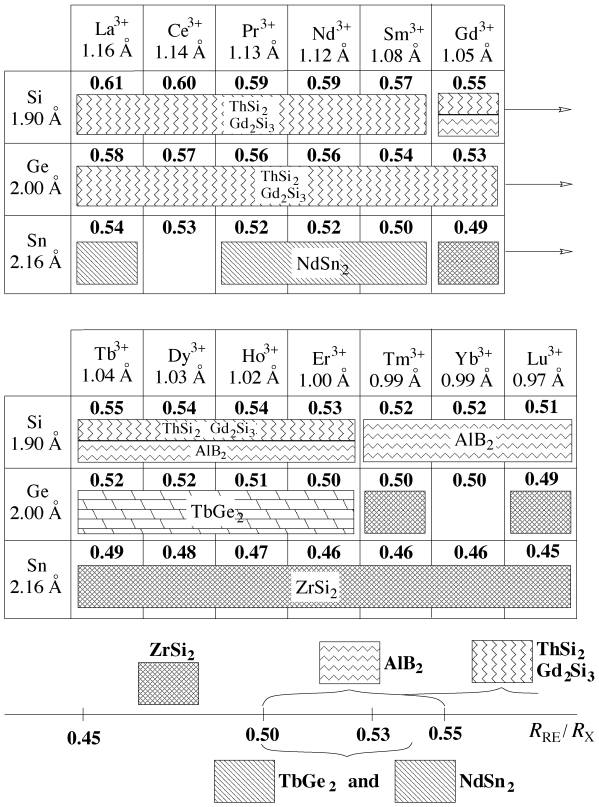


Figure 35. Crystal structure types of $M^{III}X_2$ compounds, where X = Si, Ge, Sn.[156, 158–177] The ionic radii of M^{III} for coordination number eight (found in the $ZrSi_2$ structure) were taken from the CRC Handbook of Chemistry and Physics.[155] The ionic radii ratio R_M/R_X is given for each pair.

As indicated by many authors in the field,[156–163] the ratio of ionic sizes and the degree of nonstoichiometry (defects on X sites) are the most important factors in stabilizing various structure types. Our calculated R_{RE}/R_X ionic ratios strongly indicate that stability zones exist for all structure types (Figure 35). The $ZrSi_2$ structure type is realized for the smallest R_{RE}/R_X ratio, while the tetragonal $ThSi_2$ structure

type and the closely related orthorhombic Gd_2Si_3 structure type are realized for the largest ratio. For the small ratio range of 0.50–0.55 several structure type domains coexist, with $TbGe_2$ being a $ZrSi_2$–$ThSi_2$ hybrid structure type. Rare earth disicilicides, RE = Gd, Er, having the R_{RE}/R_X ratio at the boundary of $ThSi_2/Gd_2Si_3$ and AlB_2 stability zones, crystallize in all three structure types, depending on the temperature and other conditions (Figure 35).

A simplistic approach to understanding the structural domain formation in Figures 32 and 35 may be obtained from perusal of the coordination polyhedra of rare earth metals in these structure types (Table 5). We have taken into account only the closest bonding rare earth–element contacts, and also for $NdSn_2$ two strong Nd–Nd interactions have been considered. By comparing the data from Table 5 with the structure maps in Figures 32 and 35, one observes a reasonable correlation between the ionic size ratio and the higher coordination number of the rare earth atoms.

Table 5. Coordination number of metal ions in various ME_2 structure types presented as a sum of the number of neighboring atoms + the number of atoms in the next shell, located approximately 10% further away than the closest atoms. The Nd atoms in $NdSn_2$ are connected to two other Nd atoms (6* = 4 M-X + 2 M-M).

Structure type	$CrSi_2$, $TiSi_2$	$ZrSi_2$	$NdSn_2$	AlB_2	$ThSi_2$
coordination polyhedron	4 + 6	8 + 2	6* + 6	12 + 0	12 + 0

To further rationalize these observations we notice that the $ThSi_2$ structure obeys Zintl–Klemm electron counting rules only for divalent metals, that is, the three-connected X^- network is electronically saturated in $M^{2+}(X^-)_2$ (with a lone pair of electrons at each Si atom). An extra electron is introduced by trivalent rare earth metals; this electron could either reduce the rare earth ions or enter the σ* antibonding orbitals of the X framework. There is neither direct evidence for the reduction of the rare earth ions nor for significant weakening of X–X bonding (the Si–Si bond lengths are 2.31 and 2.42 Å in $Eu^{2+}Si_2$ and 2.28 and 2.43 Å in $La^{3+}Si_2$; 2.35 Å is a normal Si–Si single bond length).

Still another way to stabilize the system when extra electrons are present is to introduce defects into the anionic sublattice. Dangling bonds on the X atoms adjacent to the defect sites are created in this way; these dangling bonds could in turn become lone pairs by absorbing additional electrons.

The explanation given above is consistent with the X atom deficiency most commonly reported for these compounds.[162, 163] Rare earth disilicides with the $ThSi_2$ structure type are often found with a $REX_{1.7-1.8}$ stoichiometry. The number of X vacancies is even higher for the compounds with the AlB_2 structure type, for which the X stoichiometry is often less than $REX_{1.7}$.[161, 163] Several authors have argued that the AlB_2 structures should be stable at even lower electron counts than the $ThSi_2$ ones,[170, 178] which might be one of the explanations of the higher X deficiency in these compounds.

By considering the data in Figures 32 and 35 we conclude that for ion size ratios R_M/R_X between 0.40 and 0.50, $ZrSi_2$ is the only structure type that is available to MX_2 compounds. This postulation is supported by the existence of the $TbGe_2$ structure type (Figure 36) at the boundary of $ZrSi_2$–$ThSi_2$ stability zones. In the $TbGe_2$ crystal structure half of the square Ge sheets from the $ZrSi_2$ structure type undergo a puckering distortion and merge with the Ge zig-zag chains above and below, which creates finite slabs of the $ThSi_2$ structure type sandwiched between square Ge sheets. By assigning a −2 charge to two-connected Ge atoms and a −1 charge to three-connected Ge atoms in the slabs, we arrive at a −1 charge on Ge atoms in the square sheets of $(Tb_2)^{6+}(Ge_3^{slab})^{4-}(Ge^{square})^{2-}$.

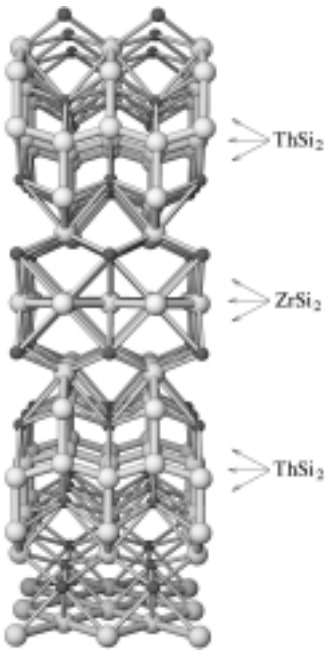


Figure 36. a) A perspective view of the crystal structure of $TbGe_2$. Tb = small dark spheres; Ge = large light spheres.

The electron count of six electrons per atom in square Ge sheets in the $TbGe_2$ structure is reduced to five for REX_2 compounds with the $ZrSi_2$ structure type. Thus square sheets of Group 4 elements may also exist for that electron count. Are there any structural consequences of the five electron count, since the nonbonding or slightly antibonding region of square sheet hypervalent bands are emptied in this case (see the discussion in Section 5)?

We have only the $ErSn_2$[156]structure to go by. One observes the following difference between the crystal structures of $ThSn_2$ ($ZrSi_2$ type) and $ErSn_2$ ($ZrSi_2$ type): the distance between the Sn atoms in the square sheets and Sn atoms in the zig-zag chains is reduced from 3.90 Å in $ThSn_2$ to 3.67 Å in $ErSn_2$, although Th^{4+} and Er^{3+} have comparable ionic sizes (see Figures 32 and 35). Moreover, the same distance in the "electronically saturated" $TbGe_2$ crystal structure is 3.81 Å, in spite of Ge being smaller than Sn. We believe that oxidation of the square sheet from six to five electrons per atom results in the tendency of "unsaturated" square sheet atoms to form secondary interactions with the zig-zag chains.

This conclusion is further supported by the light rare earth stannides crystallizing with the $NdSn_2$ structure type.[166, 168] In these compounds the square sheets merge fully with the zig-zag chains, simultaneously breaking bonds between the zig-zag chain atoms (Figure 37). This results in a remarkable layered structure of vertex-sharing octahedra, separated by rare earth ions.

Vajenine and Hoffmann recently demonstrated that the electron count in 2D sheets of vertex-sharing Al octahedra should be around 10–12 electrons per octahedron, which is significantly less than 22 electrons found in Nd_2Sn_4 (six electrons coming from Nd_2 and sixteen electrons from Sn_4).[179] Preliminary calculations indicate that the contraction of s

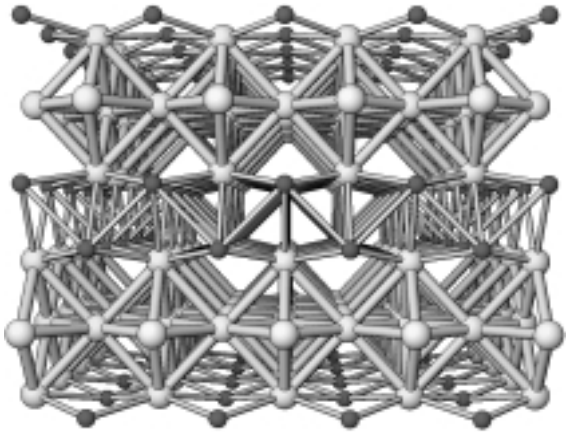


Figure 37. a) A perspective view of the crystal structure of $NdSn_2$. Nd = small dark spheres; Sn = large light spheres.

orbitals and the relative unimportance of π bonding for the heavier elements (see the earlier discussion in this paper) could substantially increase the magic electron count for such networks of condensed octahedra.[180] We expect a 2D lattice of vertex-sharing octahedra of heavy main group elements to be stable around 18 electrons per octahedron.[180] The existence of short Nd – Nd contacts (3.15 Å) in $NdSn_2$ implies that each Nd atom donates less than three electrons to the Sn subnetwork, which brings down the number of electrons per octahedron from 22 to 20 or, perhaps, 18.

11.3. Compounds with the $CeNiSi_2$ Structure Type

In the discussion above we concluded that when tetravalent metal atoms in the $ZrSi_2$ structure are substituted by trivalent rare earth ones the electron count in square sheets reduces from six to five, which induces certain secondary interactions with zig-zag chains. If it were possible to fill the square-pyramidal voids in the $RESn_2$ series of compounds ($ZrSi_2$ type) with metal cations, then the electron count in Sn square sheets could, in principle, be brought back from five to six, or perhaps even seven electrons per sheet atom. Gladyshevskii, Bodak, and co-workers reported the synthesis and characterization of several $RELiSn_2$ ternary phases (RE = La, Ce, Pr, Nd, Sm, Gd, Tb, Dy, Ho, Er, Tm, Lu) which crystallize with the $CeNiSi_2$ structure, a filled version of the $ZrSi_2$ structure.[181] A perspective view of the isostructural $BaCuSn_2$ is shown in Figure 38. For the purpose of simplicity we have not drawn connections between Ba/rare earth atoms and the Sn sublattice, as was shown above for the $ZrSi_2$ structure (see Figure 33a).

The magnetic susceptibility measurements indicate that all rare earth atoms are tripositive in $RELiSn_2$.[181] Given the plausible assumption of Li being monopositive, we are led to the $RE^{3+}Li^{+}(Sn^{zig\text{-}zag})^{2-}(Sn^{square})^{2-}$ formulation, namely, once again six electrons per square sheet atom. Schäfer and co-workers prepared some isostructural LaT_xSn_2 compounds (T being a transition metal atom; T = Cu: $x = 0.56$, T = Ni: $x = 0.74$, T = Co: $x = 0.52$, T = Fe: $x = 0.34$).[182] According to the authors, if all these compounds were to be isoelectronic, then Cu should be 2+ in $LaCu_{0.56}Sn_2$, Ni 1.33+ in $LaNi_{0.74}$, Co 2+ in $LaCo_{0.52}Sn_2$, and Fe 3+ in $LaFe_{0.34}Sn_2$[182] This line of reasoning is consistent with Cu sites being fully occupied in $BaCuSn_2$, since the substitution of La^{3+} by Ba^{2+} and the simultaneous enhancement of the Cu^{2+} occupation from 0.56 to 1 would keep the number of electrons approximately constant.

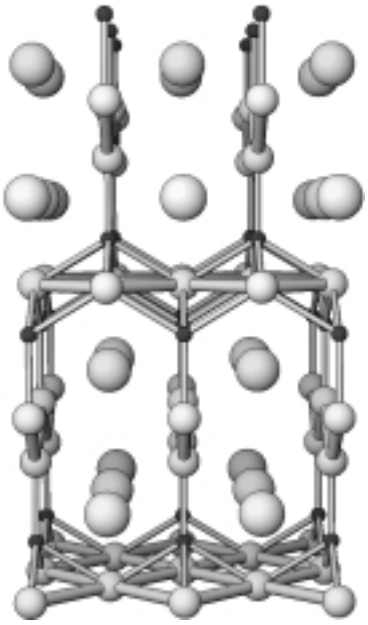


Figure 38. a) A perspective view of the crystal structure of $BaCuSn_2$ ($CeNiSi_2$ type). Cu = small dark spheres; Sn = larger light spheres; Ba = the largest light spheres.

The proposed trivalency of Fe[182] is supported by the results of Bodak and co-workers who reported $REFe_{0.33}Si_2$ compounds with other rare earth elements (RE = Y, Tb, Ho, Er, Tm, Lu).[183] It is interesting to note that $REFeSi_2$ compounds with full Fe stoichiometry crystallize with an alternative $TbFeSi_2$ structure type.[184] The Ni occupation value in $RENi_xE_2$ (E = Si, Ge, Sn) compounds varies from 1.5 to 2, which renders the determination of its oxidation state difficult.[182, 185–189] Kumigashira and co-workers have concluded from a high-energy-resolution photoemission study of $CeNiSi_2$ and $CePtSi_2$ that the d bands of Ni and Pt are, respectively, 2.0 eV and 4.4 eV below the Fermi level. If one assumes that Ni does not contribute any electrons to the Si sublattice, and given the valence fluctuation of Ce (from 3.35 at 300 K to 3.65 at 50 K, as indicated by magnetic susceptibility measurements), one is led to 5.35 – 5.65 electrons per square Si atom in this compound.[187, 185] Extensive reviews of the $CeNiSi_2$ type compounds are given by Parthé and Chabot[190] and Rogl.[191] Proserpio, Chacon, and Zheng[189] provide an alternative theoretical view of Ge subnetworks in $LaNiGe_2$ as donor layers and acceptors which lead to chain formation.

Now we are ready to examine if the square sheets can be reduced to have more than six electrons per atom.

11.4. Square Sheets of Group 4 Elements in Compounds Having $ZrSi_2$-Related Structures

If one takes as a starting point the $ZrSi_2$ binary phase, then an obvious way to introduce extra electrons into the structure is to replace Group 4 Si by a Group 5 or 6 element. Indeed, Si

may be replaced by more electron-rich Se in the ZrSiSe ternary compound shown in Figure 39a.[192] In principle there are two anionic subnetworks in the $ZrSi_2$ crystal structure that could absorb these two extra electrons: square sheets and zig-zag chains. We encountered a similar situation earlier in the paper when contemplating the consequences of the replacement of divalent Yb in $YbSb_2$ (also the $ZrSi_2$ structure type)

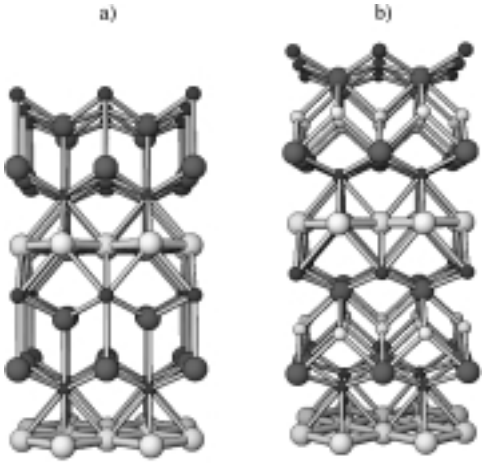


Figure 39. a) A perspective view of the crystal structure of ZrSeSi (PbFCl type). Zr = small dark spheres; Si = large light spheres; Se = large dark spheres. b) A perspective view of the crystal structure of ZrCuAsSi (ZrCuAsSi type). Zr = small dark spheres; Cu = small light spheres; Si = large light spheres; As = large dark spheres.

by a trivalent cation. In that case, it turned out that zig-zag Sb^- chains got reduced and broke into isolated Sb_2^{4-} pairs, as in $SmSb_2$ (see Figures 8 and 9).

A similar pattern is found also for the ZrSiSe crystal structure (the PbFCl structure type, sometimes referred to as the anti-Cu_2Sb type, as well as by other names[193]). The Se atoms occupy positions related to zig-zag Si positions in the $ZrSi_2$ structure, but the zig-zag chains disintegrate into isolated atoms. Hence, to complete an octet around each Se we assign charges to ZrSiSe as $Zr^{4+}(Si^{square})^{2-}(Se^{atom})^{2-}$. Therefore, the electron count of six electrons per square sheet atom in $ZrSi_2$ is preserved as well in ZrSiSe. Isoelectronic compounds having the same PbFCl structure type have been reported for most of the chalcogen-Group 4 element-tetravalent metal combinations (see Table 6). The same number of electrons is also preserved when both the chalcogen and the Group 4 element are simultaneously replaced by a Group 5 element. The resulting pnictide square sheets then carry six electrons per atom as well ($Th^{4+}(Pn^{atom})^{3-}(Pn^{square})^-$; Pn = As, Sb, Bi).[194–196] We will return to PbFCl type compounds in the next section when considering rare earth dichalcogenides.

In an isoelectronic substitution of ZrSiSe, tetravalent Zr is replaced by pentavalent Nb or Ta, and, simultaneously, Se by As.[197, 198] These compounds also crystallize with the same Cu_2Sb structure type, with the As atoms being found in isolated positions. The assignment of formal charges as $M^{5+}(Si^{square})^{2-}(As^{atom})^{3-}$ (M = Nb, Ta) still suggests an electron count of six electrons per atom in square Si sheets.

The next step in elaboration of these compounds was taken by Johnson and Jeitschko, who substituted isoelectronically pentavalent Nb atoms in NbSiAs by tetravalent Zr or Hf and monovalent Cu atoms.[201] The crystal structure of ZrCuAsSi is shown in Figure 39b. Cu atoms insert themselves inbetween isolated As atoms in a tetrahedrally coordinated environment. One may also think of the ZrCuAsSi crystal structure as being derived from a $ZrSi_2$ crystal structure by first replacing Si atoms in the zig-zag chains by As atoms, then inserting a plane of Cu atoms so as to break zig-zag chains into isolated atoms (compare Figures 33a and 39b).[204] Thus, the electron count of six electrons per atom in square Si sheets persists for these quaternary phases as well.

It turns out that it is possible to replace Group 5 As atoms in ZrCuAsSi and HfCuAsSi back by a Group 4 element.[202–204] The resulting $CuME_2$ (M = Hf, Zr; E = Si, Ge) ternary phases crystallize with the same ZrCuAsSi structure type, thus having one electron less per formula unit. If one assumes that an octet around each isolated Si or Ge atom, then a -1 charge has to be assigned to the Si and Ge atoms in the square sheets. In discussing the $ErSn_2$ crystal structure we have suggested that "electronically unsaturated" Sn^- square sheets develop secondary interactions with zig-zag Sn chains. One observes here a similar trend as well: the $Si^{square}-X^{atom}$ distance shrinks gradually as the electron count of the square sheet diminishes from 6 to 5.5 and then to 5. For instance, the Cu–As and Cu–Si bond lengths are similar in CuZrAsSi and $CuZrSi_2$, while the $Si^{square}-X^{atom}$ distance shrinks from 3.58 to 3.37 Å.

An intermediate electron count of 5.5 per square sheet atom is found in a series of compounds with the $CuHf_2Ge_4$ and $Cu_4Zr_3Si_6$ structure types (Table 6). As pointed out by Thirion and co-workers, one may imagine these compounds as being derived from the $ZrSi_2$ crystal structure by inserting Cu planes into the zig-zag chains in $ZrSi_2$.[204] In the $CuHf_2Ge_4$ crystal structure, for example, Cu planes break half of the zig-zag chains rendering the $Cu^+(Hf_2)^{8+}(Ge^{atom})^{4-}(Ge^{zig\text{-}zag})^{2-}$-$(Ge_2^{square})^{3-}$ assignment of charges. The $Cu_4Zr_3Si_6$ crystal structure is somewhat further modified, having Si_2 pairs in addition to square Si sheets and isolated atoms (Figure 40). The short Si–Si bond in the Si_2 pairs (2.29 Å) suggests that

Table 6. Compounds containing Group 4 elements which crystallize in structure types related to $ZrSi_2$.

Structure type	Compounds	Electrons per atom^{square}
Cu_2Sb	HfGeS,[192] HfGeSe,[192] HfGeTe,[192] HfSiSe,[192] HfSiTe,[192] ZrGeS,[199] ZrGeSe,[199] ZrGeTe,[199] ZrSiS,[199] ZrSiSe,[192] ZrSiTe,[199] UGeS,[200] USiS,[200] USnTe,[200] NbAsSi,[197] TaAsSi[198]	6
ZrCuAsSi	ZrCuAsSi,[201][a] HfCuAsSi,[201][a] $CuHfGe_2$,[202][b] $CuZrGe_2$,[202][b] $CuHfSi_2$,[202, 203][b] $CuZrSi_2$[202–204][b]	6[a]/5[b]
$CuHf_2Ge_4$	$CuHf_2Ge_4$, $CuHf_2Si_4$,[204] $CuZr_2Ge_4$,[205] $CuZr_2Si_4$[204]	5.5
$Cu_4Zr_3Si_6$	$Cu_4Zr_3Si_6$[204]	5.5 (see the text)

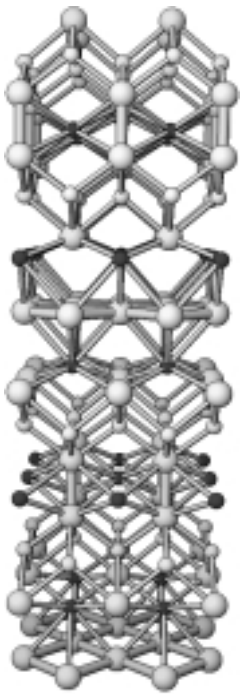


Figure 40. A perspective view of the crystal structure of $Cu_4Zr_3Si_6$. Zr = small dark spheres; Cu = small light spheres; Si = large light spheres.

they are oxidized relative to the single bond Si_2^{6-} formulation, perhaps to Si_2^{5-} (the Si–Si bond length in elemental Si with the diamond structure is 2.35 Å; the Si–Si bond in Si_2^{6-} pairs in $BaMg_2Si_2$ is 2.48 Å[206]). Assuming the −5 charge on Si_2 pairs, the remaining formal charges may be assigned as $(Cu_4)^{4+}(Zr_3)^{12+}(Si_2^{atom})^{8-}(Si_2^{pair})^{5-}(Si_2^{square})^{3-}$, namely, 5.5 electrons per Si atom in the square sheet. The Si^{square}–Si^{atom} distance of 3.47 Å is intermediate between six (CuZrAsSi) and five ($CuZrSi_2$) electrons per atom in the square sheet compounds (Table 7).

Upon substituting the Group 4 elements by chalcogens in the $ZrSi_2$ structure, two additional electrons enter the zig-zag chains and break them into isolated chalcogen atoms. A multitude of other substitutions of the resulting ZrSiS-like structures by various elements demonstrates clearly that the electron count of six electrons per square sheet atom is really dominant in related crystal structures. However, reduced electron counts of 5.5 and 5 electrons per square sheet atom are realized as well. For these compounds, "electronically unsaturated" square sheets come closer in distance to the isolated element atoms, as demonstrated earlier for the $RESn_2$ compounds. In the following subsection, which wraps up our discussion of the square sheets of Group 4 elements, we consider a group of ternary compounds with the $BaAl_4$ structure type.

11.5. Square Sheets of Group 4 Elements in the $BaAl_4$-Derived Compounds

Two common ternary derivatives of the $BaAl_4$ structure are the $ThCr_2Si_2$ and $CaBe_2Ge_2$ structure types (Figure 41). In the former one, the most electronegative element X occupies a single crystallographic site, forming X···X pairs, which may

Table 7. Selected geometrical data for various $ZrSi_2$-related crystal structures containing square Si sheets.

	Si^{square}-$X^{[a]}$ [Å]	Si^{square}-Si^{square} [Å]	M^{IV}-Si^{square} [Å]	M^{IV}-$X^{[a]}$ [Å]	Cu-$X^{[a]}$ [Å]	Electrons per $atom^{square}$
HfSeSi	3.68	2.57	2.82	2.77	–	6
ZrSeSi	3.64	2.56	2.81	2.75	–	6
CuZrAsSi	3.58	2.60	2.83	2.76	2.51	6
$CuZr_3Si_6$	3.47	2.64	2.84	2.76	2.44	5.5
$CuZrSi_2$	3.37	2.63	2.86	2.71	2.53	5
$CuHfSi_2$	3.36	2.64	2.86	2.71	2.52	5

[a] X = Se^{atom} for HfSeSi and ZrSeSi; X = As^{atom} for CuZrAsSi; X = Si^{atom} for $CuZr_3Si_6$, $CuZrSi_2$, and $CuHfSi_2$.

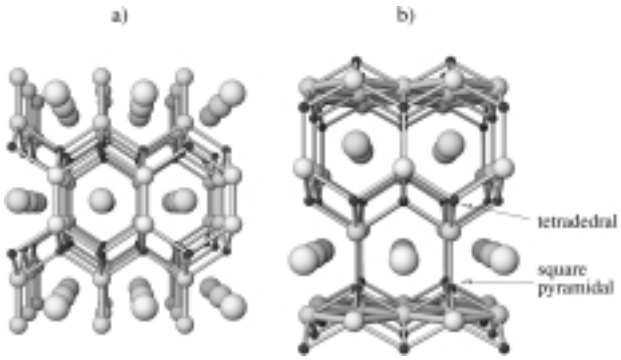


Figure 41. a) A perspective view of the crystal structure of $BaMg_2Ge_2$ ($ThCr_2Si_2$ type). Mg = small dark spheres; Ge = larger light spheres; Ba = the largest light spheres. b) A perspective view of the crystal structure of $BaZn_2Sn_2$ ($CaBe_2Ge_2$ type). Zn = small dark spheres; Sn = larger light spheres; Ba = the largest light spheres.

be bonded. In the $CaBe_2Ge_2$ crystal structure, X atoms occupy two distinct crystallographic sites, which results in square sheets and isolated atoms. Hoffmann and Zheng have analyzed the variation in X–X interactions in X_2 dumbbells in the $ThCr_2Si_2$ compounds as a function of the filling of the X_2 σ* orbital for various transition metals.[207] They have also considered the formation of $CaBe_2Ge_2$ structures as a consequence of donor–acceptor interactions.[208]

In this review we are led to still another perspective on this fascinating structure. Since X square sheets are present only in the $CaBe_2Ge_2$-type phases we are going to concentrate only on those. Furthermore, we ignore, for the moment, the interactions between the anionic X subnetwork and the remaining cations (which was the focus of the previous work). From this simplified point of view, the assignment of charges to alkaline earth members of this structural family is rather straightforward: $Ca^{2+}(Be^{2+})_2(Ge^{atom})^{4-}(Ge^{square})^{2-}$, that is, again six electrons per atom in square Ge sheets. The rather long Ge–Ge bond length of 2.84 Å within square Ge^{2-} sheets[209] is consistent with the hypervalent nature of those bonds.

The same electron count is present for other alkaline earth compounds, namely $BaMg_2Pb_2$ (Pb–Pb bond length is 3.54 Å in square sheets) and $BaZn_2Sn_2$ (Sn–Sn bond length is 3.32 Å in square sheets), assuming Zn is divalent in the latter compound.[209] The $BaMg_2Sn_2$ crystal structure (Figure 42) is an intergrowth of $ThCr_2Si_2$ and $CaBe_2Ge_2$ structure types, namely, square Sn

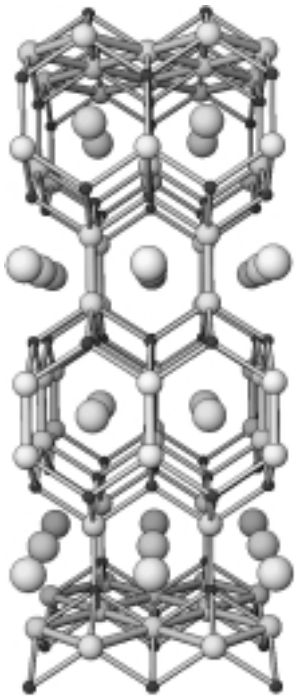


Figure 42. A perspective view of the crystal structure of $BaMg_2Sn_2$. Mg = small dark spheres; Sn = larger light spheres; Ba = the largest light spheres.

sheets, Sn_2 dumbbells, and isolated Sn atoms are present simultaneously.[206] If we follow our usual path and assign a -4 charge to isolated Sn, a -6 charge to Sn_2 pairs, then we are led again to square Sn^{2-} sheets ($(Ba_2)^{4+}(Mg_4)^{8+}(Sn^{atom})^{4-}(Sn_2^{pair})^{6-}(Sn^{square})^{2-}$). The Sn–Sn distance of 3.46 Å within square Sn^{2-} sheets, although within a hypervalent bonding range, is noticeably longer than the Sn–Sn distance of 3.13 Å found in square Sn^{2-} sheets in $ThSn_2$. It is not clear at present if such a difference in Sn–Sn bond lengths is caused by electronic or by electrostatic and size factors.

A few MM'_2X_2 compounds (M = U, La, Ce, Sm; M′ = Ni, Cu, Rh, Pd, Ir, Pt) with the $CaBe_2Ge_2$ structure type have been reported.[182, 191, 210–212] Here we concern ourselves only with the Cu-containing compounds, where we could possibly speculate about the possible formal oxidation states of the Cu atoms. In the MCu_2X_2 ($CaBe_2Ge_2$-type) structure there are two distinct types of Cu atoms, those having tetrahedral and square-pyramidal coordinations (Figure 41 b). We discussed earlier the proposition of Schäfer and co-workers to consider Cu as dipositive in $LaCu_{0.56}Sn_2$,[182] the Cu atoms also having a square-pyramidal coordination. If one extends this line of reasoning and assumes square-pyramidal Cu atoms to be dipositive, and the tetrahedral Cu atoms to be monopositive, then the following picture emerges for Cu ternary phases with the $CaBe_2Ge_2$ structure.

Purwanto and co-workers have reported the $UCu_{1.5}Sn_2$ crystal structure, in which the Cu deficiency is fully concentrated in square-pyramidal sites.[213] If U is assumed to be tetravalent, one arrives at the $U^{4+}(Cu^{tetr.})^{+}(Cu_{0.5}^{sq\text{-}pyr.})^{+}(Sn^{atom})^{4-}(Sn^{square})^{2-}$ formulation. This interpretation is consistent with Cu having a full occupancy in related rare earth compounds ($RECu_2Sn_2$, RE = La, Ce, Sm), as the loss of a single electron in the U/RE substitution is compensated by additional 0.5 Cu^{2+} square-pyramidal ions.[182, 214–217] Although our suggestion of mixed Cu^{2+}/Cu^{+} oxidation states is consistent both with the earlier work of Schäfer and co-workers,[182] as well as with the stoichiometries of reported experimental compounds, it remains somewhat speculative. Unfortunately, we can say even less about $CaBe_2Ge_2$-type compounds containing Ir, Rh, Ni, Pd, and Pt—a common difficulty in determining formal oxidation states of these nonmagnetic transition metal atoms.[211, 215, 216, 218, 219] Another interesting complication of many of these phases is the rich interplay of Kondo-like and heavy fermion behavior.[211, 214–216]

Ternary alkaline earth compounds having the $CaBe_2Ge_2$ crystal structure contain square sheets of Group 4 elements which carry six electrons per square sheet atom. If one assumes a mixed Cu^{+}/Cu^{2+} valence in the ternary U/rare earth compounds, then one is led to six electrons per square sheet atom in these compounds as well. The difficulty of assigning a formal charge to other transition metals in $CaBe_2Ge_2$-type phases renders it difficult to make the electron counting in square sheets of these phases definitive.

11.6. Summary

We have looked in this section at binary, ternary, and quaternary compounds of Group 4 elements which contain square sheets as a structural motif. Square sheets carry six electrons per atom in $M^{IV}X_2$ compounds having the $ZrSi_2$ crystal structure, which is consistent with our hypervalent bonding scheme. When the tetravalent metal is replaced by a trivalent rare earth one, then square sheets are realized in two structure types: $TbGe_2$ and $ZrSi_2$. The electron count of six electrons per atom in compounds of the $TbGe_2$ type is reduced to five in $ZrSi_2$-type compounds. In the latter, the "electronic unsaturation" of square sheets leads to secondary interactions of the sheets with zig-zag chains. The ultimate manifestation of this extra bonding is the structural collapse of square sheets and zig-zag chains into two-dimensional sheets of vertex-sharing Sn octahedra in the $NdSn_2$ structure.

When square-pyramidal voids in the $ZrSi_2$ structure are filled by metal ions, a $CeNiSi_2$ structure type is formed. It is suggested that in most of these compounds the square sheets of Group 4 elements carry six electrons per atom.

If a substitution is made in the $ZrSi_2$ structure so as to inject more electrons into the anionic subnetwork, then these extra electrons enter the zig-zag chains, breaking them apart. The resulting ternary and quaternary phases crystallize in several structure types, having six electrons per square sheet atom in most of the compounds. Reduced electron counts of 5 and 5.5 electrons per atom are realized as well, which result again in certain secondary interactions between square sheets and zig-zag chains or isolated atoms.

Square sheets of Group 4 elements are also found in the $CaBe_2Ge_2$ structure type, a ternary derivative of the well-known $BaAl_4$ structure. For those compounds where the assignment of oxidation states to metal cations is unambiguous, we find an electron count of six electrons per atom in square sheets. For the Cu-containing ternary phases we have proposed a mixed Cu^{2+}/Cu^{+} valence, which would also result in six electrons per square sheet atom in these compounds. The oxidation states of other transition metals with the $CaBe_2Ge_2$ structure type have not been determined.

The overall analysis of the compounds containing square sheets of Group 4 elements strongly indicates a preferred electron count of six electrons per square sheet atom. However, electron counts between five and six electrons per square sheet atom are realized as well. In certain cases these unsaturated square sheets develop secondary interactions with other anionic subnetworks.

Having looked at a large number of compounds containing square sheets of Group 4 and 5 elements, we have not found any that carry more than six electrons per square sheet atom. Square chalcogen sheets provide an opportunity to examine square sheets which are electron rich relative to our formulation, the last topic of our paper.

12. Square Chalcogen Sheets

In applying our electron counting scheme to square sheets of chalcogen atoms one is immediately faced with the following problem: chalcogen atoms carrying six electrons (the magic number for the square sheet) would be neutral. We have not really stressed the significance of ionic interactions in this paper, but it is self-evident that Madelung energies

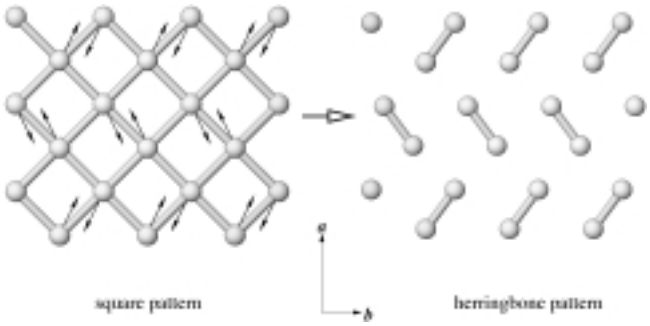
influence critically the stability of a particular crystal structure relative to other alternatives. Given that the square sheets of chalcogen atoms would be immersed in the matrix of surrounding cations, their charge neutrality would undermine ionic forces which would otherwise strongly bind anionic sheets in the lattice. A possible way to overcome the charge neutrality problem is to place additional negative charge on the square chalcogen sheets. However, by thus solving one difficulty we have simultaneously created another one: those additional electrons would enter square sheet states which are strongly antibonding, thus weakening the bonding between the square sheet chalcogen atoms. In the extreme case, no bonding interactions are expected between Te^{2-} ions.

In the following discussion we examine in some detail square sheets of chalcogen atoms in a variety of binary, ternary, and quaternary phases. Our goal is to assess empirically what might be the maximum negative charge which may be placed on chalcogen atoms in square sheets. Almost all chalcogen square sheets that we have looked at are susceptible to a CDW formation, a feature critical for our subsequent analysis.

12.1. Binary RES_2, $RESe_2$, and $RETe_2$ Phases

We have discussed the PbFCl structure in some detail when considering the ZrSiSe ternary phase (Figure 39a). If tetravalent Zr is replaced by trivalent Nd and, in addition, Si and Se are replaced by Te, then the $NdTe_2$ structure is obtained (Figure 43).[220, 221] This structure consists of Te square sheets as well as isolated Te atoms. The Te–Te distance within Te square sheets is 3.10 Å, a typical hypervalent Te–Te bond length (3.05 Å in hypervalent Te_5^{2-} in Cs_2Te_5.[113])

The electron count of six electrons per square sheet Si atom was established for the ZrSiSe phase $(Zr^{4+}(Si^{square})^{2-}$-$(Se^{atom})^{2-}$; see Section 11.4). When Zr is substituted by Nd, one electron is lost, which in turn is over-compensated by two electrons as Group 4 Si atoms are replaced by Group 6 Te atoms (the replacement of Se by Te is isoelectronic). The resulting assignment of charges, $Nd^{3+}(Te^{atom})^{2-}(Te^{square})^{-}$, seems to imply the existence of square sheets of main group elements with the electron count of seven electrons per atom. However, the story is not so simple. A closer look at the $NdTe_2$ crystal structure data reveals very large in-plane pancakelike parameters of anisotropic displacement for the square Te atoms, a feature seen also in the $LaTe_2$ and $CeTe_2$ crystal structures.[221, 222] The in-plane Te anisotropy, combined with the reported Te deficiency for many $RETe_2$ phases, points to possible distortions of square sheets in these compounds.[220, 223–225] These distortions are more clearly pronounced for similar rare earth diselenides, so we take a look at them first. Rare earth diselenides have been reported with various degrees of nonstoichiometry, which critically influences their corresponding crystal structures. The stoichiometric $RESe_2$ phases crystallize in a derivative of the PbFCl structure, in which the square Se sheets are distorted into a herringbone network of Se_2 pairs ($CeSe_2$[226]; $LaSe_2$[227, 228]; $PrSe_2$[229]). A schematic diagram of the distortion pathway is given below (Scheme 22). If the Se lattice were undistorted,



Scheme 22.

the Se–Se distance would be a uniform 2.98 Å, while in the real herringbone lattice ($CeSe_2$[226]) there are Se–Se short intrapair (2.47 Å) and long interpair (3.06 Å, 3.06 Å, 3.40 Å) distances. Lee and Foran rationalized the Se herringbone pattern in terms of maximum HOMO–LUMO interactions between the lone pair on Se_2 (HOMO) with the Se_2 σ* orbital (LUMO).[20]

Pair formation from square Se^{-} sheets is perhaps an indication of the instability of square sheets carrying seven electrons per atom. It is remarkable that the resulting "classical" $RE^{3+}(Se^{atom})^{2-}(Se^{pair})^{-}$ compounds obey Zintl–Klemm electron counting rules. Chen and Dorhout have prepared rare earth disulfides with the same $CeSe_2$ crystal structure (RE = La, Pr).[229] As we have mentioned earlier, the crystal structures of rare earth ditellurides have been refined so as to produce undistorted square Te lattices. This, however, leads to strong in-plane anisotropies.[221, 222] DiMasi, Lee, and co-workers examined $LaTe_2$ crystals with a transmission electron microscopy, and they observed superstructure reflections corresponding to the wave vector $q = a^*/2$. Since a similar doubling of the *a* axis also occurs in the distortion of

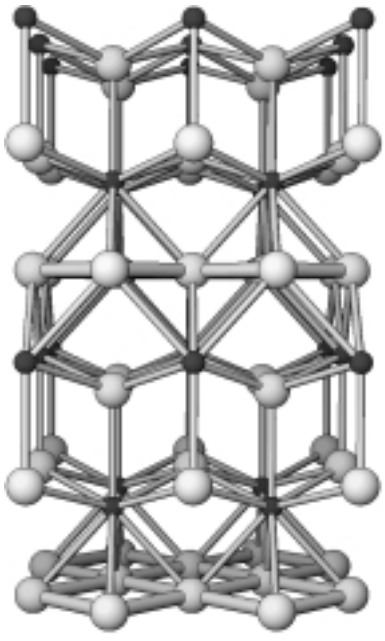


Figure 43. A perspective view of the crystal structure of $NdTe_2$ (PbFCl type). Nd = small dark spheres; Te = large light spheres.

square Se sheets to the herringbone network discussed above, the authors examined and found a general agreement between the experimental diffraction pattern and a simulated diffraction pattern resulting from a CDW similar to $LaSe_2$.[20] Consequently, their study (combined with earlier discovery of strong square Te anisotropy) points to the instability of square sheets of seven electrons per atom with respect to a CDW formation.

This conclusion is further supported by the physical property measurements on $LaTe_2$ and $CeTe_2$, carried out by Kwon and co-workers.[222, 230, 231] The electrical resistivity data indicates that $CeTe_2$ is a semimetal with "extremely low carrier concentration".[231] This picture is consistent with a CDW formation in conducting square Te sheets, which in turn would open gaps in most parts of the Fermi surface.

In summary, stoichiometric rare earth diselenides and disulfides form herringbonelike distorted square sheets, which indicates that the pair formation from a seven electron per atom square sheet is a strongly favorable process. The same conclusion applies to Te^- square sheets as demonstrated by the CDW formation in $LaTe_2$ and $CeTe_2$. The instability of square sheets carrying seven electrons per atom manifests itself in another yet way: by creating vacancies in square sheets. This subject has been discussed in some detail for the $RESe_{2-x}$ and $RETe_{2-x}$ phases by Lee and co-workers,[21, 22, 232–234] following earlier structural work.[235–237]

12.2. Binary $RETe_3$ and RE_2Te_5 Phases

The $NdTe_3$ structure may be thought of as being derived from the $NdTe_2$ structure by doubling all square Te sheets in the latter (compare Figures 43 and 44). As a result nonbonding contacts develop between neighboring square Te sheets.[238] One may assign charges to $NdTe_3$ as $Nd^{3+}(Te^{atom})^{2-}(Te_2^{square})^-$, that is, only 6.5 electrons reside in square Te sheets. Since this is intermediate between the presumably stable six electrons per atom and the unstable seven electrons per atom electron counts, one would expect a higher degree of stability from square Te sheets in $NdTe_3$.

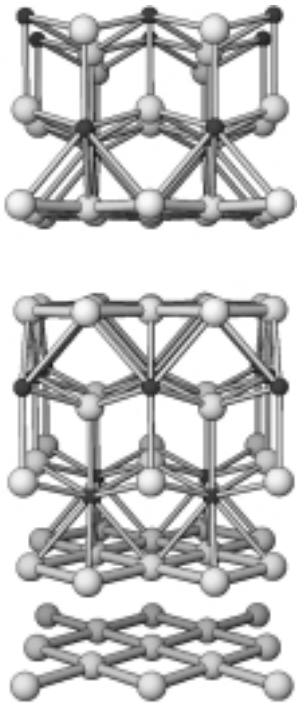


Figure 44. A perspective view of the crystal structure of $NdTe_3$. Nd = small dark spheres; Te = large light spheres.

This is indeed what happens. An X-ray structural analysis of $SmTe_3$ by Lee and co-workers indicated only a slight anisotropy of the square Te atoms, which points to a smaller amplitude of the square sheet distortion.[239] Transmission electron microscopy measurements on a number of rare earth tritellurides (RE = La, Sm, Gd, Tb, Dy, Ho, Er, Tm) demonstrated incommensurate CDW distortions in the square Te sheets, with a sinusoidal modulation of square Te atomic positions.[23] The experimentally observed superlattice wave vector agrees well with the Fermi surface nesting vector determined from extended Hückel calculations.[23] The resulting partial band gap opening was measured directly by angle-resolved photoemission spectroscopy (ARPES), which provided direct evidence of the Fermi surface nesting picture.[240] Since some of parts of the Fermi surface persist, these compounds exhibit metallic properties.[239]

Noël and Levet reported the β-UTe_3 crystal structure to be isostructural to $NdTe_3$.[241] Magnetic susceptibility measurements were consistent with a +4 oxidation state for the U atoms, which would correspond to the $U^{4+}(Te^{atom})^{2-}(Te_2^{square})^{2-}$ assignment of charges.[241] CDW distortion of the resulting square Te^- sheets was not examined, a possibility which would be anticipated from the discussion above.

Consecutive single and double square Te sheets are separated by isolated SmTe slabs in another related rare earth–Te binary phase, Sm_2Te_5. This compound may be thought of as an intergrowth of $NdTe_2$ and $NdTe_3$ crystal structures (not shown here).[239] The Sm_2Te_5 crystal structure refinement by Lee and co-workers showed that Te atoms in single square sheets were partially occupied and possessed anisotropic thermal parameters.[239] One could speculate that the metallic conductivity demonstrated by Sm_2Te_5 occurs predominantly through less-distorted double sheets of Te atoms.

The $KCuCeTe_4$ quaternary phase is also an intergrowth compound consisting of $CeTe_3$-like layers and $(CuTe^{atom})^-$ layers isolated by K^+ layers (Cu^+ is implied).[242] Charges may be assigned to the overall neutral $CeTe_3$ layer as $Ce^{3+}(Te^{atom})^{2-}(Te_2^{square})^-$, that is, 6.5 electrons per square sheet atom. Kanatzidis and co-workers found an incommensurate CDW distortion of square Te nets, which, however, does not completely destroy the Fermi surface of this material.[242]

Given the discussion above, one may draw the conclusion that an electron count of 6.5 electrons per square sheet Te atom stabilizes somewhat those square sheets, producing only small amplitude incommensurate CDW. However, strong distortions are observed in the relatively isolated square $Te^{2/3-}$ sheets in quaternary $K_{0.33}Ba_{0.67}AgTe_2$.[24] We examine this next, as well as the highly unusual zig-zag Te chain formation from defect square Te sheets found in the ternary ARE_3Te_8 series of compounds (A = K, Cs, Rb; RE = Ce, Nd).[243]

12.3. $K_{0.33}Ba_{0.67}AgTe_2$ and ARE_3Te_8 Phases

A perspective view of the $K_{0.33}Ba_{0.67}AgTe_2$ crystal structure is shown in Figure 45.[24] The layered structure consists of square Te sheets and isolated AgTe slabs sandwiched between K/Ba layers. The assignment of formal charges, $(K_{0.33})^{0.33+}(Ba_{0.67})^{1.34+}Ag^+(Te^{atom})^{2-}(Te^{square})^{0.67-}$, suggests 6.67 electrons in the square Te sheets. A remarkable feature of the $K_{0.33}Ba_{0.67}AgTe_2$ crystal structure is the isolated character of the square Te sheets which neighbor only K/Ba atoms. Thus,

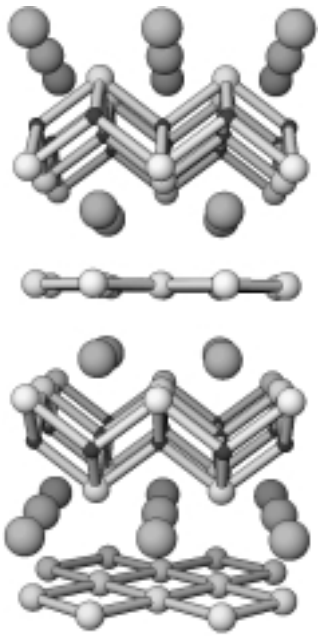
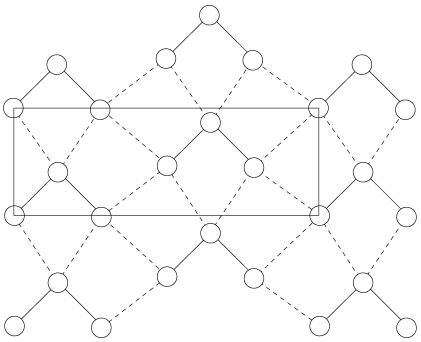


Figure 45. A perspective view of the crystal structure of $K_{0.33}Ba_{0.67}AgTe_2$. Te = medium light spheres; Ag = small light spheres; $K_{0.33}/Ba_{0.67}$ = large light spheres.

these square sheets provide a good opportunity to examine distortions of the square Te sheet free from the interference of other interactions.

The crystal structure refinement of $K_{0.33}Ba_{0.67}AgTe_2$ (carried out by Lee, Kanatzidis, and co-workers) indicated anisotropic thermal parameters for the Te atoms in the square, elongated along Te–Te bonds.[24] Electron diffraction studies revealed a CDW formation, consistent with the semiconducting nature of this compound (namely, completely destroyed Fermi surface).[24] Second moment scaled extended Hückel calculations suggested several distortion pathways; the lowest energy structure is shown in Scheme 23. The simulated diffraction pattern calculated for this distortion agreed well with the experimental one.[24] Although Te_3^{2-} trimers are engaged in strong secondary interactions which maximize their HOMO–LUMO interactions,[24] they are essentially classical Zintl–Klemm anions. It is remarkable that square Te^- sheets oligomerize into Te_2^{2-} pairs while square $Te^{2/3-}$ sheets distort into Te_3^{2-} trimers.



Scheme 23.

Another peculiar distortion of defect square Te sheets is observed in ARE_3Te_8 ternary phases (A = K, Cs, Rb; RE = Ce, Nd).[243] Their corresponding structures, not shown here, consists of defect $RETe_3$ layers (see Section 12.2) sandwiched between alkali cations. Te defects occur in square sheets, which leads to the assignment of charge as $A^+(RE_3)^{9+}(Te_3^{atom})^{6-}(Te_5^{square})^{4-}$. The authors were able to refine further the Te positions in distorted square sheets, which produced the superstructure shown in Figure 46. This

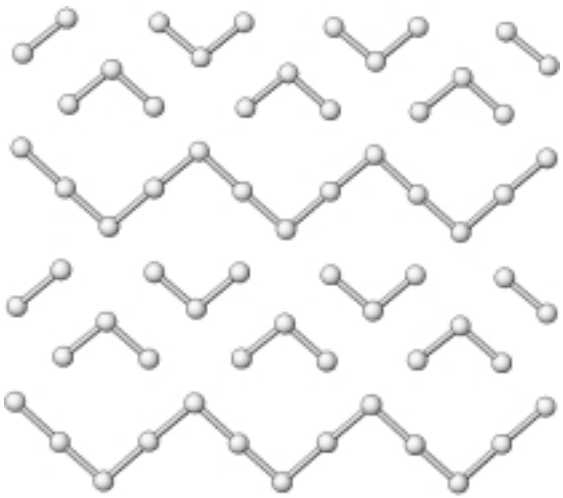


Figure 46. The defect-distorted square Te lattice in KNd_3Te_8.

square lattice distortion was predicted earlier by Lee and coworkers on theoretical grounds.[232]

Defect square Te_5^{4-} sheets in ARE_3Te_8 break into Te_3^{2-} classical trimers and infinite zig-zag Te_2^{2-} chains (see Figure 46). We examine the electron counting in the latter zig-zag chains using the following simple arguments: Te zig-zag chains consist of two types of Te atoms—those having bent and linear local geometries. Two-connected bent Te atoms are classical, thus, carry six electrons (no charge). Two-connected linear Te atoms should be compared to Xe (as in XeF_2), therefore, they carry a -2 charge. On adding up the charges on two Te atoms one arrives at the Te_2^{2-} formulation, which agrees with the experimental assignment of charges. The semiconducting behavior of these compounds is consistent with the strongly distorted nature of square Te sheets.

Square $Te^{2/3-}$ sheets in $K_{0.33}Ba_{0.67}AgTe_2$ are strongly distorted into classical Te_3^{2-} trimers, which demonstrate semiconducting properties. Defect square Te_5^{4-} sheets in the ARE_3Te_8 series of compounds are also oligomerized into Te_3^{2-} classical trimers and unusual infinite zig-zag Te_2^{2-} chains. The electron count in the latter may be derived by taking into account the local bonding environment of Te atoms. Considering all the experimental evidence, one is led to believe that square sheets with an electron count of more than 6.5 electrons per atom are highly unstable with respect to a CDW formation.

12.4. Summary

One has to apply our electron counting scheme to chalcogen square sheets with caution, since six electrons per atom chalcogen atoms would have a neutral charge. Such neutrality would provide minimal interactions of these sheets to the surrounding cationic lattice. If additional negative charge is placed on square sheets, then a significant strengthening of ionic interactions is expected, at the cost of populating antibonding states of the square chalcogen sheet. The interplay between the latter two competing forces determines the narrow range of electron counts for which undistorted square sheets of chalcogen atoms are known to exist.

By analyzing compounds containing mononegative square chalcogen sheets one may draw a conclusion that these sheets are highly unstable with respect to formation of a classical dichalcogen pair. This is explicitly seen for stoichiometric rare earth diselenides and disulfides, in which case a herringbone network of Se_2^{2-} (S_2^{2-}) pairs is found. While undistorted square sheets are expected to be metallic, the latter compounds are semiconducting, which points to complete opening of the Fermi gap. Stoichiometric rare earth ditellurides are subject to CDW formation with presumably the same herringbone pattern structure, as demonstrated for $LaTe_2$.

Nonstoichiometric rare earth diselenides and ditellurides contain defective square sheets, which are strongly distorted into classical pairs and chalcogen atoms. These species are engaged in strong secondary contacts with each other, maximizing the interactions between the lone pair (HOMO) and the σ* orbital (LUMO). As we have explained elsewhere, there is a continuum of bonding between hypervalent electron-rich three-center bonding—so called "secondary interactions"—and donor–acceptor frontier orbital interaction.[59] All these compounds are semiconducting, which confirms Fermi gap opening caused by distortion of the square sheet.

Square Te sheets carrying only 6.5 electrons per atom are found in rare earth tritellurides. Although these sheets are also subject to CDW distortion, the latter turns out to be only a small amplitude sinusoidal modulation of the Te atomic positions of the square sheet. The directly measured Fermi surface of $SmTe_3$ demonstrates incomplete Fermi surface nesting, as also evidenced by its metallic properties.

The square $Te^{2/3-}$ sheets found in quaternary $K_{0.33}Ba_{0.67}AgTe_2$ are strongly distorted into classical Te_3^{2-} trimers, which suggests that the electron count over 6.5 electrons per atom causes square Te sheets to distort. Its semiconducting behavior is in agreement with this conclusion. Classical Te_3^{2-} trimer formation is also seen in defective square Te_5^{4-} sheets, found in the ARE_3Te_8 series of compounds. Another structural motif obtained from distortion of the square sheet in these compounds is an unusual infinite Te_2^{2-} zig-zag chain. The electron count in the zig-zag Te_2^{2-} chains may be rationalized by comparing local coordination of bent and linear two-connected Te atoms to molecular analogues.

Our survey of square chalcogen sheets strongly suggests the upper limit of 6.5 electrons per square sheet atom as a condition of undistorted square sheet stability. More negatively charged square chalcogen sheets oligomerize into both classical species as well as nonclassical ones (zig-zag Te_2^{2-} chains in ARE_3Te_8). On the other hand no neutral or cationic square chalcogen sheets are known, as expected from simple electrostatic and electronegativity arguments. Taking into account the earlier discussion on square sheets of Sb and Group 4 elements, we believe that the stability zone for square sheet electron counts lies between 5.5 and 6.5 electrons per atom.

13. Summary and Outlook

Heavy late main group elements tend to form unusual, if sometimes geometrically simple, extended low-dimensional networks which just do not occur "normally" in molecules. In this paper we have carried through a systematic analysis of electron-rich multi-center extended structures aimed at deriving unambiguous electron counting schemes for various topologies. In particular we looked at a linear 1D chain (seven electrons per atom), a square sheet (six electrons peratom), a cubic lattice (five electrons per atom), an 1D ladder (six electrons per atom), a 1D X_3 strip (20 electrons per three atoms), and a number of more complex networks derived from these building blocks. We also exemplified the use of these building blocks in an aufbau of more complex structures.

We have also outlined the reasons and the possible pathways of the Peierls distortions for some of these networks. Relatively weak s-p mixing for heavier main group elements, caused by the contraction of less-screened s orbitals, is one of the main reasons behind the existence of their low-dimensional Peierls-undistorted metallic networks. In contrast, we think that strong s-p mixing for light elements (for example N) makes their Peierls distortion extremely favorable, thus excluding, for instance, the possibility of the existence of hypervalent networks of N.

Combined with classical Zintl–Klemm electron counting, the hypervalent electron counting scheme derived here may be successfully applied to understand the electronic structures of a large variety of Sb compounds. Linear Sb^{2-} chains, square Sb^- sheets, and other nonclassical networks are found in a great number of seemingly unrelated Sb phases. Indeed, we have yet to encounter an Sb phase which is in a clear violation of the proposed electron counting scheme.

Actually, because of the fractional filling of hypervalent bands in these networks, we expect the numbers of electrons derived for each network to vary a little. Linear chains of elements other than Sb also indicate that seven electrons per linear chain atom is a preferred electron count; however, some linear chains have electron count of 7.25 electrons per atom. Interestingly enough, this simple linear chain electron count serves successfully as a good starting point for rationalizing the electronic structure of a nontrivial three-dimensional network, that is found in the Tl_4SnTe_3 series of compounds.

We have also examined in great detail square sheets of Group 4 and Group 6 elements. In the former case, the preferred electron count is clearly six electrons per square sheet atom. However, some square sheets of Group 4 elements are also realized with lesser electron counts of 5.5 and 5 electrons per atom, in which case secondary interactions develop between "electronically unsaturated" square sheets and other anionic subnetworks.

Six electrons per square sheet atom would render chalcogen atoms neutral, not an advantage in an anionic atmosphere. Consequently, one expects somewhat negative square chalcogen sheets to be more stable. Most of the square chalcogen sheets carrying seven electrons per square sheet atom are severely distorted into classical dichalcogen pairs (for example the Se_2^{2-} herringbone network in $LaSe_2$). The strong tendency to form defect square sheets as well as the persistence of CDW distortions also emphasizes the intrinsic instability of square sheets carrying seven electrons per atom. It appears that 6.5 electrons per chalcogen atom in the square sheets, as found in rare earth tritellurides, are less distorted,

although a small amplitude CDW formation is still observed. It is quite remarkable that in an aufbau using both classical and hypervalent building blocks, it has been possible to make sense of bonding in nontrivial intermetallic compounds as complex as $La_{12}Mn_2Sb_{30}$. We hope that with the help of the hypervalent building blocks discussed in this paper, many other intermetallic compounds of heavy late main group elements may be successfully studied as well.

14. Appendix I: Computational Details

All calculations were performed with the help of "Yet Another extended Hückel Molecular Orbital Package (YAeHMOP)", a program developed in our group by G. Landrum.[244] The standard atomic parameters were used for Sb, N, and Zr. The parameters are listed in Table 8 with the corresponding references.

Table 8. Extended Hückel parameters. The ζ values are the exponents of the Slater orbital basis set, the c_i values the coefficients in a double-ζ expansion.

Atom	Orbital	H_{ii} [eV]	ζ_1	c_1	ζ_2	(c_2)	Ref.
Sb	5s	– 18.8	2.323				[268]
	5p	– 11.7	1.999				
N	2s	– 26.0	1.95				[77]
	2p	– 13.4	1.95				
Zr	5s	– 9.87	1.817				[269]
	5p	– 6.76	1.776				
	4d	– 11.18	3.835	0.6210	1.505	0.5769	

Addendum

While this manuscript was in press we learned that Stöwe had found that TlTe undergoes a rather peculiar Pierls distortion at 172 K, where only half of the chains with "handles" are affected.[270] The pairing distortion indicates the preservation of the band structure patterns of the underlying simple linear chain in the composite chain. Stöwe has also offered direct structural evidence of the square Te sheet distortion in $LaTe_2$ and $PrTe_2$.[271] This observation is consistent with the instability of the electron count of seven electrons per atom in a square sheet, as advocated throughout this review.

We thank many former and current members of our research group, in particular, Norman Goldberg, Dong-Kyun Seo, Grigori Vajenine and Peter Kroll for helpful discussions. We also express our gratitude to Greg Landrum, Arthur Mar, and Stephen Lee for reading this manuscript and suggesting improvements. Hans Georg von Schnering made many important suggestions to us in the course of reviewing our paper. We gratefully acknowledge the National Science Foundation for its generous support of this work by Research Grant CHE-9970089 and the Cornell Theory Center for computer time. Drawings of all crystal structures were produced with the "Atoms 3.1" software package.

Received: July 6, 1999 [A 352]

[1] E. Zintl, *Angew. Chem.* **1939**, 52, 1.
[2] *Chemistry, Structure, and Bonding of Zintl Phases and Ions* (Ed.: S. M. Kauzlarich), VCH, New York, **1996**.
[3] H. Schäfer, B. Eisenmann, W. Müller, *Angew. Chem.* **1973**, *85*, 742; Ang*ew. Chem. Int. Ed.* **1973**, *12*, 694.
[4] A. Simon, *J. Solid. State Chem.* **1985**, *57*, 2.
[5] S. Lee, L. Hoistad, *J. Alloys Comp.* **1995**, *229*, 66.
[6] U. Häussermann, R. Nesper, *J. Alloys Comp.* **1995**, *218*, 244.
[7] K. Wade, *Inorg. Chem. Radiochem.* **1976**, *18*, 1.
[8] D. P. Mingos, D. J. Wales, *Introduction To Cluster Chemistry*, Prentice Hall, Englewood Clis, NJ, USA, **1990**.
[9] C. Zheng, R. Hoffmann, *Z. Naturforsch. B* **1986**, *41*, 292.
[10] C. Belin, M. Tillard-Charbonnel, *Prog. Solid State Chem.* **1993**, *22*, 59.
[11] R. Nesper, *Angew. Chem.* **1991**, *103*, 806; *Angew. Chem. Ed. Engl.* **1991**, *30*, 789.
[12] M. Brylak, W. Jeitschko, *Z. Naturforsch. B* **1994**, *49*, 747.
[13] M. Brylak, M. H. Möller, W. Jeitschko, *J. Solid State Chem.* **1995**, *115*, 305.
[14] R. Nesper, *Prog. Solid State Chem.* **1990**, *20*, 1.
[15] W. Müller, *Z. Naturforsch. B* **1977**, *32*, 357.
[16] T. Albright, J. Burdett, M.-H. Whangbo, *Orbital Interactions in Chemistry*, Wiley, New York, **1985**.
[17] R. Hoffmann, *A Chemist's View of Bonding in Extended Structures*, VCH, New York, **1988**.
[18] R. E. Peierls, *Quantum Theory of Solids*, Oxford University Press, London, **1955**.
[19] W. Tremel, R. Hoffmann, *J. Am. Chem. Soc.* **1987**, *109*, 124.
[20] E. DiMasi, B. Foran, M. C. Aronson, S. Lee, *Phys. Rev. B* **1996**, *54*, 12587.
[21] S. Lee, B. Foran, *J. Am. Chem. Soc.* **1996**, *118*, 9139.
[22] E. DiMasi, M. C. Aronson, B. Foran, S. Lee, *Physica B* **1995**, *206/207*, 386.
[23] E. DiMasi, M. C. Aronson, J. F. Mansfield, B. Foran, S. Lee, *Phys. Rev. B* **1995**, *52*, 14516.
[24] X. Zhang, J. Li, B. Foran, S. Lee, H.-Y Guo, T. Hogan, C. R. Kannewurf, M. G. Kanatzidis, *J. Am. Chem. Soc.* **1995**, *117*, 10513.
[25] N. Tokitoh, Y. Arai, T. Sasamori, R. Okazaki, S. Nagase, H. Uekusa, Y. Ohashi, *J. Am. Chem. Soc.* **1998**, *120*, 433.
[26] R. Hoffmann, *Am. Sci.* **1991**, *79*, 11.
[27] If one π bond is included in the Sb four-ring, then the corresponding electron count diminishes by two. In this treatment we neglect the possibility of π bonding between Sb atoms, a position justified by the extreme rearness of Sb–Sb π bonds.
[28] N. N. Zuravlev, G. S. Zhdanov, *Sov. Phys. Crystallogr.* **1956**, *1*, 404.
[29] S. Rundqvist, N. O. Ersson, *Ark. Kemi* **1968**, *30*, 103.
[30] D. J. Braun, W. Jeitschko, *J. Less-Common Met.* **1980**, *72*, 147.
[31] C. B. H. Evers, W. Jeitschko, L. Boonk, D. J. Braun, T. Ebel, U. D. Scholz , *J. Alloys Comp.* **1995**, *224*, 184.
[32] D. Jung, M.-H. Whangbo, S. Alvarez, *Inorg. Chem.* **1990**, *29*, 2252.
[33] T. Schmidt, G. Kliche, H. D. Lutz, *Acta Cristallogr. Sec. C* **1987**, *43*, 1678.
[34] F. Grandjean, A. Gèrard, D. J. Braun, W. Jeitschko, *J. Phys. Chem. Solids* **1984**, *45*, 877.
[35] G. P. Meisner, M. S. Torikachvili, K. N. Yang, M. B. Maple, R. P. Guertin, *J. Appl. Phys.* **1985**, *57*, 3073.
[36] B. Eisenmann, H. Jordan, H. Schäfer, *Z. Naturforsch. B* **1985**, *40*, 1603.
[37] G. Chapius, F. Hulliger, R. Schmelczer, *J. Solid. State Chem.* **1980**, *31*, 59.
[38] B. Eisenmann, *Z. Naturforsch. B* **1979**, *34*, 1162.
[39] W. Hönle, H. G. von Schnering, *Z. Kristallogr.* **1981**, *155*, 307.
[40] F. Hulliger, R. Schmelczer, *J. Solid State Chem.* **1978**, *26*, 389.
[41] N. W. Alcock, *Adv. Inorg. Radiochem.* **1972**, 15, 1.
[42] G. A. Landrum, R. Hoffmann, *Angew. Chem.*, in press.
[43] K. Deller, B. Eisenmann, *Z. Naturforsch. B* **1978**, *33*, 676.
[44] C. S. Barrett, P. Cucka, K. Haefner, *Acta Crystallogr.* **1963**, *16*, 451.
[45] L. F. Vereshchagin, S. S. Kobalkina, *Sov. Phy. JETP (Engl. Transl.)* **1965**, *20*, 274.
[46] D. Akhtar, V. D. Vankar, T. C. Goel, K. L. Chopra, *J. Mater. Sci.* **1979**, *14*, 988.
[47] J. K. Burdett, S. Lee, *J. Am. Chem. Soc.* **1983**, *105*, 1079.
[48] G. Cordier, H. Schäfer, M. Stelter, *Z. Anorg. Allg. Chem.* **1984**, *519*, 183.

[49] A. Rehr, S. M. Kauzlarich, *J. Alloys Comp*. **1994**, *207*, 424.
[50] R. F. Gallup, C. Y. Fong, S. M. Kauzlarich, *Inorg. Chem*. **1992**, *31*, 115.
[51] S. M. Kauzlarich, M. M. Thomas, D. A. Odink, M. M. Olmstead, *J. Am. Chem. Soc*. **1991**, *113*, 7205.
[52] R. E. Rundle, *J. Am. Chem. Soc*. **1963**, *85*, 112.
[53] R. E. Rundle, *J. Am. Chem. Soc*. **1979**, *101*, 5057.
[54] G. C. Pimentel, *J. Chem. Phys*. **1951**, *19*, 446.
[55] J. I. Musher, *Angew. Chem*. **1969**, *81*, 68; *Angew. Chem. Int. Ed. Engl*. **1969**, *8*, 54.
[56] M. Häser, *J. Am. Chem. Soc*. **1996**, *118*, 7311.
[57] The octahedral symmetry introduces some special features, which cause one to think about degrees of hypervalency: G. A. Landrum, H. B. Bürgi, R. Hoffmann, T. Ward, unpublished results.
[58] M. J. Ferguson, R. W. Hushagen, A. Mar, *J. Alloys Comp*. **1997**, *249*, 191.
[59] G. A. Landrum, N. Goldberg, R. Hoffmann, *J. Chem. Soc. Dalton Trans*. **1997**, 3605.
[60] P. Pyykkö, *Chem. Rev*. **1997**, *97*, 597.
[61] B. R. Wang, R. Bodnar, H. Steinfink, *Inorg. Chem*. **1966**, *5*, 1468.
[62] P. C. Canfield, J. D. Thompson, Z. Fisk, *J. Appl. Phys*. **1991**, *70*, 5992.
[63] E. Brechtel, G. Cordier, H. Schäfer, *J. Less-Common Met*. **1981**, *79*, 131.
[64] G. Cordier, H. Schäfer, P. Woll, *Z. Naturforsch. B* **1985**, *40*, 1097.
[65] O. Sologub, K. Hiebl, P. Rogl, H. Noël, O. Bodak, *J. Alloys Comp*. **1994**, *210*, 153.
[66] A. Leithe-Jasper, P. Rogl, *J. Alloys Comp*. **1994**, *203*, 133.
[67] O. Sologub, H. Noël, A. Leithe-Jasper, P. Rogl, *J. Solid State Chem*. **1995**, *115*, 441.
[68] O. Sologub, K. Hiebl, P. Rogl, O. Bodak, *J. Alloys Comp*. **1995**, *227*, 40.
[69] P. Wollesen, W. Jeitschko, M. Brylak, L. Dietrich, *J. Alloys Comp*. **1996**, *245*, L5.
[70] H. Flandorfer, O. Sologub, C. Godart, K. Hiebl, A. Leithe-Jasper, P. Rogl, H. Noël, *Solid State Commun*. **1996**, *97*, 561.
[71] O. Sologub, M. Vybornovand, P. Rogl, K. Hiebl, G. Cordier, P. Woll, *J. Solid. State Chem*. **1996**, *122*, 262.
[72] H. Holseth, A. Kjekshus, *Acta Chem. Scand*. **1968**, *22*, 3273.
[73] H. Holseth, A. Kjekshus, *J. Less-Common Met*. **1968**, *16*, 472.
[74] T. Siegrist, F. Hulliger, *J. Solid. State Chem*. **1986**, *63*, 23.
[75] G. Bruzzone, G. B. Bonino, *Atti. Accad. Naz. Lincei Cl. Sci. Fis. Mat. Nat. Rend.* **1970**, *48*, 235.
[76] C. B. Showmaker, D. P. Shoemaker, *Acta Crystallogr*. **1965**, *18*, 900.
[77] R. Hoffmann, *J. Chem. Phys*. **1963**, *39*, 1397.
[78] R. Hoffmann, *J. Chem. Phys*. **1964**, *40*, 2745.
[79] R. Hoffmann, *J. Chem. Phys*. **1964**, *40*, 2474.
[80] L. L. Lohr, *Inorg. Chem*. **1987**, *26*, 2005.
[81] T. Albright, J. Burdett, M.-H. Whangbo, *Orbital Interactions in Chemistry*, Wiley, New York, **1985**, chap. 12.
[82] R. J. Gillespie, *Molecular Geometry*, Van Nostrand-Reinhold, London, **1972**.
[83] P. Cherin, P. Unger, *Acta Cristallogr*. **1967**, *23*, 670.
[84] J. Burdett, *Chemical Bonding In Solids*, Oxford University Press, New York, **1995**.
[85] D. A. Keszler, R. Hoffmann, *J. Am. Chem. Soc*. **1987**, *109*, 118.
[86] R. Hoffmann, C. Janiak, C. Kollmar, *Macromolecules* **1991**, *24*, 3725.
[87] H. Genin, R. Hoffmann, *J. Am. Chem. Soc*. **1995**, *117*, 12328.
[88] J. K. Burdett, *Prog. Solid State Chem*. **1984**, *15*, 173.
[89] E. Canadell, M.-H. Whangbo, *Chem. Rev*. **1991**, *91*, 965.
[90] M.-H. Whangbo, E. Canadell, P. Foury, J.-P. Pouget, *Science* **1991**, *252*, 96.
[91] M.-H. Whangbo, E. Canadell, *J. Am. Chem. Soc*. **1992**, *114*, 9587.
[92] "Looking At Chemistry Through The Unifying Lens Of Molecular Orbital Theory: From Extended Hypervalent Bonding To Hydrocarbon Chemisorption And The Reactivity Of Organic Molecules": G. A. Papoian, PhD thesis, Cornell University, Ithaca, NY, USA, **1999**.
[93] A. Imamura, *Mol. Phys*. **1968**, *15*, 225.
[94] M.-H. Whangbo in *Computational Theoretical Organic Chemistry* (Eds.: I. G. Csizmadia, R. Daudel), Reidel, Boston, **1981**, p. 233.
[95] C. Froese Fischer, *At. Data* **1972**, *4*, 301.
[96] S. Lee, *J. Am. Chem. Soc*. **1991**, *113*, 8611.
[97] W. Kutzelnigg, *Angew. Chem*. **1984**, 96, 262; *Angew. Chem. Int. Ed. Engl*. **1984**, 23, 272.
[98] D.-K. Seo, R. Hoffmann, unpublished results.
[99] G. Papoian, R. Hoffmann, *J. Solid State Chem*. **1998**, *139*, 8.
[100] R. Jaggi, *Helv. Phys. Acta* **1964**, *37*, 618.
[101] T. Chattopadhyay, J. X. Boucherle, H. G. von Schnering, *J. Phys. C* **1987**, *20*, 1431.
[102] T. Chattopadhyay, R. P. Santandrea, H. G. von Schnering, *J. Phys. Chem. Solids* **1985**, *46*, 351.
[103] T. Chattopadhyay, J. Pannetier, H. G. von Schnering, *J. Phys. Chem. Solids* **1986**, *47*, 879.
[104] H. G. von Schnering, H. Wiedemeier, *Z. Kristallogr.* **1981**, *156*, 143.
[105] E. Garcia, J. D. Corbett, *J. Solid State Chem*. **1988**, *73*, 452.
[106] A. Kjekshus, *Acta Chem. Scand*. **1972**, *26*, 1633.
[107] E. Garcia, J. D. Corbett, *J. Solid State Chem*. **1988**, *73*, 440.
[108] W. S. Sheldrick, M. Wachhold, *Angew. Chem*. **1995**, *107*, 490; *Angew. Chem. Int. Ed. Engl*. **1995**, *34*, 450.
[109] W. S. Sheldrick, M. Wachhold, *Chem. Commun*. **1996**, 607.
[110] G. A. Papoian, R. Hoffmann, unpublished results.
[111] K. Anderko, K. Schubert, *Z. Metallkd.* **1954**, *45*, 371.
[112] R. V. Baranova, Z. G. Pinsker, *Sov. Phys. Crystallogr. (Engl. Transl.)* **1964**, *9*, 83.
[113] P. Böttcher, U. Kretschmann, *Z. Anorg. Allg. Chem*. **1982**, *491*, 39.
[114] I. Schewe-Miller, P. Böttcher, *Z. Kristallogr.* **1991**, *196*, 137.
[115] Yu. V. Voroshilov, M. I. Gurzan, Z. Z. Kish, L. V. Lada, *Inorg. Mater. (Engl. Transl.)* **1988**, *24*, 1265.
[116] P. Böttcher, T. Doert, C. Druska, S. Bradtmöller, *J. Alloys Comp*. **1997**, *246*, 209.
[117] K. J. Nordell, G. J. Miller, *J. Alloys Comp*. **1996**, *241*, 51.
[118] A. J. K. Haneveld, F. Jellinek, *J. Less-Common Met*. **1970**, *21*, 45.
[119] K. Stöwe, *J. Solid State Chem*. **1996**, *127*, 202.
[120] H. P. Beck, W. Dausch, *Z. Naturforsch. B* **1988**, *43*, 1547.
[121] V. K. Slovyanskikh, N. T. Kuznetsov, N. V. Gracheva, *Russ. J. Inorg. Chem. (Engl. Transl.)* **1985**, *30*, 314.
[122] A. J. K. Haneveld, F. Jellinek, *J. Less-Common Met*. **1971**, *24*, 229.
[123] S. Furuset, H. Fjellvag, *Acta Chem. Scand*. **1991**, *45*, 694.
[124] K. Stöwe, F. R. Wagner, *J. Solid State Chem*. **1998**, *138*, 160.
[125] K.-S. Choi, R. Patschke, J. L. Billinge, M. J. Waner, M. Dantus, M. G. Kanatzidis, *J. Am. Chem. Soc*. **1998**, *120*, 10706.
[126] J. A. Cody, J. A. Ibers, *Inorg. Chem*. **1996**, *35*, 3836.
[127] E. J. Wu, M. A. Pell, J. A. Ibers, *J. Alloys Comp*. **1997**, *255*, 106.
[128] A. A. Narducci, J. A. Ibers, *Inorg. Chem*. **1998**, *37*, 3798.
[129] O. Tougait, A. Daoudi, M. Potel, H. Noël, *Mater. Res. Bull.* **1997**, *32*, 1239.
[130] N.-H. Dung, M.-P. Pardo, P. Boy, *Acta Cristallogr. Sec. C* **1983**, *39C*, 668.
[131] F. Q. Huang, S. Lee, W. Choe, C. Auriel, *Inorg. Chem*., submitted.
[132] T. Yamauchi, S. Zaima, K. Mizuno, H. Kitamura, Y. Koide, Y. Yasuda, *J. Appl. Phys*. **1991**, *69*, 7050.
[133] M. Setton, J. Van der Spiegel, *J. Appl. Phys*. **1991**, *70*, 193.
[134] T. Yamauchi, S. Zaima, K. Mizuno, H. Kitamura, Y. Koide, Y. Yasuda, *Appl. Phys. Lett*. **1990**, *57*, 1105.
[135] A. Bourret, F. M. d'Heurle, F. K. Le Goues, A. Charai, *J. Appl. Phys*. **1990**, *67*, 241.
[136] H. Schachner, H. Nowotny, H. Kudielka, *Monatsh. Chem*. **1954**, *85*, 1140.
[137] J. F. Smith, D. M. Bailey, *Acta Crystallogr*. **1957**, *10*, 341.
[138] P. G. Cotter, J. A. Kohn, A. Potter, *J. Am. Ceram. Soc*. **1956**, *39*, 11.
[139] O. G. Karpinskiy, B. A. Evseyev, *Russ. Metall. (Engl. Transl.)* **1969**, *3*, 128.
[140] A. Brown, *Acta Crystallogr*. **1962**, *15*, 652.
[141] A. Brown, *Acta Crystallogr*. **1961**, *14*, 860.
[142] S. Cirafici, A. Palenzona, P. Manfrinetti, *J. Less-Common Met*. **1983**, *90*, 49.
[143] A. E. Dwight, *Argonne Nat. Lab. Rep. ANL* **1982**, 1.
[144] M. V. Rudometkina, Yu. D. Seropegin, A. V. Griobanov, L. S. Gusei, *J. Less-Common Met*. **1989**, *147*, 239.
[145] E. S. Makarov, V. N. Bykov, *Kristallografiya* **1959**, *4*, 164.
[146] H. Boller, H. Nowotny, A. Wittmann, *Monatsh. Chem*. **1960**, *91*, 1174.
[147] H. Nowotny, H. Schachner, *Monatsh. Chem*. **1953**, *84*, 169.
[148] P. Villars, K. Mathis, F. Hullinger in *The Structures of Binary Compounds, Vol. 2* (Eds: F. R. de Boer, D. G. Pettifor), North-Holland, Amsterdam, **1989**, chap. 1.

[149] P. Villars, *J. Less-Common Met*. **1984**, *99*, 33.
[150] J. Evers, G. Oehlinger, A Weiss, F. Hulliger, *J. Less-Common Met*. **1983**, *90*, L19.
[151] R. Nesper, H. G. von Schnering, J. Curda, *Solid Compounds of Transition Elements VI, International Conference* (Stuttgart, Germany) **1979**, p. 150.
[152] J. Evers, *J. Solid. State Chem*. **1979**, *28*, 369.
[153] J. Evers, G. Oehlinger, A Weiss, *J. Solid. State Chem.* **1977**, *20*, 173.
[154] K. Janzon, H. Schäfer, A Weiss, *Angew. Chem*. **1965**, *77*, 258; *Angew. Chem. Int. Ed. Engl*. **1965**, *4*, 245.
[155] *CRC Handbook of Chemistry and Physics*, 79th ed. (Ed.: D. R. Lide), CRC Press, Washington, DC, USA **1979**.
[156] A. Iandelli, A. Palenzona, *Atti Accad. Naz. Lincei Cl. Sci. Fis. Mat. Nat. Rend*. **1966**, *40*, 623.
[157] F. A. Schidt, O. D. McMasters, O. N. Carlson, *J. Less-Common Met*. **1972**, *26*, 53.
[158] I. Mayer, Y. Eshdat, *Inorg. Chem*. **1968**, *7*, 1904.
[159] I. Mayer, E. Yanir, I. Schidlovsky, *Inorg. Chem*. **1967**, *6*, 842.
[160] I. Binder, *J. Am. Ceram. Soc*. **1960**, *43*, 287.
[161] A. Iandelli, A. Palenzona, G. L. Olcese, *J. Less-Common Met*. **1979**, *64*, 213.
[162] J. Pierre, B. Lambert-Andron, J. L. Soubeyroux, *J. Magn. Magn. Mater*. **1989**, *81*, 39.
[163] P. Schobinger-Papamantellos, D. B. De Mooij, K. H. J. Buschow, *J. Magn. Magn. Mater*. **1989**, *79*, 231.
[164] G. Borzone, A. Borsese, R. Ferro, *Z. Anorg. Allg. Chem*. **1983**, *501*, 199.
[165] G. Borzone, A. Borsese, R. Ferro, *J. Less-Common Met*. **1982**, *85*, 195.
[166] F. Weitzer, K. Hiebl, P. Rogl, *J. Solid. State Chem*. **1992**, *98*, 291.
[167] F. Weitzer, K. Hiebl, P. Rogl, *Solid State Commun*. **1992**, *82*, 353.
[168] A. Palenzona, P. Manfrinetti, *J. Alloys Comp*. **1993**, *201*, 43.
[169] E. I. Gladyshevskii, *J. Struct. Chem. (Engl. Transl.)* **1964**, *5*, 523.
[170] K. Sekizawa, *J. Phys. Soc. Jpn*. **1966**, *21*, 274.
[171] P. Schobinger-Papamantellos, D. B. De Mooij, K. H. J. Buschow, *J. Less-Common Met*. **1988**, *144*, 265.
[172] V. N. Eremenko, K. A. Meleshevich, Yu. I. Buyanov, P. S. Martensyuk, *Poroshk. Metall. (Kiev)* **1989**, *28*, 543.
[173] V. N. Eremenko, X. Q. Che, Yu. I. Buyanov, A. M. Khar'kova, *Inorg. Mater. (Engl. Transl.)* **1975**, *11*, 133.
[174] J. Perry, I. Binder, B. Post, *J. Phys. Chem*. **1959**, *63*, 616.
[175] J. Perry, E. Banks, B. Post, *J. Phys. Chem*. **1959**, *63*, 2073.
[176] A. Iandelli, A. Palenzona in *Handbook of the Physics and Chemistry of Rare Earths*, *Vol. 2* (Eds.: K. A. Gscheidner, Jr., L. Eyring), North-Holland, Amsterdam, **1979**, chap. 13.
[177] J. Pierre, E. Slaud, D. Frachon, *J. Less-Common Met*. **1988**, *139*, 321.
[178] S. Lee, *J. Am. Chem. Soc*. **1991**, *113*, 101.
[179] G. V. Vajenine, R. Hoffmann, *J. Am. Chem. Soc*. **1998**, *120*, 4200.
[180] G. A. Papoian, M. D. Bojin, R. Hoffmann, unpublished results.
[181] V. V. Pavlyuk, O. I. Bodak, V. K. Pecharskii, R. V. Skolozdra, E. I. Gladyshevskii, *Inorg. Mater. (Engl. Transl.)* **1989**, *25*, 962.
[182] W. Dörrscheidt, G. Savelsberg, J. Stöhr, H. Schäfer, *J. Less-Common Met*. **1982**, *83*, 269.
[183] L. V. Krivulya, O. I. Bodak, Yu. K. Gorelenko, *Inorg. Mater. (Engl. Transl.)* **1986**, *22*, 1685.
[184] G. Venturini, B. Malaman, M. Meot-Meyer, D. Fruchart, G. Le Caer, D. Malterre, B. Roques, *Rev. Chim. Miner.* **1986**, *23*, 162.
[185] V. K. Pecharsky, K. A. Gschneidner, Jr., L. L. Miller, *Phys. Rev. B* **1991**, *43*, 10906.
[186] W. Bazela, J. Leciejewicz, K. Maletka, A. Szytula, *J. Magn. Magn. Mater*. **1992**, *109*, 305.
[187] H. Kumigashira, A. Chainani, T. Yokoya, O. Akaki, T. Takahashi, M. Ito, M. Kasaya, O. Sakai, *Phys. Rev. B* **1996**, *53*, 2565.
[188] P. Schobinger-Papamantellos, K. H. J. Buschow, C. Wilkinson, F. Fauth, C. Ritter, *J. Magn. Magn. Mater*. **1998**, *189*, 214.
[189] D. M. Proserpio, G. Chacon, C. Zheng, *Chem. Mater*. **1998**, *10*, 1286.
[190] E. Parté, B. Chabot in *Handbook of the Physics and Chemistry of Rare Earths*, *Vol. 6* (Eds.: K. A. Gscheidner, Jr., L. Eyring), Elsevier Science, Amsterdam, **1984**, chap. 48.
[191] P. Rogl in in *Handbook of the Physics and Chemistry of Rare Earths*, *Vol. 7* (Eds.: K. A. Gscheidner, Jr., L. Eyring), Elsevier Science, Amsterdam, **1984**, chap. 51.
[192] H. Onken, K. Vierheilig, H. Hahn, *Z. Anorg. Allg. Chem*. **1964**, *333*, 267.
[193] W. Tremel, R. Hoffmann, *J. Am. Chem. Soc*. **1987**, *109*, 124.
[194] R. Ferro, *Acta Crystallogr*. **1955**, *8*, 360.
[195] R. Ferro, *Acta Crystallogr*. **1956**, *9*, 817.
[196] R. Ferro, *Acta Crystallogr*. **1957**, *10*, 476.
[197] V. Johnson, W. Jeitschko, *J. Solid. State Chem*. **1973**, *16*, 306.
[198] F. Hulliger, *J. Less-Common Met*. **1973**, *30*, 397.
[199] A. J. Klein Haneveld, F. Jellinek, *Recl. Trav. Chim. Des Pays-Bas* **1964**, *83*, 776.
[200] A. J. Klein Haneveld, F. Jellinek, *J. Less-Common Met*. **1969**, *18*, 123.
[201] V. Johnson, W. Jeitschko, *J. Solid State Chem*. **1974**, *11*, 161.
[202] L. S. Andrukhiv, L. O. Lysenko, Ya. P. Yarmolyuk, E. I. Hladyshevsky, *Dopov. Akad. Nauk Ukr. RSR Ser. A* **1975**, *7*, 645.
[203] H. Sprenger, *J. Less-Common Met*. **1974**, *34*, 39.
[204] F. Thirion, G. Venturini, B. Malaman, J. Steinmetz, B. Roques, *J. Less-Common Met*. **1983**, *95*, 47.
[205] F. Thirion, B. Malaman, G. Venturini, J. Steinmetz, B. Roques, *J. Less-Common Met*. **1984**, *96*, 153.
[206] B. Eisenmann, H. Schäfer, *Z. Anorg. Allg. Chem*. **1974**, *403*, 163.
[207] C. Zheng, R. Hoffmann, *J. Phys. Chem*. **1985**, *89*, 4175.
[208] C. Zheng, R. Hoffmann, *J. Am. Chem. Soc*. **1986**, *108*, 3078.
[209] B. Eisenmann, N. May, W. Müller, H. Schäfer, *Z. Naturforsch. B* **1972**, *27*, 1155.
[210] G. Cordier, E. Czech, H. Schäfer, P. Woll, *J. Less-Common Met*. **1985**, *110*, 327.
[211] A. Dommann, F. Hulliger, H. R. Ott, V. Gramlich, *J. Less-Common Met*. **1985**, *110*, 331.
[212] A. Szytula, J. Leciejewicz in *Handbook of the Physics and Chemistry of Rare Earths*, *Vol. 1* (Eds.: K. A. Gscheidner, Jr., L. Eyring), Elsevier Science, Amsterdam, **1989**, chap. 83.
[213] A. Purwanto, R. A. Robinson, H. Nakotte, I. P. Swainson, M. S. Torikachvili, *J. Appl. Phys.* **1996**, *79*, 6411.
[214] V. V. Gridin, S. A. Sergeenkov, A. Strydom, P. de V. du Plessis, *Phys. Rev. B* **1994**, *50*, 12995.
[215] W. P. Beyermann, M. F. Hundley, P. C. Canfield, C. Godart, M. Selsane, Z. Fisk, J. L. Smith, J. D. Thompson, *Physica B* **1991**, *171*, 373.
[216] M. Selsane, M. Lebail, N. Hamdaoui, J. P. Kappler, H. Noël, J. C. Achard, C. Godart, *Physica B* **1990**, *163*, 213.
[217] U. Rauchschwalbe, U. Gottwick, U. Ahlheim, H. M. Mayer, F. Steglich, *J. Less-Common Met*. **1985**, *111*, 265.
[218] B. Lloret, B. Buffat, B. Chevalier, J. Etourneau, *J. Magn. Magn. Mater*. **1987**, *67*, 232.
[219] R. A Steeman, A. J. Dirkmaat, A. A. Menovsky, E. Frikkee, G. J. Nieuwenhuys, J. A. Mydosh, *Physica B* **1990**, *163*, 382.
[220] W. Lin, H. Steinfink, E. J. Weiss, *Inorg. Chem*. **1965**, *4*, 877.
[221] R. Wang, H. Steinfink, W. F. Bradley, *Inorg. Chem*. **1966**, *5*, 142.
[222] J.-G. Park, I. P. Swainson, W. J. L. Buyers, M. H. Jung, Y. S. Kwon, *Physica B* **1998**, *241–243*, 684.
[223] T. H. Ramsey, H. Steinfink, E. J. Weiss, *Inorg. Chem*. **1965**, *4*, 1154.
[224] M. P. Pardo, J. Flahaut, L. Domange, *Bull. Soc. Chim. France* **1964**, 3267.
[225] S.-M. Park, S.-J. Park, S.-J. Kim, *J. Solid. State Chem*. **1998**, *140*, 300.
[226] J.-P. Marcon, R. Pascard, *C. R. Seances Acad. Sci. Ser. C* **1968**, *266*, 270.
[227] P. S. Bénazeth, D. Carré, P. Laruelle, *Acta Crystallogr. Sect. B* **1982**, *38*, 33.
[228] P. S. Bénazeth, D. Carré, P. Laruelle, *Acta Crystallogr. Sect. B* **1982**, *38*, 37.
[229] J. C. Chen, P. K. Dorhout, *J. Solid State Chem*. **1995**, *117*, 318.
[230] M. H. Jung, Y. S. Kwon, T. Kinoshita, S. Kimura, *Physica B* **1997**, *230–232*, 151.
[231] M. H. Jung, Y. S. Kwon, T. Suzuki, *Physica B* **1997**, *240*, 83.
[232] B. Foran, S. Lee, *J. Am. Chem. Soc*. **1994**, *116*, 154.
[233] A. van der Lee, L. M. Hoistad, M. Evain, B. J. Foran, S. Lee, *Chem. Mater*. **1997**, *9*, 218.
[234] B. Foran, S. Lee, M. Aronson, *Chem. Mater*. **1993**, *5*, 974.
[235] P. S. Bénazeth, D. Carré, M. Guittard, M. J. Flahaut, *C. R. Seances Acad. Sci. Ser. C* **1975**, *280*, 1021.
[236] M. Grupe, W. Urland, *J. Less-Common Met*. **1991**, *170*, 271.
[237] P. Plambeck-Fischer, W. Abriel, W. Urland, *J. Solid. State Chem*. **1989**, *78*, 164.

[238] B. K. Norling, H. Steinfink, *Inorg. Chem*. **1966**, *5*, 1488.
[239] E. DiMasi, B. Foran, M. Aronson, S. Lee, *Chem. Mater*. **1994**, *6*, 1867.
[240] G.-H. Gweon, J. D. Denlinger, J. A. Clack, J. W. Allen, C. G. Olson, E. DiMasi, M. C. Aronson, B. Foran, S. Lee, *Phys. Rev. Lett*. **1998**, *81*, 886.
[241] H. Noël, J. C. Levet, *J. Solid State Chem*. **1989**, *79*, 28.
[242] R. Patschke, J. Heising, M. G. Kanatzidis, P. Brazis, C. R. Kannewurf, *Chem. Mater*. **1998**, *10*, 695.
[243] R. Patschke, J. Heising, J. Schindler, C. R. Kannewurf, M. G. Kanatzidis, *J. Solid State Chem.* **1998**, *135*, 111.
[244] G. A. Landrum, http://overlap.chem.cornell.edu:8080/yaehmop.html **1995**.
[245] E. Brechtel, G. Cordier, H. Schäfer, *Z. Naturforsch. B* **1981**, *36*, 1341.
[246] O. Liebrich, H. Schäfer, A. Weiss, *Z. Naturforsch. B* **1970**, *25*, 650.
[247] N. A. Ignat'ev, Ya. A. Ugai, K. B. Aleinikova, N. S. Rabotkina, *J. Struct. Chem. (Engl. Transl.)* **1971**, *12*, 665.
[248] H. W. Mayer, I. Mikhail, K. Schubert, J. *Less-Common Met*. **1978**, *59*, 43.
[249] K. E. Al min, *Acta Chem. Scand*. **1948**, *2*, 400.
[250] W. K. Hofmann, W. Jeitschko, *J. Less-Common Met*. **1988**, *138*, 313.
[251] K. Deller, B. Eisenmann, *Z. Naturforsch. B* **1976**, *31*, 29.
[252] H. G. von Schnering, W. Hönle, G. Krogull, *Z. Naturforsch. B* **1979**, *34*, 1678.
[253] K. Deller, B. Eisenmann, *Z. Anorg. Allg. Chem*. **1976**, *425*, 104.
[254] A. Rehr, F. Guerra, S. Parkin, H. Hope, S. M. Kauzlarich, *Inorg. Chem*. **1995**, *34*, 6218.
[255] A. Kjekshus, T. Rakke, A. F. Andresen, *Acta Chem. Scand*. **1970**, *24*, 3309.
[256] T. Rosenqvist, *Acta Metall.* **1953**, *1*, 761.
[257] A. Kjekshus, T. Rakke, A. F. Andresen, *Acta Chem. Scand. Ser. A* **1974**, *28*, 996.
[258] B. R. Wang, H. Steinfink, *Inorg. Chem*. **1967**, *6*, 1685.
[259] N. L. Eatough, T. Hall, *Inorg. Chem*. **1969**, *8*, 1439.
[260] M. N. Abdusalyamova, *J. Alloys Comp*. **1993**, *202*, 15.
[261] M. Brylak, W. Jeitschko, *Z. Naturforsch. B* **1995**, *50*, 899.
[262] J. Dünner, A. Mewis, M. Roepke, G. Michels, *Z. Anorg. Allg. Chem.* **1995**, *621*, 1523.
[263] J. Weiss, H. Schäfer, B. Eisenmann, G. Schön, *Z. Naturforsch. B* **1974**, *29*, 585.
[264] I. Schewe, P. Böttcher, H. G. von Schnering, *Z. Kristallogr.* **1989**, *188*, 287.
[265] E. W. Breeze, N. H. Brett, J. White, *J. Nucl. Mater.* **1971**, *39*, 157.
[266] J. A. Cody, J. A. Ibers, *Inorg. Chem*. **1995**, *34*, 3165.
[267] H. Noël, *Inorg. Chim. Acta* **1985**, *109*, 205.
[268] T. Hughbanks, R. Hoffmann, M.-H. Whangbo, K. R. Stewart, O. E. Eisenstein, E. Canadell, *J. Am. Chem. Soc*. **1982**, *104*, 3876.
[269] K. Tatsumi, A. Nakamura, P. Hofmann, P. Stauffert, R. Hoffmann, *J. Am. Chem. Soc*. **1985**, *107*, 4440.
[270] K. Stöwe, *J. Solid State Chem*. **2000**, *149*, 123.
[271] K. Stöwe, *Z. Anorg. Allg. Chem*. **2000**, *626*, 803.

Was Leonardo a Chemist?**

Pedro Cintas*

The inaugural editorial and the cover illustration of the first issue of *Angewandte Chemie* for January 2000 describe a famous pencil drawing—the Vitruvian man—by Leonardo da Vinci.[1] This genius of the Renaissance was admired in his lifetime for his many facets and unlimited desire for knowledge; qualities that have remained undimmed to the present day. Most biographies concentrate on Leonardo as a great artist, architect, musician, and military engineer. His varied scientific ability has also been documented, albeit largely overlooking his contributions to chemistry and physics.

The scientific achievements are contained in a large collection of manuscripts, mostly disconnected notes for his own use, which were written between 1490 and 1518. Several of his codices, especially the comprehensive *Codex Atlanticus* and the *Codex Arundel*, contain abundant drawings and descriptions of chemical preparations and apparatus such as furnaces, a mixing mill, alembics, and ingenious balances.[2–4] Many readers will know well that all these studies were written down with in Leonardo's peculiar hand: the notebooks can be read with the aid of a mirror. Contrary to a held belief, this practice should not be considered a secret handwriting. Leonardo was left handed and mirror writing came naturally to him. Unlike his artistic studies, his scientific notes are not clearly arranged. Leonardo had a remarkable and unusual power of observation combined with a strictly empirical approach to explain natural phenomena, often with the help of mechanical models. Leonardo advocated the repetition of experiments and measurement of weights, distances, and velocities entered into all of his observations. He did not invent the balance, at least in the way as we know it, but he designed several devices to compare weights.

Leonardo's scientific activity was particularly important from 1482 to 1499 (during this period he completed only six paintings) in the service of Duke Ludovico Sforza in Milan, registered as "pictor et ingeniarius ducalis" (painter and engineer of the duke). Later, in 1502, he entered the service of Cesare Borgia as a military architect and general engineer. Leonardo studied the composition of bronzes for gun casting, noting that tin can be replaced by lead; the bronze for guns should contain from six to eight percent of tin. Likewise, he described a gunpowder, which he called Greek fire, made from saltpetre (potassium nitrate), willow charcoal, spirit of wine, sulfur, pitch, frankincense, and camphor boiled together and spread over "lana etiopica" (wool). He anticipated the invention of gas warfare consisting of fumes of burnt feathers, sulfur, and realgar (arsenic sulfide), whose effects lasted for seven to eight hours. Some chemical recipes describe the preparation of "aqua fortis" (nitric acid) from equal amounts of Roman vitriol,[5] saltpetre, verdigris,[6] and cinnabar (or colcothar).[7] Such a preparation dissolved copper and Leonardo noted that pyrites do contain copper if their treatment with aqua fortis gives a green solution, from which a precipitate is obtained with saltpetre and soft soap.

Leonardo's notes on chemistry are also formulas for paints and pigments, which he used in his artistic works. Thus, the *Codex Atlanticus* contains numerous recipes: "For 'vetro giallo' (yellow glaze) take one ounce tuzia (zinc oxide), ¾ ounce Indian saffron, ¼ ounce borax, and grind it all together into a powder." Unfortunately, other notes do not include precise amounts: "To make scent take fresh rose water and moisten the hands, then take flower of lavender and rub it between the palms, and it will be good." One of his pigments, denoted as green fire, was obtained by soaking verdigris in oil of turpentine and filtering, and other colors were extracted from flowers by alcohol. Leonardo also utilized proteins, in the form of a concentrated solution of gelatin or egg white, to which pigments or plant extracts were added. Such mixtures were applied to ceramic molds which were dried and varnished, thereby making objects that imitated agate, jasper, or amber. Impregnation of paper with the same pigments gave dense plates which, after varnishing, resembled glass and were impermeable to water, an almost perfect imitation of a modern plastic material.

A significant portion of his chemical studies were devoted to combustion. A drawing of a chemist's furnace with two alembics appears in the *Codex Atlanticus.* Leonardo also invented a lamp chimney to bring fresh air to the flame as well as a lamp with constant oil level. Leonardo was aware of the

[*] Prof. Dr. P. Cintas
Departamento de Química Orgánica
Facultad de Ciencias
Universidad de Extremadura
06071 Badajoz (Spain)
Fax: (+34) 924-271-149
E-mail: pecintas@unex.es

[**] This work was supported by the Ministry of Education and Cultura (D.G.I.C.Y.T., grant PB98-0997). I am grateful to the Britannica Center, Chicago, for kindly providing further information on the biographies and scientific contributions of Leonardo da Vinci.

 © WILEY-VCH Verlag GmbH, D-69451 Weinheim, 2000 0570-0833/00/3914-2449 $ 17.50+.50/0

importance of air to make a flame bright and in the maintenance of life. He described in detail a flame with pictures showing the blue inner cone. Some scholars have interpreted that Leonardo was close to the discovery of oxygen (which was achieved by Priestley in 1774): "Where flame cannot live, no animal that draws breath can live" (*Codex Atlanticus*). However, for Leonardo, flame and breathing were two different phenomena with nothing in common and it is therefore speculative to suppose that Leonardo thought that air contained a fluid essential for life.

Even though Leonardo admired alchemy as a means of making things which not found in nature, he faced in fact many misconceptions and frauds of alchemists (*Codex Atlanticus*):

"I bugiardi interpitri di natura affermano lo argento vivo essere commune semenza a tutti i metalli, non si ricordamo che la natura varia le semenze secondo la diversitá delle cose che essa vole produrre al mondo"

("The false interpreters of nature declare that quicksilver (mercury) is the common seed of every metal, not remembering that nature varies the seed according to the variety of the things she desires to produce in the world").

Moreover, he notes "Nature does not produce gold from mercury or sulfur of any kind, but only by the fire or heat of nature giving life to the world."

Leonardo was in practice conversant with the inductive method, when so few people in the Renaissance had established a direct dialog between observation and experiment. He had studied works by Archimedes and appreciated the value of mathematics. He compared the densities of liquids by balancing columns in a U-shaped tube, noting that fresh water is lighter than salt water, the latter leaves its salt behind when filtered through clay, and water becomes denser as it becomes colder until it freezes.

Although Leonardo discussed concepts such as movement, weight, or force, all in the context of the Aristotelian elements of air, fire, water, and earth, he was also skeptical about the "spirits or fluids" in matter. He assumed that all heat in the universe comes ultimately from the sun. Heat from the sun can be reflected by a mirror and refracted by drops of water and does not heat water in passing through it. He noted that salt is not a sweat of the earth, since springs penetrating the earth are not salty. The saltness of the sea is due to springs in the earth dissolving mineral salt and carrying it into the sea.

There is no doubt that Leonardo was ahead of his time. His scientific contributions make him a man closer to the Enlightenment and not to the Renaissance. Many of his observations or descriptions are comparable to those reported by his contemporaries. If Leonardo had lived in our epoch, he would also be a chemist because he was clearly active in chemical research during his lifetime.

[1] P. Gölitz, *Angew. Chem.* **2000**, *112*, 3 – 4; *Angew. Chem. Int. Ed.* **2000**, *39*, 3 – 4.

[2] A series of classical books are focused on the scientific side of Leonardo: L. Goldscheider, *Leonardo da Vinci: Life and Work*, Graphic, New York, **1959**; I. B. Hart, *World of Leonardo da Vinci: Man of Science, Engineer and Dreamer of Flight*, Viking, New York, **1962**; J. H. Randall in *Roots of Scientific Thought* (Eds.: P. P. Wiener, A. Noland), Basic Books, New York, **1957**, pp. 207 – 218; V. P. Zubov, *Leonardo da Vinci*, Harvard University Press, Cambridge, **1962**.

[3] L. Reti, *Chim. Ind. (Milan)* **1952**, *34*, 655 – 721.

[4] F. Klemm, *Chem. Exp. Didakt.* **1976**, *2*, 361 – 365.

[5] It should be sulfuric acid, although during the Middle Age the term vitriol was also applied to different metal sulfates.

[6] A green or blue crystalline substance obtained by the action of acetic acid on copper and used as fungicide and pigment. The name derives from old French "vert de Grice" (green of Greece).

[7] Presumably both minerals were used by Leonardo in his preparations. Cinnabar corresponds to the red form of mercuric sulfide and used as a pigment. The term comes from Latin "cinnabaris" meaning "of oriental origin". Colcothar (from a French or Arabic word), denotes a finely powdered form of ferric oxide produced by heating ferric sulfate and used as a pigment as well.

 © WILEY-VCH Verlag GmbH, D-69451 Weinheim, 2000 0570-0833/00/3914-2450 $ 17.50+.50/0

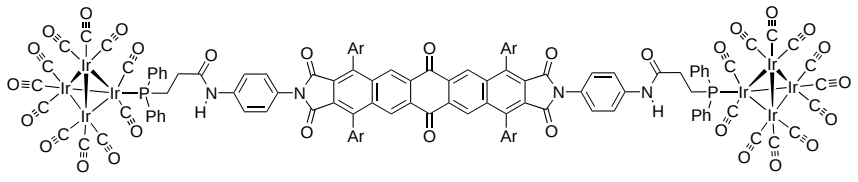
Building Photogenic Molecules—Molecules Made for Direct Individual Observation**

Harry L. Anderson*

How far away can you see a man with the naked eye? This school physics question used to irritate me. The "correct" answer is 10 km. You are meant to work it out by estimating the diffraction limit of your eye; it is the distance at which you should just be able to resolve his head from his feet (if he stands 2 m tall, your pupils are 3 mm wide, and it is a clear day). But resolving his head from his feet is not enough to distinguish him from a gatepost. On the other hand, if he is standing under a spotlight you could see him as an unresolved point of light from almost any distance (limited by the brightness of the light, the whiteness of his coat, the darkness of the background, and his ability to tolerate bright light); you might be able to tell that he is not a gatepost by watching him wander around and by the color of his coat. Looking at individual molecules raises similar issues. This article highlights the synthesis of molecules which are "big enough to see", and briefly outlines the techniques used to see them individually (in contrast to techniques such as X-ray crystallography which average over large populations).

Until about ten years ago, nobody thought it would be possible to see individual molecules with visible light but single-molecule fluorescence spectroscopy is now thriving.[1] A confocal microscope can be used to observe individual fluorescent molecules in solution, in real time, as they diffuse in and out of a focused laser beam (probe volume $\approx$ 0.5 μm^3).[2] Near-field scanning optical microscopy (NSOM) enables individual fluorescent molecules to be located with a resolution of about 50 nm, an order of magnitude better than the $\lambda/2$ diffraction limit of a conventional optical microscope.[3] This is still not enough to resolve molecular detail, except in gigantic molecules such as DNA (which can be several millimeters long). Beautiful pictures of fluorescent-labeled DNA molecules uncoiling in a shear field have enabled theories of polymer conformational dynamics to be tested with single molecules.[4]

Techniques for imaging matter with atomic resolution have advanced rapidly over the last 30 years. The first was field ion microscopy (FIM).[5] Here, the sample consists of a very sharp anode in a low pressure helium atmosphere; protruding atoms on the anode tip ionize the helium to generate cations, which are accelerated towards a fluorescent screen and create an image of the atomic arrangement on the tip. Unfortunately, organic molecules do not survive this treatment. In the late 1970s, transmission electron microscopy (TEM) became the second technique to achieve atomic resolution.[6] This method relies on the scattering of high energy electrons as they pass through a thin sample. TEM can reveal individual heavy atoms but organic molecules do not normally show up because they produce too little scattering and are damaged by electrons. Miller and co-workers evaded this problem by attaching tetrairidium clusters to each end of their molecule to give **1**; TEM images of this compound show pairs of dots at 2.7 ± 0.4 nm separation, which is the expected length (the length range is due to the flexibility of the amide linker).[7]



1 (Ar = *p*-*tert*-butylphenyl)

Recently, the same Ir_4 clusters have been used to visualize viral capsid proteins.[8] The third and most important technique for seeing atoms is scanning tunneling microscopy (STM).[5, 9] Binnig and Rohrer invented STM in 1982 and were awarded the Nobel Prize in Physics for it only four years later (together with Ruska for electron microscopy). In the simplest form of this technique, a sharp tungsten electrode is scanned over the surface of a conducting sample; feedback from the tunneling current between the electrode tip and the

[*] Dr. H. L. Anderson
University of Oxford
Department of Chemistry
Dyson Perrins Laboratory
South Parks Road, Oxford OX1 3QY (UK)
Fax: (+44) 1865-275674
E-mail: harry.anderson@chem.ox.ac.uk

[**] The author thanks Teri Odom and Charles Lieber (Harvard University), and Ken-ichi Sugiura and Yoshiteru Sakata (Osaka University) for supplying STM images for Figures 1a and 1c of this article.

 © WILEY-VCH Verlag GmbH, D-69451 Weinheim, 2000 1433-7851/00/3914-2451 $ 17.50+.50/0

surface is used to keep the tip at a fixed distance (about 0.5 nm) from the surface; this tunneling current is extremely dependent on the distance—nearly all the current flows from the most prominent atom of the tip, so atom-sized variations in the height, or the work function, of the surface can be imaged. This opened the way to direct observation of simple molecules such as benzene,[10] naphthalene,[11] phthalocyanines,[12] and porphyrins.[13, 14] The spectacular resolution which can be achieved by STM is illustrated by the image of a single-walled carbon nanotube in Figure 1 a, which reveals the hexagonal-ring structure and helicity of the nanotube; simultaneous current–voltage measurements showed that this particular nanotube has a metallic character.[15] STM also led to the invention of many other scanning probe microscopies, such as NSOM (above) and atomic force microscopy (AFM), which images surfaces by measuring the force they exert on a scanning tip.[16] AFM gives lower resolution than STM but does not require electrically conductive samples. Figure 1 b shows an AFM image of dendron-jacketed polymer **2**; comparison of the weight-averaged contour length of these wormlike objects (142 nm) with the calculated average length for an all-*trans* conformation (101 nm) shows that the backbone is almost fully extended by the dendron jacket.[17]

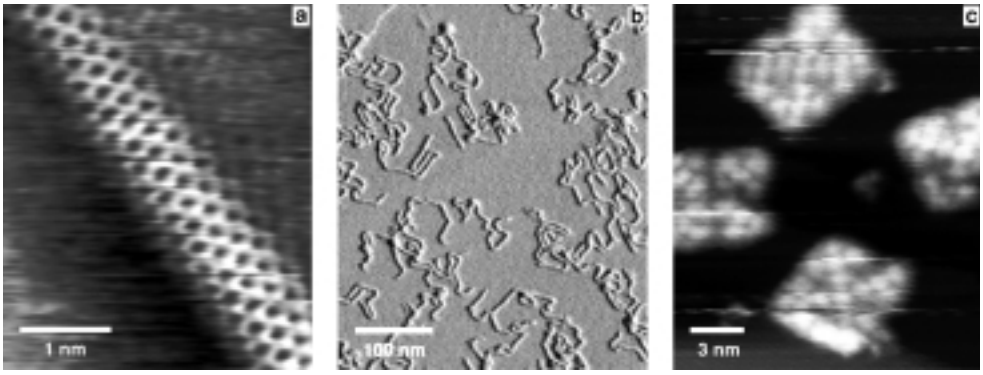
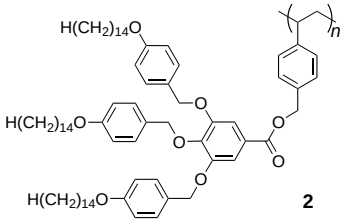
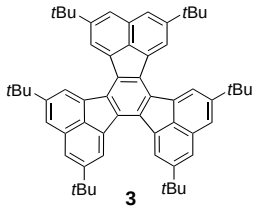


Figure 1. A triptych of molecular images: a) A single-walled carbon nanotube imaged by STM at 77 K (reproduced from ref. [15] with permission); b) AFM micrograph of dendron jacketed polymer **2** on pyrolytic graphite (reproduced from ref. [17]); c) STM image of porphyrin henicosamer **5** on a Cu(111) surface (reproduced from ref. [19] with permission).

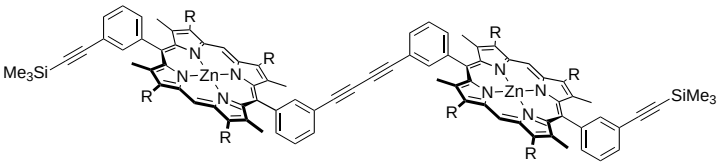


2

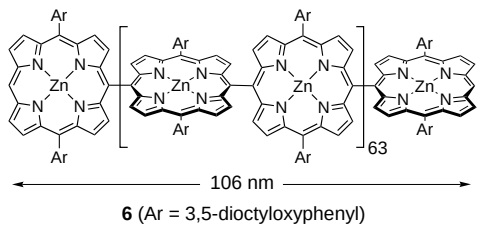


3

In order to view individual molecules by STM, it is essential to limit their motion. They need to be securely adsorbed onto a solid surface and it helps to use rigid molecules and low temperatures. Images of large symmetric molecules are easiest to interpret. Gimzewski and coworkers have reported amazing STM images of hexa-*tert*-butyl decacylene **3** on a Cu(100) surface at room temperature.[14] Steric interactions in a close-packed monolayer keep these molecules stationary and a lobe is seen for each of the six *t*Bu groups of each molecule but, at gaps in the monolayer, the molecules have space to spin, which blurs their STM images and forms "supramolecular bearings". Gimzewski's team has also used a STM tip to reposition porphyrin molecules on a surface, building supramolecular noncovalent porphyrin arrays on an individual basis.[14] Porphyrins and porphyrin oligomers are particularly suitable for STM because of their large, rigid structures. Welland, Sanders, and co-workers have used STM to observe molecules of the porphyrin dimer **4** in *cisoid* and *transoid* conformations, in which the planes of the porphyrin moieties lie perpendicular to the underlying copper surface.[18] Sakata's group have reported images of a porphyrin henicosamer **5** consisting of 20 nickel porphyrins linked by a central free-base unit (Figure 1 c).[19] Steric interactions force the *para*-phenylene linkers perpendicular to the porphyrins, so the whole molecule tends to adopt a square-planar geometry. The square pattern of 21 porphyrins is clearly visible and its size (6.5 nm × 6.5 nm) matches the expected dimensions. Even this giant porphyrin 21-mer is dwarfed by the linear porphyrin 128-mer **6** reported recently by Osuka and co-workers;[20] with a calculated length of 106 nm, this molecule should be long enough to be resolved by NSOM. Neighbouring porphyrin units in **6** are approximately orthogonal, which must contribute to its surprisingly high solubility.



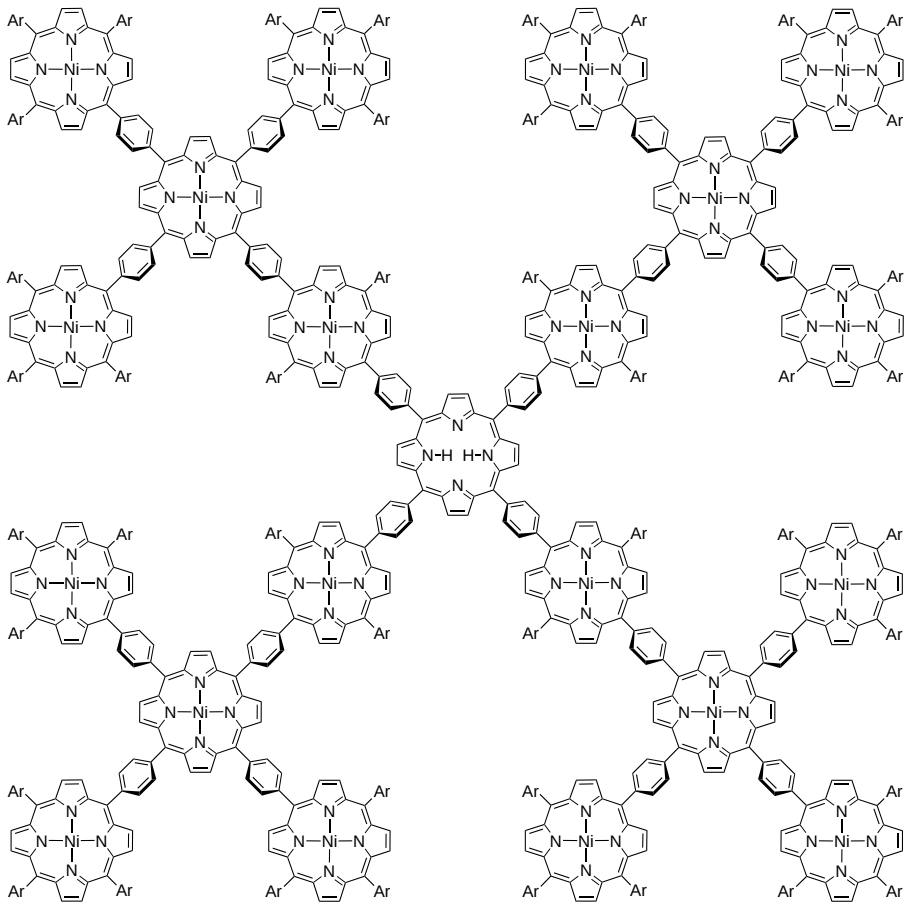
4 (R = $CH_2CH_2CO_2Me$)



6 (Ar = 3,5-dioctyloxyphenyl)

This twisted conformation prevents conjugation but energy transfer may still be efficient, so the structure may behave as a long distance "photonic molecular wire". As synthetic mol-

 © WILEY-VCH Verlag GmbH, D-69451 Weinheim, 2000 1433-7851/00/3914-2452 $ 17.50+.50/0



5 (Ar = 3,5-diisoamyloxyphenyl)

ecules grow to nanoscopic and even microscopic sizes, direct observation will become an increasingly important characterization technique because it gives information on shape without the need for crystallization and without statistical averaging.

[1] W. E. Moerner, M. Orrit, *Science* **1999**, *283*, 1670 – 1676; S. Weiss, *Science* **1999**, *283*, 1676 – 1683; Y. Ishii, T. Yanagida, *Single Mol.* **2000**, *1*, 5 – 13.

[2] S. Nie, D. T. Chiu, R. N. Zare, *Science* **1994**, *266*, 1018 – 1021.

[3] E. Betzig, R. J. Chichester, *Science* **1993**, *262*, 1422 – 1425; T. Basché, *Angew. Chem.* **1994**, *106*, 1805 – 1807; *Angew. Chem. Int. Ed. Engl.* **1994**, *33*, 1723 – 1725; R. Zenobi, V. Deckert, *Angew. Chem*. **2000**, *112*, 1814 – 1825; *Angew. Chem. Int. Ed.* **2000**, *39*, 1746 – 1756.

[4] D. E. Smith, H. P. Babcock, S. Chu, *Science* **1999**, *283*, 1724 – 1727.

[5] J. C. Rivière, *Surface Analytical Techniques*, Oxford University Press, Oxford, **1990**.

[6] E. Ruska, *Angew. Chem.* **1987**, *99*, 611 – 621; *Angew. Chem. Int. Ed. Engl.* **1987**, *26*, 595 – 605.

[7] F. R. Furuya, L. L. Miller, J. F. Hainfeld, W. C. Christopfel, P. W. Kenny, *J. Am. Chem. Soc.* **1988**, *110*, 641 – 643.

[8] N. Cheng, J. F. Conway, N. R. Watts, J. F. Hainfeld, V. Joshi, R. D. Powell, S. J. Stahl, P. E. Wingfield, A. C. Steven, *J. Struct. Biol.* **1999**, *127*, 169 – 167.

[9] G. Binnig, H. Rohrer, *Angew. Chem.* **1987**, *99*, 622 – 631; *Angew. Chem. Int. Ed. Engl.* **1987**, *26*, 606 – 614.

[10] H. Ohtani, R. J. Wilson, S. Chiang, C. M. Mate, *Phys. Rev. Lett.* **1988**, *60*, 2398 – 2401; P. S. Weiss, D. M. Eigler, *Phys. Rev. Lett.* **1993**, *71*, 3139 – 3142.

[11] V. M. Hallmark, S. Chiang, J. K. Brown, C. Wöll, *Phys. Rev. Lett.* **1991**, *66*, 48 – 51.

[12] P. H. Lippel, R. J. Wilson, M. D. Miller, C. Wöll, S. Chiang, *Phys. Rev. Lett.* **1989**, *62*, 171 – 174.

[13] M. Kunitake, U. Akiba, N. Batina, K. Itaya, *Langmuir* **1997**, *13*, 1607 – 1615.

[14] J. K. Gimzewski, C. Joachim, *Science* **1999**, *283*, 1683 – 1688.

[15] T. W. Odom, J.-L. Huang, P. Kim, C. M. Lieber, *Nature* **1998**, *391*, 62 – 64.

[16] C. F. Quate, *Surf. Sci.* **1994**, *299/300*, 980 – 995.

[17] S. A. Prokhorova, S. S. Sheiko, M. Möller, C.-H. Ahn, V. Percec, *Macromol. Rapid Commun.* **1998**, *19*, 359 – 366.

[18] N. Bampos, C. N. Woodburn, M. E. Welland, J. K. M. Sanders, *Angew. Chem.* **1999**, *111*, 2949 – 2953; *Angew. Chem. Int. Ed.* **1999**, *38*, 2780 – 2783.

[19] K. Sugiura, H. Tanaka, T. Matsumoto, T. Kawai, Y. Sakata, *Chem. Lett.* **1999**, 1193 – 1194.

[20] N. Aratani, A. Osuka, Y. H. Kim, D. H. Jeong, D. Kim, *Angew. Chem.* **2000**, *112*, 1517 – 1521; *Angew. Chem. Int. Ed.* **2000**, *39*, 1458 – 1462.

 © WILEY-VCH Verlag GmbH, D-69451 Weinheim, 2000 1433-7851/00/3914-2453 $ 17.50+.50/0

Oligopyridine Liquid Crystals—Novel Building Blocks for Supermolecular Architectures Based on Metal Coordination and Hydrogen Bonding

Carsten Tschierske*

2,2′-Bipyridines, 2,2′:6′,2″-terpyridines, phenanthrolines, and other oligopyridines are particularly attractive building blocks for the preparation of supramolecular structures.[1] This is because they easily form well-defined chelate complexes with many metals. Hence, rather complicated and exotic structures, such as catenanes, molecular knots,[2] well-defined helicates,[3] molecular grids,[4] and nanocyclic architectures[5] have been built up in recent years. Additionally, many of their transition metal complexes give rise to interesting paramagnetic, nonlinear optical, photophysical, and redox properties which can be controlled by the rational design of the ligands.

Furthermore, oligopyridines may act as efficient proton acceptors in hydrogen bonding and they can also interact through π-stacking interactions with other aromatic systems. Thus, they provide many different intermolecular interactions useful for designing well-ordered arrays of functional supramolecules. Though the stepwise construction of exotic supramolecular architectures using 2,2′-bipyridines and related oligopyridines has significantly advanced during the recent years, less progress has been achieved in obtaining macroscopic ordered structures built up by these systems. Examples are ordered arrays of molecular grids at the air–water interface[6] and self-assembled helical fibers.[7]

Liquid crystalline phases are especially challenging because they combine order and mobility on a supermolecular level. These well-defined macroscopic structures are the result of a thermodynamically controlled, dynamic self-assembly process. The molecular order provides anisotropic physical (dielectric, magnetic, optic, etc.) properties, whereas the mobility allows the switching between different well-organized states, and this combination leads to a lot of interesting applications.[8]

Many attempts have therefore been made to obtain liquid crystalline oligopyridines and to use them as ligands for the formation of metallomesogens.[9] Thus, Hanabusa et al. described linear polymers **1** comprising 2,2′-bipyridine units whose mesomorphism was however lost when significant quantities of sixfold coordinating cations were introduced.[10] Reports have also appeared of metal complexes of acylated derivatives of 6,6′-diamino-2,2′-bipyridine (**2**)[11] and lyotropic systems based on 4-alkylated 2,2′-bipyridine and 4′-alkylated 2,2′:6′,2″-terpyridine complexes of Ru^{II} and Rh^{II}, such as **3**.[12] Other examples are shown in Figure 1.

However, all these compounds have, if any, only small mesomorphic ranges and rather high melting points.[13–15]

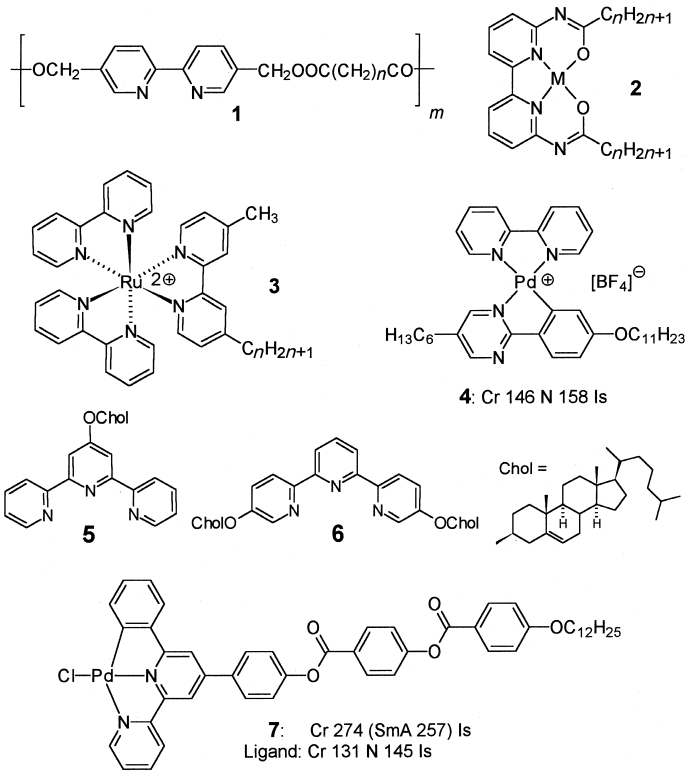


Figure 1. Representative examples of 2,2′-bipyridine mesogens;[10–15] Cr = crystalline phase; N = nematic phase; SmA = smectic A phase; Is = isotropic phase.

Bruce et al.,[16] Ziessel et al.,[17] and Attias et al.[18] have synthesized molecules incorporating linear 5,5′-disubstituted 2,2′-bipyridine units. These building blocks allow the construction of extended rodlike molecules, for which—according to classic concepts—liquid crystalline phases are likely to occur. Some examples are shown in Figure 2. Indeed broad regions of smectic (SmC, SmA) and nematic (N) phases were obtained for the free ligands **8**. However, the liquid crystalline properties of the parent bipyridines were lost when they were complexed to metal centers.[16b] Clearly, the metal atoms and the additional ligands disturb the parallel alignment of the molecules. In order to reduce this unfavorable steric disturbance it was necessary to enlarge the rigid segment to a minimum of six aromatic rings, which led to the first metallomesogens of this type (for example, **10**).[19] However, such large rodlike molecules with only two terminal alkyl chains have high melting points which inhibit more detailed investigations. Additionally, only nematic phases and layer structures (smectic phases) could be expected for such molecules. To decrease the melting points and to get other mesophases, calamitic bipyridine derivatives with up to six aliphatic chains have been synthesized.[20] Indeed, these polycatenar molecules, such as **9b** and **9c**, have lower melting points and can

[*] Prof. Dr. C. Tschierske
Institut für Organische Chemie
Martin-Luther-Universität Halle-Wittenberg
Kurt-Mothes-Strasse 2, 06120 Halle (Germany)
Fax: (+49) 345-552-7030
E-mail: Tschierske@chemie.uni-halle.de

 © WILEY-VCH Verlag GmbH, D-69451 Weinheim, 2000 1433-7851/00/3914-2454 $ 17.50+.50/0

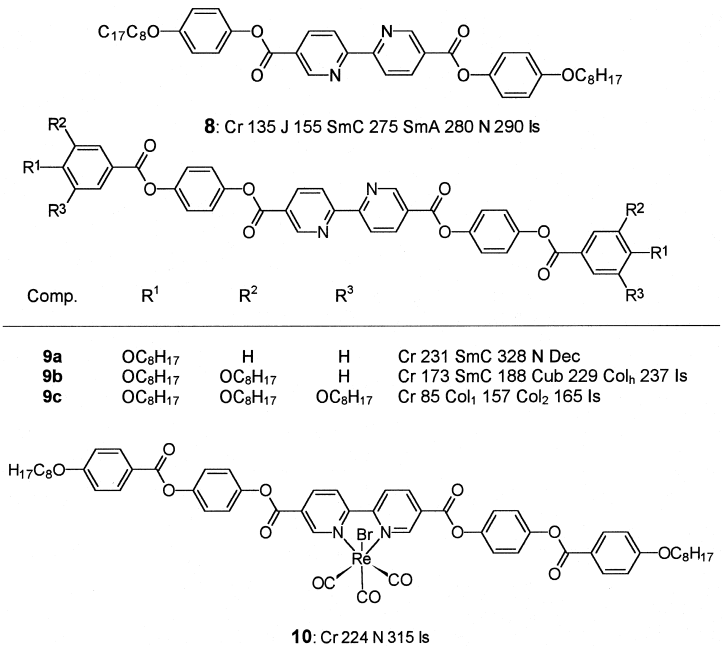


Figure 2. Representative examples of rodlike 2,2′-bipyridine mesogens[16, 17, 20] and the Re complex derived from **9a**;[19] J = crystalline J phase; SmC = smectic C phase; Cub = cubic mesophase; Col_h = hexagonal columnar phase; Col_1, Col_2 = columnar phases of unknown structure; Dec = decomposition.

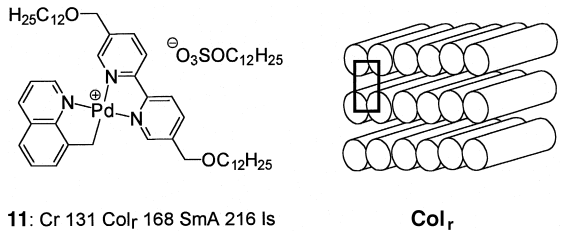


Figure 3. Structure and transition temperatures (T [°C]) of **11** and a model of the organization of the supermolecular columns in the special Col_r phase (the alkyl chains which fill the space between the layers are not shown).

form not only smectic, but also cubic (Cub) and different types of columnar (Col) mesophases.[20] The investigation of their metal coordination complexes is in progress,[20] but two promising novel types of bipyridine metallomesogens with interesting mesophase structures have been reported by Ziessel et al.

The first one is the Pd^{II} complex **11**, which consists of a positively charged central core unit connected to three flexible and lipophilic alkyl chains, two provided by the bipyridine core and one by the dodecylsulfate ion.[21, 22] Thus, a strongly amphiphilic ionic metallomesogen was obtained with a strong tendency to segregate the polar and rigid central cores from the lipophilic and rather flexible alkyl chains. This material shows a broad liquid crystalline region, whereas the parent uncharged calamitic 2,2′-bipyridine ligand is not mesogenic at all. This means that in contrast to all other earlier attempts with bipyridines, the liquid crystallinity was successfully induced in this case by metal complexation.

Two different liquid crystalline phases have been found: At lower temperatures a columnar phase occurs, in which the nearly flat aromatic central cores stack on top of each other[23] to form columns arranged in a rectangular 2D lattice (Col_r, see Figure 3). However, the structure of this Col_r phase is different from conventional columnar phases, because the columns are not completely surrounded by the alkyl chains. Instead, the polar centers of the columns are in lateral contact with each other, thereby forming layers which are separated from one another by layers of the liquidlike alkyl chains (see Figure 3).

A transition to another mesophase was observed on raising the temperature. Optical investigations indicate a smectic A phase (SmA), whereas X-ray data suggest that a local order of columns is remaining, that is, it could probably be a more disordered variant of the Col_r phase described above.[24]

A second useful approach is based on imino-substituted oligopyridines (Figure 4). These molecules are nonmesomorphic themselves, but they can act as ligands for transition metals. Bisiminobipyridines such as **12**, for example, can form stable Cu^I double helicates incorporating two tetragonal coordinated Cu^I ions. Interestingly, here the bipyridine unit is not the chelate forming unit; only one of the pyridine nitrogen atoms of each bipyridine unit and the neighboring imine group act as chelating ligands, which is in contrast to most other bipyridine complexes.[25]

Such complexes with a sufficiently large number of long alkyl chains can organize into columnar mesophases (Figure 4).[26] In these liquid crystalline phases the nonplanar, polar, and rigid helicates (carrying a positive charge at each of the Cu^I ions and also incorporating the BF_4^- counterions) organize in the centers of the columns which are surrounded by the liquidlike continuum of the nonpolar alkyl chains. This designing principle is not restricted to the bipyridine complexes **14b**, also the Cu^I complexes of the bisiminoterpyridines (for example, **14c**),[27] of the bisiminopyridines (for example, **14a**),[28] and even those of the 2-iminopyridine (**15**)[28] show liquid crystalline properties.

Only one Cu^I ion is coordinated by the two bisiminopyridine ligands in **14a** and by the two iminopyridine ligands in **15**. Hexagonal columnar phases, in which the columns are packed laterally into a two-dimensional hexagonal unit cell, were found for both mononuclear complexes (Col_h, Figure 5). However the diameters of the columns of both compounds are quite different: 60 Å for **15** and only 47 Å for **14a** with the larger ligands. The larger value found for **15** suggests that more than one molecule is located in the diameter of the columns. Since the number of alkyl chains in the complex **15** amounts to only half the number in **14a** this arrangement enables an efficient filling of the peripheral space around the columns. In this respect the organization of **15** is similar to that of the columnar phases of polycatenar liquid crystals[29] and linear stilbazole-Ag^I complexes (for example, **16**).[30] In contrast, the individual molecules of **14a** only stack one on top of the other to form the columns as known for conventional discotic liquid crystals.

However it should be pointed out that, as a result of the pseudotetrahedral coordination geometry provided by the Cu^I ions, these molecules are not flat as are conventional discotic materials. The parallel alignment of rigid discs is

 © WILEY-VCH Verlag GmbH, D-69451 Weinheim, 2000 1433-7851/00/3914-2455 $ 17.50+.50/0

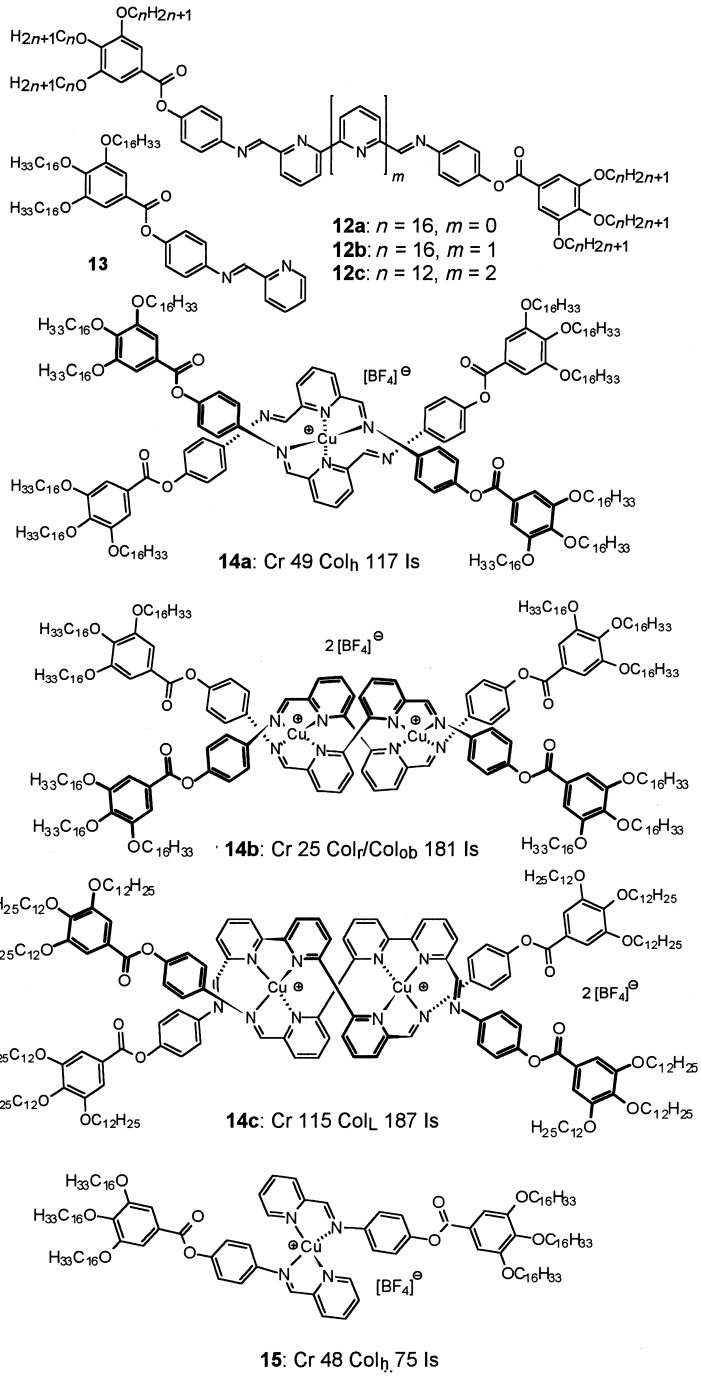


Figure 4. Structures of the nonmesogenic ligands **12** and **13** and their liquid crystalline Cu^{I} complexes **14** and **15** (T [°C]);[26–28] Col_r = rectangular columnar phase; Col_{ob} = oblique columnar phase; Col_L = lamellar phase built up by the parallel alignment of columnar aggregates.

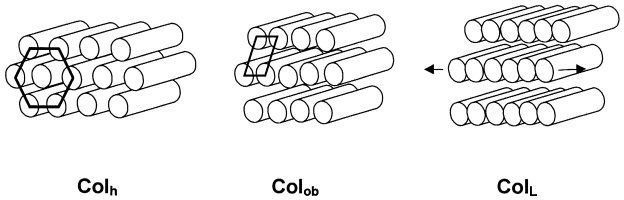
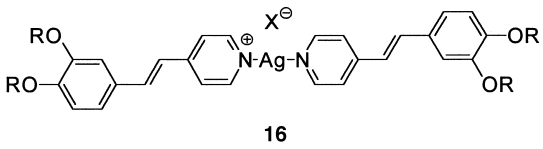
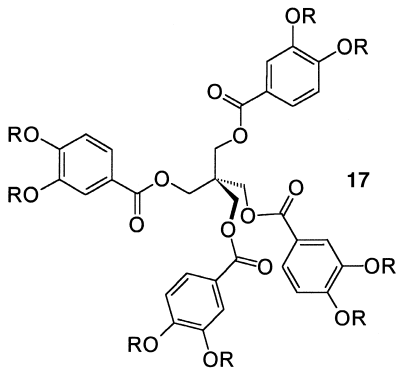


Figure 5. Organization of the Cu^{I} complexes **14** in their mesophases (only one possible structure—Col_{ob}—is shown for **14b**, the alkyl chains which fill the space between the columns are not shown).



therefore no driving force for their mesogenity.[31] In this respect the organization of the metallomesogens into columnar phases is strongly related to the organization seen in liquid crystals formed by some purely organic molecules comprising a central tetrahedral carbon atom bearing four semi-rigid subunits with peripheral alkyl chains, such as **17**[32, 33] and its



semi-fluorinated analogues.[34] For these molecules a microsegregation of incompatible structural units into different regions, separated by interfaces, was proposed to be the main driving force for mesophase formation.[32, 35] This should be even more important for the organization of **14** and **15**, because the contrast in the intramolecular polarity between the polar cores and the lipophilic chains is much larger in these molecules. Additionally, attractive ionic interactions significantly contribute to their mesophase stability, a feature that is well known for the liquid crystalline phases of anhydrous soaps and other ionic amphiphiles.[36]

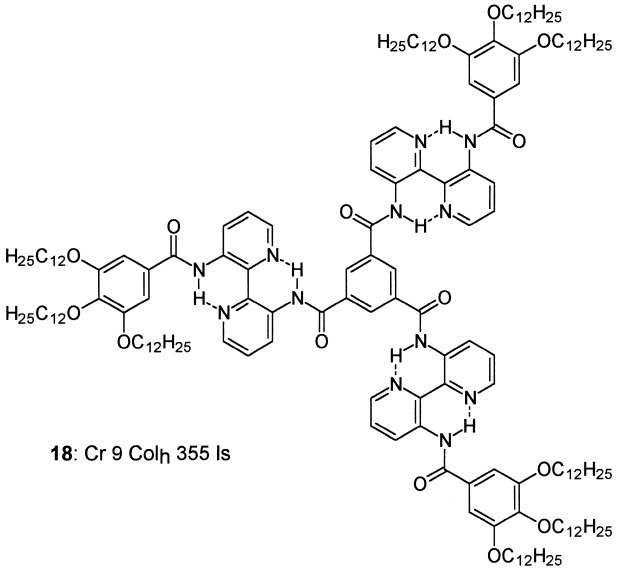
Furthermore, geometric and space-filling effects have a large influence on the mesophase structure. This is clear from the comparison of the complexes **14a–c**. In the case of the mononuclear pyridine derivative **14a** the polar rigid centers are rather small and compact. Hence, the long alkyl chains can perfectly surround the columns formed by the polar centers. This allows for the arrangement of the columns in the hexagonal lattice. A lamellar organization was found for terpyridine complex **14c** with the largest central core. In the case of the bipyridine complex **14b** a rectangular or oblique arrangement of the columns (Col_r or Col_{ob}, see Figure 5) was detected, which can be regarded as an intermediate phase between columnar and lamellar organization.

The smectic phase of **14c** is again quite unusual as the layers comprise parallel aligned columnar aggregates of the metallohelicates.[24] Hence, this smectic phase is related to the Col_r phase of the Pd complex **11**, as in both cases the layers are formed by the parallel alignment of columns. However, in the smectic phase of **14a** the correlation between the layers is lost and therefore no 2D lattice can be found. Thus, quite different organizations of columns are possible with the bipyridine-

 © WILEY-VCH Verlag GmbH, D-69451 Weinheim, 2000 1433-7851/00/3914-2456 $ 17.50+.50/0

derived metallomesogens, and the type of supermolecular self-organization can be fine-tuned by careful molecular design. It is remarkable that the unusual structure of the mesophase of **14c** resembles that of linear DNA stretched across lipid bilayers.[37]

However, coordination of metal ions is not the only feature of oligopyridines that can be used to design novel liquid crystalline materials. The ability of the nitrogen atoms to participate in hydrogen bonding has also been used to design mesomorphic materials incorporating 2,2′-bipyridine units.[38] In the 3,3′-diacylamino substituted 2,2′-bipyridine derivative **18** a high degree of planarity of the molecules is achieved by



18: Cr 9 Col$_h$ 355 Is

the large number of intramolecular hydrogen-bonding interactions. This particular shape, the polarity of the central core, and the presence of a sufficiently large number of peripheral lipophilic chains induces hexagonal columnar liquid crystalline behavior. It should be pointed out that these 2,2′-bipyridine derivatives have low melting points, extremely broad regions of liquid crystalline phases, and, additionally, the molecules retain their strong tendency to aggregate also in solutions of apolar solvents.

Thus, significant progress has been achieved in designing oligopyridine derivatives that can self-organize under ambient conditions into well-ordered supermolecular assemblies of macroscopic dimensions. Hopefully, this will allow the construction of novel and more-complex functional supermolecular systems, which are useful for future applications.

[1] J. M. Lehn, *Supramolecular Chemistry: Concepts and Perspectives*, VCH, Weinheim, **1995**; E. C. Constable, *Metals and Ligand Reactivity: An Introduction to Organic Chemistry of Metal Complexes*, VCH, Weinheim, **1995**; F. M. Raymo, J. F. Stoddart, *Curr. Opin. Colloid Interf. Sci.* **1998**, *3*, 150.

[2] J. C. Chambron, C. O. Dietrich-Buchecker, J.-P. Sauvage in *Comprehensive Supramolecular Chemistry*, *Vol. 9* (Eds.: J. L. Atwood, J. E. D. Davies, D. D. MacNicol, F. Vögtle, K. S. Suslick), Pergamon, Oxford, **1996**, p. 43; D. B. Amabilino, F. M. Raymo, J. F. Stoddart in *Comprehensive Supramolecular Chemistry*, *Vol. 9* (Eds.: J. L. Atwood, J. E. D. Davies, D. D. MacNicol, F. Vögtle, K. S. Suslick), Pergamon, Oxford, **1996**, p. 85.

[3] C. Piguet, G. Bernardinelli, G. Hopfgartner, *Chem. Rev.* **1997**, *97*, 2005; B. Hasenknopf, J. M. Lehn, N. Boumediene, A. Dupont-Gervais, A. Van Dorsselaer, B. Kneisel, D. Fenske, *J. Am. Chem. Soc.* **1997**, *119*, 10956.

[4] A. M. Garcia, F. J. Romero-Salguero, D. M. Bassani, J.-M. Lehn, G. Baum, D. Fenske, *Chem. Eur. J.* **1999**, *5*, 1803.

[5] D. P. Funeriu, J. M. Lehn, G. Baum, D. Fenske, *Chem. Eur. J.* **1997**, *3*, 99; S. Leininger, B. Olenyuk, P. Stang, *Chem. Rev.* **2000**, *100*, 853.

[6] I. Weissbuch, P. N. W. Baxter, S. Cohen, H. Cohen, K. Kjaer, P. B. Howes, J. Als-Nielsen, G. S. Hanan, U. S. Schubert, J.-M. Lehn, L. Leiserowitz, M. Lahav, *J. Am. Chem. Soc.* **1998**, *120*, 4850.

[7] L. A. Cuccia, J.-M. Lehn, J.-C. Homo, M. Schmutz, *Angew. Chem.* **2000**, *112*, 239; *Angew. Chem. Int. Ed. Engl.* **2000**, *39*, 233.

[8] *Handbook of Liquid Crystals*, *Vol. 1–3* (Eds.: D. Demus, J. W. Goodby, H.-W. Spiess, V. Vill), Wiley-VCH, Weinheim, **1998**.

[9] *Metallomesogens* (Ed.: J. L. Serrano), VCH, Weinheim, **1996**; B. Donnio, D. W. Bruce in *Structure and Bonding 95: Liquid Crystals II* (Ed.: D. M. P. Mingos), Springer, Berlin, **1999**, p. 193.

[10] K. Hanabusa, J.-I. Higashi, T. Koyama, H. Shira, N. Hojo, A. Kurose, *Makromol. Chem.* **1989**, *190*, 1.

[11] T. Kuboki, K. Araki, M. Yamada, S. Shiraishi, *Bull. Chem. Soc. Jpn.* **1994**, *67*, 984.

[12] D. W. Bruce, J. D. Holbrey, A. R. Tajbakhsh, G. J. T. Tiddy, *J. Mater. Chem.* **1993**, *67*, 984; J. D. Holbrey, G. J. T. Tiddy, D. W. Bruce, *J. Chem. Soc. Dalton Trans.* **1995**, 1769.

[13] F. Neve, M. Ghedini, A. Crispini, *Chem. Commun.* **1996**, 2463; F. Neve, M. Ghedini, O. Francescangeli, S. Campagna, *Liq. Cryst.* **1998**, *24*, 673.

[14] E. C. Constable, C. E. Housecroft, *Chimia* **1998**, *52*, 533.

[15] M. Ghedini, D. Pucci, *J. Organomet. Chem.* **1990**, *395*, 105.

[16] D. W. Bruce, K. E. Rowe, *Liq. Cryst.* **1995**, *18*, 161; D. W. Bruce, K. E. Rowe, *Liq. Cryst.* **1996**, *20*, 183.

[17] L. Douce, R. Ziessel, R. Seghrouchni, A. Skoulios, E. Campillos, R. Deschenaux, *Liq. Cryst.* **1995**, *18*, 157; L. Douce, R. Ziessel, R. Seghrouchni, A. Skoulios, E. Campillos, R. Deschenaux, *Liq. Cryst.* **1996**, *20*, 235; A. El-ghayoury, L. Douce, R. Ziessel, R. Seghrouchni, A. Skoulios, *Liq. Cryst.* **1996**, *21*, 143.

[18] A. J. Attias, C. Cavalli, B. Bloch, *J. Chim. Phys.* **1998**, *95*, 1319; A. J. Attias, C. Cavalli, B. Bloch, N. Guillou, C. Noel, *Chem. Mater.* **1999**, *11*, 2057.

[19] K. E. Rowe, D. W. Bruce, *J. Chem. Soc. Dalton Trans.* **1996**, 3913.

[20] K. E. Rowe, D. W. Bruce, *J. Mater. Chem.* **1998**, *8*, 331.

[21] A. El-ghayoury, L. Douce, A. Skoulios, R. Ziessel, *Angew. Chem.* **1998**, *110*, 1303; *Angew. Chem. Int. Ed.* **1998**, *37*, 1255.

[22] This molecule is in some respect related to compound **4** (Figure 1), which has a nonamphiphilic anion and was reported to show a nematic mesophase.[15]

[23] The polar groups of the amphiphilic anions should be located close to the central cores.

[24] Related lamellocolumnar structures have been found in other classes of compounds: P. Davidson, A. M. Levelut, H. Strzelecka, V. Gionis, *J. Phys. Fr.* **1983**, *44*, L823; G. Lattermann, S. Schmidt, R. Kleppinger, J.-H. Wendorff, *Adv. Mater.* **1992**, *4*, 30; J. Malthête, A.-M. Levelut, L. Liebert, *Adv. Mater.* **1992**, *4*, 37; D. Haristoy, S. Mery, B. Heinrich, L. Mager, J. P. Nicoud, D. Guillon, *Liq. Cryst.* **2000**, *27*, 321.

[25] R. Ziessel, A. Harriman, J. Suffert, M.-T. Youinou, A. De Cian, J. Fischer, *Angew. Chem.* **1997**, *109*, 2621; *Angew. Chem. Int. Ed. Engl.* **1997**, *36*, 2509.

[26] A. El-ghayoury, L. Douce, A. Skoulios, R. Ziessel, *Angew. Chem.* **1998**, *110*, 2327; *Angew. Chem. Int. Ed.* **1998**, *37*, 2205.

[27] R. Ziessel, L. Douce, A. El-ghayoury, A. Harriman, A. Skoulios, *Angew. Chem.* **2000**, *112*, 1549; *Angew. Chem. Int. Ed.* **2000**, *39*, 1489.

[28] L. Douce, A. El-ghayoury, A. Skoulios, R. Ziessel, *Chem. Commun.* **1999**, 2033.

[29] H. T. Nguyen, C. Destrade, J. Malthete, *Adv. Mater.* **1997**, *9*, 375.

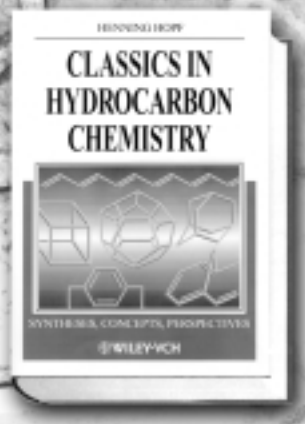
[30] D. W. Bruce, B. Donnio, D. Guillon, B. Heinrich, M. Ibn-Elhaj, *Liq. Cryst.* **1995**, *19*, 537; B. Donnio, D. W. Bruce, *New J. Chem.* **1999**, 275.

[31] Metallomesogens with an octahedral central core have also been reported: A.-M. Giroud-Godquin, A. Rassat, *C. R. Acad. Sci. Ser. 2* **1982**, *294*, 241; H. Zheng, T. M. Swager, *J. Am. Chem. Soc.* **1994**, *111*,

 © WILEY-VCH Verlag GmbH, D-69451 Weinheim, 2000 1433-7851/00/3914-2457 $ 17.50+.50/0

761; S. T. Trzaska, H.-F. Hsu, T. M. Swager, *J. Am. Chem. Soc.* **1999**, *121*, 4518.
[32] A. Pegenau, P. Göring, C. Tschierske, *Chem. Commun.* **1996**, 2563; A. Pegenau, P. Göring, S. Diele, C. Tschierske, *Chem. Eur. J.* **1999**, *5*, 1643.
[33] J. Malthête, *New. J. Chem.* **1996**, *20*, 925.
[34] A. Pegenau, X. H. Cheng, C. Tschierske, S. Diele, *New J. Chem.* **1999**, *23*, 465; X. H. Cheng, S. Diele, C. Tschierske, *Angew. Chem.* **2000**, *112*, 605; *Angew. Chem. Int. Ed.* **2000**, *39*, 592.
[35] C. Tschierske, *J. Mater. Chem.* **1998**, *8*, 1485.
[36] C. M. Paleos, *Mol. Cryst. Liq. Cryst.* **1994**, *243*, 159; J. Charvolin, *J. Chim. Phys.* **1983**, *80*, 15.
[37] T. Salditt, I. Koltover, J. O. Rädler, C. R. Safinya, *Phys. Rev. Lett.* **1997**, *79*, 2582; C. R. Safinya, I. Koltover, J. Raedler, *Curr. Opin. Colloid Interf. Sci.* **1998**, *3*, 69; C. S. O'Hern, T. C. Lubensky, *Phys. Rev. Lett.* **1998**, *80*, 4354.
[38] A. R. A. Palmans, J. A. J. M. Vekemans, H. Fischer, R. A. Hikmet, E. W. Meijer, *Chem. Eur. J.* **1997**, *3*, 300; A. R. A. Palmans, J. A. J. M. Vekemans, R. A. Hikmet, H. Fischer, E. W. Meijer, *Adv. Mater.* **1998**, *10*, 873.

CLASSICS FROM WILEY-VCH



Hopf, H.
Technical University Braunschweig, Germany
CLASSICS IN HYDROCARBON CHEMISTRY
Syntheses, Concepts, Perspectives
1999. IX, Approx 530 pages with approx 300 figures. Softcover.
Approx DM 98.-/ £ 34.95
ISBN 3-527-29606-9
Publication date: December 1999

Carbon and Hydrogen: the two basic building blocks can be combined in a million different ways to create a plethora of fascinating organic compounds. H. Hopf presents not only the most remarkable structures and properties of hydrocarbon compounds but also illustrates how molecules such as Pagodane or Dehydrobenzene challenge the synthetic skills of every organic chemist. Graduate students and researchers alike will find this book a gold mine of useful information essential for their daily work.

Nicolaou, K. C. / Sorensen, E. J.
University of California, San Diego, USA
CLASSICS IN TOTAL SYNTHESIS
Targets, Strategies, Methods
1996. XXIII, 798 pages with 444 figures. Softcover.
DM 98.-/ £ 34.95
ISBN 3-527-29231-4

This book is a must for every synthetic chemist. With didactic skill and clarity, K. C. Nicolaou and E. Sorensen present the most remarkable and ingenious total syntheses from outstanding synthetic organic chemists.

John Wiley & Sons, Ltd. • Baffins Lane
Chichester, West Sussex
PO 19 1UD, UK
Fax: +44 (0)1243-775878

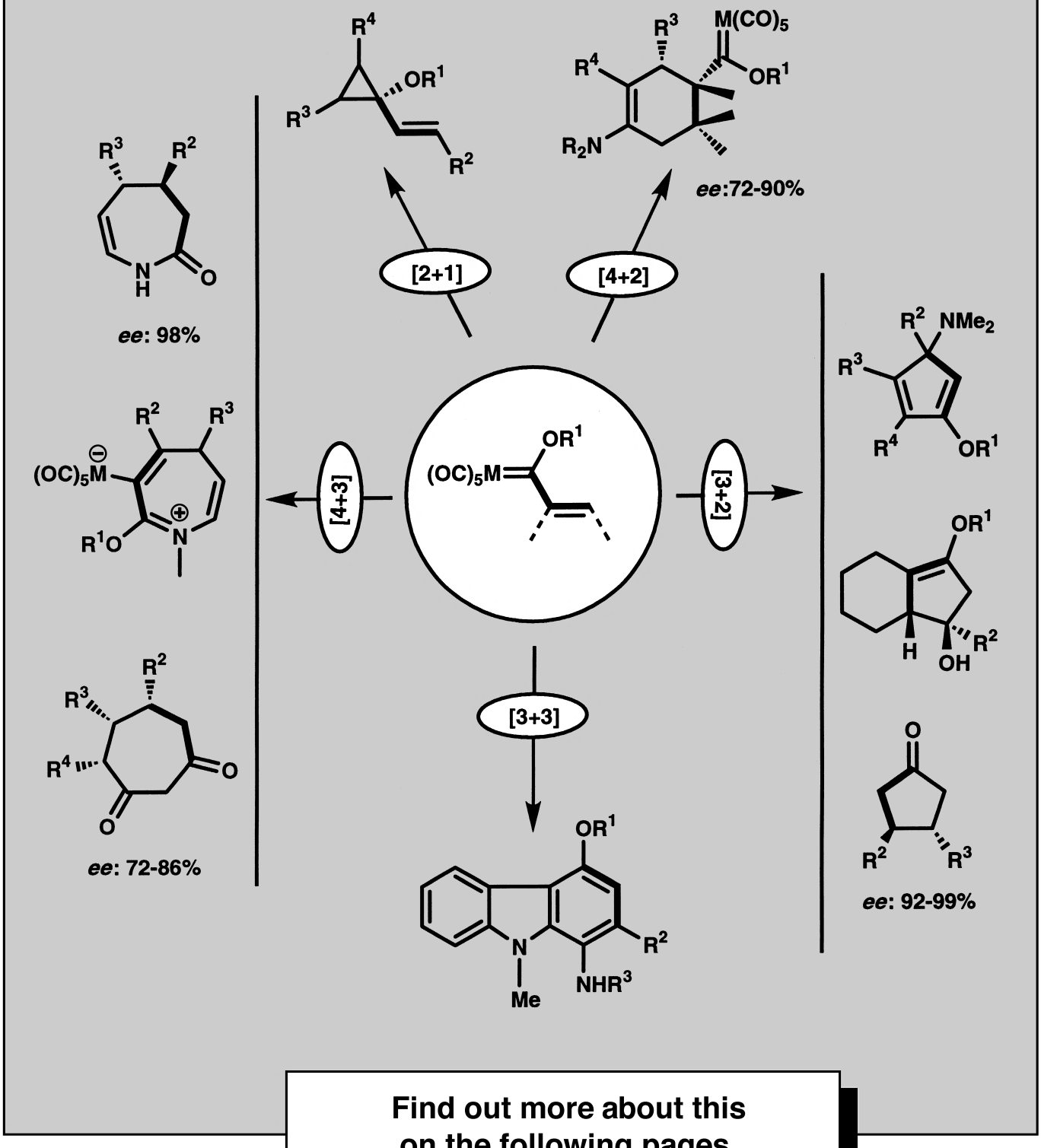
WILEY-VCH • P.O. Box 10 11 61
69451 Weinheim, Germany
Fax: +49 (0) 62 01 - 60 61 84
e-mail: sales-books@wiley-vch.de

WILEY-VCH

ZI 1199

 © WILEY-VCH Verlag GmbH, D-69451 Weinheim, 2000 1433-7851/00/3914-2458 $ 17.50+.50/0

α,β-Unsaturated Fischer Carbene Complexes: A Powerful Tool in Synthesis



Find out more about this on the following pages.

 © WILEY-VCH Verlag GmbH, D-69451 Weinheim, 2000 1433-7851/00/3914-2459 $ 17.50+.50/0

Five- and Seven-Membered Rings from Alkenyl(methoxy)carbene Complexes and Methyl Ketone Enolates**

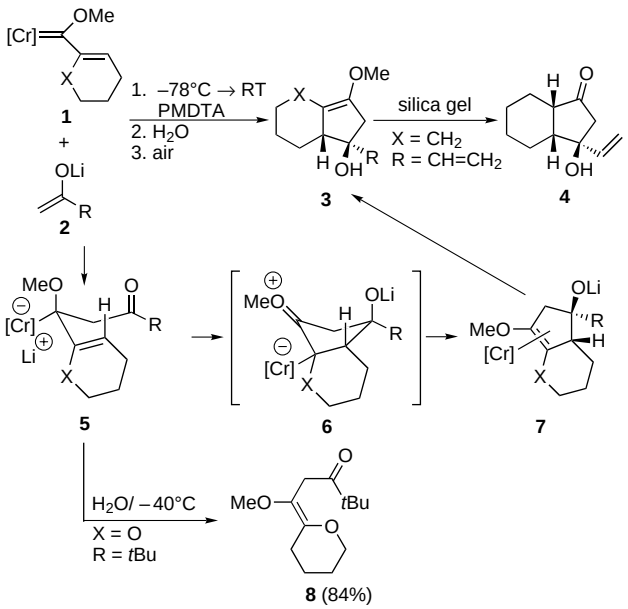
José Barluenga,* Jorge Alonso, Félix Rodríguez, and Francisco J. Fañanás

Dedicated to Professor Heinz Hoberg on the ocassion of his 75th birthday

Fischer carbene complexes have become valuable building blocks in organic synthesis.[1] In particular, they are very useful for the generation of ring systems.[2] Thus, the formal [3+2] cycloadditions of α,β-unsaturated carbene complexes to siloxy-substituted 1,3-dienes,[3] electron-poor olefins,[4] alkynes,[5] or enamines[6] give rise to functionalized five-membered carbocycles. On the other hand, the formal [4+3] cycloadditions of α,β-unsaturated carbene complexes to 1,3-dienes,[7] 1-azadienes,[8] or 2-azadienes[9] afford functionalized seven-membered rings. Although a domino cyclopropanation–Cope rearrangement[7, 9] was proposed in some cases to explain this latter type of cyclization, we demonstrated that this process involves nucleophilic attack at the carbene carbon atom followed by a cyclization that is promoted by a 1,2-$M(CO)_5$ shift.[8] Moreover, lithium enolates add to α,β-unsaturated carbene complexes in a Michael fashion,[10] and only one example has been reported in which the lithium enolate of acetone reacts with vinylcarbene complexes by 1,2-nucleophilic attack to furnish α,β-unsaturated ketones.[10a] This prompted us to study the reaction of α,β-unsaturated carbene complexes with methyl ketone enolates. Here we report a new diastereoselective route to five- and seven-membered carbocycles under very mild reaction conditions.

The treatment of alkenylcarbene pentacarbonyl complexes **1** with methyl ketone enolates **2** in THF at $-78\,^{\circ}C$ to room temperature led, after hydrolysis and metal decoordination, to the cyclopentenol derivatives **3** in low yields. However, when three equivalents of *N*,*N*,*N*′,*N*′,*N*″-pentamethyldiethylenetriamine (PMDTA) were added to the reaction mixture, compounds **3** were obtained in very good yields and as single diastereomers (Scheme 1 and Table 1). The enol ether group of **3** can be easily hydrolyzed to a carbonyl group. Thus, treatment of **3e** with silica gel quantitatively affords the bicyclic ketone **4** as a single diastereomer (Scheme 1). The relative configurations of **3** and **4** were assigned on the basis of NOESY experiments on **3f** and **4**.

The formation of cyclopentenol derivatives **3** can be explained by assuming a 1,2-addition of the lithium enolates **2** to the carbene complexes **1** to form intermediates **5**. A cyclization induced by an 1,2-migration[6, 8, 11] of the pentacarbonylchromium group leads to **6**. Subsequent elimination of the metal fragment followed by coordination of the metal



Scheme 1. Reaction of α,β-unsaturated methoxycarbene chromium complexes **1** ([Cr] = $(CO)_5Cr$) with methyl ketone enolates **2**. Formation of five-membered rings **3** and proposed mechanism.

Table 1. Formation of cyclopentenol derivatives **3** from alkenylcarbene complexes **1** and methyl ketone enolates **2**.

Entry	Complex	X	Enolate	R	Product	Yield[a]
1	**1a**	CH_2	**2a**	Me	**3a**	86
2	**1b**	O	**2a**	Me	**3b**	91
3	**1b**	O	**2b**	*t*Bu	**3c**	68[b]
4	**1b**	O	**2c**	PhC≡C	**3d**	87 (48)[c]
5	**1a**	CH_2	**2d**	CH_2=CH	**3e**	78 (28)[c]
6	**1b**	O	**2d**	CH_2=CH	**3f**	82 (34)[c]

[a] Based on starting carbene **1**. [b] Product **8** (14%) is also obtained. [c] In parentheses: yield in the absence of PMDTA.

atom to the carbon–carbon double bond furnishes intermediates **7**, which, after hydrolysis and metal decoordination, give rise to bicyclic cyclopentenol derivatives **3**. Support for the above reaction pathways, especially the 1,2-addition, was gained by studying the low-temperature hydrolysis of **5** (X = O, R = *t*Bu), which gave ketone **8**[10a] (Scheme 1). The observed diastereoselectivity in the formation of **3** can be accounted for by invoking a transition state with the same geometric disposition as **5**. Moreover, the higher yields of **3** when PMDTA was used can be rationalized in terms of coordination of the lithium atom to the triamine, which lowers the rigidity of the transition state and thus favors the approach of the allylic carbon atom of the σ-allylchromium moiety to the carbonyl carbon atom.

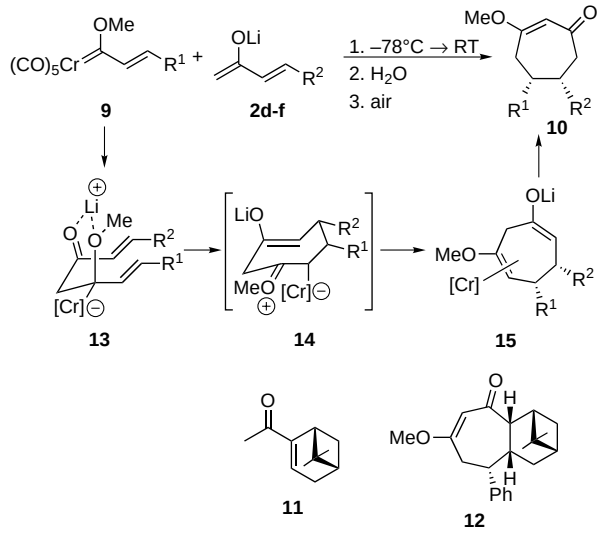
Encouraged by these good results, we extended the reaction to other alkenylcarbene complexes. Surprisingly, the reaction of complexes **9** with enolates **2a–c** under the above reaction conditions afforded an undetermined complex mixture, in which the major compound corresponds to the hydrolysis of the product of a 1,2-addition similar to that described by Casey et al.,[10a] instead of the expected cyclopentenol derivatives analogous to **3**. However, when the reaction was

[*] Prof. Dr. J. Barluenga, J. Alonso, Dr. F. Rodríguez, Dr. F. J. Fañanás
Instituto Universitario de Química Organometálica "Enrique Moles"
Unidad Asociada al CSIC, Universidad de Oviedo
Julian Clavería 8, 33071 Oviedo (Spain)
Fax: (+34) 98-510-34-50
E-mail: barluenga@sauron.quimica.uniovi.es

[**] This work was supported by DGICYT (Grant PB97-1271).

 © WILEY-VCH Verlag GmbH, D-69451 Weinheim, 2000 1433-7851/00/3914-2460 $ 17.50+.50/0

performed with enolates **2d–f**, cycloheptenone derivatives **10** were obtained as single diastereomers (Scheme 2 and Table 2). Here, the best yields were obtained when the reaction was carried out in the absence of PMDTA. The relative *cis* configuration of products **10** was determined on the basis of



Scheme 2. Reaction of α,β-unsaturated methoxycarbene chromium complexes **9** with methyl vinyl ketone enolates **2d–f**. Formation of seven-membered rings **10** and proposed mechanism.

Table 2. Formation of cycloheptenone derivatives **10** from alkenylcarbene complexes **9** and methyl vinyl ketone enolates **2d–f**.

Complex	R^1	Enolate	R^2	Product	Yield[a]
9a	Ph	**2d**	H	**10a**	46
9a	Ph	**2e**	Me	**10b**	44
9a	Ph	**2f**	Ph	**10c**	51
9b	4-$MeOC_6H_4$	**2d**	H	**10d**	52
9b	4-$MeOC_6H_4$	**2f**	Ph	**10e**	43

[a] Based on starting carbene **9**.

the coupling constant ($J_{H5,H6} = 5.5$ Hz)[3b, 12] and NOESY experiments on **10b**. Given the complete *cis* diastereoselectivity for **10** in all cases examined, we carried out a reaction with the homochiral enolate derived from ketone **11** (Scheme 2), which is easily obtained from (−)-myrtenal. The reaction of this enolate with **9a** at −78 °C to room temperature followed by hydrolysis at −78 °C with a solution of ammonium chloride afforded the fused tricyclic compound **12** in 41 % yield with diastereoselectivity greater than 99 %. The structure and absolute configuration of the new stereogenic centers were unequivocally determined by two-dimensional (COSY, HMQC, HMBC, and NOESY) NMR spectroscopic analysis.

A reasonable mechanism that accounts for the formation of cycloheptenone derivatives **10** is outlined in Scheme 2 and involves an initial nucleophilic attack of the enolates **2d–f** at the carbene carbon atom of carbene complexes **9** to give intermediates **13**. Cyclization, induced by a 1,2-migration[6, 8, 11] of the pentacarbonylchromium group leads to **14**. Subsequent elimination of the metal fragment followed by coordination of the metal atom to the carbon–carbon double bond furnishes intermediates **15**, which, after hydrolysis, metal decoordination, and double-bond isomerization, give rise to cycloheptenone derivatives **10**. The generation of the *cis* diastereomers can be explained by invoking a chairlike transition state, derived from **13**, presumably favored by the internal coordination of the oxygen atoms to the lithium atom. The different reaction courses starting from complexes **1** and **9** can be attributed to the substitution pattern in the vinyl moiety of the carbene complex (see Table 1, entries 5 and 6 and Table 2). α-Substitution seems to disfavor the chairlike approach to the seven-membered rings, presumably due to steric hindrance.

In conclusion, we have developed an interesting generalization of the sole example of 1,2-addition of enolates to alkenylcarbene complexes described by Casey et al. almost twenty-five years ago, which represents a new strategy for the diastereoselective synthesis of five- and seven-membered carbocycles. The starting materials are simple methyl ketones and vinylcarbene complexes. These cyclization processes once again demonstrate the ability of the recently described 1,2-$M(CO)_5$ migration to promote unusual umpolung annulations. Investigations to clarify the mechanism and to expand the scope of the [3+2] and [3+4] annulation methodologies to the modification of natural products such as terpenes, sugars, and α-amino acids are underway.

Experimental Section

General procedure for **3** and **10**: To a solution of lithium diisopropylamide (LDA), prepared by adding BuLi (1.1 mmol) to a solution of diisopropylamine (1.1 mmol) in THF (5 mL) at −30 °C, was added at −78 °C the appropriate methyl ketone (1.1 mmol); when PMDTA was used, it was added, freshly distilled (3 mmol), after the methyl ketone. The resulting yellow–orange solution of **2** was stirred for 30 min at the same temperature, and then a solution of the alkenylcarbene complex **1** or **9** (1 mmol) in THF (10 mL) was added dropwise at −78 °C, and stirring was continued while the temperature reached room temperature. The mixture was hydrolyzed with brine (30 mL), extracted with diethyl ether (3 × 15 mL), and the organic layer dried over anhydrous sodium sulfate. The solvent was removed at reduced pressure, and the crude product was dissolved in hexane/ethyl acetate (5/1) and subjected to air oxidation in direct sunlight. After 2–3 h the resulting brown suspension was filtered through Celite. Solvent removal on a rotary evaporator gave the crude products, which were purified by column chromatography (deactivated silica gel, hexane/ethyl acetate 20/1). All compounds gave satisfactory analytical data, including elemental analyses and mass and NMR spectra.

Received: February 11, 2000 [Z 14688]

[1] a) W. D. Wulff in *Comprehensive Organic Synthesis*, *Vol. 5* (Eds.: B. M. Trost, I. Fleming, L. A. Paquette), Pergamon, New York, **1991**, p. 1065; b) W. D. Wulff in *Comprehensive Organometallic Chemistry II*, *Vol. 12* (Eds.: E. W. Abel, F. G. A. Stone, G. Wilkinson), Pergamon, Oxford, **1995**, p. 469; c) M. P. Doyle in *Comprehensive Organometallic Chemistry II*, *Vol. 12* (Eds.: E. W. Abel, F. G. A. Stone, G. Wilkinson), Pergamon, Oxford, **1995**, p. 387; d) A. de Meijere, *Pure Appl. Chem.* **1996**, *68*, 61; e) R. Aumann, H. Nienhaber, *Adv. Organomet. Chem.* **1997**, *41*, 163.

[2] a) D. F. Harvey, D. M. Sigano, *Chem. Rev.* **1996**, *96*, 271; b) H.-W. Frühauf, *Chem. Rev.* **1997**, *97*, 523; c) H.-G. Schmalz, *Angew. Chem.* **1994**, *106*, 311; *Angew. Chem. Int. Ed. Engl.* **1994**, *33*, 303.

 © WILEY-VCH Verlag GmbH, D-69451 Weinheim, 2000 1433-7851/00/3914-2461 $ 17.50+.50/0

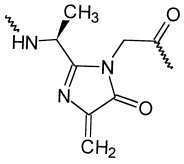
[3] a) M. Hoffmann, M. Bucher, H.-U. Reissig, *Angew. Chem.* **1997**, *109*, 281; *Angew. Chem. Int. Ed. Engl.* **1997**, *36*, 283; b) M. Hoffmann, M. Bucher, H.-U. Reissig, *Chem. Eur. J.* **1999**, *5*, 876.
[4] M. Hoffmann, H.-U. Reissig, *Synlett* **1995**, 625.
[5] B. L. Flynn, F. J. Funke, C. C. Silveira, A. de Meijere, *Synlett* **1995**, 1007.
[6] J. Barluenga, M. Tomás, A. Ballesteros, J. Santamaría, C. Brillet, S. García-Granda, A. Piñera-Nicolás, J. T. Vázquez, *J. Am. Chem. Soc.* **1999**, *121*, 4516.
[7] a) W. D. Wulff, D. C. Yang, C. K. Murray, *J. Am. Chem. Soc.* **1988**, *110*, 2653; b) J. Barluenga, F. Aznar, A. Martín, S. García-Granda, M. A. Salvadó, P. Pertierra, *J. Chem. Soc. Chem. Commun.* **1993**, 319; c) J. Barluenga, F. Aznar, C. Valdés, A. Martín, S. García-Granda, E. Martín, *J. Am. Chem. Soc.* **1993**, *115*, 4403; d) D. F. Harvey, E. M. Grenzer, P. K. Gantzel, *J. Am. Chem. Soc.* **1994**, *116*, 6719; e) J. Barluenga, F. Aznar, A. Martín, J. T. Vázquez, *J. Am. Chem. Soc.* **1995**, *117*, 9419; f) J. Barluenga, F. Aznar, A. Martín, *Organometallics* **1995**, *14*, 1429; g) J. Barluenga, F. Aznar, M. Fernández, *Chem. Eur. J.* **1997**, *3*, 1629.
[8] a) J. Barluenga, M. Tomás, A. Ballesteros, J. Santamaría, F. López-Ortiz, R. J. Carbajo, S. García-Granda, P. Pertierra, *Chem. Eur. J.* **1996**, *2*, 180; b) J. Barluenga, M. Tomás, E. Rubio, J. A. López-Pelegrín, S. García-Granda, P. Pertierra, *J. Am. Chem. Soc.* **1996**, *118*, 695; c) J. Barluenga, M. Tomás, E. Rubio, J. A. López-Pelegrín, S. García-Granda, M. Pérez-Priede, *J. Am. Chem. Soc.* **1999**, *121*, 3065.
[9] J. Barluenga, M. Tomás, A. Ballesteros, J. Santamaría, A. Suárez-Sobrino, *J. Org. Chem.* **1997**, *62*, 9229.
[10] a) C. P. Casey, W. Brunsvold, *Inorg. Chem.* **1977**, *16*, 391; b) S. Aoki, T. Fujimura, E. Nakamura, *J. Am. Chem. Soc.* **1992**, *114*, 2985; c) E. Nakamura, K. Tanoka, T. Fujimura, S. Aoki, P. G. Williard, *J. Am. Chem. Soc.* **1993**, *115*, 9015; d) J. Barluenga, J. M. Montserrat, J. Flórez, S. García-Granda, E. Martín, *Chem. Eur. J.* **1995**, *1*, 236.
[11] a) N. Iwasawa, T. Ochiai, K. Maeyama, *Organometallics* **1997**, *16*, 5137; b) N. Iwasawa, T. Ochiai, K. Maeyama, *J. Org. Chem.* **1998**, *63*, 3164; c) J. Barluenga, M. Tomás, E. Rubio, J. A. López-Pelegrín, *Angew. Chem.* **1999**, *111*, 1163; *Angew. Chem. Int. Ed.* **1999**, *38*, 1091.
[12] K. Takeda, A. Nakajima, M. Takeda, Y. Okamoto, T. Sato, E. Yoshii, T. Koizumi, M. Shiro, *J. Am. Chem. Soc.* **1998**, *120*, 4947.

Spectroscopic Evidence for a 4-Methylidene Imidazol-5-one in Histidine and Phenylalanine Ammonia-Lyases**

Dagmar Röther, Dietrich Merkel, and János Rétey*

Histidine ammonia-lyase (HAL, histidase, EC 4.3.1.3) and phenylalanine ammonia-lyase (PAL, EC 4.3.1.5) catalyse the nonoxidative deamination of their amino acid substrates to form *trans*-urocanate and *trans*-cinnamate, respectively.[1] HAL initiates histidine degradation both in bacteria and in animals.[2, 3] Its deficiency in humans causes the disease histidinemia.[4] PAL is an important plant enzyme at the crossroads of primary and secondary metabolism. Its product, cinnamate, is the precursor of lignins, flavonoids, and coumarins.

The two enzymes are highly homologous in their amino acid sequence and a prosthetic dehydroalanine was postulated at their active sites.[5–7] Overexpression in *E. coli* combined with mutagenesis experiments showed that the prosthetic group is formed autocatalytically from serines 143 and 202 of HAL and PAL, respectively.[8–10] Recently Schwede et al. solved the 3D structure of HAL by X-ray crystallography.[11] The structure revealed that the prosthetic group is not dehydroalanine but 4-methylidene imidazol-5-one (MIO, **1**). This novel electrophilic group is formed by autocatalytic cyclisation of an Ala–Ser–Gly tripeptide portion of the protein precursor, a process which is concomitant with the elimination of two molecules of water.



1

We investigated the UV spectra of wild-type HAL and of the mutant S143A which lacks the MIO group to provide spectroscopic evidence for such a chromophore. Figure 1a shows the UV difference spectra of HAL mutant S143A and wild-type HAL from 240 to 360 nm, measured at enzyme concentrations of 0.2, 0.4, 0.8, and 1.6 mg mL^{-1}. The UV spectrum of wild-type HAL exhibits a discrete maximum between 305 and 310 nm whose intensity grows with increasing enzyme concentration. We propose that this maximum originates from the MIO group, which contains a cross-conjugated double bond system. The mutant lacks this conjugated system and, therefore, it shows no absorption maximum around 308 nm.

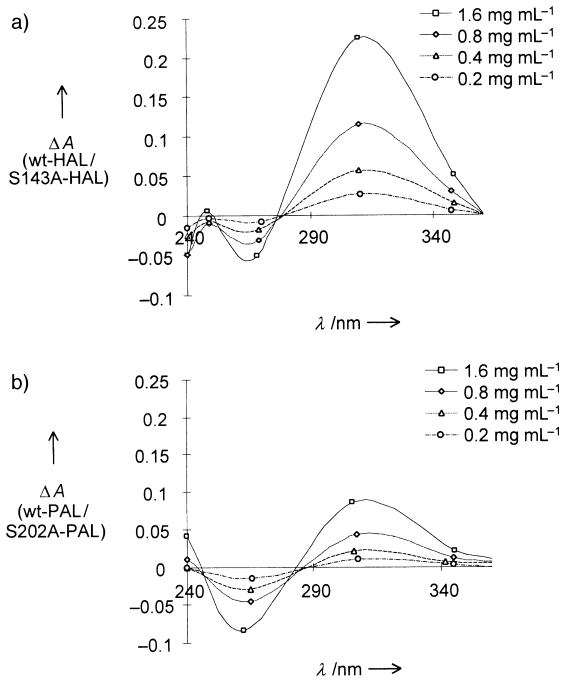


Figure 1. a) UV difference spectra of HAL mutant S143A and wild-type HAL; b) UV difference spectra of PAL mutant S202A and wild-type PAL. wt = wild-type.

[*] Prof. Dr. J. Rétey, D. Röther, Dr. D. Merkel
Institut für Organische Chemie und Biochemie der Universität
Richard-Willstätter-Allee, 76128 Karlsruhe (Germany)
Fax: (+49) 721-608-4823
E-mail: biochem@ochhades.chemie.uni-karlsruhe.de

[**] We thank Prof. G. E. Schulz and Dipl.-Chem. M. Baedeker (University of Freiburg) for providing us with the new PAL expression system and Dr. M. Stieger (Hoffmann–La Roche, Basel, Switzerland) for vector pREP4-GroESL carrying the HSP-60 system. D.R. and D.M. thank the Land of Baden-Württemberg for a scholarship for graduate students. The work was supported by the Deutsche Forschungsgemeinschaft and the Fonds der Chemischen Industrie.

 © WILEY-VCH Verlag GmbH, D-69451 Weinheim, 2000 1433-7851/00/3914-2462 $ 17.50+.50/0

The X-ray structure of PAL has not yet been solved. We performed UV spectrophotometric measurements with the wild-type enzyme and the mutant S202A to decide whether PAL also has an MIO group at the active site. Figure 1b shows the UV difference spectra of mutant S202A and wild-type PAL, measured at enzyme concentrations of 0.2, 0.4, 0.8, and 1.6 mg mL^{-1}. As in the HAL experiment one observes a maximum whose intensity grows with increasing enzyme concentration. The maximum is positioned between 305 and 310 nm.

Comparison of Figures 1a and 1b shows that the UV difference spectra of HAL and PAL are very similar, but PAL, at the same protein concentration, shows somewhat lower absorbance; this could be due to the higher molecular weight of PAL (312 relative to 215 kDa for HAL). In addition, PAL is much less stable than HAL. As a consequence, it is partially inactivated during the concentration of the solution by ultrafiltration, a process which is necessary for measuring the UV difference spectra. It has been noted that MIO, as a strong electrophile, is only stable within the intact active site. Before the concentration procedure both the wild-type and the mutant PAL samples were homogeneous in electrophoresis and were treated identically in every respect.

An absorbance maximum of wild-type HAL at approximately 315 nm was previously reported by Klee[12] but no explanation was given for this phenomenon. To exclude the possibility that the difference spectra just show relative differences in absorbance, we performed partial digestion of HAL and PAL to locate the chromophore in smaller peptides. First the enzymes were denatured with 6 M urea followed by dialysis and then incubation with pronase. The digest was applied to a reversed phase Nucleosil 100 C18 column. The peptide fragments were separated with a gradient of H_2O/CH_3CN, supplemented with 0.1% trifluoroacetic acid (TFA). In the digest of wild-type HAL we found a few peaks showing absorbance between 300 and 310 nm (Figure 2). No peptide fragment of the HAL mutant S143A showed this absorbance during the whole separation. Peptide fragments of wild-type PAL also exhibit an absorbance around wave lengths comparable to the absorbance in the UV difference spectra (Figure 2). No such maximum could be observed in any fragment of the PAL mutant S202A. Although repeated experiments led to the same results, in the case of wild-type HAL and wild-type PAL we also found peptide fragments which showed absorption maxima at higher wavelengths ($\lambda_{max} = 335$ nm). These fragments contained a modified MIO group arising from reaction with certain amino acids, such as lysine, which are present in the pronase digest.[13a] Compounds carrying a very similar chromophore to (substituted) MIO are known and exhibit λ_{max} values in the same region.[13b]

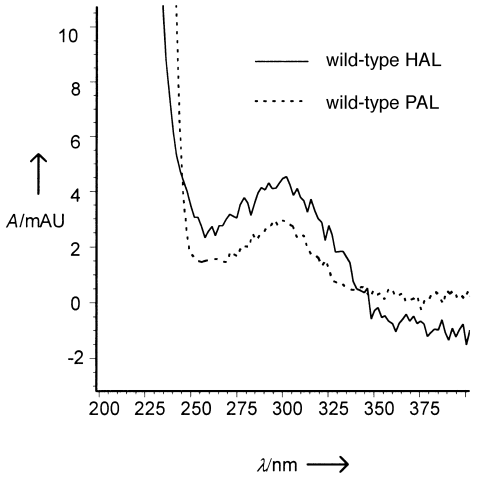


Figure 2. UV spectra of two of the peptide fragments separated after pronase digestion. The solid line shows the UV spectrum of a separated fragment (retention time of 65 min) of digested wild-type HAL. The dashed line shows the UV spectrum of a separated fragment (retention time of 14 min) of digested wild-type PAL.

We conclude that HAL and PAL are closely related enzymes which both contain the MIO group at their active sites. This also indicates that the mechanisms of action of HAL and PAL are analogous, as recently postulated.[14, 15]

Experimental Section

Bacterial strains and plasmids: HAL and PAL were overexpressed in *E. coli* BL21(DE3) cells. The gene for HAL from *Pseudomonas putida* was subcloned in the expression vector pT7-7.[8] The gene for PAL from *Petroselinum crispum* was changed to the codon usage of *E. coli* and cloned in vector pT7-7, followed by a transformation in *E. coli* BL21(DE3) cells containing vector pREP4-GroESL.[16]

Site-directed mutagenesis: HAL mutant S143A was produced by Langer et al.[8] PAL mutant S202A was produced by following the instruction manual of the QuickChange site-directed mutagenesis kit (Stratagene).[17] The oligonucleotides used in the mutagenesis reaction were as follows: S202A(+): 5′-CATCACTGCTGCCGGCGACCTGG-3′; S202A(−): 5′-CCAGGTCGCCGGCAGCAGTGATG-3′. The mutation was checked by sequence analysis using the dideoxynucleotide chain termination method.[18]

Protein expression and purification: Both HAL and PAL were expressed and purified as described in Ref. [8, 10, 16].

Enzyme activity and protein determination: The activities of HAL and PAL were measured spectrophotometrically.[19, 20] Determination of protein concentration was carried out according to Warburg and Christian[21] as modified by Layne.[22]

Spectroscopic measurements: UV difference spectra were measured at enzyme concentrations of 1.6, 0.8, 0.4, and 0.2 mg mL^{-1} in 10 mm Tris-HCl buffer (pH 7.2, Tris = Tris(hydroxymethyl)methylamine) from 240 to 360 nm using 1 cm quartz cuvettes. A blank experiment containing the mutant lacking the 4-methylidene imidazole-5-one was measured first, followed by a scan of the wild-type enzyme.

Enzyme denaturation and pronase digest: Enzyme (30 mg) was dialysed against 100 mm Tris-HCl buffer (pH 7.5) for 15 h and then denatured with 6 M urea and 0.5% sodium dodecylsulfate (SDS) for 10 min at 100 °C. The denatured enzyme was dialysed against 100 mm Tris-HCl buffer (pH 7.5) containing 10 mM $CaCl_2$, followed by concentration of the solution to 1.5 mL by ultrafiltration through a 10 kDa concentration unit (Millipore). After addition of 4 mg pronase (Roche Diagnostics), the mixture was incubated for 48 h at 37 °C. Pronase was eliminated by ultrafiltration.

Separation of the digest by HPLC: The pronase digest was separated by HPLC using a Hewlett–Packard Ti-Series 1050 liquid chromatography system. The solution was applied to a preparative-grade reverse-phase Nucleosil 100 C18 column (Macherey-Nagel) equilibrated with solvent A (twice-distilled H_2O containing 0.1% TFA). After washing with solvent A for 10 min, elution was performed at a flow rate of 5 mL min^{-1} with a linear gradient of increasing concentration of solvent B (CH_3CN containing 0.1% TFA) over a period of 90 min (0–30% B). Absorbance signals were measured at 215, 315, and 340 nm and the UV spectrum of each peak was monitored with a diode array detector.

Received: December 17, 1999
Revised: March 20, 2000 [Z14414]

 © WILEY-VCH Verlag GmbH, D-69451 Weinheim, 2000 1433-7851/00/3914-2463 $ 17.50+.50/0

[1] Review: J. Rétey, *Naturwissenschaften* **1996**, *83*, 439 – 447.
[2] H. Tabor, A. H. Mehler, O. Hayaishi, J. White, *J. Biol. Chem.* **1952**, *196*, 121 – 127.
[3] V. H. Auerbach, H. A. Waisman, *J. Biol. Chem.* **1959**, *234*, 304 – 306.
[4] R. G. Taylor, H. L. Levy, R. R. McInnes, *Mol. Biol. Med.* **1991**, *8*, 101 – 116.
[5] R. B. Wickner, *J. Biol. Chem.* **1969**, *244*, 6550 – 6552.
[6] J. L. Givot, T. A. Smith, R. H. Abeles, *J. Biol. Chem.* **1969**, *244*, 6341 – 6353.
[7] K. R. Hanson, E. A. Havir, *Arch. Biochem. Biophys.* **1970**, *141*, 1 – 17.
[8] M. Langer, G. Reck, J. Reed, J. Rétey, *Biochemistry* **1994**, *33*, 6462 – 6467.
[9] M. Langer, A. Lieber, J. Rétey, *Biochemistry* **1994**, *33*, 14034 – 14038.
[10] B. Schuster, J. Rétey, *FEBS Lett.* **1994**, *349*, 252 – 254.
[11] T. F. Schwede, J. Rétey, G. E. Schulz, *Biochemistry* **1999**, *38*, 5355 – 5361.
[12] C. B. Klee, *J. Biol. Chem.* **1970**, *245*, 3143 – 3152.
[13] a) D. Merkel, J. Rétey, *Helv. Chim. Acta* **2000**, *83*, 1151 – 1160; b) F. Campagna, A. Carotti, G. J. Casini, *Heterocycl. Chem.* **1990**, *27*, 1973 – 1977.
[14] M. Langer, A. Pauling, J. Rétey, *Angew. Chem.* **1995**, *107*, 1585 – 1587; *Angew. Chem. Int. Ed. Engl.* **1995**, *34*, 1464 – 1465.
[15] B. Schuster, J. Rétey, *Proc. Natl. Acad. Sci. USA* **1995**, *92*, 8433 – 8437.
[16] M. Baedeker, G. E. Schulz, *FEBS Lett.* **1999**, *457*, 57 – 60.
[17] C. Papworth, J. Braman, D. A. Wright, *Strategies* **1996**, *9*, 3 – 4.
[18] F. Sanger, S. Nicklen, A. Coulson, *Proc. Natl. Acad. Sci. USA* **1977**, *78*, 177 – 181.
[19] A. H. Mehler, H. Tabor, *J. Biol. Chem.* **1953**, *201*, 775 – 784.
[20] A. Zimmermann, K. Hahlbrock, *Arch. Biochem. Biophys.* **1975**, *166*, 54 – 62.
[21] O. Warburg, W. Christian, *Biochem. Z.* **1942**, *310*, 384 – 421.
[22] E. Layne, *Methods Enzymol.* **1957**, *3*, 447 – 454.

Tris(pyrazolyl)methanesulfonates: A Novel Class of Water-Soluble Ligands

Wolfgang Kläui,* Michael Berghahn, Gerd Rheinwald, and Heinrich Lang

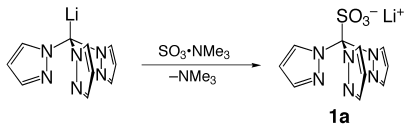
In 1966 Trofimenko introduced a new tripodal nitrogen-donating ligand, hydrotris(pyrazolyl)borate, into coordination chemistry. Soon these anions found their way into coordination chemistry as versatile nitrogen-based chelating ligands. Nowadays the substituted hydrotris(pyrazolyl)borates (in the following abbreviated as Tp) are the most important class of N_3 tripodal ligands.[1] The possibility of increasing the steric demands of the ligand through bulky substituents in the 3-position of the pyrazole ring is an important aspect in the chemistry of Tp ligands.[2] Such sterically demanding Tp ligands play an important role in the synthesis of various enzyme models.[3]

Vahrenkamp and co-workers were able to obtain a Zn–hydroxide complex with $Tp^{Cum,Me}$ ligands[4] which showed, for example, hydrolytic activity towards activated esters, amides, and nonactivated phosphate esters, and thus functioned as a stoichiometric model for esterases, peptidases, and phosphatases.[5] However, due to the insolubility of this particular complex in water it is neither possible to determine a pK_s value for a zinc-bound water molecule in aqueous solution, nor is it possible to add water during the hydrolysis reaction to regenerate the $Tp^{Cum,Me}$-Zn-OH complex. Therefore, the hydrolysis reaction shows only stoichiometric not catalytic behavior.[6] Another problem is the sensitivity of the B–N bond in hydrotris(pyrazolyl)borate ligands to hydrolysis. Even by substituting the proton in the 5-position of the pyrazolyl ring with a methyl group, the hydrolysis of the B–N bond cannot be completely avoided.[7]

Especially in the field of enzyme models it is of great interest to obtain complexes that are soluble and stable under physiological conditions. The introduction of functional groups that would generate water solubility in hydrotris(pyrazolyl)borate is still an unsolved problem to date. With this in mind, our aim was to find a ligand that would prove to be water-soluble and stable towards hydrolysis, and thus could be used as an alternative to hydrotris(pyrazolyl)borates.

A suitable ligand system should have a similar arrangement of the donor centers as in hydrotris(pyrazolyl)borate and offer the possibility to introduce hydrophilic groups in a straightforward manner. We have found that the isosteric and isoelectronic tris(pyrazolyl)methane ligand proved to be a suitable starting material. In this class of ligands, first published by Hückel and later made more easily accessible by a more facile preparation reported by Juliá, the B–N bonds are substituted by C–N bonds.[8, 9] The methine proton of tris(pyrazolyl)methane is sufficiently acidic to be removed by butyllithium, and the resulting reactive intermediate readily reacts with electrophiles.[10]

Since our goal was the introduction of a hydrophilic moiety, we added the lithiated tris(pyrazolyl)methane to a sulfurtrioxide–trimethylamine complex and obtained the lithium salt of tris(pyrazolyl)methanesulfonic acid (**1a**; LiTpms) as shown in Equation (1). A metathesis reaction of **1a** with potassium carbonate gave the corresponding potassium salt (**1b**; KTpms).



1a (1)

In contrast to tris(pyrazolyl)methane, **1b** is almost exclusively soluble in water and only moderately soluble in methanol. Another distinct difference to tris(pyrazolyl)methane[11] and especially to hydrotris(pyrazolyl)borate is the fact that the reported ligand Tpms (**1**) is stable over a wide range of pH values in aqueous solution. At pH 0 only small amounts of pyrazole—the product resulting from a hydrolysis

[*] Prof. Dr. W. Kläui, M. Berghahn
Institut für Anorganische Chemie und Strukturchemie der
Heinrich-Heine-Universität Düsseldorf
Universitätsstrasse 1, 40225 Düsseldorf (Germany)
Fax: (+49) 211-81-12287
E-mail: klaeui@uni-duesseldorf.de
Dr. G. Rheinwald, Prof. Dr. H. Lang
Institut für Chemie
Lehrstuhl für Anorganische Chemie
Strasse der Nationen 62
09107 Chemnitz (Germany)

Supporting information for this article is available on the WWW under http://www.wiley-vch.de/home/angewandte/ or from the author.

 © WILEY-VCH Verlag GmbH, D-69451 Weinheim, 2000 1433-7851/00/3914-2464 $ 17.50+.50/0

reaction—can be detected even after several weeks, at pH 13 even after weeks no signs of decomposition can be detected.

Regarding the use of tris(pyrazolyl)methanesulfonate as a novel class of ligands as enzyme models, we prepared the sterically demanding ligand tris(3-*tert*-butylpyrazolyl)methanesulfonate **2a** (LiTpms$^{t\mathrm{Bu}}$[12]), starting from tris(3-*tert*-butylpyrazolyl)methane in a reaction analogous to the synthesis of **1**. The corresponding thallium salt **2b** (TlTpms$^{t\mathrm{Bu}}$) can be obtained by a metathesis reaction with thallium nitrate in a mixture of methanol and water. Owing to the facile removal of thallium salts, **2b** is an excellent starting material for complexation reactions. The molecular structure of **2b** was solved by X-ray diffraction (Figure 1).[13] TlTpms$^{t\mathrm{Bu}}$ is stable towards protic solvents and decomposes only in the presence of mineral acids with formation of pyrazole.

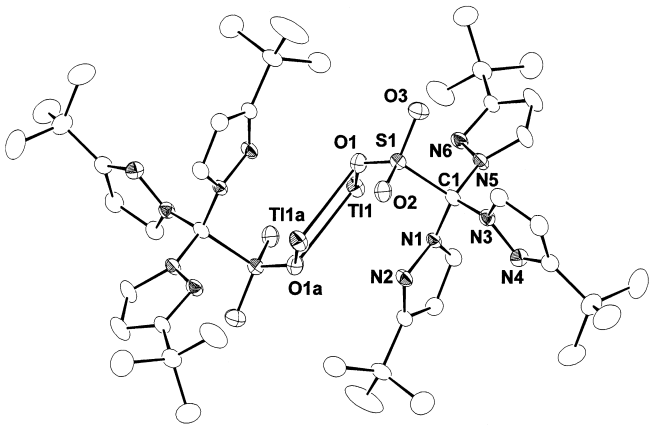


Figure 1. Crystal structure of **2b**. Selected distances [Å] and angles [°]: Tl1-O1 2.708(3), Tl1-Tl1a 4.1537(3), S1-O3 1.434(3), S1-O2 1.456(3), S1-O1 1.465(3), S1-C1 1.891(4), O1-Tl1a 2.748(3), N1-N2 1.371(4), N1-C1 1.448(5), N3-N4 1.374(5), N3-C1 1.451(5), N5-N6 1.374(5), N5-C1 1.452(5); O1-Tl1-O1a 80.86(10), O1-Tl1-Tl1a 40.79(6), O1a-Tl1-Tl1a 40.07(6), O2-S1-O1 111.72(18), O1-S1-C1 102.71(17), S1-O1-Tl1 100.26(15), S1-O1-Tl1a 135.99(17), Tl1-O1-Tl1a 99.14(10), N1-C1-N3 109.6(3), N1-C1-N5 109.5(3), N3-C1-N5 108.6(3), N1-C1-S1 110.5(2), N3-C1-S1 110.4(3), N5-C1-S1 108.2(3).

Preliminary experiments demonstrate that the ligand Tpms$^{t\mathrm{Bu}}$ (**2**) forms tetrahedral complexes with transition metals that are C_{3v}-symmetric according to spectroscopic evidence.[14] The ligand **1** forms sparingly soluble precipitates with divalent metal ions of the general composition M(Tpms)$_2$. In this respect **1** shows similar behavior as the unsubstituted Tp ligand. The solubility of Tpms in protic solvents allows, for example, the synthesis of [(Tpms)Cu(CO)], a methanol-soluble copper(I) carbonyl complex which proves to be thermally stable but sensitive towards oxidation. Evidently, Tpms (**1**) and Tpms$^{t\mathrm{Bu}}$ (**2**) serve as tripodal nitrogen-donating ligands.

Preliminary experiments have shown that it is possible to introduce hydrophilic substituents other than sulfonate. For example, the reaction of lithium tris(pyrazolyl)methanide with carbon dioxide or ethylene oxide gave the corresponding water-soluble carboxylic acid or alcohol. Numerous ways of further derivatization are possible, which should lead to stable ligands, hopefully with an even higher water-solubility, that can be used in enzyme models.

Experimental Section

1a, **b**: *n*-Butyllithium (4.7 mL of a 1.6 M solution) was added to a solution of tris(pyrazolyl)methane (1.3 g, 6.1 mmol) in THF (25 mL) at −60 °C. The solution immediately turned yellow and turbid. After one hour sulfurtrioxide-trimethylamine complex (1.0 g, 7.5 mmol) was added at −50 °C. Under constant stirring, the resulting suspension was allowed to warm to 0 °C over 90 min. After another three hours the solvent was evaporated. To remove excess tris(pyrazolyl)methane, the residue was treated with chloroform, stirred for one hour, and eventually filtered over a membrane filter. Recrystallization from hot methanol yielded colorless crystals of LiTpms (**1a**) (0.88 g, 48 %). Elemental analysis (%) calcd for $C_{10}H_9LiN_6O_3S$: C 40.0, H 3.0, N 28.0; found: C 40.0, H 3.1, N 28.2.

Alternatively, KTpms was isolated from the crude product by a metathesis reaction with potassium carbonate in a mixture of water and methanol. Evaporation of the solvent mixture and subsequent recrystallization from hot methanol gave colorless crystals of KTpms (**1b**) (0.72 g, 37 %). ^{1}H NMR (200 MHz, D_2O, 300 K): $\delta = 6.5$ (dd, $^3J(H,H) = 2.8$, 1.8 Hz, 1H; 4-H), 7.6 (dd, $^3J(H,H) = 2.8$, $^4J(H,H) = 0.6$ Hz, 1H; 3- or 5-H), 7.7 (dd, $^3J(H,H) = 1.8$ Hz, $^4J(H,H) = 0.6$ Hz, 1H; 3- or 5-H); ^{13}C{^{1}H} NMR (500 MHz, D_2O, 300 K): $\delta = 96.4$, 108.4, 132.9, 142.7; elemental analysis (%) calcd for $C_{10}H_9KN_6O_3S$: C 36.1, H 2.7, N 25.3; found: C 36.1, H 2.3, N 25.0.

2a, **b**: LiTpms$^{t\mathrm{Bu}}$ was prepared in analogy to the synthesis of LiTpms from tris(3-*tert*-butylpyrazoyl)methane.[15] The thallium salt was obtained by reaction of LiTpms$^{t\mathrm{Bu}}$ (0.23 g, 0.48 mmol) with $TlNO_3$ (0.25 g, 0.95 mmol) in a methanol/water mixture (1/1; 30 mL). Compound **2b** precipitated as an analytically pure white powder (0.25 g, 75 %). Crystallization from methanol yielded colorless crystals suitable for X-ray structure analysis. ^{1}H NMR (200 MHz, $CDCl_3$, 300 K): $\delta = 7.5$ (d, $^3J(H,H) = 2.7$ Hz, 1H, 5-H), 6.3 (d, $^3J(H,H) = 2.7$ Hz, 1H, 4-H), 1.3 (s, 9H, CH_3); ^{13}C{^{1}H} NMR (500 MHz, $CDCl_3$, 300 K): $\delta = 31.1$, 32.9, 96.8, 105.0, 134.0, 165.0; elemental analysis (%) calcd for $C_{22}H_{33}N_6O_3STl$: C 39.7, H 5.0, N 12.6; found: C 39.7, H 4.9, N 12.7.

Received: March 2, 2000 [Z 14794]

[1] a) S. Trofimenko, *J. Am. Chem. Soc.* **1966**, *88*, 1842–1844; b) S. Trofimenko, *Chem. Rev.* **1993**, *93*, 943–980; c) S. Trofimenko, *Scorpionates: The Coordination Chemistry of Polypyrazolylborate Ligands*, Imperial College Press, London, **1999**.

[2] a) S. Trofimenko, J. C. Calabrese, J. S. Thompson, *Inorg. Chem.* **1987**, *26*, 1507–1514; b) N. Kitajima, W. B. Tolman, *Prog. Inorg. Chem.* **1995**, *43*, 419–533.

[3] a) N. Kitajima, Y. Moro-oka, *Chem. Rev.* **1994**, *94*, 737–757; b) N. Kitajima, M. Osawa, Y. Moro-oka, T. Hirano, M. Hirobe, T. Nagano, *Inorg. Chem.* **1993**, *32*, 1879–1880; c) G. Parkin, *Adv. Inorg. Chem.* **1995**, *42*, 291–393.

[4] The nomenclature used for Tp is based on the one described by Trofimenko.[1b]

[5] M. Ruf, K. Weiß, H. Vahrenkamp, *J. Chem. Soc. Chem. Commun.* **1994**, 135–136.

[6] H. Vahrenkamp, *Acc. Chem. Res.* **1999**, *32*, 589–596.

[7] A. Kremer-Aach, W. Kläui, unpublished results; H. Vahrenkamp, personal communication.

[8] W. Hückel, H. Bretschneider, *Ber. Dtsch. Chem. Ges.* **1937**, *70*, 2024–2026.

[9] S. Juliá, J. M. del Mazo, L. Avila, J. Elguero, *J. Org. Prep. Proced. Int.* **1984**, *16(5)*, 299–307.

[10] P. K. Byers, A. J. Canty, R. T. Honeyman, R. M. Claramunt, C. Lopez, J. L. Lavandera, J. Elguero, *Gazz. Chim. Ital.* **1992**, *122*, 341–344.

[11] C. Tietze, J. Hermann, H. Vahrenkamp, *Chem. Ber.* **1995**, *128*, 1095–1103.

[12] The abbreviation is used in analogy to the nomenclature of Trofimenko.[1b]

[13] Crystal structure analysis of **2b**: crystal dimensions $0.45 \times 0.35 \times 0.25$ mm^3, triclinic, $P\bar{1}$, $a = 10.5675(1)$, $b = 10.7703(1)$, $c = 11.7191(2)$ Å, $\alpha = 87.3920(8)$, $\beta = 74.4663(1)$, $\gamma = 81.2366(7)°$, $V = 1270.07(3)$ Å^3, $Z = 1$, ρcalcd $= 1.741$ g cm^{-3}, $F(000) = 656$, $T = 173(2)$ K, The measurement was performed on a Bruker axs-

diffractometer with a smart CCD detector ($Mo_{K\alpha}$ radiation, $\lambda = 0.71073$ Å, ω scans, $3.6 \leq 2\theta \leq 60.74^\circ$). All in all 10263 reflections were detected (6663 independent reflections) and 5869 were classified as observed. The structure was solved by direct methods and refined against F^2. Hydrogen atoms were placed at calculated positions and refined dependent on the adjacent non-hydrogen atoms (riding model). The refinement of the 331 varied parameters converged to $R = 0.0425$ for 6663 reflections with $I > 2\sigma(I)$ and $wR2 = 0.0900$ for all reflections. Min./max. transmission 3.790/2.057 e Å^{-3}. The structure was solved with SIR-97[16] and refined with SHELXL-97.[17] Crystallographic data (excluding structure factors) for the structure reported in this paper have been deposited with the Cambridge Crystallographic Data Centre as supplementary publication no. CCDC-141108. Copies of the data can be obtained free of charge on application to CCDC, 12 Union Road, Cambridge CB21EZ, UK (fax: (+44) 1223-336-033; e-mail: deposit@ccdc.cam.ac.uk).

[14] In poorly solvating solvents the reaction of TlTpms^{rBu} with $ZnBr_2$ leads to not only the expected C_{3v}-symmetrical species but also to a C_s-symmetrical compound that has yet to be identified.

[15] D. L. Reger, J. E. Collins, D. L. Jameson, R. K. Castellano, *Inorg. Synth.* **1998**, *32*, 63–65.

[16] A. Altomare, M. C. Burla, M. Camalli, G. L. Cascarano, C. Giacovazzo, A, Guagliardi, A. G. G. Moliterni, G. Polidori, R. Spagna, *J. Appl. Crystallogr.* **1999**, *32*, 115–119.

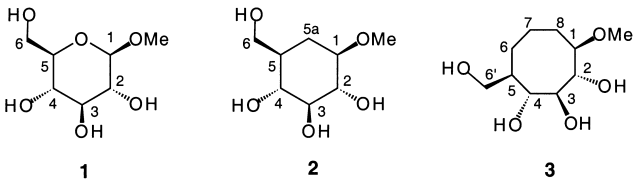
[17] G. M. Sheldrick, SHELXL 97, Programs for Crystal Structure Analysis (Release 97–2), University of Göttingen, Germany, **1997**.

From Glucose to Cyclooctanic Carbaglucose: A New Class of Carbohydrate Mimetics

Wei Wang, Yongmin Zhang, Matthieu Sollogoub, and Pierre Sinaÿ*

Synthetic oligosaccharides have recently emerged as potential therapeutic agents.[1] A possible in vivo hydrolysis of such drugs by various glycosidases has stimulated the search for nonhydrolyzable oligosaccharide mimetics. One option is to replace the endocyclic oxygen atom of aldohexopyranosyl residues by a methylene group. The resulting 5a-carbasugars are hydrolytically stable analogues, and the chemical synthesis of the 5a-carbaaldohexopyranoside family has been largely developed.[2] An intriguing alternative is to use a cyclooctane ring as a framework for the OH groups of the carbohydrate. For instance, the replacement of the endocyclic oxygen atom in methyl β-D-glucopyranoside (**1**) by one methylene group would result in a cyclohexanic mimetic **2**, whereas the replacement by three methylene groups would give a novel type of cyclooctanic carbohydrate mimetic **3** (Scheme 1).

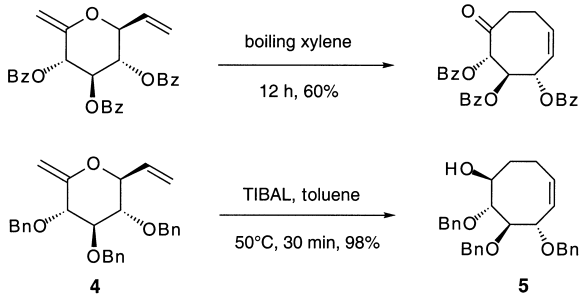
The rationale behind this proposal is that the conformation and conformational equilibration of cyclooctane derivatives[3] may offer interesting new distributions of hydroxy groups



Scheme 1. Methyl β-D-glucopyranoside (**1**) as well as the cyclohexanic (**2**) and cyclooctanic (**3**) analogues.

compared to those available through the classical pseudorotational itinerary[4] of pyranoid rings. The incorporation of these so far undescribed carbocyclic sugar mimetics in oligosaccharide chains is thus of interest in terms of the resulting biological responses, such as glycosidase inhibition, a feature which may benefit from the easy access to nonclassical conformers.

The thermal or triisobutylaluminum (TIBAL) promoted Claisen rearrangement of 2-methylene-6-vinyl-tetrahydropyran, which affords cyclooctanic derivatives by insertion of a C_2 unit, has been elegantly developed by Paquette et al.[5] for the synthesis of natural products with eight-membered rings. It has recently been applied in the carbohydrate field, either in the form of a thermal reaction,[6] or in the form of a smooth Al^{III}-catalyzed process[7] (Scheme 2).



Scheme 2. Thermal or TIBAL-catalyzed Claisen rearrangement of unsaturated monosaccharide derivatives. Bn = $PhCH_2$; Bz = PhCO.

As shown in Scheme 3, the cyclooctanol derivative **6**, the enantiomer of the previously prepared cyclooctanol **5**, was smoothly obtained in 96% yield from the TIBAL-catalyzed sigmatropic rearrangement of the gluco derivative **12**, which in turn was easily derived from methyl α-D-glucopyranoside in an eight-step sequence.

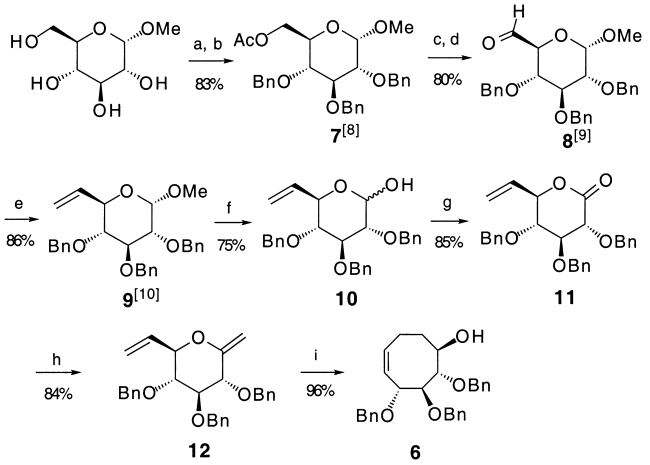
Methylation of **6** gave **13** which, upon regio- and stereoselective hydroboration, was converted in 60% yield into the cyclooctanol derivative **14** (Scheme 4). Oxidation of **14** gave the cyclooctanone **15**, and subsequent treatment with the Tebbe reagent $[Cp_2Ti(\mu\text{-}Cl)(\mu\text{-}CH_2)AlMe_2]$ generated the methylene derivative **16**. Regioselective hydroboration of **16** gave the cyclooctanic mimetic **17** and the α-L-ido isomer **18**, which were separated by flash chromatography on silica gel (Scheme 5).

The boat–chair conformation for compound **17** (Scheme 6) is assigned on the basis of the ^3J couplings in the ^{1}H NMR spectrum. The H1–H5 NOE confirms the β-D-gluco configuration. The interpretation of the NMR spectrum of the α-L-

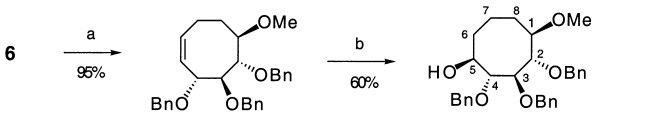
[*] Prof. P. Sinaÿ, Dr. W. Wang, Dr. Y. Zhang, Dr. M. Sollogoub
Ecole Normale Supérieure
Département de Chimie, UMR 8642,
24 rue Lhomond, 75231 Paris, Cedex 05 (France)
Fax: (+33) 1-44323397
E-mail: pierre.sinay@ens.fr

Supporting information for this article is available on the WWW under http://www.wiley-vch.de/home/angewandte/ or from the author.

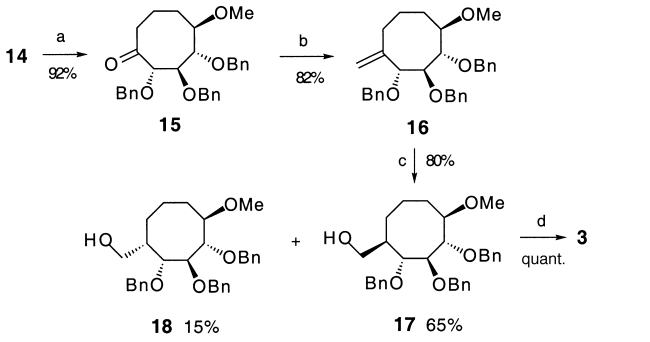
 © WILEY-VCH Verlag GmbH, D-69451 Weinheim, 2000 1433-7851/00/3914-2466 $ 17.50+.50/0



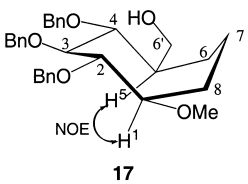
Scheme 3. a) BnBr (6 equiv), NaH (8 equiv), DMF, RT, 2.5 h, quant; b) TMSOTf (cat.), Ac_2O, CH_2Cl_2 (dry), −55 to −50 °C, 1.5 h; c) NaOMe/MeOH, 2 h, quant; d) PCC (1.1 equiv), 4 Å molecular sieves, CH_2Cl_2 (dry), 0 °C, 2 h; e) BuLi (3 equiv), Ph_3PCH_3Br (3 equiv), THF (dry), −78 °C to RT, 1.5 h; f) TfOH/AcOH/H_2O (1/28/5), 80 °C, 2.5 h; g) PCC (3 equiv), 4 Å MS, CH_2Cl_2 (dry), 0 °C to RT, 3 h; h) Tebbe reagent (3 equiv), Py/THF (1/1), −78 °C to RT, 30 min; i) *i*Bu_3Al, toluene, 50 °C, 30 min. Abbreviations: RT = room temperature; TMS = trimethylsilyl; Tf = trifluoromethanesulfonyl; PCC = pyridinium chlorochromate; Py = pyridine.



Scheme 4. a) NaH, MeI (2.8 equiv), DMF, RT, 2 h; b) 1) $BH_3 \cdot THF$ (2 equiv), THF, RT, 1 h; 2) aq. NaOH (11 %), aq. H_2O_2 (35 %), 0 °C to RT, 1.5 h.



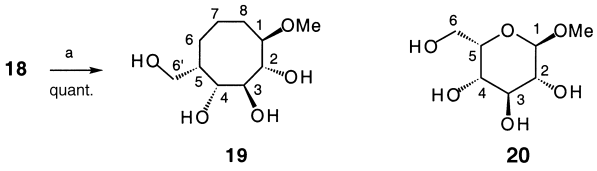
Scheme 5. a) PCC (3 equiv), dry CH_2Cl_2, 0 °C, 2 h; b) Tebbe reagent (2 equiv), Py/THF (1/1), −78 °C to RT, 20 min; c) 1) $BH_3 \cdot THF$ (2 equiv), THF, RT, 1 h; 2) aq. NaOH (11 %), aq. H_2O_2 (35 %), 0 °C to RT, 2 h; d) H_2, Pd/C, EtOAc, MeOH, RT, 2 h.



Scheme 6. The boat–chair conformation assigned to compound **17**.

ido isomer **18** is more complex and corresponds to the well known flexibility of idopyranosides.[11]

The two deprotected cyclooctanic sugar mimetics **3** and **19** were quantitatively obtained after catalytic hydrogenolysis of compounds **17** and **18** (Schemes 5 and 7), respectively. Compounds **3** and **19** represent the first two members of a new class of synthetic carbasugars, which are now available for various biological studies.



Scheme 7. Formation of **19**, a mimetic of methyl α-L-idopyranoside **20**, by deprotection of compound **18**: a) H_2 (170 kPa), Pd/C, ethyl acetate/methanol 1/1, RT, 2 h.

Received: February 11, 2000 [Z 14684]

[1] a) C. A. A. von Boeckel, M. Petitou, *Angew. Chem.* **1993**, *105*, 1741–1750; *Angew. Chem. Int. Ed. Engl.* **1993**, *32*, 1671–1690; b) *Complex Carbohydrates in Drug Research* (Eds.: K. Bock, H. Clausen), Munksgaard, **1994** (Alfred Benzon symposium 36); c) D. Zopf, S. Roth, *The Lancet* **1996**, *347*, 1017–1021; d) *Glycoscience* (Eds.: H. Driguez, J. Thiem), Springer, Berlin, **1997**; e) M. Petitou, J.-P. Hérault, A. Bernat, P.-A. Driguez, P. Duchaussoy, J.-C. Lormeau, J.-M. Herbert, *Nature* **1999**, *398*, 417–422; f) P.-A. Driguez, I. Lederman, J.-M. Strassel, J.-M. Herbert, M. Petitou, *J. Org. Chem.* **1999**, *64*, 9512–9520.

[2] a) D. H. R. Barton, S. D. Géro, J. Cléophax, A. S. Machado, B. Quiclet-Sire, *J. Chem. Soc. Chem. Commun*. **1988**, 1184–1186; b) T. Suami, S. Ogawa, *Adv. Carbohydr. Chem. Biochem*. **1990**, *48*, 21–90; c) J. Marco-Contelles, C. Pozuelo, M. L. Jimeno, L. Martinez, A. Martinez-Grau, *J. Org. Chem*. **1992**, *57*, 2625–2631; d) S. Ogawa in *Carbohydrate Mimics, Concepts and Methods* (Ed.: Y. Chapleur), WILEY-VCH, Weinheim, **1998**, pp. 87–106; e) Y.-Q. Tang, C. Maul, R. Höfs, I. Sattler, S. Grabley, X.-Z. Feng, A. Zeeck, R. Thiericke, *Eur. J. Org. Chem*. **2000**, 149–153.

[3] a) F. A. L. Anet, M. St. Jacques, *J. Am. Chem. Soc*. **1966**, *88*, 2585–2586; b) J. E. Anderson, E. S. Glazer, D. L. Griffith, R. Knorr, J. D. Roberts, *J. Am. Chem. Soc*. **1969**, *91*, 1386–1395; c) F. A. L. Anet, J. Krane, *Tetrahedron Lett*. **1973**, 5029–5032; d) D. M. Pawar, E. M. Moody, E. A. Noe, *J. Org. Chem*. **1999**, *64*, 4586–4589.

[4] J. F. Stoddart, *Stereochemistry of Carbohydrates*, Wiley-Interscience, New York, **1971**.

[5] a) L. A. Paquette, D. Friedrich, R. D. Rogers, *J. Org. Chem*. **1991**, *56*, 3841–3849; b) L. A. Paquette, C. M. G. Philippo, N. H. Vo, *Can. J. Chem*. **1992**, *70*, 1356–1365, and references therein.

[6] B. Werschkun, J. Thiem, *Angew. Chem*. **1997**, *109*, 2905–2906; *Angew. Chem. Int. Ed. Engl*. **1997**, *36*, 2793–2794.

[7] M. Sollogoub, J.-M. Mallet, P. Sinaÿ, *Angew. Chem*. **2000**, *112*, 370–372; *Angew. Chem. Int. Ed.* **2000**, *39*, 362–364.

[8] W. R. Kobertz, C. R. Bertozzi, M. D. Bednarski, *J. Org. Chem*. **1996**, *61*, 1894–1897.

[9] H. Hashimoto, K. Asano, F. Fuji, J. Yoshimura, *Carbohydr. Res*. **1982**, *104*, 87–104.

[10] K. Tatsuta, Y. Niwata, K. Umezawa, K. Toshima, M. Nakata, *J. Antibiot*. **1991**, *44*, 456–458.

[11] B. Casu, M. Petitou, M. Provasoli, P. Sinaÿ, *Trends Biochem. Sci.* **1988**, *13*, 221–225.

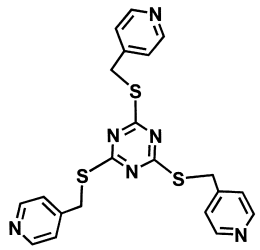
A Silver(I) Coordination Polymer Chain Containing Nanosized Tubes with Anionic and Solvent Molecule Guests**

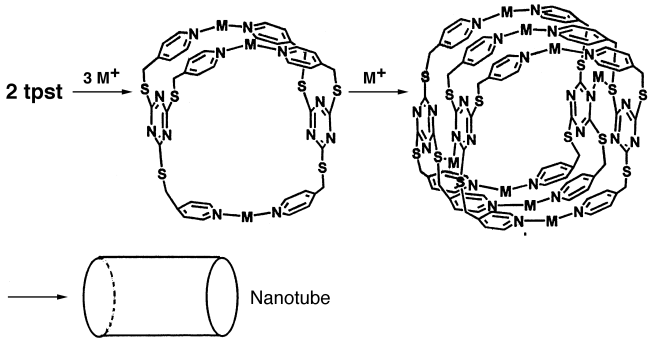
Maochun Hong,* Yingjun Zhao, Weiping Su, Rong Cao,* Makoto Fujita, Zhongyuan Zhou, and Albert S. C. Chan*

Design of and research on supramolecular architectures with inner cavities have attracted considerable current interest because of their ability to selectively include ions and molecules and catalyze specific chemical transformations.[1–6] The potential uses of such architectures, which include molecular cages, two- and three-dimensional synthetic receptors, and extended porous frameworks, largely depend on their cavity size and type, which are mainly controlled by the ligands and appropriate metal ions.[3, 7, 8] For instance, a triple-helicate (M_2L_3) or a tetrahedral (M_4L_6) cluster was obtained from the self-assembly reaction of a bis-bidentate catecholamide and metal ions in the absence or presence of Me_4N^+ ions.[8] Robson et al. reported a very large $Cu_{12}L_8$ enclosure with a cubelike cage, which was derived from the self-assembly of the tris-bidentate ligand 2,4,6-triazophenyl-1,3,5-trihydroxybenzene (H_3tapp) and copper(II) ions.[9] By using the self-assembly of molecular units driven by coordination to transition-metal ions, Stang et al. have presented NMR and MS evidence for the formation of cuboctahedral and dodecaheral cations from tridentate and bidentate subunits.[10]

A number of infinite two- and three-dimensional coordination polymers possessing a variety of cavities capable of accommodating guests have been developed.[11] Zn/tpt and Cu/tpt (tpt = 2,4,6-tris(4-pyridyl)-1,3,5-triazine) coordination polymers containing infinite two- and three-dimensional networks were generated by the assembly reaction of tpt and metal ions.[12] Recently, Goodgame et al. reported a new type of metal-organic large-pore zeotype, namely, $[Zn(dimto)_2]_n \cdot m\,DMF$ (Hdimto = 4,6-di(1-imidazolyl)-1,3,5-triazin-2-one), which was generated from zinc bromide and 2,4,6-tri(1-imidazolyl)-1,3,5-triazine (timt).[13]

We have designed two multidentate ligands, 1,2-bis-[(2-pyrimidinyl)methylsulfanyl]-benzene (bpsb) and 2,4,6-tris[(4-pyridyl)methylsulfanyl]-1,3,5-triazine (tpst), and obtained the two-dimensional lamellar network polymer $[Ag_2(bpsb)_3(ClO_4)_2]_n$ and the metallosupramolecular cube $[Ni_6(tpst)_8Cl_{12}]$.[14] Examining the geometric requirements of symmetry and sterochemistry, we expected to prepare coordination polymers with nanosized tubes of different lengths. As tpst is an exo-tridentate ligand, the N atoms of the three pyridyl groups can only bind to three different metal atoms (Scheme 1). By using metal ions with linear coordination





Scheme 1. Reaction of tpst with silver(I) salts leads to $[Ag_3(tpst)_2]^{3+}$ nanosized rings, which are linked by other silver(I) centers to form a nanosized tube. M = Ag.

geometry, such as gold(I), silver(I), and copper(I), to link tpst ligands, nanosized tubes with different lengths can be obtained. Here we report on the preparation and the structural characterization of a single-stranded one-dimensional coordination polymer, namely, compound **1**, which contains nanosized tubes.

$[Ag_7(tpst)_4(ClO_4)_2(NO_3)_5(dmf)_2]_n$ (**1**)

The reaction of $AgNO_3$ with tpst was carried out with a metal-to-ligand ratio of 2:1 in DMF/MeOH followed by addition of $AgClO_4$. Slowly diffusing diethyl ether into the reaction solution produced crystals suitable for single-crystal X-ray diffraction. The crystallographic analysis of the complex [15] revealed that its crystal structure is a one-dimensional chain polymer containing a basic nanosized tube unit, $[Ag_7(tpst)_4]$. As can be seen in Figure 1, each ligand binds to three silver(I) centers through the N atoms of the three pyridyl groups, and each silver(I) ion is in turn coordinated by the pyridyl group of another tpst ligand to form an $[Ag_3(tpst)_2]$ nanosized ring. Two such rings are linked by Ag–N and Ag–S bonds from one N and one S atom of the trithiocyanuric spacer to form the basic nanosized tube unit with the dimensions of $1.34 \times 0.96 \times 0.89$ nm, which accommodates two DMF molecules and two perchlorate ions. Figure 2 shows a space-filling representation. The tube units share Ag(1) by

[*] Prof. M. C. Hong, Prof. R. Cao, Y. J. Zhao, Dr. W. P. Su
State Key Laboratory of Structural Chemistry
Fujian Institute of Research on the Structure of Matter
Chinese Academy of Sciences, Fuzhou, Fujian 350002 (China)
Fax: (+86) 591-371-49-46
E-mail: hmc@ms.fjirsm.ac.cn
Prof. M. Fujita
Department of Applied Chemistry, School of Engineering
Nagoya University, Chikusaku, Nagoya 464-8603 (Japan)
Prof. A. S. C. Chan, Prof. Z. Y. Zhou
Open Laboratory of Chirotechnology
Department of Applied Biology and Chemical Technology
The Hong Kong Polytechnic University, Hong Hum (Hong Kong)

[**] This work was supported by the National Nature Science Foundation of China. M.C.H. thanks the Croucher Foundation of Hong Kong for financial support.

 © WILEY-VCH Verlag GmbH, D-69451 Weinheim, 2000 1433-7851/00/3914-2468 $ 17.50+.50/0

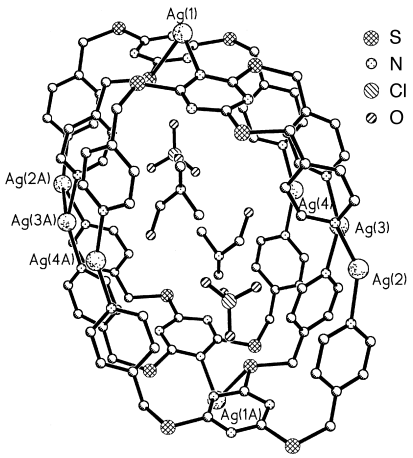


Figure 1. View of the basic nanosized tube unit in **1**.

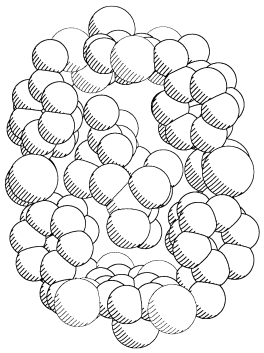


Figure 2. Space-filling representation of the nanosized tube unit in **1**.

Ag–N and Ag–S bonds to form an infinite chain (Figure 3). Such a single-stranded polymer chain with open nanosized tubes differs greatly from the usual polymer chain structures.[1] To our knowledge, the structure of **1** is a unique chain-structural motif in supramolecular coordination chemistry. The only example known to us of a larger coordinative cage that provides open framework is that in the infinite three-dimensional coordination polymer of composition $[Zn(dimto)_2]_n \cdot m\,DMF$ mentioned above.[13] Five NO_3^- ions in **1** are each located near the silver(I) centers and embedded in the polymer chain regions. The Ag···O distances are in the range of 2.65–3.10 Å.

All tpst moieties in **1** act as tetradentate ligands but with two kinds of coordination mode: one type coordinates to four silver atoms through three nitrogen atoms of different pyridyl groups and a sulfur atom of the thioether moiety, and the other through three pyridyl nitrogen atoms and one nitrogen atom of the triazine ring. The silver centers exhibit two kinds of coordination environment: one is the normal linear coordination mode of AgN_2 and the other is tetracoordinate with a slightly distorted square-planar AgS_2N_2 unit, which is seldom found in silver(I) compounds.

Further studies, such as on tubes consisting of more than two $[Ag_3(tpst)_2]$ rings, solvent- and anion-exchange properties of the polymer, and self-assembly of the ligands with other metal ions, will be reported elsewhere.

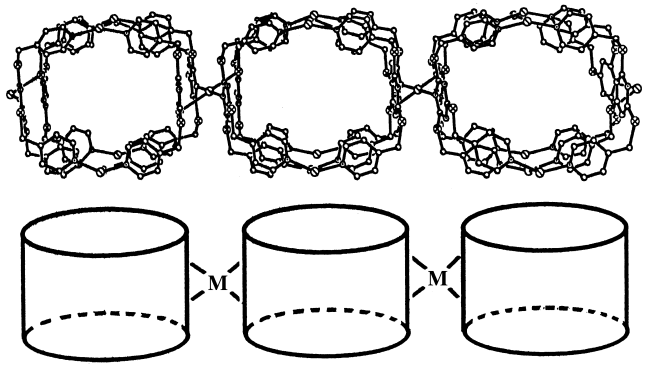


Figure 3. View of the one-dimensional polymer chain in **1** along the *b* axis.

Experimental Section

1: To a solution of tpst (1.5 mmol), prepared by heating a solution of 4-picolyl chloride hydrochloride (4.5 mmol), sodium trithiocyanurate (1.5 mmol), and NaOMe (4.5 mmol) in MeOH (25 mL) at 50 °C, a solution of $AgNO_3$ (3.0 mmol) in DMF (15 mL) was added. After the reaction mixture was stirred for 2 h, a solution of $AgClO_4$ (1.0 mmol) in DMF (10 mL) was added dropwise. The mixture was stirred for a further 2 h to give a colorless solution, which was filtered. Diffusion of diethyl ether into the resulting solution yielded a large amount of colorless needles of **1** with two water molecules per formula unit (0.76 g, 61 %). C,H,N analysis calcd for $C_{90}H_{90}N_{31}O_{27}Ag_7S_{12}Cl_2$: C 33.3, H 2.80, N 13.3; found: C 33.0, H 2.72, N 13.1; IR (KBr pellet): $\tilde{\nu} = 3450$ (m), 2929 (w), 2906 (w), 1676 (s), 1616 (s), 1479 (s), 1429 (m), 1261 (s), 1090 (s), 1028(s), 802 (s), 704 (m), 621 (m), 584 (w), 494 cm^{-1} (m).

Received: January 24, 2000 [Z 14589]

[1] a) R. W. Saalfrank, B. Demleitner in *Transition Metals in Supramolecular Chemistry*, *Perspectives in Supramolecular Chemistry*, *Vol. 5* (Ed: J.-P. Sauvage), WILEY-VCH, Weinheim, **1999**, pp. 1–51; b) O. M. Yaghi, H. Li, C. Davis, D. Richardson, T. L. Groy, *Acc. Chem. Res.* **1998**, *31*, 474–484; c) M. Fujita, *Chem. Soc. Rev.* **1998**, *27*, 417–425.

[2] G. B. Gardner, D. Venkataraman, J. S. Moore, S. Lee, *Nature* **1995**, *374*, 792–795.

[3] B. F. Abrahams, P. A. Jackson, R. Robson, *Angew. Chem.* **1998**, *110*, 2801–2804; *Angew. Chem. Int. Ed.* **1998**, *37*, 2656–2659.

[4] a) P. J. Stang, B. Olenyuk, *Acc. Chem. Res.* **1997**, *30*, 502–518; b) R.-D. Schnebeck, E. Freisinger, B. Lippert, *Angew. Chem.* **1999**, *111*, 137–139; *Angew. Chem. Int. Ed.* **1999**, *38*, 168–172; c) M. Fujita, D. Oguro, M. Miyazawa, H. Oka, K. Yamaguchi, K. Ogura, *Nature* **1995**, *378*, 469–471; d) M. Fujita, S.-Y. Yu, T. Kusukawa, H. Funaki, K. Ogura, K. Yamaguchi, *Angew. Chem.* **1998**, *110*, 2192–2196; *Angew. Chem. Int. Ed.* **1998**, *37*, 2082–2085.

[5] a) T. Shimizu, M. Koglso, M. Masuda, *Nature* **1996**, *383*, 487–488; b) S. L. James, D. M. P. Mingos, A. J. P. White, D. J. Williams, *Chem. Commun.* **1998**, 2323–2324; c) R. Vilar, D. M. P. Mingos, A. J. P. White, D. J. Williams, *Angew. Chem.* **1998**, *110*, 1323–1326; *Angew. Chem. Int. Ed.* **1998**, *37*, 1258–1261.

[6] a) M. Aoyagi, K. Biradha, M. Fujita, *J. Am. Chem. Soc.* **1999**, *121*, 7457–7458; b) M. Fujita, J. Yazaki, K. Ogura, *J. Am. Chem. Soc.* **1990**, *112*, 5645–5647.

[7] M. R. Ghadiri, J. R. Granja, R. A. Milligan, D. E. McRee, N. Khazanovich, *Nature* **1993**, *366*, 324–327.

[8] M. Scherer, D. L. Caulder, D. W. Johnson, K. N. Raymond, *Angew. Chem.* **1999**, *111*, 1690–1694; *Angew Chem. Int. Ed.* **1999**, *38*, 1588–1592.

[9] B. F. Abrahams, S. J. Egan, R. J. Robson, *J. Am. Chem. Soc.* **1999**, *121*, 3535–3536.

[10] B. Olenyuk, J. A. Whiteford, A. Fechtenkotter, P. S. Stang, *Nature* **1999**, *398*, 796–799.

[11] Examples of cavity-containing coordination polymers: a) G. B. Gardner, D. Venkataraman, J. S. Moore, S. Lee, *Nature* **1995**, *374*, 792–793; b) D. Venkataraman, G. B. Gardner, S. Lee, J. S. Moore, *J. Am. Chem. Soc.* **1995**, *117*, 11600–11601; c) O. M. Yaghi, G. Li, H. Li, *Nature* **1995**, *378*, 703–706; d) T. J. Hennigar, D. C. MacQuarrie, P. Losier, R. D. Rogers, M. J. Zaworotko, *Angew. Chem.* **1997**, *109*, 1044–1046;

Angew. Chem. Int. Ed. Engl. **1997**, *36*, 972–973; e) I. M. Müller, T. Röttgers, W. S. Sheldrick, *Chem. Commun.* **1998**, 823–824.

[12] a) S. R. Batten, B. F. J. Hoskins, R. J. Robson, *J. Am. Chem. Soc.* **1995**, *117*, 5385–5386; b) R. W. Gable, B. F. Hoskins, R. Robson, *Chem. Commun.* **1990**, 1677–1678; c) B. F. Abrahams, S. R. Batten, H. Hamit, B. F. Hoskins, R. Robson, *Angew. Chem.* **1996**, *108*, 1794–1796; *Angew. Chem. Int. Ed. Engl.* **1996**, *35*, 1690–1692.

[13] D. M. L. Goodgame, D. A. Grachvogel, D. J. Williams, *Angew. Chem.* **1999**, *111*, 217–219; *Angew. Chem. Int. Ed.* **1999**, *38*, 153–156.

[14] a) M. C. Hong, W. P. Su, R. Cao, M. Fujita, J. X. Lu, *Chem. Eur. J.* **2000**, *6*, 427–431; b) M. C. Hong, Y. J. Zhao, W. P. Su, R. Cao, M. Fujita, Z. Y. Zhou, A. S. C. Chan, unpublished results.

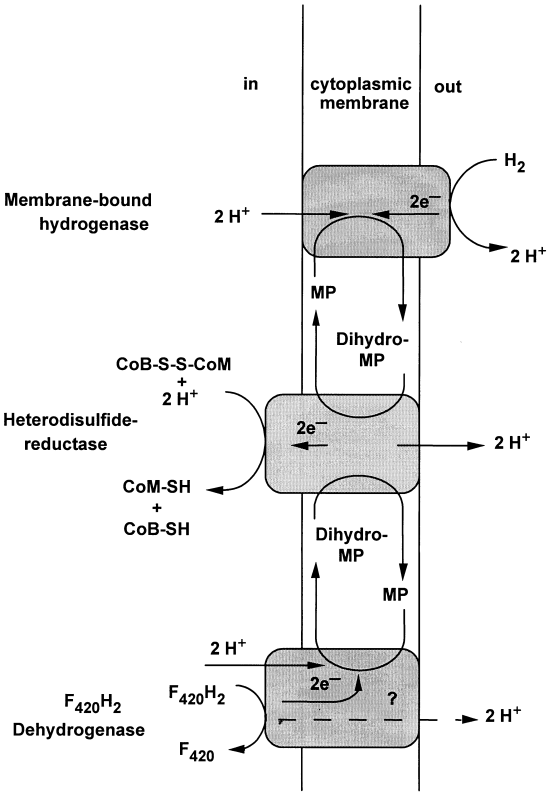
[15] Crystallography: The intensity data were collected on a Bruker CCD diffractometer with graphite-monochromated $Mo_{K\alpha}$ radiation ($\lambda = 0.71073$ Å) at room temperature. All calculations were performed by using the SHELXTL-PL version 5.10 package on an HP computer. The structure was solved by direct methods and refined by full-matrix least-squares methods. Crystal data for **1** with two water molecules per formula unit: colorless needle, dimensions $0.24 \times 0.18 \times 0.16$ mm, $C_{90}H_{90}N_{31}O_{27}Ag_7S_{12}Cl_2$, $M_r = 3248.64$, monoclinic, space group $C2/c$; $a = 28.1019(20)$, $b = 16.8556(11)$, $c = 27.9278(21)$ Å, $\beta = 117.9154(15)^\circ$, $V = 11\,689.3(25)$ Å^3; $\rho_{calcd} = 1.846$ g cm^{-3}, $Z = 4$; $F(000) = 6472$; $\mu(Mo_{K\alpha}) = 1.493$ mm^{-1}; 38 967 reflections were collected, of which 7252 with $|F_o| \geq 2.0\,\sigma(|F_o|)$ were observed; $R_1 = 0.057$; $wR_2 = 0.184$. Crystallographic data (excluding structure factors) for the structure reported in this paper have been deposited with the Cambridge Crystallographic Data Centre as supplementary publication no. CCDC-139799. Copies of the data can be obtained free of charge on application to CCDC, 12 Union Road, Cambridge CB2 1EZ, UK (fax: (+44) 1223-336-033; e-mail: deposit@ccdc.cam.ac.uk).

Methanophenazine: Structure, Total Synthesis, and Function of a New Cofactor from Methanogenic Archaea**

Uwe Beifuss,* Mario Tietze, Sebastian Bäumer, and Uwe Deppenmeier

Dedicated to Professor Sir Alan R. Battersby on the occasion of his 75th birthday

Methanogenic organisms belong to the kingdom of archaea and differ significantly from eukarya and bacteria.[1] Methanogenic archaea are widespread in anaerobic environments such as the sediments of lakes and rivers as well as the intestinal tract of ruminants. They form the end of the anaerobic food chain and transform simple substrates such as hydrogen/carbon dioxide, formic acid, methanol, methylamines, and acetic acid into methane. The latter subsequently is oxidized under aerobic conditions and is thus able to reenter the carbon cycle. Owing to the influences of civilization the amount of methane, one of the greenhouse gases, in the atmosphere has continuously increased during the last century.[2] A variety of unique enzymes and unusual cofactors contribute to its formation by methanogenic archaea. The central intermediate of all metabolic pathways of methanogens is methyl-S-CoM, which is reductively demethylated to methane under the catalytic influence of methyl-CoM-reductase.[3] The two electrons required in this process are derived from CoB-SH and lead to the formation of a heterodisulfide (CoB-S-S-CoM) from CoB-SH and CoM-SH.[4] The reduction of CoB-S-S-CoM is an energy-conserving step in the metabolism of methylotrophic methanogens (Scheme 1).[5] Two



Scheme 1. Model of the membrane-bound electron transfer of *Methanosarcina mazei* Gö1. CoM-SH = coenzyme M; CoB-SH = coenzyme B; F_{420} = coenzyme F_{420}; $F_{420}H_2$ = reduced form of the coenzyme F_{420}; MP = methanophenazine; dihydro-MP = reduced form of methanophenazine.

recently detected proton-translocating enzyme systems, the H_2:heterodisulfide oxidoreductase and the $F_{420}H_2$:heterodisulfide oxidoreductase, are involved in the membrane-bound electron transfer of *Methanosarcina mazei* Gö1.[6] The electron transport of $F_{420}H_2$ to CoB-S-S-CoM is catalyzed by an $F_{420}H_2$ dehydrogenase transferring the electrons to the heterodisulfide reductase. In the presence of molecular hydrogen a membrane-bound hydrogenase serves as an electron-feeding component to the heterodisulfide reductase (Scheme 1).

The structure of the electron carrier was not known. Recently, we have been able to isolate a phenazine ether from membranes of *Methanosarcina mazei* Gö1.[7] Detailed

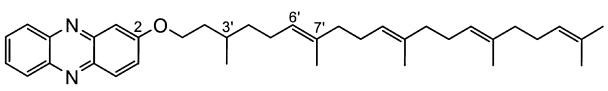
[*] Priv.-Doz. Dr. U. Beifuss, Dipl.-Chem. M. Tietze
Institut für Organische Chemie der Georg-August-Universität
Tammannstrasse 2, 37077 Göttingen (Germany)
Fax: (+49) 551-39-9660
E-mail: ubeifus@gwdg.de

Dipl.-Biol. S. Bäumer, Priv.-Doz. Dr. U. Deppenmeier
Institut für Mikrobiologie und Genetik der Georg-August-Universität
Grisebachstrasse 8, 37077 Göttingen (Germany)

[**] This work was supported by the Deutsche Forschungsgemeinschaft (Sonderforschungsbereich 416; grants De 488/6-1 and De 488/4-2) and the Fonds der Chemischen Industrie. We are grateful to Drs. J. Paust and H. Jaedicke (BASF AG, Ludwigshafen) and Dr. R. K. Müller (Hoffmann-La Roche Ltd., Basel) for generously providing chemicals.

 © WILEY-VCH Verlag GmbH, D-69451 Weinheim, 2000 1433-7851/00/3914-2470 $ 17.50+.50/0

NMR analysis of the sensitive natural product, which could only be obtained in small amounts, indicated that its lipophilic side chain, which we assume to be responsible for the anchorage in the membrane, consists of five isoprenoid units linked to each other in a head-to-tail manner. Unlike the saturated C_5 unit, which is directly linked to the 2-phenazinyl residue, the remaining four units are unsaturated. Three of them exhibit *E*-configurated double bonds. The redox-active natural product referred to as methanophenazine (MP) **1** is the first phenazine whatsoever isolated from archaea.

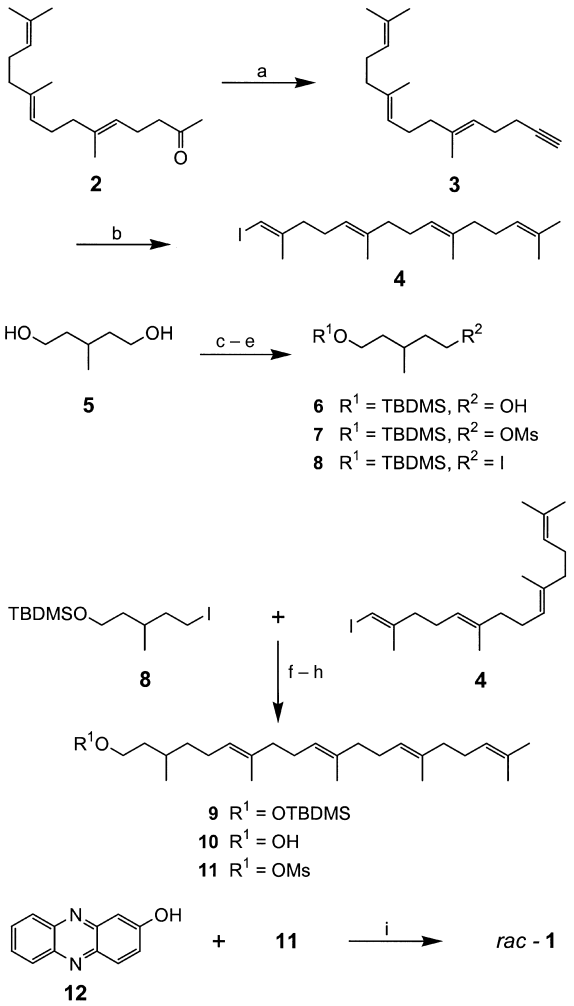


1

Sincemethanogens lack the usual quinones it was assumed that **1** functions as an electron carrier in the cytoplasmic membrane and unlike other natural phenazines takes part in the energy-conserving electron transport. Larger amounts of the natural product are necessary to determine the biological function of **1** and to elucidate the absolute configuration at C-3′. As its isolation from *Methanosarcina mazei* Gö1 is quite time-consuming the only way possible was to synthesize the natural product. For this purpose **1** was to be convergently built from the three building blocks **4**, **8**, and **12** (Scheme 2). Diastereoselective linking of **4** and **8** to give **9** and the subsequent etherification of **11** and **12** were regarded key steps. While the latter process seemed to be completely unproblematic it was unclear whether the reactivity of the alkyl metal derivative would be sufficient for the transition metal catalyzed linking to the vinyl iodide.

To prepare **4** (*E*,*E*)-farnesyl acetone (**2**) was first transformed into the terminal alkyne **3**,[8] subsequently providing the (*E*)-vinyl iodide **4** in diastereomerically pure form and 74% yield by the Zr-catalyzed carboalumination with trimethylaluminum and quenching with iodine[9] (Scheme 2). The C_5 building block *rac*-**8** required for the linking with **4** was made available by selective monofunctionalization[10] of 3-methyl-pentane-1,5-diol **5** in a few steps. The advantage of this prochiral compound is the chance to form the enantiomerically pure compounds (*R*)-**8** and (*S*)-**8** that are necessary to determine the absolute configuration of methanophenazine **1** by differentiating the enantiotopic $(CH_2)_2$-OH groups.

The coupling between the alkyl metal compounds released in situ from *rac*-**8** and the vinyl metal derivatives resulting from **4** caused considerable difficulties thus indicating that the reactivity of the sp^3 component was too low. The (*E*)-selective construction of the C-6′, C-7′ double bond[11] of the sesterterpene building block **9** could only be achieved in 65% yield when the Pd^0-catalyzed coupling of the organozinc compound derived in situ from *rac*-**8**, *tert*-butyllithium, and zinc chloride was performed with vinyl iodide **4**. Cleavage of the *tert*-butyldimethylsilyl ester and activation of the resulting alcohol **10** with methanesulfonic acid chloride provided mesylate **11**, which was etherified with 2-hydroxyphenazine **12**[12] to give *rac*-**1**.[13] When the synthesis was performed without isolation and purification of various intermediates, *rac*-**1** was produced from farnesyl acetone **2** in a total yield of more than 30%. Spectroscopic data of the synthetic methanophenazine *rac*-**1** corresponded to those of the natural product in every respect.[14] Starting from the enantiomerically pure C_5 building blocks, **1** and *ent*-**1** will be accessible as well. And in this way it will be possible to determine the absolute configuration of the natural product.



Scheme 2. a) LiTMP, THF, −78 °C; ClP=O(OEt)$_2$, −78 °C→RT; LiTMP, THF, −78 °C→RT, H_2O, 75%; b) cat. [Cp_2ZrCl_2], Me_3Al, CH_2Cl_2; I_2, THF, −30 °C→RT; K_2CO_3, H_2O, 0 °C, 74%; c) NaH, TBDMSCl, THF, 83%; d) NEt_3, MsCl, CH_2Cl_2, 0 °C; e) NaI, acetone, reflux, 93% for two steps; f) **8** + $ZnCl_2$, Et_2O, RT → −100 °C, *t*BuLi; **4** + [$Pd(PPh_3)_4$],(0.05 equiv), −70 °C→RT, 65%; g) TBAF, THF, RT; h) NEt_3, MsCl, CH_2Cl_2, 0 °C; i) KOH, aliquot, THF 90% for three steps. Aliquot = methyltrioctylammonium chloride, Ms = methanesulfonyl, TBAF = tetrabutylammonium fluoride, TBDMS = *tert*-butyldimethylsilyl, TMP = 2,2,6,6-tetramethylpiperidine.

First experiments on the biological function were performed by using the model compound 2-hydroxyphenazine **12** and its reduced form (dihydro-**12**). It was demonstrated that all key enzymes react with the artificial electron carrier.[7] After completion of the total synthesis similar tests were also performed with *rac*-**1** (Table 1). Here, washed cytoplasmic membranes of *Methanosarcina mazei* Gö1 were combined with *rac*-**1** and the activities of the respective enzymes determined. The results clearly indicated that methanophenazine **1** serves as an electron acceptor to both the membrane-bound hydrogenase and the $F_{420}H_2$ dehydrogenase if H_2 and F_{420} were added, respectively. In addition, the heterodisulfide

 © WILEY-VCH Verlag GmbH, D-69451 Weinheim, 2000 1433-7851/00/3914-2471 $ 17.50+.50/0

Table 1. Specific activities of the enzymes of the $F_{420}H_2$:heterodisulfide oxidoreductase and H_2:heterodisulfide oxidoreductase systems.

Enzyme	Electron donor	Electron acceptor	Spec. activity[a] [U mg protein^{-1}]
$F_{420}H_2$ dehydrogenase	$F_{420}H_2$	**12**	0.20
$F_{420}H_2$ dehydrogenase	$F_{420}H_2$	MP	0.15
membrane-bound hydrogenase	H_2	**12**	2.2
membrane-bound hydrogenase	H_2	MP	3.2
heterodisulfide reductase	dihydro-**12**	CoB-S-S-CoM	2.3
heterodisulfide reductase	dihydro-MP	CoB-S-S-CoM	2.6

[a] 1 U = 1 μmol substrate converted per minute.

reductase uses the reduced form of methanophenazine (dihydro MP) as an electron donor for the heterodisulfide reduction. Therefore methanophenazine is able to mediate the electron transport between the membrane-bound enzymes, so that the conversion by the proton-translocating electron transport systems[6] can be subdivided in two partial reactions each (Scheme 1). In this way methanophenazine **1** was characterized as the first phenazine derivative involved in the electron transport of biological systems. The experiments reported here suggest that its role in the energy metabolism of methanogens is similar to that of ubiquinone in mitochondria and bacteria.

Experimental Section

The growth of *Methanosarcina mazei* Gö1 and the preparation of cytoplasmic membranes was performed as previously described.[7] Photometrical analysis to determine enzymatic activities were carried out at room temperature in glass cuvettes (1.7 mL) that were gassed with N_2 or H_2 and closed with rubber stoppers. The optical-enzymatic determination of the $F_{420}H_2$-dependent reduction of MP and the dihydro-MP dependent heterodisulfide reduction was performed under a nitrogen atmosphere. The cuvette was flushed with hydrogen to determine the hydrogen-dependent reduction of MP. The reactions were initiated by adding the respective electron acceptors. Final concentrations of the reactants were: F_{420}: 25 μM; **12**: 25 μM; MP: 24 μM (stock solution in dimethylformamide), and CoB-S-S-CoM: 38 μM. Protein concentration was 7.5 μg membrane protein per mL assay. Extinction coefficients: F_{420}: $\varepsilon_{420} = 40\,mM^{-1}cm^{-1}$; MP: $\varepsilon_{414} = 3.17\,mM^{-1}cm^{-1}$; **12** $\varepsilon_{425} = 4.5\,mM^{-1}cm^{-1}$.

Received: February 1, 2000 [Z14627]

[1] C. R. Woese, O. Kandler, M. L. Wheelis, *Proc. Natl. Acad. Sci. USA* **1990**, *87*, 4576 – 4579.
[2] R. Conrad, *Microbiol. Rev.* **1996**, *60*, 609 – 640.
[3] R. K. Thauer, *Microbiology* **1998**, *144*, 2377 – 2406.
[4] R. K. Thauer, R. Hedderich, R. Fischer in *Methanogenesis* (Ed.: J. G. Ferry), Chapman & Hall, New York, **1993**, pp. 209 – 252.
[5] J. Ellermann, R. Hedderich, R. Böcher, R. K. Thauer, *Eur. J. Biochem.* **1988**, *172*, 669 – 677.
[6] U. Deppenmeier, T. Lienard, G. Gottschalk, *FEBS Lett.* **1999**, *457*, 291 – 297.
[7] H.-J. Abken, M. Tietze, J. Brodersen, S. Bäumer, U. Beifuss, U. Deppenmeier, *J. Bacteriol.* **1998**, *180*, 2027 – 2032.
[8] E. Negishi, A. O. King, W. L. Klima, *J. Org. Chem.* **1980**, *45*, 2526 – 2528.
[9] a) S. V. Ley, A. Armstrong, D. Diez-Martin, M. J. Ford, P. Grice, J. G. Knight, H. C. Kolb, A. Madin, C. A. Marby, S. Mukherjee, A. N. Shaw, A. M. Z. Slawin, S. Vile, A. D. White, D. J. Williams, M. Woods, *J. Chem. Soc. Perkin Trans. 1* **1991**, 667 – 692; b) E. Negishi, D. E. Van Horn, A. O. King, N. Okukado, *Synthesis* **1979**, 501 – 502; c) D. E. Van Horn, E. Negishi, *J. Am. Chem. Soc.* **1978**, *100*, 2252 – 2254.
[10] P. J. McDougal, J. G. Rico, Y. Oh, B. D. Condon, *J. Org. Chem.* **1986**, *51*, 3388 – 3390.
[11] A. B. Smith III, Y. Qiu, D. R. Jones, K. Kobayashi, *J. Am. Chem. Soc.* **1995**, *117*, 12011 – 12012.
[12] a) R. Ott, *Monatsh. Chem.* **1959**, *90*, 827 – 838; b) F. Kehrmann, F. Cherpillod, *Helv. Chim. Acta* **1924**, *7*, 973 – 980; c) R. Willstätter, F. Müller, *Chem. Ber.* **1911**, *44*, 2171 – 2185.
[13] A. Loupy, J. Sansoulet, F. Vaziri-Zand, *Bull. Soc. Chim. Fr.* **1987**, 1027 – 1035.
[14] $R_f = 0.51$ (diethyl ether/hexane = 1/1); ^{1}H NMR (500 MHz, C_6D_6, TMS): $\delta = 0.83$ (d, $^3J = 6.6$ Hz, 3H; 3′-CH_3), 1.14 – 1.23 (m, 1H; 4′-H_A), 1.32 – 1.39 (m, 1H; 4′-H_B), 1.44 (dt, $^2J = 13.5$ Hz, $^3J = 6.4$ Hz, 1H; 2′-H_A), 1.56 (s, 3H; 19′-CH_3), 1.60 – 1.65 (m, 1H; 3′-H) superimposed by 1.61, 1.62, 1.64 (3s, 3H each; 7′-CH_3, 11′-CH_3, 15′-CH_3), 1.68 (d, $^4J = 0.8$ Hz, 3H; 20′-H_3), 1.72 (ddt, $^2J = 13.5$ Hz, $^3J = 5.4$ Hz, $^3J = 6.8$ Hz, 1H; 2′-H_B), 1.97 – 2.27 (m, 14H; 5′-H_2, 8′H_2, 9′H_2, 12′-H_2, 13′-H_2, 16′-H_2, 17′-H_2), 3.79 (dt, $^2J = 10.7$ Hz, $^3J = 6.8$ Hz, 1H; 1′-H_A), 3.81 (dt, $^2J = 10.7$ Hz, $^3J = 6.4$ Hz, 1H; 1′-H_B), 5.25 (tt, $^3J = 6.9$ Hz, $^4J = 1.4$ Hz, 1H; 18′-H), 5.28 – 5.38 (m, 3H; 6′-H, 10′-H, 14′-H), 7.29 (ddd, $^3J = 8.6$ Hz, $^3J = 6.8$ Hz, $^4J = 1.6$ Hz, 1H; 7-H or 8-H), 7.32 (dd, $^3J = 9.6$ Hz, $^4J = 2.8$ Hz, 1H; 3-H), 7.35 (ddd, $^3J = 8.6$ Hz, $^3J = 6.8$ Hz, $^4J = 1.6$ Hz, 1H; 8-H or 7-H), 7.53 (d, $^4J = 2.8$ Hz, 1H; 1-H), 8.12 (d, $^3J = 9.6$ Hz, 1H; 4-H), 8.30 (dd, $^3J = 8.6$ Hz, $^4J = 1.6$ Hz, 1H; 6-H or 9-H), 8.31 (dd, $^3J = 8.6$ Hz, $^4J = 1.6$ Hz, 1H; 6-H or 9-H); ^{13}C NMR (125 MHz, C_6D_6): $\delta = 16.12$, 16.13, 16.15 (7′-CH_3, 11′-CH_3, 15′-CH_3), 17.73 (19′-CH_3), 19.56 (3′-CH_3), 25.78 (C-20′), 25.83 (C-5′), 27.11, 27.12, 27.23 (C-9′, C-13′, C-17′), 29.80 (C-3′), 36.01 (C-2′), 37.45 (C-4′), 40.20, 40.23 (C-8′, C-12′, C-16′), 66.91 (C-1′), 105.80 (C-1), 124.73, 124.77, 124.93, (C-10′, C-14′, C-18′), 125.04 (C-6′), 126.29 (C-3), 128.29 (C-7 or C-8), 129.58 (C-8 or C-7), 130.15 (C-6 or C-9), 130.27 (C-9 or C-6), 131.08 (C-19′), 131.30 (C-4), 134.99, 135.04, 135.09 (C-7′, C-11′, C-15′), 141.36 (C-4a), 142.63 (C-5a or C-9a), 144.12 (C-9a or C-5a), 145.89 (C-10a), 160.78 (C-2); IR (film): $\tilde{\nu} = 3059\ cm^{-1}$ (CH, olefinic), 2954, 2924, 2853 (CH, aliphat.), 1632, 1605, 1560, 1518 (C=C), 1483, 1445 (CH_2, CH_3), 1380, 1360 (CH_3), 1196 (C-O-C), 828, 757 (C=C, arom.); UV(CH_3CN): λ_{max}(lg ε) = 388 (3.72), 355 (3.78), 256 nm (4.71); MS(70 eV): *m*/*z* (%): 538 (100) [M^+], 470 (6) [$M^+ - C_5H_8$], 402 (8) [$470 - C_5H_8$], 334 (20) [$402 - C_5H_8$], 265 (4) [$334 - C_5H_9$], 196 (82) [$C_{12}H_8N_2O^+$], 168 (7) [196 – CO]; HR-MS: calcd for $C_{37}H_{50}N_2O$: 538.3923; found: 538.3923.

First Artificial Receptor for Caffeine—A New Concept for the Complexation of Alkylated Oxopurines**

Siegfried R. Waldvogel,* Roland Fröhlich, and Christoph A. Schalley

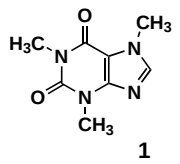
Dedicated to Professor R. R. Schmidt on the occasion of his 65th birthday

Molecular recognition and reactions with signaling ability are of potential use for the development of novel sensors.[1] The detection of small, biorelevant molecules is of particular interest because of their omnipresence in everyday life. Alky-

[*] Dr. S. R. Waldvogel, Dr. R. Fröhlich
Westfälische Wilhelms-Universität Münster
Organisch-chemisches Institut
Corrensstrasse 40, 48149 Münster (Germany)
Fax: (+49) 251-83-39772
E-mail: waldvog@uni-muenster.de
Dr. C. A. Schalley
The Scripps Research Institute, La Jolla (USA)
and Universität Bonn (Germany)

[**] This work was supported by the Fonds der Chemischen Industrie (Liebig fellowships for S.R.W. and C.A.S.) and the Deutsche Akademie der Naturforscher Leopoldina/BMBF (postdoctoral fellowship for C.A.S.). We are particularly grateful to Prof. Dr. Julius Rebek, Jr. for fruitful discussions and all his support for this project.

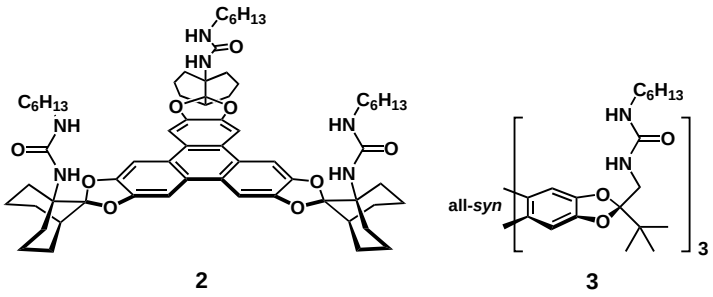
 © WILEY-VCH Verlag GmbH, D-69451 Weinheim, 2000 1433-7851/00/3914-2472 $ 17.50+.50/0



1

lated oxopurines such as caffeine (**1**), theophylline, or theobromine are among the most frequently consumed alkaloids.[2] Natural compounds like catechine[3] or cyclodextrins[4] are capable of binding caffeine or theobromine rather unspecifically through hydrophobic interactions. The tailor-made receptor by Kelly et al. for the recognition of structurally related uric acid employs only hydrogen bonds for substrate binding.[5] However, an extension of this two-dimensional recognition motif for the binding of caffeine is rendered impossible due to the presence of the methyl groups in **1**.

Here, we present a new concept for the binding of alkylated oxopurines. Our receptors **2** and **3** use the third dimension and surround the substrate as a C_3-symmetric cleft (Scheme 1).



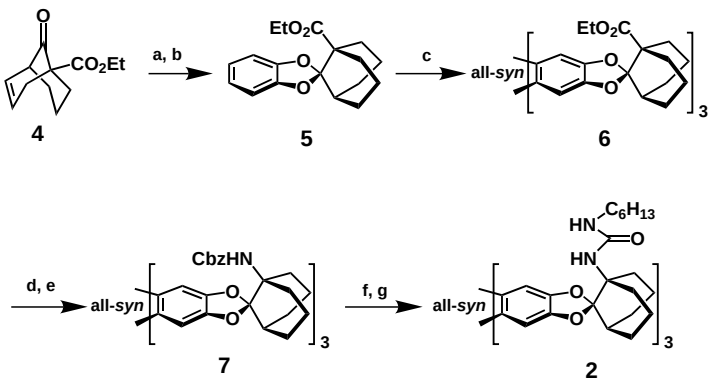
2 **3**

Scheme 1. Functionalized triphenylene ketals: rigid receptor **2** and flexible receptor **3**.

The novel receptor is based on a scaffold of trifunctionalized triphenylene ketals.[6] The combination of preorganized functional groups with a mutual distance of 11 Å and an electron-rich atomic surface in between allows C_3 or pseudo-C_3-symmetric guests to complex. Electron-deficient guest molecules are particularly suitable, because they offer the ability to interact with the host by donor–acceptor interactions in addition to the specific binding through hydrogen bonds. While the methyl groups of the caffeine block interaction with the Kelly-type receptors,[5] they fit perfectly into the free spaces between the urea anchors of our receptor.

The rigid receptor with its bicyclic spiroketal moieties has been prepared from the easily accessible precursor **4** (Scheme 2).[7] The products of the standard transformations can be separated by crystallization. Consequently, they can be synthesized by a rather simple procedure and are accessible on a large scale. The key step is the oxidative trimerization of the catechol ketals with molybdenum pentachloride.[6] Due to the rigid molecular structure, the separation of the isomers is nonproblematic, although a final chromatographic purification of **7** and **2** is recommended.[8, 9] The more flexible receptor **3** has been analogously prepared.

First, we studied the host–guest interaction of receptor and caffeine in dichloromethane solution. NMR titrations confirm a 1:1 stoichiometry of both components and show a complex formation constant of 35 600 M^{-1}. From this constant, a binding energy of approximately 6 kcal mol^{-1} can be estimated.[10] For fitting the titration data, dimerization of the receptor molecules has been taken into account with dimerization constants determined from dilution experiments.[11]



4 **5** **6** **7** **2**

Scheme 2. Synthesis of rigid receptor **2**: a) **4** (as a mixture of the double bond isomers), catechol, TsOH, Dean–Stark trap, toluene, 86%; b) H_2, Pd/C, 100%; c) $MoCl_5$, CH_2Cl_2, then separation of isomers, 18%; d) *t*BuOK, THF, H_2O; e) $(PhO)_2P(O)N_3$, NEt_3, DMF, then benzylalcohol, 49% from **6**; f) H_2, $Pd(OH)_2$, THF; g) hexyl isocyanate, CH_2Cl_2, 65% from **7**. Cbz = benzyloxycarbonyl, Ts = tosyl = toluene-4-sulfonyl.

During the ^{1}H NMR titration of **2** with caffeine, the signals for the proximal and distal (to the triphenylene plane) N–H protons shift downfield differently (Figure 1). While the signal

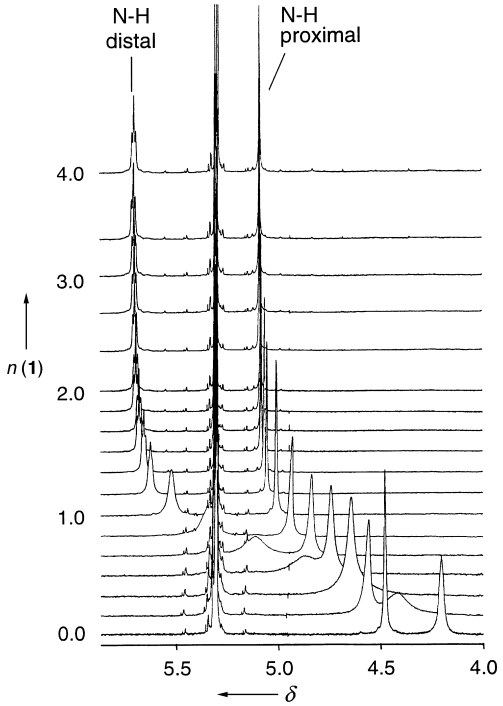


Figure 1. ^{1}H NMR titration of **2** with caffeine (N–H region). n(**1**) = number of equivalents of caffeine (**1**).

for the proximal urea protons experiences only a minor effect (+0.6 ppm), the distal counterpart shifts considerably more (+1.5 ppm). This points to stronger hydrogen bridges between the guest and the distal urea protons, while the proximal N–H atoms contribute less significantly to caffeine binding. After addition of one equivalent of caffeine, the titration curves bend rather sharply and the signals remain

 © WILEY-VCH Verlag GmbH, D-69451 Weinheim, 2000 1433-7851/00/3914-2473 $ 17.50+.50/0

more or less at a constant position in the spectrum, if more caffeine is added. Consequently, receptor **2** forms a 1:1 complex with caffeine in which the guest molecule is located between the urea functions instead of binding to the open side through $\pi-\pi$ stacking, π-donor$-\pi$-acceptor, or hydrophobic interactions.[10]

The comparison of receptors **2**, **3**, and **7** clearly shows the rigid receptor **2** has a much better performance in caffeine binding (Table 1). Urea anchors, which are well preorganized for hydrogen bonding, increase the binding constant by a factor of more than 200 relative to the flexible molecule **3**. Host **7** hardly interacts with caffeine at all, which again points to a stronger substrate binding by the distal N–H protons than the proximal ones. This result is in agreement with the crossed titration curves for both urea protons discussed above. In addition to these NMR experiments, the mass spectrometric observation of the intact caffeine–receptor complex and IR spectroscopic evidence for hydrogen bonding support complex formation.

Table 1. Binding constants K.

Entry	Receptor	Substrate	K [M^{-1}]
1	**2**	**1**	$35\,600 \pm 2000$
2	**3**	**1**	170 ± 50
3	**7**	**1**	$< 10 \pm 5$
4	**2**	**8**	$9\,240 \pm 220$
5	**2**	**9**	–[a]
6	**2**	**10**	$1\,240 \pm 115$
7	**2**	**11**	420 ± 70
8	**2**	**12**	130 ± 50

[a] Not measurable due to the insolubility of **9** in CD_2Cl_2.

Variation of the substrates for receptor **2** allows a study of the geometric and electronic fit of the substrate. The binding constant of 8-methoxycaffeine (**8**)[12] is already smaller, because the methoxy group disturbes hydrogen bonding to the urea arms of the receptor. 1,3,7-trimethyl uric acid (**9**)[12] binds strongly to **2**; unfortunately, the quantification of the binding constant is impossible due to the insolubility of free **9** in CD_2Cl_2. Addition of approximately one equivalent of **2** to a suspension of **9** in dichloromethane leads spontaneously to a clear solution, which indicates substrate binding to the receptor. *N*,*N*′,*N*″-triallylcyanuric acid (**10**) is less strongly bound due to its localized amide bonds and decreased planar systems offering $\pi-\pi$ interactions. The binding constant further decreases, if one of the nitrogen atoms is replaced by a methylene group (as in **11**) which interferes with the coplanar orientation of substrate and receptor. Finally, *N*,*N*′-dimethyl uracil (**12**) bears only two acceptor groups. This substrate is incongruent with the symmetry of the receptor—the affinity to the host decreases.

Variable-temperature ^{1}H NMR experiments give a more profound insight into the nature of caffeine binding in solution. Upon cooling to 196 K, the ^{1}H NMR spectrum of a mixture of receptor **2** and two equivalents of caffeine contains separate sets of signals for free and bound caffeine. Complexation of the guest breaks the receptor's threefold symmetry and leads to different signals for all six urea protons. The aromatic protons of the triphenylene scaffold also split into a complex pattern.

From a solution of caffeine and receptor **2** in methanol, crystals were obtained, which were appropriate for a single-crystal X-ray structure analysis (Figure 2).[13] The crystal structure exhibits a binding pattern analogous to that observed by spectroscopic methods in solution. The three distal urea protons form hydrogen bonds to the caffeine guest. The crystal structure further demonstrates caffeine to be slightly too small for the receptor and, therefore, the spiro ketals are

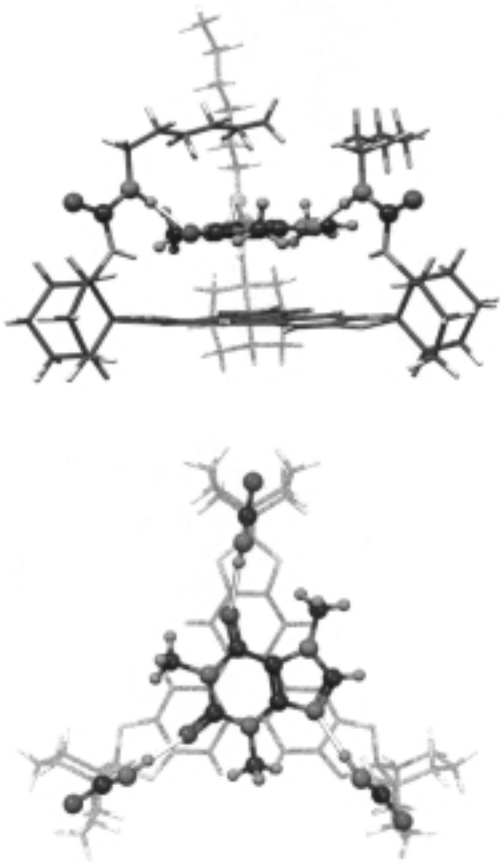
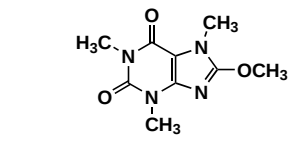
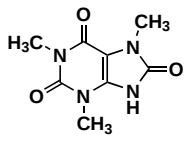


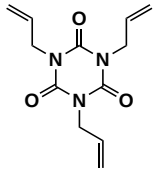
Figure 2. X-ray crystal structure of the host–guest complex of **2** with caffeine. Side and top views (above and below, respectively); caffeine and anchoring groups are emphasized as ball and stick models.



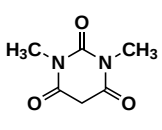
8



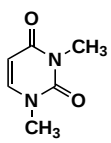
9



10



11



12

 © WILEY-VCH Verlag GmbH, D-69451 Weinheim, 2000 1433-7851/00/3914-2474 $ 17.50+.50/0

bent towards the triphenylene by approximately 11 – 15°. As a consequence, the proximal NH protons are directed towards the aromatic plane rather than the caffeine molecule and interact only weakly. The distance between the coplanar aromatic surfaces is 3.42 Å which is optimal for a donor–acceptor interaction. It turned out to be impossible to accomplish the crystallization of this receptor with sidechains shorter than *n*-hexyl. The hexyl groups must be packed in the crystal and, indeed, two of them save space by folding in, while the third alkyl chain breaks the symmetry and produces a preferred directionality. Disordered caffeine was not observed. We were even able to localize the hydrogen atoms involved in hydrogen bonding.[14] The values found are in the typical ranges.

In conclusion, rigid functionalized triketals of hexahydroxytriphenylene open up the opportunity to generate novel receptors for the selective recognition of alkylated oxopurines. For caffeine, the bonding interaction can be observed directly. Together with the results from X-ray crystallography, a consistent picture of the receptor's guest binding features evolves.

Received: February 3, 2000 [Z14639]

[1] U. E. Spichiger-Keller, *Chemical Sensors and Biosensors for Medical and Biological Applications*, WILEY-VCH, Weinheim, **1998**.

[2] N. H. Woodward, *Teas of the World*, Macmillan, New York, **1980**.

[3] Y. Cai, S. H. Gaffney, T. H. Lilley, D. M. Magnolato, R. Martin, C. M. Spencer, E. Haslam, *J. Chem. Soc. Perkin. Trans. 2* **1990**, 2197 – 2209, and references therein.

[4] H. O. Ammar, M. Ghorab, S. A. El-Nahhas, S. M. Omar, M. M. Ghorab, *Pharmazie* **1996**, *51*, 42 – 46.

[5] T. R. Kelly, M. P. Maguire, *J. Am. Chem. Soc.* **1987**, *109*, 6549 – 6551; T. R. Kelly, M. T. Bilodeau, G. J. Bridger, C. Zhao, *Tetrahedron Lett.* **1989**, *30*, 2485 – 2488.

[6] S. R. Waldvogel, A. R. Wartini, P. H. Rasmussen, J. Rebek, Jr., *Tetrahedron Lett.* **1999**, *40*, 3515 – 3517.

[7] A. C. Cope, M. E. Synerholm, *J. Am. Chem. Soc.* **1959**, *72*, 5228 – 5232; E. W. Colvin, W. Parker, *J. Chem. Soc.* **1965**, 5764 – 5766.

[8] All new compounds were obtained pure (elemental analysis (C, H, N) within ±0.4 %).

[9] Compound **2**: mp 198 °C; ^{1}H NMR (600 MHz, CD_2Cl_2, 25 °C, TMS): $\delta = 0.78$ (t, $^3J_{H,H} = 7$ Hz, 9H, CH_3), 1.06 – 1.18 (m, 24H), 1.64 – 1.73 (m, 12H), 2.12 – 2.31 (m, 21H), 2.78 – 2.88 (m, 12H), 4.51 (br., 3H, N–H distal), 4.71 (s, 3H, N–H proximal), 7.82 (s, 6H, triphenylene); ^{13}C NMR (150.8 MHz, CD_2Cl_2, 25 °C, TMS): $\delta = 14.15$, 21.45, 22.91, 26.94, 28.68, 30.44, 31.89, 34.77, 38.51, 40.51, 57.77, 101.94, 122.37, 124.97, 147.97, 157.85.

[10] The binding constants were obtained by fitting the titration curves with the Specfit program package: Specfit v.2.12, Spectrum Software Associates, Chapel Hill, NC, USA; H. Gampp, M. Maeder, C. J. Meyer, A. D. Zuberbühler, *Talanta* **1986**, *33*, 943, and references therein. The given error is systematical; multiple determination demonstrated an excellent reproducibility of the binding constants. A low mean variation is observed in the determined values.

[11] The receptors exhibit a slight tendency to self-aggregate. The Specfit program was used to determine dimerization constants from dilution experiments. These constants have been taken into account for the fit of the binding constants. For simplicity, higher aggregates have not been included. A model including receptor trimers was tested, but including these species did not change the good agreement of measured and fitted titration curve. The constants obtained from both models are the same within the error of the experiment.

[12] Syntheses of substrates: **8**: R. C. Huston, W. F. Allen, *J. Am. Chem. Soc.* **1934**, *56*, 1356 – 1358; **9**: E. Fischer, *Ann.* **1882**, *215*, 253 – 320.

[13] X-ray crystal structure analysis of **2** with caffeine: $C_{74}H_{100}N_{10}O_{11} \cdot 3.5\,CH_3OH$, $M_r = 1417.79$, light yellow crystal, $0.50 \times 0.35 \times 0.25$ mm^3, $a = 13.596(1)$, $b = 13.794(1)$, $c = 22.979(1)$ Å, $\alpha = 80.09(1)$, $\beta = 82.40(1)$, $\gamma = 67.41(1)°$, $Z = 2$, $V = 3909.2(4)$ Å^3, $\rho_{calcd} = 1.204$ g cm^{-3}, $\mu = 0.83$ cm^{-1}, absorption correction with SORTAV ($0.971 \le T \le 0.992$), triclinic, space group $P\bar{1}$ (No. 2), $\lambda = 0.71073$ Å, $T = 198$ K, ω and φ scans, 22410 reflections collected ($\pm h$, $\pm k$, $\pm l$), $[(\sin\theta)/\lambda] = 0.59$ Å^{-1}, 13700 independent ($R_{int} = 0.033$) and 8862 observed reflections [$I \ge 2\sigma(I)$], 911 refined parameters, $R = 0.094$, $wR^2 = 0.267$, max. (min.) residual electron density was 1.09(–0.69) e Å^{-3} close to the disordered solvate molecules, disorder refined with constraints, hydrogens calculated at the nitrogen atoms from difference fourier calculations, others calculated and refined as riding atoms. Crystallographic data (excluding structure factors) for the structure reported in this paper have been deposited with the Cambridge Crystallographic Data Centre as supplementary publication no. CCDC-139021. Copies of the data can be obtained free of charge on application to CCDC, 12 Union Road, Cambridge CB2 1EZ, UK (fax: (+44) 1223-336-033; e-mail: deposit@ccdc.cam.ac.uk).

Calcium-Catalyzed Selective and Quantitative Transformation of CH_4 and CO into Acetic Acid**

Mohammad Asadullah, Tsugio Kitamura, and Yuzo Fujiwara*

Methane and ethane have exerted a profound economic and sociologic influence on the world at large because of their enormous reserves.[1] However, the use of methane in the direct synthesis of functionalized products is limited by the low reactivity of methane and poor product selectivity.[2] The search for new routes of methane transformation constituted an important field of research over the last two decades.[3] Carboxylation of methane with CO to afford acetic acid is an important functionalization process that is not industrially feasible at present. In 1992 we reported the Pd-catalyzed carboxylation of methane with CO in the presence of $K_2S_2O_8$ and CF_3COOH (TFA).[4] Recently we found that systems using a $Yb(OAc)_3/Mn(OAc)_2/NaClO/H_2O$ catalyst[5] and $Mg/K_2S_2O_8$/TFA promoter[6] cause the carboxylation of methane to give acetic acid. Magic-acid-induced[7] and $RhCl_3$-catalyzed[8] reactions of methane with CO were also developed. However, these processes have several practical drawbacks, such as low yield, cost of catalyst, and product selectivity. Herein we report almost quantitative carboxylation of methane with CO to afford acetic acid (**1**) with one of the cheapest chemicals, namely, $CaCl_2$, as catalyst.

[*] Prof. Y. Fujiwara, M. Asadullah, T. Kitamura
Department of Chemistry and Biochemistry
Graduate School of Engineering, Kyushu University
Hakozaki, Fukuoka 812-8581 (Japan)
Fax: (+81) 092-642-3548
E-mail: yfujitcf@mbox.nc.kyushu-u.ac.jp

[**] This work was supported in part by the Grants-in-Aid for Scientific Research on Priority Area No. 283 "Innovative Synthetic Reactions" and Scientific Research (A) No. 09355031 from the Ministry of Education, Science, Sports, and Culture of Japan (Monbusho). M.A. thanks the Monbusho for financial support.

Our reaction of saturated hydrocarbons with CO in which Mg powder is used as a promoter[6] prompted us to investigate alkaline earth metal compounds as catalysts for the reaction of methane with CO (Table 1). In the absence of catalyst, no **1** was observed by GC analysis of the reaction mixture (entry 1), and this confirmed that the autoclave wall was not involved in the reaction of methane with CO to give any product. Addition of a catalytic amount of $CaCl_2$ gave **1** (entry 2). The other Ca compounds (entries 3–7) gave very low yields of **1**.

Table 1. Effect of calcium compounds on the carboxylation of methane with CO.[a]

Entry	Alkaline earth compound	Yield [mmol][b]	[%][c]	TON[d]
1	none	trace	–	–
2	$CaCl_2 \cdot 2H_2O$	1.05	7.1	2.1
3	CaO	0.07	0.5	0.14
4	$CaCO_3$	0.04	0.3	0.08
5	$Ca(OAc)_2 \cdot 2H_2O$	0.04	0.3	0.08
6	$[Ca(acac)_2] \cdot 2H_2O$[e]	0.03	0.2	0.06
7	$Ca(OH)_2$	0.01	0.1	0.02
8	$CaSO_4 \cdot 2H_2O$	trace	–	–

[a] 25-mL autoclave, methane (20 atm, 15 mmol), CO (30 atm), calcium compound (0.5 mmol), $K_2S_2O_8$ (5 mmol), and TFA (5 mL) at 80 °C for 15 h. [b] Determined by GC. [c] Based on methane. [d] Based on the amount of Ca. [e] acac = acetylacetonate.

The optimization of the reaction conditions is summarized in Table 2. Experiments were conducted to gain insight into the reaction conditions that would favor the formation of **1** from methane and CO. Methane reacted at temperatures as low as 60 °C in moderate yield (entry 1). Increasing the temperature increases the yield of **1**, which is highest at 85 °C (entry 2). Temperature above 85 °C resulted in low yields. In the absence of CO the reaction did not give **1** but afforded 0.2 mmol of methyl trifluoroacetate (**2**). In this case methane is first oxidized to methanol, which then reacts with TFA to yield **2**. The reaction performed under an atmospheric pressure of CO gave a low yield of **1** (entry 3). Increasing the CO pressure resulted in an increase in the yield of **1** up to 50 atm, which gave the highest yield of **1** (1.54 mmol, entry 5). In this system CO acts as a trapping agent for the methyl radical to form the acetyl radical, which forms the acetic acid in this reaction. The reaction order with respect to CO partial pressure up to 20 atm was unity. However, it became fractional beyond 20 atm of CO.

Table 2. Effect of reaction conditions on the carboxylation of methane.[a]

Entry	T [°C]	CO [atm]	$K_2S_2O_8$ [mmol]	TFA [mL]	Methane [atm]	$CaCl_2$ [mmol]	Time t [h]	Yield [mmol][b]	[%][c]
1	60	30	5	6	20	0.5	15	0.41	2.8
2	85	30	5	6	20	0.5	15	1.21	8.5
3	85	1	5	6	20	0.5	15	0.08	0.6
4	85	40	5	6	20	0.5	15	1.43	10.1
5	85	50	5	6	20	0.5	15	1.54	10.8
6	85	40	10	6	20	0.5	15	1.55	10.8
7	85	40	10	3	20	0.5	15	1.27	7.6
8	85	40	10	5	20	0.5	15	1.61	10.6
9	85	40	10	5	1	0.5	15	0.16	21.1
10	85	40	10	5	5	0.5	15	0.97	25.7
11	85	40	10	5	30	0.5	15	1.87	8.2
12	85	40	10	5	20	0.05	15	0.01	0.1
13	85	40	10	5	20	0.1	15	0.51	3.6
14	85	40	10	5	20	1	15	0.86	6.1
15	85	30	5	5	2	0.5	140[d]	1.52	93.8
16	85	40	10	5	30	0.1	200	3.05	13.5

[a] 25-mL autoclave. [b] GC yield. [c] Based on methane. [d] 2 mmol of TFAA was used.

The use of 10 mmol of $K_2S_2O_8$ resulted in a slightly higher yield than with 5 mmol (Table 2, entry 6). The number of moles of **1** formed increased up to 5 mL of TFA (entry 8). The effect of trifluoroacetic anhydride (TFAA) in the reaction mixture was also examined, and a positive effect was found with an optimum at 2 mmol of TFAA. The water of the catalyst quantitatively reacts with TFAA to give TFA. The reaction mixture thus becomes water-free, and production of **1** is improved. The use of solvents other than TFA was also investigated. Acetonitrile results in the same product distribution with significant yield (0.83 mmol), although there is an approximately twofold decrease in the amount of product formed after 15 h reaction time relative to TFA. To avoid the complexity of product analysis arising from an acetic acid solvent, ethane was used as substrate, and 0.24 mmol of propionic acid was obtained. In the case where water was used as the solvent, NaClO and H_2O_2 were used as oxidants, and lower activity was observed. No activity of the catalyst for the formation of **1** was observed in dichloromethane or 1,2-dichloroethane. Interestingly, methane underwent the reaction at atmospheric pressure and gave 21.1 % yield based on methane after 15 h (Table 2, entry 9). However, high methane pressures resulted in higher yields (1.87 mmol, entry 11). A first-order dependence of reaction rate on methane partial pressure was observed up to 5 atm. Amounts of catalyst smaller than 0.05 mmol did not give **1**. The reaction of methane with CO to give **1** is best catalyzed by 0.5 mmol of $CaCl_2$ (8.2 % yield; entry 11). Larger amounts of $CaCl_2$ also resulted in low yield (entry 14). The parameter with the largest effect was duration of the reaction. The product **1** is first observed after 2 h, after which its yield constantly increases with time. The catalyst did not lose activity even after 200 h when 0.1 mmol of $CaCl_2$ and 30 atm of methane were used, and the turnover number (TON) of the catalyst was 30.5. Selectivity for the acetic acid product in the liquid phase remained at 100 % during the entire course of the experiment. The best result was obtained with 2 atm of methane, 30 atm of CO, 0.5 mmol of $CaCl_2$, 5 mmol of $K_2S_2O_8$, 5 mL of TFA, and 2 mmol of TFAA. The reaction under these conditions gives almost quantitative yield (93.8 %, based on methane) after 140 h.[9]

We assume that the reaction proceeds through the formation of radicals ($CaO^{\bullet}$, $CH_3^{\bullet}$, and $CH_3CO^{\bullet}$). To confirm this assumption various types of radical scavengers, such as 2,4,6-tri-*tert*-butylphenol, tetrachloro-*p*-benzoquinone, and 2,2,6,6-tetramethylpiperidine, were added to the reaction mixture, and only traces or zero yield of **1** was obtained. This means that the reaction proceeds through the formation of radicals, which were trapped by the scavengers. The control reactions of ^{13}C-labeled methane with ordinary CO and of ^{13}C-labeled CO with ordinary methane were performed to investigate the

 © WILEY-VCH Verlag GmbH, D-69451 Weinheim, 2000 1433-7851/00/3914-2476 $ 17.50+.50/0 *Angew. Chem. Int. Ed.* **2000**, *39*, No. 14

actual source of the methyl and carbonyl groups of **1** and to elucidate the reaction path. From the ^{13}C NMR spectra of both the reaction mixtures it can be seen that except for two quartets of the TFA solvent, only singlet peaks are present at $\delta = 19.4$ (Figure 1a) and 182.3 (Figure 1b), and these are

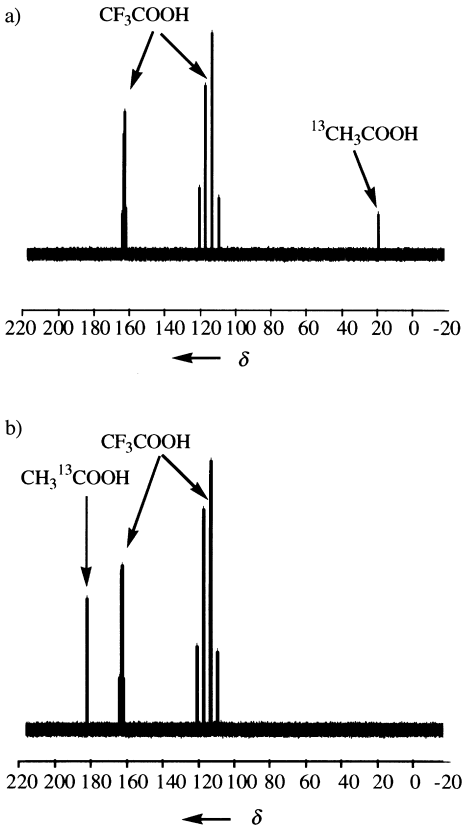


Figure 1. ^{13}C NMR spectra of the reaction mixtures after the reaction of $^{13}CH_4$ with CO (a) and of CH_4 with ^{13}CO (b), which show that the sole products are $^{13}CH_3COOH$ and $CH_3{}^{13}COOH$, respectively.

assigned to the $^{13}CH_3$ and $^{13}C{=}O$ groups of **1**, respectively. These facts confirm that the methyl and carbonyl groups of **1** are derived from $^{13}CH_4$ and ^{13}CO, respectively, and the selectivity for **1** is around 100%.

The activation parameters E_a, A, $\Delta H^{\neq}$, $\Delta S^{\neq}$, and $\Delta G^{\neq}$ at the activated state for the reaction of CH_4 (**3**) and CD_4 (**4**) with CO were calculated by using the Arrhenius and Eyring theories for first-order reaction conditions. The apparent activation energies E_{aH} and E_{aD} and frequency factors A_H and A_D were 16.9 and 19.3 kcal mol^{-1} and 1.7×10^4 and 5.4×10^5 s^{-1}, respectively. These values are reasonable for the abstraction of a hydrogen or deuteron atom from **3** and **4**, respectively, and comparable with those of the oxidation of **3** by $CuCl_2/K_2[PdCl_4]$ mixed catalyst to give methanol.[10] The thermodynamic terms $\Delta H^{\neq}$, $\Delta S^{\neq}$, and $\Delta G^{\neq}$ (253 K) had values of 16.2 and 18.6 kcal mol^{-1}, -40.6 and -34.9 cal mol^{-1} K^{-1}, and 30.5 and 31.0 kcal mol^{-1} for the reactions of **3** and **4**, respectively. In each case, the enthalpy of activation is sufficient for breaking the bond in the transition state. The entropies of activation also covered a significant range and were negative in each case. The lower $\Delta H^{\neq}$ and negative $\Delta S^{\neq}$ values suggest a greater degree of bond forming in the transition state in the case of **3** compared with **4**. From Eyring analysis, the reaction rate constants were $k_H = 9.68 \times 10^{-7}$ and $k_D = 5.63 \times 10^{-7}$ l mol^{-1} s^{-1}, from which the kinetic isotope effect k_H/k_D was calculated to be 1.82 at 80 °C (353 K).

The following evidence allows the possible path of the reaction to be inferred. The use of $^{13}CH_4$ and ^{13}CO resulted in the exclusive formation of $^{13}CH_3COOH$ and $CH_3{}^{13}COOH$, and this reveals that $CH_3^{\bullet}$ is the only methane-derived radical which is trapped by CO[11] to form $CH_3CO^{\bullet}$. The resulting acetyl radical is then converted into **1** via the mixed anhydride with TFA.[4] In the absence of $CaCl_2$, no product was formed. Furthermore, the sufficient $\Delta H^{\neq}$, negative $\Delta S^{\neq}$, and positive isotope effect indicate that the metal species is directly involved in the abstraction of hydrogen from methane to generate methyl radicals, which is the rate-determining step. In addition, in the absence of external CO, not **1** but a small amount of **2** is formed. This result means that CO is also involved in generating the active site of the metal species. The IR spectrum of the solid sample which was prepared from the reaction of $CaCl_2$ and TFA for 4 h shows peaks at 1683.6 ($\tilde{\nu}_{C=O}$) and 1209.1 cm^{-1} ($\tilde{\nu}_{C-O}$), which confirm that $CaCl_2$ is first converted into $Ca(CF_3COO)_2$. Hence, we believe that the active species that abstracts hydrogen from methane is Ca–O$^{\bullet}$, which is generated from $Ca(CF_3COO)_2$ by successive reaction with $K_2S_2O_8$ and CO.

We have discovered a new and highly efficient catalyst system that transforms simple alkanes and CO into the corresponding carboxylic acids almost quantitatively. This reaction employs a cheap catalyst, $CaCl_2$, which strongly suggest its use as a substitute for transition metal catalysts and open the door for the use of alkaline earth metals as homogeneous catalysts in C–H activation.

Experimental Section

Representative procedure: The catalyst and $K_2S_2O_8$ were placed in a 25-mL stainless steel autoclave equipped with a Teflon-coated magnetic stirring bar (12 mm, octagonal). Then TFA (5 mL) was added to the autoclave. The autoclave was closed, flushed with methane three times to dislace the air, and pressurized with the desired pressure of methane and CO. The autoclave was then heated with stirring at a fixed temperature for the desired length of time. When the reaction was complete, the autoclave was cooled in an ice bath for 15 min and then opened. About 80 mg of an internal standard (*n*-valeric acid) was added to the reaction mixture, and the content of product was analyzed by gas chromatography (Shimadzu GC-8A). The ester products of methane were analyzed by NMR spectroscopy.

After separating the solution phase from the reaction mixture, the solvent can be separated from acetic acid by distillation (the boiling point difference is sufficient for distillation). The solid spent catalyst and reagents were collected and washed with water to give a clear solution, which is now under investigation.

Received: January 24, 2000 [Z14590]

[1] a) M. G. Axelrod, A. M. Gaffney, R. Pitchai, J. A. Sofranko, *Natural Gas Conversion II* (Eds.: H. E. Cury-Hyde, R. F. Howe), Elsevier, Amsterdam, **1994**, p. 93; b) C. Starr, M. F. Searl, S. Alpert, *Science* **1992**, *256*, 981.

[2] a) *Activation and Functionalization of Alkanes* (Ed.: C. L. Hill), Wiley, New York, **1989**; b) A. E. Shilov, *Activation of Saturated Hydrocarbons by Transition Metal Complexes*, D. Reidel, Dordrecht,

1984; c) G. A. Olah, A. Molnár, *Hydrocarbon Chemistry*, Wiley, New York, **1995**; d) *Natural Gas Conversion V* (Eds.: A. Parmaliana, D. Sanfilippo, F. Frusteri, A. Vaccari, F. Arena), Elsevier, Amsterdam, **1998**.

[3] a) R. G. Bergman, *Science* **1984**, *223*, 902; b) K. Tomishige, Y. Himeno, O. Yamazaki, Y. Chen, T. Wakatsuki, K. Fujimoto, *Kinet. Catal.* **1999**, *40*, 388; c) K. Tomishige, Y. Chen, K. Fujimoto, *J. Catal.* **1999**, *181*, 91; d) A. Bagno, J. Bukala, G. A. Olah, *J. Org. Chem.* **1990**, *55*, 4284; e) R. H. Crabtree, *Chem. Rev.* **1995**, *95*, 987; f) G. V. Nizova, G. Süss-Fink, G. B. Shul'pin, *Tetrahedron* **1997**, *53*, 3603.

[4] T. Nishiguchi, K. Nakata, K. Takaki, Y. Fujiwara, *Chem. Lett.* **1992**, 1141.

[5] M. Asadullah, Y. Taniguchi, T. Kitamura, Y. Fujiwara, *Appl. Organomet. Chem.* **1998**, *12*, 277.

[6] a) M. Asadullah, T. Kitamura, Y. Fujiwara, *Appl. Organomet. Chem.* **1999**, *13*, 539; b) M. Asadullah, T. Kitamura, Y. Fujiwara, *Chem. Lett.* **1999**, 449.

[7] a) A. Bagno, J. Bukala, G. A. Olah, *J. Org. Chem.* **1990**, *55*, 4284; b) H. Hogeveen, J. Lukas, C. F. Roobeek, *J. Chem. Soc. Chem. Commun.* **1969**, 920.

[8] M. Lin, A. Sen, *Nature* **1994**, *368*, 613.

[9] The volumetric productivity of the present reaction of $6.03 \times 10^{-7}\,mol\,cm^{-3}\,s^{-1}$ is lower than that required for a practical process. Attempts to increase the volumetric productivity by optimizing the reaction conditions and the apparatus are underway.

[10] M. Lin, T. Hogan, A. Sen, *J. Am. Chem. Soc.* **1997**, *119*, 6048.

[11] a) G. V. Nizova, G. Süss-Fink, S. Stanislas, G. B. Shul'pin, *Chem. Commun.* **1998**, 1885; b) K. Nagahara, I. Ryu, N. Kambe, M. Komatsu, N. Sonoda, *J. Org. Chem.* **1995**, *60*, 7384; c) A. P. E. York, J. B. Claridge, A. J. Brungs, S. C. Tsang, M. L. H. Green, *Chem. Commun.* **1997**, 39; d) J. H. Bitter, K. Seshan, J. A. Lercher, *J. Catal.* **1997**, *171*, 279; e) Y. Lu, J. Xue, Y. Liu, S. Shen, *Chem. Lett.* **1997**, 515; f) U. Olsbye, T. Wurzel, L. Mleczko, *Ind. Eng. Chem. Res.* **1997**, *36*, 5180; g) M. C. J. Bradford, M. A. Vannice, *J. Catal.* **1998**, *173*, 157.

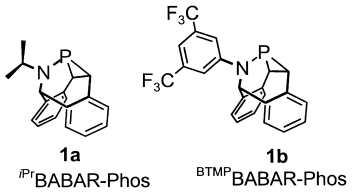
BABAR-Phos Rhodium Complexes: Reversible Metal Insertion into a Three-Membered Ring and Catalytic Hydroborations**

Jürgen Liedtke, Heinz Rüegger, Sandra Loss, and Hansjörg Grützmacher*

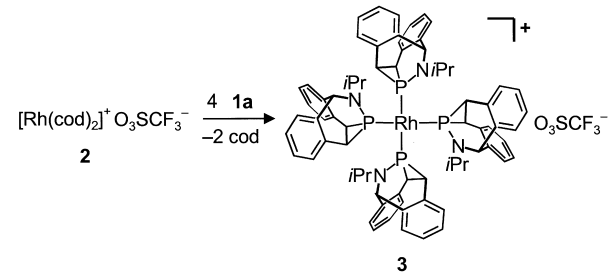
Dedicated to Professor Heinrich Vahrenkamp on the occasion of his 60th birthday

The polycyclic phosphiranes **1a** and **1b** (BABAR-Phos)[1a] are not oxidized by O_2, sulfur, and strongly alkylating agents, and they resist aqueous acids and bases. Furthermore they have electron-withdrawing properties which could make them interesting ligands for hydrosilylation and hydroboration[2] catalysts.[1b] Apart from BABAR-Phos rhodium complexes which were synthesized for this use, we describe here—to our knowledge—the first *reversible* insertion and deinsertion of a metal center into a three-membered heterocycle.[3]

As precursors for the synthesis we used either $[Rh(cod)_2]^+$-$O_3SCF_3^-$ (**2**; cod = 1,5-cyclooctadiene) containing only a weakly coordinating anion or $[Rh_2(\mu_2\text{-}Cl_2)(cod)_2]$ (**4**). Reactions of **2** with **1a** in coordinating solvents, such as acetonitrile, or with



the N-aryl-substituted phosphirane **1b** generate brown-red solutions ($\lambda_{max} > 500$ nm), whose ^{31}P NMR spectra display signals in the positive ($\delta = +20$ to $+100$) and negative ($\delta = -60$ to -150) δ range (versus 85% H_3PO_4). The signals are broadened due to chemical exchange between different species. However, when **2** is treated with **1a** in THF, product **3** is obtained almost quantitatively and independently of the initial ratio **2**:**1a** as poorly soluble, orange microcrystals (Scheme 1). The ^{31}P NMR spectrum of complex **3** shows a



Scheme 1. Synthesis of complex **3**.

doublet at $\delta(^{31}P) = -66.9$ ($^1J(Rh,P) = 170$ Hz), and the complex was structurally characterized by X-ray crystal structure analysis (Figure 1).[4] Remarkably, the Rh center, which is located on a fourfold axis of symmetry, deviates by 0.24 Å from the plane of the square planar arrangement of the four phosphorus atoms (sum of angles at P within the ligand framework: 258°). The Rh–P bond lengths in **3** (2.276(1) Å) are slightly shorter than the ones in other known rhodium phosphirane complexes.[5]

Reactions of the chloride-containing rhodium complex **4** with **1a** or **1b** in weakly coordinating solvents again give brown-red solutions containing several components (exchange-broadened ^{31}P signals in the positive or negative δ range). Only the reaction of **4** with **1b** in acetonitrile leads to one pure product **5** (formula $C_{96}H_{62}Cl_4F_{24}N_6P_4Rh_4$), which is obtained as sparingly soluble, deep brown microcrystals (Scheme 2).

Two of the Cl centers in **5** can be exchanged for poorly coordinating anions $X = O_3SCF_3^-$ or PF_6^- when it reacts with the silver salts **6a** and **6b**, respectively. Deep brown solutions ($\lambda_{max} = 660$ nm) are obtained from which the tetranuclear clusters **7a**, **b** were crystallized. Compound **7b** was also

[*] Prof. Dr. H. Grützmacher, Dipl.-Chem. J. Liedtke, Dr. H. Rüegger, Dipl.-Chem. S. Loss
Laboratorium für Anorganische Chemie, ETH-Zentrum
Universitätstrasse 6, 8092 Zürich (Switzerland)
Fax: (+41) 1-632-10-90
E-mail: gruetz@inorg.chem.ethz.ch

[**] This work was supported by the ETH Zürich and the National Swiss Science Foundation.

 © WILEY-VCH Verlag GmbH, D-69451 Weinheim, 2000 1433-7851/00/3914-2478 $ 17.50+.50/0

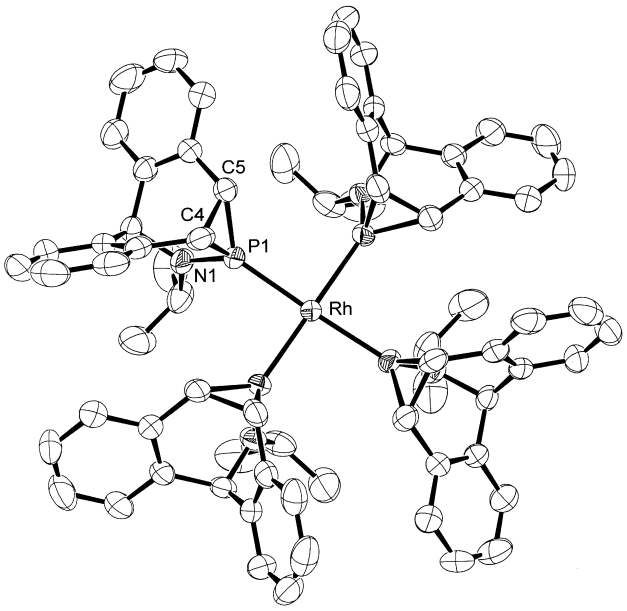


Figure 1. ORTEP plot of the cation of **3**; hydrogen atoms are omitted for clarity. Selected bond lengths [Å] and angles [°]: Rh-P1 2.279(1), P1-N1 1.650(4), P1-C5 1.810(5), P1-C4 1.813(6), P1-C4 1.813(6), C4-C5 1.576(8); P1′-Rh-P1 89.367(8), P1″-Rh-P1 167.91(8), N1-P1-C5 102.2(2), N1-P1-C4 103.5(2), C5-P1-C4 51.6(2), N1-P1-Rh 124.4(2), C5-P1-Rh 129.8(2), C4-P1-Rh 122.8(2), C5-C4-P1 64.1(3), C4-C5-P1 64.3(3).

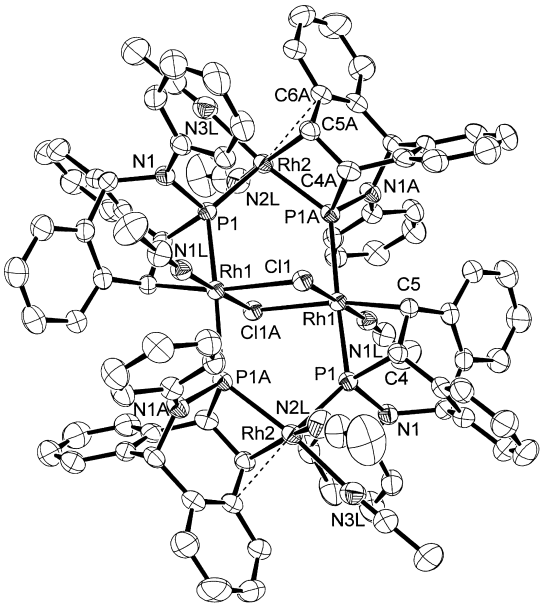
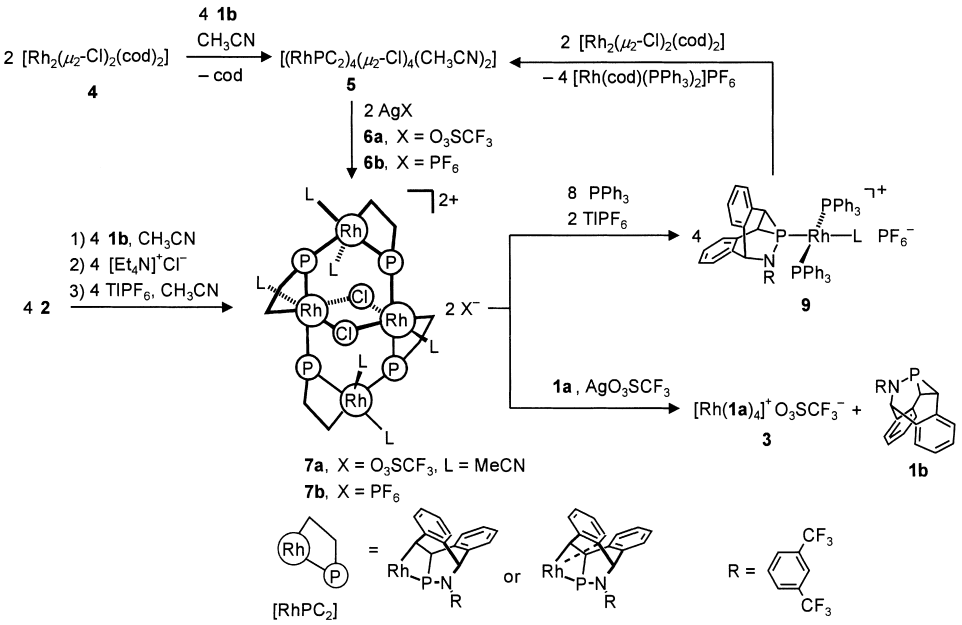


Figure 2. ORTEP plot of the centrosymmetric cation of **7b**; CF_3 groups and hydrogen atoms have been omitted for clarity. Selected bond lengths [Å] and angles [°]: Rh1-P1 2.305(1), Rh1-P1A 2.475(1), Rh1-Cl1 2.514(1), Rh1-Cl1A 2.363(1), Rh1-C5 2.131(5), Rh2-P1 2.258(1), Rh2-P1A 2.296(1), Rh2-C5A 2.082(5), P1-N1 1.705(4), P1-C4 1.857(5), C4-C5 1.557(7), P1A-N1A 1.724(4), P1A-C4A 1.865(5), C4A-C5A 1.528(7); P1-Rh1-P1A 170.61(4), P1-Rh2-P1A 95.68(5), Rh2-P1-Rh1 130.71(6), Rh2-P1A-Rh1 132.44(6), N1-P1-Rh1 110.9(2), C4-P1-Rh1 85.6(2), N1-P1-Rh2 110.1(1), C4-P1-Rh2 114.2(2), N1-P1-C4 98.0(2), N1A-P1A-Rh1 116.8(2), C4A-P1A-Rh1 112.0(2), N1A-P1A-Rh2 102.0(2), C4A-P1A-Rh2 86.5(2), N1A-P1A-C4A 98.5(2).

synthesized from **2** and **1b** in the presence of chloride ions and $TlPF_6$ (Scheme 2), and the result of a single-crystal X-ray structure analysis of **7b** is shown in Figure 2.[4]

Each rhodium center has inserted oxidatively into one of the P–C bonds of the PC_2 ring of the BABAR-Phos ligand. The resulting $[(RhPC_2)L_n]^+$ units ($RhPC_2$ denotes a Rh-inserted BABAR-Phos unit; fold angle along the P1 – C5 vector 32°; L = MeCN, see Scheme 2) are bridged by the phosphorus centers and form a planar centrosymmetric $Rh_4(\mu_2\text{-}P)_4$ ring. A planar rhombic $Rh_2(\mu_2\text{-}Cl)_2$ ring is arranged perpendicular to this ring. The Rh1 centers lie in distorted octahedral coordination spheres. The Rh2 centers show a distorted square-pyramidal (5+1) coordination with an additional long contact to one of the arene carbon atoms (Rh2–C6A 2.470(5) Å). In view of the similar colors and ^{31}P NMR spectra, we assume that **5** has a comparable structure to those of **7a**, **b** in which the four acetronitrile ligands in the latter are replaced by two chlorine centers in **5**. These probably bridge the clusters in an intermolecular fashion to give a coordination polymer.



Scheme 2. Synthesis and reactions of tetranuclear 2-rhodaphosphetanes **5**, **7a**, **b**, and complex **9**.

A simple experiment allowed the assignment of the ^{103}Rh and ^{31}P NMR chemical shifts and revealed some aspects of the reactivity of **7b**. In a CH_3CN solution containing 10% CD_3CN, one sharp resonance signal integrating for 2.7 H is observed which is assigned to the single MeCN ligand bonded to Rh1. This ligand exchanges slowly with solvent molecules.

With this information, we assigned the ^{103}Rh resonance signal at $\delta = 3308$ to Rh1 by using ^{103}Rh-^{1}H HMQC spectroscopy; the Rh2 resonance signal is observed at $\delta = 2860$. The ^{31}P resonance signals were assigned by a sequence of ^{31}P-^{1}H COSY and ^{1}H-^{1}H NOESY experiments and are listed in Table 1. The insertion products **5** and **7a**, **b** are characterized by ^{31}P NMR signals in the positive δ range; the $^{1}J(^{103}\mathrm{Rh},^{31}\mathrm{P})$ coupling constant within a $RhPC_2$ unit is generally smaller than the one between $RhPC_2$ rings.

When **7b** reacts with eight equivalents of PPh_3 in presence of $TlPF_6$, the mononuclear BABAR-Phos complex **9** is obtained quantitatively (Scheme 2). Probably, in the first reaction step each $[RhPC_2]$ unit in **7b** is transformed into a $[(Rh^{III}PC_2)(PPh_3)_2]^+$ complex.[6b] By subsequent reductive P–C bond coupling the intact BABAR-Phos ligand is reconstituted ($\delta(^{31}\mathrm{P})$ of **1b** in **9**: -60.8, $^{1}J(\mathrm{Rh,P}) = 235$ Hz). On the other hand, when **4** is added to a solution of **9** in acetonitrile (Scheme 2), the tetranuclear cluster **5** is reformed and precipitates. Also when **7b** is treated with an eightfold excess of N-isopropyl-substituted BABAR-Phos **1a** in presence of AgO_3SCF_3, ring closure regenerates **1b**, which is replaced by **1a** under formation of **3** (Scheme 2). Note that when **7b** is treated with **1b** under comparable conditions, the analogous $[Rh(\mathbf{1b})_4]^+$ complex does not form. In their pioneering work, Marinetti, Mathey, Nixon, and co-workers have shown that metal centers insert irreversibly into three-membered PC_2 heterocycles.[6] However, a reversible reaction as described here has not been observed yet to our knowledge. Comparison of the data of the isolated complexes **3**, **7a**, **b**, and **9** with the ^{31}P NMR and UV/Vis data obtained for the more complex red-brown reaction solutions mentioned above show that here also equilibria exist between compounds containing ring-opened and intact BABAR-Phos ligands. To this end we find that rhodium centers may reversibly insert into BABAR-Phos ligands **1a** and **1b**, the latter giving the more stable insertion products. The presence of "hard" donor ligands also leads to insertion products since these ligands stabilize the rhodium center in the formally +3 oxidation state.

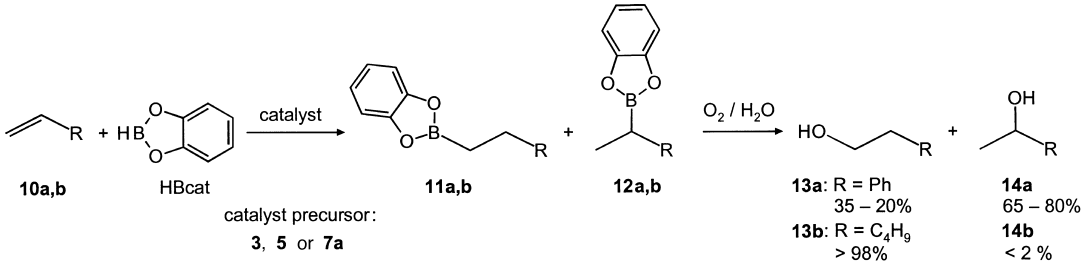
Complexes **3**, **5**, and **7a** were tested as catalyst precursors in hydroborations.[7] A solution of catechol borane (HBcat) in THF was added to a mixture of an olefin (1-hexene or styrene) and 1–0.01 mol% catalyst in THF as solvent (Scheme 3).

Table 1. Selected physical data for **3**, **5**, **7a** and **9**. *J* in Hz.

	$\delta(^{103}\mathrm{Rh})$	$\delta(^{31}\mathrm{P})$	$\delta(^{1}\mathrm{H})$ PCHCH	$\delta(^{13}\mathrm{C})$ PCHCH	λ_{max} [nm]	M.p. [°C]
3		-66.9 (d, $^{1}J(\mathrm{Rh,P}) = 170$)	3.05	23.3	382(sh)	> 230 (decomp)
5		44.0 (m, $^{1}J(\mathrm{Rh1,P1}) = 61$, $^{1}J(\mathrm{Rh2,P1}) = 206$, $^{2}J_{trans}(\mathrm{P1A,P1}) = 452$, P_1), 7.7 (m, $^{1}J(\mathrm{Rh2,P1A}) = 55$, $^{1}J(\mathrm{Rh1,P1A}) = 84$, $^{2}J_{trans}(\mathrm{P1,P1A}) = 452$, P1A)				> 185 (decomp)
7a, **b**	3308 (Rh1), 2860 (Rh2)	27.6 (m, $^{1}J(\mathrm{Rh1,P1}) = 53$, $^{1}J(\mathrm{Rh2,P1}) = 153$, $^{2}J_{trans}(\mathrm{P1A,P1}) = 443$, P1), 6.6 (m, $^{1}J(\mathrm{Rh2,P1A}) = 80$, $^{1}J(\mathrm{Rh1,P1A}) = 83$, $^{2}J_{trans}(\mathrm{P1,P1A}) = 443$, P1A)	3.75 (m, $^{2}J(\mathrm{P1,H5}) = 21$, $^{1}J(\mathrm{P1A,H5}) = 5.6$, H5), 5.98 (d, $^{1}J(\mathrm{P1,H4}) = 9$, H4), 3.98 (m, $^{2}J(\mathrm{P1,H5A}) = 12$, H5A), 7.03 (m, H4A)	18.1 (m, C5A), 53.9 (m, C4A), 24.2 (m, C5), 58.9 (d, $^{1}J(\mathrm{P1,C4}) = 83$, C4)	660	> 176 (decomp)
9		-143.3 (sept., $^{1}J(\mathrm{P,F}) = 706$), -60.8 (dt, $^{1}J(\mathrm{Rh,P}) = 235$, $^{2}J_{cis}(\mathrm{P,P}) = 62$), 30.2 (dd, $^{2}J_{cis}(\mathrm{P,P}) = 62$)	2.68 (d, $^{2}J(\mathrm{P,H}) = 4$)	26.3 (d, $^{1}J(\mathrm{P,C}) = 5$)	418	> 133 (decomp)

All catalysts show activity comparable to other rhodium complexes (turnover frequency (TOF) with 0.1 mol% **3**: > 30000 h^{-1}). In reactions with styrene, the ratio of 2-phenylethanol (**13a**) (35–20%) to 1-phenylethanol (**14a**) (65–80%) is comparable to results obtained with $[RhCl(PPh_3)_3]$ as catalyst. However, when a second catalytic run is started using $[RhCl(PPh_3)_3]$ by re-addition of **10a** and HBcat to the reaction mixture (which turned dark), almost no catalytic activity is observed. On the other hand, the BABAR-Phos complexes **3**, **5**, and **7a** showed no drop of catalytic activity even after five catalytic cycles. The reaction mixtures did not change color and the intact BABAR complexes were identified by ^{31}P NMR spectroscopy.[8]

Like the uncomplexed ligands, BABAR-Phos complexes are stable under an atmosphere of pure O_2, and even at 50 °C no destruction of **3** was observed. In contrast, $[RhCl(PPh_3)_3]$ rapidly decomposes under formation of $Ph_3P{=}O$. This re-



Scheme 3. Hydroborations with **3**, **5**, or **7b** as catalyst precursors.

 © WILEY-VCH Verlag GmbH, D-69451 Weinheim, 2000 1433-7851/00/3914-2480 $ 17.50+.50/0 *Angew. Chem. Int. Ed.* **2000**, *39*, No. 14

markable resistance to oxgen should stimulate investigations into methods to recycle BABAR-Phos complexes (e.g. by immobilization or making them water soluble).[9]

Experimental Section

3: Compound **1a** (477 mg, 1.7 mmol) was added to a solution of $[Rh(cod)_2]^+O_3SCF_3^-$ (200 mg, 0.42 mmol) in THF (3 mL). The product precipitated as a light yellow microcrystalline powder which was washed with Et_2O (2 × 1 mL) and dried in vacuum (yield 472 mg, 82 %). Crystals suitable for an X-ray analysis were grown from a CH_2Cl_2 solution layered with *n*-hexane. Elemental analysis (%) calcd for $C_{73}H_{72}F_3N_4O_3P_4RhS$: C 64.03, H 5.30, N 4.09; found: C 64.12, H 5.27, N 4.18.

5: Compound **4** (200 mg, 0.41 mmol) and **1b** (365 mg, 0.82 mmol) were combined in MeCN (3 mL). After about 1 h without stirring, the product precipitated in the form of deep brown-red crystals, which were collected by filtration and washed with MeCN (2 × 1 mL). After drying under vacuum **5** was obtained in 91 % yield (458 mg). Elemental analysis (%) calcd for $C_{96}H_{62}Cl_4F_{24}N_6P_4Rh_4$: C 47.39, H 2.57, Cl 5.83, P 5.09, N 3.45; found: C 47.39, H 2.83, Cl 5.95, P 5.10, N 3.60.

7a, b: A suspension of **5** (200 mg, 0.08 mmol) in MeCN (2 mL) was treated with $AgPF_6$ (38 mg, 0.15 mmol) or $AgSO_3CF_3$ (40 mg, 0.15 mmol), respectively. After filtration from precipitated AgCl, the solution was reduced to about about a tenth of its volume. At −25 °C, the products crystallized as brown-red rhombs; yields: **7a**: 171 mg (79 %); **7b**: 178 mg (76 %). Elemental analysis (%) calcd for $C_{104}H_{74}Cl_2F_{36}N_{10}P_6Rh_4$ (**7a**): C 44.36, H 2.65, N 4.97; found: C 44.31, H 2.59, N 5.01.

Received: December 22, 1999
Revised: February 28, 2000 [Z14445]

[1] a) J. Liedtke, S. Loss, G. Alcaraz, V. Gramlich, H. Grützmacher, *Angew. Chem.* **1999**, *110*, 1724; *Angew. Chem. Int. Ed.* **1999**, *38*, 1623; b) J. Liedtke, S. Loss, H. Grützmacher, *Tetrahedron* **2000**, *56*, 143.

[2] a) C. Widauer, H. Grützmacher, T. Ziegler, *Organometallics* **2000**, *24*, 2097; b) D. G. Musaev, A. M. Mebel, K. Morokuma, *J. Am. Chem. Soc.* **1994**, *116*, 10693; c) A. E. Dorigo, P. von R. Schleyer, *Angew. Chem.* **1995**, *107*, 108; *Angew. Chem. Int. Ed. Engl.* **1995**, *34*, 115.

[3] a) Irreversible metal insertion reactions into $(R_2C)_2X$ rings (X = CR_2; NR, O): D. Carmichael, P. B. Hitchcock, J. F. Nixon, F. Mathey, L. Ricard, *J. Chem. Soc. Dalton Trans.* **1993**, 1811; b) formation of epoxide by thermolysis of a 1-nickela-2-oxacyclobutane: A. Miyashita, J. Ishida, H. Nohira, *Tetrahedron Lett.* **1986**, *27*, 2127.

[4] Crystal structure analyses: **3**: tetragonal, space group *P*4*nc*; a = 16.5970(5), c = 11.7946(3) Å; V = 3248.9(2) Å^3; Z = 2, $Mo_{K\alpha}$ radiation, $2\Theta_{max}$ = 52.72°; 21747 reflections, 3324 independent (R_{int} = 0.0728); R_1 = 0.05, wR_2 = 0.1232 (based on F^2) for 199 parameters and 2746 reflections with $I > 2\sigma(I)$. **7b**: monoclinic, space group $P2_1/n$; a = 17.98168(5), b = 18.9535(5), c = 18.5737(4) Å, β = 104.093(1)°; V = 6139.7(3) Å^3; Z = 2, $Mo_{K\alpha}$ radiation, $2\Theta_{max}$ = 52.74°; 45154 reflections, 12557 independent ($R_{int.}$ = 0.0791); R_1 = 0.0494, wR_2 = 0.0931 (based on F^2) for 772 parameters and 8201 reflections with $I > 2\sigma(I)$. Both structures were solved by using direct methods and were refined against full matrix (versus F^2) with SHELXTL (Version 5.0). Non-hydrogen atoms were treated anisotropically, hydrogen atoms were refined on calculated positions using the riding model. The triflate anion in **3** was refined as a rigid group disordered over four equivalent positions with isotropic temperature factors. Noncoordinating acetonitrile molecules in **7b** were refined with isotropic temperature factors, one of the molecules was disordered over two equivalent positions with an occupancy factor of 0.4. Crystallographic data (excluding structure factors) for the structures reported in this paper have been deposited with the Cambridge Crystallographic Data Centre as supplementary publication no. CCDC-137943 (**3**) and CCDC-137942 (**7b**). Copies of the data can be obtained free of charge on application to CCDC, 12 Union Road, Cambridge CB21EZ, UK (fax: (+44) 1223-336-033; e-mail: deposit@ccdc.cam.ac.uk).

[5] A. Marinetti, F. Mathey, L. Ricard, *Organometallics* **1993**, *12*, 1207.

[6] a) F. A. Ajulu, P. B. Hitchcock, F. Mathey, R. A. Michelin, J. F. Nixon, A. J. L. Pombeiro, *J. Chem. Soc. Chem. Commun.* **1993**, 142; b) F. A. Ajulu, D. Carmichael, P. B. Hitchcock, F. Mathey, M. F. Meidine, J. F. Nixon, L. Ricard, M. L. Riley, *J. Chem. Soc. Chem. Commun.* **1992**, 750; c) S. S. Al Juaid, D. Carmichael, P. B. Hitchcock, A. Marinetti, F. Mathey, J. F. Nixon, *J. Chem. Soc. Dalton Trans.* **1991**, 905.

[7] a) D. Männig, H. Nöth, *Angew. Chem.* **1985**, *97*, 854; *Angew. Chem. Int. Ed. Engl.* **1985**, *24*, 878; b) Review: K. Burgess, M. J. Ohlmeyer, *Chem. Rev.* **1991**, *91*, 1179; c) J. M. Brown, G. C. Lloyd-Jones, *J. Am. Chem. Soc.* **1994**, *116*, 866, and references therein.

[8] In the presence of the olefin alone, no reaction is observed, while addition of borane alone caused a slight color change and ^{31}P NMR signals appeared in the region of the intact BABAR-Phos ligand. However, we have been unable to isolate any pure product yet.

[9] The alcohols **13a**, **b** and **14a**, **b** can be obtained by passing a stream of oxygen (or air) through the reaction mixtures. Unfortunately, although the complexes were stable under O_2 they decomposed in the presence of the organoboranes **11a**, **b**, **12a**, **b**. However, the ligands **1a**, **b** could be recovered. Workup with alkaline H_2O_2 destroys the phosphiranes as well. Probably these decomposition reactions are caused by radicals being formed from organoboranes and O_2 (see: H. J. Brown, M. M. Midland, *Tetrahedron* **1987**, *43*, 4059) or by the high oxidizing power of alkaline H_2O_2. However, one could circumvent catalyst destruction by separation before workup.

Halogen – Magnesium Exchange via Trialkylmagnesates for the Preparation of Aryl- and Alkenylmagnesium Reagents**

Kazuya Kitagawa, Atsushi Inoue, Hiroshi Shinokubo, and Koichiro Oshima*

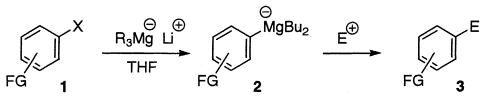
The utility of organometallic ate complexes such as R_2CuLi, R_3ZnLi, and R_4AlLi in organic synthesis is well known, and numerous studies have been devoted to the development of new methods which make use of these reagents. Several synthetic methods which utilize R_3MnLi have also been reported recently.[1] These organometallic ate complexes are known to induce halogen – metal exchange reactions in some cases.[2]

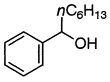
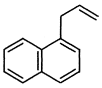
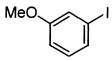
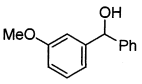
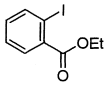
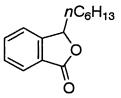
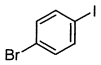
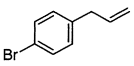
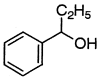
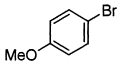
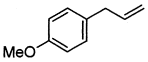
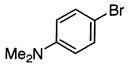
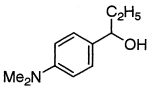
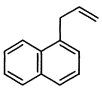
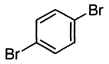
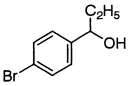
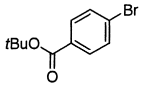
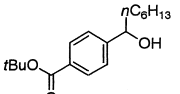
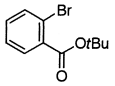
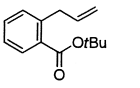
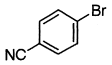
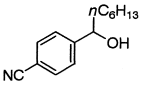
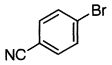
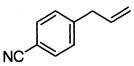
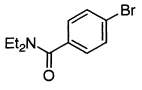
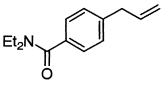
Recently, Knochel et al. have shown that polyfunctional arylmagnesium and alkenylmagnesium reagents can be prepared by an iodine – magnesium exchange reaction using RMgX.[3, 4] It then occurred to us that a magnesium-ate complex (R_3MgLi)[5] would be more effective than an alkylmagnesium halide (RMgX) for the halogen – magnesium exchange reaction. Indeed, we have found that treatment

[*] Prof. Dr. K. Oshima, K. Kitagawa, A. Inoue, Dr. H. Shinokubo
Department of Material Chemistry
Graduate School of Engineering, Kyoto University
Kyoto 606 – 8501 (Japan)
Fax: (+81) 75-753-4863
E-mail: oshima@fm1.kuic.kyoto-u.ac.jp

[**] This work was supported by a Grant-in-Aid for Scientific Research from the Ministry of Education, Science, Sports, and Culture, Japan.

Table 1. Preparation of arylmagnesates and their reaction with electrophiles.[a]



Entry	ArX	Conditions[a] Reagent	T [°C]	t [h]	Electrophile	Product	Yield [%]
1		A	0	0.5	*n*-C_6H_{13}CHO		80
2		A	0	0.5	CH_2=$CHCH_2Br$		87
3		A	−78	0.5	PhCHO		93
4		A	−78	1	*n*-C_6H_{13}CHO		60
5		A	0	0.5	CH_2=$CHCH_2Br$		73
6		A	0	0.5	C_2H_5CHO		87
7		A	0	0.5	CH_2=$CHCH_2Br$		84
8		A	0	0.5	C_2H_5CHO		94
9		A	0	0.5	CH_2=$CHCH_2Br$		97
10		B	0	0.5	C_2H_5CHO		78
11		A	−78	1	*n*-C_6H_{13}CHO		50
12		B	−78	1	*n*-C_6H_{13}CHO		71
13		B	−78	1	CH_2=$CHCH_2Br$[b]		99
14		B	−78	1	*n*-C_6H_{13}CHO		60
15		B	−78	1	CH_2=$CHCH_2Br$[b]		87
16		B	−78	1	CH_2=$CHCH_2Br$[b]		79

[a] Reagent A: *n*Bu_3MgLi, reagent B: *i*$PrBu_2MgLi$. [b] In the presence of $CuCN \cdot 2\,LiCl$.

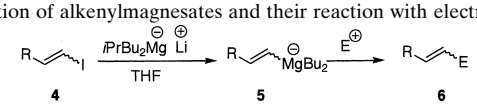
of aryl halides or alkenyl iodides with trialkylmagnesate, derived from RMgX and two equivalents of alkyllithium, provided the corresponding organomagnesium reagents in good to excellent yields. The representative results are shown in Table 1.[6] Several features of the reaction are noteworthy. Not only aryl iodides but also aryl bromides[7] can be converted into the corresponding magnesium reagents efficiently. Functional groups (FG) such as ester, amide, or cyano groups are tolerated during the exchange procedure and lead to functionalized arylmagnesates of type **2**. For the preparation of the latter, the mixed magnesate *i*$PrBu_2MgLi$ was required, which was generated from *i*PrMgBr and *n*BuLi, and was found to be more reactive than *n*Bu_3MgLi for the exchange reaction. Whereas *n*Bu_3MgLi could convert aryl iodides into the corresponding magnesate at −78 °C, the reagent could not complete the magnesiation reaction of aryl bromide at that temperature. In contrast, bromine–magnesium exchange of aryl bromides could be easily performed with *i*$PrBu_2MgLi$ at −78 °C.[8] Although the reaction of **2** with allyl bromide at 0 °C provided the allylated products in good yields, the reaction did not proceed at −78 °C. However, the addition of a catalytic amount of $CuCN \cdot 2\,LiCl$ to the reaction mixture facilitated the allylation at −78 °C, and the desired products were obtained in excellent yields (entries 13, 15, and 16; Table 1).

This new procedure was utilized for the preparation of alkenylmagnesates from alkenyl halides. The results are shown in Table 2. The iodine–magnesium exchange of alkenyl iodides proceeded with complete retention of configuration of the double bond. The reaction of (*Z*)-1-iodo-1-dodecene afforded the corresponding (*Z*)-alkenylmagnesate, and (*E*)-iodoalkene provided the *E* isomer. The resulting alkenylmagnesate could be easily trapped by various electrophiles such as chlorotrimethylsilane, allyl bromide, benzaldehyde, or acetone. The presence of an ester functionality is compatible with the formation of alkenylmagnesate at −78 °C (entry 17; Table 2).

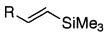
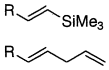
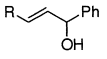
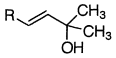
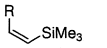
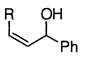
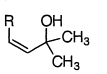
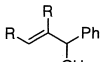
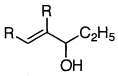
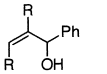
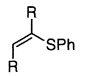
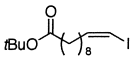
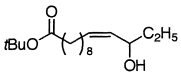
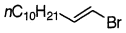
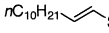
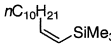
In contrast, the bromine–magnesium exchange of alkenyl bromide is not as effective. The treatment of (*E*)-1-bromo-1-dodecene with *i*$PrBu_2MgLi$ followed by an addition of chlorotrimethylsilane provided (*E*)-1-trimethylsilyl-1-dodecene in 71% yield along with 1-trimethylsilyl-1-dodecyne (29%). The alkynylsilane results from silylation of the dehydrobromination product (1-dodecyne). Meanwhile, the reaction of the *Z* isomer gave (*Z*)-1-trimethylsilyl-1-dodecene in only 27% yield in addition to 59% of the silyldodecyne (entries 18 and 19; Table 2).

 © WILEY-VCH Verlag GmbH, D-69451 Weinheim, 2000 1433-7851/00/3914-2482 $ 17.50+.50/0 *Angew. Chem. Int. Ed.* **2000**, *39*, No. 14

Table 2. Preparation of alkenylmagnesates and their reaction with electrophiles.



4 5 6

Entry	Substrate	Conditions T [°C]	t [h]	Electrophile	Product	Yield [%]
1	 R = $nC_{10}H_{21}$	0	1	D_2O		93
2		0	1	Me_3SiCl		93
3		– 78	1	Me_3SiCl		95
4		0	1	CH_2=$CHCH_2Br$[a]		70
5		0	1	PhCHO		69
6		0	1	CH_3COCH_3		75
7	 R = $nC_{10}H_{21}$	– 78	1	Me_3SiCl		83
8		0	1	CH_2=$CHCH_2Br$[a]		78
9		0	1	PhCHO		78
10		0	1	CH_3COCH_3		66
11	 R = nC_5H_{11}	0	1	D_2O		87
12		0	1	PhCHO		87
13		0	1	C_2H_5CHO		65
14		0	1	D_2O		88
15	R = nC_5H_{11}	0	1	PhCHO		70
16		0	1	PhSSPh		77
17		– 78	0.5	C_2H_5CHO		80
18		0	1	Me_3SiCl		71 (29)[b]
19		0	1	Me_3SiCl		27 (59)[b]

[a] In the presence of $CuCN \cdot 2\,LiCl$. [b] Yields of 1-trimethylsilyl-1-dodecyne in parentheses.

Experimental Section

Butyllithium (1.6 M solution in hexane, 1.5 mL, 2.4 mmol) was added to a solution of isopropylmagnesium bromide (1.0 M solution in THF, 1.2 mL, 1.2 mmol) in THF (5 mL) at 0 °C. After being stirred for 30 min, the resulting mixture was cooled to – 78 °C and a solution of *tert*-butyl *p*-bromobenzoate (0.26 g, 1.0 mmol) in THF (2 mL) was added. The mixture was stirred for 1 h at – 78 °C and then heptanal (3.0 mmol) was added. The reaction mixture was stirred for additional 1 h at – 78 °C, and then the reaction was quenched with saturated NH_4Cl and extracted with ethyl acetate (3×20 mL). The combined organic layers were dried over anhydrous Na_2SO_4 and concentrated. Purification by column chromatography (silica gel) gave *tert*-butyl 4-(1-hydroxyheptyl)benzoate as a colorless liquid (0.21 g, 71 %).

Received: February 2, 2000 [Z 14638]

[1] K. Oshima, *J. Organomet. Chem*. **1999**, *575*, 1 – 20.

[2] a) R. Inoue, H. Shinokubo, K. Oshima, *Tetrahedron Lett*. **1996**, *37*, 5377 – 5380; b) R. Inoue, H. Shinokubo, K. Oshima, *J. Org. Chem.* **1998**, *63*, 910 – 911; c) M. Hojo, H. Harada, H. Ito, A. Hosomi, *J. Am. Chem. Soc*. **1997**, *119*, 5459 – 5460; d) M. Hojo, A. Hosomi, *Chem. Commun.* **1997**, 2077 – 2078; e) M. Uchiyama, M. Koike, M. Kameda, Y. Kondo, T. Sakamoto, *J. Am. Chem. Soc.* **1996**, *118*, 8733 – 8734; f) Y. Kondo, T. Matsudaira, J. Sato, N. Murata, T. Sakamoto, *Angew. Chem.* **1996**, *108*, 818 – 820; *Angew. Chem. Int. Ed. Engl.* **1996**, *35*, 736 – 738; g) T. Harada, T. Katsuhira, D. Hara, Y. Kotani, K. Maejima, R. Kaji, A. Oku, *J. Org. Chem.* **1993**, *58*, 4897 – 4907; h) T. Harada, T. Katsuhira, K. Hattori, A. Oku, *J. Org. Chem*. **1993**, *58*, 2958 – 2965.

[3] a) C. E. Tucker, T. N. Majid, P. Knochel, *J. Am. Chem. Soc.* **1992**, *114*, 3983 – 3085; b) L. Boymond, M. Rottländer, G. Cahiez, P. Knochel, *Angew. Chem.* **1998**, *110*, 1801 – 1804; *Angew. Chem. Int. Ed.* **1998**, *37*, 1701 – 1703; c) L. Bérillon, A. Leprêtre, A. Turck, N. Plé, G. Quéguiner, G. Cahiez, P. Knochel, *Synlett* **1998**, 1359 – 1360; d) M. Rottländer, L. Boymond, G. Cahiez, P. Knochel, *J. Org. Chem*. **1999**, *64*, 1080 – 1081; e) M. Abarbi, P. Knochel, *Synlett* **1999**, 1577 – 1578; f) M. Abarbi, F. Dehmel, P. Knochel, *Tetrahedron Lett*. **1999**, *40*, 7449 – 7453.

[4] For further examples of halogen – magnesium exchange reactions, see: a) N. Furukawa, T. Shibutani, H. Fujihara, *Tetrahedron Lett*. **1987**, *28*, 5845 – 5848; b) H. Nishikawa, K. Isaka, K. Itoh, K. Ohno, H. Nagase, K. Matsumoto, H. Yoshiwara, *J. Org. Chem*. **1992**, *57*, 407 – 410; c) H. Shinokubo, H. Miki, T. Yokoo, K. Oshima, K. Utimoto, *Tetrahedron* **1995**, *51*, 11 681 – 11 692; d) F. Trécourt, G. Breton, V. Bonnet, F. Mongin, F. Marsais, G. Quéguiner, *Tetrahedron Lett*. **1999**, *40*, 4339 – 4342.

[5] The crystal structures of $[Li(TMEDA)]_2Me_4Mg$ and $[Li(TMEDA)]_2[Ph_2MgPh_2MgPh_2]$ (TMEDA = *N*,*N*,*N*′,*N*′-tetrametylethylenediamine) have been reported. a) T. Greiser, J. Kopf, D. Thoennes, E. Weiss, *Chem. Ber*. **1981**, *114*, 209 – 213; b) D. Thoennes, E. Weiss, *Chem. Ber*. **1978**, *111*, 3726 – 3731. An NMR study on CH_3Li-$(CH_3)_2Mg$ has been reported: L. M. Seitz, T. L. Brown, *J. Am. Chem. Soc*. **1966**, *88*, 4140 – 4147.

[6] The amount of the magnesate reagent can be reduced in some cases. The reaction of *p*-bromoanisole with 0.6 equivalents of nBu_3MgLi provided the corresponding product in 85 % yield upon treatment with propanal.

[7] Knochel et al. have reported that Br – Mg exchange of aryl bromides with *i*PrMgBr or iPr_2Mg is efficient when the substrate bears an electron-withdrawing group.[3f] In contrast, Br – Mg exchange with trialkylmagnesate proceeded effectively without such an activating group. For example, the corresponding phenylmagnesate species was formed quantitatively in the reaction of bromobenzen with $iPrBu_2MgLi$, whereas bromobenzene did not react *i*PrMgBr at – 78 °C.

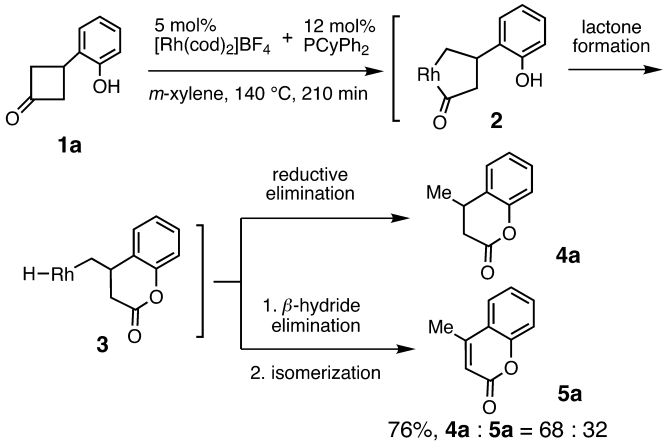
[8] The reaction of excess benzaldehyde with arylmagnesium reagent, which was derived from aryl bromide and $iPrBu_2MgLi$, provided no isopropyl-substituted alcohol. The isopropyl group was consumed for the exchange reaction. This result indicates that the isopropyl residue in the mixed ate complex is active.

Lactone Formation by Rhodium-Catalyzed C–C Bond Cleavage of Cyclobutanone**

Masahiro Murakami,* Takuo Tsuruta, and Yoshihiko Ito*

Of the variety of synthetic transformations mediated by transition metals, catalytic processes involving cleavage of C–C single bonds are among the most difficult to achieve.[1] Hence, their development remains an important challenge in organic chemistry. We recently found that the bond between the carbonyl carbon and the α-carbon atom of a cyclobutanone can be catalytically cleaved by a rhodium(I) complex.[2] Phenolic hydroxy groups have also been reported to direct intramolecular functionalization of unreactive bonds such as C–H bonds.[3] Thus we anticipated that C–C bond cleavage would be facilitated by appropriate placement of a phenol group in the substrate molecule. Here we report new lactone-forming reactions by the rhodium-catalyzed C–C bond cleavage of a cyclobutanone having a pendant phenol group.

Cyclobutanone **1a**, which has an *o*-substituted phenol group at the 3-position,[4] was heated to 140 °C in *m*-xylene in the presence of a rhodium complex prepared in situ from $[Rh(cod)_2]BF_4$ (5 mol %, cod = 1,5-cyclooctadiene) and cyclohexyldiphenylphosphane ($PCyPh_2$, 12 mol %)[5] under an argon atmosphere. The substrate **1a** was consumed after 210 min. Chromatographic purification afforded a mixture of saturated and unsaturated six-membered-ring lactones (**4a** and **5a**, 68:32) in 76% combined yield (Scheme 1).[6] The reaction occurred at 140 °C even under an atmosphere of carbon monoxide to give an analogous result.[7]

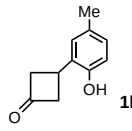
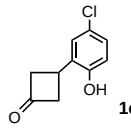
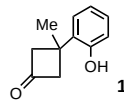


Scheme 1. Reaction of **1a** to give six-membered-ring lactones and the postulated mechanism for this reaction.

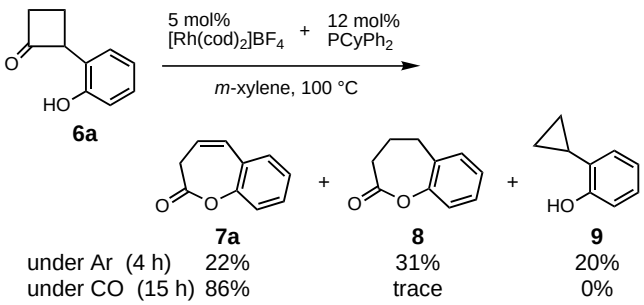
The following mechanism explains the formation of the six-membered-ring lactones from **1a**. Rhodium initially undergoes insertion between the carbonyl carbon and the α-carbon atom to afford the five-membered (acyl)rhodium intermediate **2**. The phenolic hydroxy group then reacts with the acyl group on rhodium to form the six-membered-ring lactone **3**.[8] Direct reductive elimination produces the saturated lactone **4a**. The other product, unsaturated lactone **5a**, is formed from **3** through β-hydride elimination and subsequent isomerization to an α,β-unsaturated system.

Other examples of the rhodium-catalyzed six-membered ring lactone formation are listed in Table 1. Both substrates having methyl (entry 1; Table 1) and chloro (entry 2; Table 1) groups as the phenol substituent afforded the corresponding six-membered-ring lactones as a mixture of saturated **4** and unsaturated **5** in good combined yield. In the case of **1d**, which is equipped with an additional methyl group at the 3-position, β-hydride elimination is inaccessible in the intermediate corresponding to **3**, and hence the saturated lactone was the sole product (entry 3; Table 1).

Table 1. Rhodium-catalyzed six-membered-ring lactone formation.

Entry	**1**	Time [h]	**4**:**5**	Yield of **4** + **5** [%]
1	 **1b**	9	81:19	68
2	 **1c**	4	85:15	82
3	 **1d**	24	100:0	57

A cyclobutanone possessing an *o*-substituted phenol group at the 2-position (**6a**)[9] was also examined. The reaction of **6a** proceeded under milder conditions (100 °C), and more interestingly, a mixture of the seven-membered-ring lactones **7a** and **8** was obtained together with the cyclopropane **9** (Scheme 2). When an analogous reaction was carried out under



Scheme 2. Rhodium-catalyzed reaction of **6a** under Ar and CO atmospheres.

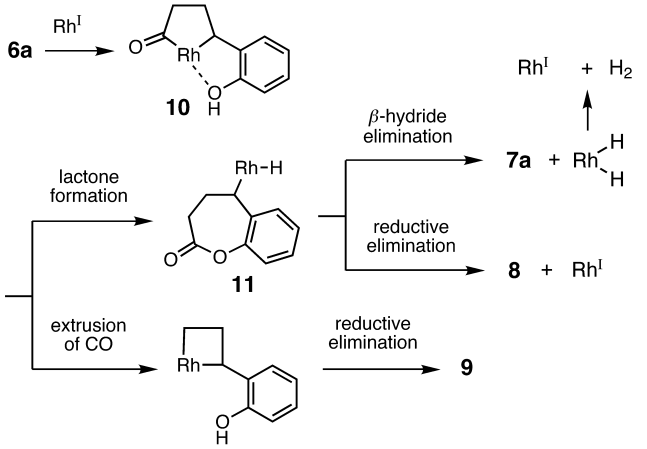
[*] Prof. M. Murakami, Prof. Y. Ito, T. Tsuruta
Department of Synthetic Chemistry and Biological Chemistry
Kyoto University
Yoshida, Kyoto 606-8501 (Japan)
Fax: (+81) 75-753-5668
E-mail: murakami@sbchem.kyoto.u.ac.jp
yoshi@sbchem.kyoto-u.ac.jp

[**] We thank Dr. T. Tanaka (Kyoto University) for GC analysis of H_2, and Dr. M. Miura (Osaka University) for helpful discussions. Support from Monbusho (Grant-in-Aid for Scientific Research on Priority Areas, No. 283: Innovative Synthetic Reactions) is gratefully acknowledged.

 © WILEY-VCH Verlag GmbH, D-69451 Weinheim, 2000 1433-7851/00/3914-2484 $ 17.50+.50/0

an atmosphere of carbon monoxide instead of an argon atmosphere, the unsaturated lactone **7a** was selectively obtained in 86% yield, [10] and only a trace of **8** was formed. The decarbonylation to **9** was completely suppressed under these conditions. In addition, nearly quantitative evolution of dihydrogen from the reaction mixture was detected by GC analysis.

A mechanistic scheme postulated to explain these results is shown in Scheme 3. Initially, the phenolic hydroxy group of **6a** coordinates to the rhodium atom, bringing it into proximity to



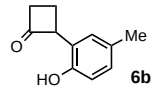
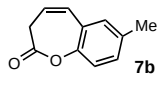
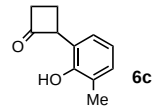
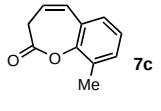
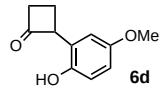
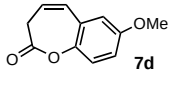
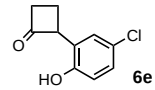
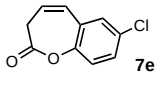
Scheme 3. The postulated mechanism for the formation of **7a**, **8**, and **9** from **6a**.

the α-C–C bond of the carbonyl group. Insertion of the rhodium atom into this bond is thus facilitated and affords the five-membered (acyl)rhodium intermediate **10**, which can react in two ways. Extrusion of the carbonyl group from the rhodacycle followed by reductive elimination affords cyclopropane **9**. It seems reasonable that this process is disfavored in a CO atmosphere. Alternatively, the hydroxy group of **10** can react intramolecularly with the (acyl)rhodium group to form the seven-membered-ring lactone **11**. Direct reductive elimination forms the saturated lactone **8**, while β-hydride elimination yields **7a**. The resulting rhodium(III) dihydride complex evolves dihydrogen by reductive elimination to regenerate the rhodium(I) catalyst. It is plausible to assume that the β-hydride elimination from **11** is intrinsically reversible and that carbon monoxide acts as a ligand for rhodium expelling the produced **7a** from the coordination sphere, and promoting this process forward irreversibly. Thus, the reaction under a CO atmosphere gives **7a** selectively.

The different rates of reactions of the substrates **1a** and **6a** are noteworthy. The reaction of **1a** at 100 °C was much slower (6% conversion under Ar after 4 h, no conversion under CO) than that of **6a**. Although the rate-determining step of the lactonization reaction has not been elucidated, it is assumed that, in the case of **6a**, the transition state of the rate-determining step is stabilized more efficiently by the phenolic hydroxy group located closer to the inserting metal, and therefore, the reaction proceeds faster.

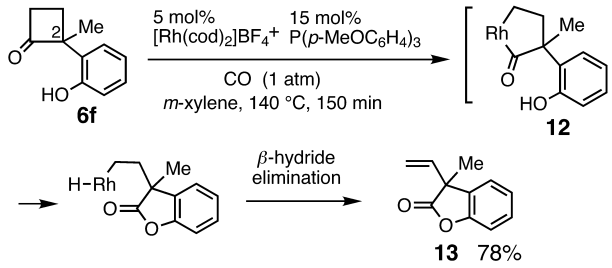
Other examples of the rhodium-catalyzed seven-membered-ring lactone formation are shown in Table 2. The use of tris(*p*-methoxyphenyl)phosphane as the ligand afforded

Table 2. Rhodium-catalyzed seven-membered-ring lactone formation.

Entry	6	Phosphane	Time [h]	7	Yield [%]
1	 **6b**	$P(p\text{-}MeOC_6H_4)_3$	6	 **7b**	91
2	 **6c**	$P(p\text{-}MeOC_6H_4)_3$	24	 **7c**	87
3	 **6d**	$PCyPh_2$	24	 **7d**	92
4	 **6e**	$PCyPh_2$	12	 **7e**	77

better results than $PCyPh_2$ in some cases. When the pendant phenol group has an additional electron-donating substituent such as methyl and methoxy, the corresponding seven-membered-ring lactone was obtained in high yield (entries 1–3; Table 2). Substrate **6e** with a *p*-chlorophenol group afforded **7e** in slightly lower yield (77%, entry 4; Table 2).

For comparison, an analogous reaction was carried out using cyclobutanone **6f** which had a methyl substituent in addition to a phenol group at the 2-position. Unlike the case of **6a**, no reaction occurred at 100 °C. The reaction at an elevated temperature (140 °C) afforded the five-membered-ring lactone **13** (Scheme 4). None of the seven-membered-ring lactone was observed. The additional steric constraints



Scheme 4. Reaction of **6f** to give five-membered-ring lactone **13** and the postulated mechanism for this reaction.

introduced by the extra methyl substituent at the 2-position hampered the cleavage of the proximal α-C–C bond. Instead the initial rhodium insertion was transposed to the less substituted C–C bond on the far side, affording rhodacycle **12**. Subsequently, a five-membered-ring lactone linkage is formed. The following β-hydride elimination produces the lactone **13**. It is likely that the assistance of the phenolic hydroxy group of **6f** coordinating to the inserting rhodium center is reduced for geometrical reasons, as with the case of **1a**. Thus, an elevated temperature was required for the insertion.

In summary, new catalytic C–C bond cleaving reactions were developed in which a phenol group serves as a coordinating ligand to facilitate the catalytic activation of a

 © WILEY-VCH Verlag GmbH, D-69451 Weinheim, 2000 1433-7851/00/3914-2485 $ 17.50+.50/0

C–C single bond. Whereas the substrates presently employed benefit from relief of the structural strain,[11] the construction of seven-membered ring lactone skeletons fused to aromatic rings is of synthetic value because of the presence of these subunits in biologically active compounds.

Experimental Section

7b: To a mixture of $[Rh(cod)_2]BF_4$ (6.0 mg, 15 μmol) and tris(*p*-methoxyphenyl)phosphane (9.6 mg, 36 μmol) in *m*-xylene (5 mL) under N_2 at room temperature were successively added 2-(2-hydroxy-5-methylphenyl)cyclobutanone (**6b**, 52.9 mg, 0.30 mmol) and *m*-xylene (5 mL). After the N_2 atmosphere was replaced with CO, the mixture was heated at 100 °C for 6 h. The reaction mixture was cooled and then passed through a pad of Florisil to remove the insoluble materials. The eluent was evaporated under vacuum, and the residue was subjected to preparative TLC (silica gel, ethyl acetate/hexane 1/5) to afford **7b** (47.3 mg, 91 %) as a colorless oil. ^{1}H NMR ($CDCl_3$, 300 MHz): $\delta = 2.36$ (s, 3H), 3.05 (d, $J = 6.6$ Hz, 2H), 6.03 (dt, $J = 9.9$, 6.6 Hz, 1H), 6.83 (d, $J = 9.9$ Hz, 1H), 7.09–7.20 (m, 3H); ^{13}C{^{1}H} NMR ($CDCl_3$, 75 MHz): $\delta = 20.6$, 34.2, 120.9, 122.8, 126.7, 129.9, 130.1, 134.5, 148.3, 169.0; IR (neat): $\tilde{\nu} = 1752\ cm^{-1}$; elemental analysis calcd for $C_{11}H_{10}O_2$: C 75.84, H 5.79; found: C 75.97, H 5.77.

Received: February 16, 2000 [Z 14720]

[1] Reviews: a) R. H. Crabtree, *Chem. Rev.* **1985**, *85*, 245; b) B. Rybtchinski, D. Milstein, *Angew. Chem.* **1999**, *111*, 918; *Angew. Chem. Int. Ed.* **1999**, *38*, 870; c) M. Murakami, Y. Ito in *Activation of Unreactive Bonds and Organic Synthesis* (Ed.: S. Murai), Springer, Berlin, **1999**, p. 97.

[2] a) M. Murakami, H. Amii, Y. Ito, *Nature* **1994**, *370*, 540; b) M. Murakami, H. Amii, K. Shigeto, Y. Ito, *J. Am. Chem. Soc.* **1996**, *118*, 8285; c) M. Murakami, K. Takahashi, H. Amii, Y. Ito, *J. Am. Chem. Soc.* **1997**, *119*, 9307; d) M. Murakami, T. Itahashi, H. Amii, K. Takahashi, Y. Ito, *J. Am. Chem. Soc.* **1998**, *120*, 9949.

[3] a) T. Satoh, J.-i. Inoh, Y. Kawamura, Y. Kawamura, M. Miura, M. Nomura, *Bull. Chem. Soc. Jpn.* **1998**, *71*, 2239; b) K. Kokubo, K. Matsumasa, Y. Nishinaka, M. Miura, M. Nomura, *Bull. Chem. Soc. Jpn.* **1999**, *72*, 303; c) T. Satoh, T. Itaya, M. Miura, M. Nomura, *Chem. Lett.* **1996**, 823; d) M. Hirano, N. Kurata, T. Marumo, S. Komiya, *Organometallics* **1998**, *17*, 501.

[4] The cyclobutanone **1a** was prepared by [2+2] cycloaddition of *o*-(methoxymethoxy)styrene with dichloroketene and the subsequent treatment with zinc in acetic acid.

[5] A cationic rhodium(I) complex having two $PCyPh_2$ ligands per rhodium atom is postulated as the catalytic species. No reaction occurred in the absence of the rhodium catalyst.

[6] The ratio of **4a** to **5a** changed little (68:32–75:25), when other catalyst systems like $[Rh(cod)_2]BF_4/PPh_3$, $[Rh(cod)_2]BF_4/P(p\text{-methoxyphenyl})_3$, and $[Rh(cod)(Ph_2PCH_2CH_2PPh_2)]BF_4$ were used.

[7] The reactions previously reported[2] normally failed to occur under a CO atmosphere.

[8] a) M. Hidai, K. Ishimi, M. Iwase, E. Tanaka, Y. Uchida, *Tetrahedron Lett.* **1973**, 1189; b) R. Grigg, T. R. B. Mitchell, S. Sutthivaiyakit, *Tetrahedron* **1981**, *37*, 4313.

[9] The cyclobutanone **6a** was prepared according to the literature procedure: B. M. Trost, M. J. Bogdanowicz, *J. Am. Chem. Soc.* **1973**, *95*, 5321.

[10] The formation of the corresponding α,β-unsaturated isomer was not observed.

[11] With less strained substrates like 2-(2-hydroxyphenyl)cyclopentanone, an analogous reaction failed to occur.

Ligand Electronic Effect in Enantioselective Palladium-Catalyzed Copolymerization of Carbon Monoxide and Propene**

Céline Gambs, Stanislav Chaloupka, Giambattista Consiglio,* and Antonio Togni*

The alternating copolymerization of olefins with carbon monoxide (CO) catalyzed by cationic palladium(II) complexes modified by diphosphane ligands has attracted considerable interest due to the potential use of the produced polyketones as new materials.[1–7] Recently, a terpolymer derived from ethene, propene, and CO has become commercially available under the trade name of Carilon.

When propene is used as the substrate, control of regio- and stereoselectivity of the olefin insertion is required to obtain stereoregular alternating copolymers.[8, 9] Recently, a few examples of successful, highly enantioselective CO/propene copolymerizations have been reported, using either in situ or preformed Pd^{II} complexes containing chiral phosphorus ligands.[10–12] Among the catalysts studied the most active ever reported to date (productivity of about $905\ g\,g(Pd)^{-1}\,h^{-1}$) contained $(R)(S_p)$-1-[2-(diphenylphosphanyl)ferrocenyl]-ethyldicyclohexylphosphane (Josiphos) as the modifying ligand.[13, 14] With this system both a very high regioregularity (>99 % head-to-tail enchainments) and stereoregularity (>96 % of isotactic diads) were achieved. Thus, despite contrasting proposals,[15] and a precedent example of a system with low catalytic activity,[16] the best combination of donor groups in the chelate diphosphane ligand seems to be that of two electronically nonequivalent ligand fragments: a basic PCy_2 group to ensure high regioselective incorporation of propene and a slightly acidic PPh_2 donor.

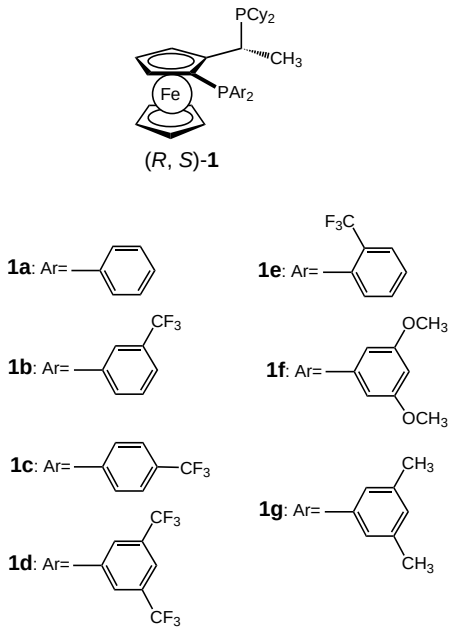
Since planar-chiral ferrocenyl ligands represent a system that is synthetically easy to modify, and 1) in view of investigating possible electronic effects on both the copolymer structure and the performance of the catalyst, and 2) to gain insight on the role of electronic differentiation of the two binding sites in these ligands,[17, 18] we prepared a series of related chiral diphosphanes **1a–g** (Scheme 1) according to already published general methods.[19–22] Here we report extremely active Pd^{II} systems bearing chiral ferrocenyl diphosphanes **1b–d** for highly enantioselective alternating copolymerization of propene and carbon monoxide.

Thus, in typical experiments, in situ Pd^{II} systems prepared by reacting $Pd(OAc)_2$ with ligands **1a–g** and $BF_3 \cdot Et_2O$ in CH_2Cl_2–MeOH were investigated (Scheme 2). In fact, ^{31}P

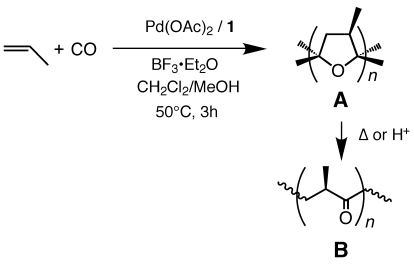
[*] Prof. G. Consiglio
Laboratorium für Technische Chemie der ETH Zürich
Universitätstrasse 6, 8092 Zürich (Switzerland)
Fax: (+41) 1-632-11-62
E-mail: consiglio@tech.chem.ethz.ch
Prof. A. Togni, C. Gambs, S. Chaloupka
Laboratorium für Anorganische Chemie der ETH Zürich
Universitätstrasse 6, 8092 Zürich (Switzerland)
Fax: (+41) 1-632-10-90
E-mail: togni@inorg.chem.ethz.ch

[**] This work was supported by the ETH Zürich. We thank Novartis AG and Solvias AG, Basel, for the donation of chemicals.

 © WILEY-VCH Verlag GmbH, D-69451 Weinheim, 2000 1433-7851/00/3914-2486 $ 17.50+.50/0



Scheme 1. Modified ferrocenyl ligands of the Josiphos-type used in the Pd-catalyzed CO/propene copolymerization.



Scheme 2. CO/propene copolymerization catalyzed by Pd^{II} systems.

NMR studies on the catalyst mixture containing Josiphos indicated first the formation of the [Pd(Josiphos)$(OAc)_2$] adduct and, following the addition of the Lewis acid $BF_3 \cdot Et_2O$, the generation of a dicationic Pd^{II} species [Pd(Josiphos)$(L)_2]^{2+}$ (L = solvent molecule).[23] Noncoordinating dichloromethane was the solvent of choice, and small amounts of methanol were required as activator. The results of CO/propene copolymerization reactions are presented in Table 1.

Table 1. CO/propene copolymerizations.[a]

Ligand	Productivity [g g(Pd)$^{-1}$ h^{-1}]	Regio-regularity [%]	Stereo-regularity (l-diads) [%]	$[\alpha]_D$[b]	$\Delta\varepsilon$ (CD)[c]	M_n[d]
1a	369	> 99	94 – 95	– 24.5	0.84	9410
1b	1044	> 99	97.5	– 27.4	1.20	14710
1c	1160	> 99	96.8	– 29.8	1.23	10670
1d	1797	> 99	97.5	– 34.6	1.26	13990
1e	–[e]	–[f]	–[f]	–[f]	–[f]	–[f]
1f	50	99	90 – 92	– 21.5	0.76	9530
1g	223	> 99	93 – 94	– 16.0	0.49	10360

[a] Reaction conditions: $Pd(OAc)_2$ (0.02 mmol), **1a – g** (0.024 mmol), $BF_3 \cdot Et_2O$ (0.040 mmol), CH_2Cl_2/CH_3OH (25/2 mL), propene (11 g), $p(CO) = 75$ bar, $T = 50\,^{\circ}C$, $t = 3$ h. [b] Measured in HFIP. [c] Measured in HFIP; 1 – 2 mg mL^{-1} concentration range. [d] Determined by integration of end groups in the ^1H NMR spectrum. [e] Very low. [f] Not determined.

Under the reaction conditions applied the copolymers grow exclusively as poly[spiro-2,5-(3-methyltetrahydrofuran)] (**A**), which is known to be formed in the presence of protic solvents (Figure 1).[10, 12] Highly regio- and stereoregular CO/Propene

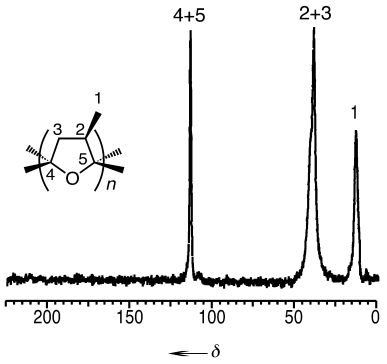


Figure 1. ^{13}C MAS solid-state NMR spectrum of poly[spiro-2,5-(3-methyltetrahydrofuran)] **A**, at room temperature.

copolymers have been obtained with all the ligands tested with the exception of **1e**. The degree of regio- and stereoselectivity was evaluated from the ^{13}C NMR spectrum in [D_2]1,1,1,3,3,3-hexafluoropropan-2-ol ([D_2]HFIP), in which the copolymer exists as a poly[2-methyl-3-oxopropane-1,3-diyl] (**B**), in the region of resonances of the carbonyl groups (Figure 2). Signals of carbonyl carbons of head-to-head and

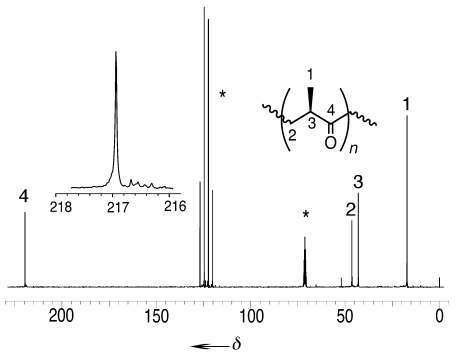


Figure 2. ^{13}C NMR spectrum of the copolymer dissolved in [D_2]HFIP (insert: CO region), indicating a highly regioselective incorporation of propene (> 99 % head-to-tail) and a very high enantioface discrimination (> 96 %). Asterisks indicate signals attributed to the solvent.

tail-to-taildiads were completely absent;[8] moreover, the sharpness of the carbonyl band, which was attributed to an isotactic pentad,[24] and the high optical activity of the copolymers are consistent with a highly isotactic structure.[25, 26]

Increasing the electronic differentiation of the two P atoms causes drastic changes in the catalyst activity. The highest productivity (1797 g polymer per gram Pd per hour [g g(Pd)$^{-1}$ h^{-1}]) is obtained with ligand **1d**, a 3,5-bis(trifluoromethyl)phenylphosphane derivative. On the other hand, its analogue **1f**, bearing the electron-donating methoxy groups instead of the electron-withdrawing trifluoromethyl groups, showed very low productivity (50 g g(Pd)$^{-1}$ h^{-1}). Thus, the effect of an enhanced π-acidity of the arylphosphane, which decreases the electron density at palladium, results in an

 © WILEY-VCH Verlag GmbH, D-69451 Weinheim, 2000 1433-7851/00/3914-2487 $ 17.50+.50/0

increase of reaction rate. Steric effects are also evident. When the trifluoromethyl substituent is located in the *ortho* position (**1e**) only low-molecular-weight oligomers are obtained in a very low yield. Thus, placing the CF_3 group in the phenyl *meta* or *para* positions (**1b**–**d**) does not drastically influence the steric properties of the ligands and constitutes the modification of choice for the formation of highly efficient systems for the CO/propene copolymerization reaction.

Whereas electronic effects on the stereoselectivity of several different catalytic asymmetric reactions have been observed before,[21, 22, 27–29] a comparable influence on the catalytic activity has been reported in particular for Rh-catalyzed hydroformylation.[30–33] Because of the C_1 symmetry of the ligands, we believe that the isomeric intermediates containing CO and/or the olefin coordinated to Pd display significantly different reactivities. When the complex $[(\mathbf{1d})PdMe]^+$ is placed under a CO atmosphere the product $[(\mathbf{1d})Pd(CO)COMe]^+$ is formed through a highly regioselective coordination of the acyl moiety *trans* to the PAr_2 group.[16] The electrophilicity of the metal center, and hence that of the coordinated substrates should be higher in the case of the ligands bearing more electron-withdrawing PAr_2 groups. This also should coincide with a lower binding energy of the substrate. In contrast to other catalytic systems,[34] in fact, the kinetic order of the copolymerization with respect to carbon monoxide is positive. The crucial assumption sustaining the electronic effect on activity is that the configurational isomers in which the monomers are coordinated *trans* to the PAr_2 groups should be more reactive by virtue of their increased electrophilicity in this position. Furthermore, it has to be noted that in catalytic polyketone synthesis the electrophilicity of the metal center needs to be carefully balanced in order for olefins to compete with CO as ligands. Thus, for ligands containing a basic PAr_2 group, such as **1f**, CO is likely to bind more strongly to the Pd^{II} center, leading to a drastic decrease of the overall rate.

In conclusion, Pd^{II} systems combined with sterically very similar chiral ferrocenyl ligands **1a**–**g** (except **1e**) produce almost completely isotactic copolymers from propene and CO in a highly enantioselective fashion. Only small variations in enantioface discrimination were observed, whereas drastic changes in catalytic activity were noted by changing the electronic properties of the PAr_2 substituent.

Received: March 10, 2000 [Z14831]

[1] F. Garbassi, *CHEMTECH* **1999**, *Oct*, 48–53.
[2] H. Seifert, *Kunstoffe* **1998**, *88*, 1154–1157.
[3] A. Gray, *Chem. Br.* **1998**, *March*, 44–45.
[4] A. Sommazzi, F. Garbassi, *Prog. Polym. Sci.* **1997**, *22*, 1547–1605.
[5] E. Drent, P. H. M. Budzelaar, *Chem. Rev.* **1996**, *96*, 663–681.
[6] A. Wakker, H. G. Kormelink, P. Verbeke, J. C. M. Jordaan, *Kunststoffe* **1995**, *85*, 1056–1064.
[7] A. Sen, *Acc. Chem. Res.* **1993**, *26*, 303–310.
[8] A. Batistini, G. Consiglio, U. W. Suter, *Angew. Chem.* **1992**, *104*, 306–3075; *Angew. Chem. Int. Ed. Engl.* **1992**, *31*, 303–305.
[9] K. Nozaki, T. Hiyama, *J. Organomet. Chem.* **1999**, *576*, 248–253.
[10] A. Batistini, G. Consiglio, *Organometallics* **1992**, *11*, 1766–1769.
[11] K. Nozaki, N. Sato, H. Takaya, *J. Am. Chem. Soc.* **1995**, *117*, 9911–9912.
[12] Z. Jiang, A. Sen, *J. Am. Chem. Soc.* **1995**, *117*, 4455–4467.
[13] S. Bronco, G. Consiglio, S. Di Benedetto, E. Drent, E. Drent, H. J. Heeres (Shell), GB-B 2 289 855, **1995**.
[14] S. Bronco, G. Consiglio, S. Di Benedetto, M. Fehr, F. Spindler, A. Togni, *Helv. Chim. Acta* **1995**, *78*, 883–886.
[15] P. W. N. M. van Leeuwen, C. F. Roobeek, H. van der Heijden, *J. Am. Chem. Soc.* **1994**, *116*, 12117–12118.
[16] K. Nozaki, N. Sato, Y. Tonomura, M. Yasutomi, H. Takaya, T. Hijama, T. Matsubara, N. Koga, *J. Am. Chem. Soc.* **1997**, *119*, 12779–12795.
[17] A. Togni, C. Breutel, A. Schnyder, F. Spindler, H. Landert, A. Tijani, *J. Am. Chem. Soc.* **1994**, *116*, 4062–4066.
[18] A. Togni, *Angew. Chem.* **1996**, *108*, 1581–1583; *Angew. Chem. Int. Ed. Engl.* **1996**, *35*, 1475–1477.
[19] A. Togni, S. D. Pastor, *Helv. Chim. Acta* **1989**, *72*, 1038–1042.
[20] A. Schnyder, L. Hintermann, A. Togni, *Angew. Chem.* **1995**, *107*, 996–998; *Angew. Chem. Int. Ed. Engl.* **1995**, *34*, 931–933.
[21] A. Schnyder, A. Togni, U. Wiesli, *Organometallics* **1997**, *8*, 255–260.
[22] G. Pioda, A. Togni, *Tetrahedron: Asymmetry* **1998**, *9*, 3903–3910.
[23] M. Sperrle, G. Consiglio, *J. Am. Chem. Soc.* **1995**, *117*, 12130–12136.
[24] S. Bronco, G. Consiglio, *Macromol. Chem. Phys.* **1995**, *197*, 355–365.
[25] S. Bronco, G. Consiglio, R. Hutter, A. Batistini, U. W. Suter, *Macromolecules* **1994**, *27*, 4436–4440.
[26] K. Nozaki, M. Yasutomi, K. Nakamoto, T. Hiyama, *Polyhedron* **1998**, *17*, 1159–1164.
[27] A. L. Casalnuovo, T. V. RajanBabu, T. A. Ayers, T. H. Warren, *J. Am. Chem. Soc.* **1994**, *116*, 9869–9882.
[28] T. V. RajanBabu, A. L. Casalnuovo, *J. Am. Chem. Soc.* **1996**, *118*, 6325–6326.
[29] D. S. Clyne, Y. C. Mermet-Bouvier, N. Nomura, T. V. RajanBabu, *J. Org. Chem.* **1999**, *64*, 7601–7611.
[30] C. P. Casey, E. L. Paulsen, E. W. Beuttenmueller, B. R. Proft, L. M. Petrovich, B. A. Matter, D. R. Powell, *J. Am Chem. Soc.* **1997**, *119*, 11817–11825.
[31] L. A. van der Veen, M. D. K. Boele, F. R. Bregman, P. C. J. Kamer, P. W. N. M. van Leeuwen, K. Goubitz, J. Fraanje, H. Schenk, C. Bo, *J. Am. Chem. Soc.* **1998**, *120*, 11616–11626.
[32] C. P. Casey, E. L. Paulsen, E. W. Beuttenmueller, B. R. Proft, B. A. Matter, D. R. Powell, *J. Am. Chem. Soc.* **1999**, *121*, 63–70.
[33] D. R. Palo, C. Erkey, *Organometallics* **2000**, *19*, 81–86.
[34] M. Brookhart, M. I. Wagner, *J. Am. Chem. Soc.* **1996**, *118*, 7219–7220.

Versatile Indole Synthesis by a 5-*endo-dig* Cyclization Mediated by Potassium or Cesium Bases**

Alain Louis Rodriguez, Christopher Koradin, Wolfgang Dohle, and Paul Knochel*

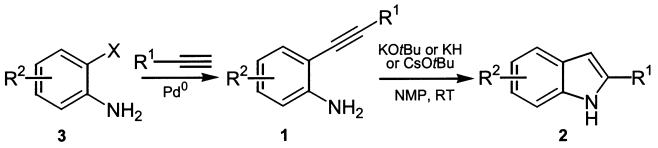
The addition of heteroatomic nucleophiles to triple bonds is an important reaction that often requires a high activation energy.[1] Intramolecular additions proceed more readily and a recent hydroamination of *o*-chlorostyrenes followed by

[*] Prof. Dr. P. Knochel, Dr. A. L. Rodriguez, Dipl.-Chem. C. Koradin, Dipl.-Chem. W. Dohle
Department Chemie, Universität München
Butenandtstraße 5–13, 81377 München (Germany)
Fax: (+49) 89-2180-7680
E-mail: Paul.Knochel@cup.uni-muenchen.de

[**] We thank the DFG (Leibniz-Programm) and the Fonds der Chemischen Industrie for generous financial support. A.L.R. and C. K. thank the Humboldt-Foundation and the BASF AG, respectively, for fellowships. W.D. was supported by the BMBF program (03 D 0056 2). We thank Dr. J. Henkelmann (BASF AG) for helpful discussions and the BASF AG for the generous gift of chemicals.

 © WILEY-VCH Verlag GmbH, D-69451 Weinheim, 2000 1433-7851/00/3914-2488 $ 17.50+.50/0

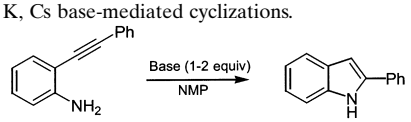
cyclization has provided an elegant access to indolines.[2] The palladium-catalyzed synthesis of indoles starting from 2-alkynylanilines of type **1**[3] or more frequently from their corresponding trifluoroacetamides has been well studied.[4] A molybdemum(0)-catalyzed cyclization of compounds **1** to indoles **2** has been reported.[5] Recently,[6] we have reported the high catalytic activity of $CsOH \cdot H_2O$[7] for promoting the addition of anilines or alcohols to alkynes or styrenes. Herein, we report a new mild synthesis of 2-substituted indoles of type **2** mediated by potassium or cesium bases in *N*-methylpyrrolidinone (NMP; Scheme 1).



Scheme 1. Base-mediated indole synthesis.

The scope of the reaction is broad and most of these ring closures are complete within a few hours at room temperature. Initial studies have shown that the strong base $CsOH \cdot H_2O$ is an effective base for the cyclization of 2-(2-phenylethynyl)aniline (**1a**); however, a reaction temperature of 90 °C was required for the completion of the reaction (Table 1). Similarly finely powdered KOH or NaOEt[8] led only to sluggish reactions below 80 °C. In strong contrast, soluble potassium or cesium alkoxides such as KO*t*Bu[9] or CsO*t*Bu[10] as well as KH[11] in NMP led to a fast reaction at room temperature (3–12 h). These mild reaction conditions allow the presence of various functionalities in the starting (2-alkynyl)anilines of type **1** and enables the preparation of a range of polyfunctional indoles (Table 2).

Table 1. Na, K, Cs base-mediated cyclizations.

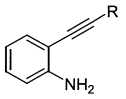
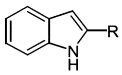
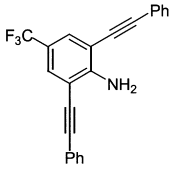
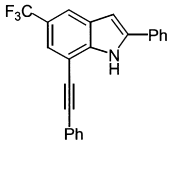
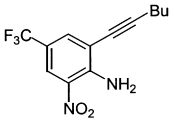
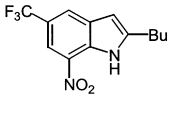
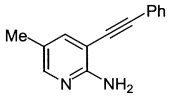
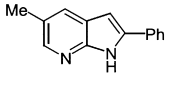
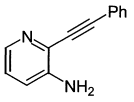
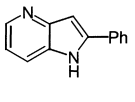
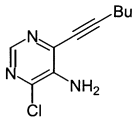
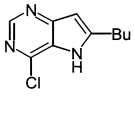
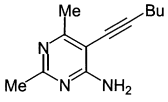
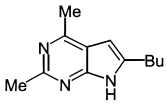
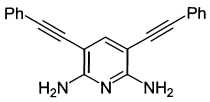
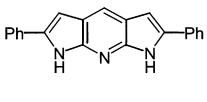
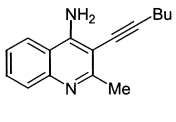
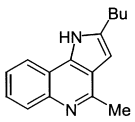


Base	*T* [°C]	*t* [h]	Yield [%][a]
NaH	60	8	< 5
NaOEt	80	15	66
KO*t*Bu	25	4	79
KH	25	5	72
CsOH	90	5	68
CsO*t*Bu	25	5	71

[a] Yield of isolated analytically pure **2a**.

The precursors **1** were prepared by the Sonogashira cross-coupling[12] of the corresponding (2-iodo- or 2-bromoanilines **3** with 1-alkynes in satisfactory to excellent yields. Various 2-substituted indoles are conveniently prepared either by using KH (1.3–2.1 equiv; Method A) or KO*t*Bu (1.3–1.7 equiv; Method B). An excess of base is necessary in these cyclizations since the final product is an unreactive potassium salt of indoles **2**. It is not basic enough to deprotonate a further molecule of starting material **1**. Several functional groups such as a hydroxy (entry 5; Table 2), an acetal (entry 6;

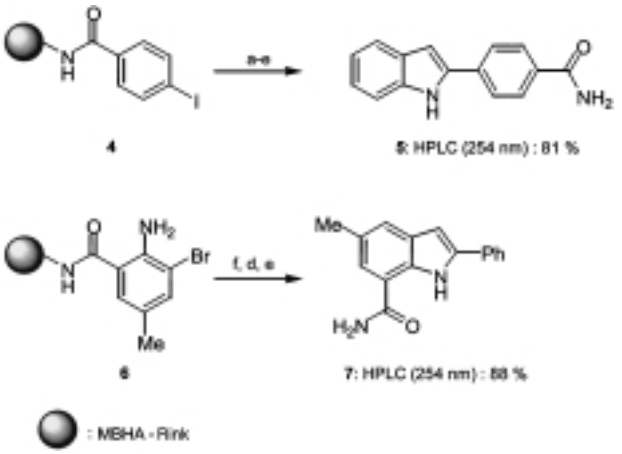
Table 2. Functionalized indoles **2a**–**r** obtained by the cyclization of the aniline derivatives **1a**–**r** in the presence of KH (Method A) or KO*t*Bu (Method B) at room temperature.

Entry	Aniline **1**	Indole **2**	Method[a]	Yield [%][b]
				
1	**1a**: R = Ph	**2a**: R = Ph	A (B)	72 (79)
2	**1b**: R = Bu	**2b**: R = Bu	A (B)	76 (78)
3	**1c**: R = 1-cyclohexenyl	**2c**: R = 1-cyclohexenyl	A	67
4	**1d**: R = H	**2d**: R = H	B	62
5	**1e**: R = $(CH_2)_2OH$	**2e**: R = $(CH_2)_2OH$	A	61
6	**1f**: R = $CH(OEt)_2$	**2f**: R = $CH(OEt)_2$	B	81
7	**1g**: R = 2-thienyl	**2g**: R = 2-thienyl	A	70
8	**1h**: R = 2-thiazolyl	**2h**: R = 2-thiazolyl	A	61
9	**1i**: R = 3-chloropropyl	**2i**: R = cyclopropyl	A	75
10	**1j**: R = 2-aminophenyl	**2j**: R = 2-aminophenyl	A	82
				
11	**1k**	**2k**	A	80
				
12	**1l**	**2l**	B	77
				
13	**1m**	**2m**	A	72
				
14	**1n**	**2n**	A	74
				
15	**1o**	**2o**	B	78
				
16	**1p**	**2p**	B	61[c]
				
17	**1q**	**2q**	B	80[d]
				
18	**1r**	**2r**	B	90[d]

[a] Method A: KH (1.3–1.7 equiv), NMP, room temperature, 3–12 h. Method B: KO*t*Bu (1.3–2.1 equiv), NMP, room temperature, 3–12 h. [b] Yields of isolated analytically pure products. [c] $T = 60$ °C, $t = 5$ h. [d] $T = 80$ °C, $t = 6$ h.

 © WILEY-VCH Verlag GmbH, D-69451 Weinheim, 2000 1433-7851/00/3914-2489 $ 17.50+.50/0

Table 2), an additional amino group (entry 10; Table 2), an alkyne (entry 11; Table 2), or a nitro group (entry 12; Table 2) are tolerated. When the alkyne bears a 3-chloropropyl substituent (entry 9; Table 2), a cyclopropanation occurs after cyclization providing 2-cyclopropylindole (**2i**) in 75% yield. Remarkably, this cyclization reaction can be extended to various heterocyclic precusors such as the aminopyridines **1m** and **1n** (entries 15 and 16; Table 2). In all cases, a smooth cyclization occurs under similar reaction conditions (Method A or Method B) providing new types of heterocycles of interest for pharmaceutical applications. It was also possible to perform this ring closure on solid phase. Thus, 4-iodobenzamide attached to a Rink–MBHA resin **4** undergoes a smooth Sonogashira reaction[13] with (trimethylsilyl)acetylene. After desilylation a second cross-coupling with 2-iodoaniline provides the expected precursor for cyclization. Treatment with KO*t*Bu (15 equiv) in NMP (25 °C, 24 h) affords the indole **5** in 81% purity after cleavage from the resin. Similarly, the Rink–MBHA resin attached 2-bromoaniline derivative **6** was converted to the 2-phenyl-substituted indole **7** (88% purity after cleavage from the resin) using an analogeous reaction sequence (Scheme 2).



Scheme 2. Solid-phase synthesis of indoles.

In summary, the combination of KO*t*Bu, KH, or CsO*t*Bu with the polar solvent NMP allows a smooth preparation of various indoles and azaindoles by a 5-*endo-dig* cyclization.[14, 15]

Experimental Section

Typical procedure for the preparation of 2-phenylindole (**2a**): Method A: To a stirred solution of potassium hydride (42 mg, 1.05 mmol) in NMP (4 mL) was added under argon (2-phenylethynyl)aniline (**1a**) (97 mg, 0.50 mmol) in NMP (1 mL). The reaction mixture was vigorously stirred for 5 h at room temperature. Water (1 mL) and dichloromethane (50 mL) were added, and the resulting solution was washed with a saturated NaCl solution, dried ($MgSO_4$), and concentrated under reduced pressure. The residue was purified by flash chromatography (silica gel, dichloromethane/pentane 7/3) to give 2-phenylindole (**2a**) (73 mg, 0.36 mmol, 72% yield; m.p. 171–175 °C).

Method B: The reaction was carried out as above using potassium *tert*-butoxide (73 mg, 0.65 mmol) instead of potassium hydride. The reaction was stirred for 4 h at room temperature. After the same workup procedure as described for method A, the product **2a** (76 mg, 0.39 mmol) was obtained in 79% yield.

Received: December 23, 1999 [Z14460]

[1] a) T. E. Müller, M. Beller, *Chem. Rev.* **1998**, *98*, 675; b) M. Beller, T. H. Riermeier in *Transition Metals for Organic Synthesis* (Eds.: M. Beller, C. Bolm), Wiley-VCH, **1998**; c) J. H. Teles, S. Brode, M. Chabanas, *Angew. Chem.* **1998**, *110*, 1475; *Angew. Chem. Int. Ed.* **1998**, *37*, 1415; d) B. F. Kukharev, V. K. Stankevich, G. R. Klimenko, *Russ. J. Org. Chem.* **1993**, *29*, 2005.

[2] M. Beller, C. Breindl, T. H. Riermeier, M. Eichberger, H. Trauthwein, *Angew. Chem.* **1998**, *110*, 3571; *Angew. Chem. Int. Ed.* **1998**, *37*, 3389; b) see also M. Beller, M. Eichberger, H. Trauthwein, *Angew. Chem.* **1997**, *109*, 2306; *Angew. Chem. Int. Ed. Engl.* **1997**, *36*, 2225; c) M. Beller, O. R. Thiel, H. Trauthwein, *Synlett* **1999**, 243.

[3] a) K. Iritani, S. Matsubara, K. Utimoto, *Tetrahedron Lett.* **1988**, *29*, 1799. For other recent indole synthesis, see: b) B. Witulski, T. Stengel, *Angew. Chem.* **1999**, *111*, 2521; *Angew. Chem. Int. Ed.* **1999**, *38*, 2426; c) M. T. Baumgartner, M. A. Nazareno, M. C. Murguia, A. B. Pierini, R. A. Rossi, *Synthesis* **1999**, 2053; d) Y. Kondo, S. Kojima, T. Sakamoto, *J. Org. Chem.* **1997**, *62*, 6507.

[4] a) A. Arcadi, S. Cacchi, F. Marinelli, *Tetrahedron Lett.* **1992**, *33*, 3915; b) S. Cacchi, G. Fabrizi, F. Marinelli, L. Moro, P. Pace, *Synlett* **1997**, 1363; c) A. Arcadi, S. Cacchi, V. Carnicelli, F. Marinelli, *Tetrahedron* **1994**, *50*, 437.

[5] a) F. E. Mc Donald, A. K. Chatterjee, *Tetrahedron Lett.* **1997**, *38*, 7687; b) F. E. Mc Donald, *Chem. Eur. J.* **1999**, *5*, 3103.

[6] a) D. Tzalis, P. Knochel, *Angew. Chem.* **1999**, *111*, 1547; *Angew. Chem. Int. Ed.* **1999**, *38*, 1463; b) D. Tzalis, C. Koradin, P. Knochel, *Tetrahedron Lett.* **1999**, *40*, 6193.

[7] a) E. E. Dueno, F. Chu, S.-I. Kim, K. W. Jung, *Tetrahedron Lett.* **1999**, *40*, 1843; b) F. Chu, E. E. Dueno, K. W. Jung, *Tetrahedron Lett.* **1999**, *40*, 1847; c) J. Busch-Peterson, Y. Bo, E. J. Corey, *Tetrahedron Lett.* **1999**, *40*, 2065.

[8] The treatment of **1a** with NaOEt in boiling ethanol does not lead to the corresponding indole **2a**, showing that the use of NMP is essential for the direct cyclization of **1a** to **2a**; see also: T. Sakamoto, Y. Kondo, H. Yamanaka, *Heterocycles* **1986**, *24*, 31.

[9] KO*t*Bu has exceptional basic properties: a) M. Schlosser, *Pure Appl. Chem.* **1988**, *60*, 1627; b) M. Schlosser, J. Hartmann, *J. Am. Chem. Soc.* **1976**, *98*, 4674; c) M. Schlosser, G. Rauchschwalbe, *J. Am. Chem. Soc.* **1978**, *100*, 3258.

[10] Cesium *tert*-butoxide is conveniently prepared by the addition of *t*BuOH to cesium in toluene at 0 °C (15 min).

[11] The suspension of KH in NMP may generate the soluble potassium enolate of *N*-methylpyrrolidinone. Reaction products derived from this enolate have been isolated in related cyclization reactions.

[12] a) S. Takahashi, Y. Kuroyama, K. Sonogashira, N. Hagihara, *Synthesis* **1980**, 627; b) T. Sakamoto, M. Shiraiwa, Y. Kondo, H. Yamanaka, *Synthesis* **1983**, 312; c) A. F. Littke, G. C. Fu, *Angew. Chem.* **1999**, *111*, 2568; *Angew. Chem. Int. Ed.* **1999**, *38*, 2411.

[13] M. D. Collini, J. W. Ellingboe, *Tetrahedron Lett.* **1997**, *38*, 7963.

[14] J. E. Baldwin, *J. Chem. Soc. Chem. Commun.* **1976**, 738.

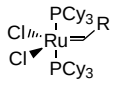
[15] A patent application with the BASF AG has been filed.

 © WILEY-VCH Verlag GmbH, D-69451 Weinheim, 2000 1433-7851/00/3914-2490 $ 17.50+.50/0

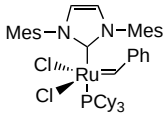
Novel Synthesis of Borane Complexes of Cyclic Phosphanes Using Ruthenium-Catalyzed Olefin Metathesis**

Marc Schuman, Michael Trevitt, Andrew Redd, and Véronique Gouverneur*

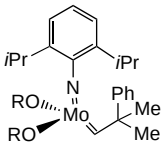
Chiral phosphane ligands are of key importance in catalytic transition metal mediated processes, which have attracted considerable attention in asymmetric synthesis.[1] It is well established that cyclic bisphosphanes and phosphanes, for example 1,2-bis(phospholanyl)benzene (DuPhos), 1,2-bis(phospholanyl)ethane (BPE), and *tert*-butyloxy or benzyloxy-substituted derivatives thereof (RoPhos), have proven to be very efficient ligands in the field of asymmetric catalysis.[2] Owing to the increasing importance of these molecules, there is an ongoing interest in the development of novel methodologies for the preparation of structurally diverse cyclic phosphanes and bisphosphanes along with their metal complexes. A survey of the literature reveals that borane complexes of phosphanes are the most versatile precursors of free phosphanes. These are sensitive to oxidation and prone to racemization if the chiral phosphane bears stereogenic phosphorus atoms.[3] We were recently attracted by the versatility and synthetic applicability of the ring-closing metathesis (RCM) reaction in the construction of functionalized carbocycles and heterocycles[4] using the well-defined ruthenium catalysts **1a**–**c**,[5] molybdenum catalyst **2**,[6] or tungsten catalyst **3**.[7] To date,



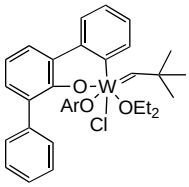
1a R = Ph, **1b** R = CHCPh$_2$



1c Mes = 2,4,6-(CH$_3$)$_3$C$_6$H$_2$



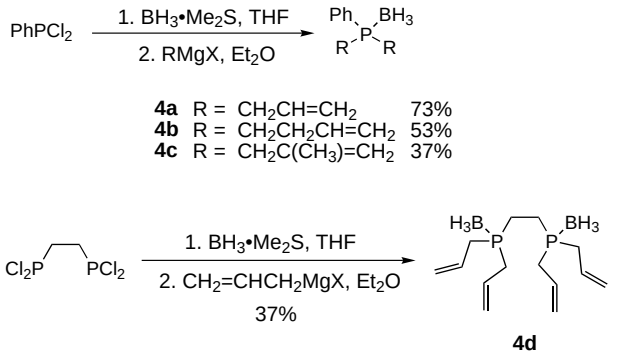
2 R = CMe(CF$_3$)$_2$



3 Ar = 2,6-Ph$_2$C$_6$H$_3$

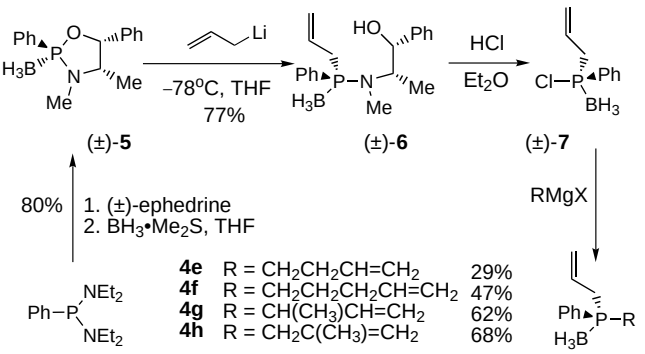
several examples of ring-closing metathesis reactions on phosphorus-containing compounds are known,[8] but only one reaction using a free phosphane as the starting diene:[9] Basset et al. reported that the ring-closing metathesis of diallylphenyl phosphane with 5 mol% of the aryloxide(neopentylidene)tungsten catalyst **3** gave the expected cyclized product in 95% yield. We have found that, on the contrary, the well explored Ru catalyst **1a** (Grubbs catalyst) was ineffective for the ring closure of diallylphenyl phosphane. Based upon these findings, we were intrigued by the possible application of transition metal alkylidene catalyzed ring-closing olefin metathesis to the general problem of constructing borane complexes of cyclic phosphanes. Herein we disclose that five-, six-, and seven-membered borane complexes of alicyclic phosphanes, as well as a bisphosphane are synthesized in good yields by metathesis of the corresponding olefinic phosphane–borane complexes.

A series of dienes **4a**–**h** was prepared by using two different strategies. The most obvious chemical problem posed in the synthesis of **4a**–**h** is the presence of double bonds that are sensitive to hydroboration. The symmetrical dienes **4a**–**c** were prepared in two steps from dichloro(phenyl)phosphane. The dichloro(phenyl)phosphane was protected by using $BH_3 \cdot Me_2S$/THF and subsequently the desired dienes were obtained in 37–73% yield by double substitution with the appropriate Grignard reagent (Scheme 1). Similarly,



Scheme 1. Synthesis of the symmetrical bis(alkenyl)phosphane–boranes **4a**–**d**.

the tetraene **4d** was prepared from commercially available 1,2-bis(dichlorophosphanyl)ethane with an overall yield of 37% after column chromatography (Scheme 1). The nonsymmetrical dienes **4e**–**h** were synthesized according to the approach of Genêt and Jugé from the known oxazaphospholidine–borane (±)-**5** (Scheme 2).[10] The diastereomerically



Scheme 2. Synthesis of nonsymmetrical bis(alkenyl)phosphane–boranes **4e**–**h**.

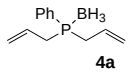
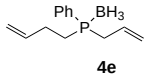
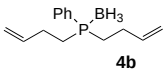
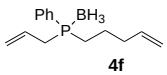
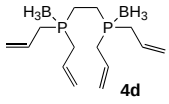
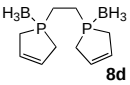
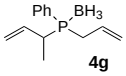
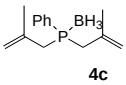
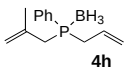
[*] Dr. V. Gouverneur, Dr. M. Schuman, M. Trevitt, A. Redd
University of Oxford
The Dyson Perrins Laboratory
South Parks Road
Oxford OX1 3QY (UK)
Fax: (+44) 1865-275-644
E-mail: veronique.gouverneur@chem.ox.ac.uk

[**] This work was supported by the European Community Training and Mobility Research Programme (COSSAC, ERBFMRXCT 980193 to M.S.) and by the Nuffield Foundation (NAL/00046/G).

pure complex (±)-**5** was obtained in one step from bis(diethylamino)phenylphosphane, (±)-ephedrine, and $BH_3 \cdot Me_2S$, and was easily isolated as a crystalline product with a chemical yield of 80%. Allyllithium [11] cleanly reacted regioselectively with (±)-**5** at low temperature in THF to give the corresponding aminophosphane–borane (±)-**6** by P–O bond cleavage with a diastereomeric ratio of 80:20 and a chemical yield of 77%. The acidic cleavage of the air-stable aminophosphane–borane (±)-**6** with HCl gas in diethyl ether led to the corresponding chlorophosphane–borane (±)-**7** which is a valuable precursor for the synthesis of a range of nonsymmetrical bis(alkene)phosphane–boranes. The final C–P bond formation was effected smoothly by addition of the appropriate organomagnesium reagent to the crude (±)-**7** to afford the expected nonsymmetrical dienes (±)-**4e–h** in moderate to satisfactory yields (29–68%; Scheme 2) after purification.

Initially, it was necessary to determine if the ruthenium alkylidene compound **1a** was active for the ring-closing metathesis of dienes containing a phosphane–borane group (Table 1). When diene **4a** was refluxed with 2% mol of catalyst **1a** for 12 h, compound **8a** was isolated in 81% yield with no side product detected in the crude mixture (entry 1, Table 1). Analogously, the reaction allowed access to the six-membered ring **8e** in very good yield (entry 2, Table 1, 95%). Formation of the seven-membered ring **8b** required 12 mol% (added sequentially in 2 mol% portions) of the catalyst **1a** and extended reaction time to achieve a 63% yield (entry 3, Table 1). Interestingly, the isomeric seven-membered ring **8f** was prepared in 94% yield after 9 h and in the presence of only 4 mol% of the catalyst **1a** (entry 4, Table 1). Mechanistically, several products were conceivable from the cyclization of substrate **4d**: A single ring-closing metathesis could lead to borane complexes of the five-membered or eight-membered cyclic phosphanes, and two ring-closing metathesis reactions could yield the desired bisphosphane–borane **8d** or a [4.4.2]bicyclo derivative. After 90 h at reflux in dichloromethane, ring-closing metathesis with 14 mol% of the catalyst **1a** afforded after purification the desired bisphosphane–borane **8d** in 55% yield along with 6% yield of a product resulting from a single ring-closing metathesis, which could be cleanly separated from **8d** by column chromatography. No eight-membered ring, bicyclic product, or dimer could be detected in the crude reaction mixture (entry 5, Table 1). The ring-closing metathesis can be extended to include borane complexes of α-substituted phosphanes, however at the expense of reduced reactivity. Indeed, the cyclization of the methyl α-substituted diene **4g** with **1a** yielded the expected five-membered cyclic compound **8g** in 61% yield (entry 6, Table 1). In contrast, alkylidene **1a** did not react with the β,β'-disubstituted diene **4c**, supporting the hypothesis that alkylidene **1a** is sensitive to steric effects (entry 7, Table 1). Moreover, the data for diene **4h** suggested that the steric influence on reactivity was equally important for borane complexes of β-monosubstituted phosphanes. Indeed, it was found that **1a** did not cyclize substrate **4h** into the corresponding β-substituted heterocycle **8h** (entry 8, Table 1).

Table 1. Ring-closing metathesis of the dienes **4a–h.**

Entry	Substrates	Amount of **1a**[a] [mol%]	t [h]	Products	Yield[b] [%]
1	 **4a**	2	14	 **8a**	81
2	 **4e**	4	9	 **8e**	95
3	 **4b**	12	49	 **8b**	63
4	 **4f**	4	9	 **8f**	94
5	 **4d**	14	90	 **8d**	55[c]
6	 **4g**	4	24	 **8g**	61[d]
7	 **4c**	8	24	 **8c**	–[e]
8	 **4h**	6	24	 **8h**	–[e]

[a] The catalyst **1a** was added sequentially by 2 % mol portions. [b] Yield after column chromatography. [c] This product is formed along with 6% of the product resulting from a single ring-closing metathesis. [d] Diastereomeric ratio 67:33. [e] Recovered starting material.

In summary, the reported synthesis of new cyclic phosphanes represents the first examples of ring-closing metathesis on bis(alkenyl)phosphane–boranes. The synthetic application of this class of compounds is well established and, by employing ring-closing metathesis, the preparation of a large variety of new cyclic phosphanes or bisphosphanes is now possible. In addition, the presence of a double bond in the products could be used for further functionalization.

Experimental Section

Typical ring-closing metathesis: The catalyst **1a** (10 mg, 4 mol%) was added to a solution of diene **4e** (70 mg) in dry and degassed CH_2Cl_2 (16 mL). The mixture was refluxed for 9 h. The solvent was then evaporated and the crude product purified by chromatography on silica gel (toluene/hexane 3/2) to yield product **8e** (59 mg; 95%) as a colorless oil; ^{1}H NMR(500 MHz,$CDCl_3$): $\delta = 7.75$ (m, 2H), 7.50 (m, 3H), 5.88 (m, 2H), 2.62 (m, 2H), 2.49 (m, 1H), 2.03 (m, 2H), 0.77 (br q, $J_{B,H} = 94.5$ Hz, 3H); ^{13}C NMR (125.7 MHz, $CDCl_3$): $\delta = 131.8$ (d, $J_{P,C} = 8.7$ Hz), 131.7 (d, $J_{P,C} = 3.3$ Hz), 129.7 (d, $J_{P,C} = 53.7$ Hz), 129.6, (d, $J_{P,C} = 12.2$ Hz), 129.2 (d, $J_{P,C} = 9.4$ Hz), 121.4 (d, $J_{P,C} = 7.8$ Hz), 21.2 (d, $J_{P,C} = 4.8$ Hz), 21.1 (d, $J_{P,C} = 36.5$ Hz), 19.8 (d, $J_{P,C} = 35.7$ Hz); ^{31}P NMR (200.4 MHz, $CDCl_3$): $\delta = -1.7$ (d, $J_{P,B} = 60.7$ Hz); ^{11}B NMR (80.2 MHz, $CDCl_3$): $\delta = -35.9$ (dq, $J_{H,B} = 95.6$, $J_{P,B} = 59.8$ Hz); positive-ion APCI MS: m/z: 177 (100%), 188.4 (50%) (APCI = chemical ionization at atmospheric pressure).

Received: March 7, 2000 [Z 14818]

[1] R. Noyori, *Asymmetric Catalysis in Organic Synthesis*, Wiley, New York, **1994**; *Catalytic Asymmetric Synthesis* (Ed.: I. Ojima), VCH, New York, **1993**.

 © WILEY-VCH Verlag GmbH, D-69451 Weinheim, 2000 1433-7851/00/3914-2492 $ 17.50+.50/0

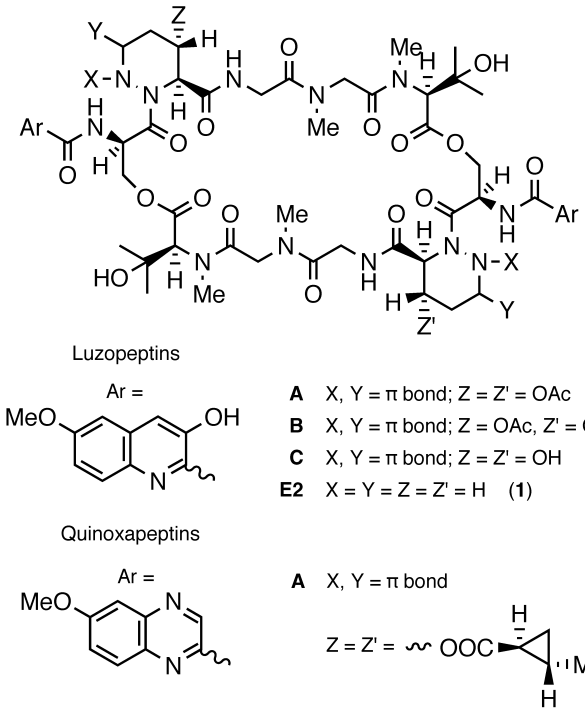
[2] M. J. Burk, *J. Am. Chem. Soc.* **1991**, *113*, 8518 – 8519; M. J. Burk, J. E. Feaster, W. A. Nugent, R. L. Harlow, *J. Am. Chem. Soc.* **1993**, *113*, 10125 – 10138; R. W. Barnhart, J. Holz, M. Quirmbach, U. Schmidt, D. Heller, R. Sturmer, A. Borner, *J. Org. Chem.* **1998**, *63*, 8031 – 8034.
[3] M. Ohff, M. Quirmbach, A. Borner, *Synthesis* **1998**, 1391 – 1415.
[4] For recent reviews on olefin metathesis see: R. H. Grubbs, S. Chang, *Tetrahedron* **1998**, *54*, 4413 – 4450; S. K. Armstrong, *J. Chem. Soc. Perkin Trans. 1* **1998**, 371 – 388; M. Schuster, S. Blechert, *Angew. Chem.* **1997**, *109*, 2124 – 2145; *Angew. Chem. Int. Ed. Engl.* **1997**, *36*, 2037 – 2056.
[5] P. Schwab, M. B. France, J. W. Ziller, R. H. Grubbs, *Angew. Chem.* **1995**, *107*, 2179 – 2181; *Angew. Chem. Int. Ed. Engl.* **1995**, *34*, 2039 – 2041; P. Schwab, R. H. Grubbs, J. W. Ziller, *J. Am. Chem. Soc.* **1996**, *118*, 100 – 110.
[6] R. R. Schrock, J. S. Murdzek, G. C. Bazan, J. Robbins, M. Dimare, M. O'Regan, *J. Am. Chem. Soc.* **1990**, *112*, 3875 – 3886.
[7] J.-L. Couturier, K. Tanaka, M. Leconte, J.-M. Basset, J. Ollivier, *Angew. Chem.* **1993**, *105*, 99 – 102; *Angew. Chem. Int. Ed. Engl.* **1993**, *32*, 112 – 114.
[8] P. R. Hanson, D. S. Stoianova, *Tetrahedron Lett.* **1998**, *39*, 3939 – 3942; M. Bujard, V. Gouverneur, C. Mioskowski, *J. Org. Chem.* **1999**, *64*, 2119 – 2123; P. R. Hanson, D. S. Stoianova, *Tetrahedron Lett.* **1999**, *40*, 3297 – 3301; M. Trevitt, V. Gouverneur, *Tetrahedron Lett.* **1999**, *40*, 7333 – 7336; L. Hetherington, B. Greedy, V. Gouverneur, *Tetrahedron* **2000**, *56*, 2053 – 2060.
[9] M. Leconte, I. Jourdan, S. Pagano, F. Lefebvre, J.-M. Basset, *J. Chem. Soc. Chem. Commun.* **1995**, 857 – 858; M. Leconte, S. Pagano, A. Mutch, F. Lefebvre, J.-M. Basset, *Bull. Soc. Chim. Fr.* **1995**, *132*, 1069 – 1071.
[10] S. Jugé, M. Stephan, J. A. Laffitte, J. P. Genêt, *Tetrahedron Lett.* **1990**, *44*, 6357 – 6360; K. M. Pietrusiewicz, M. Zablocka, *Chem. Rev.* **1994**, *94*, 1375 – 1411, and references therein.
[11] R. Taube, S. Maiwald, J. Sieler, *J. Organomet. Chem.* **1996**, *513*, 37 – 49.

Total Synthesis of Luzopeptin E2**

Marco A. Ciufolini,* Delphine Valognes, and Ning Xi

Luzopeptins are symmetric, dimeric macrocyclic depsipeptide antibiotics, which were first described in 1981.[1] Initially, these compounds attracted attention because of their antitumor activity, but the subsequent discovery of their potency as inhibitors of HIV replication in vitro at non cytotoxic doses has stimulated increased interest.[2] The biomolecular target of luzopeptins appears to be reverse transcriptase (RT). This enzyme is found only in retroviruses and it is crucial for their replication. Consequently, it is a prime target for antiretroviral therapy. Anti-HIV activity is even more pronounced in the structurally related quinoxapeptins,[3] which together with luzopeptins constitute what may be referred to as the "peptin" family of natural products. Most known RT inhibitors are nucleoside analogues (e.g, AZT); not so the peptins. This raises a number of questions concerning the mode of action and other details of their bioactivity.

Peptins exhibit an essentially invariant macrocyclic portion that incorporates two unusual components: piperazic acids (piz)[4] and *N*-methyl-3-hydroxyvaline. These delicate subunits complicate the planning of the synthesis, and indeed, peptins have remained elusive goals for a long time. Recently, Boger et al. reported total syntheses of luzopeptins A – C[5] and of the quinoxapeptins.[6, 7] Our own involvement in the peptin area has produced a number of guiding principles for the formulation of a synthetic plan[8] and it has now resulted in the total synthesis of luzopeptin E2 (**1**).[9]

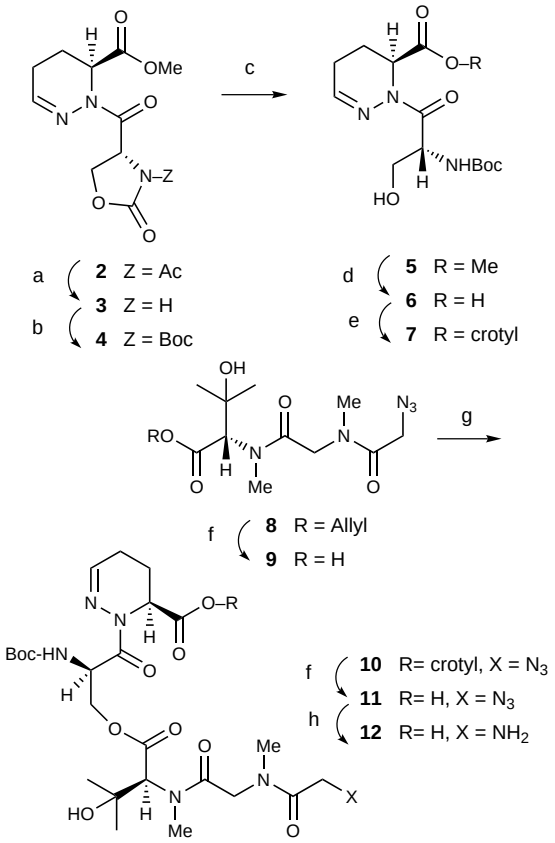


Our strategy is based on the hypothesis that the 32-membered macrocycle of the peptins may self-assemble by spontaneous cyclodimerization of a suitable monomeric precursor.[10] This goal could be accomplished in a macrolactonization (simultaneous formation of both depsi bonds) or a macrolactamization (simultaneous formation of two peptide bonds) mode. Experiment ultimately ruled in favor of the latter approach.

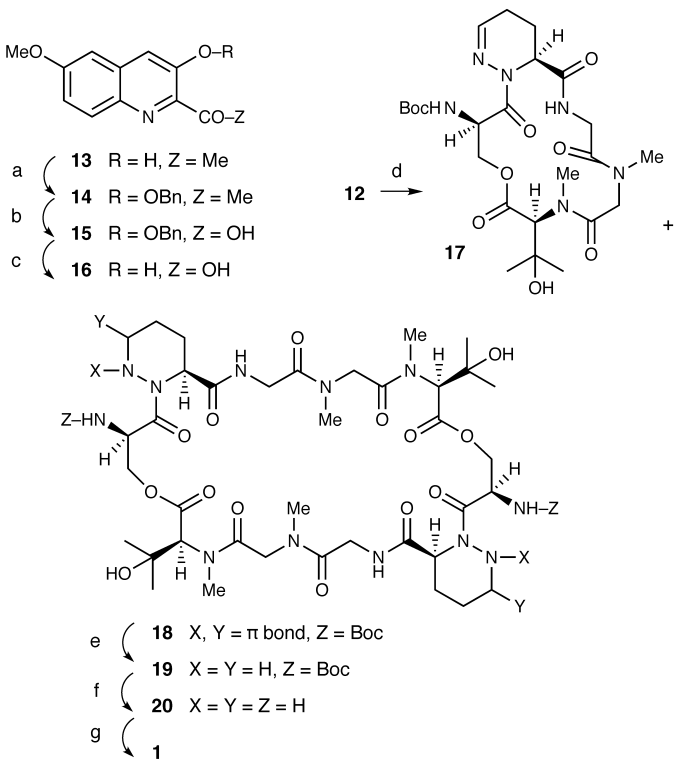
Background work identified pentapetide **10** as our primary subtarget. Oxazolone cleavage[11] of the protected serine – piperazic acid dipeptide **4** obtained from **2**[12] produced the methyl ester **5**, which was converted to the crotyl ester **7** (Scheme 1). This operation was mandated by the sensitivity of later intermediates incorporating an *N*-methyl-3-hydroxyva-

[*] Prof. Dr. M. A. Ciufolini, D. Valognes
Laboratoire de Synthèse et Méthodologie Organiques Université Claude Bernard Lyon 1
Ecole Supérieure de Chimie, Physique, et Electronique de Lyon
43, Bd. du 11 Novembre 1918, 69622 Villeurbanne cedex (France)
Fax: (+33) 4-72-43-29-63
E-mail: ciufi@cpe.fr
Prof. Dr. M. A. Ciufolini, N. Xi
Department of Chemistry, MS60
Rice University
6100 Main Street, Houston, TX 77005-1892 (USA)

[**] This work was supported by the NIH (CA-55268), the NSF (CHE 95-26183), the R. A. Welch Foundation (C-1007), the A. P.Sloan Foundation (fellowship to M.A.C., 1994 – 1998), the MENRT, the CNRS, and the Région Rhône-Alpes. We are grateful to Ms. Laurence Rousset and Dr. Denis Bouchu for recording the mass spectral data.



Scheme 1. a) N_2H_4, MeCN, room temperature, 90%; b) BOC_2O, Et_3N, cat. DMAP, CH_2Cl_2, 0°C then room temperature, 100%; c) Cs_2CO_3, MeOH, room temperature, 88%; d) LiOH, THF/H_2O, room temperature, 90%; e) crotyl-Br, Et_3N, Me_2CO, room temperature, 91%; f) [$(Ph_3P)_4Pd$], dimedone, THF, room temperature, yield of **9:** 85%; yield of **11** calculated at the stage of **18** (Scheme 2); g) **7**, DCC, DMAP, CH_2Cl_2, 0°C then room temperature, 95%; h) Ph_3P, H_2O, THF, room temperature. DCC. Abbreviations: Boc = *tert*-butoxycarbonyl; DMAP = 4-dimethylaminopyridine; dimedone = 5,5-dimethyl-1,3-cyclohexandione; DCC = dicyclohexylcarbodiimide.



Scheme 2. a) BnBr, K_2CO_3, acetone, room temperature, 82%; b) aq. NaOCl (bleach), dioxane, H_2O, room temperature, 99%; c) H_2, cat. Pd(C), EtOAc, 60%; d) EDCI, HOAt, 0°C to room temperature, yield of **17**: 10%; yield of **18**: 26% from **10** over three steps; e) H_2, 50 bar, cat. PtO_2, EtOAc, room temperature, 99%; f) TFA, CH_2Cl_2, room temperature; g) **16**, EDCI, HOBt, $NaHCO_3$, DMF, room temperature, 50% from **19** over two steps. Abbreviations: EDCI = 1-ethyl-3-[3-(dimethylamino)propyl]-carbodiimide; HOAt = 1-hydroxy-7-aza-1*H*-benzotriazole; HOBt = 1-hydroxy-1*H*-benzotriazole; TFA = trifluoroacetic acid.

line unit to the basic conditions normally employed for methyl ester cleavage,[8e] and by the consequent requirement for an ester cleavable under neutral conditions. An allyl ester, the obvious choice, was unsuitable in the present case, due to its propensity to undergo cleavage during subsequent coupling operations. The reasons for this remain unclear, but circumstantial evidence suggested that deallylation was due to S_N'-type displacement of the piz carboxylate group. Increased steric bulk at the terminal olefinic carbon atom cured the problem.[13]

The base-sensitive tripeptide **8**[8e] was selectively deblocked at the C-terminus under neutral conditions, and the resulting acid **9** was esterified[5–7] with fragment **7**. Amino and carboxy termini of the emerging product **10** were deblocked to give **12**—the monomer of the macrocyclic sector of **1**.[14]

Quinaldic acid **16** was obtained in a straightforward manner from quinoline **13**[15] (Scheme 2). Exposure of **12** to EDCI and HOAt[16] produced the desired product **18** in 26% chromatographed yield from **10** over three steps. Undesired cyclic monomer **17** (10% yield) and unreacted **12** (10–15%) were also obtained, together with a mixture of high-molecular-mass substances. The moderate yield of **18** seems acceptable in light of the conciseness of the macrocyclization sequence.

Reduction of the unsaturated piperazic acids was best effected by hydrogenation over PtO_2, which caused no damage to the potentially sensitive N–N bonds. The Boc groups in the resulting **19** were cleaved (TFA) to furnish intermediate **20**. Completion of the synthesis entailed selective acylation of the primary amino groups in **20** with **16** (EDCI, HOBt) to afford fully synthetic luzopeptin E2, whose ^1H and ^{13}C spectra were identical and superimposable with those of natural **1**.[17]

An analogue of **1** that can be considered as an "unnatural" luzopeptin was obtained from **18** by Boc release (TFA) and installation of the quinaldoyl units on the serine amino groups. Chemical reduction of this substance ($NaBH_3CN$, TFA) afforded **1** in mediocre yield, whereas attempted catalytic hydrogenation inflicted extensive damage to the quinolines. It thus appears that the E series of natural products is best accessed by adjusting the oxidation state of the macrocycle prior to introduction of the quinaldic acids.

Received: January 21, 2000 [Z 14579]

[1] a) M. Konishi, H. Ohkuma, F. Sakai, T. Tsuno, H. Koshiyama, T. Naito, H. Kawaguchi, *J. Am. Chem. Soc.* **1981**, *103*, 1241; b) E. Arnold, J. Clardy, *J. Am. Chem. Soc.* **1981**, *103*, 1243, and references therein.

 © WILEY-VCH Verlag GmbH, D-69451 Weinheim, 2000 1433-7851/00/3914-2494 $ 17.50+.50/0

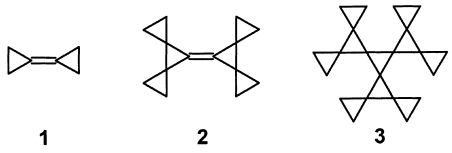
[2] a) Y. Inouye, Y. Take, S. Nakamura, *J. Antibiot.* **1987**, *40*, 100; b) Y. Take, Y. Inouye, S. Nakamura, H. S. Allaudeen, A. Kubo, *J. Antibiot.* **1989**, *44*, 107.
[3] R. B. Lingham, A. H. M. Hsu, J. A. O'Brien, J. M. Sigmund, M. Sanchez, M. M. Gagliardi, B. K. Heimbuch, O. Genilloud, I. Martin, M. T. Diez, C. F. Firsch, D. L. Zink, J. M. Liesch, G. E. Koch, S. E. Gartner, G. M. Garrity, N. N. Tsou, G. M. Salituro, *J. Antibiot.* **1996**, *49*, 253.
[4] M. A. Ciufolini, N. Xi, *Chem. Soc. Rev.* **1998**, 437.
[5] D. L. Boger, M. W. Lederboer, M. Kume, *J. Am. Chem. Soc.* **1999**, *121*, 1098.
[6] D. L. Boger, M. W. Lederboer, M. Kume, Q. Jin, *Angew. Chem.* **1999**, *111*, 2533; *Angew. Chem. Int. Ed.* **1999**, *38*, 2424.
[7] D. L. Boger, M. W. Lederboer, M. Kume, M. Searcey, Q. Jin, *J. Am. Chem. Soc.* **1999**, *121*, 11375. Boger's landmark achievement followed an earlier disclosure of the synthesis of sandramycin, a congener of the peptins that contains pipecolinic acid and valine in place of piperazic acid and *N*-methyl-3-hydroxyvaline: D. L. Boger, J. H. Chen, K. W. Saionz, *J. Am. Chem. Soc.* **1996**, *118*, 1629. The Scripps team has also explored in further detail the bioactivity of peptins and related substances: D. L. Boger, J. H. Chen, K. W. Saionz, Q. Jin, *Bioorg. Med. Chem.* **1998**, *6*, 85; D. L. Boger, K. W. Saionz, *Bioorg. Med. Chem.* **1999**, *7*, 315.
[8] See ref. [4] and [12] as well as: a) M. A. Ciufolini, N. Xi, *J. Chem. Soc. Chem. Commun.* **1994**, 1867; b) N. Xi, M. A. Ciufolini, *Tetrahedron Lett.* **1995**, *36*, 6595; c) M. A. Ciufolini, N. Xi, *J. Org. Chem.* **1997**, *62*, 2320; d) M. A. Ciufolini, T. Shimizu, S. Swaminathan, N. Xi, *Tetrahedron Lett.* **1997**, *38*, 4947; e) M. A. Ciufolini, D. Valognes, N. Xi, *Tetrahedron Lett.* **1999**, *40*, 3693.
[9] H. M. Urbanus (Bristol-Myers Co.) NL-T 84 00 237, **1984** [*Chem. Abstr.* **1985**, *102*, 22795q].
[10] Molecular mechanics calculations suggested that the strain energy present in the peptin macrocycle *per monomeric unit* is less than half of the strain energy present in the cyclic form of each monomeric segment. If the transition state for acylative cyclization reactions were sufficiently late along the reaction coordinate, it seemed plausible that the relative energy content of products might influence product distribution. Details will be provided in forthcoming full papers.
[11] T. Ishizuka, T. Kunieda, *Tetrahedron Lett.* **1987**, *28*, 4185.
[12] N. Xi, L. B. Alemany, M. A. Ciufolini, *J. Am. Chem. Soc.* **1998**, *120*, 80.
[13] a) For a valuable review of allyl-type blocking groups see: H. Kunz, *Angew. Chem.* **1987**, *99*, 297; *Angew. Chem. Int. Ed. Engl.* **1987**, *26*, 294, and references therein; b) a β,β-dimethallyl ester was also competent in later steps, but while the crotyl unit was rapidly released with dimedone/$[Pd(PPh_3)_4]$, the dimethallyl group resisted cleavage.
[14] Compounds **11** and **12** obtained in this way were contaminated with $Ph_3P{=}O$. These substances were extremely polar and difficult to purify; accordingly, they were not fully characterized. By contrast, macrocyclic materials were easily purified by chromatography. It appears that $Ph_3P{=}O$ does not interfere with subsequent coupling operations, and indeed, it might even assist them; cf.: V. A. Efimov, O. G. Chakhmakhcheva, Y. A. Ovchinnikov, *Nucl. Acids Res.* **1985**, *13*, 3651.
[15] D. W. Bayne, A. J. Nicol, G. Tennant, *J. Chem. Soc. Chem. Commun.* **1975**, 782.
[16] L. A. Carpino, *J. Am. Chem. Soc.* **1993**, *115*, 4397.
[17] The spectra of **1** are given in ref. [9].

A Third-Generation Bicyclopropylidene: Straightforward Preparation of 15,15′-Bis-(hexaspiro[2.0.2.0.0.0.2.0.2.0.1.0]pentadecylidene) and a C_{2v}-Symmetric Branched [15]Triangulane**

Malte von Seebach, Sergei I. Kozhushkov, Roland Boese, Jordi Benet-Buchholz, Dmitrii S. Yufit, Judith A. K. Howard, and Armin de Meijere*

Dedicated to Professor Paul von Ragué Schleyer on the occasion of his 70th birthday

Bicyclopropylidene (**1**), an interesting laboratory curiosity when first prepared in milligram quantities in 1970,[1] has since become easily available,[2] and due to its unique reactivity, developed into a versatile C_6 building block for organic synthesis.[3] Among other applications, it serves as the best starting material for various branched [*n*]triangulanes—hydrocarbons consisting exclusively of spiroannelated cyclopropane units.[4] The perspirocyclopropanated analogue of **1**, a second-generation bicyclopropylidene **2**, had previously been prepared along a tedious 14-step sequence,[5] and **2** had been further transformed into the perspirocyclopropanated [3]rotane **3** which, with its 10 spiroannelated cyclopropane rings, at that time was the largest achievable [*n*]triangulane.[6]

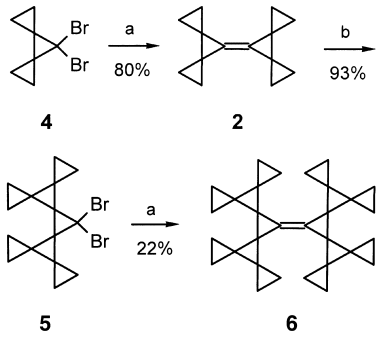


The classical approach to substituted bicyclopropylidenes by dimerization of 1-halo-1-lithiocyclopropanes generated by treatment of 1,1-dihalocyclopropanes with alkyllithium reagents,[7] has recently been significantly improved by Neu-

[*] Prof. Dr. A. de Meijere, Dipl.-Chem. M. von Seebach, Dr. S. I. Kozhushkov
Institut für Organische Chemie der
Georg-August-Universität Göttingen
Tammannstrasse 2, 37077 Göttingen (Germany)
Fax: (+49) 551-399475
E-mail: ameijer1@uni-goettingen.de
Prof. Dr. R. Boese, Dr. J. Benet-Buchholz
Institut für Anorganische Chemie der
Universität-Gesamthochschule Essen
Universitätstrasse 3–5, 45117 Essen (Germany)
Dr. D. S. Yufit, Prof. Dr. J. A. K. Howard
Department of Chemistry, University of Durham
Durham, South Road, DH1 3LE (UK)

[**] This work was supported by the Fonds der Chemischen Industrie and EPSRC (UK). M.v.S. is indebted to the Hermann-Schlosser Foundation for a Graduate Fellowship. The authors are grateful to the companies BASF AG, Bayer AG, Chemetall GmbH, Degussa AG, and Hüls AG for generous gifts of chemicals. We thank Professor H. Butenschön, TU Hannover, for his kind help in providing the DSC measurements, and Professor Burkhard König, Universität Regensburg, for cyclovoltammetric measurements. We are particularly grateful to Dr. B. Knieriem, Universität Göttingen, for his careful reading of the final manuscript.

enschwander et al. who observed that copper(II) salts assist the coupling of 1-bromo-1-lithiocyclopropanes generated from 1,1-dibromocyclopropanes to give a variety of substituted bicyclopropylidenes in well reproducible yields.[8] As we now found, this method can also be applied to 7,7-dibromodispiro-[2.0.2.1]heptane (**4**),[9] the dibromocarbene adduct of bicyclopropylidene (**1**), to yield the perspirocyclopropanated bicyclopropylidene **2** (80% isolated), making this exotic hydrocarbon easily available in preparatively useful quantities (Scheme 1). It is really spectacular that the dibromide **5**, the dibromocarbene adduct of **2**,[6] can be reductively "dimerized" again to give the third-generation bicyclopropylidene **6** (Scheme 1).[10]

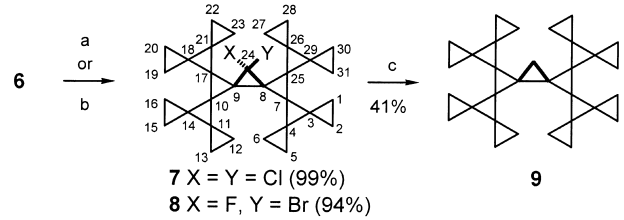


Scheme 1. Synthesis of the third-generation bicyclopropylidene **6**. a) $CuCl_2$, THF, $-95\,^{\circ}C$, addition of BuLi over 1 h, then $-95\,^{\circ}C$, 1 h; b) $CHBr_3$, KOH (powder), TEBACl, CH_2Cl_2, $0 \rightarrow 30\,^{\circ}C$, 5 h. TEBA = benzyltriethylammonium.

Although its total strain energy exceeds 517 kcal mol^{-1},[11] the new cyclopropyl-overcrowded bicyclopropylidene **6** is virtually as stable thermally (up to ca. 230 °C according to differential scanning calorimetry (DSC) measurements) as the perspirocyclopropanated bicyclopropylidene **2**. The oxidation potentials of these alkenes decrease on going from bicyclopropylidene (**1**) (1.58 V) to **2** (1.12 V, $\Delta E = 480$ mV) and further to **6** (0.98 V, $\Delta E = 140$ mV). It is remarkable that the outer sphere cyclopropyl groups in **6** still exert a significant influence, albeit a smaller one than the outer sphere groups in **2**, as indicated by the smaller difference between the values for **6** and **2** compared to that between **2** and **1**.

As expected, the steric congestion arising from the increased number of spiroannelated three-membered rings in **6** prevents certain cycloadditions. Thus, dibromocarbene did not add onto the double bond in **6**,[12] neither under phase-transfer catalysis nor under classical conditions as developed by Doering et al.[13] and Seyferth et al.[14] The addition of bromochlorocarbene also failed under all of these conditions, while 7-bromo-7-chlorodispiro[2.0.2.1]heptane was obtained from **1** in 77% yield using Doering's procedure. Also, **6** did neither react with diazocyclopropane, generated in situ from *N*-nitroso-*N*-cyclopropylurea,[15] nor with diazomethane in the presence of $Pd(OAc)_2$.[16] However, with less sterically demanding carbenes such as dichloro- and bromofluorocarbene the corresponding dihalo[15]triangulanes **7** and **8** were obtained in excellent yields (Scheme 2).[17]

For quite a while it appeared, as if the perspirocyclopropanated [3]rotane **3** would be the ultimate size achievable branched triangulane. But the current success in preparing the



Scheme 2. Preparation of the branched [15]triangulanes **7**–**9**. a) $CHCl_3$, 50% aq. NaOH, TEBACl, room temperature, 3 d; b) $CHBr_2F$, 50% aq. NaOH, TEBACl, CH_2Cl_2, room temperature, 3 d; c) Li, *t*BuOH, THF, 15–20 °C, 3 d.

dihalocarbene adducts **7** and **8** (Scheme 2) from the spirocyclopropyl-overcrowded bicyclopropylidene **6**, fuels new hope that the limits for generating even higher aggregates of spiroannelated cyclopropane rings can be pushed forward still further. Reductive dechlorination of **7** led to the hydrocarbon **9** (Scheme 2) which, with its 15 spirofused cyclopropane rings,[18] already sets a new record.

The structures of compounds **6**–**9** were confirmed by X-ray crystal structure analysis.[19] The lengths of the central double bond turned out to be essentially the same in bicyclopropylidene (**1**) (1.304(2) Å[3b]), perspirocyclopropanated bicyclopropylidene **2** (1.305(4) Å[5a]) as well as the third-generation bicyclopropylidene **6** (1.305(3) Å), and the typical difference between proximal and distal bond lengths observed for the outer spirocyclopropane rings in [3]rotane[20] and perspirocyclopropanated [3]rotane **3**[6] for **6** is observed one sphere further out (Figure 1). The structures of [15]triangulane **9** and its dihalo derivatives **7** and **8** all display a unique feature. The

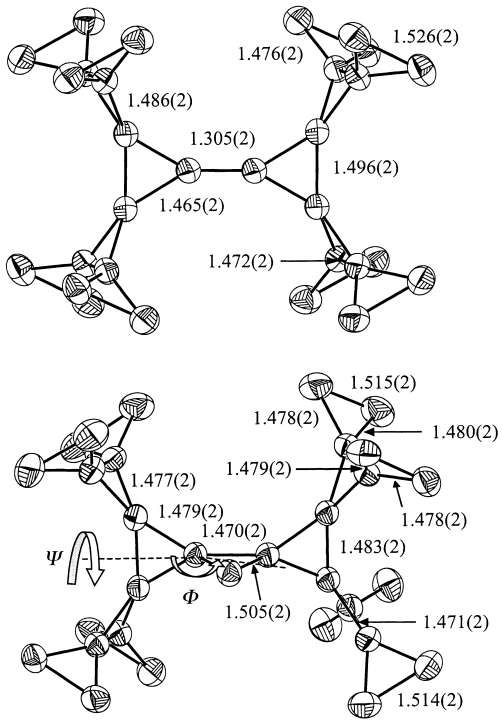


Figure 1. Crystal structures of the third-generation bicyclopropylidene **6** (top) and [15]triangulane **9** (bottom). The bond lengths [Å] are mean values based on assumed D_{2h} symmetry for **6** and C_{2v} symmetry for **9**.[19]

 © WILEY-VCH Verlag GmbH, D-69451 Weinheim, 2000 1433-7851/00/3914-2496 $ 17.50+.50/0 *Angew. Chem. Int. Ed.* **2000**, *39*, No. 14

two spiropentane moieties making up the central dispiro-[2.0.2.1]heptane units in all of them have lost their usual C_2 symmetry. In **9**, the deformation of these spiropentane units is both by twisting (i. e. rotation of the plane of one cyclopropane ring against that of the other one) by -4.3° and $+5.8^\circ$ ($\Psi = 85.7^\circ$ and 95.8°, respectively, for the left and right spiropentane unit; Figure 1) and bending (i. e. buckling the C_2 axis which usually bisects the two cyclopropane rings; Figure 1) by 11.7° ($\Phi = 168.3^\circ$ for both moieties).[21] This deformation must arise from the mutual repulsion of the two bulky branched [7]triangulane fragments spiroannelated to the central cyclopropane moiety of **9**, and it apparently goes along with a significant change in hybridization of the two central spiro carbon atoms leading to a remarkable shortening of the proximal C–C bond (1.470(2) Å) in the central ring.[22] Such a deformation was also observed in dichloro[15]triangulane **7**, but with slightly less bending ($\Phi = 169.9^\circ$) and significantly less twisting ($\Psi = 89.0^\circ$).

The structure of bromofluoro[15]triangulane **8** is one of the very few known structures of compounds containing a geminally bromofluoro-substituted carbon atom. The sterically congested [15]triangulane skeleton apparently accommodates the larger bromine and the smaller fluorine substituents at C24 best with different orientations of the C–F and C–Br bonds. The angle between the C–Br bond axis and the C9-C8-C24 plane is only 49.1°, while that between the C–F axis and the same plane is 58.2°. The crystal packing of the molecules **8** is also noteworthy. The outer-sphere three-membered rings at C4, C11, C18, and C26 form a large enough cavity which accommodates the Br substituent of the adjacent molecule quite nicely: the shortest intermolecular contact Br1···H28B 2.97(1) Å is the same as the shortest intramolecular ones Br1···H312 2.96(1) and Br1···H152 2.98(1) Å, while the sum of van der Waals radii of hydrogen (1.20 Å) and bromine (1.85 Å)[23] atoms is 3.05 Å (Figure 2).

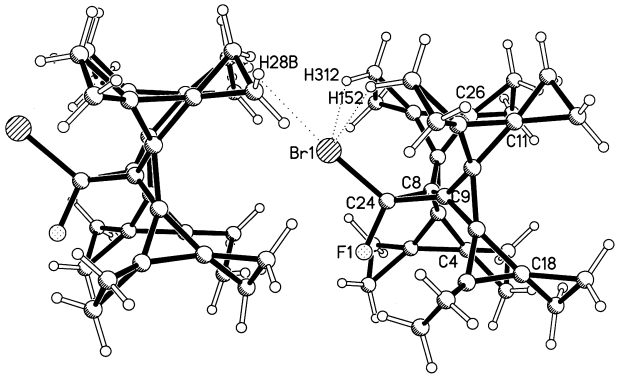


Figure 2. A section showing the crystal packing of 24-bromo-24-fluoro-[15]triangulane **8**.[19]

The central dispiro[2.0.2.1]heptane fragment in **8** is also twisted and bent, but the big bromine atom apparently causes the twisting for the two sides to be in the same direction ($\Psi =$ 96.6 and 93.3°) as opposed to compound **9** ($\Psi = 85.7$ and 95.8°), while the degree of bending ($\Phi = 169.9$ and 170.5°) is approximately the same as in **9**.

Thus, the "dimerization" of readily generated bromocuprocyclopropylidenoids has been shown to open a promising route to reasonably large aggregates of spirocyclopropane rings. It remains to be seen, whether the cuprofluorocarbenoids generated from **8** under appropriate conditions can be added to bicyclopropylidene (**1**) or even "dimerized" without rearrangement.

Received: February 16, 2000 [Z14717]

[1] P. Le Perchec, J.-M. Conia, *Tetrahedron Lett*. **1970**, 1587–1588.

[2] a) A. de Meijere, S. I. Kozhushkov, T. Spaeth, N. S. Zefirov, *J. Org. Chem*. **1993**, *58*, 502–505; b) A. de Meijere, S. I. Kozhushkov, T. Späth, *Org. Synth*. **2000**, *79*, in press.

[3] Reviews: a) A. de Meijere, S. I. Kozhushkov, A. F. Khlebnikov, *Zh. Org. Khim*. **1996**, *32*, 1607–1626; A. de Meijere, S. I. Kozhushkov, A. F. Khlebnikov, *Russ. J. Org. Chem. (Engl. Transl.)* **1996**, *32*, 1555–1575; b) A. de Meijere, S. I. Kozhushkov, A. F. Khlebnikov, *Top. Curr. Chem.* **2000**, *207*, 89–147; c) latest application in combinatorial chemistry: A. de Meijere, H. Nüske, M. Es-Sayed, T. Labahn, M. Schroen, S. Bräse, *Angew. Chem*. **1999**, *111*, 3881–3884; *Angew. Chem. Int. Ed.* **1999**, *38*, 3669–3672.

[4] Reviews: a) A. de Meijere, S. I. Kozhushkov, *Chem. Rev*. **2000**, *100*, 93–142; b) A. de Meijere, S. I. Kozhushkov in *Advances in Strain in Organic Chemistry, Vol. 4* (Ed.: B. Halton), JAI Press, London, **1995**, pp. 225–282; c) N. S. Zefirov, T. S. Kuznetsova, A. N. Zefirov, *Izv. Akad. Nauk* **1995**, 1613–1621; N. S. Zefirov, T. S. Kuznetsova, A. N. Zefirov, *Russ. Chem. Bull. (Engl. Trans.)* **1995**, 1613–1621.

[5] a) S. Zöllner, H. Buchholz, R. Boese, R. Gleiter, A. de Meijere, *Angew. Chem.* **1991**, *103*, 1544–1546; *Angew. Chem. Int. Ed. Engl.* **1991**, *30*, 1518–1520; b) S. Zöllner, Dissertation, Universität Hamburg, **1991**.

[6] S. I. Kozhushkov, T. Haumann, R. Boese, A. de Meijere, *Angew. Chem.* **1993**, *105*, 426–429; *Angew. Chem. Int. Ed. Engl*. **1993**, *32*, 401–403.

[7] W. R. Moore, H. R. Ward, *J. Org. Chem*. **1960**, *25*, 2073; W. R. Moore, H. R. Ward, *J. Org. Chem*. **1962**, *27*, 4179–4181. For a recent review on the dimerization of halometallocyclopropylidenoids from 1,1-dibromocyclopropanes see ref. [3b].

[8] a) M. Borer, T. Loosli, M. Neuenschwander, *Chimia* **1991**, *45*, 382–386; b) T. Loosli, M. Borer, I. Kulakowska, A. Minder, M. Neuenschwander, P. Engel, *Helv. Chim. Acta* **1995**, *78*, 1144–1165; c) M. Borer, T. Loosli, A. Minder, M. Neuenschwander, P. Engel, *Helv. Chim. Acta* **1995**, *78*, 1311–1324; d) M. Borer, M. Neuenschwander, *Helv. Chim. Acta* **1997**, *80*, 2486–2501; e) R. Huwyler, X. Li, P. Bönzli, M. Neuenschwander, *Helv. Chim. Acta* **1999**, *82*, 1242–1249.

[9] a) L. Fitjer, J.-M. Conia, *Angew. Chem*. **1973**, *85*, 832–833; *Angew. Chem. Int. Ed. Engl*. **1973**, *12*, 761–762; b) K. A. Lukin, N. S. Zefirov, D. S. Yufit, Yu. T. Struchkov, *Tetrahedron* **1992**, *48*, 9977–9984.

[10] Systematic name: 15,15′-bis(hexaspiro[2.0.2.0.0.0.2.0.2.0.1.0]pentadecylidene).

[11] This estimated total strain energy of **6** is based on a previously published additivity scheme for triangulanes, assuming a strain energy for the central bicyclopropylidene unit of 77.4 kcal mol^{-1}.[3b] See for example H.-D. Beckhaus, C. Rüchardt, S. I. Kozhushkov, V. N. Belov, S. P. Verevkin, A. de Meijere, *J. Am. Chem. Soc*. **1995**, *117*, 11854–11860.

[12] Several examples of attempted, but unsuccessful dibromocarbene addition to sterically congested bicyclopropylidenes have been reported: a) Y. Fukuda, Y. Yamamoto, K. Kimura, Y. Odaira, *Tetrahedron Lett*. **1979**, 877–878; b) A. Tubul, M. Bertrand, *Tetrahedron Lett*. **1984**, *25*, 2219–2222. In addition, permethylbicyclopropylidene also did not react with dibromocarbene under different conditions: c) M. von Seebach, Dissertation, Universität Göttingen, **2000**.

[13] a) W. von E. Doering; A. K. Hoffman, *J. Am. Chem. Soc.* **1954**, *76*, 6162–6165; b) W. von E. Doering, W. A. Henderson, *J. Am. Chem. Soc*. **1958**, *80*, 5274–5277.

[14] D. Seyferth, V. A. Mai, J. Y.-P. Mui, K. V. Darragh, *J. Org. Chem*. **1966**, *31*, 4079–4081. For a review on dihalocyclopropanations see: E. V.

Dehmlow, *Methoden Org. Chem. (Houben-Weyl)*, *4th ed.*, *1952–*, *Vol. E 19b*, **1989**, pp. 1461–1627.
[15] W. Kirmse, U. Jansen, *Chem. Ber.* **1985**, *118*, 2607–2625, and references therein.
[16] a) R. Paulissen, A. J. Hubert, P. Teyssie, P. *Tetrahedron Lett.* **1972**, 1465–1466; b) J. Kottwitz, H. Vorbrüggen, *Synthesis* **1975**, 636–637; c) A. J. Anciaux, A. J. Hubert, A. F. Noels, P. Teyssie, *J. Org. Chem.* **1980**, *45*, 695–702. For a review see also: Yu. V. Tomilov, V. A. Dokichev, U. M. Dzhemilev, O. M. Nefedov, *Usp. Khim.* **1993**, *62*, 847–886; Yu. V. Tomilov, V. A. Dokichev, U. M. Dzhemilev, O. M. Nefedov, *Russ. Chem. Rev.* **1993**, *62*, 799–838.
[17] All new compounds were fully characterized by spectroscopic methods (^{1}H NMR, ^{13}C NMR, MS), elemental analyses and crystal structure analyses. **6**: Colorless solid, m.p. 245–246 °C (decomp); ^{1}H NMR (250 MHz, $CDCl_3$): $\delta = 0.57–0.66$ (m, 8H), 0.73–0.90 (m, 24H); ^{13}C NMR (62.9 MHz, $CDCl_3$, additional DEPT): $\delta = 4.63$ (8 CH_2), 7.25 (8 CH_2), 21.44 (8C), 26.57 (4C), 114.17 (2C); elemental analysis (%) calcd for $C_{30}H_{32}$ (392.6): C 91.78, H 8.22; found: C 91.64, H 8.09. **7**: Colorless solid, m.p. 212 °C (decomp); ^{1}H NMR: $\delta = 0.61–0.94$ (m, 28H), 1.15–1.25 (m, 4H); ^{13}C NMR: $\delta = 4.99$, 6.78, 7.01, 7.67 (4 CH_2), 19.04 (8C), 17.85 (4C), 32.45 (2C), 37.69 (C); elemental analysis (%) calcd for $C_{31}H_{32}Cl_2$ (475.5): C 78.31, H 6.78, Cl 14.91; found: C 78.20, H 6.75, Cl 14.68. **8**: Colorless solid, m.p. 223–225 °C (decomp); ^{1}H NMR: $\delta = 0.61–1.00$ (m, 30H), 1.34–1.42 (m, 2H); ^{13}C NMR: $\delta = 4.87$, 4.98, 6.63, 6.80, 6.86, 6.98, 7.54 (2 CH_2), 6.51 (d, $^5J_{C,F} = 3.8$ Hz, 2 CH_2), 17.55, 18.08, 18.96, 32.46 (2C), 18.63 (d, $^4J_{C,F} = 3.1$ Hz, 2C), 31.88 (d, $^3J_{C,F} = 1.8$ Hz, 2C), 34.08 (d, $^2J_{C,F} = 10.6$ Hz, 2C), 90.60 (d, $^1J_{C,F} = 320.7$ Hz, C); elemental analysis (%) calcd for $C_{31}H_{32}BrF$ (503.5): C 73.95, H 6.41, Br 15.87; found: C 73.84, H 6.38, Br 15.64. **9**: Colorless solid, m.p. 191–193 °C; ^{1}H NMR: $\delta = 0.47–0.60$ (m, 8H), 0.63–0.86 (m, 24H), 0.94 (s, 2H); ^{13}C NMR: $\delta = 3.02$, 4.64, 5.99, 6.49 (4 CH_2), 5.83 (CH_2), 18.00, 18.49, 27.64, 22.55 (2C); elemental analysis (%) calcd for $C_{31}H_{34}$ (406.6): C 91.57, H 8.43; found: C 91.81, H 8.56.
[18] Systematic names: 24-dichloro- (**7**), 24-bromo-24-fluoro- (**8**), tetradecaspiro[2.0.2.0.0.0.0.0.2.0.2.0.0.0.0.2.0.2.0.0.1.0.0.2.0.2.0.0.0]untriacontane (**9**).
[19] Crystallographic data (excluding structure factors) for the structures reported in this paper have been deposited with the Cambridge Crystallographic Data Centre as supplementary publication nos. CCDC-142835 (**6**), -142836 (**7**), -142041 (**8**), and -142837 (**9**). Copies of the data can be obtained free of charge on application to CCDC, 12 Union Road, Cambridge CB21EZ, UK (fax: (+44) 1223-336-033; e-mail: deposit@ccdc.cam.ac.uk).
[20] R. Boese, T. Miebach, A. de Meijere, *J. Am. Chem. Soc.* **1991**, *113*, 1743–1748.
[21] For comparison, in spiropentane itself the angles Ψ and Φ are 90.2 and 179.6°, respectively, while in ethano-bridged spiropentane Ψ and Φ are 80.0 and 154.0°, respectively. See for example R. Boese, D. Bläser, K. Gomann, U. H. Brinker, *J. Am. Chem. Soc.* **1989**, *111*, 1501–1503.
[22] Thus, the previously published additivity Scheme for bonding parameters in [*n*]triangulanes also hold for [15]triangulane **9**. See for example R. Boese, T. Haumann, E. D. Jemmis, B. Kiran, S. Kozhushkov, A. de Meijere, *Liebigs Ann.* **1996**, 913–919.
[23] A. Bondi, *J. Phys. Chem.* **1964**, *68*, 441–451.

Cross-Linked Scandium-Containing Dendrimers: A New Class of Heterogeneous Catalysts

Manfred T. Reetz* and Dirk Giebel

Dedicated to Professor José Barluenga on the occasion of his 60th birthday

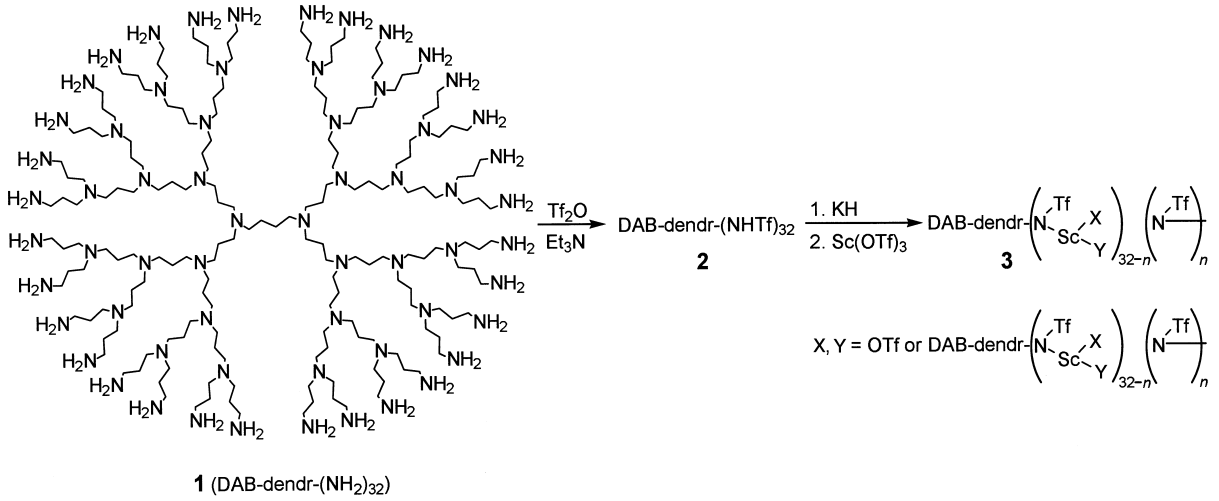
Interest in metal-containing dendrimers as catalysts[1] is increasing because in principle they combine the advantages of homogeneous and heterogeneous catalysis in one system.[1c] Nevertheless, recyclization and reuse of such catalysts is not always demonstrated, which raises the question of whether in such cases the synthetic effort necessary in their preparation is actually meaningful.[1d] Here we report on scandium-containing dendrimers, which have useful catalytic properties as Lewis acids and which can also be easily recycled and reused without any appreciable loss in activity. In contrast to soluble dendritic catalysts previously described, our materials are heterogeneous catalysts that are insoluble due to a Sc-promoted cross-linking of individual dendrimer units.[2–4] Application in catalysis is based on previous reports by Kobayashi according to which scandium salts having electron-withdrawing ligands as in $Sc(OTf)_3$ (Tf = triflate = F_3CSO_2), $ScCl_3$, $Sc(NTf_2)_3$, $Sc(PF_6)_3$, or polyallyl scandium trifylamido ditriflate (PA-Sc-TAD) are effective catalysts in Mukaiyama aldol additions to aldehydes and aldimines, Diels–Alder and Michael additions as well as Friedel–Crafts acylations.[5]

The commercially available dendrimer DAB-dendr-$(NH_2)_{32}$ **1**[6] with 32 outer primary amino groups was first subjected to sulfonylation using Tf_2O/Et_3N. The reaction afforded a solid compound **2** which turned out to be only slightly soluble in conventional solvents. The IR spectrum does not show any bands near 3359 cm^{-1} typical of primary amino groups; rather, absorption at 3489 cm^{-1} characteristic of $(R)HNSO_2CF_3$ functions is clearly visible. Thus, most of the outer amino groups appear to have been sulfonylated. We then envisioned that these functional groups can bind to scandium with concomitant cross-linking of the dendritic units **2**. For this purpose a suspension **2** in THF was treated with different amounts of the cross-linking agent $Sc(OTf)_3$ in the presence of KH as base. As a typical result the completely insoluble solid material **3** was formed, which according to elemental analysis has a Sc/N ratio of 0.2 corresponding to about 40 % Sc-loading (see Experimental Section). Although a large proportion of the outer amino groups are likely to exist as $N(Tf)[Sc(OTf)_2]$ units, some of them serve as cross-linking points with two (or three) sulfonamido ligands at scandium (symbolized by **3**). The X-ray powder diffractogram points to a completely amorphous solid. Thus, the possible presence of nonreacted $Sc(OTf)_3$ trapped in the solid matrix can be excluded.

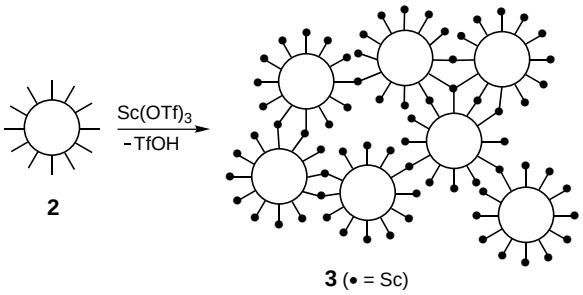
In order to obtain some information concerning the surface morphology and the actual cross-linking, a scanning electron

[*] Prof. Dr. M. T. Reetz, Dipl.-Chem. D. Giebel
Max-Planck-Institut für Kohlenforschung
Kaiser-Wilhelm-Platz 1, 45470 Mülheim an der Ruhr (Germany)
Fax: (+49) 208-306-2985
E-mail: reetz@mpi-muelheim.mpg.de

 © WILEY-VCH Verlag GmbH, D-69451 Weinheim, 2000 1433-7851/00/3914-2498 $ 17.50+.50/0



microscopic (SEM) study was undertaken. Compound **3** was first attached to an aluminum surface using conductive carbon adhesive tabs and then treated with some gold vapor in order to prevent charge buildup on the surface. The SEM pictures show the presence of a wide-meshed scalelike morphology, the individual scales being about 10–20 μm large (Figure 1a). Upon further magnification threads become visible which probably result from outer shearing forces during preparation and which speak for the polymeric nature of the material (Figure 1b). Even at maximum magnification no dendritic structures are visible on the scales, because under the conditions used maximum resolution of the instrument has been reached.



Scheme 1. Schematic representation of **3** (Sc units bear two sulfonamido groups; cross-linking Sc units bear one or no such groups).

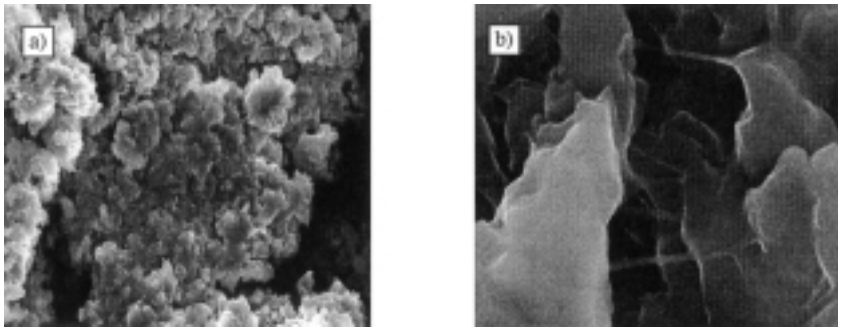
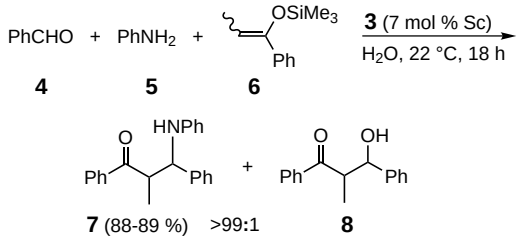


Figure 1. SEM visualization of samples of **3** at different magnification: a) ×500; b) ×10000.

The cross-linking can be represented schematically as in Scheme 1. At this point of our investigation it remained unclear whether the catalytically active Sc centers in the inner part of the solid material **3** are actually accessible for potential reaction partners.

Additional studies pertaining to the nature of the surface and the porosity of the solid **3** were performed with argon adsorption measurements. The adsorption isotherms indicate Ar adsorption only at saturation pressure. Thus, the material is not porous. The Brunauer–Emmet–Teller (BET) evaluation resulted in a value of only 9 $m^2 g^{-1}$.[7]

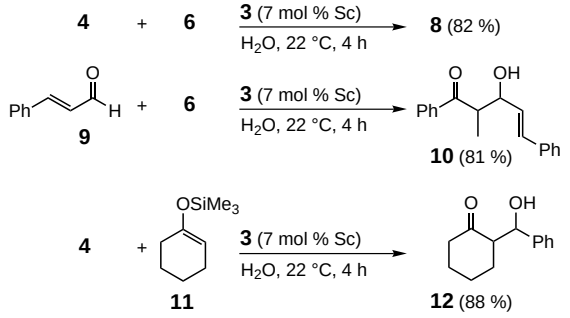
Although appreciable catalytic activity seemed unlikely in view of these results, experiments directed towards testing **3** in catalytic reactions were nevertheless performed. The three-component reaction of benzaldehyde (**4**), aniline (**5**), and enolsilane **6** with formation of the β-amino ketone **7** was tested first.[5] Accordingly, the catalyst **3** (7 mol% Sc) was added to the two-phase system composed of water and the three reaction components **4**, **5**, and **6**, and the mixture was vigorously stirred at 22°C (see Experimental Section). During this process a swelling of the solid material **3** was observed. Following separation of the solid, the aldimine adduct **7** was isolated as the only product (89%). Thus, the catalyst is highly active and completely chemoselective. It is likely that the swelling allows for efficient transport of the reaction partners and therefore enables access to the catalytically active Sc centers in the interior of the material. Moreover, the recycled catalyst showed identical performance (88–89% yield; **7**:**8** >99:1), which remained constant even after three runs.



 © WILEY-VCH Verlag GmbH, D-69451 Weinheim, 2000 1433-7851/00/3914-2499 $ 17.50+.50/0

For comparison the use of $Sc(OTf)_3$ (10 mol%) in CH_2Cl_2/CH_3CN (2/1) as solvent, this time in the presence of the usual molecular sieves (4 Å), afforded an 86:14 product mixture of **7** and **8** (90% total yield), whereas under identical conditions the polymeric catalyst PA-Sc-TAD resulted in the exclusive formation of the β-amino ketone **7**.[5] Thus, the dendritic catalyst **3** and the polymeric catalyst PA-Sc-TAD[5] have similar catalytic properties which are quite different from the "monomeric" Sc catalyst $Sc(OTf)_3$. The reason is probably not so much the so-called polymer effect,[5] but rather the influence of the ligands. On the practical side, recyclization of the solid material **3** is simpler than that of the rubberlike PA-Sc-TAD. In no case did the aqueous filtrate of the suspension of catalyst **3** turn out to be catalytically active, thereby proving that Sc leaching followed by homogeneous catalysis does not occur. Indeed, the ICP analysis of the aqueous filtrate showed essentially no scandium (< 1 ppm Sc). Hydrolysis with formation of catalytically active CF_3SO_3H, although conceivable, is also excluded.

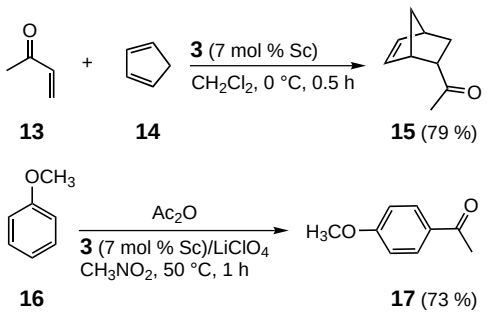
In a further test reaction the Mukaiyama aldol addition of **6** to **4** was performed in water at 22 °C (4 h) using **3** (7 mol% Sc) as the catalyst, resulting in an 82% yield of **8** as a 1:1 diastereomer mixture. Here again the multiply recycled catalyst showed no decrease in activity. Similar results were observed in the addition of **6** to cinnamaldehyde (**9**) and of **11** to benzaldehyde (**4**). In all cases the usual swelling of the



catalyst was observed, a prerequisite for the efficient transport of reaction components into the inner part of the solid catalyst. Thus, not only the outer, but also the inner Sc centers are involved in catalysis.

It is also possible to use the heterogeneous dendritic catalyst **3** in organic solvents, as in the Diels–Alder reaction of methyl vinyl ketone (**13**) with cyclopentadiene (**14**) with formation of adduct **15** (*endo*/*exo* = 85:15). Finally, the **3**-catalyzed acylation of anisol (**16**) with acetic acid anhydride and $LiClO_4$ as an additive[5] afforded *p*-methoxyacetophenone (**17**) in 73% yield. This is the first example of a Friedel–Crafts reaction induced by a dendritic catalyst.

In summary, we have shown that cross-linked Sc-containing dendrimers of the type **3** are stable, effective, and environmentally benign heterogeneous catalysts with Lewis acidic properties. They can be handled in air, used in aqueous or organic medium, and are easily recycled and reused without any appreciable loss of catalytic activity.[8] The concept of metal-induced cross-linking of appropriate dendrimers may well lead to new and efficient heterogeneous catalysts in other cases as well, for example in Al analogues of **3**.



Experimental Section

Preparation of **3**: To the solution of dendrimer **1**[6] (233 mg, 2.12 mmol) in dry 1,2-dichloroethane (5 mL) was added dropwise trifluoromethane sulfonic acid anhydride (370 µL, 2.20 mmol). Triethylamine (310 µL, 2.2 mmol) was then added dropwise and the mixture was stirred for 30 min at −20 °C. Thereafter the mixture was stirred at 60 °C for 15 h, the solvent was removed and the residue was washed three times with H_2O, 5% NaOH, dioxane, and diethyl ether, respectively, providing **2** (476 mg; > 90%) as a light brown solid. To the stirred suspension of **2** (432 mg, 1.8 mmol) in THF (10 mL) was added carefully potassium hydride (72 mg, 1.8 mmol). The mixture was stirred at 22 °C for 10 min, and the highly viscous solution was treated with scandium(III) trifluoromethane sulfonate ($Sc(OTf)_3$) (886 mg, 1.8 mmol). After the mixture had been stirred for 24 h, a brown gel had formed which was freed from the solvent in vacuo. The residue was washed three times with H_2O, diethyl ether, and H_2O/diethyl ether, respectively, to yield a light brown solid material which was dried in vacuo (0.9 g; ca. 80%).

Procedure for the three-component reaction of **4**, **5**, and **6** with **3**: To the two-phase system composed of benzaldehyde (**4**) (53 mg, 0.5 mmol), aniline (**5**) (46.6 mg, 0.5 mmol), enolsilane **6** (155 mg, 0.75 mmol), and H_2O (3 mL) was added the catalyst **3** (30 mg, 7 mol% Sc), and the mixture was vigorously stirred for 18 h at 22 °C. The catalyst was filtered off and washed with H_2O (10 mL) and twice with dichloromethane (10 mL). The aqueous phase was washed with dichlormethane (10 mL), the combined organic phases were dried over $MgSO_4$ and the residue following removal of the solvent was subjected to flash chromatography using petroleum ether/ethyl ester (9/1) on silica gel: 140 mg (89%) **7** as a 1:1 diastereomer mixture.

Received: February 17, 2000 [Z 14730]

[1] a) G. R. Newkome, C. N. Moorefield, F. Vögtle, *Dendritic Molecules: Concepts—Syntheses–Perspectives*, VCH, Weinheim, **1996**; b) F. J. Stoddart, T. Welton, *Polyhedron* **1999**, *18*, 3575–3591; c) J. W. J. Knapen, A. W. van der Made, J. C. de Wilde, P. W. N. M. van Leeuwen, P. Wijkens, D. M. Grove, G. van Koten, *Nature* **1994**, *372*, 659–663; d) M. T. Reetz, G. Lohmer, R. Schwickardi, *Angew. Chem.* **1997**, *109*, 1559–1562; *Angew. Chem. Int. Ed. Engl.* **1997**, *36*, 1526–1529; e) H. Brunner, *J. Organomet. Chem.* **1995**, *500*, 39–46; f) C. Bolm, N. Derrien, A. Seger, *Synlett* **1996**, 387–388; g) P. Bhyrappa, J. K. Young, J. S. Moore, K. S. Suslick, *J. Am. Chem. Soc.* **1996**, *118*, 5708–5711; h) G. E. Oosterom, R. J. van Haaren, J. N. H. Reek, P. C. J. Kamer, P. W. N. M. van Leeuwen, *Chem. Commun.* **1999**, 1119–1120; i) J.-J. Lee, W. T. Ford, J. A. Moore, Y. Li, *Macromolecules* **1994**, *27*, 4632–4634; j) N. J. Hovestad, E. B. Eggeling, H. J. Heidbuchel, J. T. B. H. Jastrzebski, U. Kragl, W. Keim, D. Vogt, G. van Koten, *Angew. Chem.* **1999**, *111*, 1763–1765; *Angew. Chem. Int. Ed.* **1999**, *38*, 1655–1658; k) D. de Groot, J. C. de Wilde, R. J. van Haaren, J. N. H. Reek, P. C. J. Kamer, P. W. N. M. van Leeuwen, E. B. Eggeling, D. Vogt, H. Kooijman, A. L. Spek, A. W. van der Made, *Chem. Commun.* **1999**, 1623–1624; l) C. Köllner, B. Pugin, A. Togni, *J. Am. Chem. Soc.* **1998**, *120*, 10274–10275; m) U. Lüning, T. Marquardt, *J. Prakt. Chem.* **1999**, *341*, 222–227; n) N. Brinkmann, D. Giebel, G. Lohmer, M. T. Reetz, U. Kragl, *J. Catal.* **1999**, *183*, 163–168; o) T. Mizugaki, M. Ooe, K. Ebitani, K. Kaneda, *J. Mol. Catal. A* **1999**, *145*, 329–333; p) C. Schlenk, H. Frey,

 © WILEY-VCH Verlag GmbH, D-69451 Weinheim, 2000 1433-7851/00/3914-2500 $ 17.50+.50/0

Monatsh. Chem. **1999**, *130*, 3–14; q) S. C. Bourque, F. Maltais, W.-J. Xiao, O. Tardif, H. Alper, P. Arya, L. E. Manser, *J. Am. Chem. Soc.* **1999**, *121*, 3035–3038; r) C. Bolm, N. Derriem, A. Seger, *Chem. Commun.* **1999**, 2087–2088.

[2] Cross-linked dendrimers as polymers without catalytic properties: a) N. Moszner, T. Volkel, V. Rheinberger, *Macromol. Chem. Phys.* **1996**, *197*, 621–631; b) M. Trollsås, M. A. Kelly, H. Claesson, R. Siemens, J. L. Hedrick, *Macromolecules* **1999**, *32*, 4917–4924.

[3] Cross-linked enzymes (CLECs) as catalysts: N. S. Clair, Y.-F. Wang, A. L. Margolin, *Angew. Chem.* **2000**, *112*, 388–391; *Angew. Chem. Int. Ed.* **2000**, *39*, 380–383, and references therein.

[4] a) A different concept has been used by Seebach, et al., according to which modified TADDOLs having styrene units in the outer first-generation dendritic branches are embedded in a cross-linked organic polymer by copolymerization with styrene, followed by treatment with $Ti(OiPr)_4$ with formation of recyclable Ti catalysts: H. Sellner, D. Seebach, *Angew. Chem.* **1999**, *111*, 2039–2041; *Angew. Chem. Int. Ed.* **1999**, *38*, 1918–1920. Numerous related examples of the embedment of ligands in cross-linked polymers are known, for example: b) S. J. Fritschel, J. J. H. Ackerman, T. Keyer, J. K. Stille, *J. Org. Chem.* **1979**, *44*, 3152–3157; c) S. Itsuno, Y. Sakurai, K. Ito, T. Maruyama, S. Nakahama, J. M. J. Fréchet, *J. Org. Chem.* **1990**, *55*, 304–310; d) K. Nozaki, Y. Itoi, F. Shibahara, E. Shirakawa, T. Ohta, H. Takaya, T. Hiyama, *J. Am. Chem. Soc.* **1998**, *120*, 4051–4052.

[5] a) S. Kobayashi, *Eur. J. Org. Chem.* **1999**, 15–27; b) S. Kobayashi, S. Nagayama, *J. Am. Chem. Soc.* **1996**, *118*, 8977–8978; c) S. Kobayashi, S. Nagayama, *Synlett* **1997**, 653–654; d) D. Longbottom, *Synlett* **1999**, 2023.

[6] Dendrimer **1** and other poly(amino) dendrimers are commercially available (Aldrich).

[7] Discussion concerning the limitations of the BET method: a) B. C. Gates, *Catalytic Chemistry*, Wiley, New York, **1992**; b) J. Seifert, G. Emig, *Chem. Ing. Tech.* **1987**, *59*, 475–484.

[8] In order to further increase mechanical stability, we were able to show in preliminary experiments that **3**, once ground in a mortar, can be entrapped in silica matrices using a sol–gel procedure, $Si(OCH_3)_4$ or $CH_3Si(OCH_3)_3$ serving as the precursors. Such gels are catalytically active.

A New Palladium-Catalyzed Intramolecular Cyclization: Synthesis of 1-Aminoindole Derivatives and Functionalization of their Carbocylic Rings

Makoto Watanabe,* Toshihide Yamamoto, and Masakazu Nishiyama

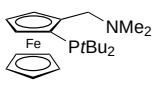
Palladium-catalyzed cyclization reactions are a versatile and efficient method for the synthesis of a large number of heterocycles.[1] The formation of the indole ring system is of interest and has been carried out by many methods[2] because indole derivatives exhibit pharmacological[3] and physiological activity.[4] The palladium-catalyzed synthesis of indoles from *o*-haloaniline precursors is one of the most useful methods for the preparation of this class of compounds.[5]

[*] Dr. M. Watanabe, T. Yamamoto, M. Nishiyama
Yokkaichi Research Laboratory
Tosoh Corporation
1–8 Kasumi, Yokkaichi, Mie 510-8540 (Japan)
Fax: (+81) 593-63-2641
E-mail: m_wata@tosoh.co.jp

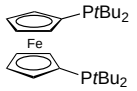
Supporting information for this article is available on the WWW under http://www/wiley-vch.de/home/angewandte/ or from the author.

Palladium-catalyzed C–N bond formation of amines with aryl halides recently proved to be a versatile method for the synthesis of a wide range of arylamines.[6] Transformation of the amination products into indole derivatives was examined. First, palladium-catalyzed cyclization of *o*-bromo-*β*-phenethylamines followed by dehydrogenation of the resulting indolines with Pd/C gave indoles with substituents in the 7-position.[7] Second, palladium-catalyzed coupling of benzophenone hydrazone with aryl bromides was also reported to give *N*-arylhydrazones, which were used as substrates for Fischer indole synthesis.[8] However, palladium-catalyzed direct formation of the indole ring by N-arylation of aryl halides has not been reported.

However, palladium catalyst systems employing P*t*Bu$_3$ and mono- and bidentate phosphanes bearing P–*t*Bu bonds were reported for amination,[9] aryl ether formation,[10] Suzuki coupling,[9b, 11] the Heck reaction,[12] and ketone arylation,[13] after we disclosed that bulky electron-rich P*t*Bu$_3$ afforded much higher catalytic activity than other phosphanes in the palladium-catalyzed amination of aryl halides with both aliphatic and aromatic amines.[14] One of the advantages of such phosphanes is the possibility of using unreactive aryl chlorides as substrates. Here we report a new method for the direct conversion of *o*-chloroarylacetaldehyde *N*,*N*-disubstituted hydrazones (**1**) into 1-aminoindole derivatives **2** and **4** by palladium-catalyzed intramolecular ring closure of **1** in the presence of P*t*Bu$_3$, 1,1′-bis(di-*tert*-butylphosphanyl)ferrocene (DB^{t}PF), and 2-(dimethylaminomethyl)-1-(di-*tert*-butylphosphanyl)ferrocene (**3**) as ligands [see Eqs. (1) and (2)].



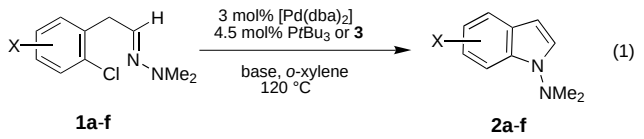
3



DB^{t}PF

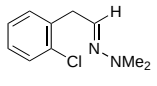
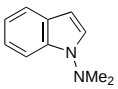
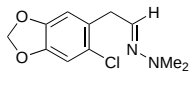
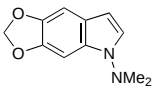
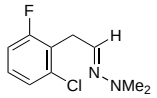
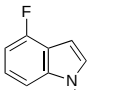
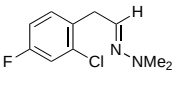
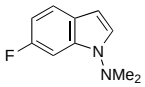
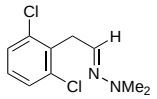
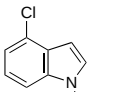
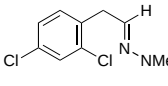
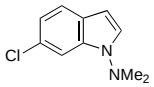
o-Chloroarylacetaldehydes can be synthesized from commercially available *o*-chloroarylmethyl chlorides.[10c] Hydrazone derivatives **1** were prepared from the above aldehydes and *N*,*N*-disubstituted hydrazines, and isolated in 90–93% yield by distillation.[15] The palladium-catalyzed cyclization of **1** gave a 1-aminoindole ring system. The results of the indolization of **1** are summarized in Table 1. The reaction with sodium *tert*-butoxide in *o*-xylene at 120 °C in the presence of [Pd_2(dba)$_3$] (dba = dibenzylideneacetone) and a bulky electron-rich phosphane gave a moderate yield of 1-(dimethylamino)indole (entry 1). A low yield was obtained in dioxane (entry 2). Whereas the yield of the reaction with the bidentate bis-phosphane DB^{t}PF[16] was lower than with P*t*Bu$_3$ (entry 3), the reaction in the presence of the P,N ligand **3** gave 78% yield (entry 4).[17] Although many P,N ligands bearing *t*Bu–P bonds are available, we chose **3** because it can be readily synthesized in one step from commercially available dimethylaminomethylferrocene.[18] Cs_2CO_3 and Rb_2CO_3 could also be used as bases (entries 5 and 6). Synthesis of indoles with substituents on the carbocyclic rings was also possible (entries 7–9). Since indole derivatives bearing a Cl substituent on the carbocyclic ring can be utilized as substrates for more elaborate indoles in palladium-catalyzed reactions such as

 © WILEY-VCH Verlag GmbH, D-69451 Weinheim, 2000 1433-7851/00/3914-2501 $ 17.50+.50/0



1a-f **2a-f**

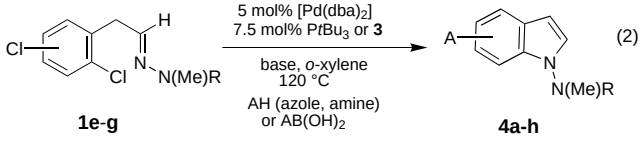
Table 1. Palladium-catalyzed intramolecular cyclization of *o*-chloroarylacetaldehyde *N*,*N*-dimethylhydrazones **1**.[a]

Entry	Substrate	Ligand	Base	Product	Yield [%][b]
1	 **1a**	P*t*Bu$_3$	NaO*t*Bu	 **2a**	39 (42)
2[c]	**1a**	P*t*Bu$_3$	NaO*t*Bu	**2a**	(7)
3	**1a**	DB^{t}PF	NaO*t*Bu	**2a**	(28)
4	**1a**	**3**	NaO*t*Bu	**2a**	73 (78)
5	**1a**	**3**	Cs_2CO_3	**2a**	(75)
6	**1a**	**3**	Rb_2CO_3	**2a**	(73)
7	 **1b**	**3**	NaO*t*Bu	 **2b**	30
8	 **1c**	**3**	NaO*t*Bu	 **2c**	60
9	 **1d**	**3**	NaO*t*Bu	 **2d**	74
10	 **1e**	P*t*Bu$_3$	NaO*t*Bu	 **2e**	46
11	**1e**	**3**	NaO*t*Bu	**2e**	34
12	**1e**	**3**	Cs_2CO_3	**2e**	33
13[d]	**1e**	**3**	NaO*t*Bu	**2e**	48
14	 **1f**	P*t*Bu$_3$	Rb_2CO_3	 **2f**	18

[a] All reactions were carried out with 3 mol% of [Pd(dba)$_2$], 4.5 mol% of **3** or P*t*Bu$_3$, 1.2 equiv of base, and 1.5–2.2 mmol of substrate at 120 °C for 2–20 h in *o*-xylene, unless otherwise noted. [b] Yield of product isolated by column chromatography on Al_2O_3 (elution with hexane/diethyl ether). Yields in parentheses were measured by GC analysis with *tert*-butylbenzene as internal standard. [c] Dioxane was used in place of *o*-xylene. [d] The reaction was carried out with 6 mol% of [Pd(dba)$_2$] and 9 mol% of **3**.

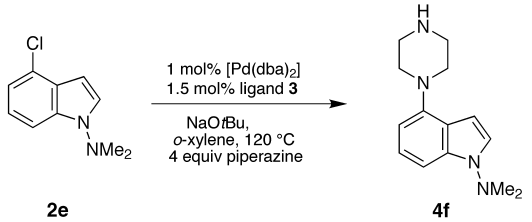
aminationand Suzuki coupling, we attempted cyclization of dichloroarylacetaldehyde hydrazones. Indeed, 4-chloro- and 6-chloro-1-dimethylaminoindoles were obtained (entries 10–14). A slightly higher yield was obtained by using P*t*Bu$_3$. The catalytic cycle is terminated when oxidative addition of these chloroindoles to Pd^0 species takes place in this reaction. Therefore, yields of chloroindoles are lower than those of unsubstituted indoles and fluoroindoles, and the yield increases with a larger amount of catalyst (entry 13).

Although chloroindole derivatives are attractive intermediates for synthesis of amino- and aryl-functionalized indoles, isolation of chloroindoles is expected to be unnecessary in the case of cyclization with coupling reagents that can react with the intermediate chloroindoles **2e–f** and **1** (X = Cl) and thus circumvent the termination of the catalytic cycle. Therefore, we examined a palladium-catalyzed cyclization of **1** (X = Cl) in the presence of phenylboronic acid, azoles, and amines to give 4- and 6-substitued indole derivatives **4** [Eq. (2)]. The



1e-g **4a-h**

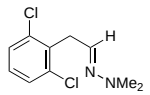
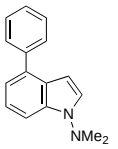
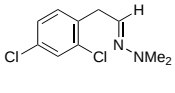
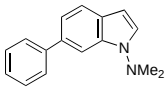
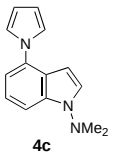
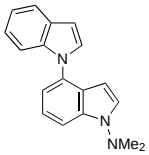
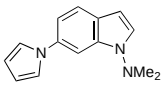
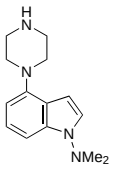
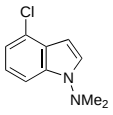
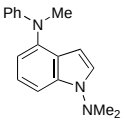
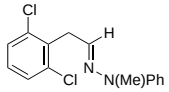
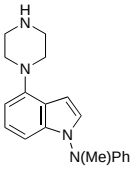
results are summarized in Table 2. Cyclization in the presence of phenylboronic acid gave 4- and 6-phenylindole derivatives **4a** and **4b** in one-pot reactions (entries 1–3). A slightly higher yield was obtained with ligand **3**. In this reaction, Suzuki coupling took place five times faster than the formation of chloroindole (2 h at 120 °C), and the conversion of the intermediate into the indole compound was then monitored by GC analysis. Reactions with azoles gave the azolylindoles **4c–e** (entries 4–7). In this case P*t*Bu$_3$ was superior to **3**, which gave only traces of **4c** and a low yield of the intermediate chloroindole **2e** (entry 4).[19] Rb_2CO_3 was preferably used because it was the most effective base in a Pd(OAc)$_2$/P*t*Bu$_3$-catalyzed synthesis of *N*-arylazoles from aryl halides and azoles.[20] Cyclization with amines was also examined. The reaction with piperazine in the presence of P*t*Bu$_3$ afforded dechlorinated derivatives of **1e** and formation of only traces of the indole nucleus (entry 9). However, the piperazinylindole **4f** was obtained with ligand **3** (entry 8). The presence of an *N*-methyl-*N*-phenylhydrazone moiety did not influence the yield (entry 12). Whereas cyclization with *N*-methylaniline gave the desired product **4g** (entry 11), the use of *N*-methylpiperazine resulted in selective formation of the 4-chloroindole derivative **2e** (entry 10). The initial formation of the chloroindole ring by C–N bond formation using azoles and amines occurred without formation of the product from the reaction of **1** with the azoles and amines. This result is in sharp contrast to C–C bond formation with phenylboronic acid. The yields obtained with amines are lower than those with phenylboronic acid and azoles. The reason might be a low tolerance of the acetaldehyde hydrazone moiety toward amines, since the reaction of isolated 4-chloro-1-dimethylaminoindole (**2e**) with piperazine at 120 °C for 2 h with palladium/**3** as catalyst furnished the desired 4-piperazinylindole (**4f**) in 94% yield [Eq. (3)].



2e **4f**

 © WILEY-VCH Verlag GmbH, D-69451 Weinheim, 2000 1433-7851/00/3914-2502 $ 17.50+.50/0 *Angew. Chem. Int. Ed.* **2000**, *39*, No. 14

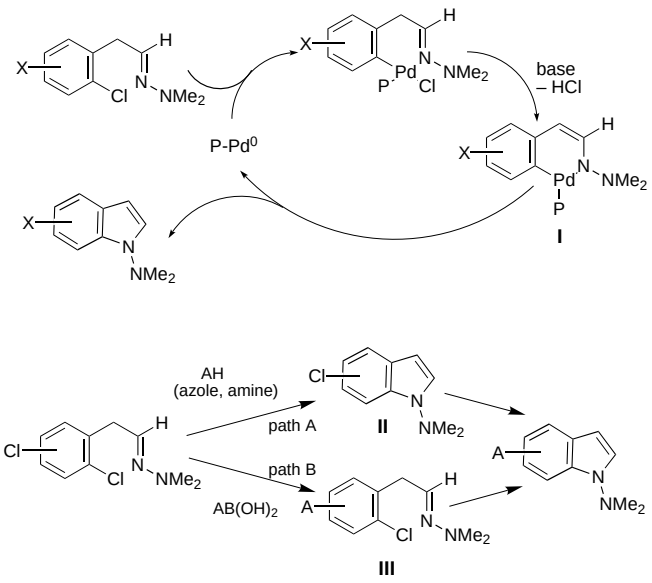
Table 2. Palladium-catalyzed synthesis of 4- and 6-substituted indoles.[a]

Entry	Substrate	Reagent	Ligand	Base	Product	Yield [%][b]
1	 **1e**	$PhB(OH)_2$	**3**	Cs_2CO_3	 **4a**	56
2	**1e**	$PhB(OH)_2$	P*t*Bu_3	Cs_2CO_3	**4a**	40
3	 **1f**	$PhB(OH)_2$	**3**	Cs_2CO_3	 **4b**	29
4	**1e**	pyrrole	**3**	Cs_2CO_3	 **4c**	Spur
5	**1e**	pyrrole	P*t*Bu_3	Rb_2CO_3	**4c**	54
6	**1e**	indole	P*t*Bu_3	Rb_2CO_3	 **4d**	40
7	**1f**	pyrrole	P*t*Bu_3	Rb_2CO_3	 **4e**	24
8[c]	**1e**	piperazine	**3**	NaO*t*Bu	 **4f**	30
9[c]	**1e**	piperazine	P*t*Bu_3	NaO*t*Bu	**4f**	trace
10	**1e**	*N*-methyl-piperazine	**3**	NaO*t*Bu	 **2e**	38
11	**1e**	PhN(Me)H	**3**	NaO*t*Bu	 **4g**	39
12[c]	 **1g**	piperazine	**3**	NaO*t*Bu	 **4h**	33

[a] All reactions were performed with 5 mol % of $[Pd(dba)_2]$, 7.5 mol % of **3** or P*t*Bu_3, 1.1 equiv of reagent, 2.2 equiv of base, and 1.5 mmol of substrate at 120 °C for 24 – 48 h in *o*-xylene, unless otherwise noted. [b] Yield of product isolated by column chromatography on Al_2O_3 (elution with hexane/diethyl ether for entries 1 – 7, 10, and 11; ethyl acetate/methanol for entries 8 and 12). [c] 4 equiv of piperazine relative to the substrate was used.

We also attempted the conversion of **1e** into 4-substituted indole derivatives using butyl acrylate and tribuyltin amides. Whereas cyclization followed by a Heck reaction took place to give approximately 10 % yield of the desired product (GC analysis), no products were obtained in the presence of the tin reagents.

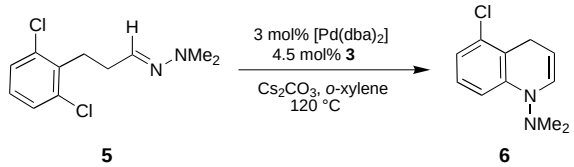
We believe that indole ring formation takes place via the aryl(enamido)palladium complex **I** (Scheme 1), although the mechanistic details of the reaction remain unknown.[21] When



Schema 1. Reaction pathways to the substituted indole derivatives and a plausible reaction sequence (neutral ligands are omitted for clarity).

coupling agents are present in the reaction mixture, the order of the cyclization and coupling reactions depends on the nature of the reagents. Chloroindole derivatives **II** were selectively formed as intermediates in the cases of azoles and amines (Scheme 1, path A), while the intermediate **III** was formed regardless of the position of the Cl substituent with phenylboronic acid (Scheme 1, path B). This means that C–C bond formation with $ArB(OH)_2$ is faster than both formation of the the indole ring and C–N bond formation with azoles and amines.

This palladium-catalyzed intramolecular indole formation could be extended to the formation of other heterocycles such as 1-amino-4*H*-quinolines. For instance, 2,6-dichlorophenylpropionaldehyde *N*,*N*-dimethylhydrazone (**5**)[22] was converted to 5-chloro-1-(dimethylamino)- 4*H*-quinoline (**6**) in 32 % yield [Eq. (4)].



5 **6** (4)

In conclusion, we have found a new palladium-catalyzed synthesis of indole rings that provides access to a wide range

of 1-aminoindoles that could formerly be synthesized by only limited methods.[23] This methodology also allows sequential reactions of this new cyclization and known palladium-catalyzed reactions with nucleophilic reagents in a single procedural operation to furnish indole derivatives with substituents on the carbocyclic rings. Indole derivatives that are not functionalized at both the 2- and 3-positions could be synthesized by using arylacetaldehyde hydrazones as substrates. Such compounds are important for the synthesis of more elaborate indole derivatives, because these positions can be easily functionalized by several methods.[5a,b] Furthermore, this methodology can be extended to the construction of six-membered ring systems such as 4*H*-quinolines.

Received: January 17, 2000 [Z14549]

[1] Reviews: S. Cacchi, *J. Organomet. Chem.* **1999**, *576*, 42 – 64; R. Grigg, V. Sridharan, *J. Organomet. Chem.* **1999**, *576*, 65 – 87; R. C. Larock, *J. Organomet. Chem*. **1999**, *576*, 111 – 124.

[2] Reviews: a) U. Pindur, R. Adam, *J. Heterocycl. Chem.* **1988**, *25*, 1 – 8; b) G. W. Gribble, *Contemp. Org. Synth.* **1994**, *1*, 145 – 172.

[3] R. J. Sundberg, *Indole*, Academic Press, London, **1996**.

[4] G. W. Gribble, *Comprehensive Heterocyclic Chemistry II*, *Vol. 2*, Pergamon, Oxford, **1996**, pp. 207 – 257.

[5] a) L. S. Hegedus, *Angew. Chem.* **1988**, *100*, 1147 – 1160; *Angew. Chem. Int. Ed. Engl.* **1988**, *27*, 1113 – 1126; b) J. Tsuji, *Palladium Reagents and Catalysis*, Wiley, Chichester, **1995**; c) C.-Y. Chen, D. R. Lieberman, R. D. Larsen, T. R. Verhoeven, P. J. Reider, *J. Org. Chem.* **1997**, *62*, 2676 – 2677; d) B. C. Söderberg, J. A. Shriver, *J. Org. Chem.* **1997**, *62*, 5838 – 5845; e) Y. Dong, C. A. Busacca, *J. Org. Chem.* **1997**, *62*, 6464 – 6465; f) Y. Kondo, S. Kojima, T. Sakamoto, *J. Org. Chem.* **1997**, *62*, 6507 – 6511; g) R. C. Larock, E. K. Yum, M. D. Refvik, *J. Org. Chem.* **1998**, *63*, 7652 – 7662.

[6] Reviews: a) J. F. Hartwig, *Angew. Chem.* **1998**, *110*, 2154 – 2177; *Angew. Chem. Int. Ed.* **1998**, *37*, 2046 – 2067; b) B. H. Yang, S. L. Buchwald, *J. Organomet. Chem.* **1999**, *576*, 125 – 146.

[7] K. Aoki, A. J. Peat, S. L. Buchwald, *J. Am. Chem. Soc.* **1998**, *120*, 3068 – 3073.

[8] S. Wagaw, B. H. Yang, S. L. Buchwald, *J. Am. Chem. Soc.* **1998**, *120*, 6621 – 6622; *J. Am. Chem. Soc.* **1999**, *121*, 10251 – 10263.

[9] a) B. C. Hamann, J. F. Hartwig, *J. Am. Chem. Soc.* **1998**, *120*, 7369 – 7370; b) J. P. Wolfe, S. L. Buchwald, *Angew. Chem.* **1999**, *111*, 2570 – 2573; *Angew. Chem. Int. Ed.* **1999**, *38*, 2413 – 2416; c) J. F. Hartwig, M. Kawatsura, S. I. Hauck, K. H. Shaughnessy, L. M. Alcazar-Roman, *J. Org. Chem.* **1999**, *64*, 5575 – 5580.

[10] a) G. Mann, C. Incarvito, A. L. Rheingold, J. F. Hartwig, *J. Am. Chem. Soc.* **1999**, *121*, 3224 – 3225; b) A. Aranyos, D. W. Old, A. Kiyomori, J. P. Wolfe, J. P. Sadighi, S. L. Buchwald, *J. Am. Chem. Soc.* **1999**, *121*, 4369 – 4378; c) M. Watanabe, M. Nishiyama, Y. Koie, *Tetrahedron Lett.* **1999**, *40*, 8837 – 8840.

[11] A. F. Littke, G. C. Fu, *Angew. Chem.* **1998**, *110*, 3586 – 3587; *Angew. Chem. Int. Ed.* **1998**, *37*, 3387 – 3388; J. P. Wolfe, R. A. Singer, B. H. Yang, S. L. Buchwald, *J. Am. Chem. Soc.* **1999**, *121*, 9550 – 9561.

[12] A. F. Littke, G. C. Fu, *J. Org. Chem.* **1999**, *64*, 10 – 11; K. H. Shaughnessy, P. Kim, J. F. Hartwig, *J. Am. Chem. Soc.* **1999**, *121*, 2123 – 2132.

[13] M. Kawatsura, J. F. Hartwig, *J. Am. Chem. Soc.* **1999**, *121*, 1473 – 1478; J. M. Fox, X. Huang, A. Chieffi, S. L. Buchwald, *J. Am. Chem. Soc.* **2000**, *122*, 1360 – 1370.

[14] M. Nishiyama, T. Yamamoto, Y. Koie, *Tetrahedron Lett.* **1998**, *39*, 617 – 620; T. Yamamoto, M. Nishiyama, Y. Koie, *Tetrahedron Lett.* **1998**, *39*, 2367 – 2370.

[15] We attempted to prepare the corresponding imine from **1** and benzylamine. However, the imine was thermally unstable and was not tolerated by the palladium-catalyzed reaction.

[16] W. R. Cullen, T. J. Kim, F. W. B. Einstein, T. Jones, *Organometallics* **1983**, *2*, 714 – 719.

[17] For a comparison between a biphenyl P,N ligand and a binaphthyl P,P ligand, see D. W. Old, J. P. Wolfe, S. L. Buchwald, *J. Am. Chem. Soc.* **1998**, *120*, 9722 – 9723.

[18] For lithiation of dimethylaminomethylferrocene at the 2-position with *n*-butyllithium, see D. W. Slocum, B. W. Rockett, C. R. Hauser, *J. Am. Chem. Soc.* **1965**, *87*, 1241 – 1246. We used *tert*-butyllithium to obtain a higher yield of **3**.

[19] The use of Cs_2CO_3 and Rb_2CO_3 with ligand **3** gave chloroindole **2e** in 4 and 21 % yield, respectively. Rb_2CO_3 also gave a trace of the desired product **4c**.

[20] M. Watanabe, M. Nishiyama, T. Yamamoto, Y. Koie, *Tetrahedron Lett.* **2000**, *41*, 481 – 483.

[21] We assume that intramolecular binding of the nitrogen atom of the imino group to the aryl(chloro)palladium complex facilitates deprotonation of the resulting complex to give **I**. Miura et al. recently reported the synthesis of benzofurans by means of a palladium-catalyzed intramolecular C–O bond formation: Y. Terao, T. Satoh, M. Miura, M. Nomura, *Bull. Chem. Soc. Jpn.* **1999**, *72*, 2345 – 2350.

[22] (2,6-dichlorophenyl)propionaldehyde was prepared from 2,6-dichlorobenzyl chloride and *N*-cyclohexyliminoacetaldehyde in diethyl ether. For the lithiation of *N*-cyclohexyliminoacetaldehyde with lithium diisopropylamide, see G. Wittig, A. Hesse, *Org. Synth. Coll. Vol. 6*, **1988**, 901 – 904.

[23] B. A. Frontana-Uribe, C. Moinet, L. Toupet, *Eur. J. Org. Chem.* **1999**, 419 – 430, and references therein.

Spin Crossover in a Supramolecular Fe_4^{II} [2 × 2] Grid Triggered by Temperature, Pressure, and Light**

Esther Breuning, Mario Ruben, Jean-Marie Lehn,* Franz Renz, Yann Garcia, Vadim Ksenofontov, Philipp Gütlich,* Elina Wegelius, and Kari Rissanen

In memory of Oliver Kahn

The development of advanced materials and devices for nanotechnology requires systems that form switchable domains on the molecular or supramolecular level, so as to

[*] Prof. Dr. J.-M. Lehn, E. Breuning, Dr. M. Ruben
Laboratoire de Chimie Supramoléculaire
ISIS-Université Louis Pasteur
4, rue Blaise Pascal, 67000 Strasbourg (France)
Fax: (+33) 388411020
E-mail: lehn@chimie.u-strasbg.fr

Prof. Dr. P. Gütlich, Dr. F. Renz, Dr. Y. Garcia, Dr. V. Ksenofontov
Institut für Anorganische Chemie und Analytische Chemie
Johannes Gutenberg-Universität Mainz
Staudingerweg 9, 55099 Mainz (Germany)
Fax: (+49) 6131-392-2990
E-mail: p.guetlich@uni-mainz.de

E. Wegelius, Prof. K. Rissanen
Department of Chemistry
University of Jyväskylä
P.O. Box 35, 40351 Jyväskylä (Finland)

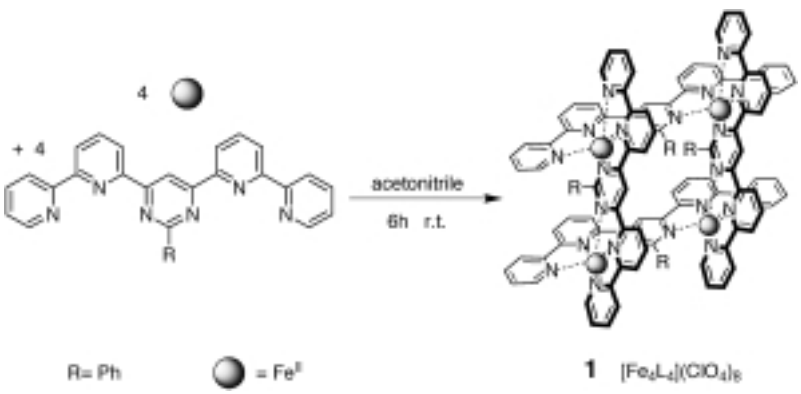
[**] This work was partly funded by the TMR Research Network ERB-FMRX-CT98-0199 entitled "Thermal and Optical Switching of Molecular Spin States (TOSS)" (Y.G., F.R.), the Fonds der chemischen Industrie, and the Universität Mainz. M.R. thanks the Deutscher Akademischer Austauschdienst (DAAD) for a postdoctoral scholarship. Financial support from Finnish Ministry of Education (E.W.) and from Ministère de l'Education Nationale, de la Recherche et de la Technologie (E.B.) is gratefully acknowledged.

 © WILEY-VCH Verlag GmbH, D-69451 Weinheim, 2000 1433-7851/00/3914-2504 $ 17.50+.50/0

enable a highly efficient information storage.[1] Towards this end, a promising and challenging field of research is the study of spin crossover (SC) compounds.[2] The phenomenon of spin crossover between low-spin (LS) and high-spin (HS) states is one of the most appealing examples of molecular bistability.[3, 4]

It has been shown that molecular systems of the [2 × 2] grid type with exactly four precisely located transition metal ions are accessible by self-organization.[5, 6] With respect to potential addressability, such architectures can be ordered on surfaces in regularly packed domains of monolayers, and even single molecules can be manipulated by means of scanning tunneling microscopy (STM).[7] The transition metal ions in [2 × 2] grid-like structures are situated in an octahedral ligand field. Introduction of sterically demanding substituents attenuates the ligand field strength to a magnitude that enables SC behavior for certain metal ions. Herein, we present the first triply switchable system, the Fe_4^{II} [2 × 2] grid **1**, in which SC can be triggered by temperature, light, and pressure.

$[Fe_4L_4](ClO_4)_8$ (**1**) was synthesized by spontaneous assembly from the ligand 4,6-bis(2′,2″-bipyrid-6′-yl)-2-phenyl-pyrimidine[8] (L) and $Fe(ClO_4)_2 \times 6H_2O$ in acetonitrile at room temperature, followed by precipitation with diethyl ether. The composition of **1** was confirmed by FAB mass spectrometry and elemental analysis.



Indications of SC behavior in solution were first obtained in the course of ^{1}H NMR investigations (Figure 1). At 308 K, **1** exhibits the number of signals expected for a symmetrically coordinated ligand, in a range from $\delta = -20$ to 130, typical for paramagnetic HS species.[9] Upon stepwise cooling to 228 K, several peaks between $\delta = 0$ and 10, that is the typical region for diamagnetic LS species, emerge at the expense of the paramagnetic peaks, ending up in a mainly diamagnetic situation.

The structure of **1** was determined by single-crystal X-ray diffraction at 293 K and 100 K (Figure 2).[10] The investigation reveals a tetranuclear complex in which each of the Fe^{II} ions is in a pseudooctahedral arrangement with a pronounced axial distortion (Δ_{ax} = ca. −0.1 Å). Each metal ion is surrounded by six nitrogen atoms arising from the pyrimidine and bipyridine units. Since the Fe–N bond lengths differ considerably between the HS and LS case ($\Delta d = 0.2 - 0.3$ Å), the averaged

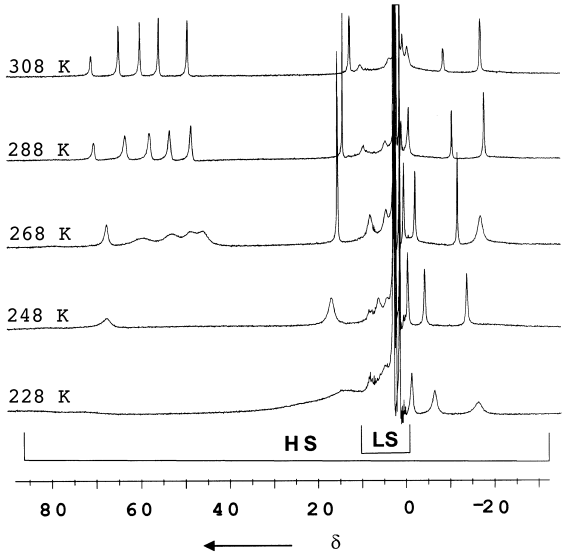


Figure 1. Variable-temperature ^{1}H NMR studies of **1** exhibiting the increase of LS fraction at the expense of the HS fraction on lowering the temperature (in [D_6]acetone/[D_6]acetonitrile).

bond lengths can be directly related to the actual spin state of each Fe^{II} ion. At room temperature, three of the Fe^{II} ions stay in the HS state (d(Fe–N) = 2.086(5) – 2.287(4) Å) with the fourth exhibiting bond lengths intermediate between both states (d(Fe–N) = 1.977(5) – 2.162(4) Å). At 100 K, three of them are between the LS and HS state but closer to the LS state (d(Fe–N) = 1.895(6) – 2.117(5) Å), while the fourth remains in the HS state (d(Fe–N) = 2.116(6) – 2.282(5) Å). This decrease in bond lengths, which is significantly larger than the thermal contraction, indicates clearly a SC behavior from HS to LS for some Fe^{II} ions. The same space group $P\bar{1}$ for **1**, is retained at both temperatures; there is no crystallographic phase transition.

The magnetic properties of **1** are represented in Figure 3a in the form of the $\chi_M T/4$ versus T curve, in which χ_M is the molar magnetic susceptibility, corrected for diamagnetic contributions ($\chi_D = -357.8 \times 10^6$ cm^3 mol^{-1}) using Pascal's constants, and T is the temperature.

At room temperature, $\chi_M T/4$ is equal to 2.5 cm^3 K mol^{-1} and thus in the range of values expected for three HS Fe^{II} ions and one LS Fe^{II} ion, since the spin-only value for a Fe^{II} ion in the HS state ($S = 2$) is 3.0 cm^3 K mol^{-1}. On lowering the temperature, $\chi_M T/4$ progressively decreases reaching a value of 1.4 cm^3 K mol^{-1} at 30 K; below this temperature, $\chi_M T/4$ drops down. This can be attributed to zero-field splitting. No hysteresis was observed.

We also investigated the magnetic properties of the BF_4^- salt of **1** under pressure (because of the hazard of explosion with perchlorate salts). Pressure dramatically affects the SC curve, decreasing the $\chi_M T/4$ values over the whole temperature range (e.g. by 0.5 cm^3 K mol^{-1} at 300 K and 8.4 kbar). This corresponds to a shift of the SC curve to higher temperatures as a result of the lower volume for the LS Fe^{II} ions.

 © WILEY-VCH Verlag GmbH, D-69451 Weinheim, 2000 1433-7851/00/3914-2505 $ 17.50+.50/0

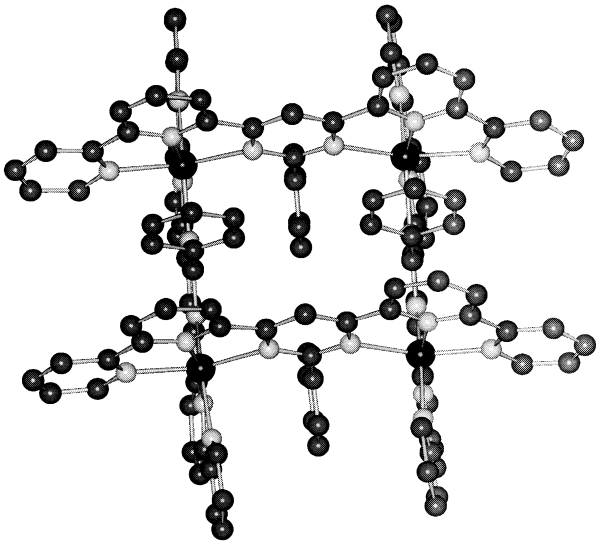


Figure 2. Molecular structure of the cation of **1** at 293 K (anions and solvent molecules are omitted for clarity). The structure of **1** has also been determined at 100 K. The averaged Fe–N distances [Å]: 1) at 293 K: 2.19(1) (HS), 2.17(1) (HS), 2.07(1) (HS/LS), 2.17(1) (HS); 2) at 100 K: 2.20(1) (HS), 2.01(1) (LS/HS), 1.99(1) (LS/HS), 2.01(1) (LS/HS).

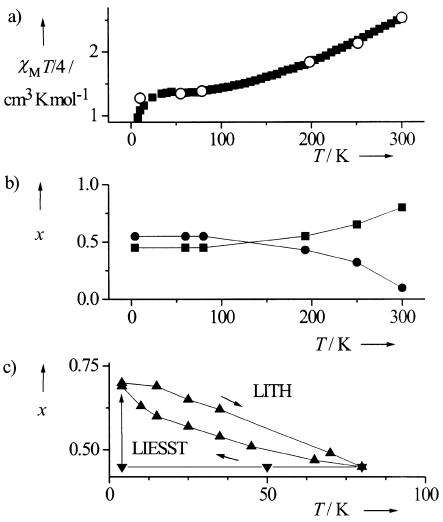


Figure 3. a) Calculated (circles) and experimental (squares) $\chi_M T/4$ versus T plots for a powder sample of **1** (calculated $\chi_M T/4$ values derived from molar fractions); b) HS (squares) and LS (points) molar fractions plotted versus T showing the thermally induced SC; c) LIESST (light-induced excited spin state trapping; irradiation at $\lambda = 514$ nm at 4.2 K) and LITH (permanent irradiation at $\lambda = 514$ nm under variation of temperature). All molar fractions are calculated from Mössbauer spectra.

The very gradual increase of $\chi_M T/4$ versus T suggests a practically noncooperative one-step SC situation with a residual HS fraction at low temperature.[2] The Mössbauer effect, a microscopic tool, has been used to probe the spin and oxidation states of the metal ions (Figure 4).[11] At 4.2 K, two doublets are found: the first one with an isomer shift of $\delta = 0.402(6)$ mm s^{-1} (relative to α-iron) and a quadrupole splitting of 1.37(1) mm s^{-1}, is typical for Fe^{II} ions in the LS state, the second one with an isomer shift of $\delta = 1.090(8)$ mm s^{-1} and a quadrupole splitting of 2.17(1) mm s^{-1} typical for Fe^{II} ions in the HS state.[11] Taking equal Lamb–Mössbauer factors for both spin states, the LS and HS molar fractions are

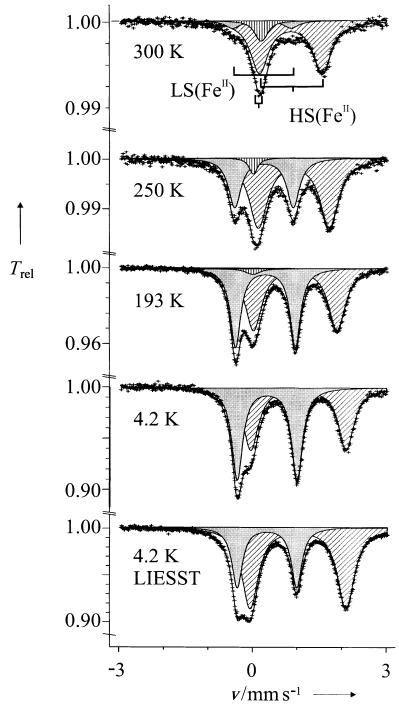


Figure 4. Selected ^{57}Fe Mössbauer spectra for **1** at various temperatures and after irradiation at $\lambda = 514$ nm at 4.2 K (LIESST).

approximately equal to the area fractions giving a population of 54 and 46%, respectively, at 4.2 K (Figure 3b). Upon increasing the temperature, the LS doublet loses intensity in favor of the HS doublet. At 300 K, the HS and LS states are observed in populations of 80 and 10%, respectively. This unambiguously indicates the occurrence of SC behavior. Above 193 K, an additional small signal appears, growing in intensity with increasing temperature. This could be attributed either to a new species, most likely Fe^{III} in the HS state, or it could be based on a texture effect,[11] where the extra signal would result from the data reduction procedure assuming equal area fractions of the Fe^{II} HS doublet.[12]

Compound **1** can also be switched by light (LIESST effect)[13] as documented in the Mössbauer spectra in Figure 4. Irradiating the sample with green light ($\lambda = 514$ nm, 15 mW cm^{-2}) at 4.2 K results in an increase of the population of the HS state from 46 to 70% (Figure 3c). Switching back to the LS state with red light, that is the reverse LIESST effect,[2] cannot be achieved because of the unfavorable position of the Fe^{II} LS MLCT bands.

Mössbauer spectra have also been recorded in the heating and cooling mode under permanent irradiation ($\lambda = 514$ nm, 15 mW cm^{-2}) and revealed a light-induced thermal hysteresis (LITH,[14] Figure 3c). The occurrence of the LITH effect implies the presence of cooperativity among the Fe^{II} centers. Therefore, the Boltzmann-shaped SC curve observed by magnetic susceptibility measurements (Figure 3a) is due to the macroscopic compensation between long-range (mainly intermolecular) and opposite directed short-range (mainly intramolecular) interactions. This indicates unambiguously intramolecular cooperativity. Therefore, the four Fe^{II} centers within the tetranuclear grid unit communicate and cannot display the same SC behavior. This excludes a single-step and

 © WILEY-VCH Verlag GmbH, D-69451 Weinheim, 2000 1433-7851/00/3914-2506 $ 17.50+.50/0

implies a multistep SC process, which has been already discussed for two-step SC compounds.[2] However, the multiple steps are not resolved macroscopically. This is attributed to the disorder of the anions and solvates around the tetranuclear grid cations, as indicated by the X-ray crystal structures, inasmuch as even the second HS Fe^{II} at 100 K is distributed over three coordination sites. This disorder contributes to a smooth SC curve, hiding the multistep character of the spin transition. We believe that this problem could be overcome by ordering the present system on a surface as a monolayer.[7]

The present results show that, in addition to the potential addressability of the $[2 \times 2]$ grid system,[7] this supramolecular entity can also be switched by several external perturbations. In particular, the Fe_4^{II} $[2 \times 2]$ grid **1** represents a unique prototype of a multiply switchable multilevel device presenting three magnetic levels (3HS/1LS, 2HS/2LS and 1HS/3LS) and driven by three different triggers (temperature, pressure, and light). Future work may allow improvements in the multistability of such systems and achieve further manipulations (e.g. applying an electric potential), in order to explore possible applications of $[2 \times 2]$ grid-type systems in information storage and nanotechnology.

Experimental Section

A solution of L[8] (20.3 mg, 44 mmol) and $Fe(ClO_4)_2 \cdot 6H_2O$ (15.9 mg, 44 mmol) in acetonitrile (5 mL) was stirred at room temperature for 6 h. Compound **1** was isolated as a dark green solid by precipitation with diethyl ether in quantitative yield. For ^{57}Fe Mössbauer experiments, samples were enriched by 33% of $^{57}Fe^{II}$. The BF_4 salt of **1** was synthesised by the same procedure using $Fe(BF_4)_2 \cdot 6H_2O$. The obtained product exhibits identical spectroscopic properties as **1**. ^1H NMR (200 MHz,[D$_3$]acetonitrile, 298 K): $\delta = 126.1, 67.6, 61.2, 55.8, 52.0, 47.1, 14.1, 9.2, 6.1, 0.3, -0.2, -8.4, -15.5$; FAB-MS (NBA): *m/z*: 2776.7 $[M-ClO_4]^+$; 2677.6 $[M-2ClO_4]^+$; 2578.6 $[M-3ClO_4]^+$; 2478.7 $[M-4ClO_4]^+$; 2378.7 $[M-5ClO_4]^+$; 2378.3 $[M-6ClO_4]^+$; 1338.8 $[M-2ClO_4]^{2+}$; 1289.3 $[M-3ClO_4]^{2+}$; 1238.8 $[M-4ClO_4]^{2+}$; 1189.4 $[M-5ClO_4]^{2+}$; 1140.9 $[M-6ClO_4]^{2+}$; UV/Vis (acetonitrile, nm): $\lambda = 379$ ($\pi-\pi^*$); 622 (MLCT); elemental analysis calcd (%) for $C_{120}H_{106}N_{24}Cl_8Fe_4O_{45}$: C 46.33, H 3.43, N 10.80; found: C 46.54, H 3.72, N 10.41.

The magnetic measurements were carried out with a Foner susceptometer working in the 4.2–300 K temperature range. The applied magnetic field was 1 Tesla. A hydrostatic high-pressure cell with silicon oil as the pressure transmitting medium has been used. The pressure determination was achieved by using the known pressure dependence of a superconducting transition of an inner tin manometer.

Mössbauer spectra were recorded in transmission geometry with a Co/Rh source kept at room temperature and a conventional spectrometer operating in the constant-acceleration mode. The samples were sealed in a plexiglass sample holder and mounted in a helium-bath cryostat for temperature variation between 4.2 and 300 K. The spectra were fitted to Lorentzian-shaped lines using a nonlinear iterative minimization routine (MOSFUN). For the LIESST experiments, approximately 20 mg of the polycrystalline compound was placed in a disc-shaped polished PMMA container (ca. 3 cm^2 surface). The sample was irradiated at 4.2 K with an Ar-ion laser (514 nm, 15 mW cm^{-2}) for 20 min within the cavity of the Mössbauer spectrometer.

Received: February 29, 2000 [Z14788]

[1] J.-M. Lehn, *Supramolecular Chemistry*, VCH, Weinheim, **1995**.

[2] P. Gütlich, A. Hauser, H. Spiering, *Angew. Chem.* **1994**, *106*, 2109–2141; *Angew. Chem. Int. Ed. Engl.* **1994**, *33*, 2024–2054, and references therein.

[3] O. Kahn, C. J. Martinez, *Science* **1998**, *279*, 44–48.

[4] W. Fujita, K. Awaga, *Science* **1999**, *286*, 261–262.

[5] G. S. Hanan, D. Volkmer, U. S. Schubert, J.-M. Lehn, G. Baum, D. Fenske, *Angew. Chem.* **1997**, *109*, 1929–1931; *Angew. Chem. Int. Ed. Engl.* **1997**, *36*, 1842–1844.

[6] a) K. L. V. Mann, E. Psillakis, J. C. Jeffery, L. H. Rees, N. M. Harden, J. A. McCleverty, M. D. Ward, D. Gatteschi, F. Totti, F. E. Mabbs, E. J. L. McInnes, P. C. Riedi, G. M. Smith, *J. Chem. Soc. Dalton Trans.* **1999**, 339–348; b) C. S. Campos-Fernàndez, R. Clérac, K. R. Dunbar, *Angew. Chem.* **1999**, *111*, 3685–3688; *Angew. Chem. Int. Ed.* **1999**, *38*, 3685–3688.

[7] A. Semenow, J. P. Spatz, M. Möller, J.-M. Lehn, B. Sell, D. Schubert, C. H. Weidl, U. S. Schubert, *Angew. Chem.* **1999**, *111*, 2701–2705; *Angew. Chem. Int. Ed.* **1999**, *38*, 2547–2550.

[8] G. S. Hanan, U. S. Schubert, D. Volkmer, E. Riviere, J.-M. Lehn, N. Kyritsakas, J. Fischer, *Can. J. Chem.* **1997**, *75*, 169–182.

[9] I. Bertini, C. Luchinat, *NMR of Paramagnetic Molecules in Biological Systems*, Benjamin/Cummings, Sydney, **1986**.

[10] X-ray structural analysis of **1**: A suitable dark green crystal ($0.5 \times 0.4 \times 0.2$ mm) of $[C_{120}H_{80}N_{24}Fe_4]^{8+} \cdot 8ClO_4^- \cdot 9CH_3CN \cdot 1.25H_2O$ was obtained from acetonitrile–diisopropyl ether. The data were measured both at 293.0(2) K and 100.0(2) K using the same crystal. Both data were recorded with a Nonius Kappa CCD diffractometer using graphite-monochromated radiation [$\lambda(MoK_\alpha) = 0.71073$ Å]. The data were processed with Denzo.[15] L_P correction was applied. The absorption correction was made with SORTAV[16]. Structure solution was done by direct methods[17] and refinement against F^2.[18] The hydrogen atoms were calculated at their idealized positions with isotropic temperature factors (1.2 or 1.5 times the C temperature factor) and were refined as riding atoms. Compound **1** at 293 K: triclinic, $P\bar{1}$, $a = 17.7037(3)$, $b = 18.4101(2)$, $c = 25.0629(4)$ Å, $\alpha = 85.7672(9)$, $\beta = 82.2308(7)$, $\gamma = 65.3290(8)^\circ$, $V = 7353.5(2)$ Å^3, $Z = 2$, $\rho_{calcd} = 1.473$ g cm^{-3}, $2\theta_{max} = 55.84^\circ$, $\mu(Mo_{K\alpha}) = 0.619$ mm^{-1}, $T_{min} = 74.7\%$, $T_{max} = 88.6\%$. A total of 87837 collected reflections, 34383 unique reflections [15896 $I > 2\sigma(I)$] were used for refinement. The final R values were $R = 0.102$, $wR^2 = 0.251$ [$I > 2\sigma(I)$], $R = 0.213$, $wR^2 = 0.314$ (all data) for 1898 parameters. A final difference map displayed the highest electron density of 1.02 e Å^{-3}, which is located near to disordered ClO_4^- ions. Compound **1** at 100 K: triclinic, $P\bar{1}$, $a = 17.2936(3)$, $b = 18.0917(3)$, $c = 24.7836(5)$ Å, $\alpha = 85.1273(11)$, $\beta = 82.0435(12)$, $\gamma = 64.9006(9)^\circ$, $V = 6951.3(2)$ Å^3, $Z = 2$, $\rho_{calcd} = 1.558$ g cm^{-3}, $2\theta_{max} = 55.84^\circ$, $\mu(Mo_{K\alpha}) = 0.655$ mm^{-1}, $T_{min} = 73.5\%$, $T_{max} = 88.0\%$. A total of 91012 collected reflections, 32258 unique reflections [19824 $I > 2\sigma(I)$] were used for refinement. The final R values were $R = 0.1150$, $wR^2 = 0.2770$ [$I > 2\sigma(I)$], $R = 0.1771$, $wR^2 = 0.3148$ (all data) for 1905 parameters. A final difference map displayed the highest electron density of 2.37 e Å^{-3}, which is located near to iron atoms, disordered ClO_4^- ions and acetonitrile molecules. Crystallographic data (excluding structure factors) for the structures reported in this paper have been deposited with the Cambridge Crystallographic Data Centre as supplementary publication nos. CCDC-140266 and CCDC-140267. Copies of the data can be obtained free of charge on application to CCDC, 12 Union Road, Cambridge CB2 1EZ, UK (fax: (+44) 1223-336-033; e-mail: deposit@ccdc.cam.ac.uk).

[11] P. Gütlich, R. Link, A. Trautwein, *Mössbauer Spectroscopy and Transition Metal Chemistry*, Springer, New York, **1974**.

[12] Work in progress.

[13] S. Decurtins, P. Gütlich, C. P. Köhler, H. Spiering, A. Hauser, *Chem. Phys. Lett.* **1984**, *105*, 1–4.

[14] A. Desaix, O. Roubeau, J. Jeftic, J. G. Haasnoot, K. Boukheddaden, E. Codjovi, J. Linares, M. Nogues, F. Varret, *Eur. Phys. B* **1998**, *6*, 183–193.

[15] Z. Otwinowski, W. Minor, *Methods Enzymol.* **1997**, *276*, 307–326.

[16] R. H. Blessing, *Acta Crystallogr. Sect. A* **1995**, *51*, 33–37.

[17] G. M. Sheldrick, SHELXS97-A Program for Automatic Solution of Crystal Structures, University of Göttingen, Germany, **1997**.

[18] G. M. Sheldrick, SHELXL97-A Program for Crystal Structure Refinement, University of Göttingen, Germany, **1997**.

Ag_3SnP_7: A Polyphosphide with a Unique $^1_\infty(P_7)$ Chain and a Novel Ag_3Sn Heterocluster**

Mikhail M. Shatruk, Kirill A. Kovnir,
Andrei V. Shevelkov,* and Boris A. Popovkin

The numerous polyphosphides known to date exhibit a variety of compositions and structures.[1] The combination of two different metals, which leads into the realm of ternary phases, is deemed an effective approach for seeking novel structure types. Here we describe the new polyphosphide Ag_3SnP_7, which possesses a unique crystal structure composed of infinite one-dimensional $^1_\infty(P_7)$ chains which are interconnected by discrete Ag_3Sn heteroclusters (Figure 1). Both

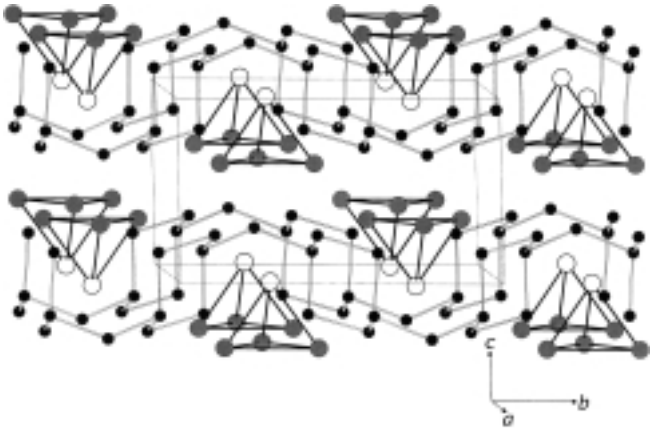


Figure 1. A view of the crystal structure of Ag_3SnP_7. Dark circles: P, white circles: Sn, shaded circles: Ag. The M–P bonds are omitted for clarity.

structural fragments were previously unknown. The compound was unexpectedly obtained during investigations of the possibility to partially substitute silver for tin in tin-based clathrates.[2] The composition Ag_3SnP_7 was established by single-crystal X-ray diffraction[3] and further confirmed by a stoichiometric synthesis of the monophase product in an ampoule.

The $^1_\infty(P_7)$ chains are built up from P_6 chair fragments that are interlinked by additional two-bonded P atoms. The linkage occurs at opposite sides of each P_6 ring. Hence, there are two three-bonded and five two-bonded phosphorus atoms per formula unit (Figure 2a). The interatomic distances within the chain lie in the range 2.18–2.20 Å, which is characteristic of conventional P–P bonding.[1] The phosphorus partial structure is therefore consistent with the formulation $^1_\infty(P_7^{5-})$: $P_7^{5-} = (3b)P_2^0(2b)P_5^{1-}$. Consequently, the formal charge on the Ag_3Sn heterocluster is +5. The tetrahedral

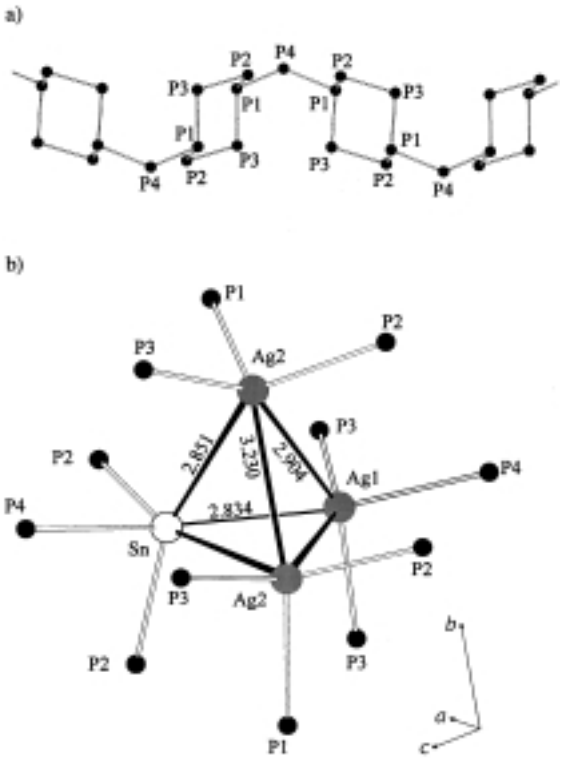


Figure 2. Fragments of the crystal structure of Ag_3SnP_7: a) a section of the polyphosphide chain; b) the $(Ag_3Sn)^{5+}$ cluster and its surrounding by phosphorus atoms. The M–P distances vary from 2.59 to 2.62 Å (Sn–P) and from 2.49 to 2.58 Å (Ag–P).

coordination of each phosphorus atom is completed by metal atoms.

The distorted tetrahedral heterocluster $(Ag_3Sn)^{5+}$ is elongated along one of its edges (Ag2–Ag2 3.23 Å) towards a butterfly shape (Figure 2b). The other edges correspond to three Sn–Ag bonds (two of 2.85 Å and one of 2.83 Å) and two Ag–Ag bonds (2.90 Å). The Ag–Ag and Sn–Ag distances are comparable with those of $SrAg_2Sn_2$[4] and Ag_3Sn.[5] The coordination number of six for each metal atom is achieved by three Sn–P or Ag–P bonds, which complete the distorted octahedral environments around the metal atoms. The M–P distances are similar to those of Ag_3P_{11}[6] and NaSnP.[7] The coordination of Ag and Sn is quite usual, and the formal oxidation states of +1 and +2, respectively, are reasonable. With such a formal charge distribution, semiconducting behavior is expected. Indeed, according to conductivity measurements, Ag_3SnP_7 is a narrow-gap semiconductor ($E_g \approx 0.2$ eV).

Molecular orbital calculations[8] at the Extended Hückel level on the discrete $(Ag_3Sn)^{5+}$ heterocluster reveal that mainly the s orbital of Sn and d orbitals of Ag contribute to bonding between the metal atoms. The contribution from the closed-shell d^{10} silver centers should not be exaggerated, even though the Ag–Ag distance of 2.90 Å, which is 0.02 Å shorter than in the metal, suggests that the d^{10}–d^{10} interactions are attractive,[9] and d electrons should be considered in the electron count. Evidently, the p orbitals of Sn and the s and p orbitals of Ag are involved predominantly in twelve external M–P bonds per cluster. Twelve electron pairs are thus

[*] Dr. A. V. Shevelkov, Dipl.-Chem. M. M. Shatruk, K. A. Kovnir, Prof. Dr. B. A. Popovkin
Inorganic Synthesis Laboratory, Department of Chemistry
Moscow State University, Moscow 119899 (Russia)
Fax: (+7) 095-939-4788
E-mail: shev@inorg.chem.msu.ru

[**] This research was supported by the Russian Foundation for Basic Research, grant no. 97-03-33275a.

 © WILEY-VCH Verlag GmbH, D-69451 Weinheim, 2000 1433-7851/00/3914-2508 $ 17.50+.50/0

donated from the 32-electron heterocluster to provide the closed-shell eight-electron configuration of the phosphorus atoms. This leaves eight electrons for internal bonding and is consistent with four 3c–2e bonds in the (distorted) tetrahedral cluster.

The only previously reported example of a mixed polyphosphide with a transition/post-transition metal heterocluster is Cu_4SnP_{10}.[10] Its crystal structure also contains distorted tetrahedral units (towards pyramidal Cu_3Sn). However, the phosphorus partial structure consists of discrete adamantane-like P_{10} cages, which are interconnected by Cu_3Sn heteroclusters and additional copper atoms. The discovery of Ag_3SnP_7 indicates that the nature of the metal atoms may play a crucial role in defining the structure of phosphorus structural fragments and their interconnection.

Experimental Section

Ag_3SnP_7: silver, tin, and red phosphorus in the stoichiometric ratio were used as starting materials (1 g in total). A few crystals of SnI_4 (ca. 0.01 g) were added to the mixture to provide effective vapor-phase transport. Annealing twice in an evacuated silica ampoule (inner diameter 6 mm; length 5 cm; 823 K for 7 d, slow cooling to ambient temperature) with intermediate grinding of the products gave a black monophase product. No impurities were detected by X-ray diffraction (as a small amount of SnI_4 was added to the original mixture this observation means that formation of iodine-containing substances is negligible). All attempts to synthesize Ag_3SnP_7 without the use of SnI_4 led to low yields.

A single crystal for the X-ray structure determination was found among the products of annealing a mixture of tin, silver, tin(IV) iodide, and red phosphorus in the ratio Sn:Ag:SnI_4:P = 17.5:4.5:2:22 (conditions were as above).

Received: January 7, 2000 [Z14511]

[1] H. G. von Schnering, W. Hönle, *Chem. Rev.* **1988**, *88*, 243.

[2] M. M. Shatruk, K. A. Kovnir, A. V. Shevelkov, I. A. Presniakov, B. A. Popovkin, *Inorg. Chem.* **1999**, *38*, 3455.

[3] Crystal structure of Ag_3SnP_7: monoclinic, space group $P2_1/m$ (no. 11), $a = 6.360(1)$, $b = 11.071(2)$, $c = 6.518(1)$ Å, $\beta = 108.17(1)^\circ$, $V = 436.1(1)$ Å^3, $Z = 2$, $\rho_{calcd} = 5.020$ g cm^{-3}. 1430 reflections, 1329 of which were independent ($R_{int} = 0.0285$), $T = 294$ K, $\omega/2\theta$ scans, $Mo_{K\alpha}$ radiation, $\lambda = 0.71069$ Å, $2\theta_{max} = 60.0^\circ$, crystal dimensions $0.12 \times 0.05 \times 0.05$ mm^3, semiempirical absorption correction (ψ scans of seven reflections, min./max. transmission: 0.6936/0.9969, $\mu = 10.668$ mm^{-1}). Structure solution: direct methods (SHELXS-86),[11a] refinement against F^2 (1186 reflections with $F > 4\sigma(F)$) by full-matrix methods (SHELXL-97)[11b] with 56 free parameters; $R1 = 0.0425$, $wR2 = 0.0930$; max./min. residual electron density: 3.775/−2.127 e Å^{-3}. Further details of the crystal structure investigation may be obtained from the Fachinformationszentrum Karlsruhe, D-76344 Eggenstein-Leopoldshafen, Germany (fax: (+49) 7247-808-666; E-mail: crysdata@fiz-karlsruhe.de) on quoting the depository number CSD-411041.

[4] W. Doerrscheidt, N. Niess, H. Schäfer, *Z. Naturforsch. B* **1976**, *31*, 890.

[5] C. W. Fairhurst, J. B. Cohen, *Acta Crystallogr. Sect. B* **1972**, *28*, 371.

[6] M. H. Möller, W. Jeitschko, *Inorg. Chem.* **1981**, *20*, 833.

[7] B. Eisenmann, U. Rössler, *Z. Kristallogr.* **1998**, *213*, 28.

[8] C. Mealli, D. M. Proserpio, *J. Chem. Educ.* **1990**, *67*, 3399.

[9] a) A. Avdeef, J. P. Fackler, *Inorg. Chem.* **1978**, *17*, 2182; b) K. M. Merz, R. Hoffmann, *Inorg. Chem.* **1988**, *27*, 2120.

[10] W. Hönle, H. G. von Schnering, *Z. Kristallogr.* **1980**, *153*, 339.

[11] a) G. M. Sheldrick in *Crystallographic Computing 3* (Eds.: G. M. Sheldrick, C. Krüger, R. Goddard), Oxford University Press, Oxford, **1985**, pp. 175–189; b) G. M. Sheldrik, SHELXL-97, Program for Crystal Structure Refinement, University of Göttingen, Germany, **1997**.

Fixation of Dinitrogen to a Mesoscale Solid Salt Using a Titanium Oxide/Conducting Polymer System**

Katsuyoshi Hoshino,* Masaki Inui, Takashi Kitamura, and Hiroshi Kokado

Since Schrauzer and Guth[1] reported the photocatalytic reduction of dinitrogen on titanium oxides under mild conditions, efforts have been devoted to prepare more effective catalysts and to understand the reaction mechanism;[2] such N_2 fixation under mild conditions is an important goal of many research groups.[3] However, the products of this reaction are gaseous ammonia (major) and hydrazine (trace); solid products which are easily isolated, manipulated, and characterized, have not been synthesized by this process. Herein, we describe a system to fix N_2 as an ammonium perchlorate salt, which has a structure of mesoscale needles. Dinitrogen fixation to this salt occurs upon white-light irradiation of a titanium oxide/conducting polymer system under ambient temperature and pressure conditions. The needles grow from the conducting polymer matrix and increase in size and abundance with irradiation time and intensity. The formation of such structures as a result of N_2 fixation is explained on the basis of ammonia synthesis on the oxide coupled with perchlorate dedoping of the conducting polymer.

The system used here is a composite of poly(3-methylthiophene) (P3MeT) and a titanium oxide, both of which were prepared electrochemically. A solution of 3-methylthiophene (3MeT, 0.08 M) and tetrabutylammonium perchlorate ($TBA^+ClO_4^-$, 0.1 M) in dichloromethane was subjected to galvanostatic electrooxidation at a temperature T of 13 °C for a time t of 400 s with a constant current density j of 1.5 mA cm^{-2} in a one-compartment cell.[4] The cell was equipped with a titanium oxide anode (2.14 cm^2) and a Pt plate cathode (2.14 cm^2). An electrochemically synthesized titanium oxide (ETO) layer on the anode was formed by the anodic oxidation[5] of a Ti plate in a CH_2Cl_2 solution containing 0.1 M of $TBA^+ClO_4^-$ under galvanostatic conditions of $j = 0.7$ mA cm^{-2}, $T = 20$ °C, and $t = 970$ s. The Ti plate (> 99.5 % purity) contained impurities such as Fe (0.250 %), K (0.013 %), O (0.200 %), and N (0.050 %); prior to the anodic oxidation the plate was degreased and etched by dipping in aqueous HF (5 %, 5 min) and then in an HF (1 %)/HNO_3 (3 %)/H_2O_2 (10 %) mixture for 30 s. In addition, prior to the deposition of P3MeT, the ETO layer was washed in trichloro-

[*] Prof. Dr. K. Hoshino, M. Inui, Prof. Dr. T. Kitamura, Prof. Dr. H. Kokado
Faculty of Engineering
Chiba University
1-33 Yayoi, Inage, Chiba 263-8522 (Japan)
Fax: (+81) 43-290-3490
E-mail: hoshino@image.tp.chiba-u.ac.jp

[**] The authors thank T. Shibuya of Idemitsu Kosan Co. for help with the XPS analyses, F. Kaneuchi of JASCO for the FTIR measurements, and T. Tohara of Edax Japan K.K. for the energy dispersive X-ray analyses. Partial support of this work was provided by The Thermal and Electric Energy Technology Foundation.

ethylene, acetone, and ethanol with sonication. After washing, the ETO-coated anode appear purplish-blue. After the electrooxidation, the plate appeared deep green, and deposition of the P3MeT (2.5 μm thick) covered about 70 % of the surface. The surface and deposition was repeatedly washed with CH_2Cl_2 and dried. The molar ratio of ClO_4^- to 3MeT was 0.16, as determined by energy-dispersive X-ray analysis coupled with a scanning electron microscope (SEM). Specimens for electron micrography were collected from the anode and characterized by SEM.

Photoirradiation experiments in a moist dinitrogen or moist argon atmosphere were carried out in a sealed box ("closed system"; fabricated from acrylic plates 10 mm thick with an inner volume of $110 \times 110 \times 80$ mm^3) equipped with stainless steel needle valves through which the passage of air and desired gases could be controlled. Illumination of samples within this closed system was made through a quartz window ($70 \times 70 \times 3$ mm) in the box. Experiments in air were conducted in a second, wooden box ("flow system"; inner volume $600 \times 500 \times 900$ mm; approximately 20 °C and 40 % relative humidity) to prevent the samples being contaminated with dust. The results from the flow system were identical to those done in the air-filled closed system and in the open air.

Immediately after the P3MeT deposition, no needle-shaped crystals could be found within the deposit (Figure 1 a). However, crystals were recognized within the deposit after 7 days (Figure 1 b). Unless otherwise noted, the deposits were stored in contact with the ETO layer under an ambient atmosphere and white-light irradiation (300 lx, Hitachi FL20SSN fluorescent lamp). After 45 days, the density and length of the needles increased (Figure 1 c). These needle structures are morphologically intriguing but the fundamental significance lies in their chemical structure. Fourier transform infrared (FTIR) spectra taken from individual needles were the same in shape and peak positions as that of $NH_4^+ClO_4^-$, which is well known from its use as a solid rocket propellant.[6] The FTIR spectrum of a needle-rich sample (taken after 180 days of white-light irradiation) was composed of the superposition of absorption bands for an undoped P3MeT[7] and those of $NH_4^+ClO_4^-$, and was entirely different from that of a needle-free sample, which was identified as a ClO_4^--doped P3MeT.[7] This result provides an important clue to the solid-state reactions during needle growth: The ClO_4^- proceeds to eliminate from the ClO_4^--doped P3MeT deposit and forms the anionic component of the needle formations. This is consistent with the SEM observations of needles growing out of the P3MeT network (Figure 1).

No needles were observed in the deposit when it was stored in the dark, even after 90 days. On the other hand, rapid and abundant needle growth was observed when the deposit was exposed to a stronger white-light irradiation (1300 lx, 7 days): The size of the needles was almost the same as those in Figure 1 c. Such rapid growth was also observed from the deposit upon irradiation (1300 lx, 7 days) after 90 days storage in the dark. In addition, immediately after the deposition, a deposit was transferred onto a carbon adhesive tape and exposed to the strong white-light irradiation: after 18 days, no needles were found. All of these observations are consistent with the photo-induced formation of needles in the solid state.

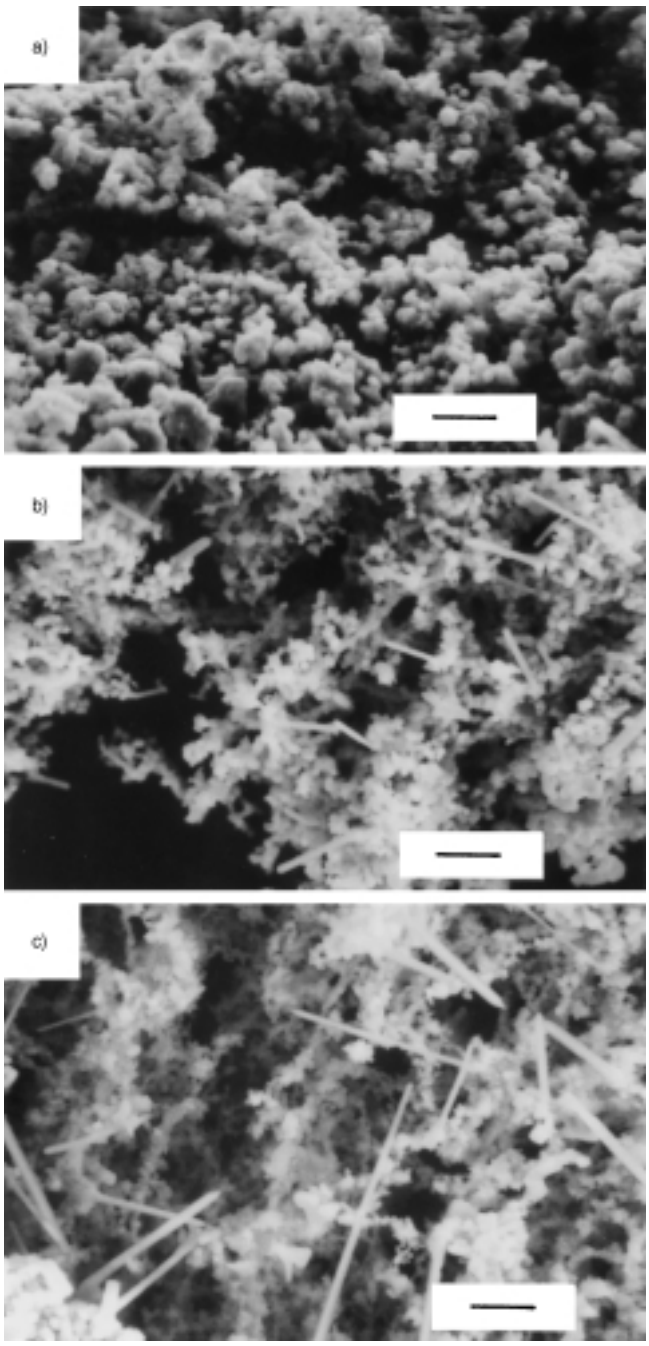


Figure 1. SEM images of the P3MeT deposit on the ETO plate show the evolution and growth of cylindrical needles with white-light irradiation under an ambient atmosphere. Images are taken after a) no exposure, b) 7 days, and c) 45 days. Irregular-shaped conglomerates are the P3MeT deposits. Note that the needles are growing off the deposits. During illumination, the deposits were allowed to stand in contact with the oxide layer. Scale bars: 10 μm.

The following experimental results indicate that the cationic (ammonium) component of the needles is photochemically synthesized from atmospheric dinitrogen. The P3MeT/ETO composite was subject to white-light irradiation (1300 lx, 7 days) in the "closed system" under atmospheres of moist argon and moist nitrogen, to result in no formation and the abundant, rapid growth of needles, respectively. The presence of large amounts of long needles in the latter P3MeT deposit

 © WILEY-VCH Verlag GmbH, D-69451 Weinheim, 2000 1433-7851/00/3914-2510 $ 17.50+.50/0 *Angew. Chem. Int. Ed.* **2000**, *39*, No. 14

is particularly intriguing: The aspect ratios of some needles were beyond ~1000:1 (Figure 2). The surface of the deposit formed under argon formed no precipitate upon treatment with Nessler's reagent whereas the other formed a brick-red

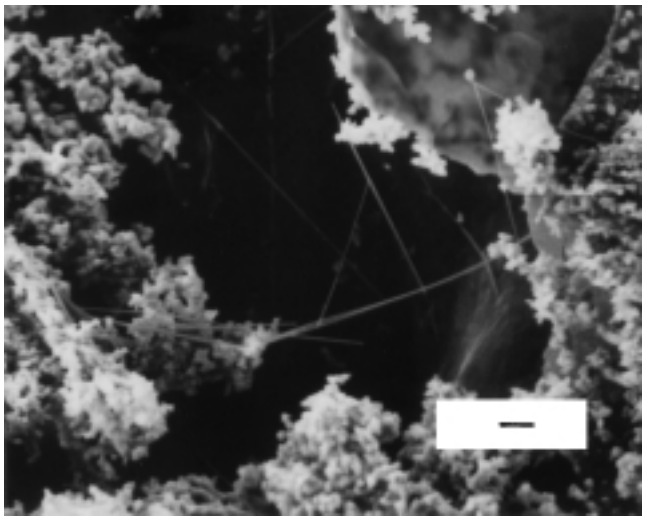


Figure 2. SEM image of a P3MeT deposit exposed to white-light irradiation (1300 lx, 7 days) under a moist N_2 atmosphere. The $NH_4^+ClO_4^-$ needles with high aspect ratios are observed. The bright conglomerates are the edges of the P3MeT deposit. The dark background is the carbon adhesive tape on which the deposit is mounted. Scale bar: 10 μm.

precipitate under the same process and thereby clearly presents evidence of N_2 fixation. X-ray photoelectron spectroscopic analyses (XPS) of a P3MeT specimen, which was prepared on the ETO and then stored in the dark (needle-free sample; Figure 3a), exhibited negligibly small signals at

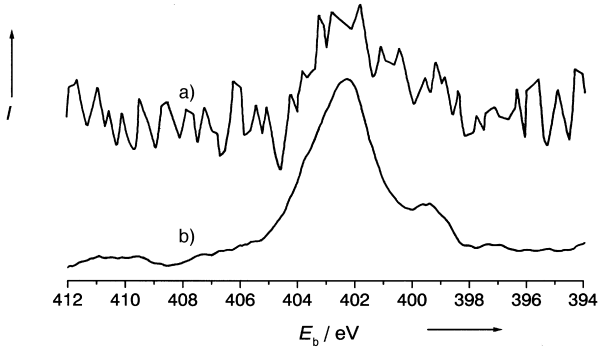


Figure 3. XPS spectra in the nitrogen 1s region for the P3MeT deposit a) stored for 7 days in the dark and b) exposed for 7 days to white-light irradiation (1300 lx). Spectrum (a) was taken under highly sensitive conditions. I = intensity; E_b = binding energy.

binding energies around $E_b = 400$ eV (N 1s), while two peaks at $E_b = 402.3$ (major) and ~399 eV (minor) were clearly exhibited by a needle-rich sample illuminated (1300 lx) for 7 days (Figure 3b). When combined with the results of the FTIR measurements, the major and minor peaks can be assigned to NH_4^+ and NH_3, respectively.[8] If this is the case, NH_3 is photosynthesized in the composite system and may be converted into NH_4^+. However, the assignment of the signal at ~399 eV is questionable, since it was reported that dinitrogen was oxidized to nitrogen oxide on a TiO_2 surface and that the XPS signal at $E_b = 399.5$ eV might originate from adsorbed nitric oxide or a diatomic nitrogen species.[9] In addition, Figure 3a implies that the P3MeT deposit is only slightly contaminated with environmental NH_3[10] and the TBA^+ ion, which was used as a supporting electrolyte cation. This Figure also indicates that the NH_4^+ does not come from chemical and/or photochemical reactions of such contamination species.

The elucidation of the detailed mechanism for needle formation or N_2 fixation awaits further research but these data lead us to speculate on the basic mechanism. Needle formation is initiated by light absorption. Photogenerated carriers at the ETO/P3MeT interface contribute to the synthesis of NH_3 [Eq. (1)] in the presence of adsorbed water according to the finding of Schrauzer and Guth,[1] In parallel with this reaction, ClO_4^--dedoping of P3MeT [Eq. (2)] and proton formation[11] may be induced by the action of photogenerated electrons and holes, respectively, leading to the formation of $HClO_4$. These are most likely followed by an acid-base reaction [Eq. (3)] to form $NH_4^+ClO_4^-$ needles.

$$2N_2 + 6H_2O \rightarrow 4NH_3 + 3O_2 \quad (1)$$

$$P3MeT^{m+}(ClO_4^-)_m + n e^- \rightarrow P3MeT^{(m-n)+}(ClO_4^-)_{m-n} + n ClO_4^- \quad (2)$$

$$NH_3 + HClO_4 \rightarrow NH_4^+ClO_4^- \quad (3)$$

How the ammonia synthesis at the interface leads to the needle formation on the free surface of P3MeT, how H^+ is (photo)chemically formed, and what enables the growth of $NH_4^+ClO_4^-$ as needles remain open questions. However, it has been clearly demonstrated that dinitrogen is fixed to a solid ammonium salt using our titanium oxide/conducting polymer system. In view of the fact that the common method of industrial dinitrogen fixation to gaseous ammonia, the Haber process,[12] requires high pressure and temperature, it seems likely that production of solid nitrogen compounds under the mild conditions of our system could become an important process.

Received: November 11, 1999
Revised: January 7, 2000 [Z 14259]

[1] G. N. Schrauzer, T. D. Guth, *J. Am. Chem. Soc.* **1977**, *99*, 7189.
[2] a) K. T. Ranjit, B. Viswanathan, *Indian J. Chem.* **1996**, *35A*, 443–453; b) A. Mills, S. Le Hunte, *J. Photochem. Photobiol. A* **1997**, *108*, 1–35; c) A. L. Linsebigler, G. Lu, J. T. Yates, Jr., *Chem. Rev.* **1995**, *95*, 735–758.
[3] a) G. J. Leigh, *Science* **1998**, *279*, 506–507; b) Y. Nishibayashi, S. Iwai, M. Hidai, *Science* **1998**, *279*, 540–542; c) M. E. Vol'pin, V. B. Shur, E. G. Berkovich, *Inorg. Chim. Acta* **1998**, *280*, 264–274; d) M. Mori, K. Hori, M. Akashi, M. Hori, Y. Sato, M. Nishida, *Angew. Chem.* **1998**, *110*, 659–661; *Angew. Chem. Int. Ed.* **1998**, *37*, 636–637; e) C. R. Dickson, A. J. Nozik, *J. Am. Chem. Soc.* **1978**, *100*, 8007–8009; f) M. Koizumi, H. Yoneyama, H. Tamura, *Bull. Chem. Soc. Jpn.* **1981**, *54*, 1682–1687.
[4] a) K. Hoshino, T. Tokutomi, Y. Iwata, H. Kokado, *J. Electrochem. Soc.* **1998**, *145*, 711–720; b) K. Hoshino, T. Ogata, H. Kokado, *Jpn. J. Appl. Phys.* **1995**, *34*, L1241–L1243.
[5] a) V. Brauer, E. Nann, *Werkst. Korros.* **1969**, *20*, 676–683; b) W. Mizushima, *J. Electrochem. Soc.* **1961**, *108*, 825–829.
[6] P. W. N. Jacobs, H. M. Whitehead, *Chem. Rev.* **1969**, *69*, 551–590.

 © WILEY-VCH Verlag GmbH, D-69451 Weinheim, 2000 1433-7851/00/3914-2511 $ 17.50+.50/0

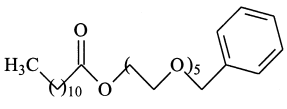
[7] a) H. Neugebauer, G. Nauer, A. Neckel, G. Tourillon, F. Garnier, P. Lang, *J. Phys. Chem.* **1984**, *88*, 652 – 654; b) G. Tourillon, F. Garnier, *J. Phys. Chem.* **1983**, *87*, 2289 – 2292.
[8] D. N. Hendrickson, J. M. Hollander, W. L. Jolly, *Inorg. Chem.* **1969**, *8*, 2642 – 2647.
[9] R. I. Bickley, V. Vishmanathan, *Nature* **1979**, *280*, 306 – 308.
[10] a) T. Okita, S. Kanamori, *Atmos. Environ.* **1971**, *5*, 621 – 627; b) H. W. Georgii, W. J. Muller, *Tellus* **1974**, *26*, 180 – 184.
[11] Different reactive species, that result from the reduction of dioxygen and from trapped photogenerated hole species, may be involved as no degassing was conducted in the experiments done under air, and in the experiments done under moist nitrogen rigorous degassing was not conducted ($\approx 10^{-3}$ Torr, $\approx 20\,^{\circ}C$) before admitting it; a) A. R. Gonzalez-Elipe, G. Munuera, J. Sorita, *J. Chem. Soc. Faraday Trans. 1* **1979**, *75*, 748 – 761; b) R. I. Bickley, F. S. Stone, *J. Catal.* **1973**, *31*, 389 – 397; c) G. Munuera, F. S. Stone, *Discuss. Faraday Soc.* **1971**, *51*, 205 – 214.
[12] F. Haber, *Chem. Z.* **1910**, *34*, 345 – 346.

Fatty Acid-Oligo(ethylene glycol) Ester Forms Ion Channels in Lipid Membranes**

Tanja Renkes, Hans J. Schäfer,* Peter M. Siemens, and Eberhard Neumann*

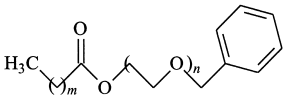
In memory of Eberhard Steckhan

Alkali and alkaline-earth ions can be selectively transported through biological cell membranes by proteins which form ion channels. The passage of ions through these channels can be controlled either by an electrical potential difference or by transmitter molecules.[1, 2] In spite of extensive knowledge on the biophysics of ion conductivity across membranes, the detailed mechanism of transport on the molecular level is still not clear.[2, 3] Since there is only limited access to chemical structures of natural ion channels, either through X-ray structure analysis or NMR spectroscopy,[4] one may identify structural elements by the synthesis and characterization of artificial ion-channel forming compounds.[5] Besides models with peptides as the main structural element, different nonpeptidic structures have been described as ion-channel forming compounds.[6, 7] Of special interest in this connection is **1**, prepared by Menger.[8] Compound **1** is reported to form proton channels by spanning, in a stretched form, the whole length of the lipid membrane. The spontaneous incorporation of **1** in lipid membranes is caused by both the hydrophobic section of the fatty acid chain and by the cationic π-interaction of the benzyl group with the choline group of the lipid. When embedded in the membrane, the oligo(ethylene glycol) chain can cause a localized increase in hydrophilicity of the membrane.[9]



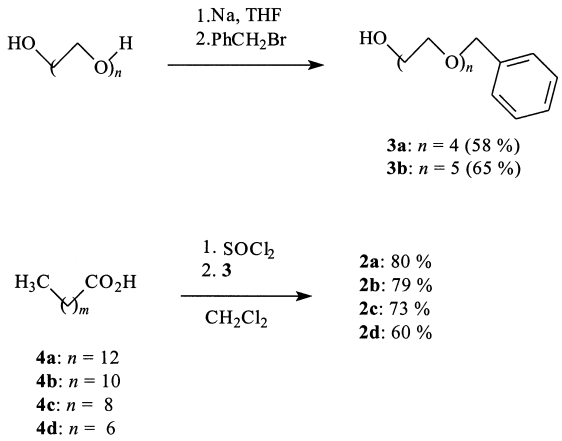
1

Here, we report the synthesis and characterization of the channel forming compounds **2a – d**, which are structurally similar to **1** but vary in the length of the fatty acid and the oligo(ethylene glycol). The activity of the channels has been analysed by fluorescence spectroscopy and, for the first time, by the electrical conductivity of single channels.



2a: $m = 12$, $n = 4$
2b: $m = 10$, $n = 4$
2c: $m = 8$, $n = 5$
2d: $m = 6$, $n = 5$

The channel-forming compounds **2a – d** are obtained in two steps. First, tetra- and pentaethylene glycol are converted by a Williamson ether synthesis into the corresponding monobenzyl ether **3a** and **3b**. These are then esterified with fatty acids **4a – d** to form **2a – d** (Scheme 1).



Scheme 1. Preparation of the channel-forming compounds **2a – d**.

In order to examine their activity as channel-forming compounds the esters **2a – d**, compound **1** and gramicidin D were integrated into lipid vesicles consisting of 1,2-dipalmitoyl-*sn*-glycero-3-phosphatidylcholin (DPPC). The rate of the ionic flux through the vesicle membrane was determined by time-resolved fluorescence spectroscopy, in which pyranine served as a pH indicator. When excited at 450 nm, pyranine exhibits a maximum in the emission spectrum at 511 nm for pH values above 7.2; this intensity maximum strongly decreases at pH values below 7.2.[10] The DPPC vesicles were prepared and suspended in a weakly buffered pyranine solution (pH 7.7).[11] Pyranine outside the vesicles was then removed by two passes through a gel filtration unit, such that the fluorescence of the probe is exclusively due to the pyranine inside the vesicles and it can therefore be used as a measure of the proton concentration. Decreasing the pH value

[*] Prof. Dr. H. J. Schäfer, Dipl.-Chem. T. Renkes
Institut für Organische Chemie der Universität Münster
Corrensstrasse 40, 48149 Münster (Germany)
Fax: (+49) 251-8339772
E-mail: schafeh@uni-muenster.de
Prof. Dr. E. Neumann, Dipl.-Chem. P. M. Siemens
Physikalische und Biophysikalische Chemie
Fakultät für Chemie
Universität Bielefeld
Postfach 10 01 31, 33501 Bielefeld (Germany)
Fax: (+49) 521-1062981
E-mail: eberhard.neumann@uni-bielefeld.de

[**] This contribution was supported by the Deutsche Forschungsgemeinschaft (SFB 424: Molekulare Orientierung als Funktionskriterium in chemischen Systemen).

 © WILEY-VCH Verlag GmbH, D-69451 Weinheim, 2000 1433-7851/00/3914-2512 $ 17.50+.50/0

outside the vesicles by only one unit leads to a fluorescence decay in the presence of an ion-channel forming compound.[12] This decay can be separated into two different phases. The initially rapid decrease results from an electrically uncompensated diffusion of protons into the vesicle, which creates a transmembrane potential difference. This potential difference induces a slow diffusion of K^+ ions to the outside and thereby allows further proton transport into the vesicle. Under these conditions, the fatty acid ester pores apparently conduct protons as well as K^+ ions.[12]

Figure 1 shows that **2a–d** form ion channels which differ in the degree of the promoted ion flux. A comparison shows that **2a** and **2d** transport protons and K^+ ions less efficiently than **1**; **2b** and **2c** exhibits a slight and significantly better ion-channel activity, respectively, than **1**.[13] These different transport properties permit some conclusions to be made on the relationship between structure and activity of the channel-forming compounds. If two compounds, like **1** and **2b** or **2a** and **2c**, are consistent in length and sufficiently hydrophobic to be incorporated into the membrane, the compound containing more oxygen atoms shows higher ion-channel activity. The length of the channel-forming compound exhibits an optimum, illustrated by the comparison of **2c** with **1** or **2a** with **2b**. The most favorable ratio between the total chain length and the number of ethylene glycol units occurs in **2c**, which exhibits the highest channel activity. In spite of the same number of ethylene glycol units, **2d** has a substantially lower ion-channel activity than **2c**. Therefore, it is assumed that the hydrophobic portion in **2d** is too small and the length too short for an ideal integration into the membrane.

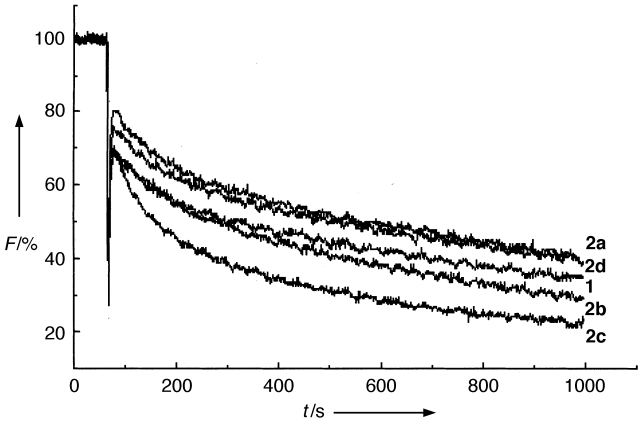


Figure 1. Fluorescence emission ($\lambda(ex) = 450$, $\lambda(em) = 511$ nm) of the vesicle suspension that contains pyranine (from 0.2 $g L^{-1}$ (0.2 mM) DPPC, $d = 100$ nm) in phosphate buffer (pH 7.7), which contains **1** or **2a–d** at a concentration of 4×10^{-3} $g L^{-1}$ (about 8 μM). At a time $t = 65$ s, the pH value was reduced from 7.7 to 6.7.

Further conclusions that concern the structure of the ion channels composed of **2a–d** can be drawn when comparing **2c** with the natural ion channel-forming compound gramicidin D (Figure 2). In contrast to **2c**, gramicidin D can significantly increase the proton concentration inside the vesicle at a concentration of only 2×10^{-3} $g L^{-1}$ (1 μM). However, a further increase of the concentration of gramicidin D, to 5 μM, barely

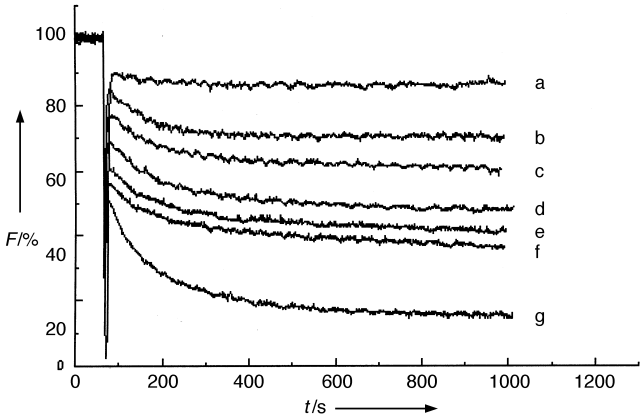


Figure 2. Fluorescence emission of pyranine in vesicles without (a) and with added gramicidin D (d: 2×10^{-3} $g L^{-1}$ (1 μM); e: 4×10^{-3} $g L^{-1}$ (2 μM); f: 1×10^{-2} $g L^{-1}$ (5 μM)) or **2c** (b: 2×10^{-3} $g L^{-1}$ (4 μM); c: 4×10^{-3} $g L^{-1}$ (8 μM); g: 1×10^{-2} $g L^{-1}$ (20 μM)) to a phosphate buffer (pH 7.7), experimental conditions are as in Figure 1.

improves the ion conductivity, which indicates a limiting value of its ion-channel activity. Raising the concentration of **2c** to 20 μM, however, leads to a further increase in the ion channel-activity. Finally, the effectiveness of the channels formed by **2c** is higher than that of channels consisting of gramicidin D. This observation indicates that **2c** does not form channels with less activity than gramicidin D but it needs, in contrast to gramicidin D, more than two molecules to assemble an ion channel.[14] With respect to pore formation, the hydrophilic part of the ion-channel forming compound must span the whole membrane. Therefore, we assume that the molecules are oriented head-to-tail.

Whereas fluorescence emission spectroscopy reflects a continuous superposition of many channel events, electrical measurements provide information on the conductance and the dynamics of a single channel event.[15] A soybean lipid with 20% phosphatidyl choline/cholesterol (9/1, w/w) was shown to be suitable as the planar membrane matrix.[16] Typical channel activities, at a transmembrane potential difference of +100 mV in the presence of 1 M KCl as supporting electrolyte, are presented in Figure 3. Under these conditions, **1** shows no channel activity and **2b** shows only a decrease of the membrane resistance but no single channel events.

In contrast, **2a**, **2c**, and **2d** clearly exhibit single channel events (Figure 3). In order to show that the ion channels formed by **2** specifically transport cations, further experiments with **2** and LiCl (Figure 4) or CsCl (Figure 5) were carried out. As before, only **2a**, **2c**, and **2d** show single channel events. The single channel currents of **2a**, as well as those of **2c** and **2d**, are significantly higher in the presence of Cs^+ ions and much lower in the presence of Li^+, as compared to KCl, as the supporting electrolyte.

The increase of the single channel currents from Li^+ through K^+ to Cs^+ correlates with the increase of the ion radii (Li^+ 78, K^+ 133, Cs^+ 169 pm),[17] as well as with the decrease of the radius of the hydrated ions (Li^+ 382, K^+ 331 pm, Cs^+ 329 pm).[17] Therefore, the cations passing through the channels have to strip off their hydration layer, at least partially. Hence, the pore diameter of such an ion channel must lie between 340 pm and 660 pm.

 © WILEY-VCH Verlag GmbH, D-69451 Weinheim, 2000 1433-7851/00/3914-2513 $ 17.50+.50/0

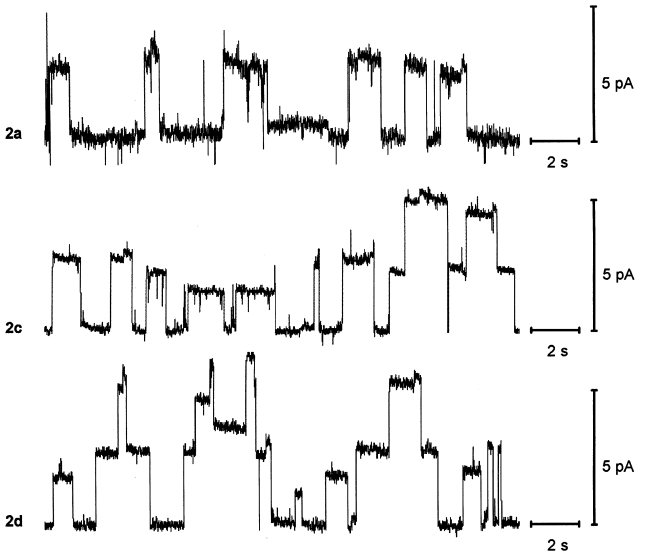


Figure 3. Single channel events (channels) of **2a**, **2c**, and **2d** in planar lipid bilayer membranes at a transmembrane voltage of $U = +100$ mV, current–time tracks (I/pA; t/s) for 20 s. Experimental conditions: membrane: soybean lipid extract with 20 % phosphatidyl choline/cholesterol (9/1, w/w) and 2.5 μM **2a**, **2c**, or **2d** in the buffer; buffer: 1M KCl; 296 K; filter frequency: 100 Hz; sample rate: 500 Hz.

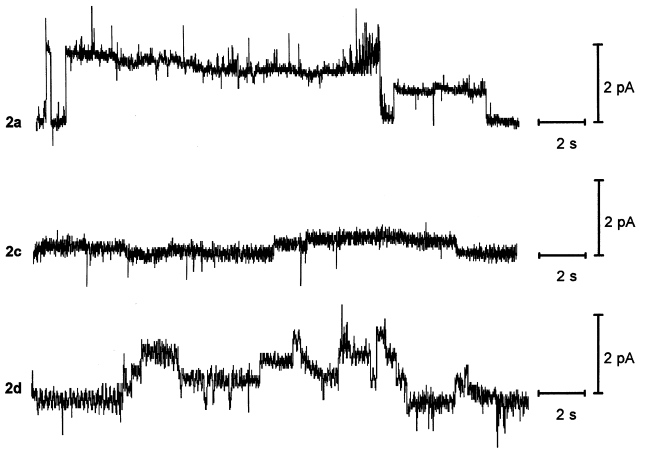


Figure 4. Single channel events (channels) of **2a**, **2c**, and **2d** in planar lipid bilayer membranes at a transmembrane voltage of $U = +100$ mV and buffer 1M LiCl; all other conditions are as in Figure 3.

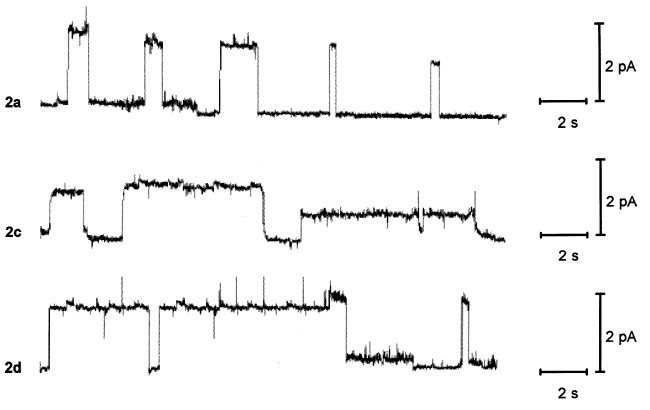


Figure 5. Single channel events (channels) of **2a**, **2c**, or **2d** in planar lipid bilayer membranes at a transmembrane voltage of $U = +100$ mV and buffer 1M CsCl; all other conditions are as in Figure 3.

At the same membrane potentials, **2c** and **2d** show several single channel events that differ in their current intensity (Figure 6). In contrast, the single channel currents of **2a** exhibit only one distinct single channel current value (Figure 6) and the current–voltage dependence is linear with a conductance of 26 ± 1.5 pS (Figure 7).

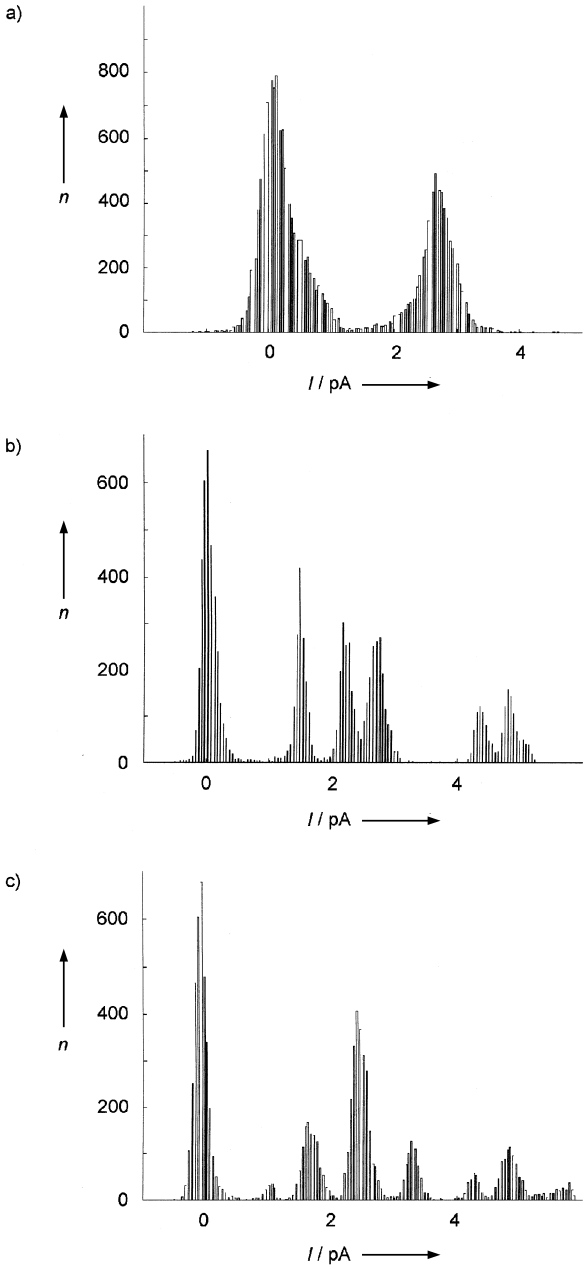


Figure 6. Amplitude histogram of the channel tracks from Figure 3 (**2a** (a), **2c** (b), and **2d** (c)) representing the frequency of the channel currents n as a function of the current (I/pA). Experimental conditions are as in Figure 3.

Apparently, the ion channels formed by the fatty acid esters differ in their constitutions. Pores formed by **2a** consist of a uniform diameter, whereas **2c** and **2d** can assemble to pores with different diameters. This difference is probably due to a variable number of molecules which form the ion channels.

 © WILEY-VCH Verlag GmbH, D-69451 Weinheim, 2000 1433-7851/00/3914-2514 $ 17.50+.50/0

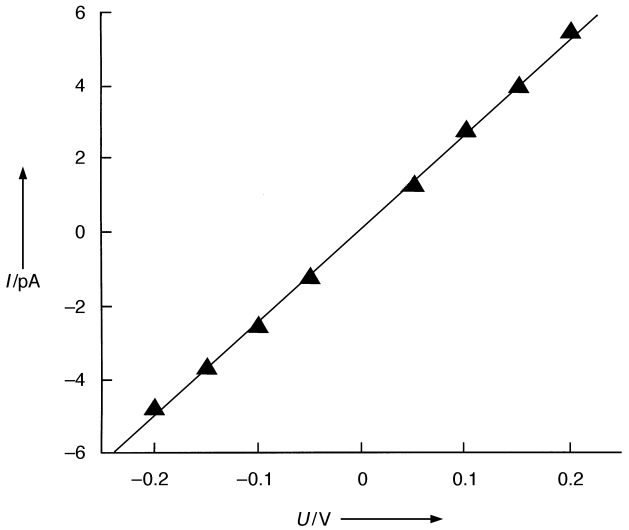


Figure 7. Symmetrical potential dependance of the single channel current of **2a**; linear regression leads to a conductance of $G = 26 \pm 1.5$ pS. Experimental conditions: membrane: soybean lipid extract with 20% phosphatidyl choline/cholesterol (9/1, w/w) and 2.5 μM **2a** in the buffer; buffer: 1M KCl; 296 K; filter frequency: 100 Hz; sample rate: 500 Hz.

In summary, based on the motif of **1**, new compounds have been prepared and identified as ion channels. They have several advantages compared to other artificial channel-forming compounds: They most probably span the membrane, their synthesis is fairly simple, and their structure provides the possibility to vary the head group, the number of the ethylene glycol units, or the ratio of the hydrophilic to hydrophobic part of the chain. The conducting pores are shown to consist of several molecules of the respective ion channel-forming compound; they require no rigid elements for ion conductivity.

Experimental Section

A) Synthesis of **2** and **3**: The purity (>99%) and structure of all new compounds have been determined by gas chromatography, ^{1}H and ^{13}C NMR spectroscopy, mass spectrometry, and elemental analysis or high resolution mass spectrometry.

3: The appropriate ethylene glycol (1 equiv) was slowly added with stirring and reflux under argon to a suspension of sodium in water-free THF (5 mL) until the sodium was totally dissolved. To this solution at 296 K, benzylbromide (1 equiv) was added and subsequently refluxed for 5 h. Water (10 mL) was then added, the aqueous phase extracted with ethyl acetate (3×5 mL), the combined organic phases dried over $MgSO_4$, and the solvent removed by rotary evaporation. Flash chromatography with ethyl acetate provided the product as colorless oil.

2: To **4a–d** (1.25 equiv) in water-free dichloromethane (10 mL) under argon, a slight excess of thionyl chloride was added and the solution refluxed until gas evolution stopped. The solvent and excessive thionyl-chloride were removed under vacuum. Thereupon the acid chloride was cautiously added, with ice-water cooling, to a solution of **3a** or **3b** (1 equiv) in water-free dichloromethane (10 mL) and triethylamine (1 mL) and was then stirred for 24 h at 296 K. Water (10 mL) was added to this solution and the mixture neutralized with dilute HCl. The aqueous phase was extracted with ethyl acetate (3×15 mL). The combined organic phases were dried over $MgSO_4$, the solvent removed under vacuum, and the product purified by flash chromatography.

B) Fluorescence emission of pyranine-containing vesicles: The vesicles were prepared from DPPC (1 mg) and phosphate buffer (pH 7.7, 293 K) containing 0.1M KCl and 5×10^{-4}M pyranine.[11] Pyranine outside the vesicles was removed by two passes through a gel filtration unit (Sephadex G-25) with a phosphate buffer (pH 7.7, 0.1M KCl) as eluent. For the fluorescence measurements (Digital Spectrofluorophotometer R-510, Shimadzu), 200 μL of this solution was diluted with the same phosphate buffer to 1 mL. Thereupon, 2–10 μL of a solution of **1**, **2a–d**, or gramicidin D in methanol are added and stirred for 5 min. (which corresponds in the vesicle solution to $2 \times 10^{-3} - 1 \times 10^{-2}$ g L^{-1}—approximately 4–20 μM **1** and **2a–d**, respectively, and 1–5 μM gramicidin D). Thereafter, by addition of HCl the pH value outside the vesicle was lowered to 6.7 and the decrease of the fluorescence was measured. Light scattering experiments show that the DPPC vesicles are not dissolved by concentrations up to 30 mol-% of **1** or **2a–d**, which is higher than the concentrations used for the fluorescence and the conductivity measurements. Additionally at room temperature, the critical micelle concentration of **2c** was determined, from the concentration dependence of the surface tension, to be 1.4×10^{-2} g L^{-1}.

C) Single channel events of the channel-forming compounds in planar lipid membranes: The planar lipid membranes are prepared using the monolayer-folding technique.[18] For that purpose, in each of the compartments of the cell, saline solution (0.7 mL, sterile filtered 1M KCl, LiCl, or CsCl, $T =$ 296 K) was added. On top of the buffer, a lipid solution (10 μL, soybean lipid extract with 20% phosphatidyl choline/cholesterol (9/1, w/w; Avanti Polar Lipids Inc., Alabaster, USA), 4 mg mL^{-1} in *n*-pentane) was added. After waiting 10 min, when the pentane had evaporated, a planar lipid membrane with a diameter of about 100 μm spontaneously formed across the hole in the teflon septum by raising and lowering the liquid level in the cell.

To both compartments of the cell, the channel-forming compounds are added as 0.5 mM solutions in ethanol. The final concentrations were 2.5–5 μM. About 2–3 min after addition of the compounds, the first single channel events were observed.

In all experiments, the sign of the potential difference refers to the side of the membrane which is connected through the Ag/AgCl electrode to the voltage supply. This side is called the *cis* side, the other the *trans* side. A positive current corresponds to a cation transfer from the *cis* to the *trans* side and is registered in the corresponding figures as an upward signal.

Received: October 25, 1999
Revised: March 28, 2000 [Z14178]

[1] B. Hille, *Ionic Channels of Excitable Membranes*, 2nd ed., Sinauer, Sunderland, **1992**.
[2] B. Eisenberg, *Acc. Chem. Res.* **1998**, *31*, 117–123.
[3] D. G. Nicholls, *Proteins, Transmitters and Synapses*, Blackwell, Oxford, **1994**.
[4] a) *Membrane Protein Structure* (Ed.: S. H. White), Oxford University Press, New York, **1994**; b) A. Kreusch, P. J. Pfaffinger, C. F. Stevens, S. Choe, *Nature* **1998**, *392*, 945–948; c) D. A. Doyle, J. M. Cabral, R. A. Pfuetzner, A. L. Kuo, J. M. Gulbis, S. L. Cohen, B. T. Chait, R. MacKinnon, *Science* **1998**, *280*, 69–77.
[5] a) U. Koert, *Chem. Unserer Zeit* **1997**, *31*, 20–26; b) G. W. Gokel, O. Murillo, *Acc. Chem. Res.* **1996**, *29*, 425–432.
[6] a) K. S. Akerfeldt, J. D. Lear, Z. R. Wassermann, L. A. Chung, W. F. DeGrado, *Acc. Chem. Res.* **1993**, *26*, 191–197; b) J. D. Lear, Z. R. Wassermann, W. F. DeGrado, *Science* **1988**, *240*, 1177–1181; c) N. Voyer, M. Robitaille, *J. Am. Chem. Soc.* **1995**, *117*, 6599–6600.
[7] a) A. Nakano, Q. Xie, J. V. Mallen, L. Echegoyen, G. W. Gokel, *J. Am. Chem. Soc.* **1990**, *112*, 1287–1289; b) Y. Kobuke, K. Ueda, M. Sokabe, *J. Am. Chem. Soc.* **1992**, *114*, 7618–7622; c) M. J. Pregel, L. Jullen, J.-M. Lehn, *Angew. Chem.* **1992**, *104*, 1695–1639; *Angew. Chem. Int. Ed. Engl.* **1992**, *31*, 1637–1639; d) K. Kaye, T. Fyles, *J. Am. Chem. Soc.* **1993**, *115*, 12315–12321; e) Y. Tanaka, Y. Kobuke, M. Sokabe, *Angew. Chem.* **1995**, *107*, 717–719; *Angew. Chem. Int. Ed. Engl.* **1995**, *34*, 693–695; f) G. Deng, M. Merritt, K. Yamashita, V. Janout, A. Sadownik, S. L. Regen, *J. Am. Chem. Soc.* **1996**, *118*, 3307–3308; g) H. Wagner, K. Harms, U. Koert, S. Meder, G. Boheim, *Angew. Chem.* **1996**, *108*, 2836–2839; *Angew. Chem. Int. Ed. Engl.* **1996**, *35*, 2643–2646; h) J. D. Mendoza, F. Cuevas, P. Prados, E. S. Meadows, G. W. Gokel, *Angew. Chem.* **1998**, *110*, 1650–1653; *Angew. Chem. Int.*

 © WILEY-VCH Verlag GmbH, D-69451 Weinheim, 2000 1433-7851/00/3914-2515 $ 17.50+.50/0

Ed. **1998**, *37*, 1534 – 1537; i) Y. Kobuke, K. Morita, *Inorg. Chim. Acta* **1998**, *283*, 167 – 174.
[8] a) F. M. Menger, D. S. Davis, R. A. Persichetti, J.-J. Lee, *J. Am. Chem. Soc*. **1990**, *112*, 2451 – 2452; b) F. M. Menger, *Bol. Soc. Chil. Quim*. **1990**, *35*(1), 33 – 38.
[9] F. M. Menger, *Angew. Chem*. **1991**, *103*, 1104 – 1118; *Angew. Chem. Int. Ed. Engl*. **1991**, *30*, 1086 – 1100.
[10] K. Kano, J. H. Fendler, *Biochim. Biophys. Acta* **1978**, *509*, 289 – 299.
[11] At first, multilamellar vesicles from DPPC films were formed: R. R. C. New, *Liposomes: A Practical Approach*, IRL Press, Oxford, **1990**; from the multilamellar vesicles, unilamellar vesicles were prepared by the membrane extrusion method: R. C. MacDonald, R. I. MacDonald, B. P. M. Menco, K. Takeshita, N. K. Subbaro, L.-R. Hu, *Biochim. Biophys. Acta* **1991**, *1061*, 297 – 303.
[12] F. M. Menger, P. Aikens, *Angew. Chem*. **1992**, *104*, 919 – 921; *Angew. Chem. Int. Ed. Engl*. **1992**, *32*, 898 – 900.
[13] The relative activity of **1**, **2a** – **d**, and Gramicidin D was reliably reproduced in several experiments.
[14] P. Läuger, *Angew. Chem*. **1985**, *97*, 939 – 956; *Angew. Chem. Int. Ed. Engl*. **1985**, *24*, 905 – 922.
[15] H. Schindler, *Methods Enzymol*. **1989**, *171*, 225 – 253.
[16] On membranes formed from pure soybean lecithin without cholesterol, no channel activity was observed. The reason could be a higher mobility of the ion channel-forming compound in the cholesterol-containing membrane: P. L. Yeagle, *Biochem. Biophys. Acta* **1985**, *822*, 267 – 287. As with amphotericin B, a specific interaction of **2a**, **2c**, and **2d** with cholesterol is also possible: D. E. Mickus, D. G. Levitt, S. D. Rychnosvsky, *J. Am. Chem. Soc*. **1992**, *114*, 359 – 360.
[17] P. K. Mondal, B. K. Seal, A. S. Basu, *Z. Phys. Chem. (NF)* **1973**, *87*, 295 – 307.
[18] M. Mantal, P. Müller, *Proc. Natl. Acad. Sci. USA* **1972**, *69*, 3561 – 3566.

Aluminum Fluoride as a Storage Matrix for Atomic Hydrogen **

Gudrun Scholz,* Reinhard Stößer, Jan Alam Momand, Andrea Zehl, and Jeannette Klein

Atomic hydrogen H• can be stabilized for years in a suitably prepared AlF_3 powder matrix at temperatures $T \geq 300$ K (Figure 1). The hydrogen atoms are formed within the matrix by γ irradiation, essential OH groups in the crystallites serve as precursors for the H•. Thus, for the first time the stabilization of the reactive H• atoms has been achieved in a fluoride of the earth metals. A prerequisite for the formation and stabilization of the H• atoms is a special preparation of AlF_3 under quasi isobaric conditions,[1] in which, in chemically and thermally controlled reactions of α- and β-trihydrates of AlF_3,

[*] Dr. G. Scholz, Prof. Dr. R. Stößer, Dr. J. A. Momand, Dr. A. Zehl, Dr. J. Klein
Humboldt-Universität zu Berlin
Institut für Chemie
Hessische Strasse 1 – 2, 10115 Berlin (Germany)
Fax: (+49) 30-2093-7378
E-mail: gs@magneton.chemie.hu-berlin.de

[**] This work was supported by Deutsche Forschungsgemeinschaft and by the Fonds der Chemischen Industrie. We thank Dr. E. Janata (HMI Berlin), Dr. B. Ziemer, Dr. M. Päch and Dr. J. Bartoll (HU Berlin) for the assistance with the experimental work.

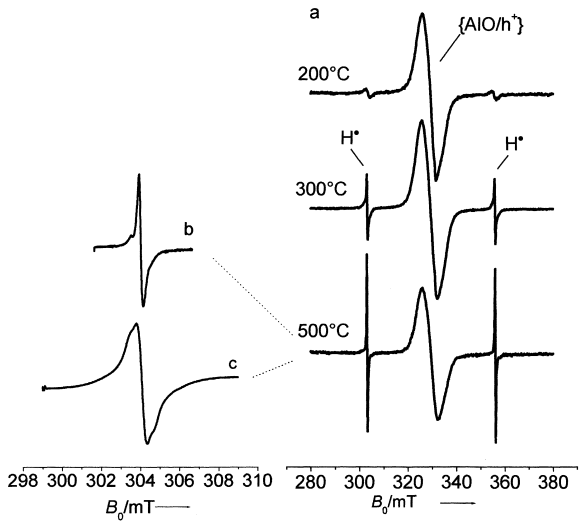


Figure 1. X-band ESR spectra (298 K) of trapped H• atoms: a) in AlF_3 powder samples of increasing crystallinity prepared from β-$AlF_3 \cdot 3H_2O$ under quasi isobaric conditions[1] at the temperatures given. b, c) Low-field signal of the trapped H• atoms in AlF_3, prepared by annealing of β-$AlF_3 \cdot 3H_2O$ at 500 °C ($P_{MW} = 2$ mW), measurement temperature 298 K (b), 4.2 K (c); the *y* axis scales are identical.

both the necessary cagelike structural elements and also the H• precursors are formed. Parallel to the long-term stability of the enclosed (trapped) H• atoms is the comparatively large values for the activation energies of their thermal decay. In addition it is noteworthy that the H• atoms fulfill the function of a spin probe in the solid-state samples. Compared to other paramagnetic dopants, such as transition metal ions,[2–5] the H• atoms are more suitable as a probe because their influence on the matrix is significantly lower. For example, both the spectral and spin dynamic ESR behavior and also the corresponding activation energies calculated from the thermal decay curves (Table 1) allow definitive conclusions to be drawn about the state of order in the matrix. These are in complete agreement with the findings from thermal analysis and X-ray diffraction. This form of direct relationship for trapped H• atoms has not been reported to date.

Table 1. Activation energies E_A and rate constants k for the thermally induced decrease in the H• signal in aluminum fluorides.

Annealing temperature [°C][a]	Annealing time [h]	k[b,c] [g mol^{-1} min^{-1}]	E_A [kJ mol^{-1}]
200	1	0.00576 (80) 0.02797 (110)	59.016
300	1	0.01148 (150) 0.08311 (200)	65.782
400	1	0.01084 (200) 0.06918 (250)	76.290
500	1	0.03668 (250) 0.11399 (280)	91.364
500	10	0.02624 (250) 0.08435 (280)	94.084

[a] The starting materials β-$AlF_3 \cdot 3H_2O$ were, in each case, annealed in a Q-crucible for 1 or 10 h under quasi isobaric conditions at the temperatures given. Following this they were subjected to γ irradiation. [b] Determined from the time dependent standard signal intensities. [c] The temperature [°C] for the decay reaction is given in each case in parentheses.

 © WILEY-VCH Verlag GmbH, D-69451 Weinheim, 2000 1433-7851/00/3914-2516 $ 17.50+.50/0

Although there are numerous results demonstrating the chemical reactions and spectroscopy of atomic hydrogen at low temperature ($4.2 \leq T \leq 100$ K), only a few systems provide direct evidence for atomic hydrogen at $T \geq 298$ K.[6–23] Of these, all but one concern the fluoride and oxide compounds of alkali and alkaline earth metals and of silicon.[24] The discovery of the trapping of H$^{\bullet}$ in $Si_8O_{12}R_8$ compounds in the solid state[14, 18] as well as in solution[18] added a new dimension to the physics and chemistry of atomic hydrogen. The unexpected long-term stability, which can run into years in the solid state and from days to weeks in the solutions, permitted a detailed analysis of the chemical and physical properties of the stabilizing $Si_8O_{12}R_8$ structural units.[18] These cages are also suitable for the investigation of hyperfine coupling in muonium.[25]

However, when atomic hydrogen is trapped in aluminum fluoride powder (AlF_3/H$^{\bullet}$), its spectral and kinetic behaviors differ greatly. This is seen in a remarkable stability at room temperature, and can be readily identified in the products of thermal decomposition of the trihydrate after γ irradiation. For the α-$AlF_3 \cdot 3H_2O$ starting material this occurs in the temperature range $250\,^{\circ}C \leq T \leq 550\,^{\circ}C$ and for β-$AlF_3 \cdot 3H_2O$ in the range $200\,^{\circ}C \leq T \leq 650\,^{\circ}C$. Three typical X-band ESR spectra of the annealed and the γ-irradiated AlF_3 samples are shown in Figure 1a. In addition to the characteristic hyperfine structure of H$^{\bullet}$ ($^{1H}A = 50.9$ mT) is, centered between these two lines, the signal of another long-lived paramagnetic AlO/h$^+$ center[26]. The degree of order in the matrix is demonstrated by the line widths and shape of the hydrogen ESR signals. Thus the physical and chemical properties of the H$^{\bullet}$ atoms are clearly influenced by the matrix. With increasing temperature the line widths ΔB_{pp} of the H$^{\bullet}$-signals becomes noticeably smaller and the intensity of the signals increase relative to that of the AlO/h$^+$ center. Both paramagnetic centers benefit, to different extents because of their differing chemical natures, from the increasing idealization of the AlF_3 structure. There is a definite correlation between the line widths of the H$^{\bullet}$ signals, the particle size of the powder sample and, its amorphous content as determined by X-ray diffraction: With increasing particle size, decreasing amorphous content and therefore the increasing crystallinity of the samples, the line width decreases (Figure 2a, b). In the amorphous sections of the samples there is a statistical distribution of bond lengths and angles. This has a direct effect on the spin coupling parameters of the trapped H$^{\bullet}$ atoms. ESR experiments at different frequencies (S-, X-, Q-band; that is at 3.8, 9.5 and 34 GHz) indicate that these statistical effects are reflected in the distributions of the anisotropic hyperfine couplings. Of the chemical aspects, a modification of the s-electron density of the H atoms as a result of discriminating repulsive interactions in the cage substructure (see Figure 3d) appears more likely than a distribution of the *g*-components, which is dependent upon the comparatively high-lying excited states.[27] Spin-flip transitions[28] are spectroscopically less well defined than those of the $Si_8O_{12}R_8$ cage (see Figure 1b,[18]). Evidently the individual line widths in AlF_3 are considerably broader as a result of the interaction with the immediately adjacent ^{19}F nuclei. The spin relaxation (microwave saturation at $T \leq 10$ K) of the trapped H$^{\bullet}$ atoms is also very different to that of the $Si_8O_{12}R_8$ cage. In the spectrum of AlF_3/H$^{\bullet}$, saturation broadening occurs as a result of magnetic dipole–dipole interactions with the ^{19}F nuclei (Figure 1b, c). This broadening is accompanied by slight changes in the signal amplitudes.

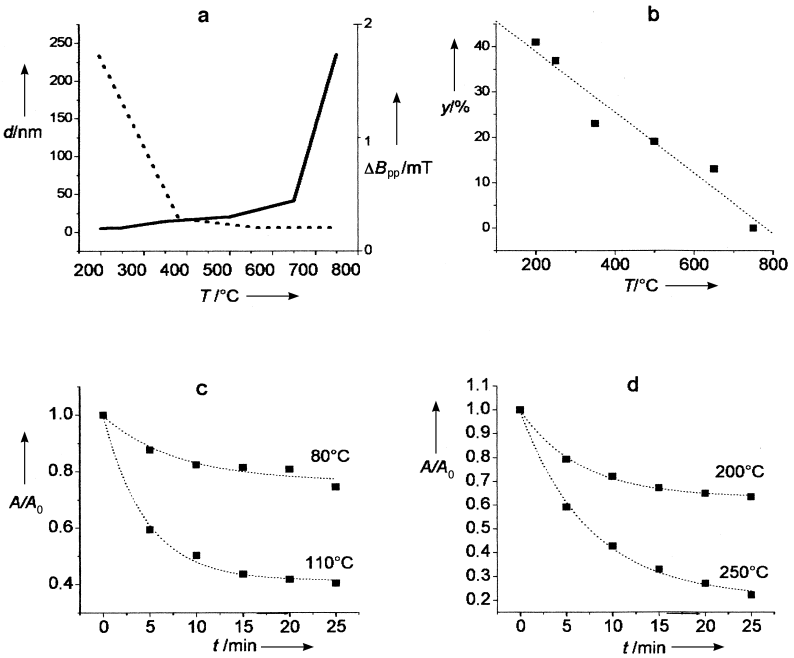


Figure 2. Annealing experiments with β-$AlF_3 \cdot 3H_2O$: a) influence of temperature on the particle size *d* of the product and on the line width ΔB_{pp} (••••) of the low-field signal of the trapped H$^{\bullet}$ atoms. b) Standardized amorphous content *y* in the annealed β-$AlF_3 \cdot 3H_2O$ samples as a function of the annealing temperature. c) Course of the decay of H$^{\bullet}$ atoms in AlF_3 against time, at 80 and 110 °C. Measurement temperature given as a function of the standard amplitude A/A_0; annealing temperature 200 °C. d) Course of the decay of H$^{\bullet}$ atoms in AlF_3 against time, at 200 and 250 °C. Measurement temperature given as a function of the standard amplitude A/A_0; annealing temperature 400 °C.

The AlF_3 matrix, because of the Pauli repulsion (see also CaF_2/H$^{\bullet}$[7, 17]), is clearly able to stabilize the H$^{\bullet}$ atoms over a wide temperature range.[29] Figures 3a–d show sections of the structures of CaF_2 and AlF_3 and of the local cages capable of incorporating H$^{\bullet}$ atoms. The time-dependent decrease of the H$^{\bullet}$ signals in AlF_3 (Figure 2c, d) demonstrate the direct dependence of the kinetic parameters of the trapped H$^{\bullet}$ atoms on the degree of order within the matrix. While in a sample annealed at 200 °C (amorphous content 41%) H$^{\bullet}$ atoms and their thermal decay can not be observed above 110 °C, in a sample annealed at 400 °C (amorphous content 20%) the H$^{\bullet}$ atoms are significantly more stable and the thermal decay can be monitored up to 250 °C (Figure 2c, d). For the macroscopic features this result is in agreement with the general observation that amorphous and structurally imperfect systems show greater chemical reactivity. An additional consideration here is that at higher temperatures, stabilized H$^{\bullet}$ atoms require a *symmetrical* environment, which, because of the repulsive

 © WILEY-VCH Verlag GmbH, D-69451 Weinheim, 2000 1433-7851/00/3914-2517 $ 17.50+.50/0

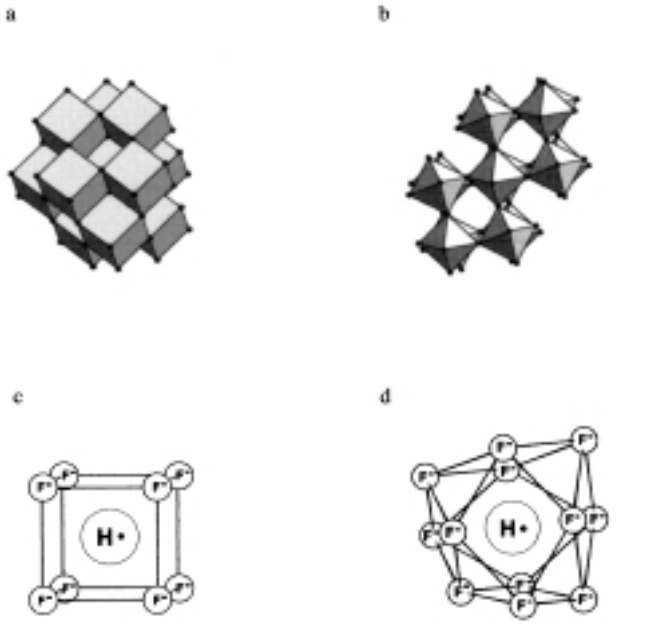


Figure 3. Sections of the structures of a) CaF_2 (space group $Fm\bar{3}m$) and b) α-AlF_3 (space group $R\bar{3}c$); local structure of the cages, formed by F atoms, which are suitable for taking up H• (from consideration of the van der Waals radius of H•): c) in CaF_2: $R_{F-F} = 2.709$ (neighboring), 4.709 Å (diagonal); d) in α-AlF_3: $R_{F-F} = 2.541$, 3.065, 4.105, 5.032 Å.

interactions, prevents the H• atoms from entering into chemical reactions or from leaving the cage. The experimental thermal decay curves (ESR intensity–time profiles, Figure 2c, d) can only be sensibly interpreted in terms of a second-order rate law leading to the rate constants and activation energies listed in Table 1. It is clear that the matrices with the greatest amorphous content give the lowest activation energies. Thus, in contrast to the molecular case[18] these experimental results support the idea that remote structural elements are involved in the stabilization of the H•. The necessary mobility of the potential reaction partners for the H• decay can be assumed.

The presence of precursors localized within the volume of the crystallites have been shown to be favorable for the long-term trapping of H• in AlF_3. Suitable prerequisites are created by the dehydration of AlF_3 hydrates under quasi isobaric conditions.[1] Treatment of the surfaces of (dehydrated) AlF_3 samples with D_2O gave the typical signals for trapped D• atoms, but only with 3–5% of the intensity of the simultaneously trapped H• atoms. Furthermore, it could be demonstrated that after γ irradiation at 300 K pure crystalline samples of CaF_2 and Na_3AlF_6 showed no trace of H•. In sharp contrast the corresponding OH contaminated powders gave, under the same conditions, intense ESR signals for trapped H• atoms. Generally the yield of H• at room temperature sinks considerably as the number of mobile H_2O molecules, OH groups, or H-bridging networks increases. H• atoms could not be trapped in the α- and β-$AlF_3 \cdot 3H_2O$ samples at $T \geq 300$ K. However, at lower temperatures ($T \leq 100$ K) even in these systems H• atoms could be stabilized in easily detectable concentrations.[26] Further support comes from the results obtained with the hydrates of calcium sulfate: At room temperature H• could only be trapped in the semi-hydrate ($CaSO_4 \cdot 0.5H_2O$).[8, 11] Similar results have so far not been reported for the dihydate.

In general the concentration of the hydrogen atoms generated and stabilized is dependent upon the nature and concentration of the transition metal ions incorporated. In AlF_3, for example, it can be shown that at Fe^{3+} concentrations above 0.1 mol% the rapid recombination of radiation defects is more effective and thus increasingly hinders the trapping of reactive species.

Experimental Section

The investigative methods used were multifrequency ESR spectroscopy (S-, X-, Q-band) in conjunction with thermal analysis, targeted chemical experiments and X-ray diffraction. ESR is the method of choice for the unambiguous detection of trapped H• atoms. In the X-band the temperature range from $4.2 \leq T \leq 600$ K can be used for the characterization of H•; that is, an observation window of over 500 degrees is available. ESR spectroscopy exploits the specific hyperfine patterns (Figure 1) to provide a simple and direct method to detect H• atoms. All ESR investigations were carried out in the μW region, or significantly below microwave saturation (max. 2 mW). A ^{60}Co source was used for the γ irradiation and an average dose of 100 kGy employed. The samples were thermally prepared in an oven by using a labyrinth Pt crucible (Q-crucible).[1] Each of the starting materials (α- and β-$AlF_3 \cdot 3H_2O$) were annealed for 1 h at temperatures between 50 and 800 °C. The results obtained were completely reproducible. Different charges of AlF_3 obtained from different preparations were employed. After appropriate thermal treatment both α- and β-$AlF_3 \cdot 3H_2O$ led to products that can, after γ irradiation, capture H• atoms. Differences occur in terms of the yields and the chemical and spin dynamic behavior of the trapped H• atoms.

Received: December 22, 1999 [Z14446]

[1] G. Scholz, R. Stösser, S. Sebastian, E. Kemnitz, J. Bartoll, *J. Phys. Chem. Sol.* **1999**, *60*, 153–162.
[2] G. Scholz, *J. Solid State Chem.* **1998**, *139*, 27–36.
[3] G. Scholz, R. Stösser, T. Grande, S. Aasland, *Ber. Bunsen-Ges. Phys. Chem.* **1997**, *101*, 1291–1296.
[4] R. Stösser, G. Scholz, *Appl. Magn. Res.* **1997**, *12*, 167–181.
[5] R. Stösser, G. Scholz, *Appl. Magn. Res.* **1998**, *15*, 449–468.
[6] E. Duval, J. Serughetti, R. Louat, *Solid State Comm.* **1970**, *8*, 1155–1158.
[7] S. L. Sligar, H. Blum, *Phys. Rev. B* **1971**, *3*, 3587–3592.
[8] H. Kon, *J. Chem. Phys.* **1964**, *41*, 573–574.
[9] R. G. Bessent, W. Hayes, J. W. Hodby, P. H. S. Smith, *Proc. R. Soc. London A* **1969**, *309*, 69–90.
[10] B. Welber, *Phys. Rev. A* **1964**, *136*, 1408–1412.
[11] A. M. Belongov, A. G. Grammakov, A. S. Serdjuk, S. A. Suppé, *Proc. Colloq. AMPERE* **1970**, *16*, 943.
[12] N. Papp, K. P. Lee, *J. Magn. Reson.* **1975**, *19*, 245–249.
[13] L. E. Iton, J. Turkevich, *J. Phys. Chem.* **1978**, *82*, 200–214.
[14] R. Sasamori, Y. Okane, T. Isobe, Y. Matsuda, *Science* **1994**, *265*, 1691–1693.
[15] K. Ogoh, S. Takaki, C. Yamanaka, M. Ikeya, E. Ito, *J. Phys. Soc. Jpn.* **1996**, *65*, 844–847.
[16] R. A. B. Devine, K. Hübner, *Phys. Rev. B* **1989**, *40*, 7281–7283.
[17] J. L. Hall, R. T. Schumacher, *Phys. Rev.* **1962**, *127*, 1892–1912.
[18] M. Päch, R. Stößer, *J. Phys. Chem. A* **1997**, *101*, 8360–8365.
[19] F. Hill, G. Lehmann, *Z. Naturforsch. A* **1978**, *33*, 1484–1486.
[20] J. M. Baker, A. Cox, A. J. O'Connell, R. C. C. Ward, *J. Phys. Condens. Matter* **1991**, *3*, 6189–6193.
[21] Y. Ueda, Y. Kazumata, M. Nishi, *Jpn. J. Appl. Phys.* **1977**, *16*, 1743–1745.
[22] A. V. Egranov, V. V. Otroshok, B. P. Chernyago, *Phys. Status Solidi B* **1991**, *167*, 451–458.
[23] A. V. Egranov, *Phys. Status Solidi B* **1993**, *179*, 323–327.

 © WILEY-VCH Verlag GmbH, D-69451 Weinheim, 2000 1433-7851/00/3914-2518 $ 17.50+.50/0

[24] LiF:OH^-,[6] CaF_2,[7, 13, 17] $CaSO_4 \cdot 0.5\,H_2O$,[8, 11] BaF_2,[9, 10] $BaSO_4$,[11] SiO_2 surface,[12] $Si_8O_{12}R_8$-cage,[14, 18] SiO_2 high-pressure modifications,[15, 16] $NaAl_3(OH)_4(PO_4)_2$,[19] Li_2O,[20, 21] LiF:H^-, Mg^{2+}.[22, 23]
[25] H. Dilger, E. Roduner, R. Scheuermann, J. Major, M. Schefzik, R. Stößer, M. Päch, D. G. Fleming, *Phys. Condens. Matter* **1999**, in press.
[26] R. Stößer, J. Bartoll, L. Schirrmeister, R. Ernst, R. Lück, *Appl. Radiat. Isot.* **1996**, *47*, 1489 – 1496.
[27] P. J. Bruna, G. H. Lushington, F. Grein, *Chem. Phys. Lett.* **1996**, *258*, 427 – 430.
[28] Detectable as satellites on the hyperfine lines of the H· atoms.[18]
[29] F. J. Adrian, *J. Chem. Phys.* **1960**, *32*, 972 – 981.

Intermediate-Range Order in Amorphous Nitridic Ceramics: Lessons from Modern Solid-State NMR Spectroscopy**

Leo van Wüllen, Utz Müller, and Martin Jansen*

Structural characterization and theoretical modeling of crystalline solids are only possible because of their translational symmetry. Once the translatorial periodicity is lost, as in quasicrystals and amorphous networks, the structural characterization of these solids, a prerequisite for a profound understanding of the physical and chemical properties, becomes a rather tedious task. This lack of routine methods for the structural characterization of amorphous solids is the reason for an only limited understanding of scientifically and industrially important systems.

Amorphous ceramics in the system boron, silicon, carbon, and nitrogen have gained considerable importance as high-performance ceramic materials due to their exceptional stability at high temperatures and their resistance to oxidation.[1] Among these ceramics, those obtained by ammonolysis, polycondensation, and subsequent pyrolysis of single-source precursors have been ascribed superior characteristics with respect to resistance to crystallization and homogeneity.[2] The ternary ceramic $Si_3B_3N_7$ and the quaternary ceramic $SiBN_3C$ are the best studied so far with respect to structural details.[3] A structural characterization of these amorphous systems can only be successful if a combination of characterization methods is used, each predominantly probing the short-, intermediate-, or long-range order. Modern solid-state NMR spectroscopy is emerging as one of the most powerful tools in this field. The short-range order in a range of 1 – 2 Å was successfully elucidated by magic angle spinning (MAS) NMR methods. These studies found trigonally planar BN_3 and tetrahedral SiN_4 polyhedra as the basic building blocks constituting the network. Transmission electron spectroscopy studies revealed[4] that the amorphous network in these ceramics is homogeneous with respect to an elemental distribution on a subnanometer scale. To date, the intermediate-range order, corresponding to a length scale of 2 – 5 Å has not yet been accessible. This gap is closed with the present study, by utilizing modern double resonance solid-state NMR methods. As a first characterization of the ceramic $Si_3B_3N_7$ the solid-state NMR single-pulse MAS solid-state spectra were recorded. The signals with isotropic chemical shifts of $\delta = -45.2$ (^{29}Si MAS-NMR) and 30.4 (^{11}B MAS NMR) indicate a local environment consisting of BN_3 and SiN_4 units, as confirmed by a comparison to the spectra of the binary model compounds h-BN and α-Si_3N_4 and β-Si_3N_4, respectively.[5]

The intermediate-range order, originating in the interconnection of the polyhedra to give the resulting amorphous network, was traced by employing rotational echo double resonance (REDOR) NMR spectroscopy.[6] In this approach, the heteronuclear dipolar interaction between two nuclear species I and S, averaged out under the conditions of the MAS experiment, is reintroduced by rotor-synchronized 180° dephasing pulses for the S spins. The signal of the first nuclear species I is detected by using a rotor-synchronized solid-state spin-echo pulse sequence. The 180° pulses for the second nuclear species (S) produce a sign shift of the heteronuclear dipolar Hamiltonian, resulting in a decreased echo amplitude *S*. A conventional spin echo experiment for the I spins provides the maximum echo amplitude S_0. Simulations of the resulting dipolar evolution curve, obtained as a plot of the normalized difference $\Delta S/S_0$ as a function of the dipolar evolution time—the product of the number of rotor cycles N and the rotor period T_R—then allows a direct determination of the ^{11}B-^{29}Si internuclear distance in the case of an isolated two-spin system. Comparing the two principally feasible experiments ^{29}Si{^{11}B}-REDOR and ^{11}B{^{29}Si}-REDOR NMR the first would be the natural choice because of the natural abundance of the two isotopes ^{29}Si (4.7 %) and ^{11}B (80.4 %). The quadrupolar nature of the isotope ^{11}B (nuclear spin = 3/2) as the dephasing nucleus however severely complicates data analysis.[7] Therefore we decided to perform the second variant, ^{11}B{^{29}Si} REDOR. This makes the use of a 100 % ^{29}Si isotopically enriched sample of $Si_3B_3N_7$ vital, since in a ^{11}B-{^{29}Si}-REDOR experiment on a sample containing ^{29}Si in natural abundance only approximately 5 % of the actual B-Si dipolar couplings would be detected.

Figure 1 contains a compilation of ^{11}B-{^{29}Si}-REDOR spectra for dipolar evolution times of 0.4, 1.2, and 2 ms together with the resulting REDOR curve. The lineshape of the ^{11}B resonance is dominated by the second-order quadrupolar interaction, which is not completely averaged out even under the conditions of fast MAS. Line shape analysis yields a quadrupolar coupling constant of 2.9 MHz and an asymmetry parameter η of 0.1. Figure 1 a shows the results of ^{11}B-spin-echo experiments, Figure 1 b the ^{11}B{^{29}Si}-REDOR spectra. The difference of the two experiments is plotted in Figure 1 c. An increase of the difference intensity $S - S_0$ with increasing dipolar evolution time becomes obvious.

[*] Prof. Dr. M. Jansen, Dr. L. van Wüllen
Max-Planck-Institut für Festkörperforschung
Heisenbergstrasse 1, 70569 Stuttgart (Germany)
Fax: (+49) 711-689-1502
E-mail: martin@jansen.mpi-stuttgart.mpg.de
Dipl.-Chem. U. Müller
Institut für Anorganische Chemie
Rheinische Friedrichs-Wilhelms-Universität Bonn
Gerhard-Domagk-Strasse 1, 53121 Bonn (Germany)

[**] This work was supported by the Deutsche Forschungsgemeinschaft (SFB 408).

 © WILEY-VCH Verlag GmbH, D-69451 Weinheim, 2000 1433-7851/00/3914-2519 $ 17.50+.50/0

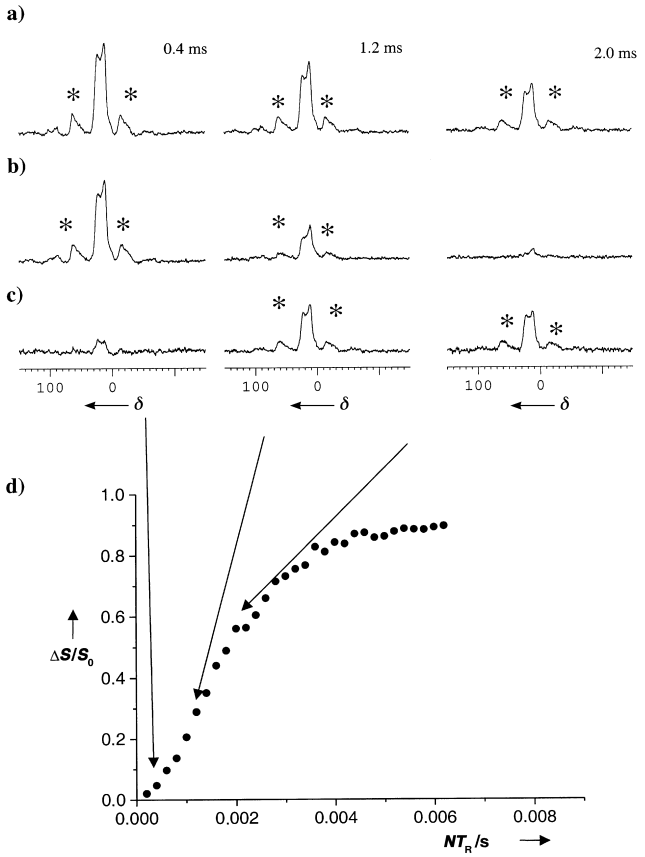


Figure 1. a) ^{11}B-spin-echo MAS spectra, b) ^{11}B{^{29}Si} REDOR NMR spectra with the 180° pulses applied on the ^{29}Si channel, c) difference spectra at evolution times of 0.4, 1.2, and 2 ms. d) Resulting REDOR curve.

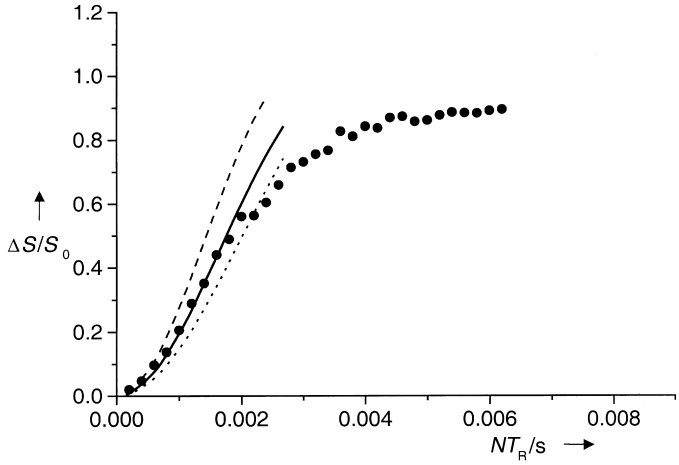


Figure 2. Experimental REDOR data (filled circles) together with simulations in which an isolated two-spin interaction (dotted curve) and a B-Si$_2$ three-spin interaction (dashed curve) are assumed. The solid line corresponds to a weighted superposition of the two simulations according to $\Delta S/S_0 = 0.38\,\Delta S/S_0(\mathrm{BSi_2}) + 0.62\,\Delta S/S_0(\mathrm{BSi})$. A B–Si internuclear distance of 2.74 Å was used in the calculations.

An analysis of the REDOR curve only succeeds when multiple spin interactions are incorporated into the simulations. Trigonally planar boron, coordinated by nitrogen, can be coordinated to up to six silicon atoms in the second coordination sphere, so that multiple spin interactions up to a seven-spin system (BSi_6 interaction) principally have to be taken into account. Moreover, distribution of bond lengths and angles in amorphous networks further complicate interpretation of the data. Both effects result in a smearing out of the oscillations of the REDOR curves characteristic for isolated two-spin systems at long evolution times. Detailed calculations, however,[8] reveal that the initial part of the REDOR curves is to a good approximation unaffected by distribution effects and exact angles in a given geometry of the multiple spin interactions. Consequently we restricted data analysis to $\Delta S/S_0$ values of up to about 0.5.

Figure 2 shows a comparison of the experimental data with simulations, obtained by assuming a B–Si two-spin system (dotted line) and a B–Si$_2$ three-spin interaction (dashed line), as well as a mean B–Si distance of 2.74 Å, a value, which is suggested by neutron diffraction data.[9] The solid line corresponds to a weighted superposition of the above-mentioned models. The simulations lead to the surprising result that the boron atoms are connected (through the three nitrogen atoms) to an average number of 1.35 ± 0.2 silicon atoms. Thus, on an intermediate length scale, the amorphous network cannot be described by a homogenous elemental distribution. This would imply an average number of three silicon neighbors in the second coordination sphere of a central boron atom. However, the results are rather consistent with a formation of silicon-rich and boron-rich islands. This connectivity motif can be explained with the help of the kinetics of the ammonolysis of the BCl_2 and $SiCl_3$ groups in the precursor molecule trichlorosilylaminodichloroborane (TADB). The higher Lewis acidity of the BCl_2 fragment implies a faster attack of ammonia at the boron site of TADB. As a consequence only B–NH_2 groups are available for the polycondensation at the beginning of the reaction, resulting in an oligomer, which is predominantly characterized by B-N-B linkages. Si–Cl bonds are not attacked by ammonia unless the local B–Cl supply is almost depleted. Thus, a network emerges, predominantly characterized by regions of B-N-B and regions of Si-N-Si linkages.

The results are supported by additional NMR experiments. Static ^{11}B spin-echo and ^{29}Si spin-echo experiments principally allow a determination of the number of homonuclear neighbors in the second coordination sphere and can therefore be used to support the double resonance data. Analysis of the ^{11}B spin-echo experiment results in an average number of 4.5 ± 0.5 boron atoms in the second coordination sphere of a central boron atom, whereas the analogous ^{29}Si spin-echo experiment indicates 6.5 ± 0.5 silicon atoms in the second coordination sphere of a central silicon atom. The single B-N-Si linkage already present in the single-source precursor molecule TADB seems to prevail during condensation and pyrolysis, while the new formed connectivities during the condensation process consist predominantly of B-N-B and Si-N-Si linkages. We emphasize the fact that the formation of the described islands is consistent with the previously found SiN_4 and BN_3 polyhedra as the short-range ordering motif and the homogenous elemental distribution down to a length scale of approximately 10 Å.

The presented results may have—apart from the structural characterization of a specific amorphous network, $Si_3B_3N_7$—a

 © WILEY-VCH Verlag GmbH, D-69451 Weinheim, 2000 1433-7851/00/3914-2520 $ 17.50+.50/0

somewhat universal character, especially in terms of attempts to model amorphous structures exclusively on the basis of the chemical composition. These calculations would inevitably produce the respective energetically most favorable ensembles. In the studied ceramic $Si_3B_3N_7$ this would imply an alternating occupation of the cation positions by silicon and boron. The need for an incorporation of the genesis of the amorphous network in the theoretical models begins to emerge.

Experimental Section

All solid-state NMR experiments were performed on a Bruker DSX400 NMR spectrometer operating at 9.4 T equipped with a 4 mm triple-resonance probe. The resonance frequencies were 128.35 MHz for ^{11}B and 79.46 MHz for ^{29}Si. All MAS measurements were performed at room temperature at a rotational frequency of 10 kHz.

^{29}Si-isotopically pure $Si_3B_3N_7$ was prepared from isotopically labeled [^{29}Si]trichlorosilylaminodichloroborane (TADB). $^{29}SiCl_4$, which was obtained by heating a mixture of elemental ^{29}Si and $Pb^{II}Cl_2$ at 600 °C, was allowed to react with hexamethyldisilazane (HMDS) in a ratio of 1:1 to give 1,1,1-trichloro-3,3,3-trimethyldisalazane (TTDS). Reaction of TTDS with BCl_3 finally led to the target molecule TADB. Condensation of TADB was performed using ammonia. Ammonium chloride, which formed as a by-product in the polymerization, was removed by sublimation at 500 °C.

Received: December 27, 1999 [Z14467]

[1] a) M. Jansen, *Solid State Ionics* **1997**, *101 – 103*, 1; b) H.-P. Baldus, M. Jansen, *Angew. Chem.* **1997**, *109*, 338 – 354; *Angew. Chem. Int. Ed. Engl.* **1997**, *36*, 328 – 343.

[2] P. Baldus, M. Jansen, D. Sporn, *Science* **1999**, *285*, 699 – 703.

[3] G. Jeschke, M. Kroschel, M. Jansen, *J. Non-Cryst. Solids* **1999**, *260*, 216 – 227.

[4] D. Heinemann, W. Assenmacher, W. Mader, M. Kroschel, M. Jansen, *J. Mater. Res.* **1999**, *14*, 3746 – 3753.

[5] a) K. R. Carduner, C. S. Blackwell, W. B. Hammond, F. Reidinger, G. R. Hatfield, *J. Am. Chem. Soc.* **1990**, *112*, 4676; b) A. H. Silver, P. J. Bray, *J. Chem. Phys.* **1960**, *32*, 288; c) P. S. Marchetti, D. Kwon, W. R. Schmidt, L. V. Interrante, G. E. Maciel, *Chem. Mater.* **1991**, *3*, 482.

[6] a) T. Gullion, J. Schaefer, *J. Magn. Reson.* **1989**, *81*, 196 – 200; b) T. Gullion, *Magn. Reson. Rev.* **1997**, *17*, 83 – 131.

[7] a) L. van Wüllen, B. Gee, L. Züchner, M. Bertmer, H. Eckert, *Ber. Bunsen Ges. Phys. Chem.* **1996**, *100*, 1539 – 1549; b) L. van Wüllen, L. Züchner, W. Müller-Warmuth, H. Eckert, *Solid State NMR* **1996**, *6*, 203 – 212.

[8] a) A. Naito, K. Nishimura, S. Tuzi, H. Saito, *Chem. Phys. Lett.* **1994**, *229*, 506 – 511; b) J. M. Goetz, J. Schaefer, *J. Magn. Reson.* **1997**, *117*, 147 – 154; c) J. C. C. Chan, M. Bertmer, H. Eckert, *J. Am. Chem. Soc.* **1999**, *121*, 5238 – 5248.

[9] R. M. Hagenmayer, U. Müller, C. J. Benmore, J. Neuefeind, M. Jansen, *J. Mater. Chem.* **1999**, *9*, 2865 – 2870.

Tecto-RNA: One-Dimensional Self-Assembly through Tertiary Interactions**

Luc Jaeger* and Neocles B. Leontis*

The pioneering work of Seeman has demonstrated the use of DNA to construct nanoscale structures.[1–3] Recent work extends these ideas to the assembly of noncovalent complexes, avoiding covalent ligation steps.[4–6] While more chemically labile than DNA, RNA appears to offer a wider range of tertiary motifs[7] that can be used as modular units for supramolecular engineering.[8, 9] "RNA-tectonics" refers to the modular character of natural RNA molecules, which can be decomposed and reassembled to create new nanoscale molecular objects. The properties of RNA that facilitate its use in exploring new paradigms in nanoscale chemical self-assembly include (1) ease of sequence-specific synthesis (using either template-driven enzymatic methods or solid-phase chemical methods); (2) amenability of secondary and, increasingly, tertiary structure to rational design;[9] (3) hierarchical folding of individual molecules;[10] and (4) ability to participate in highly specific tertiary interactions.

Here we report the modular design and synthesis of RNA molecules capable of selective dimerization and one-dimensional self-assembly (Scheme 1). In contrast to associations involving Watson – Crick pairings, association occurs by specific tertiary interactions involving hairpin tetraloops and their receptors, as confirmed by lead(II)-cleavage protection experiments and by motif-swapping experiments.

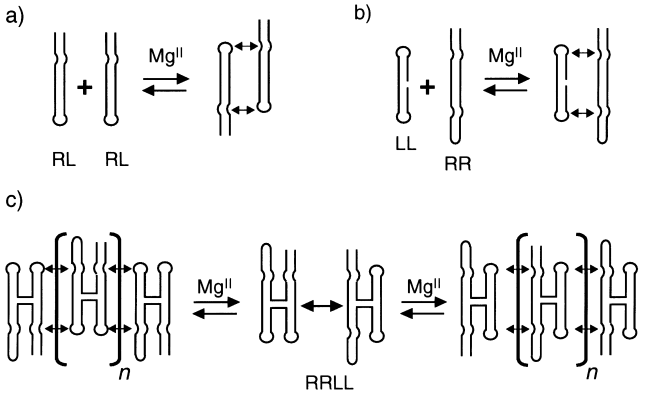
We chose the specific "11-nucleotide motif" receptor for 5′-GAAA-3′ tetraloops,[11, 12] as the primary unit to mediate specific, high-affinity intermolecular RNA interactions. We first designed the self-dimerizing molecule **1**, RL-GAAA (Figure 1). All RNA molecules were synthesized by in vitro transcription of PCR-generated DNA templates (see Supporting Information) using T7 RNA polymerase. The self-association of **1**, as monitored by nondenaturing polyacrylamide gel electrophoresis, occurred with submicromolar dissociation constants and definitely required magnesium ions. At 15 mM $Mg(OAc)_2$, **1** dimerized with $K_d = 4.3 \pm 0.4$ nM (Figure 2). The binding affinity of **1** was measured as a

[*] Dr. L. Jaeger
Institut de Biologie Moléculaire et Cellulaire
UPR 9002 du CNRS, 15 rue René Descartes
67084 Strasbourg Cedex (France)
Fax: (+33) 03-88-60-22-18
E-mail: L.Jaeger@ibmc.u-strasbg.fr

Prof. N. B. Leontis
Chemistry Department
Center for Biomolecular Sciences
Bowling Green State University
Bowling Green, OH 43403 (USA)
Fax: (+1) 419-372-9809
E-mail: leontis@bgnet.bgsu.edu

[**] This work was carried out in Strasbourg with the support of grants to N.B.L. from the NIH (1R15 GM55898) and the NIH Fogarty Institute (1-F06-TW02251-01) and the support of the CNRS to L.J. The authors wish to thank Eric Westhof for his support and encouragement of this work.

Supporting information for this article is available on the WWW under http://www.wiley-vch.de/home/angewandte/ or from the author.



Scheme 1. Assembly principles of tecto-RNA molecules based on hairpin tetraloops (L) and tetraloop receptors (R): a) Dimerization of RL molecules; b) association of LL and RR molecules; c) one-dimensional self-assembly of $n+2$ RRLL four-way junction molecules ($n=0, 1, 2, \ldots$). Self-assembly can potentially occur starting from either of two possible stacking isomers.

function of [Mg^{II}] and the data were fitted to the Hill equation.[13] $K_d(Mg^{II})$ was found to be 1 mM and the Hill coefficient was found to be 1.9 (≈ 2). In the case of all-or-none binding, the Hill coefficient corresponds to the number of magnesium ions that bind during RNA dimerization. This result is consistent with the observation of one specifically bound Mg^{II} in the crystal structure of the GAAA tetraloop/receptor interaction.[14]

Motif-swapping experiments and chemical probing with Pb^{II} were carried out to provide further evidence that dimerization of **1** was, in fact, mediated by specific tertiary interactions and not by complementary Watson–Crick base pairing between two monomers. Motif-swapping has been used to confirm tertiary interactions in natural RNA molecules.[15, 16] First, a single A→U mutation was introduced into the GAAA tetraloop to generate **2**, with a GUAA tetraloop (Figure 1). This mutation completely abolished binding even at high magnesium and RNA concentrations (see Supporting Information), most likely by disrupting the stacking of the tetraloop on the "adenosine platform". In molecule **3** the GAAA-loop receptor was replaced by one for the GUAA tetraloop,[17] while the GAAA tetraloop was retained (Figure 1). Molecule **3**, like **2**, did not self-dimerize. However, **2** and **3** bound to each other with $K_d = 153 \pm 21$ nM. Although the binding is weaker than for **1**, it is nonetheless specific and strong enough to allow dimerization at low concentrations of RNA. The weaker binding of **2** and **3** compared to **1** is consistent with previous work on the GUAA loop–receptor interaction.[17]

Computer modeling indicated that, in the homodimer of **1**, the GAAA loop of one monomer can be swapped with the receptor of the other monomer. This resulted in a heterodimer comprised of one molecule having two loops (LL in Scheme 1) and a second one having two receptors (RR). Accordingly, molecules **4** and **5**, with two GAAA loops and two GAAA-loop receptors respectively, were designed and synthesized (Figure 1). As expected, neither molecule showed any self-affinity. However, they bound to each other with $K_d = 205 \pm 85$ nM. Although the K_d was higher than for the parent **1**, it was still in the submicromolar range. Molecule **4** has a flexible single-stranded linker connecting the loop domains and thus lacks the preorganization for binding of the more rigid molecules **1**–**3** and **5**.

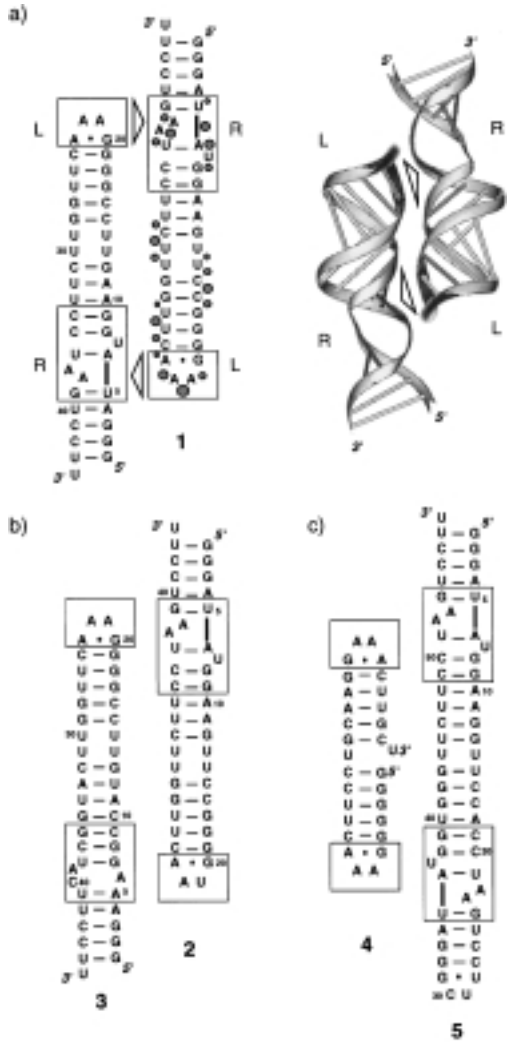


Figure 1. a) 2D diagram and 3D model of the dimer formed by **1** (RL GAAA). The boxes enclose the receptor (R) and the GAAA tetraloop (L) motifs of the molecule. The 3D modeling was done manually using MANIP[21] and the 3D view was generated with DRAWNA.[22] The dimer was assembled from two identical loop–receptor motifs, extracted from the X-ray crystal structure of the P4–P6 domain of the group I intron (NDB file URX053),[12] and separated by an A-form helix of 10 basepairs. Pb^{II} protection data are superimposed on the 2D diagram. The degree of phosphate cleavage by Pb^{II} at low RNA concentration is indicated by the size of the circles. Increasing the RNA concentration to favor dimer formation greatly reduced lead(II) cleavage at all these positions. Lead(II) cleavage was performed as follows. After being heated at 90 °C for 1 min and immediately cooled on ice, RNA samples were allowed to dimerize during 30 min at 30 °C with $Mg(OAc)_2$ (15 mM) in 2-[4-(2-hydroxyethyl)-1-piperazinyl]ethanesulfonic acid buffer (HEPES, 25 mM) at pH 7.5. Pb^{II} cleavage was induced by adding $Pb(OAc)_2$ (8 or 16 mM) and stopped after 5 min by addition of ethylenediaminetetraacetate (EDTA, 50 mM) and EtOH precipitation (see also Supporting Information). RNA fragments were separated on denaturing polyacrylamide gel (15% acrylamide, 8 M urea). b) 2D diagram of the heterodimer formed by molecules **2** and **3**. c) 2D diagram of the heterodimer formed by molecules **4** and **5**.

Lead(II)-probing experiments were carried out on **1**–**5** under conditions favoring either the monomer or the dimer

 © WILEY-VCH Verlag GmbH, D-69451 Weinheim, 2000 1433-7851/00/3914-2522 $ 17.50+.50/0

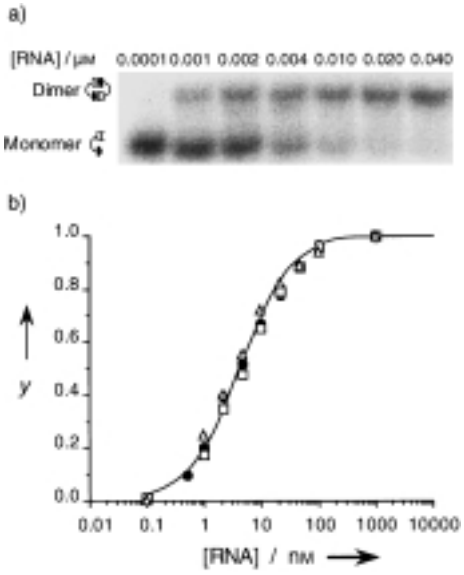


Figure 2. Self-dimerization of **1**: a) Gel electrophoresis with nondenaturing polyacrylamide gel showing the concentration dependence of the dimerization of molecule **1** at 15 mM $Mg(OAc)_2$. Samples containing the indicated total concentration of RNA (including a fixed amount of 3′-end [^{32}P]pCp labeled RNA) were heated in water at 90 °C for 1 min, immediately cooled on ice, and allowed to dimerize for 30 min at 30 °C in Tris(hydroxymethyl)methylamine (Tris) borate buffer (pH 8.3) and 15 mM $Mg(OAc)_2$. Monomers and dimers were then separated by electrophoresis at 4 °C on 9% (30:1) nondenaturing polyacrylamide gels (with the same buffer). b) Dimerization titration curves obtained from native gel-shift experiments at 15 mM $Mg(OAc)_2$. The *Y*-axis corresponds to the fraction of dimers. Quantification of gel bands was performed using a BioImager BAS2000 (Fuji). The K_d corresponds to the RNA concentration at which half of the RNA is dimerized.

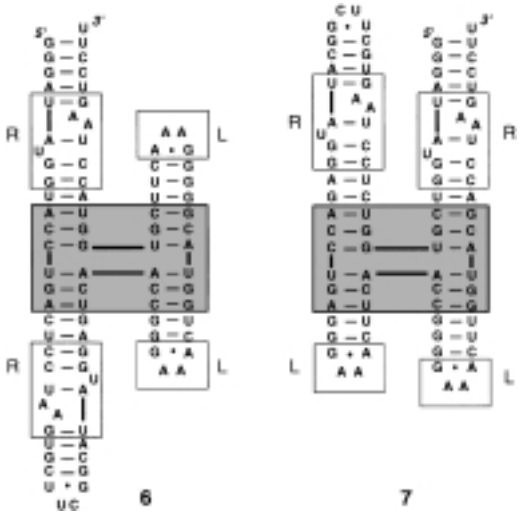


Figure 3. Secondary structure of tecto-RNA molecules **6** and **7**. The white boxes enclose the two receptors (R) and the two GAAA tetraloops (L) of each tecton. The nucleotides enclosed by the shaded boxes correspond to the sequence of the hairpin ribozyme four-way junction.[20]

states (see Supporting Information). Flexible single-stranded regions of RNA are prone to Pb^{II}-induced cleavage, whereas regular A-form helical regions are generally unreactive.[18] Moreover, Pb^{II} may substitute at specific magnesium binding sites.[19] For **1**, Pb^{II}-induced cleavage was observed within the GAAA hairpin and the GAAA receptor motif at concentrations favoring the monomer. These cleavages were dramatically reduced at higher concentrations favoring the dimer. If dimerization were occurring by complementary Watson–Crick basepairing between two molecules, the loop receptor motifs would be regenerated in the dimer and would remain exposed to solvent in the dimer. Thus, the observed Pb^{II} protections (summarized in Figure 1a) are consistent with tertiary binding to form the dimer. Similar results were obtained with the heterodimers, **2**/**3** and **4**/**5** (see Supporting Information).

The specific, high-affinity dimerization of molecules **1**–**5** provided the basis for designing bivalent molecules for linear self-assembly (RRLL in Scheme 1). Bivalent monomer units (tectons) with the potential to self-assemble into one-dimensional arrays were designed by fusing two RL-GAAA molecules at the waist, thus forming the tecto-RNA molecules **6** and **7** (Figure 3). These molecules, synthesized as single RNA transcripts, each comprise a four-way junction with an interaction module on each helical arm. They can adopt two different conformations that differ in the stacking arrangement of the helices at the four-way junction (Scheme 1). Tectons **6** and **7** were designed to favor one or other of these two conformations by incorporating, in two different ways, the four-way junction sequence from the hairpin ribozyme (Figure 3), for which the stacking preference is known.[20] In the energetically more stable conformation of **6**, the two helices with GAAA tetraloops (L) are stacked on each other. Thus, tecton **6** is preorganized to self-assemble into a one-dimensional array or to bind **4** or **5**, terminating chain propagation in one direction. In the more stable conformation of tecton **7**, each helix containing a GAAA receptor (R) is stacked on a helix terminated by a GAAA tetraloop (L). Thus, **7** is preorganized to self-assemble or to interact with **1**, which acts as a chain terminator. Both **6** and **7** can potentially isomerize between the two stacking conformations. Thus, tecton **6** can also bind **1** by isomerizing to the stacking conformation of **7**. Likewise, **7** can bind **4** or **5** by first isomerizing to the conformation of **6**.

Figure 4 shows native gels of the one-dimensional self-assembly of tectons **6** and **7**. In the upper panel, increasing amounts of unlabeled **6** were added to titrate-fixed amounts of radioactively labeled **6** or the monovalent molecules **1** or **5**. In the lower panel the same experiment was conducted with **7** substituted for **6**. These experiments showed that **6** oligomerized very efficiently in the presence of magnesium. As for **1**–**5**, **6** did not assemble in the absence of magnesium. At the highest concentrations of **6** assayed (10 μM), oligomers containing at least 15 molecules of **6** were resolved on native gels. Interestingly, **7** primarily formed dimers. Oligomers of **7** occurred in much lower yield, suggesting that **7** had to undergo a conformational change prior to oligomerization. As expected, **5** bound with higher affinity to **6** than to **7**, whereas the opposite was seen for **1**. Additional experiments were carried out in which radiolabeled **7** was titrated with **6** over the range 0.02 to 10 μM (see Supporting Information). Increasing the concentration of **6** caused radiolabeled **7** to be incorporated into higher molecular weight assemblies. Concomitant-

 © WILEY-VCH Verlag GmbH, D-69451 Weinheim, 2000 1433-7851/00/3914-2523 $ 17.50+.50/0

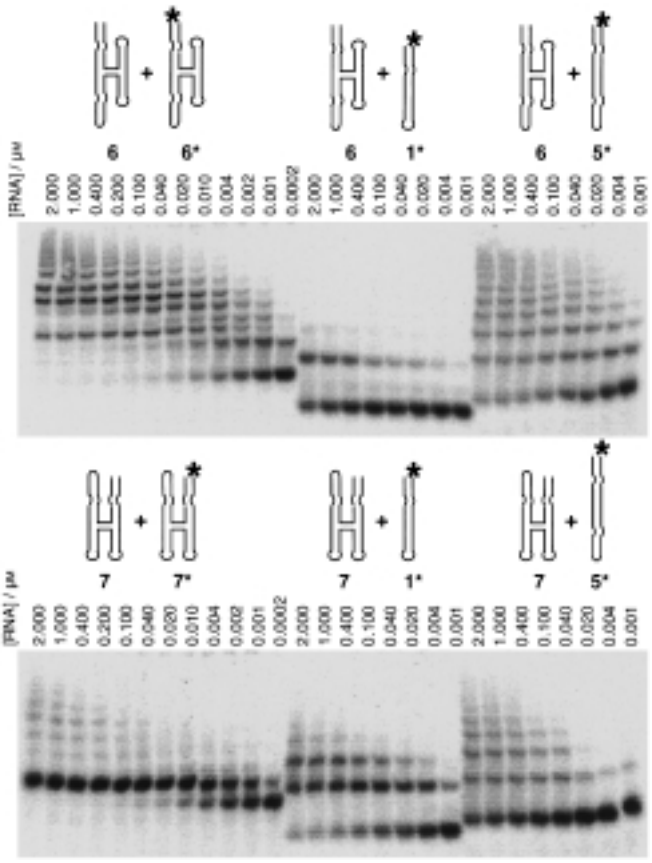


Figure 4. One-dimensional self-asssembly of molecules **6** (upper panel) and **7** (lower panel) visualized on 7% nondenaturing polyacrylamide gels (30:1). In each panel, self-assembly appears on the left and association with **1** and **5** in the center and right, respectively. The [^{32}P]pCp-labeled RNA molecule is indicated by an asterisk (*). The concentration of radiolabeled RNA is 0.1 nM. The samples were prepared and analyzed as described in Figure 2.

ly, the concentration of the dimer of **7** decreased. The simplest interpretation of these data is that **7** can only bind to **6** after isomerizing to its less favored stacking conformation. Thus added **6** shifts **7** into the conformation that can be incorporated into one-dimensional assemblies.

We have shown that RNA can be used as a medium for designing self-assembling molecular modules (tectons). In particular, we have shown that tecton **6** self-assembles into one-dimensional arrays in a conformational- and magnesium-dependent manner. As the dimensions of **6** are approximately 4×9 nm, these noncovalently bonded arrays reach nanoscale lengths of 60 nm or more. Moreover, the length is tunable, as it depends on both the concentration of RNA and Mg^{II}. Further experiments are needed to obtain more insight into the structures of these nanocomplexes. For example, the conformation favored by tecton **7** forms very stable dimers that apparently do not propagate into oligomers, even though they are capable of binding molecule **1**. Experiments are underway to elucidate the reasons for the dramatic difference in the ability of tectons **6** and **7** to self-assemble. However, this result already suggests that the self-assembly process could be potentially controlled using modular "selector" tectons that bind to and stabilize one of these two conformations. Our long-range goal is the design and assembly of two- and three-dimensional arrays using RNA. Clearly, new rules for RNA self-assembly remain to be elucidated.

Received: January 24, 2000 [Z14592]

[1] E. Winfree, F. Liu, L. A. Wenzler, N. C. Seeman, *Nature* **1998**, *394*, 539 – 544.
[2] C. Mao, W. Sun, N. C. Seeman, *J. Am. Chem. Soc.* **1999**, *121*, 5437 – 5443.
[3] N. C. Seeman, *Trends Biotechnol.* **1999**, *17*, 437 – 443.
[4] E. Protozanova, R. B. J. Macgregor, *Biochemistry* **1996**, *35*, 16638 – 16645.
[5] M. Scheffler, A. Dorenbeck, S. Jordan, M. Wüstefeld, G. von Kiedrowski, *Angew. Chem.* **1999**, *111*, 3514 – 3518; *Angew. Chem. Int. Ed.* **1999**, *38*, 3311 – 3315.
[6] R. P. Fahlman, D. Sen, *J. Am. Chem. Soc.* **1999**, *121*, 11079 – 11085.
[7] R. T. Batey, R. P. Rambo, J. A. Doudna, *Angew. Chem.* **1999**, *111*, 2472 – 2491; *Angew. Chem. Int. Ed.* **1999**, *38*, 2326 – 2343.
[8] A. R. Ferre-D'Amare, K. Zhou, J. A. Doudna, *J. Mol. Biol.* **1998**, *279*, 621 – 631.
[9] E. Westhof, B. Masquida, L. Jaeger, *Fold. Des.* **1996**, *1*, R78-R88.
[10] P. Brion, E. Westhof, *Annu. Rev. Biophys. Biomol. Struc.* **1997**, *26*, 113 – 137.
[11] J. H. Cate, A. R. Gooding, E. Podell, K. Zhou, B. L. Golden, A. A. Szewczak, C. E. Kundrot, T. R. Cech, J. A. Doudna, *Science* **1996**, *273*, 1696 – 1699.
[12] J. H. Cate, A. R. Gooding, E. Podell, K. Zhou, B. L. Golden, C. E. Kundrot, T. R. Cech, J. A. Doudna, *Science* **1996**, *273*, 1678 – 1684.
[13] A. V. Hill, *J. Physiol. (London)* **1910**, *40*, iv.
[14] J. H. Cate, R. L. Hanna, J. A. Doudna, *Nat. Struct. Biol.* **1997**, *4*, 553 – 558.
[15] M. Costa, F. Michel, *EMBO J.* **1995**, *14*, 1276 – 1285.
[16] L. Jaeger, F. Michel, E. Westhof, *J. Mol. Biol.* **1994**, *236*, 1271 – 1276.
[17] M. Costa, F. Michel, *EMBO J.* **1997**, *16*, 3289 – 3302.
[18] P. Gornicki, F. Baudin, P. Romby, M. Wiewiorowski, W. Kryzosiak, J. P. Ebel, C. Ehresmann, B. Ehresmann, *J. Biomol. Struct. Dyn.* **1989**, *6*, 971 – 984.
[19] H. Moine, B. Ehresmann, C. Ehresmann, P. Romby, in *RNA Structure and Function* (Eds.: R. W. Simons, M. Grunberg-Manago), Cold Spring Harbor Laboratory Press, Cold Spring Harbor, **1998**, pp. 77 – 116.
[20] F. Walter, A. I. H. Murchie, D. M. J. Lilley, *Biochemistry* **1998**, *37*, 17629 – 17636.
[21] C. Massire, E. Westhof, *J. Mol. Graph. Model.* **1999**, *16*, 197 – 205; C. Massire, E. Westhof, *J. Mol. Graph. Model.* **1999**, *16*, 255 – 257.
[22] C. Massire, C. Gaspin, E. Westhof, *J. Mol. Graphics* **1994**, *12*, 201 – 206.

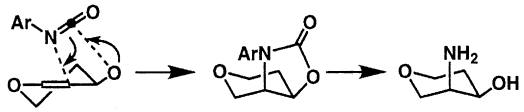
 © WILEY-VCH Verlag GmbH, D-69451 Weinheim, 2000 1433-7851/00/3914-2524 $ 17.50+.50/0

Novel IBX-Mediated Processes for the Synthesis of Amino Sugars and Libraries Thereof**

K. C. Nicolaou,* Phil. S. Baran, Yong-Li Zhong, and Juan A. Vega

Dedicated to Professor David I. Schuster on the occasion of his 65th birthday

Novel molecular diversity is one of the most hotly pursued objectives[1] of modern organic synthesis,[2] medicinal chemistry,[3] and combinatorial synthesis.[4] Amino sugars constitute integral components of a plethora of natural products and medicinally relevant compounds.[5] Several refined methods for the construction of this class of compounds have been reported and extensively reviewed.[6] We have recently reported[1f] a fundamentally new protocol for the introduction of the *N*-phenyl amino functionality into allylic alcohols using IBX (*o*-iodoxybenzoic acid; 1-hydroxy-1,2-benziodoxol-3(1*H*)-one 1-oxide)[7] as a facile reaction mediator. By capitalizing on the convenient and readily available nature of IBX, in conjunction with cheap isocyanates as a nitrogen source, we realized that a tethered approach to amino sugars would provide a distinct advantage over current methods (Scheme 1). The concept of tethering a nitrogen source to an allylic alcohol has been employed to generate amino sugars;[8] however, these conventional methods leave behind additional functionality (such as iodide) which must be dealt with in subsequent steps. For the present method to be of widespread applicability, certain criteria have to be fulfilled: (a) the stereoselectivity of the reaction must be predictable;[9] (b) the *N*-phenyl substituent should be readily removable; and (c) the reaction conditions must be mild and reliable enough to operate on a variety of carbohydrate-based scaffolds. Herein we present



Scheme 1. General concept for the IBX-mediated construction of amino sugars. Ar = aryl.

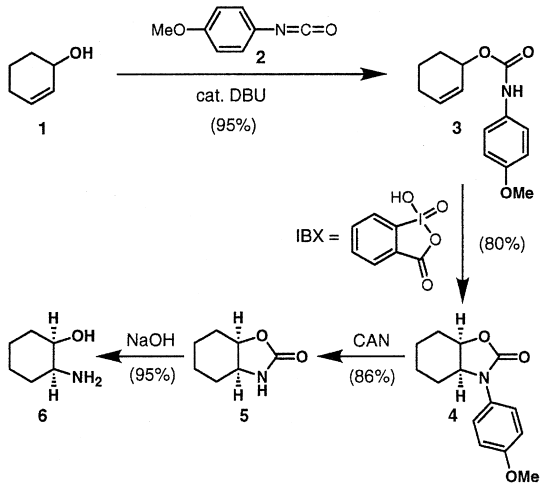
[*] Prof. Dr. K. C. Nicolaou,[+] P. S. Baran, Y.-L. Zhong, Dr. J. A. Vega
Department of Chemistry and The Skaggs Institute for Chemical Biology
The Scripps Research Institute
10550 North Torrey Pines Road, La Jolla, CA 92037 (USA)
Fax: (+1) 858-784-2469
E-mail: kcn@scripps.edu

[+] Department of Chemistry and Biochemistry
University of California San Diego
9500 Gilman Drive, La Jolla, CA 92093 (USA)

[**] We thank Dr. D. H. Huang, Dr. G. Siuzdak, and Dr. R. Chadha for NMR spectroscopic, mass spectrometric, and X-ray crystallographic assistance, respectively, and Prof. H. M. R. Hoffmann and Prof. A. Eschenmoser for helpful discussions. We also thank Dr. Maria-Rosa Rodriguez and Mr. Keith Wilcoxen of these laboratories for early intermediates leading to **9**–**12**. This work was financially supported by the National Institutes of Health (USA), The Skaggs Institute for Chemical Biology, fellowships from the Ministerio de Educacion y Cultura, Spain (J.A.V.) and the National Science Foundation (P.S.B), and grants from Array Biopharma, Pfizer, GlaxoWellcome, Merck, Schering Plough, Hoffmann-LaRoche, Boehringer Ingelheim, DuPont, and Abbott Laboratories.

(a) the realization of these goals; (b) application of the method to a concise synthesis of vancomycin's amino sugar, *l*-vancosamine (**35**, Scheme 4); (c) a revision of our previously proposed mechanism[1f] of the IBX reaction with unsaturated aryl amide carbamates and related systems; and d) the remarkable reactivity of glycals in this reaction.

We first sought a method for the efficient removal of the extraneous, but enabling, aryl moiety.[10] Using 2-cyclohexen-1-ol (**1**) we probed whether adjustment of the phenyl moiety to *p*-methoxy phenyl (pMP) would be tolerated by the IBX reaction (Scheme 2). To our delight, reaction of **1** with *p*-methoxy isocyanate (**2**) in the presence of a catalytic amount

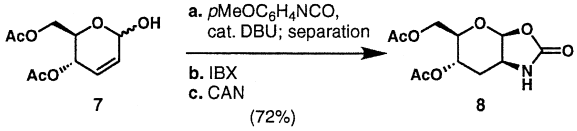


Scheme 2. IBX-Mediated synthesis of *cis*-1,2-amino alcohols (such as **6**) from allylic alcohols (like **1**) using *p*-methoxyphenyl isocyanates (such as **2**). CAN = cerium(IV) ammonium nitrate, DBU = 1,8-diazabicyclo[5.4.0]undec-7-ene.

of DBU followed by reaction with IBX furnished the bicyclic compound **4**, through urethane **3**, setting the stage for the investigation of the removal of the pMP group. In accord with literature precedent,[11] pMP cleavage using ceric ammonium nitrate (CAN), followed by treatment with 2 N NaOH led cleanly to the cis-1,2-amino alcohol **6** through the intermediacy of cyclic carbonate **5** (78% overall yield from **4**, Scheme 2).

Having established the viability of the pMP group in this reaction, we set out to explore its reactivity profile in the context of diverse carbohydrate-based scaffolds. Our first attempt (Scheme 3), which utilized the D-glucal-derived substrate **7**,[12] successfully led to protected amino sugar **8** in 72% yield over three steps.

The generality and scope of this sequence is underscored by the considerable number of substrates (**9**–**19**) successfully employed so far to prepare useful building blocks (**20**–**30**), as shown in Table 1. The reactions consistently provide one

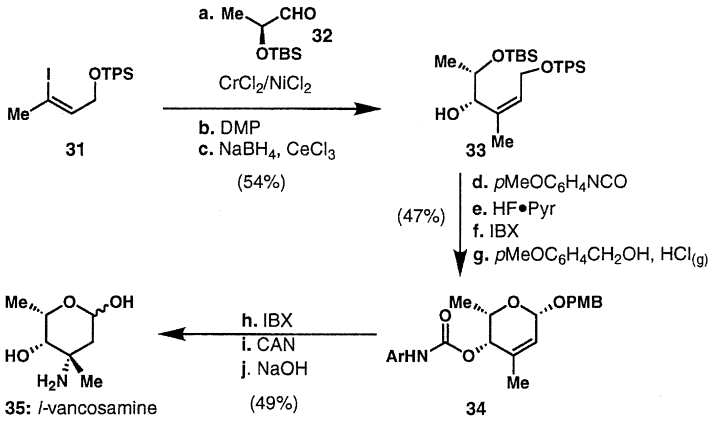


Scheme 3. IBX-Mediated synthesis of amino sugar derivative **8** from carbohydrate **7**. Reagents and conditions: a) *p*MeOC$_6$H$_4$NCO (**2**, 1.1 equiv), DBU (0.1 equiv), CH_2Cl_2, 25 °C, 1 h, 95%; b) IBX (2.0 equiv), THF:DMSO (10:1), 90 °C (sealed tube), 8 h; then IBX (2.0 equiv), 8 h, 84%; c) CAN (5.0 equiv), CH_3CN:H_2O (3:1), 25 °C, 30 min, 90%.

 © WILEY-VCH Verlag GmbH, D-69451 Weinheim, 2000 1433-7851/00/3914-2525 $ 17.50+.50/0

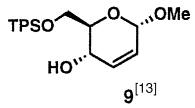
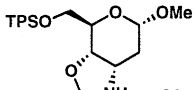
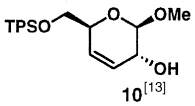
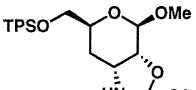
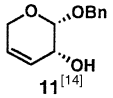
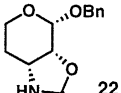
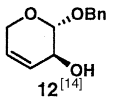
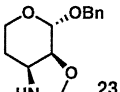
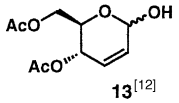
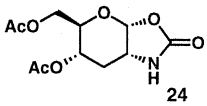
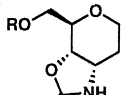
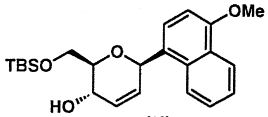
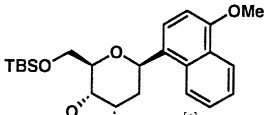
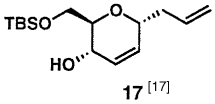
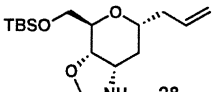
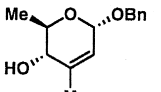
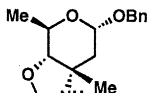
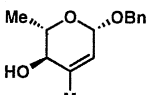
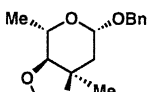
isomer (*cis*) of the protected cyclic urethane in excellent yield, and the ensuing deprotection occurs with similar efficiency to afford the parent urethanes. Base-labile (entries 5 and 6, Table 1), acid-sensitive (entries 7–11, Table 1), and sterically bulky (entry 8, Table 1) functionalities have no effect on the efficiency or stereoselectivity of the reaction. Despite the presence of an additional double bond in **17**[17] (entry 9, Table 1), the reaction proceeds with complete chemo- and stereoselectivity in high yield. In this process, rather than utilizing classical electrophiles (such as I^+, Br^+, $PhSe^+$) to invoke reactivity, the use of IBX selectively activates the nitrogen atom of anilides to react with a nearby olefin, thereby tolerating a wide range of functionalities. Enhanced substitution on the olefin does not deter the IBX-mediated cyclization, thus leading to quaternary centers with equal facility and efficiency (entries 10 and 11, Table 1).

Prompted by the obvious potential of this reaction in the construction of rare amino sugars, and in order to demonstrate its utility in natural product synthesis, we designed an expeditious synthesis of *l*-vancosamine (**35**, Scheme 4),[19] a prototypical natural amino sugar found on vancomycin's structure. Thus, intermolecular Kishi–Nozaki coupling[20] of building blocks vinyl iodide **31**[21] and **32**[22] led to a 1.3:1 mixture of alcohols which was immediately oxidized (with DMP) and subjected to Luche reduction[23] ($NaBH_4/CeCl_3$) to furnish, selectively, only the desired isomer (**33**, 54% overall from **31**). Reaction of alcohol **33** with *p*-methoxyphenyl isocyanate in the presence of catalytic amounts of DBU, followed by global deprotection (with HF·py), selective primary alcohol oxidation (by IBX), and protection of the anomeric hydroxyl group with a PMB protecting group afforded cyclization precursor **34** in 47% overall yield from **33**. IBX-induced cyclization and CAN-mediated removal of both the pMP and PMB groups, followed by basic hydrolysis, completed the stereocontrolled synthesis of *l*-vancosamine



Scheme 4. IBX-Mediated synthesis of *l*-vancosamine (**35**) from building blocks **31** and **32**. Reagents and conditions: a) $CrCl_2$ (4.0 equiv)/$NiCl_2$ (0.04 equiv), DMSO, 25 °C, 12 h, 61%; b) DMP (1.2 equiv), $NaHCO_3$ (5.0 equiv), CH_2Cl_2, 25 °C, 30 min, 98%; c) $NaBH_4$ (1.0 equiv), $CeCl_3$ (1.0 equiv), MeOH, −20 °C, 90%; d) $pMeOC_6H_4NCO$ (**2**, 2.0 equiv), DBU (0.3 equiv), CH_2Cl_2, 25 °C, 5 h, 86%; e) HF·Pyr (5.0 equiv), THF, 25 °C, 5 h, 90%; f) IBX (1.2 equiv), THF/DMSO (10:1), 25 °C, 20 min, 79%; g) $pMeOC_6H_4OH$ (**2**, 10.0 equiv), $HCl_{(g)}$, CH_2Cl_2, 0 °C, 30 min, 77%; h) IBX (4.0 equiv), $NaHCO_3$ (4.4 equiv), THF/DMSO (10:1), 90 °C (sealed tube), 24 h, 76%; i) CAN (3.0 equiv), CH_3CN/H_2O (5:1), 3 h, 92%; j) NaOH (3 N), 90 °C, 1 h, 70%. DMP = Dess–Martin periodinane, Pyr = pyridine.

Table 1. IBX-Mediated synthesis of amino sugar derivatives from allylic alcohols and aryl isocyanates (ArNCO).

Entry	Allylic alcohol	Protected amino sugar	Yield [%, overall][a]
1	 **9**[13]	 **20**	79
2	 **10**[13]	 **21**	76
3	 **11**[14]	 **22**	74
4	 **12**[14]	 **23**	83
5	 **13**[12]	 **24**	60
6	R = Bz **14**[15]	 **25**	80
7	R = TBS **15**[15]	**26**[b]	80
8	 **16**[16]	 **27**[c]	83[e]
9	 **17**[17]	 **28**	80
10	 **18**[18]	 **29**[d]	66
11	 **19**[18]	 **30**[d]	68

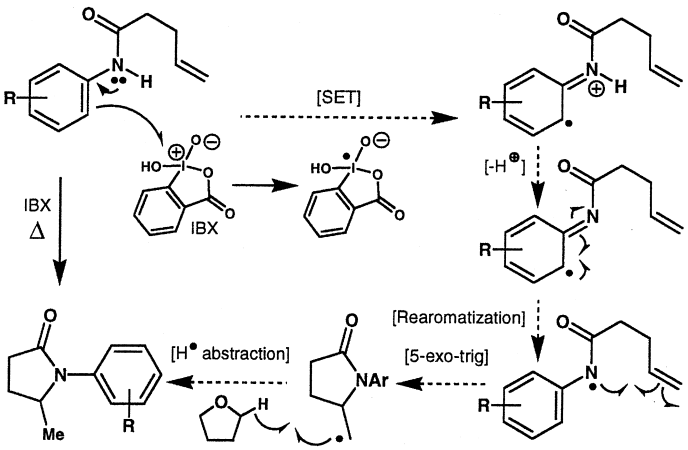
[a] Yields are for chromatographically and spectroscopically pure compounds. Reagents and conditions: a) $pMeOC_6H_4NCO$ (1.1 equiv), DBU (0.1–0.3 equiv), CH_2Cl_2, 25 °C, 5 min–8 h; b) IBX (4.0 equiv), THF:DMSO (10:1), 90 °C (sealed tube), 3–12 h, then IBX (2.0–4.0 equiv), 3–12 h; c) CAN (3.0–5.0 equiv), CH_3CN:H_2O (3–5:1), 0–25 °C. Compounds **22**–**26** were also converted to the parent amino sugars upon treatment with 2–3 N NaOH (90 °C, 30 min) in 85–95% isolated yield. [b] $NaHCO_3$ (4.0 equiv) was added to prevent TBS cleavage (approximately 10%). [c] The CAN reaction was not performed due to the presence of the napthalene ring. [d] $NaHCO_3$ (4.0 equiv) was added as a buffer to prevent cleavage of the surprisingly labile benzyl functionality. [e] Yield over two steps (see footnote [c]).

 © WILEY-VCH Verlag GmbH, D-69451 Weinheim, 2000 1433-7851/00/3914-2526 $ 17.50+.50/0 *Angew. Chem. Int. Ed.* **2000**, *39*, No. 14

(**35**; ten steps; 13% overall yield from the readily available aldehyde **32**). To the best of our knowledge, this sequence constitutes one of the shortest syntheses reported for **35** to date[24] and attests to the efficiency of the present technology for amino sugar construction.

Intrigued by the possibility of engaging glycals in this reaction, and in order to extend the scope of the present reaction technology, we proceeded to explore their reactivity towards IBX. Based on a revised mechanistic proposal for the IBX reaction[1f] with unsaturated urethane substrates and related systems, we reasoned that a prototypical glycal would undergo single electron transfer (SET), loss of a proton, rearomatization, and 5-exo-trig cyclization, as depicted for the simple substrate[1f] in Scheme 5; a glycal such as **36** would, therefore, lead to **37** (Scheme 6). In the absence of water, we expected hydrogen abstraction to proceed as usual to give deoxy amino sugar **A** (Scheme 6). However, since radical species **37** is stabilized, we entertained the possibility that SET to IBX would lead to the oxonium species **38**. In the presence of water (the efficiency of IBX is only slightly decreased in the presence of excess water) such a species would be rapidly intercepted giving rise to the amino sugar **B**. Finally, further oxidation by excess IBX could be envisioned as a conceivable entry into amino sugar lactones such as **C**.

Thus, utilizing D-glucal-derived **39**,[25] we investigated the plausibility of such a bold mechanistic hypothesis (Scheme 7).[26] As expected, the 1-deoxy amino sugar **40** was produced in excellent yield in the absence of water. Furthermore and much to our delight, reaction of **39** in the presence of water led to crystalline **41** with complete control of the two newly formed stereocenters and in 92% yield (see Figure 1



Scheme 5. Revised mechanistic considerations for the IBX reaction. SET = single electron transfer.

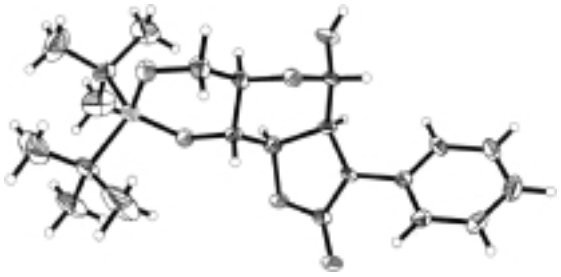
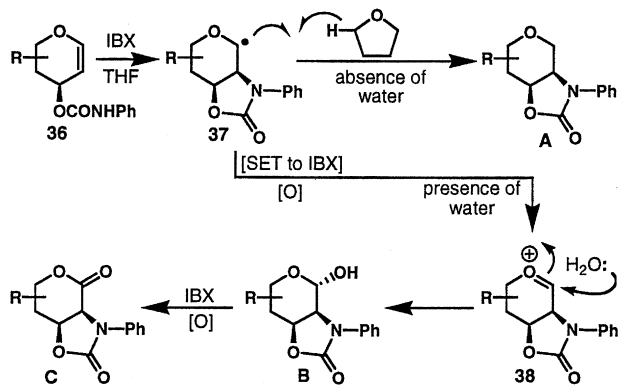
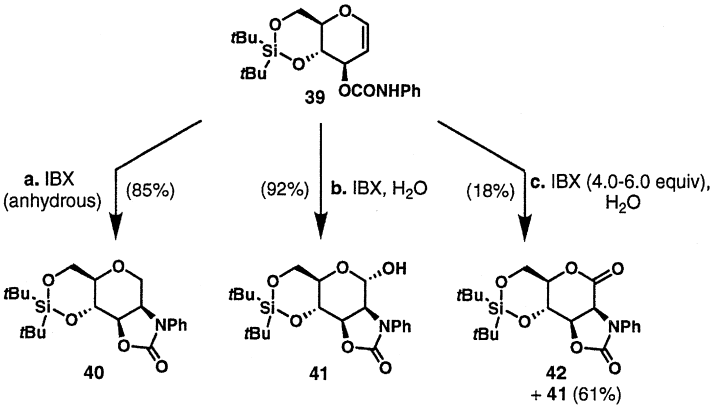


Figure 1.



Scheme 6. Mechanistic blueprint for the reactions of IBX with glycals.



Scheme 7. Formation of three different products (**41**, **42**, **43**) at will from glucal urethanes (**40**) and IBX. Reagents and conditions: a) IBX (2.0 equiv), THF, 90 °C (sealed tube), 8 h, then IBX (2.0 equiv), 8 h, 85%; b) IBX (2.0 equiv), THF:DMSO:H_2O (10:1:0.05), 12 h, 90 °C, 92%; c) IBX (6.0 equiv), THF:H_2O (100:1), 8 h, 90 °C (sealed tube), then IBX (6.0 equiv), 8 h, 73%.

for X-ray structure of **41** and Table 2 for selected physical properties of **40** and **41**). Further reaction with excess IBX furnished the lactone **42** in 18% yield (accompanied by 61% of **41**). These key observations led us to probe the generality

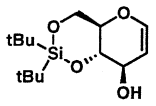
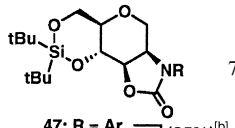
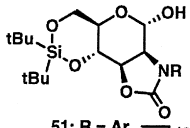
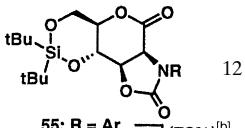
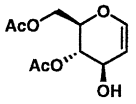
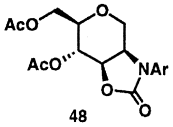
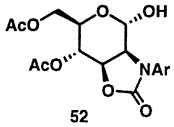
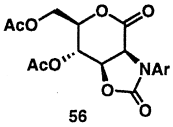
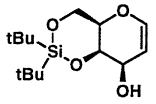
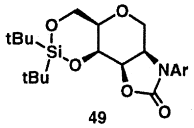
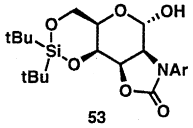
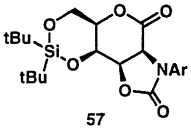
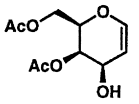
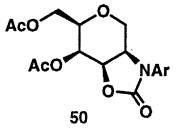
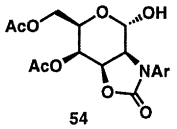
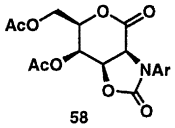
Table 2. Selected physical properties of compounds **40** and **41**.

40: $R_f = 0.31$ (silica gel, diethyl ether: hexane 1:1); $[\alpha]_D = -96.0°$ (c = 0.30, MeOH); IR (film): $\tilde{\nu}_{max} = 2921, 2851, 1680, 1651, 1453, 1394, 1132, 1103, 1016\ cm^{-1}$; ^1H NMR ($CDCl_3$, 600 MHz): $\delta = 7.45-7.41$ (m, 2H), 7.29 (brt, $J = 7.9$ Hz, 1H), 7.20–7.17 (m, 2H), 4.61 (t, $J = 7.4$ Hz, 1H), 4.38 (dd, $J = 7.4, 2.6$ Hz, 1H), 4.18 (dd, $J = 10.5, 5.3$ Hz, 1H), 4.15–4.11 (m, 2H), 3.87 (t, $J = 10.5$ Hz, 1H), 3.65 (dd, $J = 13.6, 2.6$ Hz, 1H), 3.30–3.25 (m, 1H), 1.07 (s, 9H), 1.01 (s, 9H); ^{13}C NMR ($CDCl_3$, 100 MHz): $\delta = 169.0, 137.6, 128.0$ (2C), 125.0 (2C), 124.6, 76.9, 76.0,73.6, 66.1,64.2, 57.7, 29.7, 27.4 (3C), 27.0 (3C), 22.7; HRMS (MALDI) m/z: calcd for $C_{21}H_{31}NO_5SiNa$ $[M + Na^+]$ 428.1864, found 428.1873.

41: Colorless needles; m.p. 118–119 °C; $R_f = 0.31$ (silica gel, ethyl ether: hexane 1:1); $[\alpha]_D = -133.3°$ (c = 0.09, MeOH); IR (film) $\tilde{\nu}_{max} = 3400, 2933, 2859, 1736, 1596, 1503, 1473, 1394, 1306, 1208, 1097, 1020, 971, 847, 826, 764, 694, 654\ cm^{-1}$; ^1H NMR ($CDCl_3$, 500 MHz): $\delta = 7.41$ (t, $J = 6.5$ Hz, 2H), 7.29–7.22 (m, 3H), 5.22 (s, 1H), 4.71 (t, $J = 6.4$ Hz, 1H), 4.52 (d, $J = 6.4$ Hz, 1H), 4.15–4.06 (m, 3H), 4.00 (m, 1H), 3.86–3.81 (m, 2H), 1.07 (s, 9H), 1.01 (s, 9H); ^{13}C NMR ($CDCl_3$, 125 MHz): $\delta = 159.8, 158.4, 156.2, 129.0, 125.5$ (2C), 114.8 (2C), 90.2, 84.3, 80.4, 75.6, 66.8, 65.3, 55.8, 27.8, 27.1; HRMS (MALDI) m/z: calcd for $C_{21}H_{31}NO_6Si$ $[M + H^+]$ 422.2024, found 422.2023.

 © WILEY-VCH Verlag GmbH, D-69451 Weinheim, 2000 1433-7851/00/3914-2527 $ 17.50+.50/0

Table 3. IBX-Mediated synthesis of 1-deoxy amino sugars, amino sugars, and amino sugar lactones from glycals and aryl isocyanates (ArNCO).

Entry	Glycal	1-deoxy amino sugar	Yield [%, overall][a]	Amino sugar	Yield [%, overall][a]	Amino sugar lactone	Yield [%, overall][a,c]
1	 **43**	 **47: R = Ar** **59: R = H** (85%)[b]	72	 **51: R = Ar** **60: R = H** (67%)[b]	81	 **55: R = Ar** **61: R = H** (72%)[b]	12
2	 **44**	 **48**	68	 **52**	73	 **56**	18
3	 **45**	 **49**	76	 **53**	78	 **57**	8
4	 **46**	 **50**	71	 **54**	81	 **58**	16

[a] Yields are for chromatographically and spectroscopically pure compounds. Reagents and conditions are as shown in Scheme 6 for **39**. [b] See Table 1 for reagents and conditions. [c] See text.

and scope of these controllable cascade reactions for the construction of diverse libraries of amino sugar derivatives from glycals.

As shown in Table 3 (Ar = pMP), the reaction is notably general for a range of glucal- and galactal-derived glycal substrates. Furthermore, by using pMP substitution (see above) the rapid and efficient removal of the aromatic residue is achievable (for example from **47** to **59**, **51** to **60**, and **55** to **61**; Table 3). These IBX-mediated routes to 1-deoxy amino sugar and amino sugar derivatives have been proven general and highly efficient. The direct, one-pot entry into the lactone series of compounds is, however, low yielding (Table 3); in such cases a stepwise approach is recommended. The success of this reaction, which was designed based on the mechanistic rationale shown in Schemes 6 and 7 lends credence to the proposed mechanism[1f, 26] and opens the door for further explorations.

To summarize, the cyclization of *N*-arylcarbamates onto olefins, orchestrated by IBX, exemplifies a new and general synthetic technology for the rapid and stereoselective preparation of a diverse array of amino sugar building blocks and compound libraries for biological screening. The unprecedented reactivity of IBX with glycals to allow programmable formation of three types of products from a single starting material, based merely on the presence or absence of water and the stoichiometry of the reagent, is a further demonstration of the unique and exciting potential of this reagent in organic synthesis. The amino sugar derivatives reported herein may prove interesting ligands for a variety of biological targets due to their higher lipophilicity than the naked amino sugars. Studies to elucidate the precise mechanism of these IBX-mediated processes, further exploration of DMP[1e] to generate novel carbohydrate-based polycycles, and investigations directed at the development of solid-phase versions of these new reactions suitable for high speed combinatorics (combinatorial synthesis) are in progress.

Experimental Section

CAUTION! IBX is explosive under impact or on heating to $>200\,^{\circ}C$. (See Ref. [7] and J. B. Plumb, D. J. Harper, *Chem. Eng. News* **1990**, *July 16*, 3.)

Substrates in Table 1 were prepared using the procedure reported in Ref. [7f]. Preparation of 1-deoxy amino sugar derivatives from glycals (Table 3): IBX (2.0 equiv) was added to a solution of **39** (0.1 mmol) in anhydrous THF (4 mL). The solution was placed in a sealed tube and heated for 6 h at $90\,^{\circ}C$, followed by another addition of IBX (2.0 equiv) and heating for another 6–8 h at the same temperature. The reaction mixture was diluted with EtOAc, washed with 5% aqueous $NaHCO_3$ and brine, dried over $MgSO_4$, and concentrated. After purification by flash chromatography (silica, EtOAc: hexane 1:2), compound **40** was obtained in 85% yield. We prepared **41** in an identical manner to **40**, except THF:H_2O (50:1) was employed.

Received: March 20, 2000 [Z 14870]

[1] For some recent examples, see: a) K. C. Nicolaou, S. Snyder, A. Bigot, J. Pfefferkorn, *Angew. Chem.* **2000**, *112*, 1135–1138; *Angew. Chem. Int. Ed.* **2000**, *39*, 1093–1096; b) K. C. Nicolaou, H. J. Mitchell, K. C. Fylaktakidou, H. Suzuki, R. Rodriguez, *Angew. Chem.* **2000**, *112*, 1131–1135; *Angew. Chem. Int. Ed.* **2000**, *39*, 1089–1093; c) J. A. Pfefferkorn, G.-Q. Cao, *Angew. Chem.* **2000**, *112*, 750–755; *Angew. Chem. Int. Ed.* **2000**, *39*, 734–739; d) K. C. Nicolaou, J. A. Pfefferkorn, G.-Q. Cao, *Angew. Chem.* **2000**, *112*, 755–759; *Angew. Chem. Int. Ed.* **2000**, *39*, 739–743; e) K. C. Nicolaou, Y.-L. Zhong, P. S. Baran, *Angew. Chem.* **2000**, *112*, 636–639; *Angew. Chem. Int. Ed.* **2000**, *39*, 622–625; f) K. C. Nicolaou, Y.-L. Zhong, P. S. Baran, *Angew. Chem.* **2000**, *112*, 639–642; *Angew. Chem. Int. Ed.* **2000**, *39*, 625–628; g) D. S. Tan, M. A. Foley, B. R. Stockwell, M. D. Shair, S. L. Schreiber, *J. Am. Chem. Soc.* **1999**, *121*, 9073–9087; h) D. Lee, J. K. Sello, S. L. Schreiber, *J. Am. Chem. Soc.* **1999**, *121*, 10648–10649; i) D. S. Tan,

 © WILEY-VCH Verlag GmbH, D-69451 Weinheim, 2000 1433-7851/00/3914-2528 $ 17.50+.50/0

M. A. Foley, M. D. Shair, S. L. Schreiber, *J. Am. Chem. Soc.* **1998**, *120*, 8565 – 8566; for reviews of molecular diversity, see: j) *Comb. Chem. Mol. Diversity Drug Discovery* (Eds.: E. M. Gordon, J. F. Kerwin, Jr.), Wiley, New York, **1998**, p. 516; R. E. Dolle, *Mol. Diversity* **1998**, *3*, 199 – 233; R. E. Dolle, K. H. Nelson, Jr., *J. Comb. Chem.* **1999**, *1*, 235 – 282; H. Fenniri, *Curr. Med. Chem.* **1996**, *3*, 343 – 378.

[2] For a recent review, see: K. C. Nicolaou, D. Vourloumis, N. Winssinger, P. S. Baran, *Angew. Chem.* **2000**, *112*, 46 – 126; *Angew. Chem. Int. Ed.* **2000**, *39*, 44 – 122.

[3] For a comprehensive discussion, see: *The Practice of Medicinal Chemistry* (Ed.: C. G. Wermuth), Academic Press, London, **1996**, p. 968.

[4] For selected reviews, see: a) M. S. Lee, H. Nakanishi, M. Kahn, *Curr. Opin. Drug Discovery Dev.* **1999**, *2*, 332 – 341; b) P. J. Edwards, M. Gardner, W. Klute, G. F. Smith, N. K. Terrett, *Curr. Opin. Drug Discovery Dev.* **1999**, *2*, 321 – 331; c) C. D. Floyd, C. Leblanc, M. Whittaker, *Prog. Med. Chem.* **1999**, *36*, 91 – 168; d) S. Wilson, A. W. Czarnik, *Combinatorial Chemistry: Synthesis and Application*, Wiley, New York, **1997**, p. 314.

[5] For some recent examples, see: G. W. Plant, S. Woerly, A. R. Harvey, *Exp. Neurol.* **1997**, *143*, 287 – 299; M. Chatterjee, P. J. Smith, C. A. Townsend, *J. Am. Chem. Soc.* **1996**, *118*, 1938 – 1948; G. S. Jacob, *Front. Biomed. Biotechnol.* **1993**, *1*, 74 – 86.

[6] Anonymous in *Carbohydr. Chem. Vol. 30,* Royal Society of Chemistry, London, **1998**, pp. 123 – 140; J. Jurczak, *Prep. Carbohydr. Chem*. **1997**, 595 – 614.

[7] For the first preparation of IBX, see: C. Hartman, V. Meyer, *Chem. Ber.* **1893**, *26*, 1727; for a superior route to IBX, see: M. Frigerio, M. Santagostino, S. Sputore *J. Org. Chem.* **1999**, *64*, 4537 – 4538; for the introduction of the acronym "IBX", see: A. R. Katritzky, B. L. Duell, J. K. Gallos, *Org. Magn. Reson.* **1989**, *27*, 1007 – 1011; for use as a selective oxidant for alcohols, see: M. Frigerio, M. Santagostino, *Tetrahedron Lett.* **1994**, *35*, 8019 – 8022; E. J. Corey, A. Palani, *Tetrahedron Lett.* **1995**, *36*, 7945 – 7948.

[8] For an insightful review of this approach, see: S. Knapp, *Chem. Soc. Rev.* **1999**, *28*, 61 – 72.

[9] Although, with such a mode of reaction as that shown in Scheme 1, one might expect *cis* delivery to the olefin, *trans* addition is also conceivable in certain cases. In the absence of a definitive mechanistic trend for this IBX-mediated reaction at the outset of this work, it was left to empirical observation to provide the answer as to the stereochemical outcome.

[10] The aryl moiety and nitrogen atom of the carbamate group are intimately involved in this IBX reaction, see Ref. [1f] for more details.[26]

[11] D. R. Kronenthal, C. Y. Han, M. K. Taylor, *J. Org. Chem.* **1982**, *47*, 2765 – 2768; S. Knapp, P. J. Kukkola , S. Sharma, *J. Org. Chem.* **1990**, *55*, 5700 – 5710.

[12] H. H. Baer, L. Siemsen, J. DaFaye, K. Burak, *Carbohydr Res.* **1984**, *134*, 49 – 61. The α- and β-isomers of this pyranose were separated after reaction with DBU and p-methoxyphenyl isocyanate (α-anomer used in Scheme 3; β-anomer used in entry 5, Table 1).

[13] Compounds **9** and **10** were derived from methyl-α-D-mannose pyranoside and methyl-β-D-galactose pyranoside, unpublished results.

[14] Compounds **11** and **12** were derived from *l*-arabinose, unpublished results..

[15] K. C. Nicolaou, C. K. Hwang, B. E. Marrow, S. A. DeFrees, E. A. Couladouros, Y. Abe, P. J. Carrol, J. Snyder, *J. Am. Chem. Soc.* **1990**, *112*, 3040 – 3054.

[16] M. Brakta, G. Massiot, G. D. Sinou, G. Daves, *J. Org. Chem.* **1993**, *58*, 2992 – 2998.

[17] G. F. Bordwell, S. R. Mrozack, *J. Org. Chem.* **1982**, *47*, 3802 – 3803.

[18] Compounds **18** and **19** were derived from ethyl *l*-lactate, unpublished results.

[19] A. W. Johnson, R. M. Smith, R. D. Guthrie, *J. Chem. Soc. Perkin Trans. 1* **1972**, *17*, 2153 – 2159; W. D. Weringa, D. H. Williams, J. Feeny, J. P. Brown, R. W. King, *J. Chem. Soc. Perkin Trans. 1* **1972**, *3*, 443 – 446.

[20] a) K. Takai, K. Kimura, T. Kuroda, T. Hiyama, H. Nozaki, *Tetrahedron Lett.* **1983**, *24*, 5281 – 5284; b) H. Jin, J. Uenishi, W. J. Christ, Y. Kishi, *J. Am. Chem. Soc.* **1986**, *108*, 5644 – 5646.

[21] X. Lu, G. Zhu, S. Ma, *Chin. J. Chem.* **1993**, *11*, 267 – 271.

[22] Prepared in two steps from ethyl *l*-lactate by TBS protection (TBSCl, imidazole) and DIBAL reduction (toluene, $-78\,^{\circ}C$).

[23] J.-L. Luche, *J. Am. Chem. Soc.* **1978**, *100*, 2226 – 2227.

[24] For selected syntheses of *l*-vancosamine and derivatives thereof, see: a) T. T. Thang, F. Winternitz, *J. Chem. Soc. Chem. Commun.* **1979**, 153 – 154; b) I. Dyong, H. Friege, *Chem. Ber.* **1979**, *112*, 3273 – 3281; c) T. T. Thang, F. Winternitz, *Tetrahedron Lett.* **1980**, *21*, 4495 – 4498; d) H. I. Ahmad, J. S. Brimacombe, A. S. Mengech, L. C. N. Tucker, *Carbohydr. Res.* **1981**, *93*, 288 – 293; e) I. Dyong, H. Friege, H. Luftmann, H. Merten, *Chem. Ber.* **1981**, *114*, 2669 – 2680; f) G. Fronza, C. Fuganti, P. Grasselli, G. Pedrocchi-Fantoni, *Tetrahedron Lett.* **1981**, *22*, 5073 – 5076; g) J. S. Brimacombe, A. S. Mengech, K. M. M. Rahman, L. C. N. Tucker, *Carbohydr. Res.* **1982**, *110*, 207 – 215; h) G. Fronza, C. Fuganti, P. Grasselli, G. Pedrocchi-Fantoni, *J. Carbohydr. Chem.* **1983**, *2*, 225 – 248; i) Y. Hamada, A. Kawai, T. Shioiri, *Tetrahedron Lett.* **1984**, *25*, 5413 – 5414; j) F. M. Hauser, S. R. Ellenberger, *J. Org. Chem.* **1986**, *51*, 50 – 57; k) I. Dyong, J. Weigand, J. Thiem, *Liebigs Ann. Chem.* **1986**, 577 – 599; l) A. Klemer, H. Wilbers, *Liebigs Ann. Chem.* **1987**, 815 – 823; m) Y. Hamada, A. Kawai, T. Matsui, O. Hara, T. Shioiri, *Tetrahedron* **1990**, *46*, 4823 – 4846; n) R. Greven, P. Jutten, H.-D. Scharf, *Carbohydr. Res.* **1995**, *275*, 83 – 93; o) K. C. Nicolaou, H. J. Mitchell, F. L. van Delft, F. Rübsam, R. M. Rodríguez, *Angew. Chem.* **1998**, *110*, 1972 – 1974; *Angew. Chem. Int. Ed.* **1998**, *37*, 1871 – 1874.

[25] J. O. Hoberg, *Carbohydr. Res.* **1997**, *300*, 365 – 367.

[26] Extensive mechanistic studies dealing with the interactions of periodinanes with anilides will be reported in due course.

[27] Crystallographic data (excluding structure factors) for the structure reported in this paper have been deposited with the Cambridge Crystallographic Data Centre as supplementary publication no. CCDC-142005. Copies of the data can be obtained free of charge on application to CCDC, 12 Union Road, Cambridge CB2 1EZ, UK (fax: (+44) 1223-336-033; e-mail: deposit@ccdc.cam.ac.uk).

Novel Reactions Initiated by Titanocene Methylidenes: Deoxygenation of Sulfoxides, *N*-Oxides, and Selenoxides**

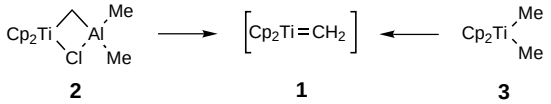
K. C. Nicolaou,* Alexandros E. Koumbis, Scott A. Snyder, and Klaus B. Simonsen

Over the course of the past several years, sulfoxides have become an increasingly important functional group in organic synthesis, particularly as chirons in asymmetric synthesis.[1] As

[*] Prof. Dr. K. C. Nicolaou, Dr. A. E. Koumbis, S. A. Snyder, Dr. K. B. Simonsen
Department of Chemistry and The Skaggs Institute for Chemical Biology
The Scripps Research Institute
10550 North Torrey Pines Road, La Jolla, CA 92037 (USA)
Fax: (+1) 858-784-2469
and
Department of Chemistry and Biochemistry
University of California San Diego
9500 Gilman Drive, La Jolla, CA 92093 (USA)
E-mail: kcn@scripps.edu

[**] We thank Drs. D. H. Huang and G. Suizdak for NMR spectroscopic and mass spectroscopic assistance, respectively. Financial support for this work was provided by The Skaggs Institute for Chemical Biology, the National Institutes of Health (USA), fellowships from the National Science Foundation (S.A.S.) and the Alfred Benzons Foundation (K.B.S.), and grants from Abbott, Amgen, Boehringer-Ingelheim, GlaxoWellcome, Hoffmann-LaRoche, DuPont, Merck, Novartis, Pfizer, and Schering Plough.

such, there has been an enduring interest among chemists in developing novel methods to effect the deoxygenation (or reduction) of sulfoxides to sulfides so that this functionality can be cleanly extruded from the molecule of interest once its presence is no longer required.[2] During the course of recent synthetic investigations, we uncovered a novel method to effect such a conversion with a titanocene methylidene complex **1** (Scheme 1), generated either from the Tebbe[3] or

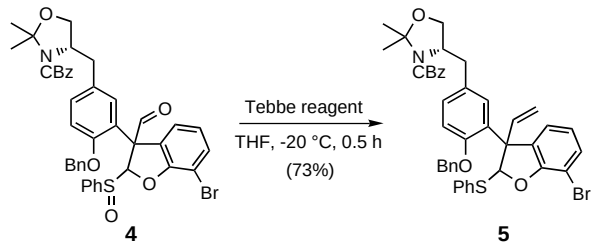


2 **1** **3**

Scheme 1. Generation of a titanocene methylidene complex **1** from the Tebbe (**2**) and Petasis (**3**) reagents. Cp = cyclopentyl.

Petasis[4] reagents (**2** and **3**, respectively). Herein we report the extension of this initial discovery to the deoxygenation of a wide range of highly functionalized sulfoxides, as well as the application of this novel methodology towards the reduction of *N*-oxides and selenoxides. Based upon these results, we propose an unprecedented carbene-initiated deoxygenation mechanism to account for our findings.

When we treated aldehyde **4** (Scheme 2) with an excess of Tebbe reagent (2.0 equivalents) at $-20^{\circ}C$, we observed not only the expected formation of the desired alkene, but also the



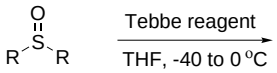
4 **5**

Scheme 2. Discovery of the sulfoxide to sulfide conversion in the presence of Tebbe reagent. CBz = benzyloxycarbonyl, Bn = benzyl.

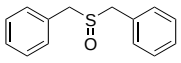
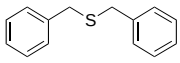
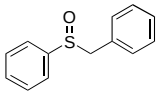
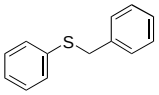
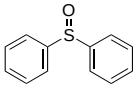
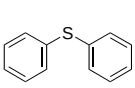
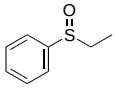
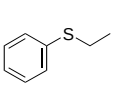
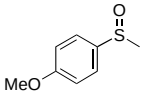
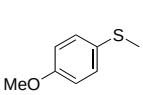
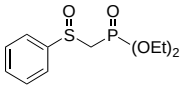
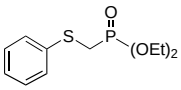
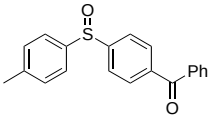
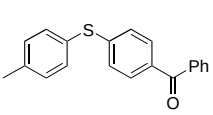
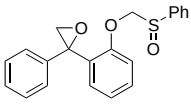
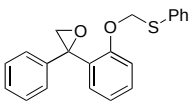
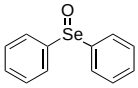
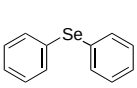
concomitant reduction of the sulfoxide group to the corresponding sulfide **5**. Although we were highly pleased with this serendipitous transformation, since we anticipated having to perform sulfoxide reduction later in our synthetic sequence, we were particularly struck by the mild conditions under which deoxygenation occurred while in the presence of numerous functionalities which survived the reaction conditions. Over the years, numerous methods have been developed to reduce sulfoxides to sulfides; however, many of these transformations require prolonged reaction times, harsh conditions, or reagents that are not readily available. Many other reported methods (see below), even if they do proceed under mild conditions with fair yields, have been explored only on a limited number of simple substrates.[5] In light of this information, we sought to explore the full utility and scope of our deoxygenation process using the Tebbe reagent.

As shown in Table 1, a wide range of diaryl, aryl – alkyl, and dialkyl sulfoxides were readily and rapidly reduced (< 3 hours) in good to excellent yields at low temperature. In particular, the reduction of dibenzylsulfoxide (entry 1)

Table 1. Conversion of sulfoxides into sulfides and the reduction of selenoxides.



(1)

Entry	Starting material	Product	Time [h]	Yield [%]
1			2	80
2			3	81
3			0.5	94
4			3	85
5			2	84
6			4	77
7			18	25
8			1	85
9			2	50
10			4	81

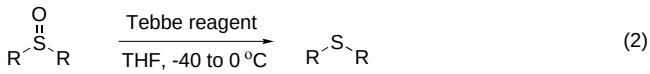
serves as a diagnostic measure of the utility of the reaction, since most methods either fail completely with this substrate or only provide poor yields of dibenzylsulfide.[6] Moreover, despite the high oxophilicity of titanocenes, sulfoxides were prefentially reduced by Tebbe reagent in the presence of both ketones (entry 8) and epoxides (entry 9).[7] We did find, however, that we could not effect selective reduction of sulfoxides in the presence of aldehydes, amides, or esters, with both sulfoxide deoxygenation and carbonyl methylenation occurring simultaneously. The only other sulfoxide substrate with which any difficulty was encountered was the sterically hindered di-*tert*-butyl sulfoxide (entry 7); after a prolonged reaction time, only a 25% isolated yield of product was obtained with recovery of a significant amount of unreacted starting material. Attempted reduction of diphenyl sulfone resulted in only the recovery of starting material, suggesting that the polarized nature of sulfoxides is critical for reactivity.

 © WILEY-VCH Verlag GmbH, D-69451 Weinheim, 2000 1433-7851/00/3914-2530 $ 17.50+.50/0 *Angew. Chem. Int. Ed.* **2000**, *39*, No. 14

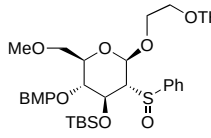
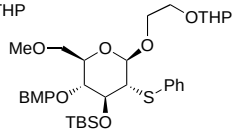
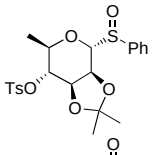
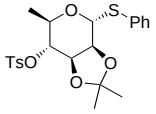
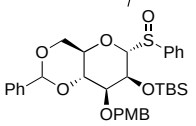
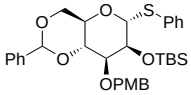
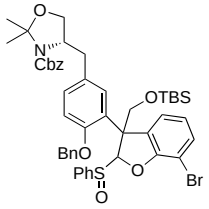
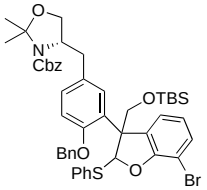
Although we found that phosphine oxides could not be deoxygenated with this protocol (neither triphenylphosphine oxide nor the phosphonate residue in entry 6 were reduced), diphenylselenoxide was readily reduced upon exposure to Tebbe reagent (entry 10).

With the scope of the reaction more clearly defined, we next sought to employ several advanced sulfoxide-containing synthetic intermediates to stringently test whether this methodology could be applied in the preparation of complex molecules (Table 2). In particular, due to their widespread use in carbohydrate chemistry, we attempted to chemoselectively reduce the sulfoxide group in several sugars. Gratifyingly, sugars containing a sulfoxide moiety in both the anomeric and the 2-position were smoothly reduced in high yield in the presence of various acetal, silyl, benzyl, THP, and tosyl protecting groups. The carbamate and aryl halide groups in entry 4 were also found to be inert under the reaction conditions. To the best of our knowledge, no other methodology currently exists where sulfur deoxygenation can occur in the presence of every one of these functional and/or protecting groups. As such, the highly selective nature of this reaction renders sulfoxides as a viable protecting group for thioethers in organic synthesis.

Table 2. Advanced examples of sulfide generation from sulfoxides.

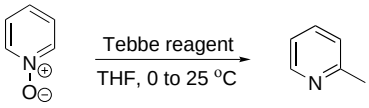


(2)

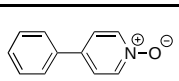
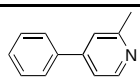
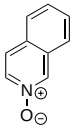
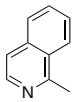
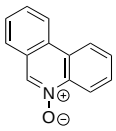
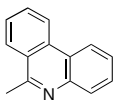
Entry	Starting material	Product	Time [h]	Yield [%]
1			3	79
2			1	76
3			0.5	84
4			1	83

Several other titanium-based reagents are known to effect the sulfoxide to sulfide conversion, such as $TiCl_4/LiAlH_4$,[6a] $TiCl_4/NaBH_4$,[8] $TiCl_4/Sm$,[9] $TiCl_4/NaI$,[10] $TiCl_3$,[11] $TiCl_2$,[12] $Cp_2Ti(CO)_2$,[13] Cp_2TiCl_2/iPrMgBr,[14] and a titanium–porphyrin complex;[15] for each of these reagent combinations, it is thought that either a low-valent Ti^{II} or Ti^{III} species is the active component, which effects deoxygenation by a redox pathway. In our case, however, since the titanocene methylidene **1** derived from Tebbe reagent is an active Ti^{IV} species, we hypothesized that sulfoxide reduction was occurring by a novel mode of action. To test this assumption, we explored the deoxygenation of pyridine *N*-oxides, a process which can be effected by several of the reagents listed above. Surprisingly, as shown in Table 3, when we subjected three different pyridine-derived *N*-oxides to Tebbe reagent, we observed the smooth formation of the corresponding 2-methylpyridines as opposed to just simple heterocycle deoxygenation. Interestingly, in the case of isoquinoline *N*-oxide (entry 2), the formation of solely one regioisomeric product was observed. Not only is this conversion of pyridine *N*-oxides to 2-methylpyridines entirely unprecedented, but this result also clearly indicates that the reaction follows a novel mechanism, different from those previously reported for titanium-mediated deoxygenation.

Table 3. Generation of 2-methylpyridines from pyridine *N*-oxides upon exposure to Tebbe reagent.



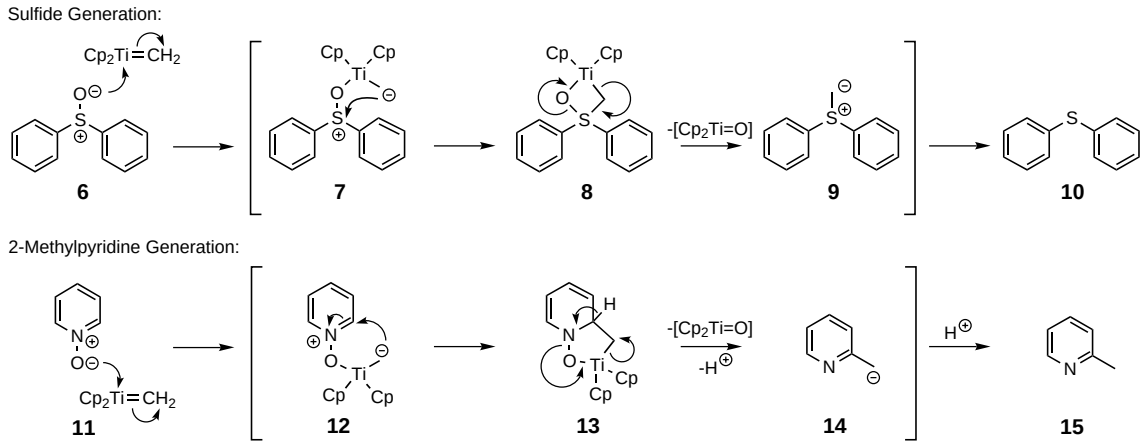
(3)

Entry	Starting material	Product	Time [h]	Yield [%]
1			2	83
2			2	90
3			2	87

To verify that a titanocene methylidene complex was indeed playing an active role in the deoxygenation process, as well as to exclude any possible role that an aluminum species derived from **2** might have in the reaction, we subjected diphenylsulfoxide, isoquinoline *N*-oxide, and diphenyl selenoxide to the Petasis reagent (**3**), readily prepared upon addition of methyl lithium to Cp_2TiCl_2.[16] Gratifyingly, as shown in Table 4, the reaction proceeded smoothly, albeit with longer reaction times at higher temperature, providing the same deoxygenated product in each case in high yield.

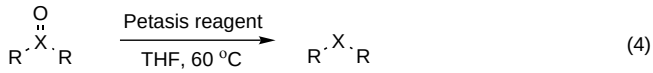
With these results in hand, the mechanism by which the titanocene methylidene exerts deoxygenation would appear to be a carbene-initiated process, as delineated in Scheme 3. For sulfoxides, initial oxygen coordination to titanium is followed by the formation of a metallacycle **8**, which then breaks down to reveal a sulfur-based ylide. Due to the inherent instability of species such as **9**, the nonstabilized ylide decomposes upon standing to provide the observed sulfide

 © WILEY-VCH Verlag GmbH, D-69451 Weinheim, 2000 1433-7851/00/3914-2531 $ 17.50+.50/0

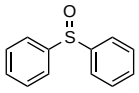
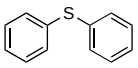
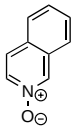
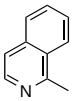
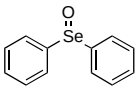
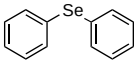


Scheme 3. Proposed carbene-based mechanisms to account for sulfur deoxygenation and 2-methylpyridine formation upon exposure to the Tebbe or Petasis reagents.

Table 4. Use of the Petasis reagent to effect sulfoxide, pyridine *N*-oxide, and selenoxide reductions.



(4)

Entry	Starting material	Product	Time [h]	Yield [%]
1			12	97
2			12	77
3			12	91

10.[17] In the pyridine *N*-oxide case, the same initial addition of oxygen to titanium is postulated to occur (to form intermediate **12**), but since the resultant alkyl anion cannot engage the nitrogen atom directly as in the sulfoxide case, it instead adds to the ortho position, forming a five-membered metallacycle in what is formally a 3+2 cycloaddition process. Once **13** has formed, hydrogen elimination results in the formation of **14** attended by the release of $Cp_2Ti{=}O$; ensuing proton capture generates the final 2-methylpyridine product **15**. In an additional experiment, the existence of intermediate **14** was confirmed by the incorporation of a single deuterium on the methyl group of **15** upon quenching the reaction with D_2O, as verified by ^1H NMR, ^{13}C NMR, and HRMS analyses.

In conclusion, we have discovered a novel methodology by which to deoxygenate sulfoxides and selenoxides as well as generate 2-methylpyridines from the corresponding *N*-oxides by an unprecedented carbene-initiated deoxygenation mechanism. Moreover, the mild conditions employed, as well as the wide range of both functional and protecting groups which have been successfully incorporated, now permits the use of sulfoxides as protecting groups and auxiliaries for complex synthetic substrates.

Experimental Section

All sulfoxides were prepared by oxidizing the precursor sulfide with *m*CPBA (1.0 equivalent) in CH_2Cl_2 at 0°C, with reaction completion typically observed within fifteen minutes. All *N*-oxides were prepared by the method of C. Copéret, H. Adolfsson, T.-A. V. Khuong, A. K. Yudin, K. B. Sharpless, *J. Org. Chem.* **1998**, *63*, 1740–1741. Diphenyl selenoxide was prepared as described by M. R. Detty, *J. Org. Chem.* **1980**, *45*, 274–279.

In a representative procedure, the sulfoxide (0.5 mmol) was dissolved in anhydrous THF (20 mL), cooled to −40°C, and then treated with Tebbe reagent (0.5 M in toluene, 0.55–0.75 mmol, 1.1–1.5 equivalents). The reaction mixture was allowed to slowly warm to 0°C if necessary, with reaction progress monitored by thin layer chromatography. Once the reaction reached completion, any excess Tebbe reagent was quenched by the addition of a few drops of 10% aqueous NaOH. The reaction mixture was then diluted with ether and, once bubbling ceased, $MgSO_4$ was added. Filtration of the solution through Celite, evaporation, and flash column chromatography furnished the pure product. In each case, the generated sulfide matched authentic material based on both thin layer chromatography and ^1H NMR analysis. For the pyridine *N*-oxide substrates, reactions were performed similarly, except the starting temperature was 0°C and the reaction was warmed to ambient temperature. For all reactions involving Petasis reagent, the reagents were refluxed for 12 hours.

Received: March 24, 2000 [Z 14895]

[1] For recent reviews in this growing area of asymmetric synthesis, see: a) M. C. Carreno, *Chem. Rev.* **1995**, *95*, 1717–1760; b) G. Solladie, A. Antonio, C. Dominguez, *Pure Appl. Chem.* **1994**, *66*, 2159–2162; c) A. J. Walker, *Tetrahedron: Asymmetry* **1992**, *3*, 961–998.

[2] M. Madesclaire, *Tetrahedron* **1988**, *44*, 6537–6580.

[3] a) F. N. Tebbe, G. W. Parshall, G. S. Reddy, *J. Am. Chem. Soc.* **1978**, *100*, 3611–3613; b) L. F. Cannizzo, R. H. Grubbs, *J. Org. Chem.* **1985**, *50*, 2316–2323; c) L. F. Cannizzo, R. H. Grubbs, *J. Org. Chem.* **1985**, *50*, 3611; d) S. H. Pine, R. J. Pettit, G. D. Geib, S. G. Cruz, C. H. Gallego, T. Tijerina, R. D. Pine, *J. Org. Chem.* **1985**, *50*, 1212–1216.

[4] a) N. A. Petasis, E. I. Bzowej, *J. Am. Chem. Soc.* **1990**, *112*, 6392–6394; b) N. A. Petasis, E. I. Bzowej, *Tetrahedron Lett.* **1993**, *34*, 943–946.

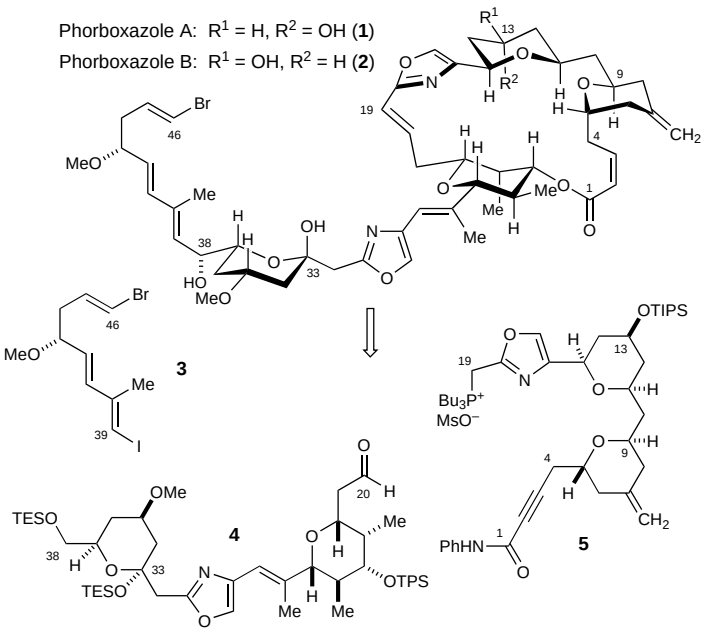
[5] For pertinent reviews of sulfoxide reductions, see: Ref. [2]; a) V. Y. Kukushkin, *Coord. Chem. Rev.* **1995**, *139*, 375–407; b) V. Y. Kukushkin, *Russ. Chem. Rev.* **1990**, *59*, 844–852; c) J. Drabowicz, T. Numata, S. Oae, *Org. Prep. Proc. Int.* **1977**, *9*, 63–83.

[6] a) J. Drabowicz, M. Mikolajczyk, *Synthesis* **1976**, 527–528; b) D. W. Chasar, *J. Org. Chem.* **1971**, *36*, 613–614; c) H. Alper, E. C. H. Keung, *Tetrahedron Lett.* **1970**, 53–56.

[7] Although the reaction with the epoxide derivative went to completion, difficulty in isolating the final product accounted for the lower yield compared to the other cases reported.

 © WILEY-VCH Verlag GmbH, D-69451 Weinheim, 2000 1433-7851/00/3914-2532 $ 17.50+.50/0

[8] S. Kano, Y. Tanaka, E. Sugino, S. Hibino, *Synthesis* **1980**, 695 – 697.
[9] J. Q. Wang, Y. M. Zhang, *Synth. Commun.* **1995**, *25*, 3545 – 3547.
[10] R. Balicki, *Synthesis* **1991**, 155 – 156.
[11] a) T.-L. Ho, C. M. Wong, *Synth. Commun.* **1973**, *3*, 37 – 38; b) H. Suzuki, H. Manabe, R. Enokiya, Y. Hanazaki, *Chem. Lett.* **1986**, 1339 – 1340.
[12] J. Drabowicz, M. Mikolajczyk, *Synthesis* **1978**, 138 – 139.
[13] T. L. Chen, A. Shaver, T. H. Chan, *J. Organomet. Chem.* **1989**, *367*, C5-C7.
[14] Y.-M. Zhang, R.-H. Lin, *Youji Huaxue* **1987**, 361 – 364.
[15] X. Wang, L. K. Woo, *J. Org. Chem.* **1998**, *63*, 356 – 360.
[16] V. K. Clauss, H. Bestian, *Liebigs Ann. Chem.* **1962**, *654*, 8 – 19.
[17] a) E. J. Corey, M. Jautelet, *J. Am. Chem. Soc.* **1967**, *89*, 3912 – 3914; b) E. J. Corey, M. Chaykovsky, *J. Am. Chem. Soc.* **1965**, *87*, 1353 – 1364; c) A. W. Johnson, V. J. Hruby, J. L. Williams, *J. Am. Chem. Soc.* **1964**, *86*, 918 – 922; d) B. M. Trost, R. LaRochelle, *Tetrahedron Lett.* **1968**, *9*, 3327 – 3330; e) J. E. Baldwin, R. E. Peavy, *Tetrahedron Lett.* **1968**, *9*, 5029 – 5031.



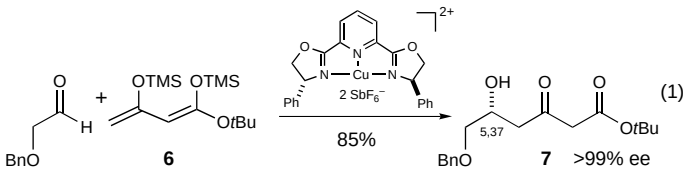
Scheme 1. Retrosynthetic analysis of phorboxazole B. (See ref. [5] for abbreviations.)

Asymmetric Synthesis of Phorboxazole B—Part I: Synthesis of the $C_{20}-C_{38}$ and $C_{39}-C_{46}$ Subunits**

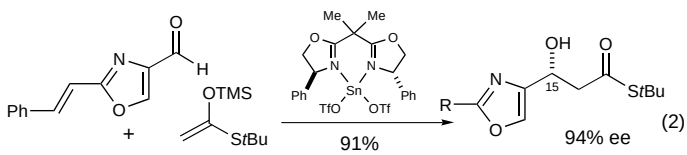
David A. Evans,* Victor J. Cee, Thomas E. Smith, Duke M. Fitch, and Patricia S. Cho

Phorboxazoles A (**1**) and B (**2**) are marine natural products isolated from a newly discovered species of Indian Ocean sponge (genus *Phorbas sp.*).[1] These substances are representatives of a new class of macrolides and are among the most cytostatic natural products known; they inhibit the growth of tumor cells at nanomolar concentrations (mean $GI_{50} = 1.58 \times 10^{-9}$ M).[2] As a result, phorboxazoles A and B have been selected by the National Cancer Institute for in vivo antitumor trials.[1b] The unique structure and impressive biological activity of these molecules have led to widespread efforts to synthesize these substances,[3] and a total synthesis of phorboxazole A has recently been reported.[3u] In this and the following communication[4] we describe our work culminating in the synthesis of phorboxazole B.

The synthesis plan (Scheme 1) calls for an early disconnection of the C_{38}–C_{39} bond to provide the triene side chain **3**, which allows the remainder of the molecule to be divided into fragments of roughly equal complexity. Disconnection through the C_{19}–C_{20} *E* olefin and macrolactone moieties provides the $C_{20}-C_{38}$ core fragment **4** and the C_1-C_{19} bispyran fragment **5**. The distinctive features of this plan include a Wittig reaction to form the C_{19}–C_{20} olefin, macrolactonization of a C_1-C_{38} seco acid, and late-stage incorporation of the fully functionalized triene side chain. The utilization of our recently developed Cu^{2+}-catalyzed enantioselective aldol reaction[6] [Eq. (1)] provides the foundation for the synthesis of two of



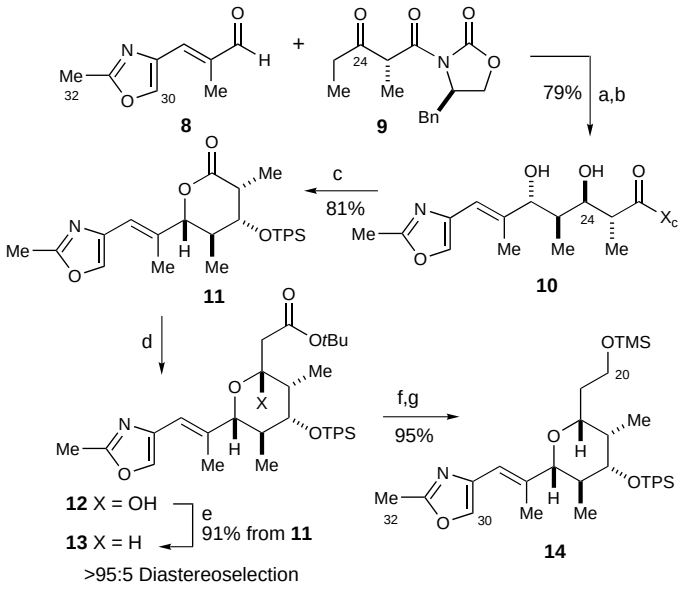
the polyacetate regions of the molecule (C_4-C_9 and $C_{33}-C_{38}$), while an enantioselective stannous triflate catalyzed aldol reaction has been employed to assemble the $C_{13}-C_{19}$ oxazole-containing subunit [Eq. (2) where R = 2-phenylethene].[4]



The synthesis of the polypropionate region of the central core fragment **4** began with the addition of the (*E*)-boron enolate of **9**[7] to the known aldehyde **8**,[8] which delivered the desired *anti* aldol adduct in 97% yield (94:6 *dr*) (Scheme 2).[9, 10] Subsequent hydroxyl-directed reduction[11] of the C_{24} ketone provided *anti* diol **10**, which was isolated in 81% yield as a single diastereomer after crystallization.[12] Cyclization of **10** under basic conditions (cat. DBU, CH_2Cl_2) followed by in situ

[*] Prof. D. A. Evans, V. J. Cee, T. E. Smith, D. M. Fitch, P. S. Cho
Department of Chemistry & Chemical Biology
Harvard University
Cambridge, MA 02138 (USA)
Fax: (+1) 617-495-1460
E-mail: evans@chemistry.harvard.edu

[**] Financial support was provided by the National Institutes of Health (GM-33328) and the National Science Foundation. An American Cancer Society Postdoctoral Fellowship to T.E.S. and an NSF Predoctoral Fellowship to V.J.C. are gratefully acknowledged. The NIH BRS Shared Instrumentation Grant Program 1-S10-RR04870 and the NSF (CHE 88-14019) are acknowledged for providing NMR facilities.



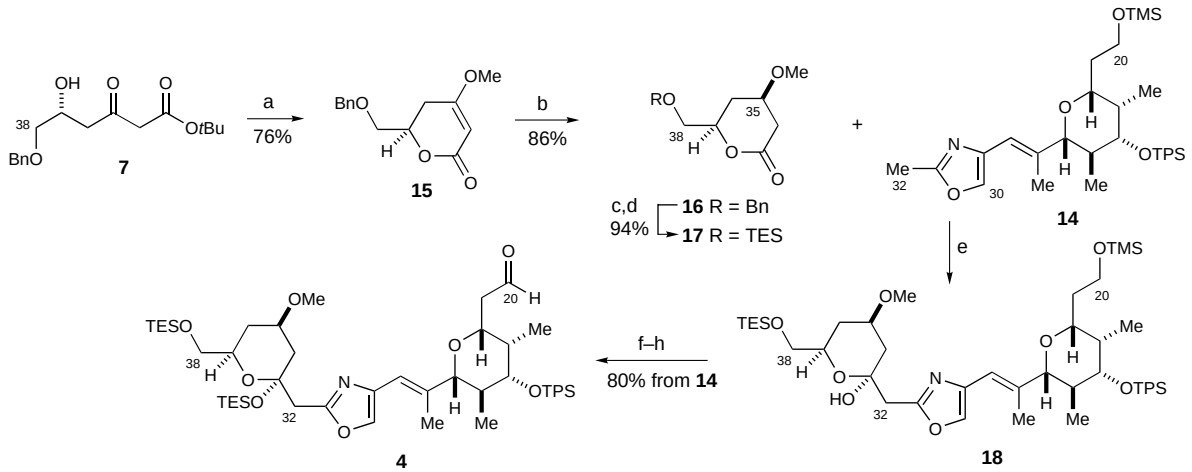
Scheme 2. Synthesis of the $C_{20}-C_{32}$ synthon. a) $(c\text{hex})_2BCl$, $EtNMe_2$, Et_2O, 0 °C; then **8**, −78 → 0 °C; 97 % (94:6 *dr*); b) $Me_4NBH(OAc)_3$, AcOH, 0 °C → RT; 81 % (> 95:5 *dr*); c) cat. DBU, CH_2Cl_2, RT; then imidazole and TPSCl, RT; 81 %; d) *tert*-butyl acetate, LDA, THF, −78 °C; e) $BF_3 \cdot OEt_2$, Et_3SiH, CH_2Cl_2, −78 → −30 °C; 91 % (2 steps); f) $LiAlH_4$, Et_2O/THF, −20 °C; 96 %; g) TMSCl, imidazole, cat. DMAP, DMF, RT; 99 %. X_c = (4R)-4-benzyl-2-oxazolidinone. (See ref. [5] for abbreviations.)

silylation (TPSCl, imidazole) yielded lactone **11**, which was subsequently alkylated with the lithium enolate derived from *tert*-butyl acetate to provide hemiketal **12**. Reduction of the unpurified hemiketal ($BF_3 \cdot OEt_2$, Et_3SiH)[13] afforded the desired *cis*-tetrahydropyran **13** (> 95:5 *dr*) in 91 % yield for the two steps.[12] Reduction of the ester ($LiAlH_4$; 96 %) and protection of the resulting primary hydroxyl group (TMSCl, imidazole; 99 %) completed the $C_{20}-C_{32}$ core pyran fragment **14** in 55 % overall yield for the eight-step sequence.

Completion of the $C_{20}-C_{38}$ core fragment **4** required the union of the $C_{33}-C_{38}$ lactone fragment **17** with methyloxazole **14**. The synthesis of the requisite lactone began with aldol adduct **7**, which was cyclized to the unsaturated lactone **15** in 76 % yield under acidic conditions (TMSCl, MeOH, CH_2Cl_2, Scheme 3).[14] Diastereoselective hydrogenation of **15** was accomplished with Raney-nickel[15] to afford methyl ether **16** containing the desired *R* configuration at the C_{35} methoxy residue (86 %; > 95:5 *dr*).[12] In two subsequent steps the benzyl group was replaced with a triethylsilyl group to provide the desired $C_{33}-C_{38}$ lactone **17**.

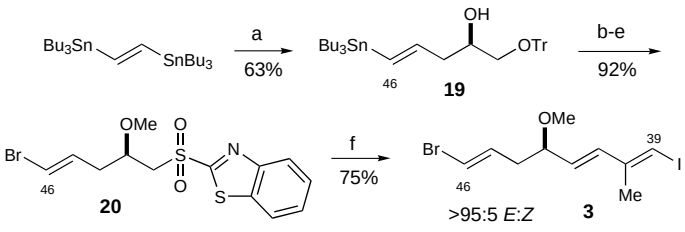
The plan for coupling lactone **17** with fragment **14** involved metalation of the C_{32} methyl group on the oxazole ring followed by alkylation with the lactone to form the C_{32}–C_{33} bond.[16] Initial attempts to selectively lithiate methyloxazole **14** using common bases (LDA, LiTMP, *n*BuLi) were thwarted by the comparable kinetic acidity of the C_{30} proton. It was eventually discovered that lithium diethylamide possessed the unique ability to provide the desired lithiated species with complete selectivity by an equilibration process that occurred at low temperatures.[3h] Lithiation of **14** with this base followed by addition of lactone **17** afforded the desired hemiketal **18** as a single regio- and stereoisomer. Although stable to silica gel chromatography, this material was carried forth through the subsequent two steps without purification for operational simplicity. While reported methods for hemiketal silylation[17] led to high levels of decomposition when applied to substrate **18**, the use of triethylsilyl trifluoromethanesulfonate and pyridine in a diethyl ether/acetonitrile mixture proved successful, providing the desired mixed-silyl ketal as a single anomer.[18] Selective cleavage of the C_{20} primary trimethylsilyl ether under basic conditions ($NaHCO_3$, MeOH) gave an intermediate alcohol (80 % from **14**), which upon subsequent oxidation with the Dess–Martin periodinane[19] provided the $C_{20}-C_{38}$ core fragment **4** in 44 % overall yield with a longest linear sequence of 12 steps from aldehyde **8**.

The synthesis of the $C_{39}-C_{46}$ triene side-chain synthon (Scheme 4) began with a $BF_3 \cdot OEt_2$-promoted alkenyllithium addition to (*R*)-3-(triphenylmethyl)-1,2-epoxypropane[20] to yield alcohol **19**.[21] Methylation of the free hydroxyl group



Scheme 3. Synthesis of the $C_{20}-C_{38}$ synthon **4**. a) TMSCl, MeOH, CH_2Cl_2, 0 °C; 76 %; b) H_2, Raney-Ni, *i*PrOH, RT; 86 % (> 95:5 *dr*); c) H_2, cat. 10 % Pd/C, EtOAc, RT; d) TESCl, imidazole, cat. DMAP, DMF, RT; 94 % (2 steps); e) **14**, $LiNEt_2$, THF, −78 °C; then **17**, −78 °C; f) TESOTf, pyr, Et_2O:CH_3CN (10:1), −50 °C; g) $NaHCO_3$, MeOH, RT; 80 % (3 steps); h) Dess–Martin periodinane, pyr, CH_2Cl_2, RT; 100 %. (See ref. [5] for abbreviations.)

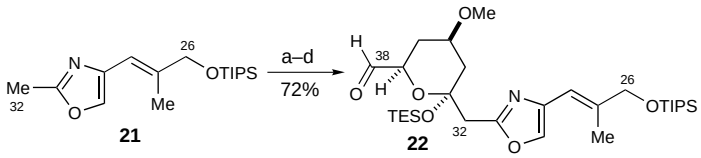
 © WILEY-VCH Verlag GmbH, D-69451 Weinheim, 2000 1433-7851/00/3914-2534 $ 17.50+.50/0 *Angew. Chem. Int. Ed.* **2000**, *39*, No. 14



Scheme 4. Synthesis of the $C_{39}-C_{46}$ synthon **3**. a) *n*BuLi, THF, $-78\,^{\circ}C$; then $BF_3\cdot OEt_2$ and (*R*)-3-(triphenylmethyl)-1,2-epoxypropane, $-78\,^{\circ}C$; 63%; b) NaH, DMF, $0\,^{\circ}C$; then MeI, RT; 96%; c) NBS, CH_3CN, $0\,^{\circ}C$; 98%; d) TsOH, Et_2O:MeOH (1:1), RT; 99%; e) 2-mercaptobenzthiazole, Ph_3P, DIAD, THF, RT; then ammonium molybdate, H_2O_2, MeOH, $0\,^{\circ}C$; 99%; f) (*E*)-3-iodo-2-methylprop-2-enal, THF, $-78\,^{\circ}C$; then NaHMDS, $-78\,^{\circ}C \rightarrow$RT; 75% (>95:5 *E*:*Z*). (See ref. [5] for abbreviations.)

(NaH, MeI; 96%), tin–bromine exchange (NBS; 98%), and deprotection of the trityl group (TsOH; 99%) provided an intermediate alcohol which was converted into the benzthiazole sulfone **20** in a one-pot procedure.[22] A subsequent Julia olefination[23] provided the desired $C_{39}-C_{46}$ side chain in 75% yield and >95:5 *E*:*Z* selectivity.[12]

At this point it was necessary to determine the feasibility of the projected late-stage side-chain addition using a model aldehyde. Aldehyde **22** (Scheme 5) was constructed in an

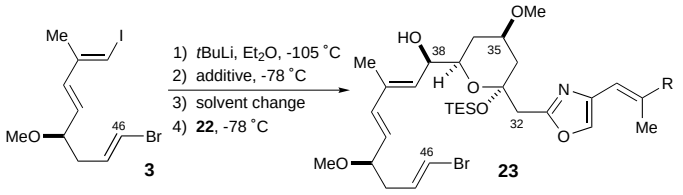


Scheme 5. Construction of a model aldehyde. a) $LiNEt_2$, THF, $-78\,^{\circ}C$; then **17**, $-78\,^{\circ}C$; 79%; b) TESOTf, pyr, 3:2 Et_2O:CH_3CN, $-50\,^{\circ}C$; 98%; c) HF·pyr, pyr, THF, $0\,^{\circ}C$; 93%; d) $SO_3\cdot$pyr, TEA, DMSO, CH_2Cl_2, $-5\,^{\circ}C$; 100%. (See ref. [5] for abbreviations.)

analogous manner to the parent hemiketal **18** by addition of the lithiated 2-methyloxazole **21**[3h] to lactone **17**. Silylation under the previously described conditions, deprotection of the primary triethylsilyl ether (HF·pyr, pyr), and Parikh–Doering oxidation[24] provided the model aldehyde **22** in four steps and 72% overall yield.

The configuration of the C_{38} hydroxyl moiety demands that the C_{38}–C_{39} bond construction be executed with chelation control.[25] Accordingly, model studies were undertaken with aldehyde **22** and the triene fragment **3** to address this coupling process (Table 1). It was first determined that site-selective metal–halogen exchange could be implemented on triene **3** at the C_{39} terminus upon treatment with *tert*-butyllithium (1.9 equiv) in ether at $-105\,^{\circ}C$ to give the desired alkenyllithium reagent.[26, 27] Not surprisingly, this organolithium species slightly favored the formation of the undesired diastereomer[12] in reactions with **22** (entry 1, Table 1), which necessitated transmetalation to a more chelate-prone alkenylmetal. The derived alkenylzincate,[28] Grignard, and aluminate,[29] each provided modest levels of diastereoselectivity in ethereal solvents (entries 2 and 4). It was found that chelate-controlled selectivity could be substantially improved by carrying out the addition in methylene chloride (entries 3, 5, and 6).[30] Ultimately, the higher yielding Grignard reagent (entry 5) derived from freshly prepared $MgBr_2$[31] was chosen for the final fragment coupling.[4]

Table 1. Side chain addition experiments.



R = CH_2OTIPS

Entry	Additive	Solvent	Yield [%]	C_{38} diastereoselectivity (*R*:*S*)
1	–	Et_2O	54	1:2
2	Me_2Zn	Et_2O	80	9:1
3	Me_2Zn	CH_2Cl_2	60	20:1
4	$MgBr_2$	Et_2O	77	5:1
5	$MgBr_2$	CH_2Cl_2	79	>20:1
6	Me_3Al	CH_2Cl_2	71	>20:1
7	$CeCl_3$	Et_2O/THF	35	1:7

The preceding discussion describes the stereoselective syntheses of the $C_{39}-C_{46}$ triene side chain and $C_{20}-C_{38}$ core fragment of the phorboxazole skeleton. In addition, a promising procedure for the projected $C_{39}-C_{46}$ side chain fragment coupling was developed on a model system. In the following communication, the synthesis of the C_1-C_{19} bispyran subunit and fragment assembly to phorboxazole B is presented.[4]

Received: April 25, 2000 [Z15024]

[1] Isolation and structure elucidation: a) P. A. Searle, T. F. Molinski, *J. Am. Chem. Soc.* **1995**, *117*, 8126–8131; b) P. A. Searle, T. F. Molinski, L. J. Brzezinski, J. W. Leahy, *J. Am. Chem. Soc*. **1996**, *118*, 9422–9423; c) T. F. Molinski, *Tetrahedron Lett.* **1996**, *37*, 7879–7880.

[2] GI_{50} is defined as the concentration at which cell growth is inhibited by 50%. See ref. [1a] and [1b]. Phorboxazoles A and B display comparable biological activities, see ref. [1a].

[3] Phorboxazole synthetic studies: a) S. D. Rychnovsky, C. R. Thomas, *Org. Lett.* **2000**, *2*, 1217–1219; b) G. Pattenden, A. T. Plowright, *Tetrahedron Lett.* **2000**, *41*, 983–986; c) J. V. Schaus, J. S. Panek, *Org. Lett*. **2000**, *2*, 469–471; d) P. Wolbers, H. M. R. Hoffmann, F. Sasse, *Synlett* **1999**, *11*, 1808–1810; e) A. B. Smith III, P. R. Verhoest, K. P. Minbiole, J. J. Lim, *Org. Lett.* **1999**, *1*, 909–912; f) A. B. Smith III, K. P. Minbiole, P. R. Verhoest, T. J. Beauchamp, *Org. Lett*. **1999**, *1*, 913–916; g) P. Wolbers, A. M. Misske, H. M. R. Hoffmann, *Tetrahedron Lett.* **1999**, *40*, 4527–4530; h) D. A. Evans, V. J. Cee, T. E. Smith, K. J. Santiago, *Org. Lett*. **1999**, *1*, 87–90; i) P. Wolbers, H. M. R. Hoffmann, *Synthesis* **1999**, *5*, 797–802; j) A. M. Misske, H. M. R. Hoffmann, *Tetrahedron* **1999**, *55*, 4315–5324; k) D. R. Williams, M. P. Clark, *Tetrahedron Lett.* **1999**, *40*, 2291–2294; l) D. R. Williams, M. P. Clark, M. A. Berliner, *Tetrahedron Lett.* **1999**, *40*, 2287–2290; m) P. Wolbers, H. M. R. Hoffmann, *Tetrahedron* **1999**, *55*, 1905–1914; n) S. D. Rychnovsky, Y. Hu, B. Ellsworth, *Tetrahedron Lett.* **1998**, *39*, 7271–7274; o) I. Paterson, E. A. Arnott, *Tetrahedron Lett*. **1998**, *39*, 7185–7188; p) G. Pattenden, A. T. Plowright, J. A. Tornos, T. Ye, *Tetrahedron Lett*. **1998**, *39*, 6099–6102; q) T. Ye, G. Pattenden, *Tetrahedron Lett.* **1998**, *39*, 319–322; r) F. Ahmed, C. J. Forsyth,

Tetrahedron Lett. **1998**, *39*, 183 – 186; s) R. D. Cink, C. J. Forsyth, *J. Org. Chem.* **1997**, *62*, 5672 – 5673; t) C. S. Lee, C. J. Forsyth, *Tetrahedron Lett.* **1996**, *37*, 6449 – 6452; u) total synthesis of phorboxazole A: C. J. Forsyth, F. Ahmed, R. D. Cink, C. S. Lee, *J. Am. Chem. Soc.* **1998**, *120*, 5597 – 5598.

[4] D. A. Evans, D. M. Fitch, *Angew. Chem.* **2000**, *112*, 2636 – 2640; *Angew. Chem. Int. Ed.* **2000**, *39*, 2536 – 2540.

[5] Abbreviations: *dr* = diastereomer ratio; TES = triethylsilyl; TPS = triphenylsilyl; TIPS = triisopropylsilyl; Ms = methanesulfonyl; Bn = benzyl; TMS = trimethylsilyl; DBU = 1,8-diazabicyclo[5.4.0]undec-7-ene; DMF = *N*,*N*-dimethylformamide; DMAP = *N*,*N*-dimethylaminopyridine; LDA = lithium diisopropylamide; TMP = 2,2,6,6-tetramethylpiperidide; NBS = *N*-bromosuccinimide; Tr = trityl = triphenylmethyl; Ts = *para*-toluenesulfonyl; DIAD = diisopropylazodicarboxylate; THF = tetrahydrofuran; HMDS = hexamethyldisilazide; pyr = pyridine; TEA = triethylamine; DMSO = dimethyl sulfoxide; Tf = triflate = trifluoromethanesulfonyl.

[6] D. A. Evans, M. C. Kozlowski, J. A. Murry, C. S. Burgey, K. R. Campos, B. T. Connell, R. J. Staples, *J. Am. Chem. Soc.* **1999**, *121*, 669 – 685.

[7] D. A. Evans, M. D. Ennis, T. Le, N. Mandel, G. Mandel, *J. Am. Chem. Soc*. **1984**, *106*, 1154 – 1156.

[8] a) D. L. Boger, T. T. Curran, *J. Org. Chem.* **1992**, *57*, 2235 – 2244; b) D. P. Provencal, C. Gardelli, J. A. Lafontaine, J. W. Leahy, *Tetrahedron Lett.* **1995**, *36*, 6033 – 6036.

[9] The product ratio was determined by HPLC analysis (Zorbax, 4.6 × 150 mm, 5 μm silica gel; 3% *i*PrOH in CH_2Cl_2, flow rate = 1 mL min^{-1}; T_r minor = 12.5 min; T_r major = 14.9 min).

[10] For examples of β-ketoimide aldol reactions, see a) D. A. Evans, H. P. Ng, J. S. Clark, D. L. Rieger, *Tetrahedron* **1992**, *48*, 2127 – 2142; b) D. A. Evans, H. P. Ng, D. L. Rieger, *J. Am. Chem. Soc.* **1993**, *115*, 11 446 – 11 459.

[11] D. A. Evans, K. T. Chapman, E. M. Carreira, *J. Am. Chem. Soc.* **1988**, *110*, 3560 – 3578.

[12] Product ratio determined by ^{1}H NMR analysis (500 MHz).

[13] M. D. Lewis, J. K. Cha, Y. Kishi, *J. Am. Chem. Soc.* **1982**, *104*, 4976 – 4978.

[14] For similar conditions employing ethylene glycol in place of methanol, see a) T. H. Chan, M. A. Brook, T. Chaly, *Synthesis* **1983**, 203 – 205; b) ref. [4].

[15] For a related reduction with Raney-Ni, see R. Bacardit, M. Moreno-Mañas, *Tetrahedron Lett.* **1980**, *21*, 551 – 554.

[16] For reports of oxazole lithiation, see ref. [3h], and references therein.

[17] A. B. Smith III, S. M. Condon, J. A. McCauley, J. L. Leazer, Jr., J. W. Leahy, R. E. Maleczka, Jr., *J. Am. Chem. Soc.* **1997**, *119*, 962 – 973; A. B. Smith III, S. M. Condon, J. A. McCauley, J. L. Leazer, Jr., J. W. Leahy, R. E. Maleczka, Jr., *J. Am. Chem. Soc*. **1995**, *117*, 5407 – 5408.

[18] Conditions were adapted from: C. H. Heathcock, S. D. Young, J. P. Hagen, R. Pilli, U. Badertscher, *J. Org. Chem*. **1985**, *50*, 2095 – 2105.

[19] D. B. Dess, J. C. Martin, *J. Am. Chem. Soc.* **1991**, *113*, 7277 – 7287.

[20] (*R*)-3-(triphenylmethyl)-1,2-epoxypropane is commercially available from Aldrich Chemical Co. and may also be prepared in 95% *ee* by Sharpless asymmetric epoxidation of allyl alcohol and in situ tritylation. Recrystallization provides the enantiomerically enriched compound: H. S. Hendrickson, E. K. Hendrickson, *Chem. Phys. Lipids* **1990**, *53*, 115 – 120.

[21] (*E*)-bis(tributylstannyl)ethylene was prepared by the following method: a) E. J. Corey, R. H. Wollenberg, *J. Am. Chem. Soc*. **1974**, *96*, 5581 – 5583; see also b) A. N. Nesmeyanov, A. E. Borisov, *Dokl. Akad. Nauk SSSR* **1967**, *174*, 96 – 99; For $BF_3 \cdot OEt_2$-promoted organolithium additions to epoxides, see c) M. J. Eis, J. E. Wrobel, B. Ganem, *J. Am. Chem. Soc.* **1984**, *106*, 3693 – 3694.

[22] Conditions were adapted from: R. Bellingham, K. Jarowicki, P. Kocienski, V. Martin, *Synthesis* **1996**, 285 – 296.

[23] Conditions were adapted from: ref. [3p]. For the synthesis of (*E*)-3-iodo-2-methylprop-2-enal, see R. Baker, J. L. Castro, *J. Chem. Soc. Perkin Trans. 1* **1990**, 47 – 65.

[24] J. R. Parikh, W. E. von Doering, *J. Am. Chem. Soc*. **1967**, *89*, 5505 – 5507.

[25] M. T. Reetz, *Angew. Chem.* **1984**, *96*, 542 – 555; *Angew. Chem. Int. Ed. Engl.* **1984**, *23*, 556 – 569.

[26] After quenching the alkenyllithium with H_2O, the selectivity of the lithium – halogen exchange was determined to be 20:1 (C_{39}I:C_{46}Br) by ^{1}H NMR spectroscopy.

[27] We are aware of few examples of this type of selective lithium – halogen exchange reaction. For a report involving bishalogenated arenes, see M. Kihara, M. Kashimoto, Y. Kobayashi, *Tetrahedron* **1992**, *48*, 67 – 78.

[28] For an example of a chelation-controlled zincate addition, see D. R. Williams, W. S. Kissel, *J. Am. Chem. Soc.* **1998**, *120*, 11 198 – 11 199.

[29] For an example of a chelation-controlled aluminate addition, see H. Imogai, Y. Petit, M. Larcheveque, *Tetrahedron Lett*. **1996**, *37*, 2573 – 2576.

[30] A similar solvent effect has been noted in additions of alkenyl Grignard reagents to α-alkoxyaldehydes: G. E. Keck, M. A. Andrus, D. R. Romer, *J. Org. Chem.* **1991**, *56*, 417 – 420.

[31] For the preparation of $MgBr_2$ as a solution in Et_2O/benzene, see M. Nakatsuka, J. A. Ragan, T. Sammakia, D. B. Smith, D. E. Uehling, S. L. Schreiber, *J. Am. Chem. Soc.* **1990**, *112*, 5583 – 5601.

Asymmetric Synthesis of Phorboxazole B—Part II: Synthesis of the $C_1 - C_{19}$ Subunit and Fragment Assembly**

David A. Evans* and Duke M. Fitch

In the preceding communication the syntheses of the $C_{20} - C_{38}$ and $C_{39} - C_{46}$ phorboxazole B subunits were presented.[1] Herein we focus on the synthesis of the final $C_1 - C_{19}$ bispyran subunit **1** and the successful assembly of these fragments into phorboxazole B.

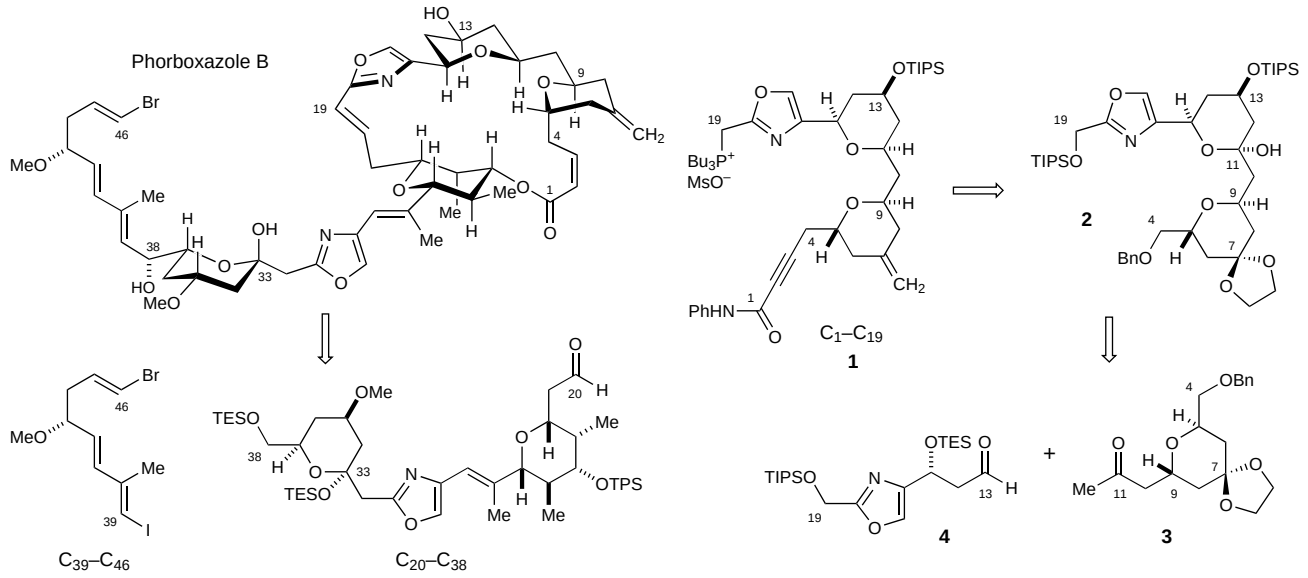
The retrosynthesis of the $C_1 - C_{19}$ region (Scheme 1)[2] began with disconnection of the peripheral functionality at C_4 and C_{19}, and the masking of leaving groups at these positions as differentially protected primary hydroxyl groups. The C_7 exocyclic olefin was masked as a protected ketone and the C_{11} stereocenter was envisioned to arrive through reduction of hemiketal **2**. Ring-chain tautomerization of **2** and aldol disconnection of the C_{12}–C_{13} bond affords the *trans* pyran methylketone fragment **3** and the oxazole aldehyde fragment **4**.

Construction of the $C_4 - C_{12}$ methylketone **3** began from the δ-hydroxy-β-ketoester **5** previously employed in the construction of the $C_{33} - C_{38}$ lactone (Scheme 2).[1, 3] Treatment of **5** with ethylene glycol and trimethylsilyl chloride[4] resulted in a simultaneous cyclization and protection of the ketone to deliver lactone **6** in good yield. Reduction (DIBAlH) and acetylation (Ac_2O, pyr, DMAP) provided **7** in quantitative

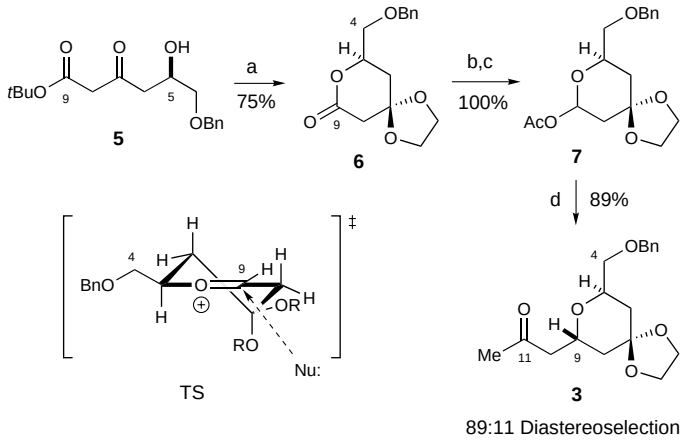
[*] Prof. D. A. Evans, D. M. Fitch
Department of Chemistry & Chemical Biology
Harvard University
Cambridge, MA 02138 (USA)
Fax: (+1) 617-495-1460
E-mail: evans@chemistry.harvard.edu

[**] Financial support has been provided by the National Institutes of Health (GM-33328) and the National Science Foundation. The NIH BRS Shared Instrumentation Grant Program 1-S10-RR04870 and the NSF (CHE 88-14019) are acknowledged for providing NMR facilities.

 © WILEY-VCH Verlag GmbH, D-69451 Weinheim, 2000 1433-7851/00/3914-2536 $ 17.50+.50/0



Scheme 1. Retrosynthetic analysis of the C_1-C_{19} fragment (See reference [2] for abbreviations.)

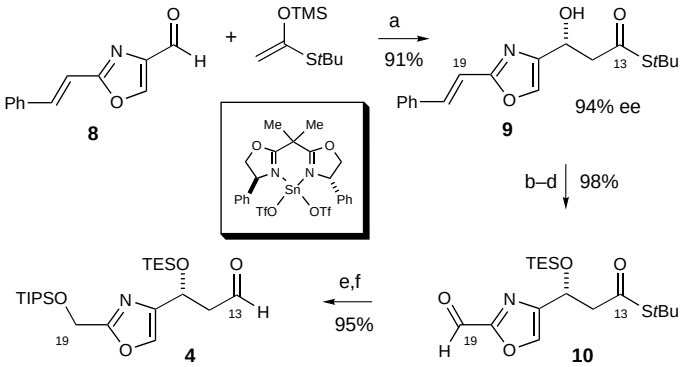


Scheme 2. Synthesis of the C_4-C_{12} *trans*-pyran **3**. a) $HO(CH_2)_2OH$, TMSCl, CH_2Cl_2, RT; 75%; b) DIBAlH, tol, $-78\,^{\circ}C$; 100%; c) Ac_2O, pyr, cat. DMAP, CH_2Cl_2, RT; 100% (92:8 β:α); d) TMSOTf, 2-(trimethylsilyloxy)propene, cat. pyr, CH_2Cl_2, $-78\,^{\circ}C$; 89%. (See ref. [2] for abbreviations.)

yield as a 92:8 mixture of β:α anomers.[5, 6] Treatment of the anomeric acetates with trimethylsilyl trifluoromethanesulfonate[7] and 2-(trimethylsilyloxy)propene resulted in an 89:11 mixture of diastereomeric tetrahydropyrans,[8] with the desired *trans* isomer favored.[9] Axial attack of the nucleophile from the bottom face of the oxocarbenium ion (as depicted in TS) via a chairlike transition structure rationalizes the formation of the major product.[10] This diastereoface is partially hindered by the axial portion of the C_7 ketal, and thus, a minor amount of the undesired *cis* isomer is observed.

The synthesis of the $C_{13}-C_{19}$ oxazole-containing aldehyde began with a Sn^{II}-catalyzed enantioselective aldol addition of the silylketene acetal derived from *tert*-butyl thioacetate to aldehyde **8**[11] (10 mol% [Sn((*S*,*S*)-Ph-box)](OTf)$_2$; box = bisoxazoline) to afford adduct **9** in excellent yield (91%) and enantioselectivity (94% ee; Scheme 3).[12, 13] This reaction is viewed as an extension of analogous aldol reactions with chelating aldehydes that we have reported previously,[14] and the high level of asymmetric induction noted in this transformation provides circumstantial evidence that aldehyde **8** is indeed chelating to the Sn^{II} catalyst. Silylation (TESCl, imidazole), osmium-mediated dihydroxylation,[15] and oxidative cleavage of the derived diol ($Pb(OAc)_4$) provided aldehyde **10** in excellent overall yield. Concomitant DIBAlH reduction of both the C_{19} aldehyde and the C_{13} *tert*-butyl thioester substituents was then accomplished in a single step, while subsequent silylation (TIPSOTf, lut) completed the synthesis of the $C_{13}-C_{19}$ oxazole aldehyde **4** in six steps and 85% overall yield from **8**.

For the important $C_{12}-C_{13}$ aldol fragment coupling, we relied upon methodology developed during our synthesis of altohyrtin C (spongistatin 2),[16] in which boron enolates of β-alkoxy methylketones were added to aldehydes with high



Scheme 3. Synthesis of the $C_{13}-C_{19}$ oxazole aldehyde **4**. a) 10 mol% [Sn((*S*,*S*)-Ph-box)](OTf)$_2$ catalyst, CH_2Cl_2, $-78\,^{\circ}C$; 91%; b) TESCl, imidazole, cat. DMAP, DMF; 100%; c) cat. $K_2OsO_4(H_2O)_2$, cat. quinuclidine, $K_3Fe(CN)_6$, K_2CO_3, methanesulfonamide, *t*BuOH:H_2O (1:1); d) $Pb(OAc)_4$, K_2CO_3, CH_2Cl_2, $0\,^{\circ}C$; 98% (2 steps); e) DIBAlH, CH_2Cl_2, $-78\,^{\circ}C$; 95%; f) TIPSOTf, lut, CH_2Cl_2, $0\,^{\circ}C$; 100%. (See ref. [2] for abbreviations.)

 © WILEY-VCH Verlag GmbH, D-69451 Weinheim, 2000 1433-7851/00/3914-2537 $ 17.50+.50/0

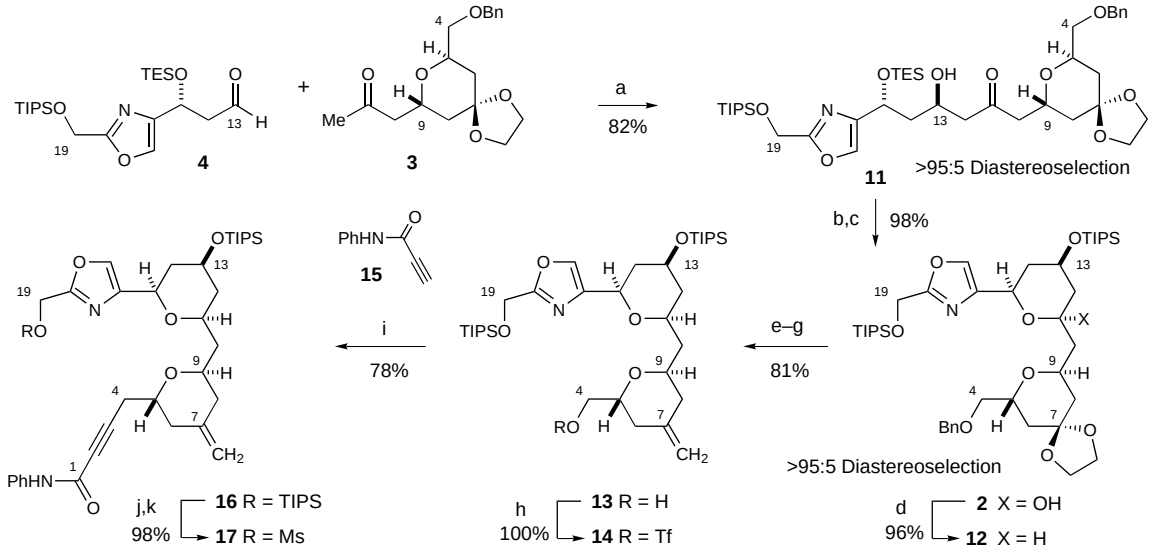
levels of 1,5-*anti* asymmetric induction, regardless of the stereochemistry of the protected β-alkoxyaldehyde substituent.[17] While the methylketones employed in the original study contained either *para*-methoxybenzyl protected β-hydroxyl groups or β-benzylidene acetals, it was unclear whether a methylketone containing a β-tetrahydropyran ring, as in **3**, would exert the same directing effect.[18] In the event (Scheme 4), treatment of the dibutylboron enolate derived from ketone **3** with aldehyde **4** in diethyl ether at $-105\,^{\circ}C$ afforded the aldol adduct **11** in good yield as a single diastereomer.[5, 19] Silylation (TIPSOTf, lut) of the resultant free C_{13} hydroxyl group followed by selective deprotection of the C_{15} triethylsilyl ether provided hemiketal **2**.[20] Axial hydride reduction of the C_{11} hemiketal ($BF_3 \cdot OEt_2$, Et_3SiH)[8] afforded bistetrahydropyran **12** in excellent yield (96%) and diastereoselectivity (>95:5).[5]

With the requisite stereochemistry incorporated into **12**, some refunctionalization was required to complete the synthesis of this subunit. Ketal hydrolysis ($FeCl_3 \cdot SiO_2$)[21] and debenzylation were followed by a Wittig olefination to install the C_7 exocyclic olefin. The C_1-C_3 fragment was incorporated by displacement of the C_4 primary trifluoromethanesulfonate **14** with the dianion of *N*-phenylpropynamide (**15**).[22] Selective deprotection of the C_{19} triisopropylsilyl ether (TBAF, $-50\,^{\circ}C$) followed by formation of the primary mesylate completed the subunit **17** in 17 steps (longest linear sequence from aldehyde **8**) and 40% overall yield.

With the three phorboxazole subunits **17**, **18**, and **26** in hand,[1] fragment coupling experiments were initiated. After some experimentation it was found that in situ formation of the phosphonium salt of mesylate **17** followed by addition of aldehyde **18** and DBU resulted in the exclusive[5] formation of the desired *E* olefin **19** (Scheme 5).[23] Pursuant to revealing the terminal carboxylic acid residue, *N*-phenylamide **19** was activated through its *N*-Boc imide and hydrolyzed with LiOH.[24] These conditions also resulted in the cleavage of the C_{38} triethylsilyl and C_{24} triphenylsilyl ethers. At this point an effort was made to execute a selective macrolactonization of diol acid **20** in the hope that conformational and entropic effects might favor cyclization onto the desired C_{24} hydroxyl moiety. Unfortunately, cyclization occurred exclusively at the less hindered C_{38} primary hydroxyl group under standard Yamaguchi conditions (2,4,6-trichlorobenzoyl chloride, Et_3N, THF; then DMAP, benzene)[25] to provide the undesired 31-membered macrocycle **21**.[26]

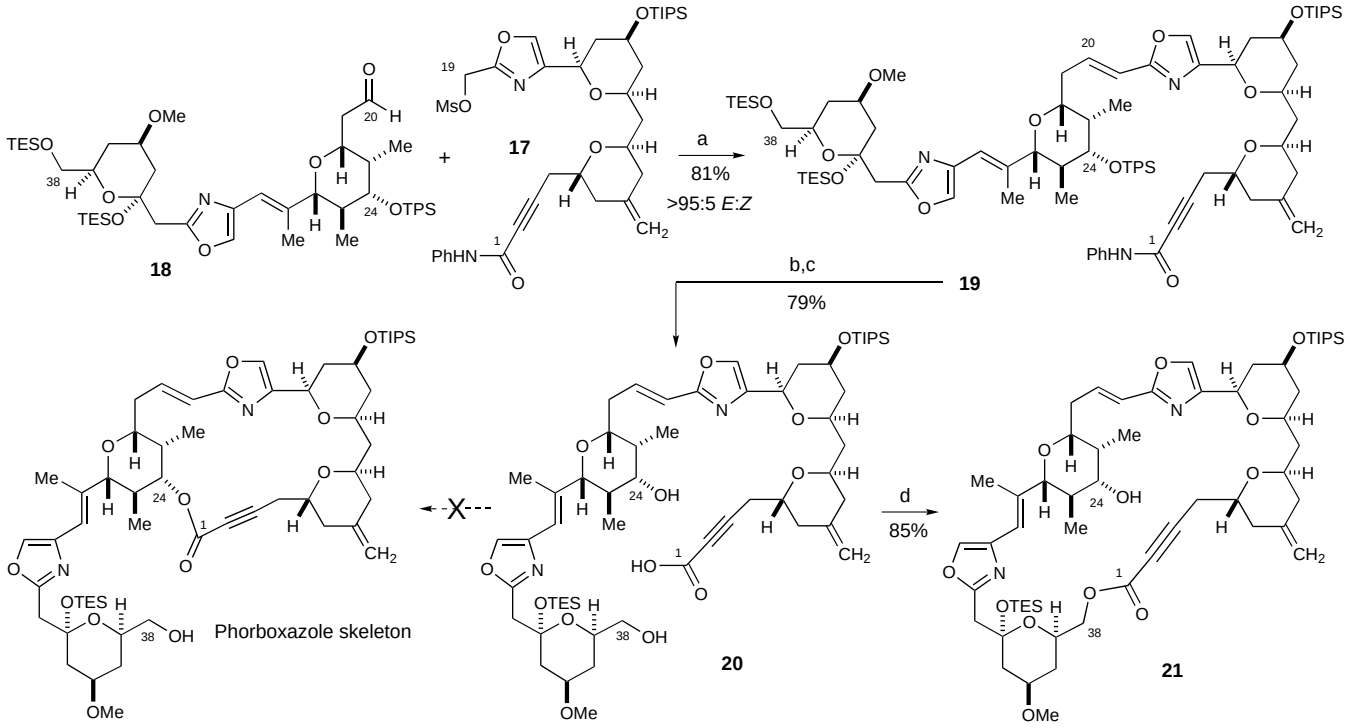
Attempts to selectively silylate the C_{38} primary hydroxyl group under standard conditions (TESCl, imidazole, CH_2Cl_2) were complicated by competitive silylation of both the C_1 carboxyl group and the C_{24} secondary hydroxyl moieties. Ultimately, a change in the base from imidazole to 2,6-lutidine led to exclusive silylation of the desired C_{38} primary hydroxyl group (Scheme 6).[27] With the C_{38} hydroxyl group now protected, macrolactonization proceeded smoothly to provide the desired 21-membered macrocycle **23** in excellent yield.[25] Lindlar reduction of the alkynoate (>95:5 *Z*:*E*)[5] led to the formation of the complete C_1-C_{38} macrocyclic region of phorboxazole B.[28] Selective deprotection of the C_{38} primary triethylsilyl ether was followed by Parikh–Doering oxidation[29] to provide the requisite α-alkoxyaldehyde **25**.

For the final fragment coupling, chelate-controlled addition of a fully functionalized $C_{39}-C_{46}$ alkenylmetal species was required. Under the previously optimized conditions,[1] site-selective lithium–halogen exchange of vinyl iodide **26**, transmetalation ($MgBr_2$), and solvent exchange ($Et_2O \rightarrow CH_2Cl_2$), followed by the addition of α-alkoxyaldehyde **25** to the alkenylmagnesium intermediate provided the protected natural product **27** in excellent yield as a single isomer.[5] Deprotection of **27** (TBAF, THF) afforded phorboxazole B in 27 steps (longest linear sequence from aldehyde **8**) and 12.6% overall yield. The synthetic phorboxazole B was identical to the natural material as judged by ^1H NMR spectroscopy (600 MHz, $CDCl_3$), HPLC, TLC R_f values,

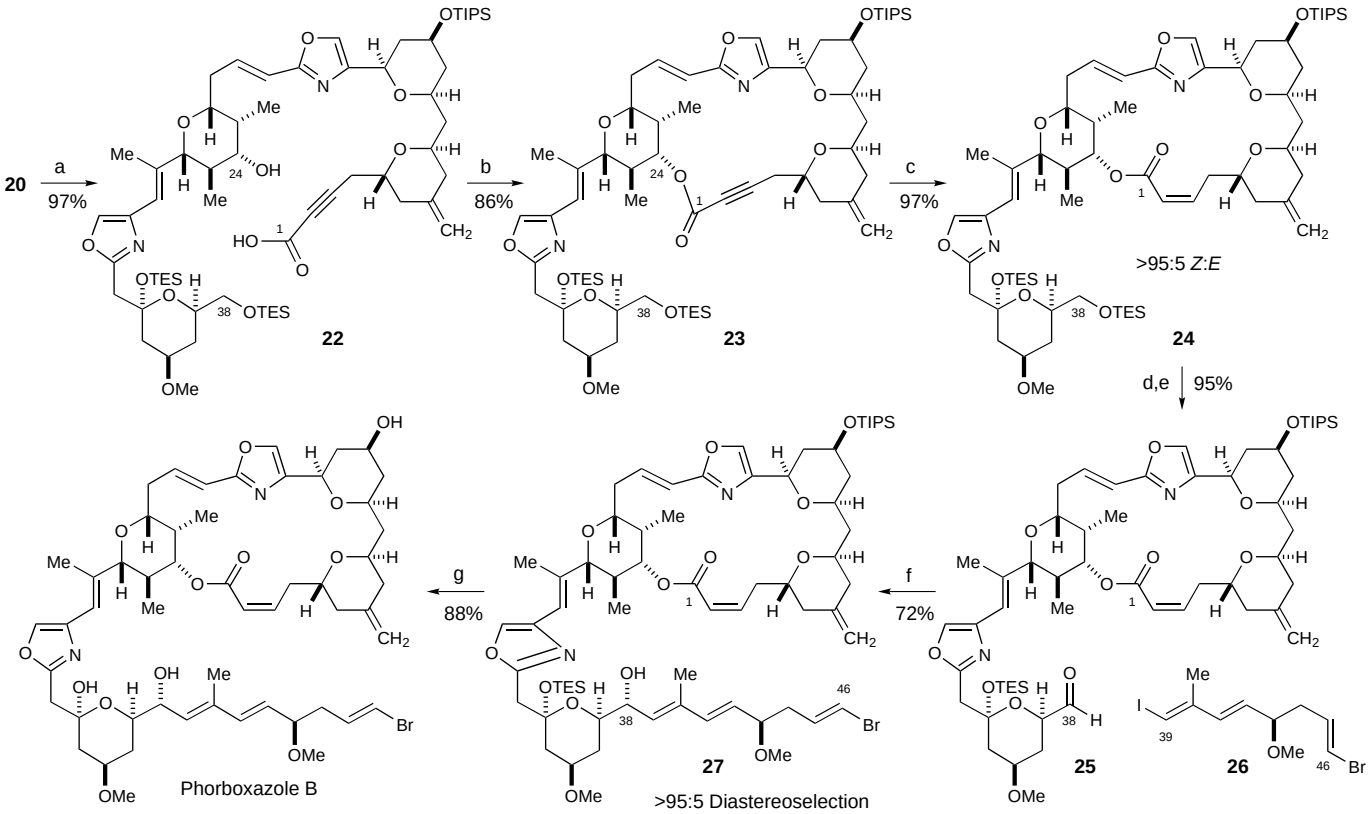


Scheme 4. Synthesis of the C_1-C_{19} bispyran **17**. a) nBu$_2$BOTf, iPr$_2$NEt, Et$_2$O, $-105\,^{\circ}C$; 82%; b) TIPSOTf, lut, CH_2Cl_2, $0\,^{\circ}C$; 99%, c) HF·pyr, pyr, THF, H_2O, $0\,^{\circ}C$; 99%; d) $BF_3 \cdot OEt_2$, Et_3SiH, CH_2Cl_2, $-78 \rightarrow -50\,^{\circ}C$; 96%; e) $FeCl_3 \cdot SiO_2$, $CHCl_3$, acetone, RT; 90%; f) 1 atm H_2, Pd/C, iPrOH; 100%; g) Ph_3PCH_3Br, PhLi, THF, $0\,^{\circ}C$; 90%; h) Tf_2O, pyr, CH_2Cl_2, $-5\,^{\circ}C$; 100%; i) **15**, nBuLi, THF, $-20\,^{\circ}C$; then **14**; 78%; j) TBAF, THF, $-50\,^{\circ}C$; 99%; k) MsCl, iPr$_2$NEt, CH_2Cl_2, $-5\,^{\circ}C$; 99%. (See ref. [2] for abbreviations.)

 © WILEY-VCH Verlag GmbH, D-69451 Weinheim, 2000 1433-7851/00/3914-2538 $ 17.50+.50/0 *Angew. Chem. Int. Ed.* **2000**, *39*, No. 14



Scheme 5. Wittig coupling and hydrolysis. a) PBu_3, DMF; DBU, RT; 81%; b) Boc_2O, DMAP, CH_3CN; 99%; c) LiOH, THF, H_2O, RT; 80%; d) 2,4,6-trichlorobenzoyl chloride, Et_3N, THF; then DMAP, benzene; 85%. (See ref. [2] for abbreviations.)



Scheme 6. Completion of the synthesis of phorboxazole B. a) TESCl, lut, CH_2Cl_2, $-78\,^{\circ}C$; 97%; b) 2,4,6-trichlorobenzoyl chloride, Et_3N, THF; then DMAP, benzene; 86%; c) 1 atm H_2, Lindlar cat., quinoline, 1-hexene, acetone; 97%; d) HF·pyr, pyr, THF, $0\,^{\circ}C$; 95%; e) SO_3·pyr, Et_3N, DMSO, CH_2Cl_2; 100%; f) **26**, *t*BuLi, Et_2O, $-105\,^{\circ}C$; then $MgBr_2$, $-78\,^{\circ}C$; then CH_2Cl_2, **25**; 72%; g) TBAF, THF, $0\,^{\circ}C$; 88%. (See ref. [2] for abbreviations.)

electrospray mass spectrometry, ultraviolet spectroscopy, infrared spectroscopy, and optical rotation values.[30]

Received: April 25, 2000 [Z15025]

[1] D. A. Evans, V. J. Cee, T. E. Smith, D. M. Fitch, P. S. Cho, *Angew. Chem.* **2000**, *112*, 2633 – 2636; *Angew. Chem. Int. Ed.* **2000**, *39*, 2533 – 2536.

[2] Abbreviations: Ac = acetyl; Ms = methanesulfonyl; TIPS = tiisopropylsilyl; TES = triethylsilyl; TMS = trimethylsilyl; DIBAlH = diisobutylaluminum hydride; Tf = trifluoromethanesulfonyl; Bn = benzyl; DMAP = 4-dimethylaminopyridine; pyr = pyridine; tol = toluene; TBAF = *tetra-n*-butylammonium fluoride; DBU = 1,8-diazabicyclo[5.4.0]undec-7-ene; lut = 2,6-lutidine; Boc = *tert*-butyloxycarbonyl.

[3] D. A. Evans, M. C. Kozlowski, J. A. Murry, C. S. Burgey, K. R. Campos, B. T. Connell, R. J. Staples, *J. Am. Chem. Soc.* **1999**, *121*, 669 – 685.

[4] T. H. Chan, M. A. Brook, T. Chaly, *Synthesis* **1983**, 203 – 205.

[5] The product ratio was determined by ^{1}H NMR analysis (500 MHz) of the unpurified reaction mixture.

[6] Although the anomers were separable by chromatography on silica gel, the mixture was generally taken on without purification.

[7] Use of stronger Lewis acids such as $BF_3 \cdot OEt_2$ or $TiCl_4$ led to high levels of decomposition.

[8] For an early example of nucleophilic addition to oxocarbenium ions in the synthesis of *C*-glycosides, see M. D. Lewis, J. K. Cha, Y. Kishi, *J. Am. Chem. Soc.* **1982**, *104*, 4976 – 4978.

[9] Optimal results were obtained when buffering the reaction with 20 mol% of pyridine. The diastereoselectivity was determined by HPLC analysis of the unpurified reaction mixture (Zorbax silica gel, 20% EtOAc in hexanes, flow rate = 1.0 mL min^{-1}, 254 nm UV cutoff, major isomer (*trans*) T_r = 11 min, minor isomer (*cis*) T_r = 13 min).

[10] E. L. Eliel, S. H. Wilen, L. N. Mander, *Stereochemistry of Organic Compounds*, Wiley, New York, **1994**, chap. 11.

[11] Aldehyde **8** was obtained from reduction (DIBAlH, CH_2Cl_2, $-91\,^\circ$C, 95% yield) of the known ethyl ester. See J. S. Panek, R. T. Beresis, *J. Org. Chem.* **1996**, *61*, 6496 – 6497.

[12] Dr. David MacMillan is gratefully acknowledged for the development of this reaction.

[13] Reported results for the reaction run on > 60 mmol scale (18.5 g isolated product). Enantiomeric excess values were determined by chiral HPLC analysis (Chiralcel OD-H column, 4% EtOH in hexanes, flow rate = 1.0 mL min^{-1}, *R* enantiomer T_r = 34.2 min, *S* enantiomer T_r = 36.8 min).

[14] D. A. Evans, D. W. C. MacMillan, K. R. Campos, *J. Am. Chem. Soc.* **1997**, *119*, 10859 – 10860.

[15] Dihydroxylation was performed using the achiral ligand, quinuclidine. For a review of asymmetric dihydroxylation under these conditions, see H. C. Kolb, M. S. VanNieuwenhze, K. B. Sharpless, *Chem. Rev.* **1994**, *94*, 2483 – 2547.

[16] D. A. Evans, B. W. Trotter, P. J. Coleman, B. Côté, L. C. Dias, H. A. Rajapakse, A. N. Tyler, *Tetrahedron* **1999**, *55*, 8671 – 8726.

[17] D. A. Evans, P. J. Coleman, B. Côté, *J. Org. Chem.* **1997**, *62*, 788 – 789. See also I. Paterson, K. R. Gibson, R. M. Oballa, *Tetrahedron Lett.* **1996**, *37*, 8585 – 8588.

[18] A model aldol reaction with ketone **3** and dihydrocinnamaldehyde under unoptimized conditions (nBu$_2$BOTf, iPr$_2$NEt, Et$_2$O, $-78\,^\circ$C) resulted in a 72% yield of the desired *anti* adduct with > 95:5 diastereoselectivity as determined by ^{1}H NMR analysis (500 MHz) of the unpurified reaction mixture. The relative stereochemistry of this product was determined by X-ray crystallography.

[19] The remainder of the material was comprised of cleanly recovered **3** and **4**.

[20] Hemiketal **2** existed as a 92:8 mixture of the closed hemiketal and open hydroxy ketone. This mixture was taken on together in the subsequent reduction.

[21] K. S. Kim, Y. H. Song, B. H. Lee, C. S. Hahn, *J. Org. Chem.* **1986**, *51*, 404 – 407.

[22] The lithium anions of methyl and ethyl propiolate failed to alkylate a model primary trifluoromethanesulfonate derived from the commercial available tetrahydropyran-2-methanol at low temperature ($-78\,^\circ$C) and decomposed upon warming, see M. M. Midland, A. Tramontano, J. R. Cable, *J. Org. Chem.* **1980**, *45*, 28 – 29. Displacement of this model trifluoromethanesulfonate with the dianion of propiolic acid was complicated by O alkylation and double alkylation, which was surpressed through use of the alternative nucleophile **15**. For a complex example of the use of an *N*-phenylamide as a carboxyl surrogate with attenuated nucleophilicity, see D. A. Evans, P. H. Carter, E. M. Carreira, A. B. Charette, J. A. Prunet, M. Lautens, *J. Am. Chem. Soc.* **1999**, *121*, 7540 – 7552. For the synthesis of **15**, see G. M. Coppola, R. E. Damon, *Synth. Commun.* **1993**, *23*, 2003 – 2010. For the alkylation of carbonyl compounds with the dianion of *N*-benzylpropynamide, see G. M. Coppola, R. E. Damon, *J. Heterocycl. Chem.* **1995**, *32*, 1133 – 1139.

[23] Similar conditions have recently appeared in the literature for an oxazole-stablized Wittig coupling, see P. Liu, J. S. Panek, *J. Am. Chem. Soc.* **2000**, *122*, 1235 – 1236.

[24] For the hydrolysis of the *N*-Boc derivatives of secondary amides and lactams with LiOH, see D. L. Flynn, R. E. Zelle, P. A. Grieco, *J. Org. Chem.* **1983**, *48*, 2424 – 2426.

[25] J. Inanaga, K. Hirata, H. Saeki, T. Katsuki, M. Yamaguchi, *Bull. Chem. Soc. Jpn.* **1979**, *52*, 1989 – 1993.

[26] The regioselectivity of the cyclization was determined by 1D ^{1}H NMR and 2D COSY experiments.

[27] The difference in the selectivity between the two bases is perhaps a result of the formation of a more active silylating agent derived from the reaction of imidazole with the silyl chloride. Presumably there is no reaction between the silyl chloride and 2,6-lutidine, which simply acts as a base.

[28] The use of 1-hexene as a co-solvent was found to effectively surpress any overreduction. For related conditions, see T.-L. Ho, S.-H. Liu, *Synth. Commun.* **1987**, *17*, 969 – 973.

[29] J. R. Parikh, W. von E. Doering, *J. Am. Chem. Soc.* **1967**, *89*, 5505 – 5507.

[30] We thank Professor T. F. Molinski for kindly providing a sample and copies of ^{1}H NMR spectra of natural phorboxazole B for comparison.

Asymmetric, Stereocontrolled Total Synthesis of Paraherquamide A**

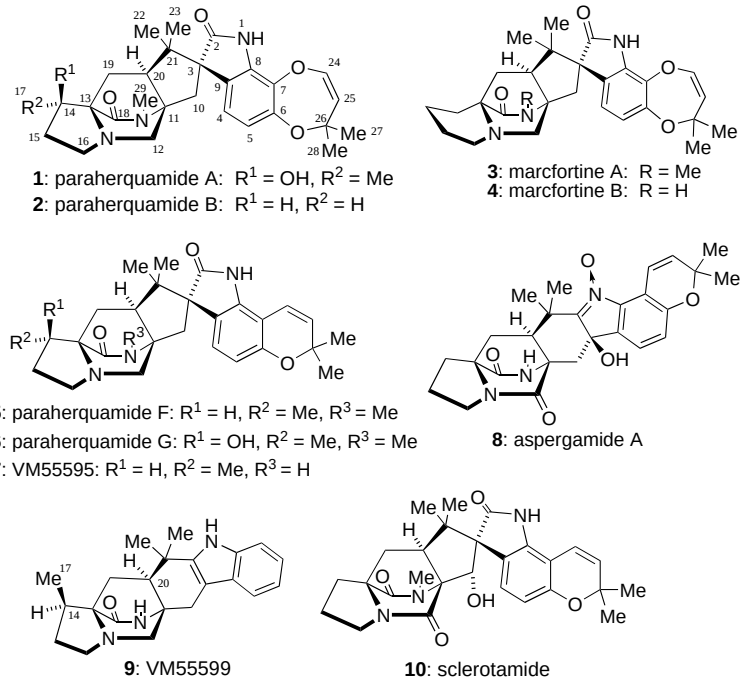
Robert M. Williams,* Jeffrey Cao, and Hidekazu Tsujishima

The paraherquamides (**1**, **2**, **5**, **6**),[1–4] marcfortines (**3**, **4**),[5] brevianamides,[6] VM55599 (**9**),[3b] and, most recently, the sclerotamides (**10**)[7] and aspergimides (**8**)[8] are indolic secondary metabolites isolated from various fungi (Scheme 1). The parent and most potent member, paraher-

[*] Prof. Dr. R. M. Williams, J. Cao, H. Tsujishima
Department of Chemistry
Colorado State University
Fort Collins, CO 80523 (USA)
Fax: (+1) 970-491-3944
E-mail: rmw@chem.colostate.edu

[**] This work was supported by the NIH (Grant CA 70375). The Japanese Society for the Promotion of Science (JSPS) is acknowledged for providing support to H.T. Mass spectra were obtained on instruments supported by the NIH Shared Instrumentation Grant (GM 49631). We also wish to thank Dr. Timothy Blizzard (Merck & Co.) for providing an authentic sample of natural paraherquamide A. We also wish to acknowledge Dr. Byung H. Lee (Pharmacia – Upjohn Co.) for providing NMR spectra and an authentic specimen of 14-oxoparaherquamide B. We also wish to thank Dr. Alfredo Vazquez for assistance with purification and characterization of synthetic paraherquamide A.

 © WILEY-VCH Verlag GmbH, D-69451 Weinheim, 2000 1433-7851/00/3914-2540 $ 17.50+.50/0



Scheme 1. Structures of the paraherquamides and related metabolites.

quamide A (**1**) was isolated from cultures of *Penicillium paraherquei*, first described by Yamazaki in 1981.[1] The simplest member, paraherquamide B (**2**), plus five other structurally related paraherquamides C–G were isolated from *Penicillium charlesii* (*fellutanum*) (ATCC 20841) in 1990 at Merck & Co.[2] and concomitantly at SmithKline Beecham.[3] Subsequently, three additional related compounds, VM55596, VM55597, and VM55599 (**9**) were discovered by the same group at SmithKline Beecham from *Penicillium* strain IMI 332995.[4] More recently, a Pfizer group[5] reported the isolation of anthelmintic metabolites VM54159, SB203105, and SB200437 along with the non-tryptophan derived metabolites, that possessing the common bicyclo[2.2.2] nucleus, aspergillimide[4] (which is identical to asperparaline A[9]) and 16-keto-aspergillimide from *Aspergillus* strain IMI 337664. This report, and a recent paper by Whyte and Gloer,[7] that described the isolation of sclerotamide (**10**) from *Aspergillus sclerotiorum*, constitute the first examples of paraherquamide derivatives isolated outside of the *Penicillia*. In addition, Zeeck et al. have isolated the interesting paraherquamide-type metabolites aspergamides A (**8**) and B.[8]

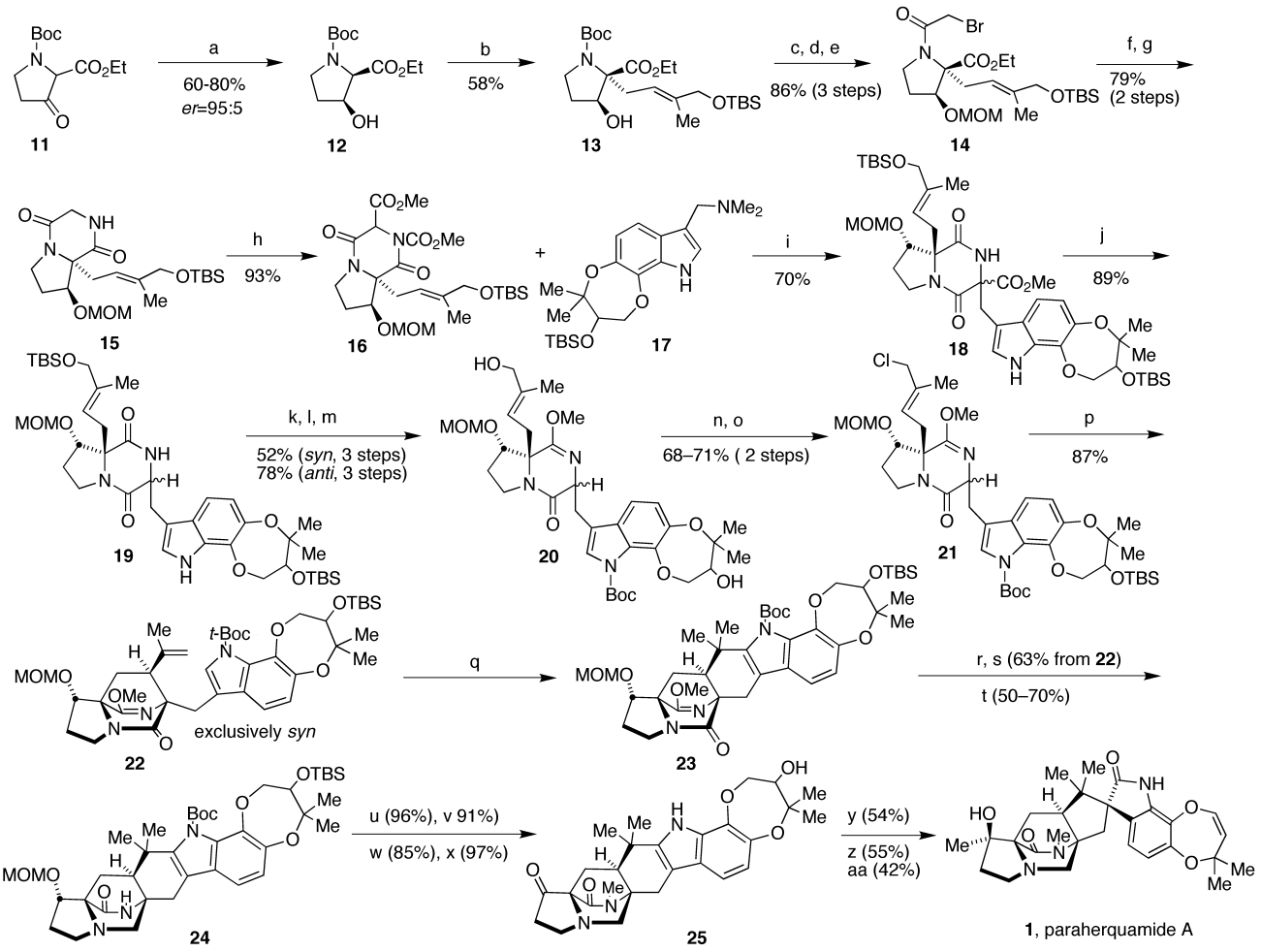
These substances have attracted considerable attention due to their molecular complexity, intriguing biogenesis,[10, 11] and some members, most notably paraherquamide A, display potent antiparasitic activity and antinematodal properties.[12] Due to the development of drug resistance by the helminths, the commonly employed broad spectrum antihelmintic agents—such as the benzimidazoles, the levamisoles/morantel, and the avermectins—are beginning to lose efficacy and there has arisen an urgent need for discovering new classes of antiparasitic agents. The paraherquamides represent an entirely new structural class of antiparasitic agents that promise to play a significant role in the near future and the derivatives of paraherquamide A hold potential as drugs for the treatment of intestinal parasites in animals.[13] The relatively low culture yields of paraherquamide A obtained for biological study have slowed the development of these agents. Recently, Lee and Clothier reported the interesting semisynthetic conversion of marcfortine A, a metabolite more readily available by fermentation, into paraherquamide A via paraherquamide B.[13] To date, a total synthesis of paraherquamide A has not been reported in the literature.

We have previously described an asymmetric synthesis of the simplest paraherquamide derivative, paraherquamide B (**2**), from (*S*)-proline.[14] In approaching the synthesis of paraherquamide A, which contains the unusual β-hydroxy-β-methyl proline residue, a new method needed to be developed to generate a suitably functionalized α-alkylated-β-hydroxyproline moiety that could be conscripted for the multistep construction of paraherquamide A. Despite the apparent similarity in the structures of paraherquamide A and B, the synthesis of the former turned out to be a significantly more challenging endeavor. We recently described a potentially general method to construct α-alkylated-β-hydroxyproline residues by the dianion alkylation of the readily available *N*-Boc-β-hydroxyproline ethyl ester derivative **12** with net retention of stereochemistry (Boc = *tert*-butylcarbonyl).[15] We have successfully applied this methodology to a concise asymmetric and stereocontrolled synthesis of paraherquamide A in 27 steps from the racemic β-keto ester **11**, as shown in Scheme 2.

As described previously,[16] β-ketoester **11** was subjected to Baker's yeast reduction to afford the optically active β-hydroxyester **12** (60–80%, *er* ~ 95:5). Dianion alkylation of **12** with (*E*)-3-methyl-4-(*O*-*tert*-butyldimethylsilyl)-2-butene afforded the desired α-alkylated product **13** in 58–70% isolated yield without attendant *O*-alkylation.[15] Protection of the secondary alcohol as the corresponding methoxy methyl (MOM) ether, followed by removal of the Boc group with $ZnBr_2$ in dichloromethane and acylation of the incipient secondary amine with bromoacetyl bromide in the presence of potassium carbonate afforded the bromoacetamide **14** in 86% overall yield from **13**. Treatment of **14** with methanolic ammonia afforded the corresponding glycinamide which was directly subjected to cyclization in the presence of sodium hydride in toluene/HMPA to afford the bicyclic substance **15** in 79% overall yield from **14**. Next, a one-pot double carbomethoxylation reaction was performed by the sequential addition of *n*BuLi in THF followed by addition of methylchloroformate, that carbomethoxylated the amide nitrogen atom. Subsequent addition of four equivalents of methylchloroformate followed by the addition of five equivalents of $LiN(TMS)_2$ afforded **16** as a mixture of diastereomers in 93% yield that were taken on directly without separation.

Somei–Kametani coupling[17] of **16** with the gramine derivative **17**[18] in the presence of tri(*n*-butyl)phosphine gave the tryptophan derivative **18** as a 3:1 mixture of diastereomers (epimeric at the newly created stereogenic center) in 70%

 © WILEY-VCH Verlag GmbH, D-69451 Weinheim, 2000 1433-7851/00/3914-2541 $ 17.50+.50/0

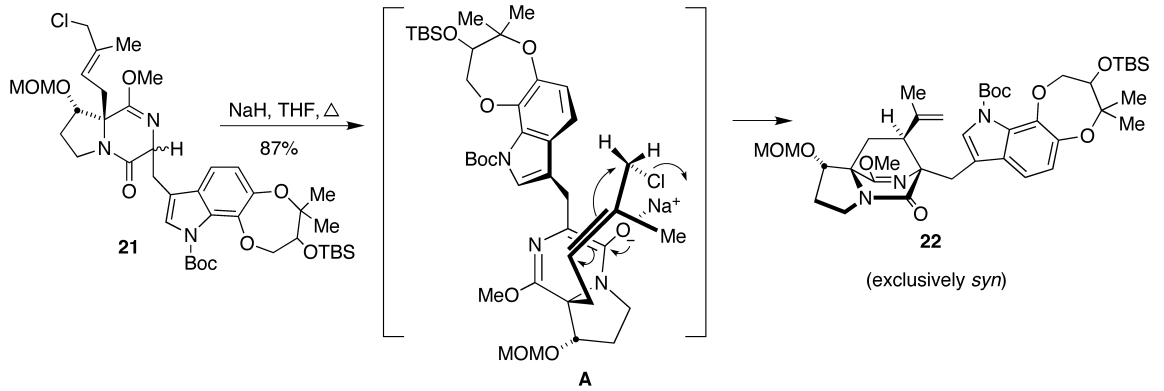


Scheme 2. Synthesis of paraherquamide A. a) Baker's yeast; b) $Li(NiPr)_2$, THF, HMPA, (*E*)-$ICH_2CH{=}C(Me)CH_2OTBS$; c) 5.7 equiv MOMCl, $(iPr)_2NEt$, CH_2Cl_2; d) 2.7 equiv $ZnBr_2$, CH_2Cl_2; e) K_2CO_3, 2 equiv $BrCH_2COBr$, CH_2Cl_2, 0 °C; f) NH_3 in MeOH (5.7 M solution), 25 °C; g) 3 equiv NaH, toluene, HMPA, 25 °C; h) 1.3 equiv *n*BuLi, THF, 1.1 equiv $ClCO_2Me$, −78 °C; then 4 equiv $ClCO_2Me$, 5 equiv $LiN(TMS)_2$, −78 °C; i) 0.7 equiv $(nBu)_3P$, MeCN; j) 5 equiv LiCl, H_2O, HMPA, 105 °C, 5 h; k) 2.5 equiv Me_3OBF_4, CH_2Cl_2, Cs_2CO_3, 25 °C; l) DMAP, 3 equiv $(Boc)_2O$, CH_2Cl_2, 0 °C; m) 3.3 equiv TBAF, THF, 25 °C; n) 1.1 equiv MsCl, collidine, CH_2Cl_2, 0 °C; o) 2 equiv TBSOTf, 2,6-lutidine, CH_2Cl_2, 0 °C; p) 20 equiv NaH, THF, reflux, 30 h; q) 3.1 equiv $AgBF_4$, 4.68 equiv $PdCl_2$, MeCN, propylene oxide; then $NaBH_4$, EtOH; r) 0.1 M HCl, THF; s) 2-hydroxypyridine, toluene, 120 °C, 2 h; t) 5 equiv $(iBu)_2AlH$, CH_2Cl_2, 0 °C; u) NaH, MeI, DMF, 0 °C; v) 6 equiv *B*-bromocatechol borane, CH_2Cl_2, 0 °C; w) 5 equiv Dess–Martin periodinane, CH_2Cl_2, 25 °C; x) TFA, CH_2Cl_2, 25 °C; y) 1.5 equiv *t*BuOCl, py; then 5 equiv *p*-TsOH, THF, H_2O, reflux; z) 5 equiv $(PhO)_3PMeI$, DMPU; aa) MeMgBr, THF. Abbreviations: HMPA = hexamethylphosphoramide; TBS = *tert*-butyldimethylsilyl; MOMCl = chloromethyl methyl ether; TMS = trimethylsilane; DMAP = 4-(dimethylamino)pyridine; $(Boc)_2O$ = dicarbonic acid bis(*tert*-butyl) ester; TBAF = tetrabutylammonium fluoride; MsCl = methanesulfonyl chloride; TBSOTf = *tert*-butyldimethylsilyl trifluoromethanesulfonate; Dess–Martin periodinane = 1,1,1-triacetoxy-1,1-dihydro-1,2-benziodoxol-3(1H)-one; TFA = trifluoroacetic acid; *t*BuOCl = *tert*-butyl hypochlorite; py = pyridine; *p*-TsOH = *para*-toluenesulfonic acid; DMPU = *N*,*N*′-dimethylpropyleneurea.

yield. Decarbomethoxylation of **18** was effected by treatment of **18** with LiCl in hot, aqueous HMPA at 105 °C providing **19** as a mixture of diastereomers that were separated and carried forward individually. Protection of the secondary amide group as the corresponding methyl lactim ether was accomplished by treating **19** with trimethyloxonium tetrafluoroborate in dichloromethane that contained cesium carbonate. Next, the indole nitrogen atom was protected as the corresponding Boc derivative by treatment with dicarbonic acid bis(*tert*-butyl) ester in the presence of DMAP and the silyl ether was removed with tetrabutylammonium fluoride to provide diol **20** in 52–78% overall yield from **19**. Selective conversion of the allylic alcohol to the corresponding allylic chloride was accomplished by mesylation in the presence of collidine. Silylation of the secondary alcohol with *tert*-butyldimethylsilyl triflate in the presence of 2,6-lutidine afforded the key allylic chloride **21** in 68–71% yield over the two steps.

The stage was now set for the critical intramolecular S_N2' cyclization that sets the relative stereochemistry at C-20 during formation of the bicyclo[2.2.2]octane ring nucleus. Based on a solid precedent from the paraherquamide B synthesis,[14] it was found that treatment of **21** with NaH in refluxing THF afforded the desired S_N2' cyclization product **22** in 87% exclusively as the desired *syn*-isomer.[19] This remarkably *syn*-selective intramolecular S_N2' cyclization reaction proceeds through a tight, intramolecular, ion-pair driven cyclization ("closed" transition state),[20] as shown in Scheme 3. Closure of the seventh ring was effected by treatment of **22** with 4.68 equivalents of $PdCl_2$ and 3.1 equivalents of $AgBF_4$[21] in acetonitrile containing propylene oxide

 © WILEY-VCH Verlag GmbH, D-69451 Weinheim, 2000 1433-7851/00/3914-2542 $ 17.50+.50/0 *Angew. Chem. Int. Ed.* **2000**, *39*, No. 14



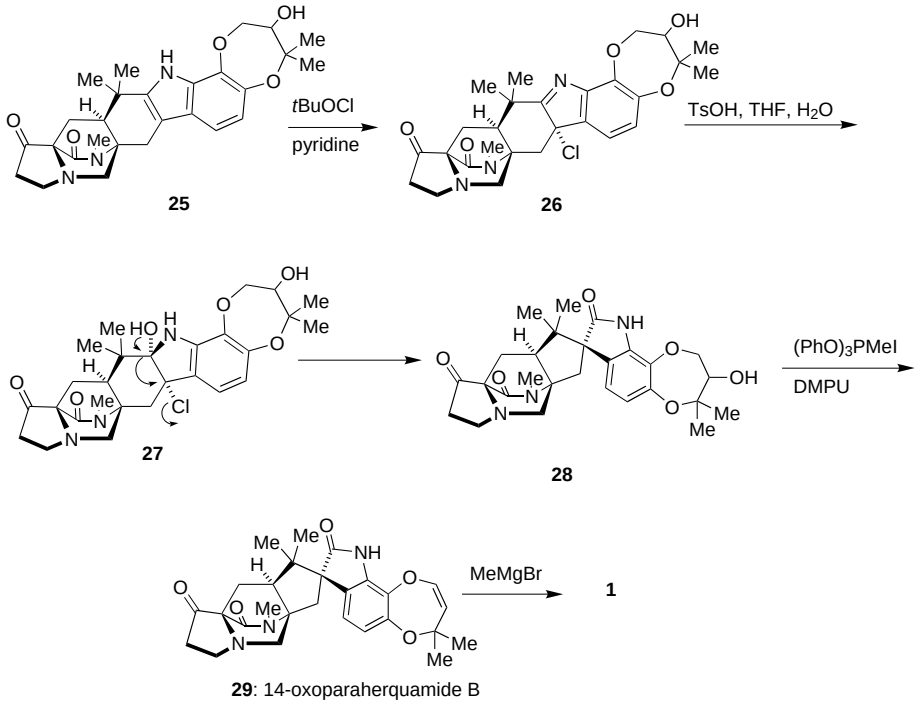
Scheme 3. Diastereoselective, intramolecular S_N2' cyclization.

as an acid scavenger. It was found that without propylene oxide to buffer this reaction, the MOM ether suffered extensive cleavage. The incipient heptacyclic σ-palladium adduct was worked up immediately by the addition of ethanol and sodium borohydride to afford the desired 2,3-disubstituted indole **23**.

Cleavage of the lactim ether of **23** was effected with 0.1M HCl to give the corresponding ring-opened amine methyl ester that was recyclized by treatment of this material with 2-hydroxypyridine in hot toluene (63% overall from **22**). Chemoselective reduction of the secondary amide in the presence of the tertiary amide was effected by treatment of the product obtained in the previous step with excess diisobutylaluminum hydride in dichloromethane (50–72%) to furnish **24**.[22] Methylation of the secondary amide of **24** proceeded in 96% yield. Cleavage of the MOM ether with bromocatecholborane[23] (91% yield) followed by oxidation of the secondary alcohol with Dess–Martin periodinane[24] (85% yield) and cleavage of the Boc group and TBS ether with TFA (97% yield) gave ketone **25**.

The final, critical oxidative spirocyclization of the 2,3-disubstituted indole to the *spiro* oxindole was effected by treatment of **25** with *tert*-butyl hypochlorite in pyridine, which provided a labile 3-chloroindolenine. It was necessary to rigorously remove all of the pyridine solvent prior to the Pinacol-type rearrangement, that was conducted by treating the incipient 3-chloroindolenine with *para*-toluenesulfonic acid in THF/H_2O. It is assumed that the chlorination of **25** proceeds from the least hindered face of the indole, to give the α-chloroindolenine **26**. The hydration of the imine functionality must, interestingly, also occur from the same α-face that is *syn* to the relatively large chlorine atom furnishing the *syn*-chlorohydrin **27**, that subsequently rearranges stereospecifically to the desired *spiro* oxindole **28** (Scheme 4).

The dioxepin ring was then formed by dehydration of the secondary alcohol of **28** with methyl triphenoxyphosphonium iodide (MTPI) in DMPU to afford 14-oxoparaherquamide B **29**, (55%).[13] This intermediate has been previously described by a Pharmacia–Upjohn group (obtained semi-synthetically from marcfortine A) and comparison of the authentic and synthetic materials (^1H and ^{13}C NMR, IR, exact mass, mobility on thin-layer chromatography (TLC)) confirmed the identity of this substance. The final step, a methyl Grignard addition to the ketone group of **29** has been previously described to give paraherquamide A along with a trace of the corresponding C-14 epimer in ~50% yield when MeMgBr was employed.[13a] Employment of this protocol using MeMgBr with our synthetic ketone gave (−)-paraherquamide A (**1**) as the exclusive product (the C-14 epimer was not detected) in 42% yield that was identical in all respects (^1H and ^{13}C NMR,



Scheme 4. Formation of the *spiro* oxindole.

 © WILEY-VCH Verlag GmbH, D-69451 Weinheim, 2000 1433-7851/00/3914-2543 $ 17.50+.50/0

IR, exact mass, mobility on TLC, m.p. (250 °C (decomp.)), $[\alpha]_D^{25} = -22$ ($c = 0.2$ MeOH)) to natural paraherquamide A.[25]

The approach developed in this study makes it feasible to examine the design and synthesis of other members of the paraherquamide family and should also permit access to structurally unique paraherquamides, which may have significant biological properties. The application of this methodology to the asymmetric, stereocontrolled, total synthesis of other members of the paraherquamide family and the evaluation of their properties is currently under study in these laboratories.

Received: March 24, 2000 [Z14890]

[1] M. Yamazaki, E. Okuyama, *Tetrahedron Lett*. **1981**, *22*, 135.

[2] a) J. G. Ondeyka, R. T. Goegelman, J. M. Schaeffer, L. Kelemen, L. Zitano, *J. Antibiot*. **1990**, *43*, 1375; b) J. M. Liesch, C. F. Wichmann, *J. Antibiot*. **1990**, *43*, 1380; c) T. A. Blizzard, H. Mrozik, M. H. Fisher, S. M. Schaeffer, *J. Org. Chem*. **1990**, *55*, 2256; d) T. A. Blizzard, G. Marino, H. Mrozik, M. H. Fisher, K. Hoogsteen, J. P. Springer, *J. Org. Chem*. **1989**, *54*, 2657; e) T. A. Blizzard, G. Margiatto, H. Mrozik, J. M. Schaeffer, M. H. Fisher, *Tetrahedron Lett*. **1991**, *32*, 2437; f) T. A. Blizzard, G. Margiatto, H. Mrozik, J. M. Schaeffer, M. H. Fisher, *Tetrahedron Lett*. **1991**, *32*, 2441.

[3] a) S. E. Blanchflower, R. M. Banks, J. R. Everett, B. R. Manger, C. Reading, *J. Antibiot*. **1991**, *44*, 492; b) S. E. Blanchflower, R. M. Banks, J. R. Everett, C. Reading, *J. Antibiot*. **1993**, *46*, 1355.

[4] R. M. Banks, S. E. Blanchflower, J. R. Everett, B. R. Manger, C. Reading, *J. Antibiot*. **1997**, *50*, 840.

[5] a) J. Polonsky, M.-A. Merrien, T. Prange, C. Pascard, *J. Chem. Soc. Chem. Commun*. **1980**, 601; b) T. Prange, M.-A. Billion, M. Vuilhorgne, C. Pascard, J. Polonsky, S. Moreau, *Tetrahedron Lett*. **1981**, *22*, 1977.

[6] a) A. J. Birch, J. J. Wright, *J. Chem. Soc. Chem. Commun*. **1969**, 644; b) A. J. Birch, J. J. Wright, *Tetrahedron* **1970**, *26*, 2329; c) A. J. Birch, R. A. Russell, *Tetrahedron* **1972**, *28*, 2999; d) B. A. Bird, A. T. Remaley, I. M. Campbell, *Appl. Environ. Microbiol*. **1981**, *42*, 521; e) B. A. Bird, I. M. Campbell, *Appl. Environ. Microbiol*. **1982**, *43*, 345; f) J. E. Robbers, J. W. Straus, *Lloydia* **1975**, *38*, 355; g) R. R. M. Paterson, D. L. Hawksworth, *Trans. Br. Mycol. Soc*. **1985**, *85*, 95; h) B. J. Wilson, D. T. C. Yang, T. M. Harris, *Appl. Microbiol*. **1973**, *26*, 633; i) J. Coetzer, *Acta Crystallogr. Sect. B* **1974**, *30*, 2254.

[7] A. C Whyte, J. B. Gloer, *J. Nat. Prod*. **1996**, *59*, 1093.

[8] "Beeinflussung der Sekundarstoffbildung bei *Aspergillus ochraceus* durch Variation der Kulturbedingungen sowie Isolierung, Strukturaufklarung und Biosynthese der neuen Naturstoffe": J. Fuchser, PhD thesis, University of Göttingen (Germany), **1995**.

[9] H. Hayashi, Y. Nishimoto, H. Nozaki, *Tetrahedron Lett*. **1997**, *38*, 5655.

[10] a) J. Baldas, A. J. Birch, R. A. Russell, *J. Chem. Soc. Perkin Trans. 1* **1974**, 50; b) A. J. Birch, *Agr. Food Chem*. **1971**, *19*, 1088; c) A. E. A. Porter, P. G. Sammes, *J. Chem. Soc. Chem. Commun*. **1970**, 1103; d) M. S. Kuo, V. H. Wiley, J. I. Cialdella, D. A. Yurek, H. A. Whaley, V. P. Marshall, *J. Antibiot*. **1996**, *49*, 1006; e) M. S. Kuo, D. A. Yurek, S. A. Mizsak, J. I. Cialdella, L. Baczynskyj, V. P. Marshall, *J. Am. Chem. Soc*. **1999**, *121*, 1763.

[11] a) E. M. Stocking, J. F. Sanz-Cervera, R. M. Williams, *Angew. Chem*. **1999**, *111*, 880; *Angew. Chem. Int. Ed*. **1999**, *38*, 786; b) R. M. Williams, J. F. Sanz-Cervera, F. Sancenón, J. A. Marco, K. Halligan, *Bioorg. Med. Chem*. **1998**, *6*, 1233; c) R. M. Williams, J. F. Sanz-Cervera, F. Sancenon, J. A. Marco, K. Halligan, *J. Am. Chem. Soc*. **1998**, *120*, 1090; d) E. Stocking, J. F. Sanz-Cervera, R. M. Williams, C. J. Unkefer, *J. Am. Chem. Soc*. **1996**, *118*, 7008; e) J. F. Sanz-Cervera, T. Glinka, R. M. Williams, *J. Am. Chem. Soc*. **1993**, *115*, 347; f) J. F. Sanz-Cervera, T. Glinka, R. M. Williams, *Tetrahedron* **1993**, *49*, 8471.

[12] a) W. L. Shoop, C. H. Eary, H. W. Michael, H. W. Haines, R. L. Seward, *Vet. Parasitol*. **1991**, *40*, 339; b) W. L. Shoop, J. R. Egerton, C. H. Eary, D. Suhayda, *J. Parasitol*. **1990**, *76*, 349; c) W. L. Shoop, B. F. Michael, H. W. Haines, C. H. Eary, *Vet. Parasitol*. **1992**, *43*, 259; d) W. L. Shoop, H. W. Haines, C. H. Eary, B. F. Michael, *Am. J. Vet. Res*. **1992**, *53*, 2032; e) D. A. Ostlind, W. G. Mickle, D. V. Ewanciw, F. J. Andriuli, W. C. Campbell, S. Hernandez, S. Mochales, E. Munguira, *Res. Vet. Sci*. **1990**, *48*, 260; f) J. M. Schaeffer, T. A. Blizzard, J. Ondeyka, R. Goegelman, P. J. Sinclair, H. Mrozik, *Biochem. Pharmacol*. **1992**, *43*, 679; for a recent review, see: g) T. G. Geary, N. C, Sangster, D. P. Thompson, *Vet. Parasitol*. **1999**, *84*, 275.

[13] a) B. H. Lee, M. F. Clothier, *J. Org. Chem*. **1997**, *62*, 1795; b) B. H. Lee, M. F. Clothier, W. W. McWhorter; PCT Int. Appl. WO 98 21, 211; [*Chem. Abstr.* **1998**, *129*, 28117z].

[14] a) T. D. Cushing, J. F. Sanz-Cervera, R. M. Williams, *J. Am. Chem. Soc*. **1993**, *115*, 9323; b) T. D. Cushing, J. F. Sanz-Cervera, R. M. Williams, *J. Am. Chem. Soc*. **1996**, *118*, 557.

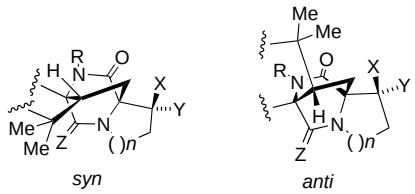
[15] R. M. Williams, J. Cao, *Tetrahedron Lett*. **1996**, *37*, 5441.

[16] a) J. Cooper, P. T. Gallagher, D. W. Knight, *J. Chem. Soc. Chem. Commun*. **1988**, 509; b) J. Cooper, P. T. Gallagher, D. W. Knight, *J. Chem. Soc. Perkin Trans. 1* **1993**, 1313; c) D. W. Knight, N. Lewis, A. Share, D. Haigh, *Tetrahedron: Asymmetry* **1993**, *4*, 625; see also: d) M. P. Sibi, J. W. Christensen, *Tetrahedron Lett*. **1990**, *31*, 5689. Compound **11** was prepared as described in ref. [16b].

[17] a) M. Somei, Y. Karasawa, C. Kaneko, *Heterocycles* **1981**, *16*, 941; b) T. Kametani, N. Kanaya, M. Ihara, *J. Chem. Soc. Perkin Trans. 1* **1981**, 959.

[18] a) R. M. Williams, T. D. Cushing, *Tetrahedron Lett*. **1990**, *31*, 6325; see also: b) B. M. Savall, W. W. McWhorter, *J. Org. Chem*. **1996**, *61*, 8696.

[19] The *syn*-/*anti*- relationship refers to the relative stereochemistry between the C-20 stereogenic center (see paraherquamide numbering) and the proline residue.



[20] a) S. A. Denmark, B. R. Henke, *J. Am. Chem. Soc*. **1991**, *113*, 2177; b) S. A. Denmark, B. R. Henke, *J. Am. Chem. Soc*. **1989**, *111*, 8032.

[21] B. M. Trost, M. D. Fortunak, *Organometallics* **1982**, *1*, 7.

[22] T. Fukuyama, G. Liu, *Pure Appl. Chem*. **1997**, *69*, 501.

[23] R. K. Boeckman, J. C. Potenza, *Tetrahedron Lett*. **1985**, *26*, 1411.

[24] a) D. B. Dess, J. C. Martin, *J. Org. Chem*. **1983**, *48*, 4155; b) D. B. Dess, J. C. Martin, *J. Am. Chem. Soc*. **1991**, *113*, 7277.

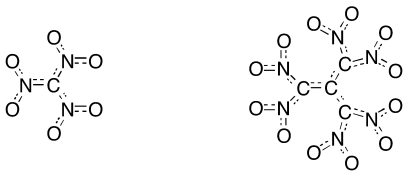
[25] The synthetic sample was recrystallized from ether. A sample of natural paraherquamide A recrystallized from ether under the same conditions rendered a sample with a m.p. = 250 °C (decomp.) and $[\alpha]_D^{25} = -21$ ($c = 0.2$ in MeOH), lit. [1] $[\alpha] = -28$ ($c = 0.43$ in MeOH). All intermediates up to the final product have an ~97.5:2.5 *er*; the final synthetic paraherquamide A upon recrystallization from ether is optically pure.

 © WILEY-VCH Verlag GmbH, D-69451 Weinheim, 2000 1433-7851/00/3914-2544 $ 17.50+.50/0

Hexanitroisobutene Dianion Salts**

Valerian M. Khutoretsky, Natalia B. Matveeva, and Andrei A. Gakh*

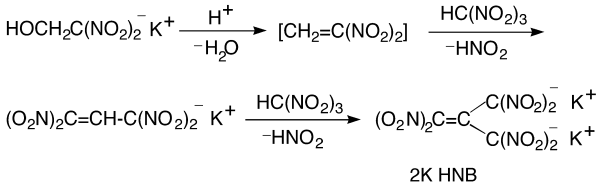
The trimethylenemethane dianion and its analogs have generated considerable interest during the last three decades, in both theoretical organic chemistry (Y-conjugation, Y-aromaticity)[1–12] and synthetic organic chemistry (ligand design).[13–15] Driven by our current interest in "dendritic" Y-conjugated anions,[16, 17] we pursued the synthesis of the hexanitroisobutene (HNB) dianion ($C_4(NO_2)_6^{2-}$; compound **II** in Scheme 1).



I **II**

Scheme 1. Sample Y-conjugated anions.

Use of a "direct" synthetic approach to HNB, via nitration of dilithium trimethylenemethanide,[2] was rejected because of the obvious problems associated with the simultaneous introduction of six nitro groups onto a chemically labile trimethylenmethane system. An alternative approach (which includes a sequence of addition–elimination reactions, that start from the potassium salt of 2,2-dinitroethanol as the 1,1-dinitoethylene precursor[18] and trinitromethane) was successful (Scheme 2). A similar approach was previously employed for the synthesis of substituted 1,1,3,3-tetranitropropanes[18] and 1,1,3-trinitropropene salts.[19] The only difference in our case was that the elimination of HNO_2 proceeds simultaneously and does not require the addition of bases.[19]



2K HNB

Scheme 2. Addition–elimination synthetic procedure.

After recrystallization from water, HNB salts can be prepared as large, deep-ruby colored crystals (which contain a single coordinated water molecule in the case of dipotassium salt 2K HNB). HNB salts are thermally unstable and tend to decompose slowly even at room temperature. The structure of the HNB dianion is depicted in Figure 1.

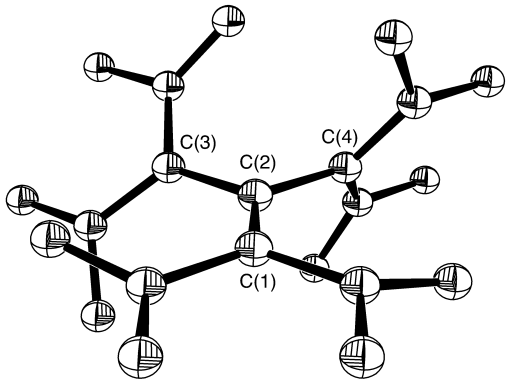


Figure 1. ORTEP representation of the HNB dianion.

The HNB dianion is a nonplanar system. Specific conformations of the anion vary from one salt to another but certain structural features remain intact. Thus, in all salts, the main plane of the molecule (C(1)-C(2)-C(3)-C(4) in Figure 1) is preserved. Dinitromethylene fragments are twisted on various angles in relations to this central plane. The C(1)–C(2) bond distance in the dipotassium salt (2K HNB · H_2O) is 1.34 Å, which is very close to a typical C=C bond distance (see the Supplementary Material). In this salt, the C(1) dinitromethylene fragment is almost coplanar to the main plane of the molecule. The other two dinitromethylene fragments (C(3) and C(4)) are twisted by substantial angles (63.5° and 40.2°, respectively).

UV/Vis spectra of the HNB salts vary from one solvent to another—an indication of the conformational mobility of the HNB dianion in solution. Thus, UV/Vis spectra of 2K HNB in acetone have two distinct absorption maxima: at 370 (19400) and 508 nm (13600 mol L^{-1} cm^{-1}). In water, these maxima shifted to 368 (21300) and 478 nm (7100 mol L^{-1} cm^{-1}), respectively. The existence of two absorption peaks in the UV/Vis spectra is a typical feature of conjugated 1,1-dinitrocabanion systems (such as 1-(*R*)-3,3-dinitropropene salts), which was attributed in the past to the presence of two types of rotamers (conjugated and nonconjugated) in solution.[20] Indeed, we found that the sum of integral intensities of these two peaks in the UV/Vis spectra of HNB salts remains constant in different solvents.

^{13}C NMR spectroscopy shows the equivalence of the dinitromethylene groups of the HNB dianion in solution (on the NMR timescale). The ^{13}C NMR spectrum of 2K HNB in [D_6]DMSO has only two signals: at $\delta = 135.3$ (dinitromethylene groups) and $\delta = 127.9$ (C(2)). These chemical shifts are very close to those observed in a similar system, the potassium salt of 1,1,3 trinitropropene ($\delta = 134.0$, 127.5, and 127.1 in [D_6]DMSO). Again, as in the case of the trinitromethanide

[*] Dr. A. A. Gakh
Chemical and Analytical Sciences Division
Oak Ridge National Laboratory
Oak Ridge, TN 37831-6197 (USA)
Fax: (+1) 865-576-5235
E-mail: gakhaa@ornl.gov
Dr. V. M. Khutoretsky, Dr. N. B. Matveeva
N. D. Zelinsky Institute of Organic Chemistry (RAS), Leninsky pr., 47
Moscow, 117913 (Russia)

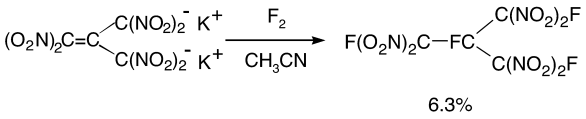
[**] This research was sponsored in part by the US Department of Energy IPP program under contract DE-AC05-96OR22464 with the Oak Ridge National Laboratory, managed by the Lockheed Martin Energy Research Corp. CNDO/2 calculations were performed by Dr. A. V. Belik and Dr. V. A. Shlyapochnikov (N. D. Zelinsky Institute of Organic Chemistry).

Supporting information for this article is available on the WWW under http://www.wiley-vch.de/home/angewandte/ or from the author.

anion (compound **I** in scheme 1),[16, 17] either the barriers of rotation of the three dinitromethylene groups in HNB dianion are too small to be detected by this method or the anion assumes an averaged symmetrical conformation in solution. Similar behavior was reported for the tris(diphenylmethylene) dianion and related systems.[3, 8]

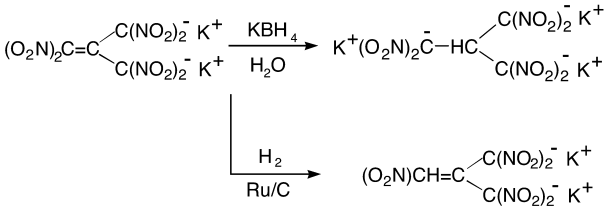
Quantum mechanical calculations show that the central carbon atom (C(2); see Figure 1 and the Supplementary Material) is postively charged, whereas the peripheral carbon atoms (C(1), C(3), and C(4)) are negatively charged. These features suggest that HNB salts can react with both nucleophilic and electrophilic agents. Unfortunately, many of the tested reactions of HNB salts proceed with the fragmentation of the carbon skeleton. Only fluorination and hydrogenation of the HNB salts were successful.

Direct fluorination of the HNB salts with elemental fluorine gave the expected, fully fluorinated product, tris-(fluorodinitromethyl)fluoromethane, albeit in a low (6.3%) yield (Scheme 3).



Scheme 3. Fluorination of HNB.

Hydrogenation of HNB salts can be achieved using elemental hydrogen (5% Ru/C) or tetrahydroborate reagents. Catalytic hydrogenation of 2K HNB yielded a substitution product, the dipotassium salt of 2-dinitromethyl-1,1,3-trinitropropene (Scheme 4). Reduction with sodium borohydride



Scheme 4. Hydrogenation of HNB.

gave the normal addition product, the tripotassium salt of tris(dinitromethyl)methane, together with the above-mentioned dipotassium salt.

In summary, we have synthesized salts of a new, fully nitrated Y-conjugated system, the hexanitroisobutene dianion. It is expected that this dianion will be useful in ligand design similar to other known Y-conjugated anions with a rich coordination chemistry, such as the hexacyanoisobutene dianion.[14, 15]

Experimental Section

Caution: all salts of polynitrocompounds should be handled as potential explosives; therefore use proper protective measures.

Dipotassium salt of hexanitroizobutene (2K HNB), monohydrate: The potassium salt of 1,1-dinitroethanol (4.1 g, 23 mmol) was added incrementally with stirring to a solution of trinitromethane (5.0 g, 33 mmol) in water (20 mL). The temperature was maintained below 25 °C during the addition. The reaction mixture was stirred for an additional 2 h and then left overnight at room temperature. Deep-ruby colored crystals of 2K HNB · H_2O were collected by filtration and were washed with a small amount of ethanol. An additional portion of the crystals was obtained from filtrate by adding KCl (1.6 g). The total yield of 2K HNB · H_2O was 1.8 g (19%). The salt can be recrystallized from warm water (45 °C). Elemental analysis: calcd for $C_4N_6O_{12}K_2 \cdot H_2O$: C 11.43, N 20.00, K 18.57, H_2O 4.29; found: C 11.29, N 19.45, K 18.62, H_2O 4.29. IR (Ge): $\tilde{\nu} = 1220\ cm^{-1}$ [$C(NO_2)_2^-$]. Other analytical data are presented in the text.

Fluorination of 2K HNB: A suspension of 2K HNB (4.2 g, 10 mmol) in CH_3CN (100 mL) was fluorinated at 0 °C using 20% F_2/N_2 until the reaction mixture became colorless. The reaction mixture was then poured into 500 g of an ice/water mixture and extracted with *n*-pentane (60 mL). The organic layer was separated and was washed several times with 5% bicarbonate until the water layer became colorless. The organic layer was finally washed with water and dried over $MgSO_4$. The pentane was evaporated at normal pressure and the residue was distilled in vacuo (48–52 °C, 0.1 mm) to yield 0.25 g (6.3%) of tris(fluorodinitromethyl)fluoromethane as a colorless liquid. Elemental analysis: calcd for $C_4F_4N_6O_{12}$: C 12.00, F 19.00, N 21.00; found: C 12.06, F 19.02, N 20.77. ^{19}F NMR (CCl_4, referenced against CF_3COOH): $\phi = 14.2$ (br m, 3F; $C(NO_2)_2F$), 87.9 (q, 1F, $J^3_{FF} = 14.8$ Hz; CF). IR (KBr): $\tilde{\nu} = 1310$, 1645 cm^{-1} [$C(NO_2)_2F$].

Hydrogenation of 2K HNB: a) A solution of 2K HNB · H_2O (0.62 g, 1.5 mmol) in water (25 mL) was hydrogenated at room temperature and normal pressure with a flow of H_2 using a 5% Ru/C catalyst (1 g). The course of the reaction was monitored by UV/Vis spectroscopy. After the reaction was complete, the catalyst was removed by filtration and washed with water (3 × 15 mL). Combined water solutions were concentrated in vacuo to 5 mL. Cesium fluoride (0.5 g) was added to the solution. The orange precipitate was removed by filtration and was washed with small amounts of water and ethanol to yield dicesium 2-dinitromethyl-1,1,3-trinitropropene (0.2 g, 25%). An analytical sample was recrystallized from hot water. Elemental analysis: calcd for $C_4HN_5O_{10}Cs$: C 8.79, H 0.37, N 12.82, Cs 48.72; found: C 8.98, H 0.41, N 12.85.77, Cs 47.9. ^1H NMR (D_2O): $\delta = 7.75$ (s; $CHNO_2$). UV/Vis (acetone): λ'_{max} (ε) = 370 (17500); λ''_{max} (ε) = 456 nm (25600 mol L^{-1} cm^{-1}). b) A solution of potassium borohydride (0.2 g, 3.7 mmol) in water (1 mL) was added with stirring to a solution of 2K HNB · H_2O (1.0 g, 2.4 mmol) in water (37 mL) at room temperature. The reaction mixture was stirred at that temperature for an additional 30 min and then was diluted with methanol (250 mL). The precipitate was filtered and was then washed with ethanol to yield 0.45 g (45%) of the tripotassium salt of tris(dinitromethyl)methane, analyzed as dipotassium monocesium salt after a partial cation exchange with CsF in water. Elemental analysis: calcd for $C_4HN_6O_{12}K_2Cs$: C 8.96, H 0.19, N 15.67, K 14.55, Cs 24.81; found: C 8.63, H 0.31, N 15.77, K 14.19, Cs 23.60; ^1H NMR (D_2O): $\delta = 7.18$ s (CH). IR (KBr): $\tilde{\nu} = 1240$, 1520 cm^{-1} [$C(NO_2)_2^-$]. UV/Vis (H_2O): λ_{max} (ε) = 373 (30500 mol L^{-1} cm^{-1}).

Received: October 29, 1999
Revised: April 25, 2000 [Z 14201]

[1] J. Klein, *Tetrahedron* **1983**, *39*, 2733–2759.
[2] J. Klein, A. Medik-Balan, *J. Chem. Soc. Chem. Commun.* **1973**, 275.
[3] A. Rajca, L. M. Tolbert, *J. Am. Chem. Soc.* **1988**, *110*, 871–876.
[4] K. B. Wiberg, *J. Am. Chem. Soc.* **1990**, *112*, 4177–4182.
[5] I. Agranat, T. P. Radhakrishnan, W. C. Herndon, A. Skancke, *Chem. Phys. Lett.* **1991**, *181*, 117–122.
[6] A. Gobbi, P. J. MacDougall, G. Frenking, *Angew. Chem.* **1991**, *103*, 1038–1040; *Angew. Chem. Int. Ed. Engl.* **1991**, *30*, 1001–1003.
[7] J. Cioslowski, S. T. Mixon, E. D. Fleischmann, *J. Am. Chem. Soc.* **1991**, *113*, 4751–4755.
[8] D. Wilhelm, H. Dietrich, T. Clark, W. Mahdi, A. J. Kos, P. von R. Schleyer, *J. Am. Chem. Soc.* **1984**, *106*, 7279–7280.
[9] A. Skancke, *J. Phys. Chem.* **1994**, *98*, 5234–5239.
[10] M. Oda, T. Kawase, C. X. Wei, *Pure Appl. Chem.* **1996**, *68*, 267–274.
[11] R. Shenhar, M. Rabinovitz, *J. Chem. Soc. Perkin Trans. 2* **1997**, 2463–2464.
[12] W. J. Middleton, E. L. Little, D. D. Coffman, V. A. Engelhardt, *J. Am. Chem. Soc.* **1958**, *80*, 2795–2806.

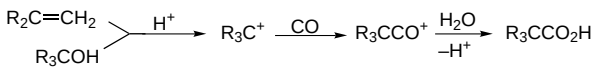
 © WILEY-VCH Verlag GmbH, D-69451 Weinheim, 2000 1433-7851/00/3914-2546 $ 17.50+.50/0

[13] G. E. Herberich, T. P. Spaniol, *J. Chem. Soc. Chem. Commun.* **1991**, 1457 – 1458.
[14] S. Triki, J. S. Pala, M. Decoster, P. Molinie, L. Toupet, *Angew. Chem.* **1999**, *111*, 155 – 158; *Angew. Chem. Int. Ed.* **1999**, *38*, 113 – 115.
[15] J. S. Miller, D. A. Dixon, J. C. Calabrese, C. Vazquez, P. J. Krusic, M. D. Ward, E. Wasserman, R. L. Harlow, *J. Am. Chem. Soc.* **1990**, *112*, 381 – 398.
[16] A. A. Gakh, M. N. Burnett, J. C. Bryan, *Acta Crystallogr. Sect. C* **1998**, *54*, 1229 – 1233.
[17] A. A. Gakh, J. C. Bryan, M. N. Burnett, P. V. Bonnesen, *J. Mol. Struct.* **2000**, *520*, 221 – 228.
[18] K. Klager, J. Kispersky, E. Hamel, *J. Org. Chem.* **1961**, *26*, 4368 – 4371.
[19] M. J. Kamlet, J. D. Dacons, J. C. Hoffsommer, *J. Org. Chem*. **1961**, *26*, 4881 – 4886.
[20] M. J. Kamlet, D. J. Glover, *J. Org. Chem*. **1962**, *27*, 537 – 543.

Superacid-Catalyzed Selective Formylation – Rearrangement of Isoalkanes with Carbon Monoxide to Branched Ketones**

George A. Olah,* G. K. Surya Prakash,* Thomas Mathew, and Eric R. Marinez

The acid-catalyzed carbonylation of olefins or alcohols to branched aliphatic acids (neo-acids) is known as the Koch – Haaf reaction.[1] It involves the intermediate formation of a trivalent alkyl cation (carbenium ion) which then alkylates CO to the corresponding acyl cation to produce, upon hydrolysis, the branched carboxylic acid (Scheme 1).

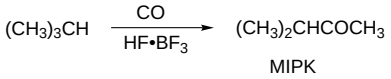


Scheme 1. Koch – Haaf reaction of alkenes and alcohols, R = CH_3.

Hopff and Nenitzescu et al.[2a] reported in 1936 that when carbon monoxide was treated with isobutane in the presence of an excess of $AlCl_3$, a mixture of products was obtained, including 31 % of methyl isopropyl ketone (MIPK) besides some *tert*-butyl isopropyl ketone and pivalic acid. Nenitzescu subsequently suggested that MIPK was formed by reaction of CO with the intermediately formed *tert*-butyl cation, followed by hydride transfer from the pivaloyl cation to give pivalaldehyde, which then rearranged to MIPK.[2b] The aluminum halide-catalyzed conversion of saturated hydrocarbons with carbon monoxide, however, as reported by Nenitzescu et al., usually gives complex mixtures of products, containing carboxylic acids and ketones.[3]

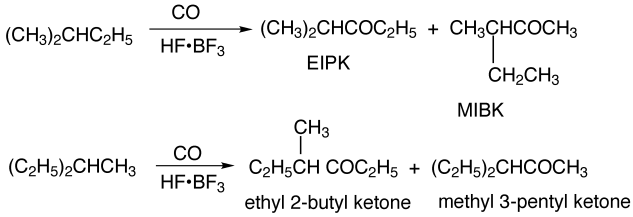
In contrast, Sommer et al.[4] treated CO with alkanes with superacidic $HF \cdot SbF_5$ as a catalyst and obtained exclusively Koch – Haaf carboxylic acid products. After studying the superelectrophilic activation of carbon monoxide and its reaction with adamantane, we reported[5] in 1988 that both the Koch type carboxylation as well as a distinctly different direct formylation to give 1-formyladamantane take place. Whereas the Koch-carboxylation involves initial formation of the 1-adamantyl cation, the formylation reaction proceeds by the activated formyl cation inserting into the tertiary C–H bond via a five-coordinate carbocation.

We now report the superelectrophilic formylation of isoalkanes, such as isobutane or isopentane (and their higher homologues), giving selectively and in high yield the corresponding rearranged branched ketones with no detectable (or minimal) branched acids, that is Koch products.[6] To achieve this remarkably efficient conversion superacids weaker than $HF \cdot SbF_5$ or $FSO_3H \cdot SbF_5$, such as $HF \cdot BF_3$ or $HF \cdot CF_3SO_3H \cdot BF_3$, are used, which do not readily oxidatively ionize isoalkanes to the corresponding alkyl cations (which would consequently lead predominantly to Koch carboxylation). They are, however, still strong enough to activate carbon monoxide to an efficient electrophilic formylating agent (that is the formyl cation protosolvated by the acid, $HCO^+ \cdots H^+A^-$). $HF \cdot BF_3$ was found to be particularly suitable to bring about the reaction. Illustrative of this in the experimental section is the example of the conversion of isobutane into MIPK (Scheme 2).



Scheme 2. Carbonylation-rearrangement of isobutane.

Other isoalkanes containing tertiary CH groups, such as isopentane, isohexanes, or isoheptanes, react under related superacidic carbonylation conditions in a similar way to give the corresponding branched ketones (Scheme 3).



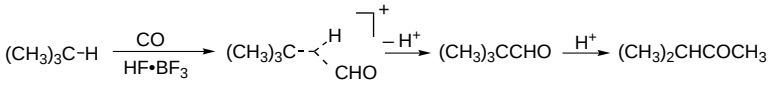
Scheme 3. Carbonylation-rearrangement of isopentane and 3-methyl pentane.

Isopentane for example is converted into methyl isobutyl ketone (MIBK) and ethyl isopropyl ketone (EIPK) in a ratio of 1:3. 3-Methylpentane gives ethyl 2-butyl ketone and methyl 3-pentyl ketone, respectively (4:1), as major products. The reaction is considered to involve electrophilic formylation of the tertiary CH bond of isobutane forming pivalaldehyde, which under the superacidic conditions rearranges to MIPK (Scheme 4).

[*] Prof. Dr. G. A. Olah, Prof. Dr. G. K. S. Prakash, Dr. T. Mathew, Dr. E. R. Marinez
Loker Hydrocarbon Research Institute and
Department of Chemistry
University of Southern California
University Park, Los Angeles, CA 90089-1661 (USA)
Fax: (+1) 213-740-5087
E-mail: olah@methyl.usc.edu, prakash@methyl.usc.edu

[**] Chemistry in Superacids, Part 51. Part 50: G. A. Olah, G. Rasul, M. Hachoumy, A. Burrichter, G. K. S. Prakash, *J. Am. Chem. Soc*. **2000**, *122*, 2737. Support of our work by the Loker Hydrocarbon Research Institute is gratefully acknowledged.

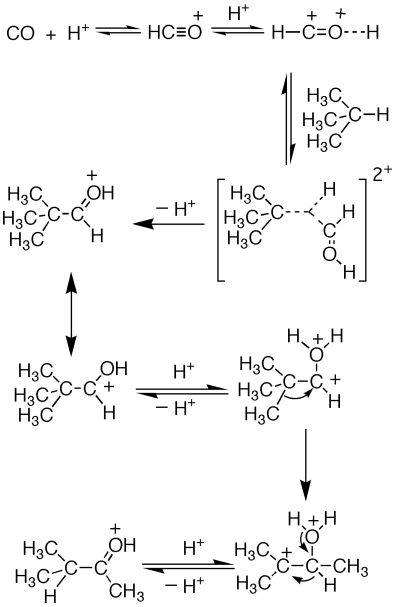
 © WILEY-VCH Verlag GmbH, D-69451 Weinheim, 2000 1433-7851/00/3914-2547 $ 17.50+.50/0



Scheme 4. Formylation of isobutane, followed by rearrangement.

The formyl cation itself is a linear carboxonium ion $HC{\equiv}O^+$ in which the charge is substantially localized on the oxygen atom. The carbocationic nature is enhanced by protosolvation that results in the decrease of neighboring oxygen participation ($HCO^+\cdots H^+A^-$, in the limiting case $HC^+{=}O^+H$) and renders the formylating species reactive enough (that is superelectrophilic) to attack the C–H bond via a five-coordinate carbocation.[7]

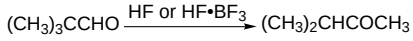
The rearrangement of pivalaldehyde again involves O protonation and protosolvation, rendering the carbonyl carbon a carbocation-like center, facilitating rearrangement (Scheme 5).



Scheme 5. Proposed mechanism for the direct formylation and rearrangement.

We indeed found that pivalaldehyde rearranges quantitatively to MIPK when treated with HF or $HF\cdot BF_3$ (Scheme 6).

The reported carbonylation rearrangement of isoalkanes to branched ketones, but not acids is fundamentally different from the Koch–Haaf type of carbonylative carboxylation



Scheme 6. Superacid-induced rearrangement of pivalaldehyde.

which exclusively gives branched carboxylic acids. Branched aliphatic ketones, such as MIPK, EIPK, MIBK, and the like are efficient high octane (>100) oxygenate additives for gasoline, without many of the detrimental effects of the methyl *tert*-butyl ether (MTBE) and, thus, have also practical significance.

Experimetal Section

Anhydrous HF (56 g, 2.80 mol) was added to a precooled (−78 °C) autoclave. Subsequently isobutane (22.04 g, 0.38 mol) was condensed into the autoclave and 5.17×10^6 Pa (750 psi) of BF_3 (170 g, 2.5 mol) was slowly introduced with thorough stirring, followed by CO (47 g, 1.7 mol) while the temperature was raised to 0 °C and the pressure to 10.34×10^6 Pa (1500 psi). The temperature of the reaction mixture increased gradually to 35 °C (pressure rose to 14.82×10^6 Pa (2150 psi)), and the reaction mixture was stirred for 14 h during which a pressure drop of 2.41×10^6 Pa (350 psi) was observed. The autoclave was cooled to −78 °C and slowly depressurized through two traps kept in an acetone/dry ice bath. The vessel was subsequently warmed to 0 °C, and after complete depressurization the liquid reaction mixture was quenched by adding in small portions of ice (400 g in total) in a polyolefin flask. The mixture was neutralized with sodium bicarbonate and extracted three times with diethyl ether (total volume 500 mL). The combined diethyl ether extracts were dried with anhydrous $MgSO_4$, filtered, and worked up by distillation in the usual way. The yield of isopropyl methyl ketone was 91% with 93% selectivity (GC, GC-MS, and NMR analysis). No isobutane was detected by GC in the condensate of the traps. At the same time the aqueous layer did not show the presence of any pivalic acid.

Received: February 1, 2000 [Z 14630]

[1] a) H. Koch, W. Haaf, *Angew. Chem.* **1960**, *72*, 628; b) G. A. Olah, A. Molnár, *Hydrocarbon Chemistry*, Wiley-Interscience, New York, **1995**, pp. 276–277, and references therein.

[2] a) H. Hopff, C. D. Nenitzescu, D. A. Isacescu, I. P. Cantuniari, *Ber. Dtsch. Chem. Ges.* **1936**, *69*, 2244–2251; b) A. T. Balaban, C. D. Nenitzescu, *Tetrahedron* **1960**, *10*, 55–64, and references therein.

[3] C. D. Nenitzescu, A. T. Balaban in *Friedel–Crafts and Related Reactions*, *Vol. 3*, *Part 2* (Ed.: G. A. Olah), Wiley-Interscience, New York, **1964**, pp. 1003–1152.

[4] J. Sommer, J. Bukala, *Acc. Chem. Res.* **1993**, *26*, 370–376.

[5] G. A. Olah, O. Farooq, M. Marcelli, G. K. S. Prakash, *J. Am. Chem. Soc.* **1988**, *110*, 864–867.

[6] G. A. Olah, US-A 6,018,088, **2000**, and related foreign applications.

[7] G. A. Olah, *Angew. Chem.* **1993**, *105*, 767–788; *Angew. Chem. Int. Ed. Engl.* **1993**, *32*, 805–827.

 © WILEY-VCH Verlag GmbH, D-69451 Weinheim, 2000 1433-7851/00/3914-2548 $ 17.50+.50/0

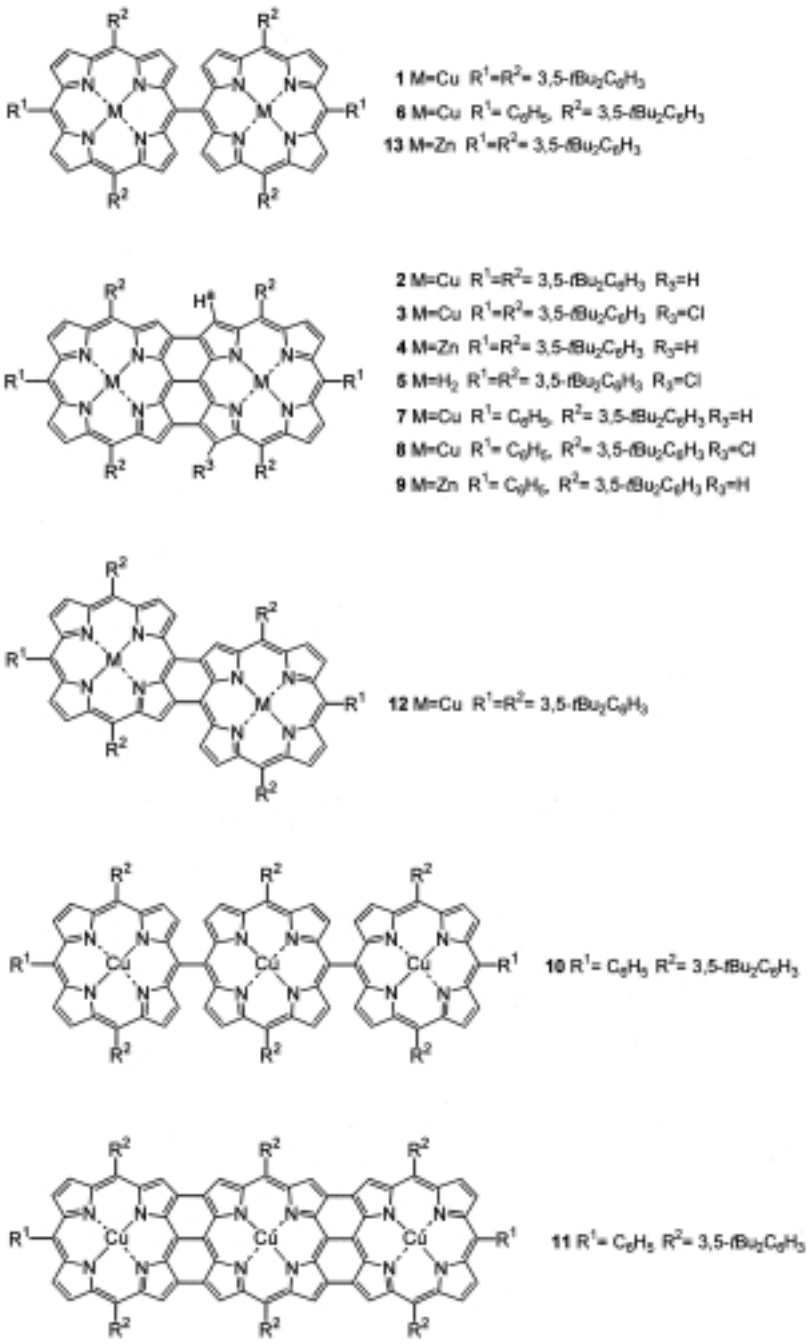
Completely Fused Diporphyrins and Triporphyrin**

Akihiko Tsuda, Hiroyuki Furuta, and Atsuhiro Osuka*

Recently, *meso*–*meso*-linked porphyrin arrays have emerged as potential photonic wires that is (capable of transmitting excitation energy over long distance) as a result of their favorable features, including a linear rodlike shape, ample electronic interactions for rapid incoherent energy hopping, and a lack of an energy sink that disrupts the energy flow along the array.[1–3] These properties originate from the orthogonal conformation of the arrays, which tends to minimize the electronic interaction between the neighboring porphyrins. If the arrays can be made planar and more electronically conjugated they will constitute a conductive electronic wire on a realistic molecular scale; the *meso*–*meso*-linked porphyrin arrays have now reached a discrete 128-mer with a molecular length of approximately 108 nm.[2]

Here, we report an effective oxidative transformation of the *meso*–*meso*-linked diporphyrins into triply linked, fused diporphyrins, which exhibit properties associated with an extremely delocalized π-electronic system as a consequence of their planar structure that is enforced by a fused connection. Fused porphyrin arrays have also attracted considerable interest in light of their application as molecular wires as well as nonlinear optical (NLO) materials, but reported examples are rather limited.[4–7]

Meso–*meso*-linked Cu^{II}-diporphyrin **1** was treated with two equivalents of tris(4-bromophenyl)aminium hexachloroantimonate (BAHA) in C_6F_6 at room temperature for two days to provide triply linked diporphyrins **2** and **3** in 62 and 6% yields, respectively. The structure of **2** has been suggested by its absorption spectrum ($\lambda_{max} = 411$, 576, and 996 nm), which is dramatically changed from that of **1**, and a parent molecular ion peak at m/z 1866 (calcd for $C_{124}H_{138}N_8Cu_2$: 1865) in its matrix-assisted laser-desorption/ionization time-of-flight (MALDI-TOF) mass spectrum, as well as by its transformation into Zn^{II}-diporphyrin **4**. The ^{1}H NMR spectrum of **4** is relatively simple (one set of mutually coupled two doublets at $\delta = 7.75$ and 7.70 for the β-protons, and a singlet at $\delta = 7.35$ for the β-protons (H^a)), which reflects its symmetric structure, and the MALDI-TOF mass spectrum shows a molecular ion at m/z 1868 in the spectrum (calcd for $C_{124}H_{138}N_8Zn_2$: 1867). Monochlorinated diporphyrin **3** exhibits a similar absorption spectrum ($\lambda_{max} = 409$, 573, and 990 nm) and has a parent peak at m/z 1900 in the MALDI-TOF mass spectrum (calcd for $C_{124}H_{137}ClCu_2N_8$: 1899).[8] The oxidation of **1** under similar



[*] Prof. A. Osuka, A. Tsuda, Prof. H. Furuta
Department of Chemistry
Graduate School of Science
Kyoto University, Sakyo-ku, Kyoto 606-8502 (Japan)
Fax: (+81) 75-753-3970
E-mail: osuka@kuchem.kyoto-u.ac.jp

[**] This work was supported by Grant-in-Aids for Scientific Research (No. 11223205) from the Ministry of Education, Science, Sports, and Culture of Japan and by CREST (Core Research for Evolutional Science and Technology) of Japan Science and Technology Corporation (JST). A.T. thanks the JSPS Research Fellowship for Young Scientists. We also thank Dr. M. Shiro of the Rigaku Corporation for his help in obtaining the single-crystal X-ray data of **5**.

Supporting information for this article is available on the WWW under http://www.wiley-vch.de/home/angewandte/ or from the author.

 © WILEY-VCH Verlag GmbH, D-69451 Weinheim, 2000 1433-7851/00/3914-2549 $ 17.50+.50/0

conditions in $CHCl_3$ led to extensive β-chlorination with production of **2** (8%), **3** (29%), and dichlorinated diporphyrin[9] (34%). This result indicates that abstraction of chlorine atoms was involved in this oxidative ring-closure process and that C_6F_6 is a better solvent than $CHCl_3$ for suppressing the β-chlorination.

In order to confirm the X-ray structure of a parent triply linked fused diporphyrin, we converted *meso*–*meso*-Cu^{II}-diporphyrin **6** into triply linked diporphyrin **7** (*m*/*z* 1645, calcd for $C_{108}H_{106}N_8Cu_2$: 1641) and **8** (*m*/*z* 1677, calcd for $C_{108}H_{105}N_8Cu_2Cl$: 1675) in 76 and 6% yields, respectively. The X-ray structure of **7** (Figure 1)[10] shows the two porphyrin

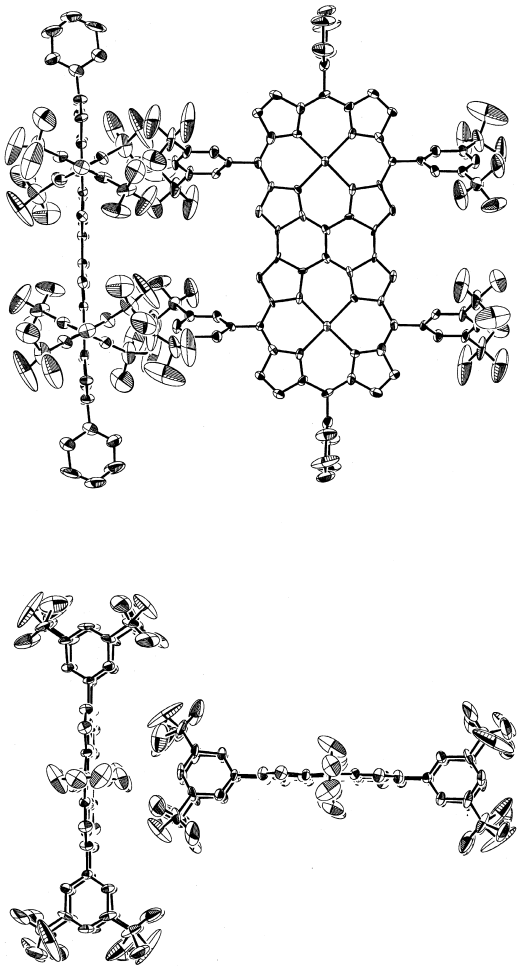


Figure 1. Molecular structure of **7**. Top: top view; bottom: side view. Hydrogen atoms and benzene molecules are omitted for clarity.

rings are fused to form an almost completely coplanar conformation with a mean plane deviation of only 0.029 Å for the 25 core atoms above and below the mean plane, and with β–β bonds of 1.41 Å and a *meso*–*meso* bond of 1.44 Å. It is interesting to note that the nearest fused diporphyrin units take an almost orthogonal arrangement, with the 3,5-di-*tert*-butylphenyl groups pointing towards the Cu^{II}-diporphyrin plane. Such crystal packing, also observed for **5**, suggests an attractive CH–π interaction between the *tert*-butyl group and the π system of the diporphyrin,[11] which may be enhanced by the larger polarizability of the π-electronic system of the diporphyrin. This type of crystal packing has been observed in neither the corresponding metal complexes of tetrakis(3,5-di-*tert*-butylphenyl)porphyrin nor in doubly *meso*–β-linked fused Ni^{II}-diporphyrin.[4, 12] We have also succeeded in obtaining the X-ray structure of the triply linked Zn^{II}-diporphyrin **9**,[13] which displays a mean plane deviation of 0.23 Å, two β–β bonds of 1.44 Å, and a *meso*–*meso* bond of 1.51 Å (Figure 2).

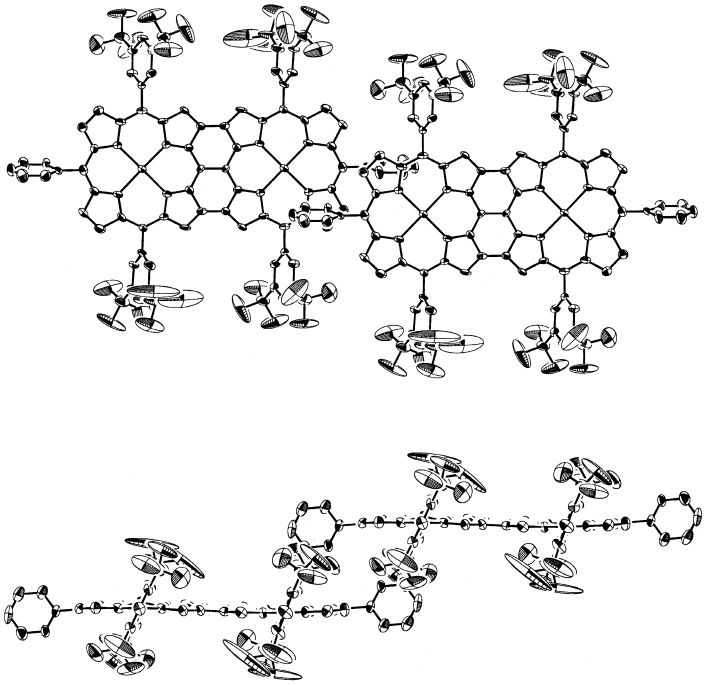


Figure 2. Molecular structure of **9**. Top: top view; bottom: side view. Hydrogen atoms, benzene, and ethanol molecules are omitted for clarity.

The crystal packing of **9** is like a parallel sheet with an interporphyrin separation of approximately 5.44 Å, which is common in porphyrin crystal structures but is entirely different from **7**. In this case, the central Zn^{II} ion is coordinated to ethanol and thus seems to be blocked from taking the orthogonal orientation found for **7**.

The *meso*–*meso*-linked Cu^{II}-triporphyrin **10** was oxidized with four equivalents of BAHA in C_6F_6 for three days to give triply linked triporphyrin **11** in 33% yield along with the recovery of **10** (30%). The fused triporphyrin **11** exhibits a parent molecular peak at *m*/*z* 2383 (calcd for $C_{156}H_{152}N_{12}Cu_3$: 2382) and an extremely red-shifted Q band at 1251 nm. Further characterization of **11** was hampered by its very poor solubility. However, this result encourages the extension of this oxidative ring-closure reaction to higher monodisperse and polymeric *meso*–*meso*-linked porphyrin arrays.[14]

It has been well established that the electronic interactions of multiply linked fused diporphyrins are strong and give rise to red-shifted intense Q bands and lower one-electron oxidation potentials.[4–6, 15] Figure 3 shows the absorption spectra of **1**, **2**, **4**, **10**, and **11**. The absorption spectrum of doubly *meso*–β-linked Cu^{II}-diporphyrin **12** is also shown for comparison. While the *meso*–*meso*-linked porphyrins **1** and **10** exhibit split Soret bands as reported previously,[1] the triply linked oligoporphyrins **2** and **11** show drastically altered absorption spectra with bands at 411, 576, and 996 nm and at

 © WILEY-VCH Verlag GmbH, D-69451 Weinheim, 2000 1433-7851/00/3914-2550 $ 17.50+.50/0

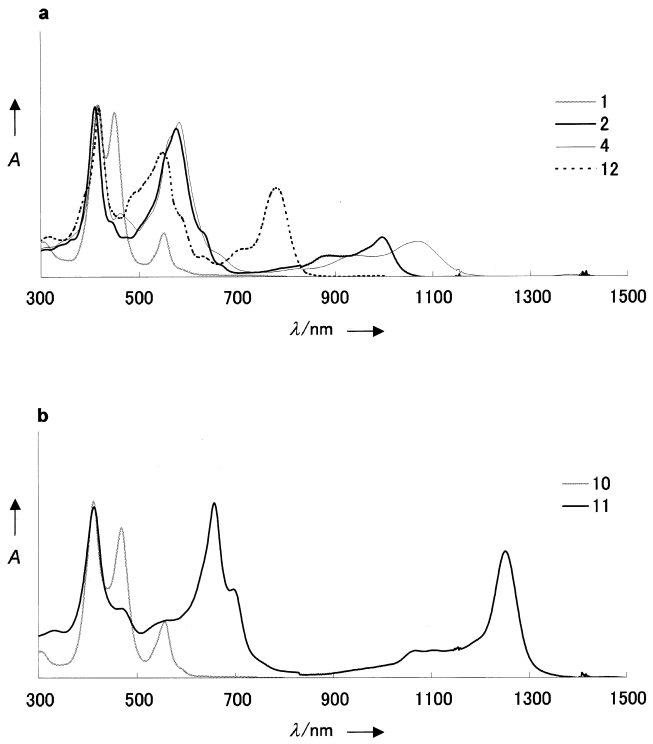


Figure 3. Absorption spectra taken in $CHCl_3$.

413, 657, and 1251 nm, respectively. Although the assignment of these absorption bands has not been done yet, it is probable that the fused connection causes a significant perturbation that breaks down the degeneracy of the e_g orbitals, and gives rise to intensified and red-shifted Q bands. The one-electron oxidation potentials were 0.69 V for **1**, 0.47 V for **12**, and 0.39 V for **2**.[16] Therefore it may be concluded that the electronic interaction in the triply linked diporphyrin **2** is much stronger than those in the fused diporphyrins (including **12**) reported before.[4–6] The effect of the central metal was preliminary examined by comparing Cu^{II}-diporphyrin **2** and Zn^{II}-diporphyrin **4**. The most red-shifted Q band is observed at 1068 nm in **4**, being red-shifted by 72 nm more than **2**, and the one-electron oxidation potential of *meso*–*meso*-linked Zn^{II}-diporphyrin **13** (0.54 V) is decreased to 0.11 V in **4** and thus the potential shift is larger in the Zn^{II} complex.

In light of the extremely strong electronic interactions, which are evidenced from the low one-electron oxidation potentials and the red-shifted intense absorption bands, the triply linked porphyrin arrays must be very promising for use as a component of an electronic molecular wire. Extension of this synthetic strategy to higher oligomeric and polymeric porphyrin arrays is a fascinating next project that is actively in progress in our laboratory. The electronic interaction in the triply-linked diporphyrins depends on the central metal and thus the incorporation of a variety of metals into this diporphyrin ligand is also an interesting project.

Experimental Section

A 50-mL round-bottomed flask was charged with a suspension of **6** (16 mg, 10 μmol) in C_6F_6 (20 mL). The reaction vessel was covered with foil and then BAHA (18 mg, 22 μmol) added in one portion. After the mixture had been stirred for 2 d at room temperature, the mixture was diluted with methanol and THF. The solvent was removed on a rotary evaporator and the residue was precipitated by treatment with benzene/methanol. The product was finally separated by flash chromatography on silica gel (Wakogel C-400). Elution with hexane/CH_2Cl_2 (95/5) gave recovered **6** (2 mg, 13 %) as the first fraction, monochlorinated **8** (1.0 mg, 6 %) as the second fraction, and **7** (12.2 mg, 76 %) as the third fraction. The triply linked Cu^{II}-diporphyrin **7** was transformed into the corresponding Zn^{II}-diporphyrin **9** in 80 % by demetalation with a mixture of conc. H_2SO_4 and TFA and the subsequent insertion of the Zn^{II} ions.

7: MALDI-TOF MS: m/z: 1645, calcd for $C_{108}H_{106}N_8Cu_2$: 1641; UV/Vis ($CHCl_3$): $\lambda_{max} = 411$ (Soret), 575 (Soret), and 994 nm.

9: ^{1}H NMR ($CDCl_3$): $\delta = {}^1$H NMR ($CDCl_3$) 1.45 (s, 72 H, *t*Bu), 7.35 (s, 4 H, Por-β), 7.56 (d, $J = 4.9$ Hz, 4 H, Por-β), 7.62 (t, $J = 1.8$ Hz, 4 H, Ar-H), 7.66 (d, $J = 1.8$ Hz, 8 H, Ar-H), 7.69 (s, $J = 1.8$ Hz, 10 H, Ar-H), and 7.80 (d, $J = 4.9$ Hz, 4 H, Por-β); MALDI-TOF MS: m/z: 1646, calcd for $C_{108}H_{106}N_8Zn_2$: 1643; UV/Vis ($CHCl_3$): $\lambda_{max} = 418$ (Soret), 581 (Soret), and 1068 nm.

Received: February 22, 2000 [Z 14751]

[1] A. Osuka, H. Shimidzu, *Angew. Chem.* **1997**, *111*, 140; *Angew. Chem. Int. Ed. Engl.* **1997**, *36*, 135; T. Ogawa, Y. Nishimoto, N. Yoshida, N. Ono, A. Osuka, *Chem. Commun.* **1998**, 337.

[2] N. Aratani, A. Osuka, Y. H. Kim, D. H. Jeong, D. Kim, *Angew. Chem.* **2000**, *112*, 1517; *Angew. Chem. Int. Ed.* **2000**, *39*, 1458.

[3] T. Ogawa, Y. Nishimoto, N. Yoshida, N. Ono, A. Osuka, *Angew. Chem.* **1999**, *111*, 140; *Angew. Chem. Int. Ed.* **1999**, *38*, 176.

[4] A. Tsuda, A. Nakano, H. Furuta, H. Yamochi, A. Osuka, *Angew. Chem.* **2000**, *112*, 572; *Angew. Chem. Int. Ed.* **2000**, *39*, 558. The analogous doubly *meso*–β-linked diporphyrin was also formed in the reaction of 5,15-diarylporphyrin with $TeCl_4$: K. Sugiura, T. Matsumoto, S. Ohkouchi, Y. Naitoh, T. Kawai, Y. Takai, K. Ushiroda, Y. Sakata, *Chem. Commun.* **1999**, 1957.

[5] M. J. Crossley, P. L. Burn, *Chem. Commun.* **1987**, 39; M. J. Crossley, P. L. Burn, *Chem. Commun.* **1991**, 1569; M. J. Crossley, L. J. Govenlock, J. K. Prasker, *Chem. Commun.* **1995**, 2379.

[6] N. Kobayashi, M. Numao, R. Kondo, S. Nakajima, T. Osa, *Inorg. Chem.* **1991**, *30*, 2241; L. Jaquinod, O. Siri, R. G. Khoury, K. M. Smith, *Chem. Commun.* **1998**, 1261; M. G. H. Vicente, M. T. Cancilla, C. B. Lebrilla, K. M. Smith, *Chem. Commun.* **1998**, 2355; M. Graca, H. Vicente, L. Jaquinod, K. M. Smith, *Chem. Commun.* **1999**, 1771.

[7] H. L. Anderson, *Chem. Commun.* **1999**, 2322.

[8] The structure of the metal-free diporphyrin **5** (m/z: 1778, calcd for $C_{124}H_{141}N_8$: 1777) including the chlorination site was confirmed by preliminary X-ray crystallography data (see the Supporting Information).

[9] The dichlorinated diporphyrin has been identified as a single product with a parent peak at m/z: 1936 (calcd for $C_{124}H_{136}Cl_2Cu_2N_8$: 1933) in the MALDI-TOF mass spectrum and an absorption spectrum ($\lambda_{max} =$ 408, 571, and 987 nm) similar to those of **2** and **3**, but the secondary chlorination site has not been determined yet.

[10] Data for the crystal structure of $\mathbf{7} \cdot 2C_6H_6$: $C_{120}H_{118}Cu_2N_8$, $M_r = 1796$, crystal obtained from C_6H_6/C_2H_5OH, crystal dimensions $0.3 \times 0.3 \times 0.1$ mm^3, space group $C2/c$, $a = 44.268(2)$, $b = 17.791(6)$, $c =$ 17.326(5) Å, $\alpha = 90$, $\beta = 98.365(2)$, $\gamma = 90°$, $V = 13500$ Å^3. $Z = 6$, $\rho_{calcd} = 1.21$ g cm^{-3}, $\mu_{Mo} = 5.26$ cm^{-1}, $\theta_{max} = 27.5°$, 15223 measured reflections, $R_1 = 0.096$ for 3555 data [$I > 3\sigma(I)$], $wR_2 = 0.137$ for all measured data. Diffraction data were collected on a RIGAKU-RAXIS imaging plate system diffractometer (296 K, $Mo_{K\alpha}$ radiation $\lambda = 0.7107$ Å). The structures were solved by direct methods and refined by F^2 with all observed reflections. All non-hydrogen atoms were refined anisotropically, and hydrogen atoms were added to calculated positions. The structure was solved using the SIR92 Program and refined by teXane for Windows.

[11] M. Nishio, M. Hirota, *Tetrahedron* **1989**, *45*, 7201; B. Aurivillius, R. E. Carter, *J. Chem. Soc. Perkin 2* **1978**, 1033.

[12] K. Sugiura, K. Ushida, T. Tanaka, M. Sawada, Y. Sakata, *Chem. Lett.* **1997**, 927.

[13] Data for the crystal structure of $\mathbf{9} \cdot C_6H_6 \cdot 2C_2H_6O$: $C_{118}H_{124}N_8O_2Zn_2$, $M_r = 1817$, crystal obtained from C_6H_6/C_2H_5OH, crystal dimensions $0.3 \times 0.2 \times 0.1$ mm^3, space group $P\bar{1}$, $a = 17.428(7)$, $b = 20.324(2)$, $c =$

8.566(2) Å, $\alpha = 91.696(2)$, $\beta = 96.988(4)$, $\gamma = 99.278(4)^\circ$, $V = 2968$ Å^3, $Z = 1$, $\rho_{calcd} = 1.02$ g cm^{-3}, $\mu_{Mo} = 4.51$ cm^{-1}, $\theta_{max} = 27.5^\circ$, 11695 measured reflections, $R_1 = 0.098$ for 4134 data [$I > 3\sigma(I)$], $wR_2 = 0.119$ for all measured data.

[14] N. Yoshida, N. Aratani, A. Osuka, *Chem. Commun.* **2000**, 197.

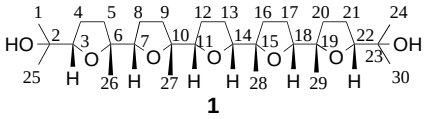
[15] T. X. Lü, J. R. Reimers, M. J. Crossley, N. S. Hush, *J. Phys. Chem.* **1994**, *98*, 11878; J. R. Reimers, T. X. Lü, M. J. Crossley, N. S. Hush, *Chem. Phys. Lett.* **1996**, *256*, 353; N. S. Hush, J. R. Reimers, L. E. Hall, L. A. Johnston, M. J. Crossley, *Ann. N.Y. Acad. Sci.* **1998**, *852*, 1; J. R. Reimers, L. E. Hall, M. J. Crossley, N. S. Hush, *J. Phys. Chem.* **1999**, *103*, 4385.

[16] Redox potentials versus $AgClO_4$/Ag were measured by cyclic voltammetry in $CHCl_3$.

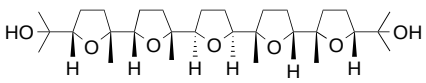
What Is the Structure of Glabrescol? Stereoselective Synthesis of Reported Glabrescol**

Hideaki Hioki, Chie Kanehara, Yumiko Ohnishi, Yukiko Umemori, Hitoshi Sakai, Suzuyo Yoshio, Masayuki Matsushita, and Mitsuaki Kodama*

Glabrescol is a triterpene isolated as a minor constituent of the branches and trunk of *Spathelia glabrescens*. Based on extensive NMR spectra analysis, as well as the symmetrical nature of the molecule, Jacobs et al. proposed a *meso*-type structure **1** containing five continuously linked tetrahydrofuran rings.[1] The novel structural features prompted us to attempt the synthesis of glabrescol.[2, 3] Furthermore, we expected that the synthesis would make it possible to examine the biological activity, including the ionophore-like character which has not yet been reported on. Herein, we describe the stereoselective synthesis of **1** and one of its diastereomers **2**,



1



2

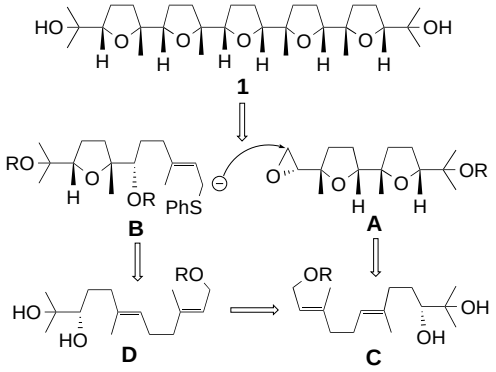
[*] Prof. Dr. M. Kodama, Dr. H. Hioki, C. Kanehara, Y. Ohnishi, Y. Umemori, Dr. H. Sakai, S. Yoshio, Dr. M. Matsushita
Faculty of Pharmaceutical Sciences
Tokushima Bunri University
Yamashiro-cho, Tokushima 770-8514 (Japan)
Fax: (+81) 88-655-3051
E-mail: kodama@ph.bunri-u.ac.jp

[**] We thank Professor Jacobs, University of the West Indies, for the NMR spectra of natural glabrescol. This work was supported by a Grant-in-Aid for Scientific Research (No. 11672132) from the Ministry of Education, Science, Sports, and Culture of Japan.

Supporting information for this article is available on the WWW under http://www.wiley-vch.de/home/angewandte/ or from the author.

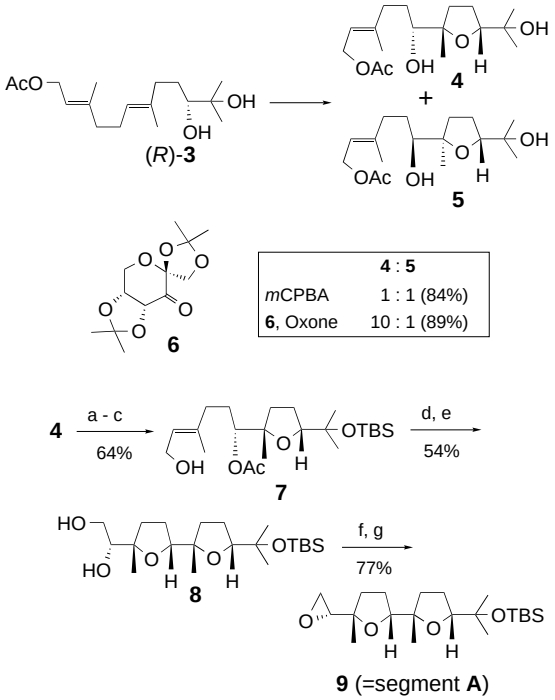
using a baker's yeast reduction as the chirality induction method.[4] Comparison of NMR spectra, however, revealed that neither compound was identical to the natural product.

The retrosynthetic analysis for **1** is illustrated in Scheme 1. Thus, compound **1** is constructed by coupling the 15-carbon segments **A** and **B**, followed by stereoselective oxygenation and tetrahydrofuran (THF) ring formation. Segments **A** and **B** can be prepared from the common (*R*)-diol **C**, obtained by baker's yeast reduction, through asymmetric oxidation.



Scheme 1. Retrosynthetic analysis of the reported glabrescol (**1**).

Segment **A** was synthesized according to Scheme 2. (*R*)-**3**[5] was first treated with *m*CPBA to yield diastereomeric THF derivatives **4** and **5** in a 1:1 ratio.[6] When the same transformation was performed using the epoxidation mediated by

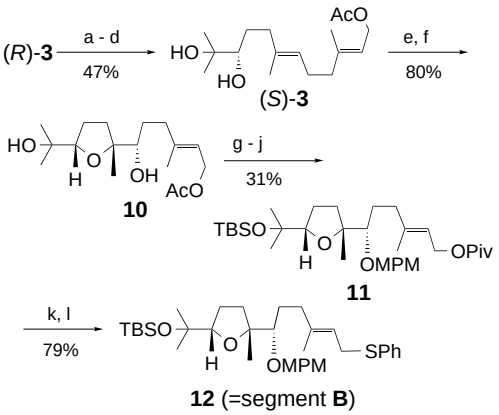


9 (=segment **A**)

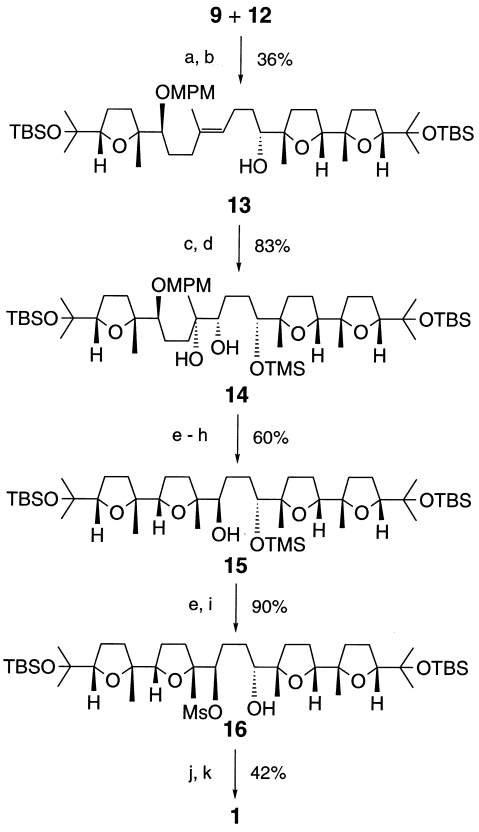
Scheme 2. Synthesis of segment **A**. a) Ac_2O, Et_3N, DMAP; b) TBSOTf, 2,6-lutidine; c) LiOH, MeOH; d) Ti(O*i*Pr)$_4$, (−)-DET, *t*BuOOH, 4 Å molecular sieves; e) 1M NaOH, MeOH; f) TsCl, Et_3N, DMAP; g) K_2CO_3, MeOH. *m*CPBA = *meta*-chloroperoxybenzoic acid, DMAP = 4-dimethylaminopyridine, TBS = *tert*-butyldimethylsilyl, Tf = triflate = trifluoromethanesulfonyl, (−)-DET = (−)-diethyl tartrate, Ts = tosyl = toluene-4-sulfonyl.

ketone (**6**), developed by Shi,[7] the ratio was increased to 10:1, favoring the desired *cis* derivative **4**. After protection of the two hydroxyl groups in **4** with acetyl and TBS groups, the terminal acetate was selectively hydrolyzed. The resulting allylic alcohol **7** was subjected to asymmetric epoxidation using (−)-DET.[8] Hydrolysis of the acetyl group in the product caused a concomitant THF ring formation to afford diol **8** as the major product (87.5% *de*). Conversion of the diol in **8** to an epoxide completed the synthesis of segment **A** (**9**).[9]

For the synthesis of segment **B**, (*R*)-**3** was first converted into (*S*)-**3** in 4 steps through an epoxide, as shown in Scheme 3. Epoxidation of (*S*)-**3** using *ent*-**6** as the chiral



Scheme 3. Synthesis of segment **B**. a) MsCl, pyridine; b) K_2CO_3, MeOH; c) Ac_2O, pyridine; d) $HClO_4$, aq. THF; e) *ent*-**6**, oxone; f) SiO_2; g) 1M NaOH, MeOH; h) PivCl, pyridine; i) MPMCl, NaH, DMF; j) TBSOTf; k) DIBAH; l) PhSSPh, Bu_3P. Ms = mesyl = methanesulfonyl, Piv = pivaloyl, MPM = *para*-methoxyphenylmethyl, DIBAH = diisobutylaluminum hydride.



Scheme 4. Completion of the synthesis of reported glabrescol (**1**). a) *n*BuLi, DABCO, THF; b) Na, *n*BuOH; c) TMSCl, imidazole; d) AD-mix-α; e) MsCl, Et_3N; f) K_2CO_3; g) DDQ; h) SiO_2; i) 1.2M HCl; j) NaH; k) nBu_4NF. DABCO = 1,4-diazabicyclo[2.2.2]octane, TMS = trimethylsilyl, DDQ = 2,3-dichloro-5,6-dicyano-1,4-benzoquinone.

catalyst,[7] followed by treatment with SiO_2, yielded the THF derivative **10** in almost the same diastereomeric selectivity as with (*R*)-**3**. The acetyl group was then changed into a pivaloyl group and the two hydroxyl groups were protected as the *p*-methoxybenzyl and TBS ethers. Finally, the pivaloyl group was reductively removed and the resulting hydroxyl group was converted into a sulfide moiety using Hata's procedure[10] to produce segment **B** (**12**).[11]

The two segments were then coupled together (Scheme 4). Reaction of the lithium anion of **12** with the epoxide **9** in the presence of DABCO ($-78 \rightarrow 0\,^{\circ}C$) afforded the desired coupling product in a rather low yield, due to the instability of **12** under the coupling conditions; the coupling product was then desulfurized with Na and *n*BuOH to give the alcohol **13**. Protection of the hydroxyl group in **13** as the TMS ether and oxidation of the double bond with AD-mix-α afforded the diol **14** in 83% yield.[12, 13] The diol in **14** was converted to an epoxide through the mesylate derivative and the MPM group was removed. Treatment of the product with SiO_2 resulted in the formation of a fourth THF ring yielding the alcohol **15**. The hydroxyl group in **15** was mesylated and the TMS group was removed to produce **16**, which was treated with NaH to yield the compound with five THF rings. Although THF ring formation is generally easily accessed, the yield of the product was unexpectedly low because of the formation of substantial amounts of the elimination product. Finally, the TBS groups were removed to achieve complete synthesis of **1**.

The ^1H and ^{13}C NMR spectra of synthetic compound **1** were compared to those of the natural glabrescol. The chemical shifts and splitting patterns were very similar to each other in the ^1H NMR spectrum, but there was a large difference in the chemical shift of the signal assigned to H-11(14) (shown in bold figures in Table 1).[14] In the ^{13}C NMR spectrum, a large difference was observed in the chemical shifts of C-10(15), C-11(14), and C-12(13). Therefore, it was concluded that the structure of glabrescol is not **1**. As the differences in the NMR spectra suggested that the stereochemistry around the central part is incorrect, we attempted the synthesis of diastereomer **2** as the possible structure of the natural product. The synthetic route was almost the same as for the synthesis of **1** (Scheme 5). Comparison of the ^1H and ^{13}C NMR spectra revealed that **2** was also not identical to natural glabrescol. The difference in the chemical shifts in the signals for **2** was even larger than in the case of **1**.

In summary, we have achieved the stereoselective synthesis of two *meso* compounds corresponding to glabrescol. Neither of them, however, were identical to the natural product and the correct structure of glabrescol remains to be clarified.

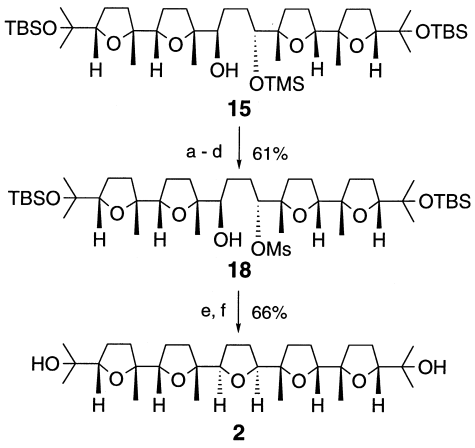
Received: February 1, 2000 [Z14632]

 © WILEY-VCH Verlag GmbH, D-69451 Weinheim, 2000 1433-7851/00/3914-2553 $ 17.50+.50/0

Table 1. Comparison of ^{1}H and ^{13}C NMR chemical shifts of natural and synthetic compounds.[a]

Compound	NMR nucleus	Chemical shift[b] at positions: 1, 30	2, 23	3, 22	4, 21	5, 20	6, 19	7, 18	8, 17	9, 16	10, 15	11, 14	12, 13	24, 25	26, 29	27, 28
natural glabrescol	^{1}H	1.05		3.79	1.80 2.08	1.39 2.23		3.97	1.48 1.72	1.53 1.96		**3.83**	1.60 1.92	1.27	1.09	1.11
	^{13}C	25.38	71.57	85.74	26.62	31.14	85.60	84.17	29.01	34.75	**85.27**	**85.01**	**28.23**	28.28	25.16	22.11
1	^{1}H	1.05		3.78	1.80 2.06	1.37 2.22		3.97	1.46 1.69	1.51 2.02		**3.70**	1.54 1.80	1.28	1.09	1.10
	^{13}C	25.26	71.57	85.59	26.48	30.88	85.49	84.20	28.98	34.52	**84.48**	**83.93**	**27.01**	28.11	24.98	22.48
2	^{1}H	1.04		3.79	1.80 2.05	1.38 2.17		3.96	1.42 1.73	1.49 2.01		3.63	1.61 1.79	1.27	1.10	1.20
	^{13}C	25.29	71.50	85.62	26.51	31.02	85.24	83.52	29.11	33.72	83.54	84.22	26.13	28.04	25.06	24.34

[a] NMR spectra were measured in $CDCl_3$:C_6D_6 (7:3). [b] Chemical shifts quoted in ppm.



Scheme 5. Synthesis of **2**. a) Ac_2O, Et_3N; b) HCl; c) MsCl, Et_3N; d) DIBAH; e) NaH; f) *n*-Bu_4NF.

[1] W. W. Harding, P. A. Lewis, H. Jacobs, S. McLean, W. F. Reynolds, L.-L. Tay, J.-P. Yang, *Tetrahedron Lett*. **1995**, *36*, 9137.

[2] For the synthetic studies of glabrescol, see: Y. Morimoto, T. Iwai, T. Yoshimura, T. Kinoshita, *Bioorg. Med. Chem. Lett*. **1998**, *8*, 2005.

[3] For the stereoselective synthesis of *trans-threo*-penta(tetrahydrofuran), see: a) U. Koert, M. Stein, K. Harms, *Angew. Chem.* **1994**, *106*, 1238; *Angew. Chem. Int. Ed. Engl.* **1994**, *33*, 1180; b) U. Koert, M. Stein, H. Wagner, *Chem. Eur. J.* **1997**, *3*, 1170.

[4] For our examples of natural product synthesis using baker's yeast reduction, see: a) M. Kodama, S. Yoshio, T. Tabata, Y. Deguchi, Y. Sekiya, Y. Fukuyama, *Tetrahedron Lett*. **1997**, *38*, 4627; b) H. Hioki, H. Ooi, Y. Mimura, S. Yoshio, M. Kodama, *Synlett* **1998**, 729.

[5] M. Kodama, H. Minami, Y. Mima, Y. Fukuyama, *Tetrahedron Lett*. **1990**, *31*, 4025. The optical purity was determined to be 98% *ee* by liquid chromatographic analysis using a chiral column.

[6] The stereochemistry of **4** and **5** was determined by a modified Mosher's method. See Ref. [4a].

[7] Z.-X. Wang, Y. Tu, M. Frohn, J.-R. Zhang, Y. Shi, *J. Am. Chem. Soc*. **1997**, *119*, 11 224.

[8] The stereochemistry of the Sharpless asymmetric epoxidation has been unambiguously established. See: a) M. G. Finn, K. B. Sharpless, *Asymmetric Synthesis* (Ed.: J. D. Morrison), Academic Press, New York, **1985**, Chap. 8, p. 247; b) T. Katsuki, V. S. Martin, *Org. React*. **1996**, *48*, 1.

[9] Compound **9**: $[\alpha]_D^{19}$ +7.69 ($c = 1.09$, $CHCl_3$); ^{1}H NMR: $\delta = 0.07$ (3H, s), 0.08 (3H, s), 0.85 (9H, s), 1.16 (3H, s), 1.18 (3H, s), 1.18 (3H, s), 1.19 (3H, s), 1.53–1.66 (2H, m), 1.79–1.97 (6H, m), 2.69–2.74 (2H, m), 3.03 (1H, dd, $J = 3.9$, 3.0 Hz), 3.71 (1H, dd, $J = 7.2$, 7.2 Hz), 3.92 (1H, dd, $J = 7.0$, 7.0 Hz).

[10] I. Nagawa, T. Hata, *Tetrahedron Lett*. **1975**, 1409.

[11] Compound **12**: $[\alpha]_D^{25.5}$ −4.19 ($c = 1.8$, $CHCl_3$); ^{1}H NMR: $\delta = 0.08$ (6H, s), 0.86 (9H, s), 1.12 (3H, s), 1.14 (3H, s), 1.22(3H, s), 1.57 (3H, br.s), 1.20–2.40 (8H, m), 3.21 (1H, dd, $J = 8.8$, 2.5 Hz), 3.54 (2H, d, $J = 7.4$ Hz), 3.74 (1H, t, $J = 7.0$ Hz), 3.80 (3H, s), 4.47 (1H, d, $J = 11.0$ Hz), 4.59 (1H, d, $J = 11.0$ Hz), 5.31 (1H, br.t, $J = 7.7$ Hz), 6.86 (2H, d, $J = 8.8$ Hz), 7.16–7.36 (7H, m).

[12] The stereochemistry of diol **14** was based on the empirical rule. See: a) K. B. Sharpless, W. Amberg, Y. L. Bennani, G. A. Crispino, J. Hartung, K.-S. Jeong, H.-L. Kwong, K. Morikawa, Z.-M. Wang, D. Xu, X.-L. Zhang, *J. Org. Chem*. **1992**, *57*, 2768; b) H. Becker, S. B. King, M. Taniguchi, K. P. M. Vanhessche, K. B. Sharpless, *J. Org. Chem*. **1995**, *60*, 3940.

[13] The AD-mix-α oxidation afforded **14** and its diastereomer in the ratio of 5.2:1.

[14] No difference was observed in ^{1}H and ^{13}C NMR spectra of **1** when they were recorded at the lower concentration.

Beneficial Effect of *ortho*-Methoxy Groups in the Asymmetric Ring Opening of *meso* Epoxides with Silicon Tetrachloride Catalyzed by Chiral *ortho*-Methoxyphenyldiazaphosphonamide Lewis Bases**

Jean Michel Brunel, Olivier Legrand, Sébastien Reymond, and Gérard Buono*

The asymmetrization of suitable *meso* compounds is an attractive approach to the synthesis of complex molecules and often greatly simplifies their preparation.[1] Numerous procedures to effect asymmetrization have been developed, including the deprotonation,[2] protonation,[3] esterification,[4] hydrolysis,[5] and ring cleavage of *meso* carboxylic anhydrides.[6]

[*] Prof. G. Buono, Dr. J. M. Brunel, O. Legrand, S. Reymond
UMR CNRS 6516, Faculté de St Jérôme
ENSSPICAM, Avenue Escadrille Normandie Niemen
13397 Marseille, Cedex 20 (France)
Fax: (+33) 4-91-02-77-76
E-mail: buono@spi-chim.u-3mrs.fr

[**] We thank the CNRS for financial support. O.L. acknowledges the CNRS and Region PACA for a doctoral fellowship. We thank Dr. M. Giorgi and Prof. M. Pierrot for their kind assistance with the X-ray analysis of compound **1** and Dr. A. Tenaglia for fruitful discussions.

Supporting information for this article is available on the WWW under http://www.wiley-vch.de/home/angewandte/ or from the author.

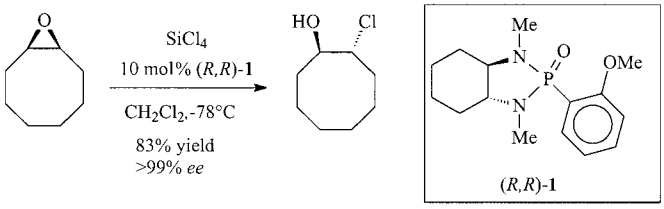
 © WILEY-VCH Verlag GmbH, D-69451 Weinheim, 2000 1433-7851/00/3914-2554 $ 17.50+.50/0

WITHDRAWAL

On the Beneficial Effect of *ortho*-Methoxy Groups in the Asymmetric Ring Opening of *meso* Epoxides with Silicon Tetrachloride Catalyzed by Chiral *ortho*-Methoxyphenyldiazaphosphonamide Lewis Bases**

Gérard Buono*

We published in this journal a communication on the enantioselective opening of *meso* epoxides with silicon tetrachloride in the presence of a catalytic amount of chiral phosphonamides.[1] In that paper we reported the asymmetric ring opening of cyclooctene oxide with $SiCl_4$ in the presence of 10 mol% of chiral phophonamide base (*R*,*R*)-**1** as a catalyst (Scheme 1).



Scheme 1.

For this reaction, we described up to 83% yield and enantiomeric excess higher than 99%. This spectacular result attracted the attention of Professor Scott E. Denmark, who pioneered this research field,[2] because it was found that cyclooctene oxide is one of the slowest acting epoxides in this catalytic system and produced the racemic chlorohydrin. However, Denmark et al. did not succeed in reproducing the results we disclosed and submitted a rebuttal to our paper.[3] We were then contacted by the Editor and Prof. Denmark and prompted to elucidate the origin of such a striking discrepancy. At this stage, I asked my co-workers[4] to check the experimental procedures and analytical conditions and to try to reproduce the described results. I was provided with experimental data and material that fully confirmed our original claims. On the basis of these results we sent a first answer to the rebuttal published in *Angewandte Chemie*, an answer that could not explain why our observation differed from Prof. Denmark's. One month later, we received a letter from the Editor who required further complementary analytical data and information. When I had these new data from my co-workers in hand, I noticed several inconsistencies with the analytical material they had previously provided. Therefore, I decided to reproduce *personally* and *independently* the whole experimental procedures from the very beginning. I was unable to observe the opening of cyclooctene oxide under the described conditions and to reproduce the analytical data (for example, NMR, retention times in chiral GPC and HPLC analyses) provided by my co-workers. Instead, I obtained results similar to those reported by Denmark et al. in their rebuttal.[3] A cross-check undertaken by several colleagues led to identical results. To date, my co-workers[4] have been unable to provide an appropriate scientific rationale for the non-reproducibility of the former results and analyses. Under these circumstances, although our communication presented several other *meso* epoxide openings with fair to high enantioselectivities, which require experimental verification, I wish to withdraw that communication.[1] Other pieces of work based on related experimental results that were published elsewhere will also be withdrawn.[5, 6]

[*] Prof. Dr. G. Buono
UMR CNRS 6516, Faculté de St Jérôme
ENSSPICAM, Avenue Escadrille Normandie Niemen
13397 Marseille, Cedex 20 (France)
Fax: (+33) 4-91-02-77-76
E-mail: buono@spi-chim.u-3mrs.fr

[**] A Response to the correspondence by Professor Scott E. Denmark et al.[3]

[1] J. M. Brunel, O. Legrand, S. Reymond, G. Buono, *Angew. Chem.* **2000**, *112*, 2654; *Angew. Chem. Int. Ed.* **2000**, *39*, 2554.
[2] S. E. Denmark, P. A. Barsanti, K.-T. Wong, R. A. Stavenger, *J. Org. Chem.* **1998**, *63*, 2428.
[3] S. E. Denmark, T. Wynn, B. G. Jellerichs, *Angew. Chem.* **2001**, *113*, 2315; *Angew. Chem. Int. Ed.* **2001**, *40*, 2255.
[4] Except O.L. who left my group in July 1999.
[5] S. Reymond, J. M. Brunel, G. Buono, *Tetrahedron: Asymmetry* **2000**, *11*, 4441.
[6] S. Reymond, O. Legrand, J. M. Brunel, G. Buono, *Eur. J. Org. Chem.* **2001**, 2819.

APOLOGY

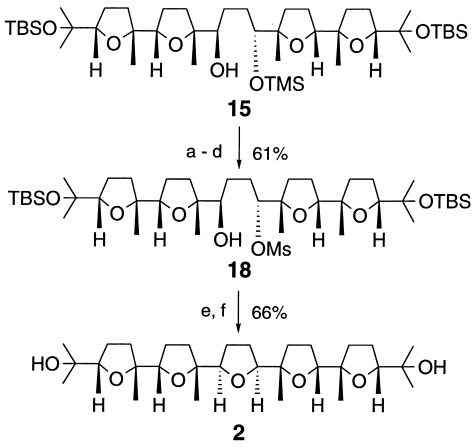
In the Communication "A Lewis Acid Catalyst Anchored on Silica Grafted with Quaternary Alkylammonium Chloride Moieties" by **M. V. Landau et al**. the authors made no reference to their thematically related communication "A comparative study of an MCM-41 anchored quaternary ammonium chloride/$SnCl_4$ catalyst and its silica gel analogue" (T. M. Jyothi, M. L. Kaliya, M. Herskowitz, M. V. Landau, *Chem. Commun.* **2001**, 992–993) and vice versa, even though both manuscripts were submitted to their respective journals at the same time. The authors apologize for this oversight.

 © WILEY-VCH Verlag GmbH, D-69451 Weinheim, 2001 1433-7851/01/4024-4536 $ 17.50+.50/0

Table 1. Comparison of ^{1}H and ^{13}C NMR chemical shifts of natural and synthetic compounds.[a]

Compound	NMR nucleus	Chemical shift[b] at positions: 1, 30	2, 23	3, 22	4, 21	5, 20	6, 19	7, 18	8, 17	9, 16	10, 15	11, 14	12, 13	24, 25	26, 29	27, 28
natural glabrescol	^{1}H	1.05		3.79	1.80 2.08	1.39 2.23		3.97	1.48 1.72	1.53 1.96		**3.83**	1.60 1.92	1.27	1.09	1.11
	^{13}C	25.38	71.57	85.74	26.62	31.14	85.60	84.17	29.01	34.75	**85.27**	**85.01**	**28.23**	28.28	25.16	22.11
1	^{1}H	1.05		3.78	1.80 2.06	1.37 2.22		3.97	1.46 1.69	1.51 2.02		**3.70**	1.54 1.80	1.28	1.09	1.10
	^{13}C	25.26	71.57	85.59	26.48	30.88	85.49	84.20	28.98	34.52	**84.48**	**83.93**	**27.01**	28.11	24.98	22.48
2	^{1}H	1.04		3.79	1.80 2.05	1.38 2.17		3.96	1.42 1.73	1.49 2.01		3.63	1.61 1.79	1.27	1.10	1.20
	^{13}C	25.29	71.50	85.62	26.51	31.02	85.24	83.52	29.11	33.72	83.54	84.22	26.13	28.04	25.06	24.34

[a] NMR spectra were measured in $CDCl_3$:C_6D_6 (7:3). [b] Chemical shifts quoted in ppm.



Scheme 5. Synthesis of **2**. a) Ac_2O, Et_3N; b) HCl; c) MsCl, Et_3N; d) DIBAH; e) NaH; f) *n*-Bu_4NF.

[1] W. W. Harding, P. A. Lewis, H. Jacobs, S. McLean, W. F. Reynolds, L.-L. Tay, J.-P. Yang, *Tetrahedron Lett*. **1995**, *36*, 9137.

[2] For the synthetic studies of glabrescol, see: Y. Morimoto, T. Iwai, T. Yoshimura, T. Kinoshita, *Bioorg. Med. Chem. Lett*. **1998**, *8*, 2005.

[3] For the stereoselective synthesis of *trans-threo*-penta(tetrahydrofuran), see: a) U. Koert, M. Stein, K. Harms, *Angew. Chem.* **1994**, *106*, 1238; *Angew. Chem. Int. Ed. Engl.* **1994**, *33*, 1180; b) U. Koert, M. Stein, H. Wagner, *Chem. Eur. J.* **1997**, *3*, 1170.

[4] For our examples of natural product synthesis using baker's yeast reduction, see: a) M. Kodama, S. Yoshio, T. Tabata, Y. Deguchi, Y. Sekiya, Y. Fukuyama, *Tetrahedron Lett*. **1997**, *38*, 4627; b) H. Hioki, H. Ooi, Y. Mimura, S. Yoshio, M. Kodama, *Synlett* **1998**, 729.

[5] M. Kodama, H. Minami, Y. Mima, Y. Fukuyama, *Tetrahedron Lett*. **1990**, *31*, 4025. The optical purity was determined to be 98% *ee* by liquid chromatographic analysis using a chiral column.

[6] The stereochemistry of **4** and **5** was determined by a modified Mosher's method. See Ref. [4a].

[7] Z.-X. Wang, Y. Tu, M. Frohn, J.-R. Zhang, Y. Shi, *J. Am. Chem. Soc*. **1997**, *119*, 11 224.

[8] The stereochemistry of the Sharpless asymmetric epoxidation has been unambiguously established. See: a) M. G. Finn, K. B. Sharpless, *Asymmetric Synthesis* (Ed.: J. D. Morrison), Academic Press, New York, **1985**, Chap. 8, p. 247; b) T. Katsuki, V. S. Martin, *Org. React*. **1996**, *48*, 1.

[9] Compound **9**: $[\alpha]_D^{19}$ +7.69 ($c = 1.09$, $CHCl_3$); ^{1}H NMR: $\delta = 0.07$ (3H, s), 0.08 (3H, s), 0.85 (9H, s), 1.16 (3H, s), 1.18 (3H, s), 1.18 (3H, s), 1.19 (3H, s), 1.53–1.66 (2H, m), 1.79–1.97 (6H, m), 2.69–2.74 (2H, m), 3.03 (1H, dd, $J = 3.9$, 3.0 Hz), 3.71 (1H, dd, $J = 7.2$, 7.2 Hz), 3.92 (1H, dd, $J = 7.0$, 7.0 Hz).

[10] I. Nagawa, T. Hata, *Tetrahedron Lett*. **1975**, 1409.

[11] Compound **12**: $[\alpha]_D^{25.5}$ −4.19 ($c = 1.8$, $CHCl_3$); ^{1}H NMR: $\delta = 0.08$ (6H, s), 0.86 (9H, s), 1.12 (3H, s), 1.14 (3H, s), 1.22(3H, s), 1.57 (3H, br.s), 1.20–2.40 (8H, m), 3.21 (1H, dd, $J = 8.8$, 2.5 Hz), 3.54 (2H, d, $J = 7.4$ Hz), 3.74 (1H, t, $J = 7.0$ Hz), 3.80 (3H, s), 4.47 (1H, d, $J = 11.0$ Hz), 4.59 (1H, d, $J = 11.0$ Hz), 5.31 (1H, br.t, $J = 7.7$ Hz), 6.86 (2H, d, $J = 8.8$ Hz), 7.16–7.36 (7H, m).

[12] The stereochemistry of diol **14** was based on the empirical rule. See: a) K. B. Sharpless, W. Amberg, Y. L. Bennani, G. A. Crispino, J. Hartung, K.-S. Jeong, H.-L. Kwong, K. Morikawa, Z.-M. Wang, D. Xu, X.-L. Zhang, *J. Org. Chem*. **1992**, *57*, 2768; b) H. Becker, S. B. King, M. Taniguchi, K. P. M. Vanhessche, K. B. Sharpless, *J. Org. Chem*. **1995**, *60*, 3940.

[13] The AD-mix-α oxidation afforded **14** and its diastereomer in the ratio of 5.2:1.

[14] No difference was observed in ^{1}H and ^{13}C NMR spectra of **1** when they were recorded at the lower concentration.

Beneficial Effect of *ortho*-Methoxy Groups in the Asymmetric Ring Opening of *meso* Epoxides with Silicon Tetrachloride Catalyzed by Chiral *ortho*-Methoxyphenyldiazaphosphonamide Lewis Bases**

Jean Michel Brunel, Olivier Legrand, Sébastien Reymond, and Gérard Buono*

The asymmetrization of suitable *meso* compounds is an attractive approach to the synthesis of complex molecules and often greatly simplifies their preparation.[1] Numerous procedures to effect asymmetrization have been developed, including the deprotonation,[2] protonation,[3] esterification,[4] hydrolysis,[5] and ring cleavage of *meso* carboxylic anhydrides.[6]

[*] Prof. G. Buono, Dr. J. M. Brunel, O. Legrand, S. Reymond
UMR CNRS 6516, Faculté de St Jérôme
ENSSPICAM, Avenue Escadrille Normandie Niemen
13397 Marseille, Cedex 20 (France)
Fax: (+33) 4-91-02-77-76
E-mail: buono@spi-chim.u-3mrs.fr

[**] We thank the CNRS for financial support. O.L. acknowledges the CNRS and Region PACA for a doctoral fellowship. We thank Dr. M. Giorgi and Prof. M. Pierrot for their kind assistance with the X-ray analysis of compound **1** and Dr. A. Tenaglia for fruitful discussions.

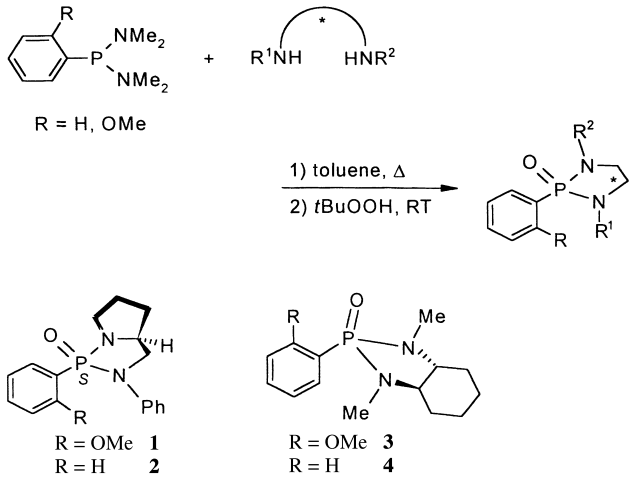
Supporting information for this article is available on the WWW under http://www.wiley-vch.de/home/angewandte/ or from the author.

 © WILEY-VCH Verlag GmbH, D-69451 Weinheim, 2000 1433-7851/00/3914-2554 $ 17.50+.50/0

Epoxides are valuable intermediates for the stereocontrolled preparation of organic compounds.[7] Thus, the desymmetrization of *meso* epoxides by enantioselective addition of nucleophiles appears to be an efficient strategy for asymmetric synthesis since it establishes two contiguous stereogenic centers.[8] In this area, halide ions have been extensively applied in the ring opening of epoxides.[9] Nevertheless, no highly efficient, catalytic methods affording enantiomerically enriched chlorohydrins have been reported. Only chiral organophosphorus Lewis bases coordinated to and thereby activating silylated nucleophiles have been introduced by Denmark et al. as catalysts in this field; these led to the formation of optically active chlorohydrins in moderate enantiomeric excess (*ee*).[10]

Recently, we have described the synthesis of new chiral *ortho*-hydroxyaryl phosphine oxides[11] and their application as chiral Lewis bases[12] in various asymmetric catalytic systems. In the context of our studies on nonorganometallic phosphorus reagents in enantioselective catalysis,[13] we report in this paper the highly efficient use of *ortho*-methoxyphenyldiazaphosphonamides in the catalytic asymmetric ring opening of *meso* epoxides with silicon tetrachloride.

Diastereomerically pure aryl phosphonic amides **1**–**4** were easily prepared in 84, 80, 91, and 80% yield, respectively, by an exchange reaction between bis(dimethylamino)aryl phosphine and the corresponding (*R*,*R*)-*N*,*N*′-dimethylcyclohexane-1,2-diamine or (*S*)-2-anilinomethyl pyrrolidine, followed by oxidation of the crude phosphines with *tert*-butyl hydroperoxide (Scheme 1). The crystalline compounds **1**–**4** were



Scheme 1. Synthesis of chiral aryl phosphonic amides **1**–**4**.

characterized by standard methods, including ^{31}P NMR spectroscopy ($\delta = 24.4$, 32.2, 32.5, and 26.5 in $CDCl_3$). The structure of **1** was unambiguously determined by a single X-ray diffraction study probing the phosphorus atom, which was shown to possess *S* absolute configuration (Figure 1).[14]

These compounds have been successfully employed as chiral Lewis bases in a catalytic asymmetric ring opening by $SiCl_4$ with cyclooctene oxide as the test substrate (Table 1). It is clear that the experimental conditions have a dramatic impact on the outcome of the reaction. In all cases, the expected chlorohydrin was obtained in good chemical yield

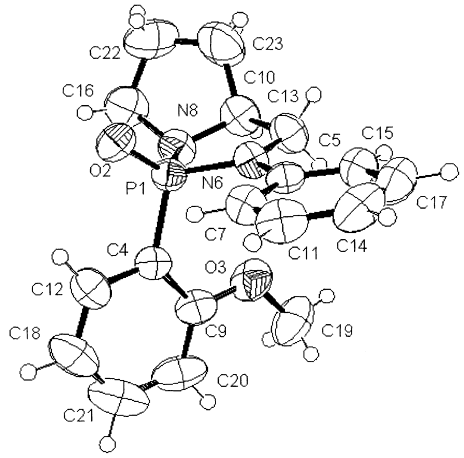
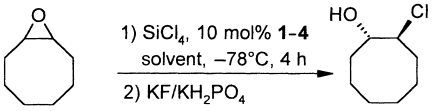


Figure 1. Structure of **1** with atom labeling. Selected bond lengths [Å] and angles [°]: P1-O2 1.466(1), P1-N6 1.669(1), P1-N8 1.648(2), P1-C4 1.788(2), N6-C5 1.414(2), C9-O3 1.372(2), O3-C19 1.410(2); O2-P1-C4 108.4(1), O2-P1-N6 116.4(1), O2-P1-N8 117.7(1), C4-P1-N6 110.3(1), C4-P1-N8 108.4(1), N6-P1-N8 94.9(1), C9-O3-C19 117.5(2), P1-C4-C9 124.3(1), P1-N8-C16 118.5(1), P1-N8-C10 113.3(1), C10-N8-C16 106.3(1).

Table 1. Catalytic asymmetric ring opening of cyclooctene oxide with $SiCl_4$.[a]



Entry	Lewis base	Solvent	Yield [%][b]	*ee* [%][c]
1	**1**	THF	68	30
2	**1**	toluene	61	98
3	**1**	DMF	–[d]	–
4	**1**	CH_2Cl_2	60	34
5	**1**	CH_2Cl_2	77	>99
6	**1**[e]	CH_2Cl_2	75	75
7	**2**	CH_2Cl_2	78	30
8	**3**	CH_2Cl_2	83	>99
9	**4**	CH_2Cl_2	78	50

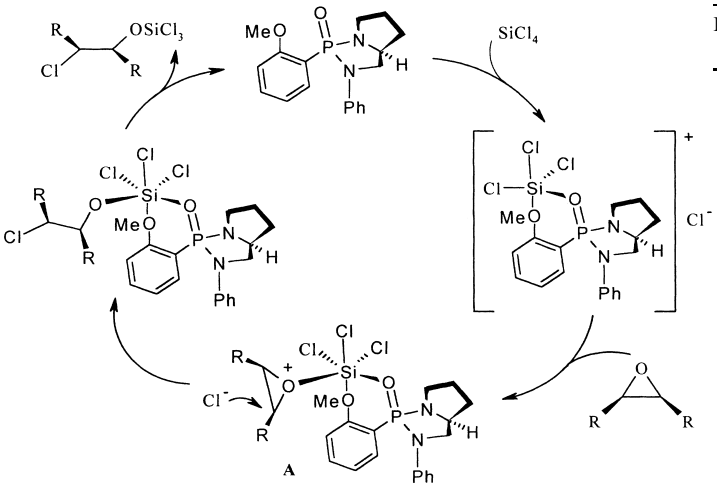
[a] Reactions were all performed on 1.2 mmol scale at −78 °C for 4 h with freshly distilled $SiCl_4$, except for the reaction in entry 4 which was performed using commercial $SiCl_4$ without any purification. [b] Yield after flash chromatography. [c] *ee* values were determined by chiral GC analysis with a Lipodex E column. [d] In this case, a low conversion (<15%) was encountered, even at room temperature. [e] Reaction was performed using 5 mol% of **1**.

(varying from 60 to 83%). Nevertheless, toluene and CH_2Cl_2 appeared to be the best solvents in terms of enantioselectivity (entries 2 and 5, 98 and >99% *ee*, respectively), whilst a polar solvent such as THF led to a poor *ee* value (entry 1, 30% *ee*). Furthermore, the use of freshly distilled $SiCl_4$ significantly enhanced the enantiomeric excess from 34 to >99% *ee* (entries 4 and 5).[15] The influence of decreasing the amount of catalyst **1** from 10 to 5 mol% was also investigated and a substantial decrease in enantioselectivity was observed (entry 6, 75% *ee*). Replacement of a methoxy group on the aromatic ring with a hydrogen atom has a detrimental effect on the enantioselectivity (entries 7 and 9, 30% and 50% *ee*, respectively).[16]

In order to explain the differences in enantioselectivity observed with the chiral base catalysts **1** and **3** relative to **2** and

 © WILEY-VCH Verlag GmbH, D-69451 Weinheim, 2000 1433-7851/00/3914-2555 $ 17.50+.50/0

4, we believe that, for **1** and **3**, the reaction with the epoxide proceeds through a hexacoordinate structure, with chelatation to the catalyst organized around a cationic silicon intermediate **A** (Scheme 2). On the other hand, for **2** and **4**, we can



Scheme 2. Proposed mechanistic rationale for the enantioselective ring opening of *meso* epoxides.

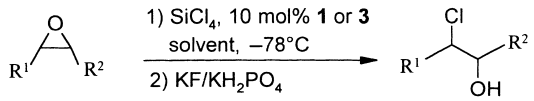
postulate a pentacoordinate intermediate in equilibrium with a hexacoordinate structure; these structures would involve one or two phosphonamide molecules, respectively, coordinated by only the oxygen of the P=O moiety.[17]

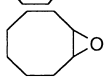
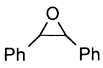
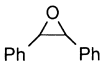
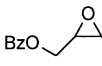
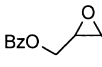
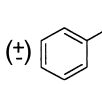
Under the best experimental conditions previously described (those in entry 5, Table 1), this study has been extended to a series of *meso* epoxides. The results are summarized in Table 2. In all cases, the chlorohydrins were obtained in good yields varying from 41 to 91%. However, the enantioselectivity of the reaction was highly substrate dependent. In the case of cyclic substrates, there is a dramatic effect with different ring sizes. Thus, using catalyst **1**, cyclopentene oxide afforded the expected product in low *ee* (entry 1, 23% *ee*) whereas cyclohexene, cycloheptene, and cyclooctene oxides led to the formation of the corresponding chlorohydrins in, respectively, 82, 98, and up to 99% *ee* (entries 5, 6, and 8). The acyclic substrates also gave good to excellent results in terms of enantioselectivity (entries 9–14, 60–94% *ee*).[19, 20]

In conclusion, a new and efficient type of chiral Lewis bases has been developed, and its utility has been demonstrated in a catalytic enantioselective ring opening of *meso* epoxides. Further studies dealing with mechanistic features of this reaction are currently under investigation.

Received: December 23, 1999
Revised: March 10, 2000 [Z14464]

Table 2. Catalytic asymmetric ring opening of various *meso* epoxides.[a]



Entry	Lewis base	Substrate	Solvent	t [h][b]	Yield [%][c]	*ee* [%] (config.)[d]
1	**1**		THF[e]	0.3	68	23 (1*R*,2*R*)[f]
2	**1**		CH_2Cl_2	3	41	48[f]
3	**3**		CH_2Cl_2	3	44	37[f]
4	**1**		CH_2Cl_2	0.3	85	62 (1*R*,2*R*)[g]
5	**3**		CH_2Cl_2	0.3	84	82 (1*R*,2*R*)[g]
6	**1**		CH_2Cl_2	3	79	98 (1*R*,2*R*)[g]
7	**3**		CH_2Cl_2	3	75	73 (1*R*,2*R*)[g]
8	**1**		CH_2Cl_2	4	77	>99 (1*R*,2*R*)[g]
9	**1**		THF[e]	3.5	68	92 (1*S*,2*S*)[h]
10	**3**		CH_2Cl_2	3.5	71	60 (1*S*,2*S*)[h]
11	**1**		CH_2Cl_2	3.5	78	94 (2*S*,3*S*)[h]
12	**3**		CH_2Cl_2	3.5	95	90 (2*S*,3*S*)[h]
13	**1**		THF	3.5	53[i]	12[j]

[a] Reactions were all performed on 1.2 mmol scale at −78 °C using freshly distilled $SiCl_4$. [b] t = reaction time. [c] Yield after flash chromatography. [d] Configuration of the product where determined. [e] A low enantiomeric excess (<20% *ee*) was encountered performing the reaction in CH_2Cl_2. [f] *ee* values were determined by chiral GC analysis with a Lipodex E column. [g] *ee* values were determined by ^{13}C NMR analysis with lactic acid derivatives as chiral shift reagents.[18] [h] *ee* values were determined by HPLC analysis on a Daicel Chiralcel OD-H column. [i] Reaction was performed using 0.5 equivalents of $SiCl_4$ and quenched after 56% conversion of the substrate. [j] *ee* values were determined by HPLC analysis on a Daicel Chiralcel OJ column.

[1] a) M. C. Wills, *J. Chem. Soc. Perkin Trans. 1* **1999**, 1765; b) E. N. Jacobsen, M. H. Wu, *Comprehensive Asymmetric Catalysis, Vol. III* (Eds.: E. N. Jacobsen, A. Pfaltz, H. Yamumoto), Springer, **1999**, Chap. 35, pp. 1309–1326; c) A. S. Rao, S. K. Paknikar, J. G. Kirtane, *Tetrahedron* **1983**, *39*, 2323.
[2] N. S. Simpkins, *J. Chem. Soc. Chem. Commun.* **1986**, 88.
[3] K. Fuji, M. Node, S. Terada, M. Murata, H. Nagasawa, *J. Am. Chem. Soc.* **1985**, *107*, 6404.
[4] a) T. Mukaiyama, I. Tomioka, M. Shimizu, *Chem. Lett.* **1984**, 49; b) J. Hiratake, K. Shibata, N. Baba, J. Oda, *Synthesis* **1988**, 278.
[5] M. Kurihara, J. Kamiyama, S. Kobayashi, M. Ohno, *Tetrahedron Lett.* **1985**, *26*, 5831.
[6] a) H. Imado, T. Ishizuka, T. Kunieda, *Tetrahedron Lett.* **1995**, *36*, 931; b) M. North, G. Zagotto, *Synlett* **1995**, 639; c) R. A. Aitken, J. Gopal, *Tetrahedron: Asymmetry* **1990**, *1*, 517; d) D. Seebach, G. Jaeschke, Y. M. Wang, *Angew. Chem.* **1995**, *107*, 2605; *Angew. Chem. Int. Ed. Engl.* **1995**, *34*, 2395; e) C. Bolm, A. Gerlach, C. L. Dinter, *Synlett* **1999**, 195.
[7] a) D. M. Hodgson, A. R. Gibbs, G. P. Lee, *Tetrahedron* **1996**, *52*, 14361.
[8] a) W. A. Nugent, *J. Am. Chem. Soc.* **1992**, *114*, 2768; b) L. E. Martinez, J. L. Leighton, D. H. Carsten, E. N. Jacobsen, *J. Am. Chem. Soc.* **1995**, *117*, 5897; c) M. Tokunaga, J. F. Larrow, F. Kakiuchi, E. N. Jacobsen, *Science* **1997**, *277*, 936; d) B. M. Cole, K. D. Shimizu, C. A. Krueger, J. P. A. Harrity, M. L. Snaper, A. H. Hoveyda, *Angew. Chem.* **1996**, *108*, 1776; *Angew. Chem. Int. Ed. Engl.* **1996**, *35*, 1668; e) W. A.

 © WILEY-VCH Verlag GmbH, D-69451 Weinheim, 2000 1433-7851/00/3914-2556 $ 17.50+.50/0

Nugent, *J. Am. Chem. Soc.* **1998**, *120*, 7139; f) N. Oguni, Y. Miyagi, K. Itoh, *Tetrahedron Lett.* **1998**, *39*, 9023.

[9] a) Y. Naruse, T. Esaki, H. Yamamoto, *Tetrahedron* **1988**, *44*, 4747; b) M. Srebnik, N. N. Joshi, H. C. Brown, *Isr. J. Chem.* **1989**, *29*, 229; c) N. N. Joshi, M. Srebnik, H. C. Brown, *J. Am. Chem. Soc.* **1988**, *110*, 6246; d) For a review, see: M. V. Bhat, S. U. Kulkarni, *Synthesis* **1983**, 249.

[10] S. E. Denmark, P. A. Barsanti, K. T. Wong, R. A. Stavenger, *J. Org. Chem.* **1998**, *63*, 2428.

[11] a) O. Legrand, J. M. Brunel, T. Constantieux, G. Buono, *Chem. Eur. J.* **1998**, *4*, 1061; b) O. Legrand, J. M. Brunel, G. Buono, *Angew. Chem.* **1999**, *111*, 1574; *Angew. Chem. Int. Ed.* **1999**, *38*, 1479; c) O. Legrand, J. M. Brunel, G. Buono, *Eur. J. Org. Chem.* **1999**, 1099; d) O. Legrand, J. M. Brunel, G. Buono, *Tetrahedron* **2000**, *56*, 595.

[12] a) J. M. Brunel, T. Constantieux, O. Legrand, G. Buono, *Tetrahedron Lett.* **1998**, *39*, 2961; b) O. Legrand, J. M. Brunel, G. Buono, *Tetrahedron Lett*. **1998**, *39*, 9419; c) J. M. Brunel, O. Legrand, G. Buono, *Tetrahedron: Asymmetry* **1999**, *10*, 1979.

[13] For a review, see: G. Buono, O. Chiodi, M. Wills, *Synlett* **1999**, 377.

[14] Single crystal X-ray analysis of **1**: $C_{18}H_{21}N_2O_2P$, $M_r = 328.35$, white plate (recrystallized in ethylacetate), $0.5 \times 0.5 \times 0.4\ mm^3$. All the measurements were made on a Rigaku diffractometer with $Cu_{K\alpha}$ radiation. Cell constants and the orientation matrix for data collection were obtained from a least square refinement using setting angles of 30 reflections in the range $1 < \theta < 25.45^\circ$; orthorhombic, $P2_12_12_1$, $a = 9.1502(2)$, $b = 10.9705(4)$, $c = 16.8227(6)$ Å, $Z = 4$, $\rho_{calcd} = 1.25\ g\,cm^{-3}$. A total of 1925 reflections were measured at $T = 298$ K. The standards were measured after every 25 reflections. Among the first 20 pairs of reflections, the signs of the corresponding calculated differences established that the molecule is described with the correct *S* absolute configuration. Moreover, the sum of the bond angles around the nitrogen atom of the pyrrolidine ring is 338.1°, showing a nonplanar configuration. Crystallographic data (excluding structure factors) for the structure reported in this paper have been deposited with the Cambridge Crystallographic Data Centre as supplementary publication no. CCDC-140554. Copies of the data can be obtained free of charge on application to CCDC, 12 Union Road, Cambridge CB2 1EZ, UK (fax: (+44) 1223-336-033; e-mail: deposit@ccdc.cam.ac.uk).

[15] It is well known that HCl easily opens epoxides. Due to this fact, it was essential to establish that the $SiCl_4$ used was free of HCl in order to obtain reproducible results. See: A. D. Cross, *Q. Rev. Chem. Soc.* **1960**, *14*, 317.

[16] For a review, see: M. Sawamura, Y. Ito, *Chem. Rev.* **1992**, *92*, 857.

[17] Cationic silicon species have been already postulated as intermediates in other Lewis base promoted reactions; see: a) S. E. Denmark, X. Su, Y. Nishigaichi, *J. Am. Chem. Soc.* **1998**, *120*, 12990; b) A. R. Bassindale, J. C. Y. Lau, P. G. Taylor, *J. Organomet. Chem.* **1995**, *499*, 137; c) A. R. Bassindale, J. C. Y. Lau, P. G. Taylor, *J. Organomet. Chem.* **1995**, *499*, 75.

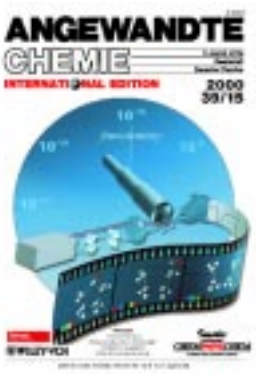
[18] a) A. Heumann, R. Faure, *J. Org. Chem.* **1993**, *58*, 1276; b) L. Tottie, C. Moberg, A. Heumann, *Acta Chem. Scand.* **1993**, *47*, 492.

[19] A careful analysis of the chlorohydrin issued from cyclohexene oxide is necessary. Indeed, a racemization occurred in CH_2Cl_2 solution, with the $[\alpha]_D^{25}$ varying from -30 to -20 after 4 hours ($c = 1.0$, $CHCl_3$). Moreover, the chlorohydrin generated in entry 11 is not very stable and a decomposition of the product has been noticed after few hours.

[20] Numerous racemic epoxides have been submitted in an attempt at an asymmetric ring opening resolution with $SiCl_4$ catalyzed by the chiral *ortho*-methoxyphenyldiazaphosphonamide Lewis bases. Whatever the experimental conditions, low enantiomeric excess values of chlorohydrins (<10% *ee*) and poor regioselectivity have been encountered, except when opening racemic phenyloxirane, where a total regioselectivity has been observed but with only 12% ee. The residual epoxide was isolated in 35% yield and 20% *ee*.

 © WILEY-VCH Verlag GmbH, D-69451 Weinheim, 2000 1433-7851/00/3914-2557 $ 17.50+.50/0

Cover Picture



Ahmed H. Zewail

The cover picture shows the experimental principles of femtochemistry, the field concerned with the real-time observation of physical, chemical, and biological changes on the femtosecond time scale. The clocking of the femtosecond events is made using laser pulses, one to initiate the change and others to take snapshots. Studies of the motion at atomic-scale resolution provide a telescopic view of the molecular world. More information about this fascinating topic is described by A. H. Zewail in his Nobel Lecture on page 2586 ff. It is quite fitting that at the back of this issue is the inaugural issue of *ChemPhysChem*, announced in earlier editorials.

ARROW OF TIME

Chemistry & Biology

femtosecond 10^{-15} — 1980 — Femtochemistry

picosecond 10^{-12} — 1970 — Picochemistry

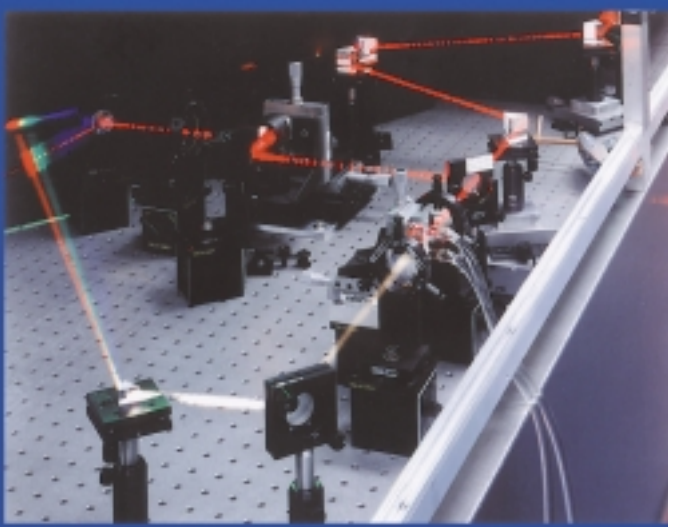
nanosecond 10^{-9} — 1960 — Laser

microsecond 10^{-6} — 1953, 1949 — Relaxation Method, Flash Photolysis

millisecond 10^{-3} — 1940, 1923 — Stopped Flow, Flow Method

seconds — Arrhenius, van't Hoff, Ostwald (Wilhelmy) — 1850 to 1900 — Kinetics

Billion seconds 10^{9} life span — 5 M years (1.6×10^{14} s) — Humans



ANGEWANDTE CHEMIE © WILEY-VCH

Femtochemistry: Atomic-Scale Dynamics of the Chemical Bond Using Ultrafast Lasers (Nobel Lecture)**

Ahmed H. Zewail*

Over many millennia, humankind has thought to explore phenomena on an ever shorter time scale. In this race against time, femtosecond resolution ($1\ \text{fs} = 10^{-15}\ \text{s}$) is the ultimate achievement for studies of the fundamental dynamics of the chemical bond. Observation of the very act that brings about chemistry—the making and breaking of bonds on their actual time and length scales—is the wellspring of the field of femtochemistry, which is the study of molecular motions in the hitherto unobserved ephemeral transition states of physical, chemical, and biological changes. For molecular dynamics, achieving this atomic-scale resolution using ultrafast lasers as strobes is a triumph, just as X-ray and electron diffraction, and, more recently, STM and NMR spectroscopy, provided that resolution for static molecular structures. On the femtosecond time scale, matter wave packets (particle-type) can be created and their coherent evolution as a single-molecule trajectory can be observed. The field began with simple systems of a few atoms and has reached the realm of the very complex in isolated, mesoscopic, and condensed phases, as well as in biological systems such as proteins and DNA structures. It also offers new possibilities for the control of reactivity and for structural femtochemistry and femtobiology. This anthology gives an overview of the development of the field from a personal perspective, encompassing our research at Caltech and focusing on the evolution of techniques, concepts, and new discoveries.

Keywords: femtobiology · femtochemistry · Nobel lecture · physical chemistry · transition states

1. Prologue

In the history of human civilization, the measurement of time and recording the order and duration of events in the natural world are among the earliest endeavors that might be classified as science. The development of calendars, which permitted the tracking of yearly flooding of the Nile valley in ancient Egypt and of the seasons for planting and harvesting in Mesopotamia, can be traced to the dawn of written language. Ever since, time has been an important concept[1] and is now recognized as one of the two fundamental dimensions in science. The concept of time encapsulates an awareness of its duration and of the passage from past to present to future and surely must have existed from the very beginning with humans searching for the meaning of birth, life, and death and—in some cultures—rebirth or recurrence.

[*] Prof. A. H. Zewail
Arthur Amos Noyes Laboratory of Chemical Physics
California Institute of Technology
Pasadena, CA 91125 (USA)
Fax: (+1) 626-792-8456
E-mail: zewail@caltech.edu

[**] Copyright© The Nobel Foundation 2000. We thank the Nobel Foundation, Stockholm, for permission to print this lecture.

My ancestors contributed to the beginning of the science of time, developing what Neugebauer[1d] has described as "the only intelligent calendar which ever existed in human history". The "Nile Calendar" was an essential part of life as it defined the state of yearly flooding with three seasons, the *Inundation* or *Flooding*, *Planting*, and *Harvesting*, each four months long. A civil year lasting 365 days was ascertained by about 3000 BC or before, based on the average time between arrivals of the flood at Heliopolis, just north of Cairo; nilometers were used in more recent times, and some are still in existence today. By the time of the First Dynasty of United Egypt under Menes in about 3100 BC, the scientists of the land introduced the concept of the "Astronomical Calendar" by observing the event of the heliacal rising of the brilliant star Sothis (or Sirius). Inscribed on the Ivory Tablet, dating from the First Dynasty and now at the University Museum in Philadelphia, were the words, "Sothis Bringer of the Year and of the Inundation".[1c] On the Palermo Stone, the annals of the kings and their time-line of each year's chief events were documented from pre-dynastic times to the middle of the Fifth Dynasty.[1a] Thus, as early as 3100 BC, they recognized a definite natural phenomenon for the accurate timing of the coming flood and recounted the observed reappearance of the star as the New Year Day—real-time observation of

daily and yearly events with the zero-of-time being well defined[*]

In about 1500 BC, another major contribution to this science was made, the development of sun-clocks, or sundials, using moving shadows (Figure 1). Now in Berlin, the sun-clock bearing the name of Thutmose III (or Thothmes after the Egyptian God Thoth of wisdom and enlightenment), who ruled at Thebes from 1447 – 1501 BC, shows the graduation of hours for daytime measurements. This clock with uneven periods for hours was man-made and transportable. For night time, the water-clock was invented, and the device provided even periods for timing. With these developments, the resolution of time into periods of year, month, day, and hour became known and has now been used for more than three millennia. The durations of minutes and seconds followed, using the Hellenistic sexagesimal system, and this division, according to Neugebauer, "is the result of a Hellenistic modification of an Egyptian practice combined with Babylonian numerical procedures." About 1300 AD, the mechanical clock[1g] was advanced in Europe, ushering in a revolution in precision and miniaturization; Galileo began studies of pendulum motions and their clocking, using his heart beat in seconds, in 1582 AD. Our present time standard is the cesium atomic clock,[**] which provides precision of about $1{:}10^{13}$, that is, the clock loses or gains one second every 1.6 million years. For this work, Norman Ramsey shared the 1989 Nobel Prize in Physics.

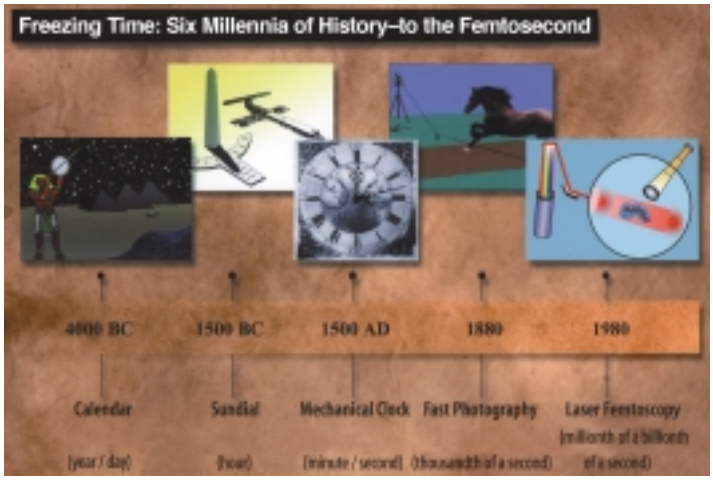


Figure 1. Timeline of some of the events in the history of the measurement of time, from yearly calendars to the femtosecond regime (see text).

Until 1800 AD, the ability to record the timing of individual steps in any process was essentially limited to time scales amenable to direct sensory perception—for example, the eye's ability to see the movement of a clock or the ear's ability to recognize a tone. Anything more fleeting than the blink of an eye (about 0.1 s) or the response of the ear (about 0.1 ms) was simply beyond the realm of inquiry. In the nineteenth century, the technology was to change drastically, resolving time intervals into the sub-second domain. The famous motion pictures by Eadweard Muybridge (1878) of a galloping horse, by Etienne-Jules Marey (1894) of a righting cat, and by Harold Edgerton (mid-1900's) of a bullet passing through an apple and other objects are examples of these developments, with millisecond to microsecond time resolution, using snapshot photography, chronophotography, and stroboscopy, respectively.[2] By the 1980's, this resolution became ten orders of magnitude better (see Section 2.2), reaching the femto-

[*] Recognizing the incommensurability of the lunar month and the solar year, they abandoned the lunar month altogether and used a 30-day month. Thus the year is made of 12 months, 30 days each, with 5 feast days at the end of the year. The "Civil Calendar" was therefore 365 days per year and differs from the astronomical calendar of Sothis by approximately a 1/4 day every year. The two calendars must coincide at intervals of $365 \times 4 = 1460$ years, and historians, based on recorded dates of the reappearance of Sothis in dynastic periods, give the four dates for the coincidence of both calendars: 139 AD, 1317 BC, 2773 BC, and 4233 BC ($+139 - 3 \times 1460 \equiv$ 4241 BC). Even though the Egyptians discovered the astronomical calendar, 365 – 1/4 days, they decided, presumably for "bookkeeping", to use the civil calendar of 365 days per year without leap years. They also divided the day into two periods of 12 hours each for day and night time. The remarkable calendar of years, months, days, and hours was adapted throughout history and formed the basis for the 365.25-day Julian (46 BC, Alexandria school) and 365.2422-day Gregorian (from 1582 AD, Pope Gregory XIII) calendars. In the words of the notable Egyptologist J. H. Breasted,[1] "It has thus been in use uninterruptedly over six thousand years." Many historians regard the date around 4241 BC as the beginning of history itself as it defines the period of written records; anything earlier is prehistory.

[**] Since 1967 one second has been defined as the time during which the cesium atom makes exactly 9 192 631 770 oscillations.



Ahmed H. Zewail was born in Egypt on February 26, 1946. He received his B.S and M.S degrees from Alexandria University, and his Ph.D from the University of Pennsylvania. After completion of his Ph.D. he went to the University of California, Berkeley, as an IBM research fellow. In 1976 he was appointed to the faculty at Caltech and in 1982 became a full professor. He is currently the first Linus Pauling Chair Professor of Chemistry and Professor of Physiscs at the California Institute of Technology, and Director of the NSF Laboratory for Molecular Sciences (LMS). His research interests center on the development of ultra-fast lasers and electrons for studies of dynamics in chemistry and biology. In the field of femtochemistry, developed at Caltech, fundamental femtosecond (10^{-15} second) processes in chemistry, physics, and biology are investigated. His outstanding contributions have been widely recognised with numerous presitigious awards and honors including the Grand Collar of the Nile, from President Murbarak, the Robert A. Welch Prize Award, the Benjamin Franklin Medal, the Leonardo Da Vinci Award of Excellence, in 1998 Egypt issued a postage stamp with his portrait, and in 1999 he received the Nobel Prize for Chemistry.

second scale,[*] the scale for atoms and molecules in motion.

The actual atomic motions involved in chemical reactions had never been observed in real time despite the rich history of chemistry over two millennia,[3] as khem became khemia, then alchemy, and eventually chemistry[3, 4] (see the Stockholm Papyrus in Figure 2). Chemical bonds break, form, or geometrically change with awesome rapidity. Whether in isolation or in any other phase, this ultrafast transformation is a dynamic process involving the mechanical motion of electrons and atomic nuclei. The speed of atomic motion is about 1 km s^{-1} and, hence, to record atomic-scale dynamics over a distance of an angström, the average time required is approximately 100 fs. The very act of such atomic motions as reactions unfold and pass through their transition states is the focus of the field of femtochemistry. With femtosecond time resolution we can "freeze" structures far from equilibrium and prior to their vibrational and rotational motions, or reactivity. The pertinent questions about the dynamics of the chemical bond are the following: How does the energy put into a reactant molecule redistribute among the different degrees of freedom, and how fast does this happen? What are the speeds of the chemical changes connecting individual quantum states in the reactants and products? What are the detailed nuclear motions that chart the reaction through its transition states, and how rapid are these motions? As pointed out by Jim Baggott, [4b] "the entire history of chemical reaction dynamics and kinetics has been about providing some approximate answers to these three questions."

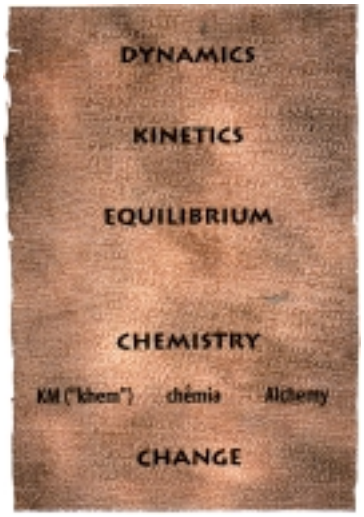


Figure 2. A picture of a page of the Stockholm papyrus (300 AD) describing the recipe for "making" (actually imitating) emerald, with key concepts overlaid. Note that "change" has been at the heart of chemistry from its millennia-old definition KM, to Chêmia and Alchemy, and to Chemistry (see ref. [B26], and references therein). Equilibrium, kinetics, and dynamics are the foundation for the description of chemical changes.

In femtochemistry, studies of physical, chemical, or biological changes are at the fundamental time scale of molecular vibrations: the actual nuclear motions (Figure 3). In this sense, femtoscience represents the end of the race against time, or, as the report of ref. [5a] puts it, "… reaching the end of the road". For this same reason, Martens stated,[5b] "all chemistry is femtochemistry". The ephemeral transition states, denoted in the past by square brackets ([TS]‡) for their elusiveness, can now be clocked as a molecular species TS‡. Moreover, on this time scale, the time-dependent description of a coherent, single-molecule trajectory represents the classical nuclear "motion picture" of the reaction as its wave packet proceeds from the initial state, through transition states, and on to final products—the language of the actual dynamics! The femtosecond time scale is unique for the creation of such coherent matter waves on the atomic scale of length, a basic problem rooted in the development of quantum mechanics and the duality of matter. Figure 4 A highlights some steps made in the desription of the duality of light-

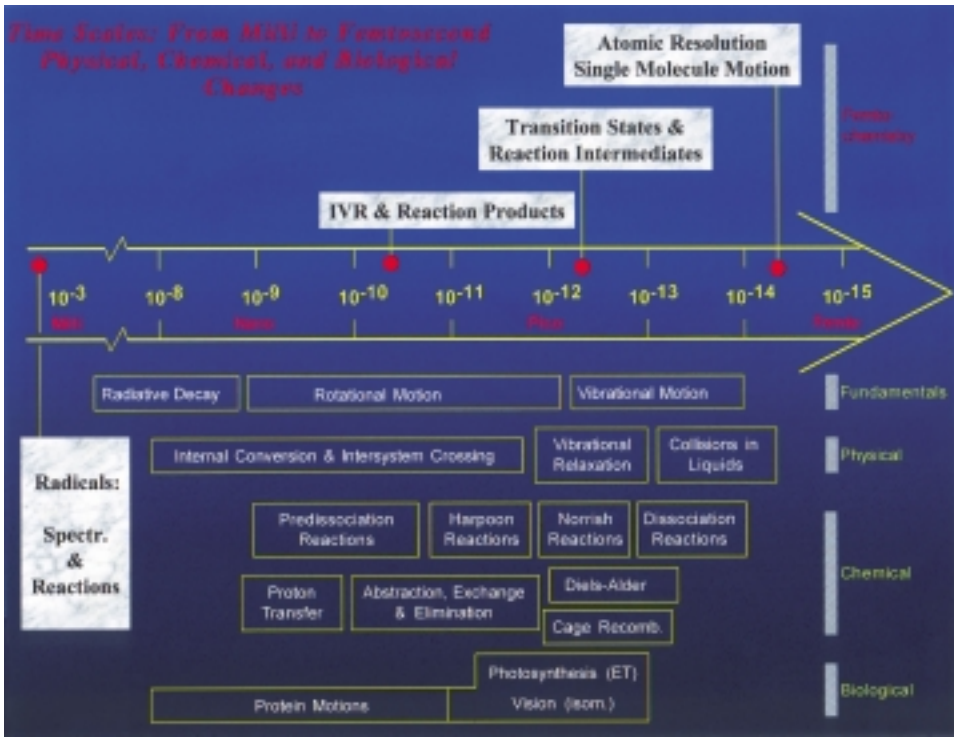


Figure 3. Time scales and their relevance to physical, chemical, and biological changes. The fundamental limit of the vibrational motion defines the regime for femtochemistry. Examples are given for each type of change and for each scale.[B4, B10]

[*] The prefix milli comes from Latin (and French), micro and nano from Greek, and pico from Spanish. Femto is Scandinavian, the root of the word for "fifteen"; nuclear physicists call femtometer, the unit for the dimensions of atomic nuclei, fermi. Atto is also Scandinavian.

A) **Matter Waves**
Particle-type Control & Dynamics

de Broglie (1924)
Einstein's light wave/particle
$E = h\nu \quad E = c\,p$
$\therefore\ \lambda = h/p$
Similarly, matter particle/wave

Schrödinger (1926)
The Wave Equation – Stationary waves
$\mathcal{H}\Psi = E\Psi$

Schrödinger (1926)
Micro- to Macromechanics
Quantum to Newton Mechanics
Ψ to wave group

Femtochemistry & Quantum Limit (h):
Particle-type
$\lambda_{\text{de Broglie}}$ (initial localization) = h/p
uncertainty in time measurement
$\Delta x\,\Delta p \geq h/(2\pi) \quad \Delta t\,\Delta E \geq h/(2\pi)$

for force free
$\Delta x = p/m\ \Delta t \equiv v\,\Delta t$

$\Delta t \sim 10$ fs $\quad \Delta x \sim 0.1$ Å
$\Delta t \sim 10$ ps $\quad \Delta x \sim 100$ Å

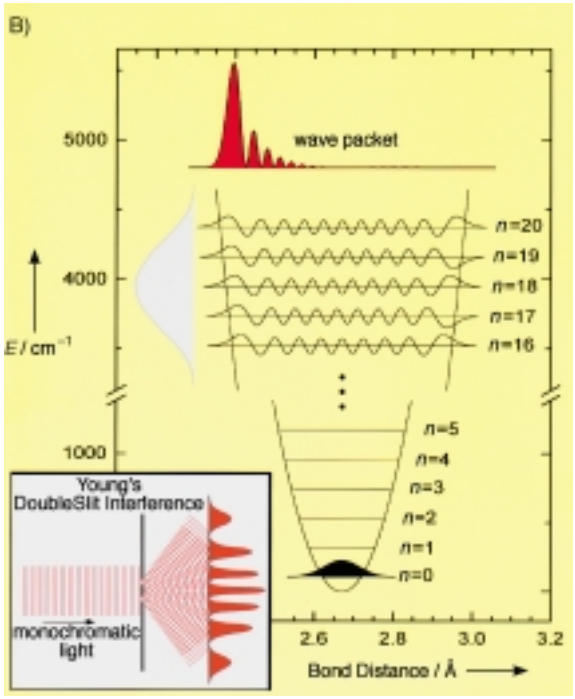


Figure 4. Matter waves and particle-type limit of dynamics. A) The atomic-scale de Broglie wavelength in the coherent preparation of a quantum system and the uncertainty of probe measurements are both reached on the femtosecond time scale. B) The limits of the wave packet and wave function for molecular systems, in this case a diatomic molecule (see Section 6). The analogy with light interference is depicted—Thomas Young's experiment of 1801.[B25]

matter and time scales, and Figure 4B shows the importance of coherence for localization (see also Section 6).

This powerful concept of coherence lies at the core of femtochemistry and was a key advance in observing the dynamics at atomic resolution. The realization of its importance and its detection by selectivity in both preparation and probing were essential in all studies, initially of states and orientations, and culminating in atomic motions in reactions. With these concepts in mind, the marriage of ultrafast lasers with molecular beams (Figure 5) proved to be essential for the initial development. Laser-induced fluorescence was the first probe used, but later we invoked mass spectrometry and nonlinear optical techniques. Now numerous methods of probing are known (Figure 6) and used in laboratories around the world; Coulomb explosion is the most recent powerful probe developed by Will Castleman[5c] for arresting reactive intermediates, as mentioned in Section 3.

Applications of femtochemistry have spanned the different types of chemical bonds—covalent, ionic, dative, and metallic, as well as the weaker ones such as hydrogen and van der Waals bonds. The studies have continued to address the varying complexity of molecular systems, from diatomics to proteins and DNA. Studies have also been made in all phases of matter: gases and molecular beams; mesoscopic phases of clusters, nanostructures, particles and droplets; condensed phases of dense fluids, liquids, solids, surfaces, and interfaces; and in sibling fields of femtoscience such as femtobiology (Figure 7).

Twenty-four centuries ago, the Greek philosopher Democritus and his teacher Leucippus gave birth to a new way of thinking about matter's invisible and elementary entity, the atom. Richard Feynman once asked, if you had only one sentence to describe the most important scientific knowledge we possess, what would that sentence be? He said, "everything is made of atoms". Democritus' atomism, which was rejected by Aristotle, was born on a purely philosophical basis, surely without anticipating some of the twentieth century's most triumphant scientific discoveries. Atoms can now be seen, observed in motion, and manipulated.[6] These discoveries have brought the microscopic world and its language into a new age, and they cover domains of length, time, and number. The length (spatial) resolution, down to the scale of atomic distance (angström), and the time resolution, down to the scale of atomic motion (femtosecond), have been achieved. The trapping and spectroscopy of a single ion (electron) and the trapping and cooling of neutral atoms have also been achieved. All of these achievements have been recognized by the awarding of the Nobel Prize to scanning tunneling microscopy (1986), to single-electron and -ion trapping and spectroscopy (1989), to laser trapping and cooling (1997), and to laser femtochemistry (1999).

2. Dynamics and Arrow of Time

2.1. Origins—From Kinetics To Dynamics

2.1.1. The Arrhenius Seminal Contribution

At the turn of the 20th century, the study of reactivity was dominated by the question:[*] How do reactions proceed and

[*] The main focus of prior studies was on the thermodynamics and equilibrium characteristics. Interestingly, chemical equilibrium was already established a century before (1798) by Claude Berthollet, during a visit to the Natron Lakes in Napoleonic times, through his studies of the reaction $Na_2CO_3 + CaCl_2 \Leftrightarrow 2\,NaCl + CaCO_3$ [S. W. Weller, *Bull. Hist. Chem.* **1999**, *24*, 61].

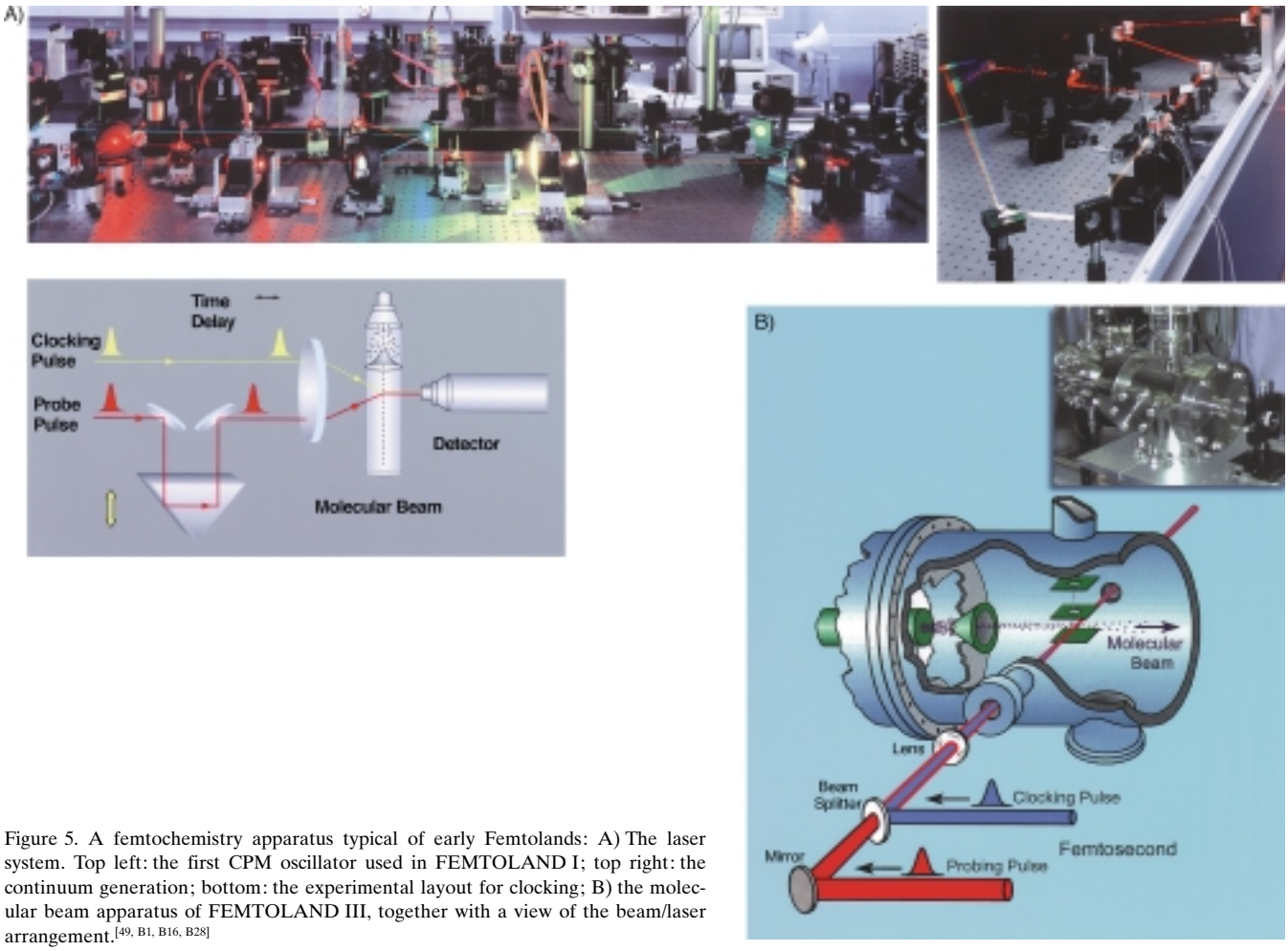


Figure 5. A femtochemistry apparatus typical of early Femtolands: A) The laser system. Top left: the first CPM oscillator used in FEMTOLAND I; top right: the continuum generation; bottom: the experimental layout for clocking; B) the molecular beam apparatus of FEMTOLAND III, together with a view of the beam/laser arrangement.[49, B1, B16, B28]

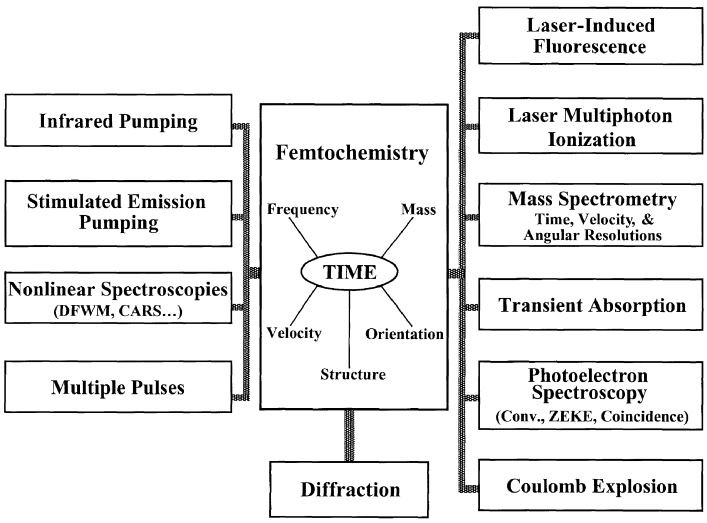


Figure 6. Techniques for probing in femtochemistry. Both excited and ground states have been probed by these methods. The correlations of time with frequency, mass, velocity, and orientation were essential in the studies of complex systems. Diffraction represents the new effort for probing structures (see text and Figure 29).

what are their kinetic rates? Svante Arrhenius gave the seminal description of the change in rates of chemical reactions with temperature and formulated in 1889 the

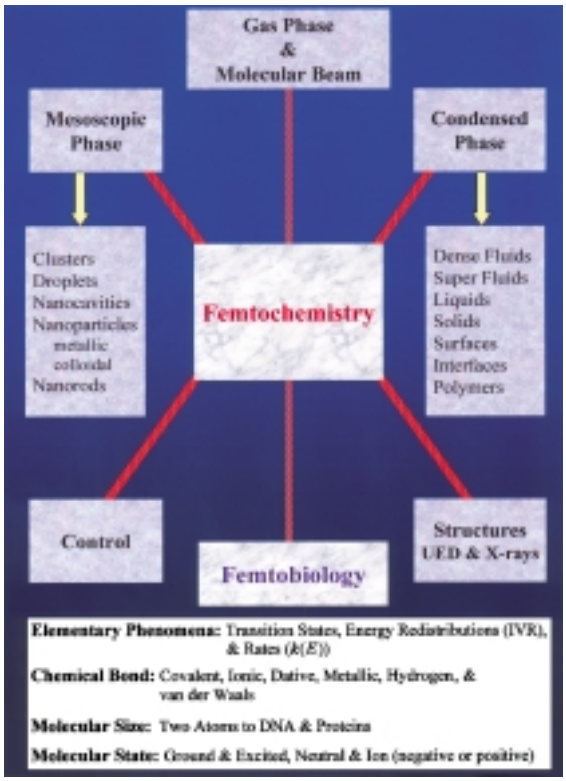


Figure 7. Femtochemistry and the scope of its applications.

familiar expression (1) for the rate constant,[7a] which, as Arrhenius acknowledged, had its roots in van't Hoff's (1884) equations.[7b] For any two reactants, the rate constant k depends on the temperature T according to an energy of

$$k = A\,e^{-E_a/RT} \quad (1)$$

activation E_a, which is different from the thermodynamic net energy change between reactants and products, and the dependence is exponential in form. R in Equation (1) is the universal gas constant. If we think of the reaction as a finite probability of reactant A colliding with B, then the rate is simply the collision frequency times the fraction of successful collisions with an energy equal to or more than E_a. The energy of activation E_a is found from the value of equation (1) through the well-known plots of "ln k versus $1/T$". Arrhenius also introduced a "hypothetical body", now known as the "activated complex", a central concept in the theory of reaction rates: the reaction, because of collisions or other means, proceeds only if the energy is sufficient to exceed a barrier whose energy is defined by the nature of the complex. Since then, various experimental data for different temperatures T were treated with Equation (1), yielding E_a and the pre-exponential factor A.

A few years after Arrhenius' contribution, Bodenstein (1894) published a landmark paper on the hydrogen/iodine system, which has played an important role in the development of gas-phase chemical kinetics, with the aim of understanding elementary reaction mechanisms.[7c] In the twenties, Lindemann (1922),[7d] Hinshelwood (1926),[7e] Tolman (1920),[7f,g] and others[8] developed, for unimolecular gas-phase reactions, elementary mechanisms with different steps describing activation, energy redistribution, and chemical rates. By 1928, the Rice-Ramsperger-Kassel (RRK) theory was formulated, and Marcus, starting in 1952, blended RRK and transition state theory in a direction which brought into focus the nature of the initial and transition-state vibrations in what is now known as the RRKM theory.[8]

The rate constant, $k(T)$, does not provide a detailed molecular picture of the reaction. This is because $k(T)$, which was obtained by analogy with van't Hoff's description of the change of the equilibrium constant K (thermodynamics) with T, is an average of the microscopic, reagent-state to product-state rate coefficients over all possible encounters. These might include different relative velocities, mutual orientations, vibrational and rotational phases, and impact parameters. A new way was needed to describe, by some quantitative measure, the process of the chemical reaction itself: How reagent molecules approach, collide, exchange energy, sometimes break bonds and make new ones, and finally separate into products. Such a description is the goal of molecular reaction dynamics.[9]

2.1.2. The London, Eyring, and Polanyi Contributions

For some time, theory was ahead of experiment in studies of microscopic molecular reaction dynamics. The effort started shortly after the publication of the Heitler–London quantum-mechanical treatment (1927) of the hydrogen molecule,[10a] a breakthrough in thinking not only about the stable structure of the chemical bond, but also about how two atoms can interact at different separations. One year later (1928), for Sommerfeld's Festschrift (60th birthday), London[10b] presented an approximate expression for the potential energy of triatomic systems, for example, H_3, in terms of the coulombic and exchange energies of the "diatomic" pairs. In 1931 Henry Eyring and Michael Polanyi, using the London equation, provided a semiempirical calculation of a potential energy surface (PES) of the $H + H_2$ reaction describing the journey of nuclei from the reactant state of the system to the product state, passing through the crucial transition state of activated complexes.[10c] The birth of "reaction dynamics" resulted from this pioneering effort and, for the first time, one could think of the PES and the trajectories of dynamics on it—in those days, often, expressed in atomic units of time! No one could have dreamed in the 1930s of observing the transient molecular structures of a chemical reaction, since the time scale for those activated complexes that were far from equilibrium in the transition state was estimated to be less than a picosecond (ps).

The time scale was rooted in the theory developed for the description of reaction rates. Building on Arrhenius' work and the work of Polanyi and Wigner (1928),[11a] in 1935, Eyring,[11b] and independently Evans and Polanyi,[11c] formulated transition-state theory, which gave an explicit expression for Arrhenius' pre-exponential factor [Eq. (2)].

$$k = \frac{k_B T}{h} K^{\neq} = \frac{k_B T}{h}\,\frac{Q^{\neq}}{Q_A\,Q_B}\,e^{-E_0/kT} \quad (2)$$

Here k_B is Boltzmann's constant, h is Planck's constant, and Q is the partition function. The key idea here is to assume the equilibration of the population between reactants and the transition state: $A + B \rightleftharpoons [TS]^{\neq} \rightarrow$ products. Thus, the rate constant can be related to the equilibrium constant for formation of the transition state $K^{\neq}$, and hence $\Delta G^{\neq}$, $\Delta H^{\neq}$, and $\Delta S^{\neq}$; physically, $\Delta G^{\neq}(\Delta H^{\neq} - T\Delta S^{\neq})$ in the exponent gives the barrier energy (through $\Delta H^{\neq}$) along the reaction coordinate and the pre-exponential entropic term, which reflects the change in vibrational modes perpendicular to the reaction coordinate. By comparing Equation (2) with Arrhenius' Equation (1), the pre-exponebtial A can be identified; E_a, the activation energy, and E_0, the barrier energy with zero-point energy corrections, are related.[8a] Kramers' (1940) classic work[11d] modified the pre-exponential factor to include friction from the surrounding medium, with transition-state theory giving an upper limit, and Casey Hynes, in the 1980s, provided a dynamical theory of friction with emphasis on time scales in the transition-state region and for solvent interaction.[11f] In the 1950s, Marcus[11e] obtained a transition-state-type expression for reactions of electron transfer in solutions with the Gibbs free energy of activation expressing the dependence on solvent reorganization energies. This work was awarded the 1992 Nobel Prize.

According to transition state theory, the fastest reaction is given by $k_B T/h$, which is basically the "frequency" for the passage through the transition state [see Eq. (2)]. At room temperature this value is $6 \times 10^{12}\ s^{-1}$, corresponding to about 170 fs; the time scale of molecular vibrations is typically 10–

100 fs. This estimate is consistent with knowledge of the speeds of nuclei and the distance change involved in the reaction. In 1936 the first classical trajectory from Hirschfelder-Eyring-Topley molecular dynamics simulations of the $H + H_2$ reaction showed the femtosecond steps needed to follow the reaction profile, albeit on the wrong PES. Later, Karplus, Bunker, and others showed a range for the time scales, picoseconds to femtoseconds, depending on the reaction and using more realistic PESs.[9, 26]

2.1.3. The Transition State and its Definition

In general, for an elementary reaction of type (3) the whole journey from reagents to products involves changes in internuclear separation totaling about 10 Å. If the atoms

$$A + BC \rightarrow [ABC]^{\ddagger} \rightarrow AB + C \quad (3)$$

moved at $10^4 - 10^5\,cm\,s^{-1}$ then the entire 10-Å trip would take $10^{-12} - 10^{-11}\,s^{-1}$. If the "transition state" $[ABC]^{\ddagger}$ is defined to encompass all configurations of ABC significantly perturbed from the potential energy of the reagents $A + BC$ or the products $AB + C$, then this period of 1 – 10 ps is the time available for its observation. To achieve a resolution of approximately 0.1 Å, the probe time window must be 10 – 100 fs.

The above definition of the transition state follows the general description given by John Polanyi and the author,[12] namely the full family of configurations through which the reacting particles evolve en route from reagents to products. This description may seem broad to those accustomed to seeing the TS symbol ‡ displayed at the crest of the energy barrier to a reaction. As stated in ref. [12], even if one restricts one's interest to the overall rates of chemical reactions, one requires a knowledge of the family of intermediates sampled by reagent collisions of different collision energy, angle, and impact parameters. The variational theory of reaction rates further extends the range of TS of interest, quantum considerations extend the range yet further, and the concern with rates to yield products in specified quantum states and angles extends the requirements most of all. A definition of the TS that embraces the entire process of bond breaking and bond making is therefore likely to prove the most enduring. This is specially important as we address the energy landscape of the reaction, as discussed in Section 4.

The cardinal choice of the transition state at the saddle point, of course, has its origin in chemical kinetics—calculation of rates—but it should be remembered that this is a mathematical "single point" with the division made to define the speed of a reaction.[8] Even in thermal reactions, there is enough of an energy distribution to ensure many types of trajectories occur. Furthermore, transition state theory is not a quantum theory, but a classical one, because of the assertion of a deterministic point. Quantum uncertainty demands some delocalization[8b] and, as mentioned above, the theory invokes the equilibration of reactants and transition-state populations, using statistical thermodynamics. In fact, the term transition state is used ambiguously to refer both to the quasi-equilibrium state of the reaction and to the molecular structure of the saddle point. As discussed in ref. [13a], perhaps the molecular species at the saddle point could be referred to as the transition structure; the activated complex is more descriptive.

The location at the saddle point provides the highest energy point that must be reached, thus defining the exponential probability factor; the dynamics (forces and time states) are governed by the nature of the transition-state region. Provided that the energy landscape of the reaction is controlled by a narrow region, the structure of the transition state becomes important in structure – reactivity correlations; rates versus Gibbs energy between the TS and the ground state. (It is also useful in designing TS analogues as enzyme inhibitors and TS complements as catalysts[13b]). The position of the TS and its energy relative to that of reactants and products along the reaction path becomes relevant. In the mid 1930s, the Bell-Evans-Polanyi principle gave a predictive correlation between the changes in barrier heights and the enthalpies of reactions, especially for a series of related reactions; the TS for exoergic or endoergic reaction is very different. In 1955, this led to Hammond's postulate which characterizes a reactantlike TS (so called "early" TS) for exoergic reactions, productlike TS (so called "late" TS) for endoergic reactions, and "central" TS for energy neutral reactions.[8d] John Polanyi, the son of Michael, formulated some concepts regarding energy disposal in relation to the position of the TS on the PES, by using molecular dynamics simulations and experimental studies of chemiluminescence.[14]

It should be recognized that selectivities, efficiencies, and stereochemistries are quantified only when the dynamics on the global energy landscape are understood. For example, the picture for simple reactions of a few (strong) bonds being made and broken is changed when the energy surface is nearly flat or there is a significant entropic contribution. Many transition states will exist in the region as in the case of protein folding.[13c] Finally, in the transition state, chemical bonds are in the process of being made and broken. In contrast, for intermediates, whose bonds are fully formed, they are in potential wells, typically "troughs" in the TS region. However, the time scale is crucial. In many cases, the residence time in intermediates approaches the femtosecond regime which is characteristic of TS structures, and the distinction becomes fuzzy. Moreover, for a real multidimensional PES, the nonreactive nuclear motions can entropically lock the system even though there is no well in the energy landscape. In addition, the presence of shallow wells in the energy landscape does not guarantee that trajectories will visit such wells.

2.1.4. The Transition State and its Spectroscopy

Various techniques have been advanced to probe transition states more directly, especially for elementary reactions. Polanyi's analogy of transition-state spectroscopy,[14] from "spectral wing emission", to (Lorentz) collisional line broadening studies, made earlier by A. Gallagher and others, set the stage for the use of continuous wave (CW) spectroscopic methods as a probe. (In this way, only about one part in a million of the population can be detected.) Emission, absorption, scattering, and electron photodetachment are

some of the novel methods presented for such time-integrated spectroscopies, and the groups of Jim Kinsey, Philip Brooks and Bob Curl, Benoit Soep and Curt Wittig, Dan Neumark, and others, have made important contributions to this area of research. The key idea was to obtain, as Kinsey[15] puts it, short-time dynamics from long-time experiments. (The renaissance of wave packet dynamics in spectroscopy, pioneered by Rick Heller, will be highlighted in Section 3.4. and 3.6.) With these spectroscopies operating in a CW mode, a distribution of spectral frequencies provides the clue to the desired information regarding the distribution of the TS over successive configurations and potential energies. Recently, this subject was reviewed by Polanyi and the author and details of these contributions are given therein,[12] and also in ref. [26].

2.2. The Arrow of Time

In over a century of development, time resolution in chemistry and biology has witnessed major strides, which are highlighted in (Figure 8).[16] As mentioned before, the Arrhenius equation (1889) for the speed of a chemical reaction

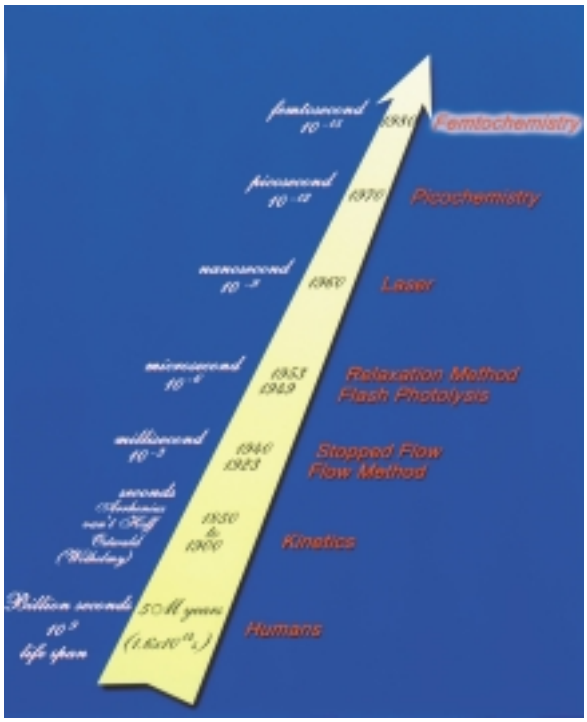


Figure 8. Arrow of time in chemistry and biology showing some of the steps over a century of development (see text).[B1]

gave information about the time scale of rates, and Eyring and Michael Polanyi's (1931) microscopic theoretical description made chemists think of the atomic motions through the transition state and on the vibrational time scale. But the focus naturally had to be on what could be measured in those days, namely the slow rates of reactions. Systematic studies of reaction velocities were hardly undertaken before the middle of the 19th century; in 1850 Ludwig Wilhelmy reported the first quantitative rate measurement, the hydrolysis of a solution of sucrose to glucose and fructose.[8a] In 1901, the first Nobel Prize for chemistry was awarded to van't Hoff for, among other contributions, the theoretical expressions (chemical dynamics), which were precursors to the important work of Arrhenius on rates. Arrhenius too received the Prize in 1903 for his work on electrolytic theory of dissociation.

A major advance in experiments involving sub-second time resolution was made with flow tubes in 1923 by H. Hartridge and F. J. W. Roughton for solution reactions. Two reactants were mixed in a flow tube, and the reaction products were observed at different distances. Knowing the speed of the flow, one could translate this into times of tens of milliseconds. Such measurements of nonradiative processes were a real advance in view of the fact that they were probing the "invisible", in contrast with radiative glows which were seen by the naked eye and measured using phosphoroscopes. Then came the stopped-flow method (B. Chance, 1940) that reached the millisecond scale. The stopped-flow method is still used today in biological kinetics.

Around 1950 a stride forward for time resolution in chemistry came about when Manfred Eigen in Germany and R. G. W. Norrish and George Porter in England developed techniques reaching the microsecond time scale.[17] For this contribution, Eigen and Norrish & Porter shared the 1967 Nobel Prize. The method of flash photolysis was developed by Norrish and Porter a few years after World War II, using electronics developed at the time. They produced an intense burst of light and created radicals in the sample, and, by using other light, they recorded the spectra of these radicals. They achieved kinetics on this time scale and observed some relatively stable intermediates.

Before the turn of the 20th century it was known that electrical sparks and Kerr cell shutters could have response times as short as ten nanoseconds. In an ingenious experiment, Abraham and Lemoine (1899)[18a] in France demonstrated that the Kerr response of carbon disulfide was faster than ten nanoseconds; it has now been measured to be about two picoseconds (with femtosecond response).[18b] Abraham and Lemoine used an electrical pulse which produced a spark and simultaneously activated a Kerr shutter. Light from the spark was collimated through a variable-delay path and through the Kerr cell (polarizer, CS_2 cell, and analyzer). The rotation of the analyzer indicated the presence of birefringence in the cell for short optical delays; this birefringence disappeared for pathlengths greater than several meters, reflecting the total optical/electrical response time of 2.5 ns. In this landmark "pump-probe" experiment, they demonstrated in 1899 the importance of synchronization. The setting of time delays was achieved by varying the light path. Bloembergen has recently given a historical perspective of short-pulse generation[18b] and Shapiro has reviewed the early developments, including mechanical, streak, spark, stroboscope, and other high-speed photography methods.[18d] As pointed out in ref. [18b, d], flash photolysis utilized the above approach but one of the flashes was made very strong to generate high concentrations of free radicals and hence enable their utility in chemical and spectroscopic applications.

Eigen developed "the relaxation method", which reached the microsecond time scale and close to the nanosecond scale.

By disturbing the equilibrium of a solution by either a heat jump, a pressure jump, or an electric field the system shifts from equilibrium. This is the point of time zero. Then the system equilibrates, and its kinetics can be followed. (At about the same time, shock-tube methods were used to provide kinetics on similar time scales.) Eigen called these reactions "immeasurably fast" in his Nobel lecture. There was a feeling that this time resolution was the fastest that could be measured or that needed to be measured for relevance to chemistry (Section 4). The invention of the laser has changed the picture.

Shortly after the realization of the first (ruby) laser by Maiman (1960), the generation of giant and short pulses became possible: nanoseconds by Q-switching (Hellwarth, 1961) and picoseconds (De Maria, et al. 1966) by mode-locking (1964). Sub-picosecond pulses from dye lasers (Schäfer and Sorokin, 1966) were obtained in 1974 by Chuck Shank and Eric Ippen at the Bell Laboratories,[19a] and in 1987 a six-femtosecond pulse was achieved.[19d] In 1991, with the discovery of femtosecond pulse generation from solid-state Ti:sapphire lasers by Sibbett and colleagues,[19e] dye lasers were rapidly replaced and femtosecond pulse generation became a standard laboratory tool; the state-of-the-art, once 8 fs,[19f] is currently about 4 fs and made it into the Guinness Book of World Records (Douwe Wiersma's group[19g]). The tunability is mastered using continuum generation[19h] and optical parametric amplification.

In the late sixties and in the seventies, ps resolution made it possible to study nonradiative processes, a major detour from the studies of conventional radiative processes to infer the nonradiative ones. As a student, I recall the exciting reports of the photophysical rates of internal conversion and biological studies by Peter Rentzepis;[20] the first ps study of chemical reactions (and orientational relaxations) in solutions by Ken Eisensthal;[21] the direct measurement of the rates of intersystem crossing by Robin Hochstrasser;[22] and the novel approach for measurement of ps vibrational relaxations (in the ground state of molecules) in liquids by Wolfgang Kaiser and colleagues.[23] The groups of Shank and Ippen[19abd] have made important contributions to the development of dye lasers and their applications in the ps and into the femtosecond regime. Other studies of chemical and biological nonradiative processes followed on the ps time scale, the scale coined by G. N. Lewis as the "jiffy"—1 jiffy is the time needed for a photon to travel 1 cm (33 picoseconds).[24]

At about the same time in the 1960s, molecular-beam studies of reactions were being developed, and, although I was not initially a member of this community, beams later became part of our effort in femtochemistry. Molecular collisions occur on a shorter time scale than a ps, and real-time studies were not possible at the time. Crossed molecular beams and chemiluminescence techniques provided new approaches for examining the dynamics of single collisions using the post-attributes of the event, the reaction products. The contributions by Dudley Herschbach, Yuan Lee, and John Polanyi[14, 25a] were acknowledged by the 1986 Nobel Prize. From the state and angular distributions of products, information about the dynamics of the collision was deduced and compared with theoretical calculations of the PES and with molecular dynamics simulations. The goal was to find self-consistency and to deduce an estimate of the lifetime of the collision complex. Laser studies using molecular beams have probed dynamics by the careful analysis of product internal energy (vibrational and rotational) distributions as well as the steady-state alignment and orientation of the products. The contributions to this important area are highlighted in the article by Dick Zare and Dick Bernstein[25b] and in the book by Raphy Levine and Bernstein.[9] An overview of femtochemistry (as of 1988) in connection with these other areas is given in a feature article[26] by myself and Bernstein.

3. Femtochemistry: Development of the Field

The development of the field is highlighted in this section, from the early years of studying coherence to the birth of femtochemistry and the explosion of research, or, as the report of ref. [5a] puts it, "… the revolution in chemistry and adjacent sciences." On the way, there were conceptual and experimental problems to overcome and many members of our Caltech group have made the successful evolution possible. The review article published in the *Journal of Physical Chemistry*[B14] names their contributions in the early stages of development. Here, references are given explicitly to the work discussed in the figures.

3.1. The Early Years of Coherence

When I arrived in the US as a graduate student in 1969, nine years after the invention of the first laser, I had no idea of what lasers were about. When appointed to the Caltech faculty as an assistant professor in 1976, I was not thinking or dreaming of femtosecond time resolution. But I had the idea of exploring coherence as a new concept in intra- and intermolecular dynamics. This proved to be vital and fruitful.

3.1.1. New Techniques for Molecules

The Caltech offer included start-up funds of 50000 $ for capital equipment (15000 $ for shop services), an empty laboratory of two rooms and an office next to it. A few months before moving to Caltech in May of 1976, I made the decision not to begin with the type of picosecond research I was doing at Berkeley as a postdoctoral fellow. Instead, the initial effort was focused on two directions: studies of coherence in disordered solids, and the development of a new laser program for the study of the phenomena of (optical) coherence. Prior to the final move, I came down from Berkeley for several visits in order to purchase the equipment and to outline the laboratories' needs for electricity, water, gases, and so on; my feeling was that of a man left out in a desert with the challenge to make it fertile. We spent a significant fraction of the 50000 $ on setting up the apparatus for the optical detection of magnetic resonance (ODMR) to study disordered solids. My experience at Penn with Professor Robin Hochstrasser and at Berkeley with Professor Charles

Harris was to culminate in these experiments. The key questions I had in mind were: What is the nature of energy migration when a crystal is systematically disordered? Is it coherent, incoherent, or partially coherent? Is there a relationship between optical and spin coherence?

While the ODMR apparatus was being built, I was thinking intensely about new laser techniques to probe the coherence of optical transitions (so-called optical coherence). I had the intuitive feeling that this area was rich and at the time had in mind several issues which were outlined in my research proposal to Caltech. Laser experiments were designed with objectives focused on the same issues outlined in the proposal. First, in the work I published with Charles Harris, and alone at Berkeley, the coherence probed had been that of spin (triplet excitons) and I felt that we should directly probe the optical coherence, that is, the coherence between the excited electronic state and the ground state, not that between two spin states of the same excited state (Figure 9). Second, I did not believe that the time scale of spin coherence was the same as that of optical coherence. Later, I wrote a paper on the subject which was published in the *Journal of Chemical Physics* (1979) with the title: "Are the homogeneous linewidths of spin resonance and optical transitions related?"

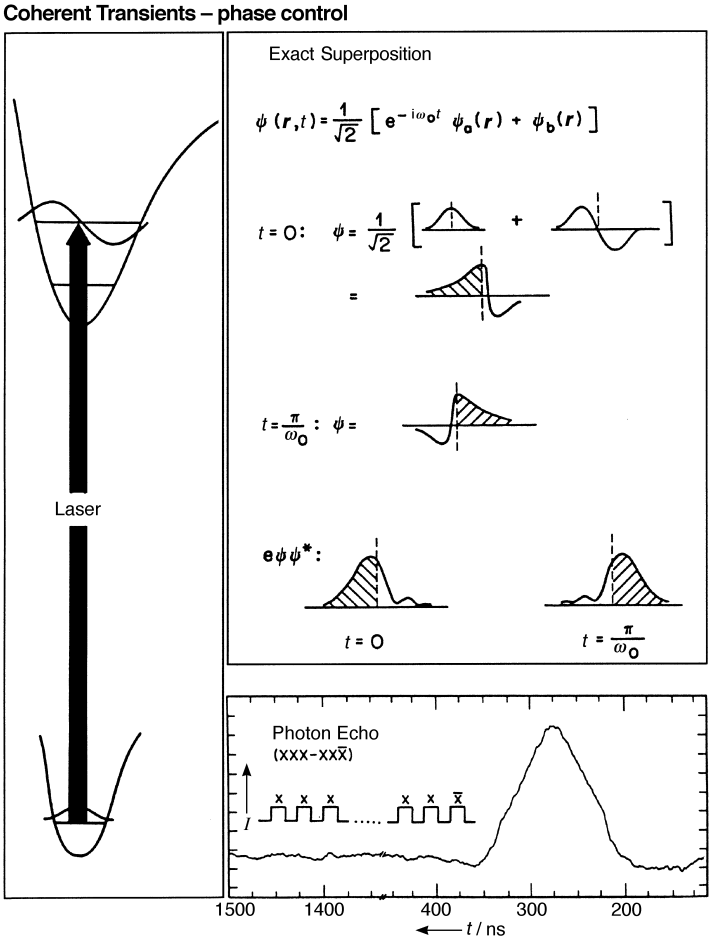


Figure 9. Molecular coherence and dephasing. Coherent transients from the superposition of states, and control of pulse phase (x or $\bar{x}$) in multiple pulse experiments, the optical analogue of NMR spectroscopy. The photon echo of iodine gas (bottom right) was observed on the spontaneous emission using the described pulse sequence.[50, B9, B13, B22, B23]

I was convinced that essentially all molecular optical transitions in solids are inhomogeneous, that is, they do not reflect the true dynamics of a homogeneous ensemble, but rather the overlapping effects of sub-ensembles. This was the key point outlined in my research proposal to Caltech. If the new set of laser experiments at Caltech proved successful, we should be able to find the answer to these important (to me) questions. However, the funds remaining were insufficient to realize our dream for the new experiments. Fortunately, Spectra Physics, started in 1961 and was now a huge laser company, was proud of a new product and was interested in helping us demonstrate the usefulness of one of the first single-mode dye lasers they produced. At Caltech, we had the argon-ion pump laser, from Wilse Robinson's Laboratory, and added the dye laser we obtained from Spectra Physics with the idea that we would purchase it if the experiments were successful. David Evans of Spectra Physics was instrumental in helping us achieve this goal. What was left were the low-temperature cryostat and electronics. We could not afford a real metal cryostat, so we custom-made a glass Dewar that could cool to 1.8 K. Most of the electronics were obtained on loan for several months. To generate laser pulses we used switching methods developed at the Joint Institute for Laboratory Astrophysics (JILA) and IBM. The work at IBM by Dick Brewer's group triggered our interest in using electro-optic switching methods.

We succeeded in making the laser perform according to specifications and began the first experiments with phenazine crystals. Phenazine has unique properties which I learned about in Robin Hochstrasser's laboratory. At Berkeley I published a paper outlining the nature of coherence in multidimensional systems and used phenazine as a prototype experimental system. Our first laser transient at Caltech was beautiful. Unfortunately, the transient was from the electronics, not from the crystal, but we soon realized this! We decided to abandon this particular system for a while and to try an impurity crystal of pentacene in a host of terphenyl. We also decided to study gases, and some success came our way.

With the theoretical knowledge acquired in handling coherence effects, which requires expertise with density matrix formalism and its manipulation in geometrical frames, I had a novel idea: we should be able to detect coherence on the incoherent emission at optical frequencies. From many discussions with Alex Pines and Charles Harris at Berkeley, I knew the power of "adding" pulses in NMR and ESR spectroscopy. This idea was successful and indeed we were able to observe the photon echo on the spontaneous emission (Figure 9) using three optical pulses. Only months after my arrival in May of 1976 we published our first scientific paper from Caltech. This success gave us confidence in the approach and in our understanding of the principles of coherence and its probing in molecular systems. We applied it to larger molecules with success but also encountered some disappointments. This work was followed by a variety of extensions to studies in gases and solids and also in a home-made (from glass) effusive molecular beam. The small group in our laboratory working on optical coherence became productive and we had an exciting time. Our group and that of Douwe Wiersma in Holland were then the two most active in these areas of chemical research.

In the meantime, the work on disorder in solids began to yield interesting results and, surprisingly, we observed an unusual change in the degree of energy transfer with concentration, which we published as evidence of Anderson localization, a hot topic in the 1970s. This was followed by detailed studies of several systems and I wrote my first research proposal to the National Science Foundation (NSF). The research was funded! The then program director at NSF, Fred Stafford, was supportive of the effort and we have maintained our support from the Division of Materials Research to this day; the NSF's Chemistry Division continues to support our research. Knowledge of energy transfer was also helpful in another area. Terry Cole, a visiting scholar at Caltech, and I initiated work on the studies of luminescent solar concentrators (LSCs) using energy transfer between dyes as a key principle. This idea, too, was successful and funding for this research came in from SERI and from ARCO. The work on LSCs resulted, ultimately, in a patent (with Sam Batchelder; issued in 1980) and in several publications. My research group was rapidly expanding.

After 18 months at Caltech, I was pleased to learn that my colleagues were considering my case for tenure. Tenure was granted a few months later, two years after my arrival at the Institute. I was both appreciative and pleased. We continued research in four areas: optical coherence phenomena and dephasing; disorder in solids; picosecond spectroscopy; and LSCs. In my own department, some colleagues were not too excited about "this stuff of coherence and dephasing"—thinking that it was not relevant to chemistry. Many chemists on the outside were also unsure what this was all about. In fact, a notable chemist once said publicly at a conference I attended that coherence and dephasing had nothing to do with chemistry. On the physics side, I was invited to numerous conferences, including one in which the Nobel Laureate Willis Lamb asked me to have dinner to discuss our research. This was a special experience.

I was not convinced by these doubts and my faith helped us to continue along with the development. The concept of coherence turned out to be fundamental in femtochemistry, and it is now well accepted that coherence is a key process in the probing and controlling of molecular dynamics. With the success we had with observations and studies of coherence in different systems, I wrote an article for *Accounts of Chemical Research*, published in 1980, with the title "Optical Molecular Dephasing—Principles of and Probings by Coherent Laser Spectroscopy". I felt that the nanosecond time scale we had mastered should be extended to the picosecond time scale, but did not wish to repeat the Berkeley experience with glass lasers. Fortunately, the design for the first sub-picosecond dye laser was reported in 1974 and we decided to build one to study the phenomena of coherence—but now on a shorter time scale.

3.1.2. The Optical Analogue of NMR Spectroscopy: Controlling the Phase

From the studies of optical transients, we learned that coherence can be probed directly in real time in gases (and solids) and that incoherent decay (for example, fluorescence) can be used to monitor such coherences provided that the laser pulse(s) is capable of forming a coherent superposition of states. For two states of a transition ψ_a and ψ_b, the coherent state can be written as Equation (4). The coefficients $a(t)$ and $b(t)$ contain in them the familiar quantum-mechanical phase factors, $\exp(-iE_at/\hbar)$ and $\exp(-iE_bt/\hbar)$, respectively (see Figure 9).

$$\Psi_{\text{coherent}}(t) = a(t)\ \psi_a + b(t)\psi_b \tag{4}$$

By using pulse sequences we could directly monitor the behavior of the ensemble-averaged coefficients of $\Psi\Psi^*$, $\langle a(t)\, b^*(t)\rangle$, which contain information on the coherence decay time (optical time T_2); they are the off-diagonal elements of a density matrix, ρ_{ab}. The term $\langle a(t)\, a^*(t)\rangle$ is the population of state ψ_a and represents the diagonal density-matrix element ρ_{aa}; $\langle a(t)\, a^*(t)\rangle$ decays with optical time T_1. We were thus able to demonstrate the power of the optical analogue of NMR pulse techniques in learning about coherence and the origin of optical dephasing in molecular systems of interest to chemical dynamics. This advance changed the thinking of many with the recognition that it was impossible to deduce T_1 and T_2 from measurements of the line width of inhomogeneous transitions.

One feature of this work which later helped us in the study of molecular reaction dynamics was the realization of the importance of the pulse phase (shape) in studies of coherence. With the acousto-optic modulation techniques we developed earlier, it became possible to make optical pulse sequences with well-defined phases. This development took us into the domain of selective and prescribed pulse sequences which could then be used to enhance coherences or suppress them—the optical analogue of NMR multiple pulse spectroscopy. We published several papers on phase control and extended the applications to include photon locking. We were eager to extend these techniques to the picosecond time domain in order to study solids, but, for several reasons, our attention was diverted to gas-phase molecular dynamics.

By this time, our group's efforts were narrowing on two major areas. (Dick Bernstein, who was on the Visiting Committee for our Division, hinted that I was doing too much in too many areas!) The work on disorder and LSCs was gradually brought to completion. Picosecond spectroscopy of rotational diffusion and energy transfer in liquids were similarly handled. I felt that the latter area of research was crowded with too many scientists, a characteristic I do not enjoy when venturing into a new area. I must add that I was not too thrilled by the exponential (or near exponential) decays we were measuring and by the lack of molecular information. Our effort began to emphasize two directions: 1) the studies of coherence and dynamics of isolated molecules in supersonic beams and 2) the development of the optical analogue of NMR spectroscopy. The low-temperature facility was put to use to study the dephasing and polarization of highly vibrationally excited molecules in the ground state. Coherence in chemical dynamics was occupying my thinking, and I made a detour in the applications that turned out to be significant.

3.2. The Marriage with Molecular Beams

The Bell Laboratories design for the dye laser (passively mode-locked, CW, and cavity dumped) was too restrictive for our use and, even though we published several papers on studies in the condensed phase with 0.6-ps resolution, we decided to change to a new system. The synchronously pumped mode-locked (CW) dye laser allowed for tunability and also detection techniques for photon counting. The power of single-photon counting became apparent, and a new laser system, a synchronously pumped, cavity-dumped dye laser was constructed for studies of gas-phase molecular dynamics, but now with the benefit of all the expertise we had gained from building the first system used for the studies in the condensed phase and for probing the torsional rigidity of DNA.

Stimulated by the work on coherence, and now with the availability of picosecond pulses, I thought of an interesting problem relating to the question of intramolecular versus intermolecular dephasing. In isolated, large molecules (as opposed to diatomics), there are the so-called heat bath modes which can be a sink for the energy. The question arose: Could these bath modes in isolated, large molecules dephase the optically excited initial state in the same way that phonons of a crystal (or collisions in gases) do? This problem has some roots in the question of state preparation, and I was familiar with its relationship to the description of radiationless transitions through the work of Joshua Jortner, Wilse Robinson, and others. There was much theoretical activity about dephasing, but I felt that they were standard extensions and they did not allow for surprises. We decided on a new direction for the studies of coherence in a supersonic molecular beam.

Rick Smalley came to Caltech in May 1980 and gave a talk entitled "Vibrational Relaxation in Jet-Cooled Polyatomics". He spoke about his exciting work on the naphthalene spectra. From the line width in the excitation spectra, he inferred the "relaxation time". At the time, the work by Don Levy, Lennard Wharton, and Smalley on CW (or nanosecond) laser excitation of molecules in supersonic jets was providing new ways to examine the spectroscopy of molecules and van der Waals complexes. Listening to Rick and being biased by the idea of coherence, I became convinced that the way to monitor the homogeneous dynamics was not through the apparent width but by using coherent laser techniques. This was further kindled by the need for direct measurement of energy redistribution rates; we were encouraged by Charlie Parmenter after he had reported on a chemical timing method using collisions as a "clock" to infer the rate of energy redistribution. The first "real" supersonic molecular beam was huge. We did not know much about this kind of technology. However, in a relatively short time, it was designed and built from scratch, thanks to the effort of one graduate student who must have consumed kilos of coffee! The molecular beam and picosecond system were interfaced with the nontrivial addition of a spectrometer to resolve fluorescence in frequency and time. This was crucial to much of the work to come.

3.2.1. The Anthracene Discovery: A Paradigm Shift

Our goal in the beginning was to directly measure the rate of intramolecular vibrational-energy redistribution (IVR), expecting to see a decrease with time (exponential decay) in the population of the initially excited, vibrational state and to possibly see a rise in the population in the state after the redistribution, thus obtaining T_1 directly. What we saw in these large systems was contrary to the popular wisdom and unexpected. The population during IVR was oscillating coherently back and forth (Figure 10) with well-defined period(s) and phases. We were very excited because the results revealed the significance of coherence at its best in a complex molecular system, now isolated in a molecular beam, with many degrees of freedom. I knew this would receive attention and skepticism. We had to be thorough in our experimental tests of the observation and three of us went to the laboratory to see how robust the observation was. We published a Communication in the *Journal of Chemical Physics* (1981). Earlier there had been attempts by another

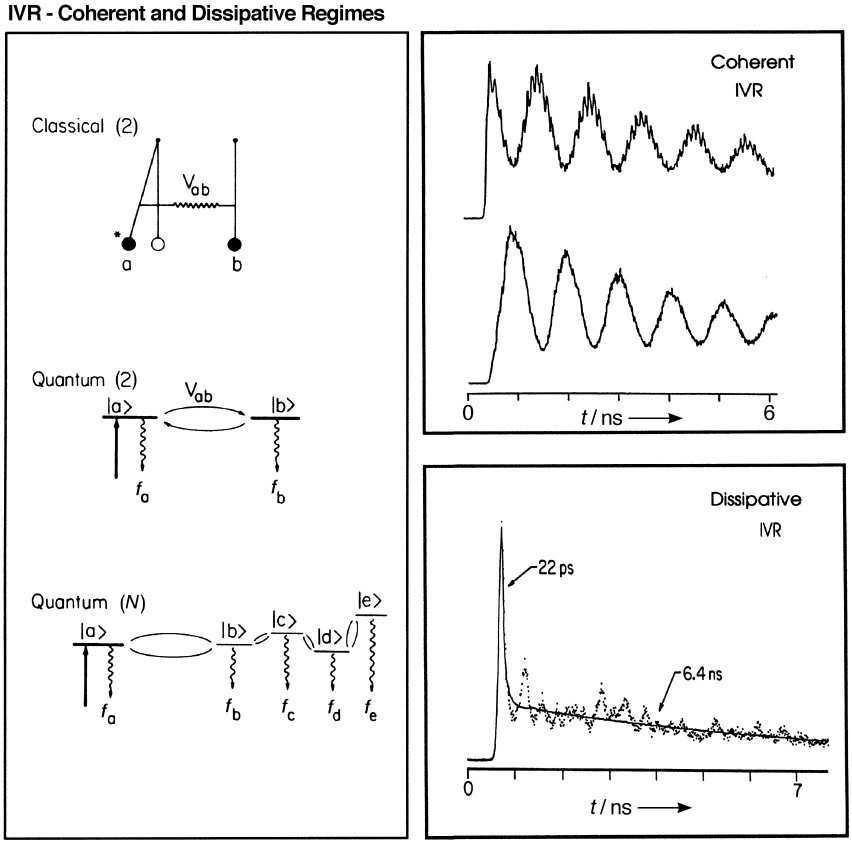


Figure 10. Dynamics of IVR showing the coherent, restricted, and the dissipative regimes. Note the exact in-phase and out-of-phase oscillatory behavior between the vibrational states of the system (anthracene in a molecular beam). The theory for classical and quantum pictures (left) has been discussed in detail in the literature.[51, B20, B21]

group to observe such a "quantum coherence effect" in large molecules, but the observation turned out to arise from an artifact. Some scientists in the field were skeptical of our new observation and the theorists argued that a molecule is too big to see such quantum coherence effects among the vibrational states. Furthermore, it was argued that rotational effects should wash out such an observation.

We followed the initial publication with several others and the effect became even more pronounced with shorter time resolution. Physicists appreciated the new results. We published an article in *Physics Review Letters* on the nature of nonchaotic motion in isolated systems, and Nico Bloembergen and I wrote a review (1984) on the relevance to laser-selective chemistry.[B21] We and other groups subsequently showed the prevalence of this phenomenon in large molecules. As is often the case in science, after the facts have been established and in retrospect, the phenomenon was clear and was soon accepted; to some it even became obvious. Looking back, this novel and unexpected observation was a *paradigm shift* of critical importance, for a number of reasons:

1. The observation was the first to clearly show the presence of a "quantum coherence effect" in isolated complex chemical systems and only among selected vibrational states. In other words, out of the expected chaotic motion in the vibrational and rotational phase space we could see ordered and coherent motion despite the presence of numerous vibrational degrees of freedom (from S_0 and S_1 states). This point was theoretically appreciated by only a few scientists. In fact, at one point Stuart Rice and I drafted a paper on the subject, thinking of clarifying the point. At the time, researchers working in the area of high-resolution spectroscopy were observing complex spectra and attributing this complexity to chaotic vibrational motion in the molecule. Stuart and I argued that spectral complexity does not mean chaos, and the anthracene experiment was a clear demonstration in real time.
2. The experiment demonstrated that coherence had not previously been detected in complex systems, not because of its absence but due to the inability to devise a proper probe. Detection of total absorption or total emission (at all wavelengths) from molecules gives a nonselective window on the dynamics and in this way coherence cannot be detected. This was a key point for the success of the anthracene experiment for which both time and wavelength were resolved and correlated. For all subsequent work on wave packet dynamics, nuclear motion in chemical reactions, and femtochemistry, this concept of "window probing" was essential. The concept was further elucidated by resolving the phase character. By probing at two different wavelengths, we found that the quantum oscillations exhibit identical periods, but were phase-shifted by exactly 180° (that is, they are out-of-phase) (Figure 10). The two wavelengths resolved were those corresponding to emission from the initial vibrational state and to that of the vibrational state to which the population goes by IVR. Thus, if "total detection" was invoked, the in-phase and out-of-phase oscillations will add up to cancel each other and coherence would have remained undiscovered.
3. The observation of phase-coherent dynamics gave us a new dimension. The phase shift indicates a true transfer of population, in contrast with conventional quantum beats, and by analyzing the phases we could understand the nature of IVR: "concerted", namely, going at the same time to all states, or "nonconcerted" that is going in a sequential redistribution of vibrational energy. We could also obtain the time scale and the effect of molecular rotations on coherence of the vibrational motion.
4. The observation of phase-coherent dynamics illustrated the importance of the "preparation of nonstationary states" in molecules. This issue was of fundamental importance in radiationless transition theories involving multiple electronic states, and experiments by Jan Kommandeur and by Doug McDonald have shown this interstate coupling. The question of interest to us was: What nuclear states do we prepare in the isolated molecule on a single surface? The anthracene experiment taught us that a coherent source spanning the stationary states can prepare a nonstationary state which evolves with time. Moreover, we can prepare molecules in-phase at time zero to observe the subsequent coherent dynamics. This concept indicates that the description, in terms of Schrödinger's molecular stationary states, is not cardinal and that the time-dependent picture is real and directly relevant to dynamics. Most textbooks describe dynamics in terms of stationary states and it took some time for this concept of a time-dependent description to be appreciated. I recently found a theoretical article by Roy Gordon published in the 1960s touching on similar issues. In femtochemistry, the concept of time-domain dynamics is what describes elementary motions.
5. By directly probing coherence and its extent in isolated, complex molecular systems we advanced some concepts regarding the nature of IVR and its regions. We divided the regions of IVR into three basic ones: no IVR, restricted IVR, and dissipative IVR. We also established that the IVR picture of one vibrational state coupled to a continuum of vibrational levels is not adequate. Instead it is a multi-tier coupling among vibrational states.

This work and its implications were published in two series of papers and reviewed in two book chapters.

3.2.2. The Successful 036 Laboratory

The laboratory known as 036 was in the sub-basement of Noyes. In this laboratory, the initial work on IVR was followed by fruitful applications spanning 1) studies of IVR in other systems, 2) radiationless transitions, and 3) reaction rates of a variety of systems. One of our first studies of reactions on the picosecond time scale, isomerization of stilbene, was stimulated by discussion with Robin Hochstrasser about his work on stilbene vapor at room temperature. He felt that if we could resolve the low-frequency modes in the molecular beam, we would derive a great deal of information on the torsional potential. We resolved these torsional modes. Furthermore, we decided to study the rates as a function of energy and in the process found the barrier for twisting

around the double bond and observed coherent IVR in reactions, the first such observation. Even now, stilbene remains a member of our molecular family and continued studies have been pursued on the femtosecond time scale by us and others.

The following list highlights some of the work (Figure 11) done in this initial period from 1981 to 1983: 1) IVR in anthracene and stilbene; 2) *trans*–*cis* isomerization of stilbene; 3) quantum beats and radiationless transitions in pyrazine; 4) intramolecular hydrogen bonding in methyl salicylate; 5) intramolecular electron transfer in donor-bridge-acceptor systems; 6) IVR and dissociation of intermolecular hydrogen-bonded complexes; and 7) isomerization of diphenylbutadiene and styrene.

Over the years, in the same laboratory (036 Noyes), members of our group have made new extensions covering the following topics: isomerization in isolated molecules versus in bulk solutions; nonchaotic multilevel vibrational energy flow; mode-specific IVR in large molecules; IVR dynamics in alkylanthracenes; isotope effects on the isomerization of stilbene; charge transfer and exciton dynamics in isolated bianthracene; isotope effects on the intramolecular dephasing and molecular states of pyrazine; IVR dynamics in alkylanilines (the "ring + tail" system); mode-specific (non-RRKM) dynamics of stilbene-rare gas van der Waals complexes; solvation effects on intramolecular charge transfer; IVR dynamics in *p*-difluorobenzene and *p*-fluorotoluene (real time versus chemical timing); IVR dynamics in deuterated anthracenes; dynamics of interstate coupling in chromyl chloride; dynamics of IVR and vibrational predissociation in anthracene-Ar_n complexes ($n = 1$–3); structural effects on the dynamics of IVR and isomerization in stilbenes; and dynamics of IVR and vibrational predissociation in *n*-hexane-solvated *trans*-stilbene. The research resulted in a series of publications.

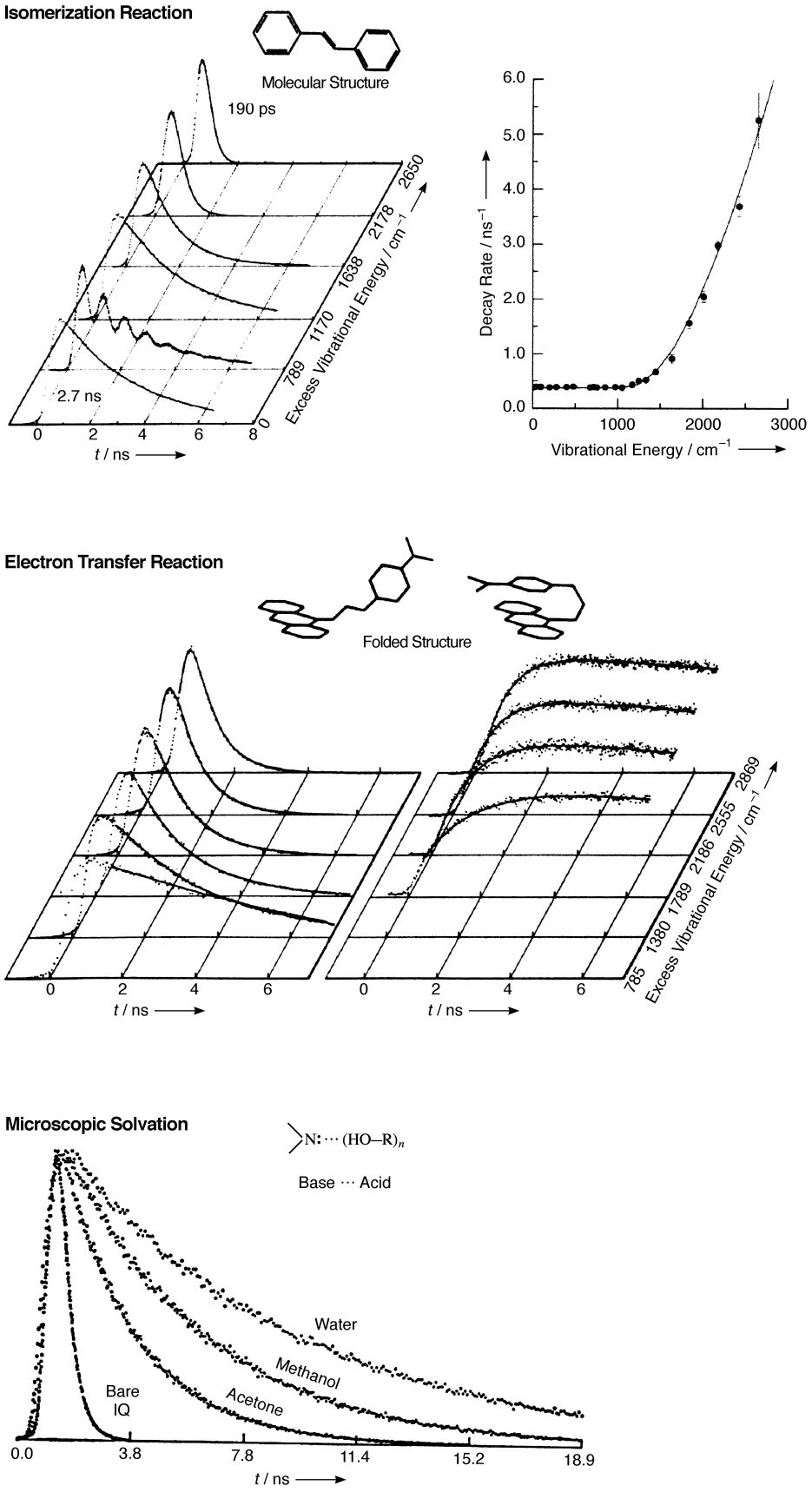


Figure 11. Some examples of studies made in the early 1980s in the 036 Laboratory: The isomerization of stilbene, intramolecular electron transfer, and solvation in clusters (see text).[52, B3] IQ = isoquinoline.

3.2.3. Changing A Dogma: Development of RCS

The success with the anthracene experiment made us ask a similar question, but now regarding the coherent rotational motion of isolated, complex molecules. There were theories around which discarded its possibility because of the general belief that Coriolis interactions, anharmonicity, and other interactions would destroy the coherence. We worked out the theoretical implications and the results suggested possibly another surprise: if we could align the molecules with a polarized picosecond pulse and probe (polarization-selective) the rotating molecules, we should be able to observe rotational recurrences which would give the full period of rotations of the isolated (large) molecule. Classically, it is as if the molecule rotated back to its initial configuration. This rotation period gives the moment of inertia and, since the masses of the atoms are known, we can deduce distances, and hence obtain information on the molecular structures of very large molecules.

Indeed the recurrences in stilbene were observed with high precision, and its molecular structure deduced. Coherence in rotational motion was clearly evident and could be probed in a manner similar to what we had done with vibrational coherence. The approach was again met with some skepticism regarding its generality as a molecular structure technique. However, it is now accepted by many as a powerful Doppler-free technique; more than 120 structures have been studied this way. The method (Figure 12) is termed "rotational coherence spectroscopy (RCS)" and is successfully used in many laboratories. Some book chapters and review articles have been published on the subject (see the Bibliography).

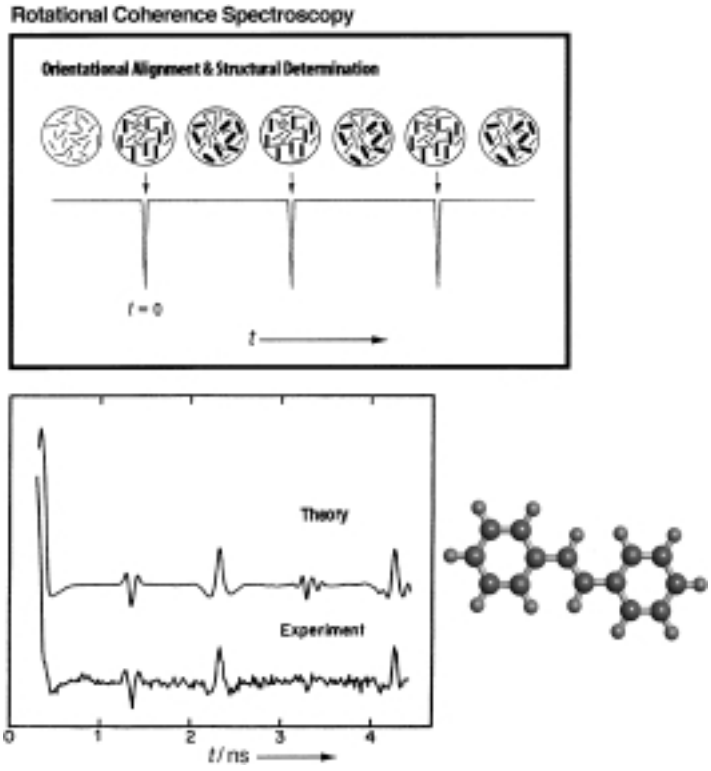


Figure 12. The concept of RCS and the first experimental observation made in a beam of *trans*-stilbene.[53, B7, B13]

Out of this first marriage between ultrafast lasers and molecular beams came the developments and concepts discussed above. We were now poised to study molecules and reactions with even shorter time resolution. We could study their vibrational and rotational dynamics and align ("orient") them by controlling time.

3.3. The Transition to the Sub-Picosecond Regime

By the early 1980s, our laser time resolution for studying molecules in supersonic jets was 15 ps and detection was made using a microchannel plate (about 40 ps). With this resolution, we had already studied reactions such as the isomerization (twisting) of stilbene, charge transfer, and intra- and intermolecular proton and hydrogen-atom transfer. How could we improve the time resolution and study, in a general way, the elementary steps of reactions? The only approach I knew of was to use two pulses, one to "pump" and the other to "probe". Unlike liquid-state studies, where the approach was proven successful, in this case, the density of a molecular beam is very low. Furthermore, it was not clear how to establish the zero of time in situ in the molecular beam and how to avoid temporal broadening as a result of propagation effects.

3.3.1. A New Beam Machine: Pump-Probe Mass Spectrometry

I thought we should build a second generation beam apparatus to house a time-of-flight mass spectrometer. From the physics literature, it was clear that single atoms could be detected using ionization techniques with lasers, and such detection had already been successful with nanosecond lasers. Unlike many nanosecond studies, we should propagate the two picosecond (and later femtosecond) pulses in the same direction, otherwise we would lose the ultrashort time resolution. The same beam machine was equipped with optics for laser-induced fluorescence detection. We began a new direction of research in a separate laboratory of our group. The new beam was built and integrated with two independently tunable dye lasers. This proved to be a precursor to the femtochemistry work as this taught us to master pump-probe picosecond and sub-picosecond experiments on chemical reactions. In this same laboratory, we studied with a resolution of a few ps: 1) dissociation reactions; 2) ground-state, overtone-initiated reactions; 3) van der Waals reactions, and others (Figure 13). We wrote a series of papers on state-to-state microcanonical rates $k(E)$, and addressed theoretical consequences and deviations from the statistical regime. It was in two of these systems (reactions of NCNO and ketene) that we found that the statistical phase-space theory (PST), although successful in describing product-state distributions, failed in describing the microcanonical rates $k(E)$ as a function of energy. Moreover, we made careful studies of the effect of rotational population on $k(E)$, and the effect was dramatic near the threshold value. Rudy Marcus, stimulated by these studies of $k(E)$, applied variational RRKM theory and we published some papers in a collaborative effort. The key point here is

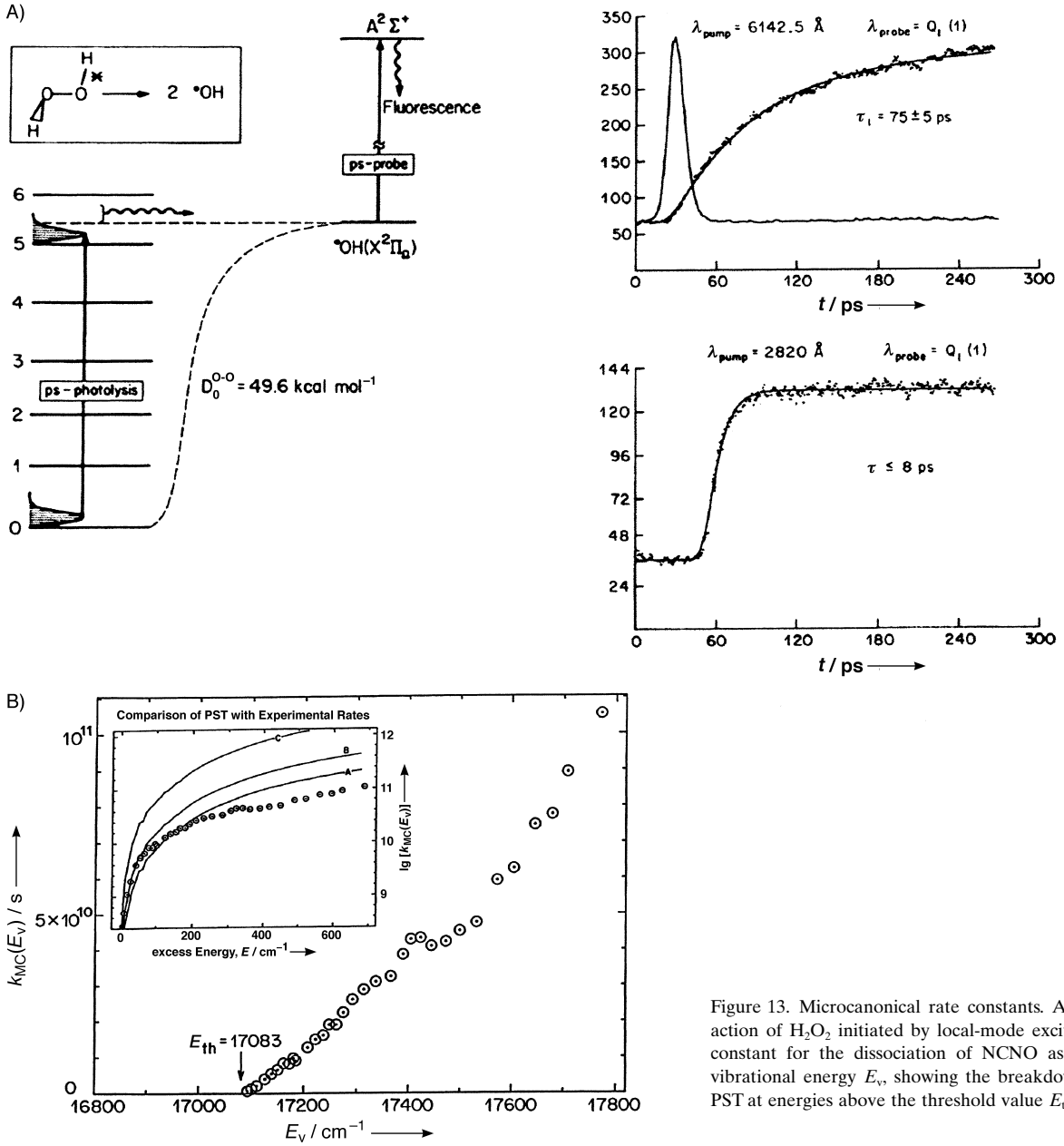


Figure 13. Microcanonical rate constants. A): Ground-state reaction of H_2O_2 initiated by local-mode excitation; B): the rate constant for the dissociation of NCNO as a function of the vibrational energy E_v, showing the breakdown of conventional PST at energies above the threshold value E_{th} (inset).[54, B1]

that the TS "moves" to different (shorter) distances along the reaction coordinate at different energies; the cardinal definition is relaxed (see Section 2). In another system (H_2O_2), we studied the ground-state ("thermal") reaction for the first time in real time by initiating the reaction with direct excitation of the overtones of the OH stretching vibration (Figure 13). The coupling between theory and experiment stimulated my interest in the nature of transition states which generally live for less than a picosecond. The thirst for even shorter time resolution became real.

3.3.2. The First Experiment on ICN: Sub-picosecond Resolution

In the early 1980s, the technology of pulse compression became available and we ordered, from Spectra Physics, a pulse compressor—a fiber optic arrangement to reduce the laser pulse width to sub-picosecond. The company indicated that it would take them several months to build one, and that the only one available was at Purdue University in the laboratory of Professor Duane Smith, one of the first two graduate students I had at Caltech. I mentioned to Duane my excitement about the experiment, which was intended to directly monitor the elementary bond breakage in a molecule, and asked if it was possible to borrow his compressor. The triatomic molecule ICN was chosen because the CN radical could be conveniently monitored by laser-induced fluorescence; we had been encouraged by the positive experience we had had with CN from NCNO and with earlier picosecond results on ICN. Also, ICN had been central to studies of dissociation reactions and to photofragment spectroscopy. Previous work, without time resolution, had provided a measurement of the so-called anisotropy parameter β and, hence, inference of the time scale.

All that we needed was a factor of 10 – 100 improvement in time resolution from what we currently had in the group. Duane shipped the compressor and joined us for two weeks. We observed the first ICN sub-picosecond transient, thus establishing the new methodology. In the same year, we wrote a paper which was accepted and published (December 1985) in the *Journal of Physical Chemistry*. We did not resolve the transition states of this reaction, but only detected the rise of the product. The last paragraph in this paper summarized what it would be possible to do if the time resolution could be improved by a further order of magnitude: "Since the recoil velocity is $\sim 2 \times 10^5$ cm s^{-1}, the fragment separation is ~ 10 Å on the time scale of the experiment (about 500 fs). With this time resolution, we must, therefore, consider the proximity of fragments at the time of probing, namely, the evolution of the transition state to final products." I wrote this sentence having in mind that the femtosecond resolution is the ideal one and that our next step in research should be in this direction.

Several factors influenced the fast entry into femtochemistry. The development in 1981 by Richard Fork, Ben Greene, and Chuck Shank of the colliding pulse mode-locked (CPM) ring dye laser took the pulse duration into the 90-fs regime. By 1985, when we were involved in the ICN experiment, 27-fs pulses were generated with the help of intracavity pulse compression. Soon after, in 1987, 6-femtosecond pulses were obtained by amplification and extracavity compression.[19d] With such short pulses, and with the help of the earlier development of continuum generation by Bob Alfano and Stanley Shapiro,[19h] continuously tunable femtosecond pulses became available and only (!) required expertise in ultrafast lasers and nonlinear optics.

The interaction with several colleagues was a stimulating force in the initial effort. With Rudy Marcus and Vince McKoy, my colleagues at Caltech, I discussed many experiments and theories, especially on our way to lunch at the Athenaeum, Caltech's faculty club. John Polanyi came to Caltech in 1982 as a Fairchild Scholar. John saw the importance of (CW) transition-state spectroscopy, and his paper in a book I edited (proceedings of the conference in Alexandria) was on this subject, focussing on the reactions of $H + H_2$ and NaI dissociation (wing emission). For some reason, we did not discuss femtosecond transition-state spectroscopy at this time, but instead we (with John providing all the notes in writing) were interested in intense-laser-field stimulated emission in the NaI system and in the field "dressing" of the potentials. I do not know why I did not think of this system as the first one for femtosecond transition-state spectroscopy. This may have been because of the earlier experience we had with the ICN picosecond experiments. Later, the potentials John sent from Toronto were helpful in my thinking of the NaI experiment.

At nearby UCLA, the arrival of Dick Bernstein to the area was a real blessing. He was extremely excited about the developments and the possibilities for real-time studies of molecular reaction dynamics. It was at his house in Santa Monica that the word *femtochemistry* was coined, helped by a discussion in the company of his wife Norma and brother Ken. Dick also came to Caltech as a Fairchild Scholar in 1986, and in 1988 we wrote a feature article together (published in *Chemical & Engineering News*[26]). We had great fun writing this article and we learned an enormous amount about molecular reaction dynamics. We also had a genuine collaboration on bimolecular reactions and published a paper in 1987. Dick came to Caltech again in 1990, but sadly died before ending his sabbatical; a number of experiments, particularly the new direction of surface femtochemistry, were designed as part of our plan. Finally, the collaboration I had with Rich Bersohn, while he was at Caltech as a Fairchild Scholar, was enlightening. We discussed the classical picture of femtosecond spectroscopy of dissociating molecules, and wrote a theoretical paper on this subject.

3.4. The Femtosecond Dream

3.4.1. A Piece of Good Fortune

To achieve the femtosecond time resolution, we needed a new laser system. A piece of good fortune came our way at a time when funding was limited and when the establishment of femtosecond lasers and molecular beam technologies required a "quantum jump" in support. Shaul Mukamel invited me to a workshop in Rochester (October 1985) on intramolecular vibrational redistribution and quantum chaos. I spoke about "IVR and chemical reactivity", and there in the audience were two program directors from the Air Force Office of Scientific Research (AFOSR): Larry Davis and Larry Burggraf. They requested a preliminary proposal immediately, and I sent one in October, followed by a complete proposal in January of 1986.

The proposal was funded and approved in August of 1986, to start in November of the same year. Larry Davis saw to it that we could order the equipment needed as soon as possible and made the necessary arrangements to do so; AFOSR continues to support our program. We did not have laboratory space to house the new equipment, but Caltech responded. Fred Anson, our Division Chairman at the time, arranged for the space (which once housed the X-ray machines of Linus Pauling) and Murph Goldberger, our President, provided funds for the renovation without delay—Murph appreciated the physics and Fred saw the importance of the new research to chemistry. By Thanksgiving (1986), we entered the new laboratory, and the CPM laser was operational at the "femtosecond party" on December 11, 1986. We focused again on the ICN reaction, but this time on the femtosecond time scale in FEMTOLAND I.

3.4.2. The Classic Femtosecond Discovery in ICN

The goal of the ICN experiment was to resolve in time the transition-state configurations en route to dissociation [Eq. (5)]. Not only did we wish to monitor the final CN

$$ICN^* \rightarrow I \cdots CN^{*+} \rightarrow I + CN \qquad (5)$$

product, free of the force field of iodine (which we did in 1985), but also the transitory species $I \cdots CN^{*+}$ (Figure 14).

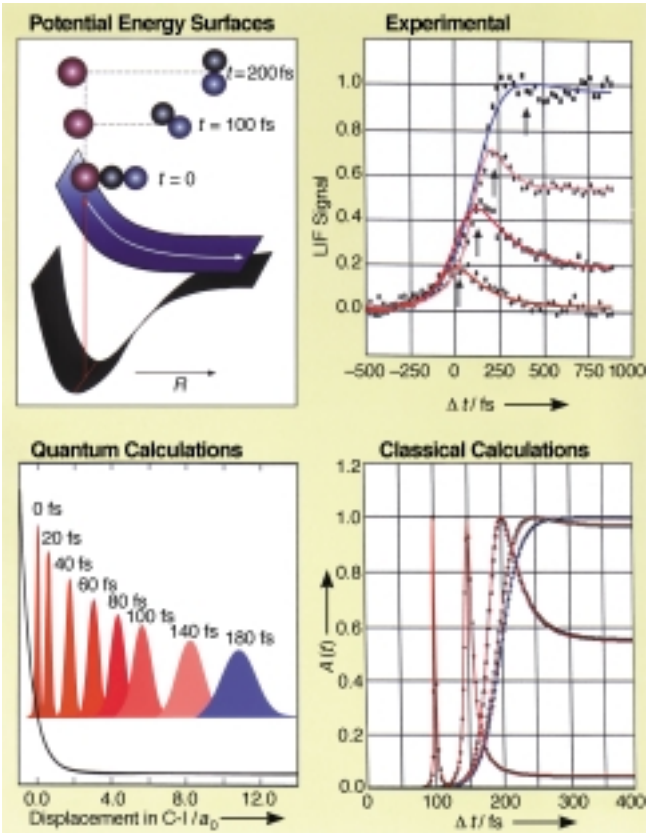


Figure 14. Femtochemistry of the ICN reaction, the first to be studied. Top right shows the experimental results for the probing of the reaction in the transition state region (rise and decay) and the final CN fragment (rise and plateau) with precise clocking of the process (Δt = time delay); the total time is 200 fs. The iodine fragment was also detected to elucidate the translational energy change with time. Classical and quantum calculations are also shown (see text).[55, B1, B4, B6, B14, B16, B18, B19, B28]

The first $I\cdots CN^{*\neq}$ transient surprised us, but after long and late hours of discussions and control experiments it became clear that, indeed, the transition configurations and the final products could be separately monitored in real time. We submitted our first communication to the *Journal of Chemical Physics* (received June 3, 1987), and it was accepted on June 15, 1987. The referee of this paper was not only prompt, but also, in retrospect, visionary. His report was ultrashort: "It (the manuscript) has the smell that the authors are onto some very exciting new stuff… This manuscript meets all requirements for a communication. It may turn out to be a classic. Publish with all dispatch."

Our thinking about the process of bond breakage was intuitive and relied on classical concepts, as discussed in the prologue. The basic observations made (Figure 14) in the ICN experiment could be related to the femtosecond nuclear dynamics; the delayed appearance of the CN (on-resonance) and the build-up and decay of transition configurations (off-resonance) was understood using simple classical mechanics and even a helpful kinetic picture of the type $A\rightarrow B\rightarrow C$, to describe the "elementary" steps of the reaction. Two papers (I and II of a series), published in the *Journal of Chemical Physics*, outlined the methodology of "femtosecond transition-state spectroscopy (FTS)" with applications to the ICN dissociation reaction. From these first experiments, we expressed the change in internuclear separation with time, namely, the reaction trajectory and the time of bond breakage, which are measured from Equations (6a) and (6b), respectively. For a given potential of interaction V, the velocity is v and the force is $F=-dV/dR$

$$\tau=\int_{R_0}^{R}\frac{dR'}{v(R')} \tag{6a}$$

$$\tau^{\neq}=\frac{\Delta V(R^{\neq})}{v(R^{\neq})|F(R^{\neq})|} \tag{6b}$$

We obtained the time of the motion to final products (τ) and during the transition state ($\tau^{\neq}$), as well as the distance of separation $R(t)$. Thus, for a given total energy E, we expressed the distance of separation between I and CN and the time of bond breakage, and compared these with experimental results, hitherto unmeasured directly. Significantly, we were able, for the first time, to observe the passage through the transition state potential energy window $\Delta V(R^{\neq})$, and measure its "lifetime" or transit time $\tau^{\neq}$ with femtosecond resolution. This experiment on the dynamics of bond breaking and another one on the dynamics of bond making ($H+CO_2\rightarrow OH+CO$) events were generally well received by colleagues in the scientific community worldwide. They even had impact on the public press with significant write-ups in popular newspapers and magazines such as New York Times, Los Angeles Times, Discover,…etc. Isaac Asimov, H. C. von Baeyer, Gary Taubes, Philip Ball, and other notable science writers gave an exposition of this published work. Many books and textbooks referred and continue to refer to this 1987 discovery.

The quantum picture was intuitive too. On the basis of the experience outlined above, we could understand that coherent preparation can lead to nonstationary states which evolve with time (motion!) (Section 2). Extension to chemical reaction dynamics gives the nonstationary wave packet shown in Equation (7), which evolves in time, similar to the two-

$$\Psi(R,t)=\sum_i c_i\psi_i(R)\,e^{-iE_it/\hbar} \tag{7}$$

level problem [Eq. (4)], but now with spatial R localization because of the sum over many energy states. This principle of superposition holds because of the linearity of the time-dependent Schrödinger equation. The phases in [Eq. (7)] give rise to the interferences (quantum coherence) and their fluctuations, arising from intrinsic anharmonicities or interactions with the environment, lead to the delocalization. Since the packet can be synthesized easily when the sum criterion is satisfied, the femtosecond pulse becomes the ideal initiator of the motion of nuclei in a reaction.

The concept of describing quantum systems using wave packets is fundamental and goes back to the 1920s (Figure 4) when the connection between quantum mechanics and classical phenomena was the subject of discussion and correspondence among many notable scientists such as Schrödinger, Lorentz, and others;[*] Sections 3.4 and 3.6

[*] Schrödinger wrote a theoretical paper (*Naturwissenschaften* **1926**, *14*, 664), pointing out the transition from micro- to macro-mechanics using the superposition of eigenstates. There was a correspondence between Schrödinger and Lorentz on this problem and the difficulty of making wave groups or wave packets.

highlight the theoretical developments since then. The ICN results demonstrated the experimental observation of wave packets in molecular systems, and since then they have been synthesized in atoms, complex molecules, and biological systems, as well as in the different phases of gases, liquids, clusters, and solids. The behavior observed for ICN was found in other studies, the most recent is an elegant series of experiments of "bubbles in solids" by Majed Chergui's group in Lausanne.

The question then was: Would quantum calculations reproduce the experimental results obtained for ICN? Dan Imre, being skeptical in the beginning, did the first of such calculations, and the results were important in showing the influence of the wave packet motion and spreading on the observed FTS transients. Horia Metiu addressed the role of rotations. We compared the quantum results with those obtained from the classical model of Bersohn and Zewail (see Figure 14). The model described the experimental trends quite well, just as did the quantum picture. This was followed by reports of trajectory calculations from Kent Wilson's group and a density-matrix description from Shaul Mukamel's group. The latter emphasized the different limits of dephasing and the time scale for nuclear motion. All theoretical results exhibited the general trends observed experimentally. In our early papers on ICN, we suggested that the δ-function limit of wave-packet dynamics could be obtained if proper deconvolution was made, when the temporal response of the pulses is known. Very recently, Volker Engel and Niels Henriksen reported a quantum theoretical agreement with this simple picture and discussed its generality.

3.4.3. The NaI Discovery: A Paradigm for the Field

There were two issues that needed to be established on firmer bases: the issue of the uncertainty principle and the influence of more complex potentials on the ability of the technique (FTS) to probe reactions. The reactions of alkali halides were thought of as perfect prototypes. Since they involve two potentials (covalent and ionic) along the reaction coordinate, I thought we would have fun with these systems. Moreover, their unique historical position in crossed molecular beam experiments ("the alkali age") made them good candidates for the "femto age". The reaction of NaI, unlike ICN, involves two electronic coordinates and one nuclear coordinate, the separation between Na and I. The resonance motion between covalent and ionic configurations is the key to the dynamics of bond breakage. How could we probe such motion in real time? We did the FTS experiments on NaI and NaBr, and the results, published in 1988, were thrilling (Figure 15) and made us feel very confident about the ability of FTS to probe transition states and final fragments. The results also illustrated the importance of coherent wave packets in quasi-bound systems. The NaI experiment was a watershed event leading to an entirely new paradigm in the field of femtochemistry and establishing some new concepts for the dynamics of the chemical bond, for several reasons:

1. We could show experimentally that the wave packet was highly localized in space (about 0.1 Å), thus establishing the concept of dynamics at atomic-scale resolution.
2. The spreading of the wave packet was minimal up to a few picoseconds, thus establishing the concept of single-molecule trajectory, that is, the ensemble coherence is induced effectively, as if the molecules are glued together, even though we start with a random and noncoherent ensemble—this is the world of dynamics, *not* kinetics.
3. Vibrational (rotational) coherence was observed during the entire course of the reaction (by the detection of products or transition states), thus establishing the concept of coherent trajectories in reactions, from reactants to products.
4. On the femtosecond time scale, the description of the dynamics follows an intuitive classical picture (marbles

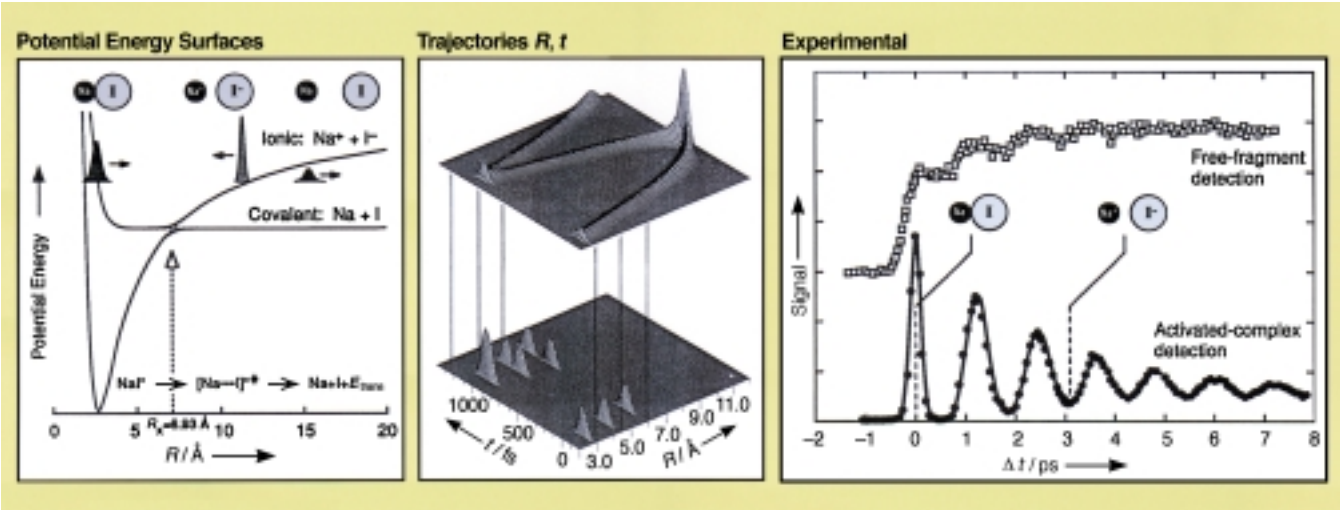


Figure 15. Femtochemistry of the NaI reaction, the paradigm case. The experimental results show the resonance motion between the covalent and ionic structures of the bond, as well as the time scales for the reaction and for the spreading of the wave packet. Two transients are shown for the activated complexes in their transition states and for the final fragments. Note the "quantized" behavior of the signal, which is not simply an exponential rise or decay of the ensemble. The classical motion is simulated as trajectories in space and time (center).[56, B1, B4, B12, B14, B17, B19, B28]

rolling on potential surfaces) since the spreading of the packet is minimal. Thus, a time-evolving profile of the reaction becomes parallel to our thinking of the evolution from reactants, to transition states, and then to products. The emerging picture is physically and chemically appealing, and compellingly demonstrated that conversion from the energy space to the time domain is not needed.

5. NaI was the first system to demonstrate the resonance behavior, in real time, of a bond converting from being covalent into being ionic.

From the results, we obtained the key parameters of the dynamics such as the time of bond breakage, the covalent/ionic coupling strength, the branching of trajectories, etc. In the 1930s, Linus Pauling's description of this bond was that it was static at equilibrium; only now can the dynamics be described in real time by preparing structures far from equilibrium. I still reflect on the beauty of these NaI experiments and the rich number of concepts they brought to dynamics. Some of the concepts were not as clear when we first made the observations as they are now. The paradigm shift in our thinking is linked and similar in value to the work on IVR (Section 3.2), but the difference is major—for IVR we studied the coherence of states, but for reactions we observed the coherence of the nuclear motion with atomic resolution.

After the initial set of experiments, we continued on this system for some time, exploring other phenomena of interest. The studies included: 1) direct observation of the reaction trajectory in R and t, and the resolution of the motion into and from the transition state (this work was first published in *Nature*); 2) direct observation of recurrences (echo-type), reflecting rephasing at long times ($t = 20-40$ ps), and their relationship to quantum interference effects as a result of the resonance behavior of the motion on the covalent and ionic potentials (this work was published in *Chemical Physics Letters*); 3) studies of the effect of the velocity of the nuclei on the crossing-to-products probability, which provided the interaction matrix element for the coupling between the covalent and ionic potentials, and the classical and quantum treatment of the dynamics (these studies were published in the *Journal of Physical Chemistry* and *Journal of Chemical Physics*).

Numerous theoretical and experimental papers have been published by colleagues and the system enjoys a central role in femtodynamics. From the beginning we understood the major features of the dynamics from the point of view of classical mechanics. The "exact" quantum calculations were first made by Volker Engel and Horia Metiu and these were important in identifying the sensitivity of the observations to details of the motion and the potential. The agreement with the experimental results was remarkable. The same agreement was found for later theoretical studies involving classical, quantum, and semiclassical approaches.

3.4.4. The Saddle-Point Transition State

Our next goal was to examine reactions governed by multidimensional (nuclear) potentials, starting with "barrier reactions" which define a saddle-point transition state, the classic case of chemistry textbooks. If the reaction dynamics involve more than one nuclear coordinate, an interesting question arises: Can one observe in real time the reactive evolution from the TS at the saddle point to final products on the global PES? The question was addressed by performing femtochemistry on ABA systems. The IHgI system was the so-called "gift experiment" I suggested to a new postdoctoral fellow in our group, who joined us in 1988 from Ken Eisenthal's group. Stunning observations were made—the product HgI was coherently formed from the transition state (Figure 16). Also, the transition state, which absorbs a probe femtosecond pulse in the red (as opposed to the HgI product which absorbs in the UV region) was found to live for only about 200 fs and this state produces different coherent product states (different periods of vibrational oscillation). It was also in this system that we studied coherence of rotational motion (real-time alignment) and learned about the geometry of the (initially prepared) transition-state, activated complex IHgI^{*+}.

With simple theoretical PES and molecular dynamics simulations we examined details of the motion, but the major features were evident in the experimental observations. Originally, we studied the TS and the evolution of HgI products by using laser-induced fluorescence. Later, we used mass spectrometry to also detect the I atoms and the translational energy; this effort triggered a great deal of theoretical work (Figure 16) in our group addressing, in depth, the actual meaning of classical TS structure (see Section 4). Features of this reaction were similarly found in other classes of reactions, including those in condensed phases and biological systems.

The studies of this ABA system were published with an emphasis on the following points: 1) coherent nuclear motion can be observed on multi-dimensional surfaces involving multiple-bond breakage (or formation); 2) coherence survives the entire reaction journey, even in multi-dimensional systems, and yields selective coherence in the products; 3) for the first time, a saddle-point TS can be seen evolving in real time; 4) the TS can be aligned (oriented) at zero time and seen evolving into rotations of the diatom (AB) and the translation of the A and AB fragments—the vibrational (scalar) and rotational (vectorial) motions were easily separated using polarized femtosecond pulses.

3.4.5. The Uncertainty Principle Paradox

At the time when I was giving lectures on the above examples of elementary reactions, some of the audience were raising a question about the "energy resolution" of the femtosecond experiments: How can a broad-energy pulse probe a sharp resonance? In the conventional teaching on spectroscopy of "eigenstates", one thinks of stationary states and their populations (diagonal elements of the density matrix [Eq. (4)], but now we must think of coherent states. All information pertinent to eigenstates is in the wave-packet structure. This point was elucidated by our experiments on a bound nonreactive system—the iodine system (Figure 17). Serendipity was at work. We were initiating studies of the FTS of CdI_2 (from the family of HgI_2) and instead observed the

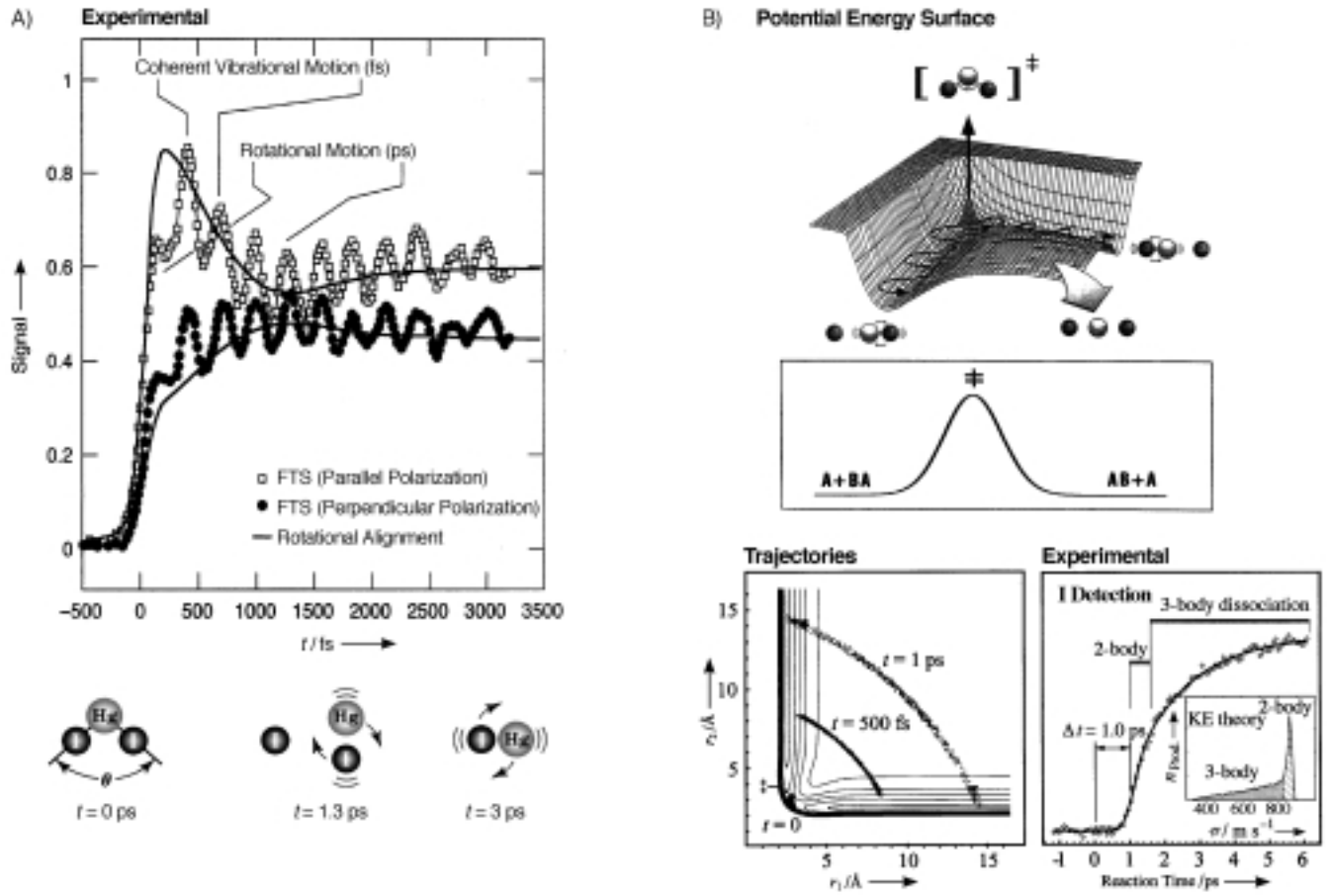


Figure 16. Femtochemistry of the IHgI reaction with a saddle-point transition state (barrier reactions). The experimental results show both the coherent vibrational and rotational motions of the reaction (A). The transition state IHgI*‡ and final fragment HgI were probed. We also probed the I fragment and the change of translational energy with time. The classical trajectory calculations are shown in (B), together with experimental results for I detection (n_{prod} in the inset corresponds to the number of atoms in the product). Both theory and experiment illustrate the family of reaction trajectories on the global PES, in time and in kinetic-energy distribution. Quantum calculations were also done (not shown). This ABA system is a prototype for saddle-point transition states.[57, B1, B4, B6, B10]

wave-packet motion of I_2, made from the samples of CdI_2 without our knowledge. It turned out that when we heated CdI_2 we made I_2, which gave us striking oscillatory transients. The oscillations directly gave the periods of the nuclear (vibration) motion, and the data could be related to the change with time of the I–I separation and the rotation of I_2; the time scales were separated (fs versus ps) and the vibrational (scalar) and rotational (vectorial) motion were clearly seen.

We used classical mechanical inversion methods, the RKR, and quantum inversion methods to characterize the potential. This was followed by a study of the ICl system. It became evident that: 1) the uncertainty in energy for short pulses works in our favor, and the shorter the pulses, the better the localization of the wave packet; and 2) we could now observe the vibrations and rotations of molecules in real time, not from energy spectra. This work was first published in *Nature* and detailed later in the *Journal of Chemical Physics.* Since the initial experiments were made on a diatomic molecule, the significance of this piece of work was originally missed, until later when many complex systems showed similar behavior. The real message of this I_2 experiment

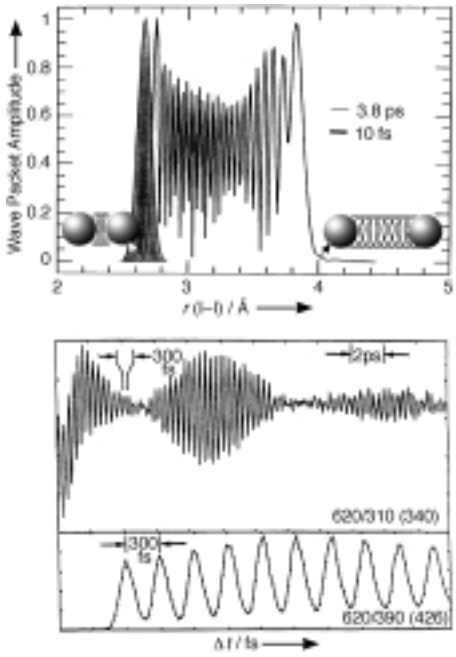


Figure 17. Femtosecond, real-time observation of the vibrational (and rotational) motion of iodine. The experiments show the anharmonic nature of the bound motion (bottom). Quantum theory (top) indicates the limit for creating a localized wave packet on the femtosecond time scale. The localized wave packet describes the classical spring motion.[58, B1, B6, B17, B18, B25]

was in its conceptual elucidation of the role of the uncertainty principle and the robustness of time, space, and energy resolutions because of coherence: Since $\Delta x \Delta p \sim \hbar$ and $\Delta t \Delta E \sim \hbar$, we can achieve localization with a very small de Broglie wavelength.

3.4.6. Bimolecular, Bond Making and Bond Breaking: Bernstein's Passion

Bimolecular reactions were ready for a femtosecond treatment, to observe the "simultaneous" processes of bonds being broken and formed. With Dick Bernstein (1987), we had studied the IH/CO_2 system. The problem was that, for bimolecular reactions, the transient time for reactants to undergo a collision is generally nanoseconds to microseconds. By using van der Waals complexes, an idea introduced for the studies of product-state distributions by Benoit Soep and Curt Wittig, we could expand HI and CO_2 in a single molecular beam. With the two reagents now within angströms of each other, we could examine the dynamics of the single collision. We used the first pulse to liberate the H atom with a given translational energy and a second pulse to probe the nascent OH product—the zero of time became well-defined and the collision was that of a limited impact parameter. The results were exciting and, in our joint paper, Dick termed this the "birth of OH from $H + CO_2$". Wittig's group improved the time resolution and studied the energy dependence of the rates. Figure 18 gives a summary of this system.

The $H + CO_2$ ground-state reaction proved to be important for a number of reasons: 1) it showed how reactive scattering resonances can be probed in real time during the collision and for a system with a complex number of degrees of freedom. 2) The experiments established that the intermediate $HOCO^{\ddagger}$ has a lifetime τ of about 1 ps and that for this reaction the OH bond making and the CO bond breaking are made in a nonconcerted pathway. The nuclear motions of HOCO thus determine the reaction mechanism. If τ had been found to be 10–100 fs, the picture would have been entirely different; bond-making and breaking would occur as a result of the electron redistribution with the nuclei essentially "frozen" in configuration. Obtaining τ directly is critical for the nature of the transition state/intermediate. This is particularly true when τ is much longer than the vibrational and rotational periods, and all other methods will fail in deducing τ. 3) The study provided a direct test of theory at the ab initio level. High quality ab initio calculations of the PES and dynamics have been made available by David Clary, George Schatz, John Zhang, and many others. Theory compares favorably with experiments, which shows that resonances must be considered—the vibrations of HOCO bottleneck the trajec-

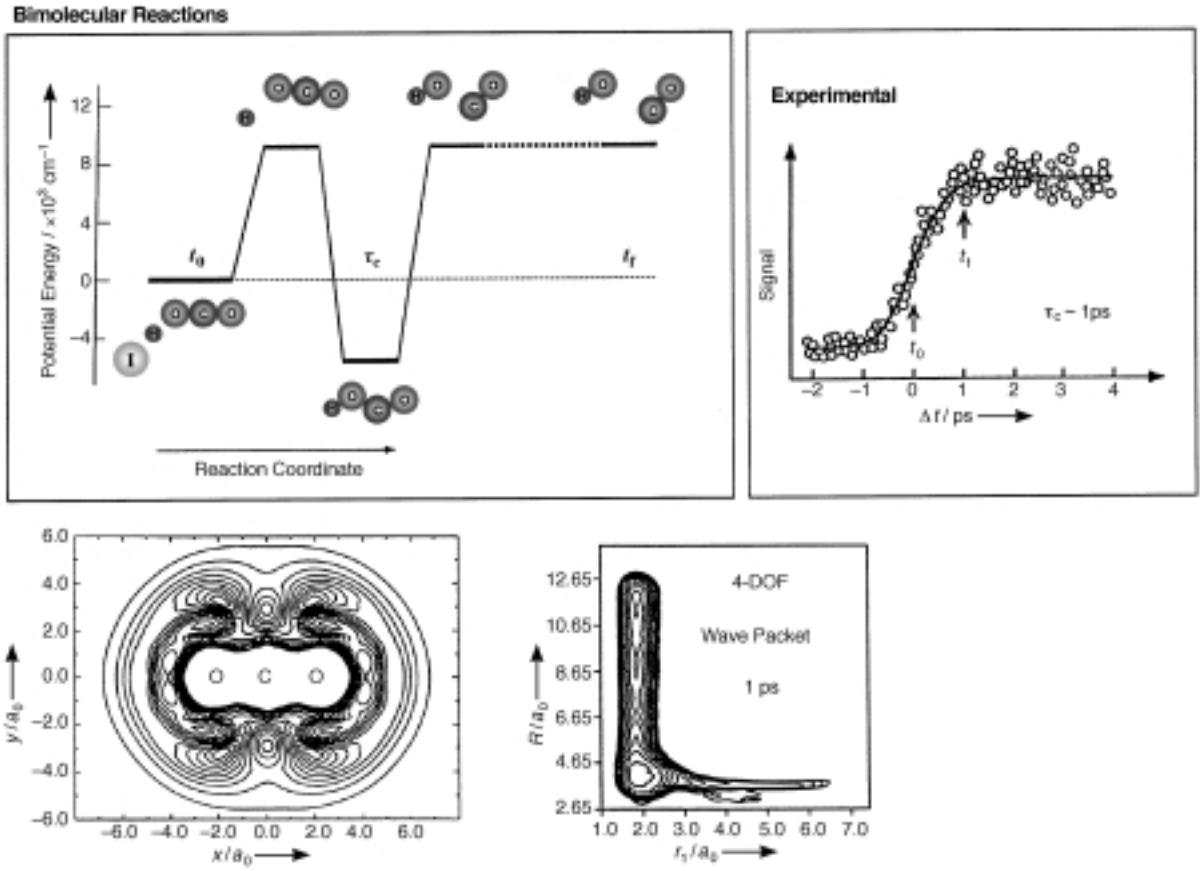


Figure 18. Femtochemistry of the bimolecular H + CO_2 reaction. The precursor in this molecular beam experiment is HI/CO_2 in a van der Waals complex. The initial experiments utilized picosecond pulses, but later sub-picosecond pulses were used (see text). Theoretical ab initio calculations of the PES and the dynamics (classical, semiclassical, and quantum wave packet) have all been reported. The PES and wave packet calculations are from the work of D. Clary, G. Schatz, and J. Zhang (see ref. [27]). The transit species $HOCO^{\ddagger}$ lives for about 1 ps. Similar studies were made on the reactive pair Br + I_2 and of the inelastic collision between I and CH_3I.[59, B1, B5, B10, B16, B19]

tories. The reaction $OH + CO \rightarrow CO_2 + H$ is one of the key reactions in both combustion and atmospheric chemistry, and represents the most studied four-atom reaction, both theoretically and experimentally.

We constructed FEMTOLAND II, and I thought it would be interesting to examine "halogen bimolecular reactions". Precursors, of which the H–Br/I–I system is a prototype, were chosen to study bimolecular halogen atom + halogen molecule reactions. Upon breaking the HBr bond, the hydrogen goes many angströms away from the field of the reaction (in femtoseconds) and we are left with the $Br + I_2$ collision. This halogen reaction had a history in crossed molecular beam experiments and comparison with real-time experimental results would be interesting. The $Br + I_2$ reaction was examined and found to occur through a sticky (approximately 50 picoseconds) collision complex. It is a stable intermediate of BrII, and there is no other way we know of determining its lifetime and dynamics. We examined classical trajectories of motion and compared them with the experimental results. In more recent work, the McDonald group obtained similar times and discussed the possibility of the involvement of ground and excited halogen surfaces. In this study of a collision between an atom and a diatom, we learned the effect of impact parameters, the influence of translational energy, and the interplay between bonding and dynamics. The analogy between full-collision ($Br + I_2$) and half-collision ($h\nu + I_2$) dynamics was based on the change in bonding, and we used frontier orbitals to describe such an analogy. Studies of bimolecular collisions in complex systems have continued in our and other laboratories; the most recent came from NIST (John Stephenson and colleagues) on the studies of $CH_4 + O \rightarrow CH_3 + OH$, using $CH_4 \cdot O_3$ as a precursor.

3.4.7. Ultrafast Electron Diffraction

FEMTOLAND III was the home of our next effort, Ultrafast electron diffraction (UED). Our goal was to complement the detection schemes of spectroscopy and mass spectrometry and to use diffraction to follow structural changes, especially for large systems. I proposed the idea in 1991 in an article for *Faraday Discussion*,[B17] and we had our first success in 1992. We were able to record structures with an electron pulse duration of a few picoseconds, but with no time scan. This was followed by other studies, both on the theoretical and experimental fronts. In our group, rumor had it that UED was a "No to the power 10 experiment!" We now have the third generation of UED machines, with a group of graduate students and post-doctoral fellows participating. In a paper published in *Nature* in 1997, we reported our state-of-the-art experimental development of the methodology. We also developed a "difference-method", which allows us to record the structure of radicals, carbenes, and intermediates, and with higher sensitivity (see Section 3.6).

3.4.8. Clusters, Dense Fluids and Liquids, and New Generations of FEMTOLANDS

With the above-mentioned spectroscopy, mass spectrometry, and diffraction techniques, it was becoming possible to study many new systems. In addition to FEMTOLANDS I to III, PICOLANDS I and II were still operational in order to cover the different time scales of reaction dynamics. We are now up to FEMTOLAND VI. Two additional beam machines, equipped with mass spectrometry and spectroscopic detectors, were added. These new FEMTOLANDS were built to accommodate the expanding scope of research, from gas phase to clusters, to liquids and dense fluids, to the world of complex organic and inorganic chemistry, and to the very complex biological systems. I find complex reactions fascinating and we have devoted significant effort to this area, studying both uni- and bimolecular reactions. We also maintain strong theoretical efforts on molecular structures and molecular dynamics to compare theory with experiment on the relevant time scale.

3.4.9. Theoretical Femtochemistry

Our involvement had roots in the study of coherence and dephasing. This line of research was initiated by using pulsed lasers to form a coherent state, [Eq. (4)]. The evolution was followed in time to obtain the pure dephasing time (T_2', which reflects the extent of phase interruptions, and the population or energy decay time (T_1). We invoked theoretical techniques such as density matrix formalism, Kubo relaxation theory, and the Bloch equations to describe the optical analogue of NMR experiments. The 1957 Feynman, Vernon, and Hellwarth paper[29] was an important contribution, as it pointed out the linkage between "spin" and "optical" coherence experiments: even in the absence of a magnetic field, used in the former, one can use a rotating frame picture to describe such optical experiments. All of this was known at the time. Our interest in theory was to relate T_1 and T_2' to molecular processes and to learn about their formal limits of applicability. We wrote a book chapter[B9] on the subject and published a number of papers relating these relaxation times to the anharmonicity of molecular vibrations, the phonon structure of solids, and collision dynamics in gases.

For collisionless, large molecules, the issue of intramolecular electronic-states coupling was, by the 1970s, well developed theoretically and heavily imbedded in theories of radiationless transitions that were formulated to explain the origin of nonradiative decays. Wilse Robinson, Joshua Jortner, Stuart Rice, and many others were involved in the early stages of this development. The Bixon–Jortner model gave the description for such coupling of inter-electronic states and the important role of preparing a doorway state which "dephases" and "relaxes" depending on the electronic coupling matrix element, Franck–Condon factors, and the density of states.[30]

For IVR processes (Section 3.2), we developed a theoretical description for the coherent preparation of a set of vibrational eigenstates on a single potential surface, defining the preparation of a nonstationary vibrational packet, with the role of rotations and vibrational couplings explicitly expressed. The probability of being in the initial state ψ_0 is given by Equation (8), where the sum is over a product of

$$P(t) = |\langle \psi_0 | \Psi(t) \rangle|^2 = \sum_{i,j} \alpha(i,j)\, e^{-(i\omega_{ij}+\Gamma)t} \quad (8)$$

coefficients α ($\alpha(i,j)$), and displays the interference of states i and j, together with their damping rate Γ. This treatment was useful because: 1) it gives a direct view of IVR, from the initial nonstationary state and as a function of time; 2) it indicates the critical role of selective probing—if all states were monitored, coherence would be obscured. On the other hand, selectivity provides rich information on the nature and extent of IVR, the level structure, and the phase changes; and 3) it shows that $P(t)$ is a measure of vibrational chaos, which defines what we called restricted or nonchaotic IVR—coherence among vibrational states of a single electronic potential. Similarly, we considered the theory for rotational coherence using polarization-analyzed probes. This topic was treated in a series of papers with focus on the phenomenon of pure rotational coherence and its utility for molecular structural determination, and the rotational dephasing time.

At the time of the first femtochemistry experiment, I was thinking of the coherent state—wave packet—as an extension of the above picture. However, the span of states is now sufficient to create a localized, in R space, atomic-scale wave packet [Eq. (7)], (see Section 3.6). We needed a classical picture to connect with Newtonian mechanics, a simplified picture of the motion. The first of such models was published after we considered the theoretical treatment of absorption of fragments during reactions. We obtained the following Equation (9a), where C is a constant and $W = V(t) - V(t^{\pm})$ is

$$A(t;R) = C\{\delta^2 + W^2(t,t^{\pm})\}^{-1} \quad (9a)$$

the potential (or more generally, the difference of the two potentials probed); δ is a half-width of the pulse (and damping). For exponential repulsion, $V = E\,\mathrm{sech}^2(vt/2L)$, with L defining the length scale and v being the speed at the total energy E.

Accordingly, the time for bond breakage τ_{BB} can be related to FTS observables [Eq. (9b)] (see Section 3.4.2). This expression defines bond breakage time when the potential drops to a

$$\tau_{BB} = \frac{L}{v}\ln\frac{4E}{\delta} \quad (9b)$$

value of δ. The model is basic and describes the reaction trajectory $R(t)$ or $\tau(R)$. It provides a simple connection between observations and the dissociation time, transition-state lifetime, and the forces of the potential [see Eq. (6) and Figure 14]. While Dick Bernstein was at Caltech, we extended the model to obtain the potential using an inversion approach. We published two papers on the subject. Peter Sorokin and colleagues at IBM have addressed different limits of the classical regime in connection with their original studies of femtosecond transient absorption of dissociation.[B50]

Next, we considered the treatment of the effect of alignment and orientation on femtochemical reaction dynamics. I considered the time evolution of alignment and coherence for a single rotational angular momentum and then averaged the different trajectories to define the coherence time τ_c; τ_c (in ps) becomes simple and equal to $2.2[B\langle E_R\rangle]^{-1/2}$, where B is the rotational constant and $\langle E_R\rangle$ is the average thermal rotational energy (in cm^{-1}) produced in the reaction fragment(s). We applied this to reactions and I wrote a paper on the subject, published in 1989.[B18] This was followed, in collaboration with Spencer Baskin, by a paper describing the details of the approach and its applications.

In quantum treatments, we have benefited greatly from the advances made in theoretical formalism and computation. A major step forward was made when Rick Heller[31a] reformulated the time-dependent picture for applications in spectroscopy, and Jim Kinsey and Dan Imre[31b] described their novel dynamical Raman experiments in terms of wave packet theory. Progress was significantly helped by advances made in the theoretical execution and speed of computation by Ronnie Kosloff[31c] and, subsequently, by many others. In Section 3.6.2, the contributions made in the 1980s in connection with quantum control are discussed.

As mentioned in Section 3.4.3, the groups of Imre and Metiu did the first "exact" quantum calculations of femtochemical dynamics (ICN and NaI). The literature is now rich with numerous theoretical studies. There is a parallelism between the experimental diversity of applications in different areas and the impressive theoretical applications to many experiments and systems. This is summarized in the (1996 Nobel Symposium) book edited by Villy Sundström on Femtochemistry and Femtobiology.[28] Jörn Manz, who has played a significant role in this field, gave an overview of developments since Schrödinger's 1926 paper, with 1500 references. Jörn classifies the field into periods of *origins*, *sleeping beauty*, *renaissance*, *and revolution*. In this Nobel Symposium book (and another one[30]) Jortner provides a unifying overview of molecular dynamics in femtochemistry and femtobiology, and Mukamel gives an exposition of a general approach using the density matrix formalism. In the same volume, Clary presents the state-of-the-art in quantum theory of chemical reaction dynamics while Marcus and Casey Hynes review transition state theories for rates and dynamics.

Theory and experiment are now hand-in-hand, and many laboratories are doing both. For elementary chemical reactions, the above classical/quantum picture captured the essence of the observation and in many cases the comparison between theory and experiment was tested critically. For complex systems, our theoretical effort has taken on a different approach. With the help of molecular dynamics (MD) simulations, we compare theory with experiments. Then we use the MD simulations as a tool and vary parameters until we reduce the problem to identify the important key forces of dynamics. At this point, we can provide a microscopic dynamic picture with focus on the relative vibrational coordinates, time scales, or system parameters. Two examples illustrate the point. The first was our study of the dynamics of a guest molecule in dense fluids, with focus on the density dependence of microscopic friction, T_1 and T_2, and of bond breaking/remaking dynamics. The second, the study of numerous organic reaction mechanisms. For the latter, we also use advanced computational methods, such as density functional theory (DFT), ab initio and CASSCF computations. For ground-state reactions, the theory can be compared in a critical way with experiment, while for excited states the situation is more challenging.[32]

3.4.10. Experimental Femtochemistry

The generation, amplification, and characterization of ultrashort pulses is a major part of femtochemistry experiments. Another is the reaction chamber: molecular-beam machine, gas cell, ultrahigh-vacuum (UHV) surface apparatus, or the high-pressure/liquid cell. Here, only the different systems designed for the studies presented in this anthology are mentioned; further details can be found in the book chapter I wrote for the volumes edited by Manz and Wöste[B6] and in the two volumes of our collected works.[16]

At Caltech, over the years, we have constructed different types of lasers depending on the particular development and the resolution needed, picosecond to femtosecond (Figure 19A); one apparatus is shown in Figure 5. Since 1976, and in evolutionary order, these are:

1) Passive mode-locked, and cavity-dumped, dye laser (pumped by a CW argon ion laser); Ippen and Shank cavity design. Pulse characteristics: 615–625 nm, 2.4 ps (and 0.7 ps), 2 nJ, 100 kHz repetition rate.
2) Synchronously pumped, mode-locked dye laser system (pumped by an actively mode-locked argon ion laser). Pulse characteristics: 550–600 nm, 3.1 ps, 1.8 nJ, 82 MHz repetition rate.
3) Mode-locked argon-ion laser. Pulse characteristics: 514.5 nm, 150 ps, 12 nJ, 82 MHz repetition rate.
4) Synchronously pumped, cavity-dumped dye laser (pumped by a mode-locked argon-ion laser). Pulse characteristics: 550–750 nm, 15 ps, 20 nJ, 4 MHz repetition rate.
5) Mode-locked (CW) Nd:YAG laser which synchronously pumps two dye lasers, with two amplifiers pumped by a 20 Hz Q-switched Nd:YAG laser. Pulse characteristics: 550–750 nm, 3–5 ps, approximately 1 mJ, 20 Hz repetition rate.
6) Dye lasers (as described in point 5) with an extra-cavity pulse compressor (using a fiber-grating optics arrangement) to obtain $\sim$0.4 ps pulses.
7) Colliding-pulse mode-locked (CPM) ring dye laser (pumped by a CW argon ion laser), and amplified in a four-stage dye amplifier pumped by a YAG laser. A compression at the output of the amplifier was also used. Pulse characteristics: 615–625 nm, 70 fs, approximately 0.5 mJ, 20 Hz repetition rate.
8) Synchronously pumped, cavity-dumped dye lasers (two), pumped by a Q-switched, mode-locked Nd:YAG laser. Pulse characteristics: 550–750 nm, 50 ps, 10 μJ, approximately 1000 Hz repetition rate.
9) Passively mode-locked, dispersion-compensated tunable dye laser (synchronously pumped by a frequency-doubled, CW, mode-locked Nd:YAG laser), amplified in a four-stage dye amplifier. The compression is after the amplifier. Pulse characteristics: 500–700 nm, 150 fs, 1 mJ, 20 Hz repetition rate.
10) CPM laser-amplifier system similar to that in point 7, used for ultrashort electron pulse generation. Pulse characteristics: 615–625 nm, 60 fs, 1 mJ, 30 Hz repetition rate.
11) Ti:sapphire laser system, Sibbett-type, argon-ion pumped; Ti:sapphire amplifier pumped by Nd:YAG laser. Pulse characteristics: 750–850 nm, 50 fs, 0.7 mJ, 1 kHz repetition rate; one optical parameter amplifier (OPA) system.
12) Ti:sapphire laser system; oscillator, diode pumped and amplifier (Ti:sapphire) Nd:YLF (2) pumped—all solid state (no gas lasers). Pulse characteristics: 750–850 nm, 50–100 fs, 2 mJ, 1 kHz repetition rate. With two OPAs, 1.1–2.6 μm tunability, with 200 nm–2.6 μm nonlinear conversions,.
13) Ti:sapphire laser system, same as in point 12, but pulse width 120 fs and 3 mJ energy, 1 kHz repetition rate.

For recording and clocking in any study, the resolution must be determined accurately, as must the zero-of-time ($t=0$). The pulses were characterized using auto-correlation and cross-correlation techniques, typically by scanning the time delay between the two pulses (of the same or different colors) in an interferometer arrangement and observing the sum- or difference-frequency generation in a nonlinear crystal. In this way, we can obtain the duration of the pulse. The central frequency of the pulse can be determined by passing the pulse through a calibrated spectrometer, while the shape of the pulse can be obtained from frequency-resolved-optical-gating (FROG) measurements, where the time and frequency components of the pulse are correlated and displayed as a 2D image (Figure 19B). In clocking experiments, the zero-of-time was precisely determined by an in situ measurement, typically using ionization techniques in beam experiments, lensing techniques in diffraction experiments, or the solvent response in condensed phase experiments.

The detection probes are numerous. Initially, we used laser-induced fluorescence for selectivity and sensitivity, and there we had a frequency-time correlation. Later, we invoked mass spectrometry (multiphoton ionization) for mass–time 2D correlations. This was followed by speed–time and angle–time correlations. All these correlations proved important in the studies of complex systems; a prime example was the application of the latter two correlations to the study of electron transfer in isolated bimolecular reactions and in clusters. For absorption-type measurements, we introduced nonlinear techniques such as degenerate-four-wave mixing. In a recent collaboration with the groups of Wolfgang Kiefer and Arnulf Materny, we also used coherent anti-Stokes Raman scattering (CARS), with frequency-time correlations to study the dynamics of ground-state systems, in this case polymers. Other detection methods are energy-resolved and ZEKE photoelectron spectroscopy, Coulomb explosion, ion–electron coincidence ionization techniques, absorption and photodetachment spectroscopy. The range of wavelengths is from the IR to the far UV. Absorption, emission, reflection, ionization, and diffraction have all been involved (see Figure 6).

3.5. Femtocopia—Examples from Caltech

The range of applications to different systems and phases in many laboratories around the world is extensive and beyond the purpose of this report. In this section I will limit the examples to those studied by the Caltech group. The details are given in the original publications and are summarized in

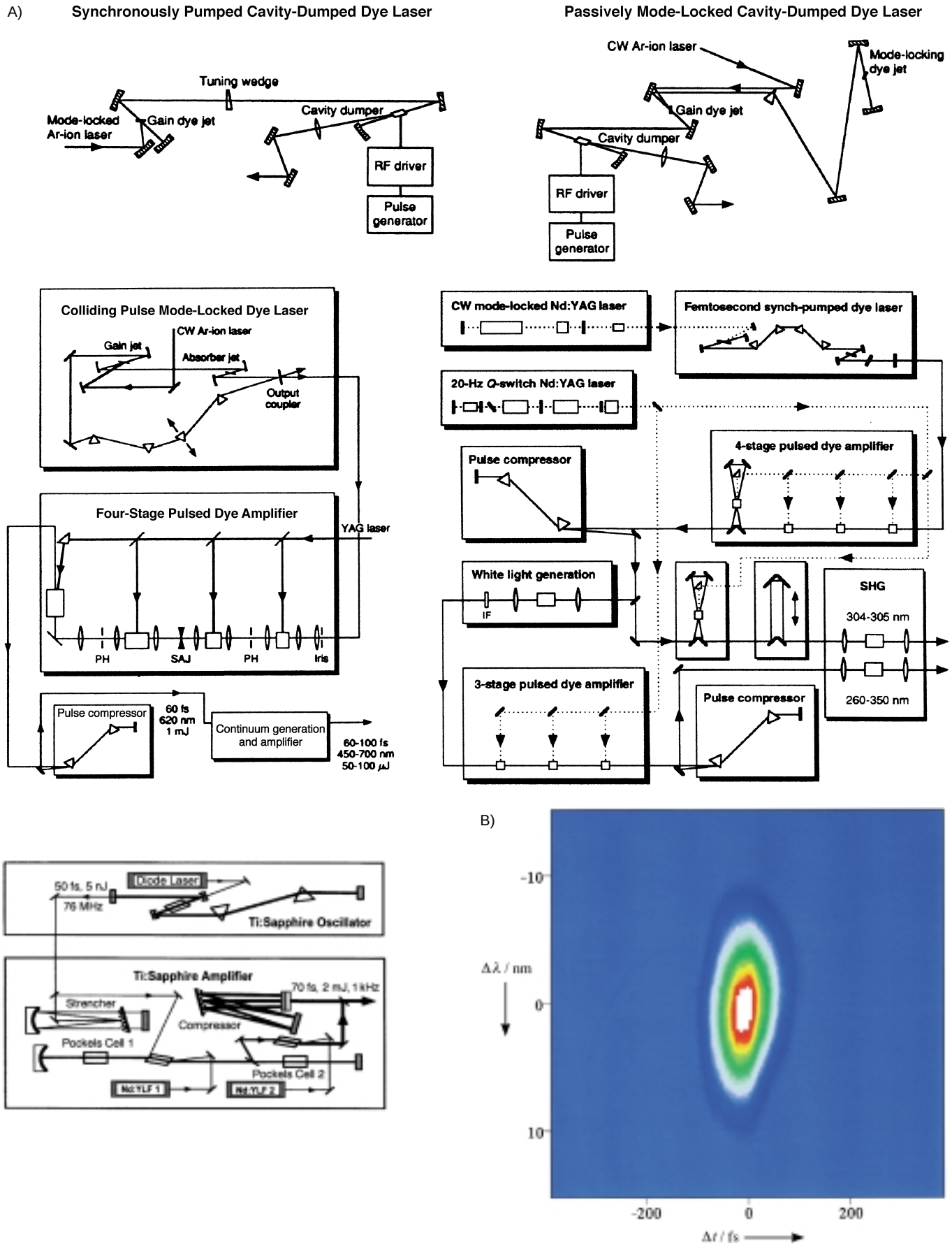


Figure 19. A) Examples of the laser systems utilized in different laboratories (for more details see text and ref. [B6]). B) The two-dimensional (time and wavelength) correlated pattern of a femtosecond pulse (M. Chachisvilis, work from this laboratory).

the reviews and books mentioned here. Figure 20 gives a summary of the different areas studied at Caltech with chronological flow from the south to the north!



Figure 20. Femtochemistry branches, from the early days of studying elementary reactions and transition states ("southern part") to the current activities ("northern part"). The flow of work has produced the different branches studied at Caltech.

3.5.1. *Elementary Reactions and Transition States*

The focus here is on the studies of elementary reactions. Some of these have already been discussed above. The dynamics are generally of three classes:

1) Dynamics of bond breakage
2) Dynamics of the (saddle) transition state
3) Dynamics of (bimolecular) bond breakage and bond formation

3.5.2. *Organic Chemistry*

With the integration of mass spectrometry into femtochemistry experiments, the field of organic reaction mechanisms became open to investigations of multiple transition states and reaction intermediates (Figure 21). The technique of femtosecond-resolved kinetic-energy-time-of-flight (KE-TOF) provided a new dimension to the experiment—correlations of time, speed, and orientation which give scalar and vectorial dynamics. The examples of reactions include (Figures 21–26):

1) Isomerization reactions
2) Pericyclic addition and cleavage reactions
3) Diels–Alder/sigmatropic reactions
4) Norrish-type I and II reactions
5) Nucleophilic substitution (S_N) reactions
6) Extrusion reactions
7) β-Cleavage reactions

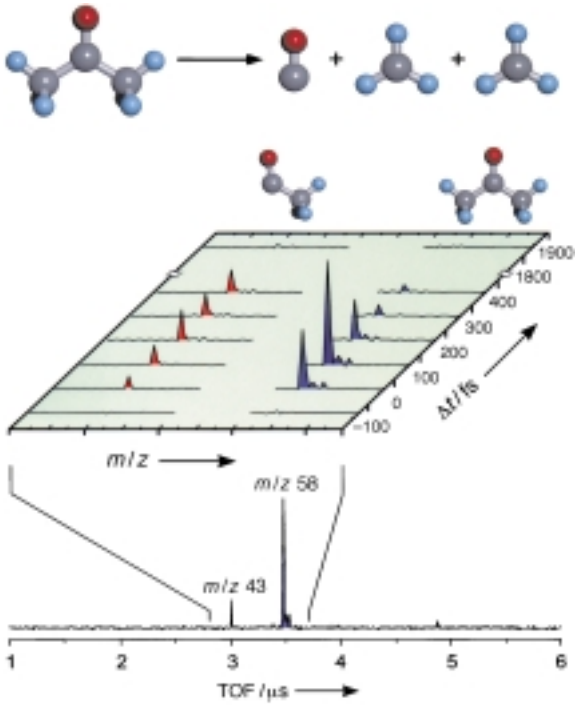


Figure 21. Femtosecond mass spectrometry, a 2D correlation important in the studies of reactive intermediates. The example given here is for the reaction of acetone (Norrish type I) and its nonconcerted behavior.[60, B10] TOF = time of flight.

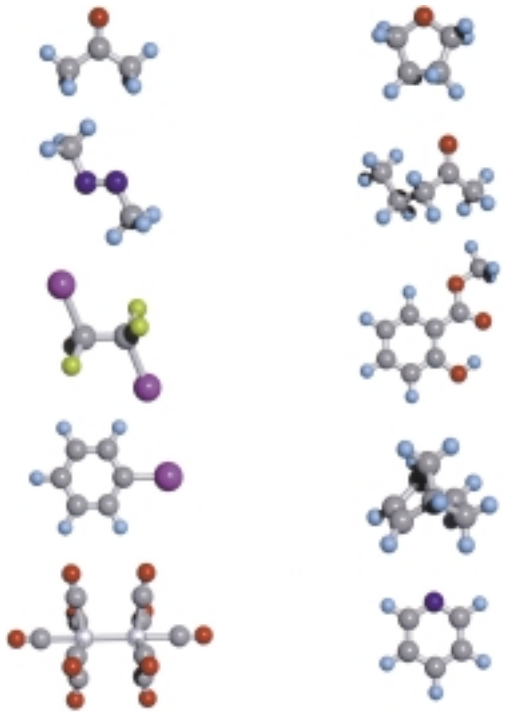


Figure 22. Molecular structures of different bond-breaking and bond-forming reactions studied, which are typical of the systems discussed in text for organic and organometallic femtochemistry: left (bond breaking): acetone,[60] azomethane,[61] diiodoethane,[62] iodobenzene,[63] [$Mn_2(CO)_{10}$];[64] right (bond breaking/bond formation): cyclic ethers,[65] aliphatic ketones for Norrish II reactions,[66] methyl salicylate,[67] one of the structures studied for addition and elimination reactions,[68] pyridine (valence isomerization).[69]

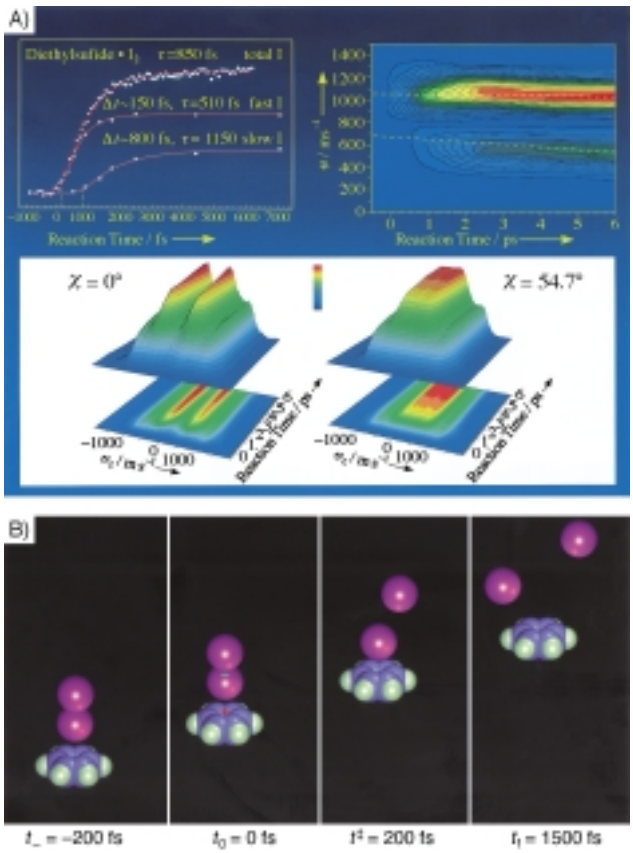


Figure 23. Femtochemistry of bimolecular electron-transfer reactions, the classic case of donors (for example, benzene or diethylsulfide) and acceptors (for example, iodine or iodomonochloride). A) The experimental results clearly show the distinct velocity and time correlations, and thus the two-speed distributions and time scales of the reaction on the global PES. B) Snapshots of the atomic motions according to experimental findings.[70]

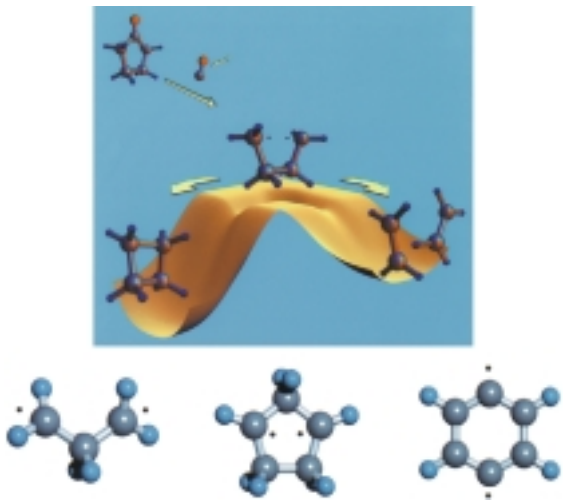


Figure 24. Reactive intermediates on the femtosecond time scale. Here, tetramethylene, trimethylene, bridged tetramethylene, and benzyne are examples of species isolated on this timescale (see Figure 22 for others).[71]

8) Elimination reactions
9) Valence-structure isomerization
10) Reactive intermediates

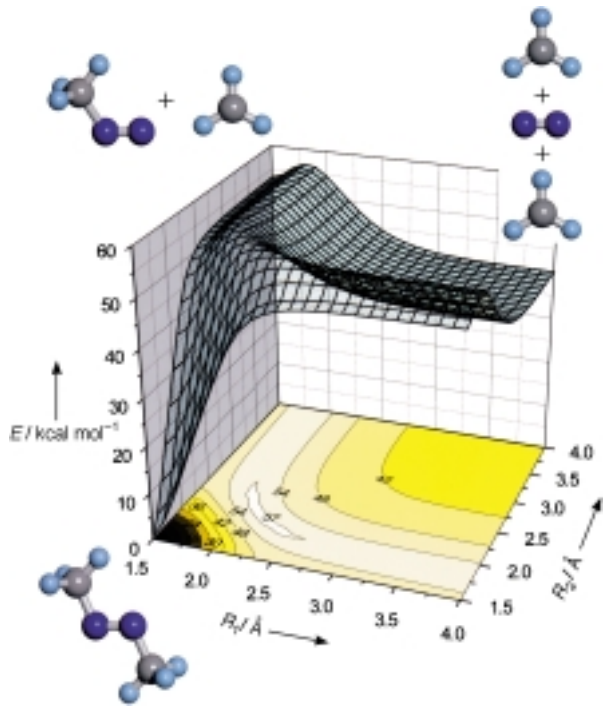


Figure 25. Reaction dynamics of azomethane, based on the experimental femtosecond studies (see Figure 22 and associated references). The ab initio PES was obtained from state-of-the-art calculations,[72] which show the two reaction coordinates (C–N distances R_1 and R_2) relevant to the dynamics. A third coordinate, which involves a twisting motion, was also studied. Note the concerted and nonconcerted pathways.

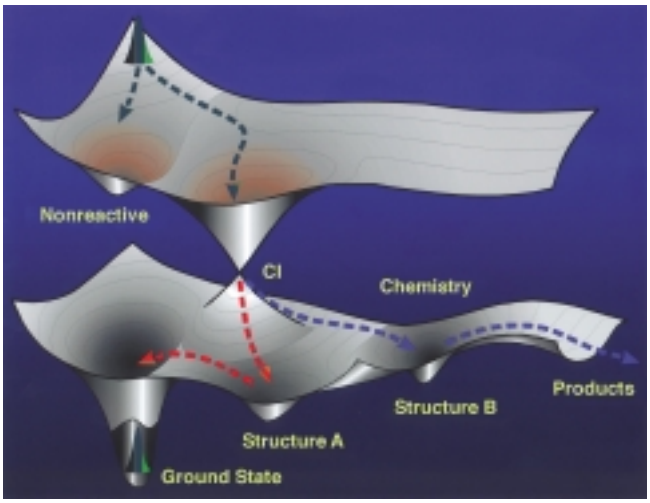


Figure 26. Generalized schematic diagram showing reactive and nonreactive pathways (bifurcation) of wave packets. Both the photophysical and photochemical processes are shown with the conical intersection (CI) playing a crucial role. Examples are given in ref. [73].

3.5.3. Electron and Proton Transfer

We examined both bimolecular and intramolecular electron transfer reactions, and these studies were the first to be made under solvent-free conditions. We also studied the transfer in clusters and in solutions (see Figures 11, 22,and 23). For proton transfer, three classes of reactions were of interest, those of bimolecular and intramolecular reactions, and those involving double proton transfer (base pair models):

1) Bimolecular electron transfer reactions
2) Intramolecular electron transfer and folding reactions
3) Acid–base bimolecular reactions
4) Intramolecular hydrogen-atom transfer
5) Tautomerization reactions: DNA mimics

3.5.4. Inorganic and Atmospheric Chemistry

We extended the applications of femtochemistry to complex inorganic reactions of organometallic compounds (see Figure 22). Organometallic compounds have unique functions and properties which are determined by the dynamics of metal–metal (M–M) and metal–ligand (M–L) bonding. The time scales for cleavage of such bonds determine the product yield and the selectivity in product channels. They also establish the nature of the reactive surface: ground-state versus excited-state chemistry. Similarly, we studied the dynamics of chlorine atom production from OClO, a reaction of relevance to ozone depletion.

3.5.5. The Mesoscopic Phase: Clusters and Nanostructures

We have studied different types of reactions under microscopic solvation conditions in clusters. These include (Figure 27):
1) Reactions of van der Waals complexes
2) Unimolecular reactions
3) Bimolecular reactions
4) Recombination, caging reactions
5) Electron and proton transfer reactions
6) Isomerization reactions

3.5.6. The Condensed Phase: Dense Fluids, Liquids, and Polymers

In this area of research, we have focused our efforts on the study of reactions in dense fluids and their comparison with dynamics in liquids. By varying the solvent density, we could study the femtosecond dynamics from gas-phase conditions to the condensed phase of liquid-state density. Accordingly, we could observe the influence of solute–solvent collisions on reaction dynamics in real time. We also did studies in liquid solutions for some of the systems examined in the gas phase: bond breakage and caging; valence structure isomerization; and double proton transfer. Similarly, we studied systems of nanocavities and polymers. Some highlights include (Figure 28):
1) Dynamics of the gas-to-liquid transition region (T_1 and T_2)
2) Dynamics of bimolecular (one-atom) caging
3) Dynamics of microscopic friction
4) Dynamics in the liquid state
5) Dynamics of energy flow in polymers
6) Dynamics of small and large molecules in cyclodextrins

3.6. Opportunities for the Future

Three areas of study are discussed.

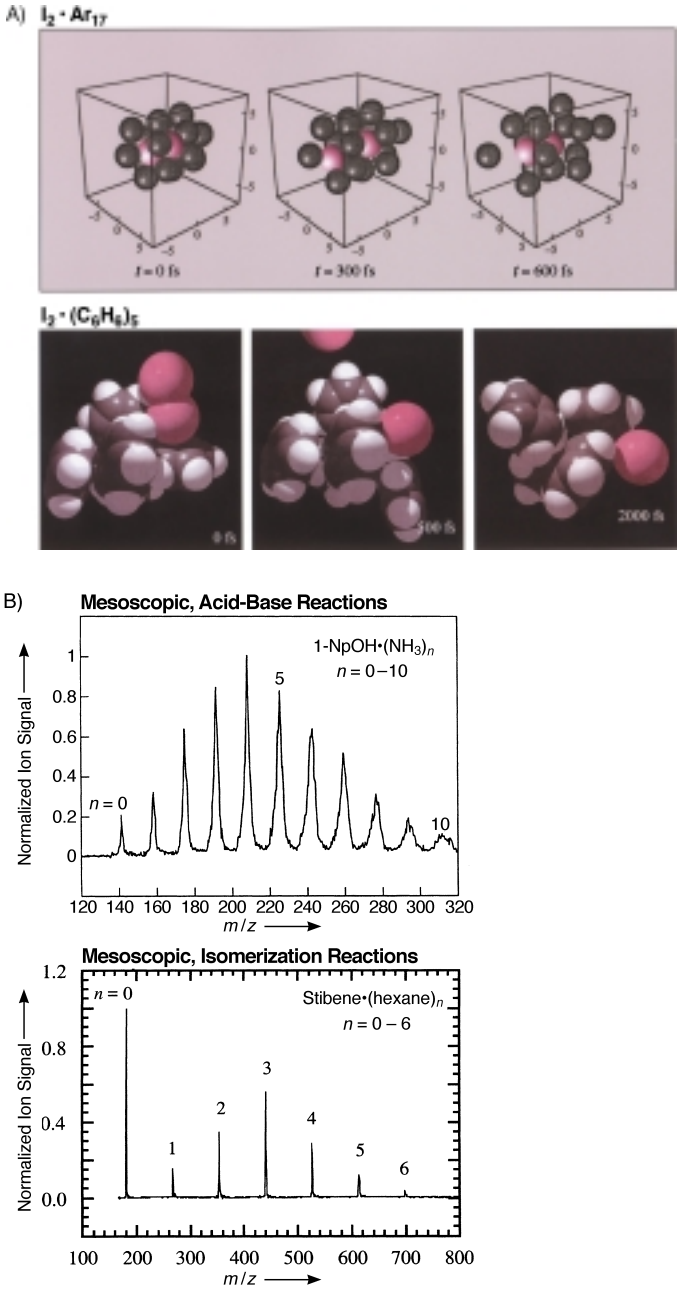


Figure 27. Femtosecond dynamics in the mesoscopic phase, reactions in solvent clusters. Several examples are given: A) The coherent nuclear dynamics of bond breakage and recombination of iodine in argon (the cage effect, top), and the dynamics of the same solute but in polyatomic solvents (benzene, bottom). It was for the I_2/Ar system that the first coherent bond breakage in the cage was observed and separated from the effect of vibrational relaxation. For the latter case, the two atoms experience different force fields and the time scales are determined by the degree of solvation. (We also studied van der Waals complexes.) B) The acid–base reactions of naphthol with ammonia is shown (top), in which the number of solvent molecules is varied from 0–10. The isomerization of stilbene was similarly studied (bottom); the number of hexane solvent molecules was varied from 0–6.[74]

3.6.1. Transient Structures from Ultrafast Electron Diffraction

Electron diffraction of molecules in their ground state has been a powerful tool over the past 50 years, and both electron

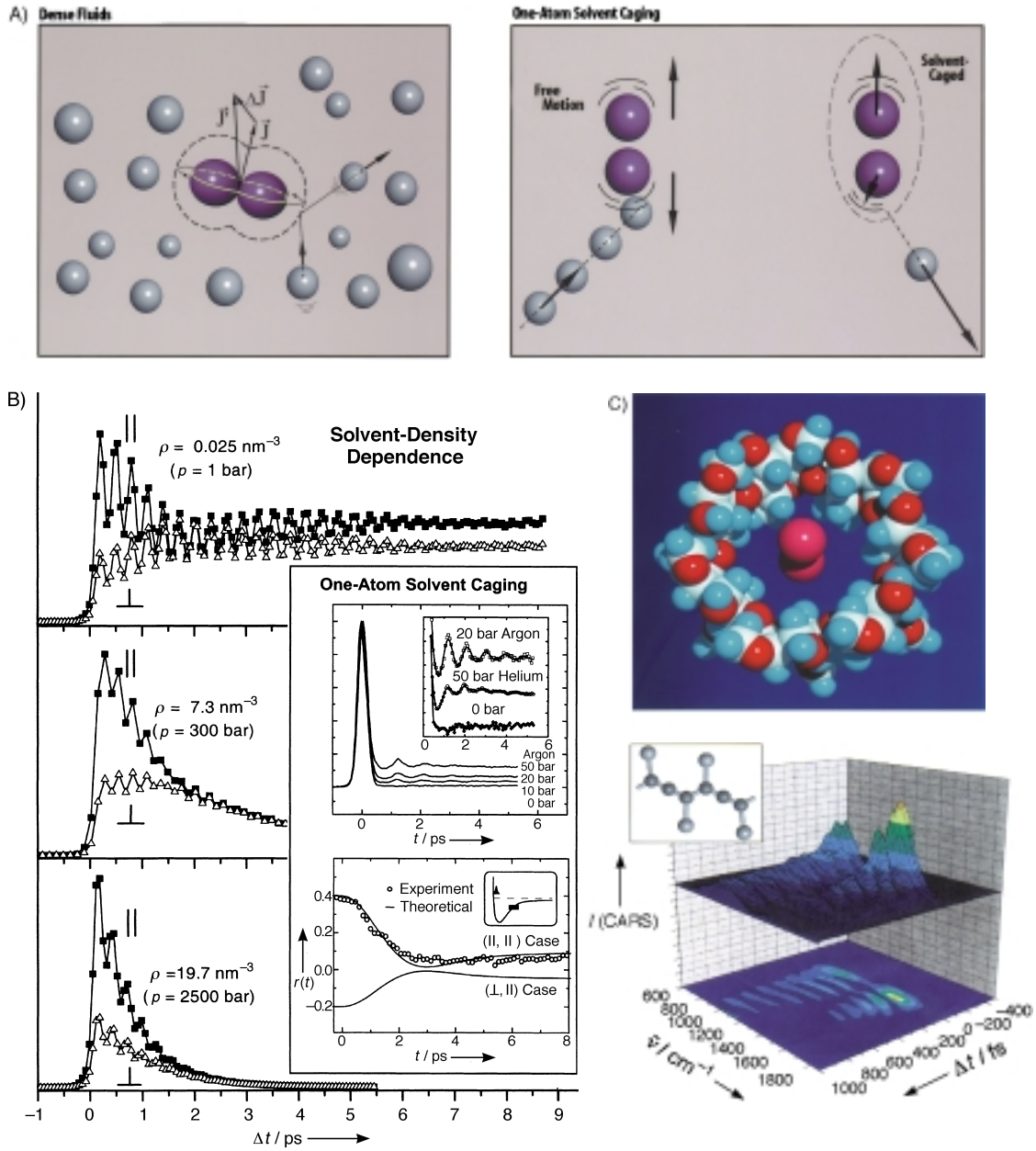


Figure 28. Femtosecond dynamics in the condensed phase: A) dense fluids; B) the coherent vibrational and rotational motions observed in dense fluids as a function of density and down to the one-atom collision with iodine; C) nanocavities in cyclodextrins (top) and polymers of polydiacetylenes (bottom) (examples of liquids are not shown, but they can be found in the literature.[75]) Studies in these media include the one-atom coherent caging, J-coherence friction model, coherent IVR in polymer chains, and anomalous T_2 behavior in dense fluids.[75]

and X-ray methods are now being advanced in several laboratories for the studies of structural changes. We have reported in *Nature* the latest advance in UED (Figure 29), by which major challenges were surmounted: the very low number of densities of gas samples; the absence of the long-range order that is present in crystals, which enhances coherent interference; and the daunting task of determining in situ the zero-of-time when diffraction changes are on the pico- and sub-picosecond time scale.

With UED, we have been able to study molecular structures and branching ratios of final products on the picosecond time scale. The change in diffraction from before to after a chemical reaction was observed. However, the direct observation of transient structural changes in the course of a reaction was published only recently (in the *Proceedings of the National Academy of Sciences*). Specifically, we observed the transient intermediate in the elimination reaction of 1,2-diiodotetrafluoroethane ($C_2F_4I_2$) to produce the corresponding ethylene derivative by the breakage of two carbon–iodine bonds (see Figure 29B and C). The evolution of the ground-state intermediate (C_2F_4I radical) was directly revealed in the population change of a single chemical bond, namely the second C–I bond. The elimination of two iodine atoms is nonconcerted, with the reaction time of the second C–I bond breakage being about 17 ps. The UED results for the short-lived C_2F_4I radical favor the classical structure over the

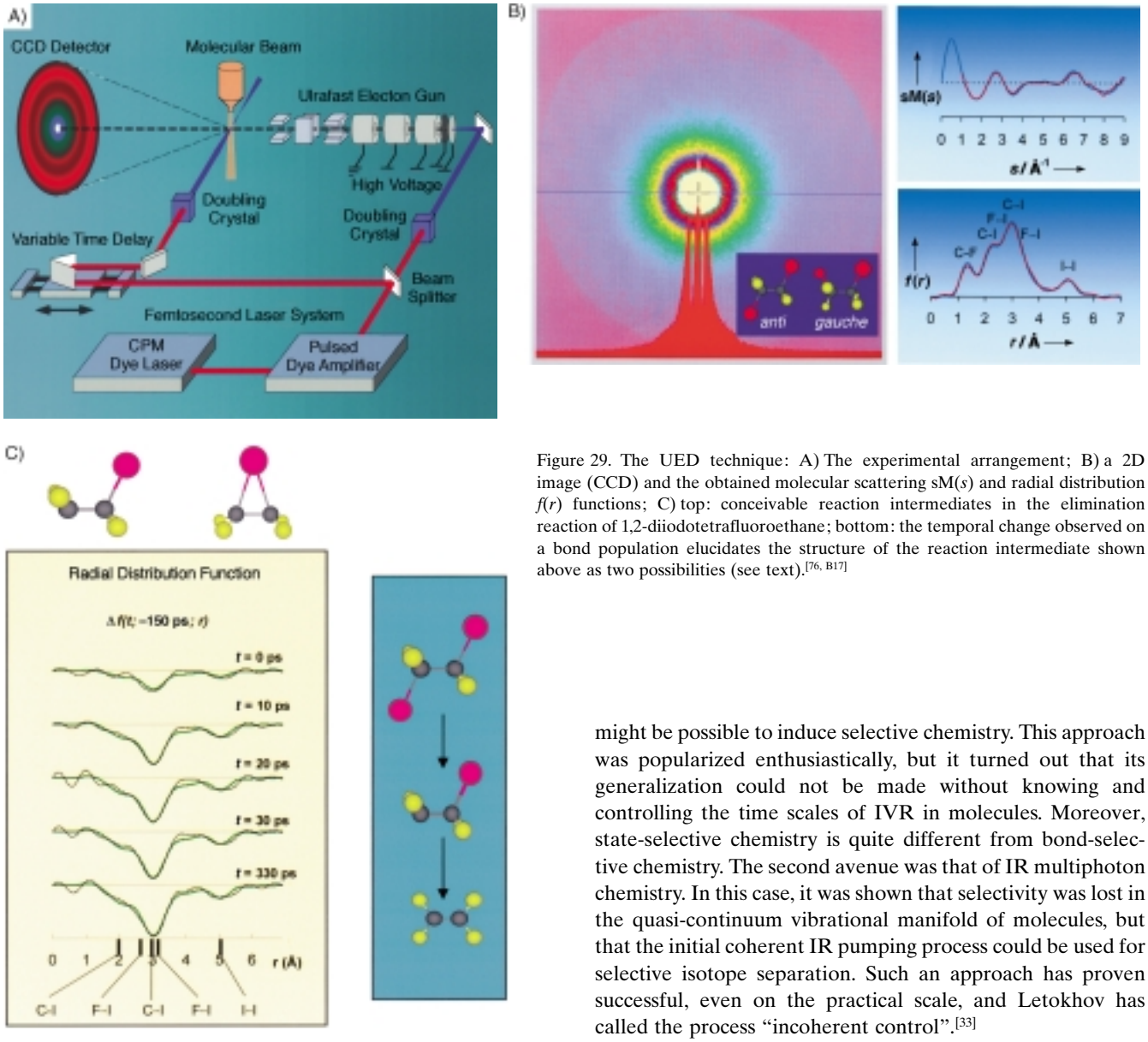


Figure 29. The UED technique: A) The experimental arrangement; B) a 2D image (CCD) and the obtained molecular scattering sM(s) and radial distribution $f(r)$ functions; C) top: conceivable reaction intermediates in the elimination reaction of 1,2-diiodotetrafluoroethane; bottom: the temporal change observed on a bond population elucidates the structure of the reaction intermediate shown above as two possibilities (see text).[76, B17]

bridged radical structure. Ab initio calculations were made to compare theory with experiments.

This leap in our ability to record structural changes on the pico- and sub-picosecond time scales bodes well for many future applications to complex molecular systems, including biological systems. We have completed a new apparatus equipped with diffraction detection and also with mass spectrometry. This universal system is capable of studying complex systems in the gas and other phases. It holds great opportunities for the future.

3.6.2. Reaction Control

Our interest in this area goes back to the late 1970s when a number of research groups were reporting on the possibility of (vibrational) mode-selective chemistry with lasers. At the time, the thinking was directed along two avenues. One of these suggested that, by tuning a CW laser to a given state, it might be possible to induce selective chemistry. This approach was popularized enthusiastically, but it turned out that its generalization could not be made without knowing and controlling the time scales of IVR in molecules. Moreover, state-selective chemistry is quite different from bond-selective chemistry. The second avenue was that of IR multiphoton chemistry. In this case, it was shown that selectivity was lost in the quasi-continuum vibrational manifold of molecules, but that the initial coherent IR pumping process could be used for selective isotope separation. Such an approach has proven successful, even on the practical scale, and Letokhov has called the process "incoherent control".[33]

The discovery (see Section 3.2) of coherent and selective vibrational oscillations (in-phase and out-of-phase) in a large molecule such as anthracene made me think of the possibility of temporally controlling the state of the system. The key idea was coherence among the vibrational degrees of freedom and its observation (published in 1981), which triggered significant interest in the issue of chaotic versus coherent "motion" of packets in isolated molecules. Some of us believed that, despite the complexity of the vibrational mode structure, coherence would be robust, provided it could be disentangled through proper preparation and probing. In fact, in a discussion with Richard Feynman (at Caltech) about the anthracene results, he informed me of a related problem noticed by Fermi, when both were at Los Alamos: A linear chain of springs (vibrations) showed recurrences when the energy was initially localized (on the computer) in one spring. They expected dissipation and not recurrences. Nico Bloembergen and I wrote a feature article (1984) emphasizing this point of coherent motion and its significance to mode-selective chemistry.[B21] Stuart Rice believed strongly in the

concept of coherence and, as I mentioned before, we even drafted a paper that was not finalized for publication.

Earlier in 1980, I wrote a *Physics Today* article in a special issue on laser chemistry suggesting the use of ultrashort pulses (not CW or long-time lasers) to control the outcome of a chemical reaction.[B24] The title of the paper was: Laser Selective Chemistry—Is it Possible? The subtitle stated the message, "With sufficiently brief and intense radiation, properly tuned to specific resonances, we may be able to fulfill a chemist's dream, to break particular selected bonds in large molecules." In this article, I was concerned with the problem of IVR and so-called chaotic behavior. Stimulated by our work on IVR and coherence (Section 3), I thought that ultrashort pulses should be used to control the system in the desired configuration by proper choice of the time duration and delay and by the preparation of the packet which is controlled by the coherence width. Experimentally, we had already developed methods for the control of the phase of the field of optical pulses with the idea of using the phase (pulse shaping) to control molecular processes—collisions, inhomogeneous broadenings, and even photon locking which could inhibit relaxation (see Section 3.1.2); the time scale was nanoseconds and for the control of IVR, femtosecond pulses were needed.

Prior to this work, the optical pulse field was simply defined by the envelope $A(t)$ and the frequency ω; the phase $\phi(t)$ was unknown [Eq. (10)]. By controlling $\phi(t)$ we were able to make

$$E(t) = E_0 A(t) \cos[\omega t + \phi(t)] \tag{10}$$

sequences of phase-coherent multiple pulses and to tailor a composite "single" pulse with a prescribed $\phi(t)$. We published a series of papers demonstrating the power of the approach, as mentioned in Section 3.1.2 (see Figure 9). In fact with composite shaped pulses, a sequence of phase segments and tilt angles (in the rotating frame) of, for example, $60_x - 300_{\bar{x}} - 60_x$, we showed experimentally that the emission of a molecule can be made twice that as when a normal single pulse was used (Figure 30). Similarly, by choosing pulse sequences such as x-y-$x(\bar{x})$ we experimentally locked the system and thus lengthened its relaxation time considerably. In theoretical papers, we examined the use of the approach for selectivity and control of molecular relaxations; in recent reviews,[34] Warren has discussed pulse shaping and its relevance to quantum control.

On the femtosecond time scale, the theoretical work of Heller (Section 3.4.9) stimulated the use of the time-dependent wave-packet picture for absorption and emission. In 1985, David Tannor and Stuart Rice, using the wave-packet picture, provided a two-photon scheme for the control of selectivity with pulse-sequence coherence being an important part of the evolution.[35a] This scheme was extended[35b] and, in their review article of 1988,[35c] they described phase-sensitive experiments such as the ones we reported earlier. An important realization was the desire to optimize the yield of a given channel. With femtosecond resolution, we began testing the idea of timing pulses on small molecular systems (see Figure 30). We first began with a single experiment on the control of the population in bound states (iodine). Then we reported results on the control of the yield in the reaction $Xe + I_2 \rightarrow XeI + I$ as a function of the delay time between the pump and control. Although the mechanism is not fully resolved, the important point is that the yield of product XeI followed the temporal motion of the iodine wave packet. In a third experiment, we used pump-control-probe femtosecond pulses to control the branching of the NaI reaction; these, together with the experiment by Gustav Gerber's group on Na_2 ($Na_2^+ + e$ versus $Na + Na^+ + e$), are prototypes for the Tannor-Rice-Kosloff scheme. Phase-locked pulses were extended to femtosecond domain by Norbert Scherer and Graham Fleming in their new studies on iodine.

Recently, we turned our attention to complex molecular systems, but this time using femtosecond pulses to implement the 1980 idea. In a series of molecules of increasing complexity, but retaining the same reaction coordinate, we illustrated selectivity by beating IVR (and entering near the transition state); the rate of reaction was two to three orders of magnitude larger than the expected statistical limit. This work was published in *Science* (see Figure 30) and promises to be significant for achieving nonstatistical chemistry at high energies. The concept suggests that control at high energies (chemical energies) is more realistic, in contrast with the conventional wisdom which asserts the need for low energies—time is of the essence! Another example of nonstatistical femtochemistry comes from the work on surfaces.[36] Recently, the group in Berlin (Ertl and Wolf[36b]) demonstrated, in an elegant experiment, the critical role of femtosecond resolution in inducing oxidation (in stead of desorption) of CO on Ru surfaces—the femtosecond nonequilibrated electron distribution of the surface gives a selective chemistry different from that of equilibrated phonon distribution, or thermal heating.

In the future, there will be extensions and new directions in light-matter control on the femtosecond time scale based on the temporal coherence of light and its interference with matter waves. One area that holds promise is the use of femtosecond pulses to induce selectivity by utilizing the three parameters of the pulse, the central frequency, the width and the "chirp", in an iterative algorithm; the chirp is, in a way, similar to a composite pulse of the type described above. The technique of liquid-crystal-display developed by Andy Weiner for femtosecond pulse shaping, combined with the evolutionary feedback idea of Herschel Rabitz, makes possible the generation of the desired complex $E(t)$ field to achieve combinatorial control. This optimal control has been demonstrated nicely for a targeted second harmonic generation or a yield of chemical reaction as reported by Gerber's group in Würzburg.[37a] Kent Wilson[37b] showed the importance of chirped pulses in focusing and reflecting wave packets and, in a more recent contribution, he, with Warren Warren, used the evolutionary feedback approach to optimize the fluorescence of a molecule in solution, reminiscent of the composite pulse experiment we described above. In pulse shaping, the field is optimized and forms a complex pattern which is used through many generations to reach the fitted, desired population.

It should be noted that all of the above schemes change the coherent composition of the initial packet and hence the evolution in different channels—but we have not changed the

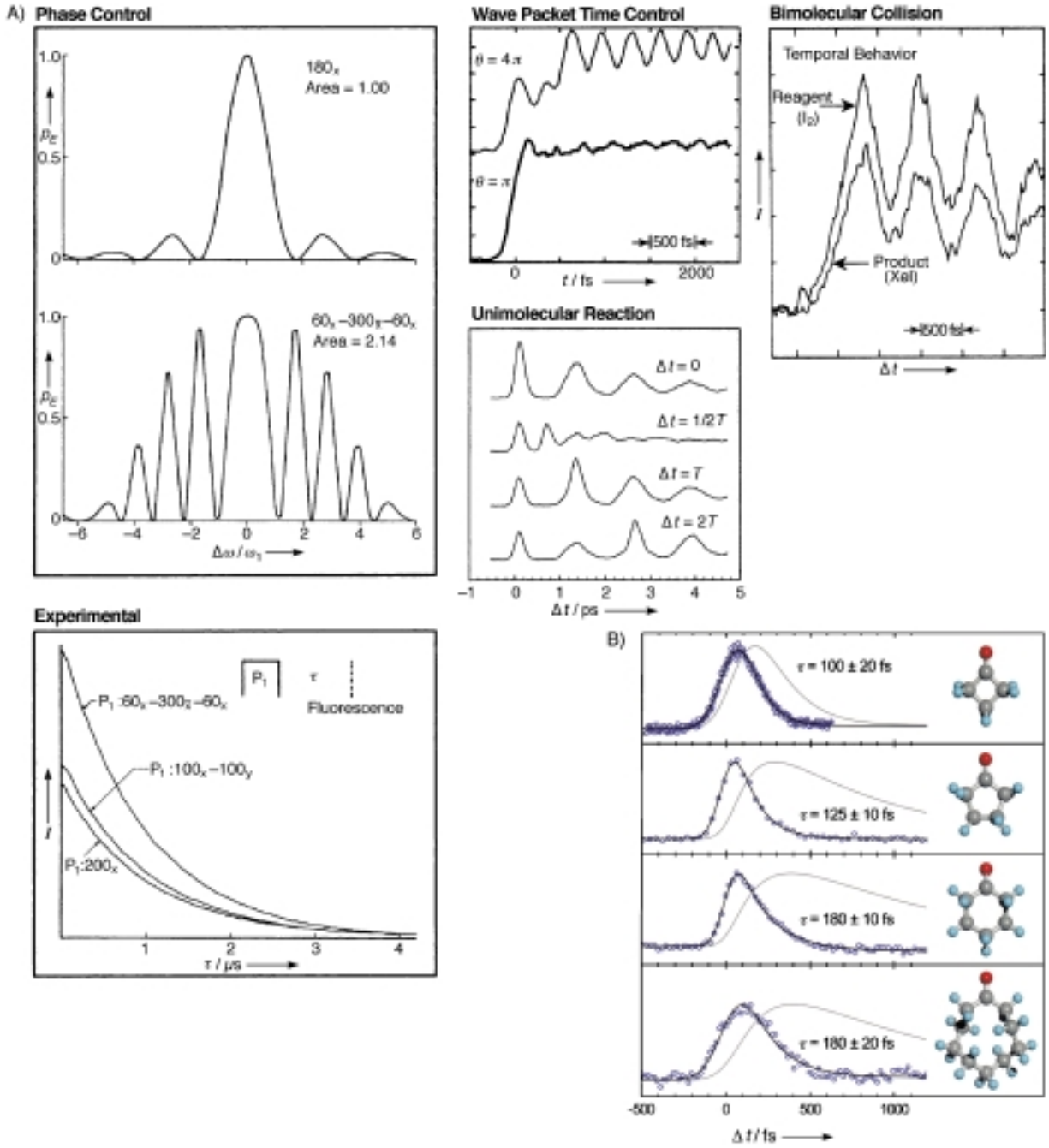


Figure 30. Control of the reaction by the phase and/or the delay, or the duration of optical pulses. A) Left: The effect of a designed composite pulse on the fluorescence of a molecule (iodine), showing the large experimental enhancement for the labeled phase-controlled sequence. Right: Control of the population (I_2), of unimolecular reactions (NaI), and of a bimolecular collision (Xe + I_2) (see text). B) Localized control of the preparation of high-energy wave packets on the femtosecond time scale, which are shorter than IVR. The series has the same reaction coordinate (C–C bond) but the molecular size has increased in complexity. The behavior is far from being statistical.[77, B20, B24]

evolution dictated by the natural forces of the atoms! Intense fields may do so. Paul Corkum, Thomas Baumert, and other colleagues have provided novel observations with intense fields.[38] Clearly these areas of control by ultrafast pulse timing (t), phase (ϕ, shape), spatial localization (R), and intensity to alter the potential (V) offer new opportunities for the future. Many theoretical efforts have already been advanced ahead of current experiments and Manz' group is providing new possibilities, including deracemization by controlled pulses—timed and shaped (see his review of 1500 references in ref. [28]). I did not discuss here the CW control scheme advanced by Paul Brumer and Moshe Shapiro, nor can I give references to all work done in this area.

3.6.3. *Biological Dynamics*

There have been important contributions to femtobiology (see ref. [28, 39], and their references) and these include: studies of the elementary steps of vision, photosynthesis,

protein dynamics, and electron and proton transport in DNA. In proteins such as those of photosynthetic reaction centers and antennas, hemoglobins, cytochromes, and rhodopsin, a femtosecond event such as bond breaking, twisting, or electron transfer occurs. There exist global and coherent nuclear motions, which can be observed in these complex systems, and it is possible that the complexity is not as complicated as we think; for the chemistry and the efficiency to be unique, the system utilizes the organized structure around the "active center" with the necessary restraint on transition states and energy flow. Thus, in my view, the early femtosecond events are critical to understanding the function of complex systems, as they reflect the important locality in biological dynamics.

Our efforts in this direction have so far focused on DNA-twisting dynamics, electron transfer in DNA assemblies, DNA base-pair mimics, and on protein–ligand dynamics. The work on the torsional rigidity of DNA was published in 1980–1982, while that relating to proton transfer in model base pairs was reported in the last few years. With donors (D) and acceptors (A) covalently bonded to DNA, studies of electron transfer on more well-defined assemblies were made possible, and the effect of distance could be addressed. With femtosecond resolution, we obtained the actual time scale of electron transfer and related the rates to the distance between D and A. In collaboration with Jackie Barton's group, we published this work in the *Proceedings of the National Acadmy of Sciences*. The time scale of orientational coherence and solvation was also examined, allowing us to elucidate the role of molecular motions, including the effect of DNA rigidity. The results reveal the nature of ultrafast electron transfer and its mechanism: in DNA, electron transfer cannot be described as in proteins simply by a phenomenological parameter β. Instead, the local involvement of the base pairs controls the time scale and the degree of coherent transport. Molecular dynamics are critical to the description of the transport. The measured rates (Figure 31) and the distance range of the transfer suggest that DNA is not an efficient molecular wire.

For proteins, our current interest is in the studies of the hydrophobic forces and electron transfer (Figure 31), and oxygen reduction in models of metalloenzymes (Figure 32). For the former, we have studied, with femtosecond resolution, the protein human serum albumin (HSA), probed with the small (ligand) molecule hydroxyphenylmethyloxazole (HPMO; see Figure 31 A); this work continues to be in collaboration with Abderrazzak Douhal. We also studied hyperthermophilic proteins. For model enzymes, we examined novel picket-fence structures which bind oxygen to the central metal with approximately 85% efficiency at room temperature. In this system (Figure 32), we observed the release of O_2 in 1.9 ps and the recombination was found to occur on a much slower time scale. These are fruitful areas for future research, especially in that they provide prototype systems for O_2 reduction with complex metalloporphyrins in the transition state, similar to the smaller systems of benzene/halogens (see Figure 23) but at room temperature. We published our first report recently in *Angewandte Chemie* in collaboration with Fred Anson's group at Caltech.

In the future, new extensions are anticipated. The nature and control of enzymatic reactions, the catalytic function of the transition state, and the design of artificial biological functions seem to be areas of great promise for dynamical studies. Also, it is envisaged that the recording of the change of a large biological structure with time and with atomic resolution may be realized. Already some success in studies of small chemical systems utilizing ultrafast electron diffraction have been reported. X-ray diffraction is another direction. The ultimate goal is the recording of all coordinates in space and time. The impact on problems such as protein folding and molecular recognition is clear.

4. Impact and Concepts—A Retrospective

In retrospect, the key to the explosion of research (see ref. [5a]) can perhaps be traced to three pillars of femtochemistry: time resolution, atomic-scale resolution, and generality of the approach.

4.1. Time Resolution—Reaching the Transition-State Limit

Three points are relevant: 1) The improvement of nearly ten orders of magnitude in time resolution, from the (milli)-microsecond time scale (Eigen and Norrish & Porter) to present femtosecond resolution, opened the door to studies of new phenomena and to new discoveries; 2) the transition state, the cornerstone of reactivity, could be clocked as a molecular species $TS^{\ddagger}$, providing a real foundation to the hypothesis of Arrhenius, Eyring, and Polanyi for ephemeral species $[TS]^{\ddagger}$, and leading the way to numerous new studies. Extensions will be made to study transition-state dynamics in complex systems, but the previous virtual status of the transition state has now given way to experimental reality;[5a] 3) inferences deduced from "rotational periods" as clocks in uni- and bimolecular reactions can now be replaced by the actual clocking of the nuclear (vibrational) motion. This is particularly important when a chemical phenomenon such as concertedness is involved or the time scale of complexes or intermediates is many vibrational periods.

In the 1960s, there was some thought that the relevant time scale for chemistry was the microsecond regime.[40a] Moreover, the uncertainty principle was thought to represent a severe limit to the utility of shorter time resolution; coherence was not part of the thinking in deciphering femtosecond nuclear motion, as discussed in Sections 3 (development of femtochemistry) and in what follows. The new vision is summarized in the following statement[40b]: "The study of chemical events that occur in the femtosecond time scale is the ultimate achievement in half a century of development and, although many future events will be run over the same course, chemists are near the end of the race against time." Manfred Eigen, who gave the 1967 Nobel Lecture with the title "Immeasurably Fast Reactions" ("Die 'Unmessbar' Schnellen Reaktionen") told me, when I teased him about the title, that nobody in the 1950s anticipated the laser and the short pulses they can provide.

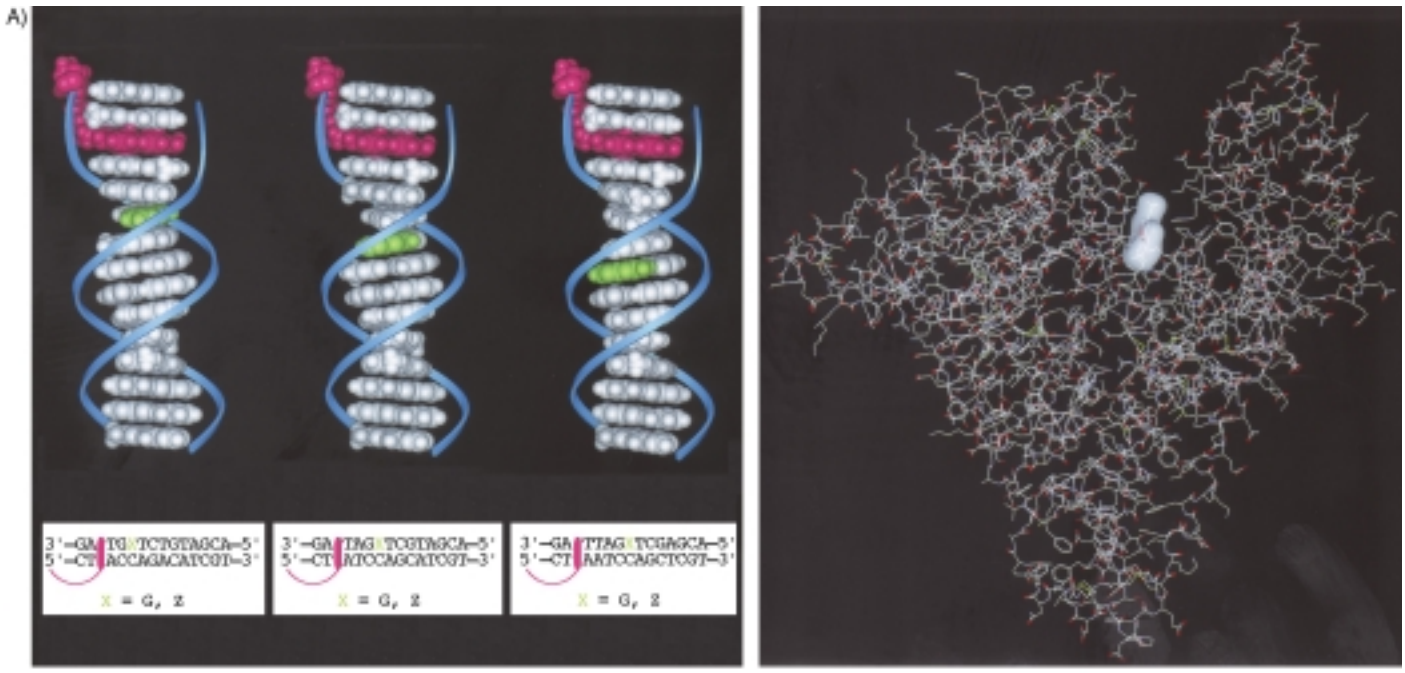


Figure 31. Femtosecond dynamics of biological systems, DNA assemblies, and protein complexes. A) The systems studied are DNA with donors and acceptors at fixed distances (left) and protein HSA with the molecule HPMO shown in the interior (right). The focus of research is on electron transfer and molecular dynamics in the former and on probing the solvation and ligand-recognition effects in the latter. B) Some illustrative femtosecond transients of DNA assemblies (A = normalized absorbance). Aminopurine was used for the initial excitation, and the effect of different bases G, C, A, and T was studied at a fixed distance. The time scale of the torsion dynamics was known from studies we and others made before.[78, 79]

4.2. Atomic-Scale Resolution

Two points are relevant: 1) The transition from kinetics to dynamics. On the femtosecond time scale, one can see the coherent nuclear motion of atoms—oscillatory or quantized steps instead of exponential decays or rises. This was proved to be the case for bound, quasi-bound, or unbound systems and in simple (diatomics) and in complex systems (proteins). Because of coherence, we can speak of the motion classically and visualize it as the change actually occurs; 2) the issue of *the* uncertainty principle. Many thought that the pulse was too short in time, thus broad in energy as described by the uncertainty principle $\Delta t \Delta E \sim \hbar$, but as discussed before, localization is consistent with the two uncertainty relationships (see Figure 4) and coherence is the key. The energy uncertainty ΔE should be compared with bond energies: ΔE is 0.7 kcal mol^{-1} for a 60 fs pulse (details are given in ref. [B17]). In the condensed phase, localiza-

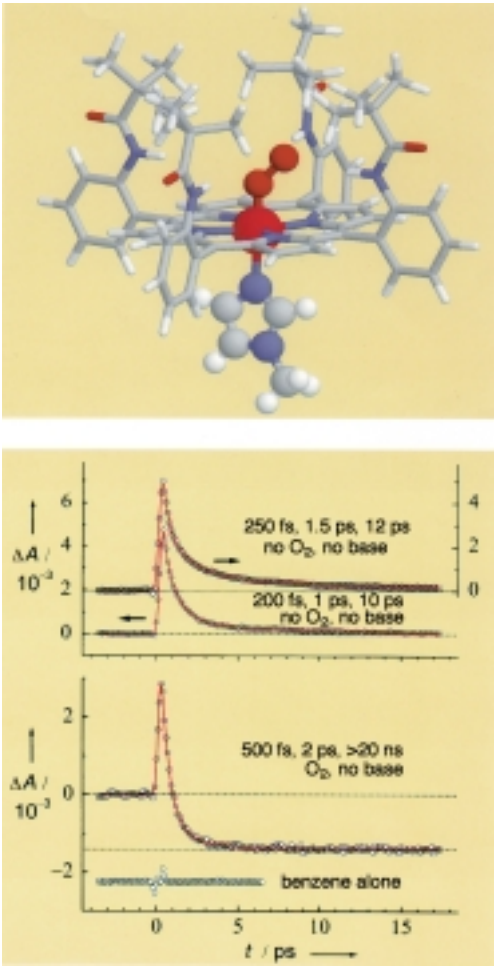


Figure 32. Femtosecond studies of model biological systems such as hemoglobin and myoglobin, DNA base pairs, and photosynthetic assemblies. Shown here are the structure of dioxygen picket fence cobalt porphyrins and the femtosecond transients which clearly show the timescales involved and the release of O_2 in 1.9 ps at room temperature. These studies on this and the other model systems (not shown) are part of the continued effort in this area.[80]

tion may become shorter lived, but the basic picture is still valid.[41]

This concept of coherence was not fully appreciated, not only among some chemists, but also among notable physicists. In 1972, at a Welch Conference, picosecond time resolution was of concern because of the perceived fundamental limitation imposed on time and energy by Heisenberg's uncertainty principle. After his lecture on lasers in chemistry, the physicist Edward Teller had a lively exchange with another physicist and friend, Eugene Wigner. Even for picosecond resolution the question was asked, is there a natural, real limit to the time…? In the Welch Prize Address (1997), I highlighted these exchanges.[42] Jacob Bigeleisen, although concerned about the uncertainty principle, asked why not venture into the "millijiffy" (femtosecond) range?[24]

4.3. Generality of the Approach

Three points are relevant: 1) In retrospect, the femtosecond time scale was just right for observing the "earliest" dynamics at the actual time scale of the chemical bond, defining the earliest time possible; 2) the methodology is versatile and general, as evidenced by the scope of applications in different phases and of different systems. Moreover, it has stimulated new directions of research in both experiment and theory in areas such as quantum control and ultrafast diffraction; 3) the time resolution offers unique opportunities when compared with other methods.

First, processes often appear complex because we look at them on an extended time scale, during which many steps in the process are integrated. On the femtosecond time scale, these steps are resolved, and the process breaks down into a series of simpler events. Second, only this time resolution can give the dynamics of transition states/intermediates in real time since for reactions neither the spectra of reactants nor those of products are directly relevant. This point was amply demonstrated in complex reactions, such as those of transient, reactive intermediates of organic compounds. Even for simple, reactive systems this is still true. For example, the spectral bandwidth of the reactant, dissociative ICN gives no information about the actual dynamics of the nuclear separation between I and CN fragments or about the transient configurations, as it only reflects the steepness of the potential at the initial nuclear configuration. For unreactive molecules, there is a different complexity; the spectra are usually inhomogenously broadened, especially in complex systems. Finally, with time resolution, we can observe the motion without resorting to a mathematical construct from eigenstates or other indirect methods.

It is worth noting that both excited and ground-state reactions can be studied. It has been known for some time that the use of multiple pulses can populate the ground state of the system and, therefore, the population and coherence of the system can be monitored.[23] The use of CARS (coherent anti-Stokes Raman spectroscopy), DFWM (degenerate four-wave mixing), SRS (simulated Raman spectroscopy), π pulses, or direct IR excitation are some of the approaches possible. Two recent examples demonstrate this point: one invokes the use of IR femtosecond pulses to study reactions involving hydrogen (bond) motions in liquid water (this work was done in France and Germany);[43] and the other utilizes CARS for the study of polymers in their ground state, which we published in collaboration with the groups of Kiefer and Materny (see Figure 28). Ground-state dynamics have also been studied by novel femtosecond photodetachment of negative ions, and the subfield of femtosecond dynamics of ions is now active in a number of laboratories.[44]

4.4. Some Concepts

New concepts and phenomena have emerged and include: Localization of wave packets; reaction path coherence; single-molecule trajectory; reaction landscapes versus path; bifurcation; chemical versus spectroscopic dynamics (time scales); concertedness; dynamical active space; nonstatistical (nonergodic) behavior; dynamical caging (by energy loss as opposed to barrier confinement); microscopic friction (energy versus mechanical); and inhomogeneous dynamics of "soft matter"

(for example, biological) systems, with a whole range of time scales. These concepts have been discussed in the original publications, and below, only a few will be highlighted:

4.4.1. Resonance (Nonequilibrium Dynamics)

The concept of resonance in the structure of the chemical bond goes back to the era of Linus Pauling and the idea of interconversion between different electronic structures. The interconversion was a hypothesis, not an observable fact. Quantum mechanically, chemists usually speak of eigenstates of the system, which are stationary with no time evolution. Resonance in dynamics is a concept which is not a stationary-state picture. With coherent preparation of molecules it is possible to prepare a nonstationary (nonequilibrium) state of a given nuclear structure and for the system to evolve in time. In our studies this was shown for vibrational redistribution, for rotational orientation, and for wave-packet nuclear motions. Such nonstationary evolution does not violate the uncertainty principle and is fundamental to chemical dynamics.

4.4.2. Coherence (Single-Molecule-Type Dynamics):

Perhaps one of the most powerful concepts in femtochemistry is coherence of the molecule, of the ensemble, and of the trajectory. First, the coherence created by a femtosecond pulse is reflected in the motion of the wave packet; for a force-free motion the group velocity is that of a free particle (p/m), a classical motion.[45] Second is the ability to "transform" the ensemble's incoherent behavior to a coherent molecular trajectory. This is achieved because on the femtosecond time scale the system can be promoted and localized in space with a localization length (ΔR) which is only limited by the uncertainty of the initial system, typically about 0.05 Å; all molecules which do not interact span this range. The chemical length scale (R) of interest is several angströms and this is why the system behaves as a single-molecule trajectory (Figure 33). Since the initial state is promoted nearly intact on the femtosecond time scale, the only dispersion is that which causes the different trajectories to spread under the influence of the new forces of the energy landscape or by external perturbations, such as solvation. If longer time pulses are used for the preparation, then ΔR is on the scale of R, and kinetics of the states are recovered. Put in time – domain language, the inhomogeneous dephasing time of the ensemble is relatively long for femtosecond preparation and the homogeneous dynamics and the actual coherence of the packet become dominant, as amply demonstrated here and elsewhere. Third, the concept of coherence is crucial for achieving a coherent trajectory of reactions. Such control projects out the non-statistical behavior through the preparation of a localized wave packet (Figure 33), as opposed to an incoherently prepared configuration (by, for example, chemical activation) or a spacially diffuse configuration (prepared by long-time experiments). The concept is powerful and basic to many phenomena: atomic-scale motion; reaction path coherence (from the transition state to products); reaction landscape trajectories as opposed to a single reaction path; energetic versus entropic structures near transition states and conical intersections; coherent caging by a solvent; bifurcation; and others.

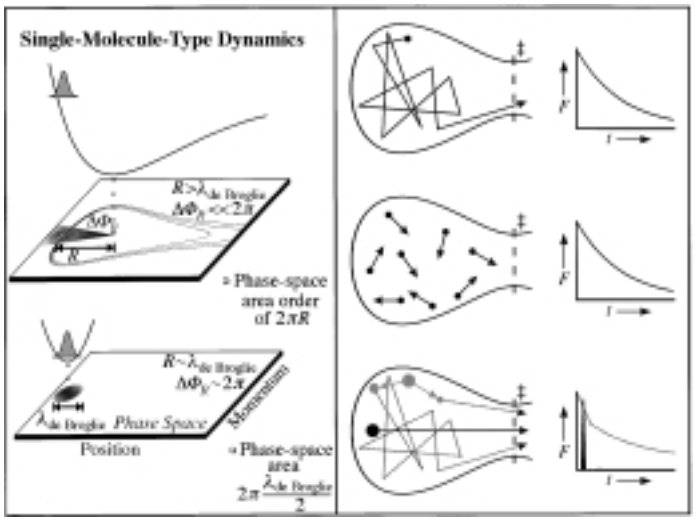


Figure 33. Concept of coherence, both in the dynamics at the atomic scale and in the control of nonstatistical behavior. Shown is the phase-space picture, describing the robustness of coherence (left); note the phase-space area of the initial state relative to that of the reaction. Right: A schematic representation of a configuration space made of the reactive coordinate and all nonreactive coordinates perpendicular to it (an equivalent phase-space picture can be made). Three cases of interest are shown: the ergodic dynamics (top); the incoherent preparation (middle); and the coherent wave packet preparation (bottom), which show the initial localization, spatially and temporally, and the bifurcation into direct and indirect reaction trajectories. Recent theoretical work (K. Møller, this laboratory) of the corresponding temporal behavior has elucidated different regimes for the influence of the initial preparation, from a wave packet to a microanonical limit.

4.4.3. Transition Structures (Landscape Dynamics):

This concept became clear to us after studies of the elementary dynamics in simple reactions of three atoms and in complex reactions of organic systems. Traditionally, one uses a reaction path and makes a distinction between a transition state and a reactive intermediate by the absence or presence of a potential well—if there is no well, bonds are not formed and thus we do not speak of a "real" structure. On the femtosecond time scale, we can isolate a continuous trajectory of transition structures; none are in a potential well. Such structures are defined by the change in bond order and lead to a family of trajectories of reaction products. Thus, the two classical pathways of either a "concerted" or "sequential" process represent a very crude approximation for the actual landscape dynamics, even in a three-atom system. There is a whole distribution of reaction times and kinetic energy releases. The problem becomes even more severe if the landscape is complex and has near-flat energy regions or entropic changes, as discussed in Section 2 for the case of complex organic reactions and protein folding. The concept of transition structures and landscape dynamics is significant to issues addressing stereochemistry, product branching, and selectivity, and to the real distinction between transition states and intermediates in many reactions. Finally, the presence of such a family of trajectories on the energy landscape makes

the restricted definition of the transition state—as only the saddle point—less clear. Concerted reactions, in the strict synchronous sense, essentially do not exist (see Sections 2 and 3).

4.4.4. Reduced Space (Directed Dynamics)

Another important concept in dynamics is the reduction of nuclear space to the sub-space critical to reactivity and nonradiative behavior in complex systems. Here, the femtosecond time scale allows one to project the primary events out of all processes possible. In complex systems with many degrees of freedom, the reduced space becomes the focus and the remaining space becomes a "continuum", thus moving the description from a multidimensional PES ($3N-6$ coordinates) to a few coordinates plus a weakly coupled continuum. This idea was central to our description of the dynamical isotope effect in elementary reactions, bifurcation to chemical and photophysical channels by conical intersections, concertedness and stereochemistry in organic reactions, nonstatistical behavior, and reaction control in large systems at high energies. The consequences to photochemistry are significant: reactions from high-energy states (π, π^*, Ryberg, etc) usually result in ground-state chemistry, and bifurcation into conical intersections is the key; for transitions involving σ^* orbitals, the time scale of rupture becomes comparable to that of the funneling, through conical intersections, and results in competitive chemical channels. It is possible that this same concept of reduced space is essential to biological dynamics. By reducing the space for dynamics, events occur efficiently and without "wasting" energy to all possible degrees of freedom. In addition, such designed local activity makes the system robust and immune to transferring "damage" over long distances. The ultrafast time scale is important because on it the system separates the important from the unimportant events—DNA bases quench their energy (nonradiatively) very rapidly, electron transfer in DNA is locally ultrafast, and the first event of vision is very efficient and occurs in 200 fs.

5. Epilogue

As the ability to explore shorter and shorter time scales has progressed from the millisecond to the present stage of widely exploited femtosecond capabilities, each step along the way has provided surprising discoveries, new understanding, and new mysteries. In their editorial on the 10th anniversary of Femtochemistry, Will Castleman and Villy Sundström put this advance in a historical perspective.[46a] The report in ref. [5a] addresses with details the field and its position in over a century of developments. Developments will continue and new directions of research will be pursued. Surely, studies of transition states and their structures in chemistry and biology will remain active for exploration in new directions, from simple systems to complex enzymes and proteins,[47] and from probing to the controlling of matter.

Since the current femtosecond lasers (4.5 fs) are now providing the limit of time resolution for phenomena involving nuclear motion, one may ask: Is there another domain in which the race against time can continue to be pushed? Subfemtosecond or attosecond (10^{-18} s) resolution may one day allow for the direct observation of the electron's motion. I made this point in a 1991 review article in *Faraday Discussions*[B17] and, since then, not much has been reported except for some progress in the generation of sub-femtosecond pulses.[46b] In the coming decades, this may change and we may view electron rearrangement, say, in the benzene molecule, in real time. Additionally, there will be studies involving the combination of the "three scales" mentioned in the prologue, namely time, length, and number. We should see extensions to studies of the femtosecond dynamics of single molecules and of molecules on surfaces (for example, using scanning tunneling microscopy). Combined time/length resolution will provide unique opportunities for making the important transition from molecular structures, to dynamics, and to functions (Section 3.6). We may also see that all of femtochemistry can be done at micro-to-nano-Kelvin temperatures, utilizing lasers and other cooling techniques.

It seems that on the femtosecond to attosecond time scale we are reaching the "inverse" of the big bang time (Figure 34), with the human heartbeat "enjoying" the geometric average of the two limits. The language of molecular dynamics is even similar to that of cosmos dynamics. Cosmologists are speaking

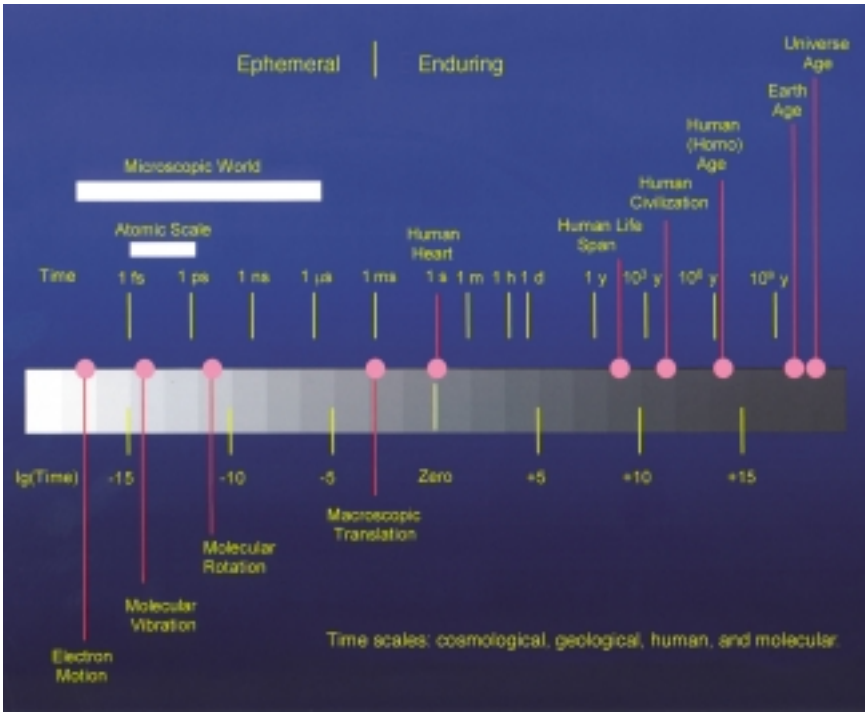


Figure 34. Timescales of cosmological, geological, human, and molecular events. Here, the timescale spans more than thirty orders of magnitude, from the big bang to the femtosecond age.[B25]

of energy landscapes and transition states for the big bang and universe inflation.[48] Perhaps we are approaching a universal limit of time!

Personally, I did not originally expect the rich blossoming in all of the directions outlined in this anthology; many more could, unfortunately, not be mentioned because of the limited space. What is clear to me is that my group and I have enjoyed the odyssey of discovery, seeing what was not previously possible, acquiring new knowledge, and developing new concepts. Perhaps the best words to describe this feeling are those of the English archaeologist, Howard Carter, on November 25, 1922 when he got his first glimpse of the priceless contents of Tutankhamen's Tomb—"At first, I could see nothing, … then shapes gradually began to emerge". Lord Carnarvon, who financed the excavation of this discovery, asked, when looking with Carter, "What do you see?" Carter replied, "Beautiful Things", "Beautiful Things". This is the thrill of discovery in science, too. It seeks to unveil the hidden simplicity and beauty of nature's truth. On a recent visit to the Los Angeles Art Museum with my wife, I stood in front of van Gogh's masterpiece—Almond Blossom (Figure 35)—and



Figure 35. The Almond Blossom (St. Rémy, 1890) of Vincent van Gogh (1853–1890). With a good beginning, even if branching is unpredictable, the blossoms are rich and the big picture is beautiful. (Los Angeles County Museum of Art).

wondered about the beauty of the big picture and the unpredictability of its details. That, also, is in the nature of scientific discoveries.

The future of femtoscience will surely witness many imaginative and unpredictable contributions. I hope that I will be able to enjoy the future as much as I have the past. Benjamin Franklin once wrote: "The progress of human knowledge will be rapid and discoveries made of which we at present have no conception. I begin to be almost sorry I was born so soon since I cannot have the happiness of knowing what will be known in years hence."

6. Appendix

6.1. A Primer for Femtoscopy, Coherence and Atoms in Motion

6.1.1. Pump–Probe Femtoscopy

In high-speed photography, a continuous motion is broken up into frames ("freezing") using a brief exposure time. For example, in Muybridge's experiment (Section 1), the shutter speed (exposure time) was about 2 ms and the speed of the motion was about $10\,m\,s^{-1}$, resulting in a well-defined resolution (speed × exposure time) of 2 cm; the number of frames per second was about twenty since the cameras were 0.5 m apart. The huge contrast with molecular experiments is due to vast differences in speed ($1\,km\,s^{-1}$), resolution (10^{-8} cm), and the number (millions) of molecules involved. Given the molecular speed and resolution, the ultrashort strobes must provide exposure time on the order of 100 fs, and in one second 10^{13} frames could be recorded! Ultrafast pulsed laser techniques have made direct exploration of this temporal realm a reality (Sections 2 and 3). Spectroscopy, mass spectrometry, and diffraction play the role of ultra-high-speed photography in the investigation of molecular processes.

A femtosecond laser pulse provides the shutter speed for freezing nuclear motion with the necessary spatial resolution. The pulse probes the motion by stroboscopy, that is, by pulsed illumination of the molecule in motion and recording or photographing the particular snapshot. A full sequence of the motion is achieved by using an accurately timed series of these probe pulses, which defines the number of frames per second. This method of probing, although different from Muybridge's, is in principle equivalent to his use of the cameras (with shutters) as probes. For molecules there exist three additional requirements in order to study the motion. First, we need to clock the motion by defining its zero of time, also accurate to tens of femtoseconds. Second, the motion must be synchronized since millions of molecules are typically used in the recording of molecular motion. Third, molecular coherence (see Section 6.1.2) must be induced to localize the nuclei. These requirements are satisfied by using a femtosecond pump (initiating) laser pulse, in what is referred to as a pump–probe configuration.

With this methodology, the process to be studied is clocked from the instant that the substance under investigation absorbs radiation from the pump pulse. Passage of a probe pulse through the sample at some later point in time provides a snapshot of the status of the system at that time. For femtosecond studies, where femtosecond control of relative timing is needed, the laser pump and probe pulses are produced in synchrony, then the probe pulse is diverted through an adjustable optical path length (see Figure 5). The finite speed of light translates the difference in path length into a difference in arrival time of the two pulses at the sample; 1 μm corresponds to 3.3 fs. The individual snapshots combine to produce a complete record of the continuous time evolution—a motion picture, or a movie—in what may be termed femtoscopy.

6.1.2. Coherence and Atomic Motion

In a classical description, the motions of nuclei would be particlelike, that is, they would behave as "marbles on a potential". At the scale of atomic masses and energies, however, the quantum mechanical wave/particle duality of matter comes into play, and the notions of position and velocity common to classical systems must be applied cautiously and in accord with the uncertainty principle, which places limits on the precision of simultaneous measurements. In fact, the state of any material system is defined in quantum mechanics by a spatially varying "wave function" with many similarities to light waves. Since the wave nature of light is a much more familiar concept than that of matter, we will use light to introduce the idea of wave superposition and interference, which plays an important role in atomic motion.

When light from two or more sources overlaps in space, the instantaneous field amplitudes (not intensities) from each source must be added together to produce the resultant light field. A well-known example is Young's two-slit experiment, in which light from a single source passes through two parallel slits in a screen to produce, in the space beyond, two phase-coherent fields of equal wavelength and amplitude. At points for which the distances to the two slits differ by $n+\frac{1}{2}$ wavelengths (for integer n) the two waves add to zero at all time, and no light is detected. Elsewhere, the amplitudes do not cancel. Thus, a stationary pattern of light and dark interference (Figure 4B, inset) fringes is produced ("light + light → darkness + more light!"). A knowledge of the wavelength of light and the spacing of fringes projected on a screen provide a measurement of the separation of the slits. In X-ray diffraction such interferences make it possible to obtain molecular structures with atomic resolution—the positions of the atoms replace the slits.

In studies of motion, we have exploited the concept of coherence among molecular wave functions to achieve atomic-scale resolution of dynamics—the change of molecular structures with time. Molecular wave functions are spatially diffuse and exhibit no motion. Superposition of a number of separate wave functions of appropriately chosen phases can produce a spatially localized and moving coherent superposition state, referred to as a wave packet (Figure 4B); constructive and destructive interference (as in the interference of light waves) is the origin of such spatial localization. The packet has a well-defined (group) velocity and position which now makes it analogous to a moving classical marble, but at atomic resolution. The femtosecond light induces the coherence and makes it possible to reach atomic-scale spatial and temporal resolution, without violation of the uncertainty principle.

In Figure 4B, a snapshot is shown of the position probability (in red) of a wave packet, formed from wave functions $n = 16-20$ with weighting according to the distribution curve(left of the figure). This was calculated for the harmonic wave functions representing the vibrational states of a diatomic molecule, in this case iodine (n is the quantum number). As time advances, the wave packet moves back and forth across the potential well. As long as the wave packet (width approximately 0.04 Å) is sufficiently localized on the scale of all accessible space (about 0.6 Å between the walls of the potential), as shown in the figure, a description in terms of the classical concepts of particle position and momentum is entirely appropriate. In this way, localization in time and in space are simultaneously achievable for reactive and nonreactive systems (Section 3.4). Note that the width of the packet prepared by a 20 fs pulse is very close to the uncertainty in bond distance for the initial $n = 0$ ground state. To prepare the packet at the inner turning point with the given phase composition, it must be launched vertically at the internuclear separation of about 2.4 Å; if launched from the shown $n = 0$ distance, the packet will have a different phase composition and will be localized initially in the center of the well.

The observation of motion in a real system requires not only the formation of localized wave packets in each molecule, but also a small spread in position among wave packets formed in the typically millions of molecules on which the measurement is performed. The key to achieving this condition is generally provided by a) the well-defined initial, equilibrium configuration of the studied molecules before excitation and b) by the "instantaneous" femtosecond launching of the packet. The spatial confinement (in this case about 0.04 Å) of the initial ground state of the system ensures that all molecules, each with its own coherence among the states which form its wave packet, begin their motion on the excited potential in a bond-distance-range much smaller than that executed by the motion. The femtosecond launching ensures that this narrow range of bond distance is maintained during the entire process of preparation (see Figure 33). Unless the molecular and ensemble coherences are destroyed by intra- and/or intermolecular perturbations, the motion is that of a classical single-molecule trajectory.

The story told here involves many dedicated students, postdoctoral fellows, and research associates. Their contributions are recognized in the publications cited. I hope that by mentioning their work, they recognize the crucial role they have played in the journey of femtochemistry at Caltech. To me the exciting time with my research group represents the highlight of the story. For 20 years I have always looked forward to coming to work with them each day and to enjoying the science in the truly international family (Figure 36). All members of the current research group have helped with the figures presented here. I particularly wish to thank Dongping Zhong for the special effort and care throughout the preparation and Ramesh Srinivasan for his devoted help with some of the figures. The artistic quality of many of the figures reflects the dedicated efforts of Wayne Waller and his staff.

There have been a number of friends and colleagues who have supported the research field and made the experience enjoyable and humanly worthwhile—to them I wish the very best. All are with us today, except one: Dick Bernstein. Caltech proved to be the ideal scientific institution for me, not only because of the strong science it radiates, but also because of its culture, the "science village". I will never forget the impact of the "round table" at the Athenaeum. Vince McKoy, friend, colleague, and neighbor at Caltech, has been the source of enjoyment and stimulation for over 20 years; Vince has taken an almost daily interest in our progress! Over the years I have enjoyed discussions with Spencer Baskin whose critical and

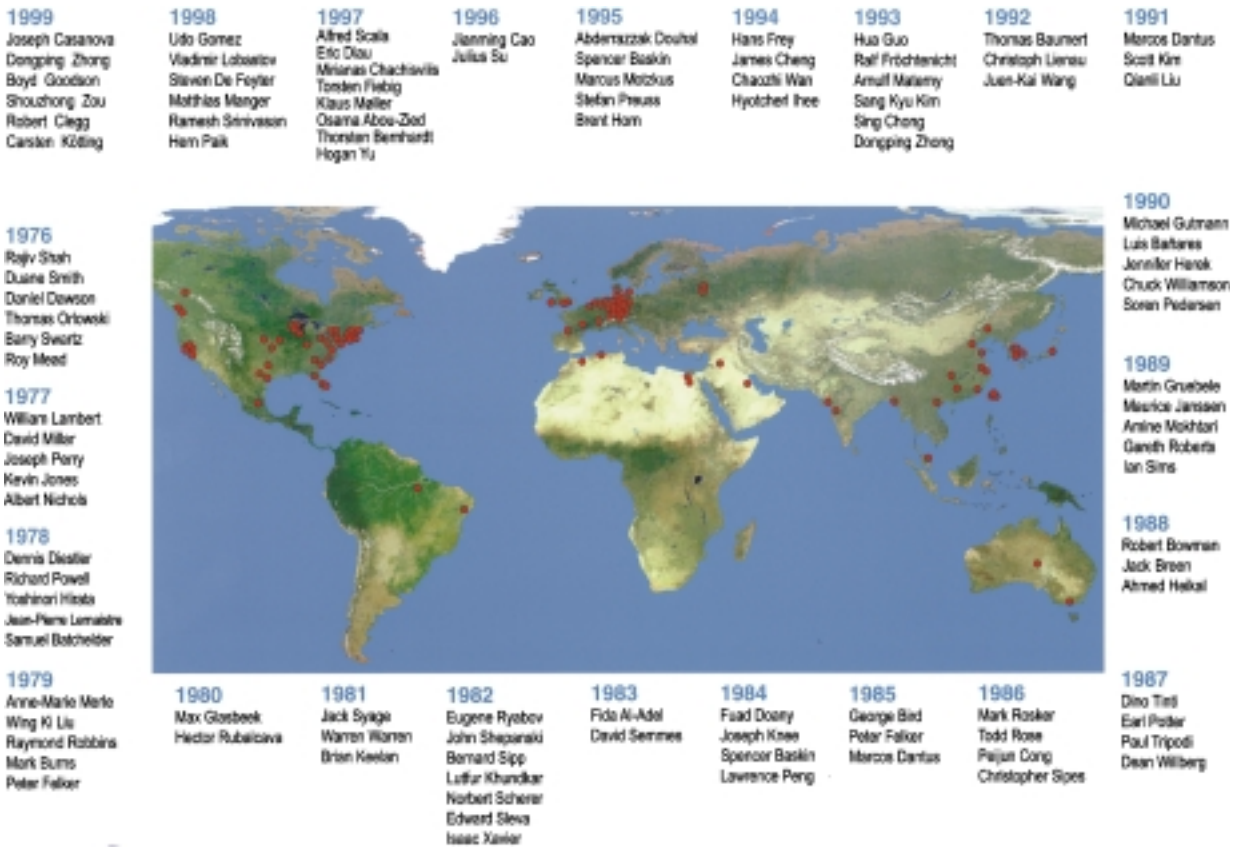


Figure 36. The International Roster of the Caltech group, 1976–1999. The red circles are usually composite of many dots, reflecting the more than one hundred graduate students, postdoctoral fellows, and visiting associates, who made up the research team over the years.

wise judgment served as a sounding board for penetrating physics concepts.

Major support of this research came from the National Science Foundation, the US Air Force Office of Scientific Research, and the Office of Naval Research, and it is a pleasure to acknowledge all of these organizations for making it possible. I take the opportunity to thank Carl and Shirley Larson for their support and friendship. Last, but not least, I wish to thank the staff of the Division and the Institute for their care and sincere efforts which have made our ship sail along with minimal resistance.

Received: March 23, 2000 [A 404]

[1] a) J. H. Breasted, *A History of Egypt*, Scribner's Sons, New York, **1909** (Renewal, **1937**); b) A. Gardiner, *Egyptian Grammar*, 3rd ed., Griffith Institute Ashmolean Museum, Oxford, **1957** (first published in **1927** and lastly in **1994**); c) "The Origin of the Ancient Egyptian Calendar": H. E. Winlock, *Proc. Am. Phys. Soc.* **1940**, *83*, 447; d) O. Neugebauer, *The Exact Sciences in Antiquity*, Brown University Press, Providence, RI, **1957**; e) R. K. Marshall, *Sundials*, McMillan, New York, **1963**; f) P. Tompkins, *The Magic of Obelisks*, Harper & Row, New York, **1981**; g) G. J. Whitrow, *Time in History*, Oxford University Press, Oxford, **1989**; i) *Encyclopedia of the History of Science, Technology, and Medicine in Non-Western Cultures* (Ed.: H. Selin), Kluwer Dordrecht, The Netherlands, **1997**; j) *A Walk Through Time*, 1998, http://physics.nist.gov/GenInt/Time/time.html,; k) M. M. Soliman, *History of Science and Technology in Ancient and Middle Ages*, Alhiaa Almasria Lelkitab, Cairo, **1995** (in Arabic); l) D. Steel, *Marking time—The Epic Quest to Invent the Perfect Calendar*, Wiley, New York, **2000**.

[2] *Sci. Am.* **1878**, *39* (Oct. 19), 241; T. K. Derry, T. I. Williams, *A Short History of Technology*, Dover, New York, **1993**; E. Jussim, G. Kayafas, *Stopping Time*, H. N. Abrams, New York, **1987**.

[3] C. A. Ronan, *Science—Its History and Development Among the World's Cultures*, Facts on File, New York, **1982**; J. R. Partington, *A Short History of Chemistry*, Dover, New York, **1989**; J. W. Servos, *Physical Chemistry from Ostwald to Pauling*, Princeton, **1990**; C. van Doren, *A History of Knowledge*, Ballantine, New York, **1991**; W. H. Brock, *Chemistry*, Norton, New York, **1992**; C. H. Langford, R. A. Beebe, *The Development of Chemical Principles*, Dover, New York, **1995**; R. Breslow, *Chemistry Today and Tomorrow*, American Chemical Society, Washington, **1997**; J. Read, *From Alchemy to Chemistry*, Dover, New York, **1995**; *Scientists—Random House Webster's Dictionary*, New York, **1997**.

[4] a) A. H. Zewail, *Cambridge Rev.* **1997**, *118*(2330), 65; b) J. Baggott, *Chemistry in a New Light*, Cambridge University Press, Cambridge, **2000**, in press.

[5] a) B. Nordén, www.nobel.se/announcement-99/chemistry99.html; b) A. Donoso, C. C. Martens, *J. Phys. Chem. A* **1998**, *102*, 4291 (introduction to this reference); c) D. E. Folmer, W. S. Wisniewski, S. M. Hurley, A. W. Castleman, Jr., *Proc. Natl. Acad. Sci. USA* **1999**, *96*, 12980, and references therein.

[6] H. C. von Baeyer, *Taming the Atom*, Random House, New York, **1992**; P. Ball, *Designing the Molecular World*, Princeton University Press, Princeton, **1994**; P. W. Atkins, *Atoms, Electrons, and Change*, Freeman, New York, **1991**.

[7] a) S. Arrhenius, *Z. Phys. Chem. (Leipzig)* **1889**, *4*, 226; b) J. H. van't Hoff in *Etudes de Dynamiques Chimiques*, F. Muller, Amsterdam, **1884**, p. 114 (translation by T. Ewan, London, **1896**); c) M. Bodenstein, *Z. Phys. Chem. (Munich)* **1894**, *13*, 56; M. Bodenstein, *Z. Phys. Chem. (Munich)* **1897**, *22*, 1; M. Bodenstein, *Z. Phys. Chem. (Munich)* **1899**, *29*, 295; d) F. A. Lindemann, *Trans. Faraday Soc.* **1922**, *17*, 598; e) C. N. Hinshelwood, *The Kinetics of Chemical Change in Gaseous Systems*, Calendron, Oxford, **1926** (second printing, **1929**;

third printing, **1933**); C. N. Hinshelwood, *Proc. R. Soc. London A* **1926**, *113*, 230; f) R. C. Tolman, *J. Am. Chem. Soc.* **1925**, *47*, 2652; R. C. Tolman, *J. Am. Chem. Soc.* **1920**, *42*, 2506; g) J. G. Kirkwood, O. R. Wulf, P. S. Epstein, *Biographical memoirs*, *Vol. 27*, National Academy of Sciences (USA), p. 139.

[8] See, for example, a) K. J. Laidler, *Chemical Kinetics*, 3rd ed., Harper Collins, New York, **1987**; b) J. I. Steinfeld, J. S. Francisco, W. L. Hase, *Chemical Kinetics and Dynamics*, Prentice-Hall, New Jersey, **1989**; c) T. Baer, W. L. Hase, *Unimolecular Reaction Dynamics*, Oxford University Press, New York, **1996**; d) S. Shaik, H. Schlegel, S. Wolfe, *Theoretical Aspects of Physical and Organic Chemistry*, Wiley, New York, **1992**; e) A. Pross, *Theoretical & Physical Principles of Organic Reactivity*, Wiley, New York, **1995**.

[9] R. D. Levine, R. B. Bernstein, *Molecular Reaction Dynamics and Chemical Reactivity*, Oxford University Press, Oxford, **1987**, and references therein.

[10] a) W. Heitler, F. London, *Z. Phys.* **1927**, *44*, 455; b) F. London, *Probleme der Modernen Physik*, Sommerfeld Festschrift, **1928**, p. 104; c) H. Eyring, M. Polanyi, *Z. Phys. Chem. B* **1931**, *12*, 279; M. Polanyi, *Atomic Reactions*, Williams, Norgate, London, **1932**.

[11] a) M. Polanyi, E. Wigner, *Z. Phys. Chem. Abt. A* **1928**, *139*, 439; b) H. Eyring, *J. Chem. Phys.* **1935**, *3*, 107; see also H. Eyring, *J. Chem. Phys.* **1935**, *3*, 492; c) M. G. Evans, M. Polanyi, *Trans. Faraday Soc.* **1935**, *31*, 875; M. G. Evans, M. Polanyi, *Trans. Faraday Soc.* **1937**, *33*, 448; d) H. A. Kramers, *Physica (Utrecht)* **1940**, *7*, 284; e) R. A. Marcus, *J. Chem. Phys.* **1956**, *24*, 966; R. A. Marcus, *J. Chem. Phys.* **1956**, *24*, 974; f) R. F. Grote, J. T. Hynes, *J. Chem. Phys.* **1980**, *73*, 2715; ref. [28].

[12] J. C. Polanyi, A. H. Zewail, *Acc. Chem. Res.* **1995**, *28*, 119, and references therein.

[13] a) I. H. Williams, *Chem. Soc. Rev.* **1993**, *22*, 277; A. Williams, *Chem Soc. Rev.* **1994**, *23*, 93; W. v. E. Doering, W. Wang, *J. Am. Chem. Soc.* **1999**, *121*, 10112; J. E. Baldwin, *J. Comp. Chem.* **1998**, *19*, 222; b) P. G. Schultz, R. A. Lerner, *Science* **1995**, *269*, 1835; c) A. R. Fersht, *Curr. Opin. Struct. Biol.* **1994**, *5*, 79.

[14] J. C. Polanyi, *Science* **1987**, *236*, 680, and references therein; J. C. Polanyi, *Faraday Discuss. Chem. Soc.* **1979**, *67*, 129.

[15] B. R. Johnson, J. L. Kinsey in *Femtosecond Chemistry* (Eds.: J. Manz, L. Wöste), VCH, Weinheim, **1994**.

[16] A. H. Zewail, *Femtochemistry—Ultrafast Dynamics of the Chemical Bond*, *Vol. I and II*, World Scientific, Singapore, **1994**. Most of the Caltech publications in this field, to be referenced here (**1976–1994**), are collected in these two volumes. References will be given for the specific topics and will be updated in the text and bibliography.

[17] M. Eigen, *Discuss. Faraday Soc.* **1954**, *17*, 194; M. Eigen in *Techniques of Organic Chemistry*, *Vol. VIII*, *Part II*, Interscience, London, **1963**; "Immeasurable Fast Reactions": M. Eigen in *Nobel Lectures (Chemistry)*, Elsevier, Amsterdam, **1972**, p. 170, and references therein; R. G. W. Norrish, G. Porter, *Nature* **1949**, *164*, 658; G. Porter in *The Chemical Bond: Structure and Dynamics* (Ed.: A. H. Zewail), Academic Press, Boston, **1992**, p. 113, and references therein.

[18] a) H. Abraham, T. Lemoine, *C. R. Hebd. Seances Acad. Sci.* **1899**, *129*, 206; for reviews, see b) N. Bloembergen, *Rev. Mod. Phys.* **1999**, *71*, S283, and references therein; c) E. N. Glezer, *Spectroscopy and Dynamics of Collective Excitations in Solids*, Plenum, New York, **1997**, p. 375; d) *Ultrashort Light Pulses* (Ed.: S. L. Shapiro), Springer, Berlin, **1977**; e) *Ultrashort Laser Pulses & Applications* (Ed.: W. Kaiser), Springer, Berlin, **1988**; *Ultrafast Phenomena*, *Vol. IX* (Eds.: P. F. Barbara, W. H. Knox, G. A. Mourou, A. H. Zewail), Springer, New York, **1994**; *Ultrafast Phenomena Vol. XI* (Eds.: T. Elsaesser, J. G. Fujimoto, D. A. Wiersma, W. Zinth), Springer, New York, **1998**, and references therein; see also ref. [2].

[19] a) C. V. Shank, E. P. Ippen, *App. Phys. Lett.* **1974**, *24*, 373; b) R. L. Fork, B. I. Greene, C. V. Shank, *App. Phys. Lett.* **1981**, *38*, 671; c) J. A. Valdmanis, R. L. Fork, J. P. Gordon, *Opt. Lett.* **1985**, *10*, 131; d) R. L. Fork, C. H. Brito Cruz, P. C. Becker, C. V. Shank, *Opt. Lett.* **1987**, *12*, 483; see also the reviews in ref. [18]; e) D. E. Spence, P. N. Kean, W. Sibbett, *Opt. Lett.* **1991**, *16*, 42; f) J. P. Zhou, G. Taft, C. P. Huang, M. M. Murnane, H. C. Kaptyn, *Opt. Lett.* **1994**, *19*, 1149; g) A. Baltuska, Z. Wei, M. S. Pshenichnikov, D. Wiersma, *Opt. Lett.* **1997**, *22*, 102; h) R. R. Alfano, S. L. Shapiro, *Phys. Rev. Lett.* **1970**, *24*, 584.

[20] P. M. Rentzepis, *Chem. Phys. Lett.* **1968**, *2*, 117; T. L. Netzel, P. M. Rentzepis, J. S. Leigh, *Science* **1973**, *182*, 238; K. J. Kaufmann, P. M. Rentzepis, *Acc. Chem. Res.* **1975**, *8*, 407.

[21] T. J. Chuang, G. W. Hoffmann, K. B. Eisenthal, *Chem. Phys. Lett.* **1974**, *25*, 201; K. B. Eisenthal, K. H. Drexhage, *J. Chem. Phys.* **1969**, *51*, 5720; K. B. Eisenthal, *Acc. Chem. Res.* **1975**, *8*, 118.

[22] R. M. Hochstrasser, H. Lutz, G. W. Scott, *Chem. Phys. Lett.* **1974**, *24*, 162; R. Anderson, R. M. Hochstrasser, H. Lutz, G. W. Scott, *Chem. Phys. Lett.* **1974**, *28*, 153; R. M. Hochstrasser, *Springer Ser. Chem. Phys.* **1978**, *3*, 98.

[23] D. von der Linde, A. Laubereau, W. Kaiser, *Phys. Rev. Lett.* **1971**, *26*, 954; A. Laubereau, D. von der Linde, W. Kaiser, *Phys. Rev. Lett.* **1972**, *28*, 1162; A. Laubereau, W. Kaiser, *Rev. Mod. Phys.* **1978**, *50*, 607.

[24] "Chemistry in a Jiffy": J. Bigeleisen, *Chem. Eng. News* **1977**, *55*, 26. In a written correspondence, Jacob emphasized that he, in contrast to the view of the 1960s (ref. [40]) understood what could be learned from time scales below the nanosecond, but that he failed to appreciate how the two uncertainties would serve to localize the length scale.

[25] a) D. R. Herschbach, *Angew. Chem.* **1987**, *99*, 1251; *Angew. Chem. Int. Ed. Engl.* **1987**, *26*, 1221, and references therein; Y. T. Lee, *Science* **1987**, *236*, 793, and references therein; b) R. N. Zare, R. B. Bernstein, *Phys. Today* **1980**, *33*, 11.

[26] A. H. Zewail, R. B. Bernstein, *Chem. Eng. News* **1988**, Nov 7, 24; also in *The Chemical Bond: Structure and Dynamics* (Ed.: A. H. Zewail), Academic Press, Boston, **1992**, p. 223.

[27] D. C. Clary, *Science* **1998**, *279*, 1879; D. C. Clary in ref. [28], and references therein.

[28] *Nobel Symposium Book: Femtochemistry and Femtobiology: Ultrafast Reaction Dynamics at Atomic-Scale Resolution* (Ed.: V. Sundström), World Scientific, Imperial College Press, London, **1997**, and references therein.

[29] R. P. Feynman, F. L. Vernon, R. W. Hellwarth, *J. Appl. Phys.* **1957**, *28*, 49.

[30] For recent reviews, see J. Jortner, M. Bixon in ref. [28]; J. Jortner, *Phil. Trans. R. Soc. Lond. A* **1998**, *356*, 477, and references therein.

[31] a) E. J. Heller, *Acc. Chem. Res.* **1981**, *14*, 368; b) D. Imre, J. L. Kinsey, A. Sinha, J. Krenos, *J. Phys. Chem.* **1984**, *88*, 3956; B. R. Johnson, C. Kittrell, P. B. Kelly, J. L. Kinsey, *J. Phys. Chem.* **1996**, *100*, 7743; c) R. Kosloff, *J. Phys. Chem.* **1988**, *92*, 2087, and references therein.

[32] B. Roos, *Acc. Chem. Res.* **1999**, *32*, 137, and references therein.

[33] V. Letokhov in ref. [28]; V. Letokhov in *Femtochemistry IV*, Leuven, Belgium, **1999**; V. Letokhov in ref. [B30]; V. Letokhov in ref. [B31].

[34] W. S. Warren, *Science* **1988**, *242*, 878; W. S. Warren, *Encyclopedia Magnetic Resonance*, Wiley, New York, **1996**.

[35] a) D. J. Tannor, S. A. Rice, *J. Chem. Phys.* **1985**, *83*, 5013; b) D. J. Tannor, R. Kosloff, S. A. Rice, *J. Chem. Phys.* **1986**, *85*, 5805; c) D. J. Tannor, S. A. Rice, *Adv. Chem. Phys.* **1988**, *70*, 44.

[36] a) H.-L. Dai, W. Ho, *Laser Spectroscopy and Photochemistry on Metal Surfaces*, *Part I & II*, World Scientific, Singapore, **1995**; b) M. Bonn, S. Funk, C. Hess, D. N. Denzler, C. Stampfl, M. Scheffler, M. Wolf, G. Ertl, *Science* **1999**, *285*, 1042; c) R. J. Finlay, T.-H. Her, C. Wu, E. Mazur, *Chem. Phys. Lett.* **1997**, *274*, 499.

[37] a) A. Assion, T. Baumert, M. Bergt, T. Brixner, B. Kiefer, V. Seyfried, M. Strehle, G. Gerber, *Science* **1998**, *282*, 919; b) B. Kohler, J. L. Krause, F. Raksi, K. R. Wilson, V. V. Yakovlev, R. M. Whitnell, Y. J. Yan, *Acc. Chem. Res.* **1995**, *28*, 133.

[38] P. B. Corkum, M. Y. Ivanov, J. S. Wright, *Annu. Rev. Phys. Chem.* **1997**, *48*, 387; T. Frohnmeyer, M. Hofmann, M. Strehle, T. Baumert, *Chem. Phys. Lett.* **1999**, *312*, 447; *Molecules in Laser Fields* (Ed.: A. D. Bandrauk), Marcel Dekker, New York, **1994**, and references therein.

[39] R. M. Hochstrasser, *J. Chem. Educ.* **1998**, *75*, 559, and references therein; V. Sundström, T. Pullerits, R. van Grondelle, *J. Phys. Chem. B* **1999**, *103*, 2327, and references therein; S. Hahn, G. Stock, *J. Phys. Chem. B* **2000**, *104*, 1146, and references therein; J.-L. Martin, M. H. Vos, *Annu. Rev. Biophys. Biomol. Struct.* **1992**, *21*, 199, and references therein; L. Zhu, J. T. Sage, P. M. Champion, *Science* **1994**, *266*, 629, and references therein; G. R. Fleming, R. van Grondelle, *Phys. Today* **1994** (February Issue), 48), and references therein; R. A. Mathies, S. W. Lin, J. B. Ames, W. T. Pollard, *Annu. Rev. Biophys. Biophys. Chem.* **1991**, *20*, 491, and references therein; R. J. D. Miller, *Annu. Rev. Phys. Chem.* **1991**, *42*, 581, and references therein; M. H. Vos, J.-L. Martin, *Biochim. Biophys. Acta* **1999**, *1411*, 1, and references

therein; U. Liebl, G. Lipowski, M. Négrerie, J.-C. Lambry, L.-L. Martin, M. H. Vos, *Nature* **1999**, *401*, 181, and references therein; *Electron Transfer—From Isolated Molecules to Biomolecules* (Eds.: J. Jortner M. Bixon), Wiley, New York, **1999**, and references therein; see also ref. [28], [79], and [80].

[40] a) *Nobel Symposium 5*, *Fast Reactions and Primary Processes in Chemical Kinetics* (Ed.: S. Claesson), Almqvist & Wiksell, Stockholm, **1967**, p. 474; b) G. Porter in *Femtosecond Chemistry*, *Vol. 1* (Eds.: J. Manz, L. Wöste), VCH, Weinheim, **1995**, p. 3.

[41] Z. Li, J.-Y. Fang, C. C. Martens, *J. Chem. Phys.* **1996**, *104*, 6919.

[42] "The 1997 Welch Prize Address, Femtochemistry": A. H. Zewail in *Proceedings of the Robert A. Welch Foundation*, 41st Conference on Chemical Research, Houston, Texas, **1997**, p. 323.

[43] G. M. Gale, G. Gallot, F. Hache, N. Lascoux, S. Bratos, J. C. Leicknam, *Phys. Rev. Lett.* **1999**, *82*, 1068; C. Chudoba, E. T. J. Nibbering, T. Elsaesser, *J. Phys. Chem. A* **1999**, *103*, 5625; for the development of methods, see J. N. Moore, P. A. Hansen, R. M. Hochstrasser, *Chem. Phys. Lett.* **1987**, *138*, 110; P. O. Stoutland, R. B. Dyer, W. H. Woodruff, *Science* **1992**, *257*, 1913; W. Kaiser, A. Laubereau in ref. [23], and references therein.

[44] A. W. Castleman, Jr., K. H. Bowen, Jr., *J. Phys. Chem.* **1996**, *100*, 12911; S. Wolf, G. Sommerer, S. Rutz, E. Schreiber, T. Leisner, L. Wöste, R. S. Berry, *Phys. Rev. Lett.* **1995**, *74*, 4177; P. Farmanara, W. Radloff, V. Stert, H. H. Ritze, I. V. Hertel, *J. Chem. Phys.* **1999**, *111*, 633; W. C. Lineberger, in ref. [28]; M. T. Zanni, B. J. Greenblatt, A. V. Davis, D. M. Neumark, *J. Chem. Phys.* **1999**, *111*, 2991, and references therein.

[45] C. Cohen-Tannoudji, B. Diu, F. Laloë, *Quantum Mechanics*, *Vol. I & II*, Wiley, New York, **1977**; J. L. Eisberg, *Fundamentals of Modern Physics*, Wiley, New York, **1964**; D. D. Fitts, *Principles of Quantum Mechanics*, Cambridge University Press, **1999**; L. Mühlbacher, A. Lucke, R. Egger, *J. Chem. Phys.* **1999**, *110*, 5851; J. Manz in ref. [28], p. 80; M. A. Morrison, *Quantum Physics*, Prentice Hall, New Jersey, **1990**.

[46] a) A. W. Castleman, Jr., V. Sundström, *J. Phys. Chem. A* **1998**, *102*, 4021 (special issue "Ten Years of Femtochemistry"); b) P. Corkum, *Nature* **2000**, *403*, 845; S. E. Harris, A. V. Sokolov, *Phys. Rev. Lett.* **1998**, *81*, 2894.

[47] A. R. Fersht, *Structure and Mechanism in Protein Science*, W. H. Freeman, New York, **1999**; W. A. Eaton, *Proc. Natl. Acad. Sci. USA* **1999**, *96*, 5897; C. L. Brooks III, M. Gruebele, J. N. Onuchic, P. G. Wolynes *Proc. Natl. Acad. Sci. USA* **1998**, *95*, 11037; D. T. Leeson, F. Gai, H. M. Rodriguez, L. M. Gregoret, *Proc. Natl. Acad. Sci. USA* **2000**, *97*, 2527.

[48] "Which way to the Big Bang?": J. Glanz, *Science* **1999**, *284*, 1448; S. Clark, *Towards the Edge of the Universe*, 2nd ed., Springer, New York, **1999**.

[49] S. Pedersen, J. L. Herek, A. H. Zewail, *Science* **1994**, *266*, 1359.

[50] A. H. Zewail, T. E. Orlowski, K. E. Jones, D. E. Godar, *Chem. Phys. Lett.* **1977**, *48*, 256; W. S. Warren, A. H. Zewail, *J. Chem. Phys.* **1981**, *75*, 5956; W. S. Warren, A. H. Zewail, *J. Chem. Phys.* **1983**, *78*, 2279; E. T. Sleva, A. H. Zewail, *Chem. Phys. Lett.* **1984**, *110*, 582; E. T. Sleva, I. M. Xavier, Jr., A. H. Zewail, *J. Opt. Soc. Am.* **1986**, *3*, 483.

[51] W. R. Lambert, P. M. Felker, A. H. Zewail, *J. Chem. Phys.* **1981**, *75*, 5958; W. R. Lambert, P. M. Felker, A. H. Zewail, *J. Chem. Phys.* **1984**, *81*, 2209; W. R. Lambert, P. M. Felker, A. H. Zewail, *J. Chem. Phys.* **1984**, *81*, 2217; P. M. Felker, A. H. Zewail, *Phys. Rev. Lett.* **1984**, *53*, 501; P. M. Felker, A. H. Zewail, *J. Chem. Phys.* **1985**, *82*, 2961; P. M. Felker, A. H. Zewail, *J. Chem. Phys.* **1985**, *82*, 2975; P. M. Felker, A. H. Zewail, *J. Chem. Phys.* **1985**, *82*, 2994; P. M. Felker, A. H. Zewail, *Adv. Chem. Phys.* **1988**, *70*, 265; P. M. Felker, A. H. Zewail in *Jet Spectroscopy and Molecular Dynamics* (Eds.: M. Hollas, D. Phillips), Chapman and Hall, Blackie Academic, **1995**, p. 222.

[52] A. H. Zewail, *Faraday Discuss. Chem. Soc.* **1983**, *75*, 315; J. A. Syage, W. R. Lambert, P. M. Felker, A. H. Zewail, R. M. Hochstrasser, *Chem. Phys. Lett.* **1982**, *88*, 266; J. A. Syage, P. M. Felker, A. H. Zewail, *J. Chem. Phys.* **1984**, *81*, 4706; P. M. Felker, A. H. Zewail, *J. Chem. Phys.* **1985**, *82*, 2961; P. M. Felker, A. H. Zewail, *J. Chem. Phys.* **1985**, *82*, 2994; P. M. Felker, J. A. Syage, W. R. Lambert, A. H. Zewail, *Chem. Phys. Lett.* **1982**, *92*, 1; J. A. Syage, P. M. Felker, A. H. Zewail, *J. Chem. Phys.* **1984**, *81*, 2233; P. M. Felker, A. H. Zewail, *Chem. Phys. Lett.* **1983**, *94*, 454; P. M. Felker, A. H. Zewail, *J. Chem. Phys.* **1983**, *78*, 5266.

[53] J. S. Baskin, P. M. Felker, A. H. Zewail, *J. Chem. Phys.* **1986**, *84*, 4708; P. M. Felker, J. S. Baskin, A. H. Zewail, *J. Phys. Chem.* **1986**, *90*, 724; P. M. Felker, A. H. Zewail, *J. Chem. Phys.* **1987**, *86*, 2460; J. S. Baskin, P. M. Felker, A. H. Zewail, *J. Chem. Phys.* **1987**, *86*, 2483; N. F. Scherer, L. R. Khundkar, T. S. Rose, A. H. Zewail, *J. Phys. Chem.* **1987**, *91*, 6478; J. S. Baskin, A. H. Zewail, *J. Phys. Chem.* **1989**, *93*, 5701.

[54] L. R. Khundkar, A. H. Zewail, *Annu. Rev. Phys. Chem.* **1990**, *41*, 15; N. F. Scherer, F. E. Doany, A. H. Zewail, J. W. Perry, *J. Chem. Phys.* **1986**, *84*, 1932; N. F. Scherer, A. H. Zewail, *J. Chem. Phys.* **1987**, *87*, 97; L. R. Khundkar, J. L. Knee, A. H. Zewail, *J. Chem. Phys.* **1987**, *87*, 77; S. J. Klippenstein, L. R. Khundkar, A. H. Zewail, R. A. Marcus, *J. Chem. Phys.* **1988**, *89*, 4761.

[55] N. F. Scherer, J. L. Knee, D. D. Smith, A. H. Zewail, *J. Phys. Chem.* **1985**, *89*, 5141; M. Dantus, M. J. Rosker, A. H. Zewail, *J. Chem. Phys.* **1987**, *87*, 2395; M. J. Rosker, M. Dantus, A. H. Zewail, *Science* **1988**, *241*, 1200; M. J. Rosker, M. Dantus, A. H. Zewail, *J. Chem. Phys.* **1988**, *89*, 6113; M. Dantus, M. J. Rosker, A. H. Zewail, *J. Chem. Phys.* **1988**, *89*, 6128; D. Zhong, A. H. Zewail, *J. Phys. Chem. A* **1998**, *102*, 4031; R. Bersohn, A. H. Zewail, *Ber. Bunsen-Ges. Phys. Chem.* **1988**, *92*, 373; G. Roberts, A. H. Zewail, *J. Phys. Chem.* **1991**, *95*, 7973; G. Roberts, A. H. Zewail, *J. Phys. Chem.* **1995**, *99*, 2520; the quantum calculations in the last reference follows the original results by D. Imre (see text).

[56] T. S. Rose, M. J. Rosker, A. H. Zewail, *J. Chem. Phys.* **1988**, *88*, 6672; T. S. Rose, M. J. Rosker, A. H. Zewail, *J. Chem. Phys.* **1989**, *91*, 7415; P. Cong, A. Mokhtari, A. H. Zewail, *Chem. Phys. Lett.* **1990**, *172*, 109; A. Mokhtari, P. Cong, J. L. Herek, A. H. Zewail, *Nature* **1990**, *348*, 225; P. Cong, G. Roberts, J. L. Herek, A. Mokhtari, A. H. Zewail, *J. Phys. Chem.* **1996**, *100*, 7832.

[57] R. M. Bowman, M. Dantus, A. H. Zewail, *Chem. Phys. Lett.* **1989**, *156*, 131; M. Dantus, R. M. Bowman, M. Gruebele, A. H. Zewail, *J. Chem. Phys.* **1989**, *91*, 7437; M. Gruebele, G. Roberts, A. H. Zewail, *Philos. Trans. R. Soc. London A* **1990**, *332*, 35; D. Zhong, A. H. Zewail, *J. Phys. Chem. A* **1998**, *102*, 4031; K. B. Møller, A. H. Zewail, *Chem. Phys. Lett.* **1998**, *295*, 1.

[58] M. Dantus, R. M. Bowman, A. H. Zewail, *Nature* **1990**, *343*, 737; M. Gruebele, G. Roberts, M. Dantus, R. M. Bowman, A. H. Zewail, *Chem. Phys. Lett.* **1990**, *166*, 459; R. B. Bernstein, A. H. Zewail, *Chem. Phys. Lett.* **1990**, *170*, 321; M. H. M. Janssen, R. M. Bowman, A. H. Zewail, *Chem. Phys. Lett.* **1990**, *172*, 99; M. Gruebele, A. H. Zewail, *J. Chem. Phys.* **1993**, *98*, 883.

[59] N. F. Scherer, L. R. Khundkar, R. B. Bernstein, A. H. Zewail, *J. Chem. Phys.* **1987**, *87*, 1451; N. F. Scherer, C. Sipes, R. B. Bernstein, A. H. Zewail, *J. Chem. Phys.* **1990**, *92*, 5239; M. Gruebele, I. R. Sims, E. D. Potter, A. H. Zewail, *J. Chem. Phys.* **1991**, *95*, 7763; I. R. Sims, M. Gruebele, E. D. Potter, A. H. Zewail, *J. Chem. Phys.* **1992**, *97*, 4127; D. Zhong, P. Y. Cheng, A. H. Zewail, *J. Chem. Phys.* **1996**, *105*, 7864; an up-to-date experimental and theoretical work is reviewed in ref. [B5] (some are adapted here) and the review by D. Clary (ref. [27]).

[60] J. L. Knee, L. R. Khundkar, A. H. Zewail, *J. Chem. Phys.* **1985**, *82*, 4715; M. Dantus, M. H. M. Janssen, A. H. Zewail, *Chem. Phys. Lett.* **1991**, *181*, 281; T. Baumert, S. Pedersen, A. H. Zewail, *J. Phys. Chem.* **1993**, *97*, 12447; S. Pedersen, J. L. Herek, A. H. Zewail, *Science* **1994**, *266*, 1359; S. K. Kim, S. Pedersen, A. H. Zewail, *J. Chem. Phys.* **1995**, *103*, 477; S. K. Kim, A. H. Zewail, *Chem. Phys. Lett.* **1996**, *250*, 279; S. K. Kim, J. Guo, J. S. Baskin, A. H. Zewail, *J. Phys. Chem.* **1996**, *100*, 9202.

[61] E. W.-G. Diau, O. Abou-Zied, A. A. Scala, A. H. Zewail, *J. Am. Chem. Soc.* **1998**, *120*, 3245.

[62] L. R. Khundkar, A. H. Zewail, *J. Chem. Phys.* **1990**, *92*, 231; D. Zhong, S. Ahmad, A. H. Zewail, *J. Am. Chem. Soc.* **1997**, *119*, 5978; D. Zhong, A. H. Zewail, *J. Phys. Chem. A* **1998**, *102*, 4031.

[63] P. Y. Cheng, D. Zhong, A. H. Zewail, *Chem. Phys. Lett.* **1995**, *237*, 399.

[64] S. K. Kim, S. Pedersen, A. H. Zewail, *Chem. Phys. Lett.* **1995**, *233*, 500.

[65] A. A. Scala, E. W.-G. Diau, Z. H. Kim, A. H. Zewail, *J. Chem. Phys.* **1998**, *108*, 7933.

[66] S. De Feyter, E. W.-G. Diau, A. H. Zewail, *Angew. Chem.* **2000**, *112*, 266; *Angew. Chem. Int. Ed.* **2000**, *39*, 260.

[67] P. M. Felker, W. R. Lambert, A. H. Zewail, *J. Chem. Phys.* **1982**, *77*, 1603; J. L. Herek, S. Pedersen, L. Bañares, A. H. Zewail, *J. Chem. Phys.* **1992**, *97*, 9046.

[68] B. A. Horn, J. L. Herek, A. H. Zewail, *J. Am. Chem. Soc.* **1996**, *118*, 8755; E. W.-G. Diau, S. De Feyter, A. H. Zewail, *Chem. Phys. Lett.* **1999**, *304*, 134; S. De Feyter, E. W.-G. Diau, A. H. Zewail, *Phys. Chem. Chem. Phys.* **2000**, *2*, 877.
[69] D. Zhong, E. W.-G. Diau, T. M. Bernhardt, S. De Feyter, J. D. Roberts, A. H. Zewail, *Chem. Phys. Lett.* **1998**, *298*, 129; M. Chachisvilis, A. H. Zewail, *J. Phys. Chem. A* **1999**, *103*, 7408.
[70] P. Y. Cheng, D. Zhong, A. H. Zewail, *J. Chem. Phys.* **1996**, *105*, 6216; D. Zhong, A. H. Zewail, *Proc. Natl. Acad. Sci USA*. **1999**, *96*, 2602; D. Zhong, T. M. Bernhardt, A. H. Zewail, *J. Phys. Chem. A* **2000**, *103*, 10093.
[71] S. Pedersen, J. L. Herek, A. H. Zewail, *Science* **1994**, *266*, 1359; S. De Feyter, E. W.-G. Diau, A. A. Scala, A. H. Zewail, *Chem. Phys. Lett.* **1999**, *303*, 249; ref. [66]; E. W.-G. Diau, J. Casanova, J. D. Roberts, A. H. Zewail, *Proc. Natl. Acad. Sci. USA* **2000**, *97*, 1376.
[72] E. W.-G. Diau, A. H. Zewail, ref. [61] and unpublished results.
[73] Ref. [69]; E. W.-G. Diau, S. De Feyter, A. H. Zewail, *J. Chem. Phys.* **1999**, *110*, 9785.
[74] Q. Liu, J.-K. Wang, A. H. Zewail, *Nature* **1993**, *364*, 427; J.-K. Wang, Q. Liu, A. H. Zewail, *J. Phys. Chem.* **1995**, *99*, 11309; Q. Liu, J.-K. Wang, A. H. Zewail, *J. Phys. Chem.* **1995**, *99*, 11321; J. J. Breen, D. M. Willberg, M. Gutmann, A. H. Zewail, *J. Chem. Phys.* **1990**, *93*, 9180; M. Gutmann, D. M. Willberg, A. H. Zewail, *J. Chem. Phys.* **1992**, *97*, 8037; J. T. Su, A. H. Zewail, *J. Phys. Chem.* **1998**, *102*, 4082; J. J. Breen, L. W. Peng, D. M. Willberg, A. Heikal, P. Cong, A. H. Zewail, *J. Chem. Phys.* **1990**, *92*, 805; S. K. Kim, J.-K. Wang, A. H. Zewail, *Chem. Phys. Lett.* **1994**, *228*, 369; S. K. Kim, J. J. Breen, D. M. Willberg, L. W. Peng, A. Heikal, J. A. Syage, A. H. Zewail, *J. Phys. Chem.* **1995**, *99*, 7421; A. A. Heikal, S. H. Chong, J. S. Baskin, A. H. Zewail, *Chem. Phys. Lett.* **1995**, *242*, 380.
[75] a) A. H. Zewail, M. Dantus, R. M. Bowman, A. Mokhtari, *J. Photochem. Photobiol. A* **1992**, *62/63*, 301; b) C. Lienau, J. C. Williamson, A. H. Zewail, *Chem. Phys. Lett.* **1993**, *213*, 289; C. Lienau, A. H. Zewail, *Chem. Phys. Lett.* **1994**, *222*, 224; C. Lienau, A. H. Zewail, *J. Phys. Chem.* **1996**, *100*, 18629; A. Materny, C. Lienau, A. H. Zewail, *J. Phys. Chem.* **1996**, *100*, 18650; Q. Liu, C. Wan, A. H. Zewail, *J. Phys. Chem.* **1996**, *100*, 18666; C. Wan, M. Gupta, J. S. Baskin, Z. H. Kim, A. H. Zewail, *J. Chem. Phys.* **1997**, *106*, 4353; J. S. Baskin, M. Gupta, M. Chachisvilis, A. H. Zewail, *Chem. Phys. Lett.* **1997**, *275*, 437; J. S. Baskin, M. Chachisvilis, M. Gupta, A. H. Zewail, *J. Phys. Chem. A* **1998**, *102*, 4158; A. Douhal, T. Fiebig, M. Chachisvilis, A. H. Zewail, *J. Phys. Chem. A* **1998**, *102*, 1657; M. Chachisvilis, I. Garcia Ochoa, A. Douhal, A. H. Zewail, *Chem. Phys. Lett.* **1998**, *293*, 153; A. Vierheilig, T. Chen, P. Waltner, W. Kiefer, A. Materny, A. H. Zewail, *Chem. Phys. Lett.* **1999**, *312*, 349; C. Wan, M. Gupta, A. H. Zewail, *Chem. Phys. Lett.* **1996**, *256*, 279; M. Chachisvilis, A. H. Zewail, *J. Phys. Chem. A* **1999**, *103*, 7408; T. Fiebig, M. Chachisvilis, M. M. Manger, I. Garcia Ochoa, A. de La Hoz Ayuso, A. Douhal, A. H. Zewail, *J. Phys. Chem A* **1999**, *103*, 7419.
[76] J. C. Williamson, A. H. Zewail, *Proc. Natl. Acad. Sci. USA* **1991**, *88*, 5021; J. C. Williamson, M. Dantus, S. B. Kim, A. H. Zewail, *Chem. Phys. Lett.* **1992**, *196*, 529; J. C. Williamson, A. H. Zewail, *Chem. Phys. Lett.* **1993**, *209*, 10; J. C. Williamson, A. H. Zewail, *J. Phys. Chem.* **1994**, *98*, 2766; M. Dantus, S. B. Kim, J. C. Williamson, A. H. Zewail, *J. Phys. Chem.* **1994**, *98*, 2782; J. C. Williamson, J. Cao, H. Ihee, H. Frey, A. H. Zewail, *Nature* **1997**, *386*, 159; H. Ihee, J. Cao, A. H. Zewail, *Chem. Phys. Lett.* **1997**, *281*, 10; J. Cao, H. Ihee, A. H. Zewail, *Chem. Phys. Lett.* **1998**, *290*, 1; J. Cao, H. Ihee, A. H. Zewail, *Proc. Natl. Acad. Sci. USA* **1999**, *96*, 338.
[77] W. S. Warren, A. H. Zewail, *J. Chem. Phys.* **1983**, *78*, 2279; W. S. Warren, A. H. Zewail, *J. Chem. Phys.* **1983**, *78*, 2298; W. S. Warren, A. H. Zewail, *J. Chem. Phys.* **1983**, *78*, 2298; J. J. Gerdy, M. Dantus, R. M. Bowman, A. H. Zewail, *Chem. Phys. Lett.* **1990**, *171*, 1; J. L. Herek, A. Materny, A. H. Zewail, *Chem. Phys. Lett.* **1994**, *228*, 15; E. D. Potter, J. L. Herek, S. Pedersen, Q. Liu, A. H. Zewail, *Nature* **1992**, *355*, 66; E. W.-G. Diau, J. L. Herek, Z. H. Kim, A. H. Zewail, *Science* **1998**, *279*, 847.
[78] D. P. Millar, R. J. Robbins, A. H. Zewail, *Proc. Natl. Acad. Sci. USA* **1980**, *77*, 5593; D. P. Millar, R. J. Robbins, A. H. Zewail, *J. Chem. Phys.* **1981**, *74*, 4200; D. P. Millar, R. J. Robbins, A. H. Zewail, *J. Chem. Phys.* **1982**, *76*, 2080.
[79] T. Fiebig, C. Wan, S. O. Kelley, J. K. Barton, A. H. Zewail, *Proc. Natl. Acad. Sci. USA* **1999**, *96*, 1187; C. Wan, T. Fiebig, S. O. Kelley, C. R. Treadway, J. K. Barton, A. H. Zewail, *Proc. Natl. Acad. Sci. USA* **1999**, *96*, 6014; the protein work involves D. Zhong of this laboratory; the work on the aminopurine system involves T. Fiebig and C. Wan of this laboratory in collaboration with Olav Schiemann and Jackie Barton.
[80] B. Steiger, J. S. Baskin, F. C. Anson, A. H. Zewail, *Angew. Chem.* **2000**, *112*, 263; *Angew. Chem. Int. Ed.* **2000**, *39*, 257; A. Douhal, S. K. Kim, A. H. Zewail, *Nature* **1995**, *378*, 260; T. Fiebig, M. Chachisvilis, M. M. Manger, I. Garcia Ochoa, A. de La Hoz Ayuso, A. Douhal, A. H. Zewail, *J. Phys. Chem. A* **1999**, *103*, 7419; B. A. Leland, A. D. Joran, P. M. Felker, J. J. Hopfield, A. H. Zewail, P. B. Dervan, *J. Phys. Chem.* **1985**, *89*, 5571; A. D. Joran, B. A. Leland, P. M. Felker, A. H. Zewail, J. J. Hopfield, P. B. Dervan, *Nature* **1987**, *327*, 508.

Bibliography: The Caltech Research

Over the past 20 years at Caltech my group and I have published some 300 scientific papers. The following list includes some reviews, feature articles, and a few books.

Books

[B1] A. H. Zewail, *Femtochemistry—Ultrafast Dynamics of the Chemical Bond*, *Vol. I and II*, World Scientific, New Jersey, Singapore, **1994**.
[B2] *The Chemical Bond: Structure and Dynamics* (Ed.: A. H. Zewail), Academic Press, Boston, **1992**.

Book Chapters

[B3] "Molecular Clusters: Real-Time Dynamics and Reactivity": J. A. Syage, A. H. Zewail in *Molecular Clusters* (Eds.: J. M. Bowman, Z. Bacic), JAI Press, London, **1998**.
[B4] "Femtochemistry: Dynamics with Atomic Resolution": A. H. Zewail in *Femtochemistry & Femtobiology* (Ed.: V. Sundström), World Scientific, Singapore, **1997**.
[B5] C. Wittig, A. H. Zewail in *Dynamics of Ground State Bimolecular Reactions*, *Chemical Reactions in Clusters* (Ed.: E. R. Bernstein), Oxford University Press, New York, **1996**, p. 64.
[B6] "Femtochemistry: Concepts and Applications": A. H. Zewail in *Femtosecond Chemistry* (Eds.: J. Manz, L. Wöste), VCH, New York, **1995**, p. 15.
[B7] "Molecular Structures from Ultrafast Coherence Spectroscopy": P. M. Felker, A. H. Zewail in: *Femtosecond Chemistry* (Eds.: J. Manz, L. Wöste), VCH, New York, **1995**, p. 193.
[B8] "Ultrafast Dynamics of the Chemical Bond—Femtochemistry": A. H. Zewail in *Ultrafast Processes in Chemistry and Photobiology*, *Chemistry for the 21st Century*, (Eds.: M. A. El-Sayed, I. Tanaka, Y. N. Molin), IUPAC, Blackwell Scientific Publishers, Oxford, **1995**, p. 1.
[B9] "Molecular Mechanisms for Dephasing: Toward a Unified Treatment of Gases, Solids, and Liquids": K. E. Jones, A. H. Zewail, *Springer Ser. Chem. Phys.* **1978**, *3*, 258 (Advances in Laser Chemistry).

Reviews

[B10] "Femtochemistry: Recent Progress in Studies of Dynamics and Control of Reactions and Their Transition States": A. H. Zewail, *J. Phys. Chem.* **1996**, *100*, 12701 (Centennial Issue).
[B11] "Proton-transfer Reaction Dynamics": A. Douhal, F. Lahmani, A. H. Zewail, *Chem. Phys.* **1996**, *207*, 477 (Special Issue).
[B12] "Direct Observation of The Transition State": J. C. Polanyi, A. H. Zewail, *Acc. Chem. Res.* **1995**, *28*, 119 (Holy-Grail Special Issue).
[B13] "Coherence—A Powerful Concept in the Studies of Structures and Dynamics": A. H. Zewail, *Laser Phys.* **1995**, *5*, 417.

[B14] "Femtochemistry": A. H. Zewail, *J. Phys. Chem.* **1993**, *97*, 12427 (Feature Article).
[B15] "Femtochemistry: Recent Advances and Extension to High-Pressures": see ref. [75a].
[B16] "Real-Time Laser Femtochemistry: Viewing the Transition States from Reagents to Products": A. H. Zewail, R. B. Bernstein, *Chem. Eng. News* **1988**, *66*(Nov 7) 24; Feature Article/Special Report in: *The Chemical Bond: Structure and Dynamics* (Ed.: A. H. Zewail), Academic Press, Boston, **1992**, p. 223.
[B17] "Femtosecond Transition-State Dynamics in Structure and Dynamics of Reactive Transition States": A. H. Zewail, *Faraday Discuss. Chem. Soc.* **1991**, *91*, 207.
[B18] "Femtochemistry: The Role of Alignment and Orientation": A. H. Zewail, *J. Chem. Soc. Faraday Trans.* **1989**, *285*, 1221.
[B19] "Laser Femtochemistry": A. H. Zewail, *Science* **1988**, *242*, 1645.
[B20] "IVR: Its Coherent and Incoherent Dynamics": A. H. Zewail, *Ber. Bunsen-Ges. Phys. Chem.* **1985**, *89*, 264.
[B21] "Energy Redistribution in Isolated Molecules and the Question of Mode-Selective Laser Chemistry Revisited": N. Bloembergen, A. H. Zewail, *J. Phys. Chem.* **1984**, *88*, 5459 (Feature Article).
[B22] "Phase Coherence in Multiple Pulse Optical Spectroscopy": W. S. Warren, A. H. Zewail in *Photochemistry and Photobiology: Proceedings of the International Conference*, *Vol. I and II* (Ed.: A. H. Zewail), Harwood Academic, Chur, Switzerland, **1983** (Alexandria, Egypt, January 5–10, **1983**); W. S. Warren, A. H. Zewail, *Laser Chem.* **1983**, *2*(1, 6), 37.
[B23] "Optical Molecular Dephasing: Principles of and Probings by Coherent Laser Spectroscopy": A. H. Zewail, *Acc. Chem. Res.* **1980**, *13*, 360.
[B24] "Laser Selective Chemistry—Is it Possible?": A. H. Zewail, *Phys. Today* **1980**, *33*, 2.
[B25] "Freezing Time—In a Femtosecond": J. S. Baskin, A. H. Zewail, *Sci. Spectra* **1998**, (14), 62.
[B26] "What is Chemistry? 100 Years After J. J. Thomson's Discovery": A. H. Zewail, *Cambridge Rev.* **1997**, *118*(2330), 65.
[B27] "Discoveries at Atomic Resolution (Small is Beautiful)": A. H. Zewail, *Nature* **1993**, *361*, 215.
[B28] "The Birth of Molecules": A. H. Zewail, *Sci. Am.* **1990**, *263*, 76. Also available in other languages: Italian, Japanese, French, Spanish, German, Russian, Chinese, Arabic, Hungarian, and Indian.

General Bibliography

Books

[B29] Nobel Symposium: *Femtochemistry & Femtobiology* (Ed.: V. Sundström), World Scientific, Singapore, **1997**.
[B30] Solvay Conference: "Chemical Reactions and Their Control on the Femtosecond Time Scale": *Adv. Chem. Phys.* **1997**, *101*.
[B31] Lausanne Conference: *Femtochemistry* (Ed.: M. Chergui), World Scientific, Singapore, **1996**.
[B32] Berlin Conference: *Femtosecond Chemistry*, *Vol. 1 and 2* (Eds.: J. Manz, L. Wöste), VCH, Weinheim, **1995**.
[B33] Amsterdam Conference: *Femtosecond Reaction Dynamics* (Ed.: D. A. Wiersma), Royal Netherlands Academy of Arts and Sciences, North Holland, Amsterdam, **1994**.
[B34] *Ultrafast Processes in Chemistry and Biology—Chemistry for the 21st Century* (Eds.: M. A. El-Sayed, I. Tanaka, Y. N. Molin), IUPAC, Blackwell Scientific, Oxford, **1994**.
[B35] *Density Matrix Method and Femtosecond Processes*, (Eds.:S. H. Lin, R. Alden, R. Isalampour, H. Ma, A. A. Villaeys), World Scientific, Singapore, **1991**.
[B36] *Principles of Nonlinear Optical Spectroscopy*, S. Mukamel, Oxford University Press, Oxford, **1995**.
[B37] *Ultrafast Dynamics of Chemical Systems* (Ed.: J. D. Simon), Kluwer, Boston, **1994**.
[B38] E. Schreiber, *Femtosecond Real-Time Spectroscopy of Small Molecules & Clusters*, Springer, New York, **1998**.

Special Issues

[B39] "Femtochemistry—Ten Years of": *J. Phys. Chem.* **1998**, *92* (June Issue).
[B40] "Femtochemistry": *J. Phys. Chem.* **1993**, *97* (December Issue).
[B41] "Ultrafast Lasers in Chemistry":, *Isr. J. Chem.* **1994**, *34*(1).

Reviews

[B42] "Chemistry in Microtime": G. Porter in *The Chemical Bond: Structures and Dynamics* (Ed.: A. H. Zewail), Academic Press, Boston, **1992**, p. 113.
[B43] "Molecular Photophysics": G. Beddard, *Rep. Prog. Phys.* **1993**, *56*, 63.
[B44] "Time-Resolved Vibrational Spectroscopy in the Impulsive Limit": L. Dhar, J. A. Rogers, K. A. Nelson, *Chem. Rev.* **1994**, *94*, 157.
[B45] "The Dynamics of Wave Packets of Highly-Excited States of Atoms and Molecules": I. Sh. Averbukh, N. F. Perel'man, *Sov. Phys. Usp. (Engl. Transl.)* **1991**, *34*, 572.
[B46] "Hot Electron Femtochemistry at Surfaces": J. W. Gadzuk in ref. [B32], Vol. 2, p. 603.
[B47] "Dynamics of Nonthermal Reactions: Surface Femtosecond Chemistry": R. R. Cavanagh, D. S. King, J. C. Stephenson, T. F. Heinz, *J. Phys. Chem.* **1993**, *97*, 786.
[B48] "Femtochemistry": J. G. Thorne, G. S. Beddard, *Chem. Ind.* **1994**, 456.
[B49] "Wave Packet Dynamics: New Physics and Chemistry in Femtotime": B. M. Garraway, K.-A. Suominen, *Rep. Prog. Phys.* **1995**, *58*, 365.
[B50] "Femtosecond Broadband Absorption Spectroscopy of Fragments Formed in the Photodissociation of Gas-phase Molecules": J. H. Glownia, R. E. Walkup, D. R. Gnass, M. Kaschke, J. A. Misewich, P. P. Sorokin in ref. [B32], Vol. 1, p. 131.
[B51] "Theory of Ultrafast Nonadiabatic Excited-State Processes and their Spectroscopic Detection in Real Time": W. Domcke, G. Stock, *Adv. Chem. Phys.* **1997**, *100*, 1.
[B52] "Femtosecond Surface Science", J. A. Misewich, T. F. Heinz, P. Weigand, A. Kalamarides in *Advanced Series in Physical Chemistry*, *Vol. 5* (Eds.: H.-L. Dai, W. Ho), World Scientific, Singapore, **1995**.
[B53] "Femtosecond Time-Resolved Photochemistry of Molecules and Metal Clusters": T. Baumert, R. Thalweiser, V. Weiss, G. Gerber in ref. [B32], Vol. 2, p. 397.

Overviews

[B54] "Pulse, Pump and Probe": R. Hoffmann, *Am. Sci.* **1999**, *87*, 308.
[B55] "Femtochemistry": Y. Tanimura, K. Yamashita, P. A. Anfinrud, *Proc. Natl. Acad. Sci. USA* **1999**, *96*, 8823; P. Anfinrud, R. de Vivie-Riedle, V. Engel, *Proc. Natl. Acad. Sci. USA* **1999**, *96*, 8328.
[B56] P. Ball, *Designing the Molecular World*, Princeton University Press, Princeton, **1994**; P. Ball, *Chemie der Zukunft—Magie oder Design?*, VCH, Weinheim, **1996**.
[B57] H. C. von Baeyer, *Taming the Atom*, Random House, New York, **1992**.
[B58] P. W. Atkins, *Atoms*, *Electrons*, *and Change*, Freeman, New York, **1991**.
[B59] "The World's Fastest Camera": V. K. Jain, *The World and I*, Washington Times Publishing, **1995**, p. 156.
[B60] see ref. [5a].
[B61] "The Classical Limit of an Atom": M. Nauenberg, C. Stroud, J. Yaezell, *Sci. Am.* **1994**, 44.
[B62] "Coherent Thinking": D. L. Smith, *Eng. Sci.* **1999**, *62*(4), 6.

ANGEWANDTE CHEMIE © WILEY-VCH



Carl Glaser was born in 1841 in Kirchheimbolanden in the Rheinpfalz. He started his chemistry studies at the University of Erlangen, where he rapidly developed an interest in the synthesis of tar dyes, which were in high industrial demand at that time. In 1864, he moved to the University of Tübingen to work with Adolph Strecker and, in the same year, obtained his doctoral degree for his experimental investigations of new derivatives of naphthalene. Upon recommendation by Strecker, a former teacher of August Kekulé, Glaser joined the group of Kekulé and participated for several years in the ongoing intensive research on benzene and its derivatives—a field that had just been started with the benzene theory. In 1867, Glaser moved with Kekulé to the Rheinische Friedrich-Wilhelms-Universität Bonn, where he continued his investigations on derivatives of cinnamic acid that he had already started in Tübingen. During this work, he discovered the oxidative coupling of copper alkynylbenzene, the reaction later named after him and which is at the center of this review. Following his habilitation in 1869, Glaser joined the Badische Anilin- & Soda-Fabrik (BASF) and became responsible first for the development, then for the direction of the technical synthesis of alizarine. During his highly successful industrial career, he was in charge of the development of technical production processes for a large series of dyes, including the milestone implementation of a technical synthesis of indigo. He joined the executive board of directors of the company in 1883 and, after his retirement from this position in 1895, was elected to the control board ("Aufsichtsrat"), which he chaired from 1912 to 1920. He died in 1935. (For a more detailed description of the scientific career of Carl Glaser see: R. Anschütz, C. Müller, *Angewandte Chemie* **1927**, *40*, 273 – 300.)

Acetylenic Coupling: A Powerful Tool in Molecular Construction

Peter Siemsen, Robert C. Livingston, and François Diederich*

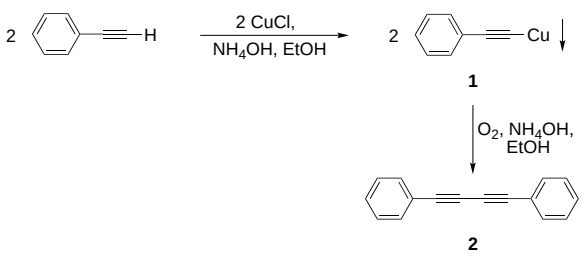
Acetylenic coupling is currently experiencing some of the most intensive study of its long history. Rigid and sterically undemanding di- and oligoacetylene moieties, which are frequently encountered in natural products, are finding increasing application as key structural elements in synthetic receptors for molecular recognition. Interesting electronic and optical properties of extensively π-conjugated systems have spurred research into new linear oligoalkynes and acetylenic carbon allotropes. The synthetic challenges associated with these efforts have in turn spawned new methods. While classical Glaser conditions are still frequently used for homocoupling, the demand for increasingly selective heterocoupling conditions has provided the focus of research over the past decades. These efforts have undoubtedly been hampered by a relatively poor mechanistic understanding of these processes. More recently, palladium-catalyzed coupling methods have led to improvements in both the selectivity and reliability of acetylenic homo- and heterocouplings and paved the way for their application to ever more complicated systems. The variety of acetylenic coupling protocols, the current mechanistic understanding, and their application in natural product and targeted synthesis are discussed comprehensively for the first time in this review, with an emphasis on the most recently developed methods, and their application to the synthesis of complex macromolecular structures.

Keywords: alkynes · C–C coupling · synthetic methods

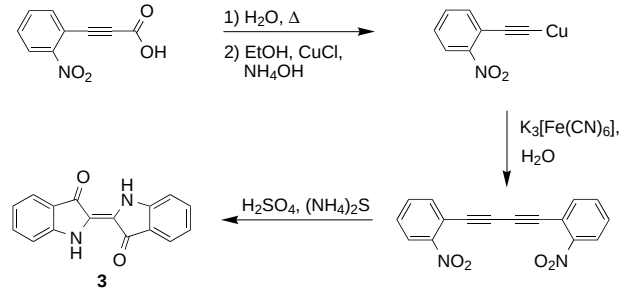
1. Introduction—A Brief Historical Survey

The history of acetylenic coupling began at the University of Bonn with the 1869 observation of Carl Glaser[1] (see p. 2632) that copper(I) phenylacetylide (**1**) exposed to air underwent smooth oxidative dimerization to diphenyldiacetylene (**2**; Scheme 1).

Later the Glaser coupling was extended to various organic compounds possessing a terminal ethynyl group. Baeyer[2a] provided an early demonstration of the synthetic utility of the method in his 1882 synthesis of indigo (**3**; Scheme 2). With the use of potassium ferricyanide as the oxidizing agent,[2b] he simultaneously showed that dioxygen itself is not necessary for the coupling process.



Scheme 1. The first acetylenic coupling described by Glaser.[1]



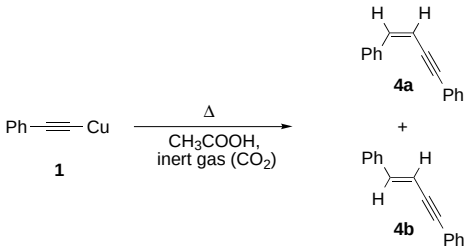
Scheme 2. Indigo synthesis by Baeyer.[2a]

In 1885, Baeyer employed this modified procedure in the preparation of diacetylene and its diiodo and dicarboxylic acid derivatives.[3] Tetraacetylene dicarboxylic acid (HOOC–(C≡C)$_4$–COOH) was also likely generated in these experiments.[3c] In the following years other groups showed that oxidizing agents besides dioxygen[4] or potassium ferricyanide[5] can be employed, including cupric salts,[6–11] potas-

[*] Prof. Dr. F. Diederich, Dipl.-Chem. P. Siemsen, Dr. R. C. Livingston
Laboratorium für Organische Chemie
ETH-Zentrum
Universitätstrasse 16, 8092 Zürich (Switzerland)
Fax: (+41) 1-632-1109
E-mail: diederich@org.chem.ethz.ch

 © WILEY-VCH Verlag GmbH, D-69451 Weinheim, 2000 1433-7851/00/3915-2633 $ 17.50+.50/0

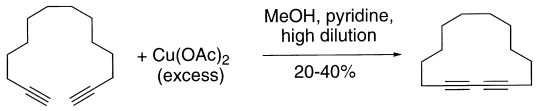
sium permanganate,[12] and peroxides.[13, 14] In 1905, Straus observed that heating copper(I) phenylacetylide (**1**) in acetic acid under inert gas (CO_2) gave linear enynes **4a** and **4b** instead of the expected diphenyldiacetylene (**2**; Scheme 3).[15] Now termed the Straus coupling, this reaction has since become quite generalized,[16, 17] and has even found industrial application in the production of vinylacetylene and divinylacetylene.[18, 19]



Scheme 3. The Straus coupling reaction.[15]

The original Glaser reaction failed to see broad application because of the apparent need to isolate the potentially explosive copper acetylide before oxidation, which was often tedious in view of the poor crystallization properties of most copper salts.[20] Particularly important then was the observation of Zalkind and Aizikovich in 1937 that tertiary alkynols coupled directly in the presence of copper(I) chloride and ammonium chloride to afford the corresponding diacetylene dicarbinols.[21] This method initially failed in the case of primary and secondary alkynols.[22] In 1955, however, Reppe succeeded in the preparation of diprimary and disecondary alkadiynediols by treating the mixture of primary or secondary alkynol, CuCl, and NH_4Cl more intensively with air or dioxygen.[23] Addition of copper(II) acetate was also found to accelerate the reaction, which indicated participation of copper(II) ions in the coupling process. The possibility of forming the copper(I) acetylide in situ paved the way for intensive investigations of the factors influencing the oxidative coupling of various substituted acetylenes,[5, 12, 13, 23–31] which ultimately led to improved convenience and scope of the reaction, and to industrial applications.

A further milestone in the evolution of oxidative acetylenic coupling was the copper(II) salt oxidation in methanolic pyridine introduced in 1956 by Eglinton and Galbraith[32] (Scheme 4). This method proved of great value within a few years of its discovery, and led to the preparation of a variety of new unsaturated macrocycles,[33] including the pioneering annulene syntheses of Sondheimer and co-workers.[34]



Scheme 4. Acetylenic coupling with copper(II) salts in pyridine according to Eglinton and Galbraith.[32]

Another important modification was reported in 1962 by Hay, who performed oxidative acetylenic couplings with O_2 in the presence of catalytic amounts of the bidentate ligand *N*,*N*,*N*′,*N*′-tetramethylethylenediamine (TMEDA) and copper(I) chloride (Scheme 5).[35] Enhanced solubility of the reactive species is one major advantage provided by this



P. Siemsen



R. Livingston

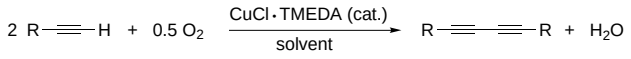


F. Diederich

Peter Siemsen, born in 1970 in Braunschweig, studied chemistry at the Technische Universität Carolo-Wilhelmina in Braunschweig, from where he received his diploma in 1995. He then joined the group of Prof. F. Diederich as a PhD student, where he is currently doing research on monodisperse platinum-bridged oligomers of tetraethynylethenes.

Robert Livingston, born in 1969 in Seattle, Washington, received his B.A. degree in chemistry from Williams College in 1992. His studies continued in the laboratory of Professor B. M. Trost at Stanford University, where he investigated the redox isomerization of propargylic alcohols. Since receiving his doctorate in 1999 he has conducted research in the group of Professor F. Diederich on the synthesis and polymerization of diethynylallenes.

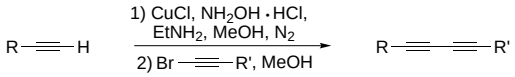
François Diederich, born in 1952 in the Grand Duchy of Luxembourg, received his Ph.D. degree in 1979 from the University of Heidelberg. Following postdoctoral studies at the University of California at Los Angeles (UCLA) from 1979–1981, he was a research associate at the Max-Planck-Institut für medizinische Forschung in Heidelberg. After his Habilitation in 1985, he joined the faculty of the Department of Chemistry and Biochemistry at UCLA where became full professor in 1989. Since April 1992, he has been a professor of organic chemistry at ETH Zürich. He is a member of the Editorial Board for Angewandte Chemie.



Scheme 5. Hay coupling conditions.[35]

method. For example, whereas the copper(I) acetylide of propargyl alcohol precipitates from solutions of copper(I)–pyridine complexes, the use of the soluble copper(I)–TMEDA complex allows the coupling reaction to proceed satisfactorily.

Parallel to the evolution of oxidative homocoupling processes, Chodkiewicz and Cadiot[36] reported in 1957 a potent heterocoupling protocol involving terminal alkyne and 1-bromoacetylene partners in the presence of an amine and catalytic amounts of copper(I) salt (Scheme 6).



Scheme 6. Cadiot–Chodkiewicz heterocoupling conditions.[36]

In Chapter 2 of this review, the scope and limitations of the various acetylenic homo- and heterocoupling methods will be discussed. It will become apparent that, despite the introduction of new methods, the variants of the Glaser homocoupling discussed above and the Cadiot–Chodkiewicz heterocoupling remain the most utilized. Chapter 3 summarizes the current mechanistic understanding of these reactions. Chapter 4 provides selected examples illustrating the wide application of acetylenic coupling in natural product synthesis, construction of molecular receptors, and formation of acetylenic all-carbon and carbon-rich matter.

2. Methods for Acetylenic Homo- and Heterocoupling: Scope and Limitations

Several reviews, now quite outdated, have been published on the Glaser and Cadiot–Chodkiewicz coupling reactions.[37–44] In the meantime, a number of new methods for the synthesis of symmetrically and unsymmetrically substituted 1,3-diynes have been described.

2.1. Copper-Catalyzed Oxidative Homocoupling Reactions—The Glaser Reaction and Related Methods

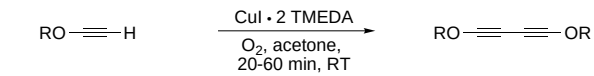
The oxidative coupling of terminal acetylenes has been most extensively investigated. In the original procedure (Scheme 1) a copper(I) acetylide was isolated and subsequently oxidized in air. The method became widely applicable with the finding that the copper(I) derivative, often characterized by poor crystallizability and a tendency to explode in the dry state, can be formed in situ. The influence of various factors, such as the proportion of copper(I) salt, oxidizing agent, pH, time, temperature, solvent, and character of the alkyne, was the subject of numerous investigations. These efforts were reviewed exhaustively by Eglinton and McCrae in 1963[37] and six years later by Cadiot and Chodkiewicz.[39]

The modification by Hay[35] (Scheme 5) presumably represents the most important method for the oxidative coupling to provide linear oligo- and polyacetylenes. In one procedure, the alkyne and catalytic amounts of a copper(I) salt (usually CuCl) are dissolved in the presence of dioxygen in a complexing tertiary amine solvent such as pyridine. More commonly, the coupling is performed in an appropriate solvent such as acetone or *o*-dichlorobenzene using catalytic amounts of the bidentate complexing ligand TMEDA. The latter protocol (O_2, CuCl, TMEDA) is commonly referred to as standard Hay coupling conditions.

By adding a small amount of the strong base 1,8-diazabicyclo[5.4.0]undec-7-ene (DBU), the reaction rate can be accelerated,[43, 45] making it possible to couple even weakly acidic terminal alkynes efficiently. For example, 5-ethynylpyrazole underwent oxidative dimerization under Hay conditions (O_2, CuCl, pyridine) whereas 2-ethynyl-1-methylpyrrole did not, presumably because of the lower acidity of its ethynyl proton.[45] In the presence of catalytic amounts of DBU, however, quantitative dimerization occurred, since the stronger base is more efficient in the deprotonation of the alkyne.

Alkoxyalkynes **5a–f** were found to undergo smooth oxidative dimerization to diynes **6a–f** when a catalyst system consisting of CuI and two equivalents (with regards to CuI) of TMEDA in acetone was used (Table 1).[46] This was attributed to the improved solubility of this catalyst in acetone. Under standard Hay conditions (O_2, CuCl, TMEDA) the conversion was quite inefficient.

Table 1. Preparation of 1,4-dialkoxybuta-1,3-diynes **6a–f** by oxidative coupling.[46]

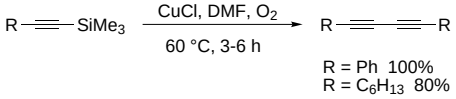


5a	R = *tert*-butyl	**6a**	77 %
5b	R = 1-adamantyl	**6b**	85 %
5c	R = decyl	**6c**	78 %
5d	R = cyclohexyl	**6d**	95 %
5e	R = L-menthyl	**6e**	76 %
5f	R = 2,6-dimethylphenyl	**6f**	65 %

In their investigations of the oxidative dimerization of heterocyclic alkynes, Fritzsche and Hünig[47] found a strong dependency between yield and solvent, and reported the advantageous use of 1,2-dimethoxyethane (DME). Havinga et al.[48] found *o*-dichlorobenzene (ODCB) to be a superior solvent for the oxidative polymerization of 1,8-nonadiyne under Hay conditions (O_2, CuCl, TMEDA) to yield polymers with a molar mass of greater than 20000. Presumably ODCB keeps higher molecular weight oligomers in solution better, thereby ensuring the growth of longer polymers. We observed a similar advantage using this solvent in the oligomerization of platinum-bridged tetraethynylethenes under Hay conditions (Section 4.3). Dichloromethane has been found to be another good solvent for both the oxidant and the polymer formed.[49] In the presence of oxygen-sensitive products or reactants, large excesses of the Hay catalyst (CuCl, TMEDA) have been used to shorten the reaction time.[43, 49]

An interesting procedure, reported by Mori, Hiyama, and co-workers, allows direct coupling of trimethylsilyl-protected

alkynes without previous removal of the protecting groups.[50] A solution of the acetylene is heated together with one equivalent of CuCl in DMF under air or dioxygen to give the coupled product in high yield (Scheme 7). No activator such as fluoride ion was needed to remove the silyl protecting group. This technique allows the efficient dimerization of alkynes which decompose after deprotection, and is also applicable to the synthesis of unsymmetrically substituted diacetylenes (Section 2.2).[51]



Scheme 7. Cu^{I}-promoted oxidative homocoupling of alkynylsilanes.[50]

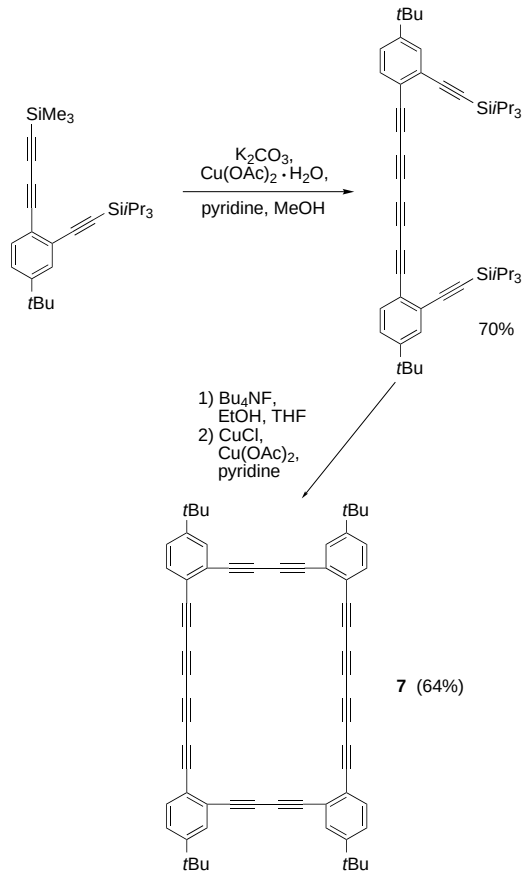
Oxidative coupling reactions are usually the method of choice for the construction of macrocyclic oligoacetylenes containing buta-1,3-diynediyl fragments. In particular the modification by Eglinton and Galbraith (Scheme 4)[32] has been heavily used for this purpose[52] (and less for the construction of linear oligomers[53, 54]). Typically copper(II) acetate is employed, either using pure pyridine as the coordinating solvent, or using cosolvents such as methanol to prevent precipitation of the copper(I) derivatives formed in the course of the reaction.[55] The rate of reaction increases with the concentration of the copper(II) salt.

Several variations of the original Eglinton protocol have been reported, and notably show that pyridine can be substituted entirely. Staab and co-workers used $Cu(OAc)_2$ in pure DMF to form buta-1,3-diynediyl linkages in the key macrocyclization step on the way to benzo-annellated [14]- and [18]annulenes.[56] Berscheid and Vögtle reported high-yielding oxidative cyclodimerizations using $Cu(OAc)_2$ in pure acetonitrile.[57]

A large excess of both CuCl and $Cu(OAc)_2$ in pyridine proved to be highly efficient in intramolecular oxidative dimerizations leading to dehydrobenzo[18]annulenes, as reported by Haley and co-workers.[58a] The same group also used potassium carbonate for the in situ deprotection and coupling of trimethylsilyl-protected alkynes. The application of both methodological advances is illustrated in the synthesis of the dehydrotetrabenzo[32]annulene **7** (Scheme 8).[58b]

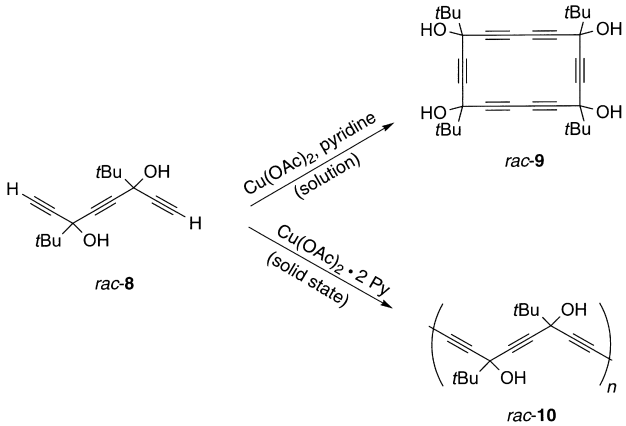
Very recently it was shown that Glaser couplings can be carried out smoothly and in high yield in supercritical carbon dioxide using solid NaOAc instead of amines.[59] Thus, the conversion of phenylacetylene (1 equiv) with $CuCl_2$ (2 equiv) and NaOAc (2 equiv) in supercritical CO_2 in the presence of methanol afforded diphenylbuta-1,3-diyne (**2**) in quantitative yield. Aliphatic alkynes also underwent homocoupling in greater than 90% yield. Control studies showed that the presence of methanol led to large rate enhancements and that reaction rates increased with higher pressures of CO_2.

Oxidative copper-mediated coupling reactions are not limited to homogeneous solutions. Toda and Tokumaru have found them to proceed efficiently and selectively in the solid state.[60] For example, keeping a mixture of powdered copper(I) phenylacetylide (**1**) and $CuCl_2 \cdot 2H_2O$ for 3 h at



Scheme 8. Synthesis of dehydrobenzo[32]annulene **7**.[58b]

room temperature gave diphenylbuta-1,3-diyne (**2**) in 60% yield, whereas the yield of the Glaser reaction in water was only 40%. A remarkable result was observed when the solid-state conditions were applied to the Eglinton procedure. Although the reaction rate was slower in the solid state than in solution, the resulting products differed in some cases. Whereas, for example, the coupling of *rac*-**8** in pyridine (Py) gave the corresponding cyclic dimer *rac*-**9**, the solid-state procedure using the $Cu(OAc)_2 \cdot 2Py$ complex afforded exclusively the linear coupling product *rac*-**10** (Scheme 9). The reaction of optically pure (−)-**8**, however, provided longer



Scheme 9. Oxidative coupling under Eglinton conditions in solution and the solid state.[60]

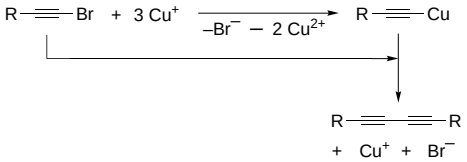
polymers (> 100 monomer units) in solution and only low molecular weight oligomers in the solid state.

In 1995, Baiker and co-workers described another heterogeneous route for the dimerization of phenylacetylene.[61] The coupling was carried out in an autoclave in the presence of sodium hydroxide under enhanced oxygen pressure using Cu-Mg-Al hydrotalcite (a hydroxycarbonate) as the catalyst. This route led, depending on the initial pressure, to yields of diphenylbuta-1,3-diyne (**2**) comparable with those achieved in the conventional Hay synthesis (> 80 %).

2.2. Heterocoupling of Alkynes with 1-Haloalkynes—The Cadiot – Chodkiewicz Reaction and Related Methods

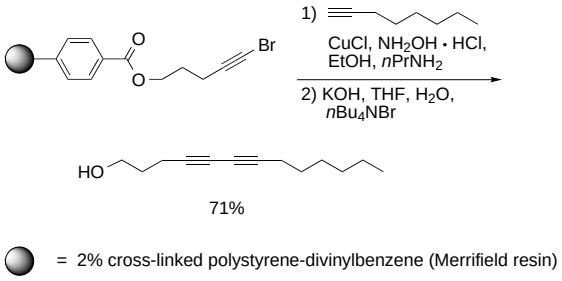
The Glaser reaction and related methods normally give unsatisfactory results for unsymmetrical coupling because of the simultaneous and rather predominant formation of the symmetrical products. Therefore, these techniques have seen little recent application in the synthesis of nonsymmetrical diynes.[62] A solution to this problem, provided by Chodkiewicz and Cadiot,[36] consists of the condensation of terminal alkynes with 1-bromoacetylenes in the presence of a copper(I) salt and a suitable amine (Scheme 6). This method has been used extensively to synthesize a wide range of diacetylenic compounds, and the influence of various factors such as the nature of the base and acetylene, solvent, time, and temperature on the reaction has been investigated in great detail.[37, 39] The method has been applied to the synthesis of numerous aliphatic and aromatic buta-1,3-diynes[63] and tolerates a wide variety of functional groups, including alcohols and polyols,[64] peroxy substituents,[65] quinols,[66] epoxides,[67] amines,[68] acetals,[69] carboxylates,[70] carboxylic esters[71] and amides,[72] disulfides,[73] acetylenic silyl-protecting groups,[74] and even nitroxyl radicals.[75]

Aromatic buta-1,3-diynes[76] are generally obtained in higher yields than their aliphatic counterparts.[39] The terminal alkyne partner for the heterocoupling is particularly suitable if it bears hydrophilic functionality such as hydroxyl, amino, or carboxylate groups.[39] Conjugated alkynes such as buta-1,3-diyne are also suitable as the terminal alkyne component. Apart from bromoalkynes, iodo derivatives[73, 77–79] have also been employed to a minor extent, whereas chloroacetylenes are of little practical importance because of their low reactivity. The former are strongly oxidizing toward copper(I) ions and normally favor self-coupling. This "secondary" Cadiot – Chodkiewicz coupling, often observed with bromoalkynes as well, is considered to proceed by halogen – metal exchange, and can be applied to the synthesis of symmetrical polyacetylenes (Scheme 10).[39]



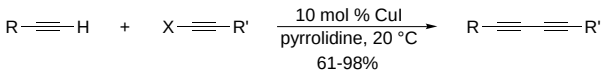
Scheme 10. Halogen – metal exchange and subsequent homocoupling are undesirable side reactions of the Cadiot – Chodkiewicz heterocoupling.[39]

This variant, which occurs primarily as a disturbing side-reaction to the heterocoupling process, can be suppressed by amines and by the use of low concentrations of the copper(I) ion and the haloacetylene.[39, 43] The separate preparation of the copper(I) acetylide proved useful in some cases.[41, 80, 81] Kurth, Schore, and co-workers recently described an interesting polymer-supported technique which inhibits the mutual interaction between haloalkynes and efficiently reduces the self-coupling.[82] The coupling of immobilized chloro- or bromoalkynes with 1-octyne under Cadiot – Chodkiewicz conditions proceeded in high yield and without formation of homocoupled product (Scheme 11), whereas the corresponding conversions in solution gave up to 34 % homocoupled side product.



Scheme 11. Polymer-supported Cadiot – Chodkiewicz heterocoupling efficiently suppresses the self-coupling of the haloacetylene as an undesirable side reaction.[82]

Besides the original Cadiot – Chodkiewicz coupling, which is still important for the synthesis of unsymmetrically substituted di- and polyynes, a number of interesting and complementary variations exist. In 1996, Alami and Ferri reported an efficient copper(I) iodide catalyzed cross-coupling reaction between 1-haloalkynes and terminal alkynes in pyrrolidine (Scheme 12).[83]



X = I, Br

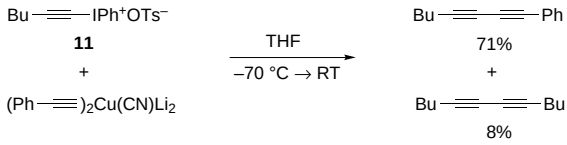
R = C_6H_5, C_5H_{11}, $C_5H_{11}CH(OH)$

R' = CH_2OH, $(CH_2)_2OH$, $(CH_2)_4OH$, $(CH_2)_3Cl$, $(CH_2)_2COOMe$, C_6H_5, C_5H_{11}, CH_2NMe_2

Scheme 12. Copper-catalyzed heterocoupling in pyrrolidine.[83]

Analogous to the Cadiot – Chodkiewicz protocol, they observed low reactivity for the chloro derivatives, whereas the corresponding iodides gave good yields. The reactivity of bromoalkynes could be enhanced by the addition of $[PdCl_2(PPh_3)_2]$ as a cocatalyst. The use of pyrrolidine as the amine solvent gave superior yields and reaction times. Other aliphatic amines gave poor yields, even in the presence of a palladium cocatalyst. The advantages of this procedure are its simplicity and high efficiency, even in the case of acetylenic alcohols, which normally give low yields of cross-coupled product.

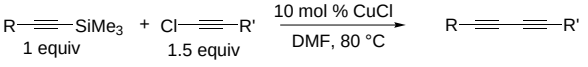
A very mild and efficient cross-coupling of alkynyl(phenyl)-iodonium tosylates such as **11** was described by Kitamura et al.[84] The addition of these tosylates to soluble lithium dialkynylcuprates led to the desired unsymmetrical diacetylenes in good yields and reasonable selectivity with respect to homocoupling (Scheme 13). This mild procedure provides a general alkynylation method for organocopper reagents and is of particular interest for the coupling of highly sensitive alkyne derivatives.



Scheme 13. Cross-coupling of alkynyl(phenyl)iodonium tosylates with alkynylcopper reagents.[84]

In addition to the homocoupling of trimethylsilyl-protected alkynes, Hiyama and co-workers described an analogous heterocoupling of alkynylsilanes and chloroalkynes.[51] The cross-coupling was carried out using catalytic amounts of CuCl and an excess of the haloalkyne in DMF at 80 °C and gave the corresponding unsymmetrically substituted diynes, by silicon to copper exchange, in moderate to high yields (Table 2). Homocoupling of the haloalkynes is clearly suppressed under these conditions and occurs only to a minor extent.

Table 2. Heterocoupling of alkynylsilanes with chloroalkynes.[51]



R	R′	Yield [%][a]
4-MeOC$_6$H$_4$	C$_6$H$_5$	90
4-MeOC$_6$H$_4$	4-MeOC$_6$H$_4$	97
4-MeCOC$_6$H$_4$	C$_6$H$_5$	69
4-MeCOC$_6$H$_4$	4-MeOC$_6$H$_4$	60
C$_6$H$_5$	4-MeCOC$_6$H$_4$	62
C$_6$H$_5$	4-MeOC$_6$H$_4$	43

[a] GC yield based on the alkynylsilane.

This result is quite remarkable considering that reactions of 1-chloroalkynes with terminal acetylenes often furnish cross-coupled products in poor yields. Since the method can be carried out under neutral conditions without base, it seems to be promising for future applications in modern acetylenic chemistry.

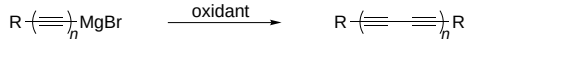
2.3. Coupling Reactions of Alkynyl Grignard Derivatives

Couplings of alkynyl Grignard reagents can be classified as oxidative homocouplings, related to the Glaser coupling, or as nonoxidative heterocouplings with a haloalkyne, analogous to the Cadiot–Chodkiewicz method. These techniques are less widely used than the classical methods, but nevertheless they have led to some significant results in specialized applications.

2.3.1. Oxidative Homocoupling Reactions of Alkynyl Grignard Derivatives

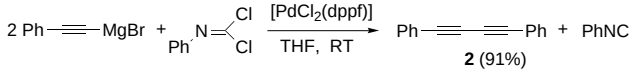
The dimerization of alkynyl Grignard reagents[8, 37–44] in the presence of oxidants such as iodine,[85–87] copper(II) and cobalt salts,[87–90] or nitrobenzene[91] is well known (Table 3), but in view of its limited scope and low tolerance to functional groups, it remains largely of theoretical interest. A small improvement of the limited applicability was reported by Luo and co-workers using 2,3-dichloropropene as the oxidizing agent.[92]

Table 3. Preparation of oligoacetylenes by the oxidative homocoupling of alkynyl Grignard derivatives.



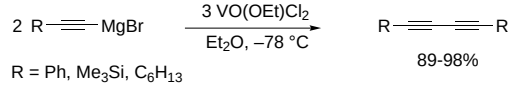
Oligoacetylene	Oxidant	Yield [%]	Ref.
H$_3$C—≡—≡—CH$_3$	C$_6$H$_5$NO$_2$	58	[91]
H$_3$C—(≡—≡)$_2$—CH$_3$	CuCl$_2$	78	[88]
H$_3$C—(≡—≡)$_2$—CH$_3$	I$_2$	66	[87]
C$_4$H$_9$—≡—≡—C$_4$H$_9$	I$_2$, CuCl	70	[89]
C$_6$H$_5$—(≡—≡)$_2$—C$_6$H$_5$	CuCl$_2$	47	[88]
C$_6$H$_5$—≡—≡—C$_6$H$_5$ **2**	CoCl$_2$	42	[88, 89]

The transition metal catalyzed oxidative homocoupling of acetylenic Grignard derivatives has opened up this concept to a larger number of alkyne derivatives. In 1988, Ito et al. described a palladium-catalyzed oxidative coupling reaction of Grignard reagents in the presence of *N*-substituted isocyanide dichlorides (R–N=CCl$_2$) as the reoxidant, which afforded conjugated diynes in high yields (Scheme 14).[93]



Scheme 14. Palladium-catalyzed dimerization of alkynyl Grignard derivatives.[93] dppf = 1,1′-bis(diphenylphosphanyl)ferrocene.

Treatment of bis(phenylethynyl)magnesium with iodine in THF in the presence of catalytic amounts of [Pd(acac)$_2$] (acac = acetylacetonate) and PPh$_3$ (4 equiv with respect to the Pd catalyst) also forms diphenylbuta-1,3-diyne (**2**) in 94% yield.[94] Quite recently, Hirao and co-workers reported that the homocoupling of various lithium (Section 2.4) and magnesium acetylides is effectively induced by oxidation with oxovanadium(V) compounds of the type VO(OR)Cl$_2$ under mild conditions (Scheme 15).[95]



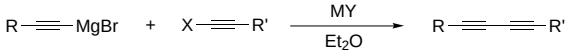
Scheme 15. Oxidative coupling of alkynyl Grignard derivatives in the presence of oxovanadium(v) compounds.[95]

None of these procedures for the oxidative coupling of alkynyl Grignard derivatives has seen widespread application to date.

2.3.2. Heterocoupling of Alkynyl Grignard Derivatives with 1-Haloalkynes

This variant of the Cadiot – Chodkiewicz coupling has been catalyzed by copper(I) and cobalt(II) salts,[37, 39] and was examined in some detail by Weedon and co-workers (Table 4).[89]

Table 4. Heterocoupling of alkynyl Grignard derivatives with 1-haloalkynes.



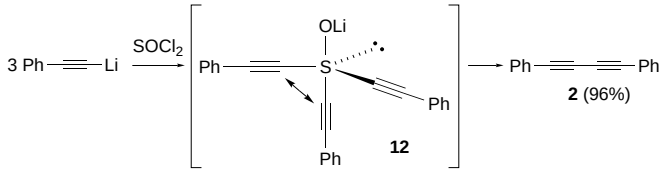
R	R′	X	MY	Yield [%]	Ref.
C_4H_9	C_6H_5	Br	$CoCl_2$	31	[89]
C_6H_5	C_4H_9	I	CuCl	35	[89]
C_6H_5[a]	Cl	Cl	–	33	[96]

[a] $C_6H_5CCMgCl$ was used as the Grignard derivative.

An interesting example was described by Viehe in which dichloroacetylene was coupled with phenylethynylmagnesium chloride to afford the corresponding chlorodiyne in the absence of a catalyst (Table 4).[96] A general problem of the method is homocoupling arising from halogen – magnesium exchange. This lack of selectivity, together with the general disadvantages inherent in the use of Grignard reagents, has hindered the wide use of this cross-coupling protocol in modern organic synthesis.

2.4. Coupling Reactions of Other Organometallic Acetylides

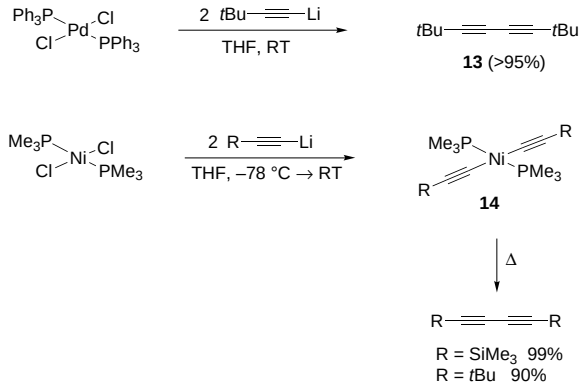
A variety of other organometallic acetylides represent interesting alternatives to the magnesium acetylides discussed in Section 2.3. For early work on oxidative dimerizations of alkali acetylides, the reader is referred to previous review articles.[37, 39] Out of the variety of oxidizing agents employed, thionyl chloride is particularly efficient for the oxidative dimerization of phenyllithium, as described by Oae et al. (Scheme 16).[97] In this conversion, the yield of diphenylbuta-1,3-diyne (**2**) is highest (96%) if the molar ratio of phenylethynyllithium to $SOCl_2$ is 3:1. This finding was explained by the formation of a hypervalent, trigonal-bipyramidal sulfurane intermediate **12** which undergoes reductive elimination



Scheme 16. The homocoupling of phenylethynyllithium in the presence of $SOCl_2$ presumably involves the intermediacy of the hypervalent sulfurane **12**.[97]

through coupling between one equatorial and one axial alkynyl ligand.

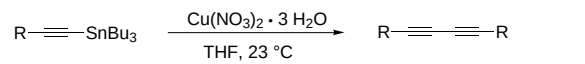
Another strategy for the dimerization of various lithium acetylides involves their addition to nickel or palladium complexes (Scheme 17). Negishi and co-workers found that the reaction of $[PdCl_2(PPh_3)_2]$ with two equivalents of *tert*-butylethynyllithium gave the desired buta-1,3-diyne **13** in greater than 95% yield.[98] Similarly high yields are obtained with nickel complexes.[99, 100] The intermediate *trans*-dialkynylnickel complexes **14a** ($R = SiMe_3$) and **14b** ($R = tBu$) can be isolated and undergo reductive elimination upon heating under argon.



Scheme 17. Homocoupling of alkynyllithium derivatives using palladium[98] and nickel[99, 100] complexes.

Lithium acetylides are often used as precursors for transmetalations which yield alkynyl derivatives that can participate in coupling reactions to provide the corresponding diacetylenes. Among the main group elements, boron,[101, 102] tin,[103] antimony,[104] selenium,[105] and tellurium[106, 107] are well known to provide metalated alkynes which subsequently undergo coupling. Some of these provide potent alternatives to the more established methods. For example, the addition of alkynylstannanes to one equivalent of $Cu(NO_3)_2 \cdot 3H_2O$ or $AgNO_3$ affords the corresponding symmetrical 1,3-diynes in good yields under mild conditions and in short reactions times (10 – 30 min; Table 5).[103] The 85% yield obtained using this procedure for the dimerization of 3-(tetrahydro-2*H*-pyran-2-yloxy)-1-propyne contrasts sharply with the 34% yield obtained under standard Glaser conditions. The Stille-type palladium-catalyzed carbon – carbon bond formation with alkynyltin compounds[108] will be presented later (Section 2.5.2).

Table 5. Formation of 1,3-diynes by a copper(II) nitrate mediated coupling of alkynyltin compounds.[103]

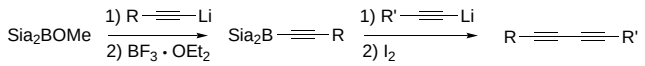


R	Reaction time [min]	Yield [%]
$THPOCH_2$[a]	10	85
C_4H_9	10	60
C_6H_5	30	50
4-MeC_6H_4	10	67

[a] THP = tetrahydro-2*H*-pyran-2-yl.

Oxidation of lithium dialkynyldialkylborates provides an efficient and selective cross-coupling method.[101b, 102] Unsymmetrical lithium dialkynyldialkylborates $Li^+[R''_2B(C{\equiv}CR)(C{\equiv}CR')]^-$ are prepared by the stepwise addition of two different lithium acetylides to dicyclohexyl(methylthio)borane.[101b] The subsequent action of iodine on the borates yields the unsymmetrically substituted conjugated diynes. Symmetrical diacetylenes can also be synthesized by this methodology.[101a] Alternatively, methyl disiamylborinate can be used for the boron-mediated cross-coupling, as demonstrated by Sinclair and Brown (Table 6).[102] This technique provides a procedurally simple alternative to the Cadiot–Chodkiewicz reaction, which requires the preparation of 1-bromoalkynes and is not efficient for the coupling of higher alkynes.

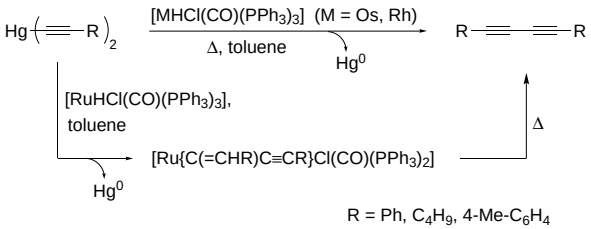
Table 6. Synthesis of conjugated diynes via disiamylalkynylboranes.[102]



R	R′	Yield [%][a]
n-C_6H_{13}	C_2H_5	95 (61)
n-C_6H_{13}	C_6H_{11}	80 (73)
n-C_6H_{13}	C_4H_9	79 (60)
n-C_6H_{13}	C_6H_5	79 (61)

[a] The first number refers to the yield obtained by isolation of the intermediate Sia_2BCCR. The yield in parenthesis refers to a one-pot procedure not involving isolation of any intermediate.

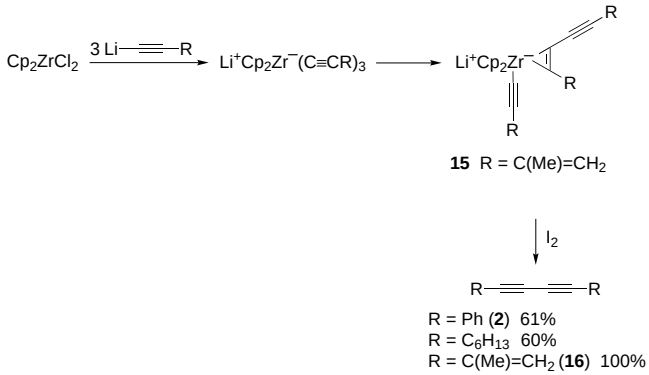
Although bis(alkynyl)mercury compounds emerged early as convenient crystalline derivatives for the characterization of terminal alkynes,[109] their deployment as alkynyl-transfer reagents started relatively late, and has not been extensively studied. Hill and co-workers noted in the course of transalkynylation experiments with bis(alkynyl)mercury compounds that certain platinum group metal complexes catalyze the elimination of mercury under mild conditions to provide buta-1,3-diynes (Scheme 18).[110]



Scheme 18. Catalytic demercuration of bis(alkynyl)mercurials to provide buta-1,3-diynes.[110]

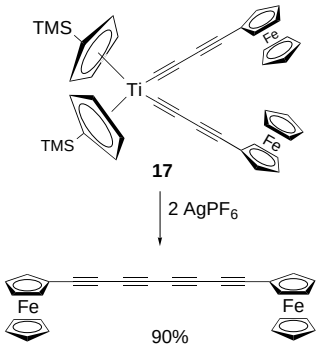
Other transition metals are also known to form alkynyl complexes possessing interesting coupling properties. As early as 1969, Tsutsumi and co-workers reported the formation of diphenylbuta-1,3-diyne in moderate to good yield by treatment of lithium phenylethynylnickel carbonylate ($Li[PhCCNi(CO)_4]$), prepared from PhCCLi and $[Ni(CO)_4]$, with iodine or bromine.[111]

The 1,2-migration reaction of alkynylzirconocenes, described by Negishi and co-workers,[112] represents an efficient carbon–carbon bond formation process which gives symmetrically substituted 1,3-diynes in good to excellent yields. Thus, reaction of zirconocene **15**, formed by treating Cp_2ZrCl_2 with three equivalents of the corresponding lithium acetylide, with iodine (2 equiv) produced buta-1,3-diyne **16** in almost quantitative yield (Scheme 19).



Scheme 19. Buta-1,3-diynes by 1,2-migration reaction of alkynylzirconocenes.[112]

The oxidation of alkynyltitanium compounds generally does not provide diacetylenes in reasonable yields.[113] Two remarkable exceptions were reported quite recently by Hayashi et al.[114] and by Lang and co-workers[115] using titanocenebis(metallocenylacetylide) complexes (metallocenyl = ferrocenyl or ruthenocenyl). The former authors found that complexes such as **17** are readily oxidized with two equivalents of $AgPF_6$ or electrochemically to yield cleanly the acetylenic coupling product (Scheme 20). The electrochemical studies suggested that the reaction is induced by initial oxidation of the metallocenyl units followed by reductive coupling of the two titanocene-bound alkynyl units.



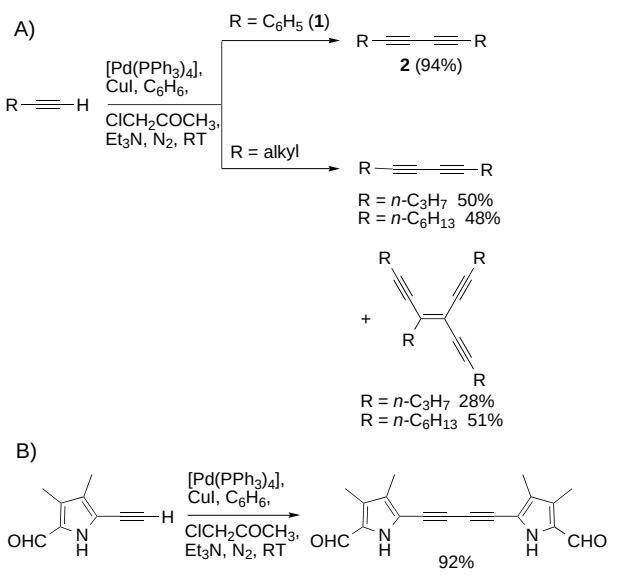
Scheme 20. Reductive coupling induced by metallocene oxidation.[114]

2.5. Palladium-Catalyzed Coupling Reactions of Alkynes and Alkynylstannanes

2.5.1. Palladium-Catalyzed Couplings of Terminal Alkynes

The discovery of palladium-catalyzed coupling reactions more than 30 years ago[116] has initiated explosive growth in the field of organometallic chemistry. An early observation was the formation of symmetric diynes, via dialkynylpalla-

dium intermediates, during couplings between terminal alkynes and aryl or vinyl halides.[117a] In 1985, Rossi et al. optimized this process as a homocoupling method for terminal acetylenes.[117b] Diaryl- and dialkylbuta-1,3-diynes were obtained in moderate to good yields using chloroacetone as the oxidant and a mixture of $[Pd(PPh_3)_4]$ and CuI as the catalyst together with triethylamine (Scheme 21). Whereas aryl-substituted alkynes react exclusively to give the corresponding

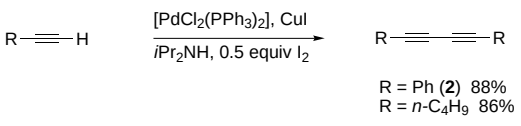


Scheme 21. A) Pd-catalyzed oxidative coupling of terminal alkynes[117b] and B) application to the oxidative dimerization of an alkynylpyrrole.[118]

diynes, aliphatic acetylenes also form 4-alkynylhexa-1,5-diyn-3-enes under these conditions (Scheme 21 A). The efficiency of this method has been underlined quite recently by Kim and co-workers, who reported the oxidative dimerization of an alkynylpyrrole in a notable 92% yield (Scheme 21 B).[118] Consequently, it may represent a good alternative to the Glaser reaction for couplings in nonpolar organic solutions.

A variant of this procedure was described by Kundu et al.[119] These authors used a mixture of $[PdCl_2(PPh_3)_2]$ and CuI as the catalyst in the presence of diisopropylamine while either 4-iodo-2-nitro-resorcinol or dimethyl sulfoxide served as the oxidant. It was found that the reaction proceeds in the absence of CuI, whereas the absence of the palladium catalyst almost completely suppressed the coupling process. Using the same catalyst system but with I_2 as the oxidant proved superior for the homocoupling of aliphatic and aromatic alkynes, as was recently described by Liu and Burton (Scheme 22).[120] A similar system was applied by Kijima and co-workers to the polycondensation of acetylene to yield carbyne fragments (-[C≡C]$_n$-).[121]

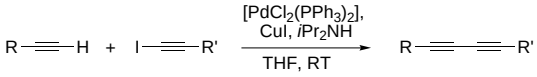
Acetylenic heterocouplings using palladium catalysis are also known. Precedence for the use of 1-haloalkynes in



Scheme 22. Convenient Pd-catalyzed oxidative coupling of both aliphatic and aromatic terminal alkynes.[120]

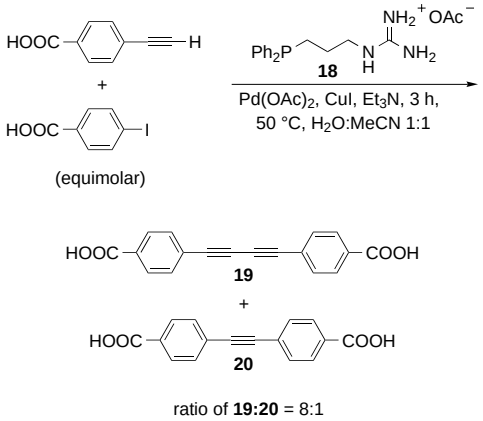
palladium-catalyzed reactions was established by Suzuki and co-workers.[122] In 1991, Wityak and Chan realized a mild and efficient palladium- and copper-mediated coupling of 1-alkynes with 1-iodoalkynes (Table 7).[123] Yields were good to excellent, without any detectable amounts of homocoupling products, even when dioxygen was not rigorously excluded.

Table 7. Pd^0-catalyzed heterocoupling in homogeneous solution.[123]



R	R′	Yield [%]
Ph	$HOCH_2$	79
C_7H_{15}	$HOCH_2$	73
$HOCH_2$	Ph	54
Me_3Si	Ph	91

The design of water-soluble catalytic systems is currently of great interest, since they offer an opportunity for simple and complete product separation from the active catalyst, which is still one of the greatest drawbacks of homogeneous catalysis using transition metals. While studying the reaction between 4-iodobenzoic acid and *p*-carboxyphenylacetylene under aqueous Heck conditions, Dibowski and Schmidtchen found that the conversion in a mixture of acetonitrile and water (1:1) in the presence of the strongly basic guanidinium phosphane ligand **18** provided mainly homocoupled product **19** and only minor amounts of heterocoupled **20** (Scheme 23).[124]

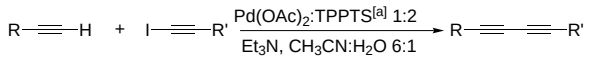


Scheme 23. Pd-catalyzed homocoupling in aqueous solution is preferred under specific conditions over the Heck cross-coupling.[124]

Amatore et al. reported in 1995 an acetylenic cross-coupling reaction with a water-soluble palladium catalyst prepared in situ from palladium(II) acetate and sulfonated triphenylphosphane $P(C_6H_4\text{-}m\text{-}SO_3Na)_3$ (TPPTS; Table 8).[125] This method works without any copper(I) promoter and is well adapted for the synthesis of unsymmetrically substituted diynes from alkynyl iodides and terminal alkynes.

There have also been a few applications of phase-transfer catalysis in the presence of Pd(0) to the synthesis of 1,3-diynes by acetylenic homocoupling.[126, 127] The use of heterogeneous catalysts is a further strategy to avoid separation problems.

Table 8. Pd-catalyzed cross-coupling in aqueous solution.[125]



R	R′	Yield [%]
$HOC(CH_3)_2$	$CH_3(CH_2)_3$	60
$HOC(CH_3)_2$	Me_3Si	57
$CH_3(CH_2)_4CHOH$	Me_3Si	43
$CH_3(CH_2)_4CHOH$	$H_2NC(C_2H_5)_2$	65

[a] TPPTS = $P(C_6H_4$-m-$SO_3Na)_3$.

Strauss and co-workers reported the homocoupling of phenylacetylene in 71 % yield using palladium on porous glass tubing.[128] This heterogenous catalyst system obviates the use of potentially air- and temperature-sensitive phosphane ligands.[129]

2.5.2. Palladium-Catalyzed Coupling of Alkynylstannanes

The palladium-catalyzed cross-coupling of organostannanes with organohalides or triflates, originally described by Stille and Groh,[130] provides a powerful method for carbon–carbon bond formation.[131] During the total syntheses of the manumycin antibiotics alisamycin[132] and limocrocin,[133] Taylor and co-workers found that the Pd-catalyzed homocoupling of vinylstannanes proceeded smoothly and in high yield under dioxygen or air.[108] This method can also be transferred to alkynylstannanes, as the authors demonstrated with the dimerization of phenylethynylstannane to give diphenylbuta-1,3-diyne (**2**) in 89 % yield (5 mol % $Pd(OAc)_2$, Me_2SO, O_2, RT).

2.6. Other Transition Metal Mediated Alkyne-Coupling Processes

Other transition metals have been applied to acetylenic couplings; however, none of these reactions has gained wide applicability so far. Only one example of a platinum-catalyzed acetylenic coupling has been reported. While investigating carbonylations of alkynyl iodides using a $[PtCl_2(PPh_3)_2]/Et_3N$ system, Watanabe and co-workers observed that 1-iodo-1-octyne underwent sp–sp homocoupling to yield hexadeca-7,9-diyne in 59 % yield.[134]

Takai et al. reported the reductive dimerization of 1-iodo- and 1-chloro-1-alkynes in the presence of two equivalents of chromium(II) chloride.[135] Thus, phenylethynyliodide gives diphenylbuta-1,3-diyne (**2**) in 66 % yield. The reaction is assumed to proceed via intermediate alkynylchromium(III) and dialkynylchromium(IV) compounds, with the latter undergoing reductive elimination to yield homocoupled products.

Conjugated diynes can also be obtained by decarbonylation of the corresponding dialkynylketones using stoichiometric amounts of $[RhCl(PPh_3)_3]$ in boiling xylene, presumably through the intermediacy of dialkynylrhodium complexes.[136] This method affords symmetrical and unsymmetrical diacetylenes, although yields are decent only if the dialkynylketone bears aromatic substituents. Thus, 1,5-diphenylpenta-1,4-diyn-3-one affords **2** in 78 % yield. A rhodium vinylidene complex has been observed to catalyze the disproportionation of phenylacetylene to give diphenylbuta-1,3-diyne (**2**) and styrene.[137, 138]

Takahashi et al. described an intramolecular zirconocene-mediated acetylenic coupling. Treatment of aryl-substituted bis(alkynyl)silanes with $[ZrCp_2Et_2]$ and subsequent addition of two equivalents of iodine provided symmetric diynes in good yields.[139] Thus, **2** was obtained in 95 % yield in the conversion of $(Ph{-}C{\equiv}C)_2SiPh_2$.

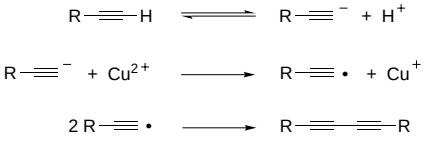
Acetylenic coupling reactions have also been observed within the coordination sphere of some organometallic clusters with the formed buta-1,3-diyne remaining bound to the metal centers.[140–142] Although of considerable mechanistic interest, these reactions have not yet found preparative use.

3. Mechanistic investigations

There have been surprisingly few mechanistic investigations of alkyne couplings, given their wide applicability in synthesis, and the potential for improved conditions that a more complete mechanistic understanding could provide. The classical oxidative alkyne couplings have been the most extensively studied, yet their exact mechanism remains unknown, and the existence of several hypotheses regarding the oxidation state and structure of the postulated intermediary copper acetylides has generated considerable discussion. Here we present an overview of the published investigations and proposed mechanisms for the most commonly employed copper- and palladium-catalyzed couplings.

3.1. Oxidative Couplings

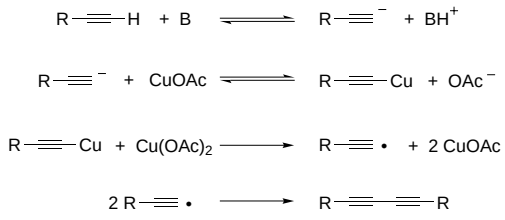
The earliest mechanistic proposals postulated the formation of acetylenic radicals which would then recombine to afford the corresponding diynes. An early kinetic investigation by Klebansky et al. demonstrated that copper(II) ions served as the direct oxidizing agent.[143] They also noted that the rate of coupling was faster in basic media and for more acidic terminal alkynes. In light of these findings, the homolytic bond cleavage proposed earlier by Zalkind and Fundyler[144] was discarded in favor of a heterolytic cleavage followed by the transfer of a single electron to the copper(II) salt (Scheme 24).



Scheme 24. Early proposal for the mechanism of the oxidative acetylenic coupling.[144]

This radical mechanism evolved further with the study of Clifford and Waters in 1963 which showed that copper(I) ions were required for the coupling using $Cu(OAc)_2$ in pyridine in the absence of O_2.[145] They proposed the formation of

copper(I) acetylides which were rapidly oxidized by the transfer of a single electron to copper(II) through an acetate ligand bridge. Decomposition of the resultant copper(II) acetylide and recombination of the free radicals would give the coupled products (Scheme 25).



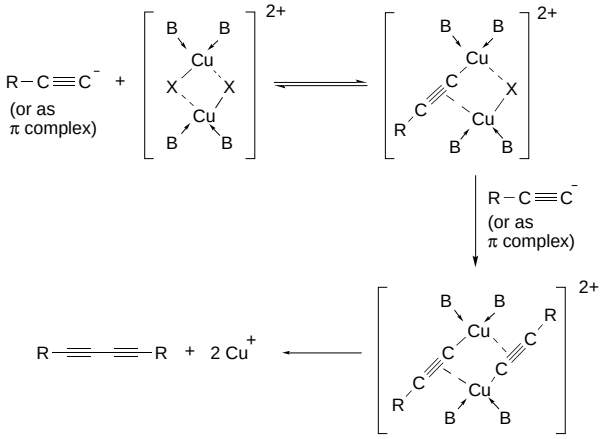
Scheme 25. Mechanism proposed for the oxidative coupling using $Cu(OAc)_2$ in pyridine in the absence of O_2.[145] The coordinating pyridine molecules are omitted.

In the following year, Bohlmann et al. published a landmark study on the rate of dimerization as influenced by the electronic nature of conjugated acetylenes.[146] They found that more acidic acetylenes underwent more rapid dimerization under alkaline conditions, which was consistent with the results of Klebansky et al. However, under acidic conditions (pH 3), an inverse relationship was observed, and the addition of a copper(I) salt became necessary. These observations were explained on the basis of the formation of π complexes between the Cu^I ions and the triple bond, which would activate the alkyne toward deprotonation (Scheme 26). This complexation would be expected to be weaker for the diffuse π systems of polyconjugated substrates, which indeed react more slowly. Klebansky et al. had previously hinted at a similar activation while Clifford and Waters invoked the reversible formation of nonreactive copper–π complexes in a competing nonproductive equilibrium to explain the observed dependence of the reaction rate on the alkyne concentration in their system.



Scheme 26. Acetylene activation by π-complex formation postulated by Bohlmann et al.[146]

Bohlmann et al. also called into question the idea of free radical intermediates, noting that mixtures of electronically different alkynes give predominantly the homocoupled products, whereas no such selectivity would be expected of free radicals. On the basis of the observed second-order dependence of the coupling rate on alkyne concentration, he proposed an alternative dinuclear copper(II) acetylide complex which would collapse directly to the coupled product (Scheme 27). Such an intermediate also rationalized the first-order dependence of the rate on the substrate concentration observed during intramolecular coupling to generate cyclic diynes. Most subsequent mechanistic proposals have discarded free radical intermediates in favor of some variant of this dimeric copper acetylide.[147, 148] Other groups have, however,



Scheme 27. Dimeric copper acetylides were first proposed by Bohlmann et al. as intermediates in the oxidative acetylenic coupling.[146] B = N ligand, for example, pyridine; X = Cl^-, OAc^-.

observed primarily monomeric species under different conditions.[149]

Studies by Fedenok et al. largely confirmed these results. They found that the oxidative coupling rate constant for a range of *para*-substituted phenylacetylenes correlated quantitatively with their Hammett σ constants;[150] that is, reactivity increases with the acidity of the ethynyl proton. The low experimentally determined activation energy of 21 kcal mol^{-1} provided an argument against radical mechanisms and in favor of the simultaneous oxidation and C–C bond formation proposed by Bohlmann et al. However, they found that copper(I) ions played no role in the reaction under their buffered conditions (Et_3N, HOAc, pyridine), and therefore proposed the formation and dimerization of Cu^{II} rather than Cu^I–π complexes.[151]

Later, the same group examined the catalytic coupling in the presence of dioxygen and found that the same mechanism was operative.[152] In buffered alkaline solution (Et_3N, HOAc, pyridine), both the reaction rate and the intensity of the ESR signal for Cu^{II} ions reached saturation above a limiting dioxygen pressure, which provided additional evidence that all the copper was present in the divalent state, with Cu^I only serving as an intermediate electron carrier. The function of dioxygen amounts to the oxidation of Cu^I and regeneration of Cu^{II} ions.

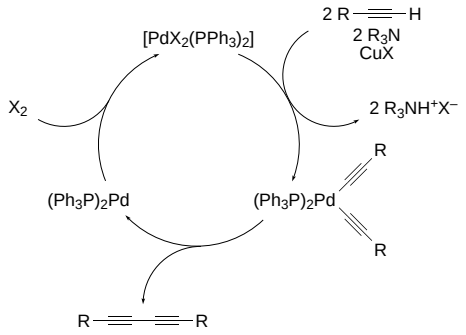
For the catalytic coupling in nonbuffered pyridine, however, they found that reoxidation of Cu^I by dioxygen was significantly slower, and that copper(I) ions were indeed involved in the reaction.[153] While the reaction started slowly, an autocatalytic effect was eventually observed, and this induction period disappeared upon addition of copper(I) chloride. They found that mixtures of copper(I) and copper(II) chloride in the absence of dioxygen in pyridine gave no coupling products unless strong base was added. The use of copper(II) ions, prepared by air oxidation of CuCl, allowed for coupling without the need of additional base. Thus some indeterminate copper(II) salt generated by dioxygen and copper(I) chloride, which the authors dubbed the "oxygen-containing part" of the copper solution, seems to act as the base during the catalytic oxidative coupling in pyridine. Fedenok et al. also noted a complex dependence of the rate

and order of the reaction on the alkyne and copper(I) chloride concentration.[153b]

Temkin and co-workers examined the kinetics of acetylene dimerization in aqueous solutions containing copper(I) and copper(II) chlorides in addition to various background electrolytes (MCl, $M = NH_4^+$, Li^+, Na^+, K^+) to ensure constant activity coefficients of all ions involved.[154] As for many reactions involving copper salts, the presence of other ions in solution had a strong effect on the reaction rate, and even the reaction path. This effect was linked to the activity of the chloride ions, which in turn affects the relative availability of Cu^I and Cu^{II} ions. The authors proposed the involvement of three copper ions (two Cu^I and one Cu^{II}) per alkyne unit in the rate-limiting stage of the oxidative dimerization.[154a] The existence of such higher order complexes has recently been demonstrated by X-ray crystallography in the solid state,[155] where an ethynyl residue was found to undergo π coordination with two Cu^I ions and to form acetylide-type bonds with two other Cu^I centers.

Clearly, the current understanding of the admittedly complex mechanism of copper-mediated oxidative acetylenic coupling remains unsatisfactory. The studies summarized above document that the mechanism is highly dependent on the experimental setup, which makes it difficult to compare the outcome of various kinetic investigations conducted under different conditions. It can be concluded that the mechanism proposed 36 years ago by Bohlmann et al. (Scheme 27) still provides the most reasonable and most accepted picture.

There have been no rigorous mechanistic investigations of the corresponding palladium-catalyzed oxidative coupling procedure. Common to all proposed mechanisms is the formation of an intermediate dialkynylpalladium(II) species and subsequent reductive elimination to generate Pd^0 and the coupled product.[156] The catalytic cycle proposed for oxidative dimerization in the presence of iodine is representative (Scheme 28).[120]

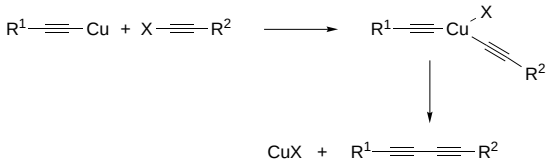


Scheme 28. Mechanism for the palladium-catalyed oxidative homocoupling of terminal alkynes.[120]

The dialkynylpalladium intermediate could conceivably be formed by direct oxidative insertion into the alkyne, ligand displacement by an acetylide anion, or by transmetalation from copper(I) acetylides. The dramatically lower reaction rates in the absence of copper(I) suggest that formation of copper(I) acetylides or alkyne activation towards deprotonation by π complexation to Cu^I ions (Scheme 26) are important processes in the catalytic cycle.[156]

3.2. Nonoxidative Heterocouplings

There have been surprisingly few mechanistic examinations of the copper-catalyzed heterocoupling of alkynes and haloalkynes. This may be due largely to the rapid reaction rates observed for the commonly employed bromoalkynes, which make classical kinetic studies difficult, although some attempts to examine the reaction using the less reactive chloroalkynes have been made.[39] It has been assumed that coupling proceeds through copper(I) acetylides that are formed through one of the mechanisms described above (Section 3.1). Subsequent oxidative addition to the alkynyl halide to generate an intermediate copper(III) species has been proposed (Scheme 29).[39] The fact that similar couplings have been observed for alkynylmagnesium halides, which cannot achieve higher oxidation states, suggests that nucleophilic addition may be a viable alternative.[96]



Scheme 29. Mechanism proposed for the Cadiot–Chodkiewicz heterocoupling.[39]

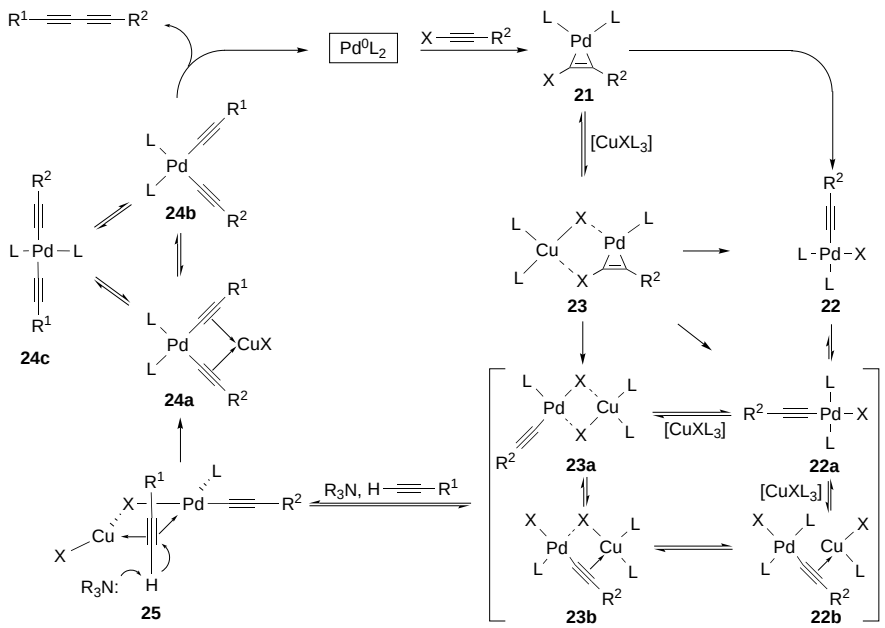
The mechanism of the palladium-catalyzed version was examined by Bugamin et al.[157] and more recently by Cai and Vasella in conjunction with the development of a binomial synthesis of acetylenic oligosaccharides (Section 4.3).[158] ^1H and ^{31}P NMR investigations in the latter study revealed that haloalkynes underwent oxidative addition to Pd(0) via the η^2-palladium complex **21** (Scheme 30). Dramatic acceleration of the rearrangement of **21** to **22** by copper(I) ions suggested the intermediacy of the bimetallic complex **23**. Formation of the dialkynylpalladium complex **24** could proceed through transmetalation of the copper(I) acetylide, for which no evidence was seen in NMR studies, or via complex **25**.

Amatore et al. proposed an alternative mechanism, which involved transmetalation of two alkynylpalladium species, for the formation of the dialkynylpalladium complex **24** in the catalytic cycle (Scheme 31).[125]

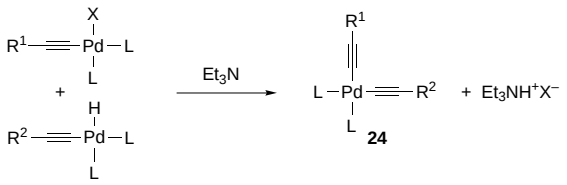
Overall, it becomes apparent that much remains to be understood about the mechanisms of both the oxidative and nonoxidative alkyne coupling processes. Although apparently highly challenging, the search for an improved mechanistic understanding could prove quite rewarding, and provide fertile ground for new method development.

4. Applications of Acetylene Couplings

The far-reaching synthetic applicability of acetylenic coupling methods is impressively demonstrated in various fields of chemistry, such as natural product synthesis, polymer chemistry, and supramolecular chemistry.[159] Because of the size of the subject, it is neither possible nor desirable to give a



Scheme 30. Mechanism proposed by Cai and Vasella for the palladium-catalyzed cross-coupling of alkynes with 1-haloalkynes.[158]



Scheme 31. Transmetalation mechanism proposed by Amatore et al. for the formation of the dialkynylpalladium complex in the palladium-catalyzed cross-coupling of alkynes with 1-haloalkynes.[125]

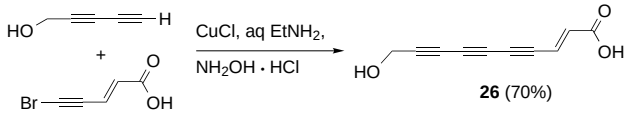
complete survey of every work involving this preparative method. Thus, this section presents only an excerpt with the aim of showing the synthetic utility of alkyne–alkyne coupling reactions, which penetrate the whole of modern chemistry. Besides natural product synthesis, we focus on the field of supramolecular chemistry, where couplings of acetylenes have proven a potent strategy for assembling complex, highly preorganized structures from relatively simple building blocks.

4.1. Synthesis of Natural Products and Analogues

Natural product synthesis was the first domain to employ oxidative coupling reactions of alkynes.[2] In the 1950s, Glaser-type reactions were used in the syntheses of a variety of naturally occurring di- and polyacetylenes.[160] A real breakthrough occurred with the invention of the Cadiot–Chodkiewicz coupling method, which provided more efficient access to unsymmetrically substituted diacetylenes.

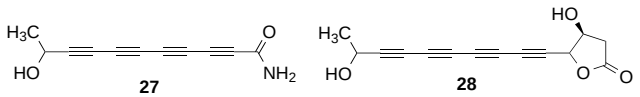
Compounds containing chains of conjugated triple bonds represent a fascinating group of natural products. They show wide distribution in higher plants, from which most natural acetylenes have been isolated,[161] but have also been found in fungi[162] and bacteria.[163] Although a number of excellent reviews have appeared,[31, 160, 164–167] the isolation and synthesis of numerous new polyacetylenic natural products with remarkably diverse functionalization patterns makes an update valuable. Many of these compounds possess interesting biological properties, such as antibacterial,[163, 168] antifungal,[163, 169] pesticidal,[72b, 170] and antitumor activity.[170, 171] For aspects related to biosynthesis and biological activity of polyacetylenic natural products, the reader is referred to the excellent reviews of Bohlmann[167] and BuLock,[165] and to the more recent review by Hansen and Boll.[172]

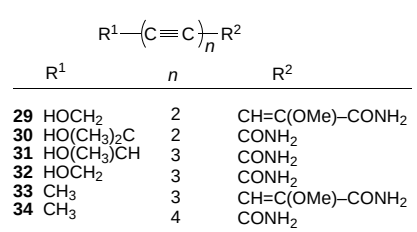
Quite often extreme instability prevents isolation or even spectroscopic investigation of natural polyacetylenes. In such cases their preparation in the laboratory is necessary for structural and biological activity studies. Before the introduction of NMR techniques, Jones and co-workers succeeded in the structure determination of various fungal polyacetylenes, such as triynoic acid **26**, which was prepared by a Cadiot–Chodkiewicz coupling reaction (Scheme 32).[173]



Scheme 32. Synthesis of *trans*-10-hydroxy-dec-2-en-4,6,8-triyn-1-oic acid (**26**).[173]

Sometimes, high instability even prevents total synthesis. In this case, chemical synthesis of more stable analogues is required to elucidate, by spectral comparison, the structure of the natural polyacetylenes. Thus, Bäuerle, Anke, and coworkers found the acetylenic metabolites tetraynamide **27** and tetrayne lactone **28** from the fungus *Mycena viridimarginata* too unstable for isolation and full characterization (Scheme 33).[174] Therefore, they synthesized stable analogues



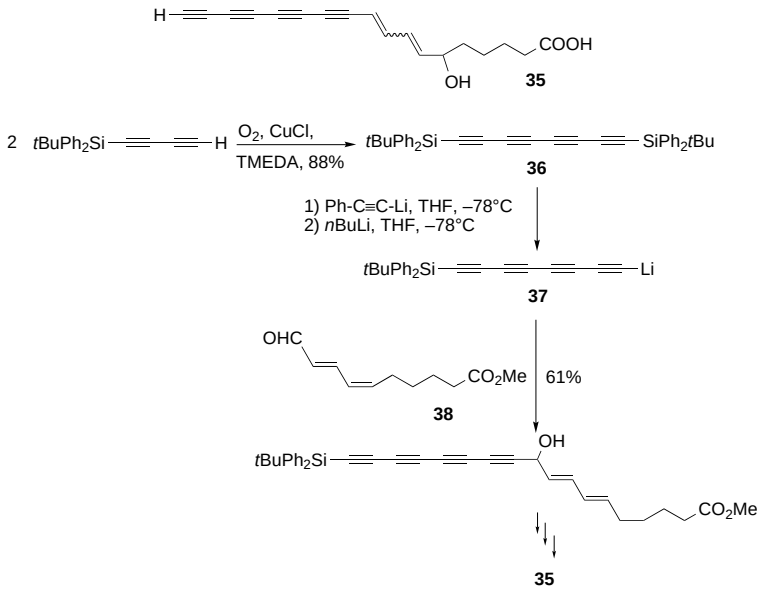


	R^1	n	R^2
29	$HOCH_2$	2	$CH=C(OMe)–CONH_2$
30	$HO(CH_3)_2C$	2	$CONH_2$
31	$HO(CH_3)CH$	3	$CONH_2$
32	$HOCH_2$	3	$CONH_2$
33	CH_3	3	$CH=C(OMe)–CONH_2$
34	CH_3	4	$CONH_2$

Scheme 33. Highly unstable fungal metabolites **27** and **28** and model compounds **29**–**34** prepared for structure elucidation (by spectral comparison).[174]

such as **29**–**34** containing substructures of **27** and **28** by oxidative cross-coupling reactions under Glaser conditions. The tetraacetylenic chromophore in **27** and **28** was subsequently established with confidence on the basis of spectral comparisons between the natural products and the model systems.

A fine example of the synthetic possibilities opened up by combination of acetylenic coupling with selective deprotection techniques was provided by Yamaguchi et al.[163] The authors achieved the total synthesis of caryoynencins (**35**), which are polyyne antibiotics with potent antibacterial activities that can be isolated from cultures of the plant pathogen *Pseudomonas caryophylli*. The tetrayne framework of these molecules was built up efficiently by Hay coupling, and resulted in the formation of the symmetrical building block **36** (Scheme 34). The full carbon skeleton of **35** was subsequently built by addition of lithium acetylide **37**, which

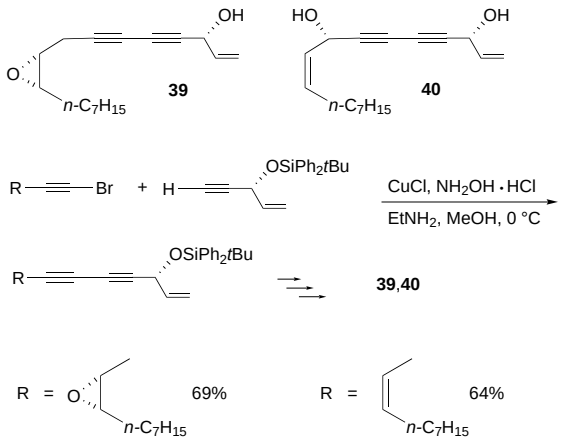


Scheme 34. Construction of the carbon skeleton in the total synthesis of the polyyne antibiotics caryoynencins (**35**).[163] TMEDA = *N*,*N*,*N*′,*N*′-tetramethylethylenediamine.

was formed by careful mono-deprotection of **36** with phenylethynyllithium, to methyl ester **38**.

The continuing importance of the Cadiot–Chodkiewicz reaction for synthetic access to unsymmetrically substituted natural acetylenes was recently demonstrated by Cai and coworkers with the syntheses of panaxydol (**39**), an antitumor constituent of the *Panax ginseng* plant,[171, 175] and (3*R*,8*S*)-falcarindiol (**40**),[168] which is found in *Umbelliferae* and *Araliaceae* and exhibits anibacterial properties (Scheme 35).

In addition to the syntheses of natural polyacetylenes shown above, alkyne coupling reactions have also been employed as key steps in the preparation of various other biologically interesting compounds, such as allylamines and alkadienylamines (antimycotics),[176] alkynylindoles[177] and indolocarbazoles (antitumor agents),[178] anacyclin and related isobutylamides (insecticides),[72b] alkynyl-substituted steroids (antigestagens),[179] natural unsaturated fatty acids (natural ionophores and defensive substances in rice plants),[180]

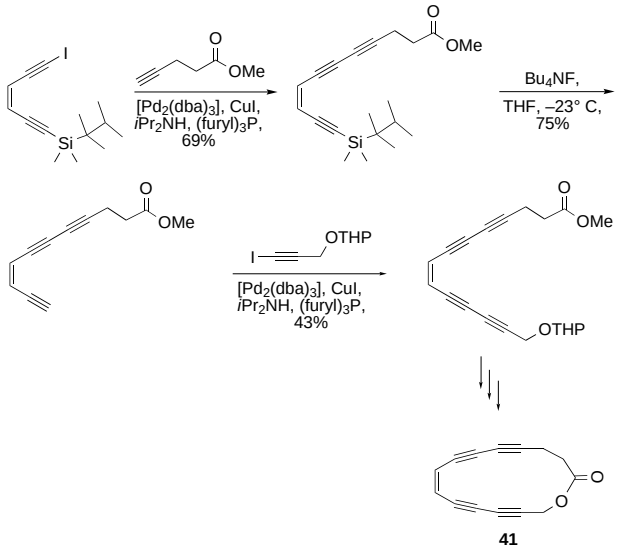


Scheme 35. The Cadiot–Chodkiewicz heterocoupling is the key step in the construction of the carbon framework of panaxydol (**39**)[171] and (3*R*,8*S*)-falcarindiol (**40**).[168]

pheromones,[181] diyne-bridged amino acids,[182] and acetylenic retinoids.[183]

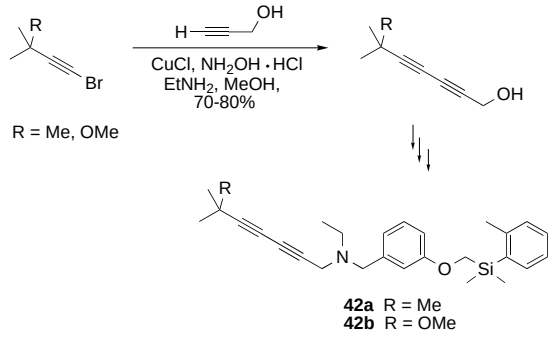
Naturally occurring *cis*-enediynes and unnatural derivatives have received special attention as potent antitumor antibiotics in recent years.[184] Schreiber and co-workers prepared a series of macrocyclic and acyclic *cis*-enetetraynes,[185] but found them remarkably unreactive with respect to the Bergman rearrangement which transforms *cis*-enediynes into benzene-1,4-diradicals, which serve as potent cytotoxic agents.[184c] The *cis*-enetetraynes, such as macrocycle **41** (Scheme 36), were obtained primarily by palladium-catalyzed alkyne cross-coupling reactions, which proved superior in this case to the classical Cadiot–Chodkiewicz conditions.

Another application of the Cadiot–Chodkiewicz cross-coupling in medicinal chemistry can be found in the preparation of the alkynylated benzylamine



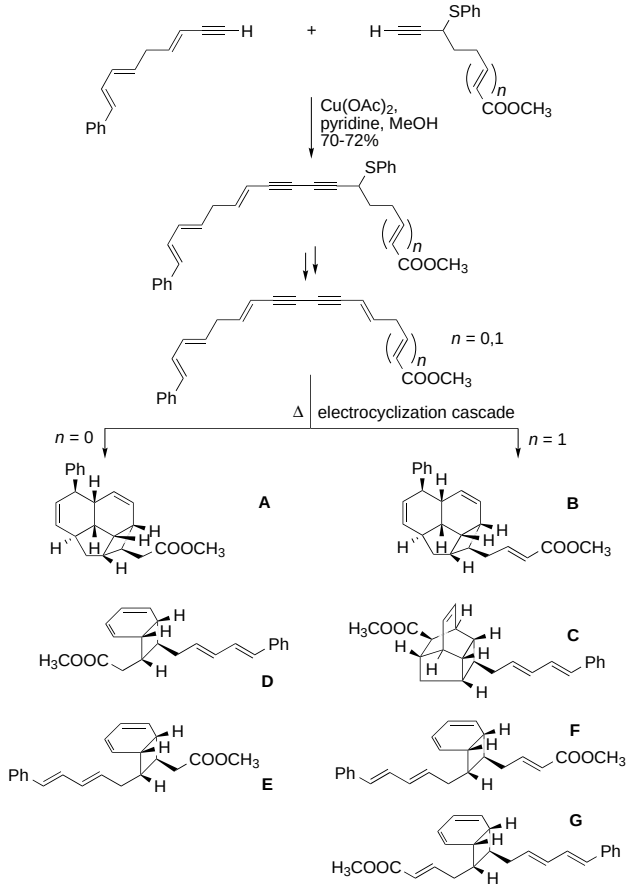
Scheme 36. Synthesis of the macrocyclic enetetrayne **41**.[185] dba = dibenzylideneacetone, THP = tetrahydro-2*H*-pyran.

derivatives **42a** and **42b** (Scheme 37),[186] which are potent inhibitors of squalene epoxidase, a key enzyme in cholesterol biosynthesis and an attractive target in cholesterol-lowering therapy.[187]



Scheme 37. Synthesis of inhibitors of squalene epoxidase.[186]

Another fine example of the use of acetylenic couplings in the preparation of natural products can be found in the synthesis of the endriandric acids, which are isolated from leaves of the Australian plant *Endiandra introrsa*. In a stereocontrolled synthesis starting from buta-1,3-diynes, Nicolaou et al. showed that the biogenesis of the endiandric acids proceeds from achiral precursors by a series of nonenzymatic electrocyclizations (Scheme 38).[188] Such a mechanism had been proposed previously by Black and co-workers.[189]

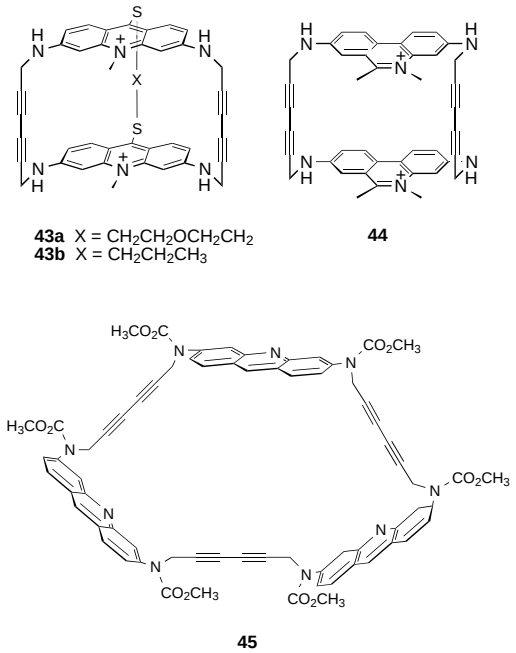


Scheme 38. Synthesis of acetylenic precursors, from which the methyl esters of endriandic acids A–G can be prepared in one step by electrocyclization cascades.[188]

4.2. Molecular Recognition—The Strategy of the Rigid Group

Synthetic cagelike molecules have received much attention as binding pockets in biomimetic systems.[159, 190] Three-dimensional macrocycles are of particular interest because their binding sites are highly defined, which often translates into enhanced affinity and substrate selectivity. Preorganization of macropolycyclic receptors is conveniently achieved by introducing rigid buta-1,3-diynediyl spacers. Furthermore, these systems can be efficiently assembled, often with remarkable yields, by macrocyclization reactions involving multiple acetylenic couplings. Breslow and co-workers reported the formation of a hydrophobic macrobicyclic receptor containing three buta-1,3-diynediyl spacers by a one-pot triple homocoupling of two ethynyl-substituted 1,1,1-triphenylethane moieties. They obtained the desired cage compound, which forms a solid-state inclusion complex with benzene, in a remarkable 35% yield by conducting the triple cyclization in O_2-free pyridine in the presence of both anhydrous CuCl and $CuCl_2$.[191] Many other groups have taken advantage of the preorganizing effect of buta-1,3-diynediyl spacers and the efficiency of acetylenic coupling for the construction of artificial receptors, and this work has been well reviewed quite recently.[159, 190c] In the subsequent survey we focus on recent examples which highlight the utility and selectivity of the most frequently used coupling methods.

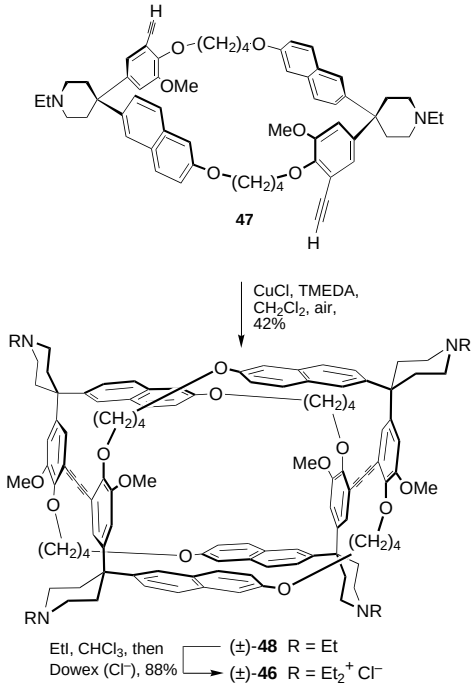
The macrocyclic receptors **43**–**45** (Scheme 39) reported by Lehn and co-workers were synthesized by homocoupling of the corresponding propargyl derivatives, by using the Eglinton method under high dilution (excess $Cu(OAc)_2$, CH_2Cl_2 or acetonitrile, with or without pyridine, under Ar, elevated temperatures).[192, 193] In these systems the buta-1,3-



Scheme 39. Macrocyclic receptors **43**–**45** prepared under Eglinton conditions for the complexation of aromatic substrates by intercalative π–π stacking and for association with nucleic acids by Coulombic and intercalative interactions.[192, 193]

diynediyl bridges serve as rigid spacers that provide cavities for aromatic substrates and nucleotides through intercalative $\pi-\pi$ stacking interactions. Some of these receptors also interact strongly with nucleic acids, presumably by Coulombic interactions with the phosphate backbone, and by intercalation into base-pair stacks.

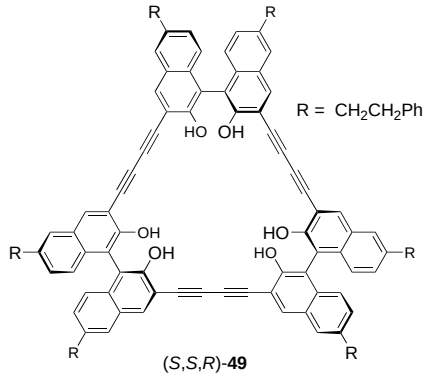
The buta-1,3-diynediyl-linked macrotricyclic receptor (±)-**46** (Scheme 40) was synthesized in our research group with the aim of providing a deep cavity capable of incorporating both the tetracyclic A – D ring system of steroids and parts of the isoprenoidal side chain at C(17).[194a] Recent comprehensive binding studies with a range of steroidal substrates showed that this objective was fully achieved.[194b] Here, the crucial ring closure was achieved by Hay coupling of the diethynylcyclophane **47**, to give (±)-**48** as a single diastereoisomer in a remarkable 42 % yield.



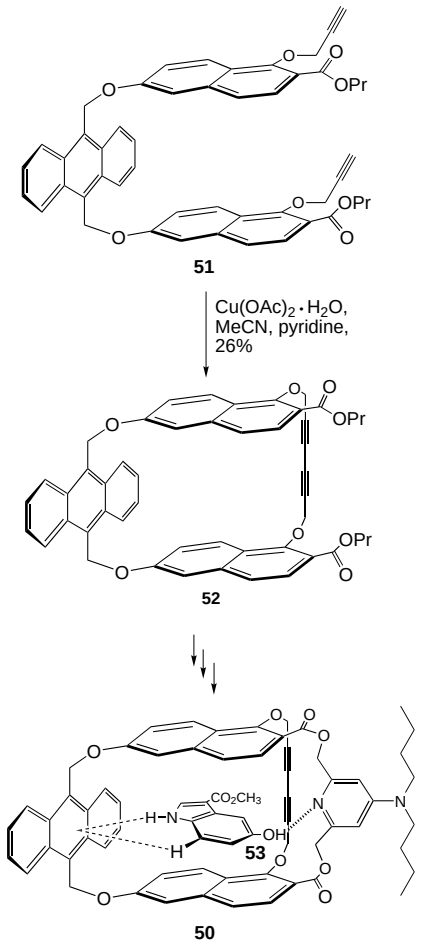
Scheme 40. The Hay coupling of **47** is the key step in the synthesis of the water-soluble steroid receptor (±)-**46**.[194]

Families of trimeric cyclophane receptors, such as (*S*,*S*,*R*)-**49** (Scheme 41) consisting of three butadiyne-bridged optically active 1,1′-binaphthalene units, were also prepared in our group.[195] The macrocyclic scaffolds were constructed using the same Hay conditions as described in Scheme 40. The cavities in these receptors are highly preorganized and (*S*,*S*,*R*)-**49** represents one of the most diastereoselective and enantioselective artificial carbohydrate receptors known. Carbohydrate recognition in these systems occurs in noncompetitive solvents by the guest hydrogen bonding to the convergent array of hydroxyl groups lining the interior of the receptor.

Whitlock and co-workers were the first to take advantage of acetylenic coupling in the construction of preorganized macrocyclic receptors.[190c] An elegant recent development from this group is shown in Scheme 42.[196] In the synthesis of



Scheme 41. The highly diastereo- and enantioselective carbohydrate receptor (*S*,*S*,*R*)-**49** was constructed under Hay conditions.[195b]



Scheme 42. Oxidative coupling under Eglinton conditions in the synthesis of receptor **50**.[196]

50, bis(propargyl) derivative **51** cyclized to **52** by intramolecular oxidative coupling under Eglinton conditions. Receptor **50** is selective for hydroxyindol **53**, which binds in the macrocyclic cavity by a combination of $\pi-\pi$ stacking, C-H $\cdots$ π(aromatic edge-to-face),[197] and OH $\cdots$ N(pyridine) hydrogen-bonding interactions.

Templates have been most successfully used to favor the formation of macrocyclic products during Glaser couplings. Their ability to control the size of macrocycles formed in oxidative alkyne coupling processes was impressively dem-

onstrated by the work of Sanders, Anderson, and Anderson.[198] McCallien and Sanders observed a dramatic influence of the template on product distribution during oligomerization of the dialkynyl-substituted zinc dioxoporphyrin **54**[199] (Scheme 43). Hay coupling of **54** in the absence of templating agents gave primarily the trimeric and tetrameric macrocycles **55b** and **55c**. The addition of bipyridine resulted in exclusive formation of dimeric **55a**, while the presence of 2,4,6-tri(4-pyridyl)triazine and 5,10,15,20-tetrapyridylporphyrin shifted the product distribution towards trimeric **55b** and tetrameric **55c**, respectively.

Macrocycle **55b** and its analogues with different solubility-providing lateral side chains on the porphyrin ring feature a variety of desirable properties, including the binding of various amine ligands,[200] stereoselective catalysis of an *exo*-selective Diels–Alder reaction,[201] and acceleration of acyl transfer in a supramolecular ternary complex.[202] The strategy of templated oxidative coupling has also been extended to the synthesis of other systems, including a ruthenium derivative of **55b**,[203] and more recently of an unusual asymmetric [2]catenane.[204]

Thus, oxidative acetylenic coupling reactions not only provide a simple and effective strategy to create highly preorganized supramolecular structures, but as well open up promising synthetic pathways towards artificial enzymes capable of recognition and catalysis, which remains one of the key objectives in supramolecular chemistry.

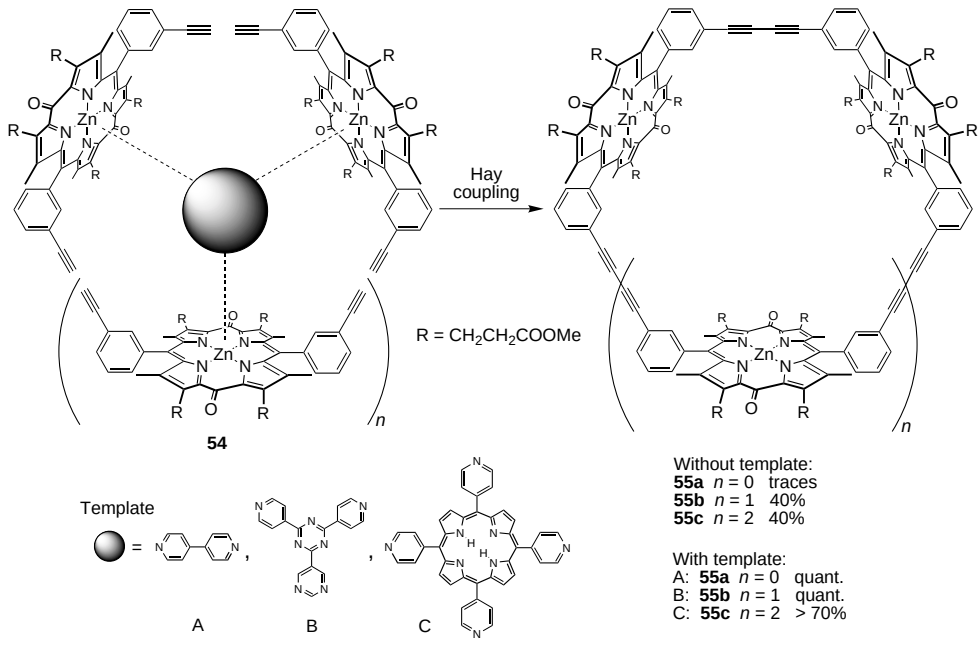
4.3. Synthesis of Linearly π-Conjugated Acetylenic Oligomers and Polymers

The synthesis and properties of conjugated organic oligomers and polymers has been the topic of two recent reviews.[205, 206] Thus, in this section we restrict ourselves to a small excerpt of this rapidly growing field, and describe only a few of the most remarkable results of recent years.

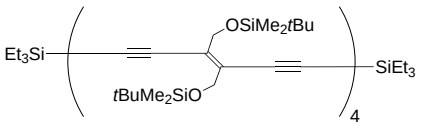
Copper-catalyzed alkyne coupling reactions have proven a potent approach to the preparation of conjugated oligo- and polyacetylenes. The most widely used procedures are oxidative processes, with a clear preference for the Hay method.[207] Controlled polymerization of diethynyl-functionalized monomers to achieve monodisperse oligomers or high molecular weight linear polymers with a well defined, rigid π-conjugated backbone is of significant interest for material scientists, since these systems feature unusual electrooptical properties.[208]

A general synthetic problem in the preparation of monodisperse oligomers and polymers is uncontrolled chain growth during the coupling process, which results in the formation of product mixtures that are difficult to separate, and frequently contain large amounts of insoluble components. Protecting group strategies need to be employed to avoid this problem. This concept was first applied by Walton and co-workers,[209] who used triethylsilyl-protected terminal alkynes in the synthesis of individual polyynes of the type H–(C≡C)$_n$–H with $n = 4-10$ and 12. Both Hay homocouplings[209a] and Cadiot–Chodkiewicz heterocouplings[209b] were successfully applied, in conjunction with protecting group methodology, to the synthesis of these carbyne fragments. Our research group succeeded in the preparation of a series of Et_3Si-endcapped monodisperse poly(triacetylene) (PTA) oligomers containing 4, 8, 12, and 16 monomeric units by a rapid and efficient statistical deprotection-Hay oligomerization sequence starting from an "extended monomer" (Scheme 44). With its 16 C=C double and 32 C≡C triple bonds, and a length of 11.9 nm, hexadecameric PTA **56** is currently the longest linearly fully conjugated molecular wire which does not contain aromatic repeat units.[210]

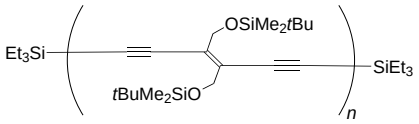
The broad functional group tolerance of oxidative alkyne dimerizations allows great flexibility in the choice of the acetylenic building blocks and easy access to multinanometer-sized structures with electron-donating and -accepting groups that have interesting nonlinear optical properties.[211] Lehn and co-workers reported the formation of reversibly reducible multinanometer-sized molecular rods consisting of poly(phenylthio)-benzene subunits linked by diacetylene bridges.[212] Their synthesis proceeded under either Eglinton or Hay coupling conditions. Wilson and Anderson used the Hay coupling method to synthesize the conjugated tetrapyridylporphyrin dimer **57**, which is capable of binding to two other metalloporphyrin dimers to generate a triple-strand array (Scheme 45).[213] Compound **57** could find interesting appli-



Scheme 43. Dramatic effects of templates on macrocyclic ring size.[199]

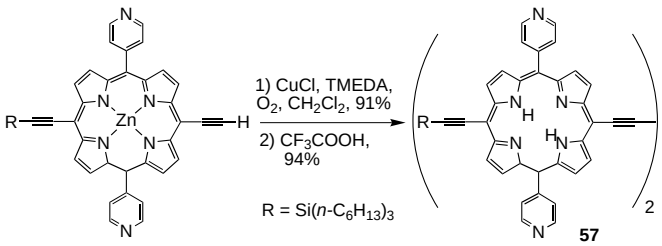


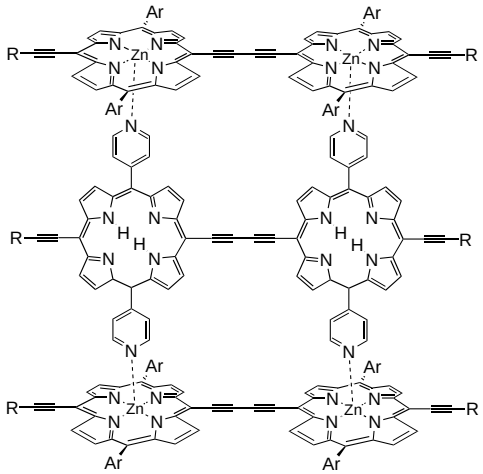
1) NaOH, THF/MeOH 1:1, 20 °C, 20 min
2) CuCl, TMEDA, toluene, molecular sieves (4Å), dry O_2 atmosphere, 2 h, reflux, 1 h



	n	yield
	4	50%
	8	20%
	12	10%
56	16	5%

Scheme 44. Synthesis of PTA oligomers by a statistical deprotection and Hay oligomerization sequence starting from an "extended monomer."[210]

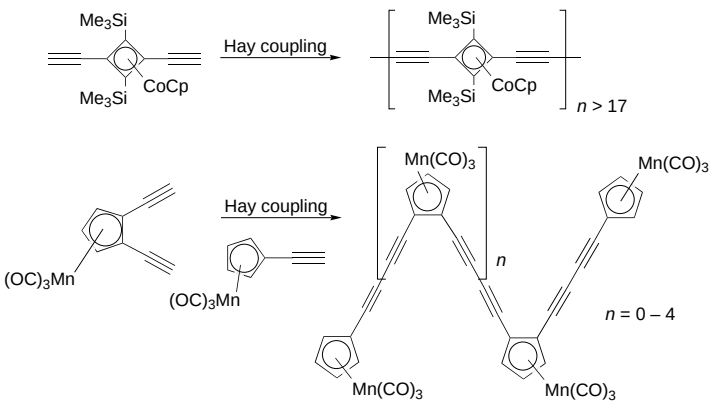




Scheme 45. A conjugated tetrapyridylporphyrin dimer for the self-assembly of a triple strand.[213]

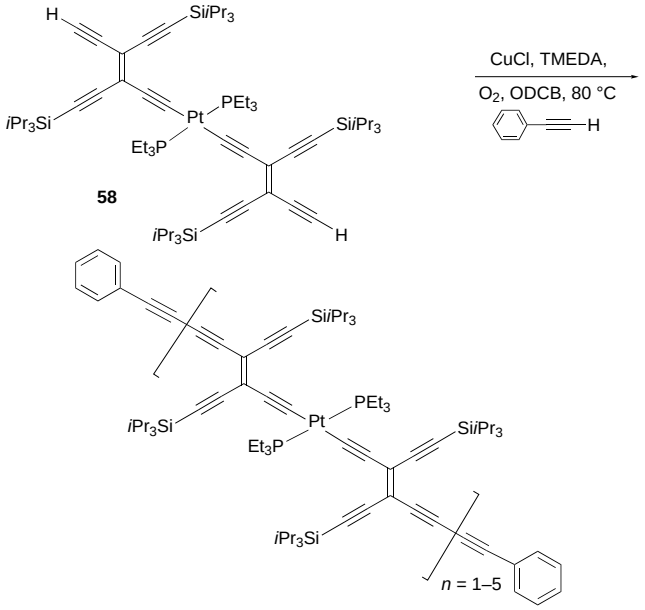
cation for templating diverse oxidative alkyne coupling processes.

Terminal alkynes in organotransition metal complexes also undergo copper-catalyzed couplings.[59, 214] Bunz has employed Hay conditions to prepare molecular rods incorporating cyclobutadiene and cyclopentadienyl–π complexes that have a variety of interesting material properties (Scheme 46).[215, 216]



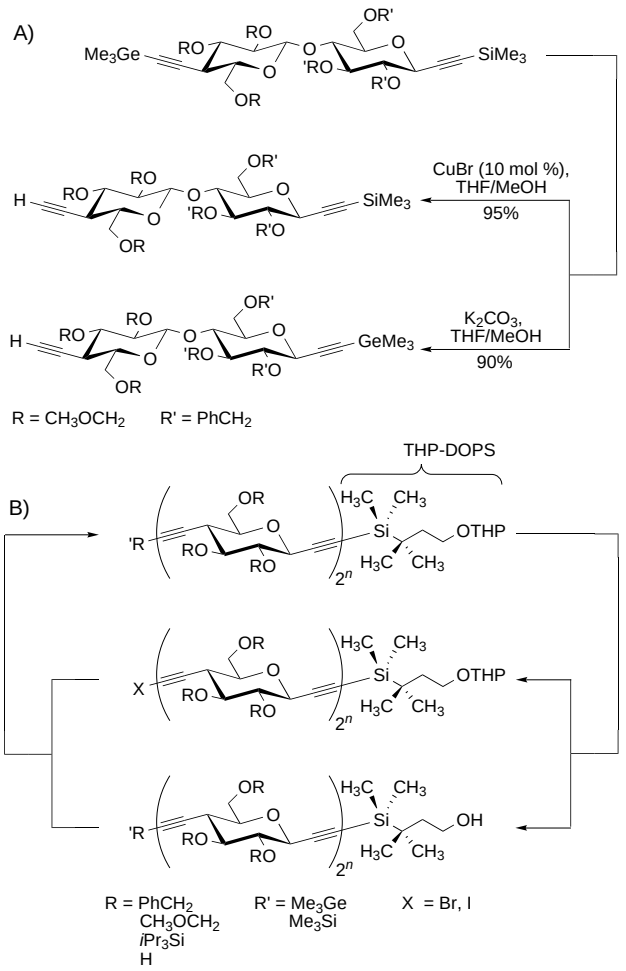
Scheme 46. Organometallic carbon chains assembled by oxidative alkyne coupling.[214–216]

By using transition metals directly as bridging units, we prepared platinum-σ-bis(acetylide) complexes of tetraethynylethenes.[217] They are potent building blocks for longer monodisperse oligomers as a result of their remarkable stability and amazing solubility. Controlled coupling of the bis-deprotected complex **58** under Hay conditions in the presence of phenylacetylene as an end-capping reagent provided oligomers up to the pentamer with a length of 10 nm (Scheme 47).[218]



Scheme 47. Oligomers with a platinum–tetraethynylethene hybrid backbone.[218] ODCB = *o*-dichlorobenzene.

A milestone in the application of copper-catalyzed acetylenic heterocouplings in oligomer preparation is the binomial synthesis of acetylenic oligosaccharides developed by Vasella and co-workers.[219] The synthetic concept consists of consecutive cycles of orthogonal dialkyne deprotection, followed by cross-coupling of the subsequently created haloalkynes with the corresponding terminal alkynes (Scheme 48A and 48B). Two useful sets of orthogonal protecting groups for diacetylenes were introduced in this work by using combinations of



Scheme 48. Two sets of orthogonal alkyne protecting groups and application to the binomial synthesis of acetylenic saccharides .[219]

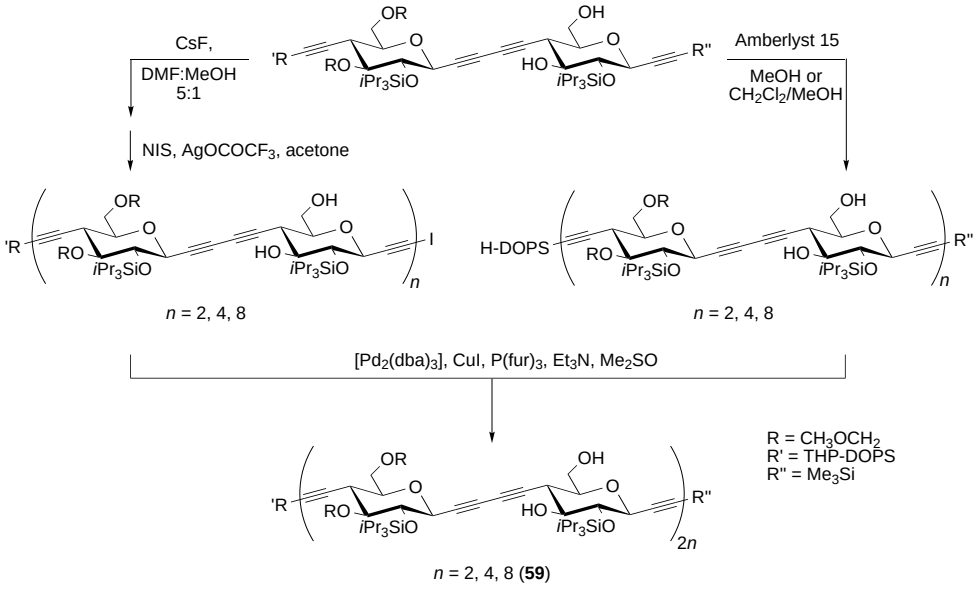
independently removable protective groups, namely Me_3Si with either [dimethyl(oxy)propyl]dimethylsilyl (DOPS)[219b,c] or Me_3Ge groups.[219d]

Quite recently, Vasella and co-workers succeeded in the binomial synthesis of a hexadecameric acetylenic saccharide (**59**), which allowed the evaluation of the structural role of intramolecular hydrogen bonds in cellulose (Scheme 49).[220] Compound **59** shows no sign of aggregation in Me_2SO since the diacetylene bridges, a previously established motif in synthetic saccharides,[221] prevent the formation of specific intramolecular interresidue hydrogen bonds. In contrast, such hydrogen bonds are present in cellulose and are responsible for the aggregation of the natural polysaccharide. This impressive example of controlled oligomerization underlines the important role of alkyne coupling reactions in modern oligomer synthesis.

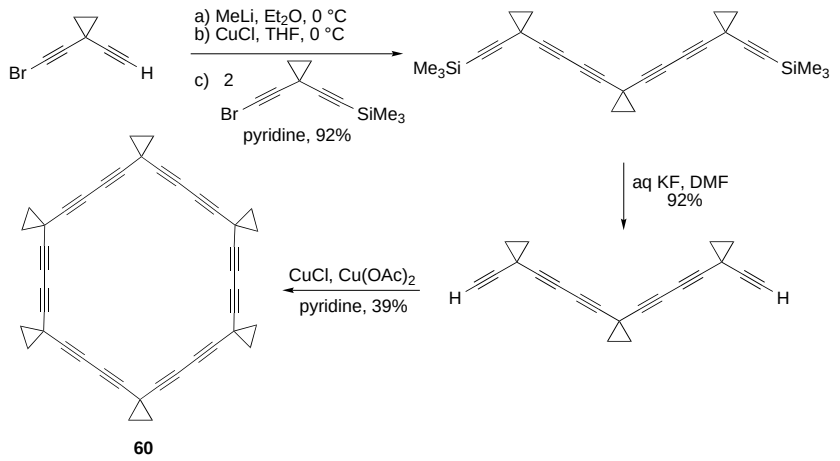
4.4. Cyclic Oligoacetylenes—Towards New Carbon Allotropes

Macrocyclic acetylenic rings have attracted considerable interest in the past. Dehydroannulenes,[34, 52b, 56, 222] and "exploded cycloalkanes" in which −C≡C− ([*n*]pericyclynes) or −C≡C−C≡C− fragments are inserted between each pair of adjacent sp^3-hybridized C atoms in *n*-membered cycloalkanes ($n = 3-6$),[52a, 223] were among the first macrocycles incorporating conjugated oligoacetylene fragments. Our contemporary knowledge of cyclic π-electron conjugation and various forms of aromaticity have been greatly influenced by fundamental studies of these compounds. The Eglinton protocol has been applied most frequently for the synthesis of cyclic oligoacetylenes, although Hay couplings are increasingly used. The size distribution of the cyclic oligomers obtained by the Eglinton or Hay coupling can vary significantly,[224a, 216b] and it is advisable to try both methods to determine which works the best for a given application. More recently, carbon-rich oligoacetylenic rings have attracted particular attention as advanced materials with interesting optoelectronic properties and as precursors to new molecular carbon allotropes. The fascinating perspectives of this research, which relies heavily on acetylenic coupling methodology, has been the subject of several reviews.[224, 225] Therefore, only a few examples of the spectacular molecular architecture generated in this field will be presented here.

In 1995, de Meijere, Scott, and co-workers reported an efficient synthesis of [*n*]rotanes, perspirocyclopropanated macrocyclic oligodiacetylenes that explode violently when struck in the solid state.[226] The synthesis of the hexameric derivative **60**, which in the solid state prefers a chair conformation, is shown in Scheme 50. The macrocyclization



Scheme 49. Binomial synthesis of a hexadecameric acetylenic saccharide.[220]

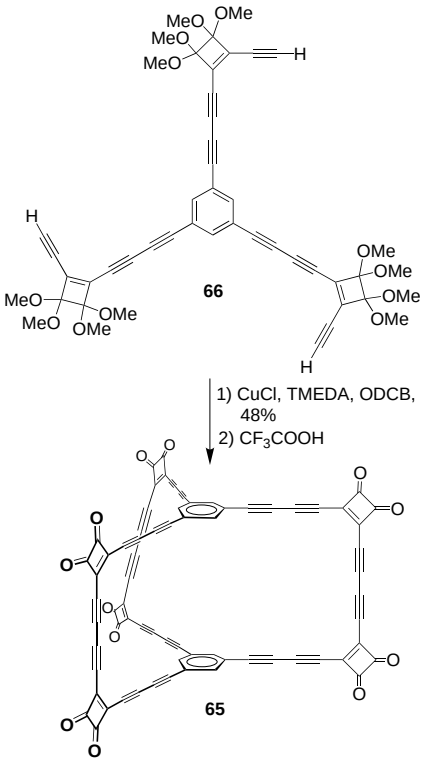


Scheme 50. Synthesis of [6]rotane **60**, a hexameric perspirocyclopropanated macrocyclic diacetylene.[226]

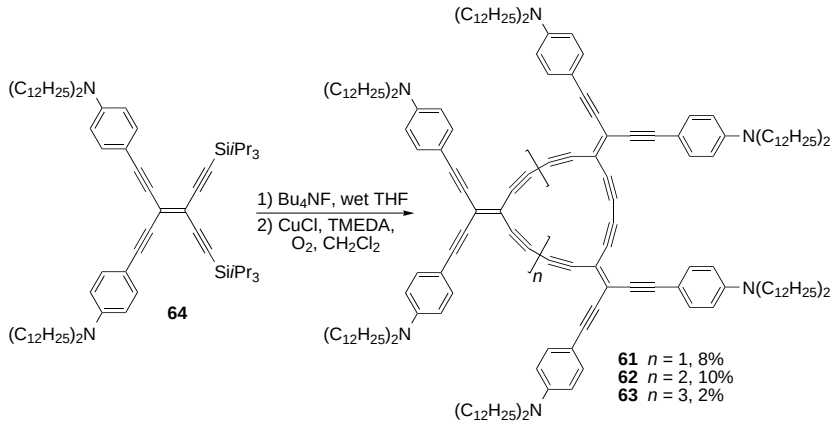
to **60** was performed under Eglinton conditions whereas the precursor alkynes were prepared through repetitive Cadiot–Chodkiewicz coupling.

A great variety of two- and three-dimensional perethynylated all-carbon chromophores have been developed during the past 15 years and are currently being investigated as precursors to all-carbon networks.[224a] Among the largest all-carbon surfaces known are the perethynylated expanded radialenes,[227] which can be conveniently functionalized at the periphery for optimization of their advanced materials properties. Thus *N*,*N*-bis(dodecyl)aniline-functionalized expanded radialenes with all-carbon cores of 30 (**61**), 40 (**62**), and 50 (**63**) C atoms, all featuring unusual electronic properties, were prepared by Hay coupling of the geminally bis-deprotected tetraethynylethene derivative **64** (Scheme 51).[228] The chromophoric properties of these and other related systems[227–229] revealed a poorly developed understanding of macrocyclic cross-conjugation.

On the way to pure molecular carbon allotropes, Diederich, Rubin, and co-workers developed a rational "precursor-approach" to the cyclo[*n*]carbons (cyclo-C_n), which are *n*-membered monocyclic rings of sp-hybridized C atoms with unique electronic structures resulting from two perpendicular systems of conjugated π orbitals. All the macrocyclic precursors to cyclo-C_{18}, cyclo-C_{24}, and cyclo-C_{30} were prepared by oxidative acetylenic coupling, and this work has been extensively reviewed.[224] Subsequent Fourier transform mass spectrometry investigations revealed that the coalescence of these cyclocarbons in ion-molecule reactions could be one pathway to the formation of fullerenes.[230] More direct "precursor-approaches" to the synthesis of buckminsterfullerene (C_{60}) and heterofullerenes were undertaken by the groups of Rubin[231] and Tobe.[232] Rubin et al. prepared macrobicyclic **65** [$C_{60}H_6(CO)_{12}$] by the high-yielding (48% yield) triple Hay coupling of **66** followed by acetal deprotection (Scheme 52). Laser desorption mass spectrometric experiments subsequently showed that the radical anion **65**$^{\bullet-}$ loses its twelve CO residues as well as the six H atoms and rearranges into the buckminsterfullerene anion $C_{60}^{\bullet-}$.



Scheme 52. High-yielding Hay coupling in the synthesis of macrobicyclic **65**, which generates C_{60} ions in mass spectrometric experiments.[231]



Scheme 51. Synthesis of perethynylated expanded radialenes.[228]

A similar "precursor-approach" was described by Tobe et al. who provided mass spectrometric evidence for formation of both $C_{60}^{\bullet-}$ [232a] and the diaza-analogue $C_{58}N_2^{\bullet-}$ [232b] in the gas phase. In these cases, precursors with the same macrobicyclic skeleton as in **65** (the dipyridine analogue was used to generate the diazafullerene) were prepared in

lower yield by Eglinton coupling, which again confirms that it cannot be predicted in advance which oxidative coupling protocol will be the highest yielding one.

These examples readily illustrate the rich variety of molecular construction based on acetylenic coupling that is currently ongoing in synthetic carbon research. A great variety of fullerene – acetylene hybrid systems, in which methanofullerenes are linked by buta-1,3-diynediyl fragments to generate linear and cyclic arrays, have been prepared.[233] Dehydrobenzoannulenes[52b] have attracted additional interest since the recent finding that they can be used for as precursors for carbon nanotubes.[234] Templates will increasingly be used in acetylenic scaffolding[198] to simplify product-purification protocols by avoiding the formation of oligomeric mixtures.[235] Clearly, many of the major research avenues in contemporary organic chemistry rely on acetylenic coupling methodology.

5. Conclusion and Outlook

The rigidity and cylindrical symmetry of oligoalkynes make them valuable as spatially and directionally well-defined structural units in diverse areas of organic chemistry, ranging from the synthesis of natural products and pharmaceuticals, to supramolecular construction, to carbon-rich and all-carbon scaffolding and networking. The applications illustrated above clearly demonstrate the versatility and high functional group tolerance which make alkyne couplings an attractive approach to the construction of complex systems. However, equally clear is that the full potential of this methodology has yet to be realized, and that more general and reliable conditions will be required to meet future synthetic challenges. The optimal conditions for the copper catalyst systems have typically been determined empirically. There is little information and virtually no predictability regarding the control of chain length and the formation of cyclic versus linear products for the oligomerization of terminal diynes. Heterocouplings are frequently complicated by poor reactivity in the case of alkynyl chlorides and by halogen – metal exchange for more reactive substrates. One key to resolving these issues may lie in an improved mechanistic understanding of these processes. Thus, alkyne couplings provide both valuable tools for synthesis as well as ample opportunities for further mechanistic and methodological work.

We thank the ETH research council for generous support of this work and Dr. E. Zass for help with the literature searches.

Received: January 20, 2000 [A 387]

[1] a) C. Glaser, *Ber. Dtsch. Chem. Ges.* **1869**, *2*, 422 – 424; b) C. Glaser, *Ann. Chem. Pharm.* **1870**, *154*, 137 – 171.

[2] a) A. Baeyer, *Ber. Dtsch. Chem. Ges.* **1882**, *15*, 50 – 56; b) Baeyer also used this oxidizing agent for the preparation of diphenyldiacetylene and its derivatives: A. Baeyer, L. Landsberg, *Ber. Dtsch. Chem. Ges.* **1882**, *15*, 57 – 61.

[3] a) A. Baeyer, *Ber. Dtsch. Chem. Ges.* **1885**, *18*, 674 – 681 (Baeyer came to the following remarkable conclusion: ".. Man sieht hieraus, dass es aller Wahrscheinlichkeit gelingen wird, noch längere Ketten von Kohlenstoffatomen aufzubauen.. Im günstigen Fall stehen jedenfalls interessante Resultate zu erwarten, da eine derartige Anhäufung von reinen Kohlenstoffatomen aller Wahrscheinlichkeit nach zu neuen Aufschlüssen über die Natur des freien Kohlenstoffs führen dürfte.."("From this one sees that the successful construction of even longer carbon chains is very likely …Even in the simplest cases interesting results can be expected, as such an accumulation of carbon atoms should lead to new insights into the nature of free carbon atoms")); b) A. Baeyer, *Ber. Dtsch. Chem. Ges.* **1885**, *18*, 2269 – 2281.

[4] M. D. Cameron, G. E. Benett, *J. Org. Chem.* **1957**, *22*, 557 – 558.

[5] F. J. Brockmann, *Can. J. Chem.* **1955**, *33*, 507 – 510.

[6] The use of copper(II) salts as oxidizing agents was first published in 1897: a) A. A. Noyes, C. W. Tucker, *Am. Chem. J.* **1897**, *19*, 123 – 128; b) see also: A. A. Noyes, C. W. Tucker, *Chem. Zentralbl.* **1897**, *68*, 582 – 583.

[7] F. Straus, L. Kollek, *Ber. Dtsch. Chem. Ges.* **1926**, *59*, 1664 – 1681.

[8] a) M. Nakagawa, *Proc. Jpn. Acad.* **1950**, *26*, 38 – 42; b) M. Nakagawa, *Proc. Jpn. Acad.* **1950**, *26*, 43 – 47.

[9] M. Nakagawa, *J. Chem. Soc. Jpn.* **1951**, *72*, 561 – 566.

[10] A. Vaitiekunas, F. F. Nord, *J. Am. Chem. Soc.* **1954**, *76*, 2733 – 2736.

[11] Y. Odaira, *Bull. Chem. Soc. Jpn.* **1956**, *29*, 470 – 471.

[12] H. H. Schlubach, V. Wolf, *Justus Liebigs Ann. Chem.* **1950**, *568*, 141 – 159.

[13] N. A. Milas, O. L. Mageli, *J. Am. Chem. Soc.* **1953**, *75*, 5970 – 5971.

[14] L. Camici, P. Dembech, A. Ricci, G. Seconi, M. Taddei, *Tetrahedron* **1988**, *44*, 4197 – 4206.

[15] F. Straus, *Justus Liebigs Ann. Chem.* **1905**, *342*, 190 – 265.

[16] a) M. Akhtar, B. C. L. Weedon, *Proc. Chem. Soc.* **1958**, 303; b) M. Akhtar, T. A. Richards, B. C. L. Weedon, *J. Chem. Soc.* **1959**, 933 – 940.

[17] N. Balcioglu, I. Uraz, C. Bozkurt, F. Sevin, *Polyhedron* **1997**, *16*, 327 – 334.

[18] a) J. A. Nieuwland, W. S. Calcott, F. B. Downing, A. S. Carter, *J. Am. Chem. Soc.* **1931**, *53*, 4197 – 4203.

[19] a) M. Rusek, V. Simame, V. Soukenik, *Czech. Pat.* 105, **1962**, 823 – 826; b) see also *Chem. Abstr.* **1964**, 60, 2751.

[20] For a recent publication on the preparation and oxidative coupling of alkynylcopper derivatives, see G. W. Ebert, R. D. Rieke, *J. Org. Chem.* **1988**, *53*, 4482 – 4488.

[21] a) Y. S. Zalkind, M. A. Aizikovich, *J. Gen. Chem. USSR* **1937**, *7*, 227 – 233; b) see also Y. S. Zalkind, M. A. Aizikovich, *Chem. Zentralbl.* **1937**, *108*, 4783.

[22] Y. S. Zalkind, I. M. Gverdtsiteli, *J. Gen. Chem. USSR* **1939**, *9*, 971 – 974.

[23] W. Reppe, *Justus Liebigs Ann. Chem.* **1955**, *596*, 1 – 224.

[24] a) K. Bowden, I. Heilbron, E. R. H. Jones, K. H. Sargent, *J. Chem. Soc.* **1947**, 1579 – 1583; b) I. Heilbron, E. R. H. Jones, F. Sondheimer, *J. Chem. Soc.* **1947**, 1586 – 1590.

[25] J. B. Armitage, C. L. Cook, N. Entwistle, E. R. H. Jones, M. C. Whiting, *J. Chem. Soc.* **1952**, 1998 – 2005.

[26] J. B. Armitage, C. L. Cook, E. R. H. Jones, M. C. Whiting, *J. Chem. Soc.* **1952**, 2010 – 2014.

[27] A. S. Hay, H. S. Blanchard, G. F. Endres, J. W. Eustance, *J. Am. Chem. Soc.* **1959**, *81*, 6335 – 6336.

[28] A. S. Hay, *J. Org. Chem.* **1960**, *25*, 1275 – 1276.

[29] R. A. Raphael, *Proc. Chem. Soc.* **1962**, 97 – 105.

[30] I. D. Campbell, G. Eglinton, *Organic Syntheses Collective Volume 5*, Wiley, New York, **1973**, pp. 517 – 520.

[31] F. Bohlmann in *Chemistry of Acetylenes* (Ed.: H. G. Viehe), Dekker, New York, **1969**, chap. 14, pp. 977 – 986.

[32] G. Eglinton, A. R. Galbraith, *Chem. Ind. (London)* **1956**, 737 – 738.

[33] A. Krebs in *Chemistry of Acetylenes* (Ed.: H. G. Viehe), Dekker, New York, **1969**, chap. 15, pp. 987 – 1062.

[34] a) Review article: F. Sondheimer, *Pure Appl. Chem.* **1963**, *7*, 363 – 388; b) F. Sondheimer, R. Wolovsky, *J. Am. Chem. Soc.* **1959**, *81*, 1771; c) F. Sondheimer, R. Wolovsky, Y. Amiel, *J. Am. Chem. Soc.* **1962**, *84*, 274 – 284.

[35] A. S. Hay, *J. Org. Chem.* **1962**,*27*, 3320 – 3321.

[36] a) W. Chodkiewicz, P. Cadiot, *C. R. Hebd. Seances Acad. Sci.* **1955**, *241*, 1055 – 1057; b) W. Chodkiewicz, *Ann. Chim. (Paris)* **1957**, *2*, 819 – 869.

[37] G. Eglinton, W. McCrae, *Adv. Org. Chem.* **1963**, *4*, 225 – 328.

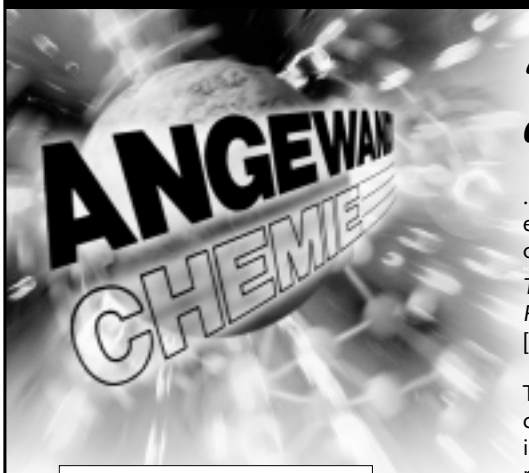
[38] T. F. Rutledge, *Acetylenic Compounds*, Reinhold, New York, **1968**, chap. 6, pp. 245 – 268.
[39] P. Cadiot, W. Chodkiewicz in *Chemistry of Acetylenes* (Ed.: H. G. Viehe), Dekker, New York, **1969**, chap. 9, pp. 597 – 647.
[40] W. G. Nigh in *Organic Chemistry*, *Vol. 5: Oxidation in Organic Chemistry*, *Part B* (Ed.: W. S. Trahanovsky), Academic Press, New York, **1973**, pp. 11 – 31.
[41] U. Niedballa, *Methoden Org. Chem. (Houben-Weyl)*, *Vol. 5/2a*, **1977**, pp. 925 – 937.
[42] L. I. Simàndi in *The Chemistry of Functional Groups Supplement C: The Chemistry of Triple-bonded Functional Groups* (Eds.: P. Patai, Z. Rappoport), Wiley, New York, **1983**, chap. 13, pp. 529 – 534.
[43] L. Brandsma, *Preparative Acetylenic Chemistry*, Elsevier, Amsterdam, **1988**, chap. 10, pp. 219 – 227.
[44] K. Sonogashira in *Comprehensive Organic Synthesis*, *Vol. 3* (Eds.: B. M. Trost, I. Fleming), Pergamon, Oxford, **1991**, pp. 551 – 561.
[45] S. F. Vasilevsky, H. D. Verkruijsse, L. Brandsma, *Recl. Trav. Chim. Pays-Bas* **1992**, *111*, 529 – 530.
[46] E. Valenti, M. A. Pericas, F. Serratosa, *J. Am. Chem. Soc.* **1990**, *112*, 7405 – 7406.
[47] U. Fritzsche, S. Hünig, *Tetrahedron Lett.* **1972**, 4831 – 4834.
[48] K. E. Knol, L. W. van Horssen, G. Challa, E. E. Havinga, *Polym. Commun.* **1985**, *26*, 71 – 73.
[49] S. Takahashi, E. Murata, K. Sonogashira, N. Hagihara, *J. Polym. Sci. Polym. Chem. Ed.* **1980**, *18*, 661 – 669.
[50] K. Ikegashira, Y. Nishihara, K. Hirabayashi, A. Mori, T. Hiyama, *Chem. Commun.* **1997**, 1039 – 1040.
[51] Y. Nishihara, K. Ikegashira, A. Mori, T. Hiyama, *Tetrahedron Lett.* **1998**, *39*, 4075 – 4078.
[52] For recent reviews on macrocyclic oligoacetylenes, see a) A. de Meijere, S. I. Kozhushkov, *Top. Curr. Chem.* **1999**, *201*, 1 – 42; b) M. M. Haley, J. J. Pak, S. C. Brand, *Top. Curr. Chem.* **1999**, *201*, 81 – 130.
[53] Y. Yto, M. Inouye, M. Murakami, *Chem. Lett.* **1989**, 1261 – 1264.
[54] For a noteworthy application of the Eglinton method in the construction of linear systems, see a) Y. Zhou, J. W. Seyler, W. Weng, A. M. Arif, J. A. Gladysz, *J. Am. Chem. Soc.* **1993**, *115*, 8509 – 8510; b) M. Brady, W. Weng, J. A. Gladysz, *J. Chem. Soc. Chem. Commun.* **1994**, 2655 – 2656; c) T. Bartik, B. Bartik, M. Brady, R. Dembinsky, J. A. Gladysz, *Angew. Chem.* **1996**, *108*, 467 – 469; *Angew. Chem. Int. Ed. Engl.* **1996**, *35*, 414 – 417; d) B. Bartik, R. Dembinski, T. Bartik, A. M. Arif, J. A. Gladysz, *New J. Chem.* **1997**, *21*, 739 – 750.
[55] G. Eglinton, A. R. Galbraith, *J. Chem. Soc.* **1959**, 889 – 896.
[56] a) U. E. Meissner, B. Meissner, H. A. Staab, *Angew. Chem.* **1973**, *85*, 957 – 958; *Angew. Chem. Int. Ed. Engl.* **1973**, *12*, 916 – 918; b) H. A. Staab, U. E. Meissner, B. Meissner, *Chem. Ber.* **1976**, *109*, 3875 – 3885; c) H. A. Staab, U. E. Meissner, W. Weinacht, A. Gensler, *Chem. Ber.* **1979**, *112*, 3895 – 3906.
[57] R. Berscheid, F. Vögtle, *Synthesis* **1992**, 58 – 62.
[58] a) J. J. Pak, T. J. R. Weakly, M. M. Haley, *J. Am. Chem. Soc.* **1999**, *121*, 8182 – 8192; b) M. M. Haley, M. L. Bell, J. C. Brand, D. B. Kimball, J. J. Pak, W. B. Wan, *Tetrahedron Lett.* **1997**, *38*, 7483 – 7486.
[59] J. Li, H. Jiang, *Chem. Commun.* **1999**, 2369 – 2370.
[60] F. Toda, Y. Tokumaru, *Chem. Lett.* **1990**, 987 – 990.
[61] S. M. Auer, M. Schneider, A. Baiker, *J. Chem. Soc. Chem. Commun.* **1995**, 2057 – 2058.
[62] In some cases, the yield of unsymmetrical product in Glaser-type couplings can be increased by using a large excess of one coupling component.[41] See for example end-capping oligomerizations under Hay conditions: A. M. Boldi, J. Anthony, V. Gramlich, C. B. Knobler, C. Boudon, J. P. Gisselbrecht, M. Gross, F. Diederich, *Helv. Chim. Acta* **1995**, *78*, 779 – 796.
[63] a) K. Naemura, Y. Hokura, M. Nakazaki, *Tetrahedron* **1986**, *42*, 1763 – 1768; b) T. Ogawa, M. Sotelo, G. Burillo, C. S. Marvel, *J. Polym. Sci. Part C* **1989**, *27*, 167 – 172.
[64] a) E. Barbu, J. Tsibouklis, *Tetrahedron Lett.* **1996**, *37*, 5023 – 5026; b) S. Okada, H. Matsuda, M. Otsuka, N. Kikuchi, K. Hayamizu, H. Nakanishi, M. Kato, *Bull. Chem. Soc. Jpn.* **1994**, *67*, 455 – 461.
[65] A. P. Yuvchenko, K. L. Moiseichuk, E. A. Dikusar, *J. Org. Chem. USSR* **1989**, *25*, 1045 – 1048.
[66] J. C. Cognacq, W. Chodkiewicz, *Bull. Soc. Chim. Fr.* **1966**, 1999 – 2005.
[67] a) D. Grandjean, P. Pale, J. Chuche, *Tetrahedron Lett.* **1992**, *33*, 5355 – 5358; b) D. Grandjean, P. Pale, J. Chuche, *Tetrahedron* **1993**, *49*, 5225 – 5236.
[68] a) S. Ohba, J. F. J. Engbersen, *Tetrahedron* **1991**, *47*, 9947 – 9952; b) R. Rodriguez-Abad, J. Tsibouklis, *Synth. Commun.* **1998**, *28*, 4333 – 4338.
[69] F. Bohlmann, R. Weber, *Chem. Ber.* **1972**, *105*, 3036 – 3040.
[70] a) B. Tieke, G. Lieser, G. Wegner, *J. Polym. Sci. Polym. Chem. Ed.* **1979**, *17*, 1631 – 1644; b) D. Villemin, P. Cadiot, M. Kuétegan, *Synthesis* **1983**, 230 – 231.
[71] a) A. G. Fallis, M. T. W. Hearn, E. R. H. Jones, V. Thaller, J. L. Turner, *J. Chem. Soc.* **1973**, 743 – 749; b) M. Rösner, G. Köbrich, *Angew. Chem.* **1975**, *87*, 715 – 717; *Angew. Chem. Int. Ed. Engl.* **1975**, *14*, 708 – 709.
[72] a) M. Ahmed, M. Y. Jarrah, E. R. H. Jones, A. F. Magalhães, M. G. Roberts, V. Thaller, *J. Chem. Res. Synop.* **1981**, 262 – 263; b) L. Crombie, A. J. W. Hobbs, M. A. Horsham, R. J. Blade, *Tetrahedron Lett.* **1987**, *28*, 4875 – 4878; c) L. Fomina, A. Vega, S. Fomine, R. Gaviño, T. Ogawa, *Macromol. Chem. Phys.* **1996**, *197*, 2653 – 2663.
[73] M. D. Mowery, C. E. Evans, *Tetrahedron Lett.* **1997**, *38*, 11 – 14.
[74] L. Blanco, H. E. Helson, M. Hirthammer, H. Mestdagh, S. Spyroudis, K. P. C. Vollhardt, *Angew. Chem.* **1987**, *99*, 1276 – 1277; *Angew. Chem. Int. Ed. Engl.* **1987**, *26*, 1246 – 1247.
[75] a) D. W. Wiley, J. C. Calabrese, R. L. Harlow, J. S. Miller, *Angew. Chem.* **1991**, *103*, 459 – 460; *Angew. Chem. Int. Ed. Engl.* **1991**, *30*, 450 – 452; b) G. P. Hamill, E. A. Yost, D. J. Sandman, *Mol. Cryst. Liq. Cryst.* **1992**, *211*, 339 – 345.
[76] A combination of the Cadiot – Chodkiewicz reaction with the Stille coupling provides a versatile protocol for the synthesis of unsymmetrical diarylbuta-1,3-diynes: A. Godt, *J. Org. Chem.* **1997**, *62*, 7471 – 7474.
[77] N. E. Porter, D. R. Magnin, B. T. Wright, *J. Am. Chem. Soc.* **1986**, *108*, 2787 – 2788.
[78] A. Singh, J. M. Schnur, *Synth. Commun.* **1986**, *16*, 847 – 852.
[79] J. Tsibouklis, C. Pearson, Y.-P. Song, J. Warren, M. Petty, J. Yarwood, M. C. Petty, W. J. Feast, *J. Mater. Chem.* **1993**, *3*, 97 – 104.
[80] R. F. Curtis, J. A. Taylor, *J. Chem. Soc. C* **1971**, 186 – 188.
[81] C. Hartbaum, H. Fischer, *Chem. Ber.* **1997**, *130*, 1063 – 1067.
[82] J. M. Montierth, D. R. DeMario, M. J. Kurth, N. E. Schore, *Tetrahedron* **1998**, *54*, 11741 – 11748.
[83] M. Alami, F. Ferri, *Tetrahedron Lett.* **1996**, *37*, 2763 – 2766.
[84] T. Kitamura, T. Tanaka, H. Taniguchi, P. J. Stang, *J. Chem. Soc. Perkin Trans. 1* **1991**, 2892 – 2893.
[85] V. Grignard, H. Perrichon, *Ann. Chim. (Paris)* **1926**, *5*, 5 – 36.
[86] H. H. Schlubach, V. Franzen, *Liebigs Ann. Chem.* **1951**, *573*, 115 – 120.
[87] J. B. Armitage, E. R. H. Jones, M. C. Whiting, *J. Chem. Soc.* **1952**, 2014 – 2018.
[88] H. H. Schlubach, V. Franzen, *Liebigs Ann. Chem.* **1951**, *572*, 116 – 121.
[89] H. K. Black, D. H. S. Horn, B. C. L. Weedon, *J. Chem. Soc.* **1954**, 1704 – 1709.
[90] J. B. Armitage, E. Entwistle, E. R. H. Jones, M. C. Whiting, *J. Chem. Soc.* **1954**, 147 – 154.
[91] J. I. Iotsitch, B. I. Orielkine, *Bull. Soc. Chim. Fr.* **1911**, *10*, 647.
[92] Y.-K. Liu, R.-T. Wang, F.-L. Chou, F.-T. Luo, *Bull. Inst. Chem. Acad. Sin.* **1990**, *37*, 43 – 48.
[93] Y. Ito, M. Inouye, M. Murakami, *Tetrahedron Lett.* **1988**, *29*, 5379 – 5382.
[94] U. M. Dzhemilev, A. G. Ibragimov, R. A. Saraev, *Izv. Akad. Nauk SSR Ser. Khim.* **1986**, *2*, 429 – 433.
[95] T. Ishikawa, A. Ogawa, T. Hirao, *Organometallics* **1998**, *17*, 5713 – 5716.
[96] H. G. Viehe, *Chem. Ber.* **1959**, *92*, 3064 – 3075.
[97] S. Oae, Y. Inubushi, M. Yoshihara, *Phosphorus Sulfur* **1995**, *103*, 101 – 110.
[98] a) E. Negishi, T. Takahashi, K. Akiyoshi, *J. Organomet. Chem.* **1987**, *334*, 181 – 194; b) E. Negishi, K. Akiyoshi, T. Takahashi, *J. Chem. Soc. Chem. Commun.* **1987**, 477 – 478.

[99] H. F. Klein, H. Beck-Hemetsberger, L. Reitzel, B. Rodenhäuser, G. Cordier, *Chem. Ber.* **1989**, *122*, 43 – 51.
[100] E. H. Smith, J. Whittall, *Organometallics* **1994**, *13*, 5169 – 5172.
[101] a) A. Pelter, K. Smith, M. Tabata, *J. Chem. Soc. Chem. Commun.* **1975**, 857; b) A. Pelter, R. Hughes, K. Smith, M. Tabata, *Tetrahedron Lett.* **1976**, 4385 – 4388.
[102] J. A. Sinclair, H. C. Brown, *J. Org. Chem.* **1976**, *41*, 1078 – 1079.
[103] S. Ghosal, G. P. Luke, K. S. Kyler, *J. Org. Chem.* **1987**, *52*, 4296 – 4298.
[104] K. Akiba, T. Okinaka, M. Nakatani, Y. Yamamoto, *Tetrahedron Lett.* **1987**, *28*, 3367 – 3368.
[105] J. V. Comasseto, V. Catani, J. T. B. Ferreira, A. L. Braga, *J. Chem. Soc. Chem. Commun.* **1986**, 1067.
[106] M. J. Dabdoub, R. Preto, J. V. Comasseto, S. M. Barros, F. Moussa, *Synth. Commun.* **1990**, *20*, 2181 – 2183.
[107] T. Murai, K. Imaeda, S. Kajita, K. Kimura, H. Ishihara, S. Kato, *Phosphorus Sulfur* **1992**, *67*, 239 – 242.
[108] L. Alcaraz, R. J. K. Taylor, *Synlett* **1997**, 791 – 792.
[109] J. R. Johnson, W. L. McEwen, *J. Am. Chem. Soc.* **1926**, *48*, 469 – 476.
[110] R. B. Bedford, A. F. Hill, A. R. Thompsett, A. J. P. White, D. J. Williams, *Chem. Commun.* **1996**, 1059 – 1060.
[111] I. Rhee, M. Ryang, S. Tsutsumi, *Tetrahedron Lett.* **1969**, 4593 – 4596.
[112] K. Takagi, C. S. Rousset, E. Negishi, *J. Am. Chem. Soc.* **1991**, *113*, 1440 – 1442.
[113] N. Krause, D. Seebach, *Chem. Ber.* **1987**, *120*, 1845 – 1851.
[114] Y. Hayashi, M. Osawa, Y. Wakatsuki, *J. Organomet. Chem.* **1997**, *542*, 241 – 246.
[115] S. Back, H. Pritzkow, H. Lang, *Organometallics* **1998**, *17*, 41 – 44.
[116] a) R. F. Heck, *J. Am. Chem. Soc.* **1968**, *90*, 5526 – 5531; b) R. F. Heck, *J. Am. Chem. Soc.* **1968**, *90*, 5518 – 5526; c) R. F. Heck, *J. Am. Chem. Soc.* **1969**, *91*, 6707 – 6714; d) T. Mizoroki, K. Mori, A. Ozaki, *Bull. Chem. Soc. Jpn.* **1971**, *44*, 581.
[117] a) K. Sonogashira, Y. Tohda, N. Hagihara, *Tetrahedron Lett.* **1975**, 4467 – 4470; b) R. Rossi, A. Carpita, C. Bigelli, *Tetrahedron Lett.* **1985**, *26*, 523 – 526.
[118] D. H. Cho, J. H. Lee, B. H. Kim, *J. Org. Chem.* **1999**, *64*, 8048 – 8050.
[119] N. G. Kundu, M. Pal, C. Chowdhury, *J. Chem. Res. Synop.* **1993**, 432 – 433.
[120] Q. Liu, D. J. Burton, *Tetrahedron Lett.* **1997**, *38*, 4371 – 4374.
[121] T. Hattori, M. Kijima, H. Shirakawa, *Synth. Met.* **1997**, *84*, 357 – 358.
[122] N. Miyaura, K. Yamada, A. Suzuki, *Tetrahedron Lett.* **1979**, 3437 – 3440.
[123] J. Wityak, J. B. Chan, *Synth. Commun.* **1991**, *21*, 977 – 979.
[124] H. Dibowski, F. P. Schmidtchen, *Tetrahedron* **1995**, *51*, 2325 – 2330.
[125] C. Amatore, E. Blart, J. P. Genêt, A. Jutand, S. Lemaire-Audoire, M. Savignac, *J. Org. Chem.* **1995**, *60*, 6829 – 6839.
[126] V. Galamb, M. Gopal, H. Alper, *Organometallics* **1983**, *2*, 801 – 805.
[127] M. Vlassa, I. Ciocan-Tarta, F. Margineanu, I. Oprean, *Tetrahedron* **1996**, *52*, 1337 – 1342.
[128] J. Li, A. W.-H. Mau, C. R. Strauss, *Chem. Commun.* **1997**, 1275 – 1276.
[129] Numerous phosphane ligands used in palladium-catalyzed processes are thermally unstable. See for example W. A. Herrmann, C. Brossmer, K. Oefele, C.-P. Reisinger, T. Priermeier, M. Beller, H. Fischer, *Angew. Chem.* **1995**, *107*, 1989 – 1992; *Angew. Chem. Int. Ed. Engl.* **1995**, *34*, 1844 – 1848.
[130] J. K. Stille, B. L. Groh, *J. Am. Chem. Soc.* **1987**, *109*, 813 – 817.
[131] a) V. Farina in *Comprehensive Organometallic Chemistry*, *Vol. 12* (Eds.: E. W. Abel, F. G. A. Stone, G. Wilkinson), Pergamon, Oxford, **1995**, 161 – 240; b) T. N. Mitchell in *Metal-catalyzed Cross-coupling Reactions* (Eds.: F. Diederich, P. J. Stang), Wiley-VCH, Weinheim, **1997**, 167 – 202.
[132] L. Alcaraz, G. Macdonald, I. Kapfer, N. J. Lewis, R. J. K. Taylor, *Tetrahedron Lett.* **1996**, *36*, 6619 – 6622.
[133] G. Macdonald, N. J. Lewis, R. J. K. Taylor, *Chem. Commun.* **1996**, 2647 – 2648.
[134] R. Takeuchi, Y. Tsuji, M. Fujita, T. Kondo, Y. Watanabe, *J. Org. Chem.* **1989**, *54*, 1831 – 1836.
[135] K. Takai, T. Kuroda, S. Nakatsukasa, K. Oshima, H. Nozaki, *Tetrahedron Lett.* **1985**, *26*, 5585 – 5588.
[136] E. Müller, A. Segnitz, *Liebigs Ann. Chem.* **1973**, 1583 – 1591.
[137] D. H. Berry, R. Eisenberg, *Organometallics* **1987**, *6*, 1796 – 1805.
[138] Ruthenium complexes have been applied to the homodimerization of terminal acetylenes to afford enynes in a reaction similar to the Straus coupling: C. S. Yi, N. Liu, *Synlett* **1999**, 281 – 287.
[139] T. Takahashi, Z. Xi, Y. Obora, N. Suzuki, *J. Am. Chem. Soc.* **1995**, *117*, 2665 – 2666.
[140] C. M. Forsyth, S. P. Nolan, C. L. Stern, T. J. Marks, A. L. Rheingold, *Organometallics* **1993**, *12*, 3618 – 3623, and references therein.
[141] a) S.-M. Yang, M. C.-W. Chan, K.-K. Cheung, C.-M. Che, S.-M. Peng, *Organometallics* **1997**, *16*, 2819 – 2826; b) Y. Chi, A. J. Carty, P. Blenkiron, E. Delgado, G. D. Enright, W. Wang, S.-M. Peng, G.-H. Lee, *Organometallics* **1996**, *15*, 5269 – 5271.
[142] C.-W. Shiu, Y. Chi, C. Chung, S.-M. Peng, G.-H. Lee, *Organometallics* **1998**, *17*, 2970 – 2976.
[143] A. L. Klebansky, I. V. Grachev, O. M. Kuznetsova, *J. Gen. Chem. USSR* **1957**, *27*, 3008 – 3013.
[144] a) Y. S. Zalkind, Fr. B. Fundyler, *Ber. Dtsch. Chem. Ges.* **1936**, *69*, 128 – 130; b) Y. S. Zalkind, B. M. Fundyler, *J. Gen. Chem. USSR* **1939**, *9*, 1725 – 1728.
[145] A. A. Clifford, W. A. Waters, *J. Chem. Soc.* **1963**, 3056 – 3062.
[146] F. Bohlmann, H. Schönowsky, E. Inhoffen, G. Grau, *Chem. Ber.* **1964**, *97*, 794 – 800.
[147] J. C. Kennedy, J. R. MacCallum, D. H. MacKerron, *Can. J. Chem.* **1995**, *73*, 1914 – 1923.
[148] a) H. J. Kevelam, K. P. de Jong, H. C. Meinders, G. Challa, *Makromol. Chem.* **1975**, *176*, 1369 – 1381; b) G. Challa, H. C. Meinders, *J. Mol. Catal.* **1977**, *3*, 185 – 190.
[149] E. G. Derouane, J. N. Brahm, R. Hubin, *Chem. Phys. Lett.* **1974**, *25*, 243 – 246.
[150] L. G. Fedenok, V. M. Berdnikov, M. S. Shvartsberg, *J. Org. Chem. USSR* **1974**, *10*, 934 – 936.
[151] L. G. Fedenok, V. M. Berdnikov, M. S. Shvartsberg, *J. Org. Chem. USSR* **1973**, *9*, 1806 – 1809.
[152] L. G. Fedenok, V. M. Berdnikov, M. S. Shvartsberg, *J. Org. Chem. USSR* **1976**, *12*, 1385 – 1387.
[153] a) L. G. Fedenok, V. M. Berdnikov, M. S. Shvartsberg, *J. Org. Chem. USSR* **1978**, *14*, 1328 – 1333; b) L. G. Fedenok, V. M. Berdnikov, M. S. Shvartsberg, *J. Org. Chem. USSR* **1978**, *14*, 1334 – 1337.
[154] a) H. M. Hoan, S. M. Brailovskii, O. N. Temkin, *Kinet. Catal. (Engl. Transl.)* **1994**, *35*, 242 – 246; b) H. M. Hoan, S. M. Brailovskii, O. N. Temkin, *Kinet. Catal. (Engl. Transl.)* **1994**, *35*, 431 – 435.
[155] B. M. Mykhalichko, *Russ. J. Coord. Chem. (Engl. Transl.)* **1999**, *25*, 336 – 341.
[156] H. Alper, M. Saldana-Maldonado, *Organometallics* **1989**, *8*, 1124 – 1125.
[157] N. A. Bumagin, A. B. Ponomarev, I. P Beletskaya, *B. Acad. Sci. USSR* **1984**, *33*, 1433 – 1438.
[158] C. Cai, A. Vasella, *Helv. Chim. Acta* **1995**, *78*, 2053 – 2064.
[159] J. Breitenbach, J. Boosfeld, F. Vögtle in *Comprehensive Supramolecular Chemistry*, *Vol. 2* (Ed.: F. Vögtle), Pergamon, Oxford, **1996**, chap. 2, pp. 29 – 67.
[160] F. Bohlmann, H. Bornowski, C. Arndt, *Fortschr. Chem. Forsch.* **1962**, *4*, 138 – 272, and references therein.
[161] F. Bohlmann, T. Burkhardt, C. Zdero, *Naturally Occurring Acetylenes*, Academic Press, New York, **1973**.
[162] E. H. R. Jones, V. Thaller in *Handbook of Microbiology*, *Vol. 3* (Eds.: A. I. Laskin, H. A. Lechevalier), CRC, Cleveland, **1973**, pp. 63 – 74.
[163] M. Yamaguchi, H.-J. Park, M. Hirama, K. Torisu, S. Nakamura, T. Minami, H. Nishihara, T. Hiraoka, *Bull. Chem. Soc. Jpn.* **1994**, *67*, 1717 – 1725.
[164] N. A. Sörensen, *Proc. Chem. Soc. London* **1961**, 98 – 110.
[165] J. D. BuLock, *Prog. Org. Chem.* **1964**, *6*, 86 – 134.
[166] E. R. H. Jones, *Chem. Br.* **1966**, 6 – 13.
[167] F. Bohlmann, *Fortschr. Chem. Forsch.* **1966**, *6*, 65 – 100.
[168] G. Zheng, W. Lu, J. Cai, *J. Nat. Prod.* **1999**, *62*, 626 – 628.
[169] S. C. Shim, T. S. Lee, *J. Org. Chem.* **1988**, *53*, 2410 – 2413.
[170] P. Quayle, S. Rahman, J. Herbert, *Tetrahedron Lett.* **1995**, *36*, 8087 – 8088.
[171] W. Lu, G. Z. Haji, A. Aisa, J. Cai, *Tetrahedron Lett.* **1998**, *39*, 9521 – 9522.
[172] L. Hansen, P. M. Boll, *Phytochemistry* **1986**, *25*, 285 – 293.
[173] J. N. Gardner, E. R. H. Jones, P. R. Leeming, J. S. Stephenson, *J. Chem. Soc.* **1960**, 691 – 697.

[174] R. Jente, F. Bosold, J. Bäuerle, T. Anke, *Phytochemistry* **1985**, *24*, 553 – 559.
[175] An earlier, less efficient synthesis of panaxydol by Cadiot – Chodkiewicz coupling has also been reported: J. Poplawski, J. T. Wrobel, T. Glinka, *Phytochemistry* **1980**, *19*, 1539 – 1541.
[176] a) A. Stütz, G. Petranyi, *J. Med. Chem.* **1984**, *27*, 1539 – 1543; b) A. Stütz, W. Granitzer, S. Roth, *Tetrahedron* **1985**, *41*, 5685 – 5696.
[177] T. A. Prikhodko, V. M. Kurilenko, Z. N. Khlienko, S. F. Vasilevskii, M. S. Shvartsberg, *Izv. Akad. Nauk. SSR Ser. Khim.* **1988**, 120 – 127.
[178] M. G. Saulnier, D. B. Frennesson, M. S. Deshpande, D. M. Vyas, *Tetrahedron Lett.* **1995**, *36*, 7841 – 7844.
[179] E. Ottow, R. Rohde, W. Schwede, R. Wiechert, *Tetrahedron Lett.* **1993**, *34*, 5253 – 5256.
[180] A. V. R. Rao, E. R. Reddy, G. V. M. Sharma, P. Yadagiri, J. S. Yadav, *Tetrahedron Lett.* **1986**, *42*, 4523 – 4532.
[181] P. I. Svirskaya, C. C. Leznoff, W. L. Roelofs, *Synth. Commun.* **1980**, *10*, 391 – 397.
[182] S. Rødbotten, T. Benneche, K. Undheim, *Acta Chem. Scand.* **1997**, *51*, 873 – 880.
[183] a) H. Hopf, N. Krause, *Tetrahedron Lett.* **1985**, *26*, 3323 – 3326; b) N. Krause, H. Hopf, L. Ernst, *Liebigs Ann. Chem.* **1986**, 1398 – 1406.
[184] a) M. D. Lee, G. A. Ellestad, D. B. Borders, *Acc. Chem. Res.* **1991**, *24*, 235 – 243; b) I. H. Goldberg, *Acc. Chem. Res.* **1991**, *24*, 191 – 198; c) K. C. Nicolaou, A. L. Smith in *Modern Acetylene Chemistry* (Eds.: P. J. Stang, F. Diederich), VCH, Weinheim, **1995**, chap. 7, pp. 203 – 283.
[185] D. Elbaum, T. B. Nguyen, W. L. Jorgensen, S. L. Schreiber, *Tetrahedron* **1994**, *50*, 1503 – 1518.
[186] J.-P. Gotteland, I. Brunel, F. Gendre, J. Désiré, A. Delhon, D. Junquéro, P. Oms, J. Halazy, *J. Med. Chem.* **1995**, *38*, 3207 – 3216.
[187] For the inhibition of HMG-CoA reductase, another important enzyme in cholesterol biosynthesis, by polyacetylenic fatty acids, see S. Y. Mhaskar, G. Lakshminarayana, *Synth. Commun.* **1990**, *20*, 2001 – 2009.
[188] a) K. C. Nicolaou, N. A. Petasis, R. E. Zipkin, J. Uenishi, *J. Am. Chem. Soc.* **1982**, *104*, 5555 – 5557; b) K. C. Nicolaou, N. A. Petasis, J. Uenishi, R. E. Zipkin, *J. Am. Chem. Soc.* **1982**, *104*, 5557 – 5558; c) K. C. Nicolaou, R. E. Zipkin, N. A. Petasis, *J. Am. Chem. Soc.* **1982**, *104*, 5558 – 5560; d) K. C. Nicolaou, N. A. Petasis, R. E. Zipkin, *J. Am. Chem. Soc.* **1982**, *104*, 5560 – 5562.
[189] W. M. Bandaranayake, J. E. Banfield, D. S. C. Black, *J. Chem. Soc. Chem. Commun.* **1980**, 902 – 903.
[190] a) J.-M. Lehn, *Supramolecular Chemistry: Concepts and Perspectives*, VCH, Weinheim, **1995**; b) C. Seel, A. Galán, J. de Mendoza, *Top. Curr. Chem.* **1995**, *175*, 101 – 132; c) B. J. Whitlock, H. W. Whitlock in *Comprehensive Supramolecular Chemistry*, *Vol. 2* (Ed.: F. Vögtle), Pergamon, Oxford, **1996**, chap. 10, pp. 309 – 324.
[191] D. O'Krongly, S. R. Denmeade, M. Y. Chiang, R. Breslow, *J. Am. Chem. Soc.* **1985**, *107*, 5544 – 5545.
[192] a) S. Claude, J.-M. Lehn, F. Schmidt, J.-P. Vigneron, *J. Chem. Soc. Chem. Commun.* **1991**, 1182 – 1185; b) P. Cudic, M. Zinic, V. Tomisic, V. Simeon, J.-P. Vigneron, J.-M. Lehn, *J. Chem. Soc. Chem. Commun.* **1995**, 1073 – 1075; c) P. Cudic, M. Zinic, V. Skaric, R. Kiralj, B. Kojic-Prodic, J.-P. Vigneron, J.-M. Lehn, *Croat. Chem. Acta* **1996**, *69*, 569 – 611.
[193] A. Lorente, M. Fernández-Saiz, J.-M. Lehn, J.-P. Vigneron, *Tetrahedron Lett.* **1995**, *36*, 8279 – 8282.
[194] a) B. R. Peterson, T. Mordasini-Denti, F. Diederich, *Chem. Biol.* **1995**, *2*, 139 – 146; b) A. Fürer, T. Marti, F. Diederich, H. Künzer, M. Brehm, *Helv. Chim. Acta* **1999**, *82*, 1843 – 1859.
[195] a) S. Anderson, U. Neidlein, V. Gramlich, F. Diederich, *Angew. Chem.* **1995**, *107*, 1722 – 1724; *Angew. Chem. Int. Ed. Engl.* **1995**, *34*, 1596 – 1600; b) A. Bähr, A. S. Droz, M. Püntener, U. Neidlein, S. Anderson, P. Seiler, F. Diederich, *Helv. Chim. Acta* **1998**, *81*, 1931 – 1963.
[196] M. J. Cloninger, H. W. Whitlock, *J. Org. Chem.* **1998**, *63*, 6153 – 6159.
[197] C. A. Hunter, *Chem. Soc. Rev.* **1994**, 101 – 109, and references therein.
[198] For review articles, see a) S. Anderson, H. L. Anderson, J. K. M. Sanders, *Acc. Chem. Res.* **1993**, *26*, 469 – 475; b) J. K. M. Sanders in *Comprehensive Supramolecular Chemistry*, *Vol. 9* (Eds.: J.-P. Sauvage, M. W. Hosseini), Pergamon, Oxford, **1996**, chap. 4, pp. 131 – 164; c) S. Anderson, H. L. Anderson in *Templated Organic Synthesis* (Eds.: F. Diederich, P. J. Stang), Wiley-VCH, Weinheim, **1999**, chap. 1, pp. 1 – 38.
[199] D. W. J. McCallien, J. K. M. Sanders, *J. Am. Chem. Soc.* **1995**, *117*, 6611 – 6612.
[200] H. L. Anderson, S. Anderson, J. K. M. Sanders, *J. Chem. Soc. Perkin Trans. 1* **1995**, 2231 – 2245.
[201] C. J. Walter, J. K. M. Sanders, *Angew. Chem.* **1995**, *107*, 231 – 233; *Angew. Chem. Int. Ed. Engl.* **1995**, *34*, 217 – 219.
[202] L. G. Mackay, R. S. Wylie, J. K. M. Sanders, *J. Am. Chem. Soc.* **1994**, *116*, 3141 – 3142.
[203] V. Marvaud, A. Vidal-Ferran, S. J. Webb, J. K. M. Sanders, *J. Chem. Soc. Dalton Trans.* **1997**, 985 – 990.
[204] D. G. Hamilton, L. Prodi, N. Feeder, J. K. M. Sanders, *J. Chem. Soc. Perkin Trans. 1* **1999**, 1057 – 1065.
[205] J. M. Tour, *Chem. Rev.* **1996**, *96*, 537 – 553.
[206] R. E. Martin, F. Diederich, *Angew. Chem.* **1999**, *111*, 1440 – 1469; *Angew. Chem. Int. Ed.* **1999**, *38*, 1350 – 1377.
[207] a) A. S. Hay, *J. Polym. Sci. Part A* **1969**, *7*, 1625 – 1634; b) for the synthesis of very long oligothiophenes using Eglinton conditions, see H. Nakanishi, N. Sumi, Y. Aso, T. Otsubo, *J. Org. Chem.* **1998**, *63*, 8632 – 8633; c) for other linear couplings under Eglinton conditions, see also reference [54].
[208] a) N. C. Greenham, S. C. Moratti, D. D. C. Bradley, R. H. Friend, A. B. Holmes, *Nature* **1993**, *365*, 628 – 630; b) J. L. Brédas, *Adv. Mater.* **1995**, *7*, 263 – 274.
[209] a) R. Eastmond, T. R. Johnson, D. R. M. Walton, *Tetrahedron* **1972**, *28*, 4601 – 4616; b) R. Eastmond, D. R. M. Walton, *Tetrahedron* **1972**, *28*, 4591 – 4599.
[210] R. E. Martin, T. Mäder, F. Diederich, *Angew. Chem.* **1999**, *111*, 834 – 838; *Angew. Chem. Int. Ed.* **1999**, *38*, 817 – 821.
[211] a) R. R. Tykwinski, F. Diederich, *Liebigs Ann. Chem.* **1997**, 649 – 661; b) R. R. Tykwinski, U. Gubler, R. E. Martin, F. Diederich, C. Bosshard, P. Günter, *J. Phys. Chem. B* **1998**, *102*, 4451 – 4465.
[212] M. Mayor, J.-M. Lehn, K. M. Fromm, D. Fenske, *Angew. Chem.* **1997**, *109*, 2468 – 2471; *Angew. Chem. Int. Ed. Engl.* **1997**, *36*, 2370 – 2372.
[213] G. S. Wilson, H. L. Anderson, *Chem. Commun.* **1999**, 1539 – 1540.
[214] a) U. H. F. Bunz, *Angew. Chem.* **1996**, *108*, 1047 – 1049; *Angew. Chem. Int. Ed. Engl.* **1996**, *35*, 969 – 971; b) F. Coat, C. Lapinte, *Organometallics* **1996**, *15*, 477 – 479.
[215] U. H. F. Bunz, *Synlett* **1997**, 1117 – 1127.
[216] a) U. H. F. Bunz, *Pure Appl. Chem.* **1996**, *68*, 309 – 312; b) U. H. F. Bunz, *Top. Curr. Chem.* **1999**, *201*, 132 – 161.
[217] a) F. Diederich, R. Faust, V. Gramlich, P. Seiler, *J. Chem. Soc. Chem. Commun.* **1994**, 2045 – 2046; b) R. Faust, F. Diederich, V. Gramlich, P. Seiler, *Chem. Eur. J.* **1995**, *1*, 111 – 117.
[218] P. Siemsen, F. Diederich, unpublished results.
[219] a) J. Alzeer, C. Cai, A. Vasella, *Helv. Chim. Acta* **1995**, *78*, 242 – 264; b) C. Cai, A. Vasella, *Helv. Chim. Acta* **1995**, *78*, 732 – 757; c) C. Cai, A. Vasella, *Helv. Chim. Acta* **1996**, *79*, 255 – 268; d) A. Ernst, L. Gobbi, A. Vasella, *Tetrahedron Lett.* **1996**, *37*, 7959 – 7962; e) T. V. Bohner, R. Beaudegnies, A. Vasella, *Helv. Chim. Acta* **1999**, *82*, 143 – 160.
[220] T. V. Bohner, O.-S. Becker, A. Vasella, *Helv. Chim. Acta* **1999**, *82*, 198 – 228.
[221] a) J. M. J. Tronchet, A.-P. Bonenfant, *Helv. Chim. Acta* **1977**, *60*, 892 – 895; b) J. M. J. Tronchet, A.-P. Bonenfant, *Helv. Chim. Acta* **1981**, *64*, 1893 – 1901.
[222] M. Nakagawa, *Angew. Chem.* **1979**, *91*, 215 – 226; *Angew. Chem. Int. Ed. Engl.* **1979**, *18*, 202 – 214.
[223] L. T. Scott, M. J. Cooney in *Modern Acetylene Chemistry* (Eds.: P. J. Stang, F. Diederich), VCH, Weinheim, **1995**, pp. 321 – 351.
[224] a) F. Diederich, L. Gobbi, *Top. Curr. Chem.* **1999**, *201*, 43 – 79; b) F. Diederich, *Nature* **1994**, *369*, 199 – 207; c) F. Diederich, Y. Rubin, *Angew. Chem.* **1992**, *104*, 1123 – 1146; *Angew. Chem. Int. Ed. Engl.* **1992**, *31*, 1101 – 1123.
[225] a) B. König, *Top. Curr. Chem.* **1998**, *196*, 91 – 136; b) U. H. F. Bunz, Y. Rubin, Y. Tobe, *Chem. Soc. Rev.* **1999**, *201*, 43 – 79.
[226] A. de Meijere, S. Kozhushkov, T. Haumann, R. Boese, C. Puls, M. J. Cooney, L. T. Scott, *Chem. Eur. J.* **1995**, *1*, 124 – 131.

[227] a) A. M. Boldi, F. Diederich, *Angew. Chem.* **1994**, *106*, 482 – 485; *Angew. Chem. Int. Ed. Engl.* **1994**, *33*, 468 – 471; b) J. Anthony, A. M. Boldi, C. Boudon, J.-P. Gisselbrecht, M. Gross, P. Seiler, C. B. Knobler, F. Diederich, *Helv. Chim. Acta* **1995**, *78*, 797 – 817.
[228] M. Schreiber, R. R. Tykwinski, F. Diederich, R. Spreiter, U. Gubler, C. Bosshard, I. Poberaj, P. Günter, C. Boudon, J.-P. Gisselbrecht, M. Gross, U. Jonas, H. Ringsdorf, *Adv. Mater.* **1997**, *9*, 339 – 343.
[229] R. R. Tykwinski, *Chem. Commun.* **1999**, 905 – 906.
[230] S. W. McElvany, M. M. Ross, N. S. Goroff, F. Diederich, *Science* **1993**, *259*, 1594 – 1596.
[231] Y. Rubin, T. C. Parker, S. J. Pastor, S. Jalisatgi, C. Boulle, C. L. Wilkins, *Angew. Chem.* **1998**, *110*, 1353 – 1356; *Angew. Chem. Int. Ed.* **1998**, *37*, 1226 – 1229.
[232] a) Y. Tobe, N. Nakagawa, K. Naemura, T. Wakabayashi, T. Shida, Y. Achiba, *J. Am. Chem. Soc.* **1998**, *120*, 4544 – 4545; b) Y. Tobe, H. Nakanishi, M. Sonoda, T. Wakabayashi, Y. Achiba, *Chem. Commun.* **1999**, 1625 – 1626.
[233] a) H. L. Anderson, R. Faust, Y. Rubin, F. Diederich, *Angew. Chem.* **1994**, *106*, 1427 – 1429; *Angew. Chem. Int. Ed. Engl.* **1994**, *33*, 1366 – 1368; b) P. Timmerman, H. L. Anderson, R. Faust, J.-F. Nierengarten, T. Habicher, P. Seiler, F. Diederich, *Tetrahedron* **1996**, *52*, 4925 – 4947; c) P. Timmerman, L. E. Witschel, F. Diederich, C. Boudon, J.-P. Gisselbrecht, M. Gross, *Helv. Chim. Acta* **1996**, *79*, 6 – 20; d) L. Isaacs, P. Seiler, F. Diederich, *Angew. Chem.* **1995**, *107*, 1636 – 1639; *Angew. Chem. Int. Ed. Engl.* **1995**, *34*, 1466 – 1469; e) L. Isaacs, F. Diederich, R. F. Haldiman, *Helv. Chim. Acta* **1997**, *80*, 317 – 342.
[234] a) R. Boese, A. J. Matzger, K. P. C. Vollhardt, *J. Am. Chem. Soc.* **1997**, *119*, 2052 – 2053; b) P. I. Dosa, C. Erben, V. S. Iyer, K. P. C. Vollhardt, I. M. Wasser, *J. Am. Chem. Soc.* **1999**, *121*, 10430 – 10431.
[235] a) S. Höger, A.-D. Meckenstock, H. Pellen, *J. Org. Chem.* **1997**, *62*, 4556 – 4557; b) S. Höger, A.-D. Meckenstock, *Tetrahedron Lett.* **1998**, *39*, 1735 – 1736.

+++ THE LINK TO INTERNATIONAL CHEMISTRY +++

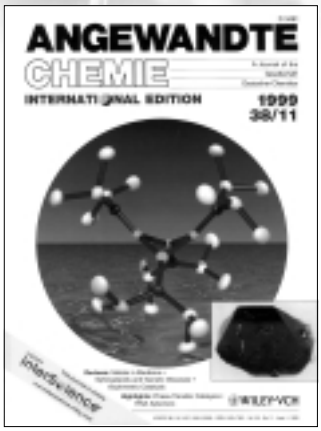


"It is a long time since I have read one issue of a journal [...] which has so much of interest...

...to process R&D chemists and engineers as issue No. 23 in Vol. 36 of *Angewandte Chemie.*

Trevor Laird, Editor of Organic Process Research & Development
[Org. Process Res. Dev. 1998, 2, 64]

The Highlights in *Angewandte* provide concise evaluations of the most important current trends in chemical research.



The most cited Highlights in 1998 are:

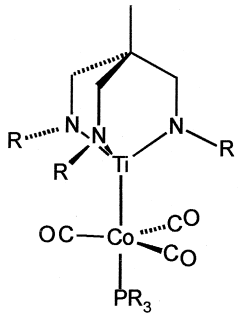
- *A.E. Rowan, R.J.M Nolte:* Helical Molecular Programming
- *N. Krause:* Copper-Catalyzed Enantioselective Michael Additions: Recent Progress with New Phosphorus Ligands
- *O. Geis, H.-G. Schmalz:* New Developments in the Pauson - Khand Reaction
- *J.E. Cosgriff, G.B. Deacon:* Another Surprise from Pyrazolate Ligands
- *C. Schneider:* New Polyol Syntheses
- *A.P. Davis:* Tilting at Windmills? The Second Law Survives
- *J.O. Metzger:* Solvent-Free Organic Syntheses
- *H. Frey:* From Random Coil to Extended Nanocylinder: Dendrimer Fragments Shape Polymer Chains
- *J.D. Smith:* Phosphanides of the Heavier Alkali Metals
- *D. Wolf :* High Yields of Methanol from Methane by C-H Bond Activation at Low Temperatures
- *P. Luger:* Large Molecules from the Virtual Bakery - Filling a Gap in Structure Research
- *V. Fehring, R. Selke:* Highly Enantioselective Complex-Catalyzed Reduction of Ketones - Now with Purely Aliphatic Derivations Too

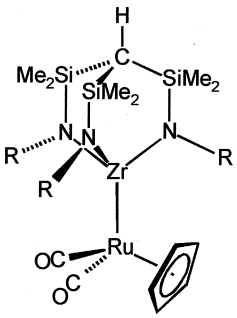
Have your own Highlights every two weeks. Subscribe to *Angewandte* with the Order Form on the last page of this issue.

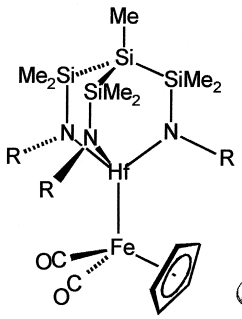
WILEY-VCH, P.O. Box 10 11 61, 69451 Weinheim, Germany
Phone +49 (6201) 606-328, Fax +49 (6201) 606-348
e-mail: sales-journals@wiley-vch.de, http://www.wiley-vch.de

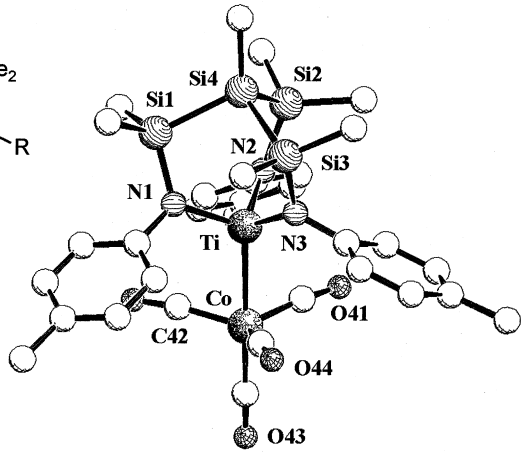
WILEY-VCH

SCHULZ1299<ACHUNK1>



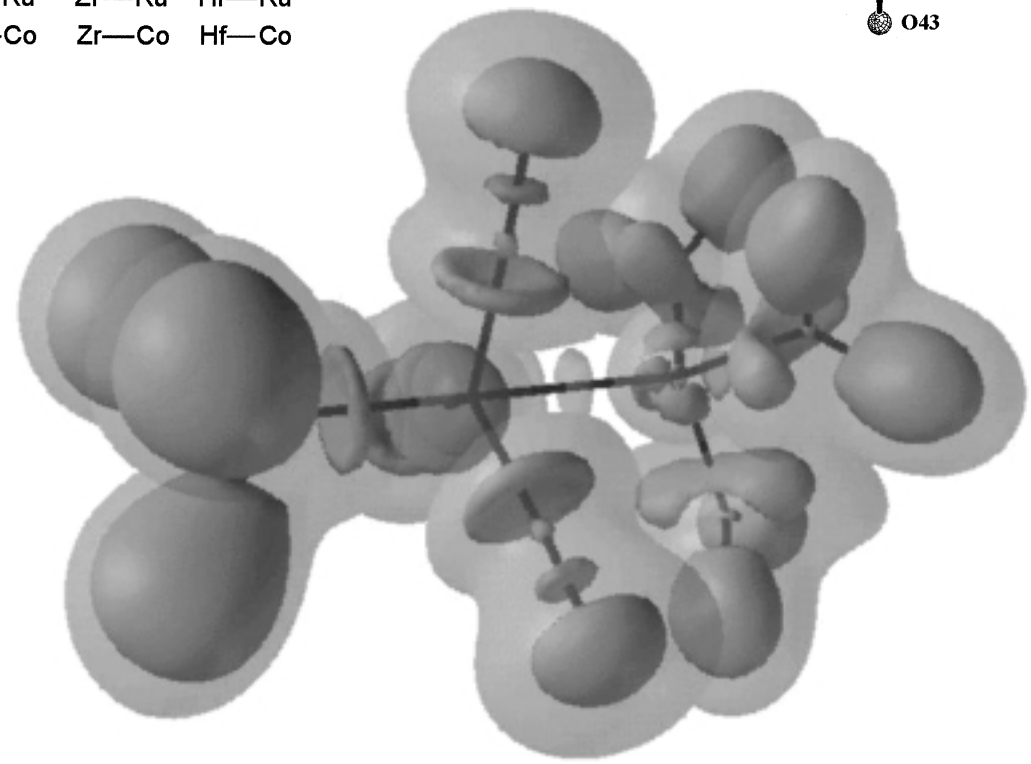


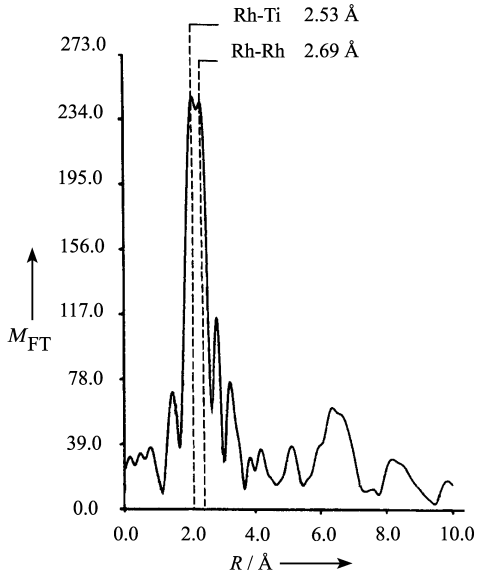


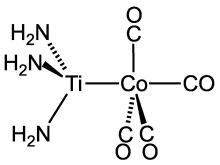


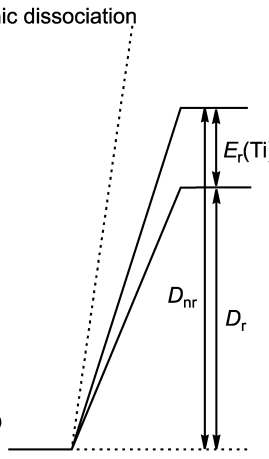
Ti—Fe Zr—Fe Hf—Fe
Ti—Ru Zr—Ru Hf—Ru
Ti—Co Zr—Co Hf—Co

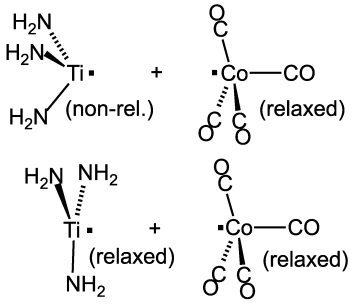
ANGEWANDTE CHEMIE © WILEY-VCH











	BLYP	B3LYP	
D_{nr}	60.0	47.2	[kcal mol^{-1}]
D_r	50.7	36.6	
E_r(Ti)	9.3	10.6	

Highly Polar Metal–Metal Bonds in "Early–Late" Heterodimetallic Complexes

Lutz H. Gade*

Dedicated to Helmut Werner

Metal–metal bond polarity in its extreme form involving transition elements is found in di- or polynuclear complexes in which molecular fragments containing metal atoms from the two ends of the d block in the periodic table are combined. This linkage by direct metal–metal bonds of metal centers having very different oxidation states has been a challenge to the synthetic chemist. The suppression of degradative reaction channels caused by intramolecular single-electron transfer and the protection of the highly Lewis acidic early transition metal center by an appropriately designed ligand shell have opened up the systematic investigation of such systems. Concomitant with this development, advances in the conceptual framework for the quantitative description of bond polarity have led to a refined understanding of the nature of this type of metal–metal bonding. The greatest stimulus for the development of this field of research is the investigation of the cooperative reactivity of two or more coordination centers in their interaction with and transformation of organic substrates. This cooperativity, which is characterized by the different functions adopted by the metal centers in these conversions offers attractive perspectives in stoichiometric or even catalytic transformations.

Keywords: cluster compounds · metal–metal interactions · organometallic compounds · transition metals

Introduction

A metal–metal bond in a di- or polynuclear complex tends to be its most characteristic structural feature and at the same time bears a reactive potential which sets it apart from the other components of the molecule.[1–3] Its chemical characteristics are not only strongly influenced by the nature of the metals involved but equally so by the set of ligands coordinated to the metals. The latter reflects the formal oxidation states of the metal centers and thus—to some extent—the charge distribution between them.

Two metal centers adjacent to each other may in principle simultaneously interact with a molecule entering the ligand sphere. Upon introducing metal–metal bond polarity, as a consequence of different metal centers or sets of ancillary ligands, this interaction with an incoming ligand or substrate will become nonsymmetrical. The greater the disparity of the electronic properties of the linked complex fragments and thus the greater the polarity of the metal–metal bond, the more clearly cut are the differences in the roles assumed by the metals involved in this interaction and in the conversion of the substrate in question. Transformations which are enhanced by the interaction with two or more coordination centers adopting different functions are frequently referred to as *cooperative*, and it is this cooperativity which offers attractive perspectives in stoichiometric or even catalytic conversions involving "dimetallic activation".[4] This concept is realized in its extreme form in the chemistry of early–late heteronuclear complexes in which complex fragments in high oxidation states with no or few d-electrons are directly linked to those of the d-electron rich late transition metals in relatively low oxidation states.[5]

The vastly different redox properties of such metal fragments combined by direct bonding have thwarted many early attempts to synthesize such heteronuclear compounds of sufficient stability to allow systematic studies of their reactivity. This has only been achieved in a systematic way during the course of this past decade. The progress which has been achieved in the exploration of the reactive potential of significantly different metal centers linked directly to each other and thus located at very close proximity to each other

[*] Prof. L. H. Gade
Laboratoire de Chimie Organométallique et de Catalyse
(CNRS, UMR 7513)
Institut Le Bel, Université Louis Pasteur
4, rue Blaise Pascal, 67000 Strasbourg (France)
Fax: (+33) 388-416045
E-mail: gade@chimie.u-strasbg.fr

 © WILEY-VCH Verlag GmbH, D-69451 Weinheim, 2000 1433-7851/00/3915-2659 $ 17.50+.50/0

will be highlighted in this article. Its principal focus, however, will be the properties of the highly polar metal–metal bonds themselves.

1.1. Direct Metal–Metal Bonding in Polynuclear Complexes: A Brief Historical Perspective

Few conceptual innovations in inorganic chemistry exemplify Thomas Kuhn's postulate of the change of paradigms[6] equally well as the formulation of covalent bonds between metal centers within polynuclear complexes which established metal–metal bonding as a structural principle in the late 1950s and early 1960s. It did not evolve as a natural extension of Alfred Werner's coordination theory[7] but rather developed in spite of it and in view of an ever growing amount of experimental data which apparently violated the accepted rules of molecular structure.[8]

The first steps in this development date back to the mid 1920s when the crystal structure analyses of the mercurous halides indicated Hg–Hg contacts of about 2.5 Å.[9] The possibility of direct metal–metal bonding in the dimercury dication was additionally supported by the report of a low-frequency band in the Raman spectrum of $Hg_2(NO_3)_2$ (171 cm^{-1}) by Woodward in 1934.[10] These early speculations, however, received little notice, and it was the report of the crystal structure of $[Fe_2(CO)_9]$ by Powell and Ewens in 1939, in which the authors invoked a metal–metal bond between the two Fe centers, which attracted greater interest.[11] This view was immediately endorsed by Pauling in the 1940 edition of his famous book "The Nature of the Chemical Bond"[12] but initially met with fierce opposition from other researchers.[13]

The importance of X-ray crystallography for the further development of the area is highlighted by the establishment of short metal–metal distances in the trianion $[W_2Cl_9]^{3-}$[14] and the metal octahedra in $[\{Mo_6Cl_8\}Cl_4(H_2O)_6]\cdot 6H_2O$ and $[Ta_6X_{14}]$ (X = Cl, Br) by C. Brosset[15] and L. Pauling[16] during the period between 1935 and 1950. In these compounds the metal–metal vectors are associated with bridging ligands thus leaving a certain degree of ambiguity as to their structural role. Metal–metal bonds between transition metal atoms which are unsupported by bridging ligands were first established for $[\{Cp(CO)_3Mo\}_2]$ and $[M_2(CO)_{10}]$ (M = Mn, Re) in 1956 and 1957, respectively.[17, 18]

From 1960 onwards there was a rapid succession of publications reporting various aspects of metal–metal bonding. The discovery of metal–metal multiple bonds by F. A. Cotton and his co-workers[19] ranks among the most important discoveries of this period and began with the report and theoretical analysis of the structure of the $[Re_3Cl_{12}]^{3-}$ cluster anion which was formulated as containing Re–Re double bonds.[20] A bond multiplicity of greater than three in the form of a Re–Re quadruple bond was established for the dinuclear complex $[Re_2Cl_8]^{2-}$ in 1964,[21] while the missing link in this series, a metal–metal triple bond, could be found for the first time in the neutral compound $[Re_2Cl_5(dth)]$ (dth = $CH_3SCH_2CH_2SCH_3$).[22]

The formulation of direct bonding between transition metal atoms is nowadays an integral part of the conceptual texture of inorganic chemistry.[23, 24] The structural characteristics and reactivity of di- and polynuclear complexes containing metal–metal bonds has been extensively reviewed and has uncovered a multitude of bonding combinations and reactive patterns.[1–3] The stabilization and unambiguous identification of complexes containing highly polar metal–metal bonds between transition metal atoms from the two ends of the d block in the periodic table has only been achieved since the late 1970s.[5] The first structural characterization of such an unsupported metal–metal bond was achieved by Schmid and co-workers for the rather complicated system $[Cp\{Co_3(CO)_9(\mu\text{-}CO)\}_2Ti{-}Co(CO)_4]$ which was isolated from the reaction of $[CpTiCl_3]$ with $Na[Co(CO)_4]$.[25] However, a systematic investigation of these "early–late" heteronuclear complexes was initially hampered by the apparent instablity of most compounds synthesized at that stage.

2. Metal–Metal Bond Polarity

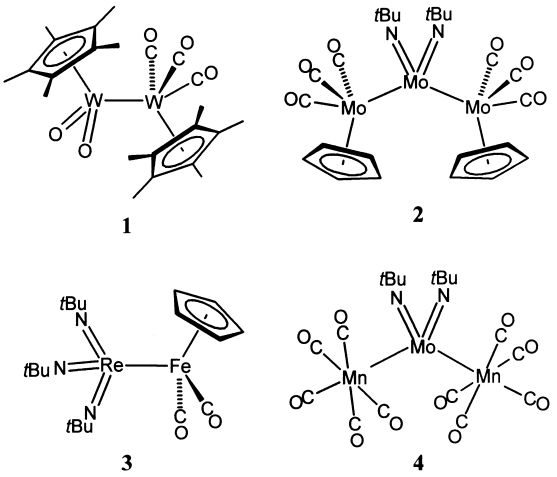
Homodinuclear complexes containing metal–metal bonds are mostly symmetrical "dimers" in which the bond linking the two metal centers is consequently nonpolar. This pattern applies to a wide range of such species and M–M bonds of different multiplicity. A certain degree of polarity of the



Lutz H. Gade, born in Bonn in 1963, received most of his school education in Johannesburg, South Africa. He carried out his undergraduate studies at the University of Bonn and the Technical University of Munich and then went to Cambridge to work for his Ph.D. with Jack Lewis where his interest in metal–metal bonding was aroused. Having returned to Germany after completing his thesis in 1991, he joined the Chemistry Department at the University of Würzburg where he finished his habilitation in 1996 and where he subsequently worked as a lecturer. In 1998 he moved to Strasbourg to take up an appointment as a professor of chemistry at the Université Louis Pasteur and as Head of the Laboratory of Organometallic Chemistry and Catalysis. His research interests are in the fields of coordination chemistry, organometallic chemistry, and catalysis and his work has found recognition through the award of the ADUC prize (1994), the Heinz-Maier-Leibnitz Preis of the DFG and the Federal Ministry of Research and Education (1997), the Gerhard-Hess-Research Award of the DFG (1998), and the Award in Chemistry of the Academy of Sciences at Göttingen (1999).

metal–metal bond may be achieved by ligand substitution at one metal center of a *homodinuclear* complex or by linking different transition metals, thus generating *heterodinuclear* complexes.

A high degree of metal–metal bond polarity is to be expected if the metal atoms in the two complex fragments have a significantly different partial atomic charges. This will be the case if their formal oxidation state differs substantially. Thus, even homodimetallic complexes may contain highly polar metal–metal bonds such as those in compounds **1** and **2** in Scheme 1.[26–28] The same applies to the high-valent–low

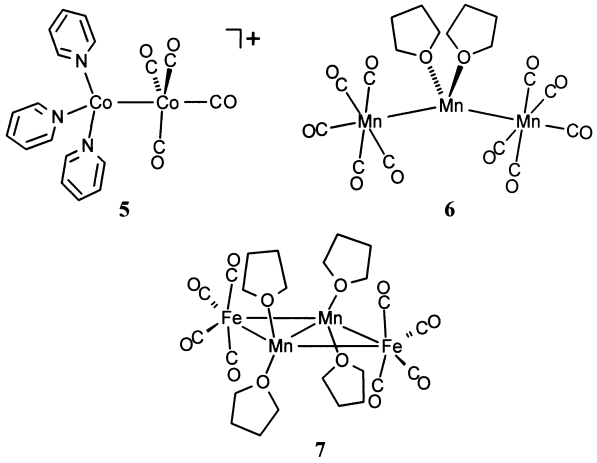


Scheme 1. Complexes with polar metal–metal bonds between metal centers in high and low formal oxidation states.

-valent complexes **3** and **4** in which the metal atoms are fairly close to each other in the periodic table but in which the different ligand spheres—imido ligands stabilizing the formal high oxidation state, CO ligand the higher electron density at the low oxidation state fragment—define the different nature of the M–M′ linked complex fragments.

A second type of complexes in which metal–metal bond polarity is due to an extreme inequality of the ligand spheres was first isolated from redox disproportionations of metal carbonyls in the presence of relatively hard donor ligands. An example for such a system is the dicobalt complex **5** which was isolated by Fachinetti et al. from the reaction of $[Co_2(CO)_8]$ with pyridine and which contains what the authors regarded as a contact ion pair between the complex ions $[Co(py)_3]^{2+}$ and $[Co(CO)_4]^-$ (Scheme 2).[29]

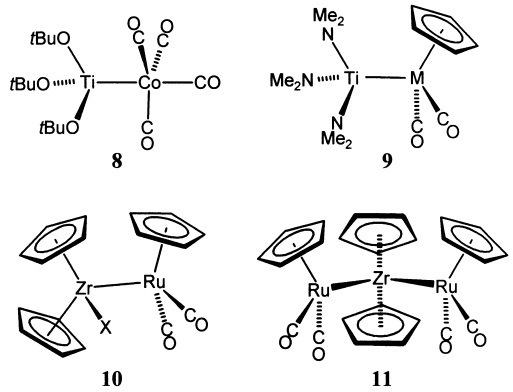
The polynuclear complexes **6** and **7**, in which "classical" Alfred Werner-type complex fragments are bonded to metal carbonyls are further examples of this class of compounds for which the term "xenophilic" ("stranger loving") has been proposed.[30–32] Their facile (though not decomposition-free) ionic dissociation in polar solvents supports the interpretation of the metal–metal bonding as being highly polar. However, a major factor in this tendency to dissociate may be the inherent weakness of the metal–metal bond between fragments with considerably divergent bonding capabilities. In the "classical" hard-donor/intermediate "oxidation state" compounds the d-orbital shell is thought to be highly contracted and barely participates in the metal–ligand bonding (which, incidentally, is



Scheme 2. "Xenophilic" clusters with polar metal–metal bonds.

the reason for the applicability of Ligand Field Theory to such systems).[33] Overlap of the d orbitals with those of a neighboring metal carbonyl fragment is expected to be very weak and thus the covalent bond order fairly low. A recent theoretical study by Xu and Lin of such "xenophilic" complexes has established high partial charges on the linked complex fragments.[34] It also successfully explained the major aspects of the interesting magnetic properties of these compounds while not directly addressing the issue of metal–metal bond strength and polarity.

The third and possibly most radical strategy to generate highly polar metal–metal bonds is based on the combination of complex fragments from the extreme ends of the d block in the periodic table (**8**–**11**, Scheme 3).[35–39, 41–44] The d-electron



Scheme 3. Early–late heterodimetallic complexes containing unsupported metal–metal bonds.

rich metal atoms in these "early–late" heterodimetallic complexes are directly bound to d-electron poor metal centers. The principle is thus closely related to that of the high-valent–low-valent complexes discussed above. In both types of compounds the frequencies of the ν(CO) infrared vibrations indicate that the negative charge at the late (low-valent) transition metal lies somewhere in the middle between those of the homonuclear dimers and the carbonyl metalate anion. An overview of the ν(CO) frequencies of the {FeCp-$(CO)_2$} fragment bonded to different metal centers is given in Table 1 and compared with those of $[CpFe(CO)_2]^-$.[40]

Table 1. Infrared carbonyl stretching frequencies of Ti–Fe, Zr–Fe, and Hf–Fe complexes containing the {CpFe(CO)$_2$} fragment.

Complex	$\tilde{\nu}_{sym}$(CO), $\tilde{\nu}_{asym}$(CO) [cm^{-1}]	Ref.
Ti–Fe		
[{MeSi[SiMe$_2$N(*p*-Tol)]$_3$}Ti–FeCp(CO)$_2$]	1978, 1931	[44]
[{HC[SiMe$_2$N(*p*-Tol)]$_3$}Ti–FeCp(CO)$_2$]	1975, 1928	[42]
[{MeC(CH$_2$NSiMe$_3$)$_3$}Ti–FeCp(CO)$_2$]	1968, 1916	[42]
[(Me$_2$N)$_3$Ti-FeCp(CO)$_2$]	1948, 1898	[35]
Zr–Fe		
[{MeSi[SiMe$_2$N(*p*-Tol)]$_3$}Zr–FeCp(CO)$_2$]	1961, 1910	[44]
[{CH$_2$(CH$_2$NSiMe$_3$)$_2$}(Cp)Zr–FeCp(CO)$_2$]	1947, 1895	[43a]
[Cp$_2$(Me)Zr–FeCp(CO)$_2$]	1937, 1872	[37]
Hf–Fe		
[{MeSi[SiMe$_2$N(*p*-Tol)]$_3$}Hf–FeCp(CO)$_2$]	1969, 1915	[44]
K[FeCp(CO)$_2$]	1866, 1772	[40]

2.1. Metal–Metal Bonding between Early and Late Transition Metals in Bare Cluster–Dimers and Intermetallic Solids

The bonding between the metals of the two ends of the d block in the periodic table was first considered and studied for solid intermetallic phases. More than 25 years ago Brewer and Wengert predicted the trends and stability of transition metal alloys.[45a] One result of their work was the postulate that particularly stable alloys were expected to be formed by the *combination of the early and late d-block elements.* The intermetallic bonding interaction determining this stability was proposed to be a type of Lewis acid/Lewis base interaction whereby paired d electrons of the late transition metal are donated to the empty acceptor orbitals of the early transition element. An optimization of this type of interaction would then result in highly negative heats of formation. The thermodynamic data reported by Topor and Kleppa for a series of binary intermetallic phases appear to support this early proposal.[45b]

The stability trends which emerged for the solids were further supported by theoretical studies reported for heterometallic transition metal dimers in the gas phase.[46] For the dimers containing iron and a second transition metal the calculated dissociation energies summarized in Table 2 indicate that an increase in the difference of the electronic structure of the atoms combined to give Fe–M leads to higher stability of the metal–metal bond with the homodimer Fe_2 being the least stable molecule.[47]

Enhanced metal–metal bonding in heterometallic solids has also been established in the bonding analysis of the large number of ternary systems, in particular in the early–late mixed metal halides and chalcogenides studied by Corbett, Hughbanks, Tremel, Harbrecht, and others.[48–52] A particularly instructive example is the ternary compound Hf_5FeTe_3 reported by Abdon and Hughbanks in which the iron atoms are situated in the center of hafnium tricapped trigonal-prismatic cages.[52] The Hf–Fe distances within the trigonal prism lie between 2.6 and 2.7 Å and indicate strong bonding interaction (Figure 1).

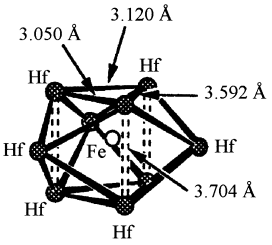


Figure 1. Arrangement of the iron atoms in the center of hafnium tricapped trigonal-prismatic cages in Hf_5FeTe_3 (from ref. [52]).

The nature of the metal–metal bonding was qualitatively established by extended Hückel (EH) band structure calculations. Crystal overlap populations were determined for the metal–metal bonded framework and the averaged curves for Hf–Fe and Hf–Hf interactions in Hf_5FeTe_3 are depicted in Figure 2. While the availability of

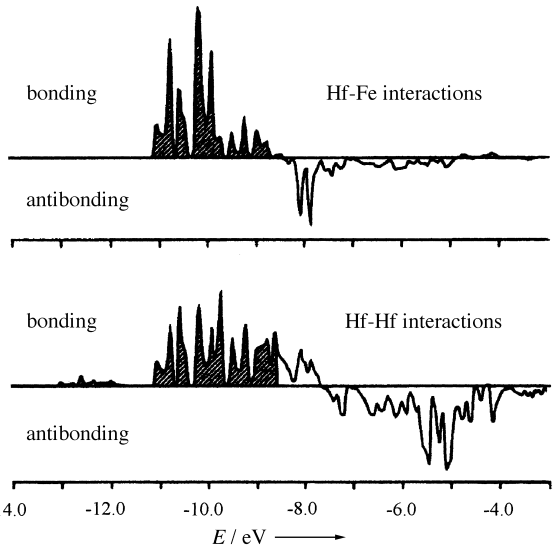


Figure 2. Average crystal orbital overlap population curves for Hf–Fe and Hf–Hf contacts in Hf_5FeTe_3 (from ref.[52]).

Hf–Hf bonding levels above the Fermi level indicate that addition of electrons would enhance the homometallic Hf–Hf bonding, the intermetallic Hf–Fe bonding is evidently optimized in the given case and it is this optimization of the heterometallic bonding which appears to stabilize the metal–metal bonded framework. Moreover, Hf–Fe bonding is polar covalent with the metal–metal bonding levels being primarily Fe localized, while the antibonding levels are unoccupied and primarily Hf localized. This result appears to be consistent with the donor–acceptor model proposed for the metal–metal bonding in intermetallic phases.

If early–late transition metal bonding appears to be particulartly favored in bare clusters and heterometallic ternary phases, why then were stable coordination compounds containing such metal–metal bonds extremely rare until recently? As high-level calculations performed for models of unsupported early–late heterodinuclear complexes have shown, their metal–metal bonds are by no means less stable

Table 2. Dissociation energies of the diatomic M–Fe molecules.

M–Fe	D°(M–Fe) [kcal mol^{-1}]	M–Fe	D°(M–Fe) [kcal mol^{-1}]
Sc-Fe	55	Fe_2	18
Ti-Fe	42	Co-Fe	30
V-Fe	44	Ni-Fe	39
Cr-Fe	32	Cu-Fe	30

than those of the homonuclear dimers.[53] However, the proximity of a high valent early transition metal and a low valent late transition metal opens up reaction channels caused by intramolecular single electron transfer which lead to a degradation of the dinuclar complex. In addition, unless the highly Lewis acidic early transition metal center is protected by an appropriately designed ligand shell, bimolecular interactions of the complexes or with the solvent may destabilize these systems.

2.2. Metal–Metal Bonds between Complex Fragments of Significantly Different Electronic Properties: Single Bonds and Formal Multiple Bonds

The complexes **8**–**11** are formally derived from tetravalent Group 4 complexes in which one anionic ligand has been replaced by a carbonyl metalate derivative. The late transition metal fragment therefore plays the role of a pseudo halide, a notion which was also put forward by Bursten and co-workers in their analysis of this type of metal–metal bonding (see Section 2.3).[54] The metal–metal bond in **1**–**4** or complexes such as **8**–**11** may therefore be interpreted as a polar single bond even though the actual covalent bond order may be well below unity as will be discussed below. However, the high-valence state of the early transition metal and the metal–metal bond polarity render these bonds remarkably short in comparison to homometallic single bonds which normally range between 2.7 and 3.0 Å. This is shown for various Ti–M complexes in Table 3.

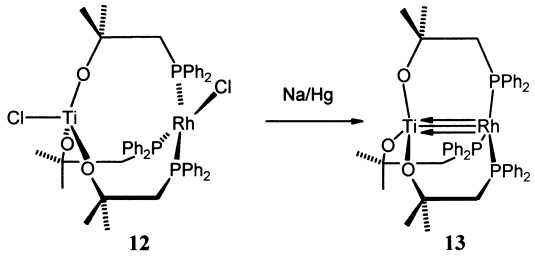
The early transition metal fragment in **8** and **9** possesses unoccupied d orbitals which would have the correct symmetry for further donor–acceptor interactions with a d-electron rich, late transition metal fragment. This additional donor–acceptor interaction would then reinforce the metal–metal bond and lead to an increased bond order, manifested in a short interatomic distance.

Table 3. Metal–metal bond lengths in Ti–M heterodinuclear complexes containing unsupported Ti–M bonds.

Complex	*d*(Ti–M)	Ref.
Ti–Mn		
$[(t\text{BuO})_3\text{Ti–Mn(CO)}_5]$	2.684(1)	[59]
Ti-Fe		
$[\{\text{MeC(CH}_2\text{NSiMe}_3)_3\}\text{Ti–FeCp(CO)}_2]$	2.433[a]	[41]
$[\{\text{MeSi[SiMe}_2\text{N(2-FC}_6\text{H}_4)]_3\}\text{Ti–FeCp(CO)}_2]$	2.433(4)	[82]
$[\{\text{MeSi[SiMe}_2\text{N}(p\text{-Tol})]_3\}\text{Ti–FeCp(CO)}_2]$	2.460(1)	[44]
$[(\text{Me}_2\text{N})_3\text{Ti–FeCp(CO)}_2]$	2.568[a]	[35]
Ti–Ru		
$[\{\text{MeC(CH}_2\text{NSiMe}_3)_3\}\text{Ti–RuCp(CO)}_2]$	2.527(1)	[41]
$[\{\text{HC[SiMe}_2\text{N}(p\text{-Tol})]_3\}\text{Ti–RuCp(CO)}_2]$	2.503(4)	[41]
$[\{\text{MeSi[SiMe}_2\text{N}(p\text{-Tol})]_3\}\text{Ti–RuCp(CO)}_2]$	2.5609(8)	[82]
$[(\text{Me}_2\text{N})_3\text{Ti–RuCp(CO)}_2]$	2.663(1)	[35]
$[(2,6\text{-Me}_2\text{C}_6\text{H}_3\text{O})_2(\text{Me}_2\text{N})\text{Ti–RuCp(CO)}_2]$	2.573(1)	[36]
Ti–Co		
$[\{\text{MeSi[SiMe}_2\text{N}(p\text{-Tol})]_3\}\text{Ti–Co(CO)}_3(\text{PTol}_3)]$	2.471(4)	[53]
$[\{\text{MeSi[SiMe}_2\text{N}(p\text{-Tol})]_3\}\text{Ti–Co(CO)}_4]$	2.5542(10)	[53]
$[(t\text{BuO})_3\text{Ti-Co(CO)}_4]$	2.565(2)	[39]
$[\text{Cp}\{\text{Co}_3(\text{CO})_9(\mu\text{-CO})\}_2\text{Ti–Co(CO)}_4]$	2.614	[25]

[a] Average value of two independent molecules in the asymmetric unit.

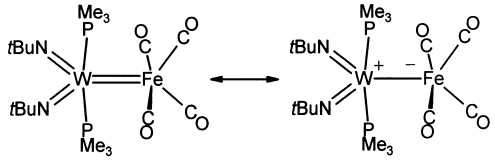
A complex containing a metal–metal bond bearing these characteristics has been reported by Slaughter and Wolczanski.[55] Reduction of the heterodinuclear complex **12** with sodium amalgam yielded the Ti–Rh bonded complex **13**. Its



12 **13**

most characteristic structural element is the extremely short Ti–Rh distance of 2.2142(11) Å which is 0.362 less than the sum of the covalent metal radii. Since the bridging ligands are fairly flexible and undistorted in complex **13**, this short metal–metal distance was interpreted as arising from additional Ti–Rh donor–acceptor interaction and thus increased metal–metal bond order.

Highly polar formal metal–metal double bonds were expected to result from the salt metathesis of an early transition metal *dihalide* with a *carbonyl metalate dianion*. A well-characterized example of this type of metal–metal bond formation is known for a high-valent–low-valent heterodinuclear complex. Reaction of the bis(imido)tungsten complex $[\text{W}(=\text{N}t\text{Bu})_2\text{Cl}_2]$ with $\text{K}_2[\text{Fe(CO)}_4]$ in the presence of trimethylphosphane yielded the W–Fe complex **14**.[56] Although



14

the structure of complex **14** is well established, the question of the W–Fe bond multiplicity is not trivial. In species of high bond polarity such as this a zwitterionic formulation leaving the covalent bond order at about unity is equally conceivable. A detailed theoretical study of this compound is clearly warranted.

2.3. Metal–Metal Bond Polarity: A Theoretical Approach

The concept of bond polarity, which is used in main group chemistry with reference to the electronegativities of the atoms involved, is less readily applied in a quantitative way to bonds between transition metals. Their nature may be more significantly influenced by the coordination spheres of the two or more metal centers involved rather than intrinsic properties of the metal itself. This increased level of sophistication required in a meaningful discussion of bond polarity in M–M′ bonds necessitates elaborate quantum-chemical methods to be used. However, this may render it difficult to extract

information from the results of such calculations which are interpretable within the established paradigms of structure and bonding familiar to the chemist.

First attempts to tackle the problem of metal–metal bond polarity in early–late heterodinuclear complexes were reported by Bursten and Novo-Gradac who applied Xα-SW molecular orbital methods to Casey's system $[Cp_2(X)Zr{-}Ru(CO)_2Cp]$ (**10**) as well as the analogous Th–Ru complex $[Cp_3(X)Th{-}Ru(CO)_2Cp]$.[54, 57] Based on an analysis of the frontier orbitals it was concluded that the nature of the M–Ru bonding is essentially the same in the two systems and that it may be described as the donation from the filled $4d_{z^2}$ orbital of ruthenium into the empty d_{z^2} orbital of Th or Zr. This results in a slightly bent M–Ru σ-bonding orbital to which the frontier orbitals of the two metal centers contribute 15% (Zr) and 72% (Ru) (Figure 3). This highly unequal contribution of the two metal centers to the metal–metal bonding orbital may be interpreted as qualitatively representing a highly polar bond.

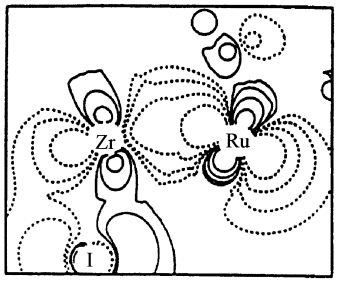
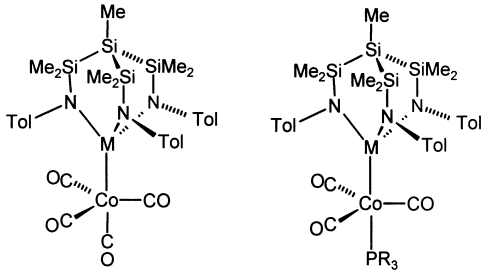


Figure 3. Contour diagram of the metal–metal bonding orbital in **10** (X = I) in the I-Zr-Ru plane.

Shortly thereafter, Wolczanski and coworkers published extended Hückel MO calculations on various early–late heterobimetallic complexes[58] and, more recently, Selent et al. reported the results of an EHMO study of $[(t\mathrm{BuO})_3Ti{-}M(CO)_n]$ (M = Co/Mn, $n = 4/5$).[59] All of these studies offered a qualitative analysis of the principal bonding interactions between the early and the late metal centers. However, the published theoretical analyses of the M–M′ bonds, based on the metric parameters derived from various crystal structures, although providing some valuable insight into the nature of this class of compounds, are unsuitable for addressing such questions as metal–metal bond polarity in even a semiquantitative way. An approach which addresses the principal difficulties of determining metal–metal bond polarity and offers a state-of-the-art theoretical analysis of the electronic structure of a suitable model complex has been reported recently and will therefore be reviewed in more detail.[53]

An important aspect governing the choice of an appropriate system of study was the molecular symmetry of the heterodinuclear complex. In order to facilitate the interpretation of the results obtained in calculations and in the experimental structural studies, both complex fragments, joined through the direct metal–metal (M–M′) bond, were required to have the same symmetry with respect to this bonding axis. Early–late heterodinuclear complexes meeting this requirement do indeed exist, such as the complexes **15** and **16** in which the *trans*-axial position at the cobalt atom is occupied either by a CO or a triarylphosphane ligand (Scheme 4).



15 **16**

Scheme 4. The Ti–Co and Zr–Co heterodinuclear complexes **15** and **16** (M = Ti, Zr, Hf; R = aryl). Tol = *p*-MeC_6H_4.

An X-ray crystallographic study of four compounds containing Ti–Co and Zr–Co bonds, with and without *trans*-axial phosphane substitution, provided the experimental "point of reference" for the metric parameters which characterize these complexes (Figure 4). The optimized structural parameters obtained by density functional theory (DFT) methods for the heterobimetallic model complexes $[(H_2N)_3Ti{-}Co(CO)_4]$ and $[(H_2N)_3Ti{-}Co(CO)_3(PH_3)]$ were compared to those obtained experimentally and good general agreement was found (Scheme 5).

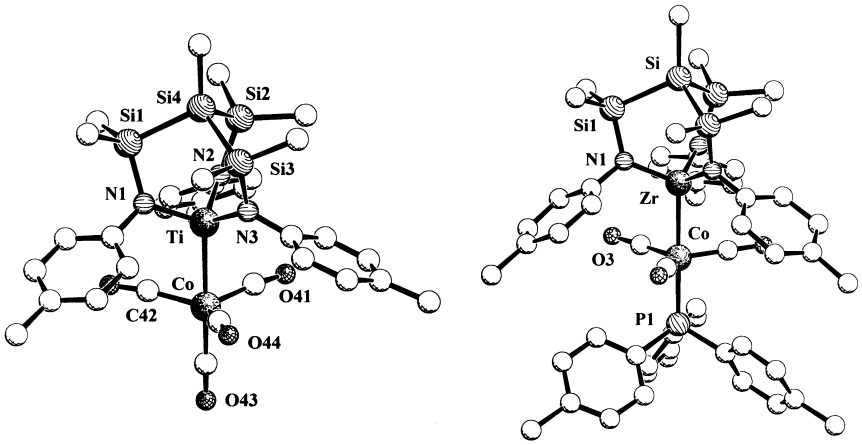
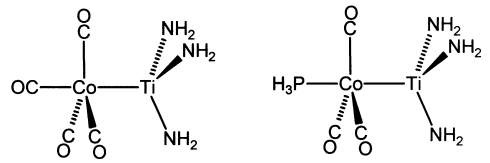


Figure 4. Molecular structures of the two M–Co heterodinuclear complexes $[\{MeSi[SiMe_2N(4\text{-}CH_3C_6H_4)]_3\}M{-}Co(CO)_3(L)]$ (M = Ti, Zr).



Scheme 5. Model compounds investigated in the theoretical study.[53]

To establish the degree of metal–metal bond polarity several independent theoretical approaches were employed. These included, on the one hand, orbital based population

analysis schemes such as natural population analysis (NPA)[60] in combination with Wiberg bond indices[61] and charge decomposition analysis (CDA).[62] On the other hand, essentially orbital independent methods such as Bader's AIM ("atoms in molecules") approach[63–65] in combination with Becke's, Edgecombe's and Savin's ELF ("electron localization function")[66, 67] were employed.

Based on these methods, in particular the combination of Bader's partitioning of the molecules into atomic domains and the localization of electron pairs using the ELF formalism, a consistent picture of the nature of the Ti–Co bonds in the dinuclear complexes was obtained: First, the covalent metal – metal bond order is less than 0.5 and influenced (b.o. ca. 0.1) by the nature of the transaxial ligand coordinated to cobalt. Second, high partial charges assigned to the complex fragments of greater than 0.5 e were established which emphasize the highly polar character of the Ti–Co bonds. A depiction of an electron density isosurface of $[(H_2N)_3$-$Ti{-}Co(CO)_3(PH_3)]$ given in Figure 5 clearly shows the low level of electron density between the metal centers if compared to the situation for the metal – ligand bonds. This is to be seen as reflecting the high Ti–Co bond polarity.[53]

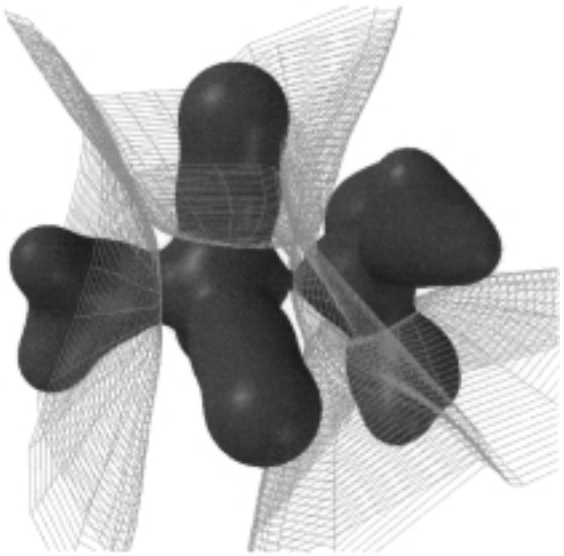


Figure 5. The isosurface of $[(H_2N)_3Ti{-}Co(CO)_3(PH_3)]$ ($\lg(\rho) = -1.3$) along with several of the Bader surfaces around the metal atoms. The molecule is depicted with the $(H_3P)(CO)_3Co$ unit pointing left and the $Ti(NH_2)_3$ unit pointing right. Note the area of low-electron density between the metal atoms.

Visualization of the nature of the Ti–Co bonds was most persuasively achieved by the representation of the ELF isosurface in relation to the AIM boundary surface between the two complex fragments bound to each other. The electron localization function (ELF) was originally introduced within the framework of Hartree – Fock theory by Becke and Edgecombe[66] as a function of the spherically averaged probability of finding an electron with a given spin in the neighborhood of another electron with the same spin which represents an indirect measure for the location of an electron pair with two electrons of opposite spin. ELF is then constructed in such a way that it assumes values of close to unity when there is a high probability of finding paired electrons (or single, unpaired electrons), and it assumes values close to zero in those regions of space where no electron pairing occurs. Figure 6 shows a superposition of a part of the

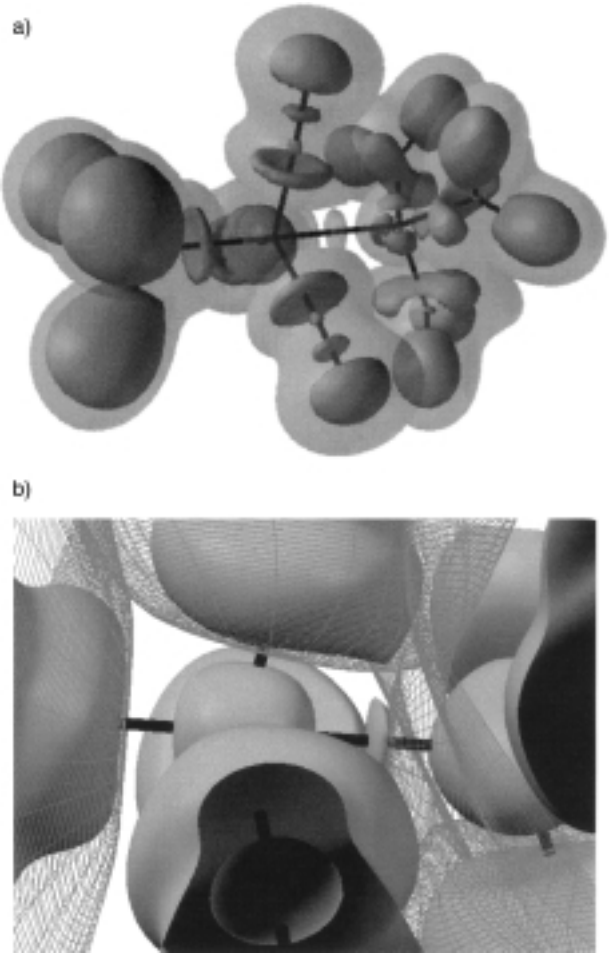


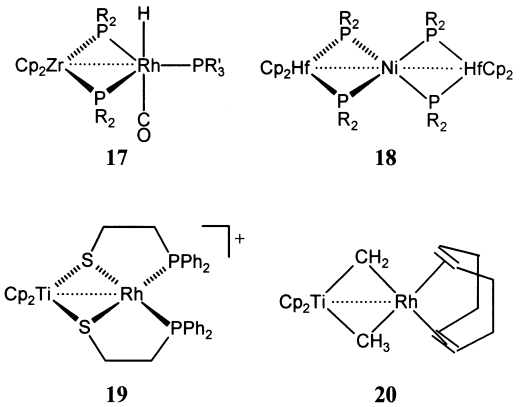
Figure 6. a) Isosurfaces of $[(H_2N)_3Ti{-}Co(CO)_3(PH_3)]$(ELF = 0.42: translucent, ELF = 0.83: solid) superimposed. The molecule is oriented in the same way as in Figure 5. b) A zoom into the Co–Ti bond region for ELF = 0.43, along with some of the Bader surfaces. This very clearly illustrates the localization of the bond electron pair close to the Co–Ti separating surface.

ELF isosurface with some of the atom-separating surfaces around the metal atoms.[53] The metal – metal bond electron pair localization domain—being disk-shaped—and very close to the separating surface between the metal atoms is essentially concentrated on the side of the Co atom and thus is mainly in the atomic domain of that metal atom towards which the bond is polarized.[67]

In summary, while molecular orbital based population analyses may provide a reliable measure of the polarity of a bond, it is only the direct analysis of electron distributions as achieved by the combination of Bader's AIM approach and the electron localization function (ELF) which achieves this independent from an MO basis set and enables us to visualize the polarization of the bonding electron pairs in real space. This theoretical approach is expected to find more widespread use in future studies of metal – metal bond polarity.

3. Directly Metal–Metal Bonded Early–Late Heterodinuclear Complexes with and without Bridging Ligands

The focus of this article is the polar metal–metal bond in early–late heterodimetallic complexes. Its importance and structural function is beyond doubt in the systems without bridging ligands and many examples of these have been introduced in the previous sections. However, by far the majority of heterodinuclear complexes synthesized and studied to date contain bridging ligands. The chemistry of these species has been reviewed first by Stephan about a decade ago[5a] and, subsequently, by Chetcuti.[68] A very recent general overview of the area has been published by Wheatley and Kalck.[5b] Typical examples for heterodimetallic complexes (**17**–**20**) stabilized by bridging ligands are summarized in Scheme 6. In all of them, the presence or absence of direct metal–metal bonding is not unambiguously clarified but all would be conceivable without there being a metal–metal bond.[69–71]

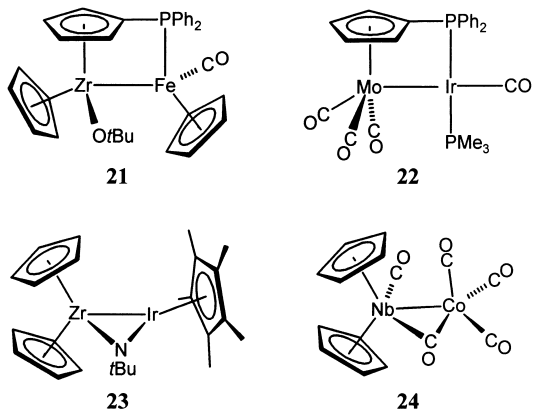


Scheme 6. Early–late heterodimetallic complexes containing bridging ligands for which direct metal–metal bonding is not unambiguously clarified but which would be conceivable without a metal–metal bond. Cp = C_5H_5; R, R′ = alkyl, aryl.

Significant metal–metal bonding between an early and a late transition metal may be assumed even in the presence of bridging ligands if the electron count and physical properties, the metal–metal distance established by X-ray crystallography and the patterns of chemical reactivity are in accord with such a bond. This is clearly the case for the complexes **21**–**24** (Scheme 7) and systems of this type will therefore be included in the following discussion of the generation and the reactivity of highly polar metal–metal bonds.[72, 73]

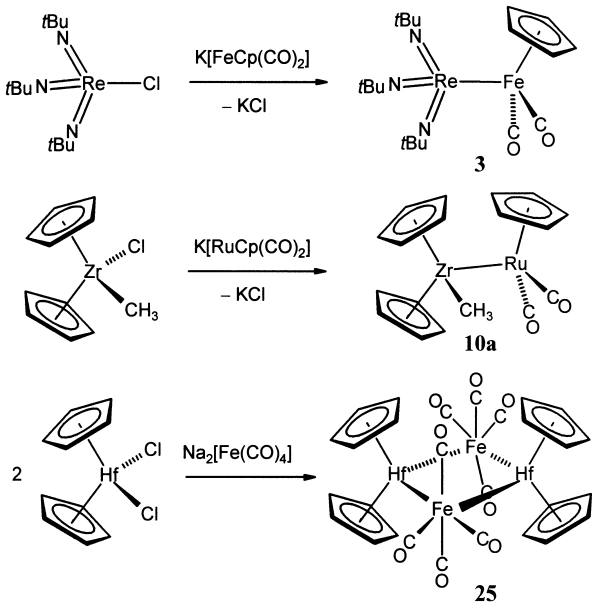
4. Synthetic Strategies for the Generation of Highly Polar Metal–Metal Bonds

The linking of the two electronically different transition metal centers to give a dinuclear complex containing a highly polar metal–metal bond may be achieved by several basic synthetic strategies. The most widely employed method is the simple salt metathesis which for early–late or high-valent–low-valent heterodinuclear complexes involves the reaction



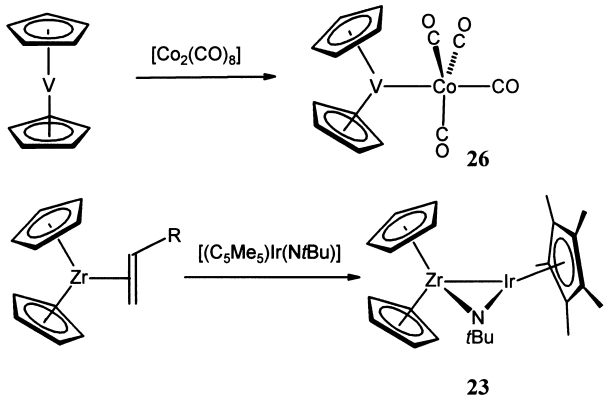
Scheme 7. Early–late heterodimetallic complexes containing bridging ligands in which the metal–metal bond is a significant structural feature.

of an early (high-valent) transition metal halide with a alkali metal salt of an anionic late (low-valent) transition metal complex (mostly carbonyl metalates). Several examples of this method, which include the reaction of a dihalide with a dianionic metal carbonylate, are summarized in Scheme 8.[27, 37, 75]



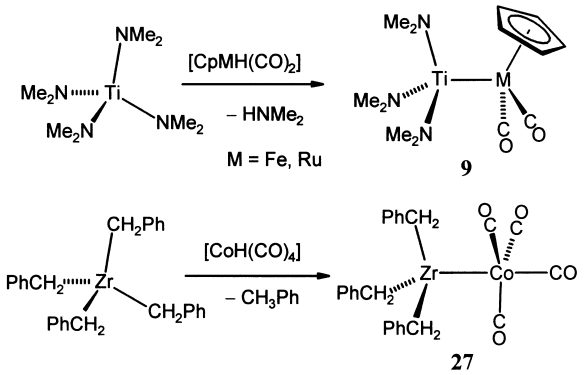
Scheme 8. Synthesis of heterodinuclear complexes by salt metathesis using alkali metal salts of the carbonyl metalates.

A severe limitation of this approach is the possibility of a single-electron transfer competing with the salt elimination and formation of the metal–metal bond. The high-valent, early transition metal complex fragments are almost always potential oxidizing agents and the carbonyl metalates reducing agents. An alternative M–M′ coupling strategy thus involves the reaction of neutral complexes and the elimination of a less polar molecule upon formation of the dinuclear complex. Examples of the former strategy are the synthesis of the unstable and thus incompletely characterized complex **26**[74] as well as the imido ligand bridged Zr–Ir complex **23** (Scheme 9).[73]



Scheme 9. Synthesis of heterodinuclear complexes by combination of neutral complex fragments.

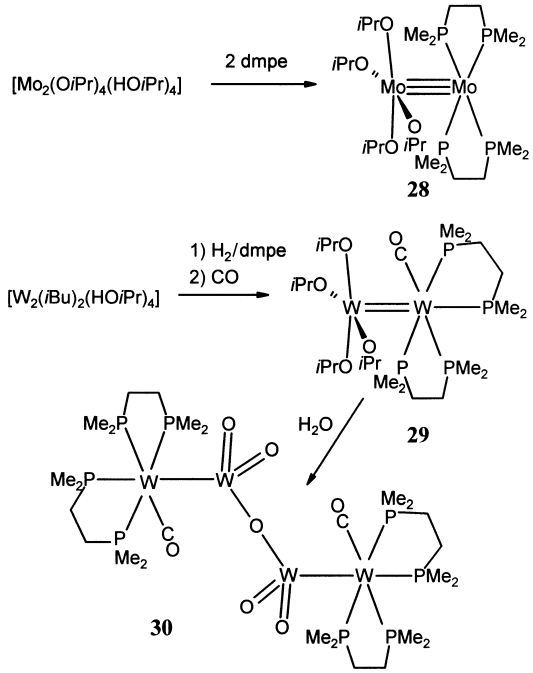
Dimetallic elimination reactions leading to metal–metal bond formation are the amine or alkane eliminations which result from the "condensation" of a late transition metal hydrido complex with an early transition metal amido or alkyl complex, respectively. Examples of this method are Selegue's synthesis of the first Ti–Fe and Ti–Ru complexes **9**[35, 36] and the reaction of $[Zr(CH_2Ph)_4]$ with $[CoH(CO)_4]$ (Scheme 10).[76]



Scheme 10. Metal–metal bond formation by bimolecular amine or alkane elimination.

A method frequently employed in the synthesis of homodinuclear complexes is the elimination of halide ligands by reduction. This strategy is applicable in the synthesis of heterodinuclear complexes if bridging ligands effect the prearrangement of the two metal centers, as is exemplified by the synthesis of the Ti–Rh complex **13** already discussed in Section 2.2 which was obtained by Na/Hg reduction of the halide precursor **12**.[55]

A remarkable synthetic strategy for homodinuclear complexes of the high-valent–low-valent type of the Group 6 metals involves the reaction of a symmetrical precursor complex containing metal centers in an intermediate oxidation state with a soft ligand such as a phosphane. Chisholm and co-workers have reported several examples of this reactive pattern. These include the reaction of the dimolybdenum complex $[Mo_2(OiPr)_4(HOiPr)_4]$ with dmpe (dmpe = $Me_2PCH_2CH_2PMe_2$) to give the unsymmetrical Mo^0–Mo^{IV} complex $[Mo_2(OiPr)_4(dmpe)_2]$ (**28**), and the hydrogenation of $[W_2(iBu)_2(OiPr)_4]$ in the presence of dmpe and subsequent carbonylation to give $[W_2(OiPr)_4(dmpe)_2(CO)]$ (**29**) (Scheme 11).[77] The latter could be hydrolyzed to give the remarkable tetranuclear complex $[W_2O_4(\mu\text{-}O)\{W(CO)(dmpe)_2\}_2]$ (**30**) with a formal W^0–W^V oxidation state pattern.



Scheme 11. Ligand rearrangement and formal redox disproportionation of the metal centers upon reaction of a symmetrical precursor complex containing metal centers in an intermediate oxidation state with a soft ligand.

This pattern of reactivity may be understood in view of the ambivalent character of the Group 6 metal with respect to their chemical hardness. Depending on the oxidation state they act as hard or soft Lewis acids and thus—at the extremes of the partial charge scale—preferentially ligate only hard or soft ligands.

4.1. Factors Influencing the Stability of "Unsupported" Metal–Metal Bonds in "Early–Late" Heterodimetallic Complexes

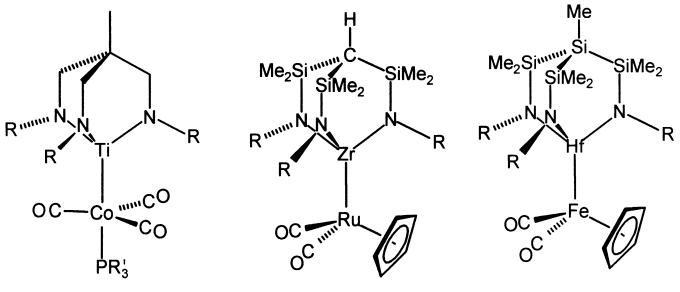
As is the case for most metal-bound molecular fragments in coordination compounds, the stabilization of the metal–metal bonds in early–late heterodimetallic complexes may be achieved by the appropriate choice of the ancillary ligands. This, in particular, applies to the early transition metal fragment which is generally highly Lewis acidic and chemically hard and thus requires an appropriate set of hard σ and π donor ligands. It is therefore not surprising that by far most of the metal–metal-bonded complexes of the early–late or high-valent–low-valent type have sets of ligands coordinated to the high-valent transition metal center which comprise alkoxy, amido, imido, and oxo ligands.[78] These chemically hard ligands not only meet the electronic demands of the Lewis acidic metal center to which they are bound but at the same time stabilize the oxidation state of this coordination

center and thus suppress degradation by single-electron transfer processes. Among other potential factors, this characterisic property of the ligands in question explains the relative stability of Selegue's Ti–Fe and Ti–Ru complexes $[(Me_2N)_3Ti{-}MCp(CO)_2]$ in comparison with the inaccessible Ti–M derivatives containing the Cp_2Ti unit. Titanocene derivatives are generally more readily reduced than the amido and alkoxy complexes of the same element.

Whereas the discussion so far has centered around the correct choice of the donor functions to stabilize the early transition metal, their integration into a polydentate ligand system and thus the design of the chemical environment of the donor atom may be of equal importance for the successful stabilization of the dinuclear complex. Amido functions (R_2N^-), which possess two substituents at the donor atom, may be readily incorporated into polydentate ligand systems which are designed to shield most of the coordination sphere of the metal center and, additionally, enforce a particular coordination geometry.[79, 80] Both aspects effect, respectively, the kinetic and an additional thermodynamic stabilization of the highly polar metal–metal bond and an example of the practical implementation of this concept is discussed in the following section.

4.2. Stabilization of Early–Late Heterodinuclear Complexes by Use of Tripodal Amido Ligands

The remarkable development which early transition metal chemistry has experienced during the past decade as a consequence of the development of many new types of polydentate amido ligands has also had its effect on the synthesis of stable early–late heterodimetallic complexes containing unsupported metal–metal bonds. The tripodal amido ligands displayed in Scheme 12[81] have provided the key to, a systematic program of complex synthesis.[41–44, 53, 82]

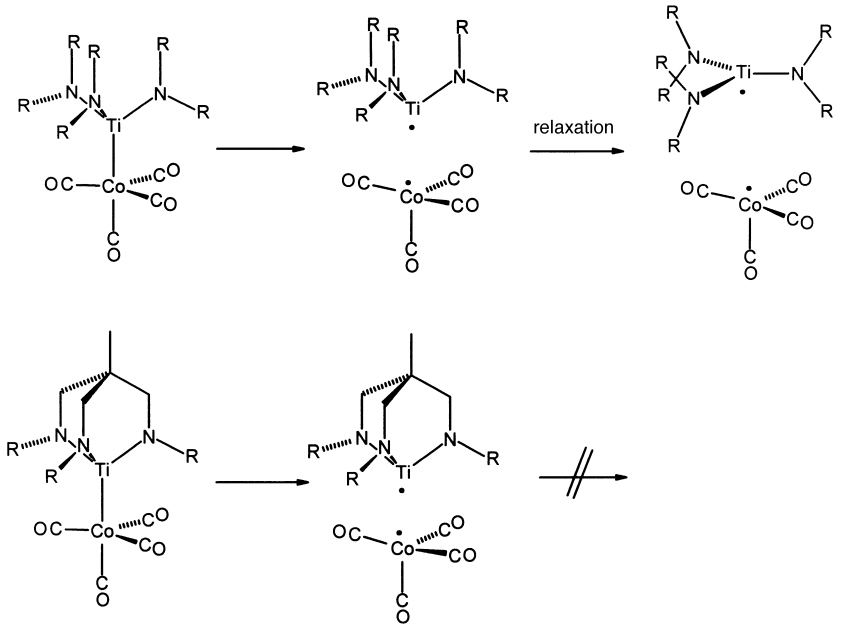


Scheme 12. Unsupported early–late heterodinuclear complexes stabilized by tripodal amido ligands. R = aryl, silyl; R′ = aryl. The metal–metal bonds displayed above were stabilized by using this approach.

While the ligand framework effectively shields the part of the coordination sphere opposite to the metal–metal bond, the latter is kinetically protected by the peripheral (silyl or aryl) substituents at the nitrogen donor functions.

At least as important as this kinetic stabilization of the dinuclear complexes is a significant thermodynamic contribution to their stability which is the result of the incorporation of the early transition metal into the rigid bicyclo[2.2.2]octane-like cage structure of the tripod–amide unit.[81, 82] This geometric fixation destabilizes the potential fragmentation product, the triamidometal fragment. In the analogous systems containing monodentate anionic ligands at the early transition metal center the $\{ML_3\}$ fragment undergoes planarization upon cleavage of the metal–metal bond, a process which stabilizes the fragment. This planarization is suppressed in the tripod cage (Scheme 13).

In order to have an estimate of the energetic contribution of this geometric relaxation of the early transition metal com-



Scheme 13. Thermodynamic stabilization of dinuclear complexes with tripodal–aminde ligands by suppression of the possible relaxation into a planar structure in systems with monodentate ligands.

plex fragment, a theoretical study was carried out on the Ti–Co model complex $[(H_2N)_3Ti{-}Co(CO)_4]$ which was already discussed in Section 2.3.[53] Figure 7 schematically represents the overall energetics for the dissociation into two neutral fragments. D_r and D_{nr} are the dissociation energies for the dissociation into, respectively, completely relaxed and partially nonrelaxed complex fragments. In the nonrelaxed case the geometry of the Ti fragment was fixed to that of $[(H_2N)_3Ti{-}Co(CO)_4]$, while in both cases the Co fragment was energetically minimized.[53]

As indicated in Figure 7 the planarization energy $E_r(Ti)$ of the Ti fragment is about 10 kcal mol^{-1}. This represents an upper boundary of the hypothetical relaxation energy of the Ti fragment containing the tripod ligand, which is unable to achieve the planar geometry of the free $[Ti(NH_2)_3]$ complex.

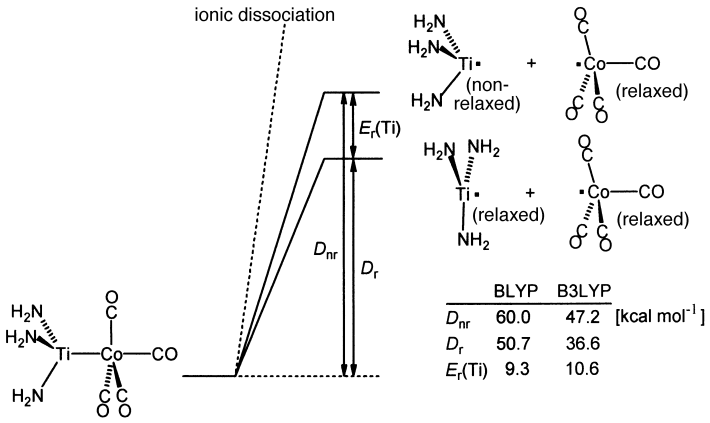


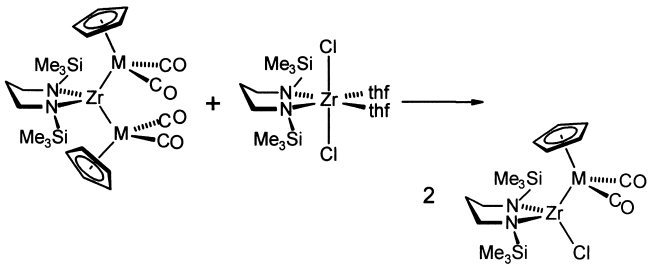
Figure 7. Energy diagram for the homolytic dissociation of the metal–metal bond in $[(H_2N)_3Ti{-}Co(CO)_4]$.

Therefore, one can estimate that the tripod ligand thermodynamically stabilizes the Co–Ti complex by about 10 kcal mol^{-1} with respect to fragmentation of the metal–metal bond. Since the early transition metal fragment is the same in the whole range of heterodinuclear complexes coordinated by tripodal amido ligands, this figure can be regarded as a general estimate of the thermodynamic stabilization of the complexes with respect to their mononuclear fragments.

5. Basic Patterns of Reactivity Observed for Metal–Metal Bonded Early–Late Heterodinuclear Complexes

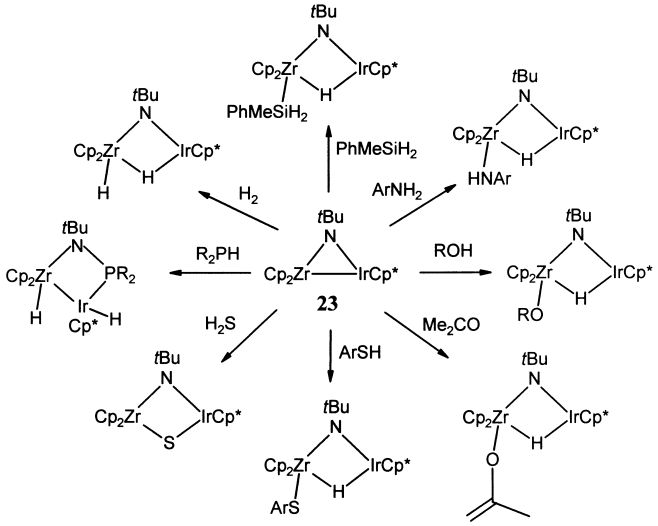
Generally, the discussion of the reactivity of metal–metal bonded polynuclear complexes may focus either on metal–ligand, that is metal–substrate interactions or the redistribution of metal complex fragments which implies cleavage and re-formation of metal–metal bonds. Most of molecular cluster complex reactivity may be described within the framework of this partitioning or by a combination of the two. Early–late heterodimetallic complexes were found to undergo redistribution reactions of their metal fragments, such as the "conproportionation" of $[Cp_2Zr\{RuCp(CO)_2\}_2]$ with $[Cp_2ZrCl_2]$ to give the dinuclear complex $[Cp_2(Cl)Zr{-}RuCp(CO)_2]$ or similar reactions involving the amido-stabilized complexes (Scheme 14).[37, 38, 83]

The scope of this complex fragment redistribution is limited. It was, for instance, not possible to obtain the heterotrimetallic complex $[\{CH_2(CH_2NSiMe_3)_2Zr\{FeCp(CO)_2\}\{RuCp(CO)_2\}]$ by reaction of the $ZrFe_2$ with the $ZrRu_2$ complex.



Scheme 14. Complex fragment redistribution in the reaction of $[\{CH_2(CH_2NSiMe_3)_2\}Zr\{MCp(CO)_2\}]$ with the dichloro complex $[\{CH_2(CH_2NSiMe_3)_2\}ZrCl_2(thf)_2]$ resulting in the formation of the corresponding dinuclear species. M = Fe, Ru.

The reactivity of the polar metal–metal bonds towards organic substrates is of more general interest. As for many other types of heterodinuclear complexes extensive reactivity studies were carried out with the aim of establishing cooperative reactivity between the electronically very different reactive sites which may interact with the substrate. Essentially two types of reaction were possible. The first involves the interaction of the metal–metal bond with substrates of no or low polarity which are fragmented and transformed to a "polarized" form at the two metal centers. For example, this is the general pattern of the addition of H_2 or a silane to the Zr–Ir bond in Bergman's heterodinuclear complex **23** (Scheme 15).[84]



Scheme 15. Cooperative reactivity of the heterodinuclear complex **23** with nonpolar and polar substrates. Cp* = C_5Me_5.

Reactivity towards substrates which match the polarity of the metal–metal bonds is far more common. Examples in Scheme 15 are the reactions of alcohols, amines, thiols, ketones, and H_2S with the Zr–Ir complex.

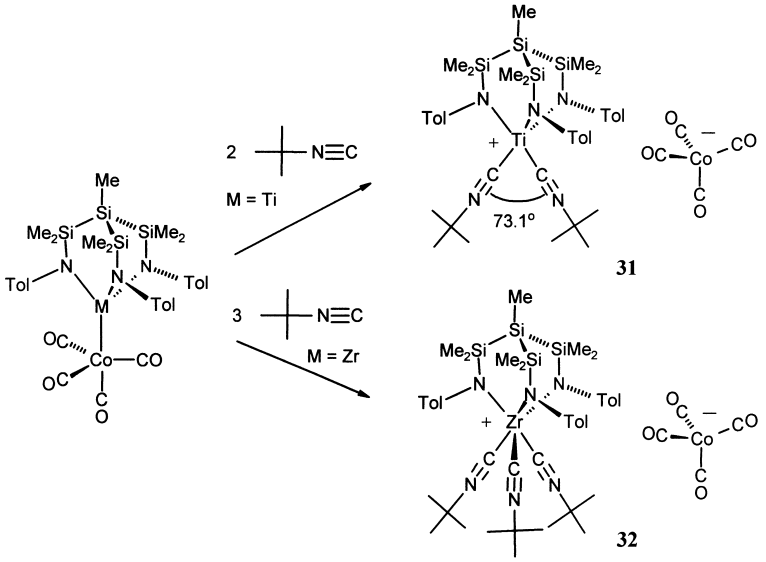
In the simplest case heterodinuclear complexes will react as pairs of metal electrophiles and nucleophiles. Cooperative reactivity is particularly likely with polar substrates. In this case the electropositive early transition metal center may react with the more Lewis basic part of the substrate, while the nucleophilic late transition metal complex fragment will attack the more Lewis acidic part of the substrate molecule. For metal–metal single bonds between the two metal centers this interaction will go along with the cleavage of the metal–metal bond. In many cases it is difficult to establish whether the cission of the metal–metal bond precedes the transformation of the substrate or whether it occurs at a later stage.

5.1. The Principle of the "Masked" Pairs of Metal Nucleophiles and Electrophiles

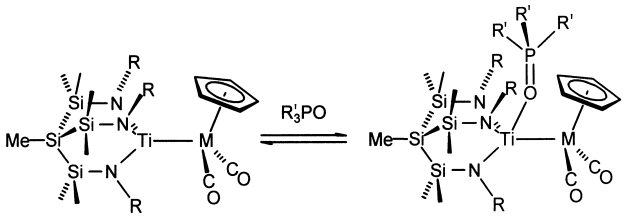
A systematic study of the reactive behavior of Ti–M and Zr–M heterodinuclear complexes (M = Fe, Ru, Co) has elucidated the early stages of the interaction of polar

substrates with the two metal centers and allowed the notion of the pair of metal electrophiles and nucleophiles to be put to a test. The initial interaction of a polar substrate with the heterodinuclear complex is the formation of a Lewis acid base adduct at the early transition metal center. In most cases this adduct formation is thought to be reversible and such intermediates of Ti–M complexes with phosphane oxides could be detected spectroscopically (Scheme 16).[85]

This adduct formation may be viewed as the first step in a solvation process of the early transition metal center which leads to the ionic dissociation of the metal–metal bond giving the solvent-stabilized early transition metal cation and the late transition metal complex anion.[86] The cleavage of metal–metal bonds yielding ionic complex fragments was already discussed in Section 2.2 in connection with the solution properties of the "xenophilic" cluster complexes.

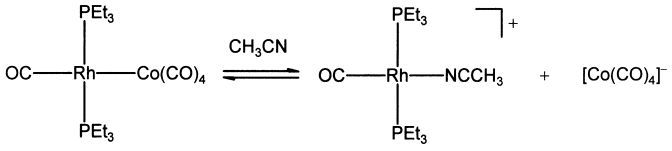


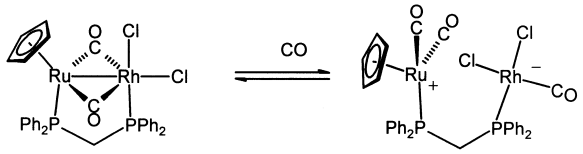
Scheme 18. Ionic cleavage of the Ti–Co and Zr–Co bonds in [{MeSi[SiMe$_2$N(4-MeC$_6$H$_4$)]$_3$}M–Co(CO)$_4$] (M = Ti, Zr).



Scheme 16. Reversible formation of a Lewis acid base adduct at an early transition metal as exemplified by the reaction of Ti–M complexes with phosphane oxides. R = aryl; R′ = alkyl, aryl.

Although ionic dissociation of metal–metal bonds has been known for some time, there are only a few well characterized examples of this behaviour in which no concomitant redox reaction is involved. (Scheme 17).[87, 88]





Scheme 17. Heterolytic dissociation of heterodinuclear complexes.

This reactive behavior is also observed for early–late heterodinuclear complexes, provided the late transition metal fragment is essentially nonnucleophilic, as is the case for $[Co(CO)_4]^-$.[89] Reaction of [{MeSi[SiMe$_2$N(4-CH$_3$C$_6$H$_4$)]$_3$}-M–Co(CO)$_4$] (M = Ti, Zr) with *t*BuNC leads to immediate dissociation of the metal–metal bonds and formation of the salts **31** and **32** (Scheme 18) both of which could be isolated and structurally characterized by X-ray crystallography (Figure 8).

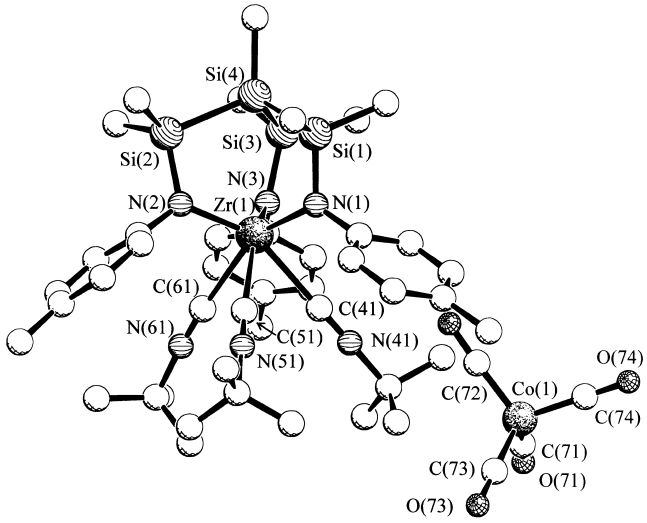


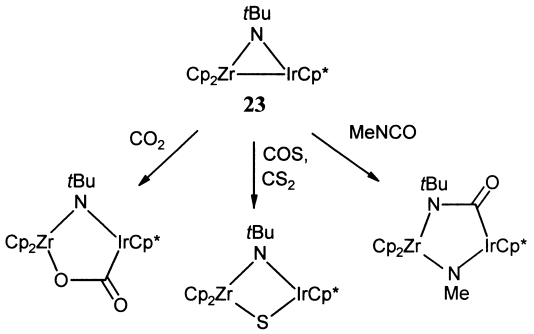
Figure 8. Molecular structure of **32** as determined by X-ray crystallography

The importance of the nucleophilicity of the complex anion could be established by the reaction of **31** with K[RuCp-(CO)$_2$], the alkali metal salt of a strongly nucleophilic metal carbonylate. Initially, immediate displacement of the isonitrile ligands at the Ti center takes place and the Ti–Ru complex thus formed is subsequently slowly converted to the product of an insertion of the isonitrile into the polar metal–metal bond. The latter reaction is reversible and the equilibrium constant was found to be 0.91 L mol^{-1} at 298 K in benzene.[89]

The insertion of an isonitrile into a polar metal–metal bond is the analogue of the polar α-addition to isonitriles, the nucleophile and electrophile being metal complexes. Insertions of substrate molecules into the metal–metal bonds are the first step in most of the reactions of polar organic molecules with the heterodinuclear complexes and thus deserved closer attention.

5.2. Insertions into Polar Metal–Metal Bonds

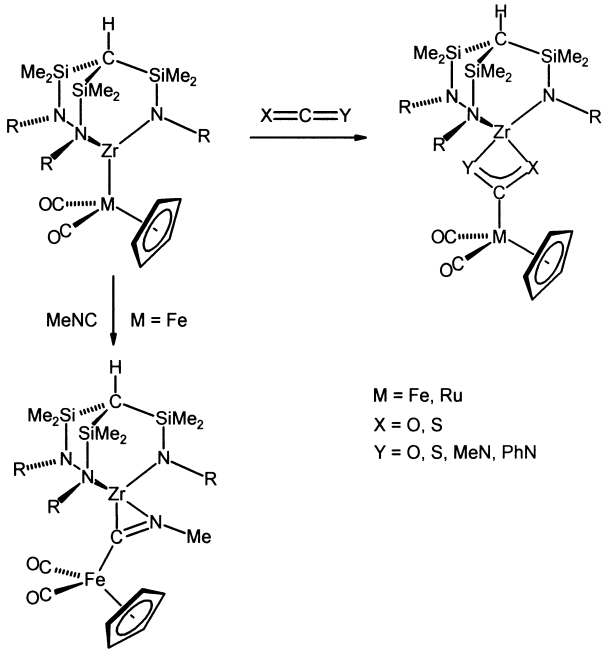
The simplest pattern of reactivity observed for early–late hereodimetallic compounds is the insertion of an unsaturated polar organic substrate into the metal–metal bond. The first such reaction was reported by Culter and co-workers who showed that Casey's Zr–M complexes insert CO_2 into their metal–metal bond[90] while Bergman et al. studied the reactions of the imido-bridged Ir–Zr complex **23** with CO_2, COS, CS_2, and MeNCS (Scheme 19).[91] While the insertion of



Scheme 19. Insertion and fragmentation of heteroallenes upon reaction with the Zr–Ir complex **23**.

CO_2 occurs in the expected fashion with the CO unit bridging the two metal centers remain still linked by the imido ligand, the other heteroallenes undergo fragmentation.

The insertion of isonitriles discussed in the previous section provides yet another example of this reactive behavior. Insertion reactions of isonitriles and heteroallenes carried out with the tripod-stabilized early–late heterodinuclear complexes which led to stable products are summarized in Scheme 20. The



Scheme 20. Insertion of isonitriles and heteroallenes into the unsupported metal–metal bond of Zr–M heterodinuclear complexes. R = 2-FC_6H_4.

molecular structure of [{HC[$SiMe_2$N(2-FC_6H_4)]$_3$}Zr(μ-CS_2)-FeCp(CO)$_2$], the product derived from the insertion of CS_2 into a Zr–Fe bond is depicted in Figure 9.[92]

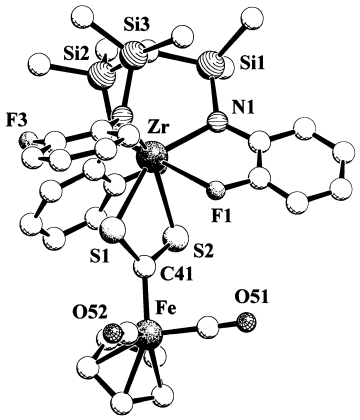
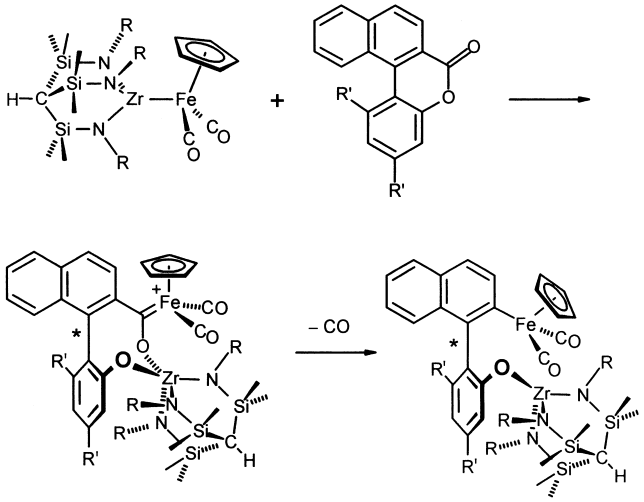


Figure 9. Molecular structure of the insertion product [{HC[$SiMe_2$N(2-FC_6H_4)]$_3$}Zr(μ-CS_2)FeCp(CO)$_2$] as determined by X-ray crystallography.

5.3. Transformations of Carbonyl Compounds in the Coordination Sphere of Zr–M Complexes

The products of the simple insertion of an organic molecule (or a functional group in it) into the polar metal–metal bond are rarely isolable and, most often, further transformations follow this initial step. In the simplest case, these subsequent transformations closely mimic those which the organic molecules undergo with "classical" nucleophiles and electrophiles. An example is the cleavage of esters RC(O)OR′ giving the early transition metal alkoxide and the acyl–metal derivative of the late transition metal complex fragment. This reaction was extended to include lactones, in particular configurationally labile prochiral biaryllactones which were readily cleaved and subsequently decarbonylated to give the ring-opened products (Scheme 21). The chiral biaryl axis in



Scheme 21. Ring opening and decarbonylation of biaryllactones. R = 2-FC_6H_4; R′ = Me, OMe.

the reaction product is evident in the view of the molecular structure of one of the product complexes shown in Figure 10.[93]

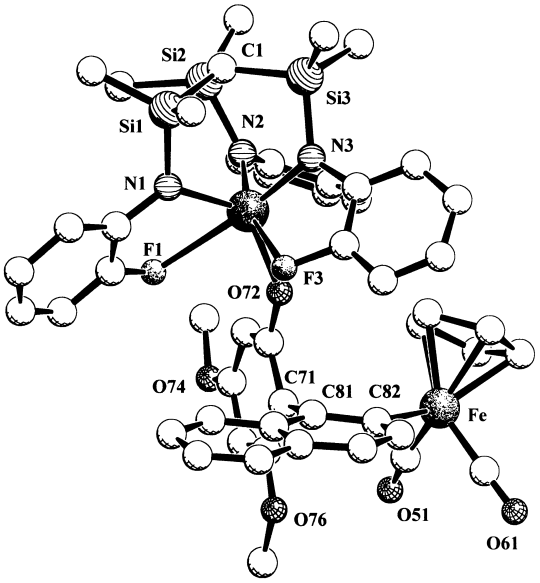


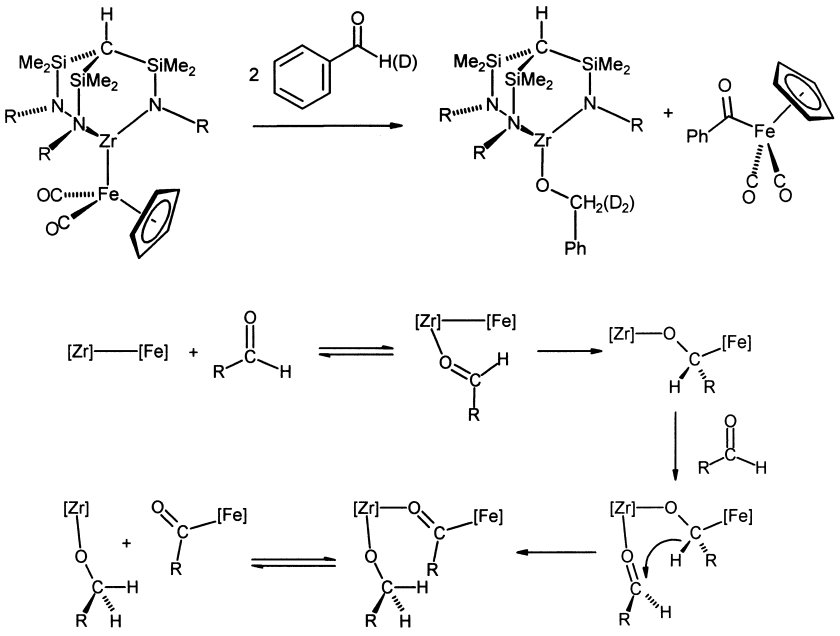
Figure 10. Molecular structure of the ring-opening product of [{HC[SiMe$_2$N(2-FC$_6$H$_4$)]$_3$}Zr–FeCp(CO)$_2$] with a biaryl lactone showing the chiral biaryl axis.

Aryl aldehydes react with Zr–M heterodinuclear complexes according to the pattern of a Cannizzaro or Tishchenkov reaction yielding the aroyl–M complex and the benzoxyzirconium derivative (Scheme 22).[94] The first step in the reaction sequence is thought to be the addition of an aldehyde molecule to the Lewis acidic early transition metal center which is followed by its insertion into the metal–metal bond. The cleavage of the Zr–Fe bond reduces the coordination number at the zirconium center which in turn facilitates the addition of the second molecule of the aldehyde. The crucial reaction step is the hydride transfer which follows and involves an analogous intermediate as proposed for the Cannizzaro disproportionation. Support for this intramolecular mechanism was obtained from the results of an isotope-labeling experiment employing C_6H_5CDO.

Finally, reaction of [{HC[SiMe$_2$N(2,3,4-F$_3$C$_6$H$_2$)]$_3$}-Zr–FeCp(CO)$_2$] with ketones gave the aldol coupling products ligated to the Zr center and equivalent amounts of the hydridoiron complex [CpFeH(CO)$_2$] (Scheme 23). The hydrido complex is thought to be formed in a first reaction step following the insertion of the carbonyl group into the metal–metal bond; the latter yields an extremely reactive enolate which in turn rapidly undergoes aldol coupling with a second molecule of ketone.[94]

5.4. Oxygen Atom Transfer within the Coordination Sphere of Zr–M Complexes

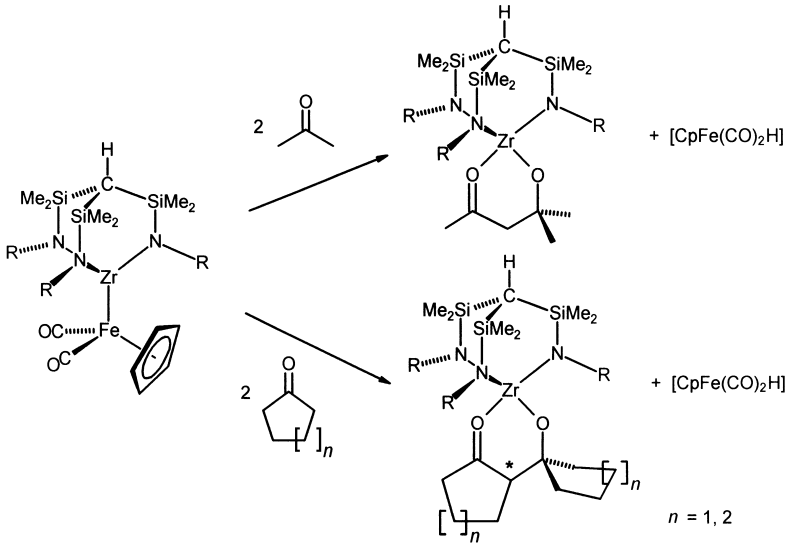
The transformations discussed so far in this section leave the ligand already present in the starting materials unchanged. The carbonyls coordinated to the late transition metal may, however, participate directly in the conversion of a substrate. The late transition metal fragment is thus not only the nucleophile in the primary reaction step with the substrate but at the same time the binding site (or source) of the second reactant. This type of cooperativity has been found in a series of oxygen-transfer reactions. The most remarkable of these is the reaction of the Zr–Fe complex **33** with 1,2-diphenylcyclopropenone giving the carbeneiron complex **34** in which the oxidized carbonyl ligand links the two metal centers as a μ-CO_2 unit (Scheme 24).[94] The result is thus formally a reduction of a ketone by CO yielding a carbene and CO_2, a reaction which is thermodynamically driven by the formation of two Zr–O bonds and the stable CO_2 unit in the product.



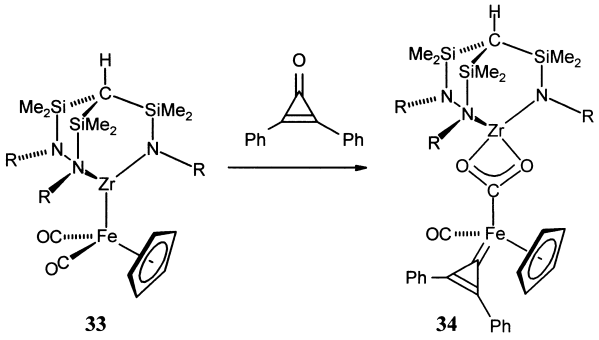
Scheme 22. Top: Cannizzaro-type disproportionation of aryl aldehydes upon reaction with a Zr–Fe heterodinuclear complex. Bottom: Proposed mechanism of the "hydride transfer".

Similar oxygen-transfer reactions have been observed with sulfoxides and other element oxides, which yielded the late transition metal bound thioethers or the corresponding reduced ligands.[95] The pattern of the oxygen transfer has been established by ^{17}O- and ^{13}C-labeling studies in all these cases.[82] That both metal centers participate in the conversion of the element oxide is evident from the inability of either of the metal complex fragments linked by the Zr–M bond to effect these tranformations on their own. These considerations led to the proposal of a reaction mechanism for the deoxygenation of the cyclopropenone given in Scheme 25 as well as analogous reaction pathways for the other oxygen transfers.[94]

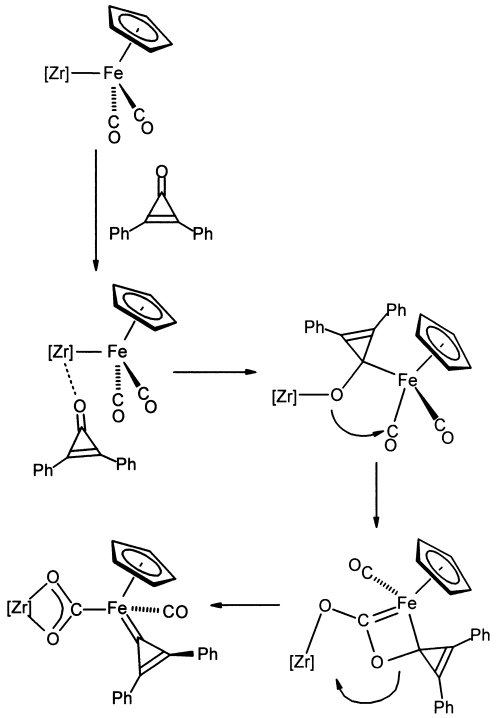
That the interaction of these substrates with only one of the mononuclear units may lead to quite different results was shown inter alia by reaction of 1,2-diphenylcyclopropenone with [CpMCO)$_2$]$^-$ (M = Fe, Ru),



Scheme 23. Aldol coupling products obtained from the reaction of $[\{HC[SiMe_2N(2,3,4\text{-}F_3C_6H_2)]_3\}Zr{-}FeCp(CO)_2]$ with ketones. R = 2,3,4-$F_3C_6H_2$.



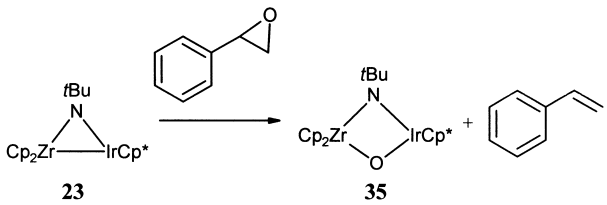
Scheme 24. Deoxygenation of 1,2-diphenylcyclopropenone giving the carbeneiron complex **34**. R = 2,3,4-$F_3C_6H_2$.



Scheme 25. Proposed reaction mechanism of the oxygen transfer in the conversion of 1,2-diphenylcyclopropenone to give the carbeneiron complex **34**.

which gave a metallacyclopentenedione instead of a carbene complex.

Rapid transfer of oxygen has been observed in reactions of **23** with pyridine *N*-oxide, nitrous oxide, and styrene oxide.[96] However, the result of these reactions is the formation of oxo-bridged heterobimetallic complexes such as **35**. Similar transfer reactions with sulfur have also been observed.



6. Strong Metal Support Interaction and the Possibility of Metal–Metal Bonding at the Surfaces of Supported Heterogeneous Catalysts

Our discussion has focussed on metal–metal bonding between early and late transition metals and its implications for the reactivity at the interface between two complex fragments of very different chemical properties. The interface character of such metal–metal interactions is thought to be important in an area of heterogeneous catalysis which superficially has little in common with the systems discussed so far. For the past two decades the interaction of late transition metals deposited on oxidic early transition metal supports, such as TiO_2, has received much attention. The phenomenon that the adsorption of H_2 and CO on the surface of Group 8–10 metals deposited on partially reduced early transiton metal oxides is partially or completely suppressed has been dubbed *strong metal-support interaction (SMSI)*.[98, 99] This suppression of the chemisorption and the decrease in the catalytic activity of such supported materials is due to a remarkable restructuring of the catalyst surface upon treatment of the early transition metal oxide carrying the late transition metal crystallites with H_2 at high temperatures. This leads to a partial reduction of the metal oxide supports, of which TiO_2 has received most attention. As a consequence of this reduced oxide surface two processes affect the deposited metal: on the one hand the oxidic material rapidly encapsulates the metal particles with a sheath of titanium oxide and thus passivates them in subsequent catalytic studies. On the other hand, the deposited metal particles may reorganize themselves to form flat, raftlike structures. Both processes lead to a maximized interface between the partially reduced early transition metal support material and the deposited late transition metal. These processes are thought to be thermodynamically driven by strong bonding forces between the two phases.[97]

The question of potential metal–metal interactions in such supported catalysts has received much attention. Whereas nowadays the concept of SMSI is referred to mostly in the phe-

nomenologigal way, relating to the difference in adsorption properties and catalytic activity believed to arise from an interaction of deposit and support, some researchers use the term in the more specific relation to structural reorganization of the interface and thus the possibility of bonding interactions.[97]

A system which was studied in particular detail is that of rhodium deposited on TiO_2 which displays all the characteristics mentioned above. There is clearly no evidence for any kind of metal–metal bonding in the system before treatment with H_2 at high temperatures as was, for example, established by X-ray photoelectron spectroscopy and UV photoelectron spectroscopy of Rh on the fully oxidized support.[100] The deposition of metallic rhodium on a reduced TiO_2 surface, for which Auger electron spectroscopy showed the presence of Ti^{3+}, led to a partial electron transfer from the trivalent titanium to the deposited rhodium, a possible indication of a polar bonding interaction.[101] This was additionally supported by an EXAFS study, by Haller and co-workers, of a Rh/TiO_2 catalyst after reduction with hydrogen at 500 °C which not only indicated Rh–Rh bonding (2.69 Å) within the deposited metal but, additionally, a metal–metal distance of 2.53–2.56 Å which was attributed to Ti–Rh bonding (Figure 11).[102] Remarkably this Rh–Ti distance is significantly shorter than the metal–metal bond found in the monoclinic alloy TiRh (2.68 Å).[103]

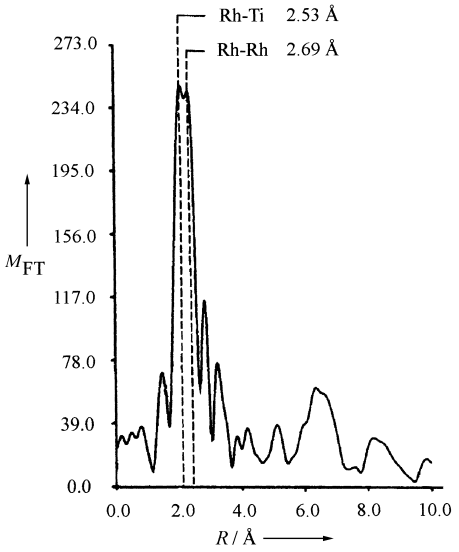


Figure 11. The k^3-weighted Fourier transform (M_{FT}) of the EXAFS spectra for a Rh/TiO_2 catalyst after in situ reduction with H_2 at 500 °C for 90 min.

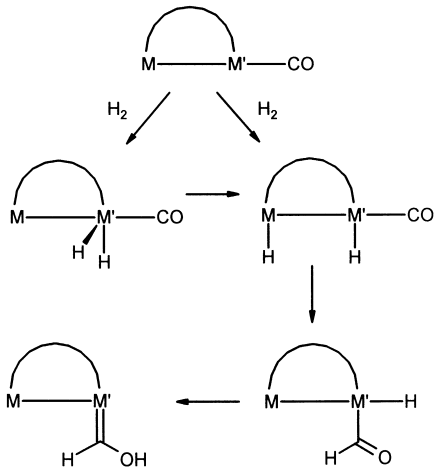
Strong metal-support interactions might have found much less attention if the interaction of TiO_x or NbO_x with deposited Ni, Pd, or Pt would not lead to a markedly increased Fischer–Tropsch activity of such supported catalysts.[104] In this industrial process synthesis gas (CO/H_2 1/3) is converted to a mixture of hydrocarbons. The rate of the hydrogenation of CO to form methane or other hydrocarbons is found to be increased by 1–2 orders of magnitude and the product distribution significatly changed. While the mechanistic details of this effect have not been established beyond doubt, it has been proposed that the activation of CO happens at the interface between the deposited late transtion metal and the reduced oxide. The CO molecule possibly "straddles" this interface with the oxygen atom coordinated to the titanium center and the carbon atom coordinated to the late transition metal in the same way as observed in early–late heterodimetallic complexes containing a bridging "isocarbonyl ligand". In addition, the presence of "spillover" hydrogen is thought to be important for the Fischer–Tropsch activity. This is H_2 which dissociates on the late transition metal surface and then "spills" into the partially reduced surrounding support to provide highly reactive reducing sites, possibly hydridic species.

6.1. Zr–M Heterodinuclear Complexes: The Quest for Homogeneous Fischer–Tropsch Catalysts

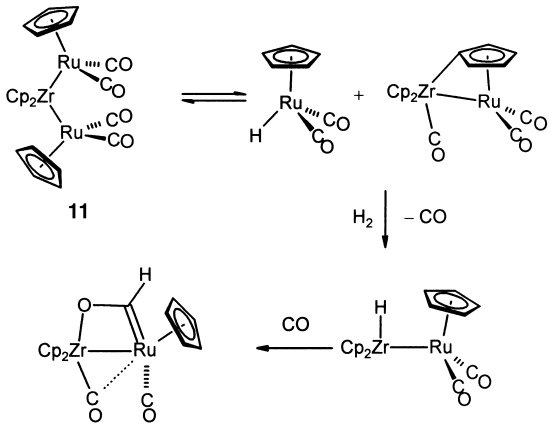
As discussed above, a direct bonding interaction between the late transition metal component in a heterogeneous catalyst and the early transition metal support material has been proposed especially for TiO_2 supported contacts. The relationship with an important industrial heterogeneous catalytic process inspired the first systematic study into the reactivity of directly metal–metal bonded early–late heterodimetallic compounds. This was carried out by Casey and coworkers in connection with the renewed interest in the chemistry of the Fischer–Tropsch process which emerged in the wake of the oil crisis in the 1970s.[105] The development of a homogeneous catalyst effecting this transformation under milder and more controlled conditions was regarded as a desirable goal and inspired a detailed investigation of the conversion of CO ligands to hydrocarbon fragments at the metal centers of organometallic complexes. Several such reactions could indeed be established although none of the systems studies showed promise for the developement of a catalyst.

A concept for a potential catalytic system was formulated in Casey's group and based on the accessibility of a heterometallic dihydrido complex containing one "hydridic" M–H bond to a high oxidation state early transition metal along with an acidic hydride at the late transition metal center. Ideally, the two metal centers were to be linked by a bridging ligand which would ensure their proximity even after the metal–metal bond was cleaved. The combination of the two differently polarized metal hydrides, generated by activation of H_2, would then provide the appropriate "reagent" for the hydrogenation of a metal-bound CO molecule, possibly along the route proposed by Casey which is outlined in Scheme 26.

The experimental study carried out throughout the 1980s mainly focussed on the unsupported Zr–Ru heterodimetallic complexes **10** and **11**. While the original objective of H_2 splitting generating a pair of hydridic and acidic hydrides and the subsequent reduction of CO was not achieved with these, the work carried out by the Madison group led to the discovery of some fascinating organometallic chemistry which has been reviewed previously in detail.[105] One example of a reaction sequence involving the conversion of CO in compound **11** is given in Scheme 27.[106]



Scheme 26. Mechanism of the nonsymmetrical activation of H_2 across a polar metal–metal bond in an early–late heterodinuclear complex (containing a bridging ligand) and the subsequent hydrogenation of coordinated CO.



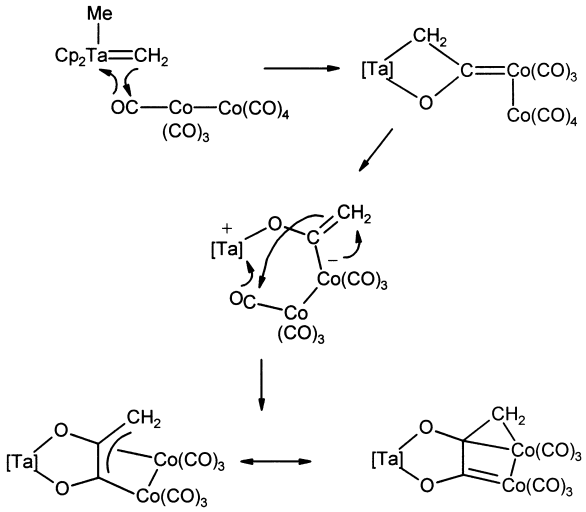
Scheme 27. Reaction of the trinuclear complex **11** with H_2 and CO resulting in the transfer of a hydride to a carbonyl ligand.

Recently, Fandos et al. reported the Ti–Rh heterometallic complex $[(C_5Me_5)Ti(\mu\text{-}O)_3\{Rh(cod)\}_3]$ (cod = 1,5-cyclooctadiene) which they regard as a molecular model for SMSI in TiO_2-supported Fischer–Tropsch catalysts. In the presence of this material, CO was indeed reduced at 250 °C and 20 bar (H_2/CO 3/1) to give, inter alia, methane and short chain alcohols. However, neither the structure of the catalytically active species nor the importance of a possible bonding interaction between the metal centers has been established.[107]

That the combination of early and late transition metal centers and the different sets of ligands they bear may induce interesting patterns of C–C bond fomation was also shown by Proulx and Bergman who reacted neutral metal carbonyls with Schrock's tantalum methylidene complex $[Cp_2(CH_3)\text{-}Ta{=}CH_2]$ (Scheme 28). It seems though that metal–metal bonding between the early and late transition metal fragments does not play a role in any of these cases.[108]

7. Conclusion and Outlook

When the chemistry of early–late heterodimetallic complexes was first reviewed comprehensively a decade ago[5] there were only a few examples for which metal–metal bonds were unambiguously established. Moreover, the nature of this type of heterometallic bonding and its implications for the chemical reactivity of such systems was barely explored. The broadening of the preparative strategies available for the generation of compounds containing highly polar metal–



Scheme 28. C–C bond formation by reaction of $[Cp_2(CH_3)Ta{=}CH_2]$ with $[Co_2(CO)_8]$.

metal bonds and in particular the availability of new types of complex fragments which may be combined to this end have significantly advanced the field.

A conceptual framework is now available for a quantitative description of metal–metal bond polarity and is accompanied by a wealth of structural data derived from several systematic studies. It is the specific use of ligand design in order to stabilize the coordination geometry and environment required for high metal–metal bond polarity which has demonstrated a strategy which has potential beyond the currently known types of structures. The quest for stable early–late heterodimetallic complexes has entailed the chemical "taming" of the early transition metal and at the same time opened up other applications of this approach in organometallic chemistry.

Early–late heterodimetallic complexes have been shown to act as homogeneous catalysts.[109] However, in none of the examples studied to date is the presence of the two *complementary* metal centers an *indispensible prerequisite* for the conversion which is effected. The usefulness of the combination of the two very different metal centers at close proximity in catalytic reactions remains to be demonstrated and it is this aspect, in particular, which will provide the challenge in future studies. This is also related to the question whether bond breaking and re-formation between early and late transition metals may be productively incorporated in a catalytic cycle.

I would like to thank my students and postdoctoral researchers who worked in the area reviewed in this article: They were, in rough chronological order, Stefan Friedrich, Harald Memmler, Martin Schubart, Bernd Findeis, Christina Platzek, Uta Kauper, Andreas Schneider, Dominique Trösch, Santiago Garcia-Yuste, Sylvie Fabre, Izoldi Bezougli, and Matthias Lutz. Our work relied heavily upon structure determinations by X-ray crystallography, and I am particularly grateful to Mary McPartlin (London) and her co-workers who not only carried out most of the X-ray diffraction studies but contributed significantly to the conceptual development. Georg Jansen (Düsseldorf/Nancy) and Catherine Housecroft (Basel) performed theoretical calculations on heterodimetallic complexes and corrected some naïve views of mine concerning metal–metal bond polarity. Georg explained the fundamentals of density functional theory to me and introduced me to Bader's AIM theory. Our research was generously supported by the Deutsche Forschungsgemeinschaft, the European Union (TMR Program MECATSYN), the Fonds der Chemischen Industrie, the British Council, and the DAAD. Most important for the author has been the unlimited support he received from Helmut Werner during his time at Würzburg.

Received: January 10, 2000 [A 385]

[1] Early Reviews: a) J. Lewis, R. S. Nyholm, *Science Progress* **1964**, *52*, 557; b) F. A. Cotton, *Q. Rev. Chem. Soc.* **1966**, *20*, 389; c) P. Chini, G. Longoni, V. G. Albano, *Adv. Organomet. Chem.* **1976**, *14*, 285.

[2] a) D. M. P. Mingos, D. Wales, *Introduction to Cluster Chemistry*, Prentice Hall, London, **1990**; b) *The Chemistry of Metal Cluster Complexes* (Eds.: D. F. Shriver, H. D. Kaesz, R. D. Adams), VCH, Weinheim, **1990**; c) M. Herberhold, G.-X. Jin, *Angew. Chem.* **1994**, *106*, 1016; *Angew. Chem. Int. Ed. Engl.* **1994**, *33*, 964.

[3] *Metal Clusters in Chemistry* (Eds.: P. Braunstein, L. A. Oro, P. R. Raithby), Wiley-VCH, Weinheim **1999**.

[4] a) D. A. Roberts, G. L. Geoffroy in *Comprehensive Organometallic Chemistry Vol. 6* (Eds.: G. Wilkinson, F. G. A. Stone, E. W. Abel) Pergamon, **1982**, p. 763; b) P. Braunstein, J. Rose in *Stereochemistry of Organometallic and Inorganic Compounds Vol. 3* (Ed.: I. Bernal), Elsevier, Amsterdam , **1989**, p. 3.

[5] a) D. W. Stephan, *Coord. Chem. Rev.* **1989**, *95*, 41; b) N. Wheatley, P. Kalck, *Chem. Rev.* **1999**, *99*, 3379.

[6] T. S. Kuhn, *The Structure of Scientific Revolutions*, Chicago, **1962**.

[7] A. Werner, *Neuere Anschauungen auf dem Gebiete der Anorganischen Chemie*, Braunschweig **1905**.

[8] An entertaining account of the development of the concept of metal–metal bonding has been given by: F. A. Cotton, *J. Chem. Educ.* **1983**, *60*, 713.

[9] R. J. Havinghurst, *J. Am. Chem. Soc.* **1926**, *48*, 2113. The history of the mercurous salts is particularly interesting and the dispute over their correct chemical formulation involved some of the most famous chemists of the 19th century: E. Mitscherlich, *Justus Liebigs Ann. Chem.* **1834**, *12*, 137 (the measurements on mercurous chloride are quoted on p. 166); H. S. Deville, L. Troost, *Justus Liebigs Ann. Chem.* **1858**, *105*, 213; R. Rieth, *Ber. Dtsch. Chem. Ges.* **1870**, *3*, 666; E. Erlenmeyer, *Justus Liebigs Ann. Chem.* **1864**, *131*, 124; A. W. Williamson, *J. Chem. Soc.* **1864**, *42*, 211; W. Harris, V. Meyer, *Ber. Dtsch. Chem. Ges.* **1894**, *27*, 1482. The matter could only be regarded as settled after the extensive thermodynamic and electrochemical studies published by Ogg in 1898: A. Ogg, *Z. Phys. Chem. Stöchiom. Verwandtschaftsl.* **1898**, *27*, 285. See also: L. H. Gade, *Angew. Chem.* **1993**, *105*, 25; *Angew. Chem. Int. Ed. Engl.* **1993**, *32*, 24.

[10] L. A. Woodward, *Philos. Mag.* **1934**, *18*, 823.

[11] H. M. Powell, R. V. G. Ewens, *J. Chem. Soc.* **1939**, 286.

[12] L. Pauling, *The Nature of the Chemical Bond*, 2nd ed., Oxford University Press, London, **1940**, p. 254.

[13] K. A. Jensen and R. W. Asmussen suggested a non-metal–metal bonded structure represented by two formally zwitterionic resonance structures (K. A. Jensen, R. W. Asmussen, *Z. Anorg. Chem.* **1944**, *252*, 234). In a reply to this proposal Ewens pointed out that this was nothing else but assuming a covalent bond without actually saying so (R. V. G. Ewens, *Nature* **1948**, *161*, 530).

[14] C. Brosset, *Ark. Kemi Mineral. Geol.* **1935**, *12B*(7).

[15] C. Brosset, *Ark. Kemi Mineral. Geol.* **1945**, *20A*(7); C. Brosset, *Ark. Kemi Mineral. Geol.* **1946**, *22A*(11).

[16] L. Pauling, *Chem. Eng. News* **1947**, *25*, 2970.

[17] F. C. Wilson, D. P. Shoemaker, *Naturwissenschaften* **1956**, *43*, 57.

[18] L. F. Dahl, E. Ishishi, R. E. Rundle, *J. Chem. Phys.* **1957**, *26*, 1750.

[19] F. A. Cotton, R. A. Walton, *Multiple Bonds Between Metal Atoms*, Oxford University Press, Oxford, **1993**.

[20] J. A. Bertrand, F. A. Cotton, W. A. Dollase, *J. Am. Chem. Soc.* **1963**, *85*, 1349.

[21] F. A. Cotton, N. F. Curtis, C. B. Harris, B. F. G. Johnson, S. J. Lippard, J. T. Mague, W. R. Robinson, J. S. Wood, *Science* **1964**, *145*, 1305.

[22] M. J. Bennett, F. A. Cotton, R. A. Walton, *J. Am. Chem. Soc.* **1966**, *88*, 3866.

[23] See for example: a) F. A. Cotton, G. Wilkinson, *Advanced Inorganic Chemistry*, 5th ed., Wiley, New York, **1988**; b) J. E. Huheey, E. A. Keiter, R. L. Keiter, *Inorganic Chemistry - Principles of Structure and Reactivity*, 4th ed., Harper Collins, New York **1993**.

[24] L. H. Gade, *Koordinationschemie*, Wiley-VCH, Weinheim **1998**.

[25] G. Schmid, B. Stutte, R. Boese, *Chem. Ber.* **1978**, *111*, 1239.

[26] a) H. G. Alt, H. I. Hayen, R. D. Rogers, *J. Chem. Soc. Chem. Commun.* **1987**, 1795; b) H. G. Alt, H. I. Hayen, R. D. Rogers, *J. Organomet. Chem.* **1989**, *366*, 287.

[27] J. Sundermeyer, D. Runge, J. S. Field, *Angew. Chem.* **1994**, *106*, 679; *Angew. Chem. Int. Ed. Engl.* **1994**, *33*, 678.

[28] J. Sundermeyer, D. Runge, *Angew. Chem.* **1994**, *106*, 1328; *Angew. Chem. Int. Ed. Engl.* **1994**, *33*, 1255.

[29] G. Fachinetti, G. Fochi, T. Funaioli, P. F. Zanazzi, *Angew. Chem.* **1987**, *99*, 681; *Angew. Chem. Int. Ed. Engl.* **1987**, *26*, 680.

[30] a) G. Fachinetti, G. Fochi, T. Funaioli, P. F. Zanazzi, *J. Chem. Soc. Chem. Commun.* **1987**, 89; b) C. Mealli, D. M. Proserpio, G. Fachinetti, T. Funaioli, G. Fochi, P. F. Zanazzi, *Inorg. Chem.* **1989**, *28*, 1122.

[31] a) G. N. Harakas, B. R. Whittlesey, *J. Am. Chem. Soc.* **1996**, *118*, 3210; b) G. Kong, G. N. Harakas, B. R. Whittlesey, *J. Am. Chem. Soc.* **1995**, *117*, 3502.

[32] L. H. Gade, *Angew. Chem.* **1996**, *108*, 2225; *Angew. Chem. Int. Ed. Engl.* **1996**, *35*, 2089.

[33] M. Gerloch, *Coord. Chem. Rev.* **1990**, *99*, 199.

[34] Z. Xu, Z. Lin, *Chem. Eur. J.* **1998**, *4*, 28.

[35] a) W. S. Sartain, J. P. Selegue, *J. Am. Chem. Soc.* **1985**, *107*, 5818; b) W. S. Sartain, J. P. Selegue, *Organometallics* **1987**, *6*, 1812.

[36] W. S. Sartain, J. P. Selegue, *Organometallics* **1989**, *8*, 2153.

[37] a) C. P. Casey, R. F. Jordan, A. L. Rheingold, *J. Am. Chem. Soc.* **1983**, *105*, 665; b) C. P. Casey, R. F. Jordan, A. L. Rheingold, *Organometallics* **1984**, *3*, 504.

[38] C. P. Casey, R. E. Palermo, R. F. Jordan, *J. Am. Chem. Soc.* **1985**, *107*, 4597.

[39] D. Selent, R. Beckhaus, J. Pickardt, *Organometallics* **1993**, *12*, 2857.

[40] M. Brookhart, W. B. Studabaker, R. Husk, *Organometallics* **1987**, *6*, 1141.

[41] S. Friedrich, H. Memmler, L. H. Gade, W.-S. Li, M. McPartlin, *Angew. Chem.* **1994**, *106*, 705; *Angew. Chem. Int. Ed. Engl.* **1994**, *33*, 676.

[42] S. Friedrich, H. Memmler, L. H. Gade, W.-S. Li, I. J. Scowen, M. McPartlin, C. E. Housecroft, *Inorg. Chem.* **1996**, *35*, 2433.

[43] a) S. Friedrich, L. H. Gade, I. J. Scowen, M. McPartlin, *Organometallics* **1995**, *14*, 5344; b) M. Galakhov, A. Martin, M. Mena, C. Yelamos, *J. Organomet. Chem.* **1995**, *496*, 217.

[44] B. Findeis, M. Schubart, C. Platzek, L. H. Gade, I. J. Scowen, M. McPartlin, *Chem. Commun.* **1996**, 219.

[45] a) L. Brewer, P. R. Wengert, *Metall. Trans.* **1973**, *4*, 83; b) L. Topor, O. Kleppa, *J. Less-Common Met.* **1989**, *155*, 61.

[46] a) A. R. Miedema, *Faraday Symp. Chem. Soc.* **1980**, *14*, 136; b) a) K. A. Gingerich, *Faraday Symp. Chem. Soc.* **1980**, *14*, 109; c) A. P. Klyagina, A. A. Levin, *Koord. Khim.* **1984**, *10*, 317.

[47] a) W. Weltner, R. J. Van Zee, *Ann. Rev. Phys. Chem.* **1984**, *35*, 291; b) R. L. Hettich, B. S. Freiser, *J. Am. Chem. Soc.* **1987**, *109*, 3537.

[48] a) T. Hughbanks, G. Rosenthal, J. D. Corbett, *J. Am. Chem. Soc.* **1986**, *108*, 8289; b) T. Hughbanks, G. Rosenthal, J. D. Corbett, *J. Am. Chem. Soc.* **1988**, *110*, 1511; c) T. Hughbanks, J. D. Corbett, *Inorg. Chem.* **1988**, *27*, 2022; d) T. Hughbanks, J. D. Corbett, *Inorg. Chem.* **1989**, *28*, 631.

[49] a) W. Tremel, *Angew. Chem.* **1992**, *104*, 230; *Angew. Chem. Int. Ed. Engl.* **1992**, *31*, 217; b) W. Tremel, *J. Chem. Soc. Chem. Commun.* **1991**, 1405; c) J. Neuhausen, E. N. Finck, W. Tremel, *Chem. Ber.* **1995**, *128*, 569.

[50] a) B. Harbrecht, H. F. Franzen, *J. Less-Common Met.* **1985**, *113*, 349; b) B. Harbrecht, *J. Less-Common Met.* **1988**, *141*, 59.

[51] a) M. E. Badding, F. J. DiSalvo, *Inorg. Chem.* **1990**, *29*, 3952; b) J. Li, R. Hoffmann, M. E. Badding, F. J. DiSalvo, *Inorg. Chem.* **1990**, *29*, 3943.

[52] R. L. Abdon, T. Hughbanks, *J. Am. Chem. Soc.* **1995**, *117*, 10035.

[53] G. Jansen, M. Schubart, B. Findeis, L. H. Gade, I. J. Scowen, M. McPartlin, *J. Am. Chem. Soc.* **1998**, *120*, 7239.

[54] B. E. Bursten, R. J. Strittmatter, *Angew. Chem.* **1991**, *103*, 1085; *Angew. Chem. Int. Ed. Engl.* **1991**, *30*, 1069.

[55] L. M. Slaughter, P. T. Wolczanski, *J. Chem. Soc. Chem. Commun.* **1997**, 2109.

[56] D. Runge, Dissertation, Universität Würzburg, **1997**.

[57] B. E. Bursten, K. J. Novo-Gradac, *J. Am. Chem. Soc* **1987**, *109*, 904.

[58] G. S. Ferguson, P. T. Wolczanski, L. Parkanyi, M. Zonnevylle, *Organometallics* **1988**, *7*, 1967.

[59] D. Selent, M. Ramm, C. Janiak, *J. Organomet. Chem.* **1995**, *501*, 235.

[60] A. E. Reed, L. A. Curtiss, F. Weinhold, *Chem. Rev.* **1988**, *88*, 899.

[61] K. A. Wiberg, *Tetrahedron* **1968**, *24*, 1083.

[62] S. Dapprich, G. Frenking, *J. Phys. Chem.* **1995**, *99*. 9352.

[63] R. F. W. Bader, *Atoms in Molecules: A Quantum Theory*, Oxford University Press, Oxford, **1990**.

[64] R. F. W. Bader, P. L. A. Popelier, T. A. Keith, *Angew. Chem.* **1994**, *106*, 647; *Angew. Chem. Int. Ed. Engl.* **1994**, *33*, 620.

[65] R. F. W. Bader, *Chem. Rev.* **1991**, *91*, 893.

[66] a) A. D. Becke, K. E. Edgecombe, *J. Chem. Phys.* **1990**, *92*, 5397; b) A. Savin, R. Nesper, S. Wengert, T. F. Fässler, *Angew. Chem.* **1997**, *109*, 1892; *Angew. Chem. Int. Ed. Engl.* **1997**, *36*, 1808.

[67] It should be noted that an interpretation of the polar metal – metal bonds as simple donor-acceptor bonds comparable to the Co – Group 13 heterobimetallics synthesized by Fischer et al.[67a] and studied theoretically by Frenking and co-workers[67b] is inappropriate as derived from the charge decomposition analysis (CDA). In other words, the Ti–Co bonds in in the systems at hand are significantly more covalent in nature. a) R. A. Fischer, A. Liehr, T. Priermeier, *Chem. Ber.* **1995**, *128*, 831; b) R. A. Fischer, M. M. Schmidt, J. Weiß, L. Zsolnai, A. Jacobi, G. Huttner, G. Frenking, C. Boehme, S. F. Vyboishchikov, *J. Am. Chem. Soc.* **1998**, *120*, 1237. Review: R. A. Fischer, J. Weiß, *Angew. Chem.* **1999**, *111*, 3002; *Angew. Chem. Int. Ed.* **1999**, *38*, 2831.

[68] M. J. Chetcuti, *Comprehensive Organometallic Chemistry Vol. X* (Eds.: G. Wilkinson, E. W. Abel, F. G. A. Stone), Pergamon, Oxford, **1995**, p. 23.

[69] a) L. Gelmini, D. W. Stephan, *Organometallics* **1988**, *7*, 849; b) G. S. White, D. W. Stephan, *Organometallics* **1988**, *7*, 903.

[70] a) R. T. Baker, W. C. Fultz, T. B. Marder, I. D. Williams, *Organometallics* **1990**, *9*, 2357; b) J. W. Park, P. B. Mackenzie, W. P. Schaefer, R. H. Grubbs, *J. Am. Chem. Soc.***1986**, *108*, 6402.

[71] a) C. P. Casey, F. Nief, *Organometallics* **1985**, *4*, 1218; b) C. P. Casey, R. M. Bullock, F. Nief, *J. Am. Chem. Soc.* **1983**, *105*, 7574.

[72] a) K. S. Wong, R. Scheidt, J. A. Labinger, *Inorg. Chem.* **1979**, *18*, 1709; b) A. A. Pasynskii, A. S. Antsyshkina, Yu. V. Skripkin, V. T. Kalinnikov, M. A. Porai-Koshits, V. N. Ostrikova, G. G. Sadikov, *Russ. J. Inorg. Chem.* **1981**, *26*, 1310; c) A. A. Pasynskii, Yu. V. Skripkin, I. L. Eremenko, V. T. Kalinnikov, G. G. Aleksandrov, V. G. Adrianov, Y. T. Struchkov, *J. Organomet. Chem.* **1979**, *165*, 49.

[73] A. M. Baranger, R. G. Bergman, *J. Am. Chem. Soc.* **1993**, *115*, 7890.

[74] J. Martin, C. Moïse, *J. Organomet. Chem.* **1982**, *232*, C55. This paper reports part of a more comprehensive early study aimed at the synthesis of early – late heterodinuclear complexes including Ti–Mo and Ti–W complexes: J. Martin, C. Moïse, P. Braunstein, unpublished results; P. Braunstein, personal communication.

[75] J. Abys, W. M. Risen, *J. Organomet. Chem.* **1981**, *204*, C5.

[76] a) T. Bartik, B. Happ, A. Sorkau, K.-H. Thiele, G. Pályi, *Organometallics* **1989**, *8*, 558; b) T. Bartik, B. Happ, A. Sieker, S. Stein, A. Sorkau, K.-H. Thiele, C. Kriebel, G. Pályi, *Z. Anorg. Allg. Chem.* **1992**, *608*, 173; c) T. Bartik, H. Windisch, A. Sorkau, K.-H. Thiele, C. Kriebel, A. Herfurth, M. Tschoerner, G. Zucchi, G. Pályi, *Inorg. Chim. Acta* **1994**, *227*, 201.

[77] a) M. H. Chisholm, J. C. Huffman, W. G. Van Der Sluys, *J. Am. Chem. Soc.* **1987**, *109*, 2514; b) M. H. Chisholm, K. S. Kramer, W. E. Streib, *Angew. Chem.* **1995**, *107*, 977; *Angew. Chem. Int. Ed.* **1995**, *34*, 891.

[78] a) M. H. Chisholm, I. P. Rothwell in *Comprehensive Coordination Chemistry, Vol. 2* (Eds.: G. Wilkinson, R. D. Gillard, J. A. McCleverty), Pergamon, Oxford, **1987**, p. 161 b) M. F. Lappert, P. P. Power, A. R. Sanger, R. C. Srivastava, *Metal and Metalloid Amides*, Ellis Horwood-Wiley, Chichester, **1980**; c) W. A. Nugent, J. M. Mayer, *Metal-Ligand Multiple Bonds*, Wiley-Interscience, New York **1988**. See also: d) T. R. Cundari, *J. Am. Chem. Soc.* **1992**, *114*, 7879; e) D. E. Wigley, *Prog. Inorg. Chem.* **1994**, *42*, 239; f) P. Mountford, *Chem. Commun.* **1997**, 2127.

[79] a) J. G. Verkade, *Acc. Chem. Res.* **1993**, *26*, 483; b) R. R. Schrock, *Acc. Chem. Res.* **1997**, *30*, 9.

[80] L. H. Gade, *Chem. Commun.* **2000**, 172.

[81] a) L. H. Gade, N. Mahr, *J. Chem. Soc. Dalton Trans.* **1993**, 489; b) L. H.Gade, C. Becker, J. W. Lauher, *Inorg. Chem.* **1993**, *32*, 2308; c) H. Memmler, L. H. Gade, J. W. Lauher, *Inorg. Chem.* **1994**, *33*, 3064; d) M. Schubart, B. Findeis, L. H. Gade, W.-S. Li, M. McPartlin, *Chem. Ber.* **1995**, *128*, 329.

[82] L. H. Gade, M. Schubart, B. Findeis, S. Fabre, I. Bezougli, M. Lutz, I. J. Scowen, M. McPartlin, *Inorg. Chem.* **1999**, *38*, 5282.

[83] a) S. Friedrich, L. H. Gade, I. J. Scowen, M. McPartlin, *Angew. Chem.* **1996**, *108*, 1440; *Angew. Chem. Int. Ed. Engl.* **1996**, *35*, 1338; b) L. H. Gade, S. Friedrich, D. J. M. Trösch, I. J. Scowen, M. McPartlin, *Inorg. Chem.* **1999**, *38*, 5295.

[84] A. M. Baranger, R. G. Bergman, *J. Am. Chem. Soc.* **1994**, *116*, 3822.

[85] M. Schubart, Ph.D. Thesis, Universität Würzburg, **1997**.

[86] See for example: J. P. Barbier, P. Braunstein, *J. Chem. Res.* **1978**, 5029.

[87] D. A. Roberts, W. C. Mercer, S. M. Zahurak, G. L. Geoffroy, C. W. DeBrosse, M. E. Cass, C. G. Pierpont, *J. Am. Chem. Soc.* **1982**, *104*, 910.

[88] P. S. Bearman, A. K. Smith, N. C. Tong, R. Whyman, *Chem. Commun.* **1996**, 2061.

[89] M. Schubart, G. Mitchell, L. H. Gade, I. J. Scowen, M. McPartlin, *Chem. Commun.* **1999**, 233.

[90] J. R. Pinkes, B. D. Steffey, J. C. Vites, A. R. Cutler, *Organometallics* **1994**, *13*, 21.

[91] T. A. Hanna, A. M. Baranger, R. G. Bergman, *J. Am. Chem. Soc.* **1995**, *117*, 665.

[92] H. Memmler, U. Kauper, L. H. Gade, I. J. Scowen, M. McPartlin, *Chem. Commun.* **1996**, 1751.

[93] A. Schneider, L. H. Gade, M. Breuning, G. Bringmann, I. J. Scowen, M. McPartlin, *Organometallics* **1998**, *17*, 1643.

[94] L. H. Gade, H. Memmler, U. Kauper, A. Schneider, S. Fabre, I. Bezougli, M, Lutz, C. H. Galka, I. J. Scowen, M. McPartlin, *Chem. Eur. J.* **2000**, *6*, 692.

[95] S. Fabre, B. Findeis, D. J. M. Trösch, L. H. Gade, I. J. Scowen, M. McPartlin, *Chem. Commun.* **1999**, 577.

[96] A. M. Baranger, T. A. Hanna, R. G. Bergman, *J. Am. Chem. Soc.* **1995**, *177*, 10041.

[97] S. J. Tauster, *Acc. Chem. Res.* **1987**, *20*, 389.

[98] *Metal-Support Interaction in Catalysis, Sintering, and Redispersion* (Eds.: S. A. Stevenson, J. A. Dumesic, R. T. K Baker, E. Ruckenstein), Van Nostrand, New York, **1987**.

[99] a) *Metal Support and Metal-Additive Effects* (Eds.: B. Imelic, C. Naccache, G. Coudurier, J. Praliaud, P. Meriaudeau, P. Gazzelot, G. A. Martin, J. C. Vedrine), Elsevier, New York, **1982**; b) K. I. Hadjiivanov, D. G. Klissurski, *Chem. Soc. Rev.* **1996**, 61.

[100] H. R. Sadeghi, V. E. Henrich, *J. Catal.* **1988**, *109*, 1.

[101] J. A. Horsley, *J. Am. Chem. Soc.* **1979**, *101*, 2870.

[102] S. Sakellson, M. McMillan, G. L. Haller, *J. Phys. Chem.* **1986**, *90*, 1733.

[103] V. N. Eremenko, T. D. Shtepa, V. G. Sirotenko, *Poroshk. Metall. (Kiev)* **1966**, *6*, 68.

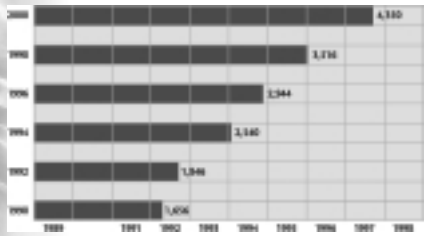
[104] See for example: a) R. A. Demmin, C. S. Ko, R. J. Gorte, *J. Phys. Chem.* **1985**, *89*, 1151; b) M. A. Vannice, C. Sudhakar, *J. Phys. Chem.* **1984**, *88*, 2429; c) M. A. Vannice, R. L. Garden, *J. Catal.* **1979**, *56*, 236; d) J. D. Bracey, R. Burch, *J. Catal.* **1984**, *86*, 384.
[105] C. P. Casey, *J. Organomet. Chem.* **1990**, *400*, 205.
[106] C. P. Casey, R. E. Palermo, *J. Am. Chem. Soc.* **1986**, *108*, 549.
[107] R. Fandos, J. L. G. Fierro, M. M. Kubicki, A. Otero, P. Terreros, M. A. Vivar-Cerrato, *Organometallics* **1995**, *14*, 2162.
[108] G. Proulx, R. G. Bergman, *Science* **1993**, *259*, 661.
[109] See for example: a) M. J. Hostetler, M. D. Butts, R. G. Bergman, *J. Am. Chem. Soc.* **1993**, *115*, 2743; b) M. J. Hostetler, M. D. Butts, R. G. Bergman, *Organometallics* **1993**, *12*, 65; c) P. Kalck, C. Serra, C. Machet, R. Broussier, B. Gautheron, G. Delmas, G. Trouvé, M. Kubicki, *Organometallics* **1993**, *12*, 1021; d) R. S. Dickson, T. De Simone, E. M. Campi, W. R. Jackson, *Inorg. Chim. Acta* **1994**, *220*, 187.

+++ THE LINK TO INTERNATIONAL CHEMISTRY +++

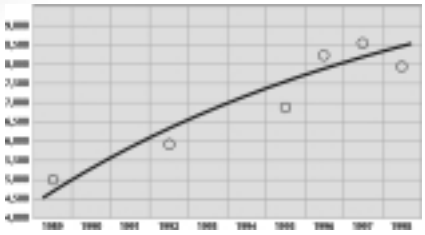


More of the Best, Every Year

More Content:



More Quality as Evidenced by the Impact Factor:



More Service:

1996: - Notification of forthcoming "Hot Papers" on the Internet
1997: - Supporting Information available on the Internet
1998: - Press releases on important communications
1999: - *Angewandte Chemie* goes Online with Wiley InterScience (www.interscience.wiley.com)
- Notification of VIPs (Very Important Papers)
- Simultaneous Publication of German and English versions
2000: - New section
- Essays has its debut
- *Angewandte* is now covered by Medline in addition to a phlethora of other databases

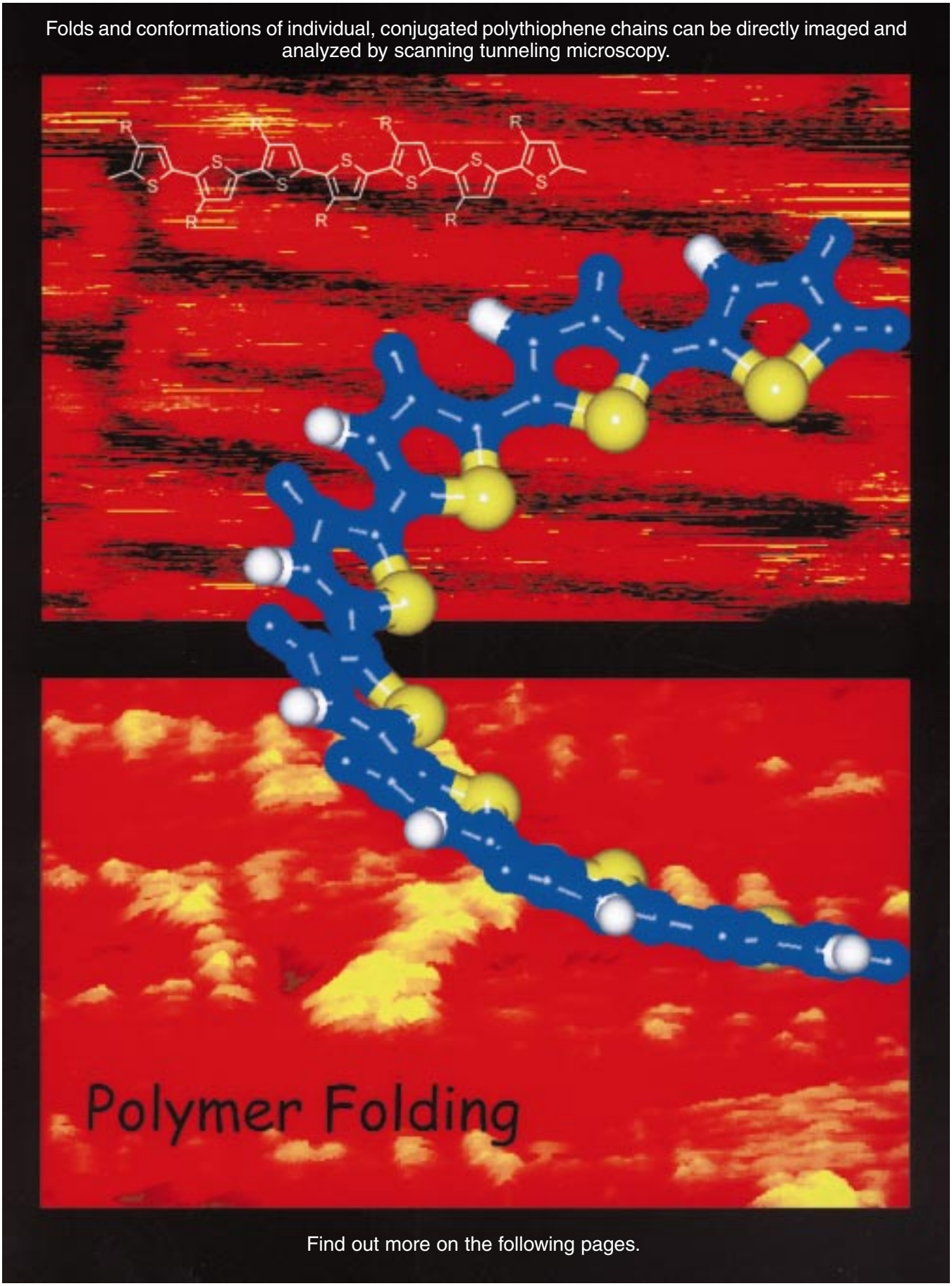
What else would you like to see in *Angewandte*?
E-mail your suggestions to:
angewandte@wiley-vch.de



WILEY-VCH, P.O. Box 10 11 61, 69451 Weinheim, Germany
Phone +49 (6201) 606-328, Fax +49 (6201) 606-348
e-mail: sales-journals@wiley-vch.de, http://www.wiley-vch.de

WILEY-VCH

Folds and conformations of individual, conjugated polythiophene chains can be directly imaged and analyzed by scanning tunneling microscopy.



Find out more on the following pages.

 © WILEY-VCH Verlag GmbH, D-69451 Weinheim, 2000 1433-7851/00/3915-2679 $ 17.50+.50/0

Two-Dimensional Crystals of Poly(3-Alkylthiophene)s: Direct Visualization of Polymer Folds in Submolecular Resolution**

Elena Mena-Osteritz, Alexander Meyer, Bea M. W. Langeveld-Voss, Rene A. J. Janssen, E. W. Meijer, and Peter Bäuerle*

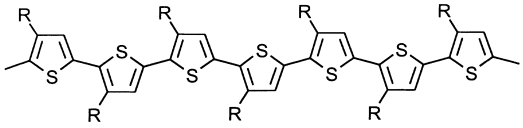
The control of structural order on the molecular level in semiconducting, self-organizing conjugated polymers has important consequences on their electronic properties.[1] In particular, X-ray diffraction (XRD) on solution-processed, semicrystalline, head-to-tail coupled poly(3-alkylthiophene)s (HT-P3ATs)[2] indicates a lamella structure with two-dimensional (2D) sheets formed by interchain stacking.[1a] Like all other synthetic polymers, chain folding is very likely and XRD on semicrystalline whiskers of regiorandom poly(3-alkylthiophene)s indicates strands 15 nm in size, in which the thiophene rings adopt an all-*trans* conformation between the polymer folds.[3] However, valuable information concerning the molecular parameters are very limited and only an educated guess of polymer conformations within folds is possible because of the lack of appropriate techniques to study these folded conformations at the atomic level.

Herein, we report the direct observation of two-dimensional crystals of HT-P3ATs at the solution/HOPG (highly oriented pyrolytic graphite) interface, by means of scanning tunneling microscopy (STM). Lamellar structures formed by interchain stacking uniformly cover wide ranges of the surface. In the in situ measurements, we achieved submolecular resolution and, besides lattice constants, various molecular parameters of the conjugated polymers were determined directly. Supported by quantum chemical calculations, interchain distances, chain lengths, conformations in linear regimes, and folding of the polymeric conjugated chains were identified and analyzed. The formation of a second layer, in which diverse, oriented polymer chains are highly resolved, provides intriguing images: Higher electronic coupling from parallel $\pi-\pi$ stacked "molecular wires" is directly visualized.

Conjugated polymers and oligomers show excellent electronic and transport properties in the solid state, which allows their application to organic electronic devices.[4] In particular, poly-[5] and oligothiophenes[6] have been intensively studied in order to understand how structural parameters affect the physical properties[7] and, consequently, the performance of the devices.[1a, 8] In this respect, we and others have developed a rational design and synthesis of model oligothiophenes that, strongly dependent upon their molecular structure, physisorb from solution either onto the basal plane of HOPG[9] or onto MoS_2[10] and form highly ordered, 2D crystalline monolayers which were imaged by STM. In particular, head-to-tail coupled oligo(3-alkylthiophene)s, that represent models for the above mentioned HT-P3ATs, show excellent self-assembly and film-forming properties.[11] In some cases, the 2D ordering at the HOPG surface is, notably, fully coincident with the molecular packing in the 3D crystal, which provides an excellent way to receive information on the molecular packing in the solid state when it is otherwise impossible to perform single-crystal X-ray analyses.[12]

Mono- and multilayers of macromolecular systems are, however, typically imaged with atomic force microscopy (AFM) on a longer length scale. Packing features have been shown for, among others, double- and single-stranded DNA,[13] nylon 6,[14] carbon nanotubes,[15] and polymeric brushes; the latter are composed of graft- or dendritic block copolymers and form cylindrical[16] or rodlike supramolecular assemblies.[17] The resolution to image polymer chain conformations, other than in extended chains of well defined linear arrays, is limited primarily due to the lack of order in regimes of high electron mobilities. Therefore, π-conjugated polymers seem to be ideal candidates to observe the chain conformations in folds. However, STM investigations undertaken so far on conducting polymers, in particular on adsorbed films of regiorandom P3ATs on gold or HOPG surfaces,[18] typically show only very small areas of ordered domains and allow only a crude determination of structural parameters. Individual strands have been recently found in STM images of the self-assembled rodlike poly(*p*-phenyleneethynylene)s, which form a nematiclike order on HOPG.[19]

Motivated by the notable self-assembly properties of head-to-tail coupled oligo(3-alkylthiophene)s, the long- and short-range ordering of the corresponding polymers were investigated in self-assembled 2D crystals at the solution/HOPG interface by means of in situ STM. Importantly, HT-coupled poly(3-hexylthiophene) (**P1**) and HT-coupled poly(3-dodecylthiophene) (**P2**) comprised high regioregularities—the



P1: R = C_6H_{13}, **P2:** R = $C_{12}H_{25}$

percentage of alkyl side chains attached stereoregularly (head-to-tail) to the 3-position of the thiophene ring—of 95% and 98%, respectively.[2] Samples of polymers with lower regioregularity could not be imaged because they do not self-assemble on the substrate surface.

In Figure 1, representative STM images of the conjugated polymers **P1** and **P2** are shown. The images are typically found on areas larger than the 1.0 μm scan range and display a long-range order with *molecularly resolved individual strands.*

[*] Prof. Dr. P. Bäuerle, Dr. E. Mena-Osteritz, Dipl.-Chem. A. Meyer
Department of Organic Chemistry II (Organic Materials and Combinatorial Chemistry)
University of Ulm
Albert-Einstein-Allee 11, 89081 Ulm (Germany)
Fax: (+49) 731-502-2840
E-mail: peter.baeuerle@chemie.uni-ulm.de
Dr. B. M. W. Langeveld-Voss, Dr. R. A. J. Janssen, Prof. Dr. E. W. Meijer
Laboratory of Macromolecular and Organic Chemistry
Dutch Polymer Institute
Eindhoven University of Technology
PO Box 513, 5600 MB Eindhoven (The Netherlands)

[**] This work was supported by the European Union in the framework of Frequent-Esprit 24793.

 © WILEY-VCH Verlag GmbH, D-69451 Weinheim, 2000 1433-7851/00/3915-2680 $ 17.50+.50/0

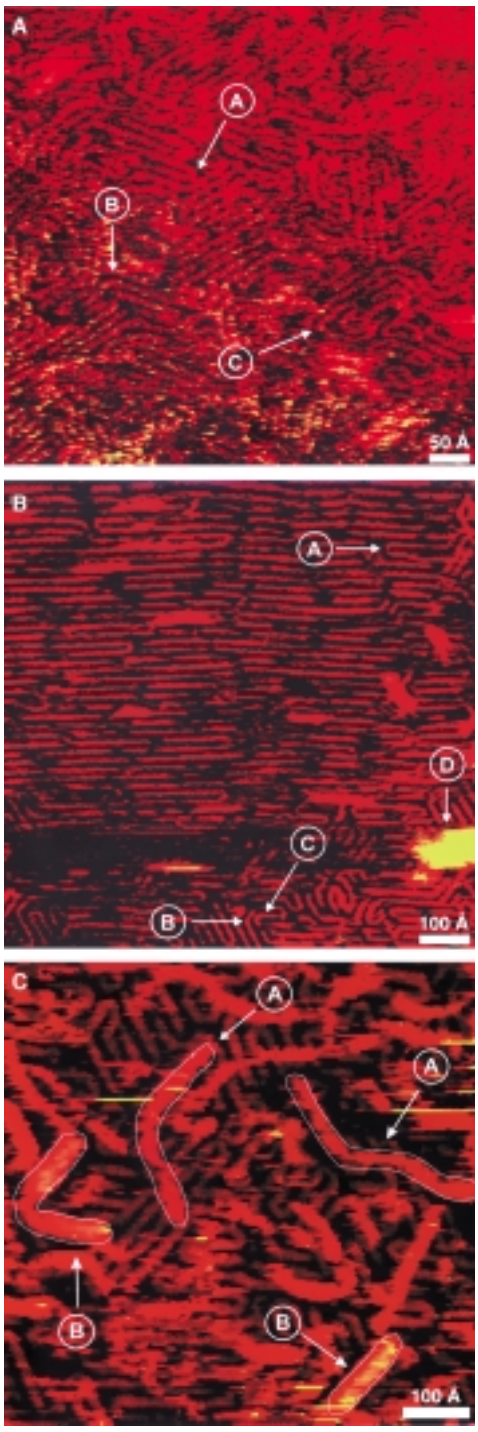


Figure 1. STM images of the long-range ordering of head-to-tail coupled poly(3-alkylthiophene)s on HOPG. A) **P1**, 600×600 Å^2; B) **P2**, 1000×1000 Å^2; C) multilayers of **P2**, 700×700 Å^2.

They are oriented according to the three crystallographic axes of the HOPG substrate, each 120° apart. Since the alkyl side chains prefer to organize in a planar, zigzag, interdigitated fashion along the three main graphite axes,[11, 12] the conjugated backbones are oriented perpendicular to them in highly ordered lamellae. Over most of the surface, the conjugated chains are linearly arranged and therefore comprise an all-*trans* conformation of the thiophene repeating units. A closer look at the images reveals that the individual strands are not only linear but chain folding is also clearly observed, in which *cis* conformations of the thiophene units are prerequisite for the fold. Regular, hair-pin folds angle can be seen (A) but also folds of 120° (B) and, rarely, of 60° (C) are evident.

STM images of the short-range ordering of the two conjugated polymers exhibit both formation of parallel lamellae and a regular folding of individual strands (Figure 2).

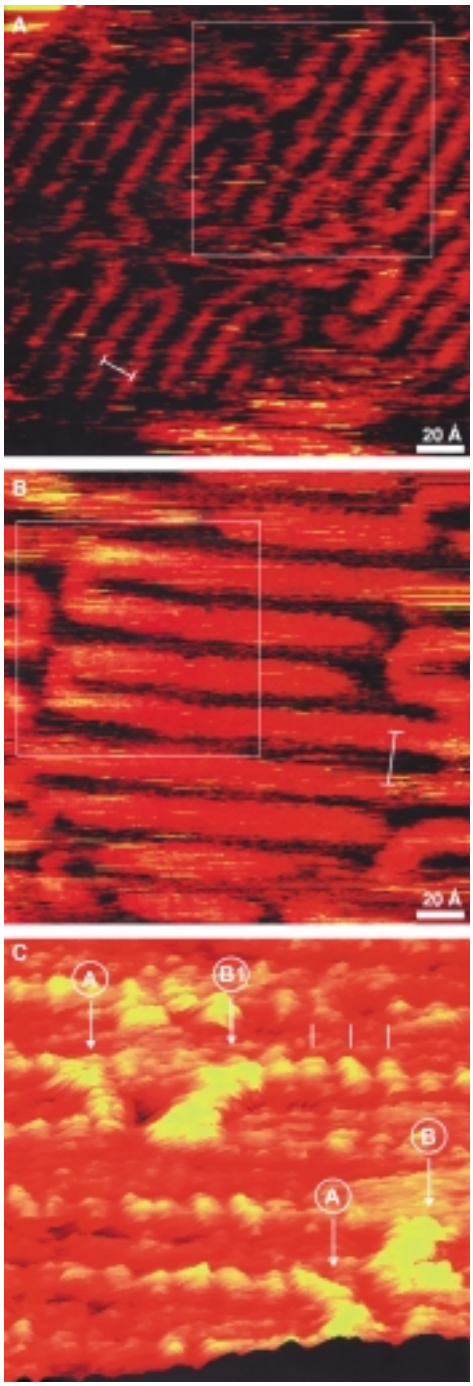


Figure 2. STM images of the short-range ordering of head-to-tail coupled poly(3-alkylthiophene)s on HOPG. A) **P1**, 200 Å $\times$ 200 Å, the chain-to-chain distance corresponds to 13 – 14 Å; B) **P2**, 200×200 Å^2, the chain-to-chain distance corresponds to 19 – 20 Å; C) individual chains and folds of **P2**, 93×93 Å^2, the periodicity of the repeating units at the submolecular resolution is 6.8 Å. The white squares in (A) and (B) correspond to the areas which are shown in Figure 3 A and 3 B.

 © WILEY-VCH Verlag GmbH, D-69451 Weinheim, 2000 1433-7851/00/3915-2681 $ 17.50+.50/0

Supported by semiempirical calculations (Figure 3), the contour length of the conjugated chains can be measured due to the submolecular resolution, which allows the determination of the number of repeating units in individual strands. Mean values are 110–130 Å (33–40 thiophene units) for **P1** and 100–150 Å (30–44 thiophene units) for **P2**. In Figure 3C, a representative histogram of the chain length distribution, here for **P2**, determined from the whole area in Figure 1B, is shown. Although the average degree of polymerization estimated from STM is lower than those of GPC and MALDI-TOF, the deviations are acceptable and comparable to those published for poly(*p*-phenyleneethynylene)s.[19]

Another important result obtained from the STM images is the chain-to-chain distance in the lamellae. Typically, distances of 13–14 and 19–20 Å for **P1** and **P2**, respectively, are found. This result is in excellent accordance with semiempirical calculations (**P1**: 13.3, **P2**: 20.8 Å; Figure 3A,B) and with highly ordered 2D crystalline monolayers of corresponding model oligomers, the head-to-tail coupled oligo(3-alkylthiophene)s on graphite (alkyl = hexyl: 12–13,[20] alkyl = dodecyl: 20–21 Å[11]) but is in contrast to XRD measurements on the same polycrystalline polymers. By XRD, a greater spacing between two individual conjugated backbones are found: 16.3 for **P1** and 27.1 Å for **P2**.[21] Two models for the side chain organization in HT-P3ATs are often used: 1) a tilted structure in which the side chains tilt away from the plane of the conjugated backbone, to nearly eliminate alkyl chain interdigitation,[21f] and 2) a structure with side-chain interdigitation.[21g] The latter model agrees in full with the STM results of polymers and oligomers and with theoretical calculations. Evidently, due to epitaxial effects of the graphite surface, the intermolecular interactions and interpenetration of the alkyl side chains is maximized and "compressed" in the monolayer whereas, in the polycrystalline bulk material, the chains are less interdigitated by two (**P1**) or four (**P2**) methylene groups (Scheme 1) when the second model is adopted. In accordance, theoretical calculations show an energy minimum in the case of maximum interdigitation.

An intriguing result comes from a detailed, calculation-supported analysis of the folds in both polymers (Figures 2 and 3). The *cis* conformations must definitely be present in a folded chain. An intramolecular hair-pin fold is composed of seven thiophene units in an all-*cis* conformation for hexyl-substituted **P1** (Figure 3A) and eight units for dodecyl-subsituted **P2** (Figure 3B). Larger curvatures include additional *cis-trans* conformations in the fold (see Figure 3A). An STM image of dodecyl-substituted **P2** at a submolecular resolution (Figure 2C) even permits conclusions about the composition of the conjugated chains to be made: chains periodicities of 6.8 Å can be observed, that corresponds to a "compressed" bithiophene repeating unit, which in the gas phase has a calculated extension of 7.4 Å. This evident compression can be rationalized by epitaxial effects of the underlying substrate surface on the alkyl side chains. Calculations show that only small variations (< 5%) of the angles and the inter-ring bonds are sufficient to achieve this 0.6 Å difference. The periodicities conform to a model, in which MOs of each second thiophene ring match a similar electronic environment on the underlying graphite

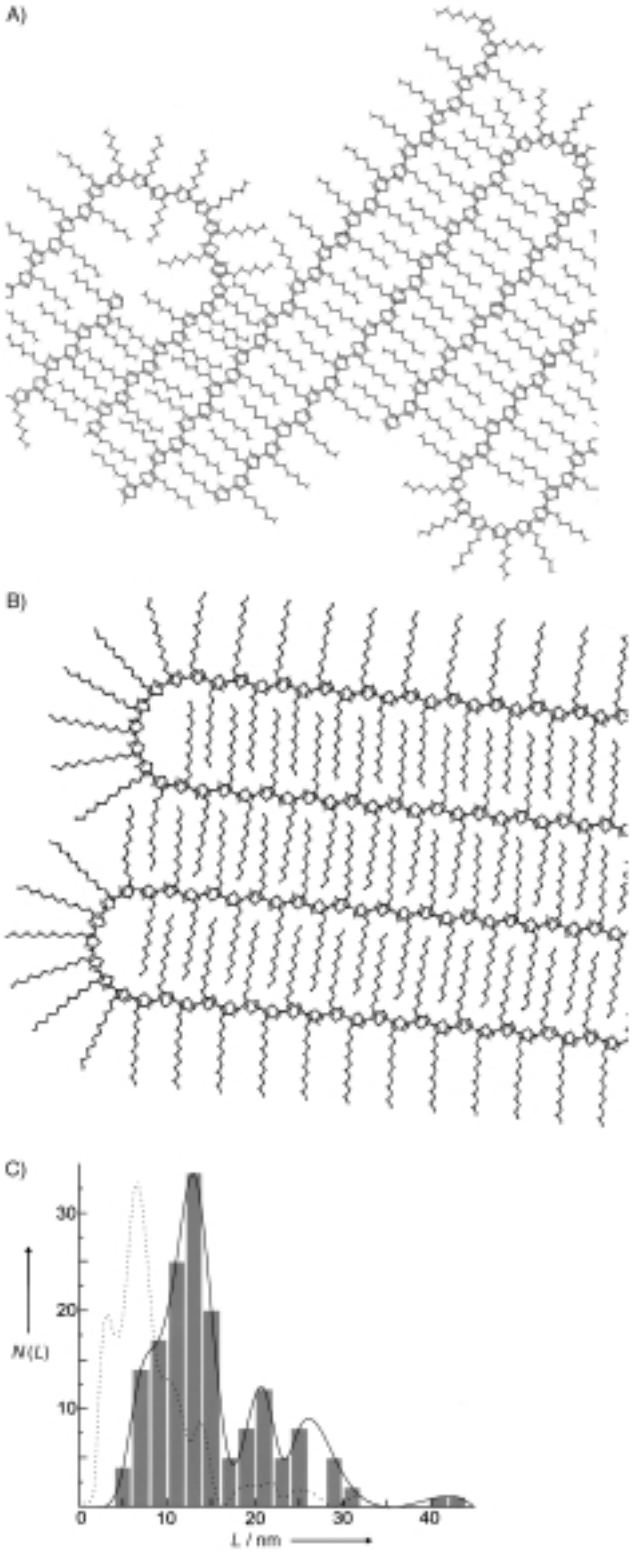
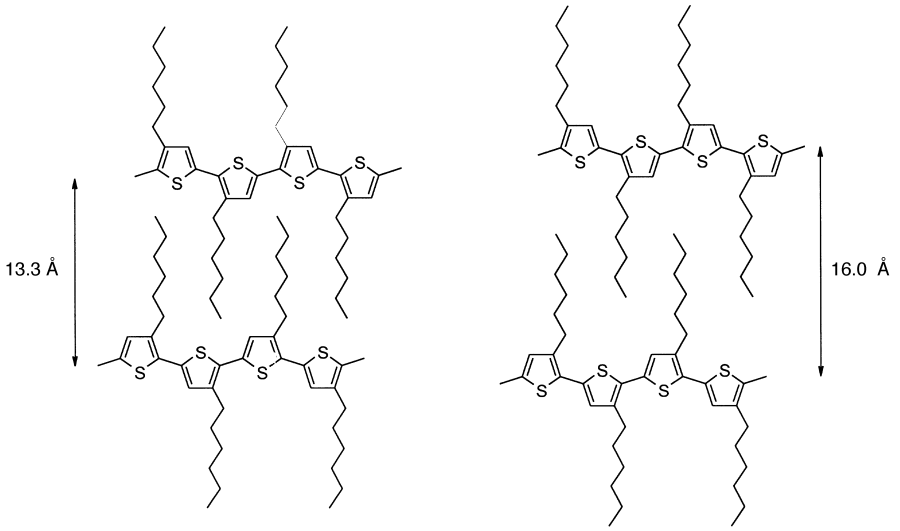


Figure 3. Semiempirical calculations of the head-to-tail coupled poly(3-alkylthiophene)s. The calculations were performed such that first chain fragments of at least ten thiophene units have been optimized in an all-*trans* or an all-*cis* conformation, the interaction of two strands was calculated subsequently, and finally the fragments were assembled in order to construct the polymer chains and to simulate the STM images. A) **P1**, the optimized chain-to-chain distance is 13.3 Å and is coincident with distances determined from STM images; B) **P2**, the optimized chain-to-chain distance is 20.8 Å and is coincident with distances determined from STM images; C) histogram of the chain length distribution (full line) and lamella thickness (dotted line) of **P2**.

 © WILEY-VCH Verlag GmbH, D-69451 Weinheim, 2000 1433-7851/00/3915-2682 $ 17.50+.50/0



Scheme 1. Schematic representations of the molecular arrangement of a monolayer of the regioregular head-to-tail coupled **P1** on graphite, derived from STM data (left) and in the bulk form derived from XRD data (right).[2c]

surface and thereby give rise to intensive tunneling currents.

Details about the adsorption process can also be deduced from Figure 2C: If two complete hair-pin folds meet on the substrate surface, one fold will lie flat on the surface (A) whereas the second one is raised due to a dynamical processes (B), as indicated from the color which represents different height profiles. In excellent accordance with the calculations in one hair-pin fold (B1), four periodic features in the fold can be identified, which correspond to eight thiophene units in an all-*cis* conformation.

The data allows a detailed analysis of the chain conformations of the polymer fold and, evidentially, the polymer adopts the *cis*-conformation to fold without disorder. In case of a fold over longer distances, in which one chain lies within the folding chain (Figure 3A), the conformation adopts a low energy, well defined, and disorder-free conformation. Furthermore, the data quantification of 7.0 nm, the length of the all-*trans* strand of the polymer between the folding points. The corresponding histogram for the all-*trans* length is given in Figure 3C for **P2**, to show the regularity of the fold, yet the length of the all-*trans* strand is only half of the whisker width in the 3D crystal.[3]

In an early stage of the adsorption process, the adsorption of individual chains and smaller aggregates onto the substrate surface may result in predominantly parallel lamellae. Because of the longer alkyl side chains, **P2** has a greater tendency to form aggregates and must therefore be used in lower concentrations. However, individual chains also seem to fold back quite regularly and bend completely by 360° without loss of interaction energy. After most parts of the surface are covered, macromolecules from the solution can only adsorb onto open areas and in the remaining gaps by randomly folding at angles of 360° or 120° (Figures 1 and 2). Interestingly for **P2**, a nearly perfect, parallel lamella-type ordering of the macromolecules is found over 70–80% of the monolayer area (Figure 2B); for the remaining 20–30% (on the bottom of the image), folding processes are commencing. Despite the fact that hair-pin folds have been discussed for liquid crystalline polymers, the chains are probably not folded before adsorption onto the surface, as the experiment is at equilibrium conditions and the behavior of poly(3-alkylthiophene)s is not liquid crystalline.

Due to the paucity of a tunneling current through nonconducting molecules, adsorbed monolayers can typically only be imaged by STM experiments. Surprisingly, in some cases at a later stage of the measurements, we observed a second layer of adsorbed macromolecules, as evident from height profiles (not shown) and the yellow areas (D) in Figure 1B. In contrast to STM experiments on oligothiophenes,[11, 12] in which a bias of about -600 mV is necessary in order allow a electron tunneling, a bias of only about -150 mV is sufficient to tunnel through two layers of these polymers. This clearly indicates superior semiconducting properties due to a more extended π-conjugation. The molecular arrangement of the second layer macromolecules can be seen in Figure 1C for **P2**. On top of the organized monolayer (red-brown region), a few individual, conjugated macromolecules are deposited in a second layer. Most chains cross the underlying molecules obliquely (A, red), however, parallel oriented molecules can be seen (B, yellow). Also in this case, chain folding of 60 and 120° turns are observed. Since the color in the image is dependent on the tunneling current, a greater tunneling current evidently passes through molecules aligned parallel rather than crossed. This is proof on a molecular scale that two conjugated molecules stacked parallel have more effective π-π interactions and, therefore, better electronic coupling than crossed ones. These results are fully consistent that macroscopic properties, such as conductivity, is better for conducting polymers which are stretched along the conjugated chains.[22]

Since the self-organization process of highly stereoregular poly(3-alkylthiophene)s to form 2D crystals proved to be only weakly influenced by the substrate surface, the visualization of polymer chain or "molecular wire" conformations at the molecular level and the subsequent determination of molecular parameters, both in extended linear arrays as well as in chain folding, provides a powerful tool to further tailor properties of conjugated materials. The variations of polymer chain folding is visualized directly and shows different conformations, dependent upon the interchain packing. Additional elucidation of the growth of 2D crystal lattices into the third dimension is of interest in order to understand the crystallization mechanism of polymers and is particularly important for the future application of π-conjugated polymers as active elements in plastic[23] and "molecular" electronic devices.[24]

 © WILEY-VCH Verlag GmbH, D-69451 Weinheim, 2000 1433-7851/00/3915-2683 $ 17.50+.50/0

Experimental Section

HT-coupled poly(3-alkylthiophene)s were synthesized according the McCullough route.[2b–d] The crude polymerization mixtures were purified by repeated Soxhlet extractions in methanol, hexane, and twice in chloroform. For the resulting fractions, a regioregularity of 95% (**P1**) and 98% (**P2**) was determined from the ^{1}H NMR signals at $\delta = 2.8$ and 2.6. Gel-permeation chromatography (GPC) measurements (polystyrene standards) gave polydispersities of 1.35 ($M_w = 28.1$, $M_n = 20.8\ kg\,mol^{-1}$; **P1**) and 1.29 ($M_w = 45.2$, $M_n = 35.1\ kg\,mol^{-1}$; **P2**). Comparison of GPC results of monodisperse model oligomers with MALDI-TOF mass spectra[25] showed that the GPC results overestimated the number-averaged molecular weight M_n by a factor of 1.6–1.9. From this, we estimate that the number-averaged degree of polymerization amounts to 70 and 80 thiophene units for the hexyl- and dodecyl-substituted polymers, respectively.

The STM images were recorded at ambient temperature with the aid of a low-current STM (RHK Rochester Hills, Michigan, USA) equipped with a mechanically cut Pt/Ir tip and regulated by a STM 1000 control system (RHK). All of the images presented were obtained at quasi-constant height in the variable current mode without using either a voltage pulse to induce sample ordering or digital image processing. The bias voltages were typically about -150 mV and the setpoint currents around 1.0 nA. A freshly cleaved surface of HOPG was first characterized under ambient conditions, then solutions of the polymers in 1,2,4-trichlorobenzene were deposited onto the substrate. In situ STM imaging of the self-assembled 2D monolayers was performed at the interface between HOPG and concentrated solutions of the polymers. Distances determined from the images are of an accuracy of ± 0.1 Å.

Received: February 11, 2000 [Z14691]

[1] a) H. Sirringhaus, J. P. Brown, R. H. Friend, M. M. Nielsen, K. Beechgard, B. M. W. Langeveld-Voss, A. J. H. Spiering, R. A. J. Janssen, E. W. Meijer, P. Herwig, D. M. de Leeuw, *Nature* **1999**, *401*, 685–688; b) R. J. O. M. Hoofman, M. de Haas, L. D. A. Siebbeles, J. M. Warmann, *Nature* **1998**, *392*, 54–56.

[2] a) T.-A. Chen, R. D. Rieke, *J. Am. Chem. Soc.* **1992**, *114*, 10087–10088; b) R. D. McCullough, R. D. Lowe, M. Jayaraman, D. L. Anderson, *J. Org. Chem.* **1993**, *58*, 904–912; c) R. D. McCullough, *Adv. Mater.* **1998**, *10*, 93–116; d) R. S. Loewe, S. M. Khersonsky, R. D. McCullough, *Adv. Mater.* **1999**, *11*, 250–253.

[3] K. J. Ihn, J. Moulton, P. Smith, *J. Polym. Sci. Polym. Phys.* **1993**, *31*, 735–742.

[4] a) M. G. Harrison, R. H. Friend in *Electronic Materials: The Oligomer Approach* (Eds.: K. Müllen, G. Wegner), Wiley-VCH, Weinheim, **1998**, pp. 515–558; b) U. Mitschke, P. Bäuerle, *J. Mater. Chem.* **2000**, *10*, 1471–1507; c) N. Tessler, G. J. Tenton, R. H. Friend, *Nature* **1996**, *382*, 695–697; d) H. Sirringhaus, N. Tessler, R. H. Friend, *Science* **1998**, *280*, 1741–1744; e) F. Garnier in *Electronic Materials: The Oligomer Approach* (Eds.: K. Müllen, G. Wegner), Wiley-VCH, Weinheim, **1998**, pp. 559–583.

[5] *Handbook of Oligo- and Polythiophenes* (Ed.: D. Fichou), Wiley-VCH, Weinheim, **1999**.

[6] P. Bäuerle, *Oligothiophenes* in *Electronic Materials: The Oligomer Approach* (Eds.: K. Müllen, G. Wegner), Wiley-VCH, Weinheim, **1998**, pp. 105–197.

[7] J. Roncali, *J. Mater. Chem.* **1999**, *9*, 1875–1894.

[8] Z. Bao, A. Dodabalapur, A. L. Lovinger, *Appl. Phys. Lett.* **1996**, *69*, 4108–4110.

[9] a) A. Stabel, J. P. Rabe, *Synth. Met.* **1994**, *67*, 47–53; b) P. Bäuerle, T. Fischer, B. Bidlingmeier, A. Stabel, J. P. Rabe, *Angew. Chem.* **1995**, *107*, 335–339; *Angew. Chem. Int. Ed. Engl.* **1995**, *34*, 303–307; c) H. Müller, J. Petersen, R. Strohmaier, B. Gompf, W. Eisenmenger, M. S. Vollmer, F. Effenberger, *Adv. Mater.* **1996**, *8*, 733–737; d) M. S. Vollmer, F. Effenberger, R. Stecher, B. Gompf, W. Eisenmenger, *Chem. Eur. J.* **1999**, *5*, 96–101.

[10] R. Azumi, G. Götz, P. Bäuerle, *Synth. Met.* **1999**, *101*, 569–572.

[11] T. Kirschbaum, R. Azumi, E. Mena-Osteritz, P. Bäuerle, *New J. Chem.* **1999**, 241–250.

[12] R. Azumi, G. Götz, T. Debaerdemaeker, P. Bäuerle, *Chem. Eur. J.* **2000**, *6*, 735–744.

[13] a) R. J. Driscoll, M. G. Youngquist, J. D. Baldeschwieler, *Nature* **1990**, *346*, 294–296; b) D. P. Allison, T. Thundat, *J. Vac. Sci. Technol. A* **1993**, *11*, 816–819.

[14] M. Sano, D. Y. Sasaki, T. Kunitake, *Science* **1992**, *258*, 441–443.

[15] L. C. Venema, J. W. G. Wildöer, J. W. Janssen, S. J. Tans, H. L. J. T. Tuinstra, L. P. Kouwenhoven, C. Dekker, *Science* **1999**, *283*, 52–55.

[16] a) V. Percec, C.-H. Ahn, G. Ungar, D. J. P. Yeardley, M. Möller, S. S. Sheiko, *Nature* **1998**, *391*, 161–164; b) P. Dziezok, S. S. Sheiko, K. Fischer, M. Schmidt, M. Möller, *Angew. Chem.* **1997**, *109*, 2894–2897; *Angew. Chem. Int. Ed. Engl.* **1997**, *36*, 2812–2815.

[17] W. Stocker, B. Karakaya, B. L. Schürmann, J. P. Rabe, A. D. Schlüter, *J. Am. Chem. Soc.* **1998**, *120*, 7691–7695.

[18] a) S. F. Bond, A. Howie, R. H. Friend, *Surf. Sci.* **1995**, *331–333*, 196–200; b) E. Lacaze, K. Uvdal, P. Bodö, J. Garbarz, W. R. Salaneck, M. Schott, *J. Polym. Sci. Part B* **1993**, *31*, 111–114; c) A. Bonfiglio, R. Paradiso, E. Di Zitti, D. Ricci, A. Bolognesi, W. Porzio, *Adv. Mater. Opt. Electron.* **1993**, *2*, 295–299.

[19] P. Samori, V. Francke, K. Müllen, J. P. Rabe, *Chem. Eur. J.* **1999**, *5*, 2312–2317.

[20] E. Mena-Osteritz, T. Kirschbaum, T. Debaerdemaeker, P. Bäuerle, unpublished results.

[21] a) R. D. McCullough, S. Tristram-Nagle, S. P. Williams, R. D. Lowe, M. Jayaraman, *J. Am. Chem. Soc.* **1993**, *115*, 4910–4911; b) T.-A. Chen, X. Wu, R. D. Rieke, *J. Am. Chem. Soc.* **1995**, *117*, 233–244; c) S. V. Meille, V. Romita, T. Caronna, A. J. Lovinger, M. Catellani, L. Belobrzeckaja, *Macromolecules* **1997**, *30*, 7898–7905; d) T. Kaniowski, W. Luzny, S. Niziol, J. Sanetra, M. Trznadel, *Synth. Met.* **1998**, *92*, 7–12; e) M. J. Winokur, T. J. Prosa, J. Moulton, P. Smith, A. J. Heeger, *Macromolecules* **1992**, *25*, 4364–4372; f) K. Tashiro, M. Kobayashi, T. Kawai, K. Yoshino, *Polymer* **1997**, *38*, 2867–2879; g) T. J. Prosa, M. J. Winokur, R. D. McCullough, *Macromolecules* **1996**, *29*, 3654–3656.

[22] S. Hotta, M. Soga, N. Sonoda, *Synth. Met.* **1988**, *26*, 267–279.

[23] C. J. Drury, C. M. J. Mutsaers, C. M. Hart, M. Matters, D. M. de Leeuw, *Appl. Phys. Lett.* **1998**, *73*, 108–110.

[24] F. Hide, M. A. Díaz-García, B. J. Schwartz, A. J. Heeger, *Acc. Chem. Res.* **1997**, *30*, 430–436.

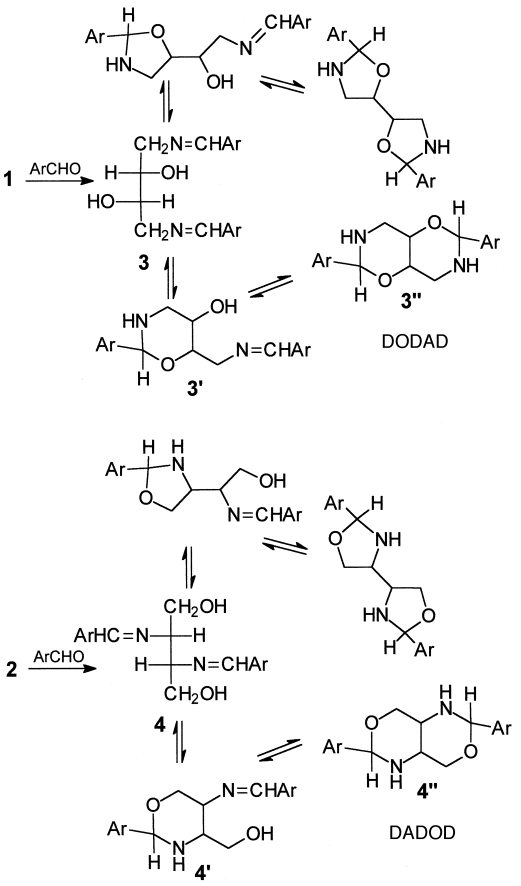
[25] a) J. Liu, R. S. Loewe, R. D. McCullough, *Macromolecules* **1999**, *32*, 5777–5785; b) B. M. W. Langeveld-Voss, R. A. J. Janssen, A. J. H. Spiering, J. L. J. van Dongen, E. W. Meijer, E. C. Vonk, H. A. Claessens, *Chem. Commun.* **2000**, 81–82; c) T. Kirschbaum, C. Briehn, P. Bäuerle, *J. Chem. Soc. Perkin Trans. 2* **2000**, 1211–1216.

 © WILEY-VCH Verlag GmbH, D-69451 Weinheim, 2000 1433-7851/00/3915-2684 $ 17.50+.50/0

Dioxadiazadecalin/Salen Tautomeric Macrocycles and Complexes: Prototypal Dynamic Combinatorial Virtual Libraries**

Alexander Star, Israel Goldberg, and Benzion Fuchs*

We recently described[1, 2] the reactions of the isomeric *threo*-1,4- and *threo*-2,3-diaminobutanediols (**1** and **2**, respectively) with aldehydes to give the new isomeric *cis*-1,5-dioxa-3,7-diazadecalin (DODAD) and *cis*-1,5-diaza-3,7-dioxadecalin (DADOD) systems,[1] out of the whole variety of possible ring–chain tautomers (Scheme 1).[2] Different 2,6-*para*-aryl substituted derivatives were investigated, and the tautomeric



Scheme 1. All possible products (diimines, mono- and diacetals) from the reaction of *threo*-1,4- and *threo*-2,3-diaminobutanediols (**1**, **2**) with aromatic aldehydes; the six-membered bicyclic systems are the *cis*-dioxadiazadecalins (DODAD) and *cis*-diazadioxadecalins (DADOD).

[*] Prof. B. Fuchs, A. Star, Prof. I. Goldberg
School of Chemistry
Raymond and Beverly Sackler Faculty of Exact Sciences
Tel-Aviv University, Ramat-Aviv
69978 Tel-Aviv (Israel)
Fax: (+972) 3-640-9293
E-mail: bfuchs@post.tau.ac.il

[**] New Supramolecular Host Systems, Part 12. Part 11: ref. [1]. We gratefully acknowledge support by a research grant from the Israel Science Foundation and by an Intel Scholarship (to A.S.), as well as the valuable assistance of Shimon Hauptman with mass spectrometry and Yuri Paskover as an undergraduate research student.

Supporting information for this article is available on the WWW under http://www.wiley-vch.de/home/angewandte/ or from the author.

ratios, which express the relative stability of these dioxadiazadecalin systems, were shown to be affected by the electronegativity of the 2,6-*p*-aryl substituents.[2a] Whereas *cis*-DADOD systems were more stable than their parent Schiff bases in all cases, the *cis*-DODADs prevailed only with electron-withdrawing substituents. In earlier detailed studies[3] of ring–chain tautomerism in 1,3-oxazanes, it was shown that *ortho*-substituted 2-aryl systems are exceptional[3c] due to hydrogen bonding in addition to electronic and steric effects. This bears upon *N*-salicylideneamino derivatives, which are related to the well-known salen systems.[4, 5]

The Schiff bases **3** and **4** (Ar = *o*-C_6H_4OH),[2b, 6] prepared by the reaction of salicylaldehyde with the L-1,4- and D-2,3-diaminobutanediols (**1** and **2**, respectively), exhibited ring–chain tautomerism,[2] with some formation of the isomeric dioxadiazadecalin systems. The open forms prevail due to strong internal hydrogen bonding involving the 2-hydroxyphenyl groups, which can be avoided[3c] by O-alkylation. Indeed,[2b] O-methylation resulted in higher dioxadiazadecalin yields in both the DODAD (**3″**, Ar = *o*-C_6H_4Me) and the DADOD (**4″**, Ar = *o*-C_6H_4OMe) series; the latter was exclusively isolated. This stability of the bicyclic forms can be partly attributed to intramolecular N–H···OR hydrogen bonds, although these are still somewhat weakened by steric interference of the two OMe groups.

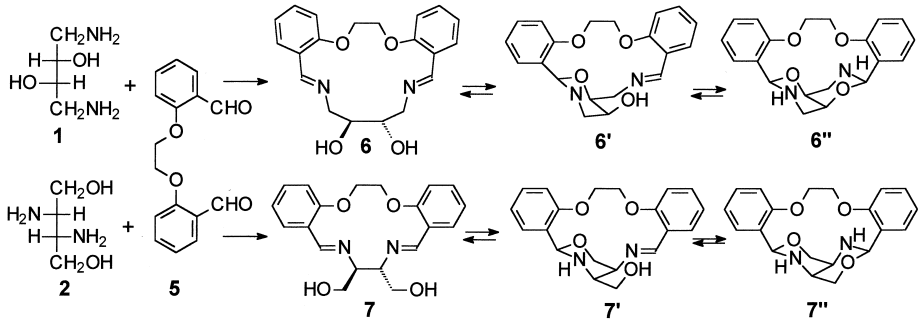
This interference can be avoided by connecting the two phenolic termini, which meets our aim of preparing macrocyclic systems from these platforms. We probed the length of the best-fitting spacer by molecular mechanics and modeling (CFF91-Insight II, MSI) of various spacers with the O···O distance as criterion. For O–CH_2–CH_2–O, this distance coincided with that of a hypothetical unsubstituted and strainless molecule.

The reaction of 1,2-bis(*o*-formylphenoxy)ethane (**5**)[7] with **1** and **2** proceeded smoothly at high dilution to give (2*R*,6*R*;9*S*;9,10-*P*)-2,6-(1′,2′;7′,8′-dibenzo-3′,6′-dioxa-1′,8′-octanylidene)-*cis*-1,5-dioxa-3,7-diazadecalin (**6″**) and (2*R*,6*R*;9*S*;9,10-*M*)-2,6-(1′,2′;7′,8′-dibenzo-3′,6′-dioxa-1′,8′-octanylidene)-*cis*-1,5-diaza-3,7-dioxadecalin (**7″**), respectively (Scheme 2), in almost quantitative yields.

The DODAD macrocycle **6″** exists in $CDCl_3$ entirely without Schiff base tautomers, even on heating. However, heating **6″** in [D_6]DMSO in a variable-temperature NMR study led to increasing formation of the open Schiff bases **6** and **6′** (3.5 and 1.5% at 298 K; 45 and 47% at 410 K, respectively) and less than 5% oxazolidine tautomers. Strong intramolecular NH···OR hydrogen bonding in **6″** and **7″** is manifested in a clear triplet for the NH group with large *anti* vicinal coupling constants, and by strong deshielding ($\Delta\delta = 2$) of these protons relative to known *p*-nitrophenyl-substituted compounds.[2] The structure of **6″**, obtained from an X-ray diffraction analysis (Figure 1), confirms the presence of these strong intramolecular hydrogen bonds, which are probably responsible in part for the smooth macrocyclization reaction.

Lehn[8a] recently introduced the concept of dynamic combinatorial chemistry/virtual combinatorial libraries (DCC/VCL).[8] These molecular or supramolecular libraries are virtual because their constituents may not necessarily exist in significant amounts in the absence of an assembling target (for

 © WILEY-VCH Verlag GmbH, D-69451 Weinheim, 2000 1433-7851/00/3915-2685 $ 17.50+.50/0



Scheme 2. The tautomeric macrocyclic products in the DODAD (**6″**) and DADOD (**7″**) series from the [1+1] reaction of 1,2-bis(*o*-formylphenoxy)ethane (**5**) with **1** and **2**, respectively.

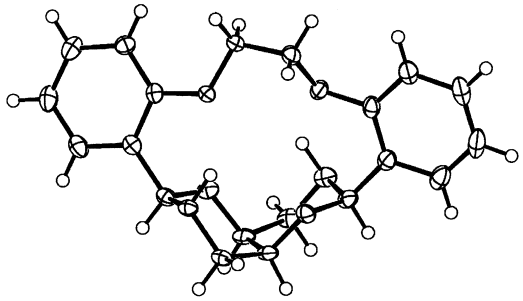


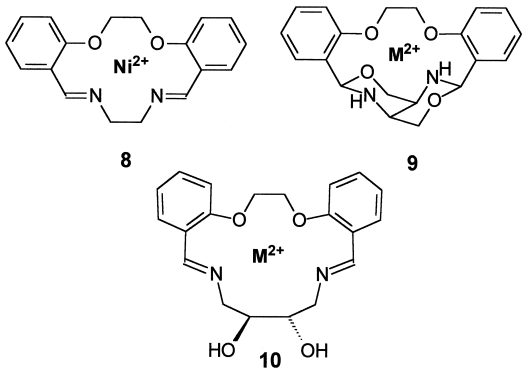
Figure 1. ORTEP plot of **6″** with 50% probability thermal ellipsoids. Crystallographic data (excluding structure factors) for the structure reported in this paper have been deposited with the Cambridge Crystallographic Data Centre as supplementary publication no. CCDC-137663. Copies of the data can be obtained free of charge on application to CCDC, 12 Union Road, Cambridge CB21EZ, UK (fax: (+44) 1223-336-033; e-mail: deposit@ccdc.cam.ac.uk). See also Supporting Information.

most recent related accounts, see ref. [9]). A pertinent passage there states: "Tautomerism, in particular in heterocyclic compounds, gives rise to dynamic diversity, allowing a shift towards one of the tautomeric states in response to interaction with the target or to environmental factors"; we now report a prototypal library of this kind.

The double Schiff base (e.g., **3**) formed in the reaction (Scheme 1) of an aromatic aldehyde with L-1,4-diamino-2,3-butanediol has two possible reaction pathways, namely, reversible consecutive ring closures to give five-membered and/or six-membered ring systems. The resulting five conceivable coexisting species can be considered a dynamic combinatorial virtual library (DCVL). The processes depicted in Scheme 2 represent only one of these options (or a subset of the above DCVL), that is, the six-membered ring closure (Scheme 1, bottom). The latter is also kinetically preferred,[2] since in accordance with Baldwin's rules,[10] the *endo-trig* ring closure is favored for 1,3-oxazanes (6-*endo-trig*), but disfavored for oxazolidines (5-*endo-trig*).

Note that we are not dealing here with an unbiased, isoenergetic DCL, as postulated by Lehn.[8a] This requirement is, after all, strongly phase- and medium-dependent and therefore of only limited pertinence. The **6** and **7** series (Scheme 2) are in fact biased libraries, in which one of the members of each series is strongly favored, such as the stable DODAD macrocycle **6″**, which can be destabilized by heating in DMSO to give **6** and **6′**. This allows the DCVL to be "scanned" for its constituents by changing the temperature and/or solvent. However, in the diazadioxadecalin series (**7**), the closed form **7″** prevails even on heating due to the intrinsic high stability of *cis*-DADOD.[2]

In a biased but target-driven library, in which one constituent is highly favored, the preferred interaction of a virtual (or minor) constituent with the target may overturn the equilibrium situation. Hence, we probed the influence of chelation of selected metal ion targets on ring–chain tautomerism in the **6** and **7** macrocyclic series. In this context, we recalled that Armstrong and Lindoy[7] had prepared the Ni^{II} complex **8** of the related diimine macrocycle (i.e., **7** without the two hydroxyethyl



pendant groups), by condensation of the dialdehyde **5** with ethylenediamine and complexation in situ. Their attempts to isolate the macrocyclic ligand by removing it from the nickel complex **8** were unsatisfactory and, in the presence of other diamines, **8** underwent amine exchange reactions to form more stable complexes of nickel.

Complexation of **7″** with $NiCl_2$ in methanol proceeded slowly at room temperature with formation of transient imine forms ($\delta = 8.5$ by NMR spectroscopy during complexation), but no evidence for a diimine macrocyclic complex similar to **8** was found in the product. The final product was clearly a DADOD complex, but it was apparently formed via **7**·Ni^{II}, which underwent tautomeric ring closure to the more stable **7″**·Ni^{II} complex. The FAB-MS spectrum of the latter has a peak at *m*/*z* 447 (20%) that fits exactly the $[NiLCl]^+$ species. All FAB-MS peak assignments were confirmed by comparison with simulated isotope patterns.

A similar complexation of **7″** with $Ni(ClO_4)_2$ in acetonitrile was carried out with UV monitoring of the complexation process (Figure 2). Addition of nickel salt affords a slight hypsochromic shift with sizable intensity increase and a 1/1 complexation stoichiometry, as determined by Job's method[11] (Figure 2, inset). Attempts to obtain a lead complex of **7″** in methanol failed. Indeed, the Ni^{2+} ion of small ionic radius (0.69 Å) can readily inhabit the DADOD **9** cavity, which the larger Pb^{2+} ion (1.18 Å) can not, and tautomeric

 © WILEY-VCH Verlag GmbH, D-69451 Weinheim, 2000 1433-7851/00/3915-2686 $ 17.50+.50/0 *Angew. Chem. Int. Ed.* **2000**, *39*, No. 15

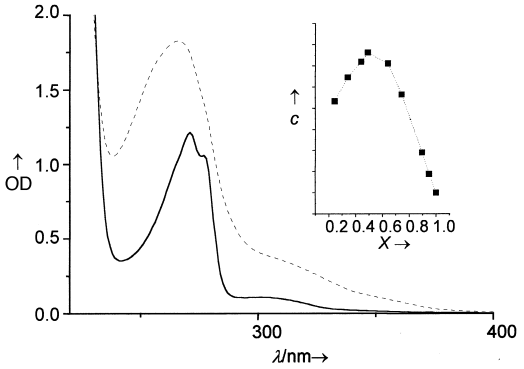


Figure 2. UV spectrometry of the complexation of **7″** with $Ni(ClO_4)_2$ (5×10^{-4} M) in MeCN: —— ligand; ---- [1:1] complex (OD = 1.82). Inset: determination of the ligand/complex ratio, by Job's method[11] (X = "molar fraction").

ring opening to give the similarly sized **7**·M^{II} (cf. **8**) is ineffective.

In the dioxadiazadecalin (DODAD) macrocyclic series (Scheme 2, top), on complexation of **6″** with $NiCl_2$, the final methanol solution shows exclusively (NMR) the dioxadiazadecalin complex. Under FAB-MS conditions, however, the occurrence of peaks at m/z 447 (30%) for $[NiLCl]^+$ and at 411 (65%) for $[NiL-H]^+$ indicate the additional presence of the tautomeric diimine complex. This general and diagnostic difference exists in all FAB mass spectra of complexes of the macrocycles in the **6** and **7** series: the complexes of both the bicyclic DODAD (**6″**) and DADOD (**7″**) exhibit $[MLX]^+$ ions, but only in the ring–chain tautomeric **6** series can one find an $[ML-H]^+$ ion, characteristic of the dimine **6**.

Interestingly and in contrast to the DADOD series (see above), addition of $Cd(ClO_4)_2$ or $Pb(ClO_4)_2$ to **6″** in methanol led to the precipitation of the complexes in each case. These could be dissolved, however, in $[D_6]$DMSO for NMR purposes. Thus, it became evident that **6″** underwent tautomeric ring opening during complexation with Cd^{2+}, and all forms (**6**, **6′**, and **6″**) are present, as is also shown by FAB-MS (peaks at m/z 567 (25%) $[CdL(ClO_4)]^+$, 467 (7%) $[CdL-H]^+$, and 465 (15%) $[CdL-3H]^+$). In the case of lead, however, the NMR spectrum in $[D_6]$DMSO shows only the diimine complex **6**·Pb^{II}, with FAB-MS peaks characteristic of the open-chain form (561 (70%) $[PbL-H]^+$ and 559 (140%) $[PbL-3H]^+$). It appears that the larger Cd^{2+} (0.97 Å) and Pb^{2+} (1.18 Å) ions are readily accomodated by **6″** (in contrast to **7″**) due to its ability to modify its cavity size by a successive ring-opening process (Scheme 2), ending with a ring expansion by two atoms to give **10** (M = Pb). Eventually, the latter may undergo gradual reverse macrocycle folding, which provides a mechanism of fine-tuning until an optimum cavity size for ion bonding is reached. Thus, Ni^{II}, Cd^{II}, and Pb^{II} are complexed by **6**–**6″** in different tautomeric modes that depend on the size of the cation.

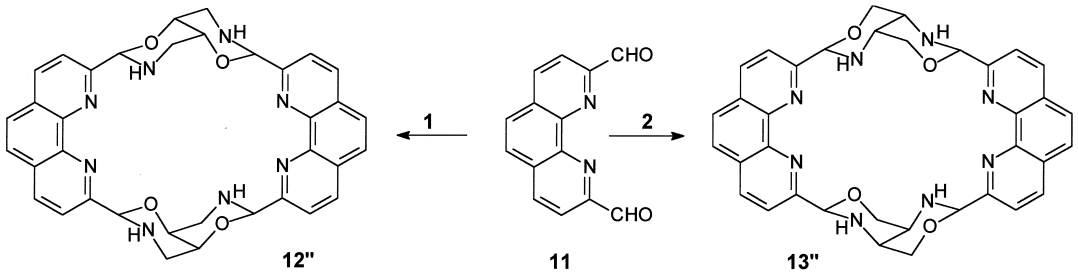
To highlight another aspect of DCVLs, the condensation of **1** and **2** with the known 1,10-phenanthroline-2,9-dicarbaldehyde (**11**)[12] was carried out in ethanol (Scheme 3) to give the macrocycles **12″** and **13″**, respectively. Evidently, a [2+2] condensation took place, since the utilization of the long and rigid dialdehyde **11** rendered the [1+1] mode improbable. In fact, according to FAB-MS, **13″** was accompanied also by some [3+3] macrocyclic product. These reactions are closely related to the previously described[13] nontemplate condensation of **11** with 1,2-diaminoethane or 1,4-diaminobutane to give the corresponding tetraimine macrocycles, except that our system has additional 2-hydroxyethyl pendant groups which turn it into a tautomeric manifold and consequently into a DCVL.

The NMR spectra of the sparingly soluble macrocycles **12″** and **13″** could be recorded in chloroform/methanol or DMSO. According to variable-temperature NMR spectra in $CDCl_3$/$[D_4]$MeOH from $-50\,^\circ$C to room temperature and in $[D_6]$DMSO from room temperature up to $120\,^\circ$C, these macrocycles exist as tautomeric mixtures, without apparent preference for any tautomer.

According to the same reasoning as in the simple cases (**3**, **4**; see above), the [2+2] macrocycles can occur in 18 tautomeric forms, with a subset of seven oxazine tautomers (**13**–**13″**, Scheme 4). In case of the [3+3] macrocyclic manifold, 67 components of the tautomeric mixture are theoretically possible, sixteen of them in the oxazine subset (Figure 3, bottom).

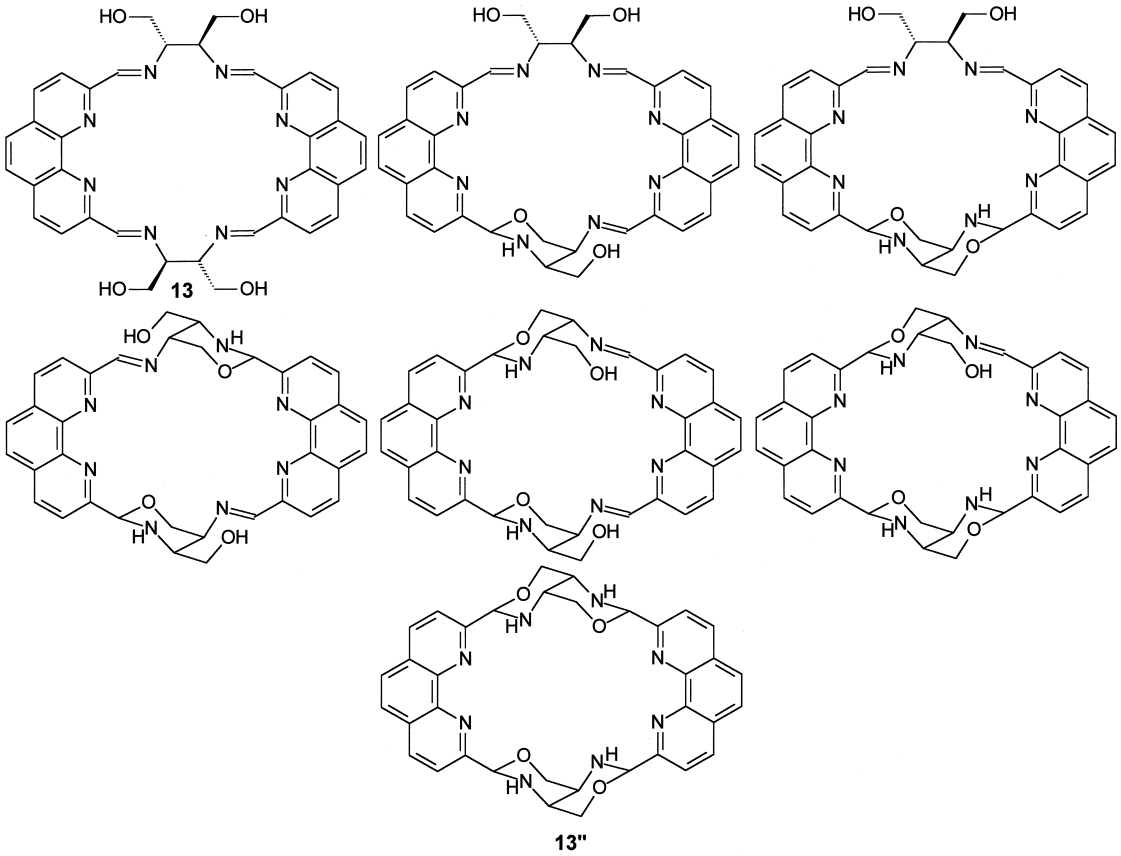
Contrary to the [1+1] macrocycles, with their strongly favored DODAD (**6″**) and DADOD (**7″**) components, the [2+2] macrocycles form partly unbiased, isoenergetic dynamic combinatorial libraries over a wide temperature range, whereby certain equilibrating constituents are of sufficiently similar free energy to generate a Boltzmann distribution with comparable populations for these constituents (states). As with the smaller [1+1] species, the [2+2] and [3+3] series are truly DCVLs (Figure 3), but with numerous components, some of which are less stable and likely absent. Further experiments are in progress to produce biased and template-induced forms.

Received: December 16, 1999
Revised: April 20, 2000 [Z14412]



Scheme 3. The fully closed macrocyclic products in the DODAD (**12″**) and DADOD (**13″**) series from the [2+2] reaction of 1,10-phenanthroline-2,9-dicarbaldehyde (**11**) with **1** and **2**, respectively.

 © WILEY-VCH Verlag GmbH, D-69451 Weinheim, 2000 1433-7851/00/3915-2687 $ 17.50+.50/0



Scheme 4. The full tautomeric set of macrocycles (**13**–**13**″) in the six-membered DADOD series.

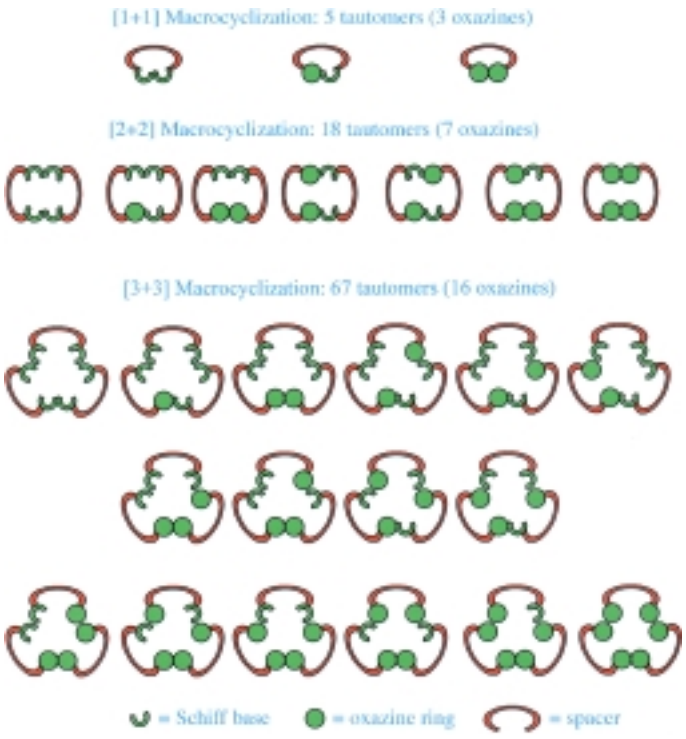


Figure 3. Schematic representation of dynamic combinatorial virtual libraries (DCVLs) comprising the macrocycles in any of the equilibria involving the six-membered DODAD and DADOD systems, bridged by ligating spacers (see Scheme 2 for the [1+1] mode and Scheme 4 for [2+2]).

[1] A. Star, I. Goldberg, N. G. Lemcoff, B. Fuchs, *Eur. J. Org. Chem.* **1999**, 2033 (see also: A. Star, N. G. Lemcoff, I. Goldberg, B. Fuchs, *Tetrahedron Lett.* **1997**, *38*, 3573).

[2] a) A. Star, B. Fuchs, *J. Org. Chem.* **1999**, *64*, 1166; b) A. Star, I. Goldberg, B. Fuchs, *J. Org. Chem.*, submitted.

[3] a) R. E. Valters, F. Fülöp, D. Korbonits, *Adv. Heterocycl. Chem.* **1996**, *66*; b) F. Fülöp, K. Pihlaja, J. Mattinen, G. Bernáth, *J. Org. Chem.* **1987**, *52*, 3821; c) F. Fülöp, L. Lázár, I. Pelczer, G. Bernáth, *Tetrahedron* **1988**, *10*, 2993.

[4] *Encyclopedia of Reagents for Organic Synthesis* (Ed.: L. A. Paquette), Wiley, Chichester, **1995**.

[5] a) E. N. Jacobsen, *Catalytic Asymmetric Synthesis* (Ed.: I. Ojima), VCH, Weinheim, **1993**, pp. 159–202; b) M. Tokunaga, J. F. Larrow, F. Kakiuchi, E. N. Jacobsen, *Science* **1997**, *277*, 936.

[6] a) M. L. Wolfrom, F. Shafizadeh, J. O. Wehrmüller, R. K. Armstrong, *J. Org. Chem.* **1958**, *23*, 571; b) F. I. Carroll, *J. Org. Chem.* **1966**, *31*, 366; c) P. W. Feit, O. T. Nielsen *J. Med. Chem.* **1967**, *10*, 927.

[7] L. G. Armstrong, L. F. Lindoy, *Inorg. Chem.* **1975**, *14*, 1322.

[8] a) J-M. Lehn, *Chem. Eur. J.* **1999**, *5*, 2455; see also: b) R. D. Cramer, D. E. Patterson, R. D. Clark, F. Soltanshahi, M. S. Lawless, *J. Chem. Inf. Comput. Sci.* **1998**, *38*, 1010; c) Y. R. de Miguel, J. K. M. Sanders, *Curr. Opin. Chem. Biol.* **1998**, 417; d) P. A. Brady, J. K. M. Sanders, *Chem. Soc. Rev.* **1997**, *26*, 327.

[9] a) I. Huc, M. J. Krische, D. P. Funeriu, J.-M. Lehn, *Eur. J. Inorg. Chem.* **1999**, 1415; b) A. V. Eliseev, J.-M. Lehn, *Curr. Top. Microbiol. Immunol. Comb. Chem. Biol.* **1999**, 159; c) V. A. Polyakov, M. I. Nelen, N. N. Nazarpack-Kandlousy, A. D. Ryabov, A. V. Eliseev, *Phys. Org. Chem.* **1999**, 357; d) B. Klekota, B. L. Miller, *Tetrahedron* **1999**, *55*, 11687; e) B. Klekota, B. L. Miller, *Trends Biotechnol.* **1999**, *17*, 205; f) P. Timmerman, D. N. Reinhoudt, *Adv. Mater.* **1999**, *11*, 71; g) M. C. Calama, R. Hulst, R. Fokkens, N. M. M. Nibbering, P. Timmerman, D. N. Reinhoudt, *Chem. Commun.* **1998**, 1021; h) S. A. Poulsen, P. J. Gates, G. R. L. Cousins, J. K. M. Sanders, *Rapid Commun. Mass Spectrom.* **2000**, *14*, 44 and previous papers; i) G. R. L. Cousins, S. A.

 © WILEY-VCH Verlag GmbH, D-69451 Weinheim, 2000 1433-7851/00/3915-2688 $ 17.50+.50/0

Poulsen, J. K. M. Sanders, *Chem. Commun.* **1999**, 1575; j) S. J. Rowan, P. S. Lukeman, D. J. Reynolds, J. K. M. Sanders, *New J. Chem.* **1998**, *22*, 1015; k) P. A. Brady, R. P. Bonar-Law, S. J. Rowan, C. J. Suckling, J. K. M. Sanders, *Chem. Commun.* **1996**, 319.
[10] J. E. Baldwin, *J. Chem. Soc. Chem. Commun.* **1976**, 734.
[11] K. A. Connors, *Binding Constants*, Wiley, New York, **1987**.
[12] C. J. Chandler, L. W. Deady, J. A. Reiss, *J. Heterocycl. Chem.* **1981**, *18*, 599.
[13] K. E. Krakowiak, J. S. Bradshaw, W. Jiang, N. K. Dalley, G. Wu, R. M. Izatt, *J. Org. Chem.* **1991**, *56*, 2675.

Lanthanide [15]Metallacrown-5 Complexes Form Nitrate-Selective Chiral Cavities

Annabel D. Cutland, Roneil G. Malkani, Jeff W. Kampf, and Vincent L. Pecoraro*

In 1989 we described a strategy using a metal salt and a bifunctional hydroxamic acid for the synthesis of metallomacrocycles known as metallacrowns.[1a] Metallacrowns are preorganised molecules that can be prepared in a variety of structure types[1b–f] in yields ranging from 60 % to quantitative. Remarkably, the molecules are robust: they retain their structure in solution and carry out cation and anion exchange reactions without decomposition.[1g,h] Recently, we have shown that resolved amino hydroxamic acids[1i–k] can be used as precursors for the preparation of macrocycles that can have molecular weights greater than 1500 Daltons,[1k] contain multiple resolved centers, and may be amphiphilic. There is current interest in developing materials capable of anion recognition, particularly through the use of macromolecules such as calixarenes,[2a,b] porphyrins,[3a,b] and macropolycyclic polyammonium molecules[4a–c] which can require multiple step syntheses. Herein we show for the first time that one can exploit the asymmetry of the chiral metallacrown motif to realize molecular cavities that are capable of selective anion recognition by using molecules that are made in a one-step reaction from simple starting materials.

The metallacrown dimer $[(\mathbf{1})Cl_2]^{4+}$[5] (Figures 1 and 2a, Table 1)[6, 7] is prepared using L-tyrosinehydroxamic acid (H_2tyrha) as a ligand.[8] The molecule contains five tyrosinehydroximate ligands and five Cu^{II} ions in each of the two [15]metallacrown-5 (15MC-5) disks, with a Gd^{III} ion captured in the core of each metallamacrocycle to give a stoichiometry of $[C_{45}H_{50}N_{10}O_{15}Cu_5Gd]^{3+}$. The metallacrowns have rotational symmetry, and therefore, the use of L-tyrosinehydroxamic acid provides face differentiation as the side chains are all oriented to the same "hydrophobic" face. The metallacrowns in the dimer are related to one another by a C_2 axis that is parallel to the plane of the disc, and thus are orientated with

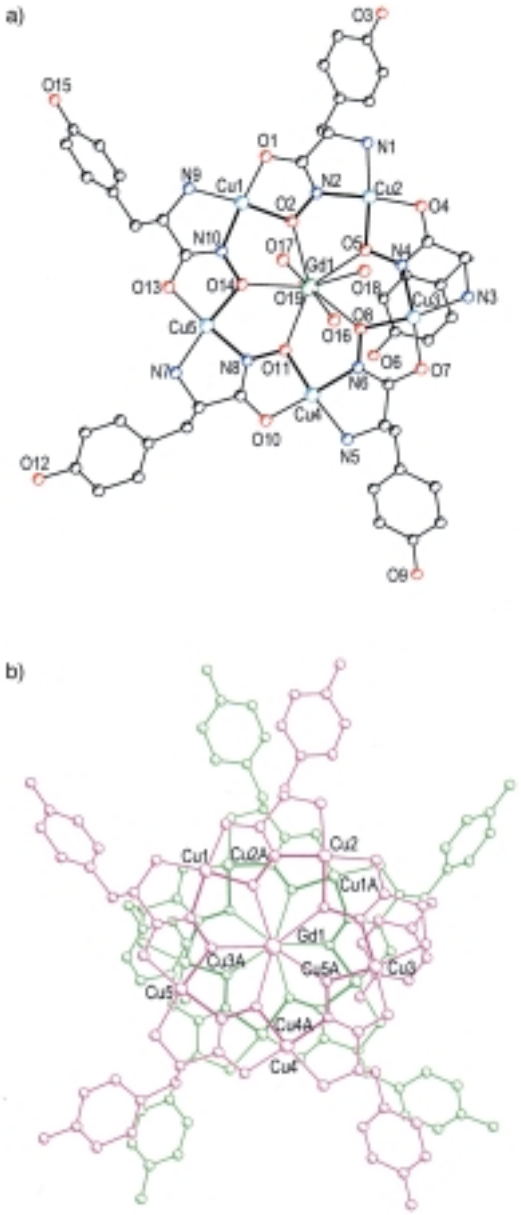


Figure 1. PLUTO diagram of $[\mathbf{1}\cdot(Cl)_2]^{4+}$ with chloride ions removed for clarity. a) Monomer and b) dimer shown looking down the psuedo fivefold axis, with the C_2 axis in the plane of the page.

the hydrophobic faces towards each other. As viewed down the pseudo fivefold axis the MC that is on top has clockwise (C) rotational symmetry (Cu-O-N-Cu); therefore, the bottom metallacrown is anticlockwise (A) when viewed from this perspective, thus giving a C/A isomer. While four phenol groups from each metallacrown are extended into solution, the remaining two wrap into the cavity and bond to a ring copper ion from the opposite metallacrown ($Cu{-}O_{tyr}$ = 2.872 Å). The ring oxygen atoms are nearly perfectly staggered, with an O–O twist angle (defined as the torsion angle O2-Gd1-Gd1A-O2A) between the two metallacrowns of the dimer of 35.7°. However, because the metallacrowns have C/A rotational symmetry, the Cu–Cu twist angle (Cu1-Gd1-Gd1A-Cu2A) is 11.4°, which makes the ring copper ions closer to being eclipsed than staggered. The result is a weakly

[*] Prof. V. L. Pecoraro, A. D. Cutland, R. G. Malkani, J. W. Kampf
Department of Chemistry
Willard H. Dow Laboratories
The University of Michigan, Ann Arbor, MI 48109-1055 (USA)
Fax: (+1) 734-647-4865
E-mail: vlpec@umich.edu

 © WILEY-VCH Verlag GmbH, D-69451 Weinheim, 2000 1433-7851/00/3915-2689 $ 17.50+.50/0

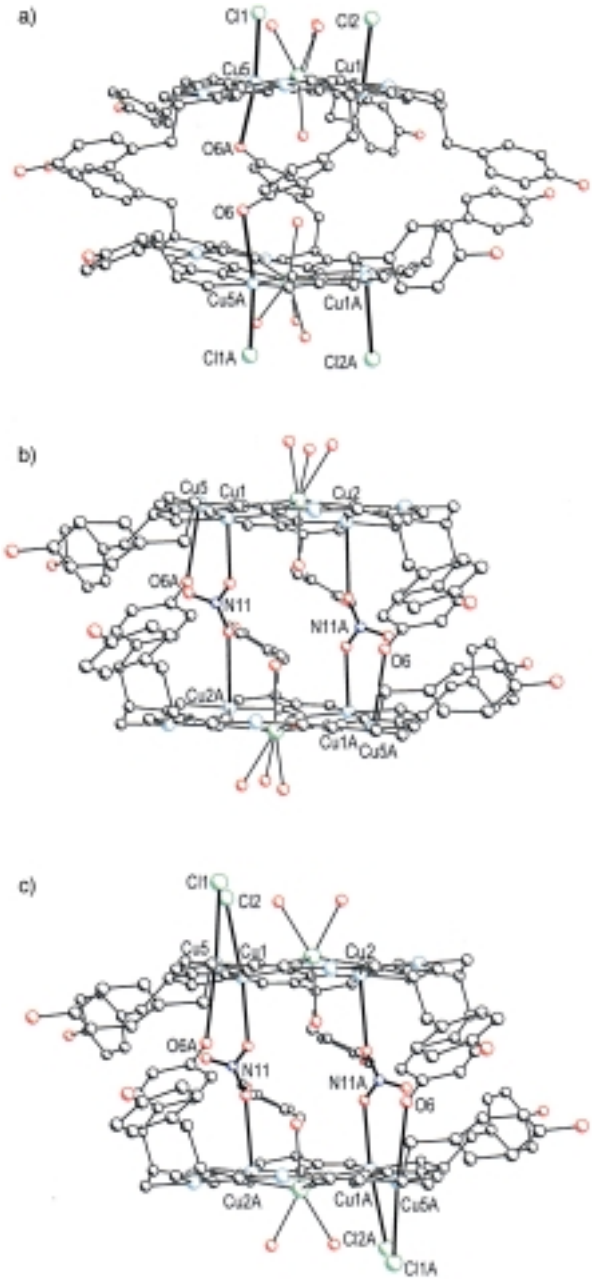


Figure 2. PLUTO diagrams of a) $[\mathbf{1}\cdot(Cl)_2]^{4+}$, b) $[\mathbf{1}\cdot(NO_3)_2]^{4+}$, and c) $[\mathbf{1}\cdot(Cl)_2(NO_3)_2]^{2+}$. The structures in b and c are viewed down the C_2 axis while a is rotated 90° from this view.

associated dimer with the Gd ions separated by 8.34 Å and a metallacrown cavity of 776 Å^3. Thus, through an exceedingly simple reaction, one can isolate a crystalline compound of molecular weight 2963 Daltons that contains 12 metal atoms, 10 defined carbon centers, and a nearly nanometer sized cavity in 60.5 % yield.

In the preceding structure there are two chloride ions per dimer that are weakly bound to ring copper ions on the outer face of each metallacrown. The same basic structure and chloride localization is obtained if La^{III} is substituted for Gd^{III} in the synthesis. We conclude that while chloride ions are capable of binding to the Cu^{II} ions, they do so only to the outer face of the metallacrown.

Table 1. Selected metrical parameters for $[\mathbf{1}\cdot(Cl)_2]^{4+}$, $[\mathbf{1}\cdot(NO_3)_2]^{4+}$, and $[\mathbf{1}\cdot(Cl)_2(NO_3)_2]^{2+}$.

Distance [Å]/angle [°]	Metallacrown		
	$[\mathbf{1}\cdot(Cl)_2]^{4+}$	$[\mathbf{1}\cdot(NO_3)_2]^{4+}$	$[\mathbf{1}\cdot(Cl)_2(NO_3)_2]^{2+}$
across the dimer cavity			
Cu1-Cu2A	7.55	7.26	7.47
Cu3-Cu5A	7.76	8.00	7.90
Cu4-Cu4A	6.68	7.90	7.26
Gd1-Gd1A	8.34	8.39	8.49
O-O twist	35.7	40.6	38.6
Cu-Cu twist	11.4	15.1	14.6
axial Cu distances			
Cu1-$O_{(tyr)}$	2.87	2.83	2.86
Cu1-$O_{(NO3)}$	N/A[a]	2.48	2.64
Cu2-$O_{(NO3)}$	N/A[a]	2.96	2.97
Cu5-Cl1	2.86	N/A[a]	2.89
Cu1-Cl2	3.14	N/A[a]	3.14
inter-dimer			
Gd1-Gd1B	8.19	8.52	8.28
Cu1-Cu1B	6.26	6.67	6.25
Cu5-Cu5B	5.71	6.07	5.77

[a] Not available.

We have also prepared $[\mathbf{1}\cdot(NO_3)_2]^{4+}$ (Figure 2b) in approximately 80 % yield.[9, 10] The basic structural features of $[\mathbf{1}\cdot(Cl)_2]^{4+}$ and $[\mathbf{1}\cdot(NO_3)_2]^{4+}$ are essentially identical except that two nitrate anions are captured in the cavity and bridge the dimer by binding to ring copper ions. The nitrate shortens the Cu1 – Cu2A distances by 0.29 Å in $[\mathbf{1}\cdot(NO_3)_2]^{4+}$ relative to that in $[\mathbf{1}\cdot(Cl)_2]^{4+}$ and the twist angles increase by 4 – 5°. Additional anions required for charge balance are found in the lattice. Thus, the cavity can act as a host for nitrate but not chloride in the solid state. We have tested the selectivity of the tyrosine metallacrown dimer for nitrate versus chloride ions in two ways. First, we assessed whether there was a binding preference for nitrate over chloride ions during the initial assembly of the metallacrown. In syntheses that contained a 10:3:1 ratio of chloride:nitrate:metallacrown a complex is isolated that contains two nitrate and two chloride ions per dimer.[11] Therefore, despite biasing the synthesis toward chloride ions, nitrate ions continue to bind inside the cavity. An X-ray analysis of $[\mathbf{1}\cdot(Cl)_2(NO_3)_2]^{2+}$ (Figure 2c)[12] reveals a hybrid structure of $[\mathbf{1}\cdot(Cl)_2]^{4+}$ and $[\mathbf{1}\cdot(NO_3)_2]^{4+}$ with metrical parameters midway between these two structures (Table 1). Of interest is the observation that the Cu1–$O_{nitrate}$ bond in $[\mathbf{1}\cdot(Cl)_2(NO_3)_2]^{2+}$ is nearly 0.16 Å longer than that in $[\mathbf{1}\cdot(NO_3)_2]^{4+}$. This difference is a result of the chloride ions binding to Cu1 in $[\mathbf{1}\cdot(Cl)_2(NO_3)_2]^{2+}$. Note that Cl1 and Cl2 are *always* bound to Cu5 and Cu1, respectively, in the presence or absence of nitrate, while the nitrate ion is *always* bound between Cu1 and Cu2A, whether or not chloride is present (see Figure 2). Next, we added four equivalents of sodium nitrate to an aqueous solution of $[\mathbf{1}\cdot(Cl)_2]^{4+}$ to test whether the metallacrown $[\mathbf{1}\cdot(Cl)_2]^{4+}$ could be converted into $[\mathbf{1}\cdot(Cl)_2(NO_3)_2]^{2+}$. A blue crystalline solid was obtained that is identical in all respects to $[\mathbf{1}\cdot(Cl)_2(NO_3)_2]^{2+}$.[13] Therefore, we have shown that the pre-formed metallacrown can selectively incorporate nitrate ions directly into the cavity with minor structural perturbations. Surprisingly, despite repeated attempts to sequester acetate, in the presence and absence of nitrate, we have not observed acetate ligands bound to **1**.

 © WILEY-VCH Verlag GmbH, D-69451 Weinheim, 2000 1433-7851/00/3915-2690 $ 17.50+.50/0

While the guest, in this case, is achiral, we hope in the future to exploit the chirality of metallacrowns by building larger cavities that may show recognition of chiral anions.

In conclusion, we have shown that a chiral metallamacrocycle can be prepared in excellent yield in a one-step synthesis using commercially available starting materials. The resultant metallacrown binds nitrate ions, complexing this anion with minor perturbations to a cavity with dimensions approaching 1 nm[3]. In contrast, acetate ions have not been seen to bind to the metallacrown, while chloride ions only bind to the outer face. These observations of the solid state are consistent with selective anion recognition; however, they do not directly address the solution behavior. Future studies to define and quantify the binding interactions of nitrate in solution are planned. We suggest that these metallacrowns form a new class of selective anion recognition agents that can be prepared by simple modification of the side chains of α-aminohydroxamic acids to alter the size, charge, or topology of the resultant supramolecular species. Through such variation, selective recognition of anions containing differing charge, shape, size, or chirality may be achieved.

Experimental Section

$[\mathbf{1}\cdot(Cl)_2]^{4+}$: Prepared by the reaction of L-tyrosinehydroxamic acid (H_2tyrha, 0.395 g, 2.00 mmol) with $CuCl_2\cdot 2H_2O$ (0.342 g, 2.00 mmol), $GdCl_3\cdot 6H_2O$ (0.150 g, 0.40 mmol), and pyridine (0.5 ml, 6.00 mmol) in water (50 mL). Blue-violet crystals of $[\mathbf{1}\cdot(Cl)_2]^{4+}$ were obtained by slow evaporation of the solvent.

$[\mathbf{1}\cdot(NO_3)_2]^{4+}$: Prepared as for $[\mathbf{1}\cdot(Cl)_2]^{4+}$ using $Gd(NO_3)_3\cdot 5H_2O$ and $Cu(OAc)_2\cdot H_2O$, without pyridine. Blue-violet crystals of $[\mathbf{1}\cdot(NO_3)_2]^{4+}$ were obtained by slow evaporation of the solvent.

$[\mathbf{1}\cdot(Cl)_2(NO_3)_2]^{2+}$: Prepared as for $[\mathbf{1}\cdot(Cl)_2]^{4+}$ using $Gd(NO_3)_3\cdot 5H_2O$ and $CuCl_2\cdot 2H_2O$ in water and methanol. Blue-violet crystals of $[\mathbf{1}\cdot(Cl)_2(NO_3)_2]^{2+}$ were obtained by slow evaporation of the solvent.

Received: October 10, 1999 [Z14099]
Publication delayed at authors' request

[1] a) M. S. Lah, V. L. Pecoraro, *J. Am. Chem. Soc.* **1989**, *111*, 7258; b) V. L. Pecoraro, A. J. Stemmler, B. R. Gibney, J. J. Bodwin, H. Wang, J. W. Kampf, A. Barwinski, *Progress in Inorganic Chemistry*, *Vol. 45* (Ed.: K. D. Karlin), Wiley, New York, **1997**, pp. 83–177; c) B. Kwak, H. Rhee, S. Park, M. S. Lah, *Inorg. Chem.* **1998**, *37*, 3599; d) G. Psomas, C. Dendrinou-Samara, M. Alexiou, A. Tsohos, C. P. Raptopoulou, A. Terzis, D. P. Kessissoglou, *Inorg. Chem.* **1998**, *37*, 6556; e) R. W. Saalfrank, N. Löw, F. Hampel, H.-D. Stachel, *Angew. Chem.* **1996**, *108*, 2353; *Angew. Chem. Int. Ed. Engl.* **1996**, *35*, 2209; f) R. W. Saalfrank, N. Löw, S. Kareth, V. Seitz, F. Hampel, D. Stalke, M. Teichert, *Angew. Chem.* **1998**, *110*, 182; *Angew. Chem. Int. Ed.* **1998**, *37*, 172; g) B. R. Gibney, H. Wang, J. W. Kampf, V. L. Pecoraro, *Inorg. Chem.* **1996**, *35*, 6184; h) A. J. Stemmler, J. W. Kampf, V. L. Pecoraro, *Angew. Chem.* **1996**, *108*, 3011; *Angew. Chem. Int. Ed. Engl.* **1996**, *35*, 2841; i) J. Halfen, J. J. Bodwin, V. L. Pecoraro, *Inorg. Chem.* **1998**, *37*, 5416; j) A. J. Stemmler, A. Barwinski, M. J. Baldwin, V. Young, V. L. Pecoraro, *J. Am. Chem. Soc.* **1996**, *118*, 11962; k) A. J. Stemmler, J. W. Kampf, M. L. Kirk, B. H. Atasi, V. L. Pecoraro, *Inorg. Chem.* **1999**, *38*, 2807.

[2] a) W. Xu, J. J. Vittal, R. J. Puddephatt, *J. Am. Chem. Soc.* **1993**, *115*, 6456; b) N. Pelixxi, A Casnati, R. Ungaro, *Chem. Comm.* **1998**, *23*, 2607.

[3] a) J. L. Sessler, M. Cyr, H. Furuta, V. Kral, T. Mody, T. Morishima, M. Shionoya, S. Weghorn, *Pure Appl. Chem.* **1993**, *65*, 393; b) R. C. Jagessar, M. Shang, W. R. Scheidt, D. H. Burns, *J. Am. Chem. Soc.* **1998**, *120*, 11684.

[4] a) S. Mason, T. Clifford, L. Seib, K. Kuczera, K. Bowman-James, *J. Am. Chem. Soc.* **1998**, *120*, 8899; b) G. Papoyan, K. Gu, J. Wiorkiewicz-Kuczera, K. Kuczera, K. Bowman-James, *J. Am. Chem. Soc.* **1996**, *118*, 1354; c) J.-M. Lehn, *Science* **1985**, *227*, 849.

[5] Compound **1** refers to the core dimer $[\{Gd15MC_{Cu(II)(L\text{-}tyrha)}\text{-}5\}_2]^{6+}$, while $[\mathbf{1}\cdot(Cl)_2]^{4+}$, $[\mathbf{1}\cdot(NO_3)_2]^{4+}$, and $[\mathbf{1}\cdot(Cl)_2(NO_3)_2]^{2+}$ indicate the anion-bound forms of the metallacrown. The empirical formula for each molecule is given with the X-ray parameters.

[6] General crystallographic data: Data were collected on a SMART-CCD 3-circle diffractometer equipped with LT-2 low-temperature device and $Mo_{K\alpha}$ ($\lambda = 0.71073$ Å) radiation. Crystals were coated with inert oil to prevent solvent loss and frozen to a teflon fiber. The data were processed using the SAINT processing package (v4.05) with a narrow-frame algorithm. A correction for absorption was performed by SADABS (R. Blessing, *Acta Cryst.* **1995**, *A51*, 33). Structure solution and refinement was performed by direct methods using the SHELXTL program suite (v5.10) operating on a SGI Octane workstation. Crystallographic data (excluding structure factors) for the structures reported in this paper have been deposited with the Cambridge Crystallographic Data Centre as supplementary publication nos. CCDC-135202–135204. Copies of the data can be obtained free of charge on application to CCDC, 12 Union Road, Cambridge CB2 1EZ, UK (fax: (+44) 1223-336-033; e-mail: deposit@ccdc.cam.ac.uk).

[7] Crystal data for $[\mathbf{1}\cdot(Cl)_2]^{4+}$: $(C_{45}H_{50}N_{10}O_{15}Cu_5GdCl\cdot 2OH\cdot 12H_2O)$, $M_r = 1731.56$, monoclinic, space group $C2$ (no. 5), $a = 18.6666(2)$, $b = 29.58500(10)$, $c = 14.58100(10)$ Å, $\alpha = 90.000$, $\beta = 122.6680(10)$, $\gamma = 90.000^\circ$, $V = 6778.59(9)$ Å^3, $Z = 4$; $\rho_{calcd} = 1.697$ g cm^{-1}; $2.44 < \theta < 26.41^\circ$; crystal dimensions, $0.22 \times 0.32 \times 0.38$ mm^3; $\mu = 26.31$ cm^{-1}; $T = 158(2)$ K; 13731 unique of 31544 reflections collected. 12844 reflections and 803 parameters were used for the full matrix, least-squares refinement on F^2, $R1 = 0.0551$, $wR2 = 0.1539$. Two hydroxide anions are inferred for charge balance, but have not been located.

[8] Elemental analysis calcd for $[\mathbf{1}\cdot(Cl)_2]^{4+}$ $(C_{45}H_{50}N_{10}O_{15}Cu_5GdCl\cdot 2OH\cdot 5H_2O)$: C 33.67, H 3.89, N 8.72; found: C 33.61, H 3.62, N 8.72. positive ion FAB-MS (in methanol with a 3-nitrobenzyl alcohol matrix): m/z: 1443.6 $[M]^+$.

[9] Elemental analysis calcd for $[\mathbf{1}\cdot(NO_3)_2]^{4+}$ $(C_{45}H_{50}N_{10}O_{15}Cu_5Gd\cdot 1.5NO_3\cdot 1.5OH\cdot 1.5H_2O)$: C 33.96, H 3.45, N 10.12; found: C 33.68, H 3.57, N 10.47. positive-ion FAB-MS (in methanol in a 3-nitrobenzyl alcohol matrix): m/z: 1443.7 $[M]^+$.

[10] Crystal data for $([\mathbf{1}\cdot(NO_3)_2]^{4+})$: $(C_{45}H_{50}N_{10}O_{15}Cu_5Gd\cdot 1.5NO_3\cdot 1.5OH\cdot 9H_2O)$, $M_r = 1726.57$, monoclinic, space group $I2$ (no. 5), $a = 15.02060(10)$, $b = 28.9110(2)$, $c = 16.42480(10)$ Å, $\alpha = 90.000$, $\beta = 103.9510(10)$, $\gamma = 90.000^\circ$, $V = 6922.24(8)$ Å^3, $Z = 4$; $\rho_{calcd} = 1.657$ g cm^{-1}; $2.47 < \theta < 29.44^\circ$; crystal dimensions, $0.14 \times 0.34 \times 0.44$ mm^3; $\mu = 25.43$ cm^{-1}; $T = 158(2)$ K; 16913 unique of 3718 reflections collected. 15095 reflections and 851 parameters were used for the full matrix, least-squares refinement on F^2, $R1 = 0.0649$, $wR2 = 0.1682$. One and a half hydroxide anions are inferred for charge balance, but have not been located.

[11] Elemental analysis calcd for $[\mathbf{1}\cdot(Cl)_2(NO_3)_2]^{2+}$ $(C_{45}H_{50}N_{10}O_{15}Cu_5Gd\cdot NO_3\cdot Cl\cdot OH\cdot 12H_2O)$: C 30.42, H 4.26, N 8.67, Cu 17.9; found: C 29.73, H 4.05, N 8.92, Cu 17.4. positive-ion FAB-MS (in methanol with a 3-nitrobenzyl alcohol matrix): m/z: 1444.6 $[M]^+$.

[12] Crystal data for $[\mathbf{1}\cdot(Cl)_2(NO_3)_2]^{2+}$: $(C_{45}H_{50}N_{10}O_{15}Cu_5Gd\cdot NO_3\cdot Cl\cdot OH\cdot 7.5H_2O)$, $M_r = 1754.59$, monoclinic, space group C2 (no. 5), $a = 19.1017(4)$, $b = 29.1994(6)$, $c = 14.7861(3)$ Å, $\alpha = 90.000$, $\beta = 123.9670(10)$, $\gamma = 90.000^\circ$, $V = 6839.8(2)$ Å^3, $Z = 4$; $\rho_{calcd} = 1.647$ g cm^{-1}; $1.39 < \theta < 26.40^\circ$; crystal dimensions, $0.38 \times 0.42 \times 0.68$ mm^3; $\mu = 26.03$ cm^{-1}; $T = 158(2)$ K; 13909 unique of 61978 reflections collected. 13354 reflections and 800 parameters were used for the full matrix, least-squares refinement on F^2, $R1 = 0.0499$, $wR2 = 0.1453$. One hydroxide anion is inferred for charge balance, but has not been located.

[13] Elemental analysis calcd for $C_{45}H_{50}N_{10}O_{15}Cu_5Gd\cdot NO_3\cdot Cl\cdot OH\cdot 10H_2O$: C 31.05, H 4.11, N 8.85, Cu 18.3; found: C 30.75, H 3.82, N 9.06, Cu 17.5. positive ion FAB-MS (in methanol with a 3-nitrobenzyl alcohol matrix): m/z: 1443.9 $[M]^+$. The structure was solved by X-ray crystallography and shown to be identical to $[\mathbf{1}\cdot(Cl)_2(NO_3)_2]^{2+}$.

 © WILEY-VCH Verlag GmbH, D-69451 Weinheim, 2000 1433-7851/00/3915-2691 $ 17.50+.50/0

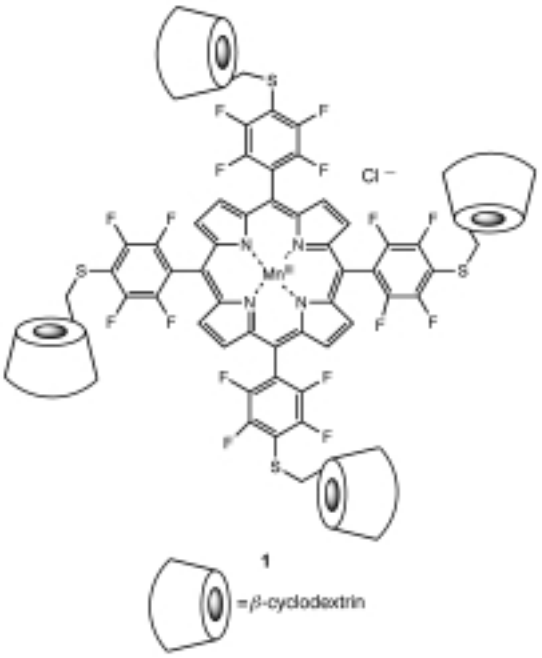
Selective Hydroxylation of a Steroid at C-9 by an Artificial Cytochrome P-450**

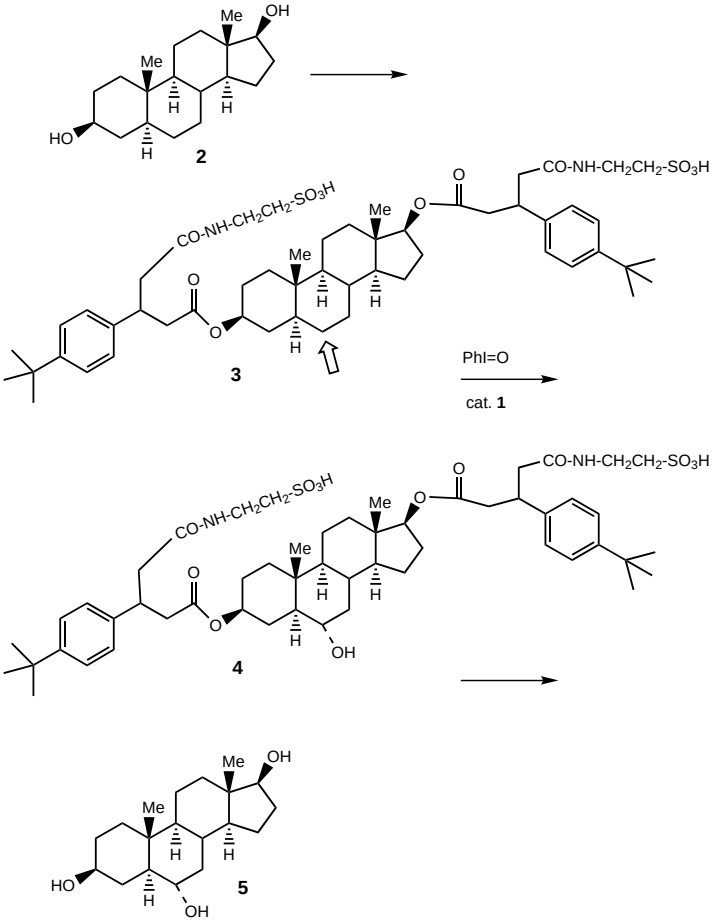
Jerry Yang and Ronald Breslow*

In contrast to the normal dependence of synthetic organic chemistry on the intrinsic reactivity of substrates, enzymatic reactions typically impose selectivity by control of the geometry in the enzyme/substrate complex. Such geometric control can override the reactivity of substrate functional groups. In the oxidation of lanosterol by P-450 enzymes, for instance, methyl groups on saturated carbons are selectively oxidized in the presence of two otherwise much more reactive double bonds and a secondary carbinol group.

We have been pursuing a program for many years to mimic such enzymes, so as to supplement the normal chemistry of functional group manipulation. The process we have termed "remote oxidation" is an example, in which a template is covalently attached to a substrate and guides free radical chlorination, by the "radical relay reaction," to positions in a substrate that are consistent with the geometry imposed by the template.[1] While the templates can then be removed, this is not a true turnover catalytic process.

Recently we reported an example in which **1**, a manganese porphyrin carrying four cyclodextrins attached to fluorinated phenyl groups, was used as a catalyst in the hydroxylation of androstane-3,17-diol (**2**).[2] The steroid **2** was converted to a diester **3** carrying *tert*-butyl groups for binding into the cyclodextrins and sulfonate groups for water solubility (Scheme 1). We saw that substrate **3** was converted to its 6α-hydroxyl derivative **4** in up to 100% yield with 95% conversion using 1 mol% of catalyst **1** and 10 equivalents of PhIO as oxidant. Ester hydrolysis afforded triol **5** (Scheme 1).





Scheme 1. Catalyst **1** converts a doubly bound substrate to the 6α-hydroxy derivative.

The reaction was completely regioselective for the C-6 position of the steroid, stereoselective in forming only the equatorial 6α-hydroxyl derivative, and chemoselective in not oxidizing the hydroxyl group further into the ketone. By contrast, without the *tert*-butylphenyl binding groups no oxidation of the steroid occurred under our conditions. When steroidal alcohols are oxidized with high concentrations of related metalloporphyrin catalysts that do not bind their substrates, we find that the dominant reaction is conversion of the alcohol group into a ketone, not hydroxylation of saturated carbons.

Corey-Pauling-Koltun (CPK) and computer molecular models suggested that our process with the enzyme mimic involves binding of the substrate to present the steroid edge on to the face of the metalloporphyrin (Figure 1). While the selectivity of the results is striking, hydroxylation of a steroid at C-6 is not intrinsically important. However, models indicated (Figure 2) that if we could bind the steroid face to face with the porphyrin we should get attack at the axial C-9α

[*] Prof. Dr. R. Breslow, J. Yang
Department of Chemistry
Columbia University
New York, NY 10027 (USA)
Fax: (+1) 212-854-2755
E-mail: rb33@columbia.edu

[**] We thank the National Institutes of Health, the National Science Foundation, and the Environmental Protection Agency for financial support of this research. J.Y. acknowledges support from an NCER-QA EPA Graduate Fellowship and a Bristol-Myers Squibb Graduate Fellowship.

 © WILEY-VCH Verlag GmbH, D-69451 Weinheim, 2000 1433-7851/00/3915-2692 $ 17.50+.50/0

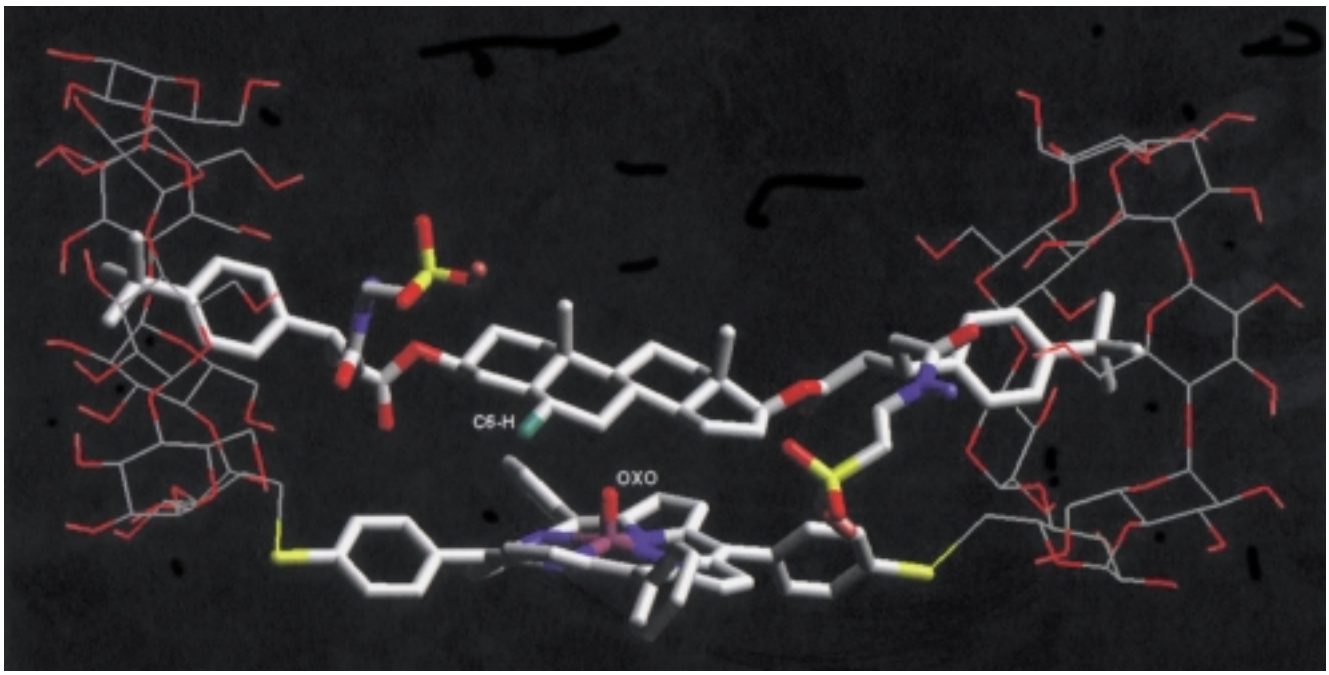


Figure 1. The computed structure of the complex of doubly bound substrate **3** with catalyst **1**, showing that the oxygen atom added to the Mn atom of **1** is in a lateral position to attack the equatorial H atom on C-6 of **3**, as observed. For details of the calculational method, which differs from that in Figure 2, see Experimental Section. For clarity the two cyclodextrins not involved in substrate binding are deleted from the figure, and those binding the substrate are shown with thin lines.

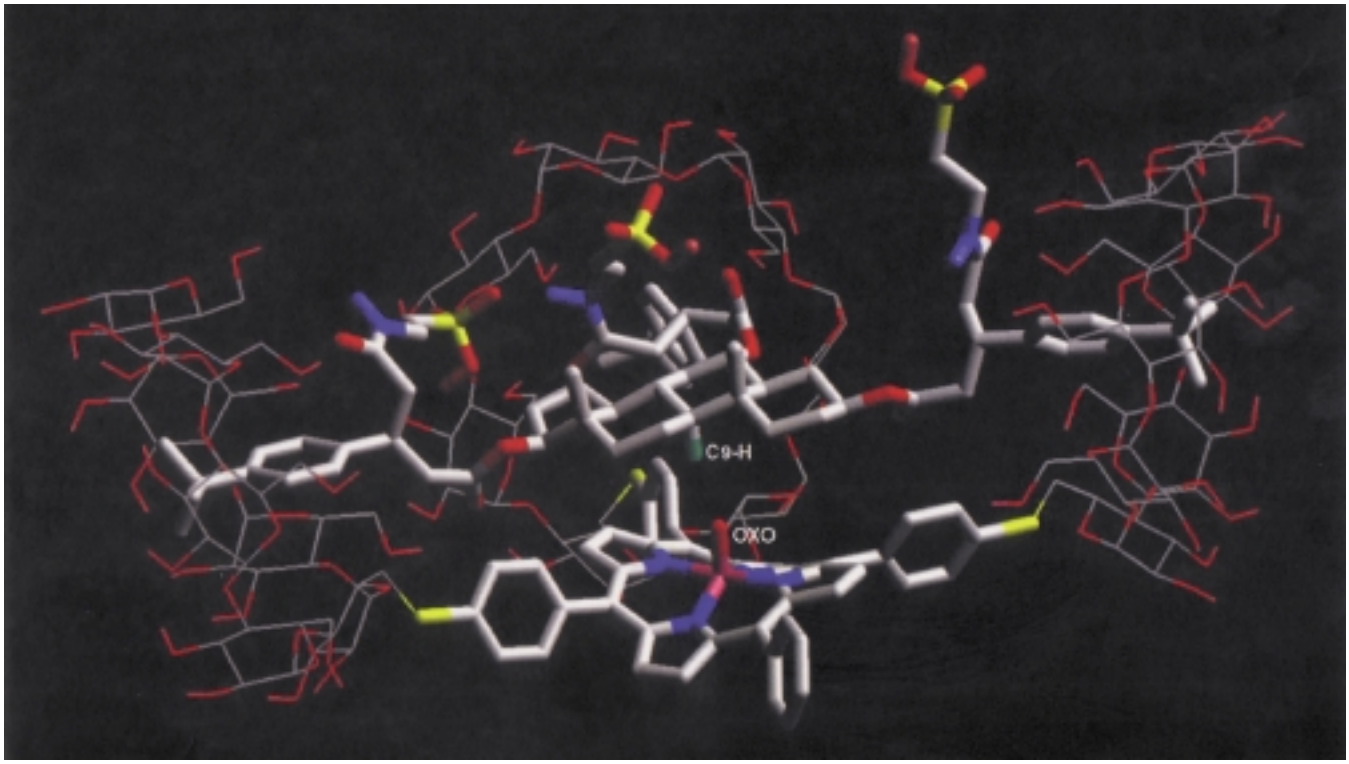


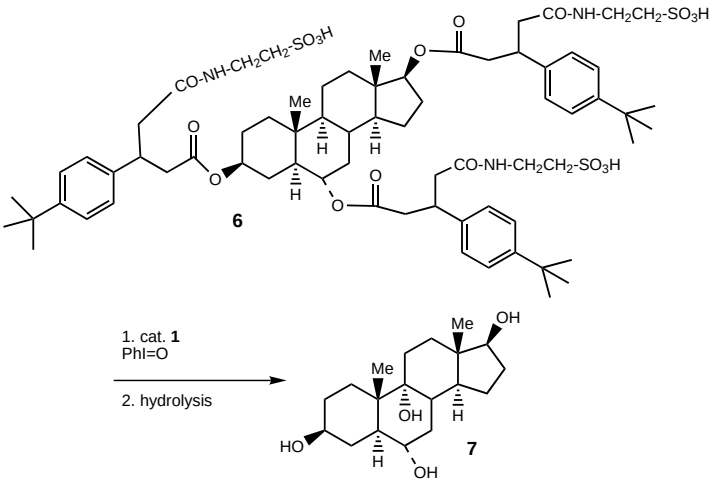
Figure 2. The computed structure of the complex of triply bound substrate **6** with catalyst **1**, showing that the oxygen atom added to the Mn atom of **1** is in a lateral position to attack the axial H atom on C-9 of **6**, as observed. For details of the calculational method, which differs from that in Figure 1, see Experimental Section. For clarity the one cyclodextrin not involved in substrate binding is deleted from the figure, and those binding the substrate are shown with thin lines.

hydrogen, a very desirable process. We have now achieved this, and find that the catalyzed reaction is indeed completely selective for hydroxylation at C-9.

To change the geometry of the complex, we introduced a third binding interaction. The 3β,6α,17β-androstantriol (**5**), synthesized on a preparative scale by our previous hydrox-

 © WILEY-VCH Verlag GmbH, D-69451 Weinheim, 2000 1433-7851/00/3915-2693 $ 17.50+.50/0

ylation reaction,[2] was converted into the triester **6** (Scheme 2), which contains binding and solubilizing groups, and oxidized with 1 equivalent of catalyst **1**, 10 equivalents of PhIO, and 10 equivalents of pyridine in pure deionized water.



Scheme 2. Catalyst **1** converts a triply bound substrate to the 9α-hydroxy derivative.

The oxidant was quenched and the ester groups removed to afford the tetraol **7** as the only detectable product in quantitative yield (Scheme 2). With only 0.1 equivalent of catalyst and excess oxidizing agent the conversion of **6** to **7** was also complete, so there are at least 10 turnovers in this catalytic hydroxylation.

As expected, **7** gave positive ion and negative ion mass spectra indicating one more oxygen than in **5**, and a ^{1}H NMR spectrum showing that there was no new CH–OH group and that the proton at C-9 in **5** was missing in **7**. Relative to **5**, the ^{1}H NMR signal (500 MHz, $CDCl_3$) for the C-18 methyl group was shifted downfield by $\Delta\delta = 0.015$ to $\delta = 0.752$, and that for the C-19 methyl group was shifted downfield by $\Delta\delta = 0.125$ to $\delta = 0.958$. This is consistent with the tabulated effect of a 9-OH group on these methyl NMR signals.[3] The COSY spectrum indicated that the C-5- and C-7α-proton signals moved downfield, as expected from their 1,3-diaxial relationship to the new C-9 hydroxyl group in **7**.

Thus we have achieved selective turnover catalytic hydroxylation of a steroid at C-9, as computer modeling suggested. Such C-9 hydroxysteroids can be dehydrated to introduce the C-9(11) double bond. As previous work shows, such a double bond permits synthesis of corticosteroids with oxygen at C-11 and fluorine at C-9, an important class of medicinal compounds.[4]

These catalytic hydroxylations in the complex of substrates with an artificial P-450 enzyme mimic thus show predictable geometric control that overwhelms intrinsic substrate reactivity, in the sense that the hydroxyl group introduced into compound **5** is not further oxidized in competition with selective hydroxylation of an unactivated methylene group. It remains to be seen how well such enzyme mimics can perform other useful oxidations, and, thus, how generally they succeed in freeing chemistry from the domination of functional group reactivities.

Experimental Section

Catalyst **1** was prepared as described in ref. [2c]. The oxidations and workup were as described in the supplementary material of ref. [2a].

The molecular models shown in Figures 1 and 2 were calculated using version 7.0 of the program MacroModel, with the inclusion of water as a continuous solvent, and with energy minimization as the geometries were varied. In both cases the cyclodextrin rings themselves were fixed in their calculated initial internal geometry before further geometry variations and energy minimizations, to cut down the calculational time required. However, there were some differences in details between the calculations resulting in Figures 1 and 2.

The model in Figure 2 was calculated by substituting a phosphorus atom for the manganese atom in catalyst **1**, since the program has no parameters for manganese. The phosphorus atom was not permitted to move, and the attached oxygen atom was held perpendicular to the porphyrin plane during geometry variation and energy minimization. Essentially the same result was obtained from a calculation using only the porphyrin system and then inserting the included metal (phosphorus atom) and its attached oxygen atom at the end of the calculation. The result was that the oxygen atom in the catalyst/substrate complex of Figure 2 was within contact distance of the hydrogen atom at C-9, consistent with the observed hydroxylation at C-9. The oxygen atom was also calculated to be within the same distance of the axial hydrogen atom on C-1, but no hydroxylation of this position was observed experimentally.

However, the model in Figure 1 was calculated with just the porphyrin system, which lacked metal or oxygen—these were later inserted after energy minimization. This shows the geometry needed to account for our finding that the doubly bound substrate is hydroxylated at C-6. However, when the calculation was done as in Figure 2, with an included phosphorus as a surrogate metal along with the oxygen atom, energy minimization did not bring the edge of the steroid near the oxygen atom, and did not account for the observed hydroxylation at C-6.

Thus, either method of calculation accounts for the observed mode of reaction at C-9 of substrate **6** with catalyst **1**; however when the full catalyst, with bound metal and attached oxygen, is included during energy minimization the calculation does not successfully account for the observed attack on C-6 in the reaction of **3** with **1**. For this reason Figure 1 should be considered simply an illustration of the geometry that explains our observed reaction, not as evidence for the success of the calculation.

Received: March 2, 2000 [Z 14798]

[1] a) R. Breslow, R. J. Corcoran, B. B. Snider, *J. Am. Chem. Soc.* **1974**, *96*, 6791 – 6792; b) R. Breslow, R. J. Corcoran, B. B. Snider, R. J. Doll, P. L. Khanna, R. Kaleya, *J. Am. Chem. Soc.* **1977**, *99*, 905 – 915; c) R. Breslow in *Comprehensive Organic Synthesis*, *Vol. 7* (Ed.: B. M. Trost), Pergamon, Oxford, **1991**, pp. 39 – 52.

[2] a) R. Breslow, X. Zhang, Y. Huang, *J. Am. Chem. Soc.* **1997**, *119*, 4535 – 4536; b) R. Breslow, Y. Huang, X. Zhang, J. Yang, *Proc. Natl. Acad. Sci. USA* **1997**, *94*, 11156 – 11158; c) R. Breslow, B. Gabriele, J. Yang, *Tetrahedron Lett.* **1998**, *39*, 2887 – 2890.

[3] N. S. Bhacca, D. H. Williams, *Applications of NMR Spectroscopy in Organic Chemistry: Illustrations from the Steroid Field*, Holden-Day, San Francisco, **1964**, p. 21.

[4] a) C. Bergstrom, R. Nicholson, R. Dodson, *J. Org. Chem.* **1963**, *28*, 2633 – 2640; b) J. Fried, E. Sabo, *J. Am. Chem. Soc.* **1954**, *76*, 1455 – 1456; c) J. Fried, E. Sabo, *J. Am. Chem. Soc.* **1957**, *79*, 1130 – 1141; d) R. Hirschmann, R. Miller, J. Wood, R. Jones, *J. Am. Chem. Soc.* **1956**, *78*, 4956 – 4959; e) R. Dodson, R. Muir, *J. Am. Chem. Soc.* **1961**, *83*, 4631 – 4635; f) R. Dodson, R. Muir, *J. Am. Chem. Soc.* **1958**, *80*, 6148.

 © WILEY-VCH Verlag GmbH, D-69451 Weinheim, 2000 1433-7851/00/3915-2694 $ 17.50+.50/0

A Porous Crystalline Molecular Solid Explored by Hyperpolarized Xenon**

Piero Sozzani,* Angiolina Comotti, Roberto Simonutti, Thomas Meersmann, John W. Logan, and Alexander Pines

Porous materials are currently of great interest to several chemical fields, including catalysis, molecular confinement, and selective absorption.[1] Such materials have been obtained synthetically in several forms in addition to those found in nature.[2] Innovative principles developed in supramolecular chemistry[3] have been of help in obtaining self-assembled porous structures that, like zeolites, absorb atoms and molecules from the gas phase.[4] These materials are generally held together by directional forces that form extended frameworks of noncovalent interactions such as hydrogen bonds, $\pi-\pi$ interactions, or coordinate bonding. Recently, steric requirements have been used in designing new host molecules that pack efficiently with a number of guests.[5] Herein the shape and symmetry of the molecule is exploited to assemble a porous crystal where open nanochannels are stable in the absence of any guests. The D_3 symmetry of tris(*o*-phenylenedioxy)cyclophosphazene[6] (TPP) allows a packing arrangement that does not satisfy the maximum filling principle.[7] Contrary to the reported examples of porous organic materials,[4] the molecular crystal of TPP does not contain stabilizing interactions except for weakly directional interactions.[8] Organic clathrates, such as perhydrotriphenylene and tri-*o*-thymotide, which are stabilized by van der Waals forces also contain sorbed molecules, but, when the guest molecules are removed the crystal structures generally collapse to a more stable crystal packing.[9] Even in some matrices where hydrogen bonding is present, such as urea, the removal of the guest molecules leads to the collapse of the crystal structure.[10] The novel polymorph of TPP absorbs guest atoms and molecules easily and when these are released the porous structure is retained (the accessible volume accounts for about 23 % of the total volume).

Continuous flow laser-polarized ^{129}Xe NMR spectroscopy is applied for the first time to investigate the open-channel structure. An anisotropic signal from the xenon atoms inside the nanochannels is detected 200 ms after contact of the polarized gas with the sample. This observation is made possible by the intense NMR response of the hyperpolarized xenon atoms[11] that are allowed to diffuse into the novel nanoporous modification of TPP. A unique case of one-dimensional diffusion of atoms into ideal, axially symmetric nanochannels is thus described.

The empty channellike structure could be obtained from the hexagonal TPP/benzene inclusion compound (IC) by mild evacuation of the volatile guest. The strategy to obtain the unusual polymorph of TPP was based on a careful study of the solid–solid transformation of the IC. The synthesis of the TPP molecule was performed as reported,[6] and the IC was prepared by crystallization from a solution in benzene. In the differential scanning calorimetric (DSC) analysis, the trace for the hexagonal phase exhibits a broad endotherm transition from 30–150 °C, an exotherm transition ($|\Delta H| = 27.7\ \mathrm{J\,g^{-1}}$) associated with the collapse to the monoclinic structure at 150 °C, and an endotherm transition (same enthalpy) at 225 °C followed by melting at 245 °C. The broad endotherm transition corresponds to the release of the volatile guests as confirmed by thermogravimetry analysis (TGA). Therefore only the thermal treatment at 75 °C (below the exotherm transition) and 10^{-2} Torr generates the empty nanoporous polymorph (pseudohexagonal) and prevents the formation of the more stable structure (monoclinic). Thermogravimetric analysis indicates no release of volatile species until the melting point.

Figure 1a shows the structure of TPP and Figure 1b (top trace) the X-ray powder diffraction pattern of the pseudo

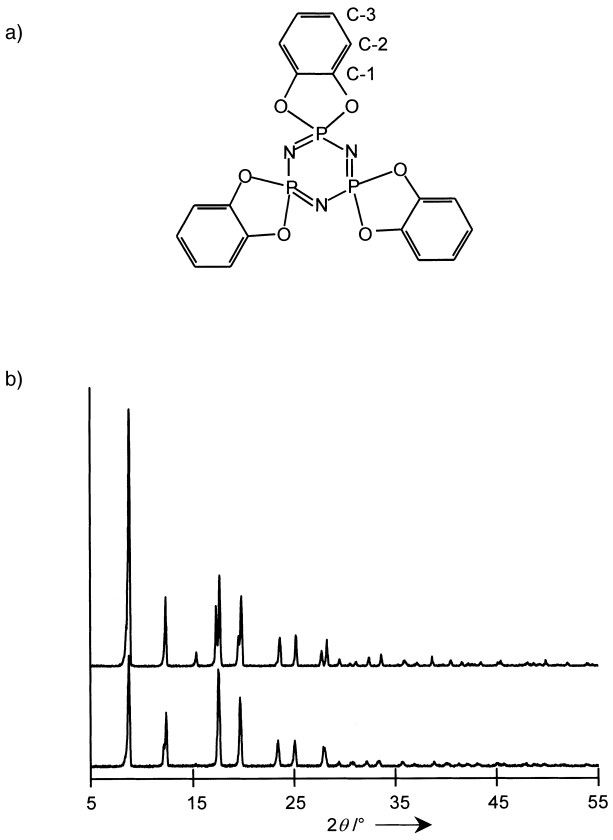


Figure 1. a) Molecular structure of TPP. b) X-ray powder diffraction pattern of the pseudohexagonal cell of the molecular zeolite TPP (top trace) and diffraction pattern of the hexagonal cell of the TPP/benzene IC (bottom trace).

[*] Prof. P. Sozzani, Dr. A. Comotti, Dr. R. Simonutti
Department of Materials Science
Universitá di Milano—Bicocca
via R. Cozzi 53, 20125 Milan (Italy)
Fax: (+39) 02-6448-5400
E-mail: Piero.Sozzani@mater.unimib.it
Dr. T. Meersmann, J. W. Logan, Prof. A. Pines
Department of Chemistry
University of California
and Materials Science Division
Lawrence Berkeley National Laboratory, Berkeley, CA 94720 (USA)

[**] We thank the Italian Ministry of Universities and Scientific Research (PRIN program) for financial support. The research with laser-polarized xenon was supported by the Director, Office of Energy Research, Office of Basic Energy Science, Materials Sciences Division of the U.S. Department of Energy. T.M. thanks the Alexander von Humboldt Foundation for a Feodor Lynen Fellowship.

 © WILEY-VCH Verlag GmbH, D-69451 Weinheim, 2000 1433-7851/00/3915-2695 $ 17.50+.50/0

hexagonalcrystal cell (space group: $P2_1/n$, $a = 11.646(1)$, $b = 10.2101(6)$, $c = 11.5106(5)$, $\beta = 119.939(5)$; $Z = 2$, $V = 1186$ Å^3, $\rho_{calcd} = 1.233$ g cm^{-3}).[12] The structure forms an empty channel surrounded by three TPP molecules at each level. For comparison, the X-ray diffraction pattern of the hexagonal packing of the TPP/benzene IC is shown in Figure 1b (bottom trace, space group $P6_3/m$, cell parameters $a = 11.6013(3)$, $c = 10.0365(9)$).[13]

The multiplicity of the ^{13}C and ^{31}P MAS NMR signals (as detected at 75.5 and 121.5 MHz, respectively, on a Bruker MSL300 spectrometer) agrees with the symmetry of the pseudohexagonal crystal cell (Figure 2). The ^{31}P MAS NMR spectrum (Figure 2a) of the pseudohexagonal structure yields

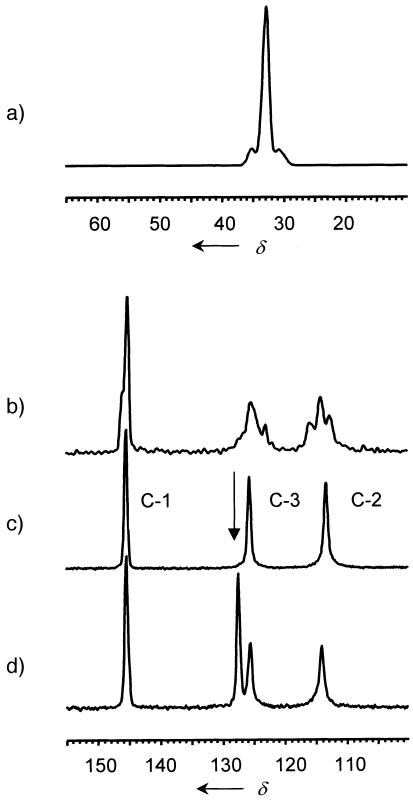


Figure 2. a) ^{31}P MAS NMR spectrum of the pseudohexagonal cell. b) ^{13}C Cross polarization (CP) MAS spectrum of the monoclinic cell (contact time of 8 ms). c) ^{13}C MAS spectrum of the pseudohexagonal cell (recycle delay of 300 s). d) ^{13}C MAS spectra of the TPP/benzene inclusion compound (recycle delay of 300 s).

one main peak at $\delta = 32.9$, which indicates that the phosphorus atoms are essentially equivalent in the unit cell.[14] The broad signals with low intensity derive from the ^{31}P–^{14}N dipolar coupling which is not completely suppressed by magic angle spinning. The ^{13}C MAS NMR spectrum (Figure 2c) also reflects the high symmetry of the crystal cell since each type of aromatic carbon atom displays a single resonance line. The arrow in the spectrum indicates the frequency at which benzene molecules would resonate if they were still present. The ^{13}C MAS NMR spectrum of the inclusion compound presents the same multiplicity as the pseudohexagonal structure, but with an additional peak at $\delta = 127.3$ for the benzene guest molecules (Figure 2d). The slight distortion of the pseudohexagonal structure, relative to the hexagonal structure, is reflected in a shift of $\delta = 1$ for the *ortho* carbon atom (C-2) resonance.[15] This shift is a result of the strong sensitivity of the chemical shift to the dihedral angle C(2)-C(1)-O-P, as already observed in tris(2,3-naphthalenedioxy)-cyclophosphazene.[16] For comparison, Figure 2b shows the ^{13}C CP MAS spectrum of the collapsed monoclinic structure devoid of channels: the presence of doublets and triplets for each type of aromatic carbon atom confirms the formation of the crystal cell with low symmetry.[17]

The above results demonstrate that the channellike structure of the TPP crystal cell with benzene is maintained after removing the guest molecules at 75 °C. It is reasonable to consider the guest-free cell as a zeolite-like structure: stable at room temperature and with channels accessible to volatile guests or even gases; xenon, in particular, is efficiently absorbed from the gas phase (Figures 3a and b).[18]

The naturally occurring ^{129}Xe isotope has a nucleus with $I = ½$ spin and ^{129}Xe NMR spectroscopy is a tool for collecting information about the cavities in porous materials. The chemical shift of ^{129}Xe is sensitive to the size of the cavities,

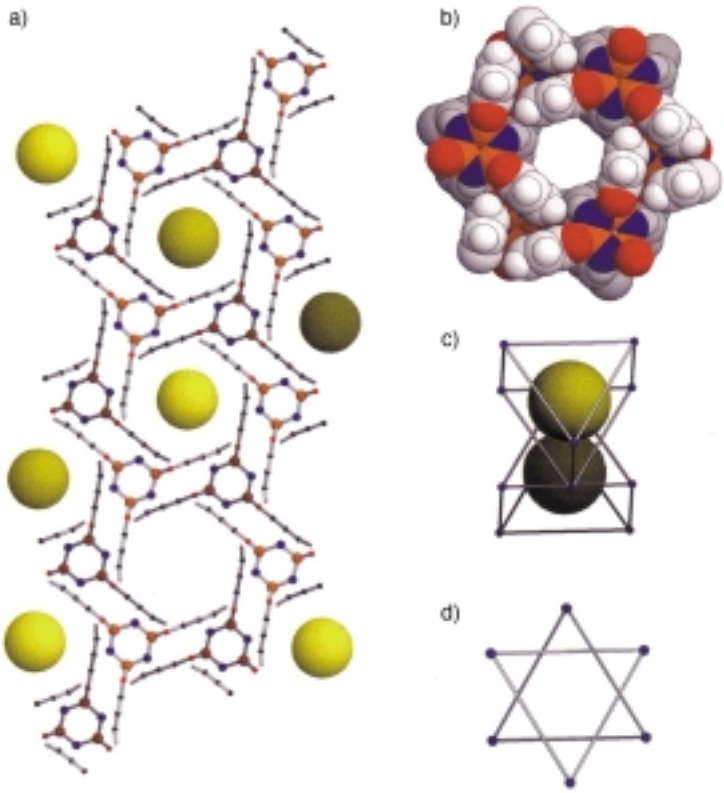


Figure 3. a) TPP channellike structure viewed along the channel axis. Colors are as follows: gray: carbon, red: oxygen, blue: phosphorus, orange: nitrogen, white: hydrogen, yellow: xenon. Broken bonds indicate an extension of the structure. The darkening of the Xe yellow color indicates the depth of the atoms along the channels. The TPP molecule packing results in the formation of cavities which are partially occupied by Xe atoms at low loading. b) The channellike structure of TPP based on the van der Waals radii viewed along the channel axis. The channel walls are formed by aromatic units parallel to the channel axis; the nitrogen atoms face the channel. c) The geometry of the cavities as viewed by perspective. d) The geometry of the cavities as viewed along the channel axis. The cavity shape corresponds to a prism with a triangular base. The prisms are stacked along the channel axis rotated by 60° with respect to the others, thus producing a hexagonal shape.

 © WILEY-VCH Verlag GmbH, D-69451 Weinheim, 2000 1433-7851/00/3915-2696 $ 17.50+.50/0

and the anisotropic profile of the confined gas atoms gives an insight into the geometry of the space explored.[19] In this particular case, the TPP nanochannels were explored by hyperpolarized xenon NMR spectroscopy.[11] This highly innovative technique gives rise to an intense NMR signal for the diffusing atoms in just one scan. Moreover, continuous-flow laser-polarized ^{129}Xe NMR spectroscopy provides a means of demonstrating the easy accessibility of the nanochannels to gas atoms, which allows an investigation of the first stages of xenon diffusion into the nanochannels.[20] The recycle time between the NMR reading pulses determines the time scale for entry of xenon into the channels. It has been possible to obtain observable ^{129}Xe NMR spectra of continuously replaced laser-polarized xenon inside the TPP channels with recycle times as short as 200 ms. This is a noteworthy result that indicates the rapid diffusion of xenon into the nanochannels.

Figure 4 shows the ^{129}Xe NMR spectra of laser-polarized xenon following diffusion into porous crystalline material (as detected at 138.3 MHz on a Chemagnetics 500 spectrometer) for several xenon/helium gas mixtures. The high sensitivity of the technique allows the detection of xenon concentrations as low as 1% diluted in helium. The laser-polarized xenon gives rise to anisotropic signals centered around $\delta = 110$, with the line shape depending on the xenon partial pressure. At a concentration of 1% xenon the line shape indicates an axially symmetric chemical shift anisotropy (CSA) with positive anisotropy.[21] Increasing the xenon partial pressure leads to an inversion of the sign of the anisotropy. The anisotropy parameter $\Delta\delta$, obtained from the numerical fitting of the CSA powder pattern,[22] ranges between $\delta = +22.1$ at 1% xenon and $\delta = -12.2$ at 100%. Although the inversion of the anisotropy was previously observed in nonaxially symmetric systems,[23] the present experiments under axial symmetry of the xenon CSA have shown the collapse of the line shape to a narrow isotropic signal at a xenon concentration of 30%. The CSA powder patterns present small values for the asymmetry parameters η of 0.12–0.14.[21, 22]

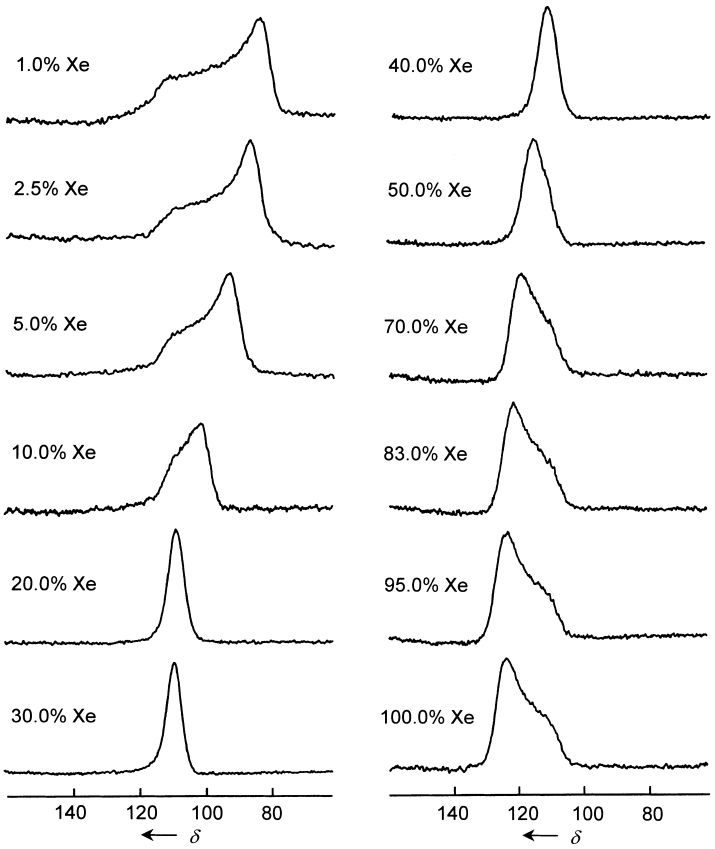


Figure 4. Continuous-flow laser-polarized ^{129}Xe NMR[20] spectra of Xe/He mixtures flowing in the TPP pseudohexagonal phase at atmospheric pressure and room temperature. The time for diffusion of the optically polarized xenon into the TPP channels was set by the recycle delay to 200 ms. The components of the CSA tensors (δ_{11}, δ_{22}, and δ_{33}) calculated by a numerical fitting procedure are reported in ref. [22].

In order to explain these results let us consider the TPP channels composed of stacked prisms with triangular bases twisted by 60° (Figure 3c), with the TPP aromatic rings constituting the vertical faces. Hexagonal restriction forms connections of about 5 Å between the prisms (Figure 3d). Within the limits of rapid diffusion the space explored by the xenon atoms appears, on average, to be a cylinder with a diameter slightly larger than the 4.4 Å diameter of the xenon atom.[12] The π electrons of the TPP aromatic units face the interior of the channel and are in close proximity to the essentially one-dimensional, fast-diffusing guest atoms. Thus, the NMR spectra suggest that the axial symmetry of the channel is imposed on the xenon atoms. Two sources for the average shape of the xenon electron cloud are the xenon–xenon interactions and the interaction of the xenon atoms with the nanochannel wall.[24] At low xenon concentrations there are fewer xenon–xenon collisions, and the xenon–wall interaction dominates the density distribution of the electron cloud of the xenon atom. At high xenon concentrations the interaction between xenon atoms is enhanced relative to the xenon–wall interaction. The change from an oblate to a prolate electronic symmetry of the electron shell is reflected in the sign change of the chemical shift anisotropy.

The unprecedented and clear evidence of a "null" (pseudoisotropic) point at a Xe concentration of 30% is consistent with the qualitative features of the model: at this point the two competing interactions (xenon–wall and xenon–xenon) are balanced, and the shape of the xenon atoms are dynamically averaged to an effectively spherical, isotropic symmetry.

The results of our experiments support the model of zeolite-like open channels that readily absorb gases that run along a one-dimensional file.[25] The structure very closely resembles that of zeolite materials containing channels of 5–8 Å.[23] In most known cases the shape of the zeolite channels deviates from a cylindrical geometry and may contain, at different levels, elliptical cross-sections.[26] The uniqueness of the system is that the nanopore shape is close to an ideal cylinder. The small values found for the asymmetry parameter η suggest only a slight distortion from the hexagonal symmetry, and this is consistent with the pseudohexagonal cell determined from the X-ray diffraction data.

In conclusion, this work describes a crystalline modification held together by weakly directional forces containing open channels. The crystal phase provides an unusual π-electron rich environment for the one-dimensional diffusion of atoms, on the other hand xenon anisotropic signals show the

squeezing of the atoms into the crystal nanochannels. In this example we were able to detect such an anisotropic xenon signal 200 ms after the gas diffusion into the aromatic nanochannel. The anisotropy of a gas diffusing into a crystal has been rarely observed, and never by advanced NMR techniques. We believe, the results are relevant to the field of supramolecular engineering, atomic confinement, and the developing of models for single-file diffusion.

Received: March 20, 2000 [Z14869]

[1] a) G. Férey, A. K. Cheetham, *Science* **1999**, *283*, 1125 – 1126; b) C. W. Jones, K. Tsuji, M. E. Davis, *Nature* **1998**, *393*, 52 – 54; c) C. N. R. Rao, *J. Mater. Chem.* **1999**, *9*, 1 – 14; d) G. A. Ozin, C. T. Kresge, S. M. Yang, N. Coombs, I. Sokolov, *Adv. Mater.* **1999**, *11*, 1427 – 1431.

[2] a) R. M. Barrer, *Zeolites and Clay Minerals as Sorbent and Molecular Sieves*, Academic Press, London, **1978**; b) D. W. Brek, *Zeolite Molecular Sieves*, Wiley, New York, **1984**; c) C. T. Kresge, M. E. Leonowicz, W. J. Roth, J. C. Vartuli, J. S. Beck, *Nature* **1992**, *359*, 710 – 712; d) T. E. Gier, X. Bu, P. Feng, G. D. Stucky, *Nature* **1998**, *395*, 154 – 157.

[3] J.-M. Lehn, *Supramolecular Chemistry: Concepts and Perspective*, VCH, Weinheim, **1995**.

[4] a) O. M. Yaghi, G. Li, H. Li, *Nature* **1995**, *378*, 703 – 706; b) P. Brunet, M. Simard, J. D. Wuest, *J. Am. Chem. Soc.* **1997**, *119*, 2737 – 2738; c) B. T. Ibragimov, S. A. Talipov, T. F. Aripov, *J. Inclusion Phenom. Mol. Recognit. Chem.* **1994**, *17*, 317 – 324; d) R. Bishop, D. C. Craig, M. L. Scudder, A. P. Marchand, Z. Liu, *J. Chem. Soc. Perkin Trans 2* **1995**, *2*, 1295 – 1300; e) K. Endo, T. Sawaki, M. Koyanagi, K. Kobayashi, H. Masuda, Y. Aoyama, *J. Am. Chem. Soc.* **1995**, *117*, 8341 – 8352; f) G. B. Gardner, Y.-H. Kiang, S. Lee, A. Asgaonkar, D. Venkataraman, *J. Am. Chem. Soc.* **1996**, *118*, 6946 – 6953.

[5] K. Kobayashi, T. Shirasaka, A. Sato, E. Horn, N. Furukawa, *Angew. Chem.* **1999**, *111*, 3692 – 3694; *Angew. Chem. Int. Ed.* **1999**, *38*, 3483 – 3486.

[6] H. R. Allcock, L. A. Siegel, *J. Am. Chem. Soc.* **1964**, *86*, 5140 – 5144.

[7] C. P. Brock, J. D. Dunitz, *Chem. Mater.* **1994**, *6*, 1118 – 1127.

[8] Weakly directional interactions are defined as in: G. R. Desiraju in *Comprehensive Supramolecular Chemistry*, *Vol. 6* (Eds.: J. L. Atwood, J. E. Davies, D. D. MacNicol, F. Vögtle), Pergamon, Oxford, **1996**, pp. 1 – 22.

[9] a) M. Farina, G. Di Silvestro, P. Sozzani in *Comprehensive Supramolecular Chemistry*, *Vol. 6* (Eds.: J. L. Atwood, J. E. Davies, D. D. MacNicol, F. Vögtle), Pergamon, Oxford, **1996**, pp. 371 – 398; b) R. Arad-Yellin, B. S. Green, M. Knossow, G. Tsoucaris in *Inclusion Compounds*, *Vol. 6* (Eds.: J. L. Atwood, J. E. D. Davies, D. D. MacNicol), Academic Press, New York, **1988**, pp. 278 – 284.

[10] M. D. Hollingsworth, K. D. Harris in *Comprehensive Supramolecular Chemistry*, *Vol. 6* (Eds.: J. L. Atwood, J. E. Davies, D. D. MacNicol, F. Vögtle), Pergamon, Oxford, **1996**, pp. 177 – 237.

[11] a) D. Raftery, H. Long, T. Meersmann, P. J. Grandinetti, L. Reven, A. Pines, *Phys. Rev. Lett.* **1991**, *66*, 584 – 587; b) D. Raftery, E. MacNamara, G. Fisher, C. V. Rice, J. J. Smith, *J. Am. Chem. Soc.* **1997**, *119*, 8746 – 8747; c) M. Haake, A. Pines, J. A. Reimer, R. Seydoux, *J. Am. Chem. Soc.* **1997**, *119*, 11711 – 11712.

[12] The X-ray powder diffraction pattern associated with the TPP/H_2O inclusion compound is absent. H. R. Allcock, M. L. Levin, R. R. Whittle, *Inorg. Chem.* **1986**, *25*, 41 – 47.

[13] H. R. Allcock, R. W. Allen, E. C. Bissell, L. A. Smeltz, M. Teeter, *J. Am. Chem. Soc.* **1976**, *98*, 5120 – 5125.

[14] The collapsed monoclinic structure shows three phosphorus peaks, according to the lower symmetry. A. Comotti, R. Simonutti, S. Stramare, P. Sozzani, *Nanotechnology* **1999**, *10*, 70 – 76.

[15] The chemical shifts of the pseudohexagonal cell are $\delta = 145.3$, 125.5, and 113.1 for the C-1, C-3, and C-2 carbon atoms, respectively. The hexagonal cell shows the following chemical shifts: $\delta = 145.3$, 125.5, and 114.1 for the C-1, C-3, and C-2 carbon atoms, respectively.

[16] a) A. Comotti, M. C. Gallazzi, R. Simonutti, P. Sozzani, *Chem. Mater.* **1998**, *10*, 3589 – 3596; b) P. Sozzani, A. Comotti, R. Simonutti in *Crystal Engineering: From Molecules and Crystals to Materials* (Eds.: D. Braga, F. Grepioni, A. G. Orpen), NATO Sciences Series, Kluwer Academic Publishers, The Netherlands, **1999**, pp. 443 – 458.

[17] The collapsed monoclinic structure (space group: $P2_1/n$) presents the following cell parameters: $a = 25.297(2)$, $b = 5.9368(4)$, $c = 26.125(2)$, $\beta = 96.211(7)$, $V = 3900.5$ Å^3, $\rho_{calcd} = 1.500$ g cm^{-3}.

[18] Empty nanoporous TPP (270.5 mg) reduced the xenon pressure in a volume of 22.1 cm^3 from 310 to 225 torr during the course of 5 min (0.17 mol Xe per mol of TPP). Microbalance measurements made it possible to follow xenon sorption with time at constant pressure: the sorption of 0.52 mol of Xe per mol of matrix is reached in a few hours at 280 Torr by the pseudohexagonal form. No gas sorption is exhibited by the monoclinc TPP form under the same conditions. As an example of volatile molecules being sorbed from the vapour phase, the benzene pressure was reduced from 15.6 to 4.5 Torr in 15 min when benzene vapours were sealed at 22 °C in a glass chamber of 22.6 cm^3 in the presence of 53 mg of TPP. No reduction of pressure within ±1 Torr was observed in the presence of the monoclinic phase.

[19] a) T. Ito, J. Fraissard, *J. Chem. Phys.* **1982**, *76*, 5225; b) J. A. Ripmeester, *J. Am. Chem. Soc.* **1982**, *104*, 289 – 290.

[20] a) A. Bifone, T. Pietrass, J. Kritzenberger, A. Pines, B. F. Chmelka, *Phys. Rev. Lett.* **1995**, *74*, 3277 – 3280; b) M. S. Albert, G. D. Cates, B. Driehuys, W. Happer, B. Saam, C. S. Springer, Jr., A. Wishnia, *Nature* **1994**, *370*, 199 – 201; c) G. Navon, T. Q. Song, T. Room, S. Appelt, R. E. Taylor, A. Pines, *Science* **1996**, *271*, 1848 – 1851.

[21] Definitions used for the CSA tensor elements: $\delta_{iso} = (\delta_{11} + \delta_{22} + \delta_{33})/3$; $|\delta_{33} - \delta_{iso}| > |\delta_{22} - \delta_{iso}| > |\delta_{11} - \delta_{iso}|$; $\Delta\delta = \delta_{33} - \delta_{iso}$; $\eta = |\delta_{22} - \delta_{11}|/|\delta_{33} - \delta_{iso}|$.

[22] The CSA tensor elements (δ_{11}, δ_{22}, δ_{33}) obtained by numerical fitting are the following: $\delta = 83.3$, 80.2, and 114.9 for 1.0% xenon; 85.1, 82.7, and 113.6 for 2.5% xenon; 91.2, 89.4, and 113.5 for 5.0% xenon; 99.6, 98.5, and 112.3 for 10% xenon; 115.4, 116.0, and 107.8 for 50.0% xenon; 119.2, 120.5, and 105.6 for 70% xenon; 121.6, 123.1, and 106.0 for 83.0% xenon; 123.6, 125.2, and 106.2 for 95.0% xenon; 124.3, 126.0, and 106.8 for 100.0% xenon. At xenon concentrations of 20%, 30%, and 40% the spectra present a lorentzian peak with the following values: $\delta = 107.9$ and line-width 332 Hz for 20% xenon; $\delta = 109.2$ and line-width 317 Hz for 30% xenon; $\delta = 111.5$ and line-width 387 Hz for 40% xenon.

[23] a) M. A. Springuel-Huet, J. Fraissard, *Chem. Phys. Lett.* **1989**, *154*, 299 – 302; b) J. A. Ripmeester, C. I. Ratcliffe, *J. Phys. Chem.* **1995**, *99*, 619 – 622.

[24] In the presence of xenon no structural changes of the matrix could be observed by X-ray diffraction analysis.

[25] V. Kukla, J. Kornatowski, D. Demuth, I. Girnus, H. Pfeifer, L. V. C. Rees, S. Schunk, K. K. Unger, J. Kärger, *Science* **1996**, *272*, 702 – 704.

[26] M. W. Anderson, J. Klinowski, *Nature* **1989**, *339*, 200 – 203.

 © WILEY-VCH Verlag GmbH, D-69451 Weinheim, 2000 1433-7851/00/3915-2698 $ 17.50+.50/0

A Three-Dimensional Polyrotaxane Network**

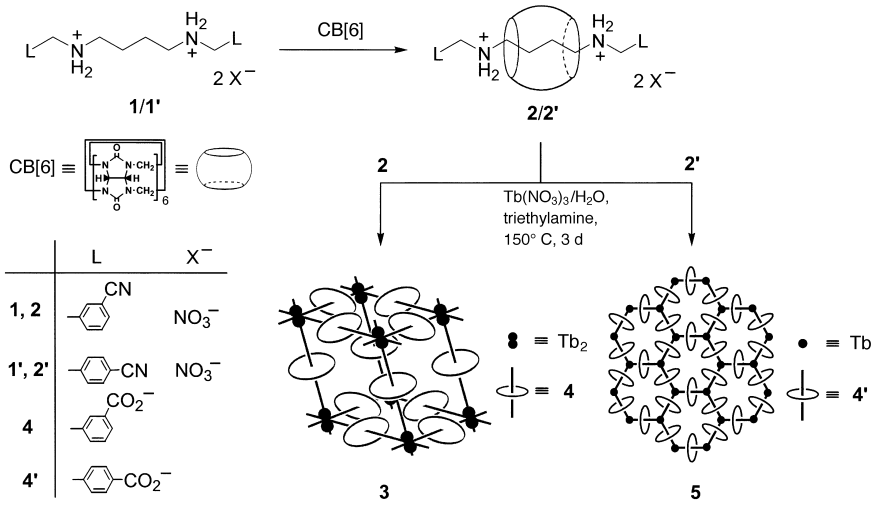
Eunsung Lee, Jungseok Heo, and Kimoon Kim*

In memory of Chung Hoe Koo

The design and synthesis of supramolecular architectures with desired structures, properties, and functions have been the subjects of intense research in recent years.[1] Polyrotaxanes[2–9]—in which many molecular "beads" are threaded on a long molecular "string"—have received much attention because of their intriguing structures as well as their potential applications.[8, 9] Our interest in interlocked structures[10] led us to develop a simple approach to one-dimensional polyrotaxanes with high structural regularity.[10b] This approach involves formation of a pseudorotaxane by threading a bead with a short string having a pyridyl group at both ends, followed by reaction of the pseudorotaxane with a transition metal ion to produce a coordination polymer. The key to the success of this approach is the use of cucurbituril (CB[6])[11, 12] as a molecular bead: It has a highly symmetric structure and is able to form exceptionally stable pseudorotaxanes with strings derived from diaminoalkanes. The versatility of this approach has been demonstrated by the fact that a variety of one-dimensional (1D) polyrotaxanes with different structures are obtained simply by changing metal ions, counterions, and the string.[10b–d] Furthermore, the same approach allowed us to construct the first 2D polyrotaxane.[10c] Immediately following our work, Robson and co-workers also reported different types of 2D polyrotaxanes.[13]

The successful construction of a 2D polyrotaxane encouraged us to pursue unprecedented 3D polyrotaxanes. At first, construction of 3D polyrotaxanes appeared to be a simple extension of the work on 2D polyrotaxanes, but it turned out to be a challenging goal. For example, all attempts to produce 3D polyrotaxanes using transition metal ions and pseudorotaxanes with pyridyl terminal groups have failed. We therefore decided to modify our approach by using the reaction between lanthanide metal ions—which in general have larger ionic radii and higher coordination numbers than transition metal ions—and pseudorotaxanes with other terminal groups such as carboxylate and cyano groups under hydrothermal conditions. This effort has successfully produced the first 3D polyrotaxane network. Here we report the self-assembly and X-ray crystal structure of the novel supramolecular 3D net.

The pseudorotaxane **2**, prepared by threading CB[6] with *N*,*N*′-bis(3-cyanobenzyl)-1,4-diammoniobutane dinitrate (**1**), was treated with $Tb(NO_3)_3$ under hydrothermal conditions to produce **3** (Scheme 1). The X-ray crystal structure of **3** reveals an unprecedented 3D polyrotaxane in which CB beads are threaded on a 3D coordination polymer network. The basic building unit of the framework consists of a binulcear Tb^{3+} center and six pseudorotaxane units (**4**), each of which contains 3-phenylcarboxylate groups at the terminals. Apparently, under the hydrothermal conditions **1** with cyano groups was first converted into **4** with carboxylate terminals,[14] which then reacted with Tb^{3+} to form **3**.



Scheme 1. Synthesis of 3D polyrotaxane **3** and 2D polyrotaxane **5**.

Two different types of pseudorotaxane **4** exist in the 3D framework: One (type I) has η^1,η'^1-bridging caroxylate terminal groups, whereas the other (type II) has η^2-chelating carboxylate moieties. The two Tb^{3+} ions, which are related to each other by an inversion center located at the midpoint between the two metal centers, are linked by four η^1,η'^1-bridging carboxylate groups of type I pseudorotaxane **4** (Tb ··· Tb 3.9774(8) Å, Figure 1). Each Tb ion is further coordinated by an η^2-carboxylate group of a type II pseudorotaxane **4** and two water molecules. The coordination geometry around the metal center is best described as a distorted square antiprism with four oxygen atoms O3, O5, O4A, and O6A forming a square base. Similar binuclear lanthanide metal centers linked by four bridging carboxylate ligands are known.[15]

The binuclear terbium centers and type I pseudorotaxanes **4** form a 2D polyrotaxane network in the *bc* plane. The 2D networks, which are stacked along the normal to the *bc* plane with a mean distance of 19.8 Å, are interconnected by η^2 coordination of the carboxylate terminals of type II pseudo-

[*] Prof. K. Kim, E. Lee, J. Heo
National Creative Research Initiative Center for Smart Supramolecules and
Department of Chemistry, Division of Molecular and Life Sciences
Pohang University of Science and Technology
San 31 Hyojadong, Pohang 790-784 (Republic of Korea)
Fax: (+82) 562-279-8129
E-mail: kkim@postech.ac.kr

[**] This paper is dedicated to the memory of Professor Chung Hoe Koo, who first introduced X-ray crystallography to Korea. We gratefully acknowledge the Korean Ministry of Science and Technology (Creative Research Initiative Program) for support of this work and the Korean Ministry of Education (Brain Korea 21 program) for graduate studentships to E.L. and J.H.

Supporting information for this article is available on the WWW under http://www.wiley-vch.de/home/angewandte/ or from the author.

 © WILEY-VCH Verlag GmbH, D-69451 Weinheim, 2000 1433-7851/00/3915-2699 $ 17.50+.50/0

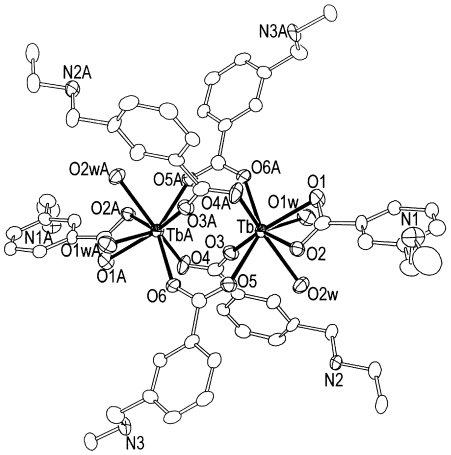


Figure 1. Coordination geometry around the binuclear terbium centers in **3**. An inversion center is located at the midpoint between the two terbium ions. The CB[6] beads are omitted for clarity. Selected bond lengths [Å]: Tb···TbA 3.9774(8), Tb–O1 2.409(6), Tb–O2 2.473(6), Tb–O3 2.349(6), Tb–O4A 2.417(6), Tb–O5 2.345(6), Tb–O6A 2.296(6), Tb–O1w 2.451(7), Tb–O2w 2.442(6).

rotaxane **4** to the terbium ions in the 2D nets to form a 3D polyrotaxane network (Figures 2 and 3). The 3D polyrotaxane has an inclined α-polonium topology with the binuclear

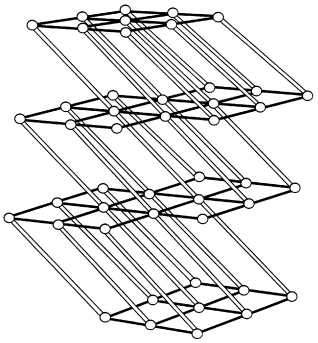


Figure 2. Schematic representation of the 3D framework in **3**. The circles represent binuclear Tb centers, and the solid and open connections represent type I and type II pseudorotaxanes, respectively.

terbium centers behaving as six-connected nodes.[16] The unit cell of the α-polonium-like net is depicted in Figure 4. The void space in the unit cell of **3** is filled with a free pseurorotaxane **4**, counteranions (nitrate and hydroxide ions), and water molecules.

A small change in the building block results in a totally different solid-state structure. For example, under the same conditions the reaction of $Tb(NO_3)_3$ with the isomeric pseudorotaxane **2′**, which has 4-cyanophenyl terminal groups, produces **5** (Scheme 1). The X-ray crystal structure of **5** reveals a polycatenated 2D polyrotaxane (see the Supporting Information) similar to that formed by the reaction of $Ag(NO_3)$ with a pseudorotaxane with pyridyl terminal groups.[10c] Here again pseudorotaxane **2′** is first converted into **4′** with carboxylate terminals under hydrothermal conditions before being coordinated to Tb metal ions to form **5**. Each Tb metal center in **5**, which is coordinated by three pseudorotaxanes **4′**, behaves as a three-connected node. The details of this structure will be reported elsewhere.

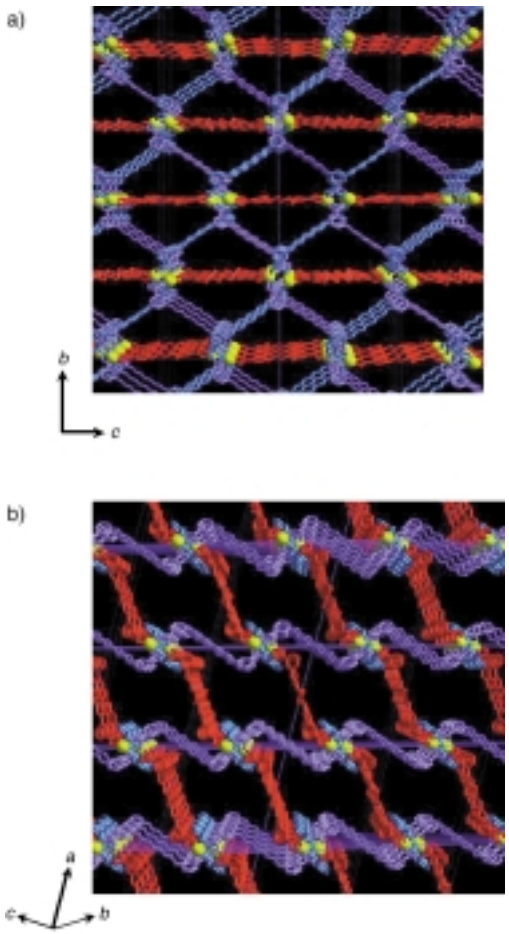


Figure 3. The 3D coordination polymer network in **3**: a) view down the *a* axis; b) view down the [011] direction. The CB[6] beads are omitted for clarity. Tb ion: yellow; type I pseudorotaxane **4**: dark and light blue; type II pseudorotaxane **4**: red.

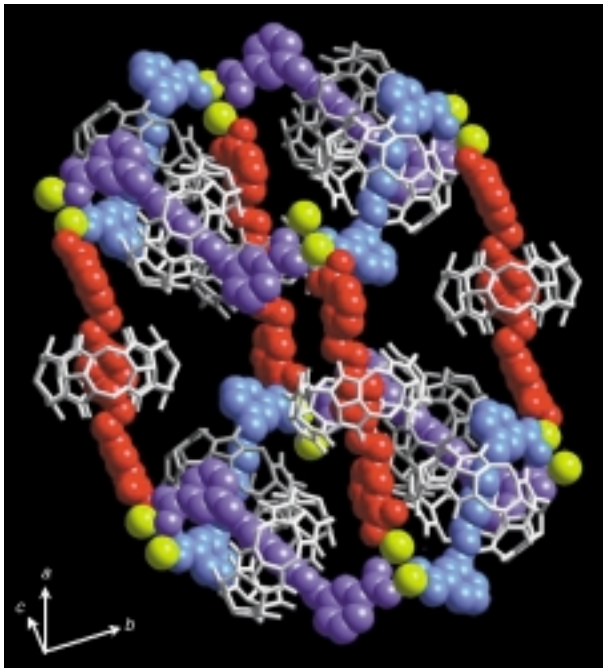


Figure 4. View of the unit cell of the α-polonium-like net in **3**. Tb ion: yellow; type I pseudorotaxane **4**: dark and light blue; type II pseudorotaxane **4**: red; CB: gray.

 © WILEY-VCH Verlag GmbH, D-69451 Weinheim, 2000 1433-7851/00/3915-2700 $ 17.50+.50/0

In conclusion, we have presented the first 3D polyrotaxane net in which beads are threaded onto 3D coordination polymer networks containing binuclear lanthanide metal centers. This novel supramolecular 3D network provides not only an intriguing example of chemical topology[17] but also new insights into the construction of solid-state materials, in particular modular open-framework or porous materials,[18] which is a subject of current intense investigation.

Experimental Section

3: Pseudorotaxane **2** (0.100 g, 0.065 mmol; see the Supporting Information), $Tb(NO_3)_3 \cdot 5H_2O$ (120 mg, 0.28 mmol), and triethylamine (0.001 mL, 0.007 mmol) were suspended in water (5 mL) in a stainless-steel bomb, which was then sealed, heated at 150 °C for 3 d, and cooled gradually to room temperature. Large, colorless crystals of **3** were collected, washed with water, and dried in air (73 mg, 68 %). Elemental analysis calcd for $C_{112}H_{123}N_{54}O_{40}Tb \cdot 20H_2O$: C 39.74, H 4.85, N 22.35; found: C 39.64, H 4.76, N 22.53.

5: Under the same conditions as for the synthesis of **3**, the reaction of **2′** and $Tb(NO_3)_3 \cdot 5H_2O$ yielded pale-yellow crystalline **5** (80 mg, 74 %). Elemental analysis calcd for $C_{168}H_{180}N_{84}O_{66}Tb_2 \cdot 24H_2O$: C 38.94, H 4.43, N 22.70; found: C 39.00, H 4.58, N 22.69.

Crystal data for **3**: $[Tb(C_{20}H_{24}N_2O_4)_{1.5}(C_{36}H_{36}N_{24}O_{12})_{1.5} \cdot 2H_2O][(C_{20}H_{26}N_2O_4)_{0.5}(C_{36}H_{36}N_{24}O_{12})_{0.5}] \cdot (NO_3)_2 \cdot (OH)_2 \cdot 20H_2O$, $M_r = 3429.92$, monoclinic, space group $P2_1/c$, $a = 19.8530(4)$, $b = 30.5734(5)$, $c = 24.1512(2)$ Å, $\beta = 109.411(1)^\circ$, $V = 13825.9(4)$ Å^3, $Z = 4$, $\rho_{calcd} = 1.643$ g cm^{-3}, $T = 243$ K, Siemens SMART CCD diffractometer, $Mo_{K\alpha}$ radiation ($\lambda = 0.71073$), $\mu = 6.33$ cm^{-1}. The structure was solved by the Patterson method (SHELXS-86). Because only two nitrate ions were found, two hydroxide ions were assumed to be present in the lattice for charge neutrality. All non-hydrogen atoms were refined anisotropically (SHELXL-93). Final block-diagonal matrix least-squares refinement on F^2 with all 21230 reflections and 2136 variables converged to $R1$ ($I > 2\sigma(I)$) = 0.0805, $wR2$ (all data) = 0.2042, and GOF = 1.108.

Crystal data for **5**: $[Tb_2(C_{20}H_{24}N_2O_4)_3(C_{36}H_{36}N_{24}O_{12})_3 \cdot 6H_2O] \cdot (NO_3)_6 \cdot 28H_2O$, $M_r = 5362.34$, rhombohedral, space group Rm, $a = b = 32.8554(2)$, $c = 17.2678(2)$ Å, $V = 16142.9(2)$ Å^3, $Z = 3$, $\rho_{calcd} = 1.655$ g cm^{-3}, $T = 243$ K, $Mo_{K\alpha}$ radiation ($\lambda = 0.71073$), $\mu = 7.77$ cm^{-1}. Final block-diagonal matrix least-squares refinement on F^2 with all 3030 reflections and 274 variables converged to $R1$ ($I > 2\sigma(I)$) = 0.1058, $wR2$ (all data) = 0.3122, and GOF = 1.129.

Crystallographic data (excluding structure factors) for the structures reported in this paper have been deposited with the Cambridge Crystallographic Data Centre as supplementary publication nos. CCDC-142050 (**5**) and CCDC-142051 (**3**). Copies of the data can be obtained free of charge on application to CCDC, 12 Union Road, Cambridge CB2 1EZ, UK (fax: (+44) 1223-336-033; e-mail: deposit@ccdc.cam.ac.uk).

Received: March 31, 2000 [Z 14929]

[1] a) J.-M. Lehn, *Supramolecular Chemistry*, VCH, Weinheim, **1995**; b) D. Philp, J. F. Stoddart, *Angew. Chem.* **1996**, *108*, 1242; *Angew. Chem. Int. Ed. Engl.* **1996**, *35*, 1154; c) S. Leininger, B. Olenyuk, P. J. Stang, *Chem. Rev.* **2000**, *100*, 853.

[2] Recent reviews: a) S. A. Nepogodiev, J. F. Stoddart, *Chem. Rev.* **1998**, *98*, 1959; b) D. B. Amabilino, J. F. Stoddart, *Chem. Rev.* **1995**, *95*, 2725; c) H. W. Gibson, M. C. Bheda, P. T. Engen, *Prog. Polym. Sci.* **1994**, *19*, 843; e) R. Jäger, F. Vögtle, *Angew. Chem.* **1997**, *109*, 966; *Angew. Chem. Int. Ed. Engl.* **1997**, *36*, 930; f) F. Vögtle, T. Dünnwald, T. Schmidt, *Acc. Chem. Res.* **1996**, *29*, 451.

[3] a) A. Harada, M. Kamachi, *Macromolecules* **1990**, *23*, 2821; b) A. Harada, J. Li, M. Kamachi, *J. Am. Chem. Soc.* **1990**, *23*, 2821; c) A. Harada, J. Li, M. Kamachi, *Nature* **1992**, *356*, 325; d) A. Harada, J. Li, M. Kamachi, *Nature* **1993**, *364*, 516; e) A. Harada, J. Li, M. Kamachi, *Nature* **1994**, *370*, 126; f) A. Harada, J. Li, M. Kamachi, *Macromolecules* **1994**, *27*, 4538.

[4] a) Y. X. Shen, H. W. Gibson, *Macromolecules* **1992**, *25*, 2058; b) Y. X. Shen, D. Xie, H. W. Gibson, *J. Am. Chem. Soc.* **1994**, *116*, 537; c) H. W. Gibson, S. Liu, P. Lecavalier, C. Wu, Y. X. Shen, *J. Am. Chem. Soc.* **1995**, *117*, 852; d) E. Marand, Q. Hu, H. W. Gibson, B. Veytsman, *Macromolecules* **1996**, *29*, 2555; e) C. Gong, H. W. Gibson, *Angew. Chem.* **1998**, *110*, 323; *Angew. Chem. Int. Ed.* **1998**, *37*, 310.

[5] a) G. Wenz, B. Keller, *Angew. Chem.* **1992**, *104*, 201; *Angew. Chem. Int. Ed. Engl.* **1992**, *31*, 197; b) G. Wenz, F. Wolf, M. Wagner, S. Kubik, *New J. Chem.* **1993**, *17*, 729.

[6] a) I. Yamaguchi, K. Osakada, T. Yamamoto, *J. Am. Chem. Soc.* **1996**, *118*, 1811; b) M. Born, H. Ritter, *Angew. Chem.* **1995**, *107*, 342; *Angew. Chem. Int. Ed. Engl.* **1995**, *34*, 309.

[7] a) C. Meschke, H.-J. Buschmann, E. Schollmeyer, *Macromol. Rapid Commun.* **1998**, *19*, 59; b) C. Meschke, H.-J. Buschmann, E. Schollmeyer, *Polymer* **1999**, *40*, 945; c) D. Tuncel, J. H. G. Steinke, *Chem. Commun.* **1999**, 1509.

[8] a) M. J. Marsella, P. J. Carroll, T. M. Swager, *J. Am. Chem. Soc.* **1994**, *116*, 9347; b) S. S. Zhu, P. J. Carroll, T. M. Swager, *J. Am. Chem. Soc.* **1996**, *118*, 8713; c) S. S. Zhu, T. M. Swager, *J. Am. Chem. Soc.* **1997**, *119*, 12568; d) J. Buey, T. M. Swager, *Angew. Chem.* **2000**, *112*, 608; *Angew. Chem. Int. Ed.* **2000**, *39*, 608.

[9] H. Fujita, T. Ooya, N. Yui, *Polym. J.* **1999**, *31*, 1099; T. Ooya, N. Yui, *J. Controlled Release* **1999**, *58*, 251; H. Fujita, T. Ooya, N. Yui, *Macromolecules* **1999**, *32*, 2534.

[10] a) Y.-M. Jeon, D. Whang, J. Kim, K. Kim, *Chem. Lett.* **1996**, 503; b) D. Whang, Y.-M. Jeon, J. Heo, K. Kim, *J. Am. Chem. Soc.* **1996**, *118*, 11333; c) D. Whang, K. Kim, *J. Am. Chem. Soc.* **1997**, *119*, 451; d) D. Whang, J. Heo, C.-A. Kim, K. Kim, *Chem. Commun.* **1997**, 2361; e) D. Whang, K.-M. Park, J. Heo, P. Ashton, K. Kim, *J. Am. Chem. Soc.* **1998**, *120*, 4899; f) S.-G. Roh, K.-M. Park, G.-J. Park, S. Sakamoto, K. Yamaguchi, K. Kim, *Angew. Chem.* **1999**, *111*, 672; *Angew. Chem. Int. Ed.* **1999**, *38*, 638; g) S. I. Jun, J. W. Lee, S. Sakamoto, K. Yamaguchi, K. Kim, *Tetrahedron Lett.* **2000**, *41*, 471.

[11] Reviews: a) W. L. Mock in *Comprehensive Supramolecular Chemistry*, *Vol. 2* (Ed.: F. Vögtle), Pergamon, Oxford, **1996**, p. 477; b) W. L. Mock, *Top. Curr. Chem.* **1995**, *175*, 1; c) P. Cintas, *J. Inclusion Phenom. Mol. Recognit. Chem.* **1994**, *17*, 205.

[12] The new cucurbituril homologues CB[5], CB[7], and CB[8]—which are pentameric, heptameric, and octameric species, respectively—have been recently reported: J. Kim, I. S. Jung, S. Y. Kim, E. Lee, J.-K. Kang, S. Sakamoto, K. Yamaguchi, K. Kim, *J. Am. Chem. Soc.* **2000**, *122*, 540.

[13] a) B. F. Hoskins, R. Robson, D. A. Slizys, *J. Am. Chem. Soc.* **1997**, *119*, 2952; b) B. F. Hoskins, R. Robson, D. A. Slizys, *Angew. Chem.* **1997**, *109*, 2402; *Angew. Chem. Int. Ed. Engl.* **1997**, *36*, 2336.

[14] The conversion of the cyanophenyl group into phenylcarboxylate under hydrothermal conditions is known: O. R. Evans, Z. Wang, W. Lin, *Chem. Commun.* **1999**, 1903. Attempts to synthesize **3** by allowing **4** and $Tb(NO_3)_3$ to react under hydrothermal conditions have been unsuccessful, presumably due to the extremely poor solubility of **4**.

[15] a) Z.-B. Daun, Z.-S. Jin, N.-H. Hu, J.-Z. Ni, *J. Struct. Chem.* **1989**, *8*, 168; b) J.-F. Ma, Z.-S. Jin, J.-Z. Ni, *Acta Crystallogr. Sect. C* **1994**, *50*, 1010.

[16] A. F. Wells, *Three-dimensional Nets and Polyhedra*, Wiley-Interscience, New York, **1977**.

[17] a) J.-P. Sauvage, *Acc. Chem. Res.* **1990**, *23*, 319; b) G. A. Breault, C. A. Hunter, P. C. Mayers, *Tetrahedron* **1999**, *55*, 5265.

[18] Representative examples: a) B. F. Abrahams, B. F. Hoskins, D. M. Michail, R. Robson, *Nature* **1994**, *369*, 727; b) R. Robson in *Comprehensive Supramolecular Chemistry*, *Vol. 6* (Eds.: D. D. MacNicol, F. Toda, R. Bishop), Pergamon, Oxford, **1996**, 733; c) S. Subramanian, M. J. Zawarotko, *Angew. Chem.* **1995**, *107*, 2295; *Angew. Chem. Int. Ed. Engl.* **1995**, *34*, 2127; d) O. M. Yaghi, H. Li, C. Davis, D. Richardson, T. L. Groy, *Acc. Chem. Res.* **1998**, *31*, 474; e) H. Li, M. Eddaoudi, M. O'Keeffe, O. M. Yaghi, *Nature* **1999**, *402*, 276; f) M. Fujita, Y. J. Kwon, S. Washizu, K. Ogura, *J. Am. Chem. Soc.* **1994**, *116*, 1151; g) S. Kitagawa, M. Kondo, *Bull. Chem. Soc. Jpn.* **1998**, *71*, 1739; h) J. Heo, S. Y. Kim, D. Whang, K. Kim, *Angew. Chem.* **1999**, *111*, 675; *Angew. Chem. Int. Ed.* **1999**, *38*, 641; i) S. S.-Y. Chui, S. M.-F. Lo, J. P. H. Charmant, A. G. Orpen, I. D. Williams, *Science* **1999**, *283*, 1148; j) J.-S. Seo, D. Whang, H. Lee, S. I. Jun, J. Oh, Y. J. Jeon, K. Kim, *Nature* **2000**, *404*, 982.

Ordered Hierarchical Porous Materials: Towards Tunable Size- and Shape-Selective Microcavities in Nanoporous Channels**

Yongsoon Shin, Jun Liu,* Li-Qiong Wang, Zimin Nie, William D. Samuels, Glen E. Fryxell, and Gregory J. Exarhos

Size and shape selectivity plays a very important role in a wide range of industrial and biological processes involving molecular transport, adsorption, catalysis, and separation. In industrial processes, the most widely used approach towards selectivity is to take advantage of well-defined cage structures in microporous zeolites.[1] Zeolites are made of three-dimensional crystalline frameworks containing interpenetrating pore channels, usually less than 10 Å in size. The crystalline structure and the pore size depend on the chemical composition as well as the processing conditions. A wide range of cations and polycations is known to stabilize certain pore structures, but a one-to-one "templating" relationship between the cations and the pore size is normally not apparent.[1] Selective transport and separation in biological processes are usually performed by soft lipid membranes containing microporous channels and pores.[2] These membrane channels and pores are self-regulated through conformational changes of membrane proteins that precisely control the ion and molecular permeability across the membrane surfaces. The self-regulating (or responsive) properties of the membrane transport process are not commonly observed in zeolites or other synthetic microporous materials.

Since 1992, the synthesis of ordered mesoporous materials using surfactants as pore-directing agents has attracted wide attention.[3] Precise control of the pore size and the ability to vary the pore size and pore geometry are highly desirable for many applications. A wide range of mesoporous materials have been synthesized as demonstrated by the large number of papers published in this area.[4] However, few reports have been published concerning the size and shape selectivity of these mesoporous materials because of the large pore size and the amorphous nature of the materials. The efforts to synthesize bimodal mesoporous materials (mesoporous materials with microporous walls) have met with limited success.

Functional groups and molecules can be incorporated into mesoporous materials to modify the surface properties for a wide range of applications, as extensively review by Möller and Bein.[5] Several approaches have been reported, including direct silanation,[6, 7] surface rehydration and silanation,[8] co-condensation,[9] and molecular imprinting.[10] A mesoporous organosilicate with bridge-bonded ethene (and other) groups was also synthesized with the co-condensation method.[11]

Recently, Katz and Davis reported molecularly imprinted bulk microporous silica using a series of imprinting molecules (carbamate bound with one, two, or three aminopropyltriethoxysilane groups).[12] The imprinted microporous material showed novel selective catalytic properties as well as selective adsorption, compared to previous molecular imprinting studies on silica materials.[13, 14]

Herein, we report on a new approach to synthesize a hierarchical porous material containing a rigid mesoporous oxide frame coated by a soft, "microporous" molecular monolayer (Figure 1). Unlike in zeolite and microporous materials, the size and the shape of the cavities embedded in the long-chain molecular monolayers determine the size and shape selectivity of the new material. The size and shape of the cavities can be systematically varied by properly choosing the template molecules. Zeolite-like properties, such as size and shape selectivity have been demonstrated. Furthermore, we can take advantage of the conformational changes of the long-chain molecules in the monolayer coating to regulate the accessibility of the microporous cavities, a property usually observed in biomembranes, but not in inorganic microporous materials. The microcavities are accessible in the open position and partially accessible or inaccessible in the closed position.

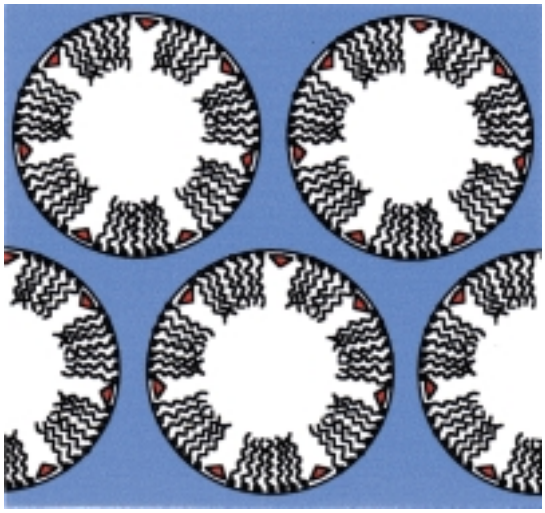


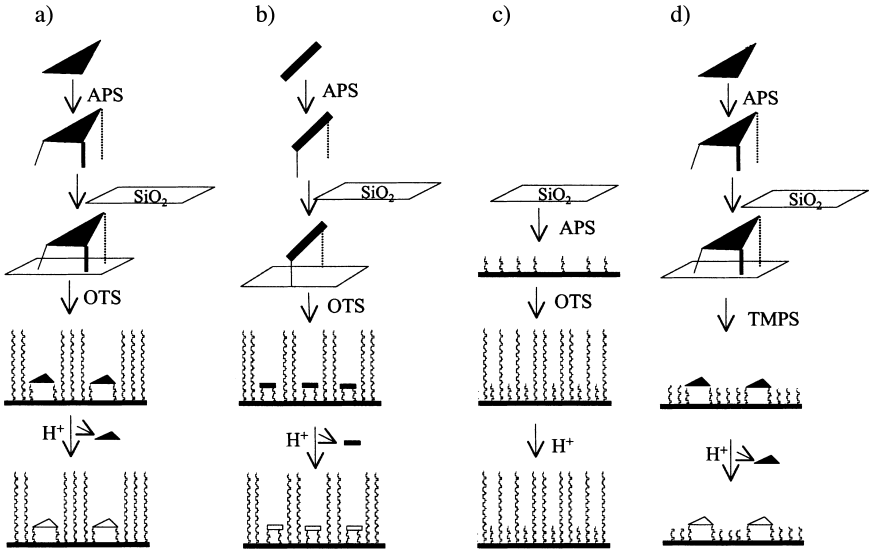
Figure 1. Schematic representation of the hierarchical porous materials with ordered nanoporosities and microcavities in the long-chain molecular monolayer coatings. The red triangular shape in the cavity represents the template molecules, or the idealized shape of the cavity.

The synthetic procedure is illustrated schematically in Scheme 1. This process was developed from widely investigated molecular imprinting techniques[15, 16] and involves the formation of heterogeneous molecular monolayers. Selectively removing the template molecules gives rise to cavitated patterns within the organic coating material. Nominally triangular, linear, and point cavities were created by first binding short aminopropyltrimethoxysilane (APS) chains to the template molecules, followed by the deposition of the template-bound silanes. Subsequently, long-chain molecules

[*] Dr. J. Liu, Dr. Y. Shin, Dr. L.-Q. Wang, Z. Nie, Dr. W. D. Samuels, Dr. G. E. Fryxell, Dr. G. J. Exarhos
Pacific Northwest National Laboratory
Richland, WA 99352 (USA)
Fax: (+1) 509-375-2186
E-mail: jun.liu@pnl.gov

[**] The Pacific Northwest National Laboratory is operated by Battelle for the U.S. Department of Energy under Contract DE-AC06-76RL0 1830. This work is supported by the Office of Basic Energy Sciences, Division of Materials Sciences, of the U.S. Department of Energy.

 © WILEY-VCH Verlag GmbH, D-69451 Weinheim, 2000 1433-7851/00/3915-2702 $ 17.50+.50/0



Scheme 1. Molecular imprinting approach for creating microcavities in the monolayer with controlled shape and size: a) triangular cavities, b) linear cavities, c) point cavities, d) triangular binding sites with short-chain capping layers. The solid triangular and rectangular shapes represent the template molecules, and the empty triangular and rectangular shapes represent the shape of the cavities after the template molecules are removed.

were deposited on the unoccupied surface of the silica substrates. The template molecules were later removed from the substrates with a mild acid wash to leave the desired cavities in the monolayer coating.

The mesoporous silica was prepared according to a method[17] using a triblock copolymer surfactant (Pluronic P123, $EO_{20}PO_{70}EO_{20}$, M.W. 5800), tetraethyl orthosilicate (TEOS). The block copolymers give more uniform pore channels for large pore sizes than the MCM-41-type mesoporous materials using a cationic surfactant. A mesoporous silica with a surface area of 517 $m^2 g^{-1}$ (corrected for microporosity) and an average radius of 48 Å was obtained. Triangular template molecules (tripod, 2,4,6-tris(*p*-formylphenoxy)-1,3,5-triazine) were synthesized by the reaction of cyanuric chloride with three equivalents of *p*-hydroxybenzaldehyde, a procedure first reported by Tahmassebi and Sasaki.[18] Linear template molecules (dipod, 2,4-bis(*p*-formylphenoxy)-6-methoxy-1,3,5-triazine) were synthesized by the same procedure using 2,4-dichloro-6-methoxy-1,3,5-triazine instead of cyanuric chloride as a starting material with two equivalents of *p*-hydroxybenzaldehyde (see the Experimental Section).

The tripod or dipod molecules were then treated with 3-aminopropyltrimethoxysilane (APS) to form tripod-APS or dipod-APS through the formation of Schiff bases.[18] The Schiff base was added to a suspension of mesoporous silica in toluene. The tripod templates should bind to the substrate with a face-on conformation through the amine groups on the three corners, and the dipod templates should bind to the substrate through the amine groups on the two ends. Long-chain organic silanes, such as octadecyltrimethoxysilane (OTS), were then added to the solution mixture to form the long-chain molecular monolayer coating.[8] The template molecules were subsequently removed by acid hydrolysis.

Ideally, these procedures should produce triangular cavities (10 Å wide, based on the dimension of the template[18]) and linear cavities (10 Å long). Gravimetric measurement suggested complete removal of the template molecules by the acid wash. For point cavities, APS molecules were first deposited on the porous substrate, followed by the deposition of OTS. The dimension of the point cavities was determined from the area an APS molecule would occupy on the surface (about 4.5 Å for one point cavity).[8] The concentrations of the template molecules (or the APS) were controlled during the sample preparations so that about 20% of the available surfaces was covered, which corresponds to 1.5 mmol APS per gram of silica. A full surface coverage would give a surface concentration of 7.5 mmol g^{-1} (SiO_2), based on the closest packing of the APS molecules.[8]

A Quantachrome instrument was used to measure the Brunauer-Emmett-Teller (BET) surface area and pore size. The pore-size distributions were obtained from the adsorption branches using the standard Barrett-Joyner-Halenda (BJH) method.[19] The adsorption branch is found to give representative results about the pore-size distribution of ordered mesoporous materials.[20] The N_2 adsorption isotherms, as well as the pore-size distributions of several samples, are plotted in Figure 2. The nitrogen adsorption usually shows a typical rectangular hysteresis loop, as previously reported.[17] This hysteresis shape represents a uniform tubular capillary pore geometry with wide and narrow regions in the pore channels.[19]

After the deposition of the templates, or the long-chain molecular coatings, the hysteresis loops were shifted to smaller pore sizes. The surface area A was also reduced, depending on the amount of silane molecules incorporated and the remaining pore diameter. Figure 2b also includes the idealized monolayer structure of the corresponding samples in a vacuum environment. The thickness of the monolayer can be estimated from the chain lengths. Here a collapsed conformation is assumed for the long-chain molecules with the triangular cavities and an extended conformation assumed for those over the point cavities on the basis of packing considerations and the space available in the nearest neighbor. The final pore radius R_e (estimated) is the difference between the initial pore radius (48 Å) and the monolayer thickness. The expected pore radii (R_e; Figure 2b) are very close to the pore radii derived from the adsorption branches. These results confirm that the suggested monolayer structures are reasonable. The desorption branches also provide useful information about the uniformity of the monolayer. The results will be published separately with more detailed analysis of the N_2 adsorption data.

 © WILEY-VCH Verlag GmbH, D-69451 Weinheim, 2000 1433-7851/00/3915-2703 $ 17.50+.50/0

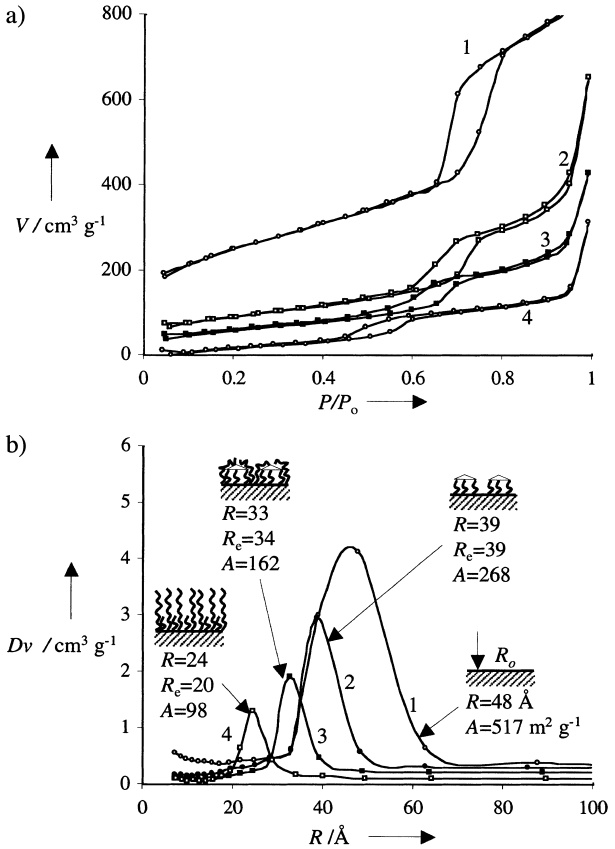


Figure 2. N_2 adsorption results: a) N_2 adsorption volume V as a function of the relative pressure P/P_o, b) pore-size distributions (incremental pore volume Dv as a function of the pore radius R): 1: native mesoporous silica, 2: mesoporous silica templated by the tripod, without OTS chains, 3: mesoporous silica with triangular cavities in OTS monolayer, and 4: mesoporous silica with APS and OTS (point cavities). The solid triangular shape represents the space initially occupied by the templates. The template molecules were removed in these samples. The expected monolayer conformations, the measured pore radii R, the expected pore radii R_e, and the measured surface area A are also included.

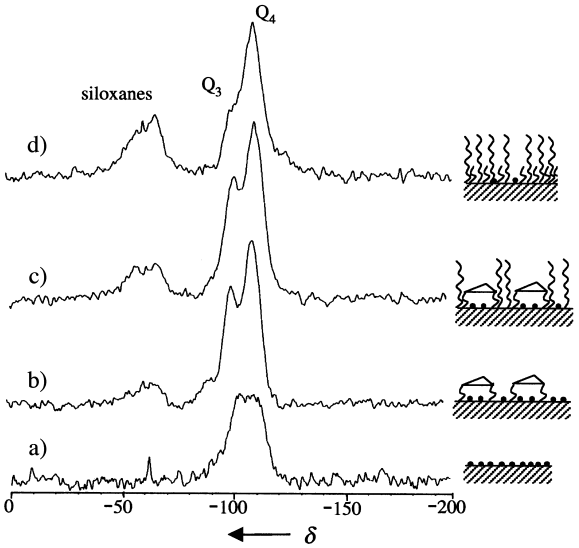


Figure 3. Single-pulse ^{29}Si spectra: a) native mesoporous silica; b) mesoporous silica templated by the tripod, without OTS chains; c) mesoporous silica with triangular cavities in the OTS monolayer; d) mesoporous silica with APS and OTS (point cavities). The triangular shape represents the space initially occupied by the templates. The template molecules were removed in these samples. The solid dots represent the surface hydroxy groups.

Single-pulse ^{29}Si NMR studies (Figure 3) provide further information about the resident chemical environments on the surfaces. A Bloch decay-pulse sequence (single-pulse excitation) with long recycle times (30 s) was used to obtain the spectra. The initial silica substrate contains significant contributions from both Si atoms with one free hydroxy group (Q_3) at -100 ppm and cross-linked silicon atoms (Q_4) at -110 ppm ($Q_3/Q_4 \approx 0.87$). The high Q_3 component is typical of the mesoporous materials prepared following ref. [17]. The deposition of silanes (APS or OTS) is accompanied by the appearance of additional siloxane peaks from -50 to -80 ppm, and reduction (for partial-surface coverage) (Figure 3b and c, $Q_3/Q_4 \approx 0.55$) or significant reduction (for high-surface coverage) of the peak for Q_3 (Figure 3d, $Q_3/Q_4 \approx 0.27$).

Part of the silica surface in both the dipod- and tripod-templated monolayers was covered with the template molecules, so that part of the surface was not available for surface silanation with OTS (Figure 3c). Therefore, Q_3 is still present in significant amounts. The shape of the siloxane peaks from $\delta = -50$ to -80 also suggests a mixture of terminal and cross-linked siloxane chains.[8] The APS molecules have less tendency to block silanation with OTS in the mixed monolayer with APS and OTS (point cavities). Q_3 is significantly reduced. The concentration of siloxane peaks from $\delta = -50$ to -80 was also found to be higher, with a more significant contribution from the cross-linked siloxane chains. These results suggest a higher packing density of OTS and a higher degree of cross-linking. In such closely packed monolayers, the molecular chains are more likely to be vertically oriented, giving a monolayer thickness roughly corresponding to the chain length. This result is consistent with the N_2 adsorption data. However, even in this case, a considerable number of free-silanol groups are still on the surface ($Q_3/Q_4 = 0.27$). The sites occupied by the template molecules in the tripod- and dipod-templated monolayers were not accessible to OTS. The OTS molecules are flexible and will give a monolayer thickness less than the full chain length unless the chains are supported and fully extended, such as in a good solvent.

The tripod and dipod molecules, which were used as the templates to create the microcavities in the monolayers, were used as probe molecules to test the size and shape selectivity of the material. Figure 4a shows the adsorption of tripod molecules onto the three cavitated substrates in toluene. The adsorption of tripod molecules on the triangular cavities (tripod templated) is two times higher than the adsorption of the same molecules on the linear cavities (tripod templated), or the substrate with point cavities (formed by APS). Similar results were also observed for the dipod adsorption studied (Figure 4b).

There are several noticeable features of these adsorption results. First is the precise nature of the selectivity. The difference between the tripod and dipod molecules is not great. The former has three benzaldehyde arms and the latter two. The rest of the molecular structures are similar. In

 © WILEY-VCH Verlag GmbH, D-69451 Weinheim, 2000 1433-7851/00/3915-2704 $ 17.50+.50/0

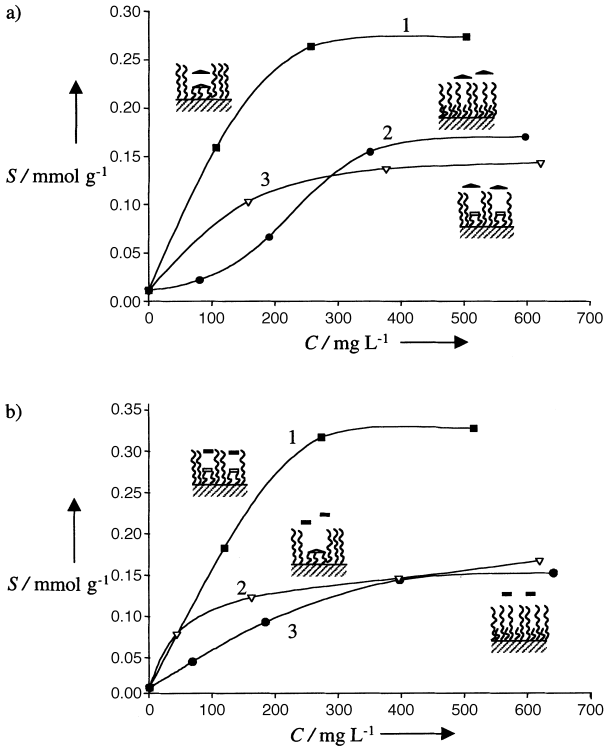


Figure 4. Specific adsorption S of dipod or tripod molecules as a function of equilibrium concentration C. a) Tripod molecules on triangular cavities (1), linear cavities (2), and point cavities (3). b) Dipod molecules on linear cavities (1), triangular cavities (2), and point cavities (3).

principle, the dipod molecules can easily fit into the triangular cavities and conform to the majority of the cavities nicely. The two aldehyde groups can also bind with the two amine groups at the corner of the cavity (through hydrogen bonding or formation of a Schiff base). We would expect the dipod molecules to adsorb on triangular cavities as well as on linear cavities. The large difference in the adsorption behavior of dipod molecules on triangular and linear cavities demonstrated that the shapes of the cavities are very important.

Second, the three-dimensional nature (arising from the long-chain molecule coating) of the cavities is critical. A one-to-one correspondence of the binding sites alone does not give any selectivity. Materials have been prepared using the same procedure without the long-chain molecule monolayer coating or with a coating layer made of small molecules (hexamethyldisilazane, or trimethoxypropylsilane (TMPS)) (Scheme 1 d). These materials contain exactly the same bindings sites (amine groups from the APS) arranged in the same way as in the long-chain monolayers. No selectivity was observed on any of these materials without the long-chain capping. If the selectivity were just attributed to the matching of the binding sites, the materials without capping or with the short-chain capping layer should have a similar selectivity as the long-chain materials. Therefore, we can conclude that the steric effect of the cavities in the long-chain monolayers largely contributed to the selectivity of such materials.

One unique feature of the new material is that the accessibility of the microcavities can be changed. This property is demonstrated with adsorption studies conducted in mixed solutions of toluene and ethanol. Pure ethanol was not used because most of the probe molecules studied were not soluble in ethanol. Generally, whether the long-chain molecules assume an extended or a collapsed conformation depends on the inter- and intramolecular forces. Toluene and long-chain hydrocarbons are hydrophobic molecules and have similar dielectric constant (ε) and refractive indices (n) ($\varepsilon_{toluene} \approx 2.37$, $\varepsilon_{C18} \approx 2.0$, $n_{toluene} \approx 1.49$, $n_{C18} \approx 1.44$). The interactions within and between the hydrocarbon chains in toluene are greatly reduced.[21] Therefore, the hydrocarbon chains will assume a more extended conformation, thus making the microcavities accessible. However, ethanol is a hydrophilic solvent and has a different dielectric constant and refractive index ($\varepsilon_{EtOH} \approx 26$, $n_{EtOH} \approx 1.36$).

The attractive forces within and between the hydrocarbon chains increases in a solvent containing ethanol.[21] This will cause the hydrocarbon chains to form a more-compact (collapsed) conformation, which blocks the microcavities from molecules in the solvent. This kind of change in molecular conformation when the solvency of the solution is changed is well documented in textbooks.[22] Figure 5 a compares the results of tripod adsorption on triangular cavities in toluene and in toluene/ethanol mixture. The adsorption in the mixture is greatly reduced. It is interesting to compare Figure 5 a with Figure 5 b (dipod adsorption on linear cavities): in the latter the adsorption in the mixture was nearly turned off. The linear cavities are much narrower than the triangular cavities and when the hydrocarbon chains curl over, the accessibility to the linear cavities can be completely shut off.

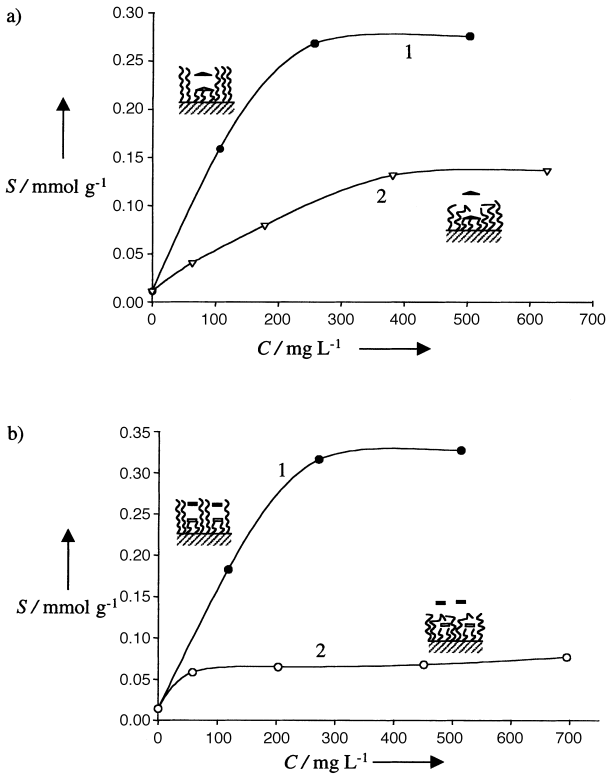


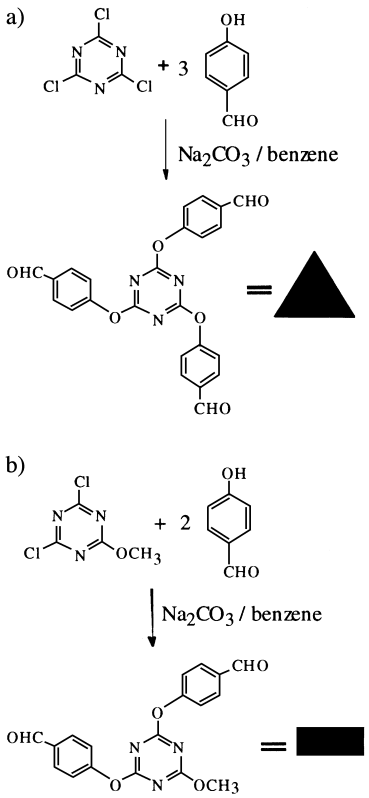
Figure 5. Solvent effects on adsorption behavior on adsorption isotherms. a) Tripod molecules on triangular cavities in toluene (1) and in toluene/ethanol (2). b) Dipod molecules on linear cavities in toluene (1) and in toluene/ethanol (2).

 © WILEY-VCH Verlag GmbH, D-69451 Weinheim, 2000 1433-7851/00/3915-2705 $ 17.50+.50/0

We should point out that the molecular conformation and the monolayer chemistry discussed herein are still under more detailed investigation. The drawings in the figures are meant to be schematic, not mechanistic or quantitative. For example, we can easily speculate that dimers, trimers, or even high-order clusters could form when APS or the template molecules were initially deposited, rather than being uniformly distributed on the surface. The aggregation of these molecules on the surface would have a negative effect on the selectivity, based on the size and shape of the cavities. The possibility also exists of forming more than one molecular layer, or aggregation of the monolayer molecules. There is also evidence that the deposition of OTS molecules can be affected by the predeposited template molecules, and therefore the long-chain monolayers may not be as well organized. Furthermore, the exact shape and size of the cavities should also be the subject of a future study, maybe using techniques such as atomic force microscopes (AFM) and flat substrates as model systems. The shape and the size of the cavities described here are based on the shape and size of the templates, and may not reflect the exact size and shape of the cavities.

The fact that we indeed observed significant selectivity and the consistency between the N_2 adsorption, NMR results, and many other properties of the materials suggests that the material does behave as we expected, and the rationale used is reasonable. This new class of hierarchical porous materials with tunable microporosities are attractive for many applications. The principles used in the synthesis should be applicable to the creation of a wide range of microcavities and patterns within a confined space. The combination of tailored nanoporosity and tunable micropatterns within the nanoporosity may lead to novel properties and applications that will even mimic the structures and functions of sophisticated biological materials.

Finally, we would like to discuss the possibility of selective catalysis based on the size of the micropores. Preliminary results on the Knoevenagel condensation[23–26] between malononitrile and benzaldehyde or 3-pentanone showed that a larger microcavity size (triangular cavities) favored the reaction of the large molecule (benzaldehyde). Although further research is needed to understand the reaction pathways and to optimize the materials properties, we believe that we can selectively enhance or reduce the reaction rate by manipulating the monolayer chemistry and the size and shape of the cavities.



Scheme 2. a) Synthesis of the triangular template (tripod). b) Synthesis of the rectangular template (dipod).

Experimental Section

Synthesis of the tripod and dipod:[18] The tripod and dipod were synthesized as illustrated in Scheme 2. The tripod: cyanuric chloride (1.20 g, 6.50 mmol) and *p*-hydroxybenzaldehyde (3.20 g, 26.2 mmol) were added to a suspension of Na_2CO_3 (20.0 g) in benzene (100 mL). After the reaction mixture had refluxed for 24 h at 100 °C, the white solid was removed by filtration and washed with ethyl acetate (EtOAc) three times. The filtrate was washed with 10 % Na_2CO_3 and H_2O three times. The organic layer was dried over $MgSO_4$ and then concentrated under reduced pressure. The crude white powder was recrystallized from EtOAc (30 mL). The dipod: the synthesis was identical to the tripod, but using 2,4-dichloro-6-methoxy-1,3,5-triazine (3.0 g, 16.7 mmol) and *p*-hydroxybenzaldehyde (4.50 g, 36.8 mmol) in a suspension of Na_2CO_3 (30.0 g) in benzene (200 mL) instead of cyanuric chloride.

Synthesis of mesoporous materials: The mesoporous silica was prepared according to a method[17] using a triblock copolymer surfactant (Pluronic P123, $EO_{20}PO_{70}EO_{20}$, M.W. 5800), tetraethyl orthosilicate (TEOS). The sample was treated at 40 °C and 100 °C and then calcined at 500 °C.

Imprinting approach for microporous monolayers in mesoporous silica: The tripod or dipod molecules were treated with 3-aminopropyltrimethoxysilane (APS) at room temperature to form tripod-APS or dipod-APS through formation of Schiff bases.[18] This Schiff base was added to a suspension of mesoporous silica in toluene and refluxed at 150 °C for 6 h. The long-chain organic silanes, such as octadecyltrimethoxysilane (OTS), were then added to the mixture to form the long-chain molecular monolayer coating.[8] The template molecules were subsequently removed by acid hydrolysis (HCl) of the Schiff bases with aqueous methanol (1/1 (v/v)) over a period of 4 h at room temperature.

Adsorption study of the tripod and dipod: The adsorption capacity toward the dipod or tripod was determined on a UV/Vis spectrophotometer. In all experiments, each sample (0.02 g) was equilibrated with different concentration solutions (10.0 mL) of dipod or tripod in toluene in stoppered glass vials, and these mixtures were stirred for 4 h on the Environ Shaker at room temperature. The difference in the template concentrations before and after equilibrium gave the adsorbed amount on the solid samples. The adsorption study of the tripod and dipod in mixed solvents was performed similarly to the above, except that a mixture of ethanol and toluene (50/50 (wt/wt)) was used as the solvent.

Knoevenagel condensation on tripod and dipod:[23] In a typical procedure, each catalyst (0.05 g) and benzaldehyde (0.212 g, 2.0 mmol) were stirred in dry toluene (10.0 mL). To this solution malononitrile (0.126 mL, 2.0 mmol) was added, and the mixture was stirred at room temperature. The reaction was monitored periodically on a UV/Vis spectrophotometer (285 nm for benzaldehyde and 314 nm for product). A similar procedure was used for 3-pentanone, except that the reaction was carried out at 110 °C.

Received: February 22, 2000 [Z 14753]

 © WILEY-VCH Verlag GmbH, D-69451 Weinheim, 2000 1433-7851/00/3915-2706 $ 17.50+.50/0

[1] a) R. M. Barrer, *Hydrothermal Chemistry of Zeolites*, Academic Press, New York, **1982**; b) M. E. Davis, *Ind. Eng. Chem. Res.* **1991**, *30*, 1675; c) F. R. Ribeiro, F. Alvarez, C. Henriques, F. Lemos, J. M. Lopes, M. F. Ribeiro, *J. Mol. Catal. A* **1995**, *96*, 245.
[2] R. B. Gennis, *Biomembranes*, *Molecular Structure and Function*, Springer, New York, **1989**, chap. 8, p. 270.
[3] a) J. S. Beck, J. C. Vartuli, R. J. Roth, M. E. Leonowicz, C. T. Kresge, T.-W. Chu, D. H. Olson, *J. Am. Chem. Soc.* **1992**, *114*, 10834; b) C. T. Kresge, M. E. Leonowicz, W. J. Roth, J. C. Vartuli, J. S. Beck, *Nature* **1992**, *359*, 710.
[4] The following review articles are available: a) J. S. Beck, J. C. Vartuli, *Curr. Opin. Solid State Mater. Sci.* **1996**, *1*, 76; b) J. Liu, A. Y. Kim, L. Q. Wang, B. J. Palmer, Y. L. Chen, P. Bruinsma, B. C. Bunker, G. J. Exarhos, G. L. Graff, P. C. Rieke, G. E. Fryxell, J. W. Virden, B. J. Tarasevich, L. A. Chick, *Adv. Colloid Interface Sci.* **1996**, *69*, 131; c) N. K. Raman, M. T. Anderson, C. J. Brinker, *Chem. Mater.* **1996**, *8*, 1682; d) U. Ciesla, F. Schuth, *Microporous Mesoporous Mater.* **1999**, *27*, 131.
[5] K. Möller, T. Bein, *Chem. Mater*. **1998**, *10*, 2950.
[6] a) D. Cauvel, G. Renard, D. Brunel, *J. Org. Chem.* **1997**, *62*, 749; b) S. L. Burkett, S. D. Simms, S. Mann, *Chem. Commun*. **1996**, 1367.
[7] a) L. Mercier, T. J. Pinnavaia, *Adv. Mater*. **1997**, *9*, 500; b) L. Mercier, T. J. Pinnavaia, *Environ. Sci. Technol*. **1998**, *32*, 2749.
[8] a) X. Feng, G. E. Fryxell, L. Q. Wang, A. Y. Kim, J. Liu, K. M. Kemner, *Science* **1997**, *276*, 923; b) J. Liu, X. Feng, G. E. Fryxell, L. Q. Wang, A. Y. Kim, M. Gong, *Adv. Mater.* **1998**, *10*, 161; c) G. E. Fryxell, J. Liu, T. A. Hauser, Z. Nie, K. F. Ferris, *Chem. Mater.* **1999**, *8*, 2148.
[9] M. H. Lim, C. F. Blanford, A. Stein, *Chem. Mater*. **1998**, *10*, 467.
[10] S. Dai, M. C. Burleigh, Y. Shin, C. C. Morrow, C. E. Barnes, Z. Xue, *Angew. Chem.* **1999**, *111*, 1314; *Angew. Chem. Int. Ed.* **1999**, *38*, 1235.
[11] a) S. Inagaki, *J. Am. Chem. Soc*. **1999**, *121*, 9611; b) B. J. Elde, B. T. Holland, C. F. Blanford, A. Stein, *Chem. Mater*. **1999**, *11*, 3302; c) T. Asefa, M. J. MacLachlan, N. Coombs, G. A. Ozin, *Nature* **1999**, *402*, 867.
[12] A. Katz, M. E. Davis, *Nature* **2000**, *403*, 286.
[13] F. H. Dickey, *J. Phys. Chem*. **1955**, *59*, 695.
[14] G. Wulff, B. Heide, G. Helfmeier, *J. Am. Chem. Soc.* **1986**, *108*, 1089.
[15] a) G. Wulff, *Angew. Chem.* **1995**, *107*, 1958; G. Wulff, *Angew. Chem. Int. Ed. Engl.* **1995**, *34*, 1812; b) G. Wulff, A. Sarhan, K. Zabrocki, *Tetrahedron Lett.* **1973**, 4329; c) K. J. Shea, E. A. Thompson, *J. Org. Chem.* **1978**, *43*, 4253; d) D. Spivak, K. J. Shea, *J. Org. Chem.* **1999**, *64*, 4627.
[16] a) G. M. Whitesides, *Sci. Am.* **1995**, *273*(9), 146; b) A. Ulman, *Chem. Rev.* **1996**, *96*, 1533; c) B. C. Bunker, P. C. Rieke, B. J. Tarasevich, A. A. Campbell, G. E. Fryxell, G. L. Graff, L. Song, J. Liu, J. W. Virden, G. L. McVay, *Science* **1994**, *264*, 48.
[17] a) D. Zhao, Q. Huo, J. Feng, B. F. Chmelka, G. D. Stucky, *J. Am. Chem. Soc.* **1998**, *120*, 6024; b) D. Zhao, J. Feng, Q. Huo, N. Melosh, G. H. Fredrickson, B. F. Chmelka, G. D. Stucky, *Science* **1998**, *279*, 548.
[18] a) D. C. Tahmassebi, T. Sasaki, *J. Org. Chem.* **1994**, *59*, 679; b) K. O. Hwang, Y. Yakura, F. S. Ohuchi, T. Sasaki, *Mater. Sci. Eng. C* **1995**, *3*, 137.
[19] B. G. Linsen, A. van den Heuvel in *The Solid Gas Interface*, *Vol. 2* (Eds.: E. A. Flood), Mercel Dekker, New York, **1967**, p. 1025.
[20] M. Kruk, M. Jaroniec, Y. Sakamoto, O. Terasaki, R. Ryoo, C. H. Ko, *J. Phys. Chem. B* **2000**, *104*, 292.
[21] J. N. Israelachvili, *Intermolecular and Surface Forces*, 2nd ed., Academic Press, San Diego, **1992**, p. 99.
[22] F. W. Billmeyer, Jr., *Textbook of Polymer Science*, 3rd ed., Wiley, New York, **1984**, p. 154.
[23] F. A. Carey, R. J. Sundberg, *Advanced Organic Chemistry B: Reactions and Synthesis*, 2nd ed., Plenum, New York, **1983**, p. 57.
[24] E. Angeletti, C. Capena, G. Martinetti, P. Venturello, *J. Chem. Soc. Perkin Trans. 1* **1989**, 105.
[25] a) B. M. Choudary, M. L. Kantam, P. Sreekanth, T. Bandopadhyay, F. Figueras, A. Tuel, *J. Mol. Catal. A* **1999**, *142*, 361; b) I. Rodriguez, S. Iborra, A. Corma, F. Rey, J. L. Jorda, *Chem. Commun.* **1999**, 592.
[26] H. O. House, *Modern Synthetic Reactions*, 2nd ed., W. A. Benjamin, Menlo Park, CA, **1972**, p. 648.

Hierarchical Pore Structures through Diatom Zeolitization**

Michael W. Anderson,* Stuart M. Holmes, Noreen Hanif, and Colin S. Cundy

There has been considerable effort recently to devise routes to hierarchical porous structures, which aid the diffusion of guest species through an inorganic network of pores and channels. In order to optimize the performance of a material for a specific application, it is desirable to combine different levels of porosity into one hierarchical porous material. In applications such as catalysis, where the diffusion of molecules through the pore structure, called "molecular traffic control",[1] is vital for optimum performance, a highly ramified network of macro- and micropores is desired. Further, for bulk processes, again such as catalysis or ion-exchange, then any hierarchical porous material must be both facile and cheap to construct. Herein, we report the use of diatomaceous earth for the controlled synthesis of ordered mesoporous/microporous composites which may have considerable utility for bulk industrial processes.

Diatoms are single-celled algae,[2] microscopic plants which secrete and are enclosed by an intricate silica shell. When these aquatic plants die, their shells collect on the ocean or lake floor, eventually forming the material called diatomaceous earth (kieselguhr) or the more light weight rock called diatomite. Diatomite is used in sound and heat insulation, as filters, abrasives, and in the manufacture of explosives. One unique feature of diatoms is their macroporous channel structure with pore sizes ranging from the submicron to tens of microns scale. As diatoms make up about a quarter of plant life by weight, they are an extremely abundant and cheap source of silica. The purpose of this work is to try to utilize the inherent macroporosity of diatoms in the construction of hierarchical composite materials by their "zeolitization".

Hierarchical pore networks have been predicted for some time to have enhanced diffusion properties, whether the networks are ordered or disordered.[3] Indeed, much of the preparation of working catalyst particles involves the treatment of the active component with a suitable binder (usually a form of clay) such that good diffusion is maintained. However, the control over the level and degree of porosity is somewhat arbitrary and depends upon processing conditions. Recently, elegant efforts to synthesize controlled hierarchical materials have resulted in composites with a pore size distribution spread over up to three orders of magnitude. However, the processing conditions are complicated and

[*] Prof. M. W. Anderson, S. M. Holmes, N. Hanif, C. S. Cundy
UMIST Centre for Microporous Materials
Department of Chemistry
University of Manchester
P.O. Box 88, Manchester M60 1QD (UK)
Fax: (+44) 161-2004527
E-mail: m.anderson@umist.ac.uk

[**] We are grateful to BNFL, BOC, Engelhard, ICI, and EPSRC for financial support and to Richard Plaisted and James Forrest for providing the colloidal silicalite. We would also like to thank Micromeritics Ltd. for their help in obtaining the sorption and porosimetry data.

 © WILEY-VCH Verlag GmbH, D-69451 Weinheim, 2000 1433-7851/00/3915-2707 $ 17.50+.50/0

require the inclusion of latex spheres within the product, which subsequently have to be removed.[4, 5] Alternatively, complex silica forms (mimicking, to some extent, diatoms) have been synthesised using pattern replication of self-organised organic assemblies, such as micelles, vesicles, and foams.[6–8] A "biomimetic" approach to porous materials using a technique called Replamineform[9] has been used to fabricate orthopedic prosthetic devices by deposition of a range of materials[10, 11] on a cast produced from the pore structures of marine invertebrate skeletal materials, such as echinoid spines and coral. However, such forms in themselves do not have suitable active sites for catalysis or ion exchange. In this work, we have developed a simple, cheap, and one-step process to the formation of a stable micro/macroporous composite material where the active component is based upon a zeolite catalyst.

One of the methods we have used to zeolitize the diatomaceous earth involves coating the diatoms with zeolite nanoparticles followed by subsequent attachment and hydrothermal growth of zeolite crystals.[12]

Most diatom shells are essentially composed of silica with traces of other oxides—the diatomaceous earth used in this study contained about 2 wt % alumina. Consequently, these initial studies concentrated on zeolitization with the high-silica zeolite ZSM-5, which in the siliceous limit is called silicalite (both structures belong to the MFI structural type).[13] ZSM-5 is one of the most important commercial zeolites and is used for a wide variety of catalytic transformations including the one-step conversion of methanol into gasoline.[14] The MFI structure consists of a two-dimensional array of intersecting micropores with pore diameter of about 5.5 Å.

Figure 1 shows the progress of diatom zeolitization by X-ray diffraction (XRD). The initial diatom has an XRD pattern which is consistent with the crystalline silica form cristobalite (probably arising from heat treatment during the manufacture of the commercial product). First, silicalite nanoparticles (dimension of approximately 80 nm) are dispersed on the surface of the diatoms and this is followed by a hydrothermal growth process inside an autoclave. The XRD patterns reveal an increase in the intensity of the reflections corresponding to the MFI structure at the expense of the reflections corresponding to cristobalite. The synthesis continued for a total of 72 h.

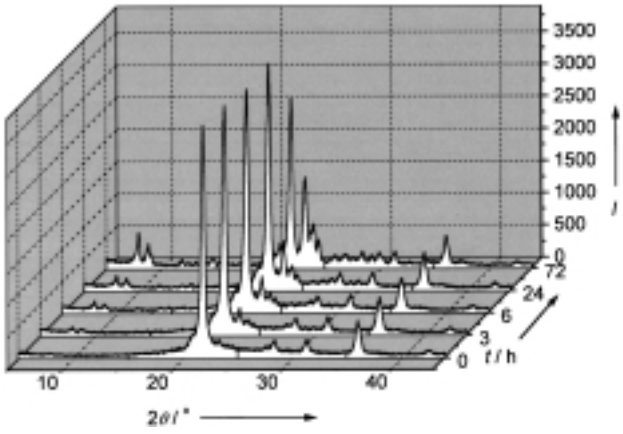


Figure 1. Powder XRD patterns show the development of an MFI phase on the surface of the diatoms. Before growth, the diatoms show reflections characteristic of a cristobalite phase. It is not clear whether the cristobalite phase is homogeneously dispersed through the diatoms or whether parts are essentially amorphous. Electron microscopy shows no indication of opaline regions often associated with diatoms. Subsequent XRD spectra show the growth of reflections characteristic of the MFI phase. The initial nanoparticles are (aluminum free) silicalite. However, an energy-dispersive X-ray spectroscopic (EDAX) analysis of the zeolite layer shows the crystals have about 2% alumina which originates from the low aluminum concentration in the diatoms.

The details of the morphological changes occurring during these growth steps are most clearly revealed by scanning electron microscopy (SEM; Figure 2). The initial diatoms consist of shell forms, which can be described as hollow tubes

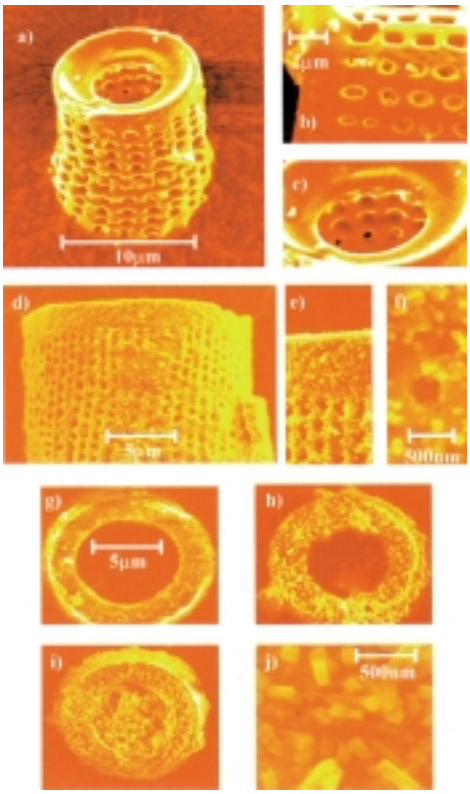


Figure 2. SEM (field emission) of the diatoms before and after growth of the MFI zeolite crystals. a)–c) The parent diatom with overall dimension of about 10×20 μm; in b) the diatom porosity is clearly shown, where the subpores are of dimensions about 0.5 μm. d)–f) The diatoms after 3 h hydrothermal growth. That zeolite nanoparticles are firmly attached is shown in g), by treatment of the same material with boiling water for 1 h. e) The diatom subpores remain free at this stage of hydrothermal growth, and f) the lip of these subpores is lined with nanoparticles. h) After 24 h growth and a calcination step, the interior of the diatoms is still clear and the zeolite nanoparticles have not grown substantially. i), j) After 72 h hydrothermal growth, the interior of the diatoms has become filled with zeolite and the crystals have grown to about 300 nm in length.

of length 15–20 μm and an internal pore diameter of about 4 μm. The walls of the tubes consist of a regular array of submicron pores (about 0.5 μm) with around 0.5 μm of silica between the pores. These pores are continuous into the internal pore space of the hollow diatom tubes. After dispersing the MFI nanoparticles on the diatoms followed by a short subsequent hydrothermal growth step (3 h, Fig-

 © WILEY-VCH Verlag GmbH, D-69451 Weinheim, 2000 1433-7851/00/3915-2708 $ 17.50+.50/0

ure 2d–f), the diatoms have an even coating and the nanoparticles have not grown to any great extent. It is also clear at this stage, that all the macroporosity of the diatoms remains intact (Figure 2g). Further hydrothermal growth (6 h total) enlarges the MFI nanoparticles only slightly. The tube wall openings of the diatom become somewhat restricted but the internal void space remains clear. For up to 24 h, the morphology does not change significantly and the diatom interior remains clear (Figure 2h). However, after 72 h growth, the MFI nanoparticles have grown into typical boat-shaped MFI crystallites of length 300 nm and width 80 nm (Figure 2j). At this stage, it is clear from the electron micrograph that some of the macroporosity of the diatoms is lost, although the basic diatom form remains intact. This image also illustrates the random orientation of the MFI crystals on the surface of the diatoms after 72 h; prior to 72 h, it is not possible to describe the orientation of the crystals since the colloidal seeds appear spherical due to their small size. Most significantly, the internal void space of the diatoms becomes filled with zeolite crystals (Figure 2i).

In order to determine how securely the MFI nanocrystallites are attached to the diatoms, the composite materials after 3 h growth were boiled in water for 1 h followed by examination by SEM. Figure 2g shows that the nanocrystallites are indeed extremely well bound to the diatoms after fixing through short hydrothermal growth steps. The thermal stability of the materials is in excess of 1000 °C and Figure 2h indicates that the composite material is intact after such a treatment. The evolution of the porosity in the composite products was followed by nitrogen sorption/desorption and mercury porosimetry. Whereas the starting material was dominated by macroporosity, zeolite crystal growth introduced a well defined secondary structure that contains both mesopores and micropores. Figure 3 shows the sorption/desorption isotherm for the calcined material which had been

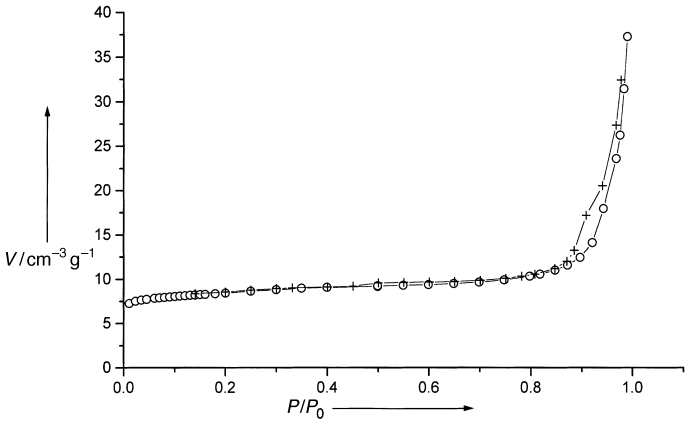


Figure 3. The sorption/desorption isotherm (relative N_2 pressure (P/P_0) against adsorbtion volume (V)) for the calcined material which had been zeolitized for 1 h. ○ desorption, + sorption.

zeolitized for 1 h. This type IV isotherm is indicative of the newly generated porosity in the material, the steep rise followed by the flat section at low relative pressures corresponds to the filling of the micropores (volume 6.7 $cm^3 g^{-1}$ N_2 at STP), while the upturn and hysteresis loop at higher relative pressures reflect the intercrystalline mesoporosity of the zeolitized diatomic structure. The Brunauer-Emmet-Teller (BET) surface area obtained for this material was 29.2 $m^2 g^{-1}$, while the unreacted, calcined, diatomaceous earth had a surface area of only 0.58 $m^2 g^{-1}$ and a micropore volume of 0.13 $cm^3 g^{-1}$. The surface area compares with a value of 421 $m^2 g^{-1}$ given by Stein and co-workers[5] for a macroporous/microporous composite synthesised using latex spheres. The larger surface area in that case is attributable to the higher concentration of zeolite per unit mass of the material. The zeolitized diatom sample had a zeolite content of only about 5% (w/w) at this stage of the reaction. Higher surface area composites can be obtained by zeolitization for longer times.

The diffusion of water through packed columns of the composite materials was tested and compared with that of a packed bed of silicalite crystallites. Figure 4 shows how a very high flow rate is maintained in the composite material.

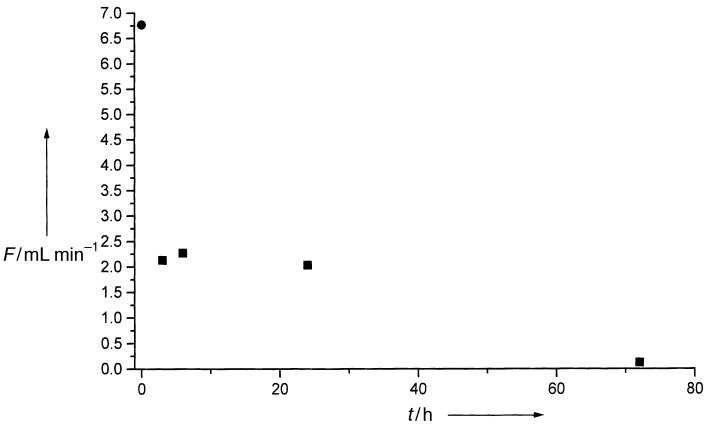


Figure 4. Diffusion rate of water through a packed column at 22 °C. F = flow rate, ● pure diatoms, ■ zeolitized diatoms.

In conclusion, the surface of a diatom structure has been successfully zeolitized to provide a micro/macroporous composite material. One can envisage zeolitizing a range of similar structures, dependent on the physical characteristics of the active bed which are required. As there are over 70000 known diatom species and over 100 zeolite types, the possibility for tailoring both the macroporous and microporous component by this method is almost limitless.

Experimental Section

Diatoms were obtained from Aldrich (Celatom FW80) and used without further treatment. Diatoms were seeded with zeolite nanoparticles (crystallite size about 80 nm) by sonication in a colloidal suspension. This had the effect of fixing the seeds to the surface of the diatoms.[12] The seeded diatoms were then placed in a synthesis mixture of total composition (including the diatoms) SiO_2:Na_2O:EtOH:H_2O:TPABr = 1:0.06:0.43:100:0.04 (TPABr = tetrapropylammonium bromide). A majority (90%) of the silica was provided by the seeded diatoms, the remainder by tetraethyl orthosilicate. The reaction mixture was equilibrated overnight, under stirring, prior to the addition of the seeded diatoms and was then divided between a series of autoclaves and heated to 175 °C.

Received: January 31, 2000 [Z14617]

 © WILEY-VCH Verlag GmbH, D-69451 Weinheim, 2000 1433-7851/00/3915-2709 $ 17.50+.50/0

[1] E. G. Derouane, Z. Gabelica, *J. Catal.* **1980**, *65*, 486.
[2] E. G. Vrieling, T. P. M. Beelen, R. A. van Santen, W. W. C. Gieskes, *J. Biotechnol.* **1999**, *70*, 39.
[3] U. A. El Nafaty, R. Mann, *Chem. Eng. Sci.* **1999**, *54*, 3475.
[4] P. D. Yang, T. Deng, D. Y. Zhao, P. Y. Feng, D. Pine, B. F. Chmelka, G. M. Whitesides, G. D. Stucky, *Science* **1998**, *282*, 2244.
[5] B. T. Holland, L. Abrams, A. Stein, *J. Am. Chem. Soc.* **1999**, *121*, 4308.
[6] S. Mann, G. A. Ozin, *Nature* **1996**, *382*, 313.
[7] H. Yang, N. Coombs, G. A. Ozin, *Nature* **1997**, *386*, 692.
[8] G. A. Ozin, *Chem. Commun.* **2000**, 419.
[9] R. A. White, J. N. Weber, E. W. White, *Science* **1972**, *176*, 922.
[10] J. N. Weber, E. W. White, J. Lebiedzik, *Nature* **1971**, *233*, 337.
[11] D. M. Roy, S. K. Linnehan, *Nature* **1974**, *247*, 220.
[12] S. M. Holmes, C. Markert, R. J. Plaisted, J. O. Forrest, J. R. Agger, M. W. Anderson, C. S. Cundy, J. Dwyer, *Chem. Mater.* **1999**, *11*, 3329.
[13] G. T. Kokotailo, S. L. Lawton, D. H. Olson, W. M. Meier, *Nature* **1978**, *272*, 437.
[14] C. D. Chang, A. J. Silvestri, *J. Catal.* **1977**, *47*, 249.

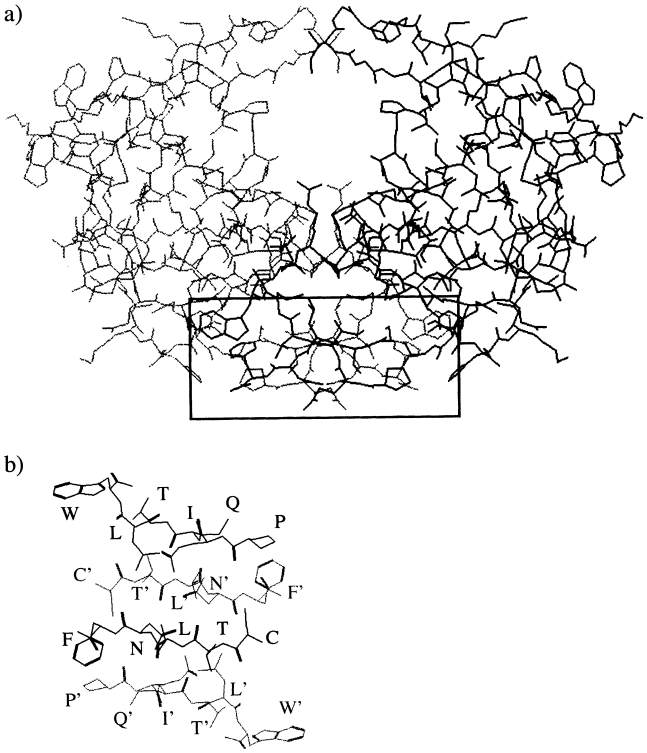


Figure 1. a) Dimeric structure of HIV-1 protease. The area of the N- and C-terminal dimerization interface is indicated by the box. b) The N- and C-terminal dimerization interface of the protease.[10]

Small-Molecule Inhibitors of HIV-1 Protease Dimerization Derived from Cross-Linked Interfacial Peptides**

Michael D. Shultz, Michael J. Bowman, Young-Wan Ham, Xuimin Zhao, George Tora, and Jean Chmielewski*

As more information on macromolecular structure unfolds, it has become obvious that interprotein interactions are a ubiquitous and fundamental aspect of biological activity.[1] Whereas the nature of these protein–protein interactions is becoming better understood, rational approaches to inhibiting these interactions are still in their infancy.[2] Using dimeric HIV-1 protease (Figure 1 a) as a template, we have developed a strategy to inhibit dimerization based on the cross-linking of interfacial peptides derived from the protease.[3] In the current study, we endeavored to identify the essential residues of a cross-linked, interfacial peptide inhibitor of HIV-1 protease, and obtain a minimal structure that maintains the essential features of dimerization inhibition.

The pivotal role of HIV protease in viral replication has made it a prime target for drug design, and there is currently a wide range of potent, active-site inhibitors of HIV-1 protease spanning a number of classes of compounds, including peptide mimetics, C_2-symmetric compounds, and non-peptidic agents.[4] To date five protease inhibitors have been approved by the Food and Drug Administration (FDA) for treatment of HIV infection,[5] but problems of drug resistance due to selection of viruses with specific mutations within protease have been discovered with these inhibitors.[6] Fortunately, results with multidrug approaches made up of protease and reverse transcriptase inhibitors have been promising. Other side effects, however, have also been identified with the current protease inhibitor drugs, including peripheral lipodystrophy,[7] central adiposity,[8] breast hypertrophy in women,[9] hyperlipidemia,[7] and insulin resistance.[7]

The problems that have been identified with the current group of protease inhibitor drugs serve to underscore the need for novel approaches to inhibitor design. One such approach would be to target the dimerization interface of HIV protease.[2] The main dimerization region of HIV-1 protease is found in an interdigitating N- and C-terminal four-stranded, antiparallel β sheet (Figure 1 b).[10] The area centered around the N and C termini accounts for approximately half of the interfacial contact area of the protease homodimer, and the contacts in this area account for greater than 75 % of the free energy of dimerization.[11] This region is also highly conserved among HIV-1 isolates and some HIV-2 isolates, presumably due to the fact that a mutation in the C terminus would necessitate a concomitant mutation in the N terminus to avoid loss of high-affinity dimerization.[12]

Taking advantage of the dimeric nature of HIV protease, Craik and co-workers developed mutant forms of HIV protease for use in a dominant-negative strategy of inhibition; incubation of wild-type protease with monomers that have mutated active-site residues (fourfold molar excess) led to

[*] Prof. J. Chmielewski, M. D. Shultz, M. J. Bowman, Y.-W. Ham, X. Zhao, G. Tora
Department of Chemistry
Purdue University
West Lafayette, IN 47907 (USA)
Fax: (+1) 765-494-0135
E-mail: chml@purdue.edu

[**] This work was supported by NIH (GM52739) and NSF (9457372-CHE).

Supporting information for this article is available on the WWW under http://www.wiley-vch.de/home/angewandte/ or from the author.

 © WILEY-VCH Verlag GmbH, D-69451 Weinheim, 2000 1433-7851/00/3915-2710 $ 17.50+.50/0

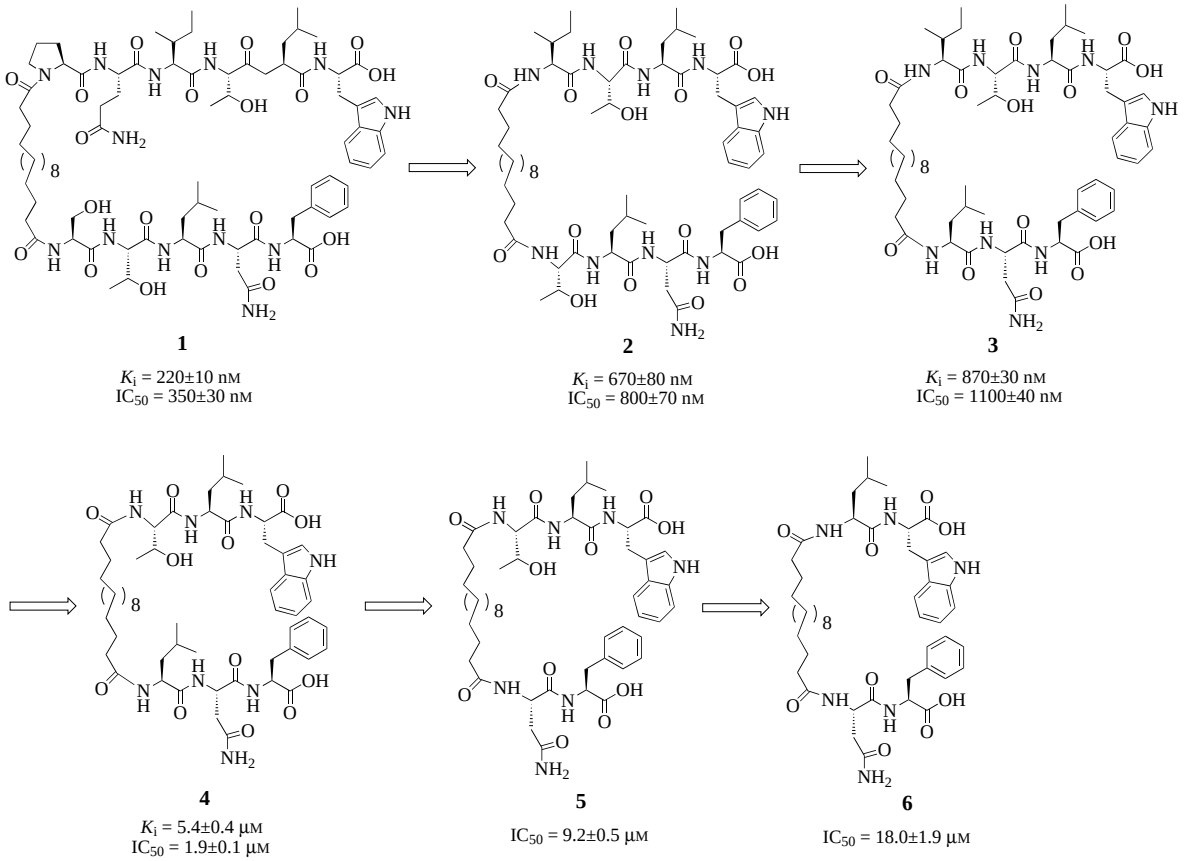
80% reduction in enzyme activity.[13] The features of the dimerization interface of HIV protease have also led to the design of inhibitors that target this portion of the enzyme; interfacial peptides derived from the N and C termini of HIV-1 protease show inhibitory activity,[14] and subunits of the natural product didemnaketal A are protease inhibitors whose kinetic profile suggests a dissociative mechanism of inhibition.[15]

Studies from our group have demonstrated that cross-linking the N termini of interfacial peptides of HIV protease (**1**) can significantly improve the potency of dimerization inhibitors.[3] In the current study we have taken a reductionist approach to developing inhibitors based on agent **1** by removing less essential residues. In this way we hoped to identify a minimal structure that maintains the essential features of dimerization inhibition, and that serves as a core structure for the development of more potent dimerization inhibitors.

An analysis of the contribution of each amino acid within **1** toward inhibition demonstrated the importance of the C-terminal residues, Trp1 and Phe11.[16] Since these residues of **1** were determined to be essential for inhibition, truncated agents (**2**–**6**; see Scheme 1) were prepared in which the peptides were shortened from the N termini. These compounds were synthesized by either a solution- or solid-phase strategy as previously described.[3]

The extent of HIV-1 protease inhibition by the truncated and cross-linked interfacial peptides was evaluated using the fluorogenic substrate developed by Toth and Marshall [17] and the kinetic analysis developed by Zhang et al.[14a] As was anticipated, removal of residues from the N termini of the peptides of **1** led to reduced potencies, with the largest losses observed with removal of Ile4 and Leu9, two hydrophobic residues whose importance was also identified from our alanine scanning experiments (Scheme 1).[16] Overall, a 25- and 50-fold loss in potency was observed from truncation of **1** (11 amino acids) to **5** (five amino acids) and **6** (four amino acids), respectively. More significantly, however, truncation to **5** and **6** led to a change in the mechanism of inhibition.

Dimerization inhibitors are easily identified using a Zhang–Poorman plot as they provide lines that are parallel to those for data with protease alone, whereas competitive and noncompetitive inhibitors provide nonparallel lines.[14a] The parent inhibitor (**1**) displayed a parallel line in the Zhang–Poorman plot (Figure 2a), indicating that this compound inhibited the dimerization of HIV-1 protease with a K_i value of 220 nM. Truncation of the parent compound **1** by three residues had no effect on the mechanism of inhibition, as parallel lines were also obtained for the truncated inhibitor **2**. As more residues were truncated from the N termini of the peptides, there was a small shift in the slope of the lines for compounds **3** and **4** (Figure 2b), indicating that inhibition was not occurring through a purely dissociative mechanism. In contrast, larger shifts in the slope were obtained with the smallest inhibitors **5** and **6** (Figure 2c), indicating a change in the mechanism of inhibition. Since compounds **5** and **6** did not inhibit HIV-1 protease through a dissociative mechanism, a double reciprocal plot was used to probe their inhibitory



Scheme 1. Results of truncating the N-terminal residues from the peptides of dimerization inhibitor **1**.

 © WILEY-VCH Verlag GmbH, D-69451 Weinheim, 2000 1433-7851/00/3915-2711 $ 17.50+.50/0

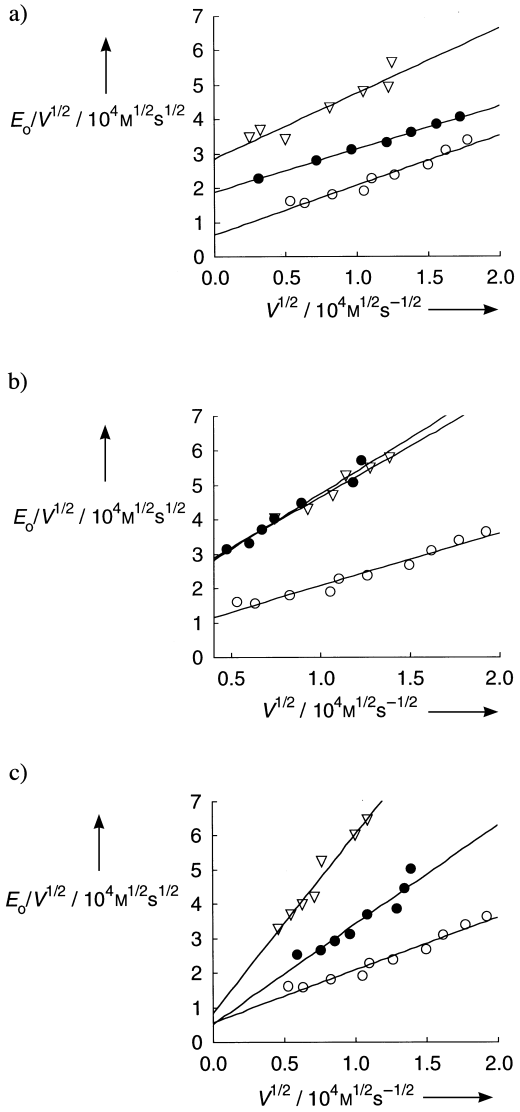
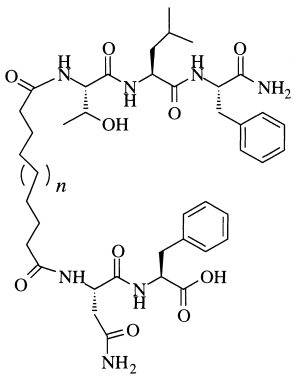


Figure 2. Zhang–Poorman plots[14a] for a) compounds **1** (●, 0.5 μM) and **2** (▽, 3.0 μM) with uninhibited protease (○), b) compounds **3** (●, 2.0 μM) and **4** (▽, 4.0 μM) with uninhibited protease (○), and c) compounds **5** (●, 20 μM) and **6** (▽, 40 μM) with uninhibited protease (○). E_o is the total enzyme concentration, and V is the initial velocity.

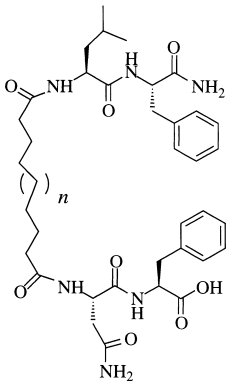
pathway. In both cases linear reciprocal plots were obtained that intersected on the $1/V$ axis, pointing to purely competitive inhibition.

Previous experiments in our laboratory had found that replacing the Trp-OH residue of **1** with Phe-NH_2 led to a threefold increase in HIV-1 protease inhibition.[18] This modification was also incorporated into compounds **5** and **6** in an attempt to increase potency (**7d** and **8d**, respectively). With both compounds this change led to approximately a twofold increase in inhibition (Table 1). A Zhang–Poorman plot was again used to probe the mechanism of inhibition by **7d** and **8d**. In this case parallel lines were obtained with compound **7d**, indicating dissociative inhibition ($K_i = 3.0 \pm 0.1$ μM), whereas nonparallel, intersecting lines were obtained with compound **8d**, indicating that inhibition did not occur by disruption of the dimerization of HIV-1 protease. A double reciprocal plot was used to determine the mechanism of

Table 1. HIV-1 protease inhibition with modified inhibitors.



7a-e (n=3, 6-9)



8a-e (n=3, 6-9)

Compound	Tether length[a]	IC_{50} [μM]
7a	9	54 ± 4
7b	12	28 ± 2
7c	13	9.7 ± 0.3
7d	**14**	**5.9 ± 0.5**
7e	15	5.0 ± 0.8
8a	9	101 ± 5
8b	12	18 ± 2
8c	13	14.1 ± 1.5
8d	**14**	**11 ± 1**
8e	15	8.2 ± 1.4

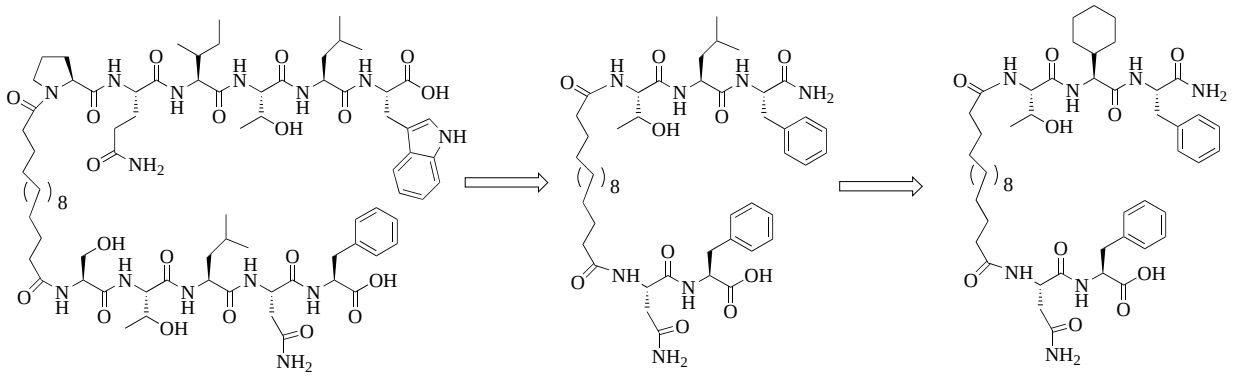
[a] Number of (CH_2) units.

protease inhibition by **8d**, and the compound was found to act as a competitive inhibitor as had been found for its analogue **6**.

The optimum tether length for inhibitor **1** was found to be 14 methylene units,[3] and further studies pointed to a potential binding interaction between the hydrophobic tether of **1** and a hydrophobic cleft formed by Phe99 and Leu97 in the interfacial region of a protease monomer.[19] While amino acid residues were removed from the N termini of compound **1**, the $(CH_2)_{14}$ tether was maintained since molecular modeling predicted that the distance to be spanned between the amino termini of the peptides in **1** and **5**, for instance, was fairly constant (9.3 Å and 9.8 Å, respectively). To test this prediction, the optimum tether length for compounds **7** and **8** was evaluated (Table 1). In both cases, decreasing the tether length to nine methylene units (**7a** and **8a**), a length that molecular modeling predicted to be too short for the two peptides to bind within the β sheet dimerization interface, led to approximately a tenfold decrease in inhibitor potency as compared to the $(CH_2)_{14}$ tether (**7d** and **8d**). Increasing the tether length to 12–15 methylene units (**7b–e**, **8b–e**) resulted in increased inhibition, although in both cases the $(CH_2)_{12}$ tether had the lowest activity, as had been observed with compound **1**.[3]

Calorimetric experiments with HIV-1 protease previously identified the four residues that contribute the most to the stability of the protease dimer: Phe99, Asn98, Leu5, and Leu97.[11] Interestingly, three of these residues occur in the smallest dimerization inhibitor identified in this study, **7d** (Phe5, Asn4, and Leu2). The current truncation strategy,

 © WILEY-VCH Verlag GmbH, D-69451 Weinheim, 2000 1433-7851/00/3915-2712 $ 17.50+.50/0 *Angew. Chem. Int. Ed.* **2000**, *39*, No. 15



1 K_i = 220 ± 10 nM (MW=1586) **7d** K_i = 3000 ± 120 nM (MW=907) **9** K_i = 310 ± 4 nM (MW=933)

Scheme 2. The development of small-molecule dimerization inhibitors of HIV-1 protease derived from the cross-linked interfacial peptide inhibitor **1**.

therefore, has identified the minimal structure (**7d**) that maintains the essential features of dimerization inhibition, and this information correlates well with known stability data with HIV-1 protease. Using **7d** as a starting structure for molecular modeling with HIV-1 protease, we identified a compound (**9**) that was predicted to have increased interactions with HIV-1 protease within the binding pocket normally occupied by the isobutyl group of Leu2 (Scheme 2). The Zhang–Poorman analysis confirmed that **9** inhibited HIV-1 protease through a dissociative mechanism with a K_i value of 310 ± 4 nM ($IC_{50} = 680 \pm 10$ nM). Interestingly, compound **9** was an order of magnitude more potent than its precursor, **7d**, and was only 1.4-fold less potent than the full-length inhibitor, **1**, the compound that was the starting point for the truncation study. These data, therefore, confirm that the core structure, **7d**, is an ideal starting point for our efforts at identifying more potent agents through a focused library approach. The β sheet motif is also commonly found at dimerization interfaces, and the inhibition strategy developed with HIV-1 protease could be extended to a wide range of dimeric protein systems.

Experimental Section

Enzyme assay: For standard inhibition determination, 50 μL of HIV-1 protease (50 nM in buffer A)[3] was incubated with 10 μL of the inhibitor solution in DMSO for 1 h. The solution was added to 40 μL of the substrate[17] solution (buffer A with 10% DMSO) to yield a final substrate concentration of 60 μM. The final concentration of DMSO was kept constant at 14%. The change in fluorescence at 430 nm ($\lambda_{ex} = 360$ nm) was monitored at 30 °C. For the determination of K_i values, all parameters were identical with the following exceptions: enzyme concentrations ranged from 5 to 160 nM and the final substrate concentration was kept constant at 25 μM. For the determination of K_m and V_{max}, the substrate concentration ranged from 5 to 200 μM and the final enzyme concentration was kept constant at 25 nM. All experiments were performed in triplicate.

Received: February 17, 2000 [Z14722]

[1] a) W. Stites, *Chem. Rev.* **1997**, *97*, 1233; b) S. Jones, J. M. Thornton, *Prog. Biophys. Mol. Biol.* **1995**, *63*, 31.

[2] R. Zutshi, M. Brickner, J. Chmielewski, *Curr. Opin. Chem. Biol.* **1998**, *2*, 620.

[3] R. Zutshi, J. Franciskovich, M. Shultz, B. Schweitzer, P. Bishop, M. Wilson, J. Chmielewski, *J. Am. Chem. Soc.* **1997**, *119*, 4841.

[4] a) D. W. Norbeck, D. J. Kempf, *Annu. Rep. Med. Chem.* **1991**, *26*, 141; b) R. A. Chrusciel, K. R. Romines, *Expert Opin. Ther. Pat.* **1997**, *7*, 111; c) A. Wlodawer, J. Vondrasek, *Ann. Rev. Biophys. Biomol. Struct.* **1998**, *27*, 249.

[5] D. R. Kaul, S. K. Cinti, P. L. Carver, P. H. Kazanjian, *Pharmacotherapy* **1999**, *19*, 281.

[6] S. G. Deeks, M. Smith, M. Holodniy, J. O. Kahn, *Am. Med. Assoc.* **1997**, *227*, 145.

[7] A. Carr, K. Samaras, D. J. Chisholm, D. A. Cooper, *Lancet* **1998**, *352*, 1881.

[8] K. D. Miller, E. Jones, J. A. Yanovski, R. Shankar, I. Feuerstein, J. Falloon, *Lancet* **1998**, *351*, 871.

[9] I. Herry, L. Bernard, P. de Truchis, C. Perronne, *Clin. Infect. Dis.* **1997**, *25*, 937.

[10] A. Wlodawer, A. Miller, M. Jaskolski, B. Sathyanarayana, E. Baldwin, I. Weber, L. Selk, L. Clawson, J. Schneider, S. Kent, *Science* **1989**, *245*, 616.

[11] M. J. Todd, N. Semo, E. Freire, *J. Mol. Biol.* **1998**, *283*, 475.

[12] A. Gustchina, I. T. Weber, *Proteins Struct. Funct. Genet.* **1991**, *10*, 325.

[13] a) J. R. Rose, L. M. Babe, C. S. Craik, *J. Virology* **1995**, *69*, 2751; b) L. M. Babe, J. R. Rose, C. S. Craik, *Proc. Natl. Acad. Sci. USA* **1995**, *92*, 10069.

[14] a) Z. Zhang, R. Poorman, L. Maggiora, R. Heinrikson, F. Kezdy, *J. Biol. Chem.* **1991**, *266*, 15591; b) H. J. Schramm, H. Nakashima, W. Schramm, H. Wakayama, N. Yamamoto, *Biochem. Biophys. Res. Comm.* **1991**, *179*, 847; c) L. M. Babe, J. Rose, C. S. Craik, *Protein Sci.* **1992**, *1*, 1244; d) J. Franciskovich, K. Houseman, R. Mueller, J. Chmielewski, *Bioorg. Med. Chem. Lett.* **1993**, *3*, 739; e) H. Schramm, A. Billich, E. Jaeger, K. Rucknagel, G. Arnold, W. Schramm, *Biochem. Biophys. Res. Commun.* **1993**, *194*, 595; f) H. J. Schramm, J. Boetzel, J. Buttner. E. Fritsche, W. Gohring, E. Jaeger, S. Konig, O. Thumfart, T. Wenger, N. E. Nagel, W. Schramm, *Antiviral Res.* **1996**, *30*, 155.

[15] X. Fan, G. R. Flentke, D. H. Rich, *J. Am. Chem. Soc.* **1998**, *120*, 8893.

[16] M. Shultz, J. Chmielewski, *Bioorg. Med. Chem. Lett.* **1999**, *9*, 2431.

[17] M. V. Toth, G. R. Marshall, *Int. J. Pept. Protein Res.* **1990**, *36*, 544.

[18] R. Zutshi, M. Shultz, L. Ulysse, R. Lutgring, P. Bishop, B. Schweitzer, K. Vogel, J. Franciskovich, M. Wilson, J. Chmielewski, *Synlett* **1998**, 1040.

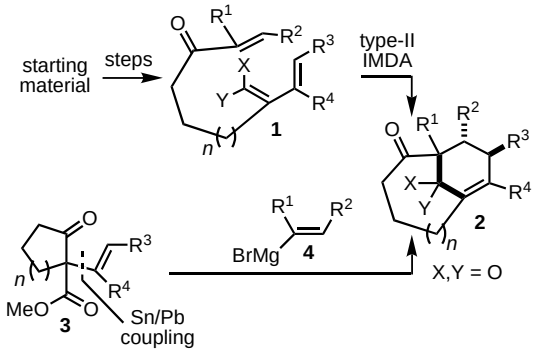
[19] M. Shultz, J. Chmielewski, *Tetrahedron: Asymmetry* **1997**, *8*, 3881.

 © WILEY-VCH Verlag GmbH, D-69451 Weinheim, 2000 1433-7851/00/3915-2713 $ 17.50+.50/0

A Highly Efficient and Convergent Reaction for the Synthesis of Bridgehead Enone-Containing Polycyclic Ring Systems**

Scott M. Sheehan, Gojko Lalic, Jason S. Chen, and Matthew D. Shair*

The development of reactions that efficiently generate complex polycyclic molecules from easily accessible starting materials continues to be an important endeavor in organic synthesis. Bridged ring structures represented by **2**[1] (Scheme 1) constitute a particularly challenging system to construct in a short number of steps. One method of assembling ring structures related to **2** is the type-II intramolecular Diels–Alder (IMDA) reaction[2] (**1** →**2**, Scheme 1), a [4+2] cycloaddition that involves tethering the dienophile to an internal position on the diene.[3]



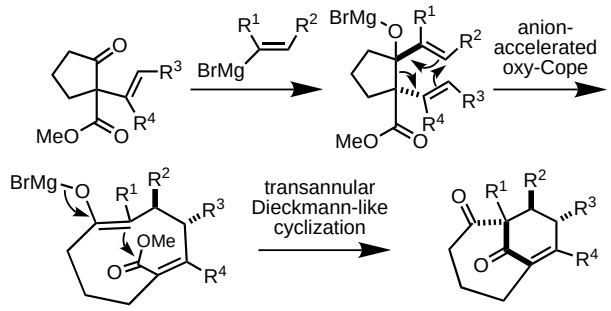
Scheme 1. A comparison of the type-II IMDA and the tandem fragment-coupling/polycyclization approach to olefin-containing bridgehead carbocycles.

Herein multiple examples of a new reaction (**3** + **4** → **2**) that also afforded complex ring systems related to **2** are reported. An attractive feature of this reaction was the ability to combine complex fragments in a stereospecific reaction to give compound **2** directly. Compound **3** was accessed, in most cases, by a convergent Pb^{IV}-promoted coupling reaction between vinylstannanes and cyclic β-ketoesters.[4] The reaction (Scheme 2) that afforded **2** comprised a tandem alkylation, an anion-accelerated oxy-Cope rearrangement,[5] and a transannular Dieckmann-like cyclization. This triple-domino reaction was based upon a transformation we reported earlier that enabled the rapid assembly of the core structure of CP-263,114.[6]

[*] Prof. Dr. M. D. Shair, Dr. S. M. Sheehan, G. Lalic, J. S. Chen
Department of Chemistry & Chemical Biology
Harvard University
12 Oxford St., Cambridge, MA 02138 (USA)
Fax: (+1) 617-496-4591
E-mail: shair@chemistry.harvard.edu

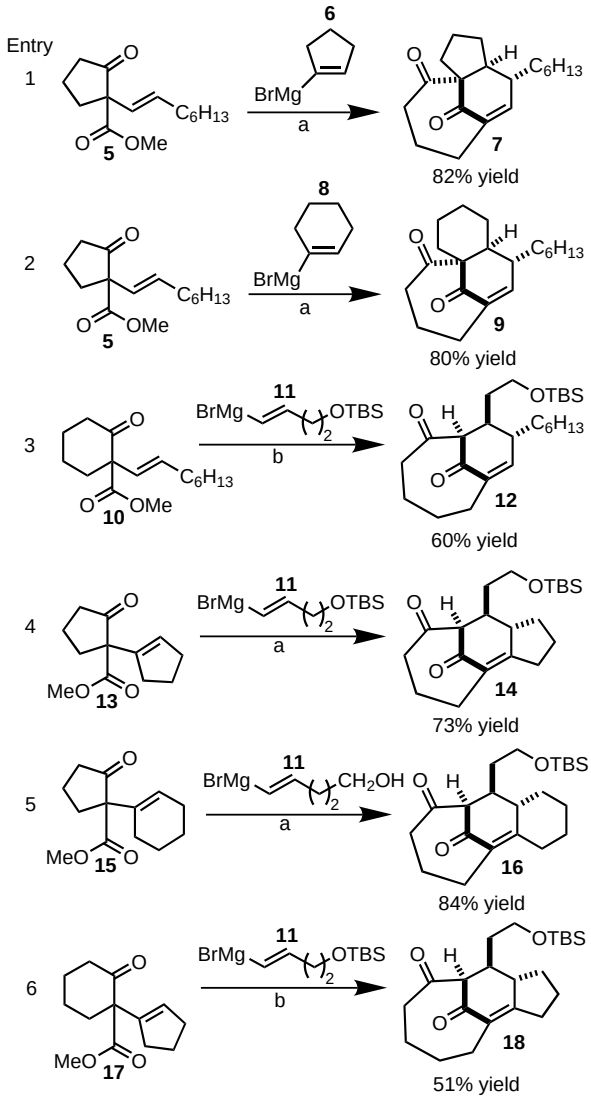
[**] Financial support from the NIH (GM59403–01A1), Bristol-Myers Squibb, Merck Research Laboratories, Pharmacia & Upjohn, Smith-Kline Beecham, the Corning Fund, and the Research Corporation is gratefully acknowledged. G.L. acknowledges Eli Lilly for a graduate fellowship.

Supporting information for this article is available on the WWW under http://www.wiley-vch.de/home/angewandte/ or from the author.



Scheme 2. Mechanism of the tandem reaction.

We began our investigation of the generality of the triple-domino reaction by exploring the synthesis of tricyclic structures using cyclic Grignard reagents (Scheme 3; entries 1 and 2). Exposure of **5** to **6** directly afforded tricycle **7** in 82% yield as a single diastereomer.[7] Treatment of **5** with the



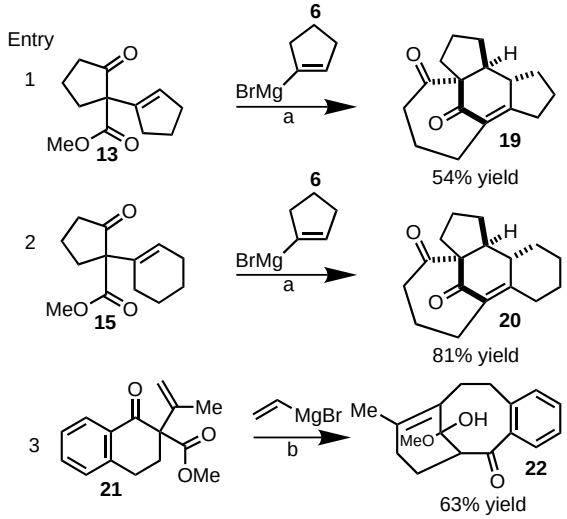
Scheme 3. The tandem fragment-coupling/polycyclization reaction provides a variety of olefin-containing bridgehead polycycles. a) Vinyl Grignard (1.4 equiv), −78 °C, $PhCH_3$/THF (3/1), −78 →25 °C, dilute to 0.01 M, 14 h; b) vinyl Grignard (1.4 equiv), −78 °C, $PhCH_3$/THF (3/1), −78 →60 °C, dilute to 0.01 M, 11 h.

 © WILEY-VCH Verlag GmbH, D-69451 Weinheim, 2000 1433-7851/00/3915-2714 $ 17.50+.50/0

cyclohexene-based nucleophile **8** delivered the 6-6-7 ring system **9** in 80% yield, again as a single diastereomer. To demonstrate that this reaction was not limited to five-membered-ring β-ketoesters, compound **10** (entry 3) was exposed to Grignard reagent **11** and afforded the 8-6 ring system **12** in 60% yield. Compound **12** corresponds to the product of a type-II IMDA reaction which uses a five-atom tether between the diene and dienophile.

The experiments depicted in entries 4–6 of Scheme 3 were performed to explore the result of placing a ring system on the olefin unit of the β-ketoester. The reactions proceeded smoothly in all three cases, to afford tricycles **14** (73% yield), **16** (84% yield), and **18** (51% yield). The 7-6-5 (**14**), 7-6-6 (**16**), and 8-6-5 (**18**) ring systems were produced as single diastereomers in each case.

The successful triple-domino reactions depicted in Scheme 3 that used ring systems on the nucleophile and, in separate experiments, on the electrophile led to the investigation of transformations using ring systems on both reaction partners simultaneously (Scheme 4). Treatment of cyclopentanone **13** with a cyclopentene-based Grignard reagent afforded tetracycle **19**, a 7-6-5-5 ring system, in 54% yield as a single diastereomer. Three contiguous chiral



Scheme 4. Additional complexity is tolerated in the tandem reaction sequence. a) Vinyl Grignard (1.4 equiv), $-78\,^{\circ}C$, $PhCH_3$/THF (3/1), $-78 \rightarrow 25\,^{\circ}C$, dilute to 0.01M, 14 h; b) $MgBr_2$ (1.0 equiv), $-78 \rightarrow -42\,^{\circ}C$, vinylmagnesium bromide (1.4 equiv), $68\,^{\circ}C$, 2 h.

centers, including one quaternary carbon center, were controlled during this transformation. Entry 2 of Table 4 depicts a second example of a tetracycle-forming reaction using a cyclohexyl ring on the electrophile. The 7-6-6-5 tetracycle **20** was formed in 81% yield upon exposure of **15** to a cyclopentene-based Grignard reagent. As a final demonstration of the generality and utility of this reaction, we sought to construct a C-aryl core structure of the taxanes from tetralone-based β-ketoester **21**. Treatment of **21** with vinylmagnesium bromide initiated the triple-domino cyclization, and directly afforded the taxane core structure **22** with an aryl C-ring in 63% yield.[8] Curiously, compound **22** existed as an isolable hemiketal that resisted conversion into the ketone.

In summary, a triple-domino reaction has been developed that affords a wide range of complex polycyclic bridgehead enone-containing molecules. Precursors for the triple-domino reaction were rapidly accessed, with each of the cyclization products provided in at most four steps from commercially available reagents. In essence, the triple-domino reaction is a fragment-coupling reaction combined with a polycyclization reaction. As a result, fragments of comparable complexity can be combined and rearranged, thus offering a highly convergent, flexible, and stereospecific route to diverse polycyclic molecules. This reaction may be useful for rapidly assembling complex naturally occurring structures. In addition, this transformation may be useful in diversity-oriented synthesis where a premium is placed on reactions that greatly increase molecular complexity while simultaneously accessing a diverse set of complex molecules.[9] Our efforts to use this reaction for target-oriented and diversity-oriented synthesis will be reported shortly.

Received: April 12, 2000 [Z14980]

[1] Naturally occurring molecules that contain this ring system include: a) CP-263,114 and CP-225,917: T. T. Dabrah, H. L. Harwood, L. G. Huang, N. D. Jankovich, T. Kaneko, J.-C. Li, S. Lindsey, P. M. Moshier, T. A. Subashi, M. Therrien, P. C. Watts, *Antibiotics* **1997**, *50*, 1; T. T. Dabrah, T. Kaneko, W. Massefski, Jr., E. B. Whipple, *J. Am. Chem. Soc.* **1997**, *119*, 1594; b) taxol and taxus terpenes: M. C. Wani, M. E. Taylor, P. Coggon, A. T. McPhail, *J. Am. Chem. Soc.* **1971**, *93*, 2325; c) welwitindolinone: K. Stratmann, D. L. Burgoyne, R. E. Moore, G. M. L. Patterson, *J. Org. Chem.* **1994**, *59*, 7219; K. Stratmann, R. E. Moore, R. Bonjouklian, J. B. Deeter, G. M. L. Patterson, S. Shaffer, C. D. Smith, T. A. Smitka, *J. Am. Chem. Soc.* **1994**, *116*, 9935.

[2] For a review of the intramolecular Diels–Alder reaction, see W. R. Roush in *Comprehensive Organic Synthesis*, *Vol. 5* (Eds.: B. M. Trost, I. Fleming, L. A. Paquette), Pergamon, Oxford, **1991**, p. 513.

[3] a) K. J. Shea, P. D. Davis, *Angew. Chem.* **1983**, *95*, 422; *Angew. Chem. Int. Ed. Engl.* **1983**, *223*, 419; b) K. J. Shea, J. W. Gilman, C. D. Haffner, T. K. Dougherty, *J. Am. Chem. Soc.* **1986**, *108*, 4953; c) K. J. Shea, C. D. Haffner, *Tetrahedron Lett.* **1988**, *29*, 1367; d) K. J. Shea, S. T. Sakata, *Tetrahedron Lett.* **1992**, *33*, 4264; e) R. W. Jackson, R. G. Higby, J. W. Gilman, K. J. Shea, *Tetrahedron* **1992**, *48*, 7013; f) R. W. Jackson, K. J. Shea, *Tetrahedron Lett.* **1994**, *35*, 1317; g) K. J. Shea, C. D. Haffner, *Tetrahedron Lett.* **1998**, *29*, 1367.

[4] a) M. G. Moloney, J. T. Pinhey, M. J. Stoermer, *J. Chem. Soc. Perkin Trans. 1* **1990**, 2645; b) C. J. Parkinson, J. T. Pinhey, M. J. Stoermer, *J. Chem. Soc. Perkin Trans. 1* **1992**, 1911.

[5] D. A. Evans, A. M. Golob, *J. Am. Chem. Soc.* **1975**, *97*, 4765.

[6] C. Chen, M. E. Layton, M. D. Shair, *J. Am. Chem. Soc.* **1998**, *120*, 10784.

[7] Each of the new compounds reported in this article was fully characterized, see the Supporting Information for details.

[8] For the synthesis of taxanes with aryl C-rings, see a) K. C. Nicolaou, W. M. Dai, R. K. Guy, *Angew. Chem.* **1994**, *106*, 15; *Angew. Chem. Int. Ed. Engl.* **1994**, *33*, 15, and references therein; b) W. B. Young, J. J. Masters, S. Danishefsky, *J. Am. Chem. Soc.* **1995**, *117*, 5228; c) K. C. Nicolaou, C. G. Claiborne, K. Paulvannan, M. A. D. Postema, R. K. Guy, *Chem. Eur. J.* **1997**, *3*, 399; d) A. G. Fallis, *Acc. Chem Res.* **1999**, *32*, 464; e) see also ref. [3].

[9] For an article discussing diversity-oriented synthesis, see S. L. Schreiber, *Science* **2000**, *287*, 1964.

 © WILEY-VCH Verlag GmbH, D-69451 Weinheim, 2000 1433-7851/00/3915-2715 $ 17.50+.50/0

Hydrogen-Bonded Molecular Ribbons as Templates for the Synthesis of Modified Mineral Phases**

Simon Champ, John A. Dickinson, Philip S. Fallon, Brigid R. Heywood,* and Mark Mascal*

The remarkable structural diversity and mechanical strength of mineral phases associated with living organisms ("biominerals") has prompted substantial effort towards synthetically reproducing the conditions under which such materials are created.[1] Since it is known that this involves the participation of biomacromolecules as templates, a number of ingenious means of presenting an organized array of polar functions to a crystallization medium have been developed, such as nucleation at the surfaces of proteins and glycoproteins,[2] bacterial filaments,[3] micelles,[4] vesicles,[5] polymers,[6] organic crystal faces,[7] inorganic particles[8] and monolayers at the air–water interface,[9] on gold,[10] or on silicon substrates.[11] Crystal growth has also been examined in structured three-dimensional media such as microemulsions,[12] foam lamellae,[13] and reverse micelles.[14] All of these approaches have resulted in the production of ionic solids in which some degree of control over size, morphology, texture, crystallographic orientation, and/or polymorph selection has been exercised. Since the principle in operation is one of epitaxial correspondence between the mineral lattice and the template, the better the design of the template in terms of spatial definition, the greater the likelihood of developing a working model for the targeted synthesis of a specific crystalline phase.

The prospect therefore of combining two well-established organizational principles, that is surfactant monolayer assembly with that of the hydrogen bonding "molecular ribbon",[15] and their application to biomimetic crystal synthesis, was an attractive one. The overall concept is well supported in literature precedent, both in the preparation of hydrogen-bonding aggregates at the air–water interface,[16] and in the ability of Langmuir monolayers to influence crystal growth.[9] The experiment consists of the following: A monolayer is cast at the air–water interface from the amphiphile *N*,*N*′-dioctadecyltriazine-2,4,6-triamine (**1**)[17] whose polar headgroup doubles as a constituent of the molecular ribbon. Its counterpart, cyanuric acid derivative **2**,[18] is dissolved in the aqueous subphase and binds to the monolayer by hydrogen-bonding recognition. The resulting assembly has the organizational characteristics shown in Figure 1. Compound **2** possesses a tailgroup R terminated by an ionophoric functionality (carboxy, amino, or phosphate group), and is represented by the unshaded pips in the view normal to the surface (Figure 1, top). The shaded pips are the surfactant component **1**. The spatial interval between like components along the hydrogen-bonded ribbon axis is fixed at 9.5 Å.[15] In the second dimension however, individual ribbons associate at the van der Waals separation of about 4.5 Å, governed by the closest approach of the hydrocarbon chains to each other.[19] The intercomponent distance here is more flexible due to the absence of strong interactions in this dimension, and can vary from the minimum of 4.5 Å (at superimposition of the headgroups) to a maximum of 6.5 Å (where like components are completely "out-of-phase" with each other).

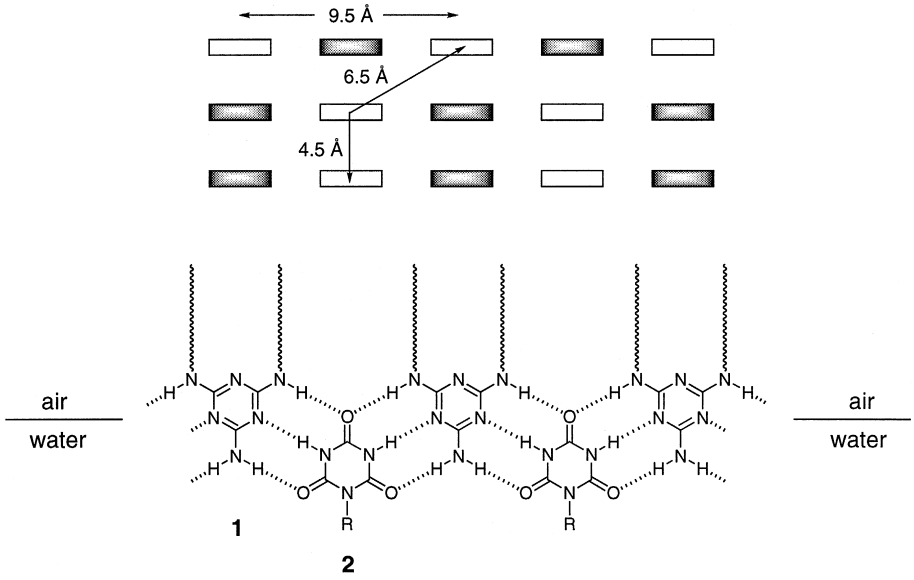


Figure 1. Representations of the melamine–cyanuric acid monolayer normal (top) and parallel (bottom) to the air–water interface. R = $CH_2CH_2CO_2H$, $CH_2CH_2CH_2OPO_3H_2$, $CH_2CH_2CH_2NH_2$.

An in-depth analysis of the structure of hydrogen-bonding molecular ribbons at the air–water interface was recently published by Kunitake et al.,[20] in which it was demonstrated that components related to **1** and **2** self-associate in a 1:1 ratio to form stable, well-defined monolayer assemblies. For this reason, discussion of the physical properties of our monolayer and the synthesis of the template components is deferred until the work is presented in full.[21]

The ensembles of polar functionalities produced by the association of **1** and **2** have been evaluated for their effect on the nucleation of calcium carbonate, the preliminary results of

[*] Dr. M. Mascal, J. A. Dickinson, P. S. Fallon
Department of Chemistry
University of Nottingham
Nottingham NG7 2RD (UK)
Fax: (+44) 115-951-3564
E-mail: mark.mascal@nottingham.ac.uk
Dr. B. R. Heywood,[+] S. Champ
Department of Chemistry and Applied Chemistry
University of Salford
Salford M5 4WT (UK)
E-mail: cha42@chem.keele.ac.uk
[+] Present address:
School of Chemistry and Physics
Keele University, Keele, ST5 5BG (UK)
Fax: (+44) 1782-583-508

[**] This work was supported by the ICI Strategic Research Fund, the EPSRC, and the Wellcome Trust.

 © WILEY-VCH Verlag GmbH, D-69451 Weinheim, 2000 1433-7851/00/3915-2716 $ 17.50+.50/0

Table 1. Data for nucleation experiments.[a]

Tailgroup (R) in **2**	Molar ratio **1**:**2**[b] ([**2**])	$CaCO_3$ polymorph[c]	Orientation[d]	Mean size [μm ± s.d]	Nucleation density [crystals mm^{-2}]	Induction time
control	–	calcite	dendritic, intergrown {10.4} rhombs	30 (10)	> 300	> 4 h
$(CH_2)_3OH$	up to 1:10000 (20.6 mM)	calcite	discrete, nonoriented {10.4} rhombs	68 (24)	20	3 h
$(CH_2)_2CO_2H$	1:750 (1.55 mM)	calcite	< 01.2 >	79 (23)	12	< 1 h
$(CH_2)_3OPO_3H_2$	1:500 (1.03 mM)	calcite	[001]	59 (15)	17	< 1 h
$(CH_2)_3NH_3^+Cl^-$	1:1000 (2.06 mM)	vaterite	< 11.0 > and [001]	204 (45)	2	< 1 h

[a] Standard calcium hydrogen carbonate solution prepared as described by Kitano (Y. Kitano, *Bull. Chem. Soc. Jpn.* **1962**, *35*, 1980); $T = 20\,^\circ C$; pH 6.5. [b] Minimum ratio necessary to provide a sufficient concentration of the soluble component in bulk solution to promote nucleation within the stated induction time. Higher ratios had little advantageous effect. Crystallization in the presence of the stated concentrations of **2** without **1** resemble the control study. [c] By powder X-ray diffraction. [d] Crystallographic orientation at the monolayer/subphase interface.

which are presented in Table 1. Thus, when an assembly incorporating the soluble component **2** with R = $CH_2CH_2CO_2H$ is organized at the surface of a supersaturated aqueous calcium hydrogen carbonate solution, oriented nucleation of habit-modified calcite is observed. The crystals are distinguished by the occurrence of a single triangular facet truncating the vertex of three intersecting {10.4} faces (Figure 2b). This unique face was resolved to be of the negative rhomohedral {01.2} form and its development here indicates that nucleation occurred through this lattice plane.[22] This contrasts with previous work in which monolayers of long-chain carboxylate surfactants induced the orientation of calcite on the < 10.0 > axis.[23] The climax morphology of the mature crystals arises from the development of the stable {10.4} faces as the < 01.2 > oriented crystallites grow along the [001], < 11.0 >, and < 10.0 > axes.

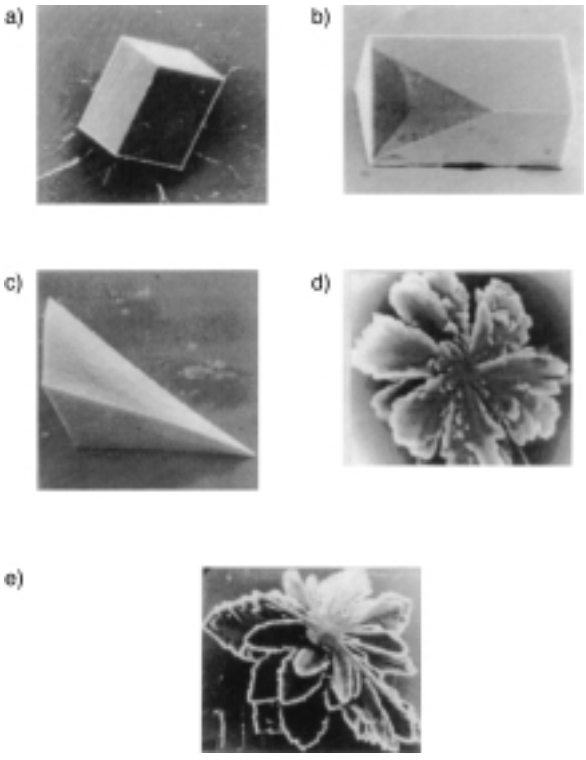


Figure 2. a) Calcite control crystal, 1 cm = 5 μm; b) {01.2}-oriented calcite grown under monolayer **1**·**2** (R = $CH_2CH_2CO_2H$), 1 cm = 5 μm; c) [001]-oriented calcite grown under monolayer **1**·**2** (R = $CH_2CH_2CH_2OPO_3H_2$), 1 cm = 15 μm; d) [001]-oriented vaterite and e) < 11.0 > oriented vaterite, both grown under monolayer **1**·**2** (R = $CH_2CH_2CH_2NH_3^+Cl^-$), 1 cm = 25 μm.

As predicted, the crystallographic orientation and morphology could be altered by employing a solution component **2** with a different tailgroup. In the case where R = $CH_2CH_2CH_2OPO_3H_2$, calcite nucleation in [001] orientation was favored. Pyramidal evolution from a triangular (001) basal face was observed, terminating at an apex formed by the intersection of three {10.4} faces (Figure 2c).

In both of the above examples, the achievement of oriented nucleation can be rationalized by invoking a stereochemical correspondence between the monolayer template and the relevant crystal face. In the case of < 01.2 >-oriented calcite, the carboxylate functions of the template coincide with lattice positions occupied by carbonate groups. Unlike the {10.4} face, which is neutral, calcite < 01.2 > consists of segregated layers of calcium and carbonate ions. The stabilization of this high-energy, homoatomic face is proposed to be the result of charge neutralization coupled with ligand binding of the calcium by the carboxylate group of **2** (R = $CH_2CH_2CO_2H$), with the 5.0×9.8 Å 75/105° rhomboidal carbonate array in calcite (Figure 3a) commensurate with a 4.7×9.5 Å 75/105° template assembly. The question arises as to why the {01.2} face is selected in preference to the other homoatomic facets, the (001), in which an appropriate lattice match also exists (vide infra). Here, however, the full effect of stereochemical homology between the mineral lattice and the template is realized: The carbonate anions are tilted by about 64° out of the crystal plane in {01.2}, whereas they lie parallel to the (001) face. This means that the carboxylate tailgroups of **2**, with their twofold axes approximately perpendicular to the aqueous surface due to the conformational requirements of the chain, are a much closer steric match to the {01.2} calcite face.[24]

In the case of the (001)-oriented calcite, four in-plane carbonate anions occupy the corners of a 60/120° rhomboid of dimensions 5.0×10.0 Å (Figure 3b) in the unique (001) face. A mimetic register of phosphate groups with their C_3 axes also aligned to [001] is presented by **2** (R = $CH_2CH_2CH_2OPO_3H_2$) which displays closely matching dimensions (5.2×9.5 Å). This favors nucleation on (001) and rapid growth along the

 © WILEY-VCH Verlag GmbH, D-69451 Weinheim, 2000 1433-7851/00/3915-2717 $ 17.50+.50/0

a)

b)

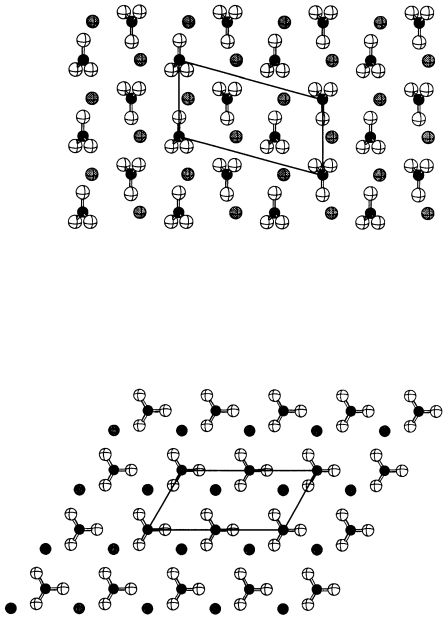


Figure 3. a) View of calcite normal to the (012) face; b) view of calcite normal to the (001) face.

[001] and <11.0> directions which determines the evolution of the unique pyramidal morphology.[25]

The use of a soluble molecular ribbon component incorporating an amine functionality ($R = CH_2CH_2CH_2NH_2$) resulted in the observation of the metastable $CaCO_3$ polymorph, vaterite. Morphological analysis revealed two distinct crystal populations; one group oriented on the [001] axis (Figure 2d) and the other aligned with the <11.0> axis perpendicular to the template (Figure 2e). The proportion of <11.0>-oriented crystals was significantly greater than the [001]-oriented form (<11.0>:[001] = 18:1). In this case, it is more appropriate to reserve comment on the reasons for the selection of this polymorph, since no definitive crystal structure of vaterite exists.[26] However, vaterite crystals displaying these distinct morphologies and specific orientations have been reported in earlier related work with simple amine surfactant monolayers (e.g. octadecylamine).[23]

On the basis of these results it can be assumed that the failure of the soluble component terminated by a hydroxy group (**2**, $R = CH_2CH_2CH_2OH$) to influence the growth of calcium carbonate relates in the first instance to its neutrality under the conditions of the assay, and second to the absence of any meaningful congruity with the ionic lattice.

Thus we have been able to demonstrate a transfer of information from a self-organized surface assembly to the nascent inorganic phase which develops from the crystallization medium. Hydrogen bonding and the hydrophobic effect work together to produce a hybrid assembly in which noncovalent aggregates pack into a monolayer at the air–water interface, directing an array of potential nucleating functions into the aqueous subphase. The basic concept is firmly grounded in work by Kunitake, Ringsdorf, and coworkers,[16] and the combination of order and mobility in this system is highly relevant to its application as a "biomimetic" mineral template.

Most importantly, the morphology and crystallographic orientation of the resulting inorganic solid can be modeled against a reciprocal geometric and functional register in the template, indicating that a systematic approach to the targeted production of specific crystalline phases can be developed. The advantages of the system described here over standard amphiphile monolayers are the following: First, systematic variation of the chemical identity of the ionophoric functions of the template is a simple matter of altering the tailgroup of the solution component **2**, without regard to whether such functionality at the end of a hydrocarbon chain would be capable of producing a stable monolayer. Second, the spatial distribution of ionophores in the monolayer is unique and more flexible than the hexagonal closest-packed arrangement of simple monolayers. Finally, the **1**·**2** monolayer does not require external compression to function as a template for crystal nucleation, whereas surfactant monolayers often do. This allows the practical extension of template-mediated crystallization to a wider range of media and removes the requirement for a dedicated Langmuir trough.

With these principles now established, there is clearly scope for modification of the above system. Most simply, the ionophoric functionality of component **2** can be further varied, as can the length of the hydrocarbon spacer between the functionality and the headgroup and/or the inorganic phase under investigation, giving new mineral–template conjugates whose analysis will also contribute to resolving the fundamentals of targeted crystal synthesis. Perhaps most interestingly, it has been shown that mixed cyanuric acid/melamine lipid systems related to **1** and **2** self-organize into disklike aggregates formed from bilayers of hydrogen-bonding ribbons,[27] leaving open the potential for extending this work into a third dimension.

Received: February 4, 2000 [Z14653]

[1] This area is replete with insightful reviews and monographs: a) S. Mann, *J. Chem. Soc. Dalton Trans.* **1997**, 3953; b) S. Mann, S. L. Burkett, S. A. Davis, C. E. Fowler, N. H. Mendelson, S. D. Sims, D. Walsh, N. T. Whilton, *Chem. Mater.* **1997**, *9*, 2300; c) S. Weiner, L. Addadi, *J. Mater. Chem.* **1997**, *7*, 689; d) *Biomimetic Materials Chemistry* (Ed.: S. Mann), VCH, Weinheim, **1996**; e) S. Mann in *Comprehensive Supramolecular Chemistry*, *Vol. 9* (Eds.: J. L. Atwood, J. E. D. Davies, D. D. MacNicol, F. Vögtle, J.-M. Lehn, J. P. Sauvage, M. W. Hosseini), Pergamon, Oxford, **1996**, pp. 529–564; f) S. Mann, G. A. Ozin, *Nature* **1996**, *382*, 313; g) B. C. Bunker, P. C. Rieke, B. J. Tarasevich, A. A. Campbell, G. E. Fryxell, G. L. Graff, L. Song, J. Liu, J. W. Virden, G. L. McVay, *Science* **1994**, *264*, 48; h) A. H. Heuer, D. J. Fink, V. J. Laraia, J. L. Arias, P. D. Calvert, K. Kendall, G. L. Messing, J. Blackwell, P. C. Rieke, D. H. Thompson, A. P. Wheeler, A. Veis, A. I. Caplan, *Science* **1992**, *255*, 1098; i) H. A. Lowenstam, S. Weiner, *On Biomineralization*, Oxford University Press, Oxford, **1989**.

[2] a) J. Aizenberg, J. Hanson, T. F. Koetzle, L. Addadi, *J. Am. Chem. Soc.* **1997**, *119*, 881; b) G. Falini, S. Fermani, M. Gazzano, A. Ripamonti, *Chem. Eur. J.* **1997**, *3*, 1807; c) R. Kniep, S. Busch, *Angew. Chem.* **1996**, *108*, 2787; *Angew. Chem. Int. Ed. Engl.* **1996**, *35*, 2624; d) G. Falini, S. Albeck, S. Weiner, L. Addadi, *Science* **1996**, *271*, 67.

[3] S. A. Davis, S. L. Burkett, N. H. Mendelson, S. Mann, *Nature* **1997**, *385*, 420.

[4] a) G. S. Attard, M. Edgar, C. G. Göltner, *Acta Mater.* **1998**, *46*, 751; b) P. V. Braun, P. Osenar, S. I. Stupp, *Nature* **1996**, *380*, 325; c) I. A.

 © WILEY-VCH Verlag GmbH, D-69451 Weinheim, 2000 1433-7851/00/3915-2718 $ 17.50+.50/0

Aksay, M. Trau, S. Manne, I. Honma, N. Yao, L. Zhou, P. Fenter, P. M. Eisenberger, S. M. Gruner, *Science* **1996**, *273*, 892; d) P. Behrens, *Angew. Chem.* **1996**, *108*, 561; *Angew. Chem. Int. Ed. Engl.* **1996**, *35*, 515.
[5] G. A. Ozin, *Acc. Chem. Res.* **1997**, *30*, 17.
[6] a) K. Schwarz, M. Epple, *Chem. Eur. J.* **1998**, *4*, 1898; b) H. Cölfen, M. Antonietti, *Langmuir* **1998**, *14*, 582; c) R. L. Reis, A. M. Cunha, M. H. Fernandes, R. N. Correia, *J. Mater. Sci. Mater. Med.* **1997**, *8*, 897; d) P. Calvert, P. Rieke, *Chem. Mater.* **1996**, *8*, 1715; e) J. Lin, E. Cates, P. Bianconi, *J. Am. Chem. Soc.* **1994**, *116*, 4738; f) A. Berman, D. J. Ahn, A. Lio, M. Salmeron, A. Reichert, D. Charych, *Science* **1995**, *269*, 515.
[7] S. J. Bonafede, M. D. Ward, *J. Am. Chem. Soc.* **1995**, *117*, 7853.
[8] I. ul Haq, E. Matijevic, K. Akhtar, *Chem. Mater.* **1997**, *9*, 2659, and references therein.
[9] a) A. L. Litvin, S. Valiyaveettil, D. L. Kaplan, S. Mann, *Adv. Mater.* **1997**, *9*, 124; b) J. Lahiri, G. Xu, D. M. Dabbs, N. Yao, I. A. Aksay, J. T. Groves, *J. Am. Chem. Soc.* **1997**, *119*, 5449; c) R. Tang, C. Jiang, Z. Tai, *J. Chem. Soc. Dalton Trans.* **1997**, 4037; d) B. R. Heywood, S. Mann, *Adv. Mater.* **1994**, *6*, 9.
[10] a) J. Aizenberg, A. J. Black, G. M. Whitesides, *J. Am. Chem. Soc.* **1999**, *121*, 4500; b) J. Küther, R. Seshadri, W. Tremel, *Angew. Chem.* **1998**, *110*, 3196; *Angew. Chem. Int. Ed.* **1998**, *37*, 3044; c) J. Küther, R. Seshadri, W. Knoll, W. Tremel, *J. Mater. Chem.* **1998**, *8*, 641; d) D. B. Wurm, S. T. Brittain, Y.-T. Kim, *J. Mater. Sci. Lett.* **1996**, *15*, 1285.
[11] B. J. Tarasevich, P. C. Rieke, J. Liu, *Chem. Mater.* **1996**, *8*, 292.
[12] D. Walsh, J. D. Hopwood, S. Mann, *Science* **1994**, *264*, 1576.
[13] B.-D. Chen, J. J. Cilliers, R. J. Davey, J. Garside, E. T. Woodburn, *J. Am. Chem. Soc.* **1998**, *120*, 1625.
[14] P. K. Dutta, M. Jakupca, K. S. N. Reddy, L. Salvati, *Nature* **1995**, *374*, 44.
[15] a) J.-M. Lehn, M. Mascal, A. DeCian, J. Fischer, *J. Chem. Soc. Chem. Commun.* **1990**, 479; b) J. A. Zerkowski, C. T. Seto, D. A. Wierda, G. M. Whitesides, *J. Am. Chem. Soc.* **1990**, *112*, 9025.
[16] a) K. Kurihara, K. Ohto, Y. Honda, T. Kunitake, *J. Am. Chem. Soc.* **1991**, *113*, 5077; b) R. Ahuja, P.-L. Caruso, D. Möbius, W. Paulus, H. Ringsdorf, G. Wildburg, *Angew. Chem.* **1993**, *105*, 1082; *Angew. Chem. Int. Ed. Engl.* **1993**, *32*, 1033.
[17] W. Zerweck, K. Keller (I.G. Farbenindustrie), US-A 2228161, **1938** [*Chem. Abstr.* **1941**, *35*, P2531].
[18] These were prepared by adaptations of known methods: D. A. Dunnigan, W. J. Close, *J. Am. Chem. Soc.* **1953**, *75*, 3615; W. J. Close, *J. Am. Chem. Soc*. **1953**, *75*, 3617.
[19] The mean $CH_2 \cdots CH_2$ distance in adjacent chains of solid octadecanoic acid is 4.2 Å: CSD refcode STARAC05, The Cambridge Structural Database, F. H. Allen, O. Kennard, *Chemical Design Automation News* **1993**, *8*, 3. Note that Kunitake et al. propose a distance of 5 Å for the inter-ribbon contact.[20]
[20] H. Koyano, P. Bissel, K. Yoshihara, K. Ariga, T. Kunitake, *Chem. Eur. J.* **1997**, *3*, 1077.
[21] In the present work, studies of ribbon assembly at the air–water interface and on a range of subphases reflecting the composition of the crystallization media confirm the auto-assembly of a robust monolayer with a structure commensurate with the model presented in Figure 1.
[22] The preferred orientation of the inorganic particles was confirmed by an analysis of the crystallographic ultrastructure of immature crystallites harvested 60 min after the induction of template assembly using established techniques for the collection and analysis of crystals which mitigate against any disruption of their alignment relative to the template.[23] In the present case, all crystals produced single-crystal electron diffraction patterns corresponding to the $<01.2>$ zone of calcite, thereby confirming the morphological assignment.
[23] B. R. Heywood, S. Rajam, S. Mann, *J. Chem. Soc. Faraday Trans.* **1991**, *87*, 735.
[24] Interestingly, preferential orientation of calcite on the {01.2} face has been reported for other self-assembled systems.[6f, 10a] The collective results suggest that while homologous geometric packing is important, it is a less critical molecular determinant of oriented nucleation than electrostatic or stereochemical directors. This is supported here by the inclusion of different structural motifs (phosphate, amino) in the ribbon and the observed sensitivity of the system to changes in the identity of the chemical functionality presented to the crystallization medium (Table 1).
[25] This is consistent the results of earlier studies in which compressed monolayers of alkyl phosphonate or sulfate amphiphiles favored the oriented nucleation of calcite on the (001) face: a) B. R. Heywood, S. Mann, *Chem. Mater.* **1994**, *6*, 311; b) B. R. Heywood, S. Mann, *J. Am. Chem. Soc.* **1992**, *114*, 4681.
[26] The three published single-crystal X-ray studies of vaterite (ICSD refcodes 6082, 7307, 12947) do not come to a consensus with regard to crystal system, unit cell, or space group. The presence of disorder and the further complication of a super-cell mean that the structure cannot be assigned unambiguously.
[27] N. Kimizuka, T. Kawasaki, K. Hirata, T. Kunitake, *J. Am. Chem. Soc.* **1998**, *120*, 4094.

Interanionic O–H···O Interactions: The Charge Density Point of View**

Piero Macchi,* Bo B. Iversen, Angelo Sironi, Bryan C. Chakoumakos, and Finn K. Larsen*

Interanion $^{\delta-}O–H \cdots O^{\delta-}$ interactions in the solid state have been the subject of recent scientific discussion. On the basis of in vacuo calculations on isolated anions and on the global repulsion between a pair of them, Braga et al.[1] suggested that the H···O "contacts" should be regarded as pseudo hydrogen bonds, in spite of the very short O···O and H···O distances.[2–5] In their view, the conformation adopted by two anions in the solid state minimizes the repulsion[6] but does not produce a chemical bond, and the stability of the crystal structure is due only to cation–anion attractions (the overall effect was called a tugboat effect). If confirmed, this hypothesis would have far-reaching implications for the understanding of hydrogen bonds (HB) and intermolecular

[*] Dr. P. Macchi,[+] Prof. F. K. Larsen, Dr. B. B. Iversen
Department of Chemistry
University of Aarhus
8000 Aarhus C (Denmark)
Fax: (+45) 86-19-6199
E-mail: piero@csmtbo.mi.cnr.it, kre@kemi.aau.dk
Prof. A. Sironi
Dipartimento di Chimica Strutturale e Stereochimica Inorganica
Via Venezian 21, 20133 Milano (Italy)
Dr. B. C. Chakoumakos
Solid State Division, Oak Ridge National Laboratory
Oak Ridge, TN 37831 (USA)
[+] Permanent address:
Dipartimento di Chimica Strutturale e Stereochimica Inorganica
Via Venezian 21, 20133 Milano (Italy)
Fax: (+39) 02-7063-5288

[**] The Oak Ridge National Laboratory is managed by Lockheed Martin Energy Research Corporation for the US Department of Energy (DE-AC05-96OR22464). Prof. M. Moret and Dr. L. Carlucci are thanked for help in crystallizing large samples suitable for the neutron study. P.M. gratefully acknowledges DANSYNC center under the Danish Natural Science Research Council for a post-doctoral grant.

Supporting information for this article is available on the WWW under http://www.wiley-vch.de/home/angewandte/ or from the author.

interactions. However, Steiner, who used the structure correlation method,[7] did not find reasons for considering these interactions significantly different from other O–H···O hydrogen bonds; in fact, IR absorption spectra, intermolecular distances, and structural changes occurring in the anion skeleton conform with the expectations for classical HBs. Thus, he dismissed the hypothesis of an H···O repulsion and focused instead on the covalent nature of this type of "charge-assisted" HB.[8]

In our opinion, the controversy can be well assessed by studying the electron-density distribution of a pertinent crystal, since unambiguous HBs can be characterized in detail with this technique.[9] It is now well established[10] that atomic multipolar expansions can be used to reconstruct the charge density $\rho(\boldsymbol{r})$, through reciprocal space fitting[11] of structure factors derived from accurate low-temperature X-ray diffraction data.[12] The advantage of this method is that a molecule can be modeled within the crystal and subsequently "extracted" (pseudomolecule); thus, each molecular building block can be studied in isolation from the others but with the same *shape* that it has in the crystal. Properties of the pseudomolecule such as the electrostatic potential can be calculated and compared with the corresponding values of the isolated molecule. Alternatively, the total $\rho(\boldsymbol{r})$ can be partitioned according to the quantum theory of atoms in molecules (QTAM),[13] which provides an unambiguous definition of chemical bonding by means of the bond path.[14] Having this in mind, we performed extensive X-ray ($T = 11$ K) and neutron ($T = 15$ K) diffraction measurements on single crystals of potassium hydrogenoxalate,[15] the most widely addressed example of $^{\delta-}$O–H···O$^{\delta-}$ so far.[1a],[7] KHC_2O_4 crystallizes in infinite chains of $HC_2O_4^-$ with short interanion H···O and O···O distances; the cations are coordinated to oxygen atoms of different chains (Figure 1). The optimized geometry of the isolated anion calculated at the HF level[16] shows important differences to that measured in the solid state: a) the O–H distance is 0.945 Å (0.968 Å at the MP2 level), much shorter than our neutron-diffraction value (1.060(2) Å); b) the HB acceptor C=O bond is shorter than in the crystal, while the C–O(H) bond is longer (Figure 1). Therefore, in agreement with the observations of Steiner,[7] a detailed comparison of geometrical features does not support the hypothesis of a pseudo hydrogen bond.[17]

A major point in the work of Braga et al.[1a] was the shape of the computed electrostatic potential $\Phi(\boldsymbol{r})$[18] of the isolated anion. Since a negative envelope completely surrounds $HC_2O_4^-$, an electrostatic repulsion was expected to exist in intermolecular contacts between two neighboring hydrogenoxalate anions. However, in the experimental pseudomolecule, $\Phi(\boldsymbol{r})$[19] is clearly different. In the vicinity of the hydrogen atom, the negative lobe is absent, and at the (expected) position of the HB acceptor oxygen atom, $\Phi(\boldsymbol{r})$ is positive (Figure 2d). It is also important to note that the atomic charges are unevenly distributed both in the isolated $HC_2O_4^-$ and in the dianionic dimer $[(HC_2O_4)_2]^{2-}$. No matter what partitioning is applied to the theoretical density, the H atom is always positively charged;[20] indeed, this is confirmed by the

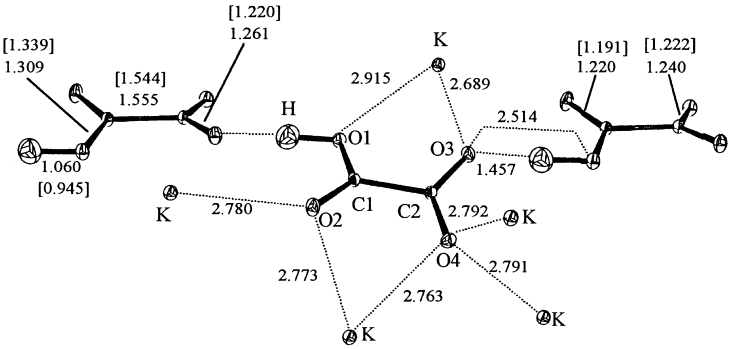


Figure 1. ORTEP view of the surrounding of a $HC_2O_4^-$ ion in the crystal (atomic ellipsoids at 70% probability level for all atoms). Distances from the X-ray/neutron model are reported in Å (standard uncertainties are less than 0.002 Å for all bonds). Figures in brackets are the distances of the HF/6-31 + G(2d,2p) optimized geometry of the isolated anion.[17]

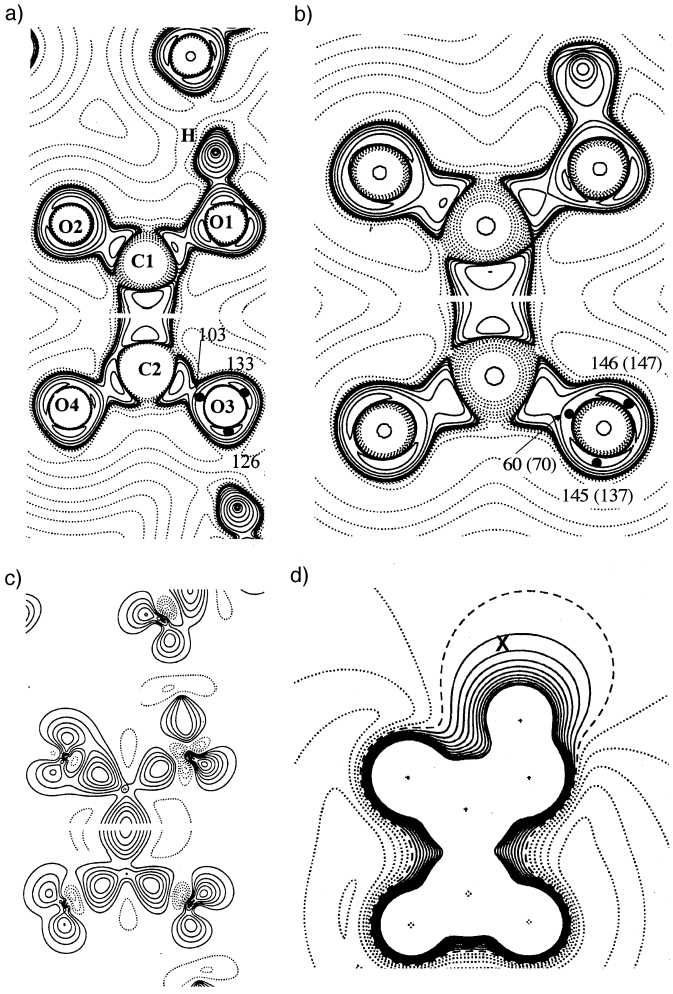


Figure 2. Drawings are composites of two molecular planes (O1-O2-H and O3-C2-O4) intersecting perpendicular to the C1–C2 bond; solid lines are positive contours. a) Experimental $L(\boldsymbol{r}) = -\nabla^2\rho(\boldsymbol{r})$ distribution (contours at $\pm 2.0, 4.0, 8.0 \times 10^x$ e Å^{-5}, $x = -2, -1, 0, 1$); maxima of $L(\boldsymbol{r})$ for O2 and O3 are reported. b) Theoretical $L(\boldsymbol{r})$ of the isolated anion (HF/6-31 + G(2d,2p)) in the solid state conformation; maxima for O2 and O3 are indicated (in parenthesis: those of O3 in the dimer). c) Static deformation map (contour intervals 0.1 e Å^{-3}); d) Electrostatic potential of the $HC_2O_4^-$ pseudomolecule from the refined X-ray model (contour intervals 0.05 e Å^{-1}, truncated at 0.5 e Å^{-1}; $\Phi(\boldsymbol{r}) = 0$ contour is a dashed line); the position of O3′ in the crystal orientation is marked by **X**.

 © WILEY-VCH Verlag GmbH, D-69451 Weinheim, 2000 1433-7851/00/3915-2720 $ 17.50+.50/0

experimental monopolar charge.[21] On the basis of atomic electrostatic moments, a global anion–anion repulsion was calculated theoretically for $[(HC_2O_4)_2]^{2-}$;[1c] however, using the experimental multipoles,[22] we found that this is mainly due to O···O contributions, whereas the H···O3′ interaction is attractive. (Because atomic pairwise terms are not reported in ref. [1c], a complete comparison with the theoretical calculations in that paper is not possible.) Thus, according to all the partitioning schemes adopted, no electrostatic H···O repulsion can be anticipated.

The most substantial evidence of a "true" HB between the H and O atoms comes from the topological analysis of $\rho(\boldsymbol{r})$ in the crystal. Indeed, for all models tested, a bond path between H and O was always found. The quantities calculated at the bond critical point (bcp, a saddle point of $\rho(\boldsymbol{r})$ necessarily found along a bond path) indicate a rather large electron density and an incipient covalency (Table 1). The total energy density $H(\boldsymbol{r})$ is negative and relatively large; at the same time, the kinetic energy density is much smaller ($G(\boldsymbol{r}_{bcp}) = 0.381\ h\,Å^{-3}$) than what would be predicted for closed-shell type HBs (for $d_{H\cdots O} = 1.457$ Å, $G(\boldsymbol{r}_{bcp}) = 0.577\ h\,Å^{-3}$ [9e]). However, the features of $L(\boldsymbol{r}) = -\nabla^2\rho(\boldsymbol{r})$ (Figure 2a) suggest that considerable electrostatic interaction must also take place. In agreement with what is indicated by the geometry, the intramolecular O–H bond is clearly weakened: $\rho(\boldsymbol{r}_{bcp})$, $|\nabla^2\rho(\boldsymbol{r}_{bcp})|$, and $|H(\boldsymbol{r}_{bcp})/\rho(\boldsymbol{r}_{bcp})|$ are smaller than in the isolated molecule, whereas $G(\boldsymbol{r}_{bcp})/\rho(\boldsymbol{r}_{bcp})$ is larger.

Table 1. Properties at the bond critical point (bcp) of the HB system in the crystal (from the experimental X-ray model) and theoretical results for the isolated anion and the dianionic dimer, both calculated on the solid-state conformation.[a]

	O–H			H···O	
distance		1.060(2) Å		1.457(2) Å	
	monomer	dimer	crystal	dimer	crystal
$\rho(\boldsymbol{r})$ [e Å^{-3}]	1.97	1.81	1.89(5)	0.51	0.54(3)
$\nabla^2\rho(\boldsymbol{r})$ [e Å^{-5}]	−39.9	−38.4	−30.4(3)	4.16	2.03(10)
$H(\boldsymbol{r})/\rho(\boldsymbol{r})$ [h e^{-1}]	*−1.58*	*−1.71*		*−0.27*	
	[−1.73]	[−1.69]	[−1.60]	[−0.32]	[−0.44]
$G(\boldsymbol{r})/\rho(\boldsymbol{r})$ [h e^{-1}]	*0.16*	*0.22*		*0.85*	
	[0.32]	[0.20]	[0.48]	[0.89]	[0.71]

[a] The exact $H(\boldsymbol{r})$ and $G(\boldsymbol{r})$ can be evaluated only from the theoretical wavefunction (in italics); alternatively, these quantities can be estimated semiempirically[25] for both the theoretical and the experimental density (in square brackets).

The polarization of lone pairs involved in hydrogen bonds has been widely studied in the past (see refs. [3, 5c] for work on O–H···$O^{\delta-}$ and $^{\delta-}$O–H···$O^{\delta-}$ systems). This feature is recognized in the deformation maps (Figure 2c) and also in the $L(\boldsymbol{r})$ distribution. In fact, relative to the isolated molecule, both lone pairs of O3 are associated with smaller $L(\boldsymbol{r})$ maxima (Figures 2a and 2b); that pointing toward H is more polarized than that pointing toward K^+.[23] The calculated dianionic dimer shows the same feature, but, of course, only in the direction of the H atom (Figure 2b, values in parentheses).[24] We may conclude that many features of the topological analysis of the charge density indicate that $^{\delta-}$O–H···$O^{\delta-}$ behaves as a strong HB.

According to the above results, a polarization of the electron density in the $HC_2O_4^-$ molecular fragment occurs in the crystal by two mechanisms: 1) mainly electrostatic (the K···O interactions); 2) partially covalent (the HB). It can be concluded that when a molecule undergoes such a strong polarization, gas-phase calculations cannot predict its "properties" in the crystal, even if the solid-state conformation is used. A more empirical structural correlation is a better alternative for examining the chemical bonding, because suitable indexes are retrieved in the correct phase. Moreover, global (interfragment) interaction energies may fail to explain local parameters such as interatomic distances, and this can be particularly misleading in crystal engineering terms. A cluster of anions is obviously unstable, and only the addition of cations eventually allows the formation of a bound state; however, this does not hamper the formation of a bond between atoms of different anions, that is, a local atom–pair attractive interaction in the context of a global repulsion (when only the anions are considered). In view of the experimental observations reported here and using a more adequate definition of a chemical bond, we find no basis for claiming "the break-down of the strength/length analogy", as advocated in reference [1].

Received: March 9, 2000 [Z14827]

[1] a) D. Braga, F. Grepioni, J. J. Novoa, *Chem. Commun.* **1998**, 1959; b) D. Braga, F. Grepioni, E. Tagliavini, J. J. Novoa, F. Mota, *New J. Chem.* **1998**, 755; c) J. J. Novoa, I. Nobeli, F. Grepioni, D. Braga, *New J. Chem.* **2000**, *24*, 5.

[2] a) B. F. Pedersen, *Acta Chem. Scand.* **1968**, *22*, 2953; b) H. Einspahr, R. E. Marsh, J. Donohue, *Acta Crystallogr. Sect. B* **1972**, *28*, 2194.

[3] a) J. O. Thomas, *Acta Crystallogr. Sect. B* **1975**, *31*, 2156; b) J. O. Thomas, S. Pramatus, *Acta Crystallogr. Sect. B* **1975**, *31*, 2159.

[4] F. H. Moore, L. F. Power, *Inorg. Nucl. Chem. Lett.* **1971**, *7*, 873.

[5] a) H.-P. Weber, R. K. McMullan, S. Swaminathan, B. M. Craven, *Acta Crystallogr. Sect. B* **1984**, *40*, 506; b) F. Takusagawa, T. F. Koetzle, *Acta Crystallogr. Sect. B* **1979**, *35*, 867; c) O. J. Thomas, *Acta Crystallogr. Sect. B* **1977**, *33*, 2867.

[6] $E = 39$ and 46 Kcal mol^{-1} (at HF and DFT levels, respectively); see ref. [1c].

[7] T. Steiner, *Chem. Commun.* **1999**, 2229.

[8] V. Bertolasi, P. Gilli, V. Ferretti, G. Gilli, *Chem. Eur. J.* **1996**, *2*, 925.

[9] Experimental electron-density studies on very strong O–H···O HBs were recently reported: a) C. Flensburg, S. Larsen, R. F. Stewart, *J. Phys. Chem.* **1995**, *99*, 10130 (the bond between the two methyl succinate anions is an interanion HB, albeit stabilized by resonance; in refs. [1a] and [7], this case was not discussed); b) D. Madsen, C. Flensburg, S. Larsen, *J. Phys. Chem.* **1998**, *102*, 2177; c) G. K. H. Madsen, B. B. Iversen, F. K. Larsen, M. Kapon, G. M. Reisner, F. H. Herbstein *J. Am. Chem. Soc.* **1998**, *120*, 10040; d) T. Koritsanszky, D. Zobel, P. Luger, *J. Phys. Chem. A* **2000**, *104*, 1549 (the bond found between two hydrogentartrate anions is an interanion HB; however, the main subject of this work was not related to hydrogen bonding, which is only marginally reported). Results of experimental QTAM analysis on several HB systems were recently studied: e) E. Espinosa, E. Molins, C. Lecomte, *Chem. Phys. Lett.* **1998**, *285*, 170.

[10] P. Coppens, *X-Ray Charge Densities and Chemical Bonding*, Oxford University Press, Oxford, **1997** (IUCr Texts on Crystallography).

[11] T. Koritsanszky, S. T. Howard, Z. Su, P. R. Mallinson, T. Richter, N. K. Hansen, *XD, Computer Program Package for Multipole refinement and Analysis of Electron Densities from Diffraction Data*, Free University of Berlin, Germany, June **1997**.

[12] F. K. Larsen, *Acta Crystallogr. Sect. B* **1995**, *51*, 468.

[13] R. F. W. Bader, *Atoms in Molecules: A Quantum Theory*, Oxford University Press, Oxford, **1990**.

[14] R. F. W. Bader, *J. Phys. Chem. A* **1998**, *102*, 7314.

 © WILEY-VCH Verlag GmbH, D-69451 Weinheim, 2000 1433-7851/00/3915-2721 $ 17.50+.50/0

[15] X-ray diffraction on a Huber four-circle diffractometer ($Ag_{K\alpha}$ radiation): $T = 11(1)$ K, $a = 4.265(1)$, $b = 12.796(1)$, $c = 7.490(1)$ Å, $\beta = 100.77(1)^\circ$, $V = 401.6(1)$ Å^3, monoclinic, space group $P2_1/c$, 12997 reflections measured (4911 independent reflections, $R_{int} = 0.0169$), absorption correction, $(\sin\theta/\lambda)_{max} = 1.4$ Å^{-1}; after multipolar refinement (4830 reflections with $I > 0$): $R1 = 0.0202$, $wR2 = 0.0410$, GOF: 1.10. Multipole expansions were extended up to $l = 4$ for C, O, and K, and $l = 2$ for H; isotropic extinction was included; positional and thermal parameters for H were fixed at neutron-diffraction positions. Neutron diffraction at the High Flux Isotope Reactor (Oak Ridge National Laboratory): $T = 15(1)$ K, $a = 4.267(1)$, $b = 12.816(7)$, $c = 7.501(6)$ Å, $\beta = 100.82(6)^\circ$, $V = 402.9(3)$ Å^3; $\lambda = 1.008(2)$ Å. 2991 reflections measured (1436 independent reflections, $R_{int} = 0.0585$); $(\sin\theta/\lambda)_{max} = 0.8$ Å^{-1}; absorption correction; agreement indexes (1082 reflections with $I > 2\sigma(I)$): $R1 = 0.0438$, $wR2 = 0.0892$, GOF: 1.03. Positional and anisotropic thermal parameters were refined for all atoms; isotropic extinction was included. Crystallographic data (excluding structure factors) for the structures reported in this paper have been deposited with the Cambridge Crystallographic Data Centre as supplementary publication no. CCDC-141183. Copies of the data can be obtained free of charge on application to CCDC, 12 Union Road, Cambridge CB2 1EZ, UK (fax: (+44) 1223-336-033; e-mail: deposit@ccdc.cam.ac.uk).

[16] Gaussian 98, M. J. Frisch, G. W. Trucks, H. B. Schlegel, G. E. Scuseria, M. A. Robb, J. R. Cheeseman, V. G. Zakrzewski, J. A. Montgomery, R. E. Stratmann, J. C. Burant, S.Dapprich, J. M. Millam, A. D. Daniels, K. N. Kudin, M. C. Strain, O.Farkas, J. Tomasi, V. Barone, M. Cossi, R. Cammi, B. Mennucci, C. Pomelli, C. Adamo, S. Clifford, J. Ochterski, G. A. Petersson, P. Y. Ayala, Q. Cui, K. Morokuma, D. K. Malick, A. D. Rabuck, K. Raghavachari, J. B. Foresman, J. Cioslowski, J. V. Ortiz, A. G. Baboul, B. B. Stefanov, G. Liu, A. Liashenko, P. Piskorz, I. Komaromi, R. Gomperts, R. L. Martin, D. J. Fox, T. Keith, M. A. Al-Laham, C. Y. Peng, A. Nanayakkara, C. Gonzalez, M. Challacombe, P. M. W. Gill, B. Johnson, W. Chen, M. W. Wong, J. L. Andres, C. Gonzalez, M. Head-Gordon, E. S. Replogle, J. A. Pople, Gaussian, Inc. Pittsburgh, PA, **1998**. The calculations of ref. [1a] were reproduced and repeated with the best X–N geometry (Table 1 and Figure 1). The geometry optimization of the anion was performed at the same level of theory, as well as with correlated methods (at the MP2 level, all distances are larger than at the HF level). Topological analysis of the theoretical density was computed with PROAIM (F. W. Biegler-König, R. F. W. Bader, T. Ting-Hua, *J. Comput. Chem.* **1982**, *3*, 317).

[17] Due to strong $O(sp^2)-O(sp^2)$ repulsion, the conformation of the isolated anion is nonplanar and the optimized torsion about C1–C2 bond is 90° (in contrast to the observed 13.2(1)°). The COO^- group is symmetric; therefore, the molecular symmetry is C_s.

[18] $\Phi(\boldsymbol{r}) = \sum_M \frac{Z_M}{|R_M - r|} - \int \frac{\rho(r')}{|r - r'|} d\boldsymbol{r}'$ ($\boldsymbol{R}_M$ are nuclear positions, and Z_M nuclear charges).

[19] Calculated according to Z. Su, P. Coppens, *Acta Crystallogr. Sect. A* **1992**, *48*, 188.

[20] $q(H) = 0.58$ (QTAM); 0.29 (Mulliken); 0.41 (charge fitting the potential); 0.51 (NBO). Similar charges are found in the dimer. Note that in ref. [1a] Mulliken charges of O(H) and H were given as a single charge ($q(OH) = -0.19$).

[21] $q(H) = 0.38(2)$. In addition, a significant population was refined in the 4s orbital of K (0.51(5)e), which implies a partial charge transfer. A model with constrained molecular charges (+1 for K, −1 for HC_2O_4) did not show significant differences in the HB region.

[22] M. A. Spackman, *J. Phys. Chem.* **1987**, *91*, 3179, and references therein.

[23] K···O bond paths were found in mainly closed-shell type interactions.

[24] The presence of an H···O bond path in the dianionic dimer cannot be defined as a chemical bond within QTAM because the structure is not at equilibrium; however, this means that the instability of the species should not be attributed to an H···O repulsion.

[25] Y. A. Abramov, *Acta Crystallogr. Sect. A* **1997**, *53*, 264.

A New Kinetic Template Synthesis of Triphosphacyclodecanes**

Peter G. Edwards,* Paul D. Newman, and David E. Hibbs

Although the first macrocycles containing solely phosphorus atoms in the ring were reported nearly thirty years ago, there are surprisingly few studies on the coordination chemistry of these potentially very interesting ligands, especially when compared to the intensely studied nitrogen analogues. Early preparations including those of Horner et al.[1] and Kyba et al.[2] were by metal-free solution or high dilution methods, and were nonstereoselective giving a mixture of all possible isomers of the macrocycles. For the smallest triphosphorus macrocyclic ring system ([11]aneP_3) known to date, Kyba et al. achieved the separation and characterization of all isomers; for the *syn*,*syn*,*anti* ligand isomer vigorous conditions (boiling xylenes) were required for the inversion of the phosphorus center and formation of facially coordinated complexes.[3] More recently, metal template approaches by Horner and Kunz,[4] Stelzer et al.,[5] Norman et al.,[6] and us[7] have been studied in order to direct the cyclization step. For facially capping triphosphanes, the template allows control of the stereochemistry at the phosphorus centers; however, liberation of the macrocycle is commonly nontrivial and to date, only 12-membered triphosphamacrocycles have been obtained as the free ligands by this method, albeit stereospecifically.[7] Variations in ring size are difficult to achieve by the established $M(CO)_3$ templates (M = Group 6 metal) which does not allow manipulation and control of steric (or electronic) influences upon the cyclization step; the 12-membered ring is the smallest obtained by this method and attempts to decrease ring size by cyclization of vinyl phosphanes have failed in our hands.[8] We are interested in facially capping triphosphanes in which the phosphorus lone pairs are fixed in the favored all-*syn* orientation forcing remaining coordination sites in their complexes into mutually *cis* orientations.

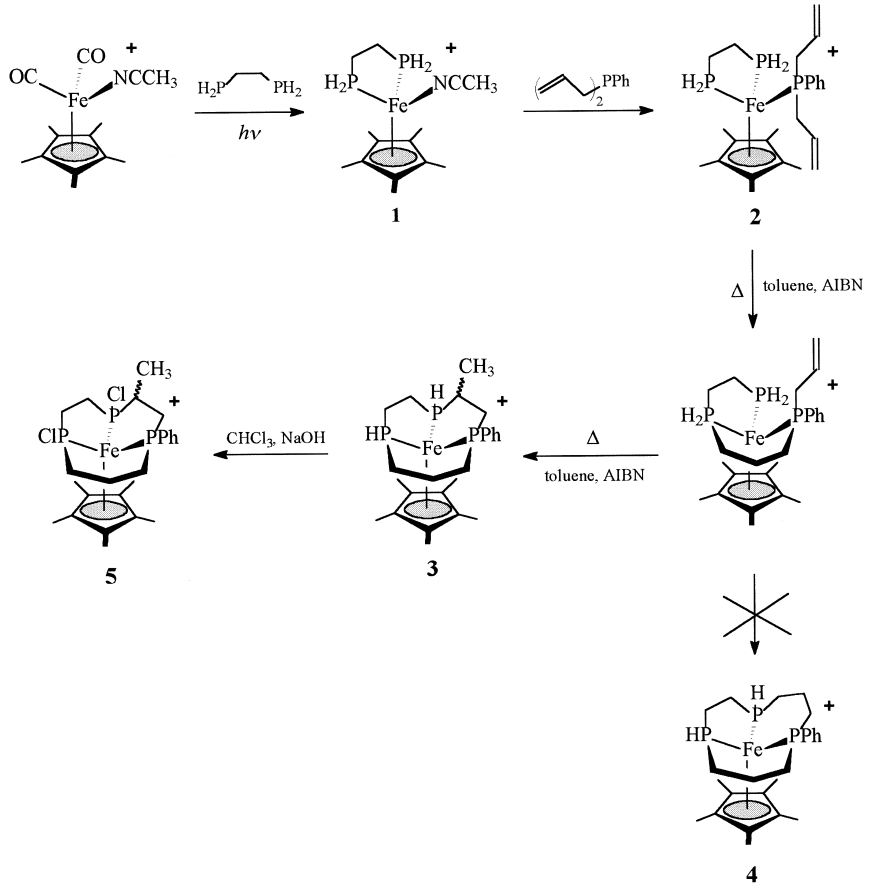
This has prompted us to seek new template methods for the formation of triphosphamacrocycles to allow access to smaller ring sizes and rational high-yield routes to selectively functionalized ligands. We have chosen to investigate $[\eta^5\text{-}CpFe(L)_3]^+$ (L = monodentate or arene ligand; Cp = η^5-C_5Me_5) complexes as potential templates since they are readily prepared and form facial trisphosphane complexes which tend to have good air-stability.[9] Of particular interest is that substituents on the Cp ring may be widely varied which may allow manipulation of steric influences upon the *trans*-coordinated phosphanes. Herein we report the synthesis of

[*] Prof. P. G. Edwards, Dr. P. D. Newman, Dr. D. E. Hibbs
Department of Chemistry
Cardiff University
PO Box 912
Park Place, Cardiff, CF10 3TB (UK)
Fax: (+44) 2920-874-030
E-mail: Edwardspg@cardiff.ac.uk

[**] This work was funded by the EPSRC.

Supporting information for this article is available on the WWW under http://www.wiley-vch.de/home/angewandte/ or from the author.

 © WILEY-VCH Verlag GmbH, D-69451 Weinheim, 2000 1433-7851/00/3915-2722 $ 17.50+.50/0



Scheme 1. Kinetic template synthesis of triphosphacyclodecanes.

the first [10]aneP_3 macrocycle by the Fe^{II}-template cyclization of a coordinated di-primary phosphane (1,2-diphosphanylethane, 1,2-dpe) and diallylphenylphosphane (Scheme 1).[10]

The hitherto unknown $[(\eta^5\text{-}C_5Me_5)Fe(1,2\text{-dpe})(CH_3CN)]BF_4$ (**1**) is readily prepared by photolysis of a 1:1 mixture of $[(\eta^5\text{-}C_5Me_5)Fe(CO)_2(CH_3CN)]BF_4$ and 1,2-dpe in acetonitrile. The coordinated acetonitrile in **1** is substituted with diallylphenylphosphane on heating in 1,2-dichloroethane to give complex **2** in quantitative yield. The $^{31}P\{^1H\}$ NMR spectrum of **2** shows the expected triplet ($\delta = 45.4$) and doublet ($\delta = 11.9$, $J_{PP} = 51$ Hz). Heating **2** in toluene at 80 °C in the presence of azobisisobutyronitrile (AIBN) gives a mixture from which complex **3** can be obtained as air- and moisture-stable yellow needles in 35 % yield after chromatography and anion exchange. The $^{31}P\{^1H\}$ NMR spectrum of **3** consists of an ABX pattern with a low-field triplet at $\delta =$ 111.7 ($J_{PP} = 25$ Hz), and two doublets of doublets at $\delta = 65.7$ and 61.7 ($J_{PP} = 54$ and 25 Hz). The resonance signals at $\delta =$ 111.7 and 61.7 in the ^{31}P NMR spectrum were attributed to secondary phosphanes ($^1J_{PH} = 348$ and 340 Hz, respectively). This pattern precludes structure **4** (Scheme 1), as a simple AX_2 ^{31}P NMR spectrum would be expected for this complex. The ^{31}P NMR spectrum is compatible with structure **3**; the low-field resonance signal is assigned to the secondary phosphane α to the C-methyl carbon atom as it is a component of two five-membered chelates which are known to cause low-field ^{31}P shifts relative to six-membered chelates;[11] the presence of the exocyclic methyl- and methine-carbon atoms are confirmed in the ^{13}C DEPT NMR spectrum. The ^1H NMR spectrum is complex but consistent with the structure, the exocyclic CH_3 group is observed as a doublet of doublets at $\delta =$ 1.46 ($J = 12$ and 7 Hz).

Attempts to grow crystals of **3** suitable for single-crystal X-ray analysis were unsuccessful. This prompted a search for a derivative of the parent macrocyclic complex that could be crystallized in an appropriate form. Following our recent observation of the halogenation of coordinated secondary phosphane macrocycles by halocarbons in the presence of base,[12] the reaction of **3** with NaOH in chloroform gave rise to a new complex **5** in high yield. The ^{31}P NMR spectrum of **5** showed new resonance signals at $\delta = 222.6$ and 202.5 and the loss of peaks attributable to secondary phosphanes. In addition, the appearance of the resonance signal from the tertiary phosphorus had changed to a doublet of doublets at $\delta =$ 59.8 ($J_{PP} = 13.5$ and 6 Hz). The IR spectrum of **5** showed an absence of bands attributable to ν_{PH} stretches. The structure of **5** was determined by a single-crystal X-ray diffraction study of a sample recrystallized from methanol in air. Orange crystals of the complex were obtained as the hemihydrate of the hexafluorophosphate salt.[13] Two views of the cation **5** are shown in Figure 1.

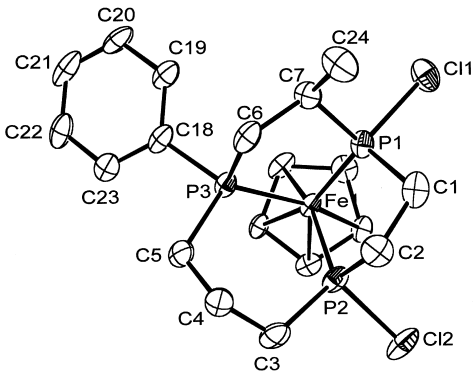


Figure 1. An Ortep[19] representation of the cation **5**. The cyclopentadienyl methyl groups have been removed for clarity. Selected bond lengths [Å] and angles [°]: Fe-P1 2.153(2), Fe-P2 2.148(2), Fe-P3 2.210(2), P1-Cl1 2.061(2), P2-Cl2 2.084(2); P1-Fe-P2 84.51(8), P1-Fe-P3 86.77(7), P2-Fe-P3 89.00(6).

It is clear from Figure 1 that both secondary phosphane groups in **3** have been converted to P–Cl functions as indicated by the spectroscopic data for **5**. In addition, the original characterization of **3** is confirmed by analogy with that of **5**, in which a ten-membered macrocycle containing two five-membered chelates (one with a methyl substituent) are present. The six-membered chelate adopts a chair conforma-

 © WILEY-VCH Verlag GmbH, D-69451 Weinheim, 2000 1433-7851/00/3915-2723 $ 17.50+.50/0

tion and both five-membered chelates have an envelope conformation. The methyl group projects equatorially from its chelate but is orientated almost perpendicular to the P_3 plane. The crystal is racemic, with both enantiomers Fe(*R*), P1(*R*), P2(*R*), P3(*S*), C1(*R*) and Fe(*S*), P1(*S*), P2(*S*), P3(*R*), C1(*S*)[17] being present in the asymmetric unit; only the former is shown in Figure 1. The Fe–P(Cl) bonds (av 2.151(2) Å) are both shorter than the Fe–P(Ph) bond length (2.210(2) Å) which is comparable to that in other related systems.[18] In addition, the P1-Fe-P3 and P1-Fe-P2 angles (84.51(8)°and 86.77(7)°, respectively) are significantly less than that of P2-Fe-P3 (89.00(6)°) or corresponding angles in related 12-aneP_3 complexes (e.g. P-Cr-P av 91.09(5)° in [(12aneP_3H_3)Cr-$(CO)_3$]).[8] It is noteworthy that the nonbonded P···P distances in **5** are significantly shorter (P1–P2 2.892(2), P1–P3 2.997(2), P2–P3 3.054(2) Å) than those observed in [(12-aneP_3H_3)Cr$(CO)_3$] (3.321(4) Å). The methyl groups of the cyclopentadienyl ring in **5** are bent slightly out of the Cp plane, suggesting some steric congestion about the metal center which may be responsible for the formation of the 10-membered as opposed to the 11-membered macrocycle (**4**) as a result of the compression of the P-Fe-P angles and corresponding reduction of the nonbonded P–P distances. These data support the view that introduction of steric control over these types of template cyclization may indeed be very valuable in enabling the formation of smaller ring systems than has previously been achieved.

The formation of **3** presumably involves coupling of the terminal carbon atom of the first allyl group with one of the primary phosphanes in **2** to produce a three-carbon bridge in the intermediate (Scheme 1). The second hydrophosphination, however, occurs at the internal carbon atom of the remaining allyl function to give **3**. As the precursor complex **2** is achiral, there is no control of the stereochemistry and complex **3** is formed as a racemate.

Thus this pentamethylcyclopentadienyliron template provides, as well as a new template system for the synthesis of triphosphorus macrocycles, the first complexes to contain a ten-membered triphosphamacrocycle and a novel example of a metal-templated internal hydrophosphination of an allyl function. Preliminary attempts to liberate the macrocycle from the metal center by reduction are encouraging. We are also investigating the influences of variations of the Cp substituents upon the outcome of the cyclization step and with alternative di-primary phosphane and alkenyl phosphane precursor ligands.

Received: March 10, 2000 [Z14838]

[1] L. Horner, P. Walach, H. Kunz, *Phosphorus Sulfur Rel. Elem.* **1978**, *5*, 171.

[2] E. P. Kyba, A. M. John, S. B. Brown, C. W. Hudson, M. J. McPhaul, A. Harding, K. Larsen, S.Niedzwiecki, R. E. Davis, *J. Am. Chem. Soc.* **1980**, *102*, 139.

[3] a) E. P. Kyba, R. E. Davis, S-T Liu, K. A. Hassett, S. B. Brown, *Inorg. Chem.* **1985**, *24*, 4629; b) E. P. Kyba, S. B. Brown, *Inorg. Chem.* **1980**, *19*, 2159.

[4] L. Horner, H. Kunz, *Chem. Ber.* **1971**, *104*, 717.

[5] T. Lebbe, P. Machnitzki, O. Stelzer, W. S. Sheldrick, *Tetrahedron* **2000**, *56*, 157; D. J. Brauer, F. Dörrenbach, T. Lebbe, O. Stelzer, *Chem. Ber.* **1992**, *125*, 1785; D. J. Brauer, T. Lebbe, O. Stelzer, *Angew. Chem.* **1988**, *100*, 432; *Angew. Chem. Int. Ed. Engl.* **1988**, *27*, 438.

[6] B. N. Diel, P. F. Brandft, R. C. Haltiwanger, A. D. Norman, *J. Am. Chem. Soc.* **1982**, *104*, 4700.

[7] P. G. Edwards, J. S. Fleming, S. S. Liyanage, *Inorg. Chem.* **1996**, *35*, 4563.

[8] P. G. Edwards, J. S. Fleming, S. S. Liyanage, S. J. Coles, M. B. Hursthouse, *J. Chem. Soc. Dalton Trans.* **1996**, 1801.

[9] D. Catheline, D. Astruc, *Organometallics* **1984**, *3*, 1094; G. T. Crisp, G. Salem, S. B. Wild, *Organometallics* **1989**, *8*, 2360; D. C. R. Hockless, Y. B. Kang, M. A. McDonald, M. Pabel, A. C. Willis, S. B. Wild, *Organometallics* **1996**, *15*, 1301.

[10] Satisfactory analytical and spectroscopic data was obtained for all new compounds and are deposited in the Supporting Information.

[11] P. S. Pregosin, R. W. Kunz, *^{31}P and ^{13}C NMR of Transition Metal Complexes*, Springer, Berlin, **1979**.

[12] P. G. Edwards, D. J. Jones, R.P Tooze, T. Albers, *J. Chem. Soc. Dalton Trans.* **1999**, 1045.

[13] Crystal data for complex **5**, $C_{24}H_{37}Cl_2F_6O_{0.5}P_4Fe$, $M_r = 698.16$, $T = 150(2)$ K, monoclinic, space group $C2/c$, $a = 30.071(2)$, $b = 9.947(3)$, $c = 20.199(10)$ Å, $\beta = 104.13(2)^\circ$, (by least-squares refinement of the setting angles for 25 reflections within $\theta = 3.05 - 26.29^\circ$), $V = 5859(3)$ Å^3, $Z = 8$, $\rho_{calcd} = 1.585$ g cm^{-3}, $\mu(Mo_{K\alpha}) = 0.971$ cm^{-1}, $F(000) = 2880$, crystal size $= 0.2 \times 0.2 \times 0.15$ mm. All crystallographic measurements were made on an Enraf Nonius CAD4 diffractometer. The structure was solved by direct methods[14] and refined on F_o^2 by full-matrix least-squares[14] using all unique data corrected for Lorentz and polarization factors. All non-hydrogen atoms were anisotropic. The hydrogen atoms were inserted in idealized positions with U_{iso} set at 1.5 times the value of U_{eq} of the parent. The weighting scheme used was $w = 1/[\sigma^2(F_o)^2 + (0.0999P)^2]$, where $P = [\mathrm{Max}F_o^2 + 2F_c^2]/3$; this gave satisfactory agreement analyses. Final R_1 (on F) and wR_2 (on F_o^2) values were 0.1410 and 0.2010 for all 5935 data and 345 parameters. The corresponding R values were 0.0777 and 0.1803 for 3545 data with $I > 2\sigma(I)$. Sources of scattering factors as in ref. [15]. Empirical absorption corrections were carried out by the DIFABS method.[16] The numbering of the atoms is shown in Figure 1. Crystallographic data (excluding structure factors) for the structure reported in this paper have been deposited with the Cambridge Crystallographic Data Centre as supplementary publication no. CCDC-133102. Copies of the data can be obtained free of charge on application to CCDC, 12 Union Road, Cambridge CB2 1EZ, UK (fax: (+44) 1223-336-033; e-mail: deposit@ccdc.cam.ac.uk).

[14] G. M. Sheldrick, *Acta Crystallogr. Sect. A* **1990**, *46*, 467.

[15] G. M. Sheldrick, SHELXL-93, Program for Crystal Structure Refinement, University of Göttingen, Germany, **1993**.

[16] N. P. C. Walker, D. Stuart, *Acta Crystallogr. Sect. A* **1983**, *39*, 158.

[17] The CIP priorities of the phosphorus centers are altered on chlorinating the P-H groups, and the stereochemical descriptors change accordingly.

[18] C.-Y. Liu, M.-C. Cheng, S.-M. Peng, S.-T. Liu, *J. Organomet. Chem.* **1994**, *468*, 199.

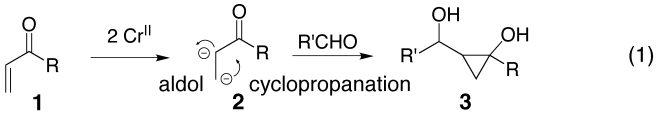
[19] Ortep for Windows, Version 1.0, L. J. Farrugia, University of Glasgow, **1997**.

 © WILEY-VCH Verlag GmbH, D-69451 Weinheim, 2000 1433-7851/00/3915-2724 $ 17.50+.50/0

Cross-Coupling Reactions between α,β-Unsaturated Ketones and Aldehydes with $CrCl_2$: Aldol Condensation and Cyclopropanol Formation**

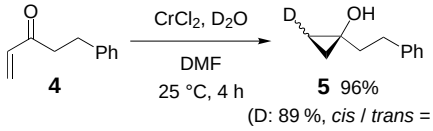
Chika Toratsu, Takafumi Fujii, Takuma Suzuki, and Kazuhiko Takai*

The reduction of carbon–carbon unsaturated bonds by chromium(II) has been observed since the 1920s,[1] and in some cases dianionic species have been postulated.[2] However, most of these reactions were conducted in protic solvents, and protonated anionic species were produced which cannot be employed for carbon–carbon bond formation except in a few cases.[3, 4] We report here that the α,β-unsaturated ketone **1** is reduced with chromium(II) in an aprotic solvent to give the ketone α,β-dianion equivalent **2**, which reacts with an aldehyde at the α position (aldol condensation) followed by intramolecular cyclopropanation to afford *cis*-2-(1-hydroxyalkyl)-substituted cyclopropanol **3** in a stereoselective manner [Eq. (1)].



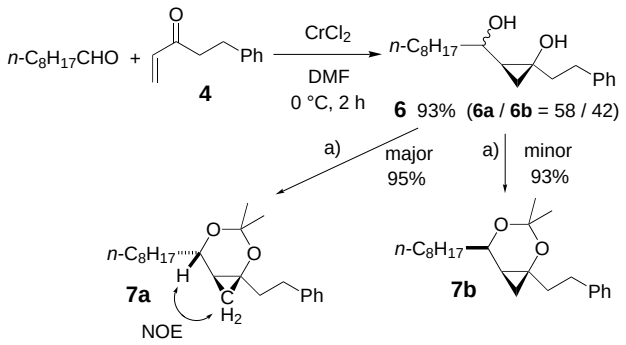
(1)

Treatment of enone **4** [see Eq. (2)] with $CrCl_2$ in DMF under strictly water-free conditions did not give cyclopropanol **5**, but instead resulted in a complex mixture.[5] However, when water was added to the reaction mixture before addition of the enone, the cyclopropanol formation proceeded smoothly.[6] For example, treatment of enone **4** with a mixture of $CrCl_2$ (4 equiv) and D_2O (2 equiv) in DMF at 25 °C for 4 h gave cyclopropanol **5** in 96% yield, and deuterium was incorporated in 89% content [Eq. (2)].



(2)

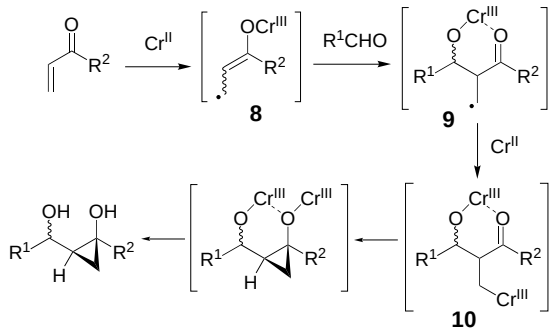
To clarify the reactivity of the nucleophilic position, the reaction was conducted in the presence of an aldehyde under water-free conditions. A solution of enone **4** and nonanal in dry DMF was added at 0 °C to a blue-green solution of $CrCl_2$ in DMF, and the resulting mixture was stirred for 2 h at 0 °C to give diol **6** in 93% yield (Scheme 1). The two isomers **6a** and **6b** (**6a**/**6b** = 58/42)[7] were produced selectively out of four



Scheme 1. Sequential aldol condensation and cyclopropanol formation followed by acetalization. a) $Me_2C(OMe)_2$, cat. PPTS, acetone, 25 °C, 2 h.

possible diastereomers, and the relative configuration of the cyclopropane rings was shown to be *cis* by quantitative transformation to the corresponding acetonides **7a** and **7b** with 2,2-dimethoxypropane and pyridinium *p*-toluenesulfonate (PPTS). The NOE experiments of the acetonides showed that the octyl group and the cyclopropane ring of the acetonide **7a**, derived from the major adduct **6a**, had a *trans* configuration of the acetonide ring.

A possible mechanism which explains the configuration of the cyclopropane rings is shown in Scheme 2. One-electron reduction of an enone with chromium(II) gives the enolate



Scheme 2. Mechanism of the coupling reaction

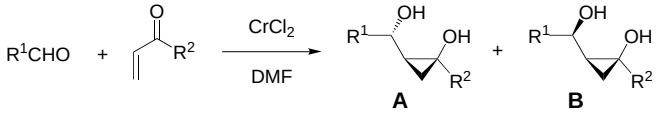
radical **8**,[2] which reacts with an aldehyde to give **9**.[8] Reduction of the radical **9** with chromium(II)[9] followed by intramolecular addition gives a cyclopropanol.[10] Because the reducing power of chromium(II) is moderate, the first one-electron transfer proceeds selectively to the enone without affecting the coexistent aldehyde.[11] Coordination of both the alkoxy and carbonyl groups to chromium(III) in **10** fixes the conformation leading to the *cis* cyclopropane ring. The Lewis acidity of the chromium salt could also facilitate the first electron transfer to the enone as well as the cyclopropanation.

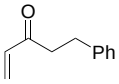
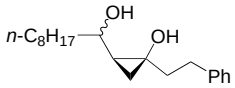
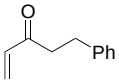
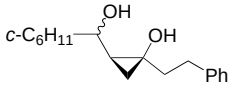
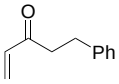
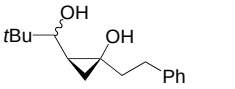
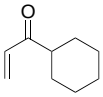
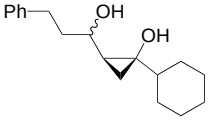
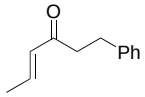
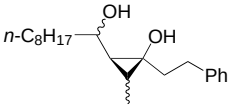
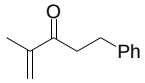
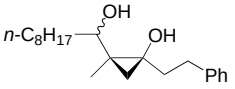
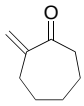
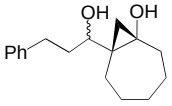
Several products resulting from the coupling reactions between α,β-unsaturated ketones and aldehydes are summarized in Table 1. Diastereomers having a *trans* configuration at

[*] Prof. Dr. K. Takai, C. Toratsu, T. Fujii, T. Suzuki
Department of Applied Chemistry, Faculty of Engineering
Okayama University
Tsushima, Okayama 700-8530 (Japan)
Fax: (+81) 86-251-8094
E-mail: ktakai@cc.okayama-u.ac.jp

[**] Financial support by a Grant-in-Aid for Scientific Research on Priority Area No. 706 from the Ministry of Education, Science, Sports and Culture of Japan is gratefully acknowledged. We would also like to thank Professor Ilhyong Ryu of Osaka Prefecture University for helpful discussions, and Dr. Teruhiko Ishikawa of Okayama University for conducting the NOE experiments.

Table 1. Sequential aldol-cyclopropanation of α,β-unsaturated ketones and aldehydes.[a]

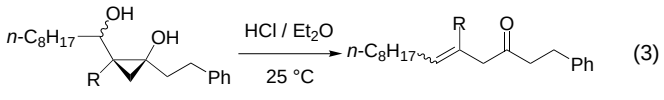


Entry	R^1	Enone	t [h]	Products	Yield [%] [b]	**A**:**B**[c]
1	n-C_8H_{17}		2		93	58:42 (**6a**:**6b**)
2	c-C_6H_{11}		2		89	79:21
3	tBu		2		76	51:49
4	$Ph(CH_2)_2$		2		62	74:26
5	n-C_8H_{17}		2		28	–[d]
6	n-C_8H_{17}		18		78	91:9 (**11a**:**11b**)
7	$Ph(CH_2)_2$		24		54	85:15

[a] The reaction was conducted on a 1.0-mmol scale. Chromium(II) chloride (8.0 mol) and enone (2.0 mol) were used per mole of aldehyde. [b] Yields of isolated products. [c] Isomer ratios were determined by isolation, GLPC, and/or NMR spectroscopy. [d] Mixture of diastereomers. The configuration of the methyl group on the cyclopropane was not determined.

the cyclopropane ring were not obtained in all cases. Substituents at the olefin positions of the enones retarded the coupling reactions, especially in the case of a β-substituted enone (Table 1, entries 5 and 6). An enone fixed to s-*cis* could also be used for the coupling reaction (entry 7).

The produced diols **6** and **11** could be transformed to the β,γ-unsaturated ketones **12**[12] and **13**[13] by treatment with hydrochloric acid in diethyl ether in 93% and 96% yields, respectively [Eq. (3)].[13] The ketones underwent an exchange



(3)

6: R = H
11: R = Me

12: 93% (*E* / *Z* = 89 / 11)
13: 96%[13]

between the α and β carbon atoms from the starting enones, and displayed alkylidenation at the α-carbon atom.

Experimental Section

Representative procedure for the reaction in Table 1, entry 1: To a mixture of $CrCl_2$ (0.98 g, 8.0 mmol)[14] in dry, oxygen-free DMF (10 mL)[15] was added a solution of nonanal (0.14 g, 1.0 mmol) and 5-phenyl-1-penten-3-one (**4**, 0.32 g, 2.0 mmol) in DMF (10 mL) at 0 °C. After stirring for 2 h at 0 °C, the reaction mixture was poured into water (20 mL). The mixture was extracted with diethyl ether (4×15 mL), and the organic extracts were dried over anhydrous magnesium sulfate and concentrated. Purification by column chromatography on silica gel (hexane/ethyl acetate, 50/1) gave 2-(1-hydroxynonyl)-1-(2-phenylethyl)-cyclopropanol in 93% yield (**6**, 0.28 g; **6a**/**6b** = 58/42).

Received: February 23, 2000 [Z 14758]

[1] J. B. Conant, H. B. Cutter, *J. Am. Chem. Soc.* **1926**, *48*, 1016–1030.

[2] a) K. D. Kopple, *J. Am. Chem. Soc.* **1962**, *84*, 1586–1589; b) C. E. Castro, R. D. Stephens, S. Mojé, *J. Am. Chem. Soc.* **1966**, *88*, 4964–4969; c) J. R. Hanson, E. Premuzic, *J. Chem. Soc. C* **1969**, 1201–1202; d) H. O. House, E. F. Kinloch, *J. Org. Chem.* **1974**, *39*, 1173–1182; e) C. E. Castro, R. D. Stephens, *J. Am. Chem. Soc.* **1964**, *86*, 4358–4363.

[3] Reduction of α,β-unsaturated ketones with other low-valent metals: a) Na: K. W. Bowers, R. W. Giese, J. Grimshaw, H. O. House, N. H. Kolodny, K. Kronberger, D. K. Roe, *J. Am. Chem. Soc.* **1970**, *92*, 2783–2799; b) H. O. House, R. W. Giese, K. Kronberger, J. P. Kaplan, J. F. Simeone, *J. Am. Chem. Soc.* **1970**, *92*, 2800–2810; c) Sm: A. Cabrera, R. Le Lagadec, P. Sharma, J. L. Arias, R. A. Toscano, L. Velasco, R. Gaviño, C. Alvarez, M. Salmón, *J. Chem. Soc. Perkin Trans. 1* **1998**, 3609–3617; d) low-valent Ti and V: J.-M. Pons, J.-P. Zahra, M. Santelli, *Tetrahedron Lett.* **1981**, *22*, 3965–3968.

[4] Intramolecular carbon–carbon bond formation between α,β-acetylenic ketones and carbonyl groups with chromium(II) was reported: A. B. Smith III, *Strategies and Tactics in Organic Synthesis* (Ed.: T. Lindberg), Academic Press, Orlando, **1984**, p. 252; see also A. B. Smith III, P. A. Levenberg, J. Z. Suits, *Synthesis* **1986**, 184–189.

[5] 2-(1-Oxo-3-phenylpropyl)-1-(2-phenylethyl)cyclopentanol was obtained as a major product (44% yield); see also ref. [3c].

[6] In 1993 Stevenson et al. first observed formation of a cyclopropanol by treatment of α,β-unsaturated aldehydes with $CrCl_2$ and a catalytic amount of $NiCl_2$: D. Montgomery, K. Reynolds, P. Stevenson, *J. Chem. Soc. Chem. Commun.* **1993**, 363–364. Our observations[5] suggest that the presence of water is necessary to promote the cyclopropanol formation. Also, in our experiments the presence of a catalytic amount of the nickel salt did not affect the transformation.

[7] When the reaction was conducted at 25 °C, the diastereomeric ratio **6a**/**6b** changed from 58/42 to 80/20 with a decrease in the total yield to 57%. This is because the minor product **6b** is more unstable than **6a** under the slightly acidic reaction conditions.

 © WILEY-VCH Verlag GmbH, D-69451 Weinheim, 2000 1433-7851/00/3915-2726 $ 17.50+.50/0

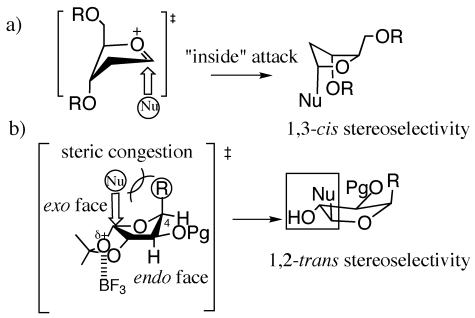
[8] a) J.-E. Dubois, G. Axiotis, E. Bertounesque, *Tetrahedron Lett.* **1985**, *26*, 4371 – 4372; b) L. Wessjohann, T. Gabriel, *J. Org. Chem.* **1997**, *62*, 3772 – 3774.
[9] a) J. K. Kochi, J. W. Powers, *J. Am. Chem. Soc.* **1970**, *92*, 137 – 146; b) R. Sustman, R. Altevogt, *Tetrahedron Lett.* **1981**, *22*, 5167 – 5170; c) T. Lübbers, H. J. Schäfer, *Synlett* **1992**, 743 – 744; d) K. Takai, N. Matsukawa, A. Takahashi, T. Fujii, *Angew. Chem.* **1998**, *110*, 160 – 163; *Angew. Chem. Int. Ed.* **1998**, *37*, 152 – 155.
[10] For cyclopropanation of enones mediated by zinc and BF_3, see I. Elphimoff-Felkin, P. Sadra, *Tetrahedron* **1975**, *31*, 2781 – 2784.
[11] The following functional substrates were recovered under the standard reaction conditions (Table 1, entry 1) due to the mild nucleophilicity of the organochromium reagent: 1-dodecene (97 %), 1-dodecyne (93 %), 1-chlorododecane (91 %), ethyl octanoate (93 %), nonanenitrile (93 %), 3-phenylpropyl acrylate (95 %), nonanal ethylene acetal (94 %), 4-phenyl-2-butanone (96 %).
[12] Both diastereomers of **6** gave an *E* isomer of **12** as a major product. This is probably due to the stability of a carbocation adjacent to the cyclopropane ring; see H. Maeta, T. Nagasawa, Y. Handa, T. Takei, Y. Osamura, K. Suzuki, *Tetrahedron Lett.* **1995**, *36*, 899 – 902.
[13] The β,γ-unsaturated ketone **13** was obtained as a mixture of geometrical isomers.
[14] Chromium(II) chloride (99.9 % purity, anhydrous powder, <100 ppm H_2O) was purchased from Aldrich Chemical Co.
[15] Dehydrated DMF was purchased from Wako Pure Chemical Industries Ltd., and stored with 4-Å molecular sieves.

Highly 1,2-*trans* Stereoselective Allylations of 1,2-*O*-Isopropylidene-Protected Glycofuranosides**

Fernando García-Tellado,* Pedro de Armas,* and José Juan Marrero-Tellado*

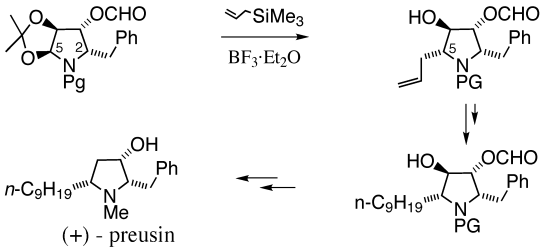
Dedicated to Professor Antonio González on the occasion of his 83rd birthday

Lewis acid mediated cleavage of chiral cyclic acetals is a useful synthetic tool for the asymmetric synthesis of C–C bonds.[1] Specifically, one of the most widely used methods for the formation of C-glycosides involves a glycosidic acetal, a Lewis acid, and a carbon nucleophile.[2] The reaction proceeds via a cyclic oxocarbenium ion, which undergoes nucleophilic attack in a stereoelectronically controlled manner to provide the product with high stereoselectivity.[3–5] Conformational effects have been invoked to explain the stereoselective reactions of substituted five-membered-ring oxocarbenium ions (Scheme 1 a).[4]



Scheme 1. a) The postulated stereoelectronic model for reactions of substituted five-membered-ring oxocarbenium ions. Nucleophilic attack occurs by a stereoelectronically controlled "inside attack" on the lower energy conformer of the cation to provide the product in its lower energy form. b) Schematic representation of the *exo* facial template effect exercised by the 1,2-*O*-isopropylidene protecting group. The nucleophilic attack is directed by the acetal onto the *exo* face of the molecule to give the 1,2-*trans* product.

Because of the biological and chemical importance of C-glycofuranosides,[2, 6] we undertook a study of the Lewis acid promoted cleavage of 1,2-*O*-isopropylidene-protected glycofuranosides by allyltrimethylsilane as a feasible and stereoselective route to these structures.[7] This procedure was introduced by us in the formal synthesis of the antibiotic (+)-preusin to install the C5 nonyl chain with the required *R* configuration (Scheme 2).[8] We hypothesized that the high



Scheme 2. The formal stereoselective synthesis of (+)-preusin. The alkyl chain at C5 is introduced with the required *R* configuration by diastereoselective allylation of the bicyclic 1,2-*O*-isopropylidene-protected dihydroxypyrrolidine intermediate. PG = protecting group.

diastereoselectivity obtained in this experiment was due to the bicyclic nature of these acetals, which confers an intrinsic and general *exo*-facial bias to the incoming nucleophile, regardless of the other substituents on the heterocyclic ring (Scheme 1 b). If this were the case, then this template effect of the bicyclic acetal should be general for any 1,2-*O*-isopropylidene-protected glycofuranoside, and thus provide invariable 1,2-*trans* stereoselectivity for nucleophilic substitution at the anomeric center. Here we present experimental evidence to confirm our initial hypothesis and establish the generality of this remarkable *exo*-facial template effect exercised by the 1,2-*O*-isopropylidene protecting group.

[*] Dr. F. García-Tellado, Dr. P. de Armas
CSIC-Instituto de Productos Naturales y Agrobiología
ASTROFÍSICO Francisco Sánchez 3
38206 La Laguna-Tenerife (Spain)
Fax: (+34)922260135
E-mail: fgarcia@ipna.csic.es
parmas@ipna.csic.es
Dr. J. J. Marrero-Tellado
Instituto Universitario de Bioorgánica Antonio González
Universidad de La Laguna
Astrofísico Francisco Sánchez 2
38206 La Laguna-Tenerife (Spain)
Fax:(+34)922260135
E-mail: jtellado@ull.es

[**] This work was supported by the Canary Islands Consejería de Educación y Ciencia (PI1998/109), the Spanish Comisión Interministerial de Ciencia y Tecnología (PB98-0443-C02-02), and the FEDER (1SD97-0747-C04-01).

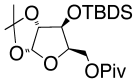
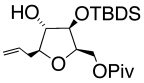
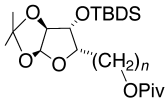
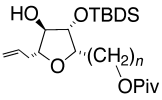
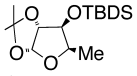
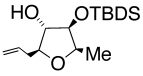
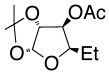
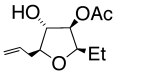
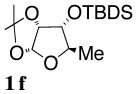
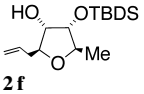
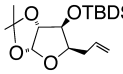
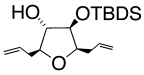
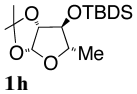
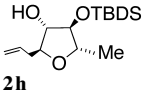
We prepared the structurally related 1,2-*O*-isoprolylidene-protected furanosides **1a**–**h**[9] and carried out a systematic study of their allylation reactions (Table 1). Remarkably, 1,2-*trans* selectivity was achieved in all of the experiments carried out with $BF_3 \cdot Et_2O$ or $TiCl_4$ as the Lewis acid and allyltrimethylsilane as the nucleophile (Scheme 3; Table 2).[10] In general, the yields ranged from modest to good and the reaction conditions were sufficently mild to be supported by other acid-sensitive groups present in the molecule. The reduced reactivity of these acetals with regard to other anomeric activating groups[2c, 6a] meant that the reaction had to be conducted at room temperature in the case of $BF_3 \cdot Et_2O$ and at 0 °C for $TiCl_4$.

Examination of the results depicted in Table 1 reveals the following features: 1) the nucleophile always adds to the *exo* face of the bicyclic acetal; 2) the stereochemical outcome of the reaction depends on neither the size nor the configuration of the substituents on the ring; 3) the yield of the reaction decreases with the bulkiness of the C4 alkyl group (compare **1a** and **1e** with **1d**) and increases with the length of the alkyl chain (compare **1a**, **1b**, and **1c**); and 4) the C3 alkoxy group behaves as a mere spectator, in sharp contrast with the well-established influence of this group for the 1,3-*syn* stereoselectivity found in the C-glycosidation of ribose derivatives.[4]

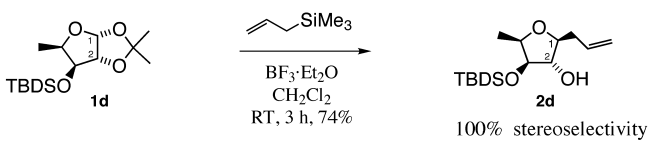
The effect of the C4 alkyl substituents on the yield of the reaction can be interpreted in terms of the destabilizing 1,3-diaxial interaction beteween the nucleophile and the alkyl group. From the model illustrated in Scheme 1b, it is clear that an increase in the size of the alkyl group at C4 produces greater steric congestion on the *exo* face of the bicyclic molecule. Lengthening of the alkyl chain places the bulky pivaloyloxy group further away from the anomeric position, reducing the steric congestion at this center.

The combined use of trimethylsilyl triflate and $BF_3 \cdot Et_2O$ as the Lewis acid (applied for the substrate **1a**, see Table 1) deserves comment. The strong Lewis acid character of this mixture is benficial for the reaction (the yield increases to about 20%), but disadvantageous for the diastereoselctivity (25%). If the starting bicyclic acetal is cleavaged before nucleophilic attack can take place, no template effect can be exercised and the stereochemical outcome of the reaction would be directed by the conforma-

Table 1. Lewis acid promoted allylation of the 1,2-*O*-isopropylidene protected glycofuranosides **1a**–**h** with allyltrimethylsilane.

Substrate	Lewis acid	Method[a]	Yield [%][b]	Product[c]
	$BF_3 \cdot Et_2O$	A	40[d]	
1a	$BF_3 \cdot Et_2O$/TMSOTf (8/2)	A	59 (α/β = 1/3)	**2a**
	$BF_3 \cdot Et_2O$	A	42[d]	
1b (n = 2)	$BF_3 \cdot Et_2O$	B	62	**2b** (n = 2)
1c (n = 3)	$BF_3 \cdot Et_2O$	A	89	**2c** (n = 3)
	$BF_3 \cdot Et_2O$	A	74	
1d	$TiCl_4$	C	83	**2d**
	$BF_3 \cdot Et_2O$	A	39[e]	
1e	$BF_3 \cdot Et_2O$	D	39[f]	**2e**
	$BF_3 \cdot Et_2O$	A	47	
1f				**2f**
	$BF_3 \cdot Et_2O$	A	55	
1g				**2g**
	$BF_3 \cdot Et_2O$	A	68	
1h				**2h**

[a] See the Experimental Section. [b] Yields of isolated compounds. [c] All the new compounds gave physical and spectroscopic data in accordance with the proposed structures. [d] Starting material was recovered (38%). [e] Starting material was recovered (25%). [f] Starting material was recovered (56%). TBDS = *tert*-butyldimethylsilyl, Piv = trimethylacetyl, TMSOTf = trimethylsilyl trifluoromethanesulfonate.



Scheme 3. Stereoselective Lewis acid catalyzed C-glycosidation of the D-xylofuranoside derivative **1d** using the 1,2-*O*-isopropylidene acetal group as the anomeric activator and stereochemical controller and allyltrimethylsilane as the nucleophile. See Table 2 for physical data of the product **2d**.

Table 2. Selected physical data for **2d** (diacetate).

$[\alpha]_D^{20} = -27.8$ (c = 0.56 in chloroform); ^{1}H NMR (500 MHz, $CDCl_3$): δ = 0.05 (s, 3H; MeSi), 0.10 (s, 3H; MeSi), 0.90 (s, 9H; tBuSi), 1.21 (d, J = 6.2 Hz, 3H; Me), 2.04 (s, 3H; AcO), 2.44 (m, 2H; CH_2–CH=CH_2), 3.80 (td, J = 6.9, 2.2 Hz, 1H; H-1), 3.88 (dd, J = 3.2, 0.9 Hz, 1H; H-3), 4.00 (qd, J = 6.2, 3.2 Hz, 1H; H-4), 4.77 (dd, J = 2.2, 0.9 Hz, 1H; H-2), 5.07 (m, 2H; CH_2=CH–), 5.81 (m, 1H; –CH=CH_2); ^{13}C NMR (100 MHz, $CDCl_3$): δ = −5.4, −4.9, 14.3, 18.0, 21.0, 25.7, 38.4, 77.5, 77.6, 82.5, 83.1, 117.1, 134.4, 170.0; IR (chloroform): $\tilde{\nu}$ = 3080, 1735, 1643 cm^{-1}; MS (870 eV): m/z (%): 299 ($M^+ - 15$, 0.5), 273 (9.3), 257 (52.8), 197 (15.4), 123 (18.4), 117 (100), 75 (41.4), 73 (31.6), 57 (8); elemental analysis calcd for $C_{16}H_{30}O_4Si$: C 61.11, H 9.61; found: C 61.40, H 9.78. The configuration assigned at C1 was confirmed by a NOESY experiment which showed nOes between H-2 and allylic protons, and between H-1 and H-3, H-4 and AcO

 © WILEY-VCH Verlag GmbH, D-69451 Weinheim, 2000 1433-7851/00/3915-2728 $ 17.50+.50/0 *Angew. Chem. Int. Ed.* **2000**, *39*, No. 15

tion of the 2-trimethylsilyoxy-substituted five-membered-ring oxocarbenium ion. We believe that this is the case as the low stereoselectivity is in good accordance with those reported for some C2-substituted furanosides[11] and γ-lactols.[4b]

To the best of our knowledge, this is the first case in which a 1,2-*O*-isoprolylidene group is used to activate the carbohydrate anomeric position and to direct the stereochemical outcome of the reaction on this center.[13] From a synthetic point of view, the easy access to these 1,2-*O*-isopropylidene-protected glycofuranosides and the intrinsic and complete 1,2-*trans* stereoselectivity of the reaction makes this strategy a very interesting and solid alternative to the established C-glycosidation methods. Despite the moderate reactivity of the bicyclic acetals, we believe that they are reactive enough to allow the use of other π nucleophiles.

Experimental Section

Method A: Under a nitrogen atmosphere, the 1,2-*O*-isopropylidene glycofuranoside (0.1 mmol) was dissolved in dry CH_2Cl_2 (1 mL) and cooled to 0 °C, and allyltrimethylsilane (0.4 mmol) was added. The homogeneous solution was stirred for 10 min, and $BF_3 \cdot Et_2O$ (0.2 mmol) was added. The resulting solution was stirred at 0 °C for 15 min, warmed to room temperature, and stirred for 3 h. After quenching with aqueous saturated sodium bicarbonate (0.1 mL) the reaction mixture was poured into more aqueous saturated sodium bicarbonate and extracted with CH_2Cl_2. The organic phases were combined, washed with aqueous saturated sodium chloride, dried over sodium sulfate, filtered, and concentrated to give an oily residue, which was purified by flash chromatography.

Method B: Under a nitrogen atmosphere, the 1,2-*O*-isopropylidene glycofuranoside (0.1 mmol) was dissolved in dry CH_2Cl_2 (1 mL) and cooled to 0 °C, and allyltrimethylsilane (0.1 mmol) was added. The homogeneous solution was stirred for 10 min, and $BF_3 \cdot Et_2O$ in dry CH_2Cl_2 (0.5 M, 0.1 mL) was added. The resulting solution was stirred at 0 °C for 15 min, warmed to room temperature, and stirred for 0.5 h. Three more portions of allyltrimethylsilane (0.1 mmol) and $BF_3 \cdot Et_2O$ in CH_2Cl_2 (0.1 mL) were added at intervals of 0.5 h, and the solution was stirred at room temperature for a further 2 h. More allyltrimethylsilane (4×0.1 mmol) and $BF_3 \cdot Et_2O$ in CH_2Cl_2 (4×0.1 mL) were sequentially added every 0.5 h, and the reaction mixture was stirred overnight. The reaction was quenched and worked up as in method A.

Method C: Under a nitrogen atmosphere, the 1,2-*O*-isopropylidene glycofuranoside (0.1 mmol) was dissolved in dry CH_2Cl_2 (1 mL) and cooled to 0 °C, and allyltrimethylsilane (0.4 mmol) was added. The homogeneous solution was stirred for 10 min and $TiCl_4$ (0.2 mmol) in CH_2Cl_2 (1 mL) was added through a cannula. The reaction mixture was stirred for 10 min at this temperature and then quenched and worked up as in method A.

Method D: Under a nitrogen atmosphere, the 1,2-*O*-isopropylidene glycofuranoside (0.1 mmol) was dissolved in dry CH_2Cl_2 (1 mL) and cooled to 0 °C, and allyltrimethylsilane (0.4 mmol) was added. The homogeneous solution was stirred for 10 min, and $BF_3 \cdot Et_2O$ in dry CH_2Cl_2 (0.5 M, 0.1 mL) was added. The resulting solution was stirred at 0 °C for 15 min, warmed to room temperature, and stirred for 0.5 h. Three more portions of $BF_3 \cdot Et_2O$ in CH_2Cl_2 (0.1 mL) were added at intervals of 0.5 h, and the solution was stirred at room temperature for a further 1 h. The reaction mixture was quenched and worked up as in method A.

Received: March 28, 2000 [Z14906]

[1] I. Fleming, *Comprehensive Organic Synthesis, Vol. 2* (Ed.: B. M. Trost), Pergamon, Oxford, **1991**, pp. 576 – 594; b) P. Mangeney, *Tetrahedron: Asymmetry* **1990**, *8*, 477.

[2] M. H. D. Postema, *C-glycoside synthesis*, CRC, Boca Raton, FL, **1995**; b) E. D. Levy, C. Tang, *The chemistry of C-glycosides*, Pergamon, Oxford, **1995**; c) For the synthesis of 2,5-disubstituted tetrahydrofurans, see J. C. Harmange, B. Figadere, *Tetrahedron: Asymmetry* **1993**, *4*, 1711 – 1754.

[3] For six-membered-ring oxocarbenium ions, see T. Harada, T. Nakamura, M. Kinugasa, A. Oku, *J. Org. Chem*. **1999**, *64*, 7594 – 7600, and references therein; T. Sammakia, R. S. Smith, *J. Am. Chem. Soc*. **1992**, *114*, 10998 – 10999; S. E. Denmark, N. G. Almstead, *J. Am. Chem. Soc.* **1991**, *113*, 8089 – 8110.

[4] For five-membered-ring oxocarbenium ions, see a) C. H. Larsen, B. H. Ridway, J. T. Shaw, K. A. Woerpel, *J. Am. Chem. Soc.* **1999**, *121*, 12208 – 12209; J. T. Shaw, K. A. Woerpel, *Tetrahedron* **1999**, *55*, 8747 – 8756; b) A. Schmitt, H.-U. Reissig, *Synlett* **1990**, 40 – 42.

[5] For acyclic acetals, see K. Manju, S. Trehan, *Chem. Commun.* **1999**, 1929 – 1930.

[6] P. Collins, R. Ferrier, *Monosacharides: Their chemistry and their roles in Natural Products*, Wiley, New York, **1995**; b) A. Cavé, D. Cortés, B. Frigadere, R. Hocquemiller, O. Laprévot, A. Laurens, M. Leboeuf, *Phytochemical Potential of Tropical Plants*; *Recent Advances in Phytochemistry*, *Vol. 27* (Eds.: K. R. Bownum, J. Romeo, H. H. A. Stafford), Plenum, New York, **1993**.

[7] Many stereocontrolled approaches to these structures have been reported. Among them, nucleophilic substitution at the anomeric center of a furanoid glycal or a furanosyl halide appears to be a general strategy for preparing the corresponding 2-substituted tetrahydrofuran (see ref. [2]).

[8] P. Armas, F. García-Tellado, J. J. Marrero-Tellado, J. Robles, *Tetrahedron Lett.* **1998**, *39*, 131 – 134.

[9] The 1,2-*O*-isopropylidene group is easily introduced in the carbohydrate either by direct treatment of the free sugar with acetone (or a suitable derivative) and acid[4a] or by using the protocal of Suárez et al., which entails the rearrangement of a suitable 2,3-O-isopropylidene-protected furanoside to the required 1,2-protected one.[12]

[10] After work-up and chromatography no other diastereomers could be isolated or detected. The configuration assigned to each newly created stereogenic center was confirmed by nOe spectroscopic analysis.

[11] P. Kozikowski, K. L. Sorgi, *Tetrahedron Lett.* **1983**, *24*, 1563 – 1566.

[12] P. Armas, C. G. Francisco, E. Suárez, *J. Am. Chem. Soc*. **1993**, *115*, 8865 – 8866.

[13] A series of 3-alkoxymethyl-5-alkoxy-2,7-dioxabicycle[2.2.1]heptane acetals derived from 6-O-protected D-galactal have been used as electrophilic substrates for C-glycosidation.[14] The bicycle does not seem to play a special role in the stereochemical outcome of these reactions, and the 1,3-*syn* stereoselectivity observed is in total accordance with the stereoelectronic model proposed by Woerpel et al.[4b]

[14] V. Jaouen, A. Jégou, L. Lemée, A. Veyrières, *Tetrahedron* **1999**, *55*, 9245 – 9260.

 © WILEY-VCH Verlag GmbH, D-69451 Weinheim, 2000 1433-7851/00/3915-2729 $ 17.50+.50/0

A Hexagonal Perovskite Intergrowth Compound: $La_2Ca_2MnO_7$**

Yingxia Wang, Jianhua Lin,* Yu Du, Ruiwen Qin, Bin Han, and Chun K. Loong

Perovskite and related compounds have attracted considerable interest during the last two decades because of their extraordinary physical properties. High-T_C cuprate superconductors and colossal magnetoresistance (CMR) manganese oxides are just two examples of a number of interesting materials with such perovskite-related structures.[1–4] Although diverse compositions and structure types have been identified for perovskite-related compounds, they primarily involve alternate stacking of the perovskite layers with layers of other structural types. The Ruddlesden–Popper phases $(ABO_3)_nAO$ [5, 6] are a well-known family of perovskite intergrowth compounds; in these compounds, multiple perovskite layers *n* octahedra thick alternate with single AO rock salt layers. The perovskite-related AO-rich intergrowth compounds $(AO)_nABO_3$ have also been obtained in cuprate systems such as $Bi_2Sr_2CuO_6$ and $Tl_2Sr_2CuO_6$.[1, 5]

In the known perovskite-related intergrowth compounds, tetragonal perovskite layers (that is, the (001) plane of cubic perovskite) are most frequently observed, and hexagonal perovskite layers (that is, the (111) plane of cubic perovskite) are rare. This structural preference clearly originates from the synergistic relationship between the interfacial structures adopted by the perovskite layers and other intergrowth components. For example, both cubic perovskite and rock salt structures have identical (001) planes with the composition "AO"; therefore, the topology of the interfacial structure remains unchanged or undergoes only a small distortion when they form an intergrowth compound. In contrast, the surface of the (111) perovskite block is a close packed AO_3 layer, and a hexagonal intergrowth compound can form only when the insert layer fits into this particular structural arrangement with favorable energy over the perovskite structure. One example of what can be regarded as hexagonal perovskite intergrowth compounds is the $BaNiO_3$ type and its derivatives. $BaNiO_3$ is a hexagonal modification of the perovskite structure in which AO_3 forms a hexagonal close packing and the NiO_6 octahedra share two opposite faces to form one-dimensional chains along the *c* axis. The intergrowth of cubic perovskite and the $BaNiO_3$ type with variable periodicities of the cubic and hexagonal layer results in various polytype structures.[5, 7] However, these compounds are generally considered to belong to the perovskite family rather than being new intergrowth compounds. Owing to the distinctive contribution of perovskite layers to the physical properties, such as superconductivity and colossal magnetoresistance, it is of interest to search for hexagonal perovskite intergrowth compounds and to see how the physical properties are influenced by different kinds of perovskite layers.

During studies on the Ca/La/Mn/O system, we identified the new compound $La_2Ca_2MnO_7$. The empirical formula of this phase was established initially by a systematic synthetic study in the phase diagram. Chemical analysis indicated that the formal oxidation state of manganese in this compound is Mn^{IV}. Crystallographic studies confirmed the composition of the compound and further established that it is an intergrowth compound formed by hexagonal perovskite and "Ca_2O" layers.[8]

The crystal structure of $La_2Ca_2MnO_7$ is composed of nearly ideal close-packed $[LaO_3]$ arrays, which are stacked in sequence AABBCC along the *c* axis. The Mn and Ca atoms, respectively, occupy the octahedral and trigonal-prismatic sites between the closed-packed $[LaO_3]$ sheets. Figure 1 shows the structure of $La_2Ca_2MnO_7$; the Mn atoms lie within the octahedra. Scheme 1 shows the packing sequence in the structure of $La_2Ca_2MnO_7$.

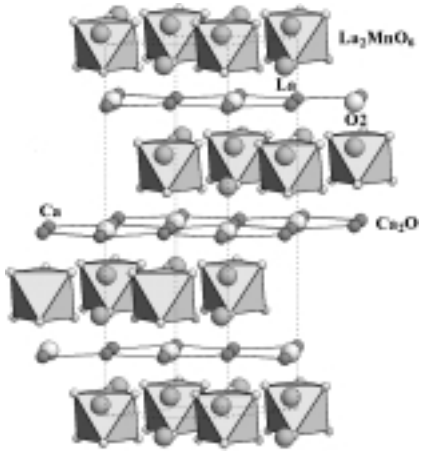
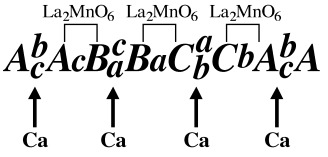


Figure 1. Crystal structure of $La_2Ca_2MnO_7$; Mn1 atoms lie within the octahedra, the vertices of which are formed by the O1 atoms. La1 atoms are shown as isolated dark circles. The Ca1 atoms form a graphite-like network, and the O2 atoms are located at the centers of the hexagons. For clarity, the distortion of the O2 site is not shown.



Scheme 1. The packing sequence in the structure of $La_2Ca_2MnO_7$. The capital letters represent the close-packed $[LaO_3]$ layers, and the small letters the positions of the Mn and Ca atoms. The Ca atoms are represented by two letters, because the Ca positions are divided into two groups.

[*] Prof. J. Lin, Dr. Y. Wang, Yu. Du, R. Qin, B. Han
State Key Laboratory for Rare Earth Materials Chemistry and Applications
Department of Materials Chemistry, Peking University
Beijing 100871 (P.R. China)
Fax: (+86) 10-6275-1708
E-mail: jhlin@chem.pku.edu.cn
Dr. C. K. Loong
Intense Pulsed Neutron Source Division
Argonne National Laboratory
Argonne, IL 60439 (USA)

[**] We are thankful for financial support from the Youth Scientist Excellency Foundation (29625101), NSFC (29731010), and State Key Basic Research Program. Work performed at Argonne is supported by US DOE-BES under Contract No. W-31-109-ENG-38.

Supporting information for this article is available on the WWW under http://www.wiley-vch.de/home/angewandte/ or from the author.

 © WILEY-VCH Verlag GmbH, D-69451 Weinheim, 2000 1433-7851/00/3915-2730 $ 17.50+.50/0

The Mn octahedra form a single hexagonal (111) perovskite layer with the composition of La_2MnO_6. The Ca atoms are located between the hexagonal perovskite blocks and form a graphite-like sheet. The coordination polyhedron of the Ca atoms is a trigonal prism formed by six oxygen atoms in the perovskite layers. The Ca layer contains an additional oxygen atom (O2); hence, the overall composition is "Ca_2O". Therefore, $La_2Ca_2MnO_7$ can be considered as an intergrowth compound in which single hexagonal perovskite (111) layers (La_2MnO_6) stack alternately with "Ca_2O" layers and can be described as $(La_2MnO_6)(Ca_2O)$. Only the early rare earth elements (Ln = La to Sm) form such compounds; the others form mixed oxides at this composition.

The Ca atoms in the "Ca_2O" layer form a graphite-like hexagonal network, in which the additional oxygen atom (O2) is located with a sixfold distortion. This distortion can be clearly seen in the difference Fourier map shown in Figure 2. The distortion of the oxygen atoms in the Ca layer can be

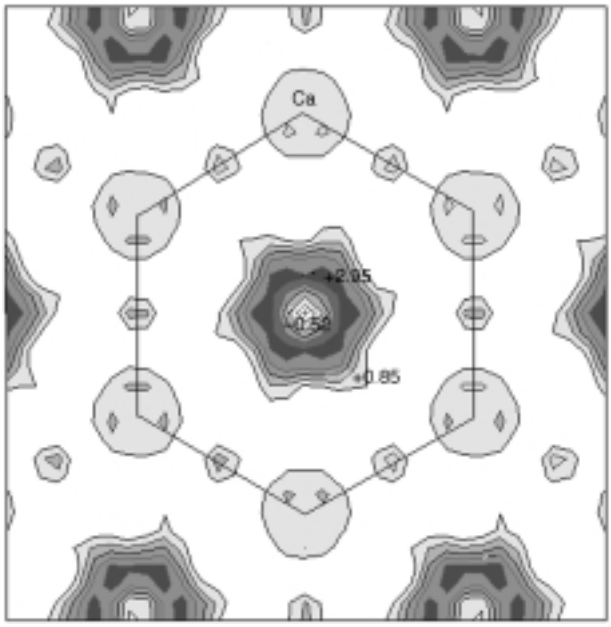


Figure 2. Electron density of the O2 position calculated from difference Fourier maps; some typical values of the electron density are shown. The Fourier map calculation was carried out by including all atoms except O2.

understood by considering their coordination environment. All of the Ca hexagonal nets are bicapped by La atoms to give hexagonal-bipyramidal polyhedra. The center of the hexagonal bipyramid is not suitable for the oxygen atom, because the distance between the opposite La atoms is too short (4.2 Å). Two other vacancies, namely, tetrahedral and triangular, are present in the hexagonal bipyramid. The triangular site is a little too small for the oxygen atoms and, from the difference Fourier map, the O2 atoms prefer to occupy the tetrahedral sites. The Ca–O2 bond length is about 2.65 Å, which is comparable with those within the trigonal prism (2.43 and 2.38 Å); therefore, the O2 atoms are capped on the rectangular faces of the Ca trigonal prisms. On average, the coordination polyhedron of the Ca atoms is a monocapped trigonal prism. In the space group $R\bar{3}$, the O2 atom can approximately be represented by a general position (0.0, 0.132(2), 0.5), and the refined occupation factor is about 0.17, which agrees very well with that expected from the empirical formula (⅙).

In the $La_2Ca_2MnO_7$ structure, the MnO_6 octahedra are isolated; hence, we could expect rather localized physical properties for this compound. $La_2Ca_2MnO_7$ shows Curie–Weiss paramagnetic behavior above $-233\,^{\circ}C$ (40 K) and a weak antiferromagnetic interaction was observed at low temperature ($\theta = 42.5$). The effective magnetic moment in the high-temperature range is $\mu_{eff} = 4.0\,\mu_B$, which agrees with that of a spin-only isolated Mn^{IV} ion ($3.87\,\mu_B$). The conductivity of $La_2Ca_2MnO_7$ increases from $\sigma = 1.0 \times 10^{-4}\,\Omega^{-1}\,cm^{-1}$ at 200 °C to about $2.3 \times 10^{-2}\,\Omega^{-1}\,cm^{-1}$ at 770 °C.

$La_2Ca_2MnO_7$ is a novel example of a hexagonal perovskite intergrowth compound, formed by alternative stacking of hexagonal perovskite (La_2MnO_6) and "Ca_2O" layers. Unlike the $BaNiO_3$ derivatives, the building blocks in this compound are of two distinct structure types, and it therefore provides a new principle for rational synthesis of perovskite-related compounds. Comparison with the Ruddlesden–Popper phases $(ABO_3)_nAO$ suggests the existence of the hexagonal perovskite intergrowth analogue $(La_{n+1}Mn_nO_{3n+3})(Ca_2O)$. According to this formula, $La_2Ca_2MnO_7$ is the $n = 1$ member of this hexagonal perovskite intergrowth family. Accordingly, the cubic perovskite or $BaNiO_3$-type structure is the end-member with $n = \infty$ in this family. The compounds of $n > 1$ in this family should contain two-dimensional hexagonal perovskite blocks formed by corner-sharing Mn octahedra; we could therefore expect stronger magnetic interactions between the transition metal atoms, which may lead to interesting physical properties.

Experimental Section

A stoichiometric mixture of $La(NO_3)_3$, $Ca(NO_3)_2$, and $Mn(NO_3)_2$, and an excess of citric acid (1:1.2) were dissolved in water. After removing H_2O, the mixture was heated at about 600 °C in a furnace, and a fine powder of the mixed oxides was obtained. The product $La_2Ca_2MnO_7$ was obtained by further heating the mixed oxides at 900 °C for 2 d. X-ray powder diffraction on a Rigaku D/Max-2000 diffractometer indicated that single-phase products can be obtained as long as a stoichiometric mixture of starting materials is used. The formal oxidation state of manganese, as determined by the oxalate titration method, is 3.99(2).

Received: February 21, 2000 [Z 14743]

[1] J. B. Goodenough, A. Manthiram in *Chemistry of High Temperature Superconductors* (Ed.: C. N. R. Rao), World Scientific, London, **1991**, p. 1.
[2] H. Müller-Buschbaum, *Angew. Chem.* **1989**, *101*, 1503; *Angew. Chem. Int. Ed. Engl.* **1989**, *28*, 1472.
[3] R. von Helmolt, J. Wecker, B. Holzapfel, L. Schultz, K. Sanwer, *Phys. Rev. Lett.* **1993**, *71*, 2331.
[4] B. Raveau, A. Maignan, C. Martin, M. Hervieu, *Chem. Mater.* **1998**, *10*, 2641.
[5] C. N. R. Rao, B. Raveau, *Transition Metal Oxides*, 2nd ed., Wiley-VCH, Weinheim, **1998**, p. 61.
[6] P. D. Battle, W. R. Branford, A. Mihut, M. J. Rosseinsky, J. Singleton, J. Sloan, L. E. Spring, J. F. Vente, *Chem. Mater.* **1999**, *11*, 674.
[7] G. B. Hyde, S. Andersson, *Inorganic Crystal Structures*, Wiley, New York, **1989**, p. 74.
[8] The crystal structure of $La_2Ca_2MnO_7$ was solved by direct methods (Sirpow92)[9] on X-ray powder diffraction data and refined by the

 © WILEY-VCH Verlag GmbH, D-69451 Weinheim, 2000 1433-7851/00/3915-2731 $ 17.50+.50/0

Rietveld method (GSAS)[10] on both X-ray and neutron diffraction data ($Rp = 0.058$, $Rwp = 0.084$). $La_2Ca_2MnO_7$ crystallizes in the space group $R\bar{3}$ (no. 148), $Z = 3$, with the lattice constants $a = 5.62176(4)$, $c = 17.3161(2)$, $V = 473.968(7)$. The refined atomic coordinates are Mn1: (3a) 0, 0, 0; La1: (6c) 0, 0, 0.37757(3); Ca1: (6c) 0, 0, 0.82745(7); O1: (18f) 0.0148(4), 0.502(3), 0.6024(1); O2: (18f) 0, 0.128(1), 0.5. The refined x and z values of the O2 position were $x = -0.026(15)$ and $z = 0.499(3)$, which are very close to 0 and ½, they were therefore fixed to improve the displacement parameters. The occupation factor of O2 was refined and fixed to ⅙ in the final refinement. The refinement also indicates mutual replacement of La and Ca atoms at the La1 and Ca1 positions, and the ratio was refined and fixed to La1: La/Ca = 0.933/0.077 and Ca1: Ca/La = 0.933/0.077 in the final refinement.

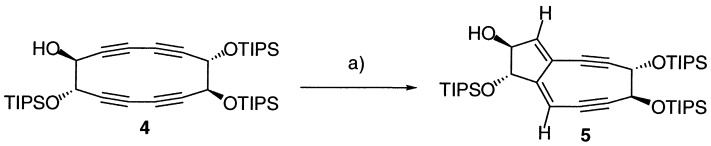
[9] A. Altomare, M. C. Burla, M. Camalli, G. Cascarano, C. Giacovazzo, A. Guagliardi, G. Polidori, *J. Appl. Crystallogr.* **1994** *27*, 435.

[10] A. C. Larson, R. B. von Dreele, Report LAUR 86-748, Los Alamos National Laboratory, **1985**.

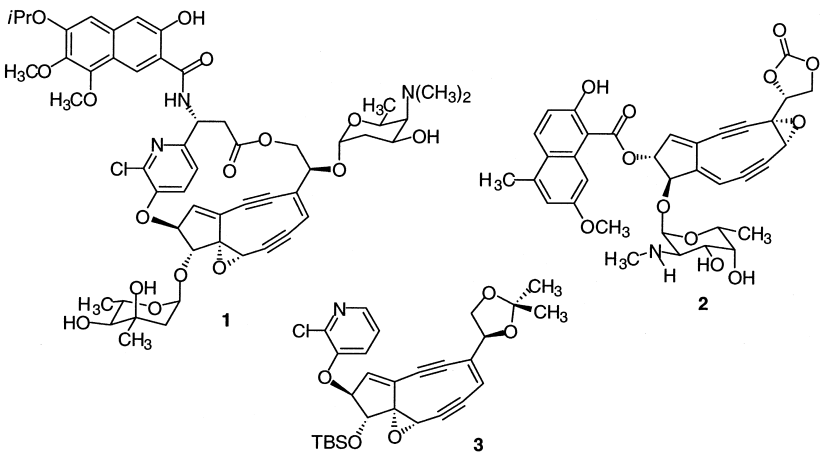
Synthesis of the Kedarcidin Core Structure by a Transannular Cyclization Pathway**

Andrew G. Myers* and Steven D. Goldberg

Kedarcidin is a chromoprotein enediyne antibiotic that is marked by the structural complexity and extraordinary reactivity of its chromophore component (**1**).[1] Like the related chromoprotein natural product neocarzinostatin,[1, 2] kedarcidin exhibits potent antitumor activity. The kedarcidin chromophore (**1**) and neocarzinostatin chromophore (**2**) share a common bicyclic carbon skeleton, but the site of epoxidation in the two structures is different (Scheme 1). As a result of this difference **1**, which contains a conjugated (*Z*)-enediyne group, is capable of cycloaromatization upon mild thermal activation alone (facile at 37 °C), whereas **2** requires nucleophilic activation for biradical formation.[2, 3] The reactivity of compound **1** and also its many unusual structural features—a highly unsaturated and strained core, bridging macrolactone, 2-chloro-3-pyridyl ether, and β-amino ester functionalities, as well as uncommon carbohydrate residues—make it an exceedingly challenging synthetic problem. Outstanding progress toward this goal has been achieved in Hirama's laboratory, including the preparation of a functional core model.[4] Recently, we described a new strategic approach to the synthesis of the common bicyclic carbon skeleton of **1** and **2** that featured the reductive transannular cyclization of a tetrayne precursor promoted by hydride addition (**4** → **5**, Scheme 2).[5] Unresolved issues regarding the adaptation of this approach to the synthesis of the kedarcidin core structure were the compatibility of the hydride reagent with a more highly functionalized substrate that would be suitable for the synthesis of **1**, the problem of regio- and stereoselective epoxidation of the diene product, and the introduction of the central olefin of the (*Z*)-enediyne group. These problems have been addressed, as described herein, within the context of an enantioselective synthesis of the kedarcidin core structure **3** (Scheme 1).



Scheme 2. Reductive transannular cyclization of the tetrayne **4**. a) KHMDS, $NaAlH(OCH_2CH_2N(CH_3)_2)_3$, THF, −78 °C, 50–54 %.[5]



Scheme 1. The structures of kedarcidin chromophore (**1**), neocarzinostatin chromophore (**2**), and the synthetic kedarcidin core structure **3**.

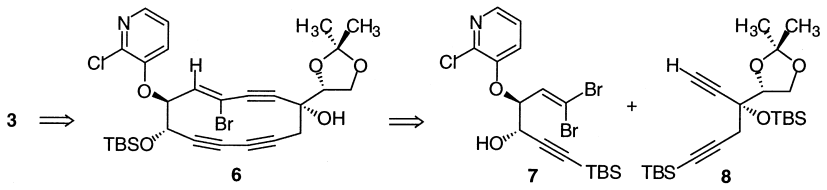
The prior reductive cyclization (**4** → **5**) was problematic with regard to a synthesis of **1** from two standpoints: (1) the requirement for a free propargylic hydroxyl group to direct the hydride addition meant that introduction of the pyridyl ether of **1** must occur after formation of the reactive core, and (2), as discussed, functional group compatibility was limited by the strongly reducing hydride reagent. To address these problems we considered an alternative strategy for the generation of the vinyl–metal intermediate believed to mediate the transannular ring closure, one involving low-temperature lithium–halogen exchange within a vinyl halide precursor such as the bromide **6**. To test this hypothesis, precursor **6** was synthesized, using as starting materials the dibromoolefin **7** and the diyne **8**,[6] two optically pure components of similar size and complexity (Scheme 3).

The enantioselective synthesis of the dibromoolefin **7**, a molecule with a latent C_2-symmetry axis, evolved from the exploration of several different synthetic routes, and ulti-

[*] Prof. A. G. Myers, S. D. Goldberg
Department of Chemistry and Chemical Biology
Harvard University
Cambridge, MA 02138 (USA)
Fax: (+1) 617-495-4976
E-mail: myers@chemistry.harvard.edu

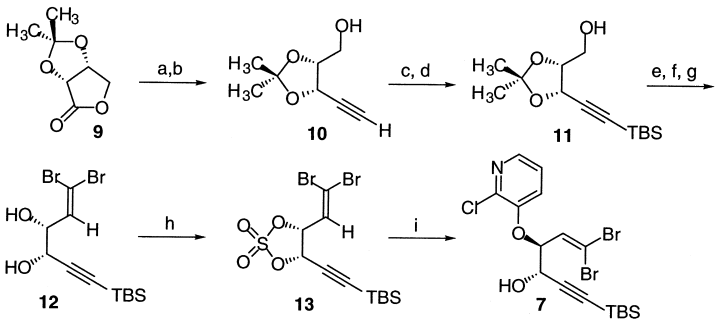
[**] Financial support from the National Institutes of Health is gratefully acknowledged.

 © WILEY-VCH Verlag GmbH, D-69451 Weinheim, 2000 1433-7851/00/3915-2732 $ 17.50+.50/0



Scheme 3. Retrosynthetic analysis of **3**.

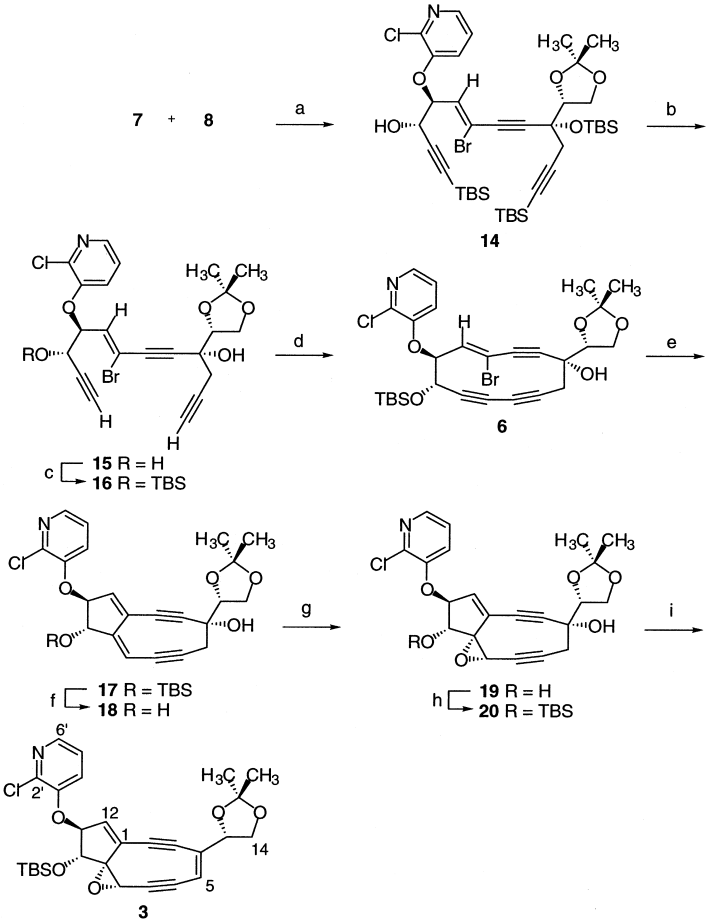
mately relied upon a subtle difference in the reactivity of the allylic and propargylic C–O bonds of the cyclic sulfate **13**, which was prepared using 2,3-*O*-isopropylidene-D-erythronolactone (**9**) as starting material (Scheme 4). A useful new



Scheme 4. Synthesis of the dibromide **7**. a) DIBAL (1.15 equiv), toluene, −78 °C, 96 %; b) LDA (2.4 equiv), $TMSCHN_2$ (1.2 equiv) THF, −78 →23 °C, 81 %; c) [LHMDS (1.25 equiv); TBSOTf (1.25 equiv)] × 2, THF, −78 °C; d) $Et_3N \cdot 3HF$ (2.5 equiv), THF, 23 °C, 82 % (from **10**); e) $(COCl)_2$ (2.0 equiv), DMSO (4.0 equiv), Et_3N (4.0 equiv), CH_2Cl_2, −78 →0 °C; f) PPh_3 (4.0 equiv), CBr_4 (2.0 equiv), Et_3N (4.0 equiv), CH_2Cl_2, 0 °C, 86 % (for 2 steps); g) TsOH (0.5 equiv), EtOH, reflux, 95 %; h) SO_2Cl_2 (1.8 equiv), Et_3N (4.0 equiv), DMAP (0.4 equiv), CH_2Cl_2, −78 °C, 50–70 %; i) NaH (2.0 equiv), 2-chloro-3-pyridinol (2.5 equiv), CH_3CN, −40 °C, 82 %. TMS = trimethylsilyl, LHMDS = lithium hexamethyldisilazanide, TBS = *tert*-butyldimethylsilyl, tf = triflate = trifluoromethanesulfonyl, Ts = toluene-4-sulfonyl.

homologative alkynylation sequence[7] was developed to transform the lactone **9** into the acetylene **10**. Reduction of **9** with diisobutylaluminum hydride (DIBAL, 1.15 equiv)[8] in toluene (−78 °C), followed by addition of a solution of the resultant lactols in tetrahydrofuran (THF) to a mixture of lithium diisopropylamide (LDA, 1.2 equiv) and (trimethylsilyl)diazomethyllithium[9] (1.2 equiv, formed from LDA and $TMSCHN_2$) in THF (−78 → 23 °C), provided **10** in 77 % yield. Iterative silylation of the hydroxyl and alkynyl groups of **10**, respectively, followed by selective cleavage of the Si–O bond with $Et_3N \cdot 3HF$ afforded the C-protected product **11** (82 % overall). Oxidation of **11** under Swern conditions, dibromoolefination[10] of the resultant aldehyde, and acidic hydrolysis of the acetonide protective group within the olefinic product furnished the diol **12** in 82 % yield for the three-step sequence. Activation of **12**, in the form of the corresponding cyclic sulfate **13** (50–70 % yield), was then accomplished by the slow addition of a solution of freshly distilled sulfuryl chloride (1.8 equiv, 79 mM, approximately 0.3 mL min^{-1}) in dichloromethane to a cold (−78 °C) solution of **12** (44 mM) in dichloromethane containing triethylamine (4.0 equiv) and 4-(dimethylamino)pyridine (DMAP, 0.4 equiv).[11] Addition of a solution of **13** in acetonitrile to a suspension of 2-chloro-3-pyridinol (2.5 equiv) and sodium hydride (2.0 equiv) in acetonitrile at −40 °C, followed by a brief acidic work-up to hydrolyze the intermediate sulfate ester,[11] afforded the pyridyl ether **7**, in which the allylic sulfate had been displaced selectively, in 82 % yield. The selectivity observed in this reaction (approximately 11:1 favoring allylic displacement) is noteworthy. Although allylic halides undergo solvolysis more readily than propargylic halides,[12] prediction of the outcome of the present transformation, with its greater S_N2 character and substituent effects (1,1-dibromoolefin, silylacetylene), was not obvious.

Palladium-mediated coupling of the dibromoolefin **7** and the diyne **8**[6] in diethyl ether in the presence of cuprous iodide (0.3 equiv) and triethylamine (2.0 equiv) proceeded optimally using tetrakis(triphenylphosphine) palladium(0) (0.1 equiv)



Scheme 5. Synthesis of the kedarcidin core structure **3**. a) $Pd(PPh_3)_4$ (0.1 equiv), Et_3N (2.0 equiv), CuI (0.3 equiv), Et_2O, 23 °C, 61 %; b) TBAF (4.0 equiv), 2-nitrophenol (4.5 equiv), THF, 0 →23 °C, 87 %; c) TBSOTf (1.2 equiv), 2,6-lutidine (2.4 equiv), CH_2Cl_2, 0 °C, 95 %; d) $Cu(OAc)_2$ (30 equiv), pyridine, THF, then CuI (5 equiv), 60 °C, then **16**, 74–86 %; e) 3 Å molecular sieves, 23 °C; LHMDS (1.05 equiv), THF, −96 °C; *t*BuLi (1.05 equiv), −96 °C; HOAc (12 equiv), 44–60 %; f) $Et_3N \cdot 3HF$ (20 equiv), THF, 23 °C; g) $VO(acac)_2$ (1.0 equiv), TBHP (2.0 equiv), EtOAc, 23 °C; h) TBSOTf (17 equiv), 2,6-lutidine (30 equiv), EtOAc, 23 °C, 53 % (from **17**); i) MsCl (4 equiv), Et_3N (8 equiv), CH_2Cl_2, 0 °C; DBU (12 equiv), 23 °C, 78 %.[4]

 © WILEY-VCH Verlag GmbH, D-69451 Weinheim, 2000 1433-7851/00/3915-2733 $ 17.50+.50/0

as catalyst and afforded the (*Z*)-vinyl bromide **14** exclusively, in 61% yield (Scheme 5). The selectivity of this coupling reaction is presumably steric in origin[13] and involves oxidative addition of Pd^0 into the less-hindered carbon–bromine bond. There is precedence for (*E*)-selective coupling (replacement of the more hindered (*Z*)-halide within a 1,1-dibromoolefin) in a related system, a result which was attributed, in that case, to internal delivery of Pd^0 by prior coordination to a tethered terminal acetylene.[14] The presence of the bulky *tert*-butyldimethylsilyl group in the present case may preclude such a directing effect.

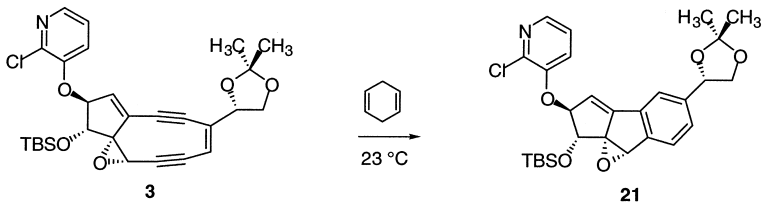
Attempted cleavage of the silyl protective groups within **14** using tetrabutylammonium fluoride (TBAF) was complicated by the concurrent elimination of hydrogen bromide (to afford the corresponding tetrayne). This undesired pathway was found to be minimized in the presence of phenolic additives, but only those that fell within a narrow range of acidity.[15] Under optimum conditions, involving the addition of TBAF (4.0 equiv) to a solution of **14** and 2-nitrophenol (4.5 equiv, $pK_a = 7.22$)[16] in THF at 0 °C, followed by warming of the resultant solution to 23 °C over 17 h, the desilylated product **15** was formed cleanly, in 87% yield. The incorporation of less acidic additives, such as phenol ($pK_a = 10.0$) or 2-bromophenol ($pK_a = 8.42$),[16] led to greater amounts of the elimination product and correspondingly lower yields of the desired product, whereas more acidic additives, such as 2,6-dichlorophenol ($pK_a = 6.79$) or pentachlorophenol ($pK_a = 4.4$),[16] retarded the rate of desilylation to such an extent as to be impractical.

With the development of an efficient procedure for the cleavage of both silicon–carbon bonds (as well as the tertiary silyl ether) within **14**, the secondary hydroxyl group of the product (**15**) was protected, selectively, using TBSOTf (1.2 equiv) and 2,6-lutidine (2.4 equiv, 95%),[17] primarily to lend stability to the macrocyclic intermediate that is formed in the next step. Many experiments were necessary before efficient, reproducible, and scalable reaction conditions were found to achieve the oxidative coupling (Glaser reaction)[18] necessary for this transformation (**16** → **6**). The optimized procedure, a modification of Eglinton conditions,[19] involved the addition of a dilute solution of **16** in pyridine:THF (2:1, 4.0 mM, approximately 1 mL min^{-1}) to a mixture of copper(II) acetate ($Cu(OAc)_2$, 30 equiv) and copper(I) iodide (CuI, 5.0 equiv) in pyridine:THF (2:1, $[Cu]_{total} = 0.15$ M) at 60 °C under an argon atmosphere. For successful coupling it was essential to prepare the mixture of copper salts by an exacting protocol. Specifically, it was necessary to age the copper(II) acetate in pyridine:THF at 23 °C (5 min), forming a (sparingly soluble) royal-blue precipitate,[20] prior to the addition of the (more soluble) copper(I) iodide, heating to 60 °C (20 min), and addition of substrate **16**. Co-mixing of the solid reagents, by contrast, gave lower yields of product.[21] After an aqueous work-up and isolation by flash column chromatography the macrocycle **6** was obtained in 74–86% yield. This procedure deviates from the standard Eglinton conditions by the incorporation of a Cu^I salt and by the use of an inert atmosphere (as opposed to oxygen). Breslow and co-workers have already described such a modification, but used a mixture of CuCl and $CuCl_2$,[22] a reagent combination which did not lead to successful coupling within **16**. As anticipated, the product **6** exhibited greater stability than the cyclic tetraynes (such as structure **4**) that were prepared in our earlier route but did decompose if held in neat form.

In preparation for the key step of the synthetic sequence, a dried solution (3 Å molecular sieves, THF, 23 °C, 20 min) of the macrocyclic bromo alcohol **6** was cooled to −96 °C, then was treated with a solution of lithium hexamethyldisilazanide (LHMDS) in THF (0.5 M, 1.05 equiv) to deprotonate the tertiary hydroxyl group. Subsequent addition of a solution of *tert*-butyllithium (1.47 M in pentane, 1.05 equiv) at −96 °C and immediate quenching with acetic acid (12 equiv) then afforded the bicyclic product **17** in 44–60% yield after aqueous work-up and chromatographic isolation. A small amount (approximately 20%) of the product of protonation of the putative vinyllithium intermediate was also isolated. This side-product, undiminished by delaying the acid quench, is believed to arise by proton transfer with hexamethyldisilazane, formed stoichiometrically in the reaction. The proposed transannular cyclization is evidently quite rapid to compete with such a process.[23]

Completion of the core synthesis was achieved by hydroxyl-directed epoxidation and elimination of the tertiary hydroxyl group within the substrate **18**, which was prepared by desilylation of **17** with triethylamine trihydrofluoride ($Et_3N \cdot 3HF$, 20 equiv) in THF at 23 °C. Treatment of **18** with vanadyl acetoacetonate ($VO(acac)_2$, 1.0 equiv) and *tert*-butyl hydroperoxide (TBHP, 2.0 equiv) at 23 °C in ethyl acetate provided the desired epoxide **19** as a single regio- and stereoisomer in good yield (determined at a later stage, see below). In contrast to this, attempts to epoxidize **18** using 4-chloroperoxybenzoic acid (*m*CPBA) or dimethyldioxirane were not successful. These findings are in excellent agreement with proposed transition-state models for hydroxyl-directed epoxidations.[24, 25] The optimum dihedral angle formed by the hydroxyl group and the olefinic plane (∢ O-C-C=C) in the directed epoxidation of allylic alcohols is proposed to be 50° for the vanadium catalyst,[24] approximately 120° for *m*CPBA,[24] and about 130° for dimethyldioxirane;[25] we estimate this dihedral angle to be approximately 60° in the lowest energy conformer of **18**. Selective protection of the secondary hydroxyl group of **19** (TBSOTf (17 equiv), 2,6-lutidine (30 equiv), ethyl acetate, 23 °C) then afforded the product **20** in 53% yield (from **17**, three steps). Finally, the central olefin (C4-C5) of **3** was introduced by elimination of the tertiary hydroxyl group of **20** under conditions developed by Hirama and co-workers in their kedarcidin core synthesis (methanesulfonyl chloride (MsCl, 4 equiv), triethylamine (8 equiv), CH_2Cl_2, 0 °C; 1,8-diazabicyclo[5.4.0]undec-7-ene (DBU, 12 equiv), 23 °C),[4] providing the kedarcidin core structure (**3**) in 78% yield. This product proved to be sufficiently stable for chromatographic isolation and full characterization (^1H NMR, ^{13}C NMR, and IR spectroscopy and high resolution mass spectrometry),[26] but it did undergo cycloaromatization upon standing at ambient temperature (18 h, 1,4-cyclohexadiene) to form the tricyclic epoxide **21** (21% yield from **20**, Scheme 6). The latter product (**21**) was also unstable, particularly toward silica gel, presumably due to

 © WILEY-VCH Verlag GmbH, D-69451 Weinheim, 2000 1433-7851/00/3915-2734 $ 17.50+.50/0 *Angew. Chem. Int. Ed.* **2000**, *39*, No. 15



Scheme 6. Cycloaromatization of **3**.

facile solvolytic cleavage of the benzylic C–O bond of the epoxide ring.

The synthetic route described provides the fully functionalized core of kedarcidin chromophore (**3**) in 18 linear steps with an average yield of 81% per step (overall yield 2.3%) and demonstrates the feasibility of the transannular cyclization approach in this context. In addition, we have established a viable protocol for epoxidation of the product and have shown that all intermediates in the synthetic sequence are sufficiently stable to be isolated. On the basis of these findings, a parallel approach to the synthesis of **1** itself, in which transannular cyclization is conducted within a substrate containing the macrolactone ring, now appears feasible. Findings of potentially general value in synthesis include the development of a two-step sequence for the homologative alkynylation of lactones, new and mild conditions for the cleavage of acetylenic Si–C bonds, and a new procedure for oxidative acetylenic coupling.

Received: April 14, 2000 [Z15004]

[1] J. E. Leet, D. R. Schroeder, D. R. Langley, K. L. Colson, S. Huang, S. E. Klohr, M. S. Lee, J. Golik, S. J. Hofstead, T. W. Doyle, J. A. Matson, *J. Am. Chem. Soc.* **1993**, *115*, 8432 – 8443.

[2] *Neocarzinostatin: The Past, Present, and Future of an Anticancer Drug* (Eds.: H. Maeda, K. Edo, N. Ishida), Springer, Tokyo, **1997**.

[3] There is evidence that the kedarcidin chromophore is subject to nucleophilic activation as well. For example, it has been shown that **1** undergoes reduction/cycloaromatization with sodium borohydride; see: Ref. [1].

[4] a) K.-i. Iida, M. Hirama, *J. Am. Chem. Soc.* **1995**, *117*, 8875 – 8876; b) S. Kawata, F. Yoshimura, J. Irie, H. Ehara, M. Hirama, *Synlett* **1997**, 250 – 252.

[5] A. G. Myers, S. D. Goldberg, *Tetrahedron Lett.* **1998**, *39*, 9633 – 9636.

[6] Diyne **8** was prepared according to the protocol of Hirama for a closely related compound, differing from **8** only in the nature of the silyl protective groups; see: K.-i. Iida, M. Hirama, *J. Am. Chem. Soc.* **1994**, *116*, 10310 – 10311.

[7] An alternative two-step protocol involving dichloroolefination/reduction (Li sand) was not successful with substrate **9** (J. S. Yadav, V. Prahlad, M. C. Chander, *J. Chem. Soc. Chem. Commun.* **1993**, 137 – 138).

[8] N. Cohen, B. L. Banner, R. J. Lopresti, F. Wong, M. Rosenberger, Y.-Y. Liu, E. Thom, A. A. Liebman, *J. Am. Chem. Soc.* **1983**, *105*, 3661 – 3672.

[9] For the use of (trimethylsilyl)diazomethyllithium in the alkynylation of aldehydes, see: K. Miwa, T. Aoyama, T. Shioiri, *Synlett* **1994**, 107 – 108.

[10] E. J. Corey, P. L. Fuchs, *Tetrahedron Lett.* **1972**, 3769 – 3772.

[11] The conversion of a diol to a cyclic sulfate is typically conducted in a two-step procedure, by cyclic sulfite formation, then sulfite oxidation (Y. Gao, K. B. Sharpless, *J. Am. Chem. Soc.* **1988**, *110*, 7538 – 7539). In the present case, decomposition occurred during oxidation of the diastereomeric cyclic sulfite intermediates. Sharpless and co-workers have shown that electron-deficient vicinal diols can be transformed into the corresponding cyclic sulfates directly, in one step, using sulfuryl chloride (K. P. M. Vanhessche, K. B. Sharpless, *Chem. Eur. J.* **1997**, *3*, 517 – 522). The conditions developed here were optimal for substrate **12** and differ significantly from those described by Sharpless and co-workers.

[12] T. W. Bentley, J.-P. Dau-Schmidt, G. Llewellyn, H. Mayr, *J. Org. Chem.* **1992**, *57*, 2387 – 2392; for related calculations, see: Y.-R. Luo, J. L. Holmes, *J. Phys. Chem.* **1994**, *98*, 10368 – 10372.

[13] a) A. Minato, K. Suzuki, K. Tamao, *J. Am. Chem. Soc.* **1987**, *109*, 1257 – 1258; b) W. R. Roush, K. J. Moriarty, B. B. Brown, *Tetrahedron Lett.* **1990**, *31*, 6509 – 6512.

[14] a) J. M. Nuss, R. A. Rennels, B. H. Levine, *J. Am. Chem. Soc.* **1993**, *115*, 6991 – 6992; b) S. Torii, H. Okumoto, T. Tadokoro, A. Nishimura, Md. A. Rashid, *Tetrahedron Lett.* **1993**, *34*, 2139 – 2142.

[15] For other examples of the use of acidic additives in TBAF-mediated desilylations, see: a) AcOH: C. M. Hayward, D. Yohannes, S. J. Danishefsky, *J. Am. Chem. Soc.* **1993**, *115*, 9345 – 9346; b) AcOH: A. B. Smith III, S. S.-Y. Chen, F. C. Nelson, J. M. Reichert, B. A. Salvatore, *J. Am. Chem. Soc.* **1995**, *117*, 12013 – 12014; c) NH_4Cl: D. F. Taber, T. E. Christos, A. L. Reingold, I. A. Guzei, *J. Am. Chem. Soc.* **1999**, *121*, 5589 – 5590.

[16] S. R. Holmes-Farley, *Langmuir* **1988**, *4*, 766 – 774.

[17] E. J. Corey, H. Cho, C. Rucker, D. H. Hua, *Tetrahedron Lett.* **1981**, *22*, 3455 – 3458.

[18] C. Glaser, *Ber. Dtsch. Chem. Ges.* **1869**, *2*, 422 – 424.

[19] G. Eglinton, A. R. Galbreath, *J. Chem. Soc.* **1959**, 889 – 896.

[20] The royal-blue precipitate is proposed to be $Cu(OAc)_2(pyr)_4$; see: a) J. H. Mathews, E. B. Benger, *J. Phys. Chem.* **1914**, *18*, 264 – 268; b) E. Kokot, R. L. Martin, *Inorg. Chem.* **1964**, *3*, 1306 – 1312.

[21] When copper(I) acetate was used instead of copper(I) iodide compound **6** was still not formed, which may explain the failure of the co-mixing experiment.

[22] D. O'Krongly, S. R. Denmeade, M. Y. Chiang, R. Breslow, *J. Am. Chem. Soc.* **1985**, *107*, 5544 – 5545.

[23] Mechanisms involving single-electron transfer, although felt to be less likely, cannot be ruled out; see: W. F. Bailey, J. J. Patricia, *J. Organomet. Chem.* **1989**, *352*, 1 – 46, and references therein.

[24] B. E. Rossiter, T. R. Verhoeven, K. B. Sharpless, *Tetrahedron Lett.* **1979**, 4733 – 4736.

[25] W. Adam, A. K. Smerz, *Tetrahedron* **1995**, *51*, 13039 – 13044.

[26] Physical Data for compound **3** (see Scheme 5, Scheme 6 for proton numbering): ^{1}H NMR (500 MHz, [D$_6$]benzene, 25 °C): $\delta = 7.78$ (dd, $^3J_{H,H} = 1.5$, 1H, 4.9 Hz; 6′-H), 6.39 (dd, $^3J_{H,H} = 4.9$, 8.3 Hz, 1H; 5′-H), 6.13 (dd, $^3J_{H,H} = 1.0$, 8.3 Hz, 1H; 4′-H), 5.79 (br. s, 1H; 5-H), 5.62 (d, $^3J_{H,H} = 2.0$ Hz, 1H; 12-H), 4.68 (dd, $^3J_{H,H} = 1.5$, 4.9 Hz, 1H; 11-H), 4.30 (d, $^3J_{H,H} = 4.9$ Hz, 1H; 10-H), 4.26 (dd, $^3J_{H,H} = 6.3$, 6.8 Hz, 1H; 13-H), 3.79 (dd, $^3J_{H,H} = 6.3$, 8.3 Hz, 1H; 14-H), 3.74 (dd, $^3J_{H,H} = 6.8$, 8.3 Hz, 1H; 14-H), 3.67 (d, $^3J_{H,H} = 1.5$ Hz, 1H; 8-H), 1.50 (s, 3H; CH_3), 1.28 (s, 3H; CH_3), 0.86 (s, 9H; $SiC(CH_3)_3$), −0.03 (s, 3H; $SiCH_3$), −0.05 (s, 3H; $SiCH_3$); ^{13}C NMR (100 MHz, [D$_6$]benzene, 25 °C): $\delta = 149.7$, 143.4, 141.5, 141.3, 137.3, 125.9, 123.0, 121.6, 120.1, 110.6, 105.5, 102.2, 100.6, 89.4, 84.2, 76.5, 75.9, 69.5, 69.0, 47.8, 26.9, 26.0, 25.9, 18.3, −4.2, −4.9; FTIR (neat): $\tilde{\nu} = 2930$ (m), 2858 (m), 2280 (w, C≡C), 2186 (w, C≡C), 1566 (m), 1420 (s), 1287 (s), 1253 (m), 1207 (m), 1157 (m), 1085 (m), 840 (s), 781 (m) cm^{-1}; HR-MS (FAB): m/z calcd for $C_{28}H_{32}O_5ClNSiNa$ [M+Na$^+$]: 548.1636; found: 548.1630.

 © WILEY-VCH Verlag GmbH, D-69451 Weinheim, 2000 1433-7851/00/3915-2735 $ 17.50+.50/0

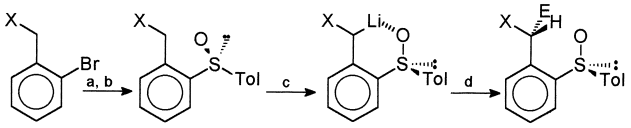
Enantioselective Generation of Benzylic Stereocenters Mediated by a Remote Sulfoxide**

José L. García Ruano,* M. Carmen Carreño,*
Miguel A. Toledo, José M. Aguirre, M. Teresa Aranda, and Jean Fischer

Enantioselective C–C bond formations via benzyllithium derivatives generated by deprotonation with organolithium bases has attracted the interest of several groups in the past two decades.[1] High asymmetric inductions were achieved by using the lithiation–substitution sequence when chiral auxiliaries are located in a remote position of the aliphatic chain[2] or by starting from tricarbonyl chromium arene complexes.[3] (−)-Sparteine[4] has been effectively used as chiral ligand to promote enantioselective synthesis of benzylic carbanions from alkylbenzenes bearing *ortho* substituents such as R_2NCO[5] and *t*BuCONH.[6] Enantiopure bis(oxazolines)[7] have also been applied with variable success.

In our continuing search for new applications of sulfoxides in asymmetric synthesis,[8] we found that association of the sulfinyl oxygen atom with lithium was essential to achieve highly diastereoselective 1,2-induction processes such as aldol-type reactions.[9] These results prompted us to investigate whether enantiopure *ortho*-sulfinyl groups[10] can stabilize benzyllithium carbanions and promote diastereoselective reactions with electrophiles by a 1,4-induction process.

This possibility was evaluated for (*S*)-2-ethylphenyl *p*-tolylsulfoxide (**3**) and (*S*)-2-(triisopropylsiloxymethyl)phenyl *p*-tolylsulfoxide (**4**; Scheme 1), which are easily accessible in high *ee* (98% by ^{1}H NMR) by Andersen synthesis[11] from *ortho*-bromo derivatives of ethylbenzene (**1**) and triisopropylsilyloxymethylbenzene (**2**). Organomagnesium reagents were used for the reaction with menthyl *p*-toluene sulfinate despite the better yields obtained with lithium analogues, since these afforded partially racemized **3** and **4**.



Scheme 1. Synthesis of **3** and **4** and reaction of their benzyllithium derivatives with electrophiles. a) Mg/diethyl ether, RT, for **1**; 1) *n*BuLi/THF, −78 °C; 2) $MgBr_2$, RT, for **2**. b) (*S*,*S*)- $TolSO_2$Menthyl, THF, −78 °C. c) LDA, THF, −78 °C. d) Electrophile, THF, −78 °C. OTIPS = OSi*i*Pr$_3$.

[*] Prof. J. L. García Ruano, Prof. M. C. Carreño, Dr. M. A. Toledo, M. T. Aranda
Departamento de Química Orgánica (C-I)
Universidad Autónoma
Cantoblanco, 28049-Madrid (Spain)
Fax: (+349) 1-397-3966
E-mail: joseluis.garcia.ruano@uam.es
carmen.carrenno@uam.es
Prof. J. M. Aguirre
Universidad de Lujan, Lujan (Argentina)
Prof. J. Fischer
Lab. de Cristallochimie, Université Louis Pasteur
67070-Strasbourg (France)

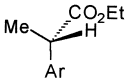
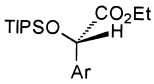
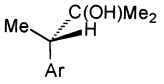
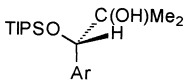
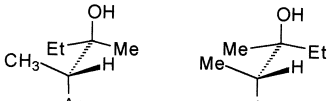
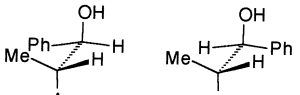
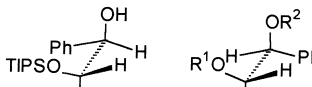
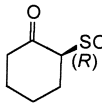
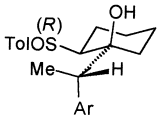
[**] This work was supported by the Dirección General de Investigación Científica y Técnica (Grants PB98-0062 to M.C.C. and PB98-0078 to J.L.G.R.).

Supporting information for this article is available on the WWW under http://www.wiley-vch.de/home/angewandte/ or from the author.

Regioselective deprotonation of **3** and **4** at the benzylic position with lithium diisopropylamide (LDA) at −78 °C[12] gave carbanions **A**. Quantitative formation of LDA was essential to avoid the partial racemization of the sulfoxide that occurred when traces of BuLi were present. Intermediates **A** reacted with electrophiles to give **a** as the major diastereomers (Scheme 1, Table 1).

As shown in Table 1, reaction of carbanions derived from **3** and **4** with ethyl chloroformate afforded diastereomerically pure esters **5a**[13] and **6a** (entries 1 and 2). In a similar way, acetone yielded pure diastereomers **7a** and **8a** from **3** and **4**, respectively (entries 3 and 4).[14] With asymmetrically substituted electrophiles, such as 2-butanone, compound **3** evolved

Table 1. Reactions of carbanions derived from **3** and **4** with electrophiles (Scheme 1).

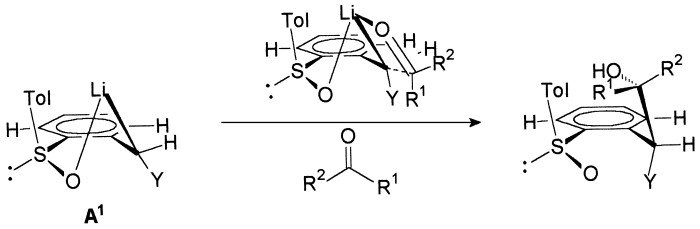
Entry	Carbanion Precursor	Electrophile	Products (diastereomer ratio)[a]	Yield [%]
1	**3**	$ClCO_2Et$	 **5a**	75
2	**4**	$ClCO_2Et$	 **6a**	75
3	**3**	MeCOMe	 **7a**	81
4	**4**	MeCOMe	 **8a**	78
5	**3**	MeCOEt	 **9a** (50) **9b** (50)	81
6	**3**	PhCHO	 **10a** (85) **10b** (15)	65[b]
7	**4**	PhCHO	 **11a** (78) **11b** (22)[c]	57[d]
8	**3**	 **12**	 **13a**	75

[a] Ar = (*S*)-2-*p*-tolylsulfinylphenyl. [b] Yield of pure **10a**. [c] Characterized as 50:50 mixture of R^1 = OTIPS; R^2 = H and R^1 = H; R^2 = OTIPS. [d] Yield of pure **11a**.

 © WILEY-VCH Verlag GmbH, D-69451 Weinheim, 2000 1433-7851/00/3915-2736 $ 17.50+.50/0

into a 1:1 mixture of carbinols **9a** and **9b**, which are epimers at the hydroxy-bearing carbon atom (entry 5). The stereogenic benzylic center showed the *S* absolute configuration. Reactions of **3** and **4** with benzaldehyde were more stereoselective. Starting from **3**, an 85:15 mixture of epimeric carbinols **10a** and **10b** was formed (entry 6); pure **10a** was isolated by chromatography. Under similar conditions, **4** yielded a 78:22 mixture of diol derivatives **11a** and **11b** (entry 7). The latter was characterized as a 50:50 regioisomeric mixture of 1- and 2-TIPS derivatives, which evolved into the diol after treatment with nBu$_4$NF. The rearrangement of silyl groups in similar 1,2-diols has already been reported.[15] To control the absolute configuration of both new stereogenic centers, a double asymmetric induction was performed in the reaction between **3** and [2*S*,(S)*R*]-2-(*p*-tolylsulfinyl)cyclohexanone (**12**).[9] The exclusive formation of diastereoisomer **13a** (entry 8) was consistent with the known stereochemical behavior of **12** in nucleophilic additions.

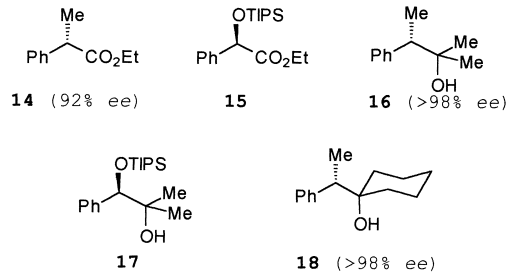
According to these results, the new benzylic stereogenic centers were always generated in a highly diastereoselective manner and with the same asymmetric induction, independent of the electrophile. When additional stereogenic centers were created, the stereoselectivity of the process was electrophile-dependent. A plausible mechanism that accounts for our current observations is shown in Scheme 2. Benzyllithium



Scheme 2. Favored transition state for reaction of intermediates **A** with electrophiles.

derivative $\mathbf{A^1}$ must be the most stable among all diastereomers and conformers since it lacks allylic strain.[16] The metal-assisted pseudoequatorial approach of the electrophile would yield the observed *S* configuration at the benzylic center if the configuration of the carbanion were retained. When the electrophile is prochiral, the stabilities of the transition states depend on the relative size of R^1 and R^2. When they are similar, equimolar mixtures of two epimers are formed (entry 5), while higher diastereoselectivies are observed when R^1 and R^2 are very different (entries 6 and 7).

Important for preparative applications of this methodology is the removal of the auxiliary. This was quantitatively achieved in compounds **5a**–**8a** and **13a** by reaction with Raney nickel, which gave **14**–**18** (Scheme 3). Formation of known **14**[17] and **16**[18] confirmed the absolute configuration of **5a** and **7a**. The enantiomeric purity of desulfurized products **14**, **16**, and **18** was identical to that of the starting materials. For OTIPS derivatives **6a** and **8a** the enantiomeric excess of the resulting compounds **15** and **17** could be determined neither by ^{1}H NMR spectroscopy nor by HPLC.



Scheme 3. Products of desulfurization of **5a**, **7a**, and **13a**. For **14** and **16**, the *ee* was determined by comparison with reported $[\alpha]_D^{20}$ values.[17, 18]

Received: February 4, 2000
Revised: April 3, 2000 [Z14652]

[1] Review: "Stereoselective Synthesis": H. Ahlbrecht, *Methods of Organic Chemistry (Houben-Weyl) 4th ed. 1952–*, *Vol. E21a*, **1995**, pp. 645–696.
[2] For recent references, see a) M. Magnus, P. Magnus, *Nature* **1997**, *38*, 3491; b) A. G. Myers, B. H. Yang, H. Chen, L. McKistry, D. J. Kopecky, J. L. Gleason, *J. Am. Chem. Soc.* **1997**, *119*, 6496–6511; c) D. J. Pippel, M. D. Curtis, H. Du, P. Beak, *J. Org. Chem.* **1998**, *63*, 2–3.
[3] T. Geller, H. G. Schmalz, J. Bats, *Tetrahedron Lett.* **1998**, *39*, 1537–1540, and references therein.
[4] Reviews: a) D. Hoppe, T. Hense, *Angew. Chem.* **1997**, *109*, 2376–2410; *Angew. Chem. Int. Ed. Engl.* **1997**, *36*, 2282–2316; b) P. Beak, A. Basu, D. J. Gallagher, Y. S. Park, S. Thayumanavan, *Acc. Chem. Res.* **1996**, *29*, 552–560.
[5] S. Thayumanavan, A. Basu, P. Beak, *J. Am. Chem. Soc.* **1997**, *119*, 8209–8216, and references therein.
[6] a) A. Basu, P. Beak, *J. Am. Chem. Soc.* **1996**, *118*, 1575–1576; b) A. Basu, D. J. Gallagher, P. Beak, *J. Org. Chem.* **1996**, *61*, 5718–5719.
[7] a) N. Komine, L.-F. Wang, K. Tomooka, T. Nakai, *Tetrahedron Lett.* **1999**, *40*, 6809–6812; b) N. Komine, L.-F. Wang, K. Tomooka, T. Nakai, *Tetrahedron Lett.* **1999**, *40*, 6813–6816.
[8] Reviews: a) M. C. Carreño, *Chem. Rev.* **1995**, *95*, 1717–1760; b) J. L. García Ruano, M. B. Cid, *Top. Curr. Chem.* **1999**, *204*, 1–126.
[9] a) J. L. García Ruano, I. Fernández, M. del Prado, J. A. Hermoso, J. Sanz Aparicio, M. Martínez-Ripoll, *J. Org. Chem.* **1998**, *63*, 7157–7161; b) J. L. García Ruano, D. Barros, M. C. Maestro, R. Araya-Maturana, J. Fischer, *J. Org. Chem.* **1996**, *61*, 9462–9470.
[10] *ortho*-Lithium heteroaromatic sulfoxides react diastereoselectively with aldehydes: P. Pollet, A. Truck, N. Plé, G. Quéguiner, *J. Org. Chem.* **1999**, *64*, 4512–4515.
[11] K. K. Andersen, W. Gaffield, N. E. Papanikolau, J. W. Foley, R. I. Perkins, *J. Am. Chem. Soc.* **1964**, *86*, 5637–5646.
[12] *ortho*-Lithiation was not observed despite the *ortho*-directing character of the sulfoxide group; see V. Snieckus, *Chem. Rev.* **1990**, *90*, 879–933.
[13] Characterization of **5a** was carried out immediately after crystallization since it readily epimerizes at C-2.
[14] The structures of **8a** and **10a** were established by X-ray diffraction. Crystallographic data (excluding structure factors) for the structures reported in this paper have been deposited with the Cambridge Crystallographic Data Centre as supplementary publications nos. CCDC-139404 and -139405. Copies of the data can be obtained free of charge on application to CCDC, 12 Union Road, Cambridge CB21EZ, UK (fax: (+44) 1223-336-033; e-mail: deposit@ccdc.cam.ac.uk).
[15] See M. Lalonde, T. H. Chan, *Synthesis* **1985**, 817.
[16] The chelate structure proposed for $\mathbf{A^1}$ is consistent with the result observed when reaction of **3** with acetone (entry 3) was conducted in the presence of hexamethylphosphoric triamide (6 equiv). Under these conditions, an 87:13 mixture of **7a** and its epimer at the benzylic carbon atom was isolated.
[17] C. Kashima, I. Fukuchi, A. Hosomi, *J. Org. Chem.* **1994**, *59*, 7821–7824.
[18] F. D. Greene, *J. Am. Chem. Soc.* **1959**, *81*, 2688–2691.

 © WILEY-VCH Verlag GmbH, D-69451 Weinheim, 2000 1433-7851/00/3915-2737 $ 17.50+.50/0

Continuous Reactions in Supercritical Water: A New Route to La_2CuO_4 with a High Surface Area and Enhanced Oxygen Mobility**

Alexander A. Galkin,* Boris G. Kostyuk, Valery V. Lunin, and Martyn Poliakoff*

Perovskite-type complex oxides have been investigated intensively in recent years because of their potential as catalysts for oxidation processes.[1, 2] Their catalytic properties are principally associated with oxygen nonstoichiometry, oxygen storage capacity, oxygen mobility, and the electronic properties of the perovskites themselves.[3] The attraction of such materials is that these properties can be tuned through variation of the metals within the structure. Additionally, they have high thermal stability and relatively low cost compared to noble metal oxidation catalysts.[1]

La_2CuO_4 is an important, catalytically active perovskite. It has the K_2NiF_4 structure with alternating layers of the ABO_3 perovskite and the AO salt.[3] La_2CuO_4 and its derivatives catalyse a wide variety of reactions including the oxidation of CO[4–7] and CH_4,[5], decomposition of NO and N_2O,[8, 9] and NO reduction with CO.[3, 10, 11] Furthermore, catalysts such as $La_{2-x}Sr_xCuO_{4-\delta}$ and $La_2Cu_{1-x}Pd_xO_4$ exhibit a catalytic activity comparable to that of $Pt\text{-}Rh/CeO_2\text{-}Al_2O_3$ for three-way automotive catalysis.[3, 8]

Usually, single-phase perovskites are synthesized by annealing stoichiometric mixtures of metal oxides or other suitable precursors at very high temperatures.[4–6, 8, 12] For example, La_2O_3 heated with CuO at 1000–1200 °C leads to the formation of La_2CuO_4 but its surface area[4, 6, 12] is $\leq 1\ m^2 g^{-1}$ and too low for use as a catalyst. However, surface areas as high as $13\ m^2 g^{-1}$ [13] can be obtained through a number of "wet chemical" routes including sol–gel processes,[3, 13] co-precipitation,[7, 9, 11] inverse microemulsion techniques,[14] and combustion synthesis,[15] all of which involve lower annealing temperatures, about 600–800 °C. Unfortunately, these "wet" routes are often complicated or involve large quantities of toxic or inflammable compounds.

Herein, we describe a relatively simple route to La_2CuO_4, the initial stage of which involves the simultaneous hydrolysis of lanthanum(III) and copper(II) acetates in supercritical water, scH_2O. There has been a considerable amount of research into the reactions of metals in scH_2O,[16] while Arai and co-workers have pioneered the use of scH_2O for hydrolysis of metal salts.[17–18] They showed that continuous hydrolysis of metal nitrates in scH_2O ($T > 374$ °C) generated the corresponding metal oxides for a wide range of different metals. Recently, we showed that decomposition of metal acetates in scH_2O was an even more facile route to metal oxides.[19] Here, we report how the decomposition of $La(CH_3COO)_3$ and $Cu(CH_3COO)_2$ in a continuous scH_2O reactor leads to the formation of an intimate mixture of $La(OH)_3$ and CuO, which can then be sintered to form single phase La_2CuO_4 with a high surface area.

Our continuous reactor is shown schematically in Figure 1. Briefly, a cold solution, which contained both La^{III} and Cu^{II} acetates, was mixed with scH_2O at 400–500 °C and at 25 MPa.

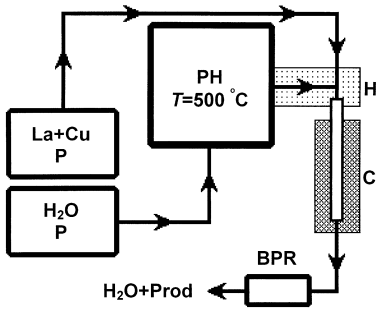


Figure 1. Continuous, supercritical water flow reactor. Abbreviations are backpressure regulator (BPR), cooling area (C), heating area (H), pumps (P), water preheater (PH), and hydrolysis products (Prod). The reactor is constructed from 316 stainless steel components (Swagelok).

The resulting colloidal suspension of $La(OH)_3$ and CuO was quenched and evaporated (see the Experimental Section). The gray, solid product was then annealed at 600 °C and La_2CuO_4 formed within 5 h.

X-ray diffraction (XRD) spectra showed the product, $(La_2CuO_4)_{sc}$ to be of a single phase;[11, 13, 14] see Figure 2. Brunauer-Emmet-Teller (BET) surface area measurements gave surface areas of up to $19\ m^2 g^{-1}$, very high for this type of material. By comparison, only $0.4\ m^2 g^{-1}$ was obtained with ceramic La_2CuO_4 prepared from La_2O_3 and CuO (see the Experimental Section). A scanning electron microscopy (SEM) examination of $(La_2CuO_4)_{sc}$ and ceramic La_2CuO_4

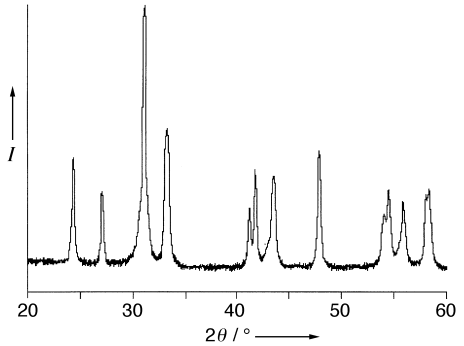


Figure 2. XRD pattern of a sample of $(La_2CuO_4)_{sc}$ synthesized in scH_2O, which shows the absence of reflections attributable to other phases or to the $CuO/La(OH)_3$ precursors.

[*] Prof. M. Poliakoff
Clean Technology Group
School of Chemistry
The University of Nottingham
University Park, NG72RD Nottingham (UK)
Fax: (+44) 115-951-3058
E-mail: Martyn.Poliakoff@nottingham.ac.uk
Dr. A. A. Galkin, Dr. B. G. Kostyuk, Academician V. V. Lunin
Physical Chemistry Department
Moscow State University
119899 Moscow (Russia)
Fax: (+7) 095-939-4575
E-mail: galkin@kge.msu.ru

[**] We thank Ms. E. P. Chinennikova, Dr. A. Cabañas, Dr. J. A. Darr, Dr. D. A. Graham, and Mr. M. Guyler for their help. We are grateful to EPSRC (grant no. GR/K84929), the Royal Society, NATO, the Royal Academy of Engineering, and the Russian Foundation for Basic Research for support.

 © WILEY-VCH Verlag GmbH, D-69451 Weinheim, 2000 1433-7851/00/3915-2738 $ 17.50+.50/0

showed that the $(La_2CuO_4)_{sc}$ material has much smaller and more uniform particle sizes (Figure 3a). More detailed SEM studies showed that the morphology of the $La(OH)_3$/CuO

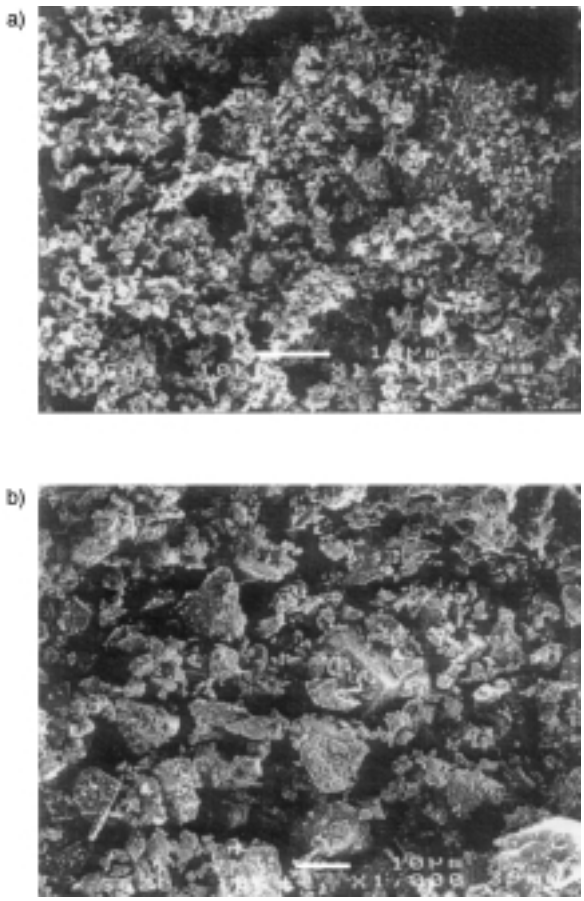


Figure 3. SEM micrographs for La_2CuO_4 samples prepared using the a) scH_2O or b) conventional ceramic method. Scale bars = 10 μm.

precursor was largely unaffected by annealing to 600 °C. Energy-dispersive X-ray microanalysis (EDX) of both La_2CuO_4 samples confirmed the correct 2:1 La:Cu ratio. La_2CuO_4 may possibly be formed by annealing the supercritical hydrolysis product at temperatures as low as 400 °C but the XRD peaks are so broadened by the small particle size that positive identification of La_2CuO_4 has not been possible.

Temperature programmed reduction (TPR) is a key indicator of potential catalytic activity and Figure 4 compares the TPR profiles for the La_2CuO_4 samples prepared using scH_2O or the ceramic method. The higher temperature peak in both traces corresponds to bulk reduction with the formation of a mixture of Cu, CuO, and La_2O_3 phases, which occurs at almost the same temperature for both samples. In contrast, the first reduction peak, assigned to loss of weakly bound oxygen, occurs 100 K cooler for $(La_2CuO_4)_{sc}$. This shift towards a lower temperature indicates a much increased bulk oxygen mobility, a crucial factor for effective oxidation catalysis. This striking difference in the TPR occurred even though the overall hydrogen takeup for the two samples was essentially identical, 5.747 and 5.736 mmol g^{-1} for the scH_2O and ceramic samples, respectively.

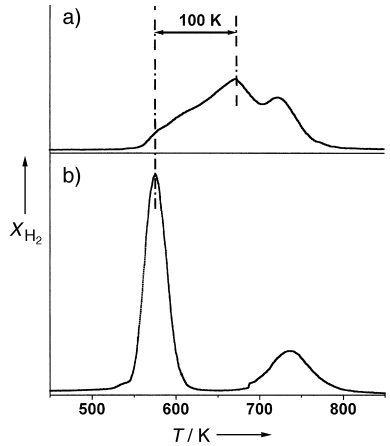


Figure 4. TPR curves for La_2CuO_4 samples prepared using the a) conventional ceramic method or b) scH_2O. x_{H_2} = hydrogen consumption.

The higher catalytic activity of $(La_2CuO_4)_{sc}$ was demonstrated by the oxidation of CO. Two independent series of pulsed microcatalytic experiments were carried out. First, with a stoichiometric $CO:O_2$ mixture, we found that the efficiency of the $(La_2CuO_4)_{sc}$ catalyst was about 2.5 times higher per unit mass compared to the ceramic sample. Second, the O_2 and CO pulses were separated in time with the catalyst heated to 270 °C, where, according to the TPR data (Figure 4), the weakly bound oxygen is mobile in $(La_2CuO_4)_{sc}$ but still inactive in the ceramic phase. Both $(La_2CuO_4)_{sc}$ and ceramic La_2CuO_4 were oxidized initially by a pulse of O_2, which was then followed by alternating pulses of CO and O_2. The rates of CO oxidation reaction were 73.5 and 9.1 μL s^{-1} m^{-2} for the scH_2O and ceramic catalysts, respectively. Thus, the $(La_2CuO_4)_{sc}$ is eight times more effective per unit area of surface. However, this difference in reaction rates may not be solely due to higher rates of oxygen diffusion in $(La_2CuO_4)_{sc}$. The large difference in the surface areas between the samples of La_2CuO_4 means that the reaction conditions are not identical and the higher "total" surface area of the $(La_2CuO_4)_{sc}$ sample may result in significant O_2 adsorption by the surface with consequently higher concentrations of active oxygen for the subsequent CO oxidation. Nevertheless, $(La_2CuO_4)_{sc}$ is a more effective catalyst.

In conclusion, our supercritical water method has produced, at a cooler reaction temperature, high surface area La_2CuO_4 with enhanced oxygen mobility, probably because the $La(OH)_3$/CuO precursor was produced as an intimate nanoparticulate mixture. The preliminary catalytic tests showed the activity of $(La_2CuO_4)_{sc}$ towards CO oxidation is considerably higher compared to the ceramic La_2CuO_4 phase. A detailed study of the catalytic activity in other oxidation reactions, as well as the investigation of the oxygen adsorption kinetics, for $(La_2CuO_4)_{sc}$ is currently in progress.

Experimental Section

Caution: These experiments involve high pressures.

The synthesis of La_2CuO_4 was performed using a particle flow reactor (Figure 1). To obtain supercritical conditions (T_c = 374 °C, P_c = 22.1 MPa), water was pumped continuously through a preheater and oven to reach a final temperature of 400 – 500 °C before mixing with a solution of La^{III} and

 © WILEY-VCH Verlag GmbH, D-69451 Weinheim, 2000 1433-7851/00/3915-2739 $ 17.50+.50/0

Cu^{II}. A backpressure regulator at the end of the system maintained the system pressure close to 25 MPa. At the mixing point, a cold solution of stoichiometric amounts of Cu^{II} and La^{III} acetates (0.01 M each) was rapidly hydrolysed by scH_2O stream. The temperature at the mixing point was in the range of 350 – 400 °C and the residence time was only a few seconds. The hot water and dispersed hydrolysis products (CuO and $La(OH)_3$) were cooled and collected after the BPR. A gray solid was recovered from the mixture by complete evaporation of water and was annealed at 600 °C for 5 h to form single-phase La_2CuO_4.

Ceramic La_2CuO_4 was synthesized by annealing a stoichiometric mixture of CuO and La_2O_3 at 1100 °C for 48 h with two intermediate grinding sessions.

The phase composition of all the materials was determined by XRD (Phillips XPERT, $Cu_{K\alpha}$ radiation), at a scan rate of 1 min^{-1} over the range $20 < 2\theta < 60°$. The microstructure of the samples was investigated by SEM (JEOL Winsem JSM-6400, acceleration voltage 10 kV) after the deposition of a gold layer (15 nm thick) on the specimen. The BET surface area was measured by N_2 adsorption at 77 K. TPR profiles were recorded at a heating rate of 10 K min^{-1}; prior to the TPR experiments, the samples were pretreated in an O_2 flow at 600 °C for 1 h and allowed to cool in oxygen until, when at room temperature, the O_2 flow was replaced with an Ar/H_2 flow (95 %/5 %).

The catalytic activity of La_2CuO_4 towards CO oxidation was studied by a pulsed microcatalytic technique over the temperature range 200 – 400 °C.[20] The composition of the gas phase was monitored by an LHM-8MD gas chromatograph (Carbosieve-B column, $l = 1$ m, $\phi = 2$ mm) with a catharometer detector and He carrier gas (70 mL min^{-1}, $P = 1$ atm). The reactant pulse was 1 mL, which contained 7.5 % v/v of the stoichiometric $CO:O_2$ mixture. Before the activity measurements, the catalysts were pretreated in a He flow.

Received: February 15, 2000 [Z14712]

[1] K. Tabata, M. Misuno, *Catal. Today* **1990**, *8*, 249 – 253.
[2] Y. Teraoka, W. F. Shangguan, K. Jansson, M. Nygren, S. Kagawa, *Bull. Chem. Soc. Jpn.* **1999**, *72*, 133 – 137.
[3] N. Guilhaume, S. D. Peter, M. Primet, *Appl. Catal. B* **1996**, *10*, 325 – 344.
[4] S. Rajadurai, J. J. Carberry, B. Li, C. B. Alcock, *J. Catal.* **1991**, *131*, 582 – 589.
[5] R. Doshi, C. B. Alcock, N. Gunasekaran, J. J. Carberry, *J. Catal.* **1993**, *140*, 557 – 563.
[6] N. Gunasekaran, A. Meenakshisundaram, V. Srinivasan, *Indian J. Chem. Sect. A* **1982**, *21*, 346 – 349.
[7] H. Yasuda, Y. Fujiwara, N. Mizuno, M. Misono, *J. Chem. Soc. Faraday Trans.* **1994**, *90*, 1183 – 1189.
[8] S. Subramanian, C. S. Swamy, *Catal. Lett.* **1995**, *35*, 361 – 372.
[9] H. Yasuda, T. Nitadori, N. Mizuno, M. Misono, *Bull. Chem. Soc. Jpn.* **1993**, *66*, 3492 – 3502.
[10] C. Oliva, L. Forni, A. M. Ezerets, I. E. Mukovozov, A. V. Vishniakov, *J. Chem. Soc. Faraday Trans.* **1998**, *94*, 587 – 592.
[11] S. D. Peter, E. Garbowski, N. Guilhaume, V. Perrichon, M. Primet, *Catal. Lett.* **1998**, *54*, 79 – 84.
[12] R. Jeyalakshmi, B. Jagannadhaswamy, B. Sivasankar, *Indian J. Chem. Sect. A* **1989**, *28*, 508 – 509.
[13] J. Mahia, J. L. Martinez-Lorenzo, M. C. Blanco, M. A. Lopez-Quintela, *J. Solid State Chem.* **1997**, *131*, 246 – 251.
[14] L. M. Gan, L. H. Zhang, H. S. O. Chan, C. H. Chew, B. H. Loo, *J. Mater. Sci.* **1996**, *31*, 1071 – 1079.
[15] S. S. Manoharan, V. Prasad, S. V. Subramanyam, K. C. Patil, *Physica C* **1992**, *190*, 225 – 228.
[16] J. A. Darr, M. Poliakoff, *Chem. Rev.* **1999**, *99*, 495 – 541.
[17] T. Adschiri, K. Kanazawa, K. Arai, *J. Amer. Ceram. Soc.* **1992**, *75*, 1019 – 1022.
[18] Y. Hakuta, H. Terayama, S. Onai, T. Adschiri, K. Arai, *Proc. 4th Int. Symp. Supercritical Fluids*, Sendai, Japan **1997**, pp. 255 – 258.
[19] A. Cabañas, J. A. Darr, E. Lester, M. Poliakoff, *Chem. Commun.* **2000**, 901 – 902.
[20] A. A. Galkin, Ph.D. dissertation, Moscow State University, Russia, **1998**.

Evidence for Dangling Bond Mediated Dimerization of Furan on the Silicon (111)-(7 × 7) Surface**

Yong Cao, Zhonghai Wang, Jing-Fa Deng, and Guo Qin Xu*

The binding of organic molecules on silicon surfaces has recently become an increasingly important aspect of surface modification in microelectronics and sensing technology.[1, 2] To gain the control needed for incorporating organic functionalities into existing technologies, there are growing efforts dedicated to the fundamental understanding of molecular adsorption on silicon surfaces.[3, 4] One central focus in this area is the covalent attachment of olefins to the Si dangling bonds at silicon surfaces.[5–7]

Experimental and theoretical results suggest that [4+2] or [2+2] cycloadditions of conjugated dienes with Si=Si dimers proceed by a diradical mechanism on the Si(100) surface.[6, 7] Recently, we showed that the radical nature of the electron-deficient Si dangling bonds plays an essential role in the [4+2] cycloaddition of thiophene to the Si(111)-(7 × 7) surface.[8] These studies implied that the Si dangling bonds can be alternatively viewed as reactive "free radicals" involved in the surface-attachment reactions. On the other hand, organic radical based C–C bond formation[9] was recently shown to be highly selective in enantioselective synthesis[10] or preparation of controlled macromolecular architectures.[11] Therefore, it is of significant interest to investigate whether this radical-based C–C formation is feasible on silicon surfaces in association with Si dangling bonds. Such a study may offer new insight into the covalent attachment of molecular functionalities onto the silicon surface.

We report here on the Si dangling bond mediated dimerization of furan molecules on the Si(111)-(7 × 7) surface. Through the use of thermal desorption spectroscopy (TDS) and vibrational high-resolution electron energy loss spectroscopy (HREELS), the structure and bonding of the adsorbed furan species on Si(111)-(7 × 7) have been investigated. The structure of the Si(111)-(7 × 7) unit cell (Figure 1) is well known,[12] and the unique Si(111)-(7 × 7) surface offers an excellent opportunity to examine the surface chemistry associated with the Si dangling bonds at the silicon surface. Furan was chosen for this study because it is one of the basic building blocks for conducting polymers.[13, 14]

[*] Prof. Dr. G. Q. Xu, Y. Cao, Z. Wang
Department of Chemistry
National University of Singapore
10 Kent Ridge 119260 (Singapore)
Fax: (+65) 779-1691
E-mail: chmxugq@nus.edu.sg
Y. Cao, Prof. J.-F. Deng
Department of Chemistry, Fudan University
Shanghai 200433 (China)

[**] This work was supported by the National University of Singapore (grant no. 3970612).

Supporting information for this article is available on the WWW under http://www.wiley-vch.de/home/angewandte/ or from the author.

 © WILEY-VCH Verlag GmbH, D-69451 Weinheim, 2000 1433-7851/00/3915-2740 $ 17.50+.50/0

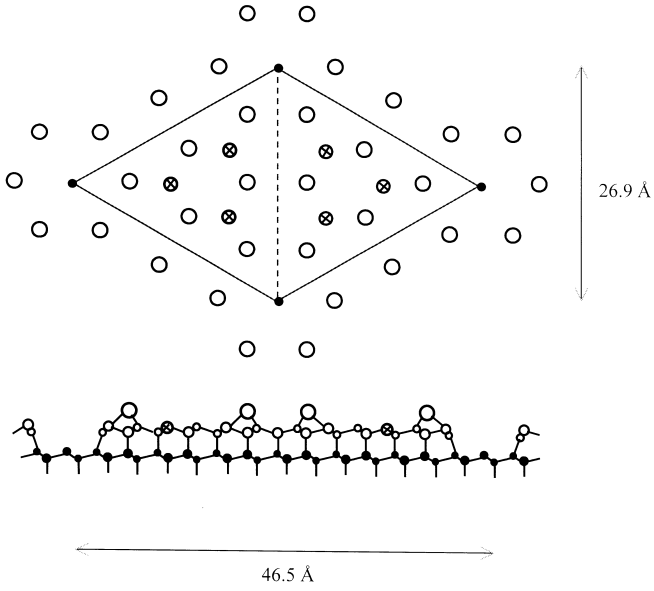


Figure 1. Schematic diagram of the Si(111)-(7 × 7) unit cell (one unit cell is within the borders; only the adatoms (first layer) and the rest atoms (second layer) with dangling bonds along the surface normal are shown). Open circles (12 per unit cell) represent the adatoms. Crossed circles (6 per unit cell) represent the rest atoms with dangling bonds that are located one atomic layer below the adatoms. The small solid circles (1 per unit cell) represent the corner-hole rest atoms at two atomic layers below the adatoms.

The temperature-programmed desorption (TPD) spectra of furan (*m*/*z* 68; see the Experimental Section), collected for various initial exposures of furan at 300 K, are displayed in Figure 2a. At low exposures, a single desorption peak with a slight tailing at the high temperature side is observed at about

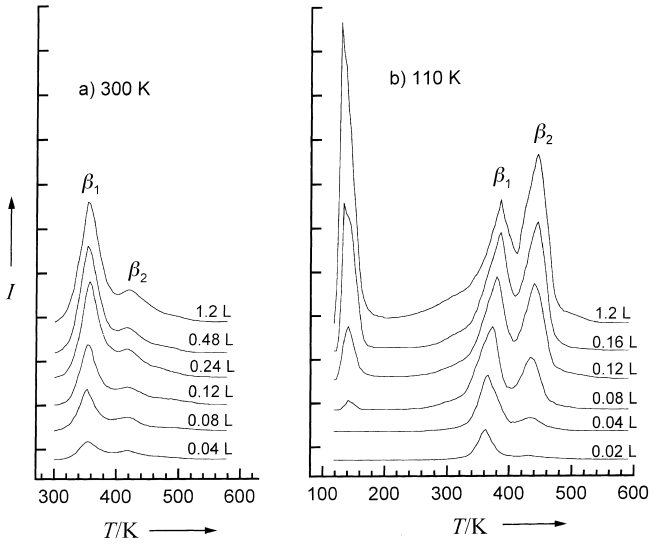


Figure 2. TPD spectra of furan (*m*/*z* 68) as a function of exposure to Si(111)-(7 × 7) at a) 300 K and b) 110 K. The heating rate for all spectra was 2 K s^{-1}.

360 K, which is labeled as β_1 and corresponds to molecular desorption of chemisorbed furan. Increasing the furan exposure causes the gradual development of a weak feature at 420 K, labeled as β_2. The intensity of the β_1 peak reaches a maximum at an exposure of about 1.2 L. In contrast, the population of the β_2 peak remains very low even at this saturation exposure.

Figure 2b shows the TPD spectra collected as a function of furan exposure at a low adsorption temperature (110 K). An increased desorption yield is observed after dosing furan at 110 K, compared to the same exposure at 300 K, implying that the chemisorption of furan on Si(111) is precursor-mediated. At low exposures, the desorption profiles (Figure 2b) are identical to those for exposure at 300 K (cf. Figure 2a), with the β_1 state being the predominant state. With increasing furan exposure, a physisorbed state at about 120 K appears. In addition, the population of the β_2 state grew much faster than that of the β_1 state. Upon saturation of the β_1 peak, the β_2 peak becomes the predominant state, as shown in the thermal desorption spectrum corresponding to an exposure of 1.2 L. This surprising change in the relative intensities of the β_1 and β_2 peaks as a function of adsorption temperature implies the formation of a unique chemisorbed state (see below).

To gain further insight into the adsorption behavior of furan on Si(111), a vibrational HREEL spectrum was taken after exposing furan to the silicon surface at 300 K (Figure 3a). Two separate vibrational features at 2886 and 3080 cm^{-1}, corresponding to sp^3 and sp^2 C–H stretching modes, respectively,

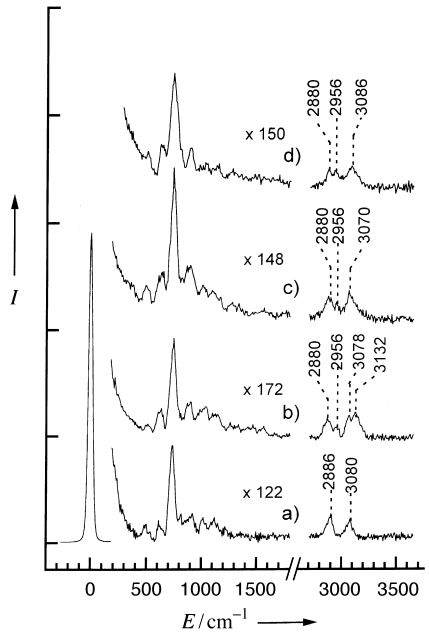


Figure 3. HREEL spectra obtained after exposing 1.20 L of furan to the Si(111)-(7 × 7) surface a) at 300 K, b) at 110 K, c) after annealing the sample from b) to 300 K, and d) after annealing the sample from b) to 360 K. The primary electron beam with an energy of 5.0 eV impinges on the surface at 60° from the surface normal. The scattered electrons were detected at the specular direction. The resolution of the spectrometer (FWHM) is 6–7 meV. *E* indicates energy loss.

indicate rehybridization in the chemisorbed furan.[16] This is in good agreement with the [4+2] cycloaddition reaction of thiophene[8] on the Si(111) surface. Considering that the β_1 state is the predominant state at 300 K, the features in Figure 3a are mainly attributed to the vibrational structure of the β_1 furan. The electronic structure of furan is similar to that

 © WILEY-VCH Verlag GmbH, D-69451 Weinheim, 2000 1433-7851/00/3915-2741 $ 17.50+.50/0

of thiophene.[17] In addition, it is well documented that furan easily undergoes cycloaddition reactions in the solution phase.[18] Thus, the β_1 state observed in our experiment is assigned to the [4+2] cycloadduct formed upon the bonding of the C2 and C5 carbon atoms in furan to a pair of adjacent adatom and rest atoms on the Si(111)-(7 × 7) surface.

The HREEL spectrum corresponding to exposure of 1.20 L of furan at 110 K is shown in Figure 3b. Four overlapping, but still resolvable features associated with C–H stretching modes can be identified. The loss feature at 3132 cm^{-1} is associated with the molecular furan[19] physisorbed on the chemisorbed monolayer, which is in good accordance with the results for thermal desorption (Figure 2b). The additional three peaks at 3078, 2956, and 2880 cm^{-1} are attributable to the chemisorbed furan on Si(111). To focus our study on chemisorbed furan, physisorbed molecules were desorbed from the surface by annealing to 300 K. Figure 3c shows the combined vibrational features contributed from the β_1 and β_2 states of chemisorbed furan. Three vibrational loss features at 3070, 2956, and 2880 cm^{-1} associated with C–H stretching motions can be resolved. Compared to the spectrum obtained for the sample in Figure 2a, in which the β_1 state predominates, it is concluded that the additional weak feature at 2956 cm^{-1} arises from the β_2 state.

Upon a progressive annealing to 360 K, only the β_2 state of chemisorbed furan is retained on the Si(111) surface (Figure 3d). Three loss bands at 3086, 2956, and 2880 cm^{-1} corresponding to C–H stretching modes are observed; these bands have comparable peak intensities. The presence of two loss features at 2956 and 2880 cm^{-1} corresponding to sp^3 C–H stretching suggests that there are two kinds of sp^3-hybridized carbon atoms in the more strongly bonded β_2 state of chemisorbed furan. In the temperature range studied, no energy losses around 2055 cm^{-1} (Si–H) were observed,[20] suggesting the nondissociative nature of furan adsorption.

According to the stepwise, diradical mechanism proposed for the [4+2] cycloaddition of thiophene on Si(111)-(7 × 7),[8] the initial molecular adsorption of furan would lead to the formation of a mono-σ-bonded surface complex involving a linkage between the electron-rich α-carbon atom in furan and the electron-deficient Si dangling bond at an adatom site. Apparently, the short-lived radical-like mono-σ-bonded complex can serve as the precursor for the subsequent chemisorption reaction. At room temperature, the radical-like precursor state readily reacts with a nearby dangling bond at a rest atom site, leading to the predominant formation of the β_1 state corresponding to a [4+2] cycloadduct. Owing to the short residence time of the precursor at room temperature, the surface concentration of this species remains very low during the adsorption process, which prohibits dimerization to form the β_2 state.

However, for furan adsorbed at 110 K, our TPD and HREELS results strongly suggest the formation of a dimer complex in addition to the [4+2] cycloadduct on the Si(111)-(7 × 7) surface. At a cryogenic temperature of 110 K, the mono-σ-bonded precursor state is thermally stablized and a high population of the state can be built up on the silicon surface. Two radical-like mono-σ-bonded species resting on two adjacent adatom sites can readily recombine to form a C–C bond; the dimensions of two furan molecules[21] are comparable with the distance between two nearest (6.9 Å) and next nearest (7.7 Å) Si atoms on the Si(111)-(7 × 7) surface.[12] This combination reaction would lead to the formation of a covalently C–C-linked, dimerlike furan adsorption complex through C_α–C_α coupling. This state of chemisorbed furan is more stable than the corresponding [4+2] product due to the formation of an additional C–C linkage between two mono-σ-bonded species. In addition, the chemical environment of the two C–C-linked α carbon atoms is clearly different from that of carbon atoms directly bonded to the silicon atoms.

The formation of the more strongly bound dimer complex for furan adsorption on Si(111) has been further supported by a PM3 semiempirical calculation using the Spartan 5.1.1 program.[22] A five-layer $Si_{51}H_{40}$ cluster containing two adatoms, two rest atoms, and three dimers as proposed by Takayanagi et al.[12] was employed in the calculation. Because of the large number of atoms involved, it was not possible to perform the calculation at a higher level. The results indicate that the proposed dimerized state (β_2) is about 93 kJ mol^{-1} more stable than the β_1 state corresponding to the [4+2] cycloadduct associated with a single furan molecule.

In summary, we have demonstrated the dimerization of adsorbed furan on the Si(111)-(7 × 7) surface. This facile reaction is attributed to the recombination of pairs of adjacent mono-σ complexes at low temperature. The clarification of the microscopic molecular mechanism involved in the chemisorption of furan on Si(111)-(7 × 7) as well as the nature of the radical precursor state during the chemisorption process can provide further insight into the attachment of molecules on semiconductor surfaces. Moreover, the present approach may open up new routes for the creation of molecular species with novel structures on silicon surfaces by organic radical based reactions.

Experimental Section

The experiments were conducted in an ultrahigh vacuum chamber equipped with facilities for temperature-programmed desorption (TPD) and HREELS.[15] The base pressure was kept below 3×10^{-10} Torr during the experiments. An n-type (P-doped) silicon wafer (1–30 Ω cm) with dimensions of $16 \times 8 \times 0.38$ mm^3 was used as the substrate. The clean Si(111)-(7 × 7) surfaces were prepared by cycles of Ar-ion bombardment (500 eV, 30 min, 20 $\mu A\,cm^{-2}$) and final annealing at 1200 K for 10 min in UHV. During the experiment, the sample can be cooled to 110 K with liquid nitrogen. Gaseous furan molecules were delivered to the sample surface through a stainless steel doser (diameter 6 mm). The furan-covered sample was subsequently subjected to TPD and HREELS investigations. The purity of furan was verified in-situ using an UTI-100 mass spectrometer.

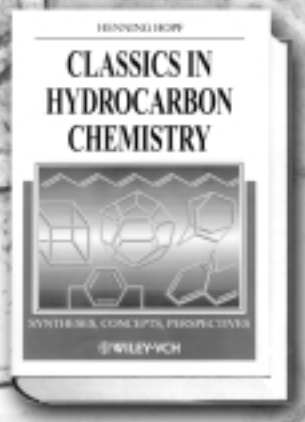
Received: February 28, 2000 [Z14771]

[1] J. T. Yates, Jr., *Science* **1998**, *279*, 335–336.
[2] G. P. Lopinski, D. J. Moffatt, D. D. M. Wayner, R. A. Wolkow, *Nature* **1998**, *392*, 909–911.
[3] R. A. Wolkow, *Annu. Rev. Phys. Chem.* **1999**, *50*, 413–441.
[4] H. N. Waltenberg, J. T. Yates, Jr., *Chem. Rev.* **1995**, *95*, 1589–1673.
[5] a) A. V. Teplyakov, M. J. Kong, S. F. Bent, *J. Am. Chem. Soc.* **1997**, *119*, 11100–11101; b) R. Konecny, D. J. Doren, *J. Am. Chem. Soc.* **1997**, *119*, 11098–11099.

 © WILEY-VCH Verlag GmbH, D-69451 Weinheim, 2000 1433-7851/00/3915-2742 $ 17.50+.50/0

[6] J. S. Hovis, H.Liu, R. J. Hamers, *J. Phys. Chem. B* **1998**, *102*, 6873 – 6879.
[7] C. H. Choi, M. S. Gordon, *J. Am. Chem. Soc.* **1999**, *121*, 11311 – 11317.
[8] Y. Cao, K. S. Yong, Z. Q. Wang, W. S. Chin, Y. H. Lai, J. F. Deng, G. Q. Xu, *J. Am. Chem. Soc.* **2000**, *122*, 1812 – 1813.
[9] J. Fossey, D. Lefort, J. Sorba, *Free Radicals in Organic Chemistry*, Wiley, New York, **1995**, p. 265.
[10] M. P. Sibi, N. A. Porter, *Acc. Chem. Res.* **1999**, *32*, 163 – 171.
[11] C. J. Hawker, *Acc. Chem. Res.* **1997**, *30*, 373 – 382.
[12] K. Takayanagi, Y. Tanishiro, S. Takahashi, M. Takahashi, *Surf. Sci.* **1985**, *164*, 367 – 392.
[13] J. P. Ferraris, D. J. Guerrero in *Handbook of Conducting Polymers* (Ed.: T. Skotheim), 2nd ed., Marcel Dekker, New York, **1986**, pp. 259 – 276.
[14] S. Glenis, M. Benz, E. LeGoff, J. L. Schindler, C. R. Kannewurf, M. G. Kanatzidis, *J. Am. Chem. Soc.* **1993**, *115*, 12519 – 12525.
[15] Y. Cao, X. M. Wei, W. S. Chin, Y. H. Lai, J. F. Deng, S. L. Bernasek, G. Q. Xu, *J. Phys. Chem. B* **1999**, *103*, 5698 – 5702.
[16] Additional losses at 1220, 1112, 1017, 920, 818, 737, 620, and 500 cm^{-1} are assigned to C–C stretching, C–H bending, C–H rocking, ring deformation, C–O stretching, C–H bending, ring torsion, and C–Si stretching modes, respectively.
[17] T. Eicher, S. Hauptmann, *The Chemistry of Heterocycles: Structure, Reactions, Synthesis and Applications*, Thieme, Stuttgart, **1995**, p. 52.
[18] C. O. Kappe, S. S. Murphree, A. Padwa, *Tetrahedron* **1997**, *53*, 14179 – 14233.
[19] A. A. El-Azhary, R. H. Hilal, *Spectrochim. Acta. Part A* **1997**, *53*, 1365 – 1373.
[20] H. Kobayashi, K. Edamoto, M. Onchi, M. Nishijima, *J. Chem. Phys.* **1983**, *78*, 7429 – 7436.
[21] A planar furan molecule is about 2.2 Å in width (spacing between two α carbon atoms). If the formation of an additional C–C bond between adjacent mono-σ precursors is considered, the overall dimension of the dimer complex is comparable to the distance between two neighboring Si adatoms.
[22] SPARTAN, Wavefunction, Irvine, CA.

CLASSICS FROM WILEY-VCH



Hopf, H.
Technical University Braunschweig, Germany
CLASSICS IN HYDROCARBON CHEMISTRY
Syntheses, Concepts, Perspectives
1999. IX, Approx 530 pages with approx 300 figures. Softcover.
Approx DM 98.-/ £ 34.95
ISBN 3-527-29606-9
Publication date: December 1999

Carbon and Hydrogen: the two basic building blocks can be combined in a million different ways to create a plethora of fascinating organic compounds. H. Hopf presents not only the most remarkable structures and properties of hydrocarbon compounds but also illustrates how molecules such as Pagodane or Dehydrobenzene challenge the synthetic skills of every organic chemist. Graduate students and researchers alike will find this book a gold mine of useful information essential for their daily work.

Nicolaou, K. C. / Sorensen, E. J.
University of California, San Diego, USA
CLASSICS IN TOTAL SYNTHESIS
Targets, Strategies, Methods
1996. XXIII, 798 pages with 444 figures. Softcover.
DM 98.-/ £ 34.95
ISBN 3-527-29231-4

This book is a must for every synthetic chemist. With didactic skill and clarity, K. C. Nicolaou and E. Sorensen present the most remarkable and ingenious total syntheses from outstanding synthetic organic chemists.

John Wiley & Sons, Ltd. • Baffins Lane
Chichester, West Sussex
PO 19 1UD, UK
Fax: +44 (0)1243-775878

WILEY-VCH • P.O. Box 10 11 61
69451 Weinheim, Germany
Fax: +49 (0) 62 01 - 60 61 84
e-mail: sales-books@wiley-vch.de

WILEY-VCH

ZI 1199

Lord of the Rings: An Octameric Lanthanum Pyrazolonate Cluster**

Jide Xu and Kenneth N. Raymond*

A continuing project in our laboratory has been the development of chelating agents for the lanthanide and actinide ions.[1] The special spectroscopic and magnetic properties of lanthanide complexes have prompted their use as luminescent probes, NMR shift agents, and as magnetic resonance imaging (MRI) agents.[2, 3] These applications rely on the precise control of the structural and electronic features of the metal coordination site(s).

The incorporation of trivalent lanthanide ions into self-assembling molecular architectures is currently also of great interest in supramolecular chemistry.[4] However, the trivalent lanthanide ions generally display variable and high (8, 9, or more) coordination numbers and the energy difference between the various coordination geometries is small; therefore they show low stereochemical preferences.[5] These factors make the rational design for the construction of supramolecular lanthanide complexes quite challenging. A better control of the coordination environment can be achieved through the use of highly predisposed ligands.[4a,b] These lead to a host of interesting and successful approaches but generally they also lead to enormously increased synthetic challenges.

Supramolecular helical species incorporating lanthanide ions were first reported in 1992 and have subsequently been prepared.[4c–g] A series of poly-*N* donor ligands of the 2,6-bisbenzimidazol-2-yl-pyridines has been studied in depth by the groups of Bünzli, Piguet, and Williams. The appeal of the helicate approach towards the preparation of well-defined coordination geometries lies in the fact that relatively simple ligands may be used. Given the right conditions, they will self-assemble into a large and predetermined structure. This process is crucially dependent on the geometry intrinsic to the particular metal–ligand interaction.

Bidentate 4-acyl-3-methyl-1-phenyl-2-pyrazolin-5-ones are β-diketonate chelators which were first synthesized at the turn of the last century.[6] Their complexing abilities, especially towards lanthanide and actinide ions, have also been long recognized and they are widely used for the separation of trace metals.[7] However it was not until 1983 that the tetradentate 4-acyl-2-pyrazolin-5-one ligands were synthesized and their coordination chemistry with lanthanide ions studied.[8a] These ligands form dinuclear lanthanide complexes which have interesting fluorescent properties.[8b–d] For example, the tetradentate ligand 3LIPYZL (1,5-Bis(1-phenyl-3-methyl-5-pyrazolone-4)-1,5-pentadione, H_2L) forms helical lanthanide(III) complexes with the stoichiometry $[Ln_2L_3]\cdot 4\,DMF$.[8b, 9] In contrast to the helical complexes formed with the six-coordinate d-block metal ions, the three tetradentate ligands can not saturate all the coordination sites of the two eight-coordinate lanthanide metal ions. Two solvent molecules fill the coordiation sites of each lanthanide ion. These structures reveal that lanthanide ions may form highly symmetric clusters with relatively simple 4-acyl-2-pyrazolin-5-one ligands, and leave some coordination vacancies for the solvent molecules to occupy. This is the guideline of our design of pyrazolonate-based lanthanide clusters.

Following the principles developed by our research group for the design of coordination clusters,[10] a tris-bidentate 4-acyl-2-pyrazolin-5-one ligand 4-(1,3,5-benzenetricarbonyl)-tris(3-methyl-1-phenyl-2-pyrazolin-5-one) (H_3L^1) was designed and synthesized. This rigid threefold-symmetric ligand forms a unique supramolecular three-dimensional ring architecture with first- and second-row transition metal ions such as Ga^{III},[11] V^{III}, Fe^{III}, and In^{III}.[12] These complexes have $[M_6L^1_6]$ architecture, which leads to three distinct environments for the three identical pyrazolone components of the ligand. The signals in the ^1H and ^{13}C NMR spectra of the Ga^{III} and In^{III} complexes show a characteristic triple splitting.[11, 12]

Based on the formation of these $[M_6L^1_6]$ three-dimensional ring structures it was reasoned that discrete supramolecular species might form with lanthanide ions, since the ligands do not necessarily have to saturate all of the coordination sites of the lanthanide ions. Indeed when the rigid threefold ligand H_3L^1 and lanthanum acetylacetonate $[La(acac)_3]$ were heated in DMSO, a high-yielding, self-assembly of a single species was observed (Scheme 1). The ^1H NMR spectra showed the characteristic triple splitting mode in the aliphatic as well as the aromatic regions (Figure 1). Similar phenomena were previously observed in $[M_6L^1_6]$ systems, which suggests that the lanthanum atoms may be located in similar coordination environments, and that the lanthanum complex may also have a three-dimensional ring structure. An X-ray crystallographic analysis[13] unambiguously revealed this complex to have a unique square-antiprismatic, three-dimensional ring structure $[La_8L^1_8]$ with idealized D_{4d} symmetry (Figure 2). Eight lanthanum atoms occupy the eight vertices of the polyhedron, while each ligand occupies one of the eight trianglar faces. Each lanthanum atom is coordinated by three ligands and each ligand coordinates to three lanthanum ions (Scheme 1). In this cluster nine-coordinate lanthanum atoms are linked by six-coordinate chelate ligands; this is a good example of coordination number residuum cluster formation. The residual coordination sites of the lanthanum ions are occupied by solvent molecules, some of which point into the cavity of the ring, as shown in Figure 2.

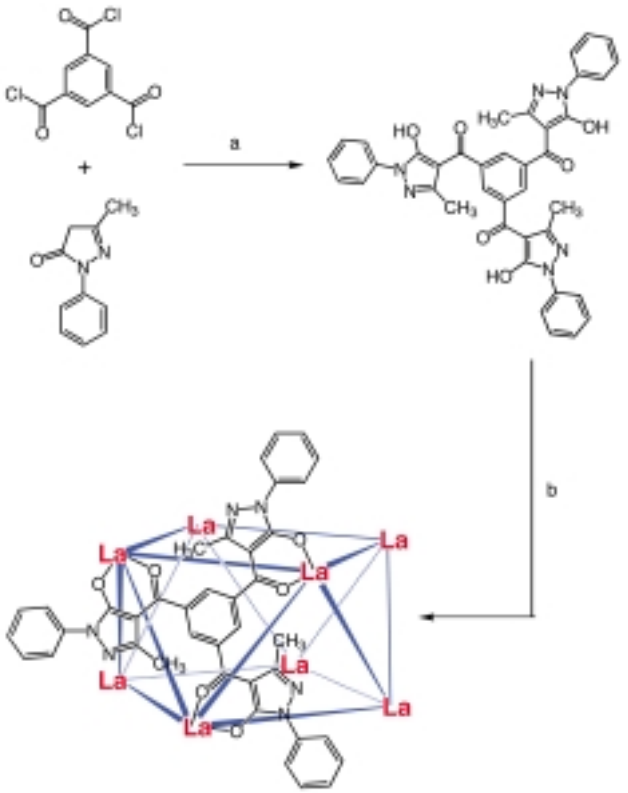
The coordinated DMSO solvent molecules can be easily replaced by other molecular donors such as alcohols, terpyridine, etc. In fact, when the complex that freshly precipitated from a DMSO solution was washed with methanol the complex dissolved and then re-precipitated. A batch of the

[*] Prof. Dr. K. N. Raymond, Dr. J. Xu
Department of Chemistry
University of California
Berkeley, CA 94720 (USA)
Fax: (+1) 510-486-1460
E-mail: raymond@socrates.berkeley.edu

[**] Coordination Number Incommensurate Cluster Formation, Part 14. This research was supported by the NSF (CHE-9709621 and INT-9603212) and by NATO (SRG951516). We gratefully acknowledge Dr. Frederick J. Hollander for help in the crystal structure determination. Part 13: T. N. Parac, M. Scherer, K. N. Raymond, *Angew. Chem.* **2000**, *112*, 1288–1291; *Angew. Chem. Int. Ed.* **2000**, *39*, 1239–1242.

Supporting information for this article is available on the WWW under http://www.wiley-vch.de/home/angewandte/ or from the author.

 © WILEY-VCH Verlag GmbH, D-69451 Weinheim, 2000 1433-7851/00/3915-2745 $ 17.50+.50/0



Scheme 1. Synthesis of the octomeric Lanthanide cluster $[La_8L_8^1]$. a) CaO/dioxane; b) $[La(acac)_3]$/DMSO, 100 °C, yield 81 %. The coordinated DMSO molecules are omitted for clarity.

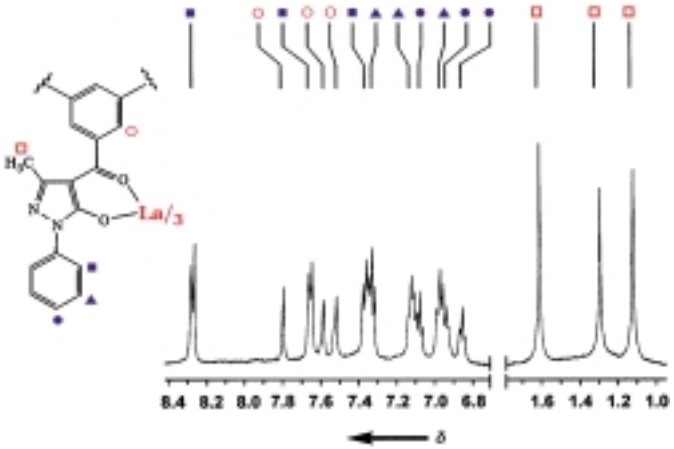


Figure 1. ^{1}H NMR spectrum of $[La_8L_8^1]$ in $[D_6]$DMSO. Only one of the three chemically inequivalent 4-acyl-pyrazolone moeities of the C_3-symmetric ligand is shown in the structure.

re-precipitated complex was dissolved in DMSO to grow crystals for X-ray structural analysis. Both MeOH and DMSO molecules were found in the structure.

The eight lanthanum atoms form a "regular" square-antiprism, both the upper and bottom sets form regular squares, and are offset by 45°. All of the distances between neighboring La atoms are equal within experimental error (10.1 and 10.3 Å). There are two lanthanum atoms (La1 and La2) in each asymmetric unit. Both lanthanum ions are nine-coordinate. The two possible ground-state geometries for nine-coordination polyhedra are the symmetrical tricapped trigonal prism with D_{3h} symmetry and the monocapped square antiprism with C_{4v} symmetry. The polyhedron of the La1 coordination sphere is best described as a slightly distorted monocapped square antiprism. The coordination polyhedron of La2 can be described as a distorted tricapped trigonal prism, in which the coordination polyhedron is distorted and has a lower symmetry (between the regular D_{3h} and C_{4v} structures).

In summary, a new lanthanum supramolecular architecture has been achieved in which nine-coordinate lanthanum centers are coordinated by three bidentate pyrazolone chelating units. These centers have been combined with a rigid C_3-symmetric ligand system to drive the formation of a square-antiprismatic cluster $[La_8L_8^1]$. This is the first example of a cyclic lanthanide cluster complex with a three-

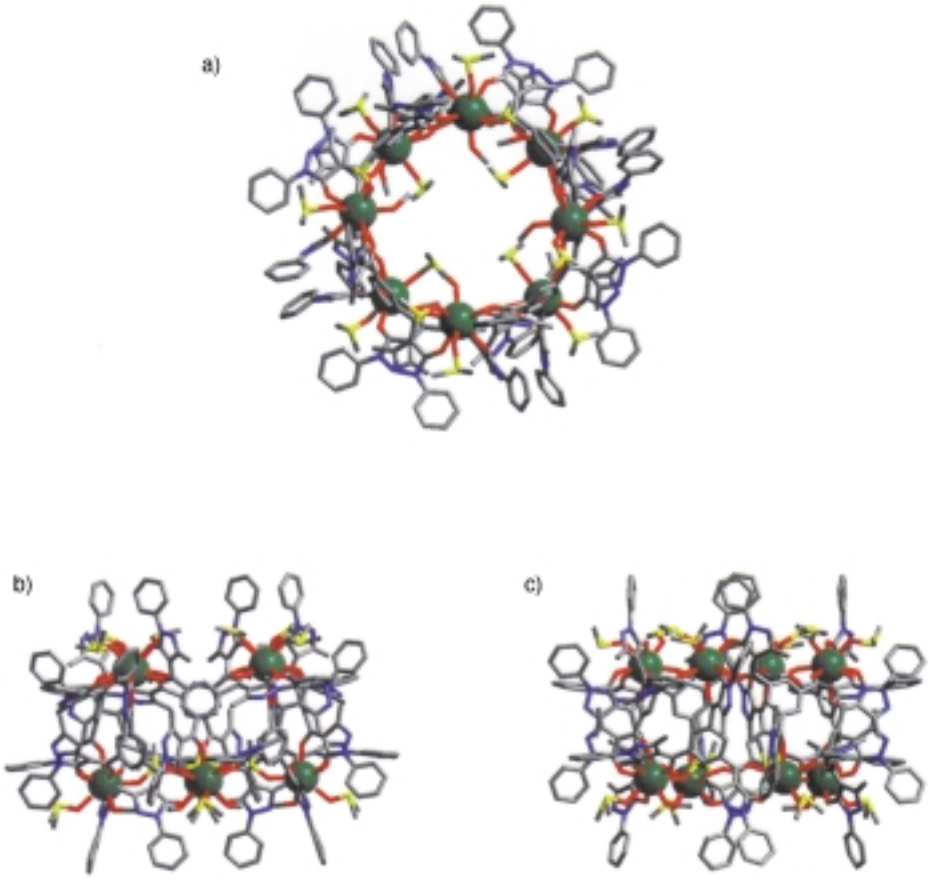


Figure 2. The X-ray crystal structure of $[La_8L_8^1]$, a) top view; b) and c) side views.

 © WILEY-VCH Verlag GmbH, D-69451 Weinheim, 2000 1433-7851/00/3915-2746 $ 17.50+.50/0

dimensional and highly symmetric ring structure, and is an extraordinary example of symmetry-driven cluster formation.

Experimental Section

General: All chemicals were used as received from Aldrich unless otherwise noted. The ^{1}H and ^{13}C NMR spectra were obtained on a Bruker DRX-500 spectrometer. Mass spectra and elemental analyses were performed at the MICRO-MASS Facility and the Elemental Analysis Facility, College of Chemistry, UC Berkeley, respectively.

H_3L^1: A suspension of 3-methyl-1-phenyl-2-pyrazolin-5-one (10.5 g, 0.06 mol) and calcium oxide (7.0 g, 0.12 mol) in dry dioxane (40 mL) was heated at 85 °C under nitrogen. A solution of 1,3,5-benzenetricarbonyl trichloride (5.0 g, 0.019 mol) in dry dioxane (10 mL) was added to this warm suspension over 1 min. The reaction mixture became a thick paste and the temperature increased immediately. The mixture was heated at reflux for 1 h, during which time the thick paste solidified. The dioxane solution was discarded and the solid was treated with 2 M HCl (250 mL). A beige solid was isolated by filtration, washed with cold water, and dried in vacuo at 60 °C overnight (yield 10.3 g, 82 %). Elemental analysis calcd for $C_{39}H_{30}N_6O_6 \cdot H_2O$ (%): C 67.23, H 4.62 N 12.06; found: C 67.01, H 4.61, N 12.06; ^{1}H NMR (500 MHz, [D$_6$]DMSO): $\delta = 2.32$ (s, 9H), 7.29 (t, $J = 7.6$ Hz, 3H), 7.43 (t, $J = 7.6$ Hz, 6H), 7.65 (d, $J = 7.9$ Hz, 6H), 8.30 (s, 3H); ^{13}C NMR (500 MHz, [D$_6$]DMSO): $\delta = 14.21$, 104.35, 121.31, 121.41, 126.31, 129.03, 131.79, 136.66, 138.68, 150.77, 188.72; positive-ion FAB-MS: *m*/*z*: 679 [$H_3L^1 + H^+$].

$La_8L^1_8$: Lanthanum acetylacetonate hydrate (94 mg, 0.2 mmol) was added to a suspension of $H_3L^1 \cdot H_2O$ (154 mg, 0.22 mmol) in DMSO (10 mL). The reaction mixture was heated with stirring under nitrogen at 100 °C for 16 h. Upon cooling the mixture down to room temperature, the yellow powdery solid precipitate was collected by filtration and dried in a vacuum oven at 80 °C overnight (170 mg, 81 %, 0.20 mmol). Elemental analysis calcd for $La_8C_{360}H_{360}N_{48}O_{72}S_{24}$ ([$La_8L^1_8$(DMSO)$_{24}$]) (%): C 51.53, H 4.32, N 8.01; found: C 51.50, H 4.21, N 8.39; ^{1}H NMR (500 MHz, [D$_6$]DMSO): $\delta = 1.12$ (s, 3H), 1.30 (s, 3H), 1.61 (s, 3H), 6.86 (t, $J = 7.4$ Hz, 1H), 6.94 (t, $J = 7.4$ Hz, 1H), 6.98 (t, $J = 8.0$ Hz, 2H), 7.08 (t, $J = 7.8$ Hz, 1H), 7.11 (t, $J = 7.6$ Hz, 2H), 7.34 (t, $J = 7.8$ Hz, 2H), 7.37 (d, $J = 8.0$ Hz, 2H), 7.52 (s, 1H), 7.59 (s, 1H), 7.66 (d, $J = 7.9$ Hz, 2H), 7.80 (s, 1H), 8.28 (d, $J = 8.0$ Hz, 2H); positive-ion FAB-MS: *m*/*z*: 6518 [$La_8L^1_8 + H^+$]; exact mass calcd for $La_8C_{312}H_{316}N_{48}O_{48}$: 6513.57.

Received: November 5, 1999
Revised: May 15, 2000 [Z14236]

[1] a) J. Xu, S. J. Franklin, D. W. Whisenhunt, Jr., K. N. Raymond, *J. Am. Chem. Soc.* **1995**, *117*, 7245; b) J. Xu, P. W. Durbin, B. Kullgren, K. N. Raymond, *J. Med. Chem.* **1995**, *38*, 2606; c) S. J. Franklin, K. N. Raymond, *Inorg. Chem.* **1994**, *33*, 5794.

[2] a) J.-C. G. Bünzli in *Lanthanide Probes in Life, Chemical and Earth Sciences*, Elsevier, Amsterdam, **1989**, chap. 7; b) P. G. Sammes, G. Yahioglu, *Nat. Prod. Rep.* **1996**, *13*, 1; c) P. Guerriero, S. Tamburini, P. A. Vigato, *Coord. Chem. Rev.* **1995**, *139*, 17.

[3] R. B. Lauffer in *MRI Clinical Magnetic Resonance Imaging*, *Vol. 1*, 2nd ed., W. B. Sauders Co., Philadelphia, **1996**, chap. 5.

[4] a) J.-M. Lehn, *Supramolecular Chemistry, Concepts and Perspectives*, VCH, Weinheim, **1995**; b) S. Petoud, J.-C. G. Bünzli, F. Renaud, C. Piguet, K. J. Schenk, G. Hopfgartner, *Inorg. Chem.* **1997**, *36*, 5750; c) G. Bernardinelli, G. Hopfgartner, S. Petoud, O. Schaad, *J. Am. Chem. Soc.* **1996**, *118*, 6681; d) J.-C. G. Bünzli, P. Froidevaux, C. Piguet, *New J. Chem.* **1995**, *19*, 661; e) N. Sabbatini, M. Guardigli, J.-M. Lehn, *Coord. Chem Rev.* **1993**, *123*, 201; f) G. Bernardinelli, C. Piguet, A. F. Williams, *Angew. Chem.* **1992**, *104*, 1626; *Angew. Chem. Int. Ed. Engl.* **1992**, *31*, 1622; g) C. Piguet, G. Bernardinelli, G. Hopfgartner, *Chem. Rev.* **1997**, *97*, 2005.

[5] a) D. Kepert, *Inorganic Stereochemistry*, Springer, Berlin, **1982**, chap. 2 and 12–16; b) J.-C. G. Bünzli in *Basic and Applied Aspects of Rare Earths*, Editional Complutense, Madrid, **1997**.

[6] a) F. Stoltz, *J. Prakt. Chem.* **1897**, *55*, 145; b) A. Michaelis, F. Engelhardt, *Chem. Ber.* **1908**, *41*, 2668; c) W. Wislicenus, H. Elvert, *Chem. Ber.* **1913**, *46*, 3395.

[7] a) B. S. Jensen, *Acta Chem. Scand.* **1959**, *13*, 1347; b) B. S. Jensen, *Acta Chem. Scand.* **1959**, *13*, 1668; c) L. Lakov, P. Vassileva, E. Gocheva, Z. Fresenius, *Anal. Chem.* **1995**, *351*, 583; d) M. O. C. Ogwuegbu, N. C. Oforka, *Hydrometallurgy* **1994**, *34*, 359; e) O. Todorova, P. Vassileva, L. Lakov, Z. Fresenius, *Anal. Chem.* **1993**, *346*, 943; f) P. K. Mohapatra, V. K. Manchanda, *Radiochim. Acta* **1992**, *57*, 25.

[8] a) X. C. Dong, F. C. Liu, Y. L. Zhao, *Acta Chim. Sin.* **1983**, *41*, 848; b) L. Yang, R. Yang, *Polyhedron* **1995**, *14*, 507; c) Y. Xing, X. Li, L. Yan, R. Yang, *Chem. J. Chin. Univ.* **1992**, *13*, 14; d) D. Zhou, Q. Li, C. Huang, G. Yao, S. Umetani, M. Matsui, L. Ying, A. Yu, X. Zhao, *Polyhedron* **1997**, *16*, 1381.

[9] J. Xu, S. Petoud, C. Brückner, K. N. Raymond, unpublished results.

[10] a) D. L. Caulder, K. N. Raymond, *J. Chem. Soc. Dalton Trans.* **1999**, 1185; b) D. L. Caulder, K. N. Raymond, *Acc. Chem. Res.* **1999**, 975; c) T. Beissel, R. E. Powers, K. N. Raymond, *Angew. Chem.* **1996**, *108*, 1166; *Angew. Chem. Int. Ed. Engl.* **1996**, *35*, 1084; d) C. Brückner, R. E. Powers, K. N. Raymond, *Angew. Chem.* **1998**, *110*, 1937; *Angew. Chem. Int. Ed.* **1998**, *37*, 1837; e) D. L. Caulder, R. E. Powers, T. N. Parac, K. N. Raymond, *Angew. Chem.* **1998**, *110*, 1940; *Angew. Chem. Int. Ed.* **1998**, *37*, 1840.

[11] D. Johnson, J. Xu, R. Saalfrank, K. N. Raymond, *Angew. Chem. Int. Ed.* **1999**, *111*, 3058; *Angew. Chem. Int. Ed.* **1999**, *38*, 2882.

[12] J. Xu, S. Petoud, D. Johnson, K. N. Raymond, unpublished results.

[13] Crystal data for [$La_8(C_{39}H_{37}N_6O_6)_8 \cdot 9.3\,CH_3OH \cdot 10.7\,DMSO \cdot 4\,H_2O$]$\cdot 20\,CH_3OH \cdot 12\,H_2O \cdot x$solvent: tetragonal, space group *P*4/*n* (Nr. 85), $a = 31.5567(3)$, $b = 31.5567(3)$, $c = 28.8080(5)$ Å, $V = 28687.7(6)$ Å^3, $Z = 2$, $\rho_{calcd} = 0.993$ g cm^{-3}, $\mu = 0.681$ mm^{-1}, $T = -115$ °C, $F(000) = 17088$. Crystal size $0.30 \times 0.20 \times 0.12$ mm^3. Data were collected using a Siemens SMART diffractometer equipped with a CCD area detector $2\theta_{max} = 40.36°$, ω scans, graphite-monochromated $Mo_{K\alpha}$ radiation ($\lambda = 0.71073$ Å). Of the 79543 reflections collected, 13351 were unique ($R_{int} = 0.1686$). The structure was solved by direct methods (SHELXL-97) and refined against F^2. Data were corrected for Lorentz and polarization effects. An empirical absorption correction was applied using SADABS (ellipsoidal model, $T_{max} = 0.900$, $T_{min} = 0.730$). $R_1 = 0.1274$, $wR_2 = 0.2428$, $GOF = 1.380$ for 6072 reflections $F_o > 4\sigma(F_o)$ (6072 Friedel unique data, 838 parameters, 48 restraints, $3.66° < 2\theta < 40.36°$); and for all 13351 data $wR_2 = 0.2990$, $GOF = 1.378$. Max/min residual density $+0.648/-0.456$ e Å^{-3}. The low density of the structure probably reflects the presence of additional solvent molecules. Unfortunately we were unable to locate these, as a result of the low quality of the crystal data. Details of the disorder in the structure are obtained in the Supporting Information. Crystallographic data (excluding structure factors) for the structure reported in this paper have been deposited with the Cambridge Crystallographic Data Centre as supplementary publication no. CCDC-141567. Copies of the data can be obtained free of charge upon application to CCDC, 12 Union Road, Cambridge CB2 1EZ, UK (fax: (+44) 1223-336-033; e-mail: deposit@ccdc.cam.ac.uk).

 © WILEY-VCH Verlag GmbH, D-69451 Weinheim, 2000 1433-7851/00/3915-2747 $ 17.50+.50/0

Evidence for Scattering Resonances in the $H + D_2$ Reaction**

Félix Fernández-Alonso, Brian D. Bean, James D. Ayers, Andrew E. Pomerantz, Richard N. Zare,* Luis Bañares, and F. J. Aoiz

The concept of scattering resonances in chemical reactions was extensively discussed[1, 2] in the early 1970s to explain oscillations in the reaction probability calculated for collinear encounters of H with H_2. Since then, the nature of resonance behavior and its observation in this prototypical reaction system have been a topic of intense and sometimes heated interest. Scattering resonances were first introduced to explain sharp features in the collision cross-section of neutrons with heavy nuclei as a function of collision energy[3] and then in the elastic scattering of electrons in atoms.[4] These (Feshbach) resonances are associated with a quasibound complex formed by the collision partners. Thus, it is common to associate the width of the resonance with the lifetime of the compound system, and the location of the resonance with the energy of the quasibound state. This semiclassical picture was the basis for the explanation that Levine and Wu[2] gave to the collinear $H + H_2$ system. Subsequently, theory was extended to three dimensions[5] and resonance features were shown to persist, but to be less pronounced.

Experimental observation of resonance behavior in the hydrogen exchange reaction has lagged behind theoretical efforts. In the late 1980s, Nieh and Valentini[6] reported scattering resonances in the integral cross-section (ICS) for the $H + H_2$ reaction. Subsequent theoretical[7] and experimental[8] work, however, showed that resonances are not observable in the ICS, but should be detectable in the energy dependence of the state-resolved differential cross-section (DCS)[9, 10] for the $H + H_2$ and $D + H_2$ reactions. The past ten years have witnessed considerable progress on the experimental front with the first fully state-resolved DCS measurements in the $H + D_2$ reaction by Schnieder and co-workers[11, 12] and by Zare and co-workers.[13–15] Aided by the theoretical predictions of Wu and Kuppermann,[16] Wrede and Schnieder[17] attempted to observe resonances in the $H + D_2$ reaction by tuning the collision energy between 1.27 and 1.30 eV, but their experimental data did not show any resonance structure, which caused them to question the theory. Recently, Shafer-Ray and co-workers[18] have found experimental and theoretical evidence for resonance signatures in the integral cross-section for $H + D_2 \rightarrow HD(v' = 0, j' = 7) + D$ at 0.94 eV, while they are absent in its isotopic cousins $H + H_2$ and $D + H_2$.

Herein we report signatures of resonances in the state-resolved DCS for the $H + D_2 \rightarrow HD(v' = 3, j') + D$ reaction at a center-of-mass (CM) collision energy of 1.64 ± 0.05 eV (158 ± 5 kJ mol^{-1}). We also complement these measurements with simulations of the experimental results using the quasiclassical trajectory (QCT) method. Experimentally we find sharp forward scattering for the lowest j' rotational levels of the $HD(v' = 3)$ product, which we attribute to the formation of short-lived reaction intermediates, the classical analogue of quantum mechanical scattering resonances. To the best of our knowledge resonances have not been previously reported in the state-resolved differential cross-sections for any chemical reaction system.

Figure 1 shows a comparison between the experimental results and QCT calculations for the $HD(v' = 3, j' = 0-7)$ ICS. The error bars in both theory and experiment represent 1σ (67%) confidence bands. The QCT calculations incorporate an initial D_2 rotational distribution characterized by a

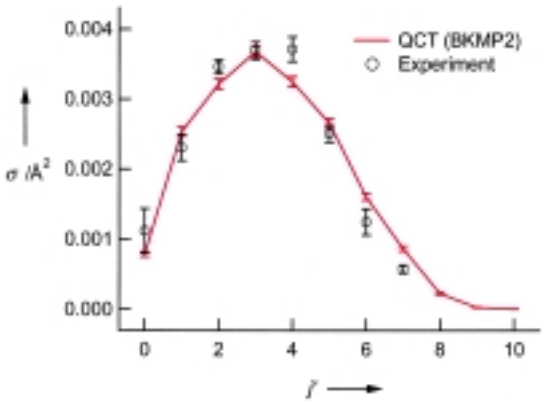


Figure 1. Reactive cross-section σ as a function of the $HD(v' = 3)$ product rotational state j'. The ordinate scale shown is for quasiclassical trajectory calculations (QCT, shown in red). The experimental points (open circles) have been normalized to the same total area as the QCT curve.

temperature of 300 K. The experimental technique employed in this study is sensitive only to the relative populations in different rotational levels. The experimental cross-sections have been scaled such that they have the same cumulative area from $j' = 0$ to 7 as the QCT calculations. No further scaling of the ICS or DCSs has been performed in the remainder of this work. Note the small reaction probabilities leading to the $HD(v' = 3, j')$ product. The scale on this plot ($0.000 - 0.004$ Å^2) should be compared with the total cross-section of 1.253 ± 0.001 Å^2 for the reaction obtained from the QCT calculations. The agreement between experiment and

[*] Prof. R. N. Zare, Dr. F. Fernández-Alonso, B. D. Bean, J. D. Ayers, A. E. Pomerantz
Department of Chemistry
Stanford University
Stanford, CA 94305-5080 (USA)
Fax: (+1) 650-725-0259
E-mail: zare@stanford.edu

Prof. L. Bañares, Prof. F. J. Aoiz
Departamento de Química Física
Facultad de Química
Universidad Complutense
28040 Madrid (Spain)

[**] We thank Donald G. Truhlar, Patrick Brown, Zee Hwan Kim, and Stephen Cho for careful and critical reading of the manuscript prior to publication. We also thank Andrew J. Alexander for his assistance in the preparation of the polar plots. Elf-Atochem (B.D.B.), the Hertz Foundation and Stanford University (J.D.A.), and the National Science Foundation (A.E.P.) are gratefully acknowledged for their support in the form of Graduate Fellowships. This work was supported at Stanford University by the U.S. National Science Foundation under Grant Number CHE-99-00305 and at Universidad Complutense by DGCYT PB98-0762-C03-01.

 © WILEY-VCH Verlag GmbH, D-69451 Weinheim, 2000 1433-7851/00/3915-2748 $ 17.50+.50/0

theory at this level of detail is excellent. Small discrepancies might be removed when a full quantum mechanical scattering calculation is completed.[19]

Qualitatively, the shape of the rotational distribution is quite similar to what has been found for HD($v'=1,j'$) and HD($v'=2,j'$) at similar collision energies.[20] The highest rotational quantum number produced in this reaction is dictated by impact parameter constraints rather than energy conservation. (The impact parameter is defined as the distance of closest approach of the reagents in the absence of the interaction potential.) In a simple-minded model for this reaction the initial impact parameter for reaction is channeled into rotational excitation of the product, that is, glancing collisions are more likely to produce rotationally excited products than head-on collisions.

Apart from the measurement of the product yield in a particular quantum state, we have also measured the state-resolved DCS in the CM frame. A DCS provides information about the preferred direction of HD product scattering (v_{HD}) with respect to the velocity of the incoming hydrogen atom (v_H). Backward scattering corresponds to an angle of 180° between v_H and v_{HD} (the two vectors being antiparallel). The opposite case (parallel velocity vectors) corresponds to forward scattering. In Figure 2 we present polar plots of the

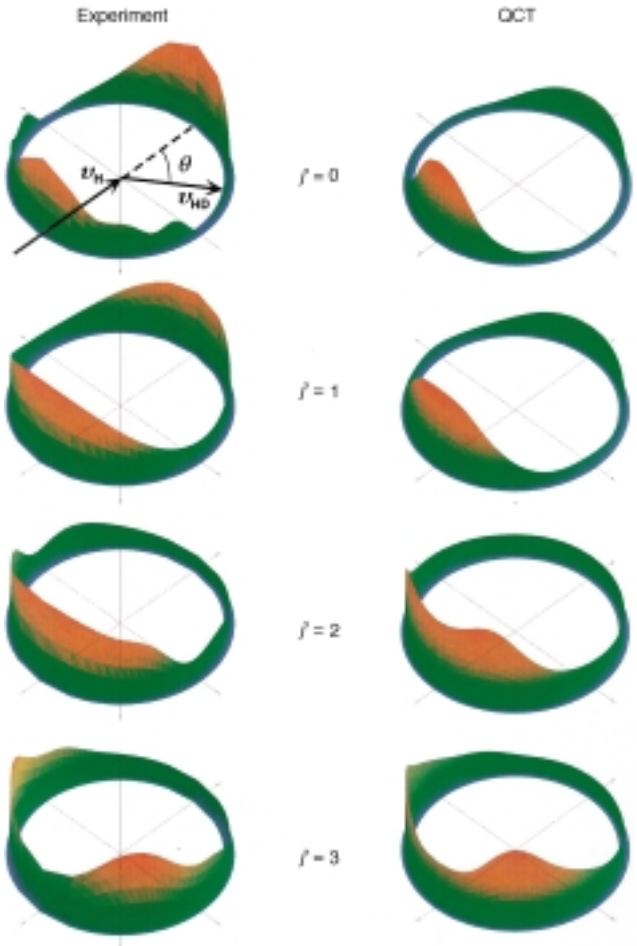


Figure 2. Polar plots of the HD($v'=3,j'=0-3$) CM differential cross-sections from experiment (left) and QCT calculations (right). The H atom reactant (v_H) and HD product (v_{HD}) CM velocities are indicated with arrows (see text for details).

experimental and QCT DCSs for HD($v'=3,j'=0-3$). In these plots the chemical reaction takes place in the plane of the figure, with the directions of v_H and v_{HD} defined as shown. The height around each circle is proportional to the probability of scattering into an angle θ, where θ is defined as the angle between v_H and v_{HD}.

The polar plots generated from the experimental data are shown on the left and have been obtained from a spline representation of a total of twelve experimental points across the whole angular range. The QCT DCSs shown on the right have been convolved with the instrumental function to provide the best simulation of the experimental results. In both cases, the DCSs show a similar dependence on j'. In the backward hemisphere ($\theta > 90°$) the DCSs move away from complete backward scattering as j' increases. This finding is also in qualitative agreement with previous findings for lower vibrational levels.[11, 13] The most striking feature in this figure is the peak in the forward direction which is most prominent for the rotationless state $j'=0$. The experimental and QCT polar plots in Figure 2 differ in regard to the ratio of forward to backward scattering. This finding suggests that the observations cannot be described solely by quasiclassical mechanics.

Despite the disagreement in the magnitude of the forward scattering peak between experiment and the QCT method, the fact that the calculations do actually show the same qualitative trends as the experiment caused us to examine the QCT reactive trajectories more closely. Figure 3 shows some of the attributes characterizing the reactive collisions that lead to HD($v'=3,j'=0-3$). The left panel shows the state-resolved reaction probabilities sorted in terms of those scattering in the forward ($\theta < 90°$) and backward hemispheres ($\theta > 90°$). The reaction cross-section is proportional to the integral of the reaction probability (opacity function) $P(b)$ × the impact parameter b. Therefore, the larger the impact parameter the larger the cross-section will be for a given value of $P(b)$. For backward scattering, the reaction probability shifts in b as the amount of product rotation increases. This trend is consistent with our previous interpretation of the shape and extent of the ICS (Figure 1). In contrast, the forward-scattering reaction probability peaks at 0.7–0.8 Å. This value for the impact parameter is close to the internuclear distance for molecular hydrogen and its isotopomers. Moreover, its shape and position seem not to depend strongly on the product rotational quantum number. This figure helps to explain why forward scattering has been observed primarily for low j' states. It is seen that the $j'=0$ back-scattered reaction probability peaks at lower b values than for $j'=1-3$. Very similar reaction probability distributions have been previously observed in QCT trajectory calculations of the $D+H_2$ reaction between 0.30 and 1.25 eV by Aoiz and co-workers.[21] The contribution of the high impact parameter to the DCS in the $D+H_2$ reaction was associated with the "E-θ ridge" which also appeared in the quantum mechanical calculations of Miller and Zhang and was associated with resonance scattering.[10] Prior to these studies, Muga and Levine[22] had proposed a classical mechanism for resonances in $H+H_2$ collisions that involved high impact parameters as well as long collision times. As shown below, we also find that our

 © WILEY-VCH Verlag GmbH, D-69451 Weinheim, 2000 1433-7851/00/3915-2749 $ 17.50+.50/0

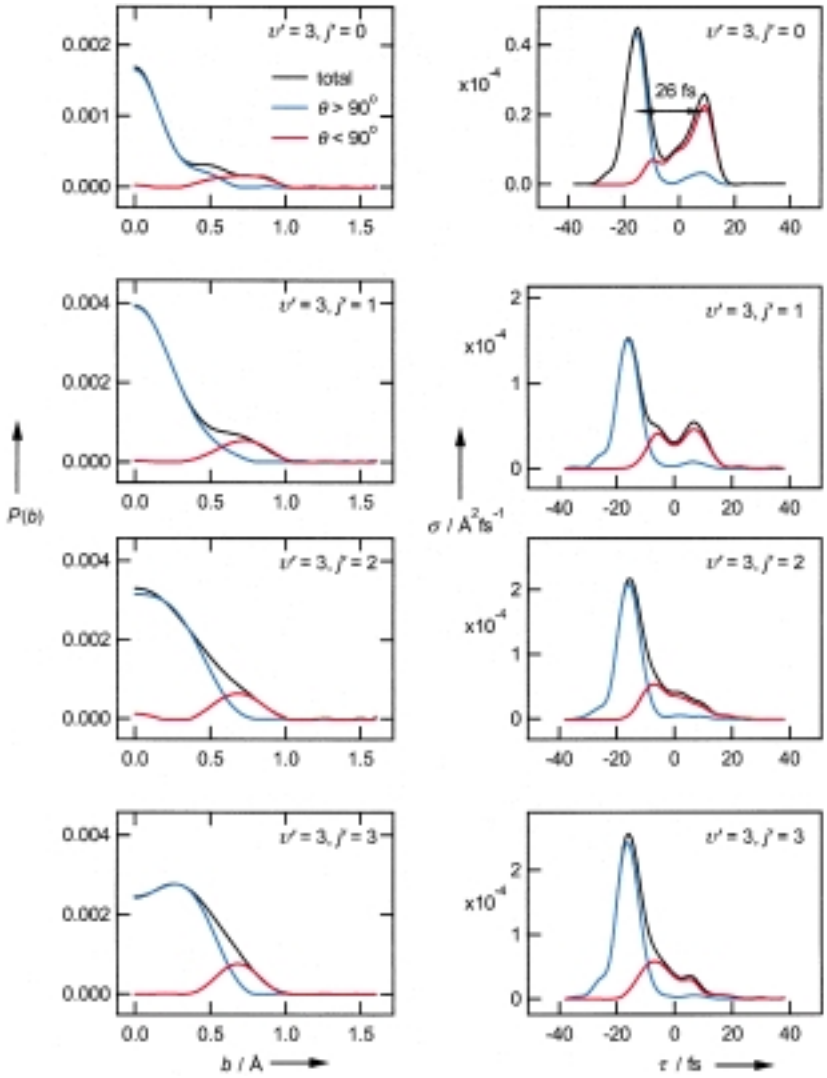


Figure 3. QCT trajectory details for HD($v'=3,j'=0-3$). The plots on the left show the reaction probability $P(b)$ as a function of impact parameter b for all, backward, and forward reactive trajectories. The plots on the right show the reactive cross-sections σ as a function of time delay τ for all, backward, and forward trajectories (see text for further details).

forward-scattering peak is associated with long-lived trajectories.

We also show the distribution of time delays (a measure of the reaction time) corresponding to the forward- and backward- scattering products that accompany the reaction probabilities in Figure 3. The classical time delay τ is defined as the time difference for trajectories with and without the potential present.[21–23] We observe negative time delays (typical for direct reactions) for the back-scattered classical trajectories, whereas the forward-scattering ones appear at more positive time delays. An approximate time difference of 26 fs between direct (backward) and indirect (forward) trajectories is calculated for the HD($v'=3,j'=0$) state (Figure 3). This time difference is considerably shorter than the classical period for the first rotational state of the HD product (120 fs) and HDD complex (480 fs). Therefore, the observed forward–backward scattering does not arise from a complex that lives for one or more rotational periods.

Distinct forward and backward contributions are most prominent for the HD($v'=3,j'=0$) product state. The peak at positive time delay has decreased considerably for the HD($v'=3,j'=1-3$) states relative to the backward (direct) contribution. Moreover, the forward-scattering time delay gradually decreases in going from $j'=0$ to $j'=3$. This finding further corroborates the conclusion that long-lived trajectories appear most prominently in the DCS for the HD($v'=3$, $j'=0$) product state.

It is possible to offer a tentative explanation for the resonance behavior based on our previous analysis of reactive trajectories and on the features of the potential energy surface. The top panel in Figure 4 shows two typical trajectories corresponding to the indirect/forward (left) and direct/backward (right) scattering mechanisms. The numbered dots indicate particular collision times for each trajectory (1 = earliest, 4 = latest). The inset defines the entrance-channel Jacobi coordinates R and γ used in this figure to plot the trajectories and potential energy contours. Here R is the distance between the H atom and the center of mass of the D_2 molecule, and γ is the angle between R and the D_2 bond axis. The middle and bottom panels show contours of the BKMP2[24] potential energy surface with the D_2 bond distance fixed at the equilibrium distance of 0.74 Å (middle) and at 1.21 Å (bottom). The trajectory dots corresponding to the elongation of each diatom bond are overlaid on these contours. The H atom approaches the diatom almost collinearly ($\gamma \approx 180^\circ$) in the direct, back-scattered trajectory. As a result, a minimum value of R is reached (dot 2 on the right) without the D_2 molecule adjusting its internuclear distance. Immediately after this "hard" knock, the D_2 bond breaks giving rise to vibrationally excited HD product (dot 3 on the right). The initial geometry of the three atoms for the indirect/forward trajectory tends to be L-shaped ($\gamma = 30-60^\circ$) and the angular variable γ changes rapidly as the H atom approaches the D_2 molecule. This deflection is mainly caused by the large barrier to insertion located at $\gamma \approx 90^\circ$ (see bottom contour plot). During this time, the D_2 molecule elongates its bond. By the time R approaches its minimum value, the topology of the potential energy surface displays two deep wells about the collinear configuration. The red dots 2–4 in the bottom panel appear to rattle around these minima for a few femtoseconds. Although this picture is only qualitatively correct, namely, the width and depth of the wells is continuously being modulated by the changing diatomic bond length, it shows what features of the underlying energy surface give rise to our observations. The presence of relatively long-lived trajectories that correlate with observed forward-scattering features is likely to give rise to quasibound states in full quantum-mechanical calculations for this reaction system, and will hopefully account for the quantitative differences between experiments and QCT

 © WILEY-VCH Verlag GmbH, D-69451 Weinheim, 2000 1433-7851/00/3915-2750 $ 17.50+.50/0

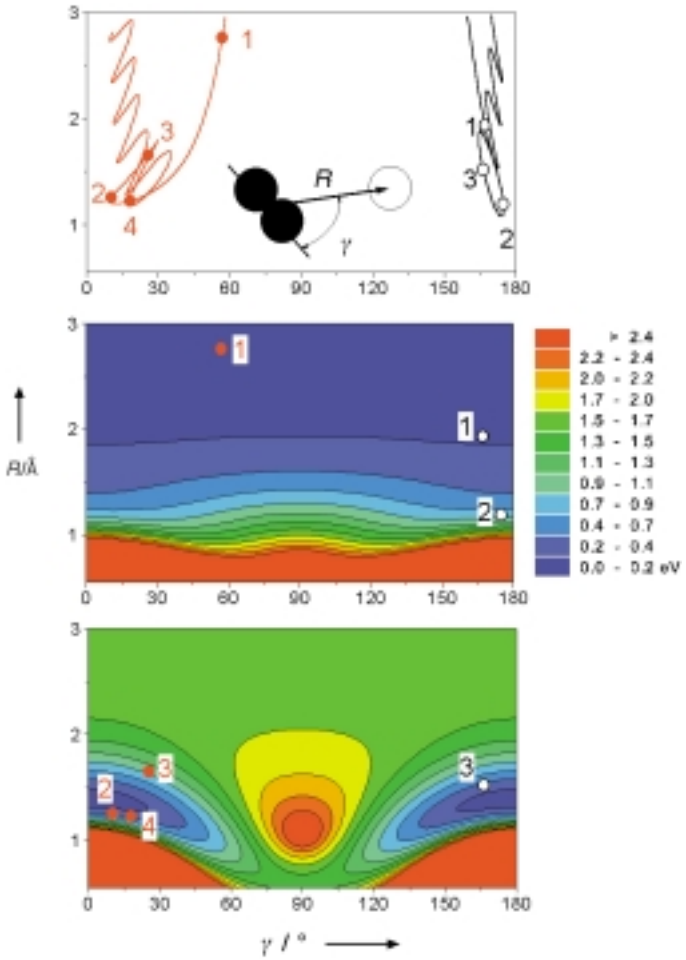


Figure 4. Top panel: R-γ plots of typical indirect (red line on the left) and direct (black line on the right) trajectories. Middle and bottom panels: potential energy contours of the BKMP2 potential energy surface with the D_2 bond length fixed at 0.74 Å (middle plot) and 1.21 Å (bottom). The trajectory dots have been overlaid on the potential energy contours corresponding to the instantaneous D_2 bond length. The color scale shown applies to both the middle and bottom contour plots.

calculations. Clearly resonance features provide detailed information on how this most elementary of chemical reactions can be understood.

Experimental Section

State-resolved DCS measurements: A mixture of HBr:D_2 (1:9) held at a stagnation pressure of 330 Torr was expanded into a high-vacuum chamber with a pulsed solenoid valve. HBr is photolyzed by the fifth harmonic of a Nd:YAG laser at 212.8 nm. Photolysis of this molecule generates two single-speed populations of "hot" hydrogen atoms. Only those hydrogen atoms corresponding to the fast photolysis channel contribute to our measured reaction signal. The HD($v'=3, j'=0-7$) reaction product is subsequently ionized 15 ns later by 2+1 resonance-enhanced multiphoton ionization (REMPI) through the $EF\,^1\Sigma_g^+ - X\,^1\Sigma_g^+$ electronic transition. Photolysis and reaction take place inside a velocity-sensitive, Wiley–McLaren time-of-flight apparatus. State-resolved CM DCSs can be directly inferred from an analysis of the time-of-flight profiles. Zare and co-workers have discussed in detail the experimental setup as well as the procedure to invert the experimental data into CM DCSs.[14]

QCT calculations: A total of five million trajectories were run on the BKMP2[24] potential energy surface at a relative translational energy of 1.64 eV. Each trajectory was initiated at a distance of 5 Å and numerically integrated in increments of 5.0×10^{-17} s using Hamming's fourth-order, predictor-corrector method. A trajectory was considered complete once the collision partners were also 5 Å apart. Asymptotic product analysis was performed at this final interparticle separation. Conservation of energy of 1 part in 10^5 and total angular momentum of 1 part in 10^6 in each trajectory was enforced throughout the calculation. No reactive trajectories were observed above 1.39 Å. Product quantization was performed by equating the internal energy of the HD product to the full Dunham expansion of rotational-vibrational levels and rounding these real values to the nearest integer.[25] The experimental rotational distribution of D_2 ($T=300$ K) was simulated by weighted sampling of the first nine rotational levels of this molecule. DCSs, reaction probabilities, and other reaction attributes were fit to a series in Legendre polynomials to provide a convenient functional representation of the computational results.[25, 26]

Received: March 31, 2000 [Z14928]

[1] a) D. G. Truhlar, A. Kuppermann, *J. Chem. Phys.* **1972**, *56*, 2232; b) G. C. Schatz, A. Kuppermann, *J. Chem. Phys.* **1973**, *59*, 964.
[2] R. D. Levine, S.-F. Wu, *Chem. Phys. Lett.* **1971**, *11*, 557.
[3] a) H. A. Bethe, *Phys. Rev.* **1935**, *47*, 747; b) N. Bohr, *Nature* **1936**, *137*, 344.
[4] a) E. Baranger, E. Gerjouy, *Phys. Rev.* **1957**, *106*, 1182; b) G. J. Schulz, *Phys. Rev. Lett.* **1962**, *10*, 104.
[5] G. C. Schatz, A. Kuppermann, *Phys. Rev. Lett.* **1975**, *35*, 1266.
[6] a) J. C. Nieh, J. J. Valentini, *Phys. Rev. Lett.* **1988**, *60*, 519; b) J. C. Nieh, J. J. Valentini, *J. Chem. Phys.* **1990**, *92*, 1083.
[7] a) M. Mladenovic, M. Zhao, D. G. Truhlar, D. W. Schwenke, Y. Sun, D. J. Kouri, *Chem. Phys. Lett.* **1988**, *146*, 358; b) J. Z. H. Zhang, W. H. Miller, *Chem. Phys. Lett.* **1988**, *153*, 465; c) D. E. Manolopoulos, R. E. Wyatt, *Chem. Phys. Lett.* **1989**, *159*, 123; d) J. Z. H. Zhang, W. H. Miller, *Chem. Phys. Lett.* **1989**, *159*, 130; e) M. Zhao, M. Mladenovic, D. G. Truhlar, D. W. Schwenke, *J. Am. Chem. Soc.* **1989**, *111*, 852; f) J. M. Launay, M. LeDourneuf, *Chem. Phys. Lett.* **1989**, *163*, 178.
[8] D. A. V. Kliner, D. E. Adelman, R. N. Zare, *J. Chem. Phys.* **1991**, *94*, 1069.
[9] R. E. Continetti, J. Z. H. Zhang, W. H. Miller, *J. Chem. Phys.* **1990**, *93*, 5356.
[10] W. H. Miller, J. Z. H. Zhang, *J. Phys. Chem.* **1991**, *95*, 12.
[11] a) L. Schnieder, K. Seekamp-Rahn, E. Wrede, K. H. Welge, *J. Chem. Phys.* **1997**, *107*, 6175; b) E. Wrede, L. Schnieder, K. H. Welge, F. J. Aoiz, L. Bañares, J. F. Castillo, B. Martínez-Haya, V. J. Herrero, *J. Chem. Phys.* **1999**, *110*, 9971.
[12] L. Schnieder, K. Seekamp-Rahn, J. Borkowski, E. Wrede, K. H. Welge, F. J. Aoiz, L. Bañares, M. J. D'Mello, V. J. Herrero, V. Sáez Rábanos, R. E. Wyatt, *Science* **1995**, *269*, 207.
[13] a) F. Fernández-Alonso, B. D. Bean, R. N. Zare, *J. Chem. Phys.* **1999**, *111*, 1035; b) F. Fernández-Alonso, B. D. Bean, R. N. Zare, *J. Chem. Phys.* **1999**, *111*, 2490.
[14] F. Fernández-Alonso, B. D. Bean, R. N. Zare, *J. Chem. Phys.* **1999**, *111*, 1022.
[15] H. Xu, N. E. Shafer-Ray, F. Merkt, D. J. Hughes, M. Springer, R. P. Tuckett, R. N. Zare, *J. Chem. Phys.* **1995**, *103*, 5157.
[16] A. Kuppermann, Y. S. M. Wu, *Chem. Phys. Lett.* **1995**, *241*, 229.
[17] E. Wrede, L. Schnieder, *J. Chem. Phys.* **1997**, *107*, 786.
[18] B. K. Kendrick, L. Jayasinghe, S. Moser, M. Auzinsh, N. Shafer-Ray, *Phys. Rev. Lett.* **2000**, *84*, 4325.
[19] J. F. Castillo, L. Bañares, F. J. Aoiz, unpublished results.
[20] B. D. Bean, F. Fernández-Alonso, R. N. Zare, *J. Phys. Chem.*, submitted.
[21] a) F. J. Aoiz, V. J. Herrero, V. S. Rábanos, *J. Chem. Phys.* **1991**, *95*, 7767; b) F. J. Aoiz, V. J. Herrero, V. S. Rábanos, *J. Chem. Phys.* **1992**, *97*, 7423.
[22] J. G. Muga, R. D. Levine, *Chem. Phys. Lett.* **1989**, *162*, 7.
[23] a) L. Eisenbud, PhD thesis, Princeton University (USA), **1948**; b) E. P. Wigner, *Phys. Rev.* **1955**, *98*, 145; c) F. T. Smith, *Phys. Rev.* **1960**, *118*, 349; d) J. W. Duff, D. G. Truhlar, *Chem. Phys.* **1974**, *4*, 1; e) P. Brumer, D. E. Fitz, D. Wardlaw, *J. Chem. Phys.* **1980**, *72*, 386;

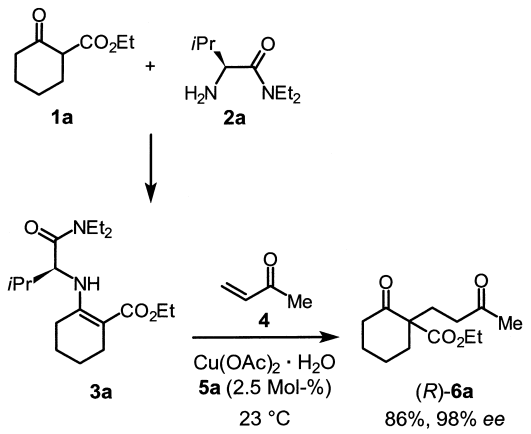
f) A. Kuppermann in *Potential Energy Surfaces and Dynamics Calculations* (Ed.: D. G. Truhlar), Plenum, New York, **1981**, pp. 375.
[24] A. I. Boothroyd, W. J. Keogh, P. G. Martin, M. R. Peterson, *J. Chem. Phys.* **1996**, *104*, 7139.
[25] F. J. Aoiz, L. Bañares, V. J. Herrero in *Advances in Classical Trajectory Methods, Vol. 3* (Ed.: W. L. Hase), JAI, New York, **1998**, pp. 121.
[26] F. J. Aoiz, L. Bañares, V. J. Herrero, *J. Chem. Soc. Faraday Trans.* **1998**, *94*, 2483.

New Chiral Auxiliaries for the Construction of Quaternary Stereocenters by Copper-Catalyzed Michael Reactions**

Jens Christoffers* and Alexander Mann

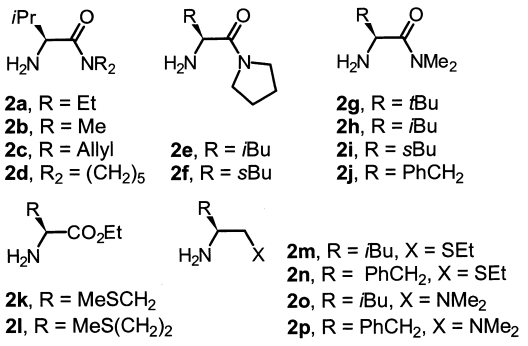
The enantioselective construction of quaternary stereocenters is still a challenging goal in synthetic organic chemistry.[1] Herein we report a new copper(II)-catalyzed and auxiliary-based Michael reaction which allows the construction of quaternary carbon centers with *ee* values in excess of 95% at ambient temperature (see Scheme 1). The Michael reaction is an established method for C–C bond formation and is commonly catalyzed by a strong Brønstedt base.[2] In order to avoid the disadvantages of basic reaction conditions, a number of transition metal catalyzed procedures has been published in recent years; this has resulted in improved chemoselectivity due to the milder reaction conditions.[3] Moreover, chiral ligands can be utilized here to achieve asymmetric catalysis of the Michael reaction. In the recent years a number of chiral catalysts has been reported for the conversion of 1,3-dicarbonyl compounds with α,β-unsaturated ketones.[4] In particular, the introduction of the heterobimetallic lanthanum/sodium/[1,1′-binaphthyl]-2,2′-diol (LSB) catalyst by Shibasaki and co-workers has to be mentioned here as it defines the state of the art in this field.[5] However, the reaction conditions are also Brønstedt basic, and the enantioselective construction of quaternary stereocenters requires low temperatures.

Another strategy is the derivatization of the Michael donor with a chiral amine as an auxiliary to give an imine or enamine, which is subsequently converted with the Michael acceptor.[6] If enamines derived from β-oxoesters are applied according to this method, further activation, by addition of a stoichiometric amount of Lewis acid or by high pressure and low temperature, is required in order to achieve reasonable yields and selectivity.[7] Recently we reported on the Ni-catalyzed conversion of cyclic β-oxoesters in the presence of 1,2-diaminocyclohexane.[8] We were able to prepare the Michael product **6a** in 91% *ee* at ambient temperature and without exclusion of moisture. Similar results can only be achieved with the LSB catalyst at $-50\,^{\circ}C$ (93% *ee*).[9] Koga and co-workers obtained *ee* values of 90% by using a chiral auxiliary and a stoichiometric amount of a Brønstedt base at $-100\,^{\circ}C$.[10] In this work we report on a new class of auxiliaries for the transition metal catalyzed reaction of β-oxoesters **1** with simple enones, such as methyl vinyl ketone (MVK, **4**), and the synthesis of the Michael product **6a** (Scheme 1) with up to 99% *ee* at ambient temperature and without inert conditions, a reaction which is unprecedented in the literature.



Scheme 1. Synthesis of **3a** and the copper(II)-catalyzed conversion with MVK (**4**).

In the course of a combinatorial search,[11] we have investigated a number of chiral amines **2a**–**p** derived from α-amino acids which bear either a thioether, a tertiary amine, or an amide group as an additional donor function.[12, 13] In an



acid-catalyzed reaction with the Michael donor **1a**, these amines yield the corresponding imines, which exist completely as the tautomeric enamines **3a**–**p**; these enamines are isolable, after chromatography, in good to excellent yields (85–95%).

In a primary screening the enaminoesters **3a**–**p** were each converted in the presence of catalytic amounts of 14 different metal salts **5a**–**n**[14] with MVK (**4**) in CH_2Cl_2. If a positive effect was observed relative to the noncatalyzed reaction, with regard to the selectivity of the formation of Michael product **6a**, we started to optimize the reaction parameters. At this first stage of the screening, we did not pay attention to the

[*] Dr. J. Christoffers, Dipl.-Chem. A. Mann
Technische Universität Berlin
Institut für Organische Chemie, Sekretariat C3
Strasse des 17. Juni 135, 10623 Berlin (Germany)
Fax: (+49) 30-723-12-33
E-mail: jchr@wap0105.chem.tu-berlin.de

[**] This work was supported by the Deutsche Forschungsgemeinschaft and the Fonds der Chemischen Industrie. We are also grateful to the Degussa-Hüls AG for gifts of amino acids and to Prof. Dr. S. Blechert for his support.

 © WILEY-VCH Verlag GmbH, D-69451 Weinheim, 2000 1433-7851/00/3915-2752 $ 17.50+.50/0

Table 1. Selected results for the screening of enaminoesters **3** with MVK (**4**) in the presence of different metal salts **5**.[a]

Enamine	*ee* (**6a**) [%][b] without metal salt	Metal salt (mol%)	*ee* (**6a**)[b] [%]	Metal salt (mol%)	*ee* (**6a**)[b] [%]
3c	28	$Cu(OAc)_2 \cdot H_2O$ (10)	59	$SnCl_2$ (5)	43
3d	47	$Cu(OAc)_2 \cdot H_2O$ (5)	57	$FeCl_3$ (5)	59
3e	53	$Cu(OAc)_2 \cdot H_2O$ (10)	73	$FeCl_3$ (5)	50
3g	78	$Cu(OAc)_2 \cdot H_2O$ (20)	86	$Cu(OTf)_2$[c] (10)	68
3h	72	$Cu(OAc)_2 \cdot H_2O$ (5)	76	$FeCl_3$ (5)	77
3i	66	$Cu(OAc)_2 \cdot H_2O$ (20)	86	$FeCl_3 \cdot 6H_2O$ (10)	73
3l	33	$Cu(OAc)_2 \cdot H_2O$ (5)	20	$SnCl_2$ (15)	50
3m	29	$NiCl_2$ (5)	37	$SnCl_2$ (17.5)	35
3o	20	$Ni(OAc)_2 \cdot 4\,H_2O$ (5)	23	$FeCl_3$ (5)	21

[a] Reaction conditions: Scale = approximately 0.20 mmol of **3**; **3**:**4** = 1:2; solvent = CH_2Cl_2. [b] The *ee* value of **6a** was determined by GC on a chiral phase.[15] The yields were not determined. [c] Tf = F_3CSO_2.

yield. Selected results are given in Table 1. Auxiliaries derived from valine and iso- or *tert*-leucine with an additional amide function (**2a**–**i**), when attached to the Michael donor, induced selectivities up to 78% *ee* even without any metal salt. In every case the *R* isomer was found to be the major enantiomer.[8] When $Cu(OAc)_2 \cdot H_2O$ was applied as the catalyst, the *ee* values were clearly improved by about 20%. Auxiliaries with a thioether or tertiary amino function did not show promising results and, for this reason, were not considered for further optimizations.

Improvement in selectivity was also achieved by variation of the solvent: With acetone as the solvent the enantioselectivity for the copper(II) catalysis was dramatically raised. Greater than 95% *ee* values were obtained with the enaminoesters **3a**, **c**, **d**, **f**, **g**, and **i** (Table 2). In particular, when

Table 2. Asymmetric Michael reactions of enaminoesters **3** with MVK (**4**) in the presence of $Cu(OAc)_2 \cdot H_2O$ (**5a**) in acetone.[a]

Enamine	*ee* (**6a**) [%][b] amount of **5a** [mol%]				
	0	2.5	5	10	20
3a	57	98	98	98	98
3b	65	83	84	85	85
3c	55	93	95	94	92
3d	55	95	97	98	92
3f	76	93	97	90	93
3g	85	96	96	97	99
3i	70	91	92	92	91

[a] Reaction conditions: Scale = approximately 0.20 mmol of **3**; **3**:**4** = 1:2; solvent = acetone. [b] For enantioselectivities of greater than 95% the *ee* values were additionally checked after derivatization to **7a**.[15]

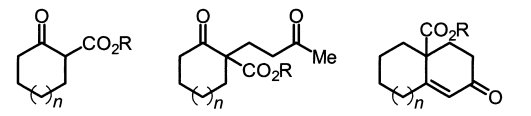
compounds **3a** and **3d** were used with 2.5 or 10 mol% of catalyst, selectivities of up to 98% *ee* were achieved. An increase to 99% *ee* resulted when compound **3g** was used in the presence of 20 mol% $Cu(OAc)_2 \cdot H_2O$. With these results, the protocol presented here is the most selective method known so far for the stereoselective generation of quaternary carbon centers by Michael reactions of β-oxoesters with MVK. However, only the auxiliaries derived from valine and iso- or *tert*-leucine show such high selectivities. The yields are dependent upon the reaction time and the amount of catalyst applied. The use of 2.5 mol% of catalyst gives 65–75% yield after 12–14 h. If more catalyst is employed, the yields rise to 80–90%. Without any catalyst the yield is less than 15% after 12–14 h. We were further interested in whether our method could be transferred to cyclic Michael donors with different ring sizes. As shown in Table 3, the Michael product **6b** can be prepared with an *ee* value of greater than 98% from the five-membered ring β-oxoester **1b** attached to auxiliary **2g**.[15] The seven-membered ring compound **1c** can be converted into

Table 3. Variation of the Michael donor **1** in acetone.

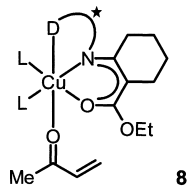
Michael donor	Auxiliary	Catalyst [mol%]	Product	*ee* [%]	Yield [%]
1b	**2g**	5	**6b**[a]	≥ 98	40
1c	**2g**	10	**6c**	74[b]	84

[a] *R* enantiomer.[8] [b] The *ee* of **6c** was determined after derivatization to **7b**.[15]

product **6c** in 74% *ee* by use of the same auxiliary **2g** (*ee* value determined after derivatization to compound **7b**).[15]



1b, *n* = 0, R = Et; **1c**, *n* = 2, R = Me; **6b**, *n* = 0, R = Et; **6c**, *n* = 2, R = Me; **7a**, *n* = 1, R = Et; **7b**, *n* = 2, R = Me



8

Regarding the mechanism of the reaction we can only speculate at the moment. However, we suppose that this Cu-catalyzed variant of an auxiliary-mediated Michael reaction does not proceed via a cyclic transition state as proposed by d'Angelo and co-workers,[6] but instead through an intermediate **8**, in which the enamine **3** coordinates as a tridentate ligand to the copper center and, thereby, effects a diastereofacial differentiation. At the same time the enone is activated by coordination to the metal center.[8]

The copper-catalyzed auxiliary-mediated Michael reaction of cyclic β-oxoesters with MVK introduced herein allows, for the first time, the construction of quaternary stereocenters in 80–90% yield with up to 99% *ee*. The reaction proceeds at ambient temperature and under mild conditions. Exclusion of air or moisture is not necessary. As chiral auxiliaries α-amino acid amides, which are readily available by standard transformations from α-amino acids, are applied; they are almost quantitatively recoverable after the reaction.

 © WILEY-VCH Verlag GmbH, D-69451 Weinheim, 2000 1433-7851/00/3915-2753 $ 17.50+.50/0

Experimental Section

3g (representative procedure): A mixture of (*S*)-*tert*-leucine dimethylamide (**2g**; 696 mg, 4.40 mmol), oxoester **1a** (749 mg, 4.40 mmol), and molecular sieves (4 Å, 2.5 g) in toluene (6 mL) under nitrogen was treated with a catalytic amount of concentrated HCl. After stirring for 14 h at 60 °C, the reaction mixture was filtered and the residue washed with CH_2Cl_2. All volatile materials were removed in vacuo and the residue was chromatographed on Al_2O_3 90 (Activity II–III; eluent = methyl *tert*-butylether/petroleum ether 3/1; $R_f = 0.45$) to yield **3g** as a colorless solid (1.17 g, 3.78 mmol, 86 %). m.p. 104 °C; $[\alpha]_D^{20} = +194$ ($c = 5.8$, $CHCl_3$); ^{1}H NMR (400 MHz, $CDCl_3$): $\delta = 1.05$ (s, 9H), 1.25 (t, $J = 7.1$ Hz, 3H), 1.47–1.58 (m, 2H), 1.58–1.67 (m, 2H), 1.99–2.09 (m, 1H), 2.22–2.34 (m, 3H), 2.97 (s, 3H), 3.11 (s, 3H), 4.09–4.20 (m, 2H), 4.24 (d, $J = 9.9$ Hz, 1H), 9.45 (d, $J = 9.8$ Hz, 1H); ^{13}C{^{1}H} NMR (50 MHz, $CDCl_3$): $\delta = 14.61$ (CH_3), 22.43 (CH_2), 22.55 (CH_2), 23.97 (CH_2), 26.66 (CH_3), 26.76 (CH_2), 35.74 (CH_3), 35.96 (C), 37.90 (CH_3), 57.75 (CH), 58.72 (CH_2), 91.27 (C), 156.47 (C), 170.41 (C=O), 171.67 (C=O); HR MS (EI, 70 eV): calcd: 310.2256, found: 310.2249; elemental analysis (%): calcd for $C_{17}H_{30}N_2O_3$ (310.44): C 65.77, H 9.74, N 9.02; found: C 65.94, H 9.76, N 9.16.

Copper(II)-catalyzed Michael reaction of **3a** (representative procedure): Enaminoester **3a** (0.216 mmol, 70.1 mg) and $Cu(OAc)_2 \cdot H_2O$ (**5a**; 0.0054 mmol, 1.1 mg) were stirred in acetone (1 mL) at 23 °C for 1 h. MVK (**4**; 0.43 mmol, 30 mg) was added and the mixture was stirred for additional 12–14 h at 23 °C. All volatile materials were removed in vacuo and the residue was treated with 2 N HCl. The mixture was stirred vigorously for 4–5 h and subsequently extracted with methyl *tert*-butylether.[16] After washing (saturated aqueous $NaHCO_3$) und drying ($MgSO_4$) of the combined extracts, the solvent was evaporated and the residue was chromatographed on SiO_2 (methyl *tert*-butylether/petroleum ether 1/2, $R_f = 0.19$). Compound **6a** (0.186 mmol, 44.6 mg, 86 %) was obtained as a colorless oil. The *ee* value of 98 % was determined by GC with a chiral column after derivatization to compound **7a**.[15]

Received: February 25, 2000 [Z14769]

[1] Reviews: a) E. J. Corey, A. Guzman-Perez, *Angew. Chem.* **1998**, *110*, 402–415; *Angew. Chem. Int. Ed.* **1998**, *37*, 388–401; b) K. Fuji, *Chem. Rev.* **1993**, *93*, 2037–2066.

[2] Reviews: a) E. D. Bergmann, D. Ginsburg, R. Pappo, *Org. React.* **1959**, *10*, 179–555; b) D. A. Oare, C. H. Heathcock in *Topics in Stereochemistry*, *Vol. 19* (Eds.: E. L. Eliel, S. H. Wilen), Wiley Interscience, New York, **1989**, pp. 227–407; c) P. Perlmutter, *Conjugate Addition Reactions in Organic Synthesis*, *Tetrahedron Organic Chemistry Series Vol. 9*, Pergamon, Oxford, **1992**.

[3] a) J. Christoffers, *J. Chem. Soc. Perkin Trans. 1* **1997**, 3141–3149; b) review: J. Christoffers, *Eur. J. Org. Chem.* **1998**, 1259–1266.

[4] a) H. Brunner, B. Hammer, *Angew. Chem.* **1984**, *96*, 305–306; *Angew. Chem. Int. Ed. Eng.* **1984**, *23*, 312–313; b) G. Desimoni, G. Dusi, G. Faita, P. Quadrelli, P. Righetti, *Tetrahedron* **1995**, *51*, 4131–4144; c) N. End, L. Macko, M. Zehnder, A. Pfaltz, *Chem. Eur. J.* **1998**, *4*, 818–824.

[5] a) H. Sasai, T. Arai, Y. Satow, K. N. Houk, M. Shibasaki, *J. Am. Chem. Soc.* **1995**, *117*, 6194–6198; b) review: M. Shibasaki, H. Sasai, T. Arai, *Angew. Chem.* **1997**, *109*, 1290–1310; *Angew. Chem. Int. Ed. Eng.* **1997**, *36*, 1236–1256.

[6] a) M. Pfau, G. Revial, A. Guingant, J. d'Angelo, *J. Am. Chem. Soc.* **1985**, *107*, 273–274; reviews: b) J. d'Angelo, D. Desmaële, F. Dumas, A. Guingant, *Tetrahedron: Asymmetry* **1992**, *3*, 459–505; c) J. Leonard, E. Díez-Barra, S. Merino, *Eur. J. Org. Chem.* **1998**, 2051–2061.

[7] A. Guingant, H. Hammami, *Tetrahedron: Asymmetry* **1991**, *2*, 411–414.

[8] J. Christoffers, U. Rößler, T. Werner, *Eur. J. Org. Chem.* **2000**, 701–705.

[9] H. Sasai, E. Emori, T. Arai, M. Shibasaki, *Tetrahedron Lett.* **1996**, *37*, 5561–5564.

[10] a) K. Tomioka, W. Seo, K. Ando, K. Koga, *Tetrahedron Lett.* **1987**, *28*, 6637–6640; b) K. Ando, W. Seo, K. Tomioka, K. Koga, *Tetrahedron* **1994**, *50*, 13081–13088.

[11] a) J. Christoffers, A. Mann, J. Pickardt, *Tetrahedron* **1999**, *55*, 5377–5388; b) J. Christoffers, A. Mann, *Eur. J. Org. Chem.* **1999**, 1475–1479; c) J. Christoffers, *J. Prakt. Chem.* **1999**, *341*, 495–498; d) J. Christoffers, U. Rößler, *Tetrahedron: Asymmetry* **1999**, *10*, 1207–1215.

[12] Syntheses of auxiliaries **2a**–**j** were accomplished in three steps from the appropriate α-amino acids: a) Boc_2O, DMAP (3 mol %), H_2O/MeOH 1/1, 70–80 %; b) DCC, HNR'_2, CH_2Cl_2, 65–85 %; c) CF_3CO_2H, CH_2Cl_2, 90–99 %. Boc = *tert*-butoxycarbonyl, DMAP = 4-dimethylaminopyridine, DCC = dicyclohexylcarbodiimide.

[13] Syntheses of auxiliaries **2m**–**p** were accomplished in four steps from the appropriate amino alcohols: a) Boc_2O, CH_2Cl_2, quantitative; b) TosCl, pyridine, 65–90 %; c) for **2m**, **n**: NaSEt, DMF, 90–95 %; for **2o**, **p**: $HNMe_2$, pyridine, 75–95 %; d) CF_3CO_2H, CH_2Cl_2, 90–99 %. Tos = *p*-$H_3CC_6H_4SO_2$.

[14] Applied metal salts: $Cu(OAc)_2 \cdot H_2O$ (**5a**), $Cu(OTf)_2$ (**5b**), $FeCl_3$ (**5c**), $FeCl_3 \cdot 6\,H_2O$ (**5d**), $NiCl_2$ (**5e**), $Ni(OAc)_2 \cdot 4H_2O$ (**5f**), $SnCl_2$ (**5g**), AgOAc (**5h**), $CoCl_2 \cdot 6H_2O$ (**5i**), $CrCl_3 \cdot 6H_2O$ (**5j**), $MgBr_2$ (**5k**), $Pb(OAc)_2 \cdot 3H_2O$ (**5l**), $ZnBr_2$ (**5m**), $ZnCl_2$ (**5n**). Tf = F_3CSO_2.

[15] Details about GC analysis and derivatization procedures have recently been reported by us.[8]

[16] Auxiliary **2** can be almost quantitatively recovered from the aqueous layer after basic workup.

Detection of a 2,3-Aminomutase in the Mushroom *Cortinarius violaceus***

Peter Spiteller, Matthias Rüth, Franz von Nussbaum, and Wolfgang Steglich*

Recently, we discovered the new natural β-amino acid (*R*)-3,4-dihydroxy-β-phenylalanine ((*R*)-β-dopa, (*R*)-**3**) in the mushroom *Cortinarius violaceus*.[1] (*R*)-**3** is present in the mushroom as the iron(III)–catechol complex, which gives the fruit bodies their blue-purple color.

In this communication we report on the biosynthesis of (*R*)-β-dopa. For this purpose, suitable precursors were applied to young fruit bodies of *C. violaceus*, which were then harvested 5 to 7 days later. All mushrooms showed normal growth and became double their original size. After extraction of the fruit bodies with methanol, the amino acids were isolated by ion exchange chromatography and further investigated by GC/MS as their trimethylsilyl derivatives. The incorporation of ^{13}C-labeled precursors was determined by NMR spectroscopy.

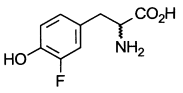
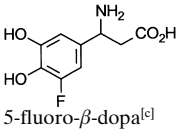
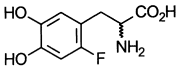
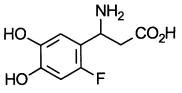
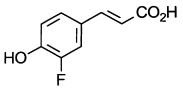
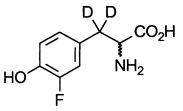
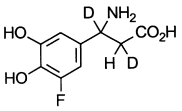
After feeding with *rac*-3-fluorotyrosine, we were able to detect the formation of 5-fluoro-β-dopa as well as traces of 3-fluoro-β-tyrosine (Table 1, entry 1).[2] This proves that tyrosine (**1**) is the biosynthetic precursor of β-dopa (**3**). This result is confirmed by the successful conversion of *rac*-[3′-

[*] Prof. Dr. W. Steglich, Dipl.-Chem P. Spiteller, Dipl.-Chem. M. Rüth, Dr. F. von Nussbaum
Department Chemie der Ludwig-Maximilians-Universität
Butenandtstrasse 5–13, Haus F, 81377 München (Germany)
Fax: (+49) 89-2180-7756
E-mail: wos@cup.uni-muenchen.de

[**] This contribution was supported by the Deutsche Forschungsgemeinschaft (SFB 369).

 © WILEY-VCH Verlag GmbH, D-69451 Weinheim, 2000 1433-7851/00/3915-2754 $ 17.50+.50/0

Table 1. Incorporation results after feeding labeled precursors to *C. violaceus*.

entry	precursor[a]	expected product	incorporation [%][b] (method)
1			3.5 (GC/MS)
	3-fluorotyrosine	5-fluoro-β-dopa[c]	
2	[3′-^{13}C]tyrosine	[3′-^{13}C]β-dopa	1.4 (^{13}C NMR)
3			0.0 (GC/MS)
	6-fluorodopa	6-fluoro-β-dopa	
4	[3′-^{13}C]dopa	[3′-^{13}C]β-dopa	0.0 (^{13}C NMR)
5	3-fluoro-β-tyrosine	5-fluoro-β-dopa	1.2 (GC/MS)
6		5-fluoro-β-dopa	0.0 (GC/MS)
	3-fluoro-4-hydroxycinnamic acid		
7	3-fluoro[^{15}N]tyrosine	5-fluoro[^{15}N]β-dopa	3.7 (GC/MS)
8			3.2 (GC/MS)
	3-fluoro[3′,3′-^{2}H$_2$]tyrosine	5-fluoro[2′,3′-^{2}H$_2$]β-dopa	
9	(*S*)-3-fluorotyrosine	(*R*)-3-fluoro-β-tyrosine[d]	1.4 (GC/MS)
10	3-fluoro-β-tyrosine	(*R*)-5-fluoro-β-dopa	1.5 (GC/MS)

[a] Racemic unless otherwise indicated. [b] In the GC/MS experiments the ratio of the base peaks of the labeled and unlabeled compounds is given in percent. In the ^{13}C NMR experiments the incorporation rate is defined as percentage of atom excess. [c] As well as 3-fluoro-β-tyrosine. [d] As well as (*R*)-5-fluoro-β-dopa.

^{13}C]tyrosine into β-dopa (Table 1, entry 2). In contrast, neither feeding with *rac*-6-fluoro-dopa nor with *rac*-[3′-^{13}C]dopa gave any labeled β-dopa (Table 1, entries 3 and 4). Therefore, we conclude that the biosynthesis of β-dopa (**3**) proceeds through β-tyrosine (**2**) which is then hydroxylated. This assumption was confirmed by a successful feeding experiment with *rac*-3-fluoro-β-tyrosine (Table 1, entry 5). In addition, traces of β-tyrosine were detected in the fruit bodies by GC/MS, after suitable derivatization.

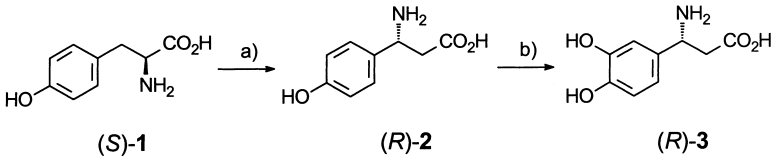
(*S*)-β-Tyrosine (**2**) is a constituent of the edein complex of antibiotics formed by *Bacillus brevis*. In this bacterium **2** is produced from tyrosine through 4-hydroxycinnamic acid by ammonia elimination and subsequent lyase-catalyzed reintroduction of the amino group in the β-position.[3] In contrast, we were unable to recognize any incorporation of 3-fluoro-4-hydroxycinnamic acid into β-dopa with *C. violaceus* (Table 1, entry 6). In order to exclude the elimination–addition sequence unambiguously, *C. violaceus* was fed with 3-fluoro[^{15}N]tyrosine. The successful incorporation of this compound into (*R*)-β-dopa verifies that the amino shift proceeds with retention of the nitrogen (Table 1, entry 7). Therefore, the biosynthesis of (*R*)-β-dopa in *C. violaceus* follows the sequence depicted in Scheme 1.

The tyrosine-2,3-aminomutase from *C. violaceus* is comparable to the enzyme discovered by Floss[4] in extracts of *Taxus brevifolia*. This aminomutase catalyses the transformation of (*S*)-α-phenylalanine into (*R*)-β-phenylalanine during the side-chain construction of paclitaxel.

In aminomutase-catalyzed reactions the pro-3*S* hydrogen is usually substituted by the migrating amino group, under retention of configuration at C-3, and concomitant intramolecular transfer of a hydrogen atom from C-3 to C-2.[5–8] This reaction was shown to occur also in *C. violaceus*: after feeding with 3-fluoro[3′,3′-^{2}H$_2$]tyrosine, the formation of 5-fluoro[2′,3′-^{2}H$_2$]β-dopa could be recognized by mass spectrometry (Table 1, entry 8).

In order to investigate the specificity of the enzyme, (*S*)-3-fluorotyrosine, as well as the racemic mixture, was applied to *C. violaceus*. The stereochemistry of the resulting 3-fluoro-β-tyrosine was determined by GC after derivatization with Mosher's acid chloride.[9] Since in both experiments only the (*R*)-enantiomer of 3-fluoro-β-tyrosine was detected, the tyrosine-2,3-aminomutase transforms exclusively (*S*)-3-fluorotyrosine (Table 1, entry 9). Likewise, the hydroxylation of 3-fluoro-β-tyrosine to 5-fluoro-β-dopa is strictly stereospecific (Table 1, entry 10).

The tyrosine-2,3-aminomutase from *C. violaceus* is the first aminomutase detected in a fungus. The transfer of the amino group in all known enzymes of this type occurs via radical



Scheme 1. Biosynthesis of (*R*)-β-dopa in *C. violaceus*: a) tyrosine-2,3-aminomutase; b) monooxygenase.

intermediates,[10] whereby either adenosylcobalamin[11] or S-adenosylmethionine (SAM)[6, 11, 12] serve as cofactors. Since corrinoids are not produced by fungi,[13] adenosylcobalamin is excluded as a cofactor in our case. At present it is not possible, however, to decide whether the tyrosine-2,3-aminomutase of *C. violaceus* is a SAM-dependent enzyme or an aminomutase of a new type.[4]

Experimental Section

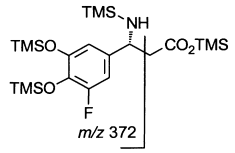
The labeled α-amino acids were synthesized according to the phthalimidomalonic ester method; 3-fluoro-4-hydroxycinnamic acid was prepared by Knoevenagel condensation. 3-Fluoro-β-tyrosine was synthesized according to the method of Rodionov and Postovskaja,[14] commencing with 3-fluoro-4-methoxybenzaldehyde, diethyl malonate, and ammonium acetate.

Feeding experiments: Each of the labeled compounds (50 mg) was dissolved in water (0.2 mL) and injected into between one and five fruit bodies of *C. violaceus* in their natural environment.[15] The mushrooms were harvested after 5–7 d and immediately frozen. The finely crushed fruit bodies (50 g) were thoroughly extracted with a mixture of methanol (250 mL) and 2 N HCl (2 mL) at room temperature. The extract was filtered

 © WILEY-VCH Verlag GmbH, D-69451 Weinheim, 2000 1433-7851/00/3915-2755 $ 17.50+.50/0

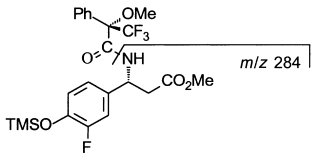
and the solvent completely removed in vacuo. The residue was dissolved in water (5 mL) and subjected to ion-exchange chromatography (Dowex 50W X8, eluent 4 N HCl) to remove the nonbasic components. The eluent was lyophilized and the residue dissolved in methanol (2 mL). In order to remove Fe^{III} ions, NaSCN (50 mg) was added. Chromatography on Sephadex LH-20 yielded 45 mg of the amino acids (0.09 % of fresh weight).

Determination of the incorporation of labeled precursors: The isolated amino acids were silylated with *N*-methyl-*N*-(trimethylsilyl)trifluoroacetamide (MSTFA) and subsequently analyzed by GC/MS. The incorporation of single fluoro-labeled precursors was determined by measuring the ion current of the base peak derived from **4** (*m*/*z* 372). In the case of double-labeled precursors the ion *m*/*z* 373 was used. If ^{13}C-labeled precursors were used the incorporation rates were determined by ^{13}C NMR measurements.



4

In order to determine the configuration of the derived 3-fluoro-β-tyrosine, the amino acid (0.5 mg) was esterified with methanol (0.5 mL) and Me_3SiCl (100 μL). After removal of the solvent, the residue was dissolved in pyridine (100 μL). (*R*)-(−)-α-Methoxy-α-(trifluoromethyl)phenylacetic acid chloride (2 μL) and a catalytic amount of 4-dimethylaminopyridine (DMAP) were added, and the mixture was kept at room temperature for 12 h. The solvent was then removed and the residue treated with MSTFA (40 μL). The amino acid derivative **5** was identified by GC/MS monitoring of the ion *m*/*z* 284. Temperature program: 2 min isotherm at 50 °C, then 10 K min^{-1} to 300 °C, followed by 15 min isotherm at 300 °C. Column: fused-silica capillary column (DB-5 ms, J&W, 30 m × 0.25 mm × 0.25 μm). The Kováts indices were determined by coinjection with a mixture of straight chain saturated hydrocarbons (C_{10}–C_{36}). (2′*S*,3*R*)-**5**: GC: $R_i = 2622$; (2′*S*,3*S*)-**5:** GC: $R_i = 2649$.



(2′*S*,3*R*)-**5**

Received: March 7, 2000 [Z14815]

[1] F. von Nussbaum, P. Spiteller, M. Rüth, W. Steglich, G. Wanner, B. Gamblin, L. Stievano, F. E. Wagner, *Angew. Chem.* **1998**, *110*, 3483–3485; *Angew. Chem. Int. Ed.* **1998**, *37*, 3292–3295.

[2] The use of fluorine for labeling of biosynthetic precursors has many advantages. The label is tolerated by many enzymes, and the detection of the metabolites is very sensitive. Thus, one single fruit body of a mushroom is sufficient for determining the incorporation; see, for example: E. Leete, G. B. Bodem, M. F. Manuel, *Phytochemistry* **1971**, *10*, 2687–2692.

[3] R. J. Parry, Z. Kurylo-Borowska, *J. Am. Chem. Soc.* **1980**, *102*, 836–837.

[4] K. D. Walker, H. G. Floss, *J. Am. Chem. Soc.* **1998**, *120*, 5333–5334.

[5] D. J. Aberhart, S. J. Gould, H.-J. Lin, T. K. Thiruvengadam, B. H. Weiller, *J. Am. Chem. Soc.* **1983**, *105*, 5461–5470.

[6] P. A. Frey, *FASEB J.* **1993**, *7*, 662–670.

[7] P. C. Prabhakaran, N.-T. Woo, P. S. Yorgey, S. J. Gould, *J. Am. Chem. Soc.* **1988**, *110*, 5785–5791.

[8] I. Freer, G. Pedrocchi-Fantoni, D. J. Picken, K. H. Overton, *J. Chem. Soc. Chem. Commun.* **1981**, 80–82.

[9] J. A. Dale, L. Dull, H. S. Mosher, *J. Org. Chem.* **1969**, *34*, 2543–2549.

[10] W. Buckel, B. T. Golding, *FEMS Microbiol. Rev.* **1999**, *22*, 523–541.

[11] Review on aminomutases: P. A. Frey, C. H. Chang in *Chemistry and Biochemistry of B_{12}* (Ed.: R. Banerjee), Wiley, New York, **1999**, pp. 835–857.

[12] Review: P. A. Frey, G. H. Reed, M. L. Moss, R. M. Petrovich, M. D. Ballinger, K. W. Lieder, W. Wu, C. H. Chang, V. Banderian, F. J. Ruzicka, R. Lo Brutto, H. Beinert in *Vitamin B_{12} and B_{12} Proteins* (Eds.: B. Kräutler, D. Arigoni, B. T. Golding), Wiley-VCH, Weinheim, **1998**, pp. 435–446.

[13] J. R. Roth, J. G. Lawrence, T. A. Bobik, *Annu. Rev. Microbiol.* **1996**, *50*, 137–181.

[14] W. M. Rodionov, E. A. Postovskaja, *J. Am. Chem. Soc.* **1929**, *51*, 841–847.

[15] The feeding experiments were performed in Autumn 1998 and 1999 near Breitbrunn and Gilching in Bavaria, Germany.

Demonstration of Chiral Enantiomerization in a Four-Atom Molecule**

Paul von Ragué Schleyer* and Michael Mauksch

In 1997, we presented the first example of the enantiomerization of a chiral five-atom molecule, *cyclo*-SeSSOS, via a completely asymmetric reaction path in a single-step process.[1] Is it possible for a chiral molecule with only four atoms to enantiomerize via a chiral pathway? The answer is "no" if all four atoms are different. Oddly, the answer may be "yes" if two of the four atoms are the same.

In 1992 and 1993, Mislow et al. presented an elegant proof that fully chiral paths might be involved in the interconversion of mirror images of asymmetric (geometrically distorted) tetrahedra, *which are not fully labeled*.[2, 3] In contrast, Mislow demonstrated in 1995 that this is an exception: No path for interconverting mirror images can preserve chirality for fully labeled, three-dimensional, four-vertex simplexes.[4] These must pass through a two-dimensional boundary in order to reach the enantiomorphic forms.[5–7] Later in 1995, Mezey explained this conundrum, "Mislow's Labeling Paradox",[8, 9] by showing, in an abstract form (Figure 1), that chiral four-vertex simplexes, in which at least two identically labeled vertices can switch roles (for example, as a permutation of sites), may be transformed to their enantiomorphs on a fully asymmetric reaction path.[10] In tetraatomic molecules, such a "permutation of sites", which leads to an enantiomer, can occur only if two atoms of the same chemical element and isotope have distinguishable sites and exchange their chemical and spatial environments.

Weinberg and Mislow's 1996 dimensional analysis[11] showed that all submaximally labeled chiral simplexes are chirally connected (for example, asymmetric tetrahedrons with at least two identical atoms can be converted into their

[*] Prof. Dr. P. von R. Schleyer
Computational Chemistry Annex
University of Georgia
Athens, GA 30602-2525 (USA)
Fax: (+1) 706-542-7514
E-mail: schleyer@uga.ed

Dr. M. Mauksch
Computational Chemistry Center
Institute of Organic Chemistry
University of Erlangen-Nuremberg
91052 Erlangen (Germany)

[**] This work was supported at Erlangen by the Deutsche Forschungsgemeinschaft and the Fond der Chemischen Industrie. We thank Prof. K. Mislow (Princeton) and Prof. P. Mezey (Saskatoon, Saskatchewan) for helpful discussions.

 © WILEY-VCH Verlag GmbH, D-69451 Weinheim, 2000 1433-7851/00/3915-2756 $ 17.50+.50/0

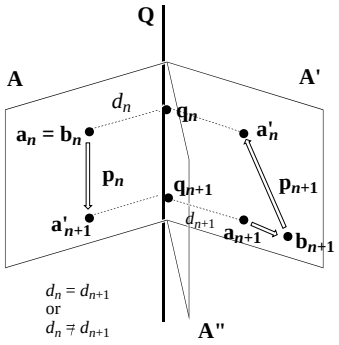
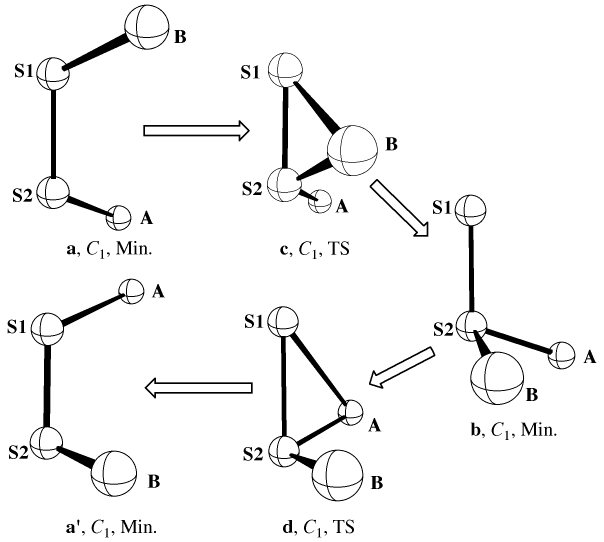


Figure 1. Illustration of the "Labeling Paradox" process, taken from ref. [8] (see therein for further details). Only if $\mathbf{a}_n = \mathbf{a}_{n+1}$ is a completely asymmetric transformation of the n-chiral $\mathbf{S} = \{\mathbf{a}_1,\mathbf{a}_2,\mathbf{a}_3,\ldots\mathbf{a}_{n-1},\mathbf{a}_n,\mathbf{a}_{n+1}\}$ into $\mathbf{S}'$ possible. The combination of $\mathbf{p}_n$ and $\mathbf{p}_{n+1}$ then constitutes the reaction coordinate for the enantiomerisation of a real molecule. The distances $\mathbf{d}_n$ and $\mathbf{d}_{n+1}$ will generally be different in actual chemical examples.

mirror image forms without encountering achiral configurations).[11] Can the abstract Mislow–Mezey solution be realized in tetraatomic molecules? Is it possible, in an intramolecular process and by purely chemical means, to exchange the sites of two atoms without transposing them? The theoretical proofs are general and do not specify the potential-energy surface (PES), that is, whether the process proceeds, for example, by one or by two steps. The independent internal motions in a two- or multistep enantiomerization should, in principle, permit the occurrence of an asymmetric path comprising different sequential steps. All instantaneous configurations on the enantiomerization path must be chiral—which includes transition states and minimum energy conformations. As discussed above, this rules out the enantiomerization of a fully labeled molecule with four different atoms (which must pass through a coplanar arrangement).

Exemplary molecular systems of the X_2AB type are easy to visualize: S_2ClF **1**, S_2BrF **2**, and S_2BrCl **3**, with branched S=SAB and linear ASSB isomers; all have the ability to enantiomerize in two steps via fully asymmetric paths (Scheme 1 and Table 1). The unimolecular chiral process can take place by two consecutive 1,2-halogen shifts through C_1 transition states (TS) **c** and **d** (Scheme 1).[12] The two asymmetric enantiomerization itineraries have different initial stages (enantiomers are denoted by primes; Scheme 2): **a** → **c** → **b** → **d** → **a′** and **a** → **d′** → **b′** → **c′** → **a′**.[13] Mezey's "role switch" of identical atoms takes place because the mono- and tricoordinate sulfur atoms S1 and S2 in **a** (Scheme 1) have exchanged their role in the enantiomers **a′**. These simple S_2AB systems illustrate that chiral enantiomerizations in tetraatomic molecules are possible.

However, these examples have practical drawbacks in experimental realization. Our computations (Table 1) confirm expectations based on earlier results[14] on related systems, that achiral pathways may be more favorable. Indeed, planar transition states with *cis*- (**1e**–**3e**) and with *trans*-configurations (**1f**–**3f**), as well as those that involve inversion at one sulfur center (TS **g**), are prefered energetically over the asymmetric paths involving **c** and **d** (Scheme 2). The energies of **c** and **d** are not lowered below those of **e**–**g** with the heavier halogens (Table 1).

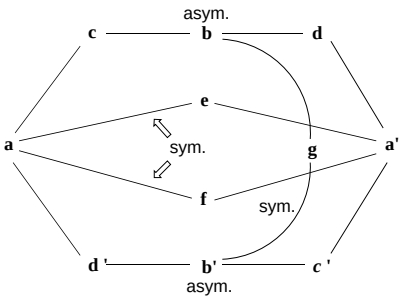


Scheme 1. Schematic representation of the S_2AB structures **a**–**d** involved in the enantiomerization of **1a**,**b**–**3a**,**b** (**1**: A = Cl, B = F; **2**: A = Br, B = F; **3**: A = Br, B = Cl). The S–S bonds are always in the paper plane. For relative energies, see Table 1.

Table 1. Zero-point energy (ZPE) corrected relative energies E_{rel} of S_2AB species at the B3LYP/6-31G* level. The stationary points of S_2F_2 at the same level of theory are included for comparison.

Structure, point group	Nature of the stationary point[a]	E_{rel}[b] [kcal mol^{-1}] S_2ClF **1**	S_2BrF **2**	S_2BrCl **3**	S_2F_2 **4**
a, C_1	Min.	0.0	0.0	0.0	0.0 (C_2)[c]
b, C_1	Min.	9.8	8.8	14.6	0.1 (C_s)
c, C_1	TS	45.3 (Cl)[d]	54.4 (F)	39.4 (Cl)	49.6 (C_1)
d, C_1	TS	36.6 (F)	36.4 (Br)	40.1 (Br)	–
e, C_s	TS	24.9	21.7	18.8	25.7 (C_{2h})
f, C_s	TS	21.6	19.3	15.7	–
g, C_s	TS	36.5	37.5	36.5	33.7 (C_{2v})

[a] Based on vibrational analysis at the B3LYP/6-31G* level. [b] With respect to the (most stable) 1,2-isomers **1a**–**3a**. [c] The point groups in parenthesis refer to S_2F_2 alone. [d] Migrating atom.



Scheme 2. Possible reaction paths in the intramolecular enantiomerization of **1a**,**b**–**3a**,**b**. Two asymmetric (asym.) and three symmetric (sym.) alternatives exist. For relative energies, see Table 1.

The ClSSCl[15] and BrSSBr[16, 17] forms are well known experimentally.[18] The thio-thionyl isomers S=SCl_2 and S=SBr_2 are much less stable (Table 1) but there is at least experimental evidence for S=SCl_2.[19] In contrast, S=SF_2 is -2.7 ± 0.4 kcal mol^{-1} [20a] more stable than the corresponding FSSF isomer.[20] Experimentally, FSSF isomerizes slowly to S=SF_2 above $-100\,^{\circ}C$,[21] which indicates a much lower

activation barrier than the 40 – 60 kcal mol^{-1} computed for the TS of the intramolecular isomerization at various levels (such as 46.1 kcal mol^{-1} at the B3LYP/6-311 + + G(3df) level[22a]).[22, 23] However, according to Seel, Budenz, and Werner,[21] a bimolecular complex [FSSF · S=SF_2]$_{(g)}$ forms at temperatures below − 80 °C; this suggests that the actual isomerisation mechanism may not be unimolecular. Possible associative or dissociative mechanisms[14, 21] would complicate experimental studies of these systems further.

Density functional theory seems to overestimate somewhat the relative stability of the C_2 (FSSF) over the C_s (S=SF_2) conformer (Table 1).[23] In contrast, the C_s form is preferred over the C_2 form by 3.0 kcal mol^{-1} at the MP4(SDTQ)/6-311G(2d)//MP2/6-311G(2d) level (including zero-point energy corrections at the MP2/6-31G* level),[23] which agrees well with the experimental value.[20a] At the same (MP4(SDTQ)) level of theory, the FSSF → S=SF_2 isomerization barrier is 46.6 kcal mol^{-1}, which is close to the value calculated at the B3LYP/6-311 + + G(3df) level.[22a] Hence, we believe that the use of density functional theory in this paper is justified.

Measurements of the He-I photoelectron spectra of a S=SF_2 sample at two different temperatures gave a first-order rate law with an activation barrier of 24.1 kcal mol^{-1} for an alleged S=SF_2 → FSSF isomerization (with reversed order of stability!).[24] However, our computation of the vertical ionization potentials for S=SF_2, FSSF, and SF_4 suggested the occurrence of a disproportionation 2 S=SF_2 → ⅜ S_8 + SF_4 rather than the purported isomerization.[25]

To conclude, we have shown the feasibility of "Mislow's Labeling Paradox" in molecular systems. However, other achiral paths are lower in energy for the illustrative cases reported here. A remaining challenge is in the identification of tetraatomic systems comprised of a different set of elements, which enantiomerize preferentially via unimolecular asymmetric rather than achiral paths, as well as the demonstration of a single step example. Other enantiomerizations might involve a similar "role switch".

Received: December 10, 1999
Revised: March 6, 2000 [Z12767]

[1] M. Mauksch, P. von R. Schleyer, *Angew. Chem.* **1997**, *108*, 1976; *Angew. Chem. Int. Ed. Engl.* **1997**, *108*, 1856.
[2] K. Mislow, P. Poggi-Corradini, *J. Math. Chem.* **1993**, *13*, 209.
[3] A. B. Buda, K. Mislow, *J. Am. Chem. Soc.* **1992**, *114*, 6006.
[4] K. Mislow, *Proceedings of the 6th International Conference on Mathematical Chemistry* (Pitlochry, Scotland), **1995**.
[5] P. G. Mezey, *J. Math. Chem.* **1995**, *17*, 185.
[6] K. Mislow in *Fuzzy Logic in Chemistry* (Ed.: D. H. Rouvray), Academic Press, New York, **1996**.
[7] The two-dimensional boundary thus splits the three-dimensional space into two subsets containing the enantiomorphs. Maximally labeled simplexes (for dimensions greater than two) can therefore be partitioned into heterochiral subsets, identified as *R* and *L*.[6]
[8] a) P. G. Mezey, *J. Math. Chem.* **1995**, *18*, 133; b) P. G. Mezey, *Chirality* **1998**, *10*, 173.
[9] P. Mezey, *Proceedings of the 6th International Conference on Mathematical Chemistry* (Pitlochry, Scotland), **1995**.
[10] Mezey stated: "By allowing an exchange of roles between points of equivalent labels, an abandoning of the unique labeling … provides additional chances for a deformed point set to become the mirror image of its original *n*-chiral arrangement."[8a]
[11] N. Weinberg, K. Mislow, *Theor. Chim. Acta* **1997**, *95*, 63.
[12] Simultaneous 1,2-migrations of both halogens are much higher in energy (93.1 (**1**), 92.6 (**2**), and 78.7 kcal mol^{-1} (**3**)); the pertinent stationary points have two imaginary frequencies.
[13] In a private communication, Mezey remarked: "These two enantiomeric paths constitute a closed chiral loop on the potential surface. Such circular processes allows one to make predictions on the presence of critical points of both ground and excited state potential energy surfaces." See also: P. G. Mezey, *J. Am. Chem. Soc.* **1990**, *112*, 3791.
[14] a) R. S. Steudel, Y. Drozdova, K. Miaskiewicz, R. H. Hertwig, W. Koch, *J. Am. Chem. Soc.* **1997**, *110*, 1980; b) Y. Drozdova, K. Miaskiewicz, R. S. Steudel, *Z. Naturforsch. B* **1995**, *50*, 889.
[15] a) R. D. Brown, F. R. Burden, G. P. Pez, *J. Chem. Soc. Chem. Commun.* **1965**, 277; b) E. Hiruta, *Bull. Chem. Soc. Jpn.* **1958**, *31*, 130.
[16] a) R. D. Brown, G. P. Pez, *Aust. J. Chem.* **1967**, *20*, 2305; b) R. D. Brown, G. P. Pez, M. F. O'Dwyer, *Aust. J. Chem.* **1965**, *18*, 627.
[17] F. Seel, *Chimia* **1968**, *22*, 79.
[18] R. Kniep, L. Koorte, D. Z. Mootz, *Z. Naturforsch. B* **1983**, *38*, 1.
[19] a) M. Feuerhahn, G. Vahl, *Chem. Phys. Lett.* **1979**, *65*, 322; b) G. Holzmann, M. Feuerhahn, R. Minkwitz, G. Vahl, *J. Chem. Res. Synop.* **1980**, 71; c) B. M. Chadwick, J. M. Crzybowski, D. A. Long, *J. Mol. Struct. (THEOCHEM)* **1978**, *48*, 139.
[20] a) O. Lösking, H. Willner, H. Baumgaertel, H. W. Jochim, Z. Rühl, *Z. Anorg. Allg. Chem.* **1985**, *530*, 169; b) C. J. Marsden, H. Oberhammer, O. Lösking, H. Willner, *J. Mol. Struct. (THEOCHEM)* **1989**, *193*, 233; c) A. Haas, H. Willner, *Spectrochim. Acta A* **1979**, *35*, 953.
[21] F. Seel, R. Budenz, D. Werner, *Chem. Ber.* **1964**, *97*, 1369.
[22] a) B. S. Jursic, *J. Comput. Chem.* **1996**, *17*, 835; b) M. Torrant, M. Duran, M. Sola, *J. Mol. Struct. (THEOCHEM)* **1996**, *362*, 163.
[23] F. M. Bickelhaupt, M. Sola, P. von R. Schleyer, *J. Comput. Chem.* **1995**, *16*, 445, and references therein.
[24] Ionization peaks characteristic of the alleged product FSSF could not be found in the reported PES spectrum; SF_4 peaks appear instead. Hence, we regard this work as highly questionable: X. Y. Cao, X. M. Qian, C. H. Qiao, D. X. Wang, *Chem. Phys. Lett.* **1999**, *299*, 322.
[25] SSF_2 disproportionates rapidly in the presence of acid catalysts (for example, HF or BF_3), see: M. V. Carlowitz, H. Oberhammer, H. Willner, J. E. Boggs, *J. Mol. Struct. (THEOCHEM)* **1983**, *100*, 161.

1,3-Stereoinduction in Radical Reactions

Ahlke Hayen, Rainer Koch, and Jürgen O. Metzger*

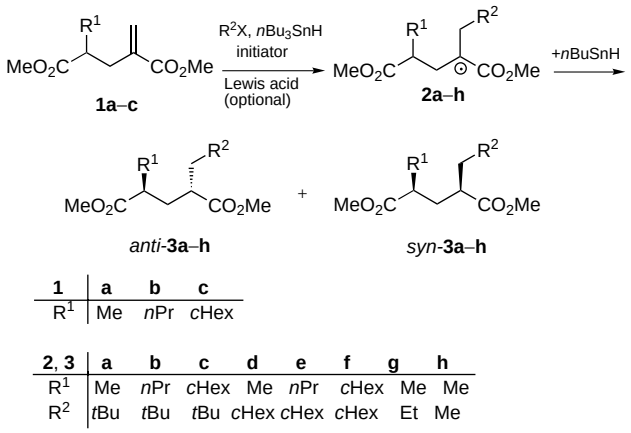
Dedicated to Professor Gerhard Zimmermann on the occasion of his 70th birthday

The possibility of steering the stereoselectivity of the trapping reactions of acyclic radicals possessing a stereogenic center in the 3-position is of great importance, both with respect to the synthesis of natural products bearing stereogenic centers in the 1,3-position and to the free radical polymerization of vinyl monomers. However, most radical polymerizations are more or less unselective,[1a] with the exception of a few sterically highly demanding methacrylates.[2] On the other hand it has been shown during the last few years that acyclic radicals can react with high stereoselectivity;[1, 3] the addition of Lewis acids has proved to be

[*] Prof. Dr. J. O. Metzger, Dipl.-Chem. A. Hayen, Dr. R. Koch
Fachbereich Chemie der Carl-von-Ossietzky Universität Oldenburg
Carl-von-Ossietzky-Strasse 9 – 11, 26129 Oldenburg (Germany)
Fax: (+49) 441-798-33-29
E-mail: juergen.metzger@uni-oldenburg.de

 © WILEY-VCH Verlag GmbH, D-69451 Weinheim, 2000 1433-7851/00/3915-2758 $ 17.50+.50/0

particularly important for controlling the configuration.[4] Until now, attention has focused on stereocontrol by 1,2- or 1,4-induction, while 1,3-stereoinduction has rarely been examined,[5] and when, the examples chosen were less interesting as models for radical polymerization. Porter et al. reported on the allyltributyltin-mediated addition of iodoalkanes to oxazolidinonacrylamides, which afforded 1,3-disubstituted products with good stereoselectivity.[6] Remarkable effects in chelation-controlled reactions of γ-alkoxy-α-ester radicals were observed by Nagano et al.[7] For the first time now, we have examined the chelation-controlled 1,3-stereoinduction of the trapping reaction of γ-alkyl-α-ester radicals **2** (Scheme 1), which are also of interest as models for radical polymerizations of acrylic esters. As trapping reaction we chose hydrogen transfer, and assumed that the stereochemical effects observed in this process should be transferable to the radical addition reaction in the chain propagation step of polymerizations.[1, 8]



1	a	b	c
R^1	Me	*n*Pr	*c*Hex

2, 3	a	b	c	d	e	f	g	h
R^1	Me	*n*Pr	*c*Hex	Me	*n*Pr	*c*Hex	Me	Me
R^2	*t*Bu	*t*Bu	*t*Bu	*c*Hex	*c*Hex	*c*Hex	Et	Me

Scheme 1. Tributyltin hydride mediated additions of haloalkanes R^2X (X = Br, I; R^2 = *t*Bu, *c*Hex, Et, Me) to methyl γ-alkyl-α-methyleneglutarates **1** via radicals **2** affording products *anti*-**3** and *syn*-**3**.

Addition of an alkyl radical R^2 to alkenes **1** generated radicals **2**, which were then trapped by tributyltin hydride to yield a mixture of diastereomeric products *anti*-**3** and *syn*-**3**. Usual processing of the addition reaction of *t*BuI to alkene **1a** at $-78\,^\circ$C afforded product **3a** unselectively (Table 1, entry 1). Addition of chelating Lewis acids such as $LiClO_4$ (Table 1, entry 2), $Sc(OTf)_3$ (Table 1, entry 3, Tf = F_3CSO_2), and especially $MgBr_2 \cdot OEt_2$ (Table 1, entry 4) provided product **3a** at $-78\,^\circ$C in good yields and excellent *syn*-selectivities of [*anti*-**3a**]:[*syn*-**3a**] = 2:98. Considering selectivity, conversion, yield, and costs $MgBr_2 \cdot OEt_2$ was chosen as the most suitable additive for further studies. With increasing reaction temperature, the stereoselectivity of the trapping reaction decreases as expected, but even at 70 °C the observed ratio is still [*anti*-**3a**]:[*syn*-**3a**] = 39:61 (Table 1, entry 5). Remarkably, the stereoselectivity is largely independent of the steric effect of the γ-alkyl group R^1. Thus, also for radicals **2b** (Table 1, entry 6) and **2c** (Table 1, entry 7) high *syn*-selectivity is observed at $-78\,^\circ$C. In contrast, alkyl substituent R^2 exerts a remarkable influence on the stereoselectivity. Addition of R^2 = cyclohexyl to alkene **1a** to give radical **2d** and subsequent hydrogen transfer yields products **3d** unselectively at

Table 1. Results of the reactions of **1a–c** with R^2X: Yields and product ratios [*anti*-**3**]:[*syn*-**3**].

Entry	R^1	R^2	Lewis acid (equiv)	T[b] [°C]	Yield[c] [%]	[*anti*-**3**]:[*syn*-**3**][d]
1	Me	*t*Bu	–	−78	81[e]	52:48
2	Me	*t*Bu	$LiClO_4$ (2)	−78	93	18:82
3	Me	*t*Bu	$Sc(OTf)_3$ (2)	−78	58	1:99
4	Me	*t*Bu	$MgBr_2 \cdot OEt_2$ (2)	−78	83	2:98
5	Me	*t*Bu	$MgBr_2 \cdot OEt_2$ (2)	70	44	39:61
6	*n*Pr	*t*Bu	$MgBr_2 \cdot OEt_2$ (1)	−78	92	2:98
7[f]	*c*Hex	*t*Bu	$MgBr_2 \cdot OEt_2$ (1)	−78	50	3:97
8[f]	Me	*c*Hex	$MgBr_2 \cdot OEt_2$ (1)	−78	64	53:47
9[f]	Me	*c*Hex	$MgBr_2 \cdot OEt_2$ (2)	70	58	65:35
10	*n*Pr	*c*Hex	$MgBr_2 \cdot OEt_2$ (1)	−78	98	53:47
11	*n*Pr	*c*Hex	$MgBr_2 \cdot OEt_2$ (2)	70	95	73:27
12[f]	*c*Hex	*c*Hex	$MgBr_2 \cdot OEt_2$ (1)	−78	62	52:48
13[f]	*c*Hex	*c*Hex	$MgBr_2 \cdot OEt_2$ (2)	70	58	81:19
14	Me	Et	$MgBr_2 \cdot OEt_2$ (2)	−78	100[e]	85:15
15	Me	Et	$MgBr_2 \cdot OEt_2$ (2)	40	53[e]	81:19
16[f]	Me	Me	$MgBr_2 \cdot OEt_2$ (2)	−78	58[e]	85:15
17	Me	Me	$MgBr_2 \cdot OEt_2$ (2)	40	50[e]	85:15

[a] The relative configuration of the free acids of *syn*-**3a** and *syn*-**3d** was confirmed by single-crystal X-ray analysis.[13]. The relative configurations of all other products **3** were assigned on the basis of their ^{1}H NMR, ^{13}C NMR, and GC data. [b] Alkyl iodides were employed at −78 °C or 40 °C, alkyl bromides at 70 °C. [c] Yield of isolated product, unless specified otherwise. [d] Diastereomeric ratio was determined by capillary gas chromatography of crude reaction material. [e] Yield was determined by capillary gas chromatography. [f] Incomplete conversion at time of analysis or workup.

−78 °C (Table 1, entry 8). Contrary to this, at 70 °C *anti*-selectivity [*anti*-**3d**]:[*syn*-**3d**] = 65:35 (Table 1, entry 9) is observed. The same applies to radicals **2e** (Table 1, entries 10, 11) and **2f** (Table 1, entries 12, 13). Overall, in the reaction series at 70 °C the *anti*-selectivity increases slightly with increasing steric demand of substituent R^1 = Me < *n*Pr < *c*Hex (Table 1, entries 9, 11, 13), reaching [*anti*-**3f**]:[*syn*-**3f**] = 81:19 (Table 1, entry 13).

The addition reactions of ethyl and methyl to alkene **1a** show high *anti*-selectivity for the radicals **2g** (Table 1, entry 15) and **2h** (Table 1, entry 17) at 40 °C as well, but remarkably also at −78 °C (Table 1, entries 14, 16).

The effects, surprising at first glance, can be rationalized as follows: The steric 1,3-interaction in the transition state is negligible in the case of the nonchelated radical **2a** due to the conformational flexibility of the alkyl chain, resulting in a practically unselective reaction.[1a, 7] By complexation of the two 1,3-carboxy functionalities of radicals **2** with the Lewis acid, an eight-membered ring system is formed, thus inhibiting the conformational flexibility (Figure 1). Semiempirical calculations[9] with $[Li(OH_2)_2]^+$ as Lewis acid reveal that the eight-membered ring system depicted in Figure 1 is the most stable conformation, irrespective of R^1, although it is not the only one. The ring shows a concave and a convex side (upper side and bottom side in Figure 1, respectively).

The ground states of radicals **2a**, **2d**, **2g**, and **2h**, chelated by $[Li(OH_2)_2]^+$ as Lewis acid were calculated by using the semiempirical PM3 method.[9] The resulting energy differences of conformations A–D are compiled in Table 2.

Bu_3SnH as radical scavenger can transfer hydrogen via transition states A^+ and D^+ leading to *syn*-**3** or via B^+ and C^+ resulting in *anti*-**3** (Figure 2). Radicals **2a–c** (Table 1, en-

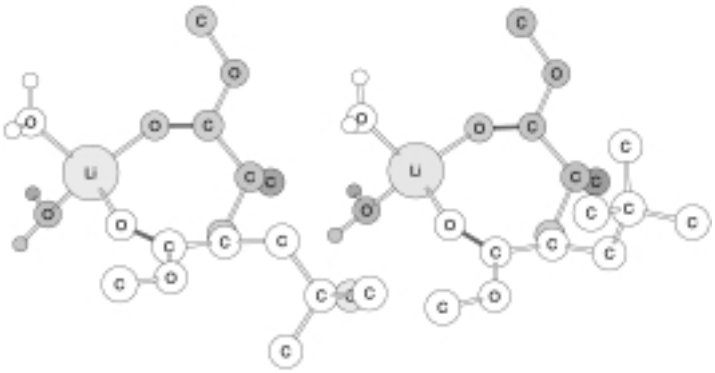


Figure 1. PM3-calculated minimum conformations A (left) and B (right) of radical **2a** (for details see text).

Table 2. Results of PM3 calculations of radicals **2a** ($R^2 = t$Bu), **2d** ($R^2 = c$Hex), **2g** (R^2 = Et), and **2h** (R^2 = Me). Relative energies [kJ mol^{-1}] of conformers A – D.[a]

R^2	A	B[b]	C	D
*t*Bu (**2a**)	0	9.2 (38)	9.6	22.6
*c*Hex (**2d**)	0	3.8 (17)	10.5	17.2
Et (**2g**)	0	– 0.5 (11)	8.0	11.0
Me (**2h**)	0	0.3 (11)	11.0	11.6

[a] For conformers A and B, see Figure 1, C and D can be derived analogously from C^+ and D^+ (Figure 2). [b] The rotational barrier for R^2 [kJ mol^{-1}] is given in parentheses.

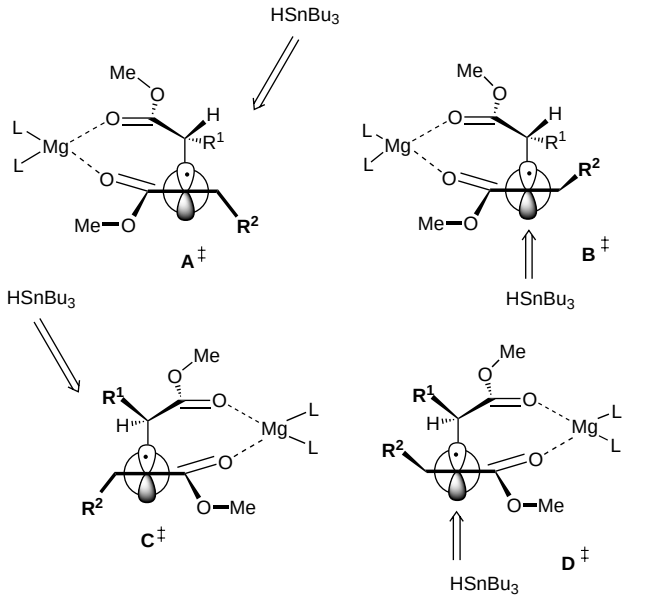


Figure 2. Possible transition states of the hydrogen transfer from Bu_3SnH to radicals **2**. Transition states A^+ and D^+ lead to *syn*-**3**, B^+ and C^+ to *anti*-**3**.

tries 2 – 7) are trapped *syn*-selectively. Evidently, this takes place via transition state A^+, because in this case steric interactions of the hydrogen donor with the concave side of the chelate-ring system are weaker than those in C^+, taking into account the additional effect of R^1, and also weaker than those of the *t*Bu group with the chelate-ring system in transition state B^+ and even more so in D^+. This interpretation also explains the low influence of R^1 on the stereoselectivity and is supported—in compliance with the Curtin – Hammett principle—by the results of the calculations of radical **2a**, which reveal A as the most stable conformer (Table 2). Furthermore, Table 2 shows that in radicals **2** the energy differences both between conformations A and B and between C and D become smaller with decreasing steric effect of $R^2 = t$Bu > *c*Hex > Et > Me, which should also apply to the corresponding transition states. Accordingly, radicals **2g** and **2h** bearing less sterically demanding R^2 groups are trapped with negligible (**2g**, Table 1, entries 14, 15) or without temperature dependence (**2h**, Table 1, entries 16, 17), but with remarkable *anti*-selectivity. These results support entropic reasons for the observed *anti*-selectivity. The most favorable transition state with the highest activation entropy should be B^+ on account of the attack of the hydrogen donor from the free convex side of **2**—compared to A^+ and C^+—and because of the unhindered rotation of R^2—compared to D^+. Radicals **2d – f** with $R^2 = c$Hex, a medium steric impact substituent, represent the transition from **2a – c** with *syn*-selectivity to **2g** and **2h** with *anti*-selectivity. While these radicals are trapped nearly unselectively at – 78 °C (Table 1, entries 8, 10, 12), at + 70 °C, the reactions take place with remarkable *anti*-selectivity (Table 1, entries 9, 11, 13). Thus, the activation enthalpy of the reaction providing the *anti* product must be higher than that of the one leading to the *syn* product. The same evidently applies to the activation entropies. At – 78 °C the compensation of activation enthalpies and entropies leads to an unselective reaction.[10] Contrary to this, by increasing the temperature *anti*-**3d – f** are formed with considerable preference due to the dominating entropic effect, evidently—as for **3g** and **3f**—via transition state B^+. The increasing *anti*-selectivity with increasing steric demand of R^1 (Table 1, entries 9, 11, 13) indicates that transition state D^+ contributes decreasingly with increasing steric impact of R^1 to the generation of the *syn* product.

We have shown that γ-alkyl-α-ester radicals **2d – h** can be trapped with remarkable *anti*-selectivity at relatively high temperatures of 40 and 70 °C. In contrast to this, high *syn*-selectivity is observed at – 78 °C with radicals **2a – c** bearing the sterically demanding neopentyl moiety at the radical center. These results imply that related radicals with 1,3-substituents such as acyloxy, alkoxy, or cyano possibly can also be trapped in a highly selective manner in the presence of Lewis acids, which should be of great interest for the polymerization of, for example, vinyl acetate, vinyl ethers, and acrylonitrile.

Experimental Section

The experiments at – 78 °C and 40 °C were performed in dichloromethane, at 70 °C benzene was employed as solvent. In the case of additional $MgBr_2 \cdot OEt_2$, diethyl ether (1/3 of solvent volume) was added. In a typical run, the Lewis acid (see Table 1) was initially stirred with the alkene (0.5 M) for at least 45 min at ambient temperature in the respective mixture of solvents, then the reaction temperature was adjusted to the desired level. At conditions of – 78 °C and 40 °C, alkyl iodide (3 equiv) and tributyltin hydride (3 equiv) were added and finally triethylborane (1 M solution in hexane, 1 equiv with respect to alkene) and O_2[11] were injected over a period of 2 – 4 h. When the reaction was run at 70 °C, the alkyl bromide (3 equiv) was added, followed by a dropwise addition of a solution of tributyltin hydride (3 equiv) and 2,2′-azobisisobutyronitrile (AIBN;

 © WILEY-VCH Verlag GmbH, D-69451 Weinheim, 2000 1433-7851/00/3915-2760 $ 17.50+.50/0 *Angew. Chem. Int. Ed.* **2000**, *39*, No. 15

20 mol %, with respect to alkene) in benzene over 3 h. Workup was performed according to usual methods.[12]

Received: December 3, 1999 [Z14352]
publication delayed at authors' request

[1] D. P. Curran, N. A. Porter, B. Giese, *Stereochemistry of Radical Reactions*, VCH, Weinheim, **1996**; a) D. P. Curran, N. A. Porter, B. Giese, *Stereochemistry of Radical Reactions*, VCH, Weinheim, **1996**, pp. 203 – 208.
[2] T. Nakano, M. Mori, Y. Okamoto, *Macromolecules* **1993**, *26*, 867 – 868.
[3] N. A. Porter, B. Giese, D. P. Curran, *Acc. Chem. Res.* **1991**, *24*, 296 – 304.
[4] P. Renaud, M. Gerster, *Angew. Chem.* **1998**, *110*, 2704 – 2722; *Angew. Chem. Int. Ed.* **1998**, *37*, 2562 – 2579.
[5] a) J. O. Metzger, R. Mahler, *Angew. Chem.* **1995**, *107*, 1012 – 1014; *Angew. Chem. Int. Ed. Engl.* **1995**, *34*, 902 – 904; b) J. O. Metzger, R. Mahler, G. Francke, *Liebigs Ann.* **1997**, 2303 – 2313; c) S. Hanessian, H. Yang, R. Schaum, *J. Am. Chem. Soc.* **1996**, *118*, 2507 – 2508; d) P. Garner, J. T. Anderson, *Tetrahedron Lett.* **1997**, *38*, 6647 – 6650; e) M. P. Bertrand, L. Feray, R. Nouguier, L. Stella, *Synlett* **1998**, 780 – 782.
[6] R. Radinov, C. L. Mero, A. T. McPhail, N. A. Porter, *Tetrahedron Lett.* **1995**, *36*, 8183 – 8186.
[7] H. Nagano, S. Toi, T. Yajima, *Synlett* **1999**, 53 – 54.
[8] W. Smadja, *Synlett* **1994**, 1 – 26.
[9] UHF calculations were performed using MOPAC 93 (J. J. P. Stewart, QCPE 455, version 93, **1993**) with the PM3 Hamiltonian (J. J. P. Stewart, *J. Comput. Chem.* **1989**, *10*, 209 – 220; Li parameters: E. Anders, R. Koch, P. Freunscht, *J. Comput. Chem* **1993**, *14*, 1301 – 1312). A calculation of transition states was renounced due to insufficient quality of the Sn parameters for PM3. Ab initio calculations are not feasible because of the magnitude of the systems to be calculated.
[10] a) B. Giese, *Angew. Chem.* **1977**, *89*, 162 – 173; *Angew. Chem. Int. Ed. Engl.* **1977**, *16*, 125 – 136; b) B. Giese, *Acc. Chem. Res.* **1984**, *17*, 438 – 442.
[11] K. Nozaki, K. Oshima, K. Utimoto, *Bull. Chem. Soc. Jpn.* **1991**, *64*, 403 – 409.
[12] P. Renaud, E. Lacôte, L. Quaranta, *Tetrahedron Lett.* **1998**, *39*, 2123 – 2126.
[13] Crystallographic data (excluding structure factors) for the structures reported in this paper have been deposited with the Cambridge Crystallographic Data Centre as supplementary publication no. CCDC-137280 (*syn*-**3a**) and CCDC 137281 (*syn*-**3d**). Copies of the data can be obtained free of charge on application to CCDC, 12 Union Road, Cambridge CB2 1EZ, UK (fax: (+44) 1223-336-033; e-mail: deposit@ccdc.cam.ac.uk).

Carbohydrate Derivatives for Use in Drug Design: Cyclic α_v-Selective RGD Peptides**

Elisabeth Lohof, Eckart Planker, Christian Mang, Fred Burkhart, Michael A. Dechantsreiter, Roland Haubner, Hans-Jürgen Wester, Markus Schwaiger, Günther Hölzemann, Simon L. Goodman, and Horst Kessler*

The improvement of pharmacokinetic and dynamic properties of pharmaceutically active compounds with retention of activity and selectivity is an important task in modern drug design. The potential of carbohydrates for the development of new drugs is not yet fully exploited. Here we will show that the modification of peptides with carbohydrate derivatives leads to an improvement of the properties of the peptides. Sugar derivatives can be incorporated in the peptide backbone and/or in the side chains. Both strategies and the different influences on structure and activity of the modified peptides are exemplified for biologically active, cyclic RGD peptides.

Earlier work in our lab demonstrated that the use of sugar amino acids (SAA) makes it possible to predict the conformation of cyclic peptides.[1] Now we show for the first time how this knowledge can be used to obtain high-affinity peptidic compounds. As a lead structure for the derivatization of the RGD motif the cyclic pentapeptide *cyclo*(-Arg-Gly-Asp-D-Phe-Val-) was chosen, which binds selectively $\alpha_v\beta_3$-integrins.[2] Integrins are located at the cell surface of a number of different cell types and play a major role in cell – matrix interactions and in tumorgenesis. This aroused pharmaceutical interest in $\alpha_v\beta_3$ antagonists, especially with regard to blocking tumor-induced angiogenesis.[2] The cyclic peptide *cyclo*(-Arg-Gly-Asp-D-Phe-*N*(Me)Val-),[3] which was the best hit in an extensive screening of peptidomimetics,[2e] is now being tested for its potency as an antitumor drug in phase II clinical trials as EMD121974 from Merck KGaA (Germany).

In earlier attempts the modification of cyclic RGD peptides with carbohydrates impaired the biological activity of the compounds.[4] In order to match the receptor's steric demands, a structurally modified sugar amino acid was incorporated into the sequence of the above-mentioned cyclic peptide. The sugar amino acid was intended to replace the two amino acids D-Phe-Val (Figure 1). From structure – activity investigations

[*] Prof. Dr. H. Kessler, Dr. E. Lohof, E. Planker, C. Mang, Dr. F. Burkhart, Dr. M. A. Dechantsreiter
Institut für Organische Chemie und Biochemie
Technische Universität München
Lichtenbergstrasse 4, 85747 Garching (Germany)
Fax: (+49) 89-289-13210
E-mail: kessler@ch.tum.de
Dr. R. Haubner, Dr. H.-J. Wester, Prof. Dr. M. Schwaiger
Nuklearmedizinische Klinik und Poliklinik
Klinikum rechts der Isar
Ismaniger Strasse 22, 81675 München (Germany)
Dr. G. Hölzemann, Dr. S. L. Goodman
Merck KGaA, Präklinische Forschung
Frankfurter Strasse 250, 64271 Darmstadt (Germany)

[**] This work was supported by the Fonds der Chemischen Industrie, the Deutsche Forschungsgemeinschaft, and the Sanderstiftung. The authors thank M. Urzinger, B. Cordes, M. Kranawetter, M. Wolff, and A. Zeller for technical assistance.

 © WILEY-VCH Verlag GmbH, D-69451 Weinheim, 2000 1433-7851/00/3915-2761 $ 17.50+.50/0

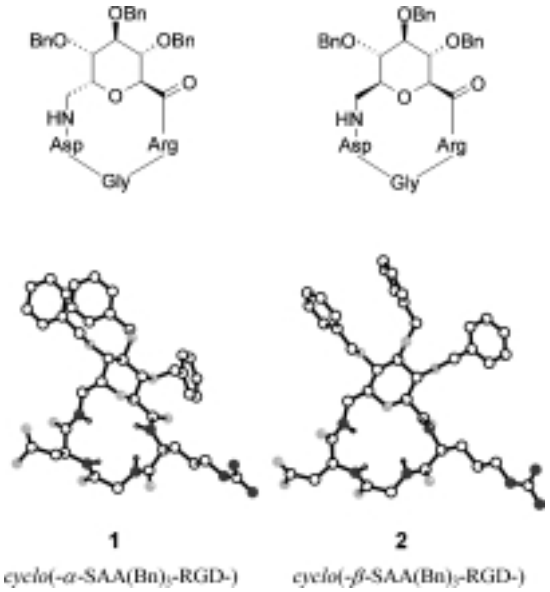


Figure 1. The benzyled sugar amino acid (SAA) built in as scaffold mimetic in the cyclic RGD peptides **1** and **2**. The conformations in DMSO were resolved by NMR spectroscopy and molecular dynamics calculations.[7]

of the lead structure it is known that the hydrophobic character of the phenylalanine improves activity,[2d] and that the backbone conformation of the residues D-Phe-Val should resemble a βII′-turn to force the RGD sequence, which acts as pharmacophore, into a kinked, $\alpha_v\beta_3$-selective conformation (Figure 2).[2, 3] Both demands are met by the new sugar amino acid,[5] whose structure is given in Figure 1: the SAA is a hydrophobic β-turn mimetic. Peptides with both SAA anomers[5] were synthesized (Figure 1, **1** and **2**), the respective structures were determined by NMR spectroscopy, and the biological activity was tested.[2d]

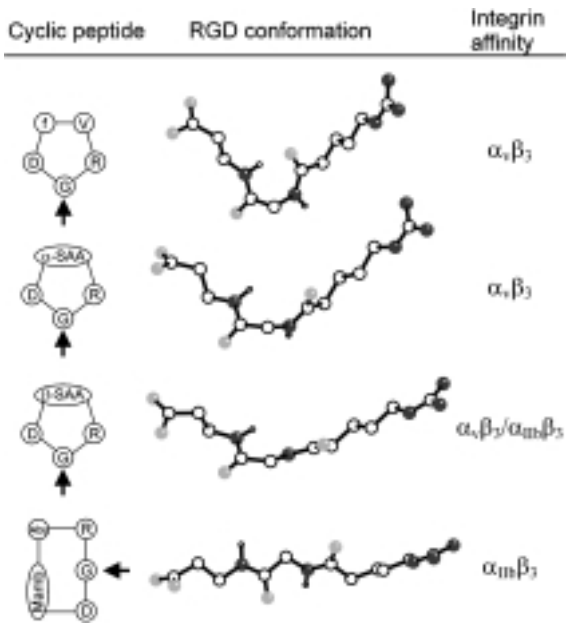


Figure 2. Structure–activity relationship of cyclic RGD peptides. The RGD conformations of the α (**1**) and β compounds (**2**) are compared with typical representatives of $\alpha_v\beta_3$- and $\alpha_{IIb}\beta_3$-antagonists, the lead peptide *cyclo*(-RGDfV-), and the compound *cyclo*(-D-Abu-*N*MeArg-Gly-Asp-Mamb-) (Abu = *A*-aminobutyric acid, Mamb = *m*-(anminomethyl)benzoic acid. [6] The view along the pharmacophoric RGD moiety (center; direction indicated by an arrow in the left-hand column) is oriented parallel to the ring plane of the cyclic peptide.

As hoped, the SAA-modified cyclic peptides exhibit a high $\alpha_v\beta_3$ activity ($IC_{50} = 150$ nM (**1**) and 25 nM (**2**); Table 1). In contrast, the high activity of **2** against the $\alpha_{IIb}\beta_3$ receptor ($IC_{50} = 13.4$ nM) was unexpected. $\alpha_{IIb}\beta_3$-selective antagonists typically adopt a stretched RGD conformation (Figure 2).[6] Structure analysis and molecular dynamics simulations[7] of both the SAA peptides provided an explanation for this unexpected behavior: whereas the conformation of the α-compound is similar to that of the lead structure (the peptidomimetic adopts the $\alpha_v\beta_3$-selective kinked conformation), the conformation of the β-SAA-peptide **2** is in between the conformations of the selective $\alpha_v\beta_3$ and $\alpha_{IIb}\beta_3$ antagonists. In addition, differences in the dynamic behavior of the two compounds are observable. For instance, the β-SAA peptide **2** is more flexible than the α-SAA peptide **1**. Therefore a kinked as well as a stretched conformation can be realized in solution. The compound is therefore able to re-adjust its conformation, matching the steric demands of both the receptor pockets: high activity with a loss of selectivity is the consequence.

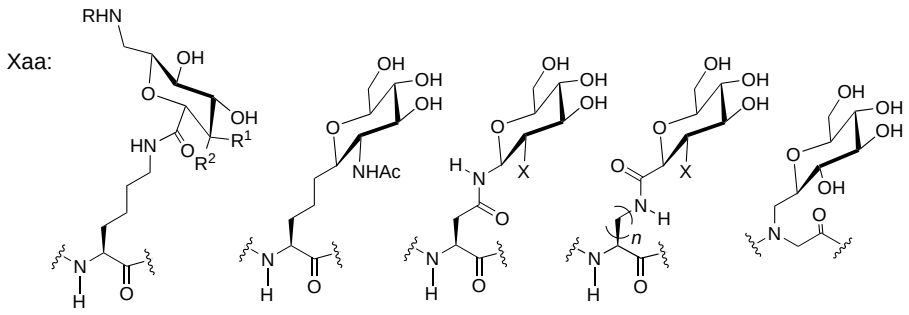
Table 1. Inhibition behavior of the different RGD peptides with regard to binding of vitronectin to the isolated $\alpha_v\beta_3$ receptor as well as the binding of fibrinogen to the isolated $\alpha_{IIb}\beta_3$ receptor. The linear peptide GRGDSPK was chosen as standard.

Compound	IC_{50} [nm]		
	$\alpha_v\beta_3$	$\alpha_{IIb}\beta_3$	$\alpha_v\beta_5$
GRGDSPK	210	1700	> 10000
cyclo(-RGDfV-)	2.5	8000	320
1	150	720	935
2	25	13.4	> 10000
11	55	> 10000	2750
12	0.8	1910	24.7
13	15	450	> 10000
14	21	5000	970
15	30	> 10000	1000
16	5.9	> 10000	4000
17	6.9	6000	6000
18	2.7	6000	480
19	15	> 10000	6000
20	1.4	> 10000	> 10000
21	1.0	> 10000	610
22	1.8	7300	260

A further possibility to modify the lead peptide is by the glycosylation of the side chains of the peptide. The main focus here is the modification of the pharmacokinetic properties[8] with retention of activity and selectivity. In contrast to the above-introduced scaffold mimetica **1** and **2**, the structure-inducing effects of the side chain modifications on the RGD entity should be negligible. Nonconserving substitutions of the valine residue in the lead peptide diminish activity only slightly, as shown in earlier studies.[2d]

Systematic substitutions of the side chain of the valine residue with carbohydrates of differing length and functionality were intended to elucidate the influence of these substitutions on the biological properties of the peptide. Scheme 1 shows the novel compounds **11**–**14**,[9a] **15**, **16**–**17**,[9b]

 © WILEY-VCH Verlag GmbH, D-69451 Weinheim, 2000 1433-7851/00/3915-2762 $ 17.50+.50/0 *Angew. Chem. Int. Ed.* **2000**, *39*, No. 15



Scheme 1. *C*- and *N*-glycosylated RGD peptides *cyclo*(-Arg-Gly-Asp-D-Tyr-Xaa-) **11**–**14**, and *cyclo*(-Arg-Gly-Asp-D-Phe-Xaa-) **15**–**22**. Shown are the structural formulas of the side chain modified residue Xaa.

18–**21**,[9c, 9f, 10] and **22**[9e]. The syntheses of compounds **12**, **14**, and **16** are modeled on the natural *N*-glycosidic protein glycosylation with glucosamine. To study a possible influence of the *N*-acetyl moiety, the glucose derivatives **11**, **13**, and **15** were incorporated. Especially the C-glucosidic derivatives **11**–**15** and **18**–**22** should be pharmacologically interesting, as this link is expected to be enzymatically very stable.

All compounds exhibit a very high $\alpha_v\beta_3$ affinity ($IC_{50} = 0.8$ to $IC_{50} = 1.8$ nM) and selectivity; some even outperform the lead structure. Noteworthy is the very high selectivity of compound **20** and the high activity of compound **12** against the $\alpha_v\beta_5$ receptor. This might indicate an otherwise unnoticed interaction of the side chain with the appropriate subtype of the receptor. Meanwhile it has also been shown that the side chain glycosylation improves the pharmacokinetic properties of peptides which have been used as tracer substances in nuclear medicinal applications.[11] In **20** D-Phe was substituted by D-Tyr to enable radioactive labeling with iodine isotopes. Pharmacokinetic studies demonstrate that the uptake in the liver was reduced compared to that of the nonglycosylated compound, the initial concentration in the blood was doubled, and, the accumulation of the tracer in tumor tissues was dramatically enhanced. Furthermore the first γ-camera pictures of osteosarcom-carrying mice with the ^{123}I-marked peptide revealed images in which the tumor could be clearly delimited from the surrounding tissue.[11]

The presented studies demonstrate that new areas in drug design can be exploited by the incorporation of sugar amino acids in biologically active peptidic compounds. We have illustrated that sugar amino acids as a part of the peptidic backbone broaden the dynamic spectrum and widen the conformational space of this class of peptidomimetics. In the process of direct drug design they help to structurally adjust the bioactive moiety to the appropriate subtypes of the receptor. Additionally they assist in tracing bioactive conformations. Derivatization of side chains with sugars can also influence activity and selectivity, though the main purpose of this kind of modification remains the improvement of pharmacokinetic properties. The results shown here lead to the assumption that the application of sugar amino acids will be used in future as a standard tool in the optimization of peptidic drugs.

Received: February 14, 2000 [Z14693]

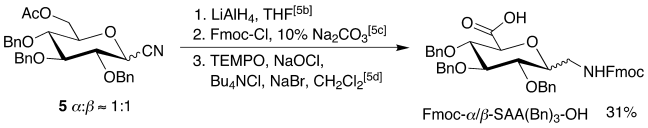
[1] a) E. Graf von Roedern, H. Kessler, *Angew. Chem.* **1994**, *106*, 684–686; *Angew. Chem. Int. Ed. Engl.* **1994**, *33*, 687–689; b) E. Graf von Roedern, E. Lohof, G. Hessler, M. Hoffmann, H. Kessler, *J. Am. Chem. Soc.* **1996**, *118*, 10156–10167; c) K. Burgess, Y. Feng, *Chemtracts: Org. Chem.* **1997**, *10*, 1054–1057.

[2] a) M. Aumailley, M. Gurrath, G. Müller, J. Calvete, R. Timpl, H. Kessler, *FEBS Lett.* **1991**, *291*, 50–54; b) M. Gurrath, G. Müller, H. Kessler, M. Aumailley, R. Timpl, *Eur. J. Biochem.* **1992**, *210*, 911–912; c) M. Pfaff, K. Tangemann, B. Müller, M. Gurrath, G. Müller, H. Kessler, R. Engel, *J. Biol. Chem.* **1994**, *269*, 20233–20238; d) R. Haubner, R. Gratias, B. Diefenbach, S. Goodman, A. Jonczyk, H. Kessler, *J. Am. Chem. Soc.* **1996**, *118*, 7461–7472; e) R. Haubner, D. Finsinger, H. Kessler, *Angew. Chem.* **1997**, *109*, 1440–1456; *Angew. Chem. Int. Ed. Engl.* **1997**, *36*, 1374–1389.

[3] a) M. Dechantsreiter, Ph.D thesis, Technische Universität München, **1998**; b) M. Dechantsreiter, E. Planker, B. Mathä, E. Lohof, G. Hölzemann, A. Jonczyk, S. L. Goodman, H. Kessler, *J. Med. Chem.* **1999**, *42*, 3033–3040.

[4] a) H. Kessler, B. Diefenbach, D. Finsinger, A. Geyer, M. Gurrath, S. L. Goodman, G. Hölzemann, R. Haubner, A. Jonzcyk, G. Müller, E. Graf von Roedern, J. Wermuth, *Lett. Pept. Sci.* **1995**, *2*, 155–160; b) K. C. Nicolaou, J. I. Trujillo, K. Chibale, *Tetrahedron* **1997**, *53*, 8751–8778.

[5] Synthesis was performed starting from **5** (Scheme 2): a) Y. Araki, N. Koboyashi, K. Watanabe, Y. Ishido, *J. Carbohydr. Chem.* **1985**, *4*, 565–585; b) M.-T. Garcia Lopez, F. G. de Las Heras, A. San Felix, *J. Carbohydr. Chem.* **1987**, *6*, 273–279; c) L. A. Carpino, G. Y. Han, *J. Org. Chem.* **1972**, *37*, 3404–3409; d) N. J. Davis, S. L. Flitsch, *Tetrahedron Lett.* **1993**, *34*, 1181–1184.



Scheme 2. Synthesis of Fmoc-α/β-SAA$(Bn)_3$-OH. Fmoc = 9-fluorenylmethoxycarbonyl, TEMPO = 2,2,6,6-tetramethylpiperidinoxyl radical.

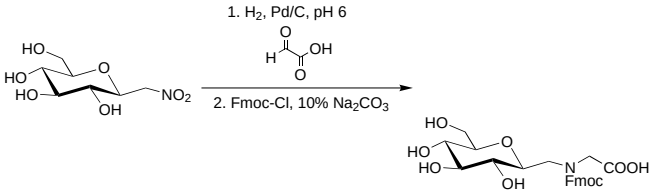
[6] A. C. Bach II, J. R. Espina, S. A. Jackson, P. F. W. Stouten, J. L. Duke, S. A. Mousa, W. F. DeGrado, *J. Med. Chem.* **1996**, *118*, 293–294.

[7] For a review on NMR-spectroscopic conformational analysis and molecular dynamics calculation see: H. Kessler, R. Konat, W. Schmitt, *NMR in Drug Design, CRC Series in Analytical Biotechnology*, CRC Press, Boca Raton, FL, USA, **1996**, pp. 215–244.

[8] K. Michael, V. Wittmann, W. König, J. Sandow, H. Kessler, *Int. J. Pept. Protein Res.* **1996**, *48*, 59–70.

[9] a) **11**–**14:** In this case the cyclic peptide *cyclo*(-Arg-Gly-Asp-D-Tyr-Lys-) was synthesized first, followed by glycosylation of the amino moiety of the lysine. **11, 12**: ref. [1a]; **13**–**14**: ref. [9f] followed by an oxidation as described in ref. [5d]; b) F. Burkhart, M. Hoffmann, H. Kessler, *Angew. Chem.* **1997**, *109*, 1240–1241; *Angew. Chem. Int. Ed. Engl.* **1997**, *36*, 1191–1192; c) H. Paulsen, S. Peters, T. Bielefeldt, *New Compr. Biochem.* **1995**, *29a*, 87–121; d) M. Hoffmann, F. Burkhart, G. Hessler, H. Kessler, *Helv. Chim. Acta* **1996**, *79*, 1519–1532; e) glycopeptoid: by reductive amination of the nitro sugar[9f] with glyoxylic acid, followed by a Fmoc derivatization (Scheme 3); f) L. Petrus, S. Bystricky, T. Sticzay, V. Bilik, *Chem. Zvesti* **1982**, *36*, 103–110.

 © WILEY-VCH Verlag GmbH, D-69451 Weinheim, 2000 1433-7851/00/3915-2763 $ 17.50+.50/0



Scheme 3. Synthesis of a glycopeptoid building block.

[10] The building blocks **15**–**22** were made as Fmoc derivatives, and were as such used under standard solid-phase conditions with TBTU/HOBt [R. Knorr, A. Trzeciak, W. Bannwarth, D. Gillessen, *Tetrahedron Lett.* **1989**, *30*, 1927–1930].

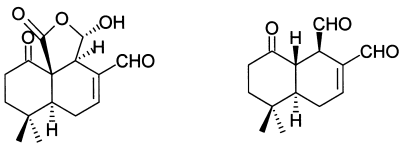
[11] a) R. Haubner, H. J. Wester, R. Senekowitsch-Schmidtke, B. Diefenbach, H. Kessler, G. Stöcklin, M. Schwaiger, *J. Labelled Compd. Radiopharm.* **1998**, *40*, 853–856; b) R. Haubner, H. J. Wester, R. Senekowitsch-Schmidtke, B. Diefenbach, H. Kessler, G. Stöcklin, M. Schwaiger, *J. Nucl. Med.* **1999**, *40*, 1061–1071.

A Short Total Synthesis of Kuehneromycin A**

Johann Jauch*

Dedicated to Professor Volker Schurig on the occasion of his 60th birthday

The kuehneromycins were isolated from the fermentation broth of the basidiomycete *Kuehneromyces* sp. 8758 in 1995.[1] Kuehneromycin A (**1**) is a noncompetitive inhibitor of avian myeloblastosis virus reverse transcriptase[2] as well as moloney murine leukemia virus reverse transcriptase.[2] Kuehneromycin B (**2**) is a strong inhibitor of platelet aggregation and both compounds show cytotoxic and antimicrobial activities. Structurally, the kuehneromycins are related to the mniopetals,[3] which inhibit HIV reverse transcriptase.



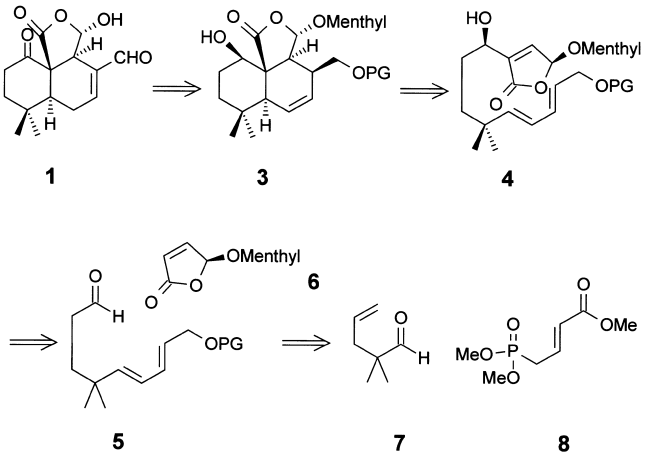
1 **2**

[*] Dr. J. Jauch
Institut für Organische Chemie und Biochemie
Technische Universität München
Lichtenbergstrasse 4, 85747 Garching (Germany)
Fax: (+49) 89-289-13-329
E-mail: jjauch@nucleus.org.chemie.tu-muenchen.de

[**] This work was generously supported by the Deutsche Forschungsgemeinschaft and the Fazit-Stiftung. We are grateful to Prof. W. Steglich, Ludwig-Maximilians-Universität München, for copies of spectra of natural kuehneromycin A and for recording 600 MHz ^{1}H NMR spectra of our synthetic sample. We thank BASF AG, Ludwigshafen, Germany, Pfizer AG, Karlsruhe, Germany, Haarmann & Reimer GmbH, Holzminden, Germany, Wacker GmbH, Burghausen, Germany, DEGUSSA AG, Frankfurt a. M., Germany and Bayer AG, Leverkusen, Germany, for chemicals and laboratory equipment.

In the course of our project towards the synthesis of new sesquiterpenoids[4] with interesting biological activities we decided to synthesize kuehneromycin A and here we report the first synthesis of naturally occurring (−)-kuehneromycin A.

Retrosynthetic analysis of kuehneromycin A (**1**) leads to the protected alcohol **3** which should readily be obtainable from the trienolide **4** in an *endo*-selective intramolecular Diels–Alder reaction (IMDA reaction; Scheme 1). Trienolide **4** is the result of a Baylis–Hillman reaction of aldehyde **5** and Feringa's butenolide **6**.[5] Aldehyde **5** is disconnected into aldehyde **7** and phosphonate **8** through retrosynthetically applying a hydroboration/oxidation Horner–Wadsworth–Emmons sequence.

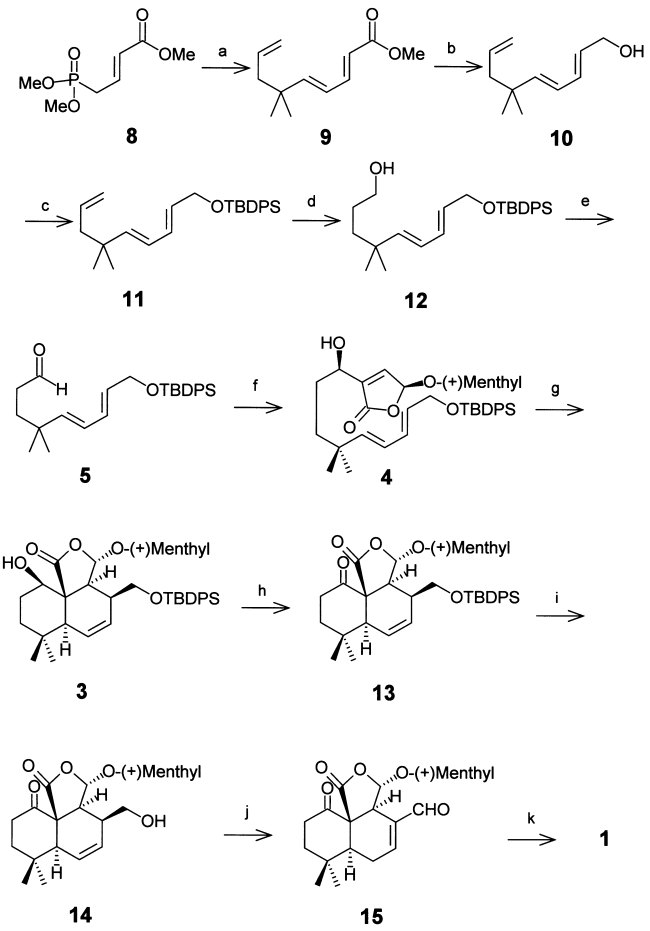


Scheme 1. Retrosynthetic analysis of kuehneromycin A (**1**). PG = protecting group.

Our synthesis (Scheme 2) started with a Horner–Wadsworth–Emmons reaction[6] of 2,2-dimethyl-4-pentenal (**7**)[7] and phosphonate **8**[8] from methyl *E*-4-bromobutenoate, which afforded a mixture of triene esters (*trans*:*cis* > 20:1) from which **9** was readily separated in 85% yield by flash chromatography. Reduction of the ester functionality with diisobutylaluminum hydride (DIBALH)[9] gave the alcohol **10** in 97% yield, which subsequently was protected as the *tert*-butyldiphenylsilyl (TBDPS) ether **11**[10] in quantitative yield. Hydroboration[11] with 9-borabicyclo[3.3.1]nonane (9-BBN), followed by oxidation with H_2O_2/NaOH under standard conditions led regioselectively to alcohol **12** in 91% yield. Oxidation of the primary alcohol with 2,2,6,6-tetramethylpiperidin-*N*-oxyl (TEMPO)/diacetoxyiodobenzene[12] gave exclusively the aldehyde **5**, which served as the starting material for the planned Baylis–Hillman reaction.[13]

The Baylis–Hillman reaction under standard conditions using 1,4-diazabicyclo[2.2.2]octane (DABCO) as a nucleophile was not applicable in our case since Feringa's butenolide[5] **6** is highly base sensitive and the DABCO-catalyzed reaction only works well for β-unsubstituted acrylic acid derivatives. Therefore we developed a new and highly diastereoselective variant[14] of the Baylis–Hillman reaction that used lithium phenylselenide as a strong but only weakly basic nucleophile. PhSeLi was readily prepared from diphenyl diselenide through reductive cleavage with either *n*BuLi[15] or

 © WILEY-VCH Verlag GmbH, D-69451 Weinheim, 2000 1433-7851/00/3915-2764 $ 17.50+.50/0



Scheme 2. Synthesis of kuehneromycin A (**1**). a) LiHMDS, **7**, THF, $-40\,^{\circ}C$, 85%, *trans:cis* > 20:1; b) DIBALH, Et_2O, $0\,^{\circ}C$, 30 min, 97%; c) TBDPSCl, imidazole, DMF, RT, 2 h, quant.; d) 9-BBN, THF, RT, 4 h, H_2O_2, NaOH, EtOH, $0\,^{\circ}C$, 4 h, 91%; e) TEMPO/diacetoxyiodobenzene, CH_2Cl_2, RT, 90 min, 98%; f) PhSeLi, THF, **6**, $-60\,^{\circ}C$, 6 h, 88%; g) xylene, silylated flask, $140\,^{\circ}C$, 60 h, 68%; h) PDC, MS 3 Å, 2 h, 95%; i) TBAF, THF, RT, 1 h, 93%; j) DMSO, $Py \cdot SO_3$, NEt_3, RT, 14 h, 69%; k) TFA/H_2O, (80/20 v/v) 4 h, 94%. LiHMDS = lithium 1,1,1,3,3,3-hexamethylsilazide.

elemental lithium, catalyzed by benzophenone under sonication.[16] Reaction of PhSeLi with aldehyde **5** and **6** at $-60\,^{\circ}C$ for 6 h gave trienolide **4** in a highly diastereoselective tandem-Michael-aldol-retro-Michael reaction in 88% yield. The configuration of the newly formed secondary alcohol is the result of chirality transfer from the acetal carbon atom in **6** to the new chirality center via a Zimmermann–Traxler like transition state in the aldol addition step.[17]

The IMDA reaction[18] of **4** gave after 60 h at $140\,^{\circ}C$ in xylene the desired cyclization product **3** (68%) along with some unidentified side products and about 20% recovered starting material. The structure of **3** was determined by NMR spectroscopy (TOCSY, HMQC, and NOESY).

In the next step, **3** was oxidized to the ketone **13** by pyridinium dichromate (PDC) in the presence of 3 Å molecular sieves in 95% yield. Deprotection of the primary alcohol by tetrabutylammonium fluoride (TBAF; 93%) was followed by Parikh–Doering oxidation[19] with concomitant double bond shift leading to the α,β-unsaturated aldehyde **15** (69%). To obtain reproducible good yields it is important to conduct the reaction under an inert atmosphere and to add the pyridine–sulfur trioxide complex very slowly with a syringe pump.

In the last step, the menthyl residue was removed through action of trifluoroacetic acid (TFA)/H_2O[20] to give kuehneromycin A (**1**) in 94% yield, identical in all respects with the natural product.[21] Thus, we were able to synthesize kuehneromycin A (**1**) in a total of 11 steps in 25–26% yield. Furthermore, our synthesis confirms the absolute configuration of kuehneromycin A (**1**) as determined already by Steglich et al.[1, 3c] for structurally related substances.

Received: March 10, 2000 [Z14830]

[1] G. Erkel, K. Lorenzen, T. Anke, R. Velten, A. Gimenez, W. Steglich, *Z. Naturforsch. C* **1995**, *50*, 1–10.

[2] *Retroviruses* (Eds.: J. M. Coffin, S. H. Hughes, H. E. Varmus), Cold Spring Harbor Laboratory Press, New York, **1997**.

[3] a) A. Kuschel, T. Anke, R. Velten, D. Klostermeyer, W. Steglich, B. König, *J. Antibiot.* **1994**, *47*, 733–739; b) R. Velten, D. Klostermeyer, B. Steffan, W. Steglich, A. Kuschel, T. Anke, *J. Antibiot.* **1994**, *47*, 1017–1024; c) R. Velten, W. Steglich, T. Anke, *Tetrahedron: Asymmetry* **1994**, *5*, 1229–1232.

[4] J. Jauch, *Synlett* **1999**, 1325–1327.

[5] B. L. Feringa, J. C. de Jong, *Bull. Soc. Chim. Belg.* **1992**, *101*, 627–640, and references therein.

[6] W. R. Roush, *J. Am. Chem. Soc.* **1980**, *102*, 1390–1404.

[7] a) K. C. Brannock, *J. Am. Chem. Soc.* **1959**, *81*, 3379–3383; b) G. Salomon, S. Ghosh, *Org. Synth.* **1984**, *62*, 125–133.

[8] P. Baeckström, U. Jacobsson, T. Norin, C. R. Unelius, *Tetrahedron* **1988**, *44*, 2541–2548.

[9] E. Winterfeldt, *Synthesis* **1975**, 617–630.

[10] S. Hanessian, P. Lavallee, *Can. J. Chem.* **1975**, *53*, 2975–2977.

[11] a) A. Pelter, K. Smith, H. C. Brown, *Borane Reagents*, Academic Press, London, UK, **1988**; b) M. J. Kurth, J. O'Brien, H. Hope, M. Yanuck, *J. Org. Chem.* **1985**, *50*, 2626–2632.

[12] A. De Mico, R. Margarita, L. Parlanti, A. Vescovi, G. Piacantelli, *J. Org. Chem.* **1997**, *62*, 6974–6977.

[13] E. Ciganek in *Organic Reactions*, *Vol. 51* (Ed.: L. A. Paquette), Wiley, New York, **1997**, pp. 201–350, and references therein.

[14] J. Jauch, *J. Org. Chem.* in press.

[15] H. J. Reich, R. R. Dykstra, *Organometallics* **1994**, *13*, 4578–4585.

[16] S. V. Ley, I. A. O'Neil, C. M. R. Low, C. *Tetrahedron* **1986**, *42*, 5363–5368.

[17] Vgl. z. B. P. Arya, H. Qin, *Tetrahedron* **2000**, *56*, 917–947, and references therein.

[18] W. R. Roush in *Comprehensive Organic Synthesis*, *Vol. 5* (Eds.: B. M. Trost, I. Fleming), Pergamon, Oxford, **1991**, pp. 513–550, and references therein.

[19] T. T. Tidwell in *Organic Reactions Vol. 39* (Ed.: L. A. Paquette), Wiley, New York, **1990**, pp. 297–572, and references therein.

[20] J. W. J. F. Thuring, G. H. L. Nefkens, R. Schaafstra, B. Zwanenburg, *Tetrahedron* **1995**, *51*, 5047–5056.

[21] ^{1}H NMR (600 MHz, [D$_6$]benzene, TMS): $\delta = 8.90$ (s, 1H), 6.46 (br. s, 1H), 5.85 (d, $^3J(H,H) = 6.8$ Hz, 1H), 5.47 (s, 1H), 3.35 (m, 1H), 2.42 (ddd, $^3J(H,H) = 15.9$, 11.5, 4.6 Hz, 1H), 1.89 (ddd, $^3J(H,H) = 3.6$, 7.0, 15.2 Hz, 1H), 1.82 (ddt, $^3J(H,H) = 2.7$, 12.5, 19.1 Hz, 1H), 1.54 (ddd, $^3J(H,H) = 3.7$, 7.0, 19.1 Hz, 1H), 1.50 (ddd, $^3J(H,H) = 4.6$, 7.0, 13.9 Hz, 1H), 1.19 (s, 3H), 1.03 (ddd, $^3J(H,H) = 3.7$, 11.4, 14.8 Hz, 1H), 0.90 (dd, $^3J(H,H) = 3.4$, 12.5 Hz, 1H), 0.54 (s, 3H); ^{13}C NMR (90 MHz, [D$_6$]benzene, TMS): $\delta = 209.6$, 191.5, 170.5, 151.8, 137.5, 101.5, 62.1, 47.6, 46.3, 37.6, 36.0, 31.7, 31.1, 24.9, 22.9; $[\alpha]_D^{21} = -53$ ($c = 0.2$ in ethanol); (ref. [1] $[\alpha]_D^{21} = -55$ ($c = 0.2$ in ethanol)).

The First Low Molecular Weight Antibiotic from Lactic Acid Bacteria: Reutericyclin, a New Tetramic Acid

Alexandra Höltzel, Michael G. Gänzle, Graeme J. Nicholson, Walter P. Hammes, and Günther Jung*

Based on a screening of lactic acid bacteria from cereal fermentations, an inhibitory effect of *Lactobacillus reuteri* LTH2584 against Gram-positive bacteria has been demonstrated.[1] This strain had been isolated as one of the strains dominating the flora of a sourdough which is prepared for the production of a commercial baking aid.[2] Here, we describe for the first time a low molecular weight antibiotic, reutericyclin (**1**), which is produced by lactic acid bacteria.

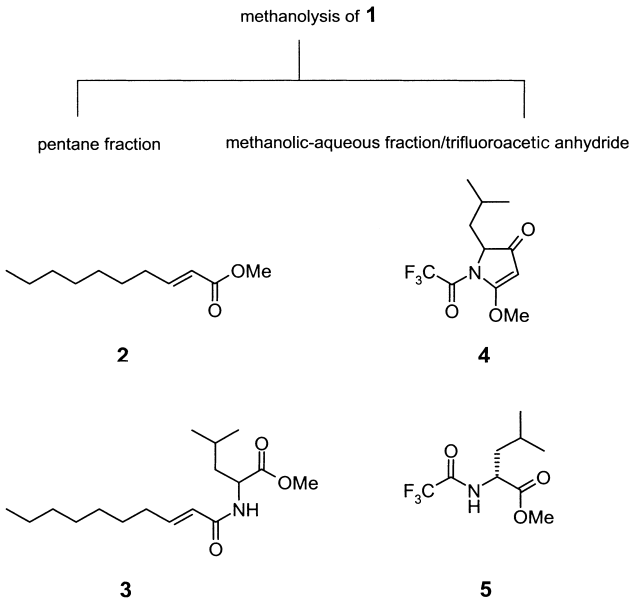
Compound **1** was purified as a yellow-brown oil from cell extracts and culture filtrate of *L. reuteri* LTH2584 with a yield of approximately 1 mg L^{-1}.[3] The elemental formula of **1** was determined by high-resolution ESI-FT-ICR mass spectrometry (ICR = ion cyclotron resonance; $[M + H^+]$ for $C_{20}H_{31}NO_4$: calculated *m*/*z* 350.23257, experimental *m*/*z* 350.23210). The UV/Vis spectrum (acetonitrile) showed absorption maxima at 238 and 286 nm. An intense absorption at 1726 cm^{-1}, as well as several strong bands between 1657 cm^{-1} and 1617 cm^{-1}, in the IR spectrum (film) pointed to the presence of several carbonyl groups in the molecule. The structure of **1** was elucidated by NMR spectroscopy and GC-MS analysis of methanolysis products.

The HSQC spectrum showed that **1** consists of four methyl and seven methylene groups as well as two aliphatic and two olefinic methine groups. Signals for five quarternary carbons were identified in the ^{13}C NMR spectrum, two of which were classified as carbonyl carbons of acid, ester, or amide functionalities, and two as ketone carbons (Table 1). TOCSY spectra (acquired with short and long mixing times) exhibited signals for two distinct spin systems, the first one including 5-H to 9-H and the second one 13-H to 21-H. The *E* configuration of the double bond between C-13 and C-14 was reflected by the vicinal coupling constant ^3J(13-H, 14-H) = 15.4 Hz. Connectivities observed in the HMBC spectrum (Table 1) confirmed the assignments within the spin systems and enabled the addition of the quarternary carbons C-4 and C-12 to the respective structural fragments. A third fragment was established from the HMBC connectivities of the methyl protons 11-H to the quarternary carbons C-3 and C-10; the ^1H NMR signal for 11-H appeared at $\delta = 2.51$, suggesting the vicinal connectivity of methyl group and keto function. HMBC connectivities were not observed between the three structural fragments established so far or to the carbonyl carbon C-2.

Table 1. ^1H and ^{13}C NMR chemical shifts for compound **1**, as well as observed HMBC correlations ([D_3]acetonitrile, 298 K). Due to keto–enol tautomerism two signal sets were detected for several nuclei (**1a** to 60%, **1b/1c** up to 40%).

	$\delta(^{13}C)$		$\delta(^1H)$		HMBC
	1a	**1b/1c**	**1a**	**1b/1c**	correlations
2	167.3	174.8	–		–
3	106.1	103.6	–		11-H
4	199.2	194.5	–		5-H, 6-H
5	60.2	64.1	4.68	4.41	6-H
6	39.8		1.81	1.76	5-H, 7-H, 8-H, 9-H
7	25.2		1.82		5-H, 6-H, 8-H, 9-H
8	23.8		0.88		9-H
9	22.6		0.93		8-H
10	195.6	189.3	–		11-H
11	22.8	20.2	2.51		–
12	165.9	165.5	–		13-H, 14-H
13	124.2		7.29	7.22	15-H
14	150.7	151.8	7.06	7.10	15-H, 16-H
15	33.3	33.2	2.28	2.29	13-H, 14-H, 16-H
16	28.8		1.50		14-H, 15-H
17	29.8		1.34		15-H, 16-H, 18-H
18	29.8		1.34		16-H, 17-H
19	32.5		1.30		20-H, 21-H
20	23.3		1.32		19-H, 21-H
21	14.3		0.90		20-H

The acid methanolyzate of **1** (formed by treatment with CH_3OH/1.5 N HCl, 110 °C, 15 min) was, after addition of water, extracted with *n*-pentane (Scheme 1). The MeOH/H_2O fraction was derivatized with trifluoroacetic anhydride. The GC-MS of the pentane fraction showed two major peaks. The peak at *m*/*z* 184 was identified as 2-decenoic acid methyl ester (**2**) while the second peak at *m*/*z* 297 was assigned to *N*-(2-decenoyl)leucine methyl ester (**3**), on the basis of character-



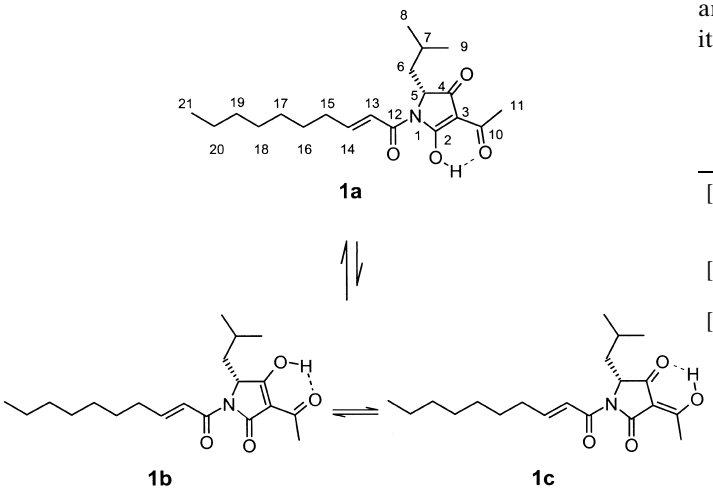
Scheme 1. Methanolysis products of reutericyclin, detected by GC-MS analysis at *m*/*z* 184 (**2**), 297 (**3**), 265 (**4**), and 241 (**5**).

[*] Prof. Dr. G. Jung, Dr. A. Höltzel, G. J. Nicholson
Institut für Organische Chemie der Universität Tübingen
Auf der Morgenstelle 18, 72076 Tübingen (Germany)
Fax: (+49) 7071-29-5560
E-mail: guenther.jung@uni-tuebingen.de
Dr. M. G. Gänzle,[+] Prof. Dr. W. P. Hammes
Institut für Lebensmitteltechnologie
der Universität Hohenheim (Germany)
[+] Current Address:
Lehrstuhl für Technische Mikrobiologie
Institut für Brauereitechnologie und Mikrobiologie
TU München in Freising-Weihenstephan (Germany)

 © WILEY-VCH Verlag GmbH, D-69451 Weinheim, 2000 1433-7851/00/3915-2766 $ 17.50+.50/0 *Angew. Chem. Int. Ed.* **2000**, *39*, No. 15

istic fragmentations. The identification of **3** in the acid methanolyzate of **1** suggested that C-5 and C-12 are connected by N-1 in the native molecule. The observed ^{13}C NMR signals left but one possibility for the arrangement of the third fragment and the carbonyl group at C-2 in the molecule. The formulation of **1** as 3-acyltetramic acid was confirmed by the identification of compound **4** as the main component of the MeOH/H_2O fraction of the acid methanolyzate. The deacylation of 3-acyltetramic acids under acidic conditions has long been known,[4] and similarly the O-alkylation of tetramic acids.[5] The MeOH/H_2O fraction also contained *N*-trifluoroacetylleucine methyl ester **5**. From the absolute configuration of **5**, as determined by GC-MS analysis with a Chirasil-Val column,[6] the (5*R*)-configuration of **1** was concluded. The methanolysis products **3** and **5**, the identification of which was essential for the structure elucidation of **1**, are unusual in that their formation requires the cleavage of a C–C bond. Up to now the release of an amino acid from 3-acyltetramic acids has only been reported upon treatment with oxidative reagents.[4] The structure and the results of the acid methanolysis of **1** were validated by the synthesis of racemic **1**.[7]

The formulation of **1** as (5*R*)-3-acyl-1-(2-decenoyl)-2-hydroxy-5-isobutyl-Δ^2-pyrroline-4-one refers to tautomer **1a** (Scheme 2), which analysis of the ^{13}C NMR signals (Table 1) revealed to be the major tautomer (60%) in acetonitrile



Scheme 2. Reutericyclin is subjected to keto–enol tautomerism in solution. In [D_3]acetonitrile **1a** is present to 60% and **1b** and **1c** in up to 20% each.

solution. The ^{13}C NMR data for the minor signal set indicate equal contributions (20% each) from the internal tautomers **1b** and **1c**. In this respect, **1** differs from all other naturally occurring 3-acyltetramic acids. These prefer almost exclusively the pyrrolidine-2,4-dione form in solution.[8, 9] The exceptional preference for the Δ^2-pyrroline-4-one form in **1** is brought about by the 2-decenoyl substituent at N-1, which not only reduces the hydrogen bridge acceptor ability of the carbonyl group at C-2, but also stabilizes the endocyclic double bond by conjugation.

Among the naturally occurring tetramic acids,[9, 10] which display a remarkable spectrum of biological activity, the structure of **1** is chemically interesting because of the unprecedented N-1 substitution with an α,β-unsaturated fatty acid. For a possible application of **1** as an antibiotic, it is noteworthy that *L. reuteri* is utilized in food fermentations[2] and has been described as a stable constituent of the intestinal microflora of both humans and animals.[11] Investigations on the inhibitory spectrum of **1** and its production by *L. reuteri* LTH2584 support the conclusion that inhibitory concentrations of the amphiphilic compound are present in sourdough fermentations with *L. reuteri*.[1, 12] Lactic acid bacteria produce a multitude of unspecific low molecular weight compounds, mainly side products of carbohydrate metabolism, which contribute to the inhibitory effect of lactic acid.[13] However, all antibiotics from lactic acid bacteria known to date are bacteriocins. The inhibitory effect of bacteriocins is restricted to closely related species and their potential for application to foods is therefore limited.[14] In recent years, a considerable amount of research has focused on the positive effect of lactic acid bacteria on human health (probiotics). In animal tests, a protective effect of antimicrobial substances from lactobacilli against *Helicobacter* and *Salmonella* infections has been demonstrated,[15] but an active substance has not been chemically characterized to date. As **1** differs in its chemical and biological properties from all other active substances produced by lactic acid bacteria, the structure elucidation of this natural compound adds a new dimension to the discussion regarding the application of lactic acid bacteria and their antimicrobial metabolites for food preservation or for positively influencing the human intestinal microflora.

Received: February 11, 2000 [Z14692]

[1] M. G. Gänzle, C. Hertel, W. P. Hammes in *Beijerinck Centennial. Microbial physiology and gene regulation* (Eds.: W. A. Scheffers, J. P. van Dijken), Delft University Press, **1995**, pp. 380–381.

[2] G. Böcker, P. Stolz, W. P. Hammes, *Getreide Mehl Brot* **1995**, *49*, 370–374.

[3] The isolation of **1** from cell extracts involved extraction with a 70/30 mixture of phosphate buffer (50 mM, pH 6.5) and isopropanol, gel filtration on Superdex S30 (Pharmacia, 75/25 mixture of triethylamine buffer (50 mM, pH 7.2) and isopropanol), and medium-pressure reversed-phase chromatography (Pharmacia, 15 μm, eluent A: H_2O/0.1% trifluoroacetic acid (TFA) solution, eluent B: isopropanol/0.1% TFA solution, gradient: from 25% to 50% B in 20 min). The isolation of **1** from culture filtrate followed a slightly modified protocol. In both cases, HPLC (Advanced Separation Technologies, C_{18} column, 5 μm, eluent A: acetonitrile/0.1% TFA solution, eluent B: H_2O/0.1% TFA solution, A/B = 85/15) was used as a final purification step.

[4] C. E. Stickings, *Biochem. J.* **1959**, *72*, 332–340.

[5] a) H.-D. Stachel, K. K. Harigel, H. Poschenrieder, H. Burghard, *J. Heterocycl. Chem.* **1980**, *17*, 1195–1199; b) K. Inami, T. Shiba, *Tetrahedron Lett.* **1984**, *25*, 2009–2012. Both, the 4-methoxy- and the 2-methoxy derivatives have been reported as the methylation products of tetramic acids. The formulation of 2-methoxy-Δ^2-pyrroline-4-one as the methanolysis product of **1** is based on the mass spectrum of **4** in which the base peak at *m*/*z* 209 originates from a McLafferty rearrangement which would require the carbonyl group at position 4.

[6] H. Frank, G. J. Nicholson, E. Bayer, *J. Chromatogr.* **1978**, *167*, 187–196.

[7] U. Marquardt, D. Schmid, G. Jung, *Synlett*, in press.

[8] The naturally occurring 3-acyltetramic acids known to date are—with the exception of magnesidins A and B—either unsubstituted or alkylated at N-1. For these compounds the dominance of the exocyclic pyrrolidine-2,4-dione form, in which the amide carbonyl group acts as

 © WILEY-VCH Verlag GmbH, D-69451 Weinheim, 2000 1433-7851/00/3915-2767 $ 17.50+.50/0

a hydrogen bond acceptor, has been deduced from a comprehensive analysis of the ^{13}C NMR spectra: a) P. S. Steyn, P. L. Wessels, *Tetrahedron Lett.* **1978**, *47*, 4707 – 4710; b) M. J. Nolte, P. S. Steyn, P. L. Wessels, *J. Chem. Soc. Perkin Trans. 1* **1980**, 1057 – 1065.

[9] The major tautomers of magnesidins A and B in solution are the Δ^3-pyrroline-2-one forms: N. Imamura, K. Adachi, H. Sano, *J. Antibiot.* **1994**, *47*, 257 – 261.

[10] B. J. L. Royles, *Chem. Rev.* **1995**, *95*, 1981 – 2001. So far, the naturally occurring *N*-acyltetramic acids known are only 4-methoxy-Δ^3-pyrroline-2-ones (with the exception of magnesidins A and B).

[11] I. A. Casas, W. J. Dobrogosz, *Microecol. Ther.* **1997**, *26*, 221 – 231.

[12] a) The optimal conditions with respect to temperature, pH, and substrate supply correspond to the conditions during sourdough fermentations: M. G. Gänzle, PhD. thesis, Universität Hohenheim, **1998**; b) additionally, it has been shown that reutericyclin-sensitive strains are inhibited in their growth or killed during cofermentation in sourdough containing *L. reuteri* LTH2584: W. P. Hammes, J. Walter, unpublished results; M. G. Gänzle, R. Vogel, unpublished results.

[13] a) P. A. Vandenbergh, *FEMS Microbiol. Rev.* **1993**, *12*, 221 – 337; b) M.-L. Niku-Paavola, A. Laitila, T. Mattila-Sandholm, A. Haikara, *J. Appl. Microbiol.* **1999**, *86*, 29 – 35.

[14] a) R. W. Jack, J. R. Tagg, B. Ray, *Microbiol. Rev.* **1995**, *59*, 171 – 200; b) R. W. Jack, F. Götz, G. Jung in *Biotechnology*, *Vol. 7*, 2nd edition (Eds.: H. Kleinkauf, H. von Döhren), VCH, Weinheim, **1997**, pp. 325 – 368.

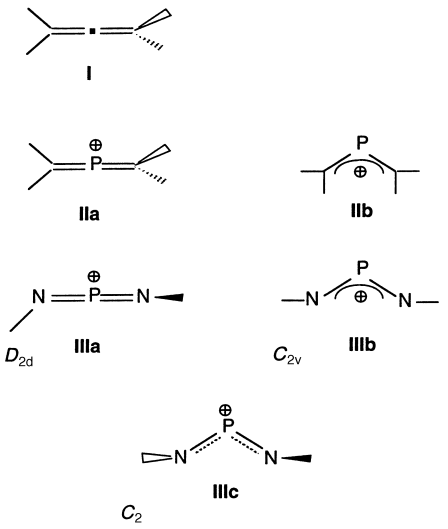
[15] a) M.-H. Coconnier, V. Liévin, E. Hemery, A. L. Servin, *Appl. Environ. Microbiol.* **1998**, *64*, 4573 – 4580; b) M.-F. Bernet-Camard, V. Liévin, D. Brassart, J.-R. Neeser, A. L. Servia, S. Hudault, *Appl. Environ. Microbiol* **1997**, *63*, 2747 – 2753.

Synthesis of the Adduct DMAP · BrP(=N-Mes*)$_2$ and of the Salt [(DMAP)$_2$P(=NMes*)$_2$]$^+$Br**

Markus Blättner, Martin Nieger, Alexander Ruban, Wolfgang W. Schoeller, and Edgar Niecke*

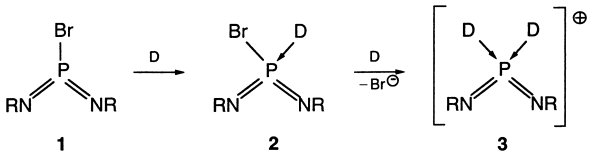
Dedicated to Professor Reinhard Schmutzler on the occasion of his 65th birthday

Allenes **I** are fundamental compounds with a linear structure (D_{2d} symmetry). This implies sp hybridization at the central carbon atom.[1] The hypothetical 2-phosphonio-allenic cation **IIa** is isovalent to **I**, but its central phosphorus atom is not sp hybridized.[2] The s orbital at the phosphorus atom becomes stereochemically active under formation of a "bent" 2-phosphaallyl cation **IIb**.[3] According to ab initio calculations[5] this geometry is favored over that of **IIa**.



Quantum-chemical calculations predict a linear arangement of atoms (D_h) for the cations PO_2^+ and PS_2^+.[6] For these cations a bis-donor adduct has been obtained recently.[7] Here we report on the first synthesis and crystal structure analysis of a bis-donor adduct of the imine analogue of **II** as well as on ab initio calculations on model compounds that support the findings.

Treatment of the bromobis(arylimino)phosphorane **1** (R = Mes* = 2,4,6-tBu$_3$C$_6$H$_2$)[8] with one equivalent of *p*-dimethylaminopyridine (DMAP = D) in CH_2Cl_2 furnished the donor/acceptor adduct **2** in good yield (75 %) in the form of air- and moisture-sensitive light yellow crystals. Subsequent reaction of **2** with a second equivalent of DMAP proceeded by halogen/nucleophile exchange to give the cation **3**, whose bromide was isolated at low temperature as yellow crystals from a little CH_2Cl_2.



Initial information concerning the constitution of **2** and **3** · Br$^-$ was obtained from multinuclear NMR investigations. The ^1H and ^{13}C NMR data clearly indicated the presence of Mes* substituents at the nitrogen atoms as well as the attachment of one (**2**) or two donor molecules (DMAP) (**3**) to the phosphorus atom. As expected the ^{31}P NMR signals appeared at higher fields ($\delta = -93.2$ (**2**), -57.2 (**3**)) than those of bis(imino)phosphoranes,[9] indicating an increase of coordination number at the phosphorus atom.

Crystal structure analyses of **2** and **3** · Br$^-$ gave evidence for the formation as a monoadduct of the bromobis(imino)phosphorane and as a bisadduct of the bis(imino)phosphonium cation (Figures 1 and 2).[10] In both compounds the phosphorus atoms adopt a strongly distorted tetrahedral geometry. The N-P-N bond angle at the phosphorus atom (N1-P1-N2

[*] Prof. Dr. E. Niecke, Dr. M. Blättner, Dr. M. Nieger, Dr. A. Ruban
Anorganisch-Chemisches Institut der Universität
Gerhard-Domagk-Strasse 1, 53121 Bonn (Germany)
Fax: (+49) 228-73-5327
E-mail: e.niecke@uni-bonn.de
Prof. Dr. W. W. Schoeller
Fakultät für Chemie der Universität Bielefeld (Germany)

[**] This work was supported by the Fonds der Chemischen Industrie and the Deutsche Forschungsgemeinschaft (SFB 334). Part of this work was reported at the International Conference on Phosphorus Chemistry, Cincinnati, USA, **1998**. DMAP = *p*-dimethylaminopyridine; Mes* = 2,4,6-tBu$_3$C$_6$H$_2$.

 © WILEY-VCH Verlag GmbH, D-69451 Weinheim, 2000 1433-7851/00/3915-2768 $ 17.50+.50/0

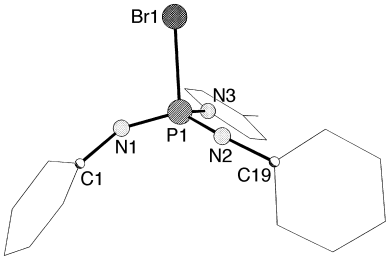


Figure 1. Molecular structure of **2** (solvent, hydrogen atoms, and peripheral groups omitted for clarity). Selected distances [pm] and angles [°]: P1-Br1 231.9(2), P1-N1 152.8(5), P1-N2 148.6(5), P1-N3 181.5(5); N2-P1-N1 130.6(3), N2-P1-N3 107.8(2), N1-P1-N3 103.6(2), N2-P1-Br1 113.2(2), N1-P1-Br1 102.5(2), N3-P1-Br1 92.2(2).

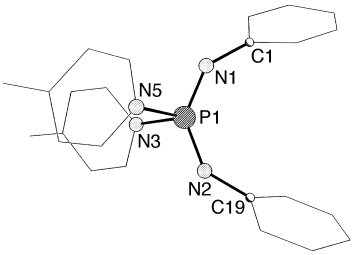
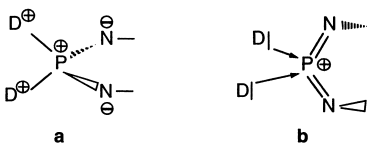


Figure 2. Molecular structure of **3** (solvent, anion, hydrogen atoms, and peripheral groups omitted for clarity). Selected bond lengths [pm] and angles [°]: P1-N1 152.8(4), P1-N2 152.6(4), P1-N3 183.0(4), P1-N5 181.2(4); N1-P1-N2 135.9(2), N1-P1-N3 110.3(2), N1-P1-N5 100.6(2), N2-P1-N3 100.9(2), N2-P1-N5 110.7(2), N3-P1-N5 88.7(2).

130.6(3)° (**2**), 135.9(3)° (**3**)) is widened with respect to that in the bis(imino)phosphorane IP(=NMes)$_2$ (121.9(2)°[8]), while the angle Br1-P1-N3 (92.2(2)°) in **2** and N1-P1-N5 (88.7(2)°) in **3** are more compressed. The sterically demanding aryl substituents at N1 and N2 are arranged differently to each other (**2**: *exo/endo*, **3**: *endo/endo*). The different conformations may be attributed to a delicate balance of steric hindrance between the crowded donor ligands (DMAP) and the bulky substituents at the nitrogen substituents (Mes*). Remarkably, in comparison with **3** the bis-donor adduct $Py_2[PS_2]^+$ is less tetrahedrally distorted (S-P-S 124°, N-P-N 94°[7b]). The dihedral angle between the planes of both aryl rings and the N1-P-N2 unit is 16°. The P–N(aryl) distances (148.6(5), 152.8(5) pm (**2**); 152.6(4), 152.8(4) pm (**3**)) correspond to those in bis(imino)phosphoranes,[9] and indicate the high degree of P–N double-bond character in **2** and **3**. On the contrary the P–N(DMAP) bond lengths (181.5(5) pm (**2**); 181.2(4), 183.0(4) pm (**3**)) are longer than the P–N single bond in the amionobis(imino)phosphorane $(Me_3Si)_2NP(=NSiMe_3)_2$ (164.6 pm[14]). The P – Br distance in **2** (231.9(2) pm) corresponds to those of a typical single bond between these atoms. The shortest contact between the anion and the electrophilic phosphorus center in the bis-donor adduct **3** is 719 pm and indicates the formation of a salt.

The structure of **3** can be described by the two limiting structures **a** and **b**. The limiting structure **a** with a strong charge separation corresponds to a classical multipolar phosphonium structure with tetrahedral coordination at the phosphorus atom. The limiting structure **b** describes the cation as a donor–acceptor complex between a heteroallenic cation and two Lewis donors. Each of the two nitrogen donor ligands transfers electron density into the two approximately orthogonal π-orbitals of the 2-phospha-heteroallene. This results in a geometry which strongly deviates from an ideal tetrahedral environment.



a **b**

According to quantum-chemical calculations (MP2(fc)/6-31g*),[15] the parent cation $[P(=NMe)_2]^+$ displays the structure **III c** with C_2 symmetry and the following parameters: P–N 153.6 pm, N-P-N 137.5°, H-N-P 142.4°). This structure is slightly lower in energy than linear structure (D_{3d} symmetry (**III c**), $\Delta E = 7.2$ kcal mol^{-1}[16]). In other words the "donor-free" cation is a highly flexible structure. The addition of two nitrogen donor ligands to the cation $[P(=NMe)_2]^+$ is strongly exothermic (e.g., $\Delta E = -64.3$ kcal mol^{-1} for the addition of two molecules of NH_3). The bond lengths and angles show a significant dependence on the basicity of the donor ligands, whereas with increasing strength of the P–N(donor) bond in the series $NH_3 < Py < DMAP$ (N–P: 195.9, 191.3, 187.9 pm, respectively) the distortion of the tetrahedral geometry dimishes (N(donor)-P-N(donor) 90.0, 89.4, 91.2, respectively, N(Me)-P-N(Me) 146.2, 142.6, 140.4°, respectively).

The peculiar bonding situation is reflected in the Laplacian distribution of the electron density of the MP2 wavefunction.[17] Figure 3 shows the electron density distribution for

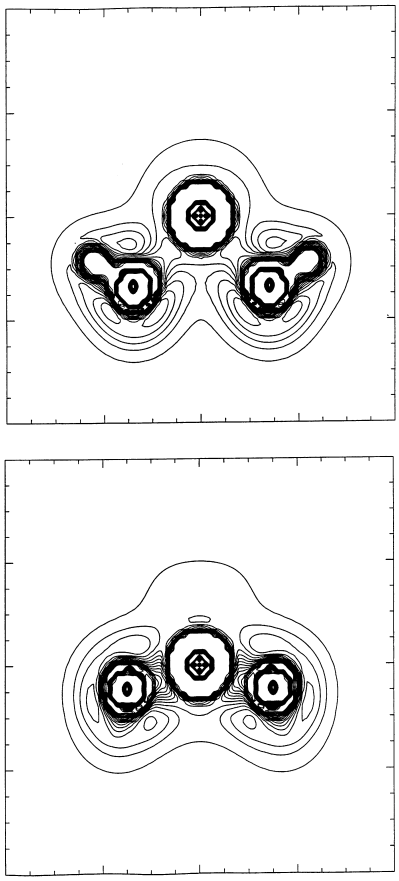
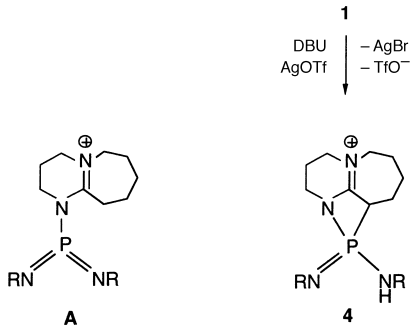


Figure 3. Laplacian of the electron density distribution in the cation $[(H_3N)_2P(=NMe)_2]^+$ in the N-P-N planes $(H_3)N$-P-$N(H_3)$ (top: P–N(imine) bonds) and (Me)N-P-N(Me) (bottom: donor–acceptor bonds). A large scale unit corresponds to 3.75 Bohr.

 © WILEY-VCH Verlag GmbH, D-69451 Weinheim, 2000 1433-7851/00/3915-2769 $ 17.50+.50/0

the cation $[(NH_3)_2P(=NMe)_2]^+$ in the N-P-N planes (H_3)N-P-N(H_3) (top) and (Me)N-P-N(Me) (bottom). In the former case electron density is predominantly localized at the nitrogen atoms of the donor ligands (NH_3) which point towards the phosphorus atom. For the latter the electron density is distributed equally between the central phosphorus atom and the two nitrogen atoms. The two donor ligands interact only weakly with the cationic heteroallene. The bonding features of the "free cation" $[P(=NMe)_2]^+$, namely the large N-P-N angle and the P–N double-bond character, are preserved.

It should be mentioned that the product of the reaction of **1** with 1.8-diazabicyclo[5.4.0]undec-7-ene (DBU) in the presence of AgOTf ($Tf = F_3CSO_2$) was described as the onio-substituted bis(imino)phosphorane **A**.[18] However, as we have proven by NMR spectroscopy as well as by a single-crystal X-ray diffraction study,[10] the reported cation is not the donor adduct **A**, but the onio-substituted iminophosphorane **4**.[19]



Experimental Section

2: A solution of **1** (1.0 g, 1.58 mmol) in toluene (25 mL) was treated with DMAP (0.19 g, 1.58 mmol) dissolved in toluene (10 mL). After the mixture had been stirred at room temperature for 30 min, the solvent was removed under reduced pressure and the remaining solid residue was recrystallized from CH_2Cl_2 at $-24\,^\circ$C. Yield: 78.4%; m.p. 112–114 °C (decomp); ^{31}P NMR (ext.; C_6D_6): $\delta = -93.2$; ^{1}H NMR ($CDCl_3$): $\delta = 1.23$ (s, 18H; *p*-tBu), 1.25 (s, 18H; *o*-*t* Bu), 1.52 (s, 18H; *o*-tBu), 3.31 (s, 6H; NMe_2), 6.71 (br., 2H; *m*-C_2H_4N), 7.06 (s, 2H; C_6H_2), 8.53 (br., 2H; *o*-C_2H_4N); ^{13}C NMR ($CDCl_3$): $\delta = 31.9$ (s; *p*-CCH_3), 32.2 (s; *o*-CCH_3), 34.8 (s; *p*-CCH_3), 36.9 (s; *o*-CCH_3), 41.2 (s; NCH_3), 107.2 (s; *m*-Py), 122.8 (s; *m*-Ar), 138.1 (d, ^2J(P,C) = 28.1 Hz; *ipso*-Ar), 139.9 (d, ^3J(P,C) = 12.8 Hz; *o*-Ar), 140.8 (s; *o*-Py), 143.4 (s; *p*-Ar), 156.8 (s; *p*-Py).

3: A solution of **1** (0.19 g, (1.58 mmol) in CH_2Cl_2 (15 mL) was treated with DMAP (0.38 g, 3.17 mmol) dissolved in CH_2Cl_2 (5 mL). After the the mixture had been stirred at room temperature for 30 min, the solvent was removed under reduced pressure and the remaining solid residue was recrystallized from CH_2Cl_2 at $-24\,^\circ$C. Yield: 84.5%, m.p. 124–125 °C (decomp); ^{31}P NMR (ext.; CH_2Cl_2): $\delta = -57.2$; ^{1}H NMR ($CDCl_3$): $\delta = 1.07$ (s, 36H; *o*-*t*Bu), 1.20 (s, 18H; *p*-*t*Bu), 3.29 (s, 12H; NMe_2), 6.71 (br., 4H; *m*-C_2H_4N), 7.03 (d, *J*(P,H) = 7.6 Hz, 2H; C_6H_2), 8.53 (br., 4H; *o*-C_2H_4N); ^{13}C NMR ($CDCl_3$): $\delta = 31.9$ (s; *p*-CCH_3), 32.9 (s; *o*-CCH_3), 34.7 (s; *p*-CCH_3), 36.9 (d, *J*(P,C) = 0.8 Hz; *o*-CCH_3), 107.2 (s; *m*-Py), 122.8 (s; *m*-Ar), 139.9 (d, ^1J(P,C) = 30.2 Hz; *ipso*-Ar), 140.0 (d, ^2J(P,C) = 8.0 Hz; *o*-Ar), 141.7 (d, *J*(P,C) = 7.9 Hz; *o*-Py), 143.4 (s; *p*-Ar), 156.8 (s; *p*-Py).

4: A solution of **1** (1.0 g, 1.58 mmol) in toluene (40 mL) was treated with DBU (0.24 g, 1.58 mmol) dissolved in toluene (5 mL). After the mixture had been stirred at room temperature for 30 min, it was treated with $AgOSO_2CF_3$ (0.40 g, 1.58 mmol) and then stirred for a further 30 min at room temperature. After separation of the AgBr, the filtrate was concentrated and the product crystallized at $-30\,^\circ$C. Yield: 67.6%, m.p. 138–140 (decomp); ^{31}P NMR (ext.; C_6D_6) $\delta = -11.7$; ^{1}H NMR (C_6D_6): $\delta =$ 1.20 (s, 9H; *p*-tBu), 1.22 (s, 9H; *p*-*t*Bu), 1.25 (s, 18H; *o*-*t*Bu), 1.27 (s, 9H; *o*-*t*Bu), 1.49 (s, 9H; *o*-tBu), 4.12 (s, 1H; NH), 7.05 (d, *J*(P,H) = 5.1 Hz, 2H; C_6H_2), 7.16 (s, 2H; C_6H_2), [DBU signals: 1.15–1.30 (m), 1.50–1.54 (m), 2.36–2.79 (m), 3.32–3.36 (m)].

Received: June 9, 1999 [Z13536]
publication delayed at authors' request

[1] "The Chemistry of Ketenes, Allenes, and Related Compounds": *The Chemistry of Functional Groups* (Ed.: S. Patai), Wiley, New York, **1980**.

[2] See for example: a) W. Kutzelnigg, *Angew. Chem.* **1984**, *96*, 262–286; *Angew. Chem. Int. Ed. Engl*. **1984**, *23*, 272–296; b) "Bonding Properties of Low Coordinated Phosphorus Compounds": W. W. Schoeller in *Multiple Bonding and Low Coordination in Phosphorus Chemistry* (Eds.: M. Regitz, O. J. Scherer), Thieme, Stuttgart, **1989**, pp. 5–32.

[3] Compounds with a bent structure **IIb** have been well known for more than three decades,[4] however, they are extended π systems.

[4] K. Dimroth, P. Hoffmann, *Angew. Chem.* **1964**, *76*, 433; *Angew. Chem. Int. Ed. Engl.* **1964**, *3*, 379.

[5] W. W. Schoeller, W. Haug, J. Strutwolf, T. Busch, *J. Chem. Soc. Faraday Trans.* **1996**, *92*, 1751–1755.

[6] The equilibrium geometry at the MP2(fc)/6-31g* level is as follows: P–O 1.467 Å, O-P-O 180°. For the corresponding radical see: a) C. Xu, E. de Beer, D. M. Neumark, *J. Chem. Phys.* **1996**, *104*, 2749–2751; b) Z.-L.Lai, G. Hirsch, R. J. Buenker, *Chem. Phys. Lett.* **1996**, *225*, 350–356.

[7] a) $[(DMAP)_2PO_2]^+$: R. Weiss, R. Engel *Angew. Chem.* **1992**, *104*, 239–240; *Angew. Chem. Int. Ed. Engl.* **1992**, *31*, 216–217; b) $[Py_2PS_2]^+$: M. Meisel, P. Lönnecke, A. R. Grimmer, D. Wulff-Molden, *Angew. Chem.* **1997**, *109*, 1940–1942; *Angew. Chem. Int. Ed. Engl.* **1997**, *36*, 1869–1870.

[8] A. Ruban, M. Nieger, E. Niecke, *Angew. Chem.* **1993**, *105*, 1544–1545; *Angew. Chem. Int. Ed. Engl.* **1993**, *32*, 1419–1420.

[9] "Bis(imino)phosphoranes": E. Niecke, D. Gudat in *Multiple Bonding and Low Coordination in Phosphorus Chemistry* (Eds.: M. Regitz, O. J. Scherer), Thieme, Stuttgart, **1990**, pp. 392–404.

[10] X-ray structure analysis of **2** ($C_{43}H_{68}BrN_4P \cdot 0.5$ toluene): yellow crystals, crystal dimensions $0.20 \times 0.40 \times 0.53$ mm^3; $M_r = 797.96$; monoclinic, space group $P2_1/c$ (no. 14), $a = 11.041(1)$, $b = 20.605(4)$, $c = 19.996(5)$ Å, $\beta = 94.68(1)^\circ$, $V = 4.534(2)$ nm^3, $Z = 4$, $\mu(Cu_{K\alpha}) = 1.817$ mm^{-1}, $T = 208(2)$ K, $F(000) = 1716$. A total of 6951 reflections up to $2\theta_{max.} = 120^\circ$ were measured on an Enraf-Nonius CAD4 diffractometer with $Cu_{K\alpha}$ radiation, 6731 of which were independent and used for all calculations. The structure was solved by direct methods (SHELXS-86[11]) and refined to F^2 anisotropically, the H atoms were refined with a riding model (SHELXL-93[12]). The final quality coefficient $wR2(F^2)$ was 0.2508, with a conventional $R(F) = 0.0808$ for 456 parameters and 22 restraints. An empirical absorption correction on the basis of ψ scans was applied (min/max transmission 0.410/0.842). One of the *p*-*t*Bu groups and the toluene molecule are disordered. X-ray structure analysis of $\mathbf{3} \cdot Br^-$ ($C_{50}H_{78}BrN_6P \cdot 3CH_2Cl_2$): yellow crystals, crystal dimensions $0.10 \times 0.28 \times 0.43$ mm^3; $M_r = 1128.84$; monoclinic, space group $P2_1/n$ (no. 14), $a = 10.542(2)$, $b = 11.213(2)$, $c = 51.27(2)$ Å, $\beta = 91.96(2)^\circ$, $V = 6.057(3)$ nm^3, $Z = 4$, $\mu(Cu_{K\alpha}) = 3.895$ mm^{-1}, $T = 200(2)$ K, $F(000) = 2384$. A total of 9715 reflections up to $2\theta_{max} = 120^\circ$ were measured on an Enraf-Nonius CAD4 diffractometer with $Cu_{K\alpha}$ radiation, 8998 of which were independent and used for all calculations. The structure was solved by direct methods (SHELXS-86[11]) and refined to F^2 anisotropically, the H atoms were refined with a riding model (SHELXL-93[12]). The final quality coefficient $wR2(F^2)$ was 0.2397, with a conventional $R(F) = 0.0744$ for 603 parameters and 141 restraints. An empirical absorption correction was applied[13]. One *p*-*t*Bu group is disordered. X-ray structure analysis of $\mathbf{4} \cdot TfO^-$ ($[C_{45}H_{74}N_4P][SO_3CF_3] \cdot$ toluene): colorless crystals, crystal dimensions $0.13 \times 0.20 \times 0.20$ mm^3; $M_r = 943.26$; triclinic, space group $P\bar{1}$ (no. 2), $a = 10.075(2)$, $b = 15.041(4)$, $c = 19.398(4)$ Å, $\alpha = 104.98(2)^\circ$, $\beta = 98.79(2)^\circ$, $\gamma = 100.13(2)^\circ$, $V = 2.734(1)$ nm^3, $Z = 2$, $\mu(Cu_{K\alpha}) = 1.227$ mm^{-1}, $T = 200(2)$ K, $F(000) = 1020$. A total of 7346 reflections up to $2\theta_{max} = 110^\circ$ were measured

 © WILEY-VCH Verlag GmbH, D-69451 Weinheim, 2000 1433-7851/00/3915-2770 $ 17.50+.50/0

on an Enraf-Nonius CAD4 diffractometer with $Cu_{K\alpha}$ radiation, 6856 of which were independent and used for all calculations. The structure was solved by direct methods (SHELXS-86[11]) and refined to F^2 anisotropically, the H atoms were refined with a riding model (SHELXL-93[12]). The final quality coefficient $wR2(F^2)$ was 0.2540, with a conventional $R(F) = 0.0780$ for 545 parameters and 91 restraints. One *p*-*t*Bu group and the triflate are disordered. Crystallographic data (excluding structure factors) for the structures reported in this paper have been deposited with the Cambridge Crystallographic Data Centre as supplementary publication no. CCDC-132812 (**2**), CCDC-132813 (**3**·Br^-), and CCDC-132814 (**4**·TfO^-). Copies of the data can be obtained free of charge on application to CCDC, 12 Union Road, Cambridge CB21EZ, UK (fax: (+44) 1223-336-033; e-mail: deposit@ccdc.cam.ac.uk).

[11] G. M. Sheldrick, SHELXS-86, *Acta Crystallogr. Sect. A* **1990**, *46*, 467–473.

[12] G. M. Sheldrick, SHELXL-93, University of Göttingen, **1993**.

[13] N. Walker, D.Stuart, *Acta Crystallogr. Sect. A* **1983**, *39*, 158–166.

[14] S. Pohl, B. Krebs, E. Niecke, *Angew. Chem.* **1975**, *87*, 284–285; *Angew. Chem. Int. Ed. Engl.* **1975**, *14*, 261–262.

[15] M. J. Frisch, G. W. Trucks, H. B. Schlegel, P. M. W. Gill, B. G. Johnson, B. G. M. A. Robb, J. R.Cheeseman, T. A. Keith, G. A. Petersson, J. A. Montgomery, K. Raghavachari, M. A. Al-Laham, V. G. Zakrewski, J. V. Ortiz, J. B. Foresman, J. Cioslowski, B. B. Stefanov, A. Nanayakkara, M. Challacombe, C. Y. Peng, P. Y. Avala, W. Chen, M. W. Wong, J. L. Andres, E. S. Replogle, R. Gom-perts, R. L. Martin, D. J. Fox, J. S. Binkley, D. J. Defrees, J. Baker, J. P. Stewart, M. Head-Gordon, C. Gonzalez, J. A. Pople, Gaussian 94 (Revision A.1), Gaussian, Inc., Pittsburgh, PA, **1995**.

[16] Calculated at the CCSD(t)/6-31g*//MP2(fc)/6-31g* level with zero-point vibrational energy correction at the MP2(fc) level.

[17] R. F. W. Bader, *Atoms in Molecules: A Quantum Theory*, Oxford University Press, Oxford, **1990**.

[18] V.Romanenko, M. Sanchez, *Coord. Chem. Rev.* **1997**, *158*, 275–324.

[19] Representative structural data for **4**·TfO^- $[CF_3SO_3]^-$: P–N(Mes*) 153.5(5), P–N(H,Mes*) 162.7(5), P–N(heterocycle) 174.4(5), P–C 188.3(6) pm.

$(2,6\text{-}Mes_2H_3C_6)_2BiH$, a Stable, Molecular Hydride of a Main Group Element of the Sixth Period, and Its Conversion to the Dibismuthene $(2,6\text{-}Mes_2H_3C_6)BiBi(2,6\text{-}Mes_2C_6H_3)$**

Ned J. Hardman, Brendan Twamley, and Philip P. Power*

Element derivatives of hydrogen are an important and fundamental compound class.[1] This is especially true for main group element hydrides, which are widely used as reducing agents. However, many such hydrides are currently unknown as stable species. For example, there are no stable hydride derivatives of members of the sixth period of the p-block (e.g., Tl, Pb, or Bi[2]). It is doubtful that their lack of stability is due to inherent weakness in the element–hydrogen bonds since these are comparable in strength to element–carbon bonds[3] and alkyl and aryl derivatives of these elements are already well-known. It is more probable that coordinative unsaturation in the hydrides provides a relatively low-energy decomposition pathway unavailable in the alkyl or aryl derivatives. If this hypothesis is correct it should be possible to synthesize stable hydrides of these metals by using sterically encumbering groups to hinder decomposition. It is now shown that the use of the sterically encumbering properties of terphenyl substituents enables the first stable hydride of bismuth to be prepared and characterized.

Treatment of the very crowded diarylbismuth halide $(2,6\text{-}Mes_2H_3C_6)_2BiCl$ (**1**) with $LiAlH_4$ in Et_2O/PhMe solution affords the hydride derivative $(2,6\text{-}Mes_2H_3C_6)_2BiH$ (**2**) in about 30% yield. The corresponding reaction using $LiAlD_4$ gave the deuteride $(2,6\text{-}Mes_2H_3C_6)_2BiD$ (**3**). The compounds **1**–**3** were characterized by C,H elemental analysis, ^1H NMR, ^2H NMR (**3** only), ^{13}C NMR, and IR spectroscopy and by X-ray crystallography in the case of **1** and **2**.[4] The structure of **1** (Figure 1) provides evidence of high steric congestion at the bismuth center. Although the bismuth center remains pyramidally coordinated (sum of angles at Bi 309.26°), there are very large distortions in the geometry at the C(*ipso*) carbon atoms bound to bismuth. Thus, the Bi-C(*ipso*)-C(*ortho*) angles in the C(1) and C(25) terphenyl groups differ by 28.6 and 34.8°, respectively. In addition, the C(1) and C(25) aromatic ring planes deviate by 27 and 10° from the extended line of the Bi(1)–C(1) and Bi(1)–C(25) bonds. The Bi–C bond lengths of 2.337(7) and 2.418(8) Å are also quite long (cf. ca. 2.28, 2.328(13), and 2.357(14) Å in the crowded molecules $BiMes_3$[5], $Bi[CH(SiMe_3)_2]_3$[6] and $Bi[2,4,6\text{-}Ph_3C_6H_2]_3$[7]) and the C(1)-Bi-C(25) angle (123.9(3)°) is very wide in comparison to the usual angles seen in trivalent bismuth com-

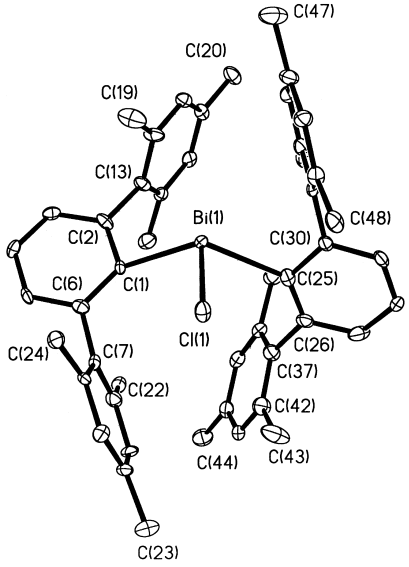


Figure 1. Structure of **1** (H atoms not shown). Selected bond lengths [Å] and angles [°]: Bi(1)-C(1) 2.337(7), Bi(1)-C(25) 2.418(8), Bi(1)-Cl(1) 2.483(3); C(1)-Bi(1)-C(25) 123.9(3), C(1)-Bi(1)-Cl(1) 98.43(19), C(25)-Bi(1)-Cl(1) 86.93(17).

[*] Prof. P. P. Power, N. J. Hardman, Dr. B. Twamley
Department of Chemistry
University of California
Davis, CA 95616 (USA)
Fax: (+1) 530-752-8995
E-mail: pppower@ucdavis.edu

[**] This work was supported by the National Science Foundation. The Bruker SMART 1000 difractometer was funded in part by NSF Instrumentation Grant CHE-9808259. Mes = 2,4,6-$Me_3C_6H_2$.

pounds.[5–7] The Bi–Cl distance (2.483(3) Å) is not greatly lengthened in comparison to that in $[2,4,6\text{-}(CF_3)_3H_2C_6]_2BiCl$ (2.463(3) Å).[8] Another interesting feature of the structure is the large difference of about 11.5° between the two C-Bi-Cl angles which is almost identical to that in $[2,4,6\text{-}(CF_3)_3H_2C_6]_2$-BiCl.[8]

Replacement of the chlorine atom by a hydrogen atom results in **2** whose structural parameters suggest that it is significantly less crowded than **1**. The molecule is characterized by the presence of a twofold rotational axis of symmetry through the bismuth atom which bisects the C-Bi-C angle (Figure 2). The C-Bi-C angle is 114.9(3)° which is 9° less than

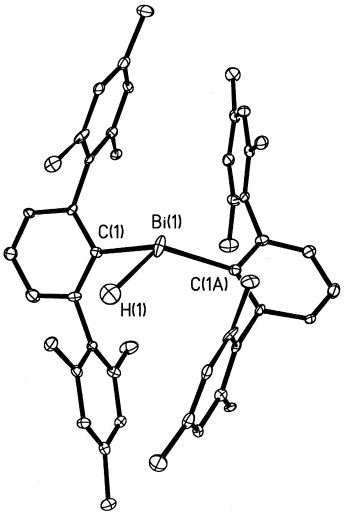
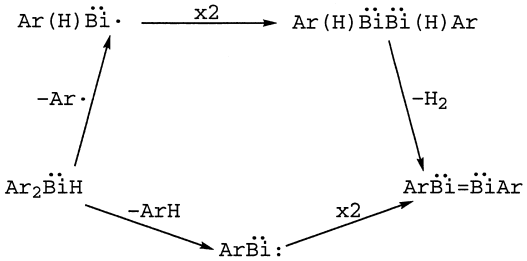


Figure 2. Structure of **2** (only H attached to Bi is shown). Selected bond lengths [Å] and angles [°]: Bi(1)-C(1) 2.314(7), Bi(1)-H(1) 1.94(2); C(1)-Bi-C(1A) 114.9(3).

the corresponding angle in **1**. In addition, the Bi–C bond (2.314(7) Å) is slightly shorter than those in **1**. Moreover, the difference between the Bi-C(*ipso*)-C(*ortho*) angles is just 6.5° and the deviation of the Bi–C(*ipso*) vector from the plane of the C(*ipso*) ring is 12.4°. Peaks which correspond to the disordered hydrogen atom could be located at two disordered positions with respect to the axis 1.94 Å distant from bismuth. Although this distance is comparable to the 1.865 Å calculated for BiH_3[9], the difference in the scattering power of bismuth and hydrogen is such that the reliability of such assignments is limited.[10]

The presence of a Bi–H moiety in **2** is proven by a strong IR absorption band at 1759 cm^{-1} which is in remarkably good agreement with the theoretically predicted value (1760 cm^{-1}) for BiH_3.[11] In contrast, the IR spectrum of **3** displayed no absorbance at this frequency. Instead, a strong peak was observed at 1260 cm^{-1} which is close to the value predicted (1248 cm^{-1}) on the basis of the difference in reduced mass between **2** (Bi–H) and **3** (Bi–D). Unfortunately, ^1H or ^2H NMR spectra of **2** or **3** did not display signals that could be assigned to the hydrogen or deuterium attached to bismuth. Possibly, the large quadrupole moment of the ^{209}Bi nucleus (100%, $I = 9/2$, quadrupole moment -0.4×10^{-28} m^{-2}) and the low local symmetry at the bismuth center broaden these peaks to such an extent that they are not observable under these conditions.

Heating of **2** or **3** led to an interesting elimination reaction. In contrast to the precursor **1**, which melts without noticeable decomposition at 203–204 °C, **2** and **3** undergo a rapid color change at 135–136 °C for **1**, and at 138–139° for **2**. In both cases a purple solid is produced which has identical spectroscopic properties to those previously described for the dibismuthene $(2,6\text{-}Mes_2C_6H_3)BiBi(2,6\text{-}Mes_2C_6H_3)$. X-ray data also afforded cell constants and a structure that were essentially the same as those previously observed.[12] The yield of the dibismuthene in this reaction is quite high (80%) so that this elimination reaction represents an alternative synthetic route to dibismuthenes.[12, 13] At least two plausible mechanisms for the decomposition of **2** and **3** to the dibismuthene product may be envisaged as shown in Scheme 1. One (top pathway) involves initial cleavage of



Scheme 1. Two possible mechanisms for the transformation of Ar_2BiH to ArBi=BiAr ($Ar = 2,6\text{-}Mes_2C_6H_3$).

the bismuth–aryl bond, followed by dimerization of the bismuth fragments to form a dibismuthane, which then eliminates hydrogen to form the dibismuthene. The second (bottom pathway) involves the concerted elimination of the arene followed by rapid dimerization of the bismuthenes to give the product. However the obervation of a deuterated arene coproduct upon heating a solution of **2** or **3**, combined with the lack of visually observable H_2 evolution, favors the pathway involving the initial elimination of ArH (ArD).

Experimental Section

All work was carried out under anaerobic and anhydrous conditions.

1: A solution of $Li(2,6\text{-}Mes_2C_6H_3)$ (1.35 g, 4.21 mmol)[14] in toluene (20 mL) was added dropwise to a suspension of $BiCl_3$ (0.66 g, 2.1 mmol) in toluene (10 mL) at about 0 °C. The mixture was warmed to room temperature and stirred overnight. The mixture was filtered through celite and the solvent was removed under reduced pressure. The residue was extracted with hexane (80 mL) and the pale yellow solution was warmed to dissolve the precipitates. Cooling to room temperature over a period of 2 h afforded X-ray diffraction quality, pale yellow crystals of **1**. Yield 0.69 g, 36%. M.p. 203–204 °C (decomp); IR: $\tilde{\nu} = 288$ cm^{-1} (Bi–Cl); ^1H NMR (300 MHz, $CDCl_3$): $\delta = 1.74$ (s, 12H; *o*-CH_3), 1.82 (s, 12H; *o*-CH_3), 2.33 (s, 12H; *p*-CH_3), 6.82 (s, 8H; *m*-Mes), 7.17 (d, $^3J_{H,H} = 7.8$ Hz, 4H; *m*-C_6H_3), 7.33 (t, $^3J_{H,H} = 6.9$ Hz, 2H; *p*-C_6H_3); ^{13}C {^1H} NMR (75 MHz, C_6D_6): $\delta = 21.47$ (*p*-CH_3), 22.48 (*o*-CH_3), 22.50 (*o*-CH_3), 128.6 (*m*-Mes), 129.1 (*p*-C_6H_3), 134.0 (*m*-C_6H_3), 136.5 (*o*-C_6H_3), 137.0 (*o*-Mes), 137.4 (*o*-Mes), 140.2 (*i*-Mes), 149.6 (*p*-Mes), 201.5 (*i*-C_6H_3); satisfactory C,H analysis.

2: A solution of $LiAlH_4$ (1.5 g, 39.5 mmol) in Et_2O (30 mL) was added to a rapidly stirred solution of **1** (3.41 g, 3.75 mmol) in toluene (40 mL) with cooling to about 0 °C. The solution immediately became black on addition of $LiAlH_4$. Stirring was continued overnight at room temperature, where-

 © WILEY-VCH Verlag GmbH, D-69451 Weinheim, 2000 1433-7851/00/3915-2772 $ 17.50+.50/0 *Angew. Chem. Int. Ed.* **2000**, *39*, No. 15

upon the solvent was removed under reduced pressure. The residue was extracted with C_6H_6 (50 mL), and the resultant red supernatant liquid was decanted. The red solution was concentrated to about 5 mL at which point a colorless solid precipitated. Hexane (50 mL) was added and the solution was heated to dissolve the majority of the precipitates. The solution was then decanted (60 °C) and allowed to cool slowly to room temperature affording X-ray diffraction quality, colorless crystals of **2**. Yield 0.96 g, 29.3 %. M.p.: on heating the crystals became red at 130 °C and purple at 139 °C (decomp); IR: $\tilde{\nu} = 1759$ cm^{-1} (s, Bi–H); ^{1}H NMR (400 MHz, C_6D_6): $\delta = 1.85$ (s, 12H; *o*-CH_3), 1.88 (s, 12H; *o*-CH_3), 2.24 (s, 12H; *p*-CH_3), 6.81, 6.82 (8H; *m*-Mes), 6.84 (d, $^3J_{H,H} = 7.2$ Hz, 4H; *m*-C_6H_3), 7.01 (t, $^3J_{H,H} = 7.6$ Hz, 2H; *p*-C_6H_3); ^{13}C {^{1}H} NMR (100 MHz, C_6H_6): $\delta = 21.29$ (*p*-CH_3), 21.87 (*o*-CH_3), 126.396 (*m*-C_6H_3), 128.306 (*p*-C_6H_3), 129.09 (*m*-Mes), 135.79 (*o*-Mes), 136.62 (*o*-C_6H_3), 144.3 (*i*-Mes), 150.9 (*p*-Mes), 153.2 (*i*-C_6H_3); satisfactory C,H analysis.

3: $LiAlD_4$ (0.25 g, 5.95 mmol) was added by using a solids addition tube to a solution of **1** (5.27 g, 5.8 mmol) in toluene (40 mL) at about −78 °C. The solution was allowed to warm slowly to room temperature overnight and stirring was continued for 30 h by which time the supernatant liquid had become red. This solution was filtered and the supernatant liquid was pumped to dryness. The resulting solid was extracted with hexane/toluene (3/1) (3 × 80 mL). Colorless, X-ray diffraction quality, crystals of **3** were obtained from these solutions upon cooling to −20 °C. Yield 0.52 g, 10 %. M.p.: on heating the crystals became red at 132 °C and purple at 139 °C;. IR: $\tilde{\nu} = 1260$ cm^{-1} (s, Bi–D); ^{1}H NMR (400 MHz, C_6D_6): $\delta = 1.85$ (s, 12H; *o*-CH_3), 1.88 (s, 12H; *o*-CH_3), 2.24 (s, 12H; *p*-CH_3), 6.81, 6.82 (8H; *m*-Mes), 6.84 (d, $^3J_{H,H} = 7.2$ Hz, 4H; *m*-C_6H_3), 7.01 (t, $^3J_{H,H} = 7.6$ Hz, 2H, *p*-C_6H_3); ^{13}C {^{1}H} NMR (100 MHz, C_6D_6): $\delta = 21.29$ (*p*-CH_3), 21.87 (*o*-CH_3), 126.396 (*m*-C_6H_3), 128.306 (*p*-C_6H_3), 129.09 (*m*-Mes), 135.79 (*o*-Mes), 136.62 (*o*-C_6H_3), 144.3 (*i*-Mes), 150.9 (*p*-Mes), 153.2 (*i*-C_6H_3); satisfactory C,H analysis.

Received: March 13, 2000 [Z14843]

[1] N. N. Greenwood, A. Earnshaw, *Chemistry of the Elements*, 2nd ed., Butterworth-Heinemann, Oxford, **1987**, Chapter 3.

[2] For example bismuthane, BiH_3, is unstable at temperatures above −60 °C and its chemistry has not been developed: S. M. Godfrey, C. A. McAuliffe, A. G. Mackie, R. G. Pritchard, *Chemistry of Arsenic, Antimony and Bismuth* (Ed.: N. C. Norman), Blackie-Chapman Hall, London, **1998**, Chapter 3.

[3] J. Huheey, E. A. Keiter, R. L. Keiter, *Inorganic Chemistry Principles of Structure and Reactivity*, 4th ed., Harper Collins, New York, **1993**, Appendix E; W. E. Dasent *Inorganic Energetics*, 2nd ed., Cambridge University Press, Cambridge, **1982**; J. F. Liebman, J. A. M. Simoes, S. W. Slayden; "Thermochemistry of organo-arsenic, antimony and bismuth compounds": *The Chemistry of organic arsenic, antimony and bismuth compounds* (Ed.: S. Patai), Wiley, Chichester, **1994**, Chapter 4, pp. 153–168.

[4] Crystal data for **1** and **2** at 90 K with $Mo_{K\alpha}$ radiation ($\lambda = 0.71073$ Å): **1**, $a = 12.3231(8)$, $b = 20.3292(14)$, $c = 16.137(11)$ Å, $\beta = 102.977(2)°$, $Z = 4$, space group $P2_1/n$, $R1 = 0.0596$ for 3994 data with $I > 2(\sigma)I$; **2**, $a = 21.0073(12)$, $b = 44.156(3)$, $c = 8.1877(5)$ Å, $Z = 8$, space group *Fdd*2, $R1 = 0.046$ for 2402 data with $I > 2\sigma(I)$. Crystallographic data (excluding structure factors) for the structures reported in this paper have been deposited with the Cambridge Crystallographic Data Centre as supplementary publication no. CCDC-143879 and CCDC-143880. Copies of the data can be obtained free of charge on application to CCDC, 12 Union Road, Cambridge CB2 1EZ, UK (fax: (+44) 1223-336-033; e-mail: deposit@ccdc.cam.ac.uk).

[5] D. M. Hawley, G. Ferguson, *J. Chem. Soc. A* **1968**, 2059.

[6] B. Murray, J. Hvoslef, H. Hope, P. P. Power, *Inorg. Chem.* **1983**, *22*, 3421.

[7] X.-W. Li, G. Lorberth, W. Massa, S. Wocadlo, *J. Organomet. Chem.* **1995**, *485*, 141.

[8] K. H. Whitmire, D. Labahn, H. W. Roesky, M. Noltemeyer, G. M. Sheldrick, *J. Organomet. Chem.* **1991**, *402*, 55.

[9] K. Balasubramanian, D. Dai, *J. Chem. Phys.* **1990**, *93*, 1837.

[10] Attempts to grow crystals suitable for neutron diffraction studies are in progress.

[11] P. Schwerdtfeger, L. J. Laakkonen, P. Pyykkö, *J. Chem. Phys.* **1992**, *96*, 6807.

[12] B. Twamley, C. D. Sofield, M. M. Olmstead, P. P. Power, *J. Am. Chem. Soc.* **1999**, *121*, 3357.

[13] N. Tokitoh, Y. Arai, R. Okazaki, S. Nagase, *Science* **1997**, *277*, 78.

[14] K. Ruhlandt-Senge, J. J. Ellison, R. J. Wehmschulte, F. Pauer, P. P. Power, *J. Am. Chem. Soc.* **1993**, *115*, 11353.

Synthesis of (*E*)-α,β-Unsaturated Esters and Amides with Total Selectivity Using Samarium Diiodide**

José M. Concellón,* Juan A. Pérez-Andrés, and Humberto Rodríguez-Solla

The development of methods for the stereoselective formation of carbon–carbon double bonds could be considered one of the most important challenges in organic synthesis.[1] The synthesis of α,β-unsaturated esters[2] is generally achieved by C=C bond formation with Wittig,[3] Horner–Emmons,[4] Heck,[5] or Peterson[6] reactions, or with the Cope rearrangement,[7] from acetylenic compounds[8] or α-sulfanyl-ester derivatives.[9] However, in most of these papers, total control of the stereoselectivity of the carbon–carbon double bond formation remained unresolved.[3a, b, d, 4–6c, 8a, 9b,c, 10] Some methodologies are limited by their poor generality,[7, 8b, 9a, 11] and other papers describe the preparation of α,β-unsaturated esters in which the substitution pattern of the olefin is quite simple (monosubstituted or 1,2-disubstituted).[3c, 6d] Only a few examples of the synthesis of α-substituted α,β-unsaturated esters in which the C=C bond is trisubstituted have been reported.[12]

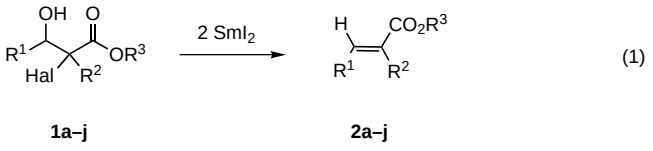
Recently, we described a stereoselective synthesis of (*Z*)-vinyl halides by treatment of O-acetylated 1,1-dihaloalkan-2-ols with samarium diiodide; this was the first general stereoselective β-elimination reaction promoted by SmI_2.[13, 14] Here we report a new methodology to obtain α,β-unsaturated esters **2** with total stereoselectivity, by treatment of the easily available 2-halo-3-hydroxyesters **1** with samarium diiodide [Eq. (1)]. We also describe preliminary results of the synthesis of related α,β-unsaturated amides.

When a solution of SmI_2 in THF was added dropwise to several 2-halo-3-hydroxyesters **1** (prepared by reaction between the corresponding lithium enolates of α-haloesters and

[*] Dr. J. M. Concellón, Dr. J. A. Pérez-Andrés, H. Rodríguez-Solla
Departamento de Química Orgánica e Inorgánica
Facultad de Química, Universidad de Oviedo
33071 Oviedo (Spain)
Fax: (+349) 8-510-34-46
E-mail: jmcg@sauron.quimica.uniovi.es

[**] We thank the II Plan Regional de Investigación del Principado de Asturias (PB-PGI99-01) and the Ministerio de Educación y Cultura (PB97-1278) for financial support. J.M.C. thanks Carmen Fernández for her help. H.R.S. thanks the Universidad de Oviedo for a predoctoral fellowship.

Supporting information for this article is available on the WWW under http://www.wiley-vch.de/home/angewandte/ or from the author.



(1)

1a–j **2a–j**

Table 1. Synthesis of α,β-unsaturated esters with SmI_2 [Eq. (1)].

entry	**1**	R^1	R^2	R^3	Hal	*de* [%][a]	yield [%][b]
1	**1a**	C_7H_{15}[c]	H	Me	Cl	63	20
2	**1a**	C_7H_{15}[d]	H	Me	Cl	88	30
3	**1a**	C_7H_{15}	H	Me	Cl	>98	70
4	**1b**	C_7H_{15}	Me	Et	Cl	>98	75
5	**1c**	cyclohexyl	Me	Et	Cl	>98	90
6	**1d**	*p*-ClC_6H_4	H	*t*Bu	Cl	>98	72
7	**1e**	Ph	Bu	Et	Br	>98	86
8	**1f**	*p*-CNC_6H_4	Me	Et	Cl	>98	84
9	**1g**	*p*-$MeOC_6H_4$	Me	Et	Cl	>98	91
10	**1h**	$Me_2C{=}CH(CH_2)_2CH(Me)CH_2$	Ph	*i*Pr	Cl	>98	84
11	**1i**	MeCH(Ph)	C_6H_{13}	Et	Br	>98	87
12	**1j**	(*E*)-MeCH=CH	C_6H_{13}	Et	Br	>98	90

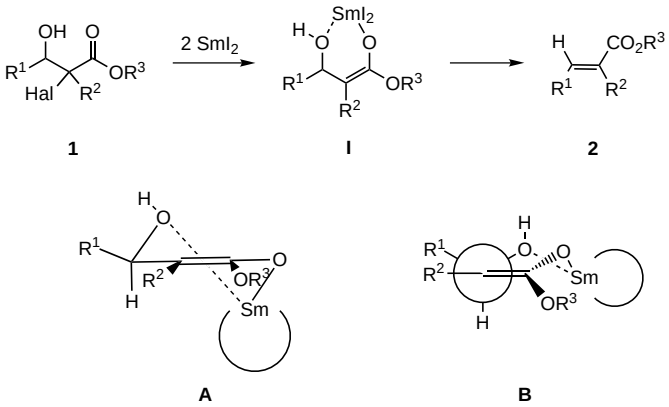
[a] Determined from crude reaction products with GC-MS. [b] Yield of isolated products. [c] Performed with Zn rather than SmI_2. [d] Performed with O-acetylated compound **1** rather than the unprotected alcohol.

aldehydes at $-78\,^{\circ}C$), the corresponding α,β-unsaturated esters **2** were isolated, after hydrolysis, with total stereoselectivity and in high yield (Table 1). The transformation was completed in a few minutes at room temperature, and addition of the SmI_2 was carried out dropwise until the blue-green color was persistent (approximately 2.1 equivalents).

The diastereoisomeric excess (*de*) was determined on the crude reaction products by ^1H NMR spectroscopy (300 MHz) and GC–MS,[15] and only a single stereoisomer was shown. When the same β-elimination reaction was carried out using Zn, a lower steroisomer ratio was obtained (entry 1). The *E* stereochemistry in the double bond C=C of α,β-unsaturated esters **2** was assigned on the basis of the value of the ^1H NMR coupling constant between the olefinic protons of compounds **2a** and **2d**[16] or by NOE experiments. In the case of compounds **2a**,[9a] **2b**,[17] **2c**,[18] **2e**,[12] and **2g**[12] comparison with the ^1H and ^{13}C NMR values described in the literature has also been carried out. It is noteworthy that although the 2-halo-3-hydroxyesters **1** were prepared and used as mixtures of diastereoisomers (roughly 1:1), the corresponding α,β-unsaturated esters **2** were obtained with total stereoselectivity.

This proposed methodology to obtain α,β-unsaturated esters is general, and R^1, R^2, and R^3 can be varied widely. Aliphatic (linear, branched, or cyclic), unsaturated, or aromatic (electron rich or deficient) aldehydes could be used to introduce different R^1 groups. Substitution at the C2 position could also be changed using different α-haloesters (again, aliphatic and aromatic groups are allowed). The stereoselectivity and yield were also unaffected by the presence of bulky groups R^3 on the carboxyl ester (entries 6 and 10), in contrast to the Wittig olefination reaction.[10] Although not only chloro- but also bromohydroxyesters can be used as the starting material (entries 7, 11, and 12), the elimination reaction has mainly been carried out using α-chloro-β-hydroxyesters, which are more accessible than the equivalent bromo derivatives.[19]

The observed stereochemistry of products **2** may be explained by assuming a chelation-control model (Scheme 1). Thus, metalation and removal of the halogen generates the enolate intermediate **I**. Chelation of the oxophilic Sm^{III} center with the oxygen atom of the alcohol group produces a six-membered ring and increases the ability of the hydroxyl group



Scheme 1. Mechanistic proposal for the synthesis of (*E*)-α,β-unsaturated esters **2** through intermediate **I**. **A** is the proposed transition state model, **B** is a Newman projection of **A** through atoms C2 and C3. Hal = Cl, Br.

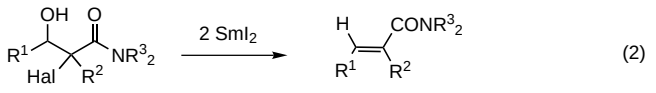
as a leaving group.[20] Indirect support for this is provided by the lower stereoselectivity obtained with an O-acetylated starting compound (entry 2). Tentatively, we propose a transition state model **A** with an equatorial R^1 group (to avoid interactions with the samarium coordination sphere). As depicted in **B**, R^1 and R^2 show a *cis* relationship. Consequently, elimination from **A** affords (*E*)-α,β-unsaturated esters. Synthesis of **2** with total stereoselectivity from a mixture of diastereoisomers of **1** could be explained by an epimerization of the $C(R^2)$ carbon center after the reaction of **1** with SmI_2, affording the diastereoisomer with the appropriate conformation for coordination of the samarium center with the alcohol oxygen.

Different behavior was observed when esters **1** derived from ketones instead of aldehydes and α-chloroesters were used. In addition to the α,β-unsaturated ester analogue of **2** the corresponding β-hydroxyester was obtained. In this case, coordination of samarium(III) with the hydroxyl oxygen could be disfavored by the higher substitution of the β-carbon, with hydrolysis of the samarium enolate by the hydroxyl group preferred to the elimination.[21]

Attempts have been made towards extending this methodology to the synthesis of α,β-unsaturated amides. Treatment of 2-chloro-3-hydroxyamides **3** (obtained from the lithium enolate of α-chloroamides with different aldehydes) with a solution of SmI_2 in THF at room temperature [Eq. (2)] afforded, in a few minutes, the corresponding α,β-unsaturated amides **4** with total *E* stereoselectivity[22] in high yield (Table 2). Generalization of this synthesis of (aliphatic and aromatic) α,β-unsaturated amides is currently under examination.

In conclusion, an easy, simple, and general methodology, promoted by samarium diiodide, has been developed to

 © WILEY-VCH Verlag GmbH, D-69451 Weinheim, 2000 1433-7851/00/3915-2774 $ 17.50+.50/0 *Angew. Chem. Int. Ed.* **2000**, *39*, No. 15



(2)

3a–c **4a–c**

Table 2. Synthesis of α,β-unsaturated amides with SmI_2 [Eq. (2)].

entry	**4**	R^1	R^2	R^3	Hal	*de* [%][a]	yield [%][b]
1	**4a**	C_7H_{15}	H	Et	Cl	> 98	89
2	**4b**	Ph	H	Et	Cl	> 98	90
3	**4c**	MeCH(Ph)	H	Et	Cl	> 98	82

[a] Determined from crude reaction products with GC-MS. [b] Yield of isolated products.

synthesize α,β-unsaturated esters and amides with total *E* stereoselectivity from the easily available 2-halo-3-hydroxy-esters or amides.

Experimental Section

A solution of SmI_2 (1 mmol) in THF (12 mL) was very slowly added dropwise, under a nitrogen atmosphere, to a stirred solution of halohydroxyester **1** (0.4 mmol) in THF (2 mL) at room temperature, until the reaction mixture turned permanently blue. The reaction mixture was quenched with aqueous HCl (1M, 5 mL). Standard work-up and filtration through a pad of Celite provided pure α,β-unsaturated esters **2** (> 98 %).

Received: January 24, 2000 [Z14593]

[1] *The Chemistry of Alkenes*, *Vol. 2* (Ed.: S. Patai), Interscience, New York, **1968**.

[2] For recent reviews on the synthesis of α,β-unsaturated esters, see: a) A. S. Franklin, *J. Chem. Soc. Perkin Trans. 1* **1998**, 2451 – 2465; b) Y. Shen, *Acc. Chem. Res.* **1998**, *31*, 584 – 592.

[3] a) V. J. Patil, U. Mävers, *Tetrahedron Lett.* **1996**, *37*, 1281 – 1284; b) A. Spinella, T. Fortunati, A. Soriente, *Synlett* **1997**, 93 – 94, and references therein; c) Y. Shen, Y. Xin, J. Zhao, *Tetrahedron Lett.* **1988**, *29*, 6119 – 6120; d) Y. Shen, Y. Zhou, *Tetrahedron Lett.* **1991**, *32*, 513 – 514.

[4] a) K. Ando, *J. Org. Chem.* **1999**, *64*, 6815 – 6821; b) K. Ando, *J. Org. Chem.* **1997**, *62*, 1934 – 1939; c) K. Ando, *Tetrahedron Lett.* **1995**, *36*, 4105 – 4108; d) W. C. Still, C. Gennari, *Tetrahedron Lett.* **1983**, *24*, 4405 – 4408.

[5] a) M. Moreno-Mañas, M. Pérez, R. Pleixants, *Tetrahedron Lett.* **1996**, *37*, 7449 – 7452; b) M. Beller, T. H. Riermeier, *Tetrahedron Lett.* **1996**, *37*, 635 – 638.

[6] a) A. C. Guevel, D. J. Hart, *J. Org. Chem.* **1996**, *61*, 465 – 472; b) J. T. Welch, R. W. Herbert, *J. Org. Chem.* **1990**, *55*, 4782 – 4784; c) B. Chenera, C. Chuang, D. J. Hart, C. Lai, *J. Org. Chem.* **1992**, *57*, 2018 – 2029; d) C. Palomo, J. M. Aizpurua, J. M. García, I. Ganboa, F. P. Cossio, B. Lecea, C. López, *J. Org. Chem.* **1990**, *55*, 2498 – 2503.

[7] a) K. Tamooka, A. Nagasawa, S. Wei, T. Nakai, *Tetrahedron Lett.* **1996**, *37*, 8895 – 8898; b) K. Tamooka, A. Nagasawa, S. Wei, T. Nakai, *Tetrahedron Lett.* **1996**, *37*, 8899 – 8900.

[8] a) A. R. Katrizky, D. Feng, H. Lang, *J. Org. Chem.* **1997**, *62*, 715 – 720; b) M. Perisamy, U. Radhakrishnan, C. Rameshkumar, J. Brunet, *Tetrahedron Lett.* **1997**, *38*, 1623 – 1626.

[9] a) B. M. Trost, J. R. Parquette, *J. Org. Chem.* **1993**, *58*, 1579 – 1681; b) R. Tanikaga, K. Miyashita, N. Ono, A. Kaji, *Synthesis* **1982**, 131 – 132; c) K. Tanaka, H. Uneme, N. Ono, A. Kaji, *Chem. Lett.* **1979**, 1039 – 1040.

[10] One of the great challenges associated with the Wittig reaction in the preparation of α,β-unsaturated esters relates to stereocontrol: B. E. Maryanoff, A. B. Reitz, *Chem. Rev.* **1989**, *89*, 863 – 927.

[11] Synthesis of α,β-unsaturated esters by the Peterson reaction is limited by the use of non-enolizable carbonyl compounds and *tert*-butyl bis(trimethylsilyl)acetate; see ref. [6d].

[12] J. Castells, F. López-Calahorra, Z. Yu, *Tetrahedron* **1994**, *50*, 13765 – 13774.

[13] J. M. Concellón, P. L. Bernad, J. A. Perez-Andrés, *Angew. Chem.* **1999**, *111*, 2528 – 2530; *Angew. Chem. Int. Ed.* **1999**, *38*, 2384 – 2386.

[14] For recent reviews on the application of SmI_2 in organic synthesis, see: a) A. Krief, A. M. Laval, *Chem. Rev.* **1999**, *99*, 745 – 777; b) G. A. Molander, C. R. Harris, *Tetrahedron* **1998**, *54*, 3321 – 3354.

[15] GC-MS was carried out with HP-5MS (60 m) and/or DB-5MS capillary columns (30 m).

[16] The coupling constants between the olefinic protons of compounds **2a** and **2d** were 15.7 and 16.3 Hz, respectively, in accordance with the average literature values for J_{trans}.

[17] N. Asao, T. Uyehara, Y. Yamamoto, *Tetrahedron* **1988**, *44*, 4173 – 4180.

[18] O. Piva, *Tetrahedron* **1994**, *50*, 13687 – 13696.

[19] Condensation of the ester bromoenolate with aldehydes affords a mixture of compounds **1** and the corresponding α,β-epoxy ester (Darzens' reaction), even at low temperatures.

[20] Similar six-membered ring transition state models have been proposed to explain the selectivity in other reactions of SmI_2: a) G. A. Molander, J. B. Etter, P. W. Zinke, *J. Am. Chem. Soc.* **1987**, *109*, 453 – 463; b) D. Urban, T. Skrydstrup, J. M. Beau, *J. Org. Chem.* **1998**, *63*, 2507 – 2516.

[21] When these reaction mixtures were hydrolyzed with D_2O, no deuterium was incorporated into the isolated α-hydroxyesters.

[22] The coupling constants between the olefinic protons of compounds **4a**, **4b**, and **4c** were 14.9, 15.3, and 15.2 Hz, respectively, in accordance with the average literature values for J_{trans}.

Investigations of Lipid – Protein Interactions on Monolayers of Chain-Substituted Phosphatidylcholines**

Ursula Dahmen-Levison,* Gerald Brezesinski, Helmuth Möhwald, Jens Jakob, and Peter Nuhn

Polarization-modulated infrared reflection absorption spectroscopy (PM-IRRAS, Figure 1) is a versatile method for studying the hydrolysis of long-chain lipids at the air/water interface and the influence of phase separations on the activity of proteins.[1, 2] Our investigations using this method were performed on phospholipase A_2 (PLA_2). PLA_2 cleaves selectively the *sn*-2 ester linkage of phospholipids, leading to a fatty acid and a lysophospholipid. PLA_2 plays an important role in the arachidonyl cascade, since arachidonyl is the main group found in the 2-position at the glycerol of the phospholipids in mammal cells. PLA_2 is an interfacially active enzyme, whose activity is strongly dependent on the physical-chemical structure of the substrate, which makes it very difficult to develop inhibitors. The investigations at the air/water inter-

[*] Dr. U. Dahmen-Levison, Dr. habil. G. Brezesinski, Prof. Dr. H. Möhwald
Max-Planck-Institut für Kolloid- und Grenzflächenforschung
Am Mühlenberg 1, 14476 Golm/Potsdam (Germany)
Fax: (+49) 331 567-9202
E-mail: dahmen@mpikg-golm.mpg.de
brezesinski@mpikg-golm.mpg.de
Dr. J. Jakob, Prof. Dr. P. Nuhn
Institut für Pharmazeutische Chemie
Martin-Luther-Universität Halle-Wittenberg
Wolfgang-Langenbeck-Strasse 4, 06099 Halle (Saale) (Germany)

[**] This work was supported by the Deutsche Forschungsgemeinschaft.

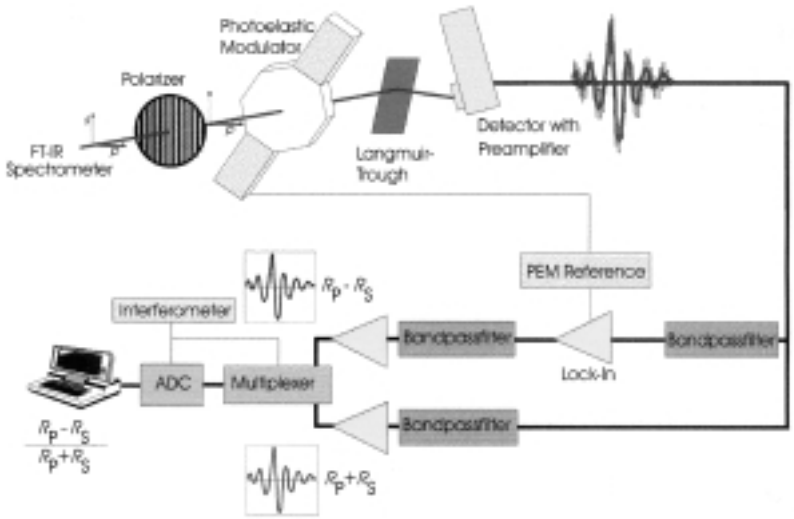


Figure 1. Schematic setup of the PM-IRRA spectrometer.

face have some clear advantages over common techniques. Only very small amounts of phospholipids and enzymes are needed and the physical conditions of the reaction can be varied easily. In many cases phospholipid monolayers with similar thermodynamic and structural parameters can be considered as a single leaflet of a biological bilayer membrane. Especially for interfacial reactions the monolayer offers a reductionistic model.

In an earlier PM-IRRAS study[3] we showed that the enzyme exerts maximal activity in the coexistence region between condensed and liquid-expanded phases. Fluorescence microscopy demonstrated that the enzyme is enriched at the phase boundaries[4] and that this is also the location where the reaction is first detectable.[5] These findings indicate two important features for the PLA_2 activity. First the preorientation of the substrate in the gel phase facilitates the enzyme reaction (Figure 2), and second the reaction can



Figure 2. Model of the preorientation of the substrate induced by enzyme adsorption and of the preferred reaction at defects.

only take place at defects within the membrane. In biological membranes (multicomponent systems) such defects can be created by lipids which are in a condensed state in the vicinity of membrane proteins[6] and by local differences in lipid composition. The turnover rate at high lateral pressures is close to zero.

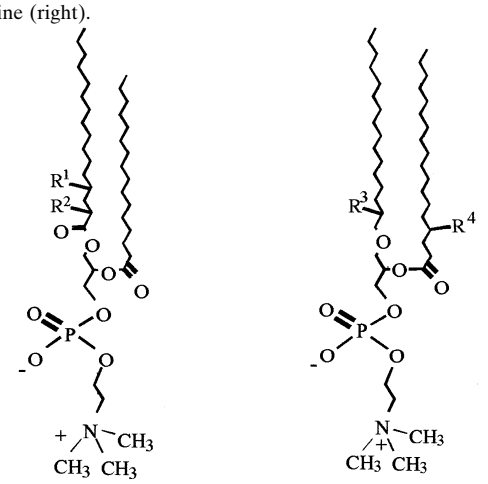
The present investigations were performed with diester and 1-ether-2-ester-glycerophosphocholines (Table 1). The latter were included since they are precursors for plasmalogen and the platelet-activating factor (PAF). Since chain-substituted glycerophosphocholines (PC) have been reported to inhibit the PLA_2 reaction,[7] we introduced lateral branches of various length at different positions into the lipophilic chains.

Monolayers of ether–ester–PC are in general in a more condensed state than those of diester–PC.[8] From the pressure/area diagrams of the chain-substituted PCs the following tendencies were determined:

1) Short-chain branching leads to an increased fluidity in the monolayer. The short chain disturbs the lateral packing of the molecules.[9]
2) A tetradecyl side chain leads to a triple-chain PC. In the compressed state the area per molecule is about 0.62 nm^2. The phase transition pressure (π_c) is shifted to larger values compared to the double-chain analogue.[10]

Figure 3 shows the PM-IRRAS spectrum of a L-DPPC (**1**) monolayer; several characteristic bands can be assigned. The band at 1734 cm^{-1} represents the carbonyl stretching vibration and that at 1469 cm^{-1} the methylene scissoring vibration. Bands at 1230 cm^{-1} and at 1088 cm^{-1} are attributed to antisymmetric and symmetric phosphate stretching vibrations.[11] The phosphate stretching vibrations comprise at least two frequencies. The occurrence of multiple bands indicate the appearance of a heterogenous population of protonated and nonprotonated groups. The broad band at 1159/1170 cm^{-1} and at 1059 cm^{-1} can be assigned to the antisymmetric and symmetric ester stretching vibrations, respectively. Furthermore the band at 971 cm^{-1} is attributed to a vibration of the $C–N^+–C$ group. Carboxylate bands at 1540 and 1581 cm^{-1} with a slight shoulder at 1562 cm^{-1} appear during hydrolysis (Figure 4). They are due to the product (fatty acid) which accumulates in the monolayer during the reaction. In the spectrum of the

Table 1. Diester-glycerophosphocholine (left) ether-ester-glycerophosphocholine (right).



Compd	R^1	R^2	Compd	R^3	R^4
1	H	H	**6**	H	H
2	H	$CH_3(CH_2)_{13}$	**7**	$CH_3(CH_2)_{13}$	H
3	H	CH_3	**8**	CH_3	H
4	CH_3	H	**9**	H	CH_3
5	$CH_3(CH_2)_{13}$	H	**10**	H	$CH_3(CH_2)_{13}$

 © WILEY-VCH Verlag GmbH, D-69451 Weinheim, 2000 1433-7851/00/3915-2776 $ 17.50+.50/0 *Angew. Chem. Int. Ed.* **2000**, *39*, No. 15

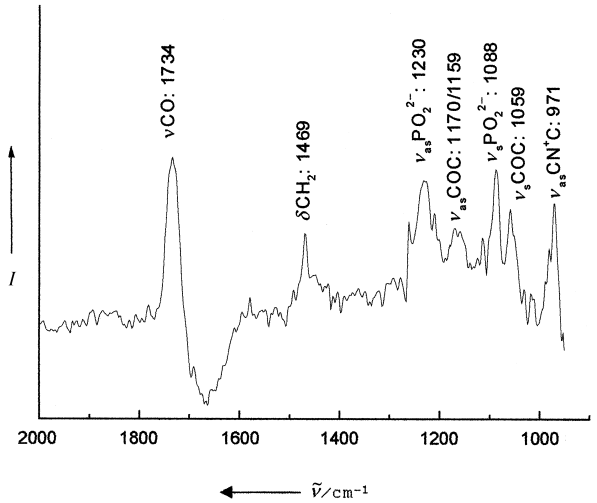


Figure 3. PM-IRRA spectrum of a pure DPPC (**1**) monolayer at a lateral pressure of 40 mN m^{-1}; $T = 20\,^{\circ}$C.

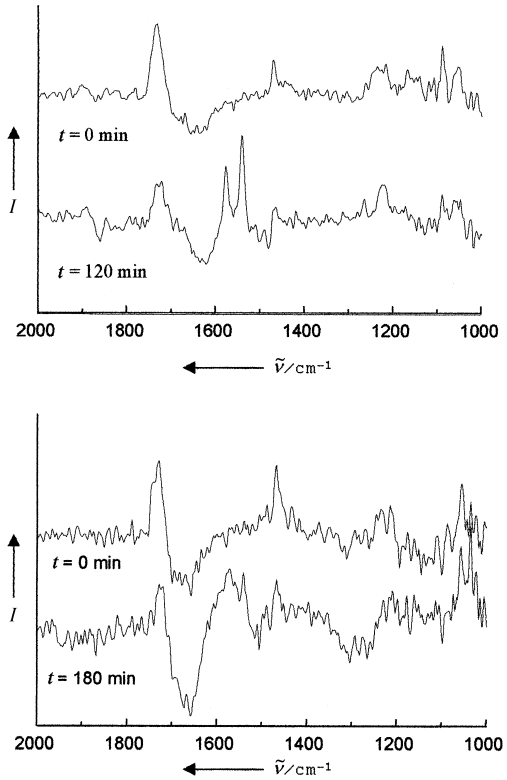


Figure 4. PM-IRRA spectra before ($t = 0$ min) and after a certain reaction time t. Top: **3**, bottom: **5**. $T = 20\,^{\circ}$C, reaction pressure = 8 mN m^{-1}, spectra recorded at 40 mN m^{-1}.

pure fatty acid monolayer one band is observed at 1563 cm^{-1}, which is assigned to the Ca^{2+}-associated carboxy group, and additionally a weak band is observed at 1540 cm^{-1}, which is attributed to a small amount of free carboxylate. The appearance of a band at 1581 cm^{-1} must be caused by an interaction between the protein and fatty acid. The high wavenumber of the band can be explained by a very strong association of the protein with the fatty acid (e.g. partial product inhibition) or by a protein-induced highly condensed state of the calcium carboxylate. In both cases enzyme domains, which build up underneath fatty acid enriched areas, should be responsible for the position of the band. The high intensity of the band at 1540 cm^{-1} can also be explained by a Ca^{2+}-shielding effect of these enzyme domains.

The decrease in intensity of the carbonyl band was used for the quantitative investigation of the hydrolysis reaction. Contrary to the results from Menger et al.,[7] all investigated chain-substituted lipids were catalytically cleaved. The hypotheses that alcylations in the chain region of phospholipids should lead to an inhibitory effect are not supported. From the determined relative hydrolysis rates (see Table 2) the following tendencies are apparent:

1) Phospholipids with unbranched alkyl chains are better hydrolyzed than branched ones.
2) Diester-glycerophosphocholines are cleaved easier than ether-ester-glycerophosphocholines.
3) Methyl-branched phospholipids are hydrolyzed faster than tetradecyl-branched ones.
4) Phospholipids branched at the *sn*-2 chain are cleaved more slowly than those branched at the *sn*-1 chain.

Table 2. Monolayer phase state at 20 °C and 8 mN m^{-1} and yields [%] of the PLA_2-catalyzed hydrolysis after a reaction time t.

Compd	Phase state	t [min]		
		60	120	180
1	con	80	–	–
2	le	ca. 20	–	40
3	con/le	55	70	–
4	le	45	60	–
5	con/le	ca. 20	–	55
6	con	30	–	-
7	con	0	40	85
8	con/le	≤ 10	50	–
9	le	0	0	ca. 20
10	con	0	0	ca. 20

[a] The error in the yield is about 5 to 10% and becomes larger for small reaction rates as well as for the ether – ester and the triple-chain compounds as a result of the smaller intensity; con = condensed, le = liquid-expanded, con/le = two-phase coexistence region.

In analogy to findings for DPPC monolayers, one can assume that also branched PCs have their activity maximum in the two-phase region. Therefore it is important for the present investigation to take the phase properties of each monolayer into consideration. At the chosen reaction pressure (8 mN m^{-1}) the compounds investigated are in different phase states (see Table 2). The increase in reactivity of **3** compared to **4** and of **2** compared to **5** could be explained considering their phase properties. Further investigations performed at the same reduced pressure (π/π_c) are necessary before final conclusions can be drawn about the influence of the substitution position (2 or 4) on the reaction rates.

Experimental Section

L-Dipalmitoylphosphatidylcholine (L-DPPC, **1**) was purchased from Sigma (Taufkirchen, Germany). Diester-glycerophosphocholines were synthesized from 2,5-di-*O*-benzyl-D-mannitol. In the final reaction steps, 2-*O*-benzyl-*sn*-glycerophosphocholine was acylated with the desired branched acid anhydride. The benzylic group was subsequently removed from the 1-acyl-2-*O*-benzyl-*sn*-glycerophosphocholines which were then acylated with stearic acid anhydride to form **2**–**5** (recovered yields between 60–

 © WILEY-VCH Verlag GmbH, D-69451 Weinheim, 2000 1433-7851/00/3915-2777 $ 17.50+.50/0

75%). The 1-ether-2-ester-glycerophosphocholines (**6**–**10**) were synthesized starting with *R*-(−)-1,2-isopropylideneglycerol. The obtained 1-*O*-alkyl-2-*O*-benzyl-*sn*-glycerophosphocholines were in the last step debenzylated and immediately acylated with the desired acid anhydride (recovered yields between 60–75%). Purification was performed by column chromatography.

2: $C_{56}H_{112}NO_8P$ (M_r = 958.48); calcd: P 3.23; found: P 3.40; ES-MS (*m*/*z*): 959.1 [*M*+H$^+$], 981.0 [*M*+Na$^+$]. **3**: $C_{43}H_{86}NO_8P$ (M_r = 776.13); calcd: P 3.99; found: P 4.15; ES-MS (*m*/*z*): 777.9 [*M*+H$^+$], 799.6 [*M*+Na$^+$], 815.9 [*M*+K$^+$], 1552.3 [2*M*+H$^+$]; ^{1}H-NMR (500 MHz, $CDCl_3$): δ = 3.51 (m, 2H; glycerol-*sn*-1-CH_2), 3.75–3.79 (s, 2H; NCH_2), 4.10 (m, 2H; glycerol-*sn*-3-CH_2), 5.00 (m, 1H, glycerol-*sn*-2-CH). **4**: $C_{45}H_{90}NO_8P$ (M_r = 804.18); calcd: P 3.85; found: P 3.71; ES-MS (*m*/*z*): 805.6 [*M*+H$^+$]; ^{1}H-NMR (500 MHz, $CDCl_3$): δ = 3.5 (m, 2H; glycerol-*sn*-1-CH_2), 3.75–3.80 (s, 2H; NCH_2), 4.02 (m, 2H; glycerol-*sn*-3-CH_2), 5.03 (m, 1H; glycerol-*sn*-2-CH). **5**: $C_{58}H_{116}NO_8P$ (M_r = 986.53); calcd: P 3.14; found: P 3.29; ES-MS (*m*/*z*): 987.5 [*M*+H$^+$], 1010.4 [*M*+Na$^+$], 1026.6 [*M*+K$^+$]. **6**: $C_{42}H_{86}NO_7P$ (M_r = 748.12); calcd: P 4.14; found: P 4.02); ES-MS (*m*/*z*): 749.5 [*M*+H$^+$], 771.3 [*M*+Na$^+$], 787.3 [*M*+K$^+$]; ^{1}H-NMR (500 MHz, $CDCl_3$): δ = 3.6 (m, 2H; glycerol-*sn*-1-CH_2), 3.75–3.80 (s, 2H; NCH_2), 4.02 (m, 2H; glycerol-*sn*-3-CH_2), 5.07 (m, 1H; glycerol-*sn*-2-CH). **7**: $C_{56}H_{114}NO_7P$ (M_r = 944.49); calcd: P 3.28; found: 3.21; ES-MS (*m*/*z*): 945.4 [*M*+H$^+$], 967.4 [*M*+Na$^+$], 983.3 [*M*+K$^+$]. **8**: $C_{43}H_{88}NO_7P$ (M_r = 762.14); calcd: P 4.06; found: 3.99; ES-MS (*m*/*z*): 763.0 [*M*+H$^+$], 785.0 [*M*+Na$^+$]; ^{1}H-NMR (500 MHz, $CDCl_3$): δ = 3.6 (m, 2H; glycerol-*sn*-1-CH_2), 4.05 (m, 1H; OCH_2CH), 4.15 (m, 2H; glycerol-*sn*-3-CH_2), 4.55 (s, 2H; CH_2CH_2N), 5.05 (m, 1H; glycerol-*sn*-2-CH). **9**: $C_{43}H_{88}NO_7P$ (762.24); calcd: P 4.06; found: 3.99); ES-MS (*m*/*z*): 763.3 [*M*+H$^+$], 1525.2 [2*M*+H$^+$]; ^{1}H-NMR (500 MHz, $CDCl_3$): δ = 3.6 (m, 2H; glycerol-*sn*-1-CH_2), 3.75–3.80 (s, 2H; NCH_2), 4.1 (m, 2H; glycerol-*sn*-3-CH_2), 4.54 (s, 2H; CH_2CH_2N), 5.10 (m, 1H; glycerol-*sn*-2 CH). **10**: $C_{56}H_{114}NO_7P$ (944.49); calcd: P 3.28; found: 3.35; ES-MS (*m*/*z*): 945.2 [*M*+H$^+$], 967.2 [*M*+Na$^+$], 983.0 [*M*+K$^+$].

Monolayer experiments: A buffer of NaCl (150 mM), $CaCl_2$ (5 mM), and Tris (10 mM) at a pH of 8.9 was utilized as the subphase. The film balance (R&K ,Wiesbaden, Germany) was equipped with an Wilhelmy-type pressure measuring system. Phospholipase A_2 of the venom from *Crotalus Atrox* was used for hydrolysis (660 units per mg protein, Sigma, Germany). The enzyme was dissolved in buffer, at 40 mN m^{-1} injected underneath the monolayer (6 ng protein per mL subphase) and carefully stirred. The hydrolysis was monitored at a constant lateral pressure of 8 mN m^{-1}. After 60, 120, or 180 min the monolayer was compressed to 40 mN m^{-1} and a spectrum was recorded. All experiments were performed at 20 °C.

PM-IRRAS experiments: The IR beam was decoupled from a Bruker IFS66 spectrometer (Bruker, Karlsruhe, Germany), linearly polarized (KRS5, Specac, Orpington, UK) and passed through a photoelastic modulator (ZnSe, Type II, Hinds). The beam was then reflected from the water surface and focused with a ZnSe lense on the nitrogen-cooled MCT detector (Figure 1). With the polarization modulation one can nearly fully delete the influence of isotropic water absorption since the parallel (R_p) and the normal (R_s) to the plane of incidence polarized reflectivity was determined simultaneously. With the electronic setup one can obtain (bandpassfilter: 300–1200 Hz, Stanford Research System, model SR 650; EG&G lock-in amplifier, model 5209) the differential signal $(R_p - R_s)/(R_p + R_s)$, with a contribution from only the anisotropic absorption of the monolayer.

Received: December 14, 1999
Revised: Febrary 23, 2000 [Z14393]

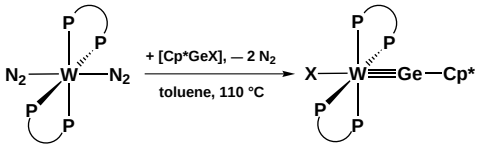
[1] D. Blaudez, T. Buffeteau, J. C. Cornut, B. Desbat, M. Pezolet, J. M. Turlet, *Appl. Spectrosc.* **1993**, *47*, 869–874.
[2] A. Gericke, A. Hühnerfuss, *Chem. Phys. Lipids* **1994** , *74*, 205–210.
[3] U. Dahmen-Levison, G. Brezesinski, H. Möhwald, *Progr. Colloid Polym. Sci*. **1998**, *110*, 269–274.
[4] U. Dahmen-Levison, G. Brezesinski, H. Möhwald, *Thin Solid Films* **1998**, *329*, 616–620.
[5] D. W. Grainger, A. Reichert, H. Ringsdorf, C. Salesse, *Biochim. Biophys. Acta* **1990**, *1023*, 365–379.
[6] D. Marsh, *Curr. Opin. Colloid Interface Sci.* **1997**, *2*, 4–14.
[7] F. M. Menger, M. G. Wood, *Angew. Chem.* **1989**, *101*, 1277–1278; *Angew. Chem. Int. Ed. Engl.* **1989**, *9*, 1218–1219.
[8] G. Brezesinski, A. Dietrich, B. Struth, C. Böhm, W. G. Bouwman, K. Kjaer, H. Möhwald, *Chem. Phys. Lipids* **1995**, *76*, 145–157.
[9] F. Bringezu, G. Brezesinski, H. Möhwald, *Chem. Phys. Lipids* **1998**, *94*, 251–260.
[10] G. Brezesinski, A. Dietrich, B. Dobner, H. Möhwald, *Progr. Colloid Polym. Sci*. **1995**, *98*, 255–262.
[11] R. D. Hunt, M. L. Mitchell, R. A. Dluhy, *J. Mol. Struct*. **1989**, *214*, 93–109.

Synthesis and Structure of the Germylyne Complexes *trans*-[X(dppe)$_2$W≡Ge(η^1-Cp*)] (X = Cl, Br, I) and Comparison of the W≡E Bonds (E = C, Ge) by Density Functional Calculations **

Alexander C. Filippou,* Athanassios I. Philippopoulos, Peter Portius, and Dirk U. Neumann

A large number of transition metal carbyne complexes have been described and their reactions investigated in depth.[1] However, complexes containing a triple bond between a transition metal and a heavier element of the fourth main group (E = Si, Ge, Sn, Pb) are very rare. To the best of our knowledge silylyne,[2] stannylyne and plumbylyne complexes are unknown, and for germylyne complexes there are only the compounds [(η^5-C_5H_5)(CO)$_2$M≡GeR] (M = Cr, Mo, W) containing a sterically very demanding substituent R (R = 2,6-$Trip_2C_6H_3$, 2,6-$Mes_2C_6H_3$; Trip = 2,4,6-*i*$Pr_3C_6H_2$; Mes = 2,4,6-$Me_3C_6H_2$).[3] Here we report a new route to germylyne complexes carrying a pentamethylcyclopentadienyl group on the germanium atom. Our route exploits the thermal elimination of N_2 from *trans*-[W(dppe)$_2$(N_2)$_2$] (dppe = $Ph_2PCH_2CH_2PPh_2$) (**1**).[4]

The reaction of **1** with the germylenes [Cp*GeX] **2a**–**c** (X = Cl, Br, I)[5] in boiling toluene leads smoothly to the germylyne complexes **3a**–**c**, respectively [Eq. (a)]. The complexes **3a**–**c** which each contain one equivalent of



1 **3a-c**

X = Cl, Br, I; P⌒P = dppe; Cp* = C_5Me_5

[*] Prof. Dr. A. C. Filippou, Dr. A. I. Philippopoulos, Dipl.-Chem. P. Portius, Dipl.-Chem. D. U. Neumann
Institut für Chemie der Humboldt-Universität zu Berlin
Hessische Strasse 1–2, 10115 Berlin (Germany)
Fax: (+49) 30-2093-6939
E-mail: filippou@chemie.hu-berlin.de

[**] This work was supported by the Deutsche Forschungsgemeinschaft and by the Fonds der Chemischen Industrie. We thank Dr. B. Ziemer and P. Neubauer for the X-ray structure analysis. dppe = $Ph_2PCH_2CH_2PPh_2$.

 © WILEY-VCH Verlag GmbH, D-69451 Weinheim, 2000 1433-7851/00/3915-2778 $ 17.50+.50/0

toluene were isolated as orange–brown to red–brown solids of remarkable thermal stability in 65–80% yields and fully characterized. The molecular structure of **3a**·toluene was determined by X-ray diffraction of dark red single crystals obtained upon slow cooling of a toluene solution of **3a** to −30 °C (Figure 1).[6] The structure shows a distorted octahedral complex with C_1 symmetry and a *trans* orientation of the chloro and germylyne ligands (Figure 1). The W−Ge bond (2.302(1) Å) is significantly shorter than W−Ge single bonds (2.493(2)–2.681(3) Å)[3b, 7] and slightly longer than the W−Ge triple bond in $[(\eta^5\text{-}C_5H_5)W(CO)_2{\equiv}Ge\text{-}2,6\text{-}Mes_2C_6H_3]$ (2.277(1) Å).[3b] The angle of 172.2(2)° at the Ge atom indicates a nearly linear W-Ge-C(Cp*) atom sequence. Furthermore, the Cp* substituent is η^1 bound as shown by the Ge−C1 bond (2.038(5) Å) which is in the range expected for Ge−C σ bonds. Additionally this bond is shorter than the Ge−C2/C5 bonds (2.739/2.812 Å) and shorter than the average Ge−C bond in **2a** (2.217(3) Å), which contains a η^2-bound Cp* ligand.[5] Finally the bond angles indicate sp^3 hybridization of the C1 atom, and the different C−C bond lengths within the five-membered Cp* ring point to localized π bonds (C2−C3 and C4−C5).[8]

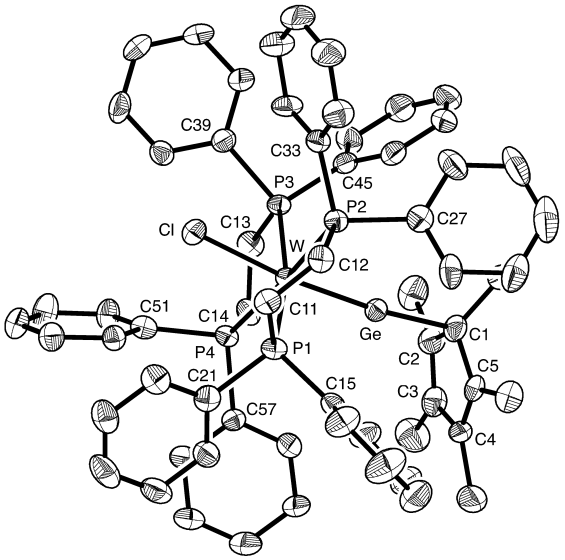


Figure 1. ZORTEP plot of the molecular structure of **3a**. The thermal ellipsoids are set at the 50% probability level. Hydrogen atoms are omitted for clarity. Selected bond lengths [Å] and angles [°]: W-Ge 2.302(1), W-Cl 2.486(1), W-P1 2.469(1), W-P2 2.489(1), W-P3 2.455(1), W-P4 2.446(1), Ge-C1 2.038(5), C1-C2 1.500(8), C2-C3 1.367(8), C3-C4 1.451(8), C4-C5 1.372(7), C1-C5 1.477(8); Ge-W-Cl 174.04(3), Ge-W-P1 101.81(4), Ge-W-P2 94.16(5), Ge-W-P3 87.80(4), Ge-W-P4 92.11(5), Cl-W-P1 81.85(5), Cl-W-P2 81.87(5), Cl-W-P3 88.91(5), Cl-W-P4 92.17(5), W-Ge-C1 172.2(2), Ge-C1-C2 100.3(3), Ge-C1-C5 105.2(3), Ge-C1-C6 111.7(4), C2-C1-C5 104.7(4), C2-C1-C6 117.1(5), C5-C1-C6 116.1(4).

The structural analogy of the complexes **3a**–**c**·toluene is demonstrated by the following properties: the IR spectra in KBr are practically identical and the ^{31}P NMR spectra display a singlet for the chemically equivalent diphosphane ligands that is flanked by tungsten satellites (see Experimental Section). In addition the ^1H and $^{13}C\{^1H\}$ NMR spectra of **3a**–**c**·toluene display the signals expected for complexes of the type *trans*-$[W(dppe)_2LL']$, that is doublets for the diastereotopic methylene protons and the phenyl groups of the dppe ligands and a singlet each for the methyl groups and ring carbon atoms of the Cp* substituent. The latter finding in conjunction with the solid-state structure of **3a** and density functional theory (DFT) calculations on **5a**–**7a** (see below) suggest a haptotropic shift of the Cp* group, which is fast on the NMR time scale, [9] and occurs via a transition state with an η^2-bound Cp* substituent.

To clarify the bonding in the germylyne complexes **3a**–**c** density functional calculations were performed (Table 1) on

Table 1. Bonding parameters, dissociation energies, CDA, and NBO results for the complexes *trans*-$[Cl(L)_4W{\equiv}ECp]$ (**4/5**: L = CO, E = C/Ge; **6/7**: L = PH_3, E = C/Ge) (BP86/II).[11]

Complex[a]			Length/angle			BDE[b]	CDA[c]			Charge (NPA[d])			W−E bond (NBO[d])				
	symm.	*n*	W−E [Å]	E−Cp [Å]	W-E-Cp [°]	[kJ mol^{-1}]	*d*	*b*	*b*/*d*	W	E	ECp	occ.[e]	*x*(W) [%]	hybrid	*x*(E) [%]	hybrid
4a	C_1	0	1.855	1.476	178.9	468.1	0.509	0.652	1.28	−0.33	0.06	0.08	σ: 1.95	32.6	$sd^{2.27}$	67.4	$sp^{0.75}$
													π1: 1.80	62.4	d	37.6	p
													π2: 1.80	62.2	$sd^{91.5}$	37.8	p
4b	C_s	1	1.911	1.625	152.3	391.2	0.506	0.534	1.06	−0.27	−0.08	0.07					
5a	C_s	0	2.374	2.091	178.5	273.2	0.371	0.617	1.66	−0.87	1.04	0.71	σ: 1.70	37.8	$sd^{1.17}$	62.2	$sp^{1.05}$
													π1: 1.70	79.9	d	20.1	p
													π2: 1.67	82.8	$sd^{56.1}$	17.2	p
5b	C_s	1	2.385	2.222	160.6	269.5	0.376	0.608	1.62	−0.86	1.04	0.72					
6a	C_s	0	1.831	1.495	178.6	466.1	0.570	0.767	1.35	−0.80	−0.05	−0.10	σ:1.94	33.7	$sd^{3.02}$	66.3	$sp^{0.71}$
													π1: 1.91	59.8	d	40.2	p
													π2: 1.90	59.5	$sd^{80.0}$	40.5	p
6b	C_s	1	1.864	1.646	153.0	370.8	0.582	0.657	1.13	−0.72	−0.13	−0.20					
7a	C_s	0	2.335	2.087	177.7	228.9	0.306	0.778	2.54	−1.47	0.92	0.50	σ: 1.76	38.3	$sd^{1.92}$	61.7	$sp^{0.81}$
													π1: 1.87	77.9	d	22.1	p
													π2: 1.85	75.6	$sd^{98.3}$	24.4	p
7b	C_s	1	2.347	2.262	160.9	218.1	0.311	0.749	2.41	−1.49	0.93	0.52					

[a] Symmetry of the complex and number *n* of the imaginary vibrational frequencies. [b] Bond dissociation energy ($L_nW{\equiv}ECp \rightarrow L_nW + ECp$) (BP86/III//BP86/II) plus ZPE(BP86/II);[11] the fragments L_nW and ER have doublet ground states. [c] Donation *d* ($[ECp]^+ \rightarrow [L_nW]^-$) and back donation *b* ($[L_nW]^- \rightarrow [ECp]^+$) in elemental charges; the residual term (interaction of unoccupied fragment orbitals) is in every case near to zero, the repulsive polarization *r* has values from −0.171 to −0.327. [d] NBO analysis (natural bond orbital) and NPA (natural population analysis) are integrated into the Gaussian program. [e] Occupancies.

 © WILEY-VCH Verlag GmbH, D-69451 Weinheim, 2000 1433-7851/00/3915-2779 $ 17.50+.50/0

the model complexes *trans*-[Cl(L)$_4$W≡ECp] (Cp = C_5H_5; **4/5**: L = CO, E = C/Ge; **6/7**: L = PH_3, E = C/Ge).[10, 11] All complexes have a minimum structure with an η^1-bound Cp substituent (**4a**–**7a**). In contrast, the structures with η^2 coordination of the Cp unit (**4b**–**7b**) are transition states for the haptotropic shift of the Cp ring.[9] Calculated and experimentally determined bond lengths and angles are in good agreement, as shown, for example, by the similar W–Ge, W–Cl, and Ge–C bond lengths of **3a**·toluene and **7a** (W–Ge 2.302(1) and 2.335 Å, W–Cl 2.486(1) and 2.485 Å, Ge–C 2.038(5) and 2.087 Å, respectively). A change in the hapticity of the Cp substituent from η^1 (**4a**–**7a**) to η^2 (**4b**–**7b**) leads to significant bending of the carbyne/germylyne ligand at the E atom, which is more pronounced in the carbyne complexes (compare for example **6a/6b** with **7a/7b**). Accordingly the barrier for the haptotropic shift of the Cp ring is significantly higher for the carbyne complexes **4a/6a** (76.9/95.3 kJ mol^{-1}) than for the germylyne complexes **5a/7a** (3.7/10.8 kJ mol^{-1}).

In all the complexes the W≡E triple bond is composed of a σ and two π bonds. The σ is polarized towards the ligand, whereas the π bonds are polarized towards the metal. The dissociation energies of the W–C bonds are significantly higher. The strength of the W–E bond is also reflected in the occupancies of the σ and π orbitals. These are higher for the carbyne complexes than for the germylyne complexes and higher for the phosphane complexes than for the carbonyl complexes.

The results of the charge–decomposition analysis (CDA) indicate that the germylyne ligand is a poorer σ donor than the carbyne ligand but an equally good π acceptor. The acceptor capability of the germylyne ligand is weakened by the presence of other π-acceptor ligands (for example CO). Accordingly the acceptor/donor ratio (*b*/*d*; see Table 1) of the germylyne ligand is greater than that of the carbyne ligand and increases on going from the carbonyl to the phosphane complexes. Finally the NPA results (Table 1) indicate a positive partial charge on the germanium atom, while the carbyne carbon is almost electroneutral. This charge distribution could be the basis for targeted reactivity studies of germylyne complexes.

Considering the large number of dinitrogen complexes that are known of the Group 6 transition metals and the possibility of utilizing the Cp* substituent as a leaving group,[12] then the synthetic method described here opens up very promising opportunities for developing the chemistry of germylyne complexes.

Experimental Section

NMR spectra were recorded at room temperature in [D$_8$]THF (Bruker AM 300 Spectrometer); the δ_H values are calibrated against the residual proton signal of the deuterated solvent at $\delta_H = 1.73$ and the δ_C values against the ^{13}C signal of the solvent at $\delta_C = 25.3$.

3a·toluene: compound **1** (0.464 g, 0.448 mmol) and **2a** (0.119 g, 0.489 mmol) were weighed into a Schlenk tube and suspended in toluene (50 mL). The orange suspension was heated, in an oil bath preheated to 120 °C, so that the reaction mixture boiled gently. On boiling the reaction mixture a clear orange solution was obtained that over the course of the reaction turned dark red–brown. Completion of the reaction (after ca. 20 min) was indicated by the disappearance of the $\nu(N_2)$ absorption bands of **1** at 2010 and 1949 cm^{-1} from the IR spectrum of the reaction mixture. The mixture was cooled to room temperature, filtered, and the volume of the filtrate was reduced to about 10 mL. Crystals of **3a**·toluene formed overnight at −78 °C. The supernatant solution was decanted, and the crystals were washed with pentane (2 × 20 mL) and dried under high vacuum at room temperature for 1 h. Yield 0.396 g (67 % from **1**) as an orange–brown powder, m.p. 248 °C (decomp). Elemental analysis calcd (%) for $C_{69}H_{71}ClGeP_4W$ (1316.11): C 62.97, H 5.44, Cl 2.69; found: C 62.64, H 5.58, Cl 2.83; ^{1}H NMR: $\delta = 1.42$ (s, 15 H; C_5Me_5), 2.31 (s, 3 H, Ph*Me*), 2.42 (m, 4 H, 4 × H_ACH$_B$), 2.86 (m, 4 H, 4 × H$_A$CH_B), 6.86–7.67 (m, 45 H, 4 × PPh_2 and *Ph*Me); ^{31}P{^{1}H} NMR: $\delta = 46.3$ (^1J(W,P) = 264.7 Hz); ^{13}C{^{1}H} NMR: $\delta = 12.7$ (C_5Me_5), 21.5 (Ph*Me*), 36.6 (m, 4 × *C*H$_2$), 126.0 (*p*-C, *Ph*Me), 127.1 (C_5Me$_5$), 127.2 and 128.0 (m, *m*-C, 4 × Ph_APPh_B), 128.3 and 129.1 (*p*-C, 4 × Ph_APPh_B), 128.9 (*m*-C, *Ph*Me), 129.7 (*o*-C, *Ph*Me), 134.8 and 135.2 (m, *o*-C, 4 × Ph$_A$PPh_B), 138.4 (*ipso*-C, *Ph*Me), 138.9 and 147.6 (m, *ipso*-C, 4 × Ph_APPh_B).

3b·toluene: Yield 78 % as an orange–brown powder, m.p. 236 °C (decomp). Elemental analysis calcd (%) for $C_{69}H_{71}BrGeP_4W$ (1360.57): C 60.91, H 5.26, Br 5.87; found: C 60.54, H 5.48, Br 6.49; selected spectroscopic data: ^{1}H NMR: $\delta = 1.37$ (s, 15 H, C_5Me_5), 2.31 (s, 3 H, Ph*Me*), 2.46 (m, 4 H, 4 × H_ACH$_B$), 2.95 (m, 4 H, 4 × H$_A$CH_B), 6.89–7.70 (m, 45 H, 4 × PPh_2 and *Ph*Me); ^{31}P{^{1}H} NMR: $\delta = 43.9$ (^1J(W,P) = 262.3 Hz).

3c·toluene: Yield 65 % as a red–brown powder, m.p. 221 °C (decomp). Elemental analysis calcd (%) for $C_{69}H_{71}GeIP_4W$ (1407.56): C 58.88, H 5.08, I 9.02; found: C 58.79, H 5.20, I 9.23; ^{1}H NMR: $\delta = 1.31$ (s, 15 H, C_5Me_5), 2.31 (s, 3 H, Ph*Me*), 2.54 (m, 4 H, 4 × H_ACH$_B$), 3.09 (m, 4 H, 4 × H$_A$CH_B), 6.89–7.72 (m, 45 H, 4 × PPh_2 and *Ph*Me); ^{31}P{^{1}H} NMR: $\delta = 38.7$ (^1J(W,P) = 258.8 Hz); ^{13}C{^{1}H} NMR: 12.6 (C_5Me_5), 21.5 (Ph*Me*), 38.4 (m, 4 × CH$_2$), 127.0 (C_5Me$_5$).

Received: April 11, 2000 [Z 14971]

[1] a) E. O. Fischer, *Adv. Organomet. Chem.* **1976**, *14*, 1; b) R. R. Schrock, *Acc. Chem. Res.* **1986**, *19*, 342; c) W. R. Roper, *J. Organomet. Chem.* **1986**, *300*, 167; d) H. Fischer, P. Hofmann, F. R. Kreißl, R. R. Schrock, K. Weiss, *Carbyne Complexes*, VCH, Weinheim, **1988**; e) F. G. A. Stone, *Adv. Organomet. Chem.* **1990**, *31*, 53; f) A. Mayr, H. Hoffmeister, *Adv. Organomet. Chem.* **1992**, *32*, 227.

[2] A donor-stabilized silylyne complex with a four-coordinate silicon atom, [Cp*Ru(PMe$_3$)$_2$Si{(2,2′-bipy)(4-MeC$_6$H$_4$S)}][OTf]$_2$ (2,2′-bipy = 2,2′-bipyridine; Tf = F_3CSO_2), has been described: S. D. Grumbine, R. K. Chadha, T. D. Tilley, *J. Am. Chem. Soc.* **1992**, *114*, 1518.

[3] a) R. S. Simons, P. P. Power, *J. Am. Chem. Soc.* **1996**, *118*, 11966; b) L. Pu, B. Twamley, S. T. Haubrich, M. M. Olmstead, B. V. Mork, R. S. Simons, P. P. Power, *J. Am. Chem. Soc.* **2000**, *122*, 650, and references therein.

[4] a) J. Chatt, J. R. Dilworth, R. L. Richards, *Chem. Rev.* **1978**, *78*, 589; b) J. Chatt, R. L. Richards, *J. Organomet. Chem.* **1982**, *239*, 65; c) R. L. Richards, *Chem. Br.* **1988**, *24*, 133.

[5] Ebullioscopic measurements show that the complexes **2a**–**c** are monomeric in solution. In the solid state **2a** is monomeric, whereas **2b** is a Br-bridged dimer and **2c** forms a ladderlike coordination polymer linked by I bridges: J. G. Winter, P. Portius, G. Kociok-Köhn, R. Steck, A. C. Filippou, *Organometallics* **1998**, *17*, 4176.

[6] Crystal structure determination of **3a**·toluene ($C_{69}H_{71}ClGeP_4W$): $M_r = 1316.03$; triclinic, space group $P\bar{1}$, $a = 10.524(3)$, $b = 16.117(4)$, $c = 17.875(5)$ Å, $\alpha = 96.86(3)$, $\beta = 96.67(3)$, $\gamma = 102.86(3)°$, $V = 2902.4(14)$ Å^3, $Z = 2$, $\rho_{calcd} = 1.506$ g cm^{-3}, STOE-IPDS diffractometer with area detector, $T = 180(2)$ K, $\lambda(Mo_{K\alpha}) = 0.71073$ Å, $\mu = 2.697$ mm^{-1}, $F(000) = 1336$, 24651 measured reflections, 10539 independent reflections, 686 parameters, GOF = 0.951, $R_1 = 0.0508$ [$I > 2\sigma(I)$], $wR2 = 0.1225$, min./max. residual electron density −2.046/1.916 e Å^{-3}. Crystallographic data (excluding structure factors) for the structure reported in this paper have been deposited with the Cambridge Crystallographic Data Centre as supplementary publication no. CCDC-142852. Copies of the data can be obtained free of charge on application to CCDC, 12 Union Road, Cambridge CB2 1EZ, UK (fax: (+44) 1223-336-033; e-mail: deposit@ccdc.cam.ac.uk).

[7] a) A. C. Filippou, J. G. Winter, G. Kociok-Köhn, I. Hinz, *J. Chem. Soc. Dalton Trans.* **1998**, 2029; b) A. C. Filippou, J. G. Winter, G. Kociok-Köhn, C. Troll, I. Hinz, *Organometallics* **1999**, *18*, 2649.

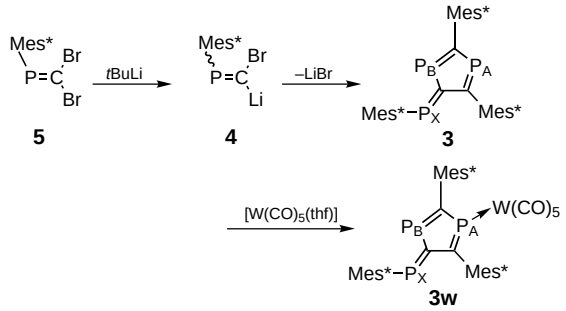
 © WILEY-VCH Verlag GmbH, D-69451 Weinheim, 2000 1433-7851/00/3915-2780 $ 17.50+.50/0

[8] R. Steck, thesis, Humboldt-Universität, Berlin, **1998**.
[9] a) N. Trong Anh, M. Elian, R. Hoffmann, *J. Am. Chem. Soc.* **1978**, *100*, 110; b) P. Jutzi, *Chem. Rev.* **1986**, *86*, 983, and references therein.
[10] The DFT calculations indicate no fundamental electronic differences between the complexes *trans*-[Cl(L)$_4$W≡EMe] and **4a**–**7a**.
[11] The gradient corrected functionals BP86 were used (A. D. Becke, *Phys. Rev. A* **1988**, *38*, 3098; J. P. Perdew, *Phys. Rev. B* **1986**, *33*, 8822). For the W atom and the elements Ge, Cl, and P the pseudo potentials (W: P. J. Hay, W. R. Wadt, *J. Chem. Phys.* **1985**, *82*, 299; Ge, Cl, P: G. Igel-Mann, H. Stoll, H. Preuss, *Mol. Phys.* **1988**, *65*, 1321) and corresponding valence basis sets were used (W: 441/2111/21 and 441/2111/111/1; Ge, Cl, P: 31/31/1 and 211/211/11). Together with the standard basis sets 6-31G(d) (P. C. Hariharan, J. A. Pople, *Theor. Chim. Acta* **1973**, *28*, 213) and 6-311G(2d,p) (R. Krishnan, J. S. Binkley, R. Seeger, J. A. Pople, *J. Chem. Phys.* **1980**, *72*, 650) for the remaining elements the combinations II and III were obtained (Table 1). The calculations were performed with Gaussian 98 (Gaussian 98, Revision A.7, M. J. Frisch, G. W. Trucks, H. B. Schlegel, G. E. Scuseria, M. A. Robb, J. R. Cheeseman, V. G. Zakrzewski, J. A. Montgomery, Jr., R. E. Stratmann, J. C. Burant, S. Dapprich, J. M. Millam, A. D. Daniels, K. N. Kudin, M. C. Strain, O. Farkas, J. Tomasi, V. Barone, M. Cossi, R. Cammi, B. Mennucci, C. Pomelli, C. Adamo, S. Clifford, J. Ochterski, G. A. Petersson, P. Y. Ayala, Q. Cui, K. Morokuma, D. K. Malick, A. D. Rabuck, K. Raghavachari, J. B. Foresman, J. Cioslowski, J. V. Ortiz, A. G. Baboul, B. B. Stefanov, G. Lui, A. Liashenko, P. Piskorz, I. Komaromi, R. Gomperts, R. L. Martin, D. J. Fox, T. Keith, M. A. Al-Laham, C. Y. Peng, A. Nanayakkara, C. Gonzalez, M. Challacombe, P. M. W. Gill, B. Johnson, W. Chen, M. W. Wong, J. L. Andres, M. Head-Gordon, E. S. Replogle, J. A. Pople, Gaussian, Inc., Pittsburgh, PA, **1998**) and CDA 2.1 (charge decomposition analysis; S. Dapprich, G. Frenking, CDA 2.1, Marburg, **1994**).
[12] P. Jutzi, *J. Organomet. Chem.* **1990**, *400*, 1.

Isolation of a Kinetically Stabilized 1,3,6-Triphosphafulvene**

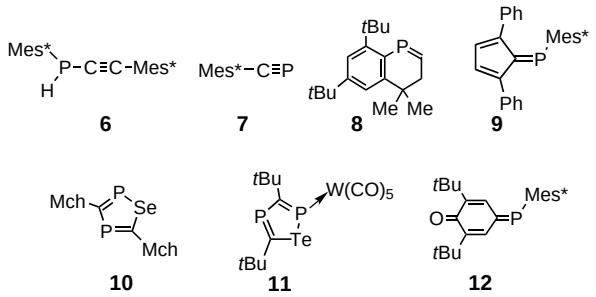
Shigekazu Ito, Hiroki Sugiyama, and Masaaki Yoshifuji*

Substitution of some of the sp^2-hybridized carbon atoms in conjugated systems with heavier main-group elements, such as phosphorus atoms, is of interest but requires kinetic stabilization with bulky substituents. In 1995, 2,4,6-tri-*tert*-butyl-1,3,5-triphosphabenzene (**1**) was first reported, prepared through the trimerization of *tert*-butylphosphaacetylene (or 3,3-dimethyl-1-phospha-1-butyne), together with its valence isomer **2**;[1] the structure of **1** was established in 1998.[2, 3] Oligomerization of *tert*-butylphosphaacetylene has been utilized for the construction of various types of five-membered heterocyclic systems containing polycyclic systems.[4] We now report one of the valence isomers of triphosphabenzene, utilizing the 2,4,6-tri-*tert*-butylphenyl group (Mes*). 2,4,6-Tris(2,4,6-tri-*tert*-butylphenyl)-1,3,6-triphosphafulvene (**3**) was formed by the trimerization of lithium phosphanylidene carbenoid **4** (Scheme 1).[5–7]



Scheme 1. Preparation of **3** and **3w**. Mes* = 2,4,6-*t*Bu$_3$C$_6$H$_2$.

Dibromophosphaethene **5**[8] was allowed to react with two equivalents of *tert*-butyllithium at −78 °C to afford the phosphanylidene carbenoid **4**, after which the reaction mixture warmed gently to 25 °C. After purification (silica-packed column chromatography), **3** was obtained as a deep red solid together with trace amounts of 2-(2,4,6-tri-*tert*-butylphenyl)-1-(2,4,6-tri-*tert*-butylphenylphosphanyl)acetylene (**6**), 1-(2,4,6-tri-*tert*-butylphenyl)-1-phosphaacetylene (**7**),[5–7, 9] and 6,8-di-*tert*-butyl-4,4-dimethyl-1-phospha-3,4-dihydronaphthalene (**8**).[5, 6, 10] The ^{31}P NMR spectrum of **3**



shows an ABX system. The signal of the exocyclic phosphorus atom P$_X$ (δ_{P_X} = 313.8) is positioned downfield compared to ring atoms P$_A$ and P$_B$ but similar to that found for **9** (δ = 321.5),[11] due to the electron-withdrawing effects of the 1,3-diphosphacyclopentadiene moiety.[12] The chemical shifts of the ring phosphorus atoms in **3** (δ_{P_A} = 291.3, δ_{P_B} = 264.7) are close to those for 1,2,4-selenadiphosphole **10** (Mch = 1-methylcyclohexyl).[13] Their coupling constant, J(P$_A$,P$_B$), is 32 Hz, which is also similar to that found for **10**;[13] values of the exocyclic coupling constants are 120 and 44 Hz for J(P$_A$,P$_X$) and J(P$_B$,P$_X$), respectively. The UV/Vis spectrum of

[*] Prof. Dr. M. Yoshifuji, Dr. S. Ito, H. Sugiyama
Department of Chemistry
Graduate School of Science
Tohoku University
Aoba, Sendai 980-8578 (Japan)
Fax: (+81) 22-217-6562
E-mail: yoshifj@mail.cc.tohoku.ac.jp

[**] This work was supported in part by a Grant-in-Aid for Scientific Research (No. 09239101) from the Ministry of Education, Science, Sports and Culture, Japan.

 © WILEY-VCH Verlag GmbH, D-69451 Weinheim, 2000 1433-7851/00/3915-2781 $ 17.50+.50/0

3 has a maxima λ_{max} at 429 nm ($\lg \varepsilon = 3.48$, in hexanes), which is at a longer wavelength than that for **9** ($\lambda_{max} = 358$ nm).[11]

Compound **3** was treated with excess amount of $[W(CO)_5(thf)]$ to afford the pentacarbonyltungsten complex **3w** as a deep red solid (Scheme 1). An ABX system was also observed in the ^{31}P NMR spectrum of **3w** and the signal for the P_A atom shifted remarkably ($\delta_{P_A} = 268.4$) relative to that found in **3**.

Complex **3w** was recrystallized from toluene at 0 °C to afford a suitable crystal for its structural determination. Figure 1 shows an ORTEP drawing of the molecular structure of **3w** together with some selected bond lengths and angles, unambiguously indicating that the metal center coordinates to

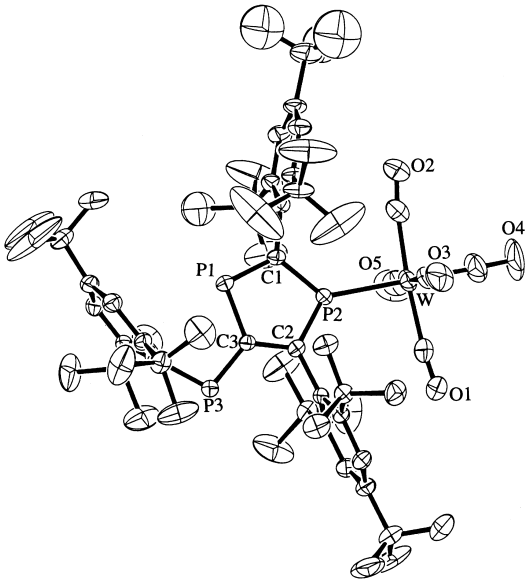
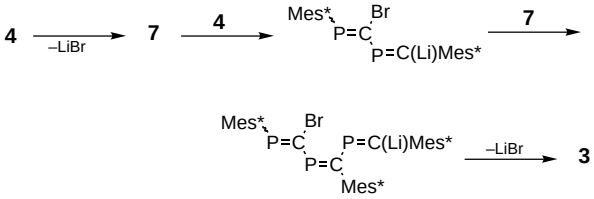


Figure 1. An ORTEP representation of the molecular structure of **3w** with 30% probability ellipsoids. Hydrogen atoms are omitted for clarity. Selected bond lengths [Å] and angles [°]: W-P2 2.480(2), P1-C1 1.689(7), P1-C3 1.815(6), P2-C1 1.801(7), P2-C2 1.703(7), P3-C3 1.710(6), C2-C3 1.447(8), C1-C_{ipso}(Mes*) 1.518(9), C2-C_{ipso}(Mes*) 1.525(8), P3-C_{ipso}(Mes*) 1.857(7); W-P2-C1 129.9(2), W-P2-C2 129.9(2), C1-P1-C3 96.6(3), P1-C1-P2 113.7(4), C1-P2-C2 100.2(3), P2-C2-C3 112.8(4), C2-C3-P1 116.8(5), P1-C3-P3 120.0(3), C2-C3-P3 123.3(5), C3-P3-C_{ipso}(Mes*) 101.7(3).

the P2 (P_A) atom. The exocyclic $\lambda_3\sigma_2$ phosphorus atom takes a *cis* configuration, probably due to the steric congestion. The triphosphafulvene framework (P1 – P3,C1 – C3), W atom, and three *ipso* carbon atoms of the Mes* groups are coplanar to within 0.074(8) Å. This plane lies at angles of 84.5° (P3), 90.0° (C1), and 90.0° (C2) to the mean aromatic rings of the three Mes* groups. The W–P2 distance is 2.480(2) Å, while the P1–C1 and P2–C2 distances (1.689(7) and 1.703(7) Å, respectively) are close to the P=C lengths of tungsten-complexed 1,2,4-telluradiphosphole **11** (1.695(7) and 1.702(7) Å).[14] The P3–C3 distance is 1.710(6) Å, which is close to the P=C length in *p*-phosphaquinone **12** (1.705(2) Å).[15] The C2–C3 distance (1.447(8) Å) is similar to the C–C length in the 1,4-diphospha-1,3-butadiene system.[16] The P1–C3 length (1.815(6) Å) is shorter than the P–C single bond in the straight-chain 1,3-diphospha-1,3-butadiene system.[17] Both of the P–C single bonds in the triphosphafulvene system are shorter than the average P–C_{sp^2} distance (1.836 Å),[18] which indicates the delocalized π system. The C1-P1-C3 and C1-P2-C2 angles are 96.6(3) and 100.2(3)°, respectively, which are smaller than those found in **11** (101.7(3) and 106.3(3)°).[14]

Compound **3** is regarded as a trimer of the phosphanylidene carbene. As depicted in Scheme 2, phosphaalkyne **7** is first generated from **4** through elimination of LiBr, followed by a



Scheme 2. Proposed mechanism for the formation of **3**.

[1,2] Fritsch – Buttenberg – Wiechell-type migration.[9] The phosphanylidene carbenoid **4** reacts with two equivalents of **7** in succession and, finally, another LiBr unit was eliminated upon annelation to **3**.[19] The presence of traces of the phosphanylacetylene **6** could be regarded as a reaction product arising from a dimerization of **4** with expulsion of one phosphorus atom.[20]

As reported previously, after the reaction of dibromophosphaethene **5** with *n*BuLi, **3** was not detected but **8** was obtained as a major product.[10a] Although it is difficult to rationalize this observation on the basis of reactivity differences between *n*BuLi and *t*BuLi,[21] the aggregation of **4** generated with *t*BuLi may be dissimilar as that generated with *n*BuLi. The formation of "free" phosphaalkyne **7** via a [1,2] migration would be preferred if *t*BuLi was employed for the reaction; on the other hand, the intramolecular cyclization would become more facile if *n*BuLi was used. Such effects were observed in the rearrangement reaction to afford phosphaalkyne **7** from (*E*)-2-chloro-1-(2,4,6-tri-*tert*-butylphenyl)-2-phosphaalkene and various butyllithium species.[9a, b]

As stated, 1,3,6-triphosphafulvene **3** is one of the valence isomers of triphosphabenzenes. Compound **3** is deeply colored compared to **1**, which correspond to the properties of fulvene versus benzene.[22] Neither the isomerization of **3** nor the trimerization of **7** affording the corresponding triphosphabenzene derivative has been previously observed. An ab initio calculation (RHF/3-21G* level)[23, 24] on non-substituted systems indicated that 1,3,6-triphosphafulvene is less stable by 20.9 kcal mol^{-1} than 1,3,5-triphosphabenzene. We postulate that the bulky Mes* groups play an important role in controlling the framework of the molecule.

Experimental Section

3: A solution of **5** (500 mg, 1.12 mmol) in THF (40 mL) was treated with *tert*-butyllithium (2.25 mmol, 1.50 mol L^{-1} in *n*-pentane) at −78 °C and allowed to warm to 25 °C. The reaction mixture was stirred for 1 h and the solvent was removed in vacuo. The residue was extracted with *n*-hexane and, in the ^{31}P NMR spectrum of the extract, mainly **3** was observed together with trace amounts of **6**,[25] **7**, and **8**. **3** was isolated by column chromatography (SiO_2, cyclohexane); yield: 57.2 mg (18%). **3**: Red plates, m.p. 93 – 95 °C (dec.); ^1H NMR (200 MHz, $CDCl_3$): $\delta = 7.54$ (m, 2H; H_{arom}),

 © WILEY-VCH Verlag GmbH, D-69451 Weinheim, 2000 1433-7851/00/3915-2782 $ 17.50+.50/0 *Angew. Chem. Int. Ed.* **2000**, *39*, No. 15

7.43 (m, 2H; H_{arom}), 7.25 (m, 2H; H_{arom}), 1.45 (s, 18H; *o*-C(CH_3)$_3$), 1.38 (s, 36H; *o*-C(CH_3)$_3$), 1.33 (s, 9H; *p*-C(CH_3)$_3$), 1.28 (s, 9H; *p*-C(CH_3)$_3$), 1.26 (s, 9H; *p*-C(CH_3)$_3$); $^{31}P\{^1H\}$ NMR (81 MHz, $CDCl_3$): $\delta = 313.8$ (P_X), 291.3 (P_A), 264.7 (P_B) ($^2J(P_A,P_B) = 32$, $^2J(P_A,P_X) = 120$, $^3J(P_B,P_X) = 44$ Hz); UV/Vis (hexanes): λ_{max} ($\lg\varepsilon$) = 429 nm (3.48); FAB-MS: *m*/*z* (%): 864 (19) [M^+], 275 (100) [Mes*P^+ − H]. **6**: Colorless needles (MeOH), m.p. 173–174 °C (dec.); ^1H NMR (200 MHz, $CDCl_3$): $\delta = 7.44$ (d, 2H, $^4J(P,H) = 2.5$ Hz; H_{arom}, PMes*), 7.25 (s, 2H; H_{arom}, CMes*), 6.13 (d, 1H, $^1J(P,H) = 244.2$ Hz; PH), 1.62 (s, 18H; *o*-C(CH_3)$_3$, PMes*), 1.35 (s, 9H; *p*-C(CH_3)$_3$, PMes*), 1.29 (s, 18H; *o*-C(CH_3)$_3$, CMes*), 1.27 (s, 9H; *p*-C(CH_3)$_3$, CMes*); $^{13}C\{^1H\}$-NMR (151 MHz, $CDCl_3$): $\delta = 155.3$ (d, $^2J(P,C) = 9.2$ Hz; *o*-C_{arom}, PMes*), 153.2 (d, $^4J(P,C) = 1.2$ Hz; *o*-C_{arom}, CMes*), 150.2 (s; *p*-C_{arom}, PMes*), 149.6 (s; *p*-C_{arom}-CMes*), 124.9 (d, $^1J(P,C) = 24.7$ Hz; C_{ipso}, PMes*), 122.3 (d, $^3J(P,C) = 4.3$ Hz; *m*-C_{arom}, PMes*), 120.6 (s; *m*-C_{arom}, CMes*), 117.4 (s, C_{ipso}, *C*Mes*), 105.3 (s; P−C≡*C*), 98.7 (d, $^1J(P,C) = 17.3$ Hz; P−*C*≡C), 38.2 (s; *o*-*C*(CH_3)$_3$-PMes*), 36.3 (s; *o*-*C*(CH_3)$_3$-CMes*), 35.1 (s; *p*-*C*(CH_3)$_3$-CMes*), 35.0 (s; *p*-*C*(CH_3)$_3$, PMes*), 32.6 (d, $^4J(P,C) = 7.2$ Hz; *o*-C(*C*H_3)$_3$, PMes*), 31.4 (s; *p*-C(*C*H_3)$_3$-PMes*), 31.2 (s; *p*-C(*C*H_3)$_3$-CMes*), 30.5 (s; *o*-C(*C*H_3)$_3$-CMes*); ^{31}P NMR (81 MHz, $CDCl_3$): $\delta = -98.6$ (d, $^1J(P,H) = 244.2$ Hz); IR (KBr): $\tilde{\nu} = 2378$, 2148 cm^{-1}; MS (70 eV, EI): *m*/*z* (%): 546 (69) [M^+], 489 (100) [$M^+ - t$Bu]; elemental analysis calcd for $C_{38}H_{59}P$: C 83.46, H 10.87; found: C 82.68, H 10.99.

3w: A solution of **3** (30.7 mg, 35.5 μmol) in THF (5 mL) was treated with [W(CO)$_5$(thf)] (about 0.143 mmol, prepared in situ by irradiation of a THF solution of [W(CO)$_6$] for 8 h with a medium-pressure Hg lamp). The reaction mixture was stirred for 12 h and the solvent was removed in vacuo. The residue was treated with column chromatography (SiO_2, *n*-hexane) affording **3w** as deep red crystals. Yield 5.5 mg (13%); m.p. 176–179 °C (dec.); ^1H NMR (200 MHz, $CDCl_3$): $\delta = 7.54$ (m, 2H; H_{arom}), 7.43 (m, 2H; H_{arom}), 7.25 (m, 2H; H_{arom}) 1.45 (s, 18H; *o*-C(CH_3)$_3$), 1.37 (s, 36H; *o*-C(CH_3)$_3$), 1.33 (s, 9H; *p*-C(CH_3)$_3$), 1.28 (s, 9H; *p*-C(CH_3)$_3$), 1.26 (s, 9H; *p*-C(CH_3)$_3$); $^{31}P\{^1H\}$ NMR (81 MHz, $CDCl_3$): $\delta = 318.7$ (P_X), 268.4 (P_A), 260.4 (P_B) ($J(P_A,P_B) = 54$, $J(P_A,P_X) = 140$, $J(P_B,P_X) = 71$, $J(P_A,W) = 277$ Hz); IR (KBr): $\tilde{\nu} = 2071$, 1944 cm^{-1}; FAB-MS: *m*/*z* (%): 1188 (2) [$M^+ + H$], 864 (13) [M^+ − W(CO)$_5$], 545 (100) [Mes*$_2C_2P^+$].

Crystal data for **3w** ($C_{62}H_{87}O_5P_3W$): $M_r = 1189.14$, deep red prisms crystallized from toluene at 0 °C, dimensions $0.30 \times 0.20 \times 0.20$ mm^3, monoclinic, space group $P2_1/n$ (no. 14), $a = 10.776(5)$, $b = 20.961(2)$, $c = 28.372(5)$ Å, $\beta = 91.43(3)°$, $V = 6406(3)$ Å^3, $Z = 4$, $\rho_{calcd} = 1.233$ g cm^{-3}, $F(000) = 2472.00$, $\mu = 1.923$ mm^{-1}, $T = 298(1)$ K. A Rigaku RAXIS-IV imaging plate detector with graphite-monochromated $Mo_{K\alpha}$ radiation ($\lambda = 0.71070$ Å) was used. Of 9153 reflections measured ($2\theta_{max} = 50.0°$), 6240 were observed ($I > 3.0\sigma(I)$). The structure was solved by direct methods (SIR 92),[26] expanded using Fourier techniques (DIRDIF 94),[27] and refined by full-matrix least squares on *F* for 628 variable parameters. The non-hydrogen atoms, except the disordered C atoms, were refined anisotropically. The disordered C atoms of the methyl groups at the *p*-position of the C1-bonded Mes* group were refined isotropically. Hydrogen atoms were included but not refined. $R = 0.049$ for $I > 3.0\sigma(I)$ and $R_w = 0.110$ for all data. Goodness of fit $S = 1.30$ for all observed reflections. Max./min. electron density = 0.77/ − 0.73 e Å^{-3}. Structure solution, refinement, and graphical representation were carried out using the teXsan package.[28] Crystallographic data (excluding structure factors) for the structure reported in this paper have been deposited with the Cambridge Crystallographic Data Centre as supplementary publication no. CCDC-140669. Copies of the data can be obtained free of charge on application to CCDC, 12 Union Road, Cambridge CB2 1EZ, UK (fax: (+44) 1223-336-033; e-mail: deposit@ccdc.cam.ac.uk).

Received: February 22, 2000 [Z14754]

[1] a) P. Binger, S. Leininger, J. Stannek, B. Gabor, R. Mynott, J. Bruckmann, C. Krüger, *Angew. Chem.* **1995**, *107*, 2411; *Angew. Chem. Int. Ed. Engl.* **1995**, *34*, 2227; b) F. Tabellion, A. Nachbauer, S. Leininger, C. Peters, F. Preuss, M. Regitz, *Angew. Chem.* **1998**, *110*, 1318; *Angew. Chem. Int. Ed.* **1998**, *37*, 1233.

[2] R. Gleiter, H. Lange, P. Binger, J. Stannek, C. Krüger, J. Bruckmann, U. Zennek, S. Kummer, *Eur. J. Inorg. Chem.* **1998**, 1619.

[3] A theoretical investigation for (HC≡P)$_3$ has been reported: M. Hoffmann, P. von R. Schleyer, M. Regitz, *Eur. J. Org. Chem.* **1999**, 3291.

[4] a) K. B. Dillon, F. Mathey, J. F. Nixon, *Phosphorus: The Carbon Copy*, Wiley, Chichester, **1998**; b) J. F. Nixon, *Chem. Soc. Rev.* **1995**, 319; c) A. Mack, M. Regitz, *Chem. Ber.* **1997**, *130*, 823.

[5] M. Yoshifuji, *J. Chem. Soc. Dalton Trans.* **1999**, 3343, and references therein.

[6] S. Ito, K. Toyota, M. Yoshifuji, *Phosphorus Sulfur Silicon* **1999**, *147*, 441.

[7] E. Niecke, M. Nieger, O. Schmidt, D. Gudat, W. W. Schoeller, *J. Am. Chem. Soc.* **1999**, *121*, 519.

[8] a) R. Appel, C. Casser, M. Immenkeppel, *Tetrahedron Lett.* **1985**, *30*, 3551; b) S. J. Goede, F. Bickelhaupt, *Chem. Ber.* **1991**, *124*, 2677.

[9] a) M. Yoshifuji, T. Niitsu, N. Inamoto, *Chem. Lett.* **1988**, 1733; b) M. Yoshifuji, H. Kawanami, Y. Kawai, K. Toyota, M. Yasunami, T. Niitsu, N. Inamoto, *Chem. Lett.* **1992**, 1053; c) R. Appel, M. Immenkeppel, *Z. Anorg. Allg. Chem.* **1987**, *553*, 7; d) V. D. Romanenko, M. Sanchez, T. V. Sarina, M.-R. Mazierès, R. Wolf, *Tetrahedron Lett.* **1992**, *33*, 2981; e) H. Jun, V. G. Young, R. Angelici, *Organometallics* **1994**, *13*, 2444.

[10] a) S. Ito, K. Toyota, M. Yoshifuji, *Chem. Commun.* **1997**, 1637; see also: b) R. A. Aitken, P. N. Clasper, N. J. Wilson, *Tetrahedron Lett.* **1999**, *40*, 527l.

[11] G. Märkl, K. M. Raab, *Tetrahedron Lett.* **1989**, *30*, 1077.

[12] a) R. Bartsch, P. B. Hitchcock, J. F. Nixon, *J. Chem. Soc. Chem. Commun.* **1987**, 1146; b) A. H. Cowley, S. W. Hall, *Polyhedron* **1989**, *8*, 849; c) N. Maigrot, L. Ricard, C. Charrier, F. Mathey, *Angew. Chem.* **1990**, *102*, 575; *Angew. Chem. Int. Ed. Engl.* **1990**, *29*, 534.

[13] S. M. F. Asmus, U. Bergsträßer, M. Regitz, *Synthesis* **1999**, 1642.

[14] M. D. Francis, D. E. Hibbs, P. B. Hitchcock, M. B. Hursthouse, C. Jones, T. Mackewitz, J. F. Nixon, L. Nyulaszi, M. Regitz, N. Sakarya, *J. Organomet. Chem.* **1999**, *580*, 156.

[15] S. Sasaki, F. Murakami, M. Yoshifuji, *Angew. Chem.* **1999**, *111*, 351; *Angew. Chem. Int. Ed.* **1999**, *38*, 340.

[16] a) S. Ito, K. Toyota, M. Yoshifuji, *Chem. Lett*. **1995**, 747; b) S. Ito, M. Yoshifuji, *Chem. Lett.* **1998**, 651; c) M. Yoshifuji, N. Yamada, A. Maack, K. Toyota, *Tetrahedron Lett.* **1998**, *39*, 9481; d) W. W. Schoeller, U. Tubbesing, *Chem. Ber.* **1996**, *129*, 419.

[17] a) R. Appel, P. Fölling, W. Schuhn, F. Knoch, *Tetrahedron Lett.* **1986**, *27*, 1661; b) S. M. Bachrach, M. Liu, *J. Org. Chem.* **1992**, *57*, 2040.

[18] F. H. Allen, O. Kennard, D. G. Watson, *J. Chem. Soc. Perkin Trans.* **1987**, S1.

[19] Taking this reaction mechanism into account, we hoped to obtain **3** in a better yield by a direct treatment of **4** with **7**. Thus, we examined the reaction of **4**, prepared from **5** and *t*BuLi, with **7**. In fact, 1,3,6-triphosphafulvene **3** was observed in the reaction mixture (^{31}P NMR) and could be was isolated by column chromatography (silica gel) with a little improvement of the yield (20%).

[20] We have previously demonstrated the additions of halocarbenes to phosphaalkyne **7** affords haloacetylenes which involves an elimination step of a phosphorus atom: M. Yoshifuji, Y. Kawai, M. Yasunami, *Tetrahedron Lett.* **1990**, *31*, 6891.

[21] A.-M. Sapse, P. von R. Schleyer, *Lithium Chemistry: A Theoretical and Experimental Overview*, Wiley, New York, **1995**.

[22] J. H. Day, *Chem. Rev.* **1953**, *53*, 167.

[23] J. S. Binkley, J. A. Pople, W. J. Hehre, *J. Am. Chem. Soc.* **1980**, *102*, 939.

[24] An ab initio calculation was performed using a PC-SPARTAN program package available from Wavefunction, Inc (Irvine, CA).

[25] A separate reaction of **5** (143 mg, 0.319 mmol) with *t*BuLi (0.630 mmol) in THF (12 mL) under similar conditions afforded **6** (12% yield) together with **8** (2% yield), **3**, and **7** (trace amounts, only observed in ^{31}P NMR spectra).

[26] A. Altomare, M. C. Burla, M. Camalli, M. Cascarano, C. Giacovazzo, A. Guagliardi, G. Polidori, *J. Appl. Crystallogr.* **1994**, *27*, 435.

[27] P. T. Beurskens, G. Admiraal, G. Beurskens, W. P. Bosman, R. de Gelder, R. Israel, J. M. M. Smits, DIRDIF 94, Technical Report of the Crystallography Laboratory, University of Nijmegen (The Netherlands), **1994**.

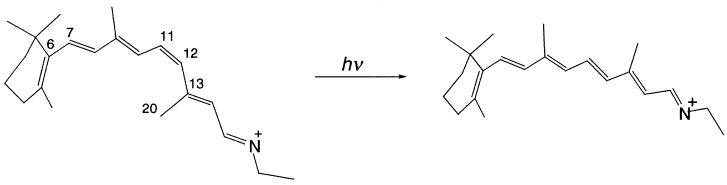
[28] TeXsan: Crystal Structure Analysis Package, Molecular Structure Corporation (The Woodlands, TX), **1985** and **1999**.

Fast Photoisomerization of a Rhodopsin Model—An Ab Initio Molecular Dynamics Study**

Volker Buß,* Oliver Weingart, and Minoru Sugihara

Dedicated to Professor Paul von Ragué Schleyer on the occasion of his 70th birthday

The protonated Schiff base (PSB) of 11-*cis*-retinal is the chromophore of rhodopsin, the photoreceptor in the retina of the vertebrate eye (Scheme 1). The photochemical isomerization to the all-*trans* form triggers a series of enzymatic



Scheme 1. Photoisomerization of the chromophore of rhodopsin, 11-*cis*-12-s-*trans*-retinal PSB (left), into the all-*trans* form (right). The structures are DFT-optimized geometries.[13b]

reactions known as the visual cascade which eventually leads to a neural signal.[1] Central for understanding the molecular basis of these processes is the geometry of the retinal chromophore which is derived from the 11-*cis*-12-s-*trans* conformer[2] and becomes twisted as a consequence of steric interaction. Evidence for this comes from resonance Raman[3] and, more directly, from circular dichroism (CD) spectroscopy:[4] after binding by the protein the optically inactive 11-*cis*-retinal displays distinct positive CD absorption bands corresponding to the absorption maximum of the chromophore in the UV/Vis region at 500 nm and at 340 nm. With different solid-state NMR techniques it has been possible to directly determine torsional angles of the chromophore[5] and distances between specific isotopically labelled positions[6] from which an approximate angle of 42° has been deduced between the C7-C8-C9–C10 and C13-C14-C15 planes.

Steric interaction with the protein and ensuing chromophore distortion is believed to be responsible for the extremely fast kinetics and the efficiency of the rhodopsin photoreaction which yields the first photoproduct after only 200 fs:[7] removal of the C13 methyl group, which according to spectroscopic data results in a flattening of the chromophore, reduces the quantum efficiency significantly from 0.65 to 0.47 or even less.[8, 9] With a methyl group in the 10-position the steric interaction is reintroduced; the quantum efficiency of this latter mutant is still subject to debate.[9, 10]

[*] Prof. Dr. V. Buß, O. Weingart, Dr. M. Sugihara
Institut für Physikalische und Theoretische Chemie
Theoretische Tieftemperaturphysik
Gerhard-Mercator-Universität
47048 Duisburg (Germany)
Fax: (+49) 203-379-2772
E-mail: theobuss@uni-duisburg.de

[**] This work was supported by the Deutsche Forschungsgemeinschaft (Graduate College "Struktur und Dynamikheterogener Systeme").

In the absence of detailed knowledge about the kind of interaction present in the protein binding pocket, it is difficult to derive a theoretical description of the chromophore conformation. The results differ already for the uncomplexed PSB depending on the model used: according to high-quality ab initio calculations (RHF,[11] CASSCF,[12] and DFT[13]) the chromophore is planar. Car–Parrinello type molecular dynamics calculations, on the other hand, converge on a geometry with a 38° twist angle about the C12–C13 bond.[14] In the following we show that a very unspecific steric strain imposed on the chromophore induces a highly specific nonplanar deformation in the region from C11 to C13, and then demonstrate that it is exactly the deformation about these bonds which is the prerequisite for fast photoisomerization of a small retinal model system.

We assume that the retinal chromophore, as a consequence of the steric fit into the protein binding pocket, undergoes some kind of conformational change. To study with the least possible bias what this change might be we have introduced a nonspecific strain into the molecule, by widening all external bond angles (C7-C8-C9, C9-C10-C11, etc.) and contracting all internal bond angles (C6-C7-C8, C8-C9-C10, etc.) by the same amount, 2.5°. This makes the banana-shaped molecule slightly shorter (the C6–N^+ distance is reduced from 11.535 to 10.966 Å), but it is still approximately planar.[15] We then performed molecular dynamics calculations[16] with free optimization of all nuclear coordinates, keeping only the C6–N^+ distance fixed. The dynamics was monitored until all bond lengths and angles, including dihedral angles, had equilibrated. The relaxed structure (Figure 1) begins to establish after 200 fs, when both the C11–C12 and the C12–C13 bonds simultaneously start to twist.[17] Except for the helical geometry resulting from this twist in the region from C11 to C13 the chromophore is essentially planar from C7 to C12 and (slightly less) from C13 to N^+. The structure is remarkably similar to one found by Bifone et al.[18, 19] from

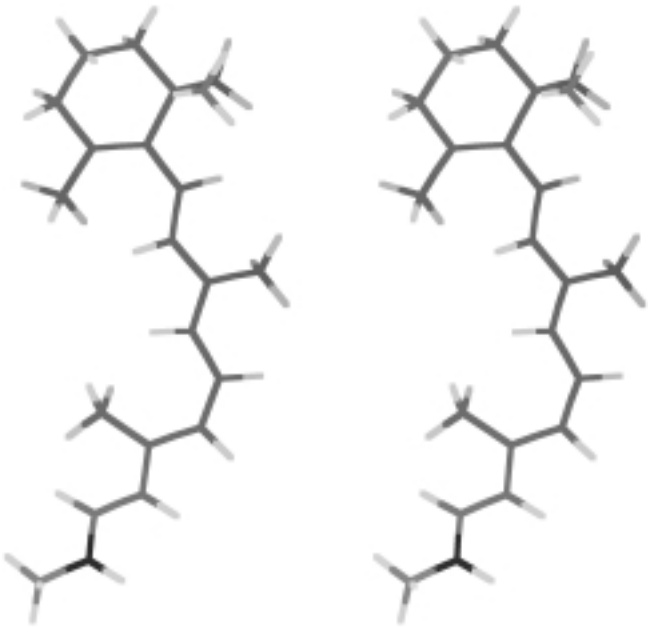


Figure 1. The relaxed geometry of 11-*cis*-retinal PSB after a molecular dynamics calculation with a fixed C6–N^+ distance of 10.966 Å (stereoview).

 © WILEY-VCH Verlag GmbH, D-69451 Weinheim, 2000 1433-7851/00/3915-2784 $ 17.50+.50/0

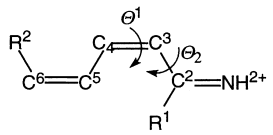
molecular dynamics calculations using experimentally determined constraints for the distance between the C13 methyl group and the C10 and C11 carbon atoms in rhodopsin. The structure they obtained is also highly twisted about the C11–C12 and the C12–C13 bonds.

The molecular dynamics calculations indicate that this geometry, in which the dihedral angle strain is concentrated in exactly the region where the photoisomerization is going to take place, does not require a highly specific protein interaction site; rather it is a consequence of the inherent tendency of the chromophore to twist about these bonds. Note that the geometry displayed in Figure 1 is without relevance to the question of absolute configuration of the chromophore since in the absence of chiral discrimination the molecular dynamics could have produced the mirror image with the same probabilty. We have established independently, based on the quantum-mechanical calculation of chiroptical data, the absolute sense of twist of the C12–C13 bond of the retinal chromophore in rhodopsin as positive, that is opposite to the one shown in Figure 1, with the 13-methyl group projecting towards the observer.[20] This conformation is the result of the chiral nature of the protein binding pocket.

The planar 11-*cis*-13-demethyl-retinal PSB, with the methyl group in the 13-position missing, stays planar and does not relax into a nonplanar conformation when subjected to the external strain. This agrees with the experimental finding that the chromophore of 13-demethylrhodopsin is less distorted in the region from C10 to C13 than the native chromophore.[9]

The excited state dynamics of the isomerization of 11-*cis*-retinal PSB has been studied recently by Robb and coworkers[21] with high-quality ab initio methods on a model chromophore, 3,5-pentadienal PSB. They found that the initial reaction of the Franck–Condon excited molecule on the S_1 surface is dominated by in-plane bond stretching before torsion of the molecule around the central *cis*-configured double bond sets in, followed by fast decay via a conical intersection. These calculations provide for the first time a realistic model including a time estimate for the photoisomerization of rhodopsin. A puzzle remains, however, which concerns the role of the methyl group: except for a slightly steeper initial slope at the beginning of the dynamic almost no acceleration was found in the α-methyl-substituted model compound compared to the unsubstituted one.

We have studied the effect of methyl substitution and dihedral distortion on this chromophore using ab initio molecular dynamics (AIMD). In this method quantum-mechanically derived forces are used to integrate Newton's equations of motion in the full space of $3N-6$ internal coordinates on the Born–Oppenheimer potential energy surface.[22] The successful application to ground-state dynamics has been described recently.[23] Our quantum-mechanical treatment of the excited state is essentially the same as Robb's, and so the results are directly comparable. The systems we have studied are shown in Scheme 2: ① is the parent PSB, twisted about the central C3–C4 bond by 10°, in ② there is an additional twist of 10° about the C2–C3 bond, ③ and ④ are the corresponding α-methyl-substituted derivatives, and ⑤ is the dimethyl derivative with dihedral angles taken from the central part of the strained 11-*cis*-retinal PSB



	R^1	R^2	Θ_1	Θ_2
①	H	H	10°	0°
②	H	H	10°	−170°
③	CH_3	H	10°	0°
④	CH_3	H	10°	−170°
⑤	CH_3	CH_3	14°	−167°

Scheme 2. Substitution pattern and starting geometries (dihedral angles Θ_1 and Θ_2) of the five pentadienal PSBs of this study.

shown in Figure 1. Except for ⑤ all systems were geometry-optimized in the ground state with only the dihedral angles shown kept constant. After excitation to the S_1 surface the trajectory was followed for simulation times between 50 and 80 fs.

The results are shown in Figure 2, where the change of the central dihedral angle Θ_1 is plotted against the simulation time. All systems need a certain amount of time before the

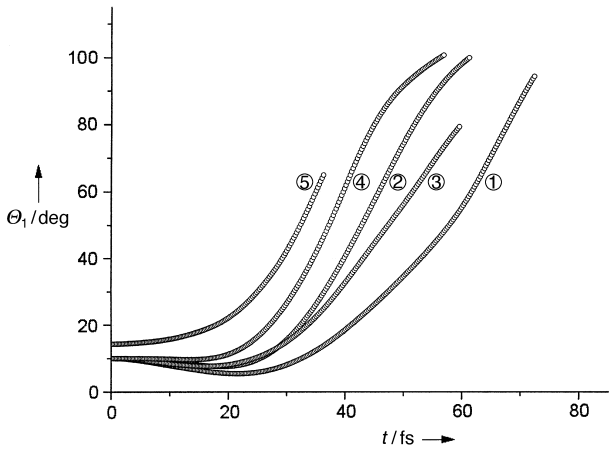


Figure 2. Comparison of the excited state dynamics of the five dienal PSBs of Scheme 2. The plot shows how the dihedral angle Θ_1 of the central double bond changes as a function of time.

torsional mode is activated; however, there are significant differences. The unsubstituted singly twisted PSB ① needs 62 fs to reach an (arbitrary) twist angle of 60°; this time is comparable to the one calculated by Robb[21c] for the same system. The additional twist in ② accelerates the torsion more (60° reached after 46 fs) than the α-methyl group in ③ with which this torsion is reached after 52 fs. When the doubly twisted PSB is methyl-substituted in the α-position we observe the strong rate acceleration in accord with the experimental evidence: ④ and ⑤ need only 39 and 35 fs, respectively, for the 60° torsion angle. Comparison of the latter two reveals in addition that the second methyl substituent (which stands for the C9 methyl group in retinal) is of less influence on the dynamics of the molecule than the higher initial torsion.

 © WILEY-VCH Verlag GmbH, D-69451 Weinheim, 2000 1433-7851/00/3915-2785 $ 17.50+.50/0

The reason for the fast photoisomerization of ④ and ⑤ is the rotation about the C3–C4 and the C2–C3 bonds in opposite directions (Figure 3) coupled very efficiently by the α-methyl group: in the excited state the double-bond character is shifted from the C3–C4 bond to the C2–C3 (and the

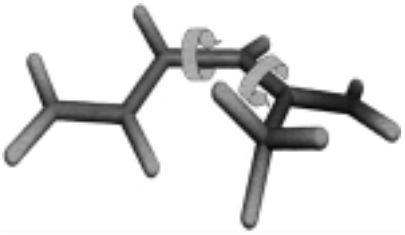


Figure 3. Coupled rotation about the C2–C3 and the C3–C4 bonds of the Schiff base ④ in the electronically excited state. The molecule is shown 20 fs into the simulation when the twist about both bonds as indicated by the two arrows has gained already considerable momentum.

C4–C5) bond. As a consequence the twisted CH_3-C2-N^+ fragment begins to rotate back into the plane of the C2–C3 bond with the methyl group pushing against the hydrogen atom at C5. Because the C3–C4 bond is torsionally softened this leads to a rapid increase of the twist of this bond. In effect the methyl group acts as a lever to set the inherently slow torsion of the central bond into motion, with the electronic excitation acting as a release mechanism.

We have shown that the photoisomerization of a short methyl-substituted pentadienal PSB twisted in a specific way that corresponds to the probable conformation of the 11-*cis*-12-s-*trans*-retinal PSB in rhodopsin is significantly enhanced over the unsubstituted PSB. Moreover, our calculations have shown that this conformation does not need a specific protein–chromophore interaction, but is realized as a result of a very general externally applied strain. Whether methyl torsion is sufficient to bring about fast excited state isomerization of larger rhodopsin models is the subject of on-going investigations.

Received: December 10, 1999
Revised: June 6, 2000 [Z14383]

[1] a) R. Hubbard, A. Kropf, *Proc. Natl. Acad. Sci. USA* **1958**, *44*, 130; b) T. Yoshizawa, G. Wald, *Nature* **1963**, *197*, 1279.
[2] W. K. Chan, K. Nakanishi, T. G. Ebrey, B. Honig, *J. Am. Chem. Soc.* **1974**, *96*, 3642.
[3] S. W. Lin, M. Groesbeek, I. van der Hoef, P. Verdegem, J. Lugtenburg, R. A. Mathies, *J. Phys. Chem.* **1998**, *102*, 2787.
[4] For a summary, see B. Honig, A. Warshel, M. Karplus, *Acc. Chem. Res.* **1975**, *8*, 92; see also B. Honig, P. Kahn, T. G. Ebrey, *Biochemistry* **1973**, *12*, 1637.
[5] P. J. E. Verdegem, P. H. M. Bovee-Geurts, W. J. de Grip, J. Lugtenburg, H. J. M. de Groot, *Biochemistry* **1999**, *38*, 11316.
[6] P. J. E. Verdegem, M. Helmle, J. Lugtenburg, H. J. M. de Groot, *Biochemistry*, in press.
[7] a) R. W. Schoenlein, L. A. Peteanu, R. A. Mathies, C. V. Shank, *Science* **1991**, *254*, 412; b) Q. Wang, R. W. Schoenlein, L. A. Peteanu, R. A. Mathies, C. V. Shank, *Science* **1994**, *266*, 422.
[8] W. Gärtner, S. Ternieden, *J. Photochem. Photobiol. B* **1996**, *33*, 83.
[9] G. G. Kochendoerfer, P. J. E. Verdegem, I. van der Hoef, J. Lugtenburg, R. A. Mathies, *Biochemistry* **1996**, *35*, 16230.
[10] D. Koch, W. Gärtner, *Photochem. Photobiol*. **1997**, *65*, 181.
[11] F. Terstegen, V. Buss, *J. Mol. Struct. (Theochem)* **1996**, *369*, 53.
[12] M. Garavelli, F. Negri, M. Olivucci, *J. Am. Chem. Soc.* **1999**, *121*, 1023.
[13] a) R. D. J. Froese, I. Komaromi, K. S. Byun, K. Morokuma, *Chem. Phys. Lett.* **1997**, *272*, 335; b) F. Terstegen, V. Buss, *J. Mol. Struct. (Theochem)* **1998**, *430*, 209.
[14] A. Bifone, H. J. M. de Groot, F. Buda, *Chem. Phys. Lett.* **1996**, *248*, 165.
[15] The chromophore is not perfectly planar, because the geometry of 11-*cis*-retinal PSB was reoptimized by the same molecular dynamics procedure used later for relaxing the bent structure. The reoptimized geometry showed dihedral angles differing from 0 or from 180° by less than 2°, except for the C10–C11 bond (2.0°) and the C15–N^+ bond (3.2°).
[16] For the molecular dynamics calculations the Vienna ab initio simulation package (VASP) was used which is a program designed for molecular dynamics simulations based on density functional theory (DFT) (G. Kresse, J. Furthmüller, *Phys. Rev. B* **1996**, *54*, 11169). We used Vanderbilt's ultrasoft inner core pseudo-potentials and treated the valence electrons in a plane-wave basis set with an energy cut-off of 261.072 eV. The calculations were performed in a periodic boundary box of $24 \times 18 \times 13$ Å^3 with a background charge of $-e$, and the time step was 0.5 fs.
[17] Note that these results, including the 200 fs time reference, relate to ground-state structural optimization and not to the excited state dynamics of the molecule!.
[18] A. Bifone, H. J. M. de Groot, F. Buda, *Pure Appl. Chem.* **1997**, *69*, 2105.
[19] A. Bifone, H. J. M. de Groot, F. Buda, *J. Phys. Chem. B* **1997**, *101*, 2954.
[20] V. Buss, K. Kolster, F. Terstegen, R. Vahrenhorst, *Angew. Chem*. **1998**, *110*, 1997; *Angew. Chem. Int. Ed.* **1998**, *37*, 1893. For a differing viewpoint, see Q. Tan, J. Lou, B. Borhan, E. Karnaukhova, N. Berova, K. Nakanishi, *Angew. Chem*. **1997**, *109*, 2190; *Angew. Chem. Int. Ed.* **1997**, *36*, 2089.
[21] a) M. Garavelli, P. Celani, F. Bernardi, M. A. Robb, M. Olivucci, *J. Am. Chem. Soc.* **1997**, *119*, 6891; b) M. Garavelli, F. Bernardi, M. Olivucci, T. Vreven, S. Klein, P. Celani, M. A. Robb, *Faraday Discuss.* **1998**, *110*, 51; c) T. Vreven, F. Bernardi, M. Garavelli, M. Olivucci, M. A. Robb, H. B. Schlegel, *J. Am. Chem. Soc.* **1997**, *119*, 12687.
[22] a) D. A. Gibson, I. V. Ionova, E. A. Carter, *Chem. Phys. Lett*. **1995**, *240*, 261; b) Z. Liu, L. E. Carter, E. A. Carter, *J. Phys. Chem*. **1995**, *99*, 4355; c) D. A. Gibson, E. A. Carter, *Chem. Phys. Lett*. **1997**, *271*, 266; d) A. J. R. da Silva, H.-Y. Cheng, D. A. Gibson, K. L. Sorge, Z. Liu, E. A. Carter, *Spectrochim. Acta Part A* **1997**, *53*, 1285.
[23] a) F. Terstegen, E. A. Carter, V. Buss, *Int. J. Quantum Chem.* **1999**, *75*, 141; b) S. Falzewski, F. Terstegen, V. Buss, *Chem. Phys.* **1999**, *243*, 179.

 © WILEY-VCH Verlag GmbH, D-69451 Weinheim, 2000 1433-7851/00/3915-2786 $ 17.50+.50/0